BIJOAK 349(1) 1–384 2000 • ISSN 0264-6021
Volume 349 • Part 1 • 1 July 2000

BIOCHEMICAL JOURNAL

review

DNA replication and damage checkpoints and meiotic cell cycle controls in the fission and budding yeasts

by H. Murakami
and P. Nurse

Biochemical Journal
VOL: 349
Part: 1,2
July
2000

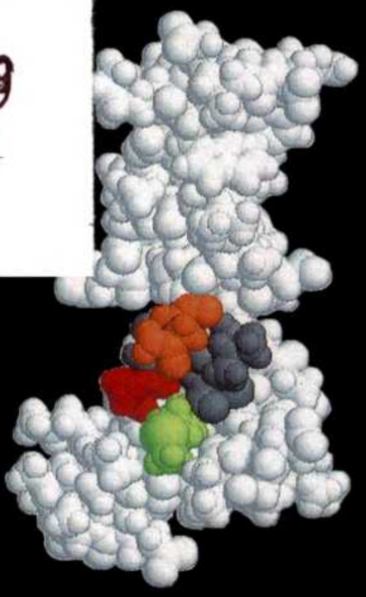

Available 1 week earlier on the Internet

The Biochemical Society, London © 2000

Essays in Biochemistry from Portland Press

Portland Press

Essays in Biochemistry: Molecular Trafficking

Edited by P Bernstein, The Journal of Experimental Medicine, New York, USA

1 85578 131 X Paperback July 2000 200 pages £19.00

This volume of Essays in Biochemistry is a collection of review articles describing how molecules (proteins and nucleic acids) are targeted to, and transported across, various membrane-bound organelles within eukaryotic cells.

The 1999 Nobel Prize in Physiology or Medicine was awarded to Dr Gunter Blobel "for the discovery that proteins have intrinsic signals that govern their transport and localization in the cell". The award acknowledges the importance of the study of how newly synthesized protein and RNA find their correct destination within the cell. This volume summarises advances being made in this field of research.

Students (and their teachers) who are undertaking advanced studies in cell biology will find this book extremely useful.

Essays in Biochemistry: Molecular Motors

Edited by SJ Higgins, University of Leeds, UK and G Banting, University of Bristol, UK

1 85578 103 4 Paperback March 2000 200 pages £19.00

Biological systems abound with examples of molecular motors — biological machines for converting the chemical energy of ATP into mechanical movement by cells — they play pivotal roles in diverse cellular function.

This volume, covers many of the most exciting developments in the field.

- All of the main motor systems are featured, giving wide coverage.
- Consists of short punchy review articles, making it easy to read.
- The application of gene-cloning methods and the recent advances are described.
- Human disorders involving defects in molecular motor systems such as hearing loss and heart disease are covered.

The Nobel Prize for Chemistry was awarded to John Walker and Paul Boyer in 1997 for their work in elucidating the mechanism of the rotary generator of ATP in the mitochondrion, the F_1-ATPase. This brought the new developments in the field of molecular motors to the attention of the whole scientific community and, via the media, to a wider world audience.

This volume aims to inspire young scientists to want to work in this area.

Essays in Biochemistry: Metalloproteins

Edited by D Ballou, University of Michigan, USA

1 85578 106 9 Paperback July 1999 200 pages £19.00

Metals are involved in most segments of the chemistry of life, including respiration, numerous steps of metabolism, photosynthesis, nitrogen fixation, nerve transmission, signal transduction, muscle contraction, oxygen transport and protection from xenobiotic compounds. In addition, metals are used in medicine as therapeutic agents. This volume describes many of the roles of metals in a variety of circumstances that are used widely in biology.

The 12 chapters of this volume are written by several of the best-known experts in their specialities.

Essays in Biochemistry: Gene Regulation

Edited by K Chapman, The University of Edinburgh, UK

1 85578 138 7 Paperback October 2000 200 pages £19.00

Contents: Transcriptional regulation, a unifying mechanism, M Ptashne and A Gann; Regulation of eukaryotic transcription initiation, G Gill; Activation and repression of transcription initiation in bacteria, G Lloyd, P Landini and S Busby; Signalling from the cell surface to the nucleus, M Lee and S Goodbourn; Cell cycle control of transcriptional activity, N La Thangue and N Shikama; Transcriptional regulation in the context of chromatin structure, A Wolffe; Methylation in the control of gene expression in vertebrate development, R Meehan and I Stancheva; Translational control in the regulation of gene expression, C Proud; Cellular choices: to die or not to die, D Harrison; Future perspectives, N Hastie

Orders:

www.portlandpress.com/books/orderinfo.htm

*Portland Press, Commerce Way,
Colchester, CO2 8HP
t: 01206 796351
f: 01206 799331
e: sales@portlandpress.com

Please add £2.50 per book to a maximum of £7.50

In the USA and Canada
Princeton University Press
c/o California/Princeton Fulfillment Services, Inc
1445 Lower Ferry Road,
Ewing, New Jersey 08618
t: 1-800-777-4726
f: 1-800-999-1958
e: orders@cpfs.pupress.princeton.edu

Postage: Please add $3.75 for first book and $1.00 for each additional book

BXS/0500/E

Biochemistry

The Biochemical Society, London © 2000

Biochemical Journal

Volume 349, part 1
1 July 2000

First published on the Internet
26 June 2000
http://www.BiochemJ.org

CULK-H04425-2-P32197

Editorial Board

Chairman
P. J. Parker • London

Deputy Chairmen
G. E. Blair • Leeds
D. N. Brindley • Edmonton
R. A. J. Challiss • Leicester
P. Ferré • Paris
J. T. Gallagher • Manchester
R. A. John • Cardiff
H. Nagase • London
J. D. Pearson • London
M. H. Rider • Bruxelles
S. B. Shears • Research Triangle Park

Reviews Editor
R. D. Burgoyne • Liverpool

Managing Editor
P. J. Starley

Deputy Managing Editor
S. E. Dilley

Senior Staff Editor
S. M. Hobday

Staff Editors
L. Johnson
W. J. Watkins
M. R. Thorne
N. B. Prowse
S. J. Cubie

Editorial Assistants
N. J. Lamb
C. L. Jeeves

R. L. P. Adams (Glasgow)
J.-W. N. Akkerman (Utrecht)
D. R. Alessi (Dundee)
D. Attaix (Ceyrat)
S. A. Baldwin (Leeds)
F. J. Ballard (Adelaide)
G. J. Barritt (Adelaide)
N. C. Bruce (Cambridge)
A. Clerk (London)
G. M. Cohen (Leicester)
P. Crine (Montreal)
D. Cutler (London)
D. A. Day (Nedlands)
H. Deckmyn (Kortrijk)
K. Docherty (Aberdeen)
B. K. Drøbak (Norwich)
J. M. East (Southampton)
K. R. F. Elliott (Manchester)
B. Engelmann (Munich)
C. Forest (Meudon)
M. J. Fry (Reading)
A. Galione (Oxford)
D. A. F. Gillespie (Glasgow)
S. Goodbourn (London)
G. W. Gould (Glasgow)
S. V. Graham (Glasgow)
S. Gutteridge (Newark, DE)
Y. A. Hannun (Charleston)

P. I. Haris (Leicester)
M. M. Harnett (Glasgow)
J. D. Hayes (Dundee)
P. C. Heinrich (Aachen)
R. Heinrich (Berlin)
B. Henrissat (Marseille)
R. C. Hider (London)
S. High (Manchester)
M. B. Hodgins (Glasgow)
D. Hoekstra (Groningen)
N. M. Hooper (Leeds)
E. F. Hounsell (London)
W. Jessup (Sydney)
J. P. Kehrer (Austin)
K. I. Kivirikko (Oulu)
B. L. Knight (London)
R. G. Knowles (Stevenage)
H. Kresse (Münster)
P. W. Kuchel (Sydney)
C. MacKintosh (Dundee)
A. I. Magee (London)
T. J. Mantle (Dublin)
P. Maurel (Montpellier)
A. J. Meijer (Amsterdam)
F. Michelangeli (Birmingham)
G. Milligan (Glasgow)
B. P. Morgan (Cardiff)
J. S. Mort (Montreal)

S. E. Moss (London)
K. J. Murray (Harlow)
A. C. Newby (Bristol)
F. Paltauf (Graz)
N. J. Pyne (Glasgow)
C. I. Ragan (Windlesham)
P. R. Rich (London)
N. J. P. Ryba (Bethesda)
G. Salvesen (San Diego)
M. F. Scully (London)
S. Shenolikar (Durham, NC)
A. G. Smith (Cambridge)
M. C. Sugden (London)
P. H. Sugden (London)
R. Sundler (Lund)
J. M. Tavaré (Bristol)
K. F. Tipton (Dublin)
M. A. Titheradge (Brighton)
A. B. Tobin (Leicester)
S. A. Tooze (London)
W. J. van Blitterswijk (Amsterdam)
R. Virden (Newcastle upon Tyne)
H. M. Wallace (Aberdeen)
M. P. Walsh (Calgary)
L. A. Witters (Hanover)
J. F. Woessner (Miami)
S. J. Yeaman (Newcastle upon Tyne)
S. Yoshikawa (Akoh-Hyogo)

- The *Biochemical Journal* (ISSN 0264-6021 for print journal; ISSN 1470-8728 for online journal) is published and distributed by Portland Press Ltd on behalf of the Biochemical Society, and appears twice monthly.
- **Editorial and publishing offices:** *Biochemical Journal*, 59 Portland Place, London W1N 3AJ, U.K.
- Royal Mail International, c/o Yellowstone International, 87 Burlews Court, Hackensack, NJ 07061, U.S.A.
- **Subscriptions department:** Portland Press Ltd, P.O. Box 32, Commerce Way, Colchester CO2 8HP, U.K.

- All rights reserved. Apart from any fair dealing for the purposes of research or private study, or criticism or review, as permitted under the Copyright, Designs and Patents Act, 1988, this publication may be reproduced, stored or transmitted, in any forms or by any means, only with the prior permission in writing of the publishers, or in the case of reprographic reproduction in accordance with the terms of permissions granted by copyright clearing houses such as the Copyright Licensing Agency (U.K.) or the Copyright Clearance Center (U.S.A.). The CCC item-fee code for this publication is 0264-6021/2000/$16.00+0.00. Inquiries concerning reproduction outside those terms should be sent to the publishers at the above-mentioned address.
- Although, at the time of going to press, the information contained in this publication is believed to be correct, neither the authors nor the editors nor the publisher assume any responsibility for any errors or omissions herein contained.

- Periodicals postage paid at Rahway, NJ, and at additional mailing offices.
- **Postmaster:** send address changes to *Biochemical Journal*, c/o Mercury International, 365 Blair Road, Avenel, NJ 07001.
- **Cover illustration:** Space-filling representation of the solvent accessible structure of human epidermal growth factor [see van de Poll et al. (2000) Biochem. J. **349**, 267–274, and http://www.BiochemJ.org/349/bj3490267add.htm].

Instructions to Authors

● **General policy** The *Biochemical Journal* publishes papers in English in all fields of biochemistry and cellular and molecular biology, provided that they make a sufficient contribution to biochemical knowledge. Papers may include new results obtained experimentally, descriptions of new experimental methods of biochemical importance, or new interpretations of existing results. Novel theoretical contributions will be considered equally with papers dealing with experimental work. All work presented should have as its aim the development of biochemical concepts rather than the mere recording of facts. Preliminary, confirmatory or inconclusive work will not be published. The *Biochemical Journal* will not publish material that has been wholly or largely published elsewhere, even as a preliminary communication or in unrefereed symposium proceedings or on the World Wide Web (WWW); equally, fragmentation of research into the 'least publishable unit' is discouraged.

Submission of a paper implies that it has been approved by all the named authors, that all persons entitled to authorship have been so named, that it reports unpublished work that is not under consideration elsewhere, and that if the paper is accepted for publication the authors will transfer to the Biochemical Society the copyright in the paper, which will then not be published elsewhere in the same form, in any language, without the consent of the Society. Authors will be required to sign an undertaking to these effects.

Authors may suggest potential reviewers for their papers, but the journal is under no obligation to follow such suggestions. Authors may also specify the names of those they wish to be excluded from the review process, and such wishes are usually respected unless, in the opinion of the journal, such a request unreasonably excludes all the expertise available to it in that scientific area.

To allow the reviewers to assess possible overlap with previous work, all submitted papers must be accompanied by duplicate copies of the author's relevant published work, including that on the WWW, and of all related papers in press or under editorial consideration in this or other journals.

The paragraphs below are a summarized version of the journal's complete Instructions to Authors (see http://www.BiochemJ.org), copies of which are available free of charge from the editorial office.

The following types of paper are included in the journal.

Research Papers are the normal form of publication, and may be of any length that is justified by their content. However, because of pressure for space in the journal, no paper, whatever its scientific merits, will be accepted if it exceeds the minimum length required for precision in describing the experiments and clarity in interpreting them. As a guide, most Research Papers published in the *Biochemical Journal* are of between six and eight printed pages. A concise well-written paper tends to be published more rapidly.

Research Communications are short (maximum four printed pages) papers bringing particularly novel and significant findings to the attention of the research community. It is intended that a decision on acceptance or rejection will be made within 10 working days of receipt, and publication of accepted Communications will follow within 2 months. Research Communications receive full but accelerated reviewing. The criteria of 'novelty and significance' are strictly enforced, and papers may be rejected solely on the grounds of lack of novelty and significance. Communications are not a path to accelerated publication of sound but non-urgent material. Authors must include in their letter of submission a brief statement of why they believe their Communication merits accelerated treatment. Papers reporting nucleotide sequences only are not acceptable as Research Communications. One colour figure will be published free of charge in Research Communications; subsequent figures will cost £300 each.

Reviews will usually be solicited, although unsolicited reviews will be considered for publication. Prospective writers of reviews should first consult the Reviews Editor, via the editorial office, and should enclose a short (one typed page) summary of the area they propose to cover.

● **Procedure for submission** Before preparing papers for the journal, authors should consult a current issue to make themselves familiar with the general format, such as the use of cross-headings, layout of tables and figures and citation of references. A full page of text in the *Biochemical Journal* contains approximately 1200 words; when calculating the printed length of papers, allowance must be made for the space occupied by tables and figures and the number of text words reduced accordingly.

The numerical system of references must be used. A reference to 'unpublished work' must be accompanied by the names of all persons concerned; a reference to a 'personal communication' must be supported by written permission for the quotation from the person or persons concerned; both of these types of citation are permitted in the text only, not in the list of references.

Three copies of the typescript (four copies for Research Communications), with a brief covering letter to which should be attached an additional copy of the synopsis, should be sent to: **The Managing Editor, *Biochemical Journal*, 59 Portland Place, London W1N 3AJ, U.K.** (telephone 020 7637 5873; fax 020 7323 1136; from overseas the international code for the U.K. is 44 and the leading 0 should be omitted; e-mail editorial@portlandpress.com).

The typescript should indicate the name, address, telephone number, fax number and e-mail address of the person to whom all correspondence should be addressed. The top copy of the typescript should be marked as such and should have attached to it the original figures; for the other copies of the typescript, glossy prints (not photocopies) of the half-tone figures should be provided, but photocopies of line drawings will suffice. A short (page-heading) title of not more than 75 characters and a maximum of five key words that do not appear in the title, should be provided.

● **Submission by fax** Research Communications that do not contain half-tone or colour figures may be submitted by fax to the number above. Only one copy of the typescript need be transmitted. The current Instructions to Authors contains full details of this procedure.

● **Electronic submission** Manuscripts may be submitted as a **single** Adobe Acrobat PDF file either: (i) as a uuencoded attachment to the e-mail address: editorial@portlandpress.com; or (ii) uploaded to the ftp site: ftp.portlandpress.com in the directory /incoming/BiochemJ [N.B. Authors using route (ii) are advised to alert us to any incoming documents via our regular e-mail address.]

● **Colour figures** The first colour figure is published at no charge provided that one author has been a member of the Biochemical Society for at least 2 years and that the use of colour is deemed scientifically necessary by the reviewers. Subsequent colour figures in the same paper cost £300 each.

● **Multimedia adjuncts** The Biochemical Journal Online is now able to offer authors the opportunity to enhance their papers with multimedia adjuncts (e.g. time-lapse movies, three-dimensional structures). These will be submitted to peer review alongside the manuscript. To submit a paper with a multimedia adjunct, please contact the Managing Editor (editorial@portlandpress.com). There is no extra charge associated with the publication of a multimedia adjunct online.

● **Use of authors' diskettes** Authors should submit diskettes of revised articles to the editorial office. Every effort will be made to use the diskette during typesetting, but this cannot be guaranteed. Authors must ensure that files have been updated to incorporate all revisions, and hence that the version on the diskette matches the revised hard copy. Our preferred word-processing format is Word for Windows version 6. Submission of manuscripts in other word-processing formats may lead to delays in processing. The diskette should be accompanied by a covering letter specifying manuscript number, operating system and software program. Files should be formatted double-spaced with no hyphenation and automatic wordwrap (no hard returns within paragraphs).

Other information

P 32197

The *Biochemical Journal* is published and distributed by Portland Press Ltd on behalf of the Biochemical Society. It is published twice monthly; in 2000 volumes 345–352 (three parts each) will appear. The subscription also includes an author and key-word index.

● **Subscription rates** Institutional subscription rates for 2000 are shown below. Subscribers to the *Biochemical Journal* can subscribe additionally to *Biochemical Society Transactions* and *Biotechnology and Applied Biochemistry* on a joint subscription at a reduced rate. Terms are cash with order (US$ in N. America, £ sterling for rest of the world, or US$ equivalent at current rate of exchange; subscribers in the EU may pay in £ sterling or Euros), or against pro forma invoice. Orders should be sent to the address below, or through your usual agent.

	N. America	Rest of world	Euro price
One yr (8 vols)	US$1950	£1110	€1776
Single issues	US$97	£56	€90

Dollar prices include airspeeded delivery. Sterling and Euro prices include airspeeded delivery in Europe and delivery by surface mail elsewhere. Airspeeded delivery is available to countries other than America and Europe at an additional cost of £50.

● **Biochemical Journal Online** Access to the Biochemical Journal Online is restricted to institutions that have a subscription to the print version. It will be free to such institutions during 2000. URL: http://www.BiochemJ.org

● **Microfiche and back issues** Volumes 102–296 of the *Biochemical Journal* are available on microfiche. Back issues are also available. Further details may be obtained from the address below.

● **Subscription department**

Portland Press Ltd
P.O. Box 32, Commerce Way
Colchester CO2 8HP, Essex, U.K.
(telephone 01206 796351; fax 01206-799331; e-mail sales@portlandpress.com).

● **Advertising** Advertising is accepted in the *Biochemical Journal*. For information contact the Advertising Department, Portland Press Ltd, 59 Portland Place, London W1N 3AJ (telephone 020 7580 5530; fax 020 7323 1136; e-mail editorial@portlandpress.com).

Biochemical Journal
Volume 349, part 1
1 July 2000
First published on the Internet
26 June 2000
http://www.BiochemJ.org

Review

DNA replication and damage checkpoints and meiotic cell cycle controls in the fission and budding yeasts
***by* H. Murakami and P. Nurse** 1–12

Research Communication

Regulation of sterol regulatory-element binding protein 1 gene expression in liver role of insulin and protein kinase B/cAkt	M Fleischmann and P.B. Iynedjian	13–17

Research Papers

Activation of extracellular signal-regulated protein kinase1,2 results in down-regulation of decorin expression in fibroblasts	P Laine, N Reunanen, L Ravanti, M Foschi, M. Santra, R V Iozzo and V-M Kahari	19–25
Characterization and regulation of *Leishmania major* 3-hydroxy-3-methylglutaryl-CoA reductase	A. Montalvetti, J Peña-Díaz, R Hurtado, L M. Ruiz-Pérez and D González-Pacanowska	27–34
Oxidation of ubiquinol by peroxynitrite implications for protection of mitochondria against nitrosative damage	F Schopfer, N. Riobó, M.C. Carreras, B. Alvarez, R. Radi, A Boveris, E Cadenas and J.J. Poderoso	35–42
Acylphosphatase possesses nucleoside triphosphatase and nucleoside diphosphatase activities	P. Paoli, G. Camici, G. Manao, E Giannoni and G Ramponi	43–49
Processing of N-linked oliosaccharide depends on its location in the anion exchanger, AE1, membrane glycoprotein	J. Li, J Quilty, M. Popov and R.A F Reithmeier	51–57
Activation of phosphatidylinositol 3-kinase is required for transcriptional activity of F-type 6-hosphofructo-2-kinase/fructose-2,6-sphosphatase assessment of the role of protein nase B and p70 S6 kinase	S F. Fernández de Mattos, E de los Pinos, M Joaquin and A Tauler	59–65
entification of a nucleoside/nucleobase ansporter from *Plasmodium falciparum*, a novel rget for anti-malarial chemotherapy	M.D. Parker, R J Hyde, S Y.M. Yao, L McRobert, C.E Cass, J D Cass, J.D. Young, G.A McConkey and S A Baldwin	67–75
polipoprotein E includes a binding site which is cognized by several amyloidogenic polypeptides	M H Baumann, J. Kallijarvi, H Lankinen, C. Soto and M. Haltia	77–84
dox equilibria of manganese peroxidase from *anerochaetes chrysosporium* functional role of sidues on the proximal side of the haem pocket	R Santucci, C Bongiovanni, S Marini, R Del Conte, M. Tien, L Banci and M Coletta	85–90
ucocorticoids induce a near-total suppression of aluronan synthase mRNA in dermal fibroblasts d in osteoblasts a molecular mechanism ntributing to organ atrophy	W. Zhang, C E Watson, C Liu, K J Williams and V P Werth	91–97
ndirect induction of suppressor of cytokine signalling-1 in macrophages stimulated with acterial lipopolysaccharide partial role of utocrine/paracrine interferon-α/β	A Crespo, M.B Filla, S.W Russell and W.J. Murphy	99–104
haracterization of the actin filament capping ate in human erythrocyte ghost and cytoskeletal eparations	P.A Kuhlman	105–111

$p40^{phox}$ participates in the activation of NADPH oxidase by increasing the affinity of $p47^{phox}$ for flavocytochrome b_{558}	A R Cross	**113–117**
Mitochondrial ATP production is necessary for activation of the extracellular-signal-regulated kinases during ischaemia/reperfusion in rat myocyte-derived H9c2 cells	L Abas, M.A. Bogoyevitch and M Guppy	**119–126**
The role of phosphatidylcholine in fatty acid exchange and desaturation in *Brassica napus* L leaves	J.P. Williams, V Imperial, M.U Khan and J.N Hodson	**127–133**
The short prodomain influences caspase-3 activation in HeLa cells	T. Meergans, A-K Hildebrandt, D Horak, C. Haenisch and A Wendel	**135–140**
Expression, purification and characterization of recombinant human choline acetyltransferase phosphorylation of the enzyme regulates catalytic activity	T Dobransky, W L Davis, G.-H Xiao and R.J Rylett	**141–151**
Idenitification and characterization of a novel cytochrome c_3 from *Shewanella frigidimarina* that is involved in Fe(III) respiration	E.H.J Gordon, A.D. Pike, A E Hill, P M. Cuthbertson, S.K. Chapman and G A. Reid	**153–158**
Identification of three human type-II classic cadherins and frequent heterophilic interactions between different subclasses of type-II classic cadherins	Y Shimoyama, G Tsujimoto, M Kitajima and M Natori	**159–167**
The pepsin residue glycine-76 contributes to active-site loop flexibility and participates in catalysis	M. Okoniewska, T. Tanaka and R.Y. Yada	**169–177**
Reconstitution of purified, active and malonyl-CoA-sensitive rat liver carnitine palmitoyltransferase I: relationship between membrane environment and malonyl-CoA sensitivity	J D McGarry and N F. Brown	**179–187**
Lithocholic acid and sulphated lithocholic acid differ in the ability to promote matrix metalloproteinase secretion in the human colon cancer cell line CaCo-2	B Halvorsen, A C Staff, S Ligaarden, K Prydz and S.O Kolset	**189–193**
Pyruvate dehydrogenase kinase from *Arabidopsis thaliana*. a protein histidine kinase that phosphorylates serine residues	J J Thelen, J.A. Miernyk and D D. Randall	**195–201**
Unifying mechanism for *Aplysia* ADP-ribosyl cyclase and CD38/NAD$^+$ glycohydrolases	C. Cakir-Kiefer, H Muller-Steffner and F Schuber	**203–210**
Investigation of the slow inhibition of almond β-glucosidase and yeast isomaltase by 1-azasugar inhibitors evidence for the 'direct binding' model	A Lohse, T Hardlei, A. Jensen, I.W. Plesner and M Bols	**211–215**
Interaction of C3b$_2$–IgG complexes with complement proteins properdin, factor B and factor H implications for amplification	E. Jelezarova, A Vogt and H.U. Lutz	**217–223**
Epidermal growth factor regulation of glutathione S-transferase gene expression in the rat is mediated by class PI glutathione S-transferase enhancer I	M Matsumoto, M Imagawa and Y Aoki	**225–230**
Low-density lipoprotein activates the small GTPases Rap1 and RAl in human platelets	C M Hackeng, B. Franke, I A M Relou, G. Gorter, J L Bos, H J M van Rijn and J-W N Akkerman	**231–238**
Regulation of ecdysteroid signalling molecular cloning, characterization and expression of 3-dehydroecdysone 3α-reductase, a novel eukaryotic member of the short-chain dehydrogenases/reductases superfamily from the cotton leafworm, *Spodoptera littoralis*	H. Takeuchi, J.-H Chen, D.R. O'Reilly, H H Rees and P C Turner	**239–245**
Definition of Munc13-homology-domains and characterization of a novel ubiquitously expressed Munc13 isoform	H. Koch, K. Hofmann and N. Brose	**247–253**
FM1-43 reports plasma membrane phospholipid scrambling in T-lymphocytes	A Zweifach	**255–260**

A single amino acid substitution (Trp^{666}→Ala) in the interbox1/2 region of the interleukin-6 signal transducer gp130 abrogates binding of JAK1, and dominantly impairs signal transduction	C Haan, H M. Hermanns, P C Heinrich and I. Behrmann	**261–266**
Non-linear antigenic regions in epidermal growth factor (EGF) and transforming growth factor (TGFα) studied by EGF–TGFα—chimaeras	M L M van de Poll, W. van Rotterdam, M.M Gadellaa, C Stortelers, M.J H. van Vugt and E.J J van Zoelen	**267–274**
Kinetic properties of missense mutations in patients with glutathione synthetase deficiency	R Njålsson, K. Carlsson, B Olin, B. Carlsson, L Whitbread, G Polekhina, M.W. Parker, S Norgren, B Mannervik, P.G. Board and A. Larsson	**275–279**
Targeting motifs and functional parameters governing the assembly of connexins into gap junctions	P E.M. Martin, J. Steggles, C Wilson, S. Ahmad and W H Evans	**281–287**
Heterologous expression, functional characterization and localization of two isoforms of the monkey iron transporter Nramp2	L Zhang, T Lee, Y Wang, T W. Soong	**289–297**
Oligomerization of β-amyloid of the Alzheimer's and the Dutch-cerebral-haemorrhage types	A K Sian, E.R. Frears, O.M A El-Agnaf, B P Patel, M F Manca, G. Siligardi, R Hussain and B M Austen	**299–308**
Oxalate oxidases and differentiation surface structure in wheat. germins	B G Lane	**309–321**
Ca^{2+} signals mediated by Ins(1,4,5)P_3-gated channels in rat ureteric myocytes	F-X. Boittin, F. Coussin, J.-L Morel, G Halet, N Macrez and J Mironneau	**323–332**
Molecular modelling and site-directed mutagenesis of the inositol 1,3,4,5-tetrakisphosphate-binding pleckstrin homology domain from the Ras GTPase-activating protein GAP1$^{\text{IP4BP}}$	G Cozier, R Sessions, J R Bottomley, J.S. Reynolds and P J Cullen	**333–342**
Identification and expression of NEU3, a novel human sialidase associated to the plasma membrane	E. Monti, M T. Bassi, N Papini, M Riboni, M Manzoni, B Venerando, G. Croci, A Preti, A Ballabio, G Tettamanti and G Borsani	**343–351**
Impaired nitric oxide production in coronary endothelial cells of the spontaneously diabetic BB rat is due to tetrahydrobiopterin deficiency	C J Meininger, R S. Marinos, K. Hatakeyama, R Martinez-Zaguilan, J.D. Rojas, K.A. Kelly and G Wu	**353–356**
Inhibition of Ca^{2+} signalling by p130, a phospholipase-C-related catalytically inactive protein. critical role of the p130 pleckstrin homology domain	H Takeuchi, M Oike, H F Paterson, V Allen, T Kanematsu, Y. Ito, C. Erneux, M. Katan and M Hirata	**357–368**
Deactivation of neutrophil NADPH oxidase by actin-depolymerizing agents in a cell-free system	M. Tamura, M. Kanno and Y. Endo	**369–375**
Sj-FABPc fatty-acid-binding protein of the human blood fluke *Schistosoma japonicum*. structural and functional characterization and unusual solvent exposure of a portal-proximal tryptophan residue	M W Kennedy, J C Scott, S. Lo, J Beauchamp and D P McManus	**377–384**

Index of Authors

PAGE

Abas, L. 119
Ahmad, S. 281
Akkerman, J.-W. N. 231
Allen, V. 357
Alvarez, B. 35
Aoki, Y. 225
Austen, B. M. 299

Baldwin, S. A. 67
Ballabio, A. 343
Banci, L. 85
Bassi, M. T. 343
Baumann, M. H. 77
Beauchamp, J. 377
Behrmann, I. 261
Board, P.G. 275
Bogoyevitch, M. A. 119
Boittin, F.-X. 323
Bols, M. 211
Bongiovanni, C. 85
Borsani, G. 343
Bos, J. L. 231
Bottomley, J. R. 333
Boveris, A. 35
Brose, N. 247
Brown, N. F. 179

Cadenas, E. 35
Cakir-Kiefer, C. 203
Camici, G. 43
Carlsson, B. 275
Carlsson, K. 275
Carreras, M. C. 35
Cass, C. E. 67
Chapman, S. K. 153
Chen, J.-H. 239
Coletta, M. 85
Coussin, F. 323
Cozier, G. 333
Crespo, A. 99
Croci, G. 343
Cross, A. R. 113
Cullen, P. J. 333
Cuthbertson, P. M. 153

Davis, W. L. 141
Del Conte, R. 85
de los Pinos, E. 59
Dobransky, T. 141

El-Agnaf, O. M. A. 299
Endo, Y. 369
Erneux, C. 357
Evans, W. H. 281

Fernández de Mattos, S. F. 59
Filla, M. B. 99
Fleischmann, M. 13
Foschi, M. 19
Franke, B. 231
Frears, E. R. 299

PAGE

Gadellaa, M. M. 267
Giannoni, E. 43
González-Pacanowska, D. 27
Gordon, E. H. J. 153
Gorter, G. 231
Guppy, M. 119

Haan, C. 261
Hackeng, C. M. 231
Haenisch, C. 135
Halet, G. 323
Haltia, M. 77
Halvorsen, B. 189
Hardlei, T. 211
Hatakeyama, K. 353
Heinrich, P. C. 261
Hermanns, H. M. 261
Hildebrandt, A.-K. 135
Hill, A. E. 153
Hirata, M. 357
Hodson, J. N. 127
Hofmann, K. 247
Horak, D. 135
Hurtado, R. 27
Hussain, R. 299
Hyde, R. J. 67

Imagawa, M. 225
Imperial, V. 127
Iozzo, R. V. 19
Ito, Y. 357
Iynedjian, P. B. 13

Jelezarova, E. 217
Jensen, A. 211
Joaquin, M. 59

Kähäri, V.-M. 19
Kallijärvi, J. 77
Kanematsu, T. 357
Kanno, M. 369
Katan, M. 357
Kelly, K. A. 353
Kennedy, M. W. 377
Khan, M. U. 127
Kitajima, M. 159
Koch, H. 247
Kolset, S. O. 189
Kuhlman, P. A. 105

Laine, P. 19
Lane, B. G. 309
Lankinen, H. 77
Larsson, A. 275
Lee, T. 289
Li, J. 51
Ligaarden, S. 189
Liu, C. 91
Lo, S. 377
Lohse, A. 211

PAGE

Lutz, H. U. 217

Macrez, N. 323
Manao, G. 43
Manca, M. F. 299
Mannervik, B. 275
Manzoni, M. 343
Marini, S. 85
Marinos, R. S. 353
Martin, P. E. M. 281
Martinez-Zaguilan, P. 353
Matsumoto, M. 225
McConkey, G. A. 67
McGarry, J. D. 179
McManus, D. P. 377
McRobert, L. 67
Meergans, T. 135
Meininger, C. J. 353
Miernyk, J. A. 195
Mironneau, J. 323
Montalvetti, A. 27
Monti, E. 343
Morel, J.-L. 323
Muller-Steffner, H. 203
Murakami, H. 1
Murphy, W. J. 99

Natori, M. 159
Njålsson, R. 275
Norgren, S. 275
Nurse, P. 1

Oike, M. 357
Okoniewska, M. 169
Olin, B. 275
O'Reilly, D. R. 239

Paoli, P. 43
Papini, N. 343
Parker, M. D. 67
Parker, M. W. 275
Patel, B. P. 299
Paterson, H. F. 357
Peña-Díaz, J. 27
Pike, A. D. 153
Plesner, I. W. 211
Poderoso, J. J. 35
Polekhina, G. 275
Popov, M. 51
Preti, A. 343
Prydz, K. 189

Quilty, J. 51

Radi, R. 35
Ramponi, G. 43
Randall, D. D. 195
Ravanti, L. 19
Rees, H. H. 239
Reid, G. A. 153
Reithmeier, R. A. F. 51

PAGE

Relou, I. A. M. 231
Reunanen, N. 19
Reynolds, J. S. 333
Riboni, M. 343
Riobó, N. 35
Rojas, J. D. 353
Ruiz-Pérez, M. 27
Russell, S. W. 99
Rylett, R. J. 141

Santra, M. 19
Santucci, R. 85
Schöpfer, F. 35
Schuber, F. 203
Scott, J. C. 377
Sessions, R. 333
Shimoyama, Y. 159
Sian, A. K. 299
Siligardi, G. 299
Soong, T. W. 289
Soto, C. 77
Staff, A. C. 189
Steggles, J. 281
Stortelers, C. 267

Takeuchi, H. 239, 357
Tamura, M. 369
Tanaka, T. 169
Tauler, A. 59
Tettamanti, G. 343
Thelen, J. J. 195
Tien, M. 85
Tsujimoto, G. 159
Turner, P. C. 239

van de Poll, M. L. M. 267
van Rijn, H. J. M. 231
van Rotterdam, W. 267
van Vugt, M. J. H. 267
van Zoelen, E. J. J. 267
Venerando, B. 343
Vogt, A. 217

Wang, Y. 289
Watson, C. E. 91
Wendel, A. 135
Werth, V. P. 91
Whitbread, L. 275
Williams, J. P. 127
Williams, K. J. 91
Wilson, C. 281
Wu, G. 353

Xiao, G.-H. 141

Yada, R. Y. 169
Yao, S. Y. M. 67
Young, J. D. 67

Zhang, L. 289
Zhang, W. 91
Zweifach, A. 255

Biochemical Journal

The Biochemical Society, London © 2000

Volume 349, 2000

Editorial Board

Chairman
P. J. Parker • London

Deputy Chairmen
G. E. Blair • Leeds
D. N. Brindley • Edmonton
R. A. J. Challiss • Leicester
P. Ferré • Paris
J. T. Gallagher • Manchester
R. A. John • Cardiff
H. Nagase • London
J. D. Pearson • London
M. H. Rider • Bruxelles
S. B. Shears • Research Triangle Park

Reviews Editor
R. D. Burgoyne • Liverpool

Managing Editor
P. J. Starley

Deputy Managing Editor
S. E. Dilley

Senior Staff Editor
S. M. Hobday

Staff Editors
L. Johnson
W. J. Watkins
M. R. Thorne
N. B. Prowse
S. J. Cuble

Editorial Assistants
N. J. Lamb
C. L. Jeeves

R L. P. Adams (Glasgow)
J.-W. N. Akkerman (Utrecht)
D R Alessi (Dundee)
D Attaix (Ceyrat)
S A. Baldwin (Leeds)
F J Ballard (Adelaide)
G J Barritt (Adelaide)
N C Bruce (Cambridge)
A Clerk (London)
G. M Cohen (Leicester)
P Crine (Montreal)
D Cutler (London)
D A Day (Nedlands)
H. Deckmyn (Kortrijk)
K Docherty (Aberdeen)
B K Drøbak (Norwich)
J M East (Southampton)
K R F Elliott (Manchester)
B Engelmann (Munich)
C Forest (Meudon)
M J Fry (Reading)
A Galione (Oxford)
D. A. F Gillespie (Glasgow)
S Goodbourn (London)
G W Gould (Glasgow)
S V Graham (Glasgow)
S Gutteridge (Newark, DE)
Y A Hannun (Charleston)
P I Harris (Leicester)
M M. Harnett (Glasgow)
J D Hayes (Dundee)
P. C Heinrich (Aachen)
R Heinrich (Berlin)
B Henrissat (Marseille)
R C Hider (London)
S High (Manchester)
M B Hodgins (Glasgow)
D Hoekstra (Groningen)
N M Hooper (Leeds)
E F Hounsell (London)
W Jessup (Sydney)
J P. Kehrer (Austin)
K I Kivirikko (Oulu)
B. L Knight (London)
R. G Knowles (Stevenage)
H. Kresse (Munster)
P W Kuchel (Sydney)
C MacKintosh (Dundee)
A I Magee (London)
T. J Mantle (Dublin)
P Maurel (Montpellier)
A J Meijer (Amsterdam)
F Michelangeli (Birmingham)
G. Milligan (Glasgow)
B P Morgan (Cardiff)
J S Mort (Montreal)
S E Moss (London)
K J. Murray (Harlow)
A C Newby (Bristol)
F. Paltauf (Graz)
N J. Pyne (Glasgow)
C I Ragan (Saffron Walden)
P. R Rich (London)
N. J P Ryba (Bethesda)
G. Salvesen (San Diego)
M F Scully (London)
S Shenolikar (Durham, NC)
A. G. Smith (Cambridge)
M. C. Sugden (London)
P H Sugden (London)
R Sundler (Lund)
J. M Tavaré (Bristol)
K. F. Tipton (Dublin)
M A. Titheradge (Brighton)
A B Tobin (Leicester
S A Tooze (London)
W J van Blitterswijk (Amsterdam)
R Virden (Newcastle upon Tyne)
H M Wallace (Aberdeen)
M P Walsh (Calgary)
L. A. Witters (Hanover)
J F. Woessner (Miami)
S J Yeaman (Newcastle upon Tyne)
S Yoshikawa (Akoh-Hyogo)

PORTLAND PRESS Ltd

59 Portland Place
London
W1N 3AJ U.K.

ISSN 0264-6021

Printed in Great Britain by the University Press, Cambridge

Biochem. J. (2000) 349, 1–12 (Printed in Great Britain)

REVIEW ARTICLE

DNA replication and damage checkpoints and meiotic cell cycle controls in the fission and budding yeasts

Hiroshi MURAKAMI[1] and Paul NURSE
Imperial Cancer Research Fund, Cell Cycle Laboratory, 44 Lincoln's Inn Fields, London WC2A 3PX, U.K.

The cell cycle checkpoint mechanisms ensure the order of cell cycle events to preserve genomic integrity. Among these, the DNA-replication and DNA-damage checkpoints prevent chromosome segregation when DNA replication is inhibited or DNA is damaged. Recent studies have identified an outline of the regulatory networks for both of these controls, which apparently operate in all eukaryotes. In addition, it appears that these checkpoints have two arrest points, one is just before entry into mitosis and the other is prior to chromosome separation. The former point requires the central cell-cycle regulator Cdc2 kinase, whereas the latter involves several key regulators and substrates of the ubiquitin ligase called the anaphase promoting complex. Linkages between these cell-cycle regulators and several key checkpoint proteins are beginning to emerge. Recent findings on post-translational modifications and protein–protein interactions of the checkpoint proteins provide new insights into the checkpoint responses, although the functional significance of these biochemical properties often remains unclear. We have reviewed the molecular mechanisms acting at the DNA-replication and DNA-damage checkpoints in the fission yeast *Schizosaccharomyces pombe*, and the modifications of these controls during the meiotic cell cycle. We have made comparisons with the controls in fission yeast and other organisms, mainly the distantly related budding yeast.

Key words: cell cycle, checkpoint, meiosis, cdc2/CDK, yeasts.

INTRODUCTION

In eukaryotes the cell cycle is divided into two phases, interphase and mitosis [1]. Interphase consists of G1, S and G2 phases. Mitosis can be sub-divided into prophase, metaphase, anaphase and telophase. Chromosomes condense during prophase, align during metaphase, separate during anaphase and decondense during telophase. There are several control points during the cell cycle: in late G1, called Start in yeast or the Restriction point in mammals, in late G2 and just prior to anaphase. To pass each point, cells have to fulfil several prerequisites. Before passing Start, cells can undergo two developmental programmes, i.e. entry into the mitotic cell cycle or sexual development. Adequate nutritional conditions and a critical cell size are required to traverse Start. During G2, cells have to check whether DNA replication is completed and ensure that DNA is not damaged. Before chromosome separation cells also examine whether chromosomes are aligned and spindles are formed properly. These cell-cycle checkpoints are the mechanisms that govern the order of the cell-cycle events, because if the order of the events is incorrect then a full complement of genetic information is not transmitted at cell division, which may lead to cancer in higher eukaryotes.

Much is now known about regulation of the eukaryotic cell cycle but two areas have yet to be fully understood. The first area is concerned with the molecular mechanisms acting during the DNA-replication and DNA-damage checkpoints, which block mitosis if DNA replication is incomplete or DNA is damaged. The second concerns the controls which operate during the meiotic cell cycle. In recent years, some progress has been made in both of these areas and the purpose of the present review is to summarize our current knowledge. The major focus will be on the yeasts, in which most work has been done, with emphasis on the fission yeast *Schizosaccharomyces pombe* and comparison with the budding yeast *Saccharomyces cerevisiae*. Work with other organisms such as *Xenopus* will also be discussed where particularly relevant, but for more detailed reviews of work on other organisms see [2–8].

REGULATION OF MITOTIC CELL CYCLE BY CYCLIN-DEPENDENT KINASE (CDK) IN FISSION YEAST

There are a number of proteins which are required for cell-cycle progression. Among these, Cdc2 protein kinase (CDK1) plays a central role in the control of the mitotic cell cycle in fission yeast [9]. Loss of Cdc2 kinase activity arrests cells both before Start in G1 and in late G2 before M phase [10], and dominant forms of Cdc2 advance entry into mitosis [11]. Furthermore, Cdc2 is essential for viability and no suppressor mutations in other genes have been identified that completely rescue the disruptant of Cdc2. Based on these facts, initiation of DNA synthesis and nuclear divisions are attributed to the activity of a single CDK catalytic sub-unit encoded by *cdc2*$^{+}$ [12]. The equivalent gene in budding yeast is *CDC28* [13,14].

After passing Start, Cdc2 becomes complexed with B-type cyclins Cdc13 and Cig2 and the Cdc2 complex is phosphorylated on tyrosine-15 by both the Wee1 and Mik1 tyrosine kinases [15–17]. This tyrosine phosphorylation is maintained until the onset of mitosis [16,17]. Dephosphorylation of this residue is carried out by the Cdc25 tyrosine phosphatase and to a lesser

---

Abbreviations used: APC, anaphase-promoting complex; Cln, G1 cyclin; FHA, forkhead associated; PCNA, proliferating-cell nuclear antigen; SPB, spindle-pole body; CDK, cyclin-dependent kinase; RFC, replication factor C; MCM, minichromosome maintenance; ORC, origin-recognition complex.

[1] To whom correspondence should be addressed (e-mail murakami@icrf.icnet.uk).

extent by the Pyp3 phosphatase [18,19]. Full activation of Cdc2 by tyrosine dephosphorylation brings about entry into mitosis. The kinase activity of tyrosine-15 phosphorylated Cdc2 is about 30 % compared with that of the dephosphorylated form in starfish [20], which is consistent with its observed activities in fission yeast interphase cells [21]. This activity is sufficient to bring about DNA replication but not mitosis [22,23]. An analogous inhibitory pathway of tyrosine-19 phosphorylation of Cdc28 (equivalent to tyrosine-15 of Cdc2 in fission yeast) has been described in budding yeast. This residue is phosphorylated by Swe1 (a homologue of fission yeast Wee1) and dephosphorylated by Mih1 (a homologue of fission yeast Cdc25) [24,25]. When a bud is not formed properly or the actin cytoskeleton is defective, a morphogenesis checkpoint, which requires Swe1-mediated phosphorylation of Cdc28, operates to delay nuclear division [26–28]. However, there is no evidence that tyrosine phosphorylation determines the cell-cycle timing of mitosis as in fission yeast.

DNA-REPLICATION AND DNA-DAMAGE CHECKPOINTS

DNA replication is accurately and temporally regulated during the cell cycle in all eukaryotes. In budding yeast, each chromosome contains multiple discrete replication origins called autonomously replicating sequences, where prereplicative complexes are assembled during M and G1 phase [29–31]. The prereplicative complexes includes the origin–recognition complex (ORC), the minichromosome-maintenance (MCM) complex and Cdc6 [29,30]. The six proteins that form the ORC bind to the autonomously replicating sequences and this binding persists throughout the cell cycle [32]. In late M phase, Cdc6 is recruited by the ORC, which in turn promotes loading of MCM proteins on to chromatin [33–38]. Activation of two protein kinase complexes, Cdc28–B cyclins and Cdc7–Dbf4, is likely to serve as the final signal activating replication fork movement [39–42]. Then the DNA-replication machinery, including DNA polymerases and proliferating-cell nuclear antigen (PCNA), initiates DNA synthesis. Similar mechanisms are likely to operate in other organisms, including fission yeast, since homologues of prereplicative-complex proteins and its regulators have been identified in many organisms [29].

In addition to the roles in DNA replication, many components of the DNA-replication machinery are required for restraining mitosis during S phase in fission yeast. These proteins are mainly involved in the initiation of DNA synthesis, including Polα [43], Cdc18 (a counterpart of budding yeast Cdc6) [44], Cdt1 [45], Cut5/Rad4 [46], Orp proteins (a counterpart of ORC proteins) [47–50], MCM proteins [51], Hsk1–Dfp1/Him1 complex (a counterpart of Cdc7–Dfb4) [52–54], and replication factor C (RFC), which is required for loading of PCNA on to DNA [55,56]. The Cdt1 protein is required for recruiting the MCM proteins on to DNA [57], whereas the biochemical function of Cut5 is not known. The checkpoint function of the temperature-sensitive strains generally remains intact, whereas the complete deletion of these genes eliminates their checkpoint function, suggesting that the formation of a complex of these proteins is important for the checkpoint. However, DNA-replication proteins involved in progression of DNA synthesis are not required for this checkpoint. These include Polε [58], Polδ complexes [59,60], fission yeast PCNA homologue [61], and PCNA interacting protein Cdc24 [62,63].

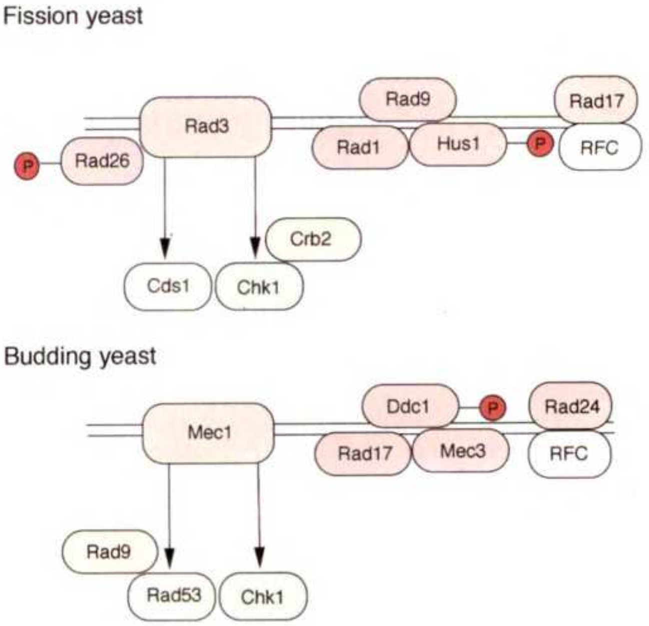

Figure 1 Complex formation of the yeast checkpoint proteins

Fission yeast Rad1, Hus1 and probably Rad9 form a complex regardless of the checkpoint signal. Rad3 kinase associates with and phosphorylates Rad26. These proteins are required for transmitting the checkpoint signal to the Cds1 and Chk1 kinases. Budding yeast Rad17, Mec3 and Ddc1 form a complex and Mec1 transmits the checkpoint signal to Rad53 and Chk1.

Apart from the essential DNA-replication proteins, several non-essential proteins have been identified which are specifically involved in the DNA-replication and DNA-damage checkpoints. Five proteins, Rad1, Rad3, Rad9, Rad17 and Hus1, are required for both the DNA-replication and DNA-damage checkpoints in fission yeast [64–68]. From their structural or functional similarities, these proteins correspond to budding yeast Rad17, Mec1, Ddc1, Rad24 and Mec3 respectively [69]. Since the phenotypes of mutants in these genes, including sensitivity to DNA damaging agents, and the kinetics of their checkpoint defects are almost identical, these fission yeast proteins are called checkpoint Rad proteins. The fission yeast Rad26 is also a member of the family of checkpoint Rad proteins but the counterpart of this protein has not been found in budding yeast [65]. Fission yeast Rad1 is structurally similar to exonucleases, and the putative human homologue has nuclease activity [70,71] and also has a structural motif closely related to the DNA sliding-clamp protein PCNA, suggesting that it could provide processivity for DNA-repair and replication enzymes [72]. Fission yeast Rad17 has a limited homology to RFC [73]. The similarities of the checkpoint proteins to the DNA-replication proteins could indicate that they are components of complexes which interact with DNA to act as sensors for detecting DNA damage or blocks in DNA replication.

Fission yeast Hus1 and Rad1 proteins associate physically in a manner dependent on Rad9, and Hus1 is phosphorylated in a checkpoint Rad-protein-dependent manner (Figure 1) [74]. Complex formation and phosphorylation are conserved, since budding yeast Rad17, Mec3 and Ddc1 form a complex and Ddc1 phosphorylation is dependent on Mec1 (Figure 1) [75,76]. The human homologue of Rad1 also interacts physically with Rad17 [77]. However, the functional significance of these complex formations has not been found. Recently, a link between the checkpoint Rad and the DNA-replication proteins has been identified in both yeasts through the RFC protein, which physically associates with fission yeast Rad17 [56] and with

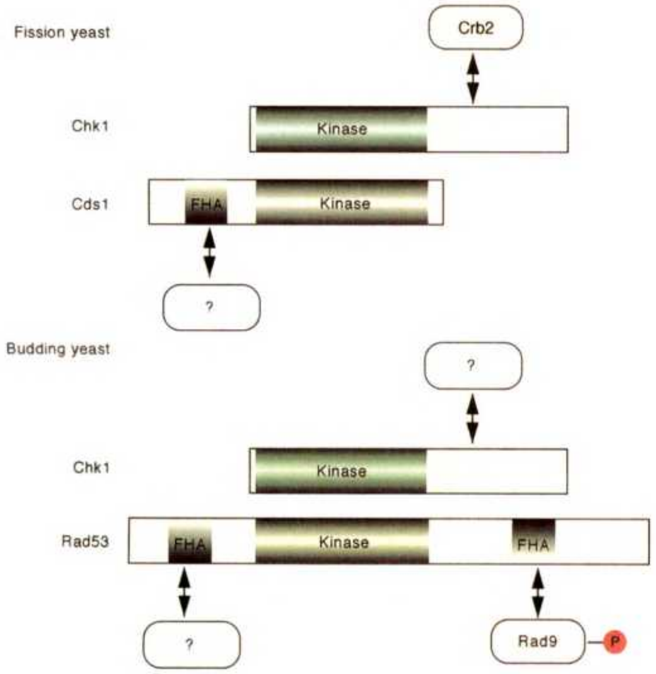

Figure 2 Schematic representation of the yeast checkpoint kinases

In fission yeast, Chk1 has a kinase domain in the N-terminal region, whereas in Cds1 the domain is in the C-terminal region. Cds1 has a FHA domain in the N-terminal region. Budding yeast Chk1 also has a kinase domain in the N-terminal region. Budding yeast Rad53 has two FHA domains, and Rad9 interacts with the FHA domain in the C-terminal region. Further interacting proteins have yet to be identified.

budding yeast Rad24 [78]. The fission yeast Rad3 kinase associates with Rad26, and Rad3 phosphorylates Rad26 independently of the other checkpoint Rad proteins, suggesting that Rad26 phosphorylation might be an initial response to DNA damage, although the functional significance of the Rad26 phosphorylation is not yet known (Figure 1) [79]. Rad3 is a member of the evolutionarily conserved subfamily of phosphatidylinositol 3-kinases, which includes fission yeast Tel1, budding yeast Mec1, Tel1, mammalian ATR and ATM and DNA-dependent protein kinase [80,81].

Two protein kinases, Chk1 and Cds1, provide a link between the checkpoint Rad proteins and the machinery which controls mitosis [82,83]. The Cds1 kinase is required specifically for proper recovery from a DNA-replication block, since *cds1Δ* cells stop cell-cycle progression when DNA replication is completely inhibited, but subsequently enter a premature mitosis when released from the replication block [83,84]. Cds1 also acts redundantly with Chk1 in the DNA-replication checkpoint [85–87], and Chk1 kinase itself is primarily involved in the DNA-damage checkpoint [82]. The protein kinase activity of Cds1 and the phosphorylation of Chk1 are dependent on the checkpoint Rad proteins [82,86]. Cds1 kinase is structurally similar to budding yeast Rad53 [83] and has a FHA (forkhead-associated) domain in the N-terminal region [88] (Figure 2). Budding yeast Rad53 kinase, which is required for both the DNA-replication and DNA-damage checkpoints, has two FHA domains and budding yeast Rad9 binds to the C-terminal FHA domain of Rad53, suggesting that this association is required for transduction of the DNA-damage checkpoint signal (Figure 2) [89]. The FHA domain of Rad53 in the N-terminal region is mainly involved in the DNA-replication checkpoint [90]. Budding yeast Rad9 has a region called the BRCT domain (the C-terminus of the breast cancer susceptibility gene 1 product), which is found in fission yeast Crb2/Rhp9, the tumour suppressor gene *BRCA1* and the p53 interacting protein 53BP1 [91–93]. Furthermore, Crb2 interacts with Chk1 as demonstrated by both genetic and two-hybrid analysis, although Chk1 lacks an obvious FHA domain [92]. Based on these facts, it is possible that an unknown protein binds to the N-terminal FHA domain of Rad53 or Cds1 and mediates the DNA-replication checkpoint signal. Crb2 is phosphorylated by the Cdc2 kinase not only in response to DNA damage but also during the normal cell cycle [94]. Cells having a non-phosphorylatable form of Crb2 fail to re-enter the cell cycle after DNA damage, suggesting the existence of a feedback regulation between the checkpoint protein and the cell-cycle machinery [94].

Cds1 and Chk1 play central roles in transducing the checkpoint signal from the checkpoint Rad proteins to the cell-cycle machinery (Figure 3A). The Cds1 kinase is activated by the inhibition of DNA replication [86] and then stops cell-cycle progression by acting through Wee1 [85] and Cdc25 [87]. The Chk1 kinase appears to phosphorylate Cdc25 [95] and Wee1 [96,97]. Thus both Cds1 and Chk1 phosphorylate Cdc25 and inhibit its activity [98]. Furthermore, the Chk1 phosphorylation of Cdc25 results in the physical association of Cdc25 with fission yeast Rad24 [99,100]. Fission yeast Rad24 is a member of the 14-3-3 family of proteins [101] which bind to phosphoproteins. Cdc25 complexed with fission yeast Rad24 is excluded from the nucleus in response to incomplete DNA replication and damaged DNA, suggesting that spatial organization is part of the DNA-replication and DNA-damage checkpoints [99,100].

Both the DNA-replication and DNA-damage checkpoint controls block entry into mitosis via the Cdc2 kinase [102–104], and both controls can be abolished by: (1) overexpressing *cdc25*$^+$ to reduce the level of phosphorylation of Cdc2 on tyrosine-15 [102,105], (2) inactivating the Wee1 and Mik1 kinases [17,103] or (3) the use of a Cdc2-Y15F mutant [103,104,106]. These studies strongly suggest that the DNA-replication and the DNA-damage checkpoints act through tyrosine-15 phosphorylation of Cdc2, although this conclusion has been controversial [104,107]. In contrast, tyrosine-19 phosphorylation of budding yeast Cdc28 is not important in the DNA-replication and DNA-damage checkpoint controls, because Cdc28-Y19F mutants arrest cell-cycle progression before nuclear division following DNA damage or inhibition of DNA replication [108–110]. In response to a DNA-replication block or DNA damage, budding yeast cells arrest with high Cdc28 protein kinase activity, short microtubule spindles and separated spindle-pole bodies (SPBs) [108–110]. If Cdc28 activity is not maintained at a high level, cells proceed through mitosis even though DNA damage is present [111]. These results suggest that the DNA-replication and DNA-damage checkpoints in budding yeast arrest cells in a metaphase-like state rather than in interphase, as is the case for most other organisms, including fission yeast.

In budding yeast, the DNA-damage checkpoint communicates to the mitotic apparatus through Pds1 and Cdc5 (Figure 3B). Pds1 is an anaphase inhibitor which is required for the DNA-damage and spindle checkpoints [112]. Pds1 is phosphorylated in response to DNA damage, a phosphorylation which is dependent on budding yeast Chk1 and Mec1 but not Rad53 [75,113]. Furthermore, budding yeast Chk1 phosphorylation depends on Mec1, and the Chk1 protein binds and phosphorylates Pds1 [114]. These studies suggest that Pds1 acts downstream of Chk1 and that Chk1 acts downstream of Mec1. Budding yeast Cdc5, a member of the polo-like family of kinases, is mainly involved in the exit from mitosis [115,116]. Overproduction of Cdc5 drives

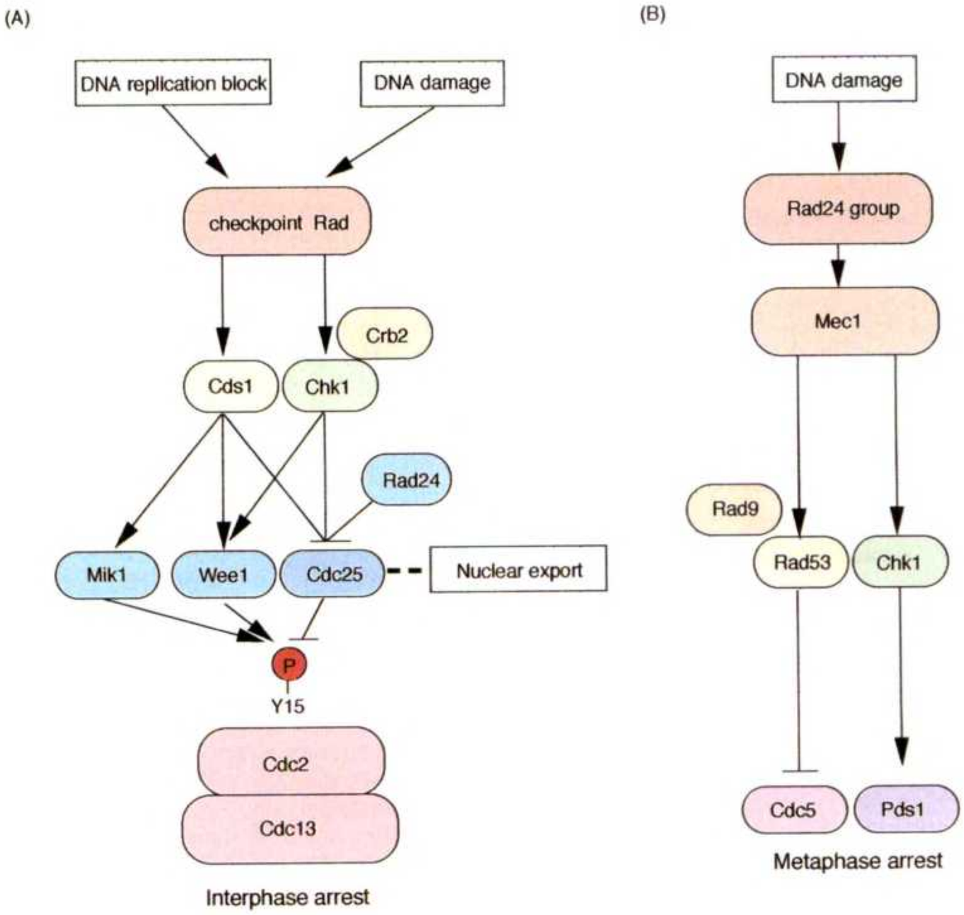

Figure 3 Model showing how the DNA-replication and DNA-damage checkpoint signals are transmitted to the cell-cycle machinery in yeast mitotic cell cycle

(**A**) The DNA-replication and DNA-damage checkpoints in fission yeast. (**B**) The DNA-damage checkpoints in budding yeast. See text for detailed explanations.

cells through anaphase so that they complete mitosis in the presence of damaged DNA, and inactivation of Cdc5 delays anaphase entry in *rad53* mutant cells after DNA damage [114]. It is interesting to note that the budding yeast Cdc5 kinase appears to have no obvious role for entry into anaphase during the normal cell cycle and that Cdc5 is phosphorylated in a Rad53-dependent manner after DNA damage, suggesting that Cdc5 acts downstream of the Rad53 kinase [117].

INTRODUCTION TO MEIOSIS

In eukaryotes, meiosis not only plays a central role in the life cycle of sexual reproduction, but it is also essential for generating genetic diversity within species [118–122]. During meiosis, haploid gametes are produced from a parental diploid cell or zygote. Two successive nuclear divisions occur without S phase which halves the number of chromosomes. Fusion of two gametes restores the diploid chromosome complement. There are a number of important differences between meiosis and mitosis. The S phase in meiosis, called premeiotic DNA replication, usually takes two to five times longer than S phase in mitotic cycles [123,124]. In addition, premeiotic DNA synthesis depends on several proteins that are dispensable for mitotic DNA synthesis in both the fission yeast [6,120] and budding yeast [118]. During meiotic prophase, homologous recombination occurs about a hundred to a thousand times more frequently than during mitosis [119]. The first division of meiosis is quite different from a mitotic cell division. Sister chromatids remain associated with each other and the two copies of the same chromosome (called homologues) segregate to opposite sides of the cell. The second meiotic division immediately follows the first meiotic division without an intervening S phase. In the second meiotic division, sister chromatid disjunction takes place, as in mitosis.

CONTROL OF ENTRY INTO MEIOSIS

In fission yeast, entry into meiosis requires a pheromone signal and nutritional starvation, primarily for nitrogen [120] (Figure 4A). Both pheromone and nitrogen starvation induce G1 arrest by inhibiting the activity of Cdc2. Pheromone inhibits the Cig2- and Cdc13-dependent Cdc2 kinase activities and induces the CDK inhibitor Rum1, which also promotes APC (anaphase-promoting complex)-dependent degradation of Cdc13 [125,126]. Nitrogen starvation enhances the degradation of both Cdc13 and Cig2, and the Cdc13 degradation is dependent on Srw1/Ste9 [127,128]. Srw1 is a regulator of the APC and is homologous to budding yeast Hct1/Cdh1 [129].

In both mitotic and meiotic cycles, periodic expression of DNA-replication genes is required for S phase. However, different components of the S phase transcriptional machinery are required to bring this about in the two cell cycles [6,130–135].

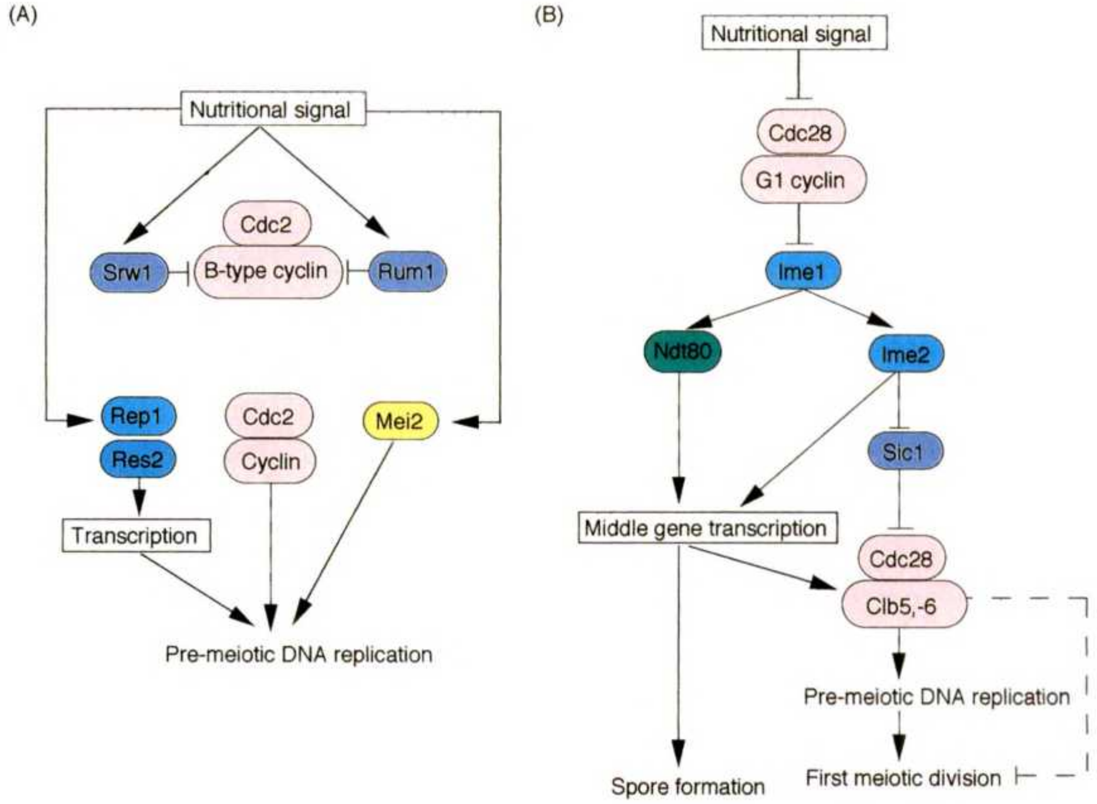

Figure 4 Model of cell-cycle regulation in yeast meiosis

(**A**) Entry into meiosis and premeiotic DNA replication in fission yeast. (**B**) Entry into meiosis and premeiotic DNA replication in budding yeast. See text for detailed explanations.

Activation of both the Cdc10–Res1 and Cdc10–Res2–Rep2 complexes is required for gene expression in the mitotic S phase, whereas the Cdc10–Res2 complex, possibly with Rep1, appears to play a similar role during meiosis (Figure 4A).

Rep1 is required specifically for premeiotic DNA replication, since *rep1*Δ cells arrest before premeiotic DNA replication but show no significant phenotype during mitotic cycles [136–138]. Rep1 is a zinc-finger protein with limited homology to Rep2 [134,136], and acts as an activator of the Res2–Cdc10 or Res1–Cdc10 complexes, since overexpression of *rep1*$^+$ rescues growth defects of *res1*Δ, *res2*Δ, *rep2*Δ and weakly rescues *cdc10*^{ts} cells [136]. In addition, *res2*$^+$ mRNA induction is dependent on Rep1 function [136]. However, the meiotic defect of *rep1*Δ cells is not rescued by overexpression of either *res1*$^+$ or *res2*$^+$, suggesting that the Res1/Res2–Cdc10 complex is not the sole target of Rep1 [133]. Further support for this notion comes from the observation that the induction of recombination genes requires the Rep1 protein [137,138].

Interestingly, the inability of *rep1*Δ cells to carry out premeiotic DNA replication is partially suppressed if rapidly growing cells are induced to undergo meiosis [136]. After starvation, *rep1*Δ cells are completely unable to undergo meiosis. This suggests that a substitute for Rep1, probably Rep2, complements its function and allows premeiotic DNA replication to take place in these circumstances. Consistent with these results, double mutants of *rep2*Δ*rep1*Δ cells are unable to initiate meiosis [134]. In *res2*Δ cells, the premeiotic DNA-replication defect is also rescued if meiosis is induced without starvation [133]. The fact that similar proteins act in mitosis and meiosis suggests that initiation of premeiotic DNA replication might be regulated in a similar manner to initiation of DNA replication in mitotic cycles [6].

In budding yeast, Swi6, Swi4 and Mbp1 have extensive homology to fission yeast Cdc10, Res1 and Res2 respectively [6]. However, in contrast to fission yeast, double homozygous diploid mutants of either *swi4*Δ*swi6*Δ or *swi4*Δ*mbp1*Δ proceed through meiosis [139], although spore viability is low even in single *swi4*Δ or *swi6*Δ cells [140]. Very low activity of these transcriptional factors may be sufficient for progression through meiosis, but not for spore viability.

REGULATION OF CDK IN MEIOSIS

In fission yeast, Cdc2 kinase plays a central role in the control of the mitotic cycle. Similarly to the situation in the mitotic cycle [10,141], Cdc2 is also required for premeiotic DNA synthesis [142], the second meiotic division [143–147] and possibly the first meiotic division [142] (Figure 4A). Cdc2 kinase activity increases around the beginning of premeiotic DNA replication and peaks around meiotic nuclear division [148,149]. Tyrosine-15 phosphorylation of Cdc2 appears around premeiotic DNA replication, with a concomitant increase in Wee1 protein levels [149], and decreases during meiotic nuclear divisions [148,149]. Cdc13 and Cdc25 are essential for both the first [142] and second meiotic divisions [144,145]. In fission yeast, the RNA binding protein Mei2 has a central role in the onset and progression through meiosis [120,150–152], but the relationship between Cdc2 and Mei2 is not known (Figure 4A).

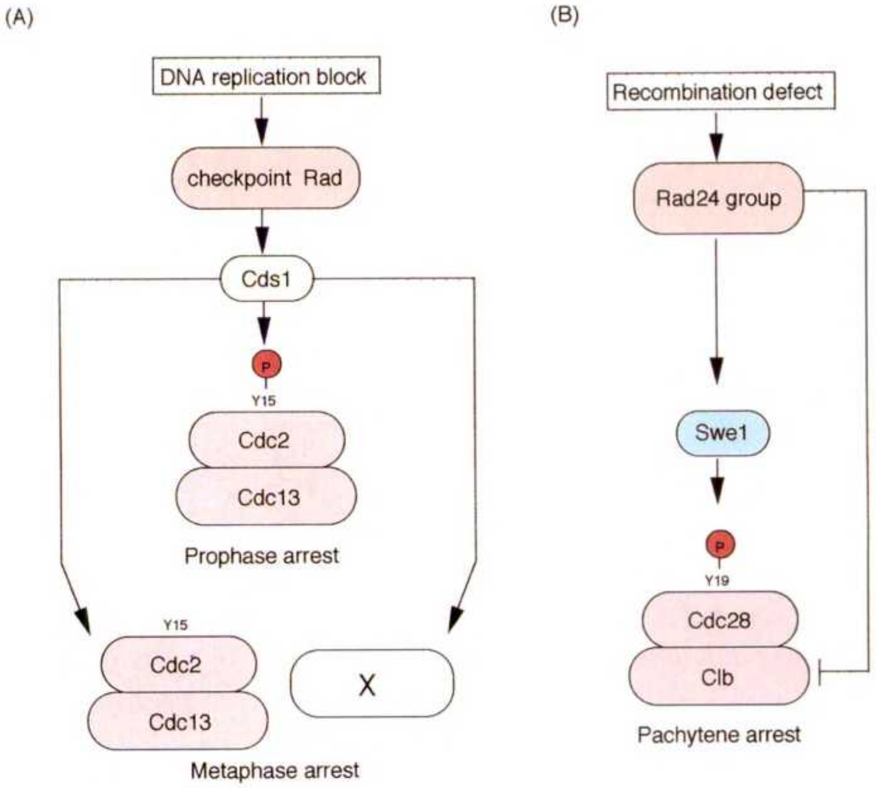

Figure 5 Model of checkpoint regulation in yeast meiosis

(**A**) The meiotic DNA-replication checkpoint in fission yeast. X represents an as-yet unidentified interacting protein. Reproduced from [148] with permission ©1999 Cold Spring Harbor Laboratory Press. (**B**) The recombination or pachytene checkpoint in budding yeast. See text for detailed explanations.

In contrast to the situation in fission yeast, using a temperature-sensitive budding yeast *cdc28* mutant, Cdc28 appears dispensable for premeiotic S phase but is required for meiotic nuclear divisions [153]. This seems inconsistent with the observation that overproduction of the CDK inhibitor Sic1 prevents premeiotic DNA replication [154]. It is possible that Cdc28 in this experiment is not sufficiently compromised to block premeiotic DNA replication because of the temperature-sensitive mutant, or that Sic1 may inhibit not only the Cdc28 protein kinase but also other proteins required for DNA replication. In budding yeast, G1 cyclin (Cln)-deficient cells enter meiosis regardless of nutrient conditions [155] and produce viable spores, suggesting that Clns are not required for meiosis [139]. Furthermore, Clns negatively regulate entry into meiosis by down-regulating both Ime1 transcription and protein levels (Figure 4B) [155]. Ime1 is a transcriptional activator of early genes that are essential for premeiotic DNA replication, homologous chromosome pairing and recombination [156]. As cells enter meiosis the level of the Clns decreases [155]. This negative regulation of entry into meiosis by Clns may be related to the fact that meiosis proceeds without bud formation, since Cln1 and Cln2 are involved in bud formation during mitotic cycles. The lack of Cln1 and Cln2 involvement also suggests that cell size may not regulate Start in meiosis. In meiosis, the target of Sic1 seems to be the B-type cyclins Clb5 and Clb6, because *clb5*Δ*clb6*Δ double mutants are unable to initiate premeiotic DNA replication [139,154] (Figure 4B). Surprisingly, the mutant cells proceed through meiosis with unreplicated chromosomes [154]. These facts suggest that Clb5 and Clb6 are essential for the activation of the meiotic DNA-replication checkpoint. The regulation of Sic1 degradation is different between mitosis and meiosis (Figure 4B) [139]. In mitotic cycles, Sic1 is phosphorylated by Cln-dependent CDK activity, which results in the degradation of Sic1 [157]. In meiosis, the double mutant *sic1*Δ*ime2*Δ undergoes premeiotic DNA replication, suggesting that degradation of Sic1 requires the meiosis-specific protein kinase Ime2 [139]. Ime2, which has sequence similarity to Cdc28, is essential for premeiotic DNA replication [156,158–160] and may phosphorylate Sic1 to target it for degradation. Ime2 is required to activate the early and middle meiotic genes, and is itself an early meiotic gene activated by Ime1. Middle gene products are required for the morphogenetic pathway that leads to spore formation [156]. Ndt80 is a transcription factor also required for the expression of middle and middle/late genes, as well as five of the six *CLB* genes, except *CLB2* (Figure 4B) [161,162]. All the *CLB* genes, except *CLB2*, are induced by ectopic expression of Ndt80 during the mitotic cell cycle. The fact that both *CLB* and middle gene expression are dependent on Ndt80 ensures that meiotic progression and ascospore formation are properly co-ordinated.

MEIOTIC DNA-REPLICATION CHECKPOINT

A DNA-replication checkpoint control also operates during meiosis in fission yeast (Figure 5A) [148]. When meiotic DNA replication is inhibited with hydroxyurea, cells arrest with no spindle, unseparated SPBs and decondensed chromosomes [148].

This arrest requires the mitotic-checkpoint Rad proteins and the Cds1 protein kinase [148]. As discussed earlier, during mitotic cycles the role of Cds1 is restricted to recovery from a DNA-replication block [83]. In meiosis, Cds1 appears to play a more prominent role equivalent to that played by the checkpoint Rad proteins, since cells defective in any of these proteins proceed through meiotic nuclear divisions [148]. When DNA replication is blocked, the checkpoint maintains Cdc2 tyrosine-15 phosphorylation [148] just as in mitotic cycles [16,104,107].

Meiotic cells blocked by hydroxyurea, which harbour dephosphorylated tyrosine-15 of Cdc2, arrest with high Cdc2 protein kinase activity, separated SPBs and spindle formation [148]. This metaphase-like arrest is at a later stage of nuclear division than that seen in cells in which Cdc2 tyrosine-15 is phosphorylated, and is similar to that observed in mitotic budding yeast cells when DNA replication is inhibited [110]. The fact that certain processes occur only during meiosis, such as increased recombination rates or homologue chromosome pairing, may mean that a second checkpoint, which blocks cells in metaphase, is required during meiosis. Like the DNA-damage checkpoint in *S. cerevisiae*, counterparts of the budding yeast Cdc5 or Pds1 proteins might be downstream targets of meiotic DNA-replication checkpoint signals. Even in the fission yeast mitotic cycle there may be another DNA-replication checkpoint mechanism independent of Cdc2 regulation on tyrosine-15. Supporting this notion is the observation that the DNA-replication checkpoint remains intact in the absence of both Cdc25 and Wee1 [67]. However, it is possible that Mik1 or Pyp3 carry out this function in the absence of Wee1 or Cdc25.

In *Drosophila*, 13 rapid syncytial nuclear divisions lacking G1 and G2 phases occur during early embryogenesis. When DNA is damaged during this period, chromosome segregation but not entry into mitosis is delayed [163]. This is similar to budding yeast in which a defined G2 phase is lacking. In post-blastoderm division cycles which include a G2 phase, DNA damage delays entry into mitosis [164]. This delay requires tyrosine phosphorylation of Cdc2 as in fission yeast and other higher eukaryotes. From these observations, it is likely that, in all eukaryotes, mitosis and meiosis can be arrested either before entry into mitosis or before chromosome segregation.

In *Aspergillus nidulans*, two DNA-replication checkpoint systems have also been reported [165]. In this organism, if DNA replication is incomplete, cells harbouring non-tyrosine phosphorylated forms of Cdc2 arrest before mitosis with high Cdc2 kinase activity. At this stage, neither chromosome condensation nor spindle formation are observed. This contrasts with the situation during meiosis of fission yeast in which chromosome condensation and spindle formation occur in the presence of hydroxyurea if Cdc2 tyrosine-15 is dephosphorylated. Mutation of an APC component, BIME, in combination with non-tyrosine-phosphorylated Cdc2 can overcome the DNA-replication checkpoint. It is likely that co-ordination of both Cdc2 and APC functions is important for the DNA-replication checkpoint in this organism, and this may have some relevance to the analogous checkpoint during fission yeast meiosis.

In *Xenopus* egg extracts, non-tyrosine phosphorylatable forms of Cdc2 show a limited capacity to induce mitosis in the presence of a DNA synthesis inhibitor [166]. In addition, *Xenopus* Chk1, which is capable of phosphorylating the mitotic inducer Cdc25, is partially involved in the DNA-replication checkpoint pathway [167]. Similarly, in human cells, regulation of Cdc2 tyrosine-15 is important in the DNA-replication and DNA-damage checkpoints but is not the sole mechanism for restraining mitotic progression [168,169]. Spatial compartmentation of cell-cycle regulators is one of the mechanisms that prevent mitosis. In fact, it has been shown that exclusion of B-type cyclin from the nucleus is required for blocking mitosis after DNA damage [170,171]. At least two different mechanisms of the DNA-replication and DNA-damage checkpoints may exist in all organisms, but they may be regulated in different ways in different organisms.

RECOMBINATION OR PACHYTENE CHECKPOINT

In many organisms, cells defective in recombination or synaptonemal complex formation arrest at the pachytene stage of meiotic prophase [121,172,173] This arrest is called the recombination checkpoint or the pachytene checkpoint (Figure 5B) [174,175]. Pachytene is the stage of the meiotic cell cycle when premeiotic DNA synthesis is completed, the SPB is duplicated but not separated and the cell is committed to recombination. This arrest requires the DNA-damage checkpoint Rad17, Rad24, Ddc1 and Mec1 proteins in budding yeast, ensuring the order of meiotic events by preventing chromosome segregation when recombination is incomplete or the synaptonemal complex is defective [121,173,174,176] (Figure 5B). Pch2 and the silencing factor Sir2 are also required for the pachytene checkpoint but are not required for the DNA-damage checkpoint in mitotic cycles [176]. The meiosis-specific Red1 and Mek1 proteins are also required for pachytene arrest [173]. Mek1 is a protein kinase and associates with Red1, which is an essential component of the meiotic chromosomes [177,178]. However, in fission yeast there are no mutants that arrest with recombination intermediates and the recombination checkpoint has not been identified [119].

Interestingly, budding yeast Rad9, which is essential for the DNA-damage checkpoint is not required for the recombination checkpoint [174]. However, this protein is required for the arrest in meiosis imposed by inactivation of a telomeric DNA binding protein [179]. This arrest point in meiosis is at a stage that follows premeiotic DNA replication but is prior to commitment to recombination. These facts indicate that Rad9 has stage-specific roles during meiosis, although the exact mechanisms of its action or regulation are not known.

Tyrosine-19 phosphorylation of Cdc28 is also required for pachytene arrest in budding yeast, since both *swe1*Δ and Cdc28-F19 cells proceed through meiosis in the presence of double-strand breaks, although the segregation of chromosomes is delayed [175] (Figure 5B). Clb1 overproduction in *swe1*Δ or Cdc28-F19 cells eliminates this delay, suggesting that the regulation of B-type cyclin synthesis is also important in this checkpoint [175] (Figure 5B) In contrast, the budding yeast Mih1 phosphatase is required neither for mitosis, meiotic progression nor the pachytene checkpoint [175]. Upon activation of the pachytene checkpoint, the Swe1 kinase accumulates and is hyperphosphorylated; this phosphorylation is dependent on budding yeast Rad24 checkpoint protein. These facts suggest that Swe1 is a target of the pachytene checkpoint control. It is of interest that these meiotic controls are similar to those operating during the DNA-replication and DNA-damage checkpoints in fission yeast.

COHESIN IN MEIOSIS

Physical association between sister chromosomes is required for their proper segregation during mitosis and meiosis. This attachment is provided by a molecular 'glue' called cohesin. The cohesin complex is composed of at least four proteins, Scc1/Mcd1, Scc3, Smc1 and Smc3, in budding yeast [180–183]. Similar proteins and their regulators exist in fission yeast and other eukaryotes, indicating that this mechanism is conserved [184,185]. Loss of any of these proteins brings about premature chromosome separation even if the APC is inactivated. At the metaphase-to-anaphase transition, Scc1 is cleaved by Esp1 (Cut1 in fission yeast), resulting in sister chromatid separation [186]. Esp1 is kept inactive by binding to Pds1 (Cut2 in fission yeast) until the onset of anaphase [187], when Pds1 (Cut2) is destroyed by the APC [184,188,189].

In meiosis, after premeiotic DNA replication, homologous chromosomes are held together by recombination between homologues [180,190]. The physical attachment between homologues is provided by chiasmata, which are sites of reciprocal recombination between homologous chromosomes. Meiotic cohesin, located in the arm regions of sister chromatids, is also important for this attachment to keep the recombined chromosomes tightly connected. In addition, meiotic cohesin, located in the vicinity of the centromeric regions, is required to hold sister chromatids together. Two sister kinetochores, held by the cohesin, move to the same pole in the first meiotic division. After disappearance of the cohesin at the centromeric region, sister chromatid disjunction occurs during the second meiotic division. This step-wise loss of cohesion is essential for an orderly progression through the two meiotic divisions.

In fission yeast, one of the candidates of the meiotic cohesin is the Rec8 protein since *rec8* mutants show precocious separation of sister chromatids [191]. Fission yeast Rec8 shares homology with the budding yeast mitotic cohesin Scc1 protein [182,192,193]. The Rec8 protein is absent in mitotic cycles, but its level increases during premeiotic DNA replication and decreases around the second meiotic division [192]. During prophase I Rec8 is distributed along the length of the chromosome. Around the first meiotic division Rec8 is lost in the arm regions but is retained at the centromeres until metaphase of the second meiotic division [192,193]. This localization may explain why recombination is reduced only at the centromere regions in *rec8* mutants [191,193]. Loss of Rec8 function causes premature separation of chromosomes [191], and a detailed analysis of the *rec8* mutant revealed that the reductional segregation pattern of the first meiotic division is shifted to an equational segregation pattern [192]. This switch to an equational segregation pattern rather than random segregation is partially explained if Rec8 has an additional role in directing sister-chromatid kinetochores to the same pole [192]. In contrast, budding yeast *rec8* mutants undergo random segregation in the first meiotic division [194].

TELOMERES

Telomeres are essential for blocking the degradation of linear chromosome ends in all eukaryotes. Telomeres have additional roles in the pairing of homologous chromosomes during the early stages of meiosis. The fission yeast Taz1 and Lot2 proteins have a critical role for the maintenance of telomere length and telomeric silencing, although disruptants of these genes can grow normally [195,196]. During meiosis in *taz1* and *lot2* mutants, telomeres fail to cluster at the SPB, resulting in a low recombination rate [196,197]. In fission yeast, the nucleus is highly mobile moving back and forth during the early stages of meiosis [198–200], a movement which is likely to be required for homologous chromosome pairing and recombination. At this stage, telomeres cluster at the SPB instead of the centromeres and reside at the leading edge of the chromosome with the rest of the chromosomes trailing behind [198,199]. Therefore the Taz1 and Lot2 proteins help chromosome pairing through telomere clustering at the SPB.

SUPPRESSION OF DNA REPLICATION BETWEEN THE FIRST AND SECOND MEIOTIC DIVISION

One of the hallmarks of meiosis is suppression of DNA replication between the first and second meiotic division. So far, there are no mutants that can initiate DNA replication during this period in either fission yeast or budding yeast. In *Xenopus* and starfish oocytes, inhibition of the Cdc2 kinase or of the Mos function can induce DNA replication during this period [201,202]. A partial fall in Cdc2 kinase activity occurs between the two meiotic divisions, concomitant with the appearance of threonine-161-dephosphorylated forms of Cdc2 [201]; threonine-161 phosphorylation of Cdc2 is essential for its activity [12]. During this period, no tyrosine-15 phosphorylation of Cdc2 was observed [201,203]. Inactivation of Mos leads to the partial phosphorylation of Cdc2 tyrosine-15 and the dephosphorylation of Cdc2 threonine-161 [201] These observations imply that the activity of Cdc2 between the two meiotic divisions is regulated by the phosphorylation status of both tyrosine-15 and threonine-161. Supporting this notion, ectopic induction of Wee1 induces DNA replication after the first meiotic division [204]. The regulation of Cdc2 complexes appears to be required for the suppression of DNA replication between the two meiotic divisions, and it is important to know how Cdc2 activity is regulated during this period.

CONCLUDING REMARKS

Recent studies have revealed that mitosis and meiosis share common pathways to undergo DNAreplication and chromosome segregation. Distinctive mechanisms also exist in meiosis, probably because of high rates of recombination and suppression of DNA replication before the second meiotic division. In the near future, the whole genome sequence of several organisms, including fission yeast and humans will be known A comparison with the budding yeast sequence will be revealing with regard to what differs and what is conserved between organisms. In particular, the comparison of the two yeasts during the mitotic and meiotic cell cycles will continue to help our understanding of the cell-cycle regulation in all eukaryotes.

We thank Jacky Hayles, Emma Greenwood, Chris Lehane, Stephanie Yanow, Annie Borgne and Takashi Toda for a critical reading of this review H M was supported, in part, by the Imperial Cancer Research Fund

REFERENCES

1 Murray, A and Hunt, T (1993) The Cell Cycle, An Introduction Oxford University Press Inc, New York
2 Roberts, J M (1999) Evolving ideas about cyclins Cell **98**, 129–132
3 Sherr, C J and Roberts, J M (1999) CDK inhibitors: positive and negative regulators of G1-phase progression Genes Dev **13**, 1501–1512
4 Osmani, S A and Ye, X S (1996) Cell cycle regulation in *Aspergillus* by two protein kinases Biochem J **317**, 633–641
5 Swanton, C, Card, G. L, Mann, D, McDonald, N. and Jones, N (1999) Overcoming inhibitions. subversion of CKI function by viral cyclins Trends Biochem Sci. **24**, 116–120
6 Okayama, H, Nagata, A, Jinno, S, Murakami, H, Tanaka, K and Nakashima, N (1996) Cell cycle control in fission yeast and mammals identification of new regulatory mechanisms Adv Cancer Res **69**, 17–62
7 Sagata, N. (1997) What does Mos do in oocytes and somatic cells? Bioessays **19**, 13–21
8 Kishimoto, T (1999) Activation of MPF at meiosis reinitiation in starfish oocytes Dev Biol **214**, 1–8
9 Nurse, P (1990) Universal control mechanism regulating onset of M-phase Nature (London) **344**, 503–508
10 Nurse, P and Bissett, Y (1981) Gene required in GI for commitment to cell cycle and in G2 for control of mitosis in fission yeast Nature (London) **292**, 558–560

11 Nurse, P. and Thuriaux, P (1980) Regulatory genes controlling mitosis in the fission yeast *Schizosaccharomyces pombe*. Genetics **96**, 627–637

12 MacNeill, S A and Nurse, P (1997) In Cell Cycle Control in Fission Yeast, *Schizosaccharomyces pombe* (Pringle, J. R, Broach, J. R and Jones, E W, eds), pp 697–763, Cold Spring Harbor Laboratory, Cold Spring Harbor, New York

13 Lew, D J, Weinert, T and Pringle, J R (1997) In Cell cycle control in *Saccharomyces cerevisiae* (Pringle, J. R., Broach, J. R and Jones, E. W., eds), pp 607–695, Cold Spring Harbor Laboratory, Cold Spring Harbor, New York

14 Mendenhall, M. D. and Hodge, A. E. (1998) Regulation of Cdc28 cyclin-dependent protein kinase activity during the cell cycle of the yeast *Saccharomyces cerevisiae* Microbiol. Mol Biol Rev **62**, 1191–1243

15 Martin-Castellanos, C, Labib, K. and Moreno, S (1996) B-type cyclins regulate G1 progression in fission yeast in opposition to the p25rum1 cdk inhibitor. EMBO J **16**, 839–849

16 Hayles, J. and Nurse, P (1995) A pre-start checkpoint preventing mitosis in fission yeast acts independently of p34cdc2 tyrosine phosphorylation EMBO J. **14**, 2760–2771

17 Lundgren, K, Walworth, N, Booher, R., Dembski, M, Kirschner, M. and Beach, D (1991) mik1 and wee1 cooperate in the inhibitory tyrosine phosphorylation of cdc2 Cell **64**, 1111–1122

18 Millar, J B and Russell, P (1992) The cdc25 M-phase inducer an unconventional protein phosphatase. Cell **68**, 407–410

19 Millar, J B, Lenaers, G and Russell, P (1992) Pyp3 PTPase acts as a mitotic inducer in fission yeast EMBO J. **11**, 4933–4941

20 Borgne, A. and Meijer, L (1996) Sequential dephosphorylation of p34(cdc2) on Thr-14 and Tyr-15 at the prophase/metaphase transition J Biol Chem. **271**, 27847–27854

21 Moreno, S, Hayles, J and Nurse, P (1989) Regulation of p34cdc2 protein kinase during mitosis Cell **58**, 361–372

22 Fisher, D. L and Nurse, P (1996) A single fission yeast mitotic cyclin B p34cdc2 kinase promotes both S-phase and mitosis in the absence of G1 cyclins. EMBO J. **15**, 850–860

23 Stern, B. and Nurse, P (1996) A quantitative model for the cdc2 control of S phase and mitosis in fission yeast Trends Genet **12**, 345–350

24 Booher, R N, Deshaies, R J and Kirschner, M. W (1993) Properties of *Saccharomyces cerevisiae* wee1 and its differential regulation of p34CDC28 in response to G1 and G2 cyclins EMBO J. **12**, 3417–3426

25 Russell, P, Moreno, S and Reed, S. I. (1989) Conservation of mitotic controls in fission and budding yeasts Cell **57**, 295–303

26 Lew, D. J. and Reed, S I. (1995) A cell cycle checkpoint monitors cell morphogenesis in budding yeast J. Cell Biol **129**, 739–749

27 Sia, R A., Herald, H A and Lew, D J (1996) Cdc28 tyrosine phosphorylation and the morphogenesis checkpoint in budding yeast Mol. Biol Cell **7**, 1657–1666

28 McMillan, J N, Sia, R A., Bardes, E S and Lew, D J (1999) Phosphorylation-independent inhibition of Cdc28p by the tyrosine kinase Swe1p in the morphogenesis checkpoint. Mol Cell. Biol. **19**, 5981–5990

29 Dutta, A and Bell, S. P (1997) Initiation of DNA replication in eukaryotic cells. Annu Rev Cell Dev Biol **13**, 293–332

30 Donaldson, A. D. and Blow, J J (1999) The regulation of replication origin activation. Curr. Opin Genet Dev. **9**, 62–68

31 Newlon, C. S. (1997) Putting it all together: building a prereplicative complex. Cell **91**, 717–720

32 Bell, S P and Stillman, B (1992) ATP-dependent recognition of eukaryotic origins of DNA replication by a multiprotein complex Nature (London) **357**, 128–134

33 Rowles, A, Chong, J. P, Brown, L, Howell, M., Evan, G I and Blow, J. J (1996) Interaction between the origin recognition complex and the replication licensing system in *Xenopus* Cell **87**, 287–296

34 Romanowski, P., Madine, M A, Rowles, A., Blow, J. J and Laskey, R. A (1996) The *Xenopus* origin recognition complex is essential for DNA replication and MCM binding to chromatin Curr Biol **6**, 1416–1425

35 Coleman, T R., Carpenter, P. B and Dunphy, W G (1996) The Xenopus Cdc6 protein is essential for the initiation of a single round of DNA replication in cell-free extracts Cell **87**, 53–63

36 Donovan, S, Harwood, J, Drury, L S and Diffley, J F (1997) Cdc6p-dependent loading of Mcm proteins onto pre-replicative chromatin in budding yeast Proc Natl Acad Sci USA **94**, 5611–5616

37 Tanaka, T, Knapp, D. and Nasmyth, K (1997) Loading of an Mcm protein onto DNA replication origins is regulated by Cdc6p and CDKs Cell **90**, 649–660

38 Aparicio, O M., Weinstein, D. M and Bell, S P (1997) Components and dynamics of DNA replication complexes in *S cerevisiae* redistribution of MCM proteins and Cdc45p during S phase Cell **91**, 59–69

39 Zou, L and Stillman, B (1998) Formation of a preinitiation complex by S-phase cyclin CDK-dependent loading of Cdc45p onto chromatin Science **280**, 593–596

40 Hua, X H and Newport, J (1998) Identification of a preinitiation step in DNA replication that is independent of origin recognition complex and cdc6, but dependent on cdk2 J Cell Biol **140**, 271–281

41 Bousset, K and Diffley, J. F (1998) The Cdc7 protein kinase is required for origin firing during S phase Genes Dev. **12**, 480–490

42 Donaldson, A D, Fangman, W L and Brewer, B J. (1998) Cdc7 is required throughout the yeast S phase to activate replication origins Genes Dev **12**, 491–501

43 D'Urso, G, Grallert, B and Nurse, P (1995) DNA polymerase alpha, a component of the replication initiation complex, is essential for the checkpoint coupling S phase to mitosis in fission yeast J Cell Sci **108**, 3109–3118

44 Kelly, T J, Martin, G S, Forsburg, S. L., Stephen, R J, Russo, A and Nurse, P (1993) The fission yeast cdc18+ gene product couples S phase to START and mitosis. Cell **74**, 371–382

45 Hofmann, J F and Beach, D. (1994) cdt1 is an essential target of the Cdc10/Sct1 transcription factor requirement for DNA replication and inhibition of mitosis. EMBO J **13**, 425–434

46 Saka, Y and Yanagida, M. (1993) Fission yeast cut5+, required for S phase onset and M phase restraint, is identical to the radiation-damage repair gene rad4+ Cell **74**, 383–393

47 Leatherwood, J, Lopez-Girona, A. and Russell, P (1996) Interaction of Cdc2 and Cdc18 with a fission yeast ORC2-like protein. Nature (London) **379**, 360–363

48 Grallert, B and Nurse, P (1996) The ORC1 homolog orp1 in fission yeast plays a key role in regulating onset of S phase Genes Dev **10**, 2644–2654

49 Lygerou, Z and Nurse, P (1999) The fission yeast origin recognition complex is constitutively associated with chromatin and is differentially modified through the cell cycle. J Cell Sci **112**, 3703–3712

50 Muzi-Falconi, M and Kelly, T J (1995) Orp1, a member of the Cdc18/Cdc6 family of S-phase regulators, is homologous to a component of the origin recognition complex Proc Natl. Acad Sci USA. **92**, 12475–12479

51 Maiorano, D., Van Assendelft, G. B and Kearsey, S E (1996) Fission yeast cdc21, a member of the MCM protein family, is required for onset of S phase and is located in the nucleus throughout the cell cycle EMBO J **15**, 861–872

52 Masai, H, Miyake, T and Arai, K. (1995) hsk1+, a *Schizosaccharomyces pombe* gene related to Saccharomyces cerevisiae CDC7, is required for chromosomal replication EMBO J **14**, 3094–3104

53 Takeda, T, Ogino, K, Matsui, E., Cho, M K., Kumagai, H., Miyake, T, Arai, K and Masai, H. (1999) A fission yeast gene, him1(+)/dfp1(+), encoding a regulatory subunit for Hsk1 kinase, plays essential roles in S-phase initiation as well as in S-phase checkpoint control and recovery from DNA damage Mol. Cell Biol **19**, 5535–5547

54 Brown, G W and Kelly, T. J. (1999) Cell cycle regulation of Dfp1, an activator of the Hsk1 protein kinase Proc Natl Acad. Sci USA **96**, 8443–8448

55 Reynolds, N, Fantes, P A and MacNeill, S A (1999) A key role for replication factor C in DNA replication checkpoint function in fission yeast Nucleic Acids Res **27**, 462–469

56 Shimada, M., Okuzaki, D, Tanaka, S, Tougan, T., Tamai, K K, Shimoda, C and Nojima, H (1999) Replication factor C3 of *Schizosaccharomyces pombe*, a small subunit of replication factor C complex, plays a role in both replication and damage checkpoints Mol Biol Cell **10**, 3991–4003

57 Nishitani, H, Lygerou, Z, Nishimoto, T and Nurse, P (2000) The Cdt1 protein is required to license DNA for replication in fission yeast Nature (London) **404**, 625–628

58 D'Urso, G and Nurse, P (1997) *Schizosaccharomyces pombe* cdc20+ encodes DNA polymerase epsilon and is required for chromosomal replication but not for the S phase checkpoint Proc. Natl Acad Sci. USA **94**, 12491–12496

59 Francesconi, S, De Recondo, A M and Baldacci, G. (1995) DNA polymerase delta is required for the replication feedback control of cell cycle progression in *Schizosaccharomyces pombe* Mol Gen. Genet **246**, 561–569

60 MacNeill, S A, Moreno, S, Reynolds, N, Nurse, P and Fantes, P A (1996) The fission yeast Cdc1 protein, a homologue of the small subunit of DNA polymerase delta, binds to Pol3 and Cdc27. EMBO J **15**, 4613–4628

61 Waseem, N. H, Labib, K, Nurse, P. and Lane, D P (1992) Isolation and analysis of the fission yeast gene encoding polymerase delta accessory protein PCNA EMBO J **11**, 5111–5120

62 Gould, K L, Burns, C G, Feoktistova, A, Hu, C. P., Pasion, S G and Forsburg, S L (1998) Fission yeast cdc24(+) encodes a novel replication factor required for chromosome integrity Genetics **149**, 1221–1233

63 Tanaka, H, Tanaka, K, Murakami, H and Okayama, H (1999) Fission yeast cdc24 is a replication factor C- and proliferating cell nuclear antigen-interacting factor essential for S-phase completion Mol Cell. Biol. **19**, 1038–1048

64 al-Khodairy, F and Carr, A M. (1992) DNA repair mutants defining G2 checkpoint pathways in *Schizosaccharomyces pombe* EMBO J. **11**, 1343–1350

65 al-Khodairy, F, Fotou, E, Sheldrick, K S, Griffiths, D. J, Lehmann, A R and Carr, A M (1994) Identification and characterization of new elements involved in checkpoint and feedback controls in fission yeast Mol Biol Cell **5**, 147–160

66 Rowley, R, Subramani, S. and Young, P G (1992) Checkpoint controls in *Schizosaccharomyces pombe* *rad1* EMBO J **11**, 1335–1342

67 Enoch, T, Carr, A. and Nurse, P (1992) Fission yeast genes involved in coupling mitosis to completion of DNA replication Genes Dev **6**, 2035–2046

68 Jimenez, G, Yucel, J, Rowley, R and Subramani, S (1992) The *rad3*$^+$ gene of *Schizosaccharomyces pombe* is involved in multiple checkpoint functions and in DNA repair Proc Natl Acad Sci U.S.A **89**, 4952–4956

69 Weinert, T (1998) DNA damage checkpoints update getting molecular. Curr Opin Genet. Dev **8**, 185–193

70 Long, K E, Sunnerhagen, P and Subramani, S (1994) The *Schizosaccharomyces pombe* rad1 gene consists of three exons and the cDNA sequence is partially homologous to the Ustilago maydis REC1 cDNA Gene **148**, 155–159

71 Parker, A E, Van de Weyer, I, Laus, M C, Oostveen, I, Yon, J., Verhasselt, P and Luyten, W H (1998) A human homologue of the *Schizosaccharomyces pombe* rad1 + checkpoint gene encodes an exonuclease J Biol Chem. **273**, 18332–18339

72 Thelen, M P, Venclovas, C and Fidelis, K (1999) A sliding clamp model for the Rad1 family of cell cycle checkpoint proteins Cell **96**, 769–770

73 Griffiths, D J, Barbet, N. C., McCready, S, Lehmann, A R and Carr, A M. (1995) Fission yeast rad17: a homologue of budding yeast RAD24 that shares regions of sequence similarity with DNA polymerase accessory proteins EMBO J **14**, 5812–5823

74 Kostrub, C F, Knudsen, K, Subramani, S and Enoch, T (1998) Hus1p, a conserved fission yeast checkpoint protein, interacts with Rad1p and is phosphorylated in response to DNA damage EMBO J **17**, 2055–2066

75 Paciotti, V, Lucchini, G, Plevani, P and Longhese, M P (1998) Mec1p is essential for phosphorylation of the yeast DNA damage checkpoint protein Ddc1p, which physically interacts with Mec3p EMBO J **17**, 4199–4209

76 Kondo, T, Matsumoto, K and Sugimoto, K (1999) Role of a complex containing Rad17, Mec3, and Ddc1 in the yeast DNA damage checkpoint pathway Mol Cell Biol **19**, 1136–1143

77 Parker, A E, Van de Weyer, I, Laus, M C, Verhasselt, P and Luyten, W H (1998) Identification of a human homologue of the *Schizosaccharomyces pombe* rad17 + checkpoint gene J Biol Chem **273**, 18340–18346

78 Shimomura, T., Ando, S, Matsumoto, K. and Sugimoto, K (1998) Functional and physical interaction between Rad24 and Rfc5 in the yeast checkpoint pathways Mol Cell Biol **18**, 5485–5491

79 Edwards, R J, Bentley, N J and Carr, A M (1999) A Rad3-Rad26 complex responds to DNA damage independently of other checkpoint proteins Nat Cell Biol **1**, 393–398

80 Naito, T, Matsuura, A and Ishikawa, F (1998) Circular chromosome formation in a fission yeast mutant defective in two ATM homologues Nat Genet **20**, 203–206

81 Bentley, N J, Holtzman, D. A, Flaggs, G, Keegan, K S, DeMaggio, A, Ford, J C, Hoekstra, M and Carr, A M (1996) The *Schizosaccharomyces pombe* rad3 checkpoint gene EMBO J **15**, 6641–6651

82 Walworth, N, Davey, S and Beach, D (1993) Fission yeast chk1 protein kinase links the rad checkpoint pathway to cdc2. Nature (London) **363**, 368–371

83 Murakami, H and Okayama, H (1995) A kinase from fission yeast responsible for blocking mitosis in S phase Nature (London) **374**, 817–819

84 Murakami, H and Okayama, H (1997) Cell cycle checkpoint control Exp Mol. Med **29**, 1–11

85 Boddy, M N, Furnari, B, Mondesert, O. and Russell, P (1998) Replication checkpoint enforced by kinases Cds1 and Chk1 Science **280**, 909–912

86 Lindsay, H D., Griffiths, D J, Edwards, R J, Christensen, P U, Murray, J M, Osman, F, Walworth, N and Carr, A M (1998) S-phase-specific activation of Cds1 kinase defines a subpathway of the checkpoint response in Schizosaccharomyces pombe Genes Dev **12**, 382–395

87 Zeng, Y, Forbes, K C, Wu, Z, Moreno, S, Piwnica-Worms, H and Enoch, T (1998) Replication checkpoint requires phosphorylation of the phosphatase Cdc25 by Cds1 or Chk1 Nature (London) **395**, 507–510

88 Hofmann, K and Bucher, P (1995) The FHA domain a putative nuclear signalling domain found in protein kinases and transcription factors Trends Biochem Sci **20**, 347–349

89 Sun, Z, Hsiao, J, Fay, D S and Stern, D F (1998) Rad53 FHA domain associated with phosphorylated Rad9 in the DNA damage checkpoint Science **281**, 272–274

90 Fay, D S, Sun, Z and Stern, D F (1997) Mutations in SPK1/RAD53 that specifically abolish checkpoint but not growth-related functions Curr Genet **31**, 97–105

91 Bork, P, Hofmann, K, Bucher, P., Neuwald, A. F, Altschul, S F. and Koonin, E V (1997) A superfamily of conserved domains in DNA damage-responsive cell cycle checkpoint proteins Faseb J. **11**, 68–76

92 Saka, Y, Esashi, F, Matsusaka, T, Mochida, S and Yanagida, M (1997) Damage and replication checkpoint control in fission yeast is ensured by interactions of Crb2, a protein with BRCT motif, with Cut5 and Chk1 Genes Dev. **11**, 3387–3400

93 Willson, J, Wilson, S, Warr, N and Watts, F Z (1997) Isolation and characterization of the *Schizosaccharomyces pombe* rhp9 gene a gene required for the DNA damage checkpoint but not the replication checkpoint Nucleic Acids Res **25**, 2138–2146

94 Esashi, F and Yanagida, M (1999) Cdc2 phosphorylation of Crb2 is required for re-establishing cell cycle progression after the damage checkpoint. Mol Cell **4**, 167–174

95 Furnari, B, Rhind, N and Russell, P (1997) Cdc25 mitotic inducer targeted by chk1 DNA damage checkpoint kinase. Science **277**, 1495–1497

96 O'Connell, M J, Raleigh, J M, Verkade, H M and Nurse, P (1997) Chk1 is a wee1 kinase in the G2 DNA damage checkpoint inhibiting cdc2 by Y15 phosphorylation EMBO J **16**, 545–554

97 Nurse, P (1997) Checkpoint pathways come of age Cell **91**, 865–867

98 Furnari, B., Blasina, A, Boddy, M N, McGowan, C H. and Russell, P (1999) Cdc25 inhibited in vivo and in vitro by checkpoint kinases Cds1 and Chk1 Mol Biol Cell **10**, 833–845

99 Zeng, Y and Piwnica-Worms, H (1999) DNA damage and replication checkpoints in fission yeast require nuclear exclusion of the Cdc25 phosphatase via 14–3-3 binding Mol Cell Biol **19**, 7410–7419

100 Lopez-Girona, A, Furnari, B, Mondesert, O and Russell, P (1999) Nuclear localization of Cdc25 is regulated by DNA damage and a 14–3-3 protein Nature (London) **397**, 172–175

101 Ford, J C, al-Khodairy, F, Fotou, E, Sheldrick, K S, Griffiths, D J and Carr, A M (1994) 14–3-3 protein homologs required for the DNA damage checkpoint in fission yeast. Science **265**, 533–535

102 Enoch, T and Nurse, P (1990) Mutation of fission yeast cell cycle control genes abolishes dependence of mitosis on DNA replication Cell **60**, 665–673

103 Rhind, N, Furnari, B and Russell, P. (1997) Cdc2 tyrosine phosphorylation is required for the DNA damage checkpoint in fission yeast Genes Dev **11**, 504–511

104 Rhind, N and Russell, P (1998) Tyrosine phosphorylation of cdc2 is required for the replication checkpoint in *Schizosaccharomyces pombe* Mol Cell Biol **18**, 3782–3787

105 Rowley, R, Hudson, J and Young, P G (1992) The wee1 protein kinase is required for radiation-induced mitotic delay Nature (London) **356**, 353–355

106 Enoch, T, Gould, K L and Nurse, P (1991) Mitotic checkpoint control in fission yeast Cold Spring Harbor Symp Quant Biol **56**, 409–416

107 Knudsen, K E, Knudsen, E S, Wang, J Y and Subramani, S (1996) p34^{cdc2} kinase activity is maintained upon activation of the replication checkpoint in *Schizosaccharomyces pombe* Proc Natl Acad Sci U S A **93**, 8278–8283

108 Amon, A, Surana, U, Muroff, I and Nasmyth, K (1992) Regulation of p34CDC28 tyrosine phosphorylation is not required for entry into mitosis in *S cerevisiae* Nature (London) **355**, 368–371

109 Sorger, P K and Murray, A W (1992) S-phase feedback control in budding yeast independent of tyrosine phosphorylation of p34cdc28 Nature (London) **355**, 365–368

110 Stueland, C S., Lew, D J, Cismowski, M J and Reed, S I (1993) Full activation of p34CDC28 histone H1 kinase activity is unable to promote entry into mitosis in checkpoint-arrested cells of the yeast *Saccharomyces cerevisiae* Mol Cell Biol **13**, 3744–3755

111 Li, X and Cai, M (1997) Inactivation of the cyclin-dependent kinase Cdc28 abrogates cell cycle arrest induced by DNA damage and disassembly of mitotic spindles in *Saccharomyces cerevisiae* Mol Cell Biol **17**, 2723–2734

112 Yamamoto, A, Guacci, V and Koshland, D (1996) Pds1p, an inhibitor of anaphase in budding yeast, plays a critical role in the APC and checkpoint pathway(s) J Cell Biol. **133**, 99–110

113 Cohen-Fix, O and Koshland, D (1997) The anaphase inhibitor of *Saccharomyces cerevisiae* Pds1p is a target of the DNA damage checkpoint pathway Proc Natl Acad Sci U.S.A **94**, 14361–14366

114 Sanchez, Y, Bachant, J, Wang, H, Hu, F, Liu, D, Tetzlaff, M and Elledge, S J (1999) Control of the DNA damage checkpoint by chk1 and rad53 protein kinases through distinct mechanisms Science **286**, 1166–1171

115 Glover, D M, Hagan, I M. and Tavares, A A (1998) Polo-like kinases a team that plays throughout mitosis Genes Dev **12**, 3777–3787

116 Nigg, E A (1998) Polo-like kinases positive regulators of cell division from start to finish Curr Opin Cell Biol **10**, 776–783

117 Cheng, L, Hunke, L and Hardy, C F. J (1998) Cell cycle regulation of the *Saccharomyces cerevisiae* polo-like kinase cdc5p Mol Cell Biol **18**, 7360–7370

118 Esposito, R E and Klapholz, S (1981) Meiosis and Ascospore Development (Strathern, J N, Jones, E W. and Broach, J R, eds), pp. 211–287, Cold Spring Harbor Laboratory, Cold Spring Harbor, New York

119 Fox, M E and Smith, G R (1998) Control of meiotic recombination in *Schizosaccharomyces pombe* Prog Nucleic Acid Res Mol Biol. **61**, 345–378

120 Yamamoto, M, Imai, Y. and Watanabe, Y (1997) Mating and Sporulation in *Sclizosaccharomyces pombe* (Pringle, J R, Broach, J R and Jones, E W, eds) 1035–1106, Cold Spring Harbor Laboratory, Cold Spring Harbor, New York

121 Roeder, G S (1997) Meiotic chromosomes it takes two to tango. Genes Dev **11**, 2600–2621

122 Kleckner, N. (1996) Meiosis how could it work? Proc Natl Acad Sci U S A **93**, 8167–8174

123 Williamson, D H, Johnston, L H, Fennell, D J and Simchen, G (1983) The timing of the S phase and other nuclear events in yeast meiosis Exp Cell Res **145**, 209–217

124 Callan, H G (1974) DNA replication in the chromosomes of eukaryotes Cold Spring Harb Symp Quant Biol **38**, 195–203

125 Stern, B and Nurse, P (1997) Fission yeast pheromone blocks S-phase by inhibiting the G1 cyclin B-p34cdc2 kinase EMBO J **16**, 534–544

126 Stern, B and Nurse, P. (1998) Cyclin B proteolysis and the cyclin-dependent kinase inhibitor rum1p are required for pheromone-induced G1 arrest in fission yeast Mol Biol Cell **9**, 1309–1321

127 Yamaguchi, S, Murakami, H and Okayama, H (1997) A WD repeat protein controls the cell cycle and differentiation by negatively regulating Cdc2/B-type cyclin complexes Mol Biol Cell **8**, 2475–2486

128 Kitamura, K, Maekawa, H and Shimoda, C (1998) Fission yeast Ste9, a homolog of Hct1/Cdh1 and Fizzy-related, is a novel negative regulator of cell cycle progression during G1-phase Mol Biol Cell **9**, 1065–1080

129 Morgan, D O (1999) Regulation of the APC and the exit from mitosis Nat Cell Biol **1**, E47–E53

130 Aves, S J, Durkacz, B W, Carr, A and Nurse, P (1985) Cloning, sequencing and transcriptional control of the *Schizosaccharomyces pombe* cdc10 'start' gene EMBO J **4**, 457–463

131 Tanaka, K, Okazaki, K, Okazaki, N, Ueda, T, Sugiyama, A, Nojima, H and Okayama, H (1992) A new cdc gene required for S phase entry of *Schizosaccharomyces pombe* encodes a protein similar to the cdc 10+ and SWI4 gene products EMBO J. **11**, 4923–4932

132 Caligiuri, M and Beach, D (1993) Sct1 functions in partnership with Cdc10 in a transcription complex that activates cell cycle START and inhibits differentiation Cell **72**, 607–619

133 Miyamoto, M, Tanaka, K and Okayama, H (1994) res2+, a new member of the cdc10+/SWI4 family, controls the 'start' of mitotic and meiotic cycles in fission yeast EMBO J **13**, 1873–1880

134 Nakashima, N, Tanaka, K, Sturm, S and Okayama, H (1995) Fission yeast Rep2 is a putative transcriptional activator subunit for the cell cycle 'start' function of Res2-Cdc10 EMBO J **14**, 4794–4802

135 Zhu, Y., Takeda, T, Nasmyth, K and Jones, N (1994) pct1+, which encodes a new DNA-binding partner of p85cdc10, is required for meiosis in the fission yeast *Schizosaccharomyces pombe* Genes Dev **8**, 885–898

136 Sugiyama, A, Tanaka, K, Okazaki, K, Nojima, H and Okayama, H (1994) A zinc finger protein controls the onset of premeiotic DNA synthesis of fission yeast in a Mei2-independent cascade EMBO J **13**, 1881–1887

137 Ding, R and Smith, G R (1998) Global control of meiotic recombination genes by *Schizosaccharomyces pombe* rec16 (rep1) Mol Gen Genet **258**, 663–670

138 Li, Y F and Smith, G R (1997) The *Schizosaccharomyces pombe* rec16 gene product regulates multiple meiotic events Genetics **146**, 57–67

139 Dirick, L, Goetsch, L., Ammerer, G and Byers, B (1998) Regulation of meiotic S phase by Ime2 and a Clb5,6-associated kinase in *Saccharomyces cerevisiae* Science **281**, 1854–1857

140 Leem, S H, Chung, C N, Sunwoo, Y and Araki, H (1998) Meiotic role of SWI6 in *Saccharomyces cerevisiae* Nucleic Acids Res. **26**, 3154–3158

141 Nurse, P, Thuriaux, P and Nasmyth, K (1976) Genetic control of the cell division cycle in the fission yeast *Schizosaccharomyces pombe* Mol Gen Genet **146**, 167–178

142 Iino, Y, Hiramine, Y and Yamamoto, M (1995) The role of *cdc2* and other genes in meiosis in *Schizosaccharomyces pombe* Genetics **140**, 1235–1245

143 Beach, D, Rodgers, L and Gould, J (1985) ran1+ controls the transition from mitotic division to meiosis in fission yeast Curr Genet **10**, 297–311

144 Grallert, B and Sipiczki, M (1989) Initiation of the second meiotic division in *Schizosaccharomyces pombe* shares common functions with that of mitosis Curr Genet **15**, 231–233

145 Grallert, B and Sipiczki, M (1991) Common genes and pathways in the regulation of the mitotic and meiotic cell cycles of *Schizosaccharomyces pombe* Curr Genet **20**, 199–204

146 Grallert, B and Sipiczki, M (1990) Dissociation of meiotic and mitotic roles of the fission yeast cdc2 gene Mol Gen Genet **222**, 473–475

147 Nakaseko, Y, Niwa, O and Yanagida, M (1984) A meiotic mutant of the fission yeast *Schizosaccharomyces pombe* that produces mature asci containing two diploid spores J Bacteriol **157**, 334–336

148 Murakami, H and Nurse, P (1999) Meiotic DNA replication checkpoint control in fission yeast Genes Dev **13**, 2581–2593

149 Daya Makin, M., Szankasi, P, Tang, L, MacRae, D and Pelech, S. L (1992) Regulation of $p105^{wee1}$ and $p34^{cdc2}$ during meiosis in *Schizosaccharomyces pombe* Biochem Cell Biol **70**, 1088–1096

150 Yamamoto, M (1996) The molecular control mechanisms of meiosis in fission yeast Trends Biochem Sci **21**, 18–22

151 Watanabe, Y, Shinozaki-Yabana, S, Chikashige, Y, Hiraoka, Y and Yamamoto, M (1997) Phosphorylation of RNA-binding protein controls cell cycle switch from mitotic to meiotic in fission yeast Nature (London) **386**, 187–190

152 Watanabe, Y and Yamamoto, M (1994) *S pombe mei2*$^{+}$ encodes an RNA-binding protein essential for premeiotic DNA synthesis and meiosis I, which co-operates with a novel RNA species meiRNA Cell **78**, 487–498

153 Shuster, E O and Byers, B (1989) Pachytene arrest and other meiotic effects of the start mutations in *Saccharomyces cerevisiae* Genetics **123**, 29–43

154 Stuart, D and Wittenberg, C. (1998) CLB5 and CLB6 are required for premeiotic DNA replication and activation of the meiotic S/M checkpoint Genes Dev **12**, 2698–2710

155 Colomina, N, Gari, E, Gallego, C, Herrero, E and Aldea, M (1999) G1 cyclins block the Ime1 pathway to make mitosis and meiosis incompatible in budding yeast EMBO J **18**, 320–329

156 Kupiec, M, Byers, B, Esposito, R E and Mitchell, A P (1997) Meiosis and Sporulation in *Saccharomyces cerevisiae* (Pringle, J R., Broach, J R and Jones, E W, eds), pp 889–1036, Cold Spring Harbor Laboratory, Cold Spring Harbor, New York

157 Schneider, B L, Yang, Q H and Futcher, A B (1996) Linkage of replication to start by the Cdk inhibitor Sic1 Science **272**, 560–562

158 Yoshida, M, Kawaguchi, H, Sakata, Y, Kominami, K., Hirano, M, Shima, H, Akada, R and Yamashita, I. (1990) Initiation of meiosis and sporulation in *Saccharomyces cerevisiae* requires a novel protein kinase homologue Mol Gen Genet **221**, 176–186

159 Foiani, M., Nadjar-Boger, E, Capone, R, Sagee, S, Hashimshoni, T and Kassir, Y (1996) A meiosis-specific protein kinase, Ime2, is required for the correct timing of DNA replication and for spore formation in yeast meiosis Mol Gen Genet **253**, 278–288

160 Kominami, K, Sakata, Y, Sakai, M and Yamashita, I (1993) Protein kinase activity associated with the IME2 gene product, a meiotic inducer in the yeast *Saccharomyces cerevisiae* Biosci Biotechnol Biochem **57**, 1731–1735

161 Chu, S and Herskowitz, I (1998) Gametogenesis in yeast is regulated by a transcriptional cascade dependent on Ndt80 Mol Cell **1**, 685–696

162 Grandin, N and Reed, S I (1993) Differential function and expression of *Saccharomyces cerevisiae* B-type cyclins in mitosis and meiosis Mol Cell Biol **13**, 2113–2125

163 Fogarty, P, Campbell, S D., Abu-Shumays, R, Phalle, B S, Yu, K R, Uy, G L, Goldberg, M L and Sullivan, W (1997) The *Drosophila* grapes gene is related to checkpoint gene chk1/rad27 and is required for late syncytial division fidelity Curr Biol **7**, 418–426

164 Su, T T, Walker, J. and Stumpff, J (2000) Activating the DNA damage checkpoint in a developmental context Curr Biol **10**, 119–126

165 Ye, X S, Fincher, R R, Tang, A., O'Donnell, K and Osmani, S A (1996) Two S-phase checkpoint systems, one involving the function of both BIME and Tyr15 phosphorylation of $p34^{cdc2}$, inhibit NIMA and prevent premature mitosis. EMBO J **15**, 3599–3610

166 Kumagai, A and Dunphy, W G (1995) Control of the Cdc2/cyclin B complex in *Xenopus* egg extracts arrested at a G2/M checkpoint with DNA synthesis inhibitors Mol Biol Cell **6**, 199–213

167 Kumagai, A, Guo, Z, Emami, K H, Wang, S X and Dunphy, W G (1998) The *Xenopus* Chk1 protein kinase mediates a caffeine-sensitive pathway of checkpoint control in cell-free extracts J Cell Biol **142**, 1559–1569

168 Blasina, A, Paegle, E S and McGowan, C H (1997) The role of inhibitory phosphorylation of CDC2 following DNA replication block and radiation-induced damage in human cells Mol Biol Cell **8**, 1013–1023

169 Jin, P, Gu, Y and Morgan, D O (1996) Role of inhibitory CDC2 phosphorylation in radiation-induced G2 arrest in human cells J Cell Biol **134**, 963–970

170 Toyoshima, F, Moriguchi, T, Wada, A, Fukuda, M and Nishida, E (1998) Nuclear export of cyclin B1 and its possible role in the DNA damage-induced G2 checkpoint EMBO J **17**, 2728–2735

171 Jin, P, Hardy, S and Morgan, D O (1998) Nuclear localization of cyclin B1 controls mitotic entry after DNA damage J Cell Biol **141**, 875–885

172 Bishop, D K, Park, D, Xu, L and Kleckner, N (1992) DMC1: a meiosis-specific yeast homolog of *E coli* recA required for recombination, synaptonemal complex formation, and cell cycle progression Cell **69**, 439–456

173 Xu, L, Weiner, B M and Kleckner, N (1997) Meiotic cells monitor the status of the interhomolog recombination complex Genes Dev **11**, 106–118

174 Lydall, D, Nikolsky, Y, Bishop, D K and Weinert, T (1996) A meiotic recombination checkpoint controlled by mitotic checkpoint genes Nature (London) **383**, 840–843

175 Leu, J-Y and Roeder, G S (1999) The pachytene checkpoint in *S. cerevisiae* depends on Swe1-mediated phosphorylation of the cyclin-dependent kinase Cdc28 Mol Cell **4**, 805–814

176 San-Segundo, P A and Roeder, G S (1999) Pch2 links chromatin silencing to meiotic checkpoint control. Cell **97**, 313–324

177 Smith, A V. and Roeder, G S. (1997) The yeast Red1 protein localizes to the cores of meiotic chromosomes J Cell Biol. **136**, 957–967

178 Bailis, J M and Roeder, G S (1998) Synaptonemal complex morphogenesis and sister-chromatid cohesion require Mek1-dependent phosphorylation of a meiotic chromosomal protein. Genes Dev **12**, 3551–3563

179 Weber, L and Byers, B (1992) A RAD9-dependent checkpoint blocks meiosis of cdc13 yeast cells Genetics **131**, 55–63

180 Nasmyth, K (1999) Separating sister chromatids Trends Biochem Sci **24**, 98–104

181 Guacci, V., Koshland, D and Strunnikov, A (1997) A direct link between sister chromatid cohesion and chromosome condensation revealed through the analysis of MCD1 in *S cerevisiae* Cell **91**, 47–57

182 Michaelis, C., Ciosk, R and Nasmyth, K (1997) Cohesins chromosomal proteins that prevent premature separation of sister chromatids Cell **91**, 35–45

183 Toth, A, Ciosk, R, Uhlmann, F., Galova, M, Schleiffer, A and Nasmyth, K. (1999) Yeast cohesin complex requires a conserved protein, Eco1p(Ctf7), to establish cohesion between sister chromatids during DNA replication Genes Dev **13**, 320–333

184 Yanagida, M (2000) Cell cycle mechanisms of sister chromatid separation; Roles of Cut1/separin and Cut2/securin Genes Cells **5**, 1–8

185 Hirano, T (1999) SMC-mediated chromosome mechanics: a conserved scheme from bacteria to vertebrates? Genes Dev. **13**, 11–19

186 Uhlmann, F, Lottspeich, F and Nasmyth, K (1999) Sister-chromatid separation at anaphase onset is promoted by cleavage of the cohesin subunit Scc1 Nature (London) **400**, 37–42

187 Ciosk, R, Zachariae, W, Michaelis, C, Shevchenko, A, Mann, M and Nasmyth, K. (1998) An ESP1/PDS1 complex regulates loss of sister chromatid cohesion at the metaphase to anaphase transition in yeast. Cell **93**, 1067–1076

188 Cohen-Fix, O, Peters, J M., Kirschner, M W and Koshland, D (1996) Anaphase initiation in *Saccharomyces cerevisiae* is controlled by the APC-dependent degradation of the anaphase inhibitor Pds1p. Genes Dev **10**, 3081–3093

189 Visintin, R, Prinz, S and Amon, A. (1997) CDC20 and CDH1 a family of substrate-specific activators of APC- dependent proteolysis Science **278**, 460–463

190 Bickel, S E and Orr-Weaver, T L (1996) Holding chromatids together to ensure they go their separate ways Bioessays **18**, 293–300

191 Molnar, M, Bahler, J., Sipiczki, M and Kohli, J (1995) The rec8 gene of *Schizosaccharomyces pombe* is involved in linear element formation, chromosome pairing and sister-chromatid cohesion during meiosis Genetics **141**, 61–73

192 Watanabe, Y. and Nurse, P (1999) Cohesin Rec8 is required for reductional chromosome segregation at meiosis Nature (London) **400**, 461–464

193 Parisi, S, McKay, M. J., Molnar, M, Thompson, M A, van der Spek, P J, van Drunen-Schoenmaker, E, Kanaar, R, Lehmann, E., Hoeijmakers, J H and Kohli, J. (1999) Rec8p, a meiotic recombination and sister chromatid cohesion phosphoprotein of the Rad21p family conserved from fission yeast to humans Mol Cell Biol **19**, 3515–3528

194 Klein, F, Mahr, P, Galova, M, Buonomo, S. B., Michaelis, C, Nairz, K. and Nasmyth, K. (1999) A central role for cohesins in sister chromatid cohesion, formation of axial elements, and recombination during yeast meiosis Cell **98**, 91–103

195 Cooper, J. P., Nimmo, E R, Allshire, R. C. and Cech, T R (1997) Regulation of telomere length and function by a Myb-domain protein in fission yeast Nature (London) **385**, 744–747

196 Nimmo, E. R., Pidoux, A L, Perry, P E and Allshire, R C (1998) Defective meiosis in telomere-silencing mutants of *Schizosaccharomyces pombe*. Nature (London) **392**, 825–828

197 Cooper, J P, Watanabe, Y and Nurse, P (1998) Fission yeast Taz1 protein is required for meiotic telomere clustering and recombination Nature (London) **392**, 828–831

198 Hiraoka, Y (1998) Meiotic telomeres a matchmaker for homologous chromosomes Genes Cells **3**, 405–413

199 Chikashige, Y, Ding, D Q, Funabiki, H, Haraguchi, T, Mashiko, S., Yanagida, M and Hiraoka, Y (1994) Telomere-led premeiotic chromosome movement in fission yeast Science **264**, 270–273

200 Chikashige, Y, Ding, D Q, Imai, Y, Yamamoto, M, Haraguchi, T and Hiraoka, Y (1997) Meiotic nuclear reorganization: switching the position of centromeres and telomeres in the fission yeast *Schizosaccharomyces pombe* EMBO J. **16**, 193–202

201 Furuno, N, Nishizawa, M, Okazaki, K, Tanaka, H, Iwashita, J., Nakajo, N., Ogawa, Y. and Sagata, N (1994) Suppression of DNA replication via Mos function during meiotic divisions in *Xenopus* oocytes EMBO J **13**, 2399–2410

202 Picard, A, Galas, S, Peaucellier, G. and Doree, M (1996) Newly assembled cyclin B-cdc2 kinase is required to suppress DNA replication between meiosis I and meiosis II in starfish oocytes EMBO J **15**, 3590–3598

203 Ohsumi, K, Sawada, W. and Kishimoto, T (1994) Meiosis-specific cell cycle regulation in maturing *Xenopus* oocytes J. Cell Sci. **107**, 3005–3013

204 Nakajo, N, Yoshitome, S., Iwashita, J, Iida, M, Uto, K., Ueno, S, Okamoto, K and Sagata, N (2000) Absence of Wee1 ensures the meiotic cell cycle in *Xenopus* oocytes Genes Dev **14**, 328–338

Biochem J (2000) 349, 13–17 (Printed in Great Britain)

RESEARCH COMMUNICATION

Regulation of sterol regulatory-element binding protein 1 gene expression in liver: role of insulin and protein kinase B/cAkt

Mark FLEISCHMANN and Patrick B. IYNEDJIAN[1]

Division of Clinical Biochemistry and Experimental Diabetes Research, University of Geneva School of Medicine, 1 Rue Michel-Servet, CH-1211 Geneva 4, Switzerland

Insulin stimulates the transcription of the sterol regulatory-element binding protein (*SREBP*) 1/*ADD1* gene in liver. Hepatocytes in primary culture were used to delineate the insulin signalling pathway for induction of *SREBP1* gene expression. The inhibitors of phosphoinositide 3-kinase (PI 3-kinase), wortmannin and LY 294002, abolished the insulin-dependent increase in SREBP1 mRNA, whereas the inhibitor of the mitogen-activated protein kinase cascade, PD 98059, was without effect. To investigate the role of protein kinase B (PKB)/cAkt downstream of PI 3-kinase, hepatocytes were transduced with an adenovirus encoding a PKB–oestrogen receptor fusion protein. The PKB activity of this recombinant protein was rapidly activated in hepatocytes challenged with 4-hydroxytamoxifen (OHT), as was endogenous PKB in hepatocytes challenged with insulin. The addition of OHT to transduced hepatocytes resulted in accumulation of SREBP1 mRNA, with a time-course and magnitude similar to the effect of insulin in non-transduced cells. The level of SREBP1 mRNA was not increased by OHT in hepatocytes expressing a mutant form of the recombinant protein whose PKB activity was not activated by OHT. Thus acute activation of PKB is sufficient to induce SREBP1 mRNA accumulation in primary hepatocytes, and might be the major signalling event by which insulin induces *SREBP1* gene expression in the liver.

Key words: hepatocytes, PKB/cAkt, sterol regulatory-element binding protein (SREBP).

INTRODUCTION

The sterol regulatory-element binding proteins (SREBPs) are microsomal proteins which serve as precursors to transcriptional activators of the basic helix-loop-helix leucine zipper family. In mammals, two distinct genes termed *SREBP1* [or adipocyte determination and differentiation factor 1 (*ADD1*)] and *SREBP2* have been identified [1–3]. The *SREBP1* gene is transcribed from optional promoters, giving rise to two mRNAs encoding precursors for SREBP1a and SREBP1c respectively [1]. The N-terminal moiety of each SREBP form, which harbours the transactivation and basic helix-loop-helix leucine zipper DNA-binding domains, is released from the full-length precursor by a two-step proteolytic cleavage, and is imported into the nucleus to activate the transcription of specific genes. The cleavage process is known to be activated when intracellular level of sterols are low, and inhibited when levels are high [4].

The three forms of SREBP bind *cis*-acting elements of the SRE or E-box types [5], and are collectively involved in the transcriptional regulation of genes, encoding the low-density lipoprotein receptor and key enzymes of cholesterol and triacylglycerol biosynthesis [4]. Enzymes of fatty acid synthesis such as acetyl-CoA carboxylase and fatty acid synthase appear to be preferentially regulated by the products of the *SREBP1* gene, in particular by SREBP1c in liver and adipose tissue [6,7]. This factor might also be a critical transcriptional activator of the gene for the regulatory enzyme of hepatic glucose metabolism, glucokinase [8].

Because glucokinase and the enzymes of triacylglycerol synthesis are inducible, the question arose whether *SREBP1* gene expression might itself be hormonally regulated. Indeed, insulin was recently shown to stimulate the accumulation of SREBP1 mRNA in adipocytes and hepatocytes [7,9]. The present study addresses the mechanism of insulin signalling for induction of *SREBP1* gene expression in hepatocytes. The effects of inhibitors of individual signal transduction pathways are reported. In addition, the specific role of protein kinase B (PKB)/cAkt, a protein kinase critically involved in the metabolic actions of insulin [10,11], is analysed in cultured hepatocytes transduced with an adenovirus vector encoding a conditionally active form of PKB.

EXPERIMENTAL

Hepatocyte culture and transduction with adenovirus

Hepatocytes were isolated and cultured as described previously [12], except that the dexamethasone concentration in the medium was reduced to 10^{-8} M. Transduction with adenoviral vectors was performed 4 h after placing cells in culture The hepatocytes, in 10-cm dishes, were exposed to recombinant viruses in 3 ml of culture medium for 1 h. The medium was removed and the hepatocytes were cultured in 10 ml of virus-free medium for 15 h. The culture medium was replaced once more and the desired effectors were supplied to the cells 2 h after the last medium change Inhibitors were supplied to cells 30 min before insulin, and in the case of wortmannin again at 2 h and 4 h after insulin. Cells were harvested at specified times after effector addition for isolation of total RNA as described [12].

Abbreviations used SREBP, sterol regulatory-element binding protein; ADD1, adipocyte determination and differentiation factor 1; OHT, 4-hydroxytamoxifen, PI 3-kinase, phosphoinositide 3-kinase; PKB, protein kinase B or cAkt, MER, myristoylated AktΔ4–129–oestrogen receptor or myrAktΔ4–129-ER, A2ER, A2myrAktΔ4–129-ER, HA, haemagglutinin

[1] To whom correspondence should be addressed (e-mail iynedjian@medecine unige ch)

Adenovirus vectors

Recombinant DNA fragments encoding the fusion proteins myrAktΔ4–129-ER (MER) and A2myrAktΔ4–129-ER (A2ER) were isolated by *Bam*HI/*Sal*I digestion of pWZLneo retroviral vector plasmids, generously provided by Dr Richard A. Roth (Department of Molecular Pharmacology, Stanford University School of Medicine, Stanford, CA, U.S.A.) [13]. After blunt-ending with the Klenow enzyme, the fragments were inserted into *Swa*I site of the cosmid pAdexCAG [14]. Adenoviral vectors were produced by *in vivo* homologous recombination in 293 cells. Transfection of these cells was performed as described by Miyake et al. [15]. Cloning, propagation and titration of the desired recombinant viruses were according to published procedures [14,15].

Northern-blot assay of mRNAs

Blotting and hybridization with ^{32}P-labelled cDNA probes was performed by described methods [16]. The amounts of probe hybridized to specific RNA bands were quantified by phosphorimaging of the membranes. The rat SREBP1/ADD1 cDNA was kindly made available by Dr Bruce M. Spiegelman (Dana-Farber Cancer Institute, Harvard Medical School, Boston, MA, U.S.A.) [2], and the rat glyceraldehyde 3-phosphate cDNA by Dr Philippe Fort (CRBM-CNRS, Montpellier, France) [17].

Immunoblotting and immunoprecipitation assays of PKB

For detection of MER and A2ER proteins expressed in virally transduced hepatocytes, total protein extracts were prepared as described previously [18]. Known amounts of protein were resolved by SDS/PAGE in 10% polyacrylamide separation gels and transferred to nitrocellulose membranes. Immunoblotting was performed using monoclonal antibodies (12CA5; Roche Molecular Biochemicals) against the haemagglutinin (HA) tag present in the middle of the recombinant proteins.

The protein kinase activity of authentic or recombinant PKB was assayed by immunoprecipitate enzyme assay. Hepatocytes in 10-cm dishes were lysed in 1 ml of cell lysis buffer (New England Biolabs). Precipitation of endogenous PKB was with solid-phase antibodies to PKB (immobilized Akt1G1 monoclonal; New England Biolabs). Precipitation of the recombinant PKBs was with anti-HA immobilized on Protein A–Sepharose as described by Kohn et al. [10]. Precipitates were resuspended in a kinase assay mixture containing a glycogen synthase kinase (GSK)-3 fusion protein (New England Biolabs) as substrate and non-radioactive ATP. The specific PKB reaction product was detected after SDS/PAGE by immunoblotting with Phospho-GSK-3 (Ser21/9) antibodies (New England Biolabs). Secondary antibodies conjugated with horseradish peroxidase were used for detection and revealed by enhanced chemiluminescence.

RESULTS

Insulin induction of SREBP1 mRNA is suppressed by inhibitors of phosphoinositide 3-kinase (PI 3-kinase)

The kinetics of effect of insulin on hepatic SREBP1 mRNA was studied using primary cultures of rat hepatocytes. As shown in Figure 1(A), the level of SREBP1 mRNA began to increase at 4 h after hormone addition and plateaued after 24 h of treatment. Mean increases of SREBP1 mRNA were 6- and 20-fold of the starting level at 8 h and 24 h respectively in four separate hepatocyte experiments.

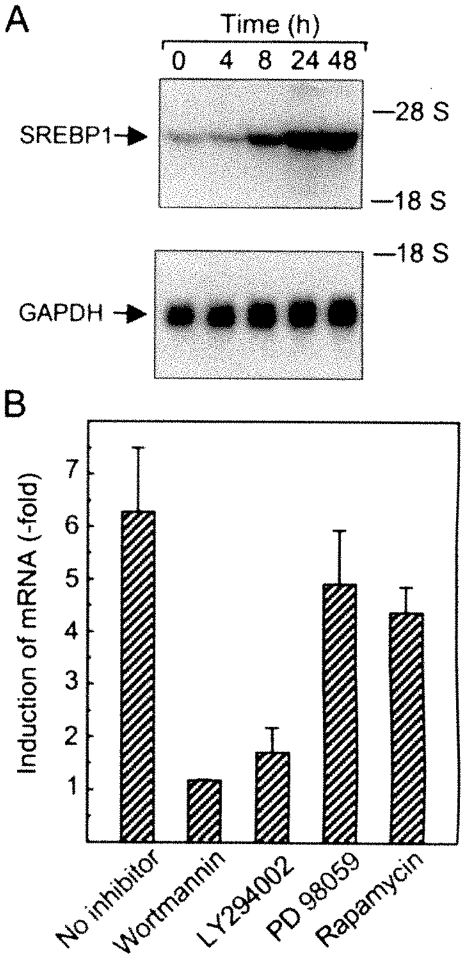

Figure 1 Insulin effect on SREBP1 mRNA: time course and effects of inhibitors

(**A**) Regular human insulin (3×10^{-8} M) was added to hepatocytes at zero time (0) and total cell RNA was extracted at the indicated time points. Autoradiographs of Northern blots using 20 μg RNA per lane hybridized with SREBP1 cDNA or glyceraldehyde-3-phosphate dehydrogenase (GAPDH) cDNA. (**B**) Inhibitors [150 nM wortmannin (3 ×), 50 μM LY 294002, 50 μM PD 98059, 200 nM rapamycin] were added 30 min before insulin, and RNA was extracted 8 h after insulin addition. Levels of SREBP1 mRNA were measured by phosphorimaging of Northern blots. The results are presented as ratios of mRNA in the presence of insulin plus inhibitor over the value with inhibitor alone. The left-most bar shows the increase induced by insulin in the absence of inhibitor. Data are means ± S.E.M. of four independent culture experiments.

The level of SREBP1 mRNA in hepatocytes was investigated 8 h after the addition of insulin to hepatocytes incubated with various inhibitors of insulin signalling pathways (Figure 1B). The inhibitor of PI 3-kinase, wortmannin, abolished the inductive effect of insulin. The insulin-dependent increase in SREBP1 mRNA was also suppressed by LY 294002, a structurally distinct inhibitor of PI 3-kinase. In contrast, the response to insulin was essentially unaffected by PD 98059, an inhibitor of mitogen-activated protein kinase activation, and by rapamycin, an inhibitor of the protein kinase mTOR (mammalian target of rapamycin). With the latter inhibitor, the effect of insulin appeared to be slightly diminished, although the difference did not reach statistical significance. However, the absolute levels of SREBP1 mRNA in both the basal and insulin-stimulated states

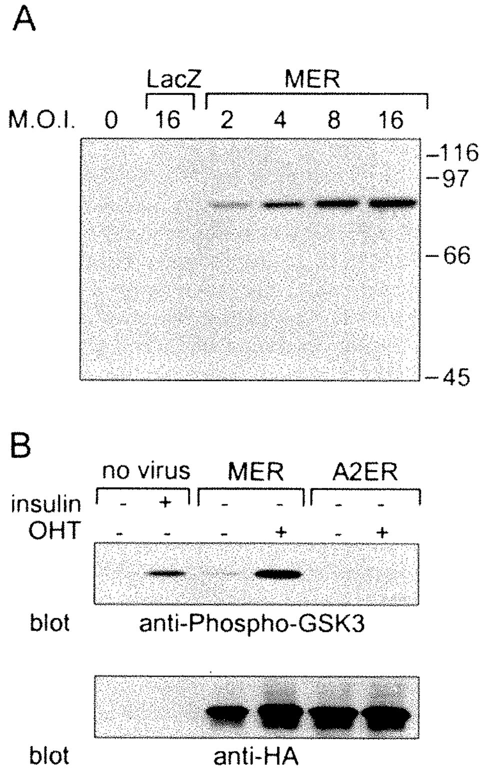

Figure 2 Expression and activation by OHT of PKB–oestrogen receptor fusion protein in adenovirus-transduced hepatocytes

(**A**) Hepatocytes were left uninfected or infected with adenovirus encoding LacZ or MER at the indicated multiplicity of infection (M.O.I.). Cell extracts were prepared 16 h after transduction and samples containing 30 μg protein were subjected to immunoblotting using antibodies to the HA tag. (**B**) Hepatocytes were not infected or infected at an M.O.I. of 4 with virus encoding MER or A2ER. Hepatocytes were left untreated or treated with insulin or OHT for 1 h. Cell extracts from equivalent number of cells were immunoprecipitated using antibodies to PKB (uninfected cells) or HA (cells infected with MER and A2ER viruses). Portions of the immunoprecipitates were assayed for PKB as described in the Experimental section. The phosphorylated GSK3 reaction product was revealed by immunoblot with phospho-specific antibodies. Portions of the immunoprecipitates were separately electrophoresed and blotted with antibodies to HA, to verify similar expression of MER and A2ER.

were reduced to approx. 50 % in presence of rapamycin. The inhibitor effects shown in Figure 1(B) were maximal effects for all of the drugs tested, a point that was verified by dose-response experiments (results not shown).

Expression of a conditionally activatable PKB fusion protein in cultured hepatocytes

The previous results suggested that insulin-dependent induction of SREBP1 required the activation of the PI 3-kinase. The role of PKB, a protein kinase downstream of PI 3-kinase, was investigated next. To this effect, hepatocytes were transduced with an adenoviral vector encoding a conditionally active form of PKB designed by Roth and colleagues [13]. This protein, termed MER (myristoylated AktΔ4–129–oestrogen receptor), is a chimaeric protein made up of a PKB moiety and an oestrogen receptor moiety, with an HA tag inserted to facilitate detection and immunoprecipitation. The expression of MER in transduced hepatocytes was quantified by immunoblotting with anti-HA antibodies (Figure 2A). Transduction with increasing numbers of viral particles resulted in dose-related expression of a recombinant protein with an apparent M_r of 89000, in agreement

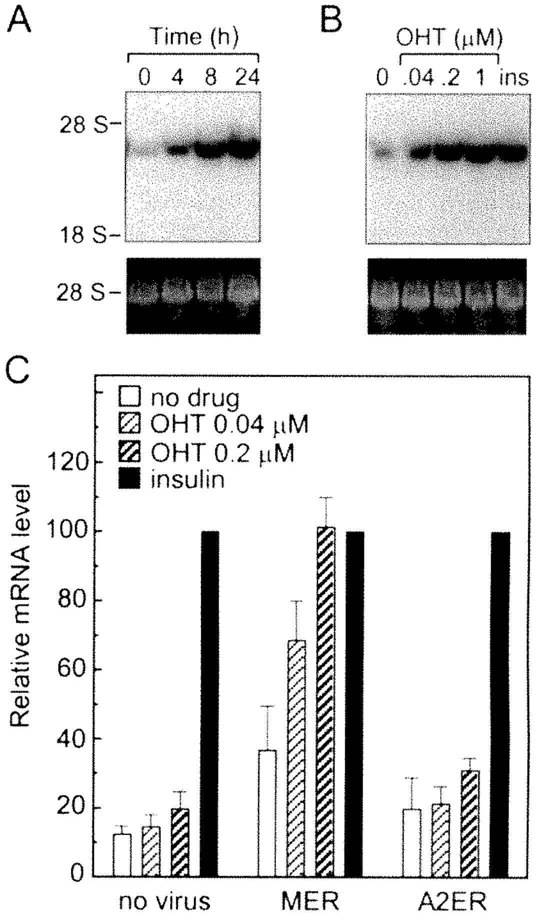

Figure 3 Induction of SREBP1 mRNA by OHT in hepatocytes expressing MER

Hepatocytes were infected with adenovirus encoding MER at a M.O.I. of 4 and were challenged with OHT 16 h after infection. (**A**) Time-course of change in SREBP1 mRNA in hepatocytes incubated with 0.2 μM OHT. (**B**) Dose-response of SREBP1 mRNA with the indicated concentrations of OHT 8 h after drug addition. The right-most lane shows the effect of 3×10^{-8} M insulin (ins) at 8 h. Lower panels in (**A**) and (**B**) depict the 28 S rRNA in the Acridine-Orange stained gel. (**C**) Uninfected hepatocytes or hepatocytes infected with adenovirus encoding MER or A2ER were left untreated, or exposed for 8 h to OHT at the doses indicated or to insulin (3×10^{-8} M). After Northern blotting, SREBP1 mRNA was quantified by phosphorimaging. In each group of cells, mRNA amounts were expressed as a percentage of the amount in cells incubated with insulin. Data are means ± S.D. of values in three independent culture experiments.

with the sequence of MER. This protein was absent both in non-transduced hepatocytes and in control hepatocytes transduced using a lacZ recombinant adenovirus. Staining the latter cells for β-galactosidase activity indicated that the transduction efficiency was 50–80 % at a multiplicity of infection of 4 and ≥ 80 % at a multiplicity of infection of 8 (results not shown).

The ability of the synthetic oestrogen 4-hydroxytamoxifen (OHT) to activate the chimaeric PKB was tested by immunoprecipitate kinase assay. The effect of OHT was compared with that of insulin on authentic PKB in non-transduced hepatocytes. As may be seen in Figure 2(B), hepatocytes transduced with the MER vector and incubated with OHT for 1 h exhibited strong activation of PKB activity of MER immunoprecipitated with anti-HA antibodies. The effect was comparable with the insulin stimulation of authentic PKB precipitated with anti-PKB antibodies in extracts of non-transduced hepatocytes.

For control purposes, hepatocytes were also transduced with a vector encoding a form of the PKB fusion protein termed A2ER, in which the N-terminal myristoylation signal of the fusion protein is inactivated by a Cys-2 → Ala mutation [13] As illustrated in Figure 2(B), the PKB activity of this protein assayed in anti-HA immunoprecipitates was not affected by incubation of the hepatocytes with OHT. Both the mutated and unaltered fusion proteins were expressed at similar levels, as verified by immunoblotting with anti-HA antibodies (bottom panel). The lack of OHT activation of the A2ER protein is consistent with the earlier results of Kohn et al. [13].

Induction of *SREBP1* gene expression by OHT in hepatocytes expressing MER

The effect of OHT on the level of SREBP1 mRNA in hepatocytes transduced with the MER adenovirus was investigated. A time-dependent accumulation of SREBP1 mRNA was noted from 4–24 h after the addition of OHT (0.2 μM), as shown by Northern blotting (Figure 3A). The increase in specific mRNA was dose-related between 0.04 μM and 1 μM OHT (Figure 3B). Data from three separate experiments (Figure 3C) showed that OHT at 0.2 μM was as efficacious for *SREBP1* induction as a maximal concentration of insulin (3×10^{-8} M). Importantly, induction of SREBP1 mRNA by OHT was restricted to hepatocytes expressing MER. A similar effect did not take place in non-transduced hepatocytes, or in hepatocytes transduced with the control A2ER adenovirus.

DISCUSSION

Using the run-on assay, Foretz et al. [7] have shown that insulin stimulates the transcription of the *SREBP1* gene in rat liver cells. Therefore we infer that the regulation of SREBP1 mRNA in our experiments resulted mostly from regulation at a transcriptional level. The predominant transcript of the *SREBP1* gene in liver is by far SREBP1c mRNA, and this form was the major insulin-regulated SREBP1 mRNA identified by RNAse protection assay in hepatocytes [19]. On this basis, the effects reported herein most likely pertain to SREBP1c mRNA, although Northern blotting with SREBP cDNA probes actually does not discriminate between the two mRNAs.

The availability of the OHT-activated PKB fusion protein, and the use of adenovirus vectors to perform gene transfer in a very high percentage of primary hepatocytes, has allowed us to investigate the possible role of PKB in hepatic *SREBP1* gene expression by a direct approach. The data conclusively establish that acute stimulation of PKB activity in isolated hepatocytes is sufficient to cause an increase in SREBP1 mRNA levels. Non-transduced hepatocytes did not induce SREBP1 mRNA in response to OHT. More importantly, SREBP1 mRNA was not increased in hepatocytes expressing a recombinant PKB refractory to activation by OHT. This provides stringent proof that the accumulation of SREBP mRNA after OHT addition to the hepatocytes expressing MER was specifically due to PKB activation. Furthermore, the effect elicited by OHT in cells expressing MER was similar in time-course and magnitude to the effect of insulin in non-transduced hepatocytes.

The insulin effect on *SREBP1* gene expression was virtually unaffected by the MEK inhibitor, PD 98059, and thus does not appear to require activation of the mitogen-activated protein kinase cascade. By contrast, results with wortmannin and LY 294002 clearly implicated the PI 3-kinase signalling pathway. A major consequence of the activation of PI 3-kinase by insulin in many cell types, including hepatocytes, is a stimulation of PKB activity [20,20a]. The collective results of experiments using inhibitors of PI 3-kinase, on the one hand, and conditional activation of PKB, on the other hand, lead us to propose that induction of *SREBP1* gene expression in the liver is most likely mediated via the PI 3-kinase/PKB branch of the insulin signalling pathways. Rapamycin, an inhibitor of mTOR, significantly reduced both induced and basal levels of SREBP1 mRNA, such that a strong insulin stimulation was conserved. However, a possible role of mTOR, which was recently shown to be a substrate for PKB [21], in maintaining basal *SREBP1* gene expression would deserve further investigation.

The PI 3-kinase/PKB signalling pathway is thought to be involved in the insulin regulation of several genes, notably the gene for the insulin-like growth-factor binding protein (IGF-BP) 1 [22] Recently, PKB was shown to phosphorylate several transcriptional activators of the forkhead family, including FKHR, AFX and FKHRL1, *in vitro* and in intact cells. The phosphorylation of specific residues in these factors inhibited their ability to activate transcription of target genes as a result of the sequestration of the phosphorylated factors in the cytoplasm [23–25]. Thus, the insulin-dependent repression of the *IGF-BP1* gene, which harbours a *cis*-acting element capable of binding FKHR in its promoter, might depend, at least in part, on PKB-mediated phosphorylation and inactivation of this forkhead transactivator [22]. However, recent evidence has suggested that additional signals by-passing the PKB pathway might contribute to down-regulate the transactivating potential of FKHR [26]. Similarly, two distinct experimental systems using hepatoma cells have provided data either in favour of or against a critical role of PKB in the negative regulation of the phosphoenolpyruvate carboxykinase gene by insulin [27,28].

Evidence for a role of PKB in the positive regulation of specific gene expression by insulin is more limited. Recent publications suggest that GLUT1 and fatty acid synthase might be induced via PKB activation [29,30]. The transcription factors which might be affected directly or indirectly by PKB and transduce positive effects of insulin on gene expression are currently unknown. With respect to *SREBP1* gene expression, the present data strongly suggest that the insulin effect might be mediated by PKB. A proof for this conclusion will require evidence for the abolition of the effect of insulin after complete and specific suppression of PKB activation. Moreover, insulin signalling via several, possibly redundant, pathways remains an intriguing possibility.

We thank Dr Richard A Roth for the gift of plasmids encoding MER and A2ER, and Dr Bruce M Spiegelman for the SREBP1/ADD1 cDNA plasmid The advice on the production and use of recombinant adenoviruses by Hisamitzu Ishihara, and his gift of the *Swa*I linearized pAdexCAG vector and the Ad5–dlX DNA-terminal protein complex, are gratefully acknowledged We thank Asllan Gjinovci for assistance, and Patrick Muzzin for access to his P2 culture facility. This research was supported by grant 32-52455 97 from the Swiss National Science Foundation.

REFERENCES

1 Yokoyama, C , Wang, X , Briggs, M R , Admon, A., Wu, J , Hua, X , Goldstein, J L and Brown, M S (1993) SREBP-1, a basic-helix-loop-helix-leucine zipper protein that controls transcription of the low density lipoprotein receptor gene Cell **75**, 187–197

2 Tontonoz, P , Kim, J B , Graves, R A and Spiegelman, B M (1993) ADD1 a novel helix-loop-helix transcription factor associated with adipocyte determination and differentiation Mol Cell Biol **13**, 4753–4759

3 Hua, X , Yokoyama, C , Wu, J , Briggs, M R , Brown, M S , Goldstein, J L and Wang, X. (1993) SREBP-2, a second basic-helix-loop-helix-leucine zipper protein that stimulates transcription by binding to a sterol regulatory element Proc Natl Acad Sci U.S A **90**, 11603–11607

4 Horton, J D and Shimomura, I (1999) Sterol regulatory element-binding proteins activators of cholesterol and fatty acid biosynthesis Curr Opin Lipidol **10**, 143–150

5 Kim, J B, Spotts, G D, Halvorsen, Y D, Shih, H M, Ellenberger, T, Towle, H C and Spiegelman, B M (1995) Dual DNA binding specificity of ADD1/SREBP1 controlled by a single amino acid in the basic helix-loop-helix domain Mol Cell Biol **15**, 2582–2588

6 Shimano, H, Yahagi, N, Amemiya-Kudo, M, Hasty, A H, Osuga, J, Tamura, Y, Shionoiri, F, Iizuka, Y, Ohashi, K, Harada, K et al (1999) Sterol regulatory element-binding protein-1 as a key transcription factor for nutritional induction of lipogenic enzyme genes J Biol Chem **274**, 35832–35839

7 Foretz, M, Pacot, C, Dugail, I, Lemarchand, P, Guichard, C, Le Liepvre, X, Berthelier-Lubrano, C, Spiegelman, B, Kim, J B, Ferre, P and Foufelle, F (1999) ADD1/SREBP-1c is required in the activation of hepatic lipogenic gene expression by glucose Mol Cell Biol **19**, 3760–3768

8 Foretz, M, Guichard, C, Ferre, P and Foufelle, F (1999) Sterol regulatory element binding protein-1c is a major mediator of insulin action on the hepatic expression of glucokinase and lipogenesis-related genes Proc Natl Acad Sci U S A **96**, 12737–12742

9 Kim, J B, Sarraf, P, Wright, M, Yao, K M, Mueller, E, Solanes, G, Lowell, B B and Spiegelman, B M (1998) Nutritional and insulin regulation of fatty acid synthetase and leptin gene expression through ADD1/SREBP1 J Clin Invest **101**, 1–9

10 Kohn, A D, Kovacina, K S and Roth, R A (1995) Insulin stimulates the kinase activity of RAC-PK, a pleckstrin homology domain containing ser/thr kinase EMBO J **14**, 4288–4295

11 Coffer, P J, Jin, J and Woodgett, J R (1998) Protein kinase B (c-Akt) a multifunctional mediator of phosphatidylinositol 3-kinase activation Biochem J **335**, 1–13

12 Iynedjian, P B, Jotterand, D, Nouspikel, T, Asfari, M and Pilot, P-R (1989) Transcriptional induction of glucokinase gene by insulin in cultured liver cells and its repression by the glucagon-cAMP system J Biol Chem **264**, 21824–21829

13 Kohn, A D, Barthel, A, Kovacina, K S, Boge, A, Wallach, B, Summers, S A, Birnbaum, M J, Scott, P H, Lawrence, Jr, J C and Roth, R A (1998) Construction and characterization of a conditionally active version of the serine/threonine kinase Akt J Biol Chem **273**, 11937–11943

14 Kiwaki, K, Kanegae, Y, Saito, I, Komaki, S, Nakamura, K., Miyazaki, J I, Endo, F and Matsuda, I (1996) Correction of ornithine transcarbamylase deficiency in adult spf(ash) mice and in OTC-deficient human hepatocytes with recombinant adenoviruses bearing the CAG promoter Hum Gene Ther **7**, 821–830

15 Miyake, S, Makimura, M, Kanegae, Y, Harada, S, Sato, Y, Takamori, K, Tokuda, C and Saito, I (1996) Efficient generation of recombinant adenoviruses using adenovirus DNA-terminal protein complex and a cosmid bearing the full-length virus genome Proc Natl Acad Sci U S A **93**, 1320–1324

16 Iynedjian, P B, Marie, S, Gjinovci, A, Genin, B, Deng, S-P, Buhler, L, Morel, P and Mentha, G (1995) Glucokinase and phosphoenolpyruvate carboxykinase (GTP) in the human liver Regulation of gene expression in cultured hepatocytes J Clin Invest **95**, 1966–1973

17 Fort, P, Marty, L, Piechaczyk, M, el Sabrouty, S, Dani, C, Jeanteur, P and Blanchard, J M (1985) Various rat adult tissues express only one major mRNA species from the glyceraldehyde-3-phosphate-dehydrogenase multigenic family Nucleic Acids Res **13**, 1431–1442

18 Bosco, D, Meda, P and Iynedjian, P B (2000) Glucokinase and glucokinase regulatory protein mutual dependence for nuclear localization Biochem J **348**, 215–222

19 Shimomura, I, Bashmakov, Y., Ikemoto, S, Horton, J D, Brown, M S and Goldstein, J L (1999) Insulin selectively increases SREBP-1c mRNA in the livers of rats with streptozotocin-induced diabetes Proc Natl Acad Sci U S A **96**, 13656–13661

20 Shepherd, P R, Withers, D J and Siddle, K (1998) Phosphoinositide 3-kinase the key switch mechanism in insulin signalling Biochem J **333**, 471–490

20a Shepherd, P R, Withers, D J and Siddle, K (1998) Erratum Biochem J **335**, 711

21 Navé, B T, Ouwens, M, Withers, D J, Alessi, D R and Shepherd, P R. (1999) Mammalian target of rapamycin is a direct target for protein kinase B identification of a convergence point for opposing effects of insulin and amino-acid deficiency on protein translation Biochem J **344**, 427–431

22 Guo, S, Rena, G, Cichy, S, He, X, Cohen, P and Unterman, T (1999) Phosphorylation of serine 256 by protein kinase B disrupts transactivation by FKHR and mediates effects of insulin on insulin-like growth factor-binding protein-1 promoter activity through a conserved insulin response sequence J. Biol Chem **274**, 17184–17192

23 Biggs, W. H, Meisenhelder, J, Hunter, T, Cavenee, W K and Arden, K C (1999) Protein kinase B/Akt-mediated phosphorylation promotes nuclear exclusion of the winged helix transcription factor FKHR1 Proc Natl Acad Sci U S A **96**, 7421–7426

24 Takaishi, H, Konishi, H, Matsuzaki, H, Ono, Y, Shirai, Y, Saito, N, Kitamura, T, Ogawa, W, Kasuga, M, Kikkawa, U and Nishizuka, Y (1999) Regulation of nuclear translocation of forkhead transcription factor AFX by protein kinase B Proc Natl Acad Sci U S A **96**, 11836–11841

25 Brunet, A, Bonni, A, Zigmond, M. J, Lin, M Z, Juo, P, Hu, L S, Anderson, M J, Arden, K C, Blenis, J. and Greenberg, M E (1999) Akt promotes cell survival by phosphorylating and inhibiting a Forkhead transcription factor Cell **96**, 857–868

26 Tomizawa, M, Kumaro, A, Perrot, V, Nakae, J, Accili, D and Rechler, M M (2000) Insulin inhibits the activation of transcription by a C-terminal fragment of the forkhead transcription factor FKHR A mechanism for insulin inhibition of insulin-like growth factor-binding protein-1 transcription J Biol Chem **275**, 7289–7295

27 Liao, J, Barthel, A, Nakatani, K and Roth, R A (1998) Activation of protein kinase B/Akt is sufficient to repress the glucocorticoid and cAMP induction of phosphoenolpyruvate carboxykinase gene J Biol Chem **273**, 27320–27324

28 Kotani, K, Ogawa, W, Hino, Y, Kitamura, T, Ueno, H, Sano, W, Sutherland, C, Granner, D K and Kasuga, M (1999) Dominant negative forms of Akt (protein kinase B) and atypical protein kinase Clambda do not prevent insulin inhibition of phosphoenolpyruvate carboxykinase gene transcription J Biol Chem **274**, 21305–21312

29 Barthel, A, Okino, S T, Liao, J, Nakatani, K, Li, J, Whitlock, Jr, J P and Roth, R A (1999) Regulation of GLUT1 gene transcription by the serine/threonine kinase Akt1 J Biol Chem **274**, 20281–20286

30 Wang, D and Sul, H S (1998) Insulin stimulation of the fatty acid synthase promoter is mediated by the phosphatidylinositol 3-kinase pathway Involvement of protein kinase B/Akt J Biol Chem **273**, 25420–25426

Received 3 April 2000/25 April 2000, accepted 3 May 2000

Activation of extracellular signal-regulated protein kinase1,2 results in down-regulation of decorin expression in fibroblasts

Pauliina LAINE*†, Niina REUNANEN*‡, Laura RAVANTI*‡, Marco FOSCHI§, Manoranjan SANTRA||, Renato V. IOZZO|| and Veli-Matti KÄHÄRI*‡¶[1]

*MediCity Research Laboratory and Department of Medical Biochemistry, University of Turku, FIN-20520 Turku, Finland, †Department of Periodontology, University of Turku, FIN-20520 Turku, Finland, ‡Department of Dermatology, University of Turku, FIN-20520 Turku, Finland, §Department of Medicine, University of Florence, Florence 50134, Italy, ||Department of Pathology and Cell Biology, and Kimmel Cancer Center, Thomas Jefferson University, Philadelphia, PA 19107, U.S.A., and ¶Turku Centre for Biotechnology, University of Turku and Åbo Akademi University, FIN-20520 Turku, Finland

Decorin is a small leucine-rich extracellular matrix proteoglycan, the expression of which is down-regulated in proliferating and malignantly transformed cells. In the present study we show that the expression of decorin in fibroblasts is suppressed by epidermal growth factor (EGF) and PMA, and that the effect of both is potently inhibited by blocking the extracellular signal-regulated protein kinase (ERK)1,2 signalling pathway (Raf/MEK1,2/ERK1,2) with the specific MAPK/ERK kinase (MEK)1,2 inhibitor, PD98059. In addition, specific activation of ERK1,2 by adenovirus-mediated expression of constitutively active MEK1 in dermal fibroblasts results in marked reduction in decorin mRNA abundance and production. Co-transfection of NIH-3T3 fibroblasts with human decorin promoter/chloramphenicol acetyltransferase (CAT) construct (pDEC−879/CAT) in combination with the expression vectors for constitutively active Raf-1 and MEK1 markedly suppressed decorin promoter activity. Co-transfections of human decorin promoter 5′-deletion constructs with constitutively active MEK1 expression vector identified the region -278 to -188 as essential for ERK1,2 mediated down-regulation of decorin promoter activity. These results show that activation of the ERK1,2 signalling pathway by a mitogenic growth factor, a tumour promoter or transformation suppresses decorin gene expression in fibroblasts, which in turn may promote proliferation and migration of normal and malignant cells.

Key words: adenovirus, biglycan, EGF, proteoglycan, mitogen-activated protein kinase.

INTRODUCTION

Decorin is a chondroitin/dermatan sulphate proteoglycan, which belongs to the gene family of small leucine-rich proteoglycans that also includes biglycan, fibromodulin and lumican [1,2]. Decorin is an abundant component of the extracellular matrix (ECM) of skin and bone and it associates with type I, II and VI collagen fibrils, and fibronectin *in vivo* [1,2]. In addition, decorin can inhibit the biological activity of transforming growth factor-β (TGF-β) by binding it with the core protein [3].

Decorin is abundantly expressed by normal fibroblasts in which its expression is enhanced by interleukin-1 [4,5] and dexamethasone [6], and inhibited by TGF-β [7], tumour necrosis factor-α (TNF-α) [8] and retinoic acid [6]. The expression of decorin in fibroblasts is cell cycle-dependent; it is low in proliferating cells and high in quiescent cells [8]. Decorin inhibits proliferation of A431 squamous carcinoma cells by binding to epidermal growth factor (EGF) receptors (EGFRs), activating EGFR signalling, including the extracellular signal-regulated protein kinase (ERK)1,2 pathway, and expression of p21 [9–11]. Furthermore, overexpression of decorin in fibroblasts inhibits their proliferation (L. Häkkinen, S. Strassburger, F. Scott, V.-M. Kähäri, K. G. Danielsson, R. V. Iozzo and H. Larjava, unpublished work). These findings are in accordance with previous observations showing that malignant transformation of cells results in loss of decorin expression and that restoration of decorin expression causes growth arrest in malignant cells [12–14]. In addition, viral transformation of human fibroblasts by the v-*src* oncogene results in marked reduction of decorin expression [15].

In the present study we show that in fibroblasts, suppression of decorin expression by EGF and tumour promoter PMA is mediated by the ERK1,2 signalling cascade, and that activation of ERK1,2 by constitutively active MEK1 potently suppresses decorin expression at the transcriptional level. These results show that activation of the ERK1,2 pathway by mitogenic growth factors, tumour promoters or transformation suppresses decorin expression in fibroblasts, which may in turn promote proliferation and migration of normal and malignant cells and play a role in malignant transformation.

MATERIALS AND METHODS

Materials

MEK1,2 inhibitor PD98059 (2′-amino-3′-methoxyflavone) [16], p38 inhibitor SB203580 [4-(4-fluorophenyl)-2-(4-methylsulphinylphenyl)-5-(4-pyridyl)-1*H*-imidazole] [17] and human recombinant EGF were obtained from Calbiochem (San Diego, CA, U.S.A.). PMA was obtained from Sigma (St. Louis, MO, U.S.A.).

Abbreviations used. CAT, chloramphenicol acetyltransferase; CMV, cytomegalovirus, CS, calf serum, DMEM, Dulbecco's modified Eagle's medium, ECM, extracellular matrix, EGF, epidermal growth factor; EGFR, EGF receptor, ERK, extracellular signal-regulated protein kinase, FBS, fetal bovine serum, FCS, fetal CS; GAPDH, glyceraldehyde-3-phosphate dehydrogenase, JNK, c-Jun N-terminal kinase, MAPK, mitogen-activated protein kinase, MEK, MAPK/ERK kinase; MKK, MAPK kinase; MOI, multiplicity of infection, pfu, plaque-forming units, RSV, Rous sarcoma virus, TGF-β, transforming growth factor-β, TNF-α, tumour necrosis factor-α.

[1] To whom correspondence should be addressed (e-mail veli-matti kahari@utu fi)

Cell culture

Normal human skin fibroblasts established by explantation from punch biopsy were obtained from a healthy male volunteer (age 23), and human gingival fibroblasts were derived from healthy gingiva of a 25-year old female. The fibroblasts were cultured in Dulbecco's modified Eagle's medium (DMEM) supplemented with 10 % (v/v) fetal bovine serum (FBS), 2 mM glutamine, 100 units/ml penicillin-G and 100 μg/ml streptomycin Mouse NIH-3T3 fibroblasts (from A.T.C.C.; Rockville, MD, U.S.A.) were cultured in DMEM supplemented with 10 % (v/v) calf serum (CS), 2 mM glutamine, 100 units/ml penicillin-G and 100 μg/ml streptomycin. For experiments, human skin and gingival fibroblasts were maintained in culture medium supplemented with 0.5 % fetal CS (FCS) for 18 h. EGF or PMA was added and incubations were continued for 24 h. In experiments with mitogen-activated protein kinase (MAPK) inhibitors, these were added 1 h prior to the addition of EGF or PMA.

Assay of MAPK activation

The activation of ERK1,2 and p38 MAPK was determined by Western-blotting using antibodies specific for phosphorylated, activated, forms of the corresponding MAPKs (New England Biolabs, Beverly, MA, U.S.A.). Fibroblasts were treated with EGF and PMA in DMEM supplemented with 0 5 % FCS for different periods of time, and lysed in 100 μl of Laemmli sample buffer. The samples were then sonicated, separated by SDS/PAGE (10 % polyacrylamide) and transferred to Hybond ECL® membrane (Amersham, Little Chalfont, Bucks., U K) Western-blotting was performed as described previously [18], with phospho-specific antibodies against ERK1,2 and p38 at 1:1000 dilution, using ECL® for detection (Amersham). As loading controls Western-blots were also performed using antibodies against total p38 (New England Biolabs) at 1·1000 dilution.

Infection of fibroblasts with recombinant adenoviruses

Recombinant replication-deficient adenovirus RAdLacZ (RAd35) [19], which contains the *Escherichia coli* β-galactosidase gene (*LacZ*) driven by the cytomegalovirus (CMV) IE promoter was kindly provided by Dr Gavin W. G. Wilkinson (University of Cardiff, Cardiff, Wales). Construction and characterization of recombinant adenovirus RAdMEK1CA, coding for constitutively active MEK1, driven by the CMV IE promoter, has been described previously [20]. Recombinant adenoviruses RAdMKK3bE [21] and RAdMKK6bE [21], coding for constitutively active MKK3b and MKK6b (where MKK is MAPK kinase), respectively, were kindly provided by Dr Jiahuai Han (Scripps Research Institute, La Jolla, CA, U.S.A.).

Human skin and gingival fibroblasts (5×10^5) in suspension were infected with recombinant adenoviruses RAdLacZ, RAdMEK1CA, RAdMKK3bE or RAdMKK6bE at a multiplicity of infection (MOI) of 500 plaque-forming units (pfu)/cell, plated and incubated for 18 h, as described in [18,22]. Culture medium (DMEM supplemented with 1 % FCS) was changed and conditioned media was collected after 24 h for assay of decorin production. The cell layers were harvested for extraction of total RNA or determination of activation of ERK1,2 and p38 MAPK, as described above.

RNA analysis

Total cellular RNA was isolated from cells using the single-step method [23]. Northern-blot hybridizations were performed as described previously [6,7], using a 1.8 kb human decorin cDNA [24] (kindly provided by Dr Tom Krusius, Finnish Red Cross, Helsinki, Finland), a 1.6 kb human biglycan cDNA [25] (kindly provided by Dr Larry Fisher, NIDR, Bethesda, MD, U.S.A), and a 1.3 kb rat cDNA for glyceraldehyde-3-phosphate dehydrogenase (GAPDH) [26]. The $[^{32}P]$cDNA–mRNA hybrids were visualized by autoradiography Decorin and biglycan mRNA levels were quantified by scanning densitometry, and corrected for the levels of GAPDH mRNA in the same samples.

Assay of decorin production

Equal aliquots of conditioned media were analysed by Western-blotting, as described previously [7] with rabbit antiserum against human decorin (kindly provided by Dr Tom Krusius) at 1·500 dilution Specific binding of antibodies was detected by horseradish peroxidase-conjugated secondary antibodies, followed by ECL® (Amersham). The levels of immunoreactive decorin were quantified by densitometric scanning of the X-ray films.

Transient transfections and chloramphenicol acetyltransferase (CAT) assays

Confluent NIH-3T3 fibroblast cultures were transiently transfected with 5 μg of human decorin promoter/CAT 5′-deletion constructs (pDEC−879/CAT, pDEC−480/CAT, pDEC−326/CAT, pDEC−278/CAT, pDEC−222/CAT, pDEC−188/CAT or pDEC−140/CAT) [8,27] In co-transfections the cells were transfected with pDEC−879/CAT in combination with 5 μg of expression vectors for wild-type MEK1, constitutively active MEK1 [28] (kindly provided by Dr Natalie Ahn, University of Colorado, Boulder, CO, U.S.A.), wild-type ERK1 and ERK2 [29] (kindly provided by Dr Melanie Cobb, Southwestern Medical Center, Dallas, TX, U.S.A.), or constitutively active Raf-1 [30] (kindly provided by Dr Ulf Rapp, University of Würtzburg, Germany). Control cultures were co-transfected in parallel with the respective empty expression vectors.

Transfections were performed using the calcium phosphate/DNA co-precipitation method, followed by a 2 min glycerol shock [31]. The cells were maintained in DMEM and 1 % FBS for 48 h, and CAT activity was measured as described previously [31]. The transfection efficiency was monitored by co-transfecting the cells with 2 μg of Rous sarcoma virus (RSV)/β-galactosidase construct and correcting the CAT activities for β-galactosidase activity [31].

RESULTS

Suppression of decorin expression by EGF and PMA in fibroblasts is mediated by ERK1,2

To examine the regulation of fibroblast decorin gene expression by mitogenic stimuli, we first studied the effect of EGF and protein kinase C activator, phorbol ester PMA, on the expression of decorin mRNA levels by Northern-blot hybridizations. Treatment of dermal fibroblasts with EGF (25 ng/ml) resulted in rapid activation of ERK1,2 and this activation was potently inhibited by blocking the ERK1,2 pathway (Raf/MEK1,2/ERK1,2) by a specific MEK1,2 inhibitor, PD98059 (20 μM) (Figure 1, left-hand upper panel) EGF also rapidly and transiently activated p38 MAPK in fibroblasts, but this activation was not altered by co-treatment with PD98059. As shown in the left-hand middle and lower panels of Figure 1, EGF treatment of cells resulted in the suppression (60 %) of decorin mRNA expression. Interestingly, co-treatment of cells with MEK1,2 inhibitor PD98059 (40 μM) prevented the inhibitory effect of EGF on decorin mRNA expression (left-hand middle and lower panels of Figure 1). In contrast, inhibition of p38 MAPK activity

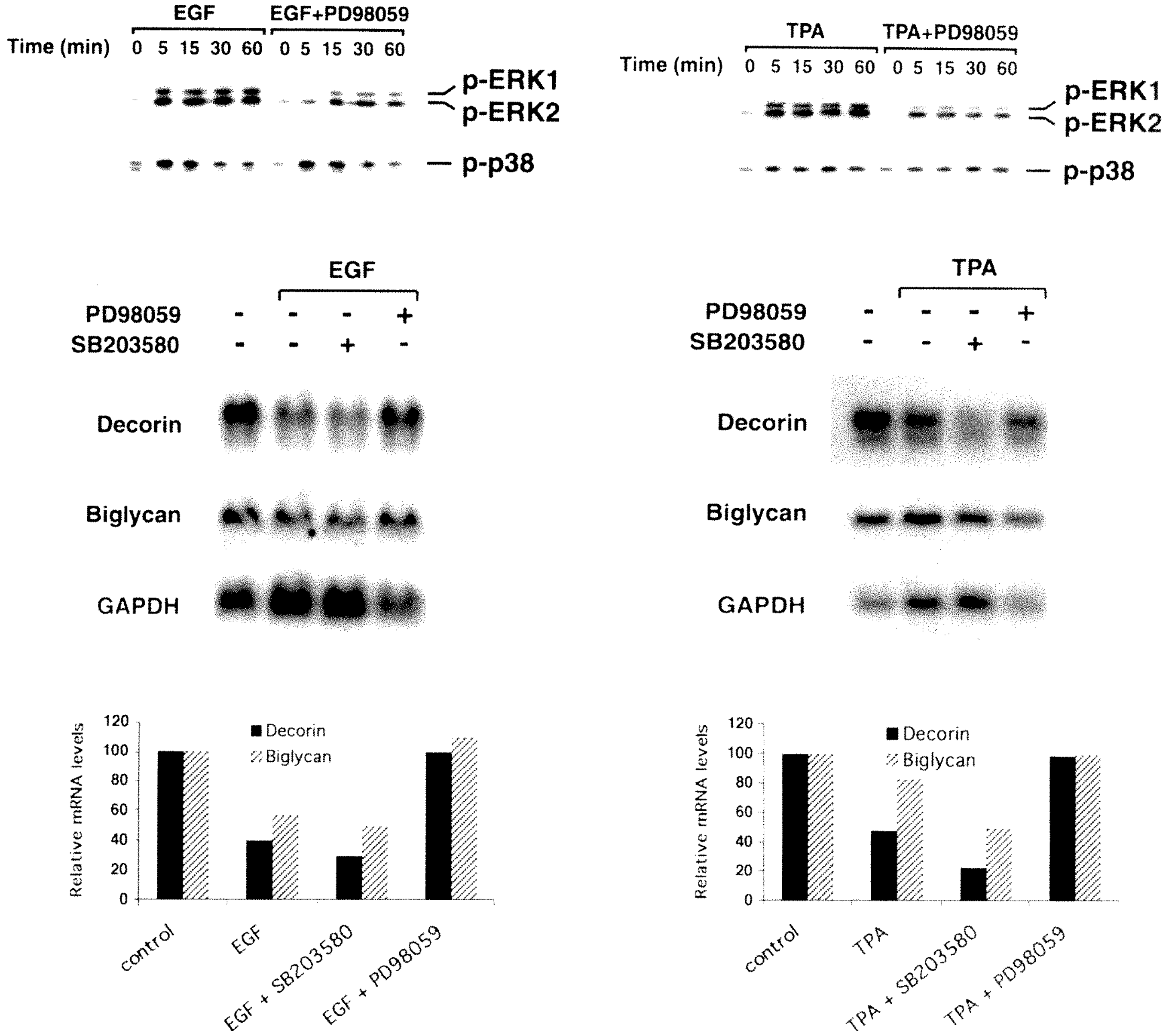

Figure 1 Suppression of decorin expression by EGF and TPA is mediated by ERK1,2

P32197

Upper panels: Confluent cultures of human skin fibroblasts were incubated with (left panel) EGF (25 ng/ml) or (right panel) PMA (60 ng/ml) alone or in combination with MEK1,2 inhibitor PD98059 (20 μM) in DMEM supplemented with 0.5% FCS for different periods of time, as indicated. The levels of activated ERK1 and ERK2 (p-ERK1, p-ERK2), and p38 (p-p38) were determined by Western-blot analysis using phosphospecific antibodies for the corresponding MAPKs. Middle and lower panels: Confluent cultures of human skin fibroblasts in DMEM supplemented with 0.5% FCS were incubated for 24 h with (left panel) EGF (25 ng/ml) or (right panel) PMA (60 ng/ml) alone or in combination with PD98059 (40 μM with EGF and 20 μM with PMA), or with SB203580 (20 μM with EGF and 10 μM with PMA), a selective p38 MAPK inhibitor. The expression of decorin, biglycan and GAPDH mRNAs was analysed by Northern-blot hybridizations of total RNA (12 μg). Densitometric quantifications of decorin and biglycan mRNA levels corrected for GAPDH mRNA levels are shown relative to the levels in untreated control cells (100) (histograms). TPA ≡ PMA.

by SB203580 (20 μM) slightly augmented the down-regulatory effect of EGF on decorin mRNA expression (left-hand middle and lower panels of Figure 1). In the same cultures biglycan mRNA levels were also decreased (by 43%) by EGF and this reduction was inhibited by PD98059 (left-hand middle and lower panels of Figure 1). EGF treatment also inhibited decorin mRNA expression by 78% in human gingival fibroblasts, and the inhibition was in part prevented by PD98059 (results not shown).

Treatment of dermal fibroblasts with PMA (60 ng/ml) also resulted in rapid activation of ERK1,2, and p38 MAPK in dermal fibroblasts, and the activation of ERK1,2 was potently inhibited by PD98059 (right-hand upper panel of Figure 1). PMA also rapidly and transiently activated p38 MAPK in these cells (right-hand upper panel of Figure 1). Treatment of dermal fibroblasts with PMA also resulted in the suppression of the abundance of decorin mRNA (by 52%) and the down-regulation was entirely prevented by PD98059 (20 μM), but not by SB203580 (10 μM) (right-hand middle and lower panels of Figure 1). Similarly, PMA treatment also inhibited decorin mRNA expression (by 78%) in human gingival fibroblasts, and the inhibition was in part prevented by PD98059 (results not shown). The inhibitory effect of PMA on biglycan expression was minimal

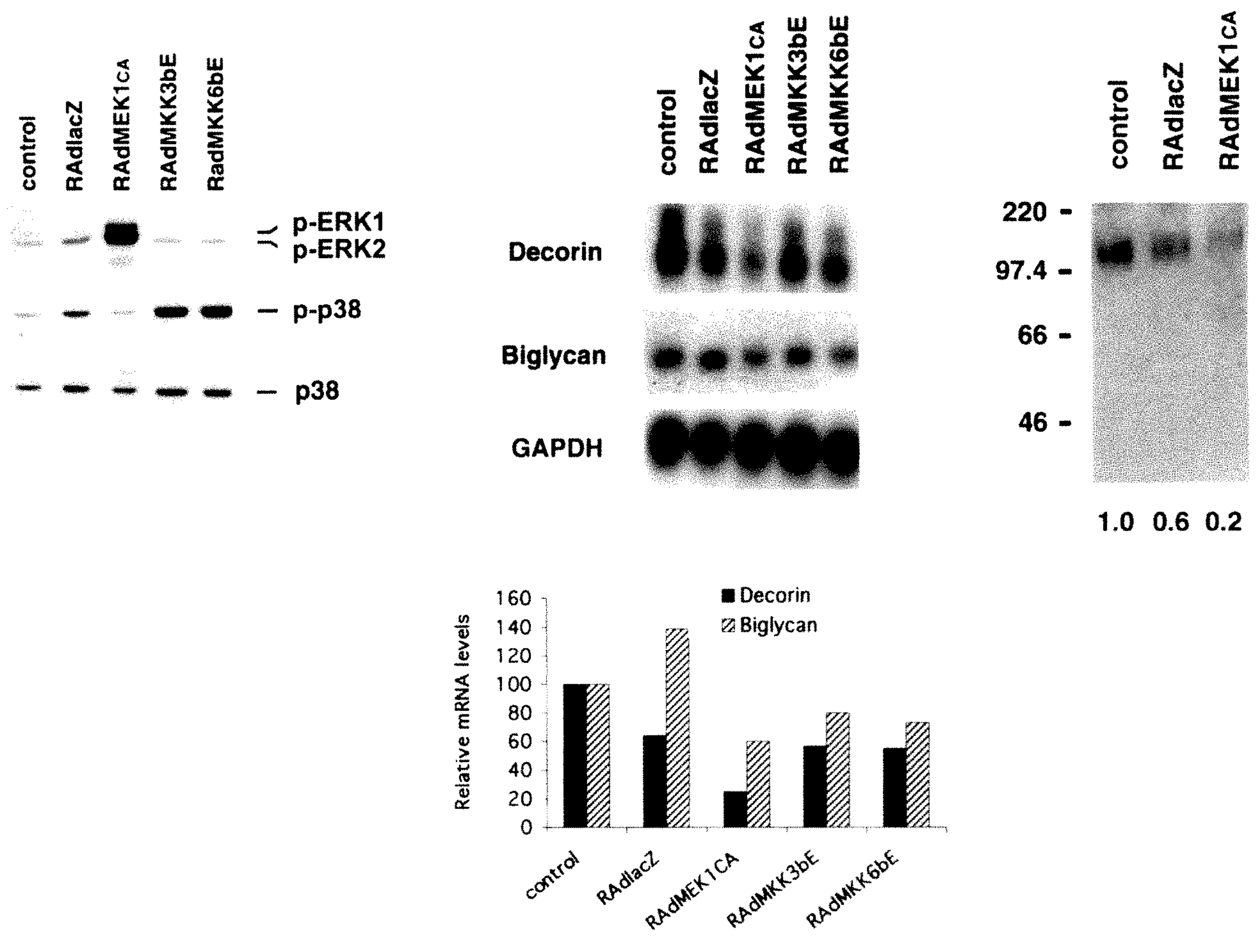

Figure 2 Activation of ERK1,2 results in suppression of decorin expression by dermal fibroblasts

Confluent human skin fibroblast cultures were transduced at a MOI of 500 pfu/ml with recombinant adenoviruses harbouring β-galactosidase (RAdLacZ), constitutively active MEK1 (RAdMEK1CA), MKK3b (RAdMKK3bE) or MKK6b (RAdMKK6bE), and incubated for 18 h. The media were changed and the incubations continued for another 24 h. Left panel: the levels of activated ERK1 and ERK2 (p-ERK1, p-ERK2), and p38 (p-p38) in cell lysates were determined by Western-blot analysis using phoshospecific antibodies for the corresponding MAPKs. As loading control, the levels of total p38 MAPK were determined in the same samples using a specific antibody. Middle panel: the levels of decorin, biglycan and GAPDH mRNAs were measured by Northern-blot hybridizations in aliquots (15 μg) of total RNA from uninfected (control) and adenovirally infected cells. Decorin and biglycan mRNA levels were quantified by scanning densitometry, corrected for the levels of GAPDH mRNA, and shown relative to the levels in untreated control cells (100) (histogram). Right panel: aliquots of conditioned media of uninfected dermal fibroblasts (control) or cells infected with RAdLacZ or RAdMEK1CA were assayed for the levels of decorin by Western-blot analysis using a decorin antiserum. The migration positions of molecular-mass markers ($M_r \times 10^{-3}$) are shown on the left. The values below the panel represent the levels of decorin relative to the uninfected control cultures (1.0) determined by densitometric scanning of the X-ray films.

(17%), but was augmented to 50% by SB203580 (right-hand middle and lower panels of Figure 1). Together these results show that inhibition of decorin expression in fibroblasts by both EGF and PMA is mediated via ERK1,2, whereas blocking the p38 pathway does not prevent down-regulation of decorin expression. In addition, the suppression of biglycan expression by EGF is mediated by the ERK1,2 signalling cascade.

Activation of ERK1,2 inhibits decorin expression in fibroblasts

To directly examine the role of ERK1,2 and p38 MAPK signalling pathways in the regulation of decorin gene expression we infected fibroblasts with recombinant adenoviruses; RAdMEK1CA, coding for constitutively active MEK1 (the activator of ERK1,2), RAdMKK3bE or RAdMKK6bE, harbouring constitutively active p38 activators MKK3b and MKK6b, respectively. Cells were infected at a MOI of 500 pfu/cell, which results in nearly 100% transduction efficiency of human primary fibroblasts [18]. As shown in the left panel of Figure 2, infection of fibroblasts with adenovirus for constitutively active MEK1 (RAdMEK1CA) resulted in activation of ERK1,2, but not p38 MAPK. In parallel, adenovirus-mediated expression of constitutively active MKK3b (RAdMKK3bE) or MKK6b (RAdMKK6bE) resulted in activation of p38, but not ERK1,2 (left panel of Figure 2). Expression of constitutively active MEK1, MKK3b or MKK6b had no effect on the total cellular levels of p38, determined as loading control (left panel of Figure 2). Infection of cells with control virus RAdLacZ did not result in sustained activation of ERK1,2 but slightly activated p38 (left panel of Figure 2).

As shown in the middle panel of Figure 2, adenovirus-mediated expression of constitutively active MEK1 resulted in a marked (61%) reduction in decorin mRNA abundance, as compared with cells infected with the control virus (RAdLacZ). In contrast, infection of parallel cultures with adenoviruses for constitutively active MKK3b or MKK6b had no marked effect on decorin mRNA levels (middle panel of Figure 2). Adenovirus-mediated expression of constitutively active MEK1 also suppressed biglycan mRNA levels (by 57%), and infection with

RAdMKK3bE or RAdMKK6bE up-regulated biglycan mRNA levels by 33 % and 22 %, respectively, compared to RAdLacZ infected cells (middle panel of Figure 2). Transduction of fibroblasts with control virus RAdLacZ also down-regulated decorin mRNA levels (by 36 %) and up-regulated biglycan mRNA expression (by 39 %), as compared to uninfected cells (middle panel of Figure 2). The effect of RadLacZ on decorin expression may be due to rapid and transient activation of the ERK1,2 pathway by adenoviral infection [32] Transduction of human gingival fibroblasts with RAdMEK1CA also suppressed decorin mRNA abundance (by 77 %), in comparison to RAdLacZ infected cells (results not shown).

Assay of the levels of immunoreactive decorin in the conditioned media of human dermal fibroblasts showed that infection of these cells with RAdMEK1CA also resulted in 67 % reduction in decorin production, as compared to RadLacZ infected cells (right panel of Figure 2). Infection of fibroblasts with RAdLacZ also reduced decorin production by 40 % (right panel of Figure 2), again possibly due to transient activation of ERK1,2 by adenovirus infection [32]. Together these results clearly show that activation of ERK1,2 by constitutively active MEK1 results in potent suppression in decorin gene expression by primary fibroblasts.

Activation of ERK1,2 results in down-regulation of decorin promoter activity in fibroblasts

To examine whether activation of ERK1,2 resulted in the suppression of decorin promoter activity we transiently transfected NIH-3T3 fibroblasts with the human decorin promoter/CAT construct, pDEC−879/CAT, in combination with the expression vector for constitutively active Raf-1. As shown in the upper panel of Figure 3 co-expression of constitutively active Raf-1 with its substrate, wild-type MEK1, resulted in potent (67 %) inhibition of decorin promoter activity, as compared to cells co-transfected with the empty expression vectors. Co-transfection of pDEC−879/CAT with wild-type MEK1 alone also inhibited decorin promoter activity by 41 %, possibly due to auto-activation of the wild-type MEK1 (upper panel of Figure 3). Similarly, co-transfection of pDEC−879/CAT with the expression vector for constitutively active MEK1 suppressed decorin promoter activity by 53 % (middle panel of Figure 3). In addition, simultaneous expression of constitutively active MEK1 with its substrates, wild-type ERK1 and ERK2 resulted in even more potent (71 %) suppression of the activity of pDEC-879/CAT (middle panel of Figure 3). These transfections show that activation of the ERK1,2 signalling cascade at the level of Raf-1 or MEK1 results in potent inhibition of decorin promoter activity in fibroblasts.

Next, we co-transfected NIH-3T3 fibroblasts with different human decorin promoter/CAT 5′-deletion constructs spanning the region from −879 to −140 in combination with the expression vector for constitutively active MEK1. Elimination of the human decorin promoter region between −278 and −188 resulted in loss of down-regulation of promoter activity by

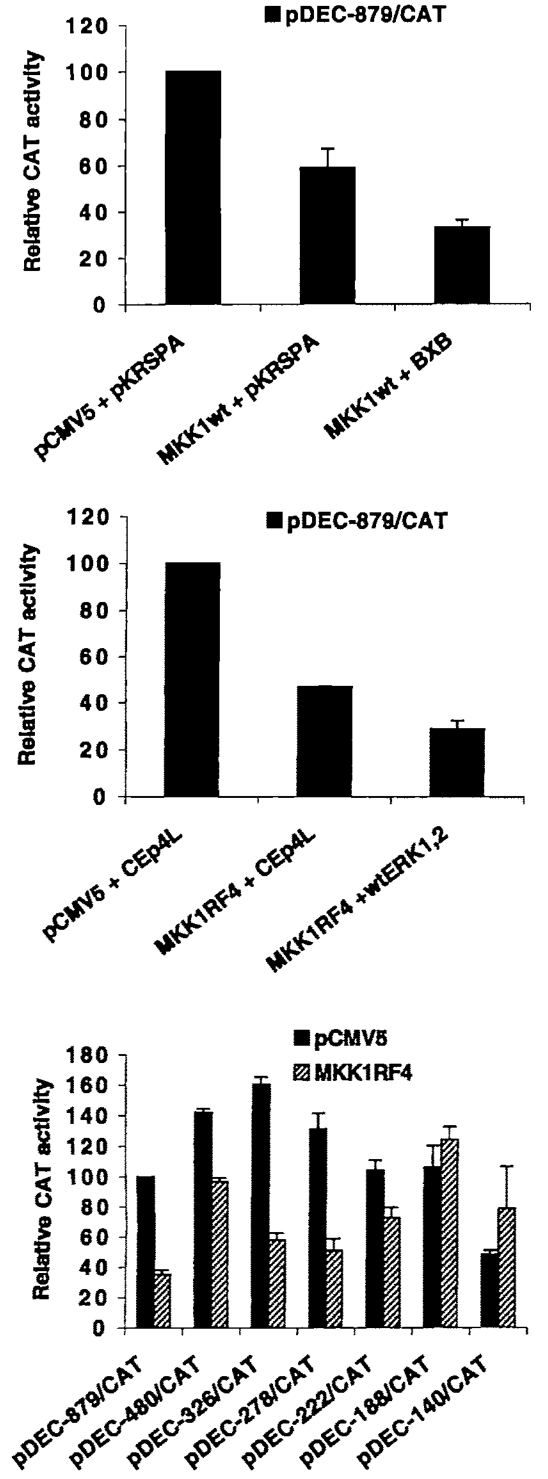

Figure 3 Activation of ERK1,2 results in down-regulation of decorin promoter activity in fibroblasts

Upper panel confluent NIH-3T3 fibroblast cultures were transiently transfected with 5 µg of human decorin promoter/CAT construct (pDEC−879/CAT) in combination with 5 µg of expression vectors for wild-type MEK1 (MKK1wt) alone or together with expression vectors for constitutively active Raf-1 (BXB) Middle panel· NIH-3T3 fibroblast cultures were co-transfected with pDEC−879/CAT in combination with the expression vector for constitutively active MEK1 (MKK1RF4) alone or together with the expression vectors for wild-type ERK1 and ERK2 (wtERK1,2) (2 5 µg each). Lower panel NIH-3T3 fibroblasts were transfected with different decorin promoter/CAT 5′-deletion constructs (5 µg) in combination with the expression vector for constitutively active MEK1 (MKK1RF4) (5 µg) For all experiments shown in this figure control cultures were co-transfected with 5 µg of the respective empty expression vectors (pCMV5, pKRSPA or CE4pL). After the glycerol shock the cultures were maintained for 48 h in DMEM containing 1 % FBS, the cells were harvested, and CAT activity was measured as an indicator of decorin promoter activity. Transfection efficiency was monitored by co-transfecting the cells with 2 µg of RSV/β-galactosidase construct The values represent the means of two or three independent transfections each performed in duplicate and are shown relative to the activity of pDEC−879/CAT co-transfected with the empty expression vectors (100) Values are means ± S E.M. (where S E M is less than 16 % for each transfection; except 35 % for pDEC−140/CAT) constitutively active MEK1 (lower panel of Figure 3). These observations show that down-regulation of decorin expression as a result of ERK1,2 activation is mediated by *cis*-elements distinct from those mediating the inhibition of decorin gene transcription by TNF-α, which involves *cis*-elements in the region -188 to -140 and in the 5′-untranslated region of exon Ib [8].

DISCUSSION

It has been shown that decorin expression is suppressed in proliferating and malignantly transformed cells [8,12–14] and that decorin itself can activate EGFR signalling, leading to activation of ERK1,2 [9–11,13]. The aim of the present study was to elucidate the role of MAPK signalling pathways in mediating the inhibition of decorin expression in proliferating fibroblasts. We demonstrate that decorin expression in primary human fibroblasts is inhibited by a mitogenic growth factor, EGF, and by tumour promoter, PMA, via the ERK1,2 pathway. In addition, our results show that activation of the ERK1,2 signalling cascade results in suppression of decorin production by human skin and gingival fibroblasts, and that the inhibition takes place at the transcriptional level.

It has been shown previously that the expression of constitutively active MEK1 results in transformation of fibroblasts [28]. Using adenovirus-mediated gene delivery, we show in the present study that the expression of constitutively active MEK1 also results in inhibition of decorin expression in normal human fibroblasts. Our recent observations show that adenovirus-mediated expression of constitutively active MEK1 in gingival fibroblasts results in the activation of c-Jun N-terminal kinase (JNK)1, as detected by Western-blot analysis using a phospho-JNK specific antibody [18]. It is therefore possible that in the experiments with constitutively active MEK1 the inhibition of decorin expression also involves activation of JNK1, which may play a role in transformation of fibroblasts by constitutively active MEK1 together with ERK1,2.

As decorin can serve as a ligand for the EGFR and activate its downstream signalling pathways, including the ERK1,2 cascade [10,11], the results of the present study suggest that decorin inhibits its own expression in fibroblasts via the ERK1,2 pathway. This suggests that the expression of decorin in normal cells is under strict control by contact with the surrounding ECM. Furthermore, these observations showing that activation of the ERK1,2 cascade in fibroblasts by mitogenic growth factors, tumour promoters or transformation potently inhibits decorin expression, provide an explanation why decorin does not belong to the cluster of genes expressed by proliferating cells. Interestingly, it was shown recently that decorin can also inhibit cell migration, an important aspect of cell invasion [33]. It is therefore probable that inhibition of decorin production, as a result of ERK1,2 activation, promotes cell proliferation and favours cell migration.

Although the inhibition of decorin expression, obtained by activation of ERK1,2, was consistent from one experiment to another, it should be noted that the maximal suppression of decorin gene expression was approximately 70%. This is in accordance with the level of suppression obtained with other inhibitors of decorin expression [6–8], and provides further evidence that decorin gene expression in normal fibroblasts is under strict control. It was also interesting to note that activation of the ERK1,2 signalling cascade suppressed expression of biglycan by dermal fibroblasts. However, biglycan does not induce phosphorylation of the EGFR [10]. In addition, the 5′-regulatory regions of human decorin and biglycan genes are quite different [27,34,35], reflecting the differential expression patterns and regulation of these two proteoglycans [1,2,4–8]. In conclusion, these observations identify a novel mechanism for suppression of decorin expression in proliferating and transformed cells and offer a new therapeutic approach for modulating decorin expression in fibroblasts.

The expert technical assistance of Hanna Haavisto, Tarja Heikkila, Marita Potila and Leila Saarinen is gratefully acknowledged This work was supported by grants from the Academy of Finland, the Sigrid Jusélius Foundation, the Cancer Research Foundation of Finland, Turku University Central Hospital and NIH (R01 CA39481)

REFERENCES

1 Iozzo, R V and Murdoch, A (1996) Proteoglycans of the extracellular environment clues from the gene and protein side offer novel perspectives in molecular diversity and function. FASEB J **10**, 598–614

2 Iozzo, R V (1998) Matrix proteoglycans from molecular design to cellular function Annu Rev Biochem **67**, 609–652

3 Yamaguchi, Y., Mann, D and Ruoslahti, E (1990) Negative regulation of transforming growth factor-β by the proteoglycan decorin Nature (London) **346**, 281–284

4 Heino, J, Kahari, V-M, Mauviel, A and Krusius, T. (1988) Human recombinant interleukin-1 regulates cellular mRNA levels of dermatan sulphate proteoglycan core protein Biochem. J. **262**, 309–312

5 Mauviel, A, Korang, K, Santra, M, Tewari, D, Uitto, J and Iozzo, R V (1996) Identification of a bimodal regulatory element encompassing a canonical AP-1 binding site in the proximal promoter region of the human decorin gene J Biol Chem **271**, 24824–24829

6 Kahari, V-M, Hakkinen, L, Westermarck, J and Larjava, H (1995) Differential regulation of decorin and biglycan gene expression by dexamethasone and retinoic acid in cultured human skin fibroblasts J Invest Dermatol **104**, 503–508

7 Kahari, V-M, Larjava, H and Uitto, J (1991) Differential regulation of extracellular matrix proteoglycan (PG) gene expression. Transforming growth factor-β1 up-regulates biglycan (PGI), and versican (large fibroblast PG) but down-regulates decorin (PGII) mRNA levels in human fibroblasts in culture J Biol Chem **266**, 10608–10615

8 Mauviel, A, Santra, M, Chen, Y Q, Uitto, J and Iozzo, R V (1995) Transcriptional regulation of decorin gene expression. Induction by quiescence and repression by tumor necrosis factor-α J Biol Chem **270**, 11692–11700

9 De Luca, A, Santra, M, Baldi, A, Giordano, A and Iozzo, R V (1996) Decorin-induced growth suppression is associated with up-regulation of p21, an inhibitor of cyclin-dependent kinases J. Biol Chem **271**, 18961–18965

10 Moscatello, D K, Santra, M, Mann, D M, McQuillan, D J, Wong, A J and Iozzo, R V (1998) Decorin suppresses tumor cell growth by activating the epidermal growth factor receptor J. Clin Invest **101**, 406–412

11 Iozzo, R V, Moscatello, D K, McQuillan, D J and Eichstetter, I (1999) Decorin is a biological ligand for the epidermal growth factor receptor J. Biol Chem **274**, 4489–4492

12 Adany, R, Heimer, R, Caterson, B, Sorrell, J M and Iozzo, R V (1990) Altered expression of chondroitin sulfate proteoglycan in the stroma of human colon carcinoma. Hypomethylation of PG-40 gene correlates with increased PG-40 content and mRNA levels J Biol Chem **265**, 11389–11396

13 Iozzo, R V, Chakrani, F, Perrotti, D, McQuillan, D J, Skorski, T, Calabretta, B and Eichstetter, I (1999) Cooperative action of germ-line mutations in decorin and p53 accelerates lymphoma tumorigenesis Proc Natl Acad Sci. USA **96**, 3092–3097

14 Santra, M, Skorski, T, Calabretta, B, Lattime, E C and Iozzo, R V (1995) De novo decorin gene expression suppresses the malignant phenotype in human colon cancer cells Proc Natl Acad Sci USA **92**, 7016–7020

15 Kolettas, E and Rosenberger, R F (1998) Suppression of decorin expression and partial induction of anchorage-independent growth by the *v-src* oncogene in human fibroblasts Eur J Biochem **254**, 266–274

16 Dudley, D T., Pang, L, Decker, S T, Bridges, A J and Saltiel, A R (1995) A synthetic inhibitor of the mitogen-activated protein kinase cascade Proc Natl Acad Sci USA **92**, 7686–7689

17 Kumar, S, Orsini, M J, Lee, J C, McDonnell, P C, Debouck, C and Young, P R (1996) Activation of the HIV-1 long terminal repeat by cytokines and environmental stress requires an active CSBP/p38 MAP kinase J Biol Chem **271**, 30864–30869

18 Ravanti, L, Hakkinen, L., Larjava, H., Saarialho-Kere, U, Foschi, M, Han, J and Kahari, V-M (1999) Transforming growth factor-β induces collagenase-3 expression by human gingival fibroblasts via p38 mitogen-activated protein kinase J Biol Chem. **274**, 37292–37300

19 Wilkinson, G W. and Akrigg, A (1992) Constitutive and enhanced expression from the CMV major IE promoter in a defective adenovirus vector Nucleic Acids Res **20**, 2233–2239

20 Foschi, M, Chan, S, Dunn, M J and Sorokin, A (1997) Biphasic activation of $p21^{ras}$ by endothelin-1 sequentially activates the ERK cascade and phosphatidylinositol 3-kinase EMBO J **16**, 6439–6451

21 Wang, Y, Huang, S, Sah, V P, Ross, J, Brown, J H, Han, J and Chien, K R (1998) Cardiac muscle cell hypertrophy and apoptosis induced by distinct members of the p38 mitogen-activated protein kinase family J Biol Chem **273**, 2161–2168

22 Ahonen, M, Baker, A H and Kahari, V-M (1998) Adenovirus-mediated gene delivery of tissue inhibitor of metalloproteinases-3 inhibits invasion and induces apoptosis in melanoma cells Cancer Res **58**, 2310–2315

23 Chomczynski, P and Sacchi, N (1987) Single-step method of RNA isolation by acid guanidinium thiocyanate-phenol-chloroform extraction Anal. Biochem **162**, 156–159

24 Krusius, T and Ruoslahti, E (1986) Primary structure of an extracellular matrix proteoglycan core protein deduced from cloned cDNA Proc Natl Acad Sci U S A **83**, 7683–7687

25 Fisher, L W, Termine, J D and Young, M F (1989) Deduced protein sequence of bone small proteoglycan I (biglycan) shows homology with proteoglycan II (decorin) and several nonconnective tissue proteins in a variety of species J Biol Chem **264**, 4571–4576

26 Fort, P, Marty, L, Piechaczyk, M, el Sabrouty, S, Dani, C, Jeanteur, P and Blanchard, J M (1985) Various rat adult tissues express only one major mRNA species from the glyceraldehyde-3-phosphate-dehydrogenase multigenic family. Nucleic Acids Res **13**, 1431–1442

27 Santra, M, Danielson, K G and Iozzo, R V (1994) Structural and functional characterization of the human decorin gene promoter. A homopurine-homopyrimidine S1 nuclease-sensitive region is involved in transcriptional control J Biol Chem **269**, 579–587

28 Mansour, S J, Matten, W T, Hermann, A S, Candia, J M, Rong, S, Fukasaw Vande Woude, G F and Ahn, N (1994) Transformation of mammalian cells by constitutively active MAP kinase kinase Science **265**, 966–970

29 Frost, J A, Geppert, T. D, Cobb, M H and Feramisco, J R (1994) A requirem for extracellular signal-regulated kinase (ERK) function in the activation of AP-1 Ha-Ras, phorbol 12-myristate 13-acetate, and serum Proc Natl Acad Sci U S A 3844–3848

30 Bruder, J T, Heidecker, G and Rapp, U R (1992) Serum-, TPA-, and Ras-induc expression from Ap-1/Ets-driven promoters requires Raf-1 kinase Genes Dev **6**, 545–556

31 Reunanen, N, Westermarck, J, Hakkinen, L, Holmstrom, T H, Elo, I, Eriksson, and Kahari, V-M (1998) Enhancement of fibroblast collagenase (matrix metalloproteinase-1) gene expression by ceramide is mediated by extracellular si regulated and stress-activated protein kinase pathways J Biol. Chem **273**, 5137–5145

32 Bruder, J T and Kovesdi, I (1997) Adenovirus infection stimulates the Raf/MAP signaling pathway and induces interleukin-8 expression J Virol **71**, 398–404

33 Merle, B, Durussel, L, Delmas, P. D. and Clezardin, P (1999) Decorin inhibits migration through a process requiring its glycosaminoglycan side chain J Cell Biochem **75**, 538–546

34 Fisher, L W, Heegaard, A M, Vetter, U, Vogel, W, Just, W, Termine, J D. an Young, M F (1991) Human biglycan gene Putative promoter, intron-exon junctio and chromosomal localization J Biol Chem **266**, 14371–14377

35 Heegaard, A M., Gehron Robey, P, Vogel, W, Just, W, Widom, R L, Scholler, Fisher, L W and Young, M F (1997) Functional characterization of the human biglycan 5′-flanking DNA and binding of the transcription factor c-Krox J Bone Miner Res **12**, 2050–2060

Received 11 January 2000/23 March 2000, accepted 18 April 2000

Biochem J (2000) **349**, 27–34 (Printed in Great Britain)

Characterization and regulation of *Leishmania major* 3-hydroxy-3-methylglutaryl-CoA reductase

Andrea MONTALVETTI, Javier PEÑA-DÍAZ, Ramón HURTADO, Luis Miguel RUIZ-PÉREZ and Dolores GONZÁLEZ-PACANOWSKA[1]

Instituto de Parasitología y Biomedicina 'López-Neyra', Consejo Superior de Investigaciones Científicas, C/Ventanilla 11, 18001-Granada, Spain

In eukaryotes the enzyme 3-hydroxy-3-methylglutaryl CoA (HMG-CoA) reductase catalyses the synthesis of mevalonic acid, a common precursor to all isoprenoid compounds. Here we report the isolation and overexpression of the gene coding for HMG-CoA reductase from *Leishmania major*. The protein from *Leishmania* lacks the membrane domain characteristic of eukaryotic cells but exhibits sequence similarity with eukaryotic reductases. Highly purified protein was achieved by ammonium sulphate precipitation followed by chromatography on hydroxyapatite. Kinetic parameters were determined for the protozoan reductase, obtaining K_m values for the overall reaction of 40.3 ± 5.8 μM for (*R,S*)-HMG-CoA and 81.4 ± 5.3 μM for NADPH; V_{max} was 33.55 ± 1.8 units·mg^{-1}. Gel-filtration experiments suggested an apparent molecular mass of 184 kDa with subunits of 46 kDa. Finally, in order to achieve a better understanding of the role of this enzyme in trypanosomatids, the effect of possible regulators of isoprenoid biosynthesis in cultured promastigote cells was studied. Neither mevalonic acid nor serum sterols appear to modulate enzyme activity whereas incubation with lovastatin results in significant increases in the amount of reductase protein. Western- and Northern-blot analyses indicate that this activation is apparently performed via post-transcriptional control.

Key words: ketoconazole, lovastatin, mevalonic acid, sterol, trypanosomatid.

INTRODUCTION

Leishmania species are protozoan parasites that cause the leishmaniases, diseases for which there is a need of improved chemotherapy. These flagellated parasites contain sterols of fungal type such as ergosterol [1,2], which differs from cholesterol, the predominant mammalian sterol, by the presence of 24-methyl group and Δ^7 and Δ^{22} bonds. Cholesterol can be taken up in large amounts by *Leishmania* promastigotes from the medium, but cannot be further metabolized or synthesized *de novo* from exogenous mevalonic acid [3]. Sterol biosynthesis inhibitors are effective anti-proliferative agents that have been used in the treatment of diseases produced by fungi and yeast [4,5]. *Leishmania* is also highly sensitive to this class of agents and the combined administration of lovastatin, a potent competitive inhibitor of 3-hydroxy-3-methylglutaryl-CoA (HMG-CoA) reductase, and 14α-demethylase inhibitors such as miconazole or ketoconazole present synergistic effects when inhibiting growth of the parasite *in vitro* [6]. Hence, the combined use of sterol biosynthesis inhibitors that act at different steps of the pathway appears to offer a promising approach for an effective treatment of leishmaniasis.

In mammalian cells, cholesterol is either obtained by receptor-mediated uptake of plasma low-density lipoprotein (LDL) or by synthesis from acetyl-CoA through the sterol biosynthetic pathway. Each cell must balance the external and internal sources of cholesterol so as to ensure the biosynthesis of molecules produced by the isoprenoid pathway while avoiding sterol overload. Cholesterol homoeostasis is achieved through feedback regulation of at least two enzymes of sterol biosynthesis, HMG-CoA synthase and HMG-CoA reductase, as well as by means of control of LDL receptors. The key rate-limiting enzyme, HMG-CoA reductase, catalyses the conversion of HMG-CoA into mevalonate, which is required for synthesis of a large family of compounds. These include cholesterol and isoprenoids such as haem A, ubiquinone, dolichol, isopentenyl tRNA, steroid hormones and other isoprenoid groups, which are covalently linked to growth-regulating proteins and oncogenic products [7].

HMG-CoA reductase is a soluble protein in prokaryotes [8–10] and in the parasitic protozoan *Trypanosoma cruzi* [11], while in all other eukaryotic organisms characterized the enzyme presents a variable N-terminal membrane domain and its subcellular location appears to be preferentially the endoplasmic reticulum [12]. This domain is necessary and sufficient for the regulated degradation of HMG-CoA reductase. Little is known about the nature and regulation of this enzyme in protozoa, while it has been studied extensively in mammalian cells. This regulation, which is mediated by sterols and non-sterol mevalonate-derived metabolites, is complex and occurs at many levels, including transcription, translation, protein degradation and protein phosphorylation [7].

In the current studies, we describe the isolation and characterization of HMG-CoA reductase from *Leishmania major* and also demonstrate that in this protozoan the enzyme lacks the membrane-domain characteristic of eukaryotic reductases. We examine the modulation of the soluble enzyme in promastigote forms of the parasite, showing that activity is not subject to regulation by mevalonic acid or medium sterols.

EXPERIMENTAL

Materials

Restriction enzymes, T4 DNA ligase, *Taq* polymerase and the Klenow fragment of DNA polymerase were from Boehringer Mannheim. [α-^{32}P]ATP was from ICN Pharmaceuticals (Irvine, CA, U.S.A.). BSA, dithiothreitol (DTT), D,L-mevalonic acid lactone, ketoconazole and sodium phosphate were from Sigma.

Abbreviations used CHEF, contour-clamped homogeneous electric field, HMG-CoA, 3-hydroxy-3-methylglutaryl CoA, *lmhmgr* gene, *Leishmania major* HMG-CoA reductase gene; LDL, low-density lipoprotein; DTT, dithiothreitol.

[1] To whom correspondence should be addressed (e-mail dgonzalez@ipb csic es)

The nucleotide sequence data reported here appear in the GenBank nucleotide sequence database under the accession number AAF155593.

Leupeptin was purchased from Boehringer Mannheim. Lovastatin was supplied by Merck Sharp and Dohme. The pET expression system was from Stratagene. Oligonucleotides HMG1 (5′-ATGGGNATGAAYATG-3′), HMG2 (5′-GTTBGCBGCV-TGBGCGTT-3′), HMG3 (5′-TCTGCGCTTCTCTGCCTTTA-3′) and HMG4 (5′-TTACGGAGTCGGAGGCTT-3′) were synthesized in a Millipore ConSep LC500DNA synthesizer at the Analytical Services of the Instituto de Parasitología y Biomedicina 'López-Neyra', Granada, Spain.

Cell culture

L. major promastigotes were grown in tissue-culture flasks at 28 °C in filter-sterilized 199 medium supplemented with either 10 % heat-inactivated fetal calf serum (Gibco) or 10 % lipid-poor serum, which was prepared by the method of Kirsten and Watson [13]. The cultures were initiated at a cell density of 5×10^5 cells·ml^{-1}, and the drugs were added at a cell density of 1×10^6 cells·ml^{-1}. Cell densities were determined by counting with a Coulter® Z1 counter. Lovastatin and D,L-mevalonic acid lactone were added from stock solutions in ethanol, the lactone rings of the drugs were hydrolysed by a 30-min incubation in 0.2 M NaOH at 37 °C, followed by neutralization with 0.2 M HCl. Ketoconazole was added as an aqueous solution titrated to pH 2.4 with HCl.

Isolation of the *L. major* HMG-CoA reductase (*lmhmgr*) gene and DNA sequencing

The hybridization probes for screenings were obtained by the PCR technique. A fragment of 303 bp of the *lmhmgr* gene was amplified, using the degenerate oligonucleotides HMG1 and HMG2 derived from highly conserved sequences of the catalytic domain, and used as hybridization probe for screening of a cDNA library. A PCR fragment of the *lmhmgr* gene was further obtained using the oligonucleotides HMG3 and HMG4, and used as a probe to screen the library of genomic DNA. The PCR reaction mixture (50 μl) contained 25 pmol of each of the two oligonucleotide primers, 500 ng of *L. major* genomic DNA, dNTPs each at 400 μM, 50 mM KCl, 10 mM Tris/HCl (pH 8) and 1.5 mM $MgCl_2$. Amplification was initiated with 1.5 units of *Taq* polymerase. PCR parameters were 35 thermal cycles consisting of a 1-min denaturation at 94 °C followed by a 1-min annealing period at 45 °C and a 2-min extension at 72 °C. The genomic library constructed in λEMBL3 was replica plated on to nitrocellulose and screened as described in [14].

The isolated λEMBL3 DNA was digested with restriction endonucleases and a 2.4-kb *Bam*HI–*Xho*I fragment that hybridized to the PCR probe was ligated into pBSKS$^-$ and transformed into XL1-Blue *Escherichia coli*. The *Bam*HI–*Xho*I insert was sequenced in an Applied Biosystems 373 DNA sequencer.

Southern- and Northern-blot analyses

Total genomic DNA from *L. major* was isolated from *Leishmania* by phenol extraction [15], digested with different restriction enzymes using the conditions recommended by the supplier. Endonuclease-cleaved DNA was electrophoresed on 0.8 % (w/v) agarose gels. The isolation of the poly(A)$^+$ RNA was accomplished with the QuickPrep® *Micro* mRNA purification kit (Pharmacia Biotech) mRNA samples were subjected to electrophoresis on 1 % (w/v) agarose gels containing 1 × Mops buffer [20 mM Mops/0.08 M sodium acetate (pH 7.0)/1 mM EDTA] and 6.29 % (v/v) formaldehyde after the samples had been boiled for 10 min in 50 % (v/v) formamide/1 × Mops buffer/5.9 % (v/v) formaldehyde A 0.24–9.5-kb RNA ladder (Gibco) was used as a standard. The gels were transferred to a Hybond-N filter and hybridized with the probe containing the entire coding sequence of the *lmhmgr* gene obtained by PCR. All Southern and Northern blots were visualized by autoradiography. The β-tubulin gene from *L. major* was used for normalization of hybridization signals on Northern blots and the relative intensities of the bands were quantified by scanning densitometry.

Low-melting-point agarose blocks were prepared as described in [16]. Chromosomes were separated on a 1 % agarose gel in 0.5 M Tris/borate/EDTA and 0.5 mg·ml^{-1} ethidium bromide using a CHEF (contour-clamped homogeneous electric field) electrophoresis system (Pharmacia) as described previously [17]. The resulting gel was transferred to a Hybond-N (Amersham) nylon filter and subjected to Southern-blot analysis [18] with the PCR-amplified *lmhmgr* gene as a probe

Construction of expression system

For expression in *E. coli* the entire coding sequence was amplified by the PCR technique. Oligonucleotide primers for amplification of the HMG-CoA reductase coding sequence were designed so that *Nde*I and *Bam*HI restriction sites were introduced at the 5′ and 3′ ends for convenient cloning in the expression vector pET-11c to give pETLMHMG, which was cloned and propagated originally in XL1B. Double-stranded DNA sequencing was performed to confirm the correct sequence after amplification. Subsequently, pETLMHMG was used to transform the *E. coli* expression host BL21(DE3). Bacterial clones were grown in Luria–Bertani medium containing 50 mg·ml^{-1} ampicillin When induction was performed, bacterial cells transformed with pETLMHMG were first grown to an absorbance of 0.6 at 37 °C and then 1 mM isopropyl β-D-thiogalactoside was added; cultures were then grown for 6 h at 37 °C, cells were collected by centrifugation and, when not used immediately, frozen at −80 °C.

Purification of *L. major* HMG-CoA reductase overexpressed in *E. coli*

A frozen pellet from 1 l of *E. coli* BL21(DE3)/pETLMHMG cells overexpressing *L. major* HMG-CoA reductase was thawed at room temperature and resuspended in 20 ml of buffer A [100 mM sucrose/20 mM Na_2HPO_4, pH 6.75/10 mM DTT/20 μg·ml^{-1} leupeptin/10 % (v/v) glycerol]. Cells were ruptured by sonication and centrifuged at 12000 *g* for 30 min at 4 °C. The supernatant was brought to 30 % saturation with $(NH_4)_2SO_4$, maintained on ice, shaken occasionally for 20 min, and then centrifuged at 12000 *g* for 30 min The precipitate was discarded and the supernatant liquid was brought to 50 % saturation with $(NH_4)_2SO_4$. The resulting precipitate was dissolved in 5 ml of buffer A and stored overnight at −80 °C. The thawed ammonium sulphate fraction was applied to a column (1 cm × 20 cm; 9 ml) of hydroxyapatite Bio-Gel® HTP Gel (Bio-Rad) in buffer A. The column was washed with 25 ml of buffer A and the enzyme was eluted with a 300-ml gradient of 0–1.5 M NaCl in buffer A (3-ml fractions). Active fractions were combined and brought to 50 % saturation with $(NH_4)_2SO_4$. The precipitate was desalted and stored at −80 °C until use. Protein was determined by the method of Bradford [19] with BSA as a standard. In gel-filtration experiments, a Superdex® 200 HR 10/30 column attached to ÄKTA purifier 10 FPLC equipment (Pharmacia Biotech) was used.

Measurement of HMG-CoA reductase activity

The activity of the enzyme was determined either by a radiometric assay as described previously [11] or by a spectrophotometric assay based on that described by Frimpong et al. [20]. Assays were performed in a final volume of 200 μl and contained 150 mM NaPO$_4$, pH 6.75, 75 mM NaCl, 10 mM DTT, 1 mM EDTA, 270 μM (*R*,*S*)-HMG-CoA, 270 μM NADPH and 125 ng of recombinant enzyme. The kinetic parameters were determined in experiments where the non-varied substrate was kept at 270 μM. NADH oxidation was assessed using two different cofactor concentrations (350 and 700 μM) and two different enzyme concentrations (625 and 2500 ng·ml^{-1}). The analysis of HMG-CoA reductase activity in *L. major* extracts was made using the radiometric assay. *Leishmania* promastigote cells were grown to exponential phase (16×10^6 cells·ml^{-1}), collected by centrifugation, washed with PBS and resuspended in buffer A with protease inhibitors. Cells were ruptured by sonication, the resulting extract was clarified by centrifugation (12000 *g*, 15 min, 4 °C) and used as an enzyme source for determination of reductase activity. When the intracellular distribution of the enzyme was analysed, the 12000 *g* supernatant was centrifuged further at 105000 *g* for 60 min at 4 °C. The pellet was resuspended in buffer A with protease inhibitors, and both the pellet and the 105000 *g* supernatant were used for determination of HMG-CoA reductase activity. Enzyme activity (1 unit) was defined as the amount of enzyme that converts 1 nmol of [^{14}C]HMG-CoA into [^{14}C]mevalonate/min per mg of protein.

All activity measurements for the purification scheme and characterization of the enzyme were performed using the spectrophotometric assay at 340 nm in a Hewlett-Packard model 8452A diode array spectrophotometer. HMG-CoA reductase activity (1 unit) was defined as the amount of enzyme that converts 1 μmol of NADPH into NADP$^+$ in 1 min/mg of protein.

Western-blot analysis

Polyclonal anti-*L. major* HMG-CoA reductase antibody was generated by immunizing rabbits with the purified protein. Promastigotes were lysed by sonication, and cell supernatants were prepared by centrifugation at 12000 *g* for 15 min. Protein (30 μg) was subjected to electrophoresis through an SDS-polyacrylamide (12 %) gel and blotted on to Immobilon-P membranes (Millipore) at 25 V for 30 min, using a Semi-Dry Transfer Cell (Bio-Rad). Western-blot analysis of HMG-CoA reductase was performed with a 1:20000 dilution of the indicated antiserum, using anti-rabbit-IgG-conjugated alkaline phosphatase as the secondary antibody. Bound antibody was visualized with chromogenic substrates [14].

RESULTS

Isolation of the *lmhmgr* gene

The PCR probe was obtained by amplification of a fragment of the *lmhmgr* gene using as primers degenerate nucleotides complementary to highly conserved regions contained within the soluble catalytic domain, and genomic *L. major* DNA as template. A PCR product of the expected size (303 bp) was identified that showed pronounced similarity to HMG-CoA reductases. A cDNA library constructed in λZAP Express was screened with the specific PCR probe (303 bp). One clone was selected that contained a 2.3-kb insert, although the 5′ end of this cDNA was truncated and only 729 bp of the 3′ end of the *lmhmgr* gene were present. The complete coding sequence was obtained from a library of *L. major* genomic DNA constructed in λEMBL3 and screened with a PCR probe (691 bp) obtained from the cDNA sequence. Two positive plaques were carried through a tertiary screening, and one clone was selected for restriction mapping and further characterization. The clone contained a 13.5-kb *Bam*HI–*Bam*HI insert that possessed the complete coding region of the HMG-CoA reductase gene. A *Bam*HI–*Xho*I restriction fragment was identified that hybridized strongly with the PCR probe. This 2.395-kb segment was ligated into pBSKS$^-$ to give pHMG2.4 and sequenced on both strands by using universal and synthetic primers. The complete coding sequence (1302 bp), together with 500 and 593 bases of the 5′ and 3′ flanking regions, respectively, was established. Prediction of the initiation codon was based on the comparison of the *L. major* sequence with the *T. cruzi* HMG-CoA reductase sequence and the identification of non-coding regions by codon-usage studies. The nucleic acid sequence is highly conserved between these protozoan parasites (62 % identity). The open reading frame presented a codon usage that correlated closely with that determined for other *L. major* genes Translation of the open reading frame of 1302 bp yielded a polypeptide of 434 residues with an estimated molecular mass of 45953 Da. The amino acid sequence was aligned with the sequences of *T. cruzi*, human, yeast, *Arabidopsis thaliana*, *Haloferax volcanii* and *Pseudomonas mevalonii* (Figure 1). The *lmhmgr* gene encoded for a protein similar to *T. cruzi* HMG-CoA reductase (80 % similarity), that lacks the membrane N-terminal domain characteristic of other eukaryotic enzymes.

Northern-blot analysis and genomic organization of the HMG-CoA reductase gene

A Northern blot of poly(A)$^+$ RNA extracted from the promastigote form of the parasite was performed by using the *lmhmgr* gene as a probe. The analysis indicated a transcript size of 4.4 kb. A prolonged exposure of the autoradiogram did not reveal any additional bands.

Genomic DNA from *L. major* cells was digested with different endonucleases, blotted and hybridized with the HMG-CoA reductase gene probe. Digestions with enzymes that cut at sites not contained within the coding region of the HMG-CoA reductase gene gave single bands, whereas two bands were obtained with enzymes with unique restriction sites in the coding region, therefore suggesting that the gene is of single copy.

The chromosomes of *Leishmania* range in size between 200 and 2000 kb [21] and can be resolved by CHEF electrophoresis. The *Leishmania* HMG-CoA reductase probe was used to hybridize a filter replicate of chromosomes of *L. major* under conditions that favoured the separation of larger chromosomal bands As shown in Figure 2, HMG-CoA reductase sequences were located on a single chromosome of 1.4 Mb

Purification and kinetic analysis

Table 1 summarizes the results of a typical purification. The enzyme was purified approx. 6-fold and represented 28 % overall recovery of activity. The HMG-CoA reductase preparation finally obtained had a specific activity of 32.9 units·mg^{-1}. Enzyme purity was judged homogeneous by SDS/PAGE (Figure 3). The single band present on the gel had an apparent molecular mass of 46000 Da, a value in agreement with the DNA-derived protein sequence of HMG-CoA reductase. The molecular mass of the native purified protein was estimated, by exclusion chromatography, to be 184585 Da, a value consistent with a tetrameric subunit organization. Optimal activity of *Leishmania* HMG-CoA reductase was observed in the range of pH 5.7–7 K_m values for the overall reaction were 40.3 ± 5 8 μM for (*R*,*S*)-HMG-CoA

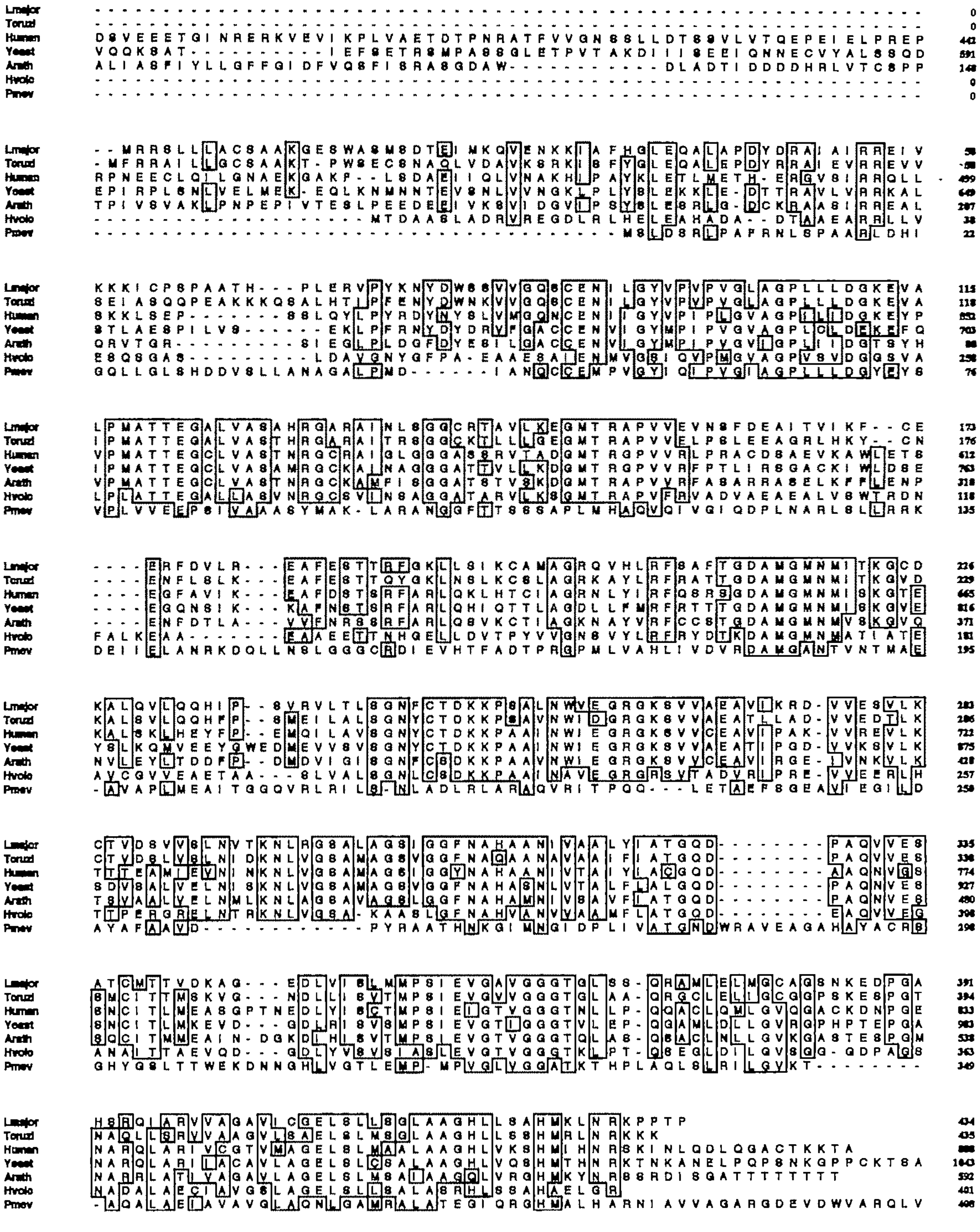

Figure 1 Comparison of the deduced amino acid sequence of *L. major* with other reductases

The deduced amino acid sequence of *L. major* HMG-CoA reductase is compared with the sequences of the *Trypanosoma cruzi* (Tcruzi, complete sequence), human (residues 383–888), yeast (yeast HMG-CoA reductase isoenzyme 2, residues 542–1043), *Arabidopsis thaliana* (Arath, residues 100–592), *Haloferax volcanii* (Hvolc, complete sequence) and *Pseudomonas mevalonii* (Pmev, residues 1–408) reductases. Solid boxes indicate regions of amino acid sequence identity.

and 81.4 ± 5.3 μM for NADPH, and the V_{max} was 33.55 ± 1.8 units·mg^{-1}. No activity was detectable when NADH was used instead of NADPH, even when high concentrations of both cofactor and enzyme were used. Lovastatin was a competitive inhibitor with respect to HMG-CoA with a K_i of 1.83 ± 0.005 nM.

Intracellular distribution of HMG-CoA reductase

The *L. major* promastigote extract was fractionated by differential centrifugation as described in the Experimental section. All of the fractions were assayed for HMG-CoA reductase activity. As

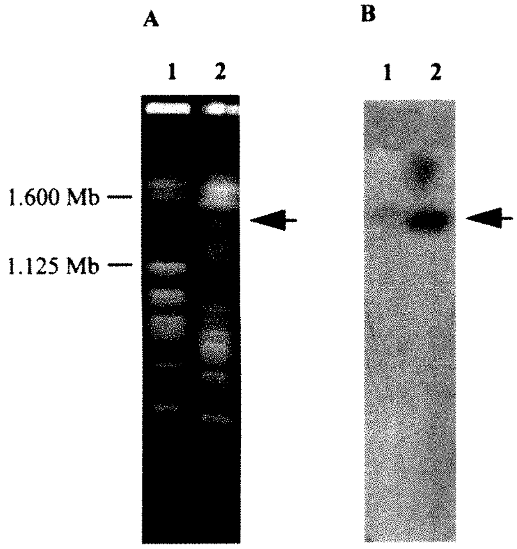

Figure 2 Chromosomal localization of the *lmhmgr* gene

(**A**) Ethidium bromide-stained gel. Lane 1, *Saccharomyces cerevisiae* as molecular-mass marker chromosomes; lane 2, *L. major* chromosomes. (**B**) Autoradiograph of a nylon transfer of the gel shown in (**A**) probed with the ^{32}P-labelled *lmhmgr* probe.

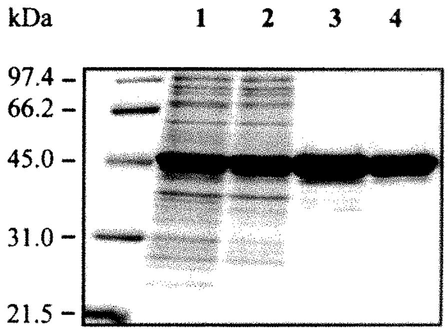

Figure 3 Purification of *L. major* HMG-CoA reductase

An SDS/polyacrylamide gel was stained with Coomassie Brilliant Blue. Lane 1, soluble extract BL21(DE3)/pETLMHMG; lane 2, ammonium sulphate 30–50% precipitate; lane 3, hydroxyapatite fraction; lane 4, ammonium sulphate 50% precipitate.

Table 2 Distribution of HMG-CoA reductase activity in *L. major* extracts

S12 refers to the whole supernatant obtained after sonication and centrifugation at 12000 ***g*** for 15 min. S105 and P105 refer to the supernatant and pellet, respectively, obtained after centrifugation of S12 at 105000 ***g*** for 60 min. Values are the means of four determinations. S.D. values did not exceed 8% of the mean value.

Fraction	Specific activity (nmol · min^{-1} · mg^{-1})	Total activity (nmol · min^{-1})
S12	8.87	77.22
S105	11.73	59.23
P105	1.82	5.12

shown in Table 2, *L. major* reductase specific activity in 105000 *g* supernatant was 6.5-fold that obtained in the pellet or 'membrane' fraction. When the total activity recovered in each fraction was calculated, 92 % of the total enzyme activity was located in the supernatant. Similar results were found with *T. cruzi* [11], in contrast with what has been observed in other eukaryotic cells.

Modulation of HMG-CoA reductase activity by mevalonate-derived products

The regulation of HMG-CoA reductase in mammalian cells has been revealed through the use of potent reductase competitive inhibitors, such as lovastatin and compactin. In cultured cells, they block the synthesis of mevalonate and trigger adaptive reactions that result in increases in reductase protein within a few hours. The increase in enzyme can be reversed by incubating compactin-treated cells with mevalonate. Large amounts of mevalonate suppress reductase activity by nearly 99 % [22,23].

To study the modulation of HMG-CoA reductase in *Leishmania*, we incubated *L. major* promastigotes with lovastatin, at concentrations near the EC$_{50}$ of the inhibitor, and/or mevalonate. As shown in Table 3, the activity of HMG-CoA reductase was increased about 2- and 3-fold in promastigotes treated for 10 h with 40 and 80 μM lovastatin respectively. In the presence of both mevalonate and lovastatin, the activity was comparable with that of control cells. The changes in HMG-CoA reductase activity were associated with changes in the amount of reductase protein, as determined by immunoblot analysis (results not shown). Protein levels were increased 2–3-fold in cells grown in the presence of 40 and 80 μM lovastatin.

We determined whether HMG-CoA reductase was regulated by exogenous mevalonate, a modulator of the mammalian enzyme. When *L. major* promastigotes were grown with different concentrations of mevalonate for 12 h, reductase activity was not suppressed significantly (Table 3). Similar results were seen when the cells were treated with mevalonate for different times of incubation.

To examine further whether activation of the HMG-CoA reductase by lovastatin and reversal by mevalonate were associated with levels of reductase mRNA, *Leishmania* promastigotes

Table 1 Purification summary of recombinant HMG-CoA reductase

Fraction	Total activity (units)	Total protein (mg)	Specific activity (units · mg^{-1})	Enrichment (-fold)	Yield (%)
Soluble extract	830.0	147.84	5.61	1.0	100
Ammonium sulphate (30–50%)	554.11	55.86	9.92	1.76	66.7
Hydroxyapatite	408.5	25.15	16.24	2.89	49.2
Ammonium sulphate (50%)	233.54	7.1	32.9	5.86	28.1

Table 3 Regulation of HMG-CoA reductase activity in *Leishmania* by lovastatin and mevalonate

A series of cultures were incubated with lovastatin and/or mevalonate for 10–12 h. Cell suspensions were harvested, washed and incubated for 1 h with fresh medium to minimize the possibility of interference by residual lovastatin or mevalonate with reductase activity. Values are the means of four determinations. S.D. values did not exceed 8% of the mean value. The experiment was repeated twice with similar results.

Addition	HMG-CoA reductase activity (nmol · min^{-1} · mg^{-1})
Lovastatin (μM)	
0	4.79
40	8.18
80	12.68
80 + Mevalonate (10 mM)	4.43
Mevalonate (mM)	
0	4.03
5	3.86
10	3.26
20	3.1

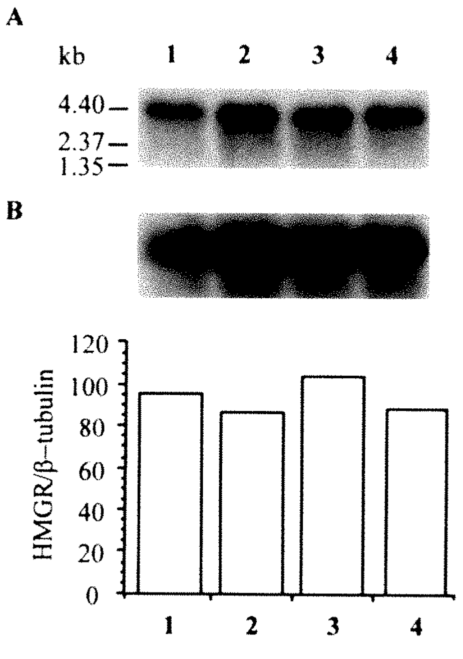

Figure 4 Analysis of HMG-CoA reductase mRNA in *Leishmania* treated with lovastatin (80 μM) and/or mevalonate (10 mM)

Northern-blot analysis of the *Leishmania* HMG-CoA reductase (**A**) and the β-tubulin (**B**) transcripts with ^{32}P-labelled specific probes. Approx. 7 μg of poly(A)$^{+}$ RNA were subjected to electrophoresis on the gel before transfer to nylon. Lanes 1, control cells; lanes 2, *L. major* grown in presence of lovastatin and mevalonate; lanes 3 and 4, cells grown in presence of lovastatin and mevalonate, respectively. The graph shows the ratio between the density of the bands corresponding to the HMG-CoA reductase and the β-tubulin transcripts. Control cells were set at a ratio of 100%. HMGR, HMG-CoA reductase.

were grown in the presence of lovastatin and/or mevalonate and poly(A)$^{+}$ RNA was prepared for hybridization analysis. As shown in Figure 4, no variations were seen in the levels of a specific HMG-CoA reductase transcript.

Table 4 Modulation of HMG-CoA reductase activity in *Leishmania* by availability of exogenous sterols and ketoconazole

To analyse the influence of lipoproteins on *Leishmania* reductase activity, promastigote forms were grown in medium containing 10% complete serum. After washing, cells were incubated in medium supplemented with 10% complete serum or 10% lipoprotein-poor serum for 24 h. Cells were treated with ketoconazole for 24 h in medium containing 10% complete serum. Values are the means of four determinations. S.D. values did not exceed 8% of the mean value.

Addition	HMG-CoA reductase activity (nmol · min^{-1} · mg^{-1})
Complete serum	6.44
Lipoprotein-poor serum	6.18
Ketoconazole (μM)	
0	8.81
0.5	10.93
1.0	13.38
1.5	13.75

Regulation of HMG-CoA reductase activity by availability of exogenous and endogenous sterols

In the absence of LDL, mammalian cells maintain high reductase activity whereas, when LDL is present, HMG-CoA reductase activity declines by more than 90%, and cells produce only the small amounts of mevalonate needed for non-sterol end-products [24]. To analyse the effect of serum sterols on reductase activity, log-phase promastigotes were harvested, washed and incubated for 24 h in medium supplemented with complete or lipoprotein-poor serum. As shown in Table 4, no differences were observed in cells grown in the presence of lipoprotein-poor serum. Similar results were obtained when promastigotes were adapted to grow in deficient medium. Consequently, serum sterol does not appear to be a regulator of the *Leishmania* enzyme, as occurs in mammalian cells.

Finally, we exploited ketoconazole as a tool to study the regulation of HMG-CoA reductase. This drug blocks ergosterol biosynthesis at the level of the cytochrome P450-dependent 14α-demethylation of lanosterol. In promastigote forms treated with different concentrations of ketoconazole for 24 h, reductase activity was increased by nearly 55% (Table 4). Similar effects were seen when cells were incubated for different time periods with ketoconazole (1 μM). The activation of the enzyme was associated with a parallel change in the amount of HMG-CoA reductase protein, as determined by Western-blot analysis (results not shown).

DISCUSSION

In the current paper we describe the isolation and characterization of the *lmhmgr* gene. The deduced amino acid sequence of the *Leishmania* enzyme was compared with other HMG-CoA reductases. Alignment analysis and hydrophobicity plots show clearly that the enzyme lacks the membrane N-terminal domain characteristic of eukaryotic enzymes. The shorter polypeptide encoded by *lmhmgr* exhibits pronounced similarity (80%) to the *T. cruzi* protein and all of the conserved residues involved in catalysis or binding identified in other HMG-CoA reductases are present in the *L. major* enzyme. The absence of a membrane-spanning domain and the existence of protease-sensitive reductase activity in the 105000 *g* supernatant firmly support that *L. major* HMG-CoA reductase is a soluble enzyme. The indications of a soluble reductase in *Leishmania* add to the observation that *T. cruzi* also lacks a membrane-spanning domain and that activity is located in the cellular soluble fraction [11] and suggest that this feature is a common characteristic of the Trypanosomatidae family. Recently, Concepción et al. have reported that the *T. cruzi* enzyme is soluble and that activity is associated mainly with the glycosomal subcellular fraction [25]. However, HMG-CoA reductase from *T. brucei*, another trypanosomatid, has been described as microsomal [26], which would contrast with what we have observed in two closely related protozoa. HMG-CoA reductase appears to be of single copy in both *T. cruzi* and *Leishmania* and Northern blots suggest the existence of only one transcript species. Therefore the existence of membrane-bound isoforms is highly improbable. More likely, the microsomal activity is unique to *T. brucei* or was an artifact, since in this organism reductase activity was two orders of magnitude lower than the values obtained in the present study. The gene coding for HMG-CoA reductase from *T. brucei* has not yet been characterized. The availability of recombinant enzyme will allow for more detailed cellular studies that would aid in establishing the definite location of the enzyme in *Leishmania*.

The purification procedure allowed for the production of highly purified protein available for structural and enzymological studies. Enzyme was relatively stable as an ammonium sulphate precipitate and could be stored as such for several weeks at −80 °C. The availability of highly stable homogeneous protein will allow for both structural and functional studies. In this sense, kinetic properties of protozoan reductase seem to resemble those of the mammalian enzyme (52 % identity with the human enzyme); however, the lack of a membrane domain is unique to this kind of organism The kinetic characterization of *L. major* HMG-CoA reductase showed that the K_m for NADPH was similar to those previously reported for other NADPH-dependent reductases. However, the K_m for HMG-CoA was one order of magnitude higher than the value described for the human enzyme [27] and the affinity for lovastatin was therefore 20000 times higher than its affinity for the natural substrate HMG-CoA

When the molecular mass was estimated by gel-filtration experiments the value obtained was 184585 Da, suggesting that *L. major* HMG-CoA reductase is a tetramer, similar to what has been described in the case of the radish seedlings enzyme [28] and the recently described catalytic portion of the human enzyme [29]

We have analysed some of the mechanisms involved in the regulation of *Leishmania* reductase. HMG-CoA reductase activity was clearly increased in promastigotes incubated with lovastatin. Inhibition of growth rate and activation of enzyme activity mediated by lovastatin was reverted by mevalonate, suggesting that exogenous mevalonate is capable of satisfying the cell requirements for non-sterol, mevalonate-derived substances that are vital for diverse cellular functions. The lovastatin-mediated increase in HMG-CoA reductase activity was associated with a increase in the amount of protein, as determined by Western-blot analysis, although no variations were determined in the levels of reductase mRNA. In *Leishmania*, control of gene expression is generally achieved through post-transcriptional regulation [30]. Our data indicate that the increase in activity is attributable solely to an increase in the amount of enzyme without parallel changes in mRNA levels; which would agree with what has been observed previously for the control of expression of other genes in this organism.

The lack of a membrane-spanning domain might account for absence of mevalonate-mediated suppression of HMG-CoA reductase activity. Studies on the mammalian enzyme have shown that the membrane domain is essential for sterol- and non-sterol-mediated degradation [31,32]. Apparently, *Leishmania* HMG-CoA reductase is a very stable protein and is not subjected to degradation regulatory mechanisms. Coppens et al. [26] have reported in *T. brucei* that HMG-CoA reductase activity is decreased 2-fold in cells incubated with mevalonate. However, the present study performed measuring soluble enzyme activity shows that the *Leishmania* enzyme is not down-regulated by the addition of exogenous mevalonate.

Serum sterols have no effect upon *L major* HMG-CoA reductase. A plausible explanation is that *Leishmania* lacks the ability to synthesize cholesterol *de novo* from mevalonate [3], thus this sterol is not a physiological regulator of the enzyme. Moreover, when ergosterol biosynthesis was inhibited by ketoconazole, HMG-CoA reductase activity was increased. Previous studies in *Leishmania* demonstrated that this drug causes accumulation of abnormal sterols with a 14α-methyl group [3]. Since ketoconazole is a cytochrome P450 inhibitor, the possibility exists that the drug prevents suppression of reductase activity from *L major* by inhibiting a cytochrome P450-dependent formation of endogenous oxysterols. Alternatively, the activation of the enzyme could be caused by inhibition of the synthesis of end-products of the sterol metabolism, such as ergosterol. The ketoconazole-mediated increase in HMG-CoA reductase activity was associated again with an increase in the amount of protein.

In summary, *Leishmania* HMG-CoA reductase is up-regulated when sterol synthesis is inhibited by drug pressure and this activation is apparently performed via post-transcriptional control. The lack of sensitivity to mevalonate and sterols is consistent with the absence of a membrane domain and may be a consequence of unique biological properties of the isoprenoid biosynthetic pathway in protozoa. Trypanosomatids are early-branching eukaryotic cells and their cell organization differs considerably from that of mammalian cells. Specific features present in trypanosomatids but absent from their hosts may be exploitable in providing targets for rational drug design. Studies are currently underway to determine the exact intracellular localization of reductase as well as the characteristics of other enzymes involved in this metabolic route.

This work was supported by grants from the United Nations Development Programme (UNDP)/World Bank/World Health Organization Program for Research and Training in Tropical Diseases (T24/181/30 ID 980139), the Spanish Programa Nacional de Biotecnología (BIO97-0659), the EC International Cooperation-Developing Countries (INCO-DC) project contract no. CT98-0371 and the Plan Andaluz de Investigación (Cod CVI-199) A.M is a fellow of the Instituto de Cooperación Internacional and J P-D and R H are fellows of the Spanish Plan de Formación del Personal Investigador of the Ministerio de Educación y Ciencia.

REFERENCES

1 Korn, E D, Von Brand, T and Tobie, E J (1969) Comp Biochem Physiol. **30**, 601–610

2 Goad, L J, Holz, Jr, G G and Beach, D H (1984) Mol Biochem Parasitol **10**, 161–170

3 Goad, L J, Holz, Jr, G G and Beach, D H (1985) Mol Biochem Parasitol **15**, 257–279

4 Ryder, N S (1988) Ann N Y Acad Sci **544**, 208–220

5 Troke, P F, Marriot, M S, Richardson, K and Tarbit, M H (1988) Ann N Y Acad. Sci **544**, 284–293

6 Haughan, P A, Chance, M. L and Goad, L J (1992) Biochem. Pharmacol **44**, 2199–2206

7 Goldstein, J L and Brown, M S (1990) Nature (London) **343**, 425–430

8 Beach, M J and Rodwell, V W (1989) J Bacteriol **171**, 2994–3001

9 Lam, W L and Doolittle, W F (1992) J Biol Chem **267**, 4223–4235

10 Takahashi, S, Kusuyama, T and Sato, H (1999) J Bacteriol **181**, 1256–1263

11 Peña-Díaz, J, Montalvetti, A, Camacho, A, Gallego, C, Ruiz-Perez, L M and Gonzalez-Pacanowska, D (1997) Biochem J **324**, 619–626

12 Olender, J L and Simoni, R D (1992) J Biol Chem **267**, 4223–4235

13 Kirsten, E S and Watson, J A (1974) J Biol Chem **249**, 6104–6109

14 Ausubel, F M, Brent, R, Kingston, R. E., Moore, D D, Seidman, J G., Smith, J A and Struhl, K (eds) (1987) Current Protocols in Molecular Biology, John Wiley and Sons, New York

15 Coderre, J. C., Beverly, S M, Schimke, R T and Santi, D. V (1993) Proc Natl Acad Sci. U.S.A **80**, 2132–2136

16 Garvey, E. P and Santi, D V (1986) Science **233**, 535–540

17 Camacho, A., Arrebola, R, Peña-Díaz, J, Ruiz-Perez, L M and Gonzalez-Pacanowska, D. (1997) Biochem. J **325**, 441–447

18 Southern, E (1975) J Mol. Biol **98**, 503–517

19 Bradford, M M (1976) Anal Biochem **72**, 248–254

20 Frimpong, K, Darnay, B G and Rodwell, V W (1993) Protein Expr Purif **4**, 337–344

21 Spithill, T W. and Samaras, N. (1987) In Molecular Strategies of Parasitic Invasion (Agabian, N., Goodman, H. and Nogueira, N, eds), pp 269–278, Alan R. Liss, New York

22 Brown, M S, Faust, J R, Goldstein, J. L, Kaneko, I. and Endo, A (1978) J Biol Chem **253**, 1121–1128

23 Nakanishi, M., Goldstein, J L and Brown, M S (1988) J. Biol Chem **263**, 8929–8937

24 Brown, M S and Goldstein, J. L (1980) J Lipid Res **21**, 505–517

25 Concepción, J L, González-Pacanowska, D. and Urbina, J A (1998) Arch Biochem Biophys **352**, 114–120

26 Coppens, I., Bastin, P., Levade, T and Courtoy, P J (1995) Mol Biochem. Parasitol **69**, 29–40

27 Mayer, R J, Debouck, C and Metcalf, B W. (1988) Arch. Biochem Biophys **267**, 110–118

28 Bach, T J., Rogers, D H. and Rudney, H. (1986) Eur. J Biochem **154**, 103–111

29 Istvan, E S, Palnitkar, M, Buchanan, S K and Deisenhofer, J. (2000) EMBO J **19**, 819–830

30 Swindle, J. and Tait, A (1996) in Molecular Biology of Parasitic Protozoa (Smith, D F. and Parsons, M, eds), pp. 6–34, Oxford University Press, New York

31 Gil, G., Faust, J R, Chin, D J, Goldstein, J L and Brown, M S (1985) Cell **41**, 249–258

32 Correll, C C. and Edwards, P A (1994) J Biol Chem **269**, 633–638

Received 15 December 1999/24 March 2000, accepted 27 April 2000

Biochem. J. (2000) **349**, 35–42 (Printed in Great Britain)

Oxidation of ubiquinol by peroxynitrite: implications for protection of mitochondria against nitrosative damage

Francisco SCHÖPFER*[1], Natalia RIOBÓ*, María Cecilia CARRERAS*, Beatriz ALVAREZ†, Rafael RADI‡, Alberto BOVERIS§, Enrique CADENAS¶ and Juan José PODEROSO*

*Laboratory of Oxygen Metabolism, University Hospital, School of Medicine, University of Buenos Aires, Córdoba 2351, Buenos Aires, Argentina (1120), †Laboratory of Enzymology, School of Science, Universidad de la República, Montevideo, Uruguay, ‡Department of Biochemistry and Laboratory of Free Radicals, School of Medicine, Universidad de la República, Montevideo, Uruguay, §Laboratory of Free Radical Biology, School of Pharmacy and Biochemistry, University of Buenos Aires, Argentina, and ¶Department of Molecular Pharmacology and Toxicology School of Pharmacy, University of Southern California, 1985 Zonal Avenue, Los Angeles, CA 90089-9121, U.S.A.

A major pathway of nitric oxide utilization in mitochondria is its conversion to peroxynitrite, a species involved in biomolecule damage via oxidation, hydroxylation and nitration reactions. In the present study the potential role of mitochondrial ubiquinol in protecting against peroxynitrite-mediated damage is examined and the requirements of the mitochondrial redox status that support this function of ubiquinol are established. (1) Absorption and EPR spectroscopy studies revealed that the reactions involved in the ubiquinol/peroxynitrite interaction were first-order in peroxynitrite and zero-order in ubiquinol, in agreement with the rate-limiting formation of a reactive intermediate formed during the isomerization of peroxynitrite to nitrate. Ubiquinol oxidation occurred in one-electron transfer steps as indicated by the formation of ubisemiquinone. (2) Peroxynitrite promoted, in a concentration-dependent manner, the formation of superoxide anion by mitochondrial membranes. (3) Ubiquinol protected against peroxynitrite-mediated nitration of tyrosine residues in albumin and mitochondrial membranes, as suggested by experimental models, entailing either addition of ubiquinol or expansion of the mitochondrial ubiquinol pool caused by selective inhibitors of complexes III and IV. (4) Increase in membrane-bound ubiquinol partially prevented the loss of mitochondrial respiratory function induced by peroxynitrite. These findings are analysed in terms of the redox transitions of ubiquinone linked to both nitrogen-centred radical scavenging and oxygen-centred radical production. It may be concluded that the reaction of mitochondrial ubiquinol with peroxynitrite is part of a complex regulatory mechanism with implications for mitochondrial function and integrity.

Key words: cytochrome oxidase, nitric oxide, superoxide anion, superoxide dismutase.

INTRODUCTION

The effects of $^{\bullet}$NO on the regulation of mitochondrial O_2 uptake are of importance for pathological conditions associated with increased levels of $^{\bullet}$NO [1]. The intramitochondrial steady-state concentration of $^{\bullet}$NO ranges from 20–500 nM depending on, on the one hand, the sources of $^{\bullet}$NO related to the activities of nitric oxide synthase (NOS) isoforms [mitochondrial (mtNOS), endothelial (eNOS), neuronal (nNOS) and inducible (iNOS)] and, on the other, the mitochondrial pathways for $^{\bullet}$NO utilization (Scheme 1). These involve reductive and oxidative decay mechanisms [2]. The former encompasses a general reduction of $^{\bullet}$NO to the nitroxyl anion (NO^-) and occurs at the expense of electron donation, mainly from ubiquinol [3] and, to a lesser extent, from cytochrome *c* [4] and cytochrome oxidase [5]. The latter, the oxidative decay mechanisms, involve the reaction of $^{\bullet}$NO with O_2^- to yield $ONOO^-$, a reaction that takes place at diffusion controlled rates ($k = 1.9 \times 10^{10}\ M^{-1} \cdot s^{-1}$) [6].

The reductive and oxidative decay pathways of $^{\bullet}$NO in mitochondria (under conditions entailing an expanded ubiquinol pool) are linked to the redox transitions of ubiquinone [2]; reduction of $^{\bullet}$NO by ubiquinol generates ubisemiquinone (eqn. 1), which decays by autoxidation to generate O_2^- (eqn. 2); the rapid reaction of the latter with $^{\bullet}$NO leads to $ONOO^-$ generation (eqn. 3):

$$^{\bullet}NO + UQH^- \rightarrow NO^- + UQ^{\bullet -} + H^+ \qquad (1)$$

$$UQ^{\bullet -} + O_2 \rightarrow UQ + O_2^{\bullet -} \qquad (2)$$

$$O_2^{\bullet -} + {}^{\bullet}NO \rightarrow ONOO^- \qquad (3)$$

where UQH^- is ubiquinol, $UQ^{\bullet -}$ is ubisemiquinone, and UQ is ubiquinone.

In agreement with these notions, it was observed that in respiring mitochondria $^{\bullet}$NO decays largely through $ONOO^-$ formation [2], and that diaphragm mitochondria undergo loss of integrity and function associated with protein nitration after exposure to increased endogenous $^{\bullet}$NO and $ONOO^-$ production [1]. Furthermore, the implications for removal of $^{\bullet}$NO (eqn. 3) are twofold: on the one hand, it releases cytochrome oxidase inhibition and, on the other hand, it leads to $ONOO^-$ formation.

In spite of its short half-life, peroxynitrite reacts with a wide range of biomolecules, such as proteins [7], nucleotides [8], lipids [9] and antioxidant molecules [10,11]. 3-Nitrotyrosine, a fingerprint of peroxynitrite reactivity towards tyrosine residues in proteins, has been found in physiological and pathological conditions [12,13]. Considering that mitochondrial membranes are permeable to $^{\bullet}$NO and impermeable to $O_2^{\bullet -}$ and that NO in mitochondria decays largely via $ONOO^-$ formation, it seems pertinent to define physiologically-relevant mitochondrial mechanisms of protection against $ONOO^-$-mediated damage. In this context, the role of ubiquinol as an antioxidant gains significance

---

Abbreviations used: NOS, nitric oxide synthase, DTPA, diethylenetriaminepenta-acetic acid, UQ_0, 2,3-dimethoxy-6-methyl-1,4-benzoquinone, UQ_2, decylubiquinone, UQ_{10}, ubiquinone-50.

[1] To whom correspondence should be addressed (e-mail fschopfer@hotmail.com)

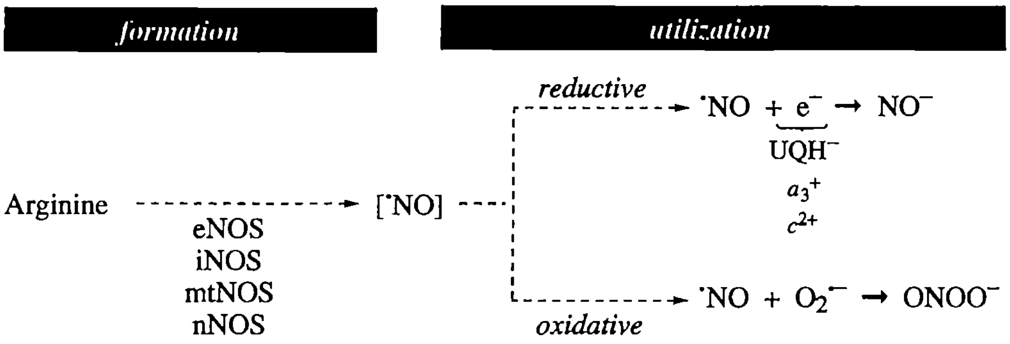

Scheme 1 Reductive and oxidative decay pathways of nitric oxide in mitochondria

UQH$^-$, ubiquinol, c^{2+}, ferrocytochrome c, a_3^+, reduced cytochrome oxidase Explanations are given in the text eNOS, endothelial NOS; iNOS, inducible NOS, mtNOS, mitochondrial NOS, nNOS, neuronal NOS

in view of its ubiquitous distribution and its effective recovery by electrons channeled through mitochondrial complexes I and II. Hence, the goals of this study were to characterize the potential reaction of ubiquinol with ONOO$^-$, examine the mitochondrial redox conditions favouring such a reaction, and to establish a role for ubiquinol in protection against ONOO$^-$-mediated nitration processes.

MATERIALS AND METHODS

Chemicals and biochemicals

2,3-Dimethoxy-6-methyl-1,4-benzoquinone (UQ$_0$), decylubiquinone, and ubiquinone-50 (Q$_{10}$), diethylenetriaminepenta-acetic acid (DTPA), H_2O_2, $NaNO_2$, KBH_4, NaCN, myxothiazol, antimycin A, fatty acid-free BSA and superoxide dismutase were from Sigma Chemical Co. (St. Louis, MO, U.S.A.). Acrylamide solutions, nitrocellulose membranes and goat anti-rabbit IgG were from Bio-Rad (Hercules, CA, U.S.A.). Specific anti-nitrotyrosine polyclonal antibody was a gift from Dr. Alvaro Estevez (University of Alabama at Birmingham, AL, U.S.A) All other reagents were of analytical grade.

Peroxynitrite was synthesized in a quenched flow reactor from 0.7 M $NaNO_2$ and 0.7 M H_2O_2, and stabilized with 1.2 M NaOH, as described previously [14]. H_2O_2 was removed by adding granular MnO_2 The solution was frozen at −70 °C. Peroxynitrite, concentrated in the yellow top layer was collected and its concentration was determined spectrophotometrically ($\epsilon_{302} = 1.67\ mM^{-1}\cdot cm^{-1}$) [14]

Chemical reduction of either UQ$_0$ or UQ$_2$ was obtained upon addition of 40 μl of KBH_4 (0.5 M dissolved in 0.1 M NaOH) to 1 ml of 20 mM quinone dissolved in either water (UQ$_0$) or ethanol (UQ$_2$); excess KBH_4 was removed by treatment with HCl [15]. Ubiquinol solutions were purged with argon for 5 min in a sealed flask.

Isolation of rat liver mitochondria, preparation of submitochondrial particles, and determination of ubiquinone content

Rat liver mitochondria were isolated in 0 23 M mannitol/70 mM sucrose/1 mM EDTA/10 mM Tris/HCl, pH 7.3, as described previously [16]. Submitochondrial particles were prepared from frozen and thawed liver mitochondria (20 mg protein/ml) placed in a small beaker in an ice bath, and disrupted by sonication for three 10 s periods with 30 s intervals at an output of 40 W using a Model W-225R sonifier (Heat Systems/Ultrasonics, Chicago, IL, U.S.A.) [17]. The submitochondrial particles were washed three times and resuspended in the above buffer at a concentration of 10 mg protein/ml. All operations were performed at 0–4 °C.

Increase in the steady-state level of endogenous ubiquinol was achieved by supplementing submitochondrial particles with succinate in the presence of complex III/IV inhibitors: antimycin A was used as a complex III inhibitor at the site of cytochromes $b_{562-566}$, myxothiazol was used as a complex III inhibitor at the Rieske Fe-S protein [18], and cyanide as a cytochrome oxidase inhibitor. Increase in the membrane ubiquinone pool was achieved by incubating submitochondrial particles (2.5 mg/ml) with various amounts of UQ$_2$ for 30 min in 100 mM phosphate buffer, pH 7.4, at 30 °C; reduction of added UQ$_2$ was accomplished upon supplementation of the membranes with 6 mM succinate and 2.4 μM myxothiazol

Rats were injected intramuscularly with a single dose of UQ$_{10}$ (20 mg/kg) suspended in aqueous soybean lecithin (1:1, v/v). Animals were killed 16 h after injection. Ubiquinone content in mitochondria (isolated as described above) was determined after extraction with cyclohexane/ethanol (5:2, v/v) (6 mg of mitochondrial protein/ml and 7 ml of cyclohexane/ethanol) [19]. Total ubiquinone content was calculated using the molecular absorption coefficient for the difference in absorption of the oxidized and reduced (obtained after addition of 0.2 mg KBH_4) forms of ubiquinone ($\epsilon_{ox}-\epsilon_{red}$) at A_{275} ($\Delta\epsilon = 12.25\ mM^{-1}\cdot cm^{-1}$) [20].

Absorption spectroscopy

Ubiquinol spectral changes were followed using a Hitachi U-3000 spectrophotometer (Hitachi Co. Ltd., Tokyo, Japan) in the 220–340 nm range ($\epsilon_{268} = 13.8\ mM^{-1}\cdot cm^{-1}$) [21]. The effect of UQ$_0H_2$ on the rate of peroxynitrite decomposition was assessed in a stopped-flow spectrophotometer (Applied Photophysics SF.17MV) with dead time of < 2 ms. The temperature was maintained at 37 0 ± 0.1 °C. A wavelength of 304 nm was used to minimize interference of UQ$_0$H$_2$ or UQ$_0$ absorbance. Changes in pH because of the addition of acidic solutions of UQ$_0$H$_2$ were counteracted by adding NaOH, and the pH was measured after the reactions. To monitor the effect of decomposition products of KBH_4 present in UQ$_0$H$_2$ solutions, peroxynitrite was mixed with control solutions prepared in the absence of UQ$_0$H$_2$. To prevent the reaction of UQ$_0$H$_2$ or semiquinone radical with oxygen, the solutions were degassed with argon for 15 min before mixing in the stopped-flow spectrophotometer. Apparent rate constants were determined by non-linear least-squares fitting of stopped-flow data to a single exponential function using the software provided with the instrument. The values reported are the average of at least seven determinations. $O_2^{\cdot-}$ production by rat liver submitochondrial particles was measured by superoxide-dismutase-sensitive cytochrome *c* reduction ($\epsilon_{550} = 21.1\ mM^{-1} \cdot cm^{-1}$, as described previously [22].

EPR spectroscopy

EPR spectra were recorded on a Bruker ECS 106 spectrometer (Bruker Analytik GmbH, Rheinstetten, Germany) equipped with a TM 8810 microwave cavity. Measurements were carried out at room temperature at a microwave frequency of 9.80 GHz and 100 kHz field modulation. Continuous-flow EPR measurements were performed with argon-purged solutions of $ONOO^-$ (400 μM in 10 mM NaOH) and UQ_0H_2 (400 μm in 200 mM phosphate buffer, pH 7.4) mixed before the cavity at a flow rate of 7 ml/min.

Immunoblotting and nitrotyrosine detection

BSA or submitochondrial particles (20 μg or 25 μg/lane respectively) were separated by electrophoresis on precast SDS 7.5 % polyacrylamide gel and transferred on to a PVDF membrane. The membranes were incubated with a rabbit anti-3-nitrotyrosine polyclonal antibody (1:2000) and blotted with a goat anti-rabbit IgG (1:3000) conjugated to alkaline phosphatase (Bio-Rad) followed by detection of immunoreactive proteins by a chemiluminescence method. BSA, exposed or not to 1 mM $ONOO^-$, was used as control.

RESULTS

Ubiquinol oxidation by peroxynitrite

Absorption spectral analysis of an anaerobic solution of UQ_0H_2 in the UV (220–340 nm) region revealed a maximum at 294 nm (Figure 1A). Addition of $ONOO^-$ (45 μM pulses) resulted in a progressive increase in absorption at 268 nm with isosbestic points at 232 and 289 nm, spectral changes ascribed to ubiquinone formation. The amount of ubiquinol oxidized was linearly related to the amount of $ONOO^-$ added, up to a ratio of $[ONOO^-]/[UQ_0H_2] \sim 4$; beyond this value, the amount of peroxynitrite required to obtain total ubiquinol oxidation did not follow a linear relationship. The amount of ubiquinol oxidized represented 22 % of $ONOO^-$ added for the first three pulses (Figure 1B).

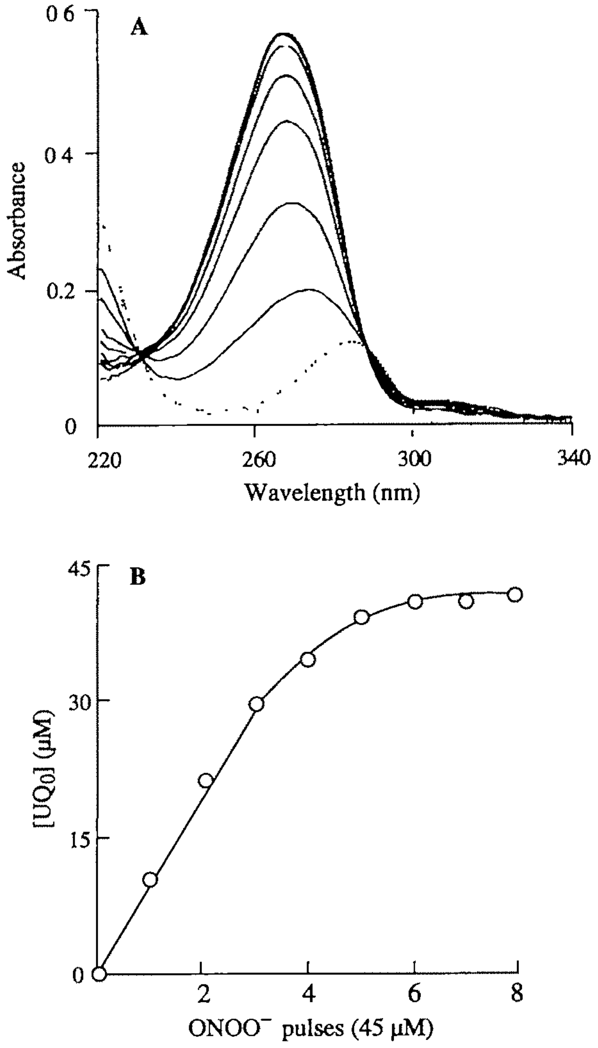

Figure 1 Oxidation of ubiquinol by peroxynitrite

(A) UV absorption spectrum. Conditions used: anaerobic solution of 45 μM UQ_0H_2 in 100 mM sodium phosphate buffer, pH 7.4, containing 1 mM DTPA was supplemented with various amounts of peroxynitrite (45 μM pulses). **(B)** Dependence of ubiquinone formation upon peroxynitrite concentration. Data were obtained from the A_{268} shown in **(A)**.

As observed in the time-dependent spectra shown in Figure 2(A), $ONOO^-$ decomposition in the presence of ubiquinol was accompanied by an increase in absorbance in the 400–450 nm region, due to quinol oxidation. However, the rate of $ONOO^-$ decomposition ($0.86 \pm 0.02\ s^{-1}$; Figure 2B) was not increased in the presence of ubiquinol ($0.82 \pm 0.03\ s^{-1}$; Figure 2C).

The kinetic pattern in Figure 1 and the time courses in Figure 2 indicate that the reactions involved in the $ONOO^-/UQ_0H_2$ interaction are first-order in $ONOO^-$ and zero-order in UQ_0H_2. This is in agreement with the rate-limiting formation of a reactive intermediate formed during the isomerization of $ONOO^-$ to NO_3^- (eqns. 4–6):

$$ONOO^- + H^+ \rightarrow ONOOH \quad (4)$$

$$ONOOH \rightarrow [HO^{\cdot} + {}^{\cdot}NO_2] \quad (5)$$

$$[HO^{\cdot} + {}^{\cdot}NO_2] \rightarrow H^+ + NO_3^- \quad (6)$$

This intermediate, which is capable of nitration, hydroxylation and oxidation, may decompose via homolytic O–O bond cleavage to yield $HO^{\cdot}$ and $NO_2^{\cdot}$ (eqn. 5); the recombination of these two radicals can result in NO_3^- formation (eqn. 6) [23–28]. The experiments in Figures 1 and 2 were carried out in argon-purged solutions, thereby ruling out a role for reactive intermediates originating from the reaction of $ONOO^-$ and CO_2.

Formation of ubisemiquinone during the oxidation of ubiquinol by peroxynitrite

The oxidation of ubiquinol by the above mentioned reactive intermediate is expected to proceed in one-electron transfer steps; this notion is strengthened by the detection by continuous flow EPR of a signal [hyperfine splitting constants: a^H (3H) = 2.14 G, a^H (1H) = 1.72 G; line intensity ratio: 13.5:5:3:1] ascribed to ubisemiquinone formed during the interaction of UQ_0H_2 and $ONOO^-$ in anaerobic conditions (Figure 3A) (eqn. 7):

$$HO^{\cdot} + {}^{\cdot}NO_2 + UQH^- \rightarrow HO^- + NO_2^{\cdot} + UQ^{\cdot-} + H^+ \quad (7)$$

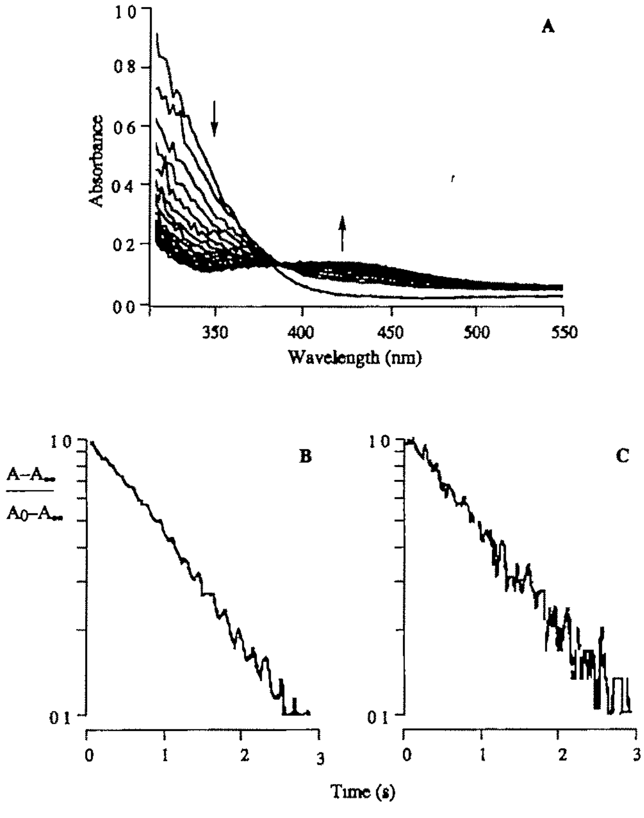

Figure 2 Time-course traces of ONOO⁻ decomposition

(**A**) Time-dependent spectra obtained for ONOO⁻ decomposition in the presence of UQ_0H_2 ONOO⁻ (1 mM) was mixed with 0.1 M phosphate buffer, pH 7.37, containing 0 1 mM DTPA in the presence of 1 mM UQ_0H_2 The time span between consecutive spectra was 346 ms The solutions were degassed with argon for 15 min before mixing (**B**, **C**). Time courses of ONOO⁻ spontaneous decomposition ONOO⁻ (0 1 mM) was mixed with 0.1 mM phosphate buffer (pH 7 37) (**B**) containing 0.1 mM DTPA at 37 °C, in the absence (**B**) or presence (**C**) of 5 mM UQ_0H_2 The solutions were degassed with argon for 15 min before mixing

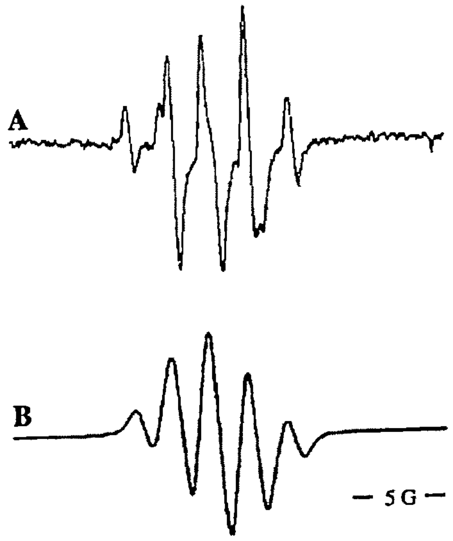

Figure 3 ONOO⁻-mediated ubisemiquinone formation

(**A**) Continuous-flow EPR spectrum of $UQ_0^{\bullet-}$ Solutions of 400 μM UQ_0H_2 and ONOO⁻ (in 10 mM NaOH) in argon-purged 0.2 M phosphate buffer, pH 7.4, were mixed at a flow rate of 7 ml/min (**B**) Simulated spectrum of (**A**) Instrument settings: modulation amplitude, 0.963 G, modulation frequency, 50.0 kHz, microwave power, 31.7 mW, sweep width, 30 G, sweep rate, 18 G/min, conversion time, 163.64 ms

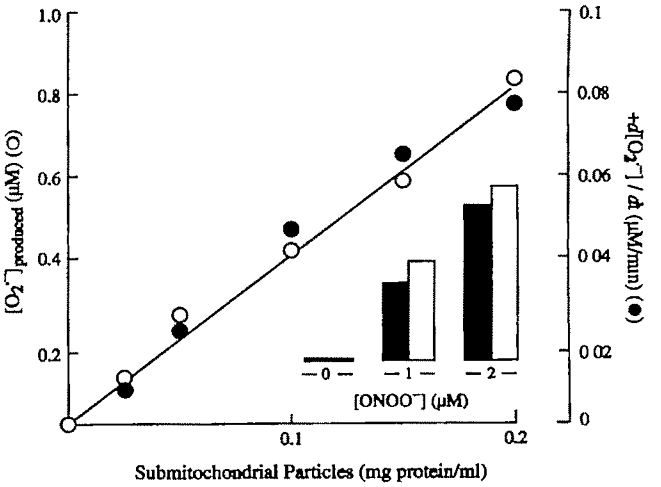

Figure 4 ONOO⁻-dependent O_2^- generation by submitochondrial particles

Assay conditions: submitochondrial particles (0 05–0.2 mg protein/ml) in 0 1 M phosphate buffer, pH 7.4, were supplemented with 6 mM succinate and 2.4 μM myxothiazol The reaction was initiated by the addition of 1 μM ONOO⁻ Inset effect of varying concentrations of ONOO⁻ on $O_2^{\bullet-}$ generation Assay conditions: submitochondrial particles (0.1 mg protein/ml) in 0.1 M phosphate buffer, pH 7.4, were supplemented with 6 mM succinate and 2.4 μM myxothiazol in the presence of various amounts of ONOO⁻ White bars, $[O_2^{\bullet-}]_{produced}$ (μM), black bars, d$[O_2^{\bullet-}]$/dt (μM/min).

The EPR signal was short lived in experiments where continuous flow was not used, probably due to the decay of the ubisemiquinone by disproportionation (eqn. 8):

$$UQ^{\bullet-} + UQH^{\bullet} \rightarrow UQ + UQH^{-} \qquad (8)$$

where UQH^- is ubiquinol, $UQ^{\bullet-}$ is ubisemiquinone, and UQ is ubiquinone. The rate of eqn. (7) is expected to be fast, assuming $HO^{\bullet}$ or $NO_2^{\bullet}$-like chemistry of the intermediate. For example, the second-order rate constant for the reaction of benzohydroquinone with $HO^{\bullet}$ and $NO_2^{\bullet}$ is $> 10^9$ $M^{-1} \cdot s^{-1}$ and $\sim 5 \times 10^8$ $M^{-1} \cdot s^{-1}$ respectively [29]. The rate of eqn. (8) depends on the relative concentrations of the anionic ($UQ^{\bullet-}$) and protonated ($UQH^{\bullet}$) forms of the semiquinone and, at pH 7.4, it occurs with a second-order rate constant of $\sim 8 \times 10^4$ $M^{-1} \cdot s^{-1}$ [30].

Peroxynitrite-dependent ubiquinol oxidation and superoxide anion formation

The formation of ubisemiquinone during the oxidation of ubiquinol by peroxynitrite (Figure 2; eqn. 7) suggests an additional source of $O_2^{\bullet-}$ in mitochondrial membranes upon autoxidation of the ubisemiquinone (eqn. 9):

$$UQ^{\bullet-} + O_2 \rightarrow UQ + O_2^{\bullet-} \qquad (9)$$

Accordingly, under conditions entailing an enhanced level of endogenous ubiquinol in mitochondrial membranes (submitochondrial particles supplemented with succinate in the presence of myxothiazol), ONOO⁻ elicited $O_2^{\bullet-}$ formation (Figure 4). The rate of $O_2^{\bullet-}$ production and total $O_2^{\bullet-}$ production were linearly related to protein (submitochondrial particles) concentration. Under these conditions, the $O_2^{\bullet-}$ production rate increased with increasing concentrations of ONOO⁻ (Figure 4 inset).

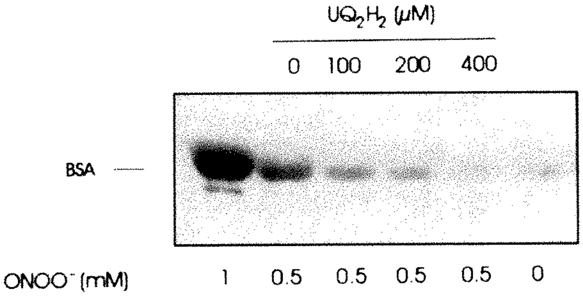

Figure 5 Effect of ubiquinol on peroxynitrite-mediated nitration of BSA

Assay conditions: BSA (2 mg protein/ml) in 0.1 M phosphate buffer, pH 7.4, was supplemented with 0.5 mM ONOO⁻ and various amounts of UQ_2H_2 (0–400 μM). The assay was performed as described in the Materials and methods section.

Effect of ubiquinol on peroxynitrite-mediated protein nitration

The reaction of ubiquinol with a reactive intermediate (eqn. 7) suggests a role for this electron donor in pathways inherent in the chemical reactivity of this intermediate, i.e. nitration, hydroxylation and oxidation. This notion was examined with experimental models involving tyrosine nitration, a fingerprint of ONOO⁻ action, in BSA and mitochondrial proteins by Western blotting.

Exposure of BSA to ONOO⁻ resulted in nitrotyrosine immunoreactivity (Figure 5); the intensity of this band was decreased with increasing amounts of ubiquinol (in the 0–400 μM range), thereby suggesting competition between ubiquinol and the tyrosine residue in the protein for the reactive intermediate involved in nitration. The reaction of ONOO⁻ with BSA proceeded with a second-order rate constant of $7.5\pm0.8\times10^3\ M^{-1}\cdot s^{-1}$ [24]; it may be inferred that, under the experimental conditions depicted in Figure 5 (30 μM BSA and 0.5 mM ONOO⁻), approx. 18% of ONOO⁻ reacted directly with BSA, and most of it decayed with production of secondary oxidants.

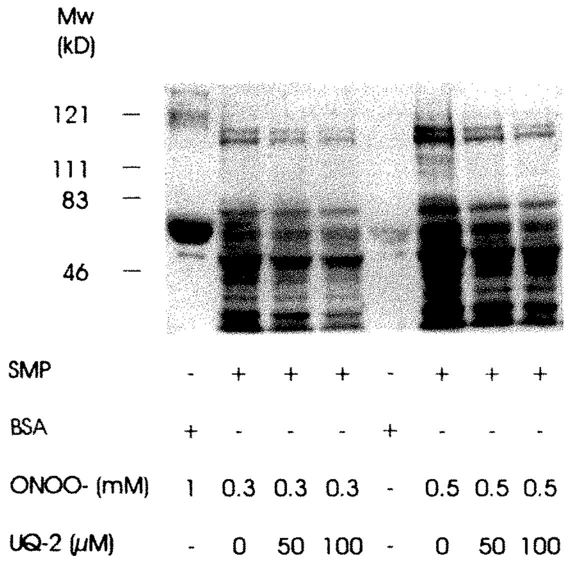
Mw (kD)
121
111
83
46
SMP - + + + - + + +
BSA + - - - + - - -
ONOO- (mM) 1 0.3 0.3 0.3 - 0.5 0.5 0.5
UQ-2 (μM) - 0 50 100 - 0 50 100

Figure 6 Effect of exogenous ubiquinone on ONOO⁻-mediated nitration of submitochondrial particles

Assay conditions: submitochondrial particles (SMP) (2.5 mg protein/ml) in 0.1 M phosphate buffer, pH 7.4, in the presence of 6 mM succinate and 2.4 μM myxothiazol were supplemented with either 0.3 or 0.5 mM ONOO⁻ and various amounts of UQ_2 (0–100 μM). Controls consisted of BSA (2 mg protein/ml) supplemented with 1 mM ONOO⁻. Molecular-mass markers in kDa (MW, kD) are shown on the left.

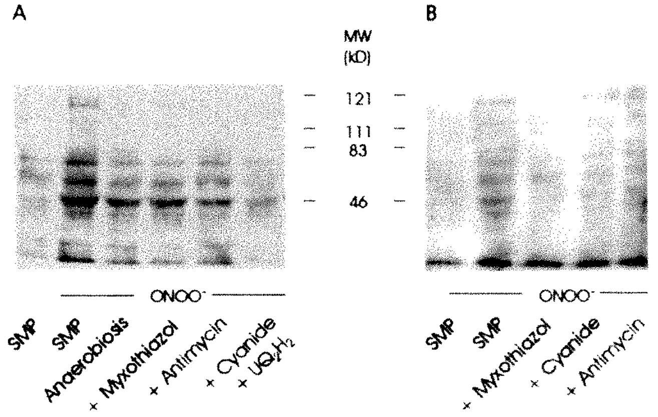

Figure 7 Effect of exogenous and endogenous ubiquinone redox status on ONOO⁻-mediated nitration of submitochondrial particles

Assay conditions: (**A**) Submitochondrial particles (SMP) (2.5 mg protein/ml) in 0.1 M phosphate buffer, pH 7.4, were supplemented with 6 mM succinate, various electron-transfer inhibitors and 20 μM UQ_2. After 30 min incubation, the samples were exposed to a single pulse of 200 μM ONOO⁻. (**B**) As in (**A**) but without the addition of UQ_2 and with 30 μM ONOO⁻; data correspond to redox changes in endogenous ubiquinol. The individual concentration of inhibitors was: 2.4 μM myxothiazol, 2.4 μM antimycin A or 1 mM KCN. The positions of molecular-mass markers in kDa (MW, kD) are shown.

When incubated with ONOO⁻, mitochondrial proteins exhibited reactivity for nitrotyrosine in numerous bands (Figure 6); the extent of tyrosine nitration was dependent on ONOO⁻ concentration (only two concentrations, 0.3 and 0.5 mM, are shown in Figure 6). The effect of ubiquinol on nitration of tyrosine residues in mitochondrial proteins was assessed with experimental models involving manipulations of the capacity and redox status of the ubiquinol pool in membranes.

First, increase in the ubiquinol pool was achieved by supplementation of submitochondrial particles with varying amounts of UQ_2 in the presence of myxothiazol, and with succinate as electron donor, thereby resulting in reduction of UQ_2 and increase of the total ubiquinol pool. Under these conditions, a progressive decrease in nitrotyrosine immunoreactivity was observed with increasing amounts of ubiquinol (Figure 6).

Secondly, the redox status of the endogenous ubiquinol pool was increased by using inhibitors of the mitochondrial complexes III and IV (myxothiazol, antimycin A and cyanide), resulting in higher levels of endogenous ubiquinone in the reduced state. Under these conditions, a decrease in nitrotyrosine immunoreactivity, elicited by supplementation of mitochondrial membranes with ONOO⁻, was observed (Figure 7).

Overall, data shown in Figures 5–7 strengthen the notion that the reaction of ubiquinol with the reactive intermediate formed in the decay of ONOO⁻ to NO_3^- prevents nitration of tyrosine residues in a concentration-dependent manner. These effects of ubiquinol also suggest that the reaction of ONOO⁻ with ubiquinol is a preferred decay pathway over the reaction of ONOO⁻ with other reduced components of the respiratory chain, such as cytochrome *c* and cytochrome oxidase [4,31]. Accordingly, the role of the latter in protection against ONOO⁻-dependent nitration may be less significant.

Table 1 Protective effects of parenteral administration of UQ_{10} on respiratory functions of rat liver mitochondria exposed to $ONOO^-$

Data are the means ± S E M from 3–4 samples .Respiratory control is the ratio between O_2 uptake rates in the presence (state 3) and in the absence (state 4) of 0.2 mM ADP with 6 mM malate/glutamate as substrate. *Denotes $P < 0.05$ with respect to control samples (determined by Student's *t* test), †denotes $P < 0.05$ with respect to basal values by analysis of variance ('ANOVA') and Dunnett's test

	Control	Injected with UQ_{10}
UQ_{10} content (μg/mg of protein)	1.29 ± 0.13	2 03 ± 0.17*
Respiratory control	8.1 ± 0.4	8 3 ± 0 4
+ 75 μM $ONOO^-$	6 1 ± 0.4	7.8 ± 0 4*
+ 150 μM $ONOO^-$	5.7 ± 0.4†	7 0 ± 0 3
+ 300 μM $ONOO^-$	4 3 ± 0.7†	4.5 ± 0 6†

Ubiquinone content and $ONOO^-$ concentration determine the oxidative damage of respiratory function in liver mitochondria

Mitochondrial content of UQ_{10} was increased ~ 57 % following the administration of the quinone to rats (Table 1), without changes in the respiratory control values. Supplementation of control mitochondria with 75, 150 or 300 μM $ONOO^-$ caused decreases in respiratory control values of ~ 25, 30, and 47 % respectively. The respiratory control values of liver mitochondria from rats injected with UQ_{10} were decreased by these $ONOO^-$ concentrations ~ 6, 15 and 45 % respectively (Table 1). It may be surmised that mitochondria with a higher content of UQ_{10} were endowed with adequate protection against damage caused by low $ONOO^-$ concentrations (e.g. 75 μM), whereas increased UQ_{10} content was apparently ineffective in protecting against functional damage caused by high $ONOO^-$ concentrations (e g. 300 μM).

DISCUSSION

This study shows that (1) ubiquinol is oxidized by reactive intermediates formed in the decay of $ONOO^-$ to NO_3^- (the reaction being zero order in peroxynitrite; Figure 2) in one-electron transfer steps, as suggested by the generation of ubisemiquinone (Figure 3). (2) $ONOO^-$ promotes the formation of $O_2^{\bullet -}$ by mitochondrial membranes (Figure 4), probably via a reaction entailing ubiquinol oxidation to ubisemiquinone (eqn. 7) followed by autoxidation of the latter (eqn. 9). (3) Ubiquinol protects against $ONOO^-$-mediated nitration of tyrosine residues in BSA (Figure 5) and mitochondrial membranes (Figures 6 and 7), as surmised from experimental designs involving the addition of ubiquinol or an expanded ubiquinol pool in mitochondria caused by the action of selective complex III/IV inhibitors. (4) Increasing membrane-bound ubiquinol upon administration of UQ_{10} to rats partially prevents the $ONOO^-$-induced loss of mitochondrial respiratory function (Table 1).

These findings may be analysed in terms of the redox transitions of ubiquinone (ubiquinol → ubisemiquinone → ubiquinone) associated with, on the one hand, scavenging of free radicals (inherent in the ubiquinol → ubisemiquinone transition) downstream of peroxynitrous acid decomposition and, on the other hand, formation of $O_2^{\bullet -}$ (inherent in the ubisemiquinone → ubiquinone transition) (Scheme 2). It may be surmised that the occurrence of a reaction between mitochondrial ubiquinol and $ONOO^-$ involves regulatory and protective aspects: first, ubiquinol scavenges free radicals derived from peroxynitrous acid decomposition, thereby protecting mitochondrial proteins against nitration. Secondly, $ONOO^-$ elicits a concentration-dependent $O_2^{\bullet -}$ formation by mitochondrial membranes; this effect is ascribed to ubiquinol oxidation followed by ubisemiquinone autoxidation; further removal of $O_2^{\bullet -}$ by matrix Mn-superoxide dismutase yields H_2O_2 in turn reduced to H_2O by mitochondrial glutathione peroxidase. The sequences entailed in these radical decay pathways ($ONOO^- \rightarrow NO_2^{\bullet} \rightarrow NO_2^-$ and $O_2^{\bullet} \rightarrow H_2O_2 \rightarrow H_2O$) suggest a strong antioxidant effect exerted by membrane ubiquinol. Thirdly, decay of $O_2^{\bullet -}$ to either H_2O_2 (by a Mn-superoxide dismutase-catalysed reaction; $k = 2.3 \times 10^{10}\ M^{-1} \cdot s^{-1}$) or $ONOO^-$ (upon its fast reaction with $^{\bullet}NO$; $k = 1.9 \times 10^{10}\ M^{-1}\ s^{-1}$) is expected to be a function of the individual mitochondrial concentrations or steady-state levels of Mn-superoxide dismutase and $^{\bullet}NO$.

It is noteworthy that the reactions of ubiquinol with $^{\bullet}NO$ (eqn. 1) and peroxynitrite-derived radicals (eqn. 7) imply paradoxical effects: on the one hand, the higher utilization of $^{\bullet}NO$ involved

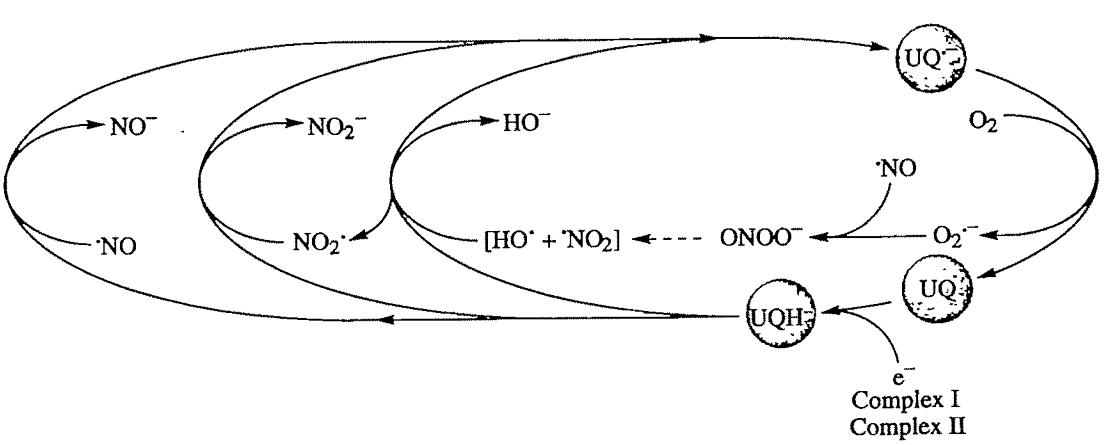

Scheme 2 Redox transitions of ubiquinol and the scavenging and formation of nitrogen- and oxygen-centred reactive species

The Scheme depicts the scavenging of nitrogen-centred species coupled to the ubiquinol (UQH^-) → ubisemiquinone ($UQ^{\bullet -}$) redox transition, the formation of the superoxide anion coupled to the ubisemiquinone → ubiquinone (UQ) transition, and the transfer of electrons from complexes I and II to ubiquinone in its reductive decay to NO^- via ubiquinol favours the release of cytochrome oxidase inhibition and thereby restores mitochondrial O_2 uptake [32]. On the other hand, the ubiquinol-centred reactions are expected to amplify the formation of $ONOO^-$ (suggested by an enhanced ubisemiquinone autoxidation to yield $O_2^{\bullet -}$ and the fast reaction of the latter with $^{\bullet}NO$). The prevalence of these pathways is partly controlled by the intramitochondrial steady-state level of $^{\bullet}NO$ (in the range 0.05–0.5 μM); high steady-state concentrations of $^{\bullet}NO$ (as during inducible-NOS induction [1]) are expected to compete efficiently with Mn-superoxide dismutase, thus favouring $ONOO^-$ formation. Furthermore, the decay of the $ONOO^-$-derived radical upon reaction with ubiquinol is relevant for mitochondrial functions, because (a) ubiquinol is a unique component of the electron transfer chain, which is efficiently and continuously recycled via electrons from complexes I and II and (b) ubisemiquinone, formed as indicated in Figure 3, is a major source of oxyradicals in mitochondria.

Understanding of the protection exerted by ubiquinol against $ONOO^-$-mediated nitration of tyrosine residues requires consideration of the mechanistic aspects of this process. Formation of nitrotyrosine is a consequence of reactive species formed during the decay of $ONOO^-$ and it entails a sequence that involves H abstraction from tyrosine to yield a tyrosyl radical ($Tyr + HO^{\bullet} \rightarrow Tyr^{\bullet} + HO^-$) followed by $NO_2^{\bullet}$ addition to the latter ($Tyr^{\bullet} + NO_2^{\bullet} \rightarrow$ 3-nitrotyrosine; $k = 3 \times 10^{10}\ M^{-1} \cdot s^{-1}$) [33]. Hence, prevention of nitrotyrosine formation by ubiquinol may involve scavenging of $HO^{\bullet}$, tyrosyl radical or $NO_2^{\bullet}$. All of these reactions are thermodynamically feasible when considering the reduction potential of the redox couples involved: ubisemiquinone/ubiquinol (+0.19 V; [34]), or $HO^{\bullet}/H_2O$ (2.3 V; [35]), $Tyr^{\bullet}Tyr$ (0.93 V; [36,37]), and $NO_2^{\bullet}/NO_2^-$ (+0.99 V; [38]).

In summary, a cohort of reactions involving mitochondrial ubiquinol with nitrogen-centred radicals have consequences for mitochondrial integrity and function and, most likely, for cellular effect signalled by mitochondrial changes. The implications of this redox network should be viewed primarily in terms of O_2 and $^{\bullet}NO$ gradients, which establish a dynamic interplay between $^{\bullet}NO$ metabolism, production of oxyradicals, regulation of O_2 uptake and scavenging of $ONOO^-$.

This work was supported by research grants from the University of Buenos Aires (TM047 and TB011), FONCYT (Agency for Promotion of Scientific and Technological Development) 02372; the Fundación Pérez Companc and CONICET (Scientific and Technological National Research Council) 0058/98 and 3110/97; ICEGEB (Italy), Sarec (Sweden), Universidad de la Republica-CSIC, and grant N° R01 AG16718 from NIH

REFERENCES

1 Boczkowski, J, Lisdero, C L, Lanone, S., Carreras, M C., Boveris, A., Aubier, M and Poderoso, J J. (1999) Endogenous peroxynitrite mediates mitochondrial dysfunction in rat diaphragm during endotoxemia FASEB J **13**, 1637–1646

2 Poderoso, J J, Lisdero, C, Schopfer, F., Riobó, N, Carreras, M. C., Cadenas, E and Boveris, A (1999) The regulation of mitochondrial oxygen uptake by redox reactions involving nitric oxide and ubiquinol J Biol Chem **24**, 37709–37716

3 Poderoso, J J, Carreras, M C., Schopfer, F, Lisdero, C, Riobó, N, Giulivi, C, Boveris, A D, Boveris, A and Cadenas, E (1999) The reaction of nitric oxide with ubiquinol kinetic properties and biological significance Free Radical Biol Med **26**, 925–935

4 Sharpe, M A and Cooper, C E (1998) Reactions of nitric oxide with mitochondrial cytochrome *c* a novel mechanism for the formation of nitroxyl anion and peroxynitrite Biochem J **332**, 9–19

5 Zhao, X, Sampath, V and Caughey, W. S. (1995) Cytochrome *c* oxidase catalysis of the reduction of nitric oxide to nitrous oxide Biochem Biophys Res Commun **212**, 1054–1060

6 Kissner, R, Nauser, T, Bugnon, P., Lye, P G. and Koppenol, W. H (1997) Formation and properties of peroxynitrite as studied by laser flash photolysis, high-pressure stopped-flow technique, and pulse radiolysis Chem Res Toxicol **10**, 1285–1292

7 Radi, R., Beckman, J S, Bush, K M and Freeman, B A (1991) Peroxynitrite oxidation of sulfhydryls The cytotoxic potential of superoxide and nitric oxide J Biol Chem **266**, 4244–4250

8 Szabó, C and Ohshima, H. (1997) DNA damage induced by peroxynitrite subsequent biological effects Nitric Oxide **1**, 373–385

9 Rubbo, H, Radi, R, Trujillo, M, Telleri, R., Kalyanaraman, B, Barnes, B, Kirk, M. and Freeman, B (1994) Nitric oxide regulation of superoxide and peroxynitrite-dependent lipid peroxidation Formation of novel nitrogen-containing oxidized lipid derivatives J. Biol Chem **242**, 26066–26075

10 Barlett, D, Church, D, Bounds, P and Koppenol, W (1995) The kinetics of the oxidation of L-ascorbic acid by peroxynitrite Free Radical Biol Med **18**, 85–92

11 Koppenol, W, Moreno, J., Pryor, W, Ischiropoulos, H and Beckman, J. S. (1992) Peroxynitrite, a cloaked oxidant formed by nitric oxide and superoxide Chem. Res Toxicol **5**, 834–842

12 Khan, J, Brennand, D M, Bradley, N, Gao, B, Bruckdorfer, R and Jacobs, M (1998) 3-Nitrotyrosine in the proteins of human plasma determined by an ELISA method Biochem J **330**, 795–801

13 Good, P, Hsu, A, Werner, P, Perl, D and Olanow, C. (1998) Protein nitration in Parkinson's disease J Neuropathol Exp Neurol **57**, 338–342

14 Beckman, J S, Chen, J, Ischiropoulos, H and Crow, J (1994) Oxidative chemistry of peroxynitrite. Methods Enzymol **233**, 229–236

15 Cadenas, E, Boveris, A, Ragan, C I. and Stoppani, A O M (1977) Production of superoxide radicals and hydrogen peroxide by NADH-ubiquinone reductase and ubiquinol-cytochrome *c* reductase from beef-heart mitochondria. Arch. Biochem Biophys **180**, 248–257

16 Chance, B. and Hagihara, B (1963) Direct spectroscopic measurements of interaction of components of the respiratory chain with adenosine triphosphate (ATP), adenosine diphosphate (ADP), phosphate, and uncoupling agents Proc Fourth Intern Congr Biochem **5**, 3–37

17 Turrens, J F. and Boveris, A (1980) Generation of superoxide anion by the NADH dehydrogenase of bovine heart mitochondria Biochem J **191**, 421–427

18 von Jagow, G and Link, T A (1986) Use of specific inhibitors on the mitochondrial bc_1 complex. Methods Enzymol **126**, 253–271

19 Ikenoya, S, Takada, M, Zuzuriha, T, Abe, K and Katayama, K (1981) Studies on reduced and oxidized ubiquinones. I Simultaneous determination of reduced and oxidized ubiquinones in tissues and mitochondria by high performance liquid chromatography Chem Pharm Bull **29**, 158–164

20 Redfearn, E R (1967) Isolation and determination of ubiquinone Methods Enzymol **10**, 381–384

21 Degli Esposti, M, Ngo, A, McMullen, L, Ghelli, A, Sparla, F, Benelli, B, Ratta, M and Linnane, A (1996) The specificity of mitochondrial complex I for ubiquinones Biochem J **313**, 327–334

22 Boveris, A, Cadenas, E and Stoppani, A O M (1976) The role of ubiquinone in the mitochondrial generation of hydrogen peroxide Biochem J **156**, 435–444

23 Beckman, J S (1990) Ischaemic injury mediator Nature (London) **345**, 27–28

24 Alvarez, B, Denicola, A and Radi, R (1995) Reaction between peroxynitrite and hydrogen peroxide formation of oxygen and slowing of peroxynitrite decomposition Chem Res. Toxicol **8**, 859–864

25 Koppenol, W H (1998) The basic chemistry of nitrogen monoxide and peroxynitrite Free Radicals Biol Med **25**, 385–391

26 Squadrito, G L and Pryor, W A. (1998) Oxidative chemistry of nitric oxide the roles of superoxide, peroxynitrite, and carbon dioxide Free Radicals Biol Med **25**, 392–403

27 Richeson, C E, Mulder, P, Bowry, V W and Ingold, K. U (1998) The complex chemistry of peroxynitrite decomposition new insights J Am Chem Soc **120**, 7211–7219

28 Beckman, J S, Beckman, T W, Chen, J, Marshall, P A and Freeman, B A (1990) Apparent hydroxyl radical production by peroxynitrite Implications for endothelial injury from nitric oxide and superoxide Proc Natl Acad U S A **87**, 1620–1624

29 Ross, A B, Bielski, B H J and Buxton, G V (1992) NIST Standard Reference Database 40 NDRL/NIST solution kinetic database Gaithersburg, MD, U S A

30 Land, E J and Swallow, A J (1970) One-electron reactions in biochemical systems as studied by pulse radiolysis 3 Ubiquinone J Biol Chem **245**, 1890–1894

31 Thomson, L, Trujillo, M., Tellen, R and Radi, R (1995) Kinetics of cytochrome c^{2+} oxidation by peroxynitrite implications for superoxide measurements in nitric oxide-producing biological systems· Arch Biochem Biophys **319**, 491–497

32 Poderoso, J J, Carreras, M C, Lisdero, C, Riobó, N, Schopfer, F and Boveris, A (1996) Nitric oxide inhibits electron transfer and increases superoxide radical production in rat heart mitochondria and submitochondrial particles Arch Biochem Biophys **328**, 85–92

33 Prutz, W A, Monig, H, Butler, J. and Land, E J (1985) Reactions of nitrogen dioxide in aqueous model systems. oxidation of tyrosine units in peptides and proteins Arch Biochem Biophys **243**, 125–134

34 Brandt, U. (1996) Bifurcated ubihydroquinone oxidation in the cytochrome bc_1 complex by proton-gated charge transfer FEBS Lett **387**, 1–6

35 Koppenol, W H. and Butler, J (1985) Energetics of interconversion reactions of oxyradicals Adv Free Radical Biol. Med. **1**, 91–131

36 DeFelippis, M R, Murthy, C. P., Broitman, F, Weinraub, D, Faraggi, M and Klapper, M H (1991) Electrochemical properties of tyrosine phenoxy and tryptophan indolyl radicals in peptides and amino-acid analogs J Phys Chem **95**, 3416–3419

37 Harriman, A (1987) Further comments on the redox potentials of tryptophan and tyrosine. J Phys Chem. **91**, 6102–6104

38 Koppenol, W H (1996) Thermodynamics of reactions involving nitrogen-oxygen compounds. Methods Enzymol **268**, 7–12

Received 17 January 200/30 March 2000, accepted 28 April 2000

Biochem J. (2000) 349, 43–49 (Printed in Great Britain)

Acylphosphatase possesses nucleoside triphosphatase and nucleoside diphosphatase activities

Paolo PAOLI, Guido CAMICI, Giampaolo MANAO, Elisa GIANNONI and Giampietro RAMPONI[1]
Dipartimento di Scienze Biochimiche, Università di Firenze, Viale Morgagni 50, 50134 Firenze, Italy

We have demonstrated that acylphosphatase possesses ATP-diphosphohydrolase (apyrase-like) activity. In fact, acylphosphatase first catalyses the hydrolysis of the γ-phosphate group of nucleoside triphosphates, and then attacks the β-phosphate group of the initially produced nucleoside diphosphates, generating nucleoside monophosphates. In constrast, it binds nucleoside monophosphates but does not catalyse their hydrolyses. The calculated k_{cat} values for the nucleoside triphosphatase activity of acylphosphatase are of the same order of magnitude as those displayed by certain G-proteins. An acidic environment enhances the apyrase-like activity of acylphosphatase. The true nucleotide substrates of acylphosphatase are free nucleoside di- and triphosphates, as indicated by the Mg^{2+} ion inhibition of the activity. We have also demonstrated that, although nucleoside triphosphates are still hydrolysed at pH 7.2 and 37 °C, in the presence of millimolar Mg^{2+} concentrations this occurs at a lower rate. Taken together with the previously observed strong increase of acylphosphatase levels during induced cell differentiation, our findings suggest that acylphosphatase plays an active role in the differentiation process (as well as in other processes, such as apoptosis) by modulating the ratio between the cellular levels of nucleoside diphosphates and nucleoside triphosphates.

Key words: acylphosphatase mutant, apyrase, ADPase, ATPase.

INTRODUCTION

Acylphosphatase (EC 3.6.1.7) catalyses the hydrolysis of the carboxyl-phosphate bond contained in metabolites such as acetyl phosphate, 1,3-bisphosphoglycerate and carbamoyl phosphate ([1], and citations therein), as well as in proteins such as the β-aspartyl phosphate intermediates formed during the actions of Na^+/K^+- ([2], and citations therein) and Ca^{2+}-membrane ion pumps ([3], and citations therein). These findings have suggested that the enzyme is involved in the control of some metabolic pathways, and in the control of the ion status of the cells.

Two isoenzymes, coded by two different genes, are expressed in vertebrate tissues. The muscle type (MT) is prevalently expressed in skeletal muscle and heart, whereas the organ common type (CT) is prevalently expressed in erythrocytes, in brain and in testis [4,5]. The three-dimensional structures of the two isoenzymes are very similar: they consist of a five-stranded anti-parallel twisted β-sheet flanked on one side by two anti-parallel α-helices running parallel to the β-sheet [6]. This peculiar acylphosphatase folding is very similar to that of the small RNA-binding domains of several RNA-binding proteins [7,8]; in fact, many RNA-binding proteins have modular structures consisting of RNA-binding modules and auxiliary domains, which perform an additional function [9]. This prompted us to investigate the involvement of acylphosphatase in polynucleotide processing. Chiarugi et al. [10] found that acylphosphatase catalyses the hydrolysis of both DNA and RNA.

This paper reports a new catalytic activity of the enzyme, demonstrating that acylphosphatase possesses nucleoside triphosphatase (NTPase) and nucleoside diphosphatase (NDPase) activities.

EXPERIMENTAL

Benzoyl phosphate was synthesized according to Camici et al. [11]. Most nucleotides were purchased from Sigma; ADP was from Boehringer Mannheim (Mannheim, Germany). The DEAE 5PW HPLC column was from Bio-Rad. The recombinant CT and MT wild-type isoenzymes of acylphosphatase were expressed and purified as described previously [12,13]. The $Arg^{23} \rightarrow Ala$ (CT acylphosphatase) and $Asn^{41} \rightarrow Gln$ (MT acylphosphatase) mutants were obtained by oligonucleotide-directed mutagenesis using a unique-site-elimination (USE) mutagenesis kit based on the USE method developed by Deng and Nickoloff [14]. The mutations were confirmed by DNA sequencing according to the method of Sanger et al. [15] and by amino acid analysis of the purified proteins. The purity of wild type and mutated acylphosphatases was checked by SDS/PAGE, staining protein with a silver nitrate-based method: in each case, a single band at about 11 kDa was present (results not shown). All other reagents were the purest commercially available.

Enzyme assays

NTPase and NDPase activities were assayed at 37 °C by adding the enzyme to test mixtures containing either one nucleoside triphosphate (NTP) or one nucleoside diphosphate (NDP) dissolved in 0.1 M buffer solutions at the indicated pH value. The buffers used were: 2.5–3.6 pH range, sodium formiate; 3.7–5.8 pH range, sodium acetate; 5.9–7.0 pH range, sodium cacodylate; 7.1–8.0 pH range, Tris/acetate. At the appropriate times, aliquots were withdrawn and the released P_i was determined as described by Baginski et al. [16]. All assays were performed at least in duplicate, taking into account the non-enzymic hydrolysis of the nucleotides. Acylphosphatase activity was determined at 25 °C using a continuous optical test and benzoyl phosphate as substrate [17].

Regression analysis

The V_{max} and K_m values were obtained by solving the equation $v = V_{max}[S]/K_m + [S]$ by non-linear regression analysis with the aid of a computer program (FigureP, BioSoft). In each determi-

---

Abbreviations used: CT, organ common type, MT, muscle type, NDPase, nucleoside diphosphatase, NTPase, nucleoside triphosphatase; NMP, nucleoside monophosphate, NDP, nucleoside diphosphate; NTP, nucleoside triphosphate

[1] To whom correspondence should be addressed (e-mail ramponi@scibio.unifi.it)

nation, the standard errors for K_m and V_{max} were calculated. In the case of inhibition studies, the linear-regression analysis of the double reciprocal plots was also performed with the FigureP program.

HPLC analysis

ATP, ADP and AMP as well as GTP, GDP and GMP were analysed by HPLC using a DEAE 5PW column (7.5 × 75 mm). Solvent A was 25 mM Tris/HCl buffer, pH 8.0; solvent B was buffer A containing 1 M NaCl. The flow rate was 0.8 ml/min The analysis program was 0–50 % solvent B in 30 min.

RESULTS

ATP, ADP and AMP behave as competitive inhibitors versus the benzoylphosphatase activity of acylphosphatase

We determined the apparent K_m and V_{max} values of acylphosphatase for benzoyl phosphate in the presence of increasing concentrations of AMP, ADP and ATP. Figure 1 shows the double reciprocal plot analyses, which demonstrate that ATP, ADP and AMP (Figures 1A, 1B and 1C respectively) apparently behave as competitive inhibitors of benzoylphosphatase activity. The actual inhibition constants, calculated by replotting the apparent K_m values against nucleotide concentration (Figure 1D), were 0.1 mM for ATP, 0 47 mM for ADP and 2 18 mM for AMP. Taken together, these findings demonstrate that acylphosphatase binds all three adenosine nucleotides at the enzyme site that also binds benzoyl phosphate, but also that binding strength increases greatly from AMP to ADP and to ATP, suggesting that the β- and γ- phosphate groups of nucleotides contribute to the binding with additional interactions.

Acylphosphatase catalyses the hydrolysis of NTPs and NDPs, but not that of NMPs

We incubated 2 mM ATP or 2 mM GTP (in separate tubes) with acylphosphatase (0.38 μM final concentration) at 37 °C in 0.1 M sodium acetate buffer, pH 5.3. At the indicated times, aliquots were taken and analysed by ion-exchange HPLC using a DEAE 5PW column. Figure 2 shows the HPLC time-course analyses. It can be seen that acylphosphatase is able to produce first ADP and, successively, AMP. Similar HPLC analyses demonstrated that when GTP was used as substrate, GDP and GMP were produced in a time-dependent manner (results not shown). The control experiments were performed under the same conditions, but without enzyme added: under the above experimental conditions very poor spontaneous NTP hydrolyses were recorded (results not shown). Similar experiments performed in the presence of 2 mM EDTA gave identical results, indicating that metal ions are not required for the activity. On the contrary, the Mg^{2+} ion behaves as an inhibitor, suggesting that the free

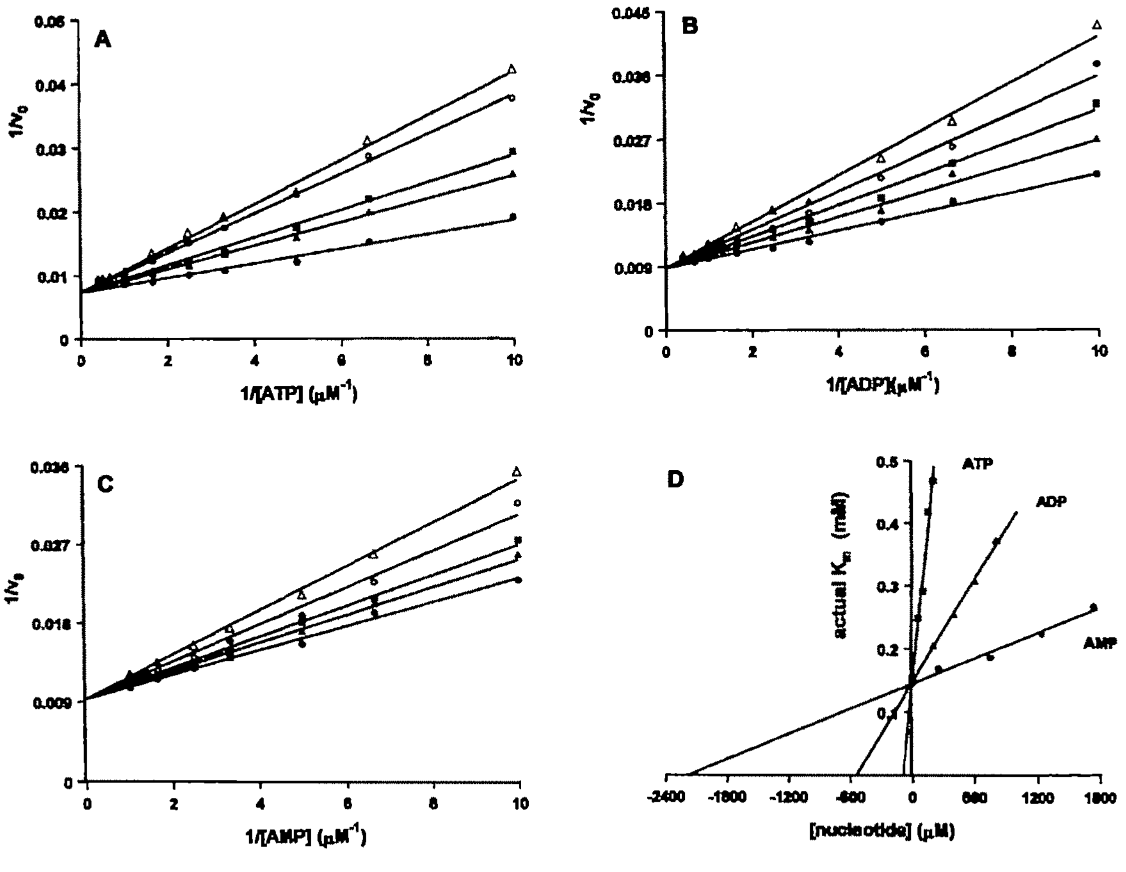

Figure 1 Inhibition of the benzoylphosphatase activity by adenine nucleotides

Experiments were performed in 0 1 M sodium acetate buffer, pH 5 3, at 25 °C The initial rates of benzoyl phosphate hydrolysis were measured in the presence of various concentrations of adenine nucleotides. The double reciprocal plots refer to (**A**) ATP, (**B**) ADP and (**C**) AMP The nucleotide concentrations were ●, 0 mM, ▲, 50 mM, ■, 100 mM, ○, 150 mM, △, 200 mM for ATP, ●, 0 mM, ▲, 200 mM, ■, 400 mM; ○, 600 mM, △, 800 mM for ADP, and ●, 0 mM; ▲, 250 mM, ■, 750 mM, ○, 1250 mM, △, 1750 mM for AMP (**D**) Replots of the actual K_m values against the nucleotide concentration

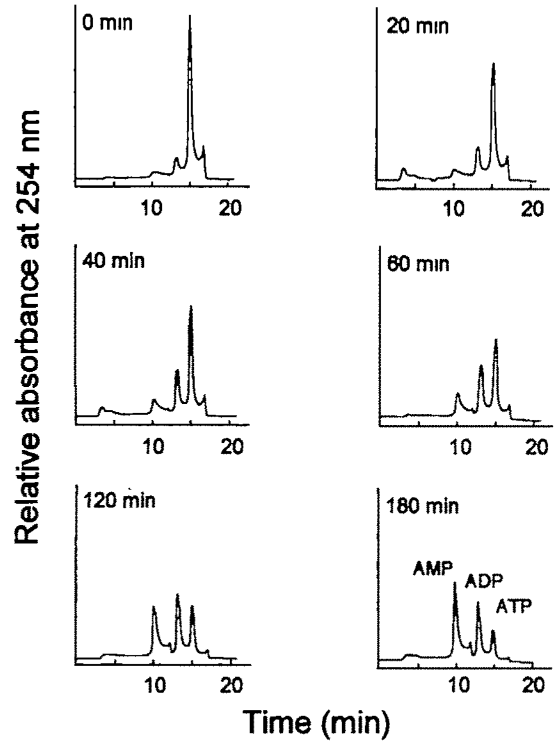

Figure 2 HPLC time-course analysis of the products released from ATP by acylphosphatase

A solution of ATP (2 mM) dissolved in 0.1 M sodium acetate buffer, pH 5.3, was incubated with acylphosphatase (0.38 μM) at 37 °C. Aliquots were withdrawn at the indicated times, and HPLC analyses were performed using a DEAE 5PW column (7.5 × 75 mm) under the conditions described in the text

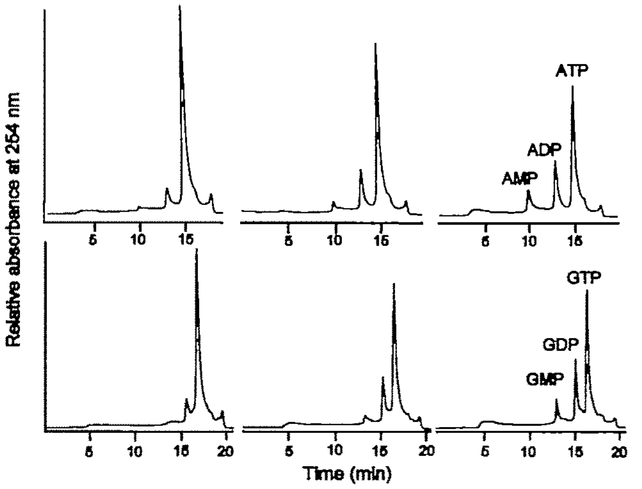

Figure 3 The HPLC time-course analysis of the products released from ATP and GTP, in the presence of Mg^{2+} ions, by acylphosphatase

Solutions of ATP or GTP (2 mM) dissolved in 0.1 M Tris/HCl buffer, pH 7.2, were incubated with acylphosphatase (1.5 μM) at 37 °C. At different times (0, 90 and 270 min, from left to right), aliquots were withdrawn and HPLC analyses were performed under the same conditions as for Figure 2

Table 1 Stability of acylphosphatase between pH 2.5 and 9.5

Acylphosphatase (0.21 μM final concentration) was incubated at the indicated pH values for 40 min at 37 °C, and then the activity was assayed at pH 5.3 and 25 °C, using 5 mM benzoyl phosphate as substrate. Specific activity is expressed as μmol of benzoyl phosphate hydrolysed/min per mg of protein (±S.E.M.)

pH	Specific activity	Buffer system
2.5	8050±210	0.1 M Formic acid/NaOH
3.5	8028±141	0.1 M Formic acid/NaOH
4.5	7891±180	0.1 M Acetic acid/NaOH
5.5	7940±126	0.1 M Acetic acid/NaOH
6.5	7066±57	0.1 M Cacodylic acid/NaOH
7.5	7592±163	0.1 M Tris/HCl
8.5	7703±63	0.1 M Tris/HCl
9.5	7743±424	0.1 M Glycine/NaOH

nucleotides are the true enzyme substrates. Nevertheless, when 2 mM ATP or GTP are incubated with acylphosphatase in 0.1 M Tris/HCl buffer, pH 7.2, and in the presence of 1 mM Mg^{2+} ions, we observe that acylphosphatase is still able to produce a time-dependent release of the respective NDP and NMP, although at lower rates (Figure 3). These findings demonstrate that acylphosphatase also displays this activity under physiological conditions. Enzymes displaying both NTPase and NDPase activities are generally classified as apyrases.

Effect of pH on the main kinetic parameters of the NTPase and NDPase activities of acylphosphatase

We first tested the stability of the enzyme activity (CT isoform) in the 2.5–9.5 pH range. This was done by incubating the enzyme (0.21 μM) in 0.1 M buffers adjusted to the appropriate pH values at 37 °C for 40 min; the activity was then assayed at pH 5.3 using 5 mM benzoyl phosphate as substrate. Table 1 shows that the enzyme is stable in the 2.5–9.5 pH range.

The main kinetic parameters (K_m and V_{max}) for the ATPase and ADPase activities displayed by acylphosphatase were determined at several pH values, and then the corresponding k_{cat}/K_m values were calculated. In general, the pK_a values derived from the pH dependence of the kinetic parameter k_{cat}/K_m reflect catalytically essential ionization of free enzyme and/or free substrate. In the present case, the substrates (ATP and ADP) can ionize in the pH range studied. In Figure 4(A), values of k_{cat}/K_m for ATP are plotted as a function of pH. The variation of k_{cat}/K_m with pH yielded a curve characterized by two plateaus and three slope changes, indicating that the reaction between free enzyme and free substrate must involve at least three ionization processes. For the analysis of k_{cat}/K_m, eqn (1) was used:

$$\frac{k_{cat}}{K_m} = \frac{A}{\left(1+\frac{K_{a1}}{[H^+]}\right)} + \frac{B}{\left(1+\frac{[H^+]}{K_{a2}}+\frac{K_{a3}}{[H^+]}\right)} \qquad (1)$$

where A is the value of k_{cat}/K_m in the plateau at pH 3–4, B is the value of k_{cat}/K_m in the plateau at about pH 6 and K_{a1}, K_{a2} and K_{a3} are the ionization constants of either free enzyme and/or free substrate (see Figure 4A). The fitting of eqn (1) was performed with the non-linear curve-fitting program FigureP (BioSoft), which enabled us to calculate the three pK_a values and their S.E.M. Figure 4(A) shows that the experimental data fit eqn (1)

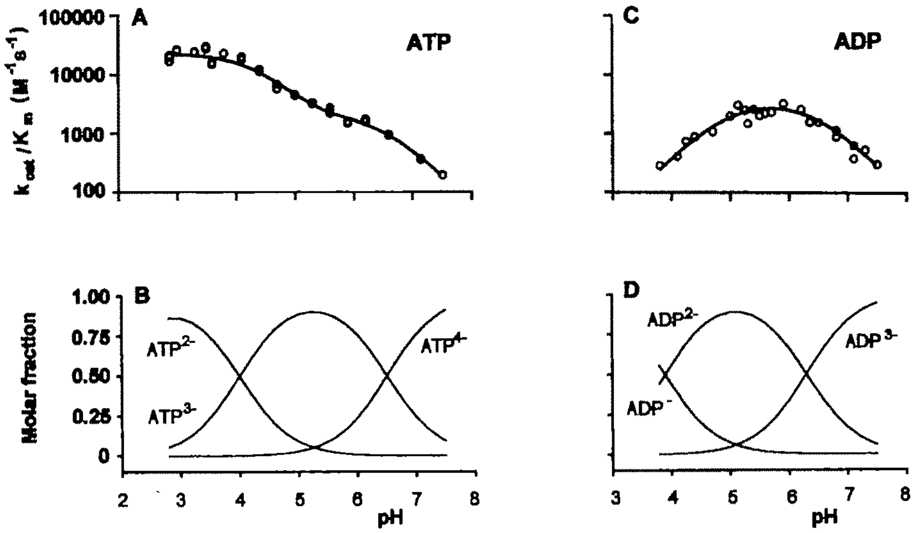

Figure 4 Effect of pH on k_{cat}/K_m for the acylphosphatase-catalysed hydrolyses of ATP and ADP

The line that is drawn through the experimental data is based on the non-linear least-squares fit of the data for (A) ATP to eqn (1), and (C) for ADP to eqn (2) (B) and (D) report the molar fractions of the different ionic forms of ATP (B) and ADP (D) as a function of pH, calculated using the known pK_a values.

very well ($r = 0$ 91). We determined the following values: pK_{a1}, 4.3±0.1; pK_{a2}, 5.3±0.2; and pK_{a3}, 6.5±0.1. These findings indicate that the pK_a values at pH 4.3 and 6.5 reflect two of the dissociation processes of ATP (pK_{a3} and pK_{a4} values for ATP determined by titration are 4–4.2 and 6.5, respectively [18]; the ATP pK_{a1} and pK_{a2} values are < 2, outside the pH range we examined [19]). We note that the maximal k_{cat}/K_m values are in the 2.9–4.0 pH range, where the most frequently represented molecular form of ATP is ATP^{2-} (Figure 4B). By increasing pH from 4 to 5, we can observe that k_{cat}/K_m decreases: the ATP^{2-} molar fraction falls while that of ATP^{3-} increases (see Figure 4B). Near pH 5.3 the slope of the curve changes suddenly, generating a shoulder. This is consistent with the presence in the free enzyme of one ionizing residue with a pK_a value of 5.3. Above pH 6, the molar fraction of ATP^{4-} increases, and this is accompanied by a decrease in k_{cat}/K_m, suggesting that the more negative species, ATP^{4-}, is a poor substrate for the enzyme.

Figure 4(C) reports the pH dependence of k_{cat}/K_m for the ADPase activity of acylphosphatase. The variation of k_{cat}/K_m with pH yielded a bell-shaped curve with a limiting slope of +1 on the acidic side and −1 on the alkaline side. This indicates that the reaction between free enzyme and free substrate must involve two ionization processes. For the analysis of k_{cat}/K_m relative to the ADPase activity of acylphosphatase, eqn (2) was used.

$$\frac{k_{cat}}{K_m}=\frac{A}{\left(1+\frac{[H^+]}{K_{a1}}+\frac{K_{a2}}{[H^+]}\right)} \qquad (2)$$

where A is the value of k_{cat}/K_m in the plateau (i e. the pH-independent second-order rate constant), and K_{a1} and K_{a2} are the ionization constants of either the free enzyme or of the free substrate. The experimental data fit eqn (2) very well ($r = 0.91$), and we determined the following values: pK_{a1}, 5.1±0.2 and pK_{a2}, 6.4±0.2. These results indicate that the pK_a value of 6 4 reflects one of the ionization processes of ADP (the pK_{a3} for ADP determined by titration is 6.3 [20]), while that of 5.1±0.2 reflects one ionization on the free enzyme. This latter value is very close to that calculated from the data of the pH dependence of k_{cat}/K_m relative to the ATPase activity displayed by acylphosphatase (5.3±0.2), indicating that the same group in the free enzyme must be deprotonated for optimal binding and catalytic hydrolysis of both ATP^{3-} and ADP^{2-}, which are the molecular forms most represented in this pH zone (see Figure 4D). The protonation of the above group does not improve the catalytic hydrolysis of the ATP^{2-} form; in fact, near pH 3, where ATP^{2-} prevails over the other molecular forms, k_{cat}/K_m has the highest values. Furthermore, it can be seen that ATP^{4-}, ADP^{3-} and ADP^{-} forms are very poor substrates for acylphosphatase All these findings indicate that the acylphosphatase catalytic pathways for ATP and ADP hydrolyses are very complicated, depending on the affinity and molar fraction of each nucleotide species that is present in solution at different pH values.

Lastly, we tested the enzymic properties of the CT and MT isoenzymes of acylphosphatase on other purine and pyrimidine nucleotides. Table 2 reports the apparent K_m and k_{cat}/K_m values for the hydrolyses of various NTPs and NDPs catalysed by the CT isoenzyme at pH 5.3 and 7.2. Taken together, these data demonstrate that acylphosphatase catalyses the hydrolysis of all nucleotides tested and that pH influences not only the kinetic parameters for adenine nucleotides but also those for the other nucleotides. The enzyme has no hydrolytic activity on NMPs. The K_m values for GTP and GDP of CT acylphosphatase are the lowest among NTPs and NDPs, at both pH 5.3 and 7.2, indicating that the CT acylphosphatase active site has the highest affinity for guanosine nucleotides. Furthermore, the k_{cat}/K_m values reported in Table 2 also indicate that GTP and GDP are among the most specific nucleotide substrates of acylphosphatase, both at acidic and neutral pHs. Table 2 also shows the kinetic properties relative to the ATPase and ADPase activities of the MT isoenzyme.

Acylphosphatase utilizes the same active site for benzoylphosphatase, ATPase and ADPase activities

In order to test whether the benzoyl phosphate, ATP and ADP hydrolyses are catalysed by the same active site, we measured the ATPase and ADPase activities of two mutants of acylphos-

Table 2 Kinetic properties of acylphosphatase versus some NDPs and NTPs

n.d., not detectable

	pH 5.3		pH 7.2	
Substrate	K_m (M × 10^{-5})	k_{cat}/K_m ($M^{-1} \cdot s^{-1}$)	K_m (M × 10^{-5})	k_{cat}/K_m ($M^{-1} \cdot s^{-1}$)
CT acylphosphatase isoenzyme				
ATP	9.5 ± 0.4	3566 ± 119	60.1 ± 4.7	208 ± 10
GTP	7 ± 0.5	3599 ± 200	7.7 ± 0.5	573 ± 27
UTP	15.8 ± 0.5	2192 ± 56	46.4 ± 3.6	167 ± 9
CTP	11.7 ± 0.6	2308 ± 93	16.5 ± 1	334 ± 18
ADP	64.1 ± 2	1550 ± 33	13.9 ± 0.6	663 ± 24
GDP	23.6 ± 1.7	2169 ± 90	12.9 ± 0.5	960 ± 30
UDP	63.7 ± 3.4	1062 ± 34	79.4 ± 5.8	138 ± 6
CDP	89.7 ± 4.3	1100 ± 28	43.6 ± 2.1	236 ± 8
MT acylphosphatase isoenzyme				
ATP	18.4 ± 0.5	1811 ± 36	38.8 ± 1.6	213 ± 6
ADP	57.5 ± 2.7	578 ± 18	31.8 ± 1.5	125 ± 4
MT acylphosphatase mutant: Asn^{41} → Gln				
ATP	26.6 ± 1.3	19.6 ± 0.6		
ADP	68.1 ± 4.9	7.2 ± 0.3		
CT acylphosphatase mutant: Arg^{23} → Ala				
ATP	–	n.d.		
ADP	–	n.d.		

phatase, i.e. Arg^{23} → Ala (CT isoenzyme) and Asn^{41} → Gln (MT isoenzyme). The two isoenzymes of acylphosphatase share 55 % sequence homology and very similar three-dimensional structures [6]. These two mutants were selected for the following experiments because both Arg^{23} and Asn^{41} are essential residues involved in the enzymic mechanism of benzoyl phosphate hydrolysis [21,22]. In particular, Arg^{23} participates in the binding of the phosphate moiety of the substrate, whereas Asn^{41} binds the nucleophilic water molecule involved in the chemical step of the catalytic pathway [6]. Table 2 shows that, like benzoyl phosphatase activity [22], both mutants show a dramatic decrease in k_{cat}/K_m values for ATPase and ADPase activities with respect to the non-mutated enzymes, indicating that these two residues are also essential for the catalytic hydrolyses of both ATP and ADP. All of the above findings, together with those concerning the competitive inhibition elicited by the adenosine nucleotides on benzoylphosphatase activity, indicate that acylphosphatase utilizes the same active site for the enzymic hydrolyses of both acylphosphates and nucleotide di- and tri-phosphates.

DISCUSSION

In this paper we have demonstrated that acylphosphatase binds NMPs, NDPs and NTPs, and that it also catalyses the hydrolysis of both NTPs and NDPs, whereas it has no activity on NMPs. Although the enzyme is inhibited by the Mg^{2+} ion (indicating that the true substrates are the free NTPs and NDPs), the HPLC time-course analyses demonstrated that, when incubated with mixtures containing both 2 mM NTPs and 1 mM Mg^{2+} ions at near-neutral pH and 37 °C, acylphosphatase causes the production of both NMPs and NDPs, although at lower rates. Both activities are pH-dependent, and have the highest values in an acidic environment. The experiments on the inhibition of benzoylphosphatase activity by nucleotides, together with those carried out with the two mutants Asn^{41} → Gln and Arg^{23} → Ala, have indicated that the enzyme utilizes the same active site to perform ATPase, ADPase and benzoylphosphatase catalyses.

Although k_{cat} values for the NTPase and NDPase activities of acylphosphatase are lower than the k_{cat} value for a typical acylphosphatase substrate such as acetyl phosphate [23], this particular enzyme activity could have relevant functions under physiological conditions. In fact, other GTPase activities, such as those elicited by the Gα subunit of heterotrimeric G-proteins, have k_{cat} values very close to the value elicited by acylphosphatase [24].

Several studies have suggested some biological roles for acylphosphatase, such as the control of the ionic conditions of the cell [2,3,25,26] or the control of the glycolytic pathway [27,28]. The control of the ionic conditions of the cell by acylphosphatase is determined by its catalytic activity on the hydrolysis of phosphorylated intermediates (β-aspartylphosphate) of membrane Na^+/K^+- and Ca^{2+}-ATPases. The findings of Riley et al. [29] suggested that acylphosphatase, which may regulate membrane ion pumps, has a role in tumourigenesis, and particularly in the determination of the metastatic phenotype. In fact these authors performed experiments of differential display comparing gene expression from cell lines (both non-metastatic and metastatic) derived from human colorectal tumours. They found that an acylphosphatase gene is expressed exclusively in a metastatic cell line, and suggested that the enzyme participates in the determination of the metastatic phenotype by altering the Na^+/K^+-ATPase pump function. They also support this hypothesis by considering the changes in the activity of this ionic pump in 1,2-dimethyhydrazine-induced colonic tumours, as reported by Davies et al. [30] Concerning the physiological significance of acylphosphatase in the regulation of membrane ion pumps, a recent paper of Nediani et al. [31] strongly supports previous findings: these authors have demonstrated that acylphosphatase behaves differently when regulating Ca^{2+} pumps of sarcoplasmic/endoplasmic reticulum of heart than when regulating fast-twitch skeletal muscle. The addition of physiological concentrations of the enzyme to a preparation of sarcoplasmic reticulum vesicles from heart exhibited a parallel increase in the rates of both ATP hydrolysis and Ca^{2+} transport. In contrast, acylphosphatase addition to sarcoplasmic reticulum vesicles from fast-twitch skeletal muscle caused the uncoupling of the pump, because the stimulation of ATP hydrolysis matched an inhibition of the calcium pump. Using controlled immunoprecipitation experiments, these authors also demonstrated the specific binding between acylphosphatase and heart sarcoplasmic reticulum Ca^{2+}-ATPase.

The present findings on the ATPase activity of acylphosphatase add further support to the previous results on the regulation of glycolysis by this enzyme, and also suggest new ideas concerning the mechanisms by which acylphosphatase controls the glycolytic pathway. In fact, the reported increase in the glycolysis rate associated with the overexpression of the enzyme in yeast [28] may be due not exclusively to the hydrolysis of 1,3-bis-phosphoglycerate (as suggested previously) but also to the hydrolysis of ATP. This idea agrees with the findings of Meyerhof [32], who reported that addition of ATPase to yeast extracts prepared by autolysis raises the glycolytic rate to that achieved by the addition of arsenate

Other cellular functions of acylphosphatase are still being debated. Previous studies have demonstrated that overexpression of acylphosphatase is accompanied by cell differentiation [33–35], and that the enzyme migrates into the nucleus during differentiation [36] as well as during apoptosis [37]. Our previous findings on the role of acylphosphatase in cell differentiation have indicated that: (i) the level of the acylphosphatase MT isoenzyme increases about 10-fold during myotube differentiation of cultured myoblasts, along with an increase in the levels of muscle-specific proteins [33]; (ii) the ectopic expression of the MT isoenzyme in K562 cells accelerates their erythrocyte differentiation [34]; (iii) tri-iodothyronine (T_3), a bland differentiating agent for K562 cells, activates the MT acylphosphatase gene, so that enzyme concentration is enhanced after hormone treatment. In contrast, T_3 has no effect on the CT isoform, indicating that the two genes are differently regulated [34].

Our findings on the NTPase and NDPase activities of acylphosphatase may support previous results on the involvement of the enzyme in differentiation and apoptosis. We suggest that the strong increase in acylphosphatase levels (by about 10-fold) during some differentiation processes causes fluctuations in the levels of NTPs and NDPs. This may result in the alteration of some biological functions, such as those mediated by G-proteins, which are relevant for the differentiation process. Dolfi et al. [25] demonstrated previously that a microinjection of acylphosphatase blocks the *Xenopus laevis* oocyte maturation induced by Ras-p21, a well-known G-protein that mediates cellular signalling processes. Although these authors have suggested a different mechanism, the observed block of this Ras-p21 biological function could be due to the acylphosphatase-induced GTP hydrolysis in this cell type. Furthermore, other authors have demonstrated that K562 cell differentiation by tiazofurin is accompanied by the early decrease of cellular GTP [38]. Similar considerations can be made for the possible changes in cellular ATP levels caused by the ATPase activity of acylphosphatase during apoptosis. Intracellular acidification is an early event associated with somatostatin-induced apoptosis [39], as well as with apoptosis induced by cytotoxic insult and by removal of growth factors ([40], and citations therein). On the other hand, the present findings demonstrate that acidification may enhance the ATPase activity of acylphosphatase through two different mechanisms: (i) acidification increases the molar fraction of free ATP^{3-} (which is a good substrate for the enzyme), which also occurs in the presence of Mg^{2+} ions (see [41]) and (ii) it causes the increase of k_{cat}/K_m value (Figure 4A). We suggest that acylphosphatase (which is activated by a pH decrease during apoptosis) causes a decrease in the ATP levels contributing to the apoptotic process. In fact, Lieberthal et al. [42] have reported that a limited depletion of ATP causes apoptosis of cultured mouse proximal tubular cells, whereas a severe depletion of ATP induces necrosis. Very recently, we have demonstrated that the transfection of an acylphosphatase gene into NIH-3T3 cell induces apoptosis (E. Giannoni, P. Cirri, P. Paoli, T. Fiaschi, G. Camici, G. Manao, G Raugei, and G. Ramponi, unpublished work).

The observed NTPase and NDPase activities of acylphosphatase are similar to those displayed by apyrases. These enzymes, which catalyse the sequential release of γ- and β-phosphate groups of NTPs and NDPs, have been found in different organisms [43]. Most of these are membrane-associated ectoenzymes; one of their putative roles is to modulate the extracellular concentrations of ATP and ADP in different physiological systems. To date, no intracellular enzyme with apyrase activity has been described in the cell

Finally, our findings suggest that acylphosphatase contains a nucleotide-binding site. A nucleotide-binding sequence motif termed the P-loop has been described for ATP- and GTP-binding proteins [44]. Its primary structure typically consists of a glycine-rich region followed by a conserved lysine. A related structure (GXXGXXK) is involved in the binding of the cofactor 3′-phosphoadenosine-5′-phosphosulphate (PAPS) in sulphotransferases [45]. We have noted that the known MT acylphosphatase isoenzymes generally contain the sequence GVVGWVK^{40} (with the exception of the fish MT isoenzyme, which contains R^{40}), whereas the known CT acylphosphatase isoenzymes contain the sequences GLVGWVQ^{40} (human, porcine and bovine), GLVGWVK^{40} (fish) and GLVGWVR^{40} (chicken) [46]. As can be seen, these sequence stretches are similar to the one involved in PAPS binding in sulphotransferases, and are located next to Asn^{41}, which is an essential residue conserved in all acylphosphatases [46]. All of these observations suggest that the sequence 34–40 of acylphosphatase is involved in nucleotide binding. Further studies, such as site-directed mutagenesis, will be required to directly localize the nucleotide-binding site of this enzyme.

This work was supported in part by the Consiglio Nazionale delle Ricerche (grants 97.03810 CT14 and 98 03276.ST74, Target Project on Biotechnology), in part by the Ministero dell'Università e della Ricerca Scientifica e Tecnologica (1997), project 'Biologia Strutturale', and in part by the Italian Association for Cancer Research

REFERENCES

1 Stefani, M and Ramponi, G (1995) Acylphosphate phosphohydrolases Life Chem Reports **12**, 271–301

2 Nediani, C., Marchetti, E, Nassi, P, Liguri, G and Ramponi, G (1991) Hydrolysis by acylphosphatase of erythrocyte membrane Na^+,K^+-ATPase phosphorylated intermediate Biochem Int **24**, 959–968

3 Nassi, P, Nediani, C, Liguri, G., Taddei, N and Ramponi, G (1991) Effects of acylphosphatase on the activity of erythrocyte membrane Ca^{2+} pump J. Biol Chem **266**, 10867–10871

4 Berti, A, Degl'Innocenti, D, Stefani, M, Liguri, G and Ramponi, G (1987) Quantitative determination of acylphosphatase levels in horse tissues by enzyme-linked immunosorbent assay Ital. J Biochem. **36**, 82–91

5 Mizuno, Y, Ohba, Y, Fujita, H, Kanesaka, Y, Tamura, T and Shiokawa, H (1990) Distribution and classification of acylphosphatase isozymes Arch Biochem Biophys **278**, 437–443

6 Thunnissen, M M G M, Taddei, N, Liguri, G, Ramponi, G and Nordlund, P (1997) Crystal structure of common type acylphosphatase from bovine testis Structure **5**, 69–79

7 Ghetti, A, Bolognesi, M, Cobianchi, F and Morandi, C (1990) Modeling by homology of RNA binding domain in A1 hnRNP protein FEBS Lett **277**, 272–276

8 Nagai, K, Oubridge, C, Jessen, T H, Li, J and Evans, P R (1990) Crystal structure of the RNA-binding domain of the U1 small nuclear ribonucleoprotein A Nature (London) **348**, 515–520

9 Nagai, K (1996) RNA-protein complexes Curr Opin Struct Biol **6**, 53–61

10 Chiarugi, P, Raugei, G., Fiaschi, T, Taddei, L, Camici, G and Ramponi, G (1996) Characterization of a novel nucleolytic activity of acylphosphatases Biochem Mol. Biol Int **40**, 73–81

11 Camici, G, Manao, G., Cappugi, G and Ramponi, G (1976) A new synthesis of benzoyl phosphate: a substrate for acylphosphatase assay Experientia **32**, 535

12 Fiaschi, T, Raugei, G, Marzocchini, R, Chiarugi, P, Cirri, P and Ramponi, G (1995) Cloning and expression of the cDNA coding for the erythrocyte isoenzyme of human acylphosphatase FEBS Lett **367**, 145–148

13 Modesti, A, Taddei, N, Bucciantini, M, Stefani, M, Colombini, B, Raugei, G and Ramponi, G (1995) Expression, purification, and characterization of acylphosphatase muscular isoenzyme as fusion protein with glutathione S-transferase Protein Expr Purif **6**, 799–805

14 Deng, W P and Nickoloff, J A (1992) Site-directed mutagenesis of virtually any plasmid by eliminating a unique site Anal Biochem **200**, 81–88

15 Sanger, F, Nicklen, S. and Coulson, A R (1977) DNA sequencing with chain-terminating inhibitors. Proc Natl Acad Sci USA **74**, 5463–5467

16 Baginski, E S, Foa, P. P. and Zak, B (1967) Determination of phosphate study of labile organic phosphate interference Clin Chim Acta **15**, 155–158

17 Ramponi, G, Treves, C and Guerritore, A (1966) Continuous optical assay of acylphosphatase with benzoyl phosphate as substrate Experientia **22**, 705–706

18 Schobert, B (1998) Do ATP^{4-} and Mg^{2+} bind stepwise to the F$_1$-ATPase of *Halobacterium saccharovorum*? Eur J Biochem **254**, 363–370

19 Symons, R H (1969) Constituents of RNA and related compounds In Data for Biochemical Research (Dawson, R M C, Elliott, D C., Elliott, W H and Jones, K M, eds), pp 145–167, Oxford University Press, Oxford

20 Pfleiderer, W (1964) in Biochemisches Tashenbuch, vol I (Rauen, H M, ed), pp 618–647, Springer-Verlag, Berlin

21 Taddei, N, Stefani, M, Vecchi, M, Modesti, A, Raugei, G, Bucciantini, M, Magherini, F and Ramponi, G (1994) Arginine-23 is involved in the catalytic site of muscle acylphosphatase. Biochim Biophys Acta **1208**, 75–80

22 Taddei, N, Stefani, M, Magherini, F, Chiti, F, Modesti, A, Raugei, G. and Ramponi, G. (1996) Looking for residues involved in the muscle acylphosphatase catalytic mechanism and structural stabilization role of Asn41, Thr42, and Thr46 Biochemistry **35**, 7077–7083

23 Paoli, P, Cirri, P, Camici, L, Manao, G, Cappugi, G, Moneti, G, Pieraccini, G., Camici, G and Ramponi, G (1997) Common-type acylphosphatase steady-state kinetics and leaving-group dependence Biochem J **327**, 177–184

24 Zerangue, N and Jan, L Y. (1998) G-protein signaling. fine-tuning signaling kinetics Curr Biol **8**, R313–R316

25 Dolfi, F, Carnero, A, Ramponi, G and Lacal, J C (1993) Microinjection of acylphosphatase bocks *Xenopus laevis* oocytes maturation induced by *ras*-p21 FEBS Lett **326**, 167–170

26 Dolfi, F, Carnero, A, Cuadrado, A, Ramponi, G and Lacal, J C (1993) Acylphosphatase synergizes with progesterone during maturation of *Xenopus laevis* oocytes FEBS Lett. **327**, 265–270

27 Baccari, V, Guerritore, A, Ramponi, G and Sabatelli, M P (1960) Azione dell'acilfosfatasi sulla glicolisi Boll. Soc Ital Biol Sper **36**, 360–361

28 Raugei, G, Modesti, A., Magherini, F, Marzocchini, R, Vecchi, M and Ramponi, G (1996) Expression of acylphosphatase in *Saccharomyces cerevisiae* enhances ethanol fermentation rate Biotechnol Appl Biochem **23**, 273–278

29 Riley, H D., Macnab, J., Farrell, T. J and Cohn, K (1997) The expression of acylphosphatase is associated with the metastatic phenotype in human colorectal tumors Carcinogenesis **18**, 2453–2455

30 Davies, R J, Sandle, G I and Thompson, S M (1991) Inhibition of the Na$^+$,K$^+$-ATPase pump during induction of experimental colon cancer Cancer Biochem. Biophys **12**, 81–94

31 Nediani, C, Fiorillo, C, Rigacci, S, Magherini, F, Francalanci, M, Liguri, G, Pacini, A and Nassi, P (1999) A novel interaction mechanism accounting for different acylphosphatase effects on cardiac and fast twitch skeletal muscle sarcoplasmic reticulum calcium pumps FEBS Lett **443**, 308–312

32 Meyerhof, O (1945) The origin of the reaction of Harden and Joung in cell-free alcoholic fermentation J Biol. Chem. **157**, 105–119

33 Berti, A, Degl'Innocenti, D, Stefani, M and Ramponi, G. (1992) Expression and turnover of acylphosphatase (muscular isoenzyme) in L6 myoblasts during myogenesis Arch Biochem Biophys **294**, 261–264

34 Chiarugi, P, Raugei, G, Marzocchini, R, Fiaschi, T., Ciccarelli, C, Berti, A and Ramponi, G (1995) Differential modulation of expression of the two acylphosphatase isoenzymes by thyroid hormone Biochem J **311**, 567–573

35 Chiarugi, P, Degl'Innocenti, D, Taddei, L, Raugei, G, Berti, A, Rigacci, S. and Ramponi, G (1997) Acylphosphatase is involved in differentiation of K562 cells Cell Death Diff **4**, 334–340

36 Raugei, G, Degl'Innocenti, D., Chiarugi, P, Solito, E, Modesti, A and Ramponi, G (1999) Preferential accumulation of muscle type acylphosphatase in the nucleus during differentiation Biochem Mol Biol Int **47**, 127–136

37 Chiarugi, P, Degl'Innocenti, D., Raugei, G, Fiaschi, T and Ramponi, G. (1997) Differential migration of acylphosphatase isoenzymes from cytoplasm to nucleus during apoptotic cell death Biochem. Biophys Res Commun **231**, 717–721

38 Olah, E, Natsumeda, Y, Ikegami, T, Kote, Z, Horanyi, M, Szelenyi, J, Paulik, E, Kremmer, T, Hollan, S R, Sugar, J and Weber, G (1988) Induction of erythroid differentiation and modulation of gene expression by tiazofurin in K-562 leukemia cells Proc Natl Acad Sci USA **85**, 6533–6537

39 Thangaraju, M, Sharma, K, Leber, B, Andrews, D W, Shen, S H and Srikant, C B (1999) Regulation of acidification and apoptosis by SHP-1 and Bcl-2. J. Biol. Chem **274**, 29549–29557

40 Li, J and Eastman, A (1995) Apoptosis in an interleukin-2-dependent cytotoxic T lymphocyte cell line is associated with intracellular acidification Role of the Na$^+$/H$^+$-antiport J Biol. Chem **270**, 3203–3211

41 O'Sullivan, W J and Smithers, G W (1979) Stability constants for biologically important metal-ligand complexes Methods Enzymol **63**, 294–336

42 Lieberthal,.W, Menza, S. A. and Levine, J S (1998) Graded ATP depletion can cause necrosis or apoptosis of cultured mouse proximal tubular cells Am J Physiol **274**, F315–F327

43 Picher, M, Côté, Y P, Béliveau, R, Potier, M and Beadoin, A R (1993) Demonstration of a novel type of ATP-diphosphohydrolase (EC 3 6 1 5) in the bovine lung J Biol Chem **268**, 4699–4703

44 Saraste, M, Sibbald, P R and Wittinghofer, A (1990) The P-loop – a common motif in ATP- and GTP-binding proteins. Trends Biochem Sci. **15**, 430–434

45 Komatsu, K, Driscoll, W. J., Koh, Y C and Strott, C A. (1994) A P-loop related motif (GxxGxxK) highly conserved in sulfotransferases is required for binding the activated sulfate donor Biochem Biophys Res Commun **204**, 1178–1185

46 Pazzagli, L, Manao, G, Cappugi, G, Caselli, A, Camici, G, Moneti, G and Ramponi, G (1998) The amino acid sequences of two acylphosphatase isoforms from fish muscle (*Lamna nasus*) Biochim Biophys Acta **1387**, 264–274

Received 20 October 1999/6 April 2000, accepted 28 April 2000

Biochem. J. (2000) 349, 51–57 (Printed in Great Britain)

Processing of N-linked oligosaccharide depends on its location in the anion exchanger, AE1, membrane glycoprotein

Jing LI, Janne QUILTY, Milka POPOV and Reinhart A. F. REITHMEIER[1]

Medical Research Council Group in Membrane Biology, Departments of Medicine and Biochemistry, Room 7344, Medical Sciences Building, University of Toronto, Toronto, Ontario M5S 1A8, Canada

The human erythrocyte anion exchanger (AE)1 (Band 3) contains a single complex N-linked oligosaccharide that is attached to Asn^{642} in the fourth extracellular loop of this polytopic membrane protein, while other isoforms (AE2, AE3 and trout AE1) are N-glycosylated on the preceding extracellular loop. Human AE1 expressed in transfected human embryonic kidney (HEK)-293 or COS-7 cells contained a high-mannose oligosaccharide. The lack of oligosaccharide processing was not due to retention of AE1 in the endoplasmic reticulum since biotinylation assays showed that approx. 30% of the protein was expressed at the cell surface. Moving the N-glycosylation site to the preceding extracellular loop in an AE1 glycosylation mutant (N555) resulted in processing of the oligosaccharide and production of a complex form of AE1. A double N-glycosylation mutant (N555/N642) contained both a high-mannose and a complex oligosaccharide chain. The complex form of the N555 mutant could be biotinylated showing that this form of the glycoprotein was at the cell surface. Pulse–chase experiments showed that the N555 mutant was efficiently converted from a high-mannose to a complex oligosaccharide with a half-time of approx. 4 h, which reflected the time course of trafficking of AE1 from the endoplasmic reticulum to the plasma membrane. The turnover of the complex form of the N555 mutant occurred with a half-life of approx. 15 h. The results show that the oligosaccharide attached to the endogenous site in extracellular loop 4 in human AE1 is not processed in HEK-293 or COS-7 cells, while the oligosaccharide attached to the preceding loop is converted into the complex form.

Key words: Band 3, endoplasmic reticulum, glycosylation, trafficking, turnover.

INTRODUCTION

The human erythrocyte anion exchanger (AE)1 (Band 3) contains a single site of N-glycosylation at Asn^{642} in the fourth extracellular loop of the protein [1–3]. This oligosaccharide consists of either an elongated polylactosaminyl structure [4] or a shorter, more typical, complex structure [5] resulting in two Band 3 glycoprotein populations [6]. In the human disease, hereditary erythroblastic multinuclearity with a positive acidified-serum lysis test (HEMPAS), the oligosaccharide on red cell glycoproteins is not completely processed but retains a high-mannose structure due to a defect in mannosidase II [7–10]. The anion transport activity of HEMPAS erythrocytes is normal showing that the high-mannose form of AE1 is fully functional [9]. Interestingly, a mannosidase II deficient mouse lacked complex N-glycans on its erythrocyte glycoproteins but contained complex glycoproteins in non-erythroid cells, resulting in a HEMPAS phenotype [11]. This suggested that an alternative oligosaccharide processing pathway not involving mannosidase II is available in cells other than those of the erythroid lineage.

Expression of human AE1 in transfected human embryonic kidney (HEK)-293 or COS-7 cells results in the production of a protein that retains a high-mannose oligosaccharide [12]. A similar observation was made previously for mouse AE1 [13]. Human AE1 is functionally expressed at the cell surface of transfected cells [14]. These results suggest that the lack of oligosaccharide processing is not entirely due to retention of the glycoprotein in the endoplasmic reticulum and that a high-mannose form of AE1 is functional. In cell-free translation studies of the topology of AE1 we found that a novel N-glycosylation acceptor site introduced at Asn^{555} in extracellular loop 3 can be N-glycosylated [15]. In the present study we report that expression of this AE1 mutant (N555) in transfected HEK-293 or COS-7 cells resulted in the production of a glycoprotein containing a complex oligosaccharide. The processing of the oligosaccharide attached to AE1 is therefore dependent on the location of the oligosaccharide in this polytopic membrane protein. The processing of the oligosaccharide on the N555 mutant allowed the study of the trafficking of human AE1 in transfected cells from its site of synthesis, in the endoplasmic reticulum, to its final destination, in the plasma membrane.

EXPERIMENTAL

Materials

Materials were purchased from the following suppliers (in parentheses): pcDNA3 (Invitrogen, San Diego, CA, U.S.A.); Transformer® site-directed mutagenesis system (ClonTech Laboratories, Palo Alto, CA, U.S.A.); T7 DNA sequencing kit, Protein G–Sepharose and restriction enzymes (Amersham Pharmacia Biotech, Baie d'Urfé, Quebec, Canada); Dulbecco's modified Eagle's medium (DMEM), calf serum, penicillin and streptomycin (Gibco BRL, Burlington, Ontario, Canada); [^{35}S]methionine, consisting of approx. 73% [^{35}S]methioinine and 27% [^{35}S]cysteine (Mandel Scientific, Guelph, Ontario, Canada); endoglycosidase H, N-glycanase F and goat peroxidase-conjugated anit-rabbit IgG (New England Biolabs, Mississauga, Ontario, Canada); octa(ethylene glycol) dodecyl ether ($C_{12}E_8$; Nikko Chemical Co., Tokyo, Japan); chemiluminescence kit

---

Abbreviations used: AE, anion exchanger; $C_{12}E_8$, octa(ethylene glycol) dodecyl ether; HEK, human embryonic kidney; HEMPAS, hereditary erythroblastic multinuclearity with a positive acidified-serum lysis test; NHS-SS-biotin, sulpho-succinimidyl 2-(biotin-amido)ethyl-1,3-dithiopropionate.

[1] To whom correspondence should be addressed (e-mail r.reithmeier@utoronto.ca).

(Boehringer Mannheim, Laval, Quebec, Canada); ImmunoPure®immobilized streptavidin and EZ-link® sulpho-succinimidyl 2-(biotin-amido)ethyl-1,3-dithiopropionate (NHS-SS-biotin; MJS BioLynx Inc., Brockville, Ontario, Canada).

Mutagenesis and DNA sequencing

The entire coding sequence for human AE1 was inserted into the *Xho*I and *Bam*HI sites of pcDNA3 [12] The following AE1 N-glycosylation mutants were constructed as described previously [15]: N642D, a non-glycosylated mutant with a mutated endogenous site; N555, a mutant with a single novel site at Asn^{555} (Y555N/V557T) and a mutated (N642D) endogenous site; and N555/N642, a double N-glycosylation mutant with a novel site at Asn^{555} (Y555N/V557T) and the endogenous site.

Expression of AE1 in transfected cells

HEK-293 or COS-7 cells were transfected with 5 μg of plasmid DNA per 10 cm diameter plate and grown in DMEM supplemented with 10 % (v/v) calf serum, 0.5 % penicillin and 0.5 % streptomycin under air/CO_2 (19:1) at 37 °C, as described previously [12]. Cell extracts were prepared by detergent solubilization of the cells 48 h after transfection, as described below.

SDS/PAGE and immunoblotting

Proteins were resolved by SDS/PAGE [16]. AE1 was detected by immunoblotting using a rabbit polyclonal antibody directed against the synthetic peptide corresponding to the C-terminal 16 residues of human AE1 [12].

Enzymic deglycosylation and lectin binding

Cell extracts (50 μl) prepared from transfected cells using 1 % (v/v) $C_{12}E_8$ were incubated for 1 h at 37 °C with no additions, 1000 units (1 μl) of endoglycosidase H (1000000 units/ml) or 500 units (1 μl) of N-glycanase F (500000 units/ml), followed by addition of 1 vol. of 2 × Laemmli sample buffer containing 4 % (w/v) SDS.

The binding of AE1 mutants to immobilized concanavalin A was determined as described previously [12]. Briefly, cell extracts (50 μl) in 1 % (v/v) $C_{12}E_8$ were incubated with 25 μl of concanavalin A–Sepharose in the absence and presence of 0.25 M methyl α-D-mannopyranoside. The supernatant represented the unbound fraction while the bound fraction was released by boiling the resin in 2 × Laemmli sample buffer. A similar binding assay was performed using wheat germ agglutinin–Sepharose in the presence and absence of 0.3 M *N*-acetyl-D-glucosamine.

Cell surface biotinylation

HEK-293 cells were grown in 6-well culture dishes for 48 h after transfection. The cells were washed once with ice-cold borate buffer (10 mM boric acid, 154 mM NaCl, 7.2 mM KCl and 1.8 mM $CaCl_2$, pH 9.0). Cells were subsequently treated with 1 ml of 0.8 mM EZ-Link® NHS-SS-biotin in borate buffer for 15 min at 0 °C. Parallel control cells were not treated with the biotinylation reagent. Cells were washed with 0.192 M glycine/25 mM Tris, pH 8.3 to quench the reaction. The cells were lysed in RIPA buffer [10 mM Tris/HCl (pH 7.5), 1 % (w/v) deoxycholate, 1 % (v/v) Triton X-100, 0.1 % SDS, 150 mM NaCl and 1 mM EDTA] containing protease inhibitors (200 μM PMSF, 2.8 μM E64, 1 μM leupeptin and 1 μM pepstatin), followed by centrifugation at 14000 g for 15 min to remove insoluble material. An aliquot of the lysate was saved for measurement of the total AE1 content. Immunopure immobilized streptavidin resin (100 μl) was added to the lysate and incubated for 1 h at 4 °C to bind biotinylated protein. Addition of a larger volume of beads did not increase the yield of bound protein. As an additional control for non-specific binding, samples were also incubated with Sepharose beads lacking streptavidin. The supernatant was removed and an aliquot saved for measurement of AE1 in the unbound fraction. The beads were washed with RIPA buffer and bound protein was eluted by addition of Laemmli sample buffer containing 5 % (v/v) 2-mercaptoethanol for 1 h at room temperature. The content of AE1 in the total, unbound and bound fractions was determined by immunoblotting.

Pulse–chase experiments

HEK-293 or COS-7 cells were grown at 37 °C in 35 mm diameter dishes for 24 h, after transfection with 0.6 μg of plasmid DNA. The cells were incubated for 45 min in methionine- and cysteine-free DMEM without calf serum. Cells were labelled with 100 μCi/ml [^{35}S]methionine for 10 min. The radioactive medium was removed and the cells were rinsed once with PBS. The cells were then chased for up to 24 h by incubation in DMEM containing 10 % calf serum, and 10 μg/ml cycloheximide to inhibit further protein synthesis. For turnover studies the cells were labelled for 90 min with 20 μCi/ml [^{35}S]methionine and then chased without cycloheximide for the indicated times up to 48 h. Cells were harvested at timed intervals, washed with PBS and then solubilized in 1 ml of RIPA buffer AE1 was immunoprecipitated using 4 μl of antibody serum directed against the C-terminal of human AE1, followed by capture on 40 μl of Protein G–Sepharose beads. The proteins were eluted from the resin using 50 μl of 2 × SDS sample buffer at room temperature for 10 min Proteins were resolved by SDS/PAGE and were detected by autoradiography.

RESULTS

AE1 N-glycosylation mutants

Human AE1 consists of 12 transmembrane segments with a single site of N-glycosylation at Asn^{642} (Figure 1A). Three mutants of AE1 (N642) were constructed that contained no N-glycosylation acceptor sites (N642D), a single novel site at Asn^{555} (N555) or a double N-glycosylation mutant with a novel site at Asn^{555} and the endogenous site at Asn^{642} (N555/N642) [15,17]. Figure 1(B) shows an immunoblot of HEK-293 cells transfected with AE1 constructs N642, N642D, N555 or N555/N642. Wild-type AE1 (lane 2) was present in transfected cells as a single band with a slightly higher molecular mass than the N642D mutant (lane 1) due to the presence of a high-mannose N-linked oligosaccharide [12]. In contrast, the N555 mutant (lane 3) was present as two closely spaced bands. The lower band was at the same position as wild-type high-mannose protein, while the second band had a higher molecular mass. These results suggest that a fraction of the N555 mutant had been processed to a high molecular mass form containing a complex oligosaccharide. Scans of the immunoblots showed that approximately one-third of the N555 mutant was present as the higher molecular mass form. The N555/N642 mutant (lane 4), with two N-glycosylation sites, also ran as two bands but with even higher molecular masses than the N555 mutant, indicating that both sites were N-glycosylated.

Enzymic deglycosylation and lectin binding

Enzymic deglycosylation was performed in order to characterize the nature of the oligosaccharide attached to the various AE1

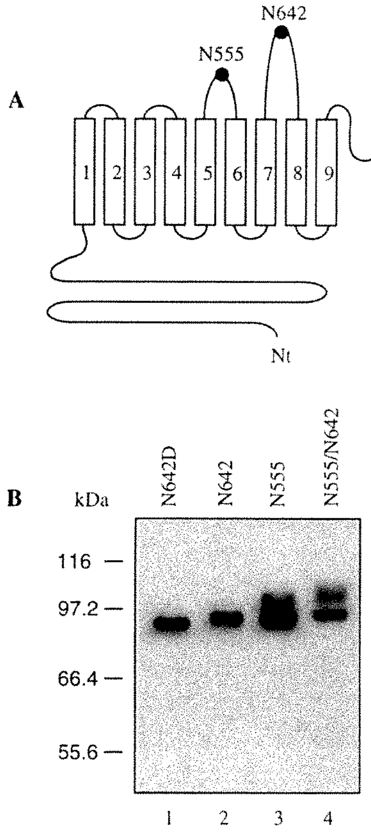

Figure 1 N-glycosylation mutants of human AE1

(**A**) Folding model of human AE1 showing the location of Asn^{555} and Asn^{642}. (**B**) Immunoblot of extracts of HEK-293 cells transfected with AE1 N-glycosylation mutants. HEK-293 cells were transfected with pcDNA3 vector containing the non-glycosylated mutant (N642D), wild-type AE1 (N642), the N555 mutant with a single acceptor site at position 555 (N555) or the N555/N642 mutant with two acceptor sites at positions 555 and 642 (N555/N642). Cell extracts were prepared by solubilizing cells with 1% (v/v) C$_{12}$E$_8$,150 mM NaCl and 5 mM sodium phosphate, pH 7.4 (PBS). Proteins were resolved by SDS/PAGE using an 8% (w/v) polyacrylamide gel, transferred to nitrocellulose and AE1 was detected by immunoblotting. Ct, C-terminus; Nt, N-terminus.

mutants (Figure 2). Wild-type AE1 was sensitive to endoglycosidase H treatment (Figure 2, lanes 1–3) consistent with a high-mannose structure [12]. The lower band of the N555 mutant was also sensitive to this enzyme (Figure 2, lanes 4–6), showing that this form of the protein contained a high-mannose oligosaccharide. The upper band, in contrast, was resistant to this enzyme treatment, but its mobility could be shifted by N-glycanase F. This suggests that the upper band contained a complex oligosaccharide. In the double mutant, the lower and upper bands were both sensitive to endoglycosidase H (Figure 2, lanes 7–9), suggesting that each contained a high-mannose oligosaccharide. The lower band shifted down to the position of the non-glycosylated AE1 showing that it contained two high-mannose oligosaccharides. In contrast, the upper band was shifted down to the position of the non-glycosylated AE1 only after treatment with N-glycanase F. This showed that the upper band contained both high-mannose and complex oligosaccharides. There was no evidence of a higher molecular mass form of this mutant that contained two complex oligosaccharide chains. The results are consistent with the oligosaccharide at position 555 being high-mannose and the oligosaccharide at position 642 of the same molecule being processed to a complex oligosaccharide.

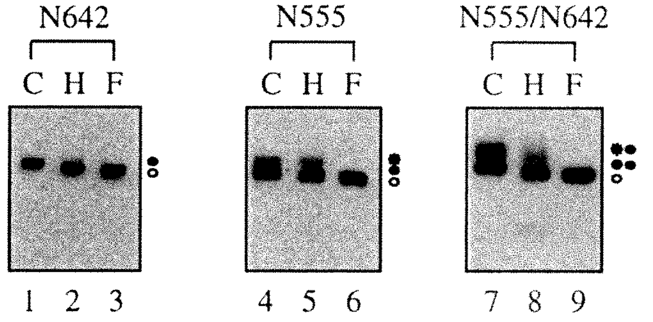

Figure 2 Immunoblot showing enzymic deglycosylation of N642, N555 or N555/N642

Cell extracts were incubated without enzyme addition (C), with endoglycosidase H (H), or with N-glycanase F (F). AE1 was detected as in Figure 1. Open circle, non-glycosylated AE1; closed circle, high-mannose form of AE1; asterisk, complex form of N555 mutant; double closed circle, double high-mannose form of N555/N642 mutant; asterisk/closed circle, high-mannose and complex form of N555/N642 mutant.

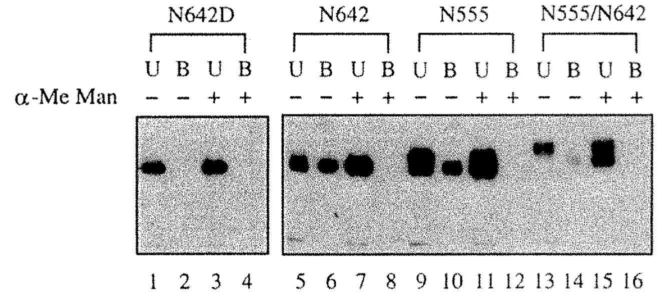

Figure 3 Immunoblot showing the concanavalin A–Sepharose binding properties of N642D, N642, N555 and N555/N642

Cell extracts of transfected HEK-293 cells were prepared by using 1% (v/v) C$_{12}$E$_8$ in lysis buffer and subjected to incubation with concanavalin A–Sepharose in the absence (−) and presence (+) of 0.25 M methyl α-D-mannopyranoside. The unbound (U) and bound (B) fractions were resolved by SDS/PAGE and AE1 was detected by immunoblotting.

Oligosaccharide chains must be accessible to the processing enzymes in the Golgi in order to be converted to a complex-type oligosaccharide [18,19]. The accessibility of the oligosaccharide chains at positions Asn^{555} and Asn^{642} of AE1 was compared by digestion of the solubilized mutant proteins with various concentrations of N-glycanase F. It was found that the oligosaccharide at position 555 was 10-fold more sensitive to enzymic deglycosylation than the site at position 642 (results not shown). This result indicates that the oligosaccharide at position 555 may also be more accessible to modification by the processing enzymes in the secretory pathway.

Lectin affinity chromatography was performed to confirm the nature of the oligosaccharide in the AE1 mutants (Figure 3). AE1 expressed in HEK-293 cells bound to concanavalin A–Sepharose (Figure 3, lanes 5–8), while the non-glycosylated N642D mutant did not (Figure 3, lanes 1–4). The binding of AE1 to concanavalin A could be blocked by methyl α-D-mannopyranoside (Figure 3, lane 7), confirming the specificity of the interaction with this lectin. In this particular experiment approximately half of the AE1 was bound to the lectin. All of the AE1 could be bound by using higher amounts of resin, however, the

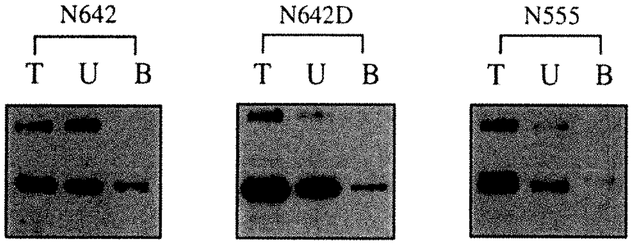

Figure 4 Immunoblot analysis of cell surface biotinylation of HEK-293 cells expressing N642 (left panel), N642D (middle panel) or N555 (right panel)

Cells extracts were prepared from biotinylated cells and incubated with streptavidin–Sepharose. The total sample (T), unbound fraction (U) and bound fraction (B) were resolved by SDS/PAGE and AE1 was detected by immunoblotting. AE1 (N642) and the N642D mutant each ran as predominantly single monomeric protein bands. The high molecular mass bands near the top of the gel represent undissociated AE1 dimers. The N555 mutant ran as two closely spaced bands. The upper band contained complex oligosaccharide while the lower band contained high-mannose oligosaccharide. The bound fraction was overloaded 12 × with respect to the total sample and the unbound fraction (i.e. the supernatant) to get comparable band densities.

protein became more difficult to elute from the lectin. The ability of wild-type AE1 to bind to concanavalin A is consistent with the presence of a high-mannose oligosaccharide. The lower band of the N555 mutant also bound to this lectin while the upper band did not (Figure 3, lanes 9–12). This is consistent with the deglycosylation results, which indicated that the upper band contained a complex oligosaccharide while the lower band retained a high-mannose oligosaccharide structure. The lower band of the double mutant was bound completely to this resin, whereas the upper band bound poorly (Figure 3, lanes 13–16). The yield of protein in the bound fraction was very low and may have been due to the high avidity of the double N-glycosylated high-mannose protein for the resin. We were surprised to find that the upper band of the double mutant bound poorly to the concanavalin A resin. This suggests that the protein has a lower avidity for the resin compared with the high-mannose protein or that the presence of the large complex chain in the neighbouring loop compromised the binding of the high-mannose chain. The upper band of the N555 mutant bound to immobilized wheat-germ agglutinin while the lower band did not (results not shown) indicating that the upper band did contain complex oligosaccharide. Thus the N555 mutant is also present in two forms in transfected cells, a lower molecular mass form containing a high-mannose oligosaccharide and a higher molecular mass form containing a complex oligosaccharide.

Cell surface biotinylation

AE1 expressed in HEK-293 cells contained a high-mannose oligosaccharide that was not processed to a complex oligosaccharide. This may be due to retention of the protein in the endoplasmic reticulum or to inefficient oligosaccharide processing as AE1 moves through the secretory pathway. Cell surface biotinylation was used to determine the level of cell surface expression of the AE1 mutants. Cells were treated with NHS-SS-biotin and the fraction of AE1 that was biotinylated was determined by binding to streptavidin beads. The total, unbound and bound fractions were analysed for AE1 by immunoblotting (Figure 4). AE1 could be biotinylated by treating intact transfected cells with the non-penetrating biotinylation reagent (Figure 4, left panel). The bound fraction of AE1 was sensitive to endoglycosidase H (results not shown). The level of cell surface expression of AE1 in HEK-293 cells, determined from the bound fraction, was only 10%. The amount in AE1 remaining in the unbound fraction relative to the total, however, indicated a decrease of 30%. This suggests that release of the biotinylated protein from the beads was not very quantitative. No AE1 bound to the resin without prior treatment of the cells with the biotinylation reagent (results not shown) and no AE1 binding to Sepharose beads lacking streptavidin was detected, confirming the specificity of the labelling. The results suggest that a significant fraction (30%) of human AE1 had moved through the secretory pathway to the plasma membrane without extensive modification to its oligosaccharide. The presence of AE1 at the cell surface is in agreement with functional assays that can measure Cl^-/HCO_3^- exchange in intact cells [14] and similar biotinylation assays [20].

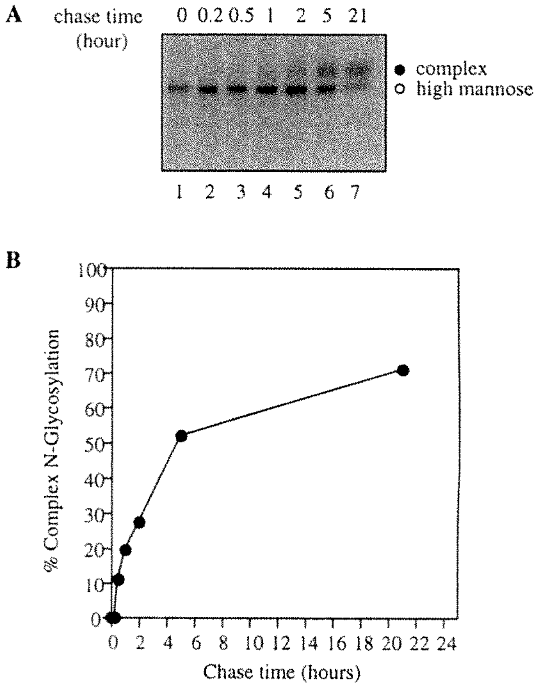

Figure 5 Pulse–chase experiments using COS-7 cells transfected with the N555 glycoform

Transfected cells were labelled with [^{35}S]methionine for 10 min followed by a chase for the indicated times. At each time point cells were lysed with RIPA buffer and AE1 was immunoprecipitated and samples were resolved by SDS/PAGE. The upper panel is an autoradiograph showing the time-dependent conversion of the high-mannose form (open circle) to the complex form (closed circle). The lower panel is a plot of the percentage of the complex oligosaccharide relative to the total oligosaccharide (complex plus high-mannose).

The N642D mutant could also be biotinylated, similarly to wild-type AE1 (Figure 4, middle panel). The amount of AE1 in the unbound fraction indicated that approx. 30% of the N642D mutant was present at the cell surface. This result suggests that N-glycosylation of AE1 is not a necessary requirement for cell-surface expression, in agreement with previous studies using AE1 expression in *Xenopus* oocytes [21].

Cell surface biotinylation assays of the cells transfected with the N555 mutant showed that the upper band could be quantitatively biotinylated while the lower band could not (Figure 4, right panel). The upper band consists of a glycoprotein that has moved through the secretory pathway and whose oligosaccharide was processed from high-mannose to complex. The lower band is AE1 that is located in the endoplasmic reticulum and contains a high-mannose oligosaccharide. Based on the decreased amount of

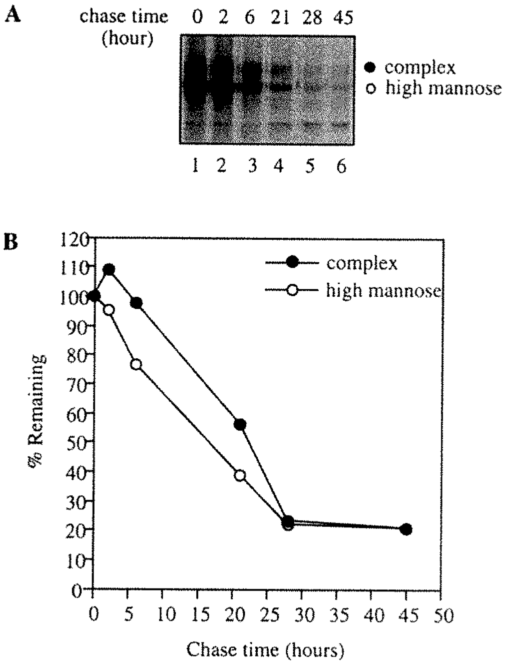

Figure 6 Turnover of the N555 mutant in transfected COS-7 cells

Transfected cells were labelled with [^{35}S]methionine for 90 min followed by a chase for the indicated times, as described in Figure 5. The upper panel is an autoradiograph showing the time-dependent loss of the high-mannose form (open circle) and the complex form (closed circle). The lower panel is a plot of the percentage of radiolabelled high-mannose and complex AE1 remaining, relative to the amount at the end of the labelling period.

AE1 in the unbound fraction, the level of cell surface expression of the N555 mutant was similar (30 %) to that of wild-type AE1.

Time course of oligosaccharide processing

The biosynthetic relationship between the high-mannose and complex forms of the N555 mutant was examined by pulse–chase experiments. Figure 5 (upper panel) shows an immunoprecipitate of a whole-cell detergent lysate of transfected COS-7 cells that were labelled with [^{35}S]methionine for 10 min and chased for the indicated intervals. The N555 mutant was initially synthesized as a lower molecular mass band that decreased in amount during the chase period with the concomitant appearance of a higher molecular mass form. The lower molecular mass form was sensitive to endoglycosidase H while the upper band was resistant (results not shown). The data indicate that there is a time-dependent conversion of a high-mannose form of the N555 mutant into a complex oligosaccharide form, with a half-time of approx. 4 h (Figure 5, lower panel). This conversion reflects the transit time of the glycoprotein from its site of synthesis in the endoplasmic reticulum to the plasma membrane. Greater than 75 % of AE1 was converted from a high-mannose form into complex form over a 21 h period. This high percentage indicates that there was nearly complete conversion of the high-mannose oligosaccharide into the complex form, and that very little degradation of the high-mannose form in the ER must have occurred over the time period. Similar pulse–chase experiments with wild-type AE1 showed that the protein ran as a single band and that there was no conversion to a higher molecular mass form (results not shown). This band remained sensitive to endoglycosidase H indicating that it contained high-mannose oligosaccharide.

Stability of N-glycosylation mutants

In order to determine the stability of the N555 mutant, cells were labelled with [^{35}S]methionine for 90 min and then chased for up to 45 h (Figure 6). The amount of the complex form of the N555 mutant initially increased due to continued conversion from the high-mannose form and then decreased with a half-life of approx. 15 h. This long half-life indicates that the mature form of human AE1 is quite stable in the plasma membrane of transfected cells. The high-mannose form of the N555 mutant also decreased during the chase period. In this case, the amount of radiolabelled high-mannose form present reflected a complex balance between conversion into the complex form, degradation within the ER and residual protein synthesis that may have occurred during the chase period.

DISCUSSION

N-glycosylation of anion exchangers

AE1 is a member of a gene family of anion exchangers responsible for the electroneutral exchange of chloride and bicarbonate across cell membranes. Mammalian AE1 proteins all contain a single site of N-glycosylation in the fourth extracellular loop, whereas AE2, AE3 and trout AE1 contain N-glycosylation sites in the preceding extracellular loop. In the present study we have shown that oligosaccharide attached to the fourth extracellular loop of human AE1 is retained as a high-mannose oligosaccharide in transfected cells. Mutants in which an N-glycosylation site is engineered into the third extracellular loop were processed to complex oligosaccharides at this site. Thus the processing of the oligosaccharide on human AE1 is dependent on its location. Murine AE2, which contains N-glycosylation sites on the third extracellular loop, was processed to a complex oligosaccharide in transfected cells [13]. This site-dependence of N-glycosylation processing has also been observed for secreted proteins that contain high-mannose and complex oligosaccharides at different sites in the same protein [19].

The results presented in this paper show that transfected HEK-293 and COS cells are unable to efficiently process the oligosaccharide on human AE1, although the protein can move through the secretory pathway to the plasma membrane. In contrast, when the oligosaccharide is attached to Asn^{555} in the third loop it is readily processed to the complex form by both of these cell types. In a double N555/N642 mutant the results indicate that the oligosaccharide chain at Asn^{555} was processed while the oligosaccharide chain at Asn^{642} was not. This result shows that although AE1 had moved through the secretory pathway to the plasma membrane, the site at Asn^{642} was refractory to modification to the complex form. An important feature of oligosaccharide processing is that cells vary in their ability to process certain glycoproteins [18]. Human AE1 is normally processed to a complex oligosaccharide during red cell development [4]. In contrast, neither HEK-293 nor COS-7 cells were capable of efficiently processing the oligosaccharide chain of AE1 at Asn^{642}. HEK-293 cells are clearly not deficient in oligosaccharide processing enzymes, since the oligosaccharide at Asn^{555} in AE1 can be converted into a complex oligosaccharide.

The ability of an oligosaccharide chain to be processed depends on the degree of accessibility of the site to the processing enzymes in the Golgi [18,19]. We found that the oligosaccharide on extracellular loop 3 is more sensitive to cleavage by N-glycanase F than the oligosaccharide on loop 4. Extracellular loop 3 in human AE1 is also accessible to cleavage by various proteases [22,23]. Moving extracellular loop 3 to other positions in AE1 also resulted in production of a high-mannose glycoprotein in transfected cells [12]. This suggests that it is the structure of loop 3 rather than its position in the protein that restricts processing. The oligosaccharide at Asn^{642} on AE1 may be a poor substrate for the processing pathway present in the transfected cells.

In the human disease HEMPAS, red cell glycoproteins retain their high-mannose oligosaccharide due to a deficiency in mannosidase II [8,10]. A mannosidase II knock-out mouse is unable to process N-linked oligosaccharide present on erythrocyte glycoproteins, but can still process glycoproteins normally in other cells [11]. This suggests that mannosidase II is essential for the processing of oligosaccharide chains on glycoproteins in the erythroid lineage. In other cells an alternative pathway is proposed which bypasses the mannosidase II step. The results suggest that mannosidase II in transfected cells may not be able to process the oligosaccharide attached to Asn^{642}. AE1 in transfected HEK-293 cells contains only high-mannose oligosaccharide and therefore resembles AE1 in HEMPAS red cells.

AE1 trafficking to the plasma membrane

The nearly complete conversion of the high-mannose form of the N555 mutant to the complex form shows that the intracellular fraction of AE1 was fully competent for trafficking to the plasma membrane. These findings are in contrast with cystic fibrosis conductance transmembrane regulator ('CFTR'), in which only a fraction of the protein moved to the plasma membrane [24,25]. The remainder was retained in the endoplasmic reticulum and degraded by a proteasome-mediated pathway [26]. The complex form of the N555 mutant present in the plasma membrane had a turnover of 15 h, showing that the mature AE1 was relatively stable in transfected cells.

The N555 mutant moved from its site of synthesis in the endoplasmic reticulum to the plasma membrane with a half-time of 4 h in transfected cells. This transit time is similar to the 2 h half-time observed for murine AE2 in transfected cells [13] Pulse–chase experiments in murine spleen cells showed that AE1 became endoglycosidase H resistant with a faster half-time of 30 min [27]. Transfected cells, unlike pre-erythroid cells, may not contain all the specific proteins required for the efficient assembly of AE1 [13]. AE1 in HEK-293 cells interacts transiently with the chaperone calnexin, which may be involved in facilitating its folding and exit from the endoplasmic reticulum [28]. Evidence suggests that other proteins present in the red cell, such as ankyrin, glycophorin A, and Band 4.2, may be required for the assembly of AE1 in the plasma membrane. Ankyrin has been reported [29] to associate with AE1 in a pre-Golgi compartment in transfected cells, which may facilitate the exit of AE1 from the endoplasmic reticulum. The trafficking of AE1 to the plasma membrane in *Xenopus* oocytes is enhanced by co-expression of glycophorin A [30] while Band 3 from glycophorin-deficient red cells has an increased level of N-glycosylation, suggesting a reduced transit time through the Golgi [31,32]. Human erythroleukemia K562 cells express endogenous glycophorin A and transfection of these cells with AE1 using a retroviral system results in functional cell surface expression of AE1 [33] Erythrocytes from AE1 knock-out mice are devoid of Band 4.2 [34] and glycophorin A [35], suggesting that both Band 4.2 and glycophorin A form a complex with AE1.

AE1 exists in mature red cells as a mixture of dimers and tetramers, the tetramers providing the binding site for ankyrin [36,37]. Ankyrin-deficient red cells lack Band 3 tetramers, suggesting that ankyrin is required for AE1 tetramer formation [38]. Murine AE1 forms dimers in transfected cells [39] and the protein is functional in the endoplasmic reticulum [13]. As HEK-293 cells are deficient in ankyrin, tetramer formation was not expected. In mouse erythroblasts AE1 tetramers are formed in early erythroblasts, are found in the microsomal fraction and are subsequently incorporated into the plasma membrane [40]. Dimers present at the late stages of erythroid maturation move rapidly to the plasma membrane and can recycle to the microsomal fractions. In chicken erythroblasts AE1 initially moves to the plasma membrane in a high-mannose form and is then internalized and recycled to the Golgi, where AE1 associates with ankyrin and the oligosaccharide is processed to a complex form [41]. The AE1–ankyrin complex then moves to the plasma membrane where the complex links to spectrin. The first stage is similar to what was observed in the present study, where the oligosaccharide on human AE1 escaped modification during the initial transit of the protein through the secretory pathway to the plasma membrane. Tetramer formation and ankyrin binding may be required for oligosaccharide processing of human AE1, which may occur during subsequent recycling of the protein from the plasma membrane to the Golgi. Tetramer formation may make human AE1 a substrate for the processing enzymes, or perhaps tetrameric AE1 follows a different processing route back to the plasma membrane. The processing of the oligosaccharide on human AE1 in transfected cells depends on the location of the oligosaccharide chain, showing that these cells contain the required processing enzymes, but that the oligosaccharide at Asn^{642} in AE1 is refractory to them.

We thank J H M Charuk and J. W Vince for providing helpful comments on the manuscript. Funding for this project was provided by a Group Grant from the Medical Research Council of Canada. M P was supported by a University of Toronto Open Fellowship and J Q by an Ontario Graduate Scholarship

REFERENCES

1 Tanner, M J A, Martin, P G and High, S (1988) The complete amino acid sequence of the human erythrocyte membrane anion-transport protein deduced from the cDNA sequence Biochem J **256**, 703–712

2 Lux, S E, John, K M and Bennett, V (1990) Analysis of cDNA for human erythrocyte ankyrin indicates a repeated structure with homology to tissue-differentiation and cell-cycle control proteins Nature (London) **344**, 36–42

3 Drickamer, L K (1978) Orientation of the Band 3 polypeptide from human erythrocyte membranes Identification of NH2-terminal sequence and site of carbohydrate attachment J. Biol Chem **253**, 7242–7248

4 Fukuda, M, Dell, A, Oates, J E and Fukuda, M. N (1984) Structure of the branched lactosaminoglycan, the carbohydrate moiety of Band 3 isolated from adult human erythrocytes J Biol Chem **259**, 8260–8273

5 Tsuji, T, Irimura, T. and Osawa, T (1981) The carbohydrate moiety of Band 3 glycoprotein of human erythrocyte membranes structures of lower molecular weight oligosaccharides J. Biol Chem **256**, 10497–10502

6 Landolt-Marticorena, C, Charuk, J H M and Reithmeier, R A F. (1998) Two glycoprotein populations of band 3 dimers are present in human erythrocytes Mol Membr Biol **15**, 153–158

7 Fukuda, M N (1990) HEMPAS disease genetic defect of glycosylation Glycobiology **1**, 9–15

8 Fukuda, M N, Masri, K A., Dell, A, Luzzatto, L and Moremen, K W (1990) Incomplete synthesis of N-glycans in congenital dyserythropoietic anemia type II caused by a defect in the gene encoding α-mannosidase II Proc Natl. Acad Sci U.S.A. **87**, 7443–7447

9 Kameh, H, Landolt-Marticorena, C, Charuk, J H M, Schachter, H and Reithmeier, R A F (1998) Structural and functional consequences of an N-glycosylation mutation (HEMPAS) affecting human erythrocyte membrane glycoproteins Biochem. Cell Biol **76**, 823–835

10 Fukuda, M N (1999) HEMPAS Biochim Biophys Acta **1455**, 231–239

11 Chui, D., Oh-Eda, M., Liao, Y-F, Panneerselvam, K., Lal, A, Marek, K. W., Freeze, H H, Moreman, K W, Fukuda, M N and Marth, J D (1997) Alpha-mannosidase-II deficiency results in dyserythropoiesis and unveils an alternate pathway in oligosaccharide biosynthesis Cell **90**, 157–167

12 Popov, M, Li, J and Reithmeier, R A F (1999) Transmembrane folding of the human erythrocyte anion exchanger (AE1, Band 3) determined by scanning and insertional N-glycosylation mutagenesis Biochem J **339**, 269–279

13 Ruetz, S, Lindsey, A. E., Ward, C L and Kopito, R R. (1993) Functional activation of plasma membrane anion exchangers occurs in a pre-golgi compartment. J Cell Biol **121**, 37–48

14 Tang, X-B, Fujinaga, J, Kopito, R and Casey, J R (1998) Topology of the region surrounding Glu681 of human AE1 protein, the erythrocyte anion exchanger J Biol Chem **273**, 22545–22553

15 Popov, M, Tam, L Y, Li, J and Reithmeier, R A F. (1997) Mapping the ends of transmembrane segments in a polytopic membrane protein Scanning N-glycosylation mutagenesis of extracytosolic loops in the anion exchanger Band 3 J Biol. Chem **272**, 18325–18332

16 Laemmli, U K (1970) Cleavage of structural proteins during assembly of the head of bacteriophage T4 Nature (London) **227**, 680–685

17 Tam, L Y, Landolt-Marticorena, C and Reithmeier, R A F (1996) Glycosylation of multiple extracytosolic loops in Band 3, a model polytopic membrane protein Biochem J **318**, 645–648

18 Williams, D B and Lennarz, W J (1984) Control of asparagine-linked oligosaccharide chain processing studies on bovine pancreatic ribonuclease B An *in vitro* system for processing of exogenous glycoproteins J Biol Chem **259**, 5105–5114

19 Faye, L, Sturm, A, Bollini, R, Vitale, A and Chrispeels, M J (1986) The position of the oligosaccharide side-chains of phytohemagglutinin and their acccessibility to glycosidases determines their subsequent processing in the Golgi Eur. J. Biochem **158**, 655–661

20 Sterling, D and Casey, J R (1999) Transport activity of AE3 chloride/bicarbonate anion-exchange proteins and their regulation by intracellular pH. Biochem J **344**, 221–229

21 Groves, J D. and Tanner, M J A (1993) Role of N-glycosylation in the expression of human band 3 mediated anion transport. Mol. Membr Biol **11**, 31–38

22 Steck, T L, Ramos, B and Strapazon, E. (1976) Proteolytic dissection of Band 3, the predominant transmembrane polypeptide of the human erythrocyte membrane Biochemistry **15**, 1154–1161

23 Jennings, M L and Nicknish, S J (1985) Localization of a site of intermolecular cross-linking in human red blood cell Band 3 protein. J. Biol Chem **260**, 5472–5479

24 Ward, C L and Kopito, R R (1994) Intracellular turnover of cystic fibrosis transmembrane conductance regulator Inefficient processing and rapid degradation of wild-type and mutant proteins J Biol. Chem **269**, 25710–25718

25 Lukacs, G L, Mohamed, A, Kartner, N, Chang, X B, Riordan, J R and Grinstein, S (1994) Conformational maturation of CFTR but not its mutant counterpart (delta F508) occurs in the endoplasmic reticulum and requires ATP EMBO J **13**, 6076–6086

26 Kopito, R R (1999) Biosynthesis and degradation of CFTR Physiol Rev **79**, S167–S173

27 Braell, W A and Lodish, H F (1981) Biosynthesis of the erythrocyte anion transport protein J Biol Chem **256**, 11337–11344

28 Popov, M and Reithmeier, R. A. (1999) Calnexin interaction with N-glycosylation mutants of a polytopic membrane glycoprotein, the human erythrocyte anion exchanger 1 (band 3) J Biol. Chem **274**, 17635–17642

29 Gomez, S and Morgans, C (1993) Interaction between band 3 and ankyrin begins in early compartments of the secretory pathway and is essential for band 3 processing J Biol Chem **268**, 19593–19597

30 Groves, J D and Tanner, M J A (1992) Glycophorin A facilitates the expression of human band 3-mediated anion transport in Xenopus oocytes J Biol Chem **267**, 11940–11948

31 Tanner, M J, Jenkins, R. E, Anstee, D J and Clamp, J R (1976) Abnormal carbohydrate composition of the major penetrating membrane protein of En(a-) human erythrocytes Biochem J **155**, 701–703

32 Tanner, M J and Anstee, D J (1976) The membrane change in En(a-) human erythrocytes Absence of the major erythrocyte sialoglycoprotein Biochem J **153**, 271–277

33 Beckmann, R, Smythe, J. S., Anstee, D J and Tanner, M J (1998) Functional cell surface expression of band 3, the human red blood cell anion exchange protein (AE1), in K562 erythroleukemia cells band 3 enhances the cell surface reactivity of Rh antigens Blood **92**, 4428–4438

34 Peters, L L, Shivdasani, R A, Liu, S-C, Hanspal, M, John, K M, Gonzalez, J M, Brugnara, C, Gwynn, B., Mohandas, N, Alper, S L et al (1996) Anion exchanger 1 (Band 3) is required to prevent erythrocyte membrane surface loss but not to form the membrane skeleton Cell **86**, 917–927

35 Hassoun, H, Hanada, T, Lutchman, M, Sahr, K E., Palek, J., Hanspal, M and Chishti, A H (1998) Complete deficiency of glycophorin A in red blood cells from mice with targeted inactivation of the band 3 (AE1) gene Blood **91**, 2146–2151

36 Jennings, M L (1984) Oligomeric structure and the anion transport function of human erythrocyte Band 3 protein J Membr Biol **80**, 105–117

37 Van Dort, H M, Moriyama, R and Low, P S (1998) Effect of band 3 subunit equilibrium on the kinetics and affinity of ankyrin binding to erythrocyte membrane vesicles. J Biol Chem **273**, 14819–14826

38 Yi, S J, Liu, S. C, Derick, L H, Murray, J., Barker, J E, Cho, M R, Palek, J and Golan, D E (1997) Red cell membranes of ankyrin-deficient nb/nb mice lack band 3 tetramers but contain normal membrane skeletons Biochemistry **36**, 9596–9604

39 Casey, J R, Ding, Y and Kopito, R R (1995) The role of cysteine residues in the erythrocyte plasma membrane anion exchange protein, AE1 J Biol Chem **270**, 8521–8527

40 Hanspal, M, Golan, D E, Smockova, Y, Yi, S J, Cho, M R, Liu, S C. and Palek, J (1998) Temporal synthesis of band 3 oligomers during terminal maturation of mouse erythroblasts Dimers and tetramers exist in the membrane as preformed stable species Blood **92**, 329–338

41 Ghosh, S, Cox, K H. and Cox, J V (1999) Chicken erythroid AE1 anion exchangers associate with the cytoskeleton during recycling to the Golgi Mol Biol Cell **10**, 455–469

Received 21 February 2000/12 April 2000, accepted 28 April 2000

Activation of phosphatidylinositol 3-kinase is required for transcriptional activity of F-type 6-phosphofructo-2-kinase/fructose-2,6-bisphosphatase: assessment of the role of protein kinase B and p70 S6 kinase

Silvia FERNÁNDEZ DE MATTOS, Elisabet DE LOS PINOS, Manel JOAQUIN and Albert TAULER[1]

Departament de Bioquímica i Biologia Molecular, Div. IV, Facultat de Farmàcia, Universitat de Barcelona, Av. Diagonal 643, E08028 Barcelona, Catalunya, Spain

---

Previous studies have demonstrated that the F isoform of 6-phosphofructo-2-kinase/fructose-2,6-bisphosphatase (6PF2K/Fru-2,6-BPase) is transcriptionally regulated by growth factors. The aim of this study was to investigate the importance of the phosphatidylinositol 3-kinase (PI 3-kinase) pathway in the regulation of *6PF2K/Fru-2,6-BPase* gene expression. We have completed studies using chemical inhibitors and expression vectors for the proteins involved in this signalling cascade. Treatment of cells with LY 294002, an inhibitor of PI 3-kinase, blocked the epidermal growth factor (EGF)-dependent stimulation of *6PF2K/Fru-2,6-BPase* gene transcription. Transient transfection of a constitutively active PI 3-kinase was sufficient to activate transcription from the F-type 6PF2K/Fru-2,6-BPase promoter. In contrast, co-transfection with a dominant-negative form of PI 3-kinase completely abrogated the stimulation by EGF, and down-regulated the basal promoter activity. In an attempt to determine downstream proteins that lie between PI 3-kinase and *6PF2K/Fru-2,6-BPase* gene expression, the over-expression of a constitutively active form of protein kinase B (PKB) was sufficient to activate *6PF2K/Fru-2,6-BPase* gene expression, even in the presence of either a dominant-negative form of PI 3-kinase or LY 294002. The over-expression of p70/p85 ribosomal S6 kinase or the treatment with its inhibitor rapamycin did not affect 6PF2K/Fru-2,6-BPase transcription. We conclude that PI 3-kinase is necessary for the transcriptional activity of F-type 6PF2K/Fru-2,6-BPase, and that PKB is a downstream effector of PI 3-kinase directly involved in the regulation of *6PF2K/Fru-2,6-BPase* gene expression.

Key words: fructose 2,6-bisphosphate, gene expression, glycolysis, LY 294002, signal transduction.

INTRODUCTION

Activation of the glycolytic pathway is common to such distinct processes as glucose metabolism in liver and cell proliferation. In all these processes, fructose 2,6-bisphosphate, a potent allosteric stimulator of 6-phosphofructo-1-kinase, determines the strength of glycolytic flux. The content of this metabolite is regulated by the bifunctional enzyme 6-phosphofructo-2-kinase/fructose-2,6-bisphosphatase (6PF2K/Fru-2,6-BPase; EC 2.7.1.105/3.1.3.46), which catalyses both its synthesis and its degradation. Various 6PF2K/Fru-2,6-BPase isoenzymes have been described in different tissues. In rat, liver, muscle and F-type isoforms are encoded by the same gene arising from distinct promoters. These isoenzymes differ in their N-terminal sequences, regulation by phosphorylation and kinetic properties (for review see [1,2]).

The expression of 6PF2K/Fru-2,6-BPase isoenzymes depends on cellular processes. The F-type isoform is more specific to proliferative tissues and is transcriptionally activated by growth factors [3–6]. In accordance with this, several binding sites for different transcription factors have been implicated in the regulation of this isoform during cell proliferation, such as binding sites for Sp1 and for members of the *ets* oncogene family located on the F promoter [4], and a binding site for the E2F transcription factor located in the first exon of F-type mRNA [5]. The signalling pathways that mediate growth-factor regulation of *6PF2K/Fru-2,6-BPase* gene expression are not fully understood. Previously we have demonstrated that activation of mitogen-activated protein kinase (MAPK) is required for the stimulation of the transcription of 6PF2K/Fru-2,6-BPase by epidermal growth factor (EGF) [6]. However, this does not rule out the possibility that other pathways could also be involved in this regulation.

A large body of evidence supports the hypothesis that the activation of the phosphatidylinositol 3-kinase (PI 3-kinase) pathway by growth factors or insulin mediates the expression of several metabolic genes [7–15]. An increase in PI 3-kinase activity occurs following ligand-induced autophosphorylation of the receptor in response to a wide range of extracellular stimuli. This results in the generation of membrane-restricted second messengers, phosphatidylinositides containing a 3′-phosphate. Recent studies have identified a number of downstream targets of these phospholipid products, including the serine/threonine kinases 3-phosphoinositide-dependent kinase 1 (PDK1), protein kinase B (PKB) and, indirectly, p70/p85 ribosomal protein S6 kinase ($p70^{S6K}$; for review see [16]).

The aim of the present study was to investigate the role of PI 3-kinase on the regulation of *6PF2K/Fru-2,6-BPase* gene expression. We now demonstrate that activation of PI-3 kinase is not only essential for the stimulation of the transcription of 6PF2K/Fru-2,6-BPase by EGF, but is also required for basal transcriptional activity. We also show that PI 3-kinase action occurs through activation of PKB, which is activated upon generation of 3-phosphorylated inositol lipids, the products of PI 3-kinase.

Abbreviations used: 6PF2K/Fru-2,6-BPase, 6-phosphofructo-2-kinase/fructose-2,6-bisphosphatase, EGF, epidermal growth factor, MAPK, mitogen-activated protein kinase; PI 3-kinase, phosphatidylinositol 3-kinase, PDK1, 3-phosphoinositide-dependent kinase 1, PKB, protein kinase B; $p70^{S6K}$, p70/p85 ribosomal S6 kinase; CAT, chloramphenicol acetyltransferase; FCS, foetal calf serum, AP-1, activator protein 1; mTOR, mammalian target of rapamycin

[1] To whom correspondence should be addressed (e-mail tauler@farmacia.far.ub.es)

EXPERIMENTAL

Materials

Foetal calf serum (FCS), Dulbecco's modified Eagle's medium, and penicillin/streptomycin were from Bio-Whittaker. [α-^{32}P]-dCTP (3000 Ci/mmol), D-*threo*-[*dichloroacetyl*-1-^{14}C]chloramphenicol (56 mCi/mmol) and Hybond-N membranes were from Amersham Pharmacia Biotech. The random-primer DNA-labelling kit was from Boehringer Mannheim. EGF was from Sigma. LY 294002 and rapamycin were from Calbiochem. Tfx-10, Transfast Reagents and luciferase assay system were from Promega. ExpressHyb Hybridization Solution was from Clontech. Phospho-specific PKB antibody was from New England Biolabs. Anti-Myc monoclonal antibody 9E10 and anti-p70^{S6K} polyclonal antibody were from Santa Cruz Biotechnology. p70^{S6K} substrate peptide was from Upstate Biotechnology. Other materials and chemicals were of the highest quality available

Plasmid constructs

The reporter-gene construct FpBLCAT3 [17] contains the *Hin*dIII/*Bsp*mI 5′-flanking region of the F isoform of *6PF2K/Fru-2,6-BPase* cloned into pBLCAT3 plasmid and was provided by Dr A. Lange (University of Minnesota, Minneapolis, MN, U.S.A.). Expression vectors for the catalytic subunit of PI 3-kinase, including constitutively active p110* and kinase-dead p110KR [18] were provided by Dr A. Klippel (Chiron Corporation, Emeryville, CA, U.S.A.). The expression vector for the constitutively active PKB/Akt, PKBgag [19], was provided by Dr G. Evan (Imperial Cancer Research Fund Laboratories, London, U.K.). Expression vector for Myc-tagged wild-type PDK1 [20] was provided by Dr B. Hemmings, and expression vectors for Myc-tagged wild-type p70^{S6K} and Myc-tagged constitutively active p70^{S6K}E389D$_3$E [20] were provided by Dr G. Thomas, both at the Friedrich-Miescher-Institut, Basel, Switzerland.

Cell cultures

Rat-1 fibroblasts and FTO-2B hepatoma cells were grown in Dulbecco's modified Eagle's medium supplemented with 10 % (v/v) FCS, 100 units/ml penicillin and 100 mg/ml streptomycin, in a 5 % CO$_2$ humidified atmosphere at 37 °C. For experimental purposes, cells were subcultured in 100-mm dishes and made quiescent by maintaining them in medium supplemented with 0.1 % FCS for 48 h. After this, cells were preincubated for 30 min in the presence of specific inhibitors, and were subsequently treated with EGF-supplemented medium plus DMSO vehicle for 6–8 h.

Transfection and chloramphenicol acetyltransferase (CAT) assays

CsCl double-gradient centrifugation was used to prepare all plasmids for transfection. Rat-1 transient transfections were performed using either the Tfx-10 or the Transfast Reagent (liposome-mediated transfections). Cells were plated at 5.8×10^5 cells/60-mm culture dish or 1.45×10^6/100-mm culture dish on the day before transfection. Transfections were performed by following the manufacturer's protocol. FTO-2B hepatoma cells were transfected using the calcium phosphate/DNA co-precipitation method as described previously [6]. Each plate contained pCMV5 luciferase expression vector as an internal control and the total amount of plasmid was adjusted with empty pCMV5 expression vector. Quiescence was achieved as described above, and the same treatment was performed before harvesting. CAT activity determinations were carried out as described by Ausebel et al. [21].

RNA isolation and analysis

Total RNA was extracted from Rat-1 cells by the LiCl/urea method [22]. The RNA was dissolved in sterile water, and the concentration and purity of each sample were assessed by absorbance at 260 nm and by the 260 nm/280 nm ratio, respectively. The abundance of 6PF2K/Fru-2,6-BPase mRNA was measured by Northern-blot analysis using ExpressHyb solution according to the instructions of the manufacturer (Clontech), and a 1-kb *Eco*RI fragment isolated from pKB plasmid [23] was used as a probe. The integrity of the RNA was verified by observing the rRNA bands in ethidium bromide-stained gel under UV irradiation. The level of mRNA was evaluated by densitometric scanning of the autoradiogram and corrected for the amount of 18 S rRNA using a ribosomal cDNA probe.

Kinase assays

The cells were harvested in ice-cold lysis buffer (50 mM Tris/HCl, pH 8.0, 120 mM NaCl, 20 mM NaF, 10 mM β-glycerol phosphate, 1 % Nonidet P40, 5 mM EGTA, 1 mM benzamidine, 0.1 mM PMSF, 15 mM sodium pyrophosphate, 1 mM dithiothreitol, 1 mM Na_3VO_4, and 1 μg/ml each of aprotinin, leupeptin and pepstatin), and kept on ice for 30 min. Endogenous or Myc-tagged p70^{S6K} was precipitated from 200 μg of cell extract by incubation for 2 h at 4 °C with 2 μg of rabbit polyclonal anti-p70^{S6K} (Santa Cruz Biotechnology) followed by 1 h at 4 °C with 40 μl of 50 % Protein A–Sepharose, or with 3 μg of Myc monoclonal antibody (9E10) and 40 μl of 50 % Protein G–Sepharose. Samples were washed three times in ice-cold PBS containing 0.1 % Nonidet P-40 and 2 mM Na_3VO_4, and once in assay buffer (20 mM Mops, pH 7.2, 25 mM β-glycerol phosphate, 5 mM EGTA, 1 mM Na_3VO_4 and 1 mM dithiothreitol). Immune-complex kinase assays were performed for 30 min at 37 °C in 40 μl of assay buffer containing 50 μM p70^{S6K} substrate peptide and 50 μM [γ-^{32}P]ATP (5 mCi/assay). Substrate-bound reactivity was collected by binding to p81 phosphocellulose paper and quantified by scintillation counting after rinsing with 0.75 % cold phosphoric acid.

Immunoblotting

Cell lysates were prepared as described above, and proteins were subjected to SDS/PAGE (10 % gels). Proteins were transferred on to PVDF membranes. The blots were blocked with blocking solution (5 % non-fat dried milk/Tris-buffered saline/Tween 20, pH. 7.5), washed with Tris-buffered saline/Tween 20 and then incubated with phospho-specific Akt antibody (1:1000 dilution) overnight at 4 °C. After extensive washing, the blots were incubated with secondary antibody (1:5000 dilution) coupled to horseradish peroxidase, and proteins were visualized with the ECL® detection kit (NEN Life Science Products). Equal loading of each lane was confirmed by immunoblotting with actin antibody.

Other methods

Protein was determined as described by Bradford [24] with BSA as standard. The statistical significance of differences was assessed by Student's unpaired *t* test.

RESULTS

The role of PI 3-kinase in the regulation of 6PF2K/Fru-2,6-BPase expression by growth factors was studied by measuring the effect of LY 294002 on the EGF-dependent stimulation of 6PF2K/Fru-2,6-BPase mRNA levels. LY 294002 is a highly specific PI 3-kinase inhibitor that directly inhibits the activity of the p110 catalytic subunit of PI 3-kinase by competing with the ATP-binding site [25]. Rat-1 fibroblasts were made quiescent by maintaining them in 0.1 % FCS medium for 48 h and were then shifted to medium supplemented with EGF at 20 ng/ml. As shown in Figure 1(A), EGF produced a 2-fold increase in the levels of 6PF2K/Fru-2,6-BPase mRNA. The addition of LY 294002 prior to EGF blocked this effect in a dose-dependent manner. To determine whether the regulation of 6PF2K/Fru-2,6-BPase mRNA levels was due to a regulation of its transcriptional rate, Rat-1 cells were transiently transfected with a *CAT* reporter gene under the transcriptional control of a 1.7-kb genomic DNA fragment that contains the F-type promoter. As shown in Figure 1(B), EGF induced up to 2-fold basal CAT activity and LY 294002 repressed this induction. In the absence of EGF, the basal levels of 6PF2K/Fru-2,6-BPase transcriptional activity were also inhibited by treatment with LY 294002. These results indicate that PI 3-kinase contributes positively to the activation of 6PF2K/Fru-2,6-BPase transcription. As a measure of the effect of LY 294002, we determined the phosphorylation state of PKB. We used Western blots probed with an antibody that specifically recognizes phosphorylation of Ser-473. As shown in Figure 1(C), EGF stimulated the phosphorylation of PKB in Ser-473 compared with non-treated cells. In contrast, cells pretreated with LY 294002 at 10 and 50 μM in the presence or absence of EGF contained no detectable phosphoprotein.

A second strategy to investigate whether PI 3-kinase is both necessary and sufficient for EGF to activate *6PF2K/Fru-2,6-BPase* gene expression involved the use of expression vectors for both the constitutively active (p110*) and the kinase-dead (p110KR) catalytic subunit of this enzyme. p110* was constructed by joining the SH2 (Src homology 2) region of p85 to its N-terminus so that it no longer requires the interaction/activation by p85, whereas p110KR carries a point mutation in the ATP-binding site [18]. Co-transfection experiments with these forms and the F-type 6PF2K/Fru-2,6-BPase promoter were performed in Rat-1 cells and CAT activity was determined in the presence or in the absence of EGF. Expression of p110* increased the transcriptional activity of F-type *6PF2K/Fru-2,6-BPase* gene in both the absence and the presence of EGF (Figure 2A). In contrast, the dominant-negative form of PI 3-kinase, p110KR, reduced both basal and EGF-induced 6PF2K/Fru-2,6-BPase promoter activity. To rule out the possibility that this

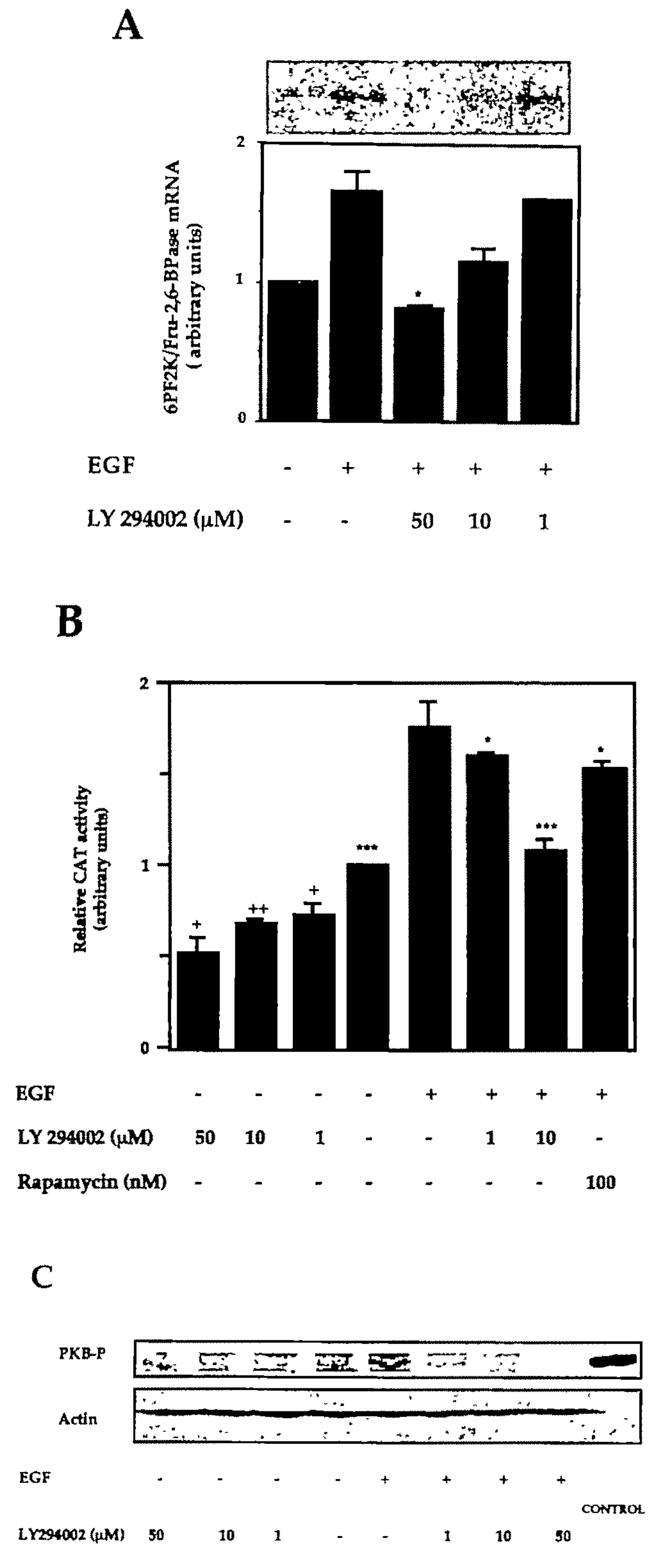

Figure 1 Effect of PI 3-kinase inhibitor LY 294002 on the stimulation of *6PF2K/Fru-2,6-BPase* gene expression by EGF

(A) Quiescent Rat-1 fibroblasts were pretreated for 30 min with the indicated concentrations of LY 294002 and then cultured for 6 h with EGF (20 ng/ml). The carrier for the inhibitors (DMSO) was added as a control. Total RNA (20 μg/lane) was extracted from cultured cells and analysed by Northern blot (a representative Northern blot is shown above the graph). The intensity of the autoradiographic signal was quantified by densitometric scanning and corrected for the amount of RNA obtained with the 18 S rRNA probe. Values are expressed relative to the value of untreated cells, which was considered as 1 arbitrary unit. Data are means ± S.E.M. from three independent experiments. Statistically significant differences are indicated by $^{*}P < 0.05$ compared with EGF-treated cells. **(B)** Quiescent Rat-1 fibroblasts transiently transfected with a *CAT* reporter gene under control of the F-type promoter were incubated for 30 min with the indicated concentrations of LY 294002 or rapamycin and then stimulated for a further 8 h with EGF (20 ng/ml)-supplemented medium carrying DMSO as a vehicle. The intensity of the autoradiographic signal was quantified by densitometric scanning. Values are normalized to luciferase activity and expressed relative to the value of untreated cells, which was considered as 1 arbitrary unit. Data are means ± S.E.M. from five independent experiments. Statistically significant differences are indicated by $^{***}P < 0.001$ and $^{*}P < 0.05$ compared with EGF-treated cells, and $^{++}P < 0.01$ and $^{+}P < 0.05$ compared with untreated cells. **(C)** Samples were obtained from cells pretreated for 30 min with the indicated concentrations of LY 294002 and activated for 10 min with EGF. Equal amounts of cell-lysate protein were subjected to SDS/PAGE followed by Western blotting as described in the Experimental section. The phosphorylated site in PKB was detected with an antibody specific to phospho-Ser-473. The control lane corresponds to Swiss 3T3 cells stimulated with platelet-derived growth factor. Equal loading was confirmed by immunoblotting with actin antibody.

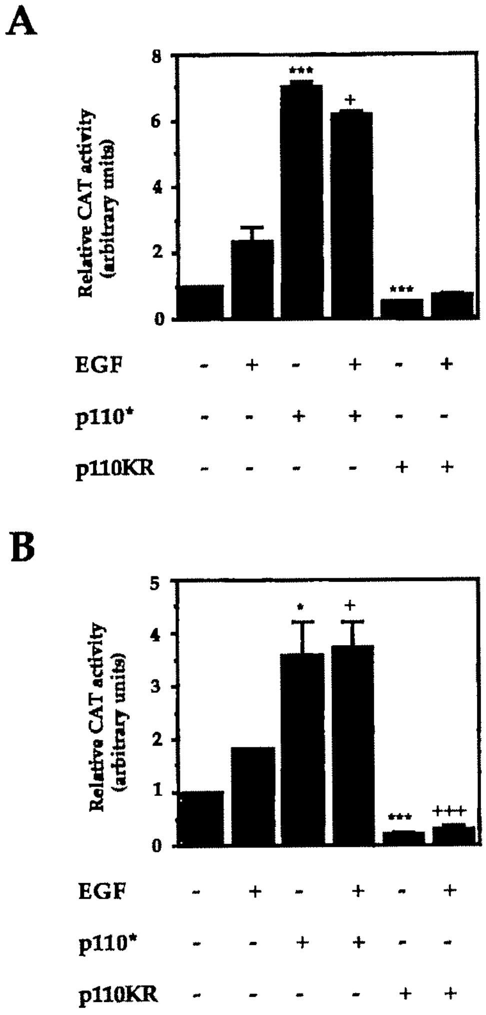

Figure 2 Effect of PI 3-kinase on EGF-stimulated 6PF2K/Fru-2,6-BPase transcriptional activity

Rat-1 cells (**A**) and FTO-2B cells (**B**) were transiently transfected in 100-mm culture dishes with 9 μg of F-type 6PF2K/Fru-2,6-BPase promoter–*CAT* fusion gene, and 2.4 μg of p110* or p110KR expression vector as described in the Experimental section. Following transfection, cells were mantained in 0.1% FCS medium for 48 h and treated with 20 ng/ml EGF. Cells were harvested 8 h after growth-factor addition. CAT activity was assayed and values corrected for luciferase activity from the co-transfected pCMV5luciferase plasmid, and expressed as arbitrary units. Data are means ± S.E.M. from three independent experiments. Statistically significant differences are indicated by $^{***}P < 0.001$ and $^{*}P < 0.05$ compared with untreated cells, and $^{+++}P < 0.001$ and $^{+}P < 0.05$ compared with EGF-treated cells

effect was cell-specific, the same experiment was performed in the FTO-2B hepatoma cell line with similar results (Figure 2B). However, the activation of p110* on PF2K/Fru-2,6-BPase was lower and, in contrast, the inhibition of p110KR was higher.

To explore the link between the activation of PI 3-kinase and the observed up-regulation of *6PF2K/Fru-2,6-BPase* gene expression, we examined the role of PKB in this stimulation. PKB is a direct target of 3′-phosphorylated phosphoinositides, the products of PI 3-kinase activity. Once targeted to the membrane via its pleckstrin homology domain, PKB becomes phosphorylated and activated by PDK1 [26]. The dominant-negative form of PI 3-kinase, p110KR, was co-transfected with F-type 6PF2K/Fru-2,6-BPase promoter, PDK1 expression vector and a constitutively active form of PKB (PKBgag), which is myristoylated and predominantly found at the plasma membrane

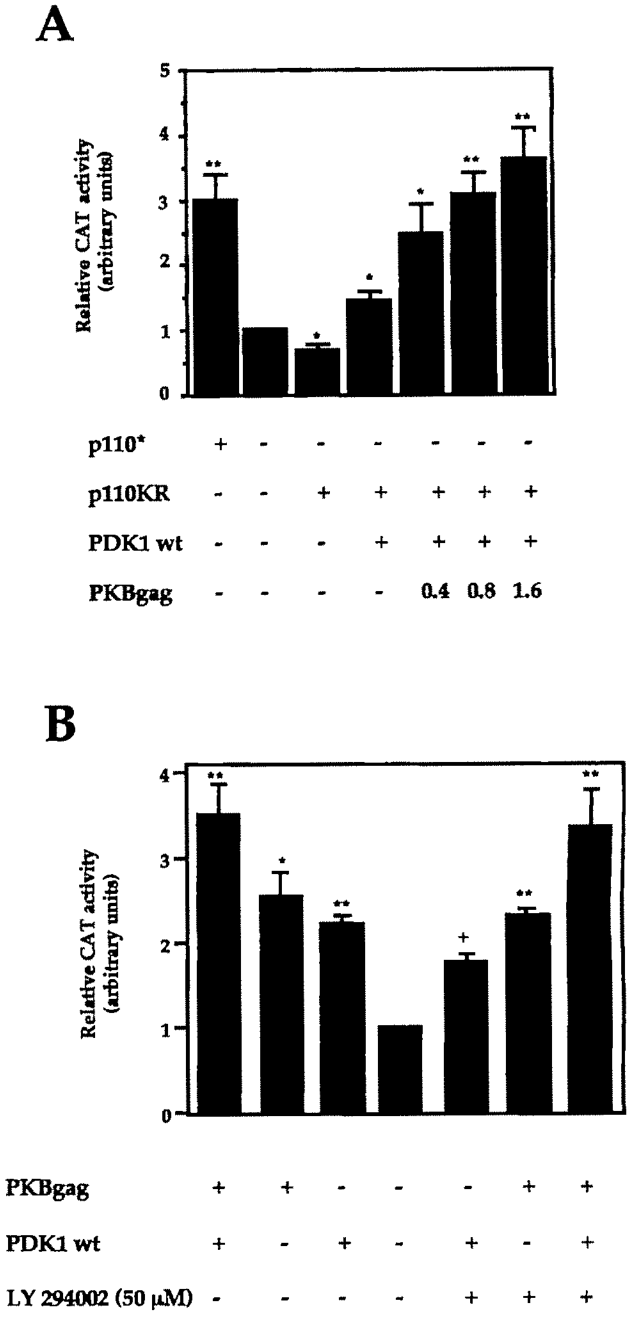

Figure 3 Effect of PKB/Akt on *6PF2K/Fru-2,6-BPase* gene expression inhibited by PI 3-kinase

Expression vectors for the constitutively active p110* or the kinase-dead p110KR (0.8 μg), wild-type (wt) PDK1 (0.8 μg) and the indicated amounts of the constitutively active PKBgag were co-transfected in Rat-1 fibroblasts (60-mm culture dish) with 3 μg of a *CAT* reporter gene under the control of the F-type promoter as described in the Experimental section. (**A**) Cell extracts for assaying CAT activity were obtained 48 h after maintaining the cells in 0.1% FCS medium. Values were normalized to luciferase activity from co-transfected pCMV5luciferase plasmid. Data are means ± S.E.M. from three independent experiments. Statistically significant differences are indicated by $^{**}P < 0.01$ and $^{*}P < 0.05$ compared with cells transfected with FpBLCAT3 plasmid alone. (**B**) Cell extracts for assaying CAT activity were obtained from quiescent transfected cells treated with the indicated amounts of LY 294002 for 8 h. Values are normalized to luciferase activity from co-transfected pCMV5luciferase plasmid. Data are means ± S.E.M. from three independent experiments. Statistically significant differences are indicated by $^{**}P < 0.01$ and $^{*}P < 0.05$ compared with untreated cells transfected with FpBLCAT3 plasmid alone, and $^{+}P < 0.01$ compared with untreated cells transfected with PDK1 wt plasmid

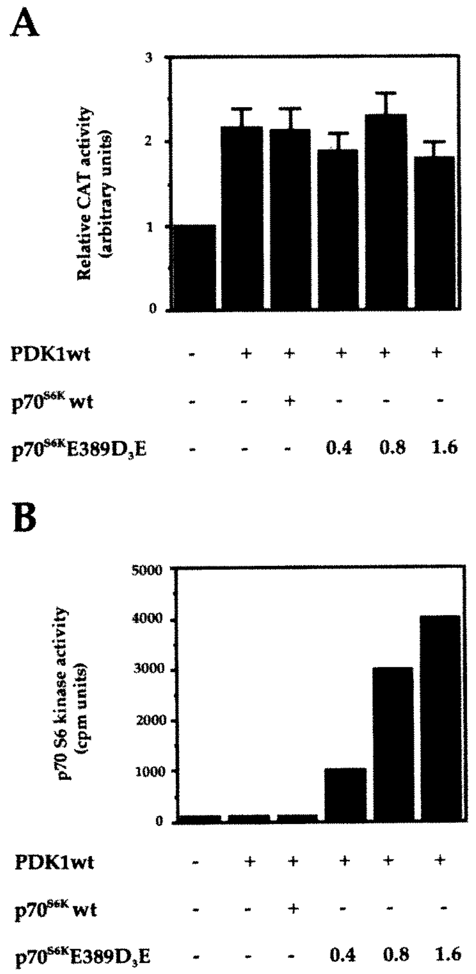

Figure 4 Effect of transfected p70^{S6K} on *6PF2K/Fru-2,6-BPase* gene expression

(**A**) Rat-1 fibroblasts (60-mm culture dish) were transiently transfected with the expression plasmids for PDK1 wild-type (wt; 0.8 μg), p70^{S6K}wt (0.8 μg), and the indicated amounts of the constitutively active p70^{S6K}E389D$_3$E, together with 3 μg of a *CAT* reporter gene under the control of F-type promoter as described in the Experimental section. CAT activity was determined 48 h after maintaining the cells in 0.1% FCS medium. Values are corrected for luciferase activity from co-transfected pCMV5luciferase plasmid. Data are means ± S.E.M. from three independent experiments. (**B**) Samples were obtained from cells transfected and treated as described above, and analysed for p70^{S6K} activity as described in the Experimental section. Values are corrected by subtracting the value for control cells.

[19]. The expression of PKBgag repressed the inhibitory effect of p110KR (Figure 3A) and LY 294002 (Figure 3B). Indeed, the rate of activation of F-type 6PF2K/Fru-2,6-BPase transcriptional activity obtained in the presence of both PKB and PDK1 was the same as with p110*. PKB and PDK1 alone were also able to increase CAT activity but to a lesser extent than when added together. Thus PDK1 and PKB can be considered as downstream effectors of PI 3-kinase directly involved in the regulation of *6PF2K/Fru-2,6-BPase* gene expression.

The ribosomal protein p70^{S6K} has also been identified as a downstream effector of the PI 3-kinase signalling pathway [27]. The precise mechanism by which p70^{S6K} is regulated by PI 3-kinase is not fully understood, but it involves at least phosphorylation by PDK1, the same kinase involved in PKB activation. To determine whether p70^{S6K} regulates *6PF2K/Fru-2,6-BPase* gene expression, the effect of the over-expression of

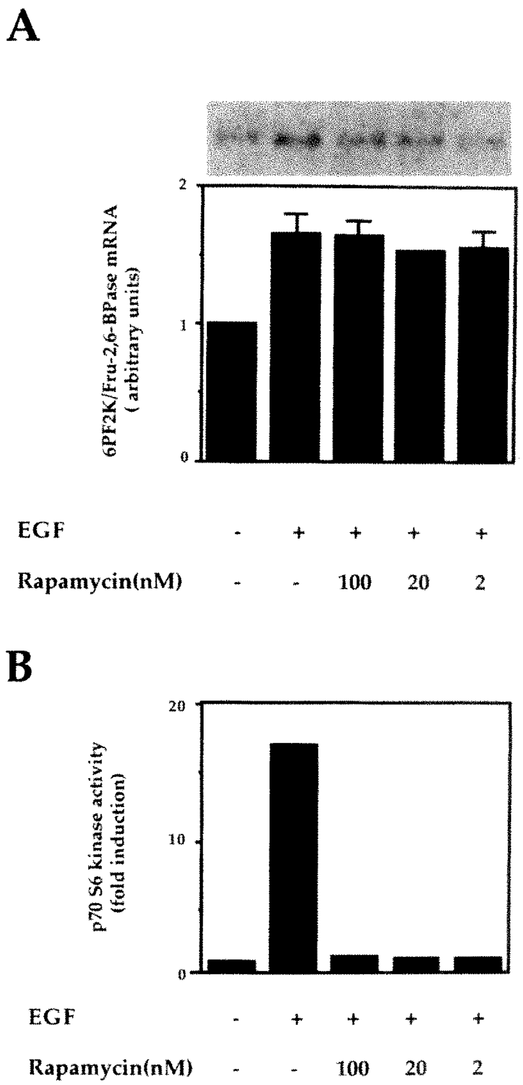

Figure 5 Effect of p70^{S6K} inhibitor rapamycin on the stimulation of *6PF2K/Fru-2,6-BPase* gene expression by EGF

(**A**) Quiescent Rat-1 fibroblasts were preincubated for 30 min with the indicated concentrations of rapamycin and then treated for 6 h with EGF (20 ng/ml). The carrier for the inhibitors (DMSO) was added as a control. Total RNA (20 μg/lane) was extracted from cultured cells and analysed by Northern blotting (a representative Northern blot is shown above the graph). The intensity of the autoradiographic signal was quantified by densitometric scanning and corrected for the amount of RNA obtained with the 18 S rRNA probe. Data are means ± S.E.M. from three independent experiments. (**B**) Samples were obtained from cells pretreated for 30 min with the indicated concentrations of rapamycin and activated for 10 min with EGF (20 ng/ml), and analysed for endogenous p70^{S6K} activity as described in the Experimental section. For both panels, values are expressed relative to the value of untreated cells which was considered as 1 arbitrary unit.

this kinase was evaluated by co-transfection experiments. For this purpose, expression vectors for the wild-type form of p70^{S6K}, p70^{S6K}wt, and for the variant with acidic residues placed at Thr-389 and at the four (Ser/Thr)-Pro sites, p70^{S6K}E389D$_3$E, were used. The p70^{S6K}E389D$_3$E variant has high basal kinase activity and is more efficiently phosphorylated by PDK1 than the wild-type enzyme, further increasing its activity. Co-tranfection with PDK1 and either the wild-type form of p70^{S6K} or the p70^{S6K}E389D$_3$E variant did not increase the transcriptional activity of the F-type promoter more than did PDK1 alone

(Figure 4A). Kinase assays *in vitro* confirm that expression of increasing amounts of p70^{S6K}E389D$_3$E increases p70^{S6K} activity in a dose-dependent fashion (Figure 4B).

A separate pathway contributing to p70^{S6K} activation involves the FKBP (FK506-binding protein) 12-rapamycin-associated protein [FRAP/mammalian target of rapamycin (mTOR)] In order to confirm the previous results, we measured the effect of the FRAP inhibitor rapamycin on the EGF-dependent stimulation of 6PF2K/Fru-2,6-BPase mRNA levels. Quiescent Rat-1 fibroblasts were preincubated for 30 min with increasing concentrations of rapamycin and then treated with medium supplemented with EGF at 20 ng/ml. EGF increased the levels of 6PF2K/Fru-2,6-BPase mRNA 2-fold (Figure 5A). The addition of rapamycin did not affect the enhancement of transcription by EGF at any of the concentrations tested. Kinase assays confirmed that rapamycin was able to block the activation of p70^{S6K} by EGF (Figure 5B). The same result was obtained in Rat-1 fibroblasts transiently trasfected with a *CAT* reporter gene under the transcriptional control of the F-type promoter; the EGF-dependent stimulation of 6PF2K/Fru-2,6-BPase transcriptional activity was insensitive to 100 nM rapamycin (Figure 1B) These results suggest that the serine/threonine kinase p70^{S6K} is not involved in the regulation of *6PF2K/Fru-2,6-BPase* gene expression.

DISCUSSION

In order to activate the glycolytic flux, transcriptional activity of the F-type isoform of 6PF2K/Fru-2,6-BPase enzyme increases during cell proliferation [5,6]. The signal-transduction pathways that lead to this activation are still unclear. Previously we reported the involvement of the MAPK cascade in this regulation [6]; however, this result does not rule out the involvement of other pathways. Here we examined the ability of PI 3-kinase pathway to regulate the transcriptional activity of the specific proliferative isoform of 6PF2K/Fru-2,6-BPase enzyme.

By using a PI 3-kinase-specific inhibitor, LY 294002, we have demonstrated that activation of this kinase was essential for the EGF-stimulated increase in 6PF2K/Fru-2,6-BPase mRNA levels. Transient transfection of a constitutively active PI 3-kinase was sufficient to activate transcription from the F-type 6PF2K/Fru-2,6-BPase promoter. In contrast, co-transfection with a dominant-negative form of PI 3-kinase completely abrogated the stimulatory effect of EGF and down-regulated the basal promoter activity. These results indicate that activation of PI 3-kinase is necessary and sufficient for activation of *6PF2K/Fru-2,6-BPase* gene expression, irrespective of the cell type. The small differences found in response to PI 3-kinase in the different cell lines could be due to the different levels of endogenous PI 3-kinase activity either in the basal or in the EGF-stimulated conditions.

In an attempt to obtain further insights into specific pathways that lie between PI 3-kinase and *6PF2K/Fru-2,6-BPase* gene expression, we evaluated the effect of p70^{S6K} and PKB, both serine/threonine kinases that are activated by PI3-kinase Our results demonstrate that over-expression of p70^{S6K} does not affect *6PF2K/Fru-2,6-BPase* gene expression. In contrast, a constitutively active form of PKB was sufficient to activate *6PF2K/Fru-2,6-BPase* gene expression, even in the presence of a dominant-negative form of PI 3-kinase. There is controversy as to the mechanism by which PKB is activated. The generation of phosphatidylinositides containing a 3′-phosphate by PI 3-kinase has been implicated not only in the translocation of PKB to the membrane, but also in the modulation of its activity [29,30]. However, other reports suggest that this modulation occurs through a phosphorylation-dependent mechanism involving a specific kinase, PDK1 [26]. In order to ensure full PKB activity, in some cases PKB was co-transfected together with PDK1. Interestingly, the finding that overexpression of PDK1 alone significantly activated the 6PF2K/Fru-2,6-BPase promoter is consistent with the role of this kinase in the activation of endogenous PKB. However, other possibilities should be considered. In fact, PDK1 can phosphorylate and activate p70^{S6K} *in vivo*, although we have shown that this kinase is not involved in the regulation of 6PF2K/Fru-2,6-BPase expression, but it could also mediate the activity of members of the AGC (protein kinases A, G and C) family of Ser/Thr kinases [20] The effect of PDK1 is partially abolished by LY 294002, suggesting that changes in the concentration of basal levels of phosphatidylinositides 3′-phosphate could regulate PDK1 activity, as has been suggested by others [31].

PI 3-kinase has recently been implicated in the regulation of enzymes that control metabolic processes In some of them, PKB is involved as a downstream effector; this is the case for fatty acid synthase [11], phosphoenolpyruvate carboxykinase [12], GLUT4 transporter [7] and glycogen synthase kinase-3 [9]. In contrast, the p70^{S6K}-dependent pathway is required for the regulation of glucose-6-phosphate dehydrogenase [14] and hexokinase II [15]. Thus PI 3-kinase is a point of divergence in metabolic signalling. The direction of divergence depends on the nature of the signal, the function of the enzyme and the cell type. From the results presented here, we have demonstrated that PI 3-kinase and PKB are involved in the transcriptional regulation of the proliferation-specific isoform of the 6PF2K/Fru-2,6-BPase enzyme. Further work is needed on the identification of proteins downstream of PKB, including transcription factors that could bind to regulatory elements of these metabolic enzymes. It has been reported that activated forms of PKB and glycogen synthase kinase-3 are translocated to the nucleus, where they may modify the activity of nuclear factors [32–34]. In concordance with this, it has been established that PKB can substitute for interleukin-2 or PI 3-kinase and induce the transcriptional activity of E2F transcription factors in Kit225 cells by regulating the cellular levels of the cyclin/cdk inhibitor p27^{kip1} [35]. In addition, expression of cyclin D1, which can modulate E2F release from the retinoblastoma protein pRB, is mediated by PI 3-kinase through mTOR-p70^{S6K}-independent signalling in growth-factor-stimulated NIH-3T3 fibroblasts [36]. Enhancement of transcriptional activity of activator protein 1 (AP-1) is also mediated by PI 3-kinase in JB6P$^+$ cells [37]. Interestingly, sequence analysis of F-type 6PF2K/Fru-2,6-BPase promoter reveals the presence of DNA-binding sites for E2F and AP-1, suggesting a hypothetical role for these sequences.

The fact that PI 3-kinase and MAPK pathways are both implicated in F-type 6PF2K/Fru-2,6-BPase trancriptional regulation is not surprising. The transcriptional activities of E2F and AP-1 are regulated by both pathways [36–40]. In addition, there is good evidence of interaction of these pathways upstream of the transcriptional response. For example, it has been shown that Ras can interact and stimulate the PI 3-kinase catalytic subunit in a GTP-dependent manner and is required for its optimal activation in response to growth factors [41]. Furthermore, the kinase activity of PI 3-kinase γ is necessary for the activation of Erk2/MAPK through MEK1 (extracellular-signal-regulated kinase/MAPK kinase) [42]. At present, it is not clear how important the synergetic interaction of PI 3-kinase and MAPK pathways is in the regulation of F-type 6PF2K/Fru-2,6-BPase enzyme. However, we cannot rule out the possibility that both pathways could act independently on the F-type 6PF2K/Fru-2,6-BPase promoter.

We thank Dr Joan Gil and Dr Ramon Bartrons for their continued interest in this work, Monste Barragan for help with immunoblotting experiments, and Dr A Lange, Dr A. Klippel, Dr G Evan, Dr B Hemmings and Dr G. Thomas for providing plasmid constructs We also thank Robin Rycroft for editorial help S F. de M is the recipient of a research fellowship from the Universitat de Barcelona, E d I P of a research fellowship from the Generalitat de Catalunya and M J of a research fellowship from the Fundació August Pi I Sunyer This work was supported by the Dirección General de Enseñanza Superior e Investigación Científica (PM-97-0111).

REFERENCES

1 Pilkis, S J, Claus, T H, Kurland, I J and Lange, A J (1995) Annu Rev Biochem **64**, 799–835
2 Uyeda, K (1991) CRC Rev. **2**, 445–456
3 Darville, M I, Antoine, I V and Rousseau, G G. (1992) Nucleic Acids Res **20**, 3572–3583
4 Dupriez, V J, Darville, M I, Antoine, I V, Gegonne, A, Ghysdael, J and Rousseau, G G (1993) Proc Natl Acad Sci USA **90**, 8224–8228
5 Darville, M I, Antoine, I V, Mertens-Strijthagen, J R, Dupriez, V J and Rousseau, G G (1995) Oncogene **11**, 1509–1517
6 Joaquin, M, Salvado, C, Bellosillo, B., Lange, A J, Gil, J and Tauler, A (1997) J Biol Chem **272**, 2846–2851
7 Summer, S A, Garza, L A, Zhou, H and Birnbaum, M J (1998) Mol Cell Biol **18**, 5457–5464
8 Ti-Zhi, S, Wang, M, Li-Jyun, S, Saltiel, A R and Oxender, D L (1998) J Biol Chem **273**, 3173–3179
9 Cross, D A E, Alessi, D R, Vandenheede, J R, McDowell, H E, Hundal, H S and Cohen, P (1994) Biochem J **303**, 21–26
10 Yamamoto-Honda, R, Tobe, K, Kaburagi, Y, Ueki, K, Asai, S, Yachi, M, Shirouzu, M., Yodoi, J, Akanuma, Y, Yokoyama, S et al (1995) J Biol Chem **270**, 2729–2734
11 Wang, D and Sul, H S (1998) J Biol. Chem **273**, 25420–25426
12 Sutherland, C, Waltner-Law, M, Gnudi, L, Kahn, B B and Granner, D K (1998) J Biol Chem **273**, 3198–3204
13 Yang, S and Dickson, A J (1995) Biochem J **310**, 375–378
14 Wagle, A, Jivraj, S, Garlock, G L and Stapleton, S R. (1998) J Biol. Chem **273**, 14968–14974
15 Osawa, H, Sutherland, C, Robey, R B, Printz, R L and Granner, D K (1998) J. Biol Chem **271**, 16690–16694
16 Coffer, P J., Jin, J and Woodgett, J R (1998) Biochem J **335**, 1–13
17 Lange, A J, Espinet, C, Hall, R., El-Maghrabi, M R, Vargas, A M, Miksicek, R J, Granner, D K and Pilkis, S J (1992) J Biol Chem **267**, 15673–15680
18 Cichy, S B., Uddin, S, Danilkovich, A, Guo, S, Klippel, A and Unterman, T. G (1998) J. Biol Chem **273**, 6482–6487
19 Kauffmann-Zeh, A, Rodriguez-Viciana, P, Ulrich, E, Gilbert, C, Coffer, P., Downward, J and Evan, G (1997) Nature (London) **385**, 544–548
20 Pullen, N, Dennis, P B, Andjelkovic, M, Dufner, A, Kozma, S. C, Hemmings, B A and Thomas, G (1998) Science **279**, 707–710
21 Ausebel, F M, Brent, R, Kington, R E, Moore, D D, Seidman, J G, Smith J. A and Struhl, K (eds) (1994) Current Protocols in Molecular Biology, John Wiley and Sons, New York
22 Auffray, C and Rougeon, F. (1980) Eur J Biochem **107**, 303–314
23 Tauler, A., Rosenberg, A H., Colosia, A, Studier, W F and Pilkis, S J (1988) Proc Natl. Acad Sci. USA **85**, 6642–6646
24 Bradford, M (1976) Anal Biochem. **112**, 195–203
25 Vlahos, C. J, Matter, W F, Hui, K. Y and Brown, R F (1994) J Biol Chem **269**, 5241–5248
26 Alessi, D R, James, S R, Downes, C P, Holmes, A B, Gaffney, P R., Reese, C B and Cohen, P (1997) Curr Biol **7**, 261–269
27 Chung, J., Grammer, T. C, Lemon, K P, Kazlauskas, A and Blenis, J (1994) Nature (London) **370**, 71–75
28 Isotani, S, Hara, K, Tokunaga, C, Inoue, H, Avruch, J and Yonezawa, K (1999) J. Biol Chem **274**, 34493–34498
29 Frech, M, Andjelkovic, M, Ingley, E, Reddy, K. K, Falck, J R and Hemmings, B A (1997) J. Biol Chem **272**, 8474–8481
30 Wijkander, J, Holst, L S, Rahn, T, Resjo, S, Castan, I, Mandaniello, V, Belfrage, P and Degerman, E (1997) J. Biol Chem **272**, 21520–21526
31 Currie, R A., Walker, K S, Gray, A, Deak, M, Casamayor, A, Downes, C. P, Cohen, P, Alessi, D R and Lucocq, J (1999) Biochem J **337**, 575–583
32 Maier, R, Alessi, D R, Cron, P., Andjelkovic, M and Hemmings, B A (1997) J Biol. Chem **272**, 30491–30497
33 Marte, B M and Downward, J (1997) Trends Biochem Sci **22**, 355–358
34 Beals, C R, Sheridan, C M, Turk, C W, Gardner, P and Crabtree, G (1997) Science **275**, 1930–1933
35 Brennan, P, Babbage, J W., Burgering, B M T, Groner, B, Reif, K and Cantrell, D A (1997) Cell **7**, 679–689
36 Takuwa, N, Fukui, Y and Takuwa, Y (1999) Mol Cell Biol **19**, 1346–1358
37 Huang, C, Wei-ya-ma, H and Dong, Z (1996) Mol Cell Biol **16**, 6427–6435
38 Albanesse, C, Johnson, J, Watanabe, G, Eklund, N., Vu, D, Arnold, A and Pestell, R G (1995) J Biol Chem **270**, 23589–23597
39 Gille, H, Sharrocks, A. D. and Shaw, P (1992) Nature (London) **358**, 414–417
40 Marais, R, Wynne, J and Treisman, R (1993) Cell **73**, 381–393
41 Rodriguez-Viciana, P, Warne, P H, Dhand, B, Vanhaesebroeck, B, Gout, I, Fry, M J, Waterfield, M D. and Downward, J (1994) Nature (London) **370**, 527–532
42 Bondeva, T, Pirola, L, Bulgarelli-Leva, G, Rubio, I, Wetzker, R and Wymann, M P (1998) Science **282**, 293–296

Received 18 October 1999/10 March 2000, accepted 26 April 2000

Biochem J (2000) **349**, 67–75 (Printed in Great Britain)

Identification of a nucleoside/nucleobase transporter from *Plasmodium falciparum*, a novel target for anti-malarial chemotherapy

Marie D. PARKER*, Ralph J. HYDE*, Sylvia Y. M. YAO†, Louisa McROBERT‡, Carol E. CASS§, James D. YOUNG†, Glenn A. McCONKEY‡ and Stephen A. BALDWIN*[1]

*School of Biochemistry and Molecular Biology, University of Leeds, Leeds LS2 9JT, U.K., †Membrane Transport Research Group, Department of Physiology, University of Alberta, Edmonton, Alberta T6G 2H7, Canada, ‡School of Biology, University of Leeds, Leeds LS2 9JT, U.K., and §Membrane Transport Research Group, Department of Oncology, University of Alberta, Edmonton, Alberta T6G 2H7, Canada

Plasmodium, the aetiologic agent of malaria, cannot synthesize purines *de novo*, and hence depends upon salvage from the host. Here we describe the molecular cloning and functional expression in *Xenopus* oocytes of the first purine transporter to be identified in this parasite. This 422-residue protein, which we designate PfENT1, is predicted to contain 11 membrane-spanning segments and is a distantly related member of the widely distributed eukaryotic protein family the equilibrative nucleoside transporters (ENTs). However, it differs profoundly at the sequence and functional levels from its homologous counterparts in the human host. The parasite protein exhibits a broad substrate specificity for natural nucleosides, but transports the purine nucleoside adenosine with a considerably higher apparent affinity (K_m 0.32 ± 0.05 mM) than the pyrimidine nucleoside uridine (K_m 3.5 ± 1.1 mM). It also efficiently transports nucleobases such as adenine (K_m 0.32 ± 0.10 mM) and hypoxanthine (K_m 0.41 ± 0.1 mM), and anti-viral 3′-deoxynucleoside analogues. Moreover, it is not sensitive to classical inhibitors of mammalian ENTs, including NBMPR {6-[(4-nitrobenzyl)thio]-9-β-D-ribofuranosylpurine, or nitrobenzylthioinosine} and the coronary vasoactive drugs, dipyridamole, dilazep and draflazine. These unique properties suggest that PfENT1 might be a viable target for the development of novel anti-malarial drugs.

Key words: adenosine, hypoxanthine, malaria, protozoa, transport.

INTRODUCTION

Malaria, resulting from infection by species of *Plasmodium*, is responsible for the highest mortality of any parasitic disease. This protozoan parasite causes more than 300 million clinical cases per annum, resulting in more than 1.5 million deaths worldwide in tropical and subtropical areas [1], with the species *Plasmodium falciparum* responsible for the majority of deaths. Unfortunately, resistance to existing anti-malarial drugs is spreading rapidly. Consequently in some areas, such as Southeast Asia, treatment options are becoming increasingly limited [2]. The identification of new drug targets is therefore an important goal, and is one of the key objectives of the Malaria Genome Sequencing Project [3].

Unlike many mammalian cells, the intra-erythrocytic stages of *Plasmodium* are incapable of *de novo* synthesis of the purine ring, and so are dependent upon salvage pathways for purine nucleotide synthesis from host precursors. The latter in particular include the nucleoside adenosine and the nucleobase hypoxanthine [4]. Purine transport and metabolism are therefore of key importance as potential targets for the development of new anti-malarial drugs. Several enzymes in the purine salvage pathway have been characterized and their genes cloned, including most recently GMP synthase [5]. However, *Plasmodium* purine transporters have not hitherto been characterized in detail.

In contrast with the dependence on purine salvage, *Plasmodia* rely on *de novo* pyrimidine synthesis and salvage has not been observed. This may be due to either lack of uptake or deficiency of salvage enzymes. Several of the currently used anti-malarial drugs target *de novo* pyrimidine metabolism in *Plasmodium* via effects on the folate pathway or upon the ubiquinone-based electron-transport system [4]. For example, sulfadoxine is an inhibitor of the protozoan dihydropteroate synthase, while pyrimethamine and cycloguanil inhibit dihydrofolate reductase.

In eukaryotes, the cellular uptake of purine nucleosides is brought about by members of the concentrative nucleoside transporter (CNT) and equilibrative nucleoside transporter (ENT) families [6]. The mammalian ENT transporters, which are more widely distributed than the CNT transporters, can be subdivided further into two subclasses on the basis of their sensitivity to the transport inhibitor 6-[(4-nitrobenzyl)thio]-9-β-D-ribofuranosylpurine (nitrobenzylthioinosine, NBMPR) [7,8]. Transporters of the *es* (equilibrative sensitive) subclass are inhibited by nanomolar concentrations of NBMPR (K_i 0.1–10 nM) In contrast, transporters of the *ei* (equilibrative insensitive) subclass are relatively insensitive to NBMPR even at micromolar concentrations. In general, transporters of the *es* type are also inhibited potently by the coronary vasodilators dipyridamole, dilazep and lidoflazine analogues, such as draflazine, whereas *ei*-type transporters are less sensitive to these inhibitors [7,8].

An equilibrative adenosine transporter related to the mammalian ENTs has recently been identified in the protozoan parasite *Toxoplasma gondii* [9]. Members of the ENT family have also been identified in the parasitic kinetoplastid protozoa *Trypanosoma* and *Leishmania*, but in these organisms they appear

---

Abbreviations used: AZT, 3′-azido-3′-deoxythymidine; CCCP, carbonyl cyanide m-chlorophenylhydrazone; CNT, concentrative nucleoside transporter; ddC, 2′,3′-dideoxycytidine; ddI, 2′,3′-dideoxyinosine; *ei*, equilibrative insensitive; ENT, equilibrative nucleoside transporter; hENT, human ENT; PfENT1, *Plasmodium falciparum* ENT 1; *es*, equilibrative sensitive; NBMPR, 6-[(4-nitrobenzyl)thio]-9-β-D-ribofuranosylpurine; TM, transmembrane segment.

[1] To whom correspondence should be addressed (e-mail s.a.baldwin@leeds.ac.uk).

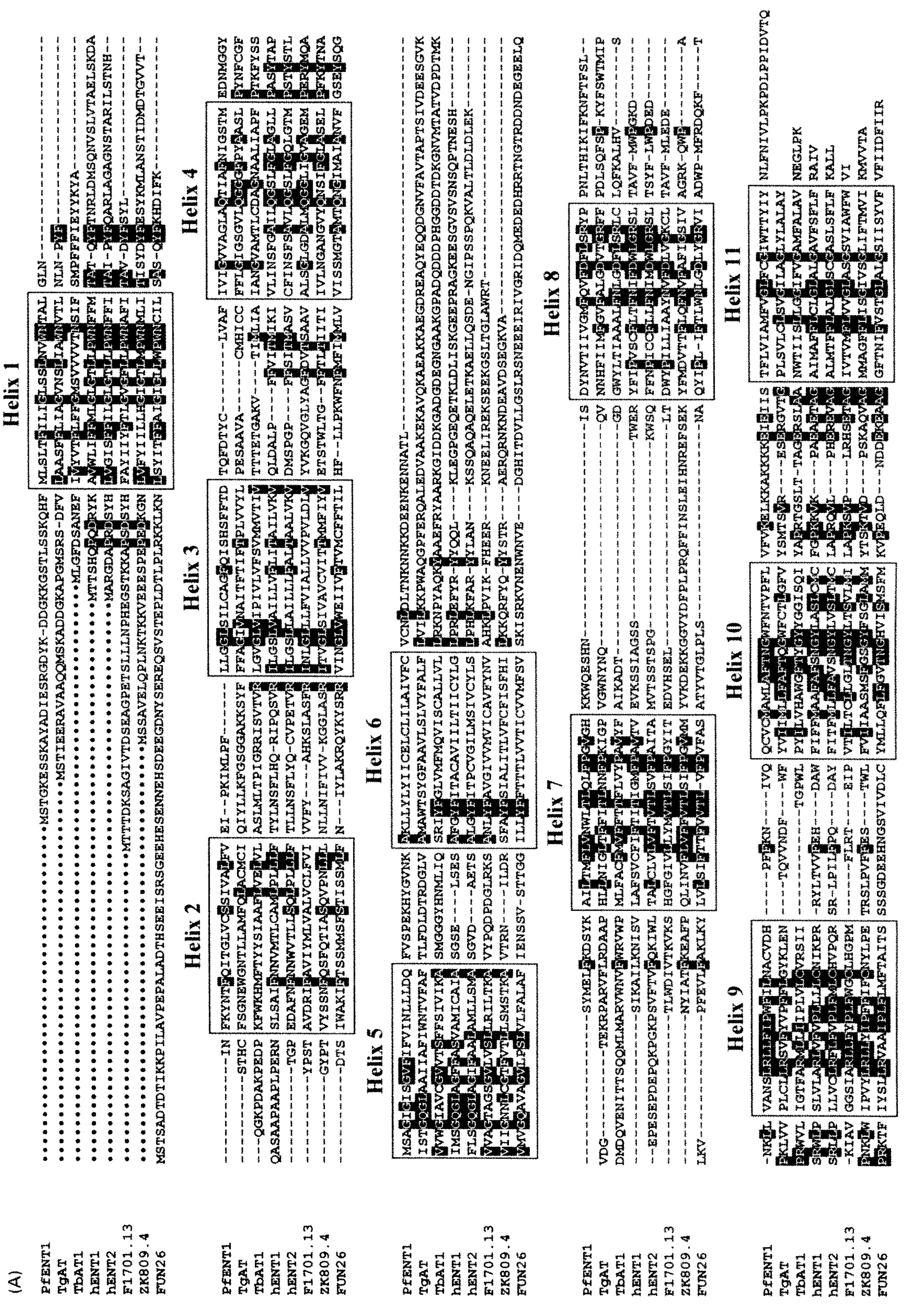

Figure 1 For legend see facing page

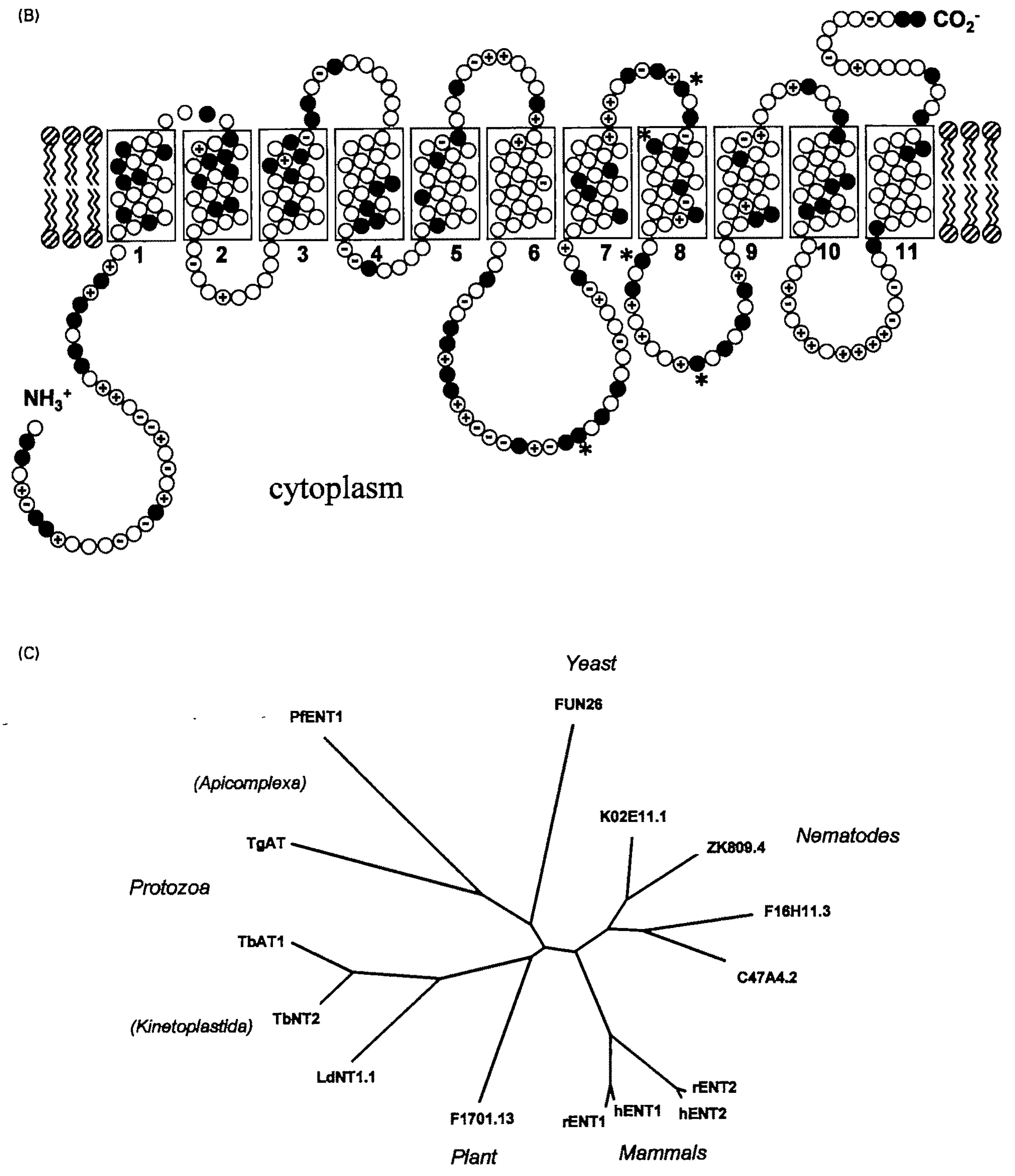

Figure 1 PfENT1 is a member of the ENT family of nucleoside transporters

(**A**) Alignment of the predicted amino acid sequence of PfENT1 with those of nucleoside transporters from *Toxoplasma gondii* (TgAT, GenBank accession no AF061580), *Trypanosoma brucei* (the P2-type transporter TbAT1, AAD45278), *Homo sapiens* (hENT1, AAC51103, and hENT2, AAC39526), *Arabidopsis thaliana* (F1701 13, AAC18807), *Caenorhabditis elegans* (ZK809 4, CAA92642) and *Saccharomcyes cerevisiae* (FUN26, S36712) The positions of putative transmembrane regions are shown by the boxes, and residues identical in four or more of the sequences are indicated by black shading (**B**) Topographical model of PfENT1 Potential membrane-spanning α-helices are numbered and the potential sites of N-glycosylation indicated by asterisks The positions of basic (Arg, Lys, His), acidic (Asp, Glu) and polar but uncharged residues (Ser, Thr, Gln, Asn) are indicated by +, − and ● respectively (**C**) Phylogenetic tree showing relationships between PfENT1 and homologues in other eukaryotes In addition to those detailed in (**A**), these include the rat transporters rENT1 (accession no AAB88049) and rENT2 (AAB88050), the P1-type transporter TbNT2 from *T brucei* (AF153409), the *Leishmania donovani* transporter LdNT1 1 (AF065311) and the putative *C elegans* transporters F16H11 3 (AAA98003), C47A4 2 (accession no for cosmid C47A4 is Z82263) and K02E11 1 (CAB01223) Genetic distances were estimated using the program Protdist (Categories model) and the phylogeny was estimated from the resultant distance matrix using the program Fitch, both programs forming part of the PHYLIP package, version 3 5c [40] to function as active transporters, catalysing the symport of nucleosides (and in some instances also nucleobases) with protons [6,10–13]. Additional transporter families specific for nucleobases have also been characterized by molecular cloning in fungi [14], but representatives of these families have not so far been identified definitively as functional nucleobase transporters in either mammals or protozoa.

In the *Plasmodium*-infected erythrocyte, the permeability of the host cell membrane to purine nucleosides and other organic solutes is markedly increased via the induction of a non-saturable permeation pathway, which has been the subject of intensive investigation [15]. Much less is known about the transport characteristics of the parasite plasma membrane itself. However, expression of mRNA from the asexual stages of *P. falciparum* in *Xenopus* oocytes has provided evidence that the parasite genome encodes nucleoside, nucleobase, monocarboxylate and hexose transporters [16], and an example of the last has recently been cloned [17]. In the present work, we have exploited the public availability of sequence information from the Malaria Genome Sequencing Project to clone, express and characterize a novel nucleoside/nucleobase transporter from *P. falciparum*. It may be possible to exploit the functional characteristics of this protein, which differ substantially from those of its mammalian counterparts, for the development of new anti-malarial drugs.

MATERIALS AND METHODS

DNA cloning and analysis

The coding region of the predicted *PfENT1* gene (coding for the *P. falciparum* ENT 1 protein) was amplified by PCR from *P. falciparum* (strain 3D7) genomic DNA using *Pwo* polymerase and primers PLFA1 (5′-CGAGGATCCAAAAATGAGTACCGGTAAAGAGTC-3′) and PLFA2 (5′-CGAGAATTCTTATTGTGTTACATCGATGGGTGG-3′), corresponding to the 5′ and 3′ ends of the region respectively. Reactions were cycled with the following parameters: 96 °C for 5 min; 96 °C for 30 s, 60 °C for 30 s, 68 °C for 3 min for 25 cycles; 68 °C for 3 min. The resultant ≈ 1.3-kb fragment was subcloned into the *Xenopus* expression vector pGEM-HE [18] using *Bam*HI and *Eco*RI restriction sites (underlined above) incorporated into the 5′ ends of PLFA1 and PLFA2 respectively to yield the construct pGEMHE-PfENT1. The entire coding region of the insert was sequenced at least once on both strands by *Taq* DyeDeoxy terminator cycle sequencing using an Applied Biosystems model 373A sequencer.

Gene organization and expression

P. falciparum (strain 3D7) was maintained in culture with human erythrocytes (5 % haematocrit) in RPMI 1640 (Life Technologies) supplemented with Hepes, sodium bicarbonate and human serum (10 %) under standard conditions [19,20]. Genomic DNA was isolated using a standard protocol from saponin-lysed infected erythrocytes [21]. For Southern blotting, samples of genomic DNA (10 μg) were digested with 30 units of the appropriate restriction enzyme and blots were hybridized, using standard protocols [21], with a probe corresponding to the coding region of the *PfENT1* gene. The [α-^{32}P]dCTP-labelled probe was prepared by random priming using the RTS RadPrime DNA Labelling System (Life Technologies). For reverse-transcriptase PCR, *Plasmodium* RNA isolation and first-strand cDNA synthesis using either random hexamers or oligo(dT) was performed as described previously [22]. PCR amplification of PfENT1 cDNA (20 ng) was then performed using *Pwo* polymerase, the primers PLFA1 and PLFA2 and the cycling parameters described above.

Xenopus expression and nucleoside/nucleobase-uptake assays

Plasmid pGEMHE-PfENT1 was linearized with *Nhe*I and transcribed with T7 polymerase in the presence of ^{m7}GpppG cap using the mMESSAGE MACHINE® (Ambion) transcription system. Remaining template was removed by digestion with RNase-free DNase 1. Oocytes were treated with collagenase to remove follicular layers [23] and then injected with 23 nl of water alone or with 23 nl of water containing 1 mg/ml PfENT1 RNA transcript. Injected oocytes were maintained for 2 days in modified Barth's medium containing 5 % horse serum, and then uptake of radiolabelled nucleoside and nucleobase compounds was measured {[5,6-^{3}H]uridine and [2,8-^{3}H]adenosine were from NEN® Life Science Products, Hounslow, Middx., U.K., [8-^{14}C]adenine and [2-^{14}C]uracil were from ICN Pharmaceuticals, Basingstoke, Hants., U.K.; [^{3}H]gemcitabine (2′,2′-difluoro-2′-deoxycytidine) was from Eli Lilley and Co., Indianapolis, IN, U.S.A.; all other compounds, Amersham, Arlington Heights, IL, U.S.A. or Moravek, Brea, CA, U.S.A.}.

Uptake assays were performed at 20 °C on groups of 10–12 oocytes in transport buffer (0.2 ml) containing 100 mM NaCl (or 100 mM choline chloride) and 2 mM KCl, 1 mM $CaCl_2$, 1 mM $MgCl_2$ and 10 mM Hepes, pH 7.5. In adenosine-uptake experiments, the transport buffer contained 1 μM deoxycoformycin to inhibit adenosine deaminase activity. For experiments involving NBMPR, dilazep, dipyridamole and draflazine, oocytes were preincubated for 1 h with inhibitor before the addition of permeant. At the end of the uptake period, extracellular label was removed by six rapid washes with ice-cold transport buffer. Individual oocytes were dissolved in 5 % (w/v) SDS for quantification of radioactivity by liquid-scintillation counting. The influx values reported represent the means ± S.E.M. for 8–10 oocytes. Each experiment was performed at least twice on different batches of oocytes, with similar results, and a representative example is illustrated. Apparent K_m and V_{max} values for substrate influx were determined by non-linear regression analysis (FigP, Elsevier-Biosoft).

RESULTS

Cloning of a *Plasmodium* ENT homologue

Nucleoside transporters do not appear to be encoded by any of the genes present in *P. falciparum* chromosomes 2 and 3, the complete nucleotide sequences of which have been published [24,25]. We therefore used the on-site BLAST server at the Sanger Centre, Cambridge, U.K., to search the unfinished sequence data arising from the Malaria Genome Sequencing Project (http://www.sanger.ac.uk/Projects/P_falciparum/) for sequences homologous to the ENT or CNT families. This approach led to the identification of fragments encoding a putative ENT homologue in the shotgun-read sequence database for chromosome 13. By searching the database for overlapping fragments it proved possible to assemble the complete coding region of a putative nucleoside-transporter gene. PCR was used to amplify the corresponding region from genomic DNA of *P. falciparum* clonal strain 3D7, yielding a fragment of apparent size ≈ 1.3 kb. Following its subcloning into the vector pGEM-HE [18], the complete nucleotide sequence of the fragment was determined (GenBank accession no. AF221844) and found to be identical to that assembled from the chromosome 13 shotgun-read sequence database.

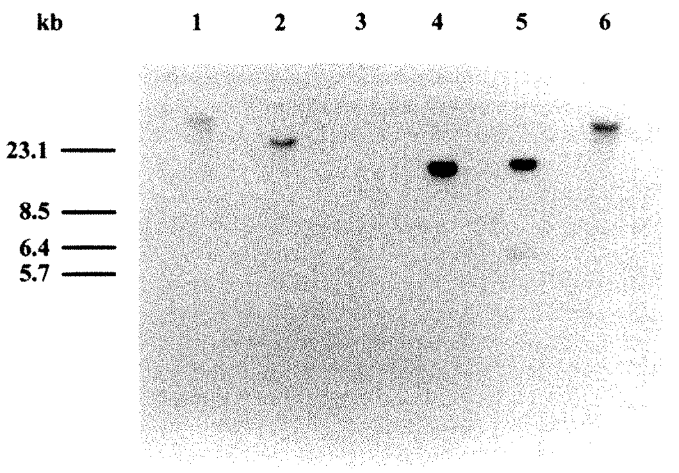

Figure 2 Southern blot of *PfENT1* in genomic DNA

P. falciparum genomic DNA (10 μg) was digested with *Eco*RI (lane 1), *Hin*dIII (lane 2), *Dra*I (lane 3), *Xba*I (lane 4), *Eco*RV (lane 5) and *Kpn*I (lane 6), and blots were hybridized with a ^{32}P-labelled probe corresponding to the coding region of *PfENT1*. The mobilities of standards of known size (kb) are indicated on the left.

In order to examine the structure of the gene encoding the transporter, which we have designated PfENT1, reverse-transcriptase PCR was used to analyse mRNA obtained from the asexual blood stages of *P. falciparum*. Amplification of cDNA, prepared by reverse transcription using either oligo(dT) or random hexamer oligonucleotides, with primers corresponding to the 5′ and 3′ ends of the predicted coding region (PLFA1 and PLFA2 respectively), yielded a product of ≈ 1.3 kb, identical with that obtained by amplification of genomic DNA (results not shown). This finding confirmed the predicted absence of introns in the *PfENT1* gene, and indicated that the gene is expressed during the intra-erythrocytic stage of the *Plasmodium* life cycle.

The *PfENT1* gene contains a 1266-bp open reading frame encoding a 422-residue protein, PfENT1, of predicted M_r 47631 (Figure 1A). PfENT1 is predicted by the hidden Markov model procedure of Sonnhammer et al. [26] to possess 11 transmembrane (TM) segments, with the hydrophilic N-terminal region of the protein and a hydrophilic central loop being cytoplasmic (Figure 1B). While two of the five potential N-glycosylation sites in the sequence are predicted to lie on the exofacial surface of the membrane, their proximity to the start of putative TM8 suggests that they are unlikely to be glycosylated *in vivo*. The presence of characteristically conserved sequence motifs, especially in the putative membrane-spanning segments (Figure 1A), confirms that PfENT1 is a distantly related member of the ENT family of equilibrative nucleoside transporters (Figure 1C), despite sharing only about 18 % amino acid sequence identity with known mammalian, nematode, yeast and protozoan nucleoside transporters. Striking differences between PfENT1 and most of the other family members are the relative shortness of the putative extramembranous regions connecting TM1 and TM2 [4 residues compared with 41 in human ENT (hENT) 1] and TM6 and TM7 (35 residues compared with 66 residues in hENT1).

In the genomes of mammals, nematodes and kinetoplastid protozoa, families containing two or more related ENT genes have been identified [6,10–12]. In order to establish whether a similar situation exists in *Plasmodium*, Southern blots of *P. falciparum* genomic DNA were hybridized with a probe corresponding to the coding region of *PfENT1*. Even at low stringency the restriction digests, with the exception of *Eco*RV, which cleaves within the gene (and *Dra*I, which generates fragments too small to be detected), yielded a single band (Figure

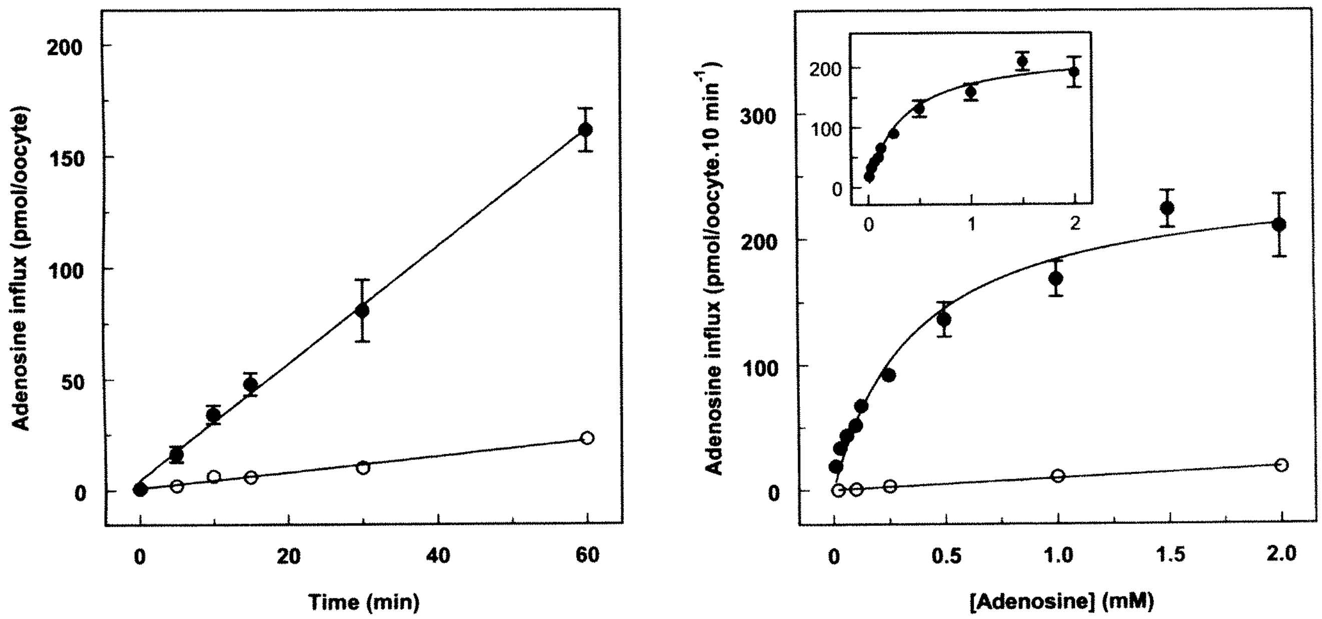

Figure 3 Functional expression of PfENT1 in *Xenopus* oocytes

(Left-hand panel) Time course for uptake of 0.1 mM [^{3}H]adenosine in oocytes injected with water alone (○) or water containing 23 ng of PfENT1 transcript (●). (Right-hand panel) Concentration dependence of [^{3}H]adenosine uptake by oocytes injected with water alone (○) or water containing PfENT1 transcript (●). Inset, mediated transport (influx of adenosine in RNA-injected oocytes minus that in water-injected oocytes).

2). This finding suggests that *PfENT1* is the sole representative of the ENT gene family in *Plasmodium*.

Functional characterization of PfENT1

To investigate functional properties, PfENT1 recombinant protein was expressed in *Xenopus* oocytes, which lack endogenous nucleoside-transport activity [27]. The rate of adenosine uptake was measured for comparison with mammalian homologues As shown in Figure 3 (left-hand panel), the initial rate of uptake of the purine nucleoside [^{3}H]adenosine (0.1 mM, 20 °C) was much greater in oocytes injected with PfENT1 RNA transcripts than in oocytes injected with water. Uptake of adenosine (and of the other nucleosides described below) was essentially linear for 1 h, and so in subsequent experiments uptake periods of either 30 min (for assessment of substrate specificity) or of 10 min (for measurement of kinetic parameters) were employed in order to approximate initial rates of transport. PfENT1-mediated influx of the purine nucleoside adenosine, defined as the difference in uptake between RNA-injected and water-injected oocytes, was saturable and conformed to simple Michaelis–Menten kinetics (Figure 3, right-hand panel). The apparent K_m value for adenosine (0.32 ± 0 05 mM) was somewhat greater than values reported previously for mammalian cells (0.05–0.15 mM) [28]. PfENT1 also mediated the uptake of the pyrimidine nucleoside uridine. Interestingly, whereas the V_{max} value for uridine uptake was somewhat greater than that for adenosine (358 ± 38 and 228 ± 13 pmol/oocyte/10 min, respectively), the apparent affinity for the pyrimidine nucleoside was considerably lower, the measured K_m for uridine uptake (3.5 ± 1.1 mM) being 10-fold greater than for adenosine (results not shown).

Substrate selectivity of PfENT1

The substrate selectivity of PfENT1 was examined further by direct measurements of the mediated influx of a range of natural nucleosides and nucleobases, which were tested at a concentration of 0.1 mM. Figure 4 (top panel) shows that, like its mammalian counterparts [6], PfENT1 exhibits a broad substrate specificity for purine and pyrimidine nucleosides, with the exception of cytidine, which is poorly transported. Cytidine has also been shown to be a relatively poor competitive inhibitor of rat ENT 2 (rENT2)-mediated uridine transport [29]. Surprisingly, PfENT1 was in addition found to transport a wide range of purine and pyrimidine nucleobases, including cytosine (Figure 4, top panel). In order to characterize this nucleobase-transport activity in more detail, the concentration dependence of PfENT1-mediated adenine transport was compared with that of the corresponding nucleoside, adenosine. As illustrated in Figure 4 (middle panel), mediated uptake of adenine was saturable, and the apparent K_m for the uptake process (0.32 ± 0.10 mM) was essentially identical with that for adenosine. The rates of adenine and adenosine uptake at a substrate concentration of 0.1 mM, measured using a single batch of oocytes, were also similar (Figure 4, top panel), suggesting that the turnover numbers for transport of the nucleobase and nucleoside are comparable. PfENT1-mediated uptake of the physiologically important nucleobase hypoxanthine was also found to be saturable (results not shown), and the apparent K_m for the uptake process (K_m 0.41 ± 0.1 mM) was similar to that for adenine. These properties of PfENT1 contrast with those of its mammalian homologues: the human erythrocyte transporter hENT1 does not transport nucleobases, and whereas the *ei*-type transporter hENT2 is capable of transporting hypoxanthine and other nucleobases, it exhibits generally lower apparent affinities for these substrates than for the corresponding nucleosides (S. Y. M. Yao, C. E. Cass, S A. Baldwin and J. D Young, unpublished work).

In addition to transporting natural nucleosides, the mammalian *es*-type transporters catalyse the cellular uptake of nucleoside analogues used in cancer chemotherapy. These include the purine nucleoside drugs fludarabine (9-β-D-arabinosyl-2-fluoroadenine) and cladribine (2-chloro-2′-deoxyadenosine) and the pyrimidine nucleoside drug gemcitabine (2′,2′-difluoro-2′-deoxycytidine) [6,30]. PfENT1 resembles the mammalian transporters in its ability to transport these anti-cancer nucleoside drugs, with an efficiency similar to that for uridine (Figure 4, bottom panel). However, unlike the mammalian transporters, it also efficiently transports the anti-viral nucleoside analogues 3′-azido-3′-deoxythymidine (AZT), 2′,3′-dideoxycytidine (ddC) and 2′,3′-dideoxyinosine (ddI) (Figure 4, bottom panel). These drugs have been reported to be very poor or negligible substrates for the mammalian *es*-type ENTs [31–35].

Cation-dependence and inhibitor-sensitivity of PfENT1

Whereas the mammalian members of the ENT family function as passive, facilitated diffusion systems, those homologues that have been cloned from the protozoan parasites *Leishmania* and *Trypanosoma* appear to act as proton symporters [10–13]. Members of the CNT family of nucleoside transporters also catalyse the symport of nucleosides with cations, these being sodium ions in the case of the mammalian transporters and protons in the case of the bacterial transporters [6]. Inwardly directed concentration gradients for both protons and sodium ions have been measured across the intra-erythrocytic *Plasmodium* plasma membrane [15], and could potentially provide a driving force for nucleoside uptake via PfENT1. To investigate this possibility, initial rates of adenosine uptake by oocytes expressing the transporter were measured in sodium-containing buffer at different pH values in the range 5.5–8.5, and also in a buffer in which sodium ions had been replaced by choline There was no significant effect of pH or of replacement of sodium ions on transport activity (Figure 5) The inclusion in the transport buffer of the uncoupler carbonyl cyanide *m*-chlorophenylhydrazone (CCCP) at a concentration of 10 μM likewise had only a slight inhibitory effect. These findings indicate that transport is not cation-dependent, and that PfENT1 is therefore unlikely to function as a symporter.

The archetypal members of the ENT transporter family in mammals are potently inhibited by a range of nucleoside analogues and other inhibitors [6]. In particular, the *es*-type transporter hENT1 of the human erythrocyte, which harbours the bloodstream form of *Plasmodium*, is very sensitive to inhibition by the thiopurine ribonucleoside NBMPR, and by the coronary vasodilators dipyridamole, dilazep and draflazine. These agents exhibit apparent K_i values for inhibition of transport in the range 0.1–10 nM [8], hence there is essentially complete inhibition at concentrations of 1 μM or above. At this concentration, none of these inhibitors had any effect on PfENT1-mediated uridine or adenosine transport (results not shown). Even when used at 10 μM, no significant inhibition of adenosine transport was observable (results not shown).

DISCUSSION

Using information from the Malaria Genome Sequencing Project, we have identified, expressed and characterized a gene encoding a novel member of the ENT family of nucleoside transporters from *P. falciparum* and the first nucleoside transporter identified in *Plasmodium*. The transporter is expressed during the asexual stages of the *Plasmodium* life cycle and catalyses the saturable uptake of nucleosides and nucleobases, as assayed by expression in *Xenopus* oocytes (Figures 3 and 4). In this respect it is completely distinct from the non-saturable permeability pathway for nucleosides induced in the infected erythrocyte plasma membrane [15]. Instead, it is likely to represent the means of nucleoside and nucleobase uptake across the parasite plasma membrane itself. Although definitive evidence will require completion of the *Plasmodium* genome sequencing project, Southern-blotting experiments suggest that PfENT1 is the sole representative of the ENT family in the parasite. This situation contrasts with that of kinetoplastid protozoa, where families of related ENT-type transporter genes have been identified [10,12]. Our failure to detect homologues of other nucleoside and nucleobase transporter families by searching the unfinished sequence data available from the Malaria Genome Sequencing Project suggests that PfENT1 may be the sole route by which the parasite takes up nucleosides and nucleobases. As purine salvage is essential in parasitic protozoa, this transporter therefore represents a potential target for therapeutic drugs. This hypothesis of a single route for nucleobase and nucleoside uptake is strengthened by previous observations that uptake of the nucleoside adenosine into oocytes injected with total mRNA isolated from *P. falciparum* can be inhibited almost completely by the presence of the nucleobase hypoxanthine [16].

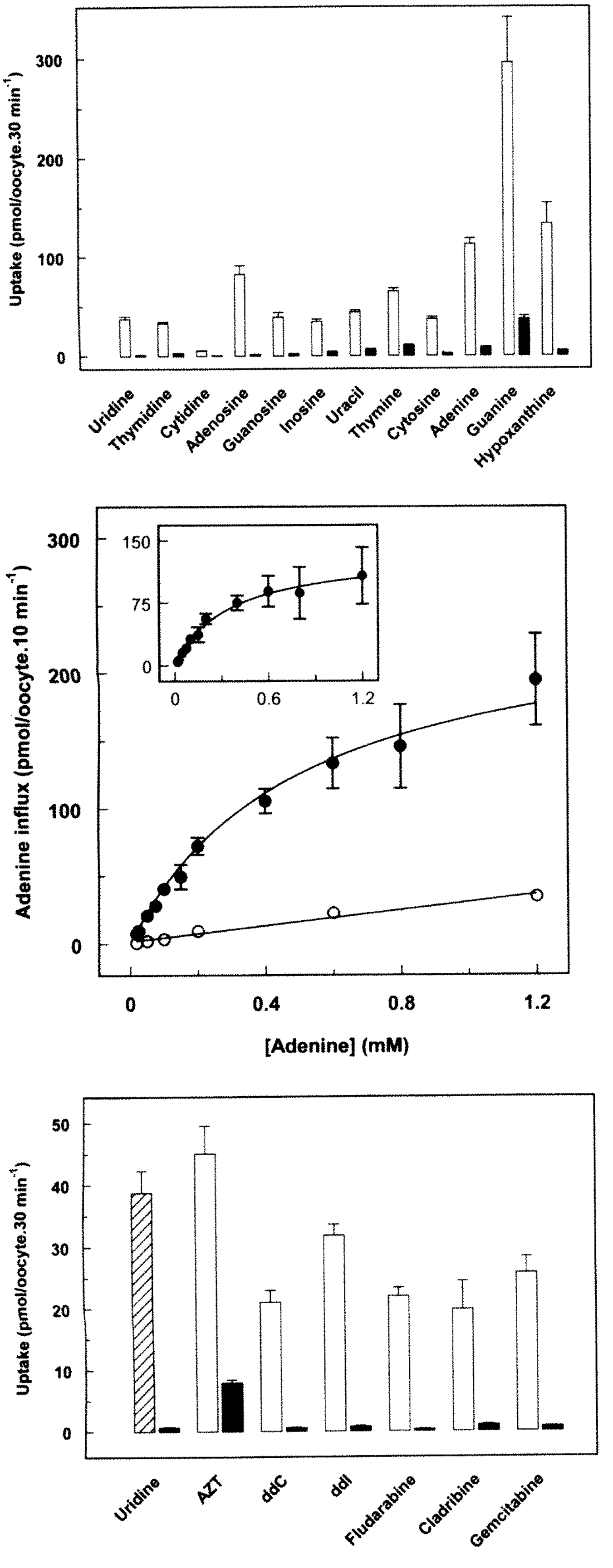

Figure 4 Substrate specificity of PfENT1

(Top panel) Influxes of radiolabelled nucleosides and nucleobases at concentrations of 0.1 mM were measured in oocytes injected with water alone (black bars) or with water containing PfENT1 RNA transcript (white bars). (Middle panel) Concentration dependence of [^{14}C]adenine uptake by oocytes injected with water alone (○) or water containing PfENT1 transcript (●). Inset, mediated transport. (Bottom panel) Influxes of radiolabelled uridine and of chemotherapeutic nucleoside analogues at a concentration of 0.1 mM were measured in oocytes injected with water alone (black bars) or with water containing PfENT1 RNA transcript (hatched and white bars).

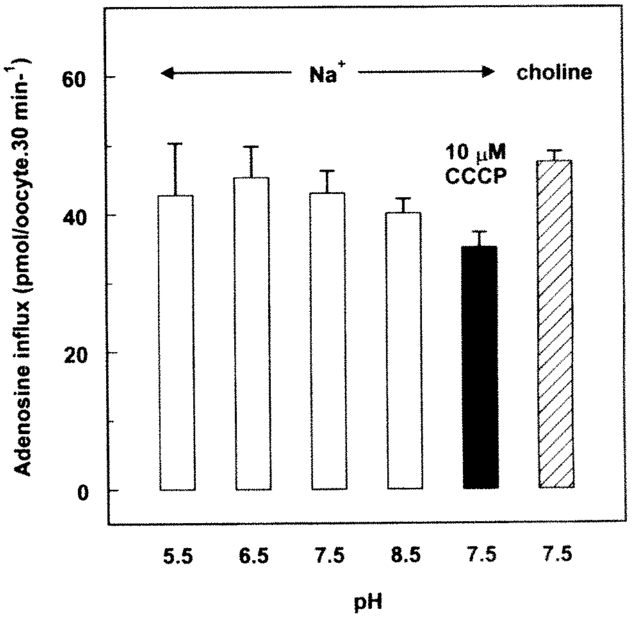

Figure 5 Cation-dependence of PfENT1

Influx of [^{3}H]adenosine (0.1 mM, 30 min) into oocytes injected with water alone or with water containing PfENT1 RNA transcript was measured in transport buffer containing 100 mM choline chloride (hatched bar) or 100 mM NaCl (white and black bars) in the presence (black bar) or absence of 10 μM CCCP at the pH values indicated. Mediated uptake was calculated as influx in RNA-transcript-injected oocytes minus influx in water-injected oocytes.

In order to exploit a parasite protein as a target for chemotherapy, it is essential that it differs functionally from analogous proteins in the host. PfENT1 differs profoundly from mammalian ENT transporters in several respects. For example, it is able to transport the anti-viral 3′-deoxynucleoside analogues ddI, ddC and AZT, the last with an efficiency equivalent to uridine. In contrast, the mammalian ENT-type transporters transport these drugs poorly (hENT2) or not at all (hENT1), probably because a ribose 3′-hydroxyl group is important for substrate recognition [36]. Moreover, unlike the mammalian transporters, which exhibit approximately equal affinities for natural purine and pyrimidine nucleosides, PfENT1 appears to be somewhat purine-selective, transporting adenosine with a 10-fold higher apparent affinity than uridine. This poor ability to transport uridine is not unexpected, given the fact that *P. falciparum* has the capacity to synthesize pyrimidines *de novo* and, with the exception of orotic acid, does not incorporate exogenous pyrimidines into nucleic acids [4] (G. A. McConkey, unpublished work). Nonetheless, the present study suggests that lack of pyrimidine salvage is not due to an inability to take up pyrimidines, but rather to the absence of salvaging enzymes. PfENT1 resembles its host counterparts in being a relatively low-affinity facilitated-diffusion system, rather than a high-affinity proton symporter like its homologues described in kinetoplastid protozoans [6,10–13]. These properties may reflect the relative abundance of host-derived purines available to *Plasmodium* from the erythrocyte.

Whereas the precise identity of the purines used by the parasite *in vivo* remains unclear, it is likely that hypoxanthine resulting from catabolism of erythrocyte ATP supplies at least a part of its requirements, and several reports show that this nucleobase enhances the growth of the organism in culture [4] The ability of PfENT1 to transport nucleobases, in particular hypoxanthine, but also adenine and guanine, is therefore likely to be of physiological importance. This ability represents another key difference between the parasite transporter and its mammalian counterparts: mammalian ENT transporters appear not to transport nucleobases [6], with the exception of hENT2, where hypoxanthine acts as an inhibitor of uridine transport [37] and is itself transported with low affinity (S. Y. M Yao, C. E. Cass, S. A. Baldwin and J D. Young, unpublished work; hypoxanthine transport via an *ei*-type transport process has also been described in human vascular endothelial cells, although the molecular identity of the nucleoside transporter responsible for this activity remains unknown [38]). Functionally, the similar affinities of adenine and adenosine suggest that the base may play the major role in substrate recognition by PfENT1, unlike the situation with the mammalian transporters.

In addition to differences in substrate specificity, PfENT1 differs from its mammalian homologues in its lack of sensitivity to classical inhibitors of nucleoside transport, such as NBMPR and coronary vasodilators. This finding suggests that it may be possible to develop inhibitors specific for the parasite transporter for use in anti-malarial chemotherapy. The reliance of the organism on purine salvage, and the fact that PfENT1 may be the major if not the sole route for purine entry into the asexual stages of the parasite, suggest that the transporter may be a worthwhile chemotherapeutic target. Alternatively, it may be possible to exploit the ability of PfENT1 to transport cytotoxic 3′-deoxynucleoside analogues that are poor substrates for the mammalian transporters. Whereas the permeability of the infected erythrocyte to such agents has not yet been tested specifically, the reported properties of the non-saturable permeation pathway induced in the host cell membrane [15] suggest that the analogues would have enhanced access to the parasite transporter. In contrast, normal host cells would be protected by the barrier to drug transport posed by the permeability properties of hENT1 and hENT2. Finally, it may be possible to potentiate the cytotoxicity of nucleoside analogues towards the parasite by using inhibitors specific for the mammalian transporters, such as lidoflazine analogues, to reversibly prevent the entry of nucleoside analogues into host cells. The feasibility of such an approach has already been explored in murine schistosomiasis, where host toxicity of the adenosine analogue tubercidin was ameliorated by co-administration of a prodrug form of NBMPR [39].

Note added in proof (received 24 May 2000)

After submission of this manuscript, a paper was published describing the cloning and characterisation of a nucleoside transporter designated pfNT1 from the W2 strain of *Plasmodium falciparum* [41]. The predicted amino acid sequences of PfNT1 and the protein encoded by strain 3D7, which we have designated PfENT1, are identical except for position 385, which contains Phe and Leu respectively. However, the reported substrate- and inhibitor-specifities of pfNT1 differ extensively from those described in the present paper. We are unsure of the origin of these differences, but results described in the present paper, namely the relatively low affinity of PfENT1 for adenosine, its ability to transport nucleobases and its insensitivity to inhibition by dipyridamole, were reproducibly and independently obtained in experiments performed in our laboratories both in Leeds and in Edmonton.

Supported by the Biotechnology and Biological Sciences Research Council, U K (studentships to M D P and L M), the Wellcome Trust, U K , the Medical Research Council, U.K., the Medical Research Council of Canada, the Alberta Cancer Board and the World Health Organization. J.D.Y is a Heritage Medical Scientist of the Alberta Heritage Foundation for Medical Research We thank Dr E R Liman for the gift of the expression vector pGEM-HE. Sequence data for *P falciparum* chromosome 13 was obtained from the Sanger Centre website at http //www sanger/ac/uk/Projects/P_falciparum/. Sequencing of *P. falciparum* chromosome 13 was accomplished as part of the Malaria Genome Project with support by the Wellcome Trust

REFERENCES

1 Trigg, P I and Kondrachine, A. V (1998) The current global malaria situation In Malaria Parasite Biology, Pathogenesis and Protection (Sherman, I W , ed), pp 11–22, ASM Press, Washington DC

2 White, N J (1996) The treatment of malaria N Engl J Med **335**, 800–806

3 Wirth, D (1998) Malaria a 21st century solution for an ancient disease Nat Med **4**, 1360–1362

4 Sherman, I W (1998) Purine and pyrimidine metabolism of asexual stages, in Malaria Parasite Biology, Pathogenesis and Protection (Sherman, I W , ed), pp 177–184, ASM Press, Washington DC

5 McConkey, G A (2000) *Plasmodium falciparum* isolation and characterisation of a gene encoding protozoan GMP synthase Exp Parasitol **94**, 23–32

6 Baldwin, S A , Mackey, J R , Cass, C E and Young, J D (1999) Nucleoside transporters molecular biology and implications for therapeutic development. Mol. Med Today **5**, 216–224

7 Cass, C E , Young, J D , Baldwin, S A , Cabrita, M A , Graham, K A , Griffiths, M , Jennings, M L, Mackey, J R., Ng, A M L , Ritzel, M W L , Vickers, M F and Yao, S Y M (1999) Nucleoside transporters of mammalian cells In Membrane Transporters as Drug Targets (Amidon, G L and Sadée, W., eds), pp 313–352, Plenum Publishing, New York

8 Griffith, D A and Jarvis, S. M (1996) Nucleoside and nucleobase transport systems of mammalian cells Biochim. Biophys Acta **1286**, 153–181

9 Chiang, C-W , Carter, N , Sullivan, W J , Donald, R G K , Roos, D. S , Naguib, F N M , el Kouni, M H , Ullman, B and Wilson, C M (1999) The adenosine transporter of *Toxoplasma gondii* identification by insertional mutagenesis, cloning and recombinant expression J Biol Chem **274**, 35255–35261

10 Sanchez, M. A , Ullman, B , Landfear, S M and Carter, N S (1999) Cloning and functional expression of a gene encoding a P1 type nucleoside transporter from *Trypanosoma brucei* J Biol. Chem **274**, 30244–30249

11 Maser, P , Sutterlin, C , Kralli, A and Kaminsky, R (1999) A nucleoside transporter from *Trypanosoma brucei* involved in drug resistance Science **285**, 242–244

12 Vasudevan, G., Carter, N. S., Drew, M. E., Beverley, S. M., Sanchez, M. A., Seyfang, A., Ullman, B. and Landfear, S. M. (1998) Cloning of *Leishmania* nucleoside transporter genes by rescue of a transport-deficient mutant. Proc. Natl. Acad. Sci. U.S.A. **95**, 9873–9878

13 De Koning, H. P., Watson, C. J. and Jarvis, S. M. (1998) Characterization of a nucleoside/proton symporter in procyclic *Trypanosoma brucei brucei*. J. Biol. Chem. **273**, 9486–9494

14 Diallinas, G., Gorfinkiel, L., Arst, H. N., Cecchetto, G. and Scazzocchio, C. (1995) Genetic and molecular characterization of a gene encoding a wide specificity purine permease of *Aspergillus nidulans* reveals a novel family of transporters conserved in prokaryotes and eukaryotes. J. Biol. Chem. **270**, 8610–8622

15 Ginsburg, H. and Kirk, K. (1998) Membrane transport in the malaria-infected erythrocyte. In Malaria: Parasite Biology, Pathogenesis and Protection (Sherman, I. W., ed.), pp. 219–232, ASM Press, Washington DC

16 Penny, J. I., Hall, S. T., Woodrow, C. J., Cowan, G. M., Gero, A. M. and Krishna, S. (1998) Expression of substrate-specific transporters encoded by *Plasmodium falciparum* in *Xenopus laevis* oocytes. Mol. Biochem. Parasitol. **93**, 81–89

17 Woodrow, C. J., Penny, J. I. and Krishna, S. (1999) Intraerythrocytic *Plasmodium falciparum* expresses a high affinity facilitative hexose transporter. J. Biol. Chem. **274**, 7272–7277

18 Liman, E. R., Tytgat, J. and Hess, P. (1992) Subunit stoichiometry of a mammalian K^+ channel determined by construction of multimeric cDNAs. Neuron **9**, 861–871

19 Trager, W. and Jensen, J. B. (1976) Human malaria parasites in continuous culture. Science **193**, 673–675

20 Trager, W. (1994) Cultivation of malaria parasites. Methods Cell. Biol. **45**, 7–26

21 Sambrook, J., Fritsch, E. F. and Maniatis, T. (1989) Molecular Cloning: a Laboratory Manual, 2nd edn., Cold Spring Harbor Press, Cold Spring Harbor

22 McConkey, G. A., Rogers, M. J. and McCutchan, T. F. (1997) Inhibition of *Plasmodium falciparum* protein synthesis. Targeting the plastid-like organelle with thiostrepton. J. Biol. Chem. **272**, 2046–2049

23 Huang, Q. Q., Harvey, C. M., Paterson, A. R., Cass, C. E. and Young, J. D. (1993) Functional expression of Na^+-dependent nucleoside transport systems of rat intestine in isolated oocytes of *Xenopus laevis*. Demonstration that rat jejunum expresses the purine-selective system N1 (*cif*) and a second, novel system N3 having broad specificity for purine and pyrimidine nucleosides. J. Biol. Chem. **268**, 20613–20619

24 Gardner, M. J., Tettelin, H., Carucci, D. J., Cummings, L. M., Aravind, L., Koonin, E. V., Shallom, S., Mason, T., Yu, K., Fujii, C. et al. (1998) Chromosome 2 sequence of the human malaria parasite *Plasmodium falciparum*. Science **282**, 1126–1132

25 Bowman, S., Lawson, D., Basham, D., Brown, D., Chillingworth, T., Churcher, C. M., Craig, A., Davies, R. M., Devlin, K., Feltwell, T. et al. (1999) The complete nucleotide sequence of chromosome 3 of *Plasmodium falciparum*. Nature (London) **400**, 532–538

26 Sonnhammer, E. L. L., von Heijne, G. and Krogh, A. (1998) A hidden Markov model for predicting transmembrane helices in protein sequences. In Proceedings of the Sixth International Conference on Intelligent Systems for Molecular Biology (Glasgow, J., Littlejohn, T., Major, F., Lathrop, R., Sankoff, D. and Sensen, C., eds.), pp. 175–182, AAAI Press, Menlo Park, CA

27 Huang, Q.-Q., Yao, S. Y. M., Ritzel, M. W. L., Paterson, A. R. P., Cass, C. E. and Young, J. D. (1994) Cloning and functional expression of a complementary DNA encoding a mammalian nucleoside transport protein. J. Biol. Chem. **269**, 17757–17760

28 Plagemann, P. G., Wohlhueter, R. M. and Woffendin, C. (1988) Nucleoside and nucleobase transport in animal cells. Biochim. Biophys. Acta **947**, 405–443

29 Yao, S. Y. M., Ng, A. L., Muzyka, W. R., Griffiths, M., Cass, C. E., Baldwin, S. A. and Young, J. D. (1997) Molecular cloning and functional characterization of nitrobenzylthioinosine (NBMPR)-sensitive (*es*) and NBMPR-insensitive (*ei*) equilibrative nucleoside transporter proteins (rENT1 and rENT2) from rat tissues. J. Biol. Chem. **272**, 28423–28430

30 Mackey, J. R., Baldwin, S. A., Young, J. D. and Cass, C. E. (1998) Nucleoside transport and its significance for anticancer drug resistance. Drug Resist. Updates **1**, 310–324

31 Zimmerman, T. P., Mahony, W. B. and Prus, K. L. (1987) 3′-Azido-3′-deoxythymidine. An unusual nucleoside analogue that permeates the membrane of human erythrocytes and lymphocytes by nonfacilitated diffusion. J. Biol. Chem. **262**, 5748–5754

32 Ullman, B., Coons, T., Rockwell, S. and McCartan, K. (1988) Genetic analysis of 2′,3′-dideoxycytidine incorporation into cultured human T lymphoblasts. J. Biol. Chem. **263**, 12391–12396

33 Chan, T. C., Boon, G. D., Shaffer, L. and Redmond, R. (1992) Antiviral nucleoside toxicity in canine bone marrow progenitor cells and its relationship to drug permeation. Eur. J. Haematol. **49**, 71–76

34 Chan, T. C., Shaffer, L., Redmond, R. and Pennington, K. L. (1993) Permeation and metabolism of anti-HIV and endogenous nucleosides in human immune effector cells. Biochem. Pharmacol. **46**, 273–278

35 Domin, B. A., Mahony, W. B. and Zimmerman, T. P. (1993) Membrane permeation mechanisms of 2′,3′-dideoxynucleosides. Biochem. Pharmacol. **46**, 725–729

36 Gati, W. P., Misra, H. K., Knaus, E. E. and Wiebe, L. I. (1984) Structural modifications at the 2′-position and 3′-position of some pyrimidine nucleosides as determinants of their interaction with the mouse erythrocyte nucleoside transporter. Biochem. Pharmacol. **33**, 3325–3331

37 Crawford, C. R., Patel, D. H., Naeve, C. and Belt, J. A. (1998) Cloning of the human equilibrative, nitrobenzylmercaptopurine riboside (NBMPR)-insensitive nucleoside transporter *ei* by functional expression in a transport-deficient cell line. J. Biol. Chem. **273**, 5288–5293

38 Osses, N., Pearson, J. D., Yudilevich, D. L. and Jarvis, S. M. (1996) Hypoxanthine enters human vascular endothelial cells (ECV 304) via the nitrobenzylthioinosine-insensitive equilibrative nucleoside transporter. Biochem. J. **317**, 843–848

39 el Kouni, M. H., Diop, D., O'Shea, P., Carlisle, R. and Sommadossi, J. P. (1989) Prevention of tubercidin host toxicity by nitrobenzylthioinosine 5′-monophosphate for the treatment of schistosomiasis. Antimicrob. Agents Chemother. **33**, 824–827

40 Felsenstein, J. (1993) PHYLIP – Phylogeny Inference Package (version 3.2) Cladistics **5**, 164–166

41 Carter, N. S., Ben Mamoun, C., Liu, W., Silva, E. O., Landfear, S. M., Goldberg, D. E. and Ullman, B. (2000) Isolation and functional characterization of the PfNT1 nucleoside transporter gene from *Plasmodium falciparum*. J. Biol. Chem. **275**, 10683–10691

Received 9 February 2000/27 March 2000, accepted 19 April 2000

Biochem J (2000) 349, 77–84 (Printed in Great Britain)

Apolipoprotein E includes a binding site which is recognized by several amyloidogenic polypeptides

Marc H. BAUMANN*[1], Jukka KALLIJÄRVI*, Hilkka LANKINEN†, Claudio SOTO‡[2] and Matti HALTIA§

*Institute of Biomedicine, Protein Chemistry Education and Research Unit, P O Box 8, FIN-00014 University of Helsinki, Finland, †Haartman Institute, Department of Virology, Peptide and Protein Laboratory, P O. Box 21, FIN-00014 University of Helsinki, Finland, ‡Department of Pathology, New York University Medical Center, New York, NY 10016, U.S.A., and §Haartman Institute, Department of Pathology, P O Box 21, FIN-00014 University of Helsinki, Finland

Inheritance of the apolipoprotein E (apoE) ϵ4 allele is a risk factor for late-onset Alzheimer's disease (AD). Biochemically apoE is present in AD plaques and neurofibrillary tangles of the AD brain. There is a high avidity and specific binding of apoE and the amyloid β-peptide (Aβ). In addition to AD apoE is also present in many other cerebral and systemic amyloidoses, Down's syndrome and prion diseases but the pathophysiological basis for its presence is still unknown. In the present study we have compared the interaction of apoE with Aβ, the gelsolin-derived amyloid fragment AGel$_{183\text{-}210}$ and the amyloidogenic prion fragments PrP$_{109\text{-}122}$ and PrP$_{109\text{-}141}$. We show that, similar to Aβ, also AGel and PrP fragments can form a complex with apoE, and that the interaction between apoE and the amyloidogenic protein fragments is mediated through the same binding site on apoE. We also show that apoE increases the thioflavin-T fluorescence of PrP and AGel and that apoE influences the content of β-sheet conformation of these amyloidogenic fragments. Our results indicate that amyloids and amyloidogenic prion fragments share a similar structural motif, which is recognized by apoE, possibly through a single binding site, and that this motif is also responsible for the amyloidogenicity of these fragments.

Key words · Alzheimer's disease, amyloidosis of the Finnish type, pathological chaperone, prion disease.

INTRODUCTION

Amyloidoses are a group of disorders characterized by the abnormal extracellular deposition of insoluble amyloid fibrils, consisting usually of soluble proteins or fragments thereof, in one or several tissues (for a review, see [1]). Although varying in their origins, the disease-state fibrils all share certain properties that include an apple-green birefringence when viewed under polarized light after Congo Red staining, a predominantly β-pleated sheet secondary structure, a typical fibrillar appearance seen in electron microscopy, and a high degree of insolubility under physiological conditions. Arrays of prion rods found in several prion disorders resemble amyloid ultrastructurally and share similar properties [2,3].

Alzheimer's disease (AD), the most common of the amyloidoses, is characterized pathologically by extracellular deposits of a fibrillar 39- to 43-amino acid-long amyloid peptide [4]. This peptide, called Alzheimer's amyloid β-peptide (Aβ), is derived by an as-yet unknown proteolytic pathway of an integral membrane protein called amyloid precursor protein (APP, for a review, see [5]). Aβ is thought to play a crucial role in the pathogenesis of AD because several mutations in the APP gene lead to the early-onset form of the disease (for a review, see [6]). Despite the fact that genetic mutations have been found to cause the disease [7–9], a vast majority seem to be sporadic cases.

Prion-related disorders (spongiform encephalopathies) are characterized by intra- and extracellular accumulation of an abnormal isoform of the cellular prion protein (PrP^{C}) called scrapie prion protein (PrP^{Sc}). The pathological form of the PrP and its cellular precursor is expressed in the brain and also, at lower concentrations, in peripheral tissues. Prion diseases in human include Kuru, Creutzfeldt–Jakob disease, Gerstmann–Straussler–Scheinker syndrome and fatal familial insomnia (for a review, see [10]). Similar to AD, prion diseases occur both as sporadic and autosomal dominant familial diseases.

Familial amyloidosis of the Finnish type (FAF) is characterized by extracellular deposition of abnormal fibrillar material derived from gelsolin, an actin-modulating protein. So far, FAF has been found to be caused by only two nucleotide substitutions, changing Asp^{187} to Asn^{187} or Tyr^{187} (for a review, see [11]), resulting in the inactivation of one of the two actin-binding domains in gelsolin [12]. The mutation leads to a misfolded protein, which becomes predisposed to an as-yet-unknown degradation pathway, finally leading to the formation of an abnormally processed amyloid peptide fragment (AGel, gelsolin-derived amyloid of the Finnish type) [13]. No sporadic cases of FAF are known.

In prion diseases and amyloidoses, the protein or a fragment thereof undergoes conformational changes involving a shift from α-helix to β-sheet. It is likely that these conformational changes are crucial for the propagation of the disease (for a review, see [14]). How such changes occur is still largely unknown.

Apolipoprotein E (apoE), a 34-kDa protein coded by a gene on chromosome 19, is produced by a polymorphic gene producing three major isoforms, E2, E3 and E4. These isoforms are coded by three *apoE* gene alleles, ϵ2, ϵ3 and ϵ4, of which the ϵ4 isoform has generated considerable interest due to genetic evidence suggesting a link between this particular apolipoprotein and the pathogenesis of late-onset AD [15–18], Lewy body dementia [19], dementia in Parkinson's disease [20] and dementia and cognitive performances in Down's syndrome patients [21,22]. Immuno-

---

Abbreviations used Aβ, A$\beta_{1\text{-}40}$, Alzheimer's amyloid β-peptide, AGel, gelsolin-derived amyloid of the Finnish type, PrP, prion protein, AD, Alzheimer's disease, APP, Alzheimer's amyloid precursor protein, FAF, familial amyloidosis of the Finnish type, apoE, apolipoprotein E, ThT, thioflavin-T

[1] To whom correspondence should be addressed (e-mail Marc Baumann@helsinki fi)

[2] Present address Ares-Serono International S.A , chemin des Mines 15, Geneva, Switzerland

logically, apoE is present in many cerebral and systemic amyloidoses, Down's syndrome and prion disorders. Recent studies support the concept that apoE would directly be involved in the amyloid deposition and fibril formation [15,17,23,24]. Complete lack of apoE has been shown to dramatically reduce Aβ and amyloid A deposition in transgenic mice overexpressing the APP^{V717F} mutation [25] or amyloid A, respectively [26]. Moreover, expressing human apoE instead of the mouse apoE in an AD mouse model results in a even more dramatic reduction of Aβ deposition [27]. These experiments indicate clearly a crucial role for this specific apolipoprotein in amyloid formation.

In the present paper we have compared four different amyloidogenic fragments, A$\beta_{1\text{-}40}$, PrP$_{109\text{-}122}$ and PrP$_{109\text{-}141}$ and AGel$_{183\text{-}210}$ for their interaction with human apoE. Here we show that, comparable with A$\beta_{1\text{-}40}$, also PrP and AGel fragments can form SDS-stable complexes with apoE Complex formation is strongest with the AGel fragments. Similar to A$\beta_{1\text{-}40}$ and AGel, apoE seems to also enhance the amyloidogenicity of the PrP fragments. Moreover, all three amyloid fragments compete for the same binding site on apoE.

To verify the unique binding properties of apoE we have performed similar experiments with a non-amyloid-associated protein, amphoterin. Amphoterin has a high capacity to bind amyloidogenic peptide fragments, but the binding properties of amphoterin are, however, completely different from those observed with apoE.

Our findings suggest that amyloids and prions share a limited structural motif which, after induction, can accelerate the adoption of a β-sheet conformation and that this motif is the same as that recognized by apoE, evidently through a common binding site. Our findings provide a possible explanation for the widespread accumulation of apoE in these diseases.

MATERIALS AND METHODS

Materials

A$\beta_{1\text{-}40}$ (DAEFRHDSGYEVHHQKLVFFAEDVGSNKGAIIGLMVGGVV), gelsolin amyloid AGel$_N$ (FNNGDCFILDLGNNIHQWCGSNSNRYER), AGel$_D$ (FNNGNCFILDLGNNIHQWCGSNSNRYER) and AGel$_Y$ (FNNGYCFILDLGNNIHQWCGSNSNRYER), corresponding to amino acids 183–210 of human plasma gelsolin [28], where N, D and Y indicate the amino acid present at position 187 of the whole protein and position 10 of the peptide, were synthesized at the Centre for the Analysis and Synthesis of Macromolecules (SUNY, Stony Brook, NY, U.S.A.). Prion peptides PrP$_{109\text{-}122}$ (PrP-H1; MKHMAGAAAAGAVV) and PrP$_{109\text{-}141}$ (PrP-H1H2; MKHMAGAAAAGAVVGGLGGYMLGSAMSRPMMHF) were purchased from Bio-Synthesis (Lewisville, TX, U.S.A.). All peptides were purified by microbore HPLC. The sequence and purity of each peptide was verified by matrix-assisted laser desorption (MALDI) MS and/or automated Edman degradation. Stock solutions of each peptide (2 mg/ml) were prepared in 50 % acetonitrile in 0.1 % trifluoroacetic acid in water and stored at −70 °C. Human plasma apoE and the recombinant apoE4 isoform, produced by the eukaryotic baculovirus expression system, were purchased from Calbiochem-Novabiochem (Läufelfingen, Switzerland) and PanVera Corp. (Madison, WI, U.S.A.), respectively. The proteins were found to be more than 95 % pure by silver staining on SDS/PAGE. Antibodies against Aβ (4G8) recognizing the 17–24 fragment were purchased from Senetek (St. Louis, MO, U.S.A.). Recombinant amphoterin was received as a kind gift from Dr H. Rauvala (Institute of Biotechnology, University of Helsinki, Helsinki, Finland). The protein was found to be more than 95 % pure by silver staining on SDS/PAGE.

Co-incubation experiments with apoE

Purified apoE or recombinant apoE4 (2 μg each, 0.72 × 10^{-10} M) were incubated at 37 °C for 16 h with Aβ (1–30 μg, 0.025–0.75 × 10^{-8} M) and/or with AGel$_{D/N/Y}$ (1-20 μg, 0.022–0.44 × 10^{-8} M) and/or PrP$_{109\text{-}141}$ (1–30 μg, 0.023–0.69 × 10^{-8} M) in 50 μl of PBS, pH 7.2. Aliquots of the peptide stock solutions were lyophilized and mixed with the desired amount of the apolipoprotein. Formed complexes were analysed by high-resolution analytical Tris/Tricine SDS/PAGE. The solubility of each peptide was tested after lyophilization by Tris/Tricine SDS/PAGE and microbore gel-filtration liquid chromatography (SMART System, Pharmacia Biotech, Uppsala, Sweden).

Competitive-inhibition experiments with amphoterin

Purified recombinant amphoterin (2 μg, 0.7 × 10^{-10} M) was incubated at 37 °C for 16 h with increasing amounts of Aβ (1–30 μg; 0.025–0.75 × 10^{-8} M) and/or with AGel$_{D/N/Y}$ (1–20 μg, 0.022–0.44 × 10^{-8} M) in 50 μl of PBS, pH 7.2. Formed complexes were analysed by high-resolution analytical Tris/Tricine SDS/PAGE.

Competitive-inhibition experiments with apoE and apoE4

apoE and apoE4 (2 μg, 0.72 × 10^{-10} M) were incubated at 37 °C for 16 h with increasing amounts of Aβ (1–20 μg, 0.025–0.5 × 10^{-8} M) and/or with AGel$_{D/N/Y}$ (1–20 μg, 0.022–0.44 × 10^{-8} M) and/or PrP$_{109\text{-}141}$ (1–20 μg, 0.023–0.46 × 10^{-8} M) in 50 μl of PBS, pH 7.2. The samples were analysed by high-resolution analytical Tris/Tricine SDS/PAGE.

Tris/Tricine SDS/PAGE

The protein–peptide complexes were analysed by Tris/Tricine SDS/PAGE according to Schaegger and von Jagow [29]. Incubations were stopped by the addition of a modified Laemmli sample buffer (without β-mercaptoethanol and only 50 % of the recommended SDS added) into each sample vial. Samples were not boiled but incubated at 37 °C for 5–10 min. Protein–peptide complexes were electrophoresed on Tris/Tricine gels (10–14.5 % T/3 % C, with a spacer gel of 10 % T/3 % C; where T is acrylamide and C is cross-linker bisacrylamide). Protein bands were visualized by Coomassie Brilliant Blue or silver staining.

Fluorometric experiments

For the fluorometric experiments, approx. 30 μg (0.66 × 10^{-8} M) of each of the AGel$_{D/N/Y}$ peptides or 30 μg (0.75 × 10^{-8} M) of Aβ or 30 μg (0.33 × 10^{-8} M) of PrP$_{109\text{-}122}$ was incubated with apoE in a ratio of 1:200 (mol lipoprotein/mol peptide) in 50 μl of PBS, pH 7.2, for 0–96 h. Incubated samples were then added to 50 mM glycine, pH 9, with 2 μM thioflavin-T (ThT; Sigma, St. Louis, MO, U.S.A.) in a final volume of 2 ml Fluorescence was measured at the excitation and emission maxima of 435 and 485 nm, respectively, in a Hitachi F-2000 fluorescent spectrophotometer. A time scan of fluorescence was performed and three values obtained after the decay reached a plateau (mostly at 300–400 s) were averaged after subtracting the background fluorescence of the ThT and buffer alone. Two identical samples were measured. The PrP$_{109\text{-}141}$ peptide could not be used in the ThT assay due to a high background variation.

CD spectroscopy

CD spectra were obtained with a JASCO spectropolarimeter J-720 at room temperature in a 0.1-cm path-length cell. Double-distilled water, 100 mM Tris/HCl, pH 7.2, and trifluoroethanol (spectroscopic grade) were used as solvents. Spectra were recorded at 1-nm intervals over the wavelength range 190–260 nm. All spectra were obtained by subtracting the buffer baseline and smoothed by using the algorithm by JASCO. The β-sheet conformation was determined following the relative change of the ellipticity at 217 nm of each identical pair of samples.

Densitometry

Each gel was scanned by a Hewlett-Packard Scanjet 4C laser scanner and each band of interest subsequently analysed by the Scion Image Program (SIP, Scion Corp., Frederick, MA, U.S.A.).

Western-blotting analysis

Western-blot analyses where performed to gels prepared as described in the section on competitive-inhibition experiments (see above). SDS/PAGE samples were transferred on to PVDF membranes. Immunoblotting was performed with anti-Alzheimer's β-amyloid peptide monoclonal antibodies (4G8). Membranes were blocked for 1 h with 3 % BSA, washed, and then incubated with the primary antibody for 2 h. This was followed by washing and incubation with alkaline phosphatase-conjugated secondary antibody (anti-mouse antibody; Bio-Rad, Richmond, CA, U.S.A.). The staining was carried out according to the manufacturer's instructions.

Surface-plasmon-resonance spectroscopy

Surface-plasmon-resonance spectroscopy measurements were made with a BIAcore 2000TM instrument (BIACORE, Pharmacia Biotech) using a CM5 sensor chip and the manufacturer's recommendations for amine coupling. Ligand levels were used that gave a clearly positive signal for the analyte binding. Aβ and AGel$_N$ were immobilized on the sensor chip, each in one channel. The running buffer (PBS) was applied at a flow rate of 20 μl/min. apoE (150 pM solution) alone, apoE (150 pM) with Aβ (1 : 10, apoE/Aβ molar ratio), and apoE (150 pM) with glycine (1 : 200, apoE/Gly molar ratio) were used as analytes. The measurements were conducted at 37 °C. The binding response of each sample solution was determined by the measurement of resonance signal units. Prior to the numerical analysis, data were adjusted to zero immediately before injection of analyte.

RESULTS

All synthetic peptides used in this study have previously been shown to be amyloidogenic [3,4,30]. Based on the fact that AD and prion disorders occur both as familial and sporadic forms, we decided to include the non-mutated form of the FAF amyloid into this study, although no sporadic cases of this disease are known. The non-mutated FAF peptides seem to be able to adopt a β-sheet structure similar to that of the mutated peptides (0.0 % α-helix, 86.7 % β-sheet) according to the predicted secondary structure by Chou and Fasman [31] and Garnier et al. [32]. Indeed, when incubated under similar conditions to Aβ, the non-mutated peptides also form amyloid fibrils indistinguishable from those formed by the mutated FAF amyloid fragments [24,33].

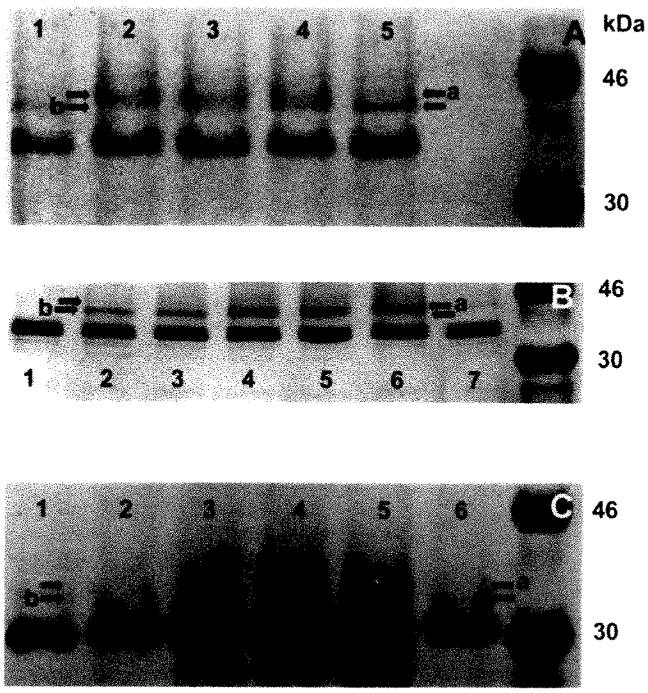

Figure 1 **Coomassie Brilliant Blue-stained 16 % Tris/Tricine polyacrylamide gels of (A) human plasma apoE, (B) apoE4 and (C) amphoterin (all 2 μg), incubated for 16 h at 37 °C with AGel$_N$ and Aβ**

(**A**) Lane 1, apoE with 0.5 μg of AGel$_N$; lane 2, apoE with 1 μg of AGel$_N$ and 20 μg of Aβ; lane 3, apoE with 2 μg of AGel$_N$ and 15 μg of Aβ; lane 4, apoE with 1 μg of AGel$_N$ and 10 μg of Aβ; lane 5, apoE with 1 μg of AGel$_N$. (**B**) Lane 1, apoE4; lane 2, apoE4 with 1 μg of AGel$_N$; lane 3, apoE4 with 1 μg of AGel$_N$ and 5 μg of Aβ; lane 4, apoE4 with 1 μg of AGel$_N$ and 10 μg of Aβ; lane 5, apoE4 with 1 μg of AGel$_N$ and 15 μg of Aβ; lane 6, apoE4 with 1 μg of AGel$_N$ and 20 μg of Aβ; lane 7, apoE4 with 1 μg of of Aβ. (**C**) Lane 1, amphoterin; lane 2, amphoterin with 1 μg of AGel$_N$ and 1 μg of Aβ; lane 3, amphoterin with 2 μg of AGel$_N$ and 5 μg of Aβ; lane 4, amphoterin with 2 μg of AGel$_N$ and 10 μg of Aβ; lane 5, amphoterin with 2 μg of AGel$_N$ and 15 μg of Aβ; lane 6, amphoterin with 1 μg of AGel$_N$. In all panels, a and b indicate complexes formed by each peptide (a, with Aβ; b, with AGel$_N$).

apoE forms SDS-stable complexes with PrP$_{109\text{-}141}$ and AGel

In order to compare the capability of apoE to form SDS-stable complexes with Aβ, AGel and PrP we incubated various amounts of these peptides under physiological conditions with apoE and apoE4. Incubation over 16 h resulted in the formation of SDS-stable complexes which could, in the case of AGel, be visualized by high-resolution Tris/Tricine SDS/PAGE as a faint band just above the major apoE band (Figure 1). Both PrP peptides turned out to be extremely difficult to visualize as a complex with apoE since they produced rather diffuse bands, probably due to the high tendency for aggregation of these particular peptides. The apoE–PrP band was almost on the same level with the native apoE, even with the 3.27-kDa PrP$_{109\text{-}144}$ peptide. Subsequently, we measured the apoE–PrP complex formation and binding competition between Aβ and PrP to apoE by indirect Western-blot analysis, as shown in Figure 2. The mutated and non-mutated gelsolin peptides revealed a higher affinity to apoE as compared with the affinity of Aβ or PrP. Densitometrical analyses indicated that the AGel peptides have an approx. 10-fold higher complex-forming affinity (Figure 3). Aβ and the PrP fragments showed only moderate differences in their capability to form complexes with apoE (Figure 2).

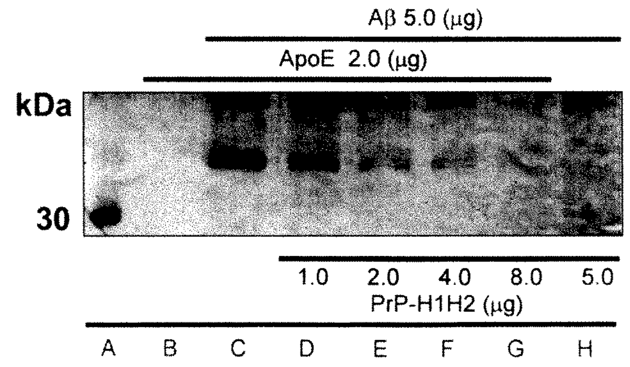

Figure 2 Western-blot analysis of apoE4 (2 μg) with Aβ (5 μg) and various amounts of $PrP_{109-141}$ (PrP-H1H2) incubated for 16 h at room temperature

The samples were blotted on to PVDF and visualized by a monoclonal anti-Aβ antibody (4G8) except lane A, which was molecular-mass standard (Coomassie Brilliant Blue-staining).

No differences could be detected in the binding of the mutated and non-mutated AGel peptides indicating that the mutation itself is not important for the binding. This is not surprising since none of the AGel mutations change the predicted β-sheet content of these peptides, a factor seemingly crucial for the binding to apoE [34].

apoE influences the fibril formation of PrP and AGel fragments

The influence of apoE on the amyloid fibril formation of these peptides was monitored by the ThT method. ThT has been shown to bind to amyloid, producing a shift in the emission spectrum and a fluorescence signal proportional to the amount of amyloid formed [35]. This measurement was mainly conducted with the $PrP_{109-122}$ (PrP-H1) peptide due to a high background drift of the $PrP_{109-141}$ (PrP-H1H2), probably caused by the high-aggregation property of this particular peptide. We have reported earlier that apoE can accelerate the fibril formation of some non-mutated and mutated AGel peptide fragments *in vitro* and here we compared the effect of apoE on Aβ, AGel and PrP. Similar to our earlier observations [24], $AGel_Y$, less amyloidogenic at pH 7.2, became highly amyloidogenic (increase approx. 4.5-fold) by the influence of this apolipoprotein. On the other hand, $AGel_N$, highly amyloidogenic at pH 7.2, was influenced less by apoE (increase approx. 1.3-fold), resembling the effect of apoE on the Dutch Aβ variant ($Aβ_{1-40Q}$; increase approx. 2-fold) [36]. Also the wild-type peptide $AGel_D$ was clearly affected (increase approx. 1.6-fold). $AGel_N$ is more amyloidogenic at pH 7.2 than $AGel_Y$

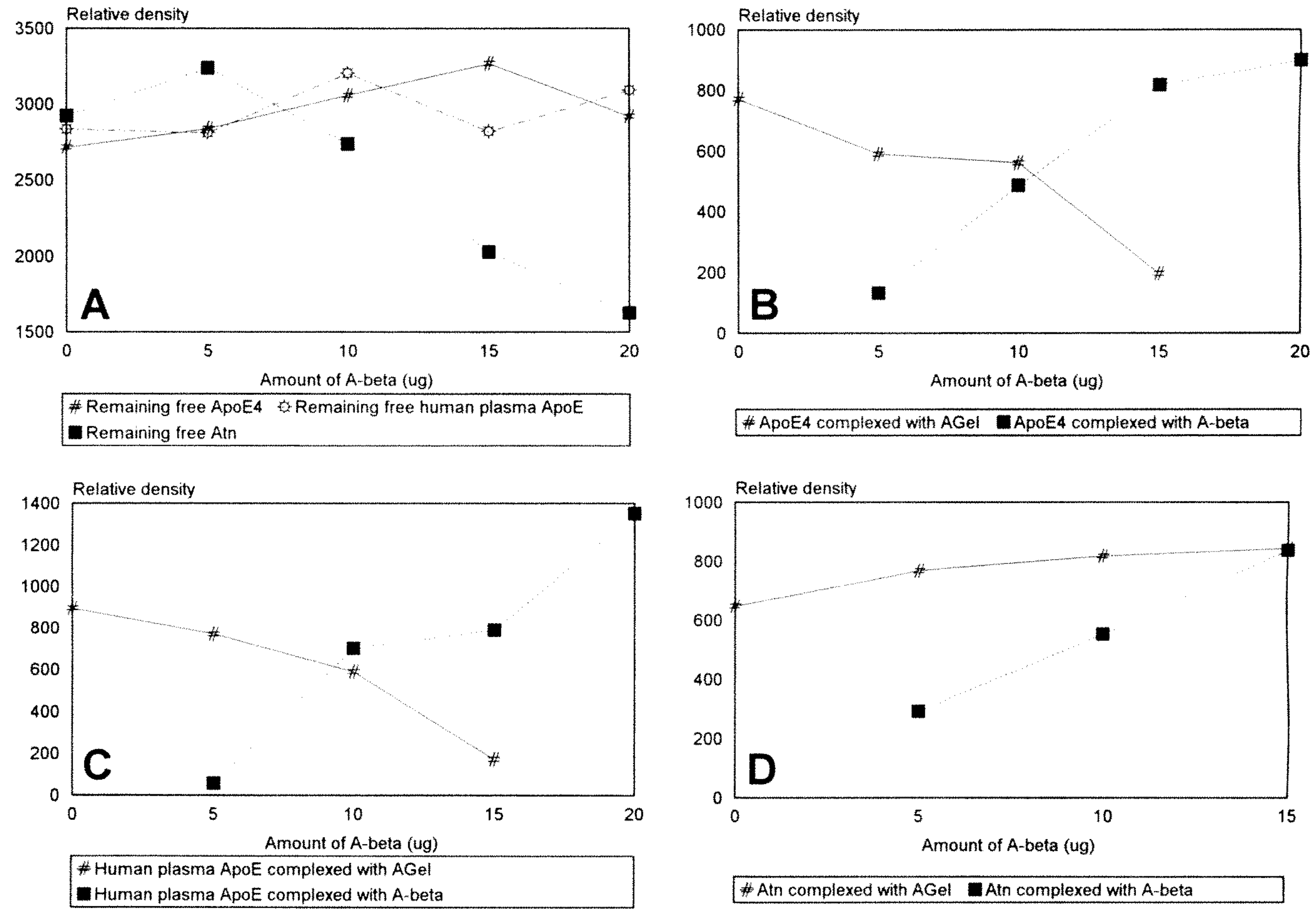

Figure 3 Densitometrical analyses of formed complexes, free apoE4, free human plasma apoE and free amphoterin (Atn) from Figure 1

(**A**) Band intensities of remaining free apoE4, free human plasma apoE and free amphoterin were measured after increasing the amount of Aβ from 0 to 20 μg. (**B**) Band intensities of $AGel_N$ and Aβ complexes with apoE4 after increasing the amount of Aβ from 0 to 20 μg. (**C**) Band intensities of $AGel_N$ and Aβ complexes with human plasma apoE after increasing the amount of Aβ from 0 to 20 μg. (**D**) Band intensities of $AGel_N$ and Aβ complexes with amphoterin after increasing the amount of Aβ from 0 to 15 μg.

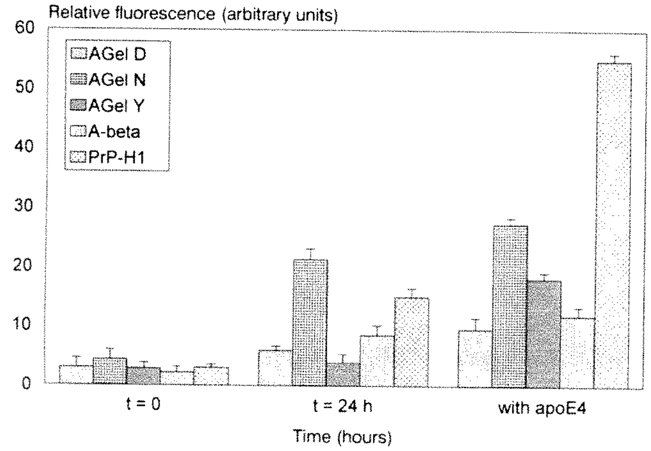

Figure 4 ThT assay of formed amyloid fibrils

Each sample was incubated for 16 h with or without human plasma apoE in duplicate (similar results were achieved with apoE4). Values are given in relative fluorescence (arbitrary units).

Table 1 Plasmon-resonance spectroscopy on the interaction and competition of Aβ and AGel$_N$ with human plasma apoE

Aβ and AGel$_N$ were bound to the matrix in one channel each. Responses were measured in real time with human plasma apoE, human plasma apoE with glycine (molar ratio 1:200) and human plasma apoE with Aβ (molar ratio 1:10) with the coupled ligands. Values are given as resonance signal units (in %, ±S.D.). The resonance signal of apoE in each channel was set at 100%.

Ligand bound to the sensor surface	apoE	apoE + glycine	apoE + Aβ
Aβ	100±5.6%	83±10.9%	30±10.0%
AGel$_N$	100±9.5%	76±5.5%	37±5.7%

and therefore probably less influenced by any external promoters. These data indicate that a peptide which is able to form amyloid fibrils rapidly does not have much help from an 'external chaperone'. As expected, apoE also enhanced the fibril formation of the PrP fragment (increase approx. 3.5-fold), resembling that of AGel$_Y$ (Figure 4).

Aβ, AGel and PrP compete for binding with apoE

The fact that Aβ, AGel and PrP were all similarly affected by apoE led us to study whether the effect of this apolipoprotein would be mediated through the same binding site on apoE. To do this we mixed various amounts of Aβ, AGel and PrP together with apoE and apoE4 for 16 h, after which time the formed complexes were analysed by Tris/Tricine SDS/PAGE (Aβ and AGel) and Western blotting (Aβ and PrP). When AGel and Aβ were incubated in a molar ratio of 1:1 no complex between Aβ and apoE was seen, only a complex between AGel and apoE could be detected; a 10-fold excess of Aβ resulted in an approx. 1:1 ratio of the formed complexes of AGel–apoE and Aβ–apoE and a 20-fold excess of Aβ washed out the AGel–apoE complex practically completely (Figures 1 and 2). The competition was independent of the peptide, e.g. each peptide could wash out the other. A molar ratio of approx. 2:1 of Aβ/PrP with apoE resulted in a 1:1 capability of complex formation, indicating that these two amyloidogenic peptides had only small differences in their complex-formation capacity with apoE under conditions used in this study (Figure 2). The formation or dissociation of the Aβ–apoE complex in the presence of AGel could be followed by Tris/Tricine SDS/PAGE, and the effect of PrP by Western-blot analysis using a monoclonal anti-Aβ antibody (Figure 2). No detectable differences in the complex-forming capacity between apoE and apoE4 were observed, indicating that different isoforms share the same binding. Human plasma apoE is a mixture of the three major isoforms, mainly composed of E3 (approx. 80%). It is worthwhile to note that experiments *in vivo* show no differences between the apoE isoforms in terms of their capability to form complexes with β-amyloid in human AD brain, e.g. each apoE isoform can form the same amount of complex *in vivo* [17,37]. In addition, there is no difference in the reduction of amyloid deposition between a mouse expressing human apoE3 or apoE4 compared with the corresponding mouse gene in an AD mouse model [27]. None of these amyloidogenic peptide fragments bound to, or accelerated the amyloid fibril formation of, the other. Pre-incubating one peptide with apoE for several hours did not effect the competitive binding. Thus the binding of amyloid peptides to apoE seems to be reversible.

Verification of the competition by surface-plasmon-resonance spectroscopy

In order to verify that the competitive inhibition of the binding of Aβ and AGel to apoE is not artificially suported by the PAGE technique, we also studied the competitive inhibition by surface-plasmon-resonance spectroscopy. Both peptides (Aβ and AGel) were coupled to the chip and the affinity of the soluble apoE in the absence and presence of Aβ to bound Aβ and AGel measured. A 200-fold molar excess of glycine was used as a control. This high amount of glycine inhibited the apoE affinity to both peptides by approx. 20–30%, presenting the quasi-maximal physical inhibition of a molecule without any affinity to the ligand. An 8-fold molar excess of Aβ in the same solution with apoE inhibited the affinity of the free apoE to Aβ by approx. 70% and to AGel by approx. 60% (Table 1). Thus the presence of Aβ together with apoE in the same solution inhibited the affinity of the free apoE in that solution to the bound Aβ and also to the bound AGel, clearly supporting our gel-electrophoresis data. If Aβ would not bind to the soluble, native apoE through the same binding site as AGel, it should not have influenced the apoE–AGel interaction. These data verify that Aβ is indeed able to inhibit the apoE interaction with an unrelated amyloidogenic protein fragment like AGel. Due to its high tendency to aggregate we could not include any of the PrP fragments in these studies.

Control studies with amphoterin

To verify the reversibility and specificity of the binding of apoE and the amyloidogenic fragments, we have performed identical competition studies with a non-amyloid associated protein, amphoterin (high-mobility group-1 protein, HMG-1). This protein features the capability to bind amyloidogenic peptide fragments although it has not been found to be associated with any of the known amyloidoses. It has, however, the capacity to accelerate the amyloidogenicity of these peptides and includes a fragment that can form amyloid-like fibrils *in vitro*. In Figures 1 and 2 we show results of a competition experiment performed between AGel, Aβ and amphoterin. Increasing the amount of Aβ in a solution with amphoterin clearly decreased the amount of soluble free amphoterin as well (Figure 3A), indicating that the binding is irreversible under conditions used in this study. On the other hand, increasing the amount of Aβ in a solution with

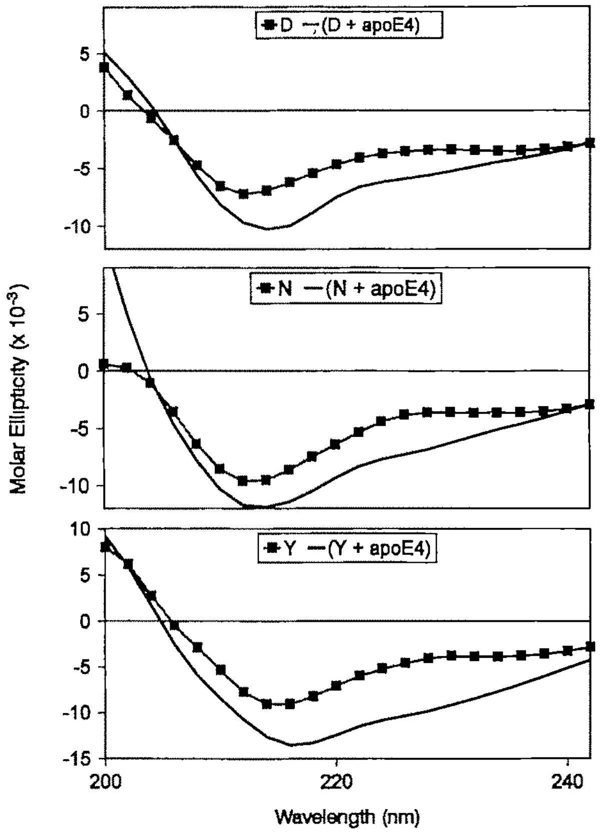

Figure 5 The effect of apoE4 on the AGel peptides as measured by CD

Each peptide (60 μg) was dissolved in 60% trifluoroethanol/100 mM Tris/HCl (pH 7.2) and immediately applied to CD measurement ($t = 0$ h). apoE4 was added to each peptide solution in a final molar concentration of 1:200 (apoE/Aβ) Each measurement was repeated after incubation overnight at 37 °C ($t = 24$ h) The CD spectrum of apoE4 alone did not deviate from the buffer alone value due to the very low amount of protein used

apoE did not reduce the amount of soluble apoE (Figures 1A, 1B and 2A). AGel and Aβ had similar effects on amphoterin and apoE (results not shown). In addition, none of the peptides competed for the binding with amphoterin, even at higher loads of one or the other (Figures 1C and 2D). Interestingly, increasing the amount of one of the peptides in a solution with amphoterin seems also to increase slightly the capacity of the other peptide to form a complex (Figure 1C and 3D). This could be due to two different binding sites, which upon single occupation can change the affinity of the other.

apoE influences the conformation of AGel

To determine whether apoE is able to induce a conformational change in the secondary structure of other amyloids, as it has been shown to do in Aβ [24], we have performed CD analyses of AGel peptides with and without apoE. Each peptide was dissolved in aqueous solution containing 60 % trifluoroethanol, a condition which optimizes the α-helix formation but does not influence the β-sheet structure. Addition of apoE (apoE/AGel, molar ratio 1:200) had a specific effect on the spectrum with principal changes observed at wavelengths of 195 and 217 nm (Figure 5; β-sheet structure maximum at 195 nm and minimum at 217 nm), similar to results obtained with e.g. Aβ and apoE [34,38] or Aβ and aluminium [39] CD spectrum of apoE alone did not deviate from the buffer alone value due to the very low amount of protein used.

DISCUSSION

Recent genetic data suggest a heterogeneity among causes and risk factors for AD. These include mutations in the APP [7], presenilin 1 [8] and 2 [9], all responsible for the familial form of this disease, and a genetic association with the apoE ε4 allele [16].

While a genetic mutation clearly leads to the disease, the role of apoE seems to be much more complicated. In fact, although many AD patients carry either one or two ε4 alleles, it is not a prerequisite, since a number of AD cases do not show any linkage to this particular allele [40]. Moreover, the effect of apoE is not limited to AD. apoE-deficient mice overexpressing amyloid A show reduced amyloid fibril formation, as well [26]. In addition, deposits in various amyloidoses and prion diseases include both biochemically and immunohistochemically detectable amounts of apoE [17,23,41–43]. Thus the molecular interaction of apoE seems not to be specific for AD but more a common characteristic in the development of other amyloidoses as well.

We have shown previously that apoE can accelerate the amyloid fibril formation of Aβ by causing a conformational change of a non-pathogenic form of the amyloid peptide to a pathogenic form of the same peptide [24]. In the present study we now show that apoE affects the amyloid fibril formation of synthetic peptides homologous to some other amyloidogenic protein fragments as well. This effect is mediated by the same mechanism, providing further evidence that apoE may indeed, act as a 'universal pathological chaperone'.

Our results indicate that the interaction of various amyloidogenic peptides with apoE is not limited to a specific amino acid sequence, but more related to the physicochemical nature of each fragment, e.g. to properties that are also responsible for the amyloidogenicity. These results are in accordance with those obtained with several mutated and non-mutated Aβ peptides [34]. The ability of any misfolded amyloidogenic intermediate to assemble into characteristic amyloid fibrils seems to depend on sequence elements that become exposed after partial or complete unfolding. A mutation may directly speed up the fibrillization or just cause a protein to misfold, subsequently leading to the release of the amyloidogenic fragment In the case of FAF, both mutations causing the disease (Asn and Tyr) lead to premature degradation of gelsolin.

It has been proposed that fragments of only 10 amino acids of AGel (^{183}FNNGDCFILD^{192}) [30] and Aβ (^{14}HQKLVFFAED^{23}) [44] would be responsible for the amyloidogenicity and amyloid fibril formation The most amyloidogenic peptide in PrP is ^{113}AGAAAAGA^{120} [45]. In addition, in several other amyloids only a short sequential stretch is responsible for the amyloidogenicity [46–49]. Thus different amyloid fragments seem to share a relatively short common motif that is responsible for the fibrillogenesis. A conformational change of such a stretch, activated by an external signal (e.g. apoE), seems to be enough to fibrillize the protein. This kind of amyloidogenic consensus sequence has been predicted to exist in various amyloids [50,51]. Observations showing that some originally non-amyloidogenic proteins form amyloid-like structures under suitable conditions support the notion that amyloidogenicity is not limited to only a few protein sequences but rather is a 'hidden' property of many proteins [52–55].

Each amyloidogenic fragment tested in this study competed on the binding to apoE with the other, suggesting that the effect of apoE is mediated through only one common binding site. This is supported further by the results obtained by quantitative N-terminal sequence analysis of each formed complex, according to which apoE can bind only one amyloid peptide at a time (results not shown). Moreover, several authors have shown *in vivo* and *in vitro* that the binding site for Aβ is located in a rather restricted area at the C-terminal domain of apoE, further limiting the possibility of several binding sites [22,56,57].

This work was supported by the National Institutes of Health, U.S.A. (C S., projects AG-10953 and NS-30455-04), the Academy of Finland (M B, project 10137556, M H and M B, project 48173), the University of Helsinki (M H and M.B., 1127/62/96), and the EVO grant from the University Hospital Helsinki (M H and M B 1997)

REFERENCES

1 Ghiso, J, Wisniewski, T and Frangione, B (1994) Unifying features of systemic and cerebral amyloidosis Mol Neurobiol **8**, 49–64

2 Prusiner, S B, McKinley, M P, Bowman, K. A., Bolton, D C, Bendheim, P E, Groth, D F and Glenner, G. G (1983) Scrapie prions aggregate to form amyloid-like birefringence rods Cell **35**, 349–358

3 Tagliavini, F, Prelli, F, Verga, L., Giaccone, G, Sarma, R, Gorevic, P, Ghetti, B, Passerini, F, Ghibaudi, E, Forloni, G, Salmona, M, Bugiani, O and Frangione, B. (1993) Synthetic peptides homologous to prion protein residues 106–147 form amyloid-like fibrils *in vitro* Proc Natl Acad Sci U S A **90**, 9678–9682

4 Glenner, G C and Wong, C. W (1984) Alzheimer's disease and Down's syndrome: sharing of a unique cerebrovascular amyloid fibril protein. Biochem. Biophys Res Commun **120**, 885–890

5 Hardy, J (1997) Amyloid, the presenilins and Alzheimer's disease Trends Neurosci. **20**, 154–159

6 Levy-Lahad, E and Bird, T. (1996) Genetic factors in Alzheimer's disease a review of recent advances Ann Neurol **40**, 829–840

7 Goate, A, Chartier-Harlin, M C, Mullan, M, Brown, J, Crawford, F, Fidani, L, Giuffra, L, Haynes, A, Irving, N, James, L et al (1991) Segregation of a missense mutation in the amyloid precursor protein gene with familial Alzheimer's disease Nature (London) **349**, 704–706

8 Sherrington, R, Rogaev, E I, Liang, Y, Rogaeva, E. A, Levesque, G, Ikeda, M, Chi, H, Lin, C, Li, G, Holman, K. et al (1995) Cloning of a gene bearing missense mutations in early-onset familial Alzheimer's disease Nature (London) **375**, 754–760

9 Levy-Lahad, E, Wasco, W, Poorkaj, P, Romano, D M, Oshima, J., Pettingell, W H, Yu, C. E., Jondro, P D, Schmidt, S D, Wang, K et al (1995) Candidate gene for the chromosome 1 familial Alzheimer's disease locus Science **269**, 973–977

10 Horwich, A and Weissman, J S (1997) Deadly conformations–protein misfolding in prion disease Cell **89**, 499–510

11 Kiuru, S (1998) Gelsolin-related familial amyloidosis, Finnish type (FAF), and its variants found worldwide Amyloid Int J. Exp Clin Invest **5**, 55–66

12 Weeds, A G, Gooch, J., McLaughlin, P. and Maury, C P J (1993) Variant plasma gelsolin responsible for familial amyloidosis (Finnish type) has defective actin severing activity FEBS Lett **335**, 119–123

13 McLaughlin, P J, Gooch, J T., Mannherz, H.-G. and Weeds, A G (1993) Structure of gelsolin segment 1-actin complex and the mechanism of filament severing Nature (London) **364**, 685–692

14 Kelly, J W (1996) Alternative conformations of amyloidogenic proteins govern their behaviour Curr Opin Struct Biol **6**, 11–17

15 Strittmatter, W. J., Saunders, A M, Schmechel, D, Pericak-Vance, M A, Enghild, J, Salvesen, G S and Roses, A D (1993) Apolipoprotein E: high-avidity binding to beta-amyloid and increased frequency of type 4 allele in late-onset familial Alzheimer disease Proc. Natl. Acad Sci U S A **90**, 1977–1981

16 Saunders, A M, Strittmatter, W J, Schmechel, D, St George-Hyslop, P. H., Pericak-Vance, M A, Joo, S H, Rosi, B. L, Gusella, J F, Crapper-MacLachlan, D R, Alberts, M J, Hulette, C., Crain, B, Goldgaber, D and Roses, A D (1993) Association of apolipoprotein E allele epsilon 4 with late-onset familial and sporadic Alzheimer's disease Neurology **43**, 1467–1472

17 Naslund, J, Thyberg, J, Tjernberg, L O., Wernstedt, C., Karlstrom, A. R, Bogdanovic, N, Gandy, S, Lanfelt, L, Terenius, L and Nordstedt, C (1995) Characterization of stable complexes involving apolipoprotein E and the amyloid beta peptide in Alzheimer's disease brain Neuron **15**, 1–20

18 Chartier-Harlin, M.-C., Parfitt, M, Legrain, S, Perez-Tur, J, Brousseau, T, Evans, A et al (1994) Apolipoprotein E, epsilon 4 allele as a major risk factor for sporadic early and late-onset forms of Alzheimer's disease. analysis of the 19q13 2 chromosomal region Hum Mol. Gen **3**, 569–574

19 Benjamin, R, Leake, A., Edwardson, J A, McKeith, I. G, Ince, P G., Perry, R H and Morris, C M. (1995) Effects of apolipoprotein E genotype on cortical neuropathology in senile dementia of the Lewy body and Alzheimer's disease Lancet **343**, 1565

20 Arai, H., Muramatsu, T, Higuchi, S, Sasaki, H and Trojanowski, J (1994) Apolipoprotein E gene in diffuse Lewy body disease with or without co-existing Alzheimer's disease. Lancet **344**, 889

21 Del Bo, R, Comi, G P, Bresolin, N, Castelli, E, Conti, E, Degiuli, A., Ausenda, C D and Scarlato, G. (1997) The apolipoprotein E epsilon4 allele causes a faster decline of cognitive performances in Down's syndrome subjects. J. Neurol Sci **145**, 87–91

22 Schupf, N, Kapell, D, Lee, J. H., Zigman, W, Canto, B, Tycko, B. and Mayeux, R (1996) Onset of dementia is associated with apolipoprotein E epsilon4 in Down's syndrome. Ann Neurol. **40**, 799–801

23 Castano, E, Prelli, F, Pras, M. and Frangione, B (1995) Apolipoprotein E carboxyl-terminal fragments are complexed to amyloids A and L Implications for amyloidogenesis and Alzheimer's disease J Biol. Chem. **270**, 1–6

24 Soto, C, Castano E. M., Prelli, F, Kumar, R A and Baumann, M (1995) Apolipoprotein E increases the fibrillogenic potential of synthetic peptides derived from Alzheimer's, Gelsolin and AA amyloids. FEBS Lett **371**, 110–114

25 Bales, K. R., Verina, T, Dodel, R C, Du, Y, Altstiel, L, Bender, M, Hyslop, P, Johnstone, E M, Little, S P., Cummins, D J et al (1997) Lack of apolipoprotein E dramatically reduces amyloid beta-peptide deposition Nat Genet. **17**, 263–264

26 Kindy, M S and Rader, D J (1998) Reduction in amyloid A amyloid formation in apolipoprotein-E-deficient mice Am J Pathol **152**, 1387–1395

27 Holtzman, D M, Bales, K R, Wu, S., Bhat, P, Parsadanian, M, Fagan, A. M., Chang, L K, Sun, Y and Paul, S. M. (1999) Expression of human apolipoprotein E reduces amyloid-beta deposition in a mouse model of Alzheimer's disease J Clin Invest **103**, R15–R21

28 Kwiatkowski, D J, Stossel, T P, Orkin, S H., Mole, J E, Colten, H R and Yin, H. L. (1986) Plasma and cytoplasmic gelsolins are encoded by a single gene and contain a duplicated actin-binding domain Nature (London) **323**, 455–458

29 Schaegger, H and von Jagow, G (1987) Tricine-sodium dodecyl sulfate-polyacrylamide gel electrophoresis for the separation of proteins in the range from 1 to 100 kDa Anal Biochem. **166**, 368–379

30 Maury, C P. J., Nurmiaho-Lassila, E-L and Rossi, H. (1994) Amyloid fibril formation in Gelsolin-derived amyloidosis Lab Invest **70**, 558–564

31 Chou, P Y and Fasman, G (1978) Empirical predictions of protein conformation Ann Rev Biochem **47**, 251–276

32 Garnier, J, Osguthorpe, D. J. and Robson, B (1978) Analysis of the accuracy and implications of simple methods for predicting the secondary structure of globular proteins J Mol Biol **120**, 97–120

33 Ratnaswamy, G, Koepf, E, Bekele, H., Yin, H and Kelly, J (1999) The amyloidogenicity of gelsolin is controlled by proteolysis and pH Chem Biol **6**, 293–304

34 Golabek, A A, Soto, C, Vogel, T and Wisniewski, T (1996) The interaction between apolipoprotein E and Alzheimer's amyloid beta-peptide is dependent on beta-peptide conformation J Biol Chem **271**, 10602–10606

35 Naiki, H., Higuchi, K, Nakakuki, K and Takeda, T (1991) Kinetic analysis of amyloid fibril polymerization *in vitro* Lab. Invest **65**, 104–110

36 Castano, E M, Prelli, F, Wisniewski, T, Golabek, A, Kumar, A, Soto, C and Frangione, B (1995) Fibrillogenesis in Alzheimer's disease of amyloid beta peptides and apolipoprotein E Biochem. J. **306**, 599–604

37 Russo, C, Angelini, G., Dapino, D, Piccini, A, Piombo, G, Schettini, G, Chen, S, Teller, J K, Zaccheo, D, Gambetti, P and Tabaton, M (1998) Opposite role of apoE in normal brains and in Alzheimer's disease Proc Natl Acad Sci U S A **95**, 15598–15602

38 Soto, C., Golabek, A, Wisniewski, T. and Castano, E M (1996) Alzheimer's beta-amyloid peptide is conformationally modified by apolipoprotein E *in vitro* Neuroreport **7**, 721–725

39 Exley, C, Price, N. C, Kelly, S M and Birchall, J D (1993) An interaction of beta-amyloid with aluminium *in vitro* FEBS Lett **324**, 293–295

40 Hyman, B T and Terry, R D. (1994) Apolipoprotein E, A beta, and Alzheimer disease. J Neuropathol Exp. Neurol **53**, 427–428

41 Dietrich, J F, Minnigan, H, Carp, R I, Whitaker, J N, Race, R, Frey, II, W and Haase, A T (1991) Neuropathological changes in scrapie and Alzheimer's disease are associated with increased expression of apolipoprotein E and cathepsin D in astrocytes J Virol **65**, 4759–4768

42 Namba, Y, Tomonaga, M., Kawasaki, H., Otomo, E and Ikeda, K (1991) Apolipoprotein E immunoreactivity in cerebral amyloid deposits and neurofibrillary tangles in Alzheimer's disease and kuru plaque amyloid in Creutzfeldt-Jakob disease Brain Res **541**, 163–166

43 Charge, S. B, Esiri, M M, Bethune, C A, Hansen, B C and Clark, A (1996) Apolipoprotein E is associated with islet amyloid and other amyloidoses Implications for Alzheimer's disease J Pathol **179**, 443–447

44 Tjernberg, L O, Callaway, D. J E, Tjernberg, A, Hahne, S, Lilliehook, C, Terenius, L, Thyberg, J and Nordstedt, C (1999) A molecular model of Alzheimer's amyloid-peptide fibril formation. J Biol Chem. **274**, 12619–12625

45 Gasset, M, Baldwin, M A, Lloyd, D H, Gabriel, J M, Holtzman, D M, Cohen, F, Fletterick, R. and Prusiner, S. B (1992) Predicted alpha-helical regions of the prion protein when synthesized as peptides form amyloid. Proc Natl Acad Sci U S A **89**, 10940–10944

46 Glenner, G G, Eanes, D E and Wiley, C A (1988) Amyloid fibrils formed from a segment of the pancreatic islet amyloid protein Biochem Biophys Res Commun **155**, 608–614

47 Westermark, P, Engstrom, U, Johnson, K H, Westermark, G T. and Betsholtz, C. (1990) Islet amyloid polypeptide pinpointing amino acid residues linked to amyloid fibril formation Proc Natl Acad. Sci U S A **87**, 5036–5040

48 Gustavsson, Å, Engstrom, U. and Westermark, P (1991) Normal transthyretin and synthetic transthyretin fragments form amyloid-like fibrils *in vitro* Biochem Biophys Res Commun **175**, 1159–1164

49 Hurle, M R, Helms, L R, Li, L, Chan, W and Wetzel, R (1994) A role for destabilizing amino acid replacements in light-chain amyloidosis Proc Natl Acad Sci U S A. **91**, 5446–5450

50 Turnell, W G and Finch, J T (1992) Binding of the dye Congo red to the amyloid protein pig insulin reveals a novel homology amongst amyloid-forming peptide sequences J. Mol Biol **227**, 1205–1223

51 Kurochkin, I. V. (1998) Amyloidogenic determinant as a substrate recognition motif of insulin-degrading enzyme FEBS Lett **427**, 153–156

52 Baumann, M, Wisniewski, T., Levy, E, Plant, G and Ghiso, J (1996) C-terminal fragments of alpha- and beta-tubulin form amyloid fibrils *in vitro* and associate with amyloid deposits of familial cerebral amyloid angiopathy, British type Biochem Biophys Res Commun **219**, 238–242

53 Guijarro, J I, Sunde, M, Jones, J A, Campell, I D. and Dobson, C M (1998) Amyloid fibril formation by an SH3 domain Proc Natl Acad. Sci U S A **95**, 4224–4228

54 Scherzinger, E, Lurz, R, Turmaine, M, Mangiarini, L, Hollenbach, B, Hasenbank, R, Bates, G P, Davies, S W, Lehrach, H and Wanker, E E (1997) Huntingtin-encoded polyglutamine expansions form amyloid-like protein aggregates *in vitro* and *in vivo*. Cell **90**, 549–558

55 Chiti, F, Webster, P, Taddei, N, Clark, A, Stefani, M, Ramponi, G and Dobson, C M (1999) Designing conditions for *in vitro* formation of amyloid protofilaments and fibrils Proc Natl Acad Sci U S A **96**, 3590–3594

56 Strittmatter, W J., Weisgraber, K J., Huang, D Y, Dong, L-H, Salvesen, G S, Pericak-Vance, M, Schmechel, D, Saunders, A M, Goldgaber, D and Roses, A D (1993) Binding of human apolipoprotein E to synthetic amyloid beta peptide· isoform-specific effects and implications for late-onset Alzheimer disease Proc Natl Acad Sci. U S A. **90**, 8098–8102

57 Pillot, T, Goethals, M, Jamilla, N, Labeur, C, Lins, L, Chambaz, J, Brasseur, R, Vandekerckhove, J and Rosseneu, M (1999) β-amyloid interacts with the carboxy-terminal domain of human apolipoprotein E relevance to Alzheimer's disease J Neurochem **72**, 230–237

Received 14 March 2000/28 March 2000, accepted 17 April 2000

Redox equilibria of manganese peroxidase from *Phanerochaetes chrysosporium*: functional role of residues on the proximal side of the haem pocket

Roberto SANTUCCI*, Cristiana BONGIOVANNI*, Stefano MARINI*, Rebecca DEL CONTE†, Ming TIEN‡, Lucia BANCI† and Massimo COLETTA*[1]

*Department of Experimental Medicine and Biochemical Sciences, Università di Roma Tor Vergata, Via di Tor Vergata 135, I-00133 Roma, Italy, †Department of Chemistry and CERM, Università di Firenze, Via Luigi Sacconi 6, I-50019 Sesto Fiorentino (FI), Italy, and ‡Department of Biochemistry and Molecular Biology, Pennsylvania State University, 16802 University Park, PA, U.S.A.

Redox potentials of recombinant manganese peroxidase from *Phanerochaetes chrysosporium* have been measured by cyclic voltammetry as a function of pH, between pH 4.5 and pH 10.5. They display a bimodal behaviour (characterized by an 'alkaline' and an 'acid' transition), which indicates that (at least) two protonating groups change their pK_b values upon reduction (and/or oxidation) of the iron atom in haem. Analogous measurements have been carried out on four site-directed mutants involving residues in close proximity to the proximal ligand, His^{173}, in order to investigate the role played by residues of the proximal haem pocket on the redox properties of this enzyme. Results obtained suggest that the protonation state of N$_\delta$ of the proximal imidazole group is redox-linked and that it is crucial in regulating the 'alkaline' transition. On the other hand, none of the proximal mutants alters the 'acid' transition, suggesting that it is modulated by groups located in a different portion of the protein.

Key words: manganese peroxidase, proximal haem pocket, site-directed mutants, redox potentiometry, pH dependence

INTRODUCTION

Manganese peroxidase (MnP) is a haem protein that was first discovered in the lignin-degrading fungus *Phanerochaetes chrysosporium* [1,2]. The enzyme utilizes H_2O_2 to oxidize divalent manganese [Mn(II)] to tervalent manganese [Mn(III)], which is a diffusible oxidant postulated to enter the lignin polymer [3]. Compound I oxidizes not only Mn(II) but also a variety of organic substrates [4]. On the other hand, compound II exhibits an absolute dependence on Mn(II) as a reductant [2,5].

The X-ray crystal structure of MnP has been solved [6,7] and it reveals similarity to other peroxidases, such as horseradish peroxidase (HRP), lignin peroxidase (LiP), the peroxidase from *Coprinus cinereus* (CIP) and cytochrome *c* peroxidase (YCcP) [8–12]. Most notably, residues in the distal haem pocket of MnP (i e. His^{46} and Phe^{45}; the latter not present in CcP) are conserved. Also conserved is Asp^{242}, which is located on the proximal side of the haem pocket, forming a hydrogen-bond with N$_\delta$ of the imidazole group of the proximal His^{173} residue [6]. There is an extensive debate in the literature about the role of this conserved hydrogen-bond in modulating the properties of the iron ion, and in particular its reduction potential, and consequently the reactivity of the protein [13–16]. An interesting structural aspect concerns the other residue located on the proximal side of the haem pocket near His^{173}, namely Phe^{190}, as it displays some variation among different peroxidases. This residue is phenylalanine in MnP (Phe^{190}), LiP and HRP [6,9,17], tryptophan in YCcP [18] and leucine in CIP [10], and either can or cannot be hydrogen-bonded to the proximal His^{173} residue. The position of this residue is close to the proximal histidine, and it suggests that it might play some role in the structural arrangement of the proximal haem pocket [6], and in particular on the orientation of the axial histidine, even though no clear evidence has been obtained for its functional role [19].

Recent studies have investigated the functional and structural properties of wild-type (wt) MnP and mutants at two residues located on the proximal side of the haem pocket, namely Asp^{242} and Phe^{190} [19–21]. The results suggest that these residues might play some role in modulating the function of MnP and prompted us to investigate the effect of these site-directed mutations on the redox properties and on the proton–electron coupling. Furthermore, the effect of Mn(II) on the redox properties has been investigated.

EXPERIMENTAL

Expression and purification

The mutagenesis, expression and purification of recombinant MnP were carried out as described previously [20,22]. The purified enzyme had an $R_z \geqslant 4.5$ (A_{407}/A_{280}), and the concentration was determined using an absorption coefficient, $\epsilon = 127$ mM$^{-1}\cdot$cm^{-1} at 407 nm [23].

Direct current (DC) cyclic voltammetry measurements

DC cyclic voltammograms were run on a pyrolytic graphite (PG) electrode coated with a polymeric film [composed of an anionic

---

Abbreviations used MnP, manganese peroxidase, LiP, lignin peroxidase; YCcP, yeast cytochrome c peroxidase; CIP, peroxidase from *Coprinus cinereus*; TBPMC, tributylmethyl phosphonium chloride polymer; SCE, saturated calomel electrode, DC, direct current, wt, wild-type, HRP, horseradish peroxidase, PG, pyrolytic graphite

[1] To whom correspondence should be addressed (e-mail coletta@seneca uniroma2 it)

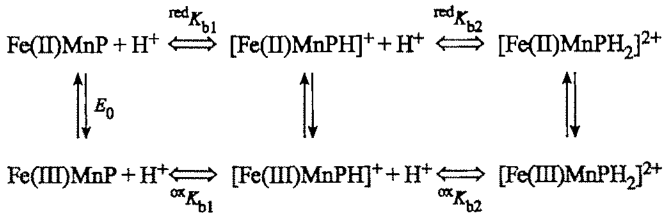

$$\begin{tikzcd}
\text{Fe(II)MnP} + \text{H}^+ \arrow[r, leftrightarrow, "{}^{\text{red}}K_{b1}"] & {[\text{Fe(II)MnPH}]^+} + \text{H}^+ \arrow[r, leftrightarrow, "{}^{\text{red}}K_{b2}"] & {[\text{Fe(II)MnPH}_2]^{2+}} \\
\text{Fe(III)MnP} + \text{H}^+ \arrow[u, shift left, "E_0"'] \arrow[r, leftrightarrow, "{}^{\text{ox}}K_{b1}"'] & {[\text{Fe(III)MnPH}]^+} + \text{H}^+ \arrow[u, shift left] \arrow[r, leftrightarrow, "{}^{\text{ox}}K_{b2}"'] & {[\text{Fe(III)MnPH}_2]^{2+}} \arrow[u, shift left]
\end{tikzcd}$$

Scheme 1 Protonation scheme of the redox equilibria

exchange resin, polystyrene cross-linked with 1 % (w/v) divinyl benzene, bound to a tributylmethyl phosphonium chloride (TBPMC) polymer, entrapping the protein.

Modified PG electrodes were prepared as previously described [24]. Briefly, TBMPC was dissolved in DMSO to give a 0.035 % (w/v) solution; a volume of 10 μl was then mixed with 40 μl of 0.2 mM MnP/water solution and deposited (by a microsyringe) on to a PG electrode surface (2 mm diameter), previously polished using an alumina (0.3 μm particle size)/water slurry, followed by extensive sonication in deionized water. Before use the modified electrode was left to dry for 2–3 days at 5 °C.

DC cyclic voltammograms were run in degassed 100 mM acetate, phosphate or carbonate buffers, depending on the pH investigated. In the electrochemical cell, the anaerobic environment was obtained by gently flowing N_2 (high-purity grade) above the surface of the solution for approx. 20 min before measurements were taken. A PG electrode (AMEL, Milan, Italy) was the working electrode, a saturated calomel electrode (SCE; AMEL) was the reference electrode and a platinum ring was the counter-electrode. A multipolarograph Amel 433 interfaced with a personal computer as the data processor was employed for cyclic voltammetry measurements.

Data analysis

The pH-dependence of the redox potential obtained by cyclic voltammograms shows that at least two protonating groups are required to account for the observed behaviour (see Scheme 1).

The pK_b [$= \log_{10}$ (K_b)] values of the controlling ionizations were calculated by fitting the data to Eqn. (1):

$$E = E_0 \cdot (1 + {}^{\text{red}}K_{b1} \cdot [\text{H}^+] + {}^{\text{red}}K_{b2} \cdot [\text{H}^+]^2) / (1 + {}^{\text{ox}}K_{b1} \cdot [\text{H}^+] + {}^{\text{ox}}K_{b2} \cdot [\text{H}^+]^2) \quad (1)$$

where E is the observed redox potential and E_0 refers to the redox potential of the unprotonated MnP. Different K_b values refer to the proton association constants for the protonating groups in the oxidized (ox) and in the reduced (red) forms.

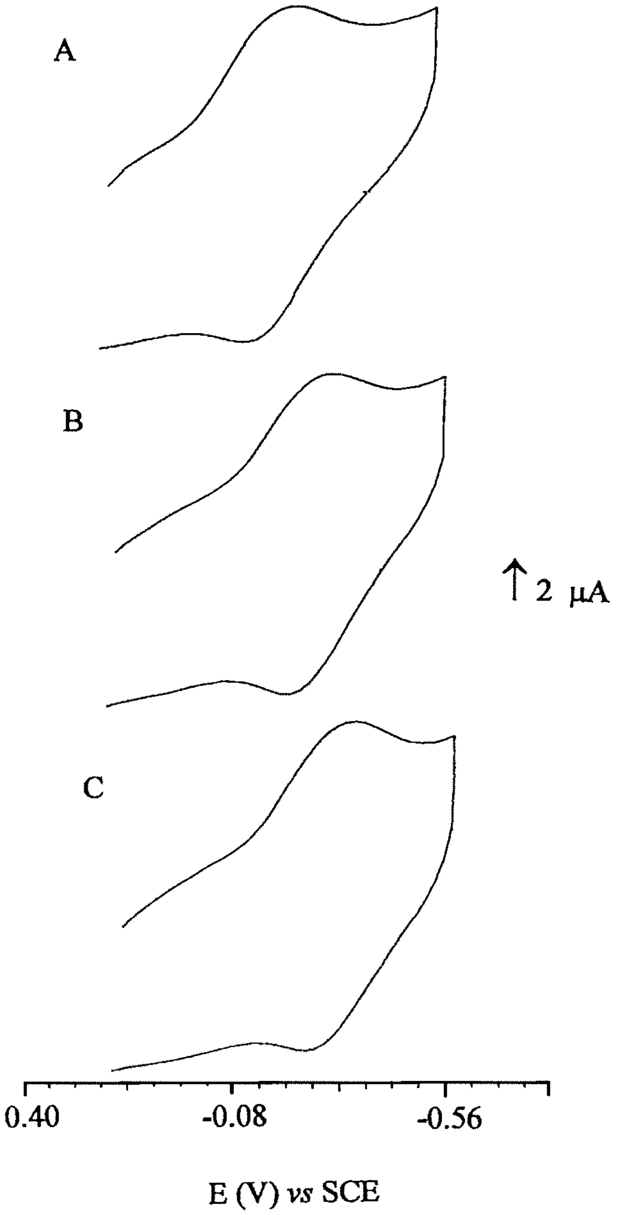

Figure 1 Cyclic voltammograms of TBMPC-embedded wt MnP at a PG electrode over the potential range between +0.4 and −0.8 V against a SCE

Cyclic voltammograms were run, at 25 °C, in 0.1 M sodium acetate buffer, pH 5.0 (**A**), and in 0.1 M sodium phosphate buffer, pH 7.0 (**B**) and pH 8.0 (**C**).

RESULTS AND DISCUSSION

Cyclic voltammetry measurements showed that in solution MnP produces no voltammetric signal at a naked PG electrode. On the other hand, rapid electron transfer is observed when the protein was embedded in a solid, inert TBMPC membrane coating the electrode (see the Experimental section). Over the whole pH range investigated (i.e. pH 4.5–10.5) the DC cyclic voltammograms of the membrane-trapped protein, dipped in the appropriate buffer, exhibited a well-defined electrochemistry for scan rates ranging between 50 and 500 mV/s. At lower scan rates the current intensity was too small to be accurately measured. Observed cathodic and anodic currents were almost identical, with an intensity ratio (i_{pa}/i_{pc}) close to unity. Such features demonstrate that the TBMPC membrane favours the direct (unmediated) electrochemistry of the protein. This explains the much sharper voltammograms obtained than those previously reported for the same protein in solution [20]. Figure 1 shows DC cyclic voltammograms for wt MnP at various pH values run at a 100 mV/s scan rate. Under the conditions investigated, the voltammetric peak current was found to depend on the square root of the scan rate, as expected for a diffusion-controlled redox process. At a scan rate of 100 mV/s, the ΔE_p values (i.e. the peak separation) were close to the theoretical value of $\Delta E_p = 57$ mV, which is expected for a one-electron-transfer reaction [25], and this was observed at all pHs investigated. At faster scan rates the

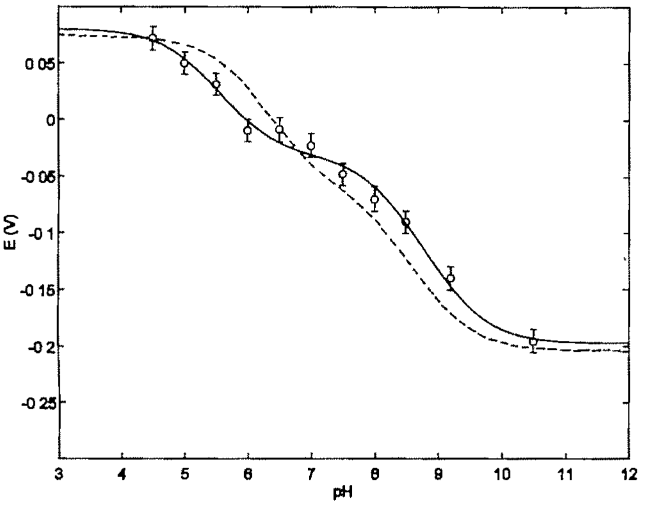

Figure 2 pH-dependence of the redox potential, E, for wt MnP

Experimental points are the average of multiple measurements (at least three) and the standard deviations are reported The continuous line was obtained by applying Eqn (1) with the parameters reported in Table 1. The dashed line corresponds to the least-squares fitting of the data according to the following equation

$$E = E_0 \cdot {}^{red}P/{}^{ox}P$$

where ${}^{red}P = 1 + ({}^{red}K_{b1} + {}^{red}K_{b2} + {}^{red}K_{b3}) \cdot [H^+] + [{}^{red}K_{b1} \cdot ({}^{red}K_{b2} + {}^{red}K_{b3}) + {}^{red}K_{b2}\ {}^{red}K_{b3}]\,[H^+]^2 + {}^{red}K_{b1} \cdot {}^{red}K_{b2}\ {}^{red}K_{b3} \cdot [H^+]^3$ and ${}^{ox}P = 1 + ({}^{ox}K_{b1} + {}^{ox}K_{b2} + {}^{ox}K_{b3}) \cdot [H^+] + [{}^{ox}K_{b1} \cdot ({}^{ox}K_{b2} + {}^{ox}K_{b1}) \cdot {}^{ox}K_{b3} + {}^{ox}K_{b2} \cdot {}^{ox}K_{b3}] \cdot [H^+]^2 + {}^{ox}K_{b1} \cdot {}^{ox}K_{b2} \cdot {}^{ox}K_{b3} \cdot [H^+]^3$, fixing ${}^{ox}K$s to pK_a values reported previously [i e. ${}^{ox}K_{a1} = 7.587 \times 10^{-10}$ M (pK_a = 9.12), ${}^{ox}K_{b1} = 1\ 318 \times 10^9\ M^{-1}$, ${}^{ox}K_{a2} = 2\ 952 \times 10^{-9}$ M (pK_a = 8.53), ${}^{ox}K_{b2} = 3.388 \times 10^8\ M^{-1}$, ${}^{ox}K_{a3} = 1.622 \times 10^{-7}$ M (pK_a = 6 79) and ${}^{ox}K_{b3} = 6.166 \times 10^6\ M^{-1}$] [21], and leaving the other parameters floating Parameters obtained from the fitting procedure were ${}^{red}K_{b1} = 3\ 31(\pm 1.35) \times 10^8\ M^{-1}$ (pK_b = 8 52±0.12), ${}^{red}K_{b2} = 1.17(\pm 0\ 41) \times 10^8\ M^{-1}$ (pK_b = 8.07±0.13), ${}^{red}K_{b3} = 6.46(\pm 1\ 86) \times 10^5\ M^{-1}$ (pK_b = 5 81±0 11) and $E_0 = -0.201 \pm 0.025$ V For further details see the text

Table 1 Redox potentials and pK_b values of redox-linked groups in wt MnP and some of its mutants

pK_b was obtained by fitting the pH-dependence of the redox potential to Eqn. (1) The reported parameters were obtained by employing different buffers at different pHs, apart from one mutant where the parameters were obtained using only phosphate buffer.

	${}^{ox}pK_{b1}$	${}^{ox}pK_{b2}$	${}^{red}pK_{b1}$	${}^{red}pK_{b2}$	E_0(V)
Wt MnP	9.39±0.16	5.95±0.13	8.17±0.13	5.13±0.11	−0.197±0 023
Asp^{242} → Glu	9 82±0.17	5 88±0.13	8 17±0.12	4.87±0.10	−0.270±0 031
Asp^{242} → Ser	8.78±0.15	5.55±0 12	7.43±0.12	4.75±0 11	−0.201±0 019
Asp^{242} → Ser only phosphate	9.10±0 17	6.12±0 16	8.29±0.14	5.44±0 12	−0.136±0.015
Phe^{190} → Val	9 27±0.17	5.73±0.16	8.11±0 14	4.92±0.12	−0.187±0 021
Phe^{190} → Leu	9.34±0.18	5.93±0.15	7.95±0 13	5.08±0.13	−0.259±0 028

ΔE_p increased (up to 140–150 mV for scan rates of 500 mV/s), indicating the occurrence of quasi-reversibility.

Figure 2 shows the pH-dependence of the redox potential for wt MnP, and the data at pH 7.0 agree with those already reported [23]. The data clearly showed that its redox behaviour was functionally modulated by the protonation of (at least) two groups, whose pK_b values were redox-linked. Fitting of data employing Eqn. (1) allowed the pK_b values to be obtained for both the oxidized (${}^{ox}pK_{b1}$ and ${}^{ox}pK_{b2}$, see Scheme 1) and the reduced (${}^{red}pK_{b1}$ and ${}^{red}pK_{b2}$, see Scheme 1) forms of the enzyme; the values obtained from the fitting of experimental data are reported in Table 1. Both ionizable groups displayed a decrease in pK_b upon reduction; the first ionization decreased it from 5.95±0.13 in the oxidized form to 5.13±0.11 in the reduced form, and the second one decreased it from 9.39±0.16 in the oxidized species to 8.17±0.13 in the reduced species (Figure 2 and Table 1). Our previous work has demonstrated that over the same pH range three pH-dependent spectroscopic transitions (observed by optical electronic absorption) were detected for oxidized wt MnP [21], and the pK_a values [$= \log_{10}(1/K_a)$] were numbered by starting from that characterized by a lower pK_a value. In the present study the equation deals with the proton association equilibrium (expressed as pK_b), and protonating groups are then numbered starting from that characterized by the highest pK_b value [see Eqn. (1)]. One of the groups responsible for a spectroscopic transition observed previously (characterized by pK_{a3} = 9.12±0.22 [21]) displayed a pK_a value similar to that corresponding to the pK_{b1} value of the oxidized molecule in our experiments (see Table 1). However, each of the other two values obtained from the spectroscopic measurements [21] differs from the other pK_b value, affecting the redox properties. This becomes evident when our data on the pH-dependence of the redox potential are fitted with the pK_a values determined by Banci et al. [21] (see Figure 2, dashed line). Findings from the two studies are not necessarily in contradiction. Indeed, only those residues whose pK_b values vary upon change of the oxidation state can affect the proton-linked redox behaviour. Therefore the two residues determining the pH-dependence of the redox potential are not necessarily the same two (out of three possible residues) modulating the pH-dependence of the wt MnP spectroscopic properties [21].

At alkaline pH values the redox potential of wt MnP was very negative ($E_0 = -0.197 \pm 0.03$ V against a normal hydrogen electrode), and as the pH was lowered, the protonation of two residues made the redox potential progressively less negative. The value became positive at pH < 6.0, with an overall change of approx. 0.3 V between pH 10.5 and pH 4.5 (see Figure 2). These results indicate that the formation of a positive charge (or the disappearance of a negative one) in these two residues brings about a condition in the haem pocket which makes the reduction of the haem's iron more favourable.

The protonation of these groups also has an effect on the heterogeneous electron transfer reaction of the protein at the electrode surface, and thus with the external environment. The rate constant for the heterogenous electron transfer (k_s) was estimated at 25 °C under acidic [i.e. in 0.1 M sodium acetate, pH 5.0; $k_s = 2.8(\pm 0.3) \times 10^{-4}$ cm/s], neutral [i.e. in 0.1 M sodium phosphate, pH 7.0; $k_s = 9.0(\pm 1.0) \times 10^{-4}$ cm/s] and alkaline [i.e. in 0.1 M sodium carbonate, pH 9.2; $k_s = 1.9(\pm 0.3) \times 10^{-4}$ cm/s] conditions according to Nicholson [26]. The values of the rate constants were calculated by using $n = 1$ (i.e. the number of electrons involved in the electron transfer process) and a diffusion coefficient, D_0, of 8.0×10^{-8} cm^2/s, calculated by applying the equation reported previously [27]. The rate constant for the heterogeneous electron transfer in the singly protonated form at neutral pH was 4–5 times faster than in the unprotonated species at alkaline pH, and approx. 3 times faster than at acidic pH. This indicates that the protonation of the residue with the higher pK_b value results in a faster rate of electron exchange, whereas the second protonation event has an opposite effect, significantly reducing the reaction rate. The addition of 1 mM MnCl$_2$, which induces the complete formation of the MnP–Mn(II) complex did not change either the observed redox potential and/or the rate of electron transfer (results not shown). This observation is sig-

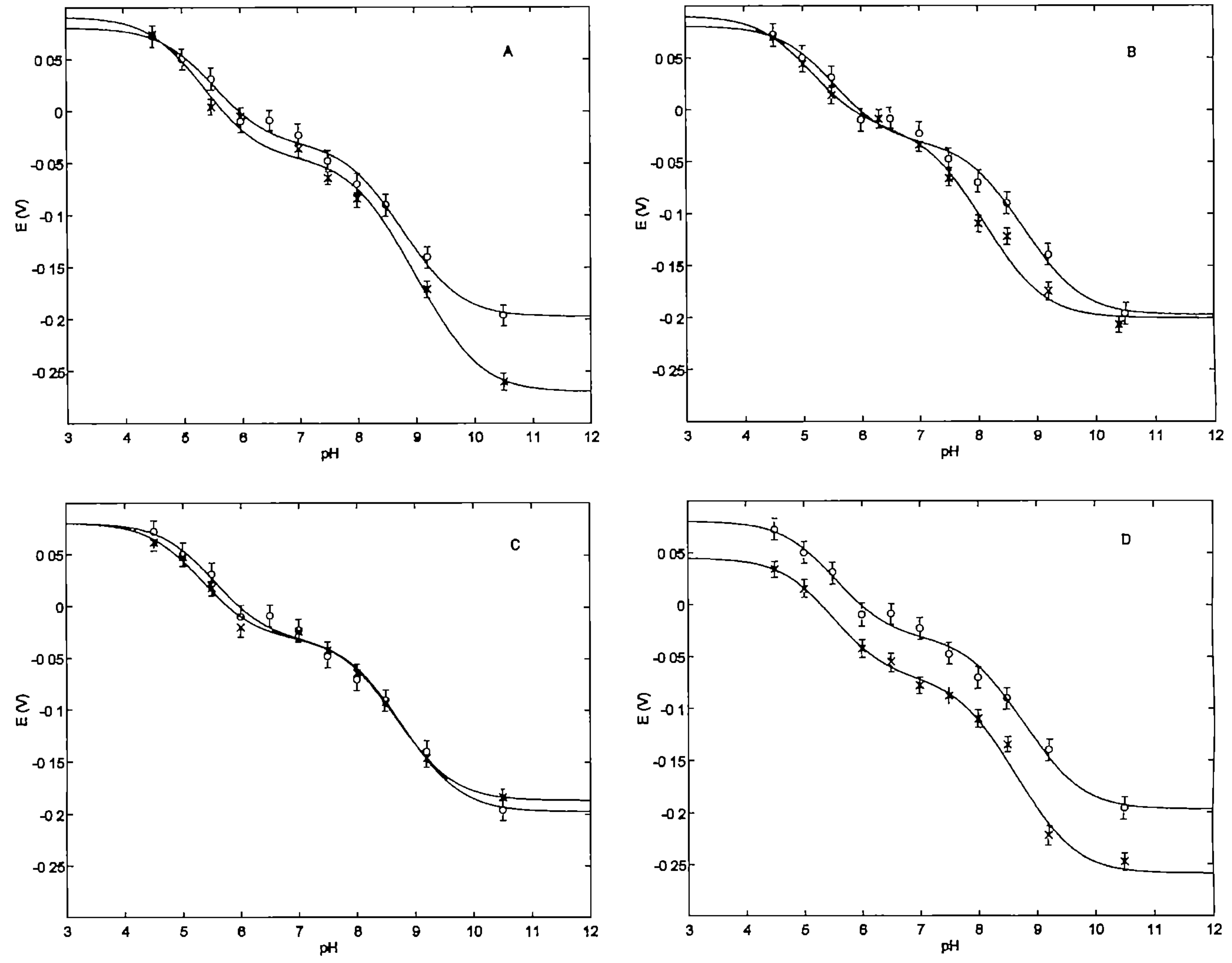

Figure 3 pH-dependence of the redox potential for mutants of MnP, namely D242E (A), D242S (B), F190V (C) and F190L (D)

Experimental points are the average of multiple measurements (at least three) and the standard deviations are reported. For clarity, in each panel the redox potentials of the mutant (×) are compared with the redox potential of wt MnP (○). Continuous lines were obtained by applying eqn (1) with the parameters reported in Table 1. For further details see the text.

nificant, since it suggests that Mn(II), which is essential in the catalytic turnover of MnP as electron donor [4,5,28], does not appreciably affect the protonation equilibria of residues modulating the oxidation state of the haem's iron and the electron exchange rates of the protein with the bulk solvent.

For the purpose of identifying the residues involved in the proton-linked modulation of both the redox potential and the heterogeneous electron transfer, we have characterized mutants in the proximal pocket of MnP, namely at Asp^{242} and at Phe^{190}. These are the same mutants previously investigated [19,21]. Two of them (i.e. D242S and D242E) display a substitution of Asp^{242}, which is hydrogen-bonded to N_{δ} of the proximal His^{173} residue [6]. Mutations concern residues, which though able to form hydrogen-bonds with the proximal histidine, show either an increased length (i.e. glutamate) or the lack of a negative charge (i.e serine). The other two mutants studied were at the Phe^{190} position (i.e. F190V and F190L), which had been substituted with other hydrophobic residues (i.e. valine or leucine) of smaller size than the aromatic ring of phenylalanine.

Figure 3 shows a comparison, as a function of pH, between the redox potential of wt MnP and those of the above mutants. It must be pointed out that results for these mutants at pH 7.0 are in agreement with those already reported [20].

The D242E mutation produced a more negative E_0 only at alkaline pH, and pK_b values were essentially the same as in the wt MnP, except for some variation of $^{ox}pK_{b1}$ (see Figure 3A and Table 1). This suggests that the increased residue length, resulting in a larger occupancy volume, has only a marginal effect on the functionally relevant proton-linked equilibria. However, the deprotonated form may impose some steric strain on the structural arrangement of the proximal side of the haem pocket, resulting in a less favourable reduction of the haem's iron. Conversely, the substitution of Asp^{242} with serine, which should produce a more dramatic change in the hydrogen-bonding network between residue 242 and His^{173}, had an effect on the first pK_b value (i.e. pK_{b1}; the residue which protonates at higher pH values); no variation was observed with either the second protonation value, pK_{a2}, or the redox potential, E_0, of the unprotonated molecule (see Figure 3B and Table 1). Thus the substitution of a negatively charged carboxy group of aspartate with the hydroxy group of serine resulted in a dramatic change in the pK_{b1} value, which turned out to be lower by approx. 0.6

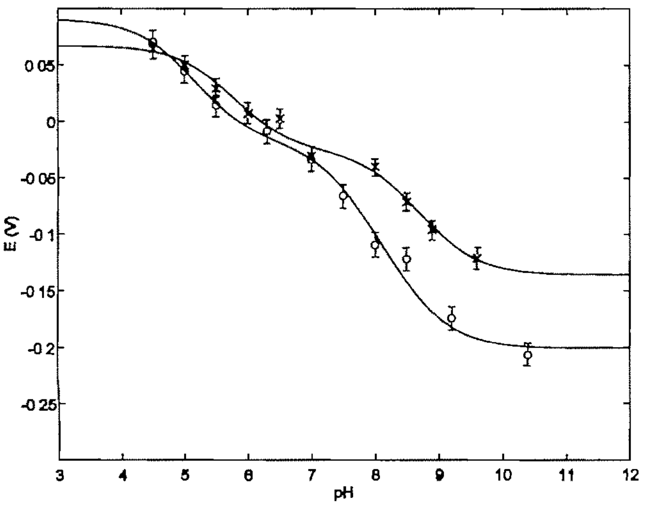

Figure 4 pH-dependence of the redox potential of the site-directed mutant D242S, employing different buffers (○) and only phosphate buffer (×)

Experimental points are the average of multiple measurements (at least three) and the standard deviations are reported Continuous lines were obtained by applying eqn (1) with the parameters reported in Table 1 For further details see the text

pH unit with respect to that of wt MnP, in both the oxidized and reduced forms (see Table 1). These results suggest that the protonation of N_δ of the proximal His^{173} residue might be responsible for the proton-linked modulatory role on the redox properties of MnP. As a matter of fact the very close proximity of a negatively charged carboxy group (of Asp^{242}) may induce an increase in the pK_b of N_δ of the imidazole group of His^{173}, and this was observed in wt MnP (i.e. 9.39$\pm$0.16 in the oxidized form and 8.17$\pm$0.13 in the reduced form, see Table 1). The substitution of aspartate with glutamate induced only a limited change and only in the oxidized form (see Table 1). This may be due to the fact that the ionic character of the interaction with N_δ was unaffected by this mutation. The interaction between N_δ of His^{173} and the residue in position 242 may still be present in the D242S mutant. This would occur through hydrogen-bonding of the imidazole N_δ with the hydroxy group of serine. Consistent with this hypothesis, the lower pK_b value for the reduced form may be related to a decreased polarizing effect of Asp^{242} on N_δ of the proximal imidazole group. This may possibly be associated to a redox-linked conformational change of the proximal portion of the haem pocket, which affects the orientation and/or the distance between the residue at position 242 and N_δ of His^{173}. The very marginal effect, if any, on the second protonation event at acid pH values upon removal of the negative carboxy group in D242S (see Table 1) rules out any possible involvement of His^{173} in the modulation of this proton-linked process. It is important to point out that the heterogeneous electron transfer (k_s) at 25 °C in the D242S mutant displayed similar values to the wt MnP (i.e. $k_s = 4.0(\pm 0.3)\times 10^{-4}$ cm/s at pH 5.0 in 0.1 M sodium acetate, $k_s = 7.5(\pm 1.0)\times 10^{-4}$ cm/s at pH 7.0 in 0.1 M sodium phosphate and $k_s = 1.9(\pm 0.3)\times 10^{-4}$ cm/s at pH 9.2 in 0.1 M sodium carbonate), suggesting that the mutation does not appreciably affect this parameter.

On the other hand, it is very interesting to remark that the nature of the buffer affected the electrochemical behaviour of the D242S mutant, such that the value of E_0 at very alkaline pH values was much less negative in the presence of phosphate (see Figure 4 and Table 1). The presence of phosphate also caused an increase in the pK_{b1} values in both the oxidized and reduced forms of the D242S mutant relative to the wt species (see Table 1). The phosphate also affected the values of pK_{b2}, rendering them even higher than that observed in the wt enzyme (see Figure 4 and Table 1) In the previous spectroscopic characterization of these mutants it was found that phosphate facilitated the removal of the distal Ca^{2+}, which occurs with a pK_a intermediate between the pK_{b1} and pK_{b2} values. Apparently this effect was not detected in our measurements, because the pK_b value of this process is the same for the oxidized and the reduced state. Alternatively, it could occur that the protein experiences slightly different pK_b values in the oxidation states with and without distal Ca^{2+}. In any event, it appears that phosphate is able to modulate, in a specific way, the redox properties of MnP, a feature which cannot be attributed to only the negative charge on the phosphate, since the E_0 value and two pK_b values are all affected.

The functional effects of mutating Phe^{190} were less apparent. As shown in Figure 3(C), the F190V mutation did not induce a significant variation in either of the pK_a values of groups, which affect the redox properties of the enzyme (see Table 1). In the case of the F190L mutant (see Figure 3D), only the redox potential E_0 was affected (see Table 1) This result suggests that the longer aliphatic chain of leucine may induce, like in the case of the glutamyl residue in position 242 (see above), some steric disturbance to the conformation of the proximal His^{173} residue. This conformational change in turn renders the reduction process less favourable. However, in both mutants the substitution of Phe^{190} did not induce any effect on the proton-linked equilibria of the oxidized and reduced forms (see Table 1). This indicates that, as expected, this residue is not involved in interactions that regulate the pK_b of functionally relevant groups.

The 'acid' transition is completely unaffected by mutations at residues 242 and 190. This proton-linked feature is most likely attributed to a group that does not interact with the proximal side of the haem pocket of MnP, and its identification must await further investigation on additional mutants in different portions of the haem pocket.

In conclusion, the comparison between wt MnP and site-directed mutants provides a significant contribution to a deeper understanding of the system through the pH-dependence of redox potentials, allowing us to discriminate between effects on pK_b values from the intrinsic redox potential(s). This confirms the requirement for a complete investigation on the electron–proton coupling in order to afford a general description of the functional modulation mechanism in an electron carrier.

This work was partially supported by the programme Progetto Finalizzato Biotechnologie of the Italian CNR (contribution 99 00286 PF49), the Department of Energy grant DEFG02-87ER13690 to M T, the Italian Ministero dell'Università e della Ricerca Scientifica e Tecnologica grant (MURST COFIN 9803184222) to M C and the European Union for the Network grant 'Foundations for controlling properties of haem proteins. structure/function relationships in archetypal systems and the development of an interdisciplinary methodology' (ERBFMRX CT 98 0218)

REFERENCES

1 Huynh, V B and Crawford, R L (1985) Novel extracellular enzymes (ligninases) of *Phanerochaete chrysosporium* FEMS Microbiol Lett **28**, 119–123
2 Glenn, J K. and Gold, M H (1985) Purification and characterization of an extracellular Mn(II)-dependent peroxidase from the lignin-degrading basidiomycete, *Phanerochaete chrysosporium*. Arch Biochem Biophys **242**, 329–341
3 Glenn, J K, Akileswaran, L and Gold, M H (1986) Mn(II) oxidation is the principal function of the extracellular Mn-peroxidase from *Phanerochaete chrysosporium* Arch Biochem Biophys **251**, 688–696
4 Wariishi, H, Dunford, H B, MacDonald, D I and Gold, M H (1989) Manganese peroxidase from the lignin-degrading basidiomycete *Phanerochaete chrysosporium*. Transient state kinetics and reaction mechanism J. Biol Chem **264**, 3335–3340

5 Kuan, I-C, Johnson, K A and Tien, M (1993) Kinetic analysis of manganese peroxidase The reaction with manganese complexes. J Biol Chem. **268**, 20064–20070

6 Sundaramoorthy, M, Kishi, K, Gold, M H and Poulos, T L (1994) The crystal structure of manganese peroxidase from *Phanerochaete chrysosporium* at 2.06-Å resolution J Biol Chem **269**, 32759–32767

7 Sundaramoorthy, M, Kishi, K, Gold, M H and Poulos, T L (1997) Crystal structures of substrate binding site mutants of manganese peroxidase J Biol Chem **272**, 17574–17580

8 Gajhede, M, Schuller, D J, Henriksen, A, Smith, A T and Poulos, T L (1997) Crystal structure of horseradish peroxidase C at 2.15 Å resolution Nat Struct. Biol **4**, 1032–1038

9 Poulos, T L, Edwards, S L, Wariishi, H. and Gold, M. H (1993) Crystallographic refinement of lignin peroxidase at 2 Å J Biol Chem. **268**, 4429–4440

10 Petersen, J W F, Kadziola, A and Larsen, S (1994) Three-dimensional structure of a recombinant peroxidase from *Coprinus cinereus* at 2.6 Å resolution FEBS Lett **339**, 291–296

11 Finzel, B C, Poulos, T. L and Kraut, J (1984) Crystal structure of yeast cytochrome c peroxidase refined at 1.7-Å resolution J Biol Chem **259**, 13027–13036

12 Wang, J, Mauro, J M, Edwards, S L, Oatley, S J, Fishel, L A, Ashford, V A, Xuong, N and Kraut, J (1990) X-ray structures of recombinant yeast cytochrome c peroxidase and three heme-cleft mutants prepared by site-directed mutangenesis Biochemistry **29**, 7160–7173

13 Banci, L, Bertini, I, Turano, P., Tien, M and Kirk, T K (1991) Proton NMR investigation into the basis for the relatively high redox potential of lignin peroxidase Proc. Natl Acad. Sci. U S A **88**, 6956–6960

14 Edwards, S L, Raag, R, Wariishi, H, Gold, M H and Poulos, T L (1993) Crystal structure of lignin peroxidase Proc Natl Acad Sci U S A **90**, 750–754

15 Goodin, D B and McRee, D E (1993) The Asp-his-Fe triad of cytochrome c peroxidase controls the reduction potential, electronic structure, and coupling of the tryptophan free radical to the heme. Biochemistry **32**, 3313–3324

16 Ferrer, J C, Turano, P, Banci, L, Bertini, I, Morris, I K, Smith, K M, Smith, M and Mauk, A G (1994) Active site coordination chemistry of the cytochrome c peroxidase Asp235Ala variant spectroscopic and functional characterization. Biochemistry **33**, 7819–7829

Received 4 January 2000/23 March 2000, accepted 25 April 2000

17 Piontek, K, Glumoff, T and Winterhalter, K (1993) Low pH crystal structure of glycosylated lignin peroxidase from *Phanerochaete chrysosporium* at 2.5 Å resolution FEBS Lett **316**, 119–124

18 Poulos, T L and Kraut, J (1980) A hypothetical model of the cytochrome c peroxidase cytochrome c electron transfer complex J. Biol Chem. **255**, 10322–10330

19 Kishi, K, Hildebrand, D. P., Kusters-van Someren, M, Gettemy, J, Mauk, A G and Gold, M H (1997) Site-directed mutations at phenylalanine-190 of manganese peroxidase effects on stability, function, and coordination Biochemistry **36**, 4268–4277

20 Whitwam, R, Kodurí, R S, Natan, M and Tien, M (1999) Role of axial ligands in the reactivity of Mn peroxidase from *Phanerochaete chrysosporium* Biochemistry **38**, 9608–9616

21 Banci, L, Bertini, I, Capannoli, C, Del Conte, R and Tien, M (1999) Spectroscopic characterization of active mutants of manganese peroxidase mutations on the proximal side affect calcium binding of the distal side Biochemistry **38**, 9617–9625

22 Whitwam, R and Tien, M (1996) Heterologous expression and reconstitution of fungal Mn peroxidase Arch Biochem Biophys **333**, 439–446

23 Millis, C D, Cai, D, Stankovich, M T and Tien, M (1989) Oxidation-reduction potentials and ionization states of extracellular peroxidases from the lignin-degrading fungus *Phanerochaete chrysosporium* Biochemistry **28**, 8484–8489

24 Santucci, R, Ferri, T, Morpurgo, L, Savini, I and Avigliano, L (1998) Unmediated heterogeneous electron transfer reaction of ascorbate oxidase and laccase at a gold electrode. Biochem J **332**, 611–615

25 Nicholson, R S and Shain, I (1964) Theory of stationary electrode polarography Single scan and cyclic methods applied to reversible, irreversible and kinetic systems Anal Chem **36**, 706–723

26 Nicholson, R S (1965) Theory and application of cyclic voltammetry for measurement of electrode reaction kinetics Anal Chem **37**, 1315–1355

27 Bard, A J and Faulkner, L R (1980) In Electrochemical Methods Fundamentals and Applications, pp 230–231, John Wiley, New York

28 Wariishi, H, Akileswaran, L and Gold, M H (1988) Manganese peroxidase from the basidiomycete *Phanerochaete chrysosporium* spectral characterization of the oxidized states and the catalytic cycle Biochemistry **27**, 5365–5370

Biochem J (2000) **349**, 91–97 (Printed in Great Britain)

Glucocorticoids induce a near-total suppression of hyaluronan synthase mRNA in dermal fibroblasts and in osteoblasts: a molecular mechanism contributing to organ atrophy

Wei ZHANG*, Catherine E. WATSON†, Connie LIU*, Kevin Jon WILLIAMS† and Victoria P. WERTH*[1]

*Department of Dermatology, University of Pennsylvania, Philadelphia V A. Hospital, 2 Rhoads Pavilion, 36th and Spruce, Philadelphia, PA 19104, U.S.A., and
†The Dorrance H Hamilton Research Laboratories, Division of Endocrinology, Diabetes & Metabolic Diseases, Department of Medicine,
Jefferson Medical College of Thomas Jefferson University, Philadelphia, PA 19107, U S A

Glucocorticoid (GC) administration induces atrophy of skin, bone, and other organs, partly by reducing tissue content of glycosaminoglycans, particularly hyaluronic acid (HA). We took advantage of the recent cloning of the three human hyaluronan synthase (HAS) enzymes (HAS1, HAS2 and HAS3), to explore the molecular mechanisms of this side effect. Northern and slot blots performed on RNA extracted from cultured dermal fibroblasts and the MG-63 osteoblast-like osteosarcoma cell line indicated that HAS2 is the predominant HAS mRNA in these cells. Incubation of both cell types for 24 h in the presence of 10^{-6} M dexamethasone (DEX) resulted in a striking 97–98 % suppression of HAS2 mRNA levels. Time-course studies in fibroblasts demonstrated suppression of HAS2 mRNA to 28 % of control by 1 h, and to 1.2 % of control by 2 h, after addition of DEX. Dose-response studies in fibroblasts indicated that the majority of the suppressive effect required concentrations characteristic of cell-surface GC receptors, a point confirmed by persistent DEX-induced suppression in the presence of RU486, an antagonist of classic cytosolic steroid hormone receptors. Nuclear run-off experiments showed a 70 % suppression of *HAS2* gene transcription in nuclei from DEX-treated fibroblasts, which is unlikely to fully explain the rapid 50–80-fold reduction in message levels. Experiments with actinomycin D (AMD) demonstrated that the message half-life was 25 min in cells without DEX, whereas the combination of AMD with DEX dramatically increased the half-life of HAS2 mRNA, suggesting that DEX acts by inducing a short-lived destabilizer of the HAS2 message. Direct assessment of HAS2 mRNA stability by wash-out of incorporated uridine label established a half-life of 31 min in cells without DEX, which substantially shortened in the presence of DEX. In conclusion, GCs induce a rapid and sustained, near-total suppression of HAS2 message levels, mediated through substantial decreases in both gene transcription and message stability. These effects may contribute to the loss of HA in GC-treated organs.

Key words: extracellular matrix, fibroblasts, hyaluronic acid.

INTRODUCTION

Hyaluronic acid (HA; also called hyaluronan) is an ancient, highly conserved, extracellular glycosaminoglycan that serves many crucial physiologic functions, including barrier effects, tissue resilience and elasticity, control of cell proliferation and migration, wound healing, and organization of hyaluronan-binding molecules, such as hyalectin-type chondroitin sulphate proteoglycans, fibrinogen, and types I and VI collagen into macromolecular assemblies [1–6]. HA is found in nearly every tissue in vertebrates. Although the amount of HA in extracellular matrix is reduced in several human conditions, including cutaneous atrophy, aging, impaired wound healing, and possibly osteoporosis, the molecular control of tissue HA content is incompletely understood [7–9].

HA is synthesized by monomeric enzymes, called hyaluronic acid synthases (HASs), that use both sugar precursors, UDP-glucuronic acid and UDP-*N*-acetyl glucosamine, to assemble the glycosaminoglycan chain. The mode of synthesis is unique amongst macromolecules since it is proposed to occur at the plasma membrane, and during its synthesis the developing HA molecule is extruded directly into the extracellular space [10]. cDNAs encoding human HAS1, human HAS2, and a partial sequence of human HAS3 have been reported [10–12], and the chromosomal locations of the three human *HAS* genes have been identified [13]. In addition, homologues in many other species have been reported, including full-length sequences encoding the murine Has1, Has2 and Has3 [13–15].

Studies using these molecular tools to examine HAS regulation have only recently begun to appear in the literature. Murine cumulus cell–oocyte complexes isolated immediately after inducing an ovulatory cycle (at which time they do not synthesize HA), showed no HAS2 mRNA by reverse-transcriptase-mediated PCR, but when HA synthesis begins 3–4 h later, HAS2 mRNA was expressed at high levels [16]. Similarly, in cultured human dermal fibroblasts and epidermal keratinocytes, transforming growth factor-β, a known stimulus for HA synthesis [17], increased the levels of HAS1 and HAS2 message (HAS3 message was not examined) [18]. These studies suggest that HAS message levels, possibly reflecting gene transcription, control HA synthesis. In addition, the promoter sequence for murine *Has1* was recently determined and found to contain several potential binding motifs for transcription factors [19].

In the present study, we sought to determine the effect of glucocorticoids (GCs) on the molecular regulation of HA synthases in skin and bone cells. GCs are widely used therapeutic

---

Abbreviations used: AMD, actinomycin D, DEX, dexamethasone, DMEM, Dulbecco's modified Eagle's medium, FBS, fetal bovine serum; GAG, glycosaminoglycan, GC, glucocorticoid, HA, hyaluronic acid; HAS, hyaluronan synthase.

[1] To whom correspondence should be addressed (e-mail werth@mail.med.upenn.edu).

agents with a serious side effect of reducing the tissue content of glycosaminoglycans, especially HA [9,20,21]. The resulting organ atrophy, particularly of skin and skeleton, produces substantial morbidity and mortality [22,23]. We found that the predominant HAS in cultured human dermal fibroblasts and osteoblast-like osteosarcoma cells is HAS2, and that GCs induce a large and rapid suppression of HAS2 expression in these cell types through effects on both transcription and mRNA stability. These molecular effects are likely to contribute to GC-induced atrophy of skin and skeleton *in vivo*.

EXPERIMENTAL PROCEDURES

Chemicals

RNAzol B was purchased from Tel-Test (Friendswood, TX, U.S.A.). Dexamethasone (DEX) was obtained from American Regent Lab, Inc. (Shirley, NY, U.S.A.). All other chemicals were obtained from Fisher and Sigma.

Cultured cells

Normal human dermal fibroblasts and the human osteosarcoma cell line, MG-63, a well-established model of osteoblasts [24], were obtained from the A.T.C.C. (Rockville, MD, U.S.A.). Cells were plated in Petri dishes (100 mm diameter; Corning, NY, U.S.A.) in Dulbecco's modified Eagle medium (DMEM) supplemented with 10% fetal bovine serum (FBS), and grown to 90% confluency, at which point the media were replaced by DMEM/10% FBS, with or without DEX (1 μM). The DEX dose-response experiment was carried out with doses of DEX ranging from 0.15 pM to 1.5 μM. Experiments with RU486, a specific antagonist of classic cytosolic steroid hormone receptors [25], were performed by pre-incubating fibroblasts for 14 h in DMEM/10% FBS, without or with this agent, followed by the addition of 1 μM DEX, and then a further 2 h incubation.

cDNA probes

The cDNA sequence in GenBank® for each human HAS enzyme was used to design specific PCR primers to amplify a segment near the 3′ end of each coding region. These segments were chosen based on their relatively poor conservation amongst HAS1, HAS2 and HAS3 cDNAs, and the fact that only the 3′ end of the human HAS3 cDNA sequence is currently available. The sequence portion and primers for each human HAS cDNA were as follows: HAS1, from bp 1116–1715 [11] using sense primer 5′-tgctactcagagacgccctc-3′ and antisense primer, 5′-ccagtacagcgtcaacatgg-3′; HAS2, from bp 1445–2016 [12] using sense primer 5′-tttatgggcaaccaatgtagc-3′ and antisense primer 5′-aaaatcacaccacccaggag-3′; and HAS3, from bp 2–490 [15] using sense primer 5′-cctactttggctgtgtgcag-3′ and antisense primer, 5′-agatcatctctgcattgccc-3′. As template for these PCR reactions, we used cDNA that we had synthesized using reverse transcriptase (Superscript II, Gibco BRL, Gaithersburg, MD, U.S.A.), oligo(dT) primers, and total RNA isolated from cultured human umbilical vein endothelial cells. Each PCR reaction generated a single band of the correct molecular mass (approx. 600 bp for each), which was then cloned into the T-tailed vector pCRII (Invitrogen, Carlsbad, CA, U.S.A.), and the identity of each insert was confirmed by sequencing.

To obtain HAS cDNA for labelling, the T-tailed vectors with the appropriate insert either were digested with *Eco*RI, or were used as template for a second PCR reaction that employed the same primers as above. As a housekeeping control, we used a probe for 18 S ribosomal RNA (1.5 kb), which was cloned into the pBluescript SK$^+$ vector, then digested with *Eco*RI to obtain an 18 S cDNA fragment for labelling. All probes were ^{32}P-labelled by random priming (Strategene, La Jolla, CA, U.S.A.) for use in Northern and slot blotting.

Northern blotting and slot blotting

Cellular RNA was extracted by adding RNAzolB (Tel-Test) directly to 100 mm Petri dishes, followed by standard RNA isolation procedures using phenol/$CHCl_3$ extraction and isopropanol precipitation. Specific binding was confirmed for each labelled probe by Northern blot. For slot blots, total fibroblast RNA was applied to nylon membranes (Magna Charge 45 μm nylon transfer membranes; MSI, Westboro, MA, U.S.A.) using a slot-blot apparatus (10 μg/slot), and then hybridized to labelled cDNA probes [26]. The level of each transcript was quantified by PhosphorImage (Molecular Dynamics, Sunnyvale, CA, U.S.A.) and normalized to 18 S RNA. In our initial experiments to compare levels of the three HAS messages in cultured cells, the mass of each HAS mRNA and of 18 S was calculated based on its PhosphorImage signal, and the specific radioactivity of the labelled cDNA probe used for hybridization.

Nuclear run-off assay

Cultured cells were treated with or without DEX for 2 h, and then nuclei were isolated, resuspended in storage buffer [50 mM Tris/HCl (pH 8.3), 5 mM $MgCl_2$, 0.1 M EDTA with 40% glycerol], and kept in liquid nitrogen until use. The run-off reaction was performed by incubating thawed nuclei with ATP, CTP, GTP, and [α-^{32}P]UTP. Newly completed, labelled RNA was isolated after 30 min, using isopropranol precipitation with Trizol (Gibco BRL). Labelled HAS2 and 18 S RNAs were quantified by hybridization to unlabelled immobilized HAS2 and 18S cDNAs on a slot-blot apparatus, followed by autoradiography on a PhosphorImager, using established procedures [27].

Assessment of HAS2 message half-life using actinomycin-D

Subconfluent fibroblasts were incubated for 30 min with 1.0 μM DEX or control media, then the cells were treated with actinomycin D (AMD; 5 μg/ml) to block further RNA synthesis. RNA was obtained upon addition of AMD, then at 20 min, 40 min, and 90 min thereafter. Quantifications of mRNA for HAS2 by slot blot were normalized to 18 S RNA, which is useful for these kinds of studies owing to its extremely long half-life [28]. Data were displayed by semi-log plot, and $t_{\frac{1}{2}}$ values were computed from linear regression of the ln of normalized mRNA values versus the time after addition of AMD, as previously described [28].

Direct assessment of HAS2 message half-life by wash-out of incorporated uridine label

Cells were labelled essentially to the steady state by incubation with [^{3}H]uridine for 2 days and then rinsed with PBS. A wash-out was performed by incubation of cells in the presence of excess unlabelled uridine for the rest of the experiment [29]. After 1 h of uridine wash-out, DEX was added to half the cells. At several time points after wells had received DEX (0, 15 and 60 min), residual tritium label in the HAS2 and 18 S RNAs was quantified. The quantification was performed by hybridization of total cellular RNA for 2 days with excess unlabelled HAS2 and 18 S cDNA probes which had been bound to nitrocellulose membranes. These membranes were washed, and then bound ^{3}H-labelled RNA was eluted with 0.5 ml of 1 M NaOH for 3 min at 95 °C. The eluate was neutralized with 1 M HCl, and radioactivity quantified using a liquid scintillation counter (Beckman LS 6000IC). Data were displayed by semi-log plot, and $t_{\frac{1}{2}}$ values were computed from linear regression of the ln of normalized mRNA values versus the time after addition of DEX.

Statistics

Unless otherwise indicated, summary statistics are reported as means ± S.E.M.; $n = 3$. Comparisons between two means were performed using the unpaired two-tailed t test. Comparisons of several groups simultaneously were performed by initially using ANOVA. When the ANOVA indicated differences among the groups, pairwise comparisons were performed using the Student–Newman–Keuls q statistic [30]. Standard errors for the differences between means of groups with equal n were calculated as the square root of the sum of the squares of the individual S.E. values. Absent error bars in graphical displays of summary statistics for $n = 3$ indicate S.E.M. values smaller than the drawn symbols.

RESULTS

Quantification of HAS messages in cultured human fibroblasts and osteosarcoma cells

Total RNA was isolated from subconfluent cultured human fibroblasts and analysed by Northern blotting using ^{32}P-labelled HAS1, HAS2 or HAS3 cDNA probes. As expected [18], HAS1 mRNA was detected as a single 2.4 kb band, and HAS2 mRNA was detected as two bands of 3.2 kb and 4.8 kb. No HAS3 message was detected in the RNA from these cells. Quantitative analysis of triplicate slot blots showed that the dominant HAS message in control fibroblasts encodes HAS2 (Figure 1). Virtually identical results were obtained in the MG-63 osteoblast line. Therefore our subsequent studies focused on the HAS2 message.

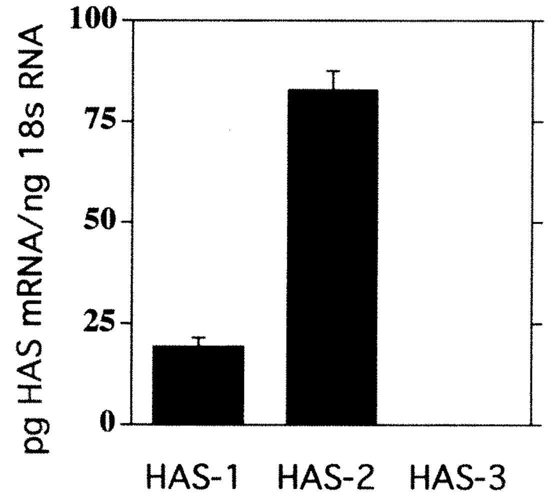

Figure 1 Quantitative comparison of HAS message levels in the absence of GCs

RNA was extracted from cultured fibroblast monolayers and analysed by slot blot. The filters were hybridized sequentially with HAS1, HAS2 and HAS3 cDNA probes and then rehybridized with the 18 S probe. The mass of each RNA was computed, based on the radioactive signal and the specific radioactivities of the labelled cDNA probes. Displayed are HAS mRNA mass data, normalized to 18 S mass. ANOVA indicated differences amongst the groups ($P < 0.0001$; Student–Newman–Keuls test indicated that the normalized HAS2 mRNA level was greater than either the HAS1 or the HAS3 signals, and that HAS1 was greater than HAS3; $P < 0.01$ for each of these pairwise comparisons).

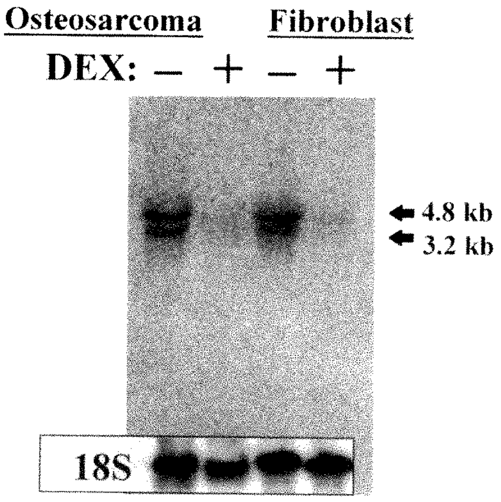

Figure 2 Effect of DEX on HAS2 mRNA levels in cultured fibroblasts and osteosarcoma MG-63 cells

90% confluent fibroblasts and osteosarcoma cells were cultured without (−) or with (+) 1 μM DEX for 24 h. Displayed is a Northern blot of total cellular RNA hybridized with ^{32}P-labelled HAS2 cDNA probe. The inset (18 S) shows the result from stripping then hybridizing the same blot with a labelled 18 S probe.

Effect of DEX on HAS2 message levels

Twenty-four hours after addition of 1 μM DEX or control buffer to cultured cells, total RNA was harvested and analysed by Northern blot. In DEX-treated fibroblasts, the 4.8 kb and 3.2 kb HAS2 mRNA bands, normalized to 18 S, were suppressed by 98 % and 97 % respectively, compared with their levels in control cells (Figure 2, fibroblast lanes, + versus −). Similarly, DEX-treated osteosarcoma cells exhibited a 98 % suppression of both HAS2 bands compared with control cells without DEX (Figure 2, osteosarcoma lanes, + versus −).

The time course of DEX-induced suppression of HAS2 mRNA was examined in fibroblasts in a long-term study, which indicated a sustained effect over 36 h (Figure 3A), and subsequently in a shorter study, which indicated near-total suppression of HAS2 message by 2 h (Figure 3B). HAS1 mRNA suppression was also observed, but to a smaller degree (by 25 % ± 7.6 % at 24 h, $P < 0.03$). Thus GCs induce a rapid, sustained, near-total suppression of HAS2 mRNA, the predominant HAS message in these cells.

Pathways for DEX signalling

GCs exert effects through three distinct pathways [31]: (i) the classic cytosolic GC hormone receptor, which is activated in more than 30 min by 1 pM–1 nM prednisone equivalents [31], i.e. between 0.14 pM and 0.14 nM DEX (0.75 mg of DEX is equivalent to 5.0 mg of prednisone, and the ratio of molecular mass is 1.09), and is inhibited by the general antagonist of cytosolic steroid hormone receptors, RU-486 [25]; (ii) putative

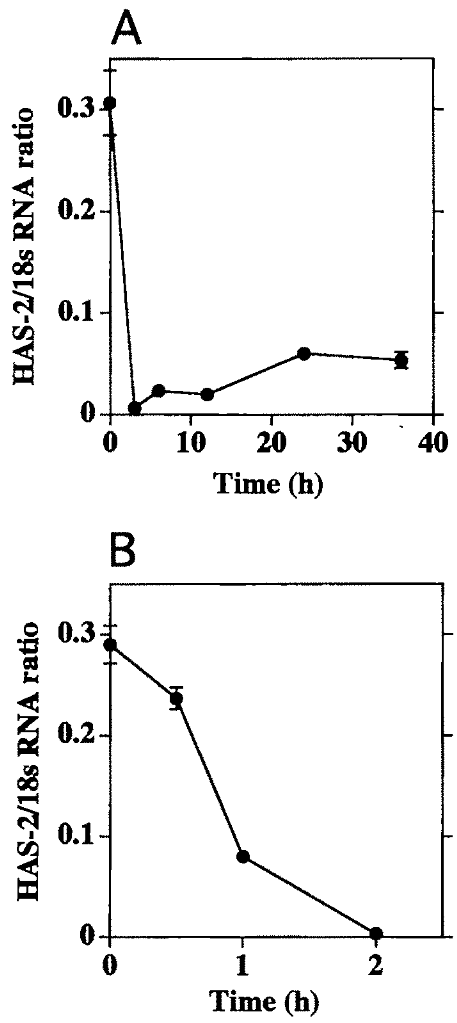

Figure 3 Time courses for DEX-induced suppression of HAS2 mRNA

Fibroblasts were incubated with DEX for the indicated times, and then RNA was harvested. Displayed are the results from triplicate slot-blot quantifications of HAS2 mRNA normalized to 18 S RNA in (**A**) long-term and (**B**) short-term incubations.

cell-surface steroid hormone receptors, which are activated within seconds to 1–2 min by 0.14 nM or greater DEX; and (iii) direct physical actions on cellular membranes, which require seconds and > 14 μM DEX [31]. Thus rapid suppression of HAS2 mRNA by 1 μM DEX is consistent with the characteristics of cytosolic and cell-surface receptors, but not direct physical effects.

Two methods were used to distinguish the roles of these different classes of receptors. First, we examined the dose response of DEX-induced suppression of HAS2 mRNA in fibroblasts. Figure 4 shows that ⩽ 45 % suppression of HAS2 mRNA occurred at 0.15 pM and 0.15 nM DEX, consistent with a limited contribution from cytosolic receptors, but the full suppression required 1.5 nM and 1.5 μM DEX, consistent with a predominant role for the cell-surface steroid hormone receptors. Secondly, blocking experiments were performed with RU486, an antagonist for cytosolic steroid hormone receptors. In the absence of DEX, RU486 produced approx. 50 % decreases in HAS2 mRNA (Figure 5), possibly because of blockage of other non-GC steroid hormones [32,33]. Addition of DEX in the absence or presence of RU486, however, produced a near-total suppression

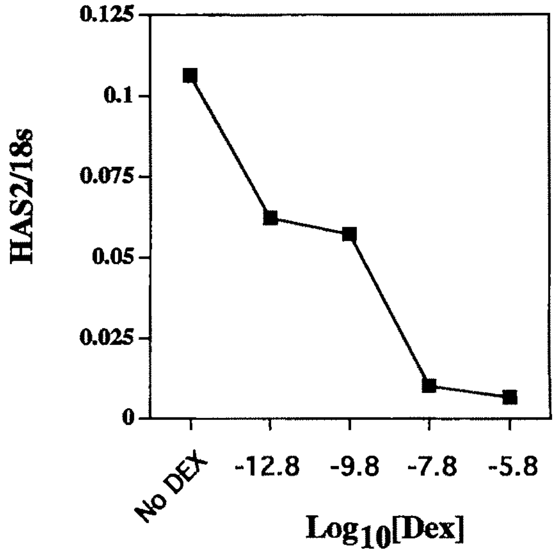

Figure 4 Dose response for DEX-induced suppression of HAS2 mRNA

Fibroblasts were incubated with the indicated concentrations of DEX, and RNA was harvested 24 h later. Displayed are the results from duplicate Northern-blot quantifications of HAS2 mRNA normalized to 18S RNA. The non-zero doses of DEX (0.15 pM, 0.15 nM, 15 nM and 1.5 μM) are indicated on the x-axis as the base$_{10}$ log.

of HAS2 mRNA levels, confirming that the majority of DEX-induced suppression is independent of cytosolic steroid hormone receptors. Taken together, these results suggest a major role for the cell-surface receptors.

Molecular mechanisms of DEX-induced suppression of HAS2 message levels

To explore the molecular basis for the large effect of GCs on HAS2 message levels, we began by examining *HAS2* transcription

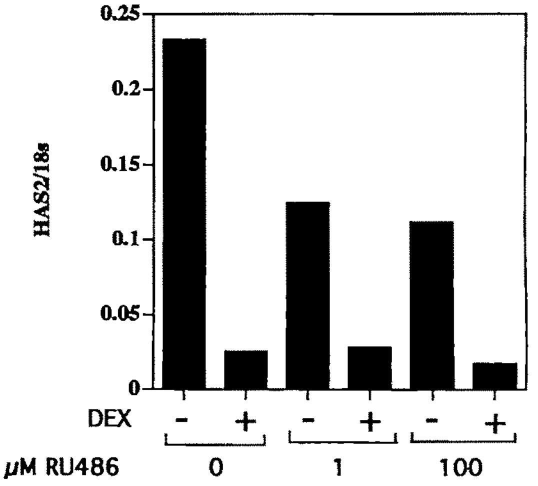

Figure 5 Lack of effect of RU486 on DEX-induced suppression of HAS2 mRNA

Fibroblasts were incubated with 1.0 or 100 μM RU486 overnight, as indicated, followed by a 2 h incubation without (−) or with (+) 1 μM DEX. RNA was harvested 2 h later. Displayed are the results from duplicate Northern-blot quantifications of HAS2 mRNA normalized to 18 S RNA.

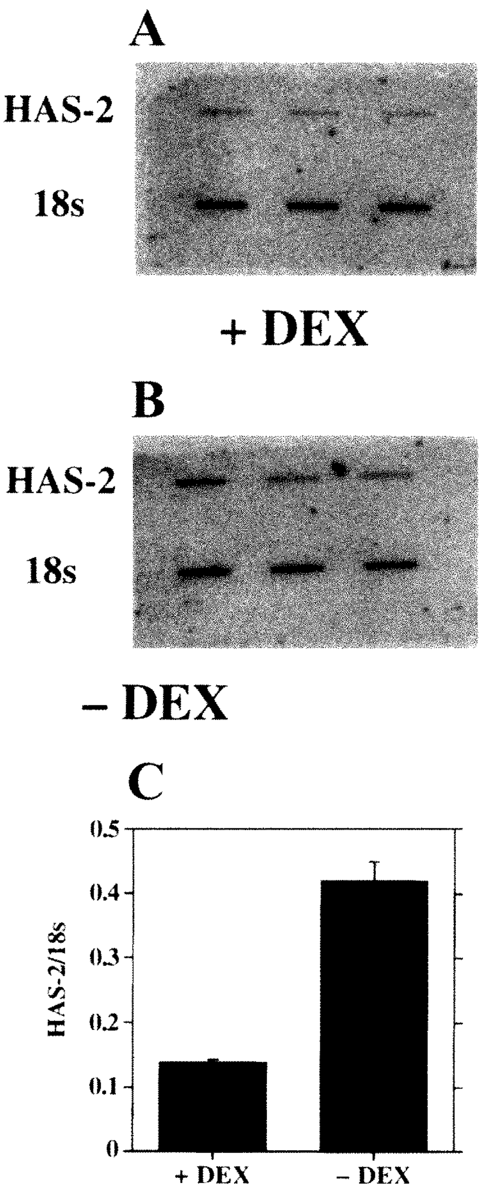

Figure 6 Effect of DEX on HAS2 gene transcription

Nuclei isolated from fibroblasts which had been pre-incubated for 2 h in the presence (A) or absence (B) of 1 μM DEX were allowed to complete the synthesis of RNA molecules during an incubation in the presence of labelled nucleotide precursors. (**A**, **B**) Autoradiograms of newly completed labelled HAS2 and 18 S RNAs, which were captured by hybridization to unlabelled, immobilized HAS2 and 18 S cDNAs on a membrane. (**C**) Graphical representation of the same information quantitatively. DEX caused a significant reduction in the ratio of labelled HAS2 to 18 S RNA made by these nuclei ($P < 0.001$).

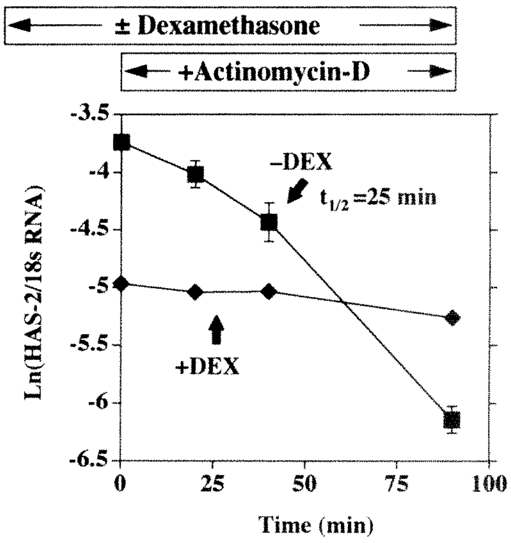

Figure 7 Assessment of HAS2 message half-life using actinomycin D

Fibroblasts were placed into media with or without DEX at $t = -30$ min (±DEX). At $t = 0$, all cells were given AMD (+AMD). Displayed is a semi-log plot of HAS2 message levels, normalized to 18 S, at the indicated times.

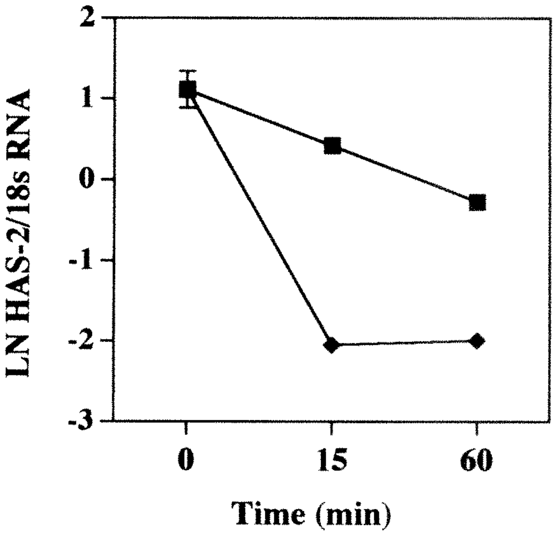

Figure 8 Direct assessment of HAS2 message half-life by wash-out of incorporated uridine label

Fibroblasts were incubated with [^{3}H]uridine for two days, and then a wash-out was performed by incubation of cells in excess unlabelled uridine. At 1 h into the wash-out, DEX was added (diamonds) or not (squares). Displayed is a semi-log plot of residual tritium label in HAS2 message, normalized to the residual label in 18S, at the indicated times.

using the nuclear run-off assay. Nuclei isolated from fibroblasts that had been pre-incubated for 2 h in medium supplemented with DEX consistently showed a 70 % reduction in HAS2 mRNA transcription rate compared with control nuclei isolated from cells pre-incubated without DEX (Figure 6). Though substantial, this suppression of transcription is inadequate to explain the rapid and large effect seen on HAS2 mRNA levels.

To examine HAS2 message stability, we used the standard approach of adding AMD, an inhibitor of RNA synthesis, to DEX-treated or control cells, then following the disappearance of specific RNAs (i.e. HAS2 mRNA and 18 S) over time. Using this approach, we determined that the half-life of HAS2 mRNA in cultured human fibroblasts in the absence of DEX was 25 min (Figure 7). Notice that this half-life will not permit 98 % of HAS2 mRNA to disappear in just 2 h (four half-lives), even if transcription completely stops. Addition of DEX 30 min before addition of AMD resulted in an initial fall in HAS2 mRNA (Figure 7; $t = 0$), consistent with our earlier results, whereas addition of AMD led to a marked decrease in rate of HAS2 mRNA degradation (Figure 7). This prolongation of mRNA half-life in the presence of DEX and AMD suggests that AMD in this circumstance may be blocking the synthesis of a destabilizing factor, such as an RNase [34] We thus sought a direct method to measure HAS2 mRNA half-life that did not require the use of metabolic inhibitors with potential secondary effects.

Our next approach was steady-state labelling of RNA by prolonged incubation of cells with $[^3H]$uridine, followed by a wash-out in the presence of excess unlabelled uridine, during which we examined the disappearance over time of labelled HAS2 and 18S RNA. In the absence of DEX, uridine-labelled HAS2 mRNA disappeared from cells with a half-life of 31 min (Figure 8), consistent with our earlier results using AMD. In contrast, uridine-labelled HAS2 mRNA in DEX-treated cells exhibited a substantially faster decline, with a half-life of less than 4 min (Figure 8; notice that by 20 min, the labelled HAS2 message was already below the limits of detection of this assay). Additional experimentation confirmed the half-life of HAS2 mRNA of just under 30 min in the absence of DEX, but with some variability in the half-life in the presence of DEX (though always below 16 min).

DISCUSSION

In this report, we have shown that GCs rapidly induce a sustained, near-total suppression of HAS2 mRNA, which we found to be the predominant HAS message in dermal fibroblasts and osteoblast-like cells. Dose–response studies in fibroblasts indicated that the majority of the suppressive effect required concentrations characteristic of cell-surface GC receptors, a point confirmed by persistent DEX-induced suppression in the presence of RU486, an antagonist of classic cytosolic steroid hormone receptors. The molecular mechanism for GC-induced suppression of HAS2 message involves a combination of decreased gene transcription and decreased message stability It is likely that these effects contribute to the substantial loss of HA from skin, skeleton and other organs during GC-induced organ atrophy *in vivo*

HA plays specific, essential roles in skin and skeleton. Skin contains about half of the total body HA [35], the major hyalectin proteoglycan in skin is versican, which assembles along strands of HA [36]. In normal skin, HA is found in the intercellular spaces of the epidermis, with the exception of the upper granular layer and stratum corneum. In the dermis, staining for HA is diffuse throughout, but is increased below the basement membrane and around the skin appendages [37]. In epidermis and dermis, large networks of HA, with versican and other molecules, form a highly charged lattice that enhances the epidermal barrier as well as tissue resiliency Regarding wound healing, the absence of cutaneous scarring in fetuses has been related to the high content of HA and cell-surface HA receptors in fetal skin [17,38]. During treatment with GCs, several changes occur in skin that contribute to atrophy of that organ [27]. Histologically, the atrophic changes in skin from GC treatment are characterized by thinning of the epidermis and a large decrease in dermal ground substance [28], which is largely composed of glycosaminoglycans (GAGs), including HA. GC treatment not only reduces the quantity of various GAGs but also changes the distribution, the relative proportion, and the structure of connective-tissue proteoglycans, partly because of the loss of HA, which ordinarily serves as a scaffold for other matrix components.

In bone and cartilage, the major hyalectin proteoglycan is aggrecan, which also assembles along strands of HA [39]. HA and proteoglycans, particularly aggrecan in the osteoid matrix, are involved in mineralization [40] The distribution of hyaluronan in vitamin D-treated chick bone and the alterations observed in rachitic tissue suggest an essential role for hyaluronan in endochondral bone formation [41].

Tissue content of HA is controlled by the synthesis and degradation of this molecule. HA has a short half-life in many tissues the $t_{\frac{1}{2}}$ is only 0.5 day in skin and joints [2,35,42]. Thus changes in HA synthesis can lead to rapid changes in tissue HA content HAS protein has an extremely short half-life of 2–4 h, and enzyme activity is 6.5 times higher in exponential growth phase versus stationary growth phase cells [3]. GCs are already known to suppress HA synthesis in dermal fibroblasts [20,21], cartilage chondrocytes [43], synovial fibroblasts [44] and palate cells [45]. Intra-articular injection of GCs into knee joints reduces the levels of proteoglycans and HA in articular cartilage [46]. Systemic administration of pharmacological doses of GCs causes significant dermal atrophy, leading to thinning of skin, easy bruising, and cutaneous ulceration [22,47]. Systemic GCs also cause atrophy of bone, leading to fractures [23] In both skin and bone, these changes involve a substantial loss of matrix, which is primarily GAGs and collagen [48]. Our results suggest that a major molecular mechanism for GC-induced organ atrophy is rapid, prolonged and near-total suppression of HAS2 message.

Our dose–response studies and the results of addition of RU486 are consistent with a major role for the putative cell-surface GC receptors (with some contribution from the classic cytosolic GC receptors) in the suppression of HAS2 message. Cell-surface GC receptors appear to act via intracellular second messengers, such as InsP_3, Ca_2^+, or protein kinase C [31] Effects mediated by cytosolic GC receptors can be direct, if there are GC response elements in the promoter of the target gene, or indirect, if the target gene responds to a protein, such as a cytokine, which is regulated by GCs. The *HAS2* promoter has not yet been characterized, but the promoter for *HAS1* contains no known GC response elements, although several motifs associated with cytokine responsiveness are present [19]. It is known that transforming growth factor-β increases HAS1 and HAS2 message [18], and that GCs suppress the effects of this cytokine [49]. Several other cytokines, including interleukin-1, tumour necrosis factor-α, epidermal growth factor and platelet-derived growth factor, also up-regulate HA synthesis [50,51], and GCs suppress many of these cytokines as well [52]. Thus it is possible that some of the effects of GCs on HAS2 mRNA levels, particularly during prolonged exposure, may involve the classic cytosolic GC receptor acting indirectly through suppression of cytokines or cytokine action We also found that AMD, an inhibitor of RNA synthesis, stabilizes the HAS2 message in the presence of DEX (Figure 7) Such findings are usually interpreted as implying the existence of a destabilizing factor, such as a specific RNase [34], which in this case would be induced by DEX and required for the effect of the drug on HAS2 message half-life.

The HAS enzymes are attractive targets for pharmacological manipulation. Enhancing levels of HAS messages, HAS enzymes, HA synthesis and tissue HA content could improve cutaneous elasticity and resiliency, skeletal integrity, and perhaps scar-free wound healing Furthermore, the devastating side effects of GC-induced organ atrophy might be lessened or averted.

This work was supported by grants from the Veterans' Administration, U S.A (Merit Review, to V P W) and from the National Institutes of Health, U.S A (HL58884 to K J W) During part of this work, K J W was an Established Investigator of the American Heart Association and Genentech

REFERENCES

1 Brecht, M, Mayer, U, Schlosser, E and Prehm, P (1986) Biochem J **239**, 445–450
2 Laurent, T. C and Fraser, J R (1992) FASEB J **6**, 2397–2404
3 Mian, N (1986) Biochem J **237**, 333–342
4 Kosaki, R, Watanabe, K and Yamaguchi, Y (1999) Cancer Res **59**, 1141–1145
5 McDevitt, C A, Marcelino, J and Tucker, L (1991) FEBS Lett **294**, 167–170
6 LeBaron, R G, Zimmermann, D R and Ruoslahti, E (1992) J Biol Chem **267**, 10003–10010
7 Meyer, L J and Stern, R (1994) J Invest Dermatol **102**, 385–389
8 Akeson, W H, Amiel, D, Abel, M F, Garfin, S R and Woo, S L (1987) Clin Orthop Relat Res **219**, 28–37
9 Lavker, R M, Kaidbey, K and Leyden, J J (1992) J Am Acad Dermatol **26**, 535–544
10 Weigel, P H, Hascall, V C and Tammi, M (1997) J Biol Chem **272**, 13997–14000
11 Itano, N and Kimata, K (1996) Biochem Biophys Res Commun **222**, 816–820
12 Watanabe, K. and Yamaguchi, Y (1996) J. Biol. Chem. **271**, 22945–22948
13 Spicer, A P, Seldin, M F, Olsen, A S., Brown, N, Wells, D E, Doggett, N A, Itano, N, Kimata, K, Inazawa, J and McDonald, J A (1997) Genomics **41**, 493–497
14 Spicer, A P and McDonald, J A (1998) J Biol Chem **273**, 1923–1932
15 Spicer, A P, Olson, J S and McDonald, J A (1997) J Biol Chem **272**, 8957–8961
16 Fulop, C., Salustri, A and Hascall, V C. (1997) Arch Biochem Biophys **337**, 261–266
17 Ellis, I R and Schor, S L (1996) Exp Cell Res **228**, 326–333
18 Sugiyama, Y, Shimada, A, Sayo, T, Sakai, S and Inoue, S (1998) J. Invest Dermatol **110**, 116–121
19 Yamada, Y, Itano, N, Zako, M, Yoshida, M, Lenas, P, Niimi, A U and Kimata, K (1998) Biochem J **330**, 1223–1227
20 Agren, U M, Tammi, M and Tammi, R (1995) J Cell Physiol **164**, 240–248
21 Smith, T J (1988) Metab Clin Exp **37**, 179–184
22 Capewell, S, Reynolds, S, Shuttleworth, D, Edwards, C and Finlay, A Y (1990) Br Med. J **300**, 1548–1551
23 Reid, I R (1997) Eur J Endocrinol **137**, 209–217
24 Melhus, H, Wilen, B, Kindmark, A and Ljunghall, S. (1997) Biochem Mol Biol Int **43**, 1145–1150
25 Burnstein, K L, Jewell, C M and Cidlowski, J A (1990) J Biol Chem **265**, 7284–7291
26 Feinberg, A P and Vogelstein, B (1984) Anal Biochem **137**, 266–267
27 Tukey, R H and Okino, S T (1991) Methods Enzymol **206**, 284–290
28 Werth, V P, Williams, K J, Fisher, E A, Bashir, M, Rosenbloom, J R and Shi, X (1997) J Invest Dermatol **108**, 290–294
29 Zhu, Y Y, Schwartz, R J and Crow, M T. (1991) J Cell Biol **115**, 745–754
30 Glantz, S A (1992) Primer of Biostatistics, McGraw Hill Inc, New York
31 Buttgereit, F, Wehling, M. and Burmester, G R (1998) Arthritis Rheum **41**, 761–767
32 Uzuka, M, Nakajima, K, Ohta, S and Mori, Y (1980) Biochim Biophys Acta **627**, 199–206
33 McCrohon, J A, Nakhla, S, Jessup, W, Stanley, K K and Celermajer, D S (1999) Circulation **100**, 2319–2325
34 Tomkins, G M, Gelehrter, T D., Granner, D, Martin, D, Samuels, H H and Thompson, E B (1969) Science **166**, 1474–1480
35 Laurent, U B G and Reed, R. K (1991) Adv Drug Delivery Rev **7**, 237–256
36 Bode-Lesniewska, B, Dours-Zimmermann, M T, Odermatt, B F, Briner, J, Heitz, P U and Zimmermann, D R (1996) J Histochem Cytochem **44**, 303–312
37 Tammi, R, Paukkonen, K, Wang, C, Horsmanheimo, M and Tammi, M (1994) Arch Dermatol Res **286**, 21–29
38 Freund, R M, Siebert, J. W, Cabrera, R C., Longaker, M T, Eidelman, Y., Adzick, N S and Garg, H G (1993) Biochem Mol Biol Int **29**, 773–783
39 Fraser, J R, Laurent, T C and Laurent, U B (1997) J Int Med **242**, 27–33
40 Robey, P G., Fedarko, N. S, Hefferan, T E, Bianco, P, Vetter, U K, Grzesik, W, Friedenstein, A, Van der Pluijm, G, Mintz, K P, Young, M F et al., (1993) J Bone Miner Res **8** (Suppl 2), S483–S487
41 Genever, P G and Dickson, I R (1996) Bone **18**, 429–435
42 Brown, T J, Laurent, U B and Fraser, J R (1991) Exp Physiol **76**, 125–134
43 Kato, Y and Gospodarowicz, D (1985) J Biol Chem **260**, 2364–2373
44 Myers, S L (1985) Arthritis Rheum **28**, 1275–1282
45 Yoshikawa, H, Tashiro, H and Kurisu, K (1986) J Craniofacial Genet Dev Biol **6**, 235–244
46 Kongtawelert, P, Brooks, P M and Ghosh, P (1989) J Rheumatol **16**, 1454–1459
47 Werth, V P, Kligman, A. M, Shi, X. and Pagnoni, A (1998) Arch Dermatol. Res. **290**, 388–393
48 Autio, P, Oikarinen, A., Melkko, J, Risteli, J and Risteli, L (1994) Br J Dermatol **131**, 660–663
49 Meisler, N, Keefer, K A, Ehrlich, H P, Yager, D R and Myers-Parrelli, J (1997) J Invest Dermatol **108**, 285–289
50 Tiedemann, K, Malmstrom, A. and Westergren-Thorsson, G (1997) Matrix Biol **15**, 469–478
51 Suzuki, M, Asplund, T, Yamashita, H, Heldin, C H and Heldin, P (1995) Biochem J **307**, 817–821
52 Cato, A C and Wade, E (1996) BioEssays **18**, 371–378

Received 15 October 1999/13 March 2000, accepted 14 April 2000

Biochem J (2000) 349, 99–104 (Printed in Great Britain)

Indirect induction of suppressor of cytokine signalling-1 in macrophages stimulated with bacterial lipopolysaccharide: partial role of autocrine/paracrine interferon-α/β

Ana CRESPO*†, Michael B. FILLA*, Stephen W. RUSSELL* and William J. MURPHY*[1]

*Wilkinson Laboratory of the Kansas Cancer Institute and the Department of Pathology and Laboratory Medicine, University of Kansas Medical Center, 1008 WHW, 3901 Rainbow Boulevard, Kansas City, KS 66160-7184, U.S.A., and †Institute of Molecular Pathology and Immunology of the University of Porto (IPATIMUP), Rua Roberto Frias s/n, 4200 Porto, Portugal

It has previously been reported by us that a brief prior exposure of mouse bone marrow culture-derived macrophages to bacterial lipopolysaccharide (LPS) resulted in a dramatic reduction in their ability to produce NO in response to a subsequent stimulus with either interferon-γ (IFN-γ) or IFN-γ plus LPS. We show here that this brief exposure to LPS results in an impaired response to subsequently added IFN-γ A 2–4 h pretreatment with LPS leads to a dramatic reduction in the IFN-γ-induced DNA-binding of the transcription factor, signal transducer and activator of transcription 1α (STAT1α). This loss in ability to activate STAT1α temporally correlates with the LPS-induced accumulation of mRNA encoding the suppressor of cytokine signalling-1 (SOCS-1). However, LPS does not directly induce the synthesis of SOCS-1. Rather, LPS induces the synthesis of autocrine/paracrine factors that are the true mediators of SOCS-1 induction. IFN-α/β is one of these mediators, but plays only a partial role in the induction of SOCS-1 because neutralization of LPS-induced IFN-α/β production incompletely inhibits the induction of SOCS-1. We show that mouse IFN-β directly induces the synthesis of SOCS-1, without the need for prior protein synthesis, and does so with faster kinetics than does LPS. Our results are consistent with the non-specific nature of LPS-induced tolerance and provide a mechanistic insight into nonspecificity; LPS indirectly induces the synthesis of a protein mediator, SOCS-1, which inhibits the signalling that is induced by IFN-γ.

Key words: cellular activation, nitric oxide, signal transduction, tolerance/suppression.

INTRODUCTION

Bacterial lipopolysaccharide (LPS) elicits a multitude of effects on the immune system and other organ systems of many vertebrates (reviewed in [1]). Systemic release of LPS induces the synthesis of numerous cytokines (including, for the purpose of our discussion, the interferons), growth factors, eicosinoids, and reactive oxygen and reactive nitrogen species [2]. While LPS may play a direct role in the induced synthesis of a number of these molecules, many of the biological effects of LPS are indirectly elicited by these secondary mediators, especially proinflammatory agents such as tumour necrosis factor-α [3], interleukin-1 (IL-1) [4], interferon-γ (IFN-γ) [5] and IL-8 [6].

Prior exposure to sublethal quantities of LPS, however, results in decreased responsiveness to a second challenge with LPS, a phenomenon referred to as 'LPS tolerance' [7]. Tolerance can be observed within hours of primary exposure to LPS and leads to a suppressed ability to produce many of the proinflammatory agents mentioned in the preceding paragraph [8]. Using whole animal models, the principal cellular mediator of tolerance has been shown to be the monocyte/macrophage lineage [9]. In fact, numerous reports support the conclusion that both macrophage cell lines [10–14] and *ex vivo* isolates of normal macrophages [12,13,15–19] can be rendered tolerant to LPS after their *in vitro* exposure to it. What is also clear is the fact that primary exposure to LPS renders macrophages tolerant not only to LPS, but to other proinflammatory mediators (see [8,9] and the Discussion section in this paper).

It has been reported by us [16] and by other investigators [12], that a brief prior exposure of mouse macrophages to LPS suppresses their responsiveness (as measured by NO production) to subsequent stimulation with either IFN-γ alone, or IFN-γ plus LPS. The goal of the work reported here was to determine whether LPS pretreatment of macrophages might lead to a suppression of cellular signalling initiated by IFN-γ. Our studies reveal that LPS treatment of mouse macrophages induce the synthesis of suppressor of cytokine signalling-1 (SOCS-1). SOCS-1 has been shown to interfere with IFN-γ signalling by inhibiting the IFN-γ receptor-directed tyrosine phosphorylation events that occur after cellular binding of IFN-γ [20]. We show that LPS does not, however, effect the direct induction of SOCS-1 mRNA synthesis. Rather, LPS first induces autocrine/paracrine mediators, including IFN-α/β, that are subsequently responsible for the induction of SOCS-1. These results provide molecular evidence for the ability of LPS to indirectly induce the negative regulatory components of distinct signalling pathways.

EXPERIMENTAL

Cells, culture medium and reagents

Male C3H/HeN mice were obtained from the National Cancer Institute (Bethesda, MD, U.S.A.). Mice were used at 6–9 weeks

---

Abbreviations used: BMCDM, bone marrow culture-derived macrophages; CHX, cycloheximide; EMSA, electrophoretic mobility-shift assay; IFN, interferon; IL, interleukin; iNOS, inducible nitric oxide synthase; JAK, Janus kinase; LPS, bacterial lipopolysaccharide; SOCS, suppressor of cytokine signalling; STAT, signal transducers and activators of transcription

[1] To whom correspondence should be addressed (e-mail bmurphy@kumc.edu)

of age to isolate bone marrow culture-derived macrophages (BMCDM), as described previously [21]. BMCDM were grown in Eagle's modified minimal essential medium supplemented with 2 mM glutamine (Flow Laboratories, McLean, VA, U.S.A.), 100 units/ml penicillin, 100 μg/ml streptomycin (Pfizer, New York, NY, U.S.A.), 15 mM Hepes (Sigma), 10 % fetal bovine serum (Hyclone, Logan, UT, U.S.A.), 5 % equine serum (Hyclone), and L-929 cell-conditioned medium (as a source of colony-stimulating factor-1). Cells were collected after 10–14 days of culture by cold PBS treatment as described in [22], centrifuged (4 °C, 250 × *g*, 10 min), and resuspended in medium without L-929 cell-conditioned medium, and were incubated for 24 h at 37 °C in 5 % CO_2 in air before treatments.

All culture media tested negative for detectable endotoxin by *Limulus amebocyte* lysate assay (Associates of Cape Cod, Woods Hole, MA, U.S.A.), at a sensitivity of 0.05 ng/ml. LPS, the lipid A-rich fraction II of phenol-extracted *Escherichia coli* O111 : B4, was purchased from List Biological Laboratories (Campbell, CA, U.S.A.). Recombinant murine IFN-γ (specific activity of 1.27×10^6 units/mg) was provided by Schering-Plough Corporation (Bloomfield, NJ, U.S.A.) through the American Cancer Society (Atlanta, GA, U.S.A.). Rabbit anti-mouse-IFN-α/β serum and normal rabbit serum were obtained from Access BioMedical (San Diego, CA, U.S.A.). Cycloheximide (CHX) was purchased from Sigma.

Electrophoretic mobility-shift assay (EMSA)

BMCDM were treated as indicated in the legend to Figure 1. Following treatment, nuclear extracts were prepared as described by Gao et al. [23,24]. The sequence of the synthetic oligonucleotide (Life Technologies) used for EMSA, which corresponded to the IFN-γ-activated site ('GAS') of the inducible NO synthase (*iNOS*) gene, was 5′-CTTTTCCCCTAACAC-3′. The pair of complementary oligonucleotides were end-labelled, using T4 polynucleotide kinase, and annealed as described in [25]. EMSA reactions were performed as described in [23,24]. A 20 μl aliquot of each reaction mixture was loaded on to a 5 % polyacrylamide gel containing 50 mM Tris/HCl, 2 mM EDTA, and 0.38 M glycine. Electrophoresis was carried out at 350 V and 4 °C for 1.5 h.

Northern-blot analysis

Monolayers containing approx. 1.7×10^7 BMCDM were prepared on 100-mm diameter cell-culture plates. After treatment (as indicated in the Figure legends), total RNA was isolated using TRI Reagent (Sigma) following the manufacturer's protocol. A 10 μg portion of total RNA from each sample were electrophoresed on a 1 % formaldehyde–agarose gel, blotted on to a Nytran nylon membrane by capillary transfer for 3 h using a TurboBlotter kit (Schleicher and Schuell, Keene, NH, U.S.A.), and baked at 80 °C for 1 h. Membranes were prehybridized for 30 min at 55 °C with QuickHyb solution (Stratagene, La Jolla, CA, U.S.A.). The cDNA probe encoding mouse SOCS-1 (generously provided by Dr Douglas Hilton, The Walter and Eliza Hall Institute for Medical Research, Parkville, Victoria, Australia) was radiolabelled using the Multiprime DNA labelling system (Amersham International). Heat-denatured probe (2.5–4×10^7 c.p.m.) and 100 μg of hearing sperm DNA were then added to the prehybridization solution. Hybridization was performed at 55 °C for 1 h, followed by four washes of 15 min each at 50 °C (twice with 0.30 M NaCl/0.03 M sodium citrate/0.1 % SDS, and twice with 0.03 M NaCl/3 mM sodium citrate/0.1 % SDS). The membranes were then subjected to autoradiography in cassettes with intensifying screens at −70 °C. To ensure that equal amounts of RNA were examined, blots were stripped and then rehybridized with a radiolabelled cDNA probe encoding human glyceraldehyde-3-phosphate dehydrogenase. Figures 2(A) and 5(A) demonstrate that BMCDM mRNA for glyceraldehyde-3-phosphate dehydrogenase was induced by both LPS and IFN-β respectively, at time points exceeding approx. 4 h. However, at shorter time intervals, mRNA encoding this enzyme provided an adequate control for mRNA loading in Northern blots.

RESULTS

Prior exposure of BMCDM to LPS inhibits the activation of transcription factor STAT1α by IFN-γ

Previous work from our laboratory [16] showed that a brief prior exposure of mouse macrophages to LPS for 2–4 h, followed by the addition of IFN-γ for 2 h, resulted in a dramatic decrease in NO production when compared with concurrent stimulation with LPS plus IFN-γ for 2 h (NO was measured 16 h after removal of LPS and IFN-γ by washing). To determine the effect of prior exposure to LPS on IFN-γ signalling, we pretreated BMCDM with LPS for 2 or 4 h, followed by washing and a subsequent 30 min treatment with LPS plus IFN-γ. Nuclear extracts were then prepared and assayed for binding of the IFN-γ-activated transcription factor, STAT1α, to the IFN-γ-activated site located in the enhancer of the mouse *iNOS* gene. As shown in Figure 1, this pretreatment protocol resulted in a dramatic, time-dependent suppression in the binding of STAT1α to the iNOS IFN-γ activated site. An average of three independent experiments revealed that STAT1α binding was reduced by 27 % after a 2 h pretreatment with LPS, and by 56 % after a 4 h pretreatment.

LPS induces the accumulation of SOCS-1 mRNA

To determine the molecular basis of LPS inhibitory effects on the subsequent stimulation by IFN-γ, we examined whether LPS could induce members of the SOCS family of suppressors during the 2–4 hour pretreatment time span. Using probes for different members of the SOCS family of inhibitors, preliminary Northern-blot analysis of total RNA isolated from LPS-stimulated and -unstimulated cell cultures revealed that SOCS-1 mRNA was induced by this treatment (results not shown).

To further elucidate the mechanisms of SOCS-1 induction by LPS, we first performed time-course and dose-dependency

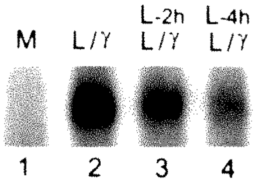

Figure 1 Brief prior exposure of macrophages to LPS suppresses the IFN-γ-induced activation of STAT1α binding to the iNOS IFN-γ activated site

Two cultures of BMCDM were incubated for 30 min with either medium alone (lane 1) or medium containing 1 ng/ml LPS + 100 units/ml IFN-γ (lane 2). An additional set of two cultures were preincubated for either 2 h (lane 3) or 4 h (lane 4) in medium containing 1 ng/ml LPS. These latter two cultures were then washed, and fresh medium containing 1 ng/ml LPS + 100 units/ml IFN-γ was added for an additional 30 min. Nuclear extracts were then prepared from each culture and EMSAs were performed using 10 μg of each nuclear extract and an oligonucleotide probe containing the IFN-γ activated site of the *iNOS* gene, as described in the Experimental section.

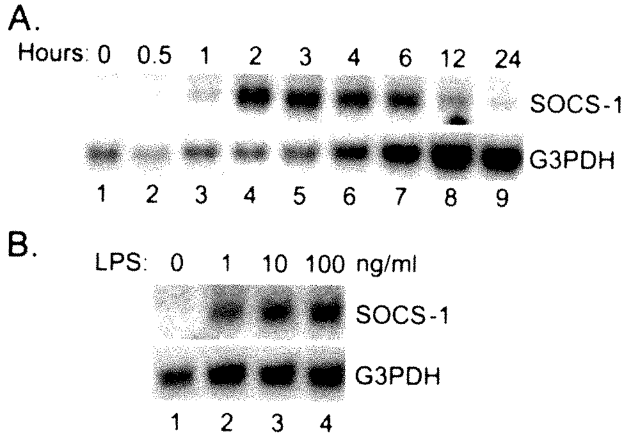

Figure 2 Time-course and dose-response analysis of the effects of LPS on SOCS-1 mRNA expression

(**A**) Total RNA was isolated from BMCDM incubated for 0–24 h in medium containing 100 ng/ml of LPS. Equal amounts of total RNA (10 μg) were electrophoretically size-separated, transferred to nylon membranes, and hybridized with a ^{32}P-labelled mouse SOCS-1 cDNA probe. After autoradiography, the nylon membrane was stripped and reprobed with a ^{32}P-labelled human glyceraldehyde-3-phosphate dehydrogenase probe. The result shown is representative of three independent experiments. (**B**) BMCDM were cultured in medium alone (lane 1) or medium containing LPS at concentrations of either 1 ng/ml (lane 2), 10 ng/ml (lane 3), or 100 ng/ml (lane 4). Total RNA was isolated after 2 h of stimulation. A 10 μg aliquot of total RNA was analysed by Northern blot as described in (**A**). The results shown are representative of three independent experiments.

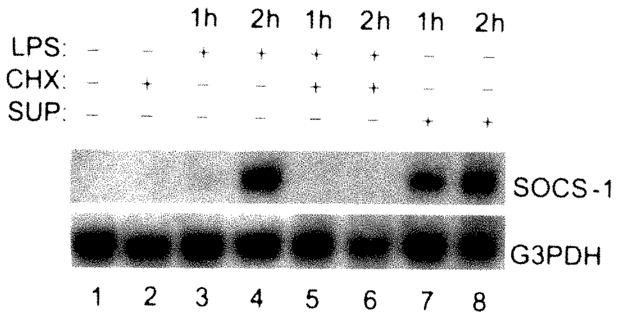

Figure 3 Indirect nature of LPS-induced SOCS-1 mRNA induction

BMCDM cultures were pre-incubated for 30 min in medium alone (lanes 1, 3 and 4) or medium containing 3 μg/ml of CHX (lanes 2, 5 and 6). Medium was then replaced with medium alone (lane 1), or medium containing either CHX alone (lane 2), 100 ng/ml of LPS alone (lanes 3 and 4), or LPS plus CHX (lanes 5 and 6). Cultures were subsequently incubated for the times indicated at the top of the Figure. Cultures represented by lanes 7 and 8 were incubated for the times indicated with cell culture supernatant (SUP), which had been transferred from primary BMCDM cultures that were treated for 2 h with 100 ng/ml of LPS. A 10 μg aliquot of total RNA, prepared from each culture, was subjected to Northern blotting as described in the legend to Figure 2.

studies. Figure 2(A) shows the time course of SOCS-1 induction in BMCDM treated with 100 ng/ml of LPS. Accumulation of SOCS-1 mRNA was evident after 1 h of cellular exposure to LPS. Maximal accumulation was observed after 2–3 h of stimulation, with mRNA levels decreasing thereafter. Accumulation of mRNA occurred in a dose-dependent fashion, as shown in Figure 2(B). The induction of SOCS-1 mRNA accumulation was observed with as little as 1 ng/ml LPS, and reached a maximum with 100 ng/ml.

Induction of SOCS-1 by LPS requires the synthesis of an autocrine/paracrine factor

It has been reported that SOCS-1 is induced by a variety of cytokines, including IL-6 [26], IFN-γ [27], and IL-4 [26,28]. Each of these cytokines signal via the Janus kinase (JAK)/STAT pathway of tyrosine kinases/transcription factors. It has been postulated that induction of SOCS-1 by these cytokines precipitates a negative-feedback loop, which tempers the strength and duration of signalling by these cytokines [28]. Because LPS does not itself elicit signalling via the JAK/STAT pathway, but does induce the *de novo* synthesis of several cytokines that do signal via the JAK/STAT pathway, we wished to determine whether LPS exerted a direct or indirect effect on the expression of SOCS-1 mRNA. To this end, we first determined the effect of the protein synthesis inhibitor, CHX, on LPS-induced accumulation of SOCS-1 mRNA. As shown in Figure 3, CHX alone did not induce the accumulation of SOCS-1 mRNA (lane 2). When BMCDM were co-incubated in the presence of LPS plus CHX for either 1 h (Figure 3, lane 5) or 2 h (lane 6), accumulation of SOCS-1 mRNA was completely abolished, in comparison with that induced by LPS alone (lanes 3 and 4).

To verify LPS-induced secretion into the culture medium of an autocrine/paracrine factor responsible for SOCS-1 induction, we also performed a culture supernatant-transfer experiment. Primary cultures of BMCDM were incubated for 2 h in the presence of 100 ng/ml of LPS, after which the culture supernatants were removed, centrifuged, and applied to fresh, secondary BMCDM cultures. RNA was extracted from these secondary cultures after 1 or 2 h of exposure and examined by Northern-blot analysis. As can be seen in Figure 3, expression of SOCS-1 mRNA could be detected after 1 h of exposure to the transferred culture supernatant (lane 7). By comparison, LPS-induced accumulation of SOCS-1 mRNA in primary cultures was undetectable after 1 h of treatment (Figure 3, lane 3). Taken together, the CHX and supernatant-transfer experiments demonstrated that LPS induced the synthesis in primary BMCDM cultures of a protein mediator that, when applied to secondary BMCDM cultures, induced a faster rate of accumulation of SOCS-1 than LPS alone.

Induction of SOCS-1 by LPS requires, at least in part, the autocrine/paracrine activity of IFN-β

Previous reports from our group demonstrated that LPS induces in mouse macrophages the production of IFN-β, which acts as a co-inducer, along with LPS, of the production of NO [29,30], and as an activator of the transcription factor, STAT1α [24]. To test the possibility that the autocrine/paracrine factor responsible for SOCS-1 induction consisted of IFN-β, we assessed the ability of LPS to induce SOCS-1 mRNA accumulation in the presence of anti-IFN-α/β serum or control antiserum. The dilution of anti-IFN-α/β serum used was determined in preliminary experiments to be that which neutralized 95% of the nitrite induced by treatment of mouse peritoneal macrophages with LPS. We have previously shown that LPS-induced production of nitrite in mouse peritoneal macrophages was completely dependent upon the autocrine/paracrine production of IFN-β [24,29]. As shown in Figure 4, the LPS-induced accumulation of SOCS-1 mRNA was suppressed by the presence of anti-IFN-α/β serum (lane 6) when compared with the accumulation observed after treatment with LPS alone (lane 4) or with that observed after treatment with LPS in the presence of a similar dilution of rabbit pre-immune serum (lane 5). In comparison with cultures treated with LPS alone, treatment in the presence of pre-immune serum resulted in a 20% reduction in SOCS-1 mRNA induction by LPS (averaged from two independent experiments). Using this

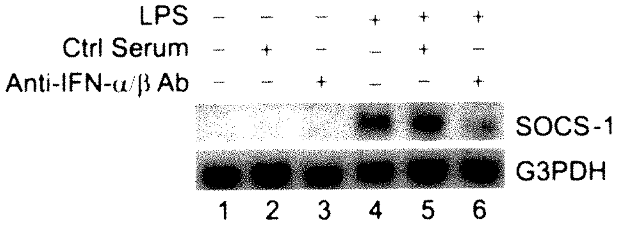

Figure 4 Effect of neutralizing anti-IFN-α/β antibodies on LPS-induced SOCS-1 mRNA accumulation

BMCDM were cultured for 3 h in medium alone (lane 1), or in medium containing either control serum (used at a 1:330 dilution, lane 2), anti-IFN-α/β serum (used at a 1:330 dilution, lane 3), LPS at 100 ng/ml (lane 4), LPS plus control serum (lane 5), or LPS plus anti-IFN-α/β serum (lane 6). A 10 μg aliquot of total RNA, prepared from each culture, was analysed by Northern blotting as described in the legend to Figure 2.

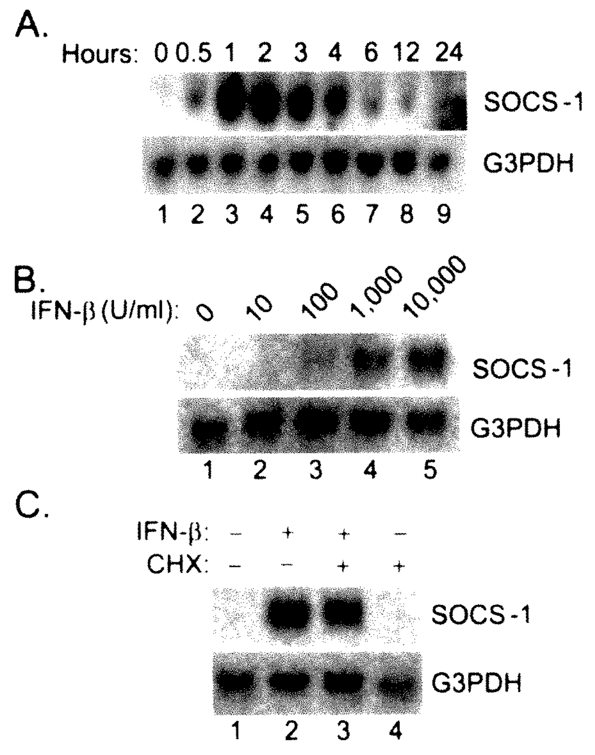

Figure 5 Analysis of SOCS-1 mRNA induction by IFN-β

(**A**) Total RNA was isolated from BMCDM treated for 0–24 h in medium containing 1000 units/ml of IFN-β. Equal amounts of total RNA (10 μg) were analysed as described in the legend to Figure 2. (**B**) BMCDM were cultured in medium alone (lane 1) or in medium containing IFN-β at concentrations of either 10 units/ml (lane 2), 100 units/ml (lane 3), 1000 units/ml (lane 4), or 10000 units/ml (lane 5). Total RNA was isolated from BMCDM after 1 h of stimulation and 10 μg aliquots were analysed by Northern blotting as described in the legend to Figure 2. (**C**) BMCDM were preincubated for 30 min in either medium alone (lanes 1 and 2) or in medium containing 3 μg/ml of CHX (lanes 3 and 4). Culture medium was then replaced with medium alone (lane 1), or with medium containing either 1000 units/ml of IFN-β alone (lane 2), IFN-β plus CHX (lane 3), or CHX alone (lane 4). Cultures were subsequently incubated for one additional hour. A 10 μg aliquot of total RNA, prepared from each culture, was subjected to Northern-blot analysis as described in the legend to Figure 2.

latter level of SOCS-1 induction as a control, the anti-IFN-α/β antibodies reduced LPS-induced expression in these two experiments by an average of 46%. Thus suppression of SOCS-1 mRNA accumulation was not complete in the presence of anti-IFN-α/β serum.

IFN-β induces SOCS-1 mRNA accumulation with faster kinetics than LPS, and in a manner independent of new protein synthesis

To provide further evidence that IFN-β induces the accumulation of SOCS-1 mRNA in BMCDM, we performed time-course and dose-dependency experiments. BMCDM were treated with 1000 units/ml of IFN-β for the times indicated in Figure 5(A), followed by preparation of RNA for Northern-blot analysis. As demonstrated in the Figure, accumulation of SOCS-1 mRNA was detectable after as little as 0.5 h of exposure to 1000 units/ml of IFN-β (Figure 5, lane 2). Accumulation reached a maximum at approx. 1 h of stimulation (Figure 5, lane 3), after which it gradually declined until it was undetectable at 24 h of stimulation (lane 9). As expected, the time course of induction of SOCS-1 mRNA by IFN-β was shifted to early time points, when compared with the time course of induction by LPS.

As shown in Figure 5(B), the accumulation of SOCS-1 mRNA could be detected after BMCDM were treated with as little as 100 units/ml of IFN-β. Maximal accumulation was detected using 10000 units/ml of IFN-β. This observation is consistent with the results of other experiments performed by us, which demonstrated maximal production of nitrite by BMCDM, using LPS plus 10000 units/ml of IFN-β (results not shown).

To verify that accumulation of SOCS-1 mRNA was a direct effect of IFN-β stimulation, we performed cellular treatments in the presence and absence of CHX, as described above for LPS. As shown in Figure 5(C), when BMCDM were incubated with both IFN-β and CHX, the level of induced SOCS-1 mRNA accumulation was equivalent to that observed using IFN-β alone (compare lane 3 with lane 2). Again, CHX alone had no effect on the expression of SOCS-1 mRNA (Figure 5, lane 4). Thus IFN-β effects the direct induction of SOCS-1 mRNA accumulation without a need for prior protein synthesis.

DISCUSSION

Numerous reports confirm the non-specific nature of LPS-induced tolerance. While prior exposure to LPS induces suppressed responsiveness to subsequent challenge with LPS, suppressed responsiveness can also be observed when the second challenge consists of either IFN-γ [12,16,31], IL-1β [8], toxic shock syndrome toxin-1 [8], tumour necrosis factor-α [31], PMA [31,32], zymosan [33], or gram positive bacterial components [33]. The results presented here are important because they demonstrate, at the molecular level, that prior exposure of mouse macrophages to LPS can effect the induction of the SOCS-1 protein, which in turn inhibits signalling via the IFN-γ pathway.

Our results also underscore the observation that many of the cellular and organismal effects of LPS are not directly due to the influence of LPS itself. Rather, secondary-response modifiers, induced by LPS, are often the true mediators of LPS action. For example, antibody-directed neutralization of IL-1β [4] and tumour necrosis factor-α [3] can mitigate some of the effects of LPS in human beings. In the case presented here, LPS induces the synthesis of IFN-α/β, which works in autocrine/paracrine fashion to induce the accumulation of SOCS-1 mRNA.

It is noteworthy that antisera to IFN-α/β do not completely abolish the induction of SOCS-1 mRNA accumulation, even though this concentration of antibody nearly completely inhibits nitrite production and autocrine/paracrine IFN-β-induced signalling in mouse peritoneal macrophages. This would indicate that other autocrine/paracrine factors induced by LPS may also play a role in the induction of SOCS-1 mRNA synthesis. Indeed, LPS is known to induce in mouse macrophages a number of cytokines that have a demonstrable effect on the induction of SOCS-1, including: IL-6, IL-10, IL-12, and colony-stimulating factors [26]. Thus induction of SOCS-1 mRNA accumulation by LPS is likely to be due to the combined effects of multiple autocrine/paracrine factors.

The question of the importance of LPS-induced, secondary-response modifiers to the induction of tolerance is an important one. Evidence would suggest that the production of tolerance is, in fact, an autocrine/paracrine effect [34,35] that may partly involve IL-10 and transforming growth factor-β [35]. Furthermore, it has been shown that pretreatment of human macrophages with both LPS and IFN-γ prevents the acquisition of the tolerant state that is induced by LPS alone. Pretreatment with LPS and IFN-β, on the other hand, promotes acquired tolerance [11]. From other studies it is clear that IFN-β by itself also induces a state of suppressed macrophage responsiveness to subsequent stimulation with LPS and IFN-γ, whereas pretreatment with IFN-γ does not [22]. Thus IFN-β may also play an important role in the production of LPS-induced tolerance.

In addition to the induction of SOCS-1 reported here, it has recently been shown that LPS can induce the synthesis of SOCS-3 in mouse macrophages [36], as well as in human and rat macrophages [37]. LPS-induced synthesis of SOCS-3 mRNA in mouse macrophages, unlike that of SOCS-1, does not require *de novo* protein synthesis [36]. Overexpression in mouse macrophages of either SOCS-1 [38] or SOCS-3 [36] results in a suppression of IFN-γ-induced signalling. Furthermore, studies of SOCS-1-deficient mice [39] have demonstrated an essential role for this suppressor protein in protection against the pathologic effects of unrestrained IFN-γ action. Thus LPS induces the synthesis of two key regulators of IFN-γ action by distinct mechanisms.

The control of host responsiveness to LPS is of paramount importance in order to protect against unrestrained inflammatory processes that may result in tissue destruction, organ dysfunction, and, in severe cases, death [1,40]. That prior exposure to low doses of LPS itself partially protects the host from subsequent challenge with greater quantities of LPS is of significant value if the molecular mechanisms that govern this protection can be uncovered and exploited In this regard, it is important to distinguish between the direct effects of LPS and those effects that are caused by secondary agents, the synthesis of which are induced by LPS.

We gratefully acknowledge Dr Jian Jun Gao for his valuable advice and other scientific contributions to the work reported here This work was supported in part by research grant P01 CA54474 (to S W R.) from the National Cancer Institute, the Wilkinson Endowment for Cancer Research, and a scholarship (BD/9586/96) from Fundação para Ciência e Tecnologia, Portugal (to A.C).

REFERENCES

1 Karima, R., Matsumoto, S, Higashi, H and Matsushima, K (1999) The molecular pathogenesis of endotoxic shock and organ failure Mol. Med Today **5**, 123–132

2 Berczi, I (1998) Neurohormonal host defense in endotoxin shock Ann N Y. Acad Sci **840**, 787–802

3 Tracey, K J, Fong, Y, Hesse, D G., Manogue, K R, Lee, A. T, Kuo, G C, Lowry, S. F. and Cerami, A (1987) Anti-cachectin/TNF monoclonal antibodies prevent septic shock during lethal bacteraemia Nature (London) **330**, 662–664

4 LeMay, L G, Otterness, I G, Vander, A J and Kluger, M. J (1990) In vivo evidence that the rise in plasma IL 6 following injection of a fever-inducing dose of LPS is mediated by IL 1β Cytokine **2**, 199–204

5 Bucklin, S. E., Russell, S W. and Morrison, D C. (1994) Augmentation of anti-cytokine immunotherapy by combining neutralizing monoclonal antibodies to interferon-γ and the interferon-γ receptor protection in endotoxin shock J Endotoxin Res **1**, 45–51

6 Carvalho, G L, Wakabayashi, G., Shimazu, M, Karahashi, T, Yoshida, M, Yamamoto, S, Matsushima, K, Mukaida, N, Clark, B D, Takabayashi, T. et al (1997) Anti-Interleukin-8 monoclonal antibody reduces free radical production and improves hemodynamics and survival rate in endotoxic shock in rabbits Surgery **122**, 60–68

7 Beeson, P B (1947) Tolerance to bacterial pyrogen. I Factors influencing its development J Exp Med **86**, 29–38

8 Granowitz, E V, Porat, R, Mier, J. W, Orencole, S F, Kaplanski, G, Lynch, E A, Ye, K, Vannier, E, Wolff, S M and Dinarello, C A (1993) Intravenous endotoxin suppresses the cytokine response of peripheral blood mononuclear cells of healthy humans J Immunol **151**, 1637–1645

9 Cavaillon, J-M (1995) The nonspecific nature of endotoxin tolerance Trends Microbiol **3**, 320–324

10 Virca, G. D, Kim, S Y, Glaser, K B and Ulevitch, R J. (1989) Lipopolysaccharide induces hyporesponsiveness to its own action in RAW 264 7 cells J Biol Chem **264**, 21951–21956

11 Haas, J G, Meyer, N, Riethmuller, G and Ziegler-Heitbrock, H W (1990) Inhibition of lipopolysaccharide-induced *in vitro* desensitization by interferon-γ Eur J Immunol **20**, 1181–1184

12 Severn, A, Xu, D, Doyle, J, Leal, L M, O'Donnell, C A, Brett, S J, Moss, D W and Liew, F Y (1993) Pre-exposure of murine macrophages to lipopolysaccharide inhibits the induction of nitric oxide synthase and reduces leishmanicidal activity. Eur. J. Immunol **23**, 1711–1714

13 Chang, C C, McCormick, C C, Lin, A W, Dietert, R. R and Sung, Y J (1996) Inhibition of nitric oxide synthase gene expression in vivo and in vitro by repeated doses of endotoxin. Am J Physiol **271**, G539–G548

14 Blackwell, T S., Blackwell, T. R and Christman, J W (1997) Induction of endotoxin tolerance depletes nuclear factor-κB and suppresses its activation in rat alveolar macrophages J Leukocyte Biol **62**, 885–891

15 Lepe-Zuniga, J L and Klostergaard, J (1990) Tolerance to endotoxin in vitro independent regulation of interleukin-1, tumor necrosis factor and interferon alpha production during in vitro differentiation of human monocytes Lymphokine Res **9**, 309–319

16 Lorsbach, R B and Russell, S W (1992) A specific sequence of stimulation is required to induce synthesis of the antimicrobial molecule nitric oxide by mouse macrophages Infect. Immun **60**, 2133–2135

17 Gonnella, P A., Starr, S, Rodrick, M L. and Wilmore, D W (1994) Induced hyporesponsiveness in rat Kupffer cells is not specific for lipopolysaccharide. Immunology **81**, 402–406

18 Li, M. H., Seatter, S. C, Manthei, R, Bubrick, M and West, M A (1994) Macrophage endotoxin tolerance. effect of TNF or endotoxin pretreatment J Surg. Res **57**, 85–92

19 Barber, S. A, Fultz, M. J, Salkowski, C A and Vogel, S N (1995) Differential expression of interferon regulatory factor 1 (IRF-1), IRF-2, and interferon consensus sequence binding protein genes in lipopolysaccharide (LPS)-responsive and LPS-hyporesponsive macrophages. Infect Immun **63**, 601–608

20 Nicholson, S E and Hilton, D J (1998) The SOCS proteins a new family of negative regulators of signal transduction J Leukocyte Biol **63**, 665–668

21 Leung, K-P., Russell, S W, LeBlanc, P A and Caballero, S (1985) Heterogeneity among macrophages cultured from mouse bone marrow Morphologic, cytochemical and flow cytometric analyses. Cell Tissue Res. **239**, 693–701

22 Pace, J L, MacKay, R. J. and Hayes, M P (1987) Suppressive effect of interferon-β on development of tumoricidal activity in mouse macrophages J. Leukocyte Biol. **41**, 257–263

23 Gao, J, Morrison, D C, Parmely, T J, Russell, S W and Murphy, W J (1997) An Interferon-γ-activated site (GAS) is necessary for full expression of the mouse *iNOS* gene in response to interferon-γ and lipopolysaccharide J Biol Chem. **272**, 1226–1230

24 Gao, J J, Filla, M B, Fultz, M J, Vogel, S. N, Russell, S. W and Murphy, W J (1998) Autocrine/paracrine IFN-$\alpha\beta$ mediates the lipopolysaccharide-induced activation of transcription factor Stat1α in mouse macrophages pivotal role of Stat1α in induction of the inducible nitric oxide synthase gene J Immunol. **161**, 4803–4810

25 Murphy, W J, Muroi, M, Zhang, C X, Suzuki, T and Russell, S W (1996) Both basal and enhancer κB elements are required for full induction of the mouse inducible nitric oxide synthase gene J Endotoxin Res **3**, 381–393

26 Starr, R., Willson, T A., Viney, E M, Murray, L J L, Rayner, J R, Jenkins, B J, Gonda, T J, Alexander, W S, Metcalf, D., Nicola, N A and Hilton, D J (1997) A family of cytokine-inducible inhibitors of signalling Nature (London) **387**, 917–921

27 Song, M M and Shuai, K (1998) The suppressor of cytokine signaling (SOCS) 1 and SOCS3 but not SOCS2 proteins inhibit interferon-mediated antiviral and antiproliferative activities J Biol Chem. **273**, 35056–35062

28 Losman, J A, Chen, X P, Hilton, D. and Rothman, P (1999) Cutting edge. SOCS-1 is a potent inhibitor of IL-4 signal transduction. J Immunol **162**, 3770–3774

29 Zhang, X., Alley, E W, Russell, S W. and Morrison, D C (1994) Necessity and sufficiency of beta interferon for nitric oxide production in mouse peritoneal macrophages Infect Immun **62**, 33–40

30 Fujihara, M, Ito, N, Pace, J L, Watanabe, Y, Russell, S W and Suzuki, T (1994) Role of endogenous Interferon-β In lipopolysaccharide-triggered activation of the inducible nitric oxide synthase gene in a mouse macrophage cell line, J774. J. Biol. Chem **269**, 12773–12778

31 Nose, M, Uzawa, A, Nomura, M, Ikarashi, Y, Nakata, Y, Akashi, M and Suzuki, G (1998) Control of endotoxin shock by the dried preparation of low virulent Streptococcus pyogenes OK-432 Cell Immunol **188**, 97–104

32 Labeta, M O, Durieux, J J., Spagnoli, G, Fernandez, N, Wijdenes, J and Herrmann, R (1993) CD14 and tolerance to lipopolysaccharide biochemical and functional analysis Immunology **80**, 415–423

33 Cavaillon, J-M, Pitton, C and Fitting, C (1994) Endotoxin tolerance is not a LPS-specific phenomenon. partial mimicry with IL-1, IL-10 and TGFβJ Endotoxin Res **1**, 21–29

34 Fahmi, H and Chaby, R (1993) Selective refractoriness of macrophages to endotoxin-induced production of tumor necrosis factor, elicited by an autocrine mechanism J Leukocyte Biol **53**, 45–52

Received 18 January 2000/9 March 2000, accepted 18 April 2000

35 Randow, F, Syrbe, U, Meisel, C, Krausch, D, Zuckermann, H, Platzer, C. and Volk, H-D. (1995) Mechanism of endotoxin desensitization involvement of interleukin 10 and transforming growth factor β J Exp Med **181**, 1887–1892

36 Stoiber, D, Kovarik, P, Cohney, S, Johnston, J A, Steinlein, P and Decker, T (1999) Lipopolysaccharide induces in macrophages the synthesis of the suppressor of cytokine signaling 3 and suppresses signal transduction in response to the activating factor IFN-γ J. Immunol **163**, 2640–2647

37 Bode, J G, Nimmesgern, A, Schmitz, J, Schaper, F, Schmitt, M, Frisch, W, Haussinger, D, Heinrich, P C and Graeve, L (1999) LPS and TNFα induce SOCS3 mRNA and inhibit IL-6-induced activation of STAT3 in macrophages FEBS Lett **463**, 365–370

38 Dickensheets, H L, Venkataraman, C, Schindler, U and Donnelly, R P (1999) Interferons inhibit activation of STAT6 by interleukin 4 in human monocytes by inducing SOCS-1 gene expression Proc Natl Acad Sci U S A **96**, 10800–10805

39 Alexander, W S, Starr, R, Fenner, J E, Scott, C L, Handman, E, Sprigg, N S, Corbin, J E, Cornish, A. L, Darwiche, R, Owczarek, C M et al (1999) SOCS1 is a critical inhibitor of interferon γ signaling and prevents the potentially fatal neonatal actions of this cytokine Cell **98**, 597–608

40 Morrison, D C and Ryan, J L (1987) Endotoxins and disease mechanisms Annu Rev Med **38**, 417–432

Biochem J (2000) 349, 105–111 (Printed in Great Britain)

Characterization of the actin filament capping state in human erythrocyte ghost and cytoskeletal preparations

Philip A. KUHLMAN[1]

Department of Biochemistry, Adrian Building, Leicester University, University Road, Leicester LE1 7RH, U K

The narrow Gaussian-length-distribution of actin filaments forming the cytoskeleton of the human erythrocyte indicates the existence of strict mechanisms for length determination and maintenance. A similar regulation is achieved in striated muscle by the capping of both the ends of the thin filaments, which consequently prevents monomer exchange. However, the ability of erythroid cytoskeletal preparations to nucleate actin polymerization has led to the proliferation of the idea that at least the barbed ends of the actin filaments are uncapped. The mechanism by which the length of the filaments is thus maintained has been left open to debate. In an effort to resolve any doubt regarding length-maintenance in human erythrocytes we have characterized the capping state of the actin filaments in a number of different ghost and cytoskeletal preparations. Under conditions of sufficiently high bivalent-cation concentration the actin filaments retain functional caps at both the barbed and pointed ends. Hence filament capping at both ends prevents redistribution of the actin monomer in a similar manner to that proposed for the thin filaments of striated muscle. Actin filament uncapping is apparently caused by the centrifugal shearing stress imposed during ghost preparation. The uncapping is more pronounced when the bivalent-cation concentration is reduced or when the membrane is removed by detergents. The effects of bivalent cations seem to be mediated through the erythroid protein spectrin, consistent with the hypothesis of Wallis et al. [Wallis, Babitch and Wenegieme (1993) Biochemistry 32, 5045–5050] that the ability of spectrin to resist shearing stress is dependent on the degree of bound bivalent cations.

INTRODUCTION

The human erythrocyte actin cytoskeleton consists of short actin filaments of well-defined length [1], cross-linked into a quasi-hexagonal lattice by long flexible spectrin molecules [1,2]. The ease of preparation of erythrocyte ghosts and the high number of filament ends, compared with total actin, provides a relatively simple system with which to investigate actin-filament length regulation and maintenance. The long-term maintenance of a narrow gaussian filament-length distribution strongly suggests the curtailment of the dynamic nature of actin by the capping of both the barbed and the pointed ends (for a fuller discussion see Fowler [3]).

The actin filaments in human erythrocytes are known to be capped at the pointed ends by tropomodulin [4,5], a protein also found at the pointed ends of the thin filaments in striated muscle, where it has been shown to be the functional capping protein and to regulate actin filament length [6]. The situation at the barbed ends of the actin filaments is less clear as two barbed-end capping proteins have been identified. The first was a non-muscle homologue of CapZ [7] that exhibited a 1 nM capping affinity *in vitro* and was down-regulated by phosphatylinositol 4,5-bisphosphate (PIP_2) in a similar manner to CapZ. However, under various lysis conditions the erythrocyte non-muscle isoform of CapZ (eCapZ) was never localized to the actin cytoskeleton. The cytosolic eCapZ exhibited capping activity, implying the presence of another barbed-end capping protein [7]. Subsequent investigation demonstrated barbed-end capping activity in the previously studied cytoskeletal protein adducin [8]. Adducin, first identified as a calmodulin binding protein [9] and later shown to be involved in the recruitment of spectrin to the short actin filaments [10,11], is stoichiometrically localized to erythrocyte actin filaments. The association of adducin with the erythrocyte actin cytoskeleton, and the concurrent loss of adducin with the availability of binding sites for eCapZ, suggested an involvement of adducin in actin filament barbed-end capping [7].

Recently DiNubile has speculated on the existence of a third barbed-end capping protein [12], due to the apparent premature cessation in pyrene-actin polymerization in the presence of erythrocyte ghosts. The increasing number of capping proteins in the erythrocyte raises the question of redundancy. Are these proteins superfluous to the cell's requirements or does the increasing number indicate a more dynamic actin filament network than currently thought?

The present study investigates the actin filament capping state of erythrocyte ghosts and actin cytoskeletons prepared under various buffer conditions. The maintenance of a sufficiently high bivalent-cation concentration during hypotonic lysis and ghost preparation leads to little uncapping of either end of the actin filaments. Actin filament uncapping can be induced by either a reduction in the bivalent-cation concentration or by extraction of the membrane with detergent. The mechanistic target of the bivalent cation is still unknown, although preliminary data suggest a role for spectrin in the uncapping event.

EXPERIMENTAL

Antibodies

Rabbit anti-human spectrin [S1515] and anti-actin [A2066] polyclonal antibodies were purchased from Sigma–Aldrich (Poole, Dorset, U.K.).

Abbreviations AEBSF, 4-(2-aminoethyl)benzenesulphonyl fluoride, eCapZ, non-muscle isoform of CapZ found in erythrocytes; 5T8 ghosts, erythrocyte membranes prepared by lysis in 5 mM Tris/HCl (pH 8.0) buffer containing protease inhibitors; Mg^{2+} ghosts, erythrocyte membranes prepared by lysis in 5 mM Tris/HCl (pH 8 0) buffer containing protease inhibitors and 3 mM Mg^{2+}, TBS, Tris-buffered saline, PIP_2, phosphatylinositol 4,5-bisphosphate, PKC, protein kinase C

[1] e-mail pak2@le ac uk

Proteins

Erythrocyte capping protein and adducin were purified essentially as described by Kuhlman and Fowler [7] and Hughes and Bennett [13], respectively. DNase I was obtained from Sigma (catalogue reference DN-EP), resuspended in storage buffer [50% (v/v) glycerol, 1 mM $CaCl_2$, 0.5 mM 4-(2-aminoethyl)-benzenesulphonyl fluoride (AEBSF), 5 μg/ml pepstatin A, 5 μg/ml leupeptin and 2% (v/v) ethanol] and kept at −20 °C as described by Podolski and Steck [14]. Actin was purified from a rabbit skeletal-muscle acetone powder, as described by Pardee and Spudich [15], with an additional purification step using a 100 cm × 1.6 cm Superose 6 (Pharmacia) gel-filtration column. Fractions were tested for the ability to produce high viscosity on polymerization (indicating lack of intrinsic nuclei) by using the falling-ball method [16,17]. Actin was pyrene-labelled with *N*-(1-pyrene)iodoacetamide (P-29; Molecular Probes Europe BV, Leiden, The Netherlands) using the method of Kouyama and Mihashi [18] with the modifications of Weber et al. [19]. Unincorporated label was removed by gel-filtration using a 30 cm × 0.5 cm Superdex 200 gel-filtration column and FPLC (Pharmacia). Actin/spectrin seeds, derived from the low ionic-strength extract of erythrocyte membranes, were prepared as described previously [20]. Protein concentrations were determined from the absorption coefficients: 26600 $M^{-1}\cdot cm^{-1}$ at 290 nm for actin; 22000 $M^{-1}\cdot cm^{-1}$ at 344 nm for pyrene, using a correction factor of $[A_{290}-(0.127\times A_{344})]/26600$ for the actin concentration; 85000 $M^{-1}\cdot cm^{-1}$ at 280 nm [21] and 100500 $M^{-1}\cdot cm^{-1}$ at 279 nm for human erythrocyte capping protein and human erythrocyte adducin respectively.

Pyrene-actin polymerization assay

Actin polymerization was monitored by observing the increase in pyrene fluorescence on polymerization using an SLM 48000 fluorimeter. Pyrene fluorescence was excited at 365 nm using a slit width of 0.5 nm. Fluorescence was detected at 407 nm using a slit width of 8 nm. To limit photobleaching the highly focused excitation beam was defocused with a convex lens (focal length of 100 mm), prior to the sample cuvette (5 mm square). All actin polymerization experiments were maintained at 25 °C by a circulating-water bath. Under low-salt conditions (2 mM KCl/0.8 mM $MgCl_2$) polymerization was primarily from the barbed filament end Other experiments were performed at higher salt concentrations (0.1 M KCl/2 mM Mg^{2+}) to detect polymerization from both the barbed and pointed filament ends. The polymerization was initiated by the addition of pyrene labelled G-actin (5% labelled; final concentration 5 μM) that had been primed with Mg^{2+} as described previously [8]. The use of DNase I to inhibit actin filament polymerization at the pointed end [14] required a 10 min incubation at 25 °C prior to initiation of actin polymerization.

Erythrocyte isolation and ghost preparation

Small amounts of human erythrocytes were prepared from 10 ml of freshly drawn blood by sedimentation, at unit gravity, through 4 vol. of 0.75% (w/v) dextran T-500 (Pharmacia) at room temperature in Tris-buffered saline [TBS; 10 mM Tris/HCl (pH 7.5)/150 mM NaCl]. The cells were then washed three times in 10 vol of TBS supplemented with 10 mM glucose, before being resuspended to a 20% (v/v) suspension, with respect to the packed-cell volume. The cells were stored on ice until required, and the erythrocyte concentration was determined by counting cells with the aid of a haemocytometer.

Erythrocyte ghosts were prepared by hypotonic lysis with an excess (30-fold) of either 5T8 buffer [5 mM Tris/HCl (pH 8.0)/5 mM β-mercaptoethanol/1 mM NaN_3/0.5 mM AEBSF; 5T8 ghosts] or the same buffer supplemented with various concentrations of $MgCl_2$ (Mg^{2+} ghosts). Following 10 min on ice, to facilitate lysis, the ghosts were collected by centrifugation at 11951 *g* in a Sorvall SS34 rotor at 4 °C for 10 min. The ghosts were washed a further three times with the same buffer, before being resuspended to a defined volume, hence defining the number of erythrocyte equivalents per ml. Ghosts prepared in the absence of Mg^{2+} were white, whereas the Mg^{2+} ghosts retained a pink hue, indicative of a small amount of retained haemoglobin.

Removal of Mg^{2+} from Mg^{2+} ghosts

Freshly prepared Mg^{2+} ghosts were either washed by repeated resuspension in 5T8 buffer and centrifugation at 11951 *g* at 4 °C for 10 min in a Sorvall SS34 rotor, or by dialysis against an excess of 5T8 buffer. Samples of ghosts were extracted after each wash or after 1 h of dialysis and tested for actin nucleation activity in the pyrene-actin polymerization assay. Samples taken during the dialysis experiment were also treated with Triton X-100 (0.1% final concentration) and centrifuged at 48700 *g* for 10 min at 4 °C in a TLA 100 rotor to remove the actin cytoskeletons. A fraction of the supernatant was solubilized in SDS sample buffer and separated by SDS/PAGE [7.5–15% (w/v) polyacrylamide] [22]. Following blotting on to nitrocellulose, the spectrin region was probed with an antibody to erythrocyte spectrin and detected using ^{35}S-labelled donkey anti-rabbit IgG serum (Amersham Pharmacia Biotech, Uppsala, Sweden). Each lane was quantified by excision of the region of nitrocellulose, solubilization in 5 ml of scintillation fluid (Optiphase 'high safe' 2; Fisher Scientific Ltd., Loughborough, U.K.) and scintillation counted.

Preparation of detergent-solubilized actin cytoskeletons

Human erythrocytes were mixed with an equal volume of 0.6% detergent (either Triton X-100 or saponin) in TBS supplemented with 0.5 mM AEBSF, 5 μg/ml pepstatin A and 5 μg/ml leupeptin. The cells were gently pipetted to aid lysis and then centrifuged, at 11600 *g* for 5 min in a microfuge, through 2 vol. of a 20% sucrose solution [TBS, 20% (w/v) sucrose, 3 mM $MgCl_2$, 0.5 mM AEBSF, 5 μg/ml pepstatin A and 5 μg/ml leupeptin]. All but 100 μl of the supernatant was carefully removed to prevent loss of cytoskeletons and then the pellet was resuspended to a final volume of 200 μl by the addition of 100 μl of similar buffer without sucrose (TBS, 3 mM $MgCl_2$, 0.5 mM AEBSF, 5 μg/ml pepstatin A and 5 μg/ml leupeptin). Hence the final sucrose concentration was 10% (w/v).

RESULTS

The actin nucleating activity was measured in a number of ghost and cytoskeletal preparations. Under low-salt conditions (2 mM KCl/0.8 mM $MgCl_2$) nucleating activity could be demonstrated with actin/spectrin seeds, 5T8 ghosts, saponin and Triton X-100 skeletons. In each case the nucleating activity could be inhibited with a saturating amount of eCapZ (30 nM), a reagent specific for the actin filament barbed-end (Figure 1A). Mg^{2+} ghosts were effectively devoid of nucleating activity. Under higher salt conditions (0.1 M KCl/2 mM $MgCl_2$) the Mg^{2+} ghosts were weak nucleators (Figure 1B), but this activity was abolished by eCapZ (15 nM), indicating the presence of a very small number of uncapped barbed ends. The nucleating activity of actin/spectrin seeds and 5T8 ghosts was identical, in so far that a

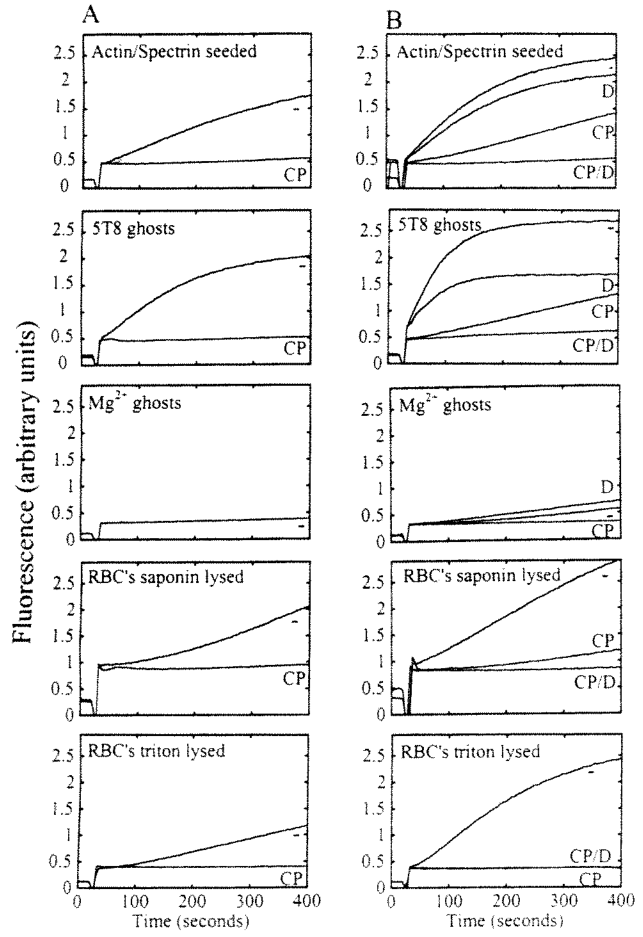

Figure 1 Actin filament capping state characterization in ghost and cytoskeletal preparations

(**A**) Raw data (non-standardized) depicting the polymerization of pyrene-labelled actin under low-salt conditions (2 mM KCl/0.8 mM $MgCl_2$) nucleated by a variety of erythrocyte preparations. (**B**) Raw data (non-standardized) of identical experiments polymerized under high-salt conditions (0.1 M KCl/2 mM $MgCl_2$). The nucleating activity of the erythrocyte preparations was modulated with erythrocyte capping protein (CP), DNAse I (D), both (CP/D) or neither (—). Concentrations of capping proteins for the different experiments were as follows: CP = 30 nM for the low-salt experiment and 15 nM for the high-salt experiment (reduction in the concentration under high-salt conditions was essential to prevent expression of its nucleating activity); D = 800 nM, except in the case of 5T8 ghosts under high-salt conditions when 2.5 μM was used in order to rule out sequestration as the mechanism of action. RBCs, red blood cells.

proportion of the nucleating activity could be abolished by eCapZ. The remainder of the activity due to polymerization from the pointed end of the filaments could be abolished by treatment with DNase I. Saponin skeletons were similar to actin/spectrin seeds and 5T8 ghosts, except that the proportion of nucleating activity due to pointed ends was smaller. The ability of eCapZ to inhibit the nucleating activity of Triton X-100 skeletons completely indicates that only the barbed ends are uncapped. To ensure complete pointed-end capping, and to demonstrate that the effects of DNase I were not through the sequestration of actin monomers, 2.5 μM DNase I was used in the high-salt experiments of the 5T8 ghosts (Figure 1B, second panel down). Note that 2.5 μM DNase I alone was unable to inhibit actin polymerization which reached an equilibrium fluorescence that was half that of the 5T8 ghosts alone, consistent with the sequestration of approx. half of the 5 μM G-actin present in the assay.

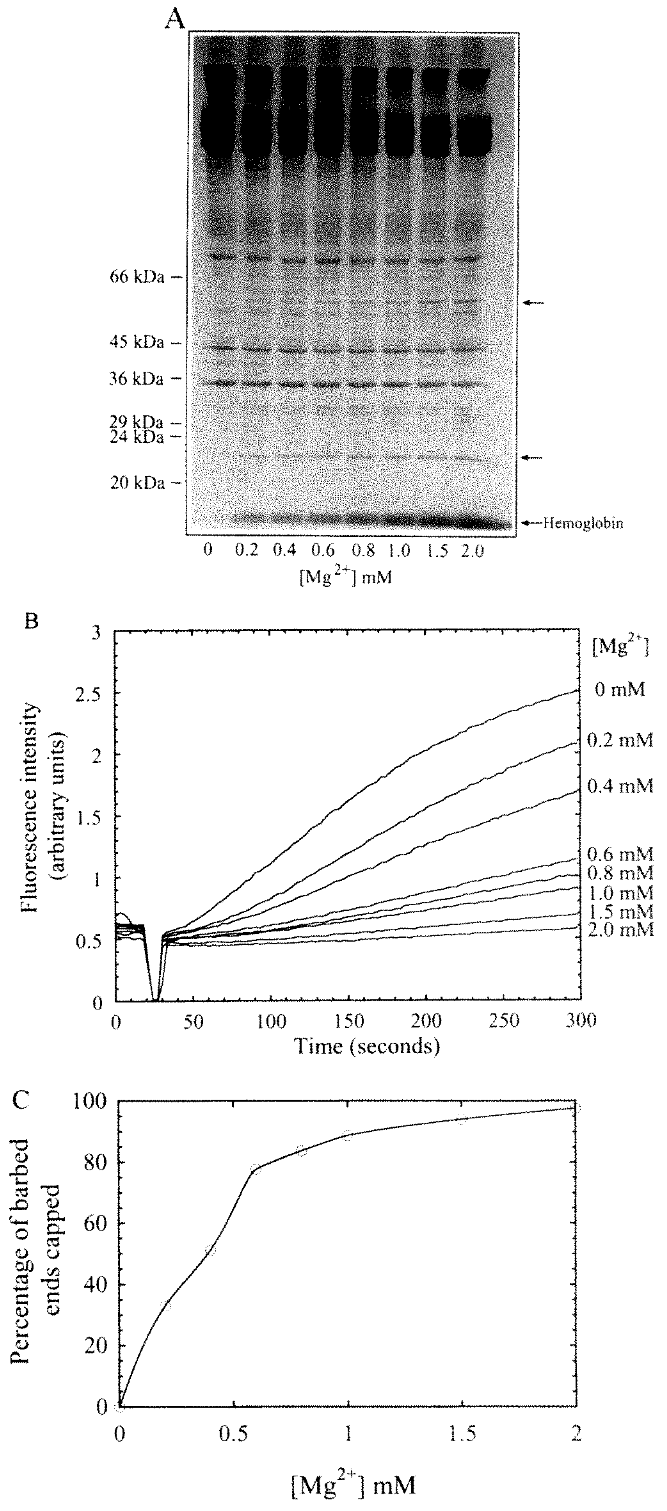

Figure 2 Effect of magnesium concentration on ghost actin filament capping state

(**A**) Equivalent samples of human erythrocyte ghosts prepared under a range of Mg^{2+} ion concentrations, separated by SDS/PAGE and stained with Coomassie Brilliant Blue R250. The positions of molecular mass standards and three proteins whose association with the erythrocyte ghosts was dependent on Mg^{2+} ion concentration are indicated. (**B**) The corresponding ghosts were also tested for their ability to nucleate actin polymerization in the pyrene-actin elongation assay (raw data). (**C**) By assuming the ghosts in the absence of Mg^{2+} were 100% uncapped, then the extent of capping in the other samples could be estimated from the initial polymerization rates.

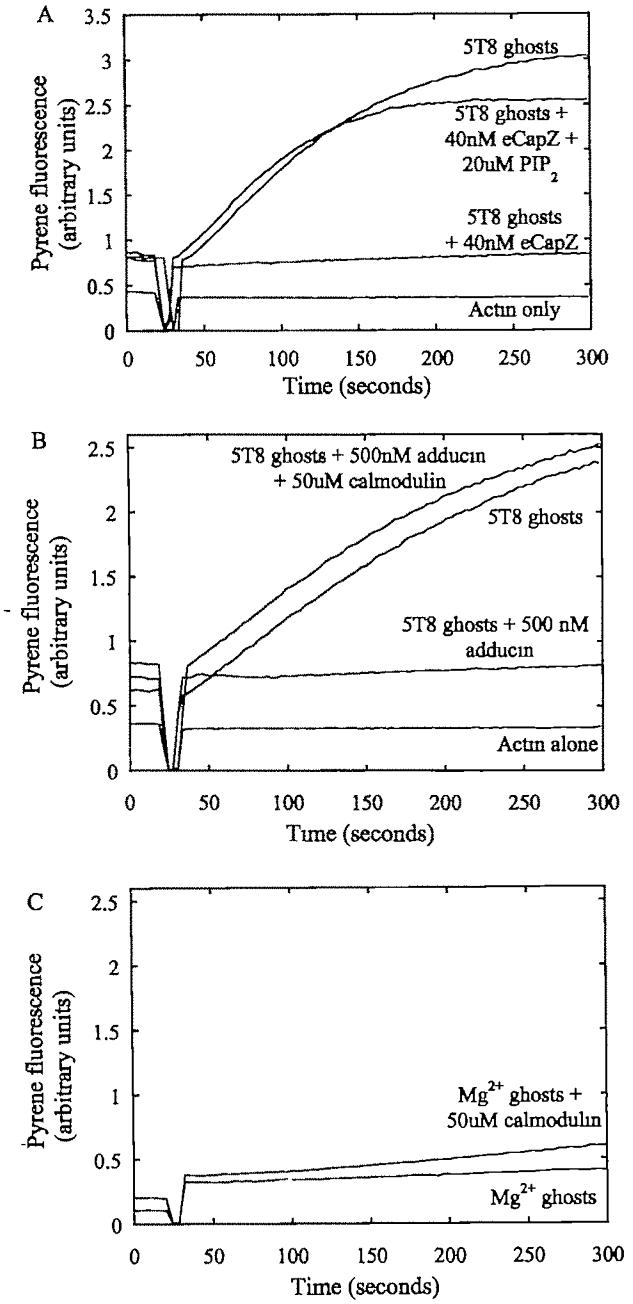

Figure 3 Comparison of actin filament barbed-end capping between 5T8 and Mg^{2+} ghosts

(A) Pyrene-actin polymerisation assay demonstrating the ability of 40 nM erythrocyte capping protein to block the polymerization from the barbed ends of 5T8 ghosts. This capping activity can be inhibited by 20 μM PIP$_2$. Actin alone has no intrinsic polymerization under these conditions. (B) The same assay demonstrating the ability of 500 nM adducin to prevent polymerization from the barbed ends of the actin filaments in 5T8 ghosts. In this case the inhibition can be relieved using 50 μM calmodulin. (C) A similar concentration of calmodulin has little effect on the nucleating activity of Mg^{2+} ghosts.

Preparation of human erythrocyte ghosts in a weak Tris buffer supplemented with increasing concentrations of MgCl$_2$ resulted in ghosts with increased actin filament capping (Figure 2). Samples of the resulting ghosts separated by SDS/PAGE (7.5–15 % polyacrylamide) and stained with Coomassie Brilliant Blue indicated at least three proteins whose association with the ghost was apparently affected by the Mg^{2+} ion concentration (Figure 2A). Haemoglobin was one such protein, although its association with the actin cytoskeleton has no effect on the capping state of the actin filament barbed-end [7]. The increasing Mg^{2+} concentration also reduced the extent to which the ghosts were able to act as nuclei in a pyrene-actin polymerization assay (Figures 2B and 2C). A repeat experiment utilizing CaCl$_2$ in place of MgCl$_2$ yielded identical results (results not shown), indicating that the effect was not specific to Mg^{2+} ions.

The actin filament barbed ends in the 5T8 ghosts were

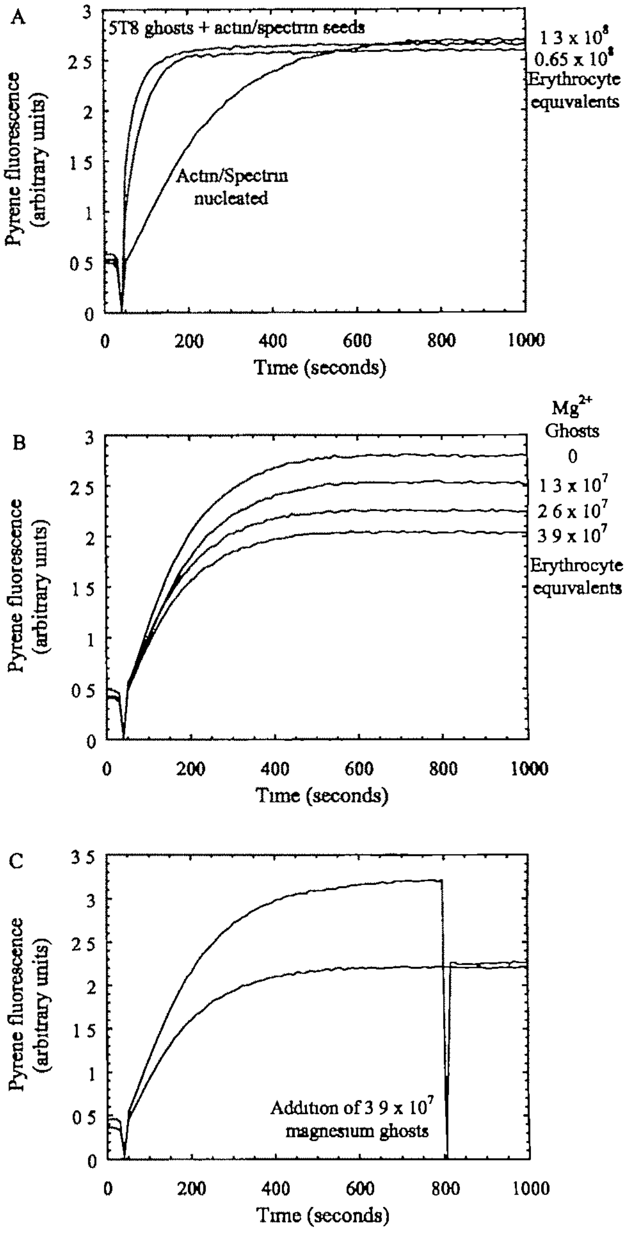

Figure 4 Effect of 5T8 and Mg^{2+} ghosts on the pyrene-actin polymerization assay

(A) 5T8 ghosts (0.65 × 10^8 or 1.3 × 10^8 cell equivalents) were added to the actin/spectrin seeded assay. Addition of polymerization salts initiated the actin polymerization. (B) Mg^{2+} ghosts (1.3 × 10^7, 2.6 × 10^7 and 3.9 × 10^7 cell equivalents) also added to actin/spectrin nucleated actin polymerization assay. (C) Addition of the Mg^{2+} ghosts (3.9 × 10^7 cell equivalents) at the end (800 s) of the polymerization assay as compared with inclusion at the start (0 s).

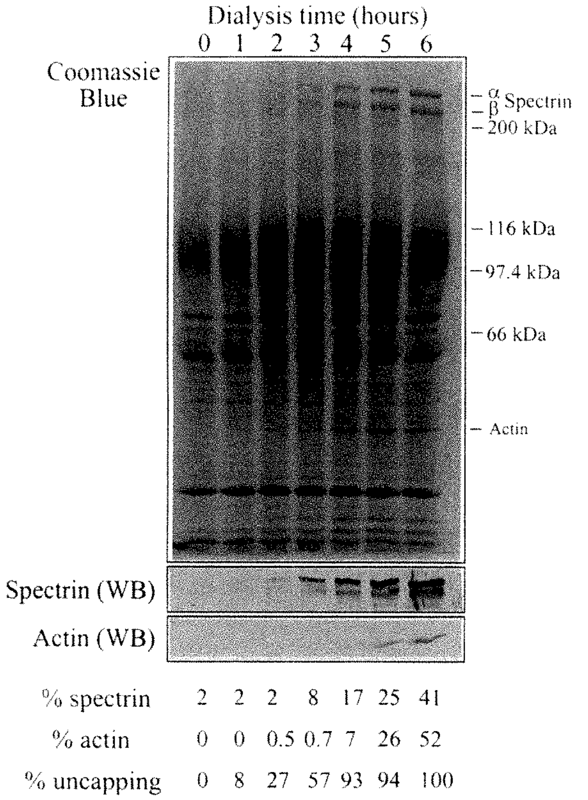

Figure 5 Conversion of Mg^{2+} ghosts into 5T8 ghosts

Samples, taken during a 6 h dialysis of Mg^{2+} ghosts with 5T8 buffer, extracted with 0.1% Triton X-100 and centrifuged to remove the actin cytoskeletons (see the Experimental section) were separated by SDS/PAGE and either stained with Coomassie Brilliant Blue or Western-blotted (WB) for spectrin and actin. The position of the alpha and beta subunits of spectrin, actin and several molecular mass markers are indicated. The percentage of spectrin and actin released has been determined against the total amounts in the sample, and the extent of barbed-end uncapping has been determined by assuming the 6 h dialysis point gave 100% uncapping.

effectively identical to those in actin/spectrin seeds with respect to the ability of both eCapZ and adducin to totally inhibit actin polymerization (Figures 3A and 3B). This inhibition could be down-regulated by PIP$_2$ and calmodulin respectively (Figures 3A and 3B). Treatment of Mg^{2+} ghosts with calmodulin under the same conditions did not yield any significant nucleating activity (Figure 3C).

In an effort to confirm the observations of DiNubile [12], both 5T8 (Figure 4A) and Mg^{2+} (Figure 4B) ghosts were added to an actin/spectrin nucleated pyrene-actin polymerization assay (Figure 4). In the case of the 5T8 ghosts, addition of 0.65×10^{8} and 1.3×10^{8} erythrocyte equivalents resulted in an increased rate of actin polymerization, consistent with the additional nuclei present (Figure 4A). The end-point of the polymerization was essentially the same, but for small effects caused by light-scattering by the ghosts, thus indicating that there was no untoward capping activity from 5T8 ghosts. The addition of Mg^{2+} ghosts did not lead to an increase in the rate of actin polymerization due to the actin filaments being capped (Figure 4B). The fluorescence at the end of the polymerization was reduced proportionally to the amount of ghosts added (Figure 4B). The fluorescence signal at the end of the polymerization assay was similar regardless of the time at which the Mg^{2+} ghosts were added (Figure 4C). The instantaneous drop in fluorescence signal on addition of the ghosts was consistent with an inner-filter effect caused by the haemoglobin in the Mg^{2+} ghost sample. Measurement of the extent of actin polymerization at the end of each reaction indicated no dramatic increase in the amount of G-actin (results not shown), a result not consistent with the idea of premature polymerization termination due to capping.

The removal of Mg^{2+} ions from Mg^{2+} ghosts by extended dialysis (Figure 5) against 5T8 buffer resulted in the uncapping of the actin filament barbed ends. Samples were taken during the dialysis, treated with 0.1% Triton X-100 and centrifuged (48 700 *g* for 10 min at 4 °C) to remove the actin cytoskeletons. The amount of spectrin and actin in the supernatants was determined empirically, by Coomassie Brilliant Blue staining, or quantitatively, by Western blotting with antibodies specific for spectrin and actin. These proteins were apparent in the supernatants after 2–3 h of dialysis, increasing thereafter until the end of the assay at 6 h. At the end of the assay approx. half of the actin and spectrin was not associated in macromolecular complexes, indicating the slow disintegration of the cytoskeleton.

DISCUSSION

Using the nucleated pyrene-actin polymerization assay, the uncapping of both actin filament ends in erythrocyte ghosts and cytoskeletons prepared in the absence of bivalent cations (Figure 1) has been confirmed. This observation is consistent with several other studies [12,14,23–29]. However, the presence of bivalent cations during ghost preparation results in actin filaments capped at both ends (Figure 2), an observation consistent with the simplest mechanism for maintaining a narrow Gaussian-length-distribution, as is thought to be the case for the thin filaments of striated muscle.

The mode of actin filament uncapping is not clear. Generally, uncapping is dependent on the degree of physical stress the cells are subjected to; this effect is amplified by treatment with detergent or by reduction in bivalent-cation concentration. During ghost isolation excessive centrifugal force results in ghost fragmentation. This was particularly true of the 5T8 ghosts which seemed to be substantially more fragile than the Mg^{2+} or Ca^{2+} ghosts (results not shown). Similar effects were observed by Das and Mukherjee [31], although they ascribed the observation to the presence of a heterogeneous population of erythrocyte ghosts. Our initial 5T8 ghost preparations when centrifuged (at 38 724 *g*) exhibited a lower packed main pellet with a diffuse pellet on top. This effect was circumvented by reducing the centrifugal force, resulting in a homogeneous pellet with no residue in the supernatant. It is likely that the two membrane populations observed by Das and Mukherjee [31] were derived from centrifugal damage during erythrocyte ghost preparation, especially due to their use of lysis and wash buffers devoid of bivalent cations.

The 5T8 ghosts act identically to actin/spectrin seeds with respect to the ability of both eCapZ and adducin to cap the barbed ends of the actin filaments and be released by PIP$_2$ and calmodulin/Ca^{2+} respectively (Figures 3A and 3B). In contrast, the actin filaments in Mg^{2+} ghosts are capped at the barbed ends, presumably by adducin [7], and at the pointed ends by tropomodulin[6]. However, treatment of Mg^{2+} ghosts with $50\,\mu$M calmodulin resulted in only a marginal increase in the nucleating activity of the ghosts (Figure 3C). Under identical conditions, $50\,\mu$M calmodulin was able to inhibit the capping activity of purified adducin on 5T8 ghosts (Figure 3B). There are two possible explanations for these observations. (1) The adducin in the Mg^{2+} ghosts is modified compared with purified adducin, possibly by phosphorylation. It is known that PKC phosphorylation of adducin on Ser^{726} prevents the binding of calmodulin

[32]. (2) Alternatively, the barbed-end capping is facilitated by an as yet undiscovered capping protein. A third barbed-end capping protein has been proposed by DiNubile [12], due to the apparent premature cessation of actin polymerization in the presence of ghosts. Addition of 5T8 (white) ghosts to actin/spectrin-seeded actin polymerization produces a higher initial polymerization rate, consistent with the increase in the number of nuclei (Figure 4A). The fluorescence end-point, however, is effectively identical to that in the absence of ghosts, apart from a small effect due to light-scattering by the ghosts. The addition of Mg^{2+} (pink) ghosts produces no real increase in the initial polymerization rate due to the ghosts being capped (Figure 4B). There is a significant reduction in the fluorescence at the end of the time course, which is dependent on the amount of ghosts added. We have ruled out the action of a capping protein for three reasons. (1) Haemoglobin in the ghosts absorbs the emitted fluorescent (407 nm) light strongly. (2) Quantification of the amount of unpolymerized actin (actin critical concentration) indicated no significant change in the presence of ghosts (results not shown). (3) Addition of the Mg^{2+} ghosts at the end of the time course led to the same final fluorescence; this instantaneous effect is unlikely to be consistent with capping protein kinetics, but simply an inner-filter effect [33]. This being the case, adducin is still the best candidate for the active barbed-end capping protein in erythrocytes.

Treatment of Mg^{2+} ghosts with bivalent cation-free buffer (5T8 buffer), either by repeated washing (results not shown) or by extended dialysis (Figure 5), renders them good nuclei in the actin polymerization assay. Efforts at reversing this uncapping event by restoring the Mg^{2+} ion concentration and/or concentrating the dialysate and readdition have been unsuccessful (results not shown). The loss of actin and spectrin during dialysis (Figure 5) indicates the disintegration of the actin cytoskeleton. However, this disruption of the actin cytoskeleton occurs under very little shearing stress, suggesting structural changes in the ghost actin cytoskeleton itself. One possible explanation would be proteolysis. To prevent this, protease inhibitors were maintained in all buffers at all times and adducin (a protein sensitive to proteolysis) was monitored for signs of degradation. Proteolytic damage to adducin was minimal during the assay, suggesting that proteolysis is not responsible for the uncapping event.

This study has confirmed the capping of both ends of the actin filaments in resting human erythrocytes and highlighted the functional significance of the bivalent-cation concentration for the structural integrity of the erythrocyte cytoskeleton. A reduction in the bivalent-cation concentration leads to changes in the actin/spectrin network, reducing its strength, rendering it prone to fragmentation, especially in the absence of the plasma membrane. This effect is likely to be derived from the dissociation of spectrin from the cytoskeleton; incubation of ghosts in low-salt buffers devoid of bivalent cations is the method by which spectrin is purified [34]. This response to bivalent cations suggests a mechanism by which the physical properties of the erythrocyte can be tailored to the varying requirements during the passage through the circulatory system, as suggested by Wallis et al. [35]. During the oxygenation/deoxygenation cycle the free Mg^{2+} ion concentration oscillates between 0.6 mM and 1.9 mM [36]. It has also been demonstrated that erythrocytes put under shearing stress leak Ca^{2+} ions [37]. Hence, the oscillating Mg^{2+} ion concentration may act as a general mechanism to modulate the physical properties of the erythrocyte during the general passage through the circulatory system, supplemented by additional fine-tuning by fluctuations in the Ca^{2+} concentration during direct application of shearing stress, such as the passage through the narrow sinusoids of the spleen. Experiments to test these hypotheses are currently underway.

This work was funded by a Wellcome Trust career development grant. I would also like to thank Clare Savage for excellent technical assistance and Dr Clive Bagshaw for critical reading of the manuscript

REFERENCES

1 Shen, B W, Josephs, R. and Steck, T L (1986) Ultrastructure of the intact skeleton of the human-erythrocyte membrane J Cell Biol. **102**, 997–1006

2 Byers, T J and Branton, D. (1985) Visualization of the protein associations in the erythrocyte-membrane skeleton Proc Natl. Acad Sci U.S A **82**, 6153–6157

3 Fowler, V M (1996) Regulation of actin filament length in erythrocytes and striated muscle. Curr. Opin Cell Biol **8**, 86–96

4 Fowler, V M, Sussman, M A., Miller, P. G., Flucher, B E and Daniels, M P (1993) Tropomodulin is associated with the free (pointed) ends of the thin-filaments in rat skeletal-muscle J Cell Biol **120**, 411–420

5 Weber, A, Pennise, C R, Babcock, G. G. and Fowler, V M (1994) Tropomodulin caps the pointed ends of actin-filaments. J Cell Biol **127**, 1627–1635

6 Gregorio, C C., Weber, A, Bondad, M, Pennise, C R and Fowler, V M (1995) Requirement of pointed-end capping by tropomodulin to maintain actin filament length in embryonic chick cardiac myocytes Nature (London) **377**, 83–86

7 Kuhlman, P A. and Fowler, V M. (1997) Purification and characterization of an alpha(1)beta(2) isoform of CapZ from human erythrocytes: cytosolic location and inability to bind to Mg^{2+} ghosts suggest that erythrocyte actin filaments are capped by adducin Biochemistry **36**, 13461–13472

8 Kuhlman, P A., Hughes, C A, Bennett, V. and Fowler, V M (1996) A new function for adducin-calcium/calmodulin-regulated capping of the barbed ends of actin filaments J Biol Chem **271**, 7986–7991

9 Gardner, K and Bennett, V (1986) A new erythrocyte membrane-associated protein with calmodulin binding-activity-identification and purification J Biol Chem **261**, 1339–1348

10 Gardner, K. and Bennett, V (1987) Modulation of spectrin actin assembly by erythrocyte adducin Nature (London) **328**, 359–362

11 Mische, S M, Mooseker, M S and Morrow, J. S. (1987) Beta-spectrin bestows protein 4.1 sensitivity on spectrin–actin interactions J Cell Biol **105**, 2837–2845

12 DiNubile, M. J (1999) Erythrocyte membrane fractions contain free barbed filament ends despite sufficient concentrations of retained capper(s) to prevent barbed end growth Cell Motil Cytoskeleton **43**, 10–22

13 Hughes, C A and Bennett, V (1995) Adducin-a physical model with implications for function in assembly of spectrin–actin complexes J Biol Chem **270**, 18990–18996

14 Podolski, J L and Steck, T L (1988) Association of deoxyribonuclease-1 with the pointed ends of actin-filaments in human red blood-cell membrane skeletons. J Biol Chem **263**, 638–645

15 Pardee, J D and Spudich, J A (1982) Purification of muscle actin. Methods Enzymol **85**, 164–181

16 Fowler, V M and Taylor, D L (1980) Spectrin plus band 4.1 cross-link actin Regulation by micromolar calcium J Cell Biol **85**, 361–376

17 Fowler, V. M and Pollard, H B. (1982) *In vitro* reconstitution of chromaffin granule–cytoskeleton interactions – ionic factors influencing the association of F-actin with purified chromaffin granule membranes J Cell Biochem **18**, 295–311

18 Kouyama, T and Mihashi, K (1981) Fluorimetry study of n-(1-pyrenyl)iodo-acetamide-labelled F-actin – local structural-change of actin protomer both on polymerization and on binding of heavy-meromyosin Eur. J Biochem **114**, 33–38

19 Weber, A., Northrop, J., Bishop, M F, Ferrone, F A and Mooseker, M S (1987) Nucleation of actin polymerization by villin and elongation at subcritical monomer concentration Biochemistry **26**, 2528–2536

20 Casella, J F, Maack, D J and Lin, S (1986) Purification and initial characterization of a protein from skeletal-muscle that caps the barbed ends of actin-filaments J Biol Chem. **261**, 10915–10921

21 Caldwell, J. E., Heiss, S. G., Mermall, V. and Cooper, J A. (1989) Effects of CapZ, an actin capping protein of muscle, on the polymerization of actin Biochemistry **28**, 8506–8514

22 Laemmli, U K (1970) Cleavage of structural proteins during the assembly of the head of bacteriophage T4 Nature (London) **227**, 680–685

23 Pinder, J C and Gratzer, W B (1982) Investigation of the actin deoxyribonuclease-I interaction using a pyrene-conjugated actin derivative Biochemistry **21**, 4886–4890

24 Pinder, J C and Gratzer, W B. (1983) Structural and dynamic states of actin in the erythrocyte J Cell Biol **96**, 768–775

25 Tsukita, S, Tsukita, S and Ishikawa, H (1984) Bidirectional polymerization of G-actin on the human-erythrocyte membrane J Cell Biol **98**, 1102–1110

26 Lin, D C and Lin, S (1979) Actin polymerization induced by a motility-related high-affinity cytochalasin binding complex from human erythrocyte membrane Proc Natl Acad. Sci. U S A. **76**, 2345–2349

27 Brenner, S L and Korn, E D (1980) Spectrin/actin complex isolated from sheep erythrocytes accelerates actin polymerisation by simple nucleation. J Biol. Chem. **255**, 1670–1676

28 Pinder, J. C., Ohanian, V. and Gratzer, W B (1984) Spectrin and protein-4.1 as an actin filament capping complex. FEBS Lett **169**, 161–164

29 Pinder, J. C, Weeds, A. G. and Gratzer, W B (1986) Study of actin filament ends in the human red-cell membrane J Mol Biol **191**, 461–468

30 Pollard, T D and Mooseker, M S (1981) Direct measurement of actin polymerization rate constants by electron-microscopy of actin-filaments nucleated by isolated microvillus cores J Cell Biol. **88**, 654–659

31 Das, S. K. and Mukherjee, S (1999) Heterogeneity of human red blood cell membrane co-existence of heavy and light membranes. Mol. Cell Biochem **196**, 141–149

32 Matsuoka, Y, Hughes, C A and Bennett, V. (1996) Adducin regulation Definition of the calmodulin-binding domain and sites of phosphorylation by protein kinase A and C J. Biol Chem. **271**, 25157–25166

33 Lakowicz, J R (1999) Instrumentation for fluorescence spectroscopy In Principles of Fluorescence Spectroscopy, pp. 52–54, Kluwer Academic/Plenum Publishers, New York

34 Gratzer, W. B (1982) Preparation of spectrin Methods Enzymol **85**, 475–480

35 Wallis, C J, Babitch, J A and Wenegieme, E F (1993) Divalent-cation binding to erythrocyte spectrin Biochemistry, **32**, 5045–5050

36 Bunn, H F, Ransil, B J. and Chao, A (1971) The interaction between erythrocyte organic phosphates, magnesium ions, and hemoglobin J. Biol Chem **246**, 5273–5279

37 Larsen, F L, Katz, S, Roufogalis, B. D. and Brooks, D. E. (1981) Physiological shear stresses enhance the Ca^{2+} permeability of human-erythrocytes Nature (London) **294**, 667–668

Received 9 February 2000/15 April 2000, accepted 4 May 2000

$p40^{phox}$ participates in the activation of NADPH oxidase by increasing the affinity of $p47^{phox}$ for flavocytochrome b_{558}

Andrew R. CROSS

Department of Molecular and Experimental Medicine, MEM-241, The Scripps Research Institute, 10550 North Torrey Pines Road, La Jolla, CA 92037, U.S.A.

NADPH oxidase is one of the major components of the innate immune system and is used by phagocytes to generate microbicidal reactive oxygen species. Activation of the enzyme requires the participation of a minimum of five proteins, $p22^{phox}$, $gp91^{phox}$ (together forming flavocytochrome b_{558}), $p47^{phox}$, $p67^{phox}$ and the GTP-binding protein, Rac2. A sixth protein, $p40^{phox}$, has been implicated in the control of the activity of NADPH oxidase principally based on its sequence homology to, and physical association with, other *phox* components, and also the observation that it is phosphorylated during neutrophil activation. However, to date its role in regulating the activity of the enzyme has remained obscure, with evidence for both positive and negative influences on oxidase activity having being reported. Data are presented here using the cell-free system for NADPH oxidase activation that shows that $p40^{phox}$ can function to promote oxidase activation by increasing the affinity of $p47^{phox}$ for the enzyme approx. 3-fold.

Key words: host defence, oxygen radicals, $p47^{phox}$, respiratory burst, superoxide.

INTRODUCTION

The NADPH oxidase of phagocytic cells plays a pivotal role in innate immunity. When activated, the function of the enzyme is to generate microbicidal reactive oxygen species derived from the primary product of NADPH oxidase, superoxide (O_2^-) (reviewed by Nauseef [1]). The active oxidase requires the participation of five gene products; two of these, $p22^{phox}$ and $gp91^{phox}$, together form flavocytochrome b_{558}, the membrane-bound core of the enzyme. $gp91^{phox}$ contains all the catalytic machinery necessary to oxidize NADPH and form O_2^-, the NADPH-binding site, one molecule of FAD and two molecules of haem ([2,3] and L. Yu, M. C. Dinauer and A. R. Cross, unpublished work). In order to convert the normally inactive oxidase into the active state, three other proteins are required, $p47^{phox}$, $p67^{phox}$ and the small GTP-binding protein Rac2. In the resting cell, these proteins are present in the cytosol and upon cellular activation associate with flavocytochrome b_{558} and convert it into a functional state in a process we have recently shown to be catalytic [4,5]. Genetic defects in any one of the $p47^{phox}$, $p67^{phox}$, $p22^{phox}$ or $gp91^{phox}$ proteins that result in the loss of their function (and failure of NADPH oxidase to generate O_2^-) cause a severe susceptibility to microbial infections, a syndrome known as chronic granulomatous disease (CGD) [6]. Recently, a description of a genetic defect in Rac2 resulting in neutrophil dysfunction and susceptibility to infection has been reported [7]. A further protein, $p40^{phox}$, has been implicated in oxidase activity, but to date its role has remained obscure $p40^{phox}$ was described independently by the groups of Segal and Someya, who identified and cloned a protein that was found to exist in a cytosolic complex with $p67^{phox}$ and $p47^{phox}$ [8,9]. These workers showed that $p40^{phox}$ had significant sequence homology to $p47^{phox}$ and $p67^{phox}$ and that its expression was reduced markedly in the cytosols of CGD patients with $p67^{phox}$ deficiency Subsequent work showed that $p40^{phox}$ becomes phosphorylated during neutrophil activation and translocates to the plasma membrane in a similar manner to $p47^{phox}$ [10–13]. These findings have prompted extensive investigations into the molecular interactions of $p47^{phox}$, $p67^{phox}$ and Rac with $p40^{phox}$ [14–20]. $p40^{phox}$ associates with $p47^{phox}$ and $p67^{phox}$ and is depleted in neutrophils of $p67^{phox}$-deficient CGD patients [8,21]. Studies of cytoskeletal associations of *phox* proteins indicate that $p40^{phox}$ and $p67^{phox}$ associate with the cytoskeletal fraction of resting cells, whereas $p47^{phox}$ only becomes associated with the cytoskeleton during activation. $p40^{phox}$ can dissociate from $p67^{phox}$ however, possibly associating with $p47^{phox}$, both in whole cells and the cell-free system [11,22]. Despite these intensive studies into the role of $p40^{phox}$, little direct evidence for a function has been found for this protein to date, and it is not required for NADPH oxidase activity in the classical cell-free system for oxidase activation. Experiments overexpressing $p40^{phox}$ in myeloid cell lines by Leto and co-workers [23] led them to conclude that $p40^{phox}$ functions to down-regulate NADPH oxidase via interactions of SH3 domains within the *phox* proteins, a finding that was supported by inhibition of cell-free NADPH oxidase activity at high (greater-than-micromolar) $p40^{phox}$ concentrations [23]. In contrast, Tsunawaki et al. [16] found that an antibody to the C-terminus of $p40^{phox}$ dissociated $p40^{phox}$ from the cytosolic *phox* complex and was inhibitory in the cell-free system, suggesting a positive role for $p40^{phox}$ in oxidase activation. Here, for the first time, we show that under appropriate conditions $p40^{phox}$ has a significant effect in enhancing the activation of NADPH oxidase in the cell-free system, probably by increasing the affinity of $p47^{phox}$ for the enzyme.

EXPERIMENTAL

Reagents

All chemicals and reagents were of reagent grade and were from Sigma unless noted otherwise. Human neutrophils and their subcellular fractions were prepared and stored as described in [24]. Recombinant *phox* proteins were generated in Sf9 or Hi5

Abbreviation used CGD, chronic granulomatous disease, O_2^-, superoxide

[1] To whom correspondence should be addressed (e-mail scross@scripps.edu)

cells and purified to homogeneity as described previously [4]. Flavocytochrome b_{558} was purified from unstimulated neutrophil membranes, and relipidated and reflavinated as described earlier [25]. Flavocytochrome b_{558} concentrations were estimated from reduced-minus-oxidized difference spectra using an absorption coefficient of 21.6 $mM^{-1} \cdot cm^{-1}$ per mol of haem (10.8 $mM^{-1} \cdot cm^{-1}$ per mol of protein) [26].

Cell-free O_2^- assay

The rate of O_2^- production was measured using the superoxide dismutase-inhibitable rate of cytochrome *c* reduction in 96-well plates using a SpectraMax kinetic microtitre plate reader (Molecular Devices, Menlo Park, CA, U.S.A.) as described previously [5]. In brief, reaction mixtures contained 0.3 pmol of purified flavocytochrome b_{558} or 2×10^6 cell equivalents of neutrophil membranes (0.2–0.3 pmol of flavocytochrome b_{558}), 15 pmol of $p40^{phox}$, 15 pmol of $p47^{phox}$, 10 pmol of $p67^{phox}$ and 4 pmol of Rac2 in a final volume of 150 μl of Mg^{2+}-free relaxation buffer containing 100 μM cytochrome *c* [25]. Where stated, 2.5×10^6 cell equivalents of neutrophil cytosol were used in place of the recombinant cytosolic *phox* proteins. This amount of cytosol contains approx. 2.5 pmol of $p40^{phox}$, 15 pmol of $p47^{phox}$, 2.5 pmol of $p67^{phox}$ and 6.5 pmol of Rac2 (A. R. Cross and P. G. Heyworth, unpublished work). Oxidase activation was initiated by the addition of 100 μM SDS, and after 5 min of incubation the reaction was started by the addition of 160 μM NADPH. Each well was paired with an otherwise identical well supplemented with 300 units of superoxide dismutase. Assays were performed in duplicate or triplicate. Titration curves were fitted to a one-site binding equation (hyperbola) using GraphPad Prism software (GraphPad Prism, San Diego, CA, U.S.A.).

RESULTS AND DISCUSSION

$p40^{phox}$ increases the activity of the cell-free system using recombinant $p47^{phox}$, $p67^{phox}$ and Rac2 when employing neutrophil membranes, but not purified material, as a source of flavocytochrome b_{558}

During routine cell-free NADPH oxidase assays using recombinant cytosolic proteins ($p47^{phox}$, $p67^{phox}$ and Rac2), we have noted that the specific activity (turnover number) of neutrophil-membrane preparations is less than that expected when compared with highly purified flavocytochrome b_{558} preparations based on their respective flavocytochrome b_{558} contents (A. R. Cross and R. W. Erickson, unpublished work). In contrast, high specific activities were obtained using neutrophil cytosol in place of recombinant $p47^{phox}$, $p67^{phox}$ and Rac2, regardless of whether the source of flavocytochrome b_{558} was crude membranes or highly purified material. As part of our studies to identify the cause of this phenomenon, the effect of $p40^{phox}$ in the two systems was examined. Addition of $p40^{phox}$ to the system consisting of recombinant *phox* proteins and neutrophil membranes consistently gave a small (10–25 %) increase in activity (Table 1). In contrast, addition of $p40^{phox}$ had little effect on the recombinant system using purified flavocytochrome b_{558}, except at high concentrations where it appeared to have a mild inhibitory effect (results not shown). Leto and co-workers have reported similar inhibitory effects at high (greater-than-micromolar) concentrations of $p40^{phox}$ [23]. We hypothesize that this inhibitory effect may be due to sequesteration of one or more of the other *phox* components in a form where they cannot interact with their partner(s) in a normal fashion. $p40^{phox}$ was not capable of supporting significant amounts of O_2^- generation in the absence of $p47^{phox}$ (see below).

Table 1 $p40^{phox}$ **increases the activity of NADPH in the cell-free system composed of neutrophil membranes and recombinant cytosolic proteins, but not in the system composed of neutrophil membranes and neutrophil cytosol**

NADPH oxidase activity was measured in the cell-free system as described in the Experimental section. Where indicated, reaction mixtures contained 2×10^5 cell equivalents of neutrophil plasma membranes (Membranes), 2.5×10^6 cell equivalents of neutrophil cytosol (Cytosol), 15 pmol of $p40^{phox}$ and/or 15 pmol of $p47^{phox}$, 10 pmol of $p67^{phox}$ and 4 pmol of Rac2 (together referred to as Recombinant cytosol). The data represent one of three experiments performed in duplicate. Values are means ± S.E.M.

Reaction mixture	$p40^{phox}$	Specific activity (nmol of O_2^-/min per pmol of flavocytochrome b_{558})
Membranes	−	0.02 ± 0.03
Cytosol	−	0.001 ± 0.001
Recombinant cytosol	−	0.001 ± 0.0005
Membranes	+	0.02 ± 0.01
Membranes + cytosol	−	7.77 ± 0.125
Membranes + cytosol	+	7.84 ± 0.175
Membranes + recombinant cytosol	−	3.91 ± 0.024
Membranes + recombinant cytosol	+	5.30 ± 0.163

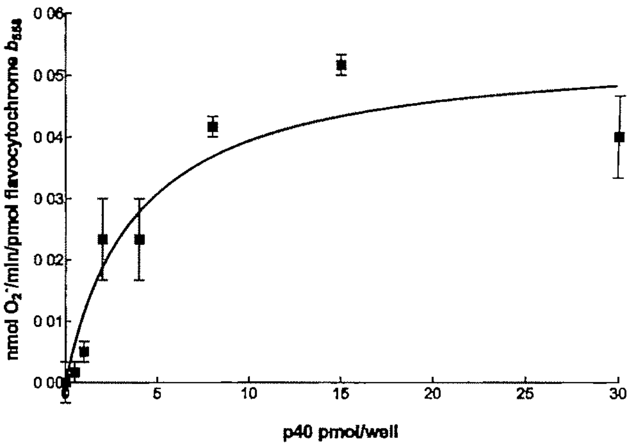

Figure 1 $p40^{phox}$ **can only weakly activate NADPH oxidase in the absence of** $p47^{phox}$

NADPH oxidase activity was measured in the cell-free system as described in the Experimental section. The reaction mixture contained 0.3 pmol of flavocytochrome b_{558}, 10 pmol of $p67^{phox}$ and 4 pmol of Rac2 and the indicated amount of $p40^{phox}$. The curve is the best fit to a one-site binding (hyperbola) equation calculated using GraphPad Prism. The data are representative of one of three experiments performed in duplicate. The error bars represent S.E.M.

$p40^{phox}$ cannot substitute for the other cytosolic *phox* components $p67^{phox}$ and Rac2

$p40^{phox}$ was incapable of supporting any O_2^--generating activity in the cell-free system using purified flavocytochrome b_{558} in the absence of either $p67^{phox}$ or Rac2 (results not shown), consistent with our previous findings [5,25]. In the absence of $p47^{phox}$, $p40^{phox}$ was capable of supporting an extremely low rate of O_2^- production, i.e. it could not effectively substitute for $p47^{phox}$ (Figure 1). Half-maximal effects were seen at 3.8 pmol of $p40^{phox}$/well (25 nM). It is suggested that this extremely small effect may be due to slightly increasing the affinity of $p67^{phox}$ and/or Rac2 for flavocytochrome b_{558} and mimicking the $p47^{phox}$-independent activity seen normally only at extremely high $p67^{phox}$

Table 2 $p47^{phox}$ is the principal limiting component in the cell-free system composed of neutrophil membranes and 'recombinant cytosol'

NADPH oxidase activity was measured in the cell-free system as described in the Experimental section. Each reaction mixture contained 2×10^5 cell equivalents of neutrophil plasma membranes. Where indicated, the membranes were supplemented with 4×10^5 cell equivalents of neutrophil cytosol ('Spike'), 15 pmol of $p47^{phox}$, 10 pmol of $p67^{phox}$ and 4 pmol of Rac2 (Recombinant cytosol), 15 pmol of $p47^{phox}$, 10 pmol of $p67^{phox}$, 4 pmol of Rac2, or 15 pmol of $p40^{phox}$. The data are representative of one of three experiments performed in duplicate. Values are means ± S.E.M.

Neutrophil membranes plus	Specific activity (nmol of O_2^-/min per pmol of flavocytochrome b_{558})
Cytosol	7.77 ± 0.125
'Spike'	0.865 ± 0.076
Recombinant cytosol	4.01 ± 0.024
'Spike' + recombinant cytosol	8.03 ± 0.024
'Spike' + $p47^{phox}$	7.4 ± 0.045
'Spike' + $p67^{phox}$	3.38 ± 0.044
'Spike' + Rac2	0.827 ± 0.055
'Spike' + $p40^{phox}$	1.91 ± 0.036

Table 3 $p40^{phox}$ augments the activity of $p47^{phox}$ in the cell-free system of NADPH oxidase activation under conditions where $p47^{phox}$ is limiting

NADPH oxidase activity was measured in the cell-free system as described in the Experimental section. The reaction mixture contained 0.3 pmol of flavocytochrome b_{558}, 10 pmol of $p67^{phox}$ and 4 pmol of Rac2, and the indicated concentrations of $p40^{phox}$ and $p47^{phox}$.

Flavocytochrome b_{558} + $p67^{phox}$ + Rac2 plus	Specific activity (nmol of O_2^-/min per pmol of flavocytochrome b_{558})
100 nM $p47^{phox}$	12.17 ± 0.4
10 nM $p47^{phox}$	3.64 ± 0.41
10 nM $p47^{phox}$ + 10 nM $p40^{phox}$	8.8 ± 0.43
10 nM $p47^{phox}$ + 100 nM $p40^{phox}$	8.27 ± 0.37

and Rac2 concentrations [4,27,28]. A maximum of 0.054 nmol of O_2^-/min per pmol of flavocytochrome b_{558} (compared with 15 nmol of O_2^-/min per pmol of flavocytochrome b_{558} or 0.4 %) was observed, with the maximum effect seen at 15 pmol/well (100 nM).

$p47^{phox}$ is the principal limiting component in the cell-free assay for oxidase activation when neutrophil membranes are used in place of purified flavocytochrome b_{558}

The difference in responses to the recombinant cytosolic factors between neutrophil membranes and purified flavocytochrome b_{558} prompted the performance of experiments testing the effects of adding the recombinant proteins individually to neutrophil membranes that had been supplemented with a small, sub-optimal amount of neutrophil cytosol that alone was only capable of eliciting a low rate of O_2^- production. As can be seen in Table 2, the greatest amount of activity was recovered by the addition of $p47^{phox}$ (15 pmol), suggesting that $p47^{phox}$ is the principal limiting component in the system when neutrophil membrane, rather than purified material, is used as a source of flavocytochrome b_{558}. Some activity was also recovered by the addition of $p67^{phox}$ (10 pmol), suggesting that it is partially limiting, whereas no further activity was obtained by the addition of Rac2 (4 pmol), suggesting that it is not limiting under these conditions. Significantly, some activity was also restored by the addition of $p40^{phox}$ (15 pmol), and it is suggested that this is due to a co-operative interaction between $p40^{phox}$ and $p47^{phox}$, described below, that increases the effective concentration of $p47^{phox}$ present in the 'spike' of cytosol.

$p40^{phox}$ functions by increasing the affinity of $p47^{phox}$ for flavocytochrome b_{558}

The experiments described above suggested that the limiting cytosolic factor in the recombinant system employing neutrophil membranes was $p47^{phox}$. Since $p40^{phox}$ augmented activity in this system, we hypothesized that $p40^{phox}$ could promote the activity of $p47^{phox}$ in some manner. Therefore, a series of experiments was designed to determine if $p40^{phox}$ could increase the effectiveness of $p47^{phox}$ in a cell-free system employing recombinant proteins and purified flavocytochrome b_{558}, under conditions where the limiting component was $p47^{phox}$. Decreasing the amount of $p47^{phox}$ in the assay from 15 pmol (100 nM final concentration) to 1.5 pmol (10 nM) reduced the amount of O_2^- activity by about 75 %. Addition of 15 pmol of $p40^{phox}$ (100 nM) restored the activity to approx. 75 % of that obtained with the near-saturating concentrations of $p47^{phox}$ (Table 3). Increasing the $p40^{phox}$ concentration 10-fold (Table 3) or 100-fold (results not shown) did not recover further activity. $p40^{phox}$ did not exhibit a co-operative effect in similar experiments where $p67^{phox}$ or Rac2 were the limiting components (results not shown).

In order to examine this co-operative effect in more detail, the concentration dependence of NADPH oxidase activity on $p47^{phox}$ in the absence or presence of 100 nM $p40^{phox}$ was measured (Figure 2, top panel). In the absence of $p40^{phox}$, half-maximal activity was observed at 2.4 ± 0.25 pmol/well (16 ± 1.7 nM final concentration), in the range that we have reported previously [5]. In the presence of $p40^{phox}$ however, $p47^{phox}$ was effective at significantly lower concentrations [half-maximal activity 0.9 ± 0.12 pmol/well (5.98 ± 0.78 nM final)]. The calculated V_{max} was similar in both cases, 12.55 and 12.81 nmol of O_2^-/min per pmol of flavocytochrome b_{558} in the absence and presence of $p40^{phox}$ respectively, demonstrating that $p40^{phox}$ increased the affinity of $p47^{phox}$ in the activation process, but did not increase the overall activity. Similar experiments determining the concentration dependence of NADPH oxidase activity on $p67^{phox}$ (Figure 2, middle panel) or Rac2 (Figure 2, lower panel) in the presence or absence of $p40^{phox}$ did not show such co-operative effects, indicating that the effect was specific for $p47^{phox}$.

Concentration dependence of the co-operative effect of $p40^{phox}$ on $p47^{phox}$

In order to estimate the concentration dependence of $p40^{phox}$ in promoting the efficiency of $p47^{phox}$ in activating NADPH oxidase, $p40^{phox}$ was titrated into the cell-free system containing a sub-optimal amount of $p47^{phox}$ as described above. The co-operative effect reached a plateau at relatively low concentrations of $p40^{phox}$ (Figure 3), with a half-maximal response at 0.23 ± 0.05 pmol of $p40^{phox}$/well (1.5 ± 0.33 nM), increasing the activity from 3 nmol of O_2^-/min per pmol of flavocytochrome b_{558} to 6.56 nmol of O_2^-/min per pmol of flavocytochrome b_{558}. This concentration of $p40^{phox}$ was much less than that present in neutrophil cytosol (460 nM; A. R. Cross and P. G. Heyworth, unpublished work). It is concluded that the function of $p40^{phox}$ is, at least in part, to promote activation of NADPH oxidase by

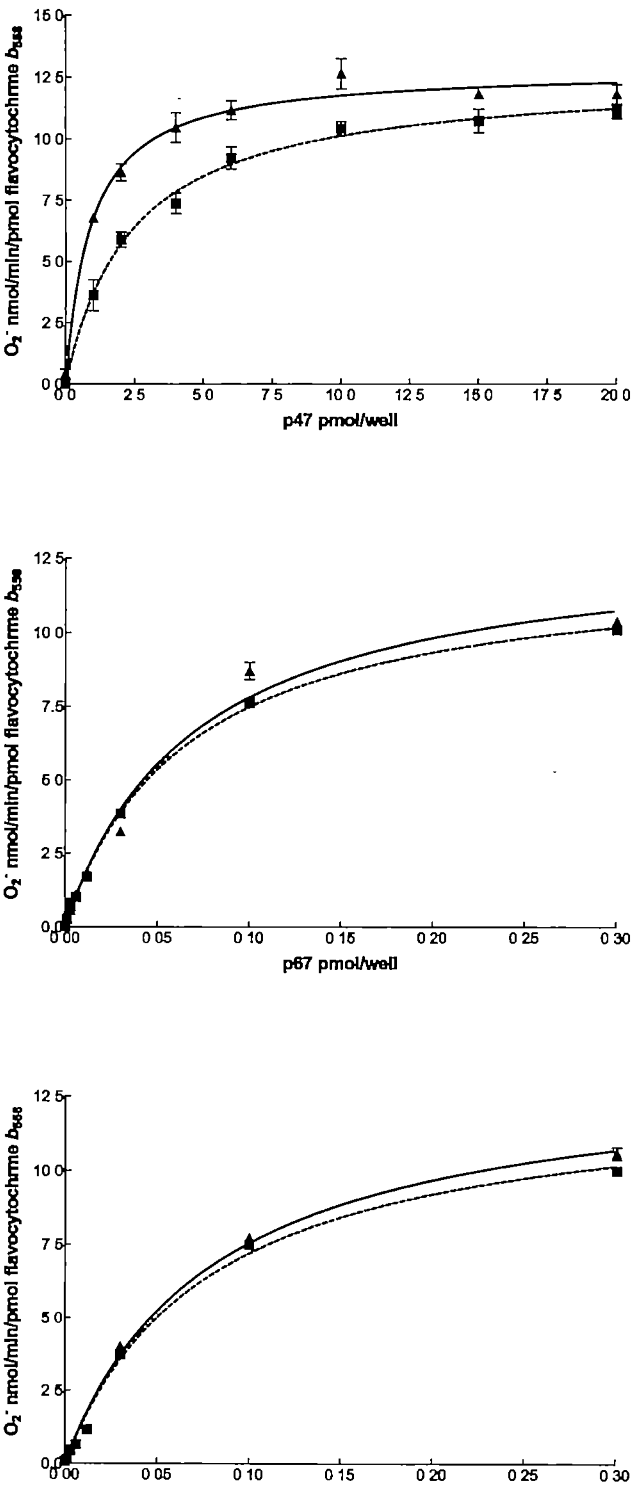

Figure 2 Concentration-dependence of NADPH oxidase activity on p47^{phox}, p67^{phox} and Rac2 in the absence and presence of p40^{phox}

NADPH oxidase activity was measured in the cell-free system as described in the Experimental section. The complete reaction mixture contained 0.3 pmol of flavocytochrome b_{558}, and 15 pmol of p47^{phox}, 10 pmol of p67^{phox} and 4 pmol of Rac2 with (▲) or without (■) 15 pmol of p40^{phox} (Top panel) Increasing concentrations of p47^{phox} were added to the complete reaction mixture lacking p47^{phox} (Middle panel) Increasing concentrations of p67^{phox} were added to the complete reaction mixture lacking p67^{phox} (Bottom panel) Increasing concentrations of Rac2 were added to the complete reaction mixture lacking Rac2. The curves are the best fits to a one-site binding (hyperbola) equation calculated using GraphPad Prism. Each data set is representative of one of two or three experiments performed in duplicate. The error bars represent S.E.M.

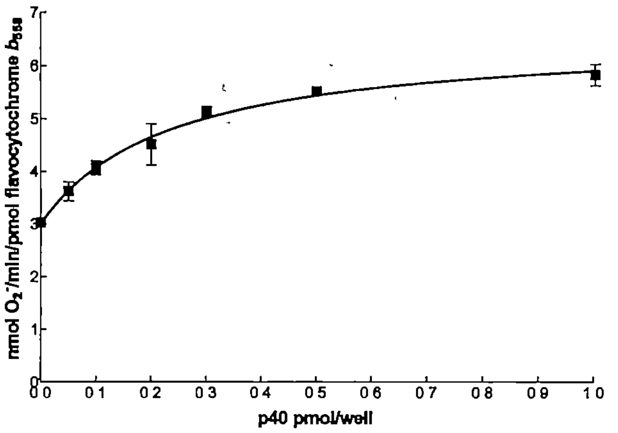

Figure 3 Concentration dependence of the co-operative effect of p40^{phox} on the ability of p47^{phox} to activate NADPH oxidase in the cell-free system

NADPH oxidase activity was measured in the cell-free system as described in the Experimental section. The reaction mixture contained 0.3 pmol of flavocytochrome b_{558}, 1.5 pmol of p47^{phox}, 10 pmol of p67^{phox}, 4 pmol of Rac2 and increasing concentrations of p40^{phox}. The curve is the best fit to a one-site binding (hyperbola) equation calculated using GraphPad Prism. The data represent one of two experiments performed in duplicate. The error bars represent S.E.M.

increasing the affinity of p47^{phox} for other oxidase components. In principle, this could be achieved in three ways. First, p40^{phox} could promote the conformational change in p47^{phox} that is believed for it to be necessary to bind to flavocytochrome b_{558} [29–31]. Secondly, p40^{phox} could bind to both flavocytochrome b_{558} and p47^{phox}, thus co-operatively increasing the binding affinity of the latter to the p40^{phox}–flavocytochrome b_{558} complex. Thirdly, p40^{phox} could bind to p67^{phox} and/or Rac2 in such a way as to increase the affinity of these components for p47^{phox}, thereby decreasing the concentration of p47^{phox} required to recruit them to flavocytochrome b_{558}. Distinguishing between these possibilities will be the focus of future work.

I am very grateful to Walter Darbonne, Rich Erickson, Jiabing Ding and John Curnutte (Genentech, South San Francisco, CA, U.S.A.) for the gift of recombinant *phox* proteins. This work was supported by National Institutes of Health grant AI24838. This is The Scripps Research Institute manuscript number 12987-MEM

REFERENCES

1 Nauseef, W. M. (1999) The NADPH-dependent oxidase of phagocytes. Proc. Assoc. Am. Physicians **111**, 373–382

2 Yu, L., Quinn, M. T., Cross, A. R. and Dinauer, M. C. (1998) Gp91^{phox} is the heme binding subunit of the superoxide-generating oxidase. Proc. Natl. Acad. Sci. U.S.A. **95**, 7993–7998

3 Yu, L., Cross, A. R., Zhen, L. and Dinauer, M. C. (1999) Functional analysis of NADPH oxidase in granulocytic cells expressing a Δ488–497 gp91^{phox} deletion mutant. Blood **94**, 2497–2504

4 Cross, A. R., Erickson, R. W. and Curnutte, J. T. (1999) Simultaneous presence of p47^{phox} and flavocytochrome b_{245} are required for activation of NADPH oxidase by anionic amphiphiles: evidence for an intermediate state of oxidase activation. J. Biol. Chem. **274**, 15519–15525

5 Cross, A. R., Erickson, R. W. and Curnutte, J. T. (1999) The mechanism of activation of NADPH oxidase in the cell-free system: the activation process is primarily catalytic and not through the formation of a stoichiometric complex. Biochem. J. **341**, 251–255

6 Heyworth, P. G., Curnutte, J. T. and Badwey, J. A. (1998) Structure and regulation of NADPH oxidase of phagocytic leukocytes. In Molecular and Cellular Basis of Inflammation (Serhan, C. N. and Ward, P. A., eds), pp. 165–191, Humana Press, Totowa

7 Ambruso, D. R., Knall, C., Panepinto, J, Kurkchubasche, A, Thurman, G, Gonzalez-Aller, C, Hiester, A, Harbeck, R J., Johnson, G and Roos, D (1999) Human Rac2 deficiency a novel syndrome of neutrophil (PMN) dysfunction and recurrent bacterial infections. Blood **94**, 615a

8 Wientjes, F B., Hsuan, J J, Totty, N F and Segal, A. W (1993) P40^{phox}, a third cytosolic component of the activation complex of the NADPH oxidase to contain *src* homology 3 domains Biochem J **296**, 557–561

9 Someya, A, Nagaoka, I and Yamashita, T (1993) Purification of the 260 kDa cytosolic complex involved in the superoxide production of guinea pig neutrophils. FEBS Lett **330**, 215–218

10 Dusi, S, Donini, M and Rossi, F (1996) Mechanisms of NADPH oxidase activation translocation of p40^{phox}, Rac1 and Rac2 from the cytosol to the membranes in human neutrophils lacking p47^{phox} or p67^{phox}. Biochem. J **314**, 409–412

11 Someya, A, Nagaoka, I., Nunoi, H. and Yamashita, T (1996) Translocation of guinea pig p40^{phox} during activation of NADPH oxidase Biochim Biophys Acta **1277**, 217–225

12 Fuchs, A, Bouin, A-P, Rabilloud, T and Vignais, P V (1997) The 40 kDa component of the phagocyte NADPH oxidase (p40^{phox}) is phosphorylated during activation in differentiated HL60 cells Eur J. Biochem **249**, 531–539

13 Bouin, A-P, Grandvaux, N, Vignais, P V and Fuchs, A (1998) P40^{phox} is phosphorylated on threonine 154 and serine 315 during activation of the phagocyte NADPH oxidase Implication of a protein kinase C-type kinase in the phosphorylation process J Biol Chem **273**, 30097–30103

14 Rinckel, L A., Faris, S L, Hitt, N D. and Kleinberg, M E (1999) Rac1 disrupts p67^{phox}/p40^{phox} binding a novel role for Rac in NADPH oxidase activation Biochem. Biophys Res Commun **263**, 118–122

15 Nakamura, R, Sumimoto, H, Mizuki, K., Hata, K, Ago, T, Kitajima, S, Takeshige, K, Sakaki, Y and Ito, T (1998) The PC motif a novel and evolutionarily conserved sequence involved in the interaction between p40^{phox} and p67^{phox}, SH3 domain-containing cytosolic factors of the phagocyte NADPH oxidase Eur J Biochem **251**, 583–589

16 Tsunawaki, S, Kagara, S, Yoshikawa, K, Yoshida, L S, Kuratsuji, T and Namiki, H. (1996) Involvement of p40^{phox} in activation of phagocyte NADPH oxidase through association of its carboxyl-terminal, but not its amino-terminal, with p67^{phox} J Exp Med. **184**, 893–902

17 Wientjes, F B, Panayotou, G, Reeves, E and Segal, A W. (1996) Interactions between cytosolic components of the NADPH oxidase p40^{phox} interacts with both p67^{phox} and p47^{phox} Biochem. J **317**, 919–924

18 Fuchs, A, Dagher, M-C, Fauré, J and Vignais, P V (1996) Topological organization of the cytosolic activating complex of the superoxide-generating NADPH-oxidase Pinpointing sites of interaction between p47^{phox}, p67^{phox} and p40^{phox} using the two-hybrid system. Biochim Biophys Acta **1312**, 39–47

19 Ito, T., Nakamura, R, Sumimoto, H., Takeshige, K and Sakaki, Y (1996) An SH3 domain-mediated interaction between the phagocyte NADPH oxidase factors p40^{phox} and p47^{phox} FEBS Lett **385**, 229–232

20 Fuchs, A., Dagher, M-C and Vignais, P V (1995) Mapping the domains of interaction of p40^{phox} with both p47^{phox} and p67^{phox} of the neutrophil oxidase complex using the two-hybrid system J Biol Chem **270**, 5695–5697

21 Tsunawaki, S, Mizunari, H, Nagata, M, Tatsuzawa, O. and Kuratsuji, T (1994) A novel cytosolic component, p40^{phox}, of respiratory burst oxidase associates with p67^{phox} and is absent in patients with chronic granulomatous disease who lack p67^{phox}. Biochem. Biophys. Res Commun **199**, 1378–1387

22 El Benna, J, Dang, P M, Andrieu, V., Vergnaud, S, Dewas, C, Cachia, O, Fay, M, Morel, F., Chollet-Martin, S, Hakim, J and Gougerot-Pocidalo, M.-A (1999) P40^{phox} associates with the neutrophil Triton X-100-insoluble cytoskeletal fraction and PMA-activated membrane skeleton a comparative study with p67^{phox} and p47^{phox} J Leukocyte Biol **66**, 1014–1020

23 Sathyamoorthy, M, de Mendez, I, Adams, A G and Leto, T L (1997) P40^{phox} down-regulates NADPH oxidase activity through interactions with its SH3 domain J Biol Chem **272**, 9141–9146

24 Curnutte, J T, Kuver, R and Babior, B M. (1987) Activation of the respiratory burst oxidase in a fully soluble system from human neutrophils. J Biol Chem **262**, 6450–6452

25 Cross, A. R, Erickson, R W, Ellis, B A. and Curnutte, J T (1999) Spontaneous activation of NADPH oxidase in a cell-free system unexpected multiple effects of magnesium ion concentrations. Biochem. J. **338**, 229–233

26 Cross, A R., Higson, F K, Jones, O T G, Harper, A M. and Segal, A W (1982) The enzymic reduction and kinetics of oxidation of the cytochrome b-245 of neutrophils Biochem J **204**, 479–485

27 Freeman, J. L and Lambeth, J D. (1996) NADPH oxidase activity is independent of p47^{phox} *in vitro* J Biol Chem **271**, 22578–22582

28 Koshkin, V, Lotan, O and Pick, E (1996) The cytosolic component p47^{phox} is not a *sine qua non* participant in the activation of NADPH oxidase but is required for optimal superoxide production. J Biol Chem **271**, 30326–30329

29 Swain, S. D, Helgerson, S L, Davis, A R, Nelson, L K and Quinn, M. T (1997) Analysis of activation-induced conformational changes in p47^{phox} using tryptophan fluorescence spectroscopy. J Biol Chem. **267**, 29502–29510

30 Park, H.-S. and Park, J-W (1998) Conformational changes of the leukocyte NADPH oxidase subunit p47^{phox} during activation studied through its intrinsic fluorescence Biochim. Biophys Acta **1387**, 406–414

31 Park, H-S and Park, J-W. (1998) Fluorescent labeling of the leukocyte NADPH oxidase subunit p47^{phox}. evidence for amphiphile-induced conformational changes Arch Biochem Biophys **360**, 165–172

Received 14 January 2000/7 April 2000, accepted 28 April 2000

Biochem J (2000) 349, 119–126 (Printed in Great Britain)

Mitochondrial ATP production is necessary for activation of the extracellular-signal-regulated kinases during ischaemia/reperfusion in rat myocyte-derived H9c2 cells

Lindy ABAS[1], Marie A. BOGOYEVITCH and Michael GUPPY

Department of Biochemistry, University of Western Australia, Nedlands, WA 6907, Australia

To search for the stimuli involved in activating the mitogen-activated protein kinases (MAPKs) during ischaemia and reperfusion, we simulated the event in a system *in vitro* conducive to continuous and non-invasive measurements of several major perturbations that occur at the time: O_2 tension, mitochondrial respiration and energy status. Using H9c2 cells (a clonal line derived from rat heart), we found that activation of the extracellular signal-regulated MAPKs (ERKs) on reoxygenation was abolished if the mitochondria were inhibited prior to and during reoxygenation. Re-introduction of O_2 *per se* is therefore not sufficient to activate the ERKs. Recovery and maintenance of cellular ATP levels by mitochondrial respiration is necessary, although ATP recovery alone is not sufficient. ERK activation by H_2O_2, but not phorbol esters, was also sensitive to mitochondrial inhibition. Thus, reoxygenation and H_2O_2-mediated oxidative stress share a mechanism of ERK activation that is ATP- or mitochondrion-dependent, and this common feature suggests that the reoxygenation response is mediated by reactive oxygen species. A correlation between ERK activity and ATP levels was also found during the anoxic phase of ischaemia, an effect that was not due to substrate limitation for the kinases. Our results reveal the importance of cellular metabolism in ERK activation, and introduce ATP as a novel participant in the mechanisms underlying the ERK cascade.

Key words: anoxia, MAPK, mitochondrial inhibitor, reactive oxygen species, oxidative stress.

INTRODUCTION

All three mitogen-activated protein kinase (MAPK) subfamilies have been implicated in the responses to ischaemia and reperfusion in heart, brain, kidney and liver [1–7]. The general pattern comprises activation of the p38 kinases during ischaemia, followed by the extracellular-signal-regulated kinases (ERKs) and the stress-activated protein kinases (SAPKs) upon reperfusion. However, it has been difficult to identify the stimuli for these signalling cascades as many changes occur during ischaemia and reperfusion, e.g. pertubations to O_2 tension (pO_2), cellular metabolism, ATP levels, pH, ion gradients and the production of reactive oxygen species (ROS). Of these events, ROS production has received particular attention as the ERKs and SAPKs are known to be activated by oxidative stresses, such as H_2O_2 [2,5,8–10]. This has led to the suggestion that the ROS produced at reperfusion [11–14] mediate the ERK/SAPK response. As H_2O_2 is easily used *in vitro*, much research on the MAPKs has been done using exposure to H_2O_2 as a model for the oxidative stress that occurs on reperfusion [2,5,9,10]. This assumes, however, that ROS are the main stimuli for these kinases. Notwithstanding the possible importance of ROS, another major event that occurs during reperfusion, and which may also have implications for MAPK activation, is metabolic recovery.

Perturbations to cellular metabolism are a distinguishing feature of ischaemia and reperfusion. Oxidative metabolism is compromised as O_2 is depleted, but recovers upon reperfusion and reoxygenation. An indication that cellular metabolism may play a role in the reperfusion activation of the MAPKs comes from studies in which the metabolic inhibitors, cyanide (CN) and 2-deoxyglucose, were used to simulate the metabolic inhibition aspect of ischaemia. Metabolic recovery following removal from such 'chemical anoxia' led to activation of the ERKs and/or the SAPKs in kidney epithelial cells [6] and cardiac myocytes [15]. This implies that metabolic recovery may contribute to the reperfusion activation of the ERKs/SAPKs in an ischaemic event, and so it may be metabolism rather than (or in combination with) ROS that activates the MAPKs. However, the chemical anoxia model cannot be used to discriminate between a metabolic- or ROS-based mechanism of MAPK activation due to the confounding factors that the application of CN in the presence of O_2 enhances the mitochondrial production of ROS [13,16], and the effect of any such ROS is potentiated as the protective enzymes catalase [17] and superoxide dismutase [18] are inhibited by CN. Also, chemical anoxia does not involve the dramatic changes in pO_2 that are such definitive events in ischaemia and reperfusion, and which may be crucial for signal transduction in terms of ROS and/or cellular O_2 sensors.

For these reasons, the activation of the MAPKs seen on metabolic recovery from chemical anoxia may not apply to the anoxia/reoxygenation situation. Here, we set out to delineate the role of metabolic inhibition and recovery in the activation of the MAPKs during ischaemia and reperfusion, and to see whether O_2 was a direct stimulus or had an indirect role via its

---

Abbreviations used CN, cyanide, ERK, extracellular-signal-regulated kinase, FCCP, carbonyl cyanide *p*-trifluoromethoxyphenylhydrazone, MAPK, mitogen-activated protein kinase, MBP, myelin basic protein, MEK, MAPK or ERK kinase, pO_2, oxygen tension, ROS, reactive oxygen species, SAPK, stress-activated protein kinase, V_{O_2}, rate of oxygen consumption

[1] To whom correspondence should be addressed (e-mail mabas@cyllene uwa edu au)

participation in the production of ROS and/or metabolic recovery. We simulated ischaemia/reperfusion *in vitro* in a physiologically meaningful sense, collected precise and accurate data on crucial parameters (pO_2, metabolic rates, ATP) and related the changes to the activity of the ERKs. The ERKs were chosen due to their known responses to metabolic and oxidative stresses, and because they are activated early in reperfusion at a time when metabolic recovery is also occurring. We also investigated a previously reported phenomenon that has never been explained, that of a decrease in basal ERK activity during ischaemia [1,10] or chemical anoxia [6,15].

EXPERIMENTAL PROCEDURES

Materials and cell culture

Bovine brain myelin basic protein (MBP), myxothiazol, antimycin A, carbonyl cyanide *p*-trifluoromethoxyphenylhydrazone (FCCP) and PMA were from Sigma.

H9c2 cells, a clonal line derived from rat heart (ATCC CRL-1446; ATCC, Rockville, MD, U.S.A.), were grown in Dulbecco's modified Eagles medium with 10 % fetal calf serum, 100 units/ml penicillin and 0.1 mg/ml streptomycin. At confluency, serum was reduced to 1 % for 24 h, then eliminated for a further 24 h. Cells were trypsinized, washed and resuspended in sterile incubation buffer (25 mM Hepes, 125 mM NaCl, 5 mM KCl, 0.5 mM $MgCl_2$, 0.9 mM $CaCl_2$, 5 mM glucose, 2 mM sodium acetate, 2 mM glutamine and 0.5 mM lactate, pH 7.4 at 37 °C, 300 mOsm) at 1×10^6–2×10^6 cells/ml and transferred to glass O_2 electrode chambers (Strathkelvin Instruments, Glasgow, Scotland, U.K.) maintained at 37 °C. Viability as measured with 0.4 % eosin was at least 85 %. Chambers typically contained 3–4 ml of cells, and were stirred continuously

Simulated ischaemia/reperfusion incubations with or without mitochondrial inhibitors

After 15–20 min of pre-incubation, an O_2 electrode (Strathkelvin Instruments) was inserted into the chamber to seal the cell suspension from air and to measure pO_2 continuously. The pO_2 data were collected using a Maclab system. During the initial period of progressive hypoxia (about 30 min) and the ensuing anoxic period, samples (cells+medium) were obtained via a stainless-steel tube built into the electrode [19] to avoid perturbing the pO_2 of the suspension. Two samples were collected at each time point, one directly into cold perchloric acid/EDTA (0.6 M/5 mM final concentrations) for ATP and lactate assays, and another frozen immediately in liquid N_2 for ERK assays. After 30 min of anoxia, the electrode was removed to bring about an immediate and spontaneous reoxygenation of the suspension and a return to normoxic pO_2 (140–160 μM) by 3 min. Incubations were continued for 30 min.

To distinguish between the effect of O_2 *per se* and metabolic recovery during reoxygenation, metabolic recovery was prevented by injecting mitochondrial inhibitors (1 μM myxothiazol or antimycin, final concentration) or solvent (0.7 mM DMSO or 0.9 mM ethanol, final concentration) into the anoxic chambers about 5 min before reoxygenation. Alternatively, the uncoupler FCCP (2 μM final concentration) was used. The possible dependence of metabolic recovery on ERK activation was also investigated by treating cells with the MEK (MAPK or ERK kinase) inhibitor PD98059 (50 μM final concentration; Calbiochem, San Diego, CA, U S.A.), or solvent (7 mM DMSO, final concentration) for 10 min, then conducting the hypoxia/anoxia/reoxygenation protocol in the continued presence of the drug.

To delineate further the role of ATP recovery in ERK activation, the period immediately following reoxygenation was investigated in more detail. Cells were subjected to hypoxia/anoxia/reoxygenation, then inhibited with 1 μM antimycin or myxothiazol at either 30, 60 or 90 s post-reoxygenation.

Normoxic incubations with mitochondrial inhibitors

All concentrations given here are final. Mitochondrial inhibitors (1 μM myxothiazol or antimycin, or 1 mM KCN) or the uncoupler FCCP (1–4 μM) were added to normoxic cells to assess the effects of the drugs on the rate of oxygen consumption (V_{O_2}), ATP levels, lactate production and ERK activity. Initial samples and intermittent V_{O_2} measurements were taken during 15–30 min of pre-incubation. Inhibitors or solvent (0.7 mM DMSO, 0.2–0.9 mM ethanol or saline) were then added and sampling continued for 40 min. V_{O_2} was remeasured to determine the effectiveness of the drugs. For the experiments with H_2O_2, cells were pre-incubated for 15 min with 1 μM antimycin or myxothiazol, or solvent, then treated with 100 μM H_2O_2 or water for 30 min. The PMA experiments were performed on cells subjected previously to the simulated ischaemia/reperfusion protocol. Cells were taken from the control and inhibited chambers about 40 min after reoxygenation (with or without inhibitors) and treated with 100 nM PMA or solvent (1.4 mM DMSO) for 30 min at 37 °C.

In-gel MBP kinase assays

After collection into liquid N_2, samples were stored at −80 °C. Cells were lysed on ice for 30–45 min in lysis buffer [final concentrations. 1 % Triton X-100, 20 mM Tris (pH 6.8), 50 mM NaF, 20 mM β-glycerophosphate, 0.1 mM $NaVO_4$, 4 mM EDTA, 2 mM EGTA, 1 mM benzamidine, 10 μg/ml aprotinin, 20 μg/ml leupeptin and 1 mM PMSF], then centrifuged (10000 *g*, 10 min, 4 °C). Supernatants were transferred to loading buffer [final concentrations: 60 mM Tris (pH 6.8), 1 % SDS, 10 % glycerol and 5 % β-mercaptoethanol] and fully denatured (90 °C, 3 min). Proteins were separated by SDS/PAGE with 10 % gels containing 0.5 mg/ml MBP. ERK activity was determined by the in-gel MBP-kinase method [2]. Dried gels were exposed to Fuji imaging plates for 6–16 h, and the plates processed in a Fuji BAS1000 Imager. Bands corresponding to ERK1 and ERK2 were quantified by densitometry using a MacBAS program. Quantification was validated by standard curves, which were linear within the range studied.

Western-blot analysis

Cell extracts were separated by SDS/PAGE (10 or 12.5 % gels) and transferred to nitrocellulose membranes (Hybond ECL, Amersham) using a semi-dry transfer apparatus (Bio-Rad). Membranes were blocked with 5 % skimmed milk and probed with primary antibodies from Zymed Laboratories (ERK1/2) or New England Biolabs (all others). Horseradish peroxidase-linked secondary antibodies (Pierce) were used for detection by enhanced chemiluminescence (LumilightPlus from Roche, or Super Signal from Pierce). Films were processed conventionally.

ATP and lactate measurement

Perchloric acid extracts were neutralized and assayed for ATP and lactate by enzyme-linked spectrophotometric assays ([20], pages 121–122 and 188–189) on a SPECTRAmax 340 microplate spectrophotometer (Molecular Devices, Sunnyvale, CA, U.S.A.). ATP levels have been presented as percentages of the initial levels (see the Figure legends). The actual ATP content of the H9c2 cells was 12.49±0.45 nmol/10^6 cells (±S.E.M.; $n = 16$), which is similar to a previous report (10 nmol/10^6 cells [21]). Using our estimated cell volume for these cells of 3 μl/10^6 cells and a cell water content of 70%, the normal intracellular concentration of ATP is about 6 mM.

Statistical analysis

All results are expressed as means±S.E.M. ($n = 3$ or more). Comparisons were made using two-tailed paired or unpaired t tests, or a one-way repeated-measures ANOVA with either Fisher's protected least-squares difference (PLSD) or Dunnett's two-tailed test of significance. Differences were considered significant at $P < 0.05$.

RESULTS

Simulated ischaemia/reperfusion affects cell metabolism and ERK activity

The simulated ischaemia/reperfusion protocol commenced with an initial normoxic/hypoxic period as the cells gradually consumed all dissolved O_2 to reduce O_2 concentration from about 140 μM down to 0 μM. During this period, ATP turnover (using a P/O_2 ratio of 4.5, and 1 mol of ATP/mol of lactate) was 1317±106 nmol of ATP/10^6 cells per h (all metabolic rates are $n = 5$), comprising 98% oxidative metabolism (285±21 nmol of O_2/10^6 cells per h) and 2% glycolytic (33±10 nmol of lactate/10^6 cells per h). Neither ATP levels (Figure 1a) nor ERK activity (Figures 1b and 1c) changed during this initial period. At the onset of anoxia, glycolysis was stimulated 8.5-fold (282±44 nmol of lactate/10^6 cells per h) to maintain ATP turnover at 21±1% of the oxidative rate. ATP levels started to decrease by 1 min of anoxia (results for 1–10 min not shown), and progressively declined over the next 15–20 min to reach 31±1% of initial levels at 30 min of anoxia (Figure 1a). ERK activity declined in a similar manner, decreasing to 30±2% (ERK1) at 30 min of anoxia (Figures 1b and 1c). This effect was specific for the ERKs as the activity of the 38-kDa MBP kinases (the p38 MAPKs) either increased or remained steady during hypoxia and anoxia (Figure 2), whereas other unidentified bands (Figure 1b) were not affected. As the pattern of activity of the p38 MAPKs was not as consistent as that of the ERKs, the results were not quantified.

Upon reoxygenation, V_{O_2} recommenced at 88±3% of the initial (normoxic/hypoxic) rate to enable ATP levels to recover to 79–88% of initial values over the next 30 min (Figure 1a). Total ATP turnover (1204±115 nmol of ATP/10^6 cells per h) and lactate production (73±40 nmol/10^6 cells per h) returned to rates that were not significantly different from initial rates. Reoxygenation also caused rapid and short-term activation of the ERKs, with a peak between 5 and 7 min and a return to initial levels by 20 min (Figures 1b and 1c). The peak activation of ERK1 was 8.6-fold higher than the immediate anoxic value, or 2.6-fold higher than the initial control level (Figure 1c).

The activity profiles of the ERKs were confirmed by changes in phosphorylation status (Figure 3b). The specific activator of the ERKs, MEK1/2, was also dephosphorylated during anoxia, and reactivated upon reoxygenation (Figure 3d). As the reactivation of MEK preceded that of the ERKs with an earlier peak at 3–5 min of reoxygenation (Figure 3d), this confirmed that MEK was responsible for the changes in the ERKs. Total expression of ERK and MEK did not change (Figures 3a and 3c).

Incubation with 50 μM PD98059 reduced basal ERK activity to 50% of the control before anoxia (results not shown, $n = 2$).

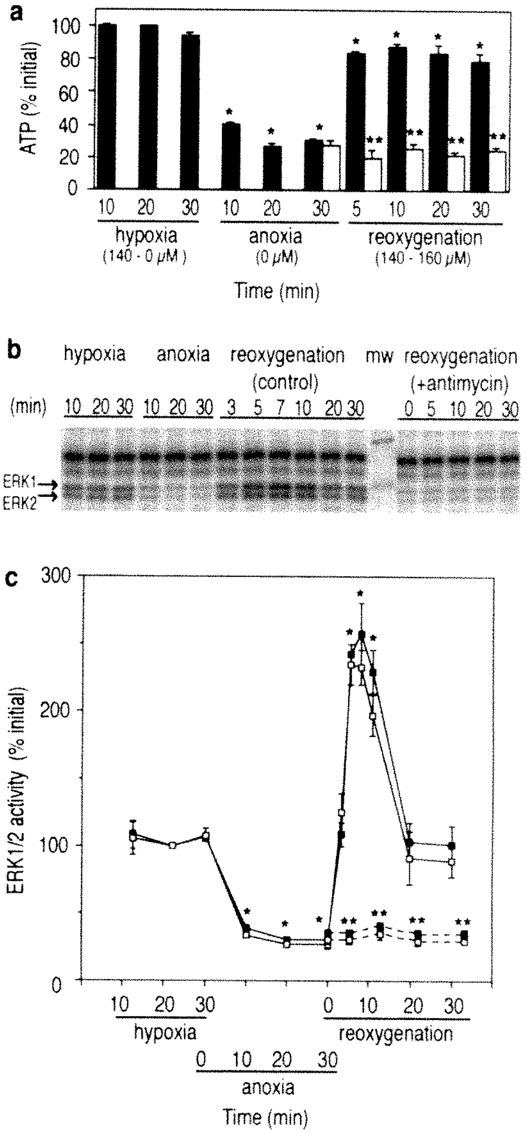

Figure 1 Effects of simulated ischaemia/reperfusion with or without mitochondrial inhibitors on ATP and ERK1/2 activity

Cells were subjected to hypoxia/anoxia/reoxygenation, ±1 μM antimycin or myxothiazol added during anoxia. Samples were assayed for ATP and ERK1/2 activity. (**a**) ATP. Black bars, control cells; white bars, cells + inhibitors; $n = 5$; the values at 20 min hypoxia were set at 100%. (**b**) Phosphorylation of MBP by ERK1/2 in an in-gel MBP kinase assay from a representative experiment with antimycin. The other bands are unidentified MBP kinases. Molecular-mass markers (mw) are 66 and 46 kDa. (**c**) Densitometric quantification ($n = 5$, from three experiments with antimycin and two with myxothiazol; 20 min hypoxia set at 100%) of ERK1 (■) and ERK2 (□) activity (solid lines, control cells; dashed lines, cells + inhibitors) from the in-gel assays. For (**a**) and (**c**), comparisons within the control time course were made using ANOVAs with a Dunnett test (*, significantly different to 10 min hypoxia, $P < 0.05$; the 20 min hypoxia time-points were discarded as they were set at 100%). Paired t tests were used to compare the inhibited cells with control values at the same time point (**$P < 0.05$).

Anoxia suppressed ERK activity in both control and PD98059-treated cells. Upon reoxygenation, the ERKs in PD98059-treated cells were activated but only to 25% of the activation seen in control cells. ATP recovery and cell metabolism (V_{O_2}, lactate production and ATP) were unaffected by PD98059 (results not shown).

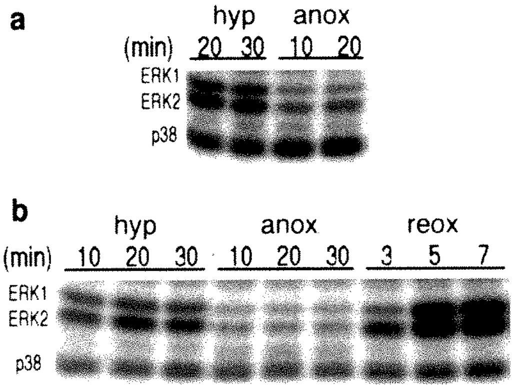

Figure 2 Effects of simulated ischaemia/reperfusion on p38 MBP kinase activity

Cells were subjected to hypoxia/anoxia/reoxygenation and samples were assayed by in-gel MBP kinase assays. The activity of the p38 MBP kinase was compared with ERK1/2 activity. Results in (**a**) and (**b**) are from separate experiments taken from those described in Figure 1, and are typical of the pattern of activity of p38 MBP kinase during the transition from hypoxia (hyp) to anoxia (anox) and reoxygenation (reox).

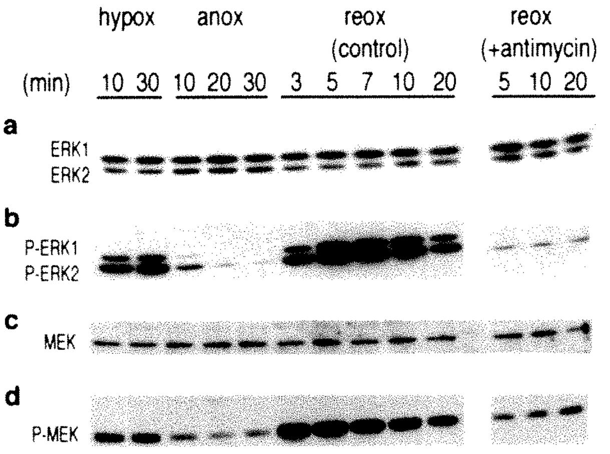

Figure 3 Effects of simulated ischaemia/reperfusion ± antimycin on the phosphorylation states of ERK1/2 and MEK

Cells were subjected to hypoxia (hypox)/anoxia (anox)/reoxygenation (reox), ±1 μM antimycin added during anoxia. Samples were extracted and analysed by Western blotting for (**a**) total ERK1/2, (**b**) phospho-ERK1/2, (**c**) total MEK1/2 and (**d**) phospho-MEK1/2. Results are representative of three experiments with antimycin and two with myxothiazol.

Mitochondrial inhibitors abolish the ERK reoxygenation response

If antimycin or myxothiazol was added prior to reoxygenation, the inhibited cells retained an anoxic pattern of metabolism despite being reoxygenated, both in terms of glycolytic rate (321 ± 57 nmol of lactate/10^6 cells per h) and ATP levels (Figure 1a). Activation (Figures 1b and 1c) and phosphorylation (Figures 3b and 3d) of the ERKs and MEK upon reoxygenation were also completely abolished in inhibited cells. Addition of FCCP prior to reoxygenation enhanced V_{O_2} by 2–3-fold (compared with initial V_{O_2}) following reoxygenation but it had the same effects on ATP and ERK activation as the inhibitors in Figure 1 (results not shown).

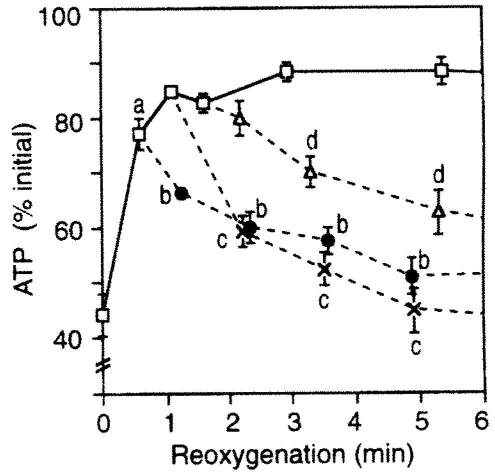

Figure 4 Recovery of ATP during early reoxygenation (0–6 min), and effects of mitochondrial inhibitors added at 30–90 s reoxygenation

Cells were subjected to hypoxia/anoxia/reoxygenation, ±1 μM antimycin or myxothiazol added after 30 s (●), 60 s (×) or 90 s (△) reoxygenation. Samples were assayed for ATP ($n = 3$–5) with the value at mid-hypoxia set at 100%. Only reoxygenation data between 0 and 6 min are shown; hypoxic and anoxic results were similar to Figure 1(a). Control cells (□) received solvent at 0 min. ANOVAs and Fisher's PLSD tests were used to compare ATP in the control time course with the control sample taken at 5 min (a, $P < 0.05$), and to compare ATP in the inhibited time courses with the sample taken at the time of initial addition of inhibitor (b, c and d, compared with appropriate control values at 30, 60 and 90 s respectively, $P < 0.05$).

ATP recovery and ERK/MEK activation during early reoxygenation

At 30–40 s following reoxygenation, levels of ATP had recovered to 77 ± 3% of initial levels, which was significantly less than the value at reoxygenation times of 60–70 s (85 ± 1%) and 5 min (88 ± 2%, Figure 4). As there was no significant difference between the latter two values, ATP recovery appeared complete by 40–60 s. Activation of the ERKs lagged behind ATP recovery, with ERK activity remaining at anoxic values up to 1.5 min after reoxygenation (Figure 5a). This was confirmed by Western-blot analysis, with phosphorylation of the ERKs seen only after 1.7 min of reoxygenation, although phosphorylation of MEK was apparent by 30 s and had increased by 1.2 min (Figure 5b). Total expression of ERK (Figure 5b) and MEK (results not shown) was unchanged.

Mitochondrial inhibition at 30, 60 or 90 s post-reoxygenation interrupted ATP recovery and immediately caused ATP to decrease towards anoxic levels (Figure 4), where it remained for the next 30 min (results not shown). Inhibition at 30 or 60 s also greatly suppressed ERK activation (Figure 5a) and resulted in less phosphorylation of ERK and MEK compared with the control (Figure 5c). When inhibitors were added at 90 s of reoxygenation, there was a more pronounced ERK activation (Figure 5a) and corresponding increases in the phosphorylation states of both ERK and MEK (Figure 5c), but levels were still lower compared with the control in both cases.

ERK activity and ATP are correlated during mitochondrial inhibition

As shown in Figure 1, both ATP levels and ERK activity decreased simultaneously during anoxia to about 30% of initial levels. This apparent relationship was investigated further using

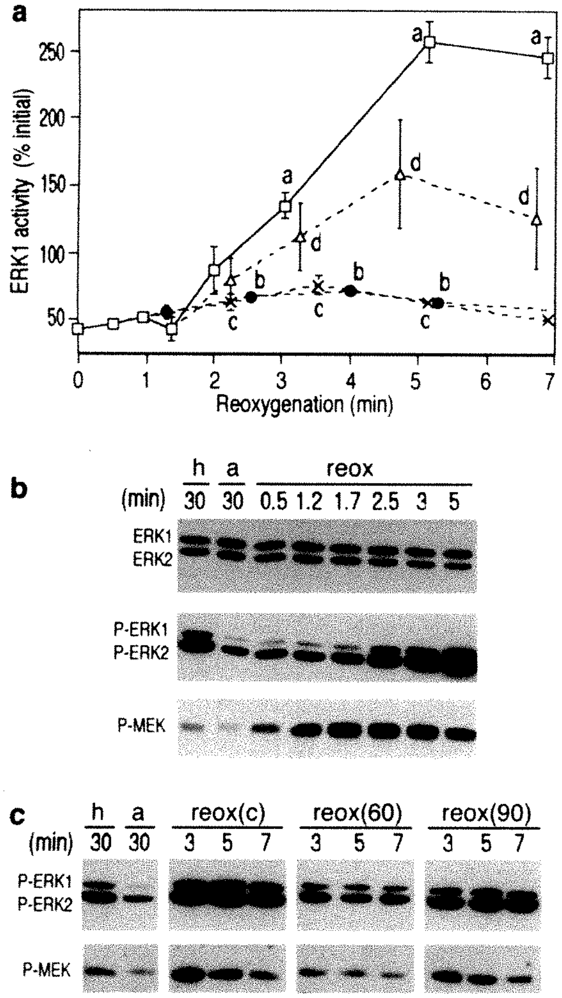

Figure 5 Activation of ERK1/2 and MEK during early reoxygenation (0–7 min), and effects of mitochondrial inhibitors added at 30–90 s reoxygenation

Cells were subjected to hypoxia (h)/anoxia (a)/reoxygenation (reox), ±1 μM antimycin or myxothiazol added after 30, 60 or 90 s of reoxygenation. (**a**) Samples were assayed for ERK1/2 activity, with activity at mid-hypoxia set at 100%. Only reoxygenation data are shown; hypoxia and anoxia were similar to Figure 1(c). Results are for ERK1 ($n = 3$–5), with inhibitors added at either 30 s (●), 60 s (×) or 90 s (△) reoxygenation. Control cells (□) received solvent at 0 s. Results for ERK2 were similar (not shown). ANOVAs and Fisher's PLSD tests were used to compare ERK activity in the control time course with control at 0 min (a, $P < 0.05$), and to compare activity in the inhibited time courses with control at the time of initial addition of inhibitor (b, c and d, compared with control values at 30, 60 and 90 s respectively, $P < 0.05$). (**b**) Western analysis of total ERK1/2 and phosphorylated ERK1/2 and MEK1/2 during hypoxia, anoxia and 0–5 min of reoxygenation in a representative experiment ($n = 3$–5). (**c**) Western analysis of phosphorylated ERK1/2 and MEK1/2 during hypoxia, anoxia and early reoxygenation in control cells [reox(c)] or in cells inhibited with 1 μM antimycin at 60 or 90 s [reox(60), reox(90)]. Data are representative of three experiments. Results for 30 s (not shown) resembled those for 60 s.

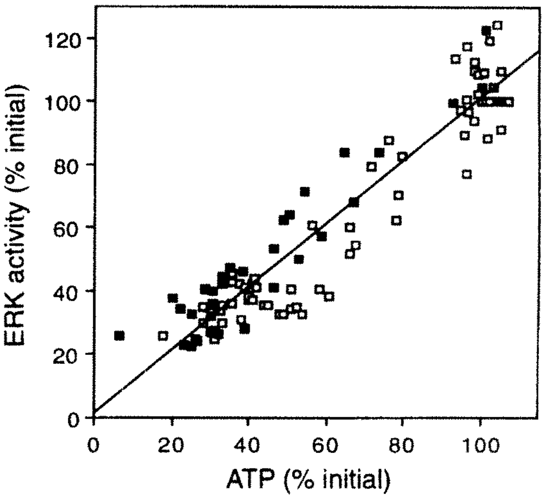

Figure 6 Correlation between ATP and ERK activity during anoxia or mitochondrial inhibition

Cells were subjected to mitochondrial inhibitors (■; from five experiments with 1 mM CN, 1 μM myxothiazol or 1 μM antimycin) or anoxia (□; from 12 experiments). Samples were collected at 1–40 min anoxia or post-inhibition, assayed for ATP and ERK1/2 activity and expressed relative to the initial values prior to inhibition or anoxia. The percentage ERK1 and ERK2 activities were combined to give an average for each point. The line was plotted using all data and has a correlation coefficient of 0.943 ($n = 98$, $P < 0.001$).

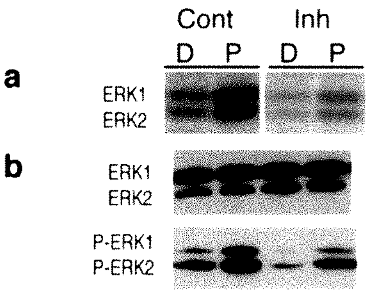

c

Treatment	PMA activation (%) ERK1	PMA activation (%) ERK2
Cont	297 ± 66	259 ± 53
Inh (MX)	262 ± 32	248 ± 17
Cont	277 ± 14	240 ± 18
Inh (AM)	353 ± 85	303 ± 40

Figure 7 ERK activation by PMA is not affected by mitochondrial inhibitors

Control (Cont) and mitochondrially inhibited (Inh) cells were stimulated for 5 min with 100 nM PMA (P) or solvent (1.4 mM DMSO, D), and assayed for ERK1/2 activity. (**a**) Phosphorylation of MBP by ERK1/2 in an in-gel MBP kinase assay. (**b**) Western analysis of total ERK1/2 and phospho-ERK1/2. Results in (**a**) and (**b**) are representative of three experiments with 1 μM myxothiazol. (**c**) Densitometric quantification ($n = 3$) of PMA-induced ERK1/2 activity from the in-gel assays. Activity in PMA-stimulated control or inhibited cells was expressed as a percentage of the activity in DMSO-treated control or inhibited cells, respectively. There were no significant differences between control and inhibited cells for either myxothiazol (MX) or antimycin (AM) (paired *t* test, $P > 0.05$).

mitochondrial inhibitors instead of anoxia to deplete ATP: 1 μM myxothiazol, 1 μM antimycin or 1 mM CN inhibited V_{O_2} immediately by 99±0.6% ($n = 7$), stimulated lactate production (results not shown) and caused progressive reductions in both ATP and ERK activity (Figure 6). The relationship between ATP and the ERKs was significant ($P < 0.001$). The decreases were not due to cell death because: first, the anoxic data were collected from cells that were subsequently reoxygenated and regained 79–88% of initial ATP (Figure 1a); secondly, the rate of lactate production was similar in anoxic and inhibited cells, and was linear throughout the incubations; and thirdly, cell viability was not different from control cells (> 85% by eosin

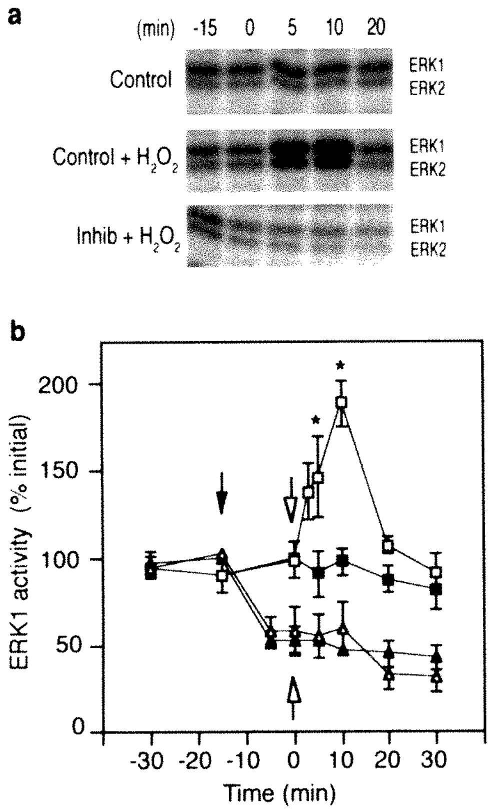

Figure 8 ERK activation by H_2O_2 is prevented by mitochondrial inhibitors

Control and mitochondrially inhibited cells were stimulated with 100 μM H_2O_2 and assayed for ERK1/2 activity. (**a**) Phosphorylation of MBP by ERK1/2 in an in-gel MBP kinase assay. Cells were treated with 0.7 mM DMSO (Control, Control + H_2O_2) or 1 μM myxothiazol (Inhib + H_2O_2) at -15 min, followed by 100 μM H_2O_2 (Control + H_2O_2, Inhib + H_2O_2) or water (Control) at 0 min. Similar results were obtained in two experiments with 1 μM antimycin. (**b**) Densitometric quantification of ERK1 activity from the in-gel assays ($n = 3$); results for ERK2 were similar (not shown). Control (□) and mitochondrially inhibited cells (△; 1 μM antimycin or myxothiazol indicated by black arrow) were stimulated with 100 μM H_2O_2 (white arrows) and compared with control (■) or mitochondrially inhibited cells (▲) that did not receive H_2O_2. Control cells at 0 min were set as 100%. At each time point, *t* tests were used to compare H_2O_2-stimulated cells (control or inhibited) with their respective non-stimulated cells ($^*P < 0.05$). Note that H_2O_2 activation at 3 min could not be compared as there was no corresponding control.

staining). Controls showed no effects of solvents on V_{O_2}, ATP or ERK activity. The uncoupler FCCP also depressed both ATP and ERK activity (results not shown).

PMA, but not H_2O_2, stimulates the ERKs in mitochondrially inhibited cells

Antimycin or myxothiazol (1 μM) did not prevent phosphorylation and activation of the ERKs by 100 nM PMA (Figure 7). The activation in inhibited cells started from a lower basal level of ERK activity due to suppression by the inhibitors (Figures 7a and 7b), but the fold activation was the same as in the control (non-inhibited) cells (Figure 7c). Total ERK levels were unchanged (Figure 7b), indicating that the differences were not due to changes in expression or degradation of the ERKs in the inhibited cells. Also, viability tests with eosin showed that the lower basal activity in inhibited cells was not due to cell death. The time course of activation by PMA was also unaffected by inhibition, with a peak at 5–10 min and a return to basal levels by 15–20 min (results not shown). Controls showed no effect of DMSO on ERK activity. In contrast to the PMA results, activation by 100 μM H_2O_2 was absent in inhibited cells, compared with maximal activation of 189 ± 13 % (ERK1) in control cells (Figure 8). ATP, V_{O_2} and lactate production were not affected by the addition of H_2O_2 (results not shown).

DISCUSSION

Following previous reports of ERK activation during metabolic recovery from chemical anoxia [6,15], we first set out to resolve whether a similar relationship exists during metabolic recovery from physical anoxia in an ischaemia/reperfusion event, and secondly what the implications are for the current theory that the reperfusion activation of the ERKs has an ROS-based mechanism. We used H9c2 cells, a myocyte line that suited our *in vitro* system, and which showed similar ERK responses to oxidative and metabolic stresses (Figures 1 and 8) to those seen in whole-organ [1,5,6] and primary cell preparations [6,9,15].

Whereas the chemical anoxia and H_2O_2 studies [5,6,8–10,15] showed that metabolic recovery and oxidative stress could individually activate the ERKs, we show here the relationship between these two stimuli and ERK activation when they occur simultaneously during reoxygenation. By preventing metabolic recovery with mitochondrial inhibitors, we found that activation of the ERKs upon reoxygenation was also completely abolished (Figures 1 and 3). This relationship was one of ERK dependence on ATP recovery as ATP recovery occurred first (Figures 4 and 5a), and the MEK inhibitor PD98059 reduced ERK activation by 75 %, yet did not affect ATP recovery. Thus recovery of ATP, or another event associated with the resumption of mitochondrial respiration, is necessary for ERK activation at reoxygenation. This shows that the physical re-introduction of O_2 is not a sufficient stimulus for the ERKs, that O_2 *per se* is not a signalling molecule and that O_2 sensors do not play a direct role in ERK activation. Instead, O_2 participates indirectly by enabling the resumption of mitochondrial respiration, and it is the latter that is required for ERK activation.

Our next step was to determine which particular aspect of mitochondrial respiration was the crucial stimulus. We have presented ATP recovery here as it is the most obvious and important aspect, and also because there appears to be a relationship between cellular ATP levels and the ERKs (Figure 6) that is not due to substrate limitation (see below). However, there are three other aspects that our data allow us to discuss: mitochondrial electron flow, pH and the production of ROS. The first of these, resumption of electron flow through the respiratory chain, may be ruled out as FCCP also suppressed ERK activation despite enhancing the respiration rate upon reoxygenation. The second event, a sudden change in pH that can occur at reperfusion following the wash-out of lactic acid accumulated during ischaemia, may also be eliminated as we did not replace the buffer upon reoxygenation.

The third aspect, the production of ROS, is important given the proposed ROS-based mechanism of ERK activation. Although the mitochondrial respiratory chain is considered the major producer of ROS during reperfusion [11,13,16], there are other possible sources, such as xanthine oxidase [12] and NADPH oxidase (present in H9c2 cells [21]). Our results (Figures 1 and 3) preclude a role for non-mitochondrial ROS in ERK activation during reperfusion as the inhibitors used would not have affected ROS from other sources. Our data are consistent with a mitochondrial source of ROS but only if it is assumed that ROS are not produced by inhibited mitochondria. However, the inhibitors used here act at different sites in the electron transport chain and so have opposite effects, i.e. antimycin and CN enhance mitochondrial ROS production [13,16], whereas myxothiazol and FCCP reduce it [11,16]. Since all these prevented ERK activation, our data would seem to suggest that mitochondrial ROS are also not the stimulus. However, the activation of the ERKs by H_2O_2 was also blocked in mitochondrially inhibited cells (Figure 8), whereas stimulation by PMA was still possible (Figure 7). This is also seen in neonatal rat cardiomyocytes, i.e mitochondrial inhibitors eliminated activation of the ERKs by H_2O_2, but did not affect activation by other stimuli such as PMA, phenylephrine or hyperosmotic shock [21a]. Taken together, the data suggest that reoxygenation and H_2O_2 share a similar pathway of ERK activation which distinguishes them from all other stimuli tested. Since the effects of H_2O_2 are thought to be mediated by oxidative stress and ROS, these results suggest strongly that ERK activation in reoxygenation is also ROS-mediated, but that the signalling mechanism is dependent on normal levels of (mitochondrially produced) ATP and/or functioning coupled mitochondria.

To confirm and look further at this dependence of ERK activation on ATP and/or the mitochondria, we added the mitochondrial inhibitors in the immediate post-reoxygenation period. Whereas the results in Figures 1 and 3 suggest that ATP recovery is necessary, we found that it was not a sufficient stimulus because inhibition at 30 or 60 s post-reoxygenation, i.e. after ATP recovery had occurred, also prevented ERK activation (Figures 4 and 5a). Since ROS are also produced early in reoxygenation (peaking at 10–40 s [12,14]), the results of the 30- and 60-s inhibition experiments (Figure 5a) indicate that ROS are not a sufficient stimulus either. This confirms that continuation of the signal-transduction mechanism requires normal ATP and/or functioning mitochondria after the initial stimulus has occurred.

Interestingly, such a requirement appears only to be necessary at a crucial period, 60–90 s post-reoxygenation. This is seen in cells inhibited at 90 s of reoxygenation (Figure 5a). Comparison of the ATP and ERK time courses in these incubations reveals that following the addition of inhibitors at 90 s, ATP decreased while ERK activity continued to rise (see the periods 2–5 min in Figures 4 and 5a) This indicates that an ATP- or mitochondrion-dependent step occurs between 60 and 90 s, but once past this critical point, ERK activation can progress without further such requirements. The long delay between the first signs of phosphorylation of MEK ($<$ 30 s) compared with ERK activation ($>$ 1.7 min; Figures 5a and 5b) indicates that such an event may be the interaction between MEK and ERK This step involves separation of ERK from its cytoplasmic anchor MEK [22], followed by translocation of phosphorylated ERK into the nucleus [23]. It has been reported recently that both the cytoplasmic localization of MEK and the nuclear translocation of ERK are sensitive to ATP depletion by mitochondrial inhibition [24].

Whereas the reoxygenation activation of the ERKs has been studied widely, much less attention has been paid to the decrease in ERK activity during anoxia, shown here (Figures 1 and 3) and in previous studies [1,6,10,15]. The ERK/ATP correlation (Figure 6) provides an explanation for these results as ATP would have decreased in each of the above cases. The effect is not due to the limited availability of ATP as a substrate for ERK or MEK as the decreases in ERK activity were always reflected by lower phosphorylation states of both these kinases (Figures 3 and 5). ATP would thus have to be substrate-limiting for kinase-activators above the level of MEK, such as the MEK kinases, Raf or MEKK. However, the correlation between ATP and ERK activity was evident at 80 % of normal ATP levels (Figure 6), at which time ATP would have been about 5 mM in these cells (assuming no compartmentation). As this is more than 10-fold the $K_{m,ATP}$ of c-Raf-1 (12 μM [25]) and MEKK (11 μM [26]), these kinases should be operating at their V_{max} and would thus be insensitive to changes in ATP concentration Substrate limitation is also unlikely to be responsible for the absence of ERK activation during reoxygenation in inhibited cells (Figure 1c), as ATP levels were still high (about 2 mM) in those cells. Also, p38 MBP kinase activity was not inhibited by anoxia (Figure 2), which showed that upstream activators and other MAPK pathways were not restricted by the lower ATP levels. Finally, mitochondrial inhibition did not prevent ERK activation by PMA (Figure 7). We emphasize here that the inhibited cells which were stimulated 3-fold by PMA were the same cells that did not respond at all to reoxygenation. Thus the effect of ATP on ERK activity appears to be specific for the ERKs and distinct from its role as a substrate in the MAPK cascade. We cannot, however, rule out the possibility of ATP compartmentation and/or substrate limitation at other steps such as the nuclear-translocation events [24].

A final interpretation of our data is that the suppression of basal ERK activity during anoxia and mitochondrial inhibition indicates a basal activity comprising two constitutive pathways, one of which is sensitive to mitochondrial inhibition. Different stimuli would then act via one or both of these pathways. Thus in inhibited cells, PMA was able to activate the ERKs by the mitochondrion-insensitive pathway (Figure 7), whereas the absence of ERK activation by reoxygenation or H_2O_2 (Figures 1 and 8) indicates that these stimuli required the mitochondrion-sensitive pathway. These results show that sensitivity to mitochondrial inhibition may distinguish between two different mechanisms of ERK activation. The broader implications are that cellular metabolism (or pertubations to it) should be considered when studying the ERKs, and that the mitochondria may be a fruitful area for future research into the mechanisms of ERK activation.

REFERENCES

1 Omura, T, Yoshiyama, M, Shimida, T, Shimizu, N, Kim, S, Iwao, H, Takeuchi, K and Yoshikawa, J (1999) Activation of mitogen-activated protein kinases in *in vivo* ischemia/reperfused myocardium in rats J Mol Cell Cardiol **31**, 1269–1279

2 Clerk, A, Fuller, S J, Michael, A and Sugden, P H (1998) Stimulation of 'stress-regulated' mitogen-activated protein kinases (stress-activated protein kinases/c-Jun N-terminal kinases and p38-mitogen-activated protein kinases) in perfused rat hearts by oxidative and other stresses J Biol. Chem. **273**, 7228–7234

3 Bogoyevitch, M A, Gillespie-Brown, J, Ketterman, A J, Fuller, S J, Ben Levy, R, Ashworth, A, Marshall, C J and Sugden, P H (1996) Stimulation of the stress-activated mitogen-activated protein kinase subfamilies in perfused heart p38/RK mitogen-activated protein kinases and c-Jun N-terminal kinases are activated by ischemia/reperfusion Circ Res **79**, 162–173

4 Bendinelli, P, Piccoletti, R, Maroni, P and Bernilli-Zazzera, A (1996) The MAP kinase cascades are activated during post-ischemic liver reperfusion FEBS Lett **398**, 193–197

5 Knight, R J. and Buxton, D B (1996) Stimulation of c-Jun kinase and mitogen-activated protein kinase by ischemia and reperfusion in the perfused rat heart Biochem Biophys Res Commun **218**, 83–88

6 Pombo, C M, Bonventre, J V, Avruch, J, Woodgett, J R, Kyriakis, J M and Force, T (1994) The stress-activated protein kinases are major c-Jun amino-terminal kinases activated by ischemia and reperfusion J Biol. Chem. **269**, 26546–26551

7 Campos-Gonzalez, R and Kindy, M S (1992) Tyrosine phosphorylation of microtubule-associated protein kinase after transient ischemia in the gerbil brain J Neurochem **59**, 1955–1958

8 Guyton, K. Z, Liu, Y, Gorospe, M., Xu, Q and Holbrook, N J (1996) Activation of mitogen-activated protein kinase by H_2O_2 J Biol Chem **271**, 4138–4142

9 Sabri, A, Byron, K. L, Samarel, A M, Bell, J and Lucchesi, P A (1998) Hydrogen peroxide activates mitogen-activated protein kinases and Na^+-H^+ exchange in neonatal rat cardiac myocytes Circ Res **82**, 1053–1062

10 Turner, N. A., Xia, F., Azhar, G., Zhang, X., Liu, L. and Wei, J. Y. (1998) Oxidative stress induces DNA fragmentation and caspase activation via the c-Jun NH_2-terminal kinase pathway in H9c2 cardiac muscle cells. J. Mol. Cell Cardiol. **30**, 1789–1801

11 Vanden Hoek, T. L., Becker, L. B., Shao, Z., Li, C. and Schumacker, P. T. (1998) Reactive oxygen species released from mitochondria during brief hypoxia induce preconditioning in cardiomyocytes. J. Biol. Chem. **273**, 18092–18098

12 Xia, Y. and Zweier, J. L. (1995) Substrate control of free radical generation from xanthine oxidase in the postischemic heart. J. Biol. Chem. **270**, 18797–18803

13 Jaeschke, H. and Mitchell, J. R. (1989) Mitochondria and xanthine oxidase both generate reactive oxygen species in isolated perfused rat liver after hypoxic injury. Biochem. Biophys. Res. Commun. **160**, 140–147

14 Zweier, J. L., Kuppusamy, P., Williams, R., Rayburn, B. K., Smith, D., Weisfeldt, M. L. and Flaherty, J. T. (1989) Measurement and characterization of postischemic free radical generation in the isolated perfused heart. J. Biol. Chem. **264**, 18890–18895

15 Bogoyevitch, M. A., Ketterman, A. J. and Sugden, P. H. (1995) Cellular stresses differentially activate c-Jun N-terminal protein kinases and extracellular signal-related protein kinases in cultured ventricular myocytes. J. Biol. Chem. **270**, 29710–29717

16 Boveris, A. (1977) Mitochondrial production of superoxide radical and hydrogen peroxide. In Tissue Hypoxia and Ischemia (Reivich, M., Coburn, R., Lahiri, S. and Chance, B., eds), pp. 67–82, Plenum Press, New York

17 Aebi, H. E. (1983) Catalase. In Methods of Enzymatic Analysis, vol. 3, 3rd edn, (Bergmeyer, J. and Graßl, M., eds), pp. 273–286, Verlag Chemie, Weinheim

18 Rotilio, G., Bray, R. C. and Fielden, E. M. (1972) A pulse radiolysis study of superoxide dismutase. Biochim. Biophys. Acta **268**, 605–609

19 Arthur, P. G., Ngo, C. T., Moretta, P. and Guppy, M. (1999) Lack of oxygen sensing by mitochondria in platelets. Eur. J. Biochem. **266**, 215–219

Received 4 January 2000/23 March 2000; accepted 27 April 2000

20 Passonneau, J. V. and Lowry, O. H. (1993) Enzymatic Analysis: a Practical Guide, Humana Press, Totowa

21 Souren, J. E. M., Van Der Mast, C. and Van Wijk, R. (1997) NADPH-oxidase-dependent superoxide production by myocyte-derived H9c2 cells: Influence of ischemia, heat shock, cycloheximide and cytochalasin D. J. Mol. Cell Cardiol. **29**, 2803–2812

21a Bogoyevitch, M. A., Ng, D. C. H., Court, N. W., Draper, K. A., Dhillon, A. and Abas, L. (2000) Intact mitochondrial electron transport function is essential for signalling by hydrogen peroxide in cardiac myocytes. J. Mol. Cell Cardiol., in the press

22 Fukuda, M., Gotoh, Y. and Nishida, E. (1997) Interaction of MAP kinase with MAP kinase kinase: its possible role in the control of nucleocytoplasmic transport of MAP kinase. EMBO J. **16**, 1901–1908

23 Lenormand, P., Sardet, C., Pagés, G., L'Allemain, G., Brunet, A. and Pouysségur, J. (1993) Growth factors induce nuclear translocation of MAP kinases ($p42^{mapk}$ and $p44^{mapk}$) but not of their activator MAP kinase kinase ($p45^{mapkk}$) in fibroblasts. J. Cell Biol. **122**, 1079–1088

24 Adachi, M., Fukuda, M. and Nishida, E. (1999) Two co-existing mechanisms for nuclear import of MAP kinase: passive diffusion of a monomer and active transport of a dimer. EMBO J. **18**, 5347–5358

25 Force, T., Bonventre, J. V., Heidecker, G., Rapp, U., Avruch, J. and Kyriakis, J. M. (1994) Enzymatic characteristics of the c-Raf-1 protein kinase. Proc. Natl. Acad. Sci. U.S.A. **91**, 1270–1274

26 Pang, L., Zheng, C. F., Guan, K. L. and Saltiel, A. R. (1995) Nerve growth factor stimulates a novel protein kinase in PC-12 cells that phosphorylates and activates mitogen-activated protein kinase kinase (MEK). Biochem. J. **307**, 513–519

Biochem J (2000) **349**, 127–133 (Printed in Great Britain) **127**

The role of phosphatidylcholine in fatty acid exchange and desaturation in *Brassica napus* L. leaves

John P. WILLIAMS[1], Valerie IMPERIAL, Mobashsher U. KHAN and Joanna N. HODSON
Department of Botany, University of Toronto, 25 Willcocks Street, Toronto, Ontario, Canada M5S 3B2

The role of phosphatidylcholine (PC) in fatty acid exchange and desaturation was examined and compared with that of monogalactosyldiacylglycerol (MGDG) in *Brassica napus* leaves using ^{14}C-labelling *in vivo*. Data are presented which indicate that in the chloroplast newly formed saturated (palmitic acid, 16:0) and monounsaturated (oleic acid, 18:1) fatty acid is incorporated into MGDG and desaturated *in situ*. In the non-plastidic compartments, however, newly formed fatty acid is exchanged with polyunsaturated fatty acid in PC, the probable major site of subsequent desaturation. The unsaturated fatty acid is released to the acyl-CoA pool, which is then used to synthesize diacylglycerol (DAG) containing a high level of unsaturated fatty acid. This highly unsaturated DAG may be the source for the biosynthesis of other cellular glycerolipids. The generally accepted pathway in which PC is synthesized from molecular species of DAG containing 16:0 and 18:1 followed by desaturation of the 18:1 to linoleic (18:2) and linolenic (18:3) acids is questioned.

Key words: acyl-CoA, ^{14}C-labelling, lipid molecular species, plant lipid.

INTRODUCTION

Phosphatidylcholine (PC) is the major phospholipid in most higher plant cells and is found in most non-plastidic membranes, endoplasmic reticulum, mitochondria, plasma membrane and tonoplast, and the outer-envelope membrane of the chloroplast. It occupies a key position in membrane structure and glycerolipid biosynthesis in leaves and the biosynthesis of triacylglycerol (TAG) in seeds of oilseed plants [1]. While it is located primarily in the non-plastidic membranes, in most plants it is believed to be a major site of fatty acid desaturation and a precursor of chloroplastic lipids in leaves [2,3]. In oilseeds PC appears to play a similar role, being largely responsible for the levels of unsaturated fatty acids in seed-oil TAGs [4]. Despite its importance in leaf chloroplast lipid and seed-oil biosynthesis, surprisingly little is known about the details of the synthesis and desaturation of fatty acids in association with PC and their transfer to the chloroplast.

There is considerable evidence that palmitoyl- and oleoyl-acyl carrier protein are the immediate products of fatty acid synthase and stearoyl-acyl carrier protein desaturase in plastids [5]. These acyl chains are exported from the plastid as free fatty acids, which are then esterified to CoA in the cytosol. The acyl-CoA thioesters exist as a soluble pool in the cytosol from which they are used in the biosynthesis of diacylglycerol (DAG) and subsequently phospholipids and TAG [1]. It is generally assumed that PC is formed from DAG containing mainly oleic acid (18:1; esterified to the *sn*-1 and -2 positions) and palmitic acid (16:0; on the *sn*-1 position) and that subsequent desaturation of the 18:1 *in situ* results in the production of linoleic (18:2) and linolenic (18:3) acids [1]. In leaves, PC containing highly unsaturated fatty acid may then be used as a structural component of cytoplasmic membranes or as a precursor to the DAG used in the production of other cytoplasmic phospholipids (e.g. phosphatidylethanolamine) and chloroplast lipids [monogalactosyldiacylglycerol (MGDG), digalactosyldiacylglycerol (DGDG) and sulphoquinovosyldiacylglycerol (SQDG)]. In seeds a similar pathway is hypothesized except that there is some exchange of fatty acid between PC and the acyl-CoA prior to DAG and TAG synthesis [6,7]. The desaturation of fatty acids in PC determines the levels of unsaturated fatty acids in the DAG precursors of seed TAG and the chloroplast lipids [8]. Despite this assumed role in chloroplast lipid biosynthesis no confirmed pathway for the transfer of the DAG moiety from PC to the chloroplast has ever been described. Recently Mongrand et al. [9] have challenged this hypothesis and proposed that the DAG from PC may not be integrated intact into the chloroplast lipids.

It has been shown that the biosynthesis of MGDG, DGDG and SQDG in chloroplasts occurs predominantly within the chloroplast envelope from DAG derived either from the chloroplast envelope itself (prokaryotic or chloroplastic pathway) or from a source outside the chloroplast (eukaryotic pathway) [1]. If the source of the DAG is from within the chloroplast, the DAG normally contains 18:1 (on the *sn*-1 position) and 16:0 (on the *sn*-2 position), a typical prokaryotic structure. If the source of the DAG is from outside the chloroplast, the molecular species of MGDG, DGDG and SQDG formed are of the eukaryotic structure, normally containing a mixture of 18:2 and 18:3 at both *sn* positions and 16:0 on the *sn*-1 position. Subsequent desaturation *in situ* of fatty acids in prokaryotic species [in hexadecatrienoic acid (16:3) plants] results in the production of mainly 18:3/16:3 molecular species of MGDG and DGDG, and 18:3/16:0 molecular species of SQDG [10]. Fatty acid desaturation in eukaryotic species results in predominantly 18:3/18:3 molecular species in MGDG and DGDG and 16:0/18:3 and 18:3/18:3 species in SQDG [10].

It is generally believed that desaturation of fatty acids on PC and MGDG in the chloroplast occurs *in situ*. Evidence for this is

---

Abbreviations used DAG, diacylglycerol; DGDG, digalactosyldiacylglycerol, lyso-PC, lysophosphatidylcholine; MGDG, monogalactosyldiacylglycerol, PC, phosphatidylcholine; SQDG, sulphoquinovosyldiacylglycerol, TAG, triacylglycerol, 16:0, palmitic acid, 16:2, hexadecadienoic acid, 16:3, hexadecatrienoic acid; 18:0, stearic acid, 18:1, oleic acid, 18:2, linoleic acid, 18:3, linolenic acid, 18:4, octadecatetraenoic acid.

[1] To whom correspondence should be addressed (e-mail williams@botany.utoronto.ca)

derived mainly from ^{14}C-labelling experiments *in vivo* and *in vitro* [1,5]. These data have been interpreted to suggest that PC and MGDG are formed from mono- and diene molecular species [18:1(16:0)/18:1 and 18:1/16:0, respectively] and that further desaturation occurs on the lipid to form the highly unsaturated fatty acids typical of PC and MGDG in different species. In 16:3 plants, only part of the DAG backbone of chloroplast lipids is thought to be derived from PC, whereas in 18:3 and octadecatetraenoic acid (18:4) plants all the DAG backbones of MGDG, DGDG and SQDG are presumed to be derived from PC [11]. In all plants it is believed that the intact lipid is the substrate for desaturases in the prokaryotic and the eukaryotic pathways [1,5] However, evidence has been presented that suggests that the acyl-CoA esters (see [5]) may also be substrates for desaturases

We undertook the experiments reported here to show in more detail the distribution of newly formed fatty acids on the molecular species of PC and MGDG with the objective of comparing the two biosynthetic pathways. While it is generally assumed that they are similar, our data show very significant differences between these pathways, suggesting that the role PC plays in fatty acid desaturation and the origin of the eukaryotic DAG in chloroplast lipid biosynthesis need to be re-examined

EXPERIMENTAL

Brassica napus plants were grown from seed in growth rooms at 20 °C under a 16-h:8-h light/dark regime with mixed fluorescent/incandescent light (approx. 200 $\mu E \cdot s^{-1} \cdot m^{-2}$) for 3–4 weeks. Mature leaves were sampled, cut into discs (1.7 cm in diameter) and the discs were fed $^{14}CO_2$ in light for 5 min. A 2-g sample of the discs was taken immediately for lipid extraction (0 h) and the remaining discs were incubated under the same light intensity and temperature for periods up to 48 h in continuous light. Samples of 2 g of discs were taken at intervals during this incubation period.

The leaf discs were extracted with chloroform/methanol (2:1, v/v) and the lipid extracts purified as described previously [12] Lipid classes were separated by TLC and molecular species of PC and MGDG were separated by argentation TLC as described previously [13]. The fatty acids of each molecular species band from the TLC plates were methanolysed using sodium methoxide [13] and the subsequent fatty acid methyl esters were analysed quantitatively using a Hewlett-Packard model 5890 gas-liquid chromatograph on a 30-m DB-23 capillary column programmed from 160 to 200 °C at 3 $°C \cdot min^{-1}$. A portion of the sample was separated in a Hewlett-Packard model 7300 gas-liquid chromatograph on a packed 1.8 m × 4 mm glass column using Reoplex 400 as stationary phase with an isothermal column temperature of 180 °C. Each fatty acid was collected and radioactivity measured by scintillation counting as described previously [14]. Each analysis was completed on at least three different samples. However, because the uptake of label from $^{14}CO_2$ is variable between experiments, it is not possible to average samples except as percentage distributions. The data presented for the quantitative distribution and radioactivity of molecular species are, therefore, results from one experiment that was typical of at least three similar analyses.

RESULTS

^{14}C Labelling of MGDG and PC

B. napus leaf discs analysed after $^{14}CO_2$ feeding showed the typical fatty acid profile of MGDG and PC in 16:3 plants with little change in the fatty acid composition during the incubation periods up to 48 h (Table 1).

Table 1 Fatty acid composition and distribution of radioactivity in MGDG and PC after ^{14}C-labelling of leaf discs and incubation for 1, 24 and 48 h in continuous light

Data are means ± S D obtained from three different experiments 16:1, palmitoleic acid, 16:2, hexadecadienoic acid, 18:0, stearic acid

	Incubation time . .	1 h		24 h		48 h	
Lipid	Fatty acid	mol%	% d.p m	mol%	% d p m	mol%	% d p m
MGDG	16:0	3±2	25±1	3±3	11±2	3±1	3±1
	16:1	1±1	2±2	1±1	1±1	0±0	1±0
	16:2	4±1	6±1	3±1	7±1	4±1	4±0
	16:3	30±1	4±2	33±1	18±1	31±1	30±1
	18:0	1±1	2±2	1±1	1±2	1±0	1±0
	18:1	1±1	27±2	1±0	4±1	1±0	2±2
	18:2	8±2	22±1	5±1	18±1	7±2	6±2
	18:3	54±0	8±1	55±1	38±2	51±3	50±2
PC	16:0	18±1	14±2	19±2	13±1	18±1	18±1
	18:0	4±1	6±1	4±1	4±1	3±1	3±0
	18:1	3±1	47±2	6±2	21±2	5±2	13±1
	18:2	30±2	19±2	31±2	43±1	32±1	47±2
	18:3	42±2	7±1	42±1	12±1	39±1	17±2

In MGDG 1 h after $^{14}CO_2$ labelling, radioactivity was found predominantly and almost equally in 16:0 and 18:1 This is consistent with the hypothesis that the initial labelling of MGDG is through the prokaryotic pathway and that the species formed is 18:1/16:0. Even at 1 h, however, there were significant levels of radioactivity in hexadecadienoic acid (16:2), 18:2 and 18:3, indicating an initial rapid desaturation phase as described previously [15]. After 24 and 48 h, progressively more of the radioactivity was converted more slowly by desaturation to 16:2 and 16:3, and 18:2 and 18:3, until after 48 h the distribution of label was similar to the mol% distribution of fatty acids (Table 1).

In PC 1 h after labelling, the majority of radioactivity was found in 18:1 and lesser amounts in 16:0, 18:2 and 18:3 (Table 1). This suggests the synthesis of PC from 18:1(16:0)/18:1 molecular species and a rapid desaturation of part of the 18:1 to 18:2 and 18:3 [15]. In contrast to MGDG, however, after 24 and 48 h incubation there is only a small increase in label in 18:3 and the levels of radioactivity are significantly lower than the mol% distribution.

Molecular species of MGDG and PC

Detailed analyses indicate that in MGDG there are two predominant molecular species (18:3/18:3 and 18:3/16:3) formed through the eukaryotic and prokaryotic pathways, respectively (Figure 1A). Pentaene and tetraene molecular species make up the bulk of the remaining molecular species The most highly labelled molecular species after $^{14}CO_2$ feeding (18:1/16:0; see below) is found in less than 1 % of the total MGDG, suggesting a transient role in the biosynthetic pathway.

The separation of molecular species of PC indicates that there are more major molecular species components (18:3/18:3, 18:3/18:2, 18:2/18:2, 16:0/18:3 and 16:0/18:2, Figure 1B) than in MGDG. The assumed initial product of biosynthesis, 18:1(16:0)/18:1 molecular species of PC, occurs in very low concentration. The major difference between MGDG and PC is that in PC there is less complete desaturation of the fatty acids and a greater array of different molecular species. This is also

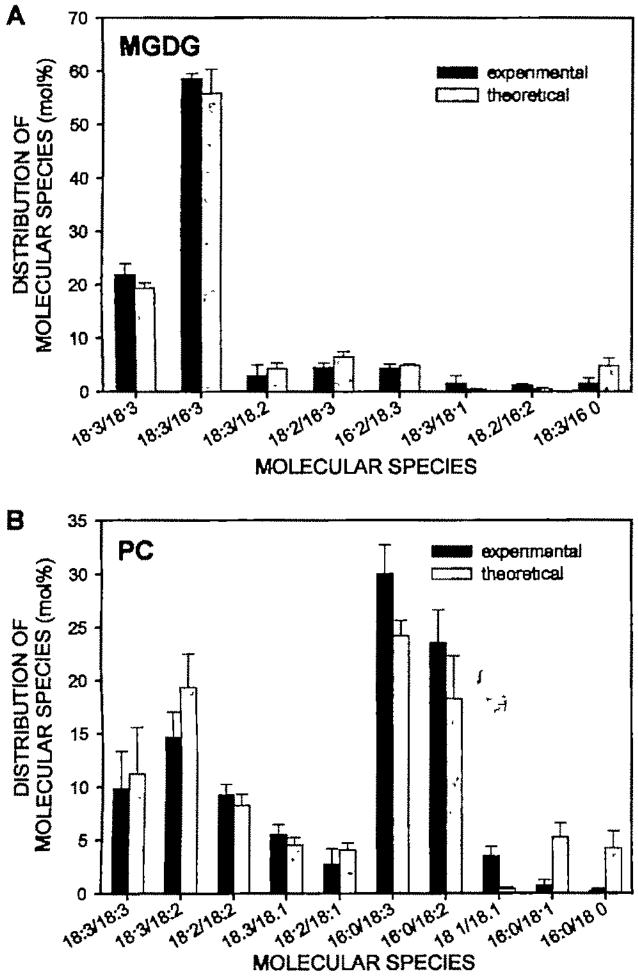

Figure 1 Distribution of molecular species of MGDG and PC determined experimentally by argentation TLC and GLC, and theoretically from the fatty acid composition of the total lipid samples analysed using a computer program to determine the theoretical distribution

The program assumes the random distribution of the fatty acids except for 16C on the *sn*-2 position of MGDG and 16 0 on the *sn*-1 position of PC The data are from labelling experiments that had been incubated for different periods up to 6 h after ^{14}C feeding ($n = 5$, ±S D) Only molecular species that are greater than 1% (either theoretical or experimental determinations) are represented

consistent with the other major lipids in the cell; the chloroplast lipids (MGDG, DGDG and SQDG) show very high levels of unsaturation and the non-chloroplastic lipids (PC, phosphatidylethanolamine) show lower, incomplete desaturation (results not shown).

Using a computer program it is possible to calculate the theoretical random distribution of molecular species from the total fatty acid composition of a DAG, assuming that all C_{16} fatty acids in MGDG are found on the *sn*-2 position and 16:0 in PC is confined to the *sn*-1 position. A comparison of the experimentally determined levels of molecular species with these theoretical random distributions shows that both MGDG and PC have close to random distribution of the fatty acid in molecular species (Figure 1). In PC, the 16:0/18:1 and 16.0/stearic acid (18:0) levels appear to be significantly below the theoretical levels. This probably results in the levels of other molecular species containing 16 0 or 18:0 (16:0/18:3, 16:0/18:2 and 18:0/18:2) being higher than the theoretical values. This suggests that some factor militates against the biosynthesis or stability of molecular species containing 0 or only 1 unsaturated bond.

^{14}C Labelling of fatty acids in molecular species of MGDG

Because of the almost equal labelling of 18:1 and 16:0 in MGDG at early feeding times it is assumed that initial synthesis occurs by the galactosylation of DAG containing 18:1 on the *sn*-1 position and 16:0 on the *sn*-2 position in the prokaryotic pathway. Analyses of the radioactive content of the fatty acids of MGDG molecular species after short-term (1 h) feeding confirm this (Figure 2A). After 1 h of incubation most of the radioactivity was found in the 18:1/16:0 molecular species with almost equal levels in each of the two fatty acids. In molecular species in which some desaturation had occurred, the levels of radioactivity in each of the two fatty acids was almost equal, even in molecular species (e.g. 18:3/16:2 and 18:2/16:3) in which unequal desaturation had occurred at the two *sn* positions. After 24 h (Figure 2B) and 48 h (results not shown), a similar pattern was found except that at these times significant desaturation had occurred and most of the radioactivity was now located in the more unsaturated species In all cases, however, the levels of radioactivity in the two fatty acids in each molecular species were similar.

In our view these data are completely consistent with the hypothesis that: (i) the majority of MGDG is synthesized through the prokaryotic pathway from 18:1/16:0 DAG, (ii) the fatty acids are desaturated *in situ* on MGDG to 18:3/16:3, and (iii) there is little or no exchange of fatty acid between molecular species

^{14}C Labelling of fatty acids in molecular species of PC

It has long been accepted that fatty acids in PC are desaturated *in situ* after the initial synthesis of PC from 18.1/18:1 and 16:0/18:1 DAG [1]. If this is the case a similar labelling pattern to that found in MGDG would be expected in PC. In other words, if PC is formed from 18:1/18:1 and 16:0/18:1 molecular species, these are the molecular species where most of the initial radioactivity would be located and the two fatty acids of all molecular species after subsequent desaturation would be similarly labelled, as shown in MGDG above.

The analyses of PC molecular species (Figure 3) show the opposite results to those found in MGDG and are, therefore, not consistent with the hypothesis that PC is formed from 18:1/18.1 and 16:0/18:1 molecular species of DAG. Most of the radioactivity was located in 18:1 1 h after ^{14}C labelling (Table 1); however, the radioactive 18:1 was not confined to 18:1/18:1 but distributed between the molecular species containing 18:1 (18:1/18:1, 18:1/18:2, 18:1/18:3, Figure 3A). Furthermore, in heterogeneous molecular species the accompanying fatty acids (18:2, 18:3) contain significantly less radioactivity and, therefore, could not be formed by desaturation of 18:1 during incubation after ^{14}C feeding. Similarly, the label found in 16:0 in the 16:0/18:3 molecular species is higher than in 18:3, and the label in 18:2 is higher than 18:3 in the 18:2/18:3 molecular species.

After 24 h of incubation, the 18:1 has been largely desaturated to 18:2 (Table 1). In molecular species that contain 18:1 the radioactive labelling pattern is similar to that found at 1 h except that the levels of radioactivity in 18:2 and 18:3 are higher (Figure 3B). In other molecular species containing 18:2 (par-

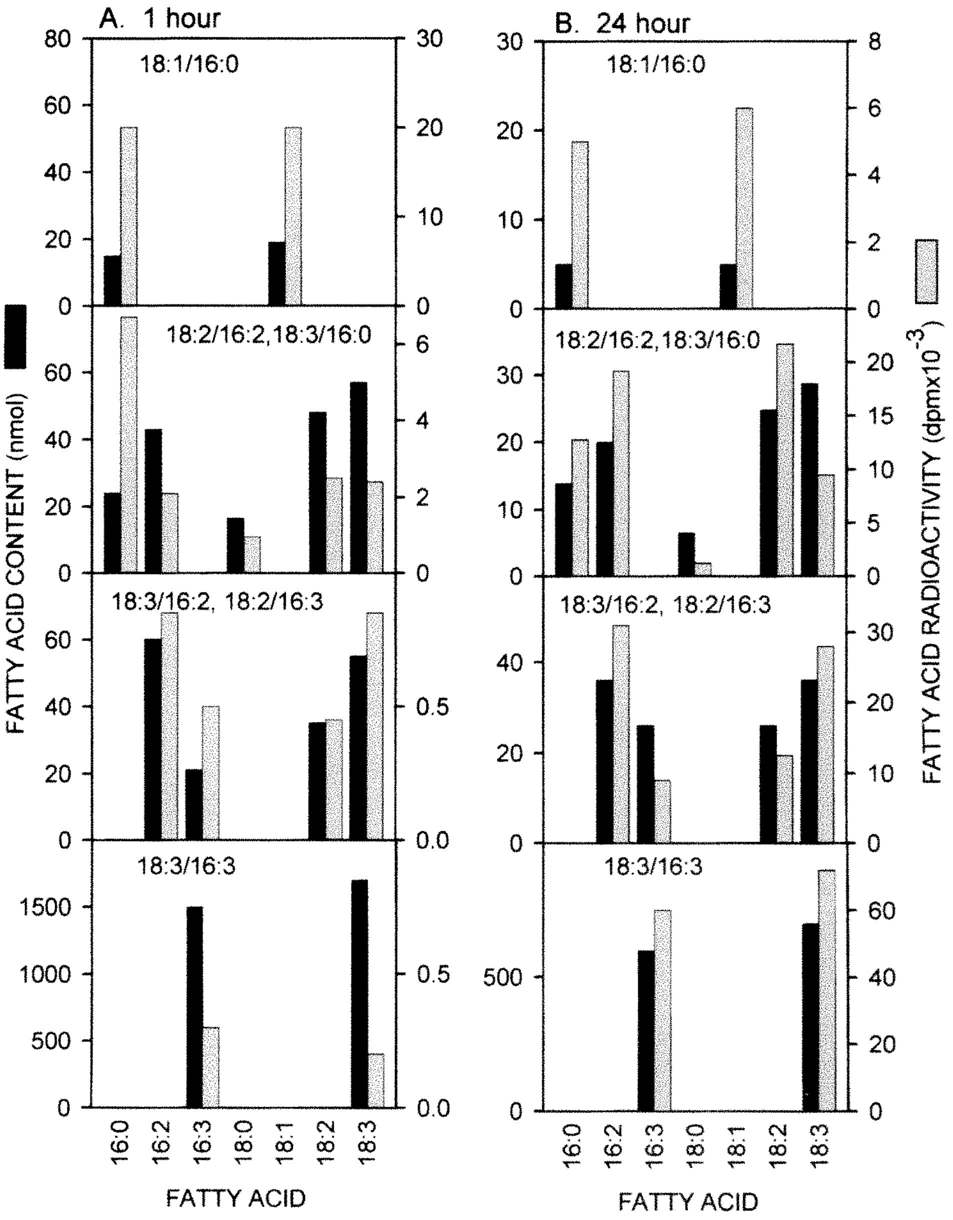

Figure 2 Fatty acid content and radioactivity of fatty acids from argentation TLC bands of prokaryotic molecular species of MGDG after ^{14}C labelling and incubation for (A) 1 and (B) 24 h

Only the major molecular species and fatty acids are presented in each band. Data are from one experiment that is typical of at least three experiments conducted at the same incubation times.

ticularly 18:2/18:3, 16:0/18:2), the higher levels of radioactivity in 18:2 also result in uneven labelling of the two fatty acids. Molecular species containing significant levels of radioactivity in 18:3 follow the same pattern of different levels of radioactivity in the two fatty acids. These data suggest that the fatty acids are continuously exchanged between all molecular species of PC and the acyl-CoA pool immediately after feeding and during longer periods of incubation. We believe this indicates that fatty acids in PC and the acyl-CoA precursor pools are in continuous flux.

Specific radioactivity of fatty acids in PC

The high levels of radioactive 18:1 found in PC immediately following feeding in association with more unsaturated fatty acid can only be interpreted as due to the exchange of newly formed fatty acid in the acyl-CoA pool with existing fatty acid in PC and not solely due to synthesis of new PC. If the fatty acids are exchanged continuously between PC and the acyl-CoA pool it would be expected that each fatty acid, irrespective of the molecular species to which it is esterified, would have the same or similar specific radioactivity. Calculations of specific radioactivity of these fatty acids from each molecular species (Table 2) indicate that the specific radioactivity of each fatty acid, while differing from other fatty acids, is similar regardless of the molecular species in which it is located. In contrast, in MGDG each fatty acid has a different specific radioactivity depending on the molecular species with which it is associated ([16], and results not shown).

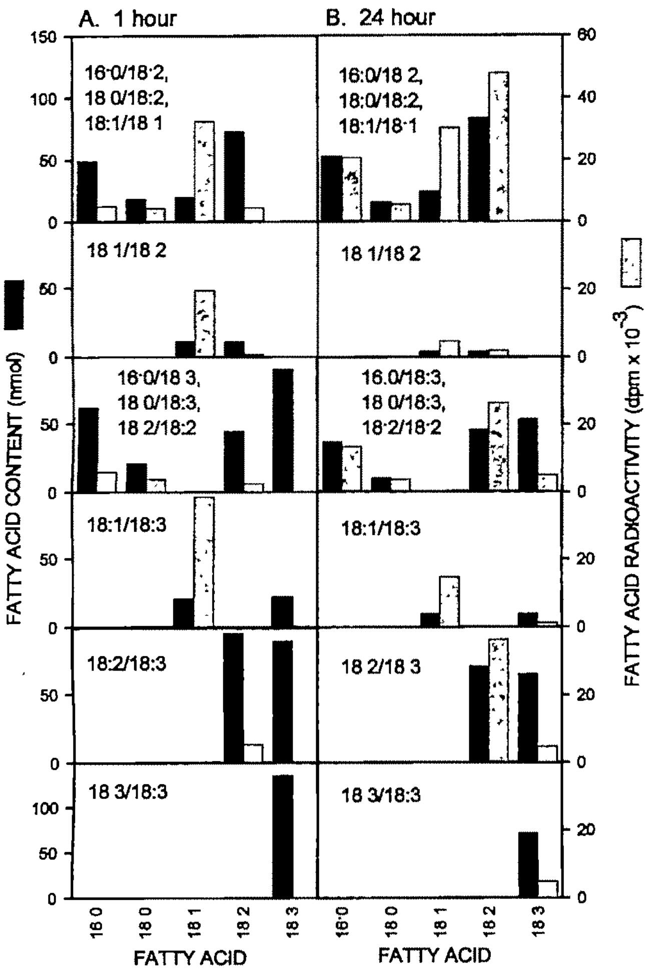

Figure 3 Fatty acid content and radioactivity of fatty acids from the major molecular species and fatty acids from argentation TLC bands of PC after ^{14}C labelling and incubation for (A) 1 and (B) 24 h

Data were obtained from the same experiments as in Figure 1 and are typical of at least three separate similar experiments

Table 2 Specific radioactivity of fatty acids from the major molecular species of PC from *B. napus* leaves after ^{14}C labelling and incubation for 0, 1 and 24 h

Molecular species were separated as bands by argentation TLC and the data for the major fatty acids in each band are presented The data are from one experiment that is typical of at least three experiments at each time

		Specific radioactivity of fatty acids (d p m /nmol)					
Incubation time	Band	16 0	18 0	18 1	18·2	18 3	Major molecular species
0 h	1					0 4	18 3/18 3
	2				3	1	18 2/18 3
	3			273		2	18 1/18 3
	4	39	106		10	1	16 0/18 3, 18 0/18 3, 18.2/18 2
	5			248	8		18 1/18 2
	6	33	105	207	11		16 0/18 2, 18 0/18 2, 18 1/18 1
1 h	1					1	18·3/18.3
	2				56	2	18 2/18.3
	3			1893		5	18 1/18 3
	4	96	178		55	2	16 0/18 3, 18:0/18 3, 18 2/18.2
	5			1720	62		18 1/18 2
	6	100	230	1618	62		16.0/18 2, 18.0/18 2, 18 1/18 1
24 h	1					69	18 3/18 3
	2				516	71	18·2/18 3
	3			1510		126	18.1/18 3
	4	362	357		575	94	16.0/18 3, 18.0/18.3, 18:2/18·2
	5			1253	576		18 1/18 2
	6	413	289	1137	514		16 0/18·2, 18 0/18 2, 18 1/18·1

Clearly the specific radioactivity of each fatty acid in PC varies with time. The specific radioactivity in 18:1 decreases with time while the specific radioactivities of 18:2 and 18:3 gradually increase. The fact that after 24 and 48 h of incubation the specific radioactivity of each fatty acid remains similar in different molecular species while changing with time is indicative of continued exchange between PC and the acyl-CoA pool.

DISCUSSION

In many ^{14}C-labelling experiments *in vivo* it has generally been assumed that ^{14}C incorporated into the fatty acids of PC and other lipids from $^{14}CO_2$ or [^{14}C]acetate occurs solely as the result of new synthesis of these lipids [1]. It has also been assumed that the first products of PC synthesis are molecular species containing predominantly 16:0 and 18:1, and that 18:1 is subsequently desaturated to form molecular species containing high levels of 18:2 and 18:3.

From the data presented here on *B. napus* leaves we can make two clear observations that are not consistent with the above assumptions. First, after $^{14}CO_2$ feeding the radioactivity of the two fatty acids on most molecular species of PC have different levels of radioactivity. This can only be the result of the mixing in PC of newly synthesized (radioactive) and existing (non-radioactive) fatty acids by deacylation/reacylation of the lipid molecule This must be a continuous process as this random mixing is also shown in the higher unsaturated species at later incubation times Secondly, the specific radioactivities of each fatty acid in different molecular species of PC are similar. This would suggest that all, or a very significant part, of the PC in the cell is involved in this process and that PC may be acting as a large pool of substrate for desaturation and a source of unsaturated fatty acid for the acyl-CoA pool. Although PC is found in most cell membranes outside the chloroplast, it is generally believed that biosynthesis and desaturation occur in the endoplasmic reticulum. However, our data suggest that the cytosolic acyl-CoA pool may exchange fatty acids with PC in many of these membranes.

Our hypothesis and the two different strategies of desaturation in the non-chloroplastic PC and chloroplastic MGDG of *B. napus* are outlined in Scheme 1. In the chloroplast, fatty acids are desaturated in a pool of MGDG predominantly in the envelope. MGDG is synthesized in the prokaryotic pathway from a small metabolic pool of MGDG molecular species containing 18:1/16:0 that represents less than 1% of the total MGDG (Figure 2A and Table 1). The small size of this pool results in the rapid desaturation and the subsequent transfer of the highly unsaturated molecular species to the thylakoid membranes forming the bulk MGDG pool. In our hypothesis the entire pool of PC,

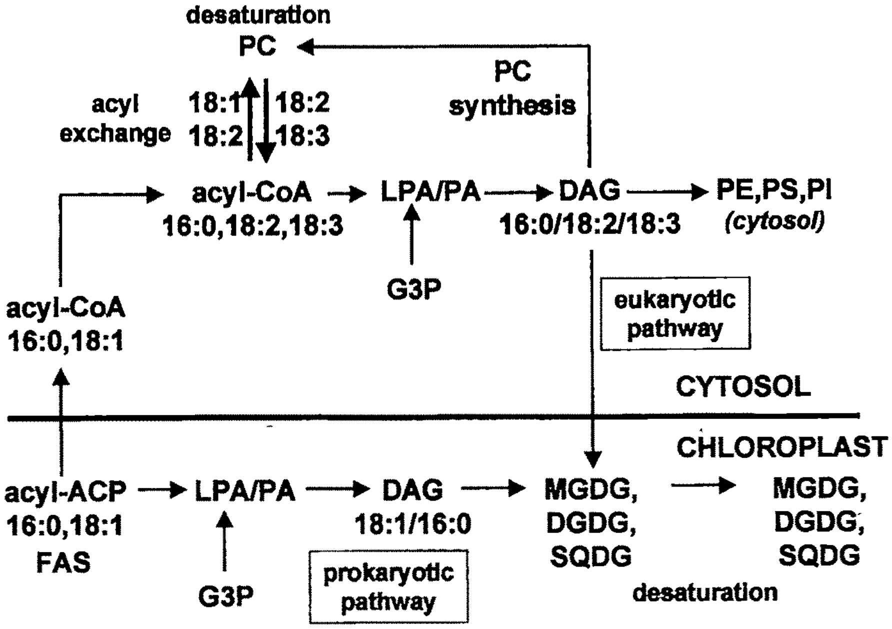

Scheme 1 Outline of the pathways of biosynthesis and desaturation of fatty acids in PC and the chloroplast lipids in *B. napus*, a 16:3 plant

The scheme illustrates the different strategies used in the non-chloroplastic compartments and chloroplast to raise and control the level of unsaturation in lipids In 18 3 and 18·4 plants the prokaryotic pathway does not participate in the synthesis of MGDG, DGDG and SQDG The major fatty acid components are indicated in each pool LPA/PA, lyso-phosphatidic acid/phosphatidic acid G3P, glycerol 3-phosphate, PS, phosphatidylserine, PI, phosphatidylinositol; PE, phosphatidylethanolamine, FAS, fatty acid synthase, ACP, acyl carrier protein

not just a small metabolic pool, is involved in the desaturation process. Through acyl exchange between PC and the acyl-CoA pool, the DAG subsequently formed from the acyl-CoA pool is maintained in a highly unsaturated state. From this pool of DAG, the other glycerolipids in the cell may be synthesized. The levels of unsaturation and rates of desaturation of fatty acid would not be tied to the rates of synthesis and degradation of PC, nor would there be a need for a separate pool of PC undergoing desaturation.

Previous reports using studies *in vitro* of developing soya bean cotyledons [17], safflower seeds [18,19], and sunflower seeds [7] have shown some exchange of fatty acids on the *sn*-2 position of PC with the acyl-CoA pool. In leaves, we believe this is a more extensive process than proposed for seeds, involving nearly all of the PC in the cell and resulting in the synthesis of highly unsaturated DAG. This DAG may be similar in fatty acid composition to the PC in the cell rather than containing just saturated (16:0) and monounsaturated (18:1) fatty acid. We have recently obtained support for the idea that the DAG precursor of PC is highly unsaturated from experiments using ^{32}P labelling in *B. napus* (16:3 plant) leaves [20], and *Vicia faba* (18:3 plant) and *Borago officinalis* (18:4 plant) leaves (J. P. Williams, M. U. Khan, J. N. Hodson and K. M. Hong, unpublished work). These data all show that PC is synthesized from highly unsaturated molecular species of DAG similar to the fatty acid composition of the bulk PC in all three types of plant.

In our experiments the apparent rate of desaturation of 18:2 to 18:3 measured by the rate of transfer of ^{14}C is slow (Table 1) and is not compatible with the rapid rates of incorporation of ^{14}C into PC The slow incorporation of ^{14}C into 18:3 may be an indication that most of the PC, which is usually high in 18:2, is the substrate for desaturation Hence the slow rate of incorporation of radioactivity into 18:3 may be due mainly to the large size and low specific radioactivity of the PC 18:2 pool and not due to slow desaturation.

Our hypothesis raises the question of whether the PC is the direct precursor of chloroplast lipids. A pathway from PC to chloroplast lipids, or TAG in seeds, involving a reversal of the CDP-choline:DAG-phosphotransferase has been used to explain how unsaturated fatty acids could be transferred from PC [1,17] in the event that newly synthesized DAG contains saturated and monounsaturated fatty acid. However, if the DAG in the non-chloroplastic compartments is largely composed of unsaturated fatty acid, as we have shown, it is unnecessary for PC to be an intermediate. The chloroplast lipids could be synthesized directly from the DAG pool that contains levels of unsaturated fatty acid generated by, and similar to those in, PC.

Our hypothesis could also explain the slow transfer of ^{14}C fatty acid from PC to MGDG even in developing leaf cells [2,3]. The exchange of radioactivity between PC and other glycerolipids through DAG is dependent not only on the rate of transfer of fatty acid but also the specific radioactivity and the pool size of the PC from which it originates. If the entire PC in the cell is involved in acyl exchange with the acyl-CoA pool, it would represent a large pool of lipid with a relatively low specific radioactivity. Consequently any fatty acid that is transferred from PC would represent only a small part of the total pool and would be low in total radioactivity. This would result in the slow transfer of radioactivity to the acyl-CoA pool and to DAG despite a fairly rapid transfer of fatty acid.

Recently Mongrand et al. [9] have also challenged the generally accepted hypothesis, suggesting that lysophosphatidylcholine (lyso-PC) instead of PC may be transferred to the chloroplast for MGDG and DGDG synthesis. Their hypothesis is partially based on the differential labelling of the fatty acids on the two *sn* positions of PC after ^{14}C-labelling [9] and the demonstration of an active acyl-CoA : lyso-PC acyl transferase [21] in leaves of leek seedlings. Stymne et al. [4] and Stobart et al. [6] also showed differential turnover or exchange of fatty acid from acyl-CoA with the *sn*-2 position of PC in microsomes from developing safflower seeds. Analyses of molecular species of PC from potato microsomes [19] and sunflower seeds [7] showed similar uneven incorporation of label *in vitro* after feeding with [^{14}C]oleoyl-CoA. Roughan et al. [22], however, showed more even labelling of the two *sn* positions of PC in spinach leaves and similar rates of desaturation on both *sn* positions after incorporation of exogenous [^{14}C]oleic acid. We have shown that in *B. napus* leaves fed $^{14}CO_2$ that the fatty acids on both *sn* positions of PC are labelled and undergo approximately equal apparent rates of desaturation (J. P. Williams and D. Wong, unpublished work). It is possible in our model that the exchange of fatty acid between PC and the acyl-CoA pool occurs unevenly on the two *sn* positions of PC. The presence of significant levels of 16:0 esterified to the *sn*-1 position must also be taken into account, as this would reduce the apparent level of desaturation on the *sn*-1 position. The relative labelling of fatty acids on the two positions would be determined by both the desaturation rates and the deacylation/reacylation rates for each *sn* position. These rates may vary between plant species, different organs and under different physiological and environmental conditions. Active lyso-PC:acyl transferase as reported by Bessoule et al. [21] and Triki et al. [7] would be an important feature of our hypothesis.

Concerning the glycerol/fatty acid labelling, Mongrand et al. [9], Slack et al. [23] and Williams et al. [3] have shown that a decrease in the labelling of glycerol and fatty acid in PC is accompanied by an increase in labelling of these moieties in MGDG. However, accurate relative labelling patterns of fatty acids and glycerol are difficult to determine and may be interpreted in different ways (see [9]). In fact, a re-examination of our data [3] in light of the recent findings suggest that the similar increase in ^{14}C labelling of glycerol and fatty acid in MGDG occurs only at early incubation times. At longer incubation times the increase in fatty acid labelling is not matched by an increase in glycerol labelling. A free exchange of fatty acid in PC with the acyl-CoA pool would mean that the glycerol and fatty acid are not continuously esterified in PC. If the glycerol and fatty acid are transferred to the chloroplast as DAG, the relative labelling of the two moieties would be a reflection of the different kinetics of glycerol and fatty acid metabolism in PC and DAG.

Our hypothesis is that at all times and under changing environmental conditions there would be a constant supply of unsaturated DAG species for lipid biosynthesis. Changes in environmental conditions would influence the fatty acid composition of these pools but would not suddenly increase or decrease the supply of unsaturated DAG. The control over the levels of unsaturated fatty acids may, therefore, be buffered from major changes in temperature and other environmental factors. In MGDG a buffering effect is also present, as the bulk of the lipid in the thylakoid is not immediately affected by environmental change. In both of these systems rapid changes in rates of desaturation are slowly reflected in changes in fatty acid composition of the lipids, thus mitigating rapid changes in unsaturation due to environmental factors.

This research was funded by a Research Grant to J.P.W. from the Natural Sciences and Engineering Research Council of Canada.

Received 23 February 2000/7 April 2000, accepted 27 April 2000

REFERENCES

1 Browse, J. A and Somerville, C R. (1991) Glycerolipid synthesis biochemistry and regulation Annu Rev. Plant Physiol. Plant Mol Biol. **42**, 467–506

2 Roughan, P G (1970) Turnover of the glycerolipids of pumpkin leaves. The importance of phosphatidylcholine Biochem J **117**, 1–8

3 Williams, J P, Watson, G R and Leung, S P K (1976) Galactolipid synthesis in *Vicia faba* leaves II Formation and desaturation of long chain fatty acids in phosphatidylcholine, phosphatidylglycerol, and the galactolipids Plant Physiol. **67**, 179–184

4 Stymne, S, Stobart, A and Glad, G (1983) The role of the acyl-CoA pool in the synthesis of polyunsaturated 18-carbon fatty acids and triacylglycerol production in the microsomes of developing safflower seeds Biochim. Biophys Acta **752**, 198–208

5 Harwood, J L (1988) Fatty acid metabolism Annu Rev. Plant Physiol **39**, 101–138

6 Stobart, A, Stymne, S and Glad, G (1983) The synthesis of linoleate and phosphatidic acid and its relationship to oil production in the microsomes of developing seeds of safflower (*Carthamus tinctorius* cultivar Gila) Biochim Biophys Acta **754**, 292–297

7 Triki, S, Demandre, C and Mazliak, P (1999) Biosynthesis of triacylglycerols by developing sunflower seed microsomes Phytochemistry **52**, 55–62

8 Williams, J. P., Khan, M U and Mitchell, K (1988) The molecular species of diacylglycerol precursors used in monogalactosyldiacylglycerol biosynthesis in the leaves of a number of higher plant species Plant Cell Physiol **29**, 849–854

9 Mongrand, S, Bessoule, J-J. and Cassagne, C (1997) A re-examination *in vivo* of the phosphatidylcholine-galactolipid metabolic relationship during plant lipid biosynthesis Biochem J **327**, 853–858

10 Bishop, D G, Sparace, S A and Mudd, J B. (1985) Biosynthesis of sulfoquinovosyldiacylglycerol in higher plants the origin of the diacylglycerol moiety Arch. Biochem Biophys **240**, 851–858

11 Williams, J. P. and Khan, M U (1996) Lipid metabolism in leaves of an 18:4-plant, *Echium plantagineum* a new model of galactolipid biosynthesis in higher plants Plant Physiol Biochem. **34**, 93–100

12 Williams, J. P and Merrilees, P A (1970) The removal of water and non-lipid contaminants from lipid extracts Lipids **5**, 367–370

13 Johnson, G and Williams, J. P (1989) The effect of growth temperature on the biosynthesis of chloroplastic galactosyldiacylglycerol molecular species in *Brassica napus* leaves. Plant Physiol **91**, 924–929

14 Watson, G R and Williams, J. P (1972) An improved method for the collection and measurement of radioactivity in compounds separated by gas-liquid chromatography J Chromatogr. **67**, 221–226

15 Williams, J P, Williams, K and Khan, M U (1992) Low temperature-induced desaturation in *Brassica napus* thermal lability of the process Biochim Biophys Acta **1125**, 62–67

16 Imperial, V (1998) Molecular species analysis of the glycerolipids involved in fatty acid desaturation in *Brassica napus*. M Sc Thesis, University of Toronto

17 Slack, C R, Campbell, L C, Browse, J A and Roughan, P G (1983) Some evidence for the reversibility of choline phosphotransferase-catalysed reaction in developing linseed cotyledons *in vivo* Biochim Biophys Acta **754**, 10–20

18 Stymne, S. and Glad, G (1981) Acyl exchange between oleoyl-coenzyme A and phosphatidylcholine in microsomes of developing soybean (*Glycine max* cultivar Fiskeby V) cotyledons and its role in fatty acid desaturation Lipids **16**, 298–305

19 Demandre, C, Tremolieres, A, Justin, A M and Mazliak, P (1986) Oleate desaturation in six phosphatidylcholine molecular species from potato (*Solanum tuberosum*) tuber microsomes Biochim Biophys Acta **877**, 380–386

20 Williams, J. P., Khan, M U, Imperial, V and Khetarpal, R (1998) Temperature regulation of desaturase activities in cytosolic and chloroplastic lipid biosynthesis, in Advances in Plant Lipid Research (Sanchez, J, Cerda-Olmedo, E and Martinez-Force, E, eds), pp 494–499, Secretariado de Publicaciones, Universidad de Sevilla, Spain

21 Bessoule, J J, Testet, E and Cassagne, C. (1995) Synthesis of phosphatidylcholine in the chloroplast envelope after import of lysophosphatidylcholine from endoplasmic reticulum membranes. Eur J Biochem **228**, 490–497

22 Roughan, P G, Thompson, Jr, G A and Cho, S H (1987) Metabolism of exogenous long-chain fatty acids by spinach leaves Arch Biochem. Biophys **259**, 481–496

23 Slack, C R, Roughan, P G and Balasingham, N (1977) Labeling studies *in vivo* on the metabolism of the acyl and glycerol moieties of the glycerolipids in the developing maize leaf Biochem J **162**, 289–296

Biochem. J. (2000) 349, 135–140 (Printed in Great Britain)

The short prodomain influences caspase-3 activation in HeLa cells

Thomas MEERGANS, Ann-Kristin HILDEBRANDT, Daniel HORAK, Christina HAENISCH and Albrecht WENDEL[1]
Biochemical Pharmacology, Faculty of Biology, University of Konstanz, POB 5560-M 668, D 78434 Konstanz, Germany

Proteolytic activation of caspases is a key step in the process of apoptosis. According to their primary structure, caspases can be divided into a group with a long prodomain and a group with a short prodomain. Whereas long prodomains play a role in autocatalytic processing, little is known about the function of the short prodomain, for example the prodomain of caspase-3. We constructed caspase-3 variants lacking the prodomain and over-expressed these in HeLa and yeast cells. We found that removal of the caspase-3 prodomain resulted in spontaneous proteolytic activation of the protein when expressed in HeLa cells. This processing was only partially autocatalytic, as demonstrated by a catalytically inactive caspase-3 mutant. Co-expression of the anti-apoptotic protein XIAP (X-chromosome-linked inhibitor of apoptosis protein) completely blocked the observed spontaneous activation, which excluded a direct involvement of caspase-8 Our findings indicate that the short prodomain of caspase-3 serves as a silencing component in mammalian cells by retaining this executioner caspase in an inactive state.

Keywords: apoptosis, TNFα, XIAP.

INTRODUCTION

Apoptosis is a process of controlled cell death that plays an important role in tissue homoeostasis of multicellular organisms. Over the last few years, it has become evident that the proteolytic activation of certain cysteine proteases, collectively called caspases [1], is a pivotal step in the apoptotic process in almost all cell types examined. Caspases-1, -4, -5 and -11 seem to function primarily in the processing of inflammatory cytokines, but the other ten known caspase species are involved in the execution of cell death in response to apoptotic stimuli. Caspases have a strict requirement for cleavage of Asp–Xaa bonds at the P_1 position The substrate specificity of the individual caspases is determined mainly by the sequence of the three amino acids preceeding the P_1 position, with P_4 being the most critical [2,3].

Caspases are synthesized as single-chain inactive zymogens with an N-terminal prodomain plus a large and a small catalytic subunit [4,5]. Activation of the zymogens is achieved through proteolytic cleavage at sites identical with the caspase-recognition motifs, generating the active heterodimeric enzyme. This suggests that caspases can process themselves or other caspase zymogens, most likely in an ordered cascade [6]. This mechanism may serve to amplify the apoptotic signal. Depending on their attributed functions within the apoptosis-related caspase cascade, these enzymes can be subdivided into a group of initiator caspases (including caspase-2, -8, -9 and -10), and a group of executioner caspases (including caspase-3, -6 and -7). The initiator group is mainly activated by an autocatalytic mechanism after a prodomain-mediated dimerization of the proenzymes, which is initiated by apoptotic stimuli. In the case of caspase-8 processing after engagement of the tumour necrosis factor-α (TNFα) receptor 1 or CD95 cell-death receptors, the procaspase is recruited to the cytosolic region of the receptor by association with the adaptor molecules Fas-associated death-domain protein (FADD)/TNFα-receptor-1-associated death-domain protein (TRADD) through homotypic interaction of their respective death-effector domains [7,8]. This aggregation is considered sufficient for procaspase-8 activation [9–11]. A different activation mechanism has been described for activation of caspase-9. Here, the ATP/cytochrome-*c*-dependent interaction of the caspase prodomain and the respective domain of the apoptotic-protease-activating factor 1 (Apaf-1) protein (CARD–CARD interaction; where CARD is caspase-recruitment domain) places the catalytic site of the caspase in close proximity to its internal cleavage site, resulting in an autocatalytic activation [12,13]. The executioner caspases act mainly downstream in the caspase pathway and they are activated, at least in part, by initiator caspases. In the execution phase, the activation of caspase-3 represents one of the key points in the transmission of the apoptotic signal because (i) caspase-3 cleavage activity results in a variety of morphological and biochemical features of apoptosis [14–16], (ii) caspase-3 seems to be able to cleave other executioner caspases, and (iii) so further amplifies the response to an apoptotic stimulus [17]. Furthermore, the central role of caspase-3 was underlined by the observation that the activated caspase-3 also cleaves the initiator caspases-9 and -2 [17], indicating its role as an amplifier in a positive-feedback loop.

Two different pathways have been described for the proteolytic activation of caspase-3: first, a direct caspase-8-mediated cleavage [18], and second, activation by caspase-9-dependent cleavage involving a cytochrome-*c*/Apaf-1-mediated oligomerization of the initiator caspase [13,19,20]. The pathway preferentially used in receptor-mediated apoptosis depends on the amount of active caspase-8 [21]. The mature caspase-3 is generated from a 32-kDa zymogen by a sequential two-step mechanism. The initial cut occurs at an IETD/S cleavage site producing the small p12 subunit and a p20 peptide. p20 is further processed at an ESMD/S site in what is most likely an autocatalytic process, whereby the prodomain is removed, resulting in the generation of the mature large p17 subunit [22]. The active enzyme is composed of two heterodimers of the generated p12 and p17 subunits [23].

In contrast with the initiator caspases, the executioner caspase zymogens contain short prodomains. Whereas the long prodomains of the initiator caspases have been ascribed an important role during the autocatalytic processing, the short prodomain

---

Abbreviations used TNFα, tumour necrosis factor-α, CARD, caspase-recruitment domain, FADD, Fas-associated death-domain protein, Apaf-1, apoptotic-protease-activating factor 1, afc, 7-amino-4-trifluoromethylcoumarin, XIAP, X-chromosome-linked inhibitor of apoptosis protein, GFP, green fluorescent protein

[1] To whom correspondence should be addressed (e-mail albrecht wendel@uni-konstanz de)

of caspase-3 was found to have no influence on the enzymic activity when expressed recombinantly in bacteria or in experiments *in vitro* using cytosolic extracts [18]. Extending these experiments, we focused our studies on the function of the short prodomain of this executioner caspase in the natural cellular environment We generated different caspase-3 expression plasmids, including truncated constructs lacking the prodomain, and expressed these in HeLa cells. Our data suggest that the prodomain suppresses the spontaneous activation of the inactive zymogen in mammalian cells.

EXPERIMENTAL

Cell culture and transfection

HeLa Tet-Off cells were obtained from Life Technologies and cultured in minimal essential medium at 37 °C with 10 % fetal calf serum in the presence of 5 % CO_2. The cells were grown to a maximum density of 1.3×10^5 cells/cm^2 Subsequently they were rinsed with PBS and treated with trypsin/EDTA (0.05 % trypsin/0.02 % EDTA in PBS) for 5 min at 37 °C. Transfection experiments were performed as described previously [24] Briefly, HeLa cells were seeded at a density of 2×10^4 cells/cm^2 into a 3.5-cm cell-culture dish 20 h prior to transfection Transfection of cells was carried out by the lipofection method using SuperFect reagent (Qiagen). For preparation of the transfection mixture for one dish, 2 μg of the respective plasmids was diluted with serum-free cell-culture medium to a total volume of 100 μl and mixed with 5 μl of SuperFect reagent. The transfection mixture was incubated at room temperature for 15 min and subsequently supplemented with 600 μl of cell-culture medium (minimal essential medium) containing 10 % fetal calf serum. After washing the cells with PBS, 700 μl of the transfection mixture was added to the cells. Following 2–3 h of incubation, transfection medium was replaced by washing with PBS and adding fresh cell-culture medium.

For tetracycline-regulated expression experiments, the antibiotic was added directly at the start of transfection using various concentrations as described below. After transfection, the cells were cultured for 16 h before further treatment. For apoptosis induction, cycloheximide was added (100 μM final concentration) 15 min prior to supplementation of the culture medium with recombinant murine TNFα (100 ng/ml final concentration). The cells were exposed to this mixture for 3.5 h. Before harvesting, the cell-culture plates were centrifuged at 900 *g* for 5 min, washed with ice-cold PBS and centrifuged again.

Cells were harvested by adding 75 μl of hypotonic lysis buffer (25 mM Hepes, pH 7.5, 5 mM $MgCl_2$, 1 mM EGTA, 1 mM Pefablock and pepstatin, leupeptin and aprotinin, 1 μg/ml each) and scraping with a rubber policeman. Cellular extracts were prepared by freezing the cells in liquid nitrogen and thawing rapidly at 37 °C (three cycles) followed by a centrifugation step (20000 *g*, 5 min).

To determine the nuclear manifestation of apoptosis, cells were stained with Hoechst 33342 (10 μg/ml in PBS) The nuclear morphology was analysed using a fluorescence microscope.

SDS/PAGE and immunoblotting

For Western blotting, cell extracts (60 μg total protein) were separated on a 4–20 % polyacrylamide gel and transferred on to a nitrocellulose membrane (Schleicher and Schuell) After blocking for 1 h at room temperature (5 % skimmed milk in Tris-buffered saline containing 0.1 % Tween 20), the membrane was incubated overnight (4 °C) with a rabbit anti-caspase-3 antibody (H277, Santa Cruz) at a 1:1000 dilution in blocking buffer followed by a horseradish-peroxidase-coupled secondary antibody (Jackson Immuno Research) at a 1:20000 dilution for 45 min at room temperature. The blot was washed with Tris-buffered saline containing 0 1 % Tween 20 for 3 × 10 min after each incubation. The immunoreactive proteins were visualized with the ECL® kit (Amersham Pharmacia Biotech). To confirm equal loading, the protein concentration was determined with the bicinchoninic acid assay (BCA, Pierce).

Measurement of caspase-3-like activity and luciferase activity

The fluorimetric DEVD-afc (7-amino-4-trifluoromethylcoumarin) cleavage assay was carried out in microtitre plates according to the method described by Thornberry [25] with following modifications: 5 μl of cytosolic extracts was diluted 1:20 with substrate buffer [55 μM fluorogenic substrate DEVD-afc (Biomol) in 50 mM Hepes, pH 7.4/1 % sucrose/0.1 % CHAPS/10 mM dithiothreitol]. Blanks contained 5 μl of extraction buffer and 95 μl of substrate buffer. Generation of free afc at 37 °C was determined by fluorescence measurement at $t = 0/t = 30$ min using the multilabel plate reader Victor II (Wallac) set at an excitation wavelength of 390 nm and an emission wavelength of 510 nm. Control experiments confirmed that the activity was linear with time and with protein concentration under the conditions described above.

The amount of recombinant expressed caspase-3 in HeLa Tet-Off cells was estimated measuring the activity of the co-expressed luciferase as described previously [24].

Construction of expression vectors

For the isolation of the human caspase-3 cDNA and cDNA of the anti-apoptotic protein XIAP (X-chromosome-linked inhibitor of apoptosis protein), total RNA was extracted from HepG2 cells (caspase-3) or Jurkat cells (XIAP) with the RNeasy kit from Qiagen. The cDNA was synthesized in an oligo(dT)-primed reaction with *MuLV* reverse transcriptase (Perkin Elmer) and amplified specifically by PCR using *Pfu* polymerase (Stratagene). The following primers were used: caspase-3 forward primer, 5′-CCCAGGCCGTGAGGAGTTAGC-3′; caspase-3 reverse primer, 5′-CAGCATCACTGTAACTTGCTAATC-3′. Isolation of XIAP cDNA was performed using primers specified by Deveraux et al. [26]. The caspase-3 amplification product was cleaved subsequently at *Ban*II/*Pst*I sites and cloned into the respective sites of a pUC19 vector. This construct served as a template for the following PCRs. Expression plasmids containing (i) or lacking (ii) the caspase-3 prodomain were generated by PCR using the forward primer (i) 5′-GAC*GATATC*ATGGAGAACACTGAAAACTCA-3′ and forward primer (ii) 5′-GTC*GATATC*ATGTCTGGAATATCCCTGGAC-3′ (*Eco*RV sites are indicated by italics, translation start codons are underlined) and the reverse-sequencing primer (Pharmacia). Subsequently, the obtained fragments were cloned into the *Eco*RV site of the pBI-luc tetracycline-dependent expression plasmid (Clontech). The XIAP PCR product was first inserted into the *Eco*RI/*Xho*I sites of the BlueScript KS II vector and then subcloned for expression as a green-fluorescent-protein (GFP)-fusion protein into the pEGFP-C1 vector (Clontech) using the *Bgl*II/*Kpn*I restriction sites.

For mutation of the caspase-3 catalytic site (substitution of Cys with Ser), the respective expression construct was subjected to site-directed mutagenesis using the QuikChange Site-Directed Mutagenesis kit (Stratagene) according to the manufacturer's instructions. The exact nucleotide sequences of the cDNA fragments were determined by automated DNA sequencing.

RESULTS

In contrast with large prodomain initiator caspases, which are prone to autoactivation, caspase-3 is only a poor inducer of cell death when overexpressed as native protein in mammalian cells [27–29]. These observations suggest that the premature zymogen is not activated by autocatalytic cleavage. To study a possible contribution of the short caspase-3 prodomain to the suppression of proteolytic activation, we expressed caspase-3 variants with or without the prodomain in HeLa cells. The peptide sequence of the construct missing the prodomain started with a Met (resulting from the ATG start codon), directly followed by a Ser, the first amino acid of the native large subunit. By using the Tet-Off tetracycline-regulated expression system and vectors that simultaneously co-express the luciferase reporter protein, we varied the amount of the expressed protein and were able to monitor and normalize the expression levels between different transfections.

As shown in Figure 1(A), a DEVD-afc cleavage activity, which was markedly higher compared with cells transfected with the control vector, was measured in caspase-3-transfected cells 20 h post-transfection. This demonstrates that the specific caspase-3 constructs were activated spontaneously. Furthermore, the construct lacking the prodomain showed a higher caspase activity (≈ 7-fold) compared with its native counterpart. Although the activation level of full-length caspase-3 is much lower compared with the protein without prodomain, the spontaneous activation is not completely blocked. Interestingly, whereas TNFα treat-

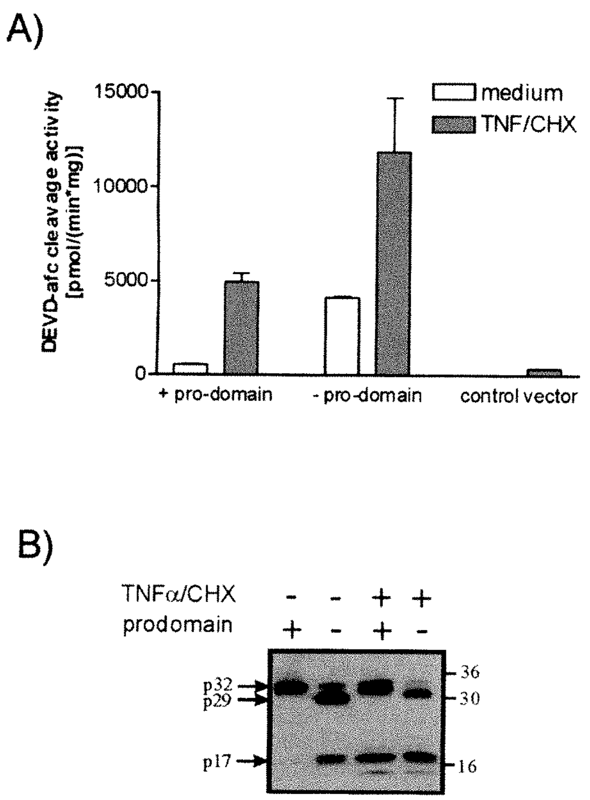

Figure 1 Expression of caspase-3 without prodomain results in spontaneous proteolytic activation

HeLa cells were transfected with various caspase-3 constructs, or with a control vector. For induction of apoptosis, cells were treated for 3 h with 100 ng of TNFα/ml in the presence of 100 μM cycloheximide (CHX). After transfection (20 h), cytosolic extracts were prepared by freeze–thawing. (**A**) For the measurement of caspase-3-like activity, 5 μl of cytosolic extract was incubated for 30 min at 37 °C with 50 μM DEVD-afc in 95 μl of assay buffer. Increase in fluorescence intensity by afc release was measured at 510 nm. Measurements were performed in triplicate, values are an average of three experiments, and error bars indicate S.E.M. (**B**) Proteolytic processing of caspase-3 constructs was analysed by immunoblotting with an antibody directed against the p17 subunit of caspase-3. Expression of the full-length construct resulted in one band (p32) representing the full-length caspase (lane 1, reading from the left). Three bands were visible when the construct lacking the prodomain was expressed (lane 2): the band at 17 kDa (p17) represents the mature large subunit, whereas the 29-kDa band (p29) shows the unprocessed recombinant protein. The band at 32 kDa represents the endogenous caspase-3 zymogen. After TNFα treatment, full-length caspase-3 was processed to the mature enzyme as indicated by the p17 subunit. An additional fragment, marginally smaller than the full-length protein, represents a partial cleavage at the Asp-9 site in the prodomain, whereas a fragment consisting of the small and the large subunit without the prodomain did not appear (lane 3). Molecular masses are depicted to the right of (**B**).

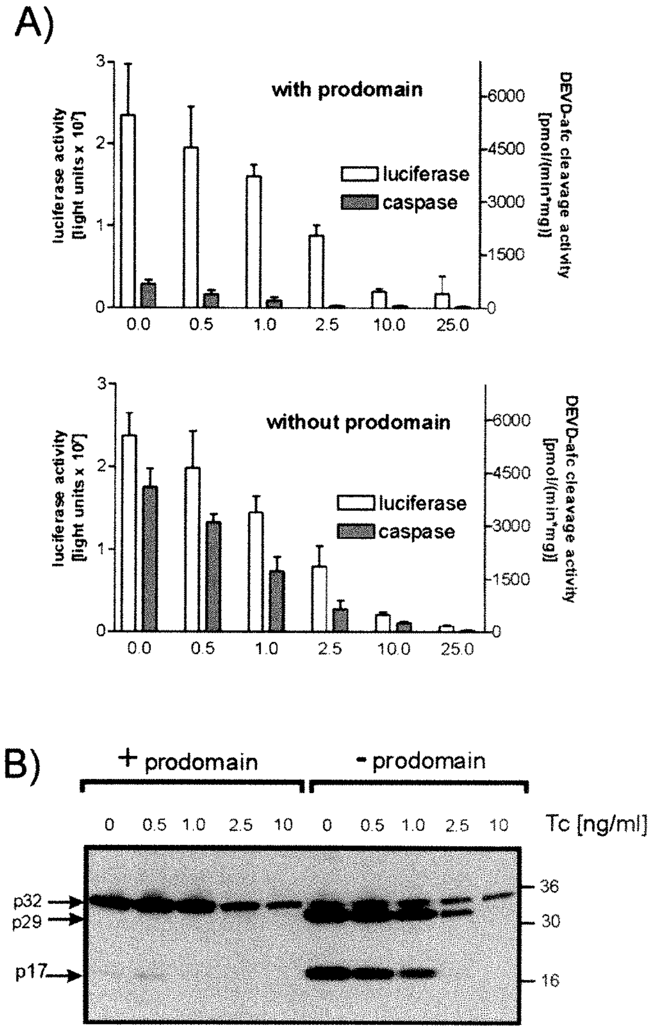

Figure 2 Effect of the prodomain is independent of expression level

HeLa cells were transfected with caspase-3 expression constructs (with or without prodomain) in a bidirectional pBI-L Tet vector which allows regulated expression by tetracycline supplementation. Tetracycline (Tc) at the concentrations indicated (0–25 ng/ml in **A**, 0–10 ng/ml in **B**) was added immediately after transfection. (**A**) Caspase-3 activity was measured in cytosolic extracts from transfected cells by DEVD-afc cleavage 20 h after transfection. Additionally, luciferase activity was measured as described in the Experimental section. Data represent means ± S.D. ($n = 2$). (**B**) Caspase-3 Western blot was used to demonstrate the expression level of the two caspase constructs and the associated spontaneous proteolytic processing. Equal amounts of cytosolic protein (30 μg) were loaded into each lane. Note that for the construct without prodomain (right half), the band at 32 kDa represents the endogenous caspase-3 zymogen.

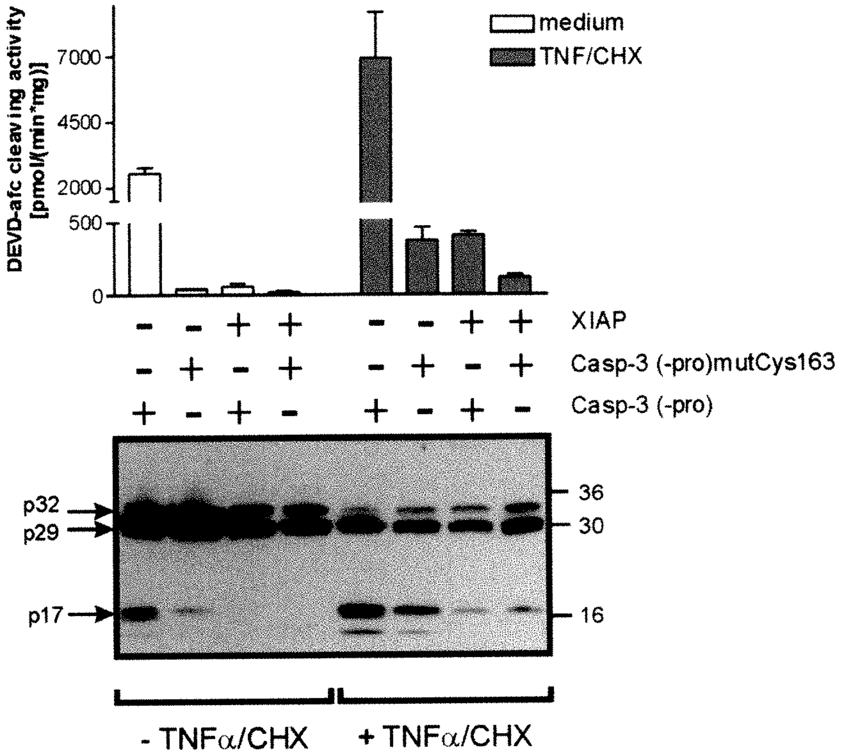

Figure 3 XIAP co-expression completely and catalytic-site mutation partially inhibit spontaneous caspase-3 activation

A caspase-3 construct without prodomain [Casp-3 (−pro)] and a catalytically inactive, mutated variant [Cys-163 changed to Ser, without prodomain, Casp-3 (−pro)mutCys163)] were transiently transfected in HeLa cells and co-expressed with XIAP as an enhanced-GFP-fusion protein. Caspase-3 activity was measured by DEVD-afc cleavage in medium alone or 3 h after apoptosis induction with TNFα (100 ng/ml) and cycloheximide (CHX, 100 μM). Note that the caspase-3 Western blotting (lower panel) reveals partial processing of the mutated caspase-3 without apoptotic stimulation (lane 2, reading from the left). Data of the DEVD-afc cleavage assay are shown as means ± S.E.M. from three independent experiments.

ment causes apoptosis in about 70% of the vector-transfected control cells, the DEVD-afc cleaving activity was similar to (with prodomain) or much lower than (without prodomain) that in untreated transfected cells. Despite the high DEVD-afc cleaving activity, only about 15% the caspase-transfected cells (determined by enhanced-GFP co-transfection) showed typical signs of apoptosis-like membrane blebbing or chromatin condensation (results not shown). When the transfected cells were exposed to TNFα/cycloheximide treatment (100 ng of TNFα/ml, 100 μM cycloheximide) for 3.5 h, the activity of both caspase-3 variants was markedly increased (Figure 1A). Although the activity of constructs lacking the prodomain was about 2.5 times stronger after TNFα treatment, the TNFα-induced relative activity shift in cells transfected with the full-length caspase was much higher (≈ 14-fold). Western-blot analysis of the two constructs with an antibody raised against the p17 subunit of caspase-3 confirmed that the prodomain-free enzyme was activated spontaneously in the transfected cells (Figure 1B).

To examine the effect of different expression levels on the spontaneous activation of the caspase-3 variants, we varied the amount of expressed protein in HeLa Tet-Off cells with different concentrations of tetracycline in the cell-culture medium. As shown in Figure 2, we observed a suppressive effect of the prodomain independent of the expression level of the recombinant caspases. At all expression levels examined (normalized to luciferase activity), the construct lacking the prodomain displayed much higher activity (6–8-fold). The largest difference was observed at a low expression level (2.5 ng of tetracycline/ml). The prodomain-dependent differences in the spontaneous activation at various expression levels were also confirmed by Western blot (Figure 2B). These data indicate a pivotal role of the prodomain in preventing caspase-3 activation in unstimulated cells.

To further investigate the mechanisms mediating the activation of the truncated caspase-3, we studied the effect of simultaneous overexpression of the caspase-3 (without prodomain) and XIAP in HeLa cells. XIAP is known to be a direct and specific inhibitor of active caspase-3. Furthermore, it also suppresses the caspase-9-dependent activation of the caspase-3 proenzyme [30]. As shown in Figure 3, the spontaneous activity of the truncated caspase-3, which was observed when the caspase was transfected alone, was strongly suppressed by co-expression of XIAP (Figure 3, lane 3 versus lane 1, reading from the left), indicating that this inhibitor can interrupt spontaneous maturation of the enzyme at the cleavage site between the large and small subunits. Interestingly, mutation of the catalytic site of the truncated caspase-3 by replacing Cys-163 with a Ser only partially inhibited the spontaneous cleavage of the subunits (Figure 3, lane 2). Although no significant caspase activity resulted from transient transfection of this mutated caspase construct, the Western-blot analysis demonstrated clearly a conversion of the zymogen into the p17 peptide, which was blocked by XIAP co-expression (Figure 3, lane 4). In addition, these data demonstrate that an intact catalytic site in the recombinant caspase is required for the observed increase in DEVD-afc cleaving activity in transfected cells. The extent of caspase-3 processing was increased after induction of receptor-mediated apoptosis by post-transfectional treatment with TNFα/cycloheximide (Figure 3, lanes 5–8). The differences between the prodomain-free native form and the inactive Cys-163 mutated form were still evident, i.e. the activation rate of the native form was higher (Figure 3, lane 5 versus lane 6). Furthermore, in TNF-treated cells, caspase-3 was processed partially in spite of XIAP overexpression (Figure 3, lanes 7 and 8). However, the amount of mature p17 and the measured caspase-3 activity in cells co-transfected with XIAP were notably lower compared with cells only overexpressing the caspase (Figure 3, lane 7 versus lane 5 and lane 8 versus lane 6). In addition, when XIAP was overexpressed, no significant differences in the proteolytic processing of the native and the mutated caspase-3 forms were observed in the Western blot (Figure 3, lanes 7 and 8). Complete suppression of the spontaneous activation of caspase-3 was achieved by adding the peptide inhibitor DEVD-fmk (fluoromethylketone; results not shown). In summary, these data suggest that caspase-3 constructs lacking the prodomain are activated in cells without apoptotic stimulation by at least two XIAP-inhibitable caspase-dependent mechanisms: (i) by autocatalytic processing and (ii) by a second process that still occurs when caspase-3 is inactivated by mutation. This second process may be mediated by a low caspase activity that is most probably related to a caspase with a small zymogenicity ratio, for example caspase-9 [31]. The XIAP-mediated inhibition of the truncated caspase-3 activation makes a direct participation of caspase-8 unlikely, as caspase-8-mediated cleavage between the large and the small subunits of caspase-3 is not inhibited by XIAP [26]. However, in the case of TNF treatment, caspase-8 activity could be responsible for the observed caspase-3 processing in cells overexpressing XIAP.

DISCUSSION

Apoptosis-associated caspases have been classified in the literature either according to their function in the caspase cascade (i e. initiators or executioners), or due to their primary structure (i.e. groups with long or short prodomains). Interestingly, in either case, the different criteria result in an almost congruent classification. This suggests that the specific function of a caspase is also determined by the structure of its prodomain. For the caspases with long prodomains, i.e. the initiator caspases, it has been shown that the N-terminal region is required for the recruitment to death-receptor complexes as well as for dimerization and autoprocessing [7,32,33]. Specific structures within the large prodomain, which are crucial for the proteolytic activation of the initiator caspases, have been characterized in detail. In case of caspase-8 activation, the death-effector domain integrated in the long prodomain mediates steric aggregation via interaction with the FADD adapter molecule, inducing autoprocessing of the procaspase-8 molecules [8,9,34]. A similar principle of long-prodomain-mediated autoactivation has been described for caspase-9. Here, procaspase-9 autoactivation is induced by interaction of the CARDs in the prodomain and the respective sequence of Apaf-1, followed by oligomerization of the Apaf-1 adapter molecule. By this mechanism, the procaspase is brought into the proximity of its catalytic sites, resulting in autoactivation of caspase-9 [20,35,36]. Although certain functions have already been attributed to the long prodomains, a function of the short prodomains (e.g. caspase-3 pro-peptide) has not been described until now.

The potential for autocatalytic activation of caspase-3 has been demonstrated by recombinant expression in *Escherichia coli* [18] and in the yeast *Saccharomyces cerevisiae* (T. Meergans and A. Wendel, unpublished work). However, in mammalian cells we found, in agreement with previous reports [37,38], that transient overexpression resulted in little native caspase-3 being processed and becoming enzymically active, indicating an important contribution to the activation process of the conditions in the specific cell. We demonstrate here that the short prodomain of caspase-3 has an inhibitory function on the activation of this executioner caspase in Hela cells. This general feature of the native full-length caspase is changed in absence of the prodomain, resulting in a proteolytic activation of the recombinant caspase. Because this inhibitory effect of the prodomain was not found in a bacterial expression system [18] or in the yeast cells (T. Meergans and A. Wendel, unpublished work), our results may indicate that factors exist that are specific for a living mammalian cell and mediate the silencing effect of the prodomain.

Spontaneous activation of caspase-3 fusion proteins has been reported previously. In this case, N-terminal fusion of the long prodomain of caspase-2 to the full-length caspase-3 resulted in caspase-3 processing most probably due to a caspase-2-prodomain-mediated oligomerization [38]. Furthermore, rearrangement of the subunits (the small subunit preceding the large subunit) generated a constitutively active enzyme that was capable of autoactivation [37]. In these preceding reports, the silencing function of the caspase-3 prodomain may have been obscured by the artificial structures resulting from these unusual fusion proteins. Our data show that deletion of the prodomain alone is sufficient for caspase-3 to become activated in the natural cellular environment. It is important to note that this finding was also valid for recombinant expression levels (regulated by the Tet-Off system) comparable with those of the endogenous zymogen.

As shown in Figure 1, the differences in the activity levels resulting from prodomain deletion were pronounced in transfected cells lacking apoptotic stimulation, but became smaller after TNFα treatment of the cells. This indicates that TNFα stimulation may initiate reactions that overcome the prodomain-associated activation barrier, whereas mechanisms responsible for processing the prodomain-free caspase may be constitutively available. Recently, Stennicke et al. described a partial activity of the caspase-9 zymogen without prior proteolytic processing [31]. Although caspase-9 activity is mainly cytochrome *c* regulated, the small remaining activity could be sufficient to activate caspase-3 lacking the prodomain. Therefore, the function of executioner caspase prodomains may consist of protection against small amounts of latent initiator caspase activity, which in turn is necessary to enable autocatalysis in response to stimulation.

The anti-apoptotic protein XIAP has been shown to specifically inhibit caspase-3 and -7 as well as caspase-9 activity. In addition, XIAP blocks the removal of the caspase-3 prodomain during caspase-8-initiated processing, but is unable to prevent caspase-8-mediated cleavage of caspase-3 between the small and the large subunit [26,30,39] Hence, the lack of caspase-3 proteolysis into the large and small subunits in unstimulated cells co-expressing XIAP and caspase-3 (without prodomain) suggests that caspase-8 is not involved in the spontaneous activation of caspase-3. Autoactivation of recombinant caspase-3 could be involved, but is unlikely to be exclusively responsible for the spontaneous activation in HeLa cells. Although we cannot exclude that the observed partial proteolysis of the mutated construct was mediated by traces of activated endogenous caspase-3, these data suggest that the spontaneous activation of caspase-3 is not only an autocatalytical process.

To our knowledge, this is the first report showing a functional role of a short caspase prodomain. Further studies will address the identification and characterization of factors mediating the silencing effect of the caspase-3 prodomain.

We thank L Haerter, H Hentze and S. von Aulock for helpful discussions and for critical comments on the manuscript This work was supported by the Deutsche Forschungsgemeinschaft (grant We 686/18-1)

REFERENCES

1 Alnemri, E S., Livingston, D J, Nicholson, D W, Salvesen, G, Thornberry, N A., Wong, W W and Yuan, J (1996) Human ICE/CED-3 protease nomenclature Cell **87**, 171

2 Talanian, R V, Quinlan, C., Trautz, S, Hackett, M, Mankovich, J. A, Banach, D, Ghayur, T, Brady, K and Wong, W W (1997) Substrate specificities of caspase family proteases J Biol Chem. **272**, 9677–9682

3 Thornberry, N. A, Rano, T A, Peterson, E P, Rasper, D M, Timkey, T, Garcia-Calvo, M, Houtzager, V. M, Nordstrom, P A, Roy, S., Vaillancourt, J P, Chapman, K T and Nicholson, D. W (1997) A combinatorial approach defines specificities of members of the caspase family and granzyme B Functional relationships established for key mediators of apoptosis. J Biol Chem **272**, 17907–17911

4 Cohen, G M (1997) Caspases the executioners of apoptosis. Biochem J **326**, 1–16

5 Nicholson, D W. and Thornberry, N A (1997) Caspases killer proteases. Trends Biochem Sci **22**, 299–306

6 Salvesen, G S and Dixit, V M (1997) Caspases Intracellular signaling by proteolysis. Cell **91**, 443–446

7 Muzio, M., Chinnaiyan, A M, Kischkel, F C, O'Rourke, K, Shevchenko, A, Ni, J, Scaffidi, C., Bretz, J D, Zhang, M, Gentz, R et al (1996) FLICE, a novel FADD homologous ICE/CED-3-like protease, is recruited to the CD95 (Fas/APO-1) death-inducing signaling complex Cell **85**, 817–827

8 Medema, J P, Scaffidi, C, Kischkel, F C, Shevchenko, A., Mann, M, Krammer, P H and Peter, M E (1997) FLICE is activated by association with the CD95 death-inducing signaling complex (DISC) EMBO J **16**, 2794–2804

9 Martin, D A, Siegel, R M, Zheng, L and Lenardo, M. J. (1998) Membrane oligomerization and cleavage activates the caspase-8 (FLICE/MACHalpha1) death signal. J. Biol Chem **273**, 4345–4349

10 Yang, X, Chang, H Y and Baltimore, D (1998) Autoproteolytic activation of pro-caspases by oligomerization Mol Cell. **1**, 319–325

11 Muzio, M, Stockwell, B R, Stennicke, H R, Salvesen, G S and Dixit, V M. (1998) An induced proximity model for caspase-8 activation J Biol. Chem **273**, 2926–2930

12 Green, D R (1998) Apoptotic pathways the roads to ruin Cell **94**, 695–698

13 Saleh, A., Srinivasula, S M, Acharya, S, Fishel, R. and Alnemri, E S (1999) Cytochrome c and dATP-mediated oligomerization of Apaf-1 is a prerequisite for procaspase-9 activation J Biol Chem. **274**, 17941–17945

14 Casciola-Rosen, L, Nicholson, D W, Chong, T, Rowan, K R, Thornberry, N A, Miller, D K and Rosen, A (1996) Apopain/CPP32 cleaves proteins that are essential for cellular repair a fundamental principle of apoptotic death J Exp Med **183**, 1957–1964

15 Kothakota, S, Azuma, T, Reinhard, C, Klippel, A, Tang, J, Chu, K, McGarry, T J, Kirschner, M W., Koths, K, Kwiatkowski, D. J and Williams, L T (1997) Caspase-3-generated fragment of gelsolin effector of morphological change in apoptosis Science **278**, 294–298

16 Cryns, V L., Bergeron, L., Zhu, H, Li, H and Yuan, J (1996) Specific cleavage of alpha-fodrin during Fas- and tumor necrosis factor-induced apoptosis is mediated by an interleukin-1beta-converting enzyme/Ced-3 protease distinct from the poly(ADP-ribose) polymerase protease. J. Biol Chem **271**, 31277–31282

17 Slee, E A, Harte, M T, Kluck, R. M., Wolf, B B, Casiano, C A, Newmeyer, D. D, Wang, H G, Reed, J C., Nicholson, D W, Alnemri, E S et al (1999) Ordering the cytochrome c-initiated caspase cascade hierarchical activation of caspases-2, -3, -6, -7, -8, and -10 in a caspase-9- dependent manner J Cell Biol **144**, 281–292

18 Stennicke, H R., Jurgensmeier, J M, Shin, H, Deveraux, Q., Wolf, B B, Yang, X, Zhou, Q, Ellerby, H M, Ellerby, L M, Bredesen, D. et al (1998) Pro-caspase-3 is a major physiologic target of caspase-8 J Biol Chem **273**, 27084–27090

19 Zou, H, Henzel, W. J, Liu, X, Lutschg, A. and Wang, X (1997) Apaf-1, a human protein homologous to *C elegans* CED-4, participates in cytochrome c-dependent activation of caspase-3 Cell **90**, 405–413

20 Li, P, Nijhawan, D, Budihardjo, I., Srinivasula, S M, Ahmad, M, Alnemri, E S and Wang, X (1997) Cytochrome c and dATP-dependent formation of Apaf-1/caspase-9 complex initiates an apoptotic protease cascade. Cell **91**, 479–489

21 Scaffidi, C, Fulda, S, Srinivasan, A., Friesen, C, Li, F, Tomaselli, K J, Debatin, K. M, Krammer, P H. and Peter, M E (1998) Two CD95 (APO-1/Fas) signaling pathways EMBO J **17**, 1675–1687

22 Han, Z, Hendrickson, E A., Bremner, T A and Wyche, J H (1997) A sequential two-step mechanism for the production of the mature p17 p12 form of caspase-3 *in vitro* J Biol Chem **272**, 13432–13436

23 Rotonda, J., Nicholson, D W, Fazil, K M, Gallant, M, Gareau, Y, Labelle, M, Peterson, E P, Rasper, D M, Ruel, R, Vaillancourt, J P, Thornberry, N. A. and Becker, J W (1996) The three-dimensional structure of apopain/CPP32, a key mediator of apoptosis Nat Struct Biol **3**, 619–625

24 Meergans, T, Albig, W. and Doenecke, D (1998) Conserved sequence elements in human main type-H1 histone gene promoters· their role in H1 gene expression Eur. J Biochem **256**, 436–446

25 Thornberry, N A (1994) Interleukin-1 beta converting enzyme Methods Enzymol **244**, 615–631

26 Deveraux, Q L, Takahashi, R., Salvesen, G S and Reed, J C (1997) X-linked IAP is a direct inhibitor of cell-death proteases Nature (London) **388**, 300–304

27 Nicholson, D W, Ali, A, Thornberry, N A, Vaillancourt, J P, Ding, C K, Gallant, M, Gareau, Y., Griffin, P. R., Labelle, M, Lazebnik, Y. A. et al (1995) Identification and inhibition of the ICE/CED-3 protease necessary for mammalian apoptosis Nature (London) **376**, 37–43

28 Dorstyn, L, Kinoshita, M and Kumar, S (1998) Caspases in cell death Results Probl. Cell Differ **24**, 1–24

29 Tewari, M, Quan, L T, O'Rourke, K., Desnoyers, S, Zeng, Z, Beidler, D R, Poirier, G G, Salvesen, G S and Dixit, V M (1995) Yama/CPP32 beta, a mammalian homolog of CED-3, is a CrmA-inhibitable protease that cleaves the death substrate poly(ADP-ribose) polymerase. Cell **81**, 801–809

30 Deveraux, Q L, Roy, N, Stennicke, H R, Van Arsdale, T, Zhou, Q, Srinivasula, S M, Alnemri, E. S, Salvesen, G S and Reed, J C (1998) IAPs block apoptotic events induced by caspase-8 and cytochrome c by direct inhibition of distinct caspases EMBO J **17**, 2215–2223

31 Stennicke, H R, Deveraux, Q L, Humke, E W, Reed, J C, Dixit, V M and Salvesen, G S (1999) Caspase-9 can be activated without proteolytic processing J Biol Chem **274**, 8359–8362

32 Boldin, M. P., Goncharov, T M, Goltsev, Y V and Wallach, D (1996) Involvement of MACH, a novel MORT1/FADD-interacting protease, in Fas/APO-1- and TNF receptor-induced cell death Cell **85**, 803–815

33 Butt, A J, Harvey, N. L., Parasivam, G and Kumar, S (1998) Dimerization and autoprocessing of the Nedd2 (caspase-2) precursor requires both the prodomain and the carboxyl-terminal regions J Biol Chem. **273**, 6763–6768

34 Chinnaiyan, A M, O'Rourke, K, Tewari, M and Dixit, V M (1995) Fadd, a novel death domain-containing protein, interacts with the death domain of fas and initiates apoptosis Cell **81**, 505–512

35 Srinivasula, S M., Ahmad, M, Fernandes-Alnemri, T and Alnemri, E S (1998) Autoactivation of procaspase-9 by Apaf-1-mediated oligomerization Mol Cell **1**, 949–957

36 Hu, Y., Ding, L, Spencer, D M. and Nunez, G (1998) WD-40 repeat region regulates Apaf-1 self-association and procaspase-9 activation J Biol Chem **273**, 33489–33494

37 Srinivasula, S M, Ahmad, M, MacFarlane, M, Luo, Z, Huang, Z, Fernandes-Alnemri, T and Alnemri, E S (1998) Generation of constitutively active recombinant caspases-3 and -6 by rearrangement of their subunits. J Biol Chem **273**, 10107–10111

38 Colussi, P A, Harvey, N L, Shearwin-Whyatt, L M and Kumar, S (1998) Conversion of procaspase-3 to an autoactivating caspase by fusion to the caspase-2 prodomain J Biol Chem **273**, 26566–26570

39 Roy, N., Deveraux, Q L, Takahashi, R, Salvesen, G S and Reed, J C (1997) The c-IAP-1 and c-IAP-2 proteins are direct inhibitors of specific caspases EMBO J **16**, 6914–6925

Received 3 December 1999/3 April 2000; accepted 25 April 2000

Expression, purification and characterization of recombinant human choline acetyltransferase: phosphorylation of the enzyme regulates catalytic activity

Tomas DOBRANSKY*†, Wanda L. DAVIS*†, Gong-Hua XIAO*†[1] and R. Jane RYLETT*†[2]

*Department of Physiology, Medical Sciences Building, University of Western Ontario, London, Ontario, Canada, N6A 5C1, and †The John P. Robarts Research Institute, London, Ontario, Canada

Choline acetyltransferase synthesizes acetylcholine in cholinergic neurons and, in humans, may be produced in 82- and 69-kDa forms. In this study, recombinant choline acetyltransferase from baculovirus and bacterial expression systems was used to identify protein isoforms by two-dimensional SDS/PAGE and as substrate for protein kinases. Whereas hexa-histidine-tagged 82- and 69-kDa enzymes did not resolve as individual isoforms on two-dimensional gels, separation of wild-type choline acetyltransferase expressed in insect cells revealed at least nine isoforms for the 69-kDa enzyme and at least six isoforms for the 82-kDa enzyme. Non-phosphorylated wild-type choline acetyltransferase expressed in *Escherichia coli* yielded six (69 kDa) and four isoforms (82 kDa) respectively. Immunofluorescent labelling of insect cells expressing enzyme showed differential subcellular localization with the 69-kDa enzyme localized adjacent to plasma membrane and the 82-kDa enzyme being cytoplasmic at 24 h. By 64 h, the 69-kDa form was in cytoplasm and the 82-kDa form was only present in nucleus. Studies *in vitro* showed that recombinant 69-kDa enzyme was a substrate for protein kinase C (PKC), casein kinase II (CK2) and α-calcium/calmodulin-dependent protein kinase II (α-CaM kinase), but not for cAMP-dependent protein kinase (PKA); phosphorylation by PKC and CK2 enhanced enzyme activity. The 82-kDa enzyme was a substrate for PKC and CK2 but not for PKA or α-CaM kinase, with only PKC yielding increased enzyme activity. Dephosphorylation of both forms of enzyme by alkaline phosphatase decreased enzymic activity. These studies are of functional significance as they report for the first time that phosphorylation enhances choline acetyltransferase catalytic activity.

Key words: acetylcholine, cholinergic, protein isoform.

INTRODUCTION

Choline acetyltransferase (ChAT; EC 2.3.1.6) catalyses synthesis of the transmitter acetylcholine (ACh) in cholinergic neurons. While only cholinergic neurons express ChAT and use ACh to communicate neurochemical information in the nervous system, recent evidence indicates that ACh is also formed in non-neuronal cells in pro- and eukaryotes ranging from bacteria and primitive plants to epithelial and immune cells in human (for review see [1,2]). The physiological role of ACh in non-neuronal tissues is unclear, and may differ from the well-studied neurotransmitter function of ACh within peripheral and central nervous systems

ChAT is encoded by a single gene for which there are multiple transcripts expressed by differential utilization and alternative splicing of three non-coding exons [3–5]. In human, three of the four transcripts identified all translate to the same 69-kDa protein (transcripts R, N1 and N2). The fourth transcript, M, has two translation-initiation sites and yields an 82-kDa enzyme in addition to the 69-kDa form. The 82-kDa form differs from 69-kDa ChAT in terms of a 118-residue N-terminal extension [3,5]. Mechanisms regulating production of the various transcripts and their physiological roles have not been elucidated, but they could vary in stability or translational efficiency or may be differentially expressed in response to trophic factors or hormones. Similarly, it has not been determined whether 82- and 69-kDa ChAT have different physiological roles or are regulated by different cellular mechanisms. We observed recently that 82-kDa ChAT is localized to nucleus, whereas the 69-kDa enzyme is in the cytoplasm of living cells transiently expressing green-fluorescent-protein conjugates of the proteins [6].

To date, there have been three reports of post-translational modification of ChAT by protein kinases [7–9]. ChAT is a substrate for calcium-dependent protein kinases [9,10], and phosphorylation *in situ* in hippocampal nerve terminals can be modulated by altering cytosolic free calcium levels [7]. The role that phosphorylation plays in regulating ChAT function is unclear, although it has been suggested that increased phosphorylation may decrease binding of the enzyme to synaptic membranes and regulate subcellular compartmentation in the nerve terminal [8]. Functional studies in which inhibitors of serine/threonine phosphoprotein phosphatases were used to modulate phosphorylation of ChAT in nerve terminals indicate that phosphorylation may play a role in its partitioning between cytoplasm and membrane, and in regulation of ACh biosynthesis under some conditions [10]. Analysis of the primary structure of ChAT indicates that it has a number of potential phosphorylation sites that could be recognized by multiple protein kinases, including protein kinase A (cAMP-dependent protein kinase, PKA), protein kinase C (PKC), protein kinase G, α-calcium/calmodulin-dependent protein kinase II (α-CaM kinase), casein kinase II (CK2) and mitogen-activated protein kinase.

Abbreviations used: ACh, acetylcholine; CK2, casein kinase II; α-CaM kinase, α-calcium/calmodulin-dependent kinase II; ChAT, choline acetyltransferase; CTab, affinity-purified anti-ChAT antibody to C-terminal peptide; His6, hexa-histidine; NTab, affinity-purified anti-ChAT antibody to N-terminal peptide; PKA, cAMP-dependent protein kinase; PKC, protein kinase C; AEBSF, 4-(2-aminoethyl)benzenesulphonyl fluoride; TRITC, tetramethylrhodamine β-isothiocyanate

[1] Present address: Department of Pharmacology, University of Louisville, Louisville, KY, U.S.A.

[2] To whom correspondence should be addressed, at the Department of Physiology (e-mail jrylett@physiology.uwo.ca)

In the present studies, recombinant 82- and 69-kDa human ChAT were prepared in baculovirus and bacterial expression systems to facilitate comparative studies of these two forms of enzyme Affinity-purified antibodies recognizing either the C-termini of both 82- and 69-kDa ChAT or only the N-terminus of the 82-kDa enzyme were generated and used as reagents for immunoblotting, immunohistochemistry and immunoprecipitation. Insect cells expressing recombinant enzymes revealed different subcellular distribution for 82- and 69-kDa forms. Proteins were analysed by two-dimensional gel electrophoresis to reveal different isoforms present in each, and were tested as substrates for a panel of protein kinases. Importantly, we report for the first time that phosphorylation of human ChAT resulted in enhanced catalytic activity.

EXPERIMENTAL

Preparation and purification of baculovirus-expressed recombinant human ChAT

Wild-type and hexa-histidine (His6) epitope-tagged recombinant 82- and 69-kDa human ChAT were produced in High-5 insect cells using a baculovirus expression system M- and N1-ChAT cDNAs were obtained as a generous gift from Dr H. Misawa (Tokyo Metropolitan Institute for Neuroscience, Tokyo, Japan). To produce 82-kDa ChAT, the M-ChAT cDNA was used as a template for the preparation of the mutant cDNA M119A in which the second translation-initiation site (ATG, Met-119) was changed to Ala (GCG) by PCR-mediated site-directed mutagenesis; the resulting mutant cDNA encodes only the 82-kDa form of ChAT, whereas wild-type M-ChAT is translated to both 82- and 69-kDa ChAT [6]. For His6-tagged proteins, cDNA inserts were modified by PCR to contain flanking 5′ *Eco*RI sites and 3′ *Sal*I restriction-endonuclease sites to facilitate ligation into the insect expression vector pBlueBacHis (Invitrogen). The translation start codons were removed during the addition of the 5′ *Eco*RI sites to allow translation to begin at the N-terminal His6-epitope tag, and result in the production of an epitope-tagged ChAT fusion protein; the 3′ *Sal*I sites were located after the stop codon of the ChAT cDNAs For wild-type proteins (non-His6-tagged proteins) cDNA inserts encoding either 69- or 82-kDa ChAT were cut out of other vectors at 5′ *Kpn*I and 3′ *Sal*I sites and ligated into the *Kpn*I/*Xho*I sites of pBlueBac4.5. Recombinant viruses for both 82- and 69-kDa ChAT were prepared from these plasmids (4 μg) and linearized Bac-N-Blue DNA (0.5 μg; Invitrogen) in High-5 cells using the liposome transfection method (Invitrogen). Following plaque purification and confirmation of the presence of the cDNA insert from viral genomic DNA by PCR, high-titre viral stocks were prepared and stored at 4 °C for use in cell infections.

High-5 cells were grown in Grace's media supplemented with yeastolate (1.7 g/500 ml; Gibco), lactalbumin hydrolysate solution (1.7 g/500 ml; Gibco), 8 % fetal bovine serum (Hyclone) and gentamicin (50 μg/ml; Gibco). Infections with recombinant baculovirus were made in monolayers of cells at the required multiplicity of infection. At 40 h after infection, High-5 cells were washed twice with PBS, scraped into PBS, then pelleted by centrifugation at 700 g for 5 min at 4 °C. Cells were lysed by incubation for 30 min at 4 °C in 5 vols of lysis buffer [20 mM Tris/HCl, pH 8.0/150 mM NaCl/2.5 mM β-mercaptoethanol/10 % ethanol/2 mM 4-(2-aminoethyl)benzenesulphonyl fluoride (AEBSF)/2 μg/ml pepstatin/2 μg/ml leupeptin/200 μg/ml aprotinin] with 0.5 % of Triton X-100. Lysates were centrifuged at 12000 g for 15 min at 4 °C with the resulting supernatant used for further protein purification.

Purification of ChAT–His6 fusion protein

ChAT–His6 proteins were purified by a two-step purification protocol with DEAE-Sepharose chromatography (Pharmacia) followed by Talon resin metal-affinity chromatography (Clontech). Supernatants from cell lysates were diluted 1:3 with buffer A (20 mM Tris/HCl, pH 7.0/150 mM NaCl/10 % ethanol/2.5 mM β-mercaptoethanol/0.5 mM AEBSF/2 μg/ml pepstatin/2 μg/ml leupeptin/20 μg/ml aprotinin) and applied to a DEAE-Sepharose column (50 mg of protein/ml of resin) at 1 ml/min. The flow-through from this column was used for the Talon metal-affinity purification step. The affinity resin was washed twice with 10 vols of buffer B (20 mM Tris/HCl, pH 8.0/150 mM NaCl), then pre-equilibrated with active fraction eluted from DEAE-Sepharose column which had been diluted 1:1 with buffer B (20 mg of total protein in active fractions/ml of resin) for 2 h at 4 °C with gentle agitation. The suspension was loaded into a chromatography column, washed with 5 column-bed vols of buffer B and 10 column vols of buffer B containing 5 mM imidazole. ChAT was then eluted with 7 column vols of buffer B containing 50 mM imidazole.

Fractionation of wild-type ChAT on DEAE-Sepharose

Wild-type 82- and 69-kDa ChAT were partially purified by fractionation on DEAE-Sepharose with an NaCl gradient. Supernatants from lysed cells were dialysed against three changes of 20 vols of buffer C (20 mM Tris/HCl, pH 8.8/10 mM NaCl/2 mM β-mercaptoethanol/0.5 mM AEBSF/2 μg/ml pepstatin/2 μg/ml leupeptin/20 μg/ml aprotinin) at 4 °C. Dialysed samples were loaded on to a DEAE-Sepharose column that had been equilibrated with buffer C. Fractions of 10 ml each were collected during stepwise elution of the column with 50, 100, 200, 300 and 1000 mM NaCl added to buffer C.

Preparation and DEAE-Sepharose fractionation of bacterially expressed recombinant human ChAT

Recombinant 82- and 69-kDa ChAT were also produced in a bacterial expression system to obtain non-phosphorylated proteins. Consequently, cDNA inserts for both 82- and 69-kDa human ChAT were ligated into 5′ *Bam*HI and 3′ *Nco*I sites of the bacterial protein expression vector pET3d (Novagen) following addition of these restriction sites by PCR. Plasmids were expressed in and isolated from DH5α cells, then used to transform BL21(DE3) bacterial cells by electroporation. Individual colonies were used to inoculate 2-ml cultures of Luria–Bertani medium containing 100 μg/ml ampicillin and grown to an A_{600} value of 0.6. This culture was used to inoculate Luria–Bertani/ampicillin medium (100–500 ml), which was grown to an A_{600} value of 0.6 before addition of 0.4 mM isopropyl β-D-thiogalactoside to induce protein formation. After 3 h of incubation, bacterial cells were harvested by centrifugation at 5000 g for 5 min at 4 °C. Cells were resuspended in 0.25 culture vol. of cold 20 mM Tris/HCl, pH 8.0, and recentrifuged. Cell pellets were sonicated in 5 vols of buffer D (buffer C supplemented with 1 mM EDTA) on ice (3 × 30 s), then centrifuged at 5000 g for 5 min. The resulting pellets were washed twice with 3 vols of buffer D and once with 1 vol of 6 M urea (this wash contained a substantial amount of ChAT activity). Supernatants were combined and centrifuged at 15000 g for 30 min, then dialysed against three changes of 20 vols of buffer D overnight. Dialysed samples were loaded on to a DEAE-Sepharose column equilibrated with buffer D. Fractions containing different forms of ChAT were collected during stepwise elution with 50, 100, 200, 300 and 1000 mM NaCl added to buffer D.

Preparation of anti-ChAT antibodies

Polyclonal antibodies to two human ChAT peptides (GeneMed Synthesis) were prepared in rabbits. The first antibody (affinity-purified anti-ChAT antibody to C-terminal peptide, CTab) was raised against the sequence CEKATRPSQGHQP [5], located at the C-termini of both 82- and 69-kDa ChAT, and recognized both forms of enzyme. The second antibody (affinity-purified anti-ChAT antibody to N-terminal peptide; NTab) was raised to the sequence CAEAAEPRRAGPH that is present in the N-terminal extension of 82-kDa ChAT (residues 87–98), and recognizes only that form of the enzyme. Both peptide immunogens were conjugated to maleimide-activated keyhole limpet haemocyanin at the N-terminal cysteine residue of the peptide. Specific immunoglobulins were purified from both antibody preparations by affinity chromatography on NHS-Sepharose columns to which the peptides used as immunogen had been coupled (4 mg/ml of resin) according to the manufacturer's instructions (Pharmacia). Antisera (25 ml) were loaded on to affinity columns (2.5 ml) pre-equilibrated with PBS at a rate of 0.5 ml/min. Following loading, columns were washed with 10 vols of PBS containing 500 mM NaCl and 0.1 % Nonidet P-40. Immunoglobulins were eluted with 100 mM glycine/HCl, pH 2.7. A volume of 1 ml of immunoaffinity-purified antibody represents 2.5 ml of crude serum.

One- and two-dimensional PAGE

One-dimensional SDS/PAGE was performed on 12 % gels according to the method of Laemmli [11]. Two-dimensional SDS/PAGE was performed by the method of Garrels [12], with isoelectric focusing gels containing 2 % ampholines pH 3.5–10 or pH 5–7 (80 % of 5–7 and 20 % of 3.5–10; Pharmacia), and the second dimension run on 10 % separating gels. To determine the pI values of different isoelectric forms of ChAT, samples were analysed by co-migration with 12 μl ($\approx$ 7.2-μg protein content) of two-dimensional SDS/PAGE standards (Bio-Rad) composed of: soya bean trypsin inhibitor, pI 4.5; bovine muscle actin, pIs 5.0 and 5.1; BSA, pIs 5.4, 5.5 and 5.6; bovine carbonic anhydrase, pIs 5.9 and 6.0; hen egg white conalbumin, pIs 6.0, 6 3 and 6.6; and equine myoglobin, pI 7.0. In some cases for ChAT pI determinations, carbamylated protein standards were used (Pharmacia) with carbonic anhydrase, pI range 4.8–6.7, and glyceraldehyde-3-phosphate dehydrogenase, pI range 4 7–8.3. After electrophoresis, proteins were either stained with Coomassie Brilliant Blue or transferred to nitrocellulose for immunoblotting. Nitrocellulose membranes were stained after protein transfer with 0.02 % Ponceau-S in 1 % acetic acid solution to visualize transferred proteins and standards.

Western-blot analysis

Proteins from one-dimensional SDS/PAGE gels were transferred to nitrocellulose membranes in a semi-dry electroblotting apparatus using transfer buffer (48 mM Tris/39 mM glycine) containing 20 % methanol. Membranes were saturated with 8 % non-fat milk powder in PBS and probed with anti-ChAT antibodies CTab (1:2000) or NTab (1:500) for 1 h at room temperature Membranes were washed with PBS containing 0.5 % Triton X-100, then bound antibodies were detected with peroxidase-coupled secondary antibodies and ECL (Amersham).

Phosphorylation of ChAT *in vivo*

^{32}P Labelling of recombinant 82- and 69-kDa ChAT expressed in High-5 cells was performed by preincubating cells for 3 h with 0.2 mCi of $^{32}PO_4^{3-}$ in 500 μl of phosphate-free culture media (MEM, Sigma) on 35-mm culture dishes. After treatment, crude cell extracts were prepared and ChAT was fractionated on DEAE-Sepharose as described above.

Phosphorylation reactions *in vitro*

Partially purified 82- or 69-kDa recombinant ChAT from *Escherichia coli* (flow through after DEAE-Sepharose fractionation step; 10 μg of total protein) was incubated at 30 °C for 15 min with PKA (10 m-units), PKC (0.4 m-unit), CK2 (1 m-unit) or α-CaM kinase (5 m-units). Incubation reactions also included 5 μCi of [γ-^{32}P]ATP in 50 μl of phosphorylation buffer comprised of: 50 mM Tris/HCl, pH 7.0, 20 mM $MgCl_2$, 50 mM KCl, 1 mM EGTA, 1 mM dithiothreitol and 25 μM ATP for PKA; 50 mM Hepes, pH 7.4, 20 mM $MgCl_2$, 1.5 mM $CaCl_2$, 0.1 mg/ml BSA, 0.05 mg/ml phosphatidylserine, 10 μg/ml 1,2-dioleoyl-*sn*-glycerol and 10 μM ATP for PKC; 50 mM Tris/HCl, pH 7.0, 10 mM $MgCl_2$, 80 mM KCl, 1 mM dithiothreitol and 10 μM ATP for CK2; and 50 mM Tris/HCl, pH 7.2, 0.4 mM dithiothreitol, 0.5 mM $CaCl_2$, 5 mM $MgCl_2$, 1 μM calmodulin and 100 μM ATP for α-CaM kinase. Reactions were stopped by the addition of sample buffer. Following electrophoresis, proteins were transferred from gels to nitrocellulose membranes, which were first exposed to film (Kodak X-OMAT or XAR-5) to identify phosphoproteins, and then immunoblotted with CTab to co-localize phosphorylated forms of ChAT with immunoreactive ChAT isoforms

For determination of the effects of phosphorylation on ChAT enzymic activity, phosphorylation reactions were carried out for 10 min under conditions as described above. Then ChAT activity was measured immediately at 37 °C in an additional 20-min incubation.

Dephosphorylation and assay of ChAT activity

Fractions eluted from DEAE-Sepharose with 200 mM NaCl containing constitutively phosphorylated 82- and 69-kDa ChAT from High-5 cells were used to study effects of dephosphorylation on enzyme activity. Samples (about 5 μg of protein) were incubated in Tris/HCl, pH 8.0, with 2 mM AEBSF and 0.5 % Triton X-100 for times up to 30 min at 37 °C with 0.5 unit of alkaline phosphatase. Separate controls were performed at each time point. ChAT activity was measured immediately at 37 °C in an additional 20-min incubation, and samples were retained for ChAT immunoblotting to determine that enzyme protein was not lost during the experimental manipulations.

ChAT activity was measured radioenzymically by a modified method of Fonnum [13] as published previously [14].

Immunohistochemistry and confocal microscopy

High-5 cells expressing either wild-type 82-kDa (M119A mutant) or 69-kDa forms of ChAT were washed three times with PBS, then fixed with 4 % paraformaldehyde in PBS for 15 min at 4 °C. Following four washes with PBS, fixed cells were incubated for 30 min at room temperature in PBS containing 1 % BSA. Cells were incubated subsequently for 1 h with CTab (1:500) or NTab (1:200) in PBS containing 1 % BSA After washing three times for 5 min with PBS, cells were incubated for 45 min with a secondary tetramethylrhodamine β-isothiocyanate (TRITC)-

coupled AffiniPure donkey anti-rabbit IgG (Jackson Immuno-Reseach Laboratories) at a 1:50 dilution. Preparations were observed with a confocal laser scanning microscope (Zeiss LSM 510).

RESULTS

Expression of recombinant human 82- and 69-kDa ChAT in High-5 cells using a baculovirus expression system

High-titre recombinant baculoviruses containing cDNA inserts encoding 82- and 69-kDa ChAT were constructed and used to infect High-5 insect cells; both wild-type and His6-tagged proteins were produced under control of the polyhedrin promoter. Maximal ChAT protein expression and enzyme specific activity were observed in crude cell extracts at 40 h post-infection, with these measures stable up to 60 h after infection (results not shown).

Purification and analysis of 82- and 69-kDa ChAT–His6

Figure 1 illustrates protein profiles on one-dimensional SDS/PAGE for 82- and 69-kDa ChAT–His6 in cell homogenates and at each purification step. This protocol yielded enzyme that was purified essentially to homogeneity. Immunoblots shown in Figure 1(B) demonstrate the specificity of the CTab anti-ChAT antibody, particularly in the case of the crude cell lysate and after the first purification step (Figure 1, lanes 1, 2, 4 and 5). A summary of the purification of His6-tagged recombinant human ChAT is presented in Table 1; comparable purification and specific activity were obtained for both forms of the enzyme. The specific activity of 69-kDa ChAT–His6 in crude extracts of High-5 cells was 425–570-fold greater than the activity found in homogenates of human placenta [15,16].

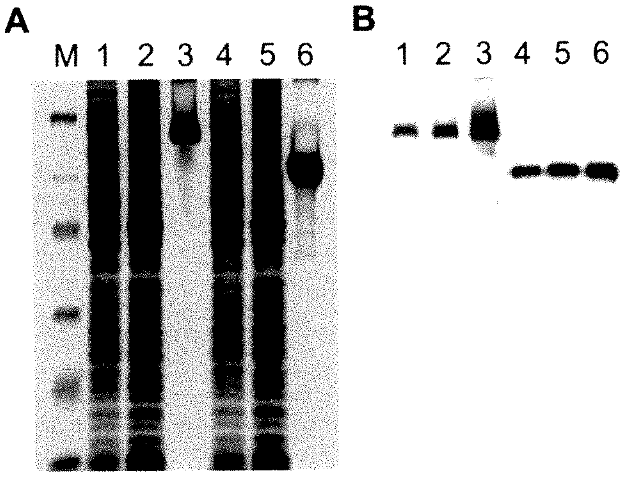

Figure 1 Purification of 82- and 69-kDa ChAT–His6

Proteins corresponding to each purification step were run on SDS/PAGE under reducing conditions. In (**A**) the gel was stained with Coomassie Brilliant Blue, and (**B**) represents the corresponding Western blot probed with CTab anti-ChAT antibody (see the Experimental section). Lane M, marker proteins (Pharmacia) from top to bottom: phosphorylase b (94 kDa), BSA (67 kDa), ovalbumin (43 kDa), carbonic anhydrase (30 kDa), trypsin inhibitor (20.1 kDa); Lanes 1–3, recombinant human 82-kDa ChAT–His6; lanes 4–6, recombinant human 69-kDa ChAT–His6; lanes 1 and 4, crude cell extract (30 μg of protein); lanes 2 and 5, fraction from DEAE-Sepharose purification step (30 μg of protein); lanes 3 and 6, Talon affinity column-purified fraction (3 μg of protein for Coomassie Brilliant Blue stain; 0.5 μg of protein for Western blot).

The DEAE-Sepharose chromatography loading buffer contained 10% ethanol. When the enzyme was purified in the absence of ethanol, a second peak of ChAT activity (17 and 20% of the total activity of 82- and 69-kDa ChAT, respectively) was eluted with 250 mM NaCl in buffer A (results not shown). This suggests that a fraction of both forms of the enzyme interacted ionically either with the column medium or with proteins retained on the column when the sample was loaded. As the column flow-through fraction was to be used for the second purification step, ethanol was included in the loading buffer to minimize ChAT bound to the column and to achieve greater recovery of enzyme in this fraction. Inclusion of ethanol in the elution buffer during ChAT purification by ion-exchange chromatography has been described previously [17].

Multiple isoforms for 82- and 69-kDa ChAT–His6 were revealed by two-dimensional SDS/PAGE

As observed with many other proteins, both 82- and 69-kDa human ChAT–His6 are comprised of multiple isoforms when the proteins were subjected to two-dimensional SDS/PAGE (Figure 2). Both forms of His6-tagged enzyme appeared as a broad smear over a pH range from 7.7 to 9.8. Also, as shown in Figure 2(A), preparations of 69-kDa ChAT–His6 contained minor protein contaminants at roughly the same apparent molecular mass that were not detected on the immunoblot with anti-ChAT antibody (Figure 2B).

DEAE-Sepharose fractionation and analysis of wild-type 82- and 69-kDa ChAT expressed in High-5 cells and in *E. coli*

Since ChAT–His6 proteins appeared as a relatively continuous smear on two-dimensional SDS/PAGE gels and immunoblots, we addressed the issue of whether the positively charged His6-epitope tag contributed to this pI distribution profile. In the first instance, recombinant viruses were prepared which encoded an enterokinase cleavage site between the N-terminal His6 tag and the ligation site for the 5′-end of the cDNA of interest. This yielded recombinant proteins from which the epitope tag could potentially be cleaved during incubation with enterokinase. In the case of both 82- and 69-kDa ChAT–His6, this was not feasible as ChAT protein was not stable during the prolonged (16-h) enterokinase cleavage step. Modification of this protocol with considerably shorter enterokinase treatment (4 h) also did not yield adequate amounts of functional ChAT (results not shown).

As an alternative strategy to obtain non-His6-tagged ChAT, we prepared high-titre recombinant baculovirus expressing wild-type 82- and 69-kDa human ChAT. Upon comparison of specific activities of wild-type and His6-tagged enzymes, it was determined that the N-terminal His6 tag significantly modified expression levels of the recombinant proteins. Specific activities of both 82- and 69-kDa ChAT–His6 were only about 50% of that measured for wild-type enzymes (Tables 1 and 2). Also by comparison, specific activity of both 82- and 69-kDa wild-type ChAT was found to be higher in crude extracts of *E. coli* expressing the enzyme compared with that measured in High-5 cell homogenates (Table 2). Specific activity of 69-kDa ChAT in crude extracts of *E. coli* was 4200–5630-fold greater than reported for human placental extracts [15,16].

Recombinant wild-type enzymes produced in High-5 cells and *E. coli* were partially purified by fractionation on DEAE-Sepharose; further purification was not carried out at this time as the enzyme preparations available allowed the questions posed to be addressed adequately. As shown in Table 2, wild-type 82-kDa ChAT produced in High-5 cells was detected

Table 1 Purification of 82- and 69-kDa ChAT–His6

His6-epitope-tagged ChAT was purified from baculovirus-infected High-5 cells expressing 82- and 69-kDa forms of the enzyme. The data are based on a starting preparation of 1.0 g (wet weight) of cells. Enzyme activity: 1 unit of enzyme catalyses the formation of 1 μmol of ACh/min at 37 °C.

Purification step	Total activity (units)	Protein (mg)	Specific activity (units/mg)	Yield (%)	Purification (-fold)
82-kDa ChAT					
Cell extract	97.3	133.2	0.7	100	1
DEAE-Sepharose	84.1	48.8	1.7	86.4	2.4
Talon column	73.7	1.6	46.1	75.7	65.9
69-kDa ChAT					
Cell extract	122.8	144.8	0.9	100	1
DEAE-Sepharose	109.7	49.4	2.2	89.3	2.4
Talon column	93.9	2.1	44.7	76.5	49.7

Table 2 Fractionation of wild-type ChAT on DEAE-Sepharose

Crude extracts of High-5 cells (1 g wet weight) expressing 82- or 69-kDa ChAT, or *E. coli* (1-g bacterial pellet) expressing 82- or 69-kDa enzyme were fractionated on a DEAE-Sepharose column using a stepwise elution with NaCl. Enzyme activity: 1 unit of enzyme catalyses the formation of 1 μmol of ACh/min at 37 °C.

Sample	Total activity (units)	Protein (mg)	Specific activity (units/mg)	Yield (%)
82-kDa ChAT (High-5 cells)				
Crude extract	78.4	52	1.5	100
DEAE-Sepharose flow-through	49.7	27.2	1.8	63.4
[NaCl]				
50 mM	–	4.1	–	–
100 mM	–	6.6	–	–
200 mM	21.6	7.2	3	27.6
300 mM	–	0.9	–	–
1 M	–	0.4	–	–
69 kDa ChAT (High-5 cells)				
Crude extract	93.8	58.2	1.6	100
DEAE-Sepharose flow-through	56.8	30.8	1.8	60.6
[NaCl]				
50 mM	12	5.2	2.3	12.8
100 mM	6.7	7.1	0.9	7.1
200 mM	13.9	11.9	1.2	14.8
300 mM	–	0.7	–	–
1 M	–	0.3	–	–
82 kDa ChAT (*E. coli*)				
Crude extract	46.3	18.6	2.5	100
DEAE-Sepharose flow-through	35.6	10.8	3.3	77
[NaCl]				
50 mM	4	4.8	0.8	8.6
100 mM	3.3	8.4	0.4	7.1
200 mM	–	9.8	–	–
300 mM	–	0.4	–	–
1 M	–	0.1	–	–
69-kDa ChAT (*E. coli*)				
Crude extract	335	21	15.9	100
DEAE-Sepharose flow-through	201	10	20.1	60
[NaCl]				
50 mM	35	2.3	15.2	10.4
100 mM	28	1.7	16.5	8.4
200 mM	58	13.2	4.4	17.3
300 mM	–	1.5	–	–
1 M	–	0.2	–	–

predominantly in the column flow-through with about 28 % of enzyme activity eluted with 200 mM NaCl. Interestingly, while this salt fraction contained substantial enzyme activity, it was represented by only a weak band on immunoblots (Figure 3A). Densitometric analysis of Western blots, in which band intensity was normalized to total protein content of crude cell extracts and fractions eluted with 200 mM NaCl, revealed that the latter represents only 4 % of total ChAT protein in crude extracts, but comprises 28 % of total enzyme activity. By comparison, a different elution profile emerged when wild-type 82-kDa ChAT expressed in *E. coli* was fractionated on DEAE-Sepharose; again, most enzyme activity was recovered in the column flow-through, with minor amounts in the low-salt fractions and no enzyme activity in the 200 mM salt fraction (Table 2). On Western blotting, immunoreactive bands at 82 kDa were observed for only the flow-through fraction and none of the salt fractions (Figure 3E). Interestingly, weak immunopositive bands with apparent molecular masses of about 47 and 30 kDa were detected in the 50 and 100 mM NaCl elution samples corresponding to a measurable amount of enzyme activity (results not shown). These bands could represent degradation products formed during fractionation; catalytically active truncated forms of rat ChAT produced by proteolytic treatment of enzyme have been described previously [18].

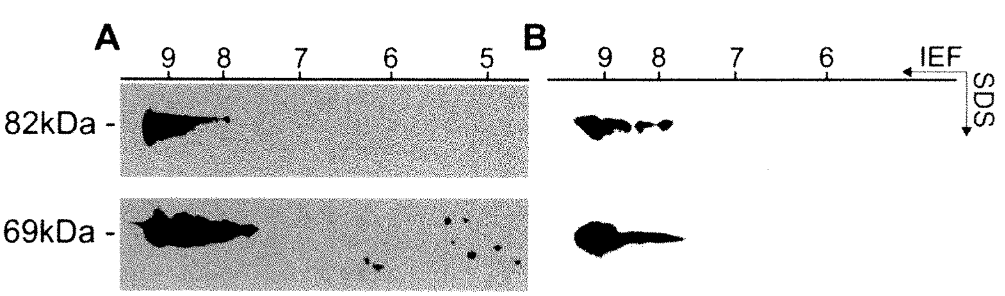

Figure 2 Two-dimensional profile of purified ChAT–His6

Recombinant 82- and 69-kDa ChAT–His6 were purified as described in the Experimental section, then analysed by two-dimensional gel electrophoresis. Proteins were separated in the first dimension (isoelectric focusing, IEF) using a pH gradient 3.5–10, then separated in the second dimension on a 10% polyacrylamide/SDS slab gel. Proteins were stained with Coomassie Brilliant Blue (**A**), or transferred to nitrocellulose membranes for Western immunoblotting (**B**). Western blots were probed with CTab anti-ChAT antibody. The upper gels show the pattern for 82-kDa ChAT–His6, and the lower gels show the pattern for 69-kDa ChAT–His6.

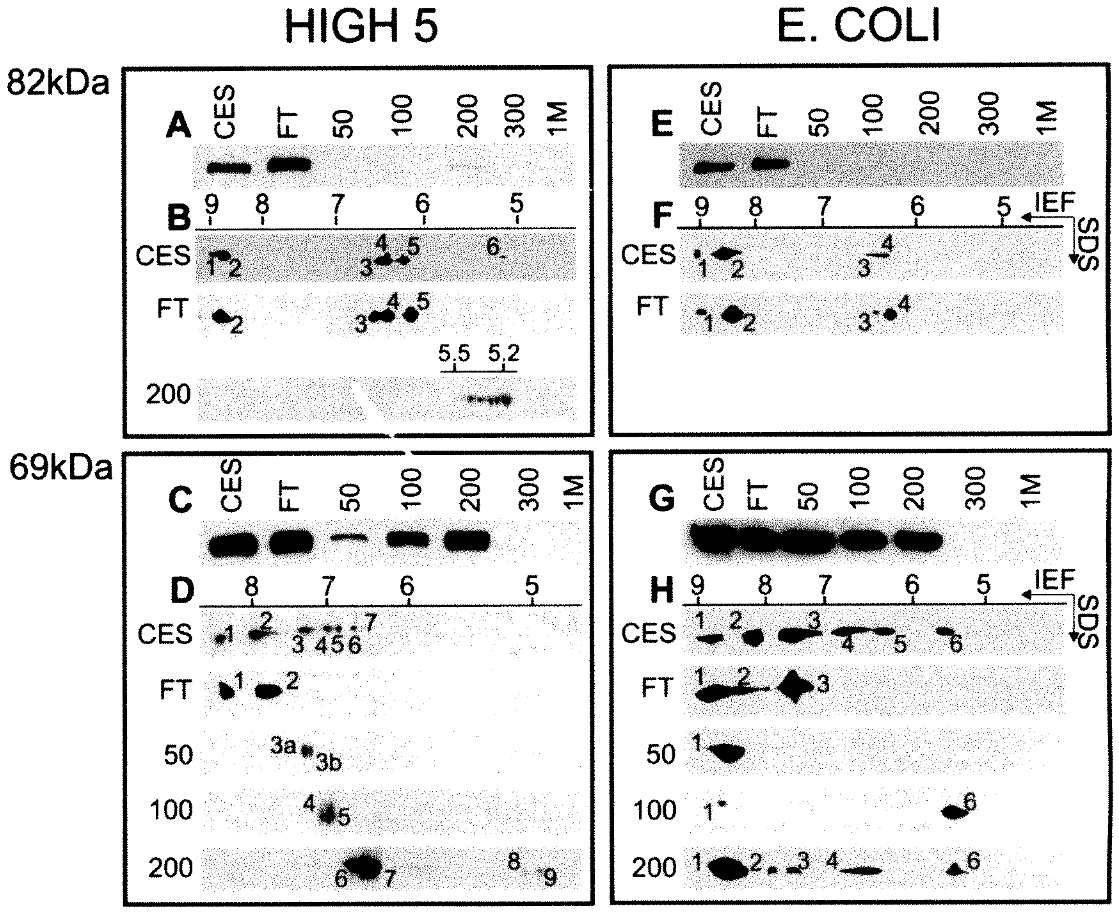

Figure 3 One- and two-dimensional profiles of wild-type 82- and 69-kDa ChAT fractionated on DEAE-Sepharose

Crude cell extracts (CES) of High-5 cells and *E. coli* expressing recombinant ChAT were fractionated on DEAE-Sepharose, as described in the Experimental section, with column flow-through (FT) and 50, 100, 200, 300 and 1000 mM NaCl elution fractions collected for analysis. Protein (50 μg) from each fraction was run on one-dimensional gels, then transferred to nitrocellulose membranes and probed with the CTab anti-ChAT antibody. (**A** and **C**) Distribution of 82- and 69-kDa ChAT proteins, respectively, in fractions from column fractionation for enzyme produced in High-5 cells. (**E** and **G**) represent distribution of 82- and 69-kDa ChAT proteins, respectively, in fractions from column fractionation for enzyme produced in bacteria. Column fractions that were determined to contain ChAT protein by immunoblot were used for further analysis of ChAT isoform profiles by two-dimensional gel electrophoresis, transferred to nitrocellulose and probed with CTab anti-ChAT antibodies. Proteins (100 μg) were separated in the first dimension using a pH gradient of 3.5–10, except in the case (**B**) where a pH 5–7 gradient was used and the sample was concentrated with 500 μg of protein loaded. (**B** and **D**) Isoform profiles present in the column fractions for 82- and 69-kDa ChAT, respectively, for enzyme produced in High-5 cells. (**F** and **H**) Isoform profiles present in the column fractions for 82- and 69-kDa ChAT, respectively, for enzyme produced in bacteria. The data are representative of at least five separate experiments.

DEAE-fractionation elution profiles for wild-type 69-kDa ChAT from both High-5 cells and *E. coli* were similar (Figures 3C and 3G), but differed substantially from that observed for the 82-kDa enzyme. ChAT activity was recovered predominantly in the column flow-through fraction, with small amounts of enzyme activity and immunoreactive protein contained in fractions eluted with up to 200 mM NaCl (Figure 3 and Table 2).

Multiple isoforms of both baculovirus- and bacterially produced wild-type human ChAT were resolved by two-dimensional SDS/PAGE, as illustrated in Figure 3, in contrast to the smears observed with His6-tagged enzymes. The 82-kDa form of ChAT produced in High-5 cells was represented by at least six isoforms detectable in the crude extract, with pI values of approx. 9.0, 8.7, 6.6, 6.5, 6.2 and 5.2 (Figure 3B). The flow-through from the DEAE-Sepharose column resolved as the first five isoforms, with isoform 6 being undetectable. The sixth isoform eluted from the column with 200 mM NaCl and, following a 5-fold concentration step, separated as seven isoforms with isoelectric points between 5.5 and 5.2 when a pH gradient of 5–7 was used in the first dimension rather than a pH gradient of 3.5–10. *E. coli*-expressed 82-kDa ChAT was represented by only four isoforms with pI values of about 9.1, 8.6, 6.5 and 6.3 (Figure 3F). It is possible that the missing isoform with a pI of 6.6 is represented with isoform 3, but their separation was not clear. Importantly, the minor acidic isoform(s) (isoform 6) found in enzyme preparations from High-5 cells were not present in bacterially produced 82-kDa ChAT; one major difference between these two protein-expression systems is that, unlike insect cells, bacterially produced proteins do not undergo post-translational modification by conventional serine/threonine/tyrosine phosphorylation.

Separation of wild-type 69-kDa ChAT produced in High-5 cells by two-dimensional gel electrophoresis yielded nine isoforms with approx. pI values of 8.3, 8.0, 7.3, 7.0, 6.8, 6.7, 6.5, 5.1 and 4.9 (Figure 3D). By comparison, *E. coli*-expressed 69-kDa ChAT was represented by six isoforms with pI values centred around pHs of about 8.9, 8.3, 7.7, 6.8, 6.3 and 5.5 (some spots were elongated; Figure 3H). Similar to the finding with 82-kDa ChAT, the most acidic isoforms of 69-kDa ChAT observed with

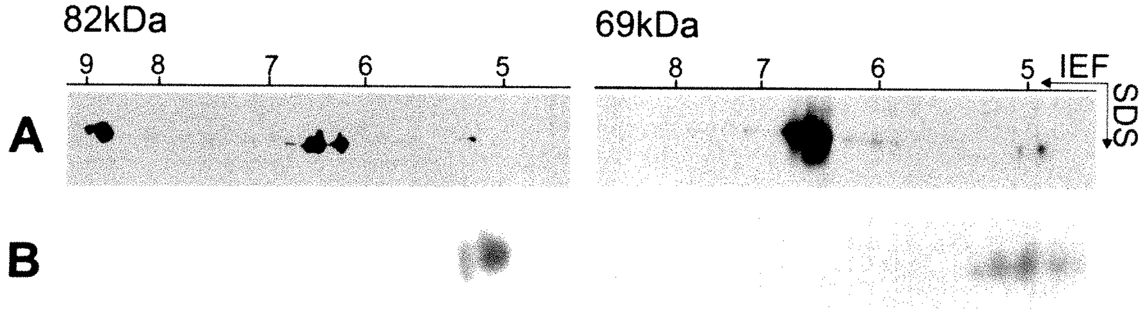

Figure 4 Phosphorylation *in vivo* of 82- and 69-kDa ChAT

High-5 cells expressing wild-type 82- and 69-kDa ChAT were pre-labelled with [^{32}P]orthophosphoric acid. Subsequently, crude lysates of cells expressing 82-kDa ChAT, and the fraction of 69-kDa ChAT eluted from DEAE-Sepharose with 200 mM NaCl, were analysed by two-dimensional PAGE. ChAT immunoblots using CTab (**A**) and autoradiographs (**B**) depicting ChAT protein distribution and ^{32}P incorporation are illustrated.

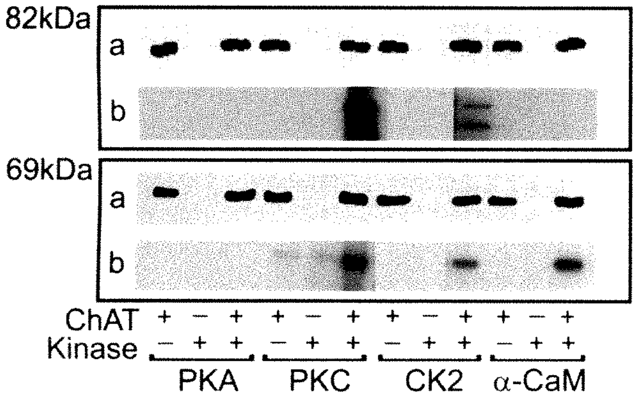

Figure 5 Phosphorylation *in vitro* of 82- and 69-kDa ChAT by multiple protein kinases

DEAE-Sepharose column flow-through fractions of wild-type 82- and 69-kDa ChAT produced in *E. coli* were incubated with PKA, PKC, CK2 or α-CaM kinase under phosphorylating conditions to test the ability of the enzymes to serve as substrates for protein kinases. Enzymes were run on one-dimensional SDS/PAGE gels, transferred to nitrocellulose membranes and analysed by autoradiography (−80 °C for 24–96 h) for incorporation of ^{32}P (**b**), then immunoblotted with CTab anti-ChAT antibody to allow co-localization with ChAT proteins (**a**). The data shown are representative of at least five separate experiments.

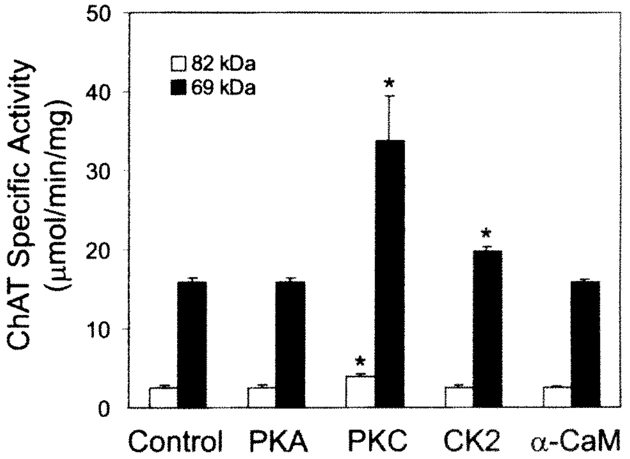

Figure 6 Phosphorylation by some kinases stimulates ChAT activity

Bacterially expressed 82- (white bars) and 69- (black bars) kDa ChAT were incubated under phosphorylating conditions with four different protein kinases, followed by measurement of ChAT enzymic activity. Statistically significant increases in catalytic activity of 82-kDa ChAT were observed following incubation with PKC, and of 69-kDa ChAT after incubation with PKC and CK2. While 82-kDa ChAT was also phosphorylated by CK2 and 69-kDa ChAT by α-CaM kinase, neither of these treatments led to enhanced ChAT activity. Data are means ± S.E.M. for $n = 5$ separate experiments. $^{*}P < 0.01$ by Student's *t* test.

enzyme produced in High-5 cells (isoforms 8 and 9) did not appear in preparations of the bacterially expressed protein.

Importantly, phosphorylation experiments *in vivo* in High-5 cells expressing wild-type 82- and 69-kDa ChAT revealed that the most acidic isoforms of the enzyme incorporated [^{32}P]phosphate (Figure 4).

Phosphorylation of ChAT by multiple protein kinases

Four protein kinases were tested for their ability to phosphorylate bacterially produced ChAT *in vitro*; DEAE-column flow-through fractions were used in these studies. Figure 5 illustrates on one-dimensional gels that 82-kDa ChAT served as a substrate for PKC and CK2, whereas 69-kDa ChAT was phosphorylated by PKC, CK2 and α-CaM kinase. Neither form of enzyme appeared to be a substrate for PKA under the experimental conditions tested.

Activity of human ChAT is enhanced by phosphorylation *in vitro*

In the present study, we began to address the functional role of phosphorylation of ChAT by protein kinases by determining whether phosphorylation altered enzyme catalytic activity. As illustrated in Figure 6, incubation of both 82- and 69-kDa ChAT produced in *E. coli* with PKC resulted in significantly increased enzyme activity by 57 ± 9 and 112 ± 17 %, respectively (means ± S.E.M.). CK2 did not alter activity of 82-kDa ChAT, but caused a small statistically significant stimulation of activity of the 69-kDa enzyme (20 ± 3 %). Interestingly, even though α-CaM kinase phosphorylated 69-kDa ChAT, activity of the enzyme was not altered relative to the control. PKA did not phosphorylate either form of the enzyme, nor was the acetylating activity of ChAT different from controls following incubation with the kinase.

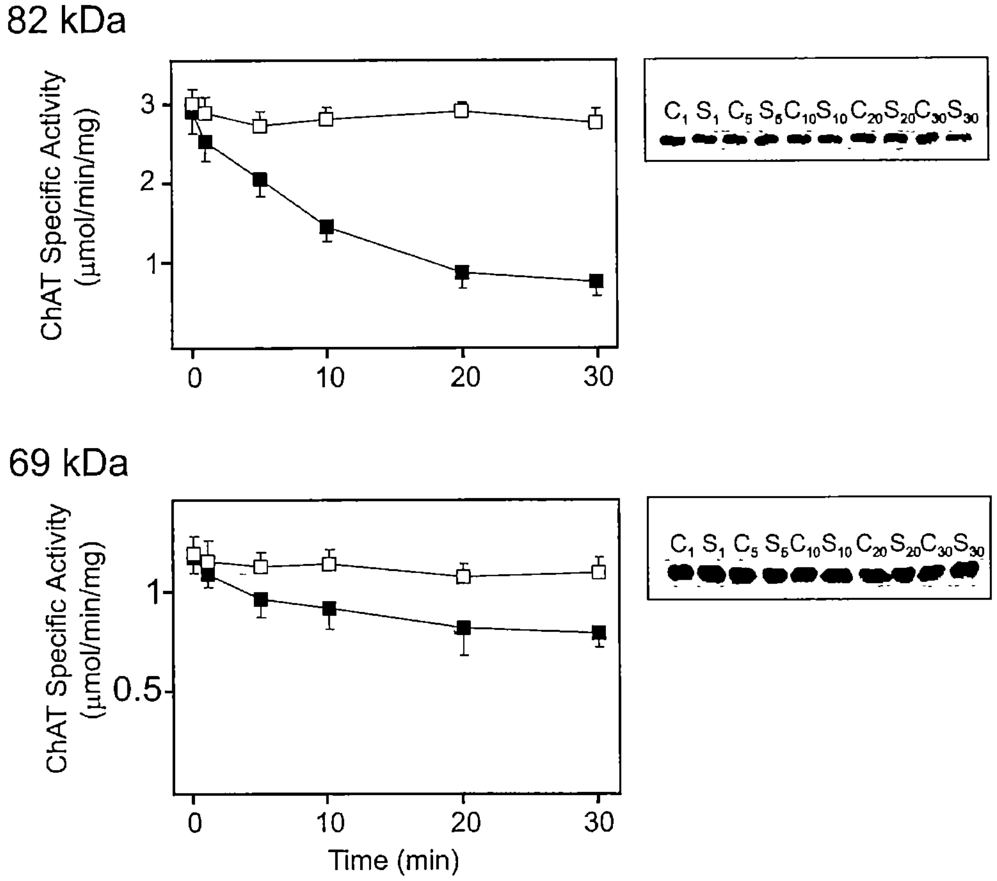

Figure 7 Dephosphorylation of ChAT decreases enzymic activity

Constitutively phosphorylated 82- and 69-kDa ChAT expressed in High-5 cells were used in these studies Aliquots of each enzyme eluted from DEAE-Sepharose with 200 mM NaCl (50 μg of protein per sample) were treated with alkaline phosphatase (0 5 units) for 1, 5, 10, 20 and 30 min at 30 °C. ChAT activity was measured in control samples (□) for comparison with those treated with alkaline phosphatase (■) Results are means±S E M for three separate experiments Western immunoblots with CTab anti-ChAT antibody of control (C) and alkaline phosphatase-treated (S) samples were performed on samples at the times indicated (subscript numbers) to determine whether dephosphorylation resulted in loss of enzyme protein

In other studies, we asked whether constitutive phosphorylation of ChAT was involved in regulating enzyme catalytic activity. Experimentally, both 82- and 69-kDa wild-type ChAT produced in High-5 cells were incubated for various times with alkaline phosphatase, then enzyme activity was measured As illustrated in Figure 7, enzymic dephosphorylation of both forms of ChAT resulted in decreased specific activity. Immunoblots, with densitometric analysis (results not shown), demonstrated that this was not the result of loss of enzyme protein during incubation with alkaline phosphatase

Subcellular localization of 82- and 69-kDa ChAT in insect cells by immunohistochemistry and confocal microscopy

Using an immunohistochemical approach, 82- and 69-kDa ChAT assume differential subcellular localizations when expressed in baculovirus-infected High-5 cells, as was noted previously in mammalian cells [6] However, in contrast to mammalian cells, at 24 h after infection 82-kDa ChAT was present in cytoplasm and concentrated in a distinct ring around the nucleus of High-5 cells, and 69-kDa ChAT was localized to plasma membrane, often at points of contact of adjacent cells, as illustrated in Figure 8(A). By 64 h after infection, ChAT proteins underwent redistribution within the High-5 cells to assume a distribution similar to that seen in mammalian cells expressing cDNAs for 82- and 69-kDa ChAT (Figure 8B). At this point, 69-kDa ChAT appeared in cytoplasm (Figure 8B, panel a) with 82-kDa ChAT localized to nucleus (Figure 8B, panel b). Use of the NTab anti-ChAT antibody produced staining in cells expressing 82-kDa ChAT, but no staining of cells producing 69-kDa ChAT (results not shown)

Polyclonal anti-ChAT antibody production

NTab anti-ChAT antibody revealed high specificity for 82-kDa ChAT and did not recognize 69-kDa ChAT (Figure 9A). When CTab antibody was used, both 82- and 69-kDa ChAT was recognized (Figure 9B). His6-tagged enzymes were detected on one-dimensional SDS/PAGE gels at slightly higher apparent molecular masses than were wild-type ChAT proteins by both CTab and NTab anti-ChAT antibodies (Figure 9). Both antibodies were capable of immunoprecipitating ChAT from crude extracts of bacteria and insect cells expressing the enzymes (results not shown).

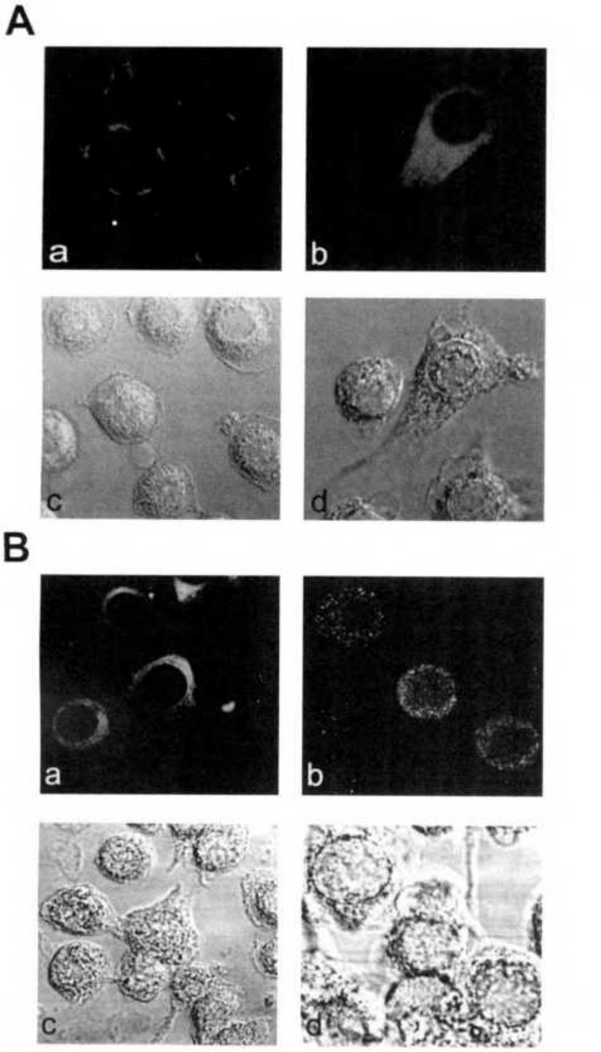

Figure 8 Immunofluorescence labelling of High-5 cells with CTab anti-ChAT antibody detected with TRITC-conjugated secondary antibody

Cells were infected with recombinant baculovirus encoding 69-kDa ChAT (**a**, **c**) or 82-kDa ChAT (**b**, **d**) at 24 h (**A**) or 64 h (**B**) prior to fixation and staining of cells. (**a**, **b**) Immunofluorescence images; (**c**, **d**) corresponding differential interference contrast images.

DISCUSSION

We describe production and purification of recombinant human 82- and 69-kDa ChAT in baculovirus and bacterial expression systems, and characterization and phosphorylation of these two forms of the enzyme. New information includes: (i) both 82- and 69-kDa ChAT are comprised of multiple isoforms which differ and can be separated by two-dimensional SDS/PAGE, (ii) both forms of enzyme serve as substrates for multiple protein kinases, (iii) phosphorylation of 69-kDa ChAT by PKC and CK2, but not α-CaM kinase, and of 82-kDa ChAT by PKC, but not CK2, led to increased catalytic activity, whereas neither form of enzyme was phosphorylated by PKA, (iv) 82- and 69-kDa ChAT were distributed differentially in cells following their synthesis with subcellular compartmentation changing over time, and (v) polyclonal antibodies generated to peptides corresponding to a portion of the N-terminus of 82-kDa ChAT and C-termini of both 82- and 69-kDa ChAT proved useful for immunoblotting, immunoprecipitation and immunohistochemistry.

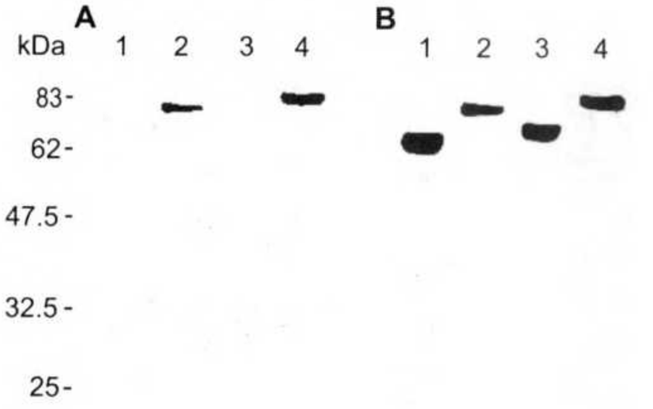

Figure 9 ChAT antibody specificity determination

Crude extracts of cellular proteins from High-5 cells expressing 82- and 69-kDa ChAT or ChAT–His6 were separated using one-dimensional SDS/PAGE. Proteins were transferred to nitrocellulose membranes and Western immunoblots were performed with (**A**) NTab anti-ChAT antibody, 1:500, then blots were stripped and reprobed with (**B**) CTab anti-ChAT antibody, 1:2000. Lanes 1, 69-kDa ChAT; lanes 2, 82-kDa ChAT; lanes 3, 69-kDa ChAT–His6; and lanes 4, 82-kDa ChAT–His6.

Recombinant ChAT proteins were produced efficiently in both High-5 cells and *E. coli*. In general, higher activities for both forms of ChAT were achieved in bacteria, with the yield of 69-kDa ChAT being greatest. Interestingly, inclusion of positively charged His6-epitope tags on the recombinant proteins decreased their yield, and also interfered with separation of protein isoforms by two-dimensional gel electrophoresis. While the epitope tag facilitated protein purification, partially purified wild-type ChAT was used in most studies to overcome problems with alteration of the charge on the proteins, and thus allow accurate determination of isoform pI values.

Using preparative isoelectric focusing to separate samples enriched in ChAT, it was reported previously that the enzyme was comprised of multiple isoforms [19–22]. However, distribution of ChAT in the resulting subfractions was determined by measuring enzymic activity rather than by documenting and comparing ChAT protein electrophoretic isoform patterns by immunoblotting, as ChAT antibodies were not generally available at that time. Measurement of ChAT activity would not distinguish and identify individual enzyme isoforms, but rather would give a relative distribution of enzyme according to fractionation condition. The present study comprises the first report of characterization of ChAT isoform patterns by two-dimensional gel electrophoresis. These data serve as an important baseline for identification and comparison of mechanisms, such as phosphorylation, which regulate the presence and/or abundance of individual enzyme isoforms.

Phosphorylation of cellular proteins by kinases is a common and important regulatory mechanism in intracellular signal transmission. Changes in the phosphorylation state of enzymes, for example, may control their biological function by altering catalytic activity and substrate specificity, or by stabilizing functional enzyme complexes. In the present study, we demonstrated that 82- and 69-kDa ChAT serve differentially as substrates for serine/threonine kinases that have significant roles in neuronal function, and in some cases, but not others, phosphorylation leads to enhanced catalytic activity for the enzymes. Whereas ChAT has consensus motifs for PKA, it was not phosphorylated by this protein kinase in the present or a previous study [8]. Whereas phosphorylation of 69-kDa ChAT by PKC has been reported [8], this is the first demonstration that 82- and 69-kDa ChAT are substrates for PKC and CK2, and that 69-kDa but not 82-kDa ChAT is phosphorylated by α-CaM kinase In the nervous system, PKC modulates neuronal plasticity and learning processes [23], with reduced levels of PKC and/or alterations in activities and distribution of isoenzymes correlating with degeneration of selective neurons during aging and Alzheimer's disease [24–26]. CK2 is also present in brain, and its activity appears to be altered in Alzheimer's disease [27] α-CaM kinase is involved in Tau protein phosphorylation and formation of paired-helical filaments in Alzheimer's disease [28].

As these kinases recognize different phosphorylation consensus motifs, it is likely that multiple residues on ChAT can be phosphorylated. This has been demonstrated for other neurotransmitter-synthesizing enzymes, such as tyrosine hydroxylase, with regulation of phosphorylation events governed by a variety of biological processes (reviewed in [29]). It is important now to identify which amino acid residues in ChAT are phosphorylated, how phosphorylation is regulated by physiological events such as neuronal activity and endogenous factors including growth and trophic factors, and whether this is modified by pathology.

The functional significance of phosphorylation of ChAT has not been determined. It is clear from the present study that phosphorylation of the enzyme by some kinases, particularly PKC, leads to enhanced catalytic activity This is the first investigation in which this parameter has been measured directly. In a previous study, using an indirect approach we determined that experimental conditions which decreased cytosolic free calcium levels in rat hippocampal nerve terminals and correlated with decreased phosphorylation of ChAT did not alter total synaptosomal ChAT activity [7]. The physiological consequence of enhanced catalytic activity for ChAT is unknown, but probably would result in increased ACh synthesis and the potential for increased neurotransmission.

Subcellular compartmentation of proteins can also be regulated by protein phosphorylation; alterations in charge on the protein brought about by addition or removal of phosphate groups could influence its ability to bind to subcellular membranes or organelles [8]. Phosphorylation can also regulate translocation of proteins bearing nuclear localization signals between cytoplasm and nucleus [30,31]. We reported recently that 69-kDa ChAT was distributed in cytoplasm of mammalian cells, whereas 82-kDa ChAT was localized to nucleus [6]. This observation was confirmed and extended in the present study where we observed a temporal shift in subcellular localization of the two forms of enzyme in High-5 cells. Regulatory events, including phosphorylation, which play a role in directing subcellular localization of ChAT, remain to be determined.

In summary, observations made in the present studies, including development of protein-isoform patterns for both 82- and 69-kDa ChAT and that human ChAT serves differentially as a substrate for multiple protein kinases, provide a basis for future functional investigations Elucidation of aspects of cellular regulation of cholinergic neurotransmission awaits identification and mutagenesis of specific residues that serve as sites for phosphorylation of ChAT. Furthermore, extension of studies at the protein level to pathology of the nervous system, such as Alzheimer's disease, may reveal important clues for modification of neurochemical transmission.

This work was supported by a grant from the Medical Research Council of Canada to R J R We are grateful for the gifts of human M- and N1-ChAT cDNAs from Dr Hideml Misawa (Tokyo Metropolitan Institute for Neuroscience, Tokyo, Japan), CK2 from Dr David Litchfield (Department of Biochemistry, University of Western Ontario, London, Ontario, Canada), and α-CaM kinase from Dr Howard Schulman (Department of Neurobiology, Stanford University, Stanford, CA, U S A). We thank Dr Ivan Lefkovits (Basel Institute for Immunology, Basel, Switzerland) for critical reading of the manuscript.

REFERENCES

1 Wessler, I, Kirkpartrick, C J and Racke, K (1998) Non-neuronal acetylcholine, a locally acting molecule, widely distributed in biological systems expression and function in humans Pharmacol Ther **77**, 59–79

2 Wessler, I, Kirkpatrick, C J and Racke, K (1999) The cholinergic 'pitfall' acetylcholine, a universal cell molecule in biological systems, including humans Clin Exp Pharmacol Physiol **26**, 198–205

3 Oda, Y, Nakanishi, I and Deguchi, T (1992) A complementary DNA for human choline acetyltransferase induces two forms of enzyme with different molecular weights in cultured cells Mol Brain Res **16**, 287–294

4 Misawa, H, Ishi, K and Deguchi, T (1992) Gene expression of mouse choline acetyltransferase Alternative splicing and identification of a highly active promoter region J Biol Chem **267**, 20392–20399

5 Misawa, H, Matsuura, J, Oda, Y, Takahashi, R and Deguchi, T (1997) Human choline acetyltransferase mRNAs with different 5′-region produce a 69-kDa major translation product Mol. Brain Res **44**, 323–333

6 Resendes, M C, Dobransky, T, Ferguson, S S G and Rylett, R J (1999) Nuclear localization of the 82-kDa form of human choline acetyltransferase J Biol Chem **274**, 19417–19421

7 Schmidt, B M and Rylett, R J (1993) Phosphorylation of rat brain choline acetyltransferase and its relationship to enzyme activity J. Neurochem **61**, 1774–1781

8 Bruce, G and Hersh, L B (1989) The phosphorylation of choline acetyltransferase Neurochem Res **14**, 613–620

9 Habert, E, Birman, S and Mallet, J (1992) High-level synthesis and fate of acetylcholine in baculovirus-infected cells characterization and purification of recombinant rat choline acetyltransferase J Neurochem **58**, 1447–1453

10 Cooke, L J and Rylett, R J (1996) Inhibitors of serine/threonine phosphatases increase membrane-bound choline acetyltransferase activity and enhance acetylcholine synthesis Brain Res **751**, 232–238

11 Laemmli, U K (1970) Cleavage of structural proteins during the assembly of the bacteriophage T4. Nature (London) **227**, 680–685

12 Garrels, J I (1979) Two-dimensional gel electrophoresis and computer analysis of proteins synthesized by clonal cell lines J Biol Chem **245**, 7961–7977

13 Fonnum, F (1969) Radiochemical microassays for the determination of choline acetyltransferase and acetylcholinesterase activities Biochem J **115**, 465–479

14 Rylett, R J., Goddard, S and Lambros, A (1993) Regulation of expression of cholinergic neuronal phenotypic markers in neuroblastoma LA-N-2 J Neurochem **61**, 1388–1397

15 Bruce, G, Wainer, B H and Hersh, L B (1985) Immunoaffinity purification of human choline acetyltransferase comparison of the brain and placental enzyme J Neurochem **45**, 611–620

16 Poethke, R, Hartig, W, Bruckner, G, Felgenhauer, K. and Mader, M (1997) Characterization of monoclonal and polyclonal antibodies to human choline acetyltransferase and epitope analysis Biol Chem **378**, 997–1004

17 Cozzari, C and Hartman, B K (1983) Choline acetyltransferase Purification procedure and factors affecting chromatographic properties and enzyme stability J Biol Chem **258**, 10013–10019

18 Wu, D, Ahmed, S N, Lian, W and Hersh, L B (1995) Activation of rat choline acetyltransferase by limited proteolysis J Biol Chem **270**, 19395–19401

19 White, H L and Wu, J C (1973) Separation of apparent multiple forms of human brain choline acetyltransferase by isoelectric focusing J Neurochem **21**, 939–947

20 Fonnum, F and Malthe-Sorenssen, D (1973) Membrane affinities and subcellular distribution of the different molecular forms of choline acetyltransferase from rat J Neurochem **20**, 1351–1359

21 Malthe-Sorenssen, D (1976) Molecular properties of choline acetyltransferase from different species investigated by isoelectric focusing and ion exchange adsorption J Neurochem. **26**, 861–865

22 Atterwill, C K and Prince, A K (1978) Multiple forms of choline acetyltransferase and the high affinity uptake of choline in brain of developing and adult rats J Neurochem **31**, 719–725

23 Akers, R F and Routtenberg, A (1985) Protein kinase C phosphorylates a 47 M_r protein (F1) directly related to synaptic plasticity Brain Res **334**, 147–151

24 Cole, G, Dobkins, K R, Hansen, L A, Terry, R D and Saitoh, T (1988) Decreased levels of protein kinase C in Alzheimer brain Brain Res **452**, 165–174

25 Erratum (1991) Brain Res. **558**, 177

26 Clark, E. A., Leach, K. L., Trojanowski, J. Q. and Lee, M. Y. (1991) Characterization and differential distribution of the three major human protein kinase C isozymes (PKC alpha, PKC beta, and PKC gamma) of the central nervous system in normal and Alzheimer's disease brains. Lab. Invest. **64**, 35–44

27 Blanquet, P. R. (1998) Neurotrophin-induced activation of casein kinase 2 in rat hippocampal slices. Neuroscience **86**, 739–749

28 Xiao, J., Perry, G., Troncoso, J. and Monteiro, M. J. (1996) α-Calcium-calmodulin-dependent kinase II is associated with paired helical filaments of Alzheimer's disease. J. Neuropath. Exp. Neurol. **55**, 954–963

29 Kumer, S. C. and Vrana, K. E. (1996) Intricate regulation of tyrosine hydroxylase activity and gene expression. J. Neurochem. **67**, 443–462

30 Jans, D. A. and Hubner, S. (1996) Regulation of protein transport to the nucleus: central role of phosphorylation. Physiol. Rev. **76**, 651–685

31 Hood, J. K. and Silver, P. A. (1999) In or out? Regulating nuclear transport. Curr. Opin. Cell Biol. **11**, 241–247

Received 19 November 1999/4 April 2000; accepted 27 April 2000

Biochem J (2000) 349, 153–158 (Printed in Great Britain) **153**

Identification and characterization of a novel cytochrome c_3 from *Shewanella frigidimarina* that is involved in Fe(III) respiration

Euan H. J. GORDON*[1], Andrew D. PIKE†, Anne E. HILL*, Pauline M. CUTHBERTSON*, Stephen K. CHAPMAN†
and Graeme A. REID*[2]

*Institute of Cell and Molecular Biology, University of Edinburgh, Mayfield Road, Edinburgh EH9 3JR, U K, and †Department of Chemistry, University of Edinburgh, West Mains Road, Edinburgh EH9 3JJ, Scotland, U K

Shewanella frigidimarina NCIMB400 is a non-fermenting, facultative anaerobe from the gamma group of proteobacteria. When grown anaerobically this organism produces a wide variety of periplasmic *c*-type cytochromes, mostly of unknown function. We have purified a small, acidic, low-potential tetrahaem cytochrome with similarities to the cytochromes c_3 from sulphate-reducing bacteria. The N-terminal sequence was used to design PCR primers and the *cctA* gene encoding cytochrome c_3 was isolated and sequenced. The EPR spectrum of purified cytochrome c_3 indicates that all four haem irons are ligated by two histidine residues, a conclusion supported by the presence of eight histidine residues in the polypeptide sequence, each of which is conserved in a related cytochrome c_3 and in the cytochrome domains of flavocytochromes c_3. All four haems exhibit low-midpoint redox potentials that range from −207 to −58 mV at pH 7; these values are not significantly influenced by pH changes. *Shewanella* cytochrome c_3 consists of a mere 86 amino acid residues with a predicted molecular mass of 11780 Da, including the four attached haem groups. This corresponds closely to the value of 11778 Da estimated by electrospray MS. To examine the function of this novel cytochrome c_3 we constructed a null mutant by gene disruption. *S. frigidimarina* lacking cytochrome c_3 grows well aerobically and its growth rate under anaerobiosis with a variety of electron acceptors is indistinguishable from that of the wild-type parent strain, except that respiration with Fe(III) as sole acceptor is severely, although not completely, impaired.

Key words: electron transfer, iron respiration, redox potentials.

INTRODUCTION

Shewanella spp. are widespread Gram-negative bacteria that have been isolated from many different habitats. This adaptability is supported by a flexible metabolic capability, particularly in the choice of respiratory electron acceptors [1,2]. Of particular note is the unusual capacity of *Shewanella* to use insoluble Fe(III) and Mn(IV) compounds as terminal oxidants, which raises important questions about how electrons are transferred to the extracellular medium. The presence of cytochromes in the outer membrane in these bacteria might provide a channel for electron transfer from the periplasm [3]. *Shewanella frigidimarina* NCIMB400 is a facultative aerobe that under anaerobic conditions produces at least nine different cytochromes in the periplasm [4]. One of these is a 64 kDa soluble flavocytochrome c_3 that functions as a respiratory fumarate reductase [5–7]. Spectroscopic analysis has shown that all four haem groups in the cytochrome domain of flavocytochrome c_3 are bis-histidine ligated and titrate at very low redox potentials [8,9]. The gene encoding this enzyme has been isolated and sequenced; its crystal structure has been determined at 1.8 Å (1Å = 0.1 nm) resolution [5,10,11]. In contrast, the structures and functions of other periplasmic components of the anaerobic respiratory chain are poorly understood.

Cytochromes *c* are common components of electron transfer pathways and, particularly in bacterial systems, are remarkably diverse in their molecular properties. Ambler [12] has classified these proteins according to sequence and structural relationships, with multihaem *c*-type cytochromes being grouped together as class III. The best characterized of these proteins are the cytochromes c_3 from obligately anaerobic, sulphate-reducing bacteria [13,14]. These are generally small, low-potential, tetrahaem proteins found in the periplasm that act as electron acceptors from hydrogenase. Related proteins with 8 and 16 haems have been found in addition to the tetrahaem cytochrome c_3 in *Desulfovibrio vulgaris*; these seem, on the basis of their amino acid sequences, to be composed of tandem tetrahaem domains [15,16]. Here we describe the purification of a low-potential, tetrahaem *c*-type cytochrome from *S. frigidimarina* and its characterization by spectroscopy, electrochemistry and sequence analysis. We have designated this protein as a cytochrome c_3 because it shares several properties with the *Desulfovibrio* proteins but the sequences are not closely related.

MATERIALS AND METHODS

Bacterial strains, growth conditions and plasmids

Escherichia coli JM109 was used for general recombinant DNA procedures and DH5α for manipulations involving the shuttle vector pJQ200KS. Growth of *S. frigidimarina* NCIMB400 was as described by Pealing et al. [5] except that Luria–Bertani broth or agar was used. When required, ampicillin was added to the medium to a final concentration of 100 μg/ml.

Purification of cytochrome c_3

S. frigidimarina NCIMB400 was grown at 23 °C without aeration in Luria–Bertani medium supplemented with 5 g/l NaCl and

---

[1] Present address Department of Biochemistry, University of Oxford, South Parks Road, Oxford, OX1 3QU, U K

[2] To whom correspondence should be addressed (e-mail graeme reid@ed ac uk).

The nucleotide sequence data reported will appear in DDBJ, EMBL and GenBank Nucleotide Sequence Databases under the accession number AJ000006

20 mM fumarate. Cells were harvested at 4 °C; all subsequent purification steps were also performed at this temperature. Harvested cells (100 g wet weight) were resuspended in 100 mM sodium phosphate buffer, pH 7.0, and lysed by sonication. The lysate was centrifuged at 39000 *g* for 1 h and the supernatant was loaded on a DE-52 anion-exchange column (5 cm × 10 cm) that had been equilibrated with 100 mM sodium phosphate, pH 7.0. Cytochrome c_3 formed a tight band at the top of the column and was eluted with 100 mM phosphate buffer containing 200–250 mM NaCl Protein fractions were pooled and concentrated before loading on a Sephadex G-50 column (2 cm × 150 cm) in 20 mM sodium phosphate buffer, pH 7.0. Further purification was achieved with a hydroxyapatite column (2.5 cm × 10 cm) with a gradient of 20–100 mM phosphate. The ratio of the Soret band at 407 nm over protein absorbance at 279 nm was used to monitor purity. Typical values of 12:1 were found. N-terminal sequencing was performed as described previously [17].

EPR spectroscopy

All measurements were made at 10 K with a Bruker ER 200D spectrometer with an Oxford Instruments cryostat and helium transfer system. Samples contained 0.2 mM protein in 100 mM sodium phosphate buffer, pH 7.0.

Redox potentials

Haem midpoint potentials were determined by protein-film voltammetry as described by Turner et al. [9]. Cytochrome c_3 was coated on a pyrolytic graphite-edge electrode, with polymyxin B as a co-adsorbate. Electrochemical studies were performed at 25 °C with a mixed buffer system of Taps, Hepes, Mes and Pipes, each at 50 mM, with 0.1 M NaCl as the supporting electrolyte. The buffers were titrated to the required pH with NaOH or HCl at 25 °C.

DNA techniques

Recombinant DNA techniques, Southern hybridization and genomic DNA library construction were performed as described by Sambrook et al. [18]. Dideoxy sequencing reactions [19] were performed with the Sequenase version 2.0 kit (USB). PCR was performed with *Tbr* thermostable polymerase (NBL Gene Sciences). Reactions typically consisted of 100 ng of *Shewanella* genomic DNA, 200 μM dNTPs and 1.5 mM $MgCl_2$ with the supplied reaction buffer; 20 ng of each oligonucleotide primer was present in each 50 μl reaction. Typically, two rounds of PCR were performed, with a 5 μl aliquot of the first-round reaction used as template in the second round. Cycles used were: 95 °C for 2 min; then 35 cycles of 95 °C for 20 s, 45 °C for 20 s and 72 °C for 10 s; and a final incubation at 72 °C for 5 min. To radiolabel DNA fragments for Southern hybridization experiments, [α-^{32}P]dCTP was included in the PCR reaction in place of unlabelled dCTP, and plasmid DNA containing cloned cytochrome c_3 PCR product was used as a template. DNA sequences were determined by the dideoxy chain termination method.

Degenerate primers

Primer sequences were designed on the basis of the N-terminal sequence of purified cytochrome c_3. The upstream primer (C31, 5′-CACGAATTCGARTTYCAYGTNGARATG-3′) contained an *Eco*RI recognition site and the codons for the sequence EFHVEM (single-letter amino acid codes). The downstream primer (C32, 5′-GCGAAGCTTYTTNARNGGYTCNCC-3′) contained a *Hin*dIII recognition site and a sequence complementary to the codons for the amino acid sequence GEPSK.

Gene knock-out

The *cctA* gene encoding cytochrome c_3 was subcloned into pK18 within a 1.7 kb fragment and disrupted by inserting the spectinomycin/streptomycin resistance cassette, isolated as a *Hin*dIII fragment from pHRP310 [20] between the *Bsa*I and *Bst*XI sites, which flank the coding sequence, by blunt-end cloning. The disrupted *cctA* sequence was transferred from the resulting plasmid, pEG801, as a 3.4 kb *Sac*I–*Pst*I fragment to the suicide vector pJQ200KS [21] to give the recombinant plasmid pEG720 This was then transferred to *S. frigidimarina* NCIMB400 by conjugation as described by Gordon et al. [7] and disruptants were selected on the basis of their resistance to streptomycin and sucrose.

Growth in liquid culture used Luria broth supplemented with 15 mM formate and 50 mM Fe(III) citrate. Bottles were filled with this medium, leaving a minimal volume of gas, before being sealed and incubated at 23 °C. Cells were prepared for ferrozine assays by growth in the same medium but lacking Fe(III). Approximately 0.5 g wet weight of cells were washed in 50 mM Hepes, pH 7.0, and resuspended in the same buffer. The rate of Fe(III) reduction was measured in 2 ml Suba-sealed cuvettes containing 350 μM ferrozine and 500 μM formate in 50 mM Hepes, pH 7.0, and with 30–100 μl aliquots of cell suspensions. After 5 min of preincubation, reactions were initiated by the addition of Fe(III) citrate to 100 μM. The appearance of the Fe(II) ferrozine complex was monitored by measurements in triplicate of A_{562}.

RESULTS

Protein purification and characterization

When separating proteins from the periplasm of *S. frigidimarina* we observed an intense red band that bound very tightly to anion-exchange resins. This protein was purified from whole cell extracts by chromatography on anion-exchange and hydroxyapatite columns with a typical yield of 25 mg from 100 g cell wet weight. The isolated protein ran as a single band on SDS/PAGE and retained the haem group, despite the presence of SDS, indicating that the protein was a *c*-type cytochrome. The apparent molecular mass on SDS/PAGE was 15 kDa, but electrospray MS

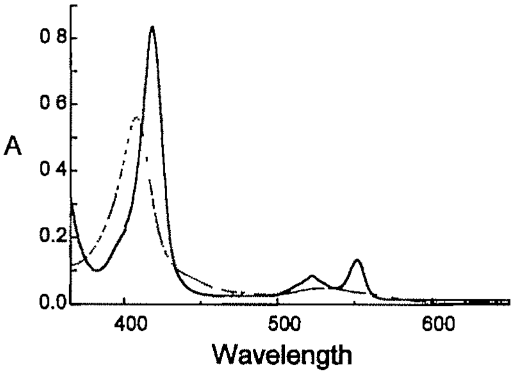

Figure 1 Absorbance spectra of *S. frigidimarina* cytochrome c_3

The protein (20 μg/ml in 10 mM Tris/HCl, pH 8.4) was reduced by the addition of dithionite (solid line) or oxidized by the addition of ferricyanide (dashed line), the absorbance was scanned at room temperature with a Shimadzu 1601 spectrophotometer

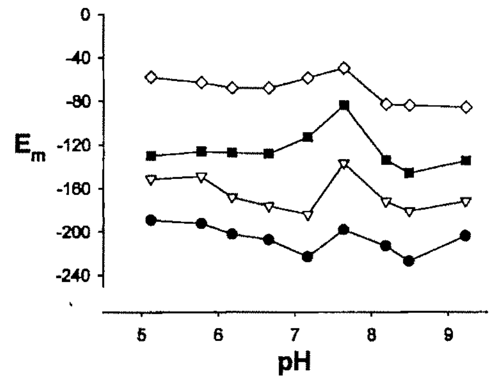

Figure 2 Midpoint potential values of cytochrome c_3 from *S. frigidimarina* NCIMB400 at 25 °C

Potentials were resolved for each of the four haems in experiments performed at several pH values The error in each of the values given is approx ±15 mV

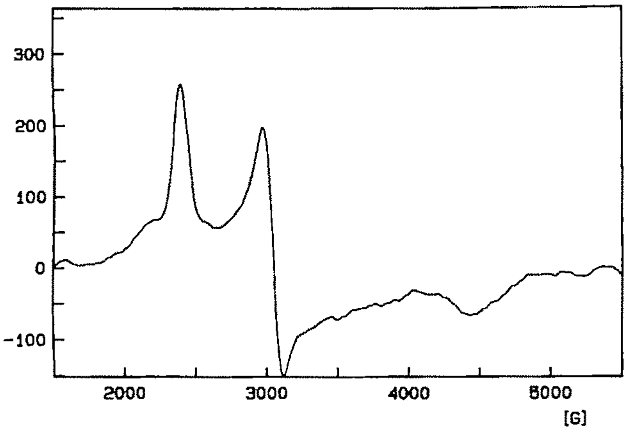

Figure 3 X-band EPR spectrum of oxidized *S. frigidimarina* cytochrome c_3, showing a single set of g values comprising $g_z = 2.83$, $g_y = 2.22$ and $g_x = 1.53$

These values are similar to those from bis-histidine-ligated haem groups in other cytochromes c_3

indicated a molecular mass of 11780 Da, in close agreement with the value expected from the sequence as described below. We presume that the protein migrates anomalously in polyacrylamide gels because the conformation is constrained by the haem groups.

The purified protein exhibited typical absorbance spectra in the reduced and oxidized forms (Figure 1). Redox potentiometry of cytochrome c_3 by conventional methods showed that the haem groups titrated at low potential but individual haem potentials could not easily be resolved. Therefore purified cytochrome c_3 was subjected to protein-film voltammetry, permitting the resolution of each of the four haem midpoint potentials (Figure 2). The potentials were low, titrating in the range from −250 to 0 mV, with no significant dependence on pH. This method had also been used successfully with flavocytochrome c_3 from the same organism and the four haem groups of this protein titrated at similar potentials to those of cytochrome c_3 (−238, −196, −146 and −102 mV at pH 7.0) [9].

The EPR spectrum of oxidized cytochrome c_3 (Figure 3) indicates a single set of g values with $g_z = 2.83$, $g_y = 2.22$ and $g_x = 1.53$. This behaviour is typical of bis-histidine-ligated haem groups.

The N-terminal amino acid sequence of purified cytochrome c_3 was determined for 26 cycles as ADETLAEFHVEMGG-EN-HADGEPSK. Cycles 15 and 18 were apparently blank, i.e. no amino acid residue was detected. This would be expected if the residues at these positions were cysteines involved in the covalent attachment of one of the haem groups.

Isolation of the gene encoding cytochrome c_3

The N-terminal amino acid sequence of the purified cytochrome c_3 was used to design degenerate oligonucleotide primers for PCR amplification of the coding sequence from *S. frigidimarina* genomic DNA. Restriction enzyme cleavage sites were included in each primer to facilitate the cloning of the resulting products. Two rounds of PCR were used to amplify the fragment of DNA encoding the N-terminus of the protein. A single product of the expected size (72 bp) was observed in the reactions. This band was excised from a 2% (w/v) agarose gel and purified with a Qiaex gel extraction kit. After digestion with *Eco*RI and *Hin*dIII, the DNA was repurified, again with Qiaex. The resulting DNA was then ligated into the vector pTZ19r [22], which had been cut with the same enzymes. Putative recombinant colonies [white on plates containing 5-bromo-4-chloroindol-3-yl β-D-galactopyranoside ('X-Gal') and isopropyl β-D-thiogalactoside ('IPTG')] were isolated and the plasmid inserts were sequenced. Plasmid DNA from one of the positive clones was then used as a template to synthesize an [α-^{32}P]dCTP-labelled probe, which was then used to probe a Southern blot of *S. frigidimarina* DNA digested with various restriction enzymes. A positive hybridization signal was seen for 4 kb *Nsi*I-digested fragments. Bands of this size range were purified from a similar gel and cloned into *Pst*I-cut pTZ18r to form a library. From 800 screened colonies, two positive clones were isolated. The DNA sequence of the insert in one of the positive recombinant plasmids, pEG700, was then determined (Figure 4).

Sequence analysis

The coding sequence of the *cctA* gene is 272 bp, including a putative signal sequence of 25 residues. Three consecutive ATG codons were found preceding the sequence encoding the N-terminus of purified cytochrome c_3. However, the predicted sequence from any of these as the initiation codon did not fit the pattern for N-terminal secretory signal sequences that are characteristic of periplasmic proteins. It seems most likely that translation was initiated at a GTG codon (Figure 4), predicting a typical signal sequence of 25 residues with a basic N-terminus and a long hydrophobic segment [23]. A putative ribosome-binding site (in capitals in Figure 4) was located just 9 bp away from this GTG codon, consistent with this being the site of translation initiation.

Examination of the DNA sequence immediately downstream of the translational stop codon revealed a region with similarity to bacterial rho-independent transcriptional terminators, implying that the *cctA* gene was not co-transcribed with any other coding sequence. Indeed, Northern blot hybridization analysis of total RNA extracted from *S. frigidimarina* cells suggested that the *cctA* mRNA was in the range of 400–600 bp in length (results not shown).

Sequencing downstream of the *cctA* gene revealed a coding sequence in the same orientation as *cctA* that encoded a putative protein product with extensive similarity to nitrate and formate reductases, both of which contain a molybdenum cofactor. This reading frame was particularly closely related to the assimilatory

```
  1 tattgtcagttaatttgagattgtttataaatctttgataaacggtttataaacaaagtt

 61 gttgaataacccttaagcaaagtgtcgtgttgcagtgtgatgatccgcgtcagataaaag

                                      M  S  N  K  L  L  S  A  L
121 aatgcggacacacactaaattGGAGGaatgaatagtgagcaataaactactaagtgcatt

     F  A  A  G  F  A  V  N  M  M  S  S  A  S  F  A  A  D  E  T
181 gtttgcggctggtttcgcggtaatgatgatgtcttctgcatcatttgctgctgatgagac

     L  A  E  F  H  V  E  M  G  G  C  E  N  C  H  A  D  G  E  P
241 cctcgcagagtttcacgttgaaatgggtggctgtgaaaactgtcacgctgatggtgaacc

     S  K  D  G  A  Y  E  F  E  Q  C  Q  S  C  H  G  S  L  A  E
301 atcaaaagatggcgcttatgaatttgaacaatgtcaaagttgtcatggttcactagctga

     M  D  D  N  H  K  P  H  D  G  L  L  M  C  A  D  C  H  A  P
361 aatggatgataaccataagccacatgatgggttacttatgtgtgctgattgtcatgcgcc

     H  E  A  K  V  G  E  K  P  T  C  D  T  C  H  D  D  G  R  T
421 acatgaagcaaaagtaggcgaaaagccaacatgtgatacatgccacgatgatggccgtac

     A  K  *
481 tgcaaaataagttatcttagatagcttgaaaataccgacataatgtcggtatttttgttt

541 ttattcctcaagagtatacatctcacttttatttttatacctctttataggtatttaaag
```

Figure 4 DNA sequence of the *cctA* gene from *S. putrefaciens*

The inferred protein sequence is shown above the DNA sequence Underlined amino acids indicate those determined by N-terminal sequencing of purified cytochrome c_3 A putative ribosome-binding site is shown in capitals, DNA sequences similar to a rho-independent terminator are overlined.

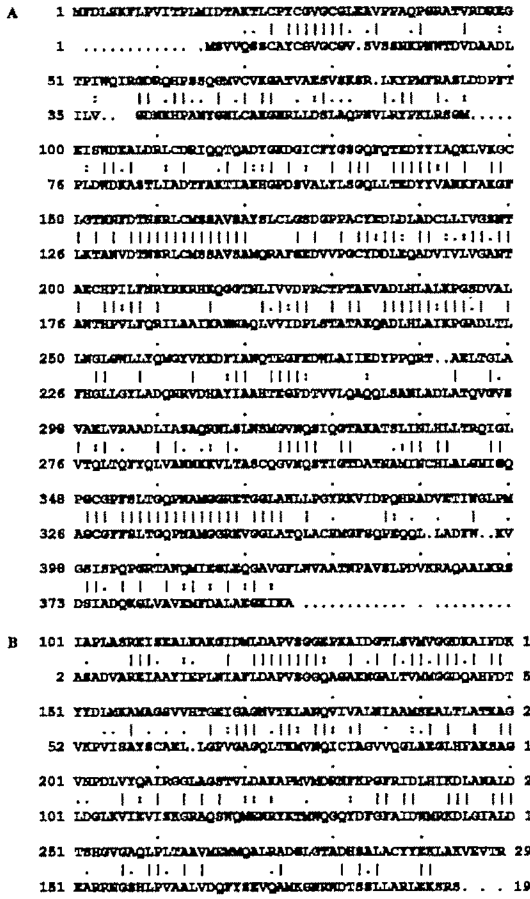

Figure 5 Alignments of the polypeptide sequences predicted by the reading frames flanking the cctA sequence with close relatives

(A) The reading frame downstream of *cctA* (bottom row of each pair) aligned with the sequence of nitrate reductase from *Synechococcus* sp (top row of each pair, Swissprot entry NARB-SYNP7 [31]) (B) The reading frame upstream of *cctA* (bottom row) aligned with the sequence of 3-hydroxyisobutyrate dehydrogenase from *Escherichia coli* (top row of each pair, Swissprot entry YHAE-ECOLI [32]) The alignments were produced with ClustalW

nitrate reductases (41 % identity with a cyanobacterial sequence) (Figure 5A), which are cytoplasmic enzymes involved in the utilization of nitrate as a nitrogen source. The nitrate reductase initiation codon was 285 base pairs downstream from the cytochrome c_3 gene termination codon. Upstream of *cctA* was a further reading frame in the same orientation as the *cctA* gene. This showed extensive similarity to 3-hydroxyisobutyrate dehydrogenases (31 % identical with the *E. coli* sequence) (Figure 5B) which, in bacteria, are cytoplasmic, NAD^+-dependent enzymes required for valine catabolism. There was a gap of 395 bp between this reading frame and the cytochrome c_3 coding sequence. These sequences are not shown here but are included in the EMBL database entry. The observation that the cytochrome c_3 gene was flanked by coding sequences clearly unrelated to anaerobic respiration indicates that *cctA* is likely to be transcribed as a monocistronic RNA

Predicted sequence of cytochrome c_3

The mature cytochrome c_3 consists of only 86 amino acid residues with a predicted molecular mass of 9316 Da excluding the haem groups. The attachment of four haems would result in a molecular mass of 11780 Da; this was the value obtained by MS of the purified protein. Cytochrome c_3 is an extremely acidic protein with a net charge of −14 (10 Asp, 10 Glu, 5 Lys and 1 Arg). In the fully oxidized state the holoprotein has a net charge of −10. The eight Cys and eight His residues are presumably all involved in haem attachment and ligation.

The cytochrome c_3 amino acid sequence was compared with sequences in the available databases. The only clear similarity was seen to other proteins from *Shewanella* or closely related organisms: the cytochrome domains of the two *S. frigidimarina* flavocytochromes c_3 [4,24], the related flavocytochrome c_3 from *S. oneidensis* MR-1 [25] and cytochromes c_3 from *S. oneidensis* MR-1 [26] and the organism H1R [27]. These sequences are aligned in Figure 6 and show a considerable degree of similarity. The relationship with cytochromes c_3 from *Desulfovibrio* species is much more distant and no significant similarity is observed outside the haem attachment sites (CXXCH) conserved in all *c*-type cytochromes.

Gene disruption

No clues to the function of cytochrome c_3 were obtained from its location in the genome (it is not encoded within an operon); we therefore constructed a null mutant to examine the phenotypic consequences of the lack of this protein. This was achieved by replacing the cytochrome c_3 coding sequence of *S. frigidimarina* NCIMB400 with a streptomycin/spectinomycin resistance cassette by homologous recombination. The presence of the expected gene disruption was verified by Southern blot hybridization; the ability of the resultant strain, AH301, to utilize a range of electron acceptors for anaerobic respiration was determined by following growth on plates and in liquid culture. The ability of AH301 to utilize nitrate, nitrite, trimethylamine *N*-oxide, DMSO, fumarate, tetrathionite and sulphite were indistinguishable from that of the parent strain, indicating that

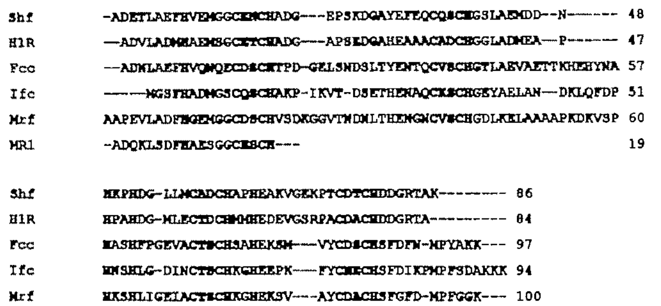

Figure 6 Alignment of amino acid sequences of cytochrome c_3 from *S. frigidimarina* (Shf) with the corresponding protein from the phototroph H1R (H1R), partial sequences of flavocytochrome c_3 and its iron-induced isoenzyme from *S. frigidimarina* (Fcc and Ifc respectively) and the flavocytochrome c_3 from *S. oneidensis* MR-1 (Mrf) corresponding to the tetrahaem cytochrome *c* domain and with the N-terminal sequence of cytochrome c_3 from *S. oneidensis* MR-1 (MR1)

The haem attachment sites (CXXCH) and the histidine ligands to the haem irons are shown in bold

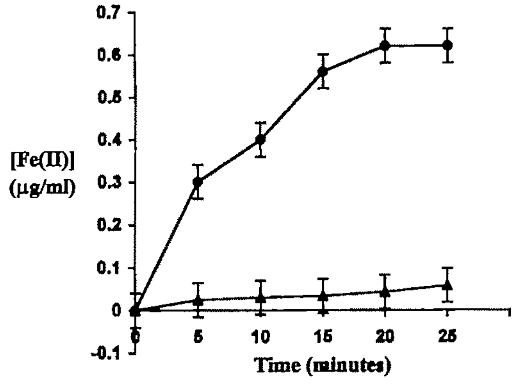

Figure 7 Reduction of Fe(III) by *S. frigidimarina* NCIMB400 and AH301(Δc_3)

Cells grown anaerobically were washed in 50 mM Hepes, pH 7.0, and resuspended in the same buffer. Equivalent aliquots from NCIMB400 (●) and AH301 (▲) were mixed anaerobically with 50 mM Hepes containing 500 μM formate and 100 μM Fe(III) citrate. The increase in A_{562} was followed and used to calculate the Fe(II) concentration. Measurements were performed in triplicate.

cytochrome c_3 is not required for electron transfer to these oxidants. In contrast, growth with Fe(III) citrate was clearly impaired. After an anaerobic incubation for 2 weeks at 23 °C in medium containing 15 mM formate and 50 mM iron (III) citrate, the parent strain, NCIMB400, grew well and completely reduced the iron to Fe(II), whereas the mutant AH301 substantially failed to dissimilate the iron, as judged by the colour of the medium. Growth of the mutant was greatly impaired, with the maximal attenuance being less than 35 % of that achieved by the wild-type parent strain. This level of growth might not have required Fe(III) reduction because a small amount of yeast extract was added; growth was extremely slow if this was omitted. To measure Fe(III) reduction more directly, we grew cultures anaerobically in the absence of Fe(III); the ability of whole cells to reduce Fe(III) was then determined spectrophotometrically with a ferrozine assay to detect Fe(II) production (Figure 7). Ferrozine forms a complex with Fe(II), with a strong absorbance maximum at 562 nm. These assays clearly showed that deletion of the cytochrome c_3 gene severely impairs the ability of *S. frigidimarina* to reduce Fe(III), although a low level of Fe(II) production remained in AH301.

DISCUSSION

During anaerobic growth, *S. frigidimarina* synthesizes several cytochromes that are absent when O_2 is available. One of these is a small acidic cytochrome that we have shown to contain four haem groups on the basis of absorption coefficients and the presence of four typical *c*-type haem attachment sites (CXXCH) in the predicted amino acid sequence. This protein shares several properties, including midpoint reduction potentials and bis-histidine ligation, with the cytochromes c_3 from sulphate reducers. We have therefore classified the *S. frigidimarina* protein also as a cytochrome c_3.

The sequence of the *cctA* gene encoding cytochrome c_3 failed to provide further clues to the function of this protein. Many respiratory proteins in bacteria are encoded in operons and are co-expressed with functionally related proteins. The cytochrome c_3 from *S. frigidimarina* NCIMB400 is produced from a small monocistronic RNA and the *cctA* gene is flanked by sequences encoding cytoplasmic enzymes with functions unrelated to anaerobic electron transfer.

The low reduction potential of this protein and its production only during anaerobiosis indicate that it is most probably involved in one or more pathways of anaerobic respiration. To address its possible function we constructed a cytochrome c_3 null mutant and showed that it has a greatly impaired ability to reduce Fe(III) to Fe(II), indicating that cytochrome c_3 is involved in the electron transfer to this respiratory oxidant. Other components of this pathway remain to be characterized, although an outer-membrane decahaem cytochrome *c* has been identified in the related freshwater *Shewanella*, *S. oneidensis* MR-1, as a component of an operon that is required for Fe(III) respiration [28], as has the inner-membrane tetrahaem cytochrome, CymA [29]. It is possible that cytochrome c_3 shuttles electrons across the periplasm between these two proteins.

A small cytochrome c_3 has also been isolated from *S. oneidensis* MR-1 (previously *S. putrefaciens* [30]). The spectroscopic and redox properties of this protein are similar to those of the cytochrome c_3 from *S. frigidimarina* NCIMB400 but the N-terminal sequences [26] show considerable divergence (Figure 6). These sequence differences could reflect different functions for these two proteins or might simply be indicative of a rather distant relationship between the two *Shewanella* strains, perhaps reflected in their different habitats. Furthermore, the genetic context of the cytochrome c_3-coding sequence in the two *Shewanella* species is quite different. In *S. frigidimarina* it is flanked by genes apparently encoding 3-hydroxyisobutyrate dehydrogenase and an assimilatory nitrate reductase, whereas in MR-1 the flanking genes encode homologues of HtpX heat-shock protease and a hydrogenase cytochrome *b* subunit. The MR-1 DNA sequence is available at www.tigr.org and this organism seems to encode only one genuine homologue of the cytochrome c_3 from *S. frigidimarina*.

The close relationship between cytochrome c_3 and the cytochrome domain of flavocytochrome c_3 from the same organism, *S. frigidimarina* NCIMB400, indicates a relatively recent duplication of this sequence. No organisms other than *Shewanella* spp. have been shown to contain a flavocytochrome c_3 type of fumarate reductase and it is probable that this protein arose by the fusion of an *FrdA* sequence (encoding the flavoprotein subunit of a typical membrane-bound bacterial fumarate reductase) with a cytochrome c_3-coding sequence. The physical and spectroscopic properties of cytochrome c_3 and the cytochrome domain of flavocytochrome c_3 are very similar but their functions are quite different. We have shown previously by gene disruption that flavocytochrome c_3 is clearly required for fumarate reduction but not for other electron transfer pathways [7]. The small cytochrome c_3 is, in contrast, involved in electron transfer to Fe(III).

We thank Andy Cronshaw (Welmet Protein Characterisation Facility, University of Edinburgh) and Phil Jackson for help with the N-terminal sequencing, Fraser Armstrong for help with the protein-film voltammetry, John Ingledew for help and guidance with the EPR spectroscopy, and Richard Ambler for advice and information This work was funded by the Biotechnology and Biological Sciences Research Council.

REFERENCES

1 Myers, C R and Nealson, K H (1988) Bacterial manganese reduction and growth with manganese oxide as a sole electron acceptor Science **240**, 1319–1321
2 Nealson, K H and Saffarini, D A (1994) Iron and manganese in anaerobic respiration. environmental significance, physiology, and regulation Annu Rev Microbiol **48**, 311–343
3 Myers, C R and Myers, J M (1992)·Localization of cytochromes to the outer-membrane of anaerobically grown *Shewanella putrefaciens* MR-1. J. Bacteriol **174**, 3429–3438
4 Morris, C J, Gibson, D. M and Ward, F B (1990) Influence of respiratory substrate on the cytochrome content of *Shewanella putrefaciens* FEMS Microbiol Lett **69**, 259–262
5 Pealing, S L, Black, A C, Manson, F. D. C, Ward, F B, Chapman, S. K and Reid, G A (1992) Sequence of the gene encoding flavocytochrome *c* from *Shewanella putrefaciens* a tetraheme flavoenzyme that is a fumarate reductase related to the membrane-bound enzymes from other bacteria Biochemistry **31**, 12132–12140
6 Morris, C J, Black, A C, Pealing, S. L, Manson, F D C, Chapman, S. K., Reid, G A, Gibson, D M and Ward, F B (1994) Purification and properties of a novel cytochrome – flavocytochrome *c* from *Shewanella putrefaciens* Biochem J **302**, 587–593
7 Gordon, E H J, Pealing, S L, Chapman, S K, Ward, F B and Reid, G A (1998) Physiological function and regulation of flavocytochrome c_3, the soluble fumarate reductase from *Shewanella putrefaciens* NCIMB400 Microbiology **144**, 937–945
8 Pealing, S L, Cheesman, M R, Reid, G A, Thomson, A J, Ward, F B and Chapman, S. K (1995) Spectroscopic and kinetic-studies of the tetraheme flavocytochrome-*c* from *Shewanella putrefaciens* NCIMB400 Biochemistry **34**, 6153–6161
9 Turner, K L, Doherty, M K, Heering, H A, Armstrong, F A, Reid, G A and Chapman, S K (1999) Redox properties of flavocytochrome c_3 from *Shewanella frigidimarina* NCIMB400 Biochemistry **38**, 3302–3309
10 Pealing, S L, Lysek, D A, Taylor, P, Alexeev, D, Reid, G A, Chapman, S. K and Walkinshaw, M D (1999) Crystallization and preliminary X-ray analysis of flavocytochrome c_3, the fumarate reductase from *Shewanella frigidimarina* J Struct Biol **127**, 76–78
11 Taylor, P, Pealing, S L, Reid, G A, Chapman, S K and Walkinshaw, M D (1999) Structural and mechanistic mapping of a unique fumarate reductase Nat Struct Biol **6**, 1108–1112
12 Ambler, R P. (1982) Structure and classification of cytochromes *c*. in From Cyclotrons to Cytochromes (Kaplan, N O. and Robinson, A B., eds), pp 263–280, Academic Press, New York
13 Higuchi, Y, Kusunoki, M., Yasuoka, N, Kakudo, M and Yagi, T (1981) On cytochrome c_3 folding J Biochem (Tokyo) **90**, 1715–1723
14 Meyer, T E (1995) Evolution and classification of *c*-type cytochromes In Cytochrome *c* a Multidisciplinary Approach (Scott, R. A. and Mauk, A G, eds), pp 33–99, University Science Books, Sausalito, CA
15 Loutfi, M, Guerlesquin, F., Bianco, P, Haladjian, J and Bruschi, M (1989) Comparative studies of polyhemic cytochromes *c* isolated from *Desulfovibrio vulgaris* (Hildenborough) and *Desulfovibrio vulgaris* (Norway) Biochem Biophys Res Commun **159**, 670–676
16 Pollock, W B R, Loutfi, M, Bruschi, M, Rapp-Giles, B. J, Wall, J D. and Voordouw, G (1991) Cloning, sequencing and expression of the gene encoding the high molecular weight cytochrome *c* from *Desulfovibrio vulgaris* Hildenborough. J Bacteriol **173**, 220–228
17 Hayes, J D, Kerr, L A and Cronshaw, A D (1989) Evidence that glutathione S-transferase B1B1 and S-transferase B2B2 are the products of separate genes and that their expression in human liver is subject to inter-individual variation molecular relationships between the B1 subunits and other α-class glutathione S-transferase Biochem J **264**, 437–445
18 Sambrook, J, Fritsch, E F and Maniatis, T (1989) Molecular Cloning A Laboratory Manual, 2nd edn, Cold Spring Harbor Laboratory, Cold Spring Harbor, NY
19 Sanger, F, Nicklen, S and Coulson, A R (1977) DNA sequencing with chain terminating inhibitors Proc Natl. Acad Sci U S A. **74**, 5463–5467
20 Parales, R E and Harwood, C S (1993) Construction and use of a new broad-host-range *lacZ* transcriptional fusion vector, pHRP309, for Gram^- bacteria Gene **133**, 23–30
21 Quandt, J. and Hynes, M F (1993) Versatile suicide vectors which allow direct selection for gene replacement in Gram negative bacteria Gene **127**, 15–21
22 Mead, D A, Szczesna-Skorpa, E and Kemper, B (1986) Single-stranded DNA 'blue' T7 promoter plasmids A versatile promoter system for cloning and protein engineering. Protein Eng **1**, 67–74
23 Nielsen, H, Engelbrecht, J, Brunak, S and von Heijne, G (1997) Identification of prokaryotic and eukaryotic signal peptides and prediction of their cleavage sites Protein Eng **10**, 1–6
24 Dobbin, P. S., Butt, J N, Powell, A. K, Reid, G. A and Richardson, D J (1999) Characterisation of a flavocytochrome that is induced during the anaerobic respiration of Fe(III) by *Shewanella frigidimarina* NCIMB400. Biochem J **342**, 439–448
25 Leys, D, Tsapin, A S, Nealson, K H, Meyer, T. E, Cusanovich, M A and van Beeumen, J J (1999) Structure and mechanism of the flavocytochrome *c* fumarate reductase of *Shewanella putrefaciens* MR-1 Nat Struct Biol **6**, 1113–1117
26 Tsapin, A I, Nealson, K H, Meyer, T, Cusanovich, M A, van Beeumen, J, Crosby, L D, Feinberg, B. A and Zhang, C (1997) Purification and properties of a low-redox-potential tetraheme cytochrome c3 from *Shewanella Putrefaciens* J Bacteriol. **178**, 6386–6388
27 Ambler, R P (1991) Sequence variability in bacterial cytochromes *c* Biochim Biophys Acta **1058**, 42–47
28 Beliaev, A. S and Saffarini, D A (1998) *Shewanella putrefaciens* MtrB encodes an outer membrane protein required for Fe(III) and Mn(IV) reduction J Bacteriol **180**, 6292–6297
29 Myers, C R and Myers, J M (1997) Cloning and sequence of *CymA*, a gene encoding a tetraheme cytochrome *c* required for reduction of iron(III), fumarate, and nitrate by *Shewanella putrefaciens* MR-1 J Bacteriol **179**, 1143–1152
30 Venkateswaran, K, Moser, D P, Dollhopf, M E, Lies, D P, Saffarini, D A, MacGregor, B J, Ringelberg, D B, White, D. C, Nishijima, M, Sano, H et al (1999) Polyphasic taxonomy of the genus *Shewanella* and description of *Shewanella oneidensis* sp nov Int J Syst Bacteriol **49**, 705–724
31 Omata, T, Andriesse, X and Hirano, A (1993) Identification and characterization of a gene cluster involved in nitrate transport in the cyanobacterium *Synechococcus* SP-PCC7942. Mol Gen Genet. **236**, 193–202
32 Komine, Y and Inokuchi, H (1991) Precise mapping of the *RnpB* gene encoding the RNA component of Rnase P In *Escherichia coli* K-12 J Bacteriol **173**, 1813–1816

Received 24 January 2000/20 March 2000, accepted 10 April 2000

Identification of three human type-II classic cadherins and frequent heterophilic interactions between different subclasses of type-II classic cadherins

Yutaka SHIMOYAMA*[1], Gozoh TSUJIMOTO†, Masaki KITAJIMA‡ and Michiya NATORI*

*Departments of Surgery and Clinical Research, National Okura Hospital, 2-10-1 Okura, Setagaya-ku, Tokyo 157-8535, Japan, †Department of Molecular Cell Pharmacology, National Children's Medical Research Center, 3-35-31 Taishido, Setagaya-ku, Tokyo 154-8509, Japan, and ‡Department of Surgery, School of Medicine, Keio University, 35 Shinanomachi, Shinjuku-ku, Tokyo 160-8582, Japan

We identified three novel human type-II classic cadherins, cadherin-7, -9 and -10, by cDNA cloning and sequencing, and confirmed that they interact with catenins and function in cell–cell adhesion as do other classic cadherins. Cell–cell binding activities of the eight human type-II classic cadherins, including the three new molecules, were evaluated by long-term cell-aggregation experiments using mouse L fibroblast clones transfected with the individual cadherins. The experiments indicated that all the type-II cadherins appeared to possess similar binding strength, which was virtually equivalent to that of E-cadherin. We next examined the binding specificities of the type-II cadherins using the mixed cell-aggregation assay. Although all of the type-II cadherins exhibited binding specificities distinct from that of E-cadherin, heterophilic interactions ranging from incomplete to complete were frequently observed among them. The combinations of cadherin-6 and -9, cadherin-7 and -14, cadherin-8 and -11, and cadherin-9 and -10 interacted in a complete manner, and in particular cadherin-7 and -14, and cadherin-8 and -11 showed an indistinguishable binding specificity against other cadherin subclasses, at least in this assay system. Although these data were obtained from an *in vitro* study, they should be useful for understanding cadherin-mediated mechanisms of development, morphogenesis and cell–cell interactions *in vivo*.

Key words: binding specificity, catenin, cell–cell adhesion, L cell.

INTRODUCTION

Classic cadherins are Ca^{2+}-dependent cell–cell adhesion molecules. They are transmembrane glycoproteins that consist of a signal peptide and a prosequence, which are both removed by intracellular proteolytic processing, a long extracellular domain, one transmembrane domain, and a rather short and highly conserved cytoplasmic domain. The cytoplasmic domain is essential for association with catenins, the ensuing linkage to the cytoskeleton, and full functioning as a cell–cell adhesion molecule [1–5]. The extracellular domain of classic cadherins serves as an interface responsible for cell–cell binding and determination of binding specificity, and can be divided into five homologous subdomains [6], which are also called cadherin repeats. Recent structural analyses have revealed that these subdomains indeed form structural units and also that the dimerization of the extracellular domain, especially the first subdomain, is crucially important for adhesive activity [7–9]. In the last decade, numerous molecules sharing this subdomain structure have been discovered, and it is generally accepted that these molecules constitute a large gene family, the cadherin superfamily [10]. Apart from the classic cadherins, however, the exact biological functions of these newly identified cadherins remain elusive.

Many classic cadherin molecules have been discovered in various vertebrates. With respect to human classic cadherins, 11 independent molecules have been identified so far by full cDNA cloning and sequencing analyses; these are E-, N- and P-cadherin, and cadherin-4 (R-cadherin), -5 (V-cadherin), -6 (K-cadherin), -8, -11 (OB-cadherin), -12, -14 and -15 [11–19]. On the basis of their overall similarities, and the conservation of several motifs and aromatic amino acid residues in the extracellular domains, Suzuki et al. [13] first proposed grouping the classic cadherins into two subgroups, type I and type II. At present, however, we consider that the human classic cadherins can be divided into more than two groups: type I, which includes E-, N- and P-cadherins and cadherin-4, type II, which includes cadherin-6, -8, -11, -12 and -14, and the others, cadherin-5 and -15, which do not show high similarities to either type-I or type-II cadherins, or to each other [19]. No subclasses with high similarity to cadherin-5 or -15 have been identified so far in humans.

As compared with non-classic-type cadherins, classic cadherins have been well characterized both functionally and structurally. However, most of these characteristics have been based on type-I classic cadherins, especially E- and N-cadherin, and it remains uncertain whether the characteristics of the type-I classic cadherins are true of the non-type-I classic cadherins. As for cell–cell binding activity, it has been suggested that some of the non-type-I classic cadherins mediate weaker cell–cell adhesion than do the type-I cadherins, since they are expressed in loosely associated cells [20]. It has also been reported that cadherin-5 and -8 did not

---

Abbreviations used CMFDA, 5-chloromethylfluorescein diacetate, DiI, 1,1′-dioctadecyl-3,3,3′,3′-tetramethylindocarbocyanine perchlorate, DMEM, Dulbecco's modified Eagle's medium, EC, extracellular subdomain

[1] To whom correspondence should be addressed (e-mail shimoyay@din or jp)

Nucleotide sequences of a human cadherin-7 cDNA, a human cadherin-9 cDNA and a human cadherin-10 cDNA have been submitted to the DDBJ/EMBL/GenBank® nucleotide sequence databases under the accession numbers AB035301, AB035302 and AB035303, respectively show significant cell-adhesion activity in cell-aggregation experiments [21,22]. These observations have led us to investigate the molecular nature of the non-type-I classic cadherins, and compare it with that of the type-I cadherins. We recently identified three human non-type-I classic cadherins, cadherin-6, -14 and -15, and characterized them using an L fibroblast cDNA transfection system [17–19,23]. In order to evaluate the binding strength of each cadherin as precisely as possible, we employed a long-term cell-aggregation assay focusing particularly on the expression level of β-catenin by the cadherin-transfected L cells, and reached the conclusion that all three non-type-I cadherins possess cell–cell binding activity similar to that of E-cadherin [19,23]. We found, however, that unlike type-I cadherins they were not protected by Ca^{2+} from trypsin degradation [19,23], although resistance to trypsin in the presence of Ca^{2+} had been considered as one of the characteristic features of classic cadherins [1]

As mentioned above, 11 classic cadherin molecules, including four type-I cadherins, five type-II cadherins and two non-type-I or -II cadherins, have been identified in humans. In addition, it is likely that there are at least three type-II cadherin molecules in humans, cadherin-7, -9 and -10, of which the full sequences are not yet available [13]. In order to analyse and clarify the molecular features of non-type-I, especially type-II, classic cadherins, in this study we first determined the full coding sequences of these three human cadherin molecules. We then assessed the cell–cell binding activities of all the eight human type-II cadherins using an L fibroblast cDNA transfection system and a long-term cell-aggregation assay. All of the cadherins exhibited cell–cell binding activity comparable with that of E-cadherin. Moreover, we frequently observed cross-reactivity of the type-II cadherins, which was incomplete or complete depending on the particular combination.

EXPERIMENTAL

cDNA cloning and DNA sequence analysis

To obtain cDNA fragments of human cadherin-9 and -10, degenerative reverse transcriptase PCR was performed using human brain poly(A)$^+$ RNA (Clontech, Palo Alto, CA, U.S.A.) as described previously [17]. The PCR products were subcloned into pCR®2.1 using a TA Cloning® kit (Invitrogen, San Diego, CA, U.S.A.). Clones were sequenced one by one, and those that corresponded with the partial nucleotide sequences of cadherin-9 and -10 reported previously [13] were selected. These clones were re-amplified by PCR with [α-^{32}P]dCTP, and used as probes for the following cDNA clonings. A human fetal brain Uni-ZAP® XR cDNA library (Stratagene, La Jolla, CA, U.S.A.), which was prepared from a pool of male and female whole brain samples ranging from 19 to 23 weeks of gestational age, was screened using the above probes by a plaque-hybridization technique as described previously [11], and positive clones were plaque-purified. The cDNA sequences of both ends of the inserts were determined by an ABI Prism® 377 DNA sequencer (Perkin-Elmer, Foster City, CA, U.S.A.) using a Dye Primer Cycle Sequencing kit (Perkin-Elmer), and compared with the cDNA sequences of known human classic cadherins. cDNA clones considered to contain start codons for complete forms of classic cadherins and to be of sufficient length were selected, and their entire nucleotide sequences were determined The sequences were determined on both strands by an ABI Prism® 377 DNA sequencer using oligonucleotide primers that annealed the cDNAs and a Prism® Ready Reaction Terminator Cycle Sequencing kit (Perkin-Elmer)

For cDNA cloning of human cadherin-7, we utilized chicken cadherin-7 cDNA [24], which we expected to cross-hybridize with the human homologue. We first obtained a 223-bp fragment of chicken cadherin-7 cDNA corresponding to nucleotide positions 429–651 of the reported cDNA [24], which encodes the signal peptide and precursor region, by PCR using chicken brain QUICK-Clone® cDNA (Clontech) as a template. The fragment was re-amplified by PCR using the same primer set with [α-^{32}P]dCTP, and used as a probe to screen the above cDNA library. A positive clone was plaque-purified, and sequenced as described above.

Other cDNAs of known human type-II cadherins, except for cadherin-6 and -14, for which we have already reported the cDNA cloning and sequencing [17,18], were obtained as follows. For cadherin-8 and -12, we prepared radiolabelled PCR probes referring to the previously reported cDNA sequences [16] as we did for the cadherin-7 cloning, and cloned each cDNA containing the entire coding sequence from the same library as above. For cadherin-11, a 2493-bp cDNA containing the whole coding region corresponding to nucleotide positions 381–2873 of the reported cDNA [15] was amplified by reverse transcriptase PCR from poly(A)$^+$ RNA of MRC-5 cells, a normal human fibroblast strain derived from embryonic lung [25] These cadherin cDNAs were also sequenced on both strands as mentioned above to confirm their integrity.

Nucleotide and deduced amino acid sequences were analysed using the GeneWorks software package (IntelliGenetics, Mountain View, CA, U.S.A.).

Expression-vector construction and transfection

For cadherin-6 and -14, we have already reported construction of the expression vectors and the establishment of L transfectant clones [23]. The transfectant clones designated L6-33 and L14-4, which express human cadherin-6 and -14, respectively, were also used in this study. To express other human type-II classic cadherins in mouse L fibroblasts that lack cadherin-mediated cell–cell adhesion activity [26] and to analyse the cell–cell adhesion properties of each cadherin, expression vectors were constructed by introducing each cadherin cDNA containing the entire open reading frame into the multicloning site of an expression vector pBAX [23] in the right direction The resulting expression vectors were cleaved by digestion with *Bgl*II, *Pvu*I or *Sca*I, and used for the following transfection.

Transfection of the expression vectors into L cells was performed using Lipofectamine® reagent (Life Technologies, Gaithersburg, MD, U.S.A.) according to the manufacturer's instructions. The transfected cells were selected in Dulbecco's modified Eagle's medium (DMEM) supplemented with 10 % calf serum in the presence of 400 μg/ml G418 in a humidified atmosphere comprising 5 % CO_2/95 % air at 37 °C for about 2 weeks Then, the G418-resistant colonies were isolated, screened for cadherin expression, and maintained under the same conditions.

Immunoblotting and immunoprecipitation

Immunoblotting of β-catenin and immunoprecipitation of the cadherin–catenin complex from cadherin-transfected L cells were performed as described previously [19,23] using an anti-β-catenin monoclonal antibody (Transduction Laboratories, Lexington, KY, U.S.A.)

Long-term cell-aggregation assay

Completely dispersed cell suspensions were obtained by treating the cells with PBS containing 0.05 % trypsin and 0.02 % EDTA at 37 °C for 15 min. The cells were washed twice with DMEM supplemented with 10 % calf serum, and then resuspended in DMEM supplemented with 10 % calf serum and 70 units/ml DNase I (Takara, Shiga, Japan) at a cell density of 2×10^6 cells/ml. The cell suspensions were added to a 24-well plastic plate (10^5 cells in 0.5 ml per well; Ultra Low Cluster, Corning Costar, Cambridge, MA, U.S.A.) and allowed to aggregate at 37 °C for 48 h at 100 rev./min in a humidified atmosphere comprising 5 % CO_2/95 % air.

To examine the heterotypic interactions between the cadherin subclasses, mixed cell-type aggregation experiments were performed using two transfectant cell lines expressing different cadherins; one line was labelled with 40 μg/ml 1,1′-dioctadecyl-3,3,3′,3′-tetramethylindocarbocyanine perchlorate (DiI; Molecular Probes, Eugene, OR, U.S.A.) in DMEM supplemented with 10 % calf serum or 10 μM 5-chloromethylfluorescein diacetate (CMFDA; Molecular Probes) in serum-free DMEM for 1 h, and the other was unlabelled. The cells were suspended as described above and equal numbers of cells of the two cell lines (5×10^4 in 0.25 ml each) were mixed, and allowed to aggregate for 12 h as described above.

RESULTS

cDNA cloning and sequence analysis of human cadherin-7, -9 and -10

cDNA clones for cadherin-7, -9 or -10, which appeared to have the complete coding regions as compared with the cDNA sequences of known human classic cadherins, were isolated. These clones were subjected to full DNA sequence analysis. The cadherin-7 cDNA consisted of 2828 nucleotides covering the complete coding region for the classic cadherin, and a poly(A)$^+$ tail. The deduced amino acid sequence comprised 785 amino acid residues. The N-terminal 47 amino acids were predicted to be removed by signal peptidases and endopeptidases [23], and the resulting mature form of 738 amino acids, which was predicted to be expressed on the cell surface and to function as a cell–cell adhesion connector, had the complete features of the type-II classic cadherin. The cadherin-9 and -10 cDNA clones consisted of 3060 and 3261 nucleotides, respectively, with poly(A)$^+$ tails, and also encoded complete forms of the typical type-II classic cadherin. The amino acid sequences of cadherin-7 and -10 exhibited high homologies, 94 and 96 %, with those of the reported chicken cadherin-7 [24] and -10 [27], respectively, indicating that these clones indeed encode human cadherin-7 and -10. The deduced amino acid sequences of the putative mature forms after post-transcriptional proteolytic processing are shown in Figure 1 together with those of other human type-II classic cadherins. Besides the above clones, we also isolated several cDNA clones for cadherin-9 and -10, which appeared to encode various truncated forms (results not shown). These are under investigation.

Comparison of deduced amino acid sequences of human type-II classic cadherins

Percentage homologies among the type-II cadherins and with E-cadherin, as a representative of the type-I cadherins, are shown in Table 1. Previously we reported the cDNA cloning and sequence determination of cadherin-6 and -14 [17,18], and these sequences are shown in Figure 1. We also obtained cDNA clones encoding the complete proteins of cadherin-8, -11 and -12 in this study, and sequenced them. Amino acid sequences deduced from those cDNA clones are also shown in Figure 1 and Table 1. Although the deduced amino acid sequence of cadherin-11 completely agreed with the reported sequence [15], the sequences of cadherin-8 and -12 differed from the previously reported ones [16] at several points, as follows. As compared with the previously reported human cadherin-8 protein, our cadherin-8 cDNA clone encoded a longer molecule at the N-terminus: seven amino acids, Met-Pro-Glu-Arg-Leu-Ala-Glu, were added. Moreover, Asp at amino acid position 348 in the third extracellular subdomain (EC3) was changed into Val, and Gln at 641 in the cytoplasmic domain was deleted in our cadherin-8 protein. As for cadherin-12, the amino acid sequence deduced from our cDNA differed from the previously reported sequence at three points. Gly at amino acid position 416 in the EC4, His at 644 and Ile at 733 in the cytoplasmic domain were replaced by Ser, Asp and Tyr, respectively, in our cadherin-12 protein.

As shown in Figure 1, the type-II cadherins share many amino acid residues. In the extracellular domains, 180 amino acid residues are conserved among the type-II cadherins, and 65 of these residues are conserved among all of the human classic cadherins (Figure 1A). These include DRE and DXND in the EC1, AXDXDD and DXNXN in the EC2, PXF at the end of EC1, 2 and 3, and four Cys residues in the EC5. On the other hand, 21 out of the 180 conserved residues are specific for the type-II cadherins, but they do not appear to form specific clusters (Figure 1A). The HAV motif, which is considered to be intimately involved in the adhesive functions of type-I classic cadherins [28–30], is replaced by a QAI tripeptide in cadherin-6, -10 and -14, a QAL tripeptide in cadherin-7, a QAV tripeptide in cadherin-8, -11 and -12, and a KAI tripeptide in cadherin-9 (Figure 1A). In the cytoplasmic domains, 52 amino acid residues are conserved among the type-II cadherins (Figure 1C). Although 26 of these residues are conserved among all of the human classic cadherins, only three residues are specific for the type-II cadherins. The alignment of amino acid sequences of the human classic cadherins revealed that the transmembrane regions of the type-II cadherins are conspicuous in comparison with those of other classic cadherins. Figure 1(B) shows the alignment of the transmembrane sequences of the type-II cadherins with other known human classic cadherins. The transmembrane domains of all of the type-II cadherins consist of exactly 33 amino acids and are well conserved, whereas those of other cadherins vary in size and do not show high similarities to each other or to those of the type-II cadherins (Figure 1B).

Expression of type-II classic cadherins

To examine the cell–cell binding activities of the type-II classic cadherins, the cadherin-7, -8, -9, -10, -11 and -12 cDNA clones, ligated into the eukaryotic pBAX expression vector, were introduced into L cells, a mouse fibroblast strain deficient in cadherin activity [26]. A lipofection method was used, and transfected clones expressing the individual cadherins were obtained. Since antibodies for these cadherins were not available, transfected clones were selected on the basis of the expression level of β-catenin, which is considered to reflect the expression level of a transfected cadherin in this system [19,23]. Establishment of the L cell clones L6-33 and L14-4, which express cadherin-6 and -14, respectively, has already been reported [23]. These clones and LE-1 cells, an E-cadherin transfectant [19], were also used in this study.

Thus transfected clones L7-3, L8-10, L11-3 and L12-6, for cadherin-7, -8, -11 and -12, respectively, were selected on the basis that they express similar amounts of β-catenin protein as the LE-1, L6-33 and L14-4 transfectants. We have reported in a previous study that LE-1, L6-33 and L14-4 cells express almost equivalent amounts of β-catenin protein. For cadherin-9 and -10, we selected over 30 transfected clones for each cadherin, but

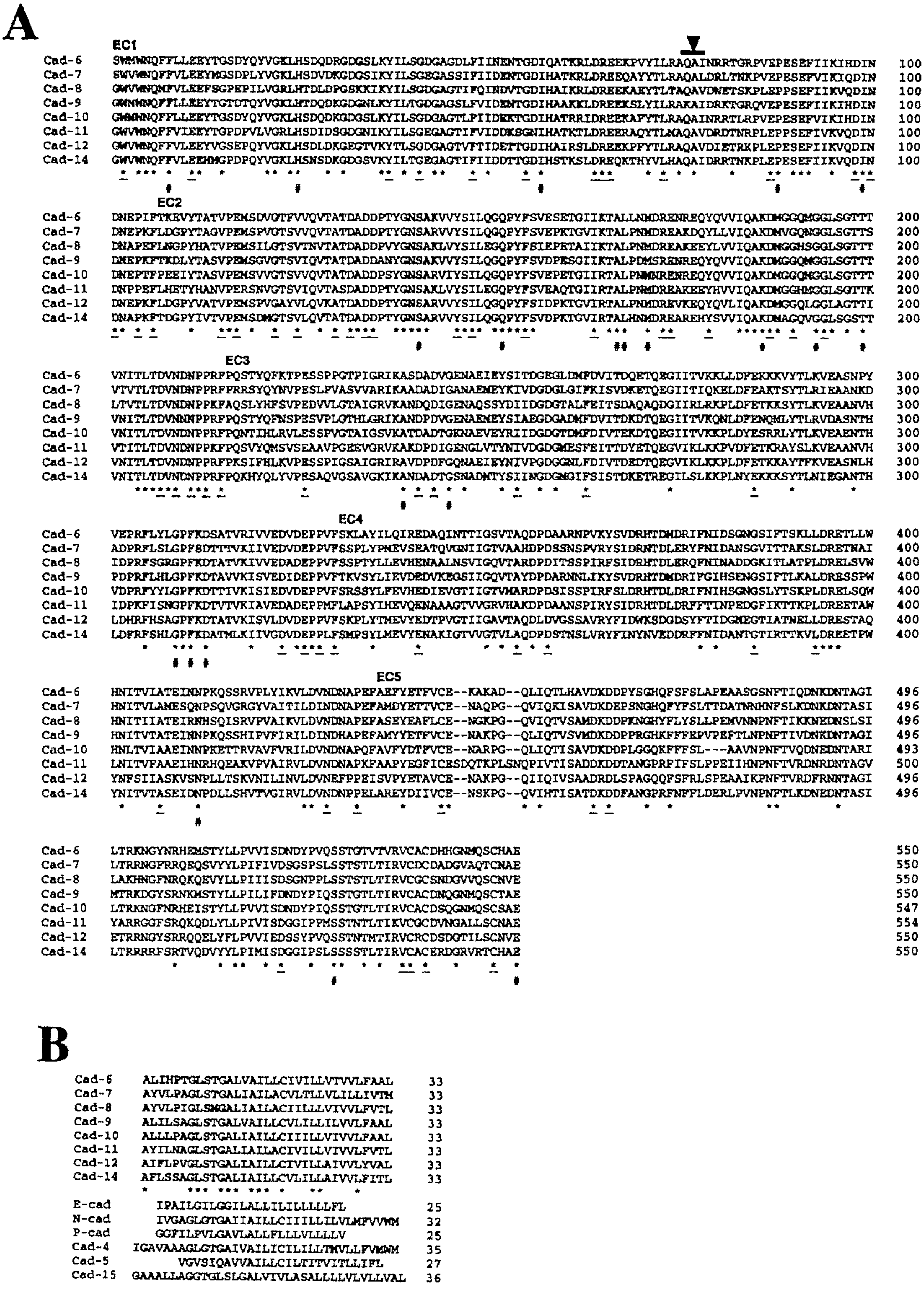

Figure 1 For legend see opposite.

C

```
Cad-6   RRQRKKEPLIISKE-DIRDNIVSYNDEGGGEEDTQAFDIGTLRNPEAIEDNKLRRDIVPEALFLPRR-TPTARDN-TDVRDFINQRLKENDTDPTAPPYDS  98
Cad-7   RRRKK-EPLIFDEERDIRENIVRYDDEGGGEEDTEAFDMAALRNLNVIRDTKTRRDVTPEIQFLSRPAFKSIPDN-VIFREFIWERLKEADVDPGAPPYDS  99
Cad-8   RRHKN-EPLIIKDDEDVRENIIRYDDEGGGEEDTEAFDIATLQNPDGINGFLPRKDIKPDLQFMPRQ-GLAPVPNGVDVDEFINVRLHEADNDPTAPPYDS  99
Cad-9   KRQRKKEPLIISKD-DVRDNIVTYNDEGGGEEDTQAFDIGTLRNPEAREDSKLRRDVMPETIFQIRR-TVPLWEN-IDVQDFIHRRLKENDADPSAPPYDS  98
Cad-10  KRQRKKEPLILSKE-DIRDNIVSYNDEGGGEEDTQAFDIGTLRNPAAIEEKKLRRDIIPETLFIPRR-TPTAPDN-TDVRDFINERLKEHDLDPTAPPYDS  98
Cad-11  RRQKK-EPLIVFEEEDVRENIITYDDEGGGEEDTEAFDIATLQNPDGINGFIPRKDIKPEYQYMPRP-GLRPAPNSVDVDDFINTRIQEADNDPTAPPYDS  99
Cad-12  RRQKKKDTLMTSKE-DIRDNVIHYDDEGGGEEDTQAFDIGALRNPKVIEENKIRRDIKPDSLCLPRQ-RPPNEDN-TDIRDFIHQRLQENDVDPTAPPYDS  98
Cad-14  RRSKK-EPLIISEE-DVRENVVTYDDEGGGEEDTEAFDITALRNPSAAEELKYRRDIRPEVKLTPRHQTSSTLES-IDVQEFIKQRLAEADLDPSVPPYDS  98
         *      *      * * *   * ********* ***   * *         * *  *      *               **  *  * * **  *****
                                 #                 #                                         #

Cad-6   LATYAYEGTGSVADSLSSLESVTTDADQDYDYLSDWGPRFKKLADMYGGVDSDKDS                                               154
Cad-7   LQTYAFEGNGSVAESLSSLDSISSNSDQNYDYLSDWGPRFKRLADMYGTGQESLYS                                               155
Cad-8   IQIYGYEGRGSVAGSLSSLESTTSDSDQNFDYLSDWGPRFKRLGELYSVGESDKET                                               155
Cad-9   LATYAYEGNDSIADSLSSLESLTADCNQDYDYLSDWGPRFKKLADMYGGDDSDRD                                                153
Cad-10  LATYAYEGNDSIAESLSSLESGTTEGDQNYDYLREWGPRFNKLAEMYGGGESDKDS                                               154
Cad-11  IQIYGYEGRGSVAGSLSSLESATTDSDLDYDYLQNWGPRFKKLADLYGSKDTFDDDS                                              156
Cad-12  LATYAYEGSGSVAESLSSIDSLTTEADQDYDYLTDWGPRFKVLADMFGEEESYNPDKVT                                            157
Cad-14  LQTYAYEGQRSEAGSISSLDSATTQSDQDYHYLGDWGPEFKKLAELYGEIESRRTT                                               154
           *  **  * * * **  *          **  *** *  *
```

Figure 1 Alignment of deduced amino acid sequences of eight human type-II classic cadherins

(A) Alignment of extracellular domains The signal peptide and precursor region of each cadherin are omitted from this Figure The position of tripeptides corresponding to the HAV motif of type-I cadherins is marked by an arrowhead (▼) and a line The beginning of each extracellular subdomain (EC) is indicated by EC1–EC5 (B) Alignment of transmembrane domains Transmembrane domains of other human classic cadherins are also shown in alignment (C) Alignment of cytoplasmic domains The amino acid residues conserved among all the type-II cadherins are marked by asterisks In (A) and (C), out of these conserved amino acid residues, those that are also conserved in the four human type-I classic cadherins and in cadherin-5 and -15, and those that are not conserved in any of them, are indicated by underlining and #, respectively

Table 1 Homologies among eight human type-II cadherins

Homologies among the putative mature forms of eight human type-II cadherins (6–14) and E-cadherin (E) were calculated and are shown as percentages

Cadherin	E	7	8	9	10	11	12	14
6	36	63	62	75	76	60	64	60
7	34	–	62	61	64	60	60	64
8	35	–	–	58	61	69	58	59
9	32	–	–	–	73	58	60	60
10	33	–	–	–	–	60	64	62
11	33	–	–	–	–	–	58	61
12	36	–	–	–	–	–	–	61
14	35	–	–	–	–	–	–	–

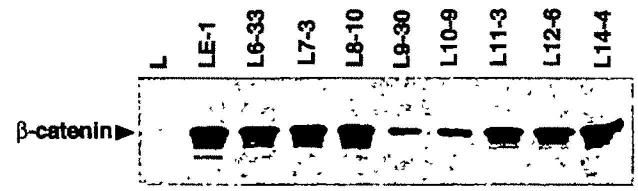

Figure 2 Immunoblot analysis of β-catenin expressed by cadherin transfectants

Whole-cell lysates of cadherin transfectants and L cells (20 μg of protein/lane) were separated by SDS/PAGE (7.5% gel) and transferred to a PVDF membrane β-Catenin was then detected with an anti-β-catenin monoclonal antibody using an ECL® system (Amersham Life Science, Bucks, U.K.) Faint bands below the main bands probably indicate degradation of β-catenin

failed to obtain any transfectant expressing β-catenin protein at a similar level to that of the other cadherin transfectants used in this study. We then used transfectant clones L9-30 and L10-9, for cadherin-9 and -10, respectively, which express the highest levels of β-catenin among each cadherin transfectant group. The levels of β-catenin expression in these cadherin transfectants, and in parental L cells, were analysed by immunoblotting, and are shown in Figure 2 As mentioned above, the cadherin-transfected clones, except for L9-30 and L10-9, expressed β-catenin at almost similar levels (Figure 2). Compared with these transfectants, L9-30 cells expressed considerably lower and L10-9 cells expressed slightly lower amounts of β-catenin, and β-catenin protein could hardly be detected in parental L cells under these experimental conditions (Figure 2).

Cadherin-7, -9 and -10 molecules, the human type-II classic cadherins newly identified in this study, were visualized as bands of approx. 116, 107 and 112 kDa, respectively, in an immunoprecipitation experiment (Figure 3). This experiment also confirmed that the three newly identified cadherins interact not only with β-catenin but also with α-catenin, similar to known classic cadherin molecules. In fact, the cadherin transfectants presented here exhibited elevated expression levels of α-catenin protein as compared with L cells, a similar result to that obtained with β-catenin (results not shown).

Cell–cell binding activities of type-II cadherins

Cell–cell binding activities of the eight human type-II classic cadherins were evaluated by long-term cell-aggregation assays using the aforementioned cadherin transfectants and the parental L cells Although cell-aggregation experiments for 30 min–3 h have been used widely to evaluate cadherin activity, we did not employ this type of short-term assay. The reason is that in the short-term assay cells are usually dispersed into single-cell suspensions by trypsin in the presence of Ca^{2+}, which is known to leave type-I cadherins intact; however, we found the functional forms of cadherin-6 and -14 to be destroyed by this treatment

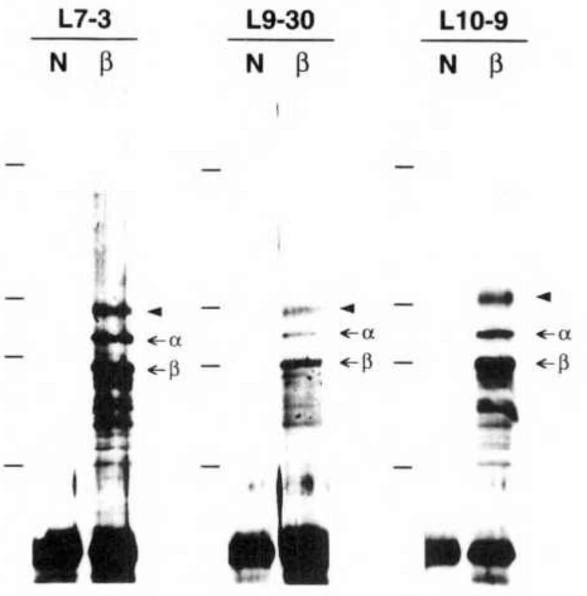

Figure 3 Immunoprecipitation of cadherin-7, -9 and -10 with an anti-β-catenin monoclonal antibody

Cadherin-7, -9 and -10 molecules were co-immunoprecipitated with an anti-β-catenin monoclonal antibody (β) from L7-3, L9-30 and L10-9 cell lysates, respectively, based on the formation of cadherin–catenin complexes in cadherin-positive cells. As a control, immunoprecipitations with normal mouse IgG (N) were performed simultaneously. The precipitates were denatured, separated by SDS/PAGE (7.5% gel), transferred on to a PVDF membrane and stained with AuroDye® forte (Amersham Life Science). Cadherins and α- and β-catenins are indicated by arrowheads and arrows, respectively. Bands below the β-catenin bands probably indicate degradation of β-catenin. Bars on the left indicate the mobilities of molecular-mass markers (200, 116, 97.4 and 66.2 kDa).

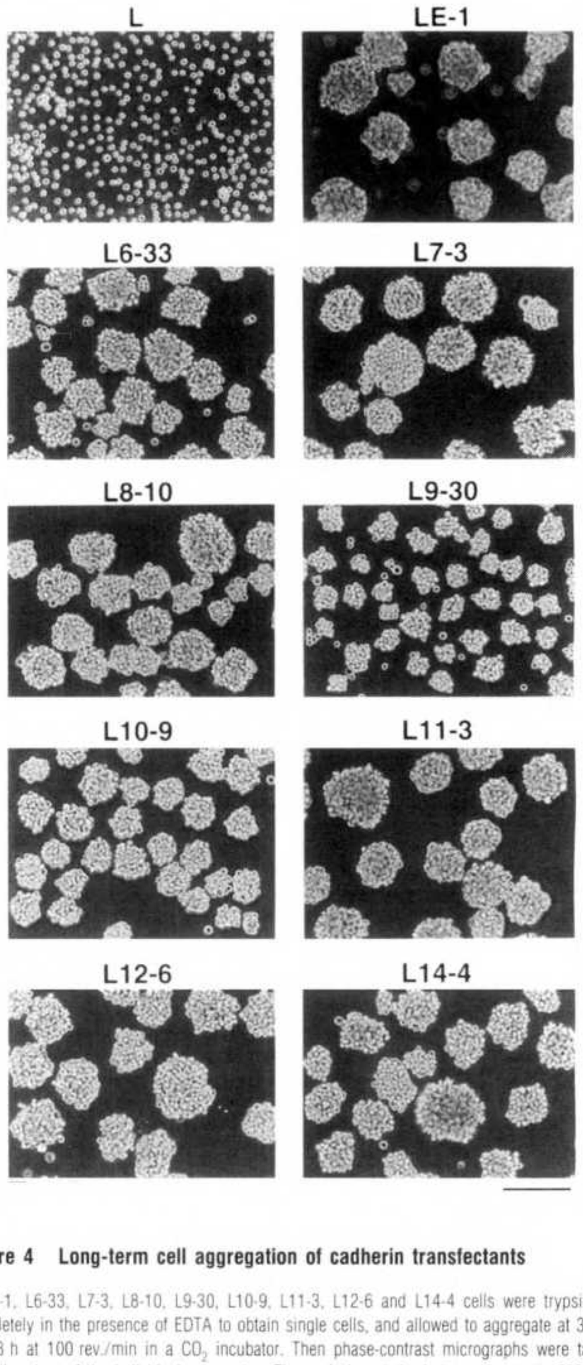

Figure 4 Long-term cell aggregation of cadherin transfectants

L, LE-1, L6-33, L7-3, L8-10, L9-30, L10-9, L11-3, L12-6 and L14-4 cells were trypsinized completely in the presence of EDTA to obtain single cells, and allowed to aggregate at 37 °C for 48 h at 100 rev./min in a CO_2 incubator. Then phase-contrast micrographs were taken. Note the sizes of the individual aggregates. The scale bar at the bottom represents 200 μm.

[23]. We therefore treated the cadherin transfectants with trypsin in the absence of Ca^{2+}, which clears the functional cadherin molecules from the external cell surface, and allowed the resulting single-cell suspensions to aggregate for 12–48 h. Since we know that expression of cadherin molecules returns to initial levels within 3 h of treatment with trypsin and EDTA [23], the influence of the trypsin pretreatment was considered to be negligible in the long-term assay. Thus the long-term assay appeared to be suitable for evaluating the cell–cell binding activities of the type-II cadherins, and also for comparison of cell–cell binding activities irrespective of cadherin type.

The results of the long-term (48 h) cell-aggregation experiments are shown in Figure 4. As can be seen, the parental L cells hardly aggregated under the assay conditions, and most of the cells remained dispersed even after incubation for 48 h. In contrast, all of the cadherin transfectants formed definite aggregates. Although these aggregates could not be discriminated from one another in terms of cell–cell adhesiveness, they varied in size. LE-1, L6-33, L7-3, L8-10, L11-3, L12-6 and L14-4 cells formed almost indistinguishable aggregates, whereas L9-30 aggregates were much smaller and L10-9 aggregates were slightly smaller, than those of other transfectants. The sizes of the aggregates corresponded well to the expression level of β-catenin protein in the individual transfectants (Figure 2).

Binding specificities of type-II cadherins

In order to elucidate the binding specificities of the type-II cadherins, one line was labelled with DiI or CMFDA fluorescent reagent, mixed with another unlabelled line, and allowed to aggregate in a similar way to the long-term assays. In these experiments, the nine cadherin transfectants mentioned above, including the E-cadherin transfectant LE-1, and the parental L cells were used, and cells were incubated for 12 h in order to provide intelligible micrographs. The results after incubation for up to 48 h were the same as those indicated here.

First, each cadherin transfectant was mixed with the parental L cells and allowed to aggregate. L cells were excluded completely from every aggregate, and chimaeric aggregates were never found (results not shown), indicating that all of the type-II cadherins mediate cell–cell adhesion in a homophilic manner but not in a ligand–receptor interaction. The results are summarized

Table 2 Interactions between eight human type-II cadherins and E-cadherin

Two out of the nine cadherin transfectants, LE-1, L6-33, L7-3, L8-10, L9-30, L10-9, L11-3, L12-6 and L14-4, which express E-cadherin and cadherin-6, -7, -8, -9, -10, -11, -12, and -14, respectively, were mixed, and allowed to aggregate for 12 h. The resultant aggregates were then observed using an Olympus IX70 phase-contrast microscope equipped with a fluorescence system. Interactions between cadherins were classified into − (no interaction), + (incomplete interaction) and ++ (complete interaction) categories.

Cadherin	E	6	7	8	9	10	11	12	14
E	++*	−*	−	−	−	−	−	−	−*
6	−*	++*	+	−	++	+	−	−	+*
7	−	+	++	−	+	−	−	+	++
8	−	−	−	++	−	−	++	−	−
9	−	++	+	−	++	++	−	−	+
10	−	+	−	−	++	++	−	−	−
11	−	−	−	++	−	−	++	−	−
12	−	−	+	−	−	−	−	++	+
14	−*	+*	++	−	+	−	−	+	++*

* These data were reported previously [23].

in Table 2. When LE-1 cells were mixed with one of the type-II cadherin transfectants, they always aggregated separately, and chimaeric aggregates were never formed. This observation indicated that all of the type-II cadherins have binding specificities distinct from that of E-cadherin, a representative of the type-I cadherins. In contrast, and surprisingly, chimaeric aggregates, which varied in their extent of heterogeneous mixing, were observed frequently when two lines of the eight type-II cadherin transfectants were mixed. In particular, with combinations of L6-33 and L9-30, L7-3 and L14-4, L8-10 and L11-3, or L9-30 and L10-9, each pair of transfectants formed the same randomly intermixed aggregates as those observed when labelled and unlabelled cells of one line were mixed (Table 2). These complete heterophilic interactions suggested that cadherin-6 and -9, cadherin-7 and -14, cadherin-8 and -11, or cadherin-9 and -10 cannot discriminate between each other, at least in this assay system. Moreover, in six other combinations, including a combination of L6-33 and L14-4 [23], incomplete heterogeneous aggregates, which were composed of clusters of each cell type, were formed (Table 2), suggesting that in these combinations the two cadherin types share part of their binding specificities, enabling incomplete heterophilic interactions. Representative results are shown in Figure 5.

DISCUSSION

In the present study, we identified three novel human type-II classic cadherins, cadherin-7, -9 and -10, by cDNA cloning and sequencing. The alignment of deduced amino acid sequences of

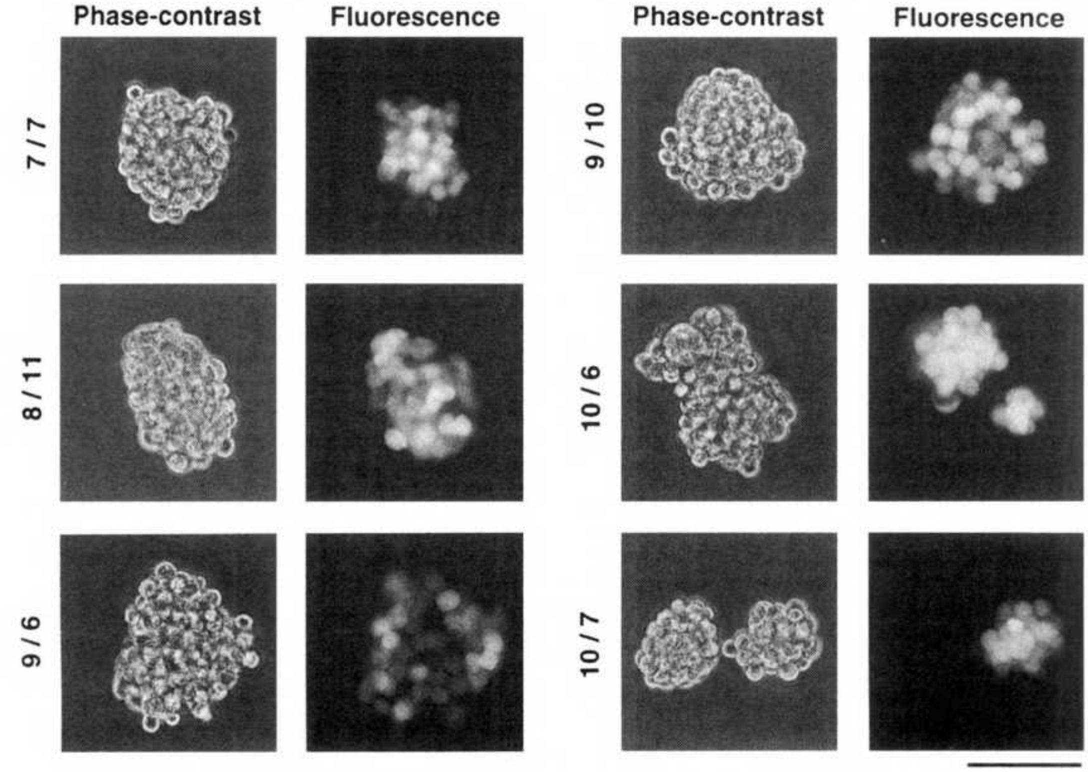

Figure 5 Mixed cell aggregation of cadherin transfectants

Equal numbers of labelled L7-3 and unlabelled L7-3 cells (7/7), labelled L8-10 and unlabelled L11-3 cells (8/11), labelled L9-30 and unlabelled L6-33 cells (9/6), labelled L9-30 and unlabelled L10-9 cells (9/10), labelled L10-9 and unlabelled L6-33 cells (10/6), and labelled L10-7 and unlabelled L7-3 cells (10/7) were mixed and allowed to aggregate for 12 h. Phase-contrast and fluorescence micrographs of the aggregates in the same fields were taken. Cells shown here were labelled with CMFDA reagent. Note that in 8/11, 9/6 and 9/10 the labelled and unlabelled cells form completely intermixed aggregates similar to that in 7/7. In contrast, the labelled and unlabelled cells were completely segregated in 10/7. In 10/6 the aggregate is composed of two clusters of labelled L10-9 cells surrounded by unlabelled L6-33 cells. This pattern of heterogeneous intermixing was interpreted as incomplete heterophilic interaction. The scale bar at the bottom represents 100 μm.

the type-II cadherins, including the three novel molecules, and comparison of the type-II cadherins with other classic cadherins confirmed the identity of this grouping. As shown in Table 1, the sequence similarities of the putative mature forms among the type-II cadherins are high, ranging from 58 to 76 %, whereas all of the type-II cadherins are less similar to every other known human classic cadherin For example, sequence similarities to E-cadherin are also shown in Table 1, and all of these are below 40 %. In the extracellular domains, which are composed of about 550 amino acids, 21 out of 180 conserved residues among the type-II cadherins are specific for type-II cadherins and are not found in any other human classic cadherin. In contrast, in the cytoplasmic domains, only three out of 52 conserved residues among the type-II cadherins are specific for type II, indicating that the type-II cadherins are more characteristic in the extracellular domains, which form interfaces for cell–cell adhesion, than in the cytoplasmic domains, which link to the cytoskeleton via catenins. However, even in the extracellular domains we could not identify any motifs specific for type-II cadherins. Unexpectedly, the most impressive sequence characteristic for the type-II cadherins was found in the transmembrane domains, which have never been considered to be of significance in the field of cadherin research. As compared with the transmembrane domains of the non-type-II cadherins, those of the type-II cadherins were markedly conserved, both in length and in amino acid sequence (Figure 1B).

To our knowledge, besides the eight molecules presented here, no other human classic cadherins of type II have been identified. Kremmidiotis et al. [31] recently reported sequencing of a partial cDNA clone homologous to chicken cadherin-7, and registered the sequence as human cadherin-7 in the GenBank® nucleotide sequence database with the accession number AF047826. However, the deduced amino acid sequence of 317 residues, corresponding to a region from the end of the EC4 to the C-terminus, shares only 54 and 53 % identities with the corresponding region of human cadherin-7 presented here and with chicken cadherin-7, respectively. In the same region, our human cadherin-7 is much more similar to chicken cadherin-7 (92 % similarity). These findings strongly suggest that the cDNA clone obtained in the present study by cross-hybridization with a chicken cadherin-7 cDNA probe actually encodes an authentic human counterpart of chicken cadherin-7, and that the cDNA fragment obtained by Kremmidiotis et al. indicates the existence of an unknown human classic cadherin. The partial amino acid sequence of clone number AF047826 shows higher similarity to the type-II cadherins (43–46 %, except for cadherin-7) than to the non-type-II cadherins (below 40 %), and possesses the 33-amino acid transmembrane domain. However, this clone, of which only a restricted sequence is available, conserves only one residue out of the five residues defined as specific for type-II cadherins in the restricted region (results not shown), and shows relatively low similarities to the type-II cadherins described above. These findings suggest that the clone is likely to encode a novel human type-II classic cadherin that is somewhat diversified from the eight type-II cadherins identified so far.

Cadherin-7, -9 and -10 were expressed in mouse L fibroblasts by a cDNA-transfection method, and the individual transfectant clones were selected. As has been demonstrated for other classic cadherins, these cadherins interacted with α- and β-catenins, and retarded their degradation (Figures 2 and 3). We obtained new L transfectant clones for cadherin-8, -11 and -12 in this study, and also used L transfectant clones for cadherin-6 and -14 that we reported previously [23]. We then evaluated cell–cell binding activities of the eight human type-II classic cadherins by cell-aggregation experiments over 48 h with particular attention to the expression level of β-catenin protein by the transfectants. As we proposed recently [19,23], the expression level of β-catenin is considered to reflect the expression level of a transfected cadherin in this system. This is based on the observation that β-catenin is hardly detectable in L cells at the protein level because of its rapid turnover rate However, once L cells begin to express classic cadherin molecules, upregulation of β-catenin protein occurs at the same time, possibly because of stabilization of the β-catenin protein by its association with the cytoplasmic domain of classic cadherin. Assuming that all classic cadherin subclasses influence the preservation of β-catenin protein in L cells to a similar extent, the relative expression level of a cadherin in an L transfectant clone could be estimated from the expression level of β-catenin protein in the clone.

As shown in Figure 4, transfectant clones for E-cadherin and cadherin-6, -7, -8, -11, -12 and -14, all of which express similar amounts of β-catenin protein (Figure 2) and therefore are expected to express a similar number of cadherin molecules per cell, formed aggregates hardly distinguishable from one another both in size and in cell–cell adhesiveness. The cadherin-9 and -10 transfectant clones, which show lower expression of β-catenin protein than the other transfectants (Figure 2), formed smaller aggregates (Figure 4). Transfectants of other cadherin types expressing similar amounts of β-catenin protein to the cadherin-9 or -10 transfectant clones formed aggregates indistinguishable from those of the cadherin-9 or -10 transfectants (results not shown). These findings strongly suggest that all of the type-II cadherins possess a similar cell–cell binding ability that is almost equivalent to that of E-cadherin.

Although Suzuki and colleagues have reported that cadherin-5 and -8 did not show significant cell-adhesion activity on cell-aggregation experiments [21,22], we demonstrated in this study that cadherin-8 mediates cell–cell binding comparable with that of other classic cadherins, and we confirmed recently that cadherin-5 also exhibits definite cell–cell binding activity in the same assay system as used in this study (Y. Shimoyama, G. Tsujimoto, M. Kitajima and M. Natori, unpublished work). This discrepancy may be explained by the difference in the assay system. Alternatively, as mentioned in the Results section, their cadherin-8 cDNA clone encoded a molecule that was seven amino acids shorter at the N-terminus as compared with the clone used in this study; this might cause derangement of the cleavage of the signal peptide and the precursor region, or of the transport of the cadherin to the cell surface, leading to malfunction of the cadherin in their study. Interestingly, a cadherin-5 cDNA clone that was isolated recently from a human adult skeletal-muscle cDNA library in our laboratory contained an open reading frame that was 12 nucleotides longer (corresponding to Met-Gln-Arg-Leu) than that previously reported by Suzuki and colleagues [16] (Y. Shimoyama, G Tsujimoto, M. Kitajima and M. Natori, unpublished work). This might suggest that the truncated N-terminal sequence was the cause of the reduced cell–cell binding activity. The nucleotide sequences of the human cadherin-5 and -8 cDNAs isolated in our laboratory have also been submitted to the DDBJ/EMBL/GenBank® nucleotide sequence databases with the accession numbers AB035304 and AB035305, respectively.

It has been postulated that some non-type-I classic cadherins, including the type-II cadherins, mediate weaker cell–cell adhesion than do type-I cadherins, since they are expressed in loosely associated cells [20]. In fact, we have confirmed recently that various human fibroblast strains express multiple cadherin molecules including type-II cadherins (Y. Shimoyama, G. Tsujimoto, M. Kitajima and M. Natori, unpublished work). It could be speculated, however, that mesenchymal cells, such as fibroblasts lack other components of the cell–cell binding machinery besides the cadherin cell-adhesion system. In any case, the data presented here indicate clearly that all of the type-II cadherins function as cell–cell binding connectors, as do type-I cadherins.

In a recent study, we found that cadherin-6 and -14 interacted with each other, although in an incomplete manner [23]. This finding prompted us to verify the heterophilic interactions among the eight type-II cadherins, and we performed aggregation experiments with mixed cell types. Surprisingly, the formation of chimaeric aggregates was observed in various combinations (Figure 5 and Table 2). Completely intermixed aggregates were formed with combinations of L transfectant clones expressing cadherin-6 and -9, cadherin-7 and -14, cadherin-8 and -11, and cadherin-9 and -10, indicating that in these combinations the two cadherin subclasses exhibit equal binding specificities. Moreover, partially intermixed aggregates similar to the heterogeneous aggregates between cadherin-6 and -14 [23] were observed with combinations of L transfectant clones expressing cadherin-6 and -7, cadherin-6 and -10, cadherin-7 and -9, cadherin-7 and -12, cadherin-9 and -14, and cadherin-12 and -14, indicating that in these combinations the two cadherin subclasses share a part of their binding specificities. In particular, either cadherin-7 and -14 or cadherin-8 and -11 showed an indistinguishable binding specificity against other cadherin subclasses, at least in this assay system (Table 2).

Similar complete and incomplete heterophilic interactions between different cadherin subclasses from the same species have been described for B-cadherin and L-CAM (liver cell-adhesion molecule) in chicken [32], for N- and R-cadherin in chicken and mouse [33,34], and for cadherin-6B and -7 in chicken [24]. However, the frequency of heterophilic interactions among the human type-II classic cadherins was unexpected. Although these results might offer significant clues for identification of the sites responsible for the binding specificities, we could not determine the sites or motifs from comparison and analysis of the primary structures. We demonstrated previously that the QAI tripeptide, corresponding to the HAV motif in type-I cadherins that is known to be intimately involved in the adhesive function and binding specificity [28–30], is itself unlikely to be responsible for the adhesive functions and binding specificities of cadherin-6 and -14 [23]. As mentioned above, cadherin-6 and -9, cadherin-7 and -14, cadherin-8 and -11, and cadherin-9 and -10 cross-reacted completely in the mixed cell-aggregation experiments; however, in every combination the tripeptide corresponding to the HAV motif of the two cadherin subclasses does not coincide (Figure 1A). Future studies on the three-dimensional structures would clarify this issue.

Although this study demonstrating frequent heterophilic interactions among the type-II classic cadherins used an assay system *in vitro*, we believe that the results presented here will be useful in the future for understanding cadherin-mediated mechanisms of development, morphogenesis and cell–cell interactions *in vivo*.

Mouse L fibroblasts and the human fibroblast strain MRC-5 were supplied by the Riken Gene Bank. This work was supported in part by Grants-in-Aid for Pediatric Research (10C-2, to M.N.) and Research on Human Genome and Gene Therapy (H10-Genome-008, to Y.S. and M.N.) from the Ministry of Health and Welfare of Japan, and in part by a Grant for Organized Research Combination System from the Science and Technology Agency of Japan (to G.T.)

REFERENCES

1 Takeichi, M. (1988) Development **102**, 639–655
2 Takeichi, M. (1991) Science **251**, 1451–1455
3 Ozawa, M., Ringwald, M. and Kemler, R. (1990) Proc. Natl. Acad. Sci. U.S.A. **87**, 4246–4250
4 Shimoyama, Y., Nagafuchi, A., Fujita, S., Gotoh, M., Takeichi, M., Tsukita, S. and Hirohashi, S. (1992) Cancer Res. **52**, 5770–5774
5 Hirano, S., Kimoto, N., Shimoyama, Y., Hirohashi, S. and Takeichi, M. (1992) Cell **70**, 293–301
6 Hatta, K., Nose, A., Nagafuchi, A. and Takeichi, M. (1988) J. Cell Biol. **106**, 873–881
7 Shapiro, L., Fannon, A. L., Kwong, P. D., Thompson, A., Lehmann, M. S., Grubel, G., Legrand, J.-F., Als-Nielsen, J., Colman, D. R. and Hendrickson, W. A. (1995) Nature (London) **374**, 327–337
8 Overduin, M., Harvey, T. S., Bagby, S., Tong, K. I., Yau, P., Takeichi, M. and Ikura, M. (1995) Science **267**, 386–389
9 Nagar, B., Overduin, M., Ikura, M. and Rini, J. M. (1996) Nature (London) **380**, 360–364
10 Suzuki, S. T. (1996) J. Cell Biochem. **61**, 531–542
11 Shimoyama, Y., Yoshida, T., Terada, M., Shimosato, Y., Abe, O. and Hirohashi, S. (1989) J. Cell Biol. **109**, 1787–1794
12 Reid, R. A. and Hemperly, J. J. (1990) Nucleic Acids Res. **18**, 5896
13 Suzuki, S., Sano, K. and Tanihara, H. (1991) Cell Regul. **2**, 261–270
14 Bussemakers, M. J. K., van Bokhoven, A., Mees, S. G. M., Kemler, R. and Schalken, J. A. (1993) Mol. Biol. Rep. **17**, 123–128
15 Okazaki, M., Takeshita, S., Kawai, S., Kikuno, R., Tsujimura, A., Kudo, A. and Amann, E. (1994) J. Biol. Chem. **269**, 12092–12098
16 Tanihara, H., Sano, K., Heimark, R. L., St. John, T. and Suzuki, S. (1994) Cell Adhes. Commun. **2**, 15–26
17 Shimoyama, Y., Gotoh, M., Terasaki, T., Kitajima, M. and Hirohashi, S. (1995) Cancer Res. **55**, 2206–2211
18 Shibata, T., Shimoyama, Y., Gotoh, M. and Hirohashi, S. (1997) J. Biol. Chem. **272**, 5236–5240
19 Shimoyama, Y., Shibata, T., Kitajima, M. and Hirohashi, S. (1998) J. Biol. Chem. **273**, 10011–10018
20 Takeichi, M. (1995) Curr. Opin. Cell Biol. **7**, 619–627
21 Tanihara, H., Kido, M., Obata, S., Heimark, R. L., Davidson, M., St. John, T. and Suzuki, S. (1994) J. Cell Sci. **107**, 1697–1704
22 Kido, M., Obata, S., Tanihara, H., Rochelle, J. M., Seldin, M. F., Taketani, S. and Suzuki, S. T. (1998) Genomics **48**, 186–194
23 Shimoyama, Y., Takeda, H., Yoshihara, S., Kitajima, M. and Hirohashi, S. (1999) J. Biol. Chem. **274**, 11987–11994
24 Nakagawa, S. and Takeichi, M. (1995) Development **121**, 1321–1332
25 Jacobs, J. P., Jones, C. M. and Baille, J. P. (1970) Nature (London) **227**, 168–170
26 Nagafuchi, A., Shirayoshi, Y., Okazaki, K., Yasuda, K. and Takeichi, M. (1987) Nature (London) **329**, 341–343
27 Fushimi, D., Arndt, K., Takeichi, M. and Redies, C. (1997) Dev. Dyn. **209**, 269–285
28 Blaschuk, O. W., Sullivan, R., David, S. and Pouliot, Y. (1990) Dev. Biol. **139**, 227–229
29 Nose, A., Tsuji, K. and Takeichi, M. (1990) Cell **61**, 147–155
30 Doherty, P., Rowett, L. H., Moore, S. E., Mann, D. A. and Walsh, F. S. (1991) Neuron **6**, 247–258
31 Kremmidiotis, G., Baker, E., Crawford, J., Eyre, H. J., Nahmias, J. and Callen, D. F. (1998) Genomics **49**, 467–471
32 Murphy-Erdosh, C., Yoshida, C. K., Paradies, N. and Reichardt, F. (1995) J. Cell Biol. **129**, 1379–1390
33 Inuzuka, H., Miyatani, S. and Takeichi, M. (1991) Neuron **7**, 69–79
34 Matsunami, H., Miyatani, S., Inoue, T., Copeland, N. G., Gilbert, D. J., Jenkins, N. A. and Takeichi, M. (1993) J. Cell Sci. **106**, 401–409

Received 16 February 2000, accepted 25 April 2000

Biochem J (2000) 349, 169–177 (Printed in Great Britain)

The pepsin residue glycine-76 contributes to active-site loop flexibility and participates in catalysis

Monika OKONIEWSKA, Takuji TANAKA and Rickey Y. YADA[1]
Department of Food Science, University of Guelph, Guelph, ON, N1G 2W1, Canada

Glycine residues are known to contribute to conformational flexibility of polypeptide chains, and have been found to contribute to flexibility of some loops associated with enzymic catalysis. A comparison of porcine pepsin in zymogen, mature and inhibited forms revealed that a loop (a flap), consisting of residues 71–80, located near the active site changed its position upon substrate binding. The loop residue, glycine-76, has been implicated in the catalytic process and thought to participate in a hydrogen-bond network aligning the substrate. This study investigated the role of glycine-76 using site-directed mutagenesis. Three mutants, G76A, G76V and G76S, were constructed to increase conformational restriction of a polypeptide chain. In addition, the serine mutant introduced a hydrogen-bonding potential at position 76 similar to that observed in human renin. All the mutants, regardless of amino acid size and polarity, had lower catalytic efficiency and activated more slowly than the wild-type enzyme. The slower activation process was associated directly with altered proteolytic activity. Consequently, it was proposed that a proteolytic cleavage represents a limiting step of the activation process. Lower catalytic efficiency of the mutants was explained as a decrease in the flap flexibility and, therefore, a different pattern of hydrogen bonds responsible for substrate alignment and flap conformation. The results demonstrated that flap flexibility is essential for efficient catalytic and activation processes.

Key words: aspartic proteinase, hinge, hydrogen bond, pepsinogen activation, substrate alignment.

INTRODUCTION

Loops represent a relatively new category of secondary structures. They reverse the direction of a polypeptide chain and are usually situated at the protein surface. Unlike α-helices and β-sheets, loop structures have no regular patterns of dihedral angles and hydrogen bonds [1,2]. Loop residues that are involved in catalysis may be more highly conserved than amino acids in surface loops whose role is purely structural. This sequence conservation can involve amino acids that interact directly with a substrate as well as amino acids that help stabilize various conformations that the loop may adopt during catalysis [3].

The hydrogen bonds to main-chain polar atoms play an important role in maintaining medium-sized loop structures. They can be formed from the loop atoms to main-chain or side-chain atoms or ligands [4]. It was observed in lactate dehydrogenase that open and closed loop conformations were facilitated by the same pattern of hydrogen bonds made among loop atoms [5]. In contrast, hydrogen bonds in triosephosphate isomerase reorganized during catalysis [6].

Loop structures have been identified in many enzymes where they have been implicated in protein function, stability and possibly in protein folding. In aspartic proteinases, a loop, commonly known as a flap, is found to extend over the active site and has been implicated in the catalytic process [7,8].

Three-dimensional structures at high resolutions have been identified for viral, fungal and mammalian aspartic proteinases. A comparison of the molecules reveals that their tertiary structures have been conserved during evolution. However, the enzymes differ in their primary structures, sequence homologies and substrate preferences. Therefore, aspartic proteinases represent an interesting group in which to study structure and function relationships [9]. Porcine pepsin is a particularly good model for these studies since its structures in zymogen, mature and inhibited forms have been determined [8,10,11].

Under physiological conditions porcine pepsin is secreted in the stomach as a zymogen, pepsinogen. In pepsinogen, a 44-residue peptide, referred to as a prosegment, blocks the entrance to the active site and is held in place by electrostatic interactions with the pepsin molecule. The acidic environment triggers the activation process. At pH values lower than 5.0, the reduction of electrostatic interactions between the pepsin molecule and the prosegment initiates a series of conformational changes and proteolytic cleavage of the prosegment or its fragments from the N-terminus of pepsin to yield a mature enzyme [10,12]. The final shape of substrate-binding subsites is gained during the activation process and residues lining the binding cleft assume positions that enable hydrogen bonding to a substrate. The hydrogen bonds align the substrate in the position most favourable for the catalysis. The crystal structures of pepsin in free and inhibited forms indicated that three flap residues, Y75, G76 and T77 (one-letter amino acid notation), contribute directly to a particular subsite specificity by hydrogen bonding to substrate residues [10,11]. Y75 was found to participate in substrate alignment; however, its influence was less pronounced than in chymosin and *Rhizomucor* pepsin, which had higher substrate specificities [13]. It was suggested that Y75 anchored the flap in pepsin. In chymosin, the residue was more mobile and therefore able to adopt more conformations that could contribute to high enzyme specificity [14]. An investigation of the role of T77 in pepsin catalysis revealed that the residue provides a catalytically essential hydrogen bond to a substrate. It was concluded that the hydrogen bond in position 77 participates in the substrate alignment and in this way is indirectly responsible for the proper geometry in the transition state [15].

Abbreviation used: Trx-PG, thioredoxin–pepsinogen fusion protein.

[1] To whom correspondence should be addressed (e-mail ryada@uoguelph.ca).

Table 1 Flap sequences of selected aspartic proteinases

Fungal pepsins are represented by endothiapepsin, penicillopepsin and rhizopuspepsin The numbering is according to porcine pepsin [36,44]

		Loop residue				
Enzyme	Position	75	76	77	78	79
Porcine pepsin		Y	G	T	G	S
Human pepsin		Y	G	T	G	S
Bovine chymosin		Y	G	T	G	S
Porcine chymosin		Y	G	T	G	S
Human cathepsin E		Y	G	T	G	S
Human cathepsin D		Y	G	S	G	S
Human gastricsin		Y	G	S	G	S
Human renin		Y	S	T	G	T
Fungal pepsins		Y	G	D	G	S

An examination of G76 atomic contacts in inhibited pepsin structure [11] indicates that main-chain hydrogen of G76 participates in hydrogen bonding to a substrate. It has also been suggested that glycine 76 is involved in the hydrogen bond stabilizing the transition state [16,17] A comparison of eukaryotic aspartic proteinases (Table 1) in the flap region demonstrates that G76 and G78 are conserved in all enzymes with the exception of renin. However, G78 is in a location too distant to interact directly with a substrate. At the same time, the greatest change in the pepsin flap structure is induced in residues G76–G78 located at the tip of the flap. C_α atoms of G76–T77–G78 move by 4.8 Å (1 Å = 0.1 nm) on average [14]. The observations suggest that G76 participates in the catalysis by direct interaction with a substrate, a transition state and/or by providing essential flap flexibility.

Glycine residues were implicated in providing conformational freedom to the polypeptide chain [18]. They have been shown to act as points of flexibility for hinge-type motions in the active-site loop of glutathione synthetase and tryptophan synthase. Some flexible loop structures identified in other enzymes that are known to change their positions during catalysis have glycines at their terminal positions, e.g. adenylate kinase, lactate dehydrogenase and Rubisco The residues probably represent flexibility points essential for the flap motions [19–23].

The present study investigated the role of G76 in pepsin's catalytic mechanism by substituting the residue in position 76 with alanine, valine and serine. These amino acids differ in their van der Waals volumes (G, 48 Å^3, A, 67 Å^3; V, 105 Å^3; S, 73 Å^3), accessible surface areas (G, 85 Å^2; A, 113 Å^2; V, 160 Å^2; S, 122 Å^2), polarities and allowable energy levels on Ramachandran plots for individual amino acids [18].

EXPERIMENTAL PROCEDURES

Materials

Restriction enzymes with corresponding buffers were purchased from New England Biolabs (Mississauga, ON, Canada) and Boehringer Mannheim Canada (Laval, QC, Canada). All the chromatography resins were purchased from Pharmacia Biotech (Uppsala, Sweden). Protein assay reagents, SDS/PAGE reagents and equipment were purchased from Bio-Rad (Hercules, CA, U.S.A.) Substrate I, Lys-Pro-Ala-Glu-Phe-Phe(NO$_2$)$_p$-Ala-Leu, was synthesized at the Institute for Molecular Biology and Biotechnology, McMaster University, Hamilton, ON, Canada. Substrate II, Leu-Ser-Phe(NO$_2$)$_p$-Nle-Ala-Leu, was purchased from Sigma (St. Louis, MO, U.S.A.). Additional materials were obtained either from Fisher Scientific (Mississauga, ON, Canada) or Sigma.

Energy minimization and molecular dynamics

Calculations were performed using Discover 2.9.5 (Biosym Technologies, San Diego, CA, U.S.A.) on an IBM Risc System/6000 computer The co-ordinates of porcine pepsin (PDB entry 4PEP by Sielecki et al. [8]) from the Protein Data Bank were used as initial data for the calculations. The residues of the wild-type protein were replaced with corresponding mutant residues and energy minimization was performed in a consistent valence force field by the steepest-descents method for 2000 iterations with 24-Å cut-off and a maximum derivative of 0.001 kcal (1 cal ≡ 4.184 J)/mol. The wild-type was minimized as the reference. Molecular-dynamics simulations were performed on the energy-minimized molecule models for 11 fs at 300 K. Co-ordinates were collected every 20 fs. Flap flexibility was determined based on the mean square deviation of the α-carbon atom displacements during the dynamics calculations.

Plasmid construction and cloning

Mutations of pepsinogen were performed according to the method of Kunkel [24]. Site-directed mutagenesis was performed using bacterial strains of *Escherichia coli* CJ236 (*dut*$^-$ *ung*$^-$), JM109 (wild-type) and bacteriophage M13mp19 RF (replicative form) DNA. The primers that introduced desired mutations and new restriction enzyme sites were for G76A, CCATCACA*TATGC*CACCGGTAG (*Nde*I); for G76V, CCATCACA*TATGT*CACCGGTAG (*Nde*I); and for G76S, CACCTATA*GT*ACT*GGTAGCATG (*Sca*I). Base replacements are indicated by asterisks, and restriction-enzyme sites are underlined. The mutations were confirmed on agarose gel after digestion with appropriate restriction enzymes and DNA sequencing by the automated M13-dideoxy method. The mutated pepsinogen genes were expressed as fusion proteins with thioredoxin (fusion protein, Trx-PG) in *E. coli* GI724 using pTFP1000 plasmid [25] by introducing a short fragment containing the mutation in place of the wild-type counterpart. Fusion-protein production was verified using Western blotting with rabbit anti-pepsinogen polyclonal antibodies and goat anti-rabbit-IgG–alkaline phosphatase conjugate. The blots were visualized using Nitro Blue Tetrazolium (NBT) and 5-bromo-4-chloroindo-3-yl phosphate toluidine (BCIP) solutions in 0.1 M Tris/50 mM MgCl$_2$/0.1 M NaCl, pH 9.5.

Protein expression and purification

Transformed cells were pre-cultured in RM media [0.8 % (w/v) casamino acids, 1 % (v/v) glycerol, 1 × M9 salt and 0 1 mM MgCl$_2$] at 30 °C for 18 h, and grown in Luria–Bertani media (1 % Bacto Tryptone, 0.5 % Bacto Yeast Extract, 1 % NaCl and 0.15 μg/ml ampicillin, pH 7.5) at 30 °C for 10 h. Cells were collected by centrifugation at 15000 g for 10 min, resuspended in 20 mM Tris/HCl, pH 8.0, and disrupted by sonication. Cell lysate was collected by centrifugation at 20000 g for 20 min. The purification procedure was performed using three ion-exchange columns Nucleic acids were precipitated from the cell lysate with protamine sulphate (10 % of protein concentration) and removed by centrifugation (20000 g, 20 min). Urea was added to the supernatant at 2 M. The supernatant was applied at a flow rate of 1 ml/min on a CM-Sepharose column (2.5 × 22 cm) connected directly to a DEAE-Sephacel column (2.5 × 30 cm) equilibrated with 0.1 M NaCl in 20 mM Tris/HCl/2 M urea (pH 8.0) buffer.

Urea was necessary to increase resolution of the fusion protein. Without urea, the fusion protein eluted as a very broad band spreading over approx 0.15–0.35 M. The two columns were disconnected after washing with 0.1 M NaCl in 20 mM Tris/HCl/2 M urea, pH 8.0, and the second column was subsequently washed with a stepwise gradient of NaCl (0.15, 0.2, 0.35 M) in 20 mM Tris/HCl/2 M urea, pH 8.0, at 1 ml/min and 4 °C. The purest fractions of the fusion protein, as detected by SDS/PAGE, were eluted with 0.35 M NaCl, pooled, and diluted three to four times to decrease the ionic strength. This preparation was applied to a DEAE-Sepharose column (2.5 × 25 cm) equilibrated with 50 mM phosphate buffer, pH 6.5, and washed with a stepwise gradient of NaCl (0.1, 0.2, 0.25, 0.3 M), at 1 ml/min and 4 °C. The Trx-PG fractions eluted with 0.3 M NaCl were subjected to further concentration on an Amicon concentrator model 8200 using a 10-kDa cut-off refined cellulose membrane (Amicon, Beverly, MA, U.S.A.) to a final volume of approx. 10 ml. The sample was then dialysed against 20 mM Tris/HCl, pH 8.0, filtered through a 0.22-μm nitrocellulose filter, and stored at 4 °C.

Protein concentration

Protein concentration was determined using two methods: (i) absorbance at 280 nm using an absorption coefficient of 27500 l/mol · cm [26]; and (ii) Bio-Rad D_C protein assay based on the Lowry method. Standard curves were generated using BSA.

SDS/PAGE and Western-blot analysis

SDS/PAGE was performed using a Bio-Rad Mini-Protean cell on a 12% acrylamide gel at 30–40 mA. Proteins were stained with Coomassie Brilliant Blue R-250. Western blots were run on a Bio-Rad Mini-Trans Blot Cell at 100 V. Proteins were transferred to a 0.2 μm PVDF membrane.

Activation of Trx-PG and purification of pepsin

Fusion protein was incubated with 0.09 M HCl for 1 h at room temperature. Activated pepsin samples were then purified from thioredoxin-activation fragments by gel-filtration chromatography on Sephadex G50 [25]. Two buffers were used: 20 mM sodium acetate, pH 5.3, for kinetic assays and 10 mM sodium acetate, pH 5.3, for far-UV CD spectroscopy analysis. Active samples were identified by milk-clotting assay [27] and only the first active fraction that eluted in the void volume was used for further pepsin analysis. For near-UV spectroscopy analysis, fusion proteins were acidified as described above, neutralized with 1 M sodium acetate buffer, pH 5.3, and then pepsins were purified from activation fragments in Centricon filtration units with a 30-kDa molecular-mass cut-off (Amicon) at 5000 *g*. The buffer was exchanged to 10 mM sodium acetate, pH 5.3, during filtration in the Centricon units.

CD spectroscopy

Far-UV CD spectra were generated using 800 μl of 0.1 mg/ml purified enzyme solutions with a Jasco 600 spectropolarimeter (Japan Spectroscopic Co., Tokyo, Japan). Pepsin samples in a 0.1-cm pathlength cuvette were scanned six times from 190 to 250 nm at room temperature under continuous nitrogen flush. The buffer blank and enzyme solutions were degassed prior to the analyses. Secondary structures were determined using the Jasco Protein Secondary Structure Estimation Program based on the method of Chang et al. [28].

Near-UV CD spectra were obtained from 1 mg/ml degassed pepsin solutions in 10 mM sodium acetate buffer, pH 5.3. Pepsin samples of 1 ml were placed in a 1-cm pathlength cuvette and scanned eight times from 320 to 240 nm at room temperature under continuous nitrogen flush. Tanaka and Yada [25] showed that properties of the wild-type and native pepsin(ogens) were the same (including N-terminal sequences). In addition, preliminary studies demonstrated that structures of the wild-type and native pepsins were the same (results not shown). Therefore, comparison of structural results for G76 mutants was performed relative to the wild-type pepsin obtained from the activation of the fusion protein in the same way as all the mutants.

Kinetic analyses

Kinetic measurements were performed on a DU 640 spectrophotometer (Beckman Instruments, Fullerton, CA, U.S.A.) with a temperature-control unit. Two synthetic substrates, as defined in the Materials section, were used. For substrate I, a change in absorbance was measured at 300 nm, 37 °C, in 100 mM sodium citrate buffer, pH 2.1 [29]. The substrate range was 2–200 μM. For substrate II, a change in absorbance was measured at 310 nm, 37 °C, in 100 mM sodium citrate buffer, pH 3.95. The second substrate range was 2–300 μM. A minimum of six concentrations for each substrate range was used to determine initial rates. All the kinetic experiments were performed within the first 3 days after the final enzyme concentration. Enzymes were activated as described in the section on activation of Trx-PG and purification of pepsin (see above). The initial slopes of progress curves were measured to give ΔA/min. The non-linear least-squares method was used to fit data and to calculate the kinetic constants K_m and k_{cat} [30]. The results were calculated based on a minimum of two measurements for each enzyme.

Trx-PG activation kinetics, and pH dependency of activation were performed as described by Okoniewska et al. [15]. Starting fusion-protein concentrations were 0.2 mg/ml for Trx-PG activation kinetics and 0.3 mg/ml for pH dependency of activation studies. In Trx-PG activation kinetics, samples were taken as follows: for the wild-type protein, every 15 s at pH 1.1 and 2.0, and every minute at pH 3.0; for G76A, every 30 s at pH 1.1 and 2.0, and every 2 min at pH 3.0; and for G76V and G76S every 2 min at pH 1.1 and 2.0, and every 5 min at pH 3.0. The activation reactions were conducted at 14 °C. Activation rate constants were calculated based on the hydrolysis of synthetic substrate I, using integrated rate law. pH dependency of activation was determined using milk-clotting assay [27]. The activity of samples was tested over ten pH values starting at pH 1.1, then 1.5, and in 0.5-pH-unit increments to 5.5, after 1 h of activation. The results were calculated based on three measurements for each enzyme

RESULTS AND DISCUSSION

Molecular-dynamics calculations (Figure 1) indicated that all the mutants in position 76 resulted in altered flexibility of the flap. G76A mutant reduced the flexibility (increased the rigidity) in position 75 less than G76S and G76V mutants. The G76S mutant reduced flexibility of the flap in position 76 slightly less than the G76A mutant. The G76V mutant resulted in the greatest reduction in flexibility in position 76 and overall flap flexibility At the same time, the G76V mutation resulted in increased flexibility of T77 and G78. This increased flexibility could have resulted from the inability of T77 to participate in certain hydrogen-bond interactions due to increased rigidity in the neighbouring position 76. Substitution of glycine 76 with serine increased flap rigidity; however, less so than in the G76V mutant. The G76A mutation resulted in increased rigidity at the tip of the flap and greater overall flap flexibility. Therefore,

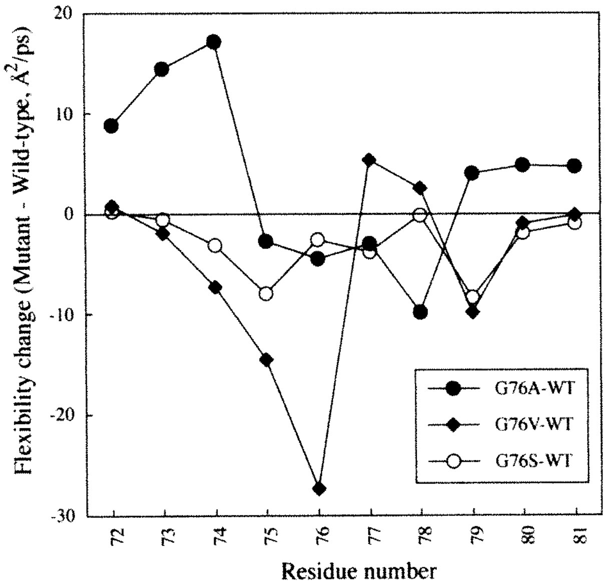

Figure 1 Evaluation of flap flexibility in pepsin G76 mutants and the wild-type (WT) using molecular-dynamics simulations

Molecular-dynamics simulations were performed on the energy-minimized molecule models. Flap flexibility was determined based on the mean square deviation of the α-carbon atom displacements during the dynamics calculations.

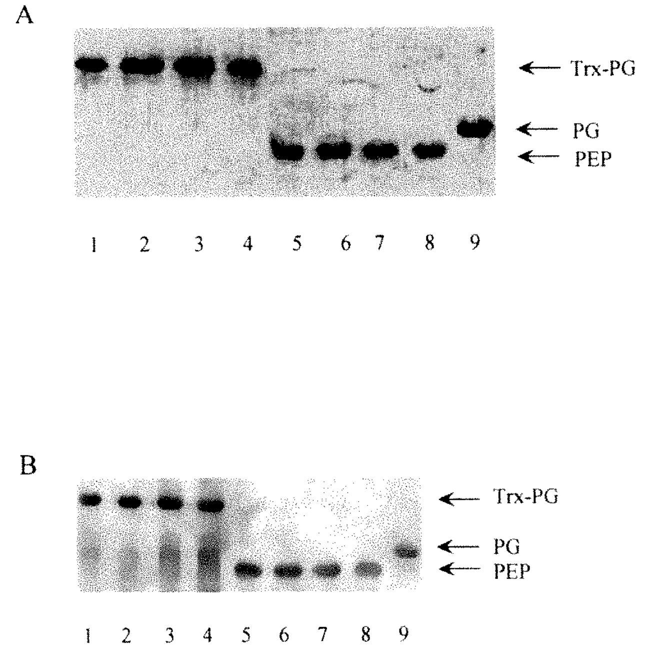

Figure 2 Electrophoresis and Western blot of mutant fusion proteins and pepsins

(**A**) SDS/PAGE (12% gel) stained with Coomassie Brilliant Blue R-250. (**B**) Western blot of the same gel. Fusion protein (Trx-PG) lanes: 1, wild-type; 2, G76A; 3, G76V; 4, G76S. Active pepsin (PEP) lanes: 5, wild-type; 6, G76A; 7, G76V; 8, G76S; lane 9, commercial pepsinogen (PG). In comparison with the results from SDS/PAGE (**A**), the Western blot (**B**) indicated that there were additional diffuse bands with mobilities similar to pepsinogen in the wild-type, G76A, G76V and G76S fusion proteins. These bands were artifacts resulting from storage. Freshly prepared protein samples did not show any of these bands. However, to run all samples on a single gel required that certain samples be stored for some months. In addition it was estimated that the amount of these faint bands was less than 0.1% of the fusion protein, and that no difference in activity should be observed.

the overall increase in flexibility could compensate for the more rigid tip of the flap. The molecular-dynamics calculations indicated that the greatest reduction of flexibility in position 76 resulted in the highest increase in flexibility of T77. It was determined previously [15] that the hydrogen bond from T77 participates in substrate alignment and indirectly positions the transition state. Consequently, the G76V mutation would be expected to have the greatest effect on enzyme kinetic parameters.

All the enzymes had similar elution profiles (results not shown) and were purified to homogeneity, as indicated by single bands on SDS/PAGE (Figure 2A). The identity of all enzyme preparations in zymogen and active forms was determined by immunoblotting (Figure 2B).

The secondary structure of all the mutants was analysed by far-UV CD spectroscopy. The results are presented in Figure 3. All the mutants had spectra overlapping with the wild-type, and their calculated secondary-structure contents were virtually the same as the wild-type (Table 2), indicating that no global secondary-structure change occurred as a result of the mutations.

Tertiary-structure analysis by near-UV CD spectroscopy (Figure 4) revealed that there were differences between mutants and the wild-type protein. The G76A mutant had a profile very similar to the wild-type. However, profiles for G76S and G76V mutants were different than the wild-type, with the greatest difference in spectral pattern seen in the G76V mutant. The near-UV CD profile differences reflect changes in the environment of aromatic residues. In the pepsin molecule, G76 is in the direct vicinity of Y75. In addition, Y75 is close to other aromatic residues in pepsin's active site, e.g. W39, F111 and F117 [8,31]. The change in environment of the active-site residues could contribute to observed differences in near-UV CD profiles. Therefore, the results indicated that mutations G76S and G76V changed the environment of aromatic residues in the vicinity of position 76. All the CD results combined suggested that the mutations did not induce dramatic conformational change and that the observed differences were caused by changes in the local conformation of the loop region (residues 71–80).

The mutants and wild-type protein were activated in ten different pH conditions from 1.1 to 5.5 over the same time of acidification to determine the pH dependence of the activation process. The amounts of pepsins formed were determined by milk-clotting assay. The activation profiles were plotted as relative amount of pepsin formed during the acidification time against pH of activation (Figure 5). The amounts of pepsin were the highest at the most acidic pH, demonstrating that all the enzymes were activated fastest in a highly acidic environment. Minimum milk-clotting activity was still observed at pH 4.5. The enzymes did not activate at pH 5.0 and 5.5. The activation profiles were similar for all the mutants and the wild-type protein, demonstrating that all the proteins reacted similarly to a change in pH environment. The mutations of G76 did not introduce any additional ionizable groups to the flap. However, the flap in pepsinogen is in a different position to that in pepsin and interacts with charged residues in the zymogen. The maximum change of the flap position is induced by residues G2-D3-E4-P5-L6-E7-N8 that insert between the flap and the E107–S110 strand in the zymogen [10,14]. In addition, Y9 has been proposed to play a critical role in the stabilization of pepsinogen [32]. If any structural changes occurred in the zymogen they should have been reflected in the interaction pattern between the flap and the G2–Y9 strand and, therefore, in the pH dependency of the activation process. The results showed that there was no change in pH dependency of activation despite the mutations.

All the mutants had similar pH activation profiles and purification chromatogram profiles (results not shown), and

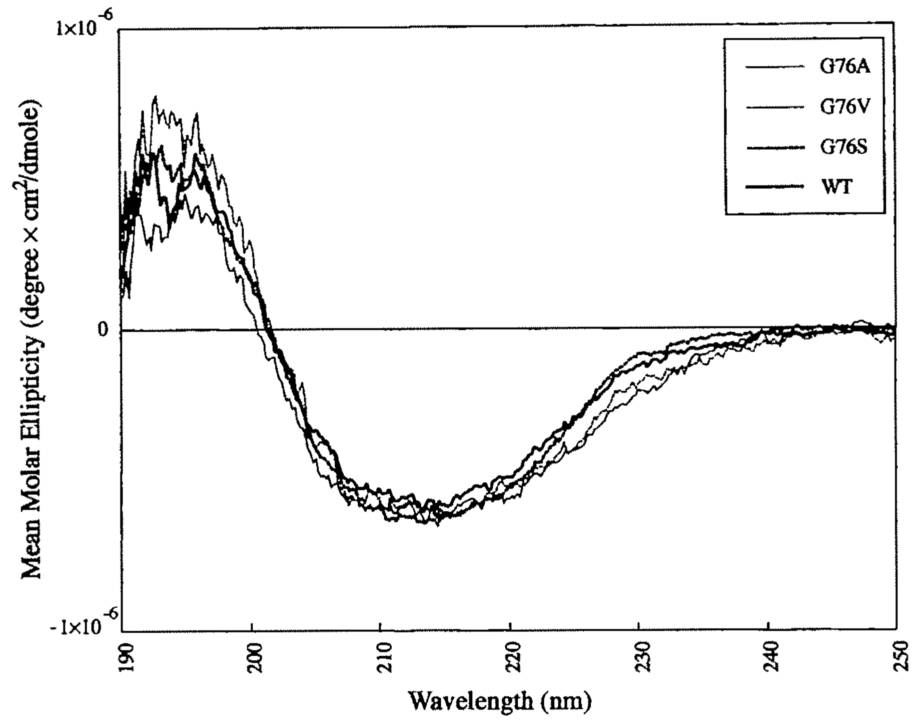

Figure 3 Far-UV CD spectra of the wild-type and mutant pepsins

Experiments were carried in 10 mM sodium acetate buffer, pH 5.3 Spectra were generated using 800 μl of 0.1 mg/ml purified enzyme solutions in a 0.1-cm pathlength cuvette after six scans from 190 to 250 nm at room temperature under continuous nitrogen flush

Table 2 Secondary-structure content of wild-type pepsin and G76 mutants determined by far-UV CD

RMS, root mean square

	Secondary-structure content (%)				
Enzyme	α-Helix	β-Sheet	β-Turn	Random coil	RMS
Wild-type	3.9	56.8	12.5	26.8	3.91
G76A	2.5	63.2	12.2	22.1	4.24
G76V	4.1	57.5	11.3	27.0	2.87
G76S	3.7	56.2	11.9	28.1	2.20

responded in the same manner to antibody binding, indicating that spatial conformation of the proteins was similar. Additionally, structural analyses indicated that the conformation of the mutants in the amide region was the same as the wild-type. Structural perturbations were observed in the aromatic region and were associated with local differences of the flap. Therefore, it was concluded that mutations in position 76 did not change overall enzyme conformations and had only regional effects.

Rate constants of the activation process were calculated for the mutants and the wild-type under three different pH conditions: pH 1.1, 2.0 and 3.0. Samples were taken at different activation times, quenched, and the amount of pepsin formed was determined with synthetic substrate I, as described in the Experimental procedures section. The activation process of pepsinogen fused with thioredoxin was shown to be unimolecular, contrary to the bimolecular activation process of native and recombinant pepsinogens [33]. Therefore, the activation rate constants, presented in Table 3, correspond to first-order reaction constants. All the mutants activated more slowly than the wild-type, regardless of amino acid size and polarity. Under all pH conditions the activation reactions were the slowest for valine and serine mutants, which had comparable reaction rates. The alanine mutant activated slower than the wild-type protein but faster than the two other mutants.

Kinetic properties of the wild-type and the mutant enzymes were determined with two synthetic substrates and the kinetic constants, K_m and k_{cat}, were calculated using the non-linear least-squares method [30]. The kinetic parameters are presented in Table 4. All the mutants, regardless of amino acid size and polarity, had lower substrate affinity and turnover numbers than the wild-type enzyme. The differences in the catalytic parameters were similar for the two synthetic substrates, indicating that the changes were not substrate-specific and that the results could, therefore, be attributed to differences in the catalytic environments of the mutants. The kinetic experiments were performed at two different pH values: pH 2.1 for synthetic substrate I and pH 3.95 for synthetic substrate II. The kinetic constants showed the same tendencies under the two different pH conditions. Therefore, it was concluded that the mutations did not change the pH dependencies of mature enzymes The above results indicated that the mutations had minimal effect on substrate binding and mainly influenced the properties of enzyme-bound species in the reaction pathway. In addition, stereochemical analysis of peptide-bond hydrolysis [16] and pepsin crystal structure [8] indicated that G76 is in a position most favourable for interactions with reaction intermediates. A possible involvement of G76 in stabilizing the transition state was indicated by the authors of the hypothetical catalytic mechanism for pepsin [17].

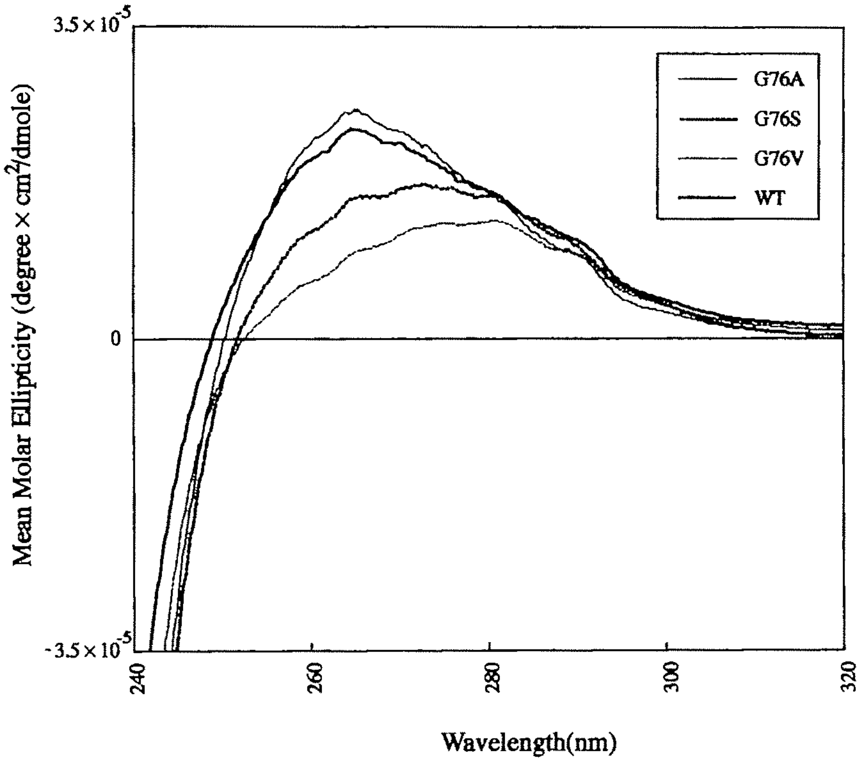

Figure 4 Near-UV spectra of the wild-type and mutant pepsins

Experiments were carried in 10 mM sodium acetate buffer, pH 5.3. Spectra were generated using 1 ml of 1 mg/ml purified enzyme solutions in a 1-cm pathlength cuvette after eight scans from 320 to 240 nm at room temperature under continuous nitrogen flush. Spectra were obtained from 1 mg/ml pepsin solution in 10 mM sodium acetate buffer, pH 5.3

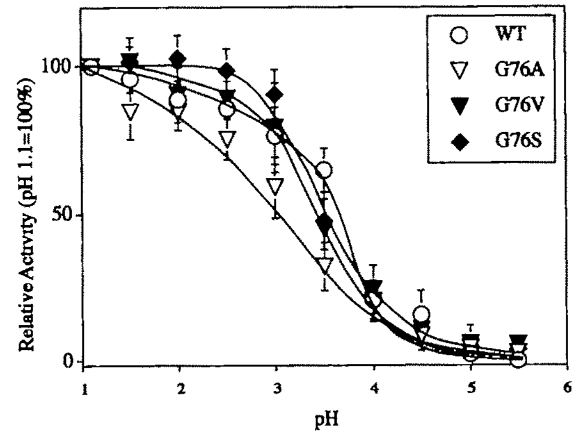

Figure 5 Relative amounts of pepsin formed during activation under different pH conditions for fusion-protein G76 mutants as determined by milk-clotting assay

Each point represents the mean ± S.D. of three measurements

Table 3 First-order rate constants for activation of Trx-PG

	k_{act} (min^{-1})		
Enzyme	pH 1.1	pH 2.0	pH 3.0
Wild-type	4.449 ± 0.262	2.819 ± 0.152	1.043 ± 0.089
G76A	0.311 ± 0.076	0.332 ± 0.014	0.104 ± 0.029
G76V	0.132 ± 0.001	0.152 ± 0.013	0.054 ± 0.001
G76S	0.13 ± 0.014	0.166 ± 0.014	0.059 ± 0.003

The trend in the activation rate constants was similar to that for the catalytic rate constants of the mutants and wild-type enzyme. All the mutants were less efficient in catalysis and activation processes than the wild-type, and the alanine mutant had higher catalytic and activation efficiency than the two other mutants, valine and serine. These results indicate that G76 plays the same role in the activation and catalytic processes. During the activation process, a prosegment represents a substrate. Therefore, the results suggest that proteolytic cleavage is a limiting step of the activation process. This is in agreement with earlier results that any changes in pepsin flap sequence in position 77 had the same effect on the activation and catalytic processes and suggested that proteolytic cleavage limits the activation process of the fusion proteins [15].

All the mutants had altered kinetic constants compared with the wild-type; however, the degree of change was different for individual enzymes. The alanine mutant was affected less than either the valine or serine mutants, which had comparable catalytic constants. Alanine has the smallest van-der-Waals volume and accessible surface area compared with valine and serine. Therefore, it places a relatively smaller restriction on a polypeptide's conformational flexibility and has relatively less contacts with surrounding atoms. Valine and serine mutants have larger volumes and their presence in a polypeptide chain results in greater conformational restrictions due to the atom-

Table 4 Kinetic parameters for wild-type pepsin and the G76 mutants

Kinetic constants were calculated based on a minimum of two measurements for each enzyme

Substrate	Enzyme	K_m (mM)	k_{cat} (s^{-1})	k_{cat}/K_m($mM^{-1} \cdot s^{-1}$)
(I) KPAEFF(NO_2)AL	Wild-type	0 043 ± 0 005	180.5 ± 10 3	4198 ± 544
	G76A	0 098 ± 0 008	47 0 ± 9 9	395 ± 96
	G76V	0 071 ± 0 011	11 1 ± 1 1	160 ± 30
	G76S	0 085 ± 0 005	2 5 ± 0 6	29 ± 7
(II) LSF(NO_2)NleAL-OCH_3	Wild-type	0 011 ± 0 002	88 7 ± 4 6	8064 ± 1525
	G76A	0 040 ± 0.009	43.4 ± 3 6	1085 ± 260
	G76V	0 044 ± 0 005	1 2 ± 0 1	28 ± 3
	G76S	0 041 ± 0 008	2 9 ± 0 3	70 ± 16

Table 5 Distances between atoms in the tip of the pepsin flap in pepsinogen, pepsin and inhibited pepsin (1.8–2.9 Å resolution)

I represents an inhibitor atom.

		Distance (Å)		
Atoms	Enzyme form ..	Pepsinogen	Pepsin	Inhibited pepsin
76 NH	75 O	2 25	2 28	2 28
	76 O	3 65	3 63	3 37
	I1 OH	–	–	3.3
	I3 O	–	–	2.9
76 O	77 NH	2 20	2 23	2 28
	77 OH	4 61	4 92	2 82
77 NH	77 OH	3 1	2 87	2 82

crowding effect. Consequently, the results suggested that all the mutations reduced polypeptide conformational freedom in the flap region. This is in agreement with molecular-dynamics calculations and structural analyses of the mutants, where the greatest local perturbations were observed for the G76V mutant. Similar observations were made in catalytic loops of other enzymes. The conversion of glycine in a flexible loop of F_1-ATPase into any residue bulkier than proline diminished the conformational mobility of the segment or destabilized β-turn [34]. Mutations of glycine 121 in the flexible loop of dihydrofolate reductase to valine and leucine modified loop flexibility and impaired its active-site lid function [35]. In glutathione synthetase, replacement of glycines and proline in the active-site loop with alanine and valine reduced flexibility of the loop [19]. Our results, combined with observations made in other loop structures, demonstrate that glycine in pepsin position 76 contributes to the flap flexibility and that this flexibility is essential for efficient catalysis.

In addition to reduced flap flexibility, the mutants could cause different distribution of hydrogen bonds in pepsin's binding cleft, especially the G76S mutant. The polar mutant had catalytic parameters lower than those of the wild-type and of a similar magnitude to the G76V mutant. However, serine's volume and accessible surface area were closer to alanine than valine. Therefore, if only reduced flap flexibility contributed to the lower catalytic parameters of G76S they should have resembled the catalytic efficiency of G76A rather than of G76V. However, the G76A mutant had catalytic parameters that were affected less than both the G76S and G76V mutants. At the same time, G76S introduced an additional polar group and, therefore, a hydrogen-bonding potential, as compared with the wild-type and the other mutants. Consequently, our results suggested that the additional hydrogen bond in the G76S mutant distorted the hydrogen-bond network in the active site in addition to the effect of reduced flap flexibility. In addition, molecular-dynamics calculation indicated that the G76V mutant would result in increased flexibility of T77 and, therefore, reduced probability of hydrogen-bond formation by the hydroxy group in position 77. Therefore, both G76S and G76V mutations would have resulted in altered hydrogen-bond distribution in comparison with the wild-type. The results support previous observations that the catalytic process in pepsin is sensitive to any changes in a delicate network of hydrogen bonds that participate in substrate alignment [10,15]. Differences in the hydrogen-bond patterns in aspartic proteinase binding clefts may contribute to substrate-specificity differences among the group members. For example, renin is the only aspartic proteinase that has serine in position 76 (Table 1) and, at the same time, it is highly specific towards angiotensinogen [36]. Consequently, S76 in renin (pepsin numbering) is likely to contribute to the lower flap mobility and different hydrogen-bond pattern and, therefore, to the high specificity of this enzyme.

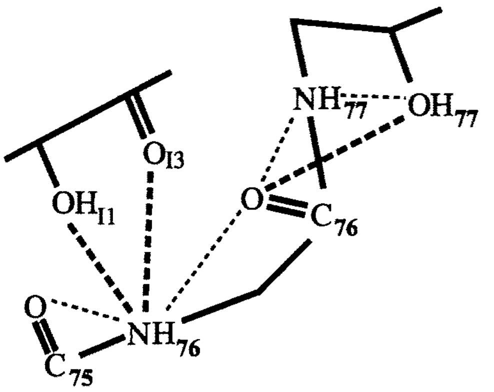

Figure 6 Schematic diagram of hydrogen bonds made by G76 and T77

Inhibitor atoms are denoted by the letter I Hydrogen bonds present in pepsinogen, pepsin and inhibited pepsin are shown as thin broken lines Distances equivalent to newly formed hydrogen bonds in inhibited pepsin are represented as thick broken lines

The reduced flexibility of the flap could indirectly affect hydrogen-bond distribution near the active site. In fungal and mammalian pepsins it has been shown that hydrogen-bonding potential in position 77 is essential for enzyme specificity and efficient catalysis [15,37]. Lower conformational freedom of the mutated flap could prohibit the residue in position 77 from forming a hydrogen bond with a substrate that was supported by energy minimization. In addition, the steric hindrance caused by overcrowding of atoms in G76 mutants could change a pattern of hydrogen bonds made by the G76 backbone and, therefore, the stability of reaction intermediates.

The distribution of hydrogen bonds in loops was thought to be responsible for their conformations [4]. Therefore, we also investigated hydrogen bonds between the flap backbone and side-chain atoms in pepsinogen, pepsin and inhibited pepsin. Table 5 lists possible distances of hydrogen bonds that were identified at the tip of the flap from crystal structures obtained at resolutions of 1.8–2.9 Å. Therefore, bond distances should be considered with a 1 8 Å confidence region. Figure 6 shows a schematic diagram of the hydrogen-bond distances at the tip of the flap in the three enzyme forms. Comparison of the three enzyme forms, i.e. zymogen, active and inhibited pepsin, revealed that during catalysis changing distances in the flap region corresponded to formation of hydrogen bonds between G76-backbone atoms and an inhibitor and T77 In the inhibited enzyme, the amide nitrogen of G76 came into hydrogen-bonding distance of the hydroxy and carbonyl oxygens of an inhibitor, and a carbonyl oxygen in position 76 came into hydrogen-bonding distance of the hydroxy group of T77. These results indicate that G76-backbone atoms participate in a hydrogen bonding to a substrate and aid in positioning the T77 hydroxy group in the most favourable conformation for substrate alignment. Similar observations were made in the flexible loop of triosephosphate isomerase, where G171 hydrogen-bonded to a ligand and in this way was essential for substrate alignment [38] Likewise, the backbone nitrogen of loop glycine in lectin formed an essential part of the monosaccharide-binding site In dihydrofolate reductase, glycine located in the catalytically important loop indirectly influenced ligand conformation by positioning the active-site loop [39–41]

The four remaining hydrogen bonds between atoms of residues 75, 76 and 77 are present in all pepsin forms, which indicates that they are responsible for the conformation of the flap tip and preservation of a turn structure. The same observations were made in fructose-1,6-bisphosphatase, dihydrofolate reductase and thymidylate synthase [41–43], where networks of hydrogen bonds have been found to stabilize conformations of catalytically important loops. This is in agreement with findings that internal-loop hydrogen bonds are essential for maintaining the conformation of these structures [4]

All the observations made of the flap hydrogen-bond patterns suggest that the carbonyl oxygen of G76 helps to position the 77 hydroxy group, and that the 76 backbone nitrogen stabilizes the transition state. All the mutants in position 76 had altered catalytic properties since T77 was not able to adopt the proper conformation and G76-backbone hydrogen bonds were impaired. This is in agreement with previous observations that preservation of hydrogen-bond potential, as in a T77S pepsin mutant, did not change enzyme catalytic properties [15]. A different distribution of hydrogen bonds in all G76 mutants and T77 apolar mutants could distort flap conformation by changing interactions of atoms that maintain the flap structure. Consequently, different distribution of the hydrogen bonds at the flap tip could affect substrate alignment, geometry of the transition state and change conformation of the flap.

In conclusion, the results indicated that G76 is involved in the catalytic process. Introduction of any additional side chain to this position, as in the G76A, G76V and G76S mutants, resulted in less efficient catalysis and a slower activation process. Alanine, which has the smallest side chain of the three substituted amino acids, had the smallest effect on enzyme catalysis and local conformation. Introduction of bulkier amino acids, serine and valine, resulted in greater decreases in catalytic parameters and activation rate constants. Therefore, it was concluded that G76 is essential for pepsin-catalysed proteolysis by contributing to the flap flexibility. We suggest that flexibility is essential for hydrogen bonding of the T77 hydroxy group to a substrate. Detailed examination of possible hydrogen-bond distances at the tip of the flap revealed that G76-backbone atoms participated in maintenance of the flap conformation and in the geometry of reaction intermediates. Based on our results and observations made of structures of other enzymes, it is postulated that terminal glycine residues in catalytically important loops and turns serve to enable movement of the residues essential in enzyme action.

All the above results and our previous studies [15] combined indicate that the tip of the flap, i.e. residues 76 and 77, participates in the catalytic and activation processes by hydrogen bonding to a substrate, or the prosegment, respectively. Binding is possible by changing the position of the flap, which is facilitated by G76 contributing to flap flexibility. It is suggested that G76 acts as a hinge at the tip of the flap and enables formation of the hydrogen bond by T77, and that G78, which is preserved in all the compared aspartic proteinases (Table 1), serves as a second hinge of the flap tip. This is in agreement with observations made in the crystal structures of aspartic proteinases [14] that the tip of the flap, residues 76–78 (pepsin numbering), is the most flexible fragment of this structure. Our hypothesis is supported further by the results of Tanaka et al [19] and Schneider et al. [20], who found that glycines act as catalytic loop hinges in glutathione synthetase and tryptophan synthase, respectively A change of the flap position enables interactions of position-76 backbone nitrogen with reaction intermediates and possibly contributes to stabilization of the transition state, which is in agreement with previous suggestions [16,17]. Additionally, we have shown that G76 and T77 contribute to the hydrogen-bond network that is responsible for substrate alignment and efficient catalysis. The flap's internal hydrogen bonds are responsible for the conformation of this structure.

REFERENCES

1 Leszczynski, J F and Rose, G. D (1986) Loops in globular proteins a novel category of secondary structures Science **234**, 849–855

2 Fetrow, J S (1995) Omega loops nonregular secondary structures significant in protein function and stability FASEB J **9**, 708–717

3 Rose, G D, Gierasch, L M and Smith, J A (1985) Turns in peptides and proteins Adv Protein Chem **37**, 1–109

4 Tramontano, A, Chothia, C and Lesk, A M (1989) Structural determinants of the conformations of medium-sized loops in proteins. Proteins **6**, 382–394

5 Gerstein, M. and Chothia, C (1991) Analysis of protein loop closure Two types of hinges produce one motion in lactate dehydrogenase J Mol Biol **220**, 133–149

6 Sampson, N. S and Knowles, J R (1992) Segmental motion in catalysis investigation of a hydrogen bond critical for loop closure in the reaction of triosephosphate isomerase Biochemistry **31**, 8488–8494

7 Kempner, E S (1993) Movable lobes and flexible loops in proteins FEBS Lett **326**, 4–10

8 Sielecki, A R, Fedorov, A A, Boodhoo, A, Andreeva, N. S and James, M N G (1990) Molecular and crystal structures of monoclinic porcine pepsin refined at 1.8 Å resolution J Mol Biol **214**, 143–170

9 Tang, J, James, M N G, Hsu, I N, Jenkins, J A and Blundell, T L (1978) Structural evidence for gene duplication in the evolution of the acid proteases Nature (London) **271**, 618–621

10 Hartsuck, J. A, Koelsch, G and Remington, J S (1992) The high-resolution crystal structure of porcine pepsinogen Proteins **13**, 1–25

11 Chen, L., Erickson, J W, Rydel, T J, Park, C H, Neidhart, D, Luly, J and Abad-Zapatero, C (1992) Structure of pepsin/renin inhibitor complex reveals a novel crystal packing induced by minor chemical alterations in the inhibitor Acta Cryst **B48**, 476–488

12 Glick, M D, Hilt, C R. and Mende-Mueller, L (1991) Conformational change that accompanies pepsinogen activation observed in real time by fluorescence energy transfer Int J Peptide Protein Res **37**, 230–235

13 Tanaka, T, Teo, K S, Lamb, K M, Harris, L and Yada, R. Y (1998) Effect of replacement of the conserved Tyr75 on the catalytic properties of porcine pepsin A Protein Peptide Lett **5**, 19–26

14 Andreeva, N, Bochkarev, A and Pechik, I (1995) A new way of looking at aspartic proteinases a comparison of pepsin structure to other aspartic proteinases in the near active site region, in Aspartic Proteinases (Takahashi, K, ed), pp 19–32, Plenum Press, New York

15 Okoniewska, M, Tanaka, T and Yada, R (1999) The role of flap residue, threonine 77, in the activation and catalytic activity of pepsin A Protein Eng **12**, 55–61

16 James, M N G and Sielecki, A R (1985) Stereochemical analysis of peptide bond hydrolysis catalyzed by the aspartic proteinase penicillopepsin Biochemistry **24**, 3701–3713

17 Pearl, L H (1987) The catalytic mechanism of aspartic proteinases FEBS Lett **214**, 8–12

18 Creighton, T E (1994) Proteins Structures and Molecular Properties, 2nd edn., W H Freeman and Company, New York

19 Tanaka, T, Yamaguchi, H, Kato, H, Nishioka, T, Katsube, Y and Oda, J. (1993) Flexibility impaired by mutations revealed the multifunctional roles of the loop in glutathione synthetase Biochemistry **32**, 12398–12404

20 Schneider, T. R., Gerhardt, E, Lee, M, Liang, P-H, Anderson, K and Schlichting, I (1998) Loop closure and intersubunit communication in tryptophan synthase Biochemistry **37**, 5394–5406

21 Fry, D C, Kuby, S A and Mildvan, A S (1986) ATP-binding site of adenylate kinase mechanistic implications of its homology with *Ras*-encoded p21, F_1-ATPase, and other nucleotide-binding proteins. Proc Natl Acad Sci U S A **83**, 907–911

22 Wilks, H M, Moreton, K M, Halsall, D J, Hart, K W, Sessions, R, Clarke, A R and Holbrook, J J (1992) Design of a specific phenyllactate dehydrogenase by peptide loop exchange on the *Bacillus stearothermophilus* lactate dehydrogenase framework Biochemistry **31**, 7802–7806

23 Larson, E M, Larimer, F W and Hartman, F C (1995) Mechanistic insights provided by deletion of a flexible loop at the active site of ribulose-1,5-bisphosphate carboxylase/oxygenase Biochemistry **34**, 4531–4537

24 Kunkel, T A (1985) Rapid and efficient site-specific mutagenesis without phenotypic selection Proc Natl. Acad Sci U S A **82**, 488–492

25 Tanaka, T and Yada, R. Y (1996) Expression of soluble cloned porcine pepsinogen A in *Escherichia coli* Biochem J **315**, 443–446

26 Lin, X-l, Wong, R N S. and Tang, J (1989) Synthesis, purification, and active site mutagenesis of recombinant porcine pepsinogen J Biol Chem. **264**, 4482–4489

27 McPhie, P. (1976) The origin of the alkaline inactivation of pepsinogen Anal Biochem **73**, 258–261

28 Chang, C T, Wu, C-S C and Yang, J T. (1978) Circular dichroic analysis of protein conformation inclusion of the β-turns Anal Biochem **91**, 13–31

29 Lin, Y, Fusek, M, Lin, X, Hartsuck, J A, Kezdy, F J. and Tang, J (1992) pH dependence of kinetic parameters of pepsin, rhizopuspepsin, and their active-site hydrogen bond mutants J Biol Chem **267**, 18413–18418

30 Sakoda, M and Hiromi, K (1976) Determination of the best-fit values of kinetic parameters of the Michaelis–Menten equation by the method of least squares with Taylor expansion J Biochem (Tokyo) **80**, 547–555

31 Andreeva, N S., Zdanov, A S, Gustchina, A E and Fedorov, A A. (1984) Structure of ethanol inhibited porcine pepsin at 2 Å resolution and binding of the methyl ester of phenylalanyl-diiodotyrosine to the enzyme J Biol Chem. **259**, 11353–11365

32 Lee, A Y, Sergei, V. G. and Erickson, J W (1998) Conformational switching in an aspartic proteinase Nat Struct Biol **5**, 866–871

33 Tanaka, T and Yada, R. Y. (1997) Engineered porcine pepsinogen exhibits dominant unimolecular activation Arch. Biochem. Biophys **340**, 355–358

34 Seeburg, P. H, Colby, W W., Capon, D J, Goeddel, D V and Levinson, A. D (1984) Biological properties of human C-Ha-ras1 genes mutated at codon 12 Nature (London) **312**, 71–75

35 Gekko, K., Yamagami, K, Kunori, Y, Ichihara, S, Kodama, M and Iwakura, M (1993) Effects of point mutation in a flexible loop on the stability and enzymatic function of *Escherichia coli* dihydrofolate reductase J Biochem **113**, 74–80

36 Fujinaga, M, Chernaia, M M, Tarasova, N. I., Mosimann, S C and James, M. N G (1995) Crystal structure of human epsin and its complex with pepstatin Protein Sci **4**, 960–972

37 Shintani, T, Nomura, K and Ichishima, E (1997) Alteration of S_1 substrate specificity of pepsin to those of fungal aspartic proteinases by site-directed mutagenesis. J Biol Chem **272**, 18855–18861

38 Pompliano, D. L., Peyman, A and Knowles, J R (1990) Stabilization of a reaction intermediate as a catalytic device definition of the functional role of the flexible loop in triosephosphate isomerase Biochemistry **29**, 3186–3194

39 Yuksel, U K, Sun, A-Q, Gracy, R W and Schnackerz, K. D (1994) The hinged lid of yeast triose-phosphate isomerase. J Biol Chem **269**, 5005–5008

40 Hoedemaeker, F J., van Eijsden, R R, Diaz, C L, de Pater, B S. and Kijne, J W (1993) Destabilization of pea lectin by substitution of a single amino acid in a surface loop Plant Mol. Biol **22**, 1039–1046

41 Miller, G P and Benkovic, S J. (1998) Deletion of highly motional residue affects formation of the Michaelis complex for *Escherichia coli* dihydrofolate reductase Biochemistry **37**, 6327–6335

42 Choe, J-Y., Poland, B W, Fromm, H J. and Honzatko, R B (1998) Role of a dynamic loop in cation activation and allosteric regulation of recombinant porcine fructose-1,6,-bisphosphatase. Biochemistry **37**, 11441–11450

43 Schiffer, C. A, Clifton, I J, Davisson, V J, Santi, D V and Stroud, R M. (1995) Crystal structure of human thymidylate synthase a structural mechanism for guiding substrates into the active site Biochemistry **34**, 16279–16287

44 Abad-Zapatero, C, Rydel, T J and Erickson, J (1990) Revised 2 3 Å structure of porcine pepsin evidence for a flexible subdomain Proteins **8**, 62–81

Received 15 December 1999/31 March 2000, accepted 25 April 2000

Biochem J (2000) 349, 179–187 (Printed in Great Britain)

Reconstitution of purified, active and malonyl-CoA-sensitive rat liver carnitine palmitoyltransferase I: relationship between membrane environment and malonyl-CoA sensitivity

J. Denis McGARRY*† and Nicholas F. BROWN*[1]

*Department of Internal Medicine, University of Texas Southwestern Medical Center, 5323 Harry Hines Boulevard, Dallas, Texas 75235-9135, U.S.A., and
†Department of Biochemistry, University of Texas Southwestern Medical Center, 5323 Harry Hines Boulevard, Dallas, Texas 75235-9135, U.S.A.

Carnitine palmitoyltransferase I (CPT I) catalyses the initial step of fatty acid import into the mitochondrial matrix, the site of β-oxidation, and its inhibition by malonyl-CoA is a primary control point for this process. The enzyme exists in at least two isoforms, denoted L-CPT I (liver type) and M-CPT I (skeletal-muscle type), which differ in their kinetic characteristics and tissue distributions. A property apparently unique to L-CPT I is that its sensitivity to malonyl-CoA decreases *in vivo* with fasting or experimentally induced diabetes. The mechanism of this important regulatory effect is unknown and has aroused much interest. CPT I is an integral outer-membrane protein and displays little activity after removal from the membrane by detergents, precluding direct purification of active protein by conventional means. Here we describe the expression of a 6 × His-tagged rat L-CPT I in *Pichia pastoris* and purification of the detergent-solubilized enzyme in milligram quantities. Reconstitution of the purified product into a liposomal environment yielded a 200–400-fold increase in enzymic activity and restored malonyl-CoA sensitivity. This is the first time that a CPT I protein has been available for study in a form that is both pure and active. Comparison of the kinetic properties of the reconstituted material with those of L-CPT I as it exists in mitochondria prepared from yeast over-expressing the enzyme and in livers from fed or fasted rats permitted novel insight into several aspects of the enzyme's behaviour. The malonyl-CoA response of the liposomal enzyme was found to be greater when the reconstitution procedure was carried out at 22 °C compared with 4 °C ($IC_{50} \approx 11\ \mu M$ versus $30\ \mu M$, respectively). When the sensitivities of L-CPT I in each of the different environments were compared, they were found to decrease in the following order: fed liver > fasted liver ≈ liposomes prepared at 22 °C ≈ *P. pastoris* mitochondria > liposomes prepared at 4 °C. In addition, pre-treatment of L-CPT I liposomes with the membrane-fluidizing reagent benzyl alcohol caused densensitization to the inhibitor. In contrast with the variable response to malonyl-CoA, the liposomal L-CPT I displayed a pH profile and kinetics with regard to the carnitine and acyl-CoA substrates similar to those of the enzyme in fed or fasted liver mitochondria. However, despite a normal sensitivity to malonyl-CoA, L-CPT I in *P. pastoris* mitochondria displayed aberrant behaviour with regard to each of these other parameters. The kinetic data establish several novel points. First, even after stringent purification procedures in the presence of detergent, recombinant L-CPT I could be reconstituted in active, malonyl-CoA sensitive form. Second, the kinetics of the reconstituted, 6 × His-tagged L-CPT I with regard to substrate and pH responses were similar to what is observed with rat liver mitochondria (whereas in *P. pastoris* mitochondria the enzyme behaved anomalously), confirming that the purified preparation is a suitable model for studying the functional properties of the enzyme. Third, wide variation in the response to the inhibitor, malonyl-CoA, was observed depending only on the enzyme's membrane environment and independent of interaction with other proteins. In particular, the fluidity of the membrane had a direct influence on this parameter. These observations may help to explain the mechanism of the physiological changes in the properties of L-CPT I that occur *in vivo* and are consistent with the current topographical model of the enzyme.

Key words: fatty acid, liposome, mitochondria.

INTRODUCTION

The carnitine palmitoyltransferase (CPT) system consists of three enzymes that operate sequentially to effect the net transport of long-chain fatty acids from the cytosol into the mitochondrial matrix, the site of β-oxidation. The first component, CPT I, an integral protein of the outer mitochondrial membrane, catalyses the transfer of a fatty acyl group from cytosolic acyl-CoA to carnitine. The acylcarnitine formed is then able to enter the mitochondrial matrix by means of a specific carnitine/acylcarnitine carrier protein. A distinct gene product, CPT II, loosely associated with the inner aspect of the inner membrane, reverses the CPT I reaction, regenerating fatty acyl-CoA and releasing free carnitine. The acetyl-CoA formed may be completely oxidized via the tricarboxylic acid cycle for the direct production of energy or, in the liver, may serve as a substrate for the synthesis of ketone bodies [1].

In addition to catalysing the first step in this transport process, CPT I plays a crucial role in the physiological regulation of fatty acid oxidation. This is mediated through potent inhibition of the enzyme by malonyl-CoA, the product of acetyl-CoA carboxylase and the first committed intermediate in the opposing pathway of fatty acid synthesis *de novo*. Thus in the liver, in the fed state, fatty acid synthesis is activated and malonyl-CoA levels

---

Abbreviations used: CPT, carnitine palmitoyltransferase, L-CPT I, liver-type CPT I, M-CPT I, skeletal-muscle-type CPT I; Ni-NTA, Ni^{2+}-nitrilotriacetate

[1] To whom correspondence should be addressed (e-mail nbrown@mednet.swmed.edu).

rise, CPT I is inhibited and futile oxidation of the newly synthesized fatty acids is prevented. Conversely, during a fast, hepatic malonyl-CoA levels fall, such that β-oxidation and ketone-body synthesis can proceed efficiently (see [1] for a review). Although first described for the liver, it now appears that this system operates in non-lipogenic tissues as well. In skeletal muscle and heart, for example, acetyl-CoA carboxylase activity is present and malonyl-CoA levels are seen to rise and fall with changes in physiological state, just as in liver [2–5]. In these tissues, it is thought that malonyl-CoA is synthesized purely as a regulator of CPT I. Because of its central role in whole-body fuel homoeostasis, CPT I has aroused interest as a target for pharmacological intervention in conditions of excessive fatty acid oxidation. For example, CPT I inhibitors are considered potentially valuable as hypoglycaemic agents in the long-term management of type-II diabetes or in the short-term reversal of diabetic ketoacidosis [6,7], as well as in the treatment of ischaemic heart disease where excessive oxidation of fatty acids is believed to exacerbate cardiac tissue damage [8–10].

Whereas CPT II, the inner-membrane (and malonyl-CoA-insensitive) form of CPT, is thought to be the same protein in all tissues of the body, CPT I is known to exist in at least two primary isoforms [1,11,12] These have been designated L-CPT I (liver type) and M-CPT I (skeletal-muscle type) since they appear to be the exclusive isoforms expressed in those organs, although each is found in a variety of other tissues [1]. In addition, based on analysis of mRNA transcripts, it has been suggested that alternatively spliced forms of M-CPT I may be expressed [13–15]. L- and M-CPT I are predicted to be proteins of 773 and 772 amino acid residues, respectively, and are 63 % identical at the amino acid level [16]. However, they differ in several important respects. Notably, the K_m for the substrate carnitine is 10–15-fold higher in the case of M-CPT I ($\approx 500\ \mu$M) and, whereas the IC_{50} for malonyl-CoA is $\approx 0.03\ \mu$M for M-CPT I, it is 100-fold higher for the liver enzyme [1]. Also, despite having almost identical predicted relative molecular masses, the two CPT I isoforms display different mobilities on SDS/PAGE [12].

An intriguing property unique to L-CPT I is that its sensitivity to malonyl-CoA changes with (patho)physiological state. When mitochondria are isolated from the livers of rats that have been fasted or rendered experimentally diabetic, L-CPT I is found to be markedly desensitized to malonyl-CoA when compared with those prepared from a fed animal [17–19]. In the case of fasting, this phenomenon of desensitization to the inhibitor is believed to act in physiological terms to amplify the effect of a decreased malonyl-CoA concentration. However, the mechanism of this change in the molecule's behaviour is unknown and remains controversial

Each of the CPT cDNAs has now been cloned from rat, human and other species [1] and this has facilitated a number of recombinant expression studies that have provided some insight into which regions and/or amino acid residues within the CPT molecules bestow particular properties. In addition, a membrane topology has been proposed that envisages CPT I as consisting of a small N-terminal domain and a larger C-terminal domain, both lying on the cytosolic aspect of the outer mitochondrial membrane and connected by two membrane spans with a short loop in the inter-membrane space [20–23]. The C-terminal region contains the active site and the determinants for whether the molecule will display L- or M-CPT I-type kinetics with regard to the K_m for carnitine or sensitivity to malonyl-CoA [23]. However, the N-terminal domain is crucial for a normal response to malonyl-CoA [23–27].

A practical problem that has hampered further progress in this area is the fact that CPT I is largely inactivated upon detergent extraction from the membrane [24,28]. This effect, presumably reflecting the necessity for a membrane environment to maintain the native tertiary structure of the protein, has made it impossible to obtain CPT I in a form that is both pure and active. In the present study we have overcome this obstacle. Rat liver CPT I, expressed at high levels in the yeast *Pichia pastoris* and purified from detergent extracts in milligram quantities, was reconstituted into artificial phospholipid liposomes with concomitant re-establishment of catalytic activity and malonyl-CoA sensitivity. This provides the first opportunity to study the properties of a CPT I isoform in active form in a defined environment free of contaminating proteins. The liposomal CPT I preparation has allowed us to demonstrate a direct effect of membrane environment on the malonyl-CoA sensitivity of the enzyme and has yielded additional insight into the relationship between the enzyme's catalytic and inhibitory sites. The data shed new light on the phenomenon of the desensitization of L-CPT I to its physiological inhibitor.

EXPERIMENTAL

Animals

Male Sprague–Dawley rats (200–250 g) were housed in a room lit from 10:00 h until 22:00 h, and maintained on a high-carbohydrate/low-fat diet [60 % sucrose/20 % protein/< 0.1 % fat (w/w)]. Fasted rats were deprived of food from 16:00 h 2 days prior to experiments (i.e. approx 42 h of fast). Animals were killed at 09 30 h by injection of Nembutal (50 mg/kg) followed by cervical dislocation. Liver mitochondria were prepared at 4 °C, as described previously ([2], method A), and resuspended in 150 mM KCl/5 mM Tris/HCl, pH 7.2.

Expression of rat L-CPT I in *P. pastoris*

Engineering of plasmid pCMV6-rL-CPT I containing the full-length cDNA for rat L-CPT I has been described [11]. With that plasmid as template, the PCR was used to amplify the coding region of the cDNA. The 5′ primer oligonucleotide, complementary to the first 21 bases of the open reading frame, contained, in addition, an *Sfu*I restriction site (CCCGAATTCGAAATAATGGCAGAGGCTCACCAAGCT) The 3′ primer encoded the last 21 bases of the coding region as well as six histidine residues, a stop codon and an *Sfu*I site (CCCGAATTCGAATTAATGGTGATGGTGATGGTGCTTTTTAGAATTGATGGTGAG). The product was ligated into the unique *Sfu*I site of plasmid pPICZA (Invitrogen, Carlsbad, CA, U.S.A.). This placed the rat L-CPT I cDNA under the control of the methanol-inducible AOX1 promoter. The fidelity of the amplification reaction was confirmed by DNA sequencing and the final product is designated pPICZA-rL-CPT I-his6. The plasmid was linearized with restriction enzyme *Pme*I and used to transform *P. pastoris* strain GS115 employing the EasyComp method (Invitrogen) to generate stable chromosomal integrants. Transformed colonies were selected using the Zeocin resistance encoded by the parent plasmid. Eight colonies were chosen for initial study and the highest-expressing strain, GS115-776-rL-1, was used for further experiments. (Growth and preparation of homogenates for characterization of these strains was essentially by a small-scale version of the procedure described below.)

Preparation of *P. pastoris* mitochondria and membrane fractions

A single colony of GS115-776-rL-1 was used to inoculate starter cultures in MGYH [minimal glycerol medium with histidine, 1.34 % (w/v) yeast nitrogen base without amino acids/1 % (v/v) glycerol/4 × 10^{-5} % (w/v) biotin/0.004 % (w/v) histidine] which were grown with shaking overnight at 30 °C. Induced cultures were inoculated from these to an initial D_{600} of 1.0 in MMH [minimal methanol medium with histidine; as MGYH, but with 1 % (v/v) methanol and without glycerol] and grown for 24 h.

A mitochondrially enriched fraction was prepared from 400-ml induced cultures as described previously for *Saccharomyces cerevisiae* [29]. Briefly, the cell wall was removed enzymically, the spheroplasts were broken using 20 cycles of a glass homogenizer fitted with a tight pestle and a mitochondrial fraction was isolated by differential centrifugation. The final product was resuspended in 150 mM KCl/5 mM Tris/HCl, pH 7.2 To obtain preparations of total *P. pastoris* membranes, six 400-ml induced cultures were harvested, after which spheroplasts were prepared and homogenized as above in a final volume of ≈ 80 ml of 0.6 M mannitol/10 mM Tris, pH 7.4/1 mM PMSF. This was divided into four equal portions and centrifuged at 100 000 *g* for 30 min at 4 °C. The resulting membrane pellets were frozen in liquid nitrogen and stored at −70 °C.

Purification of recombinant rat L-CPT I

A membrane pellet prepared as above was thawed rapidly, resuspended in 22.5 ml of 500 mM NaCl/50 mM sodium phosphate, pH 8.0/1 mM PMSF/2 mM mercaptoethanol and homogenized. To this was added 2.5 ml of 10 % (v/v) Triton X-100 to give a final detergent concentration of 1 %. Extraction of the membrane proteins was allowed to proceed with gentle stirring for 1 h at 4 °C, followed by centrifugation at 100 000 *g* for 30 min at 4 °C and collection of the supernatant (≈ 25 ml). A 50 % slurry of Ni^{2+}-nitrilotriacetate (Ni-NTA)–agarose (2 ml; Qiagen, Chatsworth, CA, U.S.A.) was washed twice with 3 ml of loading buffer (500 mM NaCl/50 mM sodium phosphate, pH 8.0/10 mM imidazole/1 % Triton X-100/2 mM mercaptoethanol) and added to the membrane extract. Imidazole (5 M, 50 μl) was also added (to give a final concentration of 10 mM) so that the preparation was now essentially in loading buffer. The mixture was again stirred gently at 4 °C for 1 h before centrifugation at 500 *g* for 5 min. The matrix was washed twice with 4 ml of loading buffer and finally resuspended in the same volume. The slurry was transferred to a glass column (1 cm diameter) fitted with a sintered glass frit and the flow rate adjusted to ≈ 0.2 ml/min. The resulting matrix bed (≈ 1 ml) was then washed sequentially with 10 ml of loading buffer/20 ml of 1 M NaCl/50 mM sodium phosphate, pH 8.0/20 mM imidazole/1 % Triton X-100/2 mM mercaptoethanol and 3 ml of 500 mM NaCl/50 mM sodium phosphate, pH 8.0/20 mM imidazole/0.1 % Triton X-100/2 mM mercaptoethanol. Elution was carried out with 2.5 ml of 500 mM NaCl/50 mM sodium phosphate, pH 8.0/250 mM imidazole/0.1 % Triton X-100/2 mM mercaptoethanol. The entire purification was performed in the cold.

Reconstitution of rat L-CPT I

For reconstitution experiments, 2 ml of the Ni-NTA–agarose column eluate was applied to a Centricon 10 microconcentrator (Amicon, Beverley, MA, U.S.A.) and centrifuged at 5000 *g* for 45 min at 4 °C, which reduced the volume to ≈ 450 μl. The reconstitution procedure was a modification of that of Garlid and co-workers [30]. To prepare the phospholipids, 50 mg of asolectin (from soya bean, primarily phosphatidylcholine) was dissolved in 500 μl of chloroform in a glass vial, dried under a stream of nitrogen, redissolved in ≈ 1 ml of diethyl ether and once again dried. It was then solubilized in 650 μl of 20 mM Hepes, pH 7.2, plus 100 μl of octyl polyoxyethylene, by heating at 50 °C with frequent mixing. The lipid was cooled to 4 °C before addition of 300 μl of the concentrated recombinant protein. To prepare the BioBeads SM2 adsorbent (Bio-Rad, Richmond, CA, U.S.A.), 1.5 g was placed in a 14-ml capped plastic tube and washed twice with 3 ml of 20 mM Hepes, pH 7.2. The washing buffer was removed to leave a final volume of ≈ 2.5 ml. The lipid/protein mixture was added and rocked for 60 min at 4 or 22 °C (see the Results section) and the contents were then transferred to a disposable spin column fitted with a paper frit. Proteoliposomes were harvested by centrifugation at 400 *g* for 2 min.

Assay of CPT activity

CPT I was assayed in the direction of acylcarnitine formation using palmitoyl-CoA and carnitine as substrates [12]. Except where noted, final concentrations in the assay were: 500 μM L-carnitine (including 0.125 μCi of L-[^{14}C]carnitine), 50 μM palmitoyl-CoA, 4 mM ATP, 4 mM $MgCl_2$, 0.25 mM glutathione, 4 mM $MgCl_2$, 40 μg/ml rotenone, 2 mM KCN, 15 mM KCl, 1 % (w/v) BSA and 105 mM Tris/HCl, pH 7.2. Malonyl-CoA was added as indicated. For pH curves, to provide buffering over a wide range, the assay was as above, but 35 mM each of Tris, Tes and Mes buffers were substituted for the 105 mM Tris. Assays were performed over 4–6 min, during which time reaction rates were linear. In certain experiments, to artificially fluidize the liposomal membrane, a portion of the proteoliposomal preparation was made 40 mM with respect to benzyl alcohol. This and a control sample were then placed at room temperature (≈ 22 °C) for 8 min before assay.

Protein measurement

The BCA (bicinchoninic acid) protein assay reagent (Pierce, Rockford, IL, U.S.A.) was used with BSA as standard. In the case of fractions from the L-CPT I purification and the proteoliposomes, interfering substances were present. To remove these, the following precipitation procedure was carried out. Samples were made up to a volume of 50 μl with 20 mM Hepes, pH 7.2, in a Microfuge tube, 250 μl of −20 °C ethanol/ether (3:1, v/v) was added and the tubes were placed at −20 °C for 30 min. They were then centrifuged at 16000 *g* for 10 min at 4 °C and the supernatant was removed. The pellet was resuspended with 250 μl of ethanol/ether (1:1, v/v) and the precipitation and centrifugation steps were performed similarly The process was then repeated with ethanol/ether (1:3, v/v) and finally with ether alone. The protein pellet was allowed to air dry for 5 min before resuspension with 50 μl of 5 % SDS in 0.1 M NaOH.

RESULTS

Plasmid pPICZA-rL-CPT I-his6 was designed for expression of recombinant rat L-CPT I in the yeast *P. pastoris*. To facilitate rapid purification of the recombinant product, bases encoding a hexahistidine tag (6 × His) were introduced at the 3′ end of the open reading frame. As a result, the expressed enzyme would possess an additional six histidine residues at its C-terminus, permitting purification over a metal-chelate affinity matrix such as Ni-NTA–agarose. After transformation of *P. pastoris* strain GS115 with plasmid pPICZA-rL-CPT I-his6, eight colonies were analysed for the presence of CPT activity. Small cultures of each were induced with methanol as sole carbon source and total homogenates prepared. All displayed significant catalytic activity, whereas a control strain transformed with the vector alone had none. The highest-expressing strain, GS115-776-rL-1, was

Table 1 Reconstitution of rat L-CPT I

Samples were prepared and assayed as described under the Experimental section. All data are the means ± S.D. of the number of independent determinations indicated in parentheses. Activity in the presence of 100 μM malonyl-CoA is given as a percentage of the value in the absence of inhibitor. n.d., not determined.

	CPT activity (nmol/min per mg of protein)	+100 μM malonyl-CoA (%)
P. pastoris membranes	14.9 ± 4.2 (6)	30.7 ± 7.3 (6)
Triton X-100 supernatant	0.23 ± 0.06 (3)	n.d.
Triton X-100 pellet	0.117 ± 0.08 (3)	n.d.
Ni-NTA–agarose eluate	1.49 ± 0.5 (5)	114.7 ± 21.2 (5)
Concentrated eluate	1.08 ± 0.7 (5)	131.0 ± 35.0 (4)
Proteoliposomes (4 °C)	245 ± 124 (5)	37.8 ± 4.3 (4)
Proteoliposomes (22 °C)	473 ± 134 (3)	22.7 ± 3.2 (3)

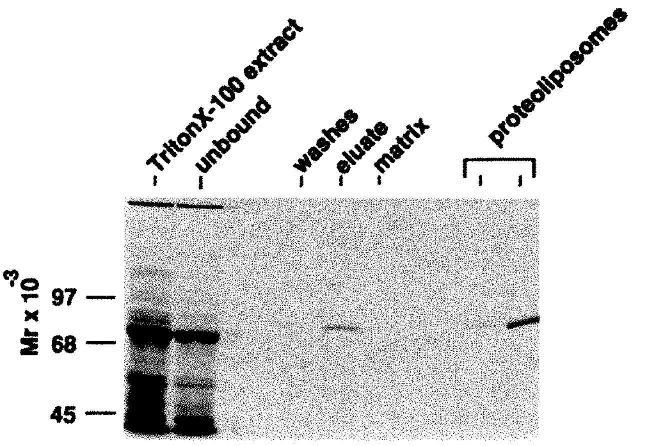

Figure 1 Purification of recombinant rat L-CPT I from *P. pastoris*

SDS/PAGE analysis of fractions from a typical purification. The same proportion of each fraction was used (0.05%), except for the right-hand proteoliposome lane where 5-fold more was loaded. Triton X-100 extract, total membrane proteins solubilized by the detergent; unbound, material remaining in solution after incubation with Ni-NTA agarose; washes, combined column washes; eluate, material eluted from the column by 250 mM imidazole; matrix, material retained by the column; proteoliposomes, material after reconstitution.

chosen for further analysis. For purification of the recombinant product, large cultures were induced and total membrane fractions prepared (see the Experimental section). Membrane pellets corresponding to 600 ml of original culture were solubilized with 1 % Triton X-100 and the insoluble material was sedimented. Western blots indicated an almost quantitative extraction of recombinant L-CPT I (results not shown). CPT I activity, both in the supernatant and pellet fractions, was largely abolished by the Triton X-100 extraction procedure (Table 1), consistent with many previous observations that L-CPT I is largely inactivated upon removal from its membrane environment. Incubation of the solubilized enzyme with Ni-NTA–agarose resulted in specific binding of the 6 × His-labelled protein. Figure 1 shows SDS/PAGE analysis of a typical purification. Comparison of lane 1 (total Triton X-100 extract) with lane 2 (unbound material) clearly shows that the band at ≈ 88 kDa corresponding to L-CPT I was removed by incubation with the matrix. The strength of binding permitted washing of the column under severe conditions (1 M NaCl/1 % Triton X-100) and the eluted product was brought to a high degree of purity in a single step (lane 4). The yield of purified recombinant L-CPT I was ≈ 2 mg/l of culture.

As shown in Table 1, despite its purified state, the eluted material retained a much lower specific activity than the original preparation of total yeast membranes. Furthermore, in contrast with the starting material, the low activity detected in the column eluate was not inhibited by malonyl-CoA. Removal of detergent and combination of the purified protein with phospholipid to generate proteoliposomes was carried out at either 4 or 22 °C. Either procedure resulted in a massive (200–400-fold) enhancement of specific activity and, additionally, resurrection of malonyl-CoA sensitivity similar to what was observed in the initial membrane preparation. (Differences shown in Table 1 between the specific activities of proteoliposomes reconstituted at different temperatures are not significant and, indeed, in two experiments in which both variations were carried out simultaneously with portions of the same purified enzyme preparation, no differences in specific activity were observed.) Interestingly, the enzyme reconstituted at 22 °C appeared to display a slightly greater sensitivity to inhibition by malonyl-CoA (Table 1). To ensure that the increase in specific activity upon reconstitution was not simply due to the removal of the detergent (rather than incorporation into phospholipid vesicles) an identical experiment was performed with the omission of the lipid component. The resulting material was totally devoid of activity and, furthermore, a visible precipitate was formed (results not shown). When account is made for sample volumes and losses of L-CPT I protein during the extraction, binding, elution, concentration and reconstitution stages, the final yield of CPT activity was ≈ 15 % of that in the starting material.

To validate that the L-CPT I had indeed been incorporated successfully into liposomes, we examined the sedimentation properties of the reconstituted product. Centrifugation of the L-CPT I proteoliposomes at 2000 *g* for 2 min resulted in almost complete retention of activity in the supernatant fraction (96.8 ± 4.4 % recovered in the supernatant and 3.1 ± 0.9 % in the pellet, relative to starting activity of 100 %). In contrast, when the proteoliposomes were subjected to high-speed centrifugation (150000 *g* for 1 h), the largely cleared supernatant contained very little activity (3.0 ± 1.7 %), most of which was recovered in the liposomal pellet (63.4 ± 8.6 %). Brief sonication of the proteoliposomes caused no change in either the activity or malonyl-CoA sensitivity of the reconstituted material (results not shown). This would suggest that (i) the majority of the enzyme was present in the correct orientation, i.e. N- and C-termini outside, or (ii) if a significant fraction of the liposomal L-CPT I had the opposite orientation, the enzyme present on the inside aspect of the phospholipid bilayer had ready access to both substrates.

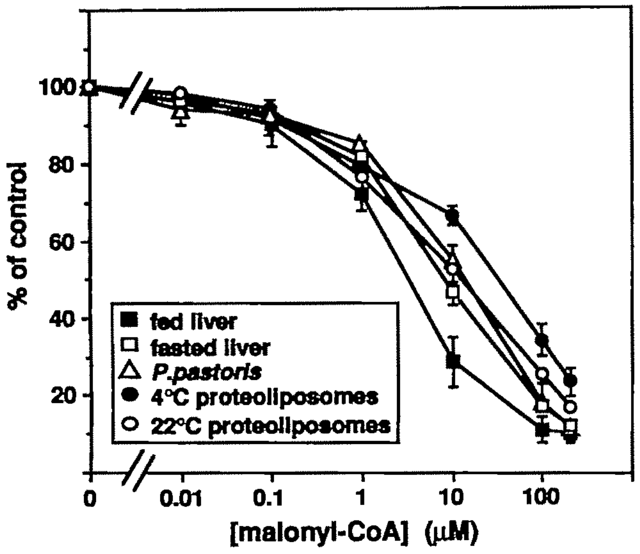

Figure 2 Effect of malonyl-CoA on L-CPT I

Values are given as percentages of the activity in the absence of inhibitor [means ± S.D. for three (or six, 4 °C liposomes only) independent preparations]. Absolute values at 0 µM malonyl-CoA were: fed liver mitochondria, 8.16 ± 1.83, fasted liver mitochondria, 20.9 ± 8.7; *P. pastoris* mitochondria, 4.39 ± 0.72, proteoliposomes prepared at 4 °C, 245 ± 124, proteoliposomes prepared at 22 °C, 473 ± 134 nmol/min per mg of protein. Note that the abscissa is on a logarithmic scale.

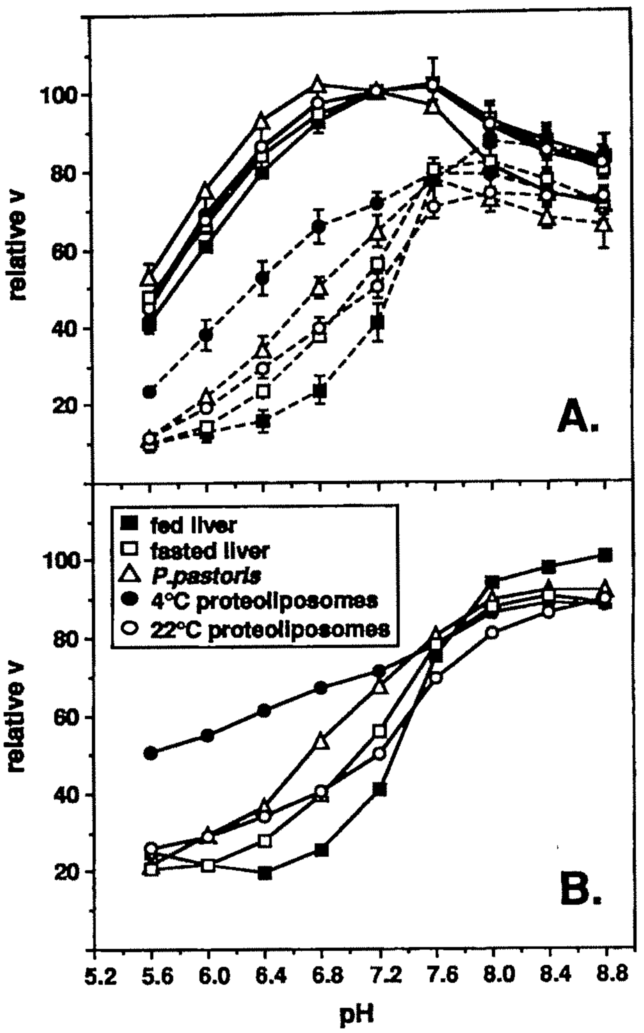

Figure 3 Effect of pH on L-CPT I activity

(**A**) Activities are normalized as percentages of those values at pH 7.2 in the absence of malonyl-CoA, solid lines, activity without malonyl-CoA, dashed lines, activity in the presence of 5 µM malonyl-CoA. (**B**) The activity in the presence of 5 µM malonyl-CoA is presented as percentages of those values in its absence. All data are means ± S.D. for three experiments with independent preparations.

In addition to a direct kinetic analysis of the L-CPT I reconstituted at 4 or 22 °C, we performed parallel experiments with a mitochondrial fraction prepared from the *P. pastoris* strain expressing the recombinant enzyme and also with mitochondria from the livers of fed and fasted rats. Figure 2 shows the effect of malonyl-CoA on each of these preparations. The IC_{50} for L-CPT I in fed liver mitochondria was ≈ 3 µM. As expected, fasted liver mitochondria were somewhat less sensitive, with an IC_{50} of ≈ 8 µM. L-CPT I *in situ* in *P. pastoris* mitochondria was slightly less sensitive than that of the fasted liver. The temperature at which reconstitution of the purified L-CPT I was performed had a marked effect on the malonyl-CoA sensitivity of the proteoliposomal enzyme. L-CPT I reconstituted at 22 °C had an IC_{50} of ≈ 11 µM but this value increased to ≈ 31 µM with material reconstituted at 4 °C. The kinetic data are summarized in Table 2.

The K_m values for carnitine of the fed and fasted rat liver mitochondrial L-CPT I were identical, at about 60 µM (Table 2). Relative to the liver mitochondria, the carnitine curve for the liposomal enzyme was slightly left-shifted with a calculated K_m of ≈ 40 µM (regardless of the reconstitution temperature). However, L-CPT I in *P. pastoris* mitochondria showed a substantially greater divergence, with a K_m of only ≈ 18 µM. As regards the response to an increasing concentration of palmitoyl-CoA,

Table 2 Kinetic characteristics of rat L-CPT I in different preparations

All data are means ± S.D. of three or six (*) independent preparations. IC_{50}, concentration of inhibitor required for 50% inhibition of enzyme activity. K_m (carnitine) data were derived from Eadie–Hofstee linearization plots of the carnitine curve data. The response to palmitoyl-CoA is presented as the concentration required for 50% of the activity at 300 µM ($S_{300/2}$).

	IC_{50} (malonyl-CoA; µM)	K_m (carnitine, µM)	$S_{300/2}$ (palmitoyl-CoA, µM)
Fed rat liver mitochondria	3.0 ± 0.2	61.9 ± 4.7	25.3 ± 4.0
Fasted rat liver mitochondria	7.8 ± 2.3	62.7 ± 1.2	34.7 ± 5.8
P. pastoris mitochondria	12.0 ± 2.6	17.9 ± 1.2	94.0 ± 2.0
Rat L-CPT I proteoliposomes (4 °C)	31.5 ± 6.0*	37.3 ± 6.0	34.0 ± 2.6
Rat L-CPT I proteoliposomes (22 °C)	11.4 ± 2.0	38.7 ± 0.4	28.2 ± 4.1

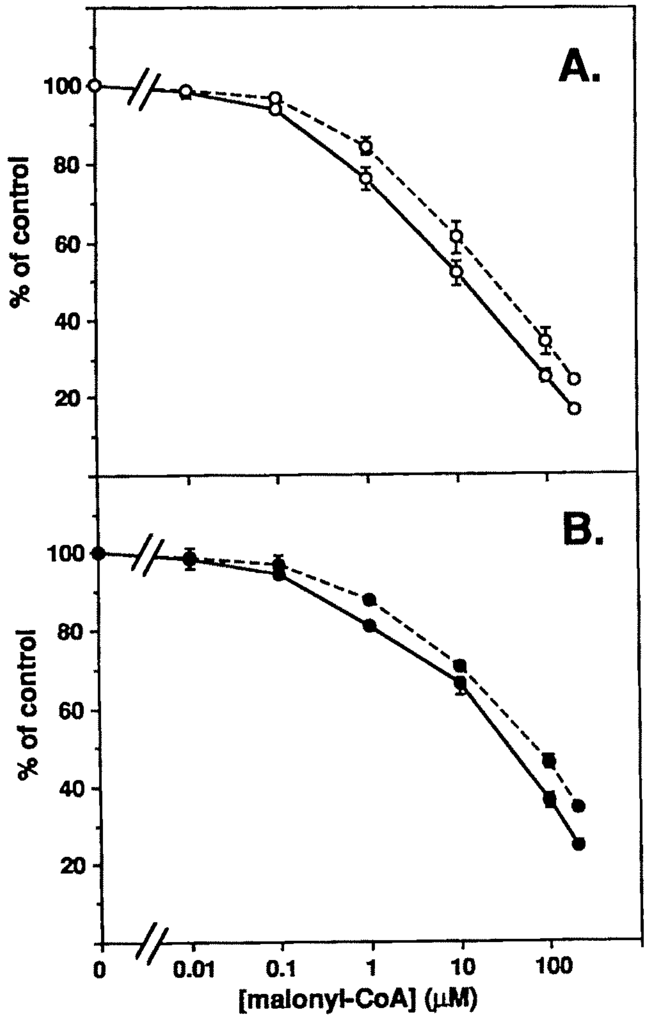

Figure 4 Effect of benzyl alcohol on malonyl-CoA sensitivity of reconstituted L-CPT I

Values are given as percentages of the activity in the absence of inhibitor (means ± S.D. for three independent preparations). Panels show L-CPT I liposomes reconstituted at (**A**) 22 °C or (**B**) 4 °C. Data are presented for samples in the absence (solid lines) or presence (dashed lines) of 40 mM benzyl alcohol (see the Experimental section). Note that the abscissa is on a logarithmic scale.

liposomal L-CPT I displayed similar characteristics to the native enzyme in rat liver mitochondria. Once again, the greatest disparity was observed with the enzyme in *P. pastoris* mitochondria, where the curve appeared to saturate much more slowly than was the case for the other preparations. Under the assay conditions used (in the presence of 1 % BSA) CPT displays non-ideal kinetics with regard to palmitoyl-CoA, making it impossible to calculate a meaningful K_m for that substrate. However, for comparative purposes, the palmitoyl-CoA responses are summarized in Table 2 as the concentration of substrate giving half the maximal activity observed at 300 μM ($S_{300/2}$).

Figure 3 shows activity for each of the L-CPT I preparations over the pH range 5.6–8.8 (Figure 3A, solid lines). Similar profiles were obtained with fed and fasted liver mitochondria and with the reconstituted protein. In contrast, the enzyme in *P. pastoris* mitochondria showed markedly altered behaviour, appearing to have a lower pH optimum and to be more sensitive to higher pH than the others. The dashed lines in Figure 3(A) represent similar experiments performed in the presence of 5 μM malonyl-CoA. At our standard assay pH of 7.2, consistent with the data in Figure 2, the different preparations of L-CPT I showed a range of inhibition levels, the enzyme in fed liver mitochondria being the most sensitive while L-CPT I reconstituted at 4 °C was the least inhibited. In Figure 3(B), activity in the presence of 5 μM malonyl-CoA is expressed as a percentage of that in the absence of the inhibitor. In all cases, malonyl-CoA became increasingly effective as the pH was lowered, consistent with earlier findings [31,32]. However, the slope of the curve in the pH range 6.5–7.5 varied markedly, fed liver showing the sharpest dependence of malonyl-CoA sensitivity on pH and liposomes generated at 22 °C being the least affected. At pH 8.0–8.8 malonyl-CoA was largely ineffective.

To assess the direct influence of membrane fluidity on the sensitivity of L-CPT I to malonyl-CoA, inhibition curves were obtained for the proteoliposomes after pretreatment with benzyl alcohol. The concentration of this agent (40 mM) and the time of exposure (8 min) have been shown to elicit a maximal effect on L-CPT I *in situ* in rat liver outer mitochondrial membranes [33]. As shown in Figure 4, fluidization of the artificial membrane environment caused a right-shift in the inhibition curve. This change (presented for clarity on a logarithmic scale) represents more than a doubling of the IC$_{50}$ for proteoliposomes made at 22 °C (Figure 4A), the value increasing from 11.4 ± 2.0 to 26.7 ± 7.6 μM. Proteoliposomes generated with the 4 °C protocol, already less sensitive compared with those manufactured at the higher temperature, were also capable of further desensitization with benzyl alcohol (Figure 4B). In this case, the IC$_{50}$ rose from 34.3 ± 6.1 to 67.7 ± 7.5 μM. Total activities in the absence of malonyl-CoA were also increased slightly by the fluidization protocol [values after treatment of 121 ± 6 and 113 ± 9 % relative to untreated controls, for liposomes produced at 4 and 22 °C, respectively ($n = 3$ in each case)].

DISCUSSION

Our primary goal here was to establish a protocol by means of which a mammalian mitochondrial CPT I isoenzyme could be obtained in pure and active form and with characteristics as close as possible to those of the enzyme in its natural environment. We chose to work with rat L-CPT I for three reasons. First, to permit direct comparison with the native protein, we preferred to work with a rat enzyme, since mitochondria from this species are readily available. Second, the enzyme as it exists in rat liver mitochondria has been studied extensively [1]. Third, we were particularly interested in a unique property of the L-isoform of CPT I, namely its changing sensitivity to malonyl-CoA under different metabolic circumstances.

In previous structure–function studies of the CPT enzymes we have used *Escherichia coli*, *S. cerevisiae* and mammalian COS cells as expression vehicles [11,12,23,24,29,34,35]. Each has its advantages. Whereas COS cells provide a mammalian mitochondrial environment for the expressed protein, they also contain an endogenous CPT activity that can complicate interpretation of the data. In contrast, the prokaryotic and yeast systems have no baseline CPT activity, and both have proved useful for expression of CPT II [29,35]. However, recombinant L-CPT I was produced only at low levels by *S. cerevisiae* [24]. By contrast, all three mitochondrial CPT isoforms, i.e. L-CPT I, M-CPT I and CPT II, were found to be expressed at high levels in *P. pastoris* [25,27,36–39]. In the present work, not only did this yeast strain synthesize the 6 × His-tagged rat L-CPT I efficiently, but purification of the recombinant product using Ni-NTA–

agarose was accomplished with relative ease and rapidity, and the yield of ≈ 2 mg of purified protein/l of *P. pastoris* culture (high for an integral membrane protein) was ample for our purposes.

As would be predicted from earlier studies with L-CPT I in rat liver mitochondria [28] or the protein expressed in *S. cerevisiae* [24], the detergent-solubilized enzyme produced by *P. pastoris* possessed very little catalytic activity. However, due to the highly purified and concentrated nature of our L-CPT I preparation, even with the very low specific activity of the solubilized enzyme, we could determine that the activity present was not sensitive to malonyl-CoA. Woldegiorgis and colleagues have previously shown that when L-CPT I is expressed in *P. pastoris*, a Triton X-100 extract of total membrane protein/lipid can be combined with additional phospholipid *in vitro* with partial restoration of catalytic activity [36]. Using a similar approach, but this time using a highly purified and lipid-free preparation of L-CPT I, when our enzyme was combined with phospholipids and the detergent removed with an adsorbent, its specific activity increased some 200–400-fold and, importantly, it proved to be malonyl-CoA-sensitive. In addition, the reconstituted material displayed properties characteristic of proteoliposomes This is the first time that a catalytically active and malonyl-CoA-sensitive CPT I enzyme has been obtained in pure form. Furthermore, as discussed in more detail below, the substrate kinetics and pH dependence of the reconstituted, 6 × His-tagged L-CPT I were similar to those of the enzyme in rat liver mitochondria.

This advance allowed us to assess the kinetic characteristics of L-CPT I in a variety of membrane environments. Specifically, we compared the properties of the purified enzyme reconstituted by two slightly different protocols with those of the protein as it exists when over-expressed in the *P. pastoris* mitochondrial membrane and, importantly, with those of the native protein in liver mitochondria taken from fed and fasted rats. The data for malonyl-CoA sensitivity of L-CPT I in intact liver mitochondria illustrate the well-established phenomenon of the enzyme's desensitization to the inhibitor that occurs with fasting. Although this observation has been made many times in different laboratories, understanding the mechanism of the change has been a major challenge and several theories have been proposed. Kolodziej and Zammit showed that when chemical reagents were used to artificially increase the fluidity of rat liver mitochondrial membranes L-CPT I became less sensitive to inhibition [33] Also, use of fluorescent probes indicated that conditions under which desensitization of hepatic L-CPT I occurs *in vivo* are associated with decreased order of the hydrophobic core of the membrane [19]. It was suggested, therefore, that the state of the membrane might significantly influence the properties of the enzyme However, in the same study, no consistent correlation could be made between changes in L-CPT I sensitivity and gross alterations in the lipid composition of the membrane. It was proposed that variations in lipid make-up could occur at the level of 'microdomains' within the outer membrane. In that context, it is interesting to note that CPT I may be concentrated at the mitochondrial membrane contact sites [40].

The idea has also been put forward that the prevailing level of malonyl-CoA itself might play a direct role, a concept suggested by the finding that pre-incubation of mitochondria with malonyl-CoA can enhance subsequent sensitivity of L-CPT I to the inhibitor [41,42]. Consistent with this notion is that physiological conditions associated with a decreased sensitivity are also those in which the malonyl-CoA levels are lowest More recently, it has been proposed that the apparent change in sensitivity on fasting may not result from a conformational change in the existing L-CPT I protein, but from the induced expression of a less-sensitive CPT I isoform [15]. Yet another possibility is that the change is the consequence of interaction of CPT I with some as-yet-unidentified regulatory protein. The protocol we have developed provided a previously unavailable purified enzyme model with which to examine the phenomenon. In particular, we have been able for the first time to study variation in the properties of the same enzyme in various environments and under conditions devoid of any putative specifically interacting regulatory proteins and in some cases entirely outside the mitochondrial milieu. This approach has permitted important new light to be shed on the likely mechanism of desensitization to malonyl-CoA.

Initial comparison of the recombinant L-CPT I over-expressed in *P. pastoris* with the native protein in liver mitochondria clearly demonstrates that the properties of both are broadly similar. In terms of malonyl-CoA sensitivity, L-CPT I present in *P. pastoris* mitochondria behaved most like the desensitized, 'fasted' version of the enzyme *in vivo*. Others have reported IC_{50} values for L-CPT I in *P. pastoris* as low as 1.9 μM [36] and as high as 54 μM [39]. The reasons for these discrepancies are unknown, but presumably reflect some differences in the details of the expression system, handling of the protein by the yeast cells under different circumstances, sample preparation or CPT assay. Hence, simple comparison of the sensitivity of the enzyme over-expressed in the yeast cell with those of L-CPT I *in situ* in the complex protein milieu of the rat liver mitochondrial outer membrane provides little clarification of the desensitization phenomenon. We were interested in determining if the membrane lipid environment could have a direct effect on the enzyme's response to malonyl-CoA. The critical observation made here is that the same recombinant L-CPT I protein that displays a certain sensitivity to malonyl-CoA when present in the *P. pastoris* mitochondrial membrane may display a similar, or markedly lower, sensitivity when reconstituted into the artificial liposomes, depending only on a slight variation in the reconstitution protocol. The physical explanation for the effect of temperature on the reconstitution is unclear, but presumably reflects differences in the structure of the liposomes formed. Although primarily phosphatidylcholine, soya bean asolectin contains a mixture of phospholipids, varying in both head group and lipid moieties, and therefore it is not surprising that the differential phase behaviours of these compounds should lead to temperature-dependent variation in the make up of the liposomes. It should be noted that desensitization of L-CPT I in liver mitochondria can occur with partial proteolysis [42,43], presumably through loss of the N-terminal domain. However, we do not believe that significant degradation of our protein occurred. Certainly, SDS/PAGE analysis of the reconstituted enzyme shows no evidence for proteolysis and, furthermore, the IC_{50} of 30 μM for the least-sensitive liposomal enzyme is much lower than that observed (80 μM) for an N-terminally truncated form of the protein [24]. Furthermore, it is the 4 °C reconstitution protocol, during which any proteolysis would be expected to be relatively slow, that yields the less sensitive product. We believe, therefore, that the identical polypeptide can assume active conformations with different levels of sensitivity. Additional evidence for this proposition comes from the experiments with benzyl alcohol Pre-treatment of rat liver outer mitochondrial membranes with the membrane-fluidizing agent had been shown to result in a relative desensitization of L-CPT I *in vitro* [33]. However, in that study, the possibility could not be excluded that the effects of changing membrane fluidity were mediated by interaction with other proteins in the mitochondrial membrane. Since we were able to reproduce this effect in the purified system, it is evident that the physical properties of the membrane/liposome directly influence the conformation of the protein in such a way as to affect malonyl-CoA sensitivity.

This is consistent with the lipid 'microdomain' theory proposed by Zammit and co-workers ([19,33], discussed above). While not immediately pertinent to the current work, it will be interesting to determine in later studies if the muscle isoform of CPT I, which does not appear to alter its malonyl-CoA sensitivity *in vivo*, can be induced to do so in an *in vitro* system.

Current understanding of CPT I topology holds that the N-terminal domain (essential for the malonyl-CoA response) and the C-terminal 'catalytic' domain both lie on the outside of the mitochondrial outer membrane, connected by a short loop in the inter-membrane space [20–23]. This model provides for an attractive, though admittedly speculative, scenario in which it is alteration in the interaction between these two domains, rather than changes within either one, that results in modulation of malonyl-CoA sensitivity. Since it is the membrane that anchors these two domains in juxtaposition, it is not surprising that changes in the physical properties of the membrane could produce the observed effects. This could also explain why the detergent-solubilized enzyme has no apparent sensitivity to the inhibitor. Such a formulation would predict that anything that affects the malonyl-CoA response need not affect the properties of the active site, and vice versa. This is also supported by the kinetic data presented here. Thus we find that the reconstituted enzyme, which displays variation in sensitivity to malonyl-CoA, retains catalytic characteristics (in terms of its interaction with the substrates) that are most similar to the enzyme in rat liver mitochondria. In contrast, L-CPT I in *P. pastoris* mitochondria, while maintaining an inhibitor sensitivity similar to that of the native rat enzyme, appears to diverge from it in its responses to carnitine and palmitoyl-CoA. This separation of catalytic and inhibitory properties is most clearly illustrated by the finding that in the absence of malonyl-CoA the pH profile for the CPT I reaction is essentially the same for the enzyme in 'fed' mitochondria, 'fasted' mitochondria and liposomes. On the other hand, once a low level of malonyl-CoA is introduced, the profiles for each of the L-CPT I preparations differ radically. The early observation that the effectiveness of malonyl-CoA as an inhibitor decreases dramatically as the pH is raised from 6.4 to 7.6 suggested that a histidine residue might be involved in the regulatory interaction with malonyl-CoA, since it would be expected to titrate over this range [31,32]. Indeed certain candidate histidines have been identified [23]. However, a detailed kinetic analysis of the mitochondrial enzyme has indicated that the interaction with malonyl-CoA has two components [44]. These most probably represent inhibition via a specific, allosteric binding site, probably involving an N-terminal histidine residue and responsible for the primary inhibitory action, and a secondary, minor inhibition effected through direct competition with the acyl-CoA substrate at the active site. Because the latter would not be predicted to have such a sharp dependence on pH, it follows that as the relationship between the two domains becomes less strong, the competitive component would account for a progressively larger proportion of the inhibition observed. As a result, the effect of pH lowering (to enhance the inhibitory effect of malonyl-CoA) should be diminished. The fact that the pH dependence of the effectiveness of a fixed concentration of malonyl-CoA decreased in the order of fed liver mitochondria > fasted liver mitochondria ≈ liposomes made at 22 °C ≈ *P. pastoris* mitochondria > liposomes made at 4 °C, and that this sequence was reversed in terms of the IC_{50} of L-CPT I for malonyl-CoA at pH 7.2, suggests that the strength of interaction between the N- and C-terminal domains of the protein also decreased in the order shown.

We conclude that the kinetic properties of L-CPT I can vary widely depending upon the membrane environment and independently of modification of the protein or its interaction with regulatory subunits. It is probable that this explains much of the variation that is observed *in vivo*. However, although alterations in the membrane may be sufficient to elicit changes in the enzyme seen *in vivo*, this does not exclude a role for other proteins in such regulation. Also, the possibility that alternative CPT I isoforms might be induced in the liver during a fast is not disproved by the present work [15]. However, that theory awaits direct demonstration of the existence of the splice variants at the protein level.

Finally, the model described provides the first opportunity to study a CPT I enzyme in a pure and active form. It has already yielded important new information about how the catalytic and allosteric properties of L-CPT I may be related and how they are influenced by the interaction of the protein with the membrane. To date, the lack of purified, active protein has severely hampered progress in CPT I structure/function research. In addition to the insights it has already provided, we believe that purified, liposomal CPT I will provide an invaluable tool to investigate the structure–function and regulatory properties of this complex enzyme that plays such a central role in the regulation of fuel metabolism.

This work was supported by a grant from the National Institutes of Health (DK18573).

REFERENCES

1 McGarry, J D and Brown, N F (1997) The mitochondrial carnitine palmitoyltransferase system from concept to molecular analysis Eur J Biochem **244**, 1–14

2 McGarry, J D, Mills, S E, Long, C. S and Foster, D W (1983) Observations on the affinity for carnitine, and malonyl-CoA sensitivity, of carnitine palmitoyltransferase I in animal and human tissues demonstration of the presence of malonyl-CoA in non-hepatic tissues of the rat Biochem J **214**, 21–28

3 Duan, C and Winder, W. W. (1992) Nerve stimulation decreases malonyl-CoA in skeletal muscle J Appl Physiol. **72**, 901–904

4 Odland, L M, Heigenhauser, G J. F., Lopaschuk, G D and Spriet, L L (1996) Human skeletal muscle malonyl-CoA at rest and during prolonged submaximal exercise Am J Physiol **270**, E541–E544

5 Prentki, M and Corkey, B E (1996) Are the β-cell signaling molecules malonyl-CoA and cytosolic long-chain acyl-CoA implicated in multiple tissue defects of obesity and NIDDM? Diabetes **45**, 273–283

6 Foley, J E (1992) Rationale and application of fatty acid oxidation inhibitors in treatment of diabetes mellitus Diabetes Care **15**, 773–784

7 Deems, R O, Anderson, R C and Foley, J E (1998) Hypoglycemic effects of a novel fatty acid oxidation inhibitor in rats and monkeys Am J Physiol **274**, R524–R528

8 Lopaschuk, G D, Belke, D D, Gamble, J, Itoi, T and Shonekess, B O (1994) Regulation of fatty acid oxidation in the mammalian heart in health and disease. Biochim. Biophys Acta **1213**, 263–276

9 Stanley, W. C, Lopaschuk, G D, Hall, J L and McCormack, J G (1997) Regulation of myocardial carbohydrate metabolism under normal and ischemic conditions. potential for pharmacological interventions Cardiovasc Res **33**, 243–257

10 Kantor, P. F, Dyck, J R and Lopaschuk, G D (1999) Fatty acid oxidation in the reperfused ischemic heart. Am J. Med Sci **318**, 3–14

11 Esser, V, Britton, C H, Weis, B C, Foster, D. W. and McGarry, J D (1993) Cloning, sequencing, and expression of a cDNA encoding rat liver carnitine palmitoyltransferase I direct evidence that a single polypeptide is involved in inhibitor interaction and catalytic function J Biol Chem **268**, 5817–5822

12 Esser, V., Brown, N F, Cowan, A T., Foster, D W and McGarry, J D (1996) Expression of a cDNA isolated from rat brown adipose tissue and heart identifies the product as the muscle isoform of carnitine palmitoyltransferase I (M-CPT-I) M-CPT I is the predominant CPT I isoform expressed in both white (epididymal) and brown adipocytes. J Biol. Chem **271**, 6972–6977

13 Yu, G-S, Lu, Y-C and Gulick, T (1998) Rat carnitine palmitoyltransferase Iβ mRNA splicing isoforms. Biochim Biophys Acta **1393**, 166–172

14 Yu, G-S, Lu, Y-C and Gulick, T (1998) Expression of novel isoforms of carnitine palmitoyltransferase I (CPT I) generated by alternative splicing of the CPT Iβ gene Biochem J **334**, 225–231

15 Yu, G-S, Lu, Y.-C. and Gulick, T (1998) Co-regulation of tissue specific alternative human carnitine palmitoyltransferase Iβ gene promoters by fatty acid enzyme substrate J Biol Chem **273**, 32901–32909

16 Yamazaki, N, Shinohara, Y, Shima, A. and Terada, H. (1995) High expression of a novel carnitine palmitoyltransferase I like protein in rat brown adipose tissue and heart: isolation and characterization of its cDNA clone FEBS Lett **363**, 41–45

17 Ghadiminejad, I and Saggerson, E D (1991) A study of properties and abundance of the components of liver carnitine palmitoyltransferases in mitochondrial inner and outer membranes Effects of hypothyroidism, fasting and a ketotic diabetic state Biochem. J **277**, 611–617

18 Zammit, V A (1996) Role of insulin in hepatic fatty acid partitioning: emerging concepts Biochem J **314**, 1–14

19 Zammit, V A, Corstorphine, C. G, Kolodziej, M. P and Fraser, F (1998) Lipid molecular order in liver mitochondrial outer membranes, and sensitivity of carnitine palmitoyltransferase I to malonyl-CoA Lipids **33**, 371–376

20 Kolodziej, M P and Zammit, V. A (1993) Mature carnitine palmitoyltransferase I retains the N-terminus of the nascent protein in rat liver FEBS Lett **327**, 294–296

21 Fraser, F, Corstorphine, C. G and Zammit, V A (1996) Evidence that both the acyl-CoA- and malonyl-CoA binding sites of mitochondrial overt carnitine palmitoyltransferase (CPT I) are exposed on the cytosolic face of the outer membrane Biochem. Soc Trans **24**, 184S

22 Fraster, F, Corstorphine, C. G and Zammit, V A. (1997) Topology of carnitine palmitoyltransferase I in the mitochondrial outer membrane. Biochem J **323**, 711–718

23 Swanson, S T., Foster, D W, McGarry, J D and Brown, N F (1998) Roles of the N- and C-terminal domains of carnitine palmitoyltransferase I isoforms in malonyl-CoA sensitivity of the enzymes insights from expression of chimeric proteins and mutation of conserved histidine residues Biochem J. **335**, 513–519

24 Brown, N F, Esser, V., Foster, D W and McGarry, J D (1994) Expression of a cDNA for rat liver carnitine palmitoyltransferase I in yeast establishes that catalytic activity and malonyl-CoA sensitivity reside in a single polypeptide J Biol Chem **269**, 26438–26442

25 Shi, J, Zhu, H, Arvidson, D N, Cregg, J M and Woldegiorgis, G (1998) Deletion of the first 18 N-terminal amino acid residues in rat liver carnitine palmitoyltransferase I abolishes malonyl-CoA sensitivity and binding Biochemistry **37**, 11033–11038

26 Cohen, I, Kohl, C, McGarry, J. D, Girard, J and Prip-Buus, C (1998) The N-terminal domain of rat liver carnitine palmitoyltransferase I mediates import into the outer mitochondrial membrane and is essential for activity and malonyl-CoA sensitivity J Biol Chem **273**, 29896–29904

27 Shi, J, Zhu, H, Arvidson, D N and Woldegiorgis, G (1999) A single amino acid change (substitution of glutamate 3 with alanine) in the N-terminal region of rat liver carnitine palmitoyltransferase I abolishes malonyl-CoA inhibition and high affinity binding J Biol. Chem **274**, 9421–9426

28 Woeltje, K F, Kuwajima, M, Foster, D W and McGarry, J D (1987) Characterization of the mitochondrial carnitine palmitoyltransferase enzyme system II Use of detergents and antibodies J Biol Chem **262**, 9822–9827

29 Brown, N F, Anderson, R C, Caplan, S L, Foster, D W. and McGarry, J D (1994) Catalytically important domains of rat carnitine palmitoyltransferase II as determined by site-directed mutagenesis and chemical modification evidence for a critical histidine residue J Biol. Chem **269**, 19157–19162

Received 9 February 2000/29 March 2000, accepted 19 April 2000

30 Garild, K D, Sun, X, Paucek, P. and Woldegiorgis, G. (1995) Mitochondrial cation transport systems Methods Enzymol. **260**, 331–348

31 Stephens, T W, Cook, G A and Harris, R A (1983) Effect of pH on malonyl-CoA inhibition of carnitine palmitoyltransferase I Biochem J **212**, 521–524

32 Mills, S E, Foster, D W. and McGarry, J D (1984) Effect of pH on the interaction of substrates and malonyl-CoA with mitochondrial carnitine palmitoyltransferase I Biochem J **219**, 601–608

33 Kolodziej, M P and Zammit, V. A (1990) Sensitivity of inhibition of rat liver mitochondrial outer-membrane carnitine palmitoyltransferase by malonyl-CoA to chemical- and temperature-induced changes in membrane fluidity Biochem J. **272**, 421–425

34 Woeltje, K F, Esser, V., Weis, B C, Sen, A, Cox, W F, McPhaul, M J, Slaughter, C. A, Foster, D W and McGarry, J D (1990) Cloning, sequencing, and expression of a cDNA encoding rat liver mitochondrial carnitine palmitoyltransferase II J. Biol Chem **265**, 10720–10725

35 Brown, N F, Sen, A, Soltis, D A, Jones, B., Foster, D. W and McGarry, J. D (1993) Expression of precursor and mature carnitine palmitoyltransferase II in *Escherichia coli* and *in vitro*. differential behaviour of rat and human isoforms Biochem J **294**, 79–86

36 de Vries, Y, Arvidson, D N., Waterham, H R, Cregg, J M and Woldegiorgis, G. (1997) Functional characterization of mitochondrial carnitine palmitoyltransferases I and II expressed in the yeast *Pichia pastoris* Biochemistry **36**, 5285–5292

37 Zhu, H, Shi, J., Cregg, J M. and Woldegiorgis, G. (1997) Reconstitution of highly expressed human heart muscle carnitine palmitoyltransferase I Biochem Biophys Res Commun **239**, 498–502

38 Zhu, H., Shi, J, de Vries, Y, Arvidson, D N., Cregg, J M and Woldegiorgis, G (1997) Functional studies of yeast-expressed human heart muscle carnitine palmitoyltransferase I Arch Biochem Biophys **347**, 53–61

39 Jackson, V N, Cameron, J M., Zammit, V A and Price, N T (1999) Sequencing and functional expression of the malonyl-CoA-sensitive carnitine palmitoyltransferase from *Drosophila melanogaster* Biochem. J **341**, 483–489

40 Fraser, F and Zammit, V A (1998) Enrichment of carnitine palmitoyltransferases I and II in the contact sites of rat liver mitochondria. Biochem J. **329**, 225–229

41 Zammit, V A. and Corstorphine, C G (1985) Effects of incubation at physiological temperatures on the concentration-dependence of [2-^{14}C]malonyl-CoA binding to rat liver mitochondria Biochem J **231**, 343–347

42 McGarry, J D, Brown, N F, Inthanousay, P P., Park, D I, Cook, B A and Foster, D W. (1992) Insights into the topography of mitochondrial carnitine palmitoyltransferase gained from the use of proteases, in New Developments in Fatty Acid Oxidation (Coates, P. M. and Tanaka, K, eds.), pp. 47–61, Wiley–Liss, New York

43 Kashfi, K and Cook, G A. (1995) Temperature effects on malonyl-CoA inhibition of carnitine palmitoyltransferase I Biochim Biophys Acta **1257**, 133–139

44 Cook, G A, Mynatt, R L. and Kashfi, K (1994) Yonetani-Theorell analysis of hepatic carnitine palmitoyltransferase-I inhibition indicates two distinct inhibitory binding sites J Biol Chem **269**, 8803–8807

Lithocholic acid and sulphated lithocholic acid differ in the ability to promote matrix metalloproteinase secretion in the human colon cancer cell line CaCo-2

Bente HALVORSEN*, Anne Cathrine STAFF*, Solveig LIGAARDEN*, Kristian PRYDZ† and Svein Olav KOLSET*[1]

*Institute for Nutrition Research, P.O. Box 1046, Blindern, University of Oslo, 0316 Oslo, Norway, and †Department of Biochemistry, P.O. Box 1041, Blindern, University of Oslo, 0316 Oslo, Norway

The human colon carcinoma cell line CaCo-2 has the ability to sulphate the secondary bile acid lithocholic acid (LA), whereas other primary or secondary bile acids were not sulphated [Halvorsen, Kase, Prydz, Gharagozlian, Andresen and Kolset (1999) Biochem. J. **343**, 533–539]. To study the biological implications of this modification, CaCo-2 cells were incubated with either LA or sulphated lithocholic acid (3-sulpholithocholic acid, SLA), and in some experiments with taurine-conjugated lithocholic acid. Increased secretion of matrix metalloproteinases (MMPs) correlates with transformation of colon epithelial cells. When CaCo-2 cells were incubated with LA, the secretion of MMP-2 was found to increase approx. 60 % when analysed by gelatin zymography, and 80 % when analysed by Western blotting. SLA, in contrast, did not affect the level of MMP-2 secretion, and after zymography the level of enzyme activity was 78 % of control values after 18 h incubation. The secretion of MMPs is linked to increased cellular invasion and, in tumours, to increased capacity for metastasis. The ability of CaCo-2 cells to invade in a chamber assay was stimulated after exposure to LA, whereas SLA-treated cells did not differ from control cells. LA therefore seems to induce a more invasive CaCo-2 cell phenotype, as judged by the two parameters tested, whereas the sulphated counterpart, SLA, did not have these effects. Sulphation of LA in the colon may be an important mechanism to decrease the potential LA has to promote a malignant epithelial phenotype.

Key words: conjugated bile acids, intestine, invasion, metastasis, sulphation.

INTRODUCTION

Absorption of dietary fat is dependent upon the secretion of bile acids from the liver. Primary bile acids are generally conjugated with taurine or glycine. Secondary bile acids, however, are formed in the large intestine as a result of bacterial dehydroxylation. The major portion of intestinal bile acids, primary and secondary, is reabsorbed through the entero-hepatic circulation. Only minor amounts of secondary bile acids escape the body through faeces elimination. Elevated levels of faecal secondary bile acids have, however, been correlated to a higher incidence of colorectal cancer [1]. The biological effects of secondary bile acids in relation to the development of colon cancer have not been defined in any great detail.

Lithocholic acid (LA) has been shown to be the most cytotoxic bile acid towards colon cells [2]. We have recently demonstrated that the secondary bile acid, LA, could be sulphated by cultured human intestinal CaCo-2 cells, whereas the secondary bile acid, deoxycholic acid, and the primary bile acids, cholic acid and chenodeoxycholic acid, were not [3]. This finding suggests that sulphation of LA by colon epithelial cells could be a protective mechanism, probably to promote increased water solubility and decreased cytotoxicity.

Several members of the matrix metalloproteinase (MMP) family are expressed at higher levels in gastrointestinal cancers than in normal tissues and benign adenomas. The most common MMPs found in colorectal or gastrointestinal cancers are gelatinase A (MMP-2), gelatinase B (MMP-9) and matrilysin (MMP-7) [4]. MMPs are important enzymes in normal processes such as development, tissue repair, wound healing and extravasation of immune cells. In malignancy, such enzymes become important for tumour cells to remodel their local environment, to ensure nutritional support through access to blood supply, and also to provide escape routes to the circulatory system for metastasis to other organs. In the latter process, the ability to migrate through matrix barriers is an important cellular property.

In the present paper we analyse the effects of exposing CaCo-2 cells to LA, 3-sulpholithocholic acid (SLA) and, in some cases, to the taurine-conjugated LA (taurolithocholic acid, TLA). We reasoned that it would be biologically relevant to test these bile acids on two parameters important to colon cancer cells: the ability to secrete MMPs, and the ability to migrate through barriers. Results presented show that SLA and LA differ in their ability to affect both parameters, suggesting that sulphation may have implications for regulating the effects of LA on human colon cells.

MATERIALS AND METHODS

Chemicals

LA, SLA, TLA and insulin were purchased from Sigma. Dulbecco's modified Eagle's medium (DMEM), non-essential

---

Abbreviations used: TLA, taurolithocholic acid; LA, lithocholic acid; SLA, 3-sulpholithocholic acid; DMEM, Dulbecco's modified Eagle's medium; FCS, fetal calf serum; MMP, matrix metalloproteinase.

[1] To whom correspondence should be addressed (e-mail s.o.kolset@basalmed.uio.no).

amino acids, penicillin, streptomycin, and fetal calf serum (FCS) were all obtained from BioWhittaker (Walkersville, MD, U.S.A.). Sulphate-free RPMI 1640 culture medium was from Gibco BRL, and trypsin was purchased from Difco (Detroit, MI, U.S.A.). Tissue culture dishes and flasks were supplied by Costar [^{35}S]Sulphate and [^{3}H]leucine were from Amersham International. [^{3}H]Thymidine and the enhanced chemiluminescence system were purchased from DuPont New England Nuclear (Boston, MA, U.S A.). Sephadex G-50 Fine was from Amersham Pharmacia Biotech. [^{14}C]LA was obtained from Amersham International, and [^{14}C]SLA was obtained by HPLC of conditioned medium from CaCo-2 cells incubated with [^{14}C]LA (described in [3]). The chromogenic peptide substrate S-2288 (*H*-D-Ile-Pro-Arg-*p*-nitroanilide) was from Chromogenix AB, Mölndal, Sweden

Cell cultures

The CaCo-2 human intestinal cell line was obtained from A.T.C.C. These cells were chosen as a model system for studying the effects and metabolism of bile acids on human intestinal cells. The cell line was maintained in DMEM medium containing 20 % FCS, 2 mM L-glutamine, insulin (10 μg/ml), penicillin (50 units/ml), streptomycin (50 μg/ml) and 1 % non-essential amino acids. For subculture, the cell medium was removed and the cells were detached with 0.25 % trypsin (in PBS containing 0.2 g/l EDTA). FCS was added to terminate trypsin treatment, and the cells were re-seeded at approx. 40000/cm^2 in new flasks. Before starting experiments, 500000 cells were seeded per well (35-mm diameter) and grown to 90 % confluence.

Bile acids

The sodium salts of LA, SLA and TLA were all solubilized in DMEM/ethanol (1:1, v/v). During experiments, control cells were exposed to the same concentration of ethanol (0.5 %) as cells treated with bile acids.

Proliferation and protein synthesis

The viability of CaCo-2 cells exposed to increasing concentrations of LA, SLA, and TLA was examined by measuring the incorporation of [^{3}H]leucine into cell-associated proteins, as previously described [3] The proliferative capacity was determined by measuring the incorporation of [^{3}H]thymidine into cell-associated DNA, as has been outlined by Staff et al. [5].

Labelling of cells

Sulphate-depleted RPMI 1640 medium containing 10 % FCS, L-glutamine and non-essential amino acids was used during [^{35}S]sulphate-labelling experiments. Before labelling, the cells were washed once with sulphate-depleted RPMI 1640. Thereafter, labelling medium with [^{35}S]sulphate (200 μCi/ml) was added to the cells. Concomitantly, the cells were exposed to LA, SLA, or TLA at concentrations from 2 to 26.6 μM. After labelling, cell and medium fractions were harvested and [^{35}S]sulphated macromolecules were recovered, as previously described [3].

In some experiments the cells were labelled with [^{3}H]glucosamine (200 μCi/ml) for 24 h with glucose-free DMEM (Gibco BRL), as described elsewhere [6]. The cells were concomitantly exposed to either LA, SLA, or TLA at concentrations from 1 to 10 μg/ml (2–26 μM), and after 24 h incubation [^{3}H]glucosamine-labelled macromolecules were isolated from the cells and the culture medium as described for isolation of [^{35}S]sulphated macromolecules [3].

Zymography

Serum-free conditioned medium from CaCo-2 cells was collected to analyse gelatinase activity, as described in [5]. Approx. 5 × 10^5 cells were seeded per 35-mm well and incubated for one or two days to approx. 90 % confluence. The cells were washed once in DMEM and incubated in 1 ml of DMEM for 9 or 18 h with all additions except serum, but also containing either LA (26.6 μM), SLA (21.9 μM), or TLA (2 μM). The conditioned media were harvested and cell debris removed by centrifugation (167 *g*, 3 min, 4 °C).

Between 60 and 75 μg of protein from conditioned media was incubated at room temperature for 10 min with non-reducing loading buffer containing 4 % SDS (w/v). The samples were then subjected to electrophoresis at 4 °C on SDS/polyacrylamide gels containing 0.1 % gelatin (w/v) (Novex, San Diego, CA, U.S.A.). High-molecular-mass markers (14.3–200 kDa; Amersham International) were used as standards. A mixture of purified human MMP-2 and human MMP-9 (Chemicon International, Temecula, CA, U.S.A.) was run in a separate lane. The gels were cleared of SDS, developed for 24 h and stained. Thereafter, the gels were scanned with a laser-scanner densitometer (Molecular Dynamics, Sunnyvale, CA, U.S.A.) and quantified using Image Quant software.

Western immunoblotting

CaCo-2 cells were incubated in medium supplemented with LA (26.6 μM), SLA (21.9 μM l), or TLA (2 μM) for 9 or 18 h. The cells were washed twice in ice-cold PBS (pH 7.2) prior to the addition of lysis buffer, consisting of 150 mM NaCl, 50 mM Tris/HCl (pH 7.6), 1 mM EDTA, 1 % Triton X-100, and protease inhibitor cocktail (Boehringer Mannheim). The samples were frozen at −70 °C until further analysis. Equal amounts of protein were subjected to SDS/10 % PAGE, and electrophoretically transferred to Immobilon PVDF filters (Millipore, Bedford, MA, U.S.A.). Filters were blocked for 1 h at room temperature with 5 % low-fat milk in Tris-buffered saline containing 0.02 % Tween (v/v), followed by incubation at room temperature for 1 h with the monoclonal anti-human MMP-2 (R & D Systems). Proteins were detected by enhanced chemiluminescence using horseradish peroxidase-labelled anti-mouse IgG (Vector Laboratories, Burlingame, CA, U.S.A.). The enhanced-chemiluminescence-exposed films were quantified by laser-scanning densitometry. To verify the presence of MMP-2 protein, another monoclonal human MMP-2 antibody from an alternative supplier (Oncogene, Cambridge, MA, U.S.A.) was also used. The two different antibodies recognized a protein band with the same molecular mass.

Transwell invasion assay

CaCo-2 cells were labelled for 72 h with [^{3}H]thymidine in medium, as previously described. The cells were trypsin-treated and washed once in DMEM. Cells (100000 in 250 μl) were seeded on 8-μm Transwell filter (24-wells; Costar) in DMEM with additions as described above but without FCS, either in the presence of ethanol (controls), LA (26 6 μM), or SLA (21.9 μM) in the upper (apical) medium. The chambers underneath the filters (basolateral) consisted of DMEM with all additions included (500 μl). After 48 h incubation, both medium fractions were discarded and adherent non-invaded cells on top of the filters were wiped off with cotton swabs. The filter membranes, containing invaded cells, were cut out and analysed for radioactivity in a scintillation counter. The counted radioactivity was regarded as a measure of invaded CaCo-2.

Enzyme assay

Trypsin-like enzyme activities were measured in serum-free conditioned media from CaCo-2 cells cultured in 16-mm wells (Costar), either untreated or exposed to either LA (26.6 μM) or SLA (21.9 μM). Media were harvested after 2, 6 and 20 h incubations. Conditioned medium (100 μl) was added to wells of 96-well microtitre plates. PBS (100 μl) was added together with 20 μl of the chromogenic substrate S-2288 (stock concentration 20 mM). The enzyme activity was recorded by using a Titertek Multiscan spectrophotometer (Flow Laboratories, Irvine, Scotland, U.K.). Media from incubations without cells were used for background subtraction. Measurements were carried out in triplicate.

Statistics

Results are presented as means ± S.E.M. The Mann–Whitney *U*-test was used to test significant differences between groups. The significance level was set at $P < 0.05$.

RESULTS

In order to compare the effects of LA and SLA on CaCo-2 cells, initial experiments were performed to measure *de novo* protein and DNA synthesis. Consequently, cells were labelled with either [^{3}H]leucine or [^{3}H]thymidine in the absence and presence of LA, SLA and TLA. The synthesis of protein and DNA was unaffected by exposure to LA (26.6 μM) and SLA (21.9 μM). In contrast the taurine-conjugated LA decreased the level of incorporation of both of [^{3}H]leucine and [^{3}H]thymidine at concentrations higher than 2.0 μM (results not shown). TLA was therefore used in 2.0 μM concentrations in further studies.

The expression level of [^{35}S]sulphated molecules was stimulated in the presence of LA, but not the other primary or secondary bile acids tested [3]. We wanted to compare the effects of LA, SLA and another modified form of LA (the taurine-conjugated form), on this particular parameter. Both LA (26.6 μM) and TLA (2.0 μM) increased the expression level of [^{35}S]sulphated molecules in the medium fractions, 3 and 1.6 times above control levels respectively (Table 1). No changes were seen in the cell fractions. In contrast, exposing the cells to SLA did not increase the level of [^{35}S]sulphated molecules, either in the medium or the cell fraction. Furthermore, the incorporation of [^{3}H]glucosamine into glycoconjugated molecules was not affected by any of the bile acids (Table 1). Consequently, we assume that LA and TLA do not affect the expression level of sulphated glycoconjugates. The lack of effect of SLA suggests that the increased level of [^{35}S]sulphated molecules after treatment with both LA and TLA is due to a sulphation of these bile acids themselves, in accordance with what has been shown for LA [3].

Table 1 Incorporation of [^{3}H]glucosamine and [^{35}S]sulphate into macromolecules in CaCo-2 cells

CaCo-2 cells were incubated in the presence of LA (26.6 μM), SLA (21.9 μM) or TLA (2.0 μM) and labelled with [^{3}H]glucosamine and [^{35}S]sulphate for 24 h. The cell and medium fractions were harvested, subjected to gel chromatography, and analysed for radioactivity as described in the Materials and Methods section. Data presented are the means ± S.E.M from three separate cell dishes. * Statistical significant difference from control ($P < 0.05$).

Fraction	[^{3}H]Glucosamine (c.p.m./100 μl)	[^{35}S]Sulphate (c.p.m./100 μl)
Medium		
Vehicle, control	2345 ± 86	1269 ± 49
LA	2257 ± 85	4038 ± 260*
SLA	2323 ± 105	1288 ± 76
TLA	2188 ± 59	2019 ± 61*
Cells		
Vehicle, control	10951 ± 135	1162 ± 104
LA	9689 ± 701	1343 ± 47
SLA	10536 ± 193	1382 ± 54
TLA	11672 ± 484	1060 ± 75

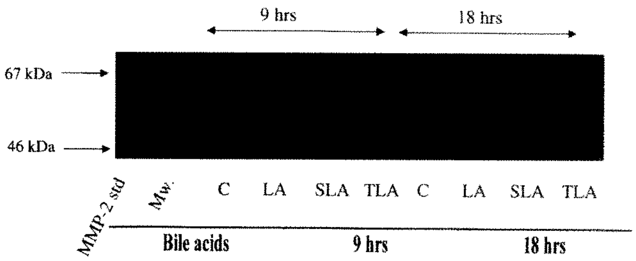

Bile acids	9 hrs	18 hrs
	% of control	*% of control*
Control	100.0	100.0
LA, 26.6 μM	170.5 (147.1 – 200.9)	155.5 (130.0 – 181.0)
SLA, 21.9 μM	50.0 (33.3 – 66.6)	78.0 (73.7 – 82.2)
TLA, 2.0 μM	90.0 (88.5 – 91.4)	132.4 (87.8 – 177)

Figure 1 Gelatinolytic activity in CaCo-2 medium

After confluence, CaCo-2 cells were incubated in the presence or absence of LA (26.6 μM), SLA (21.9 μM), or TLA (2.0 μM) for 9 h or 18 h in serum-free medium. Control cells were given ethanol (0.5%). The condition medium was harvested and subjected to zymography, as described in the Materials and methods section. The Figure shows a zymogram from one typical experiment. Each zymography was run on conditioned medium pooled from three different cell cultures. The results are calculated as percentage of controls, and data are presented as means of two experiments with ranges given in parentheses.

To compare further the effects of LA and SLA on CaCo-2 cells, conditioned media from cells cultured without serum were analysed for the content of gelatinase activity by zymography. From Figure 1 it is evident that considerable gelatinase activity is present in the medium fractions harvested. Two proteins with the ability to degrade gelatin were seen in all the medium fractions. The level of enzyme activity, however, differed to a large extent between the different conditioned media. Cells exposed to LA released 1.7 times more gelatin-degrading activity than control cells after 9 h incubation, whereas cells exposed to TLA released slightly less than control cells. Medium from cells exposed to SLA, however, contained only 50 % of the activity found in control medium after 9 h (66 % of control in the experiment shown). After 18 h this level was 78 % of the control. At this time point, LA treatment gave a 1.6-fold higher gelatinase level than in the control, whereas the effect of TLA showed a great variation with a mean slightly higher than the control. Accordingly, while LA increased gelatinase activity in the medium fractions, SLA had the opposite effect.

In order to identify the gelatinase activity seen in conditioned medium from CaCo-2 cells, the different fractions were subjected to SDS/PAGE followed by Western blotting. The activity seen after zymography in Figure 1 is clearly MMP-2, as can be seen in Figure 2. We could not detect any MMP-9 activity in these fractions with an anti MMP-9 antibody (results not shown). By scanning the blot it was possible to determine the relative level of MMP-2 protein. Figure 2 (lower panel) shows that the level of MMP-2 was significantly higher in medium from LA-treated cells than in cells exposed to SLA. The level of MMP-2 in the

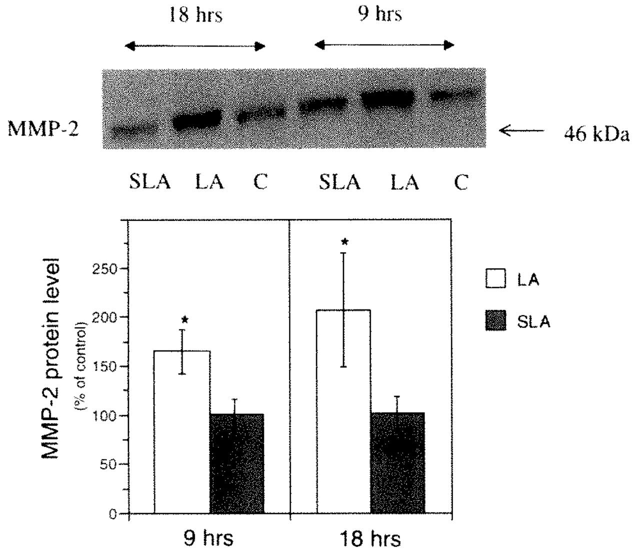

Figure 2 Effects of LA and SLA on MMP-2 expression in CaCo-2 cells

After confluence, CaCo-2 cells were incubated in the presence or absence of LA (26.6 μM), or SLA (21.9 μM) for 9 h or 18 h in serum-free medium. Control cells were given ethanol (0.5%). The cells were harvested and lysed as described in the Materials and methods section. Cell protein (20 μg) was separated on reducing SDS/PAGE, electrotransferred, and incubated with anti-human MMP-2. The results are calculated as percentage of controls. The bar graph shows the means ± S.E.M. from four separate experiments, and the immunoblot presented is from one typical experiment.

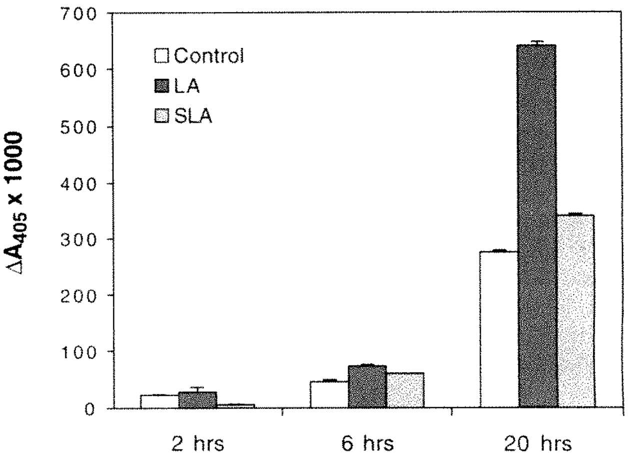

Figure 3 Effects of LA and SLA on serine protease activities in CaCo-2 cells

CaCo-2 cells were cultured under serum-free conditions in the presence or absence of LA (26.6 μM), or SLA (21.9 μM) for 2 h, 6 h and 20 h. Conditioned media were harvested, incubated with the chromogenic substrate S-2288 and the enzyme activity recorded at 405 nm in a Titertek spectrophotometer. The bar graph shows the means ± S.E.M. from three experiments.

Table 2 Effect of bile acids on the invasion of [^{3}H]thymidine-labelled CaCo-2 cells

The invasion of [^{3}H]thymidine-labelled CaCo-2 cells was performed as described in the Materials and methods section in the absence and presence of LA (26.6 μM) or SLA (21.9 μM). Results are given as means ± S. E.M from 11 to 14 separate cell cultures. The absolute values for controls ($n = 11$) were 8649 ± 2151 c.p.m./filter. * $P < 0.05$ versus control, § $P < 0.05$ versus SLA.

Bile acid	Invasion (% of control)
Control	100.0 ± 7.2
LA	163.2 ± 28.3*§
SLA	86.6 ± 7.5 *

medium from the latter cells was the same as in medium from control cells. From both zymography and Western-blot experiments we can conclude that LA treatment increases the level of MMP-2 in the medium of CaCo-2 cells, whereas the sulphated counterpart, SLA, does not have such an effect. Both in the zymography and Western-blot experiments a 45 kDa form of MMP-2 could be detected, whereas standard MMP-2 migrated as 65 kDa and 72 kDa proteins. In some experiments we could detect small levels of gelatinase activity with a molecular mass of 65 kDa (results not shown). In parallel experiments with the human trophoblastic cell line JAR MMP-2, gelatinolytic activity could only be detected at a molecular mass of 65 kDa [5]. There is evidently large differences in the processing of MMP-2 between different cell types, and the level of the 65 kDa and 45 kDa form may depend on the level of tissue inhibitor of metalloproteinase-2 in the cell type studied, as has been indicated in [7].

The difference between LA and SLA could be due to differences in the cellular uptake. CaCo-2 cells were incubated with either [^{14}C]LA or [^{14}C]SLA and the amount of cell-associated radioactivity determined. The level of [^{14}C]LA associated with the cells increased up to 2 h (1331 ± 215 c.p.m.), with no further increase at 4 h. During this incubation time the level of [^{14}C]SLA was low (115 ± 33 c.p.m.). However, in several experiments we noted that the level of MMP-2 activity was lower in CaCo-2 cells incubated with SLA for 9 h and 18 h, but significantly higher than in controls after 48h. These results indicate different rates of uptake for LA and SLA, as has been shown in hepatocytes [8]. Furthermore, in this study the uptake of LA was by simple diffusion and the uptake of SLA by Na^+-independent carrier, which may possibly lead to different intracellular routing and effects, as is indicated from our data.

Plasminogen activator and other serine proteases are important for the modulation of the cellular microenvironment, as are MMPs [9]. To investigate the effect of LA and SLA on the secretion of other proteases, serum-free supernatants from CaCo-2 cells were used to determine the level of serine proteases like plasminogen activator (tissue-type) by using the chromogenic substrate, S-2288. LA stimulated the secretion of S-2288-cleaving activity, whereas SLA did not, as can be seen in supernatants from cells incubated for 6 h (Figure 3). After 20 h incubation, cells exposed to LA released 1.8 times more enzyme activity. Interestingly, at this time point cells treated with SLA had a somewhat higher level (14 % increase) of activity in the supernatants than control cells.

Increased expression of MMPs is linked to a more migratory or invasive phenotype in many cell systems. In order to investigate a possible relation between the level of MMPs in the medium and the ability to migrate, [^{3}H]thymidine-labelled CaCo-2 cells were plated in chambers on filters with 8-μm pores. The bile acids were exposed to the cells in the upper chambers, and medium in the lower chamber contained serum as chemoattractant. Cell invasion was 1.6 times higher in cells exposed to LA compared with control cells (Table 2). Cells treated with SLA had a migratory capacity slightly lower than control cells.

DISCUSSION

The ability to catalyse sulphation reactions is an important property of all mammalian cells. The most highly sulphated macromolecules are the proteoglycans, found both in the extracellular matrix, on cell surfaces and in intracellular granules [10]. Several other glycoconjugates may also be sulphated, including glycoprotein hormones, glycolipids, secretory proteins, selectins and mucins [11–13]. Most of these sulphation reactions take place in the Golgi apparatus, whereas drugs and xenobiotic compounds are sulphated in the cytosol. The sulphation of LA in CaCo-2 cells is also a cytosolic process [3], but the biological function(s) of this bile acid modification has not been defined. It has been shown that LA has toxic effects on the liver [14], and the cytotoxicity of LA in hepatocytes was greatly reduced by either glucuronidation or sulphation of this bile acid [8]. Sulphation in the intestine could therefore reduce the detrimental effects of LA in the entero-hepatic circulation. It has been shown that SLA is present in substantial quantities in human faeces and that the LA/SLA ratio was 2.1 [15]. It has further been suggested that lowered uptake of sulphated bile acids in the ileum, and lack of uptake in the colon, may contribute to their excretion [16]. Finally, studies with mice have shown that sulphated bile acids may inhibit colon carcinogenesis [17].

In the present paper we show that LA stimulated the secretion of MMP-2 from cultured CaCo-2 cells, whereas SLA did not. Furthermore, the increased invasive capacity seen in these cells after exposure to LA was not observed in cells exposed to SLA. In addition, neither LA nor SLA were found to affect the viability or the ability of CaCo-2 cells to proliferate. From these data it is evident that sulphation of LA leads to the generation of a bile acid derivative with different effects than the parent molecule. The data presented indicate that sulphation of LA can be viewed as a biological inactivation of a compound with possible hazardous effects on colon epithelial cells. MMP-2 secretion and increased invasiveness are clearly parameters of malignant epithelial cells [4]. Our results show that LA treatment led to a stimulation of both these characteristic features in CaCo-2 cells.

The molecular mechanisms of LA effects on CaCo-2 cells or other cells types have not been the subjects of detailed investigations. There are, however, some reports on the effects of bile acids on gene expression. Recently the farnesoid X receptor, defined as an orphan receptor, was shown to bind bile acids and to repress the expression of genes regulating cholesterol metabolism [18,19]. It has furthermore been established that the expression of intestinal bile acid binding protein was promoted more efficiently with lipophilic than hydrophilic bile acids in CaCo-2 cells [20]. Bile acids may also influence cellular signalling processes by increasing the activity of protein kinase C and the transcription factor activator protein 1 in colon cells [21,22]. Although speculative, one possible scenario could be that cellular uptake or intracellular routing of LA and SLA would differ, due to differences in water solubility. SLA and LA may, furthermore, interact with different intracellular proteins or other types of ligands, and LA could reach the nucleus to modulate appropriate target genes, whereas SLA would be secreted and thereby prevented from such gene regulation. Sulphation of bile acids, and LA in particular, may turn out to have implications for the regulation of cell behaviour and development of malignancy in the large intestine.

Received 21 February 2000/23 March 2000, accepted 25 April 2000

We gratefully acknowledge the technical assistance of Tram Thu Vuong and Vivi Volden. This work was supported by grants from the Norwegian Cancer Society, the Norwegian Research Council, Novo Nordisk and the Throne-Holst Fund.

REFERENCES

1 Kishida, T, Taguchi, F, Tatsuguchi, A, Sato, J, Fujimori, S, Tashikawa, H, Tamagawa, Y., Yoshida, Y and Kobayashi, M (1997) Analysis of bile acids in colon residual liquid or fecal material in patients with colorectal neoplasia and control subjects J Gastroenterol **32**, 306–311

2 Latta, R. K, Flander, H, Ross, N W, Simpson, C and Schneider, H (1993) Toxicity of bile acids to colon cancer cell lines Cancer Lett **70**, 167–173

3 Halvorsen, B, Kase, B F, Prydz, K, Gharagozlian, S, Andresen, M S and Kolset, S O (1999) Sulphation of lithocholic acid in the colon carcinoma cell line CaCo-2 Biochem J. **343**, 533–539

4 Brown, P D (1998) Matrix metalloproteinases in gastrointestinal cancer Gut **43**, 161–163

5 Staff, A C, Ranheim, T, Henriksen, T and Halvorsen, B (2000) 8-iso-prostaglandin $F_{2\alpha}$ reduces trophoblast invasion and matrix metalloproteinase activity Hypertension, in the press

6 Salmivirta, M, Safaiyan, F, Prydz, K, Andresen, M S, Aryan, M and Kolset, S O (1998) Differentiation-associated modulation of heparan sulfate structure and function in CaCo-2 colon carcinoma cells Glycobiology **8**, 1029–1036

7 Itoh, Y, Ito, A, Iwata, K, Tanzawa, K, Mori, Y and Nagase, H (1998) Plasma membrane-bound tissue inhibitor of metalloproteinases (TIMP)-2 specifically inhibits matrix metalloproteinase 2 (gelatinase A) activated on the cell surface J Biol. Chem **273**, 24360–24367

8 Takikawa, H, Tomita, J, Takemura, T and Yamanaka, M (1991) Cytotoxic effect and uptake mechanism by isolated rat hepatocytes of lithocholate and its glucuronide and sulfate. Biochim Biophys Acta **1091**, 173–178

9 Vassalli, J-D and Pepper, M S (1994) Tumour biology Membrane proteases in focus Nature (London) **370**, 14–15

10 Kjellén, L and Lindahl, U (1991) Proteoglycans structures and interactions Annu Rev Biochem **60**, 443–475

11 Hooper, L V, Manzella, S M and Baenziger, J. U (1996) From legumes to leukocytes: biological roles for sulfated carbohydrates FASEB J **10**, 1137–1146

12 Mandon, E C., Milla, M E, Kempner, E and Hirschberg, C. B (1994) Purification of the Golgi adenosine 3′-phosphate 5′-phosphosulfate transporter, a homodimer within the membrane Proc Natl Acad Sci USA **91**, 10707–10711

13 Nieuw Amerongen, A. V, Bolscher, J. G, Bloemena, E and Veerman, E C (1998) Sulfomucins in the human body Biol. Chem **379**, 1–18

14 Palmer, R H (1972) Bile acids, liver injury, and liver disease Arch Intern Med **130**, 6066–6170

15 Podesta, M. R, Murphy, G M and Dowling, R H (1980) Measurement of faecal bile acid sulphates J Chromatogr **182**, 293–300

16 Walker, S, Stiehl, A, Raedsch, R., Kloters, P and Kommerell, B. (1986) Colonic absorption of sulfated and nonsulfated bile acids in rat Digestion **33**, 1–6

17 Takahashi, A, Tanida, N, Kawaura, A, Nishikawa, M and Shimoyama, T (1993) Sulphated bile acid per se inhibits colonic carcinogenesis in mice Eur J Cancer **2**, 161–167

18 Makishima, M, Okamoto, A. Y, Repa, J. J, Tu, H, Learned, R M, Luk, A., Hull, M V, Lustig, K D, Mangelsdorf, D. J and Shan, B (1999) Identification of a nuclear receptor for bile acids Science **284**, 1362–1365

19 Parks, D J, Blanchard, S G, Bledsoe, R K, Chandra, G, Consler, T G, Kliewer, S A, Stimmel, J B, Wilson, T M, Zavacki, A M, Moore, D. D and Lehmann, J. M (1999) Bile acids natural ligands for an orphan nuclear receptor Science **284**, 1365–1368

20 Kanda, T., Foucand, L, Nakamura, Y, Niot, I, Besnard, P, Fujita, M, Sakai, Y, Hatakeyama, K, Ono, T. and Fujii, H. (1998) Regulation of expression of human intestinal bile acid-binding protein in Caco-2 cells Biochem J **330**, 261–265

21 Pongracz, J., Clark, P, Neoptolemos, J P and Lord, J M (1995) Expression of protein kinase C isoenzymes in colorectal cancer tissue and their differential activation by different bile acids Int J Cancer **61**, 35–39

22 Hirano, F., Tanada, H, Okamoto, K, Hiramoto, M, Handa, H. and Makino, I (1996) Induction of the transcription factor AP-1 in cultured human colon adenocarcinoma cells following exposure to bile acids Carcinogenesis **17**, 427–433

Pyruvate dehydrogenase kinase from *Arabidopsis thaliana*: a protein histidine kinase that phosphorylates serine residues

Jay J. THELEN*[1], Jan A. MIERNYK† and Douglas D. RANDALL*[2]

*University of Missouri, Department of Biochemistry, 117 Schweitzer Hall, Columbia, MO 65211, U.S.A., and †Plant Genetics Research Unit, USDA, Agricultural Research Service, Columbia MO 65211, U.S.A.

Pyruvate dehydrogenase kinase (PDK) is the primary regulator of flux through the mitochondrial pyruvate dehydrogenase complex (PDC). Although PDKs inactivate mitochondrial PDC by phosphorylating specific Ser residues, the primary amino acid sequence indicates that they are more closely related to prokaryotic His kinases than to eukaryotic Ser/Thr kinases. Unlike Ser/Thr kinases, His kinases use a conserved His residue for phosphotransfer to Asp residues. To understand these unique kinases better, a presumptive PDK from *Arabidopsis thaliana* was heterologously expressed and purified for this investigation. Purified, recombinant *A. thaliana* PDK could inactivate kinase-depleted maize mitochondrial PDC by phosphorylating Ser residues. Additionally, *A. thaliana* PDK was capable of autophosphorylating Ser residues near its N-terminus, although this reaction is not part of the phosphotransfer pathway. To elucidate the mechanism involved, we performed site-directed mutagenesis of the canonical His residue likely to be involved in phosphotransfer. When His-121 was mutated to Ala or Gln, Ser-autophosphorylation was decreased by 50% and transphosphorylation of PDC was decreased concomitantly. We postulate that either (1) His-121 is not the sole phosphotransfer His residue or (2) mutagenesis of His-121 exposes an additional otherwise cryptic phosphotransfer His residue. Thus His-121 is one residue involved in kinase function.

Key words: autophosphorylation, mechanism, mitochondria, mutagenesis, transphosphorylation

INTRODUCTION

The pyruvate dehydrogenase complex (PDC) is a multienzyme structure that catalyses the oxidative decarboxylation of pyruvate, yielding CO_2, acetyl-CoA and NADH [1]. This complex is localized to the cytoplasm of bacteria and the mitochondrial matrix of eukaryotic cells. Additionally, plant cells contain a second isoform localized to the plastidial stroma [2–4]. The plastidial and mitochondrial PDCs have distinct regulatory and catalytic properties complementing their unique roles in metabolism [4]. The most striking difference is regulation by reversible phosphorylation. The mitochondrial PDC, unlike the plastid counterpart, has an associated pyruvate dehydrogenase kinase (PDK, EC 2.7.1.99) and phosphopyruvate dehydrogenase phosphatase [5]. These two enzymes catalyse the reversible phosphorylation of mitochondrial pyruvate dehydrogenase. PDK curtails mitochondrial PDC activity by catalysing the transfer of the γ-phosphate from ATP to the α subunit of the pyruvate dehydrogenase (E1) component enzyme [4,5]. Conversely, phospho-pyruvate dehydrogenase phosphatase reactivates this component by catalysing dephosphorylation in a Mg^{2+}-dependent manner [6]. The phosphorylation state, and hence the activity status, of PDC is determined by the net sum of these opposing enzyme activities.

Molecular cloning of the first PDK from mammals revealed a deduced amino acid sequence lacking typical eukaryotic Ser/Thr kinase domains but having the five domains characteristic of prokaryotic two-component histidine kinases [7]. Prokaryotic histidine kinases are multidomain polypeptides that catalyse the first step of two-component signal transduction pathways (reviewed in [8]). The sensor domain responds to a cellular signal by autophosphorylating a His residue within the transmitter domain, followed by phosphotransfer to an Asp residue within the receiver domain of a cognate response regulator protein. The activated response regulator typically functions as a specific transcription factor. Although bacterial two-component systems usually follow this reaction scheme, variations exist. Some histidine kinases contain both the histidine phosphotransfer donor domain and the aspartate receiver domain on a single polypeptide, i.e. a hybrid histidine kinase [9]. Multiple donor and receiver domains can reside on a single polypeptide with His-to-Asp phospho-relay perhaps occurring in *cis* on these kinases [10]. Regardless of mechanistic specificities, all histidine kinases characterized until now transfer phosphate from an autophosphorylated His to an Asp residue, transducing cellular signals [11,12].

On the basis of similarities to these histidine kinases [7], PDKs might also use a His for phosphotransfer. However, unlike histidine kinases, mammalian PDKs phosphorylate on Ser rather than Asp residues [13,14]. This novel class of eukaryotic protein kinases also includes the branched-chain α-keto acid dehydrogenase kinase (BCDK, EC 2.7.1.115), which regulates a related mitochondrial α-keto acid dehydrogenase complex involved in branched-chain amino acid catabolism [15]. Although not yet well understood, rat PDK and BCDK both undergo autophosphorylation [16,17]. The BCDK autophosphorylation site was mapped to a Ser residue near the N-terminus [17].

We recently reported the molecular cloning and functional expression of two PDK isoforms from *Zea mays* [18]. The deduced amino acid sequences for the plant enzymes are approx.

Abbreviations used: AtPDK, *Arabidopsis thaliana* pyruvate dehydrogenase kinase; BCDK, branched-chain α-keto acid dehydrogenase kinase; E1, pyruvate dehydrogenase; E2, dihydrolipoamide acetyltransferase; MBP, maltose-binding protein; PDC, pyruvate dehydrogenase complex; PDK, pyruvate dehydrogenase kinase.

[1] Present address: Michigan State University, Department of Botany and Plant Pathology, East Lansing, MI 48824, U.S.A.

[2] To whom correspondence should be addressed (e-mail randalld@missouri.edu).

30 % identical with those from mammals. Amino acid identity is concentrated within 11 discrete domains, of which 5 are related to the prokaryotic histidine kinases [18]. A presumptive PDK recently identified from *Arabidopsis thaliana* is approx. 70 % identical with the maize enzymes and contains the five histidine kinase and six signature PDK domains [19]. At least one of these domains was proposed to be a site for phosphotransfer owing to the presence of an invariant His residue. Here we present evidence that this *A. thaliana* cDNA encodes a genuine PDK that involves one of the conserved His residues for maximal activity.

MATERIALS AND METHODS

Bacterial expression and purification of *A. thaliana* PDK (AtPDK)

Primers DDR 229 (5′-ctcgagctgcagctattaTCAGGGTAAAGGCTCTTGCGA-3′) and DDR 230 (5′-cccgggtctagaATGGCAGTGAAGAAAGCCTGC-3′) were used to amplify the open reading frame of the AtPDK corresponding to the region between 130 and 1227 bp [19]. Restriction sites were engineered into each primer at the 5′ end (lower-case letters) to facilitate subcloning. The *Pst*I (DDR 229) and *Xba*I (DDR 230) sites were used to subclone the PCR product into the pMAL-cRI expression vector (New England Biolabs, Beverly, MA, U.S.A.). To ensure translation termination, two nonsense codons were introduced into DDR 229. Thermal cycling reactions (50 μl total volume) contained 10 mM Tris/HCl, pH 7.9, 0.5 mM $MgCl_2$, 200 μM dNTPs, 5 units of *Taq* polymerase (Promega, Madison, WI, U.S.A.), 2 ng of plasmid DNA template and 20 pmol of each primer. Cycling conditions were 94 °C for 5 min, initial denaturation, followed by 30 cycles of 30 s at 94 °C, 30 s at 50 °C, 2 min at 72 °C with 6 s extensions for the last step of each cycle.

The expression and purification of maltose-binding protein (MBP)–PDK polypeptides and the preparation of kinase-depleted PDC from maize mitochondria were performed as described elsewhere [18,20]. After purification, MBP–AtPDK was dialysed against 2 litres of 20 mM Tes/KOH (pH 7.3)/2 mM dithiothreitol for 16 h at 4 °C and was subsequently concentrated on an ultrafiltration membrane (10 kDa cut-off, Amicon, Beverly, MA, U.S.A.). Cleavage of fusion protein was performed with factor Xa protease (New England BioLabs, Beverly, MA, U.S.A.) at a 1:25 molar ratio of protease to fusion protein in 20 mM Tris/HCl (pH 8.0)/0.1 M NaCl/2 mM $CaCl_2$ for 18 h at 25 °C. Size-exclusion chromatography and native molecular mass determination were performed with a Superose 12 column (Pharmacia, Uppsala, Sweden) with thyroglobulin, ferritin, catalase, aldolase and BSA as standards. SDS/PAGE and immunoblotting were performed with standard procedures [21]. Polyclonal antibodies to PDK were characterized previously [18]. Polyclonal antibodies against MBP were affinity-purified from sera raised against a branched-chain α-keto acid dehydrogenase subunit fusion with MBP.

Mitochondria isolation and assays

Mitochondria were isolated from etiolated maize (B73; Illinois Seed Foundation, Champaign, IL, U.S.A.) shoots as described previously [21,22]. For PDC, a four-step purification procedure starting with isolated maize mitochondria yielded an 80–90 % pure preparation of PDC that was depleted of PDK activity [18,21]. This preparation was termed 'kinase-depleted PDC' and was used to assay recombinant MBP–AtPDK activity. PDC activity was monitored by the reduction of NAD^+ (ΔA_{340}) as described previously [21]. For kinase assays, MBP or MBP–AtPDK were incubated with kinase-depleted maize mitochondrial PDC for 5 min at 25 °C before the addition of $MgATP^{2-}$ to a final concentration of 0.2 mM. Phosphorylation assays proceeded for 5–60 min before PDC activity was assayed. All reported values are the means of at least three independent reactions. Protein quantification was performed by the method of Bradford [23], with BSA as standard.

Phosphorylation assays were performed by adding a known amount of $Mg[\gamma\text{-}^{32}P]ATP^{2-}$ (10 mCi/mmol) to kinase and/or PDC preparations. Reactions proceeded for 1 h at 25 °C and were stopped by the addition of an equal volume of 2 × SDS/PAGE sample buffer [8 M urea/4 % (w/v) SDS/4 % (v/v) 2-mercaptoethanol] followed by heating at 70 °C for 15 min. Denatured proteins were resolved by SDS/PAGE, electroblotted to nitrocellulose, dried and wrapped in Cellophane before exposure to X-ray film for 5–30 min. The incorporation of radiolabel into MBP–AtPDK was quantified by liquid-scintillation spectrometry of the excised MBP–AtPDK band. Relative phosphorylation efficiency was quantified with QS30 quantification software (PDI, Huntington Station, NY, U.S.A.), which accounted for band area and intensity.

Limited proteolysis of MBP–AtPDK was performed with trypsin (Sigma, St Louis, MO, U.S.A.) at a molar ratio of 3:1 fusion protein to trypsin. Protease digestion was performed in 20 mM Tes (pH 7.5)/1 mM dithiothreitol for 16 h at 25 °C and was terminated by the addition of an equal volume of 2 × SDS/PAGE sample buffer followed by heating at 70 °C for 15 min.

Site-directed mutagenesis

Mutagenesis was performed with the GeneEditor site-directed mutagenesis kit (Promega). The pMAL-cRI expression vector containing AtPDK was used as template for mutagenesis performed in accordance with the manufacturer's instructions. The oligonucleotides used for mutagenesis, synthesized at the University of Missouri DNA core facility (Columbia, MO, U.S.A.), were DDR 238 5′-GGGAACCACATTGTTA**GC**CCTTACTTTGACAGCC-3′ (His-121A oligo) and DDR 270 5′-GGGAACCACATTGTTT**T**TGCCTTACTTTGACA-3′ (His-121Q oligo). The mutated base(s) are underlined and in bold. The entire reading frames of both mutant constructs were sequenced to verify that no additional changes had been introduced.

Phosphoamino acid analyses

Protein preparations were phosphorylated with $[\gamma\text{-}^{32}P]ATP$, resolved by SDS/PAGE and transferred to PVDF membranes. Immobilized proteins were excised and phosphoamino acids released by hydrolysis in 6 M HCl for 1 h at 120 °C. The supernatants containing the phosphoamino acids were freeze-dried, then resuspended in 15 μl of pH 1.9 buffer [2.2 % (v/v) formic acid/7.8 % (v/v) acetic acid] containing phospho-Ser, phospho-Thr and phospho-Tyr standards (1 μg of each). Samples of 1.5 μl (approx. 1000 c.p.m.) were spotted on to cellulose chromatography plates (J. T. Baker, Phillipsburg, NJ, U.S.A.) in intervals. Plates were placed in a model HTLE-7000 Hunter thin-layer electrophoresis apparatus in accordance with the manufacturer's instructions (CBS Scientific Company, Del Mar, CA, U.S.A.). Electrophoresis in the first dimension with pH 1.9 buffer was performed at 1.5 kV for 20 min. After the first dimension the plates were dried and rotated through 90 ° for the second dimension. Electrophoresis in the second dimension, with pH 3.5 buffer [5 % (v/v) acetic acid/0.5 % (v/v) pyridine], was performed at 1.3 kV for 16 min. Plates were then dried and phosphoamino acid standards were detected by being stained with 0.25 % (w/v) ninhydrin in acetone, then being baked at

65 °C for 15 min. Radiolabelled amino acids were detected by autoradiography.

RESULTS

Characterization of AtPDK

When expressed as a fusion with the *Escherichia coli* MBP, AtPDK migrated as an 87±3 kDa ($n = 3$) polypeptide during SDS/PAGE (Figure 1A). This protein was absent from untransformed bacteria, determined by immunoblotting with anti-PDK antibodies (Figure 1C). Approximately 10–15 % of MBP–AtPDK was soluble under native conditions and this protein was purified to near-homogeneity by amylose affinity chromatography. Protein yields ranged from 0.1 to 0.2 mg/l of culture broth. Removal of the MBP fusion partner by cleavage with factor Xa protease was 40 % efficient after digestion for 18 h. Digestion efficiency was improved to nearly 100 % when equimolar amounts of protease and fusion protein were incubated (Figure 2C). To estimate the native size it was necessary to remove MBP because it is capable of forming dimers [24]. The factor Xa-cleaved PDK migrated at 44±2 kDa ($n = 3$) during SDS/PAGE, with a native molecular mass, as determined by size-exclusion chromatography, of approx. 86 kDa, suggesting a homodimeric native conformation. The His-121A and His-121Q mutants were identical in size with the wild-type protein (Figure 1B).

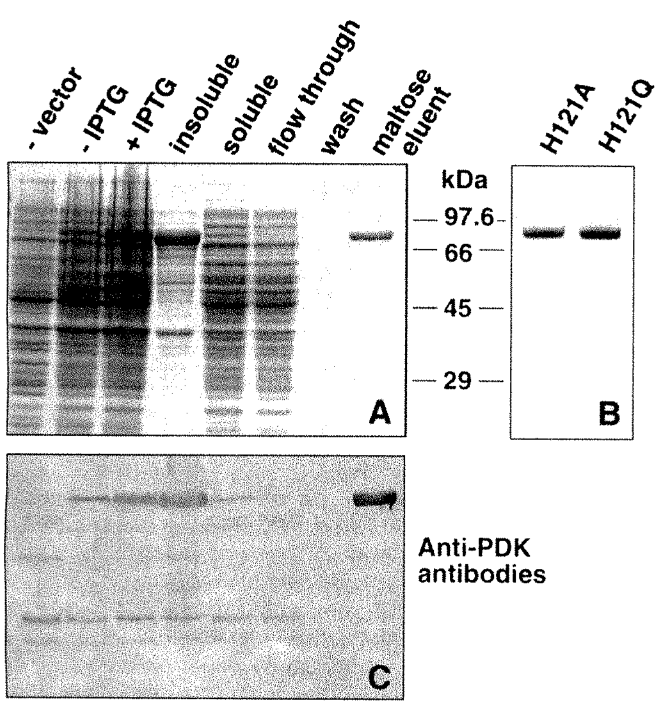

Figure 1 Expression and purification of MBP–AtPDK chimaera

(**A**) Coomassie Blue-stained SDS/PAGE of a typical expression and purification profile. Total protein fractions are shown from untransformed cells (−vector), transformed cells without (−IPTG) or with (+IPTG) the addition of the inducer isopropyl β-D-thiogalactoside at 0.5 mM. After cell disruption the 'insoluble' fraction (lane 4) was removed by centrifugation (9000 ***g***) and the supernatant was termed 'soluble' protein (lane 5). The MBP fusion bound to an amylose-affinity matrix and the unbound fraction was termed 'flow through' (lane 6). The matrix was washed with 50 column vol. of wash buffer (lane 7), after which the bound protein was eluted with maltose-containing buffer (lane 8). (**B**) The His-121A and His-121Q mutants were purified by using the same procedure; they migrated at the same position as wild-type PDK. (**C**) Immunoblot of protein from (**A**) probed with anti-PDK polyclonal antibodies. The positions of molecular mass markers are indicated for (**A**) and (**B**).

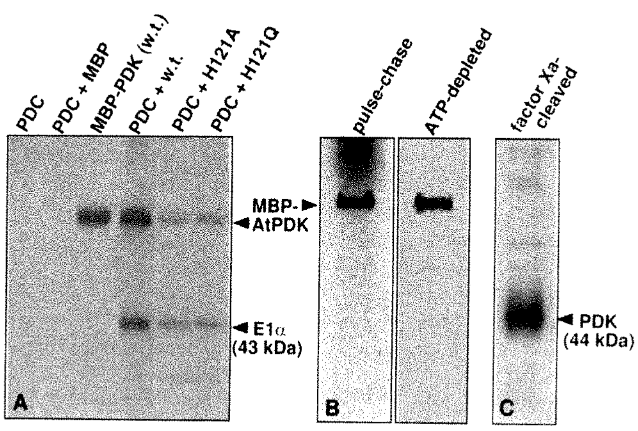

Figure 2 Autophosphorylation of MBP–AtPDK and transphosphorylation of PDC E1α

(**A**) Phosphorylation of kinase-depleted maize mitochondrial PDC by MBP–AtPDK. Kinase-depleted maize PDC (3 μg) was incubated with 2 μg of MBP or MBP–AtPDK for 30 min at 25 °C in the presence of Mg[γ-^{32}P]ATP^{2-} (5 μCi,10 mCi/mmol). Reactions were stopped by the addition of SDS/PAGE sample buffer followed by boiling. Controls lacking MBP–AtPDK (lane 1), containing maize PDC plus MBP (lane 2) and lacking maize PDC (lane 3) are also shown. Abbreviation: w.t., wild-type. (**B**) Lane 1, ^{32}P-phosphorylated MBP–AtPDK was chased with a 10-fold excess of MgATP^{2-} for 5 min before the addition of kinase-depleted maize PDC [in the same ratio as in (**A**)]; the reaction proceeded for 1 h at 25 °C before termination with SDS/PAGE sample buffer. Lane 2, ^{32}P-phosphorylated MBP–AtPDK was desalted by G-50 Sephadex chromatography and subsequently incubated with kinase-depleted maize PDC for 1 h at 25 °C. (**C**) Phosphorylated MBP–AtPDK (0.2 μg) was digested with a molar equivalent of factor Xa protease (New England Biolabs) for 18 h at 25 °C before resolution by SDS/PAGE. The position of the radiolabelled polypeptide coincided with that of AtPDK, which was detected by immunoanalysis.

AtPDK inactivates kinase-depleted maize mitochondrial PDC and phosphorylates maize pyruvate dehydrogenase on Ser residues

When incubated in the presence of MgATP^{2-}, purified MBP–AtPDK inactivated kinase-depleted maize mitochondrial PDC, whereas purified MBP had no effect on PDC activity (Table 1). Although the kinetics of inactivation were slower than observed in previous investigations of plant mitochondrial PDCs [5,6,21], recombinant AtPDK was capable of inactivating 90 % of kinase-depleted maize mitochondrial PDC. The specific activity of MBP–AtPDK was lower (10 PDC units inactivated/min per mg of PDK) than that of maize MBP–PDK2 (40 PDC units inactivated/min per mg of PDK [18]) with maize mitochondrial PDC as substrate. Inactivation of kinase-depleted PDC was coincident with the incorporation of ^{32}P from γ-labelled ATP into a 43 kDa polypeptide (Figure 2A). The radiolabelled 43 kDa polypeptide was not observed in purified MBP or MBP–PDK preparations incubated with [γ-^{32}P]ATP (Figure 2A). Addition of purified MBP to kinase-depleted PDC resulted in no phosphorylation of the 43 kDa protein (Figure 2A), demonstrating that these PDC preparations were kinase-depleted and that recombinant AtPDK was responsible for phosphorylation. The size of the radiolabelled polypeptide is identical with that of maize mitochondrial E1α [21,25]. These results clearly demonstrate that recombinant AtPDK phosphorylates the 43 kDa maize E1α subunit, concomitantly inactivating PDC. Phospho-E1α amino acid(s) were resistant to treatment with acid, indicative

Table 1 Effect of MBP–AtPDK on kinase-depleted maize PDC activity in the presence of $MgATP^{2-}$

Approximately 40 μg of kinase-depleted maize PDC was incubated with 0.2 mM $MgATP^{2-}$ plus recombinant protein at 25 °C for 5 min, then immediately assayed for activity. All rates were normalized to the rate (0.72 μmol of NADH/min per mg) in the absence of $MgATP^{2-}$ and recombinant protein activity. The final rates were obtained by incubating the sample with $MgATP^{2-}$ for 1 h before assay. All rates are means ± S.D. for three measurements.

Control contents	Relative activity (%)
$-MgATP^{2-}$, −PDK	100 ± 5
$+MgATP^{2-}$, +MBP (15 μg)	95 ± 8
With $MgATP^{2-}$; PDK added (μg)	**Relative activity (%)**
1.5	98 ± 5
3.7	84 ± 11
7.5	65 ± 4
15.0	45 ± 4
Incubation for 60 min	**Relative activity (%)**
PDK (3.7 μg)	10 ± 5
MBP (5.0 μg)	100 ± 3

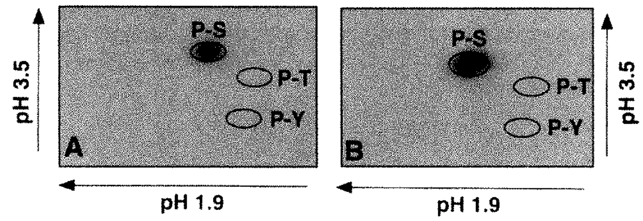

Figure 3 Phosphoamino acid analyses of radiolabelled maize mitochondrial E1α (A) and MBP–AtPDK (B)

(**A**) Kinase-depleted maize PDC was phosphorylated with MBP–AtPDK, resolved by SDS/PAGE and transferred to PVDF membrane. Radiolabelled E1α band was excised and subjected to acid hydrolysis followed by two-dimensional thin-layer electrophoresis. Phosphoamino acid standards were revealed with ninhydrin and ^{32}P-labelled amino acids were detected by autoradiography (16 h exposure). (**B**) Autoradiograph of autophosphorylated MBP–AtPDK subjected to phosphoamino acid analysis as described for (**A**). Arrows indicate the directions of electrophoretic migration; pH buffers are indicated on the axes.

of phosphoester bonds. Acid hydrolysis of the radiolabelled 43 kDa maize E1α, followed by two-dimensional thin-layer electrophoresis, indicated phosphorylation took place exclusively on Ser residues (Figure 3A).

AtPDK is autophosphorylated on Ser residues

When incubated with [γ-^{32}P]ATP, MBP–AtPDK was autophosphorylated in both the presence and the absence of PDC with similar efficiencies (Figure 2A). Autophosphorylation exhibited Michaelis–Menten kinetics, reaching saturation near 40 min. The autophosphorylation reaction was pH-dependent, with an optimum at 7.3, and was abolished when a heat-denatured sample was used. These results indicated that autophosphorylation was enzyme-catalysed and could not be attributed to non-specific binding of ATP. The stoichiometry of AtPDK autophosphorylation was approx. 0.10 mol of phosphate/mol of protein. AtPDK phosphorylation was completely stable to cleavage with 30% (w/v) trichloroacetic acid indicating that a hydroxyamino acid such as Ser, Thr or Tyr was phosphorylated (Figures 4D and 4E). Phosphoamino acid analyses indicated only Ser residues were phosphorylated (Figure 3B). Autophosphorylated AtPDK was incapable of transferring covalently bound phosphate to PDC when label was chased or when incubated with PDC after the chromatographic removal of endogenous ATP by Sephadex G-50 (Figure 2B).

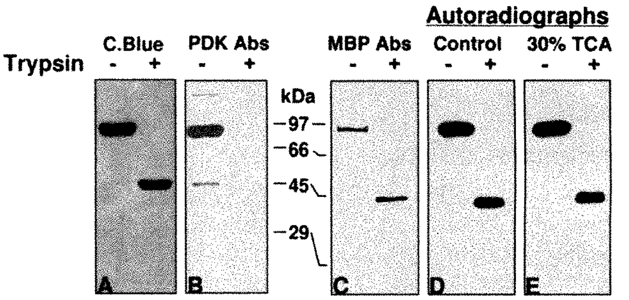

Figure 4 Autophosphorylation and tryptic digestion of MBP–AtPDK

(**A**) Coomassie Blue-stained SDS/PAGE of intact MBP–AtPDK (3 μg) and MBP–AtPDK digested with trypsin (0.5 μg) for 16 h at 25 °C. (**B**) Immunoblot of (**A**) probed with anti-PDK antibodies (PDK Abs). (**C**–**E**) MBP–AtPDK (0.5 μg) was incubated with [γ-^{32}P]ATP (1 μCi, 10 mCi/mmol) before tryptic digestion (lane 2). (**C**) Immunoblot was probed with anti-MBP antibodies (MBP Abs). (**D**, **E**) Autoradiographs of replicate-blotted ^{32}P-autophosphorylated MBP–AtPDK. The blot in (**E**) was washed with 30% (w/v) trichloroacetic acid (TCA) for 1 h at 25 °C to cleave acid-labile phosphoamino acid bonds. Both autoradiographs were exposed for 4 h. Although radiolabel migrated with the undigested N-terminal half of the fusion protein, which was predominantly composed of MBP, AtPDK was incapable of phosphorylating purified MBP. Furthermore, cleavage of the radiolabelled fusion protein at the fusion junction (with factor Xa) indicated that it was AtPDK that was phosphorylated. On the basis of these results, the phosphorylation site resides near the undigested N-terminus of AtPDK. The positions of molecular mass markers are indicated between (**B**) and (**C**).

To help to identify the site of autophosphorylation, limited proteolysis of phosphorylated MBP–AtPDK under non-denaturing conditions was employed. Digestion of MBP–AtPDK with trypsin yielded one predominant polypeptide of approx. 45 kDa (Figure 4A). Through immunoblot analyses, with anti-MBP and anti-PDK antibodies, it was determined that the 45 kDa polypeptide corresponded primarily to the MBP half of the fusion protein (Figures 4A–4C). This finding enabled us to map the autophosphorylation site coarsely to the N-terminal half of the fusion protein (Figure 4D). Because the 45 kDa N-terminal half was primarily MBP, it was necessary to determine whether AtPDK was capable of transphosphorylating purified MBP. When purified MBP was incubated with MBP–AtPDK and $MgATP^{2-}$ at a 5:1 molar ratio, no transphosphorylation of MBP was observed, though autophosphorylation of MBP–AtPDK occurred during this period (results not shown). It was therefore concluded that the autophosphorylation site was localized to the undigested N-terminus of AtPDK. This was supported by the observation that the radiolabel from factor-Xa-cleaved MBP–AtPDK co-migrated with the AtPDK polypeptide (Figure 2C).

Mechanism of phosphorylation

Because PDKs contain domains diagnostic of protein histidine kinases yet phosphorylate Ser residues in the target sequence, the mode of phosphotransfer warranted further investigation. We hypothesized that if phosphotransfer occurred through a phosphohistidine intermediate, mutating that residue should

A. thaliana	VKVR**H**^{121}NNVVP.....IRMLIGQ**H**^{168}VELHNP
Z. mays I	VKVR**H**^{117}NNVVP.....IRMLIGQ**H**^{169}VALHDP
Z. mays II	IRVR**H**^{117}TNVVP.....IRMLIGQ**H**^{169}VALHDP
D. melanogaster	IRNR**H**^{123}NDVVQ.....IRMLINQ**H**^{174}TLLFGG
A. suum	ILKR**H**^{120}SRVVE.....IRMLQNQ**H**^{169}LVVFGV
C. elegans	VLKR**H**^{120}AHVVE.....IRMLQNQ**H**^{169}LVVFGN
R. rattus	IRNR**H**^{149}NDVIP.....IRMLLNQ**H**^{198}SILFGG
H. sapiens	IRNR**H**^{149}NDVIP.....IRMLLNQ**H**^{198}SILFGG
R. rattus BCDK	LLDD**H**^{162}KDVVT.....IRMLATH**H**^{207}LALHED
Consensus	+++R**H** + VV .....IRML++Q**H** ++LHG

Figure 5 Comparison of the amino acids surrounding the two invariant His residues in PDKs and BCDKs

All sequences are PDKs except for *Rattus rattus* BCDK. The invariant His residues proposed to be involved in phosphotransfer are shown in **bold**. If five or more residues are identical in position, this residue is presented in the consensus sequence. If five or more residues are not identical, but are of the same amino acid group, this is indicated by + in the concensus sequence. Genbank accession numbers: *A. thaliana*, AF039406; *Z. mays* I, II, AF038585, AF038586; *Drosophila melanogaster*, D88814; *Ascaris suum*, U94519; *Caenorhabdhitis elegans*, M98552; *R. rattus*, L22294; *Homo sapiens*, L42450; *R. rattus* BCDK, M93271.

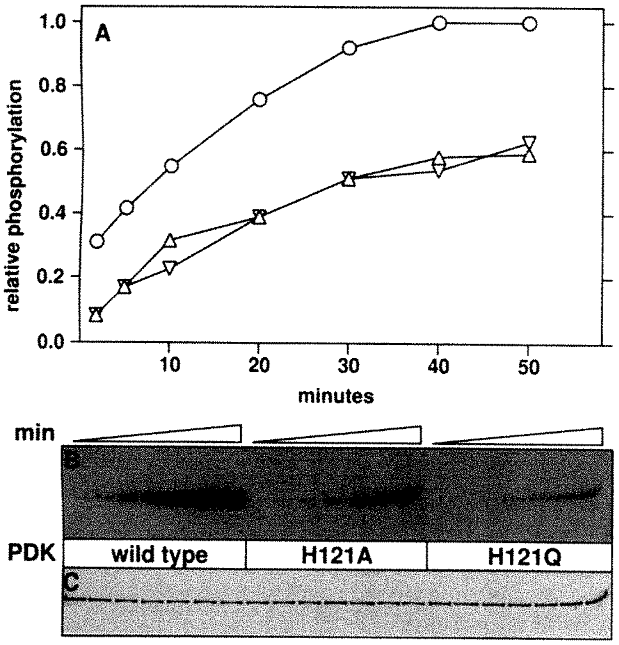

Figure 6 Kinetics of MBP–AtPDK autophosphorylation

Equal amounts (5.4 μg) of purified MBP–AtPDK were incubated with [γ-^{32}P]ATP (10 μCi, 10 mCi/mmol) at 25 °C. Samples were removed at indicated time points and mixed with an equal volume of sample buffer before analysis by SDS/PAGE. (**A**) The relative phosphorylations of MBP–PDK polypeptides [shown in (**B**): ▽, H121A; △, H121Q] were quantified with QS30 software (PDI, Huntington Station, NY, U.S.A.) and plotted relative to that of the wild-type enzyme (○). (**B**) Autoradiograph of MBP–AtPDK autophosphorylation. (**C**) Ponceau S-stained [0.1% (w/v) Ponceau S in 30% (w/v) trichloroacetic acid] loading control for (**B**).

abolish phosphorylation. Although at least three His residues are semi-conserved in all PDKs (and BCDK), only two are invariant, His-121 and His-168 (Figure 5). Because His-121 was previously proposed to be the phosphotransfer His, this residue was mutated to Ala or Gln. On an equivalent protein basis, purified His-121A and His-121Q AtPDKs were autophosphorylated at approx. 40–50% of the level of the wild-type protein during time-course studies (Figure 6). Autophosphorylation was consistent between PDK preparations, indicating that this difference was not due to recombinant expression. The lower degree to which these mutants phosphorylated maize E1α (in comparison with wild-type AtPDK) confirmed the lower $V_{\max}$ of these mutants (Figure 2A).

DISCUSSION

Reversible protein phosphorylation is a ubiquitous mechanism for signal transduction. Prokaryotic organsims use His-to-Asp phosphotransfer, whereas eukaryotic signal transduction cascades are predominantly mediated by the reversible phosphorylation of Ser, Thr and Tyr [26,27]. Examples of eukaryotic protein histidine kinases also exist, and His-to-Asp phospho-relays have been proposed [28]. So far, however, there are no conclusive examples of histidine kinases that phosphorylate Ser rather than Asp residues in Nature. Phytochrome from higher plants contains some of the hallmark histidine kinase domains yet phosphorylates Ser residues [29]. Additionally, the *E. coli* histidine kinase CheY phosphorylates hydroxyamino acids such as Ser when no Asp residue is available on its cognate response regulator, although the reaction mechanism is unknown [30]. It was later postulated that the high transfer potential of a phospho-His, the stability of a phospho-Ser and the proper positioning of the accepting amino acid collectively facilitate this unique His-to-Ser phospho-relay [28]. Although the CheY example was created artificially, the mitochondrial PDK might have evolved a similar phospho-relay system naturally.

Aside from PDK, other protein histidine-like kinases have been discovered in plants. One of these histidine-like kinases, 'ethylene triple response' (encoded by *etr1*), is involved in ethylene signal transduction and was discovered as a loss-of-function mutant responsible for a constitutive ethylene response phenotype [31]. Autophosphorylation of ETR1 is sensitive to treatment with acid, which is suggestive of His phosphorylation. Site-directed mutagenesis confirmed that this occurs on a His residue within the putative phosphotransfer domain [32]. The green algal phytochrome undergoes autophosphorylation on a His residue, determined via site-directed mutagenesis [33].

In the present study, a presumptive PDK homologue recently identified from *A. thaliana* was functionally expressed in *E. coli*. Fusing PDK with MBP obviated the difficulty in obtaining soluble AtPDK, observed previously with maize PDKs [18], and enabled the E1α subunit to be resolved from PDK during SDS/PAGE. For these two reasons intact MBP–PDK protein was used in this investigation. Autophosphorylation was not observed with MBP–AtPDK from nematodes [34]; in contrast, mammalian PDKs [16] and BCDKs [17] are capable of Ser-autophosphorylation. Here we demonstrate that the *A. thaliana* PDK is also capable of Ser-autophosphorylation. The phospho-Ser residue for AtPDK is located near the N-terminus as determined by mapping after limited proteolysis. Candidate residues include Ser-13, Ser-30 and Ser-39 because these are closest to the N-terminus on the basis of the deduced amino acid sequence. Recombinant maize PDK2 also undergoes Ser-autophosphorylation (results not shown), suggesting that this phenomenon might occur with all plant PDKs. Although the significance of Ser-autophosphorylation is not known, it is not an artifact induced by the absence of natural substrate because autophosphorylation was equivalent in the presence and in the absence of PDC (Figure 2A). Also, this phospho-Ser is not a catalytic intermediate, as evidenced by the inability to transfer this particular phosphate to maize E1α (Figure 2B). Because the stoichiometry of autophosphorylation is less than 1 mol of phosphate per mol of MBP–AtPDK, it is likely that only one phosphorylation site is present. The low stoichiometry of phosphate incorporation into purified MBP–AtPDK might indicate that autophosphorylation had taken place during bacterial expression before isolation of the protein.

Recombinant AtPDK inactivated kinase-depleted maize mitochondrial PDC by phosphorylating Ser residues on the 43 kDa E1α subunit The specific activity of recombinant MBP–AtPDK was approx. one-quarter of that for recombinant maize MBP–PDK2 [18]. This difference was surprising because maize E1α shares 80% overall identity with *A thaliana* E1α and 100% identity within the predicted phosphorylation motifs [25]. The difference in specific activities is therefore attributed either to PDK properties or docking site(s) to the dihydrolipoamide acetyltransferase (E2) core complex. Reconstitutions of mammalian PDCs have shown a 3–5-fold decrease in PDK activity (inactivation of PDC) in the absence of the E2 core [35–37]. This observation was explained by a proximity model in which the independent binding of E1 and PDK by the E2 core couples E1α phosphorylation. Recently, we demonstrated that dicotyledonous plants, such as *A. thaliana*, contain two mitochondrial E2 isoforms that share 33% amino acid identity [38], the primary difference being the presence of one compared with two lipoyl domains In contrast, monocots such as maize possess a single mitochondrial E2 that contains one lipoyl domain [21,38]. Because mammalian PDKs have been shown to bind to the E2 core via the lipoyl domains [16,36,37], perhaps the divergence between monocot and dicot E2 cores hinders AtPDK binding to maize PDC, resulting in a lower specific activity *in vitro*. Steric hindrance by the bulky fusion partner (MBP) might also contribute to the decreased activity.

The ability of a histidine-like kinase such as PDK to autophosphorylate and transphosphorylate Ser residues is enigmatic. In an attempt to explain this we employed a site-directed mutagenesis approach. Histidine kinases require a His residue for phosphotransfer. Typically the His residue lies upstream of the Gly-rich ATP-binding domains and lacks conserved flanking sequences [39]. This organization is best described as an island domain. Seven His residues in the AtPDK sequence fit this description. Of those, only His-121 and His-168 are present in all PDKs (Figure 5). Because His-121 was previously postulated as the cardinal phosphotransfer His [15,18], this site was further investigated.

Mutating His-121 to either Ala or Gln did not noticeably alter the stability or yield of recombinant protein in comparison with the wild-type control. However, on an equal protein basis both mutant PDKs had decreased activity compared with wild-type as observed by Ser-autophosphorylation and transphosphorylation of E1α. A lower V_{max} could not be attributed to the substitution of a neutral amino acid because replacement with Gln gave results similar to those with Ala The simplest interpretation is that His-121 is necessary for maximum activity but is not essential for catalysis. If His-121 is indeed a site for phosphotransfer, site-directed mutagenesis of this residue indicates either that PDKs have multiple phosphotransfer sites or that mutagenesis of His-121 exposes an otherwise cryptic site. In favour of this explanation, the covalent modification of MBP–AtPDK with two different His-modifying agents, diethyl pyrocarbonate and (2,2′ 6′,2″-terpyridine)-platinum (II) dihydrate, completely abolished activity [40]. It is therefore evident that multiple His residues are involved in kinase function. The results presented here demonstrate that His-121 is one of these functionally important His residues, although at least one other must exist because activity was not completely abolished. Resolving this issue will require the scanning mutagenesis of other His residues.

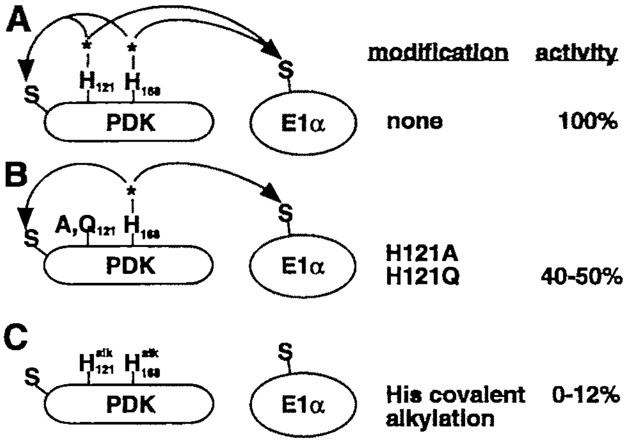

Figure 7 Model of PDK phosphorylation mechanism

The proposed model is based on the evidence that PDKs are descendants of prokaryotic protein histidine kinases, and also on the involvement of His residues in phosphotransfer and analyses revealing that PDKs autophosphorylate and transphosphorylate on Ser residues Because mutagenesis of His-121 (this paper) did not completely abolish activity, a second phosphotransfer His residue (His-168) is proposed The two conserved His residues (His-121 and His-168) are numbered in accordance with the AtPDK primary sequence Mutagenesis or covalent modification of conserved His residues and the effect on relative activity are noted Covalent modification of His was performed as described previously [40]

In summary, we have functionally expressed the *A thaliana* PDK to improve understanding of the properties of phosphorylation. Recombinant AtPDK inactivated kinase-depleted maize PDC by phosphorylating Ser residues on the E1α subunit, although the specific activity of AtPDK was one-quarter of that of maize PDK2. During phosphorylation assays it was noticed that the MBP–AtPDK fusion also underwent autophosphorylation. Analyses of phosphoamino acids after limited proteolysis revealed that this occurred on a Ser residue, most probably near the AtPDK N-terminus. The autophosphorylated Ser was stable in pulse–chase reactions and was not an intermediate for E1α phosphorylation. Site-directed mutagenesis of His-121 curtailed autophosphorylation and transphosphorylation efficiencies by approx. 50%. The results presented here support the conclusion that PDKs are protein kinases that use at least one phosphohistidine intermediate for the transfer of phosphoryl groups to Ser residues (Figure 7). In support of this model are the following data. (1) The primary amino acid sequence resembles that of prokaryotic His kinases more closely than that of eukaryotic Ser/Thr protein kinases (2) Two invariant His residues are present within the primary amino acid sequence of all PDKs and BCDKs (3) Covalent modification of His residues on AtPDK abolishes activity [40] (4) Mutagenesis of His-121 to Ala or Gln significantly decreases kinase activity. (5) PDKs autophosphorylate and transphosphorylate Ser residues. Although a phospho-His intermediate has not yet been directly defined, this might be attributed to the instability of this intermediate or to rapid phosphotransfer.

We thank Nancy David and Kevin Lease (University of Missouri-Columbia, Columbia, MO, U S A) for technical assistance with phosphoamino acid analyses, and Dr Brian Mooney for his assistance in preparing the figures. Research for this investigation was supported by National Science Foundation grant IBN-9876680

REFERENCES

1 Reed, L J (1974) Accts Chem Res **7**, 40–56
2 Williams, M and Randall, D D (1979) Plant Physiol **64**, 1099–1103

3 Camp, P J and Randall, D. D (1985) Plant Physiol. **77**, 571–577
4 Luethy, M H, Miernyk, J A, David, N. R and Randall, D D (1996) in Alpha-Keto Acid Dehydrogenase Complexes (Patel, M. S, Roche, T E and Harris, R A, eds), pp. 71–72, Birkhausen, Boston, MA
5 Randall, D D, Miernyk, J A, David, N. R., Gemel, J and Luethy, M H (1996) Proc Phytochem. Soc. Eur. **37**, 87–103
6 Miernyk, J. A. and Randall, D D (1987) Plant Physiol **83**, 311–315
7 Popov, K M, Kedishvili, N Y, Zhao, Y, Shimomura, Y, Crabb, D W and Harris, R A (1993) J Biol Chem **268**, 26602–26606
8 Robinson, V L and Stock, A. M. (1999) Structure **7**, 47–53
9 Appleby, J L, Parkinson, J. S and Bourret, R B (1996) Cell **86**, 845–848
10 Uhl, M A and Miller, J. F (1996) EMBO J **15**, 1028–1036
11 Mizuno, T (1998) J. Biochem (Tokyo) **123**, 555–563
12 Loomis, W F, Shaulsky, G and Wang, N (1997) J Cell. Sci **110**, 1141–1145
13 Yeaman, S J, Hutcheson, E T, Roche, T E, Pettit, F H, Brown, J R, Reed, L J, Watson, D C. and Dixon, G. H (1978) Biochemistry **17**, 2364–2370
14 Sugden, P. H, Kerbey, A L, Randle, P J, Waller, C A and Reid, K. B M (1979) Biochem J **181**, 419–426
15 Popov, K M, Zhao, Y, Shimomura, Y, Kuntz, M J and Harris, R A (1992) J Biol Chem **267**, 13127–13130
16 Jackson, J C, Vinluan, C C, Dragland, C J, Sundararajan, V., Yan, B, Gounarides, J S, Nirmala, N. R, Topiol, S, Ramage, P, Blume, J E. et al. (1998) Biochem J **334**, 703–711
17 Davie, J. R., Wynn, R M, Meng, M, Huang, Y, Aalund, G, Chuang, D T and Lau, K S (1995) J Biol Chem **270**, 19861–19867
18 Thelen, J J, Muszynski, M. G, Miernyk, J A and Randall, D. D. (1998) J Biol Chem **273**, 26618–26623
19 Thelen, J J., Miernyk, J A and Randall, D D (1998) Plant Physiol **118**, 1533
20 Thelen, J J, Miernyk, J A and Randall, D. D. (1998) in Proceeding of International Congress on Plant Mitochondria From Gene to Function (Moller, I M, Gardstrom, P, Glimelius, K and Glaser, E., eds), pp 417–421, Backhuys Publishers, Leiden, The Netherlands

Received 12 November 1999/20 March 2000, accepted 19 April 2000

21 Thelen, J J, Miernyk, J A and Randall, D D (1998) Plant Physiol **118**, 1443–1450
22 Fang, T K, David, N R, Miernyk, J. A. and Randall, D D (1987) Curr. Top. Plant Biochem Physiol **6**, 175
23 Bradford, M M (1976) Anal Biochem **72**, 248–254
24 Duplay, P, Bedouelle, H, Fowler, A, Zabin, I, Saurin, W. and Hofnung, M (1984) J Biol Chem **259**, 10606–10613
25 Thelen, J J, Miernyk, J A and Randall, D D. (1999) Plant Physiol **119**, 635–643
26 Stone, J M and Walker, J C (1995) Plant Physiol **108**, 451–457
27 Sopory, S. K and Munshi, M (1998) Crit Rev Plant Sci. **17**, 245–318
28 Elich, T D and Chory, J (1997) Cell **91**, 713–716
29 Yeh, K C. and Lagarias, J C (1998) Proc Natl Acad Sci USA **95**, 13976–13981
30 Bourret, R. B., Hess, J. F and Simon, M I (1990) Proc Natl Acad Sci. U.S.A. **87**, 41–45
31 Chang, C, Kwok, S F, Bleecker, A B and Meyerowitz, E. M. (1993) Science **262**, 539–544
32 Gamble, R L, Coonfield, M L and Schaller, E G (1998) Proc Natl Acad Sci USA **95**, 7825–7829
33 Yeh, K C., Wu, S H, Murphy, J T and Lagarias, J C. (1997) Science **277**, 1505–1508
34 Chen, W, Huang, X, Komuniecki, P R and Komuniecki, R (1998) Arch Biochem Biophys **353**, 181–189
35 Popov, K. M (1997) FEBS Lett **419**, 197–200
36 Radke, G. A, Ono, K, Ravindran, S and Roche, T E (1993) Biochem Biophys Res Commun **196**, 982–991
37 Liu, S, Baker, J C and Roche, T E. (1995) J Biol Chem **2**, 793–800
38 Thelen, J J, Muszynski, M G., David, N R, Luethy, M H, Elthon, T E, Miernyk, J A and Randall, D D (1999) J. Biol Chem **274**, 21769–21775
39 Stock, J B., Ninfa, A J and Stock, A M (1989) Microbiol Rev **53**, 450–490
40 Mooney, B P, David, N R, Thelen, J J, Mierynk, J A and Randall, D D (2000) Biochem Biophys Res Commun. **267**, 500–503

Unifying mechanism for *Aplysia* ADP-ribosyl cyclase and CD38/NAD$^+$ glycohydrolases

Céline CAKIR-KIEFER, Hélène MULLER-STEFFNER and Francis SCHUBER[1]
Laboratoire de Chimie Bioorganique, UMR 7514 CNRS-ULP, Faculté de Pharmacie, 74 route du Rhin, 67400 Strasbourg-Illkirch, France

Highly purified *Aplysia californica* ADP-ribosyl cyclase was found to be a multifunctional enzyme. In addition to the known transformation of NAD$^+$ into cADP-ribose this enzyme is able to catalyse the solvolysis (hydrolysis and methanolysis) of cADP-ribose. This cADP-ribose hydrolase activity, which becomes detectable only at high concentrations of the enzyme, is amplified with analogues such as pyridine adenine dinucleotide, in which the cleavage rate of the pyridinium-ribose bond is much reduced compared with NAD$^+$. Although the specificity ratio V_{max}/K_m is in favour of NAD$^+$ by 4 orders of magnitude, this multifunctionality allowed us to propose a 'partitioning' reaction scheme for the *Aplysia* enzyme, similar to that established previously for mammalian CD38/NAD$^+$ glycohydrolases. This mechanism involves the formation of a single oxocarbenium-type intermediate that partitions to cADP-ribose and solvolytic products via competing pathways. In favour of this mechanism was the finding that the enzyme also catalysed the hydrolysis of NMN$^+$, a substrate that cannot undergo cyclization. The major difference between the mammalian and the invertebrate enzymes resides in their relative cyclization/hydrolysis rate-constant ratios, which dictate their respective yields of cADP-ribose (ADP-ribosyl cyclase activity) and ADP-ribose (NAD$^+$ glycohydrolase activity). For the *Aplysia* enzyme's catalysed transformation of NAD$^+$ we favour a mechanism where the formation of cADP-ribose precedes that of ADP-ribose; i.e. macroscopically the invertebrate ADP-ribosyl cyclase conforms to a sequential reaction pathway as a limiting form of the partitioning mechanism.

Key words: cADP-ribose, cyclic ADP-ribose hydrolase, hydrolysis, methanolysis, NGD$^+$.

INTRODUCTION

cADP-ribose, a new metabolite of NAD$^+$ discovered in the late 1980s by Lee and collaborators [1], has attracted considerable attention because of its intracellular Ca^{2+}-mobilizing properties that are distinct from those of inositol 1,4,5-trisphosphate (for review see [2]). The first known enzyme able to convert NAD$^+$ into cADP-ribose was detected in invertebrates such as sea urchins [1]. Subsequently, the ADP-ribosyl cyclase from *Aplysia californica*, which is a soluble protein, was purified [3,4], cloned [5] and its three-dimensional structure determined [6]. Besides this enzyme, a cADP-ribose hydrolase that converts the cyclic metabolite into ADP-ribose has also been found in invertebrates, but much less is know about this activity [7].

In mammalian systems, the situation appeared to be quite different. First, the cloning of the *Aplysia* ADP-ribosyl cyclase revealed a striking sequence identity of this enzyme with CD38, a lymphocyte antigenic marker for which no catalytic activity was hitherto known [5]. Then an NAD$^+$ glycohydrolase, purified from canine spleen microsomes, was demonstrated to be a multifunctional enzyme. Besides its major NAD$^+$ glycohydrolase activity, this enzyme was also able to convert NAD$^+$ into cADP-ribose and to hydrolyse this molecule into ADP-ribose [8]. The same multifunctionality was established for human CD38 [9] and later for bovine spleen NAD$^+$ glycohydrolase [10,11], an archetypal representative of this class of enzymes (EC 3.2.2.6). Some topological and mechanistic problems were raised with regard to the biosynthesis of cADP-ribose in mammals. Thus CD38 and NAD$^+$ glycohydrolases, which are ecto-enzymes, transform NAD$^+$ only into small proportions of cADP-ribose (less than 2 % of the reaction products). Moreover, no intracellular equivalent of the invertebrate ADP-ribosyl cyclase, which was given to convert NAD$^+$ quasi-exclusively into cADP-ribose, has been described to date. The multifunctionality of CD38 was first invoked to explain the limited formation of the cyclic metabolite. A sequential mechanism was proposed according to which cADP-ribose, after its formation from NAD$^+$, does not accumulate because it is quickly turned over; accordingly the NAD$^+$ glycohydrolase activity of CD38 represents the sum of the ADP-ribosyl cyclase and cADP-ribose hydrolase activities [9,12]. In favour of this mechanism was the observation that nicotinamide–guanine dinucleotide (NGD$^+$), an alternative substrate which leads to the non-hydrolysable cGDP-ribose, was predominantly transformed by CD38 into the cyclic reaction product [13]. The study of the molecular mechanism of bovine spleen NAD$^+$ glycohydrolase, which we have since demonstrated to be equivalent to CD38 [14,15], led us to propose a different reaction scheme Accordingly, NAD$^+$, after cleavage of its nicotinamide-ribose bond, generates an oxocarbenium-type intermediate which then partitions between two competing pathways (Scheme 1): a reversible intramolecular reaction leading to cyclization (step k_3) and a macroscopically irreversible intermolecular hydrolysis reaction (step k_{H_2O}), generating ADP-ribose [11]. This mechanism, which links the low formation of cADP-ribose by CD38/NAD$^+$ glycohydrolases to an inefficient cyclization step relative to the capture of the oxocarbenium ion by a water molecule, was recently borne out by careful kinetic studies with a recombinant human CD38 [16].

In the present study, we have re-examined some aspects of the mechanism of *Aplysia* ADP-ribosyl cyclase. We have thus established that a highly purified form of this enzyme is also endowed with intrinsic NAD$^+$ glycohydrolase and cADP-ribose hydrolase activities. These activities are unmasked at higher enzyme concentrations, especially when using poorly hydro-

---

Abbreviations used PyAD$^+$, pyridine adenine dinucleotide, NGD$^+$, nicotinamide–guanine dinucleotide

[1] To whom correspondence should be addressed (e-mail schuber@pharma u-strasbg.fr)

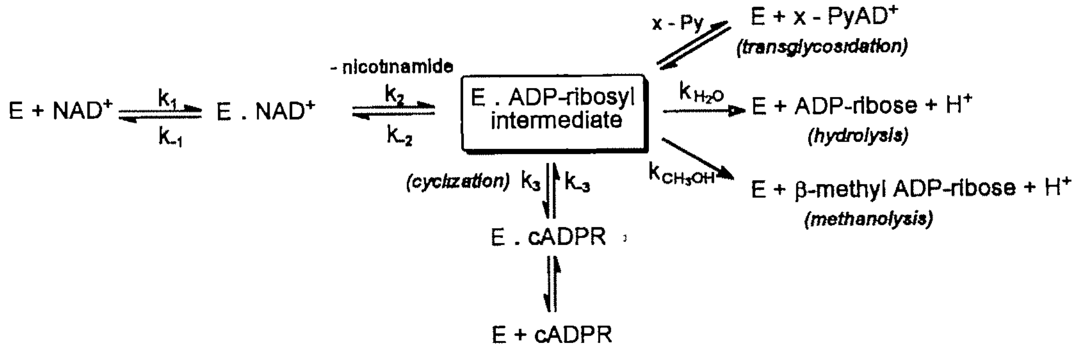

Scheme 1 Reaction mechanism of CD38/NAD$^+$ glycohydrolases

CD38/NAD$^+$ glycohydrolases catalyse the cleavage of the nicotinamide bond of NAD$^+$ leading to the formation of an E ADP-ribosyl intermediary complex (where E is the enzyme) This intermediate then partitions between competing intramolecular (ADP-ribosyl cyclase) and intermolecular (solvolysis, transglycosidation) pathways [11,14,16] (where x is the substituent of the pyridine) Note that the solvolysis reactions (hydrolysis and methanolysis) are macroscopically irreversible

lysable pyridinium analogues of NAD$^+$. Moreover this enzyme is also able to catalyse the methanolysis of both NAD$^+$ and cADP-ribose. Altogether, these reactions are very similar to the ones described for bovine and human CD38/NAD$^+$ glycohydrolases. We therefore propose a unifying mechanism for the invertebrate and mammalian enzymes, the major difference being their relative efficiencies in favouring the intramolecular reaction leading to the cyclic reaction product

EXPERIMENTAL

Materials

[*adenosine*-U-^{14}C]NAD$^+$ (567 Ci/mol) was from NEN (Boston, MA, U.S.A). NAD$^+$, NGD$^+$, 1,N^6-ethenoNAD$^+$ and cADP-ribose were from Sigma (L'Isle d'Abeau Chesnes, France) Pyridine adenine dinucleotide (PyAD$^+$) was prepared according to [17]. Hydroxylapatite (Bio-Gel HTP) and Affi-Gel Blue were obtained from Bio-Rad (Ivry-sur-Seine, France). DEAE-cellulose (DE 53) was from Whatman Laboratories (Maidstone, Kent, U K.) and CM-Sepharose CL-6B was from Pharmacia Biotech (Uppsala, Sweden).

Purification of *A. californica* ADP-ribosyl cyclase

ADP-ribosyl cyclase was purified, with some modifications, according to published procedures [3,4,18]. The soluble fraction (0.9 g) obtained from ovotestis of *A. californica* that was provided generously by Dr Bernard Poulain (CNRS-Neurochimie, Strasbourg, France) was applied to a 5 × 23-cm CM-Sepharose CL-6B column. The enzyme was eluted (flow rate, 1 ml/min) with a 0–1 M gradient of NaCl in 10 mM potassium phosphate buffer, pH 7.4 (buffer A). After dialysis against buffer A the enzyme was then purified further on a 2.5 × 60-cm DEAE-cellulose column, equilibrated and eluted with the same buffer In some experiments the cyclase was also chromatographed on Affi-Gel Blue. Briefly, a 1 × 2.5-cm column was washed with buffer A containing 1 M NaCl and then equilibrated with the same buffer. About 100 μg of the enzyme were loaded at 0.2 ml/min and the enzyme was eluted with a linear 0–1 M gradient of NaCl in buffer A. The protein concentration was determined by the BCA (bicinchoninic acid) protein assay from Pierce using BSA as standard.

Gel electrophoresis

SDS/PAGE was performed according to standard methods and the gels were silver-stained using a kit based on the technique of Heukeshoven and Dernick [19].

Enzyme assays

Cyclase activity was determined routinely using either the cyanide-addition assay [20] for ADP-ribosyl cyclase activity or continuous fluorometric assays with NGD$^+$ as substrate by estimating the appearance of cGDP-ribose (emission at 410 nm, excitation at 310 nm) [13] for GDP-ribosyl cyclase activity: NGD$^+$ (final concentration 50 μM) was incubated at 37 °C in buffer A in the presence of about 20 m-units of enzyme. To determine the kinetic parameters, ADP-ribosyl cyclase and cADP-ribose hydrolase activities were measured using, respectively, 2.5–20 μM NAD$^+$ in the presence of [*adenosine*-^{14}C]NAD$^+$ (220000 d.p.m.) and 0.025–2.25 mM cADP-ribose in 50 mM potassium phosphate buffer, pH 7.4, incubated at 37 °C in the presence of, respectively, 2 and 200 m-units of purified ADP-ribosyl cyclase. At different time points, aliquots were analysed using HPLC as described below.

Methanolysis catalysed by ADP-ribosyl cyclase

The nucleotides (NAD$^+$, PyAD$^+$ and cADP-ribose; final concentration 20 μM) or NGD$^+$ (100 μM) were incubated at 37 °C in buffer A, in the presence of 0–2 M methanol (final volume 200–500 μl) and given amounts of ADP-ribosyl cyclase At different time points, aliquots were analysed by HPLC as described below. The β-methyl ADP-ribose and β-methyl GDP-ribose standards were prepared as published previously [11,21].

Analysis of the reaction products by HPLC

Product analysis was performed by HPLC on a 300 × 3.9-mm μBondapack C_{18} column (Waters) on aliquots of the reaction medium centrifuged at 10000 *g* for 10 min at 4 °C in a Microcon microconcentrator (10-kDa cut-off; Amicon) [11]. The compounds were eluted isocratically with a 10 mM ammonium phosphate buffer, pH 5.5, containing 1.2% (v/v) acetonitrile, detected by their UV absorbance at 260 nm and/or by radiodetection (Flo-one, Packard Instruments). Standards were injected to determine the elution times and to identify the different reaction products.

Kinetic analysis

The initial rates of substrate transformation were calculated from a polynomial regression curve. Kinetic parameters were determined from the plot of initial rate as a function of substrate concentration using a non-linear regression program (GraphPad Prism).

RESULTS

When using large quantities of purified *A. californica* ADP-ribosyl cyclase to transform slow-reacting NAD$^+$ analogues into their corresponding cyclic derivatives we uncovered an apparent NAD$^+$ glycohydrolase activity, i.e. formation of ADP-ribose, which otherwise remains largely unnoticed. This observation prompted us to study the capacity of this enzyme to catalyse alternative pathways that might be useful in further delineating its molecular mechanism.

Aplysia ADP-ribosyl cyclase is also a cADP-ribose hydrolase

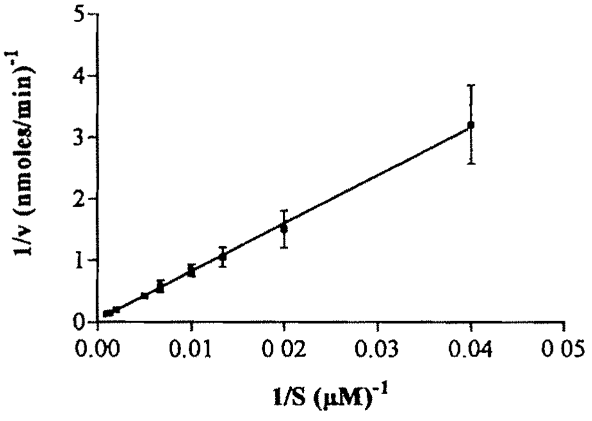

Figure 2 Double reciprocal plot of the *A. californica* ADP-ribosyl cyclase-catalysed hydrolysis of cADP-ribose

Initial rates of the hydrolysis of cADP-ribose were measured in a 50 mM potassium phosphate buffer, pH 7.4, at 37 °C

In Figure 1 are represented typical progress curves obtained by *Aplysia* ADP-ribosyl cyclase-catalysed transformations of NAD$^+$. When using intermediate amounts of enzyme (50 m-units; Figure 1A) the substrate was essentially transformed into cADP-ribose and only limited amounts of ADP-ribose were measured (less than 10% of the reaction products under these experimental conditions). This is in agreement with several authors who have also observed the limited contribution of a hydrolytic activity to the overall reaction [3,22,23]. However, with higher amounts of cyclase, the situation was quite different (Figure 1B); in this case, after a transient formation cADP-ribose declined with the concomitant formation of ADP-ribose, indicative of a hydrolytic step via either NAD$^+$ glycohydrolase or cADP-ribose hydrolase pathways, or by a combination of both.

The occurrence of a hydrolytic transformation of cADP-ribose into ADP-ribose by *Aplysia* ADP-ribosyl cyclase was then studied directly and confirmed when using high-enough concentrations of a highly purified enzyme (see below). The kinetic parameters for this newly described cADP-ribose hydrolase activity of the *Aplysia* enzyme were determined under steady-state conditions. At pH 7.4, a K_m value of 1.04±0.15 mM (±S.D.) was found (Figure 2) and the maximal rate (V_{max}) was 3.34±1.15 μmol·min^{-1}·mg of protein^{-1}. In comparison, the

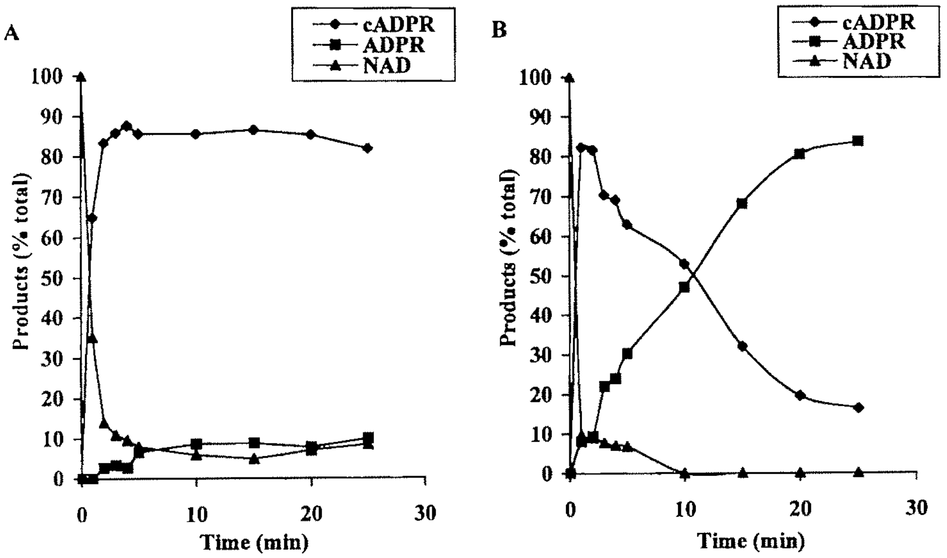

Figure 1 Transformation of NAD$^+$ catalysed by *A. californica* ADP-ribosyl cyclase

NAD$^+$ (300 μM) and [*adenosine*-^{14}C]NAD$^+$ (220000 d.p.m.) in 50 mM potassium phosphate buffer, pH 7.4, were treated with 50 m-units (**A**) or 1 unit (**B**) of highly purified *A. californica* ADP-ribosyl cyclase at 37 °C. At the given times, aliquots were taken, treated with 5% trichloroacetic acid and analysed by radio-HPLC. The reaction products formed are given as percentages of the total counts

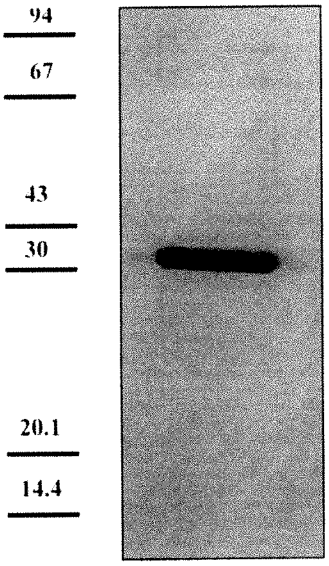

Figure 3 SDS/polyacrylamide gel of purified *A. californica* ADP-ribosyl cyclase

A heat-denatured sample of purified enzyme (2 μg) was submitted to electrophoresis under reducing conditions on a 12% polyacrylamide gel. The band was revealed by silver staining. The positions of the molecular-mass markers (kDa) are indicated.

following values were determined for NAD$^+$: $K_m = 4.6 \pm 0.4$ μM and $V_{max} = 465 \pm 57$ μmol·min^{-1}·mg^{-1}. It appears therefore that *Aplysia* ADP-ribosyl cyclase is a bifunctional enzyme that can synthesize and hydrolyse cADP-ribose. This cyclase/hydrolase ratio was not affected by temperature (down to 4 °C) and by pH (5–8; results not shown). It should be stressed that, as noted before [24], the Michaelis constants (K_m) found in the literature for NAD$^+$ and some other substrates of the cyclase vary greatly and the value determined here is among the lowest. The reason for this unusual scatter in published data is unknown, but might reflect the mode of preparation of the *Aplysia* enzyme and its propensity to oligomerize [25].

Homogeneity of the ADP-ribosyl cyclase

The enzyme used in the preliminary part of our study was purified from *A. californica* ovotestis according to the published procedures [3,4,18]. However, to ensure the homogeneity of the protein used, additional purification steps were performed such as a DEAE-cellulose column followed by pseudo-affinity chromatography on Affi-Gel Blue [26]. The first step, which is a 'negative' one, i.e. the enzyme is not retained by the gel, eliminated the small contaminating bands visible on denaturing gels. In contrast, the cyclase interacts strongly with the Blue gel and is eluted only by high monovalent-salt concentrations. The enzyme preparation thus obtained gave a single band at ≈ 29 kDa on an overloaded SDS/polyacrylamide gel (Figure 3). Microsequencing of the N-terminal region over 18 residues (IVPTRELENVFLGRXKDY) was in perfect agreement with the known sequence of the cyclase from *A. californica* [5,27] and did not reveal any additional underlying sequence when using up to 1 nmol of protein in the Edman degradation. Electrospray MS also revealed a single-molecular-mass peak of 28694.9 ± 1.3 Da. This value, which was strictly reproducible for two different batches of purified *Aplysia* ADP-ribosyl cyclase, is slightly inferior to 29539.8 Da, i.e. the theoretical molecular mass expected from the sequence based on the cloning of the *Aplysia* enzyme [5,27]. This might be related to the occurrence of isoforms, most probably at the C-terminus, as described previously by Lee et al. [18]. Heat inactivation of the enzyme was also studied by measuring both ADP-ribosyl cyclase and cADP-ribose hydrolase activities. Incubation at 60 °C over a period of 40 min led to a decrease of activity that followed pseudo-first-order kinetics and in both cases identical slopes were observed ($t_{1/2} \approx 5.75$ min; results not shown). Altogether these studies indicate that we have obtained a homogenous enzyme preparation and that the observed cADP-ribose hydrolase activity is an intrinsic property of the *Aplysia* ADP-ribosyl cyclase and is not due to a contaminating protein present in our preparation.

Further solvolysis reactions catalysed by *Aplysia* ADP-ribosyl cyclase

One of the important issues raised by the finding that *Aplysia* ADP-ribosyl cyclase is also able to hydrolyse cADP-ribose is the following: what are the reaction pathways of this multifunctional enzyme? We reasoned on the reactions illustrated in Scheme 1, which has been established for the related bovine and human CD38/NAD$^+$ glycohydrolases [10,14]. For example, is ADP-ribose obtained by the transformation of NAD$^+$ in the presence of high amounts of the enzyme (Figure 1B) originating from the hydrolysis of transiently formed cADP-ribose or from a competition between the k_{H_2O} and k_3 steps? We have addressed this question using three different tools: (i) the transformation of poorly hydrolysable pyridinium analogues of NAD$^+$, such as PyAD$^+$, (ii) the study of methanolysis of cADP-ribose, NAD$^+$ and PyAD$^+$ and (iii) the hydrolysis of NMN$^+$.

The interest of PyAD$^+$ resides in the fact that this pseudo-substrate leads, after the cleavage of its pyridinium-ribose bond, to exactly the same reaction intermediate and products as NAD$^+$ (i.e. cADP-ribose and ADP-ribose). The major difference between the two dinucleotides is that because of the higher bond energy of the scissile bond in PyAD$^+$, the k_2 step should be substantially slowed down. For example, this was the case for bovine CD38/NAD$^+$ glycohydrolase where the turnover rate was decreased 500-fold [17]. Thus if cADP-ribose is a reaction intermediate between NAD$^+$ or its pyridinium analogues and the final hydrolytic product ADP-ribose, one would expect that cADP-ribose originating from PyAD$^+$ would have a higher probability of getting hydrolysed than when originating from NAD$^+$. As a result, using such a poorly hydrolysable analogue we should amplify the importance of the cADP-ribose hydrolase pathway in the catalytic reaction, i.e. more ADP-ribose should be produced at the expense of the cyclic metabolite. This was precisely the case; we found that the *Aplysia* enzyme was able to transform PyAD$^+$ into both cADP-ribose and ADP-ribose, but at a much lower rate than NAD$^+$ (≈ 3 orders of magnitude). Moreover with e.g. a 20 μM initial concentration of the analogue, at a 10% reaction progress, the [cADP-ribose]/[ADP-ribose] ratio was about 2.2. As expected, this ratio decreased with advancement of the reaction (Figure 4), indicative of a progressive hydrolysis of cADP-ribose. In comparison, under similar conditions when using NAD$^+$ as substrate, no ADP-ribose was detectable. Importantly, the slow turnover of PyAD$^+$ indicates that, in analogy to the CD38/NAD$^+$ glycohydrolases, the formation of the ADP-ribosyl intermediary complex is also rate limiting in the *Aplysia* ADP-ribosyl cyclase-catalysed transformation of NAD$^+$ and its pyridinium analogues.

We then studied the methanolysis of cADP-ribose. By analogy to bovine and human CD38/NAD$^+$ glycohydrolases [10,14,16],

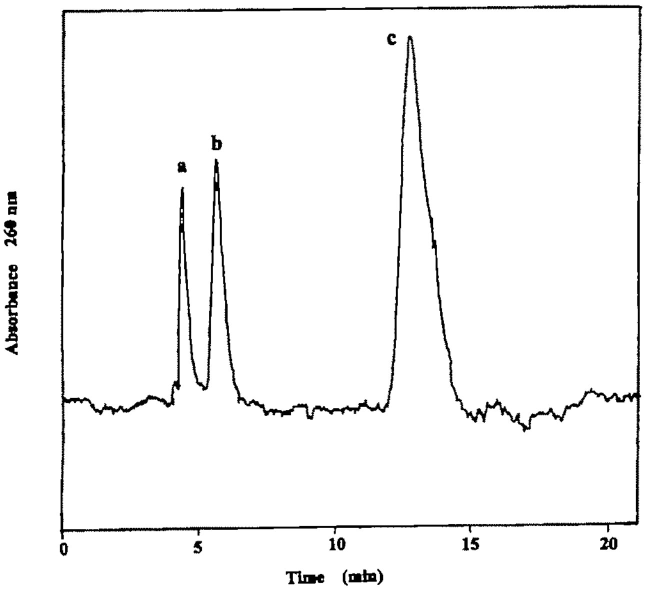

Figure 4 HPLC elution profile of the products obtained by the *A. californica* ADP-ribosyl cyclase-catalysed hydrolysis of PyAD$^+$

PyAD$^+$ (20 μM) was incubated at 37 °C in buffer A (final volume 500 μl), in the presence of 0.5 unit of enzyme. Product analysis (reaction advancement, 28%) was performed by HPLC as described in the Experimental section. (a) cADP-ribose, (b) ADP-ribose and (c) PyAD$^+$

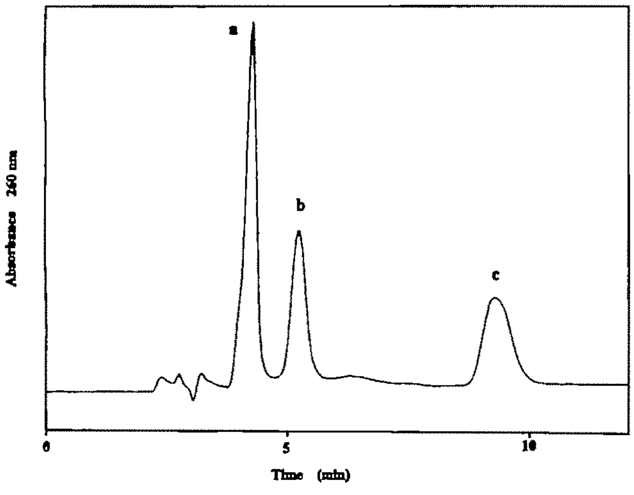

Figure 5 HPLC elution profile of the products obtained by the *A. californica* ADP-ribosyl cyclase-catalysed solvolysis of cADP-ribose in water/methanol

cADP-ribose (20 μM) was incubated at 37 °C in buffer A containing 0.5 M methanol (final volume 200 μl) in the presence of 30 m-units of enzyme. Product analysis was performed by HPLC as described in the Experimental section. (a) cADP-ribose, (b) ADP-ribose and (c) β-methyl ADP-ribose

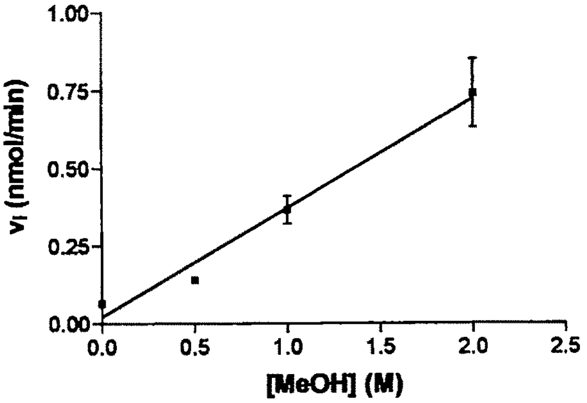

Figure 6 Dependence of the initial rate of cADP-ribose solvolysis on the concentration of methanol

Initial rates of cADP-ribose (20 μM) solvolysis catalysed by *Aplysia* ADP-ribosyl cyclase (30 m-units) at 37 °C in buffer A containing increasing concentrations of methanol (MeOH).

Aplysia ADP-ribosyl cyclase was also found to catalyse the methanolysis of the cyclic metabolite into methyl ADP-ribose. As determined by HPLC, this reaction resulted in the exclusive formation of the β-anomer, i.e. the methanolysis occurred with complete retention of configuration (Figure 5). Working with a 0–2 M range of methanol, two important parameters were established: (i) the product-partitioning ratio, i.e. $K = [\beta\text{-methyl ADP-ribose}][H_2O]/[\text{ADP-ribose}][\text{methanol}]$, which indicates the relative reactivity of the E · ADP-ribosyl intermediate (where E is the enzyme) with water and methanol, and (ii) the effect of methanol on the initial rates of cADP-ribose solvolysis (hydrolysis and methanolysis). Methanolysis/hydrolysis product ratios were found to be constant throughout the time course of the reactions and proportional to the methanol concentrations; the value of K was estimated to be 152 ± 9 (±S.D.). This indicates that, on a molar basis, methanolysis is two orders of magnitude faster than hydrolysis and points to the possible occurrence of a stabilized oxocarbenium reaction intermediate in the catalysed reaction [21]. Such a result can be used further to dissect the reaction mechanism of the cADP-ribose hydrolase activity of the enzyme from a phenomenological standpoint. Thus it was of interest to determine whether this very important acceleration of the solvolysis of the ADP-ribosyl intermediate due to methanolysis had an incidence on the turnover of the reaction. With regard to that point, one can predict that if the formation of the ADP-ribosyl intermediate from cADP-ribose is rate limiting (step k_{-3}), the addition of methanol would have no effect on the overall rate of cADP-ribose transformation, whereas if k_{H_2O} is rate limiting then the turnover would be accelerated by the solvent [28]. This latter case was observed experimentally, i.e. initial rates of cADP-ribose solvolysis were increased by the presence of methanol and a linear dependence of v_i on the concentration of this solvent was found (Figure 6), suggesting that $k_{-3} > k_{H_2O}$ in Scheme 1.

Methanolysis of NAD$^+$ catalysed by *Aplysia* ADP-ribosyl cyclase was also studied. Under the experimental conditions used, where little or no hydrolysis was observed in the absence of methanol, the addition of this solvent up to 2 M did not drastically change the product distribution. Thus at 2 M methanol, β-methyl ADP-ribose represented less than 5% of the reaction products.

The *Aplysia*-cyclase-catalysed transformation of PyAD$^+$, which leads to the formation of both cADP-ribose and ADP-ribose (see above), represents a favourable case for the study of methanolysis. In the presence of 0.5–2 M methanol, as assessed by HPLC, β-methyl ADP-ribose was also formed, mostly at the expense of cADP-ribose. In this case also, methanolysis was strictly proportional to the concentration of methanol and the partitioning ratio of 200 ± 19 is within the range of the one measured for the methanolysis of cADP-ribose. This is an important observation because it indicates that, in Scheme 1, the partitioning of the ADP-ribosyl intermediate between water and methanol is independent from its route of formation (steps k_2 or k_{-3})

ADP-ribosyl cyclase-catalysed hydrolysis of NMN$^+$ was also examined because of the great interest of this reaction for the understanding of the molecular mechanism of the enzyme. When using high amounts of enzyme (0.4 unit), we could indeed detect the hydrolysis of this mononucleotide and thus demonstrate that the cyclization step is not compulsory for the transformation of substrates by the *Aplysia* enzyme; this result is in favour of a ‘partitioning’ mechanism (Scheme 1, see the Discussion). Because NMN$^+$ cannot afford a cyclized product ($k_3 = 0$ in Scheme 1) its turnover rate should reflect $\approx k_2 + k_{H_2O}$; we found that for e.g. 1 mM NMN$^+$, which is close to the maximal velocity, the rate ratio NAD$^+$/NMN$^+$ was about 3900. This high value contrasts with the CD38/NAD$^+$ glycohydrolase-catalysed reactions, where the observed maximal velocities for NMN$^+$ and NAD$^+$ are within the same range [16,29]. It also indicates that in the *Aplysia*-enzyme-catalysed transformation of a substrate that cannot engage in a cyclization process, the slow step of the reaction pathway is most probably k_{H_2O} and not the formation of the intermediary complex resulting from the cleavage of the nicotinamide-ribose bond. This was borne out by studying the effect of methanol, which increased the turnover rate of NMN$^+$; thus for example at 1 M methanol, the initial rate of NMN$^+$ solvolysis was increased 2-fold.

Aplysia ADP-ribosyl cyclase does not catalyse methanolysis of NGD$^+$

NGD$^+$ is a useful alternative substrate because its transformation into solvolytic and cyclization reaction products occurs via dead-end (macroscopically irreversible) reactions; i.e. in contrast to cADP-ribose, cGDP-ribose is not enzymically hydrolysable (Scheme 1, $k_{-3} \approx 0$). In this respect, we have demonstrated previously that in bovine and human CD38/NAD$^+$ glycohydrolase-catalysed transformations of NGD$^+$, methanol was competing efficiently ($K \approx 50$) with the hydrolysis (k_{H_2O}) and the cyclization (k_3) steps and produced β-methyl GDP-ribose at the expense of cGDP-ribose [11,14]. This indicates that the reaction products are derived from a common oxocarbenium ion intermediate via competing intra- and intermolecular reactions [11,16]. In sharp contrast with these enzymes, and with the results obtained above with NAD$^+$, the *Aplysia* ADP-ribosyl cyclase transformed NGD$^+$ into cGDP-ribose alone; no GDP-ribose was produced and in the presence of up to 2 M methanol no β-methyl GDP-ribose became detectable. These results are important because they indicate that (i) the k_3/k_{H_2O} ratio is high enough in the *Aplysia* enzyme that $k_3/(k_{H_2O} + k_{CH_3OH})$ still macroscopically favours the cyclization reaction, and that (ii) most probably, the formation of ADP-ribose and β-methyl ADP-ribose by the *Aplysia*-enzyme-catalysed solvolysis of NAD$^+$ involves a prior formation of cADP-ribose.

DISCUSSION

The major finding of the present work was that *A. californica* ADP-ribosyl cyclase, by analogy with the multifunctional mammalian CD38/NAD$^+$ glycohydrolases, was also able to catalyse the solvolysis (hydrolysis and methanolysis) of cADP-ribose. When considering NAD$^+$ and cADP-ribose as competing substrates for the active site of the *Aplysia* enzyme, the specificity ratio, i.e. the ratio of the specificity constants V_{max}/K_m, is about 3.2×10^4 in favour of NAD$^+$. This very high value, which is due to a concomitant $2 \times \log$ increase of K_m and decrease of V_{max} values for cADP-ribose as compared with NAD$^+$, contrasts with the much lower ratio of 50 established for example for the bovine CD38/NAD$^+$ glycohydrolase [10]. From these data we can conclude that the invertebrate ADP-ribosyl cyclase is overwhelmingly a cyclase and that the cADP-ribose hydrolase activity, which becomes detectable only at very high enzyme concentrations (Figure 1B), has most probably no physiological meaning.

Nevertheless, the unravelling of this minor cADP-ribose hydrolase activity is important from a mechanistic standpoint and sheds some new light on the mode of action of the *Aplysia* cyclase. From the literature and the results obtained here we can conclude that the ADP-ribosyl cyclase and mammalian CD38/NAD$^+$ glycohydrolases, which are characterized by a great structural similarity [6], have fundamentally the following activities in common (i) transformation of NAD$^+$ into cADP-ribose, albeit with vastly different yields (see the Introduction), we have shown here that this ADP-ribosyl cyclase reaction can also be extended to pyridinium analogues of NAD$^+$ such as PyAD$^+$; (ii) transglycosidation reactions [30–32]; (iii) hydrolysis of the mononucleotide NMN$^+$; (iv) solvolysis of NAD$^+$ or its pyridinium analogues, i.e NAD$^+$ glycohydrolase activity, and (v) solvolysis of cADP-ribose, i e. cADP-ribose hydrolase activity. Interestingly, all of these reactions occur with retention of configuration at the anomeric carbon linked to the nicotinamide or other pyridinium residue, i.e. they generate β-ribosyl derivatives. Two mechanisms have been invoked for the mammalian CD38/NAD$^+$ glycohydrolases that could account for their low cyclase activities. The mechanism that was proposed first (‘sequential’ mechanism) involves an obligatory cyclization of NAD$^+$ into cADP-ribose followed by its hydrolysis into ADP-ribose [9]. Accordingly, the observed NAD$^+$ glycohydrolase activity of these multifunctional enzymes results from the sequential ADP-ribosyl cyclase and cADP-ribose hydrolase activities. The second mechanism (‘partitioning’ mechanism), which suggests that a single oxocarbenium-type intermediate partitions to cyclic and other products (solvolysis, transglycosidation), was borne out by experiment [8,11,14,16]. From the results obtained here, we can conclude that this latter mechanism also applies to *A. californica* ADP-ribosyl cyclase and therefore propose for these classes of enzymes a unifying mechanism that is illustrated in Scheme 1. The ratio [cADP-ribose]/[ADP-ribose], which is the main difference between the invertebrate and the mammalian enzymes in terms of outcome of the reaction, resides most probably in the actual values (and/or ratios) of critical rate constants that are dictated by structural contingencies.

The pathways of the *A. californica* ADP-ribosyl cyclase-catalysed reactions are nevertheless quite interesting within this context. Thus it should be noted that, from a macroscopic point of view, an apparently sequential mechanism could be explained satisfactorily according to Scheme 1 as a limiting form of the partitioning mechanism, provided that $k_3 \gg k_{H_2O}$. This seems to be the case for the *Aplysia* enzyme. Indeed, although methanolysis is much faster than hydrolysis ($k_{CH_3OH}/k_{H_2O} \approx 150$), no β-methyl GDP-ribose was formed from NGD$^+$, suggesting that methanol could not compete with the formation of cGDP-ribose and that $k_3 \gg k_{H_2O} + k_{CH_3OH}$. Moreover, only in the transformation of NMN$^+$, where solvolysis is the only possible pathway, was the capture of the intermediate by water (step k_{H_2O}) measurable and this was indeed found to be very slow. The fact that this latter step is a slow process in the pathways catalysed by the *Aplysia* enzyme can also be deduced from the increased turnover rate triggered by methanol in the solvolysis of cADP-ribose and NMN$^+$. Thus in sharp contrast to the CD38/NAD$^+$ glycohydrolases [11], because of the magnitude of k_3 it is

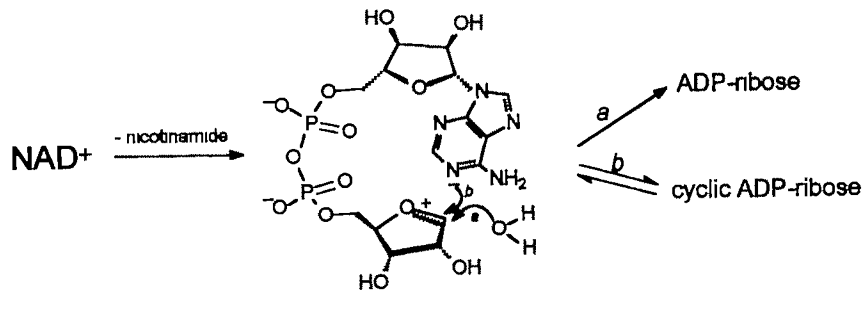

ADP-ribosyl oxocarbenium ion

Scheme 2 Partitioning of the ADP-ribosyl intermediate

The putative common ADP-ribosyl oxocarbenium ion intermediate evolves according to two competing pathways (a) An intermolecular reaction between ribosyl C-1′ and water, producing ADP-ribose This route is highly disfavoured in the *Aplysia* ADP-ribosyl cyclase (b) An intramolecular reaction between ribosyl C-1′ and N-1 of the adenine ring in the correct orientation to yield cADP-ribose This process is disfavoured in the mammalian CD38/NAD$^+$ glycohydrolases

difficult with the *Aplysia* enzyme to detect the partitioning of the ADP-ribosyl intermediate It seems therefore that the transformation of NAD$^+$ into ADP-ribose, only observed at high concentrations of ADP-ribosyl cyclase, results from the hydrolysis of cADP-ribose, which is formed first and then accumulated rather than being formed from the capture by water of the ADP-ribosyl intermediate originating from NAD$^+$. We can thus conclude that the *Aplysia* enzyme catalyses the transformation of NAD$^+$ according to an apparent sequential mechanism and that its NAD$^+$ glycohydrolase activity is due in fact to a macroscopic succession of ADP-ribosyl cyclase and cADP-ribose hydrolase activities. This conclusion is also in agreement with the observed sequential release of the reaction products nicotinamide and ADP-ribose or cADP-ribose, respectively, in the case of CD38/NAD$^+$ glycohydrolases [14,16,28] or the *Aplysia* cyclase [32].

An interesting mechanistic issue is the difference in efficiency of the k_3 and k_{H_2O} steps in the *Aplysia* cyclase and CD38/NAD$^+$ glycohydrolases. With NAD$^+$ as substrate, the turnover numbers of the ADP-ribosyl cyclase (present study) and e.g. bovine spleen NAD$^+$ glycohydrolase [26] are within the same order of magnitude and for both classes of enzymes the slow step in the formation, respectively, of cADP-ribose and ADP-ribose is the formation of the intermediary ADP-ribosyl complex. This latter point is supported by the observation that the turnover rate of both classes of enzymes is much affected by the pK_a of the leaving pyridine, i e by the bond energy of the scissile bond (this work and [17]). One would therefore expect that both classes of enzymes are equally efficient in the cleavage of the nicotinamide-ribose bond and this includes NMN$^+$. The particularly low rate of solvolysis of the latter mononucleotide by the cyclase, compared with the rate of cyclization of NAD$^+$ and to its hydrolysis catalysed by the CD38/NAD$^+$ glycohydrolases, is thus instructive. It indicates that when there is no possibility of cyclization, the turnover rate is dictated by the k_{H_2O} step, which is very low for the *Aplysia* enzyme. The same holds true in the hydrolysis of cADP-ribose. in both cases the turnover of the reaction is accelerated by methanol. Thus the characteristic of the *Aplysia* enzyme is that its k_{H_2O} step is much slower than in CD38/NAD$^+$ glycohydrolases. Altogether, this means that in the CD38/NAD$^+$ glycohydrolases the active site accommodates water molecule(s), which can react easily with the intermediary oxocarbenium to give ADP-ribose and thus efficiently compete with the cyclization process, whereas in the *Aplysia* ADP-ribosyl cyclase, water is mostly excluded from the active site, leaving the cyclization to take place.

In conclusion, the outcome of the reaction catalysed by the two classes of enzymes must reflect the partitioning of the intermediary complex (Scheme 1), where the fast steps are respectively the intramolecular cyclization in the *Aplysia* ADP-ribosyl cyclase ($k_3 \gg k_{H_2O}$) and the intermolecular reaction with water in the CD38/NAD$^+$ glycohydrolases ($k_3 < k_{H_2O}$). Within the intermediary complex of the *Aplysia* enzyme this might be due to a more favourable positioning of the N-1 of adenine with regard to the oxocarbenium ion or, more probably, because the capture by water is a highly disfavoured process, to a better shielding of this latter species from water (Scheme 2). A similar conclusion was reached recently by Munshi et al. [33]. Comparison of three-dimensional structures of the active sites of these enzymes should provide clues along these lines

The generous gift of *A californica* ovotestes from Dr Bernard Poulain is gratefully acknowledged This work was supported in part by the Centre de la Recherche Scientifique, by the Ministère de l'Education Nationale, de la Recherche et de la Technologie, by grant 1997-4053 from CNRS Programme Physique et Chimie du Vivant, and by a grant CIFRE-Institut de Recherche Jouveinal/Parke-Davis to C.C.-K. We thank Dr Charles Danzin for his support and suggestions and Dr Noelle Potier for MS determinations.

REFERENCES

1 Clapper, D L, Walseth, T F, Dargie, P J and Lee, H C (1987) J Biol Chem **262**, 9561–9568
2 Lee, H C (1997) Physiol Rev **77**, 1133–1164
3 Hellmich, M R and Strumwasser, F (1991) Cell Regul **2**, 193–202
4 Lee, H C and Aarhus, R (1991) Cell Regul **2**, 203–209
5 States, D. J., Walseth, T F and Lee, H C (1992) Trends Biochem Sci. **17**, 495
6 Prasad, G S, McRee, D E, Stura, E A, Levitt, D G, Lee, H C and Stout, C D (1996) Nat Struct Biol **3**, 957–964
7 Lee, H C, Galione, A and Walseth, T F (1994) Vitamins Hormones **48**, 199–257
8 Kim, H, Jacobson, E L and Jacobson, M K (1993) Science **261**, 1330–1333
9 Howard, M, Grimaldi, J C, Bazan, J F, Lund, F. E, Santos-Argumedo, L, Parkhouse, R M., Walseth, T F and Lee, H C (1993) Science **262**, 1056–1059
10 Muller-Steffner, H, Muzard, M., Oppenheimer, N and Schuber, F (1994) Biochem Biophys Res Commun **204**, 1279–1285
11 Muller-Steffner, H M, Augustin, A and Schuber, F (1996) J Biol Chem **271**, 23967–23972
12 Zocchi, E, Franco, L, Guida, L, Benatti, U, Bargellesi, A, Malavasi, F., Lee, H C and De Flora, A (1993) Biochem Biophys. Res Commun **196**, 1459–1465
13 Graeff, R M, Walseth, T F, Fryxell, K, Branton, W. D and Lee, H C (1994) J Biol Chem. **269**, 30260–30267

14 Berthelier, V, Tixier, J M, Muller-Steffner, H, Schuber, F and Deterre, P (1998) Biochem J **330**, 1383–1390
15 Augustin, A, Muller-Steffner, H and Schuber, F (2000) Biochem J **345**, 43–52
16 Sauve, A A, Munshi, C, Lee, H C and Schramm, V. L (1998) Biochemistry **37**, 13239–13249
17 Tarnus, C and Schuber, F (1987) Bioorg Chem **15**, 31–42
18 Lee, H C, Graeff, R M, Munshi, C B, Walseth, T F and Aarhus, R (1997) Methods Enzymol. **280**, 331–340
19 Heukeshoven, J and Dernick, R (1988) Electrophoresis **9**, 28–32
20 Schuber, F and Travo, P (1976) Eur J Biochem **65**, 247–255
21 Tarnus, C, Muller, H M and Schuber, F. (1988) Bioorg. Chem. **16**, 38–51
22 Jacobson, M K, Cervantes-Laurean, D, Strohm, M S., Coyle, D. L, Bummer, P M and Jacobson, E L (1995) Biochimie **77**, 341–344
23 Zhang, F J, Gu, Q M and Sih, C J (1999) Bioorg Med Chem **7**, 653–664
24 Migaud, M E, Pederick, R L, Bailey, V. C and Potter, B V L (1999) Biochemistry, **38**, 9105–9114
25 Munshi, C, Baumann, C, Levitt, D, Bloomfield, V A and Lee, H C (1998) Biochim Biophys Acta **1388**, 428–436
26 Muller-Steffner, H., Schenherr-Gusse, I, Tarnus, C and Schuber, F (1993) Arch Biochem Biophys **304**, 154–162
27 Glick, D L, Hellmich, M R, Beushausen, S, Tempst, P, Bayley, H and Strumwasser, F. (1991) Cell Regul **2**, 211–218
28 Schuber, F, Travo, P and Pascal, M (1976) Eur J Biochem **69**, 593–602
29 Schuber, F, Pascal, M and Travo, P (1978) Eur J Biochem **83**, 205–214
30 Anderson, B M (1982) in The Pyridine Nucleotide Coenzymes (Everse, J, Anderson, B and You, K-S, eds), pp 91–133, Academic Press, New York
31 Lee, H C, Graeff, R M and Walseth, T F (1997) Adv Exp Med Biol **419**, 411–419
32 Inageda, K, Takahashi, K, Tokita, K, Nishina, H, Kanaho, Y, Kukimoto, I, Kontani, K, Hoshino, S and Katada, T (1995) J Biochem (Tokyo) **117**, 125–131
33 Munshi, C, Thiel, D J, Mathews, I I, Aarhus, R, Walseth, T F and Lee, H C (1999) J Biol Chem **274**, 30770–30777

Received 6 January 2000/17 March 2000, accepted 17 April 2000

Investigation of the slow inhibition of almond β-glucosidase and yeast isomaltase by 1-azasugar inhibitors: evidence for the 'direct binding' model

Anders LOHSE, Tore HARDLEI, Astrid JENSEN, Igor W. PLESNER and Mikael BOLS[1]
Department of Chemistry, Aarhus University, DK-8000 Aarhus, Denmark

(−)-1-Azafagomine [(3*R*,4*R*,5*R*)-4,5-dihydroxy-3-hydroxymethylhexahydropyridazine; inhibitor **1**] is a potent glycosidase inhibitor designed to mimic the transition state of a substrate undergoing glycoside cleavage. The inhibition of glycosidases by inhibitor **1** and analogues has been found to be a relatively slow process. This 'slow inhibition' process was investigated in the inhibition of almond β-glucosidase and yeast isomaltase by inhibitor **1** and analogues. Progress-curve experiments established that the time-dependent inhibition of both enzymes by inhibitor **1** was a consequence of relatively slow dissociation and association of the inhibitor from and to the enzyme, and not a result of slow interchanges between protein conformations. A number of hydrazine-containing analogues of inhibitor **1** also inhibited β-glucosidase and isomaltase slowly, while the amine isofagomine [(3*R*,4*R*,5*R*)-3,4-dihydroxy-5-hydroxymethylpiperidine; inhibitor **5**] only inhibited β-glucosidase slowly. Inhibitor **1** and related inhibitors were found to leave almond β-glucosidase with almost identical rate constants, so that the difference in K_i values depended almost entirely on changes in the binding rate constant, k_{on}. The same trend was observed for the inhibition of yeast isomaltase by inhibitor **1** and a related inhibitor. The values of the rate constants were obtained at 25 °C and at pH 6.8.

Key words: non-steady-state kinetics, rate constants, slow binding inhibitors.

INTRODUCTION

Glycosidases are crucial in many biological processes, including breakdown of edible carbohydrates [1], eukaryotic glycoprotein processing [2], and polysaccharide and glycoconjugate anabolism and catabolism [3]. Glycosidases are also involved in a variety of metabolic disorders and other diseases such as diabetes [4], viral attachment [5], bacterial infection [6], and cancer formation [7]. Thus potent and selective glycosidase inhibitors have many interesting potential applications, such as treatment of AIDS [8], diabetes [4] and cancer [9], as well as crop protection.

Of the many potent glycosidase inhibitors the valieneamine derivatives (acarbose) and monosaccharide analogues, with nitrogen in place of ring oxygen, are the most notable [10]. A vigorous debate whether, or to what extent, the various inhibitor types are transition-state analogues has taken place [11]. It has recently been found that monosaccharide analogues with nitrogen in place of anomeric carbon is a new group of potent glycosidase inhibitors [12], in some cases having K_i values in the nanomolar range. It is of interest for future inhibitor design to understand how these molecules work, particularly if they function as transition-state analogues.

Slow binding, or slow onset of inhibition, is a widespread phenomenon among potent glycosidase inhibitors [10], where the inhibition process is relatively slow, occurring over a period of minutes and not at diffusion-controlled rates [13]. Rather than the subject of detailed study, it has often been considered as a troublesome complication in the measurement of enzyme inhibition constants. However, a study of slow inhibition may give a more detailed insight into the binding mode of potent glycosidase inhibitors. Thus it has been suggested that slow inhibition might be caused by the enzyme having two conformational states: one that binds the substrate in the ground state, and one that binds it in the transition state [13,14]. Transition state-like inhibitors bind to the latter form, which is present in small amounts, and have to be formed from the other state. The slowness of the inhibition is, according to this explanation, due to protein conformational changes which require the repositioning of a large number of atoms.

Slow-binding enzyme inhibition has been thoroughly reviewed in [13]; since this review a number of studies have appeared [15–19]. From the kinetic point of view, three possible mechanisms have been considered for the slow inhibition phenomena (Scheme 1). Binding between enzyme and inhibitor

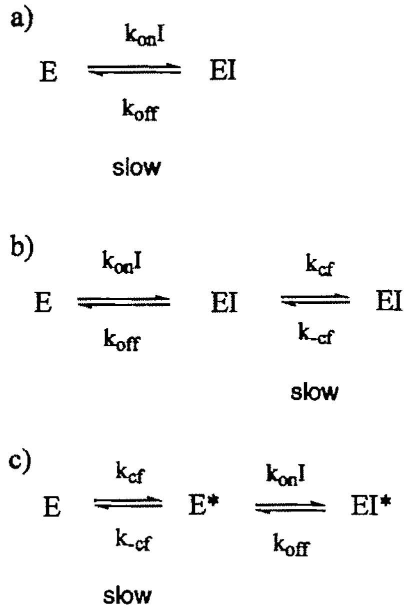

Scheme 1 Kinetic schemes for three models of slow inhibition

(**a**) 'Direct binding' model, (**b**, **c**) two 'conformational change' models

---

[1] To whom correspondence should be addressed (e-mail mb@kemi.aau dk)

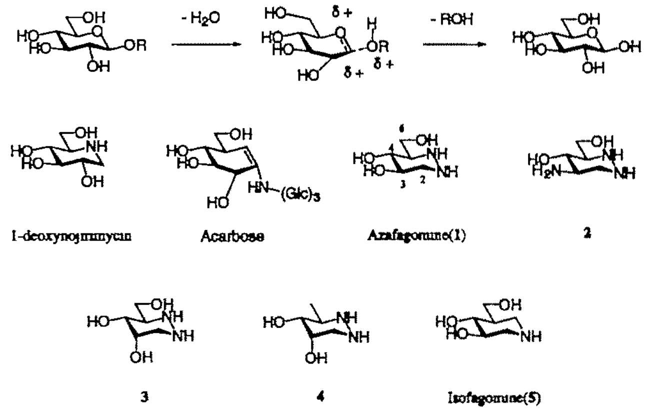

Figure 1 The strucure of the substrate, transition state and product in hydrolysis of a β-glucoside and the structures of some glycosidase inhibitors

may either involve a single step, having slow on and off rates (k_{on}[I] and k_{off} being small, Scheme 1a); have an initial fast-binding step, followed by a slow reversible transformation of EI to another entity, EI* (Scheme 1b); or have an initial slow interconversion of the enzyme E into another form E*, which binds the inhibitor by a fast step.

In our study of 1-azasugar inhibitors, we noticed that one of the inhibitors, 1-azafagomine (inhibitor **1**, see Figure 1], exhibited a time-dependent inhibition of almond β-glucosidase and isomaltase As a study of the slow inhibition process might give more insight into the binding mode of inhibitor **1** and analogues, we report here an investigation of the slow-inhibiton process of the two enzymes by inhibitors **1**–**5**. We report the finding that almond β-glucosidase and isomaltase are slowly inhibited by compounds **1**–**5** in a manner that agrees with the direct-binding model (Scheme 1a).

MATERIALS AND METHODS

Inhibitors

Compound (−)-**1** was synthesized optically pure from L-xylose [20], compounds (±)-**2**–**4** were synthesized as racemates as previously described [21,22], and racemic **5** was synthesized from arecoline [23]. All the compounds have previously been found to be competitive inhibitors of isomaltase and almond β-glucosidase [20,22]

Substrates

4-Nitrophenyl-α-D-glucopyranoside and 4-nitrophenyl-β-D-glucopyranoside were purchased from Sigma.

Enzymes

Chromatographically purified sweet almond β-glucosidase (21–25 units/mg) was obtained from Sigma SDS/PAGE showed essentially pure protein (purity > 90 %) as a 67 kDa band. This accords with the subunits of the type A isoenzyme, which has a molecular mass of 135 kDa [24,25]. Partially purified isomaltase (Sigma) was used without further treatment.

Enzyme kinetics: general conditions

All reactions were carried out in 0.05 M sodium phosphate buffer (pH 6.8) at 25 °C. When β-glucosidase was the catalyst, 4-nitrophenyl-β-D-glucopyranoside was used as substrate; when isomaltase was the catalyst, 4-nitrophenyl-α-D-glucopyranoside was used as substrate. Formation of the product, 4-nitrophenol, was measured continually at 400 nm using a Milton Roy Genesys 5 spectrometer.

Measurement of K_m

Measurements were performed in 2 ml solutions with 0.05 M buffer. Substrates were added at various concentrations (0.5, 2, 8 or 16 mM), the enzyme was mixed, and the reaction immediately monitored. From experiments ($n = 4$) with varied substrate concentrations, initial reaction rates were calculated as the slope of the product absorption versus reaction time. K_m and V_{max} were calculated by non-linear regression of the reaction rate versus substrate concentration using the graphics program Easy Plot

Progress curve determinations

Reactions with inhibitor (compounds **1**–**3**) present were carried out with and without preincubation of enzyme and inhibitor. Experiments without preincubation were carried out with 2 ml solutions (0.05 M buffer) with substrate [S] (4 mM for 4-nitrophenyl-β-D-glucopyranoside and 2 mM for 4-nitrophenyl-α-D-glucopyranoside), and the inhibitor [I] at various concentrations (0.7–14 K_i). The enzyme was mixed, and the reaction immediately monitored spectrophotometrically for 8–10 min. Experiments with preincubation were carried out with 50 μl solutions of inhibitor (10 K_i), with the enzyme being kept at 25 °C for 60 min The reaction was started by diluting to 2 ml (0.05 M buffer) with substrate solution containing variable amounts of inhibitor, so that [I] = K_i−20 K_i and [S] = 4 M or 16 M. No more than 5 % of the substrate was consumed in any single run.

Data treatment

The progress curves were fitted to eqn. (1), in the form $P(t) = at + b[\exp(-\beta t) - 1]$, using the program INRATE in the software package Simfit (developed by W. G. Bardsley, University of Manchester, U.K.).

RESULTS

Observation of slow inhibition

It was found that inhibitors **1**–**5** showed a non-instantaneous onset of inhibition of β-glucosidase, while inhibitors **1**–**4** showed similar behaviour towards isomaltase. Some representative examples of progress curves are shown in Figure 2.

For β-glucosidase, the slow inhibition was more apparent when the enzyme was incubated with the inhibitors **1**–**5** at elevated inhibitor concentrations for a period of 30 min or more. When the incubated enzyme and inhibitor were diluted with substrate and buffer, the progress curves (examples of which are shown in Figures 2C and 2D) were obtained. The time-dependent increase in reaction rate, resulting from slow release of enzyme from inhibitor, is readily recognized.

For isomaltase, preincubation was not necessary. In fact best results were obtained by directly monitoring the progress curve without preincubation.

Kinetics of slow inhibition: models and data analysis

There are in principle three ways in which a slow-binding competitive inhibitor **1** may interact with an enzyme (Scheme 1):

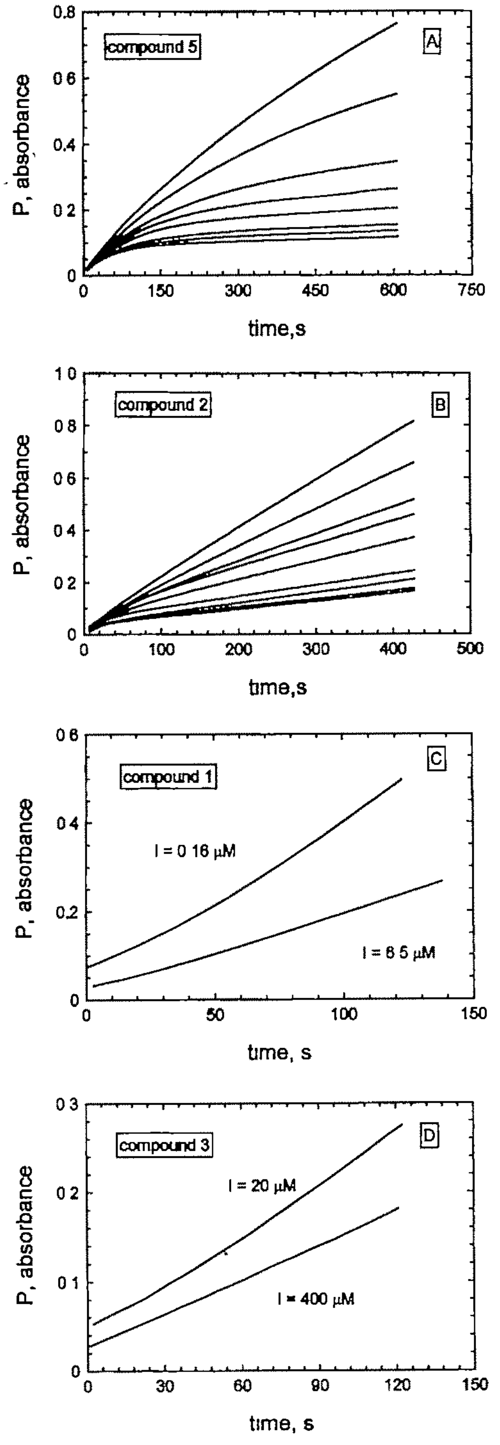

Figure 2 Representative examples of progress curves

(**A**, **B**) Solutions of phosphate-buffer (0.05 M, pH 6.8), substrate (4-nitrophenyl-β-D-glucoside), inhibitor and almond β-glucosidase were mixed to yield a final solution with [S] = 3.9 M and variable inhibitor concentrations between 0.35 μM and 4.8 μM (**A**) or 24 μM and 450 μM (**B**) (**C**, **D**) Phosphate-buffer (0.05 M, pH 6.8), almond β-glucosidase and Inhibitor ([I] = 6.5 μM) were preincubated 60 min Phosphate-buffer (0.05 M, pH 6.8), substrate (4-nitrophenyl-β-D-glucoside) and, in (D) inhibitor, were added to yield a final solution with [S] = 3.9 M and the inhibitor concentration shown

in the direct-binding model (a), the slow step is the inhibitor binding and release steps, characterized by the rate constants k_{on} and k_{off}; in model (b), the inhibitor binds rapidly to the enzyme, forming the complex EI which in turn, by a slow step, undergoes a conformational change to the species EI*; and in model (c), the slow rate is caused by a slow conformational change of the enzyme prior to binding the inhibitor. For model (a) the equations describing the time evolution are the simultaneous differential equations $dP(t)/dt$ and $dE(t)/dt$. Under steady-state conditions, with respect to substrate, these are solved in closed form to yield the progress curve:

$$P(t) = A(1-\alpha/\beta)t + (AC/\beta)[\exp(-\beta t) - 1] \qquad (1)$$

where,

$$A = V_m \times s/(1+s),\ s = [S]/K_m,\ \alpha = k_{on} \times [I]/(1+s),\ \beta = \alpha + k_{off},\ C = (ei)_{t=0} - \alpha/\beta,\ ei = [EI]/[E_0] \qquad (2)$$

Eqn. (1) has, in slightly different notation, been derived previously [13]. For model (b), the progress curve for eqn. (1) is also valid, but with altered A, α and β coefficients:

$$A = V_m \times s/(1+s+i),\ \alpha = k_{cf} \times i/(1+s+i),\ \beta = \alpha + k_{-cf},\ i = [I]/K_i \qquad (3)$$

Also, model (c) has a progress curve that follows eqn. (1), but the A, α and β coefficients are:

$$A = V_m \times s/(1+s),\ \alpha = k_{on} \times [I]/(1+s),\ \beta = [k_{cf}/(1+s)] + [k_{-cf}/(1+i)] \qquad (4)$$

For all the models the intrinsic $K_i = k_{off}/k_{on}$. Thus the progress curve data is given by the same equation for the three models, but they can be distinguished by the dependence of the coefficients on the inhibitor concentration. By fitting the data to eqn. (1) we can determine, by non-linear regression, the coefficient of the linear term, the coefficient of the exponential term, and the apparent rate constant β

Note that the appearance of the progress curve will depend on the way the kinetic experiments are carried out. If enzyme and sufficient inhibitor are first preincubated, after which substrate is added to initiate reaction, the term $(ei)_{t=0}$ is close to 1, and the constant $C > 0$. As a result the progress curve will be upwards concave (Figures 2C and 2D). In contrast, if no preincubation is performed, $C < 0$, and the progress curve will be upwards convex (Figures 3A and 3B)

From eqns (2) and (3) it is seen that for model (a) the apparent rate constant is a linear function of the inhibitor concentration, having the form:

$$\beta = k_{on} \times [I]/(1+s) + k_{off} \qquad (5)$$

From this rectilinear relationship the rate constants k_{on} and k_{off} may be determined. In contrast, from eqn (3) we see that for model (b):

$$\beta = k_{cf} \times [I]/\{(1+s)K_i + [I]\} + k_{-cf} \qquad (6)$$

The apparent rate constant is a monotonically increasing hyperbolic function of the inhibitor concentration. Finally, it can be seen from eqn. 4, that for model (c) β will also be a hyperbolic function of [I], but a decreasing one. We may thus expect that a study of the apparent rate constant (β), determined from a fit of the data to eqn. (1) can provide us with a diagnostic tool allowing a distinction between the models and a subsequent calculation of the rate constants.

Progress curve measurement

As seen earlier, the equations show that it is possible to distinguish between the three models (a), (b) and (c) by measuring β as a function of [I] For each of the inhibitors **1**–**5** a set of progress

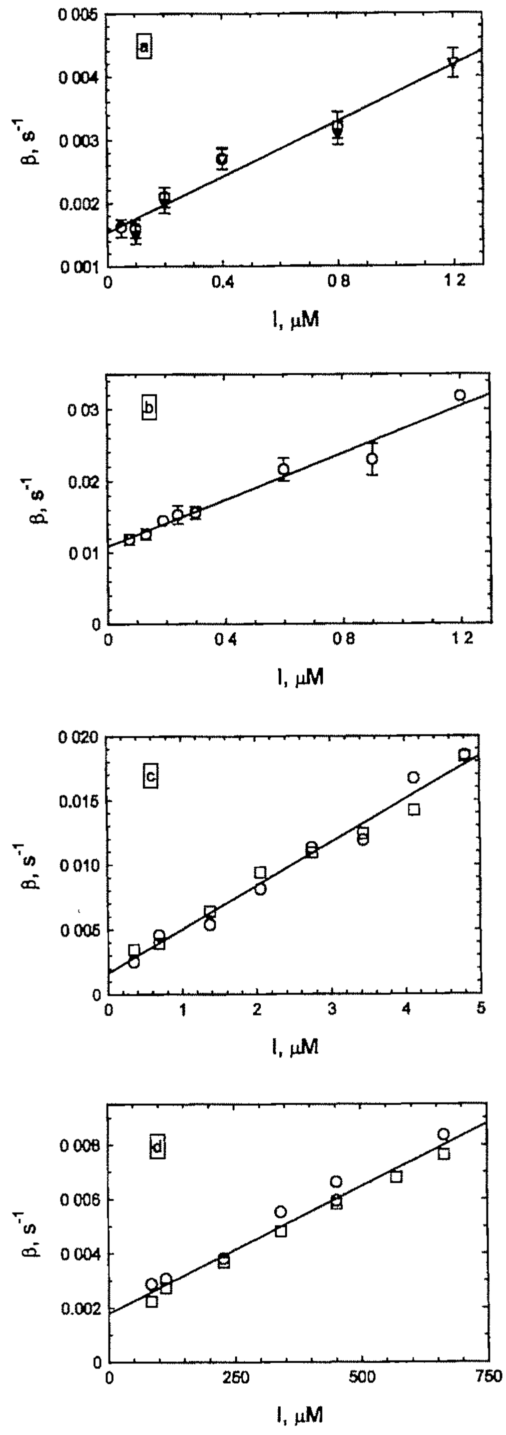

Figure 3 Representative examples of plots of the apparent rate constants β [cf. eqn. (1)] as a function of inhibitor concentration

The rate constants k_{on} and k_{off} are obtained from the slope and intercept, respectively, of the straight lines fitting the data. (**A**) Isomaltase inhibited by **1** (**B**) β-glucosidase inhibited by **1** (**C**) β-glucosidase inhibited by **5** (**D**) Isomaltase inhibited by **2**

Table 1 Dissociation constants and rate constants for inhibitors of almond β-glucosidase and isomaltase at temperature 25 °C and pH 6.8

The rate constants are the means of parameters of 2–4 weighted linear plots of β versus [I] (as in Figure 3). The weights used are determined by the S.D. of β obtained from non-linear fitting of the progress data [see eqn. (1)]. The K_i are calculated as k_{off}/k_{on} with S.D. obtained by propagation of errors

Enzyme	Inhibitor	K_i (μM)	k_{on} ($M^{-1} \cdot s^{-1}$)	k_{off} (s^{-1})
β-Glucosidase	**1**	0.33 ± 0.06	$(3.3 \pm 0.2) \times 10^4$	$(1.1 \pm 0.2) \times 10^{-2}$
β-Glucosidase	(±)-**1**	0.72 ± 0.12	$(1.4 \pm 0.2) \times 10^4$	$(1.0 \pm 0.1) \times 10^{-2}$
β-Glucosidase	(±)-**2**	56 ± 6	$(1.50 \pm 0.09) \times 10^2$	$(8.4 \pm 0.7) \times 10^{-3}$
β-Glucosidase	(±)-**3**	128 ± 17	$(1.4 \pm 0.4) \times 10^2$	$(1.8 \pm 0.4) \times 10^{-2}$
β-Glucosidase	(±)-**4**	28 ± 6	$(2.4 \pm 0.5) \times 10^3$	$(6.7 \pm 0.1) \times 10^{-2}$
β-Glucosidase	(±)-**5**	0.22 ± 0.06	$(7.3 \pm 0.3) \times 10^3$	$(1.6 \pm 0.4) \times 10^{-3}$
Isomaltase	**1**	0.27 ± 0.03	$(5.33 \pm 0.4) \times 10^3$	$(1.43 \pm 0.09) \times 10^{-3}$
Isomaltase	(±)-**2**	79 ± 10	23 ± 1	$(1.8 \pm 0.2) \times 10^{-3}$
Isomaltase	(±)-**6**	5.8	Not slow	Not slow

curves was determined at different concentrations of inhibitor. This was done with (Figures 2C and 2D) and without (Figures 2A and 2B) a preincubation of the inhibitor with the enzyme prior to experiment. If preincubation gave more curved progress curves these were used for data extraction; this was the case for inhibitor **1**. For each of the progress curves thus obtained, β values were determined. Plots of β versus [I] were made for inhibitors **1**–**5**. Typical plots of β versus [I] are shown in Figure 3, and the rate constants and inhibition constants determined from fitting the plots to eqn. (4) are collected in Table 1.

DISCUSSION

It is clear that the plots of β versus [I] for the inhibition of β-glucosidase or isomaltase show a linear relationship with all the inhibitors (Figure 3); there is no indication of a hyperbolic relationship. The data therefore exclusively suggest that the inhibition of the two enzymes by the inhibitors studied follows model (a) (Scheme 1). This is corroborated by the property observed for the progress curves without preincubation (Figures 2A and 2B): the slope of these curves at $t = 0$ is independant of [I]. If, as in model (b), the inhibitor were binding rapidly to the enzyme, the initial rate would decrease as the concentration of inhibitor increased. This means that the slow steps are the binding of the inhibitor to the enzyme and its release, and not a conformational change of the enzyme or enzyme–inhibitor complex. This seems at first sight extraordinary, because binding is commonly believed to take place nearly at diffusion-controlled rates, and indeed previous work suggests that most slow-inhibition phenomena are caused by slow conformational changes. However, a number of recent studies of slow inhibition on other systems also support model (a) [15,16,19], so there is reason to believe that this model may be widespread.

The binding constants k_{on} and k_{off} extracted from the model show some remarkable trends (Table 1). First of all, k_{on} is remarkably small even for a potent inhibitor like (−)-**1**. Furthermore, inhibitors **1**–**4** are released from almond β-glucosidase with approximately the same k_{off}. Similarly, **1** and **2** are released from isomaltase with the same rate, though k_{off} in this case is about 10 times smaller than that for β-glucosidase. So inhibitors of the same overall type, in this case hydrazines, are released from either enzyme with a fixed rate, even though their K_i values differ widely, and this variation is due exclusively to differences in the k_{on}. A similar property was observed by Hanozet et al. [26] for the inhibition of sucrase by acarbose, nojirimycin and deoxynojirimycin. Note that inhibitors (−)-**1** and (±)-**1** also have the same k_{off} from β-glucosidase, but differ in k_{on}. This value is also expected, since the (+)-**1** enantiomer has been found not to be an inhibitor [20]. Therefore twice as much racemic **1** as optically active **1** is required to get the same rates, and the k_{on}, which is multiplied with [I], will be half that of pure inhibitor.

It is, however, also clear that the release rate is not identical for all azasugar inhibitors. An inhibitor of different type, isofagomine (inhibitor **5**), has a 10-fold smaller k_{off} constant than the hydrazines, inhibitors **1–4** (Table 1). The inhibition of isomaltase by inhibitor **5** is not slow, which means that with a K_i value of 5.8 μM the release constant k_{off} must be larger than 10^{-3} s^{-1}. It is not necessarily much larger, because with a k_{off} value between 0.1 and 1 s^{-1}, the equilibration time will be less than 10–20 s, and therefore too fast to observe with the present method.

The fact that the release constant of the related inhibitors **1–4** does not vary suggests that the stereochemistry or presence of a hydroxyl group does not play a significant role in the release of the inhibitor from the enzyme.

Furthermore, the data in Table 1 show that the azasugars bind tightly and perhaps in a unique orientation with respect to the protein, compared to the possible varied orientation of binding of simple sugars, which bind with lower affinity [27]. Also the 3-hydroxyl group is important and not effectively substituted by an amino group; 3-amino-3-deoxy-D-glucose, a relatively strong inhibitor compared to glucose [27], is suggested to be oriented differently when bound to the enzyme.

We thank Mr Ib Thomsen, Mr Henrik H Jensen and Dr Steen U Hansen for providing us with inhibitor samples and the Danish Natural Science Research Council for financial support (grant no. 9502986 and THOR program)

REFERENCES

1 Marshall, J (1974) Application of enzymic methods to the structural analysis of polysaccharides. Adv Carbohydr Chem Biochem **30**, 257–370

2 Kornfeld, R and Kornfeld, S (1976) Comparative aspects of glycoprotein structure Annu Rev Biochem **45**, 217–237

3 Kobata, A. (1979) Use of endo- and exoglycosidases for structural studies of glycoconjugates Anal Biochem **100**, 1–14

4 Robinson, K M., Begovic, M E, Rhinehart, B L, Heineke, E W, Ducep, J-B, Kastner, P R, Marshall, F N and Danzin, C (1991) New potent α-glucohydrolase inhibitor MDL 73945 with long duration of action in rats Diabetes **40**, 825–830

5 Liener, I E, Sharon, N and Goldstein, I J. (1986) The Lectins Properties, Functions and Application in Biology and Medicine, Academic Press, New York

6 Paulson, J E (1985) Interactions of animal viruses with cell surface receptors In The Receptors (Cohn, P M, ed), pp 131–219, Academic Press, New York

7 Dennis, J W, Laferte, S, Waghorne, C, Breitman, M L and Kerbel, R S (1987) β-1–6 Branching of Asn-linked oligosaccharides is directly associated with metastasis Science **236**, 582–585

8 Karpas, A, Fleet, G W J, Dwek, R A, Fellows, L E, Tyms, A S, Petursson, S, Namgoong, S K, Ramsden, N G, Jacob, G S and Rademacher, T W (1988) Aminosugar derivatives as potential anti-human immunodeficiency virus agents Proc Natl Acad. Sci USA **85**, 9229–9233

9 Bernacki, R J, Niedbala, M J and Korytnyk, W (1985) Glycosidases in cancer and invasion Cancer Metastasis Rev **4**, 81–102

10 Legler, G (1990) Glycoside hydrolases mechanistic information from studies with reversible and irreversible inhibitors Advan Carbohydr Chem Biochem **48**, 319–384

11 Heightman, T D and Vasella, A T (1999) Recent insights into inhibition, structure, and mechanism of configuration-retaining glycosidases Angew Chem. Int Ed **38**, 750–770

12 Bols, M (1998) 1-Azasugars, Apparent Transition State Analogous of Equatorial Glycoside Formation/cleavage Acc Chem Res **31**, 1–8

13 Morrison, J. F and Walsh, C T (1988) The behavior and significance of slow-binding enzyme inhibitors Adv Enzymol Relat Areas Mol Biol **61**, 201–301

14 Legler, G (1999) Glycosidase Inhibition by Basic Sugar Analogs and the Transition State of Enzymatic Glycoside Hydrolysis In Iminosugars as Glycosidase Inhibitors (Stutz, A, ed.), pp 31–67, Wiley-VCH, Weinheim

15 Yiallouros, I., Vassiliou, S, Yiotakis, A, Zwilling, R, Stocker, W and Dive, V (1998) Phosphinic peptides, the first potent inhibitors of astacin, behave as extremely slow-binding inhibitors Biochem J **331**, 375–379

16 Ploux, O Breyne, O Carillon, S and Marquet, A (1999) Slow-binding and competitive inhibition of 8-amino-7-oxopelargonate synthase, a pyridoxal-5′-phophate-dependent enzyme involved in biotin biosynthesis, by substrate and intermediate analogs. Eur J Biochem **259**, 63–70

17 Merkler, D J, Brenowitz, M and Schramm, V L (1990) The Rate Constant Describing Slow-Onset Inhibition of Yeast AMP Deaminase by Coformycin Analogues Is Independent of Inhibitor Structure. Biochemistry **29**, 8358–8364

18 Pegg, M S and Itzstein, M von (1994) Slow-binding Inhibition of Sialidase from Influenza Virus Biochem Mol Biol Int **32**, 851–858

19 Kati, W M, Saldivar, A S., Mohamadi, F, Sham, H L, Laver, W G and Kohlbrenner, W E (1998) GS4071 Is a Slow-Binding Inhibitor of Influenza Neuraminidase from Both A and B Strains Biochem Biophys Res Commun. **244**, 408–413

20 Ernholt, B V, Thomsen, I B, Lohse, A, Jensen, K B, Hazell, R G, Plesner, I, Liang, X, Jacobsen, A and Bols, M (2000) 1-Azafagomine 2 Enantiospecific Synthesis of Azafagomine Chem. Eur J **6**, 278–287

21 Lohse, A, Jensen, H H, Bach, P and Bols, M (2000) Synthesis of 3-substituted isofagomine analogues using a unusual *syn* hydrogenation reaction J Chem Soc Perkin Trans **1**, 659–665

22 Bols, M, Hazell, R and Thomsen, I (1997) 1-Azafagomine A Hydroxyhexahydropyridazine that Potently Inhibit Enzymatic Glycoside Cleavage Chem Eur J **3**, 940–947

23 Hansen, S U and Bols, M (2000) Synthesis of isofagomine and its stereoisomers from Arecoline J. Chem Soc Perkin Trans **1**, 911–915

24 Kleinschmidt, T, Glossmann, H and Horst, J (1970) Zur Kenntnis des Sussmandel-Emulsins Weitere Charakterisierung der Komponenten A und B Hoppe-Seyler's Z Physiol. Chem **351**, 349–358

25 Grover, A K, Macmurchie, D D and Cushley, R J (1977) Studies on Almond Emulsin β-D-glucosidase I Isolation and Characterization of a Bifunctional Isozyme Biochim Biophys Acta **482**, 98–108

26 Hanozet, G, Pircher, H-P, Vanni, P, Oesch, B and Semenza, G (1981) An example of enzyme hysteresis The slow and tight interaction of some fully competitive inhibitors with small intestinal sucrase J Biol Chem **256**, 3703–3710

27 Dale, M P., Ensley, H E, Kern, K, Sastry, K. A R and Byers, L D (1985) Reversible Inhibitors of β-Glucosidase Biochemistry **24**, 3530–3539

Received 14 January 2000/7 April 2000; accepted 25 April 2000

Interaction of C3b$_2$–IgG complexes with complement proteins properdin, factor B and factor H: implications for amplification

Emiliana JELEZAROVA, Anna VOGT[1] and Hans U. LUTZ[2]

Institute of Biochemistry, Swiss Federal Institute of Technology, ETH-Zentrum, CH 8092, Zurich, Switzerland

Nascent C3b can form ester bonds with various target molecules on the cell surface and in the fluid phase. Previously, we showed that C3b$_2$–IgG complexes represent the major covalent product of C3 activation in serum [Lutz, Stammler, Jelezarova, Nater and Späth (1996) Blood **88**, 184–193]. In the present report, binding of alternative pathway proteins to purified C3b$_2$–IgG complexes was studied in the fluid phase by using biotinylated IgG for C3b$_2$–IgG generation and avidin-coated plates to capture complexes. Up to seven moles of properdin 'monomer' bound per mole of C3b$_2$–IgG at physiological conditions in the absence of any other complement protein. At low properdin/C3b$_2$–IgG ratios bivalent binding was preferred. Neither factor H nor factor B affected properdin binding. On the other hand, properdin strongly stimulated factor B binding. Interactions of all three proteins with C3b$_2$–IgG exhibited pH optima. An ionic strength optimum was most pronounced for properdin, while factor B binding was largely independent of the salt concentration. C3b$_2$–IgG complexes were powerful precursors of the alternative pathway C3 convertase. In the presence of properdin, C3 convertase generated from C3b$_2$–IgG cleaved about sevenfold more C3 than the enzyme generated on C3b. C3b$_2$–IgG complexes could therefore maintain the amplification loop of complement longer than free C3b.

Key words: C3 convertase, immunoglobulins, C3.

INTRODUCTION

Proteolytic activation of the third component of human complement, C3, liberates the anaphylatoxic fragment C3a and generates C3b. The reactive thioester within C3b forms a very short-lived intermediate which reacts preferentially with hydroxyl groups on target molecules and forms ester bonds [1,2]. Much effort has been focused on the binding selectivity of C3 with respect to the molecular structures in the immediate environment of the hydroxyl group [3,4] as well as at higher structural levels [4,5].

The efficiency of covalent interaction of nascent C3b is low. Only approx. 10% of the activated C3b binds covalently to target molecules on cells in the near vicinity [1]. The majority of C3b molecules remain in the fluid phase, where they react with water or form covalent complexes with serum proteins such as C4 or IgG. IgG has a measurable affinity for C3 [6] and can serve as a target for covalent attachment of C3b. It has been demonstrated that C3b in complex with IgG [7] or C4b [8] is partially protected from factor I-dependent inactivation, and therefore has a longer half-life than free C3b (30–40 min in 2% serum [7] or 3–4 min in 20% serum [9]). These properties make C3b- and IgG-containing covalent complexes (C3b$_n$–IgG complexes) powerful activators of the amplification loop [7] and efficient opsonins that bind simultaneously to C3 and Fc receptors [10]. The same complexes may be involved in systemic, excessive complement activation which initiates inflammation and contributes to persisting injury In many such cases intravenously applied IgG has beneficial effects. High-dose IgG diverts nascent C3b from immune complexes to fluid-phase IgG [11,12] by forming C3b$_n$–IgG complexes, and stimulates their factor I-dependent inactivation [9].

Though covalent complexes containing C3b and IgG appear to have important functional properties, their architecture and bonding is insufficiently understood. Evidence from several laboratories suggests that C3b is ester-bonded exclusively to IgG heavy chain [13–17], and within the heavy chain to the CH1 domain [15,17]. Some of these complexes contain not one, but two C3b molecules [9,16], most likely in the form of C3b–C3b–IgG complexes. The ester-linkage between the two C3b molecules is not arranged at random, but probably occurs between the 65 kDa fragments of α'C3 molecules This type of bonding maintains the sequential arrangement during inactivation of the complexes. The dimeric organization of the inactivated C3b molecules may increase their affinity for binding to complement receptor, CR3. A detailed analysis of the properties of these complexes was hampered by the fact that complement activation generates a whole series of complexes containing C3b, C4b and IgG The major C3b$_n$–IgG complex observed in serum, the C3b$_2$–IgG complex, can also be generated *in vitro* from C3b and IgG [16], and we have designed a new protocol to purify it In the present paper, we address the functional properties of purified C3b$_2$–IgG complexes, and study their interaction with the proteins of the alternative pathway in order to establish their potential involvement in persistent complement amplification

EXPERIMENTAL

Materials

As whole human IgG we used Sandoglobulin® (manufactured by the Central Laboratory, Blood Transfusion Service, Bern, Switzerland). Sephadex, Na^{125}I, and Bolton and Hunter Reagent {*N*-succinimidyl-3-(4-hydroxy, 5[^{125}I] iodophenyl) propionate} were from Amersham Pharmacia Biotech; factor B, properdin,

---

Abbreviations used HABA, 2-(4′-hydroxybenzeneazo)benzoic acid, HSA, human serum albumin, IgG^B, biotinylated IgG, VBS, veronal-buffered saline, GVBS, VBS containing 0.1% gelatin

[1] Present address Karolinska Institutet, Mikrobiologiskt okt Tumorbiologiskt Centrum, Parasitologen, S-17177 Stockholm, Sweden.

[2] To whom correspondence should be addressed (e-mail hlutz@bc biol ethz.ch)

and factor D, from Calbiochem–Novabiochem (San Diego, CA, U.S.A.) Complement C3 was isolated from fresh plasma as described elsewhere [9,18], and was deprived of inactivated C3 before use [19].

C3b$_2$–IgG$^{\mathrm{B}}$ complexes

Biotinylation of IgG was performed according to manufacturer's instructions. Briefly, 500 mg of whole human IgG in 50 mM bicarbonate buffer (pH 8 5) and 20 mg of sulfo-*N*-hydroxysuccinimidobiotin (Pierce, Rockford, IL, U.S.A.) were incubated at room temperature for 45 min with rotation. The reaction was stopped by dilution with cold bicarbonate buffer. Free sulfo-*N*-hydroxysuccinimidobiotin was removed by ultrafiltration in Vivaspin 15 (cut-off 100 kDa; Vivascience, Westford, MA, U.S.A.), and IgG$^{\mathrm{B}}$ was concentrated to approx 80 mg/ml.

C3b$_2$–IgG$^{\mathrm{B}}$ complexes were generated from 6 mg of C3 and 400 mg of biotinylated IgG (IgG$^{\mathrm{B}}$), using trypsin to activate C3 [7,16]. Free IgG$^{\mathrm{B}}$ was removed by ion-exchange chromatography on QAE Sephadex A-50. The sample was dialysed and loaded to a QAE Sephadex column (2.5 cm × 7 cm), equilibrated in 20 mM Tris, 140 mM NaCl, pH 8.3 (30 ml/h, 4 °C) After washing, the bound material was eluted with a stepwise gradient using 160 mM, 180 mM and 200 mM NaCl in starting buffer. C3b$_2$–IgG$^{\mathrm{B}}$ eluted at 180 mM NaCl, as judged by SDS/PAGE. Most of the free C3b was removed on a Sephacryl S 300 HR column (1.6 cm × 60 cm, FPLC) equilibrated with veronal-buffered saline (VBS), pH 7.4, containing 0.04 % sodium azide (18 ml/h, room temperature). Fractions corresponding to C3b$_2$–IgG$^{\mathrm{B}}$ complexes were dialysed and finally purified on MonoQ HR 5/5 (FPLC) using a stepwise NaCl gradient from 100 mM to 1 M NaCl in 20 mM Tris (pH 7.8). Purified C3b$_2$–IgG$^{\mathrm{B}}$ complexes were dialysed against VBS and stored at 4 °C.

The degree of biotinylation of IgG was determined by the 2-(4′-hydroxybenzeneazo)benzoic acid (HABA) method [20] using several different IgG$^{\mathrm{B}}$ concentrations and a mean value was taken. The average molecular mass of IgG was considered to be 160 kDa. The apparent degree of biotinylation of IgG was 4–5 moles of biotin per mole of IgG. Using this number, and the determined biotin concentration in the C3b$_2$–IgG$^{\mathrm{B}}$ preparation, the C3b$_2$–IgG$^{\mathrm{B}}$ concentration was calculated.

Protein iodination

Factor H, C3 and monoclonal antibody H206 were labelled by the chloramine-T procedure as previously described [21]. Properdin and factor B were labelled by the milder Bolton and Hunter method. Dimethyl formamide was evaporated from Bolton and Hunter Reagent under nitrogen. Protein, in 10 mM phosphate buffer (pH 8), 50 mM NaCl, was added and incubated for 30 min at room temperature with gentle shaking. The reaction was stopped by 0.1 M ethanolamine, and the labelled protein was purified on Sephadex G-25 in PBS (pH 7.4). Specific activity was 0.5×10^6 c.p.m./μg for properdin and 3.8×10^6 c.p.m./μg for factor B. Labelled proteins were stored in aliquots at −20 °C and used within two weeks. Prior to use, radioiodinated proteins were dialysed and centrifuged for 3 min at 14000 *g* to remove any aggregated material.

Radioimmune assay

Deglycosylated avidin (neutro-avidin; Fluka) or C3b were covalently coupled at 20 μg/ml to Chemobond® microtitre plates as described before [22]. Prior to use, the plates were blocked with 150 μl/well of blocking solution [20 mg/ml of IgG, 10 mg/ml of human serum albumin (HSA) in VBS, pH 7.4] for 1 h at room temperature, and washed with 300 μl/well of suitable buffer.

Purified C3b$_2$–IgG$^{\mathrm{B}}$ complexes in VBS (pH 7.4) were mixed with the ^{125}I-labelled protein in the presence of 10 mg/ml of HSA in a total volume of 180 μl. The samples were incubated for 2 h at 37 °C, and then loaded in triplicate on the neutro-avidin-coated plates (50 μl/well). The plates were incubated for 2 h at room temperature and washed three times with 300 μl/well of VBS (pH 7.4). Bound radioactivity in each well was determined.

Factor B binding was studied in the presence of 3 mM MgCl$_2$ and, where indicated, in the presence of 7 8 μg/ml of properdin.

Properdin molar concentration was calculated with respect to the monomer.

To study the ionic strength dependence of the binding, samples were prepared in different final NaCl concentrations in veronal buffer (pH 7 4), and corresponding buffers were used for all subsequent steps. The pH dependence of the binding was assayed in a buffer containing 1.25 mM glycine, 1.25 mM Mes, 1.25 mM Hepes and 1.25 mM Tris, which was brought to different pH values by the addition of HCl or NaOH [23]. This buffer mixture has a constant ionic strength over the whole pH interval and was supplemented with 150 mM NaCl. All incubations and washings were performed with buffer of the corresponding pH.

In the controls, C3b$_2$–IgG$^{\mathrm{B}}$ complexes were replaced by IgG$^{\mathrm{B}}$ at the same molar concentration Radioactivity bound to those wells was subtracted from the corresponding data with complexes. It was 3–5 % of that in the equivalent samples and was dependent solely on the amount of radioactive protein.

The biotin-binding capacity of the plate was determined by incubating with an excess of IgG$^{\mathrm{B}}$ under the same assay conditions. The biotin content of the solution before and after incubation was measured by the HABA method [20]. There were 109 ± 60 pM of biotin bound per well (mean from four independent measurements). The biotin content of C3b$_2$–IgG$^{\mathrm{B}}$ at the highest concentration used (12 μg/ml) was approx. 5.6 pM per well, i.e. 20-fold lower. Therefore it was assumed that most of the C3b$_2$–IgG$^{\mathrm{B}}$ complexes were trapped on the plate.

Detection of C3b$_2$–IgG$^{\mathrm{B}}$ or C3b on the plate

C3b$_2$–IgG$^{\mathrm{B}}$ was incubated at 0.05–0.6 μg/well (1.93–23.2 nM) in VBS, pH 7.0, on a neutro-avidin plate overnight at room temperature. C3b was covalently coupled to a Chemobond® plate at 0.035–0.42 μg/well (3 86–46.4 nM). The plates were blocked with 20 mg/ml of human IgG in VBS, containing 0.1 % gelatine, pH 7.0 (GVBS), and incubated with 0.03 μg/well (3.75 nM) of ^{125}I-labelled H206 for 2 h at room temperature in the same buffer. The plates were washed three times with GVBS containing 0.04 % Tween 20 and cut to determine bound radioactivity.

C3 convertase activity

C3b$_2$-IgG$^{\mathrm{B}}$ and C3b plates were prepared and blocked with human IgG as described above. C3 convertase generation was carried out in GVBS, pH 7.0, containing 3 mM MgCl$_2$ for 30 min at 37 °C (50 μl/well). Factor B was used at 50 μg/ml, factor D at 0.5 μg/ml, and properdin, where indicated, was added at a final concentration of 5 μg/ml. The plates were washed three times with GVBS containing 0.04 % Tween 20 and 20 ng/well of ^{125}I-labelled C3 (11×10^6 c.p.m./μg) was added for 30 min at 37 °C. In one series of wells C3 cleavage was performed in the presence of 0.5 M *N*-acetyl-L-tyrosine (Fluka) and aliquots from those samples were taken for SDS/PAGE prior to plate washing. The plates were washed three times with GVBS containing 0.04% Tween 20, and bound radioactivity was determined. Control wells were treated in exactly the same way except that convertase generation was omitted. The deposition of ^{125}I-labelled C3 to those wells was subtracted from the corresponding data.

SDS/PAGE

SDS/PAGE was performed according to a modified Neville gel system using 5% or 7% separating gels [24]. Gels were stained with Coomassie Brilliant Blue R250 and scanned on a laser densitometer (Molecular Dynamics, Sunnyvale, CA, U.S.A.). The amount of protein was quantified using the Image Quant program.

Protein concentration

Protein concentration was determined spectrophotometrically using the following $A^{1\%}_{280,\ 1\mathrm{cm}}$: 9.7 for C3 and C3b, 14.1 for IgG, 17.8 for properdin, 12.7 for factor B, and 13.1 for factor H Molecular masses were taken as follows: 190 kDa and 181 kDa for C3 and C3b, respectively; 53 kDa for properdin monomer, 150 kDa for factor H; 93 kDa for factor B; and 518 kDa for C3b$_2$–IgG.

RESULTS

Assay system for studying the binding of AP proteins to C3b$_2$–IgG complexes

An assay system based on the biotin–avidin interaction was developed for the purpose of this study. C3b$_2$–IgG complexes were generated from IgG^B and purified to yield a preparation containing only traces of C3b (Figure 1, lane 1). After reduction the C3b$_2$–IgG^B complex appeared on the gel as a characteristic pattern of several bands including α'-α'-heavy chain, β, heavy chain and light chain (Figure 1, lane 3). The preparation contained no detectable amount of IgG^B (Figure 1, lane 1), which at this acrylamide concentration is well separated from C3b (Figure 1, lanes 2 and 4). The presence of α' and α'-α' bands in the reduced complexes (Figure 1, lane 3) indicates the existence of free C3b and traces of C3b–C3b dimers in the preparation. Their amount was quantified from densitometric scans and was not more than 20% of the total protein.

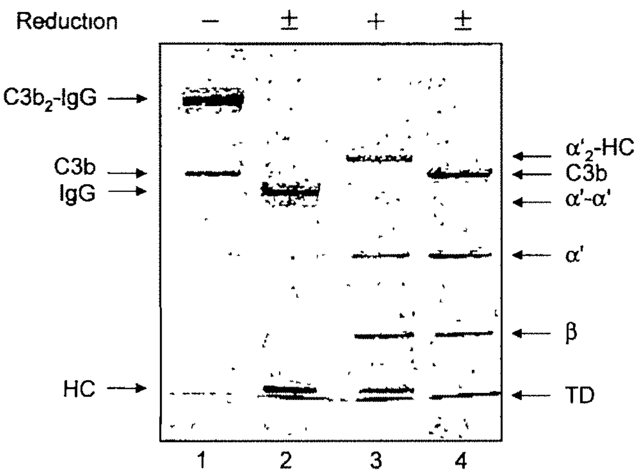

Figure 1 SDS/PAGE of purified C3b$_2$–IgG^B complexes

C3b$_2$–IgG^B complexes were boiled in sample buffer for 3 min, alkylated, and run on 5% gels (lanes 1 and 3) C3b (lane 4) and IgG^B (lane 2) were prepared reduced and non-reduced, and mixed after alkylation Note that IgG light chain migrates together with the tracking dye (TD) HC, heavy chain

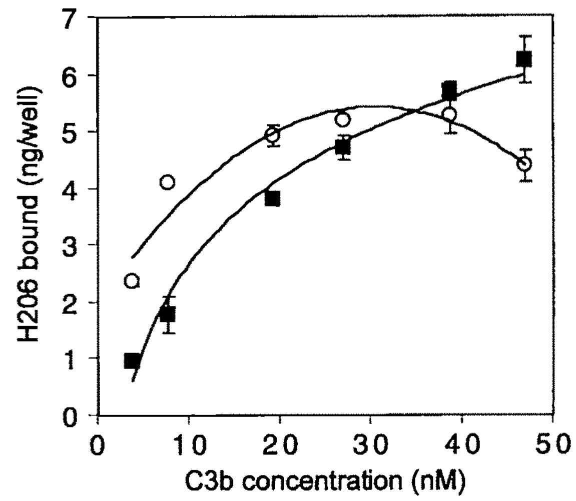

Figure 2 Immobilization of C3b$_2$–IgG^B or C3b

Increasing concentrations of C3b$_2$–IgG^B (1 93–23 2 nM, ■) or C3b (3 86–46.4 nM, ○) were immobilized on an avidin or a Chemobond® plate respectively Note that the same number of C3b molecules per well was used for coating The plates were incubated with ^{125}I-labelled monclonal antibody H206 for 2 h at 37 °C and the bound radioactivity was determined C3b$_2$–IgG^B concentration is expressed as C3b residues Data are given as means ± S D from triplicates.

The use of biotinylated complexes for binding studies has the advantage that protein–protein interactions occurred in solution rather than with immobilized ligand Once equilibrium was reached, the C3b$_2$–IgG^B complexes were captured on the avidin plate together with any other protein that specifically interacted with them. We chose to label the IgG portion of the C3b$_2$–IgG complexes for several reasons. IgG has been successfully biotinylated without any loss of functional activity [25], while C3 has proved difficult in this respect [26]. The IgG portion of the complexes was not expected to take part in the interaction with the complement proteins, whilst the C3b moieties had to be in close-to-native state. In addition, the traces of C3b and C3b–C3b dimers in the C3b$_2$–IgG^B preparation could not bind to the plate, and thus interaction of the labelled ligand with them could not contribute to bound radioactivity.

A monoclonal anti-C3 antibody (H206) directed to the C-terminal 43-kDa portion of C3 [27] was used to verify capture of C3b$_2$–IgG^B complexes on the avidin plate and to determine the relative concentration of C3b moieties on the C3b$_2$–IgG^B/avidin and on the C3b plate ^{125}I-labelled H206 binding increased with the C3b$_2$–IgG concentration (Figure 2). The same result was obtained when C3b$_2$–IgG^B complexes were incubated with the antibody in solution and then captured to the plate (results not shown). H206 binding to covalently immobilized C3b showed a different pattern, but revealed a similar number of C3b molecules per well at the corresponding concentrations

Binding of properdin to C3b$_2$–IgG complexes

Binding of labelled properdin was indistinguishable from that of the unlabelled one at 0.25–10 μg/ml (results not shown). Properdin bound to C3b$_2$–IgG complexes in the absence of any other complement protein. The degree of binding was dependent on

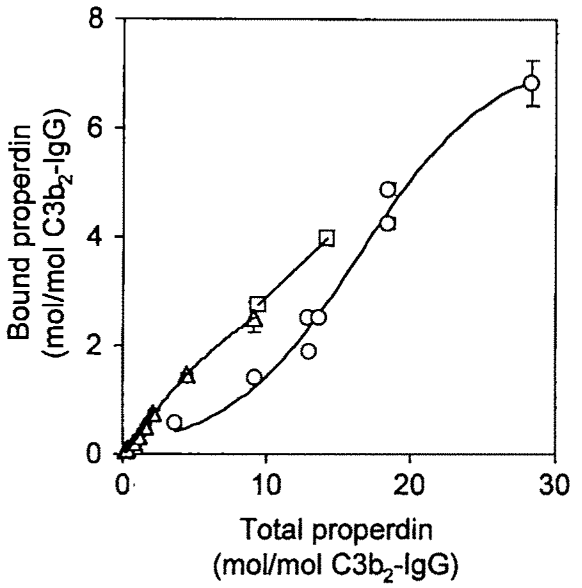

Figure 3 Concentration dependence of properdin binding to C3b$_2$–IgG^B complexes

^{125}I-labelled properdin was incubated with C3b$_2$–IgG^B complexes at increasing molar excess as described in the Experimental section The molar concentration of properdin was calculated for monomer Binding for 9 65 nM (○), 19 3 nM (□) and 23 2 nM (△) C3b$_2$–IgG^B is shown as means ± S D from at least triplicates of several independent experiments.

the concentration of both reacting species Up to seven moles of properdin ‘monomer’ bound per mole of C3b$_2$–IgG complex, provided that a large enough excess of properdin was available (Figure 3). This extent of binding corresponds to one tetramer and one trimer bound per C3b$_2$–IgG complex. On the other hand, at lower properdin/C3b$_2$–IgG ratios, 2–4 moles of properdin were bound per complex, suggesting that properdin oligomers reacted monovalently or bivalently depending on the availability of binding sites. In addition, the binding curves at higher concentrations of complexes showed higher stoichiometry of interaction at the same molar ratio of reacting species. At 10-fold molar excess of properdin, the number of bound properdin monomers increased from 1.4 to 2.7 per mole of C3b$_2$–IgG (see different curves in Figure 3). Although such behaviour is in accordance with the general predictions of the mass law, it is possible that preferential binding of a particular properdin oligomer contributes to the effect. Factor B (83 μg/ml) and factor H (117 μg/ml) had no effect on properdin binding, the differences in both cases being within one S D.

Binding of factors B and H

The same assay system was utilized to investigate the interaction between C3b$_2$–IgG^B complexes and factors B and H. Binding of factor B to C3b$_2$–IgG^B complexes in the absence of properdin was not detectable within the concentration range tested (up to 290 nM; Figure 4). Addition of 147 nM properdin resulted in binding of up to 0 25 M of factor B per mole of C3b$_2$–IgG complex The amount of bound factor B was low, but specific, since addition of factor D during incubation diminished bound radioactivity by approx. 40 %, which roughly corresponds to the portion of the released Ba fragment (results not shown).

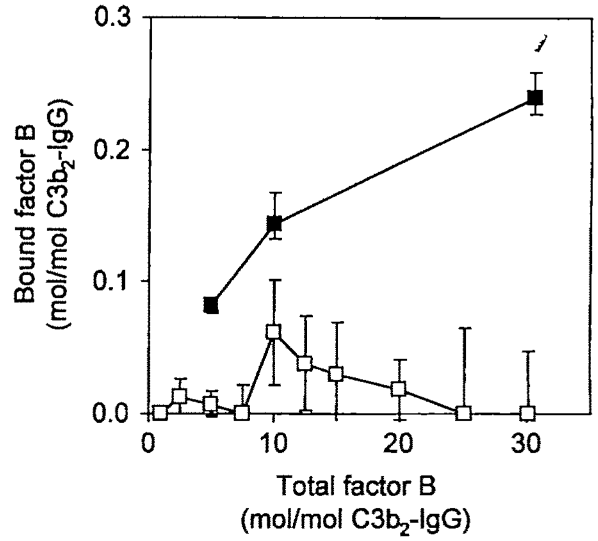

Figure 4 Binding of factor B to C3b$_2$–IgG^B complexes

^{125}I-labelled factor B (10–290 nM) was incubated with 1 93 nM C3b$_2$–IgG^B complexes without properdin (□) or in the presence of 147 nM properdin (■) in VBS (pH 7 4), containing 3 mM Mg^{2+} Results are from triplicates and are given as means ± S D

Factor H binding was also relatively low and a high excess of it was required to obtain significant binding. Therefore concentration dependence was not performed. However, it is worth mentioning that of all three proteins, factor B showed the lowest binding in the absence of a stabilizer such as properdin

Ionic strength and pH dependence

To further characterize the functional properties of C3b$_2$–IgG complexes, the ionic strength and pH dependence of their interaction with properdin, factor B and factor H was investigated under conditions giving optimal binding for each individual protein. Interaction with properdin was performed at concentrations corresponding to the steep part of the binding curve (Figure 3). For factors B and H, 1 93 nM C3b$_2$–IgG complexes were used in order to obtain high molar excess of the ligands. Binding of properdin and factor H exhibited a clear maximum at 110 mM and 60 mM NaCl respectively (Figure 5A). Factor B binding did not show a clear peak, but maximal values were approx. 120 mM NaCl and were within one S.D. in the range between 60 and 170 mM NaCl.

As the pronounced optimum of properdin and factor H binding to C3b$_2$–IgG complexes appeared rather unexpected, when compared to their binding to C3b [28], care was taken to exclude potential errors. Substitution of IgG^B in controls (see the Experimental section) with biotinylated HSA had no effect on the type of the curves. Another potential source of error was poor solubility and/or aggregation of properdin, factor B and factor H during incubation at low ionic strength. To address this issue, the proteins were incubated for 30 min at 37 °C at the corresponding salt concentration in the absence of C3b$_2$–IgG complexes and centrifuged for 30 min at 14000 *g* to separate any pelletable material. The radioactivity in the pellet was negligible except for properdin at low ionic strength. A comparison of bound/total to bound/soluble properdin showed that the impact on the binding curve was minimal. The decreased binding was therefore not due to poor solubility (Figure 5B).

The pH dependence of the interactions was studied at physiological salt concentration in the range between pH 4.5 and pH 8.5. A pH optimum of 5.5, 6 and 6.5 was observed for factor B, properdin and factor H respectively (Figure 6).

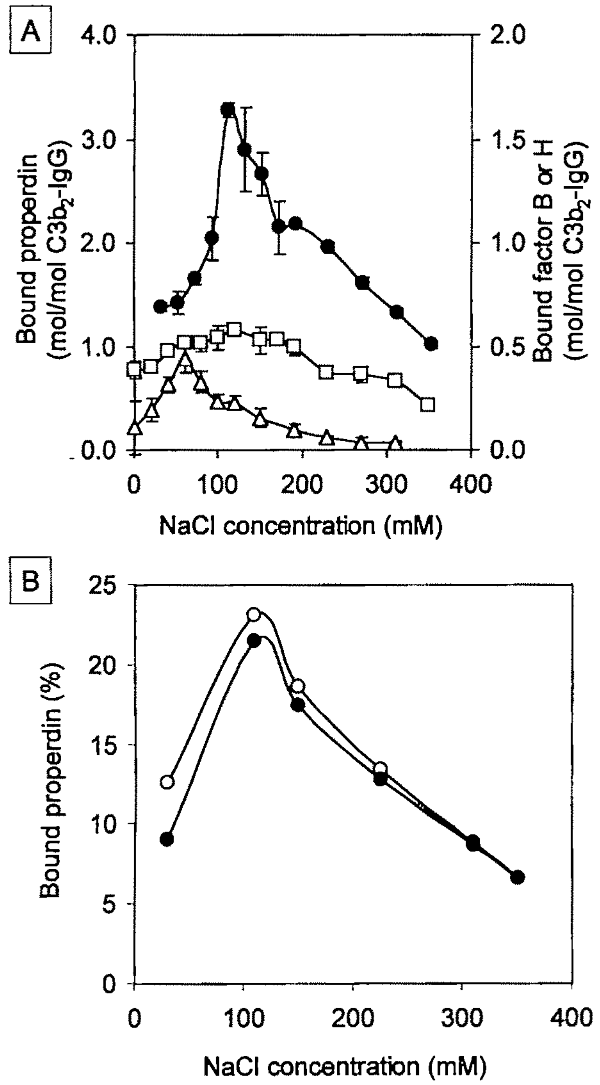

Figure 5 Effect of ionic strength on the interaction of C3b$_2$–IgG^B complexes with the alternative pathway proteins

(**A**) Ionic strength dependence. Binding of properdin (●) was studied at 9.65 nM C3b$_2$–IgG^B and 147 nM properdin. For the binding of factors B (□, 473 nM) and H (△, 147 nM) a concentration of 1.93 nM C3b$_2$–IgG^B was chosen. Binding of factor B was performed in the presence of 3 mM MgCl$_2$ and 147 nM properdin. Results are expressed as means ± S.D. from at least triplicates. (**B**) Impact of solubility on the binding of properdin. Bound properdin is expressed as percent of total (●) or as percent of soluble properdin (○).

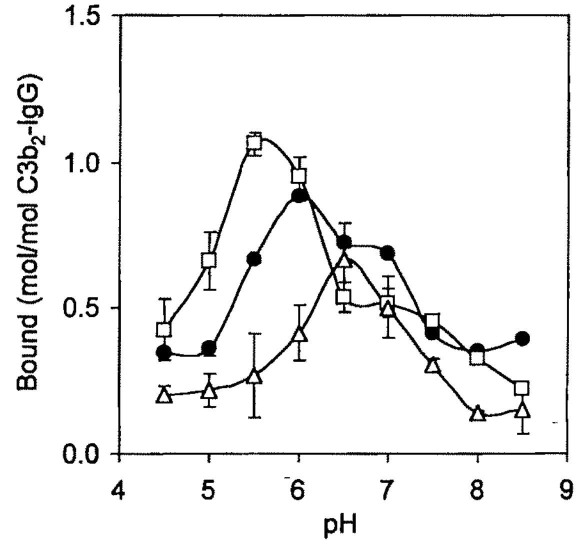

Figure 6 pH dependence of the interaction of C3b$_2$–IgG^B complexes with properdin and factors B and H

The concentration of C3b$_2$–IgG^B was 1.93 nM. Binding of factor B was performed in the presence of 3 mM MgCl$_2$ and 147 nM properdin. Labelled properdin (●), factor B (□) and factor H (△) were 29, 473 and 147 nM respectively. Results are given as means ± S.D. from at least triplicates.

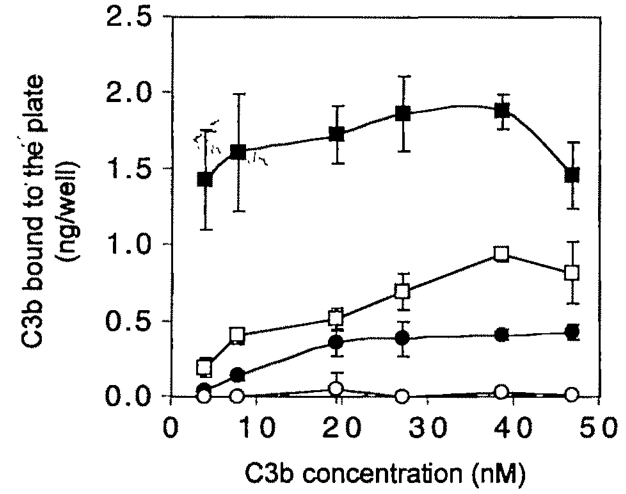

Figure 7 Comparison of C3 convertases generated from C3b or C3b$_2$–IgG^B

Complexes (squares) were immobilized on a neutro-avidin plate at 1.93 to 23.2 nM. C3b plate (circles) was prepared as described in the Experimental section using 3.86–46.4 nM C3b. Convertase was assembled by incubation with 538 nM factor B and 21 nM factor D in GVBS (pH 7.0), containing 3 mM Mg^{2+} (30 min at 37 °C). Properdin (94 nM) was added, where indicated (filled symbols). After washing, convertase activity was determined by the cleavage of ^{125}I-labelled C3 (2.1 nM, 30 min/room temperature). C3b$_2$–IgG^B molar concentration was multiplied by two in order to compare the same number of C3b molecules. Data are means ± S.D. from triplicates.

C3b$_2$–IgG complexes as precursors of a C3 convertase

In view of the possible role of C3b$_2$–IgG complexes in maintaining the amplification loop, it was of interest to verify their ability to generate C3 convertase in comparison with C3b. C3b was covalently coupled to Chemobond® plates and C3b$_2$–IgG^B complexes were immobilized on neutro-avidin plates as described in the Experimental section. The coupling concentrations were chosen to be equal with respect to the C3b moieties. As revealed by monoclonal antibody H206 binding, there were similar numbers of C3b sites on both plates (Figure 2). Convertase activity was determined by the amount of ^{125}I-labelled nascent C3b which was deposited to the plate. The specificity of C3 cleavage was verified by measuring the release of ^{125}I-C3b to the fluid phase after incubation in the presence of *N*-acetyl-tyrosine (results not shown). In the absence of properdin, convertase activity on the C3b plate was measurable, but very low (Figure 7). Cleavage of ^{125}I-labelled C3b on the C3b$_2$–IgG plate was considerably higher and showed a clear dose response. Addition of 5 μg/ml of properdin resulted in a general stimulation of convertase activity, but the absolute effect on ^{125}I-C3b cleavage was much higher in C3b$_2$–IgG plate. Thus convertase activity was 4–11-fold higher on the C3b$_2$–IgG plate over the entire concentration range tested.

DISCUSSION

In the physiological concentration range (2–15 μg/ml) properdin bound to C3b$_2$–IgG in a dose-dependent manner (Figure 3). The binding of seven properdin monomers to one molecule of C3b$_2$–IgG can be explained as the simultaneous binding of one trimer and one tetramer. Evidently, both C3b portions of the complex, each having one binding site for properdin [29], retained their binding capacity. Therefore the C3b$_2$–IgG complex as a whole can bind properdin bivalently. Since properdin oligomers are believed to possess significant flexibility [30], bivalent binding would be possible. Indeed, at low properdin/C3b$_2$–IgG ratios bivalency was favoured (Figure 4, sigmoidal curve). A bivalent contact would increase the avidity of interaction significantly, thus offering partial protection from inactivation already at low properdin concentration. It has been shown that properdin tetramers and trimers had higher affinities for C3b-coated particles than dimers [31], but the role of the different oligomers has yet to be clarified. Higher oligomers may geometrically better suit a bivalent interaction. While C3b clusters can be formed only at the cell surface, C3b$_2$–IgG complexes have the potential to bind properdin bivalently and support alternative pathway activation even in the fluid phase.

The effect of factor B and of factor H on properdin binding was studied at a properdin concentration corresponding to the steep part of the curve (Figure 4), where binding is most sensitive to modulation. Factor B and factor H did not affect properdin binding to C3b$_2$–IgG at all. In contrast, interaction of properdin with C3b bound to zymosan was augmented by factor B and inhibited in the presence of factor H [28]. This discrepancy may originate from different methods used to detect bound protein. Since we studied binding to the complexes in the fluid phase, no ligand could be entrapped by carrier material. More importantly, properdin strongly stimulated binding of factor B to C3b$_2$–IgG complexes (Figure 4). The same result was demonstrated for solid-phase immune complexes, which bound properdin in the absence of factor B [32]. Factor B is known to have a very low affinity even for zymosan-bound C3b, the K_a being in the order of 0.65 μM [28] to 2 μM [33]. These observations strongly question the sequence of events during alternative pathway convertase generation. Binding of factor B to C3b or C3b$_2$–IgG complexes is likely to be rather inefficient under physiological conditions and may require the presence of properdin. Moreover, properdin secretion by peripheral blood T cells, monocytes and neutrophils in response to inflammatory agents would result in elevated local levels of properdin, and would lead to transient amplification in sites of inflammation [34].

Interaction of properdin and factor H with C3b$_2$–IgG complexes in solution showed optima at 110 and 60 mM NaCl respectively. Binding of these proteins to C3b has been studied earlier using C3b bound to activating surfaces, like erythrocytes [35], zymosan [28], and microtitre plates [23]. Binding under those conditions did not show optima, but was favoured at low ionic strength with a sharp decrease towards physiological salt concentration, suggesting primarily ionic interactions. We think that this discrepancy originates from studying fluid-phase interactions as compared with interactions with solid supports, of which some were even highly charged. The lack of a well-defined ionic strength maximum of factor B binding to C3b$_2$–IgG is in good agreement with the proposed primarily hydrophobic nature of its interaction with C3b [36]. Maximal binding was found at pH 6 for properdin, 6.5 for factor H and 5.5 for factor B. In the interval between pH 6 and 7, where optimum of binding to C3b$_2$–IgG complexes was achieved, ionization of histidine residues is known to occur. Other groups have also indicated the importance of histidine residues for the interaction between factors H, I and C3b [23]. None of the proteins studied showed a pH optimum in the physiological range. Such a shift may contribute to the inherent regulation of the amplification loop. Whether the difference has structural reasons or originates from studying fluid-phase rather than solid-phase interactions, has to be further investigated.

C3b$_2$–IgG complexes served as precursors for C3 convertase generation and were considerably more efficient than C3b alone (Figure 7). This property can explain the correlation of complement activity in serum with the amount of C3b$_2$–IgG generated [9]. The presence of two C3b moieties within this complex did not perturb the substrate specificity of the subsequently generated convertase, although covalent C3b dimers were implicated in the C5 convertase [37]. On the other hand, recent work reported the ability of monomeric C3b to generate C5 convertase [38]. The specificity of the convertase, therefore, does not originate only from the structure of the enzyme, but has a more complex ground.

Our results altogether strengthen the conviction that properdin stabilizes C3b$_2$–IgG complexes before any other complement protein has bound to them and that, in general, the alternative pathway of convertase generation may depend on whether properdin is bound to its precursor, a C3b or a C3b$_2$–IgG complex. Since C3b$_2$–IgG complexes can bind properdin oligomers bivalently, they are far more potent activators of the alternative pathway than nascent C3b.

This work was supported by grants to H U L from the Swiss Union Bank on behalf of a client and from the Swiss National Science Foundation (grant 3200-045844) The monoclonal anti-C3 antibody (H206) was kindly provided by Professor R. Burger, Robert Koch Institute, Berlin, Germany. The excellent technical assistance of Mrs Pia Stammler is gratefully acknowledged

REFERENCES

1 Law, S K and Dodds, A W (1997) Protein Sci **6**, 263–274
2 Law, S. K, Lichtenberg, N A and Levine, R P (1979) J Immunol **123**, 1388–1394
3 Sahu, A., Kozel, T R and Pangburn, M K (1994) Biochem J **302**, 429–436
4 Pangburn, M. K (1989) J Immunol **142**, 2759–2765
5 Pangburn, M K. (1989) J Immunol **142**, 2766–2770
6 Kulics, J, Rajnavolgyi, E, Fust, G and Gergely, J (1983) Mol Immunol **20**, 805–810
7 Fries, L F, Gaither, T A, Hammer, C H and Frank, M M (1984) J Exp Med **160**, 1640–1655
8 Meri, S and Pangburn, M K (1990) Eur J Immunol **20**, 2555–2561
9 Lutz, H U, Stammler, P, Jelezarova, E, Nater, M and Spath, P J (1996) Blood **88**, 184–193
10 Fries, L F, Siwik, S A, Malbran, A and Frank, M M (1987) Immunology **62**, 45–51
11 Basta, M, Kirshbom, P, Frank, M M and Fries, L F (1989) J Clin Invest **84**, 1974–1981
12 Basta, M, Langlois, P. F, Marques, M, Frank, M M and Fries, L F (1989) Blood **74**, 326–333
13 Gadd, K J and Reid, K B (1981) Biochem J **195**, 471–480
14 Takata, Y, Tamura, N and Fujita, T (1984) J Immunol **132**, 2531–2537
15 Shohet, J M, Bergamaschini, L, Davis, A E and Carroll, M C (1991) J Biol. Chem. **266**, 18520–18524
16 Lutz, H. U., Stammler, P and Fasler, S. (1993) J Biol Chem **268**, 17418–17426
17 Sahu, A and Pangburn, M K (1994) J Biol Chem **269**, 28997–29002
18 Hammer, C H, Wirtz, G H, Renfer, L, Gresham, H D and Tack, B F (1981) J Biol Chem. **256**, 3995–4006
19 Janatova, J, Lorenz, P E, Schechter, A N, Prahl, J W and Tack, B F (1980) Biochemistry **19**, 4471–4478
20 Green, N M (1965) Biochem J. **94**, 23–24

21 Lutz, H U, Nater, M and Stammler, P. (1993) Immunology **80**, 191–196

22 Lutz, H U, Stammler, P and Fischer, E A. (1990) J. Immunol Methods **129**, 211–220

23 Soames, C J and Sim, R B (1997) Biochem J. **326**, 553–561

24 Fasler, S, Skvaril, F. and Lutz, H U (1988) Anal Biochem. **174**, 593–600

25 Gretch, D R, Suter, M and Stinski, M F (1987) Anal Biochem **163**, 270–277

26 Berger, M, Gaither, T A, Cole, R M, Chused, T M, Hammer, C H and Frank, M M (1982) Mol Immunol **19**, 857–864

27 Burger, R, Bader, A, Kirschfink, M, Rother, U, Schrod, L, Womer, I. and Zilow, G (1987) Clin. Exp. Immunol **68**, 703–711

28 DiScipio, R G (1981) Biochem. J. **199**, 485–486

29 Daoudaki, M E, Becherer, J D and Lambris, J. D (1988) J Immunol **140**, 1577–1580

30 Higgins, J M, Wiedemann, H., Timpl, R and Reid, K B (1995) J Immunol **155**, 5777–5785

31 Pangburn, M K (1989) J Immunol **142**, 202–207

32 Junker, A, Baatrup, G, Svehag, S E, Wang, P, Holmstrom, E, Sturfelt, G and Sjoholm, A G (1998) Scand J Immunol **47**, 481–486

33 Kazatchkine, M D, Fearon, D T and Austen, K F (1979) J Immunol **122**, 75–81

34 Schwaeble, W J. and Reid, K. B (1999) Immunol Today **20**, 17–21

35 Fishelson, Z, Horstmann, R. D. and Muller-Eberhard, H J (1987) J Immunol **138**, 3392–3395

36 Pryzdial, E L and Isenman, D E (1988) J. Biol. Chem. **263**, 1733–1738

37 Kinoshita, T, Takata, Y, Kozono, H, Takeda, J, Hong, K S and Inoue, K (1988) J Immunol **141**, 3895–3901

38 Rawal, N and Pangburn, M K (1998) J. Biol Chem **273**, 16828–16835

Received 2 November 1999/24 March 2000, accepted 18 April 2000

Biochem J (2000) **349**, 225–230 (Printed in Great Britain)

Epidermal growth factor regulation of glutathione S-transferase gene expression in the rat is mediated by class Pi glutathione S-transferase enhancer I

Michi MATSUMOTO*[1], Masayoshi IMAGAWA†[2] and Yasunobu AOKI*

*Environmental Health Sciences Division, National Institute for Environmental Studies, 16-2 Onogawa, Tsukuba 305-0053, Japan, and †Graduate School of Pharmaceutical Sciences, Osaka University, 1-6 Yamada-oka, Suita 565-0871, Japan

---

Using chloramphenicol acetyltransferase assays we showed that epidermal growth factor (EGF), transforming growth factor α (TGFα), and 3,3′,4,4′,5-pentachlorobiphenyl (PenCB) induce class Pi glutathione S-transferase (GSTP1) in primary cultured rat liver parenchymal cells. GSTP1 enhancer I (GPEI), which is required for the stimulation of GSTP1 expression by PenCB, also mediates EGF and TGFα stimulation of GSTP1 gene expression However, hepatocyte growth factor and insulin did not stimulate GPEI-mediated gene expression On the other hand, the antioxidant reagents butylhydroxyanisole and *t*-butylhydroquinone, stimulated GPEI-mediated gene expression, but the level of GSTP1 mRNA was not elevated. Our observations suggest that EGF and TGFα induce GSTP1 by the same signal transduction pathway as PenCB. Since the sequence of GPEI is similar to that of the antioxidant responsive element (ARE), some factors which bind to ARE might play a role in GPEI-mediated gene expression.

Key words: antioxidant responsive element, coplanar polychlorinated biphenyl, chloramphenicol acetyltransferase assay, primary culture, transfection.

INTRODUCTION

Glutathione S-transferase is one of the Phase II detoxifying enzymes involved in the defense mechanism against xenobiotics [1,2]. Class Pi glutathione S-transferase (GSTP1), which is latent in normal rat liver, is a marker enzyme for pre-neoplastic hepatic foci and hepatocarcinomas [3,4]. Previously, we showed that GSTP1 was specifically induced in primary cultured rat liver parenchymal cells by 3,3′,4,4′,5-pentachlorobiphenyl (PenCB) [5], one of the most toxic coplanar polychlorinated biphenyl congeners [6,7].

Coplanar polychlorinated biphenyl congeners and related compounds (e.g. 2,3,7,8-tetrachlorodibenzo-*p*-dioxin) are dioxin-related compounds (dioxins), which exhibit various kinds of toxicity, such as hepatocarcinogenicity [6–8] and teratogenicity [9,10]. Recently, these compounds were recognized as disruptors of the endocrine system [11,12]. We have been interested in clarifying the signal transduction pathways which may play roles in the common mechanisms involved in the induction of various toxicities by dioxins A well known mechanism for gene expression induced by dioxins involves an aryl hydrocarbon receptor (AhR)-mediated pathway [13,14]. Dioxins taken up by cells bind to AhR (a member of the per AhR nuclear translocator Sim homology region family of ligand-dependent transactivating factors), and the ligand–receptor complex translocates into the nucleus and associates with AhR nuclear translocator factor (another member of the per AhR nuclear translocator Sim homology region family). The resulting heterodimer acts on a specific region, termed the xenobiotic-responsive element, in the 5′-flanking sequences of cytochrome P450 1A1, glutathione S-transferase A2 subunit and some other Phase II enzyme genes, causing their expression [15]. However, since the 5′-flanking sequence of the *GSTP1* gene does not contain an xenobiotic-responsive element [16,17], AhR may not act directly as a transactivating factor for *GSTP1* gene expression. As PenCB is difficult to metabolize [18], its metabolite probably does not stimulate gene expression. It seems that PenCB itself stimulates some gene expression, and this gene product stimulates *GSTP1* gene expression. We expected to find a novel signal transduction pathway activated by dioxins, and by identifying its components, to reveal the mechanism for the induction of GSTP1.

Previously we have shown PenCB- and epidermal growth factor (EGF)-induced expression of GSTP1 mRNA in primary cultured rat liver parenchymal cells [19]. It was expected that PenCB and EGF induce GSTP1 by a common mechanism. Using a chloramphenicol acetyltransferase (CAT) assay we identified an enhancer element, termed GSTP1 enhancer I (GPEI), in a 5′-upstream region which is required for GSTP1 induction in rat liver parenchymal cells by PenCB [20]. The region is located 2.5 kb upstream of the transcription initiation site of the *GSTP1* gene, and was originally identified as the element necessary for GSTP1 expression in hepatocarcinoma cells [21,22]. GPEI contains a dyad of PMA-responsive element (TRE)-like elements palindromically oriented with a 3 bp interval [21,23]. This TRE-like sequence has recently been recognized to be similar to the antioxidant responsive element (ARE) consensus or nuclear factor erythroid 2 consensus which is required for gene expression in response to antioxidant reagents such as butylhydroxyanisole (BHA) and *t*-butylhydroquinone (t-BHQ) [24–26]. We determined whether GPEI is required for GSTP1

Abbreviations used AhR, aryl hydrocarbon receptor, ARE, antioxidant responsive element, BHA, butylhydroxyanisole; t-BHQ, *t*-butylhydroquinone, CAT, chloramphenicol acetyltransferase, EGF, epidermal growth factor, β-Gal, *Escherichia coli* β-galactosidase, GPEI, class Pi glutathione S-transferase enhancer I, GPEIs, 38 bp core sequence of GPEI; GSTP1, rat class Pi glutathione S-transferase; HGF, hepatocyte growth factor, MAP, mitogen-activated protein, NQO1, NAD(P)H quinone oxidoreductase 1, Nrf2, nuclear factor erythroid 2-related factor 2, PenCB, 3,3′,4,4′,5-pentachlorobiphenyl, TGFα, transforming growth factor-α, TRE, PMA-responsive element, XRE, xenobiotic-responsive element

[1] To whom correspondence should be addressed (e-mail michi@nies go jp)

[2] Present address Faculty of Pharmaceutical Sciences, Nagoya City University, 3-1 Tanabe-dori, Mizuho-ku, Nagoya 467-8603, Japan

induction by EGF, other growth factors and antioxidant reagents, and report here that EGF and transforming growth factor α (TGFα) stimulate GPEI-mediated gene expression.

MATERIALS AND METHODS

Chemicals

GPEI/Δ–56kCAT plasmid, its synthetic fragment and mutants, and pGP5 were prepared as described previously in [21,23]. Vector pSVβGAL and TransFast® transfection reagent were purchased from Promega; mouse EGF and acetyl coenzyme A were from Wako Pure Chemicals (Tokyo, Japan); recombinant human hepatocyte growth factor (HGF) was from Becton Dickinson (Bedford, MA, U.S.A.), rat TGFα was from Calbiochem; insulin, BHA, dexamethasone, and cell culture media were from Sigma; t-BHQ was from Aldrich (Milwaukee, WI, U.S.A.); fetal bovine serum was from Life Technologies; 1-deoxy[dichloroacetyl-1-^{14}C]chloramphenicol was from Amersham International; and β-galactosidase reporter gene assay kit was from Boehringer Mannheim.

Preparation of monolayer cultures of rat liver parenchymal cells

Cell culture was performed essentially as described in [19]. Liver parenchymal cells were isolated from the liver of male Wistar rats by digestion with collagenase. Cells (2.5×10^6) in 3 ml of modified Williams medium E (pH 7.4), containing 10 mM sodium pyruvate, 100 units/ml penicillin, 100 μg/ml streptomycin, 0.25 μg/ml amphotericin B, 25 mM Hepes/NaOH buffer, 1 nM insulin, 100 nM dexamethasone, and 10% (v/v) fetal bovine serum, were plated in collagen-coated 60 mm plates. After the cells had been cultured for 4 h at 37 °C in air/CO$_2$ (19:1, v/v), the medium was changed to serum-free Williams medium E, containing 1 nM insulin, 100 nM dexamethasone, and 0.1 μg/ml aprotinin, and the cells were then incubated for 20 h.

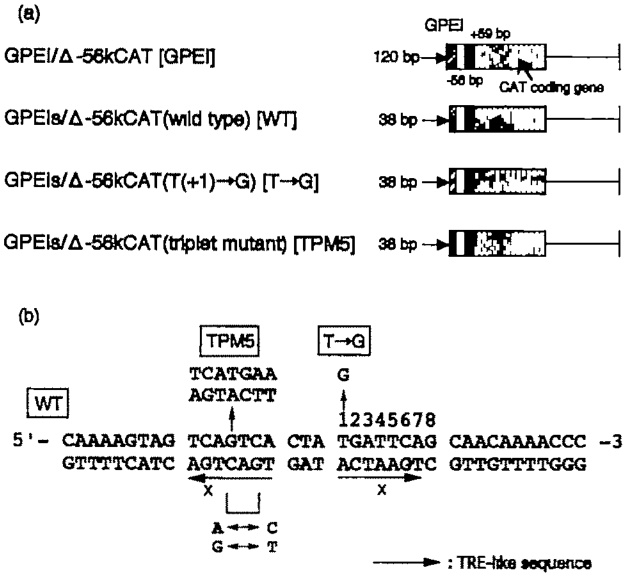
(a)
GPEI/Δ-56kCAT [GPEI]
GPEI
+69 bp
120 bp
-56 bp
CAT coding gene
GPEIs/Δ-56kCAT(wild type) [WT]
38 bp
GPEIs/Δ-56kCAT(T(+1)→G) [T→G]
38 bp
GPEIs/Δ-56kCAT(triplet mutant) [TPM5]
38 bp
(b)
TPM5
T→G
TCATGAA
AGTACTT
G
WT
12345678
5'- CAAAAGTAG TCAGTCA CTA TGATTCAG CAACAAAACCC -3'
GTTTTCATC AGTCAGT GAT ACTAAGTC GTTGTTTTGGG
X
X
A↔C
G↔T
: TRE-like sequence

Figure 1 Structures of GPEI and GPEIs–CAT fusion plasmid constructs

(**a**) Structures of the constructs used for transfections. The abbreviations in the square brackets show the plasmid DNA species used for the results shown in Figure 4 (**b**) Structures of GPEIs and its synthetic mutants [21] The TRE-like sequence is indicated by horizontal arrows The positions of nucleotides in the TRE-like sequence are numbered in accordance with Angel et al. [48]. The single point-mutated nucleotide is indicated by a vertical arrow TPM5 is the mutant in which the nucleotides as a consecutive triplet are changed to non-complementary ones (A↔C, G↔T) The TPM5 sequence is shown above the wild-type sequence The positions of nucleotides different from those of the consensus TRE are indicated by X

Construction of reporter gene plasmids

CAT fusion plasmids were constructed by the method of Sakai et al. [23]. GPEI fragments, a synthetic 38 bp fragment of the GPEI core, and its mutants were linked to Δ-56kCAT (an enhancer-negative plasmid that contains a GC box and a TATA box) by the method of Okuda et al. [21]. The structures of GPEI/Δ–56kCAT, GPEIs/Δ–56kCAT and its mutants are illustrated in Figure 1. pSVβGAL includes the SV40 promoter and enhancer [27] and *lacZ* [*Escherichia coli* β-galactosidase (β-Gal)] as a reporter gene.

DNA transfection and treatment with growth factors and antioxidant reagents

Plasmid transfections of monolayer cultures of rat liver parenchymal cells were performed by the lipofection method [28–30]. Cells were washed with 3 ml of Williams medium E without fetal bovine serum before lipofection. The plasmids were then transfected into the cells with 1 ml of Williams medium E without fetal bovine serum and 24 μl of TransFast reagent per 60 mm plate. CAT plasmids (6 μg) were transfected into the cells with 2 μg of pSVβGAL. After the cells were incubated for 1 h at 37 °C in air/CO$_2$ (19:1), 2 ml of serum-free Williams medium E, containing 10 mM sodium pyruvate, 100 units/ml penicillin, 100 μg/ml streptomycin, 0.25 μg/ml amphotericin B, 25 mM Hepes/NaOH buffer, 1 nM insulin, 0.1 μg/ml aprotinin, and 6 mM nicotinamide was added. Cells were treated with growth factors, BHA, t-BHQ or PenCB (which were added to the medium at the indicated concentrations as described in [19]), and incubated for an additional 36 h

Cells were harvested by scraping in PBS. Cell extracts were prepared by four cycles of freeze–thawing in 0.25 M Tris/HCl (pH 7.5), and their protein concentrations were determined by the procedure of Bradford [31].

Reporter gene assay

For CAT assays [32], the extracts were heated at 65 °C for 10 min, and the precipitates were removed by centrifugation at 15000 *g* for 5 min. The reaction mixtures (final volume 125 μl), containing cell extract, 210 mM Tris/HCl (pH 7.5), 11 kBq of 1-deoxy[^{14}C]chloramphenicol [33] and 80 nmol of acetyl-CoA, were incubated at 37 °C for 2 h. Reactions were terminated by the addition of 1 ml of cold ethyl acetate. The product (3-acetyl-1-deoxychloramphenicol) and unreacted substrate were extracted with ethyl acetate. After evaporation of the ethyl acetate, the residue was dissolved in 20 μl of ethyl acetate, and chromatographed on a thin layer plate (LK6D; Whatman, Maidstone, Kent, U.K.) with chloroform/methanol (94:6, v/v). The radioactivity of product and substrate was analysed using a Fuji BAS 2000 system (Fuji Photo, Tokyo, Japan). CAT activity was expressed as the ratio of radioactivity of the product to the total radioactivity. We usually use β-Gal activity to standardize CAT activity; however, the expression of plasmids that we used as controls previously [20] was stimulated in cultured liver parenchymal cells by treatment with EGF. Therefore CAT activity was standardized with protein concentration of the cell extract.

β-Gal activity in the cell extracts was measured as described previously [20].

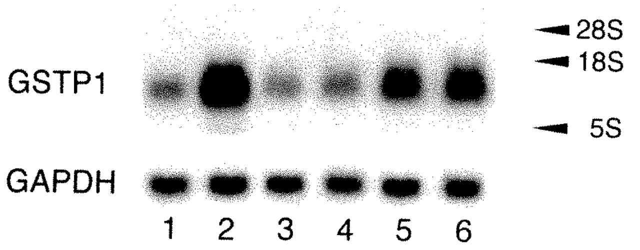

Figure 2 Induction of GSTP1 mRNA by PenCB, antioxidant reagents and growth factors

Rat liver parenchymal cells were treated with PenCB (100 nM), BHA (60 μM), t-BHQ (60 μM), EGF (10 ng/ml), or TGFα (10 ng/ml) for 36 h after being cultured for 25 h. GSTP1 and glyceraldehyde-3-phosphate dehydrogenase mRNA levels in the cells were determined by Northern-blot analysis. The lanes were loaded with 20 μg of RNA from the cells treated as follows: 1, control; 2, PenCB (100 nM); 3, BHA (60 μM); 4, t-BHQ (60 μM); 5, EGF (10 ng/ml); 6, TGFα (10 ng/ml). The positions of 28 S, 18 S, and 5 S ribosomal RNA are indicated at the right.

RNA preparation and Northern-blot analysis

When the level of GSTP1 mRNA induced in primary cultured rat liver parenchymal cells by a growth factor, BHA, t-BHQ, or PenCB was determined, untransfected cells were cultured in the presence of the inducing agent in the same manner as transfected cells. After the cells had been treated with the agent for 36 h, total RNA was extracted from the cells as described by Chomczynski and Sacchi [34]. A 20 μg portion of RNA was separated on a formaldehyde/1.2 % agarose gel containing 0.02 % ethidium bromide. After RNA was separated on the gel, the positions of ribosomal RNAs were visualized by UV illumination. The separated RNA was transferred to a nylon membrane (Amersham), and the membrane was incubated with a GSTP1 cDNA probe, which is an *Eco*RI–*Sal*I fragment of pGP5 [35], as described in [19,36]. The membrane was rehybridized with glyceraldehyde-3-phosphate dehydrogenase probe [19]. Radioactive bands on the membrane were detected by autoradiography.

RESULTS

Primary cultured rat liver parenchymal cells were treated with PenCB (100 nM), BHA (60 μM), t-BHQ (60 μM), EGF (10 ng/ml), or TGFα (10 ng/ml; a ligand of the EGF receptor) for 36 h, and the relative amounts of GSTP1 mRNA were determined by Northern blotting (Figure 2). Expression of GSTP1 mRNA was stimulated in the cells treated with EGF or TGFα, as well as with PenCB. However, it was not stimulated in the cells treated with BHA or t-BHQ.

We found previously that the expression of a CAT plasmid containing the −2.9 kb upstream region of the GSTP1 gene was stimulated in rat liver parenchymal cells by EGF as well as by PenCB [20]. Since this stimulation of CAT gene expression by PenCB was dependent on the GPEI element, we determined whether expression of the GPEI/Δ-56kCAT plasmid (120 bp region around GPEI core-ligated to Δ-56kCAT plasmid) was stimulated by EGF, as was shown with PenCB. As expected, the expression of GPEI/Δ-56kCAT was increased 1.73-fold in cells treated with EGF (Figure 3a), and the extent of the increase caused by EGF was similar to that caused by PenCB (1.52-fold) (results not shown). This is consistent with the similarity in the levels of GSTP1 mRNA after treatment with EGF or PenCB. EGF probably stimulates GPEI-mediated gene expression, suggesting that GPEI is required for the increase in GSTP1 expression caused by EGF.

To examine this possibility, CAT activities were determined in cells transfected with GPEIs/Δ-56kCAT plasmid [Figure 1, GPEI core (38 bp) conjugated to Δ-56kCAT plasmid] after treatment with EGF or TGFα (Figure 3b). CAT expression was

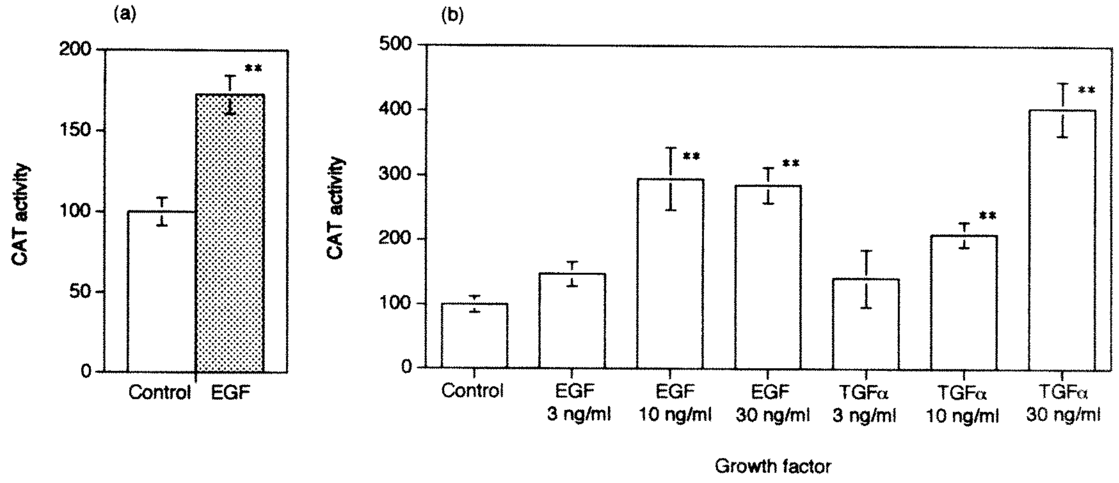

Figure 3 Effect of growth factors on the expression of *CAT* in primary cultured rat liver parenchymal cells transfected with GPEI or GPEIs (WT)–CAT construct

(**a**) Effect of EGF on the cells transfected with GPEI–CAT construct. Rat liver parenchymal cells were transfected with 6 μg of GPEI–CAT construct on each 60 mm plate, then treated with 10 ng/ml of EGF for 36 h. CAT activity was assayed and standardized with protein concentration in the cell extract. Each value is the mean ± S.E.M. for five separate experiments. Open bars show the CAT activity of the cells without EGF treatment (control); stippled bars show that of the cells treated with EGF. The activity in the cells without EGF treatment (control) is represented as 100. (**b**) Effect of the concentration of EGF and TGFα on the cells transfected with GPEIs–CAT construct. Rat liver parenchymal cells were transfected with 6 μg of GPEIs–CAT construct on each 60 mm plate, then treated with EGF or TGFα for 36 h. CAT activity was assayed and standardized as above. Each value is the mean ± S.E.M. for five separate experiments. The activity in the cells without a growth factor treatment (control) is represented as 100. $^{**}P < 0.01$ compared with control.

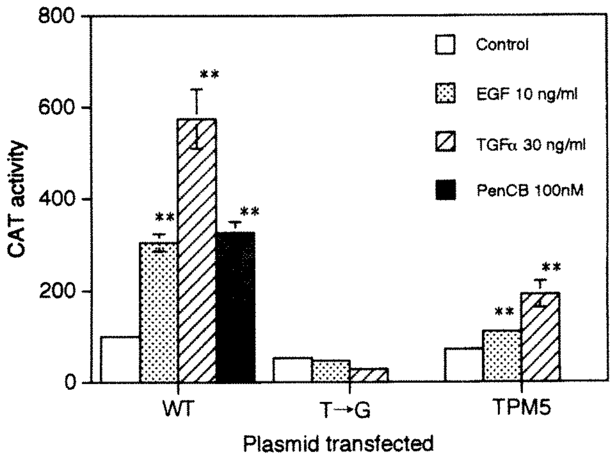

Figure 4 Effect of EGF and TGFα on the expression of *CAT* in primary cultured rat liver parenchymal cells transfected with wild-type GPEIs or mutant GPEIs–CAT constructs

Rat liver parenchymal cells were transfected with 6 μg of CAT construct on each 60 mm plate, then treated with PenCB, EGF, or TGFα for 36 h. The structures and abbreviated names of the plasmid constructs are shown in Figure 1. Each value is the mean ± S.E.M. for five separate experiments. The activity in the cells transfected with wild-type GPEIs plasmid (WT) without growth factor treatment is represented as 100. $^{**}P < 0.01$ compared with control.

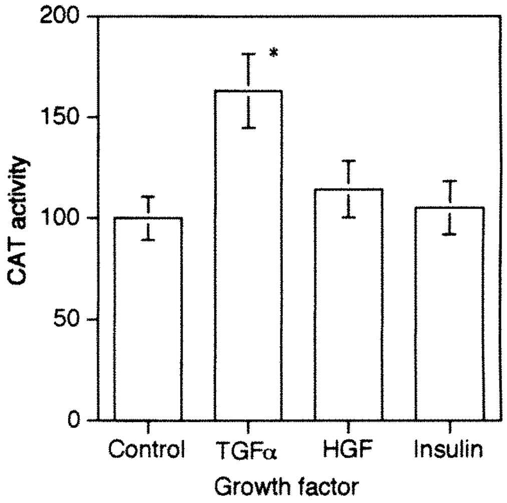

Figure 5 Effect of growth factors on the expression of *CAT* in primary cultured rat liver parenchymal cells transfected with wild-type GPEIs–CAT construct

Rat liver parenchymal cells were transfected with 6 μg of wild-type GPEIs–CAT construct on each 60 mm plate, then treated with a growth factor for 36 h. Each value is the mean ± S.E.M. for five separate experiments. The activity in the cells without growth factor treatment (control) is represented as 100. $^{*}P < 0.05$ compared with control.

stimulated in cells treated with EGF at concentrations of 10 and 30 ng/ml; TGFα also stimulated CAT expression in a dose-dependent manner at the same concentrations. At 30 ng/ml, TGFα stimulated CAT expression approx. 4-fold. In cells treated with 10 ng/ml EGF, CAT activity was the same as in cells treated with 100 nM PenCB (Figure 4, WT). The optimum concentration of EGF or TGFα for stimulating DNA synthesis in cultured liver parenchymal cells is 10–30 ng/ml, but 100 nM PenCB was not effective in this regard (results not shown).

These results show that the induction of GSTP1 in rat liver cells by EGF and TGFα is mediated by the GPEI enhancer element core. To confirm this, CAT assays were performed after treatment of cells with EGF (10 ng/ml) or TGFα (30 ng/ml), which had been transfected with the mutant plasmids of GPEIs/Δ-56kCAT (termed T → G and TPM5), which have a single point mutation in the downstream TRE-like sequence of GPEI and three consecutive point mutations in the upstream TRE-like sequence respectively (Figure 1). As shown in Figure 4, while CAT expression was stimulated by both EGF and TGFα in the cells transfected with the GPEIs/Δ-56kCAT (wild-type) plasmid, in the cells transfected with the T → G mutant plasmid CAT expression was not stimulated by either growth factor. However, in the cells transfected with the TPM5 mutant plasmid CAT expression was slightly stimulated.

CAT activities were also determined in rat liver parenchymal cells transfected with GPEIs/Δ-56kCAT (wild-type) plasmid and treated with HGF (20 ng/ml), which stimulates DNA synthesis in liver parenchymal cells [37], or with insulin (100 nM). CAT expression was stimulated in the cells transfected with GPEIs/Δ-56kCAT after treatment with TGFα, but not in those treated with HGF or insulin (Figure 5), indicating that GPEI-mediated gene expression is caused specifically by EGF and related ligands.

To examine the responsiveness of GPEI to antioxidant reagents, CAT activities were determined in rat liver cells transfected with GPEIs/Δ-56kCAT (wild-type) plasmid or its mutant plasmids (T → G, TPM5) and treated with BHA (60 μM) or t-BHQ (60 μM). At 60 μM of t-BHQ, GPEI-mediated gene expression was stimulated in HepG2 cells [26]. As shown in

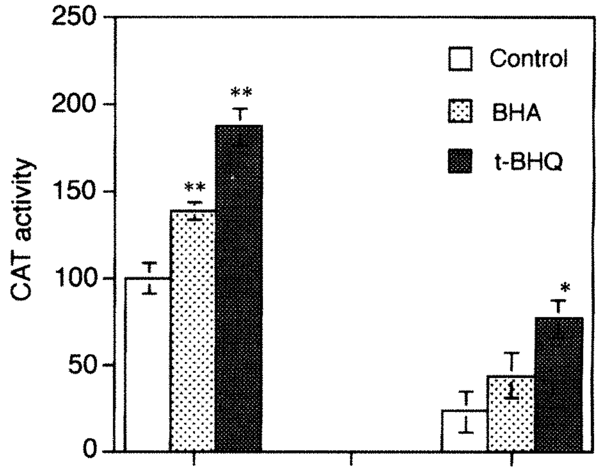

Figure 6 Effect of antioxidant reagents on the expression of *CAT* in primary cultured rat liver parenchymal cells transfected with wild-type GPEIs or mutant GPEIs–CAT constructs

Rat liver parenchymal cells were transfected with 6 μg of CAT construct on each 60 mm plate, then treated with BHA or t-BHQ for 36 h. The structures and abbreviated names of the plasmid constructs are shown in Figure 1. Each value is the mean ± S.E.M. for four separate experiments. Open bars show the CAT activity of the cells without antioxidant treatment (control); stippled bars of the cells treated with BHA (60 μM); shaded bars of the cells treated with t-BHQ (60 μM). The activity in the cells transfected with wild-type GPEIs plasmid (WT) without antioxidant treatment is represented as 100. $^{*}P < 0.05$, $^{**}P < 0.01$, compared with control.

Figure 6, CAT expression was also stimulated by both BHA and t-BHQ in rat liver cells transfected with GPEIs/Δ–56kCAT (wild-type) plasmid. The expression was stimulated more by t-BHQ than by BHA. In the cells transfected with the T → G mutant plasmid CAT expression was not stimulated by either antioxidant, but in the cells transfected with the TPM5 mutant plasmid CAT expression was slightly stimulated by both antioxidant reagents. This was similar to the results with EGF and TGFα.

DISCUSSION

We demonstrated that EGF and TGFα stimulate GPEI-mediated gene expression in primary cultured rat liver parenchymal cells, indicating that GPEI, an ARE-like enhancer element, is required for the stimulation of GSTP1 expression by EGF or TGFα. The GPEI enhancer element is located 2.5 kb upstream of the initiation site of the GSTP1 gene. Both EGF and TGFα (a ligand of the EGF receptor) activate the tyrosine kinase of the EGF receptor for potentiating signal transduction pathways, e.g. the MAP (mitogen-activated protein) kinase cascade [38]. GPEI-mediated gene expression might be stimulated by EGF through these signal transduction pathways.

We showed previously that the GPEI element is required for PenCB-induced expression of the *GSTP1* gene in liver parenchymal cells [20], as it is for GSTP1 expression in hepatocarcinoma. Since GPEI-mediated gene expression was stimulated by both EGF and PenCB, it is possible that PenCB mimics the effect of EGF by activating the same signal transduction pathway as EGF, resulting in the stimulation of the expression of the *GSTP1* gene. It is well known that EGF activates c-Jun, a transcription factor which binds to TRE as a heterodimer with c-Fos, through the phosphorylation of c-Jun by MAP kinases [39]. Previously, we showed that in cultured liver parenchymal cells phosphorylation of c-Jun was stimulated by PenCB or EGF treatment [40]. However, we have not clarified whether this stimulation by PenCB depends on stress-activated protein kinase, c-Jun N-terminal kinase, or other protein kinases. Activation of the ARE-protein complex by Phase II enzyme inducers is also regulated by signal transducing kinase cascades [2]. It has been reported that the extracellular signal-regulated protein kinase 2 kinase pathway is involved in the ARE-mediated induction of Phase II detoxifying enzymes by t-BHQ [41]. The signal transduction pathway for phosphorylating c-Jun through MAP kinases and related kinases seems to be the common pathway for stimulating GSTP1 expression by PenCB and EGF. c-Jun has been shown to regulate the expression of genes containing an ARE in co-ordination with transcription factors such as nuclear factor erythroid 2-related factor 2 (Nrf2) and c-Fos [42]. In particular, Itoh et al. reported that Nrf2 is essential for the expression of some Phase II drug-metabolizing enzymes containing an ARE [25]. Venugopal and Jaiswal [43] also showed that Nrf2 acts on the ARE of the human *NAD(P)H:quinone oxidoreductase* 1 (*NQO1*) gene along with some factors The human and rat NQO1 promoters have two AREs which are classed as 'ARE enhancers found in inverted-repeat orientation' [44]. The sequence of the GPEI is similar to those of the NQO1 promoters However, there are two nucleotide differences between the prototype ARE (5′-GTGACNNNGC-3′) [45] and the GPEI (5′-ATGATTCAGC-3′). The transcription factors such as c-Jun and Nrf2 may also contribute to GPEI-mediated gene expression by EGF, but it is not understood how *GSTP1* gene expression mediated by the GPEI element is regulated by EGF and PenCB, although the transcription factors involved in the expression of ARE-containing genes (e.g. NQO1) stimulated by xenobiotics have been examined extensively.

We have shown that the influence of EGF or TGFα on the expression of the CAT gene in the cells transfected with the mutant GPEIs/Δ–56kCAT plasmids was different from that of PenCB. While PenCB did not stimulate CAT activity in cells transfected with either of the mutant GPEIs plasmids, T → G and TPM5, EGF and TGFα did not stimulate CAT activity in the cells transfected with the T → G mutant plasmid, but did stimulate the activity a little in cells transfected with the TPM5 mutant plasmid. Since the single point mutation (T → G) is located in the downstream TRE-like sequence of GPEI, EGF seems to stimulate the expression of GSTP1 via the downstream TRE-like sequence, while both TRE-like sequences are required for the stimulation of GSTP1 expression by PenCB. In GPEI, the downstream TRE-like sequence is very close to a perfect TRE, but the upstream half-site is an imperfect TRE [22,44]. Both TRE-like sequences are required for full activity of GPEI; the downstream sequence is essential for GSTP1 expression. Therefore the T → G mutant plasmid is probably not responsive. On the other hand, the TPM5 mutant plasmid may be responsive to c-Jun because the downstream TRE-like sequence becomes a typical TRE. c-Jun might mediate the slightly stimulated CAT expression in the cells transfected with the TPM5 mutant plasmid

Since HGF or insulin did not stimulate GPEI-mediated CAT expression, EGF appears to be a growth factor which specifically effects the expression of genes containing a GPEI. We showed that EGF has the potential to activate the expression of the gene containing an ARE-like element as well as a TRE in its 5′-flanking sequence. Crosstalk between signal transduction pathways activated by EGF and an ARE might occur in liver parenchymal cells.

BHA and t-BHQ stimulated GPEI-mediated CAT expression. The effect of BHA or t-BHQ on CAT expression in the cells transfected with the GPEIs/Δ–56kCAT (wild-type) plasmid and its mutant plasmids was similar to that of EGF or TGFα. GPEI seems to be responsive to BHA or t-BHQ as well as to EGF. However, the level of GSTP1 mRNA was not elevated in the cells treated with BHA or t-BHQ. An additional pathway other than GPEI-mediated regulation may be required for elevation of GSTP1 mRNA levels by PenCB and EGF; however, BHA and t-BHQ seem to be unable to activate this additional pathway. For example, a silencer element is located in the 5′-flanking region of the *GSTP1* gene [21], and PenCB and EGF possibly abolish the effect of the silencer. Sherratt et al. showed that GSTP1 was induced in the livers of rats fed a diet containing 0.75% BHA for 14 days [46]. The expression of GSTP1 in rat liver could have been caused by a longer exposure to BHA than is the case in primary cultured liver cells.

As mentioned above, Nrf2 is thought to interact with c-Jun or the transcriptional factor, Maf [25], for the expression of ARE-containing genes. Recently, Nrf2 was shown to be located in the cytoplasm, associated with Keap1 factor which possibly binds to actin. This complex is translocated into the nucleus in response to the pro-oxidant, diethylmaleate, resulting in the expression of ARE-containing Phase II drug-metabolizing enzymes [47]. We have already shown that a signal transduction pathway including a protein kinase cascade is activated by PenCB as well as EGF for phosphorylating c-Jun [40]. Although the contribution of Nrf2 to the expression of the *GSTP1* gene is unclear, a signal transduction pathway activated by EGF or PenCB could activate the Nrf2/Keap1 system to induce the expression of GSTP1 and related ARE-containing genes Further studies are required to elucidate the mechanism by which the expression of GPEI or ARE-containing genes is regulated by EGF and PenCB.

We wish to thank Dr M Morita (NIES) for kindly donating PenCB We are also grateful to Dr C Tohyama (NIES) for his encouragement This work was supported in part by Grants-In-Aid for Scientific Research (C) from the Ministry of Education, Science, Sports and Culture of Japan.

REFERENCES

1 Ketterer, B, Meyer, D J and Clark, A. G (1988) in Glutathione Conjugation, Mechanism and Biological Significance (Sies, H and Ketterer, B, eds), pp 73–135, Academic Press, London

2 Hayes, J. D and Pulford, D J. (1995) Crit Rev. Biochem Mol Biol **30**, 445–600

3 Satoh, K, Kitahara, A, Soma, Y, Inaba, Y, Hatayama, I and Sato, K (1985) Proc Natl Acad Sci. U S A **82**, 3964–3968

4 Tsuchida, S and Sato, K. (1992) Crit. Rev. Biochem Mol Biol **27**, 337–384

5 Aoki, Y, Satoh, K, Sato, K and Suzuki, K. T (1992) Biochem J **281**, 539–543

6 Ahlborg, U G, Becking, G C, Birnbaum, L S, Brouwer, A, Derks, H J G M, Feeley, M, Golor, G, Hanberg, A, Larsen, J C et al. (1994) Chemosphere **28**, 1049–1067

7 Safe, S H. (1994) Crit Rev Toxicol **24**, 87–149

8 Kuratsune, M, Nakamura, Y, Ikeda, M and Hirohata, T (1987) Chemosphere **16**, 2085–2088

9 Couture, L A, Abbott, B D and Birnbaum, L S (1990) Teratology **42**, 619–627

10 Mayura, K, Spainhour, C B, Howie, L, Safe, S and Phillips, T D. (1993) Toxicology **77**, 123–131

11 Krishnan, V and Safe, S (1993) Toxicol Appl Pharmacol **120**, 55–61

12 Birnbaum, L S (1995) Toxicol. Lett **82–83**, 743–750

13 Hankinson, O (1995) Annu Rev Pharmacol Toxicol. **35**, 307–340

14 Schmidt, J V and Bradfield, C A (1996) Annu. Rev Cell Dev. Biol **12**, 55–89

15 Whitlock, Jr, J P, Chichester, C H, Bedgood, R. M, Okino, S. T, Ko, H P, Ma, Q, Dong, L, Li, H and Clarke-Ketzenberg, R (1997) Drug Metab Rev **29**, 1107–1127

16 Lusska, A, Shen, E. and Whitlock, Jr, J P. (1993) J Biol Chem **268**, 6575–6580

17 Yao, E F and Denison, M S (1992) Biochemistry **31**, 5060–5067

18 Koga, N, Beppu, M and Yoshimura, H (1990) J. Pharmacobio-Dyn **13**, 497–506

19 Aoki, Y, Matsumoto, M and Suzuki, K T (1993) FEBS Lett **333**, 114–118

20 Matsumoto, M, Imagawa, M and Aoki, Y (1999) Biol J **338**, 599–605

21 Okuda, A, Imagawa, M, Maeda, Y, Sakai, M and Muramatsu, M (1989) J Biol Chem **264**, 16919–16926

22 Okuda, A, Imagawa, M, Sakai, M and Muramatsu, M (1990) EMBO J **9**, 1131–1135

23 Sakai, M, Okuda, A. and Muramatsu, M (1988) Proc Natl. Acad Sci. U S A **85**, 9456–9460

24 Xie, T, Belinsky, M, Xu, Y and Jaiswal, A K (1995) J Biol Chem **270**, 6894–6900

25 Itoh, K, Chiba, T, Takahashi, S., Ishii, T, Igarashi, K, Katoh, Y., Oyake, T, Hayashi, N, Satoh, K, Hatayama, I et al (1997) Biochem Biophys. Res Commun **236**, 313–322

26 Favreau, L V and Pickett, C. B. (1995) J Biol Chem. **270**, 24468–24474

27 Subramani, S and Southern, P J (1983) Anal. Biochem **136**, 1–15

28 Felgner, P L., Gadek, T R, Holm, M, Roman, R, Chan, H. W, Wenz, M, Northrop, J. P, Ringold, G M and Danielsen, M (1987) Proc. Natl Acad Sci U S A. **84**, 7413–7417

29 Rippe, R. A., Brenner, D. A. and Leffert, H L (1990) Mol Cell Biol **10**, 689–695

30 Jarnagin, W R, Debs, R J, Wang, S S and Bissell, D M. (1992) Nucleic Acids Res **20**, 4205–4211

31 Bradford, M M (1976) Anal Biochem. **72**, 248–254

32 Gorman, C M, Moffat, L F and Howard, B H (1982) Mol Cell Biol **2**, 1044–1051

33 Murray, I A, Lewendon, A, Williams, J. A, Cullis, P M, Lashford, A G and Shaw, W V (1991) Nucleic Acids Res **19**, 6648

34 Chomczynski, P and Sacchi, N (1987) Anal Biochem. **162**, 156–159

35 Suguoka, Y, Kano, T, Okuda, A, Sakai, M, Kitagawa, T and Muramatsu, M (1985) Nucleic Acids Res **13**, 6049–6057

36 Morimura, S, Okuda, A, Sakai, M., Imagawa, M and Muramatsu, M (1992) Cell Growth Differ **3**, 685–691

37 Nakamura, T, Teramoto, H and Ichihara, A (1986) Proc Natl Acad Sci U S A **83**, 6489–6493

38 Angel, P and Karin, M (1991) Biochim Biophys Acta **1072**, 129–157

39 Kyriakis, J M, Banerjee, P, Nikolakaki, E, Dai, T, Rubie, E A, Ahmad, M F, Avruch, J and Woodgett, J R (1994) Nature (London) **369**, 156–160

40 Tanno, K and Aoki, Y (1996) Biochem J **313**, 863–866

41 Yu, R., Lei, W, Mandlekar, S, Weber, M J, Der, C J and Kong, A-N T (1999) J Biol Chem **274**, 27545–27552

42 Venugopal, R and Jaiswal, A K (1996) Proc Natl Acad. Sci U S A **93**, 14960–14965

43 Venugopal, R and Jaiswal, A K (1998) Oncogene **17**, 3145–3156

44 Hayes, J D, Ellis, E M, Neal, G E, Harrison, D J and Manson, M M (1999) Biochem Soc. Symp **64**, 141–168

45 Rushmore, T H, Morton, M R and Pickett, C B (1991) J Biol Chem **266**, 11632–11639

46 Sherratt, P J, Manson, M M., Thomson, A M, Hissink, E A M, Neal, G E, van Bladeren, P J., Green, T and Hayes, J D (1998) Biochem J **335**, 619–630

47 Itoh, K, Wakabayashi, N., Katoh, Y., Ishii, T, Igarashi, K, Engel, J D. and Yamamoto, M (1999) Genes Dev **13**, 76–86

48 Angel, P, Imagawa, M, Chiu, R, Stein, B, Imbra, R J, Rahmsdorf, H J, Jonat, C, Herrlich, P and Karin, M (1987) Cell **49**, 729–739

Received 22 November 1999/31 March 2000, accepted 18 April 2000

Low-density lipoprotein activates the small GTPases Rap1 and Ral in human platelets

Christian M. HACKENG*†[1], Barbara FRANKE*‡[1], Ingrid A. M. RELOU*, Gertie GORTER*, Johannes L. BOS‡, Herman J. M. VAN RIJN† and Jan-Willem N. AKKERMAN*[2]

*Department of Haematology, Institute for Biomembranes, University Medical Center Utrecht, P.O Box 85500, 3508 GA Utrecht, Heidelberglaan 100, 3584 CX Utrecht, The Netherlands, †Department of Clinical Chemistry, University Medical Center Utrecht, P O Box 85500, 3508 GA Utrecht, Heidelberglaan 100, 3584 CX Utrecht, The Netherlands, and ‡Laboratory for Physiological Chemistry and Centre for Biomedical Genetics, University Medical Center Utrecht, P O Box 85500, 3508 GA Utrecht, Heidelberglaan 100, 3584 CX Utrecht, The Netherlands

Physiological concentrations of low-density lipoprotein (LDL) sensitize blood platelets to α-thrombin- and collagen-induced secretion, and after prolonged contact trigger secretion independent of other agonists. Here we report that LDL activates the small GTPases Rap1 and Ral but not Ras, as assessed by specific precipitation of the GTP-bound enzymes. In unstirred suspensions, the inhibitor SB203580 blocks Rap1 activation by 60–70 %, suggesting activation via p38 mitogen-activated protein kinase and a second, unidentified route. Inhibitors of cyclooxygenase (indomethacin) and the thromboxane A_2 (TxA_2) receptor (SQ30741) induce complete inhibition, indicating that Rap1 activation is the result of TxA_2 formation. Stirring reveals a second, TxA_2-independent Rap1 activation, which correlates quantitatively with a slow induction of dense granule secretion. Both pathways are unaffected by inhibitors of ligand binding to integrin $\alpha_{IIb}\beta_3$. The results suggest that Rap1 and Ral, but not Ras, may take part in signalling routes initiated by LDL that initially enhance the sensitivity of platelets to other agonists and later trigger LDL-dependent secretion.

Key words: GTP, lipid oxidation, lipoproteins, thrombocyte, thromboxane.

INTRODUCTION

Physiological concentrations of low-density lipoprotein (LDL) increase the sensitivity of human platelets to agonist stimulation [1–4], but during 0–30 min contact with platelets LDL is not an independent inducer of shape change [4,5] and aggregation [3,4,6]. There is little insight into the mechanisms which respond to LDL. LDL receptors on platelets differ from the classical LDL receptors on hepatocytes, lymphocytes and fibroblasts [7]. Binding depends critically on intact lysine residues in LDL, suggesting that the protein moiety bears the signal-inducing elements [8]. Among the signalling steps activated by LDL are phosphoinositide turnover [3,5], Ca^{2+} mobilization [3,9], protein kinase C [5,10] and $\alpha_{IIb}\beta_3$-mediated outside-in signalling [10]. Concurrently, thromboxane A_2 (TxA_2) is formed, reflecting activation of cytosolic phospholipase A_2 ($cPLA_2$) [2,5,11]. Inhibition of this pathway reveals both TxA_2-dependent and TxA_2-independent sensitization by LDL [2]. During prolonged contact (2–4 h), LDL becomes an independent secretion-inducing agonist triggering release of dense granule contents independent of TxA_2 formation [11].

Human platelets contain several low-molecular-mass GTPases of the Ras family which are activated during stimulation [12–14]. These GTPases cycle between an active GTP-bound form and an inactive GDP-bound state, via reactions controlled by exchange factors and GTPase-activating proteins. Rap1 is abundantly expressed in platelets and accounts for 0.1 % of total platelet protein. It is approx. 50 % homologous to Ras, with the strongest similarity within the core effector domain. Rap1 is expressed as two isoforms, Rap1A and Rap1B, which are 95 % identical and differ predominantly in the C-terminal part. Human platelets contain predominantly the Rap1B isoform. In platelets stimulated by α-thrombin, collagen and platelet activating factor, Rap1 is activated within seconds, which critically depends on an increase in cytosolic Ca^{2+} [14]. Platelet inhibition by prostacyclin inactivates Rap1. Thus activation and inactivation of Rap1 closely follow the activation state of the platelet, suggesting that Rap1 contributes to the signalling mechanisms that control platelet functions.

The Ras-like GTPase Ral also exists as two isotypes, RalA and RalB [15]. It is strongly expressed in platelets, testes and brain [16–18]. In platelets, Ral and Rap1 are activated through similar pathways [12]. The small GTPase Ras is also activated in platelets, but this activation requires high concentrations of α-thrombin and TxA_2 analogue [12,13].

In the present study we investigated whether Ras, Rap1 and Ral were affected by LDL which would make them possible intermediates in the pathways that increase the sensitivity of platelets for secretion-inducing agonists, and after prolonged contact, make LDL an independent secretagogue. The active GTP-bound state of these GTPases was identified using activation-specific probes, based on the differential affinity of the GDP- and GTP-bound forms of the GTPases for their respective downstream effector molecules.

Abbreviations used BAPTA/AM, bis-(o-aminophenoxy)ethane-*N,N,N′,N′*-tetra-acetic acid tetrakis(acetoxymethyl ester), $cPLA_2$, cytosolic phospholipase A_2, ERK2, extracellular-signal-regulated protein kinase 2, LDL, low-density lipoprotein, LPA, 1-oleoyl-L-α-lysophosphatidic acid; MAPK, mitogen-activated protein kinase, TxA_2, thromboxane A_2

[1] These authors contributed equally to this work

[2] To whom correspondence should be addressed (e-mail J W N Akkerman@lab azu nl)

MATERIALS AND METHODS

Materials

Radiolabelled [5,6,8,9,11,12,14,15-^{3}H]arachidonic acid (specific radioactivity 5.5–8.5 TBq/mmol) and 5-hydroxy [side chain-2-^{14}C]tryptamine creatinine sulphate ([^{14}C] 5-hydroxytryptamine; specific activity 1.85 GBq/mmol) were from Amersham International. Silicagel 60 was from Merck, Darmstadt, Germany. RalA antibody was from Transduction Laboratories, Lexington, KY, U.S.A.; antibody 4-4B-3C against cPLA$_2$ and antibody C14 against extracellular-signal-regulated protein kinase 2 (ERK2), were from Santa Cruz Biotechnology, Santa Cruz, CA, U.S.A., and total- and dual-phosphorylated mitogen-activated protein kinase (p38^{MAPK}) antibodies were from New England Biolabs, Beverly, MA, U.S.A. The antibodies against Rap1, Ras and Rap1B were prepared in our own laboratory. 5,8,11,14-Eicosatetraynoic acid, human α-thrombin, indomethacin and 1-oleoyl-L-α-lysophosphatidic acid (LPA) were from Sigma. The inhibitor of the LPA receptor, *N*-palmitoyl-L-serine-phosphoric acid was from Biomol, Plymouth Meeting, PA, U.S.A. Iloprost was from Behring, Berlin, Germany; bisindolylmaleimide I was from Boehringer Mannheim, demineralized BSA was from Organon Teknika, Eppelheim, Germany; and bis-(*o*-aminophenoxy)ethane-*N*,*N*,*N*′,*N*′-tetra-acetic acid tetrakis(acetoxymethyl ester) (BAPTA/AM) was from Calbiochem (La Jolla, CA, U.S.A.). Fibrinogen-derived peptide GRGDS was kindly provided by Dr H. M. Verheij, department of Biochemistry, University of Utrecht. SQ30741 was from Bristol-Myers-Squibb (Maarssen, The Netherlands), and SB203580 was from Alexis Corporation (San Diego, CA, U.S.A.). The cDNA encoding Rap1B was a gift of Dr Veronique Pizon (Paris, France), and 2,2′-azobis(2-amidinopropane) dihydrochloride was a kind gift of Dr Wolfgang Sattler, Karl-Franzens University, Graz, Austria.

LDL isolation, lysine modification and oxidation

Fresh non-frozen plasma from four healthy subjects each containing less than 100 mg lipoprotein(a)/l was pooled and LDL (density range 1.019–1.063 kg/l) was isolated [10,19]. To prevent lipid modification and bacterial contamination, 0.25 mM PMSF, 0.2 mM thimerosal, 2 mM NaN$_3$ and 4 mM EDTA (final concentrations) were present during the first centrifugation. A control purification was carried out in the absence of thimerosal, which, if not fully removed, might contribute to the activating properties of LDL. Subsequent centrifugations were carried out in the absence of additives except for NaN$_3$ and EDTA; a final dialysis was done without these inhibitors. Further details have been described in [10,11]. The concentrations of LDL were expressed as g of apo B100 protein/l.

For modification of apo B100 lysines [20], LDL (20 g of apo B100/l) in 0.15 M NaCl, 0.01 % EDTA, was diluted with 0.3 M sodium borate buffer, pH 8.0 (2:1, v/v). Potassium cyanate (20 mg/mg of apo B100) was added and the mixture was incubated for 2 h at 35 °C. Excess reagent was removed by two dialysis steps against 0.15 M NaCl, 0.01 % EDTA (pH 7.0), for 12 h at 4 °C. LDL was oxidized with CuCl$_2$ [21] or 2,2′-azobis(2-amidinopropane) dihydrochloride [22]. Mildly oxidized LDL was prepared by incubation of 20 g/l of LDL with 100 μM CuCl$_2$ or 10 mM 2,2′-azobis(2-amidinopropane)dihydrochloride (2 h, 37 °C); oxidized LDL was prepared by incubation of the same amount of LDL with 750 μM CuCl$_2$ or 25 mM 2,2′-azobis(2-amidinopropane)dihydrochloride (16 h, 37 °C). Data for thiobarbituric acid-reactive substances for mildly oxidized LDL were 1.62±0.25, for oxidized LDL 5.28±3.34, and for native LDL 0.07±0.04 nmol/mg of apo B100 respectively.

Platelet isolation

Freshly drawn venous blood from healthy volunteers was collected with informed consent into 0.1 vol. of 130 mM trisodium citrate. Platelet-rich plasma was prepared by centrifugation (200 *g* for 15 min at 22 °C). Gel-filtered platelets were isolated by gel filtration through Sepharose 2B equilibrated in Ca^{2+}-free Tyrode's buffer and adjusted to 2×10^{11} platelets/l. Platelet suspensions were incubated with LDL or α-thrombin (control) at 37 °C without or with stirring (900 rev./min), as indicated.

Measurement of active GTPases and expression of recombinant GST–Rap1B

GTP-bound Rap1 was precipitated from gel-filtered platelets lysed in Ral buffer [12] with the GST-tagged Rap-binding domain of RalGDS bound to GSH–agarose beads (Sigma). GTP-bound Ral was precipitated with GST-tagged Ral-binding domain of RLIP76 [12]. Activated Ras was precipitated from platelets lysed in Ral buffer with GST-tagged Ras-binding domain of Raf1 [23]. The GTPases were identified by Western blotting with the appropriate antibodies [14]. To account for donor variation, different concentrations of recombinant GST–Rap1B were applied to PAGE and analysed densitometrically using ImageQuant software. A linear correlation was obtained between the amount of GST–Rap1B and densitometric intensities up to 7500 arbitrary units (results not shown), subsequent analysis was within this range. The cDNA encoding Rap1B was inserted into the pGEX-4T3 vector by restriction with *Sma*I and *Not*I. GST–Rap1B was expressed in *Escherichia coli* AD202 after induction with isopropyl β-D-thiogalactoside. After lysis of the bacteria, GST–Rap1B was bound to GSH–agarose beads and washed extensively. Protein concentrations were estimated by SDS/PAGE and Coomassie staining, with BSA as a standard.

Phosphorylation of cPLA$_2$, ERK2 and p38^{MAPK}

cPLA$_2$ phosphorylation [24] and ERK2 phosphorylation were measured by mobility shifts on SDS/PAGE, which accompanies phosphorylation of these proteins. Platelets were incubated with LDL, and samples were withdrawn and centrifuged (30 s, 9000 *g*). Pellets were suspended in Laemmli sample buffer, sheared through a needle, heated (5 min, 100 °C) and stored at −20 °C until analysis [24]. The running buffer for electrophoresis of cPLA$_2$ was pH 8.3, and for ERK2, pH 8.8. After separation, proteins were transferred to PVDF membranes by electroblotting. cPLA$_2$ was detected using the mouse monoclonal antibody 4-4B-3C, and ERK2 using the rabbit polyclonal antibody C14. Phosphorylated and total p38^{MAPK} were measured [24] using phosphoplus p38^{MAPK} (Thr^{180}/Tyr^{182}) or anti-p38^{MAPK} antibody for detection. For quantitative determinations, the density of the bands was analysed using ImageQuant software [24].

Analysis of [^{3}H]arachidonate release

Platelet-rich plasma was labelled with 0.01 μM [^{3}H]arachidonic acid for 60 min at 37 °C and incubated in the presence of 30 μM 5,8,11,14 eicosatetraynoic acid to prevent metabolism of released arachidonate [24]. Lipids were extracted according to Bligh and Dyer [25]. For separation of phospholipids, phosphatidic acid and free arachidonic acid, the mixture was chromatographed on Silica gel 60 at 22 °C. Spots were visualized with phosphomolybdic acid and the radioactivity measured. Release of arachidonic acid was expressed as percentage free [^{3}H]-arachidonate compared to total radioactivity.

Measurement of dense granule secretion

Platelet-rich plasma was incubated with 1 μM [^{14}C]5-hydroxytryptamine for 30 min at 37 °C followed by gel filtration. At different times, samples were collected in formaldehyde, centrifuged, and the supernatant was analysed for [^{14}C]5-hydroxytryptamine. Data were expressed as percentage of maximal secretion, as defined in [11].

Patients

Three unrelated patients with Glanzmann's thrombo-asthenia (designated Patient 1, 2 and 3) were studied and have been described in [10] The patients had a prolonged Simplate bleeding time (> 30 min; normal values < 8 min). Patient 1 suffered from a thrombocytopenia (72000 platelets/μl), and showed a faint signal for α_{IIb} and β_3 after two-dimensional electrophoresis of platelet-membrane lysates with subsequent silverstaining, as well as in lysates of ^{125}I-labelled platelets analysed by autoradiography. On FACS, the mean fluorescence of β_3-expressing cells was 0.3 % of that observed with normal platelets. Platelet fibrinogen was normal. Platelets from Patient 2 and Patient 3 were 0.7 and 0.2 % $\alpha_{IIb}\beta_3$-positive respectively.

Presentation of data

Data are expressed as means ± S.D. for the given number of observations n, and were analysed with the Student's t test for unpaired observations. Differences were considered significant at $P < 0.05$.

RESULTS

LDL activates the small GTPase Rap1 in human platelets

Unstirred platelet suspensions were incubated with LDL (1.2 g/l) or α-thrombin (0.1 units/ml) and GTP-bound Rap1 was precipitated with GST–RalGDS Rap-binding domain. Activation of Rap1 was observed 1–3 min after incubation with LDL (Figures 1A and 2B). This is relatively slow compared with α-thrombin, which activated Rap1 after approx. 5 s, and induced full activation within 30 s [14]. Figure 1(B) shows the time course of Rap1 activation by LDL and α-thrombin in platelets from five (LDL) or three (α-thrombin) different subjects. Activation of Rap1 by LDL started after 1–5 min (depending on the donor), was maximal at 5 min, and remained high for 1 h. A similar activation was observed with LDL prepared in the absence of thimerosal. Activation of Rap1 by α-thrombin was faster, showing a maximal response after 30 s. Figure 2(A) illustrates the dose-response relationship of the LDL-induced Rap1 activation after 10 min. Rap1 was activated at 0.7 g/l or more, reaching a maximum at approx. 1.2 g/l LDL. The maximal Rap1 activation by LDL (1 2 g/l, 10 min) was 69 ± 4 % of the activation induced by α-thrombin (0 1 units/ml, 1 min, $n = 3$), indicating that LDL is a slower and slightly weaker activator than α-thrombin. LDL preparations might become slightly oxidized during prolonged storage, resulting in formation of LPA [26] To investigate whether LPA contributed to the LDL-induced activation of Rap1, control experiments were carried out with LDL in the presence of N-palmitoyl-L-serine-phosphoric acid, an inhibitor of the LPA-receptor, and with LPA in the absence of LDL. As shown in Figure 2(B), this inhibitor did not change the effect of LDL, and LPA was unable to activate Rap1.

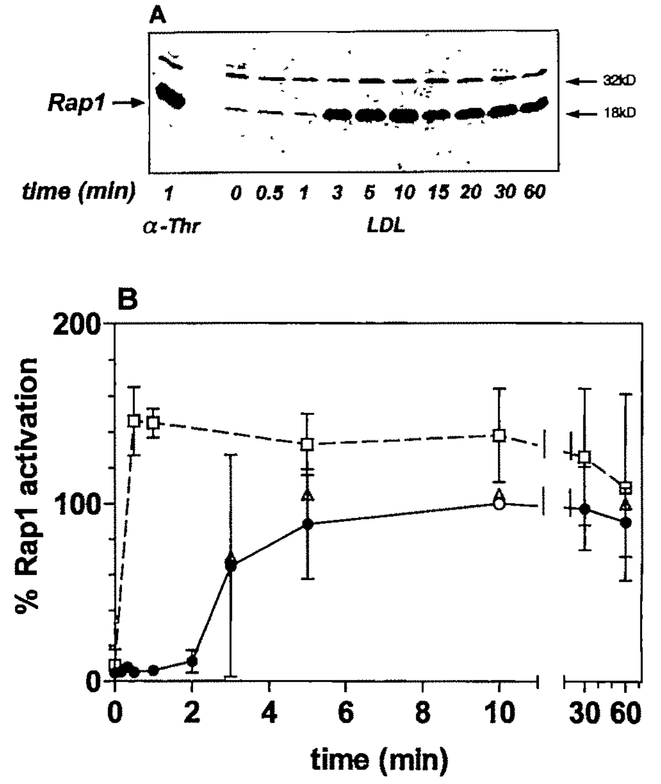

Figure 1 Time course of LDL-induced Rap1 activation

(**A**) Platelets were incubated with α-thrombin (α-Thr, 0 1 units/ml) and LDL (1 2 g/l) for the indicated time periods without stirring After lysis in Ral buffer, GTP-bound Rap1 was precipitated with GST–RBD, coupled to GSH–agarose beads, and identified by Western blotting using a polyclonal antibody against Rap1 The upper band on the immunoblot is caused by aspecific binding to the GSH–agarose beads Data are representative of 5 similar experiments (**B**) LDL- (●) and α-thrombin- (□) induced activation of Rap1 For each experiment, the band intensity at 10 min LDL-stimulation was set at 100% (○) $n \geqslant 3$, means ± S D, $P < 0\ 05$ for all LDL-incubations ≥ 2 min, and for all α-thrombin incubations ≥ 30 s compared to control Data indicated by (Δ) reflect Rap1 activation by LDL prepared in the absence of thimerosal ($n = 1$)

To get a better insight into the nature of the activating properties of LDL, studies were focused on the protein moiety (mainly apo B100) and the lipid components. Figure 3(A) shows that modification of lysine residues in apo B100, which abolishes specific LDL-platelet binding [8], blocked Rap1 activation. This indicates that the binding of the apo B100 moiety to the platelet is a crucial step in LDL signalling to Rap1 As LDL may activate cells via oxidation [26], the effect of mildly oxidized and oxidized LDL on Rap1 activation was studied. Figure 3(B) shows that with an increasing degree of CuCl$_2$-induced oxidation, the ability of LDL to activate Rap1 decreases. Similar results were obtained using 2,2′-azobis(2-amidinopropane) dihydrochloride-oxidized LDL (results not shown). Taken together, these results suggest that both protein and lipid moieties play an important role in Rap1 activation by LDL, and that LDL-induced Rap1 activation is not due to oxidative modification of the LDL preparation.

Recently [10], we reported that LDL enhances platelet sensitivity to collagen via a mechanism which involves exposure of ligand-binding sites on integrin $\alpha_{IIb}\beta_3$ (glycoprotein IIb-IIIa). To clarify the role of this complex in Rap1 activation, studies were repeated in platelets from patients with Glanzmann's thrombo-asthenia which lack integrin $\alpha_{IIb}\beta_3$ and are insensitive to LDL-induced sensitization [10]. The same activation was observed in platelets from healthy subjects (Figure 3C). Also, the presence of GRGDS, a peptide that mimicks part of the fibrinogen α-chain and inhibits fibrinogen binding [27] as well as the effect of LDL

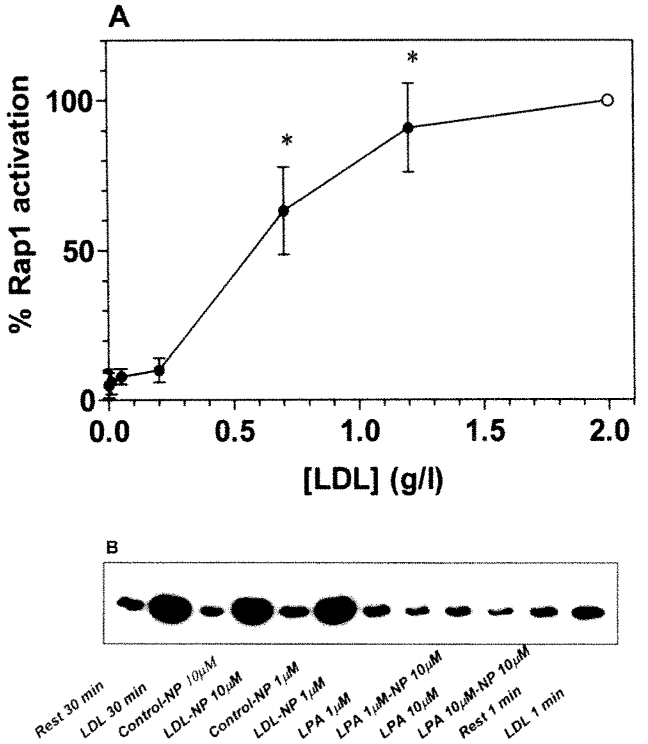

Figure 2 Dose-response relation for LDL-induced Rap1 activation

(**A**) Platelets were incubated with LDL at the indicated concentrations for 10 min without stirring (●). GTP–Rap1 was identified and band intensities were measured and expressed as percentage of the intensity at 2 g/l (○). $n = 3$; means ± S.D; $^*P < 0.05$ compared to control. (**B**) Control incubation for possible involvement of LPA in the LDL-induced activation of Rap1. Unstirred platelet suspensions were incubated without (Rest) and with 1.2 g/l LDL for 1 min and 30 min, and for 30 min with LPA in the indicated concentrations. Incubations with the inhibitor of the LPA-receptor *N*-palmitoyl-L-serine-phosphoric acid (5 min preincubation; [26]) are indicated by NP. Similar results were obtained in stirred suspensions (results not shown). Note that the blot is overexposed to reveal a possible weak activation by LPA.

on collagen-induced secretion [10], failed to change Rap1 activation by LDL (Table 1). Thus LDL-induced Rap1 activation occurred independently of integrin $\alpha_{IIb}\beta_3$.

LDL-induced Rap1 activation is mediated by TxA_2 formation

Earlier work showed that activation of Rap1 by α-thrombin depends critically on a rise in intracellular Ca^{2+} [14]. LDL-induced Rap1 activation was almost completely abolished by the Ca^{2+}-scavenger BAPTA/AM, illustrating a similar dependance on intracellular Ca^{2+} (Table 1). Since LDL induces TxA_2 formation in platelets [2,5,11], studies were performed in the presence of the cyclooxygenase inhibitor indomethacin and the thromboxane receptor antagonist SQ30741. Both inhibitors blocked Rap1 activation almost completely, suggesting that LDL signals towards Rap1 via formation of TxA_2. Thromboxane formation is the result of arachidonate release from membrane phospholipids by $cPLA_2$. Recent reports indicate that platelet $cPLA_2$ is phosphorylated and activated by the p38 mitogen-activated protein kinase ($p38^{MAPK}$). The role of this kinase in LDL-induced Rap1 activation was studied using the $p38^{MAPK}$ inhibitor SB203580 [28,29]. SB203580 binds covalently, or within close proximity, to the ATP-binding site of $p38^{MAPK}$ [30,31]. Preincubation of platelets with 10 μM inhibitor decreased the ability of LDL to activate Rap1 by approx. 70 %. In contrast, α-thrombin-induced Rap1-activation was not affected (results not shown). At 10 μM, SB203580 also inhibits kinases of the stress-activated protein kinase/c-Jun N-terminal kinases family [32]. The experiments were therefore repeated with 1 μM, which inhibits $p38^{MAPK}$ by approx. 90 % [28,29], and a similar inhibition was found compared with 10 μM (results not shown). Thus LDL activates $cPLA_2$ via $p38^{MAPK}$ and a second, unidentified pathway.

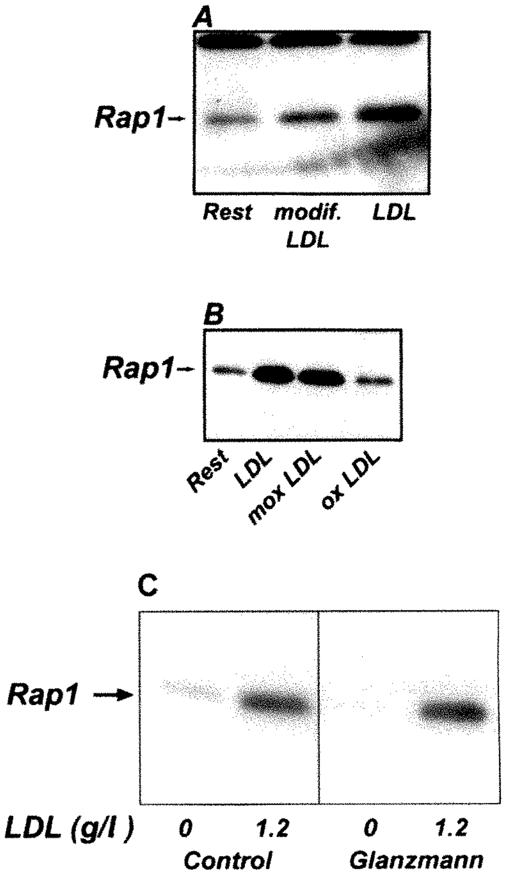

Figure 3 Effect of LDL-modification and platelet $\alpha_{IIb}\beta_3$-deficiency on Rap1 activation

(**A**) Platelets were stimulated with lysine-modified LDL or native LDL (1.2 g/l) for 10 min without stirring. (**B**) Platelets were incubated with 1.2 g/l LDL, mildly oxidized (mox) or oxidized (ox) LDL for 10 min. Shown here are the results of incubations with $CuCl_2$-oxidized LDL. Experiments with 2,2′-azobis(2-amidinopropane) dihydrochloride-oxidized material gave similar results. (**C**) Platelets from a control and a Glanzmann patient deficient in integrin $\alpha_{IIb}\beta_3$ (Glycoprotein IIb/IIIa) were incubated with vehicle or LDL (1.2 g/l). The data are from Patient 3 and are representative of the results from the two other patients

To compare the kinetics of $cPLA_2$ and Rap1 activation by LDL in more detail, enzyme phosphorylation identified by mobility shift on PAGE was compared with enzyme activation assessed by release of arachidonate [33]. $cPLA_2$ from resting platelets migrated as a single band reflecting the non-phosphorylated state (Figure 4A). LDL (1.2 g/l) induced a mobility shift starting at 1.5 min and leading to 60 % phosphorylation after 10 min. $cPLA_2$-phosphorylation was preceded by $p38^{MAPK}$-activation, which was detectable as phosphorylation of the protein after 10 s incubation with 0.1–1.0 g/l LDL (Figure 4B). The activation of $p38^{MAPK}$ was responsible for phosphorylation of $cPLA_2$, since SB203580 inhibited the mobility shift completely (results not shown). These findings are in contrast with an earlier report for collagen-

Table 1 Effect of inhibitors on LDL-induced Rap1 activation

Unstirred platelet suspensions were incubated with LDL in the absence and presence of GRGDS (100 μM, 1 min), BAPTA/AM (30 μM, 30 min), indomethacin (30 μM, 30 min), SQ30741 (400 nM, 15 min) or SB203580 (10 μM, 15 min), before addition of LDL (1.2 g/l, 10 min). In each experiment, the band intensity after LDL-incubation without inhibitors was set 100%. Data were corrected for background intensities without LDL, and expressed as means ± S.D., $n \geqslant 4$. $^*P < 0.05$ for the incubation with LDL.

Inhibitor	Rap1 activation (% of control)
None	100
GRGDS	92 ± 36
BAPTA/AM	8 ± 8*
Indomethacin	10 ± 9*
SQ30741	10 ± 10*
SB203580	32 ± 15*

Table 2 Influence of the p38^{MAPK} inhibitor SB203580 on arachidonic acid release

Unstirred [^{3}H]arachidonic acid-labelled platelets were stimulated with LDL (1.2 g/l, 10 min, 37 °C) or α-thrombin (1 unit/ml, 1 min, 37 °C) in the absence or presence of the p38^{MAPK} inhibitor SB203580, without stirring. 5,8,11,14-Eicosatetraynoic acid was added to prevent metabolism of released arachidonic acid. The release of arachidonic acid is expressed as percentage of total radioactivity (left column) and also compared between suspensions treated without and with SB203580 (right column). Values were corrected for radioactivity in resting platelets (2.7 ± 0.3%). Data are means ± S.D., $n = 5$. $^*P < 0.05$.

Stimulator	% Arachidonic acid release	% Of control
LDL	5.30 ± 1.77	100
LDL + SB203580	1.75 ± 1.09*	33 ± 21
α-Thrombin	8.00 ± 1.32	100
α-Thrombin + SB203580	8.23 ± 1.84	103 ± 23

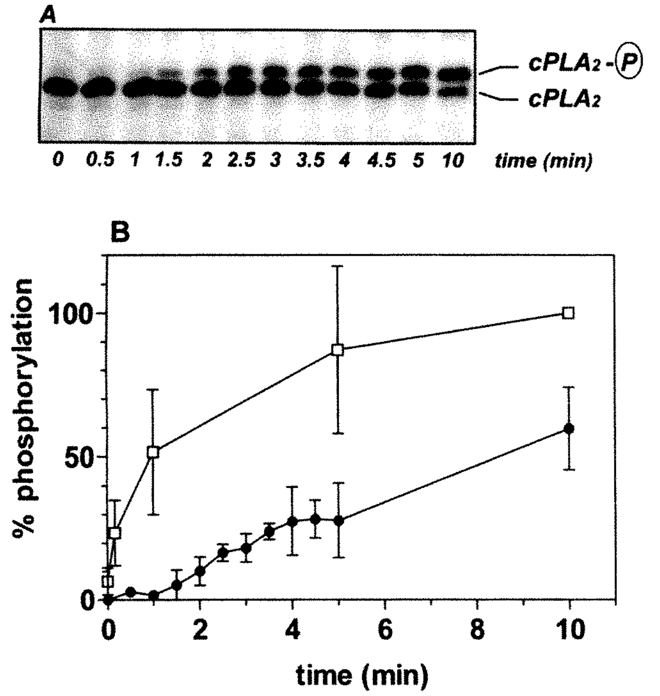

Figure 4 LDL induces phosphorylation of cPLA$_2$

(**A**) Platelets were incubated with LDL (1.2 g/l) for the indicated time without stirring. Samples were then centrifuged and pellets were dissolved in Laemmli sample buffer. cPLA$_2$ was identified by Western blotting with an antibody against cPLA$_2$. (**B**) Bands from cPLA$_2$ (●) and p38^{MAPK} phosphorylation (□) analyses of LDL-stimulated platelets were scanned and quantified using ImageQuant software. Phosphorylation of cPLA$_2$ was expressed as the intensity of the upper band compared to total cPLA$_2$. Activation of p38^{MAPK} was expressed as the percentage of LDL-induced phosphorylation after 10 min (1.2 g/l LDL, 37 °C, 100%). Analysis of p38^{MAPK} blots with an antibody recognizing both phosphorylated and unphosphorylated protein showed that protein concentration was similar in all samples (results not shown). $n \geqslant 3$; means ± S.D.

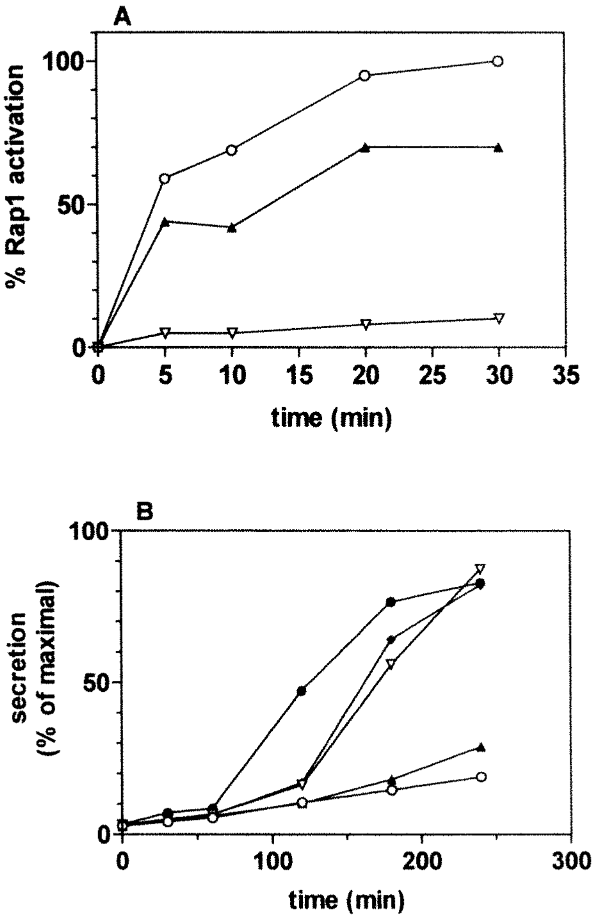

Figure 5 TxA$_2$-independent Rap1 activation by LDL

(**A**) Platelet suspensions without (○) and with (▲,▽) pretreatment with indomethacin (30 μM, 30 min) were stirred (900 rev./min) in the presence of 1.2 g/l LDL (○,▲) or buffer (▽) for 30 min, and at different time intervals GTP–Rap1 was analysed as indicated in Figure 1. (**B**) Indomethacin-treated platelet suspensions were stirred (900 rev./min) with different concentrations of LDL for 30 min and GTP–Rap1 was analysed. Concurrently, indomethacin-treated, [^{14}C]5-hydroxytryptamine-labelled platelets were stirred (900 rev./min) with different concentrations of LDL for 4 h, and at different time intervals dense granule secretion was measured using [^{14}C]5-hydroxytryptamine as a marker. LDL concentrations (g/l) and corresponding Rap1 activation (% of maximal, $n = 3$; means ± S.D.) were 0 (○, 3 ± 1%), 0.5 (▲, 24 ± 6%), 1.0 (▽, 33 ± 9%), 1.5 (◆, 41 ± 8%), and 2.0 (●, set at 100%). Data are representative for 2 similar experiments with equivalent results.

induced cPLA$_2$-phosphorylation [28]. Unstimulated platelets contained little free arachidonate, but incubation with LDL (1.2 g/l for 10 min) released approx. 5% of the incorporated [^{3}H]arachidonic acid (Table 2). SB203580 inhibited this release by more than 60%. α-Thrombin-induced arachidonate release was insensitive to SB203580, in accordance with a previous report [34]. Hence these data indicate that in unstirred suspensions LDL signals to cPLA$_2$ via p38^{MAPK} and a second,

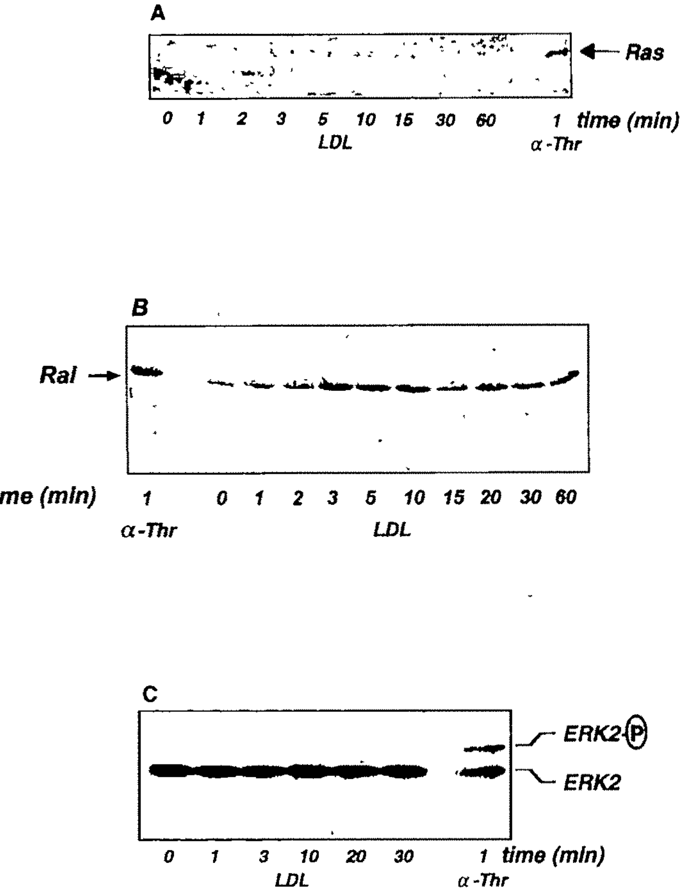

Figure 6 LDL activates the small GTPase Ral but not Ras or ERK2

(A) Platelets were incubated with α-thrombin (α-Thr, 1 unit/ml) and LDL (1.2 g/l) for the indicated time periods without stirring and lysed in Ral buffer. Activated Ras was precipitated with GST-tagged Raf1-Ras binding domain (GST–Raf1RBD) coupled to GSH–agarose beads, and identified by Western blotting using an antibody against Ras (the lower band on the immunoblot is caused by aspecific binding to the GSH–agarose beads). (B) Platelets were incubated with α-thrombin (α-Thr, 0.1 unit/ml) or LDL (1.2 g/l, 37 °C) for the indicated time periods without stirring, lysed in Ral buffer, and activated Ral was precipitated with GST–Ral-binding domain of RLIP76 coupled to GSH–agarose beads, and identified by Western blotting using an antibody against RalA. (C) Platelets were incubated with α-thrombin (α-Thr, 1 unit/ml) and LDL (1.2 g/l, 37 °C) as indicated. Samples were centrifuged and pellets were dissolved in Laemmli sample buffer. ERK2 phosphorylation was measured as a mobility shift by Western blotting with a polyclonal antibody against ERK2.

unidentified route, and that activation of cPLA$_2$ and formation of TxA$_2$ account for further Rap1 activation.

TxA$_2$-independent Rap1 activation

The observation that Rap1 activation fully depended on the formation of TxA$_2$ made it difficult to separate the roles of these molecules in LDL-induced sensitization. Earlier studies showed that the faster α-thrombin-induced secretion in LDL-treated platelets was only partly sensitive to inhibitors of TxA$_2$ formation or blockade of the TxA$_2$-receptor [2]. These conditions were therefore further explored in a search for a role for Rap1. When platelets were stirred, LDL induced a second, indomethacin-insensitive formation of GTP–Rap1 (Figure 5A). This activation was unchanged by inhibitors of ligand binding to integrin $\alpha_{IIb}\beta_3$ (95±7% compared with control), the protein kinase C inhibitor bisindolylmaleimide (110±8%), or the p38^{MAPK} inhibitor SB203580 (84±12%). The Ca^{2+}chelator BAPTA/AM (16±4%) and iloprost, which raises cAMP (6±2%; $n = 3$, $P < 0.05$), interfered with the formation of GTP–Rap1.

To investigate whether the TxA$_2$-independent Rap1 activation played a role in the secretion response, GTP–Rap1 and [^{14}C]5-hydroxytryptamine secretion were compared in stirred, indomethacin-treated platelets (Figure 5B). Although 0.5 g/l already induced 50% Rap1 activation without affecting secretion, a stepwise further increase to 2 g/l was accompanied by a dose-dependent enhancement of 5-hydroxytryptamine release. This suggests that the formation of GTP–Rap1 might play a role in the slow release of dense granule contents induced during prolonged contact with LDL.

LDL activates the small GTPase Ral but not Ras

Apart from Rap1, platelets contain the small GTPases Ral and Ras [12]. Figure 6(A,B) illustrates that Ral is activated by LDL (1.2 g/l), reaching a maximum between 3 and 10 min. Formation of GTP–Ral showed the same sensitivity to indomethacin, SB203580 and SQ30741 as formation of GTP–Rap1 (results not shown). In contrast, no significant activation of Ras was observed in LDL-treated platelets. A downstream element of Ras signalling is the serine/threonine kinase ERK2 (p42^{MAPK}) [35]. Earlier studies have shown that phosphorylation of ERK2 is a reflection of enzyme activation, and leads to a mobility shift on SDS/PAGE [36]. Figure 6(C) shows that in contrast to α-thrombin (1 unit/ml, 1 min), LDL is unable to activate ERK2 in accordance with the absence of Ras activation.

DISCUSSION

The present study shows that an LDL concentration within the physiological range (0.26–1.23 g apo B100/l) [37] activates the small GTPase Rap1, reaching maximal activation within 5 min. The activation of Rap1 by LDL probably involves both the protein and the lipid moieties of the particle. The role of apo B100 is illustrated by the loss of LDL activity after lysine-modification. The role of lipids is illustrated by the decrease in agonist activity after extensive lipid oxidation. The latter finding contrasts with results showing that mildly oxidized LDL, but not native LDL, initiates platelet shape change via formation of LPA, a product also found in atherosclerotic lesions [26].

In unstirred platelet suspensions, LDL triggered the formation of GTP–Rap1 entirely via activation of p38^{MAPK}, cPLA$_2$, and TxA$_2$ formation, and further activation via the TxA$_2$-receptor. Thus is was not possible to separate a role of Rap1 from the well known activating properties of TxA$_2$. Earlier work had shown that the secretion induced by α-thrombin in stirred platelet suspensions was faster following preincubation with LDL, and that the effect of LDL could only be inhibited in part by indomethacin or the TxA$_2$-receptor antagonist, SQ30741 [2]. The present data illustrate that stirring also introduces a TxA$_2$-independent Rap1 activation. This second pathway of Rap1 activation is followed by a slow secretion of dense granule contents. Studies with different LDL concentrations reveal that formation of GTP–Rap1 and secretion show the same dose-response relationship, suggesting, but not proving, that active Rap1 might be an intermediate in this TxA$_2$-independent secretion.

A previous study revealed an important role for platelet integrin $\alpha_{IIb}\beta_3$ in LDL-induced sensitization [10]. The sensitization was absent in normal platelets with blocked ligand-induced outside-in signalling, as well as in $\alpha_{IIb}\beta_3$-deficient platelets. The present data show that Rap1 activation by LDL occurs normally in the absence of integrin signalling, indicating that it is not a downstream event of $\alpha_{IIb}\beta_3$. Thus Rap1 may either function in pathways that control integrin activation or is independent of $\alpha_{IIb}\beta_3$. Control studies show that LDL-induced fibrinogen binding, as detected in FACS studies [10], is completely abolished by indomethacin, and the role of Rap1 in integrin regulation therefore remains uncertain (results not shown)

Both the TxA_2-dependent and the TxA_2-independent Rap1 activation are inhibited by the Ca^{2+} chelator BAPTA/AM, and by agents that raise cAMP. There are several steps in the TxA_2-dependent route both upstream and downstream of the TxA_2 receptor that involve Ca^{2+}, e.g. $cPLA_2$ and the initial activation of $p38^{MAPK}$ is extremely sensitive to cAMP [24]. The nature of the TxA_2-independent Rap1 activation remains uncertain but may involve p125 focal adhesion kinase, which is phosphorylated by LDL with little interference by indomethacin [38].

Platelet $cPLA_2$ associates with the membrane via its Ca^{2+}-dependent lipid-binding domain located at the N-terminus in a Ca^{2+}-dependent manner [39], and is phosphorylated at Ser^{505} and Ser^{727} by various agonists [40]. This finding agrees with the strong phosphorylation of $cPLA_2$ induced by LDL, which in turn depends on activation of $p38^{MAPK}$. An inhibitor of this kinase (SB203580) strongly decreased $cPLA_2$-phosphorylation and arachidonic acid release, as well as Rap1 activation by LDL. Therefore in LDL-induced signal generation, phosphorylation and activation of PLA_2 are coupled processes, leading to a release of approx. 6 % of total [^{3}H]arachidonic acid in 10 min. In contrast, α-thrombin-induced (1 unit/ml) arachidonate release is rapid (approx. 8 % in 1 min) and apparently independent of $p38^{MAPK}$-mediated phosphorylation. The same insensitivity for $p38^{MAPK}$ inhibition is observed for α-thrombin-induced Rap1 activation. Recent observations in PC12 cells suggest that activation of Rap1 may result in activation of ERK2 via B-raf [41]. Our results in LDL-stimulated platelets show that Rap1 activation is not accompanied by activation of ERK2. Apart from Rap1, the small GTPase Ral is also activated upon platelet stimulation with LDL. Activated Ral might play a role in cytoskeletal rearrangements; it has recently been shown that Ral can play a role in filopodia formation upstream of the filamin ABP280, a protein responsible for crosslinking of actin filaments [42]. Another putative effector protein of Ral, RLIP76, is a GTPase-activating protein for CDC42, a member of the Rho/Rac family. CDC42 is responsible for rearrangement of the actin cytoskeleton leading to focal contact formation and filopodia extension. Ral might also contribute to regulation of phospholipase D. In v-Src transformed cells, phospholipase D activity was precipitated with Ral, an interaction that was disturbed after deletion of an N-terminal region of Ral. Overexpression of Ral potentiated phospholipase D-activity, whereas the expression of a dominant negative mutant of Ral was inhibitory [16] The association of Ral with another small GTPase, Arf, seems necessary to render Ral able to stimulate phospholipase D activity.

In fibroblasts, Ral activation critically depends on Ras [43]. However, Wolthuis et al [12] recently reported the concurrent activation of Ral and Rap1, rather than Ras, in platelets stimulated by different agonists, suggesting that Ral might be a signalling molecule downstream of Rap1 in these cells. This also follows from our results showing that Rap1 and Ral are regulated by the same upstream signalling components activated by LDL. Indeed, Rap1 activates Ral in cotransfection experiments with the Ral exchange factor Rlf in Cos7 cells [44]. Therefore Rap1 may have taken over the function of Ras in platelets. In accordance with the absence of Ras activation by LDL, no activation of the downstream element of Ras signalling, ERK2, is observed, indicating that both Ras and ERK do not have a function in LDL-induced platelet sensitization Ras is activated in platelets stimulated by high concentrations of α-thrombin and TxA_2 analogue. One would therefore expect a similar activation of Ras in LDL-treated platelets, since this leads to TxA_2 formation and TxA_2-dependent Rap1 activation. The fact that this does not occur might be due to the relatively weak activating properties of LDL which, in contrast to α-thrombin, requires 3 min or more before activation of signalling sequences can be identified.

We thank D Rademakers and M. W. Pladet for technical assistance This study was supported by the Netherlands Organization for Scientific Research, the Netherlands Heart Foundation (grants 940.50 102/900 526.094 and 94 136) and the University Hospital Utrecht. The support by the Netherlands Thrombosis Foundation is gratefully acknowledged.

REFERENCES

1 Van Willigen, G , Gorter, G and Akkerman, J W N (1994) LDLs increase the exposure of fibrinogen binding sites on platelets and secretion of dense granules Arterioscler Thromb **14**, 41–46

2 Surya, I I , Gorter, G., Mommersteeg, M and Akkerman, J W N (1992) Enhancement of platelet functions by low density lipoproteins Biochim Biophys Acta **1165**, 19–26

3 Nofer, J R , Tepel, M., Kehrel, B , Wierwille, S , Walter, M , Seedorf, U., Zidek, W and Assmann, G (1997) Low-density lipoproteins inhibit the Na^+/H^+ antiport in human platelets A novel mechanism enhancing platelet activity in hypercholesterolemia Circulation **95**, 1370–1377

4 Weidtmann, A , Scherthe, R , Hrboticky, N , Pietsch, A , Lorenz, R and Siess, W (1995) Mildly oxidized LDL induces platelet aggregation through activation of phospholipase A_2 Arterioscler Thromb Vasc Biol. **15**, 1131–1138

5 Andrews, H E , Aitken, J W , Hassall, D G , Skinner, V O and Bruckdorfer, K R (1987) Intracellular mechanisms in the activation of human platelets by low-density lipoproteins Biochem J **242**, 559–564

6 Ardlie, N G , Selley, M L and Simons, L A (1989) Platelet activation by oxidatively modified low density lipoproteins Atherosclerosis **76**, 117–124

7 Pedreno, J , de Castellarnau, C , Cullare, C , Sanchez, J , Gomez Gerique, J , Ordonez Llanos, J and Gonzalez Sastre, F (1992) LDL binding sites on platelets differ from the 'classical' receptor of nucleated cells Arterioscler Thromb **12**, 1353–1362

8 Aviram, M., Brook, J G , Lees, A M and Lees, R S (1981) Low density lipoprotein binding to human platelets role of charge and of specific amino acids Biochem Biophys Res Commun **99**, 308–318

9 Dunn, R. C , Schachter, M , Miles, C. M , Feher, M D , Tranter, P R , Bruckdorfer, K R and Sever, P S (1998) Low-density lipoproteins increase intracellular calcium in aequorin-loaded platelets FEBS Lett **238**, 357–360

10 Hackeng, C M , Huigsloot, M , Pladet, M W , Nieuwenhuis, H K , van Rijn, H J M and Akkerman, J W N (1999) LDL enhances platelet secretion via integrin $\alpha_{IIb}\beta_3$-mediated signaling Arterioscler Thromb Vasc Biol **19**, 239–247

11 Surya, I I , Gorter, G and Akkerman, J W N (1992) Arachidonate transfer between platelets and lipoproteins Thromb Haemostasis **68**, 719–726

12 Wolthuis, R M F , Franke, B , van Triest, M , Bauer, B , Cool, R H , Camonis, J H , Akkerman, J W N and Bos, J L (1998) Activation of the small GTPase Ral in platelets. Mol Cell Biol **18**, 2486–2491

13 Shock, D D , He, K , Wencel Drake, J D and Parise, L V (1997) Ras activation in platelets after stimulation of the thrombin receptor, thromboxane A_2 receptor or protein kinase C Biochem J **321**, 525–530

14 Franke, B , Akkerman, J W N and Bos, J L (1997) Rapid Ca^{2+}-mediated activation of Rap1 in human platelets EMBO J **16**, 252–259

15 Mark, B L , Jilkina, O and Bhullar, R P (1996) Association of Ral GTP-binding protein with human platelet dense granules Biochem Biophys Res Commun **225**, 40–46

16 Jiang, H , Luo, J Q , Urano, T , Frankel, P , Lu, Z , Foster, D A and Feig, L A (1995) Involvement of Ral GTPase in v-Src-induced phospholipase D activation Nature (London) **378**, 409–412

17 Bhullar, R P , Chardin, P and Haslam, R J (1990) Identification of multiple ral gene products in human platelets that account for some but not all of the platelet G_n-proteins FEBS Lett **260**, 48–52

18 Olofsson, B , Chardin, P , Touchot, N , Zahraoui, A and Tavitian, A (1988) Expression of the ras-related ralA, rho12 and rab genes in adult mouse tissues Oncogene **3**, 231–234

19 Havel, R J, Eder, H. A and Bragdon, J. H (1955) The distribution and chemical composition of ultracentrifugally separated lipoproteins in human serum J Clin Invest **34**, 1345–1353

20 Weisgraber, K H, Innerarity, T L and Mahley, R W (1978) Role of lysine residues of plasma lipoproteins in high affinity binding to cell surface receptors on human fibroblasts J Biol Chem **253**, 9053–9062

21 Kleinveld, H A, Hak Lemmers, H L, Stalenhoef, A F and Demacker, P N (1992) Improved measurement of low-density-lipoprotein susceptibility to copper-induced oxidation application of a short procedure for isolating low-density lipoprotein Clin Chem **38**, 2066–2072

22 Sattler, W, Mohr, D and Stocker, R (1994) Rapid isolation of lipoproteins and assessment of their peroxidation by high-performance liquid chromatography postcolumn chemiluminescence Methods Enzymol **233**, 469–489

23 de Rooij, J. and Bos, J. L (1997) Minimal Ras-binding domain of Raf1 can be used as an activation-specific probe for Ras Oncogene **14**, 623–625

24 Hackeng, C M., Relou, I A M., Pladet, M. W., Gorter, G., van Rijn, H. J M and Akkerman, J W N (1999) Early platelet activation by Low Density Lipoprotein via p38^{MAP} Kinase Thromb Haemost **82**, 1749–1756

25 Bligh, E G and Dyer, W J (1959) A rapid method of total lipid extraction and purification Can J Biochem Physiol **37**, 911–918

26 Siess, W, Zangl, K J, Essler, M, Bauer, M, Brandl, R, Corrinth, C, Bittman, R, Tigyi, G and Aepfelbacher, M (1999) Lysophosphatidic acid mediates the rapid activation of platelets and endothelial cells by mildly oxidized low density lipoprotein and accumulates in human atherosclerotic lesions Proc Natl. Acad Sci U.S.A **96**, 6931–6936

27 Shattil, S J (1988) Platelet membrane receptors molecular biology, immunology, biochemistry and pathology (Jamieson, G A. ed), pp 345–380, Alan R Liss, Inc, New York

28 Borsch-Haubold, A. G, Kramer, R M and Watson, S P (1997) Phosphorylation and activation of cytosolic phospholipase A_2 by 38-kDa mitogen-activated protein kinase in collagen-stimulated human platelets Eur. J. Biochem **245**, 751–759

29 Saklatvala, J, Rawlinson, L, Waller, R J, Sarsfield, S, Lee, J C., Morton, L F., Barnes, M J and Farndale, R W (1996) Role for p38 mitogen-activated protein kinase in platelet aggregation caused by collagen or a thromboxane analogue J Biol Chem **271**, 6586–6589

30 Tong, L, Pav, S, White, D M, Rogers, S, Crane, K M, Cywin, C L, Brown, M L and Pargellis, C A (1997) A highly specific inhibitor of human p38 MAP kinase binds in the ATP pocket Nat Struct Biol **4**, 311–316

31 Young, P R, McLaughlin, M M, Kumar, S, Kassis, S, Doyle, M L, McNulty, D, Gallagher, T. F., Fisher, S, McDonnell, P C, Carr, S A et al (1997) Pyridinyl imidazole inhibitors of p38 mitogen-activated protein kinase bind in the ATP site J. Biol Chem **272**, 12116–12121

32 Clerk, A. and Sugden, P H (1998) The p38-MAPK inhibitor, SB203580, inhibits cardiac stress-activated protein kinases/c-Jun N-terminal kinases (SAPKs/JNKs). FEBS Lett **426**, 93–96

33 Borsch-Haubold, A G, Kramer, R M and Watson, S P (1995) Cytosolic phospholipase A_2 is phosphorylated in collagen- and thrombin-stimulated human platelets independent of protein kinase C and mitogen-activated protein kinase J Biol Chem **270**, 25885–25892

34 Kramer, R M, Roberts, E F., Um, S L, Borsch-Haubold, A G, Watson, S P., Fisher, M J and Jakubowski, J A (1996) P38 mitogen-activated protein kinase phosphorylates cytosolic phospholipase A_2 (cPLA$_2$) in thrombin-stimulated platelets Evidence that proline-directed phosphorylation is not required for mobilization of arachidonic acid by cPLA$_2$ J Biol Chem **271**, 27723–27729

35 Howe, L R, Leevers, S J, Gómez, N, Nakielny, S, Cohen, P and Marschall, C J (1992) Activation of the MAP Kinase pathway by the protein kinase Raf Cell **71**, 335–342

36 Kramer, R M, Roberts, E F, Hyslop, P A, Utterback, B G., Hui, K Y and Jakubowski, J A (1995) Differential activation of cytosolic phospholipase A_2 (cPLA$_2$) by thrombin and thrombin receptor agonist peptide in human platelets. Evidence for activation of cPLA$_2$ independent of the mitogen-activated protein kinases ERK1/2 J Biol. Chem **270**, 14816–14823

37 Jacobs, D S (1996) Laboratory test handbook, U S. Lexi-Comp Inc, Cleveland

38 Hackeng, C M, Pladet, M W, Akkerman, J W N and van Rijn, H J M (1999) Low Density Lipoprotein phosphorylates the focal adhesion-associated kinase p125^{FAK} in human platelets independent of integrin $\alpha_{IIb}\beta_3$ J Biol Chem **247**, 383–388

39 Nalefski, E A, Sultzman, L A, Martin, D M, Kriz, R. W, Towler, P S, Knopf, J L and Clark, J D (1994) Regulation of purified subtypes of phosphatidylinositol-specific phospholipase C-β by G-protein α and $\beta\gamma$ subunits J Biol Chem **269**, 18239–18249

40 Borsch-Haubold, A G, Bartoli, F, Asselin, J, Dudler, T, Kramer, R M, Apitz-Castro, R., Watson, S P and Gelb, M H (1998) Identification of the phosphorylation sites of cytosolic phospholipase A_2 in agonist-stimulated human platelets and HeLa cells J Biol Chem **273**, 4449–4458

41 Vossler, M R, Yao, H., York, R D., Pan, M G, Rim, C S and Stork, P J (1997) cAMP activates MAP kinase and Elk-1 through a B-Raf- and Rap1-dependent pathway Cell **89**, 73–82

42 Ohta, Y, Suzuki, N, Nakamura, S, Hartwig, J H and Stossel, T (1999) The small GTPase RalA targets filamin to induce filopodia Proc Natl Acad Sci. U S A **96**, 2122–2128

43 Wolthuis, R M F., Zwartkruis, F., Moen, T C. and Bos, J L (1998) Ras-dependent activation of the small GTPase Ral Curr Biol. **8**, 471–474

44 Zwartkruis, F J T, Wolthuis, R M F, Nabben, N M. J. M, Franke, B and Bos, J L (1998) Extracellular signal-regulated activation of Rap1 fails to interfere in Ras effector signalling EMBO J **17**, 5905–5912

Received 5 January 2000/3 April 2000, accepted 17 April 2000

Biochem J. (2000) **349**, 239–245 (Printed in Great Britain)

Regulation of ecdysteroid signalling: molecular cloning, characterization and expression of 3-dehydroecdysone 3α-reductase, a novel eukaryotic member of the short-chain dehydrogenases/reductases superfamily from the cotton leafworm, *Spodoptera littoralis*

Hajime TAKEUCHI*, Jian-Hua CHEN*, David R. O'REILLY†, Huw H. REES*[1] and Philip C. TURNER*

*School of Biological Sciences, University of Liverpool, Life Sciences Building, Crown Street, Liverpool L69 7ZB, U.K., and †Department of Biology, Sir Alexander Fleming Building, Imperial College of Science, Technology and Medicine, Imperial College Road, South Kensington, London SW7 2AZ, U.K.

One route of inactivation of ecdysteroids in insects involves ecdysone oxidase-catalysed conversion into 3-dehydroecdysone (3DE), followed by irreversible reduction by 3DE 3α-reductase to 3-epiecdysone. The 3DE 3α-reductase has been purified and subjected to limited amino acid sequencing. It occurs as two distinct forms, including a probable trimer of subunit molecular mass of approx. 26 kDa. A reverse-transcriptase PCR-based approach has been used to clone the cDNA (1.2 kb) encoding the 26 kDa protein. Northern blotting showed that the mRNA transcript was expressed in Malpighian tubules during the early stage of the last larval instar. Conceptual translation of the 3DE 3α-reductase cDNA and database searching revealed that the enzyme belongs to the short-chain dehydrogenases/reductases superfamily. Furthermore, the enzyme is a novel eukaryotic 3-dehydrosteroid 3α-reductase member of that family, whereas vertebrate 3-dehydrosteroid 3α-reductases belong to the aldo-keto reductase (AKR) superfamily. Enzymically active recombinant 3DE 3α-reductase has been produced using a baculovirus expression system. Surprisingly, we observed no similarity between this 3DE 3α-reductase and a previously reported 3DE 3β-reductase, which acts on the same substrate and belongs to the AKR family.

Key words: insect hormone, moulting hormone, steroid reductase.

INTRODUCTION

Moulting and aspects of reproduction in insects are regulated by the steroidal moulting hormones (ecdysteroids) [1]. In the immature stages of insects, the prothoracic glands are the primary source of ecdysteroids, generally ecdysone (Scheme 1; I). However, in most Lepidoptera investigated, the major product of the glands is 3-dehydroecdysone (3DE; Scheme 1, II), accompanied by varying proportions of ecdysone [2–6]. The 3DE then undergoes reduction to ecdysone by NAD(P)H-linked 3DE 3β-reductase in the haemolymph [3,4,6,7]. Ecdysone undergoes 20-hydroxylation in certain peripheral tissues, yielding 20-hydroxyecdysone, which is considered to be the major active moulting hormone in most insect species [8].

The ecdysteroid titre exhibits obligatory, distinct peaks at specific stages in development [9]. In immature stages, these arise by increased ecdysteroid synthesis in the prothoracic glands, whereas decreases in titre result from enhanced ecdysteroid inactivation reactions together with elevated excretion. A number of transformations contribute to the inactivation of ecdysteroids [8], including the formation of 3-epi(3α-hydroxy)ecdysteroids, which are regarded as hormonally inactive [10–12]. Although production of 3-epiecdysteroids occurs in many insect orders, it is apparently prominent in lepidopteran midgut cytosol and involves ecdysone oxidase-catalysed formation of 3-dehydroecdysteroid, followed by NAD(P)H-dependent irreversible reduction to 3-epiecdysteroid (Scheme 1; III) [8,11–15]. The 3-dehydroecdysteroid may also undergo NAD(P)H-dependent

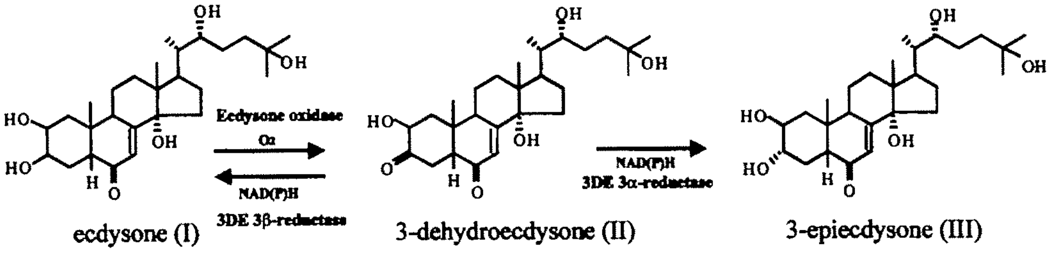

Scheme 1 Enzymic interconversions of ecdysone, 3-dehydroecdysone and 3-epiecdysone

---

Abbreviations used: 3DE, 3-dehydroecdysone; AKR, aldo-keto reductase; SDR, short-chain dehydrogenases/reductases; RACE, rapid amplification of cDNA ends; HSD, hydroxysteroid dehydrogenase.

[1] To whom correspondence should be addressed (e-mail reeshh@liv.ac.uk).

The nucleotide sequence data reported will appear in DDBJ, EMBL, GenBank and GSDB Nucleotide Sequence Databases under the accession number AF255341.

3DE 3β-reductase-catalysed reduction back to 3β-hydroxysteroid (Scheme 1, reviewed in [8,16]). Similar reactions occur with ecdysone and 20-hydroxyecdysone. The significance of reduction of 3DE back to ecdysone is uncertain. In fact, particularly puzzling is the occurrence of enzymes for reversible interconversion of ecdysteroids and their 3-dehydro-derivatives in tissues of several species that are incapable of producing 3-epiecdysteroids [16].

We recently reported the purification of 3DE 3β-reductase from haemolymph of the cotton leafworm, *Spodoptera littoralis* [6]. Based upon limited amino acid sequences in this enzyme protein, its cDNA was cloned by a PCR-based approach. Conceptual translation and amino acid sequence analysis suggested that 3DE 3β-reductase from *S. littoralis* is a new member of the aldo-keto reductase (AKR) superfamily [17]. Furthermore, Northern-blot analysis showed that 3DE 3β-reductase mRNA transcripts are widely distributed in various tissues of *S. littoralis*.

As part of our studies aimed at elucidating the regulation of ecdysteroid titre and the reactions involved in ecdysteroid inactivation, we have purified 3DE 3α-reductase from midgut with attached Malpighian tubules of last instar larvae of *S. littoralis* [18]. Two forms of 3α-reductase were detected: a 26 kDa form, which may exist as a trimer with apparent molecular mass of 76 kDa, and a monomer with approximate molecular mass of 51 kDa. Limited amino acid sequences of internal proteolytic peptides of the 26 kDa form were determined, since the N-terminus is apparently blocked.

Here we report the molecular cloning and characterization of the cDNA encoding the approx. 26 kDa 3DE 3α-reductase of the cotton leafworm, *S. littoralis*, together with heterologous expression of enzymically active recombinant enzyme. Conceptual translation and amino acid sequence analysis indicated that 3DE 3α-reductase is closely related to members of the short-chain dehydrogenases/reductases (SDR) superfamily In fact, the 3DE 3α-reductase is novel in being, hitherto, the only eukaryotic 3-dehydrosteroid 3α-reductase member of the SDR superfamily.

EXPERIMENTAL

Protein sequencing

3DE 3α-reductase (26 kDa form) from *S. littoralis* was purified as described previously [18]. To obtain limited amino acid sequences of the enzyme, purified protein was resolved by SDS/PAGE on 10 % gels, visualized by Coomassie staining, and the corresponding band was excised and cleaved with V8 proteinase. The resulting proteolytic peptides were purified by HPLC and sequenced by Edman degradation using an automated pulsed liquid-phase sequencer (Applied Biosystems 471A; Applied Biosystems, Foster City, CA, U S A.). The partial sequences of three proteolytic peptides were determined: fragment 1, SVAFVGRHQAXL (where X represents a gap); fragment 2, IAXMIVYLA; fragment 3, LAPSGVRVNXVNPGPVLTDIAAG.

cDNA cloning and sequencing

A PCR-based cloning strategy was used to clone a cDNA fragment encoding the region between internal peptides sequenced as described above. Three degenerate primers were synthesized Primer 3A26-1 was designed on the basis of a part of the internal proteolytic peptide fragment 1 amino acid sequence (5′-GCI TTY GTI GGI MGI CAY CAR GC, where I represents inosine, Y is T/C, M is A/C, and R is A/G); primer 3A26-3 and 3A26-3AS were designed according to the sequence of internal proteolytic peptide fragment 3 (3A26-3, 5′-GCI CCI WSI GGI GTI MGI GTN AA, where W represents A/T, S is C/G, N is A/T/C/G; reverse primer 3A26-3AS, 5′-GTI ARI ACI GGI CCI GGR TTN AC).

Total RNA was extracted using TRIzol® (Life Technologies) from combined midgut and Malpighian tubules dissected from larvae 42 h into the last larval instar. First strand cDNA was reverse-transcribed from the total RNA using a 1st Strand cDNA synthesis kit (Roche Molecular Biochemicals, Lewes, East Sussex, U K.) with Q_T adapter primer, 5′-CCA TCA GTG CTA GAC AGC TAA GCT TGA GCT CGG ATC $C(T)_{17}$ (modified from [19]). cDNA synthesized with Q_T primer served as template for the PCR, in which the above three degenerate primers were combined in turn with the adapter Q_0 primer, 5′-CCA TCA GTG CTA GAC AGC T (modified from [19]) PCR was carried out as follows: 1 cycle of 94 °C for 3 min and 35 cycles of 94 °C for 1 min, 50 °C for 1 min, 72 °C for 2 min and 1 cycle of 72 °C for 8 min. PCR products were analysed by electrophoresis on a 1 % agarose gel. This revealed that PCR with 3A26-1 and Q_0 yielded various lengths of product. These PCR products were used as template for the nested PCR, which was carried out as follows: 1 cycle of 94 °C for 3 min and 30 cycles of 94 °C for 1 min, 50 °C for 1 min, 72 °C for 2 min and 1 cycle of 72 °C for 8 min. The nested PCR with 3A26-3 and the other adapter $Q_{1\text{-}2}$ primer, 5′-TAA GCT TGA GCT CGG A (modified from [19]), yielded a product of approx. 550 bp, and the semi-nested PCR with 3A26-1 and 3A26-3AS yielded a product of approx. 450 bp. Both PCR products were gel-purified using a Hybaid Recovery® DNA purification kit (Hybaid, Teddington, Middx., U.K.).

The purified PCR products were cloned into pGEM®-T Easy Vector (Promega) Transformants were screened by colony-PCR using M13 forward primer and M13 reverse primer (5′-GTA AAA CGA CGG CCA G and 5′-CAG GAA ACA GCT ATG AC respectively). Those showing the correct size of insert were propagated in Luria–Bertani broth containing 100 μg/ml of ampicillin, and plasmid DNA was purified after 16 h incubation at 37 °C. Double-stranded DNA sequencing was performed by the dideoxy termination method using Sequenase Version 2.0 (USB®; Amersham Pharmacia Biotech). The sequences of three independent clones of both cloned products were compared to detect errors that could have occurred during the reverse-transcription and PCR amplification.

5′-Rapid amplification of cDNA ends (5′-RACE)

5′-RACE was carried out to obtain the 5′-end of the cDNA. For this, mRNA from total RNA was isolated using the Dynabeads® mRNA purification kit (Dynal, Bromborough, Merseyside, U K.). A 5′-RACE System Version 2.0 (Life Technologies) was used to amplify the 5′-terminus of the message for sequencing. Briefly, a gene-specific primer 1 (5′-GCA ATC TCC TCA GAC T) was hybridized to the mRNA, and cDNA was synthesized using Superscript II reverse transcriptase. The RNA was then degraded with RNase mix (RNase H and RNase T1), and the cDNA was purified using a GlassMax spin cartridge supplied with the kit. A poly(dC) tail was added to the 3′-terminus of the purified cDNA using dCTP and terminal deoxynucleotidyl transferase, and the cDNA region corresponding to the 5′-end of the mRNA was amplified by two successive rounds of PCR using additional gene-specific primers 2 and 3 (5′-CCC TGT ATC TTC AAG CAG ATC A and 5′-GAT GAG GAC AAC TGG ACG TAA AT respectively), together with the anchor primers supplied by the manufacturer. The second-round PCR yielded a product of approx. 400 bp, which was cloned into pGEM®-T Easy Vector, and the nucleotide sequences of several clones were determined.

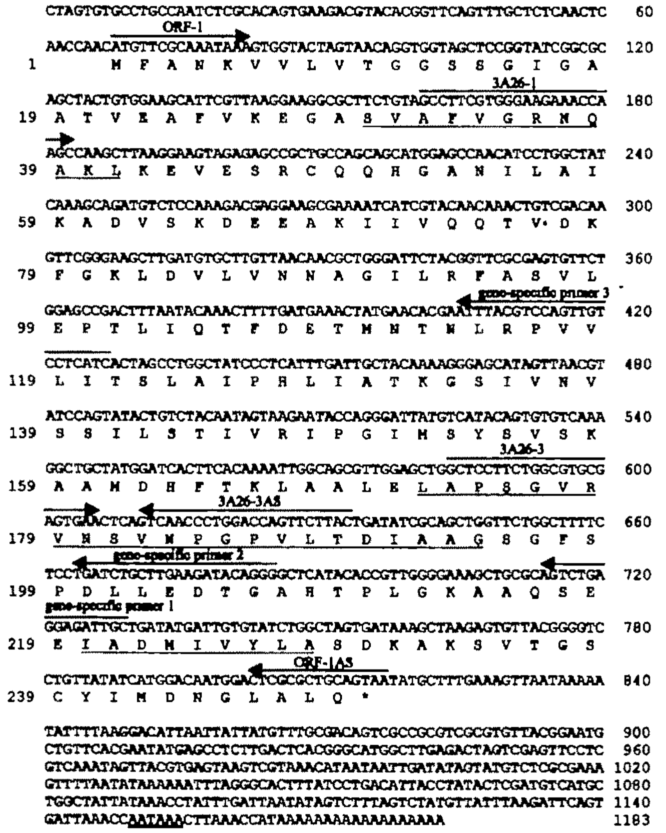

Figure 1 Nucleotide and deduced amino acid sequences of 3DE 3α-reductase

Nucleotide numbers are indicated on the right, amino acid numbers are on the left The putative polyadenylation signal is double-underlined The amino acid sequences obtained from three V8 proteolytic peptides derived from purified 3DE 3α-reductase are underlined The termination codon is indicated by an asterisk The positions and directions of primers are indicated as arrows above the nucleotide sequence

Construction of a cDNA containing an open reading frame

The cDNA sequence containing the entire open reading frame was amplified by PCR from the cDNA synthesized with primer Q_T as described above. Expand® High Fidelity PCR System (Roche Molecular Biochemicals) was used with the following gene-specific primers: ORF-1 (5′-TCA GAATTCATG TTC GCA AAT AAA) and ORF-1AS (5′-CAA AGATCTTTA CTG CAG CGC GAG). These primers were designed to incorporate *Eco*RI, and *Bgl*II sites (underlined in the primer sequences) into the 5′-end and 3′-end of the sense strand respectively. PCR was conducted as follows: 1 cycle of 94 °C for 3 min, 37 cycles of 94 °C for 1 min, 51 °C for 1 min, 68 °C for 1 min and 1 cycle of 72 °C for 10 min. The resulting PCR product was gel-purified, and cloned into pGEM®-T Easy Vector. Three independent clones were sequenced.

Northern-blot analysis

Total RNA from various tissues was isolated using TRIzol® reagent. A 10 μg aliquot of RNA was fractionated on a formaldehyde/agarose gel, transferred to Electran® nylon membrane (Merck), and hybridized with a probe corresponding to the whole open reading frame of the 3DE 3α-reductase cDNA. The probe was radiolabelled with ^{32}P using a Ready-To-Go® DNA labelling kit (-dCTP) (Amersham Pharmacia Biotech), and loading was normalized by probing with an 18 S rRNA probe from mouse (a gift from Ms Yi-Ping Bao, University of Liverpool, U.K.). Prehybridization and hybridization were carried out using QuickHyb® hybridization solution (Stratagene), under the conditions recommended by the manufacturer. The blots were washed at high stringency at 60 °C with 0.1 × SSC (where 1 × SSC is 0.15 M NaCl/0.015 M sodium citrate) containing 0.1 % SDS, and labelled bands were visualized by autoradiography.

Baculovirus expression of 3DE 3α-reductase

The cDNA containing the complete open reading frame of 3DE 3α-reductase was cut out with *Eco*RI and *Bgl*II from the plasmid as described above and transferred into pSynXIV VI$^+$X3 [20], which was digested with the same enzymes. This was cotransfected into *S. frugiperda* Sf21 cells (approx. 2×10^6 cells) with vSynVI$^-$gal DNA [20]. Recombination between viral sequences flanking the 3DE 3α-reductase cDNA in pSynXIV VI$^+$X3 and homologous sequences in the viral genome resulted in the replacement of the β-galactosidase in vSynVI$^-$gal with the entire 3DE 3α-reductase cDNA and a functional polyhedrin gene. The recombinant viruses were identified by screening based on their β-galactosidase-negative, occlusion-body-positive plaque phenotype. Their structures were confirmed by restriction-endonuclease analysis and Southern blotting. Procedures used for maintenance of Sf21 cells, for propagation of vSynVI$^-$gal, and for the construction and characterization of recombinant viruses are as described in [20].

SDS/PAGE

Total cell proteins were analysed by vertical 4–12 % gradient acrylamide gel electrophoresis using the NuPAGE Bis-Tris system (Novex, Groningen, The Netherlands). All samples (from approx. 3×10^5 cells each) were lysed in 50 μl of the NuPAGE SDS sample buffer containing NuPAGE sample reducing agent, and boiled for 5 min before loading 5 μl of each sample onto the gel. After electrophoresis, the gel was stained with Coomassie Brilliant Blue and destained to allow visualization of the proteins. The band of recombinant protein was cut out and subjected to in-gel digestion with trypsin and HPLC purification, before limited sequencing.

Enzyme assay

Assay of the recombinant 3DE 3α-reductase activity was performed in duplicate by modification of the method described in [14]. Sf21 cells (3×10^5 cells/well), infected with wild-type *Autographa californica* nuclear polyhedrosis strain baculovirus or with recombinant baculovirus, were homogenized at 68 h post-infection in 50 μl of 100 mM Tris buffer (pH 8.0) containing 0.05 % NaN_3. A 20 μl aliquot of this extract was assayed by incubation for 30 min at 37 °C in a 50 μl assay mixture consisting of 0.1 M sodium phosphate buffer (pH 7 4), 0.5 mM NADPH and 60 μM 3DE. Assays were quenched with 50 μl of methanol, and proteins were removed by centrifugation. The supernatant was analysed by reversed-phase HPLC. Protein concentration was determined by the method of Bradford using a dye-binding assay (Bio-Rad), with BSA as a standard. Three independent experiments were performed for each assay, with all assays being carried out in duplicate.

HPLC

Ecdysteroids were analysed by HPLC on a Waters instrument (Waters Associates, Northwich, Cheshire, U.K.) linked to a 440

UV detector set at 254 nm and a C_{18} Nova-Pak cartridge (10 cm × 5 mm; Waters Associates), and eluted with an isocratic solvent system consisting of acetonitrile:0.1 % (v/v) trifluoroacetic acid in water (22:78, v/v) at 1 ml/min [14].

RESULTS

Cloning of the cDNA encoding 3DE 3α-reductase

A PCR-based cloning strategy, as detailed in the Experimental section, allowed us to obtain two cDNA fragments corresponding to the sequences between nt 161–633 and 584–1183 respectively (Figure 1). Gene-specific primers derived from these sequences were synthesized and used for 5′-RACE to obtain the 5′-end of the cDNA. 5′-RACE produced a cDNA clone of 427 bp which contains a putative translation start site at position 68. Taken together, all overlapping cDNAs span a total of 1183 bp. The polyadenylation signal (AATAAA) is located at position 1150. As shown in Figure 1, using the first ATG as the start codon, the full-length 3DE 3α-reductase cDNA encodes a protein of 249 amino acids with a predicted molecular mass of 26079.09, which is almost identical to its apparent M_r observed in our SDS/PAGE analysis [18]. The protein is mildly acidic with an estimated pI of 5.82.

Similarity of the deduced amino acid sequence to proteins of the SDR family

The deduced amino acid sequence for the cDNA coding region showed similarity to enzymes in the SDR family (Figure 2), such as *Drosophila melanogaster* alcohol dehydrogenase (69 %), *Bacillus megaterium* glucose 1-dehydrogenase II (66 %), *Cuphea lanceolata* 3-oxoacyl-reductase (61 %) and *Comamonas testosteroni* 3β-hydroxysteroid dehydrogenase (58 %). The 3DE 3α-reductase amino acid sequence exhibited features characteristic of the proteins of the SDR family [21,22], such as the putative consensus sequence for the cofactor binding site [23,24], $G(X)_3GXG$ at Gly^{11}, the active site consensus sequence [25–27], $Y(X)_3K$ at Tyr^{154}, and three further residues (Gly^{133}, Ser^{140} and

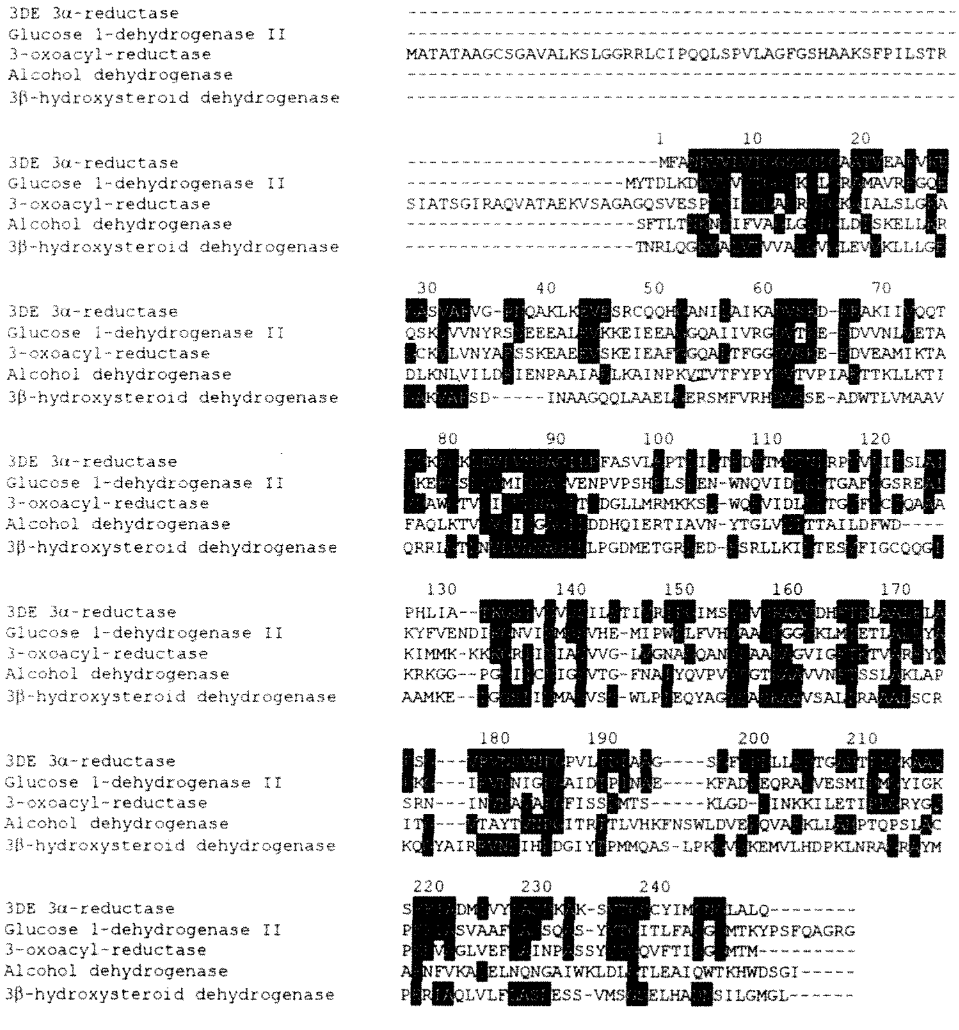

Figure 2 Alignment of the deduced amino acid sequences of 3DE 3α-reductase and the most similar database proteins

The deduced 3DE 3α-reductase sequence was compared with all sequences in the Swiss-Prot database using the BLAST programme. Only the amino acid sequences of some similar proteins representing the SDR family are shown in the alignment. Gaps introduced to optimize alignment are indicated by hyphens. Identical amino acids between 3DE 3α-reductase and at least one other sequence are indicated in black boxes. Numbers on the top refer to the amino acid residues of the 3DE 3α-reductase sequence. The accession number of each protein sequence is as follows: *B. megaterium* glucose 1-dehydrogenase II, P39483; *C. lanceolata* 3-oxoacyl-reductase, P28643; *D. melanogaster* alcohol dehydrogenase, P00334; and *C. testosteroni* 3β-hydroxysteroid dehydrogenase, P19871. The alignment was constructed by use of the CLUSTALW programme.

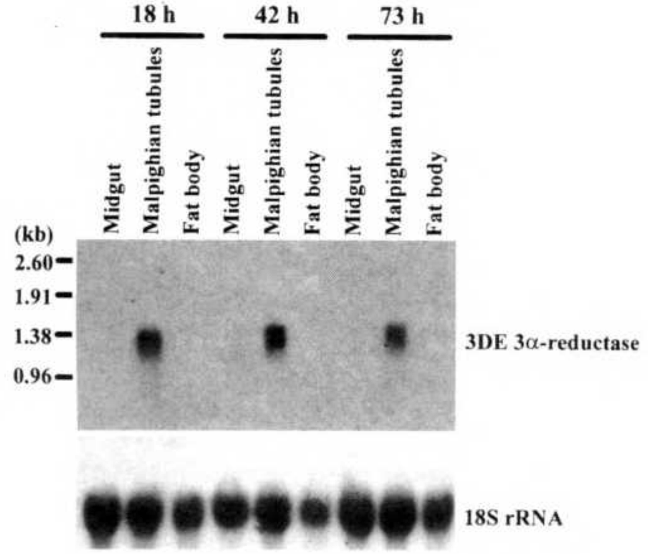

Figure 3 Northern-blot analysis of the tissue distribution and expression of 3DE 3α-reductase

A 10 μg aliquot of total RNA from various tissues at different times (top) within the last larval instar was used. The blot was hybridized with a ^{32}P-labelled 3DE 3α-reductase cDNA probe which corresponded to the whole protein coding region. The same blot was stripped and reprobed with 18 S rRNA probe. The positions of RNA size markers are shown on the left.

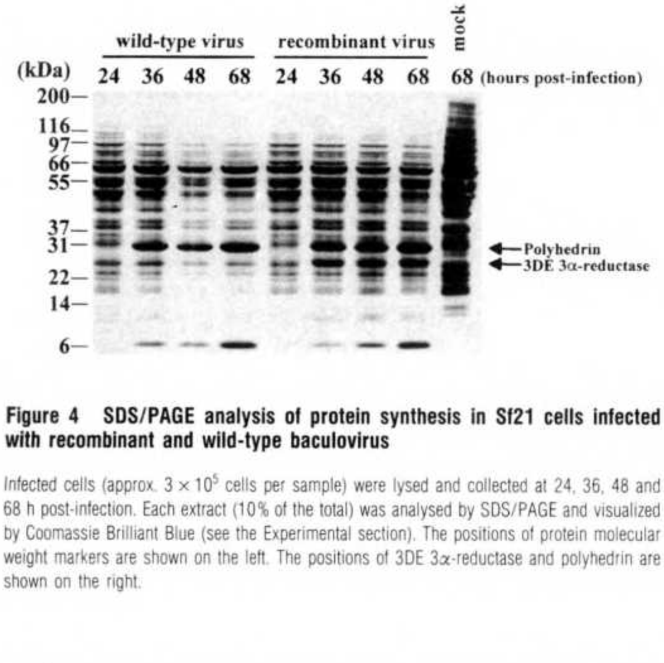

Figure 4 SDS/PAGE analysis of protein synthesis in Sf21 cells infected with recombinant and wild-type baculovirus

Infected cells (approx. 3×10^5 cells per sample) were lysed and collected at 24, 36, 48 and 68 h post-infection. Each extract (10% of the total) was analysed by SDS/PAGE and visualized by Coomassie Brilliant Blue (see the Experimental section). The positions of protein molecular weight markers are shown on the left. The positions of 3DE 3α-reductase and polyhedrin are shown on the right.

Pro^{184}) which are highly conserved in members of that superfamily [21].

Tissue distribution and developmental expression of 3DE 3α-reductase mRNA

As demonstrated in Figure 3, a cDNA probe representing the protein coding region detected a transcript of approx. 1.2 kb in the Malpighian tubules prepared from larvae at 18, 42 and 73 h into the last-larval instar. No detectable expression was found in fat body and midgut. We could not detect the mRNA of 3α-reductase in haemocytes at 42 h (results not shown).

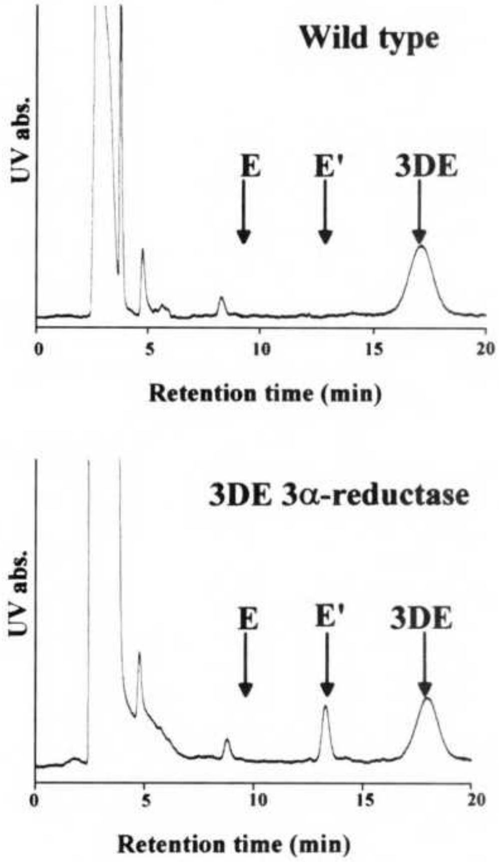

Figure 5 Enzymic activity of recombinant 3DE 3α-reductase

Sf21 cells infected with wild-type or recombinant virus were lysed, incubated with 3-dehydroecdysone in the presence of NADPH and the products were analysed by reversed-phase HPLC (see the Experimental section). The positions of elution of authentic ecdysone (E), 3-epiecdysone (E') and 3-dehydroecdysone (3DE) are shown.

Expression of 3DE 3α-reductase in Sf21 cells

Monolayers of Sf21 cells (3×10^5 cells/well) were infected with wild-type or with recombinant virus, and the cells were collected at intervals between 24 and 68 h. It was found that a polypeptide of approx. 26 kDa, as determined by SDS/PAGE, increased in intensity with time post-infection in samples infected with the recombinant baculovirus, but not in samples infected with the wild-type virus (Figure 4). This recombinant protein was confirmed to be the 3α-reductase by in-gel digestion with trypsin followed by sequencing of two internal fragments (VVLVTGGXXGIG and KXXALXLAP). These correspond to amino acids 6–17 and 166–174 in the 3DE 3α-reductase sequence. The level of expression of 3DE 3α-reductase is comparable with that of viral polyhedrin protein at approx. 30 kDa.

It was demonstrated that the recombinant protein cell lysate was enzymically functional in reduction of 3-dehydroecdysone to 3-epiecdysone in the presence of NADPH as a cofactor (Figure 5). As shown in the reversed-phase HPLC UV chromatograms (Figure 5), there was appreciable conversion of 3-dehydroecdysone into 3-epiecdysone by the NADPH-supplemented lysate from 3DE 3α-reductase recombinant virus-infected cells, with no detectable transformation in the case of wild-type virus-infected cells (Figure 5) or lysate of uninfected Sf21 cells alone (results not shown). In the case of the 3DE 3α-reductase recombinant virus-infected cell lysate, the 3DE 3α-reductase activity was absolutely dependent upon NAD(P)H cofactor and the specific activity was 2.86±0.32 nmol/min per mg of protein in the presence of NADPH (mean±S E.M. for three independent experiments), which is of the same order of magnitude as partially fractionated normal activity [18].

DISCUSSION

Using a reverse-transcription PCR-based cloning strategy, employing degenerate primers designed on the basis of the partial amino acid sequences of fragments of 3DE 3α-reductase, together with 5′-RACE, the complete cDNA encoding the enzyme was isolated and sequenced The predicted amino acid sequence of the cDNA contained the three internal peptides obtained from V8 proteinase digestion of the band corresponding to the M_r 26000 polypeptide, confirming that we had cloned the 3DE 3α-reductase cDNA.

When the cDNA encoding 3DE 3α-reductase was expressed using the baculovirus system, a polypeptide band of approx. 26 kDa was observed on SDS/PAGE which increased in intensity with time of culture (Figure 4). Limited sequencing of internal proteolytic fragments confirmed that the sequences corresponded to the conceptually translated amino acid sequence of the cDNA. Furthermore, the lysate from recombinant baculovirus-infected cells showed NADPH-dependent 3DE 3α-reductase enzymic activity. The foregoing results indicate that the cloned cDNA encodes 3DE 3α-reductase.

Database searching revealed that 3DE 3α-reductase belongs to the SDR superfamily [21,22]. It is clear that the predicted amino acid sequence of this enzyme has high similarity to other enzymes in this family; in particular, the glycine residues (Gly^{11}, Gly^{15} and Gly^{17}) involved in cofactor binding [23,24], as well as Tyr^{154} and Lys^{158} essential for catalytic function, are conserved [25–27]. Furthermore, that 3DE 3α-reductase may exist as a homotrimer of apparent molecular mass approx. 76 kDa and subunit molecular mass approx. 26 kDa [18] is in agreement with SDR proteins, which are homo-oligomers composed of subunits with molecular masses between 25 kDa and 37 kDa [22].

3DE 3α-reductase activity has been demonstrated in midgut, fat body, haemolymph and epidermis of various insect species [11,14,28,29], but hitherto, there were no data concerning this enzyme in Malpighian tubules. Our Northern-blot analysis has revealed that the mRNA for the 3α-reductase is expressed strongly in Malpighian tubules (Figure 3). Furthermore, we have detected enzymic activity of the 3α-reductase in Malpighian tubules (results not shown). Chen et al. [18] showed that there were at least two forms (26 kDa and 51 kDa) of the 3α-reductase in combined midgut and Malpighian tubules of *S. littoralis*. The current data suggest that expression of the small form of 3α-reductase occurs in the Malpighian tubules, but not in the midgut. Expression of the 3α-reductase in the Malpighian tubules may suggest a role for the enzyme in inactivation of endogenous haemolymph ecdysteroid

Northern-blot analysis (Figure 3) also revealed that the mRNA transcript for the enzyme is expressed over 18–73 h of the last larval instar. Since this expression correlates with times in development when ecdysteroid titres are minimal [14], the 3α-reductase may function in keeping the hormone levels low. In final larval instar of the Lepidoptera, *Manduca sexta* [30], *Diatraea grandiosella* [31] and *Bombyx mori* [32], very low multiple peaks in haemolymph ecdysteroid titre have been detected appreciably earlier in development than the commitment peak. Presumably, a similar situation exists in *S. littoralis* Thus expression of the mRNA encoding the small form of 3α-reductase in the early stage of the last larval instar may reflect involvement of the enzyme in inactivation of such small ecdysteroid peaks in the Malpighian tubules.

Hydroxysteroid dehydrogenases (HSDs) belong to at least two distinct protein families: the SDR and AKR families [21,22,33]. Furthermore, some 3β-HSDs belong to an additional 3β-HSD family whose members are membrane-bound proteins located in the endoplasmic reticulum and mitochondrial membranes [34]. HSDs belonging to the SDR or AKR families interconvert similar substrates, but bear no significant sequence similarity, and have completely different three-dimensional structures [35,36].

Recently, we reported [17] the deduced amino acid sequence of another reductase enzyme from *S. littoralis* that reduces 3DE to yield a 3β-hydroxy-ecdysteroid (biologically active), rather than a 3α-hydroxy-ecdysteroid (inactive), as in the case of the 3DE 3α-reductase Surprisingly, the 3DE 3β-reductase belongs to the AKR superfamily [33], whereas the current 3DE 3α-reductase belongs to the SDR superfamily [21,22]. Furthermore, there are no conserved regions between these families, resulting in no significant sequence similarity. Within the SDR superfamily, members share a consensus active site sequence Tyr-X-X-X-Lys, the tyrosine and lysine residues being essential for catalysis [21]. Thus it is envisaged that Tyr^{154} and Lys^{158} are important residues at the active site of 3DE 3α-reductase, whereas Asp^{73}, Tyr^{78}, Lys^{107}, and His^{140} in the 3DE 3β-reductase [17] are characteristic of active sites of the AKR superfamily [35]. SDR superfamily members have a Rossmann nucleotide-binding fold $[G(X)_3GXG]$ located near the N-terminus [21,24]. In contrast, AKR family members bind cofactors through interaction with residues at the C-terminus end, consisting of an α/β barrel or several β-strands and α-helix [36]. Thus, based on conserved amino acid residues in these superfamilies, we expect the structure of 3DE 3α-reductase to be very different from that of the corresponding 3DE 3β-reductase, though they catalyse reduction of an identical substrate. Furthermore, we found no nucleotide sequence similarity between the cDNA for these two reductases, which supports our view that they have evolved independently.

Surprisingly, our protein database and literature searches have revealed that no other 3-dehydrosteroid 3α-reductase enzyme hitherto reported belongs to the SDR family, except for bacterial ones [37,38]. Mammalian 3α-HSDs belong to the AKR superfamily [22,39–42], whereas carbonyl reductases from mammalian tissues belong to the SDR family [43–46]. These results may suggest that 3DE 3α-reductase from *S. littoralis* is not evolutionarily close to 3α-HSDs but to carbonyl reductases in mammals. It may be significant in the case of ecdysteroids that a specific ecdysone oxidase (i.e. oxygen-dependent), rather than an NAD(P)$^+$-dependent dehydrogenase, is responsible for oxidation of ecdysteroid to 3-dehydroecdysteroid, whereas the vertebrate 3-HSDs generally catalyse reversible reactions.

We thank Dr M C Wilkinson for peptide sequencing and Mr S G Corrigan for insect rearing We gratefully acknowledge the financial support of the Biotechnology and Biological Sciences Research Council

REFERENCES

1 Koolman, J (1989) Ecdysone, Georg Thieme-Verlag, Stuttgart, Germany
2 Warren, J T, Sakurai, S, Rountree, D B, Gilbert, L I, Lee, S S and Nakanishi, K (1988) Regulation of the ecdysteroid titer of *Manduca sexta* reappraisal of the role of the prothoracic glands Proc Natl Acad Sci U S A **85**, 958–962
3 Sakurai, S, Warren, J and Gilbert, L I (1989) Mediation of ecdysone synthesis in *Manduca sexta* by a hemolymph enzyme Arch Insect Biochem Physiol **10**, 179–197
4 Kinishi, S, Rountree, D B., Sakurai, S and Gilbert, L I (1990) Prothoracic gland synthesis of 3-dehydroecdysone and its hemolymph 3β-reductase mediated conversion to ecdysone in representative insects Experientia **46**, 57–64

5 Blais, C and Lafont, R. (1991) Biosynthesis of ecdysteroids by prothoracic glands in *Pieris brassicae* (Lepidoptera Insect) Conversion *in vitro* of radiolabelled precursor of 3-dehydroecdysone Acad Sci Paris C. R Ser III **313**, 359–364

6 Chen, J-H, Webb, T J, Powls, R. and Rees, H H (1996) Purification and characterisation of haemolymph 3-dehydroecdysone 3β-reductase in relation to ecdysteroid biosynthesis in the cotton leafworm *Spodoptera littoralis* Eur J Biochem **242**, 394–401

7 Watson, R D, Spaziani, E and Bollenbacher, W E (1989) Regulation of ecdysteroid biosynthesis in insects and crustaceans a comparison In Ecdysone (Koolman, J, ed), pp 188–196, Georg Thieme-Verlag, Stuttgart, Germany

8 Rees, H H (1995) Ecdysteroid biosynthesis and inactivation in relation to function Eur J. Entomol **92**, 9–39

9 Steel, C. G H and Vafopoulou, X (1989) Ecdysteroid titer profiles during growth and development of arthropods In Ecdysone (Koolman, J, ed), pp 221–231, Georg Thieme-Verlag, Stuttgart, Germany

10 Nigg, H N, Svoboda, J A, Thompson, M J, Kaplanis, J N, Dutky, S R and Robbins, W E (1974) Ecdysone metabolism ecdysone dehydrogenase-isomerase Lipids **9**, 971–974

11 Blais, C and Lafont, R (1984) Ecdysteroid metabolism by soluble enzymes from an insect Metabolic relationships between 3β-hydroxy-, 3α-hydroxy- and 3-oxoecdysteroids Hoppe Seyler's Z Physiol Chem **365**, 809–817

12 Milner, N P and Rees, H H (1985) Involvement of 3-dehydroecdysone in the 3-epimerization of ecdysone Biochem. J **231**, 369–374

13 Weirich, G F (1989) Enzymes involved in ecdysone metabolism. In Ecdysone (Koolman, J, ed), pp. 174–180, Georg Thieme-Verlag, Stuttgart, Germany

14 Webb, T J, Powls, R and Rees, H H (1995) Enzymes of ecdysteroid transformation and inactivation in the midgut of the cotton leafworm, *Spodoptera littoralis* properties and developmental profiles Biochem. J **312**, 561–568

15 Webb, T J, Powls, R and Rees, H H (1996) Characterization, fractionation and kinetic properties of the enzymes of ecdysteroid 3-epimerization and phosphorylation isolated from the midgut cytosol of the cotton leafworm, *Spodoptera littoralis* Insect Biochem Mol Biol **26**, 809–816

16 Lafont, R and Koolman, J (1984) Ecdysone metabolism In Biosynthesis, Metabolism and Mode of Action of Invertebrate Hormones (Hoffmann, J and Porchet, M, eds), pp 196–226, Springer-Verlag, Berlin

17 Chen, J-H, Turner, P C and Rees, H H. (1999) Molecular cloning and characterization of hemolymph 3-dehydroecdysone 3β-reductase from the cotton leafworm, *Spodoptera littoralis*. A new member of the third superfamily of oxidoreductases J. Biol Chem **274**, 10551–10556

18 Chen, J-H, Powls, R, Rees, H H and Wilkinson, M C (1999) Purification of ecdysone oxidase and 3-dehydroecdysone 3α-reductase from the cotton leafworm, *Spodoptera littoralis* Insect Biochem. Mol Biol **29**, 899–908

19 Frohman, M A (1993) Rapid amplification of complementary DNA ends for generation of full-length complementary DNAs Thermal RACE Methods Enzymol (Wu, R, ed), **218**, 340–356

20 O'Reilly, D R, Miller, L K and Luckow, V A (1994) Baculovirus Expression Vectors, Oxford University Press, New York, Oxford

21 Jornvall, H, Persson, B, Krook, M., Atrian, S, Gonzàlez-Duarte, R, Jeffery, J and Ghosh, D. (1995) Short-chain dehydrogenases/reductases (SDR) Biochemistry **34**, 6003–6013

22 Penning, T M, Bennett, M J, Smith-Hoog, S, Schlegel, B P, Jez, J M and Lewis, M (1997) Structure and function of 3α-hydroxysteroid dehydrogenase Steroids **62**, 101–111

23 Wierenga, R K, Maeyer, M C H and Hol, W G J (1985) Interaction of pyrophosphate moieties with α-helixes in dinucleotide binding-proteins Biochemistry **24**, 1346–1357

24 Rossmann, M G, Liljas, A, Brandén, C-I and Banaszak, L J (1975) Evolutionary and structural relationships among dehydrogenases In The Enzymes (Boyer, P D, ed), Vol 11, pp 61–102, Academic Press, New York

25 Ghosh, D, Weeks, C. M, Grochulski, P, Duax, W L, Erman, M., Rimsay, R L and Orr, J C (1991) Three-dimensional structure of holo 3α,20β-hydroxysteroid dehydrogenase a member of a short-chain dehydrogenase family. Proc Natl Acad. Sci USA **88**, 10064–10068

26 Ghosh, D, Wawrzak, Z, Weeks, C M., Duax, W L and Erman, M (1994) The refined three-dimensional structure of 3α,20β-hydroxysteroid dehydrogenase and possible roles of the residues conserved in short-chain dehydrogenases Structure **2**, 629–640

27 McKinley-McKee, J S, Winberg, J-O and Pettersson, G (1991) Mechanism of action of *Drosophila melanogaster* alchol-dehydrogenase Biochem Int **25**, 879–885

28 Weirich, G F, Feldlaufer, M F. and Svoboda, J A (1993) Ecdysone oxidase and 3-oxoecdysteroid reductases in *Manduca sexta* Developmental changes and tissue distribution Arch Insect Biochem Physiol **23**, 199–211

29 Thompson, M J, Weirich, G F and Svoboda, J A (1985) Ecdysone 3-epimerase Methods Enzymol **111**, 437–442

30 Wolfgang, W J and Riddiford, L M (1986) Larval cuticular morphogenesis in the tabacco hornworm, *Manduca sexta*, and its hormonal regulation. Dev Biol **113**, 305–316

31 Yin, C-M and Chaw, W-D (1984) Hemolymph ecdysteroid titer and epidermal cell commitment of the female southwestern corn borer larvae J Insect Physiol **30**, 257–263

32 Sakurai, S, Kaya, M and Satake, S (1998) Hemolymph ecdysteroid titer and ecdysteroid-dependent developmental events in the last-larval stadium of the silkworm, *Bombyx mori* role of low ecdysteroid titer in larval-pupal metamorphosis and a reappraisal of the head critical period J Insect Physiol **44**, 867–881

33 Bohren, K M, Bullock, B, Wermuth, B and Gabbay, K H (1989) The aldo-keto reductase superfamily cDNAs and deduced amino acid sequences of human aldehyde and aldose reductases J Biol Chem **264**, 9547–9551

34 Labrie, F, Simard, J, Luu-The, V, Pelletier, G, Belanger, A, Lanchance, Y., Zhao, H F., Labrie, C, Breton, N, DE Launoit Y et al (1992) Structure and tissue-specific expression of 3β-hydroxysteroid dehydrogenase/5-ene-4-ene isomerase genes in human and rat classical and peripheral steroidgenic tissues J Steroid Biochem. **41**, 421–435

35 Hoog, S S, Pawlowski, J E, Alzari, P M, Penning, T M and Lewis, M (1994) Three-dimensional structure of rat liver 3α-hydroxysteroid/dihydrodiol dehydrogenase· a member of the aldo-keto reductase superfamily Proc Natl. Acad Sci USA **91**, 2517–2521

36 Bennett, M J, Schlegel, B P, Jez, J M, Penning, T M and Lewis, M (1996) Structure of 3α-hydroxysteroid/dihydrodiol dehydrogenase complexed with NADP$^+$ Biochemistry **35**, 10702–10711

37 Suzuki, K, Ueda, S, Sugiyama, M and Imamura, S (1993) Cloning and expression of a *Pseudomonas* 3α-hydroxysteroid dehydrogenase-encoding gene in *Escherichia coli*. Gene **130**, 137–140

38 Oppermann, U C T and Maser, E (1996) Characterization of a 3α-hydroxysteroid dehydrogenase/carbonyl reductase from the gram-negative bacterium *Comamonas testosteroni*. Eur J Biochem **241**, 744–749

39 Stolz, A, Rahimi-Kiani, M, Ameis, D, Chan, E, Ronk, M and Shively, J E (1991) Molecular structure of rat hepatic 3α-hydroxysteroid dehydrogenase A member of the oxidoreductase gene family J Biol Chem **266**, 15253–15257

40 Cheng, K C, White, P C and Qin, K N (1991) Molecular cloning and expression of rat liver 3α-hydroxysteroid dehydrogenase Mol Endocrinol **56**, 823–828

41 Pawlowski, J. E, Huizinga, M and Penning, T M (1991) Cloning and sequencing of the cDNA for rat liver 3α-hydroxysteroid/dihydrodiol dehydrogenase J Biol. Chem **266**, 8820–8825

42 Penning, T M (1997) Molecular endocrinology of hydroxysteroid dehydrogenases Endocrine Rev. **18**, 281–305

43 Wermuth, B., Bohren, K M, Heinemann, G, Von Wartburg, J-P and Gabbay, K H (1988) Human carbonyl reductase Nucleotide sequence analysis of a cDNA and amino acid sequence of the encoded protein. J Biol Chem **263**, 16185–16188

44 Wei, J, Dlouhy, S R, Hara, A, Ghetti, B and Hodes, M E (1996) Cloning a cDNA for carbonyl reductase (Cbr) from mouse cerebellum murine genes that express cbr map to chromosomes 16 and 11 Genomics **34**, 147–148

45 Nakanishi, M, Deyashiki, Y, Nakayama, T, Sato, K and Hara, A (1993) Cloning and sequence analysis of a cDNA encoding tetrameric carbonyl reductase of pig lung Biochem Biophys Res Commun **194**, 1311–1316

46 Wermuth, B., Maeder-Heinemann, G. and Ernst, E. (1995) Cloning and expression of carbonyl reductase from rat testis Eur J Biochem **228**, 473–479

Received 17 January 2000/27 March 2000; accepted 11 April 2000

Biochem J (2000) 349, 247–253 (Printed in Great Britain)

Definition of Munc13-homology-domains and characterization of a novel ubiquitously expressed Munc13 isoform

Henriette KOCH*, Kay HOFMANN† and Nils BROSE*[1]

*Max-Planck-Institut fur experimentelle Medizin, AG Molekulare Neurobiologie, Hermann-Rein-Str. 3, D-37075 Gottingen, Germany, and
†MEMOREC Stoffel GmbH, Bioinformatics Group, Stoeckheimer Weg 1, D-50829 Koln, Germany

Munc13 proteins constitute a family of three highly homologous molecules (Munc13-1, Munc13-2 and Munc13-3). With the exception of a ubiquitously expressed Munc13-2 splice variant, Munc13 proteins are brain-specific. Munc13-1 has a central priming function in synaptic vesicle exocytosis from glutamatergic synapses. In order to identify Munc13-like proteins that may regulate secretory processes in non-glutamatergic neurons or non-neuronal cells, we developed protein profiles for two Munc13-homology-domains (MHDs). MHDs are present in a wide variety of proteins, some of which have previously been implicated in membrane trafficking reactions. Taking advantage of partial sequences in the human expressed sequence tag (EST) database, we characterized a novel, ubiquitously expressed, rat protein (Munc13-4) that belongs to a subfamily of Munc13-like molecules, in which the typical Munc13-like domain structure is conserved. Munc13-4 is predominantly expressed in lung where it is localized to goblet cells of the bronchial epithelium and to alveolar type II cells, both of which are cell types with secretory function. In the present study we identify a group of novel proteins, some of which may function in a Munc13-like manner to regulate membrane trafficking. The MHD profiles described in the present study are useful tools for the identification of Munc13-like proteins, that would otherwise have remained undetected.

Key words: lung, protein profile, secretion.

INTRODUCTION

Synaptic vesicles are the key organelles in neurotransmitter release at synapses. In the presynaptic terminal of a nerve cell synaptic vesicles pass through a complex cycle of membrane fusion and fission reactions that govern the release process. Vesicles are probably generated by budding from early endosomes. They are loaded with transmitter, translocate to the plasma membrane and dock at the active zone, an electron dense presynaptic membrane region where the release process is restricted to. Docked vesicles have to be primed, that is mature to a fusion competent state, before a rise in the intracellular calcium concentration can trigger fusion and secretion of the transmitter. After fusion, vesicular membrane and protein components are retrieved by clathrin-mediated endocytosis and recycled directly or via early endosomes [1].

Munc13 proteins constitute a family of three molecules (Munc13-1, Munc13-2 and Munc13-3) with homology to *Caenorhabditis elegans* unc-13p. With the exception of a ubiquitously expressed Munc13-2 splice variant, Munc13 proteins are specifically expressed in brain, where Munc13-1 has a central role in synaptic vesicle priming. Munc13 proteins contain a phorbol ester-binding C$_1$-domain and two C$_2$-domains, which are Ca^{2+}/phospholipid binding domains [2,3]. The most abundant isoform in rat brain, Munc13-1, is specifically targeted to presynaptic active zones [4]. It binds to syntaxin, a component of the synaptic vesicle fusion apparatus [5], as well as to DOC2 ('double C$_2$') [6], and acts as a phorbol ester-dependent enhancer of neurotransmitter secretion when overexpressed in *Xenopus* neuromuscular junctions [4]. Loss of Munc13-1 in deletion mutant mice leads to an arrest of the synaptic vesicle cycle of hippocampal neurons at the synaptic vesicle priming step, resulting in a functional shutdown of synapses. These contain normal numbers of docked vesicles which are not primed and therefore unable to fuse upon physiological stimulation [7], demonstrating that Munc13-1 is an essential synaptic vesicle priming protein in neurons. Interestingly, this Munc13-1 mutant phenotype is restricted to excitatory/glutamatergic neurons while inhibitory/γ-aminobutyric acid (GABA)ergic nerve cells are unaffected by the Munc13-1 deficiency [7]. Analysis of deletion mutations in the *C. elegans* and *Drosophila unc-13* genes yielded results that are very similar to those obtained in Munc13-1 mutant mice, demonstrating that the functional role of Unc-13 homologues is evolutionary conserved [8,9].

Munc13-1 is expressed in all neurons of the rat central nervous system [3]. In contrast, Munc13-2 and Munc13-3 exhibit strikingly differential expression patterns. Munc13-2 is only present in rostral brain regions, including cerebral cortex and 'cornu ammonis' regions of the hippocampus, while Munc13-3 expression is mostly restricted to the cerebellum [3]. Thus neurons in the rat brain co-express Munc13-1 with either Munc13-2 or Munc13-3, depending on the brain region under examination. On the basis of these findings and preliminary observations in deletion mutant mice [7], it was concluded that Munc13-2/Munc13-3 and Munc13-1 have partially redundant roles in neurotransmitter release. Neurons utilize transmitter-specific synaptic vesicle priming mechanisms where excitatory/glutamatergic cells are dependent on Munc13-proteins, while inhibitory/GABAergic cells are not [7].

In view of this striking differential dependence of neurons, in

---

Abbreviations used. BAI1, brain-specific angiogenesis inhibitor 1, BAP3, BAI1-associated protein 3, CAPS, Ca^{2+}-dependent activator protein for secretion, CIRL, Ca^{2+}-independent recepter for α-latrotoxin, CPD2, cerebellum postnatal development associated protein 2, EST, expressed sequence tag, GABA, γ-aminobutyric acid, GST, glutathione S-transferase, MHDs, Munc13-homology-domains; ORFs, open reading frames

[1] To whom correspondence should be addressed (e-mail brose@mail mpiem gwdg.de).

The Munc13-4 nucleotide sequence data reported here appears in the DDBJ, EMBL and GenBank Nucleotide Sequence Databases under the accession number AF159356

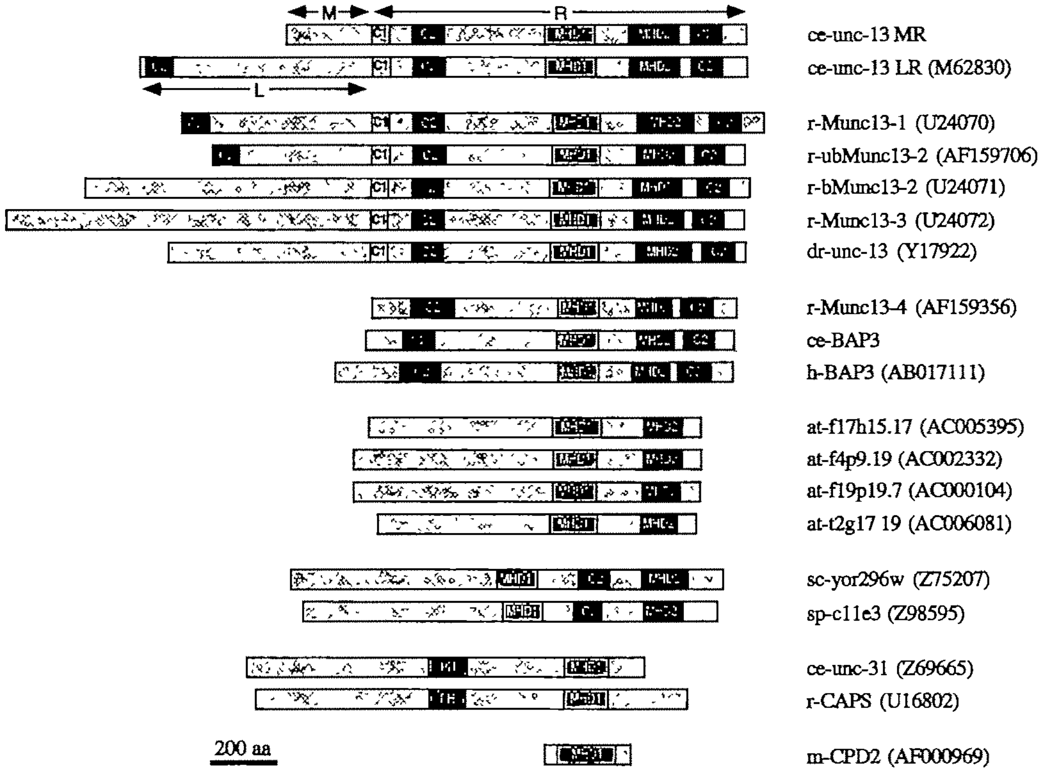

Figure 1 Proteins containing MHDs

Domain structure of proteins identified with protein profiles for two Munc13-consensus sequences Proteins are identified on the right and GenBank accession numbers are also given (ce-BAP3 was assembled manually from the genome; domain structure of the MR form of *C elegans* unc-13 from [8]) MHDs are present in a diverse set of proteins, many of which are involved in the regulation of secretory processes Note that *C elegans* unc-13 is expressed in two variants (LR and MR) The L region is conserved in rat Munc13-1 and rat ubMunc13-2, while all other unc-13 homologues have unrelated N-termini at, *A thaliana*, C1, C_1-domain; C2, C_2-domain, ce, *C elegans*, dr, *D melanogaster*, h, human; m, mouse, PH, pleckstrin-homology-domain, r, rat, sc, *S cerevisiae*, sp; *S. pombe*

the central nervous system, on vesicle priming by the three known Munc13 isoforms, we initiated a search for novel Munc13-like proteins. Based on the assumptions that (1) synaptic vesicle priming is a general feature of neurotransmitter release from all neurons, and that (2) similar priming processes may be involved in non-neuronal cells, the aim of this search was the identification of novel vesicle priming proteins with central roles in secretory processes. We used distantly related Munc13-like protein sequences from *Saccharomyces cerevisiae* and *Schizosaccharomyces pombe* to develop protein profiles for two Munc13-homology-domains (MHDs). We found that MHDs are present in a wide variety of proteins from *Arabidopsis thaliana*, *C. elegans*, *Drosophila melanogaster*, mouse, rat and human. Taking advantage of partial sequences in the human expressed sequence tag (EST) database we identified, cloned and characterized a novel, ubiquitously expressed rat protein (Munc13-4) that belongs to a subfamily of Munc13-like molecules in which the typical Munc13-like domain structure, with two C_2-domains separated by a sequence containing the two MHDs, is conserved. Munc13-4 is predominantly expressed in lung where it is localized to goblet cells of the bronchial epithelium and to alveolar type II cells, both of which are cell types with secretory function. In the present study we identify a group of novel proteins, some of which may function in a Munc13-like manner to promote vesicle priming during secretion from non-glutamatergic neurons and cells outside of the central nervous system.

MATERIALS AND METHODS

Sequence analysis and identification of Munc13-like proteins

Initial database searches for Munc13-like proteins were performed using the BLAST server at the National Center for Biotechnology Information (http://www.ncbi.nlm.nih.gov). Multiple sequence alignments were calculated with either DNASTAR (Madison, WI, U.S.A.) or the PILEUP program of the GCG program suite and improved manually [10]. Profiles for MHD consensus sequences were constructed from aligned sequences [11] using the BLOSUM45 amino acid similarity matrix [12] with a gap penalty of 2.1 and a gap-extension penalty of 0.2. These profiles were used to search the current protein and DNA database releases [13].

Cloning of Munc13-4

Initial database searches led to the identification of two yeast open reading frames (ORFs) with similarity to Munc13 proteins; yor296w from *S. cerevisiae*, and c11e3 from *S. pombe* (Figures 1 and 2). Databank searches with MHD profiles, developed on the basis of the two yeast sequences and known Munc13-sequences, identified, among other sequences (Figures 1 and 2), three ESTs with similarity to Munc13 proteins (Clone ID/GenBank accession numbers: 231903/H92853; 700912/AA287381,

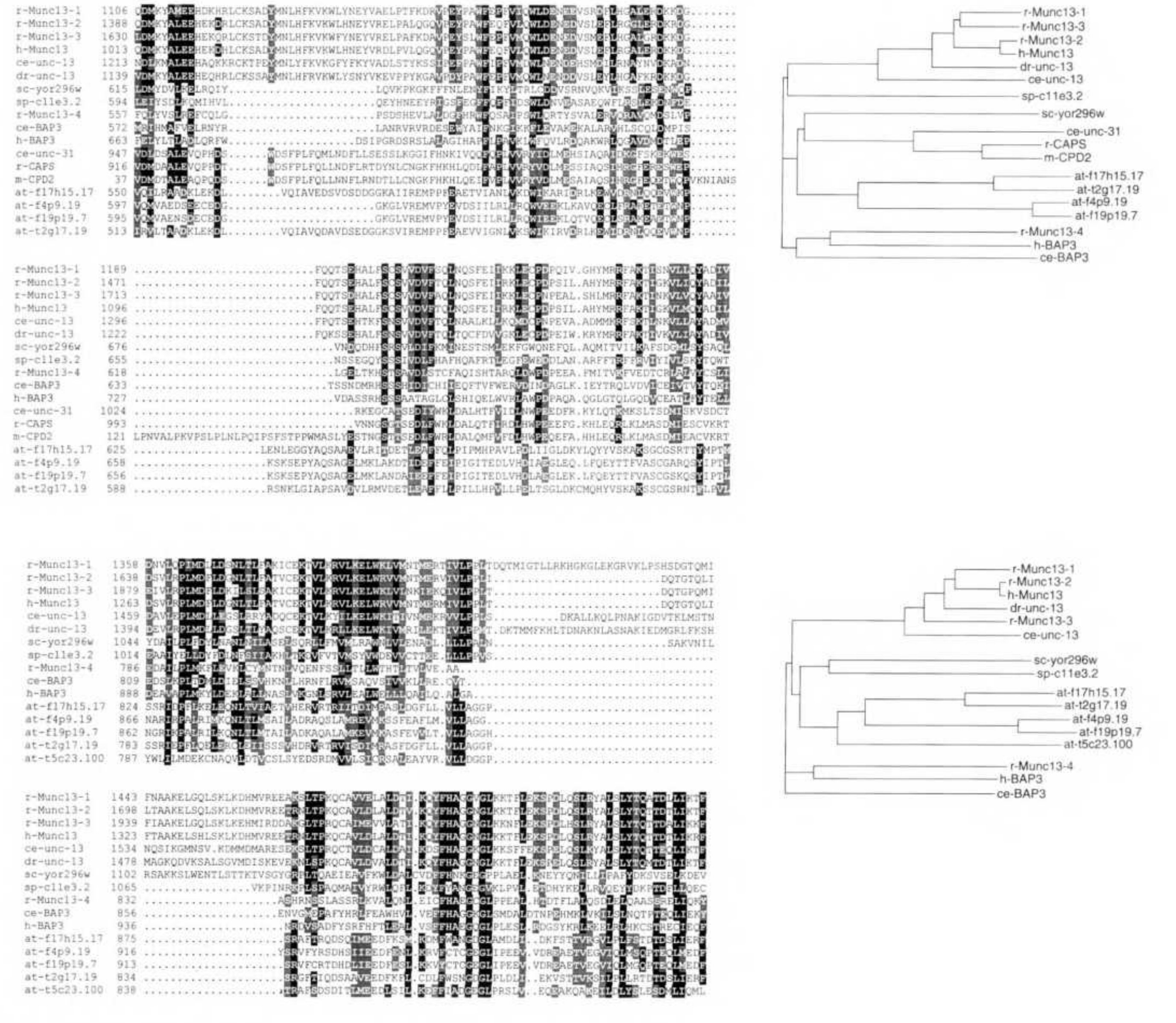

Figure 2 Conservation of MHDs

Alignments and corresponding dendrograms of MHD1 (top panels) and MHD2 (bottom panels) from the indicated proteins. Proteins and residue numbers are identified on the left. Sequences are shown in single letter amino acid code and are aligned for maximal homology. Conserved residues are shown on black background and residues that are similar are shown on shaded background [similarity groups: (F,Y,W); (I,L,V,M); (H,R,K); (D,E); (G,A); (T,S); (N,Q)]. Dots indicate gaps. at, *A. thaliana*; ce, *C. elegans*; dr, *D. melanogaster*; h, human; m, mouse; r, rat; sc, *S. cerevisiae*; sp, *S. pombe*.

1035452/AA621650). The respective clones were obtained (Research Genetics, Huntsville, AL, U.S.A.), and their inserts were used to screen a rat forebrain cDNA library in λZAPII (J. Boulter, University of California, Los Angeles, CA, U.S.A.) as well as a rat whole-brain library in λZAPII (Stratagene, Heidelberg, Germany) at high stringency. From 1×10^6 plaques, three positive clones were isolated. Rescued plasmids were sequenced using the dideoxy chain termination method with dye terminators on an Applied Biosystems 373 DNA sequencer (Applied Biosystems, Weiterstadt, Germany). All three clones overlapped with the EST clones used in the screen. Inserts of positive clones were then used in a screen of a rat lung cDNA library in λgt11 (Clontech, Heidelberg, Germany) at low stringency. From 1×10^6 plaques, 71 clones were isolated, subcloned into pBluescript (Stratagene, Heidelberg, Germany) and sequenced as described above. Of the sequenced clones, 45 contained parts of the appropriate cDNA, while the rest represented unrelated artefacts. A full-length sequence of the novel cDNA, designated Munc13-4, was assembled from multiple overlapping cDNA fragments and subcloned into pcDNA3 (pcDNA3-Munc13-4; Invitrogen, San Diego, CA, U.S.A.). A human embryonic kidney cell line (HEK-293) was transfected with this vector, using calcium phosphate [14].

Generation of antibodies to Munc13-4

Polyclonal antibodies directed against Munc13-4 were generated with a glutathione-S-transferase (GST) fusion protein as the

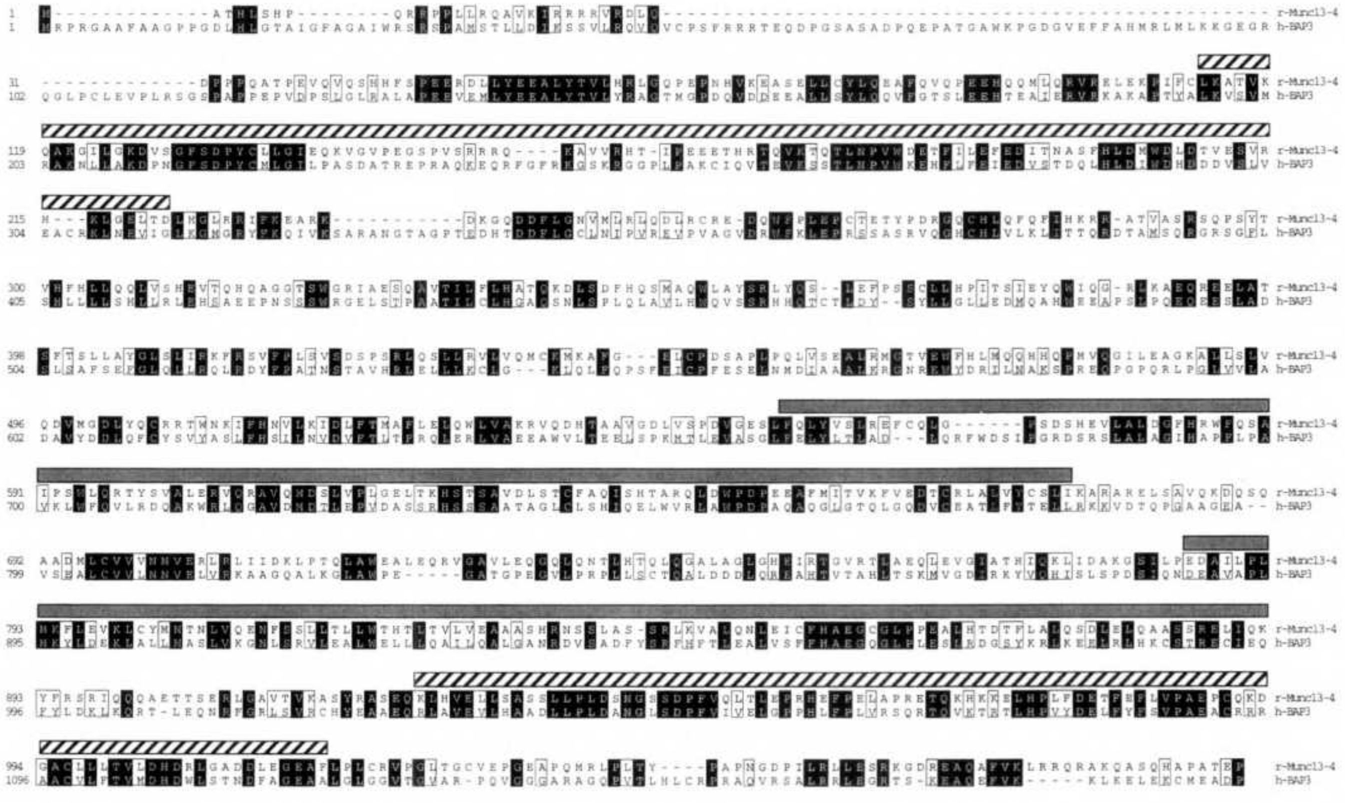

Figure 3 Primary structure of Munc13-4

The amino acid sequence of rat Munc13-4 was deduced from the nucleotide sequence assembled from multiple overlapping cDNA clones (GenBank accession number AF159356). Sequences are shown in single letter amino acid code and are aligned for maximal homology with human BAP3 (GenBank accession number AB017111). Conserved residues are shown on black background and residues that are similar are boxed [similarity groups: (F,Y,W); (I,L,V,M); (H,R,K); (D,E); (G,A); (T,S); (N,Q)]. Dots indicate gaps. C$_2$-domains are indicated by hatched bars and MHDs are indicated by shaded bars above the respective sequence stretch. Munc13-4 and BAP3 are 34% identical and form a new subfamily of Munc13-like proteins. h, human; r, rat.

antigen. Recombinant GST–Munc13-4 fusion protein was generated by using the expression plasmid pGEX-Munc13-4, which represents residues 889–1088 of Munc13-4 in the pGEX-KG vector [15]. Antisera were affinity-purified on fusion proteins that was either coupled to CNBr-activated Sepharose (Pharmacia, Freiburg, Germany) [16] or blotted to nitrocellulose [17].

Immunocytochemical detection of Munc13-4

Adult rats were anaesthetized with tribromoethanol and fixed by transcardial perfusion with 4% (w/v) paraformaldehyde/0.1 M phosphate buffer (pH 7.4). Lungs were immediately dissected, post-fixed for 1 h and cryoprotected with 30% (w/v) sucrose. On a frozen microtome, 14 μm thick sections were cut and mounted onto microscope slides for light microcopic immunocytochemistry. Endogenous peroxidase activity was blocked by incubation for 20 min at room temperature with 0.5% (v/v) H_2O_2 in methanol. Sections were probed with affinity-purified antibodies to Munc13-4 and labelled according to published procedures with the steptavidin/biotin/horseradish peroxidase ('ABC') method (Dako, Glostrup, Denmark), followed by a histochemical nickel-intensified horseradish peroxidase reaction with 3,3′-diaminobenzidine [4]. Sections were counterstained with Kernechtrot (Merck, Darmstadt, Germany).

Miscellaneous

Multiple rat tissue mRNA blots were purchased from ClonTech (Heidelberg, Germany) and hybridized at high stringency with an 0.7 kb *Sac*I-*Apa*I-fragment (bp 2851–3554) from the Munc13-4 cDNA. SDS/PAGE and immunoblotting were performed using standard procedures [18,19].

RESULTS

Identification of proteins containing MHDs

In initial cDNA database searches we identified two yeast ORFs that exhibited similarities with Munc13 proteins outside the conserved C$_2$-domains; *S. cerevisiae* yor296w, presumably involved in bud formation, and *S. pombe* c11e3 (Figures 1 and 2). Two profiles for MHD consensus sequences, designated MHD1 and MHD2 for MHDs 1 and 2, were constructed from alignments between Munc13-sequences and the novel yeast proteins. Interestingly, MHD1 and MHD2 enclose a central C$_2$-domain in the two yeast ORFs, while they are arranged between two flanking C$_2$-domains in Munc13 proteins (Figure 1). Using these profiles multiple proteins containing MHDs were detected in the current databases (Figures 1 and 2). Apart from the rat, human, *C. elegans* and *D. melanogaster* Munc13 proteins and the yeast ORFs described above, these included the following proteins: (1)

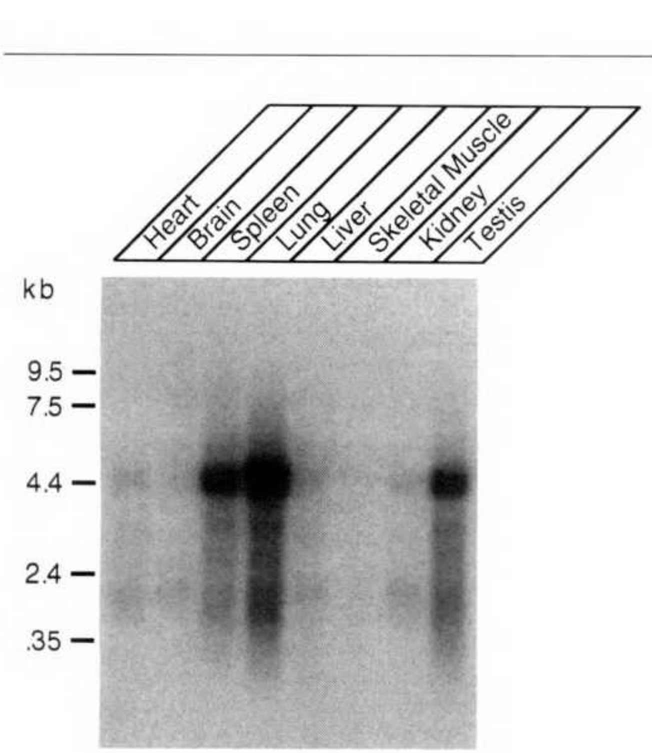

Figure 4 Tissue distribution of Munc13-4 mRNA

Blots containing polyadenylated-enriched RNA from the indicated rat tissues were hybridized at high stringency with a uniformly labelled probe from the coding region of Munc13-4 and exposed to film for 24 h. The same blots were rehybridized with a probe for glyceraldehyde-3-phosphate dehydrogenase to ensure uniform loading (not shown). Apart from skeletal muscle, Munc13-4 mRNA was expressed in all tissues examined. Strongest expression was observed in lung, spleen and testis.

C. elegans and human brain-specific angiogenesis inhibitor 1 (BAI1)-associated protein 3 (BAP3) which exhibit the typical Munc13-like domain structure with two C_2-domains flanking the two MHDs, but which lack the long N-terminus with the phorbol ester-binding C_1-domain (human BAP3 binds to BAI1, a member of the secretin-receptor family [20]); (2) rat Ca^{2+}-dependent activator protein for secretion (CAPS), a regulator of large dense-core vesicle secretion [21–23], and its *C. elegans* homologue unc-31p, both of which contain only MHD1 and are otherwise unrelated to Munc13 proteins; (3) human cerebellum postnatal development associated protein 2 (CPD2) (partial sequence which contains only MHD1), a protein with a putative role in cerebellum development; (4) four *A. thaliana* proteins of unknown function.

Cloning of Munc13-4

In addition to the above sequences our database searches resulted in the identification of several human ESTs containing MHDs. Three of these encoded parts of a protein with weak homology to human BAP3 (Clone ID/GenBank accession numbers: 231903/H92853; 700912/AA287381; 1035452/AA621650), demonstrating the existence of a family of mammalian BAP3-like proteins. Since the domain structure of BAP3 resembles that of the known Munc13 proteins, indicating that BAP3 and its homologues may also be functionally related to Munc13 proteins, we cloned the full-length sequence of the novel EST-encoded protein from rat lung cDNA. The resulting cDNA contained an ORF that encoded a protein of 1088 amino acid residues with a calculated molecular mass of 125 kDa (Figure 3). The primary structure of the novel protein was 34% identical to that of BAP3. In addition, the domain structures of the two proteins were identical, with two C_2-domains at the N- and C-termini flanking the central MHDs (Figures 1 and 3). Due to the highly conserved Munc13-like domain arrangement, and because its two C_2-domains were most closely related to the C_2-domains of Munc13 proteins (see [20] for a comparison of C_2-domains in BAP3 and Munc13), the novel protein was named Munc13-4.

Characterization of Munc13-4 mRNA and protein

RNA blots loaded with polyadenylated-enriched RNA from different tissues were hybridized at high stringency with a probe

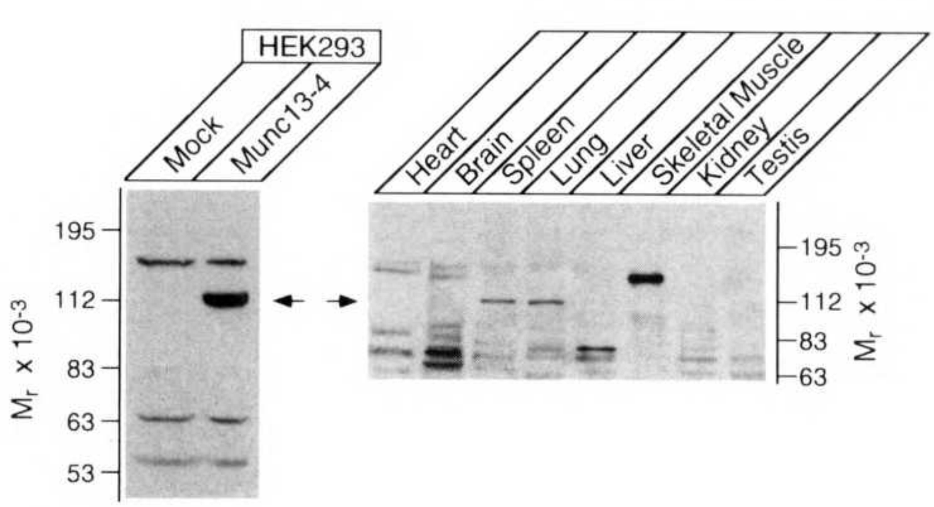

Figure 5 Tissue distribution of Munc13-4 protein

Left panel: homogenates from untransfected HEK-293 cells (Mock) and from HEK-293 cells that had been transfected with a eukaryotic expression vector encoding full-length Munc13-4 (pcDNA-Munc13-4) (20 μg/lane) were analysed by SDS/PAGE and immunoblotting using affinity-purified antibodies to Munc13-4. Full-length Munc13-4 (arrow) migrates as a 115 kDa polypeptide. Additional bands represent unidentified cross-reactive proteins. Right panel: homogenates from the indicated tissues (20 μg/lane) were analysed by SDS/PAGE and immunoblotting using affinity-purified antibodies to Munc13-4. Like Munc13-4 mRNA, Munc13-4 protein (arrow) was expressed most strongly in rat spleen and lung. Additional bands represent unidentified cross-reactive proteins.

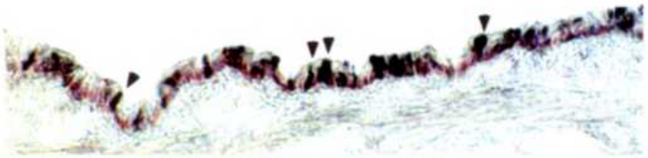

Figure 6 Munc13-4 localization in lung

Section through the bronchial epithelium of rat demonstrating the presence of Munc13-4 in goblet cells (examples are indicated by arrowheads).

specific for Munc13-4 (0.7 kb *Sac*I-*Apa*I fragment from the Munc13-4 cDNA). A 4.5 kb Munc13-4 mRNA transcript was detected in lung, spleen and testis (Figure 4). In heart muscle, kidney, liver, brain and skeletal muscle a very weak signal of similar size was detected. This demonstrates that in contrast to the brain-specific BAP3, Munc13-4 is expressed in a more ubiquitous manner.

For the basic protein chemical characterization of Munc13-4, we generated a polyclonal antibody to the C-terminus of Munc13-4 (residues 889–1088). The resulting rabbit antiserum was affinity-purified on immobilized antigen. Using the affinity-purified antibodies to Munc13-4 in Western blots of HEK-293 cells, a 115 kDa band was detected in cells transfected with the full-length eukaryotic Munc13-4 expression construct pcDNA-Munc13-4, but not in untransfected cells (Figure 5, left panel). A protein of the same size was detected by Western blot analysis in lung and spleen, confirming the non-neuronal expression pattern of Munc13-4 as determined by mRNA blotting (Figure 5, right panel). Protein levels in other tissues expressing Munc13-4 mRNA were below the detection limit of the antibody.

Munc13-4 protein was most strongly expressed in lung, and our affinity purified antibodies to Munc13-4 were essentially mono-specific for Munc13-4 in Western blots of lung homogenates (Figure 5, right panel). Therefore the distribution of Munc13-4 was examined in lung by light microscopic immunocytochemistry, employing affinity-purified antibodies to Munc13-4. We found that Munc13-4 was mainly present in goblet cells of the bronchial epithelium (Figure 6). Weaker staining was also observed in alveolar type II cells (results not shown).

DISCUSSION

With the exception of a ubiquitously expressed Munc13-2 splice variant, rat Munc13 proteins are expressed in a brain-specific manner [2,3]. Munc13-1, the most abundant isoform, is selectively targeted to presynaptic active zones where it plays an essential role in synaptic vesicle priming [4,7]. Since vesicle priming by Munc13 proteins appears to be specific for glutamatergic neurons [7], alternative pathways for (synaptic) vesicle priming have to be postulated for cells in which priming of secretory vesicles occurs (e.g. non-glutamatergic neurons or neuroendocrine cells). It is likely that some of these priming reactions, and particularly those that are taking place in neurons, are mediated by Munc13-like proteins. In addition, unrelated proteins may participate in vesicle priming reactions as exemplified by the roles of phosphatidylinositol transfer protein, phosphatidylinositol 4-kinase, and phosphatidylinositol-4-phosphate 5-kinase in the priming of chromaffin granules [24].

In the present study, we attempted to find novel Munc13-like proteins with putative roles in the regulation of membrane trafficking processes. For this purpose we developed protein profiles for two Munc13 consensus sequences (designated MHD1 and MHD2) as tools for the detection of Munc13-like proteins in database releases. Using these profiles we identified several proteins whose similarity to Munc13 proteins was highly significant but had not been detected before (Figures 1 and 2). Apart from the yeast ORFs used in the initial development of MHD profiles, four *A. thaliana* proteins of unknown function, and a human protein with a putative role in cerebellar development, our analysis identified two extremely interesting protein families with similarity to Munc13 proteins. One of these included rat CAPS and its *C. elegans* homologue unc-31p, while the other one was represented by human and *C. elegans* BAP3 and the Munc13-4 protein cloned in the present study.

Both CAPS and unc-31p contain only MHD1 and are otherwise unrelated to Munc13 proteins (Figure 1). In PC12-cells CAPS is required for a post-priming Ca^{2+}-dependent step in neurosecretion [21]. In brain CAPS is specifically localized to large dense-core vesicles whose secretion it appears to regulate in a manner similar to that in PC12-cells [22,23]. The localization and function of CAPS is different from that of Munc13-1, which is localized to presynapic active zones [4], not present on vesicles [3], and which mediates the vesicle priming step *per se* [7]. However, the involvement of CAPS and Munc13-1 in consecutive steps of vesicle secretion suggests that MHD1 has similar functions in the two proteins.

In contrast to CAPS, BAP3 and Munc13-4 share the same domain structure and exhibit significant similarity with Munc13 proteins throughout their sequence, indicating that BAP3, Munc13-4 and the three known Munc13 isoforms are evolutionary descendants of a common ancestor and have similar functional roles. Human BAP3 was originally identified as an interaction partner of BAI1, a member of the secretin-receptor family [20]. Interestingly, BAI1 is distantly related to the Ca^{2+}-independent recepter for α-latrotoxin (CIRL), which is involved in the regulation of synaptic neurotransmitter release [25,26]. This link to transmitter secretion and the brain-specific expression pattern of BAP3 raise the possibility that BAP3 mediates synaptic vesicle priming in neurons that are independent of priming by Munc13 isoforms (e.g. GABAergic neurons). Unlike BAP3, its homologue Munc13-4 is expressed in a ubiquitous fashion (Figures 4 and 5). Munc13-4 is strongly expressed in lung where it is mainly present in goblet cells of the bronchial epithelium (Figure 6) and alveolar type II cells (results not shown), suggesting a role in secretory processes. With the exception of an N-terminal splice variant of Munc13-2, which also appears to be expressed outside of the nervous system ([27] and N. Brose, unpublished work), this identifies Munc13-4 as the first bona fide ubiquitous Munc13 isoform.

Apart from the identification of novel Munc13-like proteins, an important objective of the present study was to use the newly identified molecules in order to gain insight into the molecular or enzymic function of Munc13 proteins and their relatives. Unfortunately, the function of the novel Munc13-like proteins identified here is either completely unknown (as in the case of the *A. thaliana* proteins) or has only been analysed 'phenomenologically' on the system or cellular level, but not in molecular terms. MHDs are present in organisms as phylogenetically distant as yeast and mammals, and some mammalian MHD-bearing proteins are expressed in a ubiquitous manner, suggesting that these domains take part in molecular processes common to all organisms and cells. Although Munc13 proteins (synaptic vesicle priming), CAPS/unc-31p (large dense-core vesicle exocytosis), BAP3 (CIRL-binding, neurosecretion), yor296w (bud formation) and Munc13-4 (present in secretory cells of the lung) are all linked to secretory processes of some sort, this common molecular role of MHDs remains unclear. In most of these molecules MHDs do not coincide with functionally characterized domains. Only the syntaxin-binding region of the known Munc13 proteins [5] overlaps partially with MHD1, but Munc13-4 does not bind syntaxins (H. Koch and N. Brose, unpublished work).

The MHD profiles described in the present study are very useful tools for the identification of Munc13-like proteins, that would otherwise have remained undetected. As with other conserved protein sequence domains, it is probable that the molecular role of MHDs will become evident once the 'common theme' in the known MHD-bearing proteins is recognized.

We thank S. Wenger for excellent technical assistance and I. Thanhauser and F. Benseler for DNA synthesis and sequencing. This study was supported by grant SFB406/A1 from the German Research Foundation (Bonn, Germany) and by the Max-Planck-Society (Munchen, Germany) N B is a Heisenberg Fellow of the German Research Foundation (Bonn, Germany)

REFERENCES

1 Sudhof, T C (1995) The synaptic vesicle cycle: A cascade of protein-protein interactions Nature (London) **375**, 645–653
2 Brose, N, Hofmann, K., Hata, Y. and Sudhof, T C (1995) Mammalian homologues of *C elegans* unc-13 gene define novel family of C_2-domain proteins J Biol Chem **270**, 25273–25280
3 Augustin, I, Betz, A, Herrmann, C., Jo, T. and Brose, N (1999) Differential expression of two novel Munc13 proteins in rat brain Biochem. J **337**, 363–371
4 Betz, A, Ashery, U, Rickmann, M., Augustin, I, Neher, E, Sudhof, T C, Rettig, J and Brose, N. (1998) Munc13–1 is a presynaptic phorbol ester receptor that enhances neurotransmitter release Neuron **21**, 123–136
5 Betz, A, Okamoto, M, Benseler, F and Brose, N (1997) Direct interaction of the rat unc-13 homologue Munc13–1 with the N-terminus of syntaxin J Biol Chem **272**, 2520–2526
6 Orita, S, Naito, A., Sakaguchi, G, Maeda, M, Igarashi, H., Sasaki, T and Takai, Y (1997) Physical and functional interactions of DOC2 and Munc13 in Ca^{2+}-dependent exocytotic machinery J Biol Chem **272**, 16081–16084
7 Augustin, I, Rosenmund, C, Sudhof, T C and Brose, N (1999) Munc13–1 is essential for fusion competence of glutamatergic synaptic vesicles Nature (London) **400**, 457–461
8 Richmond, J E, Davis, W S and Jorgensen, E M (1999) Unc-13 is required for synaptic vesicle fusion in *C elegans* Nature Neurosci **2**, 959–964
9 Aravamudan, B, Fergestad, T, Davis, W S, Rodech, C K and Broadie, K (1999) *Drosophila* Unc-13 is essential for synaptic transmission Nature Neurosci **2**, 965–971
10 Devereux, J, Haeberli, P and Smithies, O (1984) A comprehensive set of sequence analysis programs for the VAX. Nucleic Acids Res **12**, 387–395
11 Bucher, P, Karplus, K, Moeri, N and Hofmann, K (1996) A flexible motif search technique based on generalized profiles Comput Chem **20**, 3–24
12 Henikoff, S and Henikoff, J G. (1992) Amino acid substitution matrices from protein blocks Proc Natl Acad Sci U S A. **89**, 10915–10919
13 Benson, D., Boguski, M, Lipman, D J and Ostell, J (1994) GenBank Nucleic Acids Res **22**, 3441–3444
14 Sambrook, J, Fritsch, E F and Maniatis, T (1989) Molecular Cloning A Laboratory Manual, Cold Spring Harbor Laboratory Press, Cold Spring Harbor, NY
15 Guan, K L and Dixon, J E (1991) Eukaryotic proteins expressed in *Escherichia coli* an improved thrombin cleavage and purification procedure of fusion proteins with glutathione-S-transferase Anal. Biochem **192**, 262–267
16 Harlow, E and Lane, D (1988) Antibodies: A Laboratory Manual, Cold Spring Harbor Laboratory Press, Cold Spring Harbor, NY
17 Brose, N, Thomas, A, Weber, M G and Jahn, R. (1990) A chloride- and calcium-dependent glutamate-binding protein from rat brain identification as a ubiquitous constituent of the inner mitochondrial membrane J Biol. Chem. **265**, 10604–10610
18 Laemmli, U K (1970) Cleavage of structural proteins during the assembly of the head of bacteriophage T4 Nature (London) **227**, 680–685
19 Towbin, H, Staehelin, T and Gordon, J (1979) Electrophoretic transfer of proteins from polyacrylamide gels to nitrocellulose sheets procedure and some applications Proc Natl. Acad Sci U S.A **76**, 4350–4354
20 Shiratsuchi, T, Oda, K, Nishimori, H, Suzuki, M, Takahashi, E, Tokino, T. and Nakamura, Y (1998) Cloning and characterization of BAP3 (BAI-associated protein 3), a C2 domain-containing protein that interacts with BAI1 Biochem Biophys Res Commun **251**, 158–165
21 Ann, K, Kowalchyk, J A, Loyet, K M and Martin, T F. (1997) Novel Ca2+-binding protein (CAPS) related to UNC-31 required for Ca2+-activated exocytosis. J Biol Chem **272**, 19637–19640
22 Berwin, B, Floor, E and Martin, T F. (1998) CAPS (mammalian UNC-31) protein localizes to membranes involved in dense-core vesicle exocytosis Neuron **21**, 137–145
23 Tandon, A, Bannykh, S, Kowalchyk, J A, Banerjee, A, Martin, T F and Balch, W E (1998) Differential regulation of exocytosis by calcium and CAPS in semi-intact synaptosomes Neuron **21**, 147–154
24 Martin, T F. (1998) Mechanisms of protein secretion in endocrine and exocrine cells Vitam. Horm. (San Diego) **54**, 207–226
25 Krasnoperov, V G, Bittner, M A, Beavis, R, Kuang, Y, Salnikow, K V, Chepurny, O G, Little, A R, Plotnikov, A N, Wu, D., Holz, R W and Petrenko, A G (1997) α-Latrotoxin stimulates exocytosis by the interaction with a neuronal G-protein-coupled receptor. Neuron **18**, 925–937
26 Lelianova, V G, Davletov, B A, Sterling, A, Rahman, M. A, Grishin, E V, Totty, N F and Ushkaryov, Y A (1997) α-Latrotoxin receptor, latrophilin, is a novel member of the secretin family of G-protein-coupled receptors J Biol Chem **272**, 21504–21508
27 Song, Y, Allenberg, M. and Silverman, M (1998) Cloning of a novel gene in the human kidney homologous to rat munc13s its potential role in diabetic nephropathy Kidney Int **53**, 1689–1695

Received 4 January 2000/16 March 2000, accepted 31 March 2000

Biochem. J. (2000) 349, 255–260 (Printed in Great Britain)

FM1-43 reports plasma membrane phospholipid scrambling in T-lymphocytes

Adam ZWEIFACH[1]

Department of Physiology and Biophysics and the Department of Immunology, University of Colorado Health Sciences Center, 4200 E. 9th Ave.,
Denver, CO 80262, U.S.A.

We have found using imaging techniques that stimulating Jurkat human leukaemic T-cells with ionomycin in the presence of FM1-43, a dye used to monitor exocytosis and endocytosis, causes large (6–10-fold) increases in FM1-43 fluorescence. These responses are too large to be caused by exocytosis. Instead, three lines of evidence suggest that FM1-43 is responding to phospholipid scrambling. First, ionomycin also stimulates increases in the fluorescence of annexin V, a phosphatidylserine-specific probe, while thapsigargin does not stimulate fluorescence increases of either probe. Secondly, cells that exhibit FM1-43 fluorescence increases after ionomycin stimulation stain with annexin V once FM1-43 is washed out. Thirdly, ionomycin stimulates uptake of 7-nitrobenz-2-oxa-1,3-diazole-labelled phosphatidylcholine, a specific assay for scramblase activity, whereas thapsigargin does not. We find that FM1-43 reports phospholipid scrambling with 'better' kinetics than annexin V, and does require extracellular Ca^{2+} to report phospholipid scrambling. We suggest that FM1-43 may be a useful probe to study the dynamics of phospholipid scrambling. The results are the first demonstration that FM1-43 can respond significantly to a biological process other than vesicular trafficking.

Key words: annexin V, necrosis, phosphatidylserine exposure.

INTRODUCTION

Plasma membrane lipid composition is asymmetric in most healthy mammalian cells [1]. An aminophospholipid translocase ensures that essentially all membrane phosphatidylserine (PS) and phosphatidylethanolamine (PE) reside in the inner leaflet of the plasma membrane, while phosphatidylcholine (PC) and sphingomyelin (SM) are found in both leaflets. One of the earliest detectable events in cells undergoing apoptosis or necrosis is a disruption of normal plasma membrane lipid asymmetry, resulting in exposure of PS on the outer leaflet [2]. Exposed PS can activate the alternative pathway of complement [3,4] and act as a macrophage recognition signal [5], effects that contribute to the destruction and removal of dying cells. Phospholipid scrambling is also a key event in the normal activation of platelets [6]. Because phospholipid scrambling is an early event in apoptotic or necrotic cell death [2], the development of a specific probe, annexin V, which identifies cells exposing PS [7], has contributed enormously to our understanding of the sequence of events leading to cell death. Annexin V, a recombinant protein that can be coupled with a fluorophore, binds to PS in the presence of extracellular Ca^{2+} (Ca^{2+}_o) [8], making it possible to identify cells in the early stages of cell death and to follow the course of their progression through the process.

FM1-43 is a styryl dye that has been used widely to monitor exocytosis and endocytosis [9]. It is essentially non-fluorescent in aqueous solution. Upon binding to membranes, its quantum yield increases several-hundredfold, and it is not able to cross from the outer to the inner leaflet of intact membranes [10]. In the present report, we provide evidence that FM1-43 fluorescence is sensitive to changes in plasma membrane lipid composition that accompany phospholipid scrambling stimulated by ionomycin in Jurkat human leukaemic T-cells. FM1-43 is likely to be a useful probe for monitoring phospholipid scrambling, as it reports scrambling with 'better' kinetics than annexin V, and does not require extracellular Ca^{2+} to bind to scrambled membranes. These results are the first demonstration that FM1-43 can respond significantly to a biological process other than vesicular trafficking.

MATERIALS AND METHODS

Chemicals, reagents and cells

Salts for physiological solutions and poly-L-lysine were from Sigma–Aldrich (St. Louis, MO, U.S.A.). Fura-2 AM and FM1-43 were from Molecular Probes (Eugene, OR, U.S.A.). FITC-labelled annexin V was from R&D Systems (San Diego, CA, U.S.A.). Thapsigargin (TG) and ionomycin were purchased from Alexis Biochemicals (San Diego, CA, U.S.A.). C_6 NBD-PC was from Avanti Polar Lipids (Birmingham, AL, U.S.A.) (NBD is 7-nitrobenz-2-oxa-1,3-diazole). RPMI 1640 medium and tissue-culture plastic were obtained from Fisher Scientific (Pittsburgh, PA, U.S.A.). Fetal-calf serum, glutamine and antibiotics were purchased from Gemini Bioproducts (Calabassas, CA, U.S.A.). Jurkat E6-1 cells were provided by Dr Michael Cahalan (University of California, Irvine, CA, U.S.A.), and were maintained in RPMI medium supplemented with 2 mM glutamine, 10 % (v/v) heat-inactivated fetal-calf serum and antibiotics at 37 °C in a humidified incubator. For experiments in which Fura-2 was used to assess membrane integrity, cells were loaded by incubating them with 1 μM Fura-2 acetoxymethyl ester (Fura-2 AM) in cell-culture medium for 30 min at room temperature. Cells were washed twice with fresh medium before use. Ringer's solution contained (in mM): 145 NaCl, 4.5 KCl, 1 $MgCl_2$, 2 $CaCl_2$, 5 Hepes and 10 glucose (adjusted to pH 7.4 with NaOH). Ca^{2+}-free

---

Abbreviations used: Ca^{2+}_o, extracellular calcium, MC 540, merocyanine 540, PC, phosphatidylcholine, PE, phosphatidylethanolamine, PS, phosphatidylserine, ROI, region of interest, SM, sphingomyelin, TG, thapsigargin, Fura-2 AM, Fura-2 acetoxymethyl ester, NBD, 7-nitrobenz-2-oxa-1,3-diazole

[1] e-mail: adam.zweifach@UCHSC.edu

Ringer's solution was identical, except that CaCl$_2$ was replaced with MgCl$_2$.

Imaging

Experiments were performed at room temperature with an imaging system described previously [11]. A Nikon PlanFluor 40× oil objective (N.A 1.4) was used for all experiments. Excitation light was filtered with a 485 nm bandpass filter for FM1-43 and FITC–annexin V, and a 360 nm bandpass filter for Fura-2. Emitted light was collected with a 595 nm bandpass filter for FM1-43, a 515 nm bandpass filter for FITC–annexin V, and a 510 nm bandpass filter for Fura-2. A Fura-BCECF [2′,7′-bis-(2-carboxyethyl)-5(6)-carboxyfluorescein] dichroic mirror was used. Images were acquired with 8 × 8 binning at a rate of one frame every 15 s. Images were analysed by drawing regions of interest (ROIs) over cells, and also over a cell-free region that was used as a background for FM1-43 or FITC–annexin. The mean intensity for all the ROIs in an image was computed, and exported as a text file to Igor Pro (Wavemetrics, Lake Oswego, OR, U.S.A.) for further processing. After background subtraction, single-cell fluorescence data were normalized to each cell's pre-stimulation fluorescence intensity.

NBD-PC uptake experiments

Cells were incubated in normal Ringer's solution containing 1 μg/ml NBD-PC with or without either 1 μM ionomycin or TG for 20 min at room temperature, and then centrifuged and resuspended in Ca^{2+}-free Ringer's solution 5 % fatty-acid-free BSA for 5 min to extract outer leaflet NBD-PC. They were then washed twice with normal Ringer's solution, and examined on the imaging system using FITC filters.

RESULTS

Ionomycin, but not TG, stimulates FM1-43 fluorescence increases in Jurkat cells

Exposure of Jurkat cells to ionomycin in the continuous presence of 3.2 μM FM1-43 at room temperature caused large increases in FM1-43 fluorescence (Figure 1). On average, fluorescence increased to levels ≈ 6-fold above control levels, although in some cells fluorescence increased as much as 15-fold. There was considerable variability in the delay until cells began to respond. TG, a drug that activates Ca^{2+} influx through Ca^{2+}-release-activated channels in Jurkat cells [12], did not cause FM1-43 brightening, and brightening was not observed when cells were stimulated with ionomycin in the absence of Ca$^{2+}_{o}$. When the fluorescence of cells loaded with Fura-2 AM was monitored at an excitation wavelength of 360 nm (the Ca^{2+}-insensitive isosbestic wavelength) to assess plasma membrane integrity, a small number of cells demonstrated abrupt decreases in Fura-2 fluorescence, consistent with plasma membrane disruption, but the majority (> 99 %) did not. Ionomycin-induced fluorescence increases were also observed with two other FM analogues [10]: FM2-10, a less hydrophobic FM dye, and FM4-64, which has a red-shifted excitation spectrum (results not shown).

We investigated whether FM1-43 fluorescence increases could be reversed by removing FM1-43 from the extracellular solution. When FM1-43 was washed out of the extracellular solution 800–1000 s after ionomycin stimulation, fluorescence was reduced by 60–70 %, to levels ≈ 2-fold above unstimulated values. The ≈ 30 % of fluorescence that remains might reflect dye trapped in cells as a result of endocytosis. We found that the fluorescence of cells that did not brighten in response to ionomycin was also reduced by 60–70 % upon washout of FM1-43 (results not shown). Thus a similar fraction of FM1-43 cannot be washed out of cells, whether they brighten or not. These results are consistent with the idea that dye internalization occurs at similar rates whether cells brighten or not, and that the internalized dye in cells that brighten is brighter because the dye in the membrane that was internalized was brighter.

FM1-43 brightening is due to phospholipid scrambling

The amount of FM1-43 brightening that was observed is too large to be due to exocytosis. Jurkat cells are not known to be secretory cells, although it is possible that ionomycin stimulates some exocytosis. For example, Chinese hamster ovary cells, considered, like Jurkat cells, to be non-secretory cells, increase their surface area by ≈ 20–30 % by exocytosis when intracellular calcium levels are raised to micromolar levels [13]. Membrane capacitance, a measure of cell-surface area, increases by a similar

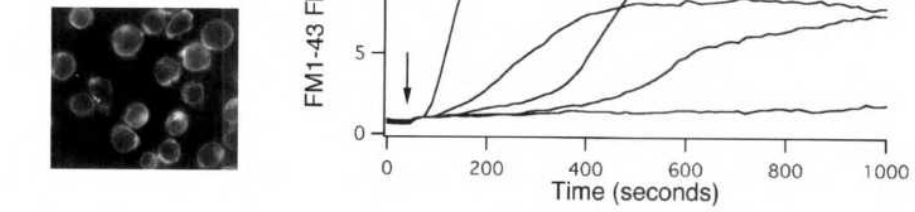

Figure 1 Ionomycin causes FM1-43 fluorescence increases

(**A**) FM1-43 fluorescence images taken before and 840 s after ionomycin stimulation. 2 × 2 binning was used for display purposes. (**B**) Representative single-cell fluorescence traces. Arrows indicate addition of ionomycin.

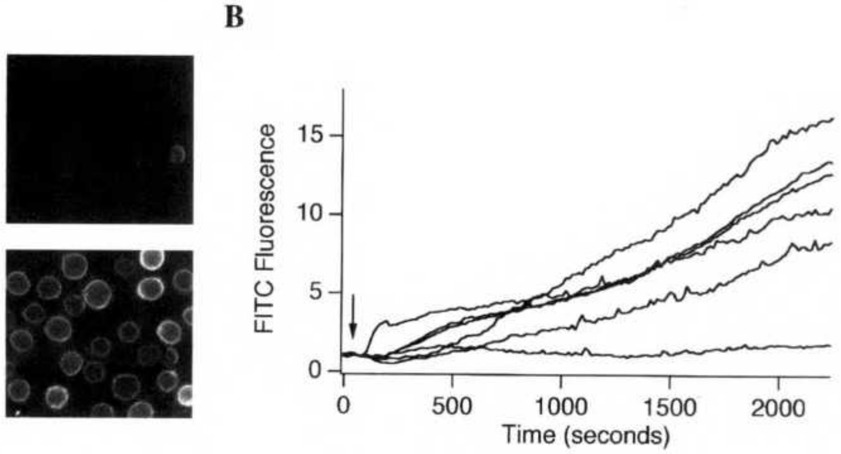

Figure 2 Ionomycin causes FITC–annexin V fluorescence increases

(**A**) Annexin V fluorescence images taken before and 1440 s after ionomycin stimulation. 2 × 2 binning was used for display purposes. (**B**) Representative single-cell fluorescence traces. Arrows indicate addition of ionomycin.

amount (15–20 %) in ionomycin-stimulated Jurkat cells (A. Zweifach and G. Burgett, unpublished work). We might therefore expect exocytosis to cause a 15–30 % increase in fluorescence, as increases in FM1-43 fluorescence are thought to correlate 1 : 1 with exocytosis when FM1-43 is present in the extracellular solution [14], except in cases in which secretory-granule contents are stained with FM1-43, casing enhanced fluorescence signals and visible single exocytic events [15,16]. Brightening of Jurkat cells in response to ionomycin was uniform, with no bright spots (Figure 1). Therefore, for exocytosis to cause 10-fold increases in FM1-43 fluorescence, Jurkat cells would have to undergo more exocytosis than is observed upon massive stimulation of secretory cells such as mast cells [17] and chromaffin cells [18], in which surface area increases 2–5-fold.

We conjectured, for the following three reasons, that the FM1-43 fluorescence increases we observed might be due to phospholipid scrambling. First, previous work using flow cytometry has demonstrated that treatment of Jurkat human leukaemic T-cells with the calcium ionophore ionomycin results in rapid phospholipid scrambling, as detected by annexin V labelling [19], consistent with the observation with Jurkat cells express high levels of the phospholipid scramblase [20]. Secondly, merocyanine 540 (or MC 540), a styryl dye that is structurally related to FM1-43, has been used to identify PS-exposing membranes [5]. MC 540 is believed to respond to decreases in lipid-packing density that accompany phospholipid scrambling. Thirdly, a recent study that examined the effect of lipid head-group charge on the apparent affinity of FM1-43 for lipid vesicles found that FM1-43 displayed increased affinity for vesicles containing PG, a phospholipid with a negatively charged head group [21]. PS exposure might cause similar effects.

To test the hypothesis that FM1-43 is responding to phospholipid scrambling, we performed the following three experiments. First, we tested whether the conditions that cause FM1-43 brightening also cause phospholipid scrambling, as assessed by the appearance of PS on the outer leaflet. We bathed cells in Ringer's solution containing 100 ng/ml FITC–annexin V, and stimulated them with 1 μM ionomycin (Figure 2). Initially, most cells exhibited little or no annexin staining, indicating normal plasma membrane asymmetry. Approx. 100 s after exposure to ionomycin, some cells began to brighten. There was considerable heterogeneity in the delay until cells began to brighten. FITC–annexin V fluorescence increased slowly and continuously in the cells that responded, with no sign of saturation over ≈ 40 min (Figure 2). As with the results described above for FM1-43, when the fluorescence of Fura-2 was monitored at an excitation wavelength of 360 nm to assess plasma membrane integrity, only a small number of cells demonstrated abrupt decreases in Fura-2 fluorescence. TG treatment did not cause increased staining with FITC–annexin over the ≈ 40-min observation time, consistent with a previous report [22], and with our results with FM1-43.

Secondly, we tested whether individual cells that display FM1-43 brightening had exposed PS (Figure 3). We stimulated cells with ionomycin in the presence of FM1-43. The extracellular solution contained 1 mM Ca^{2+} to reduce the number of responding cells. Figure 3 shows images of a cluster of five cells using this protocol. In another experiment, in which an entire field of cells was monitored, 58 cells had brightened after 840 s. We then washed off FM1-43. The chamber was perfused with solution containing FITC–annexin V, and images were acquired ≈ 1000 s later. Three FM-brightened cells washed away, but the remaining 55 were all FITC–annexin V-positive. Note that two cells that were not stained with FM1-43 were positive for FITC–annexin V. These cells may have exposed PS after FM1-43 was removed. Thus there is a good correlation between FM1-43 brightening and staining with FITC–annexin. Note that we could not perform double-labelling experiments using FM1-43 and FITC- or rhodamine-conjugated annexin V to determine whether cells that exhibited FM1-43 brightening had exposed PS, since FM1-43 exhibits a broad emission spectrum that spans FITC and rhodamine emission wavelengths (≈ 515–595 nm).

Finally, we monitored phospholipid scramblase activity directly by measuring uptake of NBD-labelled PC [6,23,24] (Figure 4). Unstimulated control cells exhibited a low level of NBD-PC fluorescence, NBD-PC stained the plasma membrane, as well as intracellular organelles, consistent with previous reports that exogenous lipids label intracellular organelles [25]. Cells stimulated with ionomycin exhibited ≈ 10-fold higher levels of NBD-PC fluorescence than controls, indicating that ionomycin treatment stimulated uptake of NBD-PC. As in the case of unstimulated cells, both the plasma membrane and intracellular

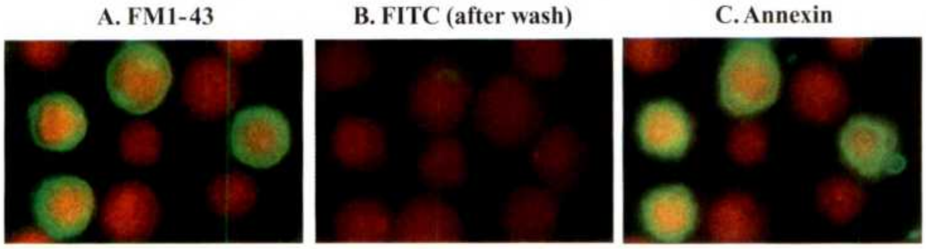

Figure 3 Cells that display FM1-43 brightening stain with annexin V

(**A**) Cells 840 s after stimulation with 2 μM ionomycin in the presence of 1 mM $Ca^{2+}{}_o$. Fura-2 fluorescence excited at 360 nm (red) and FM1-43 fluorescence (excitation at 485 nm, emission at 565 nm; green) are shown. (**B**) Cells after the washing out of FM1-43. As in (**A**), fluorescence of Fura-2 excited at 360 nm is shown, as well as FITC fluorescence (excitation at 485 nm, emission collected at 535 nm; green). (**C**) Cells after perfusion of the chamber with FITC–annexin. As in (**B**), fluorescence of Fura-2 excited at 360 nm (red), as well as FITC fluorescence (green), are shown. Cells that were FM1-43-bright were stained with FITC–annexin V. 2 × 2 binning was used for display.

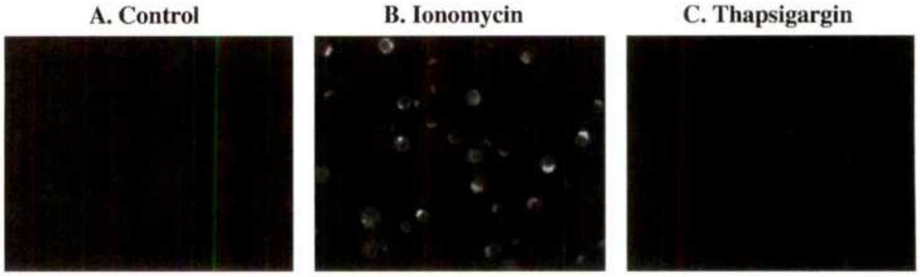

Figure 4 Ionomycin, but not TG, stimulates uptake of NBD-PC

(**A**) Fluorescence images of control cells incubated with NBD-PC in normal Ringer's solution for 20 min, followed by 5 min of albumin extraction. (**B**) Fluorescence images of cells incubated with NBD-PC in normal Ringer's solution + 1 μM ionomycin for 20 min followed by 5 min of albumin extraction. (**C**) Fluorescence images of cells incubated with NBD-PC in normal Ringer's + 1 μM TG for 20 min, followed by 5 min of albumin extraction. All images are scaled identically. 4 × 4 binning was used.

membranes were stained with NBD-PC. Consistent with the results obtained with FITC–annexin and FM1-43, TG-stimulated cells were indistinguishable from control ones, indicating that NBD-PC uptake was not stimulated by TG treatment.

FM1-43 reports the kinetics of phospholipid scrambling with higher fidelity than annexin V

A striking difference between annexin V and FM1-43 brightening is that annexin V fluorescence increases continuously, whereas FM1-43 fluorescence begins earlier and reaches a steady state after 15–20 min (compare Figures 1 and 2). Saturation of FM1-43 brightening could reflect saturation of the ability of FM1-43 to bind to scrambled membranes, or could indicate that phospholipid scrambling has resulted in a stable new phospholipid composition of the outer leaflet. We performed two experiments to distinguish between these possibilities (Figure 5). First, we stimulated cells with ionomycin in the presence of 3.2 μM FM1-43. After 1245 s, the chamber was perfused with solution containing 6.4 μM FM1-43 (Figure 5A). Fluorescence approximately doubled, indicating that the ability of FM1-43 to bind to the membrane was not saturated. Secondly, cells were stimulated with ionomycin in normal Ringer's solution containing 3.2 μM FM1-43 (Figure 5B). After 1185 s, the chamber was perfused with EGTA/Ringer's solution lacking Ca^{2+}, but containing FM1-43. Fluorescence approximately doubled following perfusion of the chamber with $Ca^{2+}{}_o$-free solution. The brightening observed following removal of $Ca^{2+}{}_o$ is consistent with the idea FM1-43 responds to phospholipid scrambling, in part due to increased negative surface charge (see above). Note that when the identical experiment was performed with annexin V, fluorescence decreased to the baseline level within 30 s (results not shown), consistent with the known Ca^{2+}-dependence of annexin V binding to PS [7]. Importantly, these results suggest that saturation of FM1-43 brightening does not reflect saturation of FM1-43 binding, but reflects rather the fact that membrane composition has reached a steady state.

The slower time course of FITC–annexin V compared with FM1-43 fluorescence increases, and the observation that FM1-43 apparently reports a stable phospholipid composition after 15–20 min while FITC–annexin V does not, can be explained if FITC–annexin V binds more slowly to scrambled membranes than FM1-43. If this is the case, the slow binding of FITC–annexin V would distort the apparent kinetics of phospholipid scrambling. To test this, we performed the experiments illustrated in Figure 5(C). Cells were stimulated with 1 μM ionomycin in normal Ringer's solution. After FM1-43 fluorescence had increased to a stable elevated value, the chamber was perfused with FM1-43-free solution. As described above, fluorescence was reduced by ≈ 70 % by the washing procedure. The chamber was then perfused with normal Ringer's solution containing either FM1-43 or FITC–annexin V, and the time course of fluorescence increases was analysed. FM1-43 fluorescence increased rapidly after re-addition, reaching a steady-state level equivalent to the pre-washout level within two frames (30 s). by contrast, when FITC–annexin V was added following washout of FM1-43, fluorescence increased extremely slowly. We conclude that FITC–annexin V binding to PS-exposing membranes is extremely

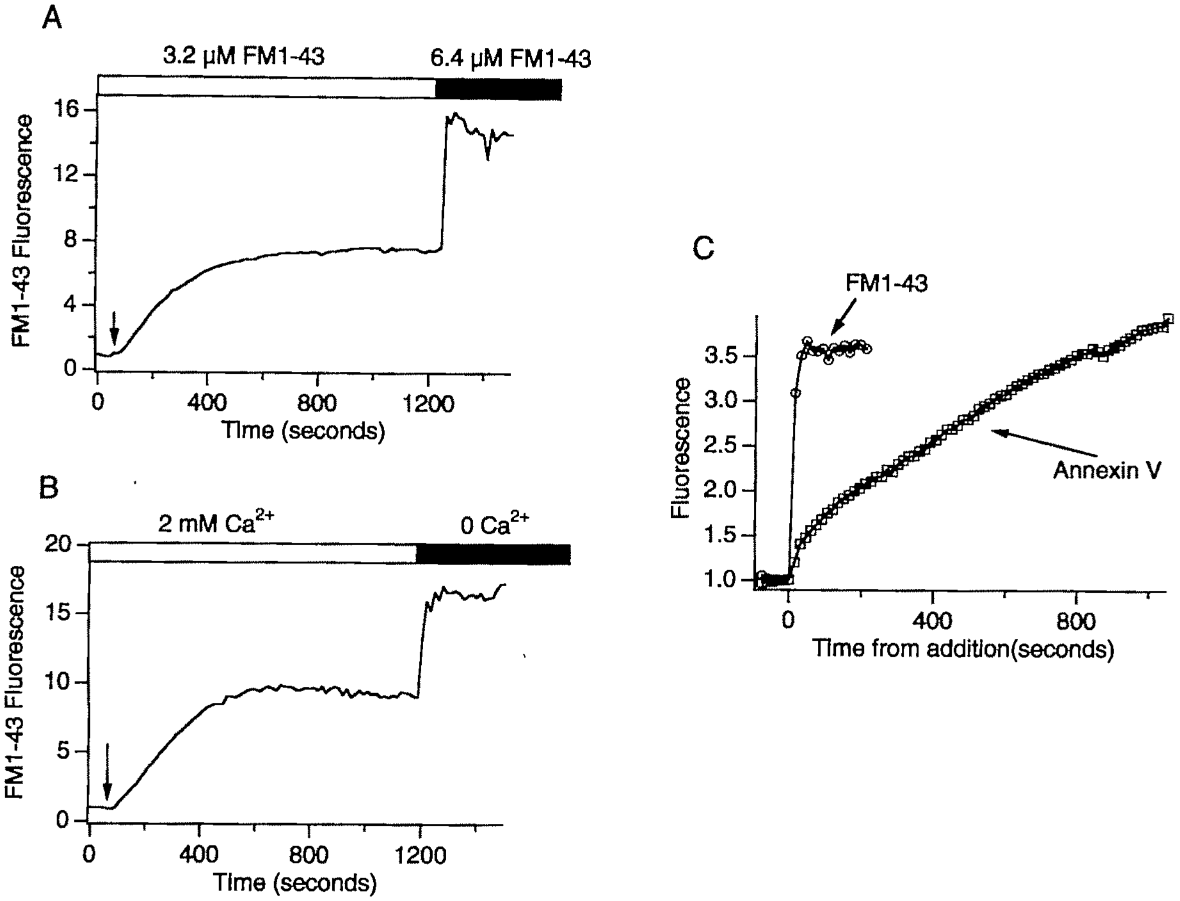

Figure 5 FM1-43 fluorescence can increase further after apparent saturation, and stains cells that have already scrambled phospholipids faster than FITC–annexin V

(**A**) Cells were stimulated with 1 μM ionomycin in normal Ringer's solution + 3.2 μM FM1-43. After stimulation (1245 s), the chamber was perfused with Ringer's containing 6.4 μM FM1-43 Fluorescence increased by ≈ 100% (**B**) Cells were stimulated with 1 μM ionomycin in normal Ringer's + 3.2 μM FM1-43 After stimulation (1140 s), the chamber was perfused with Ca^{2+}-free Ringer's containing 3.2 μM FM1-43 Fluorescence increased by ≈ 75%. (**C**) After cells were exposed to 1 μM ionomycin in the presence of FM1-43 (1140 s) the chamber was perfused with normal Ringer's solution that did not contain FM1-43 The chamber was then perfused with Ringer's solution containing FM1-43 or annexin V Traces are normalized to the fluorescence remaining after washout of FM1-43 Note that FM1-43 fluorescence increased rapidly, attaining a steady-state level after ≈ 30 s, while annexin V fluorescence increases more slowly

slow compared with FM1-43, and that the kinetics of phospholipid scrambling are faster than those reported with annexin V.

DISCUSSION

In the present paper, we provide evidence that FM1-43 is sensitive to plasma membrane phospholipid scrambling. Note that, on the basis of analogy to MC 540, we might also expect FM1-43 to respond to changes in lipid-packing density unrelated to scrambling. It seems most likely that the effects we observed were due primarily to scrambling-induced changes in packing, since conditions that cause FM1-43 fluorescence increases also cause scrambling, as assessed by either annexin staining or NBD-PC fluorescence increases. FM1-43 offers significant advantages over annexin V for the study of phospholipid scrambling FM1-43, unlike annexin V, does not require Ca^{2+}_0 to report phospholipid scrambling (Figure 5B), so studies designed to investigate the Ca^{2+}-dependence of phospholipid scrambling or apoptosis will be simpler to conduct with FM1-43 than with annexin V. FM1-43 binds more quickly to scrambled membranes than annexin V (Figure 5C), and is thus a more accurate reporter of the kinetics of phospholipid scrambling. Consistent with our results, a previous study found that annexin bound slowly to platelets that exposed POS [26]. It is possible to observe ionomycin-induced FM1-43, but not FITC–annexin V, fluorescence increases in Jurkat cells using a spectrofluorimeter (A. Zweifach, unpublished work), because the quantum yield of FM1-43 increases several-hundredfold when it partitions into lipid bilayers. In contrast, total FITC–annexin V fluorescence does not increase, but rather redistributes from the extracellular solution to membrane. FM1-43 is significantly less expensive than annexin V. FM1-43 also brightly stains cells that have been induced to undergo apoptosis by UV-irradiation (A. Zweifach, unpublished work), suggesting that FM1-43 may be used to identify cells in the earliest stages of apoptosis. Note that one disadvantage of the use of FM1-43 as a reporter of phospholipid scrambling is its broad emission spectrum (515–595 nm), which makes it difficult to use a second fluorophore that emits in either the FITC or rhodamine channels.

Our results are the first report that a process other than vesicular trafficking can cause significant increases in FM1-43 fluorescence. That FM1-43 can give large responses to phospholipid scrambling is a significant caveat for its use as an optical probe of exocytosis and endocytosis.

This work would not have been possible without the superb technical assistance of Georjeana A Burgett We thank Dr Michael Cahalan for the generous gift of Jurkat E6-1 cells. We also thank Drs Joseph K Angleson and William J Betz for critically reading a version of this work, and Donna L. Bratton and Valerie A. Fadok for helpful discussions This work was supported by NIH grant AI42964

REFERENCES

1 Bruckheimer, E. and Schroit, A (1996) Membrane phospholipid asymmetry host responses to the externalization of phosphatidylserine. J Leukocyte Biol **59**, 784–788

2 Martin, S., Reutelingsperger, C, McGahon, A, Rader, J, Van Schie, R, LaFace, D. and Green, D. (1995) Early redistribution of plasma membrane phosphatidylserine is a general feature of apoptosis regardless of the initiating stimulus: inhibition by overexpression of Bcl-2 and Abl. J Exp Med **182**, 1545–1556

3 Chonn, A, Cullis, P. and Devine, D. (1991) The role of surface charge in the activation of the classical and alternative pathway of complement by liposomes J Immunol **146**, 4234–4241

4 Wang, R, Phillips, G J, Medof, M and Mold, C (1993) Activation of the alternative complement pathway by exposure of phosphatidylethanolamine and phosphatidylserine on erythrocytes from sickle cell disease patients J. Clin Invest **92**, 1326–1335

5 Fadok, V, Voelker, D, Cambell, P, Cohen, J, Bratton, D and Henson, P (1992) Exposure of phosphatidylserine on the surface of apoptotic lymphocytes triggers specific recognition and removal by macrophages J Immunol **148**, 2207–2216

6 Chang, C-P, Zhao, J Wiedmer, T and Sims, P (1993) Contribution of platelet microparticle formation and granule secretion to the transmembrane migration of phosphatidylserine J Biol Chem **268**, 7171–7178

7 Vermes, I, Haanen, C and Steffens-Nakken, H R C (1995) A novel assay for apoptosis. flow cytometric detection of phosphatidylserine expression on early apoptotic cells using fluorescein-labelled annexin V. J. Immunol Methods **184**, 39–51

8 Andree, H, Reutelingsperger, C, Hauptmann, R, Hemker, H, Hermens, W and Willems, G (1990) binding of vascular anticoagulant alpha (VAC alpha) to planar phospholipid biolayers J. Biol. Chem **265**, 4923–4928

9 Cochilla, A, Angleson, J and Betz, W (1999) Monitoring secretory membrane with FM1-43 fluorescence. Annu Rev Neurosci **22**, 1–10

10 Betz, W., Mao, F and Smith, C (1996) Imaging exocytosis and endocytosis Curr Opin Neurobiol **6**, 363–371

11 Zweifach, A (2000) Target cell contact activates a highly selective capacitative calcium entry pathway in cytotoxic T lymphocytes J Cell Biol **148**, 603–614

Received 27 March 2000/25 April 2000; accepted 5 May 2000

12 Zweifach, A and Lewis, R. S (1993) Mitogen-regulated Ca^{2+} current of T lymphocytes is activated by depletion of intracellular Ca^{2+} stores Proc Natl. Acad Sci U.S.A. **90**, 6295–6299

13 Coorssen, J, Schmitt, H and Almers, W. (1996) Calcium triggers massive exocytosis in Chinese hamster ovary cells. EMBO J. **15**, 3787–3791

14 Smith, C. and Betz, W (1996) Simultaneous independent measurement of endocytosis and exocytosis Nature (London) **380**, 531–534

15 Haller, T, Ortmayr, J, Friedrich, F, Volkl, H and Dietl, P (1998) Dynamics of surfactant release in alveolar type II cells Proc Natl Acad Sci U S A **95**, 1579–1584

16 Angleson, J, Cochilla, A, Kilic, G, Nussinovitch, I. and Betz, W. (1999) Regulation of dense core release from neuroendocrine cells revealed by imagining single exocytic events Nat. Neurosci. **2**, 440–446

17 Neher, E (1988) The influence of intracellular calcium concentration on degranulation of dialysed mast cells from rat peritoneum J Physiol (Cambridge, U K) **395**, 193–214

18 Augustine, G. and Neher, E (1992) Calcium requirements for secretion in bovine chromaffin cells J Physiol (Cambridge, U K) **450**, 247–271

19 Li, W. and Tait, J (1998) Regulatory effect of CD9 on calcium-stimulated phosphatidylserine exposure in Jurkat T lymphocytes Arch Biochem Biophys **351**, 89–95

20 Zhao, J, Zhou, Q., Wiemer, T. and Sims, P (1998) Level of expression of phospholipid scramblase regulates induced movement of phosphatidylserine to the cell surface J Biol. Chem **273**, 6603–6606

21 Schote, U and Seelig, J (1998) Interaction of the neuronal marker dye FM1-43 with lipid membranes thermodynamics and lipid order Biochim Biophys Acta **1415**, 135–146

22 Hampton, M, Vanags, D., Porn-Ares, I and Orrenius, S (1996) Involvement of extracellular calcium in phosphatidylserine exposure during apoptosis FEBS Lett. **399**, 277–282

23 Bevers, E, Comfurius, P., Dekkers, D and Zwaal, R (1999) Lipid translocation across the plasma membrane of mammalian cells Biochim Biophys Acta **1439**, 317–330

24 Bratton, D, Fadok, V, Richter, D, Kailey, J, Guthrie, L and Henson, P. (1997) Appearance of phosphatidylserine on apoptotic cells requires calcium-mediated nonspecific flip-flop and is enhanced by loss of the aminophospholipid translocase J Biol Chem **272**, 26159–26165

25 Hanada, K and Pagano, R (1995) A chinese hamster ovary cell mutant defective in the non-endocytic uptake of fluorescent analogs of phosphatidylserine: isolation using a cytosol acidification protocol J Cell Biol **128**, 793–804

26 Dachary-Prigent, J., Pasquet, J-M, Freyssinet, J-M and Nurden, A. (1995) Calcium involvement in aminophospholipid exposure and microparticle formation during platelet activation a study using Ca^{2+} ATPase inhibitors Biochemistry **34**, 11625–11634

Biochem J (2000) 349, 261–266 (Printed in Great Britain)

A single amino acid substitution (Trp^{666} → Ala) in the interbox1/2 region of the interleukin-6 signal transducer gp130 abrogates binding of JAK1, and dominantly impairs signal transduction

Claude HAAN, Heike M. HERMANNS, Peter C. HEINRICH[1] and Iris BEHRMANN
Department of Biochemistry, RWTH Aachen, Pauwelsstr 30, 52074 Aachen, Germany

gp130 is the common signal-transducing receptor chain of interleukin (IL)-6-type cytokines. Here we describe, for the first time, a single amino acid substitution (Trp^{666} → Ala) in the membrane-proximal interbox1/2 region that abrogates activation of STAT (signal transducer and activator of transcription) transcription factors and the proliferative response of pro-B-cell transfectants. Moreover, association of the Janus kinase JAK1 is prevented. No signalling of heterodimeric IL-5 receptor (IL-5R)/gp130 chimaeras occurs in COS-7 cells, even when only a single cytoplasmic chain of a gp130 dimer contains the Trp^{666}Ala mutation, indicating that it acts dominantly.

Key words: cytokine receptor, interleukins, Jak/STAT pathway, Janus kinase.

INTRODUCTION

Interleukin (IL)-6 is a pleiotropic cytokine that plays a central role in host defence, e.g. it induces the acute-phase response and mediates proliferation and differentiation of B- and T-cells. Overexpression has been implicated in the pathology of a number of diseases, such as rheumatoid arthritis, Castleman's disease and multiple myeloma [1,2].

IL-6 belongs to a family of cytokines including IL-11, leukaemia inhibitory factor, oncostatin M, ciliary neurotrophic factor, cardiotrophin-1 and novel neurotrophin-1/B-cell-stimulating factor-3. These IL-6-type cytokines have overlapping functions, which might be explained by the fact that they all share gp130 as part of their multicomponent signalling receptor complexes. Whereas IL-6 and IL-11 induce homodimerization of gp130 after binding to their respective ligand-specific α-receptors, the others induce the heterodimerization of gp130 with the leukaemia inhibitory factor- or oncostatin M-receptor [1,3].

Like other cytokine receptors, gp130 transduces signals via the JAK/STAT (Janus kinase/signal transducers and activators of transcription) pathway. JAKs, which are cytoplasmic tyrosine kinases of the Janus family, are preassociated with the receptor. Upon cytokine-induced receptor aggregation, the JAKs are thought to transphosphorylate, and thereby autoactivate themselves. The kinases subsequently phosphorylate tyrosine residues in the receptor, providing docking sites for SH2-domain-containing signalling proteins. These include transcription factors of the STAT family. Upon phosphorylation, STATs translocate to the nucleus, where they bind to specific DNA sequences in the promoter regions of their target genes. In addition, phosphatases (SHP-1, SHP-2) and adaptor proteins, such as Shc, are recruited to certain receptors, thereby creating a link to the Ras/Raf/mitogen-activated protein kinase pathway [4,5].

The family of JAKs comprises four mammalian homologues: JAK1, JAK2, JAK3 and Tyk2. Cytokines utilizing gp130 have been reported to activate JAK1, JAK2 and Tyk2. Among these, JAK1 is essential for signal transduction, as demonstrated for JAK1-deficient fibrosarcoma cells and for cells derived from JAK1 knock-out mice [6,7]. The N-terminal half (≈ 600 amino acids) of the JAKs is involved in receptor binding, whereas the C-terminal region contains the kinase and the pseudokinase domains [8].

The membrane-proximal part of gp130 contains sequences that are conserved among various cytokine receptors and are crucial for JAK activation: box1, a proline-rich motif of eight amino acids, and box2, a cluster of hydrophobic residues followed by positively charged amino acids. Point mutations of amino acid residues in box1 of gp130 led to impaired binding [9] and activation [9,10] of JAKs, and abolished the proliferative response of stable Ba/F3 pro-B-cell transfectants after cytokine stimulation [11]. Although deletion of box2 did not abrogate binding to an overexpressed JAK2 construct [9], a truncated receptor lacking box2 was unable to sustain a proliferative response in Ba/F3 cells [11]. Apart from box1 and box2, regions N-terminally located to box1, between box1 and box2, or C-terminally located to box2 have been implicated in JAK binding and activation in certain receptors [12–19].

In the present paper, we show that an aromatic residue, Trp^{666}, in the interbox1/2 region is crucial for JAK binding to gp130. Receptor constructs with a single point mutation at this position are no longer able to associate with JAK1. Moreover, using heterodimeric receptor chimaeras, we found that Trp^{666} has to be present in both chains of a functional gp130 dimer to allow signalling to occur.

MATERIALS AND METHODS

Cell culture and transfection

Simian monkey kidney cells (COS-7 cells) were maintained in Dulbecco's modified Eagle's medium (DMEM) supplemented with 10% (v/v) fetal-calf serum (FCS), 100 mg/l streptomycin and 60 mg/l penicillin. Cells were grown at 37 °C in a water-saturated atmosphere in air/CO_2 (19:1). COS-7 cells were transiently transfected using the DEAE/chloroquine transfection method, with modifications as described previously [20].

Abbreviations used: DMEM, Dulbecco's modified Eagle's medium, EMSA, electrophoretic mobility-shift assay, EPOR, erythropoietin receptor, FCS, fetal-calf serum, JAK, Janus kinase, IL, interleukin; sIL-6R, soluble IL-6 receptor, SIE, *sis*-inducible element of the *c-fos* promoter, STAT, signal transducer and activator of transcription, WT, wild-type

[1] To whom correspondence should be addressed (e-mail heinrich@rwth-aachen de)

Ba/F3 cells were transfected by electroporation of 28 μg of either pSVLgp130 or the mutant constructs (see Figure 1), and 2 μg of pSV2neo using 3.5×10^6 cells in 0.8 ml of medium at 200 V and 70 ms. Selection with G418 (1 mg/ml) in IL-3-conditioned medium was initiated 24 h after transfection. Selected Ba/F3 clones were screened by flow cytometry for cell-surface expression of gp130. Recombinant IL-6 was prepared as described previously [21]. The specific activity was 2×10^6 B-cell stimulatory factor-2 units/mg protein Soluble IL-6 receptor (sIL-6R) was prepared in insect cells, as described previously [22].

Cell proliferation assay

Ba/F3 cells (2×10^4) expressing the receptor mutants were cultured in DMEM containing the indicated concentrations of IL-6 and 1 μg/ml sIL-6Rα, or conditioned medium from X63Ag-653 BPV-IL-3 myeloma cells as a source of IL-3. After 72 h of incubation, viable and metabolically active cells were quantified using the colorimetric cell proliferation kit, XTT (Boehringer Mannheim, Mannheim, Germany), as described by the manufacturer.

Construction of gp130 and IL-5Rα/β-gp130 mutants

Standard cloning procedures were performed throughout the present study. The mutations were introduced by the technique of PCR. The primers used were 5′-ATTGTCCTCTTTGACTA-3′(sense) and 5′-CTGGGCAAAATACCATCAC-3′ (antisense). The primers used for introducing the mutations were as follows: for the mutation Δbox1, 5′-AAAAAACACTCAAAGAGTCATATTGCCC-3′ (sense) and 5′-ACTCTTTGAGTGTTTTTTAATTAGGTCTCG-3′ (antisense); and for Trp^{666}Ala, 5′-TTGCCCAGGCGTCACCTCACACTCCTCC-3′ (sense) and 5′-TGAGGTGACGCCTGGGCAATATGACTCTTTG-3′ (antisense). The nucleotides that are underlined indicate the position where the mutation was introduced.

The restriction enzymes used for cloning the Trp^{666}Ala PCR-amplified fragment into the pSVL-based expression vector for gp130 [23] were *Eco*RI and *Asp*I. For insertion of the PCR fragments into the expression vector for IL-5Rβ/gp130 [24], *Eco*RI–*Bst*EII (Δbox1) and *Eco*RI–*Asp*I (Trp^{666}Ala) restriction sites were used. The corresponding IL-5Rα/gp130 chimaeras were generated by exchange of the *Xho*I–*Eco*RI fragment encoding the extracellular domain of IL-5Rβ with the one encoding the extracellular part of IL-5Rα. The gp130ΔMP mutant was generated by exchanging the region encoding the ectodomain of the construct IL-5Rβ/gp130ΔBB23 [25] with the region encoding the extracellular part of gp130 using *Xho*I and *Eco*RI restriction sites. The integrity of all constructs was verified by DNA sequencing.

Flow cytometry

Transiently transfected COS-7 cells or stably transfected Ba/F3-gp130 cells were resuspended in cold PBS supplemented with 5% (v/v) FCS and 0.1% (w/v) sodium azide (PBS/azide). Cells (5×10^5 to 1×10^6) in 100 μl of PBS/azide were incubated with 1 μg/ml of the corresponding monoclonal antibodies, anti-gp130 antibody BP8 (kindly provided by J. Wijdenes, Diaclone, Besançon, France), anti-IL-5Rα antibody 16-4 (kindly provided by J. Tavernier, University of Ghent, Ghent, Belgium) or anti-IL-5Rβ antibody S16 (Santa Cruz, Heidelberg, Germany) for 30 min at 4 °C. Cells were then washed with cold PBS/azide. To detect the antibodies bound to the full-length gp130, the cells were subsequently incubated in the dark with a 1:50 dilution of an *R*-phycoerythrin-conjugated anti-(mouse IgG) Fab fragment (Dianova, Hamburg, Germany) for 30 min at 4 °C. Cells were again washed with cold PBS/azide, and then were resuspended in PBS/azide with 1% (v/v) formaldehyde. From each sample, 10^4 cells were analysed by flow cytometry using a FACScalibur (Beckton–Dickinson, Heidelberg, Germany) equipped with a 488-nm argon laser.

Electrophoretic mobility-shift assays (EMSAs)

Cells were stimulated with 20 ng IL-6/ml and 1 μg sIL-6R/ml for 15 min, or with 10 ng IL-5/ml (Cell Concepts, Umkirch, Germany) for 30 min. EMSAs were performed as described previously [26]. Protein concentrations were measured with the BioRad™ protein assay. A double-stranded mutated *sis*-inducible element (SIE)-oligonucleotide from the c-*fos* promoter (m67SIE: 5′-GATCCGGGAGGGATTTACGGGAAATGCTG-3′) was labelled by filling-in 5′-protruding ends with the Klenow enzyme, using [α-^{32}P]dATP (3000 Ci/ml). This probe binds STAT1 and STAT3 homo- and hetero-dimers, resulting in retarded bands of different mobilities. Nuclear extracts containing 5 μg of protein were incubated with approx. 10 fmol (10000 c.p.m.) of probe in gel-shift incubation buffer [10 mM Hepes, pH 7.8/1 mM EDTA/5 mM $MgCl_2$/10% (v/v) glycerol/5 mM dithiothreitol/0.7 mM PMSF/0.1 mg/ml poly(dI-C)/1 mg/ml BSA] for 10 min at room temperature. The protein–DNA complexes were separated on a 4.5% (w/v) polyacrylamide gel containing 7.5% (v/v) glycerol in 0.25 × TBE (where 1 × TBE is 45 mM Tris/borate/1 mM EDTA) at 20 V/cm for 4 h Gels were fixed in an aqueous solution of 10% (v/v) methanol and 10% (v/v) acetic acid for 30 min, dried and then autoradiography was performed.

Cell lysis, immunoprecipitation and Western blot analysis

Cells were lysed on the dish with 500 μl of lysis buffer containing 1% Brij-96, 20 mM Tris/HCl, pH 7.5, 150 mM NaCl, 10 mM NaF, 1 mM sodium vanadate, 10 mM PMSF, 1 mM benzamidin, 5 μg/ml aprotinin, 3 μg/ml pepstatin, 5 μg/ml leupeptin and 1 mM EDTA. Lysates were cleared by centrifugation at 12000 ***g***. A monoclonal antibody raised against human IL5–Rβ (S16; Santa Cruz) was used for immunoprecipitation. After incubation overnight at 4 °C, the immunoprecipitates were collected by chromatography with protein A–Sepharose (1 h, 4 °C), washed three times with washing buffer (0.1% Brij 96/20 mM Tris/HCl, pH 7.5/150 mM NaCl/10 mM NaF/1 mM sodium vanadate/10 mM PMSF/1 mM benzamidin/5 μg/ml aprotinin/3 μg/ml pepstatin/5 μg/ml leupeptin/1 mM EDTA) and analysed further by SDS/PAGE The proteins were transferred to a PVDF membrane (Amersham, Braunschweig, Germany), probed with the respective antibodies and detected for signals using the ECL® system (Amersham). Anti-IL5Rβ (N20, Santa Cruz) and anti-JAK1 polyclonal antisera (kindly provided by A. Ziemicki, University of Bern, Switzerland) were used for detection. The horseradish-peroxidase-conjugated secondary antibodies were purchased from Dako (Copenhagen, Denmark).

RESULTS

A single amino acid substitution, Trp^{666}Ala, in the interbox1/2 region of gp130 leads to total abortion of the proliferative response of stably transfected Ba/F3 cells

The box1 region of gp130, comprising a number of conserved hydrophobic residues, has been shown to be involved in JAK activation and mediation of proliferative responses in Ba/F3 transfectants [10,11]. In the present work, we mutated a bulky

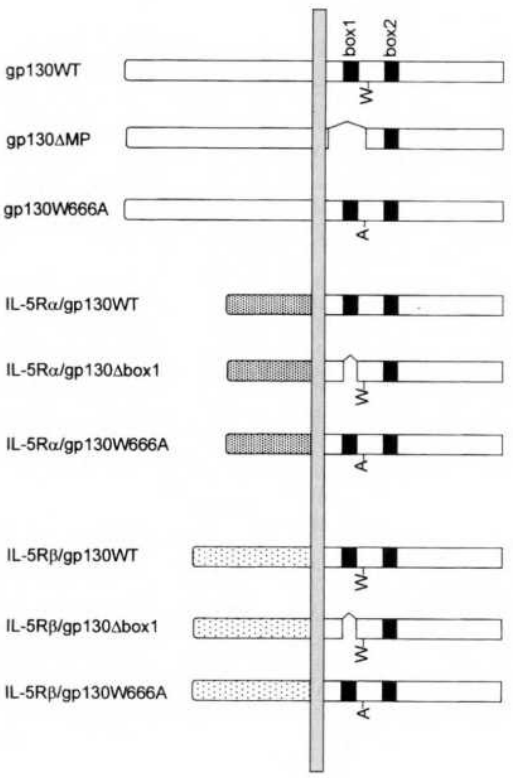

Figure 1 Schematic representation of the receptors used in the present study

The receptors consist of the extracellular region of gp130, IL-5Rα or IL-5Rβ, and the transmembrane and intracellular regions of gp130. Deletions and point mutations were introduced into the membrane-proximal part of gp130, as indicated.

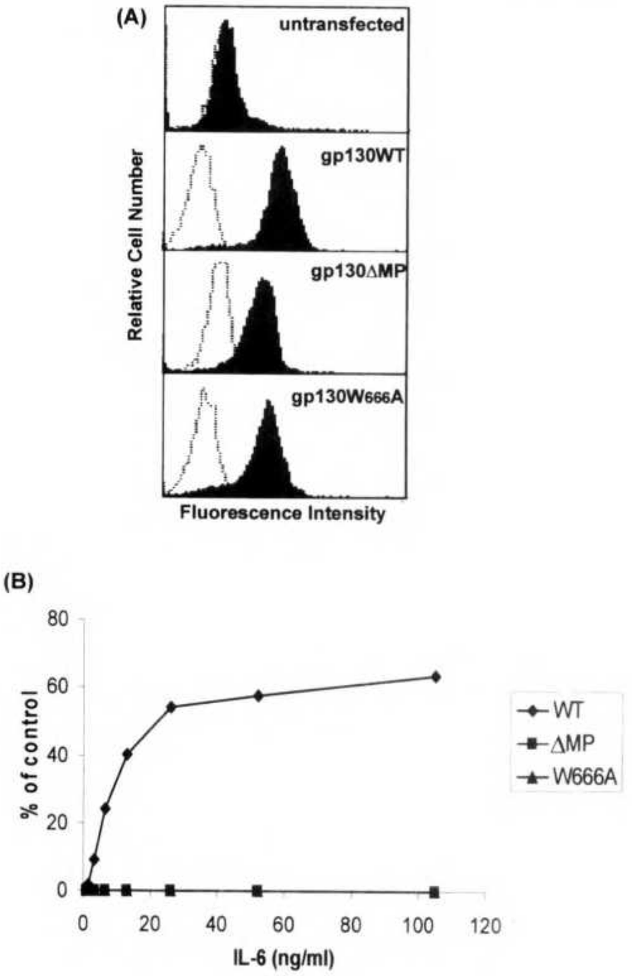

Figure 2 The mutations ΔMP and Trp^{666}Ala abrogate the gp130-mediated proliferative response in Ba/F3 transfectants

(**A**) Surface expression of gp130 on stable Ba/F3 clones. Parental cells and transfectants were incubated with the anti-gp130 monoclonal antibody BP-8, and subsequently with phycoerythrin-conjugated anti-mouse IgG(ab')2 (filled-in traces). The cells treated with secondary antibody alone are represented by dotted-line traces. (**B**) Proliferation of Ba/F3 transfectants. Cells were cultured for 4 days with increasing amounts of IL-6 in the presence of 1 μg/ml sIL-6Rα. Cell growth was assessed by an XTT test, and is represented as the percentage of the values obtained with IL-3 (set to 100%).

hydrophobic amino acid, Trp^{666}, in the inter-box1/2 region of gp130 to alanine (Figure 1), since protein–protein interactions are often mediated by hydrophobic residues. As a negative control, we constructed gp130ΔMP with a deletion of the membrane-proximal amino acids 643–666, including box1. We generated stable Ba/F3 transfectants with a similar surface expression of gp130, or the mutants thereof (Figure 2A). The gp130 wild-type (WT) and mutant (ΔMP and Trp^{666}Ala) Ba/F3 transfectants were cultured for 72 h with increasing amounts of IL-6 in the presence of the sIL-6R, which is known to act agonistically [27,28]. Subsequently, the metabolically active cells were quantified (Figure 2B). The cells expressing gp130WT proliferated at concentrations of IL-6 as low as 3.3 ng/ml, whereas the transfectants expressing the mutant receptors ΔMP and Trp^{666}Ala did not proliferate even at the highest IL-6 concentrations tested. However, all Ba/F3 clones expressing gp130WT or mutant receptors proliferated IL-3-dependently, demonstrating that their cell-growth machinery was functional. Thus the presence of Trp^{666} in the cytoplasmic region of gp130 is crucial for the proliferative response of Ba/F3-gp130 transfectants upon stimulation with IL-6/sIL-6R.

Mutation of Trp^{666} to alanine prevents the activation of STAT3 factors in stably transfected Ba/F3 cells

After having demonstrated the inability of the mutant gp130 Trp^{666}Ala to mediate proliferation of stably transfected Ba/F3 cells, we investigated its capability to activate STAT transcription factors upon cytokine treatment. STAT activation is known to be necessary for gp130-mediated proliferation of Ba/F3 tranfectants [29,30]. Three independent cell clones (Trp^{666}Ala/3, Trp^{666}Ala/6 and Trp^{666}Ala/7; Figure 3) were stimulated with 20 ng/ml IL-6 and 1 μg/ml sIL-6Rα for 30 min, nuclear extracts were prepared and analysed by EMSA with the radiolabelled SIE probe (Figure 3). In contrast with gp130WT, mutant gp130 Trp^{666}Ala was not able to induce STAT3 activation upon stimulation with IL-6/sIL-6Rα.

Mutation of Trp^{666} to alanine impairs JAK1 binding as potently as deletion of the box1 region

Since JAKs have been shown previously [4] to bind to the membrane-proximal region of cytokine receptors, the failure of the Trp^{666}Ala mutant to induce STAT3 activation might reflect its inability to bind JAKs. Because of the low expression levels of gp130WT and mutant proteins in Ba/F3 cells, co-precipitation experiments did not yield satisfactory results. Therefore we

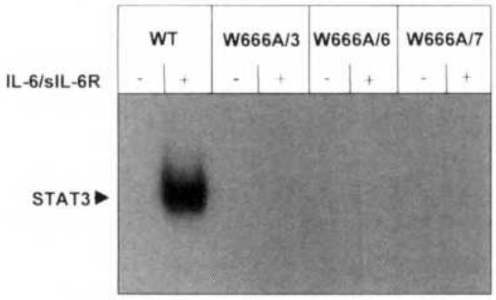

Figure 3 A single point mutation in gp130 (Trp^{666}Ala) abrogates STAT3 activation

Stable Ba/F3 transfectants expressing gp130 or the gp130Trp^{666}Ala mutant (three independent clones: Trp^{666}Ala/3, Trp^{666}Ala/6 and Trp^{666}Ala/7) were stimulated for 30 min with 20 ng IL-6/ml + 1 μg/ml sIL-6Rα. Nuclear extracts were prepared and analysed by EMSA using the SIE probe.

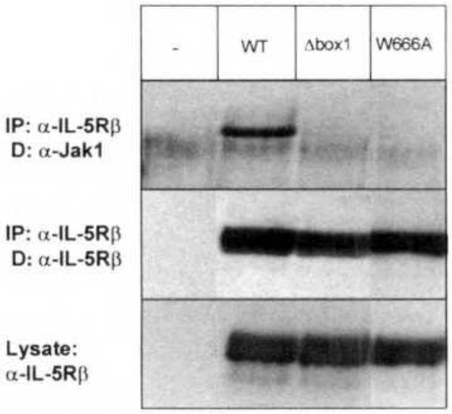

Figure 4 Gp130Δbox1 and gp130Trp^{666}Ala mutants do not associate with JAK1

Transiently transfected COS-7 cells expressing IL-5Rβ/gp130WT or mutants, as indicated, were lysed and subjected to immunoprecipitation using an anti-(IL-5Rβ) monoclonal antibody (S16), as described in the Materials and methods section.

switched to COS-7 cells, which can be efficiently transfected and yield high levels of heterologously expressed proteins. However, since COS-7 cells contain endogenous gp130, we transiently expressed chimaeric receptors consisting of the extracellular part of the IL-5Rβ chain and the transmembrane and intracellular parts of gp130WT, gp130Δbox1 or gp130 Trp^{666}Ala respectively. The chimaeric receptors were immunoprecipitated with an IL-5Rβ-specific antibody. Immunoprecipitates were analysed further by SDS/PAGE and Western blotting. Co-precipitation of JAK1 was detected using a JAK1-specific antibody. Whereas the gp130WT construct bound JAK1 efficiently, association of the kinase with the Δbox1 and Trp^{666}Ala mutants was greatly impaired (Figure 4). Therefore the inability of the Trp^{666}Ala mutant to associate with JAK1 is likely to account for the lack of receptor function.

Both chains of a functional gp130 dimer have to associate with JAKs

The use of heterodimeric receptor chimaeras on the basis of IL-5Rα- and β-chains enabled us to induce the dimerization of the cytoplasmic parts of a gp130 mutant with a WT receptor construct. Thus we could investigate whether both chains of a gp130 dimer have to associate with JAKs to activate STATs.

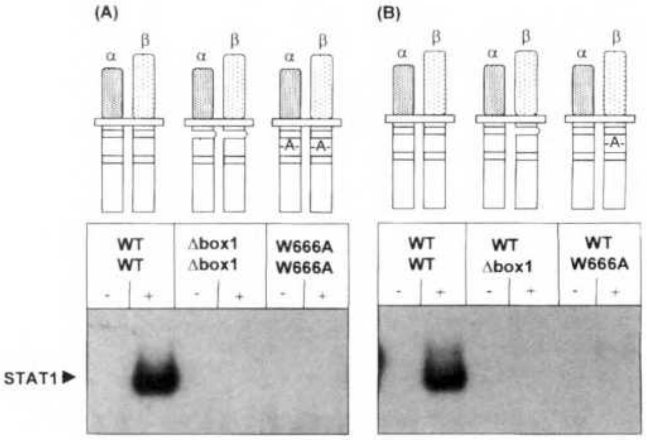

Figure 5 Gp130 mutants unable to associate with JAK1 prevent signal transduction even when dimerized with a WT gp130 construct

(**A**) Mutations were introduced into both chains of the gp130 dimer. (**B**) Dimerization of one WT with a mutant chain. COS-7 cells were transiently transfected with chimaeric expression constructs, as indicated. Post-transfection (48 to 72 h), the cells were starved (0% FCS) for 6 h, before they were stimulated with 10 ng/ml IL-5 for 30 min. Nuclear extracts were prepared and analysed by EMSA using the SIE probe. In contrast with Ba/F3 cells (Figure 2), only STAT1 was activated gp130-dependently in COS-7 cells, as observed previously [20,24].

COS-7 cells were transiently co-transfected with IL-5Rα and IL-5Rβ expression constructs, as depicted in Figure 5. WT and mutant constructs were expressed on the cell surface to a similar level, as determined by flow cytometry (results not shown). After stimulation with IL-5, nuclear extracts were analysed by EMSA. Homodimerization of two gp130WT cytoplasmic chains induced a strong STAT signal (Figure 5). Interestingly, IL-5-induced dimerization of one WT with one mutant chain that was unable to associate with JAK1 (Trp^{666}Ala or Δbox1) did not elicit a STAT signal. This shows that even a single point mutation that abrogates JAK association in one chain of a gp130 dimer is detrimental to the signalling capacity of such a receptor complex.

DISCUSSION

This is the first report showing that exchange of a single amino acid residue (Trp^{666}) in the cytoplasmic region of gp130 results in a receptor that is functionally inactive. Moreover, we have shown that a residue outside the conserved box1 and box2 regions of gp130 is important for coupling with JAKs. Finally, we provide evidence that the Trp^{666}Ala mutation even prevents receptor function when dimerized with the corresponding gp130WT cytoplasmic region.

To date, it was known that point mutations of two proline residues in box1 of gp130 led to impaired binding [9] and activation [9,10] of JAKs, and abolished the proliferative response in stable Ba/F3 pro-B-cell transfectants after cytokine stimulation [11]. In addition, combined point mutations of an isoleucine, a tryptophan and a valine residue within box1, or of five positively charged amino acid residues in the region between box1 and box2, abolished the growth response in Ba/F3 transfectants, but the cause for this was not analysed further [11]. A truncated receptor lacking box2 was also unable to mediate proliferation in Ba/F3 cells [11], although deletion of box2 did not abrogate binding to an overexpressed JAK2 construct [9].

Our data provide evidence that the gp130 region between box1 and box2 is also important for the interaction of gp130 and JAK1. The interaction of JAKs with cytokine receptors seems to be complex, and with large N-terminal portions of the kinases implicated in the mechanism. Thus it is not surprising that receptor regions in addition to box1 are necessary for JAK1 association. Hydrophobic interactions beween gp130 and JAK1 might well involve other residues in the membrane-proximal region, which is currently under investigation.

We cannot rule out, however, the possibility that Trp^{666} plays a structural role (rather than being a direct binding partner for JAKs), so that its substitution by alanine would destroy the structural interface of the receptor necessary for JAK association. The three-dimensional structure of the cytoplasmic region of gp130 (or other members of the cytokine receptor family) still awaits elucidation.

The importance of tryptophan residues in the interbox1/2 regions has been studied for other receptors: replacement of Trp^{650} with arginine for the human granulocyte colony stimulating factor receptor, or replacement of Trp^{282} of the erythropoietin receptor (EPOR) with arginine resulted in non-functional receptors [12,17]. For the EPOR mutant, association with JAK2 has been observed [18,31], or, conversely, could not be detected [32]. Mutation of Trp^{272} in the IL-2Rβ to glycine abrogated both association of JAK1 and JAK3 [19] and the ability of the mutated receptors to transmit proliferative signals [14,19]. However, replacement of Trp^{272} with alanine [16] or arginine [17] did not impair IL-2R function. Thus it seems difficult to draw general conclusions about the relevance of tryptophan residues in the interbox1/2 region for cytokine receptor function.

A further finding of this study is that mutation of Trp^{666} in just one chain of a gp130 dimer inactivates the receptor complex. The recruitment of JAKs by a single receptor chain is in itself not sufficient to induce a further downstream signal (Figure 5). Previously, we have shown that combination of an IL-5Rα/gp130 full-length chimaera with IL-5Rβ/gp130Δcyt (a mutant lacking the whole cytoplasmic region) is inactive, whereas the combination of an IL-5Rα/gp130 full-length chimaera with IL-5Rβ/gp130ΔB (a truncation mutant retaining only the membrane-proximal 68 amino acids and associating with JAKs) has the ability to activate STATs [20,24]. In addition, for other receptor systems evidence is provided that JAKs have to bind to both chains of a receptor dimer [31,33,34], thereby supporting the concept that two JAKs have to be brought into proximity upon cytokine-induced receptor dimerization to mediate their mutual activation by transphosphorylation. In addition, JAKs might have scaffolding functions, as suggested for the interferon α-receptor system [35].

The results of our study suggest that gp130 with only a single point mutation at position Trp^{666} should suppress signalling of the WT receptor in a dominant-negative fashion. This may be of interest for potential future therapeutic interventions, e.g. to inhibit the growth of IL-6-dependent plasmacytoma cells.

We thank H. Schmitz-Van de Leur for excellent technical assistance, and Dr L. Graeve for a critical reading of the manuscript We are grateful to Dr J. Wijdenes for the gift of the gp130-BP8 antibody, to Dr J Tavernier for the gift of the anti-IL-5R antibody, and to Dr A. Ziemicki for providing the JAK1-specific antiserum. This work was supported by the Deutsche Forschungsgemeinschaft (Bonn) and by Fonds der Chemischen Industrie (Frankfurt)

REFERENCES

1 Heinrich, P C., Behrmann, I, Muller-Newen, G., Schaper, F and Graeve, L (1998) Interleukin-6-type cytokine signalling through the gp130/JAK/STAT pathway Biochem J. **334**, 297–314

2 Kishimoto, T, Akira, S, Narazaki, M and Taga, T. (1995) Interleukin-6 family of cytokines and gp130 Blood **86**, 1243–1254

3 Senaldi, G, Varnum, B C, Sarmiento, U, Starnes, C, Lile, J, Scully, S, Guo, J, Elliott, G, McNinch, J, Shaklee, C L et al (1999) Novel neurotrophin-1/B cell-stimulating factor-3 a cytokine of the IL- 6 family. Proc Natl. Acad Sci. U S A **96**, 11458–11463

4 Ihle, J. N, Witthuhn, B A, Quelle, F W., Yamamoto, K and Silvennoinen, O (1995) Signaling through the hematopoietic cytokine receptors Annu. Rev Immunol **13**, 369–398

5 Darnell, Jr, J. E, Kerr, I M. and Stark, G R. (1994) JAK-STAT pathways and transcriptional activation in response to IFNs and other extracellular signaling proteins. Science **264**, 1415–1421

6 Guschin, D., Rogers, N, Briscoe, J., Witthuhn, B., Watling, D, Horn, F, Pellegrini, S, Yasukawa, K, Heinrich, P, Stark, G R et al (1995) A major role for the protein tyrosine kinase JAK1 in the JAK/STAT signal transduction pathway in response to interleukin-6 EMBO J **14**, 1421–1429

7 Rodig, S J, Meraz, M A, White, J. M, Lampe, P. A, Riley, J K., Arthur, C D., King, K L, Sheehan, K C, Yin, L, Pennica, D, Johnson, Jr, E M and Schreiber, R D. (1998) Disruption of the JAK1 gene demonstrates obligatory and nonredundant roles of the JAKs in cytokine-induced biologic responses Cell **93**, 373–383

8 Pellegrini, S and Dusanter-Fourt, I (1997) The structure, regulation and function of the Janus kinases (JAKs) and the signal transducers and activators of transcription (STATs). Eur. J Biochem. **248**, 615–633

9 Tanner, J W, Chen, W., Young, R. L, Longmore, G D and Shaw, A S. (1995) The conserved box1 motif of cytokine receptors is required for association with JAK kinases. J Biol Chem **270**, 6523–6530

10 Narazaki, M., Witthuhn, B A., Yoshida, K., Silvennoinen, O., Yasukawa, K, Ihle, J N, Kishimoto, T and Taga, T. (1994) Activation of JAK2 kinase mediated by the interleukin 6 signal transducer gp130. Proc Natl. Acad Sci. U S A. **91**, 2285–2289

11 Murakami, M, Narazaki, M, Hibi, M, Yawata, H, Yasukawa, K., Hamaguchi, M., Taga, T and Kishimoto, T. (1991) Critical cytoplasmic region of the interleukin 6 signal transducer gp130 is conserved in the cytokine receptor family Proc. Natl Acad. Sci U.S A **88**, 11349–11353

12 Barge, R M, de Koning, J. P, Pouwels, K, Dong, F, Lowenberg, B and Touw, I. P. (1996) Tryptophan 650 of human granulocyte colony-stimulating factor (G-CSF) receptor, implicated in the activation of JAK2, is also required for G-CSF-mediated activation of signaling complexes of the p21ras route Blood **87**, 2148–2153

13 Dorsch, M, Danial, N N., Rothman, P B. and Goff, S P. (1999) A thrombopoietin receptor mutant deficient in JAK-STAT activation mediates proliferation but not differentiation in UT-7 cells Blood **94**, 2676–2685

14 Goldsmith, M A, Xu, W., Amaral, M C, Kuczek, E S and Greene, W. C (1994) The cytoplasmic domain of the interleukin-2 receptor beta chain contains both unique and functionally redundant signal transduction elements. J Biol Chem **269**, 14698–14704

15 Lebrun, J J, Ali, S., Ullrich, A and Kelly, P A. (1995) Proline-rich sequence-mediated JAK2 association to the prolactin receptor is required but not sufficient for signal transduction J. Biol Chem. **270**, 10664–10670

16 Liu, K D, Lai, S Y., Goldsmith, M A. and Greene, W. C (1995) Identification of a variable region within the cytoplasmic tail of the IL-2 receptor beta chain that is required for growth signal transduction J. Biol. Chem. **270**, 22176–22181

17 Miura, O, Cleveland, J L and Ihle, J. N (1993) Inactivation of erythropoietin receptor function by point mutations in a region having homology with other cytokine receptors. Mol Cell Biol. **13**, 1788–17895

18 Witthuhn, B. A, Quelle, F W, Silvennoinen, O, Yi, T, Tang, B, Miura, O and Ihle, J N (1993) JAK2 associates with the erythropoietin receptor and is tyrosine phosphorylated and activated following stimulation with erythropoietin Cell **74**, 227–236

19 Zhu, M H, Berry, J A., Russell, S M and Leonard, W J (1998) Delineation of the regions of interleukin-2 (IL-2) receptor beta chain important for association of JAK1 and JAK3. JAK1-independent functional recruitment of JAK3 to Il-2Rbeta. J Biol Chem **273**, 10719–10725

20 Hermanns, H, Radtke, S., Haan, C, Schmitz-Van de Leur, H., Tavernier, J., Heinrich, P C. and Behrmann, I (1999) Contributions of leukemia inhibitory factor receptor and oncostatin M receptor to signal transduction in heterodimeric complexes with gp130 J Immunol **163**, 6651–6658

21 Arcone, R, Pucci, P, Zappacosta, F., Fontaine, V., Malorni, A, Marino, G and Ciliberto, G (1991) Single-step purification and structural characterization of human interleukin-6 produced in *Escherichia coli* from a T7 RNA polymerase expression vector Eur J. Biochem **198**, 541–547

22 Weiergraber, O, Hemmann, U., Kuster, A., Muller-Newen, G, Schneider, J, Rose-John, S, Kurschat, P, Brakenhoff, J. P, Hart, M H, Stabel, S and Heinrich, P C (1995) Soluble human interleukin-6 receptor Expression in insect cells, purification and characterization. Eur J. Biochem. **234**, 661–669

23 Schaper, F., Gendo, C., Eck, M., Schmitz, J., Grimm, C., Anhuf, D., Kerr, I. M. and Heinrich, P. C. (1998) Activation of the tyrosine phosphatase SHP2 via the interleukin-6 signal transducing receptor protein gp130 requires tyrosine kinase JAK1 and limits acute-phase protein expression. Biochem. J. **335**, 557–565

24 Behrmann, I., Janzen, C., Gerhartz, C., Schmitz-Van de Leur, H., Hermanns, H., Heesel, B., Graeve, L., Horn, F., Tavernier, J. and Heinrich, P. C. (1997) A single STAT recruitment module in a chimeric cytokine receptor complex is sufficient for STAT activation. J. Biol. Chem. **272**, 5269–5274

25 Thiel, S., Behrmann, I., Dittrich, E., Muys, L., Tavernier, J., Wijdenes, J., Heinrich, P. C. and Graeve, L. (1998) Internalization of the interleukin 6 signal transducer gp130 does not require activation of the JAK/STAT pathway. Biochem. J. **330**, 47–54

26 Wegenka, U. M., Buschmann, J., Lutticken, C., Heinrich, P. C. and Horn, F. (1993) Acute-phase response factor, a nuclear factor binding to acute-phase response elements, is rapidly activated by interleukin-6 at the posttranslational level. Mol. Cell. Biol. **13**, 276–288

27 Taga, T., Hibi, M., Hirata, Y., Yamasaki, K., Yasukawa, K., Matsuda, T., Hirano, T. and Kishimoto, T. (1989) Interleukin-6 triggers the association of its receptor with a possible signal transducer, gp130. Cell **58**, 573–581

28 Mackiewicz, A., Schooltink, H., Heinrich, P. C. and Rose-John, S. (1992) Complex of soluble human IL-6-receptor/IL-6 up-regulates expression of acute-phase proteins. J. Immunol. **149**, 2021–2027

29 Fukada, T., Hibi, M., Yamanaka, Y., Takahashi-Tezuka, M., Fujitani, Y., Yamaguchi, T., Nakajima, K. and Hirano, T. (1996) Two signals are necessary for cell proliferation induced by a cytokine receptor gp130: involvement of STAT3 in anti-apoptosis. Immunity **5**, 449–460

30 Schmitz, J., Dahmen, H., Grimm, C., Gendo, C., Muller-Newen, G., Heinrich, P. C. and Schaper, F. (2000) The cytoplasmic tyrosine motifs in full-length glycoprotein 130 have different roles in IL-6 signal transduction. J. Immunol. **164**, 848–854

31 Watowich, S. S., Liu, K. D., Xie, X., Lai, S. Y., Mikami, A., Longmore, G. D. and Goldsmith, M. A. (1999) Oligomerization and scaffolding functions of the erythropoietin receptor cytoplasmic tail. J. Biol. Chem. **274**, 5415–5421

32 Miura, O., Nakamura, N., Quelle, F. W., Witthuhn, B. A., Ihle, J. N. and Aoki, N. (1994) Erythropoietin induces association of the JAK2 protein tyrosine kinase with the erythropoietin receptor *in vivo*. Blood **84**, 1501–1507

33 Cornelis, S., Fache, I., Van der Heyden, J., Guisez, Y., Tavernier, J., Devos, R., Fiers, W. and Plaetinck, G. (1995) Characterization of critical residues in the cytoplasmic domain of the human interleukin-5 receptor alpha chain required for growth signal transduction. Eur. J. Immunol. **25**, 1857–1864

34 Friedrich, K., Kammer, W., Erhardt, I., Brandlein, S., Sebald, W. and Moriggl, R. (1999) Activation of STAT5 by IL-4 relies on Janus kinase function but not on receptor tyrosine phosphorylation, and can contribute to both cell proliferation and gene regulation. Int. Immunol. **11**, 1283–1294

35 Velazquez, L., Mogensen, K. E., Barbieri, G., Fellous, M., Uze, G. and Pellegrini, S. (1995) Distinct domains of the protein tyrosine kinase tyk2 required for binding of interferon-alpha/beta and for signal transduction. J. Biol. Chem. **270**, 3327–3334

Received 13 April 2000/8 May 2000; accepted 16 May 2000

Biochem J (2000) 349, 267–274 (Printed in Great Britain)

Non-linear antigenic regions in epidermal growth factor (EGF) and transforming growth factor α (TGFα) studied by EGF–TGFα chimaeras

Monique L. M. VAN DE POLL[1], Walter VAN ROTTERDAM, Mireille M. GADELLAA, Catelijne STORTELERS,
Marianne J. H. VAN VUGT and Everardus J. J. VAN ZOELEN
Department of Cell Biology, University of Nijmegen, Toernooiveld 1, 6525 ED Nijmegen, The Netherlands

With the help of 16 chimaeras between human epidermal growth factor (hEGF) and human transforming growth factor α (hTGFα), a detailed analysis was performed on the epitope recognized by two polyclonal antibodies raised against hEGF, and one polyclonal antibody raised against hTGFα. All three antibodies recognized essentially the same antigenic site, a non-linear and conformation-dependent sequence that is located near the second and fourth disulphide-bonded cysteines and that includes the start of the B-loop β-sheet. The epitope recognized by the anti-hEGF antibodies was further characterized using 8 chimaeras between hEGF and an EGF-repeat from *Drosophila* Notch and was found to include Met^{21}, Ala^{30} and Asn^{32}. All three polyclonal antibodies were able to neutralize the biological activity of the respective growth factor when tested on 32D murine haematopoietic progenitor cells transfected with ErbB-1, indicating that the receptor binding domain is shielded upon binding of the antibody.

Key words: antibodies, conformation-dependent, epitope mapping, discontinuous.

INTRODUCTION

Human epidermal growth factor (hEGF) and human transforming growth factor α (hTGFα) are single-chain polypeptides of 53 and 50 amino acids respectively [1]. The polypeptide chain is folded in a well-defined conformation, which is largely determined by the presence of six identically spaced disulphide-bonded cysteine residues and two highly conserved glycine residues. The structures of hEGF and hTGFα can be divided into three disulphide-bonded loops: the A-loop (residues 6–19) containing some α-helical structure, the B-loop (residues 20–31) forming a two-stranded anti-parallel β-sheet, and the C-loop (residues 33–42), which is part of a second β-sheet structure. Between the fourth and fifth cysteine residues a single amino acid (Asn^{32} in hEGF and Val^{33} in hTGFα) functions as a hinge. The loops are linked to linear sequences at both the N- and C-termini [1].

EGF and TGFα bind to and activate a tyrosine kinase receptor known as the EGF receptor or ErbB-1, and by virtue of this interaction they are potent mitogens that stimulate cellular proliferation and differentiation in a wide variety of cell types [2,3]. High expression of members of the EGF family, in particular TGFα, has been found in several human cancers and the co-expression of EGF receptors in these tumours increases the possibility of autocrine growth stimulation. In general, high expression of TGFα in human malignant effusions has been found to correlate with poor prognosis [4–6]. In the past, antisera have been generated as a diagnostic tool to detect EGF and TGFα expression in tissue samples. In addition, monoclonal and site-specific polyclonal antibodies have been used in fundamental research to identify functional epitopes.

Antigenic regions in TGFα have been identified in the past either by the ability of anti-peptide antisera to recognize native TGFα [7–9] or by the ability of anti-TGFα antibodies to react with linear peptide fragments that cover the entire sequence of the protein [10–12]. In this way both the N-terminal tail (residues 1–9), the B-loop (residues 22–34) as well as the C-terminus (residues 34–50) were found to be immunoreactive sites.

Similar studies on the antigenic sites in EGF have recognized the B-loop (residues 22–32) as an immunodominant region [13]. On the other hand, when polyclonal antisera were raised against the intact protein all kinds of monospecific antibodies could be identified, by affinity purification, against peptide fragments encompassing the entire EGF sequence [13]. This indicates that antigenic regions are present over the entire molecule. However, it gives no information on the most prevalent immunoreactive site in EGF.

Using linear peptide fragments to either map epitopes or identify immunodominant regions on proteins has the disadvantage that only linear, non-conformational, epitopes can be detected, whereas discontinuous or conformational epitopes remain unrevealed. Thus several monoclonal antibodies raised against native EGF or TGFα were found to be unable to bind any of the linear peptide fragments and showed no affinity for the intact protein after reduction of disulphide bridges. This indicates that they recognize a thus far unknown conformational epitope [12,13].

To identify regions important for receptor binding, we have previously constructed a large panel of hEGF–hTGFα chimaeras [14,15] as well as chimaeras between hEGF and an EGF repeat from *Drosophila* Notch, a 300 kDa transmembrane protein with no apparent growth-factor activity [16,17]. In these chimaeras domains have been exchanged at the sites of the highly conserved cysteine residues to ensure optimal protein folding and biological activity. Fine-tuning to individual amino acids was achieved by selective reintroduction of EGF-derived residues [16]. With these chimaeras we were able to identify the minimal requirements for EGF receptor recognition in terms of loop-size and amino acid identity. Several antibodies raised against native EGF or TGFα are commercially available nowadays, but the epitopes they

---

Abbreviations used hEGF, human epidermal growth factor, hTGFα, human transforming growth factor α, anti-hTGFα9129, residues 9129–8024 of mature human recombinant TGFα, IGF-1, type I insulin-like growth factor, IL-3, interleukin-3, MTT, 3-(4,5-dimethylthiazol-2-yl)-2,5-diphenyl-2*H*-tetrazolium bromide, ECL, enhanced chemiluminescence

[1] To whom correspondence should be addressed (e-mail MvdPoll@sci.kun.nl)

recognize are unknown. Since anti-EGF and anti-TGFα antibodies are usually not cross-reactive, due to the relatively low sequence similarity (42 %) between these related growth factors, EGF–TGFα chimaeras can be expected to be valuable tools for epitope mapping that will overcome the limitations encountered by using linear peptide sequences. In the present study we set out to identify the most predominant antigenic site(s), including non-linear or conformational epitopes, recognized by three commercially available polyclonal antisera, two of which were raised against native hEGF and one against native hTGFα.

EXPERIMENTAL

Antibodies

Ab-3 (Oncogene Research Products, Cambridge, MA, U.S.A.) and BT-580 (Biomedical Technologies Inc., Stoughton, MA, U.S.A.) are rabbit polyclonal antibodies raised against recombinant hEGF. They are specific for hEGF and show no cross-reactivity with hTGFα. A sheep polyclonal antibody directed against residues 9129–8024 of mature human recombinant TGFα (anti-hTGFα9129) was purchased from Biogenesis Ltd. (Poole, Dorset, U.K.). It recognizes TGFα from human, rat and bovine origin, but does not react with EGF. The monoclonal antibody 8B-2 was generously supplied by NV Organon (Oss, The Netherlands). It was raised against a synthetic circular peptide corresponding to residues 34–50 of hTGFα.

Chimaeric growth factors

EGF–TGFα chimaeras or chimaeras between hEGF and an EGF-like repeat (amino acid residues 530–560) from *Drosophila* Notch [17] were constructed by exchanging domains bordered by the highly conserved cysteine residues, as previously described by us [15,16]. The constructs were linked at the 5′ end to the sequence coding for the recognition sequence (Ile-Glu-Gly-Arg) of the proteolytic enzyme Factor X, and cloned into the *Bam*HI-*Sal*I site of the pEZZ18 expression vector (Amersham Pharmacia Biotech, Uppsala, Sweden), 3′ of the sequence encoding two synthetic IgG-binding domains (Z-domains).

Wild-type and mutant growth factors were expressed and secreted as ZZ–Factor X–growth-factor fusion proteins into the periplasmic space of *Escherichia coli* KS474 and purified as described previously [15]. The isolated fusion proteins were digested with Factor X, and an additional run on IgG–Sepharose was performed to remove the two IgG-binding domains. Finally, active growth factors were separated from inactive dimers and other disulphide mismatches by reverse-phase HPLC.

Dot-blot procedure

Nitrocellulose (Protran BA 79; 0.1 μm pore size; Schleicher and Schuell, Dassel, Germany) was pre-wetted in 25 mM Tris/HCl (pH 7.3)/192 mM glycine/20 % (v/v) methanol. Recombinant wild-type and mutant growth factors (50 ng) were dissolved in 50 μl of 1 M acetic acid and spotted on to the nitrocellulose using dot-blot apparatus. The blot was subsequently dried and incubated for 30 min in 20 mM Tris/HCl (pH 7.3)/150 mM NaCl/0.5 % (v/v) Tween-20 (TBS-T) containing 0.1 % (w/v) ovalbumin to block non-specific binding sites. Incubation with specific primary antibodies took place for 16 h at 4 °C using a 1:1000 (polyclonal antibodies) or 1:500 (monoclonal antibody) dilution in TBS-T/0.1 % ovalbumin. Probed proteins were detected by incubation for 2 h at room temperature with a secondary antibody linked to horseradish peroxidase (Nordic Immunological Lab., Tilburg, The Netherlands) at a 1:25000 dilution in TBS-T/0.1 % ovalbumin. For visualization, enhanced chemiluminescence (ECL; Boehringer Mannheim, Mannheim, Germany) was used.

Cell proliferation assay

32D murine haematopoietic progenitor cells, transfected with ErbB-1 [18], were grown in RPMI 1640 medium supplemented with antibiotics, 10 % (v/v) heat-inactivated fetal-calf serum and 0.5 ng/ml interleukin-3 (IL-3) [19]. Prior to stimulation, the cells were washed free of IL-3 and resuspended in RPMI 1640 medium at a concentration of 5×10^5 cells/well. Serial dilutions of polyclonal antibodies were added, together with 2.5 ng/ml hEGF or hTGFα. After 20 h at 37 °C, cell survival was determined using a 3-(4,5-dimethylthiazol-2-yl)-2,5-diphenyl-2*H*-tetrazolium bromide (MTT) assay [18]. For this, cells were incubated for an additional 2 h at 37 °C with MTT (0.1 mg/ml) and the formation of dark-blue formazan crystals by living cells was quantified, after lysis of the cells with acidic propan-2-ol, by reading the absorbance at 540–630 nm.

RESULTS

Chimaeric proteins

In Figure 1 a schematic presentation is given of two sets of chimaeric proteins containing hEGF sequences; EGF–TGFα chimaeras [14,15] and EGF–Notch chimaeras [16]. The EGF–TGFα chimaeras are named according to the nomenclature introduced previously [14], in which, for instance, T3E stands for a ligand with TGFα sequences N-terminal and EGF sequences C-terminal of the third cysteine residue. A similar nomenclature is used for domain exchange mutants of hEGF and an EGF-repeat from Notch [16]. In cases where hEGF-derived amino acids were reintroduced into the Notch sequence this is indicated by capitals. Thus E1N2E stands for EGF in which the entire sequence between the first and second cysteine residue has been replaced by the corresponding sequence in Notch and E1N2E/Y stands for the same mutant in which the hEGF-derived tyrosine residue (position 13 in hEGF) has been reintroduced into the Notch sequence (Figure 1).

Mapping of the epitope recognized by polyclonal antibodies raised against native hEGF

The wild-type recombinant growth factors hEGF and hTGFα, as well as 16 EGF–TGFα chimaeras, were spotted on to a nitrocellulose filter and incubated with either Ab-3 or BT-580 (both polyclonal antibodies were raised against native recombinant hEGF). Probed proteins were detected by a goat anti-rabbit antibody linked to horseradish peroxidase and were visualized by enhanced chemiluminescence. Films were exposed for different time intervals ranging from 5–120 s in order to detect small differences in the efficiency of recognizing the various epitopes presented by the chimaeras. Table 1 gives a semi-quantitive analysis of 5 (Ab-3) and 2 (BT-580) independent experiments. Representative examples are shown in Figure 2. The antibodies show no cross-reactivity with hTGFα or murine EGF, as indicated by the fact that the signal remains below the background (0.1 % BSA), even after long exposure times.

Chimaeras with hTGFα sequences N-terminal of the third cysteine residue (T1E, T3E and T3E4T) were well recognized by Ab-3 (Figure 2, top panel), although T3E generally needed longer exposure to give the same signal as native hEGF. Also the presence of hTGFα sequences C-terminal of the fourth cysteine residue (E4T, E5T, E6T, T3E4T, E4T6E, E6ET and E6TE) did not affect the ability of Ab-3 to recognize the protein. All these chimaeras contain hEGF sequences between the third and fourth

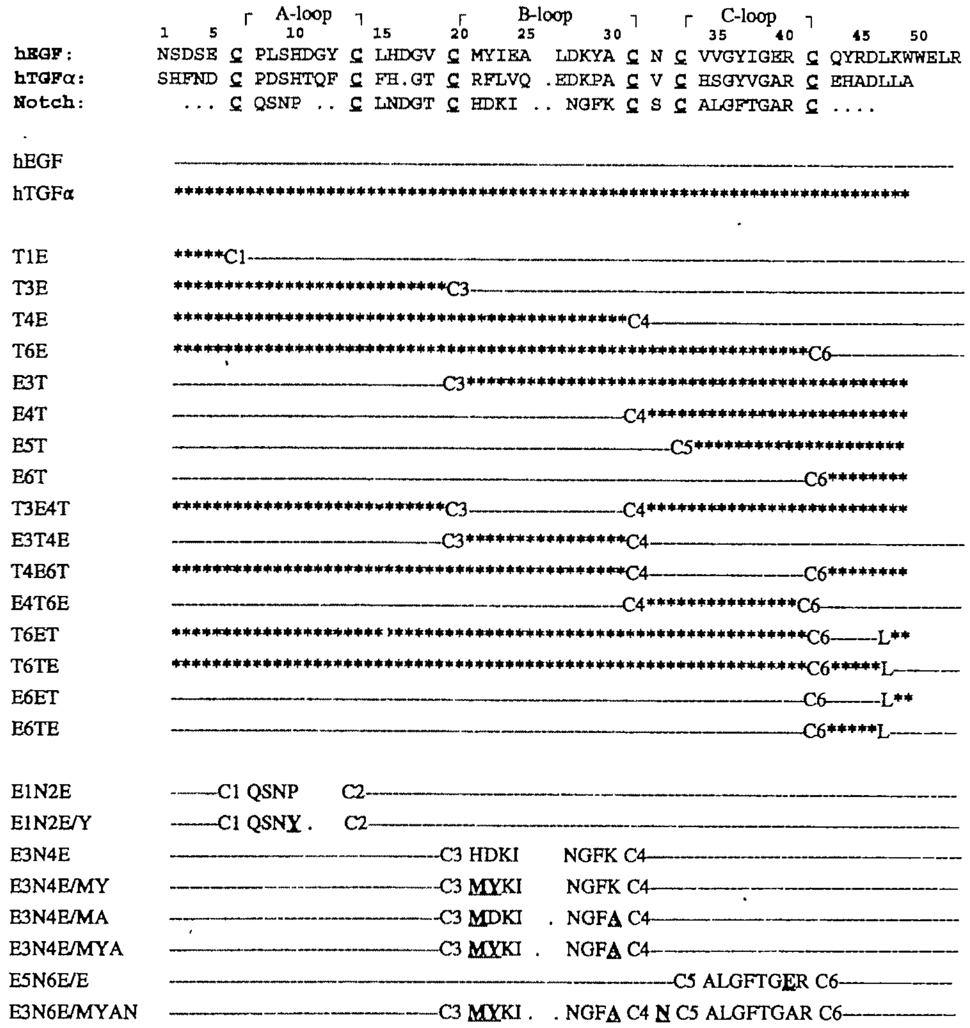

Figure 1 Sequence alignment of hEGF, hTGFα and *Drosophila* Notch EGF-like repeat 13, and schematic presentation of chimaeric growth factors

Domains exchanged are bordered by the six cysteine residues (C1–C6), which are present in hEGF, hTGFα and Notch. hEGF sequences are presented as dashed lines and hTGFα sequences as asterisks. In the EGF/Notch chimaeras the Notch sequence that is introduced in hEGF is given in capitals. In cases where hEGF-derived amino acids are reintroduced into the Notch sequence these are underlined.

cysteine residues, which indicates that the B-loop contains the main immunoreactive site. Indeed, all chimaeras that contained hTGFα sequences in this region (E3T, T4E, T6E, T4E6T, T6ET and T6TE) were not recognized by Ab-3. A notable exception, however, was E3T4E. The finding that Ab-3 reacted with both T3E4T and E3T4E could be due to the polyclonal nature of the antibody; however, when the B-loop of hEGF was replaced by the corresponding sequence of Notch EGF-repeat 13 instead of hTGFα (E3N4E), Ab-3 was unable to bind to the chimaeric protein. The difference in reactivity between E3T4E and E3N4E might be due to the higher sequence similarity between the B-loops of hEGF and hTGFα compared with that of Notch, but it also suggests that only part of the B-loop is required to bind the antibody. To investigate this, variants of E3N4E were tested in which hEGF-derived amino acids were reintroduced. Figure 2 (top panel) shows that the presence of alanine at position 30 in combination with methionine at position 21 (E3N4E/MA) especially increased the reactivity of the chimaeric protein with Ab-3. Although these two residues in the B-loop appeared to be sufficient for antibody recognition, it did not explain why E3T4E having an arginine at position 21 was recognized and other chimaeras with the same B-loop such as E3T and T4E were not. Therefore residues outside of the B-loop must also add to the epitope, and apparently these flanking regions must be present in order to recognize chimaeras with a hTGFα B-loop. In contrast with E3T, the EGF–Notch chimaera E3N6E/MYAN was well recognized. In this protein, C-terminal of the B-loop, only the asparagine at position 32 and the C-terminal tail were EGF-derived which indicated that either separately or together these residues may add to antibody recognition.

Using another polyclonal antibody (BT-580) raised against native hEGF, similar results were obtained (Table 1 and Figure 2, bottom panel). Similarly to Ab-3 this antibody recognized the chimaeras E4T, E5T, E6T, T3E4T, E4T6E, E6ET, E6TE and T1E that all have a hEGF B-loop. In addition E3T4E and the hEGF–Notch chimaeras E3N4E/MA and E3N6E/MYAN were again well recognized, whereas other chimaeras having hTGFα or Notch sequences in the B-loop were not. Small differences in the epitopes recognized by Ab-3 and BT-580 were, however, observed. Whereas T3E was slightly less recognized than T3E4T

Table 1 Semiquantative analysis of the ability of antibodies raised against native hEGF (Ab-3 and BT-580), native hTGFα (9129) or hTGFα residues 34–50 (8B-2) to recognize EGF–TGFα chimaeras or EGF–Notch chimaeras

++, well recognized, +, moderately recognized, ±, slightly recognized; −, not recognized, ND, not determined

	Anti-EGF Ab-3 ($n = 5$)	Anti-EGF BT-580 ($n = 2$)	Anti-TGFα 9129 ($n = 3$)	Anti-TGFα 8B-2 ($n = 2$)
hEGF	++	++	−	−
hTGFα	−	−	++	++
murine EGF	−	ND	ND	ND
T1E	++	+	−	ND
T3E	+	−	−	−
T4E	−	−	++	−
T6E	−	−	++	−
E3T	−	−	−	+
E4T	++	+	−	++
E5T	++	+	−	++
E6T	++	+	−	+
T3E4T	++	++	++	++
E3T4E	++	+	−	−
T4E6T	−	−	±	ND
E4T6E	++	++	−	ND
T6ET	±	−	++	ND
T6TE	−	−	++	ND
E6ET	++	++	−	ND
E6TE	++	++	−	ND
E3N4E	−	±	ND	ND
E3N4E/MY	+	±	ND	ND
E3N4E/MA	++	++	ND	ND
E3N4E/MYA	+	±	ND	ND
E3N6E/MYAN	+	++	ND	ND
E5N6E/E	++	ND	ND	ND
E1N2E	++	ND	ND	ND
E1N2E/Y	++	ND	ND	ND

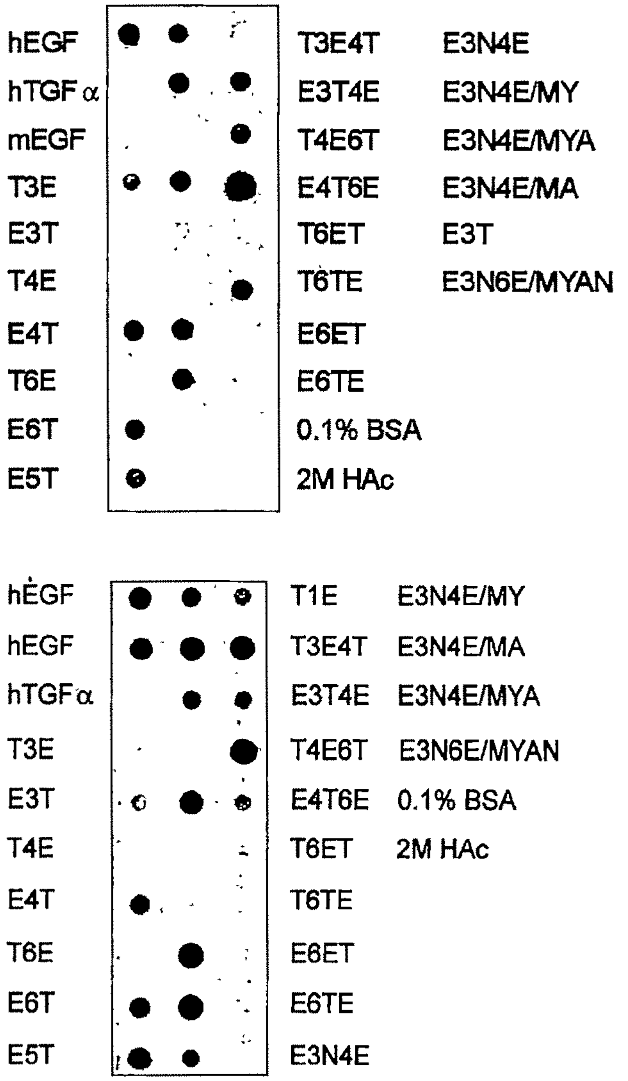

Figure 2 Representative dot-blot analysis of the ability of the anti-hEGF polyclonal antibody Ab-3 (top panel) and BT-580 (bottom panel) to recognize EGF–TGFα and EGF–Notch chimaeras

Each protein (50 ng) was spotted on to nitrocellulose and the antibody was tested at a dilution of 1 1000 The reactivity of Ab-3 was tested 5 times and the reactivity of BT-580 was tested 2 times. Visualization was by ECL and the film was exposed for 15 s mEGF, murine EGF

by Ab-3, it was not recognized at all by BT-580. In the native protein the peptide chain is folded in such a way that residues in the A-loop are in close contact to residues in the C-loop [20]. Although T3E was found to be as biologically active as hEGF and hTGFα [14], the specific combination of a hTGFα A-loop and a hEGF C-loop in T3E may have caused a slight change in the conformation of the epitope recognized by these antibodies, and the inability of BT-580 to react with T3E therefore suggests that this antibody is more sensitive to conformational changes. Furthermore, the finding that E4T6E seemed to react better with the antibody than E4T, while E6ET and E6TE (see Figure 1 for definition) also seemed to react better than E6T, suggests that the linear C-terminal tail also adds to recognition of the protein by BT-580.

The above results indicate that both polyclonal antibodies directed against native hEGF recognize essentially the same discontinuous conformational epitope. In agreement with this, reduction of hEGF by β-mercaptoethanol appeared to disrupt the epitope, causing a strong decrease in the ability of the antibodies to bind to the protein (results not shown).

Mapping of the epitope recognized by a polyclonal antibody raised against native hTGFα

The same set of hEGF–hTGFα chimaeras was used to map the epitope recognized by anti-hTGFα 9129. In Table 1 a semiquantative analysis of three independent experiments is given, and Figure 3 shows a representative dot-blot result. The antibody was unable to recognize chimaeras that had EGF sequences N-terminal of the third cysteine residue (E3T, E4T, E5T, E6T, E3T4E and E4T6E), which indicates that this region contains an important immunoreactive site. On the other hand, even when the entire sequence N-terminal of the third cysteine residue was TGFα (T3E), this was clearly not sufficient for antibody recognition. Therefore either the conformation of the epitope was changed due to the specific combination of EGF and TGFα sequences, or additional regions in TGFα needed to be present in order for the antibody to bind to the protein. These could be either residues in the B-loop or residues C-terminal of the fourth cysteine residue, since both T4E and T3E4T were well recognized.

Although fine-tuning to individual amino acids was not possible with the available chimaeras, the above results suggest that, as for the anti-EGF antibodies, the epitope recognized by anti-hTGFα9129 is a conformational non-linear epitope that containes residues lying at the start of the main B-loop β-sheet.

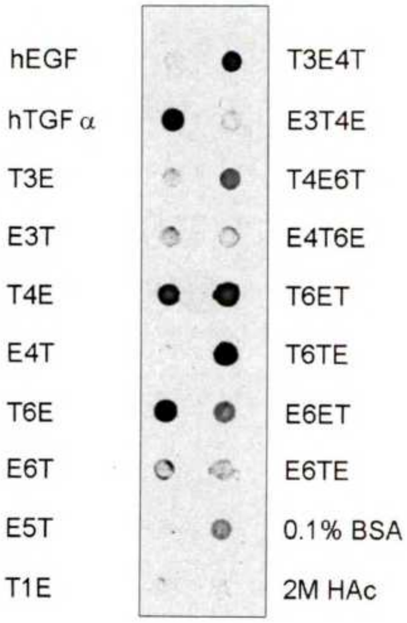

Figure 3 Representative dot-blot analysis of the ability of anti-hTGFα9129 to recognize EGF–TGFα chimaeras

Each protein (50 ng) was spotted on to nitrocellulose and the antibody was tested at a dilution of 1:1000. The experiment was repeated twice. Visualization was by ECL, and the film was exposed for 20 s.

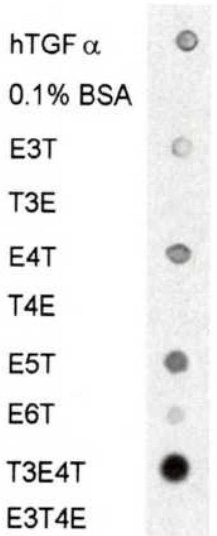

Figure 4 Representative dot-blot analysis of the ability of the monoclonal antibody 8B-2 raised against a synthetic circular peptide corresponding to residues 34–50 of hTGFα

Each protein (50 ng) was spotted on to nitrocellulose and the antibody was tested at a dilution of 1:500. The experiment was repeated once. Visualization was by ECL, and the film was exposed for 10 s.

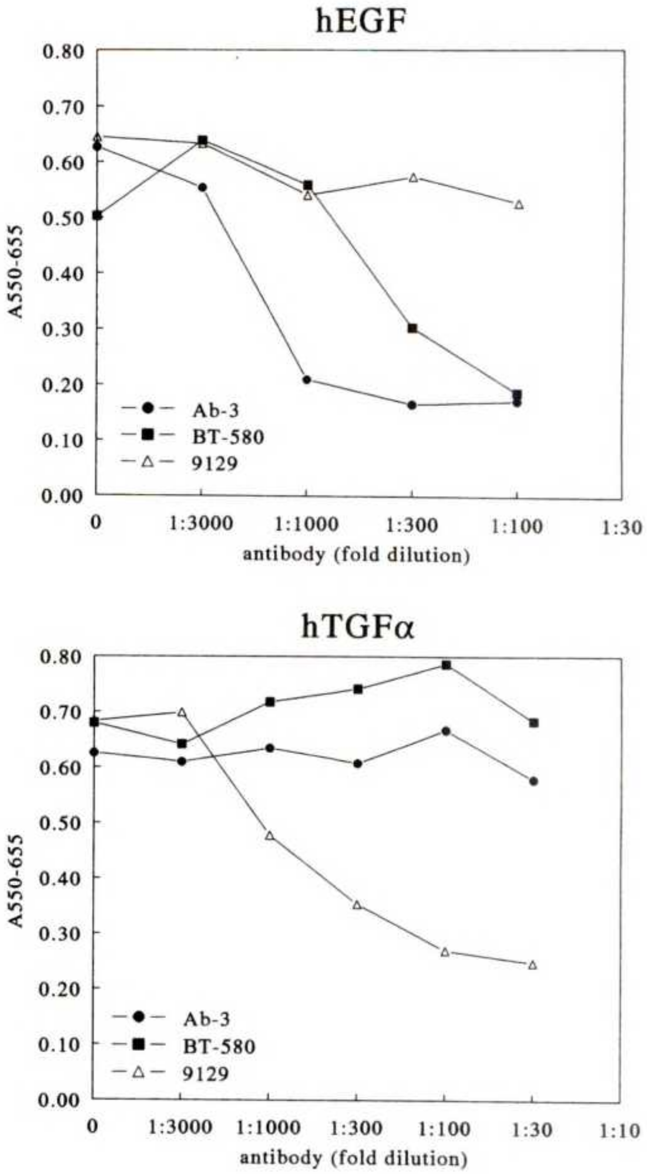

Figure 5 Inhibition of growth factor-induced cell survival by polyclonal antibodies directed against native hEGF (Ab-3 and BT-580) or hTGFα (9129)

D1 cells expressing ErbB-1 were deprived of IL-3 and subsequently incubated with 2.5 ng/ml hEGF (top panel) or hTGFα (bottom panel), together with serial dilutions of the polyclonal antibodies. Cell survival was measured after 24 h using an MTT assay, as described in the Experimental section.

Mapping of the epitope recognized by a monoclonal antibody raised against hTGFα residues 34–50

In order to validate the results obtained above with EGF–TGFα chimaeras, we performed a control experiment with 8B-2, a monoclonal antibody raised against a synthetic circular peptide corresponding to residues 34–50 of hTGFα. In spite of the fact that the peptide used as an immunogen was not linear, the antibody was found to recognize hTGFα better when the growth factor was reduced by β-mercaptoethanol than when the growth factor was its native conformation (results not shown). Therefore the chimaeric proteins were also tested under reducing conditions. As expected, 8B-2 was able to bind E3T, E4T, E5T and T3E4T, which are all chimaeras that contain TGFα residues 34–50 (Table 1 and Figure 4). In agreement with previous results obtained with an antiserum raised against the same peptide sequence [10], 8B-2 could also recognize chimaeras that contained only TGFα residues 43–50 (E6T). All other chimaeras tested were negative.

Inhibition of growth-factor-induced cell survival by polyclonal antibodies directed against hEGF or hTGFα

IL3-dependent 32D haematopoietic cells transfected with ErbB-1 (D1 cells) can survive in the absence of IL-3 through activation of ErbB-1 by one of its ligands. To investigate the ability of the above polyclonal antibodies to neutralize the biological activity of hEGF or hTGFα, D1 cells were deprived of IL-3 and subsequently incubated with the growth factors at a concentration of 2.5 ng/ml, which gave maximum growth stimulation (results not shown). Serial dilutions of the antibodies were added at the same time and their effect on growth-factor-dependent cell survival was measured in an MTT assay, as described in the Experimental section. Figure 5 shows that all three polyclonal antibodies inhibited the growth-factor-induced proliferation of D1 cells in a dose-dependent and growth-factor-specific way. This suggests that these antibodies recognize an epitope that is either part of or lies close to the binding interface.

DISCUSSION

Using synthetic peptide fragments several immunoreactive sites in EGF and TGFα have previously been identified, including the N-terminus, the B-loop β-sheet and the C-terminus [7–13]. A major disadvantage of the approach used, however, was that only linear non-conformational epitopes were identified. Discontinuous conformational epitopes may have remained undetected. Thus in previous studies several monoclonal antibodies raised against the native growth factors were unable to react with synthetic linear peptides, and the epitopes which they recognized remained unknown [12,13]. A more detailed analysis of antigen–antibody interaction can be obtained by the use of random peptide libraries, either displayed on phage or chemically synthesized [21,22]. Such peptide libraries have been used successfully to fine-tune linear epitopes at the amino acid level [23–26]. Furthermore, the large sequence diversity created in this way may result in the selection of peptides that mimic discontinuous binding sites. Although a few examples are known in which so-called 'mimotopes' were found [25,27–30], most attempts to identify discontinuous epitopes in this way have failed.

In the present study we have shown that chimaeras of hEGF and hTGFα can be used successfully to identify non-linear conformational epitopes. The most antigenic site on hEGF, which was recognized by two polyclonal antibodies raised against the native protein, was found to be discontinuous and to contain residues close to the third cysteine residue (including Met^{21} at the start of the B-loop β-sheet) and near the fourth cysteine residue (including Ala^{30} at the end of the B-loop β-sheet and the hinge residue Asn^{32}). Analysis of the epitope recognized by anti-TGFα was less detailed, but the data obtained in the present study also suggest that in TGFα the same region is immunoreactive. Although we cannot rule out the possibility that only some of the residues implicated in this study are in direct contact with the antibody and that others serve for efficient and correct presentation of the epitope, the fact that the antibodies only recognize the proteins when non-reduced (results not shown) indicates that the epitope is at least conformation-dependent. Furthermore, since two-dimensional NMR studies have shown that in the three-dimensional structure the above residues are in close contact and that Met^{21} forms a hydrogen bond with Ala^{30} in the double-stranded anti-parallel β-sheet [20] (Figure 6), this makes it likely that together these residues form the reactive site.

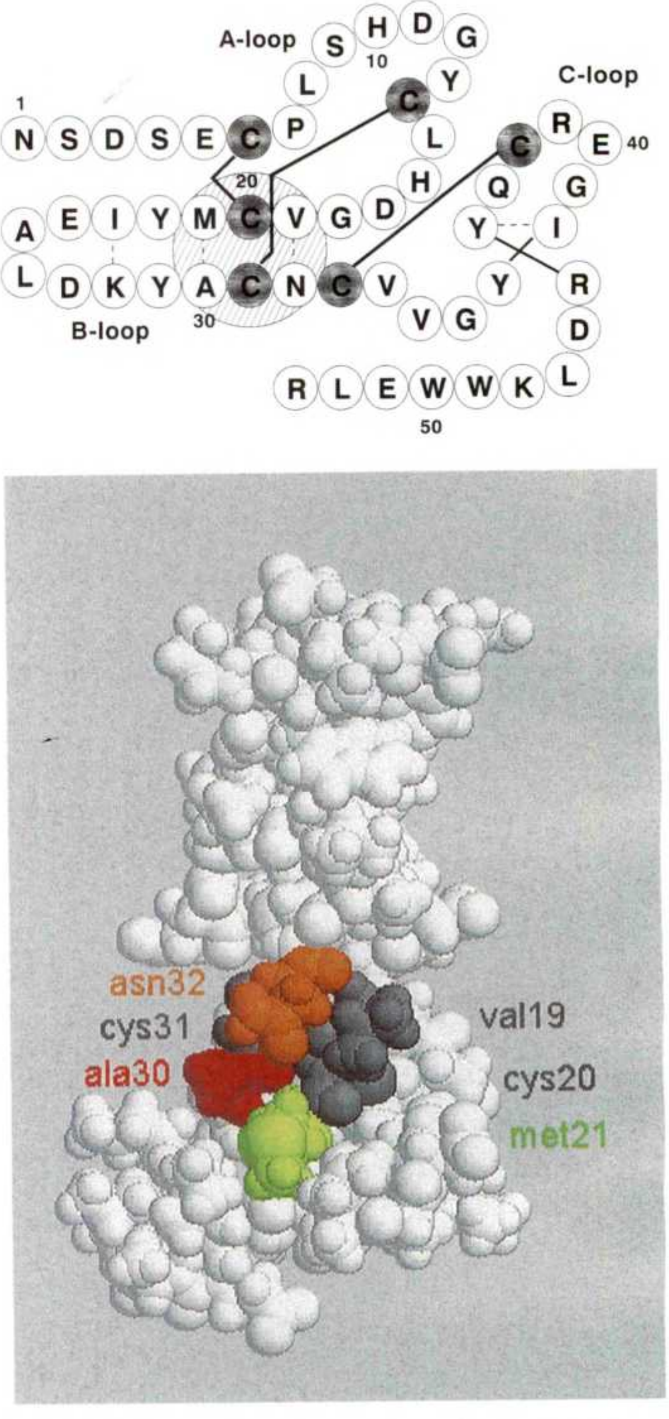
A-loop
C-loop
B-loop
1
10
20
30
40
50
N S D S E C P L S H D G Y C L C R E
A E I Y M C V G D H Q G Y I
L D K Y A C N C V V G Y R D
R L E W W K L
asn32
cys31
ala30
val19
cys20
met21

Figure 6 (Upper panel) schematic presentation of hEGF showing the B-loop β-sheet with the antigenic site and (lower panel) a space-filling representation of the solvent accessible structure of hEGF

The residues that form the antigenic site are shown in colour and are found to be clustered on the outside of the molecule. An animated version of Figure 6 can be accessed via the URL: http://www.BiochemJ.org/bj/349/bj3490267add.htm. Met^{21} is located at the start of the B-loop β-sheet near the third cysteine residue and opposite to Ala^{30}, which is located at the end of the B-loop. Together with the hinge residue, Asn^{32}, they form an important discontinuous epitope recognized by polyclonal antibodies raised against native hEGF. The residues indicated in grey may also add to the antigenic site.

All three polyclonal antisera were able to block the biological activity of the respective growth factor in a proliferation assay on D1 cells expressing ErbB-1, which indicates that the receptor binding domain is shielded upon binding of the antibody [20]. Increasing evidence exists that the binding domains of hEGF and hTGFα for ErbB-1 are non-linear and consist of residues from the A-loop, the C-loop and the C-terminal tail [16,20,31–33]. Furthermore, we have previously found that Met^{21} and Ala^{30} in the B-loop and the hinge residue, Asn^{32}, are also essential for high-affinity ligand–receptor interaction [16], probably because they guarantee the correct conformation of the binding domain. The epitope recognized in the present study clearly overlaps with the above region.

Chimaeras between related proteins that show no cross-reactivity have been successfully used in the past to map epitopes recognized by specific monoclonal antibodies [34–39]. For example, chimaeras between the human and the chicken EGF receptor have been used to map domains recognized by various monoclonal antibodies raised against the human EGF receptor [34], and chimaeras between the human type I insulin-like growth factor (IGF-1) receptor and the human insulin receptor were used to map the epitope of IGF-1-receptor-specific monoclonal antibodies to different regions of the extracellular domain [35]. More recently four chimaeras have been constructed between human E- and L-selectins through which the epitope recognized by a neutralizing antibody, directed against human E-selectin, was assigned to the lectin domain [36]. In the above studies only a limited number of chimaeras were available and relatively large domains were exchanged. Fine-tuning was eventually achieved by introducing random amino acid substitutions.

In the present study, with the help of 16 EGF–TGFα chimaeras and 8 EGF–Notch chimaeras a detailed analysis was performed on the epitopes recognized by polyclonal antibodies directed against native hEGF and hTGFα. A thus far unknown major antigenic site was identified as a non-linear and conformation-dependent region involved in receptor binding.

The current studies were carried out with financial support from the Dutch Cancer Society.

REFERENCES

1 Groenen, L C, Nice, E C. and Burgess, A. W (1994) Structure-function relationships for the EGF/TGF-alpha family of mitogens Growth Factors **11**, 235–257

2 Jones, J T, Akita, R W and Sliwkowski, M. X (1999) Binding specificities and affinities of egf domains for ErbB receptors FEBS Lett. **447**, 227–231

3 Alroy, I and Yarden, Y (1997) The ErbB signaling network in embryogenesis and oncogenesis signal diversification through combinatorial ligand-receptor interactions FEBS Lett **410**, 83–86

4 Arteaga, C. L., Hanauske, A R, Clark, G M., Osborne, C. K., Hazarika, P., Pardue, R L, Tio, F and Von Hoff, D D (1988) Immunoreactive alpha transforming growth factor activity in effusions from cancer patients as a marker of tumor burden and patient prognosis Cancer Res. **48**, 5023–5028

5 Lee, D C, Fenton, S E, Berkowitz, E A and Hissong, M A (1995) Transforming growth factor alpha expression, regulation, and biological activities Pharmacol Rev **47**, 51–85

6 Lee, D C, Luetteke, N C, and Petch, L A (1993) Oncogenes and tumor suppressor genes. In Human Malignancies (Benz, C. C and Lin, E. T., eds) pp 233–254, Kluwer Academic Publishers, Boston

7 Nestor, J. J., Newman, S R, DeLustro, B, Todaro, G J and Schreiber, A B (1985) A synthetic fragment of rat transforming growth factor alpha with receptor binding and antigenic properties Biochem Biophys Res Commun. **129**, 226–232

8 Kobrin, M S, Samsoondar, J and Kudlow, J E (1986) Alpha-transforming growth factor secreted by untransformed bovine anterior pituitary cells in culture II Identification using a sequence-specific monoclonal antibody J Biol Chem **261**, 14414–14419

9 Hazarika, P, Pardue, R L, Earls, R. and Dedman, J R. (1987) Identification and subcellular localization of a 21-kilodalton molecule using affinity-purified antibodies against alpha-transforming growth factor Biochemistry **26**, 2067–2070

10 Hazarika, P and Dedman, J R (1988) Epitope mapping of alpha-transforming growth factor evidence of an immunodominant region Life Sci **42**, 2525–2531

11 Sorvillo, J M, McCormack, E S., Yanez, L, Valenzuela, D. and Reynolds, Jr, F H (1990) Preparation and characterization of monoclonal antibodies specific for human transforming growth factor alpha Oncogene **5**, 377–386

12 Hoeprich, Jr, P D, Langton, B C, Zhang, J W and Tam, J P (1989) Identification of immunodominant regions of transforming growth factor alpha Implications of structure and function J. Biol Chem. **264**, 19086–19091

13 Katsuura, M. and Tanaka, S (1989) Topographic analysis of human epidermal growth factor by monospecific antibodies and synthetic peptides J. Biochem (Tokyo) **106**, 87–92

14 Kramer, R H, Lenferink, A E G, van Bueren-Koornneef, I L., van der Meer, A, van de Poll, M. L M and van Zoelen, E. J J (1994) Identification of the high affinity binding site of transforming growth factor-alpha (TGF-alpha) for the chicken epidermal growth factor (EGF) receptor using EGF/TGF-alpha chimeras J Biol Chem. **269**, 8708–8711

15 van de Poll, M L M, Lenferink, A E G, van Vugt, M J H, Jacobs, J J., Janssen, J W, Joldersma, M and van Zoelen, E J J (1995) A single amino acid exchange, Arg-45 to Ala, generates an epidermal growth factor (EGF) mutant with high affinity for the chicken EGF receptor J Biol. Chem **270**, 22337–22343

16 van de Poll, M L M., van Vugt, M J H, Lenferink, A E. G and van Zoelen, E J. J (1998) Identification of the minimal requirements for binding to the human epidermal growth factor (EGF) receptor using chimeras of human EGF and an EGF repeat of Drosophila Notch J Biol Chem **273**, 16075–16081

17 Wharton, K A, Johansen, K M., Xu, T and Artavanis-Tsakonas, S (1985) Nucleotide sequence from the neurogenic locus notch implies a gene product that shares homology with proteins containing EGF-like repeats Cell **43**, 567–581

18 Pinkas-Kramarski, R, Soussan, L, Waterman, H., Levkowitz, G., Alroy, I., Klapper, L, Lavi, S., Seger, R, Ratzkin, B J, Sela, M and Yarden, Y. (1996) Diversification of Neu differentiation factor and epidermal growth factor signaling by combinatorial receptor interactions EMBO J **15**, 2452–2467

19 Karasuyama, H and Melchers, F (1988) Establishment of mouse cell lines which constitutively secrete large quantities of interleukin 2, 3, 4 or 5, using modified cDNA expression vectors Eur J Immunol **18**, 97–104

20 Hommel, U., Harvey, T S., Driscoll, P. C. and Campbell, I D (1992) Human epidermal growth factor. High resolution solution structure and comparison with human transforming growth factor alpha J Mol Biol **227**, 271–282

21 Scott, J K and Smith, G P (1990) Searching for peptide ligands with an epitope library Science **27**, 386–390

22 Clackson, T and Wells, J A (1994) *In vitro* selection from protein and peptide libraries Trends Biotechnol **12**, 173–184

23 Appel, J R., Campbell, G D, Buencamino, J., Houghten, R A and Pinilla, C (1998) Characterization of antigen-antibody interactions using single substitution analogs and mixture-based synthetic combinatorial libraries J Pept. Res **52**, 346–355

24 Murthy, K K, Shen, S. H and Banville, D (1998) Epitope mapping of SHP-1 monoclonal antibodies using peptide phage display Biochem Biophys Res Commun **248**, 69–74

25 Yone, K., Bajard, S, Tsunekawa, N. and Suzuki, J. (1995) Epitopic regions for antibodies against tumor necrosis factor alpha Analysis by synthetic peptide mapping. J. Biol Chem. **270**, 19509–19515

26 Kramer, A., Vakalopoulou, E, Schleuning, W D and Schneider-Mergener, J (1995) A general route to fingerprint analyses of peptide-antibody interactions using a clustered amino acid peptide library comparison with a phage display library Mol Immunol **32**, 459–465

27 Orlandi, R, Menard, S., Colnaghi, M. I., Boyer, C M. and Felici, F (1994) Antigenic and immunogenic mimicry of the HER2/neu oncoprotein by phage-displayed peptides. Eur J Immunol **24**, 2868–2873

28 Geysen, H. M, Rodda, S. J. and Mason, T J. (1986) A prior delineation of a peptide which mimics a discontinuous antigenic determinant Mol Immunol **23**, 709–715

29 Luzzago, A, Felici, F, Tramontano, A., Pessi, A and Cortese, R (1993) Mimicking of discontinuous epitopes by phage-displayed peptides Epitope mapping of human H ferritin using a phage library of constrained peptides Gene **128**, 51–57

30 Balass, M., Heldman, Y., Cabilly, S, Givol, D, Katchalski-Katzir, E and Fuchs, S (1993) Identification of a hexapeptide that mimics a conformation-dependent binding site of acetylcholine receptor by use of a phage-epitope library Proc. Natl Acad. Sci. U S A. **90**, 10638–10642

31 McInnes, C, Hoyt, D W, Harkins, R N, Pagila, R N, Debanne, M T, O'Connor-McCourt, M and Sykes, B D (1996) NMR study of the transforming growth factor-alpha (TGF-alpha)-epidermal growth factor receptor complex Visualization of human TGF-alpha binding determinants through nuclear Overhauser enhancement analysis J Biol Chem. **271**, 32204–32211

32 Hoyt, D. W., Harkins, R. N, Debanne, M T, O'Connor-McCourt, M and Sykes, B D (1994) Interaction of transforming growth factor alpha with the epidermal growth factor receptor binding kinetics and differential mobility within the bound TGF-alpha Biochemistry **33**, 15283–15292

33 Nandagopal, K, Terzaghi-Howe, M and Niyogi, S (1999) Receptor recognition by histidine 16 of human epidermal growth factor via hydrogen-bond donor/acceptor interactions. J Cell Biochem. **72**, 16–24

34 Lax, I, Fisher, R., Ng, C, Segre, J, Ullrich, A, Givol, D and Schlessinger, J (1991) Noncontiguous regions in the extracellular domain of EGF receptor define ligand-binding specificity Cell Regul **2**, 337–345
35 Soos, M A, Field, C E, Lammers, R., Ullrich, A, Zhang, B., Roth, R. A, Andersen, A S, Kjeldsen, T and Siddle, K (1992) A panel of monoclonal antibodies for the type I insulin-like growth factor receptor Epitope mapping, effects on ligand binding, and biological activity J Biol Chem **267**, 12955–12963
36 Tsurushita, N, Fu, H, Melrose, J and Berg, E L (1998) Epitope mapping of mouse monoclonal antibody EP-5C7 which neutralizes both human E- and P-selectin. Biochem Biophys. Res Commun. **242**, 197–201
37 Kuroki, Y, McCormack, F X., Ogasawara, Y, Mason, R J and Voelker, D R (1994) Epitope mapping for monoclonal antibodies identifies functional domains of pulmonary surfactant protein A that interact with lipids J. Biol. Chem **269**, 29793–29800
38 Richardson, T H, Griffin, K J, Jung, F, Raucy, J L and Johnson, E F. (1997) Targeted antipeptide antibodies to cytochrome P450 2C18 based on epitope mapping of an inhibitory monoclonal antibody to P450 2C51. Arch Biochem Biophys **338**, 157–164
39 Nasu, T, Fukuda, Y, Hashino, J., Nagahira, K, Kawashima, H, Noguchi, C, Oika-wa, S. and Nakanishi, T (1999) Epitope mapping of monoclonal antibodies against N-domain of carcinoembryonic antigen Immunol Lett **67**, 57–62

Received 13 December 1999/25 February 2000; accepted 26 April 2000

Biochem. J. (2000) 349, 275–279 (Printed in Great Britain)

Kinetic properties of missense mutations in patients with glutathione synthetase deficiency

Runa NJÅLSSON*[1], Katarina CARLSSON*, Birgit OLIN†, Birgit CARLSSON‡, Lei WHITBREAD§, Galina POLEKHINA‖, Michael W. PARKER‖, Svante NORGREN*, Bengt MANNERVIK†, Philip G. BOARD§ and Agne LARSSON*

*Department of Paediatrics, B57, Karolinska Institutet, Huddinge University Hospital, S-141 86 Huddinge, Sweden, †Department of Biochemistry, Uppsala University, S-751 23 Uppsala, Sweden, ‡Department of Clinical Genetics, Uppsala University Children's Hospital, S-751 85, Sweden, §Molecular Genetics Group, John Curtin School of Medical Research, Australian National University, Canberra ACT 2601, Australia, and ‖The Ian Potter Foundation Protein Crystallography Laboratory, St Vincent's Institute of Medical Research, Fitzroy, Victoria 3065, Australia

Patients with hereditary glutathione synthetase (GS) (EC 6.3.2.3) deficiency present with variable clinical pictures, presumably related to the nature of the mutations involved. In order to elucidate the relationship between genotype, enzyme function and clinical phenotype, we have characterized enzyme kinetic parameters of missense mutations R125C, R267W, R330C and G464V from patients with GS deficiency. One of the mutations predominantly affected the K_m value, with decreased affinity for glycine, two mutations influenced both K_m and V_{max} values, and one mutation reduced the stability of the enzyme. This characterization agrees well with predictions based on the recently reported crystal structure of human GS. Thus our data indicate that different mutations can affect the catalytic capacity of GS by decreasing substrate affinity, maximal velocity or enzyme stability.

Key words: γ-glutamyl cycle, 5-oxoprolinuria, haemolytic anaemia.

INTRODUCTION

To date, more than 65 patients with inborn errors in the metabolism of GSH, in 56 families, have been reported [1]. Glutathione synthetase (GS) (EC 6.3.2.3) deficiency is the most common of these disorders and exhibits autosomal recessive inheritance. It is probable that homozygosity for GS alleles that results in a totally inactive enzyme or the absence of protein expression would be lethal. Clinically, two variants can be distinguished. The mild form is restricted to erythrocytes and is thought to be caused by mutations that reduce the stability of the enzyme. The patients have low GSH levels in erythrocytes, but not in nucleated cells, and often have mild haemolytic anaemia. The severe form is caused by mutations that impair the catalytic function of the enzyme. These patients are referred to as 'generalized GS deficient' and present with massive urinary excretion of 5-oxoproline, haemolytic anaemia and metabolic acidosis, often in association with progressive impairment of central nervous system function. It is unclear if there is extensive polymorphism arising from functionally normal GS sequence variants. Although the 5′ and central regions of the GS cDNA are not well represented in the expressed sequence tag ('EST') database, a search [2] has identified a number of GS sequence variants. However, most variation appears in non-coding regions, and the frequency of these potential polymorphisms has yet to be determined (P. G. Board, unpublished work). GS catalyses the final step in the biosynthesis of GSH according to:

$$\gamma\text{-glutamylcysteine} + \text{glycine} + \text{ATP} \rightarrow \gamma\text{-glutamylcysteinylglycine (GSH)} + \text{ADP} + \text{P}_i$$

The enzyme has been purified to homogeneity from several sources, e.g. rat kidney [3], *Escherichia coli* [4] and yeast [5], but until now not to homogeneity from any human tissue. The human enzyme functions as a homodimer, with subunits containing 474 amino acid residues [6], encoded by a gene located on chromosome 20q11.2 [7]. Eighteen different mutations from 16 patients with GS deficiency have been described [8–10]. Many of these mutations affect residues that are within the protein core and active-site regions [11].

The recently reported crystal structure of human GS allows some predictions of the effects of naturally occurring mutations [11]. However, characterization of the mutant proteins is required to understand the complex interactions between structure, function and clinical phenotype. Furthermore, since GSH can be critical to the disposition of a range of therapeutic agents and the development of drug resistance, knowledge gained from the analysis of natural mutants may provide avenues for therapeutic intervention. The patients are often compound heterozygotes, which complicates kinetic analyses of specific mutations of enzymes isolated from blood samples. In the present investigation kinetic parameters of four naturally occurring missense mutations from patients with GS deficiency were investigated *in vitro* and the findings were correlated with the tertiary structure of the enzyme. The positions of the mutations within the GS subunit are illustrated in Figure 1. The properties of these mutations have not previously been studied and it was possible to compare the real characteristics of the proteins with predictions derived from the structure. The recombinant enzymes were His-tagged to facilitate purification. To evaluate putative effects of the added histidine residues on enzyme activity, wild-type His-tagged enzyme was compared to wild-type enzyme isolated from erythrocytes. This is the first time the human erythrocyte enzyme has been purified to homogeneity.

Abbreviations used: GS, glutathione synthetase; BTP, Bis-Tris Propane; γ-gluABA, L-γ-glutamyl-L-α-aminobutyric acid.

[1] To whom correspondence should be addressed (e-mail runa.njalsson@mednut.ki.se).

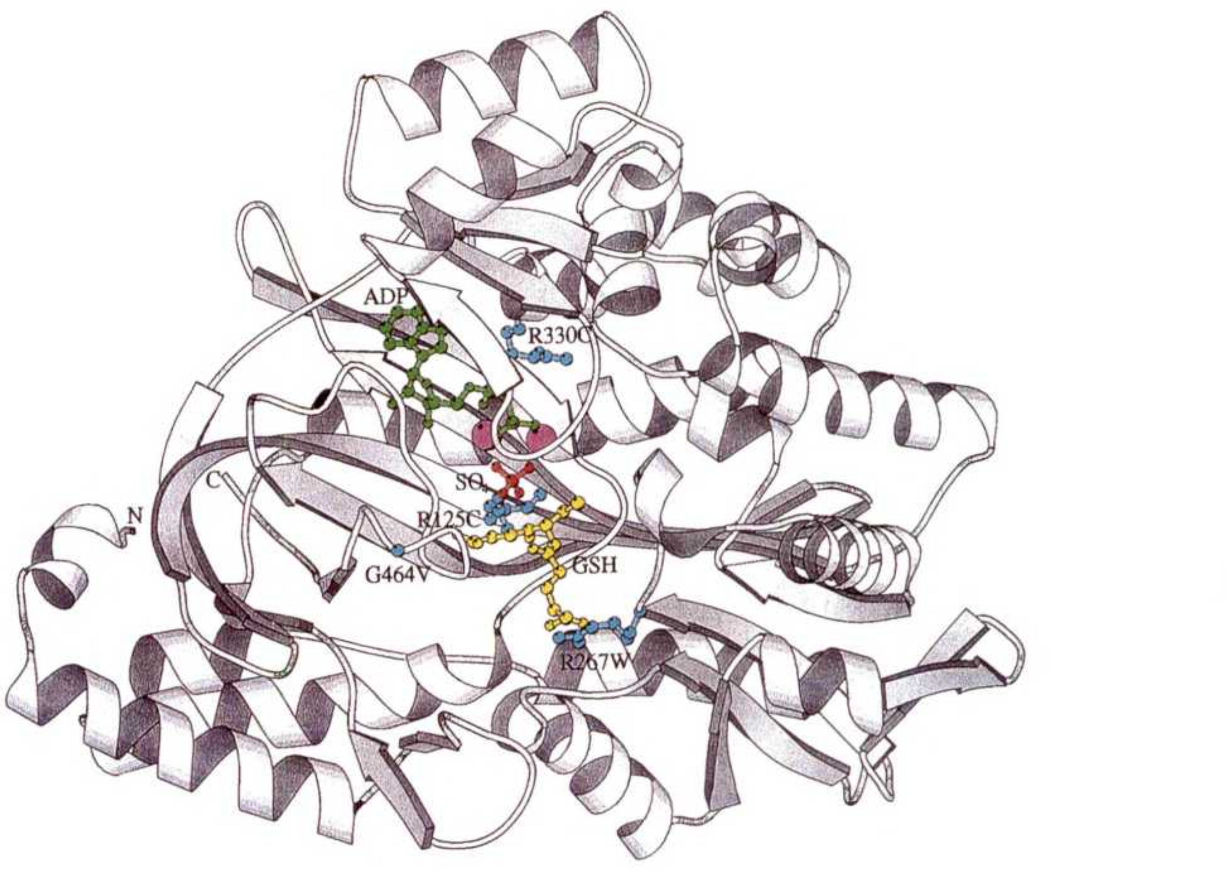

Figure 1 A ribbon representation of the human GS monomer

The GS deficiency mutations discussed in the text are shown in blue. The cofactors (ADP is green, the sulphate which mimics the γ-phosphate is red and the magnesium ions are shown as two mauve spheres) and product (GSH is yellow) are also shown. This Figure was drawn using MOLSCRIPT [15].

EXPERIMENTAL

Materials

[1-^{14}C]Glycine and the DNA Sculptor Kit were purchased from Amersham (Little Chalfont, Bucks., U.K.). DEAE-Sepharose CL-6B, thiopropyl-Sepharose 6B, Sephacryl S-300, Polybuffer (pH 6.5–4) and restriction endonucleases were obtained from Pharmacia Biotech. Bis-Tris Propane (BTP) was purchased from Sigma. Mercaptopyridine–Sepharose 6B was produced as described previously [12]. Primers coding the missense mutations R125C, R267W, R330C, and G464V were synthesized at the Australian National University Biomolecular Resource Facility (Canberra, Australia). Sequence analysis was performed using a Sequenase version 2.0 kit supplied by USB (Cleveland, OH, U.S.A.). Protein assay reagent was purchased from Bio-Rad (Sundbyberg, Sweden). All chemicals were of analytical grade. Human erythrocyte concentrates were obtained from the Blood Bank, Akademiska Hospital, Uppsala, Sweden. This study was approved by the ethical committee of the Karolinska Institute.

Preparation of haemolysate

Erythrocytes were centrifuged at 5000 ***g*** for 20 min, before washing the cells twice with six vol. of PBS. One vol. of 5 mM Tris/HCl (pH 7.4)/1 mM EDTA was then added to the packed erythrocytes, prior to sonication. Haemolysate was subsequently obtained, after centrifugation at 25000 ***g*** for 30 min.

Purification of GS

GS was purified from the haemolysate by ion-exchange chromatography, thiophilic adsorption chromatography, gel filtration, chromatofocusing and ammonium sulphate precipitation. The stepwise use of the different columns is described below. Fractions were collected throughout the purification for activity measurements. All procedures were performed at 5 °C. All column sizes are given as diameter × height.

DEAE-Sepharose

DEAE-Sepharose CL-6B (200 ml) was equilibrated with 20 mM BTP (pH 6.5), and suspended in 1000 ml of haemolysate (containing 138 g of protein). The mixture was agitated for approx. 2 h, collected in a Buchner funnel and washed with BTP buffer. The matrix was placed in a 3.2 cm × 25 cm column and washed with BTP buffer. At pH 6.5 haemoglobin did not bind to the matrix and was thus eluted. The adsorbed proteins were eluted stepwise with 0.05, 0.15 and 0.5 M KCl in BTP buffer. The enzyme activity was detected in the fractions eluted with BTP buffer containing 0.15 M KCl. These fractions were pooled (489 mg of protein), and K_2SO_4 was added to a final concentration of 0.5 M.

Table 1 Purification of GS from human erythrocytes

GS was purified from the haemolysate by ion-exchange chromatography, thiophilic adsorption chromatography, gel filtration, chromatofocusing and ammonium sulphate precipitation

Fraction	Volume (ml)	Total protein (mg)	Purification factor	Yield of activity (%)
Haemolysate	1000	138000	1	100
DEAE-Sepharose	670	490	160	56
Thiopropyl-Sepharose	102	42	1710	52
Mercaptopyridine–Sepharose	43	5.2	10600	39
Sephacryl S-300	41	3.7	11400	30

Thiopropyl-Sepharose

The sample was then applied to a 2 cm × 20 cm column of thiopropyl-Sepharose 6B equilibrated with a buffer containing 10 mM Tris/HCl (pH 7.8) and 0.5 M K_2SO_4. After washing with equilibration buffer, the enzyme was eluted with 10 mM Tris/HCl (pH 7.8)/1.5 M NaCl. Fractions with enzyme activity were pooled (42 mg of protein), and K_2SO_4 was added to a final concentration of 0.5 M.

Mercaptopyridine–Sepharose

The sample was passed through a 2 cm × 16 cm column of mercaptopyridine–Sepharose 6B equilibrated with a buffer containing 10 mM Tris/HCl (pH 7.8) and 0.5 M K_2SO_4. After washing with equilibration buffer, the enzyme was eluted with 10 mM Tris/HCl (pH 7.8)/1.5 M NaCl. The active fractions were pooled (5.2 mg of protein) and concentrated by ultrafiltration (Immersible CX-10; Millipore, Sundbyberg, Sweden).

Sephacryl

The concentrated sample (3.5 ml) was gel filtered through a 2 cm × 82 cm column of Sephacryl S-300 equilibrated with 20 mM BTP buffer. The fractions containing enzyme activity were pooled.

Chromatofocusing

The gel filtration peak containing GS was concentrated (3.7 mg of protein) and run on an FPLC Mono P HR 5/20 column (Pharmacia Biotech). Polybuffer, with pH range 6.5–4.0, was then used to elute the enzyme. The active fractions were pooled, and solid ammonium sulphate was supplemented to a concentration of 0.4 g/ml. The mixture was stirred for 30 min, before the precipitate was collected by centrifugation and dissolved in PBS. The final sample contained 0.5 mg of enzyme in 1.3 ml of buffer. The purity of the enzyme was assessed by a Pharmacia Phast System, with Phast Gel Gradient 8–25 and Phast Gel SDS Buffer Strips.

Construction and expression of mutant cDNAs

The wild-type GS cDNA was inserted into the His-tag vector pQE-31 (Qiagen, Clifton Hill, Australia), resulting in the addition of 6 histidine residues at the N-terminus of the protein [13]. Mutated cDNAs were constructed by PCR, employing mutant specific primers and the DNA Sculptor Kit. Constructs were confirmed by DNA sequencing using a Sequenase version 2.0 kit. Mutant cDNAs were expressed in *E. coli* TG1 and isolated as described previously [8]. The purity of the recombinant enzymes was determined as described above.

Enzyme assay

The enzyme activity was determined as described previously [14], with the following modifications: the total incubation volume was 100 μl, containing 12 mM L-γ-glutamyl-L-α-aminobutyric acid (γ-gluABA), 16 mM [1-^{14}C]glycine (specific activity 9.3 × 10^9 Bq/mol), 8000 units/l pyruvate kinase, 4 mM phosphoenolpyruvate, 4 mM ATP, 100 mM Tris/HCl (pH 8.6), 25 mM KCl, 6 mM $MgCl_2$ and 1 g/l BSA. Following incubation at 37 °C for 60 min the reaction was stopped by the addition of 10 μl of 20 % (v/v) perchloric acid. Denatured protein was removed by centrifugation at 17000 g for 3 min, and the supernatant was applied to a 0.5 cm × 4 cm Dowex acetate column. Remaining [1-^{14}C]glycine was eluted with 6 ml of 20 mM acetic acid. The absorbed product, ^{14}C-γ-glutamyl-aminobutyryl-glycine (ophthalmic acid), was eluted with 6 ml of 1.5 M ammonium acetate. Radioactivity was analysed by liquid scintillation counting. The kinetic constants K_m and V_{max} were determined by varying the concentrations of γ-gluABA, glycine and Mg^{2+}/ATP (concentration ratio 3:2) respectively. Enzyme activity is expressed as μmol [1-^{14}C]glycine incorporated/min per mg of protein.

K_m and V_{max} values were determined from the enzyme activity data by non-linear regression analysis, using GraFit Version 4 (Erithacus Software, Horley, Surrey, U.K.). For each substrate and enzyme, the concentration curve experiments were repeated twice. Results for V_{max} are consequently means ± S.D. of six determinations.

RESULTS

A protocol for the purification of wild-type GS from human control erythrocytes is outlined in Table 1. From 138 g of haemolysate proteins, approx. 0.5 mg of purified enzyme was obtained. The four different missense mutants R125C, R267W, R330C and G464V, as well as the wild-type enzyme, were expressed as His-tagged proteins in *E. coli*. One litre of each *E. coli* culture yielded 10–100 mg of recombinant enzyme. The purity of all isolated enzyme preparations was verified by SDS gel electrophoresis. Each preparation resulted in a single band (results not shown). The K_m and V_{max} data are shown in Table 2. Due to the high K_m for glycine in the G464V mutant, the highest velocity which could be reached in the γ-gluABA and ATP/Mg^{2+} concentration curves was only 10 % of V_{max}. The V_{max} for mutation G464V was therefore derived from the glycine con-

Table 2 The kinetic properties, V_{max} and K_m, of erythrocyte and His-tagged recombinant GS

Kinetic parameters were determined using increasing concentrations of each substrate ranging from 0.1–18 times the K_m in the presence of 12–18 times the determined K_m of the other substrates Activity data are given as means ± S.D The V_{max} for mutant R330C decreased successively Therefore the range of V_{max} is given rather than the mean

Enzyme	Mutation	V_{max} (μmol/min per mg of protein)	K_m γ-gluABA (mM)	K_m glycine (mM)	K_m ATP (mM)
Erythrocyte	–	5.676 ± 2.053	0.99 ± 0.07	1.37 ± 0.01	0.23 ± 0.03
Wild type*	–	6.014 ± 1.402	0.65 ± 0.22	1.34 ± 0.34	0.22 ± 0.03
R125C*	373C → T	0.017 ± 0.004	1.79 ± 0.45	12.39 ± 0.84	0.06 ± 0.01
R267W*	799C → T	0.008 ± 0.002	10.12 ± 2.35	8.58 ± 3.24	0.44 ± 0.30
R330C*	988C → T	4.401 ± 0.300	0.72 ± 0.36	1.51 ± 0.08	0.29 ± 0.01
G464V*	1391G → T	1.608 ± 0.169	0.22 ± 0.03	130.40 ± 12.16	0.11 ± 0.06

* Recombinant His-tagged enzyme

centration curves. The V_{max} of the mutant R330C decreased markedly with repeated freezing and thawing (the range is shown in Table 2). The R125C and R267W mutants exhibited markedly reduced but consistent V_{max} values, as well as increased K_m values for all of the substrates.

DISCUSSION

The genotype–phenotype relationship in human GS deficiency was addressed by expression of four mutants and kinetic analysis of the purified recombinant mutant enzymes. The mutations and the heterogeneous clinical symptoms of the patients studied have been described previously [8–10]. The four patients are compound heterozygotes for missense mutations affecting amino acid residues that are conserved between rats and humans.

Although kinetic properties of His-tagged recombinant enzymes have been studied previously [13], it was essential to confirm that the His-tag did not influence the catalytic properties of the enzymes. Thus comparison between wild-type His-tagged enzyme and wild-type enzyme isolated from erythrocytes demonstrated that the addition of the His-residues had minimal effects on enzyme kinetics. The experimental finding agrees with predictions from the crystal structure of His-tagged wild-type human enzyme. The His-tag is disordered in the crystal structure, as are the first two residues of the mature protein [11]. The third N-terminal amino acid residue is located on the surface of the protein and is approx. 28 Å (1 Å = 0.1 nm) from the active-site. Hence the His-tag, which is joined to the N-terminus, is not expected to influence activity. Although GS has been purified from several tissues in other species, this is the first protocol for purification of human GS to homogeneity. The results indicate that GS constitutes at least 0.01 % of the soluble protein in human erythrocytes.

As illustrated in Table 2, the R125C and R267W mutations reduced the V_{max} to 0.2 % and 0.1 % of the wild-type activity, respectively. This suggests that these residues are of critical importance for formation of the active-site and catalysis Examination of the crystal structure (Figures 1 and 2, left panel) shows that the guanidine group of Arg^{125} forms a number of important contacts in the active-site including a salt-link with Asp^{127} and hydrogen bonds to a sulphate ion, which mimics the position of the cleaved γ-phosphate, to the main-chain carbonyl of Ser^{151} and to the carbonyl of the cysteine moiety of the substrate. It has been proposed that Arg^{125} neutralizes the negative charge of the γ-phosphate group of ATP during the reaction and that the main-chain amide of Ser^{151} stabilizes a reaction intermediate [11]. Asp^{127} is engaged in a complicated hydrogen-bonding network with active-site residues. In accord with these observations, the kinetic data demonstrate that the substitution of Arg^{125} with cysteine appears to effect both the reaction mechanism and substrate binding. Although there is one direct contact between the arginine and substrate/product, it is only one of 95 interactions [11] and so the loss of one hydrogen-bonding interaction is likely to have only a limited effect on substrate binding. The

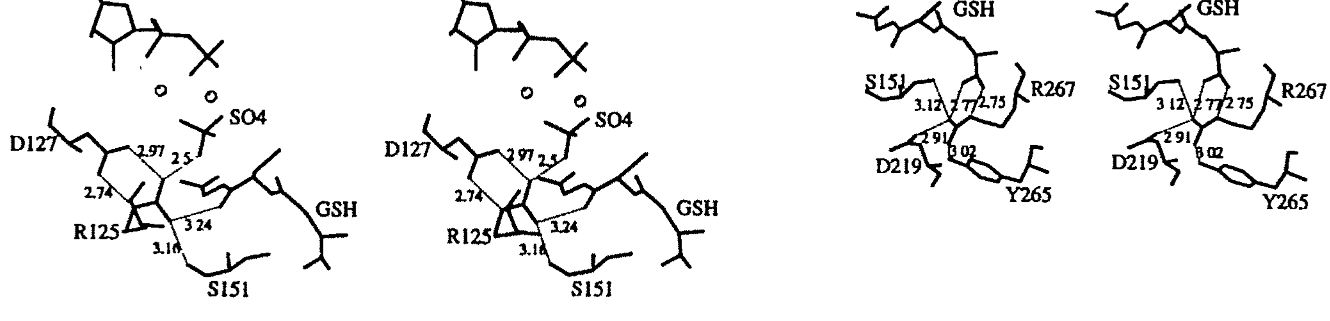

Figure 2 Stereo pictures of the micro environments around the site of two of the missense mutations

Left panel. Arg^{125} The two magnesium ions are shown as open circles. Right panel Arg^{267} The polar interactions between the side-chains of these residues and surrounding atoms are shown by the dashed lines and the distance between polar atoms is measured in Ångstroms These Figures were drawn using MOLSCRIPT [15]

R267W mutation caused a 15-fold increase in K_m for γ-gluABA and a 6-fold increase in the K_m for glycine. Arg^{267} is located in the substrate binding loop and the effect of the mutation on substrate binding is not surprising, since the bulky tryptophan substitution appears to be too large for the active-site defined in the crystal structure (Figures 1 and 2, right panel) [11]. Furthermore, the guanidine group of Arg^{267} is involved in numerous interactions such as salt-links to the γ-glutamyl moiety of the substrate and to Asp^{219}, as well as hydrogen bonds to the hydroxy groups of Ser^{151} and Tyr^{265}. These contacts would be lost in the mutants. As previously mentioned, the main-chain amide of Ser^{151} is thought to stabilize a reaction intermediate. Asp^{219} is a site of mutation for the mild form of GS deficiency and we have previously proposed that this mutation would disrupt a complicated network of hydrogen bonds in the active-site [11]. Tyr^{265} is located immediately preceding the substrate-binding loop. Hence mutation of Arg^{267} is predicted to affect both substrate binding and catalysis; this is borne out by the kinetic data. The R125C and R267W mutations can thus be classified as combined K_m and V_{max} mutations.

The kinetic data on the R330C mutant provide a new insight into the disease, because it was previously thought that it might represent a polymorphism with normal function (since the mutation occurred in a patient who also had Asp^{219} and Leu^{188} mutations). Arg^{330} is located on the surface of the protein (on helix 16, Figure 1), forming a salt-bridge with Asp^{71}, and is 22 Å distant from the active-site and hence not in a position to impact on substrate binding or catalysis. The results of the present study are in agreement with these structural observations as the R330C mutation caused insignificant changes in the K_m values for the substrates. However, as opposed to the other mutant enzymes, the V_{max} of this mutant decreased with repeated freezing and thawing. This indicates that the mutation affects the stability of the enzyme, rendering it more susceptible to oxidation or denaturation. After only one round of freezing and thawing, the V_{max} was higher than 70 % of wild-type activity, indicating that the activity of this mutant *in vivo* may be very close to or just as high as the wild-type activity. After repeated rounds of freezing and thawing, the V_{max} decreased successively to only 5 % of wild-type activity. The poor stability is probably related to the loss of the salt-bridge and the introduction of an accessible, reactive, cysteine residue. Since GS is a dimer, heterozygotes will form heterodimers between normal and mutant subunits. In examples such as the R330C mutant, it is possible that the inactivation of one subunit in a heterodimer could inactivate the complete dimer. This could lead to the loss of up to 75 % of activity in such heterozygotes. The residual 25 % of activity would result from the probability that 25 % of the enzyme in a heterozygote will be wild-type homodimer. However, it is likely that, under normal conditions, 25 % of normal activity might be sufficient to avoid the characteristic symptoms of GS deficiency. In addition to this, the Arg^{330} residue is located at the opposite end of the molecule to the dimer interface [11] so it would not be expected to destabilize the wild-type monomer in a heterodimer.

The G464V mutation clearly affected the affinity for glycine, causing an almost 100-fold increase in the K_m. The K_m values for the two other substrates were only slightly decreased. The glycine residue, shown in Figure 1, adopts main-chain phi and psi angles (96° and 7°, respectively) that are outside the allowed values for non-glycine residues, and hence replacement by any other residue is likely to impair the conformation and flexibility of the alanine-rich loop, which is involved in binding of the glycine substrate [11]. Thus the high K_m for glycine is in excellent agreement with predictions from the crystal structure. The V_{max} for this mutant was low, but might theoretically be able to reach normal levels if substrate concentrations are increased sufficiently. Thus this mutation is classified as a K_m mutation.

The present study demonstrates that specific missense mutations of GS cause distinct kinetic impairment of enzyme function, such as decreased substrate affinity, decreased maximal activity or decreased stability. We speculate that the variation in the clinical picture of patients with GS deficiency is correlated with the mutations involved. However, as many patients are compound heterozygotes with two different mutations a direct correlation between genotype and clinical phenotype may not always be evident. Further studies of natural and directed mutations of GS are required to obtain a greater understanding of the catalytic mechanism and the function of this important enzyme.

This work was supported by the Swedish Medical Research Council (project no 4792), the Swedish Natural Science Research Council, the Frimurare Barnhuset Foundation, the Wera Ekstrom Foundation, the Samariten Foundation, the Sven Jerring Foundation and the Australian Research Council

REFERENCES

1 Larsson, A and Anderson, M (2000) Glutathione synthetase deficiency and other disorders of the γ-glutamyl cycle In The Metabolic Basis of Inherited Disease, 8th edn (Scriver, C R, Beaudet, A L, Sly, W S. and Valle, D., eds), McGraw Hill, New York, in the press
2 Blackburn, A C., Tzeng, H-F., Anders, M W and Board, P G (2000) Discovery of a functional polymorphism in human glutathione transferase zeta by expressed sequence tag database analysis Pharmacogenetics **10**, 49–57
3 Oppenheimer, L, Wellner, V P, Griffith, O W and Meister, A (1979) Glutathione synthetase Purification from rat kidney and mapping of the substrate binding sites J. Biol. Chem. **254**, 5184–5190
4 Gushima, H, Miya, T, Murata, K and Kimura, A (1983) Purification and characterization of glutathione synthetase from *Escherichia coli* B J Appl. Biochem **5**, 210–218
5 Mooz, E D and Meister, A. (1967) Tripeptide (glutathione) synthetase Purification, properties, and mechanism of action Biochemistry **6**, 1722–1734
6 Gali, R. R and Board, P G (1995) Sequencing and expression of a cDNA for human glutathione synthetase Biochem. J. **310**, 353–358
7 Webb, G C, Vaska, V L, Gali, R. R., Ford, J H and Board, P G (1995) The gene encoding human glutathione synthetase (GSS) maps to the long arm of chromosome 20 at band 11.2 Genomics **30**, 617–619
8 Dahl, N., Pigg, M, Ristoff, E, Gali, R, Carlsson, B, Mannervik, B, Larsson, A. and Board, P. (1997) Missense mutations in the human glutathione synthetase gene result in severe metabolic acidosis, 5-oxoprolinuria, hemolytic anemia and neurological dysfunction. Hum. Mol Genet **6**, 1147–1152
9 Shi, Z. Z., Habib, G M, Rhead, W J, Gahl, W A, He, X, Sazer, S. and Lieberman, M. W. (1996) Mutations in the glutathione synthetase gene cause 5-oxoprolinuria Nat Genet **14**, 361–365
10 Al-Jishi, E, Meyer, B. F., Rashed, M S, Al-Essa, M, Al-Hamed, M. H, Sakati, N., Sanjad, S, Ozand, P. T. and Kambouris, M (1999) Clinical, biochemical, and molecular characterization of patients with glutathione synthetase deficiency Clin Genet **55**, 444–449
11 Polekhina, G, Board, P G, Gali, R R, Rossjohn, J. and Parker, M W (1999) Molecular basis of glutathione synthetase deficiency and a rare gene permutation event EMBO J. **18**, 3204–3213
12 Oscarsson, S and Porath, J (1989) Covalent chromatography and salt-promoted thiophilic adsorption Anal Biochem **176**, 330–337
13 Gali, R R and Board, P G (1997) Identification of an essential cysteine residue in human glutathione synthase. Biochem J **321**, 207–210
14 Wellner, V P., Sekura, R, Meister, A and Larsson, A (1974) Glutathione synthetase deficiency, an inborn error of metabolism involving the γ-glutamyl cycle in patients with 5-oxoprolinuria (pyroglutamic aciduria) Proc. Natl Acad Sci USA **71**, 2505–2509
15 Kraulis, P J (1991) MOLSCRIPT a program to produce both detailed and schematic plots of proteins J Appl Crystallogr **24**, 946–950

Received 7 February 2000/3 April 2000, accepted 18 April 2000

Biochem J (2000) 349, 281–287 (Printed in Great Britain)

Targeting motifs and functional parameters governing the assembly of connexins into gap junctions

Patricia E. M. MARTIN[1,2], James STEGGLES, Claire WILSON, Shoeb AHMAD and W. Howard EVANS[1]

Department of Medical Biochemistry, University of Wales College of Medicine, Heath Park, Cardiff CF14 4XN, U K

To study the assembly of gap junctions, connexin–green-fluorescent-protein (Cx–GFP) chimeras were expressed in COS-7 and HeLa cells. Cx26– and Cx32–GFP were targeted to gap junctions where they formed functional channels that transferred Lucifer Yellow. A series of Cx32–GFP chimeras, truncated from the C-terminal cytoplasmic tail, were studied to identify amino acid sequences governing targeting from intracellular assembly sites to the gap junction. Extensive truncation of Cx32 resulted in failure to integrate into membranes. Truncation of Cx32 to residue 207, corresponding to removal of most of the 78 amino acids on the cytoplasmic C-terminal tail, led to arrest in the endoplasmic reticulum and incomplete oligomerization. However, truncation to amino acid 219 did not impair Cx oligomerization and connexon hemichannels were targeted to the plasma membrane. It was concluded that a crucial gap-junction targeting sequence resides between amino acid residues 207 and 219 on the cytoplasmic C-terminal tail of Cx32. Studies of a Cx32E208K mutation identified this as one of the key amino acids dictating targeting to the gap junction, although oligomerization of this site-specific mutation into hexameric hemichannels was relatively unimpaired. The studies show that expression of these Cx–GFP constructs in mammalian cells allowed an analysis of amino acid residues involved in gap-junction assembly.

Key words: chimera, connexin assembly, green fluorescent protein, targeting motifs.

INTRODUCTION

Gap-junction channels are conduits for the direct exchange of ions and small molecules (< 1 kDa) between neighbouring cells and provide a potential mechanism for the intercellular propagation of signalling molecules and metabolites. Gap junctions are constructed of connexins (Cxs), a highly conserved family of proteins with 15 different isoforms identified in rodents to date. Cxs are integral membrane proteins spanning the membrane four times with two extracellular-gap-facing loops, one intracellular loop and cytoplasmically located N- and C-termini [1].

The formation of gap junctions involves a stepwise series of assembly processes. Cxs are inserted into the endoplasmic reticulum (ER) membrane where they must fold correctly prior to oligomerizing into hexameric hemichannels (connexons), an event occurring as they traffick from the ER to the Golgi via an intermediate compartment [2]. Connexons delivered to the plasma membrane then align and dock with partners in neighbouring cells to generate the gap-junction channel [3]. Gap-junction operation is regulated by transmembrane voltage [4] and chemically via cytoplasmic pH and calcium ions [5,6].

The amino acid motifs involved in assembly and targeting of Cxs to gap junctions are poorly understood. Also, channel-gating mechanisms are subject to speculation and a number of Cx mutations result in failure of gap-junction channels to operate normally [7]. Analysis of the functional consequences of these mutations is now possible owing to the increasing number of DNA mutations encoding Cxs shown to be associated with genetically inherited diseases. For example, mutations in Cx32 are associated with Charcot–Marie–Tooth X-linked disease (CMT-X disease), a peripheral neuropathy [8], mutations in Cx26 are associated with non-syndromic sensorineural deafness [9], mutations in Cx31.1 are associated with keratoderma [10] and Cx50 and Cx46 are implicated in cataract formation [11]. These missense, nonsense and frame-shift deletions are scattered throughout the Cx sequences with some also occurring in non-coding regions of the DNA. Cx mutations may radically influence hemichannel assembly processes occurring during intracellular trafficking or gap-junction channel gating, and thus can provide a biochemical explanation of the pathophysiology underlying these diseases [7]. Defects in gap-junction channel operation resulting from Cx mutations have been studied by exogenous expression and electrophysiological techniques in *Xenopus* oocytes [12,13] and by intercellular transfer in cultured mammalian cells of the fluorescent dye Lucifer Yellow [14–16]. Several Cx32 mutations associated with CMT-X disease result in aberrant protein trafficking in mammalian cells [16–18]. In-depth analysis of selected mutations should allow definition of the roles that specific amino acids and protein domains have in the biogenesis of gap junctions.

Green fluorescent protein (GFP) is used widely to study intracellular trafficking routes since its properties allow rapid visualization of cellular localization with high sensitivity [19–21]. Although chimeric proteins are likely to exhibit modified behaviour, it was shown that fusion of the reporter protein aequorin (Aeq) to the C-terminus of Cx43 or Cx32 led to the assembly of

---

Abbreviations used Cx, connexin, wtCx, wild-type Cx, ER, endoplasmic reticulum, CMT-X disease, Charcot–Marie–Tooth X-linked disease, GFP, green fluorescent protein; eGFP, enhanced GFP; TNT, coupled *in vitro* transcription/translation

[1] To whom correspondence should be addressed (e-mail martinpe@cardiff ac uk).

[2] Present address· Department of Diagnostic Radiology, Cardiovascular Sciences Research Group, University of Wales College of Medicine, Heath Park, Cardiff CF14 4XN, U K

functional chimeric gap-junction channels [22]. In the present work, we used Cx–GFP chimeras to study the assembly, intracellular trafficking and functionality of gap junctions and to define a region on the cytoplasmic C-terminal tail of Cx32 that is crucial for targeting to the gap junction.

EXPERIMENTAL

Construction of chimeric Cx–GFP cDNA

Cx cDNA was fused in-frame to the N-terminus of enhanced GFP (eGFP) in the vector pe-GFP-N1 (Clontech; Figure 1). For wild-type (wt) Cx26 [23] and Cx32 [24] the open reading frame was amplified by PCR from plasmids containing the relevant full-length cDNA [22] using appropriate oligonucleotide primers introducing *Bgl*II (for Cx26) and *Hin*dIII restriction-enzyme sites (for Cx32 constructs) at the 5′ and 3′ ends of the cDNA respectively. The primers used were as follows, with restriction-enzyme sites underlined and Cx sequences in bold. Cx32 forward primer, Cx32GF, 5′-CTC GAG CTC AAGCTT **ATG AAC TGG ACA GGT**-3′; Cx32 reverse primer, Cx32GR, 5′-CAG AAT TCG AAGCTT **GCA GGC TGA GCA TCG**-3′; Cx26 forward primer, Cx26GF, 5′-CTA CCG GAC TCAGATCTC **ATG GAT TGG GGC ACC**-3′; and Cx26 reverse primer, Cx26GR, 5′-CTT GAG CTC GAGATCTGA **GAC TGG TCT TTT GGA**-3′.

To generate truncated Cx32 proteins, Cx32Δ19, Cx32Δ93, Cx32Δ207 and Cx32Δ219, reverse primers incorporating the relevant 3′ cDNA position and a *Hin*dIII site were used. The primer sequences were as follows: Cx32Δ19 reverse primer, Δ19R, 5′-CAG AAT TCG AAGCTT **AAT GGC TGT AGA ATG**-3′; Cx32Δ93 reverse primer, Δ93R, 5′-CAG AAT TCG AAGCTT **TGC CAC GAG GAG AGC**-3′; Cx32Δ207 reverse primer, Δ207R, 5′-CAG AAT TCG AAGCTT **CGC CAC GTT GAG GAT**-3′; and Cx32Δ219 reverse primer, Δ219R, 5′-CAG AAT TCG AAGCTT **GCG GGC ACA GGC CCG GAT**-3′.

The 5′ primers were the same as the wild-type counterparts shown above. To generate the chimeric constructs the resulting PCR products were digested with *Bgl*II or *Hin*dIII and ligated into the dephosphorylated *Bgl*II or *Hin*dIII sites of pe-GFP-N1 respectively [25]. The truncated mutant Cx32Δ215 was engineered by PCR amplification of wtCx32 using the forward primer Cx32P1 [22] and a reverse primer introducing a premature stop codon at amino acid position 215. These primers contained *Bam*HI sites to enable subcloning of the PCR products into the vector pCR3 (Invitrogen) as described above.

All ligation reactions were transformed into *Escherichia coli* DH5α (Gibco-BRL) and positive clones identified by mini-plasmid preparation and restriction-enzyme analysis. Selected constructs were sequenced using the dRhodamine Dye Termination Cycle Sequencing kit (Perkin-Elmer).

In vivo expression and cellular localization of Cxs

COS-7 or HeLa cells (European Collection of Animal Cell Cultures, Salisbury, Wiltshire, U.K.) were transfected with the relevant Cx cDNA and harvested for Western-blot analysis [22]. Proteins were characterized using a primary rabbit polyclonal anti-GFP antibody, generated against a GFP–calreticulin fusion protein [26] and a secondary goat anti-rabbit antibody conjugated to horseradish peroxidase (Bio-Rad). Blots were developed using the enhanced chemiluminescence (ECL®) system (Pierce).

For cellular localization, 5×10^5 cells were transfected with 1 μg of relevant cDNA. Post-transfection (24 h) the cells were split on to four 16-mm^2 coverslips placed in 12-well dishes followed the next day by fixation in 4 % formaldehyde, and if necessary, processed for immunocytochemical analysis [22]. Co-localization of Cx and GFP was confirmed by staining the cells with the relevant primary anti-Cx antibodies: for Cx26 Gap 28H against the intracellular loop of Cx26 [27], for Cx32 a monoclonal antibody to an intracellular loop sequence was used (Chemicon) and a polyclonal rabbit antibody against calreticulin was used as an ER marker [26]. The secondary antibody was goat anti-rabbit or goat anti-mouse conjugated to Cy3 (Sigma) as required. Cells were viewed under a laser confocal microscope (Leitz) and GFP

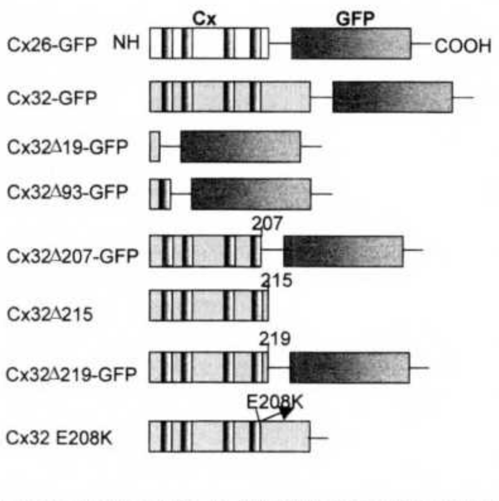

	Targets	Oligomerisation	Functionality
Cx26-GFP	Yes	Yes	Yes
Cx32-GFP	Yes	Yes	Yes
Cx32Δ19-GFP	No	ND	ND
Cx32Δ93-GFP	No	ND	ND
Cx32Δ207-GFP	No	No	No
Cx32Δ215	Yes	Yes	No
Cx32Δ219-GFP	Yes	Yes	Yes
Cx32 E208K	No	Yes	No

Figure 1 Diagramatic representation of the Cx–GFP chimeras and Cx mutants studied

Cxs were fused in-frame to the N-terminus of GFP. The Cx transmembrane domains are depicted by grey shading. The ability to target to gap junctions, whether Cxs oligomerize to connexons and whether the cells were functional according to transfer of Lucifer Yellow are indicated. ND, not determined.

expression visualized in cells using excitation (488 nm) and emission (515 nm) wavelengths. Images were processed using Adobe Photoshop 5.

Analysis of the oligomeric state of chimeric and mutated connexons

The oligomeric status of the chimeric and mutated connexons was determined by expression of the proteins in transiently transfected COS-7 cells or by cell-free synthesis using a coupled *in vitro* transcription/translation (TNT) system (Promega).

To determine the oligomeric status in cells expressing the chimeric Cx–GFP proteins, 1×10^7 cells were seeded on to 10-cm dishes and transfected with 8 μg of the relevant Cx cDNA [22]. Ten plates (1×10^8 cells) were used for each assay. Post-transfection (48 h), cells were washed in PBS, harvested in 1 ml of PBS in the presence of protease inhibitors [22], and the cells pelleted by centrifugation at 1000 ***g*** for 5 min.

For determination of the oligomeric status using the cell-free system the relevant cDNA was synthesized using the TNT system (Promega) supplemented with canine pancreatic microsomes and ^{35}S promix (Amersham) as described in [27,28]. Membrane-integrated Cxs were separated from free Cxs by centrifugation as described in [28]. In both cases, connexons were extracted from the cell pellets or the membranes in an orbital rotator at 4 °C for 1 h in 500 μl of a buffer containing 20 mM triethanolamine, pH 9.2, 20 mM EDTA, 2 % (w/v) dodecyl maltoside and 10 mM dithiothreitol, a procedure that maintains the connexons intact [29]. As a control, extraction used 20 mM triethanolamine, pH 9.2, 20 mM EDTA, 2 % (w/v) SDS and 20 mM dithiothreitol, which dissociates connexons into Cxs. Sucrose–detergent gradients were calibrated with carbonic anhydrase (29 kDa) and myosin (209 kDa) marker proteins to determine the approximate positions in the gradients where monomeric and hexameric Cxs sedimented, corresponding to 5 and 9 S, respectively [16,30–32]. Under the conditions used [10–40 % (w/v) sucrose, 20 h, 150000 ***g***], the sucrose gradient was calibrated as < 18 % (w/v; Cxs), 18–28 % (Cx oligomeric intermediates) and 28–40 % (connexons) [27,31,32]. The positions of Cxs, intermediate oligomers and connexons present in cell extracts resolved by the gradients into 11–12 fractions were analysed by SDS/PAGE and ECL® Western blotting using an antibody to GFP as described above. With Cxs synthesized *in vitro* by the TNT system [28,32a] Cx, oligomeric Cx and connexon analysis was by autoradiography of each of the gradient fractions resolved by SDS/PAGE. Densitometric analysis of the ECL® Western blots or autoradiographs was carried out using the Bio-Rad 700 densitometer and software [27,28].

Functionality of chimeric constructs

HeLa cells were transfected by calcium phosphate transfection with cDNA encoding the various Cx–GFP chimeras [22]. Stable cell populations expressing the chimeric proteins were selected by growing the transfected HeLa cells for 3 weeks in medium supplemented with Geneticin (G418 sulphate, 4 mg/ml) and GFP-positive cells were sorted using a fluorescence-activated cell sorter (Becton and Dickinson). Selected populations of cells were grown to confluency and functionality of the cell lines determined according to the ability of cells microinjected with Lucifer Yellow [5 % (w/v) in 0.3 M LiCl] to transfer dye to neighbouring cells. Prior to injection (18 h) of cells, protein expression was enhanced by addition of 5 mM sodium butyrate to the media [22].

RESULTS

Properties of the Cx–GFP constructs

The intracellular trafficking of wtCx26– and wtCx32–GFP and a series of truncated Cx32–GFP cDNAs expressed in COS-7 and HeLa cells and the functionality of gap junctions formed were examined. Cx cDNAs were fused in-frame to the N-terminus of eGFP. The Cx32–GFP chimeras examined included two constructs, encoding the N-terminal 19 and 93 amino acids, but low expression and difficulties in membrane insertion precluded further studies. Therefore, two cytoplasmic tail deletions, terminating at amino acids 207 and 219, were constructed (Figure 1). Also, the assembly, trafficking and functionality of two site-specific mutations of wtCx32, Cx32E208K and Cx32Δ215, were included as non-chimeric mutants to validate the behaviour shown by the truncated Cx–GFP chimeric proteins.

Expression of Cx–GFP chimeras in mammalian cells

Western-blot analysis of cell lysates from cells transfected with the various Cx32–GFP and Cx26–GFP constructs resulted in the detection of immunolabelled protein using an anti-GFP antibody and anti-Cx antibodies. The predicted size pattern of the expressed protein was observed, i.e. Cx32–GFP (59 kDa) Cx32Δ219–GFP (51 kDa) Cx32Δ207–GFP (50 kDa) eGFP (28 kDa; Figure 2). A further protein product, possibly a proteolytic product, migrated ahead of the full-length protein in the gels. A similar phenomenon was reported recently for Cx43–GFP [21]. A Cx26–GFP protein product of the predicted molecular mass (54 kDa) was also expressed (Figure 2).

Cellular localization of Cx–GFP chimeras

The cellular location of the recombinant chimeric proteins was determined by virtue of the inherent fluorescence of GFP (Figure 1). Analysis by confocal microscopy showed that wtCx26 and the Cx26–GFP chimera were targeted to the plasma membrane of COS-7 cells giving characteristic punctate gap-junction staining

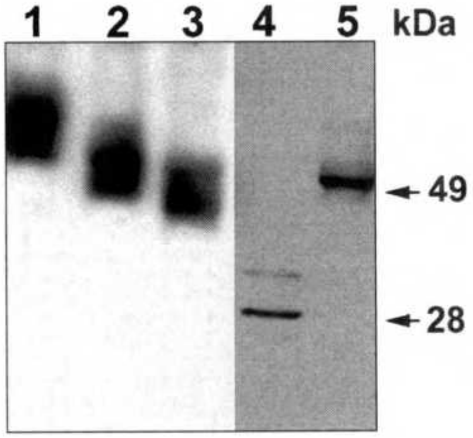

Figure 2 Western-blot analysis of Cx32–GFP chimeric proteins

COS-7 cells, transfected with the relevant cDNA, were harvested 48 h post-transfection and prepared for SDS/PAGE and Western-blot analysis as described in the Experimental section. Proteins were detected using a primary antibody against GFP. Lane 1, Cx32–GFP; lane 2, Cx32Δ219–GFP; lane 3, Cx32Δ207–GFP; lane 4, eGFP; lane 5, Cx26–GFP.

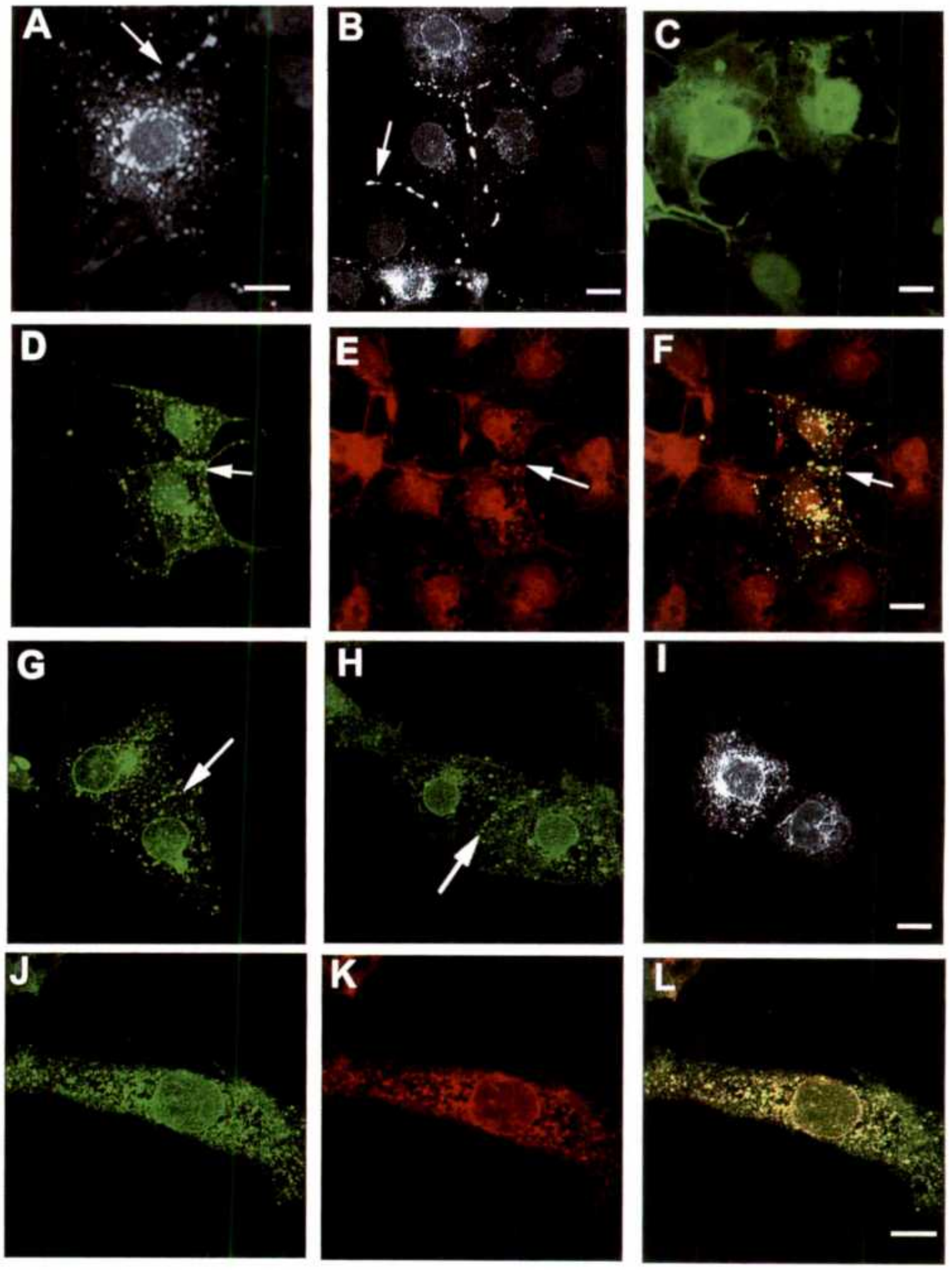

Figure 3 Localization of CxGFP chimeras

COS-7 cells were transfected with the relevant cDNA. Post-transfection (48 h), cells were fixed and either viewed for GFP autofluorescence or stained with a relevant antibody against Cx26 or Cx32 as described in the Experimental section. (**A**) wtCx26 immunostained with an antibody against the intracellular loop of Cx26; (**B**) wtCx32 stained with an antibody against the intracellular loop of Cx32; (**C**) eGFP; (**D**) Cx26–GFP viewed by GFP autofluorescence; (**E**) Cx26–GFP immunostained with the antibody Gap28H and a goat anti-rabbit Cy3-conjugated secondary antibody; (**F**) co-localization of (**D**) and (**E**); (**G**–**H**) Cx32–GFP and Cx32Δ219–GFP viewed by GFP autofluorescence; (**I**) Cx32Δ215 immunostained with an antibody against the intracellular loop of Cx32; (**J**) Cx32Δ207–GFP viewed by GFP autofluorescence; (**K**) cells transfected with Cx32Δ207–GFP immunostained with an antibody against calreticulin and a goat anti-rabbit Cy3-conjugated secondary antibody; (**L**) co-localization of (**J**) and (**K**). Arrows indicate targeting to the gap junction. Scale bars, 10 μm.

(Figures 3A and 3D, respectively). Similarly, wtCx32 and Cx32–GFP were also targeted to areas of cell contact (Figures 3B and 3G, respectively). Immunolocalization studies using a Cx26 antibody confirmed that GFP and Cx26 expression were coincident (Figures 3D–3F), showing that the proteins expressed were chimeric. In contrast, eGFP was spread diffusely throughout the cell with some cells showing intense nuclear staining (Figure 3C). A similar cellular localization was observed for the short N-terminal segments Cx32Δ19–GFP and Cx32Δ93–GFP (results not shown). Cx32Δ219-GFP was targeted to the plasma membrane (Figure 3H). However, cells expressing Cx32Δ207–GFP showed no punctate plasma membrane staining, but extensive staining of the ER was observed (Figure 3J).

Immunolocalization studies with relevant anti-Cx antibodies confirmed that the Cx component of each mutated chimera co-localized with GFP, thus confirming that the proteins were expressed together (results not shown). Immunostaining of cells expressing Cx32Δ207–GFP with an antibody to calreticulin,

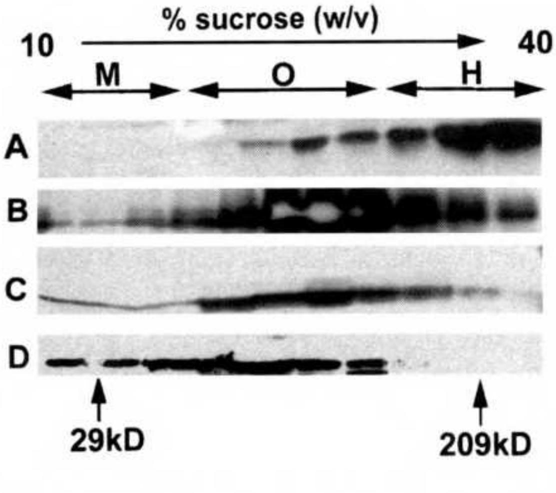

Figure 4 Analysis by rate-sedimentation of the oligomeric status of Cx32–GFP chimeras and Cx32 mutated proteins

Connexons were extracted with detergents from COS-7 cells expressing the Cx32–GFP chimeric proteins 48 h post-transfection as described in the Experimental section. After rate sedimentation in 10–40% (w/v) linear sucrose–detergent gradients, the proteins in each fraction were concentrated and prepared for SDS/PAGE and Western-blot analysis as described in the text. (**A**–**D**) Representative sucrose-gradient profiles of connexons extracted from cells with dodecyl maltoside: (**A**) wtCx32 detected with an antibody against the C-terminal tail of Cx32; (**B**–**D**) Cx32–GFP, Cx32Δ219–GFP and Cx32Δ207–GFP, respectively, detected with an antibody against GFP. For quantification, see Table 1. The positions of standard proteins that co-sediment with Cxs or connexons are indicated (29 and 209 kDa, respectively) and the positions in the gradient of monomeric (M), intermediate (O) and hexameric (H) Cxs are indicated.

a resident ER protein, confirmed the predominant ER location of this mutant (Figures 3J–3L). Similar intracellular staining was also observed when the site-specific mutation Cx32E208K was expressed in COS-7 cells [16,17]. A non-chimeric protein, truncated at position 215, i.e. Cx32Δ215, was examined by immunostaining using an antibody against the intracellular loop of Cx32, and the results also showed intracellular retention (Figure 3I).

Oligomeric status of Cx–GFP constructs

To investigate the biochemical parameters underlying targeting to ER or the gap junction, the oligomeric status of wtCx32–GFP, Cx32Δ219–GFP and Cx32Δ207–GFP expressed in COS-7 cells was determined by a velocity sedimentation procedure that separates monomeric and oligomeric Cxs [31,32]. The amount of each of the chimeric Cxs sedimenting as monomer [in the 5 S fraction, i.e. fractions $< 18\%$ (w/v) sucrose], incompletely oligomerized product [18–28 % (w/v) sucrose] and hexameric connexons [in the 9 S fractions, i.e. $> 28\%$ (w/v) sucrose] was determined by Western-blot analysis of each fraction from the gradient and subsequent densitometric analysis. The results show that when wtCx32 was extracted from COS-7 cells using dodecyl maltoside, a non-ionic detergent that extracts connexons [29], $> 70\%$ of the expressed protein sedimented as hexamer, 18 % as intermediate oligomeric products and 2 % as monomers (Figure 4A and Table 1). These results show that most of the wtCx32 expressed in cells was assembled into connexons. Chemical cross-linking studies of the 9 S fraction showed previously that hexameric connexons were present in this fraction [31]. In contrast, when wtCx32 was extracted from cells with SDS, which dissociates connexons into Cxs [31], $> 70\%$ of the protein was present as monomers (Table 1A). A study of the oligomerization status of the chimeric Cx32–GFP expressed proteins was therefore carried out. This showed that wtCx32–GFP and Cx32Δ219–GFP assembled into connexons, albeit at a reduced efficiency compared with wtCx32 (45 % compared with 70 %; Figures 4B and 4C, and Table 1A). The reduced level of connexons produced resulted in an increase in the ratio of oligomeric intermediate non-functional products, suggesting that fusion of GFP to Cxs impeded the oligomerization of Cxs into connexon hexameric hemichannels. In contrast to the oligomerization behaviour of wtCx32–GFP and Cx32Δ219–GFP, Cx32Δ207–GFP was expressed in cells mainly as monomers and intermediate oligomers with only 2 % of the protein sedimenting in the 9 S fraction (Figure 4D and Table 1A). Parallel studies using a complimentary *in vitro* oligomerization assay system were also carried out to analyse two non-chimeric mutants. These studies showed that Cx32Δ215 did not oligomerize into hexameric connexons whereas a site-specific mutation, Cx32E208K, assembled into hexameric proteins with a similar efficiency to

Table 1 Oligomeric status of Cx32–GFP chimeras and Cx32 mutated proteins

(**A**) The oligomerization assay shows the distribution of Cx constructs expressed in COS-7 cells. (**B**) The oligomerization potency of the constructs was assessed by using an *in vitro* assay system. The relative oligomeric status of Cxs in each fraction collected from the sucrose–detergent gradients was determined by densitometric analysis of ECL® Western blots (**A**) or autoradiograms (**B**). The results are represented as the percentages of Cxs present in the relevant fractions of the sucrose gradient: Cx monomer fractions, $< 18\%$ (w/v) sucrose, intermediate oligomer fractions, 18–28% (w/v) sucrose, and connexon fractions, $> 28\%$ (w/v) sucrose. Data are means ± S.E.M., $n = 3$.

(A) Construct	% Cx monomer	% Intermediate Cxs	% Connexons
wtCx32	2.2 ± 1.3	18.7 ± 2.9	79.2 ± 4.1
Cx32–GFP	17.2 ± 0.5	37.4 ± 1.0	45.4 ± 1.3
Cx32Δ219–GFP	5.3 ± 1	51.8 ± 1.7	42.9 ± 1.5
Cx32Δ207–GFP	48.6 ± 0.5	49.6 ± 1.4	1.8 ± 2 .7
wtCx32 (extracted with SDS)	72.4 ± 3.2	27.4 ± 1.3	0.2 ± 0.9

(B) Construct	% Monomer	% Intermediate Cxs	% Connexons
wtCx32	30 ± 2.6	42.3 ± 1.1	27.2 ± 1.5
Cx32E208K	39 ± 4	33 ± 5.5	27 ± 4.5
Cx32Δ215	87 ± 11	11 ± 7.8	2 ± 0.4
wtCx32 (extracted with SDS)	64 ± 3.5	33 ± 1.1	2.2 ± 2.4

Table 2 Functionality of Cx–GFP chimeric proteins

HeLa cells expressing the various Cx–GFP proteins were assessed for their ability to transfer Lucifer Yellow. The results are expressed as the percentages of cells transferring dye to 0–2 cells, 3–5 cells and to > 5 cells (± S.E.M.). Experiments were performed in triplicate and at least 20 cells were injected per experiment.

	Cells transferring Lucifer Yellow (%)		
Construct	0–2 cells	3–5 cells	> 5 cells
Cx26–GFP	53.4 ± 5.6	18.8 ± 3.5	26.3 ± 4.3
Cx32–GFP	56.8 ± 5	19.4 ± 6.5	23.7 ± 6.9
Cx32Δ219–GFP	88 ± 4.3	11.9 ± 4.8	0
Cx32Δ207–GFP	90.7 ± 7.3	6.0 ± 1.5	3.2 ± 3.2
HeLa control	96.6 ± 3.5	2.7 ± 1.4	1.0 ± 1.0

wtCx32 in this *in vitro* assay system (Table 1B). The results identify amino acids 207–219 on the C-terminal tail of Cx32 as playing an essential role in the oligomerization of Cxs into hexameric hemichannels.

Intercellular dye transfer of cells expressing chimeric Cx–GFP

To analyse further intercellular communication by gap junctions formed by the Cx–GFP chimeric proteins, HeLa cells that do not assemble gap junctions [32] were transfected stably with the various constructs (Figure 1). The functionality of gap junctions assembled by these cell lines was analysed by their ability to transfer Lucifer Yellow to 3–5, or 5 or more, neighbouring cells. The results show that cells expressing wtCx26–GFP or wtCx32–GFP efficiently formed gap-junction channels with 18.8 and 19% of injected cells transferring dye to 3–5 cells, respectively, and 26.3 and 23.7% of the cells transferring dye to 5 or more neighbouring cells, respectively. In control (non-transfected) HeLa cells only 1% transferred dye to more than 5 neighbouring cells (Table 2). The functionality of Cx32Δ219–GFP was reduced compared with wtCx32–GFP, with 11.9% of cells transferring dye to 3–5 cells, although Student's *t*-test analysis showed this not to be significantly reduced compared with wtCx32–GFP. However, communication to more than 5 cells was severely compromised ($P < 0.05$). The functionality of Cx32Δ207–GFP was reduced further, and was similar to that of the 'null' HeLa cells ($P < 0.05$) (Table 2).

DISCUSSION

The assembly of multimeric gap-junction intercellular communication channels from the constituent Cx subunits is a complex process [2]. As two or more cells contribute to the formation of the direct cell-to-cell channel, the component reactions leading to assembly can be analysed by following the formation of gap-junction hemichannels. Following insertion and correct topological folding of the Cx subunit in the ER, oligomeric association generates hexameric structures in which Cxs are arranged around a central pore [33]. Connexons may be homomeric or heteromeric in composition, which can result in varying channel permeability properties [31,34]. The position in the secretory pathway where Cx subunit association leading to channel formation occurs is unlikely to be the trans-Golgi [30], for Cx oligomerization is a progressive and sequential process initiated in the ER, and completed in the Golgi apparatus [31,32].

The current work aimed to identify specific amino acid sequences involved in targeting of Cxs/connexons from intracellular stores to the plasma membrane and gap junction. The approach taken involved analysis of the expression in mammalian cells of a range of intact and truncated Cxs with GFP attached to the Cx C-terminal tail. Chimeric Cx32–GFP or Cx26–GFP were targeted to the gap junction and studies involving intercellular transfer of Lucifer Yellow showed the intercellular channels to be functional. The experiments using chimeric Cx32 showed that most of the 78 amino acids comprising the cytoplasmic C-terminal tail were not required for intracellular trafficking to the gap junction, but a short amino acid sequence leading from the fourth membrane traverse was crucial. A truncated chimera, Cx32Δ207–GFP, which inefficiently oligomerized into hemichannels, was arrested mainly in the ER. In contrast, Cx32Δ219–GFP, which oligomerized with a similar efficiency to Cx32–GFP, trafficked along the secretory pathway and was targeted to the plasma membrane. Thus a gap-junction-targeting motif resides between amino acid residues 207 and 219 of Cx32. To analyse further this short sequence, we studied two further mutations, Cx32E208K, a point mutation, and Cx32Δ215, a truncated protein, both observed in the peripheral neuropathy, CMT-X disease [7]. The results, taken together with others [16,17], show that the Cx32E208K and Cx32Δ215 mutants accumulated primarily in intracellular membranes. Other Cx32 mutations associated with CMT-X, e.g. Y211stop, R215W, R215Q and R215stop, were shown not to form gap junctions using electrophysiological techniques in *Xenopus* oocytes [13] but their trafficking competence in mammalian cells was not studied. The Cx32E208K mutant [16] oligomerized to a similar extent as wtCx32. Although productive association of Cx subunits to generate a hexameric hemichannel is a fundamental requirement for formation of functional gap junctions, the present results suggest that targeting motifs present in this 12-amino acid region on the cytoplasmic tail can override association into hemichannels [16].

Targeting sequences of monotopic membrane proteins are invariably located at cytoplasmic areas contiguous to the membrane-traversing sequence [35], but with polytopic proteins, such as Cxs, the situation appears more complex. Further domains appear to be involved in the assembly of multimeric membrane-associated proteins. For example, both N- and C-terminal regions contribute to the assembly and functional expression of homo- and heteromeric voltage-gated K^+ channels [36]. The fifth and sixth membrane-spanning regions of the inositol 1,4,5-trisphosphate receptor have been shown recently to be key determinants in receptor oligomerization [37]. The targeting sequence now identified on the C-terminal tail of Cx32 is cytoplasmic, situated close to the membrane and coincides with one of two calmodulin-binding sites identified on Cx32 [38]. Analysis of several Cx32 mutations at the N-terminal tail suggests that targeting determinants also exist in this domain [16]. However, the truncation mutants Cx32Δ19–GFP and Cx32Δ93–GFP could not be used owing to the role of this domain in insertion into the ER [28,32a]. Furthermore, gap-junction targeting determinants may be interlinked with properties underlying association into hexamers in which Cxs are arranged around a central channel. The present data obtained in cells expressing Cx32E208K emphasize the dominant requirement for maintaining the correct amino acid sequence in this region of the protein. The accumulation mainly in the ER of Cx32E208K, where oligomerization occurred, and the limited oligomerization and intracellular location of Cx32Δ207–GFP, illustrate the complexity of the various processes that regulate intracellular trafficking and connexon hemichannel formation in the secretory pathway.

The present results illustrate the utility of GFP as a reporter protein in the study of the targeting of Cxs and their assembly into gap junctions. GFP was more resilient in the recombinant construction of Cx chimeras than other reporter proteins, such as aequorin (Aeq), used to measure the cytoplasmic calcium environment [22,40] and β-galactosidase [41]. Although a Cx26–Aeq chimera was shown not to be expressed [22], this deficiency was corrected by exchanging the short C-terminal tail of Cx26 with that of Cx43 [40]. The trafficking properties of a range of truncated and mutated Cxs in gap-junction-associated disease models such as CMT-X disease [16,27] and sensorineural deafness [27] are now open to investigation in live cells expressing Cx–GFP chimeras.

This work was supported by an M.R.C. programme grant and a Commonwealth scholarship to S. A. We thank S. Coleman for research assistance, C. George for helpful discussion and Dr David Llewellyn for the GFP and calreticulin antibodies

REFERENCES

1 Goodenough, D. A., Goliger, J. A. and Paul, D. L. (1996) Connexins, connexons, and intercellular communication. Annu. Rev. Biochem. **65**, 475–502

2 Evans, W. H., Ahmad, S., Diez, J., George, D. H., Kendall, J. M. and Martin, P. E. M. (1999) Trafficking pathways leading to the formation of gap junctions, in Gap Junction-Mediated Intercellular Signalling in Health and Disease, Novartis Foundation Symposium 219, pp. 44–59, Wiley, Chichester

3 Evans, W. H. (1994) Assembly of gap junction intercellular communication channels. Biochem. Soc. Trans. **22**, 788–792

4 Trexler, E. B., Bennett, M. V. L., Bargiello, T. A. and Verselis, V. K. (1996) Voltage gating and permeation in a gap junction hemichannel. Proc. Natl. Acad. Sci. U.S.A. **93**, 5836–5841

5 Ekvitorin, J. F., Calero, G., Morley, G. E., Coombs, W., Taffet, S. M. and Delmar, M. (1996) pH regulation of connexin43 – molecular analysis of the gating particle. Biophys. J. **71**, 1273–1284

6 Wang, X. G., Li, L. Q., Peracchia, L. L. and Peracchia, C. (1996) Chimeric evidence for a role of the connexin cytoplasmic loop in gap junction channel gating. Pflugers Arch. Eur. J. Physiol. **431**, 844–852

7 Martin, P. E. M. and Evans, W. H. (1999) Trafficking and targeting of Connexin 32 mutations to gap junctions in Charcot-Marie-Tooth-X-linked disease. Curr. Topics Membr. **49**, 461–481

8 Bergoffen, J., Scherer, S. S., Wang, S., Scott, M. O., Bone, L. J., Paul, D. L., Chen, K., Lensch, M. W., Chance, P. F. and Fischbeck, K. H. (1993) Connexin mutations in X-linked Charcot-Marie-Tooth disease. Science **262**, 2039–2042

9 Kelsell, D. P., Dunlop, J., Stevens, H. P., Lench, N. J., Liang, J. N., Parry, G., Mueller, R. F. and Leigh, I. M. (1997) Connexin 26 mutations in hereditary non-syndromic sensorineural deafness. Nature (London) **387**, 80–83

10 Xia, J. H., Liu, C. Y., Tang, B. S., Pan, Q., Huang, L., Dai, H. P., Zhang, B. R., Xie, W., Hu, D. X., Zheng, D. et al. (1998) Mutations in the gene encoding gap junction protein beta-3 associated with autosomal dominant hearing impairment. Nat. Genet. **20**, 370–373

11 Shiels, A., Mackay, D., Ionides, A., Berry, V., Moore, A. and Bhattacharya, S. (1998) A missense mutation in the human connexin 50 gene (GJA8) underlies autosomal dominant 'zonular pulverulent' cataract, on chromosome 1q. Am. J. Hum. Genet. **62**, 526–532

12 Oh, S., Ri, Y., Bennett, M. V. L., Trexler, E. B., Verselis, V. K. and Bargiello, T. A. (1997) Changes in permeability caused by connexin 32 mutations underlie X-linked Charcot-Marie-Tooth disease. Neuron **19**, 927–938

13 Castro, C., GomezHernandez, J. M., Silander, K. and Barrio, L. C. (1999) Altered formation of hemichannels and gap junction channels caused by C-terminal connexin-32 mutations. J. Neurosci. **19**, 3752–3760

14 George, C. H., Martin, P. E. M. and Evans, W. H. (1998) Rapid determination of gap junction formation using HeLa cells microinjected with cDNAs encoding wild-type and chimeric connexins. Biochem. Biophys. Res. Commun. **247**, 785–789

15 Yoshimura, T., Satake, M., Ohnishi, A., Tsutsumi, Y. and Fujikura, Y. (1998) Mutations of connexin 32 in Charcot-Marie-Tooth disease type X interfere with cell-to-cell communication but not cell proliferation and myelin-specific gene expression. J. Neurosci. Res. **51**, 154–161

16 Martin, P. E. M., Mambetisaeva, E. T., Archer, D. A., George, C. H. and Evans, W. H. (2000) Analysis of gap junction assembly using mutated connexins detected in Charcot Marie Tooth X linked disease. J. Neurochem. **74**, 711–720

17 Deschenes, S. M., Walcott, J. L., Wexler, T. L., Scherer, S. S. and Fischbeck, K. H. (1997) Altered trafficking of mutant connexin 32. J. Neurosci. **17**, 9077–9084

18 Omori, Y., Mesnil, M. and Yamasaki, H. (1996) Connexin 32 mutations from X-linked Charcot-Marie-Tooth disease patients: Functional defects and dominant negative effects. Mol. Biol. Cell **7**, 907–916

19 Kendall, J. M. and Badminton, M. N. (1998) *Aequorea victoria* bioluminescence moves into an exciting new era. Trends Biotechnol. **16**, 216–224

20 Tenjinbaru, K., Furuno, T., Hirashima, N. and Nakanishi, M. (1999) Nuclear translocation of green fluorescent protein-nuclear factor kappa B with a distinct lag time in living cells. FEBS Lett. **444**, 1–4

21 Jordan, K., Solan, J. L., Dominguez, M., Sia, M., Hand, A., Lampe, P. D. and Laird, D. W. (1999) Trafficking, assembly, and function of a connexin 43-green fluorescent protein chimera in live mammalian cells. Mol. Biol. Cell **10**, 2033–2050

22 Martin, P. E. M., George, C. H., Castro, C., Kendall, J. M., Capel, J., Campbell, A. K., Revilla, A., Barrio, L. C. and Evans, W. H. (1998) Assembly of chimeric connexin-aequorin proteins into functional gap junction channels. Reporting intracellular and plasma membrane calcium environments. J. Biol. Chem. **273**, 1719–1726

23 Zhang, J. T. and Nicholson, B. J. (1989) Sequence and tissue distribution of a second protein of hepatic gap junctions, Cx26, as deduced from its cDNA. J. Cell Biol. **109**, 3391–3401

24 Paul, D. L. (1986) Molecular-cloning of cDNA for rat-liver gap junction protein. J. Cell Biol. **103**, 123–134

25 Sambrook, J., Fritsch, E. F. and Maniatis, T. (1989) Molecular Cloning: a Laboratory Manual, 2nd edn., Cold Spring Harbor Press, Cold Spring Harbor

26 Roderick, H. L., Campbell, A. K. and Llewellyn, D. H. (1997) Nuclear localisation of calreticulin *in vivo* is enhanced by its interaction with glucocorticoid receptors. FEBS Lett. **405**, 181–185

27 Martin, P. E. M., Coleman, S. L., Casalotti, S. O., Forge, A. and Evans, W. H. (1999) Properties of connexin 26 gap junctional proteins derived from mutations associated with non syndromal hereditary deafness. Hum. Mol. Genet. **13**, 2369–2376

28 Ahmad, S., Diez, J. A., George, C. H. and Evans, W. H. (1999) Synthesis and assembly of connexins *in vitro* into homomeric and heteromeric functional gap junction hemichannels. Biochem. J. **339**, 247–253

29 Cascio, M., Kumar, N. M., Safarik, R. and Gilula, N. B. (1995) Physical characterization of gap junction membrane connexons (hemi- channels) isolated from rat-liver. J. Biol. Chem. **270**, 18643–18648

30 Musil, L. S. and Goodenough, D. A. (1993) Multisubunit assembly of an integral plasma-membrane channel protein, gap junction connexin 43, occurs after exit from the ER. Cell **74**, 1065–1077

31 Diez, J. A., Ahmad, S. and Evans, W. H. (1999) Assembly of heteromeric connexons in guinea-pig liver en route to the Golgi apparatus, plasma membrane and gap junctions. Eur. J. Biochem. **262**, 142–148

32 George, C. H., Kendall, J. M. and Evans, W. H. (1999) Intracellular trafficking pathways in the assembly of connexins into gap junctions. J. Biol. Chem. **274**, 8678–8685

32a Falk, M. M., Buehler, L. K., Kumar, N. M. and Gilula, N. B. (1997) Cell-free synthesis and assembly of connexins into functional gap junction membrane channels. EMBO J. **16**, 2703–2716

33 Unger, V. M., Kumar, N. M., Gilula, N. B. and Yeager, M. (1999) Three-dimensional structure of a recombinant gap junction membrane channel. Science **283**, 1176–1180

34 He, D. S., Jiang, J. X., Taffet, S. M. and Burt, J. M. (1999) Formation of heteromeric gap junction channels by connexins 40 and 43 in vascular smooth muscle cells. Proc. Natl. Acad. Sci. U.S.A. **96**, 6495–6500

35 Simon, S. (1993) Translocation of proteins across the endoplasmic reticulum. Curr. Opin. Cell Biol. **5**, 581–588

36 Hopkins, W. F., Demas, V. and Tempel, B. L. (1994) Both N- and C-terminal regions contribute to the assembly and functional expression of homo and heteromultimeric voltage-gated K$^+$ channels. J. Neurosci. **14**, 1385–1393

37 Galvan, D. L., Borrego-Diaz, E., Perez, P. J. and Mignery, G. A. (1999) Subunit oligomerisation and topology of the inositol 1,4,5-triphosphate receptor. J. Biol. Chem. **274**, 29483–29492

38 Torok, K., Stauffer, K. and Evans, W. H. (1997) Connexin 32 of gap junctions contains two cytoplasmic calmodulin-binding domains. Biochem. J. **326**, 479–483

39 Reference deleted

40 George, C. H., Kendall, J. M., Campbell, A. K. and Evans, W. H. (1998) Connexin-aequorin chimerae report cytoplasmic calcium environments along trafficking pathways leading to gap junction biogenesis in living COS-7 cells. J. Biol. Chem. **273**, 29822–29829

41 Sullivan, R. and Lo, C. W. (1995) Expression of a connexin-43 beta-galactosidase fusion protein inhibits gap junctional communication in NIH3T3 cells. J. Cell Biol. **130**, 419–429

Received 3 December 1999/22 March 2000; accepted 6 April 2000

Heterologous expression, functional characterization and localization of two isoforms of the monkey iron transporter Nramp2

Li ZHANG*, Timothy LEE*, Yue WANG† and Tuck W. SOONG†[1]

*Department of Surgery, National University of Singapore, S(119260), Singapore, and †Institute of Molecular and Cell Biology, 30 Medical Drive, S(117609), Singapore

Natural resistance-associated macrophage protein 2 (Nramp2) has been suggested to be involved in transferrin-independent iron uptake. Two isoforms of the Nramp2 gene generated by alternative splicing of the 3′ exons were identified in mouse, rat and human, but it is unclear if they perform distinct functions. To rationalize our previous work, which indicated an increase in iron deposition in a Parkinsonian monkey brain, two monkey Nramp2 isoforms were isolated for a comparative study to assess their relative iron-uptake abilities, tissue distribution and subcellular localization. The monkey Nramp2 isoforms, 2a and 2b, exhibit approx. 98 % identity at the amino acid level when compared with the human homologues. The Nramp2a transcript contains a canonical iron-responsive element (IRE), whereas that of Nramp2b lacks the IRE motif in the 3′ untranslated region. By reverse transcriptase (RT)-PCR, the mRNAs of both isoforms were detected in all tissues examined. The amino acid differences at the C-terminus neither affected the protein expression levels in HEK-293T and COS-7 cells nor altered the subcellular localization and tissue distribution of the isoforms. Similar levels of iron uptake were detected in the HEK-293T cells transfected with either the Nramp2a or 2b gene, and a reduction of iron from the ferric (Fe^{3+}) to the ferrous (Fe^{2+}) state is necessary before transport can take place. However, this transferrin-independent uptake of iron into the cells is not a Ca^{2+}-dependent process.

Key words: alternative splicing, gene cloning, Parkinson's disease, transferrin-independent iron uptake.

INTRODUCTION

Iron is an essential trace element that is important for many biological processes, including oxygen transport and electron transport during cellular respiration [1,2]. Iron is also important as a cofactor for enzymes involved in neurotransmitter synthesis [3,4]. Overload of free iron has been implicated in the generation of reactive oxygen species, which mediate permanent cell and tissue damage [5–7]. An increased iron concentration was found at the substantia nigra pars compacta (SNPc) in Parkinsonian brains, and it has been suggested that the iron-catalysed production of hydroxyl free radicals might be involved in the onset of the disease [8–11]. We and others have demonstrated that the levels of transferrin or its receptor did not increase in the 1-methyl-4-phenyl-1,2,3,6-tetrahydropyridine (MPTP)- or 6-hydroxydopamine (6-OHDA)-induced Parkinsonian brain, indicating that the transferrin-dependent pathway might not be responsible for the increased influx of iron into the cells [8,12]. Thus the greater iron deposition in neurons and/or glial cells in the SNPc of the Parkinsonian brain might occur by a different iron transport mechanism.

A novel non-haem iron transporter gene was identified in *mk/mk* mouse (Nramp2) by positional cloning [13] and in rat DCT1 (divalent cation transporter 1) by expression cloning in oocytes [7]. DCT1 has been shown to be a membrane-potential-dependent, proton-coupled metal-ion transporter that has a broad range of substrates, including Fe^{2+}, Zn^{2+}, Mn^{2+}, Co^{2+}, Cd^{2+}, Cu^{2+}, Ni^{2+} and Pb^{2+} [7]. By functional complementation of a *smf1* mutant yeast defective in bivalent cation transport, the mouse Nramp2 transporter was also shown to be capable of Mn^{2+} transport [14]. Heterologous expression of mouse Nramp2 in HEK-293T cells demonstrated that the Nramp2 isoform could functionally transport Fe^{2+} as well. Introduction of the mutation Gly^{185} → Arg into the protein abrogated iron-transport activity [15]. This same mutation was discovered both in the microcytic anaemia (mk) mice and in Belgrade (b)-rats, and these animals were also found to be defective in transferrin-mediated iron transport, resulting in severe iron-deficiency anaemia [13,16,17]. These previous studies seem to imply that Nramp2 could be involved in both transferrin-dependent and transferrin-independent transport of iron into the cell. There have also been some contradictory reports regarding the necessity for both a reduction of iron from the ferric to ferrous form and the presence of Ca^{2+} for the transferrin-independent iron-uptake process to occur [18–20]. Clearly, for a better understanding of its roles in iron uptake, the functions and properties of Nramp2 need to be further characterized.

Two Nramp2 isoforms, arising possibly from the alternative use of the polyadenylation signal exons, have been identified in mouse [21], rat [7] and human [22,23]. The spliced mRNA for Nramp2a, but not 2b, contains in its 3′ untranslated region a copy of the iron-responsive element (IRE) known to confer iron-dependent stability to the mRNA [24]. The two isoforms have different C-termini. However, whether the two isoforms perform

---

Abbreviations used BPS, bathophenanthroline disulphonate, DMEM, Dulbecco's modified Eagle's medium, IRE, iron-responsive element, MPTP, 1-methyl-4-phenyl-1,2,3,6-tetrahydropyridine, Nramp2, natural resistance-associated macrophage protein 2, NTA, nitrilotriacetic acid, 6-OHDA, 6-hydroxydopamine, RT, reverse transcriptase, SNPc, substantia nigra pars compacta; UTR, untranslated region

[1] To whom correspondence should be addressed, at the present address National Neuroscience Institute, Irrawaddy Block, 11 Jalan Tan Tock Seng, S(308433), Singapore (e-mail soongtw@yahoo com)

The nucleotide sequences for the monkey iron transporters Nramp2a and Nramp2b have been deposited in the GenBank® database under GenBank® accession numbers AF153279 and AF153280 respectively distinct functions is not known, because the characterization of the functions, localization and regulation of these two isoforms have not been studied in tandem.

Recently, we detected an increase in iron in the SNPc of a MPTP-induced Parkinsonian monkey by nuclear microscopy (Y. He, P.-S. Thong, T. Lee, S.-K. Leong and F. Watt, unpublished work). Meanwhile, Nramp2 mRNA was found to be expressed at a relatively high level in rat SNPc [7]. As an initial step to determine whether Nramp2 is responsible for the increased iron deposition in Parkinsonian monkey brain, we have isolated cDNAs encoding monkey Nramp2a and Nramp2b, and have carried out a comparative study of the two Nramp2 isoforms. Here, we report the characterization of the function and subcellular localization of the monkey Nramp2a and Nramp2b in transfected HEK-293T and COS-7 cells, and their distribution in various monkey tissues.

EXPERIMENTAL

Cloning of monkey Nramp2a and Nramp2b cDNA

Monkey Nramp2a and Nramp2b full-length cDNAs were isolated by reverse transcriptase (RT)-PCR. The primers used were obtained from the highly conserved sequences of the 5′ and 3′ untranslated regions (UTRs) of the Nramp2 genes of the mouse [16,21], rat [7,16] and human [22,23]. The reverse primer for Nramp2a contains an invariant sequence, Mon2aR (5′ AAA CAC ACT GGC TCT GAT GGC 3′), which includes the IRE For Nramp2b, the reverse primer was slightly degenerate, and was designated Mon2bR (5′ GAA CAA RYT CAC CTC IGA ACT AA 3′; I = deoxyinosine). A common forward primer MonF1 (5′ CT CAG GTA TCC ACC ATG GTG 3′) was used for both Nramp2a and Nramp2b (Figure 1). First, the cDNA strand was synthesized by using 1 μg of monkey kidney total RNA and the SUPERSCRIPT® II RT (Gibco BRL, Gaithersburg, MD, U.S.A.). High-fidelity PCR reactions were ensured by using 'hot-start' and a mixture of *Platinum Taq* (Gibco BRL) and *Pfu* (Stratagene, La Jolla, CA, U.S.A.) DNA polymerases in a ratio of 12.5:1. The PCR program was as follows: an initial denaturation was set up at 94 °C for 4 min, followed by 30 cycles of amplification at 94 °C for 40 s, 50 °C for 1 min, 72 °C for 2 min, and a final extension at 72 °C for 10 min. The PCR products were cloned into a pGEMTeasy vector (Promega, Madison, WI, U.S.A.), and sequenced using an ABI model 377 Automated DNA Sequencer (Perkin–Elmer, Norwalk, CT, U.S.A.).

Southern blot analysis of genomic DNA

Southern blotting for Nramp2 was performed following standard protocols [25]. The blot was hybridized to a 321-bp ^{32}P-labelled Nramp2 probe (nt 862 to 1182) at 60 °C for 16 h, and washed at 60 °C in 0.2 × SSC/0.1 % SDS (where 1 × SSC is 0.15 M NaCl/0.015 M sodium citrate).

Hemi-nested RT-PCR for detecting tissue distribution of monkey Nramp2 mRNA

Total RNA was isolated by using TRIZOL® Reagent (Gibco BRL) from frozen tissues of adult male monkeys (*Macaca fascicularis*): cerebral cortex, cerebellum, medulla, lung, liver, spleen, kidney, testis and skeletal muscle. Of each RNA, 1 μg was used for RT-PCR. In the first round of amplification, the forward primer MonF3 (5′ TGT ACC TGC ATT CTG CCT TAG 3′) was used for both Nramp2a and Nramp2b. The reverse primer for Nramp2a was 2aProbe (5′ ATC CAG TGT TAT TTA GTG TAG 3′), and the reverse primer for Nramp2b was 2bProbe (5′ AAC TAA CAG AGA TGT TAA CAG 3′). The resulting PCR products were gel-purified (Qiagen, Hilden, Germany) and 1 μl of the eluted PCR products from different tissues were used as templates for secondary PCR reactions. The forward primer for both Nramp2a and Nramp2b was changed to HybriF (5′ GAA GTT CGA GAA GCC AAT AAG 3′), which was 56 bp downstream of MonF3. The reaction mixture lacking RT was used as a negative control in the RT-PCR procedure; reaction mixture without cDNA was used as a negative control in secondary PCR. The cloned Nramp2a and Nramp2b cDNAs were used as templates for testing the specificity of the PCR amplifications.

Construction of Nramp2–c-Myc expression plasmids

The Kozak sequences (CCACC) [26] were introduced by PCR immediately upstream of the ATG start codon of Nramp2a or Nramp2b, while sequences encoding three tandem copies of the c-Myc antigenic peptide (GEQKLISEEDLN) were ligated in-frame at the 3′end. The Nramp2–c-Myc sequences were then subcloned into the eukaryotic expression vector, pRc/RSV (Invitrogen, Carlsbad, CA, U.S.A.).

Cell culture and transient transfection

COS-7 and HEK-293T cells were maintained in Dulbecco's modified Eagle's medium (DMEM) supplemented with 10 % (v/v) fetal-bovine serum, 2 mM L-glutamine, 100 units/ml penicillin, 100 μg/ml streptomycin and 0.25 μg/ml amphotericin B. These cells were grown to a density of 2×10^5 in six-well Nunclon® dishes for Western blotting, or on poly-(D-lysine)-treated cover slides for immunostaining. For iron-uptake assay, the cells were grown in 9-cm Nunclon® dishes to a density of 2×10^6. Expression plasmid (0.2 μg or 1 μg) was added to each well for transfection by using the Qiagen Effectene Transfection Kit, as described by the manufacturer. For negative controls, the cells were transfected either with vector alone or without DNA.

Western blotting and immunocytochemistry

After transfection (48 h), the cells grown in six-well dishes were trypsin-treated and collected. The cells were then resuspended in 300 μl of cell-disruption buffer [0.2 M Tris/HCl, 10 mM $MgCl_2$, 1 mM dithiothreitol, 10 % (v/v) glycerol, 2 mM PMSF and 2 μg/ml pepstatin A (pH 8.0)], and sonicated. The homogenates were centrifuged and proteins in the supernatant were collected. Upon determination of the concentration by Bradford assay, 10 μg of protein from the supernatant was loaded on to an SDS/10 %-polyacrylamide gel, and electrophoresed (SDS/PAGE) under reducing conditions. Following gel electrophoresis, the fractionated proteins were transferred in blotting buffer [20 % (v/v) methanol, 25 mM Tris base, 192 mM glycine and 0.1 % (w/v) SDS] to Hybond-C extra membrane (Amersham, Piscataway, NJ, U.S.A.) overnight at 4 °C. The blot was blocked for 1 h with PBS containing 5 % (w/v) skimmed milk and 0.1 % (v/v) Triton X-100, washed, and incubated for 2 h with an anti-(c-Myc) antibody (9E10; Santa Cruz Biotechnology Santa Cruz, CA, U.S.A) diluted 1:1000. The membranes were washed three times in 0.1 % Triton X-100 in PBS, incubated for 1 h with horseradish-peroxidase-conjugated anti-mouse IgG (Pierce, Rockford, IL, U.S.A.) diluted 1:8000, and washed three times in 0.1 % Triton X-100 in PBS. Proteins were revealed using enhanced chemiluminescence lighting system (ECL; Pierce). To detect actin protein, the membrane was reprobed with a monoclonal antibody raised against actin (Boehringer Mannheim, Mannheim, Germany) diluted 1:500.

For immunostaining, 48 h after transfection the cells growing on cover slips were washed with PBS and fixed with 3.7 % (w/v) paraformaldehyde for 10 min. After blocking with 10 % (v/v) normal sheep serum for 10 min, the cells were incubated with the anti-(c-Myc) antibody (9E10) diluted 1:1000 overnight at 4 °C. The cells were then washed three times in 0.1 % Triton X-100 in PBS, and incubated for 1 h with fluorescein-conjugated sheep anti-mouse IgG (Boehringer Mannheim) diluted to 20 μg/ml This was followed by three changes of PBS to remove unreacted secondary antibody. The cells were then counterstained with propidium iodide and viewed under a Zeiss confocal microscope.

Transferrin-independent iron-uptake assay

^{55}Fe-nitrilotriacetic acid (^{55}Fe-NTA) was prepared by addition of $^{55}FeCl_3$ (New England Nuclear, Beverly, MA, U.S.A.) to a 20-fold molar excess of the disodium salt of NTA. After transfection (48 h), the cells growing in 9-cm dishes were incubated for 1 h in serum-free DMEM to deplete cells of transferrin. The cells were then washed with PBS and washing buffer (25 mM Tris, 25 mM Mes, 140 mM NaCl, 5.4 mM KCl, 5 mM glucose, 1.8 mM $CaCl_2$ and 800 μM $MgSO_4$, pH 5.5) before incubation in a buffer (25 mM Tris, 25 mM Mes, 140 mM NaCl, 5.4 mM KCl, 5 mM glucose, 1.8mM $CaCl_2$ and 800 μM $MgSO_4$, pH 5.5) containing 1 μM ^{55}Fe-NTA at 37 °C for 20 min. For ferrous iron-uptake assay, 50 μM ascorbic acid was added in the incubation buffer to keep the iron in the ferrous state. The cells were then washed with incubation buffer and removed by digestion with 2 ml of 0.5 % trypsin/EDTA (Sigma, St. Louis, MO, U.S.A.) at 37 °C for 2 min. Cells were washed with ice-cold washing buffer and centrifuged twice. The cell pellet was dissolved in 1 ml of liquid-scintillation cocktail (ICN Biomedicals, Costa Mesa, CA, U.S.A.). Radioactivity was determined by using a Beckman LS6000 scintillation counter with a band-width of 0 to 400.

To determine whether the reduction of ferric iron is required for transport via Nramp2, the impermeable ferrous iron chelator, bathophenanthroline disulphonate (BPS), was used. After transfection (24 h), the cells grown in 9-cm dishes were split equally into four wells of the six-well multidishes pretreated with poly-(D-lysine). The cells were then cultured for a further 24 h in an air/CO_2 mixture (19:1) at 37 °C. Ferric iron-uptake assay was performed as described above, except that BPS was added in the incubation buffer. Toxicity assays of BPS on the cells were performed similarly, except that the cells were put back into culture to assess viability after exposure to various concentrations of BPS up to 10 μM. All the experiments were repeated three times.

To investigate the effects of Ca^{2+} on the function of Nramp2, cells were split and grown on poly-(D-lysine)-treated dishes 24 h after transfection. After transfection (48 h), the cells were incubated in serum-free DMEM for 1 h, and washed with PBS. The cells were then washed twice in 1 mM EGTA for 5 min. Ferrous iron uptake was measured as above, except that Ca^{2+} was removed from the washing buffer and added to the incubation buffer at various concentrations. The time for iron uptake was reduced from 20 to 10 min. The cells not washed in EGTA were used as a control; once again, three independent experiments were performed.

RESULTS

Isolation of cDNAs encoding the two isoforms of monkey Nramp2

By designing degenerate oligonucleotides that correspond to conserved regions of the Nramp2 proteins, we were able to isolate a partial cDNA from monkey-kidney and -brain mRNAs. Alignment of this monkey partial Nramp2 cDNA sequence with the mouse, rat and human DNA sequences revealed a very high homology with the Nramp2 DNA sequences among the different species (results not shown). Subsequent alignment of the DNA sequences of the 5′ and 3′ UTRs flanking the various Nramp-2a and -2b genes from mouse, rat and human helped in the design of the PCR primers for the cloning of the complete coding sequences for the two isoforms of the monkey Nramp2 genes by the RT-PCR method (Figure 1). The high fidelity in RT-PCR cloning was demonstrated by the identical sequences of six Nramp2a and seven Nramp2b clones analysed. The monkey Nramp-2a and -2b sequences have been deposited into GenBank® (accession numbers AF153279 and AF153280 respectively) and the only difference between the two isoforms is found in the C-terminus, in which there are also an extra 7 amino acids in Nramp2b (Figure 2). Both isoforms display approx. 91 % to approx. 98 % identity at the amino acid level with the mouse, rat and human Nramp2 proteins. The Kyte–Doolittle hydrophilicity

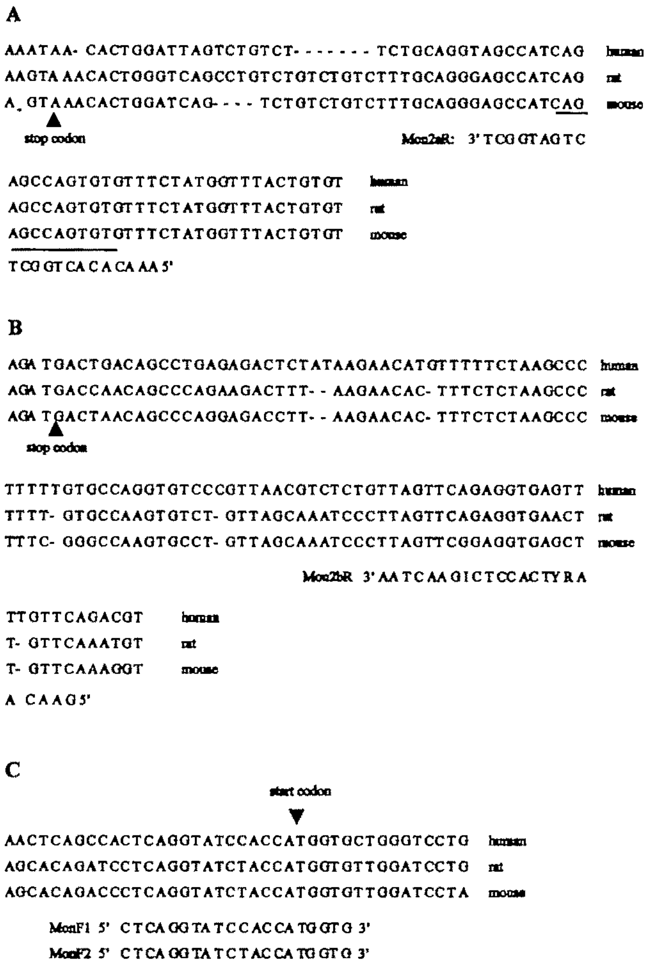
A
AAATAA- CACTGGATTAGTCTGTCT- - - - - - - TCTGCAGGTAGCCATCAG human
AAGTA AACACTGGGTCAGCCTGTCTGTCTGTCTTTGCAGGGAGCCATCAG rat
A GTA AACACTGGATCAG- - - - TCTGTCTGTCTTTGCAGGGAGCCATCAG mouse
stop codon
Mon2aR: 3' TCG GTAGTC
AGCCAGTGTGTTTCTATGGTTTACTGTGT human
AGCCAGTGTGTTTCTATGGTTTACTGTGT rat
AGCCAGTGTGTTTCTATGGTTTACTGTGT mouse
TCG GTCACACAAA 5'
B
AGA TGACTGACAGCCTGAGAGACTCTATAAGAACATGTTTTTCTAAGCCC human
AGA TGACCAACAGCCCAGAAGACTTT- - AAGAACAC- TTTCTCTAAGCCC rat
AGA TGACTAACAGCCCAGGAGACCTT- - AAGAACAC- TTTCTCTAAGCCC mouse
stop codon
TTTTTGTGCCAGGTGTCCCGTTAACGTCTCTGTTAGTTCAGAGGTGAGTT human
TTTT- GTGCCAAGTGTCT- GTTAGCAAATCCCTTAGTTCAGAGGTGAACT rat
TTTC- GGGCCAAGTGCCT- GTTAGCAAATCCCTTAGTTCGGAGGTGAGCT mouse
Mon2bR 3' AATCAAGICTCCACTYRA
TTGTTCAGACGT human
T- GTTCAAATGT rat
T- GTTCAAAGGT mouse
A CAAG 5'
C
start codon
AACTCAGCCACTCAGGTATCCACCATGGTGCTGGGTCCTG human
AGCACAGATCCTCAGGTATCTACCATGGTGTTGGATCCTG rat
AGCACAGACCCTCAGGTATCTACCATGGTGTTGGATCCTA mouse
MonF1 5' CTCAGGTATCCACCATGGTG 3'
MonF2 5' CTCAGGTATCTACCATGGTG 3'

Figure 1 Primers for cloning of monkey Nramp2a and Nramp2b cDNA

(A) The reverse primer Mon2aR was chosen by comparing the 3′ UTRs of human, rat and mouse Nramp2a transcripts The conserved IREs are underlined The nucleotide sequence for Mon2aR is shown under the alignment. (B) The reverse primer Mon2bR was designed to target a conserved sequence in the 3′ UTRs of Nramp2b transcripts The nucleotide sequence of this primer is slightly degenerate, and is shown under the alignment I, deoxyinosine. (C) Two forward primers, MonF1 and MonF2, were designed by comparing sequences across the start codon There was only a single base difference between MonF1 and MonF2

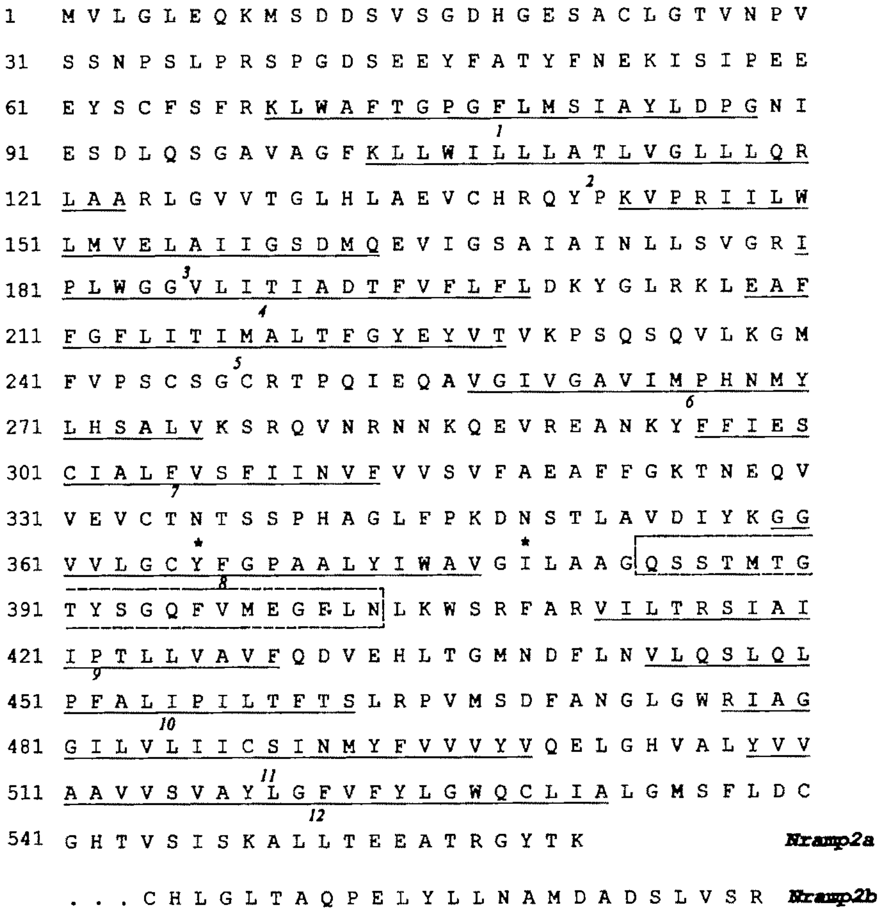
1 M V L G L E Q K M S D D S V S G D H G E S A C L G T V N P V
31 S S N P S L P R S P G D S E E Y F A T Y F N E K I S I P E E
61 E Y S C F S F R K L W A F T G P G F L M S I A Y L D P G N I
1
91 E S D L Q S G A V A G F K L L W I L L L A T L V G L L L Q R
2
121 L A A R L G V V T G L H L A E V C H R Q Y P K V P R I I L W
151 L M V E L A I I G S D M Q E V I G S A I A I N L L S V G R I
3
181 P L W G G V L I T I A D T F V F L F L D K Y G L R K L E A F
4
211 F G F L I T I M A L T F G Y E Y V T V K P S Q S Q V L K G M
5
241 F V P S C S G C R T P Q I E Q A V G I V G A V I M P H N M Y
6
271 L H S A L V K S R Q V N R N N K Q E V R E A N K Y F F I E S
301 C I A L F V S F I I N V F V V S V F A E A F F G K T N E Q V
7
331 V E V C T N T S S P H A G L F P K D N S T L A V D I Y K G G
*
*
361 V V L G C Y F G P A A L Y I W A V G I L A A G Q S S T M T G
8
391 T Y S G Q F V M E G F L N L K W S R F A R V I L T R S I A I
421 I P T L L V A V F Q D V E H L T G M N D F L N V L Q S L Q L
9
451 P F A L I P I L T F T S L R P V M S D F A N G L G W R I A G
10
481 G I L V L I I C S I N M Y F V V V Y V Q E L G H V A L Y V V
11
511 A A V V S V A Y L G F V F Y L G W Q C L I A L G M S F L D C
12
541 G H T V S I S K A L L T E E A T R G Y T K Nramp2a
. . . C H L G L T A Q P E L Y L L N A M D A D S L V S R Nramp2b

Figure 2 The deduced amino acids of the monkey Nramp2a protein

The 12 putative transmembrane regions are indicated by horizontal bars, the consensus transport motif is boxed by dashed lines Two predicted N-linked glycosylation sites are indicated by the asterisks (*) The monkey Nramp2b protein only differs from Nramp2a in the C-terminus

plot predicts that the monkey Nramp2 protein should contain 12 transmembrane domains with both N- and C-termini projecting into the cytoplasm. The monkey Nramp2 protein contains the common prokaryotic and eukaryotic transporter motif (amino acids 384–403) known as the 'binding-protein-dependent, inner-membrane-component transport signature' [27]. Between transmembrane segments 7 and 8 is a large predicted extracellular loop that contains two putative glycosylation sites. Southern blot analysis detected a single band from monkey genomic DNA digested with various restriction enzymes (results not shown), indicating that Nramp2 is a single gene.

Tissue distribution of monkey Nramp2a and Nramp2b mRNA

Previous studies have shown that the expression of mouse Nramp1 is restricted to the macrophages, whereas the mouse, rat and human Nramp2 genes are expressed ubiquitously in many tissues and cell types [7,21,28]. To date, the tissue distributions of Nramp-2a and -2b have not been compared To determine if Nramp-2a and -2b are differentially expressed in different tissues, or if there are cellular mechanisms that preferentially generate one splice form over the other, we used the RT-PCR technique to examine the expression patterns of the mRNAs for the two isoforms (Figure 3). The PCR conditions were optimized for specific amplification of each isoform. The negative control, in which no RT was added, did not yield any PCR product. The specific PCR products for both Nramp2a and Nramp2b were detected from the total RNA prepared from all the tissues examined. The aggregate levels of Nramp-2a and -2b mRNAs were uneven among different tissues. The mRNA levels in brain, kidney, testis, liver and skeletal muscle were comparable, but higher than those in lung and spleen.

Subcellular localization of Nramp-2a and -2b

We made two expression constructs where a DNA sequence encoding three tandem copies of c-Myc epitope was fused in frame to the C-terminal end of Nramp2a- and Nramp2b-coding regions. The c-Myc-tagged Nramp2 proteins were expressed in transfected cells, and their cellular localization was determined by immunostaining using an anti-(c-Myc) antibody. After transfection, the transient expression of the Nramp2 proteins was first examined by Western blot analysis (Figure 4A). A major band of approx 65 kDa, close to the predicted molecular mass of the Nramp2 proteins, was produced in the HEK-293T cells transfected with either Nramp2a (Figure 4A, lane 3) or Nramp2b (Figure 4A, lane 4) gene. Faint bands of approx. 90 kDa were also observed, which were probably the glycosylated forms of the Nramp2 proteins. No band was detected in the extracts of

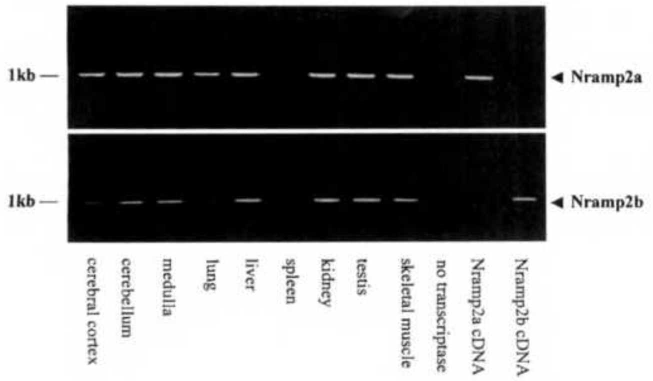

Figure 3 Hemi-nested RT-PCR for detecting tissue distribution of the two isoforms of the monkey Nramp2 gene

Total RNA (1 μg) from different monkey tissues was used. For a negative control, no RT was added. Cloned cDNA for Nramp2a or Nramp2b was also used as a control in PCR reactions.

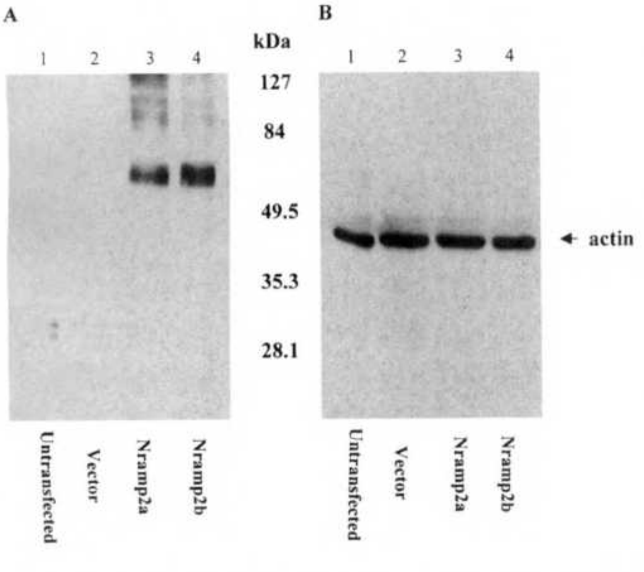

Figure 4 Western blot analysis of Nramp2 expression in HEK-293T cells transfected with c-Myc-tagged Nramp2a or Nramp2b

Each lane contains 10 μg of proteins. The blot was first probed with monoclonal anti-(c-Myc) antibody (**A**), and then reprobed with anti-actin antibody (**B**). Lanes 1, untransfected cells; lanes 2, cells transfected with pRc/RSV vector alone; lanes 3, cells transfected with Nramp2a construct; lanes 4, cells transfected with Nramp2b construct.

the untransfected cells or cells transfected with the expression vector alone. Each lane was also stained for actin to demonstrate that similar amounts of protein were used (Figure 4B).

The subcellular localization of the two Nramp2 isoforms was determined by immunostaining using c-Myc antibody. Confocal microscopy demonstrated that the localization patterns of Nramp-2a and -2b proteins were similar. Both isoforms showed strong punctate staining in the cytoplasm, and a faint staining on the plasma membrane (Figures 5C, 5D, 5G and 5H). This pattern was observed in both the COS-7 (Figure 5C and 5D) and HEK-293T (Figures 5G and 5H) cells transfected with constructs for both isoforms. Untransfected cells (Figures 5A and 5E) or cells transfected with the vector alone (Figures 5B and 5F) exhibited only propidium iodide staining for the nucleus, with no fluorescein signals at all. The punctate staining pattern suggests an endosomal localization of the Nramp2 proteins, which has also been demonstrated in other studies describing Nramp2 co-localization with transferrin receptors in endosomes and its presence in the endosomal membrane fraction [15,17]. The results above demonstrate that the different C-termini affected neither the expression levels of the two Nramp2 isoforms nor their subcellular localization in the transfected cells.

Monkey Nramp2a and Nramp2b demonstrate a similar ability in the transferrin-independent uptake of iron

The ability of Nramp2a and Nramp2b in iron transport has not been compared. Our Western blotting results above revealed similar levels of protein expression for both Nramp2 isoforms in transiently transfected HEK-293T or COS-7 cells. To determine whether the difference in the C-termini might play a regulatory role in the protein's iron transport activity, we carried out assays to measure the uptake of $^{55}Fe^{2+}$ or $^{55}Fe^{3+}$ by HEK-293T cells transfected with either Nramp2a or Nramp2b construct. Both Nramp2a and Nramp2b were found to confer on the transfected cells the same level of iron transport, giving rise to more than a 150-fold increase of $^{55}Fe^{2+}$ uptake and a 50-fold increase of $^{55}Fe^{3+}$ uptake over untransfected or vector-tansfected HEK-293T cells (Figures 6A and 6B). This result shows that the difference in the C-termini again has no detectable effect on the iron-transport efficiency of the two monkey Nramp2 isoforms, at least under the experimental conditions used. However, it should be noted that, in the overexpression system, the total effect will be largely amplified. This might be the reason why there is such a marked increase in the cross-plasma-membrane ^{55}Fe uptake via Nramp2, although most of the protein is localized in endosomes in the transfected cells. In order to investigate transferrin-independent iron transport via Nramp2 expressed on the plasma membrane, we minimized the possible contamination by transferrin in our experiments. This was done by incubating the transfected cells first in serum-free medium to deplete transferrin and at pH 5.5, a pH value at which transferrin binds iron poorly and is not internalized by the cells [18]. The stronger Nramp2 expression on the endosomal membrane (Figure 5) might result in an even higher level of iron uptake via the transferrin-dependent pathway.

Fe^{3+} reduction is a prerequisite of iron transport by monkey Nramp2

Iron uptake by Nramp2 decreased greatly (by approx. 14-fold) in transfected HEK-293T cells when $^{55}Fe^{2+}$-NTA was replaced with $^{55}Fe^{3+}$-NTA. However, iron uptake in these cells was still much higher than that of untransfected cells (Figure 6B). The higher uptake rate of Fe^{2+} over Fe^{3+} raises the question of whether Nramp2p transports Fe^{2+} more efficiently, or a reduction of Fe^{3+} to Fe^{2+} is a prerequisite for transport to happen. We addressed this question by using different concentrations of BPS, a selective impermeant Fe^{2+} chelator, to block ferrous-iron transport by Nramp2p. A decrease of Fe^{3+} transport was observed with the increase in BPS concentration. At 1 μM BPS, approx. 75% of iron uptake was inhibited and, in the presence of 10 μM BPS, Fe^{3+} transport was reduced to near-background level (Figure 7). Similar results were also obtained when another ferrous iron chelator, ferrozine, was used (results not shown). This result indicates that a reduction of Fe^{3+} to Fe^{2+} is necessary before iron uptake by Nramp2 proteins occurs.

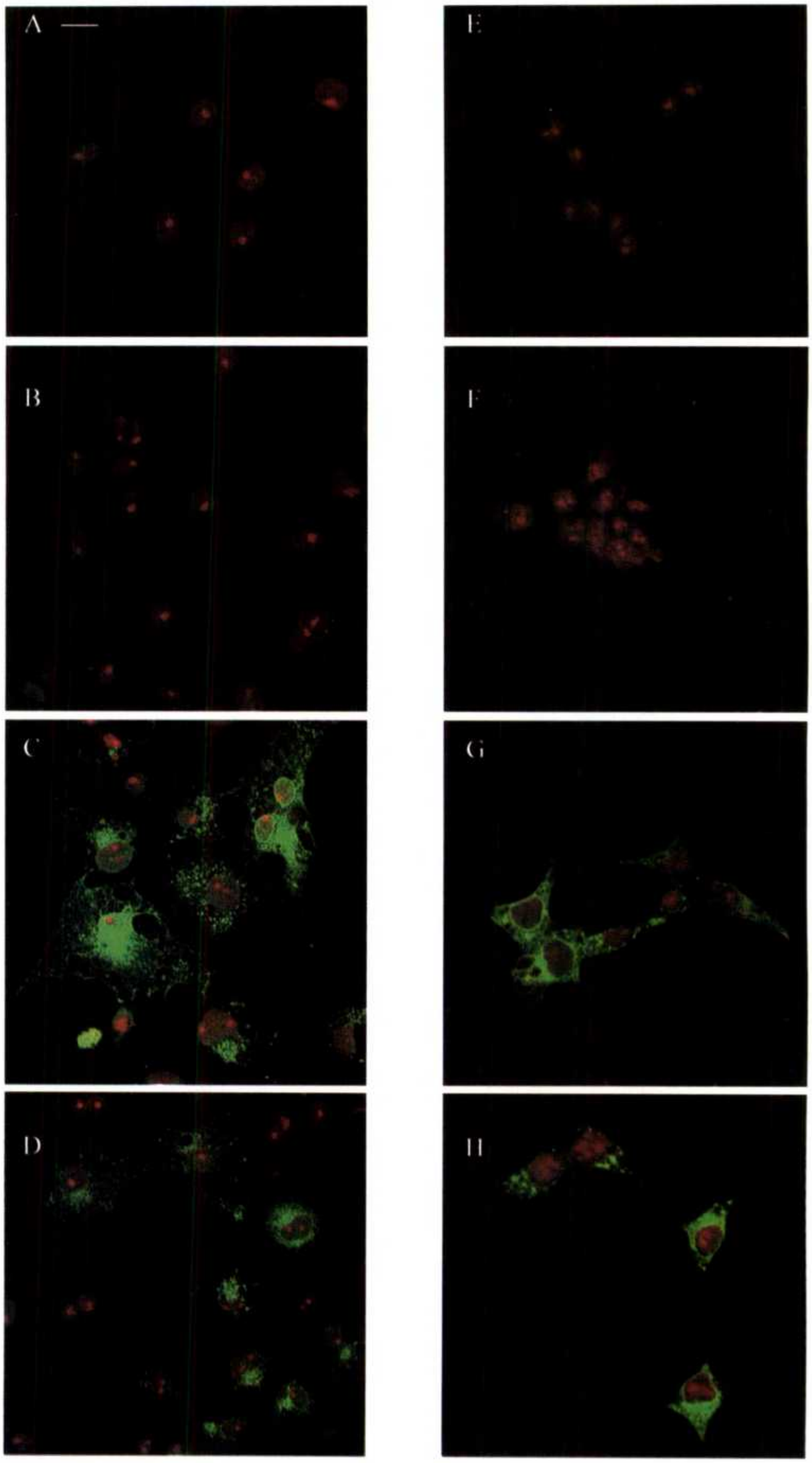

Figure 5 For legend see facing page.

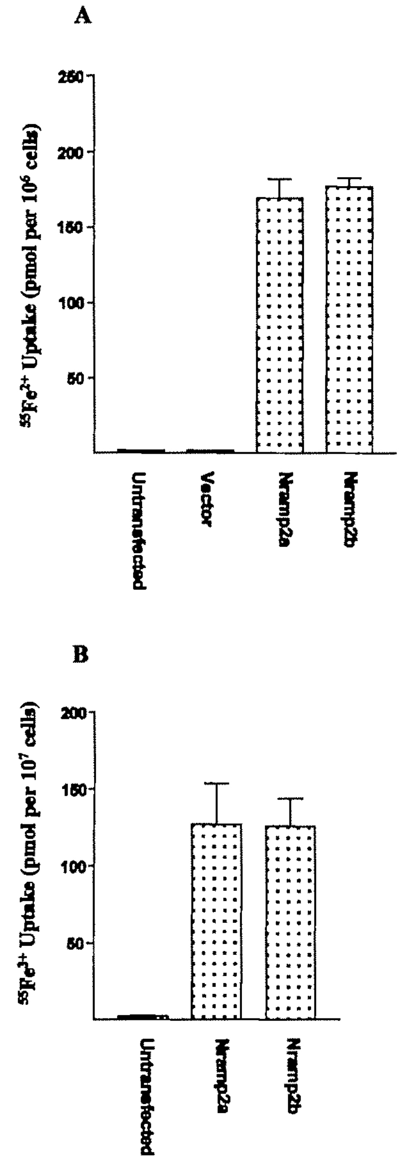

Figure 6 Iron transport activity of Nramp2a and Nramp2b

Non-transfected HEK-293T cells and cells transfected with the constructs indicated were incubated for 20 min in incubation buffer containing 1 μM ^{55}Fe^{2+}-NTA (**A**) or ^{55}Fe^{3+}-NTA (**B**) The radioactivity was then determined

Iron uptake of Nramp2 is not Ca^{2+}-dependent

Transferrin-independent iron uptake has been shown to be Ca^{2+}-dependent in most cells [20]. To determine whether Ca^{2+} has a role in regulating the iron transport by Nramp2 protein, we examined the effect of Ca^{2+} in the iron-transport process in Nramp2-transfected HEK-293T cells. Iron-uptake assay conducted in Ca^{2+}-free buffer did not show a decrease in ^{55}Fe^{2+}-NTA transport. Instead, when 10 mM Ca^{2+} was used, iron

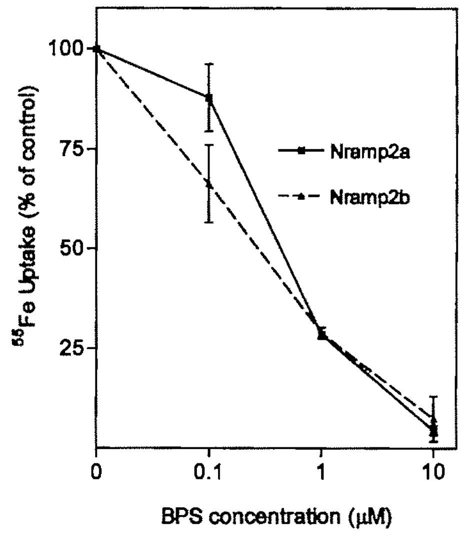

Figure 7 Effect of BPS on Fe^{2+} and Fe^{3+} uptake mediated by Nramp2 expressed in HEK-293T cells

Non-transfected HEK-293T cells and cells transfected with constructs indicated were incubated for 20 min in incubation buffer with 1 μM ^{55}Fe^{3+}-NTA and different concentrations of BPS The radioactivity was then determined Iron uptake in non-transfected cells was taken as the background level, and subtracted from that of transfected cells The amount of uptake determined in the absence of BPS was defined as 100%

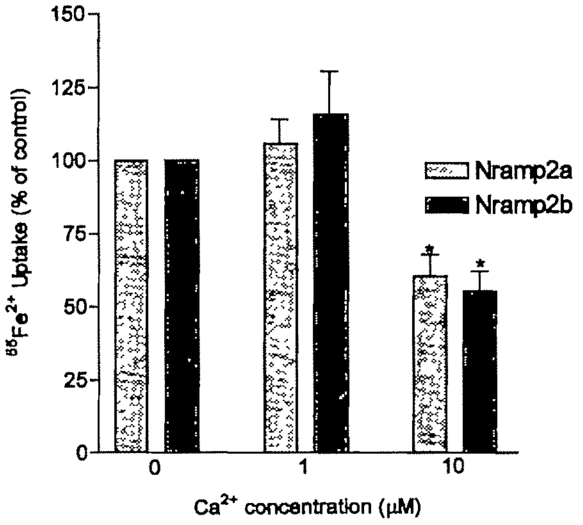

Figure 8 Effect of Ca^{2+} on iron-transport activity of Nramp2

Non-transfected cells and transfected HEK-293T cells were treated with EGTA as described in the Experimental section, and then incubated for 10 min with ^{55}Fe^{2+}-NTA and different concentrations of Ca^{2+}. The iron uptake of non-transfected cells was deducted from that of transfected cells. The amount of radioactivity accumulated in the absence of Ca^{2+} was defined as 100%. *, $P < 0.05$ compared with control, as determined by using the Mann–Whitney test

Figure 5 Subcellular localization of Nramp2a and Nramp2b proteins

Two cell lines, COS-7 (**A–D**) and HEK-293T (**E–H**), were used for this study Non-transfected cells (**A**, **E**) and cells transfected with the vector alone (**B**, **F**) serve as negative controls Both types of cell were transfected with a construct expressing either Nramp2a (**C**, **G**) or Nramp2b (**D**, **H**) Cells were stained with both the nuclear stain, propidium iodide (red), and anti- (c-Myc) antibody plus fluorescein-conjugated sheep anti-mouse IgG (green) The scale bar shown in (**A**) represents 20 μm, and is applicable for **B–H** uptake was decreased by 40 % (Figure 8). This result suggests that Ca^{2+} was not required for iron uptake.

DISCUSSION

As a first step towards an understanding of whether Nramp2 is responsible for iron accumulation in the SNPc in a Parkinsonian monkey brain, we isolated cDNAs for the two isoforms of monkey Nramp2. The study of Nramp2a of other mammalian species has been reported, with a cursory mention about the Nramp2b protein [7,16,23]. In the present study we report a comparative analysis of the functional characteristics and localization of the two monkey iron-transporter isoforms. The monkey Nramp2 proteins show the highest amino acid identity, of approx. 98 % with their human counterparts. The extremely high identity at the DNA level enabled the cloning of the complete open reading frames of the two monkey Nramp2 isoforms by RT-PCR.

Similar to the mouse and human homologues, the monkey Nramp2 gene is a single gene. It is possible that, like its counterparts, the two monkey isoforms were generated by alternative splicing of Nramp2 transcripts. The physiological significance of these two isoforms is unknown. Our attempts to address this question showed that first, the two isoforms were present ubiquitously in all the monkey tissues examined, with a putative difference in the level of expression in the cerebral cortex, lung and spleen. *In-situ*-hybridization analysis might give a better semi-quantitative measurement of the relative amounts of the two isoforms in a cell type. Secondly, the different C-termini do not seem to have any effect on the subcellular localization, the level of protein expression or iron uptake in either COS-7 or HEK-293T cells.

Previous studies showed that mouse, rat and human Nramp2 proteins could be involved in transferrin-independent iron uptake [7,15]. Our results showed that both Nramp-2a and -2b could be expressed in human HEK-293T cells to induce robust uptake of ^{55}Fe into the transfected cells via a transferrin-independent pathway. The levels of transport for both proteins were comparable, which again points towards their functional similarities, in spite of the differences in the carboxy tails.

Previous studies have not shown whether Nramp2 was able to transport Fe^{3+} [7,15]. Here, we have demonstrated by using a specific ferrous chelator, BPS, that the iron uptake by monkey Nramp2 requires the reduction of Fe^{3+} to Fe^{2+}. The dosage and time of BPS treatment were found not to be toxic to the cells (results not shown), and therefore the reduced iron uptake in the presence of BPS reflects not only the unavailability of Fe^{2+}, but also the inability of Nramp2 to transport Fe^{3+}. The effect of BPS and the higher uptake rate of Fe^{2+} over Fe^{3+} both demonstrated the requirement for the reduction of Fe^{3+} to Fe^{2+} before transport mediated by Nramp2 occurred.

In many types of cells, transferrin-independent iron uptake is Ca^{2+}-dependent [20]. Consistent with the results of Gunshin et al. [7], we have shown that, in the presence of Ca^{2+}, iron uptake was not induced, but instead, at 10 mM concentration, inhibition of transport was observed. The Ca^{2+}-independent iron transport by the monkey Nramp2p suggests that there might be other iron transporters in those cells that showed a Ca^{2+}-dependence in the transferrin-independent iron-transport processes Previous studies also showed that low-affinity, transferrin-independent iron transport in rat erythroid cells demonstrates little dependence on Nramp2 (DMT1) [29]. These studies, together with our observations, suggest that transferrin-independent iron transport in mammalian cells is mediated probably by multiple pathways via different transport proteins.

Taken together, our results have shown that Nramp2a and Nramp2b have very similar functional characteristics. The major difference in function of the Nramp2 isoforms could lie in their post-transcriptional regulation. Nramp2a contains the IRE sequence and, in mouse and rat, animals fed on iron-deficient diets showed a marked increase in Nramp2a mRNA expression levels [30]. Our attempts to study post-transcriptional regulation by iron in COS-7 cells exposed to high external iron concentrations did not detect an obvious decrease in Nramp2a mRNA level by specific RT-PCR. One possibility is that the amount of intracellular iron loaded via the transferrin-independent pathway was insufficient to generate a detectable difference in mRNA levels of the two isoforms. However, neither supplying cells with transferrin nor overexpressing the 3′UTR-truncated Nramp-2a and -2b clones in COS-7 cells produced any difference in the expression patterns of the Nramp-2a and -2b mRNAs (results not shown). Another possibility is that COS-7 cells might not contain the IRE-binding protein that is essential to stabilize the Nramp2a mRNA. To address further the question of the physiological role of the two isoforms, work is still in progress to identify the localization *in situ* of both isoforms to determine their extent and levels of expression in each cell type in the brain. The ratio of the expression of the Nramp-2a and -2b mRNAs in a cell might shed light on our understanding of the overall regulation of iron uptake, and the response to either iron deficiency or overload in an animal. Knowledge of the expression levels of the monkey Nramp2 isoforms will help to determine whether the iron deposition in the pathological area of the Parkinsonian monkey brain was due to an increased iron uptake through the Nramp2 iron transporter. Subsequently, the pathophysiological mechanisms that lead to Parkinson disease can be investigated.

This work was supported by a grant, RP3950376, from the National University of Singapore. L. Z. is a recipient of the National University of Singapore scholarship award. We thank Dr Wai-Ho Yap for reading the manuscript critically, Dr Alice Tay for sequencing the Nramp2 clones, Narendrakumar Ramanan for helpful discussions, and Dr Ratha Mahendran and Tan-Fong Yong for able technical assistance.

REFERENCES

1 Karlin, K. D. (1993) Metalloenzymes, structural motifs, and inorganic models Science **261**, 701–708

2 Aisen, P (1994) Iron metabolism: an evolutionary perspective In Iron Metabolism in Health and Disease (Brock, J. H., Halliday, J W, Pippard, M J and Powell, L W, eds), pp 1–30 W B Saunders, London

3 Beard, J D, Connor, J R and Jones, B. C (1993) Iron in the brain Nutr Rev **51**, 157–179

4 Roskams, A. J I and Connor, J. R. (1994) Iron, transferrin, and ferritin in the rat brain during development and aging J Neurochem **63**, 709–716

5 Gerlach, M, Ben-Shachar, D, Riederer, P and Youdim, M B H (1994) Altered brain metabolism of iron as a cause of neurodegenerative diseases? J Neurochem **63**, 793–807

6 Gelman, B B (1995) Iron in CNS disease J. Neuropathol Exp Neurol **54**, 477–486

7 Gunshin, H, Mackenzie, B, Berger, U V, Gunshin, Y, Romero, M F., Boron, W F, Nussberger, S, Gollan, J. L and Hediger, M A (1997) Cloning and characterization of a mammalian proton-coupled metal-ion transporter. Nature (London) **388**, 482–488

8 Goto, K, Mochizuki, H, Imai, H., Akiyama, H and Mizuno, Y (1996) An immunohistochemical study of ferritin in 1-methyl-4-phenyl-1,2,3,6-tetrahydropyridine (MPTP)-induced hemiparkinsonian monkeys Brain Res **724**, 125–128

9 He, Y, Thong, P S, Lee, T, Leong, S K, Shi, C Y, Wong, P T, Yuan, S Y and Watt, F. (1996) Increased iron in the substantia nigra of 6-OHDA induced parkinsonian rats a nuclear microscopy study Brain Res **735**, 149–153

10 Jenner, P and Olanow, C W (1996) Oxidative stress and the pathogenesis of Parkinson's disease Neurology **47**, S161–S170

11 Qian, Z M and Wang, Q (1998) Expression of iron transport proteins and excessive iron accumulation in the brain in neurodegenerative disorders Brain Res. Rev. **27**, 257–267

12 He, Y , Lee, T. and Leong, S K (1999) Time-course and localization of transferrin receptor expression in the substantia nigra of 6-hydroxydopamine-induced parkinsonian rats. Neuroscience **91**, 579–585

13 Fleming, M D , Trenor, III, C. C , Su, M. A., Foernzler, D , Beier, D R , Dietrich, W F and Andrews, N C (1997) Microcytic anaemia mice have a mutation in Nramp2, a candidate iron transporter gene. Nat. Genet **16**, 383–386

14 Pinner, E , Gruenheid, S , Raymond, M. and Gros, P (1997) Functional complementation of the yeast bivalent cation transporter family SMF by NRAMP2, a member of the mammalian natural resistance-associated macrophage protein family J. Biol Chem **272**, 28933–28938

15 Su, M. A , Trenor, C C , Fleming, J C., Fleming, M D and Andrews, N C (1998) The G185R mutation disrupts function of the iron transporter Nramp2 Blood **92**, 2157–2163

16 Fleming, M D , Romano, M. A , Su, M A , Garrick, L M , Garrick, M D and Andrews, N C (1998) Nramp2 is mutated in the anemic Belgrade (b) rat. evidence of a role for Nramp2 in endosomal iron transport Proc Natl Acad. Sci. U S A **95**, 1148–1153

17 Gruenheid, S., Canonne-Hergaux, F , Gauthier, S , Hackam, D J , Grinstein, S and Gros, P. (1999) The iron transporter protein Nramp2 is an integral membrane glycoprotein that colocalizes with transferrin in recycling endosomes J. Exp Med **189**, 831–841

18 Sturrock, A., Alexander, J , Lamb, J , Craven, C M. and Kaplan, J (1990) Characterization of a transferrin-independent uptake system for iron in HeLa cells J. Biol. Chem **265**, 3139–3145

19 Barisani, D , Berg, C. L , Wessling-Resnick, M and Gollan, J. L (1995) Evidence for a low K_m transporter for non-transferrin-bound iron in isolated rat hepatocytes Am J Physiol **269**, G570–G576

20 de Silva, D. M., Askwith, C C. and Kaplan, J. (1996) Molecular mechanisms of iron uptake in eukaryotes Physiol Rev. **76**, 31–47

21 Gruenheid, S , Cellier, M , Vidal, S and Gros, P (1995) Identification and characterization of a second mouse Nramp gene Genomics **25**, 14–25

22 Kishi, F and Tabuchi, M (1997) Complete nucleotide sequence of human NRAMP2 cDNA Mol Immunol **34**, 839–842

23 Lee, P L , Gelbart, T , West, C., Halloran, C and Beutler, E (1998) The human Nramp2 gene: characterization of the gene structure, alternative splicing, promoter region and polymorphisms Blood Cells Mol Dis **24**, 199–215

24 Casey, J L , Hentze, M. W , Koeller, D M , Caughman, S W., Rouault, T A , Klausner, R D and Harford, J. B. (1988) Iron-responsive elements regulatory RNA sequences that control mRNA levels and translation Science **240**, 924–928

25 Sambrook, J , Fritsch, E F and Maniatis, T (1989) Southern blot in Molecular cloning: a laboratory manual, pp. 11–111, Cold Spring Harbor Laboratory, Cold Spring Harbor, NY

26 Kozak, M (1991) Structural features in eukaryotic mRNAs that modulate the initiation of translation J Biol Chem **266**, 19867–19870

27 Bairoch, A (1991) PROSITE a dictionary of sites and patterns in proteins Nucleic Acids Res **19**, 2241–2245

28 Kishi, F. and Tabuchi, M (1998) Human natural resistance-associated macrophage protein 2 gene cloning and protein identification Biochem. Biophys Res. Commun **251**, 775–783

29 Garrick, M D , Gniecko, K , Liu, Y , Cohan, D S and Garrick, L M (1993) Transferrin and the transferrin cycle in Belgrade rat reticulocytes J Biol Chem. **268**, 14867–14874

30 Fleming, R E , Migas, M. C , Zhou, X Y , Jiang, J X , Britton, R. S , Brunt, E M., Tomatsu, S , Waheed, A., Bacon, B R and Sly, W S (1999) Mechanism of increased iron absorption in murine model of hereditary hemochromatosis· increased duodenal expression of the iron transporter DMT1. Proc Natl. Acad Sci U S A **96**, 3143–3148

Received 22 October 1999/14 March 2000, accepted 6 April 2000

Biochem J (2000) 349, 299–308 (Printed in Great Britain)

Oligomerization of β-amyloid of the Alzheimer's and the Dutch-cerebral-haemorrhage types

Aneet K. SIAN*, Emma R. FREARS*, Omar M. A. EL-AGNAF*, Bhroma P. PATEL*, Maria F. MANCA*, Giuliano SILIGARDI†, Rohanah HUSSAIN† and Brian M. AUSTEN*[1]

*Department of Surgery, St George's Hospital Medical School, Cranmer Terrace, London SW17 0RE, U.K., and †Department of Pharmacy, King's College, Franklin–Wilkins Building, 150 Stamford Street, London SE1 8WA, U.K.

A novel ELISA has been developed which detects oligomerization of β-amyloid (Aβ). Oligomerization, fibrillization and neurotoxicity of native Aβ associated with Alzheimer's disease (AD) type has been compared with E22Q Aβ (amyloid β-protein containing residues 1–40 with the native Glu at residue 22 changed to Gln) implicated in Dutch cerebral haemorrhage disease. Solutions of Aβ rapidly yield soluble oligomers in a concentration-dependent manner, which are detected by the ELISA, and by size-exclusion gel chromatography. Conformational changes from disordered to β-sheet occur more slowly than oligomerization, and fibrils are produced after prolonged incubation. The E22Q Aβ oligomerizes, changes conformation and fibrillizes more rapidly than the native form and produces shorter stubbier fibrils. Aged fibrillar preparations of E22Q Aβ are more potent than aged fibrils of native Aβ in inducing apoptotic changes and toxic responses in human neuroblastoma cell lines, whereas low-molecular-mass oligomers in briefly incubated solutions are much less potent. The differences in the rates of oligomerization of the two Aβ forms, their conformational behaviour over a range of pH values, and NMR data reported elsewhere, are consistent with a molecular model of oligomerization in which strands of Aβ monomers initially overcome charge repulsion to form dimers in parallel β-sheet arrangement, stabilized by intramolecular hydrophobic interactions, with amino acids of adjacent chains in register.

Key words: apoptosis, ELISA, fibril, parallel β-sheet, toxicity.

INTRODUCTION

Alzheimer's disease (AD) is a progressive degenerative disease of the brain characterized by loss of cognitive function (dementia), selective neuronal death and the abnormal formation of neuritic and core plaques throughout the cerebral cortex, predominating in the hippocampus and temporal lobe cortex, and around the blood vessels of the meninges and cerebral cortex. Deposits in brain are associated with reactive microglia, astrogliosis and neuronal loss. The major component of AD amyloid deposits is a 39–43-residue amyloid β (Aβ) peptide, which is produced as a cleavage product of a much larger transmembrane glycoprotein, encoded by the amyloid-precursor-protein (APP) gene on chromosome 21 [1].

A mutated form of Aβ is also deposited in a rare form of amyloidosis known as hereditary cerebral haemorrhage with amyloidosis Dutch type (HCHWA-D), a disease that typically manifests itself with recurring strokes and dementia. In a pathological study, both HCHWA-D and AD showed compact cerebral amyloid angiopathy (CAA) with Aβ deposits in arterial/arteriolar media and concomitant smooth-muscle cell loss, whereas only HCHWA-D CAA featured severe involvement of larger arteries and arterioles, with a single or double rings of radial deposited Aβ [2]. In contrast with AD, the neuropil of HCHWA-D patients showed diffuse rather than senile plaques, which were not associated with neuronal loss [3]. The toxicity of the HCHWA-D form of Aβ toward neurons has not previously been reported. HCHWA-D is an autosomal dominant condition associated with a point mutation at codon 693 of the gene for βAPP, which leads to the substitution of glutamic acid at position 22 of Aβ with glutamine. The mutation does not alter the ratio of secreted Aβ to p3 (peptides comprising the C-terminal residues 17–40 or 17–42 of Aβ), nor the stability of the secreted Aβ and p3 peptides, but increases the biosynthesis of Aβ peptides with N-termini of Asp^1, Val^{18} and Phe^{19} [4]. Why this single mutation leads to the extreme severity of the vascular pathology, hallmark of HCHWA-D, as well as the absence of senile plaques in the neuropil, is so far not clear.

A central question in the etiology of AD and HCHWA-D is the mechanism(s) by which soluble Aβ monomers are converted into fibrillar deposits. This question is particularly relevant because Aβ fibres, unlike soluble monomers, are neurotoxic *in vitro* [5–7] and associated with damaged neuropil *in vivo* [8]. Using optical microscopy, ultracentrifugation and electrophoresis, it was shown that only aggregated forms of Aβ peptides containing the hydrophobic region 25–35 were toxic to primary neurons [5]. Upon reversal of aggregation, neurotoxicity disappeared.

There is disagreement over the precise structure of the neurotoxic forms of Aβ. Protofibrils, distinguished from mature fibrils by their appearance under the electron microscope, were reported as toxic as mature fibrils [9]. Low-molecular-mass oligomers induced toxicity in long-term neuronal cultures, but were less toxic than fibrils [9]. Protofibrils and fibrils, but not low-molecular-mass oligomers, alter the electrical activity of neurons, and it has been suggested that preclinical and early progression

---

Abbreviations used Aβ, amyloid β-protein containing residues 1–40, p3, peptides comprising the C-terminal residues 17–40 or 17–42 of Aβ, AD, Alzheimer's disease, APP, amyloid precursor protein, HCHWA-D, hereditary cerebral haemorrhage with amyloidosis Dutch type, CAA, cerebral amyloid angiopathy, Fmoc, fluoren-9-ylmethoxycarbonyl, NTA4, a peptide containing the ten N-terminal residues of β-amyloid, E22Q Aβ, amyloid β-protein containing residues 1–40 with the native Glu at residue 22 changed to Gln, MEM, minimal essential medium, MTT, 3-(4,5-dimethylthiazol-2-yl)-2,5-diphenyltetrazolium bromide, QLS, quasi-light-scattering spectroscopy, ACTH, adrenocorticotrophic hormone

[1] To whom correspondence should be addressed (e-mail sghk200@sghms.ac.uk)

of AD is driven by accumulation of oligomeric intermediates prior to the assembly of fibrils [9]. In contrast, some authors suggest that soluble Aβ dimers, which purportedly survive SDS treatment [10], are highly toxic to neuronal cultures [11] Fluorescence measurements indicate that Aβ dimers may be stable at very low concentrations [12], and Western blotting has suggested that Aβ dimers are formed in the brains of AD patients before fibrillary tangles [13].

In order to define the structural and oligomeric changes that take place in Aβ solutions in more detail, a novel ELISA assay that monitors the formation of oligomers from monomers has been developed. We have correlated the changes found in solutions of Aβ peptides by ELISA with changes observed by gel filtration and CD. Finally, the apopototic and toxic changes induced by Aβ peptides incubated for different times have been determined. As the Q22E mutation appears to produce quite a distinct phenotype, we have compared the properties of Q22E 1–40 with native Aβ

EXPERIMENTAL

Preparation of aggregated 'aged' solutions of Aβ peptides

Aβ peptides were synthesized using fluoren-9-ylmethoxycarbonyl (Fmoc) chemistry on a Millgen 9050 synthesizer (PE Biosystems, Warrington, Cheshire, U.K.) by an optimized protocol [14], purified by acetonitrile gradients on HPLC on Vydac C_8 columns in 0.1 % (v/v) trifluoroacetic acid, and freeze-dried. Aβ peptides were shown to be homogeneous by MS. Aβ peptides were dissolved first in sterilized distilled water, then a 10 % volume of sterilized 1 M Tris/HCl, pH 7.4, was added to give a final peptide concentration of 1.16 mM. These solutions were aged by incubating them at 37 °C.

Preparation of the biotinylated antibody

Biotinamidohexanoate *N*-hydroxysuccinimide (Sigma–Aldrich, Poole, Dorset) (20 μl of a 10 mg/ml solution in DMSO) was added to anti-NTA4, an affinity-purified antibody to the N-terminal ten residues of Aβ coupled to BSA [15] in 0.1 M sodium borate, pH 8 (0.5 ml at 1 mg/ml), and incubated at 24 °C for 4 h. Ammonium chloride (20 μl of 1 M) was added, and incubation continued for 10 min. The mixture was desalted on a Sephadex G-25 column in PBS to remove excess uncoupled biotin. The biotinylated antibody was stored at −20 °C.

An ELISA to measure oligomers

An ELISA plate was coated with 5 μg/ml of non-biotinylated anti-NTA4 antibody (100 μl/well) in PBS/0.01 % (w/v) sodium azide at 4 °C for 24 h, washed twice with blocking buffer (PBS/1 % BSA/0.05 % Tween, pH 7.4), and incubated with blocking buffer for 1 h at room temperature. Peptides incubated in 0.1 M Tris were diluted to 18 nM in blocking buffer, and 100μl added to each well. The plate was incubated at 37 °C for 2 h.

After washing four times with blocking buffer, biotinylated anti-NTA4 diluted 1 to 500 in blocking buffer (100 μl) was added, and incubated at 37 °C for 1.5 h. Wells washed three times with blocking buffer were incubated with peroxidase–avidin (Sigma) (1:1000 in blocking buffer) (100 μl) at 37 °C for 1.5 h, washed three times with PBS/1 % (w/v) BSA/0.05 % (v/v) Tween, pH 7.4, and once with PBS/0.05 % (v/v) Tween, before adding substrate for peroxidase (Europa Ltd., Wicken, Ely, Cambs., U.K.) (100 μl), developing for about 5 min before adding 1 M H_2SO_4 (100 μl) and reading at 450 nm.

Size-exclusion chromatography

Aliquots (20 μl) of freshly prepared or incubated solutions of Aβ peptides at 1.16 mM in 0.1 M Tris/HCl, pH 7.4, were loaded on a Superdex 75 gel-filtration column (10 cm × 270 mm) in 0 1 M Tris/HCl, pH 7.4, with a flow rate of 0.5 ml/min. Eluate was monitored at 215 nm

CD

Spectra were recorded with nitrogen-flushed JASCO J720 and J600 spectropolarimeters using 4 s time constant, 10 nm/min scan speed and a spectral bandwidth of 2 nm. Both spectropolarimeters were calibrated with ammonium D-camphor-10-sulphonate. Quartz cells of 0.02 cm and 1 cm were used for measurements in the far-UV (185–250 nm) and near-UV (250–350 nm) regions respectively. CD spectra were reported as:

$$\Delta\epsilon = \epsilon_L - \epsilon_R \ (M^{-1}\cdot cm^{-1})$$

where $\Delta\epsilon$ is the difference between the molar absorbance of left circularly polarized light (ϵ_L) and the molar absorbance of right circularly polarized light (ϵ_R) and is based upon an average molecular mass per amino acid of 113.

Electron microscopy

Samples of precipitated peptides aged at 1.16 mM (10 μl) were fixed with glutaraldehyde, stained with uranyl acetate and examined on a Zeiss 900 transmission electron microscope [16].

Cell culture

SH-SY5Y cells (European Collection of Cell Cultures, Porton Down, Salisbury, Wilts., U.K.) were cultured in Dulbecco's minimal essential medium (MEM)/Nutrient Mix F-12 (1:1, v/v) (Gibco BRL) containing 10 i.u. of penicillin/ml and 100 μg/ml streptomycin, 15 % (v/v) foetal-calf serum, 1 % non-essential MEM amino acid supplement, and 2 mM freshly prepared glutamine at 37 °C in a humidified incubator with CO_2/room air (1:19).

Cytotoxicity assay

The cytotoxicity of Aβ peptides was assessed by measuring cellular redox activity. Cells were plated at a density of 7500 cells/well in 96-well plates in 100 μl of fresh medium. After 24 h the medium was replaced with 100 μl of OPTI-MEM (Gibco BRL) serum-free medium and aged or fresh Aβ peptides diluted in OPTI-MEM added. The positive control contained 15 μM camptothecin (Sigma) Cells were incubated at 37 °C in 5 % CO_2 for 48 h. Medium was replaced with RPMI-1640 without Phenol Red (Sigma) (100 μl), 25 μl of 3-(4,5-dimethylthiazol-2-yl)-2,5-diphenyltetrazolium bromide (MTT) (Sigma) (5 mg/ml) added to each well and the plate incubated at 37 °C for 3 h [17]. The plate was centrifuged for 5 min at 137 *g* (Sorvall RT 6000D centrifuge) and the medium/MTT solution removed. Propan-1-ol (100 μl) was added and the plate shaken for 60 min and read at 570 nm.

Apoptosis assay

Apoptosis was detected by using an annexin V/propidium iodide (Vybrant® Apoptosis Assay Kit), and mitochondrial tracker (CMXRos/Sytox; Molecular Probes, Eugene, OR, U.S.A.). An eight-well chambered coverglass (Nalge Nunc International, Naperville, IL, U.S.A.) was seeded with 0.45 ml of SH-SY5Y cells at 290 000 cells/ml and incubated for 20 h. Medium was replaced with OPTI-MEM with aged or fresh peptide solutions. Positive controls contained 15 or 50 μM camptothecin, or 100 μM H_2O_2. Chambers were incubated for 9 h at 37 °C. Adhering cells were washed twice with ice-cold PBS and Annexin-Binding Buffer (Molecular Probes) (100 μl) added. Alexa 488 annexin V (5 μl) and propidium iodide (1 μl, 100 μg/ml) (Molecular Probes) were added and cells incubated in the dark for 15 min. Alternatively, cells were incubated for 20 min at 37 °C with Mitochondrial tracker at 0.11 μg/ml and Sytox at 0.1 μM. Unbound reagents were washed out with ice-cold Annexin Binding Buffer or PBS, and cells were inspected by confocal microscopy on a Carl Zeiss laser scanning microscope, using a narrow pass 515–565 nm filter and 488 irradiation or a > 695 nm filter with 546 irradiation.

RESULTS

Oligomer formation detected by ELISA

An ELISA was developed to detect soluble oligomers of Aβ. Solutions of both Aβ and E22Q Aβ incubated at 1.16 mM at pH 7.4 in 0.1 M Tris/HCl for up to 3 h, and then immobilized on to a non-biotinylated form of the antibody anti-NTA4, showed a rapid increase in binding to the biotinylated antibody by the increase in absorbance in the ELISA assay (Figure 1). No increase in binding of biotinylated anti-NTA4 was found in control 1.16 mM pre-incubated solutions of the N-terminal ten-residue peptide of Aβ. The rate of increase was more rapid for E22Q Aβ than for the native sequence. Preincubation of the E22Q Aβ solutions for longer than 3 h gave a decrease from maximum response, and precipitates formed, which were shown by electron microscopy to contain fibrils (see below). E22Q Aβ preincubated at 0.116 mM produced soluble oligomers more slowly than at 1.16 mM, and reached a higher maximum value, possibly because fewer fibrils were formed at the lower concentration. In contrast, the increase in binding of biotinylated

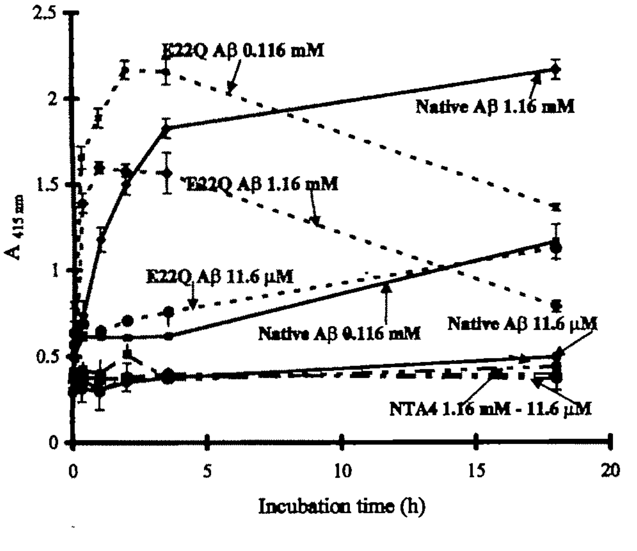

Figure 1 Oligomerization of Aβ peptides measured by ELISA

Solutions of native Aβ (continuous lines) or E22Q Aβ (variously broken lines) in 0.1 M Tris/HCl, pH 7.4, at 1.16 mM, 0.116 mM and 11.6 μM were incubated at 37 °C, diluted to 18 nM, and incubated on an ELISA plate already coated with immobilized anti-NTA4 antibody. Additional epitopes formed by oligomerization during the pre-incubation step were measured by subsequent binding to a biotinylated sample of anti-NTA4. The plots of negative controls containing the ten-residue peptide NTA4 incubated at 1.16 mM, 0.116 mM and 11.6 μM, are also shown (bottom three curves). S.E.M. values for assays performed in triplicate are shown for each point as bars above and/or below the mean. The mid-range of the assay for 18 h-oligomerized native Aβ was 0.9 nM. At 0.9 nM concentration, the within-assay variance was 5.7%. A day-to-day variance of 5.2% at 0.9 nM was found in seven assays calibrated with standard solutions of Aβ incubated in 0.1 M Tris/HCl, pH 7.4, at 1.16 mM for 18 h, diluted to 18 nM in blocking buffer, divided into aliquots and stored at −20 °C.

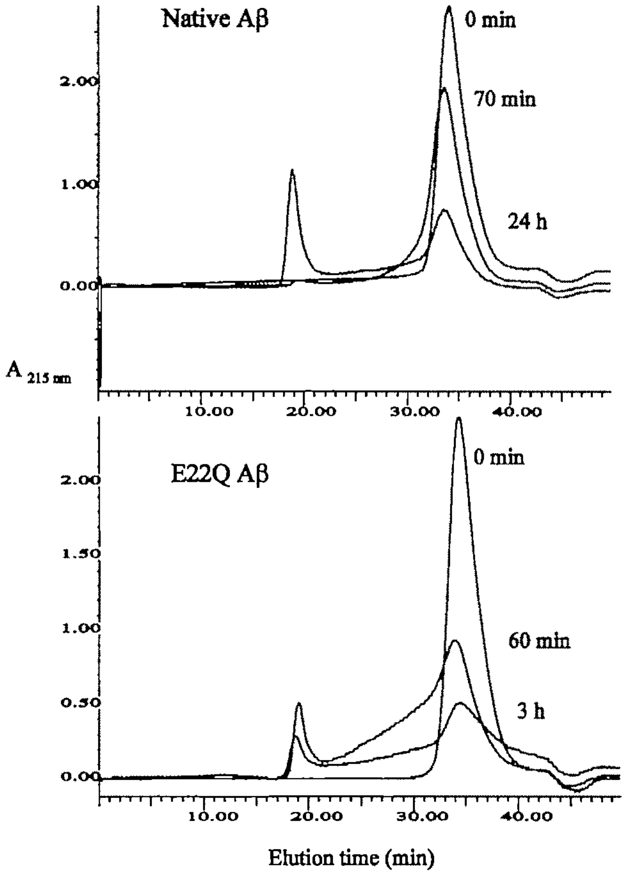

Figure 2 Size-exclusion chromatography of Aβ oligomers

Elution profiles of samples of solutions of native or E22Q Aβ pre-incubated at 1.16 mM in 0.1 M Tris, pH 7.4, at 37 °C for the times shown.

Table 1 Elution of proteins and peptides of known molecular mass from Superdex 75

Protein	Molecular mass (kDa)	Elution time (min)
BSA	68	22.7
Porcine lipotropin	9.9	29.3
Bovine aprotinin	6.5	53.4
Human ACTH	4.5	39.4
Human neuropeptide Y	4.2	64.0
MBP-TET peptide*	3.4	39.7
Tram peptide†	2.1	40.0
E22Q Aβ	4.3	34.6
Native Aβ	4.3	34.6

* A peptide containing the sequence YGGRASDYKSAHKGFKQYIKANSKFIGITE

† A peptide of the sequence LDKINRRMHFSKTKHSC

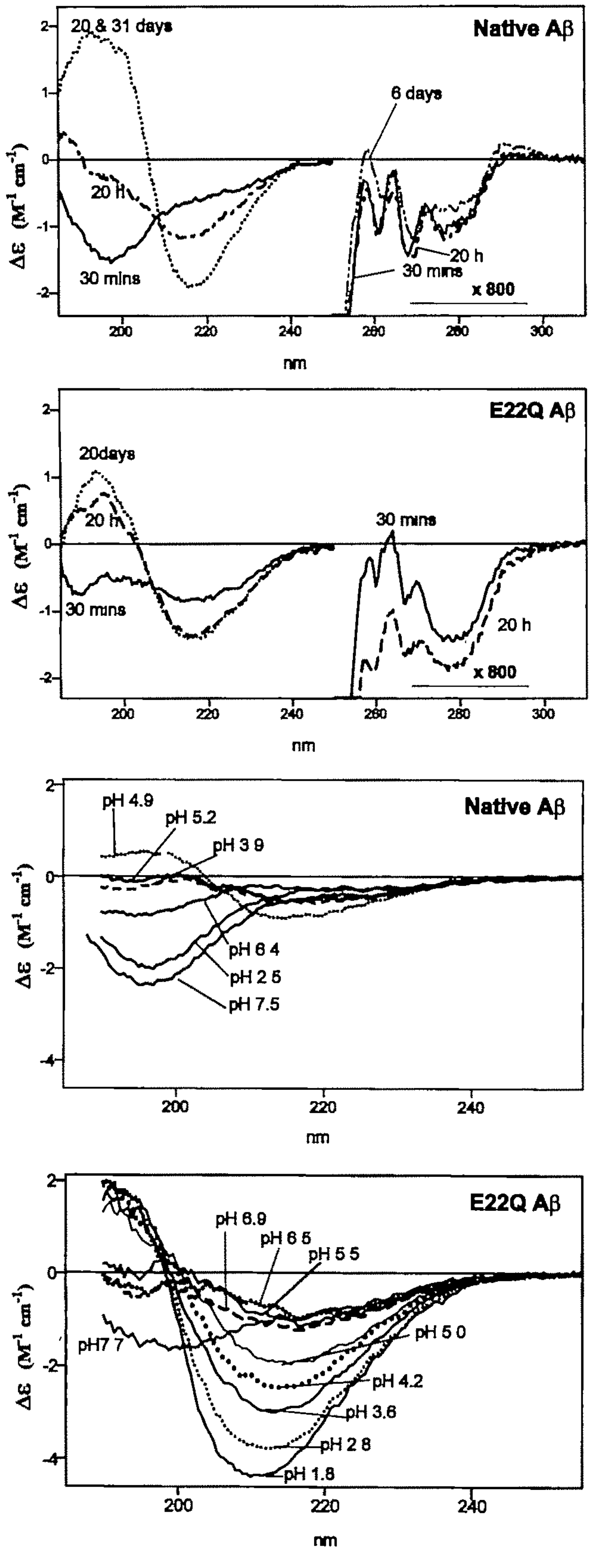

Figure 3 CD of Aβ peptide solutions

Top two panels time-induced changes in the conformation of Aβ peptides CD spectra of native (top) or E22Q (below) Aβ pre-incubated at 1.16 mM in 0.1 M Tris/HCl, pH 7.4, at 37 °C for either 30 min (continuous lines), 20 h (broken lines), 20 days (dotted lines) and 31 days (dotted line), then diluted 10-fold with water just prior to measurement. Bottom two panels pH-induced changes in the conformations of Aβ peptides CD spectra of fresh native (top) and E22Q (below) Aβ solutions in 10 mM Tris/HCl as a function of pH. The pH titration was carried out in a stepwise manner from pH 7.5 and pH 7.7 respectively by addition of aliquots of HCl. The pH was measured just before recording the spectra, and each spectrum obtained is shown marked with the pH value recorded. Sample at pH 1.8 (Figure 3, bottommost panel) was incubated for 25 h at pH 1.8 before recording spectra.

anti-NTA4 to soluble oligomers formed in preincubated solutions of native Aβ was less than with E22Q, and no precipitate was visible up to 24 h of incubation. Increases of binding to biotinylated anti-NTA4 of native Aβ preincubated at 0.116 mM and 11.6 μM were much less than with the same concentrations of E22Q Aβ. Over an 18 h incubation, about three times the amount of soluble oligomers, as judged by increase in binding to biotinylated NTA4, were produced by the E22Q mutant incubated at 0.116 mM than at 11.6 μM, whereas binding to biotinylated NTA4 caused by native Aβ oligomers produced at 11.6 μM concentration was about 4 % of the binding produced at 1.16 mM.

Size-exclusion chromatography

Changes in the state of oligomerization of the Aβ peptides were also examined by size-exclusion chromatography on Superdex 75 (Figure 2). Fresh solutions of the Aβ peptides were eluted in one symmetrical peak at 34.6 min. Between 10 and 70 min of preincubation at 37 °C in 0.1 M Tris/HCl, pH 7.4, produced changes in the elution profiles. The major peaks were eluted slightly earlier (33.2 min) and shoulders appeared before the main peak. After 60 min preincubation for E22Q Aβ or 24 h for native Aβ, a second peak appeared at the flow-through volume (19 min). Attempts to calibrate the Superdex column with proteins and peptides of known molecular mass were not satisfactory (Table 1) The elution times of the fresh Aβ peptides were between those of adrenocorticotrophic hormone (ACTH; 4.5 kDa; 39.4 min) and lipotropin (9.4 kDa; 29.3 min) and might indicate that non-incubated Aβ was behaving as a peptide of 6.5 kDa. However, both neuropeptide Y (4.2 kDa) and aprotinin (6.4 kDa) were not eluted as expected from their molecular mass (see Table 1).

CD

CD spectroscopy of solutions of the Aβ peptides preincubated at 1.16 mM and then diluted 10-fold immediately before measurement are shown (Figure 3). Substantial differences were observed in the conformational behaviour of both peptides as a function of incubation time and pH. The rates of changes from mainly random coil to conformations of the β-sheet type were more than one order of magnitude different, with no further changes being observed after 20 days of incubation for native Aβ, or 20 h for E22Q Aβ. The changes taking place in the UV region between 250 and 290 nm during incubation were significantly more enhanced in E22Q Aβ than in native Aβ (Figure 3, top two panels).

The titration from pH 7.0 to 2.0, and the reverse titration from pH 2.0 to 7.0, revealed interesting CD spectra that differentiate and discriminate between the two Aβ forms. Both peptides showed random-coil-to-β-sheet transitions on lowering the pH from 7.0 to 4.0, by 0.5 pH unit in a stepwise manner. However, below pH 4.0, native Aβ 1–40 revealed an almost reversible β-sheet–random-coil transition, whereas E22Q showed further random-coil–β-sheet transitions. At pH 1.8 this transition took 24 h to stabilize (Figure 3, bottom two panels; plot marked 'pH

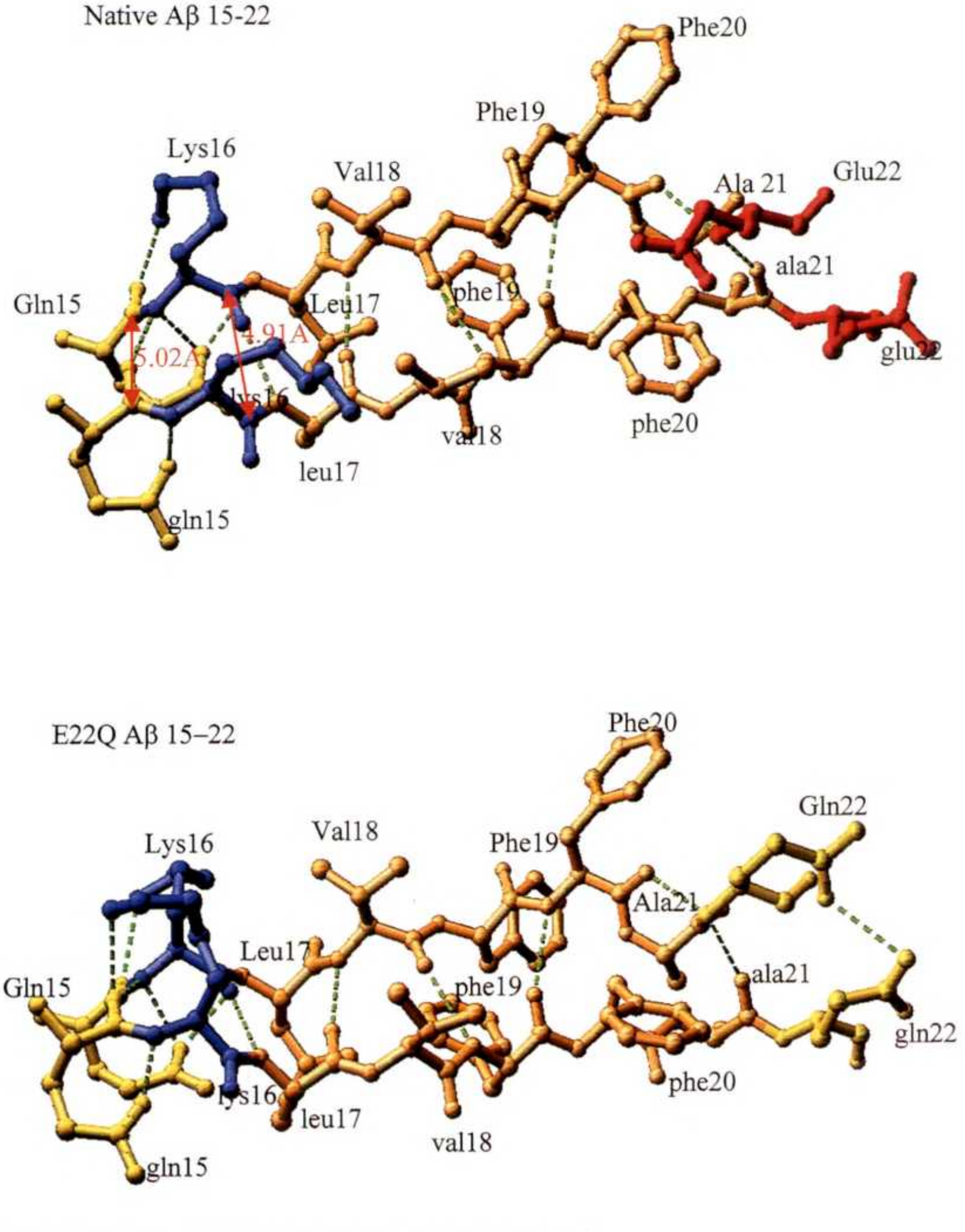

Figure 4 Energy-minimized molecular models of residues 15–22 of native and E22Q Aβ

Two strands of native or E22Q Aβ are shown modelled on Swiss-Prot PDB viewer in a parallel β-sheet arrangement, with the residues in register. Colour coding: broken lines, intermolecular hydrogen bonding; red, Glu^{22}; blue, Lys^{16}; yellow, Gln residues; brown, hydrophobic residues. Distances shown are measured between the carbonyl carbon atoms of the Gln^{15} residues and between the Lys^{16} residues.

1.8'). The rate of adoption of β-sheet at pH 2.8 was more than the rate of change monitored at pH 7.4.

Molecular modelling

Energy-minimized molecular models of dimeric sequences of residues 15–22 in the native and E22Q sequences were produced on Swiss PDB viewer. The model (Figure 4) indicated that hydrophobic interactions between the side chains in this region could be maximized by a parallel arrangement in which the β-strands were held together by hydrogen bonding between the peptide bonds, with amino acid residues on each strand in register.

Electron microscopy

Prolonged incubation of several hours for E22Q and 1 week for native Aβ yielded precipitated material. Precipitates produced from 3-week incubations were harvested, and subjected to electron microscopy. The results showed that the fibrils pro-

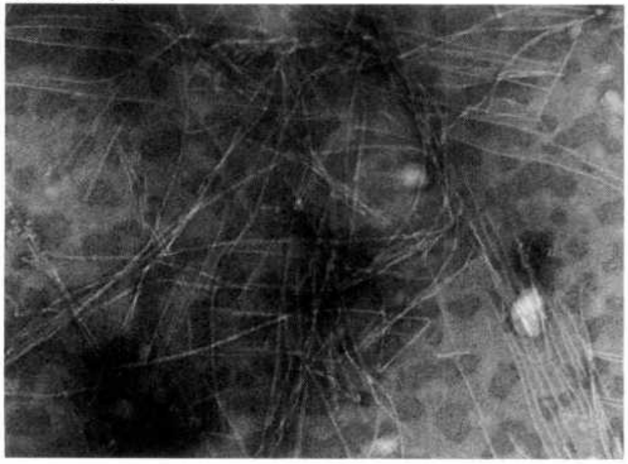

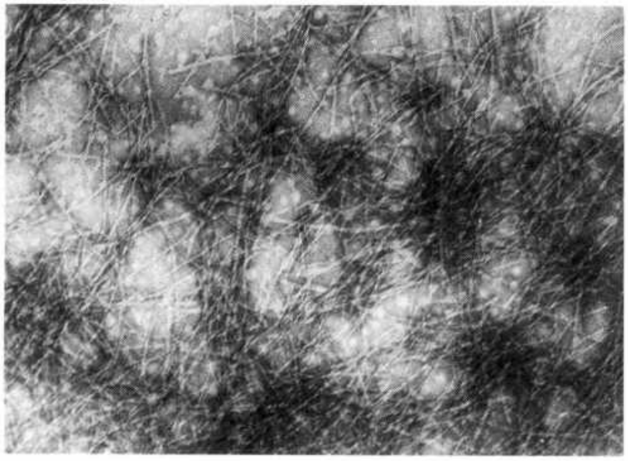

Figure 5 Transmission electronmicrographs of native and E22Q Aβ fibrils

Solutions of native or E22Q Aβ 1.16 mM were aged for 3 weeks at 37 °C in 0.1 M Tris/HCl, pH 7.4, and the precipitates fixed, stained, and examined on a Zeiss 900 transmission electron microscope. Magnification is $\approx$ 100000 ×.

duced from native Aβ were longer and thinner than those produced from E22Q Aβ (Figure 5).

Cytotoxic effect of aged and fresh βA4 peptides

The results obtained by ELISA (Figure 1) and size-exclusion chromatography (Figure 2) showed that native and E22Q peptides incubated at 1.16 mM for 1 h produced soluble oligomers. Several hours of incubation produced fibrillar forms of E22Q Aβ, whereas several days of incubation were required to fibrillize native Aβ. We then sought to find out which forms of the peptides were toxic to neuronal cells by finding out what periods of incubation time were required to produce high toxicity.

Human dopaminergic neuroblastoma SHSY-5Y cells were exposed to freshly prepared, 1-h- or 3-week-incubated solutions of E22Q Aβ and native Aβ. Camptothecin was used as a positive control. After incubation for a further 2 days, cell viability was evaluated using the MTT assay and compared with that of negative control cells incubated without peptide. Fresh native Aβ was much less toxic than fresh E22Q Aβ, whereas both solutions that had been incubated for 3 weeks showed considerable toxicity, even at concentrations below 1 μM (Figure 6A). At the highest concentrations, fresh E22Q Aβ was as toxic as aged E22Q Aβ. In contrast, there were no significant differences between toxicities of fresh solutions and those incubated at 1.16 mM for 1 h (Figure 6B); both incubates were equally toxic at high concentrations.

Apoptosis induced by Aβ peptides

In order to explore the differences between the two Aβ peptides further, SHSY-5Y cells were exposed to fibrils of native and E22Q Aβ for 10 h. Preparations of E22Q Aβ aged for 3 weeks completely ablated the mitochondrial membrane potential at 11.6 μM and 2.3 μM (Figures 7E and 7G). Aged native Aβ was also completely effective at 11.6 μM (Figure 7A), but only partly effective at 2.3 μM (Figure 7C). In contrast, freshly made solutions had little effect on mitochondrial potential (compare treated cells in Figures 7B, 7D, 7F and 7H with control cells in Figure 7I). Extensive staining of nuclei with Sytox was apparent only in cells treated with H_2O_2 (Figure 7L) or 50 μM camptothecin (Figure 7J). No nuclear staining was seen in cells treated with 15 μM camptothecin. Most (90 %) of the cells treated with E22Q Aβ stained with annexin V (Figure 7N), and about 20 % also stained with propidium iodide. About 40 % of the cells exposed to native Aβ stained with annexin V (Figure 7M), with about 10 % staining with propidium iodide. Cells treated with camptothecin (15 μM) are shown in Figure 7(O) and control untreated cells in Figure 7(P).

DISCUSSION

It has been suggested that the toxic forms of Aβ are relatively soluble dimers that might do some of the damage by forming flickering deposits on the neural membranes, with larger deposits and neuritic plaques forming later in the disease [11]. Aβ isolated from human brain varies in reported distributions of monomer, dimer, trimer, tetramer and higher-order oligomers [11]. Aβ oligomers have been identified in conditioned media of certain cell lines that constitutively secrete Aβ [10,18] and as components of cerebrospinal fluid [19]. As well as low-molecular-mass oligomers, protofibrils, sizeable (> 100000 kDa) oligomeric structures that lack the repeating structure of fibrils, have been identified as products of aged Aβ solutions [9,20,21].

In the present studies, E22Q or native Aβ in freshly prepared solutions were eluted as symmetrical peaks with elution times of 34.6 min from a column of Superdex 75 (Figure 2), a time that was not altered by preincubation of Aβ in the disaggregating solvents formic acid, DMSO or hexafluoroisopropanol [22], indicating that 34.6 min is the elution time of the monomer. After 1 h preincubation of the Aβ peptides, changes in the elution profiles were found, indicative of formation of higher-molecular-mass oligomers. Other authors have suggested that dimers exist in Aβ solutions under most aqueous conditions [11,12,21]. The characterization of dimers in previous studies rested on the behaviour of Aβ solutions on gel-filtration columns, on SDS/PAGE or in quasi-light-scattering spectroscopy (QLS), studies which required calibration with standard small proteins of known molecular mass [21,23]. However, small proteins of molecular mass similar to that of Aβ are not eluted in positions that accord to their molecular mass from Superdex 75 columns (Table 1). In particular, neuropeptide Y (4.2 kda) and bovine aprotinin (molecular mass 6.5 kDa) are much more strongly retarded on the column than other peptides and proteins of lower molecular mass. It seems likely that elution behaviour is more strongly influenced by the composition and degree of folding of the peptides than their molecular size. Similar conclusion were

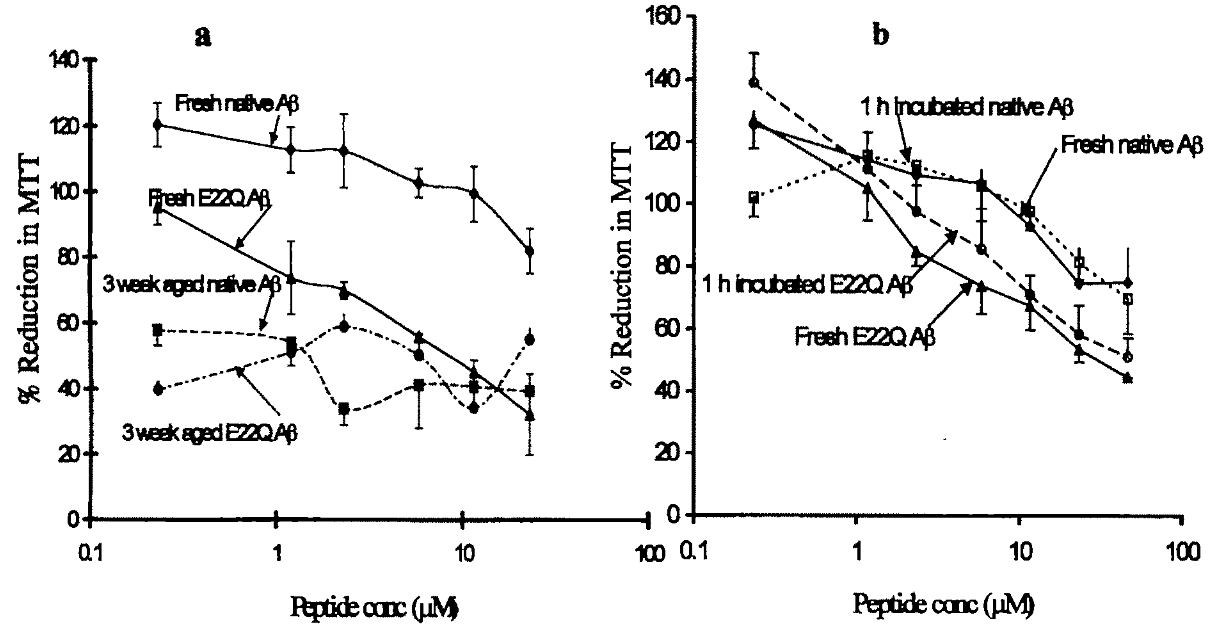

Figure 6 Cytotoxic effect of aged and fresh Aβ peptides

Shown is a comparison of the ability to reduce MTT by SH-SY5Y cells incubated for 48 h with freshly prepared native Aβ (---◆---) or E22Q Aβ (---▲---) (**a** and **b**) and aged (3 weeks) native Aβ (—■—) and E22Q Aβ (---●---) solutions (**a**) or 1 h preincubated solutions of native Aβ (—□—) and E22Q Aβ (—○—) (**b**) (preincubated at 1 16 mM and diluted into the media surrounding the cells Data shown are expressed as percentage of control values (no peptides) Under the same conditions, camptothecin incubated with the cells led to a reduction in MTT staining of 93%. S E M values for assays performed in triplicate are shown for each point as bars above and/or below the mean.

reached by others [24] who found that Aβ was not eluted as expected from a size-exclusion column calibrated with a wide range of globular proteins. These workers also found, by translational diffusion measurements using NMR, that Aβ behaves as monomers in solution. Moreover, its elution behaviour did not allow one to differentiate whether Aβ exists as an extended monomer or a compact dimer [25].

Evidence for Aβ dimers in solution has come from studies of size-exclusion chromatography in salt. High salt has previously been found to precipitate Aβ, leaving a small percentage of a species that is eluted from a column of Bio-Gel P10 as a monomer, whereas, under most other aqueous conditions, Aβ has a reduced elution time, possibly behaving as a dimer [23]. Inclusion of NaF in the elution buffer caused Aβ to be eluted later from Bio-Gel P10. However, as NaF also significantly altered the behaviour of the standard proteins used [23], the changes observed in elution behaviour of Aβ were difficult to interpret. QLS measurements made on Aβ solutions were also suggestive of dimers, but QLS is known to be less useful in studying small molecules when they exist in equilibrium with polymers [21].

An ELISA was developed to probe the oligomeric nature of native and E22Q Aβ. The formation of additional epitopes to the N-terminal specific antibody anti-NTA4 in oligomers attached to the wells by one epitope via immobilized non-biotinylated anti-NTA4 were detected by an increase in binding to a biotinylated form of the same antibody (Figure 1). The increases in binding to biotinylated-anti-NTA4 in incubated solutions of the Aβ peptides indicate that soluble oligomeric species are generated from the initially monomeric species over the course of incubation. The possibility that the fresh solutions already contain dimers in which the epitopes are so close that they cannot simultaneously bind the non-biotinylated and biotinylated forms of the anti-NTA4 antibody cannot, however, be excluded. The maximum increases in absorbance from ELISA occurred under conditions of incubation similar to those that gave rise to a decrease in the elution time (of 1 6 min) to the major peak eluted from Superdex 75, and to the appearance of shoulders on this peak (Figure 2), supporting the contention that oligomers are formed from monomers during incubation. E22Q Aβ formed oligomers, detected by the increase in biotinylated anti-NTA4 binding, more rapidly than native Aβ. Soluble protofibrils, which are eluted in the void volume from Superdex 75, in 18 h incubates of native Aβ and 60 min incubates of E22Q Aβ were also seen (Figure 2; [9]). As a control, solutions of the N-terminal ten-residue peptide, which does not contain the sequences known to be important for oligomerization [23], but contains the complete epitope for the antibody anti-NTA4 [15], did not show increased binding to the antibody upon incubation.

The binding to biotinylated-anti-NTA4 of oligomers produced in solutions of E22Q Aβ incubated at 1.16 mM and 0.116 mM reached a maximum, and then declined at a low rate, which was commensurate with the appearance of insoluble fibrils. The most likely cause of the decline is a slow occlusion of some of the binding sites to anti-NTA4 by precipitation of insoluble fibrils. In contrast, native Aβ did not show any decline in binding with incubations of up to 24 h, and did not yield fibril precipitates until after several days of aging. In keeping with these results observed on 1–40 full-length amyloid peptides, fragments 13–26 and 1–28 of E22Q mutation in Aβ have been reported to fibrillize more rapidly that fragments of native Aβ [26,27]. An ELISA similar in principle has been described [28] for the detection of inhibitors of Aβ fibrillization.. However, the changes occurring with time during incubation of Aβ peptides were not studied, and insufficient detail is given [28] to compare sensitivities of the assays.

The formation of soluble oligomers measured by ELISA was found to be dependent on the concentrations of the incubated Aβ

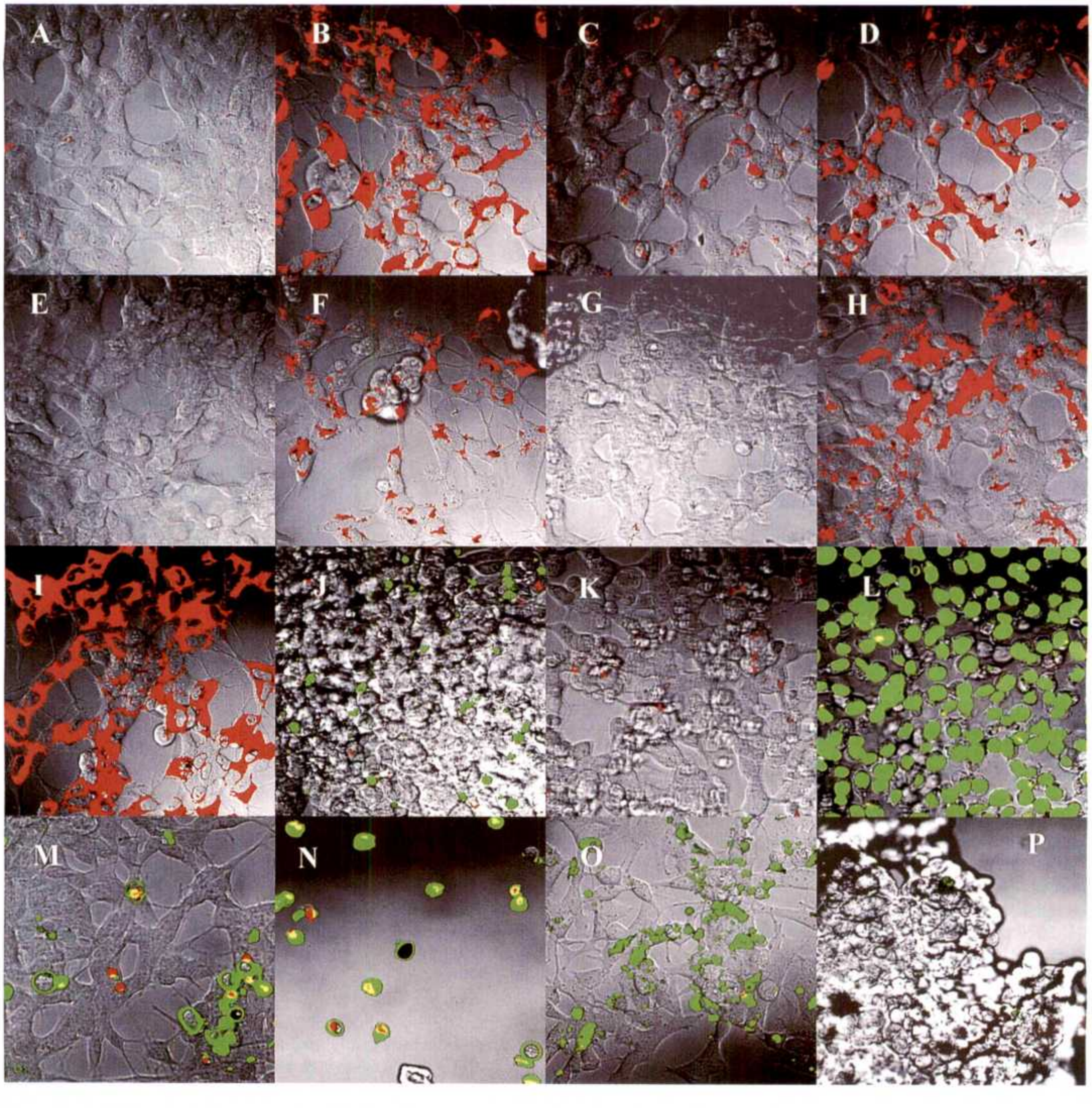

Figure 7 **Apoptotic effects of native and E22Q Aβ peptides**

Representative fluorescence photomicrographs showing the loss of mitochondrial membrane potential monitored by loss of CMXRos (red) fluorescence (**A**–**L**) or the appearance of phosphatidylserine monitored by binding with annexin V conjugated to Alexa 488 (green fluorescence) (**M**–**P**) in SHSY-5Y cells treated with aged (3 weeks) (**A**, **C** and **M**) or fresh (**B** and **D**) preparations of native Aβ, or aged (**E**, **G** and **N**) or fresh (**F** and **H**) preparations of E22Q Aβ. Peptides were incubated with cells at 11.6 μM (**A**, **B**, **E**, **F**, **M** and **N**) or 2.3 μM (**C**, **D**, **G** and **H**) for 10 h. Apoptosis induced by camptothecin is shown at 15 μM in (**J**) and 50 μM in (**K**) and (**O**), and necrosis induced by H_2O_2 is shown in (**L**). Control cells (no additions) are shown in (**I**) and (**P**). Sytox (green) (**A**–**L**) or propidium iodide (red) (**M**–**P**) detected any necrotic cells. Cells are outlined in grey as differential contrast interference images.

peptides (Figure 1). In contrast, fluorescence resonance energy transfer observed from DMSO solutions of fluorescently labelled Aβ diluted into aqueous buffers did not change over concentrations from 3 μM to 100 nM [11]. It is possible that oligomers formed from modified fluorescent peptides give rise to much more stable dimers than those of unmodified Aβ. Alternatively, the use of organic solvents [11] may have had marked effects on the behaviour of the Aβ adducts [22].

The conversion of random to β-sheet conformation of native and E22Q Aβ peptides detected by CD were an order of magnitude lower than rates at which soluble low-molecular-mass oligomers, detected by ELISA and gel filtration, are formed

(Figure 3). In the association process, Aβ molecules may be driven together in a way that retains their irregular structure, and then undertake slower conformational transitions into β-sheets in ways which are very sensitive to the amino acid change E22Q. The molecular changes that take place during the initial stages of oligomerization are clearly important in determining the kinetics and equilibrium of the fibrillar product, although precipitation of fibrils may be dependent upon a nucleation process [29]. X-ray-diffraction measurements of fibrils formed by Aβ1–28 indicated that residues LVFF$^{17-20}$ form a hydrophobic core in the fibrils [30]. The marked changes observed in the 250–288 nm region (Figure 3), associated with changes in the CD contributions of the side chains Phe^{19} and Phe^{20}, concur with the interpretations of X-ray data. A change in the environment of the Phe residues upon oligomerization is consistent with the results of peptide scanning [31,32], which showed that KLVFF$^{16-20}$ is a sequence in Aβ essential for fibril formation which efficiently binds to the total Aβ sequence.

Previous comparisons of the CD of 1–42 versions of these two peptides showed that, in 50 % acetonitrile, the E22Q sequence has a higher percentage of β-sheet than the native 1–42 [33]. These findings are here extended to show that the E22Q mutation plays an important role in altering the rates of oligomerization and random-coil-to-β-sheet transition in Aβ, and conformational changes occurring during pH change. Molecular modelling of Aβ 14–23 previously suggested that favourable hydrophobic interactions are stabilized by salt bridges between the two Aβ strands arranged anti-parallel [34]. Involvement of E22 in a stabilizing salt bridge would not account for the more rapid rate of oligomerization and fibrillization found in E22Q Aβ. The distances between isotopically labelled carbonyl carbon atoms of Gln^{15} and Lys^{16} in adjacent strands, measured by solid-state NMR to be 5.1 ± 0.2 and 4.9 ± 0.2 Å respectively, suggest that Aβ strands are aligned in a parallel β-strand with residues in register [35]. Parallel, in-register β-sheet formation is consistent with the strong 5 Å and weak 10 Å angstrom X-ray-diffraction reflections seen in fibrils [30]. An energy-minimized molecular model showing the dimeric arrangement of residues 15–22 in native and E22Q Aβ peptides (Figure 4) would satisfy these carbonyl carbon distances. Additional hydrogen bonding between Gln^{22} residues, and lack of charge repulsion between Glu^{22} side chains, would explain why E22Q Aβ oligomers form more rapidly than native Aβ.

There is increasing evidence that apoptosis plays a role in neuronal cell death in neurodegenerative disease. For example, neurons in post-mortem specimens from Alzheimer's patients show DNA damage and increased c-Jun immunoreactivity in the enterorhinal cortex [36]. Fibril-containing suspensions of native and E22Q Aβ produced by incubation at high concentrations for 3 weeks were more active than freshly prepared solutions in reducing MTT uptake (Figure 6) or inducing apoptotic changes (Figure 7), by further incubation at low concentrations with SHSY-5Y cells for 72 h (Figure 6) or 10 h (Figure 7). In contrast, there were no differences in the MTT reduction induced between freshly prepared solutions and solutions of high concentrations of native or E22Q Aβ incubated for 1 h (Figure 6). Thus fibrils are far more apoptotic and toxic than the low-molecular-mass oligomers produced in a 1 h incubation (Figures 1 and 2) The toxicity of low-molecular-mass oligomers reported previously may have been due to conversion into fibrils over the 5-day incubation period with the cells in culture [9].

Aged E22Q preparations are far more potent in inducing apoptotic changes and reducing MTT uptake than equal concentrations of aged native Aβ preparations (Figures 6 and 7). Toxicity differences may be due to the characteristic morphology of the fibrils formed [37]; the E22Q fibrils are short and stubby in appearance, whereas those formed by native Aβ are long and spindly (Figure 5). The different morphologies of the fibrils of native and E22Q Aβ peptides have been noted previously [38], although X-ray diffraction measurements of native and E22Q Aβ fibrils indicate they are both of similar crossed β-sheet structure. An E22K mutation in two Italian families apparently produces clinical and pathological findings highly similar to those of the E22Q Dutch disease [39], consistent with the notion that the clinical manifestations of the Dutch mutation are due to the molecular consequences of the replacement of Glu^{22}. In contrast with neuronal cell types, human cerebrovascular smooth-muscle cells are not killed by fully fibrillized forms of native Aβ 1–42 or E22Q Aβ [40], whereas E22Q Aβ 1–40 added in its soluble forms to these cells is highly toxic [41]. These differential effects towards different cell types may in part explain the differential pathology of HCHWA-D and AD. Modelling studies *in vitro* suggest that the propensity of E22Q to form fibrils could result in increased fibril binding to vascular-wall components, such as heparin, which would accelerate vascular amyloid deposition [4]. Furthermore, E22Q Aβ 1–40, but not wild-type Aβ 1–40, has been found to cause cellular degeneration into fibrils assembled *in situ* on smooth-muscle-cell surfaces, [41]. Degeneration has been observed in cultured brain pericytes treated with the Dutch E22Q Aβ [42]; in each case, fibril assembly was a prerequisite for toxicity. Elucidation of the molecular events which initiate oligomerization, a necessary intermediate step in the fibrillization process, are crucial to understanding the pathology and to developing potential therapeutics, not only of AD, but also for strokes caused by amyloidogenesis in cerebral vascular cell walls.

We are grateful to Research Into Ageing, CeNeS plc and the Engineering and Physical Science Research Council for their support, and Mr R. Moss in the Electron Microscopy Unit at St George's Hospital for the electron micrographs

REFERENCES

1 Muller-Hill, B and Beyreuther, K (1989) Molecular biology of Alzheimer's disease Annu. Rev Biochem 58, 287–307

2 Haan, J. Algra, P. R and Roos, R. A C (1990) Hereditary cerebral hemorrhage with amyloidosis-Dutch type Clinical and computed tomographic analysis of 24 cases Arch. Neurol 47, 649–653

3 Maat-Schieman, M L, van Duinen, S G., Rozemuller, A J., Haan, J. and Roos, R A (1994) Hereditary cerebral hemorrhage with amyloidosis (Dutch) a model for congophilic plaque formation without neurofibrillary pathology Acta Neuropathol. 88, 371–378

4 Watson, D J, Selkoe, D J and Teplow, D B (1999) Effects of the amyloid precursor protein Glu^{693} → Gln 'Dutch' mutation on the production and stability of amyloid β-protein Biochem J 340, 703–709

5 Pike, C. J, Burdick, A J, Walencewicz, C G, Glabe, C G and Cotman, C W (1993) Neurodegeneration induced by β-amyloid peptides *in vitro* the role of peptide assembly state J Neurosci 13, 1676–1687

6 Lorenzo, A and Yankner, B. A (1994) Beta-amyloid neurotoxicity requires fibril formation and is inhibited by congo red. Proc Natl Acad Sci U S A 91, 12242–12247

7 Mattson, M P, Tomaselli, K J and Rydel, R E (1993) Calcium-destabilizing and neurodegenerative effects of aggregated beta-amyloid peptide are attenuated by basic FGF Brain Res 621, 35–49

8 Younkin, S. G (1998) The role of A beta 42 in Alzheimer's disease. J Physiol (London) 92, 289–292

9 Hartley, D M, Walsh, D M, Ye, C P, Diehl, T, Vassilev, P M., Teplow, D. B and Selkoe, D J (1999) Protofibrillar intermediates of amyloid beta-protein induce acute electrophysiological changes and progressive neurotoxicity in cortical neurons J. Neurosci 19, 8876–8884

10 Podlisny, M B, Ostaszewski, B L, Squazzo, S L, Koo, E H, Rydell, R E, Teplow, D B and Selkoe, D J. (1995) Aggregation of secreted amyloid beta-protein into sodium dodecyl sulfate-stable oligomers in cell culture J Biol Chem. 270, 9564–9570

11 Roher, A. E, Chaney, M O, Kuo, Y M, Webster, S. D, Stine, W B, Haverkamp, L J, Woods, A S, Cotter, R J et al (1996) Morphology and toxicity of Aβ-(1–42) dimer derived from neuritic and vascular amyloid deposits of Alzheimer's disease J Biol Chem **271**, 20631–20635

12 Garzon-Rodriguez, W, Sepulveda-Becerra, M., Milton, S. and Glabe, C G (1997) Soluble amyloid Aβ-(1–40) exists as a stable dimer at low concentrations. J. Biol. Chem **272**, 21037–21044

13 Funato, H, Enya, M, Yoshimura, M, Morishima-Kawashima, M and Ihara, Y. (1999) Presence of sodium dodecyl sulfate-stable amyloid beta-protein dimers in the hippocampus CA1 not exhibiting neurofibrillary tangle formation. Am J Pathol **155**, 23–28

14 El-Agnaf, O M. A., Goodwin, H, Sheridan, J M, Frears, E R and Austen, B M (1999) Improved solid-phase synthesis of amyloid proteins associated with neurodegenerative diseases Pep Protein Lett **7**, 1–8

15 Stephens, D J and Austen, B M (1996) Metabolites of the beta-amyloid precursor protein generated by beta-secretase localise to the trans-Golgi network and late endosome in 293 cells J Neurosci Res **45**, 211–225

16 El-Agnaf, O M A, Jakes, R, Curran, M D, Middleton, D, Ingenito, R, Bianchi, E, Pessi, A, Neill, D and Wallace, A. (1998) Aggregates from mutant and wild-type alpha-synuclein proteins and NAC peptide induce apoptotic cell death in human neuroblastoma cells by formation of beta-sheet and amyloid-like filaments FEBS Lett **440**, 71–75

17 Denziot, F. and Lang, R (1986) Rapid colorimetric assay for cell growth and survival Modifications to the tetrazolium dye procedure giving improved sensitivity and reliability J Immunol Methods **89**, 271–277

18 Xia, W, Zhang, J, Kholodenko, D, Citron, M, Podlisny, M B, Teplow, D B, Haas, C, Seubert, P, Koo, E H and Selkoe, D J (1997) Enhanced production and oligomerization of the 42-residue amyloid beta-protein by Chinese hamster ovary cells stably expressing mutant presenilins J. Biol Chem **272**, 7977–7982

19 Pitschke, M, Prior, R., Haupt, M and Riesner, D (1998) Detection of single amyloid beta-protein aggregates in the cerebrospinal fluid of Alzheimer's patients by fluorescence correlation spectroscopy Nat Med **4**, 832–834

20 Harper, J. D, Wong, S S, Lieber, C M and Lansbury, P T (1997) Observation of metastable Abeta amyloid protofibrils by atomic force microscopy. Chem Biol **4**, 119–125

21 Walsh, D M, Lomarkin, A, Benedek, G. B., Condron, M. M and Teplow, D B (1997) Amyloid beta-protein fibrillogenesis Detection of a protofibrillar intermediate. J. Biol Chem. **272**, 22364–22372

22 Snyder, S. W., Ladror, U S., Wade, W S, Wang, G T, Barrett, L W, Matayoshi, E D, Huffaker, H J, Krafft, G A and Holzman, T F (1994) Amyloid-beta aggregation selective inhibition of aggregation in mixtures of amyloid with different chain lengths Biophys J **67**, 1216–1228

23 Hilbich, C, Kisters-Wolke, B, Reed, J, Masters, C L and Beyreuther, K (1991) Aggregation and secondary structure of synthetic amyloid beta A4 peptides of Alzheimer's disease J Mol Biol. **218**, 149–163

24 Tseng, B P., Esler, W. P, Clish, C B, Stimson, E R, Ghilardi, J R, Vinters, H V, Mantyh, P W, Lee, J P and Maggio, J E (1999) Deposition of monomeric, not oligomeric, Aβ mediates growth of Alzheimer-Disease amyloid plaques in human brain preparations Biochemistry **38**, 633–642

25 Walsh, D M, Hartley, D M, Kusumoto, Y, Fezoui, Y, Condron, M M., Lomakin, A, Benedek, G. B, Selkoe, D J and Teplow, D B (1999) Amyloid β-protein fibrillogenesis, structure and biological function of protofibrillar intermediates J Biol Chem. **274**, 25945–25952

26 Clements, A., Walsh, D M, Williams, C H and Allsop, D (1993) Effects of the mutations Glu22 to Gln and Ala21 to Gly on the aggregation of a synthetic fragment of the Alzheimer's amyloid beta/A4 peptide Neurosci Lett **161**, 17–20

27 Wisniewski, T, Ghiso, J and Frangione, B (1991) Peptides homologous to the amyloid protein of Alzheimer's disease containing a glutamine for glutamic acid substitution have accelerated amyloid fibril formation Biochem Biophys Res. Commun **179**, 1247–1254

28 Howlett, D, Cutler, P, Heales, S and Cammilleri, P (1997) Hemin and related porphyrins inhibit β-amyloid aggregation FEBS Lett **417**, 249–251

29 Lomakin, A, Teplow, D B, Kirschner, D A and Beneder, G B (1997) Kinetic theory of fibrillogenesis of amyloid beta-protein. Proc Natl Acad Sci U S A **94**, 7942–7947

30 Inouye, H and Kirschner, D A. (1996) The Nature and Origin of Amyloid Fibrils, pp 22–38, Wiley, Chichester

31 Tjernberg, L O., Naslund, J, Lindqvist, F, Johansson, J, Karlstrom, A R., Thyberg, J., Terenius, L and Nordstedt, C (1996) Arrest of beta-amyloid fibril formation by a pentapeptide ligand. J. Biol Chem **271**, 8545–8548

32 El-Agnaf, O M A, Guthrie, D J S, Walsh, D M and Irvine, G B (1998) The influence of the central region containing residues 19–25 on the aggregation properties and secondary structure of Alzheimer's beta-amyloid peptide. Eur J Biochem **256**, 560–569

33 Fabian, H., Szendrei, G I, Mantsch, H H and Otvos, L. (1993) Comparative analysis of human and Dutch-type Alzheimer beta-amyloid peptides by infrared spectroscopy and circular dichroism Biochem Biophys Res Commun **191**, 232–239

34 Tjernberg, L O, Callaway, D J E, Tjernberg, A, Hahne, S, Lilliehook, C, Terenius, L, Thyberg, J. and Nordstedt, C (1999) A molecular model of Alzheimer amyloid beta-peptide fibril formation J Biol. Chem **274**, 12619–12625

35 Benzinger, T L S, Gregory, D M, Burkoth, T S, Miller-Auer, H, Lynn, D G., Botto, R. E and Meredith, S. C (1998) Propagating structure of Alzheimer's beta-amyloid(10–35) is parallel beta-sheet with residues in exact register Proc. Natl Acad Sci U S A **95**, 13407–13412

36 Anderson, A J, Su, J. H and Cotman, C W (1996) DNA damage and apoptosis in Alzheimer's disease colocalization with c-Jun immunoreactivity, relationship to brain area, and effect of postmortem delay J. Neurosci **16**, 1710–1719

37 Seilheimer, B, Bohrmann, B, Bondolfi, L, Muller, F, Stuber, D and Dobeli, H (1997) The toxicity of the Alzheimer's beta-amyloid peptide correlates with a distinct fiber morphology J Struct Biol **119**, 59–71

38 Fraser, P. E, Nguyen, J T., Inouye, H, Surewicz, W K, Selkoe, D J, Podlisny, M B and Kirschner, D. A (1992) Fibril formation by primate, rodent, and Dutch-hemorrhagic analogues of Alzheimer amyloid beta-protein. Biochemistry **31**, 107161–10723

39 Bugiani, O., Padovani, A, Magoni, M, Andora, G, Sgarzi, M, Savoiardo, M., Bizzi, A, Giaccone, G, Rossi, G and Tagliavini, F (1998) An Italian type of HCHWA Neurobiol Aging **19**, S23

40 Davis, J and van Nostrand, W E (1996) Enhanced pathologic properties of Dutch-type mutant amyloid beta-protein Proc. Natl Acad Sci U S A **93**, 2996–3000

41 van Nostrand, W E, Melchor, J P and Ruffinini, L (1998) Pathologic amyloid beta-protein cell surface fibril assembly on cultured human cerebrovascular smooth muscle cells J Neurochem. **70**, 216–223

42 Verbeek, M M, Dewaal, R M-W, Schipper, J J and van Nostrand, W E. (1997) Rapid degeneration of cultured human brain pericytes by amyloid beta protein J Neurochem **68**, 1135–1141

Received 4 January 2000/13 March 2000, accepted 3 April 2000

Biochem. J. (2000) 349, 309–321 (Printed in Great Britain)

Oxalate oxidases and differentiating surface structure in wheat: germins

Byron G. LANE
Department of Biochemistry, University of Toronto, Toronto, Ontario, Canada M5S 1A8

Oxalate oxidases (OXOs) have been found to be concentrated in the surface tissues of wheat embryos and grains: germin is concentrated in root and leaf sheaths that surround germinated embryos; pseudogermin (OXO-ψ) is concentrated in the epidermis and bracts that 'encircle' mature grains. Most strikingly, the epidermal accumulation of OXO-ψ was found to presage the transition of a delicate 'skin', similar to the fragile epidermis of human skin, into the tough shell (the miller's 'beeswing') that is typical of mature wheat grains. A narrow range of oxalate concentration (1–2 mM) in the hydrated tissues of major crop cereals (barley, maize, oat, rice, rye and wheat) contrasted with wide variations in their OXO expression, e.g. cold-tolerant and cold-sensitive varieties of maize have similar oxalate contents but the former was found to contain approx. 20-fold more germin than did the latter. Well-known OXOs in sorghum, a minor cereal, and beet, a dicotyledon, were found to have little antigenic relatedness to the germins, but the beet enzyme did share some of the unique stability properties that are peculiar to the germin-like OXOs that are found only in the major crop cereals. Their concentration in surface structures of domesticated wheat suggests a biochemical role for germin-like OXOs: programmed cell death in surface tissues might be a constitutive as well as an adaptive form of differentiation that helps to produce refractory barriers against tissue invasion by predators. Incidental to the principal investigation, and using an OXO assay (oxalate-dependent release of CO_2) that did not rely on detecting H_2O_2, which is often fully degraded in cell extracts, it was found that OXO activity in soluble extracts of wheat was manifested only in standard solution assays if the extract was pretreated in a variety of ways, which included preincubation with pepsin or highly substituted glucuronogalactoarabinoxylans (cell-wall polysaccharides).

Key words: apoptosis, cereals, maturation, pathogenesis, seeds.

INTRODUCTION

Oxalates have been studied in the basic and applied sciences for centuries [1]. In biology, oxalates have usually been regarded as inert end products of carbon assimilation that, in the forms of their insoluble calcium salts, are well-tolerated 'storage forms' of calcium in plants, and serious contributors to chronic, sometimes acute, 'stone diseases' in humans [1]. Entrenched and traditional views of oxalate as a 'static substance' were challenged by the discovery that germin, long known as a marker of growth onset in germinating cereals [2,3] and long suspected of being an agent in host-plant resistance to disease [4], is an oxalate oxidase (OXO) [5,6]. A focused vision of plant oxalate as a dynamic resource, as a source of H_2O_2, which can, at different concentrations, mediate developmental signalling, cross-linking and defence reactions in higher plants [3], has met with increasing favour [7].

Germins are remarkable water-soluble oligomeric proteins: they are refractory to dissociation in SDS/PAGE gels [8] and to hydrolysis by known proteases under non-denaturing conditions [9]. Germins [10] and their coding elements [11] have so far been found only in what Hill dubbed the 'true cereals', the major crop cereals barley (*Hordeum*), maize (*Zea*), oat (*Avena*), rice (*Oryza*), rye (*Secale*) and wheat (*Triticum*) [12]. Wheat [5], barley [5,6], maize (the present paper), oat, rice and rye (B. G. Lane, unpublished work) germins are OXOs (EC 1.2.3.4) that generate H_2O_2 from oxalate, confirming an early suspicion [4], partly based on an association with wheat cell walls [4,13], that germins might have a role in plant defence [3] as well as development [2]. A 1.6 Å X-ray diffraction structure of barley germin is complete (J. Dunwell, personal communication) and is compatible with a proposed octahedral co-ordination of 6 mol of Mn per mol of catalytic hexamer [14].

As shown here, an OXO in a minor cereal, sorghum (*Sorghum*) [15], lacks the stability of germins, and an OXO in the garden beet (*Beta vulgaris*) [16], a dicotyledon, shares some of their stability but does not react with germin antibodies. Beginning with the most idiosyncratic sequence (PHIHPRATEI; single-letter amino acid codes) in wheat germin [11], called the 'germin box' in PROSITE analyses (PHXHPRATEI), it was shown that there is broad dispersal of coding elements for germin-like proteins (GLPs) [17–19] beyond the monocotyledons. GLPs are found in protists [11], bryophytes [20], gymnosperms [21] and dicotyledons [22–27]. Study of GLP proteins, as opposed to coding elements, has been rare, but a moss GLP has been shown to be a superoxide dismutase [20] and two *Arabidopsis thaliana* GLPs have been shown to share the stability of germins [26].

Classical botanical studies had forecast roles for oxalate and 'wound oxalate' in the germinative development of lupin ([28], cited in [1]) and in the defence responses of *Tradescantia fulminensis* [29] respectively but the possible significance of these isolated observations faded with the passage of time. More recently, projected roles of germins and germin-like OXOs (gl-OXOs) in phytopathology were proposed [3,4] and soon validated when three groups showed independently that infection with powdery mildew induces the synthesis of gl-OXOs in barley [30,31] and wheat [32]. The germinative emergence of germin in structures that envelop the embryo (3% of grain mass) [33] is

---

Abbreviations used: d.p.a., days post-anthesis; gl-OXO, germin-like OXO, i.e. an OXO oligomer that has the unique stability properties of germin (refractory to hydrolysis by all known proteases and resistant to dissociation in standard SDS/PAGE gels); GLP, germin-like protein, i.e. a protein encoded by a germin-like coding element; hsGGAX, highly substituted glucuronogalactoarabinoxylan(s); OXO, oxalate oxidase; OXO-ψ, pseudogermin; P16, insoluble (pellet) fraction after centrifugation of a homogenate at 16000 ***g***; S16, soluble (supernatant) fraction after centrifugation of a homogenate at 16000 ***g***; XG, xyloglucan.

e-mail byron.lane@utoronto.ca

broadly extended in the present study to structures comprising most of the mass of the wheat flower (embryo, grain and bracts). During maturation, there is a striking concentration of OXO-ψ in structures that tightly envelop (epidermis) and loosely surround (bracts) the wheat grain. Pseudogermin (OXO-ψ) is a uniquely stable germin [13] and its emergence in the epidermis presages the transformation of a delicate 'skin' into a tough shell that fuses with the seedcoat to form the protective outer surface in a ripened wheat grain. Implications of the findings for the biochemical importance of gl-OXOs are discussed.

EXPERIMENTAL

Plant materials

Hexaploid wheat grains of the Neepawa and Conway varieties were obtained from the Alberta Wheat Pool (Lethbridge, Alberta, Canada). Diploid wheat grains having the A (PI 119423 TR SD 1277, *Triticum monococcum*), B (CIae 64 AE SD, *Aegilops speltoides*) or D (CIae 4 AE SD 2038, *Aegilops tauschii*) genomes were supplied by Dr Harold Bockelman (Small Grains and Potato Germplasm Research Unit, USDA/ATRS, Aberdeen, ID, U.S.A.). Immature grains were harvested from Vulcan and Cheyenne cultivars of wheat by Dr William J. Hurkman (Plant Research Center, USDA/ARS Albany, CA, U.S.A.). Two varieties of maize grain, one cold tolerant (C0255) and one cold sensitive (C0286), were kindly supplied by Dr Bob Hamilton and Dr Chris Andrews (Agriculture Canada, Plant Research Centre, Ottawa, Canada). Sorghum seeds (genotype CSH-5) were kindly provided by Dr C. S. Pundir (Department of Bio-Sciences, M. D. University, Rohtak, India) through the agency of Nath Seeds Pvt. Ltd (Aurangabad, India). *Arabidopsis thalania* seeds were kindly provided by Dr François Bernier (Institut Botanique, Université de Strasbourg, Strasbourg, France). Transgenic tobacco and canola (*Brassica Napus*) seeds of the T2 generation (progeny of the primary transformants) were obtained by transforming wild-type tobacco and canola (Brutor cultivar) with an approx. 740 bp *Hind*III$_1$/*Sph*I$_2$ fragment of the *gf-2.8* germin gene [11], which contains approx. 15 bp of the 5′ untranslated region, the entire signal sequence, the entire structural-protein coding sequence and approx. 50 bp of the 3′ untranslated region. This germin-coding element, inserted between a 35 S cauliflower promoter and a Nos terminator, was ligated into a pBIN19 vector (with kanamycin selection) and the construct was transferred to *Agrobacter tumefaciens* (LBA 4404) for transformations. Beet seeds (var. Early Wonder, Ruby Queen) were purchased from a local seed supplier. Seedlings were grown by culturing mature grains or seeds on water-soaked Whatman no. 3 filter paper for 1–15 days at room temperature in laboratory light (approx. 12 h/day). Embryos were prepared from mature wheat grains (*Triticum aestivum*, var. Neepawa or Conway) [34]. Purified specimens of highly substituted glucuronogalacto-arabinoxylan(s) (hsGGAX) and xyloglucan (XG) were generously supplied by Professor Nicholas Carpita (Purdue University, West Lafayette, IN, U.S.A.).

Preparation and immunostaining of thick sections of water-cultured wheat embryos

Pre-isolated embryos (200 mg) were cultured on a disc (8.5 cm) of Whatman no. 3 filter paper that was immersed in sterile water (5 ml) at room temperature in darkness for 40 h For thick-sectioning, single embryos that seemed to be essentially intact (approx. 30 % of the total number and approx. 50 % of the total mass) were first fixed (1 h) in a solution made by mixing 7 ml of 95 % (v/v) ethanol with 2.5 ml of acetic acid, and then dehydrated successively in 70 % (v/v) ethanol (four times, 15 min), graded concentrations (70 %, 85 %, 95 % and 100 %, v/v) of aqueous 2-methylpropan-2-ol (once, for 30 min each), and finally in 100 % 2-methylpropan-2-ol (twice, 1 h), before being embedded in paraffin blocks at 60 °C. Sections (8 mm) were transferred to slides that had been cleaned for 10 min in ethanol and coated for 10 min in poly-(L-lysine) in a Coplin jar. The slides, with sections, were kept at 60 °C for 1 h before they were incubated in Histo-Clear (twice, 10 min), graded concentrations (100 %, 90 %, 70 % and 50 %, v/v) of aqueous ethanol, water, Tris-buffered saline (TBS) (once, for 3 min each), and finally for 1 h in 200 μl of 'blocking solution' [10 % (v/v) goat serum in TBS]. 'Blocked' sections were incubated for 45 min with 150 μl of germin antiserum (1:100 dilution in TBS), with or without prior pre-adsorption to remove glycan-directed antibodies [13], washed with TBS (three times, 5 min), and incubated for 45 min with alkaline-phosphatase-conjugated goat anti-rabbit IgG [1 μl in 1 ml of 1 % (w/v) BSA in TBS], before again being washed in TBS (twice, 5 min). For staining, sections were incubated for 30 min in 200 μl of substrate solution [100 mM Tris/HCl (pH 9.5)/100 mM NaCl/50 mM $MgCl_2$, containing levamisole, 1.65 mg of Nitro Blue Tetrazolium in 22 ml of 70 % (v/v) dimethylformamide and 0.82 mg of 5-bromo-4-chloroindol-3-yl phosphate in 16.5 ml of dimethylformamide], and after being washed in TBS (three times, 5 min) and water (once, 3 min), and being dehydrated in graded concentrations of ethanol (50 %, 70 %, 90 % and 100 %, v/v) (once, for 3 min each), were overlaid with Crystalmount and incubated for 20 min at 80 °C before light microscopy.

Quantitative solution assay and qualitative blot assay of OXO activity

A published method [35] was used to measure the release of $^{14}CO_2$ from [^{14}C]oxalate. Reaction mixtures containing 2 mM oxalic acid were buffered with 0.1 M sodium succinate, pH 3.5, for maximal activity. Buffers used to assess the pH dependence of OXO activity were: 0.1 M sodium acetate, pH 4.5, 0.1 M sodium phosphate, pH 6.7, 0.1 M Tris formate, pH 7.7, and 0.1 M ammonium formate, pH 9.2. The specific radioactivity of the [^{14}C]oxalate that was used in the $^{14}CO_2$ release assays was approx. 10^5 c.p.m./μmol. Soluble and pellet fractions of homogenates were prepared by homogenizing embryos, seedlings or individual organs in 100 mM potassium acetate/3 mM magnesium acetate/20 mM Hepes (pH 7.5)/1 mM dithiothreitol (1.5, 3 or 20 μl of buffer/mg of fresh mass) in a Duall homogenizer and then centrifuging homogenates at 16000 g for 10 min (all at 0–4 °C). This buffer conserves cell-free protein-synthesizing activity in the 16000 g supernatant fraction (S16) of homogenates of mature wheat embryos [36]. Pellets (P16) were suspended in the same buffer by vortex-mixing in an Eppendorf tube in the presence of a straight-pin to obtain smooth suspensions, volumes of the P16 extracts being adjusted to equal those of the corresponding S16 extracts. The quantities (20 μl) of S16 or P16 extract used in $^{14}CO_2$ release assays (total volume 0.5 ml), and for application to SDS/PAGE gels for blot assay [5], were derived from 1 mg (20 μl of buffer/mg), 6.4 mg (3 μl of buffer/mg) or 8.5 mg (1.5 μl of buffer/mg) fresh mass. Reactions were terminated by the addition of trichloroacetic acid after 20 min at 37 °C. After trichloroacetic acid-induced release of $^{14}CO_2$, released $^{14}CO_2$ was collected in a bucket of 40 % (w/v) KOH (100 μl) in a reaction vessel supplied by Kontes (cat. no. 882360-0010). The residual reaction mixture, containing H_2O_2, was neutralized (to approx. pH 4) with KOH and analysed for H_2O_2 as described in [37]. Measurements of radioactivity were made in 10 ml of CytoScint with an LKB Rackbeta liquid-scintillation counter. After separation of proteins by SDS/PAGE and transfer to nitrocellulose, germin and its isoforms were detected by reaction with a polyclonal anti-germin rabbit serum [13] or by staining for OXO activity [5].

Quantitative assay of oxalate

Fresh or frozen biological material (50–200 mg) was homogenized (1 min) in a round-bottomed 2051 Falcon tube with a Polytron blender (Brinkmann Instruments), at a speed setting of 7 (Kinematica rheostat) with 1 ml of 3 M HCl that had been supplemented with 10 μl (0.01 μM, approx. 10^5 c.p.m.) of [^{14}C]oxalic acid. Tracer oxalic acid was included to assess the percentage recovery of oxalic acid from tissue on the assumption that all tissue oxalate was equilibrated with the tracer in 3 M HCl; the tracer solution was prepared by dissolving 5.2 mg (250 mCi) of [^{14}C]oxalic acid from Sigma (cat. no. 31,391-2) in 100 μl of sterile water (solubility 9.5 g/100 ml at 15 °C). When wheat embryos had been homogenized for 1 min and the homogenate had been left at room temperature for 30 min before again being blended for 1 min, the measured amount of oxalate in the embryos was the same as that found after a single 1 min homogenization, confirming that the tracer was well equilibrated with tissue oxalate. The pH of the homogenate was adjusted to pH 7.0 with 10 M NaOH (approx. 220 μl) and the neutralized homogenate was transferred to a Microfuge tube for centrifugation (10 min, 14000 g, room temperature). The resulting supernatant (approx. 1.5 ml) was transferred to a larger tube for mixing with an equal volume of satd $CaSO_4$ and ethanol (10 ml/1.5 ml satd $CaSO_4$) and allowed to precipitate at room temperature for 24–48 h. The precipitate was suspended in 2 ml of the 1:1 diluent in the oxalate analysis kit supplied by Sigma (cat. no. 591-4) and the suspension was clarified by transfer to an Eppendorf tube for centrifugation in an Eppendorf 5415 centrifuge (14000 rev./min, 10 min, room temperature). A 50 μl aliquot of the clear supernatant solution was used to assess the recovery of [^{14}C]oxalic acid (25–40 %); separate aliquots (approx. 100–200 μl), containing the amounts of oxalate recovered from 5 and 10 mg of fresh mass, were assayed for oxalate. Potassium oxalate standards (0.18, 0.45 and 0.90 μg) and experimental samples, in a total volume of 200 μl of Sigma diluent, were mixed with 1 ml of reagent A and 100 μl of reagent B and incubated at 37 °C for 20–30 min before measurement of A_{590}. Reagent B, containing soluble barley germin and horseradish peroxidase, was obtained from Sigma (cat. no. 591-2); reagent A was prepared by dissolving 23.7 mg of 3-dimethylaminobenzoic acid (Sigma cat. no. D0787) and 2.13 mg of 3-methyl-2-benzothiazolinone hydrazone (Sigma cat. no. M 8006) in 45 ml of 0.1 M sodium succinate, pH 3.2. For a 'low-oxalate' plant (e.g. wheat), A_{590} was approx. 0.1 above background for the amount of oxalate (approx. 0.4 μg) recovered from 10 mg of fresh mass. Measurements were corrected for tracer recovery (25–40 %) and for the contribution of the tracer itself (approx. 5 %) to the total oxalate measured in the analysis.

Because it has been reported [38] that oxalate is generated when ascorbate is incubated in phosphate buffer at slightly alkaline pH (7.4) for several hours, it is significant that we observed no effect on measured oxalate if extraction with tributylphosphate [39] was used to partition the extracted oxalate at alkaline pH. Measurements were also not significantly changed if, during the neutralization of acid extracts of oxalate, the pH was adjusted to approx. 13 and the alkaline extract was incubated at room temperature for 2–3 h before being adjusted to pH 7. Linear increases were observed for aliquots containing the oxalate recovered from 5 and 10 mg of fresh mass; there was additivity when such aliquots of experimental samples were mixed with pure potassium oxalate, i.e. there was no interference with, or suppression of, OXO activity in the assay when aliquots corresponding to 10 mg of fresh mass (or less) were used for analysis. Acid extracts of tissues were stored at −20 °C for up to 3 weeks without affecting the measurements of oxalate.

RESULTS

Increased amounts of germin in pellet fractions of homogenates depend on germinative development of water-cultured mature wheat embryos

For ease of comparison of OXO activities with the oxalate contents of tissues, both are expressed as mass quantities, as in the oxalate literature [40]. As shown in Table 1, the cell walls of germinated embryos had strong OXO activity. The physical properties of the cell-wall form of germin from wheat embryos were very similar to those of a commercially available preparation of barley OXO (preparation no. 1 in Table 1): both activities were totally insoluble in water or aqueous buffers and were fully sedimented at low speeds. In contrast, it was found that the kind

Table 1 Comparison of the OXO activities in equal masses of wheat embryo cell walls and three commercially available preparations of barley OXO

Purified cell walls were prepared after preisolated embryos from mature wheat grains had been germinated by culturing them in water for 48 h [13]. Preparation no. 1 was purchased as 'oxalate oxidase' from Sigma (cat. no. O 4127) and, as with the activity in purified wheat-embryo cell walls, this activity was totally insoluble in water or aqueous buffers. Preparation no. 2 was purchased as 'oxalate oxidase' from Boehringer Mannheim (cat. no. 567 698) and the activity was totally water-soluble. Preparation no. 3 was purchased from Sigma (reagent B in their oxalate analysis kit, cat. no. 591-2) and the activity was totally water-soluble. Most of the mass in preparations no. 2 and no. 3 was due to the commercial suppliers' additions of 'stabilizers' (probably borate) to the proteins. When analysed in SDS/PAGE gels, preparation no. 2 was free of protein impurities but preparation no. 3 had precisely the same contaminants previously found in earlier lots of preparation no. 2 [5]. Protein was estimated by comparing the degree of Coomassie staining of germin oligomers and monomers with the staining of a known amount (0.5 μg) of BSA in SDS/PAGE gels. Allowance was made for the (approx. 50 %) greater staining intensity of BSA relative to known amounts (by amino acid analysis) of germin, on a mass basis. Protein was extracted from the cell-wall preparation [13] and the amount of extractable germin monomer was measured in SDS/PAGE as described (Figure 6 in [13]). These results suggest implicitly that the germin in cell walls has much greater specific activity (per mol of germin) than the more highly purified soluble germin preparations (see the discussion of GGAX 'activation' in Table 7).

Specimen	Dry mass (μg)	Germin content (μg)	OXO activity (μg of oxalate degraded in 10 min)
Wheat embryo walls (water-insoluble)	150	0.1	7.8
OXO preparation no. 1 (water-insoluble)	150	0.5	36.2
OXO preparation no. 2 (water-soluble)	150	1.7	3.7
OXO preparation no. 3 (water-soluble)	150	3.3	9.2

Table 2 Temporal emergence of OXO activity in water-cultured mature embryos prepared in bulk from two varieties of hexaploid wheat

After being purged of $^{14}CO_2$, liquid phases from reaction flasks containing insoluble P16 extract were shown to contain an amount of H_2O_2 that was equimolar to the amount of degraded [^{14}C]oxalate, e.g. for the Neepawa insoluble (P16) extract at 15 h the amount of H_2O_2, as measured by a solution assay [35], was equal to the molar amount (3.4/90 = 0.038 μmol) of [^{14}C]oxalate that was degraded (see the Experimental section). The molar equivalence between H_2O_2 release and [^{14}C]oxalate degradation was established for all reaction mixtures whenever the amount of H_2O_2 was sufficient for reliable measurement in the colorimetric assay. For flasks containing soluble (S16) extracts, the amount of H_2O_2 was too small for reliable estimation but quasi-quantitative results were compatible with expectations. Reaction mixtures (0.5 ml) contained 1.5 mM oxalate/oxalic acid (approx. 10^5 c.p.m.) in 0.1 M sodium succinate, pH 3.5, and were supplemented with 25 μl of soluble (S16) or insoluble (P16) extract from 8.5 mg (fresh mass) of embryos (see the Experimental section for further details).

	OXO activity (μg of oxalate degraded in 10 min)			
	Neepawa embryos		Conway embryos	
Time (h)	Soluble (S16)	Insoluble (P16)	Soluble (S16)	Insoluble (P16)
0	0.01	1.7	0.00	1.9
15	0.03	3.4	0.05	3.4
25	0.34	11.7	0.18	7.1
35	0.20	13.5	0.16	16.8
45	0.32	12.0	0.27	13.9

of commercially available preparations included as part of 'reagent B' in oxalate analysis kits (preparations no. 2 and no. 3 in Table 1) were freely soluble in water and they had specific activities (per μg of protein) that approached the OXO activity reported for soluble wheat germin [5].

Compatible with a prominent association of germin with wheat cell walls [13], germin activity became increasingly concentrated in the P16 fractions of homogenates made from embryos that were pre-isolated from field-ripened grains and cultured in water [41] (Table 2). Strong OXO activity in the soluble (S16) fractions of wheat homogenates was largely repressed and was undetected when OXO activity was measured by $^{14}CO_2$ release from [^{14}C]oxalate (Table 2) (see below). The striking increase in OXO activity in embryo homogenates during the temporal development of water-cultured, pre-isolated wheat embryos (Table 2) paralleled previously demonstrated increases in levels of germin, its translatable mRNA [10] and its gene expression [42] under the same conditions. The burgeoning amounts of germin made during germinative development were confirmed (results not shown) in Western (antibody) and activity blots after SDS/PAGE separation of proteins in the different extracts [5].

Localization of germin in different parts of wheat and maize seedlings

As previously defined [10], the 'stem' is that part of the plant that remains after excision of the roots and shoots from embryos or seedlings, there being little stem growth when grains are cultured on water-soaked filter-paper. Immunocytology (see below) showed that 'stem' germin was mostly localized to enveloping tissues (coleorhiza or coleoptile) [33], not the axis proper. OXO activities in fractionated homogenates of roots, 'stems', coleoptiles and leaves from hexaploid and diploid seedlings are compared in Table 3. Notably, when grown on filter paper, hexaploid roots had more OXO activity than diploid roots. Hexaploid, A-diploid and D-diploid seedlings (and parts) generally had much greater germin activity than the B diploid. It is of incidental interest that unfractionated homgenates of the A and D diploids, and of the B diploids, had approx. 30% and approx. 5% respectively of the OXO activity measured in a homogenate of hexaploid (cv. Conway) wheat. Similar large differences existed between the germin activities found in cold-sensitive and cold-tolerant maize cultivars (Table 4). The germin character [5] of the OXO activities listed in Tables 3 and 4 was confirmed in companion (Western and activity) nitrocellulose blots of SDS/PAGE separations (results not shown).

Oxalate and OXO levels during the early growth of selected plants

There have been no previously reported systematic comparisons of OXO-to-oxalate ratios in higher plants, all of which contain oxalate. To explore factors that might mitigate and/or enhance OXO activity in plants, it was of interest to know whether OXO activity and oxalate levels in wheat seedlings were related to those in (1) another cereal (sorghum) that contained an OXO that was not a gl-OXO, i.e. did not have germin-like stability [8,9], (2) a dicotyledon (*A. thalania*) that contained GLPs, i.e. non-OXO proteins encoded by germin-like coding elements, and (3) a dicotyledon (beet) that contained an OXO but was, unlike wheat, a 'high-oxalate' plant [40].

As shown in Table 5, the oxalate content (approx. 0.1 μg per mg of hydrated mass) of wheat kept pace with the approx. 100-fold increase in (hydrated) fresh mass that accompanied germinative development of a mature embryo, *in situ* (in the grain), into a 6-day seedling. Although there were only modest differ-

Table 3 Comparison of OXO activities in intact seedlings and individual organs from hexaploid and diploid wheat varieties

Mean fresh masses of seedlings at excision, after grains had been cultured in water for 9 days, were 110 mg for hexaploid (Conway), 107 mg for A diploid, 25 mg for B diploid and 24 mg for D diploid (see the Experimental section for additional details). Values of 0.14, 0.10 and 0.14 μg of oxalate/mg of fresh mass were measured for single A, B and D diploids, values similar to those found for hexaploids (see Table 5). Limited availability of materials dictated the preparation of more dilute homogenates (20 μl of S16 buffer/mg of fresh mass) than were made in the experiments shown in Table 2 (3 μl of S16 buffer/mg of fresh mass). Reaction mixtures (0.5 ml) contained 20 μl of soluble or insoluble fraction from approx. 1 mg of fresh mass.

		OXO activity (μg of oxalate degraded in 10 min)							
		Root		'Stem'		Coleoptile		Leaf	
Wheat variety	Mass distribution (%) between root, 'stem', coleoptile and leaf	S16	P16	S16	P16	S16	P16	S16	P16
Hexaploid	30, 10, 26, 34	0.23	2.0	0.53	14.9	0.11	4.0	0.01	0.25
A diploid	33, 3, 18, 46	0.01	0.05	0.42	16.0	0.02	0.91	0.01	0.004
B diploid	16, 4, 18, 58	0.01	0.09	0.05	0.88	0.004	0.11	0.01	0.01
D diploid	12, 6, 48, 34	0.01	0.33	0.71	15.4	0.11	0.40	0.01	0.01

Table 4 Comparison of OXO activities in the organs of cold-tolerant and cold-sensitive cultivars of maize

Distributions of mass between the organs of single cold-sensitive C0286 (380 mg) and cold-tolerant C0255 (431 mg) seedlings were significantly different, owing largely to limited leaf development in the C0286 seedling when grains had been cultured in water for 11 days; significantly, however, similar differences in OXO activity were obtained with pot-grown (vermiculite) cultivars, in which case leaf growth was equally luxuriant for cv. C0255 and cv. C0286. These results, with freshly harvested grain, are similar to the observations made with seedlings grown from 5-year-old grains Assays were performed at 20 °C but similar large (10–20-fold) differences were observed between the two cultivars when extracts were assayed at 37 °C. Assays were otherwise performed as in the legend to Table 2, except that these reaction mixtures (0.5 ml) contained 20 μl (rather than 25 μl) of the soluble (S16) or insoluble (P16) fractions of homogenates prepared from 6.4 mg (not 8.5 mg) of fresh mass. Germin-like properties (oligomer stability during SDS/PAGE and nitrocellulose transfer) for these OXO activities were demonstrated. SDS/PAGE mobilities of the maize germin activities were similar to that of OXO-ψ but their thermal stabilities were similar to that of germin.

		OXO activity (μg of oxalate degraded in 10 min)							
		Root		'Stem'		Coleoptile		Leaf	
Maize cultivar	Mass distribution (%) between root, 'stem', coleoptile and leaf	S16	P16	S16	P16	S16	P16	S16	P16
Cold-sensitive	27, 28, 28, 17	0.01	0.03	0.02	0.46	0.02	0.27	0.01	0.02
Cold-tolerant	12, 23, 27, 38	0.01	1.1	1.8	8.3	0.20	2.8	0.01	0.01

Table 5 Oxalate contents and OXO activities of equal fresh masses of intact seedlings and individual organs from selected higher plants

The oxalate measurement given in parentheses for the ungerminated wheat embryo allows for a degree of hydration equivalent to a germinated embryo (85%), to illustrate that there was little or no net change in oxalate content (μg/mg of hydrated mass) in the embryo when a mature embryo was germinated. As with wheat homogenates, most of the OXO activity in homogenates of sorghum and beet, as measured by $^{14}CO_2$ release from [^{14}C]oxalate, was confined to the insoluble (P16) fractions when homogenates were made in the 'S16 buffer' that was used to prepare all extracts made in this study (see the Experimental section). Reaction mixtures (0.5 ml) contained 1.5 mM oxalate/oxalic acid (approx. 10^5 c.p.m.) in 0.1 M sodium succinate, pH 3.5, and 20 μl of insoluble (P16) extract from 6.4 mg (fresh mass) of plant material (see the Experimental section for further details)

Specimen	Sample	Fresh mass (mg)	Oxalate (μg/mg)	OXO (μg/10 min per mg)	Ratio OXO to oxalate
Pre-isolated wheat embryo	Ungerminated	0.35	0.67 (0.10)	0.17	2
	Germinated (water)	1.9	0.10	1.1	11
	Germinated (5% sucrose)	2.9	0.059	0.51	9
Wheat seedling (3 days)	Overall	51	0.10	1.8	18
	Root	25	0.080	0.34	4
	'Stem'	6.4	0.085	4.6	54
	Coleoptile	19	0.12	0.65	5
	Leaf	–	–	–	–
Wheat seedling (6 days)	Overall	90	0.10	1.4	14
	Root	43	0.071	0.57	8
	'Stem'	6.2	0.073	6.2	85
	Coleoptile	22	0.11	0.65	6
	Leaf	19	0.11	0.01	0.09
Sorghum seedling (12 days)	Overall	45	0.16	0.035	0.22
	Root	10	–	0.10	–
	'Stem'	6.3	–	0.072	–
	Coleoptile	11	–	0.002	–
	Leaf	18	–	0.003	–
Beet seedling (17 days)	Overall	64	1.2	0.20	0.2
	Root	5.8	2.0	0.025	0.01
	Stem	38	0.98	0.34	0.4
	Leaf	20	1.4	0.003	0.002

ences between their oxalate contents, there were gross differences between OXO activities of different parts of the seedling; e.g. the OXO-to-oxalate ratio, as depicted in Table 5, varies more than 500-fold between leaf and 'stem' in a 6-day wheat seedling: 'stem' germin was concentrated in enveloping tissues (coleorhiza or coleoptile) in embryos or seedlings.

Sorghum analyses (Table 5) showed that the oxalate content (approx. 0.16 μg/mg) was similar but the OXO activity was approx. one-tenth of that found in hexaploid wheat. The sorghum OXO activity was not detected (results not shown) if soluble or insoluble extracts were subjected to SDS/PAGE and blotting on nitrocellulose, either at the pH optimum of the sorghum enzyme [15] or at the pH optimum (3.5) of the wheat enzyme, which was used for the assays reported in Table 5. Accordingly, although sorghum OXO is oligomeric [15], the protein and its OXO activity are not germin-like in character: they do not, as do the germin oligomer [8] and its OXO activity [5] in soluble extracts of wheat, survive SDS/PAGE and nitrocellulose blotting. Interestingly, however, a band with the expected mobility of sorghum OXO (molecular mass approx. 60 kDa) [15] was weakly antigenic to wheat germin apoprotein antiserum after SDS/PAGE and Western blotting (results not shown).

Analyses of beet (Table 5) showed that the oxalate content of this dicotyledon (approx. 1.2 μg/mg) was approx. 10-fold greater but the OXO/oxalate ratio was approx. 100-fold smaller than in hexaploid wheat. The beet OXO activity [16] had the same pH optimum as the wheat enzyme (results not shown); when beet extracts were subjected to SDS/PAGE and blotting on nitro-

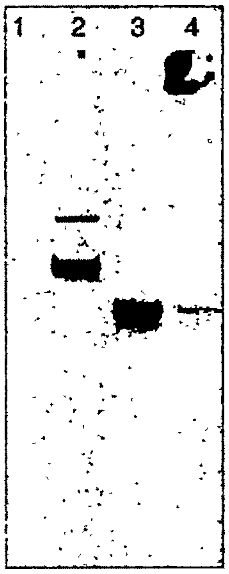

Figure 1 Beet and wheat OXO activities are detected after blotting an SDS/PAGE gel

This is an 'activity' blot [5]. Proteins (approx. 65 μg) in the soluble (S16) and insoluble (P16) fractions of wheat embryo [4] and beet homogenates were derived from 6.4 mg of fresh mass (approx. two embryos) and were separated by SDS/PAGE, they were then electroblotted on nitrocellulose and assayed for gl-OXO activity [5]. The base of each numeral marks the top of the well of the parent SDS/PAGE gel. Lanes 1, 2, 3 and 4 contained proteins derived from beet S16, beet P16, hexaploid wheat S16 and hexaploid wheat P16 fractions respectively. The gl-OXO activity bands in lanes 3 and 4 correspond to the G (the stronger, slower band; molecular mass approx. 125 kDa) and G′ glycoforms of germin [67]. The beet OXOs have not yet been similarly characterized but they were concentrated in the pellet fraction of the beet homogenate (lane 2); unlike the wheat OXOs in the pellet fraction, which were trapped in the position of the well of the parent SDS/PAGE gel, the beet OXOs entered freely into the SDS/PAGE gel.

cellulose (Figure 1), the beet OXO activity was detected by SDS/PAGE after nitrocellulose blotting but antigenicity toward wheat germin antiserum could not be detected in Western blots (results not shown). Although not explored by electrophoretic analysis, the beet OXO shared at least some of the protease resistance properties of germin in the oxalate-dependent $^{14}CO_2$ release assay.

Other selected dicotyledon seedlings that we have studied (*A. thalania*, canola, lettuce, radish and tobacco) are 'low-oxalate' plants (0.1–0.2 μg/mg). Unlike the (low-oxalate) cereals (wheat, maize and sorghum) we have studied, extracts of these dicotyledon seedlings did not have either OXO activity by $^{14}CO_2$ release assay, or gl-OXO activity by H_2O_2 release assay after SDS/PAGE and nitrocellulose blotting (results not shown).

Methodological study of the cryptic germin activity present in soluble wheat extracts

The large disparity between the OXO activities of soluble and insoluble fractions of wheat homogenates, found with the oxalate-dependent $^{14}CO_2$ release assay (Tables 2–4), was very surprising. Not only had similar amounts of the germin monomer been detected in soluble extracts [10] and (insoluble) cell-wall fractions of wheat embryos [13] before the OXO activity of germin was known [5], but, afterwards, gel-blot assays, by direct blotting on nitrocellulose or by electrophoresis in SDS/PAGE gels [5], had indicated similar amounts of OXO activity in the soluble and pellet fractions of wheat homogenates (Figure 1). However, evidence of its gl-OXO character, by mobilizing most of the putative germin oligomer in the pellet fraction in SDS/PAGE, was not obtained. Thus, although the putative germin in the wells (gel-slots) of SDS/PAGE gels (Figure 1, lane 4) could be released and mobilized as the monomer by being heated before SDS/PAGE [13], the monomer was devoid of OXO activity in SDS/PAGE blots.

In totality, our findings had suggested that, when wheat extracts were made with a buffer designed to conserve the physiological integrity of protein-synthesizing activity (see the Experimental section), the OXO activity in soluble wheat extracts was inhibited by a factor that was removed, destroyed or separated from germin during SDS/PAGE and/or nitrocellulose blotting. Because gl-OXO enzymes are refractory to treatment with pepsin, soluble fractions of wheat homogenates can be treated with pepsin to determine whether the putative inhibition might be caused by a protein. Compatible with this possibility was the observation that treatment of a soluble wheat extract with pepsin caused a marked increase in OXO activity in the $^{14}CO_2$ release assay (Table 6). A similar large increase in OXO activity was achieved when untreated soluble wheat extracts were blotted on nitrocellulose (Table 6). Although still unproved, these results were consistent with the possible existence of a protein inhibitor of OXO in soluble wheat extracts.

Table 6 Effects of treatment with pepsin and/or blotting to nitrocellulose on the cryptic OXO activity present in a soluble extract of germinated (48 h) wheat embryos

For treatment with pepsin, soluble (S16) extracts (1.2 ml) were adjusted to pH 2 by adding approx. 0.16 ml of 1 M HCl and then mixed with approx. 0.16 ml of pig pepsin (0.5 mg/ml in 0.01 M HCl) and incubated at 37 °C for 90 min before being neutralized to pH 7.5 with approx. 0.08 ml of 2.5 M Tris [10]. The pepsin treatment destroyed most proteins in the extracts, except germin [9]. Treatment of the corresponding insoluble (P16) fraction of the homogenate with pepsin led to a comparable absolute increase in OXO activity but this constituted a relatively small (50–100%) proportional increase owing to a much higher activity in the insoluble (relative to the soluble) fraction before treatment with pepsin. Reproducible results were obtained consistently if extracts of different cultivars and batches of embryos were made by homogenization in 1.5–3 μl of S16 buffer/mg of fresh mass (Table 2), but results could be capricious with more dilute homogenates, e.g. homogenization in 20 μl of S16 buffer/mg of fresh mass.

	OXO activity (μg of oxalate degraded in 10 min)	
Fraction	In solution	Dot-blotted on nitrocellulose
Untreated soluble (S16)	0.2	56.7
Untreated insoluble (P16)	59.2	–
Adjusted to pH 2.0 and readjusted to pH 7.5	0.4	41.0
Adjusted to pH 2.0, incubated at 37 °C for 90 min without pepsin and readjusted to pH 7.5	0.4	48.6
Adjusted to pH 2.0, incubated at 37 °C for 90 min with pepsin and readjusted to pH 7.5	46.6	50.4

Table 7 Effects of preincubating soluble germin and germin-containing soluble cell extracts with soluble or particulate fractions of homogenates or cell-wall polysaccharides

Assays were performed at 20 °C after test solutions or suspensions (20 μl) had been incubated, separately or mixed, for 10 min at 20 °C, then added to buffered substrate solution. The S16 homogenizing buffer, polysaccharides and all soluble and insoluble fractions of homogenates of beet, wild-type canola and maize were virtually devoid of OXO activity For further details, see the Experimental section and the legend to Table 2.

Fractions	OXO activity (μg of oxalate degraded in 10 min)
Soluble fraction of a transgenic tobacco homogenate	3.5
+ Soluble fraction of a wheat homogenate	0.2
Soluble fraction of a transgenic canola homogenate	2.2
+ Soluble fraction of a wheat homogenate	0.1
Soluble germin (dialysed, salt-free)	42.5
+ S16 homogenizing buffer	38.2
+ Soluble fraction of a beet homogenate	55.7
+ Soluble fraction of a cold-sensitive maize homogenate	52.8
+ Soluble fraction of a wheat homogenate	7.3
Soluble fraction of a wheat homogenate (with pepsin)	37.1
+ Soluble fraction of a wheat homogenate (without pepsin)	0.3
Soluble fraction of a wheat homogenate	0.3
+ Soluble fraction of homogenate of a wild-type canola	0.2
+ Insoluble fraction of homogenate of a wild-type canola	42.9
+ hsGGAX (100 μg)	6.8
+ XG (100 μg)	0.4

'Mixing experiments' were done to determine whether the OXO activities of soluble extracts of transgenic dicotyledons might be inhibited by preincubating them with soluble wheat extract. As shown in Table 7, there were notable decreases in OXO activity if (1) a soluble extract of transgenic dicotyledons, (2) a pepsin-treated soluble extract of wheat or (3) germin itself was preincubated (10 min at room temperature) with soluble wheat (but not beet or maize) extract. Moreover, the existence of a cryptic germin activity was manifested when a soluble extract of wheat was preincubated with particulate fractions of wild-type rape (devoid of germin) or with some (hsGGAX) but not other (XG) types [43,44] of cell-wall polysaccharide (Table 7).

It is germane to note that failure to detect OXO activity by $^{14}CO_2$ release assay of crude extracts is distinct from failure to detect OXO activity by H_2O_2 release in solution assays of crude extracts. In the latter instance it is common for the assay not to detect the product of OXO action on oxalate (H_2O_2) because the H_2O_2 formed from oxalate is often, if not usually fully, degraded by peroxidases and catalases in crude cell extracts. Failure to detect OXO activity by the $^{14}CO_2$ release assay of crude extracts is, in contrast, a hitherto unknown process that is reversible either by pretreatment with proteases or with (cell-wall) polysaccharide-containing specimens.

It is worth mentioning that the putative inhibitor might be (1) diffusible (dialysable), (2) able to bind and repress the activity of a pepsin-susceptible activator of OXO activity (e.g. GGAX) or (3) a pepsin-susceptible oxygen-consuming activity that deprives the OXO enzyme of an essential reactant (oxygen) needed to oxidize oxalate (see also the Discussion section).

Germin is concentrated in surface structures when 'pre-isolated' wheat embryos are germinated

In the now classical system of Marcus [41], mature embryos, pre-isolated from dry, field-ripened wheat grains, undergo a triphasic uptake of water. First, rapid hydration (0–1 h) increases the water content of the embryos (from approx. 5% to approx. 65%) and more than doubles their mass. Secondly, there is a germination period (1–5 h) during which fresh mass does not change but notable changes occur in the translatable mRNA population. Finally, there is a resumption of water uptake (5–48 h) in singular association with the conspicuous nascent synthesis of germin and its mRNA [2,3]. This latter growth process increases the water content of the embryos (to approx. 85%) and increases their mass 3–4-fold [4] (Table 5). To obtain biochemical insight into the critical changes that occur in this system, in alliance with a surge of cell-wall germin activity (Table 2), the gross anatomical distribution of germin in the germinated embryos was determined.

For this purpose, thick sections of water-cultured embryos were immunostained with an anti-germin serum [13]. Sections were virtually transparent with preimmune serum, but with anti-germin serum there was, at 40 h after imbibition, differential staining of support tissues surrounding the embryo. Immunostaining of the envelope (coleorhiza) that surrounds the embryonic roots was particularly extensive in all sections (e.g. Figures 2A and 2B) but blue staining in the sheath (coleoptile) surrounding the embryonic leaves was extensive in some (Figure 2A) and superficial in other (Figure 2B) sections, and staining near the mesocotyl was strong in some (Figure 2B) but absent from other (Figure 2A) sections. Although the cause is unknown, non-specific staining of nuclei, observed with immune serum but not preimmune serum, was useful because it provided, without counterstaining, clear rust-coloured delineation of structures (nuclei) also observed when sections were counterstained with Nuclear Fast Red.

At higher magnification it was apparent that there was, in addition to non-specific staining of nuclei in the embryonic apex, primordial roots, leaves and mesocotyl (Figure 2), some weak (blue) staining in the cytoplasm of these non-vacuolated tissues (e.g. Figure 2C, a). The higher magnification emphasizes that there was much stronger, selective staining of vacuolated cells in the enveloping tissues that were adjacent to the apex (Figure 2C, b and c) and primordial roots (Figure 2C, d–f) in Figure 2(A). Immunostaining in the region of the mesocotyl (Figure 2B) was, at higher magnification (Figure 2C, g), comparable to the intense staining seen in enveloping tissues (Figure 2C, h) and also in superficial layers of the coleoptile (Figure 2C, i) of the same

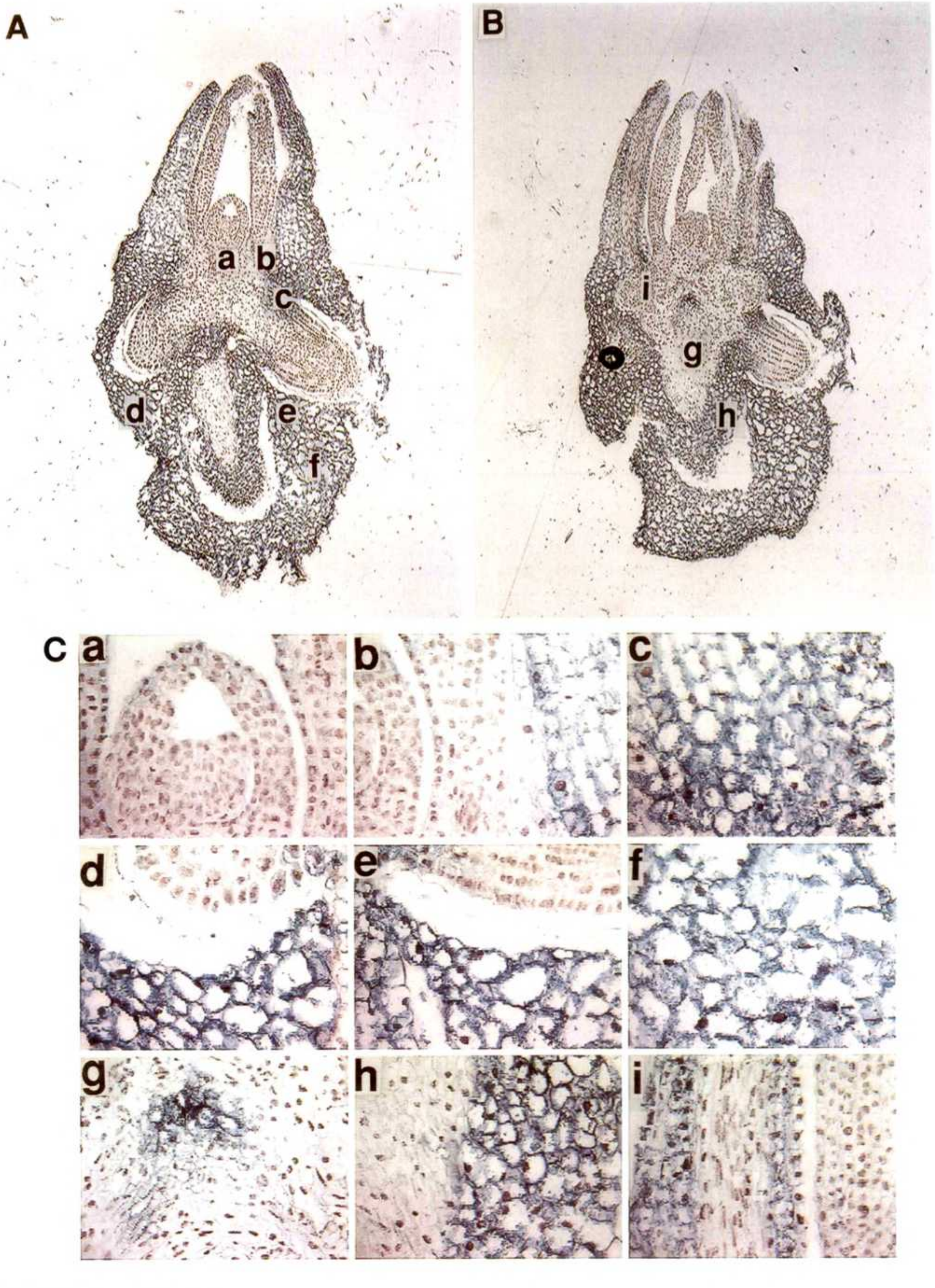

Figure 2 For legend see facing page.

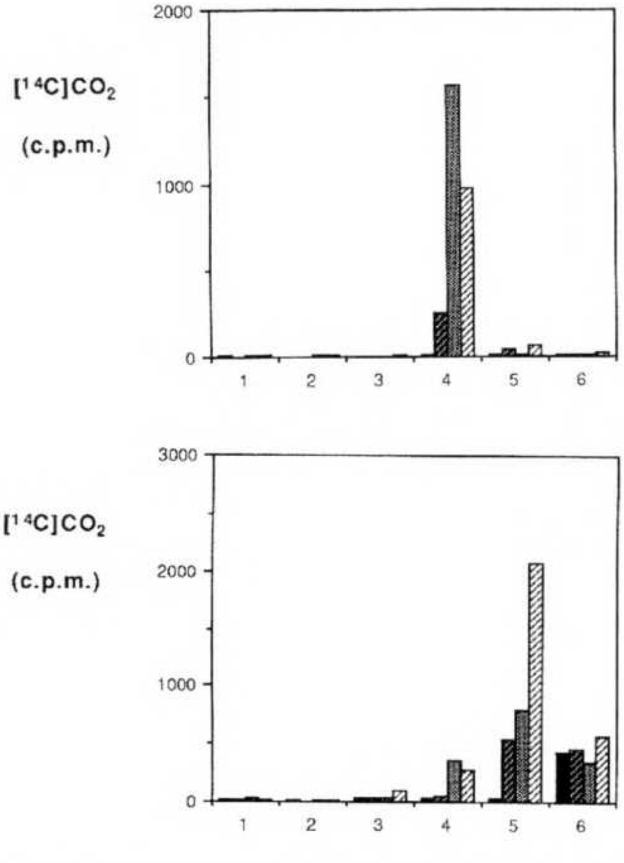

Figure 3 Temporal and spatial distributions of OXO activity in maturing wheat grains

The bar graphs show the relative release of $^{14}CO_2$ from [^{14}C]oxalate at 10 d.p.a. (black), 15 d.p.a. (dark hatching), 20 d.p.a. (stippling) and 25 d.p.a. (light hatching) when aliquots of homogenates of approx. 1 mg fresh mass of embryos, seedcoats, epidermes and bracts from developing wheat grains (cv. Vulcan) were assayed in solution/suspension [35]. Upper panel: soluble fractions of homogenates: 1, embryo; 2, endosperm; 3, seedcoat; 4, epidermis; 5, palea/lemma; 6, glumes. Lower panel: pellet fractions of homogenates: 1, embryo; 2, endosperm; 3, seedcoat; 4, epidermis; 5, palea/lemma; 6, glumes.

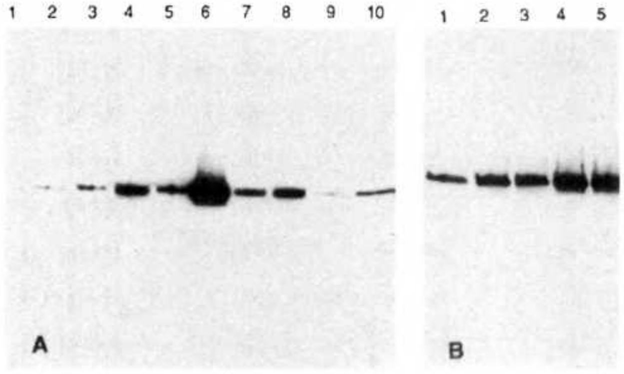

Figure 4 Temporal and spatial distributions of gl-OXO in selected parts of maturing wheat grains

'Activity' blots [5] are shown. Proteins in soluble (S16) fractions of homogenates from different parts (approx. 1 mg of fresh tissue) of developing wheat grains (cv. Vulcan) were separated by SDS/PAGE, electroblotted on nitrocellulose and assayed for gl-OXO activity [5]. (**A**) Lanes contain embryo proteins extracted at 10 (lane 1) and 20 (lane 2) d.p.a., seedcoat proteins extracted at 10 (lane 3) and 20 (lane 4) d.p.a., epidermis proteins extracted at 10 (lane 5) and 20 (lane 6) d.p.a., palea/lemma proteins extracted at 10 (lane 7) and 20 (lane 8) d.p.a. and glume proteins extracted at 10 (lane 9) and 20 (lane 10) d.p.a. (**B**) Lanes contain glume proteins extracted at 10 (lane 1), 15 (lane 2), 20 (lane 3), 25 (lane 4) and 30 (lane 5) d.p.a.

section. Neighbouring tracheid-like structures (arrowhead in Figure 2C, g) suggest that the selectively stained region near the mesocotyl might be a part of the scutellar node [45].

The dominant features of these immunostained sections of water-cultured mature wheat embryos at 48 h after imbibition were the differential immunostaining of germin in the vacuolated enveloping tissues (Figure 2C, h) and in terminally differentiated vascular tissue (Figure 2C, g). These thick sections revealed, primarily, tissue rather than subcellular distributions of germin, but there is little doubt that much of the total germin, as previously shown by electron-scanning microscopy [13], was allied with cell walls. At 10 h after imbibition, just before the onset of secondary uptake of water in concert with germin accumulation (results not shown), vacuolation was absent from the enveloping tissues of water-cultured mature embryos and there was only very weak (but still selective) immunostaining of the enveloping tissues (results not shown). Likewise, in immature [20–30 days post-anthesis (d.p.a.)] wheat embryos (results not shown) there was weak but selective immunostaining of enveloping tissues, comparable to that seen in the axial tissues of water-cultured mature embryos (Figure 2C, a).

OXO-ψ is concentrated in surface structures of the naturally maturing and mature wheat grain

The $^{14}CO_2$ release assays in Figure 3 illustrate the differential temporal accumulations of OXO-ψ that occurred in various parts of a developing wheat grain. Accumulations of soluble OXO-ψ in the epidermis (Figure 3, upper panel) and of insoluble OXO-ψ in the palea/lemma (Figure 3, lower panel) are most noteworthy. Limited availability, friability and tractability of structures enveloping the caryopsis dictated the preparation of relatively dilute extracts (i.e. 20 μl rather than 3 μl of buffer/mg of fresh mass).

Blot comparisons of release of H_2O_2 in Figure 4(A) illustrate the special character (stable to SDS/PAGE and blot transfer), temporal emergence and relative magnitudes of OXO activities

Figure 2 Germin is immunostained in thick sections of 'pre-isolated' germinated wheat embryos

(**A**) A longitudinal section of a water-cultured (40 h), mature wheat embryo was immunostained with an anti-germin rabbit serum as a source of primary antibodies, and alkaline-phosphatase conjugated goat anti-rabbit IgG as a source of secondary antibodies. A serial section from the same embryo was almost transparent when it was processed as described (see the Experimental section) with pre-immune serum in place of the anti-germin serum. The reason why all nuclei stained non-specifically is unknown. Lettering (a–f) is placed below areas shown at higher magnification in the nine-panel composite (**C**). Magn. × 37. (**B**) As in (**A**), but this longitudinal section contains a centrally located, immunostained structure that could be the scutellar node (above g). Lettering (g–i) is placed below areas that are shown at higher magnification in the nine-panel composite (**C**). Magn. × 37. (**C**) The lettered areas indicated in (**A**) and (**B**) are shown at higher magnification (× 184) The apex is shown in (**a**), and regions adjacent to the apex, including primary leaves and vacuolated enveloping tissue, are shown in (**b**) and (**c**). Primary root and adjacent enveloping tissue (coleorhiza) are shown in (**d**) and (**e**), and vacuolated enveloping tissue is again shown in (**f**). A region that might correspond to the scutellar node, with allied tracheids, is shown in (**g**), and the apposed tissues of the primary root and vacuolated envelope are shown in (**h**). The coleoptile and vacuolated enveloping tissue, possibly including the coleoptile epidermis, are shown next to primary leaf tissue in (**i**).

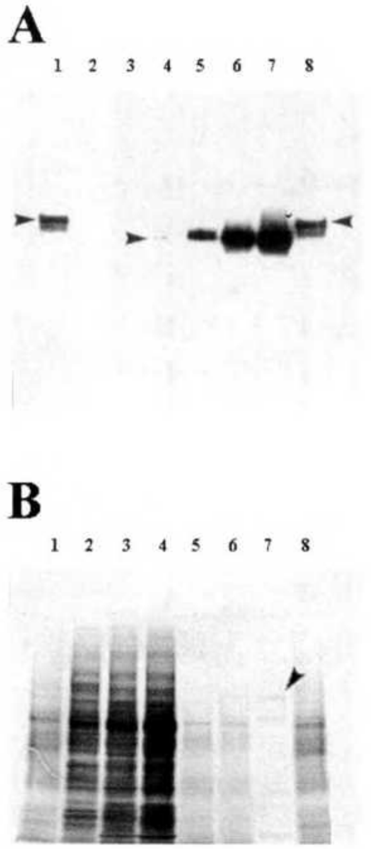

Figure 5 Comparison of gl-OXO activities and dye-stainable proteins in the embryos and epidermes of maturing wheat grains

(**A**) This shows an 'activity' blot [5]. Proteins in the soluble fractions of homogenates were prepared from approx. 1 mg of fresh tissue, separated by SDS/PAGE, electroblotted to nitrocellulose and assayed for gl-OXO activity [5]. The fresh tissues used for these analyses derived from the embryos and epidermes of developing wheat grains (cv. Cheyenne), and from the same 'pre-isolated' wheat embryos (cv. Neepawa) that had been germinated (40 h) and used for the histological studies of Figure 2. Lane 1, proteins from germinated (40 h after imbibition) wheat embryos; lane 2, proteins from developing (15 d.p.a.) wheat embryos; lane 3, proteins from developing (25 d.p.a.) wheat embryos; lane 4, proteins from developing (35 d.p.a.) wheat embryos; lane 5, proteins from developing (15 d.p.a.) wheat epidermes; lane 6, proteins from developing (25 d.p.a.) wheat epidermes; lane 7, proteins from developing (35 d.p.a.) wheat epidermes; lane 8, proteins from germinated (40 h after imbibition) wheat embryos. Arrowheads indicate the G glycoform of germin (molecular mass approx. 130 kDa) [61] in lanes 1 and 8, and OXO-ψ (molecular mass approx. 100 kDa) [67] in lane 4. (**B**) A dye-stained SDS/PAGE gel is shown. The samples analysed on this gel were identical with those on the gel that was used to obtain the activity blot in (**A**), but in (**B**) the gel was stained directly with Coomassie Blue without being blotted to nitrocellulose. Comparison of the corresponding lanes (1–8) in (**B**) with those in (**A**) illustrates the vast differences in protein content between the embryo and epidermis extracts that were assayed for gl-OXO activity in (**A**). The arrowhead indicates OXO-ψ in lane 7; i.e. OXO-ψ (molecular mass approx. 100 kDa) is visible by dye-staining and constitutes a considerable proportion of the total protein in epidermal extracts at 35 d.p.a.

in soluble extracts made from different parts of the caryopsis at 10 and 20 d.p.a. At all stages of development, the endosperm was virtually devoid of detectable OXO activity in either $^{14}CO_2$ release or H_2O_2 release assays (results not shown). The blot comparison in Figure 4(B) shows that, in spite of their toughness and resistance to disintegration, developing glumes yielded easily detected and increasing amounts of OXO in soluble extracts made between 10 and 30 d.p.a.

Further blot comparisons of H_2O_2 release (Figure 5) show the temporal emergence and relative magnitudes of OXO activities in the embryo and epidermis of the immature wheat caryopsis at 15, 25 and 35 d.p.a. Compatible with the results in Figure 3 for a more rapidly developing wheat cultivar was the observation that the soluble and insoluble fractions of homogenates of the epidermis had much greater activity than the corresponding embryo fractions at each time point (Figure 5A). Extracts applied to each gel slot in Figures 3–5 were derived from approx. 1 mg (fresh mass) of tissue. The replica dye-stained gel (Figure 5B) was not subjected to blot transfer and showed that embryo extracts contained vastly more protein than did extracts of epidermis, which tissue accumulates large amounts of 'pentosans' during this period of development [46].

The accumulation of OXO-ψ, in relation to total protein, was very much greater in the epidermis than in the embryo; it seems likely that this has a significant bearing on the profound physical change that occurred in the epidermis of this cultivar between 25 and 35 d.p.a. The epidermis of the pericarp had a pliable, rubbery consistency, similar to the peeled human-skin epidermis in appearance and texture, and it readily separated from underlying tissue at 25 d.p.a.; however, at 35 d.p.a. the epidermis had been transformed into a tough, horny layer that was difficult to separate from underlying tissue.

The OXO activities in extracts made from parts of the immature caryopsis, when assayed by $^{14}CO_2$ release from [^{14}C]oxalate or by H_2O_2 release in activity blots of SDS/PAGE gels, all had the same special properties, i.e. the OXO-ψ oligomer and its activity were both refractory to heating, diminishing only marginally after 1 min at 100 °C in aqueous SDS-containing solution [13]; however, the activity of germin was fully eradicated in less than 20 s.

DISCUSSION

Biological considerations

It is remarkable that the source of H_2O_2 used to form covalent cross-links in cell walls generally [47–49], and in the cell walls of seedcoats and pericarps in particular [50], remains unknown. The present study was initiated to address and perhaps redress some of this deficit in our understanding. Temporal and spatial correlation between the extensive vacuolation of, and the emergence of OXO enzymes in, root and leaf sheaths of the germinated embryo (germin) (Figure 2), and in epidermis and bracts of the maturing grain (OXO-ψ) (Figures 3 and 5), lend compelling support to the idea [3,33] that oxalate is a source of the H_2O_2 used to form cell-wall cross-links in the surface tissues of developing wheat.

The oxalate contents of cereals (0.1–0.2 μg/mg of fresh mass) (Table 5) correspond to mean concentrations of 1–2 mM in normally hydrated tissues. Without compartmentation of substrate and enzyme, it would be expected from the data in Table 5 that there would be rapid and complete oxidation of oxalate by germin. This could occur *in vivo* if, during the formation of the hard surface structures of ripened grains or during pathogen invasion, there were a collapse of cellular permeability barriers [51] and broad penetration of the OXO-containing extracellular matrix by oxygen and vacuolar [52] soluble oxalate at appropriately acidic pH values (see [3]). In this context, programmed cell death (apoptosis) is seen as a constitutive as well as an adaptive form of differentiation [53,54] or tissue remodelling. For example, OXO-ψ can decrease the toxic levels of oxalate secreted by predator organisms such as *Sclerotinia sclerotiorum* [55] and unlike the predator, which degrades oxalate without forming H_2O_2, OXO-ψ converts oxalate into H_2O_2, which is toxic to the predator and promotes the formation, in the host, of cross-linked wall barriers against predator penetration.

It was reported, on the basis of their superoxide dismutase and peroxidase activities, that hexaploid wheats are conspicuously deficient in their antioxidant capacities [56]. From the present study (Table 5), it seems that this 'antioxidant deficiency' of hexaploids might reflect elevated pro-oxidant capacity, to which the A and D diploid progenitors contribute most heavily (Table 3). Compatible with this is the observation that the *gf-2.8* OXO promoter occurs, minimally, in one or two, none or one, and three or four copies respectively in the A, B and D genomes, and maximally at 2–3-fold these frequencies [11]. There have been reports that oxalate might also have a role in creating pro-oxidant environments in animal cells. This seems unlikely in the case of neutrophils, in which reportedly elevated levels of oxalate [57] were probably due to a procedural artifact: the conversion of ascorbate into oxalate in blood specimens ([38,58], and B. G. Lane, unpublished work). In contrast, wheat products in the human diet could be a source of H_2O_2 in the gastrointestinal tract, where oxalate degradation ordinarily proceeds without H_2O_2 formation [59]. For example, wheat brans used to manufacture breakfast cereals are a rich source of OXO-ψ, and robust OXO-ψ-like activity has been found in several commercial products, including 'shredded wheat' (B. G. Lane, unpublished work). In view of its formidable stability, some of this OXO-ψ activity might survive in the gut and have as yet unknown but possibly significant consequences.

Molecular considerations

The stability of OXO-ψ is unusual, even for germins. Indeed, it is characteristic of the stability of enzymes in hyperthermophilic organisms [60]. Accordingly, pepsin digestion at pH 2 and extended periods (30 min) of boiling are steps used to isolate OXO-ψ from bulk, commercially accessible wheat bran and whole grains (B. G. Lane, unpublished work). It is of special interest to know what causes germin to lose its OXO activity completely after a few seconds in boiling water, whereas OXO-ψ, so closely related to germin antigenically and in its primary structure [13], is vastly more stable at 100 °C. Differences in quaternary structure and/or molecular mass (approx. 130 kDa for wheat germin; approx. 100 kDa for wheat OXO-ψ, by SDS/PAGE) might be important factors. Historically, these properties of the germins have presented knotty problems. On the basis of our comprehensive physicochemical studies, which first revealed extensive β-structure in germins, it had seemed that the 130 kDa wheat germin oligomer was homopentameric [61]; however, our subsequent X-ray diffraction study of barley germin (E. F. Pai and B. G. Lane, cited in [62]) clearly showed that the germin oligomer lacked a fivefold axis of symmetry and that it was likely to be a tetramer or hexamer, most probably a hexamer because a pentamer had been detected by cross-linking with dimethylsuberimidate [61]. This was confirmed by more complete X-ray diffraction study [63].

Transformation of oilseed rape by a full-length barley germin-coding element was first reported by Thompson et al. [64]. Transformations of dicotyledons (sunflower, tobacco, canola, soybean and potato) and a monocotyledon (maize), with a full-length wheat germin-coding element supplied by this laboratory, have also been achieved. Field trials, now under way to assess any improved host-resistance to microbial predators in the transgenics, have shown promise.

Study of the classical 'pre-isolated wheat-embryo system' [41,65] led to the discovery of germin [2,3] and later to the discovery of OXO-ψ [13] Growth in this system is 'unnatural'. Unlike 'natural' embryos, *in situ*, in wheat grains, which vigorously accumulate DNA (2-fold increase), protein (3-fold increase) and carbohydrate (5-fold increase) during the 48 h that follow the onset of germination, 'pre-isolated embryos', after their mass isolation from grains, accumulate no DNA or protein and only a modest amount of carbohydrate during the same period [66]. Growth in the 'pre-isolated wheat embryo' is due largely to water uptake. To account for a conspicuous correlation between the bulk of the water uptake in this system [65] and the nascent synthesis of germin, which was shown to be adventitiously associated with GGAX [13,67], it was proposed, after germin was found to be an OXO, that the co-transport of germin with GGAX from the Golgi network to cell walls might initiate vacuolation by enhancing wall plasticity and that, later, vacuolation might be terminated by germin-generated induction by H_2O_2 of cross-linking in cell walls [3].

The discovery that there is a concerted accumulation of OXO-ψ (this study) and 'pentosans' [46] in the maturing epidermis of the wheat grain has provided an unprecedented opportunity to study the relation between OXO accumulation and GGAX [44,67] in a natural environment, in which differentiation is allied with profound physical transformation, perhaps the H_2O_2-mediated hardening/lignification of surface structure. As we noted when the OXO activity of germins was discovered [5], the fact that peroxidases, with their reliance on H_2O_2, are a parameter of metabolic activity during growth alterations [68] gives testimony to the importance of H_2O_2 production during growth. This concept was recently well articulated [33] in the context of embryo growth during wheat germination. It is therefore tempting to speculate that hsGGAX-induced activation of OXO activity in the soluble fraction of wheat homogenates (Table 7) might reflect intimate linkage *in vivo* between H_2O_2 generation and peroxidatic activity. If, as suspected, GGAX is a natural target of the H_2O_2 generated by gl-OXO *in vivo*, perhaps in a coupled reaction sequence that involves the peroxidase-dependent cross-linking of GGAX to ferulate and hydroxycinnamate [43,44,69–71], then hsGGAX might be expected to have an idiosyncratic capacity to activate gl-OXO *in vitro*, and thereby, to contribute to order-of-magnitude variations in the OXO activities of different 'soluble' and 'insoluble' fractions of 'pre-isolated wheat embryos' (Tables 2, 5–7).

I am deeply grateful for the material assistance of many colleagues who provided or facilitated the procurement of several of the biological materials used in this study: Dr François Bernier (Institut Botanique, Université de Strasbourg, Strasbourg, France) in connection with *A thalania* seeds, Professor Nicholas Carpita (Department of Botany and Plant Pathology, Purdue University, West Lafayette, IN, U S A) in connection with specimens of hsGGAX and XG; Dr Bob Hamilton and Dr Chris Andrews (Agriculture Canada, Plant Research Centre, Ottawa, Canada) in connection with maize cultivars C0255 and C0286, Dr William Hurkman (Plant Research Center, USDA, Albany, CA, U S.A) in connection with A, B and D diploid wheats and maturing wheat stalks; Dr C S Pundir (Maharshi Dayanand University, India) in connection with sorghum grains; Dr Michel Schneider and Alain Toppan (Rustica Prograin Génétique, Mondonville, France) for seeds of transgenic (germin) tobacco and canola I gratefully acknowledge the long-term and generous financial support of these investigations by the Medical Research Council of Canada (grant MRC-MT-1226).

REFERENCES

1 Hodgkinson, A (1977) Oxalic Acid in Biology and Medicine, Academic Press, London

2 Thompson, E W and Lane, B G (1980) Relation of protein synthesis in imbibing wheat embryos to the cell-free tranlational capacities of bulk mRNA from dry and imbibing embryos J Biol Chem **255**, 5965–5970

3 Lane, B G (1994) Oxalate, germin, and the extracellular matrix of higher plants FASEB J **8**, 294–301

4 Lane, B G , Grzelczak, Z F , Kennedy, T D , Kajioka, R , Orr, J , D'Agostino, S and Jaikaran, A (1986) Germin: compartmentation of two forms of the protein by washing growing wheat embryos Biochem Cell Biol. **64**, 1025–1037

5 Lane, B. G., Dunwell, J M., Ray, J. A., Schmitt, M. R. and Cuming, A C (1993) Germin, a protein marker of early plant development, is an oxalate oxidase J Biol Chem **268**, 12239–12242

6 Dumas, B, Sailland, A, Cheviet, J.-P, Freyssinet, G and Pallett, K (1993) Identification of barley oxalate oxidase as a germin-like protein. C R Acad Sci. (Paris) **316**, 793–798

7 Franceschi, V R. and Loewus, F. A (1995) Oxalate biosynthesis and function in plants and fungi. In Calcium Oxalate in Biological Systems (Kahn, S R, ed.), pp 113–130, CRC Press, Boca Raton, FL

8 Grzelczak, Z F and Lane, B G (1983) The growth-related 28-kilodalton protein in germinating wheat Use of peptide mapping to identify cryptic forms in cell-free extracts and protein-synthesizing systems Can J Biochem. Cell Biol **61**, 1233–1243

9 Grzelczak, Z F and Lane, B G (1984) Signal resistance of a soluble protein to enzymic proteolysis An unorthodox approach to the isolation and purification of germin, a rare growth-related protein Can. J. Biochem Cell Biol **62**, 1351–1353

10 Grzelczak, Z F, Rahman, S, Kennedy, T D and Lane, B G. (1985) Germin. Compartmentation of the protein, its translatable mRNA, and its biosynthesis among roots, stems and leaves of wheat seedlings Can J. Biochem Cell Biol. **63**, 1003–1013

11 Lane, B G, Bernier, F, Dratewka-Kos, E, Shafai, R, Kennedy, T D, Pyne, C, Munro, J R, Vaughan, T, Walters, D and Altomare, F (1991) Homologies between members of the germin gene family in hexaploid wheat and similarities between these wheat germins and certain *Physarum* spherulins. J Biol Chem. **266**, 10461–10469

12 Hill, A F (1937) In Economic Botany, pp 309–333, McGraw-Hill, New York

13 Lane, B. G, Cuming, A. C, Fregeau, J., Carpita, N C., Hurkman, W J., Bernier, F, Dratewka-Kos, E and Kennedy, T D (1992) Germin isoforms are discrete temporal markers of wheat development. Pseudogermin is a uniquely thermostable water-soluble oligomeric protein in ungerminated embryos and like germin in germinated embryos, it is incorporated into cell walls Eur J Biochem **209**, 961–969

14 Requena, L and Bornemann, S (1999) Barley (*Hordeum vulgare*) oxalate oxidase is a manganese-containing enzyme Biochem. J. **343**, 185–190

15 Pundir, S. and Pundir, C S. (1993) Purification and properties of an oxalate oxidase from leaves of grain sorghum hybrid CSH-5 Biochim. Biophys. Acta **1161**, 1–5

16 Obzansky, D M and Richardson, K E (1983) Quantification of urinary oxalate with oxalate oxidase from beet stems Clin Chem **29**, 1815–1818

17 Baumlein, H, Braun, H, Kakhovskaya, I. A. and Shutov, A. D (1995) Seed storage proteins of spermatophytes share a common ancestor with desiccation proteins of fungi J. Mol Evol **41**, 1070–1075

18 Dunwell, J M and Gane, P J (1998) Microbial relatives of seed storage proteins: Conservation of motifs in a functionally diverse superfamily of enzymes J Mol. Evol **46**, 147–154

19 Dunwell, J M. (1998) Cupins: a new superfamily of functionally diverse proteins that include germins and plant storage proteins Biotechnol Genet Eng Rev **15**, 1–32

20 Yamahara, T, Shiono, T, Suzuki, T, Tanaka, K, Takio, S., Sato, K, Yamazaki, S and Satoh, T (1999) Isolation of a germin-like protein with managanese superoxide dismutase activity from cells of a moss, *Barbula unguiculata*. J. Biol Chem. **274**, 33274–33278

21 Domon, J-M, Dumas, B., Laine, E, Meyer, Y, David, A and David, H (1995) Three glycosylated polypeptides secreted by several embryogenic cell cultures of pine show highly specific serological affinity to antibodies directed against the wheat germin apoprotein monomer Plant Physiol **108**, 141–148

22 Michalowski, C. B. and Bohnert, H. J. (1992) Nucleotide sequence of a root-specific transcript encoding a germin-like protein from the halophyte *Mesembryanthemum crystallinum* Plant Physiol **100**, 537–538

23 Hofte, H, Desprez, T., Amselem, J, Chiapello, H, Caboche, M, Moisan, A, Jouron, M F, Charpenteau, J L, Berthomieu, P., Guerrier, D. et al. (1993) An inventory of 1152 expressed sequence tags obtained by partial sequencing of cDNAs from *Arabidopsis thaliana* Plant J **4**, 1051–1061

24 Delseny, M, Gaubier, P, Hull, G, Saez-Vasquez, J, Gallois, P, Raynal, M, Cooke, R and Grelle, F. (1994) Nuclear genes expressed during seed desiccation: relationship with responses to stress. In Induced Gene Expression (Basra, AS, ed), pp 25–59, Harwood Academic Publishers, Reading

25 Heintzen, C, Fischer, R, Melzer, S, Kappeler, S, Apel, K. and Staiger, D (1994) Circadian oscillations of a transcript encoding a germin-like protein that is associated with cell walls in young leaves of the long-day plant *Sinapsis alba* L (1994) Plant Physiol. **106**, 905–915

26 Membre, N, Berna, A, Neutelings, G., David, A, David, H., Staiger, D, Vasquez, J S, Raynal, M, Delseney, M and Bernier, F (1997) cDNA sequence, genomic organization and differential expression of three *Arabidopsis* genes for germin/oxalate-oxidase-like proteins. Plant Mol Biol **35**, 459–469

27 Carter, C, Graham, R. A and Thornburg, R. W. (1998) *Arabidopsis thaliana* contains a large family of germin-like proteins characterization of cDNA and genomic sequences encoding 12 unique family members Plant Mol Biol **38**, 929–943

28 Kohl, F. G (1889) Anatomisch–physiologische Untersuchung der Kalksalze und Kieselsaure in der Pflanze, N G. Elwert'sche Verlagsbuchhandlung, Marburg

29 Bloch, R (1935) Wound healing in *Tradescantia fulminensis* Vell Ann Bot **49**, 651–670

30 Zhang, Z, Collinge, D B and Thordal-Christensen, H (1995) Germin-like oxalate oxidase, hydrogen peroxide-producing enzyme, accumulates in barley attacked by the powdery mildew fungus Plant J. **8**, 139–145

31 Dumas, B, Freyssinet, G. and Pallett, K E (1995) Tissue-specific expression of germin-like oxalate oxidase during development and fungal infection of barley seedlings Plant Physiol **107**, 1091–1096

32 Hurkman, W. J. and Tanaka, C K (1996) Germin gene expression is induced in wheat leaves by powdery mildew infection Plant Physiol **111**, 735–739

33 Caliskan, M and Cuming, A C. (1998) Spatial specificity of H_2O_2-generating oxalate oxidase gene expression during wheat embryo germination. Plant J **16**, 165–171

34 Johnston, F. B. and Stern, H (1957) Mass isolation of viable wheat embryos Nature (London) **179**, 160–161

35 Chiriboga, J (1966) Purification and properties of oxalic acid oxidase Arch. Biochem Biophys **116**, 516–523

36 Kennedy, T D., Hanley-Bowdoin, L K and Lane, B G. (1981) Structural integrity of RNA and transcriptional integrity of ribosomes in nuclease-treated cell-free protein synthesizing systems prepared from wheat germ and rabbit reticulocytes. J. Biol Chem. **256**, 5802–5809

37 Sugiura, M, Yamamura, H, Hirano, K, Sasaki, M, Morikawa, M and Tsuboi, M (1979) Purification and properties of oxalate oxidase from barley seedlings. Chem Pharm. Bull. **27**, 2003–2007

38 Hallson, P C. and Rose, G A (1991) Observations on the breakdown of ascorbate to oxalate and carbon dioxide Clin. Chem Enzymol. Commun **3**, 329–340

39 Zarembski, P. M and Hodgkinson, A (1965) The fluorometric determination of oxalic acid in blood and other biological materials Biochem. J. **96**, 717–721

40 Libert, B. and Franceschi, V R (1987) Oxalate in crop plants J Agr. Food Chem. **35**, 926–938

41 Marcus, A (1969) Seed germination and the capacity for protein synthesis Symp Soc Exp Biol **23**, 143–160

42 Rahman, S, Grzelczak, Z F, Kennedy, T. D and Lane, B G (1988) Germin Molecular cloning of cDNA that selects germin mRNA from bulk wheat mRNA Biochem Cell Biol **66**, 100–106

43 Gibeaut, D M. and Carpita, N. C (1991) Tracing cell wall biogenesis in intact cells and plants. Plant Physiol **97**, 551–561

44 Carpita, N C (1993) Structural models of primary cell walls in flowering plants: consistency of primary structure with the physical properties of the walls during growth Plant J. **3**, 1–30

45 Swift, J. G and O'Brien, T P. (1972) The fine structure of the wheat scutellum during germination Aust J Biol. Sci. **25**, 469–486

46 Jennings, A C and Morton, R. K (1963) Changes in carbohydrate, protein and non-protein nitrogenous compounds of developing wheat grain Aust J Biol Sci. **16**, 318–331

47 Fry, S C (1986) Cross-linking of matrix polymers in the growing cell walls of angiosperms Annu Rev Plant Physiol **37**, 165–186

48 Iiyama, K., Lam, T B-T. and Stone, B A (1994) Covalent cross-links in the cell wall Plant Physiol **104**, 315–320

49 Richardson, A, Stewart, D and McDougall, G J (1997) Identification and partial characterization of a coniferyl alcohol oxidase from lignifying xylem of Sitka spruce (*Picea sitchensis*) Planta **203**, 35–43

50 Graven, P, De Koster, C. G, Boon, J J and Bouman, F (1996) Structure and macromolecular composition of seed coat of the the Musaceae Ann Bot **77**, 105–122

51 Wheeler, H and Hanchey, P (1968) Permeability phenomena in plant disease Annu. Rev. Phytopathol. **6**, 331–350

52 Wagner, G J (1981) Vacuolar deposition of ascorbate-derived oxalic acid in barley Plant Physiol. **67**, 591–593

53 Greenberg, J. T, Guo, A, Klessig, D F and Ausubel, F M (1994) A pathogen-triggered response activated coordinately with multiple defense functions. Cell **77**, 551–563

54 Dietrich, R A Delaney, T P, Uknes, S. J, Ward, E R., Ryals, J A and Dangl, J L (1994) *Arabidopsis* mutants simulating disease resistance response. Cell **77**, 565–577

55 Godoy, G, Steadman, J R, Dickman, M B and Dam, R (1990) Use of mutants to demonstrate the role of oxalic acid in pathogenicity of *Sclerotinia sclerotiorum* on *Phaseolus vulgaris* Physiol Mol Plant Path **37**, 179–191

56 Zhang, J and Kirkham, M. B. (1994) Drought-stress-induced changes in activities in superoxide dismutase, catalase, and peroxidase in wheat species Plant Cell Physiol **35**, 785–791

57 Albrecht, S, Brandl, H and Schonfels, C. (1994) Human oxalate – really just an end product of metabolism? Angew Chem Int Ed Engl **33**, 1780–1781

58 Hatch, M. (1990) Spectrophotometric determination of oxalate in whole blood. Clin Chim. Acta **193**, 199–202

59 Allison, M J, Daniel, S L and Cornick, N. A. (1995) Oxalate degrading bacteria In Calcium Oxalate in Biological Systems (Kahn, S R, ed.), pp. 107–168, CRC Press, Boca Raton, FL

60 Klump, H, Di Ruggiero, J, Kessel, M, Park, J-B, Adams, M. W. W and Robb, F T (1992) Glutamate dehydrogenase from the hyperthermophile *Pyrococcus furiosus* Thermal denaturation and activation. J. Biol Chem **267**, 22681–22685

61 McCubbin, W C, Kay, C M., Kennedy, T. D. and Lane, B G (1987) Germin. physicochemical properties of the glycoprotein which signals onset of growth in the germinating wheat embryo Biochem Cell Biol **65**, 1039–1048

62 Gane, P J, Dunwell, J. M and Warwicker, J (1998) Modeling based on the structure of vicilins predicts a histidine cluster in the active site of oxalate oxidase J Mol Evol **46**, 488–493

63 Woo, E-J, Dunwell, J M, Goodenough, P. W. and Pickersgill, R. W. (1998) Barley oxalate oxidase is a hexameric protein related to seed storage proteins: evidence from X-ray crystallography FEBS Lett **437**, 87–90

64 Thompson, C., Dunwell, J M, Johnstone, C. E, Lay, V., Ray, J, Schmitt, M, Watson, H and Nisbet, G. (1995) Euphytica **85**, 169–172

65 Lane, B G (1991) Cellular desiccation and hydration developmentally regulated proteins, and the maturation and germination of seed embryos. FASEB J **5**, 2893–2901

66 Lane, B G (1988) The wheat embryo, then and now In The Roots of Modern Biochemistry Energetics of the Cell: Fritz Lipmann's Squiggle and its Consequences (Kleinkauf, H, von Dohren, H. and Jaenicke, L., eds), pp. 457–476, Walter de Gruyter, Berlin

67 Jaikaran, A S I, Kennedy, T D, Dratewka-Kos, E and Lane, B G (1990) Covalently bonded and adventitious glycans in germin J Biol Chem. **265**, 12503–12512

68 van Huystee, R B. and Cairns, W L (1980) Appraisal of studies of peroxidase and associated porphyrin metabolism. Bot Rev **46**, 429–446

69 Markwalder, H U and Neukom, H. (1976) Diferulic acid as a possible crosslink in hemicelluloses from wheat germ. Phytochemistry **15**, 836–837

70 Scalbert, A, Monties, B, Lallemand, J.-Y, Guittet, L L and Rolando, C (1985) Ether linkage between phenolic acids and lignin fractions from wheat straw Phytochemistry **24**, 1359–1362

71 Zimmerlin, A, Wojtaszek, P and Bolwell, G P (1994) Synthesis of polymers of ferulic acid with high specificity by a purified cell-wall peroxidase from French bean (*Phaseolus vulgaris* L) Biochem. J. **299**, 747–753

Received 4 February 2000/22 March 2000, accepted 13 April 2000

Biochem J (2000) 349, 323–332 (Printed in Great Britain)

Ca^{2+} signals mediated by Ins(1,4,5)P_3-gated channels in rat ureteric myocytes

François-Xavier BOITTIN, Frédéric COUSSIN, Jean-Luc MOREL, Guillaume HALET, Nathalie MACREZ and Jean MIRONNEAU[1]

Laboratoire de Physiologie Cellulaire et Pharmacologie Moléculaire, CNRS UMR 5017, Université de Bordeaux II, 146 rue Léo Saignat, 33076 Bordeaux Cedex, France

Localized Ca^{2+}-release signals (puffs) and propagated Ca^{2+} waves were characterized in rat ureteric myocytes by confocal microscopy. Ca^{2+} puffs were evoked by photorelease of low concentrations of Ins(1,4,5)P_3 from a caged precursor and by low concentrations of acetylcholine; they were also observed spontaneously in Ca^{2+}-overloaded myocytes. Ca^{2+} puffs showed some variability in amplitude, time course and spatial spread, suggesting that Ins(1,4,5)P_3-gated channels exist in clusters containing variable numbers of channels and that within these clusters a variable number of channels can be recruited. Immunodetection of Ins(1,4,5)P_3 receptors revealed the existence of several spots of fluorescence in the confocal cell sections, supporting the existence of clusters of Ins(1,4,5)P_3 receptors. Strong Ins(1,4,5)P_3 photorelease and high concentrations of acetylcholine induced Ca^{2+} waves that originated from an initiation site and propagated in the whole cell by spatial recruitment of neighbouring Ca^{2+}-release sites. Both Ca^{2+} puffs and Ca^{2+} waves were blocked selectively by intracellular applications of heparin and an anti-Ins(1,4,5)P_3-receptor antibody, but were unaffected by ryanodine and intracellular application of an anti-ryanodine receptor antibody. mRNAs encoding for the three subtypes of Ins(1,4,5)P_3 receptor and subtype 3 of ryanodine receptor were detected in these myocytes, and the maximal binding capacity of [^{3}H]Ins(1,4,5)P_3 was 10- to 12-fold higher than that of [^{3}H]-ryanodine. These results suggest that Ins(1,4,5)P_3-gated channels mediate a continuum of Ca^{2+} signalling in smooth-muscle cells expressing a high level of Ins(1,4,5)P_3 receptors and no subtypes 1 and 2 of ryanodine receptors.

Key words: calcium puff, calcium-release channel, confocal microscopy, sarcoplasmic reticulum, smooth muscle.

INTRODUCTION

The release of Ca^{2+} ions from the intracellular stores into the cytosol plays a central role in the control of many cellular activities in excitable and non-excitable cells. Ins(1,4,5)P_3 receptors and ryanodine receptors represent the two major types of intracellular Ca^{2+}-release channels, and share some functional similarities. Global Ca^{2+} signals in intact cells have been reported to be due to the co-ordinated recruitment of 'elementary' Ca^{2+}-release units [1,2], inducing either Ca^{2+} sparks when the units contain mainly ryanodine receptors, i.e. in cardiac and vascular myocytes [3–5], or Ca^{2+}-release signals, or 'puffs', when the units contain mainly Ins(1,4,5)P_3 receptors, i.e. in *Xenopus* oocytes and HeLa cells [6,7]. Elementary Ca^{2+} events are spatially localized, short transient signals that dissipate rapidly due to diffusion of Ca^{2+} into the cytoplasm and sequestration into the intracellular stores.

In smooth muscles, it is believed generally that Ca^{2+} release from the intracellular store can be generated by Ins(1,4,5)P_3 and ryanodine receptors [8]. In rat portal-vein myocytes, there are indications that these two Ca^{2+}-release channels are co-localized on the same intracellular store [9]. In these myocytes, ryanodine receptors are highly expressed and organized in clustered units, so that they can generate Ca^{2+} sparks. In contrast, Ins(1,4,5)P_3 receptors are not organized in clustered units and Ins(1,4,5)P_3-evoked Ca^{2+} puffs have not been observed in portal-vein myocytes [9]. Up to now, Ca^{2+} puffs activated by Ins(1,4,5)P_3 have never been reported in any smooth muscle. On the basis of contraction and cytosolic Ca^{2+} measurements, it has been suggested recently that rat ureter myocytes may possess only an Ins(1,4,5)P_3-sensitive Ca^{2+} store [10,11] and may therefore represent a good model with which to study the hierarchy of Ca^{2+} signals evoked by Ins(1,4,5)P_3-gated channels.

The present study identifies for the first time in smooth-muscle cells Ca^{2+} puffs evoked by activation of clusters of Ins(1,4,5)P_3-gated channels in response to photorelease of Ins(1,4,5)P_3 and application of low doses of acetylcholine. Ca^{2+} puffs can be observed spontaneously in Ca^{2+}-overloaded myocytes. The Ca^{2+} puffs display some variability in size, time course and spatial spread. Increasing concentrations of Ins(1,4,5)P_3 and acetylcholine induce a spatial recruitment of localized Ca^{2+} signals leading to propagated Ca^{2+} waves. The functional experiments are supported by immunodetection of Ins(1,4,5)P_3 receptors, showing the existence of several spots of fluorescence in confocal cell sections, and by binding data indicating that the density of Ins(1,4,5)P_3 receptors is 10–12-fold higher than that of ryanodine receptors in these myocytes. These results suggest that in visceral smooth-muscle cells expressing a high level of Ins(1,4,5)P_3 receptors and no subtypes 1 and 2 of ryanodine receptors, a continuum of Ins(1,4,5)P_3-gated channel-mediating Ca^{2+} signalling can be detected.

EXPERIMENTAL PROCEDURES

Cell preparation, solutions and membrane-current recordings

Wistar rats (150–160 g) were stunned and killed by cervical dislocation. Ureters were removed quickly, cut into several pieces and incubated for 10 min in low-calcium (40 μM) physiological

---

Abbreviations used: AM, acetoxymethyl ester, $[Ca^{2+}]_i$, cytoplasmic calcium concentration, $[Ca^{2+}]_o$, external calcium concentration, FWHM, full width at half-maximal amplitude; Fluo-3, 1-[2-amino-5-(2,7-dichloro-6-hydroxy-3-oxo-3*H*-xanthen-9-yl)]-2-(2′-amino-5′-methylphenoxy)ethane-*N*,*N*,*N*′,*N*′-tetra-acetic acid penta-ammonium, Indo-1, 1-[2-amino-5-(6-carboxyindol-2-yl)phenoxy]-2-(2′-amino-5′-methylphenoxy)ethane-*N*,*N*,*N*′,*N*′-tetra-acetic acid pentasodium

[1] To whom correspondence should be addressed (e-mail jean.mironneau@umr5017.u-bordeaux2.fr)

solution; then 0.8 mg/ml collagenase, 0.25 mg/ml Pronase E and 1 mg/ml BSA were added at 37 °C for 15 min. After this time, the solution was removed and the ureter pieces were incubated again in a fresh enzyme solution at 37 °C for 15 min. Tissues were then placed in enzyme-free solution and triturated using a fire-polished Pasteur pipette to release cells. Cells were stored on glass coverslips and used within 10 h. Portal-vein myocytes were obtained as described previously [5,9].

The normal physiological solution used contained 130 mM NaCl, 5.6 mM KCl, 1 mM $MgCl_2$, 1.7 mM $CaCl_2$, 11 mM glucose and 10 mM Hepes, pH 7.4. The basic pipette solution contained 130 mM CsCl, 10 mM Hepes and 60 μM Fluo-3 {1-[2-amino-5-(2,7-dichloro-6-hydroxy-3-oxo-3*H*-xanthen-9-yl)]-2-(2′-amino-5′-methylphenoxy)ethane-*N*,*N*,*N*′,*N*′-tetra-acetic acid penta-ammonium}, pH 7.3, with CsOH. Substances were applied externally by pressure ejection from a glass pipette for the periods indicated in the relevant Figure legends. All the experiments were performed at 28 ± 1 °C.

Voltage-clamp and membrane-current recordings were made with a standard patch-clamp technique using a List EPC-7 patch-clamp amplifier (List, Darmstadt-Eberstadt, Germany). Patch pipettes had resistances of 4–6 MΩ. Membrane potential and whole-cell membrane current were stored and analysed using an IBM-PC computer (P-clamp System, Axon Instruments, Foster City, CA, U.S.A.).

Confocal microscopy and fluorescence measurements

A Bio-Rad MRC 1000 (Bio-Rad, Paris, France) confocal scanning head was coupled to a Nikon Diaphot (Nikon, Tokyo, Japan) inverted microscope. In all experiments a Nikon Plan Apo ×60, 1.4 numerical aperture objective lens was used. The iris aperture was set to 40–50 % of maximum, providing an axial (*z*) resolution of about 1.5 μm and an *x*–*y* resolution of 0.4 μm. Illumination was provided by a 25-mW argon ion laser (Ion Laser Technology, Salt Lake City, UT, U.S.A.). The excitation wavelength (488 nm) was selected using interference filters and the emitted fluorescence was collected at wavelengths greater than 515 nm. For some experiments, Fluo-3 (60 μM) was dialysed into the cells through the patch-pipette, as reported previously [9]. The fluorescence beam was filtered and detected using a photomultiplier tube. For other experiments, cells were loaded by incubation in physiological solution containing 1 μM Fluo-3 acetoxymethyl ester (AM) for 1 h at room temperature. These cells were washed and allowed to cleave the dye to the active Fluo-3 compound for at least 1 h. To compensate for uneven distribution of the Fluo-3, self ratios were calculated ($R = F/F_{rest}$, where F is fluorescence and F_{rest} is resting-level fluorescence). Note that no change in fluorescence corresponds to $F/F_{rest} = 1$ and $\Delta F/F_{rest} = 0$. Image acquisition and data analysis were performed by using COMOS, TCSM and MPL-1000 software (Bio-Rad). Images were acquired in the line-scan mode of the confocal microscope; this mode repeatedly scanned a single line through the cell every 6 ms. Spatial average fluorescence can be measured (after filtering with a 3 × 3 rank filter) in the entire line-scan image or in a 2-μm region on the *x*-axis, illustrating temporal changes of $[Ca^{2+}]_i$, the cytoplasmic calcium concentration.

In some experiments, cells were loaded by incubation in physiological solution containing 1 μM Indo-1 {1-[2-amino-5-(6-carboxyindol-2-yl)phenoxy]-2-(2′-amino-5′-methylphenoxy)-ethane-*N*,*N*,*N*′,*N*′-tetra-acetic acid pentasodium}/AM for 30 min. Measurement of fluorescence to monitor $[Ca^{2+}]_i$ using Indo-1 has been reported previously [12].

Flash photolysis

Caged Ins(1,4,5)P_3 [Ins(1,4,5)P_3, $P^{4(5)}$-1-(2-nitrophenyl) ethyl ester] was introduced into the cell via the patch pipette, allowing 3–4 min for equilibration. Photolysis was produced by a 1-ms pulse from a xenon flash lamp (Hi-Tech Scientific, Salisbury, Wilts., U.K.) focused to a spot of about 2 mm in diameter around the cell. Light was band-pass filtered with a UG11 glass between 300 and 350 nm. Flash intensity could be adjusted by varying the capacitor charging voltage between 0 and 385 V, which corresponded to a change in the energy input into the flash lamp from 0 to 240 J. Upon flash photolysis, Ins(1,4,5)P_3 was released within 2 ms. A small percentage of conversion of caged compounds (about 10 %) was useful if repetitive pulses were applied in order to obtain similar responses. Flash intensities up to 60 J could be applied repetitively without altering the reserve of caged Ins(1,4,5)P_3 (20 μM) and, consequently, the amount of photoreleased compounds.

Immunocytochemistry

Myocytes were immunostained as described previously [13], except that donkey serum was used instead of fetal calf serum. Myocytes were incubated in the presence of anti-Ins(1,4,5)P_3 receptor antibodies (at 1:200 dilution) for 20 h at 4 °C, and the secondary antibodies (donkey anti-rabbit IgG conjugated to FITC, diluted 1:200) were incubated for 3 h at 20 °C. Thereafter, cells were mounted in Vectashield.

Microsomal-membrane preparation

Microsomal membranes of ureter and cerebellum from Wistar rats were prepared by homogenization with a Kontes potter in a solution containing 20 mM Tris/HCl, 1 mM EGTA and 1 mM PMSF, pH 7.4. The homogenate was centrifuged at 170 *g* for 10 min at 4 °C. Microsomal membranes were obtained as a pellet by centrifugation of the supernatant at 185000 *g* for 90 min at 4 °C. Microsomal membranes were then resuspended in the buffer and stored at −80 °C. Protein concentration was determined according to Bradford [14].

Immunoblotting

For Western-blotting analysis, microsomal proteins were separated on SDS/PAGE (7.5 %) minigels and transferred to PVDF membranes for 16 h at 30 V in a transfer buffer containing 192 mM glycine and 25 mM Tris/HCl (pH 8.3). Membranes were blocked for 1 h in blocking buffer containing 20 mM Tris/HCl and 3 % BSA (pH 7.4) and then incubated for 5 h at room temperature with the primary anti-Ins(1,4,5)P_3 receptor antibody at 1:200 dilution. After extensive washing, membranes were incubated for 2 h with the secondary antibody coupled to horseradish peroxidase (anti-rabbit, 1:5000 dilution). Specific antigen detection was performed using H_2O_2 and diaminobenzidine to detect horseradish peroxidase activity on PVDF membranes and Kodak EDAS 120 (Kodak, Rochester, NY, U.S.A.).

[^{3}H]Ryanodine- and [^{3}H]Ins(1,4,5)P_3-binding assays

[^{3}H]Ryanodine binding to microsomal membranes of rat ureters was measured, as reported previously on rat portal vein [15], in a medium containing 1 M KCl, 25 mM Hepes (pH 7.8 at 37 °C), 1 mM dithiothreitol, 0.1 mM $CaCl_2$, 1 mg/ml BSA and 0.1 mM PMSF. [^{3}H]Ryanodine was used in the concentration range of

2–30 nM. After a 3-h incubation at 37 °C, aliquots were filtered through Whatmann GF/C fibre-glass filters and washed three times with 5 ml of ice-cold binding buffer. The filters were placed in scintillation vials filled with 4 ml of liquid-scintillation cocktail, shaken for 1 h, and counted in a Packard 1500 Tri-Carb. Non-specific binding was measured in the presence of 10 μM ryanodine and was subtracted before calculation. At 20 nM [^{3}H]ryanodine, non-specific binding was < 60 % of total binding.

[^{3}H]Ins(1,4,5)P_3 binding was measured in a medium containing 0.1 M KCl, 50 mM Tris/HCl (pH 8.3 at 2–4 °C) and 1 mM EGTA. [^{3}H]Ins(1,4,5)P_3 was used in the concentration range of 2–200 nM. After a 10-min incubation on ice, binding reactions were terminated by centrifugation (15000 g, 15 min, 4 °C). The supernatant was aspirated and the pellet was rinsed quickly with 0.2 ml of ice-cold binding buffer. Pellets were solubilized with 0.1 ml of Soluene-100 (55 °C, 30 min). After transfer into scintillation vials with 4 ml of liquid-scintillation cocktail, radioactivity was counted in a Packard 1500 Tri-Carb. Non-specific binding was measured in the presence of a 1000-fold excess of Ins(1,4,5)P_3 over [^{3}H]Ins(1,4,5)P_3 concentration. At 100 nM [^{3}H]Ins(1,4,5)P_3, non-specific binding was < 55 % of total binding.

Maximal binding capacity (B_{max}) and dissociation constant (K_d) were obtained from saturation binding experiments.

Reverse transcriptase PCR

Total RNA was extracted from about 500 cells using the RNeasy mini kit (Qiagen, Hilden, Germany). The reverse-transcription reaction was performed using the Sensiscript RT kit (Qiagen). Total RNA was incubated first with random primers (Promega, Lyon, France) at 65 °C for 5 min, then, after a cooling time of 15 min (at 25 °C), reverse transcriptase mix was added and the total mixture was incubated 60 min at 37 °C. The resulting cDNA was stored at −20 °C. PCR was performed with 2 μl of cDNA (in reverse transcriptase PCR mix), 1.25 units of HotStart *Taq* DNA polymerase (Qiagen), 1 μM of each primer and 200 μM of each deoxynucleotide triphosphate, in a final volume of 50 μl. The solution was supplemented with 2.5 mM MgCl$_2$, except for subtype 1 of Ins(1,4,5)P_3 receptors. The PCR conditions were 95 °C for 15 min, then 35 cycles at 94 °C for 1 min, 60 °C (subtypes 1 and 2 of ryanodine receptors and all subtypes of Ins(1,4,5)P_3 receptors) or 56 °C (subtype 3 of ryanodine receptor) for 1 min and 72 °C for 1.5 min and at the end of PCR, samples were kept at 72 °C for 10 min for final extension and then stored at 4 °C. Reverse transcription and PCR were performed with a thermal cycler (Techne, Cambridge, U.K.). Amplification products were separated by electrophoresis (2 % agarose gel) and vizualized by ethidium bromide staining. Gels were photographed with EDAS 120 and analysed with KDS 1D 2.0 software (Kodak Digital Science, Paris, France). Sense and antisense primer pairs used to amplify fragments of subtypes 1, 2 and 3 of Ins(1,4,5)P_3 and ryanodine receptors were designed on the basis of the known cloned receptor sequences deposited in GenBank (accession numbers J05510, X61677, L06096, X83932, X83933 and X83934, respectively) with DNASTAR software (Lasergene, DNAstar, Madison, WI, U.S.A.). The nucleotide sequences and the lengths of the expected PCR products (in parentheses) for each primer pair were as follows. Subtype 1 of Ins(1,4,5)P_3 receptor, sense, 5′-ACTGGAAGACCATAAAAGGGGTGA-3′, and antisense, 5′-TCCGTCAGCCGGCAGAAAAATGAG-3′ (368 bp); subtype 2 of Ins(1,4,5)P_3 receptor, sense, 5′-GGCACAGCCTCTCCATGTGGCAGG-3′, and antisense, 5′-TTCCTGTCTCGCTGACCCCAGTGC-3′ (197 bp); subtype 3 of Ins(1,4,5)P_3 receptor, sense, 5′-CACGGAGCTGCCACATTTATGGGC-3′, and antisense, 5′-TCCTCAGTCCGTGGTTCATGACGG-3′ (168 bp) [16]; subtype 1 of ryanodine receptor, sense, 5′-GAAGGTTCTGGACAAACACGGG-3′, and antisense, 5′-TCGCTCTTGTTGTAGAATTTGCGG-3′ (435 bp); subtype 2 of ryanodine receptor, sense, 5′-GAATCAGTGAGTTACTGGGCATGG-3′, and antisense, 5′-CTGGTCTCTGAGTTCTCCAAAAGC-3′ (635 bp); subtype 3 of ryanodine receptor, sense, 5′-CCTTCGCTATCAACTTCATCCTGC-3′, and antisense, 5′-TCTTCTACTGGGCTAAAGTCAAGG-3′ (505 bp) [17].

Chemicals and drugs

Collagenase was obtained from Worthington (Freehold, NJ, U.S.A.); Pronase E, BSA, acetylcholine, heparin and Ins(1,4,5)P_3 were from Sigma (St Louis, MO, U.S.A.). Ryanodine, Indo-1/AM and caged Ins(1,4,5)P_3 [Ins(1,4,5)P_3, $P^{4(5)}$-1-(2-nitrophenyl)ethyl ester] were from Calbiochem (Meudon, France) Caffeine was from Merck (Nogent sur Marne, France). Fluo-3 and Fluo-3/AM were from Molecular Probes Europe (Leiden, The Netherlands). Oxodipine was a gift from Dr Galiano (Instituto de Investigacion y Desarrollo Quimico Biologico, Madrid, Spain). [^{3}H]Ryanodine (68 Ci/mmol) and [^{3}H]Ins(1,4,5)P_3 (20 Ci/mmol) were from DuPont NEN (Boston, MA, U.S.A.). Primers specific for Ins(1,4,5)P_3 and ryanodine receptors were synthesized by Eurogentec (Seraing, Belgium).

Antibodies directed against Ins(1,4,5)P_3 and ryanodine receptors were added to the pipette solution to allow dialysis of the cell after a breakthrough in whole-cell recording mode for at least 5–8 min, a time longer than that expected theoretically for diffusion of substances in solutions [18]. The rabbit anti-Ins(1,4,5)P_3-receptor antibody was raised to the C-terminal amino acids (GGVGDVLRKPS) of the Ins(1,4,5)P_3 receptors (407143-S, Calbiochem). The mouse anti-(ryanodine receptor) antibody was raised to the C-terminal amino acids (DQQEQVKEDMETK) of the ryanodine receptor (559279-S, Calbiochem). For immunological detection, FITC-conjugated affinity-pure donkey anti-rabbit IgG and donkey serum were from Jackson Immunoresearch Laboratories (West Grove, PA, U.S.A.) and Vectashield was from Biosys (Compiègne, France).

Analysis of data

The results are expressed as means ± S.E.M. Significance was tested by means of Student's t test. P values of < 0.05 were considered significant.

RESULTS

Expression of Ins(1,4,5)P_3 and ryanodine receptors in rat ureteric myocytes

The expression of Ins(1,4,5)P_3- and ryanodine-receptor subtypes was examined by using subtype-specific primers designed to amplify cDNA fragments of subtypes 1, 2 and 3 of these receptors in rat ureter and cerebellum. Amplified fragments of all three Ins(1,4,5)P_3-receptor subtypes were observed (Figure 1A), indicating that the three Ins(1,4,5)P_3-receptor mRNAs were expressed in ureter and cerebellum. In contrast, amplification of fragments of mRNAs encoding the ryanodine-receptor subtypes showed that only the subtype 3 was expressed in rat ureteric myocytes, whereas all three subtypes were revealed in cerebellum (Figure 1B). Amplified products obtained with the primers designed to amplify the Ins(1,4,5)P_3- or ryanodine-receptor subtypes displayed sizes and sequences (results not shown) corresponding to those of the cloned Ins(1,4,5)P_3- or ryanodine-receptor subtypes. Scatchard analysis of [^{3}H]Ins(1,4,5)P_3 and

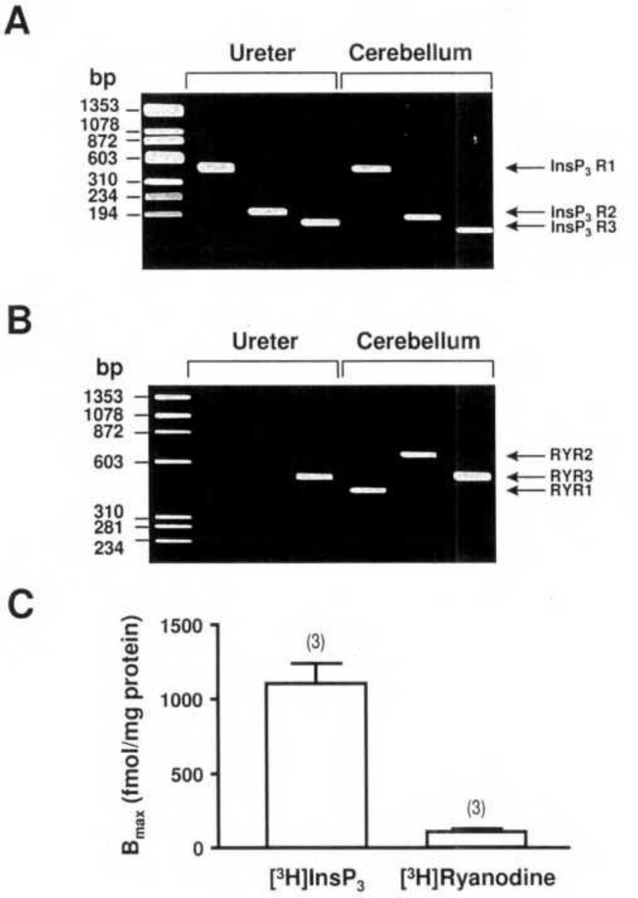

Figure 1 Expression of Ins(1,4,5)P_3 and ryanodine receptors in rat ureteric myocytes

(**A**) Amplified DNA fragments of subtypes 1, 2 and 3 (R1–3) of Ins(1,4,5)P_3 receptors were separated on a 2% agarose gel and visualized by staining with ethidium bromide using rat ureter and cerebellum RNA. Numbers on the left indicate molecular-size standards. (**B**) Amplified DNA fragments of isoforms 1, 2 and 3 of ryanodine receptors (RYR1–3) using rat ureter and cerebellum RNA. For RNA purification and PCR conditions, see the Experimental procedures section. (**C**) Specific binding of [^{3}H]Ins(1,4,5)P_3 and [^{3}H]ryanodine to ureteric smooth-muscle membranes. Maximal binding capacity (B_{max}) corresponding to the total number of binding sites (high-affinity sites for [^{3}H]ryanodine; high-affinity plus low-affinity sites for [^{3}H]Ins(1,4,5)P_3) is the mean ± S.E.M. of three experiments, each carried out in duplicate. The mean K_d values for [^{3}H]ryanodine and [^{3}H]Ins(1,4,5)P_3 (high-affinity and low-affinity) were 2.5, 5.3 and 207.5 nM, respectively.

[^{3}H]ryanodine binding on rat ureter membranes showed that the B_{max} value corresponding to the total number of Ins(1,4,5)P_3-binding sites (high-affinity plus low-affinity sites) was 1113 ± 125 fmol/mg of protein ($n = 3$), whereas the B_{max} value corresponding to the total number of ryanodine-binding sites was 109 ± 21 fmol/mg of protein ($n = 3$; Figure 1C). Finally, Western-blot detection on samples of rat ureter and cerebellum (Figure 2A) revealed a similar molecular-mass band ($\approx$ 240 kDa) corresponding to the value reported previously for Ins(1,4,5)P_3 receptors [19]. These results indicate that rat ureteric myocytes possess mainly Ins(1,4,5)P_3 receptors.

Immunodetection of Ins(1,4,5)P_3 receptors in 0.5-μm confocal sections from freshly dissociated ureteric myocytes was performed with the anti-[Ins(1,4,5)P_3 receptor] antibody (used for protein detection) and the binding sites were revealed with FITC-conjugated secondary antibody. As illustrated in Figure 2(B), Ins(1,4,5)P_3 receptors appeared to be distributed in the whole confocal section, with several marked spots of fluorescence localized near the plasma membrane and in the cytoplasm. Taken together, these results suggest that ureter smooth muscle can be a suitable model for studying Ca^{2+} signalling induced by Ins(1,4,5)P_3-gated channels.

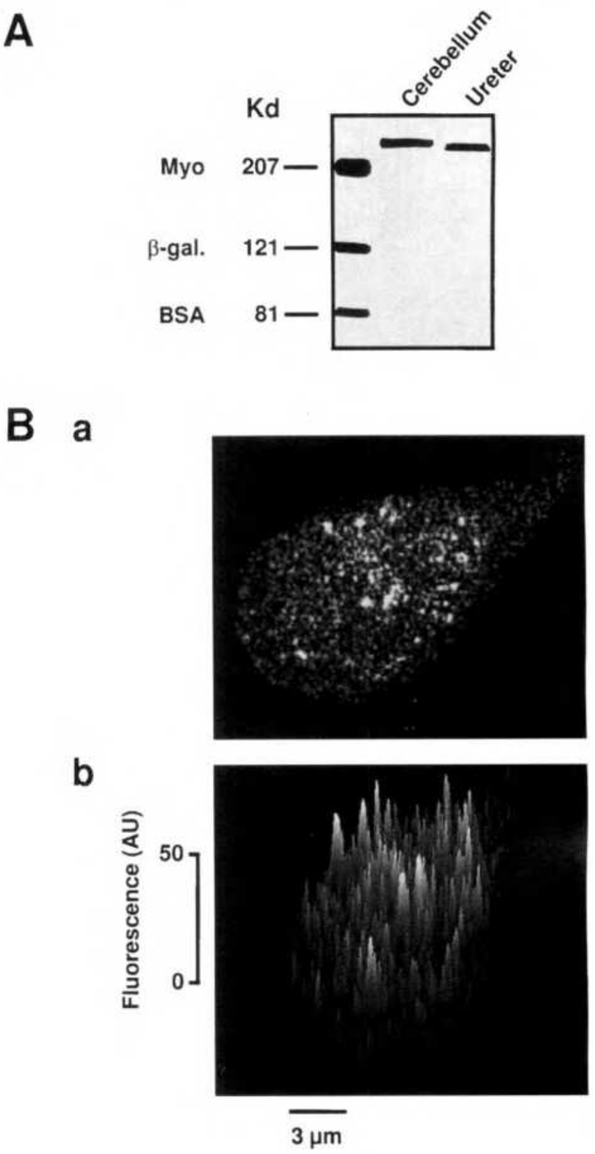

Figure 2 Immunological detection of Ins(1,4,5)P_3 receptors in rat ureteric myocytes

(**A**) Microsomes of ureter smooth muscle (200 μg) and cerebellum (100 μg) were separated by SDS/PAGE (7.5% gel) and analysed by Western blot with an anti-Ins(1,4,5)P_3-receptor antibody. Numbers on the left indicate molecular-mass standards (in kDa). Myo, myosin; β-gal, β-galactosidase. (**B**) Immunolocalization of Ins(1,4,5)P_3 receptors. (**a**) A typical confocal cell section of a freshly dissociated ureteric myocyte performed above the nucleus, showing several spots of fluorescence near the plasma membrane and in the cytoplasm. (**b**) Three-dimensional representation of the fluorescence (in arbitrary units, AU) from the same confocal cell section. In absence of primary antibody or after inactivation of the antibody with its antigen, only a faint background fluorescence was observed.

Acetylcholine- and Ins(1,4,5)P_3-induced localized Ca^{2+} signals

Line-scan images of ureteric myocytes were obtained by scanning of a single line in a confocal section. Most of the scanned lines

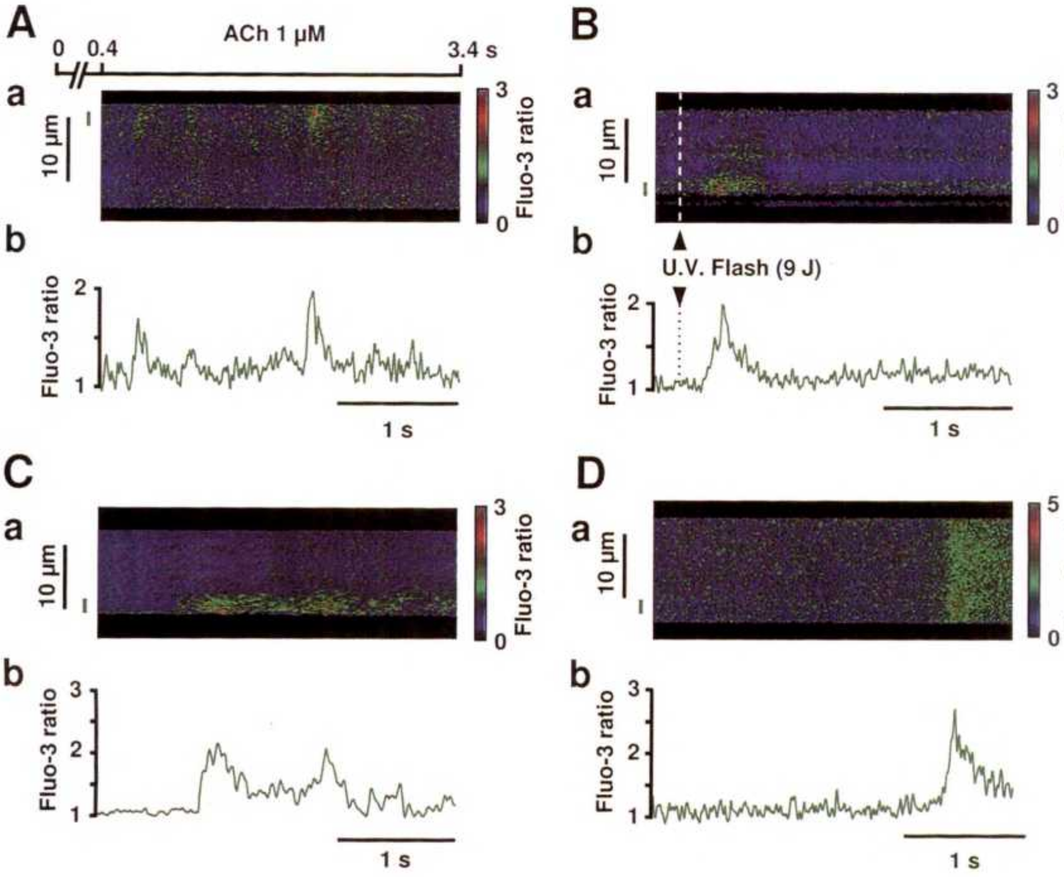

Figure 3 Triggered and spontaneous Ca^{2+}-release signals in rat ureteric myocytes

(**A**) Typical Ca^{2+} response evoked by 1 μM acetylcholine (ACh; horizontal bar) in physiological (1.7 mM Ca^{2+}) solution, shown as a line-scan image (**a**) and averaged fluorescence from a 2-μm region (**b**), indicated by the vertical bar on the line-scan image. Myocytes were loaded with Fluo-3/AM and not patch-clamped. (**B**) Ca^{2+} responses evoked by a 9-J flash pulse in physiological solution, displayed as in (**A**), indicated by the vertical bar on the line-scan image. Myocytes were loaded with Fluo-3 and caged Ins(1,4,5)P_3 through the patch-pipette and held at -50 mV. (**C**, **D**) Spontaneous Ca^{2+} puff (**C**) and Ca^{2+} spike (**D**), displayed as in (**A**), indicated by the vertical bar on the line-scan image in myocytes superfused with 10 mM Ca^{2+} from 30 min. Myocytes were loaded with Fluo-3/AM and not patch-clamped. External solution contained 10 μM ryanodine and 1 μM oxodipine. No change in fluorescence corresponds to a Fluo-3 ratio of 1.

performed above the nucleus detected Ca^{2+} signals, in agreement with immunostaining of Ins(1,4,5)P_3 receptors (Figure 2B). Experiments were performed in either voltage-clamped (holding potential, -50 mV) or non-voltage-clamped myocytes, in the continuous presence of 1 μM oxodipine (a light-stable dihydropyridine) to inhibit voltage-dependent Ca^{2+} channels. Fluorescence signals are expressed as a pseudo-ratio (F/F_{rest}) and are depicted by a pseudocolour scale as indicated by the colour bars (see Figures 3 and 5, below). The basal [Ca^{2+}]$_i$ level measured with the Indo-1 dye was 91 ± 7 nM ($n = 25$).

In non-voltage-clamped ureteric myocytes, applications of 1 μM acetylcholine induced localized and transient Ca^{2+} signals that originated from 1 or 2 initiation sites in the line-scan images and appeared after a delay of 0.55 ± 0.01 s ($n = 29$; Figure 3A). However, these signals showed some heterogeneity in amplitude, time course and spatial spread, even when they originated from the same site. The largest Ca^{2+}-release events are characterized by a relatively rapid upstroke (with time-to-peak of 93.6 ± 9.7 ms, $n = 10$) followed by a decline, with a time to decay to half-maximal amplitude of 107.4 ± 16.4 ms, and were restricted to a small area with full width at half-maximal amplitude (FWHM) of 1.89 ± 0.23 μm. The peak amplitude of such events was 1.13 ± 0.16 ($\Delta F/F_{rest}$, $n = 10$) and they appear generally similar to the Ca^{2+} puffs reported in non-excitable cells [6,7]. The smallest Ca^{2+}-release events had a lower peak amplitude ($\Delta F/F_{rest} = 0.39 \pm 0.02$, $n = 19$) and a more restricted spatial spread (1.03 ± 0.07 μm). The kinetics of these events were more rapid than those of Ca^{2+} puffs, with time-to-peak and time at half-decay of 49.2 ± 3.9 ms and 60.9 ± 8.5 ms, respectively ($n = 19$). Such small events are unlikely to be due to out-of-focus Ca^{2+} puffs, since such out-of-focus Ca^{2+} signals would exhibit a reduced amplitude and a slower time course [20], whereas the detected small events are generally much faster than the other localized Ca^{2+} events.

Distributions of peak fluorescence, time-to-peak, time at half-decay and FWHM of 29 elementary Ca^{2+} signals obtained from 11 different cells are illustrated in Figure 4. The broad range of amplitude, time-to-peak, time at half-decay and FWHM is consistent with the notion of a continuum of Ca^{2+} puffs rather than a hierarchy of discrete amplitudes. This conclusion is also supported by the localization of Ca^{2+} events of different amplitude originating from the same site (Figure 3A). In addition, a noticeable variation was also observed in spatial spread (Figure 4D). Such a variation in FWHM would be expected for Ca^{2+} events that differed in amplitude, since a high-amplitude signal should have a larger spatial spread than a signal of lower amplitude, providing the Ca^{2+} buffering and sequestration mechanisms were equal for both events. As shown in Figure 4(D)

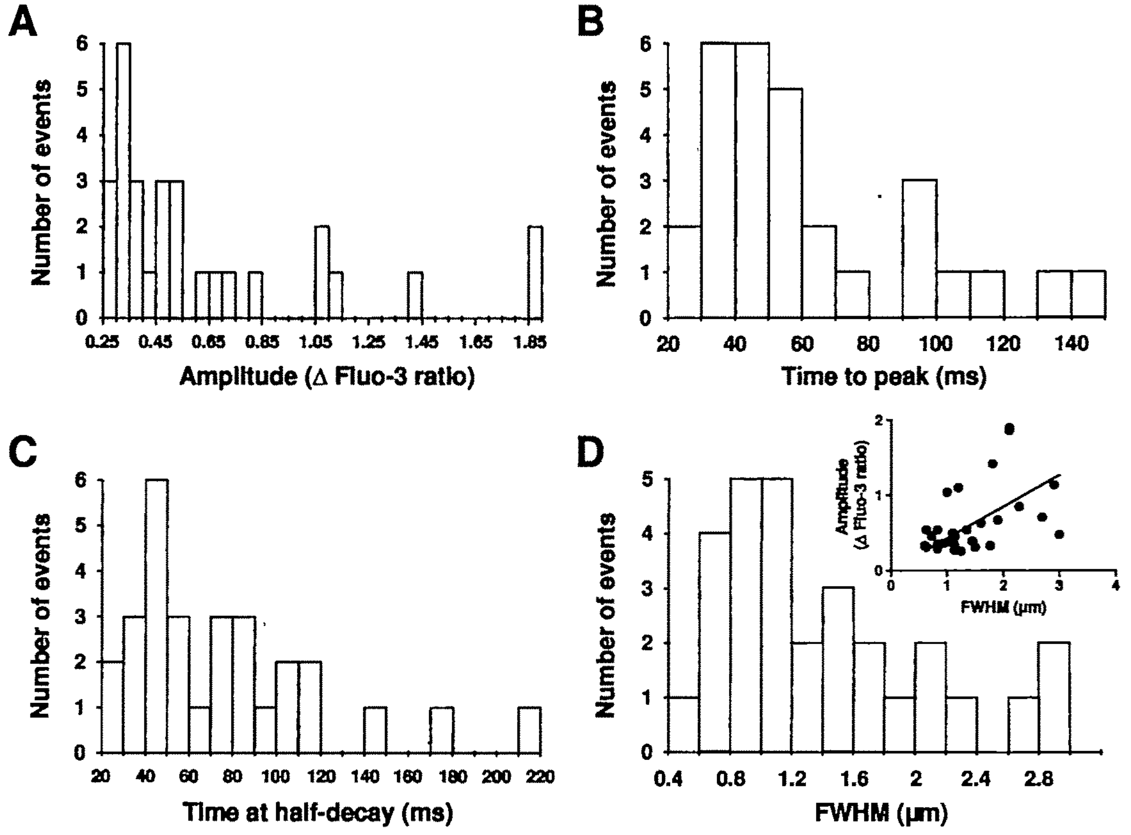

Figure 4 Characteristics of localized Ca^{2+}-release signals evoked by low concentrations of acetylcholine

(**A**) Amplitude histogram of 29 elementary Ca^{2+} signals (from 11 different cells) stimulated by 1 μM acetylcholine Distribution of the time to reach peak Ca^{2+} signals (**B**), the time to reach half-decay (**C**) and the FWHM (**D**) for the same 29 elementary Ca^{2+} signals Inset shows the correlation between amplitude of localized Ca^{2+} signals and FWHM The linear regression coefficient (r^2) was 0.72 Myocytes were loaded with Fluo-3/AM and not patch-clamped. External solution contained 1 μM oxodipine.

(inset), such a relationship between amplitude and spatial spread could be observed, although the correlation was not high (r^2 = 0.72).

In voltage-clamped myocytes, photorelease from a caged Ins(1,4,5)P_3 precursor by UV-light flashes of low-intensity (9 J) evoked localized and transient Ca^{2+} events (Figure 3B) with variable amplitudes and time courses (n = 15), similar to those obtained with 1 μM acetylcholine.

Spontaneous Ca^{2+} puffs in Ca^{2+}-overloaded myocytes

In accordance with previous data [21], the potency of muscle cells to generate spontaneous localized Ca^{2+} signals may depend on the Ca^{2+}-loading status. Superfusion of ureteric myocytes with 10 mM $[Ca^{2+}]_o$ (the external calcium concentration) for at least 30 min resulted in a significant increase in the mean amplitude ($\Delta F/F_{rest}$) of the Ca^{2+} responses evoked by 10 μM acetylcholine from 2.48 ± 0.15 (n = 32) in normal (1.7 mM Ca^{2+}) physiological solution to 2.89 ± 0.17 (n = 32) in 10 mM $[Ca^{2+}]_o$, suggesting a Ca^{2+} loading of the store. With a $[Ca^{2+}]_o$ of 1.7 mM, most ureteric myocytes had a steady-state $[Ca^{2+}]_i$ level and spontaneous Ca^{2+} signals were very scarce. With a $[Ca^{2+}]_o$ of 10 mM for at least 30 min, the basal $[Ca^{2+}]_i$ level was not significantly affected (97 ± 12 nM, n = 20) but discrete, spontaneous events occurred more frequently (Figure 3C). The majority of these localized Ca^{2+} events were not associated with Ca^{2+} waves. Occasionally, localized Ca^{2+} events appeared to spread and generate transient Ca^{2+} spikes (Figure 3D). The peak amplitude of spontaneous Ca^{2+} events was 1.24 ± 0.20 ($\Delta F/F_{rest}$, n = 31). The time-to-peak, the half-time of decay and the FWHM were 110 ± 25, 190 ± 35 and 2.51 ± 0.25 μm, respectively (n = 31). Although Ca^{2+} overload appeared to slow the time course of the Ca^{2+}-signal decline and to increase slightly the FWHM, the kinetic parameters of the spontaneous Ca^{2+} events resembled those of Ca^{2+} puffs. The frequency of spontaneous Ca^{2+} puffs increased significantly from 0.03 ± 0.01 puff·s^{-1} (n = 54) in control conditions to 0.31 ± 0.3 puff·s^{-1} (n = 31) in Ca^{2+}-loading conditions. These results show that in muscle cells overloaded with Ca^{2+}, clustered Ins(1,4,5)P_3 receptors may underlie spontaneous Ca^{2+} releases, as in non-excitable cells [22]. Spontaneous Ca^{2+} puffs were obtained in the continuous presence of 10 μM ryanodine and 1 μM oxodipine to inhibit ryanodine receptors and L-type Ca^{2+} channels, respectively. In addition, in patch-clamped myocytes intracellular applications of 1 mg/ml heparin or 10 μg/ml anti-[Ins(1,4,5)P_3 receptor] antibody for 7–8 min suppressed any spontaneous Ca^{2+}-release signals (n = 12).

Acetylcholine- and Ins(1,4,5)P_3-induced Ca^{2+} waves

It is proposed generally that the spatio-temporal summation of localized Ca^{2+} signals due to Ins(1,4,5)P_3-receptor activation gives rise to the whole-cell increase in $[Ca^{2+}]_i$. Increases in the frequency or amplitude of localized Ca^{2+} signals, or spatial recruitment of additional initiation sites, have been reported to

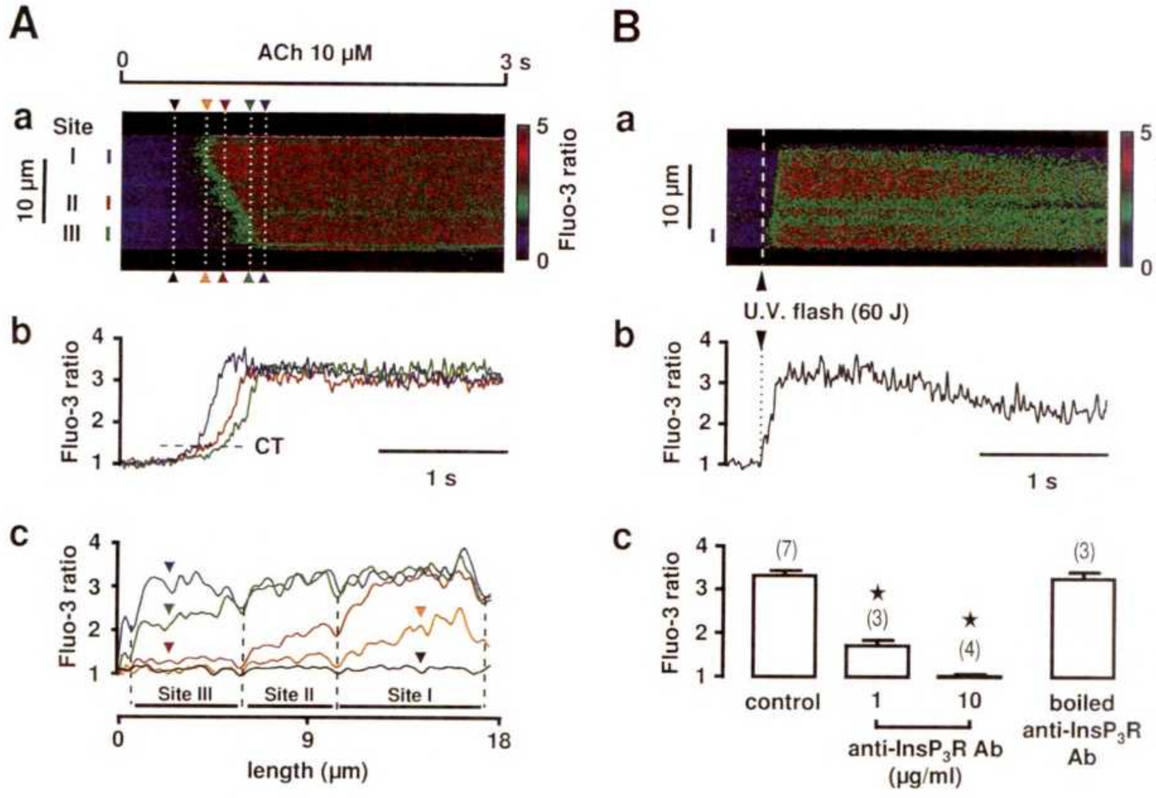

Figure 5 Activation of propagated Ca^{2+} waves by high doses of acetylcholine (ACh) and high-intensity flash photolysis of caged Ins(1,4,5)P_3

(**A**) Line-scan image (**a**) in response to the continuous application of 10 μM acetylcholine, as indicated by the horizontal bar. (**b**) Averaged fluorescence from three 2-μm regions (indicated by the vertical bars on the line-scan image). CT, control $[Ca^{2+}]_i$ threshold. (**c**) Spatial profiles (measured in 2-μm-wide areas indicated by coloured arrow heads) of the line-scan image shown in (**A**, **a**). In this myocyte, the Ca^{2+} wave started at one site (site I, yellow trace) and then propagated through the entire line-scan image by recruiting neighbouring Ca^{2+}-release sites (sites II and III). Myocytes were loaded with Fluo-3/AM and not patch-clamped. (**B**) Ca^{2+} waves evoked by flash photolysis of caged Ins(1,4,5)P_3 in voltage-clamped rat ureteric myocytes. (**a**) Line-scan image evoked by a high-intensity (60 J) flash pulse. (**b**) Averaged fluorescence from a 2-μm region indicated by the vertical bar on the line-scan image. (**c**) Compiled data showing the effects of the anti-Ins(1,4,5)P_3-receptor [anti-Ins(1,4,5)P_3R] antibody (Ab), applied intracellularly for 7–8 min. Data are means ± S.E.M. with the number of experiments indicated in parentheses. ★, Values significantly different from those obtained under control conditions ($P < 0.05$). Myocytes were loaded with Fluo-3 and caged Ins(1,4,5)P_3 through the patch-pipette and held at −50 mV. External solution contained 1 μM oxodipine. No change in fluorescence corresponds to a Fluo-3 ratio of 1.

be necessary for triggering propagated Ca^{2+} waves [23]. In all the cells tested ($n = 16$), we never observed increases in frequency or amplitude of Ca^{2+} puffs in response to 10 μM acetylcholine, which were able to initiate propagated Ca^{2+} waves. In contrast, propagated Ca^{2+} waves appeared from a first initiation site that progressively recruited neighbouring initiation sites by Ca^{2+} diffusion (Figure 5A). The delay between application of acetylcholine and the onset of the Ca^{2+} wave was estimated to be 0.50 ± 0.01 s ($n = 16$). The mean amplitude ($\Delta F/F_{rest}$) and the mean overall wave velocity of the acetylcholine-evoked Ca^{2+} waves were 2.56 ± 0.25 and 38 ± 3 μm/s ($n = 16$), respectively. The propagation velocity of Ca^{2+} waves depends on the distance between Ca^{2+}-release sites as well as their Ca^{2+} sensitivity and the amount of Ca^{2+} released. As shown in Figure 5(Ab), recordings of localized fluorescence signals at release sites activated during Ca^{2+} wave propagation showed an initial slow Ca^{2+} elevation preceding an abrupt rise. This is consistent with the triggering of regenerative Ca^{2+} release by an early rise in $[Ca^{2+}]_i$ resulting from summation of localized Ca^{2+} signals or from Ca^{2+} ions diffusing from neighbouring active sites. Fluorescence analysis in the spatial domain at different times during the onset of the Ca^{2+} wave (Figure 5Ac) revealed clearly the recruitment of neighbouring Ca^{2+}-release sites from the early initiation site (site I in Figure 5Ac). The mean number of initiation sites per line-scan image was 2.4 ± 0.4 ($n = 16$).

Photorelease of caged Ins(1,4,5)P_3 by high-intensity (30–60 J) flash pulses evoked large Ca^{2+} responses that started either from a simultaneous increase in $[Ca^{2+}]_i$ in the scanned line or from an initiation site leading to activation of a propagating wave (Figure 5B). The mean amplitudes ($\Delta F/F_{rest}$) of the Ins(1,4,5)P_3- and acetylcholine-evoked Ca^{2+} waves in voltage-clamped myocytes were 2.32 ± 0.11 and 2.48 ± 0.31 ($n = 7$), respectively.

To identify the molecular nature of the Ca^{2+}-release channels involved in both Ins(1,4,5)P_3- and acetylcholine-induced Ca^{2+} signals, we tested the effects of Ins(1,4,5)P_3- and ryanodine-receptor inhibitors. Intracellular infusion of 1 mg/ml heparin for 7–8 min through the patch-pipette suppressed both Ins(1,4,5)P_3- and acetylcholine-induced Ca^{2+} waves ($n = 5$; results not shown). Similarly, intracellular application of the anti-Ins(1,4,5)P_3-receptor antibody for 7–8 min inhibited in a concentration-dependent manner the Ca^{2+} responses evoked by flash photolysis of caged Ins(1,4,5)P_3 (Figure 5Bc) or application of 10 μM acetylcholine (Figure 6A). This antibody-induced inhibition was specific, in as much as boiled (95 °C for 30 min) anti-Ins(1,4,5)P_3-receptor antibody had no significant effect on both Ins(1,4,5)P_3-and acetylcholine-activated Ca^{2+} responses (Figures

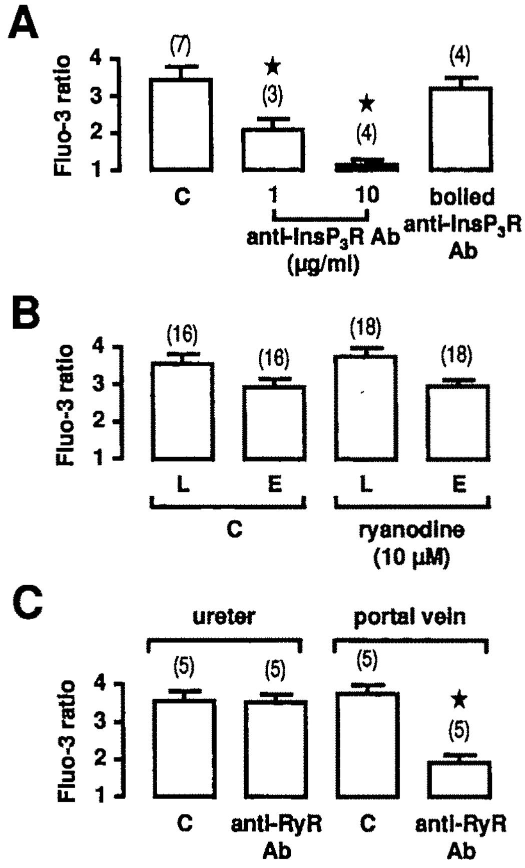

Figure 6 Effects of inhibitors of Ins(1,4,5)P_3 and ryanodine receptors on the acetylcholine-induced Ca^{2+} waves in voltage-clamped myocytes

(**A**) Compiled data showing the effects of increasing concentrations of anti-Ins(1,4,5)P_3 receptor [anti-Ins(1,4,5)P_3R] antibody (Ab) and of 10 µg/ml boiled antibody, applied intracellularly for 7–8 min on 10 µM acetylcholine-induced Ca^{2+} waves in ureteric myocytes (**B**) Compiled data showing the effect of 10 µM ryanodine (applied externally for 15–17 min) on 10 µM acetylcholine-induced Ca^{2+} waves in ureteric myocytes The fluorescence was measured either in the entire line-scan image (E) or in a localized 2-µm region of the line-scan image (L). (**C**) Compiled data showing the effect of 10 µg/ml anti-ryanodine receptor (anti-RyR) antibody, applied intracellularly for 7–8 min on 10 µM acetylcholine-induced Ca^{2+} waves in ureteric and portal-vein myocytes Data are means ± S E M with the number of cells tested indicated in parentheses ★, Values significantly different from those obtained under control conditions ($P < 0.05$). Holding potential was −50 mV External solution contained 1 µM oxodipine. No change in fluorescence corresponds to a Fluo-3 ratio of 1. C, control.

5Bc and 6A). In vascular myocytes, extracellular applications of 10 µM ryanodine have been shown to inhibit ryanodine receptors without depleting the internal Ca^{2+} store in a manner similar to that induced by an anti-ryanodine-receptor antibody [24]. Application of 10 µM ryanodine for 15–17 min in non-voltage-clamped ureteric myocytes had no significant effect on the amplitude of acetylcholine-induced global Ca^{2+} waves, measured in a 2-µm region or in the entire line-scan image (Figure 6B). Similarly, intracellular applications of 10 µg/ml anti-ryanodine-receptor antibody for 7–8 min did not affect the acetylcholine-induced Ca^{2+} wave (Figure 6C) as well as the Ins(1,4,5)P_3-induced Ca^{2+} response in ureteric myocytes. In contrast, in portal-vein myocytes, the acetylcholine-induced Ca^{2+} wave was decreased by about 60 % in the presence of 10 µg/ml of the same anti-ryanodine-receptor antibody (Figure 6C), in good agreement with previous data obtained from noradrenaline-induced Ca^{2+} response [24]. It is noteworthy that 10 µM anti-Ins(1,4,5)P_3-receptor antibody suppressed the Ca^{2+} puffs evoked by low concentrations of acetylcholine or Ins(1,4,5)P_3 using low-intensity flashes, in all the cells tested ($n = 12$). In contrast, 10 µM anti-ryanodine-receptor antibody was ineffective on Ca^{2+} puffs ($n = 9$).

DISCUSSION

This study describes for the first time in smooth-muscle cells the localized and transient Ca^{2+} events (Ca^{2+} puffs) evoked by Ins(1,4,5)P_3-gated channels in response to low concentrations of Ins(1,4,5)P_3 either released from caged Ins(1,4,5)P_3 or produced by low doses of acetylcholine. In addition, spontaneous Ca^{2+} puffs were detected frequently in myocytes overloaded with Ca^{2+}. At high concentrations of Ins(1,4,5)P_3 or acetylcholine, recruitment of several localized Ca^{2+} signals generates Ca^{2+} waves that appear to propagate between several Ca^{2+}-release sites in the scanned line. The functional results are supported by both binding and immunochemical data showing that Ins(1,4,5)P_3 receptors are highly expressed when compared with ryanodine receptors and that spots of Ins(1,4,5)P_3 receptors are detected in several areas of the cell confocal sections.

In rat ureteric myocytes, immunodetection of Ins(1,4,5)P_3 receptors in cell confocal sections showed that spots of Ins(1,4,5)P_3 receptors were detected in several areas in addition to an homogeneous distribution in the whole confocal sections. This observation is in good agreement with the fact that Ins(1,4,5)P_3 receptors are highly expressed in these smooth-muscle cells, as supported by binding experiments. The maximal binding capacity of [^{3}H]Ins(1,4,5)P_3 to ureteric microsomal preparations is 10–12 times higher than that of [^{3}H]ryanodine. The reverse-transcriptase PCR analysis showed that the RNAs encoding the three subtypes of the Ins(1,4,5)P_3 receptor and subtype 3 of the ryanodine receptor were detected in rat ureteric myocytes. However, binding experiments revealed that the level of expression of ryanodine-receptor subtype 3 was very low in these cells. This low expression level together with the fact that ryanodine-receptor subtype 3 is less sensitive to Ca^{2+}-induced channel activation than the other ryanodine-receptor subtypes [25] may explain why ryanodine and the anti-ryanodine-receptor antibody do not affect both localized and global Ca^{2+} signals evoked by flash photolysis of caged Ins(1,4,5)P_3 and acetylcholine. This is in contrast with results obtained in vascular myocytes, where both ryanodine and the anti-ryanodine-receptor antibody inhibit the Ca^{2+} responses evoked by noradrenaline [24] or acetylcholine (the present study). However, in vascular myocytes the density of ryanodine receptors is 3–4 times higher than that of Ins(1,4,5)P_3 receptors [24]. Taken together, these results indicate that in rat ureteric myocytes the Ca^{2+} responses to photorelease of Ins(1,4,5)P_3 and acetylcholine depend only on activation of Ins(1,4,5)P_3 receptors, in agreement with previous contraction experiments and [Ca^{2+}]$_i$ measurements in intact and permeabilized rat ureteric strips [10,11]. Accordingly, both Ins(1,4,5)P_3- and acetylcholine-evoked Ca^{2+} signals were blocked by heparin and by an anti-Ins(1,4,5)P_3-receptor antibody, which recognized in Western-blot analysis a molecular-mass band of about 240 kDa in rat ureter and cerebellum, but were unaffected by high concentrations of ryanodine and by an anti-ryanodine-receptor antibody.

The spatio-temporal characteristics of Ca^{2+} puffs evoked by photorelease of Ins(1,4,5)P_3 or low concentrations of acetylcholine were relatively variable, suggesting that they are not stereotypic. Therefore, the variable amplitude of Ca^{2+} puffs may depend on the number and organization of the Ins(1,4,5)P_3

receptors in the local volume as well as the local state of Ca^{2+} loading in the sarcoplasmic reticulum. Our results are compatible with a model where Ins(1,4,5)P_3-gated Ca^{2+} channels would exist in clusters containing variable numbers of channels and that within these clusters a variable number of channels could be recruited. A similar explanation has been proposed recently in non-excitable cells to account for hormone-evoked elementary Ca^{2+} signals [20,26]. In addition, successive activation of a given cluster of Ins(1,4,5)P_3 receptors may decrease the amount of Ca^{2+} locally available in this area of the sarcoplasmic reticulum and modify the amplitude of localized Ca^{2+} signals. It has been also proposed that the gating properties of Ins(1,4,5)P_3-gated channels may influence the amplitude and time course of Ca^{2+} events. An interesting possibility is that the individual clusters may be composed with different subtypes of Ins(1,4,5)P_3 receptors, which may have different sensitivity for Ca^{2+}-dependent modulation [27]. For example, subtype 3 of the Ins(1,4,5)P_3 receptor does not exhibit a Ca^{2+}-dependent inhibition, whereas subtype 1 shows a bell-shaped dependence on [Ca^{2+}]$_i$ [27,28]. Another possibility is that the gating of Ins(1,4,5)P_3 receptors may depend on the luminal Ca^{2+} concentration which may, in turn, regulate their sensitivity to Ins(1,4,5)P_3 [22,29]. In agreement with this proposal is the observation of spontaneous Ca^{2+} puffs and spikes in ureteric myocytes overloaded with 10 mM Ca^{2+} for 30 min. Spontaneous Ca^{2+} release from Ins(1,4,5)P_3-sensitive Ca^{2+} stores has been reported previously from permeabilized hepatocytes overloaded with Ca^{2+} [22]. To our knowledge, spontaneous Ca^{2+} puffs have never been described in intact cells at a basal Ins(1,4,5)P_3 level. The possibility that spontaneous Ca^{2+} puffs may activate various membrane conductances, as shown for Ca^{2+} sparks [4,5], is under investigation. It has been shown recently that co-expression of Ins(1,4,5)P_3-receptor subtypes 1 and 2 facilitates Ca^{2+} oscillations, whereas expression of Ins(1,4,5)P_3-receptor subtype 3 alone generates monophasic Ca^{2+} transients [30]. Since Ins(1,4,5)P_3-receptor subtypes 1 and 2 are more sensitive to Ins(1,4,5)P_3 and Ca^{2+} [30], it can be postulated that they are required for spontaneous Ca^{2+} puffs. In contrast, the Ins(1,4,5)P_3-receptor subtype 3 is activated by higher [Ca^{2+}]$_i$ and may participate in the acetylcholine-induced Ca^{2+} wave. Further experiments are needed to identify the expression pattern of Ins(1,4,5)P_3-receptor subtypes in ureteric myocytes and their specific roles in Ca^{2+} signalling.

As illustrated in Figure 5, Ca^{2+} waves propagate throughout ureteric myocytes by alternating between regeneration at several Ca^{2+}-release sites along the scanned line and Ca^{2+} diffusion between these release sites. In HeLa cells and *Xenopus* oocytes, Ca^{2+} wave activation has been associated with an increased frequency of elementary Ca^{2+} events at a single site, with an increased amplitude of Ca^{2+} events or with the recruitment of Ca^{2+}-release sites in the spatial domain [23,31]. In ureteric myocytes, Ca^{2+} waves were triggered by activation of an initiation site, frequently located at the edge of the cell, without any detectable increase in frequency or amplitude of preceding Ca^{2+} puffs. Diffusion of Ca^{2+} from this early initiation site activated neighbouring Ca^{2+}-release sites in the scanned lines, and this may account for wave-propagation velocity in ureteric myocytes. The notion that a sub-threshold pacemaker elevation of [Ca^{2+}]$_i$ precedes regenerative Ca^{2+} waves is not new [32], but our results emphasize further the importance of the pacemaker Ca^{2+} phase in cells expressing mainly Ins(1,4,5)P_3 receptors.

Visceral and vascular smooth muscles display a large variability in the type of intracellular Ca^{2+} store and in the role of these stores in initiating increase in [Ca^{2+}]$_i$ in response to mediators and hormones. Rat portal-vein myocytes possess a single functional intracellular Ca^{2+} store on which both ryanodine and Ins(1,4,5)P_3 receptors have been identified [9]. However, in these cells, only clusters of ryanodine receptors are present whereas Ins(1,4,5)P_3 receptors are distributed homogeneously on the sarcoplasmic reticulum, and the B_{max} value of [^{3}H]ryanodine binding is 3–4 times higher than that of [^{3}H]Ins(1,4,5)P_3 binding [24]. A physiological consequence is that a co-operativity between Ins(1,4,5)P_3- and ryanodine-sensitive Ca^{2+} channels is detected in these vascular myocytes to amplify Ca^{2+} release responsible for fast propagated Ca^{2+} waves in response to neuromediators [24]. In rat mesenteric artery myocytes, it has been proposed that Ca^{2+} stores are organized into small, spatially distinct compartments [33]. When these compartments possess only ryanodine or Ins(1,4,5)P_3 receptors, they function as separate Ca^{2+} stores and neuromediators may only activate the Ins(1,4,5)P_3-sensitive Ca^{2+} store. In contrast, when the compartments possess both ryanodine and Ins(1,4,5)P_3 receptors, they function as mixed Ca^{2+} stores and a co-operativity between Ins(1,4,5)P_3 and ryanodine receptors may be effective. In rat ureteric smooth muscle, as a consequence of the high expression of Ins(1,4,5)P_3 receptors and the absence of subtypes 1 and 2 of ryanodine receptors, Ca^{2+} release from the intracellular store is only activated by Ins(1,4,5)P_3 receptors and the amplifying mechanism is a pure Ins(1,4,5)P_3-induced Ca^{2+} release. In contrast, in guinea-pig ureter, the amplifying mechanism is described as dependent only on Ca^{2+}-induced Ca^{2+} release [11]. It can be proposed that in phasic smooth muscles showing electrical pacemaker activity, the Ca^{2+}-induced Ca^{2+}-release mechanism may play a major role in modulating contraction and cell excitability, whereas in tonic smooth muscles the Ins(1,4,5)P_3-induced Ca^{2+}-release mechanism predominantly controls Ca^{2+} release and contraction. Taken together, these data illustrate the variability of intracellular Ca^{2+} stores and Ca^{2+}-amplifying mechanisms in different cell types expressing different amounts of Ins(1,4,5)P_3 and ryanodine receptors. The results emphasize the importance of combining molecular experiments, immunostaining and functional approaches to identify the specific characteristics of Ca^{2+} signalling in each cell type studied.

In conclusion, these findings show that in rat ureteric smooth-muscle cells localized and transient Ca^{2+} events induced by the opening of clusters of Ins(1,4,5)P_3-sensitive Ca^{2+}-release channels can be triggered in response to neuromediator activation or recorded spontaneously in Ca^{2+}-overloaded myocytes. They represent a continuum of Ca^{2+} signals with variable amplitude, duration and diffusion rather than a strict hierarchy of Ca^{2+} events. Propagated Ca^{2+} waves appear to result from the spatial recruitment of several Ca^{2+}-release sites by Ca^{2+} diffusion. Both Ca^{2+} signals provide an integrated mechanism to regulate contractility in smooth-muscle cells where ryanodine receptors are not or are poorly expressed.

This work was supported by grants from the Centre National de la Recherche Scientifique, the Centre National des Etudes Spatiales, and Région Aquitaine (Pôle Médicament-Santé), France. We thank V. Carricaburu for initiating us into Western-blot experiments and N. Biendon for secretarial assistance.

REFERENCES

1 Lipp, P. and Niggli, E. (1996) A hierarchical concept of cellular and subcellular Ca^{2+}-signalling. Prog. Biophys. Mol. Biol. **65**, 265–296
2 Berridge, M. J. (1997) Elementary and global aspects of calcium signalling. J. Physiol. (London) **499**, 291–306
3 Cheng, H., Lederer, W. J. and Cannell, M. B. (1993) Calcium sparks: elementary events underlying excitation-contraction coupling in heart muscle. Science **262**, 740–744
4 Nelson, M. T., Cheng, H., Rubart, M., Santana, L. F., Bonev, A. D., Knot, H. J. and Lederer, W. J. (1995) Relaxation of arterial smooth muscle by calcium sparks. Science **270**, 633–637

5 Mironneau, J, Arnaudeau, S, Macrez-Leprêtre, N and Boittin, F. X (1996) Ca^{2+} sparks and calcium waves activate different Ca^{2+}-dependent ion channels in single myocytes from rat portal vein. Cell Calcium **20**, 153–160

6 Parker, I. and Yao, Y. (1996) Ca^{2+} transients associated with openings of inositol trisphosphate-gated channels in *Xenopus* oocytes J. Physiol. (London) **491**, 663–668

7 Bootman, M, Niggli, E., Berridge, M., and Lipp, P (1997) Imaging the hierarchical Ca^{2+} signalling system in HeLa cells J Physiol (London) **499**, 307–314

8 Somlyo, A. P. and Somlyo, A. V. (1994) Signal transduction and regulation in smooth muscle Nature (London) **372**, 231–236

9 Boittin, F X, Coussin, F, Macrez, N., Mironneau, C. and Mironneau, J (1998) Inositol 1,4,5-trisphosphate- and ryanodine-sensitive Ca^{2+} release channel-dependent Ca^{2+} signalling in rat portal vein myocytes Cell Calcium **23**, 303–311

10 Burdyga, T V, Taggart, M. J. and Wray, S. (1995) Major difference between rat and guinea-pig ureter in the ability of agonists and caffeine to release Ca^{2+} and influence force J Physiol (London) **489**, 327–335

11 Burdyga, T. V., Taggart, M. J., Crichton, C., Smith, G L and Wray, S. (1998) The mechanism of Ca^{2+} release from the SR of permeabilised guinea-pig and rat ureteric smooth muscle Biochim. Biophys Acta **1402**, 109–114

12 Morel, J L, Macrez-Leprêtre, N. and Mironneau, J. (1996) Angiotensin II-activated Ca^{2+} entry-induced release of Ca^{2+} from intracellular stores in rat portal vein myocytes. Br. J Pharmacol. **118**, 73–78

13 Macrez-Leprêtre, N, Kalkbrenner, F, Schultz, G and Mironneau, J (1997) Distinct functions of G_q and G_{11} proteins in coupling α_1-adrenoceptors to Ca^{2+} release and Ca^{2+} entry in rat portal vein myocytes J Biol. Chem **272**, 5261–5268

14 Bradford, M. M. (1976) A rapid and sensitive method for the quantitation of microgram quantities of protein utilizing the principle of protein-dye binding. Anal. Biochem **72**, 248–254

15 Morel, J. L., Boittin, F X, Halet, G, Arnaudeau, S., Mironneau, C. and Mironneau, J. (1997) Effect of a 14-day hindlimb suspension on cytosolic Ca^{2+} concentration in rat portal vein myocytes. Am J Physiol. **273**, H2867–H2875

16 Tovey, S C., Godfrey, R E, Hughes, P J, Mezna, M., Minchin, S. D., Mikoshiba, K. and Michelangeli, F. (1997) Identification and characterization of inositol 1,4,5-trisphosphate receptors in rat testis Cell Calcium **21**, 311–309

17 Neylon, C B, Richards, S M, Larsen, M A, Agrotis, A. and Bobik, A. (1995) Multiple types of ryanodine receptor/Ca^{2+} release channels are expressed in vascular smooth muscle Biochem. Biophys Res. Commun **215**, 814–821

18 Viard, P, Exner, T, Maier, U, Mironneau, J, Nurnberg, B. and Macrez, N (1999) $G\beta\gamma$ dimers stimulate vascular L-type Ca^{2+} channels via phosphoinositide 3-kinase FASEB J. **13**, 685–694

19 De Smedt, H, Missiaen, L, Parys, J B., Henning, R. H, Sienaert, I, Vanlingen, S, Gijsens, A, Himpens, B. and Casteels, R (1997) Isoform diversity of the inositol trisphosphate receptor in cell types of mouse origin Biochem. J. **322**, 575–583

20 Sun, X P, Callamaras, N, Marchant, J S. and Parker, I. (1998) A continuum of $InsP_3$-mediated elementary Ca^{2+} signalling events in *Xenopus* oocytes. J. Physiol. (London) **509**, 67–80

21 Cheng, H, Lederer, M. R., Lederer, W. J and Cannell, M B (1996) Calcium sparks and $[Ca^{2+}]_i$ waves in cardiac myocytes Am J Physiol. **270**, C148–C159

22 Missiaen, L, Taylor, C W and Berridge, M. J. (1991) Spontaneous calcium release from inositol trisphosphate-sensitive calcium stores Nature (London) **352**, 241–244

23 Bootman, M. D, Berridge, M. J and Lipp, P (1997) Cooking with calcium the recipes for composing global signals from elementary events Cell **91**, 367–373

24 Boittin, F. X, Macrez, N, Halet, G. and Mironneau, J (1999) Norepinephrine-induced Ca^{2+} waves depend on $InsP_3$ and ryanodine receptor activation in vascular myocytes. Am J Physiol. **277**, C139–C151

25 Sonnleitner, A, Conti, A., Bertocchini, F, Schindler, H and Sorrentino, V (1998) Functional properties of the ryanodine receptor type 3 (RyR3) Ca^{2+} release channel EMBO J. **17**, 2790–2798

26 Thomas, D., Lipp, P, Berridge, M J and Bootman, M. D (1998) Hormone-evoked elementary Ca^{2+} signals are not stereotypic, but reflect activation of different size channel clusters and variable recruitment of channels within a cluster J. Biol. Chem **273**, 27130–27136

27 Cardy, T. J, Traynor, D and Taylor, C W. (1997) Differential regulation of types-1 and -3 inositol trisphosphate receptors by cytosolic Ca^{2+}. Biochem J. **328**, 785–793

28 Hagar, R E, Burgstahler, A D, Nathanson, M H. and Ehrlich, B E (1998) Type III $InsP_3$ receptor channel stays open in the presence of increased calcium. Nature (London) **396**, 81–84

29 Missiaen, L., De Smedt, H, Droogmans, G and Casteels, R. (1992) Luminal Ca^{2+} controls the activation of the inositol 1,4,5-trisphosphate receptor by cytosolic Ca^{2+} J Biol. Chem **267**, 22961–22916

30 Miyakawa, T, Maeda, A, Yamazawa, T, Hirose, K., Kurosaki, T. and Iino, M (1999) Encoding of Ca^{2+} signals by differential expression of IP_3 receptor subtypes EMBO J. **18**, 1303–1308

31 Callamaras, N, Marchant, J. S, Sun, X P. and Parker, I (1998) Activation and co-ordination of $InsP_3$-mediated elementary Ca^{2+} events during global Ca^{2+} signals in *Xenopus* oocytes. J. Physiol (London) **509**, 81–91

32 Iino, M, Yamazawa, T, Miyashita, Y, Endo, M. and Kasai, H (1993) Critical intracellular Ca^{2+} concentration for all-or-none Ca^{2+} spiking in single smooth muscle cells EMBO J **12**, 5287–5291

33 Golovina, V. A and Blaustein, M. P (1997) Spatially and functionally distinct Ca^{2+} stores in sarcoplasmic and endoplasmic reticulum. Science **275**, 1643–1648

Received 18 October 1999/23 March 2000; accepted 14 April 2000

Molecular modelling and site-directed mutagenesis of the inositol 1,3,4,5-tetrakisphosphate-binding pleckstrin homology domain from the Ras GTPase-activating protein GAP1^{IP4BP}

Gyles COZIER, Richard SESSIONS, Joanna R. BOTTOMLEY, Jon S. REYNOLDS and Peter J. CULLEN[1]
Department of Biochemistry, School of Medical Sciences, University of Bristol, Bristol BS8 1TD, U K

GAP1^{IP4BP} is a Ras GTPase-activating protein (GAP) that *in vitro* is regulated by the cytosolic second messenger inositol 1,3,4,5-tetrakisphosphate [Ins(1,3,4,5)P$_4$]. We have studied Ins(1,3,4,5)P$_4$ binding to GAP1^{IP4BP}, and shown that the inositol phosphate specificity and binding affinity are similar to Ins(1,3,4,5)P$_4$ binding to Bruton's tyrosine kinase (Btk), evidence which suggests a similar mechanism for Ins(1,3,4,5)P$_4$ binding. The crystal structure of the Btk pleckstrin homology (PH) domain in complex with Ins(1,3,4,5)P$_4$ has shown that the binding site is located in a partially buried pocket between the $\beta1/\beta2$- and $\beta3/\beta4$-loops. Many of the residues involved in the binding are conserved in GAP1^{IP4BP}. Therefore we generated a model of the PH domain of GAP1^{IP4BP} in complex with Ins(1,3,4,5)P$_4$ based on the Btk–Ins(1,3,4,5)P$_4$ complex crystal structure. This model had the typical PH domain fold, with the proposed binding site modelling well on the Btk structure. The model has been verified by site-directed mutagenesis of various residues in and around the proposed binding site. These mutations have markedly reduced affinity for Ins(1,3,4,5)P$_4$, indicating a specific and tight fit for the substrate. The model can also be used to explain the specificity of inositol phosphate binding.

Key words: GAP, GTPase-activating protein, PIP$_3$, PH domain, Ras.

INTRODUCTION

Pleckstrin homology (PH) domains are independent protein modules of approximately 120 amino acids that were initially identified as regions of weak sequence similarity repeated in pleckstrin [1,2]. Subsequently more than 100 different PH domain-containing proteins have been identified, many of which are involved in intracellular signalling. These include protein kinases [Bruton's tyrosine kinase (Btk), β-adrenergic receptor kinase (β-ARK), protein kinase B and phosphomositide-dependent kinase-1], all phospholipase C (PLC) isoforms, the insulin receptor substrates (IRS-1 and -2), the phosphoinositide 3-kinase p110γ subunit, ADP-ribosylation factor (ARF) guanine nucleotide exchange factors, general receptor for phosphoinositides-1 (GRP1), cytohesin-1 and ARF nucleotide-binding site opener (ARNO) and the dynamin GTPase [3–5].

Recently our appreciation of PH domains has dramatically increased following the observation that certain PH domains contain specific binding sites for various phosphoinositides. For example, the PH domains of both PLC-δ_1 and β-spectrin specifically bind PtdIns(4,5)P$_2$ and its soluble inositol head group Ins(1,4,5)P$_3$, albeit with distinct affinities {K_d of PLC-δ_1 for Ins(1,4,5)P$_3$ is 210 nM; K_d of β-spectrin for Ins(1,4,5)P$_3$ is 40 μM [6–9]}. In the case of the PH domain from PLC-δ_1, its ability to bind PtdIns(4,5)P$_2$ results in the targeting of this protein to the plasma membrane [10]. Interestingly, since PLC-δ_1 hydrolyses PtdIns(4,5)P$_2$ to generate Ins(1,4,5)P$_3$, the *in vivo* membrane localization of PLC-δ_1 appears to be a reversible process governed by whether the PH domain is bound to PtdIns(4,5)P$_2$ or Ins(1,4,5)P$_3$ [11,12].

In contrast, the PH domain from Btk specifically binds PtdIns(3,4,5)P$_3$ and its corresponding soluble inositol head group, Ins(1,3,4,5)P$_4$ [13,14]. *In vivo* this PtdIns(3,4,5)P$_3$-binding results in the PH domain-dependent recruitment of Btk from the cytosol to the plasma-membrane following agonist stimulation [15]. A similar plasma-membrane recruitment has also been described for the PtdIns(3,4,5)P$_3$/Ins(1,3,4,5)P$_4$-binding PH domains from the ARF-exchange factors GRP1, cytohesin-1 and ARNO, and the Ras GTPase-activating protein GAP1^m ([16,17] and references therein). It is unclear, however, whether in a manner analogous to that of PLC-δ_1, the plasma-membrane association of these proteins is regulated by the interaction of their PH domains with either plasma-membrane PtdIns(3,4,5)P$_3$ or cytosolic Ins(1,3,4,5)P$_4$.

GAP1^m is a member of the GAP1 family of Ras GTPase-activating proteins (GAPs), which also contains GAP1^{IP4BP} and Ras GTPase-activating-like ('RASAL') (reviewed in [18] and see 19). As with Btk, both GAP1^{IP4BP} and GAP1^m contain C-terminal Ins(1,3,4,5)P$_4$-binding PH domains [20–22]; however, in contrast with GAP1^m, the available data suggest that the function of GAP1^{IP4BP} may be regulated not by PtdIns(3,4,5)P$_3$ but by Ins(1,3,4,5)P$_4$. For example, GAP1^{IP4BP} is predominantly a plasma-membrane-localized protein [21,23,24] which, from *in vitro* plasma-membrane-based liposomes assays, appears unable to function as a Ras GAP unless Ins(1,3,4,5)P$_4$ is present [25]. Importantly, the ability of Ins(1,3,4,5)P$_4$ to regulate the Ras GAP activity of GAP1^{IP4BP} is not affected by the presence of PtdIns(3,4,5)P$_3$ [25]. Furthermore, there is compelling evidence that GAP1^{IP4BP} is involved in what is now a well-established phenomenon whereby Ins(1,3,4,5)P$_4$ influences Ca^{2+} mobilization

---

Abbreviations used ARF, ADP-ribosylation factor, ARNO, ARF nucleotide-binding site opener, β-ARK, β-adrenergic receptor kinase; Btk, Bruton's tyrosine kinase; GAP, GTPase-activating protein, GRP1, general receptor for phosphoinositides-1, GST, glutathione S-transferase, PH, pleckstrin homology, PLC, phospholipase C; SOS1, son-of-sevenless 1, 3-D, three-dimensional.

[1] To whom correpondence should be addressed (e-mail Pete.Cullen@bristol.ac.uk)

induced by Ins(1,4,5)P_3 in permeabilized L-1210 cells [26,27]. Together these data suggest that GAP1^{IP4BP} may function *in vivo* as an unique receptor for Ins(1,3,4,5)P_4 rather than PtdIns(3,4,5)P_3.

The three-dimensional (3-D) structures of PH domains from seven different proteins have so far been determined, namely those from pleckstrin [28], β-spectrin [9,29,30], dynamin [31–34], PLC-δ_1 [7], son-of-sevenless 1 (SOS1) [35,36], Btk [37,38] and β-ARK [39]. Despite sharing sequence identity which averages only 10–20 %, all of these structures share the same overall topology, i.e. seven β-strands arranged in two almost orthogonal β-sheets (β1–β4 and β5–β7) capped on one side by a C-terminal α-helix. Each of these structures contain clusters of lysine and arginine residues that form a positively-charged surface, which interacts with the negatively-charged phosphate groups of their respective phosphoinositide ligands The precise manner of phosphoinositide binding has only been inferred from crystal structures of Ins(1,4,5)P_3 bound to the PH domains of β-spectrin [9] and PLC-δ_1 [7], and of Ins(1,3,4,5)P_4 bound to the PH domain of Btk [38]. Intriguingly whereas the Ins(1,4,5)P_3-binding site in β-spectrin comprises the β1/β2- and β5/β6-loops, the PLC-δ_1 PH domain binds Ins(1,4,5)P_3 through residues from the β1/β2- and β3/β4-loops. From studies using NMR the ligand binding described for PLC-δ_1 appears to also be present in the PH domains from dynamin [40,41] and SOS1 [35], and has also been loosely characterized on the N-terminal pleckstrin and β-ARK PH domains [42,43] A 3-D structure of the ligand-free R28C mutant of the Btk PH domain has been described, and mutational analysis has suggested an analogous phosphoinositide-binding site to that of PLC-δ_1 [37,41]. This has recently been confirmed by the structure of the wild-type Btk PH domain being solved in complex with Ins(1,3,4,5)P_4 [38]. Interestingly, although the Ins(1,3,4,5)P_4 is bound in an equivalent binding pocket to Ins(1,4,5)P_3 in PLC-δ_1, it is in a different orientation, being rotated 180 ° about the P1–P4 axis [38].

In the present study we have compared, in detail, the binding of Ins(1,3,4,5)P_4 to the PH domains of Btk and GAP1^{IP4BP}. This has established that these proteins bind Ins(1,3,4,5)P_4 with similar affinities and importantly almost identical specificities, evidence which suggests a similar mechanism of Ins(1,3,4,5)P_4-binding. Therefore we have used the 3-D structure of Btk in complex with Ins(1,3,4,5)P_4 to obtain a molecular model describing the Ins(1,3,4,5)P_4-binding site within the GAP1^{IP4BP} PH domain. This model, which has been verified through the analysis of a number of site-directed mutants, explains the molecular nature of the high-affinity isomer-specific binding of Ins(1,3,4,5)P_4 to GAP1^{IP4BP}.

EXPERIMENTAL

Expression and purification of GAP1^{IP4BP} and GAP1^{IP4BP} mutants

Both wild-type and mutagenic glutathione S-transferase (GST)–GAP1^{IP4BP} fusion proteins were isolated as follows. An overnight 20 ml culture was used to inoculate four 2.5 l conical flasks, each containing 500 ml of Luria–Bertani broth, 50 μg/ml ampicillin and 25 μg/ml kanamycin. The cells were cultured at 25 °C until D_{600} reached 0.6. Protein expression was then induced by the addition of 0.1 mM isopropyl β-D-thiogalactoside, followed by a further 4 h incubation prior to harvesting the bacteria by centrifugation (3000 g for 10 min at 4 °C). All of the subsequent steps were carried out at 4 °C. The bacterial pellet was gently resuspended in 40 ml of PBS buffer (pH 7 2), containing 1 mM EDTA, 1 mM EGTA, 1 mM β-mercaptoethanol and 0.1 mM PMSF, and sonicated for 3 periods of 15 s, with 3 min on ice between each sonication Triton X-100 [1 % (v/v), final concentration] was added and the suspension was left stirring for 45 min on ice prior to the addition of lysozyme (2 mg/ml, final concentration). This was incubated for a further 15 min, before cell debris was removed by centrifugation (36000 g for 30 min). The supernatant was removed and 2 ml of a 1:1 suspension of glutathione–agarose beads (washed and pre-swollen with several volumes of PBS buffer) was added and incubated on a rotating wheel overnight. The beads were pelleted by centrifugation and washed sequentially with 3 × 20 ml of PBS containing 0.1 % (v/v) Triton X-100, followed by 75 mM Tris/HCl (pH 8.0) containing 0.1 % (v/v) Triton X-100 and 500 mM NaCl. The beads were finally washed with 4 × 20 ml of PBS. The GST fusion protein was liberated by eluting with 3 × 1 ml of 75 mM Tris/HCl (pH 8.0), 1 M NaCl, 0.5 % (w/v) CHAPS and 20 mM glutathione at room temperature over the course of 1 h. The eluants were pooled and concentrated using a Centricon apparatus (Amicon, Conneticut, MA, U.S.A.)

Site-directed mutagenesis of the GAP1^{IP4BP} PH domain

This was performed as previously described [21,22] using the Transformer Kit® (ClonTech Laboratories, Basingstoke, Hants., U.K.) and pCIneo-GAP1^{IP4BP} as the template. Primers used were as follows· K585R, 5′-GAAGGGTTCATGATCAGGAGGGCCCAAGGACGG-3′; A587F, 5′-TTCATGATCAAGAGGTTCCAAGGACGGAAGCGC-3′; N597D, 5′-TTTGGGATGAAGGATTTTAAGAAGAGATGG-3′; F598Q, 5′-TTTGGGATGAAGAATCAGAAGAAGAGATGGTTTC-3′; R601K, 5′-GATGAAGAATTTTAAGAAGAAGTGGTTTCGTTTGACCAAC-3′; R601C, 5′-GATGAAGAATTTTAAGAAGTGCTGGTTTCGTTTGACCAAC-3′; K614E, 5′-GAATTTACCTACCACGAAAGCAAAGGGGACCAG-3′; W668F, 5′-GTGGAGGCCAAGGACTTTATCGACATTCTCACC-3′. In each case the underlined codon describes the particular mutation.

[^{32}P]Ins(1,3,4,5)P_4-binding assays

The binding of radiolabelled Ins(1,3,4,5)P_4 was performed as previously described [21]. An individual binding assay contained 100 mM KCl, 20 mM NaCl, 1 mM EDTA, 30000 d.p.m. of [^{32}P]Ins(1,3,4,5)P_4 (prepared as in [21]), 0.5 μg of GST fusion protein and various concentrations of competing unlabelled inositol phosphates in 10 mM Hepes/NaOH (pH 7.0) buffer, to a final volume of 0.5 ml. Equilibrium binding was achieved by a 15 min incubation at 4 °C, after which the receptor complex was precipitated by the addition of 100 μl of 5 mg/ml γ-globulin and 1 ml of 25 % (w/v) poly(ethylene glycol) in Hepes/NaOH buffer (pH 7.0) containing 100 mM KCl, 20 mM NaCl and 1 mM EDTA and incubated at 4 °C for 10 min. The precipitated proteins were pelleted by centrifugation (21000 g for 10 min) and washed with ice-cold water prior to counting. Non-specific binding was defined as the binding remaining in the presence of 10 μM unlabelled Ins(1,3,4,5)P_4.

Molecular modelling

All analysis and modelling of the PH domains was performed using the program packages Quanta/CHARMm and InsightII. The alignment of PLC-δ_1 and Btk was structure-based, with the GAP1^{IP4BP} PH domain being aligned by sequence, initially using Omiga and then refined by hand where necessary. Any insertions or deletions in the aligned sequences were, where possible, introduced in the loop regions, rather than in the β-sheet or α-helical regions. The backbone co-ordinates of aligned residues, and the side-chain co-ordinates of the identical amino acids, in

Btk were then mapped to the equivalent amino acids in the model. Where insertions or deletions occurred in the sequence that was being modelled, a fragment database [43] was used to search for short sequences that overlapped with the structure either side of the unknown region and which contained the same number of residues. The best-fit fragment was then used in the model structure. After defining the backbone co-ordinates the validity of the emerging structure was assessed using the Protein Health module in Quanta. The irregularities identified were either re-modelled manually or by re-using the fragment database. The non-identical amino acids were modelled in their most likely rotameric form and major side-chain clashes were removed manually.

To form the binding site, the Ins(1,3,4,5)P_4 was positioned in the same position and orientation as observed in the Btk–Ins(1,3,4,5)P_4 complex. Conserved residues in the binding site were fixed so as to retain the interactions with Ins(1,3,4,5)P_4, and other side chains were manually positioned to maximize interactions and minimize steric hindrance. The InsightII Discover program was then used to perform an energy minimization using a 5 Å (1 Å = 0.1 nm) layer of water and applying constraints to preserve the basic backbone structure as copied from Btk [the backbone constraints were 100 kcal/Å^2 for 200 iterations, 50 kcal/Å^2 for 200 iterations, 20 kcal/Å^2 for 200 iterations, 5 kcal/Å^2 for 500 iterations, 0.5 kcal/Å^2 for 500 iterations and 0 kcal/Å^2 for 4000 iterations (1 cal ≡ 4.184 J)]. The automatic parameter function of InsightII was used to assign force-field parameters to the Ins(1,3,4,5)P_4 molecule, and these were checked to ensure that appropriate potentials were used. The final structure was checked for abnormalities and inconsistencies using the Protein Health option in Quanta.

Materials

Inositol phosphates were generously given by Professor Robin Irvine (Department of Pharmacology, University of Cambridge, U.K.), Professor Barry Potter (Department of Pharmacology, University of Bath, U.K.) and Dr Young-Tae Chang (Department of Chemistry, Pohang University of Science and Technology, Pohang 790-784, South Korea).

RESULTS

Analysis of the affinity and inositol phosphate specificity of [^{32}P]Ins(1,3,4,5)P_4-binding to the PH domains from Btk and GAP1^{IP4BP}

Table 1 describes the affinity and inositol phosphate specificity of Ins(1,3,4,5)P_4-binding to the PH domain of recombinant GAP1^{IP4BP}. From these experiments the following were readily apparent. Firstly, D/L-Ins(1,3,4,5)P_4 was half as potent as D-Ins(1,3,4,5)P_4, consistent with L-Ins(1,3,4,5)P_4 being weaker than the D-isomer. Secondly, any inositol tetrakisphosphate with a phosphate on the 2-axial position was essentially inactive Thirdly, there was some tolerance for a 6-phosphate [Ins-(1,3,4,5,6)P_5 compared with Ins(1,3,4,5)P_4], and a 1-phosphate considerably strengthened binding {Ins(3,4,5,6)P_4 compared with Ins(1,3,4,5,6)P_5 [44] and also Ins(3,4,5)P_3 compared with Ins(1,3,4,5)P_4 [45]}. Finally, both a 3-, 4- and 5-phosphate were essential [Ins(1,4,5)P_3 compared with Ins(1,3,4,5)P_4, Ins(1,3,5)P_3 compared with Ins(1,3,4,5)P_4, and Ins(1,3,4)P_3 compared with Ins(1,3,4,5)P_4], although addition of a 6-phosphate slightly increased the binding affinity [Ins(1,4,5)P_3 compared with Ins(1,4,5,6)P_4]. Thus the Ins(1,3,4,5)P_4-binding site within GAP1^{IP4BP} primarily recognized the 1-, 3-, 4- and 5-phosphates, with no tolerance for a 2-axial phosphate and limited tolerance for a 6-phosphate.

Table 1 Comparison of the affinity and inositol phosphate specificity of the Ins(1,3,4,5)P_4 binding sites present within the PH domains of GAP1^{IP4BP} and Btk

[^{32}P]Ins(1,3,4,5)P_4-binding was performed as described in the Experimental section In each case IC_{50} values (means ± S E M.) were obtained from three individual experiments performed on distinct protein preparations. n.d., not determined

	IC_{50} (nM)	
Inositol phosphate	GST–Btk PH domain	GST–GAP1^{IP4BP}
D-Ins(1,3,4,5)P_4	57.2 ± 3.4	11.3 ± 3.2
D/L-Ins(1,2,4,5)P_4	4572 ± 321	2231 ± 112
D/L-Ins(1,2,4,6)P_4	2874 ± 129	1086 ± 56.1
Ins(1,2,3,5)P_4	> 10000	> 5000
Ins(1,3,4,6)P_4	> 10000	2793 ± 231
Ins(2,4,5,6)P_4	> 10000	2658 ± 321
D/L-Ins(1,2,5,6)P_4	> 10000	5000
D/L-Ins(1,2,3,4)P_4	> 10000	5000
D/L-Ins(1,4,5,6)P_4	3212 ± 235	632.9 ± 189
D/L-Ins(1,3,4,5)P_4	92.4 ± 9.4	26.4 ± 9.1
D-Ins(1,4,5)P_3	> 10000	> 5000
D-Ins(1,3,4)P_3	> 10000	> 5000
D-Ins(1,3,5)P_3	n.d.	> 1000
D-Ins(1,3,5,6)P_4 [= L-Ins(1,3,4,5)P_4]	n.d.	96.3 ± 9.1
D-Ins(1,3,4,5,6)P_5	442.3 ± 14.3	85.0 ± 4.5
InsP_6	833.2 ± 15.7	646.7 ± 28.7

Importantly, by directly comparing the pharmacological profile of Ins(1,3,4,5)P_4-binding to GAP1^{IP4BP} with that of the Btk PH domain, it was readily apparent that, of the inositol phosphates tested, a similar specificity was observed (see Table 1). This suggests that the manner through which the PH domains of GAP1^{IP4BP} and Btk bind Ins(1,3,4,5)P_4 are very similar.

Molecular modelling of the GAP1^{IP4BP} PH domain

In an attempt to explain, at the molecular level, the pharmacological details of Ins(1,3,4,5)P_4-binding to GAP1^{IP4BP} we have generated a molecular model of the GAP1^{IP4BP} PH domain in complex with Ins(1,3,4,5)P_4. As various PH domain structures have been solved, there was a choice of which structure to use as the basis for the modelling. Structures of three PH domains have been determined as complexes with inositol phosphates: PLC-δ_1 [7] and β-spectrin [9] in complex with Ins(1,4,5)P_3 and Btk [38] in complex with Ins(1,3,4,5)P_4. PLC-δ_1 and β-spectrin bound the Ins(1,4,5)P_3 in different pockets, located on opposite sides of the $\beta 1/\beta 2$ loop. In the PLC-δ_1–Ins(1,4,5)P_3 complex there are more interactions with the Ins(1,4,5)P_3 than in the β-spectrin/Ins(1,4,5)P_3 structure, an observation possibly explaining why Ins(1,4,5)P_3 binds with a much higher affinity to PLC-δ_1 than it does to β-spectrin [6–9]. In the Btk PH domain structure the Ins(1,3,4,5)P_4 was bound in an equivalent pocket with many similar interactions to that observed for Ins(1,4,5)P_3 in PLC-δ_1 [38]. However, the orientation of Ins(1,3,4,5)P_4 in the Btk structure is rotated 180 ° about the P1-P4 axis when compared with Ins(1,4,5)P_3 in PLC-δ_1 [38]. Table 2 shows that PLC-δ_1 and Btk have some residues, which interact with the substrate, that are conserved and some that are similar. Both PH domains also have additional residues that interact with the substrates, which may help to give the different specificities of the proteins. Since the data in Table 1 demonstrated that Btk interacted with Ins(1,3,4,5)P_4 with a similar affinity and pharmacology as

Table 2 Comparison of the residues involved in binding of the inositol phosphate substrates in PLC-δ_1, Btk and the model GAP1^{IP4BP}

Bold type indicates residues that interact with the substrate and normal type indicates residues that do not interact with the substrate. In parentheses are shown the phosphates with which that residue interacts and whether it is via the side chain (sc) or backbone (bb) of that residue.

PLC-δ_1	Btk	GAP1^{IP4BP}
Lys^{30} (4+5, sc)	**Lys^{12} (3+4, sc)**	**Lys^{586} (3+4, sc)**
Lys^{32} (4, sc)	Ser^{14}	Ala^{587}
Ser^{33}	**Gln^{15} (4, bb)**	**Gln^{588} (4, bb)**
Ser^{34}	**Gln^{16} (5, bb)**	**Gly^{589} (5, bb)**
–	**Lys^{17} (5, bb)**	**Arg^{590} (5, bb)**
–	**Lys^{18} (5, sc+bb)**	**Lys^{591} (5, sc+bb)**
–	Lys^{19}	Arg^{592}
–	**Ser^{21} (5, sc)**	Gly^{594}
Trp^{36} (1, sc)	**Asn^{24} (1, sc)**	**Asn^{597} (1, sc)**
Arg^{38} (1, sc)	**Lys^{26} (1, sc)**	**Lys^{599} (1, sc)**
Arg^{40} (5, sc)	**Arg^{28} (3, sc)**	**Arg^{601} (3, sc)**
Gln^{53}	**Tyr^{39} (4, sc)**	**Tyr^{612} (4, sc)**
Ser^{55} (5, sc)	Glu^{41}	Lys^{614}
Arg^{56} (5, sc)	Tyr^{42}	Ser^{615}
Lys^{57} (4+5, sc)	Asp^{43}	Lys^{616}

GAP1^{IP4BP}, and a comparison of the residues involved in binding the substrates showed that GAP1^{IP4BP} had greater similarity to Btk than PLC-δ_1 (Table 2), it was decided to use the recently solved structure of the Btk PH domain–Ins(1,3,4,5)P_4 complex (solved to 2.4 Å resolution [38]) to create the model GAP1^{IP4BP}–Ins(1,3,4,5)P_4 complex structure.

The sequences used for modelling were 1–170 of Btk and 574–714 of GAP1^{IP4BP}. Although the alignment of the sequence for the PH domain of GAP1^{IP4BP} (Figure 1) did not show a high degree of identity with Btk (32%), it was possible to produce a model structure with the typical PH domain fold (Figure 2) and similar Ins(1,3,4,5)P_4-binding sites.

As stated above, although PLC-δ_1 and Btk bound the substrates in equivalent pockets, the orientation of the inositol phosphates differed by being rotated 180° about the P1–P4 axis. Because of the symmetry of Ins(1,3,4,5)P_4 about the P1–P4 axis, either orientation would have little effect on the position of the phosphates in the Btk binding site. This is highlighted by many interactions between the protein and substrate being conserved or similar in PLC-δ_1 and Btk; that is, many interactions are conserved even though the substrates are in different orientations. It is possible to place Ins(1,3,4,5)P_4 into the GAP1^{IP4BP} model structure in either orientation and retain all of the interactions with the phosphates. However, another effect of the rotation is to swap the position of the 2- and 6-hydroxyls; as the 2-hydroxyl is axial and the 6-hydroxyl is equatorial, any interactions with the hydroxyls in one orientation of the Ins(1,3,4,5)P_4 are unlikely to be retained in the other orientation. PLC-δ_1 has no direct interactions with the hydroxyls of Ins(1,4,5)P_3, but in Btk Ser^{21} interacts with the 6-hydroxyl, and Lys^{12} and Asn^{24} interact with the 2-hydroxyl. In GAP1^{IP4BP}, Lys^{12} and Asn^{24} of Btk are conserved (Lys^{586} and Asn^{597} in GAP1^{IP4BP}), but Ser^{21} of Btk is replaced by Gly^{594} in GAP1^{IP4BP}. As two of the residues that interact with the hydroxyls in Btk are conserved in GAP1^{IP4BP}, and because the binding affinities of Btk and GAP1^{IP4BP} for Ins(1,3,4,5)P_4 are similar, it was decided to use the orientation of the Ins(1,3,4,5)P_4 in Btk for the model GAP1^{IP4BP}–Ins(1,3,4,5)P_4 complex structure.

A comparison of the residues from Btk, PLC-δ_1 and the model GAP1^{IP4BP} that are important in binding the inositol phosphates (Table 2) showed similarities between these high-affinity binding sites. Some of these residues are conserved in all three proteins (Lys^{12} and Arg^{28} of Btk; Lys^{586} and Arg^{601} of GAP1^{IP4BP}; Lys^{30} and Arg^{40} of PLC-δ_1), while others, although not identical, have similar functions (Asn^{24} and Lys^{26} of Btk; Asn^{597} and Lys^{599} of GAP1^{IP4BP}; Trp^{36} and Arg^{38} of PLC-δ_1). PLC-δ_1 has extra residues that interact with the 4- and 5-phosphates of Ins(1,4,5)P_3 that are not in Btk or GAP1^{IP4BP}, which is consistent with PLC-δ_1 having a higher affinity for Ins(1,4,5)P_3 compared with the affinity of either Btk or GAP1^{IP4BP} for Ins(1,4,5)P_3. The residues in the binding site of the model GAP1^{IP4BP} have a higher similarity to Btk than PLC-δ_1, which is consistent with the substrate specificities and, as stated above, was one of the

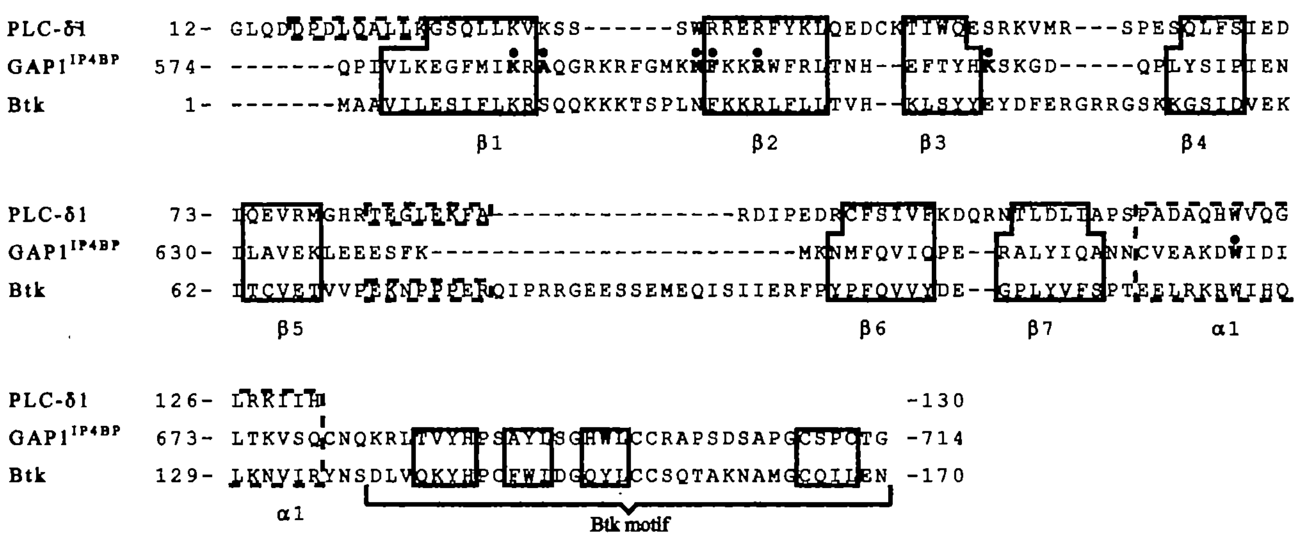
PLC-δ1 12- GLQDDEDLQALLKGSQLLKVKSS------SWRRERFYKLQEDCKTIWQESRKVMR---SPESQLFSIED
GAP1IP4BP 574- -------QPIVLKEGFMIKRAQGRKRFGMKNFKKRWFRLTNH--EFTYHKSKGD-----QPLYSIPIEN
Btk 1- -------MAAVILESIFLKRSQQKKKTSPLNFKKRLFLLTVH--KLSYYEYDFERGRRGSKKGSIDVEK
β1
β2
β3
β4
PLC-δ1 73- IQEVRMGHRTEGLEKFA----------------RDIPEDRCFSIVFKDQRNTLDLIAPSPADAQHWVQG
GAP1IP4BP 630- ILAVEKLEEESFK-----------------------MKNMFQVIQPE--RALYIQANNCVEAKDWIDI
Btk 62- ITCVETVVPEKNPPPERQIPRRGEESSEMEQISIIERFPYPFQVVYDE--GPLYVFSPTEELRKRWIHQ
β5
β6
β7
α1
PLC-δ1 126- LRKIIH -130
GAP1IP4BP 673- LTKVSQCNQKRLTVYHPSAYLSGHWLCCRAPSDSAPGCSPQTG -714
Btk 129- LKNVIRYNSDLVQKYHPCFWIDGQYLCCSQTAKNAMGCQILEN -170
α1
Btk motif

Figure 1 Sequence alignment of the PH domains from PLC-δ_1, GAP1^{IP4BP} and Btk

The alignment between PLC-δ_1 and Btk is structure based, with the GAP1^{IP4BP} PH domain being aligned based on sequence β-sheets are highlighted by solid boxes and α-helical regions by dashed boxes The secondary-structural features conserved in PH domains are labelled β1–β7 and α1 Residues mutated in GAP1^{IP4BP} are indicated by ●

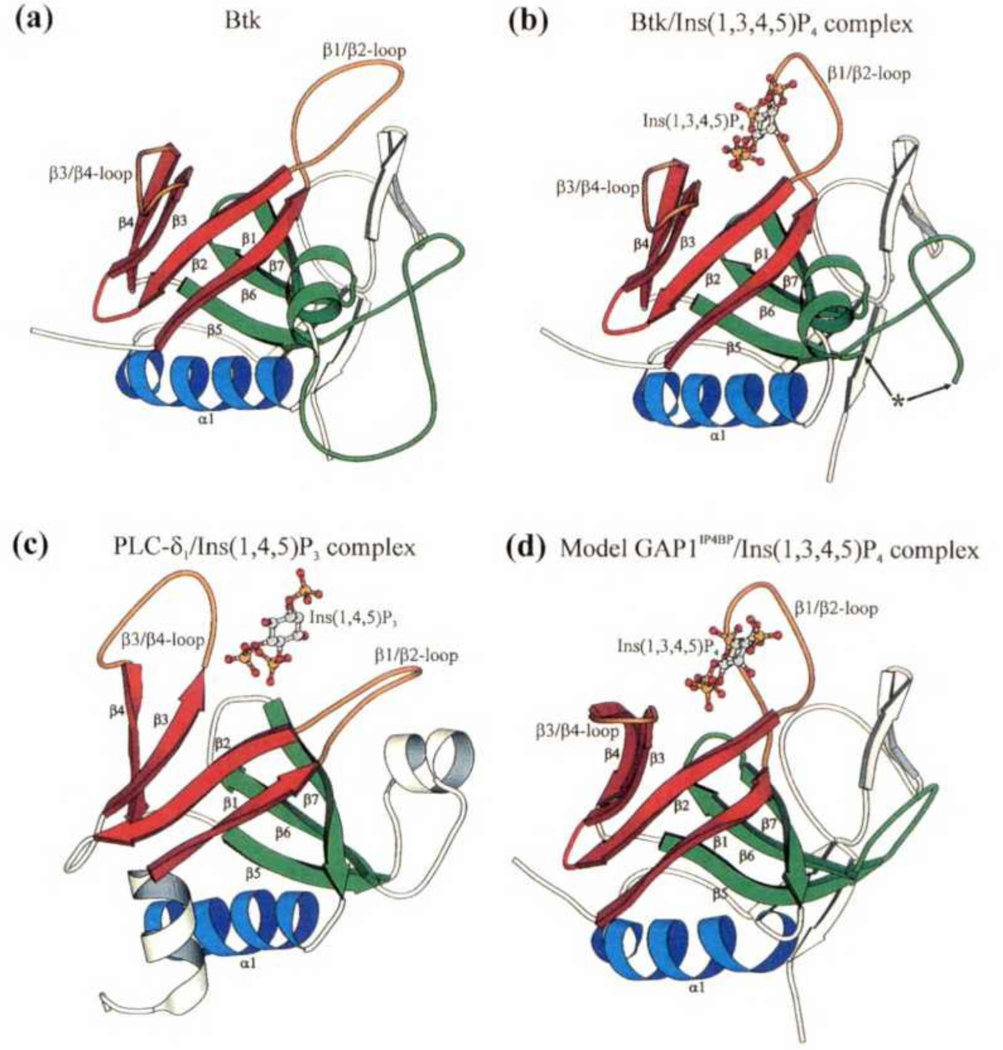

Figure 2 Schematic representation of the backbone of (a) R28C Btk crystal structure, (b) crystal structure of wild type Btk in complex with Ins(1,3,4,5)P_4, (c) crystal structure of PLC-δ_1 in complex with Ins(1,4,5)P_3 and (d) the model structure of GAP1^{IP4BP} in complex with Ins(1,3,4,5)P_4

The structural features conserved in PH domains are labelled $\beta1$–$\beta7$ and $\alpha1$. The $\beta1/\beta2$- and $\beta3/\beta4$-loops shown to be involved in Ins(1,4,5)P_3 binding by PLC-δ_1 and Ins(1,3,4,5)P_4 binding by Btk are highlighted. The Ins(1,4,5)P_3 and Ins(1,3,4,5)P_4 groups are shown as ball-and-stick structures. The Btk residues 83–88 were not clearly visible in the electron density map. The * in (**b**) indicates the gap this region would occupy. This Figure was generated using Molscript [49].

reasons for modelling the structure of GAP1^{IP4BP} on to Btk rather than PLC-δ_1.

The major differences between the model of the GAP1^{IP4BP} PH domain and the Btk crystal structure occurred in the loop regions, particularly the $\beta3/\beta4$- and $\beta5/\beta6$-loops (Figure 2). The $\beta5/\beta6$-loop in Btk has an α-helical insertion that is not found in GAP1^{IP4BP}, but instead there is just a short loop between the $\beta5$- and $\beta6$-strands. In Btk the $\beta3/\beta4$-loop is 12 residues long and forms a random coil with no interactions with the Ins(1,3,4,5)P_4. In contrast, the $\beta3/\beta4$-loop of GAP1^{IP4BP} is smaller, being only seven residues in length, and contains basic residues that could interact with the substrate. However, modelling this region on the Btk structure orientated the loop away from the Ins(1,3,4,5)P_4 binding site (Figure 2) and therefore there were no interactions between this loop and Ins(1,3,4,5)P_4 in the model structure. This is in contrast with the $\beta3/\beta4$-loop of PLC-δ_1, which forms part of the binding site and provides interactions to the bound Ins(1,4,5)P_3. The $\beta3/\beta4$-loop of GAP1^{IP4BP} is more similar in size to PLC-δ_1, which may suggest that it could interact with the substrate. However, as the binding characteristics for GAP1^{IP4BP} were very similar to Btk, it was decided to leave the $\beta3/\beta4$-loop based on the Btk structure.

To account for the much higher affinity of GAP1^{IP4BP} for Ins(1,3,4,5)P_4 than Ins(1,4,5)P_3 (K_d of 11.3 ± 3.2 compared with > 5000 nM), there must be some interactions which only occur when the 3-phosphate is present. Based on the model structure, these interactions are probably from the $\beta1/\beta2$-loop, which in the GAP1^{IP4BP} PH–Ins(1,3,4,5)P_4 model structure is adjacent to the 5-phosphate. As the structure of the PLC-δ_1–Ins(1,4,5)P_3 complex was solved prior to the Btk–Ins(1,3,4,5)P_4 structure, it was proposed that the 3-phosphate would interact with the $\beta1/\beta2$-loop. Based on this, two characteristics of the $\beta1/\beta2$-loop were proposed to play important roles in binding 3-phosphorylated inositol products [43]. Firstly a non-bulky residue at the start of the loop is required to allow space for the additional phosphate (e.g. Ser^{14} in Btk) and secondly the loop

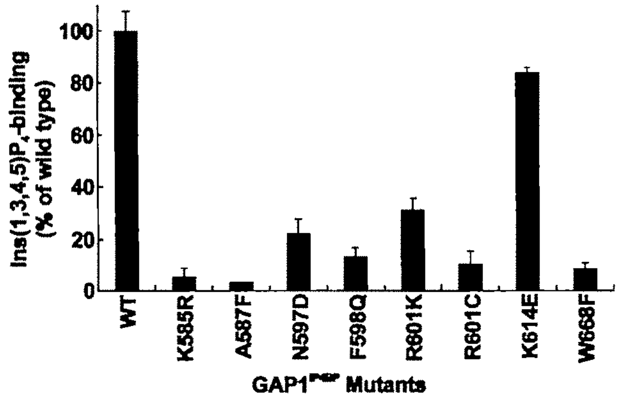

Figure 3 Mutational analysis of Ins(1,3,4,5)P$_4$-binding to the PH domain of GAP1^{IP4BP}

The ability of the GAP1^{IP4BP} mutants to bind [^{32}P]Ins(1,3,4,5)P$_4$ is shown. Binding was performed as described in the Experimental section on protein purified from prokaryotic expression. Data are means ± S.E.M. ($n = 3$)

has to be at least six residues in length to be flexible enough to bend around the 3-phosphate [43]. Although the Btk–Ins(1,3,4,5)P$_4$ structure showed that it was the 5-phosphate which was orientated towards the $\beta1/\beta2$-loop, the same characteristics of the loop would need to be fulfilled. In GAP1^{IP4BP} the $\beta1/\beta2$-loop comprises 11 amino acids, the first being an alanine residue (Ala^{587}), which allows space for the 5-phosphate. In the Btk–Ins(1,3,4,5)P$_4$ complex structure, the 5-phosphate has interactions with the backbone nitrogens of Gln^{16}, Lys^{17} and Lys^{18}, and also with the side chain of Lys^{18}. The $\beta1/\beta2$-loop of GAP1^{IP4BP} modelled well on to the Btk structure; the backbone interactions with the 5-phosphate were retained (Gly^{589}, Arg^{590} and Lys^{591} in GAP1^{IP4BP}) and Lys^{18} of Btk is conserved (Lys^{591} in GAP1^{IP4BP}).

The first structure of Btk solved was of the R28C mutant. In this structure the $\beta1/\beta2$-loop is pointing away from the binding pocket and is flush with the surface of the protein. However, in the Btk–Ins(1,3,4,5)P$_4$ complex, the loop is perpendicular to the protein surface and interacts with the 5-phosphate. The majority of the interactions with the 5-phosphate are from the backbone nitrogens, with only Lys^{18} providing a side-chain interaction. This suggests that as Ins(1,3,4,5)P$_4$ enters the binding site the 5-phosphate initially interacts with the $\beta1/\beta2$-loop main chain, causing a conformational change in this loop. This conformational change is probably similar to the difference observed in the $\beta1/\beta2$-loop between the structures of the R28C mutant and the Btk–Ins(1,3,4,5)P$_4$ complex. Based on the similarities between the Btk–Ins(1,3,4,5)P$_4$ crystal structure and the model GAP1^{IP4BP}–Ins(1,3,4,5)P$_4$ structure, a similar conformational change in the $\beta1/\beta2$-loop of GAP1^{IP4BP} may occur upon Ins(1,3,4,5)P$_4$ binding. If Ins(1,4,5)P$_3$ entered the binding site of Btk or GAP1^{IP4BP}, then, with no 3-phosphate present, a similar orientation of substrate as observed in the PLC-δ_1–Ins(1,4,5)P$_3$ complex would be likely (that is, maximize the interactions with residues already in the binding site). Therefore there would be no phosphate to cause the conformational change in the $\beta1/\beta2$-loop, and so overall there would be fewer interactions between protein and substrate. In other words the higher affinity of GAP1^{IP4BP} for Ins(1,3,4,5)P$_4$ over Ins(1,4,5)P$_3$ arises because of the interactions between the $\beta1/\beta2$-loop and the 5-phosphate of Ins(1,3,4,5)P$_4$, but the interactions will only occur if the 3-phosphate is present to allow the substrate to adopt the rotated conformation.

[^{32}P]Ins(1,3,4,5)P$_4$-binding to site-directed mutants within the PH domain of GAP1^{IP4BP}

Prior to generating the model of the GAP1^{IP4BP} PH–Ins(1,3,4,5)P$_4$ complex we have previously isolated a number of site-directed mutants within the GAP1^{IP4BP} PH domain that corresponded to mutations known to effect Ins(1,3,4,5)P$_4$-binding to Btk [37,41,46]. These mutants, expressed as full-length GST–GAP1^{IP4BP} fusion proteins, were analysed with respect to their ability to bind Ins(1,3,4,5)P$_4$. As shown in Figure 3 [^{32}P]Ins(1,3,4,5)P$_4$-binding to the GAP1^{IP4BP} K585R, A587F, F598Q, R601C and W668F mutants was dramatically inhibited whereas binding to the N597D and R601K mutants was inhibited by approximately 81.4 ± 3.1 and 75.4 ± 4.1 %, respectively ($n = 3$). The lack of Ins(1,3,4,5)P$_4$-binding to these mutants made the subsequent detailed analysis of the affinity and specificity of Ins(1,3,4,5)P$_4$ practically impossible. However, in the case of GAP1^{IP4BP} K614E, in which Ins(1,3,4,5)P$_4$-binding was only inhibited by 15.2 ± 3.1 %, a detailed pharmacological analysis of this binding activity was performed.

[^{32}P]Ins(1,3,4,5)P$_4$ bound to recombinant GAP1^{IP4BP} K614E with a K_d value for Ins(1,3,4,5)P$_4$ of 109.1 ± 5.2 nM ($n = 3$), with the other inositol phosphates tested, namely Ins(1,3,4,5,6)P$_5$, InsP$_6$, Ins(1,4,5)P$_3$ and Ins(1,3,4)P$_3$, having K_d values of 401.2 ± 8.1, > 10000 nM, > 10000 nM and > 10000 nM, respectively ($n = 3$, for each inositol phosphate). Detailed Scatchard analysis revealed a single class of binding site (results not shown). With respect to these parameters expressed GAP1^{IP4BP} K614E had approximately a 10-fold lower affinity compared with Ins(1,3,4,5)P$_4$-binding to wild-type GAP1^{IP4BP} (see Table 1).

Molecular explanation of the mutagenic studies

From Figure 3 it can clearly be seen that mutation of Arg^{601}, either R601C or R601K, had the effect of inhibiting Ins(1,3,4,5)P$_4$-binding to GAP1^{IP4BP} by greater than 75 %. This was not surprising, given that from the GAP1^{IP4BP} model structure, mutations to Arg^{601} would remove some of the interactions with the 3-phosphate of Ins(1,3,4,5)P$_4$ (Figure 4). For example, Cys^{601} would be unable to interact with the 3-phosphate, whereas Lys^{601} could retain some hydrogen bonds, explaining why R601C inhibited Ins(1,3,4,5)P$_4$-binding to a greater extent than R601K (90 % compared with 75 %). The importance of Arg^{601} in Ins(1,3,4,5)P$_4$-binding was further highlighted by the F598Q mutation. Phe^{598} of GAP1^{IP4BP}, which is conserved in Btk (Phe^{25}) and so was modelled in the same position, points away from the Ins(1,3,4,5)P$_4$-binding site and appeared to have no interaction with Ins(1,3,4,5)P$_4$ in the model complex. Therefore it was not initially obvious why mutating this residue to glutamine should dramatically reduce Ins(1,3,4,5)P$_4$-binding activity. However, the difference in size between phenylalanine and glutamine, or if glutamine hydrogen bonds to a neighbouring residue, could cause a localized conformational change. Arg^{601} is only three residues away and so any change in its conformation could cause the effects observed.

With respect to K585R, although this could retain the interaction with the 4-phosphate of Ins(1,3,4,5)P$_4$, the bulkier arginine residue may, by steric hindrance, cause the Ins(1,3,4,5)P$_4$ molecule to alter its position in the binding site, effectively having to move further out. This would weaken, or remove, the other interactions between Ins(1,3,4,5)P$_4$ and GAP1^{IP4BP}, thereby lowering the binding activity. Likewise, the mutation N597D, which

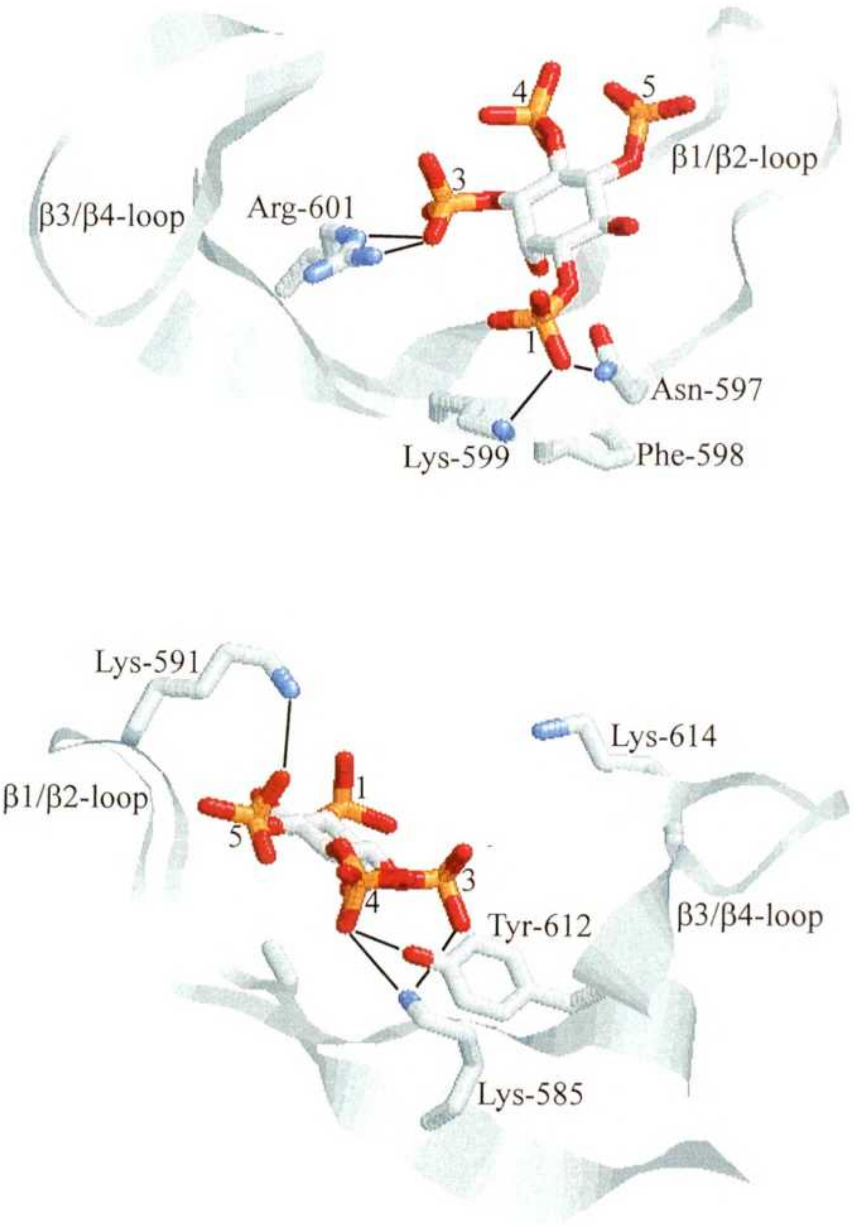

Figure 4 Two views of the $Ins(1,3,4,5)P_4$-binding site in the model $GAP1^{IP4BP}$ structure, showing the relative positions of the residues chosen to study by site-directed mutagenesis

The $\beta1/\beta2$- and $\beta3/\beta4$-loops are shown as ribbons. $Ins(1,3,4,5)P_4$ and amino acid side chains are shown as stick structures. Other residues in and around the binding site have been omitted for clarity.

inhibited $Ins(1,3,4,5)P_4$ binding by $81.4 \pm 3.1\,\%$, would not only remove hydrogen bonding with the substrate, but also, by introducing a negative charge close to the 1-phosphate, may repel the $Ins(1,3,4,5)P_4$. Similarly, although the K614E mutation only inhibited $Ins(1,3,4,5)P_4$ binding by $15.2 \pm 3.1\,\%$, the 10-fold lower affinity may indicate that either the lysine residue had a weak interaction that was removed by the mutation or, if there was no such interaction, then the introduction of a negative charge may again repel the $Ins(1,3,4,5)P_4$ molecule from the binding site. The model structure did not have any direct interactions between Lys^{614} and $Ins(1,3,4,5)P_4$ (Figure 4), indicating electrostatic repulsion between K614E and $Ins(1,3,4,5)P_4$.

In the model structure Ala^{587} of $GAP1^{IP4BP}$ corresponded to Lys^{32} of PLC-δ_1. This was interesting, since Lys^{32} of PLC-δ_1 is at the start of the $\beta1/\beta2$-loop and has been previously suggested to prevent substrates containing a 3-phosphate from binding [43,47] [based on the Btk–$Ins(1,3,4,5)P_4$ complex it is actually the 5-phosphate that will be close to Ala^{587} in $GAP1^{IP4BP}$]. Therefore although a change from Lys^{32} in PLC-δ_1 to Ala^{587} in $GAP1^{IP4BP}$ reduced the number of interactions with $Ins(1,3,4,5)P_4$, such a change may be essential for $Ins(1,3,4,5)P_4$ binding. In the model $GAP1^{IP4BP}$ structure Ala^{587} was close to the 5-phosphate (Figure 4), so it was not surprising that the A587F mutation caused steric hindrance, which inhibited $Ins(1,3,4,5)P_4$ binding by $90\,\%$.

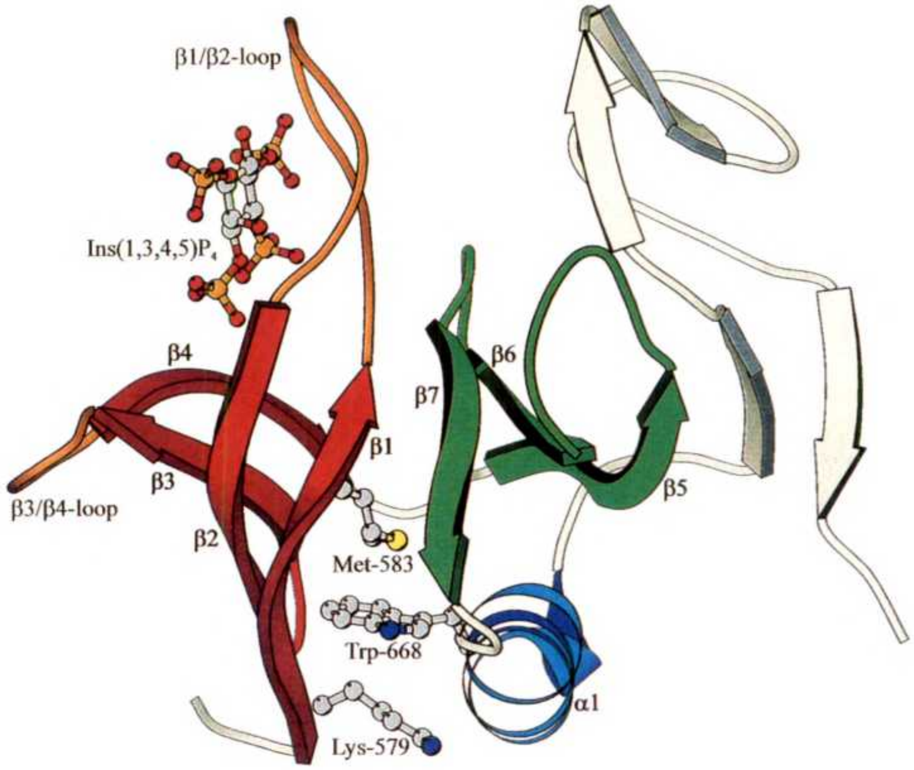

Figure 5 Schematic representation of the model GAP1^{IP4BP} PH–Ins(1,3,4,5)P$_4$ complex with Trp^{668}, and the residues Lys^{579} and Met^{583} with which it interacts, shown as ball-and-stick structures

Ins(1,3,4,5)P$_4$ is shown as a ball-and-stick structure and the structural features conserved in PH domains are labelled β1–β7 and α1. This Figure was generated using Molscript [49].

The only invariant residue in PH domains is a tryptophan in the α-helix (Trp^{668} in GAP1^{IP4BP}). This residue has been suggested to form a structural role in the orientation of the α-helix and β-sheet [48]. In the model GAP1^{IP4BP} structure, and also the Btk and PLC-δ_1 structures, this tryptophan is sandwiched between two residues (Lys^{579} and Met^{583}) from the β1-strand (Figure 5). The W668F mutation in GAP1^{IP4BP} was therefore likely to cause a structural change, probably in either the β1-strand or $\beta1/\beta2$-loop, which resulted in a reduction in the ability of the protein to bind Ins(1,3,4,5)P$_4$.

DISCUSSION

In the present study we have compared, in some detail, the Ins(1,3,4,5)P$_4$-binding sites present within the PH domains of recombinant GAP1^{IP4BP} and Btk, an approach which has highlighted that these two proteins bind Ins(1,3,4,5)P$_4$ with very similar affinities and inositol phosphate specificities. With this in mind, we have used the crystal structure of the Btk PH domain in complex with Ins(1,3,4,5)P$_4$ [38] to generate a molecular model of the potential Ins(1,3,4,5)P$_4$-binding site within GAP1^{IP4BP}.

The model structure of the GAP1^{IP4BP} PH–Ins(1,3,4,5)P$_4$ complex predicts an inositol phosphate-binding site in which the inositol ring is partially buried within a pocket comprised of the $\beta1/\beta2$- and $\beta3/\beta4$-loops. Importantly, we propose that the high-affinity binding site is formed following a conformational change in the $\beta1/\beta2$-loop that is induced upon Ins(1,3,4,5)P$_4$-binding. Our model suggests that the pharmacology of inositol phosphate-binding to GAP1^{IP4BP}, as detailed in Table 1, arises for the following reasons. Firstly, for high-affinity binding a minimum of four phosphate groups are necessary in order to induce the conformational changes required to bring crucial residues, some of which we have highlighted by mutagenesis, into proximity with the phosphates [compare the affinities of D-Ins(1,4,5)P$_3$, D-Ins(1,3,4)P$_3$ and D-Ins(1,3,5)P$_3$ with D-Ins(1,3,4,5)P$_4$]. These four phosphates need to be in equatorial positions, since any inositol tetrakisphosphate containing a phosphate on the axial 2-hydroxyl has a low affinity (see Table 1). Furthermore, three of the phosphates need to be in a row, with the fourth phosphate immediately opposite, such that the remaining hydroxyls separate it from the three phosphates {see the affinities of D-Ins(1,3,4,5)P$_4$ and D-Ins(1,3,5,6)P$_4$ [= L-Ins(1,3,4,5)P$_4$] in Table 1}. Such a requirement is predicted from the model, since the three phosphates [3-,4- and 5- in the case of D-Ins(1,3,4,5)P$_4$] are shown to interact with residues that lie in the bottom of the binding pocket and are therefore buried; the remaining phosphate [the 1-phosphate of D-Ins(1,3,4,5)P$_4$] is orientated towards the top of the binding site. In this context the high affinity of GAP1^{IP4BP} for D-Ins(1,3,4,5,6)P$_5$ (K_d = 85 ± 4.5 nM) is interesting, since we would predict from the model that this binds in the same orientation as D-Ins(1,3,4,5)P$_4$ and that sufficient space may be available to accommodate the 6-phosphate.

Both PLC-δ_1 and Btk have had their crystal structures solved in complex with inositol phosphates, and they have shown that they bind the inositol phosphates in equivalent binding sites. Of the residues involved in binding the substrates some are conserved, others although not identical do perform similar functions and there are unique residues that are probably responsible for the distinct affinities of the two PH domains. As the binding sites are similar, it is surprising that they bound the inositol phosphates in different orientations, which are rotated 180 ° about the P1–P4 axis. This gave a choice of which orientation to use for the model GAP1^{IP4BP}–Ins(1,3,4,5)P_4 structure. Based on the sequence and substrate-specificity similarities between GAP1^{IP4BP} and Btk it was decided to use the Btk orientation. However, until the crystal structure of GAP1^{IP4BP} in complex with Ins(1,3,4,5)P_4 has been solved the orientation of the Ins(1,3,4,5)P_4 will be open to debate.

Therefore, in summary, we have generated a credible model structure describing the Ins(1,3,4,5)P_4-binding site within the PH domain of GAP1^{IP4BP}. This model explains the molecular nature of the high-affinity isomer-specific binding of Ins(1,3,4,5)P_4 to GAP1^{IP4BP} and highlights important residues required for high-affinity binding, some of which we have confirmed by site-directed mutagenesis.

We thank Professor Robin Irvine and Professor Tony Clarke for helpful discussions This work is funded by Grants from the BBSRC Integration of Cellular Responses Initiative and the MRC J.S.R. is in receipt of a BBSRC Studentship. P.J.C. is a Lister Institute Research Fellow.

REFERENCES

1 Haslam, R J., Koide, H B and Hemmings, B (1993) Pleckstrin domain homology Nature **363**, 629–630

2 Mayer, B. J, Ren, R, Clark, K L and Baltimore, D (1993) A putative molecular domain present in diverse signalling proteins Cell **73**, 629–630

3 Lemmon, M A, Ferguson, K M and Schlessinger, J. (1996) PH domains diverse sequences with a common fold recruit signalling molecules to the cell surface Cell **85**, 621–624

4 Lemmon, M A, Falasca, M., Ferguson, K M and Schlessinger, J. (1997) Regulatory recruitment of signalling molecules to the cell membrane by PH domains Trends Cell Biol. **7**, 237–242

5 Bottomley, M J, Salim, K and Panayotou, G (1998) Phospholipid-binding protein domains. Biochim Biophys Acta **1436**, 165–183

6 Hirata, M., Kanematsu, T, Sakuma, K., Koga, T, Watanabe, Y, Ozaki, S. and Yagissawa, H (1994) D-myo-inositol 1,4,5-trisphosphate binding domain of phospholipase C-delta 1 Biochem Biophys. Res Commun **205**, 1563–1571

7 Ferguson, K. M., Lemmon, M A, Schlessinger, J and Sigler, P. B. (1995) Structure of the high affinity complex of inositol trisphosphate with phospholipase C PH domain Cell **83**, 1037–1046

8 Lemmon, M A, Ferguson, K. M., Sigler, P B and Schlessinger, J. (1995) Specific and high affinity binding of inositol phosphates to an isolated PH domain. Proc Natl Acad Sci. U.S.A. **92**, 10472–10476

9 Hyvonen, M., Macias, M J, Nilges, M., Oshkinat, H, Saraste, M. and Willmans, M (1995) Structure of the binding-site for inositol phosphates in a PH domain EMBO J **14**, 4676–4685

10 Paterson, H F, Savopoulos, J W, Pensic, O., Cheung, R, Ellis, M. V., Williams, R L and Katan, M (1995) Phospholipase $C_{\delta 1}$ requires a PH domain for interaction with the plasma membrane Biochem J. **312**, 661–666

11 Stauffer, T. P., Ahn, S. and Meyer, T (1998) Receptor-induced transient reduction in plasma membrane PtdIns(4,5)P_2 concentration monitored in living cells Curr Biol **8**, 343–346

12 Varnai, P and Balla, T (1998) Visualisation of phosphoinositides that bind PH domains. calcium- and agonist-induced dynamic changes and relationship to *myo*-[^{3}H]-inositol-labeled phosphoinositide pools J. Cell Biol **143**, 501–510

13 Fukuda, M, Kojima, T., Kabayama, H and Mikoshiba, K (1996) Mutation of the PH domain of Bruton's tyrosine kinase in immunodeficiency impaired inositol 1,3,4,5-tetrakisphosphate binding capacity J Biol. Chem **271**, 30303–30306

14 Rameh, L E, Arvidsson, A, Carraway, K L R., Couvillon, A. D, Rathbun, G, Crompton, A., VanRenterghem, B, Czech, M P, Ravichandran, K S, Burakoff, S J. et al (1997) A comparative analysis of the phosphoinositide-binding specificity of PH domains J Biol Chem **272**, 22059–22066

15 Varnai, P., Rother, K I and Balla, T (1999) PI 3-kinase-dependent membrane association of the Bruton's tyrosine kinase PH domain visualised in single living cells. J. Biol Chem **274**, 10983–10989

16 Venkateswarlu, K, Oatey, P. B, Tavare, J. M. and Cullen, P J. (1998) Insulin-dependent translocation of ARNO to the plasma membrane of 3T3 L1 adipocytes requires PI 3-kinase Curr Biol **8**, 463–466

17 Lockyer, P J, Wennstrom, S, Kupzig, S, Venkateswarlu, K., Downward, J and Cullen, P. J. (1999) Identification of the Ras GTPase-activating protein GAP1^m as a phosphatidylinositol 3,4,5-trisphosphate-binding protein *in vivo* Curr. Biol **9**, 265–268

18 Cullen, P J (1998) Bridging the GAP in inositol 1,3,4,5-tetrakisphosphate signalling Biochim Biophys Acta **1436**, 35–47

19 Allen, M., Chu, S., Brill, S, Stotler, C and Buckler, A (1998) Restricted tissue expression pattern of a novel human rasGAP related gene and its murine ortholog Gene **218**, 17–25

20 Fukuda, M. and Mikoshiba, K (1996) Structure-function relationships of the mouse GAP1^m J Biol Chem **271**, 18838–18842

21 Lockyer, P J, Bottomley, J. R, Reynolds, J S, Venkateswarlu, K, Potter, B V. L, Dempsey, C E and Cullen, P J (1997) Distinct subcellular distribution of the putative inositol 1,3,4,5-tetrakisphosphate receptors GAP1^{IP4BP} and GAP1^m result from the GAP1^{IP4BP} PH domain directing plasma membrane targeting Curr Biol **7**, 1007–1010

22 Bottomley, J R., Reynolds, J S, Lockyer, P J and Cullen, P J (1998) Structure and functional analysis of the putative inositol 1,3,4,5-tetrakisphopshate receptors GAP1^{IP4BP} and GAP1^m Biochem Biophys Res. Commun **250**, 143–149

23 O'Rourke, F, Matthews, E and Feinstein, M B (1996) Isolation of inositol 1,3,4,5-tetrakisphopshate and inositol hexakisphopshate binding proteins from human platelets, inositol 1,3,4,5-tetrakisphosphate promotes Ca^{2+} efflux from inside-out plasma membrane vesicles containing 104 kDa GAP1^{IP4BP} protein Biochem J **316**, 1027–1034

24 Lockyer, P J, Vanlingen, S., Reynolds, J. S, McNulty, T J., Irvine, R. F., Parys, J B and Cullen, P. J (1999) Tissue specific expression and endogenous subcellular distribution of the inositol 1,3,4,5-tetrakisphopshate-binding proteins GAP1^{IP4BP} and GAP1^m Biochem Biophys Res Commun **255**, 421–426

25 Cullen, P. J, Hsuan, J J, Truong, O., Letcher, A J, Jackson, T. R, Dawson, A P and Irvine, R. F. (1995) Identification of a specific inositol 1,3,4,5-tetrakisphosphate-binding protein as a member of the GAP1 family Nature (London) **376**, 527–530

26 Loomis-Husselbee, J W, Cullen, P. J., Dreikhausen, U E, Irvine, R F and Dawson, A P (1996) Synergistic effects of inositol 1,3,4,5-tetrakisphosphate on inositol 2,4,5-trisphosphate-stimulated Ca^{2+} release do not involve direct interaction of inositol 1,3,4,5-tetrakisphosphate with inositol trisphosphate-binding sites Biochem J. **314**, 811–816

27 Loomis-Husselbee, J W, Walker, C. D, Bottomley, J R, Cullen, P J, Irvine, R F and Dawson, A. P. (1998) Modulation of inositol 2,4,5-trisphosphate-stimulated Ca^{2+} mobilisation by inositol 1,3,4,5-tetrakisphosphate enhancement by activated G-proteins, and evidence for the involvement of a GAP1 protein, a putative inositol 1,3,4,5-tetrakisphosphate receptor Biochem J **331**, 947–952

28 Yoon, H S, Hajduk, P J, Petros, A M, Olejniczak, E T, Meadows, R P and Fesik, S W (1994) Solution structure of a PH domain Nature (London) **369**, 672–675

29 Macias, M J, Musacchio, A, Ponstingl, H, Nilges, M, Saraste, M and Oschkinat, H (1994) Structure of the PH domain from β-spectrin. Nature (London) **369**, 675–677

30 Zhang, P, Talluri, S, Deng, H. Y., Branton, G and Wagner, G (1995) Solution structure of the PH domain of *Drosophila* β-spectrin Structure **3**, 1185–1195

31 Downing, A. K, Driscoll, P C, Gout, I., Salim, K, Zvelebil, M J and Waterfield, M D (1994) Three-dimensional solution structure of the PH domain from dynamin Curr Biol **4**, 884–891

32 Ferguson, K. M, Lemmon, M. A., Schlessinger, J and Sigler, P B (1994) Crystal structure at 2.2Å resolution of the PH domain from human dynamin Cell **79**, 199–209

33 Fushman, D, Cahill, S., Lemmon, M A, Schlessinger, J and Cowburn,.D. (1995) Solution structure of the PH domain of dynamin by heteronuclear NMR spectroscopy Proc Natl. Acad Sci U S A **92**, 816–820

34 Timm, D, Salim, K, Gout, I., Guruprasad, L, Waterfield, M and Blundell, T (1994) Crystal structure of the PH domain from dynamin Nat. Struct Biol **1**, 782–788

35 Zheng, J, Chen, R H, Corbian-Garcia, S, Cahill, S M., Bar-Sagi, D and Cowburn, D (1997) The solution structure of the PH domain of human SOS1 A possible structural role for the sequential association of diffusion and PH domains. J Biol Chem **272**, 30240–30344

36 Koshiba, S, Kigawa, T, Kim, J H, Shirouzu, M, Bowtell, D. and Yokoyama, S (1997) The solution structure of the PH domain of mouse Son-of-sevenless (mSOS1) J Mol Biol **269**, 579–591

37 Hyvonen, M and Saraste, M (1997) Structure of the PH domain and Btk motif from Bruton's tyrosine kinase molecular explanation for X-linked agammaglobulinaemia. EMBO J **16**, 3396–3404

38 Baraldi, E., Carugo, K D, Hyvonen, M, LoSurdo, P, Riley, A M., Potter, B V L, O'Brien, R, Ladbury, J E and Saraste, M (1999) Structure of the PH domain from Bruton's tyrosine kinase in complex with inositol 1,3,4,5-tetrakisphosphate Structure **7**, 449–460

39 Fushman, D., Najmabadi-Haske, T., Cahill, S., Zheng, J., LeVine, H. and Cowburn, D. (1998) The solution structure and dynamics of the PH domain of G protein-coupled receptor kinase 2 (β-adrenergic receptor kinase 1) – a binding partner of G$\beta\gamma$ subunits J Biol Chem. **273**, 2835–2843

40 Zheng, J., Cahill, S. M., Lemmon, M. A., Frushman, J., Schlessinger, J. and Cowburn, D. (1996) Identification of the binding site for acidic phospholipids on the PH domain of dynamin implications for stimulation of GTPase activity. J Mol Biol **255**, 14–21

41 Salim, K., Bottomley, M. J., Querfurth, E., Zvelebil, M. J., Gout, I., Scaife, R., Margolis, R. L., Gigg, R., Smith, C. I., Driscoll, P. C. et al (1996) Distinct specificity in the recognition of phosphoinositides by the PH domains of dynamin and Bruton's tyrosine kinase EMBO J **15**, 6241–6250

42 Harlan, J. E., Yoon, H. S., Hajduk, P. J. and Fesik, S. W. (1995) Structural characterisation of the interaction between a PH domain and phosphatidylinositol 4,5-bisphosphate. Biochemistry **34**, 9859–9864

43 Bernstein, F. C., Koetzle, T. F., Williams, G. J. B., Meyer, E. F., Brice, M. D., Rogers, J. R., Kennard, O., Shimanouchi, T. and Tasumi, M. (1997) The Protein Data Bank a computer-based archival file for macromolecular structures J Mol Biol. **112**, 535–542

44 Cullen, P. J., Chung, S.-K., Chang, Y.-T., Dawson, A. P. and Irvine, R. F. (1995) Specificity of the purified inositol 1,3,4,5-tetrakisphosphate-binding protein from porcine platelets FEBS Lett **358**, 240–243

45 Bradford, P. G. and Irvine, R. F. (1987) Specific binding-sites for [^{3}H]inositol 1,3,4,5-tetrakisphosphate on membranes of HL60 cells Biochem Biophys Res Commun. **149**, 680–685

46 Kojima, T., Fukuda, M., Watanabe, Y., Haamazato, F. and Mikoshiba, K. (1997) Characterisation of the PH domain of Btk as an inositol polyphosphate and phosphoinositide binding domain. Biochem Biophys Res Commun **236**, 333–339

47 Isakoff, S., Cardozo, T., Andreev, J., Li, Z., Ferguson, K. M., Abagyan, R., Lemmon, M. A., Aronheim, A. and Skolnik, E. Y. (1998) Identification and analysis of PH domain-containing targets of phosphatidylinositol 3-kinase using a novel *in vivo* assay in yeast EMBO J **17**, 5374–5387

48 Shaw, G. (1996) The PH domain. an intriguing multifunctional protein module. BioEssays **18**, 35–46

49 Kraulis, P. J. (1991) MOLSCRIPT. a program to produce both detailed and schematic plots of protein structures J Appl. Crystallogr. **24**, 946–950

Received 24 January 2000/21 March 2000; accepted 7 April 2000

Biochem J (2000) 349, 343–351 (Printed in Great Britain)

Identification and expression of NEU3, a novel human sialidase associated to the plasma membrane

Eugenio MONTI*†[1], Maria T. BASSI*, Nadia PAPINI‡, Mirko RIBONI*, Marta MANZONI*, Bruno VENERANDO‡, Gianluigi CROCI‡, Augusto PRETI†, Andrea BALLABIO*§, Guido TETTAMANTI‡ and Giuseppe BORSANI*

*Telethon Institute of Genetics and Medicine (TIGEM), San Raffaele Biomedical Science Park, via Olgettina 58, 20132 Milan, Italy, †Department of Biomedical Science and Biotechnology, University of Brescia, via Valsabbina 19, 25123 Brescia, Italy, ‡Department of Chemistry and Medical Biochemistry, L I T A, via Fratelli Cervi 93, 20090 Segrate, Italy, and §Università Vita e Salute San Raffaele, San Raffaele Biomedical Science Park, Milan, Italy

Several mammalian sialidases have been described so far, suggesting the existence of numerous polypeptides with different tissue distributions, subcellular localizations and substrate specificities. Among these enzymes, plasma-membrane-associated sialidase(s) have a pivotal role in modulating the ganglioside content of the lipid bilayer, suggesting their involvement in the complex mechanisms governing cell-surface biological functions. Here we describe the identification and expression of a human plasma-membrane-associated sialidase, NEU3, isolated starting from an expressed sequence tag (EST) clone. The cDNA for this sialidase encodes a 428-residue protein containing a putative transmembrane helix, a YRIP (single-letter amino acid codes) motif and three Asp boxes characteristic of sialidases. The polypeptide shows high sequence identity (78 %) with the membrane-associated sialidase recently purified and cloned from *Bos taurus*. Northern blot analysis showed a wide pattern of expression of the gene, in both adult and fetal human tissues. Transient expression in COS7 cells permitted the detection of a sialidase activity with high activity towards ganglioside substrates at a pH optimum of 3.8. Immunofluorescence staining of the transfected COS7 cells demonstrated the protein's localization in the plasma membrane.

Key words: expressed sequence tag, gangliosides, gene structure, membrane-bound enzyme.

INTRODUCTION

Sialidases or neuraminidases (EC 3.2.1.18) remove sialic acid residues from various sialo derivatives such as sialo-oligosaccharides, sialoglycoproteins and sialoglycolipids (gangliosides). The biology of viral and bacterial sialidases has been extensively studied [1], whereas the study of their mammalian counterparts has been hampered for a long time by their usually low cellular content and lability during purification procedures. In mammals, several sialidases with different subcellular localizations, tissue distributions and substrate specificities have been described, suggesting great molecular variety in these proteins. In this perspective, the availability of the cDNA species encoding mammalian sialidases is an important step leading to a comprehensive picture of the relationships between the structure and function of these enzymes.

In the past decade several mammalian sialidases have been cloned. The first mammalian protein carrying this enzyme activity to be cloned and characterized at the molecular level was the rat cytosolic sialidase [2], followed by a soluble sialidase secreted into the culture medium by CHO (Chinese hamster ovary) cells [3]. Then the cDNA species encoding the human [4–6] and mouse [7–9] lysosomal sialidases were isolated, permitting the definition of the molecular basis of the human lysosomal disorder sialidosis [10] and the neuraminidase defect in the SM/J mouse [11] respectively. We recently reported the identification of a novel human gene, *NEU2*, encoding a cytosolic sialidase similar to the soluble enzyme from rat and hamster [12,13]. The last gene of the mammalian sialidase family that has so far been cloned encodes a bovine plasma-membrane-associated sialidase specific for gangliosides [14], a protein previously purified from bovine brain [15]. Membrane-associated sialidases have been described in different tissues [16–18] and cell types [19–21]; a form linked to the membrane via a glycosylphosphatidylinositol anchor has also been identified [22,23]. The main role of these forms of sialidases is thought to be the regulation of the sialic acid content of membrane-bound sialyl glycoconjugates. Among these compounds, gangliosides are the most abundant in the plasma membrane of vertebrate cells; they are involved in various biological processes including cell adhesion, cell–cell interactions and cell proliferation, differentiation and oncogenic transformation [24]. Therefore a detailed molecular characterization of membrane-associated sialidases could help in an understanding of the mechanisms underlying these different aspects of ganglioside biology. Here we report the identification of a human plasma-membrane-associated sialidase encoded by a novel human gene, *NEU3*, mapping on chromosome 11q13.

EXPERIMENTAL

General techniques

Standard molecular biological techniques were performed as described by Sambrook et al. [25]. DNA restriction and modifying enzymes were from Boehringer unless indicated otherwise.

Isolation of *NEU3* cDNA and gene

Searches of the database of expressed sequence tags (dbEST) were performed as described previously [26]. The IMAGE cDNA

Abbreviations used: dbEST, database of expressed sequence tags, EST, expressed sequence tag, HA, haemagglutinin, 4-MU, 4-methylumbelliferone, ORF, open reading frame, PAC, P1-derived artificial chromosome

[1] To whom correspondence should be addressed at TIGEM (e-mail monti@tigem.it)

The nucleotide sequence data reported will appear in DDBJ, EMBL and GenBank Nucleotide Sequence Databases under the accession number Y18563.

clones corresponding to the *NEU3* transcript were obtained from the UK Human Genome Mapping Project Resource Centre.

Phage library plating and screening conditions were performed with standard procedures [25]. Human cDNA clones were isolated from a human skeletal muscle cDNA library (Clontech; in λ GT11 vector) by using a probe derived from IMAGE clone 1041654 with primers HS1F (5′-AGGCCTCATTCTCTGATG-3′) and HS1R (5′-CTTACCACACTCCCTTGG-3′). Inserts of recombinant phages were isolated by PCR with vector oligonucleotide primers.

DNA sequencing

Automated sequencing (with an Applied Biosystems ABI 377 fluorescence sequencer) was performed with vector- and gene-specific oligonucleotide primers. The sequences of the exon–intron boundaries were determined by sequencing P1-derived artificial chromosome (PAC) clones with cDNA-specific primers.

Computer sequence analysis

Sequence assembly and editing was performed with both Auto-Assembler version 1.4 (Perkin Elmer–Applied Biosystems) and DNA Strider version 1.2 [27] programs. Multiple sequence alignment was performed with the ClustalW algorithm [28]. Nucleotide and amino acid sequences were compared with the non-redundant sequence databases present at the NCBI (National Center for Biotechnology Information) with BLAST version 2.0 [29].

Chromosomal localization and PAC library screening

For radiation-hybrid mapping we used the Genebridge 4 panel (Research Genetics, Huntsville, AL, U.S.A.), which includes 93 human and hamster clones. DNA (25 ng) for each of the hybrid clones was used for PCR amplification in 96-well microtitre plates with the HS1F and HS1R primers, at 55 °C as the annealing temperature. Results were sent to the Radiation Hybrid Mapper server at Whitehead Institute/MIT Center for Genome Research (http://www-genome.wi.mit.edu/cgi-bin/contig/rhmapper.pl).

For the RPCI-5 PAC library screening, the same set of primers was used.

Northern blot analysis

Commercial human RNA Master Blot (Clontech) containing dotted human poly(A)$^+$ RNA species from 50 different tissues was hybridized with human sialidase (HS) probe. This probe was PCR-amplified from the cDNA HSM5 clone by using the primer set HSNt (5′-ATGGAAGAAGTGACAACATG-3′) and HSCt (5′-TTAATTGCTTTTGAATTGG-3′) and spanned the entire *NEU3* open reading frame (ORF). The experiment was performed under the conditions recommended by the manufacturer.

Expression in COS7 cells

The cDNA region containing the entire *NEU3* ORF was amplified by PCR with cloned *Pfu* polymerase (Stratagene), a sense primer with a *Bgl*II site (HSNtB, 5′-GAAGATCTATG-GAAGAAGTGACAACATG-3′), an anti-sense primer with an *Eco*RI site (HSCtE, 5′-CATGAATTCTTAATTGCTTTTGA-ATTGG-3′) and HSM5 cDNA clone as template. pCDNAI-NEU3 was constructed by cloning the amplified insert 5′ in frame with the haemagglutinin (HA) epitope into plasmid pCDNAI (Invitrogen). The amplified insert was also cloned into a Rous-sarcoma-virus-promoted vector [30], yielding the pCDL-NEU3 construct. COS7 cells were grown in Petri dishes (100 mm diameter) by using Dulbecco's modified Eagle's medium with 10% (v/v) fetal calf serum. Transfections were performed overnight with 6 μg of plasmid DNA and LipofectAMINE reagent, in accordance with the manufacturer's guidelines (Life Technologies) Cells were harvested by scraping, washed in PBS and resuspended in the same buffer containing 1 mM EDTA, 1 μg/ml pepstatin A, 10 μg/ml apoprotinin and 10 μg/ml leupeptin. Total cell extracts were prepared at various times up to 72 h after transfection by sonication. The supernatant obtained after centrifugation at 800 *g* for 10 min was designated the crude cell extract and was subsequently centrifuged at 200000 *g* for 15 min on an Optima TL 100 ultracentrifuge (Beckman). Aliquots of the original crude cell extract, 200000 *g* supernatant and pellet were used for assays for protein (Coomassie Protein Assay Reagent; Pierce) and sialidase activity, and for Western blot analysis.

Western blot analysis

Protein samples corresponding to 10 μg of each cell fraction were subjected to SDS/PAGE [10% (w/v) gel] and subsequently transferred to nitrocellulose extra blotting membrane (Sartorius) by electroblotting. The membranes were incubated for 30 min in TBS/0.1% (v/v) Tween 20 (TTBS) containing 10% (w/v) dried milk (blocking buffer; BB). The primary antibody, anti-HA monoclonal antibody (Boehringer), was added at an appropriate dilution in BB and blots were incubated for 1 h. After being washed in TTBS, the membranes were incubated for 1 h with the appropriate horseradish-peroxidase-conjugated IgG (Amersham) diluted in BB. After a final wash in TTBS, detection of antibody binding was performed with enhanced chemiluminescence (Amersham) in accordance with the manufacturer's instructions. All incubations were performed at room temperature, with constant shaking.

Preparation of unlabelled and ^{3}H-labelled gangliosides and neutral glycolipids

Gangliosides GM1, GD1a, GD1b, GT1b and lactosylceramide from calf brain and GM3 (NeuAc) from human spleen were prepared and analysed structurally as described previously [31]. GM1, GM3 and GD1a were ^{3}H-labelled at C-3 of the sphingosine moiety; the separated and purified *erythro* forms were used [32]. In addition, GM3 was ^{3}H-labelled at the level of the *N*-acetyl group of sialic acid ([*NeuAc*-^{3}H]GM3) by the method of Chigorno et al. [33]. The radiochemical purity of [^{3}H]GM1, [^{3}H]GD1 and [*NeuAc*-^{3}H]GM3 was greater than 99% and the specific radioactivities were 1.25, 0.96 and 0.30 Ci/mmol respectively. Gangliosides were stored at −20 °C in propan-1-ol/water (4:1, v/v).

Sialidase assay

The enzymic activity of NEU2 in total cell lysates and in cellular subfractions was determined by various methods. The sialidase activity towards ganglioside substrates, in the presence or absence of Triton X-100 (0.1%, v/v), was determined as described by Venerando et al. [34]. All reaction mixtures were set up at least in duplicate, with 25 μg of total protein, in a final volume of 100 μl and in the presence of 12.5 mM sodium citrate/phosphate buffer, pH 3.8. In all cases 1 unit of sialidase activity is defined as the liberation of 1 μmol of NeuAc/min at 37 °C.

Fluorimetric method

Reactions were set in the presence of 400 μg of BSA, with 0.2 mM 2′-(4-methylumbelliferyl)-α-D-*N*-acetylneuraminic acid

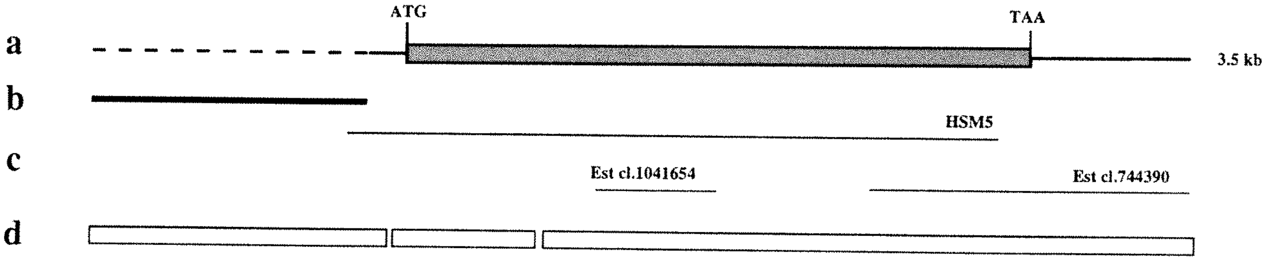

e

```
   1  tttccttttattggcgtttgtaaaatttcttcttttaaaattgttatatttagagacag  60
  61  ggtctcgctctgtcacccaggctggagtgcagtggtgcaatcacagctcaccacagcctc  120
 121  caactcctgggctcaaggcatcctcccacgtaggccttccaaagcgctgagattgtaggc  180
 181  ataagccaccaggcccagcctattacctttacgttgtacttagtcccagataaaaaatga  240
 241  ccttagatcagtcctttcctctttggctggggagagggggcttaaattccggtactgtg  300
 301  aaacagaagaatggactcagtgctatgtgacaaatctatgtatgtaaatgtgtgtatata  360
 361  cacacacataaattatatatatgaatatatttcattttcatattttgcaaggagagtag  420
 421  ccaatgctctggacctctggtcctttttgtagggtaccctctgaggccgggaacctttgc  480
 481  tcaactctcaggctgtccagggaagctttaggcggtgataccgagctacagaccaatata  540
 541  agagctcggggctgtggcactgaagagaggaggcggccgttgggaactgaggtgggccca  600
 601  gggcttgagctgagttggcgagggtggaggtggtgccggtcccacgccgtggtggggacc  660
 661  gagctgcgggctggagggaggggcagcgccgagggggcgggacgggagagggctcgcgga  720
 721  gtaggccaacggttggccccaaccgccactgactacagcctgcgcccgcctcttttcgtt  780
 781  gccgttacctgtttccggcagtcgacacgctcttcgcttctcggggcttgtctccgtgtc  840
 841  ctccgtctcagttgtttctccctctctatcctcctctgtctcagtctccccagccttggg  900
 901  gccggtgcctcttccgggcttcggcgaatgagacctgcggacctgccccgcgccccatg  960
 961  gaagaatccccggcgtccagctctgccccgacagagacggaggagccggggtccagtgca  1020
1021  gaggtcATGGAAGAAGTGACAACATGCTCCTTCAACAGCCCTCTGTTCCGGCAGGAAGAT  1080
   1        M  E  E  V  T  T  C  S  F  N  S  P  L  F  R  Q  E  D  18
1081  GACAGAGGGATTACCTACCGGATCCCAGCCCTGCTCTACATACCCCCCACCCACACCTTC  1140
  19  D  R  G  I  T  Y  R  I  P  A  L  L  Y  I  P  P  T  H  T  F  38
1141  CTGGCCTTTGCAGAGAAGCGTTCCACGAGGAGAGATGAGGATGCTCTCCACCTGGTGCTG  1200
  39  L  A  F  A  E  K  R  S  T  R  R  D  E  D  A  L  H  L  V  L  58
1201  AGGCGAGGGTTGAGGATTGGGCAGTTGGTACAGTGGGGGCCCCTGAAGCCACTGATGGAA  1260
  59  R  R  G  L  R  I  G  Q  L  V  Q  W  G  P  L  K  P  L  M  E  78
1261  GCCACACTACCGGGGCATCGGACCATGAACCCCTGTCCTGTATGGGAGCAGAAGAGTGGT  1320
  79  A  T  L  P  G  H  R  T  M  N  P  C  P  V  W  E  Q  K  S  G  98
1321  TGTGTGTTCCTGTTCTTCATCTGTGTGCGGGGCCATGTCACAGAGCGTCAACAGATTGTG  1380
  99  C  V  F  L  F  F  I  C  V  R  G  H  V  T  E  R  Q  Q  I  V  118
1381  TCAGGCAGGAATGCTGCCCGCCTTTGCTTCATCTACAGTCAGGATGCTGGATGTTCATGG  1440
 119  S  G  R  N  A  A  R  L  C  F  I  Y  S  Q  D  A  G  C  S  W  138
1441  AGTGAGGTGAGGGACTTGACTGAGGAGGTCATTGGCTCAGAGCTGAAGCACTGGGCCACA  1500
 139  S  E  V  R  D  L  T  E  E  V  I  G  S  E  L  K  H  W  A  T  158
1501  TTTGCTGTGGGCCCAGGTCATGGCATCCAGCTGCAGTCAGGGAGACTGGTCATCCCTGCG  1560
 159  F  A  V  G  P  G  H  G  I  Q  L  Q  S  G  R  L  V  I  P  A  178
1561  TATACCTACTACATCCCTTCCTGGTTCTTTTGCTTCCAGCTACCATGTAAAACCAGGCCT  1620
 179  Y  T  Y  Y  I  P  S  W  F  F  C  F  Q  L  P  C  K  T  R  P  198
1621  CATTCTCTGATGATCTACAGTGATGACCTAGGGGTCACATGGCACCATGGTAGACTCATT  1680
 199  H  S  L  M  I  Y  S  D  D  L  G  V  T  W  H  H  G  R  L  I  218
1681  AGGCCCATGGTTACAGTAGAATGTGAAGTGGCAGAGGTGACTGGGAGGGCTGGCCACCCT  1740
 219  R  P  M  V  T  V  E  C  E  V  A  E  V  T  G  R  A  G  H  P  238

1741  GTGCTATATTGCAGTGCCCGGACACCAAACAGGTGCCGGGCAGAGGCGCTCAGCACTGAC  1800
 239  V  L  Y  C  S  A  R  T  P  N  R  C  R  A  E  A  L  S  T  D  258
1801  CATGGTGAAGGCTTTCAGAGACTGGCCCTGAGTCGACAGCTCTGTGAGCCCCCACATGGT  1860
 259  H  G  E  G  F  Q  R  L  A  L  S  R  Q  L  C  E  P  P  H  G  278
1861  TGCCAAGGGAGTGTGGTAAGTTTCCGGCCCCTGGAGATCCCACATAGGTGCCAGGACTCT  1920
 279  C  Q  G  S  V  V  S  F  R  P  L  E  I  P  H  R  C  Q  D  S  298
1921  AGCAGCAAAGATGCACCCACCATTCAGCAGAGCTCTCCAGGCAGTTCACTGAGGCTGGAG  1980
 299  S  S  K  D  A  P  T  I  Q  Q  S  S  P  G  S  S  L  R  L  E  318
1981  GAGGAAGCTGGAACACCGTCAGAATCATGGCTCTTGTACTCACACCCAACCAGTAGGAAA  2040
 319  E  E  A  G  T  P  S  E  S  W  L  L  Y  S  H  P  T  S  R  K  338
2041  CAGAGGGTTGACCTAGGTATCTATCTCAACCAGACCCCCTTGGAGGCTGCCTGCTGGTCC  2100
 339  Q  R  V  D  L  G  I  Y  L  N  Q  T  P  L  E  A  A  C  W  S  358
2101  CGCCCCTGGATCTTGCACTGTGGGCCCTGTGGCTACTCTGATCTGGCTGCTCTGGAGGAG  2160
 359  R  P  W  I  L  H  C  G  P  C  G  Y  S  D  L  A  A  L  E  E  378
2161  GAGGGCTTGTTTGGGTGTTTGTTTGAATGTGGGACCAAGCAAGAGTGTGAGCAGATTGCC  2220
 379  E  G  L  F  G  C  L  F  E  C  G  T  K  Q  E  C  E  Q  I  A  398
2221  TTCCGCCTGTTTACACACCGGGAGATCCTGAGTCACCTGCAGGGGGACTGCACCAGCCCT  2280
 399  F  R  L  F  T  H  R  E  I  L  S  H  L  Q  G  D  C  T  S  P  418
2281  GGTAGGAACCCAAGCCAATTCAAAAGCAATTAAttggcttaggacccaatttccatagat  2340
 419  G  R  N  P  S  Q  F  K  S  N  *                                428
2341  gcaaatggcagttacagacaggttaacagaagctactgaagtctacagataatcaaaaaa  2400
2401  cttaatattctgttccctaccttttttcactttcctcctccaaagagcaaaatgaaaat  2460
2461  tttgccttagctactgcagtggaaagagcactgaactaggagttggaagacaaggatgtg  2520
2521  gtcctggctctgccactggcttgcttttggaccttggatgtgtcacctgaactctctgga  2580
2581  cctcaggtttccatctgtaaaatgagagtattggttctaagatttctcatcttctcatcc  2640
2641  ctaggacaagcatagtgcctgcatgcttcatgatcagtaagtcctggctgcataaaggac  2700
2701  tctgatgtcaaaatggaaaccaggggacttaccttttcacatgacttacccctcatccga  2760
2761  gtgtgaggttacaagcaggtgtcatggcaggaaggaagaccagatctgtatgatttgttc  2820
2821  catttttaataacaaaaatatccacacccttttaataatgctcagagttctgtaggctct  2880
2881  ctatcctagaggaattgagcaaaacagaagaatcatgaagtctcctaccttctacagcct  2940
2941  tgtagttctgcttaccttctcttcctcatccagaaagcatcattttctagggagaacaat  3000
3001  gagaatctcaatgccagtagtactggataatagtgcgtattgcttctggtggcattaccc  3060
3061  tgatgatgggctgaagttcatttattagggtggttcctgatgggaaaaggacatggatta  3120
3121  ggactttaaaacactggacagaatttcccacagtctttgccctcaaggagttcaccagtt  3180
3181  tatggggctagaagagcgagaaaattcaagaaaataaatgtagctggtgggagactttgt  3240
3241  agatgttgggctatatgttggggtgatggtagctcctgatgtaatttcttagttgcatc  3300
3301  ttcaatatgcctggagtcgtctgtccaaggcttgtccaggcttctgggtttctctcaagt  3360
3361  ttgtttttctcaggatattgtcctggcccagctactcctttacctgtgagaagatcttca  3420
3421  ccattaggaagatctctagacccccagatctcagaatcaggcctatttgtgtaggcccat  3480
3481  ggaaatcactacttgtgaagtagagatgcctttttgtttaaaaaaaaaaaaaaaaaaaa  3540
```

Figure 1 NEU3 cDNA contig, gene structure and translation

(**a**) Schematic representation of the *NEU3* consensus sequence; the grey box indicates the coding region. The broken line in (**a**) and the heavy bar in (**b**) represent the portion of the consensus sequence obtained from genomic DNA. (**c**) The contig of cDNA and EST clones (cl.). (**d**) The genomic structure of *NEU3*. (**e**) The *NEU3* consensus sequence and the corresponding protein translation (one-letter amino acid codes).

(4-MU-NeuAc; Sigma), and incubated at 37 °C for 25 min. Reactions were stopped by the addition of 1.5 ml of 0.2 M glycine/NaOH, pH 10.2. Fluorescence emission was measured on a Jasco FP-770 fluorimeter with excitation at 365 nm and emission at 445 nm, with the use of 4-methylumbelliferone (4-MU) to obtain a calibration curve. Determination of the kinetic parameters was performed with this artificial substrate in the concentration range 0.02–0.6 mM.

Colorimetric method

Reactions were set up with various concentrations of GD1b and GT1b, from 0.03 to 0.6 mM. After incubation at 37 °C for up to 25 min, the release of sialic acid was determined by the thiobarbituric acid method [35].

Radiochemical method

Incubation mixtures containing 0.025–0.6 mM of ^{3}H-labelled GM1, GM3 and GD1a gangliosides, carrying 100000 d.p.m. of ^{3}H label, were incubated at 37 °C for up to 25 min. The incubations were terminated by cooling the tubes in an ice bath and adding 400 μl of tetrahydrofuran. The mixtures were centrifuged at 10000 g for 5 min; 10 μl of the resulting supernatant (in triplicate) was subjected to high-performance TLC on silica-gel plates with chloroform/methanol/0.2% aqueous $CaCl_2$ (50:42:11, by vol.) as solvent system, to separate the reaction products from the substrates [36]. The separated glycolipids were quantified by radiochromatoscanning (Beta Imager 2000; Biospace Mesures, Paris, France, with the software interface Beta Vision from Dell Optiplex Systems), and the enzyme activity was calculated as described [36].

Immunofluorescence localization

For immunofluorescence studies, COS7 cells were grown in eight-well chamber slide culture chambers (Nunc). Transfections were performed as described previously, with 0.2 μg of DNA in each well. Indirect immunostaining of HA-NEU3 was performed

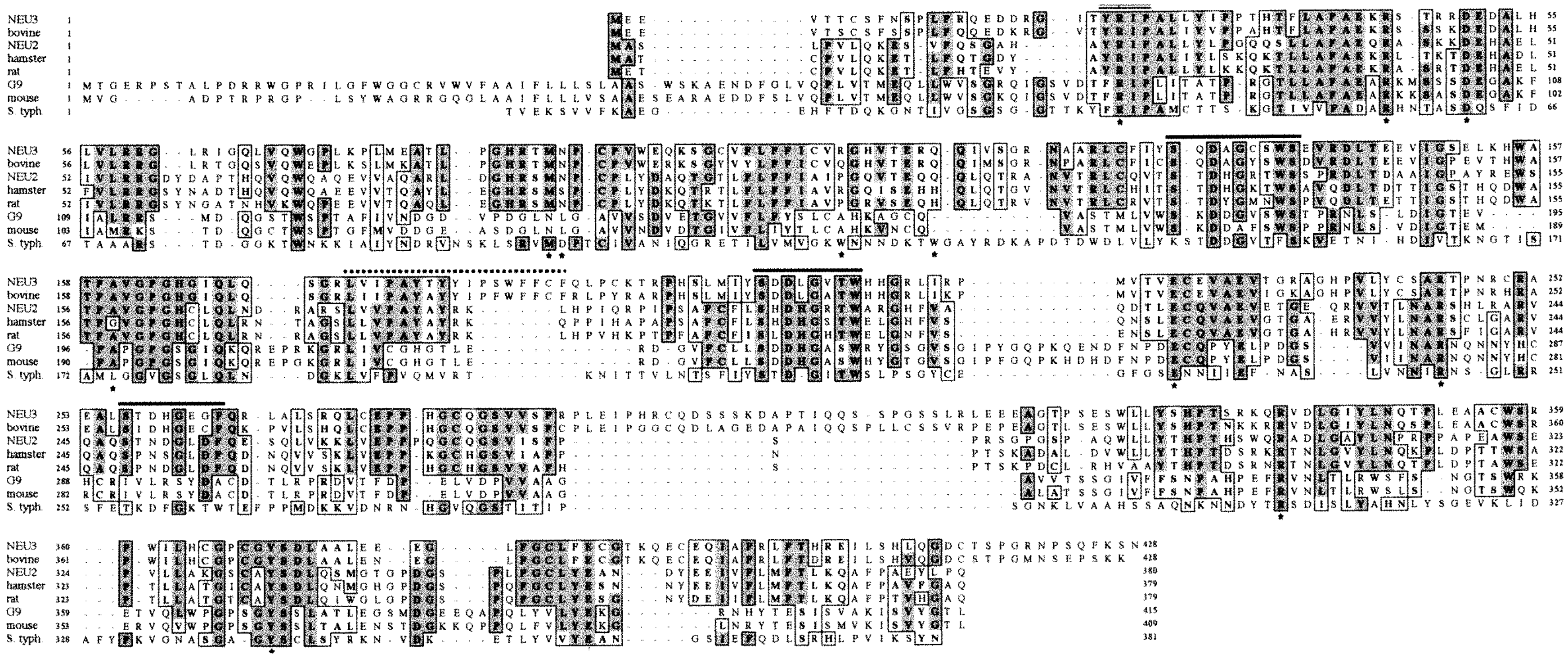

Figure 2 Multiple amino acid sequence alignment of sialidases

An alignment is shown of the amino acid sequence of human NEU3 sialidase with the sequences of the bovine plasma-membrane-associated sialidase (accession no. BAA75071.1); the cytosolic and soluble sialidases from human (NEU2) (accession no. NP-005374), hamster (accession no. A54961) and rat (accession no. A49679); the human lysosomal sialidase (G9) (accession no. NP-000425) and the mouse counterpart (accession no. CAA72215); and the *S. typhimurium* sialidase (S. typ.; accession no. P29768) as a reference. The alignment was performed with the ClustalW program. Identical residues are boxed and shown on a grey background; conservative substitutions are boxed on a white background. The conserved F(Y)RIP box, the three Asp boxes and the putative transmembrane helix are indicated by a double thin, black lines and a dotted line respectively. The active-site amino acid residues derived from crystallographic data of the enzyme from *S. typhimurium* are indicated by asterisks below the sequence.

on cells fixed with 4% (w/v) paraformaldehyde in PBS. Cells were subsequently permeabilized with 0.2% (v/v) Triton X-100, blocked with pig serum and incubated with anti-HA monoclonal antibody (4 μg/ml) (Boehringer Mannheim) in PBS plus pig serum and 0.1% (v/v) Triton X-100. Staining was obtained after incubation with FITC-conjugated isotype-specific antibodies (1:100 dilution) (Dako). Fluorescence microscopy was performed with an Axioplan microscope (Zeiss).

RESULTS

Identification and characterization of the *NEU3* gene

As a starting point for the identification of novel mammalian sialidases we searched the dbEST [37] for entries showing homology with NEU2 polypeptide. This analysis led us to the identification of a human expressed sequence tag (EST) (accession number AA578048) showing significant sequence identity with the medial part of both the query sequence and the rodent soluble sialidase. Moreover, the homology region contained an Asp box [consensus sequence S/TXD(X)GXTW/F], an amino acid motif found in all the microbial [38] and mammalian [6] sialidase enzymes cloned so far.

The sequence of the corresponding cDNA clone (IMAGE clone 1041654) revealed an insert size of 395 bp. A set of oligonucleotides (oligos) was designed on the basis of the cDNA sequence and were used for preliminary expression studies with various human RNA species as templates. Reverse-transcriptase-mediated PCR revealed a product of the expected size in heart, brain, lung and, with higher yield, in skeletal muscle (results not shown). The PCR product was used as a probe to screen a human skeletal muscle cDNA library (2×10^6 plaques); out of seven positive clones, four were characterized further and the clone containing the longest insert (HSM5) (Figure 1) was sequenced directly. A reiterated search of the EST database allowed us to identify an additional EST (IMAGE clone 744390) corresponding to the 3′ untranslated region. The cDNA consensus sequence at the 5′ end was confirmed and extended at the genomic level (as indicated in Figures 1a–1c) to build up a contig of 3540 bp. Four in-frame ATG codons were found (nt positions 424, 928, 958 and 1027 of the contig), preceded by several in-frame stop codons. Comparison of the amino acid sequence of the predicted *NEU3* protein product with its putative bovine homologue [14] revealed that the fourth ATG was the real starting codon, indicating that the human putative NEU3 protein is 428 residues long. Bioinformatic analysis of the genomic sequence upstream of the ATG, performed at http://bimas.dcrt.nih.gov/molbio/signal/, revealed the presence of several putative Sp1-binding sites and the absence of TATA and CAAT box sequences. These findings are in agreement with the expression data obtained by Northern analysis, demonstrating that *NEU3* is a ubiquitously expressed gene. During the submission of this paper a transcript corresponding to *NEU3* was isolated from human brain cDNA library and reported by Wada et al. [39].

NEU3 protein analysis

The predicted NEU3 protein has a calculated molecular mass of 48.25 kDa and a theoretical pI of 6.78. The protein contains three canonical Asp boxes (residues 131–138, 205–212 and 256–263), an F(Y)RIP (one-letter amino acid codes) motif in the N-terminal region and one potential N-glycosylation site (Asn-348). Comparison of the amino acid sequence with protein sequence databases showed the highest degree of identity (78%) with the bovine membrane-associated sialidase [14], followed by rat [2], NEU2 [12] and hamster [3] soluble enzymes (42%, 42% and 40% sequence identities respectively) and the human [4–6] and mouse [7–9] lysosomal sialidase (31 and 30% sequence identities respectively). As reported for the bovine protein, the analysis for putative transmembrane regions by using the TMpred and PHDhtm programs [40] at ISREC (Switzerland) and EMBL (Germany) revealed a hydrophobic stretch of 17 residues (174–190) that apparently divides the protein into two segments located on the opposite layers of the membrane. In

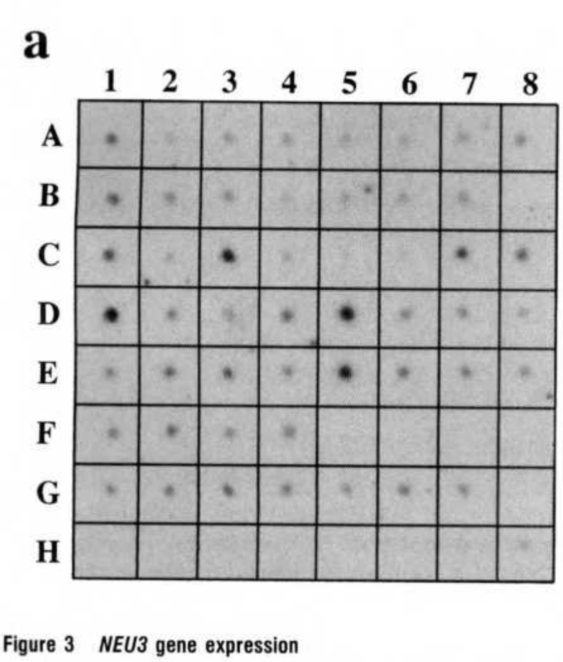

b

	1	2	3	4	5	6	7	8
A	whole brain	amygdala	caudate nucleus	cerebellum	cerebral cortex	frontal lobe	hippocampus	medulla oblongata
B	occipital pole	putamen	substantia nigra	temporal lobe	thalamus	subthalamic nucleus	spinal cord	
C	heart	aorta	skeletal muscle	colon	bladder	uterus	prostate	stomach
D	testis	ovary	pancreas	pituitary gland	adrenal gland	thyroid gland	salivary gland	mammary gland
E	kidney	liver	small intestine	spleen	thymus	peripheral leukocyte	lymph node	bone marrow
F	appendix	lung	trachea	placenta				
G	fetal brain	fetal heart	fetal kidney	fetal liver	fetal spleen	peripheral leukocyte	fetal lung	
H	yeast total RNA	yeast tRNA	*E. coli* rRNA	*E. coli* DNA	Poly r(A)	human C0t DNA	human DNA	human DNA

Figure 3 ***NEU3* gene expression**

(**a**) Human mRNA master blot (Clontech) hybridized with *NEU3* probe (exposed for 4 days). (**b**) List of the types and positions of poly(A)$^+$ RNA species and control RNA and DNA species dotted on the membrane.

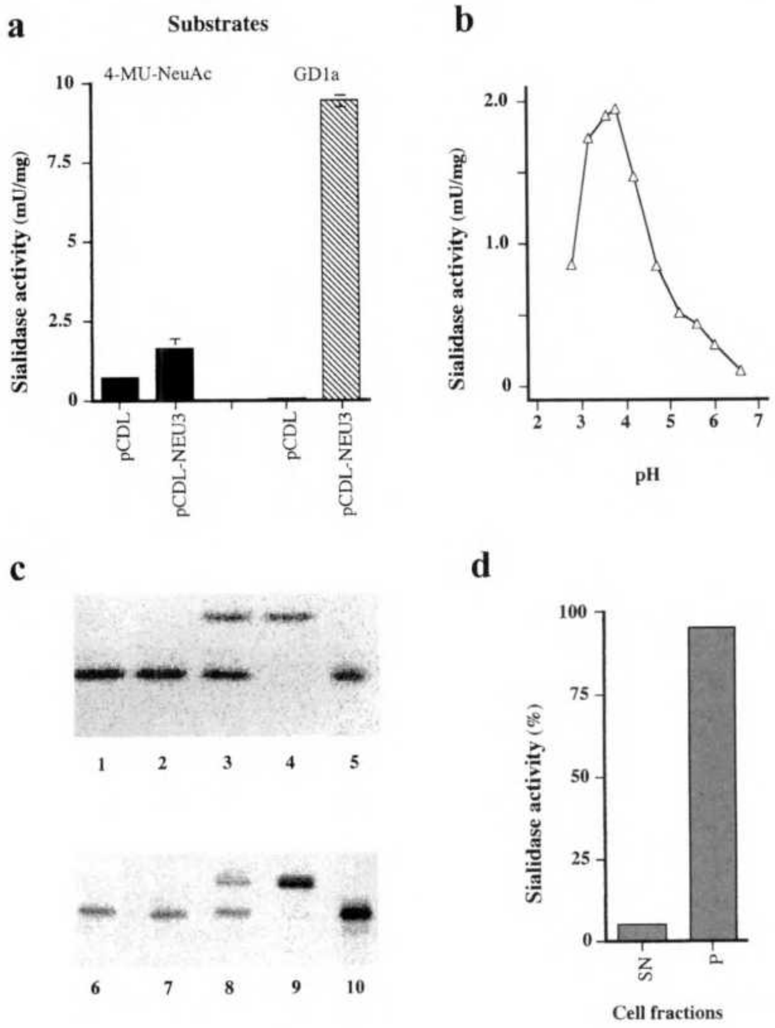

Figure 4 NEU3 expression in COS7 cells

(**a**) COS7 cells transfected overnight with pCDL vector alone or pCDL-NEU3 construct were grown for 24 h; sialidase-specific activities towards the substrate 4-MU-NeuAc and ganglioside GD1A were determined in the total cell lysate. Variation in the observed activity is indicated by the S.D. error bars ($n = 3$). (**b**) Rate of hydrolysis of 4-MU-NeuAc over the pH range 2.8–6.6 in 12.5 mM sodium citrate/phosphate buffer, with the use of aliquots of the crude cell homogenate of pCDL-NEU3-transfected cells as the enzyme source. (**c**) TLC of 10 μl of sialidase reaction mixture containing radiolabelled [^{3}H]GM3 (lanes 1–3) and [^{3}H]GD1a (lanes 6–8). Aliquots (25 μg) of the particulate material of COS7 cells transfected with pCDL (lanes 2 and 7) and pCDL-NEU3 (lanes 3 and 8) were used as enzyme sources. Standard ^{3}H-sphingolipids are loaded on the right of each TLC: GM3 (lane 5); lactosyl-ceramide (lane 4); GD1a (lane 10) and GM1 (lane 9). Detection of the ^{3}H-gangliosides was performed with a radiochromatoscanner. (**d**) Sialidase activity of the supernatant (SN) and pellet (P) obtained by ultracentrifugation at 200000 ***g*** of the total lysate of pCDL-NEU3-transfected cells. The rates of hydrolysis of 4-MU-NeuAc are expressed as percentages of the value detectable in the total cell lysate ($n = 3$).

addition, primary structure analysis revealed a high cysteine content (21 residues, 4.9% of the total), and the secondary-structure prediction performed by the PHDsec program at EMBL (Germany) showed several β-sheet regions, a characteristic common to all the sialidase enzymes studied so far. A multiple alignment of the amino acid sequences of the cloned mammalian sialidases and the protein from *Salmonella typhimurium* is shown in Figure 2. As expected, the F(Y)RIP motif is highly conserved in all the proteins, as are the three Asp boxes. In addition, the presence of the microbial sialidase, whose three-dimensional structure has been solved [41], permitted the identification of the putative amino acid residues involved in the formation of the active site of mammalian sialidases. In fact, most of the active-site residues identified in *S. typhimurium* are conserved in NEU3 as well as in the bovine counterpart, in NEU2, in the rodent enzymes (9 out of 13) and in the two lysosomal sialidases (8 out of 13). The differences are concentrated in the hydrophobic residues (Trp-121, Trp-128 and Leu-175) that in the *S. typhimurium* enzyme form the hydrophobic pocket accommodating the *N*-acetyl group of the sialic acid [41]. These discrepancies could reflect a different organization of the hydrophobic pocket and/or differences in substrate specificity.

Expression analysis of the *NEU3* gene

To ascertain the expression level of the *NEU3* gene, a dot-blot analysis was performed with a PCR product spanning the entire putative *NEU3* coding region, by using a dot-blot containing poly(A)$^+$ RNA extracted from 50 different human tissues. After exposure overnight, expression was detectable in testis, skeletal muscle, adrenal gland and thymus; several other tissues gave faint signals (Figure 3). A 4-day exposure of the membrane revealed a ubiquitous expression of the gene in all the human tissues tested, with the lowest expression detectable in bladder

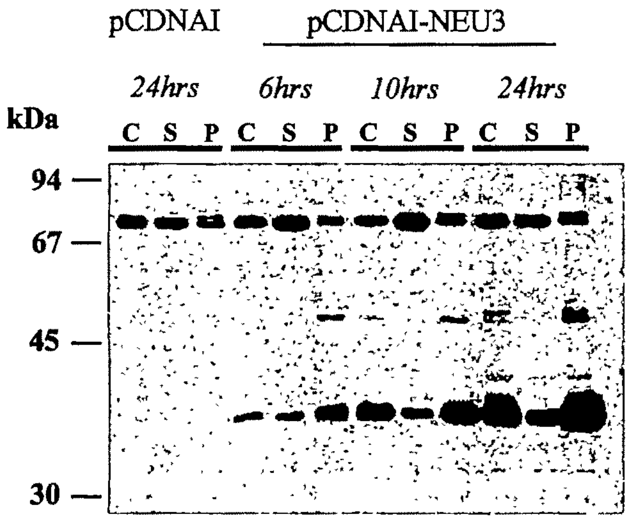

Figure 5 Western blot analysis of COS7 cells transiently expressing NEU3-tagged protein

Western blot analysis of protein samples (10 μg) obtained by cells transfected with pCDNAI-NEU3 construct at different times after transfection pCDNAI vector alone was used as a control For each time after transfection, aliquots of crude homogenate (C), and of supernatant (S) and pellet (P) obtained by ultracentrifugation, were analysed The blot was with anti-HA monoclonal antibody Detection of antibodies bound to HA epitope was performed with peroxidase-conjugated isotype-specific antibodies, followed by enhanced chemiluminescence developing reagents The positions of molecular mass markers are indicated at the left

Table 1 Kinetic constants of NEU3 expressed in COS7 cells

Aliquots corresponding to 25 μg of protein from the crude particulate fraction obtained by ultracentrifugation were used as enzyme sources Abbreviation: n d, not determined

Substrate	Presence of Triton X-100	V_{max} (m-units/mg)	K_m (μM)
GM1	−	n d	
	+	n d	
GM3	−	12.5	166
	+	92.4	158
GD1a	−	9.4	98
	+	61.6	95
GD1b	−	1.2	85
	+	3.1	81
GT1b	−	6.7	130
	+	17.9	125
4-MU-NeuAc	−	7.6	143

and uterus. In addition, *NEU3* was expressed in human fetal tissues.

Expression of *NEU3* in COS7 cells

To demonstrate that *NEU3* encodes a sialidase, the entire ORF deduced from the cDNA sequence was amplified by PCR and subcloned into a mammalian expression vector (pCDL). The recombinant vector (pCDL-NEU3) was used to transfect COS7 cells transiently. Crude homogenates from cells transfected with pCDL-NEU3 or pCDL alone were tested for sialidase activity by using the artificial substrate 4-MU-NeuAc and the ganglioside GD1a. Transfection with pCDL-NEU3 gave rise to a 2.5-fold increase in the enzymic activity detected in the crude cell extract with the artificial substrate (Figure 4a). The enzyme had an extremely low pH optimum: the pH curve revealed detectable activity from pH 2.8 and a maximum at pH 3.8 (Figure 4b). NEU3 showed a higher activity towards ganglioside GD1a than 4-MU-NeuAc (Figure 4a). In fact, in the presence of GD1a ganglioside micelles, the detected increase in sialidase activity corresponded to approx. 90-fold that observed in the pCDL-transfected cells.

To analyse the subcellular localization of *NEU3*-encoded sialidase, fractionation into soluble and particulate cell materials was performed by centrifugation, using as a starting material the crude homogenate of COS7 cells transfected with pCDL-NEU3. The experiments clearly demonstrated the particulate nature of NEU3 (Figure 4d): more than 95 % of the activity detectable in the homogenate was recovered in the pelleted material.

These results were confirmed by a Western blot analysis of COS7 cells transiently transfected with pCDNAI-NEU3. In these experiments, *NEU3* cDNA ORF was subcloned into a pCDNAI mammalian expression vector, giving rise in transfected cells to a fusion protein (HA-NEU3) carrying the HA epitope in the N-terminal region. This tagged chimaera protein was easily revealed with a commercial monoclonal antibody against the HA epitope. A protein band with a molecular mass of approx. 51 kDa, corresponding to the expected molecular mass of the tagged sialidase, was detectable in the 200000 *g* pelleted material of the transfected cells; its amount increased with the time after transfection (Figure 5). An additional band at 37 kDa was detected by the anti-HA antibody, with a much higher signal than the original transcribed chimaera protein. The finding that a longer transfection time led to an increase in the 37 kDa signal suggested that this protein band was related to a strong proteolytic degradation of the HA-NEU3. The presence of the degradation product in the soluble material might suggest a labile binding of the shortened polypeptide to the cell membranes. In addition, at 24 h after transfection, a novel band with a molecular mass of approx. 52 kDa was detectable in the crude homogenate and in the particulate fraction, possibly representing a modified form of the 51 kDa NEU3. Additional protein bands of approx 75 kDa were detected by the monoclonal antibody. The presence of the same bands in the cell fractions obtained from COS7 cells transfected with pCDNAI vector alone (Figure 5, left three lanes) indicated that they were unrelated to NEU3.

Aliquots of the crude particulate fraction obtained from pCDL-NEU3-transfected cells were used to analyse the substrate specificity of the protein enzyme. Under the experimental conditions used to measure the kinetic parameters towards ganglioside substrates, the endogenous sialidase activity detected in the particulate material of control COS7 cells transfected with pCDL vector was undetectable, as shown with the radiolabelled substrates GM3 and GD1a, and a radiochromatoscanner as detection system (Figure 4c). The results are summarized in Table 1. NEU3 hydrolysed all the gangliosides tested except GM1, which seemed to be resistant, with similar K_m values. However, a comparison between the observed values of apparent V_{max} showed that the enzyme acted preferentially on terminal sialic acid residues, linked to the oligosaccharide moiety with an α2-3 sialyl linkage. In addition, the presence of Triton X-100 led to a strong increase in the enzymic activity, as demonstrated by the increase in apparent V_{max} observed with all ganglioside substrates.

Mapping and gene structure

Mapping assignment of *NEU3* was performed with a set of primers (HS1F and HS1R) located in the coding region (see the Experimental section) on the Radiation Hybrid mapping panel

Table 2 Splice-site junctions of *NEU3*

Capital letters denote exonic sequences and lower-case letters intronic sequences.

Exon number	5′ splice site	3′ splice site	Exon size (bp)
1	–	TGCAGAgtgagcgggg	–
2	AtccttgcagAGGTCA	GTACAGgtgactcttc	211
3	CcttgtctagTGGGGG	–	–

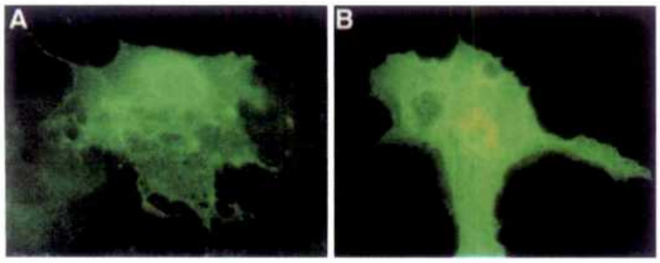

Figure 6 Immunofluorescence localization of NEU3

COS7 cells were transfected with pCDNAI-NEU3 and grown for 24 h (**A**) and 48 h (**B**) before fixation and immunofluorescence staining. Cells were fixed with paraformaldehyde and permeabilized with Triton X-100, then treated with anti-HA monoclonal antibody. Staining was performed with FITC-conjugated isotype-specific antibodies. Magn. × 230.

Genebridge 4. The results obtained indicated that *NEU3* maps to chromosome 11q13 between markers D11S916 and D11S3966.

To determine the genomic structure of *NEU3*, the RPCI-5 PAC library was screened by PCR with the same set of primers as those used for the mapping. Two positive clones (919A14 and 1039I21) were identified and then used for direct sequencing with cDNA-derived oligonucleotide primers. The locations and sequences of all exon–intron boundaries (Table 2) were therefore determined.

NEU3 gene is organized in three exons, with the ATG codon located in the second one. All the exon–intron junctions agree with the GT--AG consensus sequence. *NEU3* and *NEU2* [12] share a similar gene structure with the ORF spanning only two exons, whereas the lysosomal enzyme seems to be more complex, with the gene organized into five exons [6].

Immunofluorescence localization of NEU3

Immunofluorescence localization was studied in COS7 cells transiently transfected with pCDNAI-NEU3. Expression tested up to 72 h after transfection gave an extensive cell-surface labelling, a staining pattern typically associated with plasma membrane proteins (Figure 6). The membrane structures detected inside the cells can be related to *NEU3*-encoded protein travelling from the rough endoplasmic reticulum to the cell surface, as a consequence of the high expression level driven by the pCDNAI-NEU3 vector.

DISCUSSION

So far, three different types of mammalian sialidase have been characterized at the molecular level. They are the cytosolic, or soluble, forms [2,3,12,13], the lysosomal form [4–9] and a plasma-membrane-associated protein from *Bos taurus* [14]. Here we describe the molecular cloning and expression of a novel human sialidase, encoded by the *NEU3* gene, that is highly similar to the bovine protein.

Expression of the polypeptide in COS7 cells demonstrates the particulate nature of the enzyme. In fact, the enzymic activity is found associated with the membrane structures pelleted by ultracentrifugation. These results were confirmed by Western blot analysis, with a protein chimaera tagged at the N-terminus with the HA epitope. As already observed for HA-NEU2 [13], the chimaera is catalytically inactive, suggesting a critical role of the N-terminus in correct protein folding and/or in active-site formation. The 51 kDa HA-NEU3 chimaera is detectable only in the particulate fractions. HA-NEU3 undergoes proteolytic degradation with high efficiency, as demonstrated by the detection of a large amount of a 37 kDa protein band. This phenomenon could be explained by the high content of foreign proteins induced by the expression vector promoter that could also result in a cytotoxic effect, and/or by the presence of the HA epitope on the protein chimaera. Immunofluorescence localization of the tagged polypeptide further demonstrates the distribution of NEU3 at the cell surface.

The primary structure of these mammalian proteins reveals the presence of amino acid motifs, such as the F(Y)RIP motif and Asp boxes, which are conserved in all sialidases cloned so far. Interestingly, the plasma-membrane-associated sialidase seems to be more similar to the cytosolic sialidases than to the lysosomal forms. This can be related to the substrate specificities of these three forms of sialidase. In fact, whereas the soluble forms showed high activity towards various gangliosides [42,43], G9 is apparently unable to hydrolyse mixed gangliosides [6]. Recently, a lysosomal sialidase-mediated depletion of GM2 ganglioside in Tay–Sachs neuroglial cells was reported, demonstrating the activity of this lysosomal protein *in vivo* towards ganglioside GM2 [44]. This last finding suggests that the different degrees of sequence similarity between these forms of sialidases might be related to one or more different factors, not only to substrate specificities. Overall, a multiple alignment of the amino acid sequences of these mammalian polypeptides demonstrates that they belong to a unique protein family with highly conserved amino acid blocks throughout the primary structure. In addition, the presence in topologically equivalent positions of the F(Y)RIP motif, the Asp boxes and nine amino acid residues that are possibly involved in the active site suggests the existence of a common folding topology similar to the typical superbarrel or β-propeller described for the viral and microbial sialidases [1]. This picture strongly supports the hypothesis of a monophyletic origin of the sialidase enzymes.

By using protease digestion of a protein chimaera tagged at the C-terminus with different antibodies, it was demonstrated that the bovine plasma membrane sialidase is a classical type I membrane protein, with the N-terminus exposed to the extracellular side of the lipid bilayer [14]. In this spatial arrangement the conserved Arg-25 residue, which is located within the YRIP motif, Arg-45, Asp-50, Met-87 and the other amino acids involved in the formation of the active site hydrophobic pocket are exposed at the cell surface and thus isolated from Glu-225, Arg-245, Arg-340, Tyr-370 and Glu-387, which are located in the portion of the protein exposed to the cytosol. From the structural and functional data collected so far, it is unlikely that a sialidase with these characteristics would show catalytic activity. In addition, the detection of the 37 kDa HA-NEU3 proteolytic degradation product in the soluble fractions obtained by ultracentrifugation suggests a labile interaction of this polypeptide with the membranes. Therefore alternative model(s) must be found. One possibility is that NEU3, and its bovine counterpart, are associated with the plasma membrane via a single hydrophobic segment of 16–20 residues located within the 50 residues at the C-terminus and can either span the phospholipid bilayer or dip into the membrane in a loop structure. The Kyte–Doolittle hydrophobicity plot of the protein showed several hydrophobic regions; although those that are more consistent are located at the N-terminus and in the middle of the primary structure, a short segment can be found at the C-terminus (residues 369–387) Further experiments will be performed to elucidate this aspect of NEU3 biology.

It is noteworthy that, despite the high similarity between NEU3 and the corresponding bovine protein [14], the results obtained by transfecting mammalian cells with the corresponding cDNA suggest different biochemical behaviours of the two enzymes. In fact, whereas the activity towards the artificial substrate 4-MU-NeuAc was practically identical in COS7 cells expressing the bovine membrane sialidase, under the same experimental conditions we observed a 2–3-fold increase on NEU3 expression with a more acidic pH optimum. However, the main differences are detectable on ganglioside substrates. The observed values of apparent $V_{\max}$ indicate that the human enzyme hydrolysed ganglioside GM3 with higher efficiency, as reported for the bovine enzyme, but seemed to be much less active toward the gangliosides GT1b. Moreover, whereas the bovine enzyme showed a hydrolysis rate for the GD1b intermediate between those observed for GD1a and GT1b, NEU3 hardly acted on the α2-8 sialyl linkage of this ganglioside substrate. NEU3 activity towards the ganglioside substrate was increased by Triton X-100, demonstrating that further disaggregation of the membrane is important for substrate recognition. The detergent activation of membrane-bound sialidase has been already reported in human fibroblasts [45], neuroblastoma cells [21] and human brain tissue [46]. A rapid comparison of the substrate preferences of these different membrane-bound enzymes suggests a great molecular heterogeneity of these proteins. NEU3 is, for example, the enzyme with the most acidic pH optimum. The great variety of results available on membrane sialidase enzymes, together with the several biological roles of the gangliosides, makes the detailed characterization of these proteins an attractive field of study.

Overall, the identification of the cDNA encoding NEU3 might contribute to a better understanding of the biological functions of the different members of the sialidase enzyme family.

We thank Claudio Gattuso for graphic assistance, and the YAC Screening Center at San Raffaele Biomedical Science Park This work was partly supported by 60% MURST funds to E M and MURST Cofin 1997 (Hydrolytic enzymes in physiological and pathological metabolism of glycoconjugates) to B V The financial support of the Italian Telethon Foundation and of the BIOMED2 CT97-BMH4-2284 EC grant (EURO-IMAGE) to A.B. is gratefully acknowledged.

REFERENCES

1 Taylor, G (1996) Curr. Opin. Struct Biol **6**, 830–837

2 Miyagi, T, Konno, K, Emori, Y, Kawasaki, H, Suzuki, K., Yasui, A. and Tsuiki, S. (1993) J. Biol. Chem. **268**, 26435–26440

3 Ferrari, J, Harris, R and Warner, T G (1994) Glycobiology **4**, 367–373

4 Bonten, E, van der Spoel, A, Fornerod, M., Grosveld, G and d'Azzo, A (1996) Genes Dev **10**, 3156–3169

5 Pshezhetsky, A V, Richard, C, Michaud, L, Igdoura, S, Wang, S, Elsliger, M A, Qu, J, Leclerc, D, Gravel, R, Dallaire, L and Poher, M (1997) Nat Genet **15**, 316–320

6 Milner, C M, Smith, S V, Carrillo, M. B, Taylor, G L, Hollinshead, M and Campbell, R D. (1997) J Biol Chem **272**, 4549–4558

7 Carrillo, M. B., Milner, C M, Ball, S T, Snoek, M and Campbell, R. D. (1997) Glycobiology **7**, 975–986

8 Igdoura, S, Gafuik, C, Mertineit, C, Saberi, F, Pshezhetsky, A, Potier, M, Trasler, J and Gravel, R (1998) Hum Mol Genet **7**, 115–121

9 Rottier, R, Bonten, E and d'Azzo, A (1998) Hum Mol Genet **7**, 313–321

10 Thomas, G H and Beaudet, A L (1995) in The Metabolic and Molecular Bases of Inherited Disease (Scriver, C. R., Beaudet, A L, Sly, W S and Valle, D, eds), pp 2529–2561, Mc-Graw-Hill, New York

11 Pober, M, Lu Shun Yan, D and Womack, J E (1979) FEBS Lett **108**, 345–348

12 Monti, E, Preti, A., Rossi, E, Ballabio, A and Borsani, G (1999) Genomics **57**, 137–143

13 Monti, E, Preti, A, Nesti, C, Ballabio, A and Borsani, G (1999) Glycobiology **9**, 1313–1321

14 Miyagi, T, Wada, T, Iwamatsu, A, Hata, K, Yoshikawa, Y., Tokuyama, S and Sawada, M (1999) J Biol Chem. **274**, 5004–5011

15 Hata, K, Wada, T, Hasegawa, A., Kiso, M and Miyagi, T (1998) J Biochem (Tokyo) **123**, 899–905

16 Ohman, R, Rosenberg, A and Svennerholm, L (1970) Biochemistry **9**, 3774–3782

17 Miyagi, T, Sagawa, J, Konno, K, Handa, S and Tsuiki, S. (1990) J Biochem (Tokyo) **107**, 787–793

18 Saito, M and Yu, R. K. (1986) J Neurochem **47**, 632–641

19 Riboni, L, Prinetti, A, Bassi, R and Tettamanti, G (1991) FEBS Lett **287**, 42–46

20 Pitto, M, Giglioni, A and Tettamanti, G (1992) Neurochem Int **21**, 367–374

21 Kopitz, J, von Reitzenstein, C, Muhl, C and Cantz, M. (1994) Biochem Biophys Res Commun **199**, 1188–1193

22 Chiarini, A, Fiorilli, A., Siniscalco, C, Tettamanti, G and Venerando, B (1990) J Neurochem. **55**, 1576–1584

23 Chiarini, A, Fiorilli, A, Di Francesco, L, Venerando, B and Tettamanti, G (1993) Glycoconj J **10**, 64–71

24 Tettamanti, G and Riboni, L (1993) Adv. Lipid Res. **25**, 235–267

25 Sambrook, J, Fritsch, E F and Maniatis, T (1989) Molecular Cloning A Laboratory Manual, 2nd edn, Cold Spring Harbor Laboratory, Cold Spring Harbor, NY

26 Banfi, S., Guffanti, A. and Borsani, G. (1998) Trends Genet **14**, 80–81

27 Marck, C (1988) Nucleic Acids Res **16**, 1829–1836

28 Thompson, J D, Higgins, D G and Gibson, T J (1994) Nucleic Acids Res **22**, 4673–4680

29 Altschul, S F, Madden, T L, Schaffer, A A, Zhang, J, Zhang, Z, Miller, W and Lipman, D J (1997) Nucleic Acids Res **25**, 3389–3402

30 Takebe, Y., Seiki, M., Fujisawa, J.-I., Hoy, P., Yokota, K., Arai, K.-I., Yoshida, M. and Arai, N (1988) Mol Cell Biol **8**, 466–472

31 Tettamanti, G, Bonali, F, Marchesini, S and Zambotti, V (1973) Biochim Biophys Acta **296**, 160–170

32 Sonnino, S, Ghidoni, R, Gazzotti, G, Kirschner, G, Galli, G and Tettamanti, G (1984) J. Lipid Res. **25**, 620–629

33 Chigorno, V., Pitto, M, Cardace, G, Acquotti, D., Kirschner, G, Sonnino, S, Ghidoni, R and Tettamanti, G (1985) Glycoconj J **2**, 279–286

34 Venerando, B., Fiorilli, A, Croci, G. L and Tettamanti, G (1997) Blood **90**, 2047–2056

35 Warren, L (1963) Methods Enzymol **6**, 465–475

36 Chigorno, V., Cardace, G, Pitto, M., Sonnino, S, Ghidoni, R and Tettamanti, G (1986) Anal Biochem **153**, 283–294

37 Boguski, M S and Schuler, G D (1995) Nat Genet **10**, 369–371

38 Gaskell, A, Crennell, S and Taylor, G. (1995) Structure **3**, 1197–1205

39 Wada, T, Yoshikawa, Y, Tokuyama, S, Kuwabara, M, Akida, H. and Miyagi, T. (1999) Biochem Biophys Res Commun **261**, 21–27

40 Rost, B, Casadio, R, Fariselli, P and Sander, C (1995) Protein Sci. **4**, 521–533

41 Crennell, S J, Garman, E F, Laver, W. G., Vimr, E. R and Taylor, G. L. (1993) Proc Natl Acad Sci U S A **90**, 9852–9856

42 Miyagi, T and Tsuiki, S (1985) J Biol. Chem **260**, 6710–6716

43 Warner, T G, Chang, J, Ferrari, J., Harris, R, McNerney, T., Bennett, G., Burmer, J. and Sliwkowski, M B (1993) Glycobiology **3**, 455–463

44 Igdoura, S A., Mertineit, C, Trasler, J M and Gravel, R A (1999) Hum Mol. Genet. **8**, 1111–1116

45 Lieser, M, Harms, E, Kern, H, Bach, G and Cantz, M. (1989) Biochem. J **260**, 69–74

46 Kopitz, J, Muhl, C, Ehemann, V, Lehmann, C. and Cantz, M (1997) Eur J Cell Biol **73**, 1–9

Received 19 August 1999/8 March 2000, accepted 13 April 2000

Biochem. J. (2000) 349, 353–356 (Printed in Great Britain)

Impaired nitric oxide production in coronary endothelial cells of the spontaneously diabetic BB rat is due to tetrahydrobiopterin deficiency

Cynthia J. MEININGER*[1], Rebecca S. MARINOS*, Kazuyuki HATAKEYAMA†, Raul MARTINEZ-ZAGUILAN‡, Jose D. ROJAS‡, Katherine A. KELLY* and Guoyao WU*§

*Cardiovascular Research Institute and Department of Medical Physiology, The Texas A&M University System Health Science Center, College Station, TX 77843-1114, U.S.A., †Department of Surgery, University of Pittsburgh, Pittsburgh, PA 15213, U.S.A., ‡Department of Physiology, Texas Tech University, Lubbock, TX 79430, U.S.A., and §Department of Animal Science, Texas A&M University, College Station, TX 77843-2471, U.S.A.

Endothelial cells (EC) from diabetic BioBreeding (BB) rats have an impaired ability to produce NO. This deficiency is not due to a defect in the constitutive isoform of NO synthase in EC (ecNOS) or alterations in intracellular calcium, calmodulin, NADPH or arginine levels. Instead, ecNOS cannot produce sufficient NO because of a deficiency in tetrahydrobiopterin (BH_4), a cofactor necessary for enzyme activity. EC from diabetic rats exhibited only 12% of the BH_4 levels found in EC from normal animals or diabetes-prone animals which did not develop disease. As a result, NO synthesis by EC of diabetic rats was only 18% of that for normal animals. Increasing BH_4 levels with sepiapterin increased NO production, suggesting that BH_4 deficiency is a metabolic basis for impaired endothelial NO synthesis in diabetic BB rats. This deficiency is due to decreased activity of GTP-cyclohydrolase I, the first and rate-limiting enzyme in the *de novo* biosynthesis of BH_4. GTP-cyclohydrolase activity was low because of a decreased expression of the protein in the diabetic cells.

Key words: diabetes, GTP-cyclohydrolase, nitric oxide synthesis, vascular disease.

INTRODUCTION

Insulin-dependent diabetes mellitus is associated with severe cardiovascular complications which are responsible for most of the morbidity and mortality associated with this disease. These complications include coronary heart disease, hypertension, cerebrovascular disease, nephropathy, retinopathy, thrombosis, ischaemia and, through the reduction in blood flow, neuropathy. Much research has been devoted to understanding diabetic vascular disease. Enhanced production of vasoconstrictors or reduction in the synthesis of vasodilators could theoretically contribute to many of the vascular complications of long-term diabetes. Recently it has been shown that there is an impaired endothelium-dependent relaxation in diabetic patients [1–3] and in the spontaneously diabetic BioBreeding (BBd) rat [4–6], an animal model of human insulin-dependent diabetes mellitus [7]. Although the mechanism for this defect in blood vessels is not understood, it has been hypothesized that the abnormal endothelial function in diabetic patients may be due to a defect in the synthesis of NO [8], the so-called endothelium-dependent relaxing factor.

The production of NO is catalysed by the various isoforms of NO synthase (NOS). The constitutively active form of NOS found in endothelial cells (EC), ecNOS, requires arginine as a substrate and several cofactors {e.g. NADPH, calcium and tetrahydrobiopterin [(6*R*)-5,6,7,8-tetrahydro-L-biopterin, or BH_4]} for normal activity. We have shown previously [9] that NO synthesis is impaired in coronary EC from the BBd rat. The defect responsible for this decreased NO synthesis was not elucidated.

Currently, there is little information available in the literature concerning NOS in diabetes mellitus. A few studies suggest normal or even enhanced levels of NOS protein and mRNA in diabetic animals or in EC exposed to high concentrations of glucose [10–12]. Indeed, we have shown normal NOS activity in EC homogenates [9], suggesting that there is no intrinsic defect in ecNOS from the BBd rat. The fact that NO production *in vivo* or *in vitro* is reduced in spite of normal NOS activity (measured under optimal conditions) suggests that substrate or cofactor availability may be limiting for NOS in EC. Therefore, the objective of the present study was to investigate whether a deficiency in one or more of the cofactors of NOS is responsible for impaired NO synthesis in intact EC of the BBd rat. We demonstrate a marked decrease in BH_4 concentration in EC from the diabetic animals compared with EC from the non-diabetic animals. The concentration of BH_4 could be increased by treatment of the cells with sepiapterin, suggesting an intact salvage pathway for BH_4 synthesis. The BH_4 deficiency in the diabetic cells is the result of a reduced *de novo* synthesis of BH_4, due to decreased GTP-cyclohydrolase activity.

EXPERIMENTAL PROCEDURES

Reagents

BSA, Dulbecco's PBS, Joklik's modified minimal essential medium, Dulbecco's modified Eagle's medium, L-glutamine and penicillin/streptomycin/amphotericin B were obtained from Gibco-BRL (Gaithersburg, MD, U.S.A.). Acetylated low-density lipoprotein labelled with 1,1′-dioctadecyl-3,3,3′,3′-tetramethylindocarbocyanine perchlorate was from Biomedical Technologies (Stoughton, MA, U.S.A.); fetal bovine serum was from Summit (Greeley, CO, U.S.A.); collagenase (type II) was from Worthington Biochemical (Freehold, NJ, U.S.A.); calmodulin and mouse anti-calmodulin antibody were from Upstate Biotechnology (Lake Placid, NY, U.S.A.); sepiapterin was from

---

Abbreviations used: BH_4, (6*R*)-5,6,7,8-tetrahydro-L-biopterin; EC, endothelial cells; NOS, nitric oxide synthase; ecNOS, constitutive isoform of NOS in EC; BBd, diabetic BioBreeding; BBn, non-diabetes-prone BioBreeding.

[1] To whom correspondence should be addressed (e-mail cjm@tamu.edu).

Research Biochemicals (Natick, MA, U.S.A.) and heparin was from Elkins-Sinn (Cherry Hill, NJ, U.S.A.).

Animals

Diabetic (BBd), diabetes-prone and non-diabetes-prone (normal, BBn) BB rats were obtained from the Animal Resources Division of the Health Protection Branch (Ottawa, ON, Canada). Diabetic rats were maintained with daily subcutaneous injections of 2–4 units of Ultralente insulin (Eli Lilly, Indianapolis, IN, U.S.A.) to prevent hyperglycaemia, ketosis and hypoinsulinaemia as described previously [13]. BBd rats (95–100 days of age) 25–30 days post onset of diabetes and age-matched BBn rats were used as a source of coronary microvascular EC. Serum glucose concentrations were determined by an enzymic method involving hexokinase and glucose-6-phosphate dehydrogenase [13] and were found to be 5.64±0.43 and 6.17±0.68 mM (means ± S.E.M., $n = 30$) for BBn and BBd rats, respectively, at the time of death. Diabetes-prone animals not developing diabetes within the usual time frame (70–100 days) were maintained until 150 days of age to verify the absence of disease.

Isolation and culture of microvascular EC

Microvascular EC were isolated from BBd, age-matched BBn, and diabetes-prone but normal BB rats (i.e. those not developing the disease) by collagenase perfusion, using the method of Ford and Rovetto [14], as described previously by our laboratories [9,15]. EC were obtained free of smooth-muscle cells and myocytes. The endothelial identity of the cultured cells was confirmed by the uptake of modified low-density lipoprotein [16]. EC from three or four rat hearts were pooled into one gelatin-coated (1.5% in PBS) 60-mm culture dish. EC were cultured at 37 °C under 10% CO_2 in Dulbecco's modified Eagle's medium containing 20% fetal bovine serum, 2 mM L-glutamine, 20 mM D-glucose, 20 units/ml heparin, 1 mM sodium pyruvate, 100 units/ml penicillin, 100 μg/ml streptomycin and 0.25 μg/ml amphotericin B. After the cells neared confluence, they were passaged using 0.25% trypsin and 0.02% EDTA and used at passages 5–15. No phenotypical changes were noted in the cells in this range of passage levels.

NO synthesis by EC

For the measurement of NO synthesis, EC were rinsed with PBS and cultured for 48 h in serum-free, Phenol-Red-free Dulbecco's modified Eagle's medium containing 0.2 mM L-glutamine, 0.4 mM L-arginine, 20 mM D-glucose, 1 mM sodium pyruvate, 100 units/ml penicillin, 100 μg/ml streptomycin and 0.25 μg/ml amphotericin B. At the end of the 48-h culture period, the conditioned media were used for the determination of nitrite and nitrate (two major stable end products of NO oxidation [17]) with $NaNO_2$ and $NaNO_3$ as standards, respectively, as described previously [18], using a microplate reader. In all experiments, culture medium incubated without cells was used as the blank. Cells, harvested from the culture dish, were used for metabolite analysis and measurements of enzyme activity, as described below.

HPLC analysis of cellular BH_4, arginine and NADPH

The cellular content of BH_4 was determined using a modification of the HPLC method of Fukushima and Nixon [19] in which EC (3×10^6) were lysed in 0.3 ml of 0.1 M phosphoric acid containing 5 mM dithioerythritol (an antioxidant) and 35 μl of 2 M trichloroacetic acid. Arginine levels in EC were measured by HPLC as described previously [9]. Extraction of NADPH from EC and its analysis by HPLC were done as described previously [20], except that 1 mM bathophenanthroline-disulphonic acid (a bivalent metal chelator) was used to prevent oxidation of NADPH by iron [21] and NADPH was detected by a fluorimeter (excitation 340 nm, emission 460 nm) to improve sensitivity.

Calcium measurement *in situ*

EC grown on coverslips were co-loaded with SNARF-1 and Fura-2 (Molecular Probes, Eugene, OR, U.S.A.) to simultaneously measure intracellular pH and calcium concentration as we described previously [22,23]. Simultaneous measurements of these two ions is necessary because the K_d of Fura-2 is affected by pH. We corrected for this interaction but, for the purposes of discussion, present only the Fura-2 data.

Immunoblot procedure

Cellular protein from BBd and BBn EC was loaded on to 9.5–16% polyacrylamide gels. Separated proteins were blotted on to nitrocellulose and the blots were blocked with 5% non-fat dried milk in Tris-buffered saline with 0.1% Tween 20 (blocking buffer). For analysis of calmodulin, the primary antibody, mouse anti-bovine calmodulin (Upstate Biotechnology), was used at 1 μg/ml in blocking buffer and the secondary antibody, horseradish peroxidase-conjugated donkey anti-mouse IgG (Jackson Laboratories, West Grove, PA, U.S.A.), was used at 1:75000 in blocking buffer. For analysis of GTP-cyclohydrolase I, primary antibody (prepared against purified rat recombinant GTP-cyclohydrolase I [24]) was diluted 1:10000 in blocking buffer and the secondary antibody, peroxidase-conjugated donkey anti-rabbit IgG (Jackson Laboratories) was used at 1:100000 in blocking buffer. Bands were visualized using SuperSignal® West Dura Extended Duration Substrate (Pierce, Rockford, IL, U.S.A.) according to the manufacturer's directions with Kodak Biomax ML film (Kodak, Rochester, NY, U.S.A.). Blots were scanned using a UMAX S6E scanner (UMAX Data System, Hsinchu, Taiwan) with VistaScan software (Kodak) and analysed using Multi-Analyst software (BioRad, Hercules, CA, U.S.A.).

Determination of GTP-cyclohydrolase activity

GTP-cyclohydrolase activity in EC was determined as described by Viveros et al. [25]. The product of this enzymic reaction was converted into neopterin by alkaline phosphatase (1 unit/μl in 50 mM $MgCl_2$; 10 units/tube). Neopterin was then analysed by HPLC as described by Fukushima and Nixon [19].

Statistical analysis

Data were analysed by paired or unpaired t test using the SAS program [26]. Probability values of $P < 0.05$ were taken to indicate statistical significance.

RESULTS AND DISCUSSION

There are many pharmacological studies demonstrating impaired dilator responses to agonists in conduit and resistance blood vessels from experimental diabetic animals (see [27] for review). We have shown previously that coronary EC from the BBd rats are unable to produce as much NO as EC from non-diabetic rats [9]. The defect in the ability of these cells to produce NO, however, was not in the NOS enzyme itself. Instead, our earlier work suggested that it might be a deficiency in the amount of a cofactor necessary for full activity of ecNOS [9].

Table 1 Calcium, NADPH and arginine concentrations in BB rat EC

EC from BBn and BBd rats were analysed for calcium, NADPH and arginine concentrations. Data are means ± S.E.M., with the number of experiments given in parentheses. $^*P < 0.01$, BBd versus BBn, as analysed by unpaired *t* test

EC	Calcium (nM)	NADPH (pmol/10^6 cells)	Arginine (nmol/10^6 cells)
BBn	13.3 ± 0.96 (24)	66.3 ± 5.4 (8)	2.88 ± 0.23 (10)
BBd	15.2 ± 0.95 (29)	117.9 ± 10.8 (8)*	4.37 ± 0.31 (10)*

Table 2 BH$_4$ concentrations in BB rat EC

EC from BBn and BBd rats were analysed for BH$_4$. Data are means ± S.E.M., with the number of experiments given in parentheses. $^*P < 0.01$, BBd versus BBn, as analysed by unpaired Student's *t* test. $^†P < 0.01$, group with sepiapterin versus group with no sepiapterin, as analysed by paired *t* test

	BH$_4$ (pmol/10^6 cells)	
EC	No sepiapterin	+10 μM Sepiapterin
BBn	1.42 ± 0.22 (7)	32.1 ± 2.9 (4)†
BBd	0.17 ± 0.01 (5)*	29.9 ± 2.6 (4)†

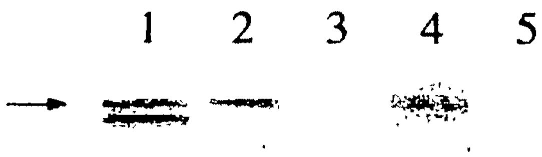

Figure 1 GTP-cyclohydrolase I immunoblot

Cellular protein from Sprague–Dawley rat liver (lane 1, 5 μg/lane, positive control), BBn EC (lanes 2 and 4, 30 μg/lane), and BBd EC (lanes 3 and 5, 30 μg/lane) was separated on a polyacrylamide gradient gel, blotted on to nitrocellulose and probed using a rabbit anti-rat GTP-cyclohydrolase I antibody. The arrow indicates a protein band corresponding to a molecular mass of approx. 29000 Da

We investigated the intracellular concentrations of calcium, NADPH and calmodulin, all required for full activity of ecNOS [28]. Steady-state intracellular calcium concentrations in unstimulated EC from BBd and BBn rats were not significantly different (Table 1) and thus would not account for the differences in NO production. The enzyme ecNOS oxidizes arginine to produce citrulline and NO in a process that consumes NADPH [28]. It is therefore possible that decreased NO production is due to decreased availability of NADPH in BBd EC. However, NADPH levels were significantly higher in the BBd EC compared with BBn EC (Table 1). This greater concentration of NADPH in BBd EC is consistent with increased activity of the pentose cycle pathway for NADPH provision in these cells (G. Wu and C. Meininger, unpublished work). Finally, calmodulin levels in BBd and BBn EC were not significantly different. Calmodulin levels were 2.80 ± 0.13 ng/μg of protein in the BBn EC (means ± S.E.M., $n = 7$) and 2.78 ± 0.13 ng/μg of protein in the BBd EC ($n = 6$; calculated by comparison of absorbance of samples with that of a standard curve). These data suggest that adequate amounts of calcium, NADPH and calmodulin exist in the EC of diabetic animals to support NO production.

Because decreased availability of substrate for ecNOS could also result in lowered production of NO, we measured arginine levels in the BBd and BBn EC. Arginine uptake was not different in the two cell types [9], yet intracellular arginine concentrations were significantly higher in the EC from diabetic animals (Table 1). We have shown previously that arginase activity is decreased in the EC from BBd rats [9], which would account for the increase in intracellular arginine concentrations and would theoretically provide more substrate for NO production by ecNOS. Thus it is unlikely that the arginine substrate was limiting for NO production in the BBd EC.

BH$_4$ plays an essential role in EC NO synthesis [29]. To determine whether the defect in NO production was due to a deficiency in this cofactor for ecNOS, we measured BH$_4$ levels in the EC. BBd EC exhibited only 12% of the BH$_4$ level found in BBn EC (Table 2). The levels found in the BBn EC were similar to those previously reported for EC from human umbilical veins [30]. Importantly, EC isolated from diabetes-prone BB rats that *did not* develop disease exhibited BH$_4$ levels equivalent to non-diabetes prone (i.e. normal) BB rats (1.45 ± 0.36 pmol/10^6 cells, mean ± S.E.M., $n = 6$). Equivalent levels were found in cells analysed immediately upon isolation from the animals without being cultured (1.51 ± 0.27 pmol/10^6 BBn EC versus 0.22 ± 0.03 pmol/10^6 BBd EC, $n = 4$, $P < 0.01$). These findings imply that the BH$_4$ deficiency is not simply an inbred defect in the diabetes-prone animals or the result of cell culturing but is somehow linked to the disease state

BH$_4$ is produced in EC by two pathways: a salvage pathway which makes BH$_4$ from dihydrobiopterin in the cell and a *de novo* synthetic pathway which generates BH$_4$ from GTP [30]. Sepiapterin is taken up by EC and utilized in the salvage pathway to generate BH$_4$. Treating EC from either the normal or diabetic rats with 10 μM sepiapterin resulted in a significant increase in BH$_4$ levels in the cells (Table 2). This result suggests that there is

Table 3 Effect of sepiapterin on NO production in BB rat EC (pmol/h per 10^6 cells)

EC from BBd and BBn rats were cultured in growth medium containing 0.2 mM L-glutamine for 48 h in the presence or absence of 10 μM sepiapterin. Conditioned media were analysed for nitrite and nitrate concentrations as a measure of NO production. Data are means ± S.E.M., $n = 8$. $^*P < 0.01$, group with sepiapterin versus group with no sepiapterin, as analysed by paired *t* test. $^†P < 0.01$, BBd versus BBn group, as analysed by unpaired *t* test

	No sepiapterin			+10 μM Sepiapterin		
	Nitrite	Nitrate	Nitrite + nitrate	Nitrite	Nitrate	Nitrite + nitrate
BBn	53.9 ± 4.1	238.9 ± 15.8	292.8 ± 18.9	107.4 ± 6.7*	406.3 ± 20.9*	514.9 ± 24.2*
BBd	17.3 ± 1.9†	35.1 ± 5.0†	52.3 ± 6.6†	46.5 ± 3.8†*	206.1 ± 11.0†*	253.8 ± 13.5†*

no defect in BH_4 synthesis via the salvage pathway in BBd EC. To determine whether there may be a defect in *de novo* synthesis of BH_4 from GTP in BBd EC, we measured the activity of GTP-cyclohydrolase I, the first and rate-limiting enzyme in this *de novo* synthetic pathway [29]. Enzyme activity was higher ($P < 0.01$) for BBn cells (0.624 ± 0.2 pmol/mg per 90 min, mean ± S.E.M., $n = 5$) than for BBd cells (0.072 ± 0.04 pmol/mg per 90 min, $n = 5$). When GTP-cyclohydrolase I levels were analysed by immunoblot, the amount of protein was found to be significantly higher in the EC from the non-diabetic animals (Figure 1). This decrease in enzyme expression would explain the deficiency in enzyme activity. Interestingly, BH_4 levels in the BBd EC were decreased to the same extent as the decrease in GTP-cyclohydrolase activity, consistent with the role of GTP-cyclohydrolase as the rate-limiting enzyme for *de novo* BH_4 synthesis. Thus the decrease in GTP-cyclohydrolase I activity is sufficient to account for the BH_4 deficiency in EC of diabetic rats.

To investigate whether increasing intracellular BH_4 levels could enhance NO production in BBd EC, we cultured EC in the presence and absence of sepiapterin. We found that 10 μM sepiapterin increased the production of NO by both BBn and BBd EC (Table 3). In the absence of sepiapterin, EC from the diabetic animals made only 18% of the NO produced by EC from the non-diabetic animals. The addition of 10 μM sepiapterin increased NO production by BBd EC to a level approximately equal to that of BBn EC in the absence of sepiapterin. Sepiapterin increased NO production by BBn EC an additional 76%. Whereas sepiapterin treatment was able to normalize BH_4 levels in EC from diabetic animals (Table 2), the nitrite/nitrate accumulation by these cells was less than that of EC from non-diabetic animals treated with sepiapterin over the same time period (Table 3). This difference in nitrite/nitrate levels was probably the result of the time necessary for BH_4 levels to increase in order to augment NO production in the BBd EC. The BBn EC did not start with a deficit in BH_4 and therefore accumulated more nitrite/nitrate during the treatment period.

In conclusion, we have shown a BH_4 deficiency in coronary EC from the diabetic BB rat due to a decreased expression of GTP-cyclohydrolase, the rate-limiting enzyme for *de novo* synthesis of BH_4. With insufficient BH_4 the cells are unable to make sufficient NO. This BH_4 deficiency may be the metabolic basis for the heretofore unexplained observation that endothelium-dependent relaxation is impaired in diabetic animals as well as diabetic patients, and may contribute significantly to the pathogenesis of diabetic vascular complications.

Funding for this study was received from the American Heart Association, National Office and Texas Affiliate, Dallas, TX, U.S.A., as well as from Interdisciplinary Research Initiative Funds from Texas A&M University. G.W is an Established Investigator of the American Heart Association We thank Tony E Haynes for his technical expertise in isolating these cell lines and Wene Yan for technical assistance with HPLC measurements.

Received 13 March 2000, accepted 17 April 2000

REFERENCES

1 Calver, A, Collier, J and Vallance, P (1992) J Clin Invest **90**, 2548–2554

2 Elliott, T G., Cockcroft, J R, Groop, P H, Viberti, C C and Ritter, J M (1993) Clin Sci **85**, 687–693

3 Johnstone, M T, Creager, S. J., Sclaes, K. M., Cusco, J A, Lee, B K and Creager, M. (1993) Circulation **88**, 2510–2516

4 Durante, W, Sen, A K and Sunahara, F A (1988) Br J Pharmacol **94**, 463–468

5 Meraji, S, Jayakody, L, Senaratne, M P, Thomson, A B and Kappagoda, T. (1987) Diabetes **36**, 978–981

6 Pieper, G M, Moore-Hilton, G. and Roza, A. M (1996) Life Sci **58**, PL147–PL152

7 Marliss, E. B., Nakhooda, A F, Poussier, P and Sima, A. A (1982) Diabetologia **22**, 225–232

8 Calver, A., Collier, J and Vallance, P. (1993) Exp Physiol. **78**, 303–326

9 Wu, G. and Meininger, C J. (1995) Am J Physiol **269**, H1312–H1318

10 Rosen, P., Ballhausen, T, Block, W and Addicks, K (1995) Diabetologia **38**, 1157–1168

11 Cosentino, F., Hishikawa, K, Katusic, Z S and Luscher, T F (1997) Circulation **96**, 25–28

12 Mancusi, G, Hutter, C, Baumgartner-Parzer, S, Schmidt, K, Schutz, W and Sexl, V (1996) Biochem J **315**, 281–287

13 Wu, G and Marliss, E B (1993) Diabetes **42**, 520–529

14 Ford, D. A and Rovetto, M J. (1987) Am J. Physiol **252**, H54–H63

15 Wu, G and Meininger, C J (1993) Am J Physiol **265**, H1965–H1971

16 Voyta, J C, Via, D P., Butterfield, C E and Zetter, B R (1984) J Cell Biol. **99**, 2034–2040

17 Ignarro, L J (1990) Ann Rev Pharmacol Toxicol **30**, 535–560

18 Wu, G and Brosnan, J T (1992) Biochem J **281**, 45–48

19 Fukushima, T and Nixon, J C (1980) Anal Biochem **102**, 175–188

20 Stocchi, V., Cucchiarini, L, Canestrari, F, Piacentini, M. P and Fornaini, G (1987) Anal Biochem. **167**, 181–190

21 Klaidman, L K., Leung, A C. and Adams, Jr, J D (1995) Anal Biochem **228**, 312–317

22 Martinez-Zaguilan, R, Martinez, G M, Lattanzio, F and Gillies, R J (1991) Am. J Physiol **260**, C297–C307

23 Martinez-Zaguilan, R, Gurule, M and Lynch, R M. (1996) Am J Physiol **270**, C1438–C1446

24 Yoneyama, Y, Brewer, J M and Katakeyama, K (1997) J Biol Chem **272**, 9690–9696

25 Viveros, O H, Lee, C-L., Abou-Donia, M M., Nixon, J. C and Nichol, C A (1981) Science **213**, 349–350

26 SAS Institute Inc (1990) SAS/SAT User's Guide, SAS Institute, Cary, NC

27 Pieper, G M (1998) Hypertension **31**, 1047–1060

28 Wu, G and Morris, Jr, S M (1998) Biochem J **336**, 1–17

29 Werner-Felmayer, G. and Gross, S S (1996) in Methods in Nitric Oxide Research (Feelisch, M and Stamler, J S, eds), pp 271–299, John Wiley & Sons, New York

30 Werner-Felmayer, G., Werner, E R, Fuchs, D, Hausen, A, Reibnegger, G, Schmidt, K, Weiss, G and Wachter, H (1993) J Biol Chem **268**, 1842–1846

Biochem. J. (2000) 349, 357–368 (Printed in Great Britain)

Inhibition of Ca^{2+} signalling by p130, a phospholipase-C-related catalytically inactive protein: critical role of the p130 pleckstrin homology domain

Hiroshi TAKEUCHI*, Masahiro OIKE†, Hugh F. PATERSON‡, Victoria ALLEN‡, Takashi KANEMATSU*, Yushi ITO†, Christophe ERNEUX§, Matilda KATAN‡ and Masato HIRATA*[1]

*Department of Biochemistry, Faculty of Dentistry, Kyushu University and Kyushu University Station for Collaborative Research, Fukuoka 812-8582, Japan, †Department of Pharmacology, Faculty of Medicine, Kyushu University, Fukuoka 812-8582, Japan, ‡CRC Center for Cell and Molecular Biology, Chester Beatty Laboratory, Institute of Cancer Research, Fulham Road, London SW3 6JB, U.K., and §Institute of Interdisciplinary Research (IRIBHN), Free University of Brussels, Campus Erasme, Bldg C, Route de Lennik 808, B-1070 Brussels, Belgium

p130 was originally identified as an Ins(1,4,5)P_3-binding protein similar to phospholipase C-δ but lacking any phospholipase activity. In the present study we have further analysed the interactions of p130 with inositol compounds *in vitro*. To determine which of the potential ligands interacts with p130 in cells, we performed an analysis of the cellular localization of this protein, the isolation of a protein–ligand complex from cell lysates and studied the effects of p130 on Ins(1,4,5)P_3-mediated Ca^{2+} signalling by using permeabilized and transiently or stably transfected COS-1 cells (COS-1^{p130}). *In vitro*, p130 bound Ins(1,4,5)P_3 with a higher affinity than that for phosphoinositides. When the protein was isolated from COS-1^{p130} cells by immunoprecipitation, it was found to be associated with Ins(1,4,5)P_3. Localization studies demonstrated the presence of the full-length p130 in the cytoplasm of living cells, not at the plasma membrane. In cell-based assays, p130 had an inhibitory effect on Ca^{2+} signalling. When fura-2-loaded COS-1^{p130} cells were stimulated with bradykinin, epidermal growth factor or ATP, it was found that the agonist-induced increase in free Ca^{2+} concentration, observed in control cells, was inhibited in COS-1^{p130}. This inhibition was not accompanied by the decreased production of Ins(1,4,5)P_3; the intact p130 pleckstrin homology domain, known to be the ligand-binding site *in vitro*, was required for this effect in cells. These results suggest that Ins(1,4,5)P_3 could be the main p130 ligand in cells and that this binding has the potential to inhibit Ins(1,4,5)P_3-mediated Ca^{2+} signalling.

Key words: Ca^{2+} release, Ins(1,4,5)P_3 receptor, phosphoinositides.

INTRODUCTION

It is now well established that the metabolism of phosphoinositides is important in a wide variety of cellular functions. The hydrolysis of PtdIns(4,5)P_2 by phospholipase C (PLC) yields the water-soluble messenger Ins(1,4,5)P_3, which binds to specific Ca^{2+}-channel receptors and mobilizes intracellular Ca^{2+}, while the hydrophobic moiety, diacylglycerol, activates protein kinase C isoenzymes [1,2]. PtdIns(4,5)P_2 can also be phosphorylated by phosphoinositide 3-kinase (type 1) to form PtdIns(3,4,5)P_3, a lipid product found in stimulated cells [3–5]. There is growing evidence that PtdIns(3,4,5)P_3, and some other products of phosphoinositide 3-kinase activation, could bind directly to specific intracellular protein targets and thus act as second messengers [4,6].

Considerable effort, with a variety of experimental approaches, has been made to identify proteins that could bind phosphoinositides and inositol phosphates and thus participate in a signalling network via these second messengers [7]. One such potential protein target, designated p130, was isolated by using affinity chromatography with an Ins(1,4,5)P_3 analogue as a ligand [7,8]. Subsequent cloning of the cDNA encoding p130 revealed extensive similarity with phosphoinositide-specific PLC enzymes and, in particular, the PLC-δ family [9]. On the basis of the crystal structure of PLC-δ1 [10], p130 protein is predicted to have the same domain organization, incorporating the pleckstrin homology (PH), EF-hand, catalytic and C2 domains [10a]. However, p130 has some distinct characteristics. It is a larger molecule than the PLC-δ isoenzymes and unique regions are present at both the N-terminus preceding the PH domain and at the C-terminus. More importantly, the residues within the catalytic domain critical for PLC activity (Glu-390 and His-356) are not conserved in p130 [9]. As expected from a mutagenesis study of PLC-δ1 [11] it has been found that p130 does indeed lack PLC activity [7,9]. Other molecules with similarity to p130 have also been described and designated human PLC-L [12] and K10F12.3 gene product from *Caenorhabditis elegans* [13]. Otsuki et al. [14] recently isolated a novel cDNA from mouse brain library with a similarity of 70% to PLC-L; they therefore designated it mouse PLC-L$_2$, calling the original PLC-L human PLC-L$_1$. Furthermore, the gene for human PLC-L$_2$ has been reported by Kazusa DNA Research Institute [15]. All these proteins have characteristic N- and C-terminal extensions, and replacements of critical catalytic residues. Finding a similar molecule in a simple organism such as *C. elegans* suggests that

---

Abbreviations used: BK, bradykinin; COS-1^{p130}, COS-1 cells stably expressing p130; EGF, epidermal growth factor; GFP, green fluorescent protein; GFP–p130(F), GFP-fused full-length p130; GFP–p130(ΔPH), GFP-fused p130 lacking the PH domain; GFP–p130PH, GFP-fused PH domain of p130; IP3R, Ins(1,4,5)P_3 receptor; p130, a new Ins(1,4,5)P_3-binding protein with a molecular mass of 130 kDa; PH, pleckstrin homology; PLC, phospholipase C; SAX, strong anion exchange.

[1] To whom correspondence should be addressed (e-mail hirata1@dent.kyushu-u.ac.jp).

this catalytically inactive branch evolved early and separated from other PLC families to form a new protein family.

Further studies of p130 demonstrated that the PH domain of this molecule is responsible for binding inositol phosphates [16], a property that could be important for the function of the entire molecule. The functions of PH domains, present in more than 100 proteins, have been extensively studied [6,17,18]. This stable structural entity incorporates variable regions that, in different proteins, can be adapted to perform a specific function through binding to phosphoinositides present in the membrane or specific proteins. Several recent examples illustrate that the function of some PH domains, which interact with phosphoinositides, is to regulate membrane attachment [19–23]. Interactions with inositol phosphates have also been reported for a number of PH domains [6,16,17,21,23]. However, inositol phosphates have often been regarded as a mimic of the cytoplasm-exposed headgroup of the membrane-bound phosphoinositides, rather than as physiological ligands for these PH domains. A possible exception could be the PH domain of GAP1^{IP4BP} (GAP being GTPase-activating protein), which was, like p130, originally purified as inositol-phosphate-binding protein [with a K_d for Ins(1,3,4,5)P_4 of approx. 6 nM] [24]. Subsequently, this protein was found to have Ras-GAP activity [25]. However, the function of Ins(1,3,4,5)P_4 binding to GAP1^{IP4BP} remains unclear. It could be required for the enhancement of GAP activity towards Ras or its functions could be related to Ins(1,3,4,5)P_4-regulated Ca^{2+} entry.

Here we describe studies aiming at the characterization of a potential physiological ligand for the p130PH domain and functional properties of p130. The results provide evidence for the involvement of p130, found exclusively in the cytoplasm, in the Ins(1,4,5)P_3-mediated Ca^{2+} signalling. They also suggest that a consequence of the binding of Ins(1,4,5)P_3 to the p130PH domain could be to sequester Ins(1,4,5)P_3 and therefore to prevent its interaction with the Ins(1,4,5)P_3 receptors and metabolizing enzymes.

EXPERIMENTAL

Materials

[^{3}H]Ins(1,4,5)P_3 (specific radioactivity 777 GBq/mmol) and *myo*-[1,2-^{3}H]inositol (specific radioactivity 2105 GBq/mmol) were obtained from Du Pont–New England Nuclear (Boston, MA, U.S.A.). phGFP-S65T and pEGFP-C1 vectors (in which GFP stands for green fluorescent protein) were from Clontech (Palo Alto, CA, U.S.A.). LipofectAMINE® reagent and Geneticin (G418) were from Gibco BRL (Gaithersburg, MD, U.S.A.). Biotinylated or fluorescein-labelled goat anti-mouse IgG antibodies were from Amersham (Little Chalfont, Bucks., U.K.). Protein G–Sepharose was from Amersham Pharmacia Biotech (Uppsala, Sweden). An alkaline phosphatase staining kit was obtained from Pierce (Rockford, IL, U.S.A.). Lipids [phosphatidylethanolamine, PtdIns and PtdIns(4,5)P_2] were from Sigma (St Louis, MO, U.S.A.). Short-chain PtdIns(4,5)P_2 [(diC$_4$)-PtdIns(4,5)P_2] and PtdIns(3,4,5)P_3 [(diC$_4$)PtdIns(3,4,5)P_3] were from Echelon Research Laboratory (Salt Lake City, UT, U.S.A.). Fura 2 (free acid), fura 2 acetoxymethyl ester and Ins(1,4,5)P_3 were from Dojindo Laboratory (Kumamoto, Japan). All other reagents were of the highest grade available

Construction of plasmids for stable expression and cell culture for establishing COS-1^{p130} cells

p130 cDNA (pcMT3; see [9]) was subcloned into BCMGSneo. The BCMGSneo/p130 was transfected into COS-1 cells with the use of LipofectAMINE reagent in accordance with the manufacturer's instructions and cultured in the presence of 0.8 mg/ml G418. Stable transfectants were established by selection with G418 and cloning.

Construction of plasmids for expression of GFP fusion proteins

GFP fusion proteins of the full-length p130 [GFP–p130(F)], the PH domain deletion mutant [GFP–p130(ΔPH)] and the p130 isolated PH domain [GFP–p130PH] were constructed with the phGFP105-C1 and phGFP105/Sse vectors, modified from phGFP-S65T vector by changing several amino acids of GFP to enhance the fluorescent intensity [26]. To construct GFP–p130(F), the phGFP105-C1 vector was digested with *Eco*RI, followed by treatment with Klenow fragment for end-filling; it was then digested with *Xho*I again. The p130 cDNA, pcMT3 [9], was digested with *Hin*dIII (end-filling) and *Xho*I; the purified insert was ligated into phGFP105-C1. GFP–p130(ΔPH) and GFP–p130PH was constructed as follows: the *Sma*I fragment of pcMT3 was introduced into the phGFP105/Sse vector digested with *Sma*I; the *Bam*HI (end-filling) and *Sma*I fragments of pcMT3 were inserted into phGFP105-C1 vector digested with *Xho*I (end-filling). To construct GFP–PLC-δ1 E341A, the full-length PLC-δ1 E341A as a glutathione S-transferase fusion protein [11] was digested with *Bam*HI and *Sma*I; the resultant fragment was subcloned into pEGFP-C1 vector digested with *Bgl*II and *Sma*I. For construction of the PLC-δ1 PH domain as a GFP fusion protein, a pGEX-2T plasmid encoding the N-terminal part of PLC-δ1 (amino acid residues 1–290) [19] was digested with *Bam*HI and *Eco*RI; the fragment was subcloned into pEGFP-C1 vector digested with *Bgl*II and *Eco*RI. GFP–PKB/Akt PH domain plasmid was generated by using a PCR fragment of bovine PKB/Akt encoding the N-terminus (residues 1–147) and subcloning into pEGFP-C1 vector.

Transfection and microinjection of GFPs for cell localization studies

COS-1, NIH 3T3 and Madin–Darby canine kidney ('MDCK') cells, cultured in Dulbecco's modified Eagle's medium with 10% (v/v) fetal bovine serum, were transiently transfected with LipofectAMINE Plus reagent, in accordance with the manufacturer's protocol Procedures for the microinjection of MDCK cells were essentially the same as described previously [19].

Immunostaining with monoclonal antibody against p130

COS-1^{p130} cells were grown on a glass coverslips for 24 h The cells were rinsed in PBS and fixed for 30 min in 4% (w/v) paraformaldehyde. All steps were performed at room temperature; coverslips were rinsed in PBS between each of the steps. Cells were permeabilized in PBS containing 0.2% (v/v) Triton X-100 for 20 min; p130 was detected with monoclonal anti-p130 antibody (2F9) and either FITC-conjugated goat anti-mouse IgG or biotinylated monoclonal antibody (biotin-2F9) and FITC-conjugated avidin. The coverslips were examined for fluorescent images with a Zeiss axiophot microscope using Zeiss 40 × 1.3 and 63 × 1.4 oil immersion objectives Untransfected COS-1 cells or mock-transfected COS-1 cells were used as a control.

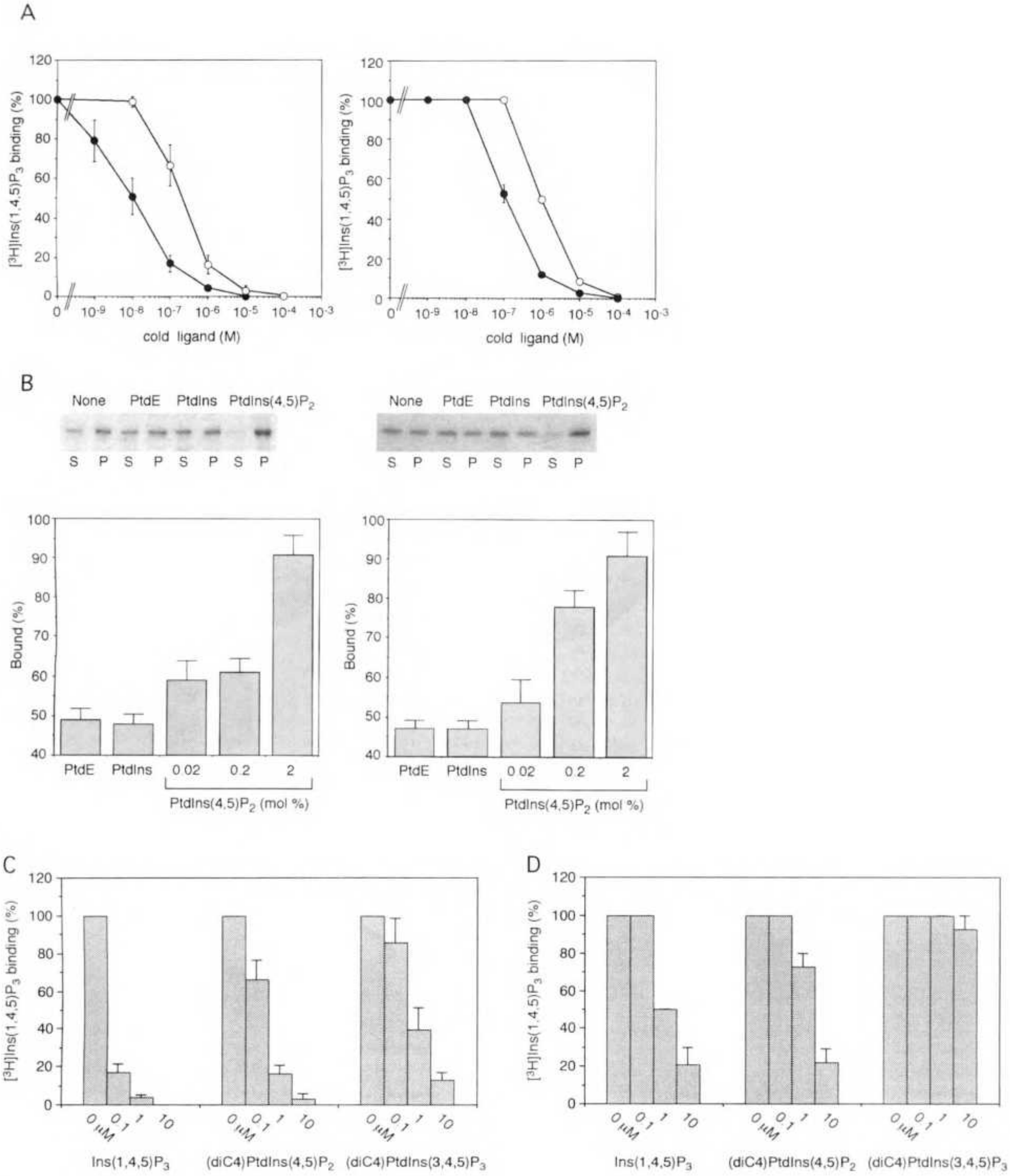

Figure 1 Binding of inositol compounds

(**A**) Displacement of [^{3}H]Ins(1,4,5)P_3 bound to p130 (left panel) and the p130PH domain (right panel) by Ins(1,4,5)P_3 (●) and water-soluble short-chain (diC$_4$)PtdIns(4,5)P_2 (○). (**B**) Binding of p130 (left panel) and p130PH domain (right panel) to liposomes containing naturally occurring PtdIns(4,5)P_2. Lanes marked S and P indicate supernatant and precipitate after centrifugation respectively. (**C**, **D**) Binding specificity of p130 (**C**) and PLC-δ1 E341A (**D**). For displacing [^{3}H]Ins(1,4,5)P_3, unlabelled Ins(1,4,5)P_3, (diC$_4$)PtdIns(4,5)P_2 and (diC$_4$)PtdIns(3,4,5)P_3 were used. Each result is the mean ± S.E.M. for five to seven experiments.

Protein expression and purification

Expression and purification of the full-length PLC-δ1 E341A and PLC-δ1 PH domain constructs were as described previously [11,19]. To prepare the full-length p130 (residues 1–1096), a baculovirus expression system was employed, with the use of standard procedures, and the fragment encoding p130 was subcloned into pAcHLT-B vector in frame with the His$_6$ tag. The recombinant PH domain of p130 was prepared as described previously [16].

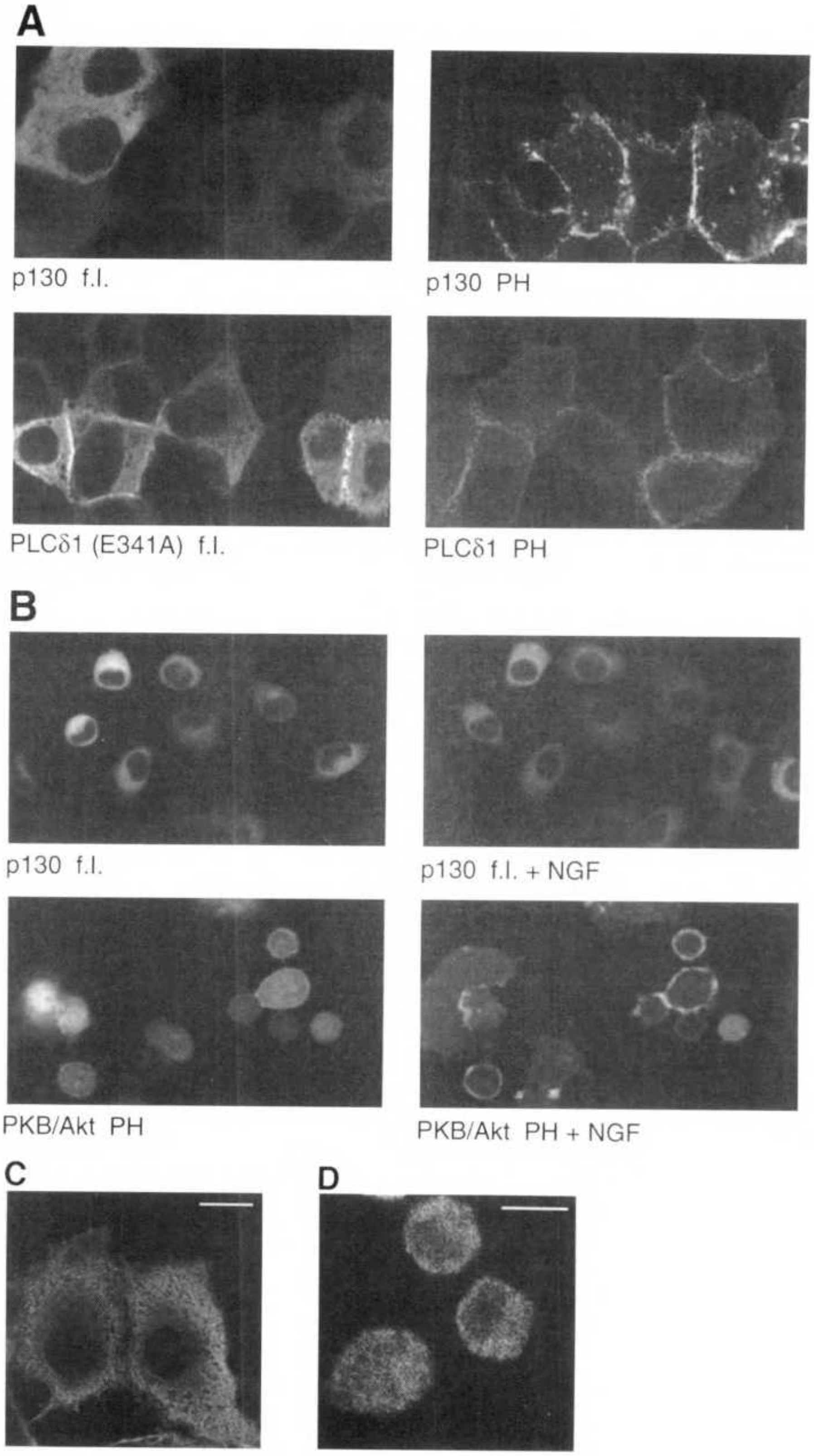

Figure 2 Cellular localization studies of p130

(**A**) The localization of the GFP fusion protein of the full-length p130 (p130 f.l.) and the isolated PH domain (p130PH) and corresponding constructs of PLC-δ1 [PLC-δ1 (E341A) f.l. and PLC-δ1 PH domain respectively] was monitored after microinjection of the plasmids into MDCK cells. The images were recorded 2.5 h after microinjection. Experiments were repeated at least 10 times, giving essentially the same results. (**B**) Localization of the full-length p130 GFP fusion protein (p130 f.l.) in the PC12 cells was analysed 2.5 h after microinjection and images were recorded before

Binding assay of recombinant proteins to [^{3}H] Ins(1,4,5)P_3 or to liposomes

The [^{3}H]Ins(1,4,5)P_3 binding assay was performed as described previously [27], except that the pH was 7.4. Binding to liposomes was assayed with the method described previously [28].

Measurement of changes in free Ca^{2+} concentration of the intact cells

Intracellular free Ca^{2+} concentration was measured in COS-1 cells by using an Attofluor digital fluorescence microscopy system in combination with fura 2 (Atto Instruments, Rockville, MD, U.S.A.). Cells were loaded with fura 2 by incubation with fura 2 acetoxymethyl ester for 20 min at room temperature, then for a further 20 min at 37 °C. For measurement with control COS-1 or COS-1^{p130}, fura 2 was excited alternately at two wavelengths (340 and 380 nm) and the fura 2 fluorescence from a single cell was measured. For measurement with COS-1 cells transfected with the GFP-fused version of p130, successful transfection of the plasmid into the cell was confirmed by GFP fluorescence. Fura 2 fluorescence from a single cell in the same microscopic field was measured. Thus it was possible to measure Ca^{2+} concentrations from only the vector-transfected, GFP-positive cells. All experiments were performed at room temperature (20–25 °C).

Measurement of production of Ins(1,4,5)P_3

The cellular content of Ins(1,4,5)P_3 was measured by a radioreceptor competition assay by the method of Palmer et al. [29]. Cell labelling experiments were also performed with the method described by Shears [30], with a minor modification for the separation of labelled inositol phosphates by a strong anion exchange (SAX) column (Whatman) mounted on an HPLC system.

Assay of Ca^{2+} release from permeabilized cells by Ins(1,4,5)P_3

The procedures for obtaining and analysing permeabilized COS-1 cells were essentially the same as those previously described for other cell types [31]. The COS-1 cells were harvested 4–5 days after plating, then permeabilized with saponin. Ca^{2+} uptake and release by saponin-permeabilized cells were assayed as described previously [31].

Assay of Ins(1,4,5)P_3-metabolizing activity

Assays of Ins(1,4,5)P_3 metabolizing enzymes were performed as described previously, with recombinant enzymes [8].

Binding of inositol phosphate in living cells to p130

COS-1^{p130} cells were incubated for 48 h in inositol-free medium supplemented with *myo*-[^{3}H]inositol (50 μCi/ml) and dialysed fetal bovine serum. The labelled cells were stimulated with bradykinin (BK) or epidermal growth factor (EGF) and then lysed with a buffer containing 1 % (v/v) Triton X-100/50 mM Hepes/NaOH (pH 7.2)/150 mM NaCl/5 mM EDTA. After centrifugation at 12000 g for 30 min at 4 °C, the resulting supernatant was incubated with 20 μg/ml anti-p130 monoclonal antibody (2F9), followed by the addition of 20 μl of a 50 % (w/v) slurry of Protein G–Sepharose for 2 h at 4 °C. Immunoprecipitate was treated with 5 % (w/v) trichloroacetic acid to release the radioactivity bound to p130 After neutralization of the sample, it was analysed by applying to a SAX column as described above.

RESULTS

Purified p130 and its isolated PH domain have a preference for Ins(1,4,5)P_3 over inositol lipids

The Ins(1,4,5)P_3-binding properties of p130 have previously been mapped to the N-terminus containing the PH domain [16]. Further characterization has also been performed with different inositol phosphates [32]. To compare the binding of p130 to both inositol phosphates and inositol lipids, short-chain water-soluble (diC$_4$)PtdIns(4,5)P_2 was directly compared with Ins(1,4,5)P_3 in competition experiments with radiolabelled [^{3}H]Ins(1,4,5)P_3 (Figure 1A). Both the full-length p130 and the N-terminal construct containing the PH domain had a higher binding affinity for Ins(1,4,5)P_3 than for PtdIns(4,5)P_2. {Previously we reported that the isolated PH domain of p130 showed approx. 3500-fold lower affinity for Ins(1,4,5)P_3 than did the full-length p130 [16]. We later noticed that this was simply because of the pH when assayed. At pH 7.4, which was used in the present study, only an approx. 10-fold difference in the apparent affinity was observed (Figure 1A). An alkaline pH (e.g. pH 8.3, used previously) significantly decreased the affinity of the isolated PH domain but not that of the full-length p130 } Calculated K_d values for the full-length p130 were 3 nM for Ins(1,4,5)P_3 and 100 nM for PtdIns(4,5)P_2. Binding to PtdIns(4,5)P_2, isolated from natural sources, incorporated into liposomes was also observed for both the full-length p130 and the isolated PH domain. Figure 1(B) shows a typical SDS/PAGE pattern of the pellets and supernatants obtained with p130 and the PH domain and a summary of the liposome binding study. Although some protein was found in the pellet even in the absence of liposomes (lanes labelled ‘none’) [28] and associated with liposomes containing phosphatidylethanolamine or PtdIns, the inclusion of PtdIns(4,5)P_2 into liposomes resulted in a significant increase in the amount of bound protein. Binding of PLC-δ1 to PtdIns(4,5)P_2 was also confirmed with the same assay (results not shown).

The binding properties of full-length p130 were directly compared with those of full-length PLC-δ1 E341A by using Ins(1,4,5)P_3 and short-chain (diC$_4$)PtdIns(4,5)P_2 and (diC$_4$)-PtdIns(3,4,5)P_3 as ligands. The mutation E341A in PLC-δ1 greatly decreases PLC activity from approx. 1000 units/mg, determined for the wild type, to 0.004 unit/mg [11]. This virtually catalytically inactive mutant was therefore suitable for comparison with p130, preventing the hydrolysis of PtdIns(4,5)P_2. As shown in Figures 1(C) and 1(D), p130 bound all three ligands more strongly than did PLC-δ1. Furthermore, differences in relative specificities have been observed. A preference for Ins(1,4,5)P_3 over PtdIns(4,5)P_2 or PtdIns(3,4,5)P_3 was clearly demonstrated for p130 (30-fold or 130-fold respectively), whereas PLC-δ1 demonstrated similar binding to both Ins(1,4,5)P_3 and PtdIns(4,5)P_2 (Figure 1D). However, PLC-δ1 bound PtdIns(4,5)P_2 preferentially when compared with PtdIns(3,4,5)P_3 (30-fold difference), while p130 showed less selectivity.

and after the addition of nerve growth factor (NGF) for 10 min The same conditions were used to analyse the localization of the GFP fusion protein of the PKB/Akt PH domain **(C)** The localization of p130 in the stably transfected cell line COS-1^{p130} was revealed with a monoclonal anti-p130 antibody Experiments were repeated at least five times, giving essentially the same results **(D)** Staining of PC12 cells with a monoclonal anti-p130 antibody Experiments were repeated at least three times, giving essentially the same results

p130 is present in the cytoplasm

The ability of a number of PH domains to interact with phosphoinositides has been related to membrane localization [19,23]. To test the localization of p130, the microinjection or transfection of expression plasmids encoding GFP fusion proteins has been performed in several cell lines. Figure 2 shows a direct comparison of GFP–p130(F) and GFP–p130PH with the corresponding constructs of PLC-δ1. Localization of all constructs was monitored after microinjection into MDCK cells. As assessed by GFP fluorescence, the preferential localization of GFP–p130PH to the plasma membrane was observed, whereas GFP–p130(F) was found throughout the cytoplasm (Figure 2A). In contrast, membrane localization could be detected for both the full-length E341A and the PH domain of PLC-δ1 protein (Figure 2A). This observation was confirmed by using other cell types (COS-1 and NIH 3T3) in transient transfection experiments (results not shown).

Because p130 also binds PtdIns(3,4,5)P_3 with a high affinity (Figure 1C), we tested whether stimulation of cells, leading to the activation of type 1 phosphoinositide 3-kinase, could cause the translocation of p130 to the membrane. Using the PH domain of PKB/Akt as a positive control, we demonstrated that this did not occur (Figure 2B).

In addition to GFP fluorescent studies, we performed immunostaining of p130 with a monoclonal anti-p130 antibody. Because COS-1 cells contain no endogenous p130, COS-1 cells stably expressing p130 (COS-1^{p130}) were established. As shown in Figure 2(C), expressed p130 was abundant in the cytoplasm; no enrichment at the plasma membrane was observed. PC12 cells, the only cell line containing endogenous p130 among cell lines described in this study (PC12, MDCK, COS-1, NIH 3T3, rat basophilic leukaemic cells), also exhibited preferential localization in the cytoplasm as assessed by immunostaining (Figure 2D), indicating that the presence of p130 in the cytoplasm observed after transfection or microinjection was not caused by artificial or forced expression of p130. (We have found recently that GH3 cells also contain endogenous p130.)

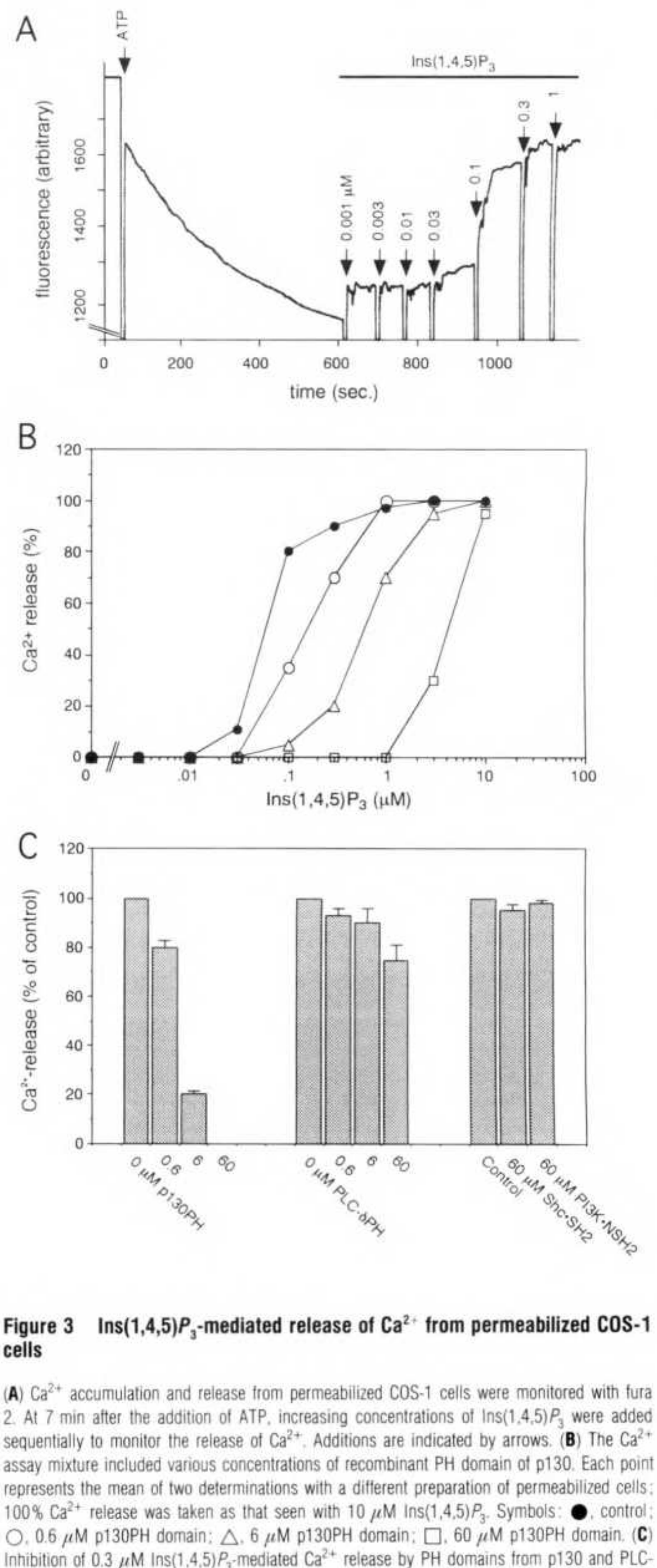

Figure 3 Ins(1,4,5)P_3-mediated release of Ca^{2+} from permeabilized COS-1 cells

(**A**) Ca^{2+} accumulation and release from permeabilized COS-1 cells were monitored with fura 2. At 7 min after the addition of ATP, increasing concentrations of Ins(1,4,5)P_3 were added sequentially to monitor the release of Ca^{2+}. Additions are indicated by arrows. (**B**) The Ca^{2+} assay mixture included various concentrations of recombinant PH domain of p130. Each point represents the mean of two determinations with a different preparation of permeabilized cells; 100% Ca^{2+} release was taken as that seen with 10 μM Ins(1,4,5)P_3. Symbols: ●, control; ○, 0.6 μM p130PH domain; △, 6 μM p130PH domain; □, 60 μM p130PH domain. (**C**) Inhibition of 0.3 μM Ins(1,4,5)P_3-mediated Ca^{2+} release by PH domains from p130 and PLC-δ1, or by SH2 domains. Each result is the mean for two determinations, relative to the Ca^{2+} release caused by 0.3 μM Ins(1,4,5)P_3 (taken as 100%).

Addition of p130 to permeabilized cells inhibits Ins(1,4,5)P_3-triggered Ca^{2+} release

Studies of cellular localization demonstrating the presence of p130 in cytoplasm, and the ability of p130 to bind strongly to Ins(1,4,5)P_3, suggested that it might be involved in the regulation of inositol signalling through binding to the soluble inositol phosphates rather than inositol lipids in the membrane. To test this possibility, Ca^{2+} release in response to the addition of Ins(1,4,5)P_3 was analysed by using reconstitution experiments with permeabilized COS-1 cells (Figure 3). Permeabilized COS-1 cells were incubated in the presence of ATP and NaN_3, an inhibitor of mitochondrial Ca^{2+} accumulation, but in the absence of EGTA and exogenously added Ca^{2+}. Thus the endoplasmic reticulum of permeabilized cells accumulated the water-contaminating Ca^{2+} with the coupling of ATP hydrolysis. The amount of Ca^{2+} outside the endoplasmic reticulum was monitored by the fluorescence changes of fura 2. The addition of ATP together with Mg^{2+} caused a decrease in the fura 2 fluorescence due to the decrease in the Ca^{2+} concentration, as shown in Figure 3(A). Neither ATP nor Mg^{2+} alone could cause the observed decrease in fluorescence, demonstrating that the decrease in the fluorescence was most likely to have been due to the accumulation of Ca^{2+} in the endoplasmic reticulum of permeabilized cells coupled to ATP hydrolysis. The sequential addition of Ins(1,4,5)P_3 caused a stepwise increase in the fluorescence, demonstrating that Ins(1,4,5)P_3 triggered a dose-dependent release of Ca^{2+} accumulated in the endoplasmic reticulum (Figure 3A). When the recombinant PH domain of p130 at various concentrations (0.6–60 μM) was included in the assay mixture, the dose-dependent release of Ca^{2+} by Ins(1,4,5)P_3 shifted to the

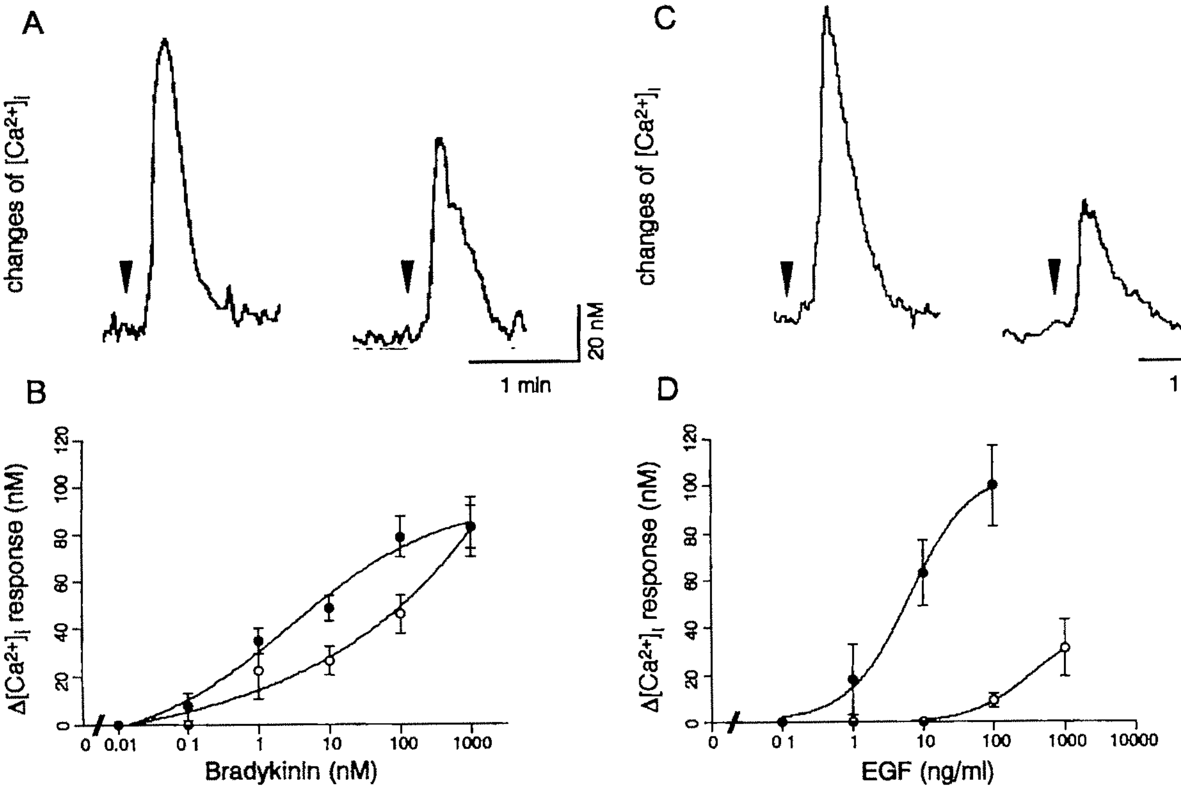

Figure 4 Effects of extracellular stimulation with either BK (A, B) or EGF (C, D) on the change in free Ca^{2+} concentration ($[Ca^{2+}]_i$) of COS-1^{p130}

Control cells (left traces) or COS-1^{p130} (right traces) were stimulated with BK (**A**) or EGF (**C**) after being loaded with fura 2. Arrowheads indicate the addition of agonist. The traces are representative of more than 300 cells examined. (**B**, **D**) The respective dose–response relationships. Symbols ●, control cells, ○, COS-1^{p130}. Each point is the mean ± S.E.M. for at least five determinations.

right (Figure 3B). This shift was correlated with the amount of PH domain added, demonstrating that the PH domain of p130 was able to compete with the receptor involved in the Ca^{2+} release for the Ins(1,4,5)P_3. Figure 3(C) also shows some inhibition of Ca^{2+} release by the PH domain of PLC-δ1 at high protein concentrations, presumably due to the binding of added Ins(1,4,5)P_3. This observation is consistent with the previous studies of PLC-δ1 PH domain demonstrating that Ins(1,4,5)P_3 can compete for PtdIns(4,5)P_2 binding in permeabilized cells [33], and a recent study suggesting Ins(1,4,5)P_3-mediated membrane detachment of PLC-δ1 PH domain after the microinjection of Ins(1,4,5)P_3 [23]. However, the potency of the PLC-δ1 PH domain in inhibiting Ca^{2+} release was much lower than that observed for the p130PH domain. This is in agreement with a higher binding affinity of p130 for Ins(1,4,5)P_3 and its preference for Ins(1,4,5)P_3 over PtdIns(4,5)P_2 observed in binding studies *in vitro* (Figure 1). In addition, recombinant SH2 domains of Shc and the 85 kDa subunit of type 1 phosphoinositide 3-kinase, proteins of similar molecular mass to the p130PH domain that are incapable of binding Ins(1,4,5)P_3, were also examined and had no effects on the Ca^{2+} release (Figure 3C).

p130 inhibits the agonist-induced rise in Ca^{2+} concentrations when expressed in COS-1 cells

Further experiments were performed with COS-1 cells stably expressing p130 (COS-1^{p130}). To determine the concentration of p130 in this cell line, a direct comparison with PC12 cells containing endogenous p130 and known amounts of purified p130 was performed. The calculated concentration of p130 expressed in COS-1^{p130} (40 ± 6 μM) was approx. 5-fold that of the endogenous p130 present in PC12 cells (8 ± 1 μM). As described previously, in control COS-1 cells we were unable to detect any p130 protein.

To analyse the involvement of p130 in Ca^{2+} signalling, three extracellular agonists were chosen: BK and ATP as stimulators of PLC-β isoforms, and EGF as a stimulator of the γ-isoforms of PLC. COS-1 cells lack the δ subtype of PLC as assessed by Western blotting with a specific polyclonal antibody (T. Kanematsu, H. Taneuchi and M. Hirata, unpublished work).

After the loading of cells with fura 2, COS-1^{p130} and control COS-1 cells were stimulated with either BK or EGF and changes in free Ca^{2+} concentration were monitored, in the absence of extracellular Ca^{2+}, indicating that the increase in free Ca^{2+} concentration was a reflection of the release from intracellular store site(s), most probably the endoplasmic reticulum. The increase in free Ca^{2+} concentration caused by either BK or EGF was lower in COS-1^{p130} than in control cells (Figure 4). A trace from a single cell shown in Figures 4(A) and 4(C) is representative of more than 80 % of over 300 cells examined. The dose–response curve to increasing concentrations of BK and EGF was also shifted to the right in COS-1^{p130} (Figures 4B and 4D). A higher concentration of BK (1 μM) restored the Ca^{2+} response to the maximal level, whereas the decrease in Ca^{2+} response caused by EGF was not restored to the control level even at 1000-fold higher agonist concentrations. The Ca^{2+} response in the cells stimulated with ATP through the P2-purinergic receptor was

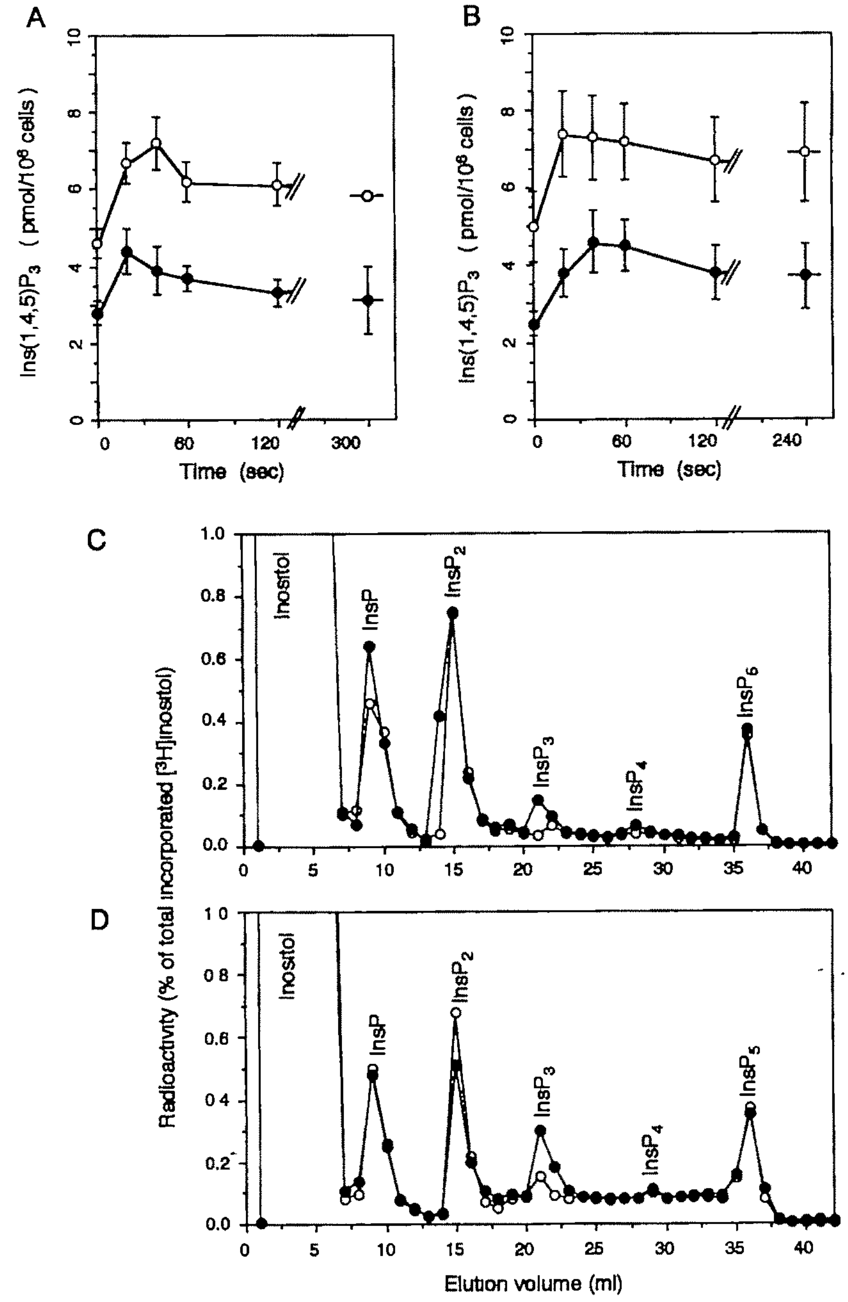

Figure 5 Production of Ins(1,4,5)P_3

The production of Ins(1,4,5)P_3 in control (●) or COS-1^{p130} (○) cells stimulated with BK at 100 nM (**A**) or EGF at 100 ng/ml (**B**) was measured by a radio-receptor competition assay. Each point is the mean ± S.E.M. for at least five determinations. (**C**, **D**) The determination of Ins(1,4,5)P_3 after labelling of cells and the separation of [^{3}H]inositol phosphates by a SAX column of the cellular extract from control (**C**) or COS-1^{p130} cells (**D**), either non-stimulated (○) or stimulated with 100 nM BK for 60 s (●). The results are expressed as percentages of total [^{3}H]inositol incorporated into inositol phosphates and phosphoinositides, and are representative of five experiments. Note that the radioactivities of Ins(1,4,5)P_3 in both non-stimulated and BK-stimulated control cells were lower than those in COS-1^{p130} cells, consistent with the measurements described in (**A**).

also inhibited, as in cells with EGF stimulation (results not shown).

Decrease in agonist-induced Ca^{2+} concentration increase in COS-1^{p130} is not caused by inhibition of PtdIns(4,5)P_2 hydrolysis

The possibility of an inhibitory interaction at the level of PtdIns(4,5)P_2 hydrolysis and Ins(1,4,5)P_3 production was analysed by measurements of total Ins(1,4,5)P_3 concentrations in the control and COS-1^{p130} cells stimulated with BK or EGF. Consistent results were obtained with two different methods (Figure 5). The radio-receptor competition assay (Figures 5A and 5B) demonstrated that the production of Ins(1,4,5)P_3 was not inhibited (rather, a slight enhancement was observed) in COS-1^{p130} cells stimulated with BK or EGF. The measurements made with the standard separation of radiolabelled inositol phosphates showed a similar accumulation of [^{3}H]Ins(1,4,5)P_3 in cells stimulated with BK (Figures 5C and 5D). Stimulation with EGF was

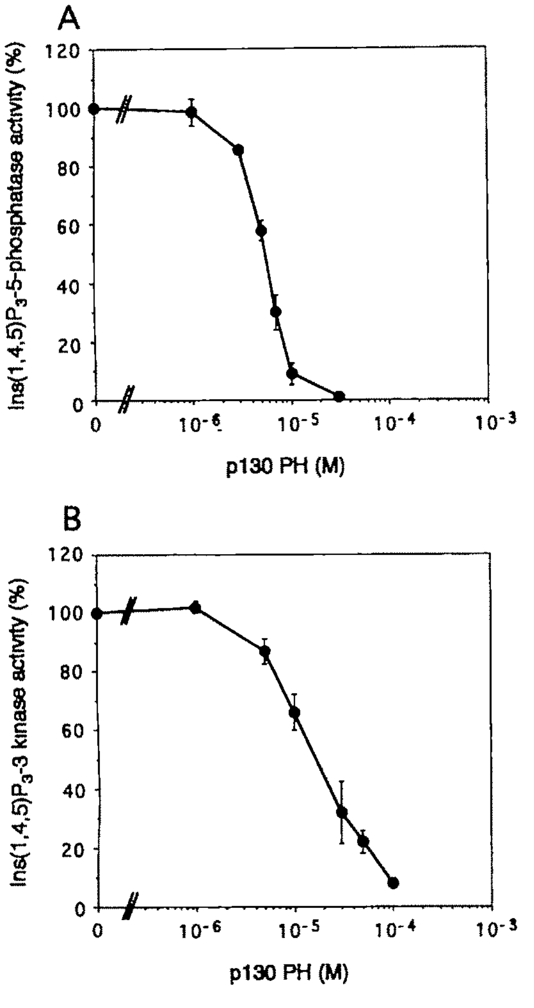

Figure 6 Effect of p130 on Ins(1,4,5)P_3 metabolism by Ins(1,4,5)P_3-5-phosphatase (A) or Ins(1,4,5)P_3-3-kinase (B)

Recombinant enzymes were incubated in the presence of increasing amounts of p130PH domain as described in the Materials and methods section. Each point is the mean ± S.E.M. for at least five determinations.

also performed and gave essentially the same results in the labelling experiments. The basal level of Ins(1,4,5)P_3 in COS-1^{p130} was 1.5–2-fold that in the control cells, whereas the amount of Ins(1,4,5)P_3 produced after stimulation with BK or EGF was slightly higher than that in the control cells. In addition, a return to the basal level of Ins(1,4,5)P_3 produced by the stimulation was hardly observed, particularly after stimulation with BK. Although the basal level of Ins(1,4,5)P_3 in COS-1^{p130} was maximally 2-fold that in the control cells, the basal concentration of free Ca^{2+} in COS-1^{p130} was the same as that seen in the control cells (results not shown). This was probably due to the competition for the binding of Ins(1,4,5)P_3, between p130 and the Ins(1,4,5)P_3 receptor on the endoplasmic reticulum. A similar explanation could apply to the inhibition of metabolism by p130 after agonist stimulation. The formation of a stable complex between Ins(1,4,5)P_3 and p130 might prevent not only the interaction with the receptor, as suggested by Figures 3 and 4, but also its further metabolism by either or both of Ins(1,4,5)P_3-5-phosphatase and Ins(1,4,5)P_3-3-kinase or other effects attributed to this inositol phosphate.

To test the possibility described above, we examined the effect of the p130PH domain on Ins(1,4,5)P_3 metabolism by Ins(1,4,5)P_3-5-phosphatase and Ins(1,4,5)P_3-3-kinase. Recombinant 5-phosphatase and 3-kinase enzymes were analysed *in vitro* with [^{3}H]Ins(1,4,5)P_3 as a substrate in the presence of various amounts of the p130PH domain. As shown in Figure 6, the p130PH domain inhibited both Ins(1,4,5)P_3-5-phosphatase (Figure 6A) and Ins(1,4,5)P_3-3-kinase (Figure 6B) activity in a dose-dependent manner.

Ins(1,4,5)P_3 is bound to p130 in cells

In vitro, p130 is also able to bind to other inositol polyphosphates (InsP_5 and InsP_6), which are abundant in the resting cells [7,34], indicating the possibility that the binding capacities of cellular p130 are saturated by these inositol polyphosphates inside cells. However, the affinities for these inositol polyphosphates were approx. 100-fold lower than that for Ins(1,4,5)P_3 [7], indicating that above notion is unlikely. To obtain direct evidence that cellular p130 forms a complex with Ins(1,4,5)P_3 in living cells, COS-1^{p130} cells were labelled with *myo*-[^{3}H]inositol. Cellular p130 was subsequently immunoprecipitated from the lysate of the labelled cells. Analysis of the protein content of the immunoprecipitates (Figure 7A) shows that p130 was a major protein. Labelled inositol phosphates bound to p130 were then analysed (Figure 7B). Under standard conditions of immunoprecipitation, Ins(1,4,5)P_3 was clearly identified as one of the peaks of radioactivity. Peaks of the abundunt free inositol and Ins$P$ could also be detected but were completely removed by stringent washing and therefore represented contaminants in p130 immunoprecipitates. The immunoprecipitation of p130 was not quantitative; five experiments performed under stringent conditions provided a minimum value for bound Ins(1,4,5)P_3. When cells were stimulated with BK, the radioactivity of only Ins(1,4,5)P_3 bound to p130 increased up to 2-fold, supporting a possibility that cellular p130 sequesters Ins(1,4,5)P_3 produced in response to cell stimulation.

PH domain is required for the effect of p130 on Ca^{2+} signalling

To examine whether the PH domain of p130 is involved in the decrease in the Ca^{2+} response as shown in Figure 4, GFP–p130(F) and GFP–p130(ΔPH) were made. The use of GFP-fused proteins permitted the identification of living cells that expressed p130 in a transient expression system. After the transfection of COS-1 cells with the plasmid harbouring GFP–p130(F) or GFP–p130(ΔPH), cells were loaded with fura 2 for Ca^{2+} measurement and then revealed by fluorescent microscopy. Almost all cells were fluorescent for fura 2, whereas approx. 30 % of cells were transfected and fluorescent for GFP. Stimulation of COS-1 cells was performed with BK, EGF and also with ATP through P2-purinergic receptors with essentially the same results; responses to stimulation of the P2-purinergic receptor are summarized in Figure 8. The increase in free Ca^{2+} concentration in response to ATP was observed in COS-1 cells that were fluorescent only for fura 2 (Figure 8A) and was similar to Ca^{2+} responses in untransfected COS-1 cells (results not shown). Figures 8(B)–8(D) show the ATP-induced Ca^{2+} response in cells with GFP alone, with GFP–p130(F) and with GFP–p130(ΔPH) respectively. Ca^{2+} responses were not altered by GFP alone, whereas GFP–p130(F) caused 70–80 % inhibition, as expected from results in COS-1^{p130} cells. In contrast, GFP–p130(ΔPH) was not capable of mediating such a decrease in Ca^{2+} responses. Figure 8(E) summarizes these results, showing clearly that the inhibition of the Ca^{2+} response required the presence of the PH domain of p130.

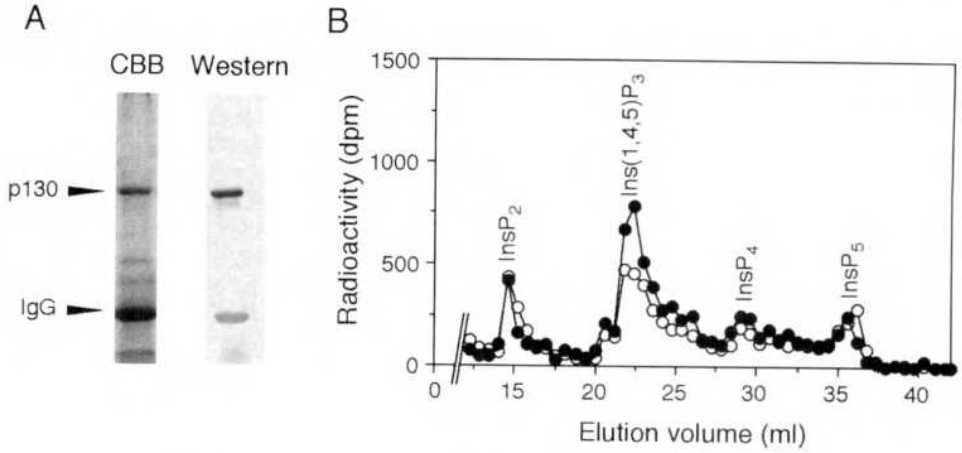

Figure 7 Immunoprecipitation from the lysate of COS-1^{p130} cells labelled with *myo*-[^{3}H]inositol by monoclonal anti-p130 antibody

(**A**) Labelled COS-1^{p130} cells were lysed and subjected to immunoprecipitation with monoclonal anti-p130 antibody (2F9) and Protein G–Sepharose. The immunoprecipitates were analysed by SDS/PAGE followed by CBB staining or Western blotting with monoclonal anti-p130 antibody. (**B**) The inositol phosphates bound to the immunoprecipitate were extracted by treatment with trichloroacetic acid and analysed by application to a SAX column. Results are representative of five experiments. Because there was much variation in labelling efficiency and immunoprecipitation, it was impossible to show statistical values. Symbols: ○, non-stimulated; ●, stimulated with 100 nM BK.

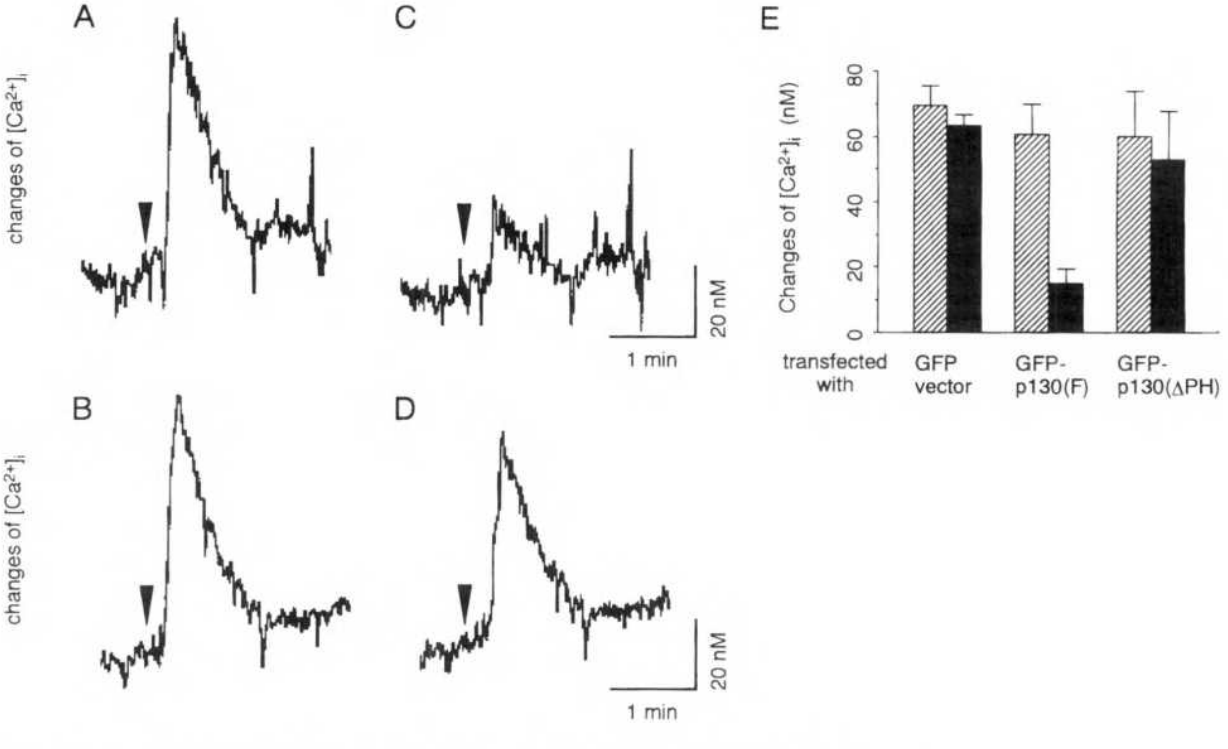

Figure 8 Ca^{2+} response by ATP stimulation in COS-1 cells transfected with GFP–p130(F) or GFP–p130(ΔPH)

COS-1 cells were transfected with either plasmid encoding GFP–p130(F) or GFP–p130(ΔPH), followed by loading with fura 2. By using fluorescent microscopy, cells were selected for those with fura 2 but without GFP fluorescence (**A**) or those with fura 2, and GFP alone (**B**), GFP–p130(F) (**C**) or GFP–p130(ΔPH) (**D**). Cells were stimulated with 10 μM ATP as indicated by the arrowhead. Each trace is typical of at least 10 cells examined. The summary of the changes in Ca^{2+} concentrations after ATP stimulation (**E**) shows mean values from cells without (hatched) or with (black) GFP fluorescence.

DISCUSSION

In the present study we analysed the functional properties of p130 protein, which was originally isolated as a protein with high affinity for Ins(1,4,5)P_3 [7,35]. We have extended our analysis of ligand binding *in vitro*, used a combination of approaches to identify which of the potential ligands could interact with p130 in cells and further considered the implications of this binding for cellular function.

Studies of ligand binding *in vitro* have previously shown that the PH domain of p130 is responsible for the high-affinity binding of Ins(1,4,5)P_3 by the full-length protein [16]. The binding *in vitro* is not restricted to this ligand: a few other inositol phosphates [Ins(1,4,5,6)P_4 and, to a smaller extent, Ins(1,3,4,5)P_4] can also bind to p130 through the PH domain [7,9,16,32,35]. Here we have also demonstrated that p130 can bind short-chain inositol lipids [(diC_4)PtdIns(4,5)P_2 and (diC_4)PtdIns(3,4,5)P_3], although with lower affinity than for Ins(1,4,5)P_3; the affinity for PtdIns(4,5)P_2 isolated from natural sources is even lower (Figure 1). Nevertheless, affinities for short-chain versions of PtdIns(4,5)P_2 and PtdIns(3,4,5)P_3 estimated in this study (K_d values of 100 and 500 nM respectively) are comparable with those reported for proteins in which these phosphoinositides have been accepted as physiological ligands. For example, the K_d for binding of PKB/Akt to (diC_8)PtdIns(3,4,5)P_3 was approx. 400 nM [36] and that for the binding of PLC-δ1 to PtdIns(4,5)P_2 was approx. 1.7 μM [37]. Therefore, on the basis of the studies of ligand binding *in vitro*, several inositol compounds could potentially be physiological ligands for p130.

Factors that have to be considered when searching for a physiological ligand include the relative concentration of the free ligand and the cellular localization of both the ligand and the binding protein. Free concentrations of inositol lipids are difficult to measure; however, estimated concentrations in the inner leaflet of plasma membrane are within the millimolar range for PtdIns(4,5)P_2 and up to 200 μM for PtdIns(3,4,5)P_3 [38]. The cellular levels of Ins(1,4,5)P_3 are lower, ranging from 1 μM (in 'resting' cells) to 10 μM (in receptor-activated cells) [34]. Therefore, in spite of the higher affinity for Ins(1,4,5)P_3, the inositol lipids could possibly be bound to p130 in cells. This has been clearly shown for PLCδ1 in non-stimulated cells, in which the full-length and isolated PH domains reside in the membrane [19–22] (Figure 2). Studies with several cell types have demonstrated that the isolated p130PH domain was associated with the membrane (Figure 2A). However, the full-length p130 was present only in the cytoplasm of cells endogenously expressing this protein or when introduced into a range of different cell types (Figures 2A, 2C and 2D). There are several possibilities for explaining why the PH domain within the entire p130 molecule and in the cellular context cannot act as a determinant of cellular localization through phosphoinositide binding. The possibility that other domains of p130 mask the PH domain is unlikely because the full-length p130 binds the ligands *in vitro* (Figure 1) and, as discussed below, also in cells. On the basis of the observation that the isolated PH domain can interact with the membrane (Figure 2A), it is also unlikely that the p130PH domain interacts with other cellular molecules that could block PtdIns(4,5)P_2 binding. One possible explanation could be that other region(s) of p130, outside the PH domain, make interactions that determine its presence in the cytoplasm. Although this remains to be clarified, the experiments presented here strongly support inositol phosphates rather than phosphoinositides as physiological ligands for the PH domain in p130. Evidence supporting this was provided by the isolation of a complex between p130 and Ins(1,4,5)P_3 after the immunoprecipitation of p130 from COS-1 cells that stably express this protein (Figure 7). As shown with some other proteins, this is not an ideal, quantitative, type of analysis. Nevertheless, we clearly demonstrated that the amounts of bound Ins(1,4,5)P_3 increase after stimulation with agonist.

To establish the identity of the ligand and the possible implications of the binding for cell function, the effects of p130 on Ca^{2+} signals were monitored in permeabilized and transfected cells. We demonstrated that p130, through the function of the PH domain, was capable of attenuating the Ins(1,4,5)P_3-triggered and the agonist-induced increase in Ca^{2+} concentrations (Figures 3, 4 and 8). Furthermore, experimental support has been provided for an interaction of p130 with Ins(1,4,5)P_3, rather than an inhibitory interaction at the level of PtdIns(4,5)P_2 hydrolysis as described for some related proteins [22,39]. Measurements of the production of Ins(1,4,5)P_3 in the control and COS-1^{p130} cells stimulated with BK or EGF demonstrated that the production of Ins(1,4,5)P_3 was not inhibited (Figure 5). A possible role for p130, suggested by the results presented here, is to provide a level of control in Ca^{2+} signalling through competition with Ins(1,4,5)P_3 receptor (IP3R) for Ins(1,4,5)P_3 binding. However, for this function to be fulfilled in cells one would expect that both affinities and concentrations of these proteins were comparable. The IP3Rs are a family of tetrameric ligand-gated Ca^{2+} channels and the complete cDNA sequences encoding three distinct receptors (IP3R1, IP3R2 and IP3R3) have been determined. The affinities of three types of IP3R for the ligand are reported to be in the nanomolar range, with K_d values of 1.5 nM (IP3R1), 2.5 nM (IP3R2) and 22 nM (IP3R3) [40]. These values are similar to those measured for p130 (2–5 nM) [7,16,35]. Therefore, on the basis of affinity, p130 could effectively compete for the Ins(1,4,5)P_3 ligand Regarding their expression, both p130 and IP3Rs are expressed in a range of tissues, with high concentrations present in brain [41,42]. As described in the Results section, the concentrations of endogenous p130 measured in PC12 are approx. one-fifth of those in COS-1^{p130} cells but are higher than the concentrations of protein that could inhibit Ca^{2+} release in permeabilized cells triggered by physiological amounts of Ins(1,4,5)P_3 (Figure 3). These results therefore do not rule out the suggested function of p130. However, to obtain direct proof, further studies are clearly required.

The results described here can be summarized as follows. (1) p130 expressed in cells was mainly localized in the cytoplasm, although the PH domain of p130 is capable of binding PtdIns(4,5)P_2. (2) p130 did not inhibit the formation of Ins(1,4,5)P_3 from PtdIns(4,5)P_2 by PLC activation. (3) Most importantly, p130 attenuated the increase in free Ca^{2+} concentration, possibly through binding to Ins(1,4,5)P_3 via the PH domain. p130 is therefore the first example of a PH-domain-containing molecule that might have a physiological role in Ins(1,4,5)P_3 binding and inhibition of the Ins(1,4,5)P_3-mediated signalling, suggesting that the amount of p130 present in cells could be one of the factors that determine the effectiveness of Ca^{2+} signalling. Although these experiments argue that p130 could bind Ins(1,4,5)P_3 in cells, other experiments (currently in progress) focusing on endogenous p130 and the use of knock-out cells are needed to further our insights into the physiological role of this molecule.

We thank Dr T Tsukamoto and Professor T. Osumi (Himeji Institute of Technology, Hyogo, Japan) for providing us with the plasmid for GFP-fused protein that was modified to increase its fluorescence This work was funded by a Grant-in-Aid for Scientific Research from the Ministry of Education, Science, Sports and Culture of Japan (to M O, Y. I. and M H.) and by Kyushu University Interdisciplinary Programs in Education and Projects in Research Development (to M. H), the Ryoichi Naito Foundation for Medical Research (to M. H), the Fukuoka Cancer Society (to M H.), the Naito Foundation (to M H), the Uehara Memorial Foundation (to T K.) and the Cancer Research Campaign (to M. K).

REFERENCES

1 Berridge, M J (1993) Inositol trisphosphate and calcium signalling. Nature (London) **361**, 315–325

2 Katan, M (1998) Families of phosphoinositide-specific phospholipase C structure and function. Biochim Biophys Acta **1436**, 5–17

3 Hawkins, P. T., Welch, H , McGregor, A , Eguinoa, A , Gobert, S , Krugmann, S , Anderson, K , Stokoe, D and Stephens, L (1997) Signalling via phosphoinositide 3OH kinases Biochem Soc Trans **25**, 1147–1151

4 Rameh, L E and Cantley, L C (1999) The role of phosphoinositide 3-kinase lipid products in cell function J. Biol. Chem **274**, 8347–8350

5 Leevers, S J, Vanhaesebroeck, B and Waterfield, M. D. (1999) Signalling through phosphoinositide 3-kinases: the lipids take centre stage Curr Opin Cell Biol **11**, 219–225

6 Bottomley, M J, Salim, K and Panayotou, G (1998) Phospholipid-binding protein domains Biochim Biophys Acta **1436**, 165–183

7 Kanematsu, T, Takeya, H, Watanabe, Y., Ozaki, S, Yoshida, M, Koga, T, Iwanaga, S and Hirata, M (1992) Putative inositol 1,4,5-trisphosphate binding proteins in rat brain cytosol J Biol Chem **267**, 6518–6525

8 Hirata, M, Watanabe, Y, Ishimatsu, T, Yanaga, F, Koga, T and Ozaki, S (1990) Inositol 1,4,5-trisphosphate affinity chromatography Biochem Biophys Res Commun **168**, 379–386

9 Kanematsu, T, Misumi, Y, Watanabe, Y, Ozaki, S, Koga, T, Iwanaga, S, Ikehara, Y and Hirata, M (1996) A new inositol 1,4,5-trisphosphate binding protein similar to phospholipase C-δ1 Biochem. J. **313**, 319–325

10 Essen, L-O., Perisic, O, Cheung, R., Katan, M. and Williams, R L (1996) Crystal structure of a mammalian phosphoinositide-specific phospholipase Cδ Nature (London) **380**, 595–602

10a Kanematsu, T., Yoshimura, K., Hidaka, K, Takeuchi, H, Katan, M and Hirata, M (2000) Eur J Biochem. **267**, 2731–2737

11 Ellis, M V, James, S. R, Perisic, O, Downes, C P, Williams, R L and Katan, M (1998) Catalytic domain of phosphoinositide-specific phospholipase C J Biol Chem **273**, 11650–11659

12 Kohno, T, Otsuka, T, Takano, H, Yamamoto, T, Hamaguchi, M, Terada, M and Yokota, J (1995) Identification of a novel phospholipase C family gene at chromosome 2q33 that is homozygously deleted in human small cell lung carcinoma Hum Mol Genet. **4**, 667–674

13 Koyanagi, M, Ono, K, Suga, H., Iwabe, N and Miyata, T. (1998) Phospholipase C cDNAs from sponge and hydra antiquity of genes involved in the inositol phospholipid signaling pathway FEBS Lett **439**, 66–70

14 Otsuki, M., Fukami, K., Kohno, T, Yokota, J and Takenawa, T (1999) Identification and characterization of a new phospholipase C-like protein, PLC-L$_2$ Biochem Biophys Res Commun **266**, 97–103

15 Kikuno, R, Nagase, T, Ishikawa, K, Hirosawa, M, Miyajima, N., Tanaka, A, Kotani, H, Nomura, N. and Ohara, O (1999) Prediction of the coding sequences of unidentified human genes XIV The complete sequences of 100 new cDNA clones from brain which code for large proteins in vitro DNA Res **6**, 197–205

16 Takeuchi, H, Kanematsu, T, Misumi, Y, Yaakob, H B, Yagisawa, H, Ikehara, Y, Watanabe, Y, Tan, Z, Shears, S B. and Hirata, M (1996) Localization of a high affinity inositol 1,4,5-trisphosphate/inositol 1,4,5,6-tetrakisphosphate binding domain to the pleckstrin homology module of a new 130-kDa protein characterization of the determinants of structural specificity Biochem J **318**, 561–568

17 Hirata, M, Kanematsu, T., Takeuchi, H and Yagisawa, H (1998) Pleckstrin homology domain as an inositol compound binding module Jpn J Pharmacol **76**, 255–263

18 Lemmon, M A, Falasca, M, Ferguson, K M and Schlessinger, J (1997) Regulatory recruitment of signalling molecules to the cell membrane by pleckstrin homology domains Trends Cell Biol. **7**, 237–242

19 Paterson, H F, Savopoulos, J W, Perisic, O, Cheung, R, Ellis, M V, Williams, R L and Katan, M (1995) Phospholipase C-δ1 requires a pleckstrin homology domain for interaction with the plasma membrane. Biochem J **312**, 661–666

20 Staufer, T P., Ahn, S and Meyer, T (1998) Receptor-induced transient reduction in plasma membrane PtdIns(4,5)P_2 concentration monitored in living cells Curr. Biol. **8**, 343–346

21 Yagisawa, H, Sakuma, K, Paterson, H. F., Cheung, R, Allen, V, Hirata, H, Watanabe, Y, Hirata, M, Williams, R L and Katan, M (1998) Replacements of single basic amino acids in the pleckstrin homology domain of phospholipase C-δ1 alter the ligand binding, phospholipase activity and interaction with the plasma membrane J. Biol Chem **273**, 417–424

22 Varnai, P and Balla, T (1998) Visualization of phosphoinositides that bind pleckstrin homology domains calcium- and agonist-induced dynamic changes and relationship to *myo*-[^{3}H]inositol-labeled phosphoinositide pools J Cell Biol **143**, 501–510

23 Hirose, K, Kodowaki, S, Tanabe, M, Takeshima, H and Iino, M (1999) Spatiotemporal dynamics of inositol 1,4,5-trisphopshate that underlie complex Ca^{2+} mobilization patterns Science **284**, 1527–1531

24 Cullen, P J, Dawson, A P and Irvine, R F (1995) Purification and characterization of an Ins(1,3,4,5)P_4 binding protein from pig platelets possible identification of a novel non-neuronal Ins(1,3,4,5)P_4 receptor Biochem J **305**, 139–143

25 Cullen, P. J., Hsuan, J J, Truong, O, Letcher, A J, Jackson, T R, Dawson, A P and Irvine, R F (1995) Identification of a specific Ins(1,3,4,5)P_4-binding protein as a member of the GAP1 family Nature (London) **376**, 527–530

26 Yamasaki, M, Hashiguchi, N, Tsukamoto, T and Osumi, T (1998) Variant forms of green and blue fluorescent proteins adapted for the use in mammalian cells Bioimages **6**, 1–7

27 Hirata, M., Watanabe, Y, Ishimatsu, T, Ikebe, T, Kimura, Y, Yamaguchi, K, Ozaki, S and Koga, T (1989) Synthetic inositol trisphosphate analogs and their effects on phosphatase, kinase, and the release of Ca^{2+} J Biol Chem **264**, 20303–20308

28 Takeuchi, H, Matsuda, M, Yamamoto, T, Kanematsu, T, Kikkawa, U, Yagisawa, H, Watanabe, Y and Hirata, M. (1998) PTB domain of insulin receptor substrate-1 binds inositol compounds Biochem. J **334**, 211–218

29 Palmer, S., Hughes, K. T, Lee, D Y and Wakelam, M V O (1989) Development of a novel, Ins(1,4,5)P_3-specific binding assay Its use to determine the intracellular concentration of Ins(1,4,5)P_3 in unstimulated and vasopressin-stimulated rat hepatocytes Cell Signal **1**, 147–156

30 Shears, S B (1997) Measurement of inositol phosphate turnover in intact cells and cell-free systems In A Practical Approach in Signalling by Inositides (Shears, S B, ed), pp 33–52, Oxford University Press, Oxford

31 Matsuki, N, Tateishi, K, Takeuchi, H, Yagisawa, H, Kanematsu, T, Oishi, M and Hirata, M (1999) Antibodies against the PH domain of phospholipase C-δ1 inhibit Ins(1,4,5)P_3-mediated Ca^{2+} release from the endoplasmic reticulum Biochem Biophys Res Commun **260**, 42–47

32 Takeuchi, H, Kanematsu, T, Misumi, Y, Sakane, F., Konishi, H, Kikkawa, U, Watanabe, Y, Katan, M and Hirata, M (1997) Distinct specificity in the binding of inositol phosphates by pleckstrin homology domains of pleckstrin, RAC-protein kinase, diacylglycerol kinase and a new 130-kDa protein Biochim Biophys Acta **1359**, 275–285

33 Allen, V., Swigart, P, Cheung, R, Cockcroft, S and Katan, M (1997) Regulation of inositol lipid-specific phospholipase Cδ by changes in Ca^{2+} ion concentrations Biochem J **327**, 545–552

34 Shears, S B (1992) Metabolism of inositol phosphates Adv Second Messenger Phosphoprotein Res **26**, 63–92

35 Yoshida, M, Kanematsu, T., Watanabe, Y, Koga, T., Ozaki, S, Iwanaga, S and Hirata, M (1994) D-*myo*-Inositol 1,4,5-trisphosphate binding proteins in rat brain membranes J Biochem (Tokyo) **116**, 973–980

36 Frech, M, Andjelkovic, M, Ingley, E, Reddy, K K, Falck, J R and Hemmings, B A (1997) High affinity binding of inositol phosphates and phosphoinositides to the pleckstrin homology domain of RAC/protein kinase B and their influence on kinase activity J Biol Chem. **272**, 8474–8481

37 Lemmon, M A, Ferguson, K M, O'Brien, R, Sigler, P B and Schlessinger, J (1995) Specific and high affinity binding of inositol phosphates to an isolated PH domain Proc. Natl Acad Sci USA **92**, 10472–10476

38 Stephens, L R, Jackson, T R and Hawkins, P T (1993) Agonist-stimulated sythesis of phosphatidylinositol (3,4,5)-trisphosphate a new intracellular signalling system? Biochim Biophys Acta **1179**, 27–75

39 Nagano, K, Fukami, K, Minagawa, T, Watanabe, Y, Ozaki, C and Takenawa, T (1999) A novel phospholipase C δ4 (PLCδ4) splice variant as a negative regulator of PLC. J Biol Chem **274**, 2872–2879

40 Wilcox, R A, Primrose, W U, Nahorski, S R. and Challiss, R A J (1998) New developments in the molecular pharmacology of the *myo*-inositol 1,4,5-trisphosphate receptor Trends Pharmacol Sci **19**, 467–475

41 Matsuda, M, Kanematsu, T., Takeuchi, H., Kukita, T. and Hirata, M. (1998) Localization of a novel inositol 1,4,5-trisphosphate binding protein, p130 in rat brain. Neurosci Lett **257**, 97–100

42 Furuichi, T, Yoshikawa, S, Miyawaki, A., Wada, K., Maeda, N and Mikoshiba, K (1989) Primary structure and functional expression of the inositol 1,4,5-trisphosphate-binding protein P400 Nature (London) **342**, 32–38

Received 7 January 2000/15 March 2000, accepted 10 April 2000

Deactivation of neutrophil NADPH oxidase by actin-depolymerizing agents in a cell-free system

Minoru TAMURA[1], Masamichi KANNO and Yaeta ENDO
Department of Applied Biochemistry, Faculty of Engineering, Ehime University, Matsuyama, Ehime 790-8577, Japan

The cell-free activation of human neutrophil NADPH oxidase (O_2^--generating enzyme) is enhanced by actin [Morimatsu, Kawagoshi, Yoshida and Tamura (1997) Biochem. Biophys. Res Commun. **230**, 206–210]. In an attempt to elucidate the mechanism, we examined the effect of actin-depolymerizing agents on the duration of NADPH oxidase in a cell-free system. The addition of DNase I, an F-actin-depolymerizing protein, caused an accelerated deactivation of the oxidase. The deactivation was also facilitated by latrunculin A, a sponge toxin that depolymerizes F-actin. Exogenously added actin prevented the deactivation by DNase I or latrunculin A, whereas EDTA accelerated a dilution-induced deactivation of the oxidase and Mg^{2+} ions retarded it. The stability in dilution was found to correlate well with free Mg^{2+} concentration. Estimation of F-actin in the system showed that F-actin increased during the oxidase activation and that DNase I or EDTA decreased F-actin content in parallel with the activity. Treatment of the cell-free mixture with a chemical cross-linker prevented the deactivation and F-actin decrease by EDTA. Taken together, these results suggest that actin filaments which grow during the activation of NADPH oxidase prolong the lifetime of the oxidase.

Key words. cytoskeleton, F-actin, magnesium ion, phagocytosis, superoxide

INTRODUCTION

Superoxide (O_2^-) generation by neutrophils has an important role in host defence against microbial infection [1]. The enzyme responsible for O_2^- generation is called NADPH oxidase (or respiratory burst oxidase), which is dormant in resting cells and becomes active upon cell activation [2]. The oxidase can also be activated in a cell-free system including plasma membrane and cytosol in the presence of an anionic amphiphile [2]. The oxidase consists of membrane cytochrome b_{558} ($gp91^{phox}$ and $p22^{phox}$) and cytosolic proteins ($p47^{phox}$, $p67^{phox}$ and Rac) [3], which assemble into an active complex upon activation. Recently $p40^{phox}$, which is bound to $p67^{phox}$, has been suggested as a regulator [3]. The oxidase is extremely labile when activated either *in vivo* [4] or *in vitro* [5] and the deactivation is assumed to involve the dissociation of a cytosolic component or components from cytochrome b_{558}.

Actin, a major component of cytoskeleton, is abundantly present in neutrophils [6]. Approx. one-third of the total actin is present in polymeric form (F-actin) in resting neutrophils [7] and upon cell activation additional monomer actin (G-actin) polymerizes into F-actin. Actin polymerization has long been related to neutrophil chemotaxis or phagocytosis [6], probably because they involve motion and shape change. However, the relation to O_2^- generation has not been considered.

Quinn et al. [8] reported that NADPH oxidase activity from phorbol ester-stimulated neutrophils co-sediments with heavy plasma-membrane fraction that includes actin and fodrin. Woodman et al. [9] found that the activated oxidase is restricted to the membrane cytoskeleton. We showed previously that the labile enzyme is remarkably stabilized by chemical cross-linking [4,5]. However, the stabilized activity cannot be extracted, even by Triton, suggesting that the enzyme complex is linked to the cytoskeleton.

Recently we found that actin, either endogenous or exogenous, enhances the activation of the oxidase in a cell-free system [10]. In the present study, to elucidate the mechanism for the phenomenon we examined several F-actin-depolymerizing agents on the stability of the oxidase. We found that actin-depolymerizing agents markedly facilitated the deactivation of NADPH oxidase, and suggested a role of F-actin to prolong the lifetime of NADPH oxidase.

EXPERIMENTAL

Materials

DNase I (molecular-biology grade) was obtained from Worthington Biochemical Corp. (Lakewood, NJ, U.S.A.) Actin (rabbit skeletal muscle, AKL95) was purchased from Cytoskeleton (Denver, CO, U.S.A.). Latrunculin A was obtained from Wako Pure Chemicals (Osaka, Japan). E64 [*trans*-epoxysuccinyl-L-leucylamido-(4-guanidino)butane] was a product of Peptide Institute (Osaka, Japan). Phalloidin, tetramethylrhodamine isothiocyanate (TRITC)-phalloidin and guanosine 5′-[γ-thio]triphosphate (GTP[S]) were purchased from Sigma Aldrich (St. Louis, MO, U.S.A.). All other reagents were of the best grade commercially available.

Neutrophil preparation and subcellular fractionation

Isolation of human neutrophils and subcellular fractionation were carried out as described previously [5]. The isolated cells were suspended in buffer A [100 mM KCl, 3 mM NaCl, 3.5 mM $MgCl_2$, 1 mM ATP, 10 mM potassium phosphate buffer (KPB), pH 7.3] and subjected to nitrogen cavitation. After sucrose-gradient separation, the plasma membrane fraction was diluted with 1 vol. of buffer B (100 mM KCl, 3 mM NaCl, 4 mM $MgCl_2$,

---

Abbreviations used E64, *trans*-epoxysuccinyl-L-leucylamido-(4-guanidino)butane; KPB, potassium phosphate buffer, TRITC, tetramethylrhodamine isothiocyanate; GTP[S], guanosine 5′-[γ-thio]triphosphate, EDC, 1-ethyl-3-(3-dimethylaminopropyl)carbodi-imide

[1] To whom correspondence should be addressed (e-mail miketamu@en3.ehime-u.ac.jp)

1 mM EGTA, 10 mM Pipes, pH 7.0), sedimented by centrifugation at 200000 *g* for 1 h, and resuspended in modified buffer B (with all the concentrations given above halved) containing 0.34 M sucrose.

Cell-free activation and assay for O_2^- generation

The standard conditions for assay were as follows. Plasma membrane (15 μg of protein, 5×10^6 cell equivalents) and cytosol (210 μg of protein, 9×10^6 cell equivalents) were mixed per 100 μl in 20 mM KPB (pH 7.0) supplemented with SDS (final concentration 240 μM), and incubated for 10 min at 25 °C. An aliquot (10 μl) of the mixture was mixed with 240 μl of 20 mM KPB (pH 7.0) containing 80 μM cytochrome *c* and 200 μM NADPH, and the mixture (120 μl each) was transferred into two cuvettes, one of which (reference) contained superoxide dismutase (80 μg/ml). O_2^--generating activity was assayed at 25 °C as described previously [11]. O_2^--generating activities were expressed as nmol of O_2^- formed/min per mg of plasma-membrane protein.

Pretreatment of DNase I

Because DNase I prepared from pancreas contains trace amounts of chymotrypsin and other proteases, and because NADPH oxidase activity is inhibited by some protease inhibitors at high concentrations, we treated DNase I with irreversible inhibitors prior to the experiments and then removed unreacted reagents by dialysis. DNase I preparation was incubated with 500 μM di-isopropyl fluorophosphate, 500 μM PMSF and 10 μM E64 at 0 °C for 20 min and then dialysed against 20 mM KPB (pH 7.0) for 4 h at 0 °C.

Measurement of F-actin content

F-actin content was measured following the method of Redmond et al. [12] with modifications. The cell-free activated mixture containing plasma membrane (15 μg) and cytosol (210 μg) per 100 μl was fixed with 1 % glutaraldehyde at 0 °C for 1 h and treated with 0.2 μM TRITC-phalloidin with or without 2 μM phalloidin at 0 °C for 1 h. The mixture was centrifuged at 340000 *g* at 4 °C for 15 min with a compact ultracentrifuge (Hitachi CS150GX), and the pellets were extracted with 1 ml of methanol for 48 h. The supernatant was obtained by centrifugation at 2000 *g* at 4 °C for 5 min. The fluorescence of the supernatant was measured with a spectrofluorimeter (Shimadzu RF-5300 PC; excitation at 540 nm and emission at 565 nm). The difference in fluorescence intensity between TRITC-phalloidin-treated sample and phalloidin + TRITC-phalloidin-treated sample was calculated and expressed as ΔRFI (relative fluorescence intensity), which reflects the specific binding of phalloidin to F-actin.

Dilution experiments

In dilution experiments, the activated mixture was diluted with 10 mM Pipes (pH 7.0) alone or the same buffer containing EDTA and/or $MgCl_2$ and incubated at 0 °C. In some experiments, EDTA and $MgCl_2$ were included in the dilution buffer to afford an indicated free Mg^{2+} concentration. After the incubation, the mixture was supplemented with cytochrome *c* and NADPH, warmed up to 25 °C for 30 s, and assayed for O_2^- generation without further dilution. The standard cell-free system contained 0.2 mM ATP and 0.8 mM $MgCl_2$ brought from cytosol and plasma membrane preparations.

Calculation of free Mg^{2+} concentration

Free Mg^{2+} concentration $[Mg^{2+}]$ in the system was calculated using the equation described by Sunyer et al. [13]:

$$[Mg^{2+}]_t = [Mg^{2+}]\{1 + [EDTA]_t/([Mg^{2+}] + K_{EDTA}) + [ATP]_t/([Mg^{2+}] + K_{ATP}) + [GTP[S]]_t/([Mg^{2+}] + K_{GTP[S]})\}$$

where $[Mg^{2+}]_t$, $[EDTA]_t$, $[ATP]_t$ and $[GTP[S]]_t$ are the total concentrations of those compounds. K_{EDTA}, K_{ATP}, and $K_{GTP[S]}$ are the dissociation constants (K_d) of the Mg^{2+}–EDTA (0.4 μM) [13], Mg^{2+}–ATP (40 μM) [14] and Mg^{2+}–GTP[S] (60 μM) [13] complexes, respectively.

RESULTS

Effect of DNase I

DNase I is known to depolymerize F-actin by binding G-actin tightly [15] and shifting the equilibrium from F- to G-actin [16]. Therefore, we examined the effect of DNase I on the stability of NADPH oxidase activity. As shown in Figure 1(A), DNase I markedly accelerated the deactivation of the oxidase at 4 °C. The activity fell to 54 % in the first 10 min and then gradually decreased. In a first-order plot of the data, the deactivation was biphasic (results not shown) and the half-life ($t_{1/2}$) for the first phase was 8 min (Table 1), which was much shorter than that for the control (160 min). In contrast, the second-phase decay ($t_{1/2}$ = 165 min) was similar to that for control. The deactivation by DNase I was prevented by addition of actin (100 μM). When actin was added to the mixture by itself, the oxidase activity was stabilized further (Figure 1A). These results suggest that actin filaments play a role in maintaining the oxidase activity, although some subpopulation of the oxidase seems unrelated to actin filaments

Figure 1(B) shows the concentration dependence for DNase I in the deactivation of NADPH oxidase. The deactivation by DNase I occured in a dose-dependent manner, and when DNase I was used at 2.5 mg/ml, the activity was decreased to 47 %. At higher concentrations the activity was not much changed (results not shown). The addition of actin (100 μM) completely prevented the deactivation by DNase I.

The prevention by actin of the DNase I-induced deactivation was examined in more detail. When different amounts of actin were used, the activity was restored in a concentration-dependent manner (Figure 1C), whereas ovalbumin showed no such effect, indicating that it was not a general protein effect (results not shown). Interestingly when F-actin, actin polymerized before addition, was added to the incubation mixture, a similar effect was obtained. Although F-actin does not inhibit DNase I, it could be a source of G-actin when endogenous G-actin is captured by DNase I, protecting endogenous F-actin from depolymerization. These results indicate that F-actin has an ability to sustain the oxidase activity.

Effect of latrunculin

To ascertain a role of F-actin, we examined another F-actin-depolymerizing agent. Latrunculin A, a marine toxin, is known to depolymerize F-actin by a mechanism similar to DNase I. Figure 2 shows the time course of the oxidase activity in the incubation with or without latrunculin A. Latrunculin apparently accelerated the deactivation, and at 30 min the activity was 55 % of the control. The first-order plot of the deactivation curve was biphasic and the $t_{1/2}$ value for the first phase was estimated to be 13 min (Table 1), which is much less than that for the control

Table 1 Half-lives of O_2^--generating activity in the cell-free activation mixture under various conditions

Half-lives ($t_{1/2}$) were estimated from a first-order plot of the data described in Figures 1(A), 2 and 4 using linear least-squares regression analysis. Incubation conditions not specified are provided in each Figure legend. The values in parentheses are the half-lives for the 1-ethyl-3-(3-dimethylaminopropyl)carbodi-imide (EDC)-treated sample described in Table 3 (see below).

		$t_{1/2}$ (min)	
Temperature	Conditions	First phase	Second phase
4 °C	None	160	–
	DNase I	8	165
	DNase I + actin	180	–
0 °C	None (DMSO)	310	–
	Latrunculin	13	300
	Latrunculin + actin	460	–
	Dilution	12	200
	Dilution + EDTA	4 (190)	60
	Dilution + Mg^{2+}	26 (> 350)	320

(310 min). The $t_{1/2}$ value for the second phase (300 min) was similar to that for the control. The deactivation by latrunculin was prevented by addition of actin in a dose-dependent manner and at 100 μM actin completely prevented the deativation by latrunculin (results not shown).

F-actin content

To confirm that F-actin was actually decreased by DNase I or latrunculin A, F-actin content was measured with fluorescently labelled phalloidin, which selectively binds to F-actin. As shown in Table 2, either DNase I or latrunculin decreased F-actin content in the system. F-actin levels were 56 and 63 % of the control after the incubation with DNase I and latrunculin, respectively. The result supports the concept that actin depolymerization deactivates the oxidase.

In the course of the experiment, we noticed that F-actin level increased in the cell-free activation with SDS. Therefore we next examined the relationship between the activation and F-actin level. F-actin level was measured after incubation with or without SDS (Figure 3). The incubation with SDS resulted in a 70 % increase in F-actin level. When the activation was performed with sub-optimal concentrations of SDS, F-actin level increased almost in parallel with the oxidase activity over a threshold of

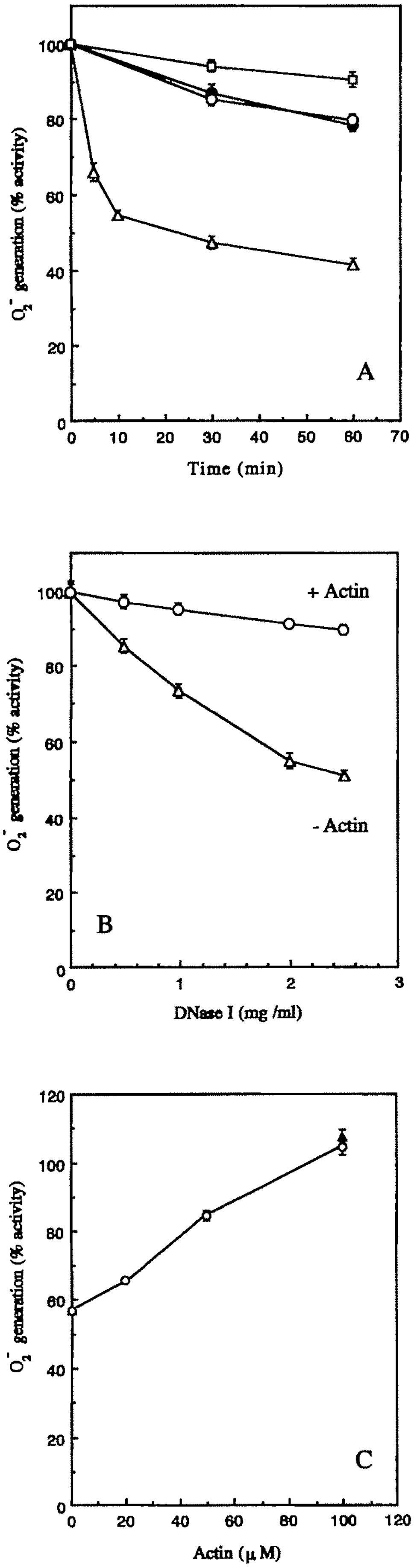

Figure 1 The deactivation of NADPH oxidase in the presence and absence of DNase I and/or actin

(**A**) Time course. After cell-free activation, the mixture was incubated at 4 °C for 0–60 min in the absence (●) or presence of 2.5 mg/ml DNase I (△), 2.5 mg/ml DNase I + 100 μM actin (○) and 100 μM actin (□) in a total of 75 μl. After incubation, an aliquot of the mixture was assayed for O_2^- generation as described in the Experimental section. Data are expressed as means ± S.D. of three determinations. The initial activities of the control and the samples with DNase I, DNase I + actin and actin were 952 ± 9.2, 904.8 ± 17.5, 943.8 ± 18.9 and 1079.4 ± 12.8 nmol/min per mg of plasma-membrane protein, respectively. (**B**) Concentration-dependence of DNase I. The cell-free activation mixture was incubated with various amounts of DNase I in the presence and absence of 100 μM actin. The control activities (100 %) with and without actin were 742.9 ± 15.1 and 651.6 ± 13.4 nmol/min per mg of plasma-membrane protein, respectively. (**C**) Effect of actin concentration on DNase I-induced deactivation. The activation mixture was incubated for 1 h with DNase I (2.5 mg/ml) plus 0–100 μM actin in a total of 60 μl. In some experiments, actin (100 μM) was polymerized before addition by incubating in 8 mM $MgCl_2$/20 mM KPB (pH 7.0) at 0 °C for 1 h (▲). The control activity at 60 min was 727 ± 10.5 nmol/min per mg of plasma-membrane protein.

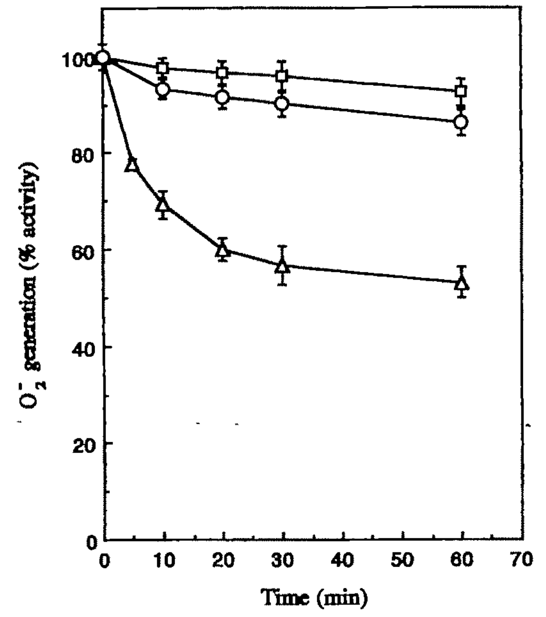

Figure 2 Effect of latrunculin A on the time course of NADPH oxidase activity

After cell-free activation the mixture was incubated with DMSO (○), 50 μM latrunculin (△) or 50 μM latrunculin + 100 μM actin (□) at 0 °C for 0–60 min and assayed for O_2^- generation. Data are expressed as means ± S.D. of three determinations. The initial activity of the control was 994.1 ± 19.8 nmol/min per mg of plasma-membrane protein.

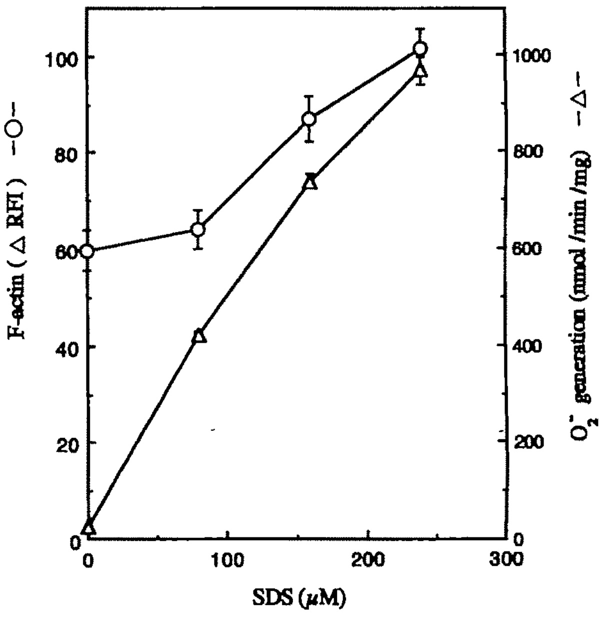

Figure 3 The oxidase activation and F-actin content using different concentrations of SDS

The cell-free activation was performed with 0, 80, 160 and 240 μM SDS, and the mixture was assayed for O_2^- generation and subjected to F-actin measurement as described in the Experimental section. Data are expressed as means ± S.D. of three determinations. ΔRFI, relative fluorescence intensity.

Table 2 Effect of DNase I or latrunculin on NADPH oxidase and F-actin content

The cell-free activated mixture was incubated at 4 °C for 1 h in the presence and absence of DNase I (2.5 mg/ml) or incubated at 0 °C for 30 min in the presence and absence of latrunculin A (100 μM). After the incubation, the mixture was assayed for O_2^- generation and subjected to F-actin estimation. The values in parentheses are the data as percentages relative to the respective controls (set at 100%). ΔRFI, relative fluorescence intensity.

Addition	O_2^--generating activity (nmol/min per mg)	F-actin content (ΔRFI)
None	783 ± 18.2 (100%)	97.1 ± 8.4 (100%)
DNase I	490 ± 9.9 (51%)	54.0 ± 7.6 (56%)
None	955 ± 21.3 (100%)	97.0 ± 7.9 (100%)
Latrunculin A	604 ± 11.4 (63%)	61.5 ± 8.1 (63%)

80 μM. The result suggests that actin polymerization takes place during the oxidase activation.

Effects of Mg^{2+} and EDTA

F-actin starts to depolymerize when actin concentration is lowered to the critical concentration [17], and critical concentration is drastically decreased by the presence of Mg^{2+} ions [18]. Here we diluted the activated mixture 25-fold with 10 mM Pipes buffer (pH 7) with or without 8 mM $MgCl_2$, or 2 mM EDTA, and examined the time course of the oxidase activity. It should be noted that the control mixture contained 32 μM $MgCl_2$ when diluted 25-fold (see the Experimental section). Dilution made the deactivation curve biphasic (Figure 4)

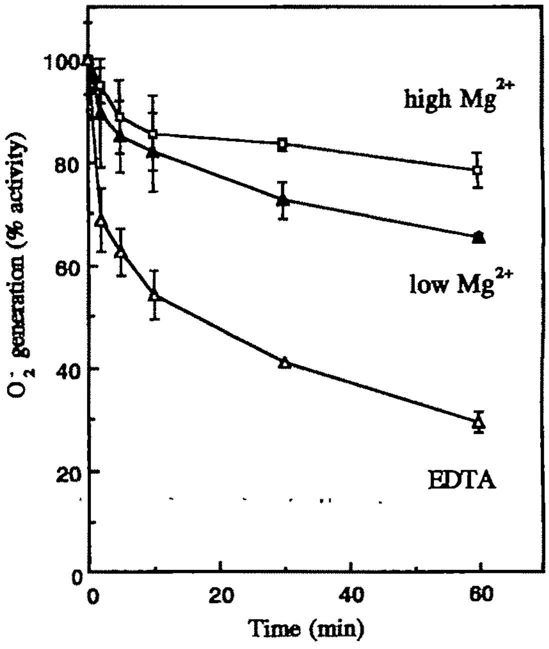

Figure 4 Time course of NADPH oxidase in dilution with Mg^{2+} or EDTA

After the cell-free activation the mixture was diluted 25-fold with 10 mM Pipes (pH 7.0) in the absence (low Mg^{2+}) and presence of 8 mM $MgCl_2$ (high Mg^{2+}) or 2 mM EDTA (EDTA) and incubated for 0–60 min at 0 °C. Then the mixture was assayed for O_2^- generation. Data are expressed as means ± S.D. of three determinations. Initial activities of the diluted mixture with the buffer, the buffer with 8 mM $MgCl_2$, and 2 mM EDTA were 654.7 ± 44.3, 789.1 ± 58.6 and 558.6 ± 38.7 nmol/min per mg of plasma-membrane protein, respectively.

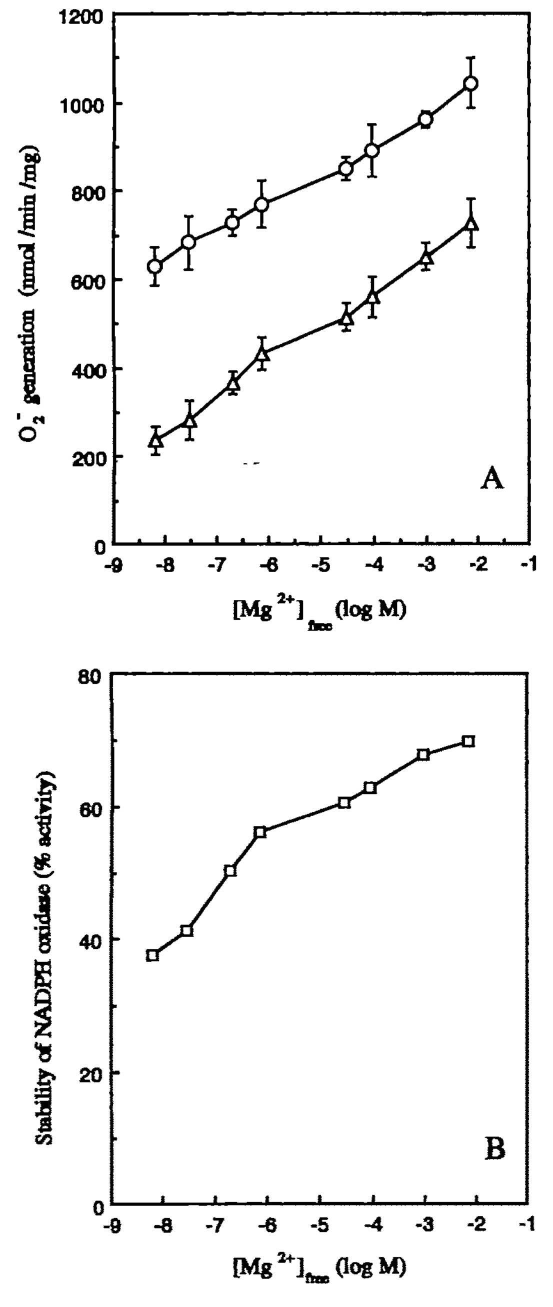

Figure 5 The effect of free Mg^{2+} concentration on NADPH oxidase stability

(A) NADPH oxidase activity immediately or 30 min after dilution Cell-free activation was performed in 10 mM Pipes buffer (pH 7.0) containing 0 8 mM $MgCl_2$, and the mixture was diluted 25-fold with the same buffer containing $MgCl_2$ or EDTA to afford 6.7 nM–7 99 mM free Mg^{2+} concentration and assayed immediately (○) or after 30 min (△) Data are expressed as means ± S.D of three determinations (B) Correlation between free Mg^{2+} concentration and enzyme stability The stability was estimated from the data in (A) using the following equation stability (%) = activity (t = 30 min)/activity (t = 0) × 100

Table 3 Prevention by cross-linking against EDTA-induced NADPH oxidase deactivation and F-actin depolymerization

The cell-free activation mixture was stirred with 20 mM EDC at 0 °C for 30 min The control mixture (Native) or EDC-treated mixture (EDC) was diluted 25-fold with 20 mM KPB (pH 7) containing 8 mM $MgCl_2$ or 2 mM EDTA and incubated at 0 °C for 30 min After the incubation, the mixture was assayed for O_2^- generation and subjected to F-actin estimation. Data are expressed as means ± S.D. of three determinations. The values in parentheses are the data as percentages relative to the control activity (960 ± 44.5 nmol/min per mg, set at 100%) or F-actin content of the non-cross-linked, non-diluted, sample (relative fluorescence intensity, ΔRFI, 89 6 ± 5 3, set at 100%)

Sample	Additives in dilution	O_2-generating activity (nmol/min per mg)	F-actin content (ΔRFI)
Native	EDTA	243 ± 23 3 (25%)	27 0 ± 5 4 (30%)
	$MgCl_2$	758 ± 29 6 (79%)	68.9 ± 6.5 (77%)
EDC	EDTA	615 ± 40 2 (64%)	103 ± 6 6 (115%)
	$MgCl_2$	834 ± 29.5 (87%)	92.2 ± 3 5 (103%)

and the lifetime shorter than that without dilution (Table 1). The $t_{1/2}$ values for the first and second phases were 12 and 200 min, respectively. When $MgCl_2$ was added in the dilution the half-lives for the first and second phases increased to 26 and 320 min. On the other hand, EDTA markedly accelerated the deactivation and the half-lives for the first and second phases decreased to 4 and 60 min, respectively. These results indicate clearly that Mg^{2+} has an ability to prolong the lifetime of the oxidase, although some populations of the oxidase are relatively stable under the conditions for actin depolymerization.

Effect of free Mg^{2+} concentration

Next we examined the correlation between free Mg^{2+} concentration and oxidase stability. Figure 5(A) shows the oxidase activities at zero time (t = 0) and 30 min after dilution at various concentrations of free Mg^{2+}. The activity at t = 0 increased as free Mg^{2+} concentration was increased. The activity with 7.99 mM Mg^{2+} was about 1.7-fold that with 6.7 nM Mg^{2+}. When the stability was defined as activity (t = 30)/activity (t = 0) × 100 and plotted against free Mg^{2+} concentration, the stability correlated well with free Mg^{2+} concentration (Figure 5B). On the other hand, when Ca^{2+} was used instead of Mg^{2+} the stabilizing effect was hardly observed (results not shown). These results suggest that the effect of Mg^{2+} on the stability of the oxidase is related to the stabilization of actin filaments.

Effect of 1-ethyl-3-(3-dimethylaminopropyl)carbodi-imide (EDC) on deactivation and F-actin loss by dilution with EDTA

To confirm the concept mentioned above, we estimated F-actin content in the diluted mixture in the presence and absence of Mg^{2+}. Dilution itself lowered F-actin level to 61% and it was decreased to 30% by addition of EDTA, where the oxidase activity fell to 25% (Table 3). Our earlier study showed that the oxidase activity was remarkably stabilized by cross-linking with EDC. Therefore we examined the effect of EDC on EDTA-induced deactivation and F-actin depolymerization. When the activated mixture was cross-linked with EDC before dilution, F-actin content was not decreased by dilution with EDTA and the activity was largely preserved. The $t_{1/2}$ values were much extended in both the presence and absence of Mg^{2+} (Table 1). These results further support the relationship between oxidase stability and F-actin content.

Effect of GTP[S]

Mg^{2+} is known to influence the activation of small GTPases including Rac, Rho and rap1A. Rac is an essential component and rap1A is a possible regulator of the oxidase that is associated with cytochrome b_{558}. Therefore, we examined whether the effect of Mg^{2+} on stabilization is related to these small GTPases.

GTP[S], a well-established activator for small GTPases (a non-hydrolysable analogue of GTP), was added to the dilution and the stability of the enzyme was examined. The stability was not increased but, in fact, it was somewhat decreased by GTP[S]. The stabilities at 6.6 nM, 0.7 μM and 7.76 mM free Mg^{2+} were 29, 40 and 56 %, respectively, whereas those without GTP[S] were 38, 56 and 70 %, respectively (Figure 5B)

DISCUSSION

Neutrophils contain high concentrations of actin (approx. 40 μM in total) [7], and it is actually the most abundant protein in neutrophil cytosol preparation. In the resting cells one-third of total actin is present as F-actin and upon cell activation further polymerization takes place. Actin polymerization has been related to chemotaxis and phagocytosis, both of which are accompanied by motion, but not to the respiratory burst (O$_2^-$ generation).

In the present study, we propose that actin polymerization regulates the lifetime of NADPH oxidase based on the following. (i) DNase I or latrunculin A facilitated the deactivation of NADPH oxidase and actin prevented it. (ii) EDTA accelerated the deactivation in a diluted mixture and Mg^{2+} prevented the deactivation. (iii) The treatment with these agents diminishes the F-actin content. (iv) EDC, a cross-linker, prevents the deactivation and F-actin depolymerization induced by EDTA It should be stressed that actin polymerization is not essential for the oxidase activation, but is required for the duration of the oxidase.

The biphasic deactivation induced by DNase I, latrunculin or dilution showed that some part of the oxidase activity was resistant to these agents or the condition. This implies the presence of sub-populations of the oxidase complex that do not require or do not depend very much on F-actin for stabilization. It cannot be ruled out, however, that these agents did not depolymerize all the F-actin involved in the oxidase stabilization. Whichever is the case, the contribution of F-actin to the respiratory burst seems important because the net amount of O$_2^-$ generated is governed by the lifetime of the oxidase as well as the catalytic rate.

In the cell-free system, it has been pointed out that there is a requirement for Mg^{2+} at a concentration of several millimolar [19,20]. However, recently it was shown that the optimal Mg^{2+} concentration is much lower (0.1 μM) when recombinant cytosol phox proteins are used instead of cytosol [21] and, more dramatically, Mg^{2+} is not required when purified cytochrome b_{558} was used instead of the membrane [22]. Thus it seems that Mg^{2+} is not required for the activation in a purified reconstitution system, but is necessary for the maximal activation in a crude system. We speculate that Mg^{2+} is required for F-actin-involved stabilization of the oxidase.

Mg^{2+} ions are thought to stabilize F-actin by shifting the equilibrium from G- to F-actin. The equilibrium between G- and F-actin depends critically on the concentration of bivalent cations such as Mg^{2+} and Ca^{2+} [16]. In the absence of bivalent cations, actin is essentially monomeric. Addition of bivalent cations markedly decreases the critical concentration for actin polymerization. For example, the critical concentration is approx. 0.05 μM for Mg^{2+}-bound actin and approx. 0.3 μM for Ca^{2+}-bound actin [18]. In our system, total actin concentration was estimated to be 2 μM in the activation mixture and 0.08 μM after dilution, which is higher than the critical concentration with Mg^{2+} and lower than that with Ca^{2+}. This is consistent with the result that Mg^{2+}, and not Ca^{2+}, had a significant effect on the oxidase stability.

As Mg^{2+} facilitates the GDP/GTP exchange reaction on small GTPases at a low concentration (< 0.1 μM), additional activation of Rac might stabilize the oxidase. However, the Mg^{2+} concentrations used in our system are much higher (> 1 mM) and at such a concentration the nucleotide exchange is not facilitated [23]. Thus it is unlikely that Rac is involved in Mg^{2+}-supported stabilization. Actually, the addition of GTP[S] to the dilution mixture did not increase, but rather decreased, the enzyme stability to some extent.

We used SDS as an activator for cell-free activation of NADPH oxidase. Since the system was established, the anionic amphiphile has often been used for the activation system, as well as arachidonate [3]. Nevertheless, the exact role of SDS in the activation is not clear. It has been suggested that SDS mimics p47^{phox} phosphorylation catalysed by a protein kinase by providing negative charges to the protein. However, a pure system, which includes a large excess of p67^{phox} and Rac over cytochrome b_{558}, does not need p47^{phox} but needs SDS to be activated [24], suggesting that SDS also acts on other phox protein(s).

One of the most interesting findings here is that F-actin increases during NADPH oxidase activation. Although the exact mechanism for the phenomenon is not clear, the conditions for the oxidase activation could be suitable for actin polymerization, i.e. the requirement of Mg^{2+}, GTP, small GTPase such as Rac, and high concentrations of G-actin (cytosol). It was reported that Rho GTPases, including Rac, Rho or Cdc42, induce actin polymerization in neutrophils or other cells [25,26]. Thereby it is plausible that the activated Rac or other GTPase may induce actin polymerization. In this context, it is of interest that SDS is able to activate Rho GTPases by dissociating the complex with Rho GDI (GDP-dissociation inhibitor) [27,28] because in the cytosol Rac GTPase is complexed with Rho GDI [29].

Cytochalasins, which are often used to depolymerize F-actin, had no effect on the oxidase stability (results not shown). In contrast, latrunculin A facilitated the deactivation of the oxidase. It is known that latrunculin, and not cytochalasin, depolymerizes F-actin that lies beneath the plasma membrane, i.e. cortical actin [30,31]. This might be due to the difference in action mechanism between cytochalasin and latrunculin. Cytochalasins bind to the barbed end of F-actin to block filament elongation while latrunculin depolymerizes F-actin by a similar mechanism to DNase I [31]. Thus the difference in the effects of cytochalasins and latrunculin may suggest that the F-actin that stabilizes the oxidase is cortical actin.

How can actin filaments stabilize neutrophil NADPH oxidase? The interaction between cytoskeleton and the oxidase components has been reported, which include p47^{phox}, p67^{phox}, [9,32], Rac [33] and cytochrome b_{558} [9]. Coronin, an actin-binding protein, was also reported to interact with p67^{phox} and p40^{phox} [34]. So it is reasonable to speculate that the cytosol phox proteins link to actin filaments, either directly or indirectly. On the other hand, cortical actin anchors to the plasma membrane through ERM proteins (ezrin, radixin and moesin) and a membrane-spanning protein, CD44 [35]. Therefore, actin filaments may stabilize and immobilize the oxidase complex as a scaffold on the plasma membrane.

In summary, the present work indicates that during the activation of the oxidase actin filaments grow on the plasma membrane and stabilize the oxidase complex This suggests that actin polymerization and depolymerization regulate the lifetime of the oxidase in neutrophils.

Finally what is the physiological significance of actin regulation of NADPH oxidase? Active oxygen species, such as O$_2^-$ and its derivatives, are microbicidal but also toxic to the host cells. Complex formation on the membrane cytoskeleton may help to restrict the area of the respiratory burst and avoid unfavourable 'firing'. On the physiological relevance of actin in the respiratory burst, it is of interest that Nunoi et al. reported recently of a patient with a mutated β-actin gene showing impaired O_2^- generation in neutrophils [36].

We are grateful to Shogo Murakami and Tomomi Morimatsu for technical assistance. We thank Dr Dave Lambeth (Department of Biochemistry, Emory University, Atlanta, GA, U S A), Dr Kathy Griendling and Dr Masuko Fukai (Emory University School of Medicine, Atlanta, GA, U S A) for valuable discussions We are indebted to Dr Keiichi Kato (Department of Applied Chemistry, Ehime University, Matsuyama, Ehime, Japan) and Dr Yoshihiko Sadaoka (Faculty of Engineering, Ehime University, Matsuyama, Ehime, Japan) for fluorimetric measurement and Dr Syuichi Saeki and Kazue Murakami (Health Care Center, Ehime University, Matsuyama, Ehime, Japan) for obtaining blood We also thank Mr Ronald P Murphy for careful reading of the manuscript

REFERENCES

1 Babior, B M (1978) Oxygen-dependent microbial killing by phagocytes N Eng J Med **298**, 659–668

2 Rossi, F (1986) The O_2-forming NADPH oxidase of the phagocytes nature, mechanism of activation and function Biochim Biophys Acta **853**, 65–89

3 Thrasher, A J., Keep, N H , Wientjes, F and Segal, A. W (1994) Chronic granulomatous disease Biochim Biophys Acta **1227**, 1–24

4 Tamura, M , Tamura, T , Burnham, D. N., Uhlinger, D J and Lambeth, J D (1989) Stabilization of the superoxide-generating respiratory burst oxidase of human neutrophil plasma membrane by crosslinking with EDC Arch Biochem. Biophys **275**, 23–32

5 Tamura, M , Takeshita, M , Curnutte, J T , Uhlinger, D J and Lambeth, J D (1992) Stabilization of human neutrophil NADPH oxidase activated in a cell-free system by cytosolic proteins and by 1-ethyl-3-(3-dimethylaminopropyl) carbodiimide J Biol Chem **267**, 7529–7538

6 Stossel, T P (1992) Basic principles and clinical correlates, in Inflammation (Gallin, J I , Goldstein, I M and Snyderman, R , eds), pp 459–475, Raven Press, New York

7 Yassin, R , Schfcyk, J., White, J R , Tao, W , Volpi, M , Molski, T. F P , Naccache, P. H , Feinstein, M. B and Sha'afi, R. I (1985) Effects of chemotactic factors and other agents on the amounts of actin and 65kd protein associated with the cytoskeleton of rabbit and human neutrophils J Cell Biol **101**, 182–188

8 Quinn, M T , Parkos, C A and Jesaitis, A J (1989) The lateral organization of components of the membrane skeleton and superoxide generation in the plasma membrane of stimulated human neutrophils. Biochim Biophys Acta **987**, 83–94

9 Woodman, R C , Ruedi, J M , Jesaitis, A J., Okamura, N , Quinn, M T , Smith, R M , Curnutte, J. T and Babior, B M (1991) Respiratory burst oxidase and three of four oxidase-related polypeptides are associated with the cytoskeleton of human neutrophils J Clin. Invest **87**, 1345–1351

10 Morimatsu, A , Kawagoshi, A , Yoshida, K. and Tamura, M (1997) Actin enhances the activation of human neutrophil NADPH oxidase in a cell-free system Biochem Biophys Res Commun **230**, 206–210

11 Ogata, K , Nishimoto, Y , Uhlinger, D J , Igarashi, K , Takeshita, M. and Tamura, M (1996) Spermine suppresses the activation of human neutrophil NADPH oxidase in cell-free and semi recombinant systems Biochem J **313**, 549–554

12 Redmond, T , Trdif, M and Zigmond, S H. (1994) Induction of actin polymerization in permeabilized neutrophils role of ATP J Biol Chem **269**, 21657–21663

13 Sunyer, T , Codina, J and Birnbaumer, L (1984) GTP hydrolysis by pure Ni, the inhibitory regulatory component of adenylcyclases. J. Biol. Chem **259**, 15447–15451

14 Nakayama, S and Tomita, T (1990) Depletion of intracellular free Mg^{2+} in Mg^{2+} and Ca^{2+}-free solution in the taenia isolated from guinea-pig caecum J Physiol **421**, 363–378

15 Kabsch, W , Mannherz, H G , Suck, D , Pai, E F and Holmes, K C. (1990) 3D-structure of actin-DNase I complex Nature (London) **347**, 37–44

16 Steinmetz, M O , Stoffler, D and Hoenger, A (1997) Actin from cell biology to atomic detail J Struct Biol **119**, 295–320

17 Cano, M L , Cassimeris, L , Joyce, M and Zigmond, S H (1992) Cell motility and cytoskeleton Cell Motil. Cytoskel **21**, 147–158

18 Khaitlina, S Y , Moraczewska, J and Strzelecka-Golaszewska, H (1993) The actin/actin interactions involving the N-terminus of the DNase-I-binding loop are crucial for stabilization of the actin filament Eur J Biochem **218**, 911–920

19 Gabig, T G , English, D , Akard, L P. and Schell, M J (1987) Regulation of neutrophil NADPH oxidase activation in a cell-free system by guanine nucleotides and fluoride evidence for participation of PT insensitive G protein J Biol Chem **262**, 1685–1690

20 Babior, B M , Kuver, R. and Curnutte, J T (1988) Kinetics of activation of the respiratory burst oxidase in a fully soluble system from human neutrophils J Biol Chem **263**, 1713–1718

21 Aoyagi, K , Takeshige, K , Sumimoto, H , Nunoi, H and Minakami, S (1992) Role of Mg in activation of NADPH oxidase of human neutrophils evidence that Mg^{2+} acts through G-protein. Biochem Biophys Res. Commun **186**, 391–397

22 Cross, A R , Erickson, R W , Ellis, B A and Curnutte, J T (1999) Spontaneous activation of NADPH oxidase in a cell-free system unexpected multiple effects of Mg ion concentrations. Biochem J **338**, 229–233

23 Knaus, U G , Heyworth, P. G , Kinsella, B T , Curnutte, J T and Bokoch, G M (1992) Purification and characterization of rac 2 J Biol Chem **267**, 23575–23582

24 Freeman, J L and Lambeth, J D (1996) NADPH oxidase activity is independent of p47*phox* *in vitro* J Biol. Chem **271**, 22578–22582

25 Zigmond, S H , Joyce, M , Borleis, J , Bokoch, G M and Devreotes, P N (1997) Regulation of actin polymerization in cell-free systems by GTPγS and cdc42 J Cell Biol **138**, 363–374

26 Tapon, N and Hall, A (1997) Rho, Rac and Cdc42 GTPases regulate the organization of the actin cytoskeleton Curr Opin Cell Biol **9**, 86–92

27 Chuang, T-H , Bohl, B P and Bokoch, G. M. (1993) Biologically active lipids are regulators of rac GDI complexation J Biol Chem. **268**, 26206–26211

28 Pick, E , Gorzalczany, Y. and Engel, S (1993) Role of the rac p21-GDI for rho heterodimer in the activation of the superoxide-forming NADPH oxidase of macrophages Eur J Biochem. **217**, 441–455

29 Kwak, J Y , Lopetz, I , Uhlinger, D J , Ryu, S H. and Lambeth, J D (1995) RhoA and cytosolic 50-kDa factor reconstitute GTPγS-dependent phospholipase D activity in human neutrophil subcellular fraction J Biol Chem **270**, 27093–27098

30 Cassimeris, L , McNeill, H and Zigmond, S. H. (1990) Chemoattractant-stimulated polymorphonuclear leukocytes contain two populations of actin filaments that differ in their spatial distributions and relative stabilities J Cell Biol **110**, 1067–1075

31 Lamaze, C , Fujimoto, L M , Yin, H L and Schmid, S L (1997) The actin cytoskeleton is required for receptor-mediated endocytosis in mammalian cells. J Biol Chem **272**, 20332–20335

32 Nauseef, W. M , Volpp, B D , McCormick, S , Leidal, K G and Clark, R A (1991) Assembly of the neutrophil respiratory burst oxidase J Biol Chem **266**, 5911–5917

33 Wientjes, F B , Segal, A W and Hartwig, J H (1997) Immunoelectron microscopy shows a clustered distribution of NADPH oxidase components in the human neutrophil plasma membrane J Leukocyte Biol **61**, 303–312

34 Grogan, A , Reeves, E , Keep, N., Wientjes, F , Totty, N F , Burlingame, A. L., Hsuan, J J and Segal, A W (1997) Cytosolic phox proteins interact with and regulate the assembly of coronin in neutrophils J Cell Sci. **110**, 3071–3081

35 Hall, A (1998) Rho GTPases and the actin cytoskeleton Science **279**, 509–514

36 Nunoi, H , Yamazaki, T., Tsuchiya, H , Kato, S , Malech, H L , Matsuda, I. and Kanegasaki, S (1999) A heterozygous mutation of β-actin associated with neutrophil dysfunction and recurrent infection Proc Natl Acad Sci U S A. **96**, 8693–8698

Received 29 November 1999/20 March 2000, accepted 16 April 2000

Biochem J (2000) 349, 377–384 (Printed in Great Britain)

Sj-FABPc fatty-acid-binding protein of the human blood fluke *Schistosoma japonicum*: structural and functional characterization and unusual solvent exposure of a portal-proximal tryptophan residue

Malcolm W. KENNEDY*[1], Julie C. SCOTT†, Steven LO*, Jeremy BEAUCHAMP‡ and Donald P. McMANUS†

*Division of Infection and Immunity, Institute of Biomedical and Life Sciences, Joseph Black Building, University of Glasgow, Glasgow G12 8QQ, Scotland, U.K., †Molecular Parasitology Unit, Australian Centre for International and Tropical Health and Nutrition, and the Cooperative Research Centre for Vaccine Technology, The University of Queensland and The Queensland Institute of Medical Research, Post Office Royal Brisbane Hospital, Herston, Queensland 4029, Australia, and ‡Protein Crystallography Group, Department of Chemistry, Joseph Black Building, University of Glasgow, Glasgow G12 8QQ, Scotland, U.K.

Sj-FABPc of the blood fluke of humans, *Schistosoma japonicum*, is a member of the FABP/P2/CRBP/CRABP family of β-barrel cytosolic fatty-acid-binding and retinoid-binding proteins. Sj-FABPc has at least eight different variants encoded by a single-copy polymorphic gene. In fluorescence-based assays, recombinant Sj-FABPc was found to bind 11-(dansylamino)undecanoic acid (DAUDA), inducing a shift in peak fluorescence emission from 543 to 493 nm. A similar spectral change was observed in dansyl-amino-octanoic acid (in which the dansyl fluorophore is attached at the α-carbon rather than the ω-carbon of DAUDA), indicating that the ligand enters entirely into the binding site. Sj-FABPc also bound the naturally fluorescent *cis*-parinaric acid, as well as oleic acid and arachidonic acid, by competition, but not all-*trans*-retinol. Dissociation constants were, for *cis*-parinaric acid, $K_d = 2.5 \pm 0.1$ μM (mean ± S.E.M.) and an apparent stoichiometry consistent with one binding site per molecule of Sj-FABPc and, for oleic acid, $K_i \approx 80$ nM. A deletion mutant from which α-II was absent failed to bind ligand. Sj-FABPc modelled well to known structures of the protein family, an unusually solvent-exposed Trp side chain was evident adjacent to the presumptive portal through which ligand is thought to enter and leave. Intrinsic fluorescence analyses of Sj-FABPc and of the deletion mutant (from which Trp-27 is absent) confirmed the unusual disposition of this side chain. Virtually all members of the FABP/P2/CRBP/CRABP protein family have prominent hydrophobic side chains in this position, with the exception of liver FABP and ileal FABP, which instead have charged side chains. Liver FABP is known to be distinct from other members of the protein family in that it does not seem to contact membranes to collect and deposit its ligand. It is therefore postulated that the unusually positioned apolar side chains in Sj-FABPc and others in the family are important in interactions with membranes or other cellular components.

Key words: cytosolic lipid-binding proteins, fluorescent lipid analogues, polymorphism, portal region, tryptophan fluorescence.

INTRODUCTION

Schistosoma japonicum and *Schistosoma mansoni* are blood flukes of humans that cause chronic, highly debilitating diseases involving extensive liver damage [1]. These parasites are unable to synthesize fatty acids or sterols, so are entirely dependent on their hosts for these and other complex lipids [2–4]. Moreover, these flukes are unique in their possession of a double outer membrane in the blood-parasitic stage, there are indications of a highly active membrane-processing system in the outer syncitial layer of the organism [2,3,5]. The acquisition, retention, storage and internal transport of lipids are therefore of particular importance to the survival of these organisms; the proteins involved in lipid transport and exchange provide potential targets for chemotherapy and immunotherapy.

Fatty-acid-binding proteins (FABPs) of the FABP/P2/CRABP/CRBP family (the cytosolic FABP/myelin P2/cellular retinoic-acid-binding protein/cellular retinol-binding protein family) of cytosolic lipid-binding proteins (cLBPs) have been described in both of the above species of schistosome as important immune targets in infected individuals [6,7]. Both proteins are currently under investigation as vaccine components and are among a set of antigens that have been selected by the World Health Organization for inclusion in human immunization trials [8]. The subject of this report, the cytosolic FABP of *S. japonicum* (Sj-FABPc), seems not to be widely distributed within the worms, as might otherwise be expected for a generalized intracellular lipid-binding transporter. Instead, it is confined to lipid droplets of male worms (which are thought to assist nutritionally the females they enfold), and, crucially, also to the vitelline structures of the female parasites [9]. The protein might therefore be essential to the production and provisioning of the parasites' eggs; it is these that cause the pathology of schistosomiasis [1].

Despite the importance of Sj-FABPc and the similar protein from *S. mansoni* (Sm14) [7,10], no detailed structural and functional analysis of the proteins has appeared. The two seem to have different distributions within their respective organisms, so might have different biological roles [7,9]. We provide here a

---

Abbreviations used: cLBP, cytosolic lipid-binding protein; DACA, dansyl-D,L-α-amino-octanoic acid; DAUDA, 11-(dansylamino)undecanoic acid; F10, recombinant Sj-FABPc; F25, deletion mutant of Sj-FABPc; FABP, fatty-acid-binding protein; FABP/P2/CRABP/CRBP, proteins of the cytosolic FABP/myelin P2/cellular retinoic-acid-binding protein/cellular retinol-binding protein family; GdmCl, guanidinium chloride; LBP, lipid-binding protein; retinol, all-*trans*-retinol; Sj-FABPc, cytosolic fatty-acid-binding protein homologue of *Schistosoma japonicum*.

[1] To whom correspondence should be addressed (e-mail malcolm.kennedy@bio.gla.ac.uk).

The nucleotide sequence data for F10 and F25 will appear in DDBJ, EMBL and GenBank Nucleotide Sequence Databases under the accession numbers AF044409 and AF0444410 respectively. The coordinates of the structural model are available by e-mail from the corresponding author.

biochemical, biophysical and structural analysis of Sj-FABPc that additionally revealed unexpected features with implications for the functioning of the cLBPs of humans. In particular, we provide evidence that Sj-FABPc has an unusually disposed bulky hydrophobic side chain, which we postulate to be involved in cLBP–membrane interactions, adjacent to the presumptive portal of ligand entry and exit. We additionally propose that this amino acid position differentiates those cLBPs that interact directly with membranes in ligand exchange and trafficking from those that act as holding proteins to regulate the intracellular levels of unbound fatty acids.

MATERIALS AND METHODS

cDNA encoding Sj-FABPc sequences

DNA encoding the FABP was obtained by antibody screening of a *S. japonicum* (Philippines strain) cDNA expression library (Uni-ZAP XR; Stratagene, La Jolla, CA, U.S.A.) constructed using poly(A)$^+$ mRNA isolated from mixed-sex adult worms obtained from the Mindoro region of the Philippines. The antibody for screening was raised in rabbits against soluble *S. japonicum* proteins [11]. Initial sequencing was performed with the pBluescript (pBSK) SK primer and a *Taq* DyeDeoxy Terminator Cycle Sequencing Kit (Applied Biosystems, Foster City, CA, U.S.A.). Clones identified as having full-length open reading frames encoding proteins similar to cytosolic FABPs were further sequenced in both directions with pBSK M13 forward and reverse direction primers. Further FABP-encoding cDNA species were isolated by DNA hybridization screening with a previously isolated cDNA encoding the FABP obtained from the mainland Chinese strain of the parasite [6]. This provided seven new Sj-FABPc sequences in addition to the original one, the encoded proteins differing by a few amino acid positions (see Figure 1). Southern blot analysis showed that the encoding gene was in single copy, so the variants were true alleles. Two clones were selected for protein expression, one encoding a complete Sj-FABPc (F10), and one encoding a deletion mutant (F25).

Expression and purification of recombinant Sj-FABPc

The cDNA inserts of clones F10 and F25 were subcloned into a pQE31 expression vector (Qiagen, Venlo, The Netherlands) and used to transform *Escherichia coli* SG13009[pREP4] competent cells (Qiagen). To enhance protein expression, the PCR used to produce amplicons for insertion into expression vectors was designed to omit most of the 5′ untranslated regions of both F10 and F25. After the bulk culture of transformed bacteria from single colonies and the induction of expression with 2 mM isopropyl β-D-thiogalactoside, recombinant His-tagged protein was isolated from clarified soluble cell extracts by metal-affinity chromatography (Talon resin; Clontech, Palo Alto, CA, U.S.A.). After release from the resin with buffer containing imidazole [0.05 M $NaHPO_4$/0.3 M NaCl/0.5 M imidazole (pH 7.2)], recombinant protein was further purified by ion-exchange FPLC. Protein purity was monitored by SDS/PAGE and Coomassie Brilliant Blue staining or analysed by Western blotting with the use of the rabbit antiserum as primary antibody; the protein was concentrated with Centriprep-10 centrifugal concentrators (Amicon, Beverly, MA, U.S.A.). As has frequently been found for proteins of this family (particularly over-expressed recombinants) [7,12], both F10 and F25 proteins tended to precipitate after storage at low temperatures, so they were solubilized in 2.0 M guanidinium chloride (GdmCl). For the fluorescence studies, small quantities of this solution were added to buffer in the fluorescence cuvette, diluting the GdmCl and allowing the proteins to refold without precipitation (see results below). Far-UV CD analysis of F10 and F25 showed them to be similarly rich in β structure, to a degree expected for this type of protein, and indicated that the F25 deletion mutant had a decreased helical content. Analysis of the spectra over the range 240–200 nm by the CONTIN program [13] indicated that the β-sheet contents of both the full-length and truncated proteins were of the order of 50% and that the helical contents of these proteins were of the order of 15% and 5% respectively. The concentrations of the recombinant proteins were estimated from A_{280}, with an ϵ_{280} of 12660 $M^{-1}\cdot cm^{-1}$ for F10 and 6970 $M^{-1}\cdot cm^{-1}$ for the F25 deletion mutant, on the basis of the amino acid compositions of the recombinant proteins [14].

Spectrofluorimetry and fluorescence-based ligand binding

Fluorescence emission spectra were recorded at 20 °C with a SPEX FluorMax spectrofluorimeter (Spex Industries, Edison, NJ, U.S.A.), with 2 ml samples in a silica cuvette. Raman scattering by solvent water was corrected for where necessary by the use of appropriate blank solutions. The fluorescent fatty-acid analogues 11-(dansylamino)undecanoic acid (DAUDA), and dansyl-D,L-α-amino-octanoic acid (DACA) were obtained from Molecular Probes and Sigma respectively. all-*trans*-Retinol (referred to hereafter simply as retinol) and oleic acid were also obtained from Sigma; *cis*-parinaric acid was a gift from Dr Bruce Hudson (University of Oregon, Eugene, OR, U.S.A.) or obtained from Molecular Probes. The excitation wavelengths used for DAUDA, DACA, retinol and *cis*-parinaric acid were 345, 345, 350 and 319 nm respectively. The dansylated fatty acids were stored as stock solutions of approx. 1 mg/ml in ethanol, in the dark at −20 °C, and freshly diluted in PBS [171 mM NaCl/3.35 mM KCl/10 mM Na_2HPO_4/1.8 mM KH_2PO_4 (pH 7.2)] to 1 μM before use in the fluorescence experiments. Competitors of fluorescent fatty-acid binding were prepared as stock solutions in ethanol at approx. 10 mM and diluted in PBS or ethanol for use. Free retinol is poorly soluble and unstable in aqueous solution, so it was dissolved and diluted in ethanol immediately before use; binding to proteins was tested by addition of typically 5 μl of this directly to a cuvette containing protein in PBS. The following reference proteins were obtained from Sigma and prepared as stock solutions at 10 mg/ml in PBS: BSA, β-lactoglobulin (bovine), ribonuclease A, ovalbumin (chicken) and transferrin (bovine).

For the estimation of dissociation constants for protein–fatty-acid binding, 5 or 10 μl samples of *cis*-parinaric acid in ethanol were added successively to 2 ml of protein at 2.49 μM; the fluorescence emission was measured at 408 nm, with an excitation wavelength of 319 nm. The concentration of the ethanol stock solution of *cis*-parinaric acid was checked by measuring the A_{303} of an appropriate dilution in ethanol, using an ϵ_{303} of 76000 $M^{-1}\cdot cm^{-1}$ [15]. Fluorescence data were corrected for dilution where necessary, and fitted by standard non-linear regression techniques (with Microcal ORIGIN software) to a single non-competitive binding model to give estimates of the dissociation constant (K_d) and maximal fluorescence intensity (F_{max}). Similar non-linear regression methods were used to analyse results of competition experiments in which oleic acid was progressively added to a preformed complex of *cis*-parinaric acid and protein. A stock solution of oleic acid in ethanol was freshly diluted to 1 mM in PBS, increasing concentrations of oleic acid were added to a mixture containing 2.43 μM *cis*-parinaric acid and 3.29 mM protein.

Structural predictions and modelling

Protein sequence comparisons and alignments were performed with the BLAST program to search the protein sequence database (blastp) or MaxHom, both accessed through PHD on the ExPASy server (http://www.expasy.ch/) at SwissProt. Predictions of secondary structure and searching for structural analogues were made using the PHD program on the PredictProtein server (http://cubic.bioc.columbia.edu/predictprotein/) at SwissProt [16–18]. Molecular mass and theoretical molar absorption values were calculated with the ProtParam program through ExPASy. Searching for protein motifs such as hydrophobic leader sequences and protein family signatures were performed with Signalp (trained on eukaryotic sequences) and PROSITE programs. The Sj-FABP structure was modelled using SwissModel, and refined with the CHARMM forcefield [19,20], using for templates either the five most similar proteins of known structure as identified by PHD, or with a set of five structures (Protein Database codes 1HMR, 1PMP, 1ADL, 1ABO and 1ACD) automatically selected by SwissModel as a composite template. Model geometries were checked with the PROCHECK suite of programs.

RESULTS AND DISCUSSION

cDNA analysis and sequence variants

Screening of the *S. japonicum* cDNA library provided a set of seven protein sequences that differed at a only few amino acid positions (Figure 1) and exhibited sequence similarities to proteins of the FABP/P2/CRABP/CRBP family of cLBPs. The sequences are closest to the Sm14 protein of *S. mansoni* (89 % pairwise sequence identity), and showed substantially lower similarities to other proteins of the family, sequences of which are mainly derived from mammals. Together with a Sj-FABPc described previously from the Chinese strain of *S. japonicum* [6], this provided eight different sequences for the Sj-FABPc protein (Figure 1). Southern and Northern blotting analysis showed that the encoding gene was in single copy (results not shown), which is consistent with the variants' being alleles of a polymorphic gene.

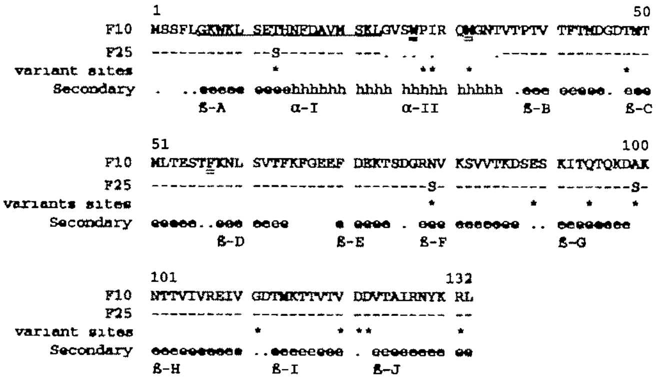
1
50
F10 MSSFLGKWKL SETHNFDAVM SKLGVSWPIR QMGNTVTPTV TFTMDGDTMT
F25 ---------- --S------- ---. .. . .----- ----------
variant sites * ** * *
Secondary . ..eeeee eeeehhhhhh hhhh hhhhh hhhhh .eee eeeee. eee
ß-A
α-I
α-II
ß-B
ß-C
51
100
F10 MLTESTFKNL SVTFKFGEEF DEKTSDGRNV KSVVTKDSES KITQTQKDAK
F25 ---------- ---------- --------S- ---------- --------S-
variants sites * * * *
Secondary eeeee..eee eeee e eeee . eee eeeeeee .. eeeeeeee
ß-D
ß-E
ß-F
ß-G
101
132
F10 NTTVIVREIV GDTMKTTVTV DDVTAIRNYK RL
F25 ---------- ---------- ---------- --
variant sites * * ** *
Secondary eeeeeeeeee ..eeeeeeee . eeeeeeee ee
ß-H
ß-I
ß-J

Figure 1 Amino acid sequences of Sj-FABPc F10 and F25 proteins of *S. japonicum*

Identical amino acids are indicated with dashes, the deleted amino acids in the F25 mutant are indicated with full stops The secondary structure according to the molecular modelling analysis is indicated as follows h, helix, e, β/extended, full stop, no prediction/loop. The FABP signature sequence identified by PROSITE is underlined The Trp-27, Met-32 and Phe-57 positions discussed in the text are doubly underlined in the F10 sequence line The 'variant sites' line shows where differences exist between between the eight Sj-FABPc sequences obtained (see the text) Most of the variant sites are on α-II or loop regions, and all except one (Gln-94 → His) are of outwardly projecting side chains according to the model (Figure 2)

The Signalp program [21] trained on eukaryotic sequences found no evidence of a cleavable signal peptide in the amino acid sequence of any of the encoded proteins. This is also true for other members of the cLBP family, with the exception of an unusual subfamily from nematodes [22,23]. PROSITE identified a signature sequence for cytosolic FABPs (GKWKLSETHNFDAVMSKL; single-letter amino acid codes) in addition to two potential glycosylation sites and several consensus protein kinase sites. The latter two motifs are common by chance in protein sequences but have no functional relevance, although it is pertinent to note that the phosphorylation of one human cLBP at least has been suggested to regulate its ligand-binding activities [24,25].

One of the cDNA clones, F25, has an in-frame deletion of DNA encoding 12 residues that fall within the predicted helical region of the protein (see below). Southern and Northern blotting analysis (results not shown) showed no difference in banding patterns when DNA encoding either the complete F10 protein or F25 was used as a probe, suggesting that the deletion was caused by misprocessing of F25's precursor mRNA or that it represents a rare deletion allele. From an alignment (results not shown) of the F25 cDNA with the genomic DNA sequences encoding rat liver FABP, human intestinal FABP and human cellular retinol-binding protein II, the deletion in F25 begins precisely at the expected exon–intron junction of intron 1 (results not shown). It is therefore likely that the F25 deletion is indeed an artifact of misprocessing, but an analytically useful one. F25 is distinctive in that the deletion has removed α-II (which forms one side of the putative portal for entry of the ligand; Figure 2) rather than both α-I and α-II as examined previously in intestinal FABP [26–28]. Deletions and mutations in the helical 'lid' region of cLBPs have proved instructive in understanding the mode of ligand binding in these proteins [27–30]. F25 is additionally useful because it provides information on the environments of the Trp side chains of the complete F10 protein (see below).

Ligand binding in wild-type protein and deletion mutant

Previous preliminary work on an F10-like protein from *S. japonicum* showed that it binds ^{14}C-labelled palmitic acid [6]. The fatty-acid-binding activities of F10 and F25 were examined here by using environment-sensitive fluorescent fatty acid analogues that alter their fluorescence emission spectra and intensities on entry into binding proteins [31–36]. Binding of DAUDA to F10 was accompanied by a substantial increase in both fluorescence intensity and a shift in the fluorescence emission maximum from 543 to 493 nm (Figure 3A), indicative of entry into an apolar environment [37]. To place this blue shift in context, rat liver FABP, rat intestinal FABP (both structural analogues of Sj-FABPc), BSA and the ABA-1 lipid-binding polyprotein of nematodes all produce shifts in DAUDA emission to 500, 496, 492 and 475 nm respectively [31,32,34,38]. The degree of blue shift in fluorescence emission with F10 was therefore typical for a member of the β-barrel cLBPs; we have found a similar shift in cLBP family proteins from other invertebrates [22]. F10 was also found to bind the naturally fluorescent *cis*-parinaric acid, as with DAUDA, the addition of oleic acid (Figure 4) or arachidonic acid (results not shown) displaced the fluorescent probe from the protein.

Fluorimetric titration of F10 with *cis*-parinaric acid yielded an apparent dissociation constant in the micromolar range (K_d = 2.5±0.1 μM; Figure 4A) and was consistent with 1:1 binding. The progressive addition of oleic acid to the mixture caused a

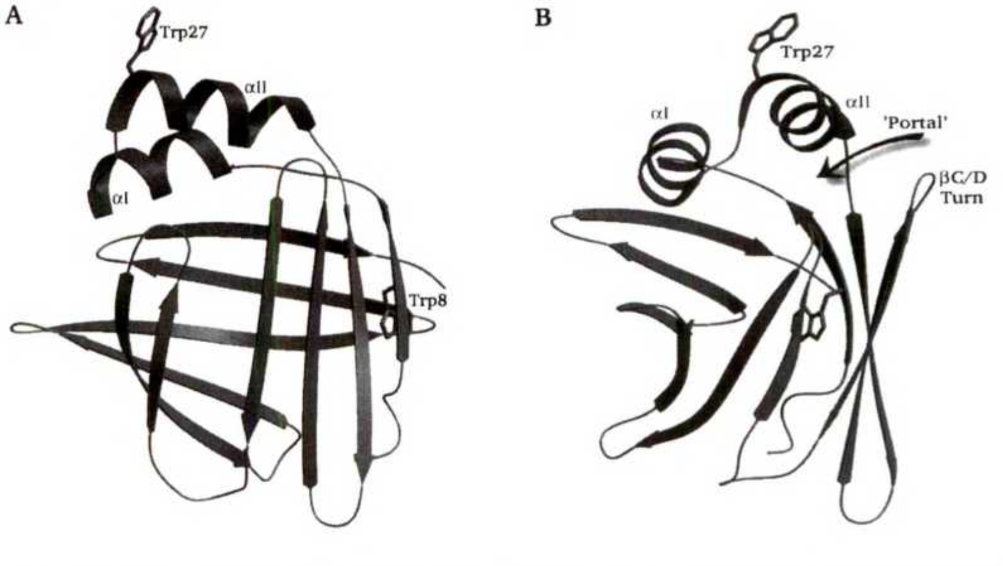

Figure 2 Two orientations of a molecular model of F10 to show the general structure and predicted dispositions of Trp-8 and Trp-27

The model was created by SwissModel (CHARMM refined) on the basis of five known crystal structures of cLBPs (see the text). The ribbon representation was created with Setor [70].

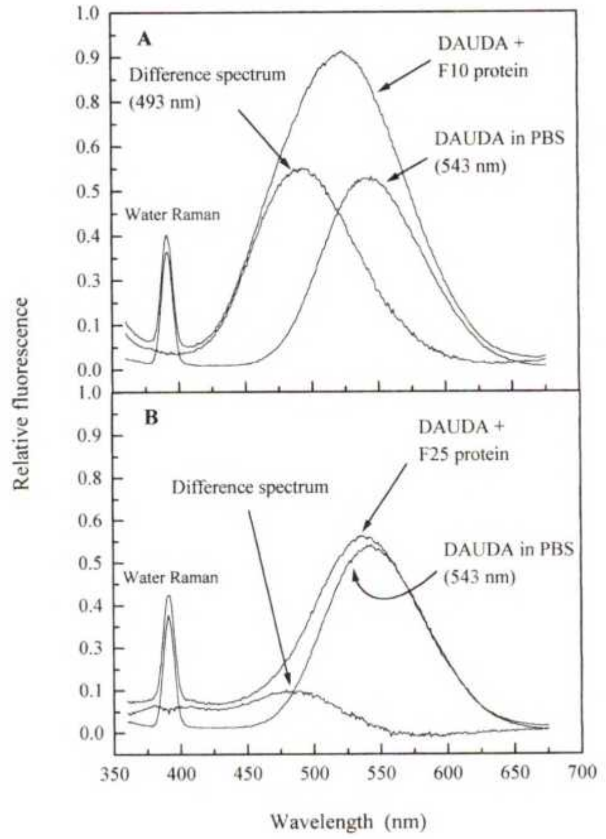

Figure 3 Fatty-acid binding by the Sj-FABPc F10 protein but not by the deletion mutant F25

Fluorescence emission spectra (λ_{ex} 345 nm) of approx. 1 μM DAUDA alone or on the addition of 2.1 μM F10 (**A**) or 4.1 μM F25 (**B**). The emission spectrum of DAUDA alone in PBS is also given, as is the spectrum of DAUDA when in the protein-binding site (difference spectra).

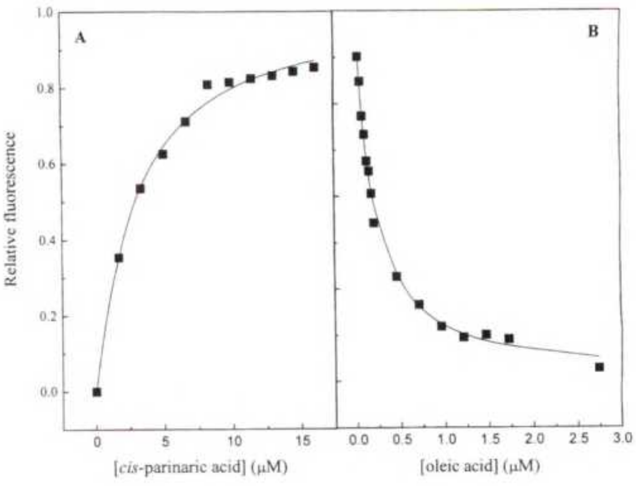

Figure 4 Titration curves for the binding of *cis*-parinaric acid and oleic acid to Sj-FABPc F10 protein

(**A**) Change in relative fluorescence intensity at 408 nm (corrected for dilution; λ_{ex} 319 nm) of 11.6 μM *cis*-parinaric acid on the addition of increasing concentrations of F10 protein. The solid line is the theoretical binding curve for complex formation with a dissociation constant K_d of 2.5 ± 0.1 μM and an apparent stoichiometry consistent with one binding site per molecule of protein. (**B**) Decrease in relative fluorescence due to the displacement of *cis*-parinaric acid from F10 by oleic acid. Increasing concentrations of oleic acid were added to a mixture containing 2.43 μM *cis*-parinaric acid and 3.29 μM F10. The solid line is a theoretical curve for the simple competitive binding of oleic acid in the DAUDA-binding site of F10, with an apparent dissociation constant K_i^{oleic} of approx. 80 nM.

stoichiometric reversal of the fluorescence enhancement effect; analysis of the titration curve yielded an apparent K_i^{oleic} of approx. 80 nM (Figure 4B), which is within the range of K_d values found for other cLBPs [33,38]. The tighter binding observed with oleic acid is presumably because oleic acid is more representative of the natural ligand than is the highly conjugated *cis*-parinaric acid. Similar titrations with DAUDA, and competitive titrations with oleic acid, provided K_d values of a similar order of magnitude to the above.

We also investigated the binding of F10 to a fluorescent fatty acid (DACA) in which the dansyl fluorophore is attached at the α-carbon rather than at the hydrocarbon terminal, as in DAUDA. The DACA probe was found to alter its fluorescence characteristics when mixed with F10 in a similar way to that with DAUDA, with a similar enhancement of fluorescence intensity and peak emission occurring at 489 nm (results not shown). The similar changes in emission spectrum of the dansyl fluorophore when positioned at either end of a fatty acid indicate that the entire ligand is taken into the protein and shielded from solvent. This is consistent with crystal and NMR structures of cLBP and other lipid-transporter proteins in complex with fatty acids or retinoids in which they are wholly internalized [39–42]. The single exception to this is liver FABP, which is unusual in binding two ligand molecules, one fully internalized and the other with its carboxylate exposed to solvent [43]. Isolation of ligand from solvent in F10 would serve to protect oxidation-sensitive (or otherwise sensitive) ligands during transport.

Several of the cLBPs bind retinol, so F10 was also tested for retinol binding by exploiting the intrinsic fluorescence of this lipid. Because retinol is highly unstable in water, the binding assay was modified: retinol was added as a solution in ethanol directly to protein solution in the fluorescence cuvette [36,44]. This yielded no evidence of binding, although control proteins (BSA, bovine β-lactoglobulin and recombinant ABA-1 allergen) all showed strong binding as manifested by a marked increase in the intensity of emission by retinol (results not shown).

Neither DAUDA nor DACA was found to bind to the deletion mutant F25 (Figure 3B). This was unexpected given that a previous deletion analysis of human intestinal FABP in which the entire helical portion of the protein was removed and replaced by a short linker peptide (rather than the deletion of only α-II as in F25) did not abrogate binding, although there was a change in the dynamics of ligand binding [26,27]. The difference between the two cases might lie in a distortion of the structure of the portal and binding cavity by F25's remaining section of helix.

Structural model

The sequence of F10 aligns well with cLBPs whose structures are known from X-ray crystallographic studies, although the amino acid sequence similarity between them is typically low for this family of proteins. These cLBPs are β-strand-rich and have ten anti-parallel β-strands forming a flattened β-barrel, with two short helices closing one end of the barrel [38,42,45]. The point of entry and exit of ligand (the portal) is thought to be between α-II and the loops between β-C and β-D, and β-E and β-F. Consistent with this are results from NMR studies showing that this region is the most flexible and becomes more ordered in the holoprotein [46]. The ligand is held within a cavity in the centre of the barrel, where it is isolated from solvent and is only in contact with structured water molecules [38,42,45].

The PHD program predicts F10 to be β-rich (6.1 % helix, 64.4 % extended/β structures and 29.5 % loop/remainder) on the basis of multiple alignments assembled from the F10 sequence and similar mammalian proteins by the MaxHom routine SwissModel was used to create a three-dimensional model based on the coordinates of four experimentally derived structures of cLBPs identified by PHD as being most similar to F10 in sequence, and another based on a multiple comparison of five known structures (Protein Data Bank accession codes 1HMR, 1PMP, 1ADL, 1ABO and 1ACD). All the models were checked by the PROCHECK suite of programs, the best proving to be that based on the five structures; all checks showed better than average geometry, and the Ramachandran plot showed 90.9 % of residues in the most favoured areas, 5.8 % in additional allowed regions, 3.3 % in generously allowed regions, 0 % in disallowed regions and an acceptable overall geometry. The protein is modelled closely on the 1HMR structure (human muscle FABP) [47]; the three-dimensional coordinates of the α-carbon atoms match to about 0.1 Å root-mean-square deviation. The model is probably therefore faithful to the structure of Sj-FABPc and the following predictions are warranted, although limited by current uncertainties inherent in structural modelling. With the use of Voidoo [48], the volume of the cavity in the protein is 968 Å^3, which is substantially larger than usually found for cLBPs. 1HMR includes several internal structured water molecules and a bound fatty-acid ligand. Removing these gives a cavity of approx. 760 Å^3, which is in the same order of magnitude as the F10 model, the difference probably arising from side-chain movements in the absence of ligand. In 1HMR the fatty-acid carboxy group draws two Arg side chains into the cavity, thus decreasing its size. In the F10 model the ligand is not present and so the Arg side chains are free to move and form interactions with the wall of the cavity, thus increasing the apparent size. There are three charged residues pointing towards the centre of the cavity; the conserved arginines described above (Arg-107 and Arg-127) seem to be in a very similar environment to that in the 1HMR structure and so probably have the same role in interacting with ligand carboxylate; Glu-79 also points towards the centre of the cavity but is in a relatively hydrophilic environment (as in 1HMR) and so, as in 1HMR, is probably not able to form strong polar interactions.

Mapping the variant sites observed for the set of Sj-FABPc sequences (Figure 1) showed that four out of eight were confined to loop regions of the molecule, with all but one of the others lying in α-II. The latter site and the turn between β-I and β-J seem to be unusally endowed with variant positions, which might be functionally significant given the strategic positions of this helix and the apposition of the β-turn to α-I. It might be pertinent that α-I is also notable for being poorly antigenic in epitope mapping experiments [11]. Most variant sites involve amino acid side chains that are modelled to be directed to the outside of the protein, the single exception being a substitution of a side chain projecting into the binding cavity (Gln-94 → His). There has so far been insufficient sampling of cLBP genes from other sources, including human cLBPs, to generalize about clustering of polymorphic sites. The variant sites known so far for human cLBPs cluster differently from those of Sj-FABPc, which might mean that the latter is under immune selection, driving a balanced polymorphism in immunologically important parts of the molecule.

α-II, but not the adjacent α-I, is unusual in possessing hydrophobic side chains that are predicted to protrude directly into solvent, rather than being directed internally. These are Trp-27 and Met-32, the former being most notable for its predicted degree of exposure and the latter being slanted towards the portal of the protein. A similarly exposed hydrophobic side chain (Phe-57) is positioned on the turn between β-C and β-D, opposing Met-32. Adipocyte lipid-binding protein also has a Phe residue in the same position as modelled for Phe-57 in Sj-FABPc; this is known from crystallography to alter its orientation markedly on the binding of ligand to the protein such that it comes to be directed into solvent.

Many proteins that bind fatty acids have a tryptophan residue in or near the binding pocket [12,39,49,50]. In some proteins (e.g.

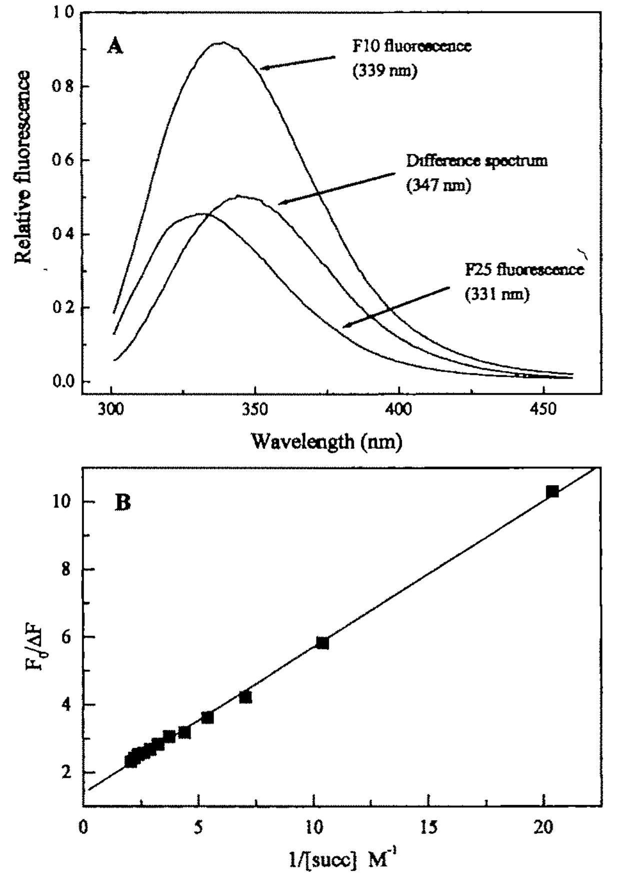

Figure 5 Heterogeneity in the solvent environments of Trp-8 and Trp-27 in the F10 protein

(**A**) Intrinsic fluorescence emission spectra of equivalent quantities of F10 and F25 proteins, with the wavelengths of peak emission as indicated, λ_{ex} was 285 nm The spectrum of F10 is a composite of the emission of Trp-8 and Trp-27, whereas that of F10 (from which Trp-8 has been deleted) is of Trp-8 only A difference spectrum (with spectra corrected for protein concentration) is also given, which approximates to the emission spectrum of Trp-27 of F10 in isolation (**B**) Modified Stern–Volmer plot [56] showing the effect on the intrinsic fluorescence emission spectrum of F10 protein after successive additions of succinimide (succ) to the fluorescence cuvette The inverse of the intercept with the $F_0/\Delta F$ axis is taken as an estimate of the proportion of Trp side chains exposed to solvent, that value here being 0 72 λ_{ex} was 285 nm

β-lactoglobulin and serum albumin), the fluorescence emission spectrum of such side chains is observed to alter on the binding of lipid, presumably through direct interaction between the tryptophan residue and the ligand, alteration in the environment of the side chain, or local changes in protein conformation [34,51,52]. F10 has two tryptophan residues, one being the putatively exposed Trp-27, the other being Trp-8, which is positioned on β-A with its side chain angled into the cavity at the opposite end to the portal. Excitation of F10 at 287 nm produced an emission spectrum that peaked at 339 nm (Figure 5) but there was no change on the addition of oleic acid (results not shown). This probably indicates that Trp-8 does not interact with ligand and that there is no change in the disposition of Trp-27 on the binding of ligand.

Unusual solvent exposure of Trp-27 adjacent to presumptive ligand portal

An unusual feature of the model is the predicted orientation of Trp-27 in projecting directly into solvent. Tryptophan side chains are usually buried within proteins unless they are in sites of interaction between a protein and a membrane or with another protein [53–55]. The predicted disposition of Trp-27 was therefore tested by intrinsic fluorescence of the protein and by succinimide quenching, a combination of which is used to discriminate between exposed and buried tryptophan side chains [56–58].

The fluorescence emission spectrum of F10 excited at 285 nm showed a maximum at 339 nm (Figure 5A). Denaturation in 6 M GdmCl to unfold the protein shifted the fluorescence emission to that expected of Trp fully exposed to solvent water (356 nm; results not shown). The availability of F25 (from which Trp-27 was absent) permitted the examination of Trp-8 in isolation; the value of 331 nm for its fluorescence emission maximum was indicative of a buried side chain (Figure 5). Subtraction of the spectra of F10 and F25 gives an emission at 347 nm, which should approximate to that of Trp-27 in isolation, assuming that the deletion in F25 had not altered the emission characteristics of Trp-8. This wavelength of emission would indicate a considerable degree of exposure to solvent water.

The solvent exposure of the Trp side chains was examined further by fluorescence quenching with succinimide. When quencher was progressively added to a solution of F10, the fluorescence emission of the protein decreased progressively, and the wavelength of maximum emission shortened (results not shown). When these results were analysed with a conventional Stern–Volmer plot, the resulting plot was non-linear. Both of these effects are indicative of differences in the solvent environments of the two tryptophan residues. Analysis with a modified Stern–Volmer plot, however, yielded a straight line (Figure 5B) with an estimate for the fraction of exposed tryptophan residues of 0.72 [56]. Taken together, these results are consistent with a distinctiveness of Trp-27 in its exposure to solvent.

The Trp-27 position in F10 is usually occupied in crystallographic structures of mammalian cLBPs by prominent hydrophobic amino acids (frequently Phe, but also Met, Leu, Ile and Val), which project directly into solvent. This applies to intestinal, brain, heart and adipocyte FABPs, among others (group 1), but not to liver FABP or ileal lipid-binding protein (LBP) (group 2) in which the Trp-27 position is occupied by a charged residue (Asp or Glu in liver FABP; Asp or Ser in ileal LBP). Liver FABP is considered to be functionally distinct from group 1 cLPBs in two respects (there is little comparable information yet for ileal LBP). First, it can hold two ligand molecules simultaneously, whereas all those proteins with prominent apolar amino acids in the 27 position hold only one, and it binds a wider range of ligand types [59]. Secondly, the group 1 human adipocyte, heart and intestinal FABPs are considered to exchange ligand by collisional contact with artificial membrane vesicles, whereas ligand must enter the aqueous phase to pass to and from liver FABP [60,61]. Moreover, also unlike liver FABP, these proteins exhibit exposed bulky hydrophobic side chains protruding from α-II and the turn between β-C and β-D, which are in similar positions to Met-32 and Phe-57 of F10. These flank the presumptive portal for ligand entry and exit in these proteins [59] and, together with the position 27 side chain, might be crucially involved in interactions between cLBPs and membranes or receptor proteins.

Site-directed mutagenesis of surface-exposed lysine residues on α-II of H-FABP and on the βC/D turn have demonstrated that these residues are important to interactions between the protein and phospholipid vesicles [29,30]. F10 has lysine residues in similar positions and orientations (Lys-22 and Lys-58). The unusual exposure of the nearby hydrophobic residues (especially at position 27) might, however, be a second feature adjacent to the portal that is important in interaction between cLBPs and cellular components. This possibility is strengthened by the existence of similarly exposed bulky hydrophobic side chains in other proteins that interact with membranes [62–64]. It is therefore feasible that Trp-27 of Sj-FABPc could be involved in transient, shallow interaction with membranes, and that similar side chains in other cLBP proteins have a similar role. There is spectroscopic evidence that tryptophan residues and simple indole analogues partition preferentially into the interfacial region of phospholipid bilayers (specificially the region that includes the glycerol backbone and the esters that link the fatty-acid chains) and that phenylalanine residues penetrate more deeply [65,66]. It could therefore be envisaged that the protruding apolar side chain dips into the membrane, whereas the external lysine residues interact with the charged head groups of membrane phospholipid. This would allow the proteins to associate with a membrane until encountering ligand dissolved in the membrane itself or a transmembrane fatty acid transporter protein.

Could the protruding apolar side chains instead be involved in protein–protein interactions? Examples in which isolated, protruding bulky hydrophobic residues are crucial to protein–protein interactions would include the phenylalanine residue involved in 43% of the intermolecular interactions between CD4 of the human lymphocyte surface and gp120 of HIV [67]. Of pertinence to cLBPS, it has recently been demonstrated that adipocyte lipid-binding protein interacts with hormone-sensitive lipase and possibly also with lipid droplets with which the lipase associates [68]. It might therefore be that the site on adipocyte lipid-binding protein at which this takes place involves the phenylalanine residue of adipocyte lipid-binding protein that replaces the Trp-27 of F10.

It is only in the cLBPs of schistosomes and nematodes that the 27 position is held by a tryptophan residue, so F10 could prove to be of value in the fluorescence-based investigation of interactions between cLBPs and membranes or (membrane) proteins, as has been exploited for the study of amphipathic peptides interacting with artifical membrane vesicles [69]. If the Trp-27 feature is predictive of function, then Sj-FABPc might be one with the cLBPs that actively transfer proteins within the cytoplasm rather than acting as a holding/storage proteins, as liver FABP is thought to do [27,59,60]. The fact that both Sj-FABPc and adipocyte lipid-binding protein both seem to associate with lipid droplets [9,68] might also be more than mere coincidence.

In Glasgow, we are indebted to Lindsay McDermott, Jamie Crawford and Alan Cooper for assistance with the ligand binding assays and their analysis, and to Alan Cooper and Judith Storch of Rutgers University for valuable discussions We thank Mary Duke for excellent technical support in Brisbane, and also Sharon Kelly and Nicholas Price at the BBSRC-funded CD facility at Stirling University for performing the CD analysis This work was funded by a grant (number 044156) from the Wellcome Trust to M W K and Alan Cooper We also acknowledge the financial support of the Cooperative Research Centre for Vaccine Technology, the National Health and Medical Research Council of Australia and the UNDP/World Bank/WHO Special Programme for Research and Training in Tropical Diseases

REFERENCES

1 Wiest, P M, Wu, G, Zhang, S, Yuan, J, Peters, P A S, McGarvey, S T, Tso, M, Olveda, R and Olds, G R (1992) Morbidity due to schistosomaisis japonica in the People's Republic of China Trans R Soc Trop Med Hyg **86**, 47–50

2 Brouwers, J. F. H M., Smeenk, I M B., van Golde, L M G and Tielens, A G M (1997) The incorporation, modification and turnover of fatty acids in adult *Schistosoma mansoni*. Mol Biochem Parasitol. **88**, 175–185

3 Brouwers, J F H M, Skelly, P J and van Golde, L M G, Tielens, A G M (1999) Studies on phospholipid turnover argue against sloughing of tegumental membranes in adult *Schistosoma mansoni* Parasitology **119**, 287–294

4 Meyer, F, Meyer, H and Bueding, E (1970) Lipid metabolism in the parasitic and free-living flat worms *Schistosoma mansoni* and *Dugesia dorotocephala* Biochim Biophys Acta **210**, 256–266

5 McLaren, D J and Hockley, D J (1977) Blood flukes have a double outer membrane Nature (London) **269**, 147–149

6 Becker, M M, Kalinna, B H, Waine, G J and McManus, D P (1994) Gene cloning, overproduction and purification of a functionally active cytoplasmic fatty acid-binding protein (Sj-FABPc) from the human blood fluke *Schistosoma japonicum* Gene **148**, 321–325

7 Moser, D, Tendler, M, Griffiths, G and Klinkert, M-Q (1991) 14-kDa *Schistosoma mansoni* polypeptide is homologous to a gene family of fatty acid binding proteins J Biol Chem **266**, 8447–8454

8 Bergquist, N R. and Colley, D G (1998) Schistosomiasis vaccines research and development Parasitol Today **14**, 99–104

9 Gobert, G N, Stenzel, D J, Jones, M K and McManus, D P (1997) Immunolocalisation of the fatty acid-binding protein Sj-FABPc within adult *Schistosoma japonicum* Parasitology **115**, 33–39

10 Tendler, M, Brito, C A., Vilar, M M, Serra-Freire, N, Diogo, C M, Almeida, M S, Delbem, A C B, Figueiredo da Silva, J, Savino, W, Garratt, R C et al (1996) A *Schistosoma mansoni* fatty acid binding protein, Sm-14, is the potential basis of a dual-purpose anti-helminth vaccine Proc Natl Acad Sci U S A **93**, 269–273

11 Waine, G J, Scott, J C, Mazzer, D and McManus, D P (1998) Mapping of linear epitopes on the 14-kDa fatty-acid binding protein of Chinese *Schistosoma japonicum* Int J Parasitol **28**, 303–308

12 Zimmerman, A W, Rademacher, M, Ruterjans, H, Lucke, C and Veerkamp, J H (1999) Functional and conformational characterization of new mutants of heart fatty acid-binding protein Biochem J **344**, 495–501

13 Provencher, S W and Glockner, J (1981) Estimation of globular protein secondary structure from circular dichroism Biochemistry **20**, 33–37

14 Gill, S. C. and von Hippel, P H (1989) Calculation of protein extinction coefficients from amino acid sequence data Anal Biochem **182**, 319–326

15 Haughland, R. P. (1992) Handbook of Fluorescent Probes and Research Chemicals, Molecular Probes, Eugene, OR

16 Rost, B (1996) PHD predicting one-dimensional protein structure by profile based neural networks Methods Enzymol. **266**, 525–539

17 Rost, B and Sander, C (1993) Prediction of protein structure at better than 70% accuracy. J Mol Biol **232**, 584–599

18 Rost, B and Sander, C (1994) Combining evolutionary information and neural networks to predict protein secondary structure Proteins **19**, 55–72

19 Guex, N., Diemand, A and Peitsch, M C (1999) Protein modelling for all Trends Biochem Sci **24**, 364–367

20 Brunger, A T (1987) X-PLOR Manual, version 3 1, Yale University Press, New Haven, CT

21 Nielsen, H, Engelbrecht, J, Brunak, S and von Heijne, G (1997) Identification of prokaryotic and eukaryotic signal peptides and prediction of their cleavage sites Protein Eng **10**, 1–6

22 Mei, B., Kennedy, M W, Beauchamp, J, Komuniecki, P R and Komuniecki, R (1997) Secretion of a novel, developmentally regulated fatty acid binding protein into the perivitelline fluid of the parasitic nematode, *Ascaris suum* J Biol Chem. **272**, 9933–9941

23 Plenefisch, J, Xiao, H, Mei, B., Geng, J, Komuniecki, P R and Komuniecki, R (2000) Secretion of a novel class of iFABPs in nematodes coordinate use of the *Ascaris/Caenorhabditis* model systems Mol Biochem Parasitol **105**, 223–236

24 Buelt, M K, Shekels, L L, Jarvis, B W and Bernlohr, D. A (1991) In vitro phosphorylation of the adipocyte lipid-binding protein (p15) by the insulin receptor effects of fatty acid on receptor kinase and substrate phosphorylation J Biol Chem **266**, 12266–12271

25 Buelt, M. K, Xu, Z, Banaszak, L J and Bernlohr, D A. (1992) Structural and functional characterization of the phosphorylated adipocyte lipid-binding protein (pp15). Biochemistry **31**, 3493–3499

26 Cistola, D P, Kim, K, Rogl, H and Frieden, C (1996) Fatty acid interactions with a helix-less variant of intestinal fatty acid-binding protein Biochemistry **35**, 7559–7565

27 Corsico, B, Cistola, D P, Frieden, C and Storch, J (1998) The helical domain of intestinal fatty acid binding protein is critical for collisional transfer of fatty acids to phospholipid membranes Proc Natl Acad Sci U S A **95**, 12174–12178

28 Kim, K, Cistola, D P and Frieden, C (1996) Intestinal fatty acid-binding protein the structure and stability of a helix-less variant Biochemistry **35**, 7553–7558

29 Herr, F H, Matarese, V., Bernlohr, D A and Storch, J (1995) Surface lysine residues modulate the collisional transfer of fatty acid from adipocyte fatty acid binding protein to membranes Biochemistry **34**, 11840–11845

30 Herr, F M, Aronson, J and Storch, J (1996) Role of portal lysine residues in electrostatic interactions between heart fatty acid binding protein and phospholipid membranes Biochemistry **35**, 1296–1303

31 Wilton, D C (1990) The fatty acid analogue 11-(dansylamino)undecanoic acid is a fluorescent probe for the bilirubin-binding sites of albumin and not the high affinity fatty acid-binding sites Biochem J **270**, 163–166

32 Wilkinson, T C I and Wilton, D C (1986) Studies on fatty acid-binding proteins The detection and quantification of the protein from rat liver using a fluorescent fatty acid analogue. Biochem J **238**, 419–424

33 Thumser, A E A, Evans, C., Worrall, A F. and Wilton, D C (1994) Effect on ligand binding of arginine mutations in recombinant rat liver fatty acid-binding proteins Biochem J **297**, 103–107

34 Kennedy, M W, Brass, A, McCruden, A B, Price, N C, Kelly, S. M and Cooper, A (1995) The ABA-1 allergen of the parasitic nematode *Ascaris suum* fatty acid and retinoid binding function and structural characterization Biochemistry **34**, 6700–6710

35 Kennedy, M W., Britton, C, Price, N C, Kelly, S M and Cooper, A (1995) The DvA-1 polyprotein of the parasitic nematode *Dictyocaulus viviparus* a small helix-rich lipid-binding protein J Biol Chem **270**, 19277–19281

36 Kennedy, M W, Garside, L H, Goodrick, L E, McDermott, L, Brass, A, Price, N C, Kelly, S M, Cooper, A and Bradley, J E (1997) The Ov20 protein of the parasitic nematode *Onchocerca volvulus* A structurally novel class of small helix-rich retinol-binding protein J Biol Chem. **272**, 29442–29448

37 Macgregor, R B and Weber, G (1986) Estimation of the polarity of the protein interior by optical spectroscopy Nature (London) **319**, 70–73

38 Veerkamp, J H, van Moerkerk, H T B., Prinsen, C F. M and van Kuppevelt, T H (1999) Structural and functional studies on different FABP types Mol. Cell Biochem **192**, 137–142

39 Papiz, M Z, Sawyer, L, Eliopoulos, E. E, North, A C. T, Findlay, J B C, Sivaprasadarao, R, Jones, T. A, Newcomer, M. E and Kraulis, P J (1986) The structure of beta-lactoglobulin and its similarity to plasma retinol-binding protein Nature (London) **324**, 383–385

40 LaLonde, J M, Levenson, M A, Roe, J. J, Bernlohr, D A and Banaszak, L. J. (1994) Adipocyte lipid-binding protein complexed with arachidonic acid titration calorimetry and X-ray crystallographic studies J Biol Chem **269**, 25339–25347

41 Wu, S-Y, Perez, M D, Puyol, P and Sawyer, L (1999) β-Lactoglobulin binds palmitate within its central cavity J Biol Chem **274**, 170–174

42 Coe, N R and Bernlohr, D A (1998) Physiological properties and functions of intracellular fatty acid-binding proteins Biochim Biophys Acta **1391**

43 Thompson, J, Winter, N, Terwey, D, Bratt, J and Banaszak, L (1997) The crystal structure of the liver fatty acid-binding protein a complex with two bound oleates J Biol Chem **272**, 7140–7150

44 Cogan, U, Kopelman, M, Mokady, S and Shinitzky, M (1976) Binding affinities of retinol and related compounds to retinol binding proteins. Eur. J Biochem **65**, 71–78

45 Sacchettini, J C and Gordon, J I (1993) Rat intestinal fatty acid binding protein. a model system for analyzing the forces that can bind fatty acids to proteins J Biol Chem **268**, 18399–18402

46 Hodsdon, M E and Cistola, D P (1997) Ligand binding alters the backbone mobility of intestinal fatty acid-binding protein as monitored by ^{15}N NMR relaxation and ^{1}H exchange Biochemistry **36**, 2278–2290

47 Zanotti, G, Scapin, G, Spadon, P, Veerkamp, J H. and Sacchettini, J C. (1992) Three-dimensional structure of recombinant human muscle fatty acid-binding protein J Biochem (Tokyo) **267**, 18541–18550

48 Kleywegt, G T and Jones, T A (1994) Detection, delineation, measurement and display of cavities in macromolecular structures Acta Crystallogr D **50**, 178–185

49 Curry, S, Mandelkow, H, Brick, P and Franks, N (1998) Crystal structure of human serum albumin complexed with fatty acid reveals an asymmetric distribution of binding sites Nat. Struct Biol **5**, 827–835

50 He, X. M and Carter, D C (1992) Atomic structure and chemistry of human serum albumin Nature (London) **358**, 209–215

51 Frapin, D, Dufour, E and Haertle, T (1993) Probing the fatty acid binding site of β-lactoglobulins J Protein Chem **12**, 443–449

52 Thumser, A E and Wilton, D C. (1994) Characterization of binding and structural properties of rat liver fatty-acid-binding protein using tryptophan mutants Biochem J **300**, 827–833

53 Bogan, A A and Thorn, K S. (1998) Anatomy of hot spots in protein interfaces J Mol Biol **280**, 1–9

54 Janin, J (1979) Surface and inside volumes in globular proteins Nature (London) **277**, 491–492

55 Rose, G., Geselowitz, A, Lesser, G, Lee, R and Zehfus, M (1985) Hydrophobicity of amino acid residues in globular proteins Science **229**, 834–838

56 Lehrer, S S (1971) Solute perturbation of protein fluorescence The quenching of the tryptophyl fluorescence of model compounds and of lysozyme by iodide ion Biochemistry **10**, 3254–3263

57 Eftink, M R and Ghiron, C A (1976) Exposure of tryptophanyl residues in proteins quantitative determination by fluorescence quenching studies Biochemistry **15**, 672–679

58 Eftink, M R and Ghiron, C A (1984) Indole fluorescence quenching studies on proteins and model systems use of the efficient quencher succinimide Biochemistry **23**, 3891–3899

59 Bernlohr, D A, Coe, N R and LiCata, V J. (1999) Fatty acid trafficking in the adipocyte. Cell Dev Biol **10**, 43–49

60 Hsu, K-T and Storch, J (1996) Fatty acid transfer from liver and intestinal fatty acid-binding proteins to membranes occurs by different mechanisms J Biol Chem **271**, 13317–13323

61 Storch, J and Bass, N M (1990) Transfer of fluorescent fatty acids from liver and heart fatty acid-binding proteins to model membranes J Biol Chem **265**, 7827–7831

62 Gelb, M H, Cho, W and Wilton, D C (1999) Interfacial binding of secreted phospholipase A_2: more than electrostatics and a major role for tryptophan Curr Opin Struct Biol **9**, 428–432

63 Doyle, D A, Cabral, J M, Pfuetzner, R A, Kuo, A., Gulbis, J M, Cohen, S L, Chait, B T and MacKinnon, R. (1998) The structure of the potassium channel molecular basis of K^{+} conduction and selectivity Science **280**, 69–77

64 Baker, S F, Othman, R and Wilton, D C. (1998) Tryptophan-containing mutant of human (Group IIa) secreted phospholipase A_2 has a dramatically increased ability to hydrolyze phosphatidylcholine vesicles and cell membranes Biochemistry **37**, 13203–13211

65 Kachel, K, Asuncionpunzalan, E and London, E (1995) Anchoring of tryptophan and tyrosine analogs at the hydrocarbon polar boundary in model membrane-vesicles – parallax analysis of fluorescence quenching induced by nitroxide-labelled phospholipids Biochemistry **34**, 15475–15479

66 Yau, W M, Wimley, W C, Gawrisch, K and White, S H (1998) The preference of tryptophan for membrane interfaces Biochemistry **37**, 14713–14718

67 Kwong, P. D, Wyatt, R, Robinson, J, Sweet, R W, Sodroski, J and Hendrickson, W. A (1998) Structure of an HIV complex with the CD4 receptor and a neutralizing human antibody Nature (London) **393**, 648–659

68 Shen, W-E, Sridhar, K, Bernlohr, D A and Kraemer, F B (1999) Interaction of rat hormone-sensitive lipase with adipocyte lipid-binding protein Proc Natl Acad Sci U S A. **96**, 5528–5532

69 Perez-Mendez, O, Vanloo, B, Decout, A, Goethals, M, Peelman, F, Vandekerckhove, J, Brasseur, R and Rosseau, M (1998) Contribution of the hydrophobicity gradient of an amphipathic peptide to its mode of association with lipids Eur J Biochem. **256**, 570–579

70 Evans, S V (1993) SETOR Hardware lighted three-dimensional solid model representations of macromolecules. J Mol Graphics **11**, 134–138

Received 9 February 2000/30 March 2000, accepted 17 April 2000

Essential Reading from Portland Press

Portland Press

The Biology of Nitric Oxide Part 7

Edited by S Moncada, Cruciform Project, London, UK, L Gustafsson, Karolinska Institute, Stockholm, Sweden, P Wiklund, Karolinska Hospital, Stockholm, Sweden and EA Higgs, Cruciform Project, London, UK

1 85578 142 5 Hardback March 2000 400 pages £110.00

The proceedings of the *Sixth International Meeting on the Biology of Nitric Oxide* held at Stockholm, Sweden on 5-8 September 1999.

This book provides an up-to-date overview of the current status of the field with contributions from over 400 specialists covering the following areas:

Molecular Biology, Biochemistry, Physiology, Pathophysiology, Inflammation, Tumours, Apoptosis, Novel Compounds and Clinical Aspects.

Nitric Oxide and the Peripheral Nervous System

Edited by N Toda, Shiga University of Medical Science, Ohtsu, Japan, S Moncada, Cruciform Project, London, UK, R Furchgott, State University of New York, USA and EA Higgs, Cruciform Project, London, UK

1 85578 139 5 Hardback June 2000 200 pages £85.00

This volume provides an overview of NO in the peripheral nervous system, covering aspects ranging from the molecular biology and distribution of neuronal nitric oxide synthase, through the physiological and pathophysiological roles of NO in various nitrergic systems (systems of nerves whose transmitter function depends on the release of NO).

Potential therapies that may arise from our increasing knowledge of this fascinating field of research are also reviewed.

Eicosanoids and Related Compounds in Plants and Animals

Edited by AF Rowley, University of Wales, Swansea, UK, H Kühn, Humboldt University of Berlin, Germany, and T Schewe, Free University of Berlin, Germany

1 85578 108 5 Hardback October 1998 240 pages £65.00

This book provides an up-to-date overview of the nature, modes of biosynthesis, and functions of eicosanoids and related compounds in plants and animals.

This volume draws together, for the first time, overviews describing the importance of eicosanoids in plants and animals. No other volume has attempted to consolidate such a diverse approach in a single volume. The uniformity of presentation is an unusual feature with the volume divided into two main sections: biochemical and functional sections. The first section deals with the diversity of eicosanoids generated and the nature of the enzymes and other factors associated with their biosynthesis. The second deals largely with the more functional aspects of eicosanoids. The volume should be of great interest to researchers in diverse fields including lipid biochemistry, molecular evolution, plant and animal physiology, and general biology.

Landmarks in Intracellular Signalling

Edited by RD Burgoyne and OH Petersen, University of Liverpool, UK

1 85578 101 8 Paperback 1997 278 pages £20.00

The idea behind Landmarks in Intracellular Signalling is to provide full reproductions of a set of key papers which have been chosen as landmark papers in the various aspects of intracelllular signalling. The selected papers have all resulted in significant advances in one or other aspect of intracellular signalling.

Readers of *Landmarks in Intracellular Signalling* will now have easy, ready available access to the original literature from one source. The papers are accompanied by commentaries that describe why the papers were significant, how the work came about and summarize the advances that have been made up to the present time as a consequence of the original paper.

Orders:
www.portlandpress.co.uk/books/orderinfo.htm

*Portland Press, Commerce Way,
Colchester, CO2 8HP
t: 01206 796351
f: 01206 799331
e: sales@portlandpress.co.uk

Please add £2.50 per book to a maximum of £7.50

In the USA and Canada
Princeton University Press
c/o California/Princeton Fulfillment Services, Inc
1445 Lower Ferry Road,
Ewing, New Jersey 08618
t: 1-800-777-4726
f: 1-800-999-1958
e: orders@cpfs.pupress.princeton.edu

Postage: Please add $3.75 for first book and US$1.00 for each additional book

BXT/0500/E

Essential Life Sciences Online

Biochemical Journal

Chairman of Editorial Board: ***Peter Parker*** *(ICRF, London, UK)*

http://www.BiochemJ.org

The Biochemical Journal is available online offering many additional advantages:

- **New** – Every year in January the online content for the previous years will become free • Published online one week early • Electronic multi-media adjuncts • Medline and Inter-journal linking

Subscription – 2000: Volumes 345–352 (24 issues)
North America: US$1950.00 Rest of World: £1110.00

Biotechnology and Applied Biochemistry

Editor-in-Chief: ***Roger Lundblad*** *(Chapel Hill, USA)*

http://bab.portlandpress.com

In addition to the features of the Biochemical Journal Online, the full text of papers for *Biotechnology & Applied Biochemistry* are now published online as soon as they are ready, several weeks before the printed edition.

It includes scholarly articles and reviews concerning the expression, purification, characterization and application of biological macromolecules in therapeutics and diagnostics.

Subscription – 2000: Volumes 31–32 (6 issues)
North America: US$250.00 Rest of World: £143.00

Clinical Science

Editor-in-Chief: ***Kim Bartlett*** *(Newcastle-upon-Tyne, UK); Associate Editor Americas:* ***Aubrey Taylor*** *(Mobile, USA); Associate Editor Pacific Rim:* ***Stephen Harrap*** *(Melbourne, Australia)*

http://cs.portlandpress.com

Full access to online papers from 1998, abstracts from 1997 plus full text of papers published online as soon as they are ready.

Publishes articles and reviews on all aspects of clinical investigation, including biochemical, physiological, immunological, cellular, molecular biological and other approaches of relevance to disease in man.

Subscription – 2000: Volumes 98–99 (12 issues)
North America: US$525.00 Rest of World: £290.00

Biochemical Society Transactions

http://bst.portlandpress.com

Missed the Biochemical Society Meeting? - Don't Miss the Science

The Biochemical Society's conferences bring together some of the best biochemical and life-science research by international speakers. *Biochemical Society Transactions* contains the scientific reports and poster abstracts from these meetings. The prestigious medal lectures are also published.

New for 2000 full papers will be published online as well as speaker abstracts.

Subscription - 2000: Volume 28 (6 parts)
North America: US$305.00 Rest of World: £178.00

Free to subscribers

Full free online access to the current year of these journals is restricted to institutions that have a subscription to the printed version. Ask your subscribing library to contact us to ensure you have access to papers in these online journals as soon as they are available.

Contact: support@portlandpress.com

Portland Press

Back

Next

.pdf

Home

Join the email current awareness service for these important journals

Enquiries to:

Portland Press Ltd,
59 Portland Place,
London W1N 3AJ
Tel: +44 020 7580 5530
Fax: +44 020 7323 1136
sales@portlandpress.com
www.portlandpress.com

Portland Press is the not-for-profit subsidiary of the Biochemical Society publishing journals and books in the life sciences.

BVV/0200/S

Printed in Great Britain by the University Press, Cambridge

BIJOAK 349(2) 385-656 2000 • ISSN 0264-6021
Volume 349 • Part 2 • 15 July 2000

BIOCHEMICAL JOURNAL

review

Sphingosine 1-phosphate signalling in mammalian cells

by S. Pyne
and N. J. Pyne

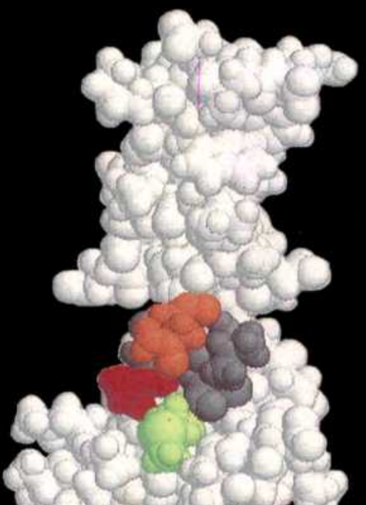

Available 1 week earlier on the Internet

The Biochemical Society, London © 2000

Essays in Biochemistry
from Portland Press

Portland Press

Essays in Biochemistry: Molecular Trafficking

Edited by P Bernstein, The Journal of Experimental Medicine, New York, USA

1 85578 131 X Paperback July 2000 200 pages £19.00

This volume of Essays in Biochemistry is a collection of review articles describing how molecules (proteins and nucleic acids) are targeted to, and transported across, various membrane-bound organelles within eukaryotic cells.

The 1999 Nobel Prize in Physiology or Medicine was awarded to Dr Gunter Blobel "for the discovery that proteins have intrinsic signals that govern their transport and localization in the cell". The award acknowledges the importance of the study of how newly synthesized protein and RNA find their correct destination within the cell. This volume summarises advances being made in this field of research.

Students (and their teachers) who are undertaking advanced studies in cell biology will find this book extremely useful.

Essays in Biochemistry: Molecular Motors

Edited by SJ Higgins, University of Leeds, UK and G Banting, University of Bristol, UK

1 85578 103 4 Paperback March 2000 200 pages £19.00

Biological systems abound with examples of molecular motors — biological machines for converting the chemical energy of ATP into mechanical movement by cells — they play pivotal roles in diverse cellular function.

This volume, covers many of the most exciting developments in the field.

- All of the main motor systems are featured, giving wide coverage.
- Consists of short punchy review articles, making it easy to read.
- The application of gene-cloning methods and the recent advances are described.
- Human disorders involving defects in molecular motor systems such as hearing loss and heart disease are covered.

The Nobel Prize for Chemistry was awarded to John Walker and Paul Boyer in 1997 for their work in elucidating the mechanism of the rotary generator of ATP in the mitochondrion, the F_1-ATPase. This brought the new developments in the field of molecular motors to the attention of the whole scientific community and, via the media, to a wider world audience.

This volume aims to inspire young scientists to want to work in this area.

Essays in Biochemistry: Metalloproteins

Edited by D Ballou, University of Michigan, USA

1 85578 106 9 Paperback July 1999 200 pages £19.00

Metals are involved in most segments of the chemistry of life, including respiration, numerous steps of metabolism, photosynthesis, nitrogen fixation, nerve transmission, signal transduction, muscle contraction, oxygen transport and protection from xenobiotic compounds. In addition, metals are used in medicine as therapeutic agents. This volume describes many of the roles of metals in a variety of circumstances that are used widely in biology.

The 12 chapters of this volume are written by several of the best-known experts in their specialities.

Essays in Biochemistry: Gene Regulation

Edited by K Chapman, The University of Edinburgh, UK

1 85578 138 7 Paperback October 2000 200 pages £19.00

Contents: Transcriptional regulation, a unifying mechanism, M Ptashne and A Gann; Regulation of eukaryotic transcription initiation, G Gill; Activation and repression of transcription initiation in bacteria, G Lloyd, P Landini and S Busby; Signalling from the cell surface to the nucleus, M Lee and S Goodbourn; Cell cycle control of transcriptional activity, N La Thangue and N Shikama; Transcriptional regulation in the context of chromatin structure, A Wolffe; Methylation in the control of gene expression in vertebrate development, R Meehan and I Stancheva; Translational control in the regulation of gene expression, C Proud; Cellular choices: to die or not to die, D Harrison; Future perspectives, N Hastie

Orders:

www.portlandpress.com/books/orderinfo.htm

***Portland Press, Commerce Way,**
Colchester, CO2 8HP
t: 01206 796351
f: 01206 799331
e: sales@portlandpress.com

Please add £2.50 per book to a maximum of £7.50

In the USA and Canada
Princeton University Press
c/o California/Princeton Fulfillment Services, Inc
1445 Lower Ferry Road,
Ewing, New Jersey 08618
t: 1-800-777-4726
f: 1-800-999-1958
e: orders@cpfs.pupress.princeton.edu

Postage: Please add $3.75 for first book and $1.00 for each additional book

BXS/0500/E

Bio Chemical Sc

Biochemical Journal

The Biochemical Society, London © 2000

Volume 349, part 2
15 July 2000

First published on the Internet
10 July 2000
http://www.BiochemJ.org

Editorial Board

Chairman
P. J. Parker • London

Deputy Chairmen
G. E. Blair • Leeds
D. N. Brindley • Edmonton
R. A. J. Challiss • Leicester
P. Ferré • Paris
J. T. Gallagher • Manchester
R. A. John • Cardiff
H. Nagase • London
J. D. Pearson • London
M. H. Rider • Bruxelles
S. B. Shears • Research Triangle Park

Reviews Editor
~~**R. D. Burgoyne** • Liverpool~~

Managing Editor
P. J. Starley

Deputy Managing Editor
S. E. Dilley

Senior Staff Editor
S. M. Hobday

Staff Editors
L. Johnson
W. J. Watkins
M. R. Thorne
N. B. Prowse
S. J. Cuble

Editorial Assistants
N. J. Lamb
C. L. Jeeves

R. L. P. Adams (Glasgow)
J.-W. N. Akkerman (Utrecht)
D. R. Alessi (Dundee)
D. Attaix (Ceyrat)
S. A. Baldwin (Leeds)
F. J. Ballard (Adelaide)
G. J. Barritt (Adelaide)
N. C. Bruce (Cambridge)
A. Clerk (London)
G. M. Cohen (Leicester)
P. Crine (Montreal)
D. Cutler (London)
D. A. Day (Nedlands)
H. Deckmyn (Kortrijk)
K. Docherty (Aberdeen)
B. K. Drøbak (Norwich)
J. M. East (Southampton)
K. R. F. Elliott (Manchester)
B. Engelmann (Munich)
C. Forest (Meudon)
M. J. Fry (Reading)
A. Galione (Oxford)
D. A. F. Gillespie (Glasgow)
S. Goodbourn (London)
G. W. Gould (Glasgow)
S. V. Graham (Glasgow)
S. Gutteridge (Newark, DE)
Y. A. Hannun (Charleston)

P. I. Haris (Leicester)
M. M. Harnett (Glasgow)
J. D. Hayes (Dundee)
P. C. Heinrich (Aachen)
R. Heinrich (Berlin)
B. Henrissat (Marseille)
R. C. Hider (London)
S. High (Manchester)
M. B. Hodgins (Glasgow)
D. Hoekstra (Groningen)
N. M. Hooper (Leeds)
E. F. Hounsell (London)
W. Jessup (Sydney)
J. P. Kehrer (Austin)
K. I. Kivirikko (Oulu)
B. L. Knight (London)
R. G. Knowles (Stevenage)
H. Kresse (Munster)
P. W. Kuchel (Sydney)
C. MacKintosh (Dundee)
A. I. Magee (London)
T. J. Mantle (Dublin)
P. Maurel (Montpellier)
A. J. Meijer (Amsterdam)
F. Michelangeli (Birmingham)
G. Milligan (Glasgow)
B. P. Morgan (Cardiff)
J. S. Mort (Montreal)

S. E. Moss (London)
K. J. Murray (Harlow)
A. C. Newby (Bristol)
F. Paltauf (Graz)
N. J. Pyne (Glasgow)
C. I. Ragan (Windlesham)
P. R. Rich (London)
N. J. P. Ryba (Bethesda)
G. Salvesen (San Diego)
M. F. Scully (London)
S. Shenolikar (Durham, NC)
A. G. Smith (Cambridge)
M. C. Sugden (London)
P. H. Sugden (London)
R. Sundler (Lund)
J. M. Tavaré (Bristol)
K. F. Tipton (Dublin)
M. A. Titheradge (Brighton)
A. B. Tobin (Leicester)
S. A. Tooze (London)
W. J. van Blitterswijk (Amsterdam)
R. Virden (Newcastle upon Tyne)
H. M. Wallace (Aberdeen)
M. P. Walsh (Calgary)
L. A. Witters (Hanover)
J. F. Woessner (Miami)
S. J. Yeaman (Newcastle upon Tyne)
S. Yoshikawa (Akoh-Hyogo)

- The *Biochemical Journal* (ISSN 0264-6021 for print journal; ISSN 1470-8728 for online journal) is published and distributed by Portland Press Ltd on behalf of the Biochemical Society, and appears twice monthly
- **Editorial and publishing offices:** *Biochemical Journal*, 59 Portland Place, London W1N 3AJ, U.K.
- Royal Mail International, c/o Yellowstone International, 87 Burlews Court, Hackensack, NJ 07061, U.S.A.
- **Subscriptions department:** Portland Press Ltd, P.O. Box 32, Commerce Way, Colchester CO2 8HP, U.K.

- All rights reserved. Apart from any fair dealing for the purposes of research or private study, or criticism or review, as permitted under the Copyright, Designs and Patents Act, 1988, this publication may be reproduced, stored or transmitted, in any forms or by any means, only with the prior permission in writing of the publishers, or in the case of reprographic reproduction in accordance with the terms of permissions granted by copyright clearing houses such as the Copyright Licensing Agency (U.K.) or the Copyright Clearance Center (U.S.A.). The CCC item-fee code for this publication is 0264-6021/2000/$16.00+0.00. Inquiries concerning reproduction outside those terms should be sent to the publishers at the above-mentioned address.
- Although, at the time of going to press, the information contained in this publication is believed to be correct, neither the authors nor the editors nor the publisher assume any responsibility for any errors or omissions herein contained

- Periodicals postage paid at Rahway, NJ, and at additional mailing offices
- **Postmaster:** send address changes to *Biochemical Journal*, c/o Mercury International, 365 Blair Road, Avenel, NJ 07001
- **Cover illustration:** Space-filling representation of the solvent accessible structure of human epidermal growth factor [see van de Poll et al. (2000) Biochem. J. **349**, 267–274, and http://www.BiochemJ.org/349/bj3490267add.htm].

Instructions to Authors

● **General policy** The *Biochemical Journal* publishes papers in English in all fields of biochemistry and cellular and molecular biology, provided that they make a sufficient contribution to biochemical knowledge Papers may include new results obtained experimentally, descriptions of new experimental methods of biochemical importance, or new interpretations of existing results Novel theoretical contributions will be considered equally with papers dealing with experimental work All work presented should have as its aim the development of biochemical concepts rather than the mere recording of facts Preliminary, confirmatory or inconclusive work will not be published The *Biochemical Journal* will not publish material that has been wholly or largely published elsewhere, even as a preliminary communication or in unrefereed symposium proceedings or on the World Wide Web (WWW), equally, fragmentation of research into the 'least publishable unit' is discouraged

Submission of a paper implies that it has been approved by all the named authors, that all persons entitled to authorship have been so named, that it reports unpublished work that is not under consideration elsewhere, and that if the paper is accepted for publication the authors will transfer to the Biochemical Society the copyright in the paper, which will then not be published elsewhere in the same form, in any language, without the consent of the Society Authors will be required to sign an undertaking to these effects

Authors may suggest potential reviewers for their papers, but the journal is under no obligation to follow such suggestions Authors may also specify the names of those they wish to be excluded from the review process, and such wishes are usually respected unless, in the opinion of the journal, such a request unreasonably excludes all the expertise available to it in that scientific area

To allow the reviewers to assess possible overlap with previous work, all submitted papers must be accompanied by duplicate copies of the author's relevant published work, including that on the WWW, and of all related papers in press or under editorial consideration in this or other journals

The paragraphs below are a summarized version of the journal's complete Instructions to Authors (see http //www BiochemJ org), copies of which are available free of charge from the editorial office

The following types of paper are included in the journal

Research Papers are the normal form of publication, and may be of any length that is justified by their content However, because of pressure for space in the journal, no paper, whatever its scientific merits, will be accepted if it exceeds the minimum length required for precision in describing the experiments and clarity in interpreting them As a guide, most Research Papers published in the *Biochemical Journal* are of between six and eight printed pages A concise well-written paper tends to be published more rapidly

Research Communications are short (maximum four printed pages) papers bringing particularly novel and significant findings to the attention of the research community It is intended that a decision on acceptance or rejection will be made within 10 working days of receipt, and publication of accepted Communications will follow within 2 months Research Communications receive full but accelerated reviewing The criteria of 'novelty and significance' are strictly enforced, and papers may be rejected solely on the grounds of lack of novelty and significance Communications are not a path to accelerated publication of sound but non-urgent material Authors must include in their letter of submission a brief statement of why they believe their Communication merits accelerated treatment Papers reporting nucleotide sequences only are not acceptable as Research Communications One colour figure will be published free of charge in Research Communications, subsequent figures will cost £300 each

Reviews will usually be solicited, although unsolicited reviews will be considered for publication Prospective writers of reviews should first consult the Reviews Editor, via the editorial office, and should enclose a short (one typed page) summary of the area they propose to cover

● **Procedure for submission** Before preparing papers for the journal, authors should consult a current issue to make themselves familiar with the general format, such as the use of cross-headings, layout of tables and figures and citation of references A full page of text in the *Biochemical Journal* contains approximately 1200 words, when calculating the printed length of papers, allowance must be made for the space occupied by tables and figures and the number of text words reduced accordingly

The numerical system of references must be used. A reference to 'unpublished work' must be accompanied by the names of all persons concerned, a reference to a 'personal communication' must be supported by written permission for the quotation from the person or persons concerned; both of these types of citation are permitted in the text only, not in the list of references

Three copies of the typescript (four copies for Research Communications), with a brief covering letter to which should be attached an additional copy of the synopsis, should be sent to · **The Managing Editor, *Biochemical Journal*, 59 Portland Place, London W1N 3AJ, U.K.** (telephone 020 7637 5873, fax 020 7323 1136, from overseas the international code for the U K is 44 and the leading 0 should be omitted, e-mail editorial@portlandpress com)

The typescript should indicate the name, address, telephone number, fax number and e-mail address of the person to whom all correspondence should be addressed The top copy of the typescript should be marked as such and should have attached to it the original figures, for the other copies of the typescript, glossy prints (not photocopies) of the half-tone figures should be provided, but photocopies of line drawings will suffice A short (page-heading) title of not more than 75 characters and a maximum of five key words that do not appear in the title, should be provided

● **Submission by fax** Research Communications that do not contain half-tone or colour figures may be submitted by fax to the number above Only one copy of the typescript need be transmitted The current Instructions to Authors contains full details of this procedure

● **Electronic submission** Manuscripts may be submitted as a **single** Adobe Acrobat PDF file either (i) as a uuencoded attachment to the e-mail address editorial@portlandpress com, or (ii) uploaded to the ftp site ftp portlandpress com in the directory /incoming/BiochemJ [N B Authors using route (ii) are advised to alert us to any incoming documents via our regular e-mail address]

● **Colour figures** The first colour figure is published at no charge provided that one author has been a member of the Biochemical Society for at least 2 years and that the use of colour is deemed scientifically necessary by the reviewers Subsequent colour figures in the same paper cost £300 each

● **Multimedia adjuncts** The Biochemical Journal Online is now able to offer authors the opportunity to enhance their papers with multimedia adjuncts (e g time-lapse movies, three-dimensional structures) These will be submitted to peer review alongside the manuscript To submit a paper with a multimedia adjunct, please contact the Managing Editor (editorial@portlandpress com) There is no extra charge associated with the publication of a multimedia adjunct online

● **Use of authors' diskettes** Authors should submit diskettes of revised articles to the editorial office Every effort will be made to use the diskette during typesetting, but this cannot be guaranteed Authors must ensure that files have been updated to incorporate all revisions, and hence that the version on the diskette matches the revised hard copy. Our preferred word-processing format is Word for Windows version 6 Submission of manuscripts in other word-processing formats may lead to delays in processing The diskette should be accompanied by a covering letter specifying manuscript number, operating system and software program Files should be formatted double-spaced with no hyphenation and automatic wordwrap (no hard returns within paragraphs)

Other information

The *Biochemical Journal* is published and distributed by Portland Press Ltd on behalf of the Biochemical Society It is published twice monthly, in 2000 volumes 345–352 (three parts each) will appear The subscription also includes an author and key-word index

● **Subscription rates** Institutional subscription rates for 2000 are shown below Subscribers to the *Biochemical Journal* can subscribe additionally to *Biochemical Society Transactions* and *Biotechnology and Applied Biochemistry* on a joint subscription at a reduced rate Terms are cash with order (US$ in N America, £ sterling for rest of the world, or US$ equivalent at current rate of exchange, subscribers in the EU may pay in £ sterling or Euros), or against pro forma invoice. Orders should be sent to the address below, or through your usual agent

	N America	Rest of world	Euro price
One yr (8 vols)	US$1950	£1110	€1776
Single issues	US$97	£56	€90

Dollar prices include airspeeded delivery Sterling and Euro prices include airspeeded delivery in Europe and delivery by surface mail elsewhere Airspeeded delivery is available to countries other than America and Europe at an additional cost of £50

● **Biochemical Journal Online** Access to the Biochemical Journal Online is restricted to institutions that have a subscription to the print version It will be free to such institutions during 2000 URL. http//www BiochemJ org

● **Microfiche and back issues** Volumes 102–296 of the *Biochemical Journal* are available on microfiche Back issues are also available Further details may be obtained from the address below

● **Subscription department**
Portland Press Ltd
P O. Box 32, Commerce Way
Colchester CO2 8HP, Essex, U K
(telephone 01206 796351, fax 01206-799331, e-mail sales@portlandpress com)

● **Advertising** Advertising is accepted in the *Biochemical Journal* For information contact the Advertising Department, Portland Press Ltd, 59 Portland Place, London W1N 3AJ (telephone 020 7580 5530, fax 020 7323 1136, e-mail editorial@portlandpress com)

Biochemical Journal
Volume 349, part 2
15 July 2000

First published on the Internet
10 July 2000
http://www.BiochemJ.org

Review

Sphingosine 1-phosphate signalling in mammalian cells ***by* S. Pyne and N. J. Pyne**		**385–402**

Research Communications

Cloning and mapping of human *PKIB* and *PKIG*, and comparison of tissue expression patterns of three members of the protein kinase inhibitor family, including PKIA	L Zheng, L Yu, Q Tu, M. Zhang, H. He, W Chen, J Gao, J. Yu, Q Wu and S. Zhao	**403–407**
HSP43, a small heat-shock protein localized to specific cells of the vulva and spermatheca in the nematode *Caenorhabditis elegans*	L Ding and E P M Candido	**409–412**
Ascorbate oxidation is a prerequisite for its transport into rat liver microsomal vesicles	M Csala, V. Mile, A Benedetti, J. Mandl and G Bánhegyi	**413–415**

Research Papers

Evidence for phosphorylation and ubiquitinylation of the turnip yellow mosaic virus RNA-dependent RNA polymerase domain expressed in a baculovirus–insect cell system	F. Héricourt, S Blanc, V. Redeker and I Jupin	**417–425**
Interferons activate the p42/44 mitogen-activated protein kinase and JAK-STAT (Janus kinase-signal transducer and activator transcription factor) signalling pathways in hepatocytes: differential regulation by acute ethanol via a protein kinase C-dependent mechanism	V-A.T. Nguyen, J Chen, F Hong, E.J.N Ishac and B Gao	**427–435**
Sp1-like activity mediates angiotensin-II-induced plasminogen-activator inhibitor type-1 (*PAI-1*) gene expression in mesangial cells	M. Motojima, T Ando and T Yoshioka	**435–441**
Tissue-specificity, functional characterization and subcellular localization of a rat ubiquitin-specific processing protease, UBP109, whose mRNA expression is developmentally regulated	K C Park, E J. Choi, S.W. Min, S.S. Chung, H Kim, T Suzuki, K. Tanaka and C.H Chung	**443–453**
Glutathione peroxidase-1 but not -4 is involved in the regulation of cellular 5-lipoxygenase activity in monocytic cells	D. Straif, O. Werz, R Kellner, U Bahr and D Steinhilber	**455–461**
Esterification of free fatty acids in adipocytes a comparison between octanoate and oleate	W Guo, J.-K Choi, J.L Kirkland, B E Corkey and J.A. Hamilton	**463–471**
Link peptide cartilage growth factor is degraded by membrane proteinases	M F Dean and P. Sansom	**473–479**
Evidence that 12-lipoxygenase product 12-hydroxyeicosatetraenoic acid activates p21-activated kinase	Y Wen, J Gu, U.G Knaus, L Thomás, N Gonzales and J.L Nadler	**481–487**
Activation of protein kinase C alters $P34^{cdc2}$ phosphorylation state and kinase activity in early sea urchin embryos by abolishing intracellular Ca^{2+} transients	F.A. Suprynowicz, L Groigno, M. Whitaker, F.J. Miller, G. Sluder, J. Sturrock and T. Whalley	**489–499**
Identification of active-site residues in *Bradyrhizobium japonicum* malonamidase E2	H.M Koo, S.-O. Choi, H.M. Kim and Y S Kim	**501–507**

NIMA-related kinase 2 (Nek2), a cell-cycle-regulated protein kinase localized to centrosomes, is complexed to protein phosphatase 1	N.R. Helps, X. Luo, H M Barker and P T W Cohen	**509–518**
Kinetics and control of oxidative phosphorylation in rat liver mitochondria after chronic ethanol feeding	A. Marcinkeviciute, V Mildaziene, S Crumm, O. Demin, J B Hoek and B Kholodenko	**519–526**
Isolation and characterization of casein kinase I from *Dictyostelium discoideum*	G. Moreno-Bueno, C. Calés, M M Behrens and M. Fernández-Renart	**527–537**
Hepatic intralobular mapping of fructose metabolism in the rat liver	S P Burns, H C. Murphy, R.A Iles, R A. Bailey and R D Cohen	**539–545**
Regulation of BAD by cAMP-dependent protein kinase is mediated via phosphorylation of a novel site, Ser^{155}	J M Lizcano, N. Morrice and P Cohen	**547–557**
The human breast carcinoma cell line HBL-100 acquires exogenous cholesterol from high-density lipoprotein via CLA-1 (CD-36 and LIMPII analogous 1)-mediated selective cholesteryl ester uptake	P J Pussinen, B. Karten, A. Wintersperger, H. Reicher, M McLean, E. Malle and W. Sattler	**559–566**
Novel application of *S*-nitrosoglutathione–Sepharose to identify proteins that are potential targets for *S*-nitrosoglutathione-induced mixed-disulphide formation	P. Klatt, E. Pineda Molina, D Pérez-Sala and S Lamas	**567–578**
Effect of inhibition of glutathione synthesis on insulin action: *in vivo* and *in vitro* studies using buthionine sulfoximine	M. Khamaisi, O. Kavel, M Rosenstock, M Porat, M. Yuli, N Kaiser and A Rudich	**579–586**
N-arginine dibasic convertase (nardilysin) isoforms are soluble dibasic-specific metalloendopeptidases that localize in the cytoplasm and at the cell surface	V. Hospital, V. Chesneau, A. Balogh, C. Joulie, N G Seidah, P Cohen and A Prat	**587–597**
Recovery of active medium-chain-length-poly-3-hydroxyalkanoate polymerase from inactive inclusion bodies using ion-exchange resin	Q Ren, G de Roo, B. Kessler and B. Witholt	**599–604**
Phosphoinositide 3-kinase-dependent phosphorylation of the dual adaptor for phosphotyrosine and 3-phosphoinositides by the Src family of tyrosine kinase	S. Dowler, L Montalvo, D. Cantrell, N. Morrice and D R Alessi	**605–610**
Targeting and insertion of C-terminally anchored proteins to the mitochondrial outer membrane is specific and saturable but does not strictly require ATP or molecular chaperones	L Lan, S Isenmann and B W Wattenberg	**611–621**
pH-dependence of the fast step of maltose hydrolysis catalysed by glucoamylase G1 from *Aspergillus niger*	U Christensen	**623–628**
Identification of the differential distribution patterns of mRNAs and consensus binding sequences for mouse DAF-16 homologues	T Furuyama, T. Nakazawa, I Nakano and N. Mori	**629–634**
Substrate specificity of the expressed carotenoid 3,4-desaturase from *Rubrivivax gelatinosus* reveals the detailed reaction sequence to spheroidene and spirilloxanthin	S. Steiger, C. Astier and G. Sandmann	**635–640**
Cloning and characterization of the 5′ flanking region of the sialomucin complex/rat *Muc4* gene: promoter activity in cultured cells	S.A. Price-Schiavi, A Perez, R Barco and K.L Carraway	**641–649**
Enhancement of the thermostability and hydrolytic activity of xylanase by random gene shuffling	H Shibuya, S Kaneko and K. Hayashi	**651–656**

Index of Authors

PAGE
Alessi, D R 605
Ando, T. 435
Astier, C. 635

Bahr, U. 455
Bailey, R. A. 539
Balogh, A 587
Bánhegyi, G 413
Barco, R 641
Barker, H M 509
Behrens, M M 527
Benedetti, A 413
Blanc, S 417
Burns, S P 539

Calés, C. 527
Candido, E P M 409
Cantrell, D 605
Carraway, K L 641
Chen, J. 427
Chen, W. 403
Chesneau, V. 587
Choi, E. J. 443
Choi, J.-K. 463
Choi, S.-O 501
Christensen, U. 623
Chung, C H 443
Chung, S S. 443
Cohen, P 547, 587
Cohen, P T. W. 509
Cohen, R D 539
Corkey, B E. 463
Crumm, S 519
Csala, M 413

Dean, M F 473
Demin, O. 519
de Roo, G. 599

PAGE
Ding, L. 409
Dowler, S. 605

Fernández-Renart, M 527
Furuyama, T 629

Gao, B 427
Gao, J 403
Gonzales, N 481
Groigno, L 489
Gu, J 481
Guo, W. 463

Hamilton, J. A. 463
Hayashi, K. 651
He, H. 403
Helps, N. R 509
Héricourt, F 417
Hoek, J. B 519
Hong, F. 427
Hospital, V. 587

Iles, R. A. 539
Isenmann, S. 611
Ishac, E. J N. 427

Joulie, C 587
Jupin, I. 417

Kaiser, N. 579
Kaneko, S 651
Karten, B 559
Kavel, O. 579
Kellner, R 455
Kessler, B 599
Khamaisi, M 579
Kholodenko, B. 519
Kim, H. 443
Kim, H. M. 501
Kim, Y. S 501

PAGE
Kirkland, J L. 463
Klatt, P 567
Knaus, U G 481
Koo, H M 501

Lamas, S 567
Lan, L. 611
Lizcano, J M 547
Luo, X 509

Malle, E 559
Mandl, J 413
Marcinkeviciute, A 519
McLean, M 559
Mildaziene, V 519
Mile, V. 413
Miller, F. J. 489
Min, S W. 443
Montalvo, L. 605
Moreno-Bueno, G. 527
Mori, N. 629
Morrice, N. 547, 605
Motojima, M 435
Murphy, H. C. 539

Nadler, J. L. 481
Nakano, I. 629
Nakazawa, T. 629
Nguyen, V-A T 427

Park, K C. 443
Perez, A. 641
Pérez-Sala, D 567
Pineda Molina, E 567
Porat, M 579
Prat, A 587
Price-Schiavi, S A 641
Pussinen, P J 559
Pyne, N. J 385
Pyne, S 385

PAGE
Redeker, V. 417
Reicher, H. 559
Ren, Q 599
Rosenstock, M. 579
Rudich, A. 579

Sandmann, G 635
Sansom, P. 473
Sattler, W. 559
Seidah, N. G. 587
Shibuya, H 651
Sluder, G 489
Steiger, S 635
Steinhilber, D. 455
Straif, D 455
Sturrock, J 489
Suprynowicz, F. A. 489
Suzuki, T 443

Tanaka, K 443
Thomas, L 481
Tu, Q 403

Wattenberg, B W. 611
Wen, Y 481
Werz, O 455
Whalley, T 489
Whitaker, M 489
Wintersperger, A 559
Witholt, B. 599
Wu, Q 403

Yoshioka, T 435
Yu, J. 403
Yu, L. 403
Yull, M. 579

Zhang, M 403
Zhao, S 403
Zheng, L 403

Editorial Advisory Panel

C Abell (Cambridge)
M Abrahamson (Lund)
B A C Ackrell (San Francisco)
L Agius (Newcastle)
L Alhonen (Kuopio)
N G Anderson (Manchester)
C Anthony (Southampton)
G J Arlaud (Grenoble)
F A Armstrong (Oxford)
O I. Aruoma (London)
B Ashby (Philadelphia)
K S Authi (London)

A Baici (Zurich)
A J Bailey (Langford)
A J Baines (Canterbury)
D Barford (London)
M P Barrett (Glasgow)
K Bartlett (Newcastle)
J F Bateman (Melbourne)
G Baverel (Lyon)
J H Beattie (Aberdeen)
C Beaumont (Paris)
D R Bell (Nottingham)
D S Bendall (Cambridge)
A Benedetti (Siena)
J P Bennett (London)
M. J Berridge (Cambridge)
A Berry (Leeds)
R J Beynon (Liverpool)
C D Bingle (Sheffield)
I Bjork (Uppsala)
J L Blank (Leicester)
N Blau (Zurich)
P G Board (Canberra)
M. A. Bogoyevitch (Perth, West Aus.)
G B Bolger (Salt Lake City)
M Bollen (Leuven)
G. P. Bolwell (London)
A R Boobis (London)
K M Botham (London)
M J. Brammer (London)
P. Brickell (London)
K M. Brindle (Cambridge)
K. Brocklehurst (London)
E Brot-Laroche (Paris)
A J P Brown (Aberdeen)
G. Brown (Birmingham)
B. Brune (Erlangen)
N J Bulleid (Manchester)
N W Bunnett (San Francisco)
A Burchell (Dundee)
B Burchell (Dundee)
S J W Busby (Birmingham)
P. J. Butterworth (London)

J J Calvete (Valencia)
M J Carden (Canterbury)
E A. Carrey (London)
C Casals (Madrid)
A M Caswell (Leeds)
A F Chaffotte (Paris)
K E. Chapman (Edinburgh)
F. Checler (Valbonne)
P K Chiang (Silver Spring)
E R Chilvers (Cambridge)
M Claret (Orsay)
P Cohen (Dundee)
J Colyer (Leeds)
S J Cook (Cambridge)
R. A. Cooper (Leicester)
A P Corfield (Bristol)
A Cornish-Bowden (Marseille)
M W. H Coughtrie (Dundee)
D A Cowan (London)
C. M Cuchillo (Barcelona)
J. M. Cuezva (Madrid)
P Cullen (Bristol)
N P Curthoys (Fort Collins)
W Cushley (Glasgow)

R M Daniel (Hamilton)
M J Davies (Sydney)
F C de Beer (Lexington)
H de Groot (Essen)
H R De Jonge (Rotterdam)
L Dekker (London)
P N M Demacker (Nijmegen)
M Dickens (Leicester)
C Dingwall (Harlow)
C J Dorman (Dublin)
R Douce (Lyon)
K T Douglas (Manchester)
C. P Downes (Dundee)
K Drickamer (Oxford)
M J Dufton (Glasgow)

Y Edwards (London)
J M Edwardson (Cambridge)
J P Eiserich (Birmingham, AL)
C Erneux (Bruxelles)
C T Evans (Melbourne, FL)
R W Evans (London)

T Feizi (London)
R C Feldhoff (Louisville, KT)
L M Field (Harpenden)
M C Field (London)
L M Fisher (London)
P R Flatt (Coleraine)
K R Fox (Southampton)
M H Fukami (Bergen)
S J Fuller (London)

T G Gabig (Indianapolis)
C. G Gahmberg (Helsinki)
V Gerke (Munster)
C. S. Gillespie (Edinburgh)
D. B Glass (Atlanta)
L Graeve (Aachen)
A Graham (London)
J C Gray (Cambridge)
P A Grimaldi (Nice)
S Grinstein (Toronto)

H P Haagsman (Utrecht)
P A Halban (Genève)
A. Hall (London)
R A P Harrison (Cambridge)
P Hawkins (Cambridge)
F G Hegardt (Barcelona)
A. C. Herington (Brisbane)
J Higgins (Sheffield)
A. A Holder (London)
G D Holman (Bath)
M J Holness (London)
N A Hotchin (Birmingham)
M D. Houslay (Glasgow)
C Howe (Cambridge)
H Hundal (Dundee)
J C Hutton (Denver)
E Hyde (Birmingham)

Y Ikehara (Fukuoka)
R A Iles (London)
R E Isaac (Leeds)
C M Isacke (London)
T Ishikawa (Yokohama)
P B. Iynedjian (Geneva)

K H Jakobs (Essen)
S. M Jarvis (Canterbury)
P Johnson (Vancouver)
N Jones (London)

M A Kaderbhai (Aberystwyth)
K E. Kadler (Manchester)
H Kanoh (Sapporo)
J H Kaplan (Portland, OR)
P Karran (South Mimms)
D J Keeling (Molndal)
C Kennedy (Norwich)
C M Kielty (Manchester)
T M Kitson (Palmerston North)
L Kjellen (Uppsala)
E Knecht (Valencia)
J Knudsen (Odense)
W Kolch (Glasgow)
I M Kovach (Washington, DC)
Y Kuroki (Sapporo)
J Kuznicki (Warsaw)

A Lane (London)
D A Lane (London)
P J Large (Hull)
P J Lea (Lancaster)
D S Leake (Reading)
C C Leslie (Denver)
R E Lewis (Omaha, NE)
J E Lillehaug (Bergen)
D. M. J Lilley (Dundee)
M Liscovitch (Rehovot)
J M Lord (Coventry)
M G Low (New York)
P A Lund (Birmingham)

C C Malbon (Stony Brook, NY)
W Maltese (Toledo, OH)
J P. G. Malthouse (Dublin)
G E Mann (London)
B Mannervik (Uppsala)
D Martin (Oslo)
G G F Mason (Bristol)
R. W. Mason (Wilmington)
P Masson (La Tronche)
B. Mayer (Graz)
K H Mayo (Minneapolis)
M J. McConville (Melbourne)
A McEuen (Southampton)
J D McGivan (Bristol)
M McGrane (Storrs)
R A. J McIlhinney (Oxford)
A G. McLennan (Liverpool)
L C McPhail (Winston-Salem)
P A Meacock (Leicester)
D W Meek (Dundee)
P. J. Meier-Abt (Zurich)
E Melendez-Hevia (Tenerife)
H Mellor (Bristol)
A K Menon (Madison)
D J Meyer (London)
P A Millner (Leeds)
J L A Mitchell (DeKalb, IL)
T J Monks (Austin)
A Morgan (Liverpool)
H W Morgan (Hamilton)
I Morgan (Glasgow)
M. Mori (Kumamoto)
S Morley (Brighton)
S Morris (Pittsburgh)
N Moustaid Moussa (Knoxville, TN)
M Mueckler (St Louis)
B Mulloy (Potters Bar)
G Murphy (Cambridge)
M E Murphy (Durham, NC)

T Nagatsu (Aichi)
I A Nieduszynski (Lancaster)
M Nishijima (Tokyo)
R I Norman (Leicester)

S Olsnes (Oslo)
L A J O'Neill (Dublin)

M G P Page (Basel)
M I Page (Huddersfield)
F Palmieri (Bari)
G Panayotou (Vari)
M Parenti (Milano)
M Paulsson (Koln)
T M Penning (Philadelphia)
K C Persaud (Manchester)
L Persson (Lund)
J M. Pfeilschifter (Frankfurt)
T Pihlajaniemi (Oulu)
T S Pillay (Nottingham)
J Pines (Cambridge)
C Ponzetto (Torino)
F Possmayer (London, Ont.)
A. D. Postle (Southampton)
D Poyner (Birmingham)
N C Price (Stirling)
S A Prigent (Leicester)
D. Prockop (Philadelphia)
D Pruss (Salt Lake City)
M Puceat (Montpellier)
S. Pyne (Glasgow)

D. M. Raben (Baltimore)
Z Radić (La Jolla)
D. P. Ramji (Cardiff)
M Rattray (London)
F. X Real (Barcelona)
C C Reddy (Penn State)
C P F Redfern (Newcastle upon Tyne)
M J Reed (London)
R. A. F. Reithmeier (Toronto)
P S Rennie (Vancouver)
C. Rice-Evans (London)
P J Richardson (Cambridge)
C. C. Rider (London)
A Ridley (London)
H Rosen (Rahway)
G Rotilio (Roma)
F Russo-Marie (Paris)
G A Rutter (Bristol)

EDITORIAL ADVISORY PANEL (continued)

K S Sakariassen (Uppsala)
J P Salier (Rouen)
J Savill (Edinburgh)
M F. G Schmidt (Berlin)
N S Scrutton (Leicester)
K Seedorf (Hamburg)
A W. Segal (London)
S D Shapiro (St. Louis)
D. Sheehan (Cork)
P. R Shepherd (London)
Y Shimomura (Nagoya)
H Sies (Dusseldorf)
H. Sjostrom (Copenhagen)
D M Smith (London)
F. Spener (Munster)
A. K Stobart (Bristol)
W Stocker (Munster)
G J Strous (Utrecht)
T. W. Sturgill (Charlottesville)
K Suckling (Welwyn)
B. Svensson (Copenhagen)

M. J. A Tanner (Bristol)
C W Taylor (Cambridge)
A Tepikin (Liverpool)
M Thelen (Bellinzona)
N. S B Thomas (London)
D. Thornton (Manchester)
C Tickle (Dundee)
D Tosh (Bath)
P. Trayhurn (Oslo)
A J. Trewavas (Edinburgh)
J T Triffit (Oxford)
J Turnbull (Birmingham)
B. M Turner (Birmingham)

B Ullman (Portland, OR)

G van de Werve (Montréal)
L M G. van Golde (Utrecht)
S van Heyningen (Edinburgh)
E van Schaftingen (Bruxelles)

G Vassart (Bruxelles)
P. F. T Vaughan (Leeds)
A Veillette (Montreal)
G Verhoeven (Leuven)
D A Vessey (San Francisco)
H Vidal (Lyon)
J F. G Vliegenthart (Utrecht)

M J. Warren (London)
N J Watmough (Norwich)
S P Watson (Oxford)
A Watts (Oxford)
D. J Waxman (Boston)
K G Welinder (Copenhagen)
R E Wettenhall (Melbourne)
R. Wever (Amsterdam)
M Wheatley (Birmingham)
C Wheeler-Jones (London)
D G Wilkinson (London)
D C Wilton (Southampton)
J -O. Winberg (Tromsø)

S J Winder (Glasgow)
C C Winterbourn
(Christchurch, NZ)
S G Withers (Vancouver)
P Wojtaszek (Poznan)
A. Wolffe (Bethesda, MD)
J M Woof (Dundee)
J M Wrigglesworth (London)
M C Wright (Southampton)
S Wright (Leeds)
G Wu (College Station)
F Wuytack (Leuven)
M. P Wymann (Fribourg)

I Young (Belfast)
L S. Young (Birmingham)
S. P Young (Birmingham)

I Zachary (London)
R Zamoyska (London)

Biochem J (2000) 349, 385–402 (Printed in Great Britain)

REVIEW ARTICLE

Sphingosine 1-phosphate signalling in mammalian cells

Susan PYNE[1] and Nigel J. PYNE[1]

Department of Physiology and Pharmacology, Strathclyde Institute for Biomedical Sciences, University of Strathclyde, 27 Taylor Street, Glasgow G4 0NR, Scotland, U.K.

Sphingosine 1-phosphate is formed in cells in response to diverse stimuli, including growth factors, cytokines, G-protein-coupled receptor agonists, antigen, etc. Its production is catalysed by sphingosine kinase, while degradation is either via cleavage to produce palmitaldehyde and phosphoethanolamine or by dephosphorylation. In this review we discuss the most recent advances in our understanding of the role of the enzymes involved in metabolism of this lysolipid. Sphingosine 1-phoshate can also bind to members of the endothelial differentiation gene (EDG) G-protein-coupled receptor family [namely EDG1, EDG3, EDG5 (also known as H218 or AGR16), EDG6 and EDG8] to elicit biological responses. These receptors are coupled differentially via G_i, G_q, $G_{12/13}$ and Rho to multiple effector systems, including adenylate cyclase, phospholipases C and D, extracellular-signal-regulated kinase, c-Jun N-terminal kinase, p38 mitogen-activated protein kinase and non-receptor tyrosine kinases. These signalling pathways are linked to transcription factor activation, cytoskeletal proteins, adhesion molecule expression, caspase activities, etc. Therefore sphingosine 1-phosphate can affect diverse biological responses, including mitogenesis, differentiation, migration and apoptosis, via receptor-dependent mechanisms. Additionally, sphingosine 1-phosphate has been proposed to play an intracellular role, for example in Ca^{2+} mobilization, activation of non-receptor tyrosine kinases, inhibition of caspases, etc. We review the evidence for both intracellular and extracellular actions, and extensively discuss future approaches that will ultimately resolve the question of dual action. Certainly, sphingosine 1-phosphate will prove to be unique if it elicits both extra- and intra-cellular actions. Finally, we review the evidence that implicates sphingosine 1-phosphate in pathophysiological disease states, such as cancer, angiogenesis and inflammation. Thus there is a need for the development of new therapeutic compounds, such as receptor antagonists. However, identification of the most suitable targets for drug intervention requires a full understanding of the signalling and action profile of this lysosphingolipid. This article describes where the research field is in relation to achieving this aim.

Key words: endothelial differentiation gene (EDG), lipid phosphate phosphatase, lysosphingolipid, sphingosine kinase, sphingosine 1-phosphate lyase.

INTRODUCTION

Sphingosine 1-phosphate (S1P) is a polar sphingolipid metabolite which has been proposed to act both as an extracellular mediator and as an intracellular second messenger. Extracellular effects are mediated via a recently identified family of plasma membrane G-protein-coupled receptors (GPCRs), whereas specific intracellular sites of action remain to be defined. S1P is stored and released from platelets upon their activation, but can also be synthesized in a wide variety of cell types in response to extracellular stimuli, such as growth factors and cytokines. S1P affects diverse biological processes, including cell growth, differentiation, migration and apoptosis, and may have an important role in pathophysiological disease states, such as atherosclerosis and cancer.

SPHINGOLIPID METABOLISM

It is beyond the scope of this review to describe sphingolipid metabolism in detail, and the reader is referred to more specific articles on this subject [1,2]. However, a brief overview is provided, with details of several useful compounds for the selective inhibition of key enzymes, which may be used to ultimately modulate S1P metabolism in cells (Schemes 1a and 1b).

Ceramide may be important in determining apoptotic responses to stress [1,2]. However, it may also serve as a precursor for the synthesis of S1P, which, in certain cell types, is implicated in cell survival. This suggests that the metabolic conversion of ceramide into S1P could switch cells from an apoptotic state to a proliferative one. Therefore inhibition of the conversion of ceramide into S1P might be usefully exploited to induce cell death in disease, such as cancer. Ceramide can be synthesized either in response to the agonist-dependent activation of sphingomyelinases or *de novo*. Agonist-dependent activation of sphingomyelinases has been observed in response to growth factors, cytokines and arachidonic acid [3]. Additionally, cellular stress and changes in the redox state of the cell can result in sphingomyelinase activation [4,5]. To date, five distinct sphingomyelinases have been identified, based on their pH optima, cellular localization and cation dependence [2,3]. Ceramidase catalyses the deacylation of ceramide to produce non-esterified fatty acid and sphingosine. Both an acidic ceramidase [6,7] (deficient in Farber's disease and inhibited by the ceramide analogue *N*-oleoylethanolamine) and an alkaline ceramidase [8]

Abbreviations used: BAPTA/AM, bis-(*o*-aminophenoxy)ethane-*N*,*N*,*N*′,*N*′-tetra-acetic acid tetrakis(acetoxymethyl ester); EDG, endothelial differentiation gene; EGF, epidermal growth factor; ERK, extracellular-signal-regulated kinase; EST, expressed sequence tag; FAK, focal adhesion kinase; GPCR, G-protein-coupled receptor; IGF, insulin-like growth factor; JNK, c-Jun N-terminal kinase; LDL, low-density lipoprotein; LPA, lysophosphatidic acid; LPP, lipid phosphate phosphatase; MAPK, mitogen-activated protein kinase; NGF, nerve growth factor; PA, phosphatidic acid; PDGF, platelet-derived growth factor; PI3K, phosphoinositide 3-kinase; PKC, protein kinase C; PLC/D, phospholipase C/D; SH2, Src homology 2; SPC, sphingosylphosphocholine; S1P, sphingosine 1-phosphate; SPHK, sphingosine kinase; SRE, serum response element; SRF, serum response factor; TNFα, tumour necrosis factor α.

[1] Correspondence may be addressed to either author (e-mail susan.pyne@strath.ac.uk or n.j.pyne@strath.ac.uk).

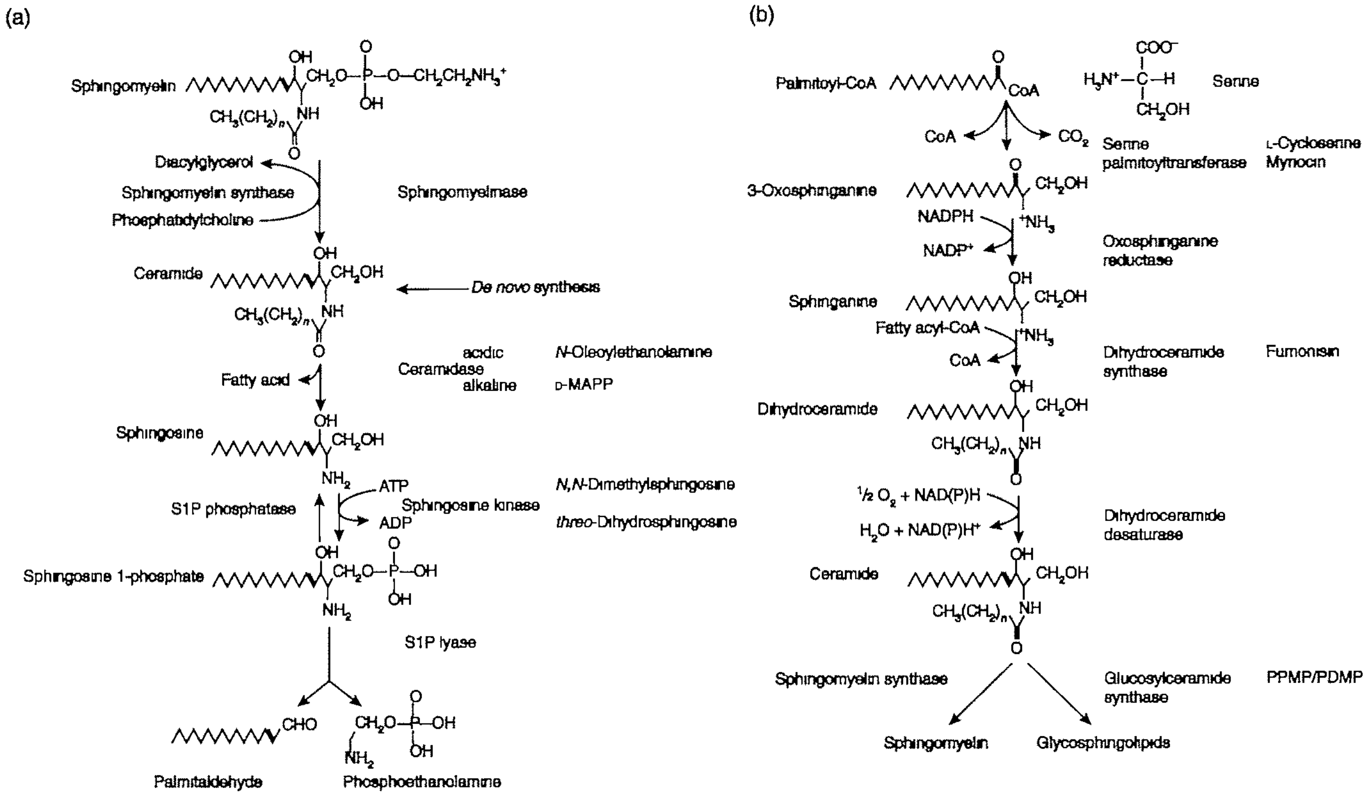

Scheme 1 Sphingolipid metabolism

(a) S1P biosynthesis and degradation, (b) *de novo* ceramide biosynthesis Structural formulae of the sphingolipids are shown, with enzymes denoted in green and their inhibitors in red Abbreviations D-MAPP, D-*erythro*-2-(*N*-myristoylamino)-1-phenylpropanol; PPMP, D-*threo*-1-phenyl-2-palmitoylamino-3-morpholino-1-propanol, PDMP, D-*threo*-1-phenyl-2-decanoylamino-3-morpholino-1-propanol

[inhibited by D-*erythro*-2-(*N*-myristoylamino)-1-phenylpropanol (D-MAPP)] exist. The resulting sphingosine may act as the substrate for sphingosine kinase (SPHK) to produce S1P. This is cleaved by S1P lyase (to produce palmitaldehyde and phosphoethanolamine) or dephosphorylated by S1P phosphatase. Alternatively, ceramide can be converted back into sphingomyelin by the addition of a phosphocholine headgroup (donated by phosphatidylcholine), catalysed by sphingomyelin synthase [9] (Scheme 1a)

De novo ceramide synthesis (which occurs in the endoplasmic reticulum) is initiated by the condensation of serine and palmitoyl-CoA to produce 3-oxosphinganine and CO_2, catalysed by serine palmitoyltransferase. 3-Oxosphinganine is rapidly reduced to dihydrosphingosine (sphinganine) by an NAD(P)H-dependent reductase which is stereospecific for the D-isomer. Subsequently, dihydrosphingosine is N-acylated to dihydroceramide, catalysed by dihydroceramide synthase. Dihydroceramide desaturase catalyses the subsequent introduction of a *trans* double bond at C-4–C-5 to produce ceramide. *De novo* ceramide synthesis can be blocked at serine palmitoyltransferase by L-cycloserine [10] or by the fungal metabolite myriocin [11], whereas the mycotoxin fumonisin inhibits dihydroceramide synthase [12].

Ceramide produced *de novo* can be metabolized to glycosphingolipids, the first step of which is catalysed by a glucosylceramide synthase [13] (Scheme 1b). This enzyme is inhibited by the ceramide analogues D-*threo*-1-phenyl-2-palmitoylamino-3-morpholino-1-propanol (PPMP) and D-*threo*-1-phenyl-2-decanoylamino-3-morpholino-1-propanol (PDMP), a potential anti-cancer agent [14]. Alternatively, ceramide can be phosphorylated by a calcium-activated ceramide kinase to produce ceramide 1-phosphate [15,16].

SPHK

SPHK was originally purified from rat kidney as a 49 kDa protein, with K_m values of 5 μM and 93 μM for sphingosine and ATP respectively [17]. The enzyme binds calmodulin in the presence of calcium. Subsequently two SPHKs have been cloned [18]. Kohama and colleagues [18] trypsin-treated the purified kidney form and obtained amino acid sequences of eight peptides. Using tBLASTn algorithm searches they identified several expressed sequence tags (ESTs) which yielded predicted amino acid sequences similar to those of three of the peptides obtained by trypsin treatment of purified kidney SPHK. Subsequently, two clones from mouse were obtained with apparent open reading frames of 381 and 388 amino acids containing homologous sequence encoding seven of the eight peptides obtained from the rat kidney form. The enzymes were designated SPHK1a and SPHK1b. Their predicted molecular masses were 42.3 and 43.2 kDa. These isoforms differ in only a few amino acids at the N-terminus, suggesting that they may be derived by alternative splicing of the same mRNA transcript. However, since both cDNAs lacked Kozak sequences [19], the suggestion is that they may represent only partial cDNAs. Therefore, until upstream sequence at the 5′ end is obtained, the exact relationship of the two forms is unknown.

SPHK mRNA expression has been detected as a 2.4 kb mRNA species in most tissues, with abundant expression in lung and spleen, and barely detectable levels in skeletal muscle and liver.

A SPHK gene family has been identified which includes LCB4 and LCB5 from *Saccharomyces cerevisiae* [20]. Other potential SPHKs were identified in the genomic sequences of *Caenorhabditis elegans* and *Schizosaccharomyces pombe*. Five critical regions of highly conserved amino acids (C1–C5) have been identified in all the forms, including the mammalian enzymes. Regions C1 and C3 of SPHK show 35 % and 58 % identity with residues 296–315 and 378–389 respectively of human diacylglycerol kinase ζ [21], which are present in the conserved subdomain 1 of all diacylglycerol kinase isoforms. Subdomain 1 is believed to contain the ATP-binding site that is distinct from that present in protein-specific protein kinases [22] Therefore, because of the close similarity with diacylglycerol kinase, Kohama et al. [18] have suggested that C1 and C3 in SPHK might also constitute an ATP-binding domain. More specifically, the invariant sequence, Gly-Gly-Lys-Gly-Lys, within the C1 domain of SPHK is suggested to form part of the ATP-binding site.

The cloned murine SPHK isoforms contain at least three calcium/calmodulin-binding consensus sequences and several potential protein kinase phosphorylation sites: one for protein kinase A, two for casein kinase II and eight for protein kinase C (PKC). The presence of the latter is of interest because SPHK in intact cells has been shown to be stimulated by PKC activators, such as PMA [23]. Furthermore, inhibition of ceramide-induced apoptosis by PKC activation is associated with the stimulation of SPHK and S1P formation [23]. The mammalian SPHKs also lack Src homology 2 (SH2), SH3 and pleckstrin homology domains, suggesting that they do not interact with phosphotyrosine-containing adaptor proteins, G-protein $\beta\gamma$ subunits or phospholipids, such as phosphatidylinositol 3,4,5-trisphosphate. Earlier *in vitro* studies demonstrated that the enzyme could be activated by acidic phospholipids such as phosphatidate, phosphatidylinositol, phosphatidylinositol 4,5-bisphosphate and especially phosphatidylserine [24], suggesting a possible relationship between S1P levels and glycerophospholipid signalling.

SPHK1a activity, measured in lysates of transiently transfected HEK 293 cells, has specificity for the *trans* isomer of D-*erythro*-sphingosine (K_m 2.15 μM). The enzyme can also phosphorylate D-*erythro*-dihydrosphingosine, but to a lesser extent. Ceramide, diacylglycerol, phosphatidylinositol and phytosphingosine were not substrates. *N*,*N*-Dimethylsphingosine and D,L-*threo*-dihydrosphingosine were confirmed as inhibitors of SPHK, with K_i values of 2.64 and 2.15 μM respectively.

Transient transfection of HEK 293, NIH 3T3 and Swiss 3T3 cells with SPHK1a resulted in a 400–800-fold increase in SPHK activity [18,25]. The transfected SPHK activity partitioned into both cytosolic and membrane fractions (approx. 70–80 % cytosolic and 20–30 % particulate) Indeed, the lack of hydrophobic-enriched domains and of a signal peptide in the protein are consistent with its predominantly cytosolic localization. Platelet-derived growth factor (PDGF) stimulated a 2-fold increase in the specific activity of cytosolic SPHK1a, but did not induce significant translocation to the membrane fraction [25]. Other studies support the presence of both membrane and cytosolic SPHK activities. Notably, in platelets, 70 % of total activity was particulate and 30 % cytosolic [26]. Chromatographic fractionation of the cytosol resolved two distinct SPHK activities. Therefore multiple isoforms of SPHK may exist, with different physiological roles and possibly derived from distinct genes.

Transfection of NIH 3T3 cells with SPHK1a resulted in a marked (21-fold) increase in S1P mass, with 67 % and 29 % decreases in sphingosine and ceramide repsectively. However, the net increase in S1P (0.95 pmol/nmol of total phospholipid) did not equate with the observed decrease in ceramide and sphingosine (which totalled 6.23 pmol/nmol of total phospholipid) [18]. This suggests the concomitant removal of S1P by, for instance, S1P lyase and/or S1P phosphatase and/or efflux.

S1P lyase

S1P lyase catalyses the cleavage of S1P at the C-2–C-3 bond to produce hexadecanal (palmitaldehyde) and phosphoethanolamine [27,28]. The enzyme requires the coenzyme pyridoxal 5′-phosphate, has a pH optimum of 7.4–7.6 and is inhibited by heavy-metal ions. Activity is specific for the D-*erythro* isomers (in common with SPHK) of phosphorylated sphingoid bases, including S1P, dihydrosphingosine 1-phosphate and phytosphingosine 1-phosphate, although chain length can vary. The enzyme is ubiquitously expressed with regard to species and mammalian tissues, with the notable exception of platelets, where it is absent. S1P lyase activity was present in cultured human fibroblasts to which [^{3}H]dihydroS1P (1 μM) was added [29]. [^{3}H]DihydroS1P was rapidly taken up by the fibroblasts and converted, in part, into [^{3}H]palmitaldehyde, which was further metabolized into glycerophospholipids and alk(en)yl-phospholipids.

S1P lyase was first cloned by D-*erythro*-sphingosine selection of *Saccharomyces cerevisiae* transformed with yeast genomic library carried on the pRS202 high-copy shuttle vector [30]. The most highly represented insert was subcloned and sequenced to identify a novel gene termed *BST1* (bestower of sphingosine tolerance). BST1 (since renamed DPL1) is a 65.5 kDa protein comprising 589 amino acids, and is 23 % identical with *gadA* and *gadB* of *Escherichia coli*, which encode glutamate decarboxylase, another pyridoxal 5′-phosphate-dependent enzyme that catalyses the synthesis of γ-aminobutyric acid. Deletion of *BST1*/*DPL1* resulted in increased sensitivity to exogenous D-*erythro*-sphingosine and phytosphingosine. In addition, the *bst1*/*dpl1*Δ deletion mutant accumulated S1P upon exposure to exogenous sphingosine.

A mammalian S1P lyase gene has also been identified [31] using a BLAST search of the Genbank EST database for sequence similarity with the S1P lyase gene of *Caenorhabditis elegans*. An EST with an open reading frame of 1707 nucleotides was found which encodes a protein of 568 amino acids and a predicted molecular mass of 63.7 kDa. Hydropathy analysis indicates that the enzyme contains a single 20-amino-acid transmembrane domain close to the N-terminus. Indeed, the enzyme is located in membranes within mammalian cells. Comparison of the deduced amino acid sequence of the mouse S1P lyase with that of *Saccharomyces cerevisiae* BST1/DPL1 and *C. elegans* revealed 59 %/62 % similarity and 40 %/39 % identity respectively. Furthermore, the mouse gene encodes S1P lyase activity, confirmed by its expression in the *Saccharomyces cerevisiae bst1*/*dpl1*Δ deletion mutant. Under these conditions, the sphingosine-sensitive phenotype was reversed, demonstrating that the mouse gene can complement the yeast defect when expressed. Analysis of S1P lyase mRNA levels was consistent with previously reported S1P lyase activity levels, being most abundant in liver, followed by kidney, lung, heart and brain.

S1P phosphatase

Several lipid phosphate phosphatases (LPP1/1a/2/3) have been cloned and exhibit a broad substrate specificity which includes S1P, lysophosphatidic acid (LPA), phosphatidic acid (PA) and ceramide 1-phosphate [32]. A mammalian S1P-specific phosphatase has yet to be cloned. However, a S1P phosphatase which is distinct from the LPP activities has been detected in mammalian cells. Dephosphorylation of S1P to sphingosine has been observed in tissue homogenates [33] and whole cells [29]. For example, human fibroblasts incorporated exogenous $[^3H]$dihydroS1P (1 μM) and, in part, dephosphorylated it to $[^3H]$sphingosine, which was subsequently metabolized to $[^3H]$ceramide and $[^3H]$sphingomyelin. The rate of dephosphorylation of S1P by this phosphatase was calculated to be at least the same as that of its degradation by S1P lyase. A later study by the same group identified both high- and low-K_m dihydroS1P phosphatase activities in liver homogenate [34]. The high-affinity enzyme was predominantly associated with the plasma membrane and exhibited a pH optimum of 7.5. Significantly, the activity was distinguished from that of LPP (and other phosphatases) by the differential effects of bivalent cations, chelators, water-soluble and amphiphilic phosphate esters and detergents

Two specific genes (*YSR2/LBP2* and *YSR1/LBP1*, where *YSR* stands for yeast sphingosine resistance) have been identified in *Saccharomyces cerevisiae* which encode a dihydrosphingosine/phytoS1P phosphatase [35,36]. Thus a *ysr2*Δ deletion mutant accumulated dihydroS1P, whereas overexpression of YSR2 conferred sphingosine resistance to a dihydroS1P lyase-defective mutant, which is hypersensitive to sphingosine [35]. Similarly, deletion of LBP2 resulted in the accumulation of long-chain sphingoid bases and lowered ceramide levels [36]. Furthermore, YSR2 and LBP1 specifically dephosphorylated dihydrosphingosine/phytosphingosine phosphate and S1P, but not ceramide 1-phosphate or PA [35,36]. Deletion of LBP1 and LBP2 dramatically enhanced cell survival upon severe heat shock, suggesting that phosphorylated sphingoid bases modulate stress responses in yeast in a manner similar to that observed in mammalian cells.

MEASUREMENT OF S1P

A number of methods are available to measure S1P levels in tissue and cell samples. S1P exhibits unusual solubility for a lipid due to its polar headgroup. S1P (and ceramide 1-phosphate) can be selectively separated from other phospholipids and sphingolipids when an alkaline lipid extraction is used. Under these conditions, S1P partitions into the aqueous phase. S1P can be quantified by its chemical modification to ^{3}H-labelled ceramide 1-phosphate [37] or by dephosphorylation to sphingosine followed by rephosphorylation (in the presence of $[\gamma\text{-}^{32}P]$ATP) to $[^{32}P]$S1P [38]. Alternatively, relative changes in the S1P content of cells can be measured by incorporating radiolabelled palmitate, serine or sphingosine into cellular sphingolipids.

Yatomi et al. [37] obtained quantitative measurements of S1P by its extraction from cells and chemical conversion into N-$[^3H]$acetylated S1P (i.e. $[^3H]C_2$-ceramide 1-phosphate) by N-acylation with $[^3H]$acetic anhydride. The assay detects between 30 pmol and 10 nmol. Using this technique, S1P was quantified in human platelets, plasma and serum and in all rat tissues examined, being most abundant in testis and intestine (see Table 1; [37–40]). The biological significance of the observed S1P tissue distribution is yet to be determined. However, a correlation exists between the S1P content in the plasma of platelet concentrates, poor platelet increments and the occurrence of transfusion reactions in patients [41].

Alternatively, SPHK preparations can be used to quantify S1P (in the range 0.25 pmol–2.5 nmol) in biological samples [38] (Table 1). S1P of cell extracts, prepared under alkaline conditions, is dephosphorylated with alkaline phosphatase to produce sphingosine, which is then incubated with a SPHK preparation, i.e. the cytosol from cells transfected with cloned mammalian SPHK [38]. The cytosol of Swiss 3T3 cells [24] or partially purified enzyme [17,42] can also be used. Chain length and degree of saturation also affect activity, which can be promoted by the inclusion of phospholipids [24].

Table 1 S1P and sphingosine levels

Values are means, means ± S D or ranges

Species	Plasma/serum	S1P (μM)	Sphingosine (μM)	Ref
Human	Plasma	0 19 ± 0 08	–	[39]
Human	Serum	0 48 ± 0 08	–	[39]
Bovine (foetal)	Serum	0 34	0.05–0 1	[38]
Bovine (calf)	Serum	0 11	0 05–0 1	[38]
Bovine (calf)	Serum*	Negligible	0 05–0 1	[38]
Horse	Serum	0 68	0 05–0 1	[38]

Tissue (rat)	S1P (pmol/mg wet wt)	Sphingosine (pmol/mg wet wt)	Ref
Testis	98	–	[40]
Testis	0 5	6 5	[38]
Spleen	39	–	[40]
Spleen	2 4	22	[38]
Brain	37	–	[40]
Brain	5 8	8	[38]
Heart	8	–	[40]
Heart	0 6	6	[38]
Liver	1	–	[40]
Liver	0.7	9	[38]
Kidney	12	–	[40]
Kidney	0 6	8	[38]
Eye	2 1	1	[38]
Intestine	90	–	[40]
Lung	18	–	[40]
Muscle	3	–	[40]

Cell type	S1P (pmol/10^8 cells)	Sphingosine (pmol/10^8 cells)	Ref
Platelets	141 ± 4	37 ± 6	[37]
Neutrophils	150 ± 28	–	[39]
Erythrocytes	7 17 ± 1 66	–	[39]
Swiss 3T3	1600 ± 200	–	[43]
HL60	111 ± 10	2500 ± 280	[38]
Jurkat	40 ± 10	610 ± 60	[38]
U937	2030 ± 160	1380 ± 120	[38]
C6 glioma	1670 ± 390	414 ± 860	[38]
MCF7	1140 ± 140	11000 ± 570	[38]
PC12	860 ± 60	12100 ± 710	[38]

* Denotes charcoal-stripped

A comparison between these two methods (Table 1) shows an approximate 10-fold difference in the chemical amounts of S1P detected. The reasons for this are not clear. However, SPHK selectively phosphorylates only D-*erythro*-sphingosine and to a lesser extent D-*erythro*-dihydrosphingosine, whereas the acylation method would detect other lysolipids containing an amino group that might be present in the alkaline lipid extract.

AGONIST-STIMULATED S1P FORMATION

A wide variety of stimuli have been shown to increase SPHK activity and elevate S1P levels (Table 2). These include growth factors, GPCR agonists, cytokines, phorbol esters, vitamin D_3 and antigen.

PDGF and serum stimulated a rapid activation of SPHK (1.4–1.5-fold at 10–15 min) and transient production of S1P (maximum of 2.2–2.8-fold increase over basal at 3 min) in Swiss

Table 2 Agonist-stimulated S1P production

Abbreviations FMLP, formyl-Met-Leu-Phe, HUVEC, human umbilical-vein endothelial cells

(a) Acute and transient

Cell type	Stimulus	Ref
Swiss 3T3	PDGF/foetal calf serum	[43]
Airway smooth muscle	PDGF	[44]
M_2/M_3-transfected HEK 293	Carbachol	[45]
RBL-2H3 mast cells	Antigen	[46]
U937	Antigen	[47]
HL60	FMLP	[48]
HUVEC	TNFα	[49]
HEK 293	EGF	[51]

(b) Chronic and sustained

Cell type	Stimulus	Ref
HEL	PMA	[53]
PC12	NGF	[54]
HL60	Vitamin D_3	[55]
Vascular smooth muscle	Oxidized LDL	[56]
RP11 periosteal cells	Forskolin	[57]

3T3 fibroblasts [43]. PDGF also stimulated transient S1P formation in airway smooth-muscle cells [44]. Similar kinetics and magnitude of response were observed for carbachol stimulation of M_2 and M_3 muscarinic receptors in transfected HEK 293 cells [45], and antigen-stimulated clustering of high-affinity IgE receptors (FcεRI) in a rat mast cell line (RBL-2H3) [46] and of IgG receptors in cytokine-primed U937 cells [47], formyl peptide receptor-stimulated HL60 cells [48] and tumour necrosis factor α (TNFα)-stimulated human umbilical vein endothelial cells [49] These rapid and transient kinetics are consistent with a second messenger action and/or an autocrine/paracrine role. Epidermal growth factor (EGF) also stimulates SPHK, although this varies between different cell types. For example, EGF is without effect in Swiss 3T3 cells [50] and HEK2 clones, but is effective in a HEK3 clone [51].

The regulatory mechanisms governing SPHK activity have not been fully defined. The presence of calcium/calmodulin-binding domains and PKC phosphorylation sites in the protein suggest that receptor activation linked via phospholipase C (PLC) to inositol 1,4,5-trisphosphate and diacylglycerol formation may represent an acute mechanism for increasing activity of the kinase. Indeed, this appears to be the case for PDGF which has engaged PDGF receptor β. Using various mutants of PDGF receptor β, Olivera and colleagues [52] demonstrated that phenylalanine substitution of tyrosine-1021, which acts as a docking site for PLCγ, blocked PDGF-induced activation of SPHK. In contrast, mutation of tyrosine-740/751 and -1009, which are responsible for binding of phosphoinositide 3-kinase (PI3K) and SHP-2 respectively, did not abrogate PDGF-stimulated SPHK activity. Calcium-dependent activation of SPHK was supported by the inhibitory effects of intracellular Ca^{2+} chelators, such as BAPTA/AM [bis-(*o*-aminophenoxy)ethane-*N*,*N*,*N*′,*N*′-tetra-acetic acid tetrakis(acetoxymethyl ester)]. Whilst this supports a model in which Ca^{2+} mobilization by PDGF may activate SPHK, other studies suggest that SPHK activation *precedes* Ca^{2+} mobilization, e.g. in FcεRI-stimulated rat mast cells [46]. Other signalling pathways have also been implicated in the regulation of SPHK. For instance, in cytokine-primed U937 cells, SPHK activation was shown to be dependent upon the tyrosine kinase-mediated activation of phospholipase D (PLD) [47]. Furthermore, in HL60 cells, SPHK was stimulated by direct G-protein activation [48]. The mechanism underlying TNFα activation of SPHK remains undefined, but does not require prior sphingomyelinase and ceramidase activities [49].

SPHK can also be regulated chronically (hours/days), e.g. by PMA [53], nerve growth factor (NGF) [54], vitamin D_3 [55] and oxidized low-density lipoprotein (LDL) [56]. PMA-induced increases in SPHK activity in HEL cells were dependent upon both transcription and translation [53] and may be involved in differentiation. For instance, the NGF-stimulated differentiation of PC12 neuronal cells correlates with a 4-fold increase in the V_{max} of SPHK, an effect which required protein kinase activity and protein synthesis [54]. In HL60 cells, SPHK activation by vitamin D_3 supports a cytoprotective role for S1P [55]. Similarly, cAMP suppression of apoptosis in RP-11 periosteal cells is mediated by activation of SPHK [57]. Stimulation of S1P production by oxidized LDL, which occurs downstream of sphingomyelinase and ceramidase, has also been implicated in smooth-muscle cell proliferation [56].

EXTRACELLULAR VERSUS INTRACELLULAR ACTIONS

A key question is whether S1P formed intracellularly in response to extracellular agonists is released from cells to act on cell-surface GPCRs. In this manner, S1P would act as either an autocrine or a paracrine factor. Alternatively, S1P may function as a second messenger for growth factors, by altering the activity of specific intracellular target proteins (Figure 1). In the following, we have reviewed the evidence for both extracellular and intracellular actions of S1P.

Identification of GPCRs for S1P

To date, five closely related GPCRs of the EDG (endothelial differentiation gene) family (EDG1, EDG3, EDG5/AGR16/H218, EDG6 and EDG8/*nrg-1*) have been identified as high-affinity S1P receptors [58–64]. They are integral membrane proteins that are probably glycosylated, predicted to have seven transmembrane domains and exhibit approximately 50 % amino acid sequence identity.

EDG1 was identified as an immediate-early gene product in phorbol ester-differentiated human umbilical vein endothelial cells, and was suggested to play a role in the morphogenetic differentiation of vascular endothelial cells into capillary-like tubules and in angiogenesis [58]. Amino acid sequence analysis of EDG1 showed that it is a 380-amino-acid protein containing seven hydrophobic transmembrane-spanning domains and significant sequence similarity with the GPCR family [58]. Fusion of the third intracellular loop of EDG1 with glutathione S-transferase polypeptide was used to make an affinity matrix to which members of the G_i family could bind [65]. Indeed, overexpression of EDG1 in HEK 293 cells led to association with $G_{i\alpha1}$ and $G_{i\alpha3}$ polypeptides [65]. Furthermore, EDG1-induced activation of extracellular-signal-regulated kinase (ERK) was blocked by pertussis toxin (which ADP-ribosylates and inactivates G_i/G_o) [65]. A high similarity (25 %) between EDG1 and the cannabinoid receptor suggested that the EDG1 ligand may be a lipid. This was confirmed in assays of morphogenetic differentiation, which was dependent on EDG1 expression and the presence of serum-borne lipid, S1P. Further characterization studies confirmed EDG1 to be a GPCR with high affinity for S1P (measured K_d values of 8.1 nM [66] and 13.2 nM [67]). A variety of sphingolipids and lysolipids failed to significantly displace [^{32}P]S1P in EDG1-transfected cells [66,67].

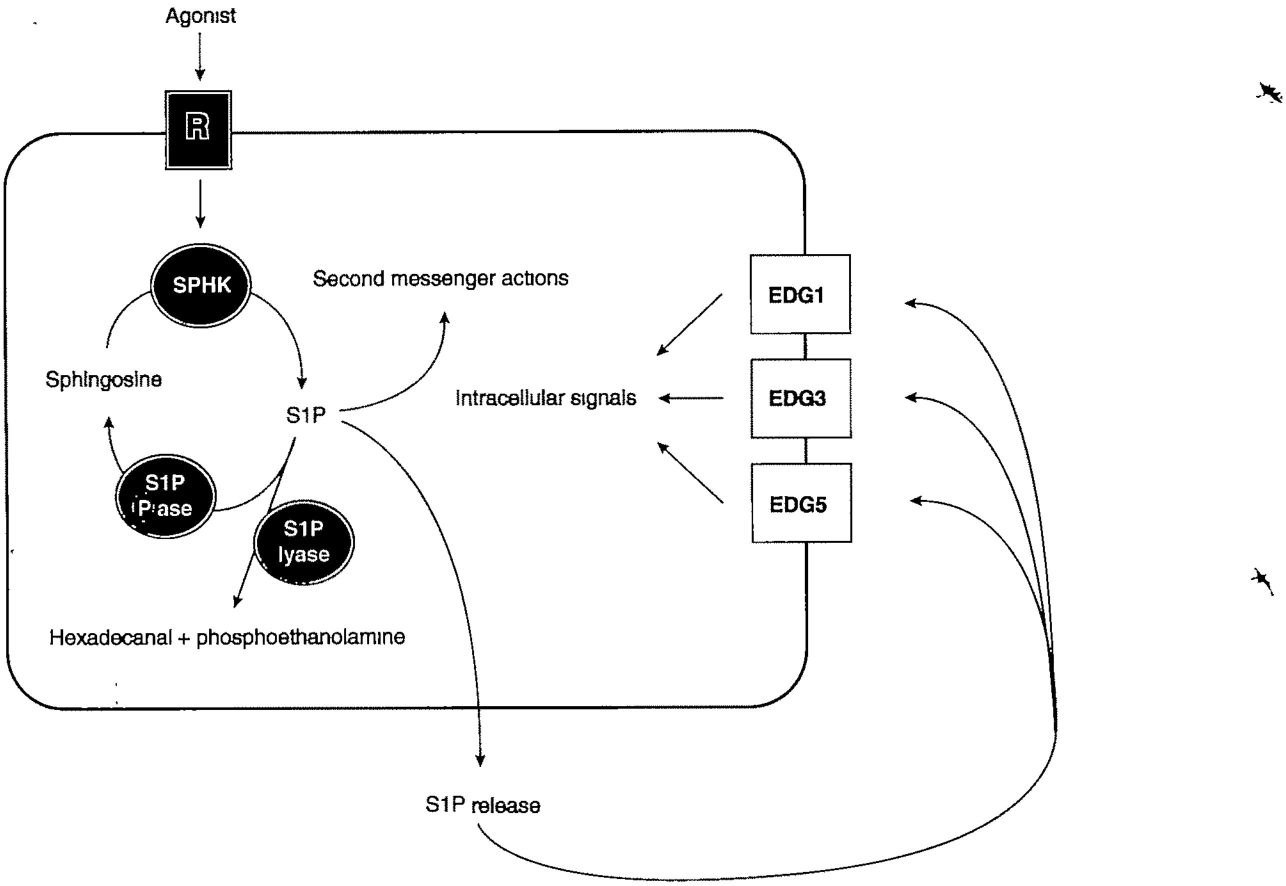

Figure 1 Extracellular versus intracellular role of S1P

S1P produced in response to agonist stimulation may elicit second messenger actions before its removal by S1P phosphatase and/or S1P lyase In addition, S1P may be released from cells to act in a paracrine and/or autocrine manner at EDG receptors R, receptor

Other studies using transfected CHO, HEL, Cos-7 and Sf9 cells have all confirmed that EDG1 functions as a high-affinity S1P receptor which couples to a number of signalling pathways via G_i/G_o [68,69]. More recently, EDG1-transfected Sf9 cells were used to establish that S1P binding to this receptor in fact activates several members of the G-protein family, including G_{i1}, G_{i2}, G_{i3}, G_o and G_z, but not G_s, G_q, G_{12} or G_{13} [70]. Others have also shown that EDG1 receptors can utilize Rho-dependent signalling. For instance, S1P-stimulated morphogenetic differentiation of EDG1-transfected HEK 293 cells was shown by Lee et al. [66] to be G_i-independent and blocked by the C3 exoenzyme, a specific inhibitor of the small GTPase Rho, which regulates stress fibre formation and focal adhesions [71]. Recent studies have confirmed these findings in T lymphoma cells, where Rho and Rac appear to be involved in S1P-induced migration [72].

EDG1 has also been reported to act as a low-affinity receptor for LPA (K_d 2.3 μM), the binding of which induces EDG1 receptor phosphorylation [73]. However, no effects of LPA were evident in membranes of Sf9 cells co-expressing EDG1 and G_{i2}, whereas S1P was effective [70].

EDG3 and EDG5 also have high affinity for S1P (measured K_d values of 23 nM and 27 nM respectively [74] and 26.2 nM and 20.4 nM respectively [67]), which is poorly displaced by other sphingolipids and lysolipids, including LPA, sphingosylphosphocholine (SPC), cyclic S1P, C_8-ceramide 1-phosphate, ceramide and sphingosine [74]. DihydroS1P (K_i 15 nM [75]) and SPC are most effective. The K_d for S1P binding at EDG6 is 12–19 nM [62], with SPC exhibiting an approx. 50-fold lower binding affinity, whereas LPA was ineffective. The recently cloned EDG8 has a K_d of 2 nM for S1P, dihydroS1P was equipotent, whereas SPC was relatively ineffective [63].

EDG3 and EDG5 communicate not only via G_i, but also through G_q, G_{12} and G_{13} [76–78]. Interestingly, in transfected Sf9 cells, the expression of EDG3 and EDG5 also produced constitutive activation of G_{12} and G_{13} respectively [70]. Several studies are consistent with the use of G_q, G_{12} and G_{13} by these EDG receptors. Co-expression of a G_q/G_i α subunit chimaera ($G\alpha_{qi}$) with EDG3 or EDG5 potentiated S1P-stimulated rises in intracellular Ca^{2+}. Furthermore, co-expression of $G\alpha_{qi}$ with EDG1 allowed S1P-stimulated coupling to the G_q pathway [78]. In addition, it was also shown that suramin acts as a subtype-specific functional antagonist of EDG3 (IC_{50} 22 μM) [78]. EDG6 couples via $G_{i/o}$, whereas a role for G_q, $G_{12/13}$ and/or Rho has yet to be addressed [62]. EDG8 couples via $G_{i/o}$, but not through G_q [63].

As a general paradigm, the role of Rho in EDG receptor signalling has still to be fully defined. For EDG3 and EDG5 receptors, coupling to $G_{12/13}$ may be the predominant route of Rho activation [79,80]. Indeed, $G\alpha_{12/13}$ has been shown to initiate RhoGTP regulation of serum response element (SRE)-mediated transcription, cytoskeletal rearrangement, PLD and PI3K [81]. Moreover, RhoGEF, which promotes guanine nucleotide exchange in Rho, is stimulated by G_{13} [82,83]. The mechanism for this remains to be determined. One possibility is that the

$G\beta\gamma_{13}$ dimer may act as an adaptor for Rho. As mentioned above, EDG1 receptor signalling has also been shown to be Rho-dependent [66], e.g. S1P stimulates morphogenetic changes in EDG1-transfected HEK 293 cells. However, studies by Windh et al. [70] demonstrated that EDG1 does not functionally couple to G_{12} or G_{13} Therefore EDG1 must activate Rho by a different mechanism.

These observations support the conclusion that S1P-specific EDG GPCRs couple productively to different types of G-protein α subunits, $\beta\gamma$ subunits and Rho (Figure 2).

A second group of EDG receptors (EDG2, EDG4 and EDG7) have high affinity for LPA (35 % identity with EDG1, 3, 5 and 8). EDG2 (or Vzg-1) was the first EDG family member to have its ligand identified. EDG2 overexpression in a neuronal-like cell (TSM) exaggerated LPA-stimulated cytoskeletal changes (Rho-mediated) and inhibition of adenylate cyclase (G_i-mediated) [84] A sequence-based search subsequently identified EDG4 [85]. EDG2- and EDG4-transfected HTC4 hepatoma cells (which have a LPA-null background) exhibit LPA-stimulated calcium transients [86], and EDG2 expression in yeast confers LPA responsiveness [87]. EDG7-transfected Sf9 cells exhibit LPA-stimulated calcium mobilization and increased cAMP levels [88]. These effects are similar to those elicited by stimulation of S1P-specific EDG receptors, and suggest that the two lysolipids may signal via common pathways.

Extracellular GPCR-mediated actions of S1P

Many signalling pathways are activated in response to stimulation of cells by S1P. An S1P-dependent decrease in forskolin- and cholera toxin-stimulated intracellular cAMP levels has been observed in several cell types (see Figure 2). This has been correlated with EDG1 expression [67–69,75,89]. The effect is blocked by pertussis toxin pretreatment and is probably mediated by a typical G_i/adenylate cyclase interaction. More recently, S1P has been shown to inhibit forskolin-stimulated cAMP formation in EDG3-transfected CHO cells [90] and EDG8-transfected Rh7777 hepatoma cells [63] via a pertussis toxin-sensitive mechanism. In contrast, there are a number of cell types in which stimulation by S1P produces an increase in intracellular cAMP [67,91,92]. For example, S1P-stimulated cAMP formation is pertussis toxin-insensitive in EDG3- and EDG5-transfected CHO cells [67,92]. Since EDG receptors appear not to couple to G_s, it is probable that increased cAMP synthesis is mediated by cross-talk via the G_q/PLC signalling pathways. In this case the activation of calcium/calmodulin-sensitive or PKC-stimulated adenylate cyclase isoforms might be involved.

There are a number of studies in which S1P has been shown to activate PLC-catalysed inositol phosphate formation [67,68,91–93]. The EDG1-mediated response was blocked by pertussis toxin [68], whereas that mediated by EDG5 was only reduced by 30 % [92]. For EDG1, this effect may be mediated by $G\beta\gamma_i$ subunit regulation of PLCβ. More recently, EDG1-, EDG3- and EDG5-transfected CHO cells have been compared [67]. S1P-stimulated inositol phosphate production was observed in EDG3- and EDG5-transfected cells, which in both cases was moderately inhibited but not abolished by pertussis toxin. In contrast, S1P binding to EDG1 did not produce a response [67]. EDG6-transfected cells also exhibit a S1P-stimulated PLC activity that is blocked by pertussis toxin [62]. Consistent with the production of diacylglycerol and Ins(1,4,5)P_3-sensitive Ca^{2+} mobilization, conventional isoforms of PKC (α and β) translocate to the membrane in response to S1P, as does the atypical PKCϵ [93]. Regulation of other glycerophospholipid signalling pathways by S1P also appears to be mediated by both G_i-independent and G_i-dependent routes. S1P-dependent activation of PLD was reported to be independent of EDG1 expression [75] and insensitive to pertussis toxin [75,93].

Stimulation of Ca^{2+} mobilization by S1P (EC_{50} 1 nM) has also been correlated with EDG1 expression [68]. High concentrations of S1P (10 μM) were required for Ca^{2+} mobilization in EDG1-transfected HEK 293 cells [75] and in the rat mast cell line RBL-2H3 [46]. EDG3- and EDG5-transfected cells also exhibit pertussis toxin-sensitive S1P-stimulated Ca^{2+} mobilization {reported EC_{50} values of $\approx$ 2 nM and 20 nM respectively [67], and of $\approx$ 3 nM (EDG5) [92]}. However, others have shown the Ca^{2+} response in EDG3- and EDG5-transfected cells to be largely pertussis toxin-insensitive [90]. In oocytes microinjected with EDG3 and EDG5 mRNA, S1P stimulated Ca^{2+} mobilization via a G_q-dependent mechanism, although both receptors were also shown to couple to G_i [78]. S1P mobilizes intracellular Ca^{2+} in EDG6-transfected CHO cells in a pertussis toxin-sensitive manner [62], whereas S1P stimulation of EDG8-transfected Rh7777 cells failed to mobilize intracellular Ca^{2+} [63]. Therefore EDG-receptor-dependent Ca^{2+} mobilization appears to be differentially regulated by G_i- and G_q-linked pathways.

The S1P-stimulated activation of ERK1/ERK2 has been widely observed Using cultured airway smooth muscle cells, which express EDG1 but not EDG3, we were one of the first to show that activation of ERK by S1P is pertussis toxin-sensitive [94,95], clearly implicating the involvement of a GPCR acting via G_i (airway smooth muscle cells do not express G_o). Several others have shown that the S1P-stimulated activation of ERK is pertussis toxin-sensitive in EDG1-transfected cells [66,68,69]. Studies on GPCR signalling to ERK have identified the involvement of $G\beta\gamma_i$ dimers [96,97], which regulate non-receptor tyrosine kinase-catalysed phosphorylation of Shc and the sequential recruitment of Grb-2 and mSos. In airway smooth muscle cells, S1P activates c-Src tyrosine kinase via a pertussis toxin-sensitive mechanism. Furthermore, c-Src inhibitors abrogated the S1P-dependent activation of ERK [89]. Thus S1P signalling via EDG1 may involve the generation of free $G\beta\gamma_i$ subunits, which may stimulate c-Src to initiate activation of the ERK cascade.

$G\beta\gamma_i$ subunits have also been shown to regulate PI3K, which has been identified as playing a critical role in linking GPCRs to the stimulation of ERK [98,99]. We have shown that the S1P-dependent activation of ERK via EDG1 was inhibited by two structurally dissimilar PI3K inhibitors (LY294002 and wortmannin). Moreover, PI3K activity was present in immunoprecipitates of Grb-2 (an intermediate in the ERK pathway) prepared from S1P-stimulated cells, an effect which was pertussis toxin-sensitive. These findings support a model whereby the EDG1 receptor is coupled via G_i to Grb-2/PI3K complex-formation [89]. This is similar to observations made in Rat-1 and Cos-7 cells with LPA, which also acts via PI3K [100]. Kranenberg et al. [100] also showed that LPA stimulated the tyrosine phosphorylation of dynamin II, which binds to the C-terminal SH3 domain of Grb-2 in an agonist- and G_i-dependent manner. PI3K inhibitors prevented LPA-stimulated dynamin II tyrosine phosphorylation and ERK activation. The latter suggests that PI3K regulates an unidentified novel tyrosine kinase which phosphorylates dynamin II. These studies, together with those on S1P, suggest that LPA and S1P might utilize similar signalling pathways to regulate ERK.

The interaction between Grb-2 and PI3K is entirely consistent with studies demonstrating that insulin and insulin-like growth factor-I (IGF-I) receptors stimulate ERK via a PI3K-dependent pathway involving the tyrosine phosphorylation of Gab1 (Grb-2-associated binder-1 protein), which has been shown to activate

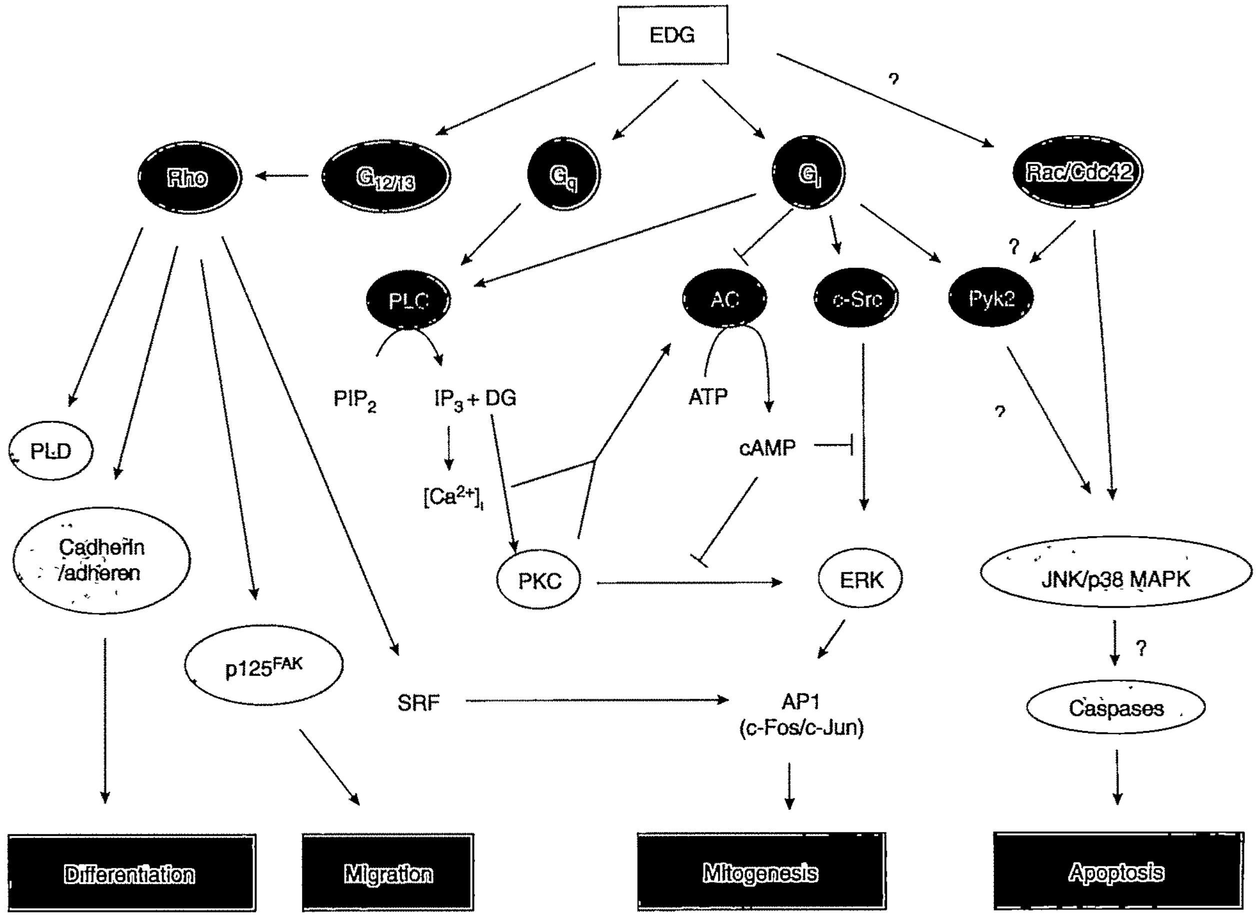

Figure 2 S1P-stimulated signal transduction

Diagram showing the known signalling pathways activated by S1P binding to EDG receptors regulating mitogenesis, chemotaxis, differentiation and apoptosis It should be noted that this encompasses all EDG receptors However, differential coupling to G-proteins and effectors may be apparent for EDG1, EDG3 and EDG5 Levels of cAMP can be increased indirectly via G_q or reduced via G_i to limit the mitogenic pathway However, in some cell types (e g Swiss 3T3 cells), cAMP increases mitogenesis Abbreviations AC, adenylate cyclase, PIP_2, PtdIns(4,5)P_2, IP_3, Ins(1,4,5)P_3, DG, diacylglcerol; AP1, activator protein 1

p85/p110 PI3K1a [101,102]. It remains to be determined whether S1P can induce stimulation of Gab1 tyrosine phosphorylation (c-Src mediated) as a possible mechanism for Grb-2-associated PI3K activation. The stimulation of certain GPCRs (e.g. β-adrenergic) induces binding of β-arrestin I and II to receptors and sequential phosphorylation of the Grb-2 adaptor protein, dynamin II (molecular mass 100 kDa), which mediates clathrin-dependent GPCR internalization by endocytosis [103]. Recent studies have shown that β-arrestin I/II- and dynamin II-mediated internalization of MEK-1 [mitogen-activated protein kinase (MAPK)/ERK kinase] is a mandatory stimulatory signal required for the GPCR-dependent activation of ERK. Thus inhibitors of clathrin-mediated endocytosis or the expression of dominant-negative mutants of β-arrestin I/II or dynamin II abrogate GPCR-stimulated activation of this kinase [104,105]. Significantly, using HEK 293 cells, Lee et al. [66] showed that expression of EDG1 fused with a C-terminal green fluorescent protein was localized primarily on the plasma membrane, but that this construct was internalized upon stimulation with 100 nM S1P for 2 h.

In general terms, the activation of the ERK pathway by S1P shows differential sensitivity to pertussis toxin [106,107]. In C6 cells, the pertussis toxin-insensitive component was abolished by inhibition of PKC, and was attributed to EDG5 linked to G_q/PLC. In contrast, S1P-induced ERK activation occurs entirely through a $G_{i/o}$-dependent pathway in EDG5-transfected CHO cells [92] and in HTC4 cells transfected with either EDG3 or EDG5 [108]. Interestingly, in the HTC4 cells, the concentration-dependence for S1P activation of ERK differs for EDG3 and EDG5, being maximal at 10 nM and 100 nM respectively [108], suggesting that the efficiency of coupling to G_i differs.

S1P can activate a number of non-receptor tyrosine kinases in order to transmit signals to well defined effector systems. For example, S1P activates Pyk2, which has been identified as a Ca^{2+}- and PKC-regulated effector of GPCRs, resulting in the activation of ERKs [106,109]. However, in rat aortic smooth muscle cells, S1P-activated Pyk2 and ERK were not linked, since Pyk2 activation was pertussis toxin-sensitive, while that of ERK was not [106]. Other non-receptor tyrosine kinases which are activated by S1P include Syk [110], Crk [111] and $p125^{FAK}$ (where FAK is focal adhesion kinase) [75,112]. Syk requires PKC and transmits signals to Ras, PI3K and PLCγ. Crk activation correlates with increased mitogenesis, while $p125^{FAK}$ phosphorylation is associated with cytoskeletal changes and formation of focal adhesions. S1P-stimulated $p125^{FAK}$ phosphorylation is EDG1-

LPP1 : 118-KYSIGRLRP--37--SFYSGHS--38--IYVGLSRISDYKHHWSD-227
LPP1a : 121-KYSIGRLRP--37--SFYSGHS--38--IYVGLSRVSDYKHHWSD-228
LPP2 : 117-KYMIGRLRP--37--SFYSGHA--38--LYVGYTRVSDYKHHWSD-224
LPP3 : 148-KVSIGRLRP--37--SFFSGHA--38--FYTGLSRVSDHKHHPSD-255

LBP-1 : 128-KDYWCLPRP--18--GAPSSHT--36--MTLVFGRIYCGMHGILD-214
LBP-2 : 129-KDYWCLPRP--18--GAPSSHS--36--LTLVFGRVYCGMHGMLD-215

Consensus KXXhXXXRP--X_{12-54}-XXXSnHn-X_{31-54}-XXXXXnRhXXXXHXXXD

Figure 3 Conserved phosphatase motif of lipid phosphate phosphatases and S1P phosphatase

Amino acid sequence alignment of mammalian LPP isoforms (LPP1, LPP1a, LPP2 and LPP3) and *Saccharomyces cerevisiae* LBP1/LBP2 (S1P phosphatases). Fully conserved residues are indicated in red in the consensus sequence X, any amino acid, h, hydrophobic amino acid, n, neutral amino acid (Ala, Cys, Gly, Ser)

independent [75,112] and is not inhibited by suramin [75] (an EDG3 antagonist [78]), thereby implicating EDG5 (or EDG6) as the probable GPCR involved. Furthermore, S1P-stimulated p125^{FAK} phosphorylation was inhibited by C3 exoenzyme, suggesting the involvement of Rho [75,112].

The regulation of PLD by Rho family members, such as Rho, Rac and Cdc42, is well established [113]. Therefore the S1P-dependent activation of PLD might be mediated by these low-molecular-mass G-proteins. Other effector systems which involve Rac and Cdc42 and which are activated by S1P include the stress-activated protein kinases c-Jun N-terminal kinase (JNK) and p38 MAPK, as demonstrated in EDG5-transfected CHO cells [92]. Both p38 MAPK and JNK have been implicated in the regulation of apoptosis.

Gene transcription is also activated in response to stimulation by S1P. For example, S1P stimulates the induction of the AP1 transcription factors c-Jun and c-Fos [114]. This has recently been shown to be mediated by both EDG3 and EDG5 [108]. The induction of other immediate-early genes is mediated by the promoter SRE in a Rho-dependent manner. SRE is activated co-operatively by the transcription factors serum response factor (SRF) and Elk-1 [115,116]. Both of these transcription factors can be activated by S1P via EDG3 or EDG5 [108].

Bunemann et al. [117] have shown activation of the muscarinic K^+ current by S1P in isolated cultured guinea-pig atrial myocytes. Desensitization of the muscarinic receptor did not affect the response to S1P, which was blocked by pertussis toxin. These results were interpreted as reflecting S1P binding to a GPCR that could activate a K^+ channel normally linked to other GPCRs, such as muscarinic receptors. Others have shown that S1P increases the minimum stimulus current needed to induce an action potential in isolated myocytes. S1P reversibly inhibited the peak Na^+ current by 50 pA, while the inward rectifier K^+ current was unaffected [118].

S1P signal termination at EDG receptors

The termination of EDG receptor signal transduction has not been established. We are focusing on a mechanism that involves the dephosphorylation of S1P to sphingosine. This could be catalysed by S1P phosphatase (an integral membrane protein with seven predicted transmembrane domains) [35] and/or a lipid phosphate phosphatase [LPP1, or type 2 PA phosphatase (PAP2), an integral membrane protein with six transmembrane domains] [32]. S1P phosphatase and members of the LPP family, including LPP1, contain a novel phosphatase motif [KXXXXXXXRP(X_{12-54})PSGH(X_{31-54})SRXXXXXXHXXXD] which is found in a superfamily of phosphatases [119] (Figure 3). Recently, site-directed mutagenesis has been used to establish that the conserved residues Lys, Arg, Pro, Ser, Gly, His, Arg and His are obligatory for the catalytic activity of LPP1 [120]. Significantly, the LPP1 isoform is located at the plasma membrane, with an externally oriented catalytic site [121]. Thus LPP1 may decrease extracellular S1P levels to limit its bioavailability at EDG receptors (Figure 4). This might require a co-ordinated mechanism that enables S1P to induce 'downstream' signalling responses before LPP1 is activated to reduce the extracellular concentration of S1P. This could involve an intracellular phosphorylation/dephosphorylation mechanism. In this regard LPP1 has putative cytoplasmic-facing phosphorylation sites for ERK, casein kinase, PKC and protein kinase A [122]. Overexpression of LPP1 has been shown to block LPA-stimulated ERK activation and DNA synthesis in Rat-1 cells [121].

Evidence for an intracellular role for S1P

A second messenger role for S1P was first proposed when a kinase-dependent sphingosine-stimulated release of Ca^{2+} from intracellular stores was observed [123,124]. In addition, mitogenesis of Swiss 3T3 cells in response to sphingosine was shown to be mimicked by S1P. The effect of sphingosine was believed to occur through its rapid conversion into S1P [125]. Furthermore, DNA synthesis in Swiss 3T3 cells was increased by microinjection of S1P [75]. Moreover, stimulation of cells with various mitogens elicits the production of S1P (see Table 2). However, many of the functions of S1P previously attributed to a second-messenger role may be due to its action at EDG receptors, especially since a large number of studies invoking intracellular actions involve the application of exogenous S1P to cells (see below; Figure 5).

Evidence to support an intracellular role for S1P has been based mainly on the stimulation of SPHK by agonists, the use of SPHK inhibitors and, more recently, transfection of SPHK.

Exogenous-S1P-stimulated activation of the ERK1/2 pathway in Swiss 3T3 cells was observed to be partially (70–80 %) inhibited by pertussis toxin [95]. Thus it was proposed that S1P acts both extracellularly (pertussis toxin-sensitive) and intracellularly (pertussis toxin-insensitive) to regulate the ERK1/2 pathway [126]. In hindsight, one cannot exclude a role for G_q-linked activation of ERK, which would be pertussis toxin-insensitive. In contrast with Swiss 3T3 cells, S1P-stimulated ERK1/2 activity in ASM

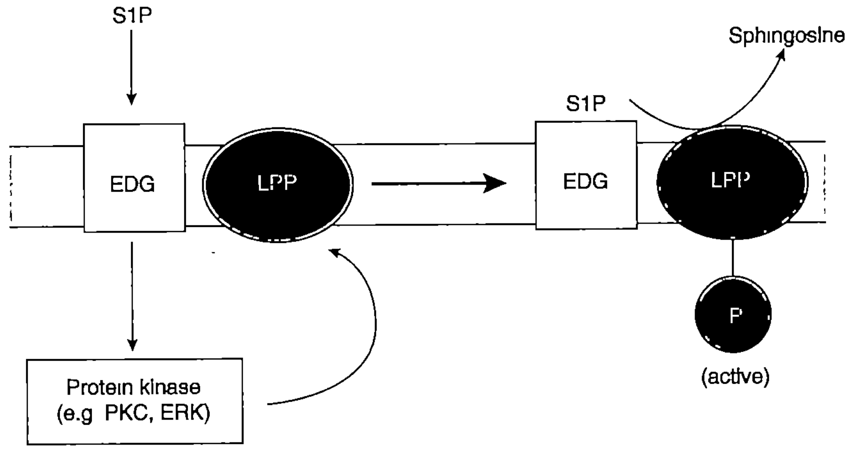

Figure 4 Model for signal termination at EDG receptors

S1P binding to the EDG receptor activates protein kinases which phosphorylate the ecto-lipid phosphate phosphatase (LPP) Activated LPP dephosphorylates extracellular S1P and thereby terminates its signalling and/or limits its bioavailability

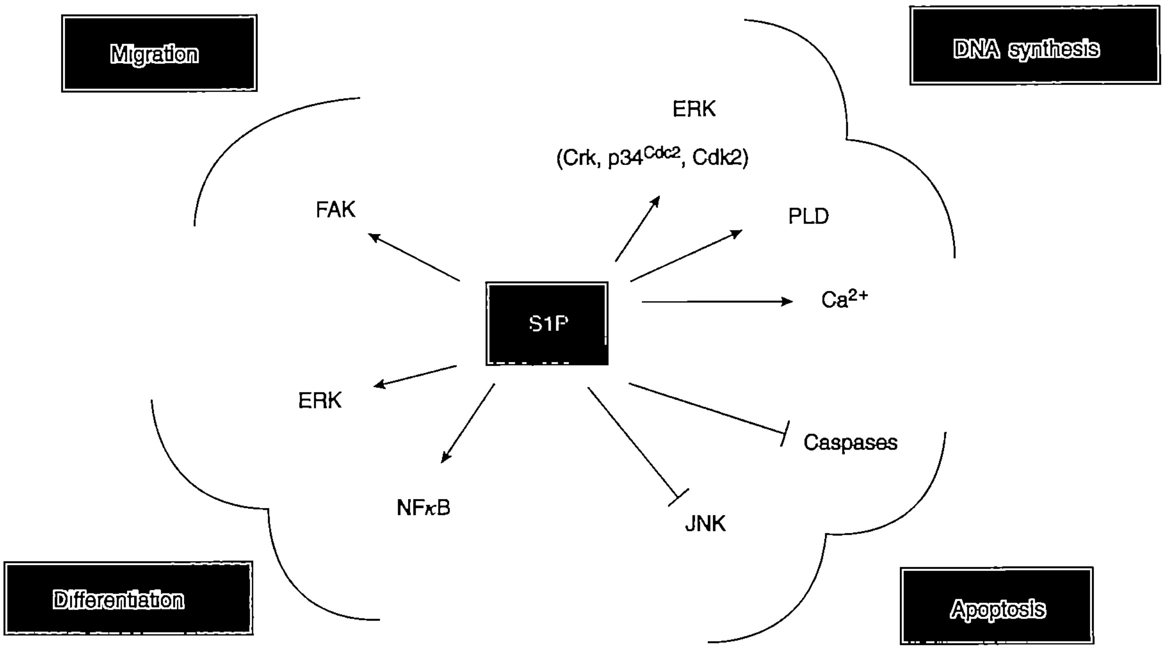

Figure 5 Possible intracellular actions of S1P

Diagram showing possible intracellular actions of S1P affecting DNA synthesis, apoptosis, differentiation and cell motility Abbreviation NFκB, nuclear factor κB

cells was completely abrogated by pertussis toxin [94]. In this case, an entirely extracellular action of S1P was corroborated by studies which showed that the addition of sphingosine to cells and its intracellular conversion into S1P failed to support ERK1/2 activation in C6 glioma cells [107]. Thus intracellular increases in S1P do not support activation of this kinase in this case.

More recently, Van Brocklyn and colleagues [75] examined the effects of exogenous S1P in HEK 293 cells transfected with EDG1. S1P-stimulated calcium mobilization, $p125^{FAK}$ phosphorylation and activation of PLD were shown to be independent of EDG1 expression. Furthermore, mitogenesis and the prevention of apoptosis were correlated with S1P uptake into cells, but not with EDG1 expression. These observations were interpreted as evidence for an intracellular role for S1P. However, one cannot exclude the possibility that additional types of S1P receptor are expressed which were not detected in ligand binding assays. In this regard, An et al. [108] have correlated the expression of EDG3 and EDG5 in HTC4 hepatoma cells with S1P-induced proliferation and survival. A receptor-dependent action of S1P was supported by reporter gene assays in EDG3- and EDG5-transfected Jurkat cells. These effects were inhibited by abrogation of $G_{i/o}$- and Rho-dependent pathways [108]. Therefore partial pertussis toxin sensitivity can no longer be presumed to reflect a receptor-independent, intracellular site of action of S1P. However, the intracellular action is supported by experiments which showed that dihydroS1P (sphinganine 1-phosphate) competes with S1P for binding to EDG1 [75], EDG3 and EDG5 [74], but lacks a cytoprotective effect.

Using Swiss 3T3 fibroblasts, Rani et al. [50] proposed that S1P formed in response to PDGF can function as a second messenger. This was based upon experiments which showed that the SPHK inhibitor D,L-*threo*-dihydrosphingosine abrogated PDGF-stimulated S1P formation and ERK1/2, Crk, $p34^{cdc2}$ and Cdk2 kinase activation. We obtained identical results for inhibition of PDGF-stimulated ERK1/2 activity with D,L-*threo*-dihydrosphingosine in cultured ASM cells [127,128]. However, D,L-*threo*-dihydrosphingosine is also a PKC inhibitor [129], and this might represent an alternative route through which ERK1/2 activation is abrogated, especially as PKC is an intermediate in the ERK1/2 cascade activated by PDGF [130,131]. This was further supported by studies which showed that other sphingoid bases, such as *N,N*-dimethylsphingosine and D,L-*erythro*-sphingosine (the substrate of SPHK), which also inhibit PKC [129], blocked ERK1/2 activation with identical concentration-dependence [130]. Thus inhibition by dihydrosphingosine or *N,N*-dimethylsphingosine should not be presumed to be at the level of SPHK alone. In contrast, Edsall et al. [132] reported that, in PC12 cells, 10 μM *N,N*-dimethylsphingosine had no effect on PMA- and NGF-stimulated PKC activity or on PMA-induced PKCα and PKCδ translocation to membranes, despite competitively inhibiting SPHK. However, PKC was assayed using a commercial PKC kit which is not optimized for individual PKC isoforms. Furthermore, the PKC isoforms translocated in response to NGF and the effects of *N,N*-dimethylsphingosine were not established.

N,N-Dimethylsphingosine has also been used to implicate S1P as an intracellular signal involved in the inhibition of apoptosis and the promotion of cell survival. For example, Cuvillier et al. [133] showed that activation of JNK and apoptosis of promyelocytic HL60 and U937 monoblastic leukaemia cells induced by TNFα, sphingomyelinase, cell-permeable ceramide or PKC inhibitors was prevented by the addition of exogenous S1P. Similarly, the cell survival effect of 1α,25-dihydroxyvitamin D_3 in HL60 cells is via a mechanism involving activation of SPHK and S1P formation, whereas cytoprotection against ceramide-induced cell death was blocked by *N,N*-dimethylsphingosine [55]. Additionally, S1P inhibits various caspase activities and protects against ceramide- and Fas-induced apoptosis [23,133]. However, the sensitivity of these effects to pertussis toxin and C3 exoenzyme and, therefore, the involvement of EDG receptors was not investigated.

Inhibition of SPHK by dihydrosphingosine (K_i 5–18 μM) has also been used to support a second-messenger role for S1P in antigen clustering of FcεRI and subsequent intracellular calcium mobilization in a rat mast cell line (RBL-2H3) [46]. In oligodendroglial cells, PDGF-BB stimulates SPHK and induces oscillatory and non-oscillatory calcium signals. The oscillatory signal is due to the action of sphingosine, while the non-oscillatory component is mediated by S1P. Thus dihydrosphingosine was shown to increase the percentage of cells producing Ca^{2+} spikes in response to PDGF-BB. This effect was correlated with a decrease in PDGF-stimulated S1P formation and elevated levels of sphingosine [134,135]. Similarly, stimulation of muscarinic M_2 and M_3 receptors expressed in HEK 293 cells also induced calcium signals that were blocked by dihydrosphingosine and *N,N*-dimethylsphingosine [45]. A general role for S1P in Ca^{2+} mobilization has been suggested for some, but not all, GPCRs [45]. Furthermore, microinjection of S1P induced rapid, transient Ca^{2+} mobilization which was not antagonized by heparin, thereby excluding a role for inositol trisphosphate and its receptor [45]. Similarly, heparin did not block the S1P-induced mobilization of Ca^{2+} in a microsomal preparation [124]. However, intracellular release of caged dihydrosphingosine has also been shown to mobilize Ca^{2+} from ryanodine-sensitive intracellular stores in cultured neurons [136]. Moreover, SPC also releases microsomal Ca^{2+} [124,137], thereby questioning the specificity of the S1P effect. In addition, others have failed to detect S1P-induced mobilization of intracellular calcium [138,139].

Sphingosine-stimulated increases in intracellular Ca^{2+} appear to be mediated by PA. This may involve PA species derived from a PLC/diacylglycerol kinase pathway. Thus the diacylglycerol kinase inhibitor R59002 decreased both PA formation and Ca^{2+} mobilization [139]. S1P does not appear to activate this pathway, but instead can stimulate the formation of distinct PA species via a PLD route. Thus the effect of sphingosine on calcium mobilization is not due to its conversion into S1P. Other effects of sphingosine include a PKC-dependent action on Ca^{2+} dynamics [140] and blockade of ryanodine receptors [141]. Additionally, SPC releases Ca^{2+} from isolated sarcoplasmic reticulum in a ryanodine-receptor-dependent manner [142] and activates GPCR-mediated Ca^{2+} mobilization [143,144]. The advent of caged sphingolipids, including caged S1P [145,146], should progress this area of research, which remains controversial.

Cloning of SPHK [18] has led to an alternative approach to investigate the intracellular role of S1P. A 500-fold overexpression of SPHK in NIH 3T3 cells and HEK 293 cells resulted in a 4–8-fold increase in S1P levels, and promoted growth in low-serum medium, the G1/S transition, DNA synthesis and increased cell number. Overexpression of SPHK also protected against apoptosis induced by serum deprivation or ceramide in NIH 3T3 and HEK 293 cells, and reduced that in Jurkat T cells stimulated with anti-Fas. The protective effects of SPHK were blocked by *N,N*-dimethylsphingosine [25]. An autocrine role for S1P was not apparent, since S1P was not detected in the extracellular medium. Furthermore, the protective effect of S1P was not blocked by pertussis toxin, thereby eliminating a role for EDG1. However, signalling via pertussis toxin-insensitive pathways involving EDG3 and EDG5 receptors remains a possibility. Indeed, S1P-induced proliferation and survival have recently been demonstrated in EDG3- and EDG5-transfected HTC4 hepatoma cells [108]. Additionally, other effects of SPHK overexpression may play a role, e.g. a concomitant decrease in cellular ceramide levels.

THE CERAMIDE/S1P RHEOSTAT

The balance between cellular concentrations of ceramide and S1P has been proposed to determine the physiological fate of the cell. Generally, S1P and ceramide elicit opposing cellular fates, e.g. proliferation and survival versus growth arrest and apoptosis. However, it should be noted that there is considerable controversy as to whether ceramide is a physiological mediator of apoptosis [147,148], as most studies have either correlated increased intracellular ceramide with apoptosis or have used exogenous short-chain ceramides (which may have non-specific membrane-perturbing effects). The rheostat model is, therefore, currently based on the assumption that ceramide does indeed induce apoptosis. This is believed to be due to the differential regulation by ceramide and S1P of members of the ERK and stress-activated protein kinase families and caspase proteases [23,44,149]. Importantly, the rheostat model for controlling the ceramide/S1P balance and cell fate does not rely upon whether S1P acts intracellularly or as an EDG receptor agonist (Figure 6).

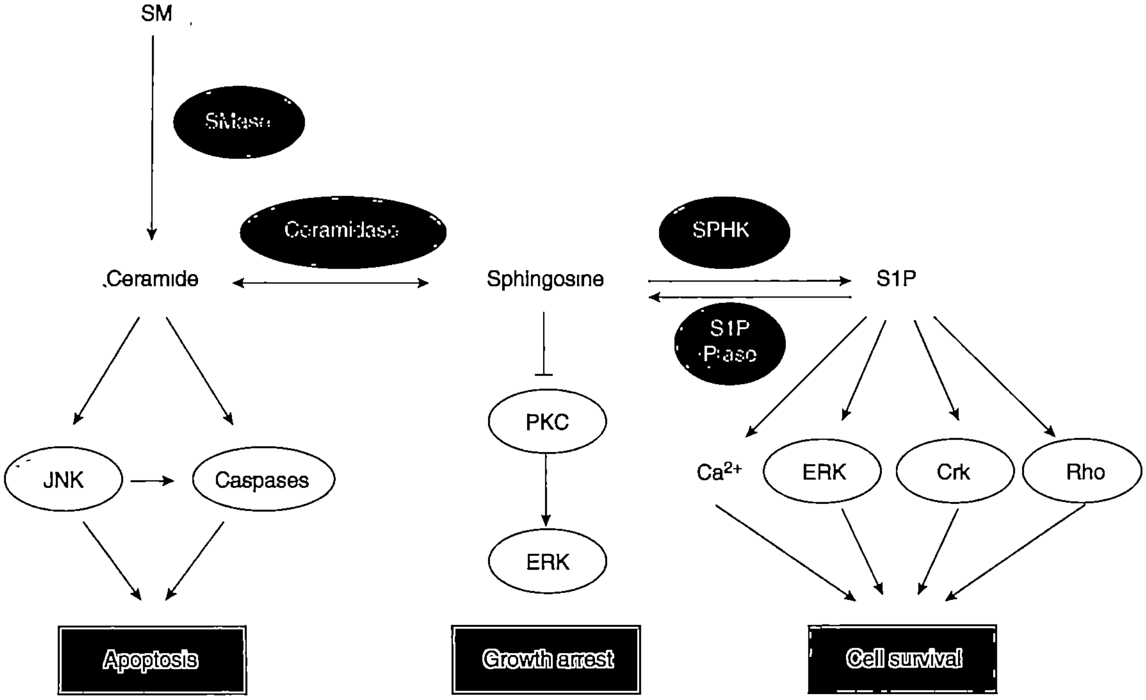

Figure 6 The rheostat model

The conversion of ceramide into sphingosine and S1P determines cell fate, based upon data which show that, as a general rule, ceramide induces apoptosis (caspase activation), whereas S1P induces cell survival Agonists differentially regulate the rheostat enzymes, ceramidase and SPHK Abbreviation. SM, spingomyelin

Cell-permeant ceramides strongly activate JNK in cultured airway smooth muscle cells, but are weak or ineffective with regard to activation of ERK1/2 [44]. Sphingosine inhibits ERK1/2 activation by PDGF, S1P and bradykinin, and is anti-proliferative in airway smooth muscle cells [128]. In contrast, exogenously applied S1P activates the ERK1/2 cascade and is co-mitogenic. Furthermore, ceramide/sphingosine and S1P elicit opposing effects on cAMP levels which might also contribute to their differential outcomes on DNA synthesis [94]. Similar observations have been made in glomerular mesangial cells [149], where cell-permeable ceramides activate JNK and inhibit PDGF-stimulated DNA synthesis. However, sphingosine stimulates ERK1/2 and proliferation. Thus the effect of sphingosine varies between cell types. This may depend on the metabolism of sphingosine, e.g. to S1P in glomerular mesangial cells.

A key piece of evidence to support the rheostat hypothesis is that ceramide-mediated programmed cell death is suppressed by the addition of S1P [23]. Thus ceramide-induced JNK activation and apoptosis were prevented by the addition of S1P. Furthermore, the PKC-mediated activation of SPHK and the concomitant increase in S1P levels were shown to have a similar inhibitory effect on ceramide-mediated apoptosis. Subsequently, Fas ligation or C_2-ceramide-mediated caspase-3/CPP32 and caspase-7/Mch3 activation and resulting poly(ADP-ribose) polymerase cleavage were shown to be blocked by PKC activation and attenuated by the addition of exogenous S1P (0.5–5 μM) [133]. Similarly, either S1P or PKC activation inhibited C_2-ceramide-mediated caspase-6/Mch2 activation and subsequent lamin B cleavage. However, neither S1P nor PKC stimulation were effective at blocking Fas-induced caspase-8/FLICE (Fas-associated death domain-like interleukin-1β converting enzyme) activation. Thus S1P/PKC activation probably acts downstream of caspase-8/FLICE activation and ceramide formation, and upstream of caspases-3 (CPP32), -6 (Mch2) and -7 (Mch3) [133]. Similarly, S1P promotes survival of neuronal cells [150].

Further support for the rheostat model comes from studies showing that growth factors and cytokines tend to differentially regulate sphingomyelinase/ceramidase and SPHK activities and, consequently, ceramide and S1P levels. For example, alkaline membrane-associated ceramidase is up-regulated (within 1 h) by growth factors, including PDGF, fibroblast growth factor, IGF and EGF, in a tyrosine kinase-dependent manner, with a concomitant increase in sphingomyelinase activity. In contrast, cytokines such as TNFα and interleukin-1 activated sphingomyelinase but not ceramidase activity, thereby resulting in the accumulation of ceramide within cells. Inhibition of ceramidase activity by *N*-oleoylethanolamine reduced PDGF-stimulated DNA synthesis, but was without effect upon the proliferative response to endothelin, which failed to modulate ceramidase and sphingomyelinase activities [151].

Furthermore, manipulation of intracellular S1P levels can also affect the levels of ceramide and sphingosine. For example, NIH 3T3 cells transfected with SPHK1a exhibit a substantial decrease in their ceramide content [18]. This correlates with increased survival upon serum depletion, which usually induces apoptosis [25]. Therefore the concomitant removal of ceramide upon SPHK overexpression may prevent ceramide-induced apoptosis. Additionally, the subsequently formed S1P may promote cell survival by inducing mitogenic signalling pathways that counteract the effects of ceramide.

CELL PROLIFERATION, DIFFERENTIATION, MIGRATION AND APOPTOSIS

S1P appears to be both a full mitogen and a co-mitogen in different cell systems. For instance, in Swiss 3T3 cells it elicits a marked increase in DNA synthesis [95], whereas in airway smooth muscle cells S1P is co-mitogenic with PDGF and non-mitogenic alone [89,94]. In Swiss 3T3 cells, S1P-stimulated PLD-derived PA [152] and Ca^{2+} mobilization [125] were proposed to be key events in the regulation of DNA synthesis. In contrast, PA failed to mimic the effects of S1P in thyroid FRTL5 cells, thereby excluding a role for PLD. In that study, S1P activated the Na^+/H^+ exchanger, which promotes a subsequent increase in intracellular calcium, an important commitment step in the stimulation of DNA synthesis [153].

The mitogenic efficacy of growth factors has been correlated with the magnitude and kinetics of ERK activation [154]. Sustained ERK activation is thought to govern the amount of kinase translocating to the nucleus, the extent of subsequent transcription factor activation and, therefore, the magnitude of DNA synthesis. We have demonstrated that a greater activation of ERK occurs over 30 min in airway smooth muscle cells when S1P and PDGF are applied together than is observed with either agonist alone [89]. These results suggest that the amount of DNA synthesis might be governed by various 'threshold' levels of ERK activation throughout the 30 min stimulation. The extent to which these levels are exceeded at each time point might explain why combined stimulation with PDGF/S1P produced more DNA synthesis than stimulation with PDGF alone. S1P alone produces much weaker ERK activation via EDG1, which is probably below the 'threshold' levels and is therefore non-mitogenic.

Another possible mechanism to explain the co-mitogenic action of S1P is its synergism with choline phosphate. This was observed in NIH 3T3 fibroblasts, where a combination of the two lipids elicited a synergistic increase in DNA synthesis [155]. This was reported to involve amplification at the level of $p70^{S6K}$ and to a lesser extent PI3K, based on the use of rapamycin (inhibitor of $p70^{S6K}$) and wortmannin (PI3K inhibitor) and dominant-negative p85 PI3K, which block synergism. Choline phosphate and S1P also elicited synergistic stimulation of DNA synthesis in Swiss 3T3 fibroblasts, an effect mediated by amplification of ERK activation. In these experiments, high concentrations of ethanolamine also potentiated the synergism on DNA synthesis, via an unidentified mechanism [156]. In contrast, low concentrations of ethanolamine actually inhibited choline phosphate/S1P-induced DNA synthesis [157]. Therefore the action of PLD on phosphatidylethanolamine might result in a bimodal regulation of S1P stimulation of DNA synthesis. In this case, the specificity of action may be dependent upon the extent of PLD activation. S1P can also mobilize intracellular calcium and promote activation of the transcription factor nuclear factor κB, which was blocked by BAPTA/AM [158]. Therefore this action of S1P may involve calcium-dependent phosphatases and redox potential changes in the cell, which could affect mitogenesis.

S1P can both stimulate and inhibit chemotactic responses in different cell types. For instance, high concentrations (micromolar) of S1P inhibited, whereas low concentrations (10–100 nM) stimulated, the migration of EDG1-transfected HEK 293 cells [159]. S1P also stimulated the migration of endothelial cells [159] and CHO cells overexpressing EDG1 or EDG3 [67]. In contrast, EDG5-transfected CHO cells were unaffected [67]. S1P also inhibited PDGF-stimulated chemotaxis of aortic smooth muscle cells, via a calcium- and cAMP-dependent mechanism [91]. Furthermore, S1P stimulation of $p125^{FAK}$ may be involved in the inhibition of breast cancer cell motility [160]. Indeed, S1P inhibits integrin-dependent cell motility, by affecting actin filament re-organization. In contrast, formyl-Met-Leu-Phe stimulates SPHK in HL60 cells, and may play a role in promoting chemotaxis of these cells [48].

S1P is also implicated in differentiation processes. For instance, NGF-induced neural differentiation correlates with increased SPHK activity [54]. Both were blocked by the inhibitor K252a. In endothelial cells, TNFα-stimulated ERK, nuclear factor κB activation and VCAM-1 (vascular cell-adhesion molecule-1)/E-selectin expression were mediated by SPHK activation and S1P production. This was established using *N*,*N*-dimethylsphingosine, which blocked the effects of TNFα. Furthermore, S1P, but not ceramide or sphingosine, mimicked the effect of TNFα [161]. Expression of E-selectin and, to a lesser extent, VCAM were also increased by S1P in human aortic endothelial cells [162]. S1P may also affect differentiation processes indirectly by inducing the release of cytokines. For instance, in osteoblast-like MC3T3-E1 cells, S1P appears to be involved in TNFα-induced interleukin-6 synthesis [163].

S1P can both promote and protect against apoptosis in mammalian cells. For instance, in human hepatoma cells, S1P up-regulates Bax expression, which is a pro-apoptotic protein belonging to the Bcl-2 family. This was shown to be independent of p53-mediated transcription and growth arrest [164]. In neuronal cells, neurite retraction is one of the first steps in the apoptotic process. S1P induced neurite retraction in N1E-115 cells via a GPCR- and Rho-dependent pathway that involves contraction of the actin cytoskeleton [165]. Others have confirmed that the action of S1P is confined to an extracellular receptor, by using S1P immobilized on glass beads that fail to penetrate the cells [166]. Recent studies have shown that S1P-induced neurite retraction involves EDG5 and, possibly, EDG3 [74]. In contrast, agonist stimulation of SPHK protects against apoptosis, as observed in TNFα-stimulated endothelial cells [49] and vitamin D_3-stimulated HL60 cells [55]. In osteoblastic cells, prostaglandin E_2 stimulates cAMP formation and inhibits apoptosis. This appears to be mediated by a cAMP-dependent modulation of SPHK and S1P production [57]. Furthermore, protection of T lymphocytes from apoptosis by S1P was associated with suppression of Bax expression via an EDG5- and EDG3-dependent mechanism [167].

S1P AND DISEASE

S1P may have an important role in a number of disease states. A particular focus is to determine whether EDG receptor levels and signalling via heterotrimeric G-proteins and Rho are altered in disease. A recent study by Goetzl et al. [168] identified EDG4 as a marker for ovarian cancer cells. A similar situation may exist for S1P-specific EDG receptors in other cancers. S1P has also been implicated in breast cancer. For example, S1P induces the secretion of type II IGF (IGF-II), which increases proliferation [169]. In contrast, S1P inhibits chemo-invasiveness of an oestrogen-independent breast cancer cell line, MDA-MB-231, through a $p125^{FAK}$-dependent pathway [160].

The role of S1P in angiogenesis (the formation of new blood vessels) is another key area. This involves endothelial-cell differentiation and increased motility/mitogenesis of smooth muscle cells, which may be influenced by lipoproteins, such as oxidized LDL [56]. Several reports of the angiogenic role of S1P have been published [159,170,171]. Leucocyte migration is also affected by S1P, which may play a role in inflammation. For example, S1P inhibits neutrophil motility [172] and modulates adhesion molecule expression [162]. Additionally, the relative levels of sphingosine and S1P in mast cells may determine, in part, their allergic responsiveness [173]. Thus changes in the phenotypic expression of EDG receptors, SPHK, S1P lyase and LPPs may have a critical role in governing the intracellular/extracellular concentration of S1P and its efficacy at EDG receptors, and this may impact upon a number of disease processes.

Essential studies are required to produce gene knockouts, to establish the effect of abolishing the expression of EDG receptors, SPHK and other metabolizing enzymes. Deficiency in enzymes involved in S1P production and action may be associated with defects in important cellular processes, such as neuronal differentiation and apoptosis. It will be interesting to see whether these knockout animals exhibit neurological disorders, such as Alzheimer's disease and Parkinson's disease, which are associated with de-regulated apoptosis.

There are a number of potential approaches in the area of therapeutics. These include the development of selective EDG receptor antagonists, discrete inhibitors of enzymes involved in S1P metabolism and gene therapy. It may be possible to produce drugs or antisense oligonucleotides that can be delivered specifically to tumours to prevent growth and cell motility. Alternatively, it may be possible to overexpress enzymes which destroy S1P, such as LPP and S1P lyase, in order to prevent proliferation.

FUTURE STUDIES

The biology of S1P has advanced considerably over the past 3–5 years. However, there are many questions still to be answered, promising further exciting and interesting developments in this area of lipid biology.

There are likely to be novel EDG receptors expressed in cells that remain to be identified. Whether these all conform to classical GPCR signalling will be of interest. Certain ligands can bind to both GPCRs and receptor ion channels, e.g. the 5-hydroxytryptamine receptors 5-HT$_1$, 5-HT$_2$, 5-HT$_4$ and 5-HT$_5$ are GPCRs, while 5-HT$_3$ is a receptor ion channel, more closely related to the nicotinic acetylcholine receptor. It will also be of interest to determine whether there is an intracellular S1P receptor, analagous to that for inositol 1,4,5-trisphosphate. Once the entire complement of receptors has been established, the evolutionary processes that governed their biology can be defined. Identification of members of this family in lower organisms should provide details regarding their divergence and functional heterogeneity. Moreover, the structure/functional properties of identified EDG receptors need to be fully characterized. This will be achieved over the next few years and will involve site-directed mutagenesis studies to define the amino acids involved in binding S1P and the molecular basis for divergent signalling from a single receptor subtype via G$_i$, G$_q$ and G$_{12}$/G$_{13}$. Hopefully, characterization of the functional groups in each receptor will allow rational drug design for the production of receptor antagonists.

Receptor signalling mechanisms

Although a large number of effector systems that are regulated by the binding of S1P to EDG receptors have been identified, the molecular organization of signalling events downstream of these receptors has not been fully defined. In this regard, a large amount of information can be borrowed from general paradigms of GPCR signalling, and future research will proceed down these lines. There are many questions to be answered. For instance, how do the different EDG receptors activate Rho-dependent signal transduction? Is this via the intermediacy of G$_{12}$/G$_{13}$ and RhoGEF? Do EDG receptors communicate with JNK via a Rac/Cdc42-dependent mechanism? Do the G$_i$-linked EDG receptors utilize $\beta\gamma$ subunits to regulate non-receptor tyrosine kinases, and how does this initiate activation of the ERK pathway? What is the role of PI3K in this pathway, and does this involve endocytic signalling mediated by β-arrestins and dynamin II? Is there potential cross-talk with other growth factor receptors, such as the PDGF receptor? In certain cases, growth factor receptors (e.g. those for insulin, IGF-I and PDGF) appear to utilize G$_i$ to signal downstream to ERK [101,131]. It would be very interesting to know whether G$_i$ activated by EDG receptors can be used by growth factor receptor tyrosine kinases. This may allow the PDGF receptor, for example, to signal more efficiently, and could provide the basis for co-mitogenicity. Certain GPCR agonists have also been shown to transactivate growth factor receptors, by stimulating their tyrosine phosphorylation. These tyrosine-phosphorylated receptors can then scaffold with signalling proteins. The best example of this is LPA, which stimulates tyrosine phosphorylation and transactivation of the EGF receptor [174]. It remains to be determined whether S1P stimulates tyrosine phosphorylation and transactivation of growth factor receptors.

Another important question is: what are the factors that enable S1P binding to EDG5 receptors to elicit opposite cellular outcomes, e.g. proliferation versus apoptosis? This may be dependent upon specific localization of EDG5 with the appropriate signalling machinery. Certain, but not all, JNK isoforms have been purported to be upstream of caspases, which play a key role in cell death. Therefore the specificity of signalling from EDG5 might be achieved by co-expression of the relevant JNK isoform in these cells. It is also important to determine whether the EDG5 receptor has functional determinants, distinct from those of other EDG receptors, that allow selective activation of JNK and cell death.

Finally, Rho-dependent kinase activation plays a key role in calcium sensitization of smooth muscle contractility. It remains to be determined whether S1P binding to EDG receptors can elicit contraction of smooth muscle via this Rho-dependent mechanism. This is important because S1P is released by platelets at atherosclerotic plaques, and this might contribute to increased vasoconstriction leading to hypertension in patients with atherosclerosis.

Intracellular versus autocrine role of S1P

Perhaps the key question is whether S1P can also function as an intracellular second messenger. This is still controversial, because of the uncertainty as to whether S1P is released from cells to act at EDG receptors. Although there are many studies which support a second messenger role, these are based upon the use of inhibitors of SPHK, which at best are only selective for this enzyme. In our opinion, the question of an intracellular role for S1P has to be redefined, especially as unequivocal proof would place S1P in a rather unique position as a signalling molecule with both intracellular and extracellular actions. In this regard, it will be necessary to develop more sensitive assays to measure extracellular S1P (e.g. in the presence of LPP inhibitors), in order to establish whether certain growth factors and cytokines can stimulate its release. The molecular cloning of SPHK offers another approach to addressing this question. Increased S1P levels have been correlated with enhanced cell growth and survival in cells transfected with SPHK. In cells with a null background for EDG receptors, this might be indicative of an intracellular action of S1P. PDGF stimulates SPHK and S1P formation. Therefore, if S1P is released, it can be predicted that PDGF-stimulated signalling might be modified by altered EDG receptor expression. These experiments would distinguish between intracellular and autocrine models. Further information on the role of SPHK in cells might also be obtained by using antisense deoxyoligonucleotides to ablate expression of the protein.

Further studies are required to clone and characterize mammalian forms of SPHK and S1P lyase. These enzymes are likely to have a very significant role in regulating the kinetics of S1P formation. Both intra- and ecto-sphingosine 1-phosphate lyase activities may be expressed in cells, and these might serve as markers for extracellularly and intracellularly acting S1P. A similar paradigm has already been established for the LPPs, which exist as a family of isoforms. Some of these enzymes have ecto-activity against S1P, LPA, PA and ceramide 1-phosphate. As explained above, these ecto-enzymes may limit S1P bioavailability at EDG receptors. The best approach here would be to evaluate the mechanisms regulating ecto-LPP and to establish a structure/function relationship. Such regulatory mechanisms could serve as a feedback route for lowering the extracellular concentration of S1P after the cellular response has occurred.

CONCLUSION

S1P is an important bioactive lysolipid that appears to have duality in its function, since it may act as both an extracellular and an intracellular mediator. It has profound biological activity, and aberrant regulation is implicated in certain disease states. Recent advances in this area have identified many potential targets for therapeutic intervention, such as EDG receptors and S1P-metabolizing enzymes. This suggests that further research may yield compounds that have clinical benefit.

We acknowledge the support of the Wellcome Trust and the BBSRC. S P is a Wellcome Trust Senior Fellow

REFERENCES

1 Mathias, S , Pena, L A and Kolesnick, R N (1998) Signal transduction of stress via ceramide Biochem J **335**, 465–480

2 Perry, D K and Hannun, Y A (1999) The role of ceramide in cell signalling Biochim. Biophys Acta **1436**, 233–243

3 Levade, T and Jaffrezou, J.-P. (1999) Signalling sphingomyelinases which, where, how and why? Biochim Biophys Acta **1438**, 1–17

4 Liu, B and Hannun, Y A (1997) Inhibition of the neutral magnesium-dependent sphingomyelinase by glutathione J. Biol Chem **272**, 16281–16287

5 Liu, B., Andrieu-Abadie, N , Levade, T , Zhang, P , Obeid, L M. and Hannun, Y. A (1998) Glutathione regulation of neutral sphingomyelinase in tumor necrosis factor-α-induced cell death J Biol Chem. **273**, 11313–11320

6 Bernardo, K , Hurwitz, R , Zenk, T , Desnick, R J , Ferlinz, K , Schuchman, E H and Sandhoff, K (1995) Purification, characterization, and biosynthesis of human acid ceramidase J Biol Chem **270**, 11098–11102

7 Koch, J., Gartner, S , Li, C. M , Quintern, L E , Bernardo, K , Levran, O., Schnabel, D , Desnick, R. J., Schuchman, E H. and Sandhoff, K (1996) Molecular cloning and characterization of a full-length complementary DNA encoding human acid ceramidase Identification of the first molecular lesion causing Farber disease J Biol Chem **271**, 33110–33115

8 Sugita, M , Williams, M., Dulaney, J T and Moser, H W (1975) Ceramidase and ceramide synthesis in human kidney and cerebellum Description of a new alkaline ceramidase Biochim Biophys Acta **398**, 125–131

9 Ullman, M D and Radin, N S (1974) The enzymatic formation of sphingomyelin from ceramide and lecithin in mouse liver J Biol Chem. **249**, 1506–1511

10 Sundaram, K S and Lev, M (1984) Inhibition of sphingolipid synthesis by cycloserine *in vitro* and *in vivo*. J. Neurochem **42**, 577–581

11 Miyake, Y., Kozutsumi, Y , Nakamura, S , Fujita, T and Kawasaki, T (1995) Serine palmitoyltransferase is the primary target of a sphingosine-like immunosuppressant, ISP-1/myriocin Biochem Biophys Res Commun **211**, 396–403

12 Wang, E , Norred, W P , Bacon, C W., Riley, R T and Merrill, Jr , A H (1991) Inhibition of sphingolipid biosynthesis by fumonisins. Implications for diseases associated with *Fusarium moniliforme* J Biol Chem **266**, 14486–14490

13 Jeckel, D., Karrenbauer, A , Burger, K. N., van Meer, G and Wieland, F (1992) Glucosylceramide is synthesized at the cytosolic surface of various Golgi subfractions J Cell Biol **117**, 259–267

14 Vunnam, R. R. and Radin, N S (1980) Analogs of ceramide that inhibit glucocerebroside synthetase in mouse brain Chem. Phys Lipids **26**, 265–278

15 Bajjalieh, S. M , Martin, T F and Floor, E (1989) Synaptic vesicle ceramide kinase. A calcium-stimulated lipid kinase that co-purifies with brain synaptic vesicles J Biol Chem **264**, 14354–14360

16 Kolesnick, R. N and Hemer, M R (1990) Characterization of a ceramide kinase activity from human leukemia (HL-60) cells Separation from diacylglycerol kinase activity J Biol Chem **265**, 18803–18808

17 Olivera, A , Kohama, T , Tu, Z., Milstein, S. and Spiegel, S. (1998) Purification and characterization of rat kidney sphingosine kinase J Biol. Chem **273**, 12576–12583

18 Kohama, T , Olivera, A , Edsall, L., Nagiec, M M., Dickson, R and Spiegel, S (1998) Molecular cloning and functional characterisation of murine sphingosine kinase J Biol Chem. **273**, 23722–23728

19 Kozak, M (1986) Point mutations define a sequence flanking the AUG initiator codon that modulates translation by eukaryotic ribosomes. Cell **44**, 283–292

20 Nagiec, M M , Skrzypek, M , Nagiec, E E , Lester, R. L and Dickson, R L (1998) The LCB4 (YOR171c) and LCB5 (YLR260w) genes of *Saccharomyces* encode sphingoid long chain base kinases J Biol Chem **273**, 19437–19442

21 Bunting, M , Tang, W , Zimmerman, G A , McIntyre, T M and Prescott, S M. (1996) Molecular cloning and characterization of a novel human diacylglycerol kinase ζ J Biol. Chem **271**, 10230–10236

22 Schaap, D., Van der Wal, J. and Van Blitterswijk, W J (1994) Consensus sequences for ATP-binding sites in protein kinases do not apply to diacylglycerol kinases. Biochem J. **304**, 661–662

23 Cuvillier, O , Pirianov, G , Kleuser, B , Vcanek, P. G , Coso, O A , Gutkind, S and Spiegel, S (1996) Suppression of ceramide-mediated programmed cell death by sphingosine 1-phosphate Nature (London) **381**, 800–803

24 Olivera, A., Rosenthal, J and Spiegel, S (1994) Sphingosine kinase from Swiss 3T3 fibroblasts a convenient assay for the measurement of intracellular levels of free sphingoid bases Anal. Biochem **223**, 306–312

25 Olivera, A , Kohama, T , Edsall, L , Nava, V , Cuvillier, O., Poulton, S and Spiegel, S (1999) Sphingosine kinase expression increases intracellular sphingosine 1-phosphate and promotes cell growth and survival J. Cell Biol **147**, 545–557

26 Banno, Y , Kato, M , Hara, A and Nozawa, Y (1998) Evidence for the presence of multiple isoforms of sphingosine kinase in human platelets Biochem. J. **336**, 301–304

27 Van Veldhoven, P P and Mannaerts, G P (1991) Subcellular localization and membrane topology of sphingosine-1-phosphate lyase in rat liver J Biol Chem. **266**, 12502–12507

28 Van Veldhoven, P P and Mannaerts, G P (1993) Sphingosine-phosphate lyase Adv. Lipid Res **26**, 69–98

29 Van Veldhoven, P P and Mannaerts, G P. (1994) Sphinganine 1-phosphate metabolism in cultured skin fibroblasts evidence for the existence of a sphingosine phosphatase Biochem J **299**, 597–601

30 Saba, J D , Nara, F., Bielawska, A , Garrett, S and Hannun, Y A (1997) The *BST1* gene of *Saccharomyces cerevisiae* is the sphingosine 1-phosphate lyase J Biol Chem. **272**, 26087–26090

31 Zhou, J and Saba, J D (1998) Identification of the first mammalian sphingosine phosphate lyase gene and its functional expression in yeast Biochem Biophys Res Commun **242**, 502–507

32 Brindley, D N. and Waggoner, D. W (1998) Mammalian lipid phosphate phosphohydrolases J Biol. Chem **273**, 24281–24284

33 Stoffel, W , LeKim, D. and Sticht, G. (1969) Distribution and properties of dihydrosphingosine-1-phosphate aldolase (sphinganine-1-phosphate alkanal-lyase) Hoppe-Seyler's Z Physiol Chem. **350**, 1233–1241

34 De Ceuster, P , Mannaerts, G P and Van Veldhoven, P P. (1995) Identification and subcellular localization of sphinganine phosphatases in rat liver Biochem J **311**, 139–146

35 Mao, C , Wadleigh, M , Jenkins, G M , Hannun, Y A and Obeid, L M (1997) Identification and characterization of *Saccharomyces cerevisiae* dihydrosphingosine-1-phosphate phosphatase J. Biol. Chem **272**, 28690–28694

36 Mandala, S M , Thornton, R., Tu, Z , Kurtz, M. B., Nickels, J , Broach, J , Menzeleev, R. and Spiegel, S (1998) Sphingoid base 1-phosphatase a key regulator of sphingolipid metabolism and stress response Proc. Natl Acad Sci U S A **95**, 150–155

37 Yatomi, Y , Ruan, F , Ohta, H., Welch, R J , Hakomori, S -I and Igarashi, Y. (1995) Quantitative measurement of sphingosine 1-phosphate in biological samples by acylation with radioactive acetic anhydride Anal. Biochem **230**, 315–320

38 Edsall, L C and Spiegel, S (1999) Enzymatic measurement of sphingosine 1-phosphate Anal. Biochem **272**, 80–86

39 Igarashi, Y and Yatomi, Y (1998) Sphingosine 1-phosphate is a blood constituent released from activated platelets, possibly playing a variety of physiological and pathological roles Acta Biochim Polon **45**, 299–309

40 Yatomi, Y , Igarashi, Y., Yang, L , Hisano, N , Qi, R , Asazuma, N , Satoh, K., Ozaki, Y. and Kume, S (1997) Sphingosine 1-phosphate, a bioactive sphingolipid abundantly stored in platelets, is a normal constituent of human plasma and serum. J. Biochem (Tokyo) **121**, 969–973

41 Igarashi, Y, Yatomi, Y and Kickler, T S (1998) Sphingosine-phosphate content in the plasma of platelet concentrates correlates with poor platelet increments after transfusion and with occurrences of transfusion reactions in patients. Am J Hematol **57**, 261–262

42 Buehrer, B M and Bell, R M (1992) Inhibition of sphingosine kinase in vitro and in platelets Implications for signal transduction pathways. J. Biol. Chem **267**, 3154–3159

43 Olivera, A. and Spiegel, S (1993) Sphingosine 1-phosphate as a second messenger in cell proliferation induced by PDGF and FCS mitogens Nature (London) **365**, 557–560

44 Pyne, S, Chapman, J, Steele, L and Pyne, N J (1996) Sphingomyelin-derived lipids differentially regulate the extracellular signal-regulated kinase 2 (ERK-2) and c-Jun N-terminal kinase (JNK) signal cascades in airway smooth muscle Eur. J Biochem **237**, 819–826

45 Meyer zu Heringdorf, D, Lass, T, Alemany, R, Laser, K T, Neumann, E, Zhang, C., Shmidt, M, Rauen, U, Jakobs, K. H. and Van Koppen, C J. (1998) Sphingosine kinase-mediated Ca^{2+} signalling by G-protein-coupled receptors. EMBO J **17**, 2830–2837

46 Choi, O H, Kim, J. H and Kinet, J P (1996) Calcium mobilisation via sphingosine kinase in signalling by the FcϵRI antigen receptor Nature (London) **380**, 634–636

47 Melendez, A, Floto, R. A, Gillooly, D J, Harnett, M M. and Allen, J M (1998) FcγRI coupling to phospholipase D initiates sphingosine kinase-mediated calcium mobilization and vesicular trafficking J. Biol Chem **273**, 9393–9402

48 Alemany, R, Meyer zu Heringdorf, D, van Koppen, C. J. and Jakobs, K H (1999) Formyl peptide receptor signaling in HL-60 cells through sphingosine kinase J Biol Chem **274**, 3994–3999

49 Xia, P, Wang, L, Gamble, J R and Vadas, M A (1999) Activation of sphingosine kinase by tumor necrosis factor-α inhibits apoptosis in human endothelial cells J Biol Chem **274**, 34499–34505

50 Rani, C S, Berger, A, Wu, J, Sturgill, T. W., Beitner-Johnson, D, Le Roith, D, Varticovski, L and Spiegel, S (1997) Divergence in signal transduction pathways of platelet-derived growth factor (PDGF) and epidermal growth factor (EGF) receptors. involvement of sphingosine 1-phosphate in PDGF but not EGF signalling J Biol Chem **272**, 10777–10783

51 Meyer zu Heringdorf, D, Lass, H., Kuchar, I, Alemany, R, Guo, Y, Schmidt, M and Jakobs, K H (1999) Role of sphingosine kinase in Ca^{2+} signalling by epidermal growth factor receptor FEBS Lett **461**, 217–222

52 Olivera, A., Edsall, L, Poulton, S, Kazlauskas, A and Spiegel, S (1999) Platelet-derived growth factor-induced activation of sphingosine kinase requires phosphorylation of the PDGF receptor tyrosine residue responsible for binding of PLCγ FASEB J **13**, 1593–1600

53 Buehrer, B M, Bardes, E S and Bell, R M (1996) Protein kinase C-dependent regulation of human erythroleukemia (HEL) cell sphingosine kinase activity Biochim. Biophys Acta **1303**, 233–242

54 Rius, R A, Edsall, L C and Spiegel, S. (1997) Activation of sphingosine kinase in pheochromocytoma PC12 neuronal cells in response to trophic factors FEBS Lett **417**, 173–176

55 Kleuser, B, Cuvillier, O and Spiegel, S. (1998) 1α,25-Dihydroxyvitamin D_3 inhibits programmed cell death in HL60 cells by activation of sphingosine kinase Cancer Res **58**, 1817–1824

56 Augé, N, Nikolova-Karakahian, M., Carpentier, S, Parthasarathy, S, Negre-Salvayre, A, Salvayre, R, Merrill, Jr, A H. and Levade, T (1999) Role of sphingosine 1-phosphate in the mitogenesis induced by oxidized low density lipoprotein in smooth muscle cells via activation of sphingomyelinase, ceramidase, and sphingosine kinase. J. Biol. Chem. **274**, 21533–21538

57 Machwate, M, Rodan, S. B, Rodan, G A and Harada, S-I (1998) Sphingosine kinase mediates cyclic AMP suppression of apoptosis in rat periosteal cells Mol Pharmacol **54**, 70–77

58 Hla, T and Maciag, T (1990) An abundant transcript induced in differentiating human endothelial cells encodes a polypeptide with structural similarities to G-protein-coupled receptors J Biol Chem **265**, 9308–9313

59 Okazaki, H, Ishizaka, N, Sakurai, T, Kurokawa, K, Goto, K, Kumada, M and Takuwa, Y (1993) Molecular cloning of a novel putative G protein-coupled receptor expressed in the cardiovascular system Biochem Biophys Res Commun **190**, 1104–1109

60 MacLennan, A J, Browe, C S, Gaskin, A A, Lado, D C and Shaw, G (1994) Cloning and characterisation of a putative G-protein coupled receptor potentially involved in development Mol Cell Neurosci **5**, 201–209

61 Graler, M H, Bernhardt, G and Lipp, M. (1998) A lymphoid tissue-specific receptor, EDG6, with potential immune modulatory functions mediated by extracellular lysophospholipids Genomics **53**, 164–169

62 Yamazaki, Y, Kon, J, Sato, K, Tomura, H, Sato, M, Yoneya, T, Okazaki, H, Okajima, F and Ohta, H (2000) EDG6 as a putative sphingosine 1-phosphate receptor coupling to Ca^{2+} signalling pathway Biochem Biophys Res Commun **268**, 583–589

63 Im, D.-S, Heise, C E, Ancellin, N, O'Dowd, B F, Shei, G-J, Heavens, R P, Rigby, M R, Hla, T, Mandala, S, McAllister, G et al (2000) Characterisation of a novel sphingosine 1-phosphate receptor, EDG8 J Biol Chem **275**, 14281–14286

64 Glickman, M, Malek, R. L, Kwitek-Black, A E, Jacob, H J and Lee, N H (1999) Molecular cloning, tissue-specific expression, and chromosomal localisation of a novel nerve growth factor-regulated G-protein-coupled receptor, *nrg-1* Mol Cell Neurosci. **14**, 141–152

65 Lee, M.-J, Evans, M and Hla, T (1996) The inducible G protein-coupled receptor *edg-1* signals via the G_i/mitogen-activated protein kinase pathway J Biol Chem **271**, 11272–11279

66 Lee, M-J, Van Brocklyn, J R, Thangada, S., Liu, C H, Hand, A R, Menzeleev, R, Spiegel, S and Hla, T (1996) Sphingosine-1-phosphate as a ligand for the G protein-coupled receptor EDG-1. Science **279**, 1552–1555

67 Kon, J, Sato, K, Watanabe, T, Tomura, H, Kuwabara, A, Kimura, T, Tamama, K-I, Ishizuka, T., Murata, N, Kanda, T et al (1999) Comparison of intrinsic activities of the putative sphingosine 1-phosphate receptor sub-types to regulate several signalling pathways in their cDNA-transfected Chinese hamster ovary cells J Biol Chem **274**, 23940–23947

68 Okamoto, H, Takuwa, N, Gonda, K., Okazaki, H, Chang, K, Yatomi, Y, Shigematsu, H. and Takuwa, Y (1998) EDG1 is a functional sphingosine-1-phosphate receptor that is linked via a G(i/o) to multiple signalling pathways, including phospholipase C activation, Ca^{2+} mobilization, ras-mitogen-activated protein kinase activation and adenylate cyclase inhibition J Biol Chem **273**, 27104–27110

69 Zondag, G C, Postma, F R, Van Etten, A, Verlaan, I and Moolenaar, W H (1998) Sphingosine 1-phosphate signalling through the G-protein-coupled receptor Edg-1 Biochem J **330**, 605–609

70 Windh, R. T., Lee, M-J, Hla, T, An, S, Barr, A J and Manning, D R (1999) Differential coupling of the sphingosine 1-phosphate receptors EDG1, EDG3 and H218/EDG5 to the G_i, G_q, and G_{12} families of heterotrimeric G proteins J Biol Chem **274**, 27351–27358

71 Hall, A, Paterson, H F, Adamson, P and Ridley, A J (1993) Cellular responses regulated by rho-related small GTP-binding proteins Philos Trans R Soc London B Biol Sci **340**, 267–271

72 Stam, J C, Michiels, F, van der Kammen, R. A, Moolenaar, W H and Collard, J (1998) Invasion of T-lymphoma cells co-operation between Rho family GTPases and lysophospholipid receptor signalling EMBO J **17**, 4066–4074

73 Lee, M.-J., Thangada, S, Liu, C H, Thompson, B D and Hla, T (1998) Lysophosphatidic acid stimulates the G-protein-coupled receptor EDG-1 as a low affinity agonist. J. Biol Chem **273**, 22105–22112

74 Van Brocklyn, J R, Tu, Z, Edsall, L, Schmidt, R. R and Spiegel, S (1999) Sphingosine 1-phosphate-induced cell rounding and neurite retraction are mediated by the G protein-coupled receptor H218 J Biol Chem **274**, 4626–4632

75 Van Brocklyn, J R, Lee, M-J, Menzeleev, R, Olivera, A, Edsall, L, Cuvillier, O, Thomas, D M, Coopman, P J P, Thangada, S, Liu, C H et al (1998) Dual actions of sphingosine 1-phosphate extracellular through the G_i-coupled receptor EDG1 and intracellular to regulate proliferation and survival J Cell Biol **142**, 229–240

76 An, S, Bleu, T. and Zheng, Y (1999) Transduction of intracellular calcium signals through G protein-mediated activation of phospholipase C by recombinant sphingosine 1-phosphate receptors Mol Pharmacol **55**, 787–794

77 An, S., Goetzl, E J and Lee, H (1998) Signalling mechanisms and molecular characteristics of G protein-coupled receptors for lysophosphatidic acid and sphingosine 1-phosphate J Cell Biochem Suppl **30/31**, 147–157

78 Ancellin, N and Hla, T (1999) Differential pharmacological properties and signal transduction of the sphingosine 1-phosphate receptors EDG-1, EDG-3, and EDG-5. J Biol Chem **274**, 18997–19002

79 Buhl, A M, Johnson, N L, Dhanasekaran, N and Johnson, G L (1995) $G\alpha_{12}$ and $G\alpha_{13}$ stimulate Rho-dependent stress fibre formation and focal adhesion assembly J Biol Chem **270**, 24631–24634

80 Kozasa, T, Jiang, X, Hart, M. J., Sternweis, P. M, Singer, W D, Gilman, A G, Bollag, G and Sternweis, P C (1998) p115 RhoGEF, a GTPase activating protein for $G\alpha_{12}$ and $G\alpha_{13}$ Science **280**, 2109–2111

81 Karnam, P, Standaert, M L, Galloway, L and Farese, R V. (1997) Activation and translocation of Rho (and ADP ribosylation factor) by insulin in rat adipocytes apparent involvement of phosphatidylinositol 3-kinase J Biol Chem **272**, 6136–6140

82 Mao, J., Huan, H, Xie, W and Wu, D (1998) Guanine nucleotide exchange factor GEF115 specifically mediates activation of Rho and serum response factor by the G protein α subunit $G_{\alpha13}$ Proc Natl Acad Sci U S A **95**, 12973–12976

83 Hart, M J, Jiang, X, Kozasa, T, Roscoe, W, Singer, W D, Gilman, A G, Sternweiss, P C and Bollag, G (1998) Direct stimulation of the guanine nucleotide exchange activity of p115 RhoGEF by $G_{\alpha13}$. Science **280**, 2112–2114

84 Hecht, J H, Weiner, J A, Post, S R and Chun, J. (1996) *Ventricular zone gene-1* (*vzg-1*) encodes a lysophosphatidic acid receptor expressed in neurogenic regions of the developing cerebral cortex J Cell Biol **135**, 1071–1083

85 An, S., Bleu, T, Hallmark, O. G and Goetzl, E J (1998) Characterisation of a novel subtype of human G protein-coupled receptor for lysophosphatidic acid. J. Biol Chem. **273**, 7906–7910

86 An, S, Bleu, T, Zheng, Y and Goetzl, E J (1998) Recombinant human G protein-coupled lysophosphatidic acid receptors mediate intracellular calcium mobilization Mol. Pharmacol **54**, 881–888

87 Erickson, J R, Wu, J. J, Goddard, J G, Tigyi, G, Kawanishi, K, Tomei, L D. and Kiefer, M. C (1998) Edg-2/Vzg-1 couples to the yeast pheromone response pathway selectively in response to lysophosphatidic acid J Biol Chem. **273**, 1506–1510

88 Bandoh, K., Aoki, J, Hosono, H, Kobayashi, S, Kobayashi, T, Murakami-Murofushi, K, Tsujimoto, M, Arai, H and Inoue, K (1999) Molecular cloning and characterization of a novel human G-protein-coupled receptor, EDG7, for lysophosphatidic acid J. Biol Chem **274**, 27776–27785

89 Rakhit, S, Conway, A-M, Tate, R, Bower, T, Pyne, N. J. and Pyne, S (1999) Sphingosine 1-phosphate stimulation of the p42/p44 mitogen-activated protein kinase pathway in airway smooth muscle. role of endothelial differentiation gene-1, c-Src tyrosine kinase and phosphoinositide 3-kinase Biochem. J. **338**, 643–649

90 Okamoto, H, Takuwa, N., Yatomi, Y, Gonda, K, Shigematsu, H and Takuwa, Y (1999) EDG3 is a functional receptor specific for sphingosine 1-phosphate and sphingosylphosphorylcholine with signalling characteristics distinct from EDG1 and AGR16. Biochem. Biophys Res Commun. **260**, 203–208

91 Bornfeldt, K, Graves, L M, Raines, E. W, Igarashi, Y, Wayman, G., Yamamura, S, Yatomi, Y., Sidhu, J S., Krebs, E G, Hakomori, S-I. and Ross, R. (1995) Sphingosine-1-phosphate inhibits PDGF-induced chemotaxis of human arterial smooth muscle cells spatial and temporal modulation of PDGF chemotactic signal transduction J. Cell Biol **130**, 193–206

92 Gonda, K., Okamoto, H, Takuwa, N., Yatomi, Y, Okazaki, H., Sakura, T, Kimura, S., Sillard, R., Hani, K. and Takuwa, Y (1999) The novel sphingosine 1-phosphate receptor AGR16 is coupled via pertussis toxin-sensitive and -insensitive G-proteins to multiple signalling pathways. Biochem J **337**, 67–75

93 Banno, Y., Fujita, H, Ono, Y, Nakashima, S, Ito, Y, Kuzumaki, N. and Nozawa, Y (1999) Differential phospholipase D activation by bradykinin and sphingosine 1-phosphate in NIH 3T3 fibroblasts over-expressing gelsolin J Biol. Chem **274**, 27385–27391

94 Pyne, S and Pyne, N J. (1996) The differential regulation of cyclic AMP by sphingomyelin-derived lipids and the modulation of sphingolipid-stimulated extracellular signal regulated kinase-2 in airway smooth muscle. Biochem. J **315**, 917–923

95 Wu, J, Spiegel, S. and Sturgill, T W (1995) Sphingosine 1-phosphate rapidly activates the mitogen-activated protein kinase pathway by a G-protein-dependent mechanism J Biol Chem. **270**, 11484–11488

96 Koch, W J, Hawes, B. E., Allen, L F and Lefkowitz, R J (1994) Direct evidence that G_i-coupled receptor stimulation of mitogen-activated protein kinase is mediated by $G\beta\gamma$ activation of $p21^{ras}$ Proc. Natl. Acad Sci U S A **91**, 12706–12710

97 Crespo, P, Xu, N, Simonds, W F and Gutkind, J S (1994) Ras-dependent activation of MAP kinase pathway mediated by G-protein $\beta\gamma$ subunits Nature (London) **369**, 418–420

98 Stephens, L R, Smrcka, A., Cooke, F T, Jackson, T. J., Sternweis, P and Hawkins, P T. (1994) A novel phosphoinositide 3 kinase activity in myeloid-derived cells is activated by G protein $\beta\gamma$ subunits Cell **77**, 83–93

99 Lopez-Ilasaca, M., Crespo, P, Pellici, P. G, Gutkind, J S and Wetzker, R. (1997) Linkage of G protein-coupled receptors to the MAPK signalling pathway through PI 3-kinase γ Science **275**, 394–397

100 Kranenburg, O, Verlaan, I, Hordijk, P L and Moolenaar, W. H (1997) G_i-mediated activation of the Ras/MAP kinase pathway involves a 100 kDa tyrosine-phosphorylated Grb2 SH3 binding protein, but not Src nor Shc EMBO J **16**, 3097–3105

101 Luttrell, L M, van Biesen, T, Hawes, B E, Koch, W. J., Tohura, K and Lefkowitz, R J. (1995) $G\beta\gamma$ subunits mediate mitogen-activated protein kinase activation by the tyrosine kinase insulin-like growth factor 1 receptor J Biol Chem **270**, 16495–16498

102 Holdago-Madruga, M, Emlet, D. R, Moscatello, D K, Godwin, A. K and Wong, A J (1996) A Grb2-associated docking protein in EGF- and insulin-receptor signalling Nature (London) **379**, 560–564

103 Lin, F. T., Kreuger, K M, Kendall, H. E., Daaka, Y, Fredericks, Z L, Pitcher, J A and Lefkowitz, R J. (1997) Clathrin-mediated endocytosis of the β-adrenergic receptor is regulated by phosphorylation/dephosphorylation of β-arrestin 1 J. Biol Chem. **272**, 31051–31057

104 Luttrell, L M., Daaka, Y, Della Rocca, G J. and Lefkowitz, R J (1997) G protein-coupled receptors mediate two functionally distinct pathways of tyrosine phosphorylation in rat 1a fibroblasts Shc phosphorylation and receptor endocytosis correlate with activation of ERK kinases J Biol Chem **272**, 31648–31656

105 Daaka, Y., Luttrell, L M, Ahn, S., Della Rocca, G J, Ferguson, S. S. G., Caron, M G and Lefkowitz, R J (1998) Essential role for G protein-coupled receptor endocytosis in the activation of mitogen-activated protein kinase J Biol Chem. **273**, 685–688

106 Guo, C, Zheng, C, Martin-Padura, I., Bian, Z C and Guan, J.-L (1998) Differential stimulation of proline-rich tyrosine kinase 2 and mitogen-activated protein kinase by sphingosine 1-phosphate Eur J Biochem **257**, 403–408

107 Sato, K, Tomura, H., Igarashi, Y, Ui, M and Okajima, F (1999) Possible involvement of cell surface receptors in sphingosine 1-phosphate-induced activation of extracellular signal-regulated kinase in C6 glioma cells Mol Pharmacol. **55**, 126–133

108 An, S, Zheng, Y. and Bleu, T (2000) Sphingosine 1-phosphate-induced cell proliferation, survival and related events mediated by G protein-coupled receptors EDG3 and EDG5 J. Biol Chem. **275**, 288–296

109 Dikic, I., Tokiwa, G., Lev, S, Courtneidge, S A and Schlessinger, J (1996) A role for Pyk2 and Src in linking G-protein-coupled receptors with MAP kinase activation Nature (London) **383**, 547–550

110 Yang, L, Yatomi, Y., Hisano, N, Qi, R, Asazuma, N, Satoh, K, Igarashi, Y, Ozaki, Y and Kume, S (1996) Activation of protein-tyrosine kinase Syk in human platelets stimulated with lysophosphatidic acid or sphingosine 1-phosphate. Biochem Biophys Res. Commun **229**, 440–444

111 Blakesley, V. A, Beitner-Johnson, D., Van Brocklyn, J R., Rani, S, Shen-Orr, Z, Stannard, B, Spiegel, S. and LeRoith, D (1997) Sphingosine 1-phosphate stimulates tyrosine phosphorylation of Crk J Biol Chem **272**, 16211–16215

112 Wang, F, Nobes, C D, Hall, A and Spiegel, S (1997) Sphingosine 1-phosphate stimulates Rho-mediated tyrosine phosphorylation of focal adhesion kinase and paxillin in Swiss 3T3 fibroblasts Biochem J **324**, 481–488

113 Exton, J H (1999) Regulation of phospholipase D Biochim Biophys Acta **1439**, 121–133

114 Su, Y, Rosenthal, D, Smulson, M. and Spiegel, S (1994) Sphingosine 1-phosphate, a novel signalling molecule, stimulates DNA binding activity of AP-1 in quiescent Swiss 3T3 fibroblasts. J. Biol Chem **269**, 16512–15517

115 Hill, C S, Marais, R., John, S., Wynne, J., Dalton, S and Treisman, R (1993) Functional analysis of a growth factor-responsive transcription factor complex Cell **73**, 395–406

116 Hill, C S, Wynne, J and Treisman, R (1995) The Rho family GTPases RhoA, Rac1, and CDC42Hs regulate transcriptional activation by SRF. Cell **81**, 1159–1170

117 Bunemann, M., Brandts, B, Meyer zu Heringdorf, D, Van Koppen, C J, Jakobs, K. H. and Pott, L (1995) Activation of muscarinic K^+ current in guinea-pig atrial myocytes by sphingosine-1-phosphate J Physiol (London) **489**, 701–707

118 MacDonell, K L, Severson, D L and Giles, W R (1998) Depression of excitability by sphingosine 1-phosphate in rat ventricular myocytes. Am. J Physiol **275**, H2291–H2299

119 Stukey, J and Carmen, G M (1997) Identification of a novel phosphatase sequence motif Protein Sci **6**, 469–472

120 Zhang, Q-X., Pilquil, C S, Dewald, J., Berthiaume, L G and Brindley, D N (2000) Identification of structurally important domains of lipid phosphate phosphatase-1. Implications for sites of action. Biochem J **345**, 181–184

121 Jasinska, R, Zhang, Q-X, Pilquil, C, Singh, I, Xu, J, Dewald, J, Dillon, D. A, Berthiaume, L. G., Carman, G M, Waggoner, D W and Brindley, D N (1999) Lipid phosphate phosphohydrolase-1 degrades exogenous glycerolipid and sphingolipid phosphate esters Biochem. J. **340**, 677–686

122 Tate, R J, Tolan, D. and Pyne, S (1999) Molecular cloning of magnesium-independent type 2 phosphatidic acid phosphatase from airway smooth muscle Cell. Signalling **11**, 515–522

123 Ghosh, T. K, Bian, J. and Gill, D L (1990) Intracellular calcium release mediated by sphingosine derivatives generated in cells. Science **248**, 1653–1656

124 Ghosh, T K, Bian, J. and Gill, D. L (1994) Sphingosine 1-phosphate generated in the endoplasmic reticulum membrane activates release of stored calcium J Biol Chem **269**, 22628–22635

125 Zhang, H., Desai, N N, Olivera, A., Seki, T, Brooker, G. and Spiegel, S (1991) Sphingosine-1-phosphate, a novel lipid, involved in cellular proliferation J. Cell Biol **114**, 155–167

126 Goodemote, K A, Mattie, M. E., Berger, A and Spiegel, S (1995) Involvement of a pertussis toxin-sensitive G protein in the mitogenic signalling pathways of sphingosine 1-phosphate. J. Biol Chem **270**, 10272–10277

127 Tolan, D., Conway, A-M, Pyne, N. J and Pyne, S. (1997) Sphingosine prevents diacylglycerol signalling to mitogen-activated protein kinase in airway smooth muscle Am J Physiol **273**, C928–C936

128 Tolan, D, Conway, A-M, Steele, L, Pyne, S and Pyne, N J (1996) The identification of DL-*threo* dihydrosphingosine and sphingosine as novel inhibitors of extracellular signal-regulated kinase signalling in airway smooth muscle Br J Pharmacol **119**, 185–186

129 Hannun, Y A and Bell, R. M. (1989) Functions of sphingolipids and sphingolipid breakdown products in cellular regulation Science **243**, 500–507

130 Tolan, D, Conway, A-M, Rakhit, S, Pyne, N J and Pyne, S. (1999) Assessment of the extracellular and intracellular actions of sphingosine 1-phosphate by using the p42/p44 mitogen-activated protein kinase cascade as a model Cell Signalling **11**, 349–354

131 Conway, A-M, Rakhit, S, Pyne, S. and Pyne, N J (1999) Platelet-derived growth factor-stimulation of the p42/p44 mitogen-activated protein kinase pathway in airway smooth muscle· role of pertussis toxin-sensitive G-proteins, c-Src tyrosine kinases and phosphoinositide 3-kinase Biochem J **337**, 171–177

132 Edsall, L C., Van Brocklyn, J R, Cuvillier, O, Kleuser, B and Spiegel, S (1998) *N,N*-dimethylsphingosine is a potent competitive inhibitor of sphingosine kinase but not of protein kinase C modulation of cellular levels of sphingosine 1-phosphate and ceramide Biochemistry **37**, 12892–12898

133 Cuvillier, O, Rosenthal, D. S., Smulson, M E and Spiegel, S (1998) Sphingosine 1-phosphate inhibits activation of caspases that cleave poly(ADP-ribose) polymerase and lamins during Fas- and ceramide-mediated apoptosis in Jurkat T lymphocytes J Biol. Chem **273**, 2910–2916

134 Fatatis, A and Miller, R J (1996) Sphingosine and sphingosine 1-phosphate differentially modulate platelet-derived growth factor-BB-induced Ca^{2+} signalling in transformed oligodendrocytes J. Biol Chem **271**, 295–301

135 Fatatis, A and Miller, R J. (1999) Cell cycle control of PDGF-induced Ca^{2+} signalling through modulation of sphingolipid metabolism FASEB J **13**, 1291–1301

136 Ayar, A, Thatcher, N M, Zehavi, U, Trentham, D. R and Scott, R H (1998) Mobilization of intracellular calcium by intracellular flash photolysis of caged dihydrosphingosine in cultured neonatal rat sensory neurones Acta Biochim. Polon **45**, 311–326

137 Huang, W-C and Chueh, S-H (1996) Calcium mobilization from the intracellular mitochondrial and non-mitochondrial stores of the rat cerebellum Brain Res. **718**, 151–158

138 Durieux, M E, Carlisle, S J, Salafranca, M N and Lynch, K R (1993) Responses to sphingosine-1-phosphate in *X. laevis* oocytes similarities with lysophosphatidic acid signaling Am J Physiol **264**, C1360–C1364

139 Orlati, S, Hrelia, S and Rugolo, M (1997) Pertussis toxin- and PMA-insensitive calcium mobilization by sphingosine in CFPAC-1 cells evidence for a phosphatidic acid-dependent mechanism Biochim Biophys Acta **1358**, 93–102

140 Sabala, P, Wiktorek, M., Czarny, M, Chaban, V and Baranska, J (1996) Sphingosine stimulates calcium mobilization and modulates calcium signals evoked by thapsigargin in glioma C6 cells Acta Neurol Exp. **56**, 507–513

141 Needleman, D H, Aghdasi, B, Seryshev, A B., Schroepfer, G J and Hamilton, S L (1997) Modulation of skeletal muscle Ca^{2+}-release channel activity by sphingosine Am J Physiol **272**, C1465–C1474

142 Betto, R, Teresi, A, Turcato, F, Salviati, G, Sabbadini, R A, Krown, K, Glembotski, C C, Kindman, L A, Dettbarn, C, Pereon, Y et al (1997) Sphingosylphosphocholine modulates the ryanodine receptor/calcium-release channel of cardiac sarcoplasmic reticulum membranes Biochem J. **322**, 327–333

143 Orlati, S., Porcelli, A M, Hrelia, S, Lorenzini, A and Rugolo, M (1998) Intracellular calcium mobilization and phospholipid degradation in sphingosylphosphorylcholine-stimulated human airway epithelial cells Biochem J **334**, 641–649

144 Orlati, S, Porcelli, A M, Hrelia, S. and Rugolo, M (1998) Sphingosylphosphorylcholine and sphingosine-1-phosphate mobilise cytosolic calcium through different mechanisms in human airway epithelial cells Cell Calcium **23**, 387–394

145 Zehavi, U (1997) Synthesis of potentially caged sphingolipids, possible precursors of cellular modulators and second messengers Chem Phys Lipids **90**, 55–61

146 Qiao, L, Kozikowski, A P, Olivera, A and Spiegel, S (1998) Synthesis and evaluation of a photolyzable derivative of sphingosine 1-phosphate – caged SPP Bioinorg. Med Chem Lett **8**, 711–714

147 Hofmann, K and Dixit, V M (1998) Ceramide in apoptosis – does it really matter? Trends Biochem Sci. **23**, 374–377

148 Kolesnick, R J and Hannun, Y A (1999) Ceramide and apoptosis Trends Biochem Sci **24**, 224–225

149 Coroneos, E, Wang, Y, Panuska, J R, Templeton, D J. and Kester, M (1996) Sphingolipid metabolites differentially regulate extracellular signal-regulated kinase and stress-activated protein kinase cascades Biochem J **316**, 13–17

150 Edsall, L C, Pirianov, G G and Spiegel, S. (1997) Involvement of sphingosine 1-phosphate in nerve growth factor-mediated neuronal survival and differentiation. J Neurosci **17**, 6952–6960

151 Coroneos, E, Martinez, M, McKenna, S and Kester, M (1995) Differential regulation of sphingomyelinase and ceramidase activities by growth factors and cytokines Implications for cellular proliferation and differentiation J Biol Chem **270**, 23305–23309

152 Zhang, H., Desai, N. N, Murphey, J M. and Spiegel, S (1990) Increases in phosphatidic acid levels accompany sphingosine-stimulated proliferation of quiescent Swiss 3T3 cells J Biol Chem **265**, 21309–21316

153 Tornquist, K, Saarinen, P., Vainio, M and Ahlstrom, M (1997) Sphingosine 1-phosphate mobilizes sequestered calcium, activates calcium entry and stimulates DNA synthesis in thyroid FRTL-5 cells. Endocrinology **138**, 4049–4057

154 Marshall, C J (1995) Specificity of receptor tyrosine kinase signaling transient versus sustained extracellular signal-regulated kinase activation. Cell **80**, 179–185

155 Chung, T, Crilly, K S, Anderson, W H and Kiss, Z (1997) ATP-dependent choline phosphate-induced mitogenesis in fibroblasts involves activation of p70 S6 kinase and phosphatidylinositol 3′-kinase through an extracellular site Synergistic mitogenic effects of choline phosphate and sphingosine 1-phosphate J Biol Chem **272**, 3064–3072

156 Kiss, Z and Mukherjee, J J (1997) Phosphocholine and sphingosine 1-phosphate synergistically stimulate DNA synthesis by a MAP kinase-dependent mechanism FEBS Lett **412**, 197–200

157 Kiss, Z, Crilly, K S and Anderson, W H (1997) Extracellular sphingosine 1-phosphate stimulates formation of ethanolamine from phosphatidylethanolamine modulation of sphingosine 1-phosphate-induced mitogenesis by ethanolamine, Biochem J **328**, 383–391

158 Shatrov, V A, Lehmann, V. and Chouaib, S (1997) Sphingosine-1-phosphate mobilizes intracellular calcium and activates transcription factor NF-κB in U937 cells Biochem Biophys. Res Commun **234**, 121–124

159 Wang, F, Van Brocklyn, J R, Hobson, J P, Movafagh, S, Zukowska-Grojec, Z, Milstien, S and Spiegel, S (1999) Sphingosine 1-phosphate stimulates cell migration through a G_i-coupled cell surface receptor. Potential involvement in angiogenesis. J Biol Chem **274**, 35343–35350

160 Wang, F., Nohara, K, Olivera, A, Thompson, E W and Spiegel, S (1999) Involvement of focal adhesion kinase in inhibition of motility of human breast cancer cells by sphingosine 1-phosphate Exp Cell Res **247**, 17–28

161 Xia, P, Gamble, J R, Rye, K-A, Wang, L., Hii, C S T, Cockerill, P, Khew-Goodall, Y, Bert, A G, Barters, P J and Vadas, M A (1998) Tumor necrosis factor-alpha induces adhesion molecule expression through the sphingosine kinase pathway. Proc Natl Acad Sci U S A **95**, 14196–14201

162 Rizza, C, Leitinger, N., Yue, J, Fischer, D J, Wang, D.-A, Shih, P T, Lee, H, Tigyi, G and Berliner, J A (1999) Lysophosphatidic acid as a regulator of endothelial/leukocyte interaction Lab Invest. **79**, 1227–1235

163 Kozawa, O, Suzuki, A, Kaida, T, Tokuda, H and Uematsu, T (1997) Tumor necrosis factor-alpha autoregulates interleukin-6 synthesis via activation of protein kinase C Function of sphingosine 1-phosphate and phosphatidylcholine-specific phospholipase C J. Biol Chem **272**, 25099–25104

164 Hung, W-C and Chuang, L-Y (1996) Induction of apoptosis by sphingosine 1-phosphate in human hepatoma cells is associated with increased expression of bax gene product Biochem Biophys Res Commun. **229**, 11–15

165 Postma, F R, Jalink, K, Hengeveld, T and Moolenaar, W H (1996) Sphingosine 1-phosphate rapidly induces Rho-dependent neurite retraction action through a specific cell surface receptor EMBO J **15**, 2388–2392

166 Sato, K, Tomura, H, Igarashi, Y, Ui, M and Okajima, F (1997) Exogenous sphingosine l-phosphate induces neurite retraction possibly through a cell surface receptor in PC12 cells Biochem Biophys Res Commun **240**, 329–334

167 Goetzl, E J, Kong, Y and Mei, B (1999) Lysophosphatidic acid and sphingosine 1-phosphate protection of T cells from apoptosis in association with suppression of Bax J Immunol **162**, 2049–2056

168 Goetzl, E J, Dolezalova, H., Kong, Y, Hu, Y-L, Jaffe, R B., Kalli, K R. and Conover, C A (1999) Distinctive expression and functions of the type 4 endothelial differentiation gene-encoded G protein-coupled receptor for lysophosphatidic acid in ovarian cancer Cancer Res **59**, 5370–5375

169 Goetzl, E. J, Dolezalova, H, Kong, Y and Zeng, L (1999) Dual mechanisms for lysophospholipid induction of proliferation of human breast carcinoma cells Cancer Res. **59**, 4732–4737

170 Lee, M J, Thangada, S, Claffey, K P, Ancellin, N, Liu, C. H, Kluk, M, Volpi, M., Sha'afi, R I and Hla, T (1999) Vascular endothelial cell adheren junction assembly and morphogenesis by sphingosine 1-phosphate Cell **99**, 301–312

171 Lee, O-H., Kim, Y-M, Lee, Y M, Moon, E-J, Lee, D-J, Kim, J-H, Kim, K-W and Kwon, Y-G (1999) Sphingosine 1-phosphate induces angiogenesis: its angiogenic action and signalling mechanism in human umbilical endothelial cells Biochem. Biophys Res Commun **264**, 743–750

172 Kawa, S, Kimura, S, Hakomori, S.-I. and Igarashi, Y (1997) Inhibition of chemotactic motility and trans-endothelial migration of human neutrophils by sphingosine 1-phosphate FEBS Lett **420**, 196–200

173 Prieschl, E E, Csonga, R, Novotny, V and Baumruker, T (1999) The balance between sphingosine and sphingosine 1-phosphate is decisive for mast cell activation after Fcε receptor I triggering J Exp. Med **190**, 1–8

174 Zwick, E, Hackel, P O, Prenzel, N and Ullrich, A (1999) The EGF receptor as a central transducer of heterologous signalling systems Trends Pharmacol Sci **20**, 408–412

RESEARCH COMMUNICATION

Cloning and mapping of human *PKIB* and *PKIG*, and comparison of tissue expression patterns of three members of the protein kinase inhibitor family, including PKIA

Lihua ZHENG, Long YU[1], Qiang TU, Min ZHANG, Hua HE, Wengjie CHEN, Jie GAO, Jianqiang YU, Qianhong WU
and Shouyuan ZHAO

State Key Laboratory of Genetic Engineering, Institute of Genetics, School of Life Science, Fudan University, Shanghai 200433, People's Republic of China

Two novel members of the human cAMP-dependent protein kinase inhibitor (PKI) gene family, *PKIB* and *PKIG*, were cloned. The deduced proteins showed 70% and 90% identity with mouse PKIβ and PKIγ respectively. Both the already identified pseudosubstrate site and leucine-rich nuclear export signal motifs were defined from the 11 PKIs of different species. The *PKIB* and *PKIG* genes were mapped respectively to chromosome 6q21-22.1, using a radiation hybrid GB4 panel, and to chromosome 20q13.12-13.13, using a Stanford G3 panel. Northern-blot analysis of three PKI isoforms, including the PKIA identified previously, revealed significant differences in their expression patterns. *PKIB* had two transcripts of 1.9 kb and 1.4 kb. The former transcript was abundant in both placenta and brain and the latter was expressed most abundantly in placenta, highly in brain, heart, liver, pancreas, moderately in kidney, skeletal muscle and colon, and very little in the other eight tissues tested. *PKIG* was widely expressed as a 1.5-kb transcript with the highest level in heart, hardly detectable in thymus and peripheral blood leucocytes and was moderately expressed in the other tissues, with slightly different levels. However, PKIA was specifically expressed as two transcripts of 3.3 kb and 1.5 kb in heart and skeletal muscle. The distinct expression patterns of the three PKIs suggest that their roles in various tissues are probably different.

Key words: human *PKIB* and *PKIG*, protein kinase inhibitor motif, tissue-expression pattern.

INTRODUCTION

The protein kinase inhibitors (PKIs) are a class of proteins that can inhibit the activity of cAMP-dependent protein kinase (PKA), a complex composed of two regulatory subunits (R-subunits) and two catalytic subunits (C-subunits). The function of PKA mainly depends on its free C-subunits, which leave the inactive tetrametric complex in the cytoplasm in response to an increase in intracellular cAMP concentration [1]. The PKI binds the C-subunits of PKA in the nucleus and carries them into the cytoplasm to reform the inactive PKA complex with R-subunits. Studies on the molecular structure of human and/or mouse PKA, have shown that the R-subunit includes four isoforms (RIα, RIβ, RIIα and RIIβ) and the C-subunit contains three isoforms (Cα, Cβ and Cγ) [2]. To date, three mouse *Pki* genes encoding three isoforms (PKIα, PKIβ and PKIγ) have been cloned [3–5]. Although all three PKI proteins can inhibit PKA activity, they may act by preferentially inhibiting different C-subunits [6]. However, only one human *PKI* gene (termed *PKIA*), which is homologous to mouse *Pkiα*, has been cloned and its protein product inhibits the activity of PKA [1]. Thus it is speculated that other PKI members might also exist in humans. Before the inhibition of the various C-subunits by different PKIs in humans can be elucidated, the identification of additional human *PKI* genes is necessary. In the present study, the isolation of two novel human *PKI* genes (*PKIB* and *PKIG*) is described, and a comparison of the expression patterns of the genes in the *PKI* family, including *PKIA*, is made.

EXPERIMENTAL

The cDNA sequences of mouse *Pkiβ* (GenBank accession number L02241) and *Pkiγ* (GenBank accession number U97176) were used to search the Human EST (expressed sequence tag) division of GenBank. Homologous ESTs were obtained and assembled into two EST contigs using Assembly Machine (http://gcg.tigem.it/cgi-bin/uniestass.pl). Two pairs of primers, LZB$_1$ (5′-GCCAGGGACAGGAAAGATAGGAG-3′) and LZB$_2$ (5′-CACATGCTGCTTAGGGCTGCAATG-3′); LZG$_1$ (5′-ACAGGCCTGAGGAGCGATGCAC-3′) and LZG$_2$ (5′-GGAGCTCAGAGAAGAGGCTGCTG-3′) were designed based on the contig sequences, and custom-made by ShengGong Inc. (Shanghai, China). The primers were used to amplify several human tissue cDNA λgt11 libraries (Clontech, Palo Alto, CA, U.S.A.). PCR conditions with primers LZB$_1$ and LZB$_2$, and primers LZG$_1$ and LZG$_2$ were as follows: 1 μl template ($> 10^8$ plaque-forming units/ml) was amplified in a final volume of 50 μl containing 5 μl of 10 × PCR buffer, 1 μl of 20 mM dNTPs, 1.5 μl of 2.5 mM MgCl$_2$, 2 units *Taq* polymerase (Promega) and 1 μl of 25 mM of each specific primer. PCR reactions were run on a PTC-200 DNA Engine (MJ Research, Watertown, MA, U.S.A.) for 34 cycles (1 min at 93 °C, 1 min at 60 °C and 1 min

---

Abbreviations used: EST, expressed sequence tag; PKA, cAMP-dependent protein kinase; PKI, protein kinase inhibitor; RH, radiation hybrid; UTR, untranslated region.

[1] To whom correspondence should be addressed (e-mail longyu@fudan.edu.cn).

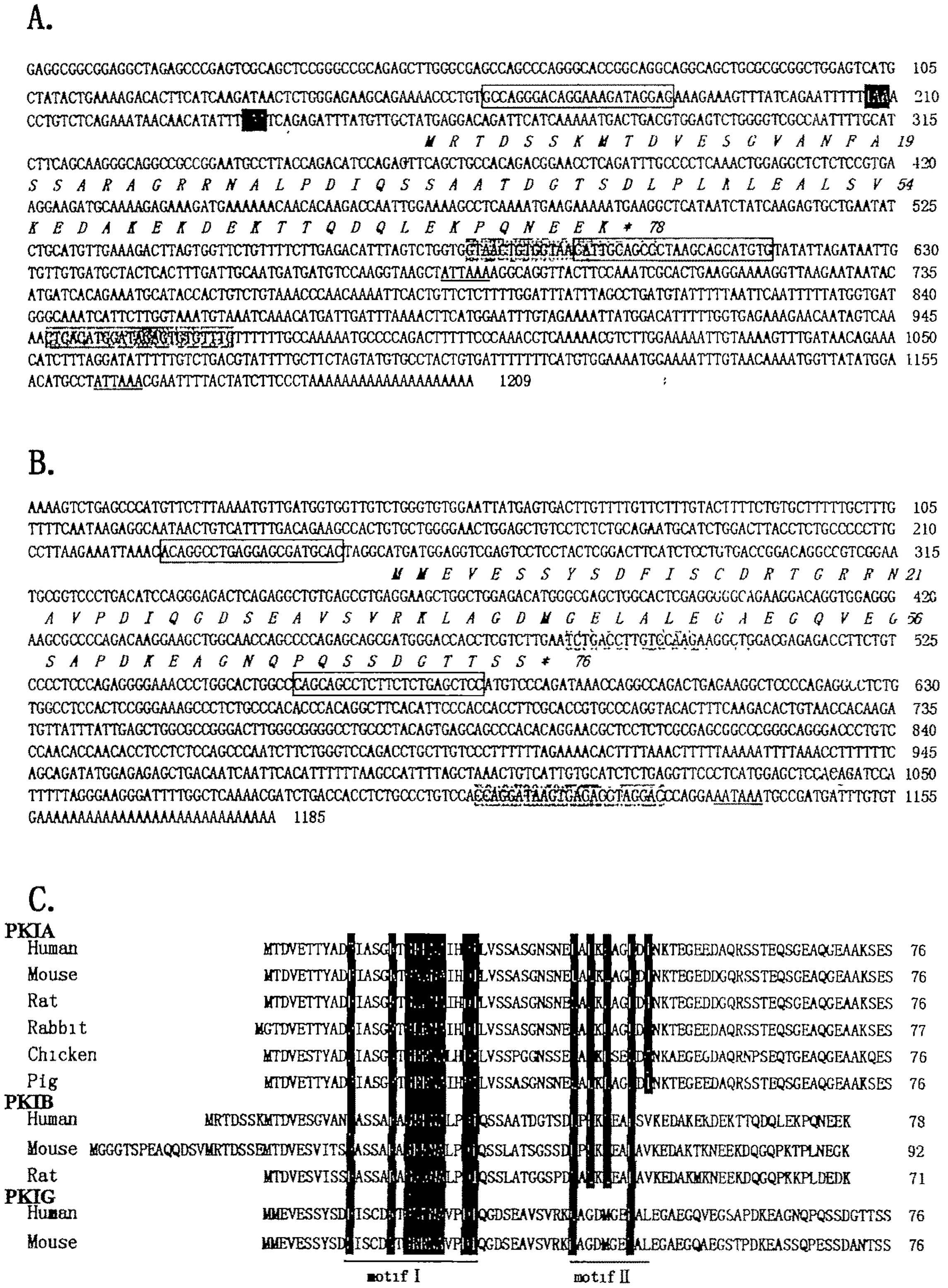

Figure 1 cDNA and deduced amino acid sequences of human *PKIB* (A) and *PKIG* (B), and multiple alignment of PKIs from different species to show PKI motifs (C)

(**A**) and (**B**) Primers for PCR amplification (LZB_1 and LZB_2, LZG_1 and LZG_2) are boxed, and for RH mapping (LZB-RH_1 and LZB-RH_2, LZG-RH_1 and LZG-RH_2) are shown with grey shading. Polyadenylation signal sequences (ATTAAA) are underlined. In-frame stop codons (TAA) in the upstream of the start codon of *PKIB* are shown with a black background. (**C**) PKIs from different species were aligned using the CLUSTAL program. The pseudosubstrate site (motif I) and leucine-rich nuclear export signal (motif II) are shown with a black background. The GenBank accession numbers of the PKI sequences are as follows PKIA Human, S76965, Mouse, M63554, Rat, L02615, Rabbit, M23079, Chicken, U19496; Pig, AF132737 PKIB Human, AF087873, Mouse, L02241, Rat, M64092 PKIG Human, AF115966; Mouse, U97170 at 72 °C) after an initial denaturation at 93 °C for 3 min, and were followed by incubation at 72 °C for 5 min. Based on the human *PKIA* sequence reported previously [1], a pair of primers, LZA$_1$ (CCTGCTATGTGGATATTTGGTAG) and LZA$_2$ (GGTTCCTGCAATGCAGCACAGCCA) was designed and used to amplify cDNA libraries as described above. The PCR products were subcloned into the pGEM-T vector and sequenced using the BigDye terminator sequencing kit and ABI377 sequencer (Perkin-Elmer Applied Biosystems, Foster City, CA, U.S.A.).

The protein sequences of PKI isoforms from other organisms were searched for in Entrez (National Center for Biotechnology Information) and motif analysis was performed using the MEME program (Multiple EM for Motif Elicitation; http://www.sdsc.edu/MEME/meme/website/) [7].

Radiation hybrid (RH) mapping of *PKIB* was performed using a GB4 panel (GeneBridge4 Human/Hamster RH Panel; Research Genetics Inc., Huntsville, AL, U.S.A.) and PCR primers LZB-RH$_1$ (5′-GTAACTGTGGTAACATTGCAGCC-3′) and LZB-RH$_2$ (5′-CAAACACACTCTATCCATGTGAG-3′). The primers were designed, based on the 3′-untranslated region (UTR) sequence of *PKIB* cDNA. The PCR conditions were as above and the reactions were run for 40 cycles (1 min at 94 °C, 1 min at 63 °C and 40 s at 72 °C) after initial denaturation at 94 °C for 3 min, and were followed by incubation at 72 °C for 10 min. The PCR products, amplified with DNA samples from five Chinese subjects, were sequenced to confirm that they were identical to the 3′-UTR sequence of *PKIB* cDNA. The PCR results were graded (0 if two duplicate PCRs showed a negative signal, 1 if both showed a positive signal and 2 if they showed a different signal) and were sent to the Sanger RH Mapping Server (http://www.sanger.ac.uk/RHserver/RHserver.shtml) for statistical analysis. RH mapping of *PKIG* was determined using a G3 panel (Stanford G3 Human/Hamster RH Panel; Research Genetics Inc.). The PCR primers used were LZG-RH$_1$ (5′-TCTGACCTTGTCCAAGAAGGCTG-3′) and LZG-RH$_2$ (5′-GTCCTAGGTGTCACTTATCCTGG-3′); the annealing temperature for each PCR amplification cycle was 60 °C. The procedure was then the same as for the RH mapping of *PKIB* described above. The recorded PCR results of *PKIG* were sent to the Stanford RH mapping server (http://www-shgc.stanford.edu/RH/rhserverformnew.html) for statistical analysis. The chromosome locus was determined using the GDB database (http://gdbwww.gdb.org/gdb/).

Northern hybridizations of *PKIA*, *PKIB* and *PKIG* were performed on multiple-tissue Northern (MTN) membranes (MTNI and MTNII; Clontech Inc.) with mRNA samples from 16 adult human tissues. The probes were prepared by labelling the cDNA fragments (amplified from human cDNA libraries as described above) with [α-^{32}P]dATP (Amersham) using the PCR method and were purified on a Sepharose-G50 column. The MTN membranes were prehybridized in hybridization/prehybridization solution {5 × SSPE [1 × SSPE = 0.15 M NaCl/10 mM sodium phosphate (pH 7.4)/1 mM EDTA], 50 % formamide, 10 × Denhart's (1 × Denhardt's = 0.02 % Ficoll 400/0.02 % polyvinylpyrrolidone/0.002 % BSA), 2 % (w/v) SDS, 100 μg/ml calf-thymus DNA} at 42 °C for 16 h, and hybridized in a hybridization oven (Hybaid Interactive, Teddington, Middx., U.K.) with the labelled probe for a further 24 h, with continuous shaking. The membranes were then washed several times with 0.1 × SSC (1 × SSC = 0.15 M NaCl/0.015 M sodium citrate) containing 0.1 % SDS at 42 °C and were exposed to X-ray film at −80 °C for 5 days. Northern blotting of human β-actin was performed as described above, except that the membranes were exposed to the X-ray film for 8 h. The intensities of the bands were determined using the Complete Gel Documentation and Analysis System (GDS 8000; Gene Company Limited, Shanghai, China).

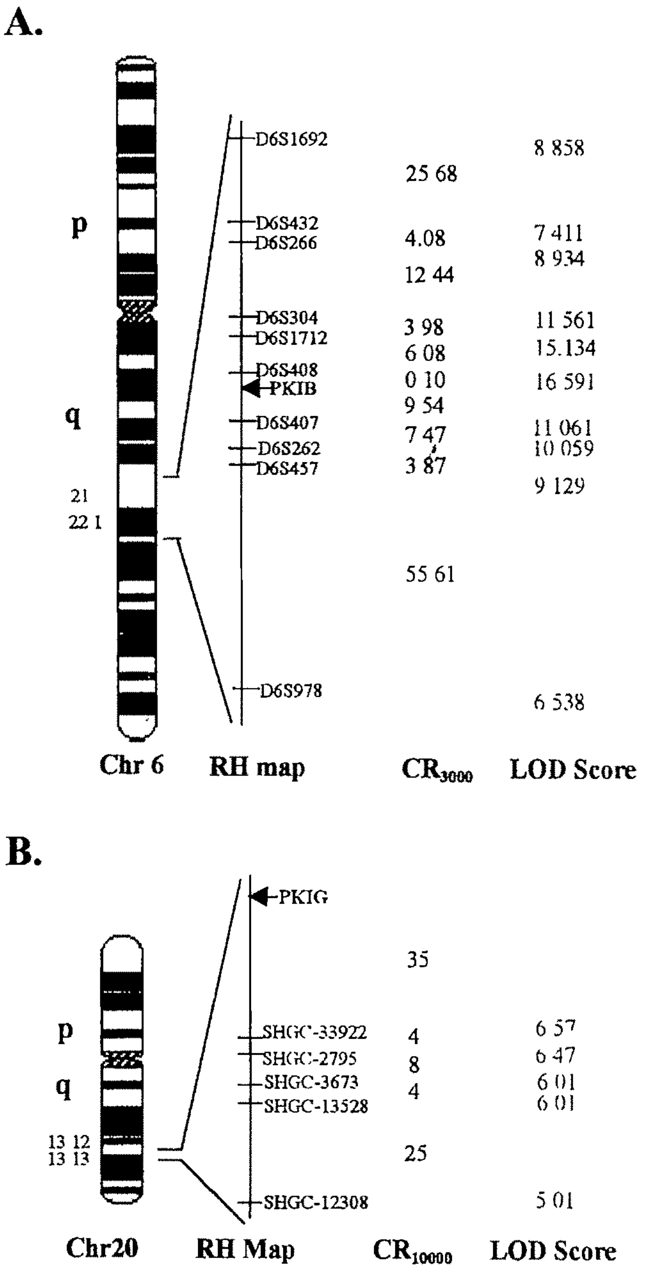

Figure 2 Mapping of *PKIB* (A) and *PKIG* (B)

(A) *PKIB* was localized to chromosome 6q21-22.1 between marker D6S408 and D6S407 **(B)** *PKIG* was localized to 20q13 12-13 13 and 35 cR$_{10000}$, proximal to marker SHGC-33922 Centiray (cR = CR) distances between the markers and the lod score scores associated with each marker are also indicated on the map

RESULTS AND DISCUSSION

Twenty eight human ESTs with high homology with mouse *PKIβ* (GenBank accession number L02241) and 18 human ESTs homologous to mouse *PKIγ* (GenBank accession number U97176) were obtained and assembled into two EST contigs,

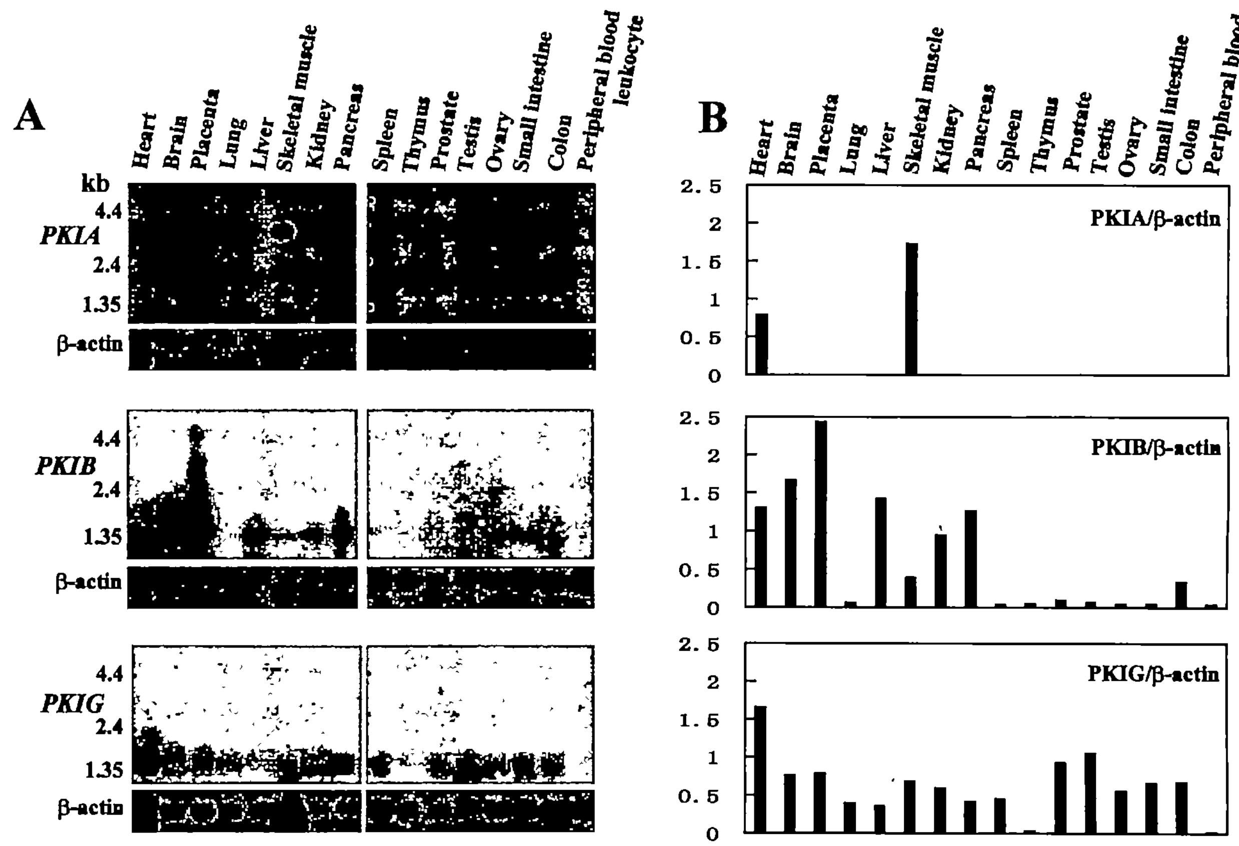

Figure 3 Northern blots of three human *PKI* isoforms in 16 adult human tissues and comparison of tissue expression patterns

(**A**) The membranes (MTNI and MTNII) were hybridized with *PKIA*, *PKIB* and *PKIG*. The Northern blots were also hybridized with the β-actins corresponding to the genes, to allow normalization for differences in loading. (**B**) Ratios of the autoradiographic intensities of the three *PKI* isoforms with those of the corresponding β-actins. The intensities of β-actin expression in heart and skeletal muscle are given as the average of that in brain, placenta, lung, liver, kidney and pancreas. Both long and short forms are included in the intensities of *PKIA* in heart and skeletal muscle, and *PKIB* in brain and placenta. The molecular-size markers (kb) are shown on the left of the panels in (**A**).

each 1.2 kb long. A fragment amplified from a human heart cDNA library was obtained with primers LZB_1 and LZB_2. Another specific fragment amplified from a human testis cDNA library was derived with primers LZG_1 and LZG_2. The two DNA fragments were sequenced and confirmed to be identical with the two contig sequences homologous to mouse *PKIβ* and *PKIγ* respectively. These two cDNAs were later respectively named PKIβ (cAMP-dependent, catalytic; *PKIB*) and PKIγ (cAMP-dependent, catalytic; *PKIG*) by the Human Nomenclature Committee. The *PKIB* cDNA contains an open reading frame (nt 258–494) coding for a peptide of 78 amino acids and a 3′-UTR sequence comprising two polyadenylation signals (ATTAAA; nt 681–686 and nt 1164–169) followed by a poly(A)$^+$ tail (Figure 1A). In the 5′-UTR sequence of *PKIB* cDNA there are two in-frame stop codons (TAA; nt 207–209 and nt 237–239) upstream of the start codon. The putative protein shows 70% homology with mouse PKIβ [4] but only 26% identity with the human PKI (i.e. PKIA) reported previously [1]. The *PKIG* cDNA comprises an open reading frame (nt 254–484) which encodes a peptide of 76 amino acids (Figure 1B). The polyadenylation signal (AATAAA; nt 1134–1139) and a poly(A)$^+$ tail are present in the 3′-UTR of human *PKIG*. The deduced protein of *PKIG* shows 90% homology with mouse PKIγ but only 25% identity with the previously reported human PKIA and 18% identity with the PKIB protein.

Notably, the PKI consensus pseudosubstrate site (FxxxxRxGRRNA), which is essential for binding and inhibiting C-subunits of PKA [8–10], exists in PKIB and PKIG (aa 18–29 in PKIB and aa 11–22 in PKIG) (Figures 1A and 1B). Additionally, the leucine-rich nuclear export signal (LxLxLxxLxHy) [11] is highly conserved in PKIB (aa 45–54) (Figure 1A). A segment similar to the nuclear export signal is also present in PKIG (Figure 1B). These conserved sequences found in PKIB and PKIG suggest that they are both novel members of human PKI. To learn more about the structural characteristics of the proteins, the amino acid sequences of PKIs from other organisms were obtained by searching the GenBank database. As expected, the conserved pseudosubstrate site and leucine-rich nuclear export signal motifs (Figure 1C) were defined from the 11 existing PKIs using the MEME program (bits > 3.0), also each of the 11 sequences had an e-value much less than 10 (from 8.1e-8 to 2e-32). The e-value of a sequence is given as the expected number of sequences in a random database of the same size that would match the motifs as well as the sequence does.

The *PKIB* gene was located on a human chromosome using the RH GB4 panel with primers LZB-RH_1 and LZB-RH_2. The results were recorded as follows. 1011100100-1210000100-0000010000-0000100000-1011001000-1010000000-0100100010-1011100100-2010001001-000. The statistical analysis using the Sanger RH server showed the *PKIB* gene was mapped between marker D6S408 (lod score = 16.6, $cR_{3000} = 0.10$) and D6S407 (lod score = 11.1, $cR_{3000} = 9.54$). These two markers were located between 6q21–22.1 according to the Genome Database comprehensive map. Hence, human *PKIB* was assigned to chromosome 6q21–22.1 (Figure 2A). Similarly, the chromosome localization of human *PKIG* was determined with the G3 panel and primers LZG-RH_1 and LZG-RH_2. The recorded PCR results were 0000000000-0001000000-0000001010-0000010002-0000000000-0000000000-0001010000-0100010000-000 and, after statistical analysis, revealed that *PKIG* was 35 cR_{10000} proximal to SHGC-33922 (lod score = 6.57) and 40 cR_{10000} to SHGC-2795 (lod score = 6.01). The markers were located in chromosome 20q13.12–13.13 according to the GDB database. Therefore human *PKIG* was mapped to 20q13.12–13.13 (Figure 2B).

Northern-blot hybridizations of human *PKIA*, *PKIB* and *PKIG* were performed and their expression patterns were compared. The Northern blot of *PKIA* cDNA, which was obtained by amplifying a human skeletal muscle cDNA library with primers LZA_1 and LZA_2, revealed that *PKIA* was specifically expressed in heart and skeletal muscle as two transcripts of 3.3 kb and 1.5 kb (Figure 3A). Hybridization with the *PKIB* probe detected two transcripts of 1.9 kb and 1.4 kb. The widely expressed 1.4 kb transcript was most abundant in placenta, abundant in brain, heart, liver, and pancreas, moderate in kidney, skeletal muscle and colon, and very weak in lung, spleen, thymus, prostate, testis, ovary, small intestine and peripheral blood leucocytes. The 1.9 kb transcript of *PKIB* was abundant in both placenta and brain. The two transcripts may be attributed to alternative polyadenylation at its two different polyadenylation signal positions. A 1.5 kb transcript of *PKIG* was identified in all tissues examined, with the highest level in heart, lowest in thymus and peripheral blood leucocytes and moderate expression in the other tissues at slightly different levels.

Comparison of tissue expression patterns of the three human PKI isoforms was performed using the ratios of the autoradiographic intensities of *PKI* and β-actin in the 16 tissues tested. As shown in Figure 3(B), both *PKIB* and *PKIG* were widely expressed (all 16 tissues), whereas *PKIA* was only expressed in two tissues, heart and skeletal muscle. The ratio of autoradiographic intensities of PKIs and the corresponding β-actins indicated that PKIB was abundant in placenta (2.43), brain (1.68), liver (1.43), heart (1.30), pancreas (1.27) and kidney (0.95); PKIG was abundant in heart (1.66), testis (1.05), prostate (0.93), placenta (0.79), brain (0.77) and skeletal muscle (0.69). It was also shown (Figure 3B) that heart and skeletal muscle, in which *PKIA* was specifically expressed, were the only tissues in which all three *PKI*s were expressed. In addition, the predominant PKI isoforms were distinct in different tissues. In brain, placenta, liver, kidney and pancreas, PKIB was the predominant PKI isoform. In heart, lung, spleen, prostate, testis, ovary, small intestine and colon, PKIG was the predominant isoform, and PKIA was predominant in skeletal muscle. Interestingly, in thymus and peripheral blood leucocytes the three PKI isoforms were undetectable or showed only trace expression levels. The differences in tissue expression patterns of human *PKIA*, *PKIB* and *PKIG* suggest that they might play different roles in various tissues, individually or co-operatively.

In conclusion, there are at least three PKI isoforms in human tissues, including PKIB, PKIG and the already known PKIA, and two PKI motifs, including the pseudosubstrate site and the nuclear export signal defined with 11 PKIs from six different species. The *PKIB* gene is localized on chromosome 6q21–22.1 and *PKIG* on 20q13.12–13.13. The tissue expression patterns of human *PKIA*, *PKIB* and *PKIG* are obviously different, which might be helpful in the further investigation and understanding of their functions.

This work was supported by the National 973 and 863 High Technology Programmes (863-Z-102-19-04-04) and the National Science Foundation of China (39525015, 39680019).

REFERENCES

1 Olsen, S R and Uhler, M D (1991) Inhibition of protein kinase-A by overexpression of the cloned human protein kinase inhibitor Mol Endocrinol **5**, 1246–1255

2 Tasken, K, Skalhegg, B S, Tasken, K A, Solberg, R, Knutsen, H K, Levy, F O, Sandberg, M., Orstavik, S., Larsen, T, Johansen, A K et al (1997) Structure, function and regulation of human cAMP-dependent protein kinases Adv Second Messenger Phosphoprotein Res **31**, 191–204

3 Olsen, S R and Uhler, M D (1991) Isolation and characterization of cDNA clones for an inhibitor protein of cAMP-dependent protein kinase J Biol Chem **266**, 11158–11162

4 Scarpetta, M A and Uhler, M D (1993) Evidence for two additional isoforms of the endogenous protein kinase inhibitor of cAMP-dependent protein kinase in the mouse J Biol Chem. **268**, 10927–10931

5 Collins, S P and Uhler, M D (1997) Characterization of PKI-gamma, a novel isoform of the protein kinase inhibitor of cAMP-dependent protein kinase J Biol Chem. **272**, 18169–18178

6 Beebe, S J (1994) The cAMP-dependent protein kinase and cAMP signal transduction Semin Cancer Biol **5**, 285–294

7 Bailey, T L and Elkan, C (1994) Fitting a mixture model by expectation maximization to discover motifs in biopolymers pp 28–36 Proceedings of the Second International Conference on Intelligent Systems for Molecular Biology, AAAI Press, Menlow Park

8 Gamm, D M and Uhler, M D (1995) Isoform-specific differences in the potencies of murine protein kinase inhibitors are due to nonconserved amino-terminal residues J Biol Chem **270**, 7227–7232

9 Scott, J D, Glaccum, M B, Fischer, E H and Krebs, E G (1986) Primary-structure requirements for inhibition by the heat-stable inhibitor of the cAMP-dependent protein kinase Proc Natl Acad Sci U.S.A **83**, 1613–1616

10 Glass, D B, Cheng, H C, Mende-Mueller, L, Reed, J and Walsh, D A. (1989) Primary structural determinants essential for potent inhibition of cAMP-dependent protein kinase by inhibitory peptides corresponding to the active portion of the heat-stable inhibitor protein J Biol Chem **264**, 8802–8810

11 Wen, W, Meinkoth, J L, Tsien, R Y. and Taylor, S S (1995) Identification of a signal for rapid export of proteins from the nucleus Cell **82**, 463–473

Received 4 April 2000/17 May 2000; accepted 30 May 2000

Biochem J (2000) 349, 409–412 (Printed in Great Britain)

RESEARCH COMMUNICATION

HSP43, a small heat-shock protein localized to specific cells of the vulva and spermatheca in the nematode *Caenorhabditis elegans*

Lily DING and E. Peter M. CANDIDO[1]
Department of Biochemistry and Molecular Biology, University of British Columbia, Vancouver, BC, Canada V6T 1Z3

Heat-shock protein 43 (HSP43) of *Caenorhabditis elegans* is prominently expressed in the utse cell, which attaches the uterus to the hypodermis, the uv1 cells joining the vulva and the uterus, the spermathecal valve and junctions between cells of the spermathecal cage. In body-wall muscle, HSP43 forms a punctate pattern of circumferential lines, probably corresponding to regions where the hypodermis contacts the muscle cells.

Key words: α-crystallin, immunocytochemistry, reproductive organs, stress protein, tissue specificity.

INTRODUCTION

Small heat-shock proteins (smHSPs) belong to the α-crystallin family [1–3]. Whereas the subunit molecular masses of these proteins range from approx. 12000 to 43000, they generally exist as large complexes in their native forms. The best characterized smHSP structure, that of HSP16.5 from the thermophilic archaeon *Methanococcus jannaschii*, consists of a spherical assembly of 24 subunits [4]. Some smHSPs are strictly stress-inducible, whereas others may be constitutively expressed, developmentally regulated or up-regulated under stress. Although the functions of smHSPs *in vivo* are poorly understood, they show an ATP-independent chaperone activity *in vitro*, i.e. the ability to inhibit aggregation and precipitation of substrate proteins [5]. SmHSPs have been found to be associated with specific structures in some cells, such as intermediate filaments [6], adherens junctions of desmosomes [7] or co-localized with muscle components [7,8]. A mixed complex between the small heat-shock proteins myotonic dystrophy protein kinase-binding protein/HSPB2 and HSPB3 is formed during muscle differentiation in rat [8] These findings suggest that smHsps may serve a variety of specific functions in different tissues and cell types. Here we report the characterization of a new smHSP, HSP43, the largest identified member of this protein family encoded in the genome of the nematode *Caenorhabditis elegans*. HSP43 is constitutively expressed, developmentally regulated and shows striking localization to specific somatic cells of the vulva and spermatheca, and to body-wall-muscle cell contacts.

MATERIALS AND METHODS

Cloning and expression of HSP43

To generate the expression vector pRSET43, the HSP43 cDNA was amplified from phagemid pRATII-CM14F11 (a gift from Dr Chris Martin, Genome Sequencing Center, Washington University, St. Louis, MO, U.S.A.) with primers LD1 (5′ tga catATG ACT CTT GCA ACC CGT CAT 3′, forward primer) and LD2 (5′ cga ctgcag TTA ATA TGT CTT GCG GAG 3′, reverse primer). The amplified HSP43 sequence (nucleotides 1–1107 of the coding region) was cloned into the *Nde*I–*Pst*I sites of pRSET (Invitrogen). The vector pET43H$_6$ encoding HSP43 with a C-terminal His$_6$ tag (HSP43H$_6$) was prepared by amplifying and subcloning the HSP43 coding region from pRSET43 into the *Nco*I–*Hin*dIII sites of pET28a(+) (Novagen) using primers LD20 (5′ aat ccatgg gc ACT CTT GCA ACC CGT CAT 3′, forward primer) and LD14 (5′ ccgaagctt ATA TGT CTT GCG GAG AAT 3′, reverse primer). HSP43H$_6$ was produced in *Escherichia coli* BL21(DE3) cells as described previously [7]. Bacterial cell pellets were suspended in 20 ml of Denaturing Buffer (6 M guanidinium chloride/50 mM Tris, pH 7.5), centrifuged at 12000 *g* for 10 min, and the supernatant was loaded onto a Ni^{2+}-nitrilotriacetate–agarose column (Qiagen; 1 cm × 6.5 cm; 5 ml bed volume). The column was washed with 50 ml of Denaturing Buffer containing 10% (v/v) glycerol and 1% (v/v) Triton X-100, followed by 10 ml of Denaturing Buffer, and eluted with 0.5 M imidazole in Denaturing Buffer. After dialysis against PBS (137 mM NaCl/2.7 mM KCl/4.3 mM $Na_2HPO_4 \cdot 7H_2O$/1.4 mM KH_2PO_4, pH 7.4), HSP43H$_6$ precipitated from solution. The insoluble protein was collected by centrifugation, and an aliquot was analysed by SDS/PAGE to confirm purity [9]. The HSP43H$_6$ was then used for antibody production as described in [7].

Developmental expression profile

Western blots of proteins from control and heat-shocked wild-type *C. elegans* were carried out as described in [7]. Immobilon-P membranes were probed with rabbit anti-HSP43 antibody {1:10000 dilution, pretreated with 1% (w/v) *E. coli* acetone-dried powder [10]} or with an anti-actin monoclonal antibody (Clone 4, 1:10000 dilution; ICN), followed by the appropriate secondary antibody [horseradish peroxidase-conjugated donkey anti-rabbit secondary antibody, 1:10000 dilution (Amersham) or horseradish peroxidase-conjugated mouse anti-rabbit secondary antibody, 1:10000 dilution (Promega)]. Protein–antibody complexes were detected by enhanced chemiluminescence (ECL®; Amersham). For comparison of different developmental stages, samples were adjusted so as to yield approximately equal signals with the anti-actin antibody.

Abbreviations used (sm)HSP, (small) heat-shock protein, HSP43H$_6$, HSP43 with a C-terminal His$_6$ tag, DAPI, 4,6-diamidino-2-phenylindole; RNAi, RNA-mediated interference

[1] To whom correspondence should be addressed (e-mail epmc@interchange ubc ca)

Size-exclusion column chromatography

Nematode extract (100 μl) was loaded onto a Superdex 200 column (24 ml bed volume; Amersham Pharmacia Biotech) and chromatographed on an AKTA system (Amersham Pharmacia Biotech) at a flow rate of 0.7 ml/min. Fractions (0.25 ml each) were collected, and aliquots were analysed by SDS/PAGE, followed by Western blotting with the anti-HSP43 antibody

Immunocytochemistry

Mixed populations of N2 nematodes were cultured at 20 °C [11] or heat-shocked at 33 °C as described previously [12]. Immunofluorescence staining was a modification of the method of Loer and Kenyon [13], as previously described [7]. After blocking in BSA at room temperature for 1 h, permeabilized nematodes were incubated with rabbit anti-HSP43 antibody (pre-treated with 1 % *E. coli* acetone-dried powder) at 1:250 dilution, and/or mouse monoclonal antibodies MH27 [14] or DM5.6 [16] at 1:250 dilution at room temperature for 2 h. Samples were washed and incubated with fluorescent secondary antibodies at 1:250 dilution (Alexa™488 anti-rabbit conjugate from Molecular Probes, Inc. and/or Texas Red dye-conjugated anti-mouse IgG from Jackson Immunoresearch Laboratories, West Grove, PA, U.S.A.) at room temperature for 2 h. In combination with antibody staining, some nematodes were also stained with 4,6-diamidino-2-phenylindole (DAPI) and Texas Red-X–phalloidin (Molecular Probes). In control experiments, anti-HSP43 antibody was pre-incubated with 1 mg/ml of recombinant HSP43H_6 prior to use. After staining, nematodes were mounted as described in [7] and viewed by fluorescence microscopy on an Axioplan 2 microscope (Zeiss).

Double-stranded-RNA-mediated interference (RNAi) assays of HSP43

Double-stranded RNA was prepared from phagemid pRATII-CM14F11 (nucleotides 1–1107 of the HSP43 coding region) or cDNA clone YK275 (phagemid pBluescript SK–; nucleotides 117–1107 of the HSP43 coding region; a gift from Dr. Yuji Kohara, National Institute of Genetics, Mishima, Japan). Double-stranded RNA was synthesized as described by Fire et al. [17] and microinjected into nematodes as previously described [7].

RESULTS AND DISCUSSION

Polyclonal antibodies produced to recombinant HSP43 reacted with a single major protein species with an apparent molecular mass of 43 000, and was present at similar levels in both control and heat-shocked animals (Figure 1A). To investigate the developmental expression of HSP43, nematode extracts were prepared from all life-cycle stages and probed with anti-HSP43 antibody (Figure 1B). HSP43 was detected at all developmental stages in animals growing at normal temperature, although levels in embryos were somewhat lower. HSP43 was surprisingly unstable in nematode extracts (even when stored on ice in SDS loading buffer, with protease inhibitors), levels becoming almost undetectable within 15 min. In contrast, actin was stable under the same conditions (Figure 1C). Given this finding, quantitative comparisons of HSP43 levels at different developmental stages must be interpreted with caution, since it is possible that the half-life of HSP43 in extracts could vary at different stages.

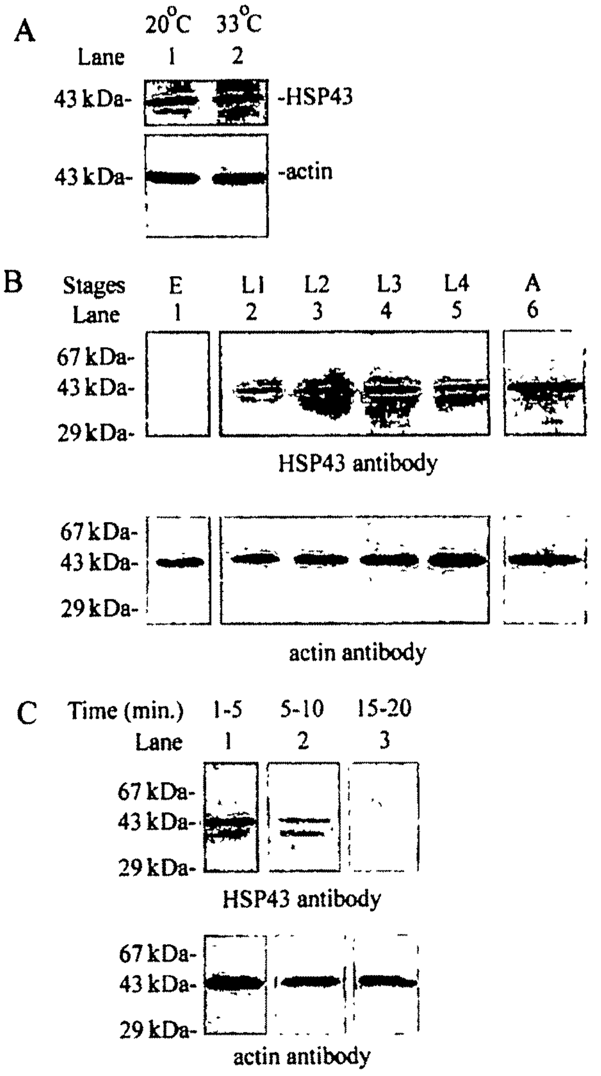

Figure 1 Expression of HSP43

(**A**) Effect of heat shock on HSP43 synthesis *C. elegans* was cultured either at 20 °C (lane 1) or heat-shocked at 33 °C (lane 2) Extracts were analysed by SDS/PAGE and Western blotting (upper panel, antibody to HSP43, lower panel, antibody to actin) (**B**) Extracts were prepared from *C. elegans* at each developmental stage and analysed by SDS/PAGE and Western blotting as in (**A**) Lane 1, embryo, lanes 2–5 (L1–L4 larval stages), lane 6, adult (**C**) Degradation of HSP43 Fresh nematode extracts in 1 × SDS/PAGE loading buffer were treated as described in the Materials and methods section and incubated on ice for the indicated times before SDS/PAGE analysis

We attempted to estimate the size of the HSP43 complex in fresh nematode extracts by size-exclusion chromatography. HSP43 was eluted in the void volume from a column of Superdex 200, as shown by Western blotting of column fractions with the HSP43 antibody. The size of the complex was estimated to be more than 670 kDa (results not shown), suggesting that HSP43 forms multimers of at least 16 subunits.

The tissue specificity of HSP43 in larval and adult nematodes was examined by immunofluorescence staining. In both control and heat-shocked adult and L4 larvae (the fourth larval stage) a low level of staining was seen throughout the body, together with very strong, specific, staining in the vulva and spermatheca (Figure 2A). In the vulval region, HSP43 was localized in the adherens junctions of vulval epithelial cells (Figure 2B), but absent from vulval muscle (Figure 2C). Images taken in different focal planes of the vulval region revealed HSP43 staining in the utse cells, which attach the uterus to the seam cells of the

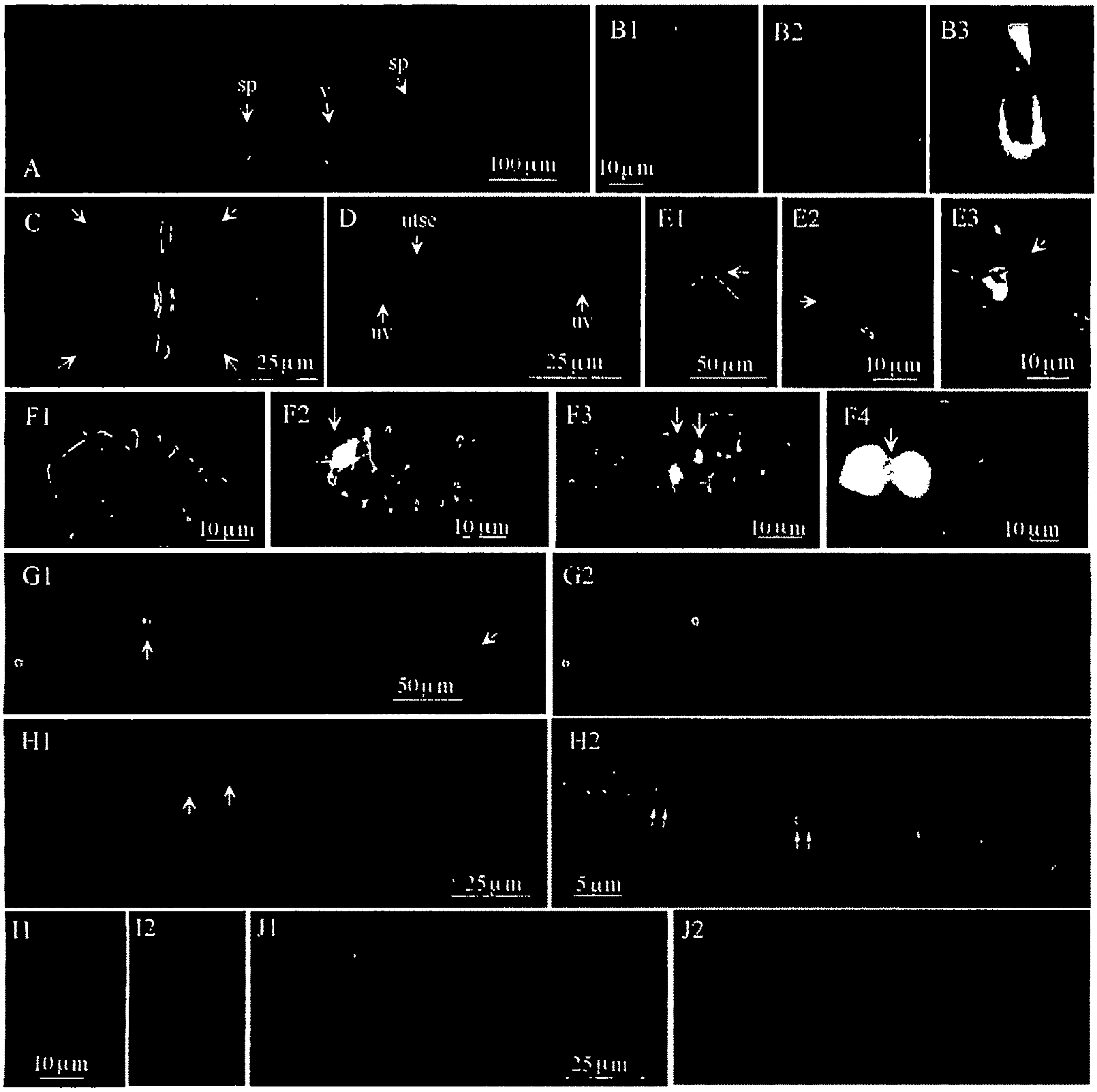

Figure 2 Immunocytochemistry of HSP43

All animals orientated with anterior to the left unless otherwise mentioned. In all images, HSP43 staining is shown in green (**A**) Young adult HSP43 is concentrated in the vulva (v) and spermathecae (sp) (**B**) HSP43 expression in the adherens junctions of vulval epithelia (ventral view) HSP43 (**B1**) and MH27, which stains desmosomes (**B2**), are partially co-localized (**B3**) (**C**) Ventral view. The relative position of HSP43 in vulva (green) is compared to vulval muscle (red, arrows, phalloidin). (**D**) Overview of HSP43 staining in vulval region (adult, lateral view) Arrows indicate utse and 2 uv1 cells (**E1**) H-shaped utse, ventro-lateral view (**E2**) and (**E3**) uv1 cells, with adjacent DAPI-stained gonadal nuclei (shown in red). (**F**) Spermathecal expression of HSP43 (**F1**) HSP43 staining in the spermathecal cage (green) with DAPI-stained sperm nuclei (shown in blue) (**F2**) HSP43 (green) is co-localized with desmosomes (red, MH27), except in spermathecal valve (arrow) (**F3**) More lateral view of a spermathecal cage, with HSP43 staining in green and nuclei (DAPI) in red (**F4**) HSP43 staining in spermathecal valve region (green) compared with valve-muscle staining (red, phalloidin), HSP43 labels both ends of the phalloidin pattern (**G1**) and (**G2**) L2 showing staining of muscle in red (phalloidin, **G1**) and nuclei in blue (DAPI, **G2**) The pharyngeal–intestinal valve (left arrow, **G1**) and intestinal–anal valve (right arrow, **G1**) are labelled by HSP43 (**H**), HSP43 staining over body-wall muscle (**H1**) L3 larva The signal is more intense where muscle cells contact one another (arrows). (**H2**) magnified region of L3-larval muscle surface, showing punctate pattern of HSP43 staining forming columns running circumferentially over muscle cells, probably at sites of hypodermal contacts Columns can be resolved as doublets of elongated spots (arrows). (**I**) and (**J**) Specificity of anti-HSP43 No HSP43 signal was seen in spermatheca (**I**) or vulva (**J**) when antiserum was pre-incubated with excess pure HSP43 DAPI staining (blue) shows location of nuclei (**I1** and **J1**), and co-staining with MH27 (red, **I2**) or DM5 6 (red, **J2**) indicates efficient permeabilization of the animals hypodermis (Figures 2D and 2E1) and in the uv1 cells which form the junction between the vulva and uterus [18] (Figures 2D, 2E2 and 2E3). At the same developmental stages, HSP43 staining was seen in desmosomes of cells which make up the spermathecal cage (Figure 2, F1–F4) and the spermathecal valve (Figure 2, F2–F4). L2 larvae, which lack vulva and spermatheca, showed prominent HSP43 staining anteriorly in the pharyngeal–intestinal valve, a structure made up of six cells coupled by a system of desmosomes [19], and posteriorly in a discreet region probably corresponding to the intestinal–rectal valve (Figure 2, G1 and G2).

In all post-embryonic stages, HSP43 staining was observed in a very regular punctate pattern over body-wall muscle, the columns of labelled spots running circumferentially along the muscle quadrant and the signal being more intense where the muscle cells contact each other (Figure 2, H1, arrows). Individual bands could be resolved as doublets separated by a narrow space (Figure 2, H2, arrows). This pattern appears identical with that reported for monoclonal antibody MH5 [20], which labels fibrous organelles containing hemidesmosomes associated with the hypodermis, where it contacts the muscle cells. Similar patterns, but differing in some details, were noted with monoclonal antibodies MH4 and MH46 [20]. Interestingly, the monoclonal antibody IFA, which defines an epitope conserved on all classes of mammalian intermediate filments [21], also reacts with arrays of filaments in *C. elegans* [20] and *Ascaris* [22], and yields an immunofluorescence pattern very similar to those of MH4 and MH5 [20]. The specificity of the antiserum for HSP43 is demonstrated by the loss of signal when the antibody is pre-incubated with excess pure recombinant HSP43 (Figure 2, I1–J2).

Recently a number of associations between smHSPs and cytoskeletal elements have been noted. α-Crystallins have been implicated in modulating intermediate-filament assembly [23] and actin polymerization [24], and HSP27 is associated with glial fibrillary acidic protein (a class of intermediate filament), vimentin and keratin filaments in various mammalian cell lines [6]. Characterization of five of the six known mammalian smHSPs revealed that only muscle-related tissues expressed all types [8]. Our recent studies of HSP25, another *C. elegans* smHSP, showed it to be localized to dense bodies and M lines in body muscle, and to junctions between cells of the spermathecal wall [7]. The latter resembled the pattern seen here with HSP43. Thus an increasing body of evidence implicates the smHSPs in managing interactions between protein components of filamentous networks in cells.

To examine the possible phenotype of an HSP43 knock-out mutation, we carried out RNAi experiments. This technique, which involves micro-injection of double-stranded RNA corresponding to a given gene sequence, results in potent and specific inhibition of gene expression in the F1 progeny of the injected animal, and often mimics the null phenotype of the gene [17,25]. Under conditions which produced suppression of a control myosin–green fluorescent protein fusion gene in approx. 90% of the progeny of injected animals, no effect of HSP43 RNAi on embryo viability was seen, and the progeny of the injected nematodes developed normally (results not shown). The lack of a conspicuous phenotype in these RNAi experiments suggests, but does not prove, that the function of HSP43 is non-essential in normal *C. elegans* growth and development. Other possibilities are that up-regulation of another member of the smHSP family might be able to compensate for a decrease in HSP43, or that HSP43 might be essential only under specific physiological conditions. It is unlikely that RNAi experiments would reveal a moderate selective advantage conferred by HSP43 function, which could be of great significance under natural conditions.

We have shown that HSP43 expression shows remarkable tissue specificity in *C. elegans*, being localized prominently to the utse and uv1 cells of the vulva, the somatic cells forming the spermatheca and the spermathecal valve. HSP43 is also found at sites of contact between body-wall muscle cells and, tentatively, between muscle cells and overlying hypodermis. In the light of demonstrated associations between smHsps and intermediate filaments [6,23], one might envisage, for instance, that HSP43 is particularly well adapted for chaperoning intermediate-filament assembly ↔ disassembly in the above tissues.

We thank Chris Martin for cDNA clone pRATII-CM14F11 and Yuji Kohara for cDNA clone YK275. We are very grateful to John G White (Laboratory of Molecular Biology, University of Wisconsin, Madison, WI, U.S.A.) for help in interpreting vulval staining patterns, to Donald Jones for a critical review of the manuscript before its submission and helpful discussions, to Richard Pfuetzner for FPLC analysis and James DeCesare for technical support This research was supported by the Medical Research Council and the Natural Sciences and Engineering Research Council of Canada.

REFERENCES

1 Gething, M.-J. (ed.) (1997) Guidebook to Molecular Chaperones and Protein-Folding Catalysts, pp 269–290, Oxford University Press, New York

2 de Jong, W. W., Caspers, G.-J. and Leunissen, J A M (1998) Int J Biol Macromol **22**, 151–162

3 Ehrnsperger, M., Buchner, J and Gaestel, M. (1997) In Molecular Chaperones in the Life Cycle of Proteins (Fink, A. L. and Goto, Y., eds.), pp. 533–575, Marcel Dekker, New York

4 Kim, K K., Kim, R and Kim, S.-H (1998) Nature (London) **394**, 595–599

5 Horwitz, J (1992) Proc Natl Acad Sci. U.S.A. **89**, 10449–10453

6 Perng, M D., Cairns, L., van den IJssel, P., Prescott, A., Hutcheson, A. M and Quinlan, R. A. (1999) J Cell Sci. **112**, 2099–2112

7 Ding, L and Candido, E. P M (2000) J Biol. Chem **275**, 9510–9517

8 Sugiyama, Y., Suzuki, A., Kishikawa, M., Akutsu, R., Hirose, T., Waye, M M. Y., Tsui, S. K W., Yoshida, S and Ohno, S (2000) J Biol Chem **275**, 1095–1104

9 Laemmli, U K (1970) Nature (London) **227**, 680–685

10 Harlow, E. and Lane, D (1988) Antibodies A Laboratory Manual, p 633, Cold Spring Harbor Laboratory Press, Cold Spring Harbor, NY

11 Brenner, S. (1974) Genetics **77**, 71–94

12 Stringham, E. G., Jones, D and Candido, E P. M (1992) Mol Biol Cell **3**, 221–233

13 Loer, C M and Kenyon, C J. (1993) J Neurosci. **13**, 5407–5417

14 Francis, G. R and Waterston, R. H (1985) J Cell Biol. **101**, 1532–1549

15 Reference deleted

16 Miller, III, D M., Ortiz, I., Berliner, G C and Epstein, H F. (1983) Cell **34**, 477–490

17 Fire, A., Xu, S., Montgomery, M. K., Kostas, S A., Driver, S E. and Mello, C C (1998) Nature (London) **391**, 806–811

18 Sharma-Kishore, R., White, J. G., Southgate, E and Podbilewicz, B (1999) Development **126**, 691–699

19 White, J. (1988) In The Nematode *Caenorhabditis Elegans* (Wood, W. B., ed.), pp 103–105, Cold Spring Harbor Laboratory Press, Cold Spring Harbor, NY

20 Francis, R and Waterston, R H (1991) J Cell Biol. **114**, 465–479

21 Pruss, R M., Mirsky, R., Raff, M C., Thorpe, R., Dowding, A J and Anderton, B. H (1981) Cell **27**, 419–428

22 Bartnik, E., Osborn, M and Weber, K (1986) J Cell Biol. **102**, 203–2041

23 Nicholl, I D. and Quinlan, R A (1994) EMBO J **13**, 945–953

24 Arrigo, A.-P. and Landry, J (1994) in The Biology of Heat Shock Proteins and Molecular Chaperones (Morimoto, R I., Tissières, A. and Georgopoulos, C., eds.), pp 335–373, Cold Spring Harbor Laboratory Press, Cold Spring Harbor, NY

25 Fire, A. (1999) Trends Genet **15**, 358–363

Received 25 April 2000; accepted 21 May 2000

Biochem. J (2000) 349, 413–415 (Printed in Great Britain)

RESEARCH COMMUNICATION

Ascorbate oxidation is a prerequisite for its transport into rat liver microsomal vesicles

Miklós CSALA*, Valéria MILE*, Angelo BENEDETTI†, József MANDL* and Gábor BÁNHEGYI*[1]

*Department of Medical Chemistry, Semmelweis University, P.O.B. 260, H-1444 Budapest, Hungary, and †Dipartimento di Fisiopatologia e Medicina Sperimentale, Università di Siena, Siena, Italy

Oxidation and uptake of ascorbate show similar time courses in rat liver microsomal vesicles: a rapid burst phase is followed by a slower process. Inhibitors of ascorbate oxidation (proadifen, econazole or quercetin) also effectively decreased the uptake of ascorbate. The results show that dehydroascorbate is the transport form of ascorbate at the membrane of the endoplasmic reticulum.

Key words: dehydroascorbate, endoplasmic recticulum, protein disulphide.

INTRODUCTION

The concentration of ascorbate is markedly different in the extracellular space, in the cytoplasm and in subcellular compartments of various cells, both in ascorbate-synthesizing and non-ascorbate-synthesizing species [1]. Ascorbate and its oxidized form, dehydroascorbate, are charged and are water-soluble compounds, and therefore their uneven distribution can be explained by the different rates and capacities of transport processes in the membrane. The ascorbate-transport systems of the plasma membrane are the best known; the intracellular accumulation of ascorbate is due to the Na$^+$-dependent co-transport of ascorbate and the facilitated diffusion and cytosolic reduction of dehydroascorbate [2–4]. Besides Na$^+$-dependent co-transport, it is questionable whether or not other forms of ascorbate transport exist. However, the intracellular and subcellular accumulation of ascorbate suggest that the facilitated diffusion of ascorbate can be absent, or minimally represented, in most membranes.

The lumen of the hepatic endoplasmic reticulum (ER) and of the vesicular structures of the secretory pathway is characterized by high (millimolar) ascorbate concentrations [5–7]. Ascorbate, in addition to its antioxidant properties, has another function: its accumulation creates a cofactor pool for several ascorbate-dependent intraluminal enzymes of the ER, such as prolyl hydroxylase and lysyl hydroxylase [1]. However, the mechanism of ascorbate accumulation is unknown. Although ascorbate transport seems to be less effective and can be inhibited by reducing agents, the facilitated diffusion of dehydroascorbate has been described in rat liver microsomes. It is presumably mediated by a glucose transporter, the T3 subunit of the glucose-6-phosphatase system [8]. These observations might suggest that ascorbate transport is dependent on its prior oxidation; that is, dehydroascorbate is the obligatory transport form in the ER. This mechanism is not unprecedented: superoxide anion produced by neutrophil granulocytes oxidizes ascorbate in the medium, dehydroascorbate is transported into the cells and it is reduced back to ascorbate in the cytosol. The whole process results in the intracellular accumulation of ascorbate [9]. Since ascorbate oxidation also takes place at the ER membrane [10,11], we considered the possibility that a similar mechanism might be responsible for ascorbate uptake and accumulation in this subcellular compartment. The aim of the present work, therefore, was to explore the role of ascorbate oxidation in intraluminal ascorbate accumulation in rat liver microsomal vesicles.

EXPERIMENTAL

Preparation of microsomes

Liver microsomal vesicles were prepared from Wistar male rats (250–300 g body weight) [12]. Microsomes were resuspended, frozen, and stored as described previously [8]. The intactness of microsomal vesicles was checked by measuring the latency of mannose-6-phosphatase and *p*-nitrophenol:UDP-glucuronosyltransferase [8].

Uptake measurements

Ascorbate transport was measured by a rapid-filtration method [8]. Inhibitors were added 10 min before the experiments. Ascorbate transport was also evaluated by the light-scattering method detailed in [8].

Ascorbate oxidation

For the determination of ascorbate oxidation, microsomal vesicles (1 mg of protein/ml) were incubated in the presence of 0.1 mM ascorbate at room temperature. Reactions were terminated and ascorbate contents were measured as described elsewhere [10]. Protein concentrations were measured with the Bio-Rad protein assay using BSA as standard.

Materials

Ascorbate, proadifen, econazole and quercetin were obtained from Sigma. l-[*carboxy*-^{14}C]Ascorbic acid (13.7 mCi/mmol) was from Amersham, Little Chalfont, Bucks., U.K. Cellulose acetate/nitrate filter membranes were from Millipore. All other chemicals were of analytical grade.

Abbreviation used ER, endoplasmic reticulum.

[1] To whom correspondence should be addressed (e-mail banhegyi@puskin.sote.hu)

RESULTS

Ascorbate oxidation in rat liver microsomal vesicles

Rat liver microsomal vesicles were incubated in the presence of 0.1 mM ascorbate. On account of the instability and rapid re-reduction of dehydroascorbate, the oxidation of ascorbate was measured on the basis of decreases in its concentration. In the microsomal system the only likely metabolism of ascorbate is its oxidoreduction; the ascorbate consumption measured in our experiments represents a balance of oxidation and re-reduction [10]. An 'oxidative burst' was observed in the first 30 s of the incubation: approx. 15 % of added ascorbate disappeared. This period was followed by a phase of slow, but continuous, ascorbate oxidation (Figure 1). In incubations carried out in the presence of inhibitors (proadifen, econazole or quercetin) the rate of ascorbate oxidation was significantly slower (Table 1).

Ascorbate transport into rat liver microsomal vesicles

Ascorbate (0.1 mM, plus radiolabelled tracer) was added to rat liver microsomal vesicles and its intravesicularly accumulated radioactivity was measured by a rapid-filtration method. Ascorbate uptake showed a biphasic behaviour – an initial fast phase (in the first minute of measurement) was followed by a second phase of slow transport (Figure 1). During the 10 min detection period, ascorbate uptake did not reach equilibrium; ascorbate occupied about 60 % of the intravesicular water space (3.5 μl/mg of protein; see [8]). Addition of the inhibitors of ascorbate oxidation (proadifen, econazole or quercetin) inhibited ascorbate uptake (Table 1).

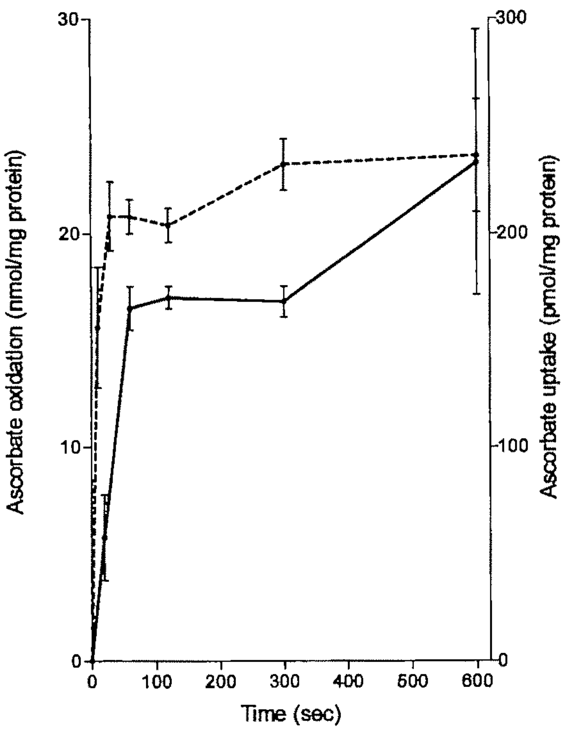

Figure 1 Time course of ascorbate oxidation and uptake in rat liver microsomal vesicles

Microsomes (1 mg of protein/ml) were incubated in the presence of 0.1 mM ascorbate at room temperature. At the indicated times the decrease in ascorbate concentration (broken line) was measured and ascorbate uptake (continuous line) was detected by a rapid-filtration method. Results are expressed as means ± S.D. for four to six experiments.

Table 1 Effect of the inhibitors of ascorbate oxidation on ascorbate uptake in rat liver microsomal vesicles

Microsomes (1 mg of protein/ml) were incubated in the presence of 0.1 mM ascorbate and the indicated inhibitors of ascorbate oxidation (0.1 mM each) at room temperature for 10 min. The decrease in ascorbate concentration was measured and ascorbate uptake was detected by a rapid-filtration method. The half-time of ascorbate transport was also calculated from the light-scattering traces shown in Figure 2. Results are expressed as means ± S.D. for four to six experiments. Abbreviation used: NM, not measured.

	Ascorbate uptake or oxidation (nmol/10 min per mg of protein)		
Addition	Oxidation	Uptake	Ascorbate uptake half-time (s)
None	23.6±2.6	0.23±0.06	5±2
Econazole	4.5±3.9	0.06±0.01	29±5
Proadifen	1.7±1.4	0.05±0.02	20±5
Quercetin	10.4±8.9	0.05±0.01	NM

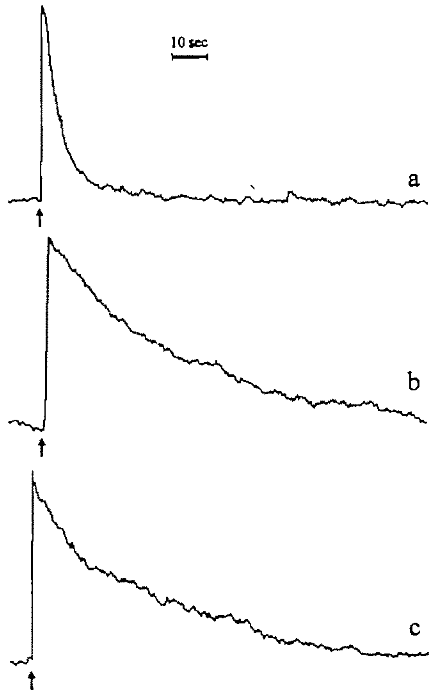

Figure 2 Ascorbate permeation in rat liver microsomes detected by a light-scattering technique

Microsomes (0.1 mg of protein/ml) were preincubated in the presence or absence of the inhibitors of ascorbate oxidation (trace a, control; trace b, 0.1 mM econazole; trace c, 0.1 mM proadifen) for 10 min. At the indicated time (arrow), 50 mM ascorbate was added and the osmotically induced changes in light-scattering were recorded. Representative traces from four experiments are shown.

Ascorbate uptake was also detected by a light-scattering technique. Ascorbate (50 mM) addition, in accordance with previous observations [8], resulted in the temporary shrinkage of rat liver microsomal vesicles, followed by a swelling phase, indicating the equalization of osmolarity on the two sides of the ER membrane due to ingress of osmolyte into the lumen. In the presence of econazole or proadifen the swelling phase became extended, showing a hindered permeation (Figure 2), with the half time of ingress increasing approx. 4–6-fold (Table 1).

These two compounds did not affect the permeation of other investigated molecules (glucose or sucrose; results not shown)

DISCUSSION

The transport of ascorbate and dehydroascorbate through the membrane of the ER has been described in rat liver microsomal vesicles [8]. The results presented here suggest that genuine ascorbate transport is negligible, or even absent, in microsomal vesicles, and the oxidation of ascorbate to dehydroascorbate is a prerequisite for the uptake. This assumption is supported by the following observations: (i) ascorbate oxidation and uptake display a similar time course in microsomes (Figure 1); (ii) inhibitors of oxidation also inhibit uptake (Table 1 and Figure 2); (iii) reducing agents decrease ascorbate uptake [8]; (iv) non-specific anion-transport inhibitors were only marginally effective in respect to ascorbate uptake [8].

The uptake did not reach equilibrium, even after 1 h incubation [8]; the concentration gradient for dehydroascorbate was therefore continuous. However, transport slowed down after the first minute, which can be attributed to the similar behaviour of ascorbate oxidation. A possible explanation for the slowing of ascorbate oxidation could be that the redox potential of the ascorbate–dehydroascorbate conjugate pair at this point approaches the redox potential value of the enzyme responsible for the oxidation.

The results indicate that ascorbate always arrives into the lumen of the ER in an oxidized form. Therefore, this transport process may be an important source of the oxidizing environment of the ER necessary for protein disulphide formation and protein folding. Dehydroascorbate can oxidize GSH or directly the protein thiol groups non-enzymically or by the mediation of protein disulphide-isomerase [15,16]. The reactions result in the reduction of dehydroascorbate and in the intraluminal entrapping of ascorbate.

The poor permeability of the ER membrane to ascorbate can explain the high ascorbate concentrations found in microsomal preparations or in the vesicular structures of the secretory pathway. The intraluminal entrapping of ascorbate creates a cofactor pool for ascorbate-dependent enzymes of the ER; moreover, it can be the source of ascorbate secretion by the hepatic exocytotic pathway, even in species unable to synthesize ascorbate [17].

In summary, the present results support the transport-based hypothesis for the generation of the oxidizing environment in the ER lumen. Ascorbate is able to promote protein thiol oxidation in microsomes; agents inhibiting microsomal ascorbate oxidation also inhibit its uptake and protein thiol oxidation. Altogether these findings strongly suggest that dehydroascorbate could be an oxidizing agent in the mechanism of protein disulphide formation.

This work was supported by Ministry of Welfare Grants (ETT 448 and 449), Ministry of Education Grant (FKFP 0652/97), Országos Tudományos Kutatási Alap Grant (T 032873), Hungarian Academy of Sciences Grant (F-226/98) by the Hungarian–Italian Intergovernmental S&T Co-operation Programme and by a NATO Linkage Grant (to A B and G B.).

REFERENCES

1 Harris, J R (ed.) (1996) Ascorbic Acid Biochemistry and Biomedical Cell Biology (Subcellular Biochemistry, vol 25), Plenum Press, New York

2 Goldenberg, H and Schweinzer, E J (1994) Transport of vitamin C in animal and human cells. J. Bioenerg. Biomembr **26**, 359–367

3 Vera, J C., Rivas, C. I, Fischbarg, J and Golde, D W. (1993) Mammalian facilitative hexose transporters mediate the transport of dehydroascorbic acid Nature (London) **364**, 79–82

4 Washko, P. and Levine, M. (1992) Inhibition of ascorbic acid transport in human neutrophils by glucose. J Biol Chem **267**, 23568–23574

5 Daniels, A J, Dean, G, Viveros, O H. and Diliberto, Jr, E J (1982) Secretion of newly taken-up ascorbic acid by adrenomedullary chromaffin cells Science **216**, 737–739

6 von Zastrow, M, Tritton, T R and Castle, J D (1984) Identification of L-ascorbic acid in secretion granules of the rat parotid gland J. Biol Chem **259**, 11746–11750

7 von Zastrow, M., Tritton, T R and Castle, J. D (1986) Exocrine secretion granules contain peptide amidation activity Proc Natl Acad Sci U S A **83**, 3297–3301

8 Bánhegyi, G., Marcolongo, P, Puskás, F., Fulceri, R, Mandl, J and Benedetti, A (1998) Dehydroascorbate and ascorbate transport in rat liver microsomal vesicles J. Biol Chem **273**, 2758–2762

9 Thomas, E. L., Learn, D. B, Jefferson, M M and Weatherred, W (1988) Superoxide-dependent oxidation of extracellular reducing agents by isolated neutrophils J. Biol Chem **263**, 2178–2186

10 Csala, M, Braun, L, Mile, V, Kardon, T, Szarka, A, Kupcsulik, P, Mandl, J and Bánhegyi, G (1999) Ascorbate-mediated electron transfer in protein thiol oxidation in the endoplasmic reticulum FEBS Lett **460**, 539–543

11 Sun, I. L, Morrè, D J, Crane, F L, Safranski, K and Croze, E M (1984) Monodehydroascorbate as an electron acceptor for NADH reduction by coated vesicle and Golgi apparatus fractions of rat liver Biochim Biophys Acta **797**, 266–275

12 Henne, V and Soling, H D. (1986) Guanosine 5′-triphosphate releases calcium from rat liver and guinea pig parotid gland endoplasmic reticulum independently of inositol 1,4,5-trisphosphate FEBS Lett **202**, 267–273

13 Freedman, R. B, Dunn, A D and Ruddock, L W (1998) Protein folding a missing redox link in the endoplasmic reticulum Curr Biol **8**, R468–R470

14 Huppa, J B and Ploegh, H. L (1998) The eS-Sence of -SH in the ER Cell **92**, 145–148

15 Venetianer, P and Straub, F B (1964) The mechanism of action of the ribonuclease-reactivating enzyme Biochim. Biophys. Acta **89**, 189–190

16 Wells, W W., Xu, D P., Yang, Y. and Rocque, P A (1990) Mammalian thioltransferase (glutaredoxin) and protein disulphide isomerase have dehydroascorbate reductase activity J Biol. Chem **265**, 15361–15364

17 Upston, J M, Karjalainen, A, Bygrave, F L and Stocker, R (1999) Efflux of hepatic ascorbate a potential contributor to the maintenance of plasma vitamin C Biochem. J **342**, 49–56

Received 27 March 2000/25 April 2000, accepted 18 May 2000

Biochem. J. (2000) 349, 417–425 (Printed in Great Britain)

Evidence for phosphorylation and ubiquitinylation of the turnip yellow mosaic virus RNA-dependent RNA polymerase domain expressed in a baculovirus–insect cell system

François HÉRICOURT*, Stéphane BLANC†, Virginie REDEKER‡ and Isabelle JUPIN*[1]

*Laboratoire de Virologie Moléculaire, Institut Jacques Monod, UMR 7592, CNRS – Universités Paris 6 – Paris 7, 2 place Jussieu, 75251 Paris Cedex 05, France, and †Laboratoire de Biologie Moléculaire et Cellulaire, Station de Recherches de Pathologie Comparée, CNRS- INRA, 30380 Saint Christol-lez-Alès, France, and ‡Laboratoire de Neurobiologie et Diversité Cellulaire, Ecole Supérieure de Physique et Chimie Industrielles de la Ville de Paris, CNRS UMR 7637, 75231 Paris Cedex 05, France

---

All RNA viruses known to date encode an RNA-dependent RNA polymerase (RdRp) that is required for replication of the viral genome. We have expressed and purified the turnip yellow mosaic virus (TYMV) RdRp in insect cells using a recombinant baculovirus, either in its native form, or fused to an hexa-histidine tag. Phosphorylation of the protein was demonstrated by labelling experiments *in vivo*, as well as phosphatase treatment of the purified protein *in vitro*. Phospho amino acid analysis and immunoblotting experiments identified serine and threonine residues as being the subject of phosphorylation. Peptide mass mapping using MS analysis of a protein digest revealed that phosphorylation sites are localized within a putative PEST sequence [a sequence rich in proline (P), glutamic acid (E), serine (S) and threonine (T) residues] in the N-terminal region of the protein. Using monoclonal antibodies specific for ubiquitin conjugates, we were able to demonstrate that the TYMV RdRp is conjugated to ubiquitin molecules when expressed in insect cells. These observations suggest that the TYMV RdRp may be processed selectively by the ubiquitin/proteasome degradation system upon phosphorylation of the PEST sequence.

Key words: PEST sequence, positive-strand RNA virus, TYMV, viral replication

---

INTRODUCTION

Turnip yellow mosaic virus (TYMV), a member of the tymovirus group, is a plant RNA virus that belongs to the 'alpha-like' super-group of viruses [1], which also comprises Sindbis virus. TYMV possesses a monopartite positive-strand genomic RNA of 6.3 kb, which directs the expression of two overlapping non-structural proteins of 69 and 206 kDa [2]. A third open reading frame encodes the 20-kDa coat protein which is expressed from a subgenomic RNA. The longer 206-kDa (206K) protein has considerable amino acid sequence similarities with non-structural putative replication proteins of several positive-strand RNA viruses (reviewed in [3]) and it has been shown to be necessary for TYMV RNA replication [4]. Upon expression *in vitro*, the 206K protein undergoes proteolytic maturation events [5], resulting in the synthesis of N-terminal 140 kDa (140K) and C-terminal 66 kDa (66K) proteins [6,7].

Replication of TYMV occurs in membrane-associated replication complexes [8]. Within these, the genomic plus-strand RNA is transcribed into minus-strand RNA, which in turn can be used as a template for synthesis of progeny genomic and subgenomic plus strands. At least the two viral proteins 140K and 66K appear to be involved in this reaction [9]. While the role in RNA replication of the 140K protein, which carries methyltransferase and NTPase/putative RNA helicase motifs, is less clear, the 66K protein is obviously the key enzyme responsible for synthesis of progeny RNA strands because it contains several motifs considered to be signature sequences for RNA-dependent RNA polymerases (RdRps) [10]. It has been suggested that these motifs may co-operate to form an ordered domain, which constitutes a 'polymerase module' implicated in template interaction and polymerase activity [11]. All RNA viruses known to date encode an RdRp that is required for replication of the viral genome. Some events of TYMV genome replication have been elucidated by mutagenesis of cloned genomes [9] whereas purification of active replication complexes from infected plants [12,13] has allowed the characterization of some of their enzymic properties [13–15]. However, the low amounts of non-structural viral proteins produced during viral infection precluded any biochemical and structural analyses.

Such studies can be greatly facilitated by the use of RdRp purified from recombinant sources. This approach has been successfully used in earlier experiments including poliovirus $3D^{pol}$ [16], tobacco vein mottling potyvirus NIb [17] and hepatitis C virus NS5B protein [18]. Purification and characterization of poliovirus $3D^{pol}$ from different sources showed that recombinant enzyme preparations from bacteria or insect cells are indistinguishable by all measured criteria from the RdRp synthesized in the natural host cell [19].

In order to study the properties of the TYMV RdRp, we report the expression of the TYMV 66K protein (RdRp domain) in insect cells using recombinant baculoviruses. Using a rapid purification procedure by means of an engineered N-terminal hexa-histidine tag, we show that the protein is phosphorylated *in vivo* on serine and threonine residues. Using matrix-assisted laser-desorption ionization–time-of-flight (MALDI–TOF) MS,

---

Abbreviations used: MALDI–TOF, matrix-assisted laser-desorption ionization–time-of-flight; Ni-NTA, Ni^{2+}-nitrilotriacetate; RdRp, RNA-dependent RNA polymerase; TYMV, turnip yellow mosaic virus; a.m.u., atomic mass units.

[1] To whom correspondence should be addressed (e-mail jupin@ccr.jussieu.fr).

phosphorylated peptides were localized to a putative PEST region [a region enriched in proline (P), glutamic acid (E), serine (S) and threonine (T) residues]. In addition, higher-molecular-mass products were identified as ubiquitin–66K conjugates. We discuss the possible role of these post-translational modifications in the regulation of the protein's metabolic stability.

EXPERIMENTAL

Plasmid constructions

All DNA manipulations were performed using standard techniques [20,21]. The DNA fragment encoding the TYMV 66K protein (nt 3872–5629 according to [2]) was amplified by PCR using *Pfu* DNA polymerase (Stratagene) and primers 1, 5′-CGGAATTCCATGGGCACCCCCAGCGCATCCCCCACCCACC-3′, and 3, 5′-CGGGATCCGGTACCCTATTGGACGTAGTGAAGCAATTC-3′, which provided *Nco*I and *Kpn*I restriction sites (underlined) at the 5′ and 3′ termini of the gene, respectively. The 1766-nt-long *Nco*I–*Kpn*I fragment was cloned in the similarly restricted baculovirus transfer vector p10-119pst (kindly provided by M. Cerutti, Station de Recherches de Pathologie Comparée CNRS-INRA, Saint Christol-lez-Alès, France), a modified version of pGm8022, which allows expression under the control of the late p10 gene promoter [22], to give the construct p17AE. The ATG codon in the engineered *Nco*I site serves as an artificial start codon for translation. In the following, the protein expressed by this construct will be referred to as 66K.

To create the construct p8AF, the same procedure was used with the combination of primers 2, 5′-CGGAATTCCATGGGC(CACCAT)$_3$ACCCCCAGCGCATCCCCCACCCACCGTTCG-3′ (with the *Nco*I site underlined), and 3. This construct gives rise to a 66K protein with an N-terminal hexa-histidine tag, which will be referred to as His-66K. The transferred PCR fragments were sequenced completely on an ABI Prism 377 DNA sequencer (Applied Biosystems) using a BigDye Terminator Sequencing kit (Applied Biosystems) and specific primers. Due to the engineering of the start codon within an *Nco*I cloning site in the DNA sequence, the N-termini of both recombinant proteins differed from the authentic viral protein by the presence of a methionine followed by a glycine residue instead of the threonine residue at position 1. The amino acid numbering starts at T^{1}PSA ... 7, i.e. at the genuine N-terminus of the viral 66K protein [6,7], so that residue positions of recombinant and native 66K proteins correlate.

Expression of 66K and His-66K in insect cells

Recombinant baculoviruses Bac17AE and Bac8AF were generated by co-transfection of *Spodoptera frugiperda* (Sf9) lepidopteran cells with AcSLP10 DNA [22] and the p17AE and p8AF constructs respectively. The growth of Sf9 cell cultures and propagation of recombinant baculoviruses were carried out as described previously [23]. For the expression of 66K or His-66K proteins in insect cells, monolayers of Sf9 cells were infected with recombinant baculovirus Bac17AE or Bac8AF and incubated at 28 °C for 48 to 64 h. When tested, tunicamycin dissolved in DMSO was added to the cell cultures (final concentration, 10 μg/ml) at 7 or 20 h post-infection. As controls, cells were incubated with DMSO alone. The cells were harvested 52 h post-infection and the recombinant proteins were detected as described below.

Purification of His-66K

Bac8AF-infected Sf9 cells were harvested 64 h post-inoculation, pelleted at 500 *g* for 5 min, washed with PBS, and resuspended in buffer A (6 M guanidinium hydrochloride/0.1 M sodium phosphate/10 mM Tris/HCl, pH 8) at 10^6 cells/ml. Cells were incubated for 1 h at room temperature and the lysate was centrifuged at 10000 *g* for 15 min. Then, 1 ml of a 50 % slurry of Ni^{2+}-nitrilotriacetate (Ni-NTA) Superflow resin (Qiagen) previously equilibrated in buffer A was added to 10 ml of the supernatant and incubated for 45 min at room temperature with occasional shaking. The mixture was then loaded on a 0.5-cm-diameter column, washed with six column volumes of buffer A, three column volumes of buffer B (8 M urea/0.1 M sodium phosphate/10 mM Tris/HCl, pH 8) and three column volumes of buffer C (8 M urea/0.1 M sodium phosphate/10 mM Tris/HCl, pH 6.3). The recombinant protein was eluted with buffer C containing 300 mM imidazole.

Protein gel electrophoresis and staining

Proteins were separated by electrophoresis through SDS/polyacrylamide gels (12.5 or 7 %) according to the procedure described in [24]. After staining with Coomassie Brilliant Blue, the amount of protein was estimated by comparison with known amounts of BSA analysed on the same gel. Alternatively, proteins were detected by reverse staining using imidazole-zinc salts according to [25].

Western-blot analysis

After separation by SDS/PAGE, the proteins were electrotransfered to nitrocellulose BA83 (Schleicher and Schuell) or to PVDF membrane (Millipore). Polyclonal antibodies raised against the C-terminal region of TYMV 66K expressed in *Escherichia coli* as a fusion protein [26] were provided kindly by Dr K. Séron (Institut Jacques Monod, Paris, France) and were used at 1/500 dilution in PBS/5 % dried skimmed milk/0.05 % Tween 20. Antibodies raised against phosphoserine, phosphothreonine and phosphotyrosine were obtained from Zymed and were used at 1/200, 1/200 and 1/400 dilutions, respectively, in 10 mM Tris/HCl, pH 7.5/150 mM NaCl/6 % BSA. Monoclonal antibodies against ubiquitin conjugates (FK2) [27] were provided kindly by Dr R. Haguenauer-Tsapis (Institut Jacques Monod, Paris, France) and were used at 1/1000 dilution in PBS/5 % dried skimmed milk/0.05 % Tween 20. The blots were developed using alkaline phosphatase-conjugated secondary antibodies and Nitro Blue Tetrazolium/5-bromo-4-chloroindol-3-yl phosphate (NBT-BCIP) as substrates.

Labelling *in vivo*

Sf9 cells (2×10^6 cells in a 25-cm^2 culture flask) were infected with the recombinant baculovirus Bac8AF, and 24 h post-infection the growth medium was replaced with phosphate-free medium containing 25 μCi/ml of [^{32}P]orthophosphate (ICN). After a labelling period of 18 h, the cells were collected and washed with PBS. Total cell proteins were analysed by SDS/PAGE after lysis of 4×10^5 cells in SDS sample buffer. The remaining cells were used to purify the labelled His-66K protein under denaturing conditions as described above.

Phospho amino acid analysis

Phospho amino acid analysis was performed as described in [28] after transfer of ^{32}P-labelled purified His-66K to a PVDF membrane. The protein was subjected to hydrolysis in 200 μl of 6 M HCl for 2 h at 110 °C, after which the supernatant was transferred to a new tube and lyophilized. The pellet was dissolved in 3 μl of water containing 2 μg each of phosphoserine, phosphothreonine and phosphotyrosine, and was spotted on to a thin-layer cellulose plate (Kodak). The first-dimension ascending chromatography was carried out for 13 h in solvent A (isobutyric acid/0.5 M NH_4OH, 5:3, v/v) followed by 6 h of chromatography in the second dimension in solvent B (2-propanol/HCl/H_2O, 14:3:3, v/v) according to [29]. Phospho amino acids were visualized by spraying with ninhydrin (0.25%, w/v, in acetone) while radioactive molecules were revealed by autoradiography.

Protein phosphatase treatment

Purified His-66K protein (50 ng) was incubated with 400 and 800 units of λ protein phosphatase (New England Biolabs) as recommended by the supplier for 30 min at 30 °C.

Trypsin digestion

Purified His-66K protein (6 μg) was reduced by a treatment with 10 mM dithiothreitol/0.1 M NH_4HCO_3 for 45 min at 56 °C, followed by alkylation with 55 mM iodoacetamide/0.1 M NH_4HCO_3 for 30 min. After electrophoresis on a 7% SDS/polyacrylamide gel and reverse staining, the bands containing the proteins of interest were excised from the gel, and rinsed twice in 1 ml of 50 mM Tris, pH 8/0.3 M glycine/30% acetonitrile and twice in water. Proteins were digested in-gel with sequencing-grade trypsin (Boehringer) according to published procedures [30]. The reaction was stopped by freezing the samples at −20 °C. The supernatant containing tryptic peptides was collected for MS analysis. Further peptide extraction was also performed as described previously [30].

MS analysis

The tryptic peptides were acidified with aqueous trifluoroacetic acid to a final concentration of 0.1% and mixed with a saturated solution of 2,5-dihydroxybenzoic acid (Sigma) in 0.1% aqueous trifluoroacetic acid. The samples were then analysed by MALDI–TOF MS. Ionization was accomplished with a 337-nm beam from a nitrogen laser. Mass spectra of positive ions were recorded in reflectron mode with a single-stage reflectron mass spectrometer (Voyager Elite, PerSeptive Biosystems, Framingham, MA, U.S.A.) equipped with a delayed extraction device. Delayed extraction time was set at 100 ns. Typically, 200–250 shots were averaged for each acquired spectrum. Internal calibration was performed using peptides generated by autoproteolysis of trypsin and corresponding to the protonated peptides 132–142, 56–75 and 76–85 with mono-isotopic mass-to-charge (m/z) ratios of 1153.57, 2163.06 and 2273.16, respectively. Only the mono-isotopic m/z ratio of the protonated peptides are given in the Results section.

RESULTS

Expression and purification of the TYMV 66K protein in insect cells

In order to develop an *in vitro* system for analysis of the viral RdRp domain structure and function, the entire TYMV 66K protein was expressed in insect cells using a recombinant *Autographa californica* nuclear polyhedrosis virus (AcNPV). For this purpose, two different recombinant baculoviruses were constructed: Bac17AE directs the expression of the TYMV 66K protein, hereafter called 66K, while Bac8AF allows the expression of an extended version of this protein, hereafter called His-66K, bearing a hexa-histidine affinity tag at the N-terminus. This tag was designed to permit the rapid purification of the protein by affinity chromatography on immobilized metal [31]. *S. frugiperda* (Sf9) lepidopteran cells were infected with the recombinant baculoviruses Bac17AE or Bac8AF, or a control recombinant baculovirus containing TYMV-unrelated sequences [23]. After incubation for 48 h at 28 °C, the total protein content of these cells was analysed by SDS/PAGE (12.5% gel). Coomassie Brilliant Blue staining of this gel (Figure 1A) revealed that a prominent band with a molecular mass of about 69 kDa was present in the protein extracts from Bac17AE- and Bac8AF-infected Sf9 cells (Figure 1A, lanes 2 and 3), but was absent from control extracts (Figure 1A, lane 1). These major proteins were confirmed as being the TYMV 66K protein and its tagged derivative by immunoblot analysis using an antiserum raised against a bacterial fusion protein containing the C-terminal part of the TYMV 66K protein (Figure 1B, lanes 1–3). In addition, a set of bands of lower molecular masses was also visible in the total protein extracts, that may correspond to degradation products of the TYMV 66K protein.

Despite the fact that the His-66K protein synthesized in Bac8AF-infected insect cells appeared mostly insoluble, the use of strong denaturing agents coupled with affinity purification on Ni-NTA resin allowed the rapid purification of significant quantities of this protein. After purification, analysis by SDS/PAGE and Coomassie Brilliant Blue staining, the protein was estimated to be more than 90% pure (Figure 1A, lane 4) Its identity was confirmed by immunoblotting using the anti-66K antiserum (Figure 1B, lane 4). Since the putative degradation products were not retained on Ni-NTA resin, it is likely that the N-terminal hexa-histidine tag was absent from these species.

When the protein extracts from Bac17AE- and Bac8AF-infected cells were analysed on a 7% acrylamide gel, the prominent bands corresponding to 66K and His-66K, as well as the purified fraction of the latter, were resolved into two close bands of similar intensity (Figure 1C, lanes 2–4). Both bands were recognized equally by the anti-66K antiserum (Figure 1D, lanes 2–4). Because there are no other in-frame initiation codons or suppressible stop codons in the surrounding sequences that would allow the expression of a protein product different from the genuine 66K protein, we speculated that the protein species with a shifted electrophoretic mobility may rather correspond to a post-translationally modified version of the TYMV 66K protein.

The TYMV 66K amino acid sequence contains several potential N-glycosylation sites. We therefore investigated the effects of the fungal antibiotic tunicamycin, which inhibits an early step in the N-glycosylation of proteins, on the pattern of expression of His-66K in insect cells. We observed no change in the total amount of recombinant proteins produced, nor a shift in the migration of the proteins synthesized in the presence of tunicamycin relative to the control samples (results not shown). Consequently, the TYMV 66K protein does not appear to be N-glycosylated in insect cells.

Evidence for the phosphorylation of the TYMV 66K protein

The phosphorylation status of the 66K protein was examined by labelling the Bac8AF-infected cells with $[^{32}P]$orthophosphate for 18 h. Total protein extracts were analysed by SDS/PAGE (12.5% gel), and the labelled proteins were visualized by autoradiography. A radioactive protein of apparent molecular mass 69 kDa was detected in the Bac8AF-infected cell extracts (Figure 2A, lane 2), which was absent in cells infected with the control baculovirus (Figure 2A, lane 1). This labelled protein is likely to correspond to the TYMV His-66K protein because it could be purified from the pool of proteins present in the metabolically

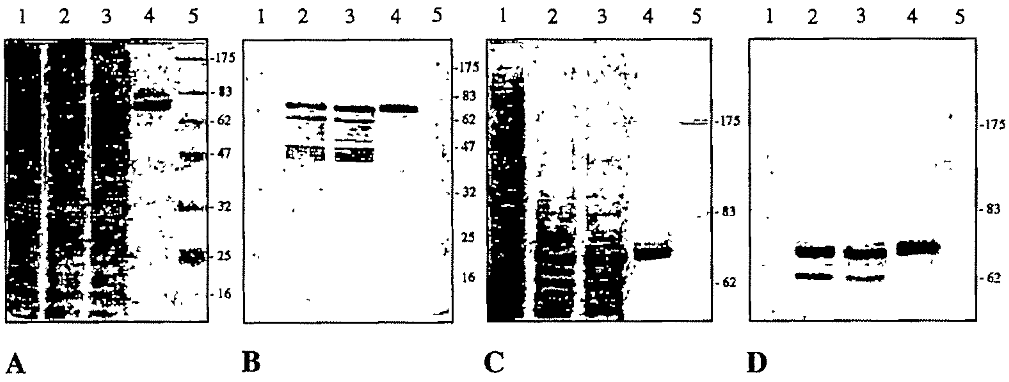

Figure 1 Expression and purification of TYMV 66K in baculovirus-infected insect cells

Total proteins from control baculovirus-infected cells (lanes 1), Bac17AE-infected cells (lanes 2), Bac8AF-infected cells (lanes 3), purified His-66K (lanes 4) and molecular-mass markers (lanes 5) were analysed by SDS/PAGE on 12.5% (**A** and **B**) or 7% (**C** and **D**) gels. The gels were stained with Coomassie Brilliant Blue (**A** and **C**) or electroblotted on to a nitrocellulose filter that was revealed by Western blotting using the anti-66K antiserum (**B** and **D**). The positions of molecular-mass markers are indicated.

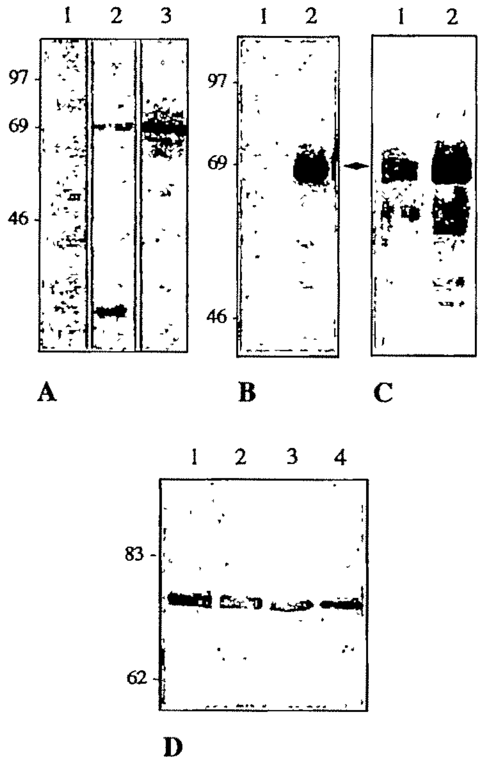

Figure 2 Phosphorylation of TYMV 66K protein expressed in baculovirus-infected insect cells

(**A**) Following metabolic labelling with [^{32}P]orthophosphate, total proteins from control baculovirus-infected cells (lane 1), Bac8AF-infected cells (lane 2) and purified His-66K (lane 3) were analysed by SDS/PAGE (12.5% gel) and revealed by autoradiography. (**B**) Following metabolic labelling with [^{32}P]orthophosphate, 50 and 150 ng of purified His-66K protein (lanes 1 and 2, respectively) were analysed by SDS/PAGE (7% gel), electroblotted on to a nitrocellulose filter and revealed by autoradiography. (**C**) The same blot as in (**B**) was revealed by Western blotting using the anti-66K antiserum. (**D**) Purified His-66K protein (50 ng) was treated with 400 and 800 units of protein phosphatase λ (lanes 3 and 4, respectively). Lanes 1 and 2 contain identical amounts of protein before or after incubation in the reaction buffer in the absence of phosphatase. The proteins were then subjected to SDS/PAGE followed by immunoblotting with the anti-66K antiserum. The positions of molecular-mass markers are indicated.

labelled cells by affinity chromatography on Ni-NTA resin under denaturing conditions (Figure 2A, lane 3).

To investigate whether both bands of the doublet were similarly labelled, different amounts of the purified labelled His-66K protein were separated on a 7% acrylamide gel, followed by transfer to a nitrocellulose membrane. The membrane was first subjected to autoradiography (Figure 2B), and was then probed with the antiserum raised against the 66K protein (Figure 2C). Careful alignment of the signal from the anti-66K antibody with the autoradiograph of the same blot revealed that most of the radioactivity was incorporated in the upper band of the doublet, which therefore corresponded to the phosphorylated form of the TYMV 66K protein. Accordingly, treatment of purified His-66K protein with protein phosphatase λ resulted in the disappearance of the shifted band (Figure 2D, lanes 3 and 4), whereas control incubation of the protein in the absence of phosphatase had no effect on its mobility (Figure 2D, lane 2).

Taken together, these experiments demonstrate that the TYMV RdRp domain is produced in insect cells as a phosphoprotein whose phosphorylation reduces its electrophoretic mobility in SDS/PAGE, resulting in an increased apparent molecular mass.

Phosphorylation occurs on serine and threonine residues

Determination of the amino acid residue subjected to phosphorylation was performed by TLC. The ^{32}P metabolically labelled protein His-66K was purified, totally hydrolysed and the resulting phospho amino acids were mixed with standard phospho amino acids and subjected to two-dimensional TLC according to [29]. Figure 3(A) shows that a unique spot that co-migrated with phosphoserine and phosphothreonine species was detected after autoradiography of the TLC plate.

Because these two species were resolved poorly, the identity of the amino acid subjected to phosphorylation was confirmed by performing immunoblot experiments using antibodies directed against each phospho amino acid. Figure 3(B) shows that the upper band was recognized by the antisera directed against phosphoserine and phosphothreonine residues, whereas the band with the faster mobility was recognized by the antiserum raised against phosphoserine. This demonstrates that both serine and threonine residues are the target residues for phosphorylation of

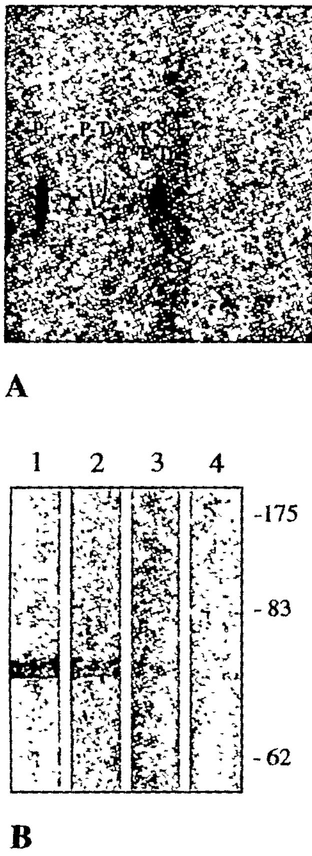

Figure 3 TYMV 66K protein contains both phosphoserine and phosphothreonine residues

(**A**) Purified *in vivo* ^{32}P-labelled His-66K was subjected to phospho amino acid analysis After hydrolysis of the protein with 6 M HCl, the products were spotted together with standard phospho amino acids and subjected to two-dimensional TLC The positions of standard phospho amino acid phosphoserine (P-Ser), phosphothreonine (P-Thr) and phosphotyrosine (P-Tyr), as revealed by ninhydrin reactions, are indicated by dotted circles First and second dimensions are indicated, as well as the location of free phosphate (Pi) (**B**) Purified His-66K protein was analysed by SDS/PAGE (7% gel) and was revealed by Western blotting using antibodies raised against phosphoserine (lane 2), phosphothreonine (lane 3) and phosphotyrosine (lane 4) Lane 1 was revealed using anti-66K antibodies The positions of molecular-mass markers are indicated

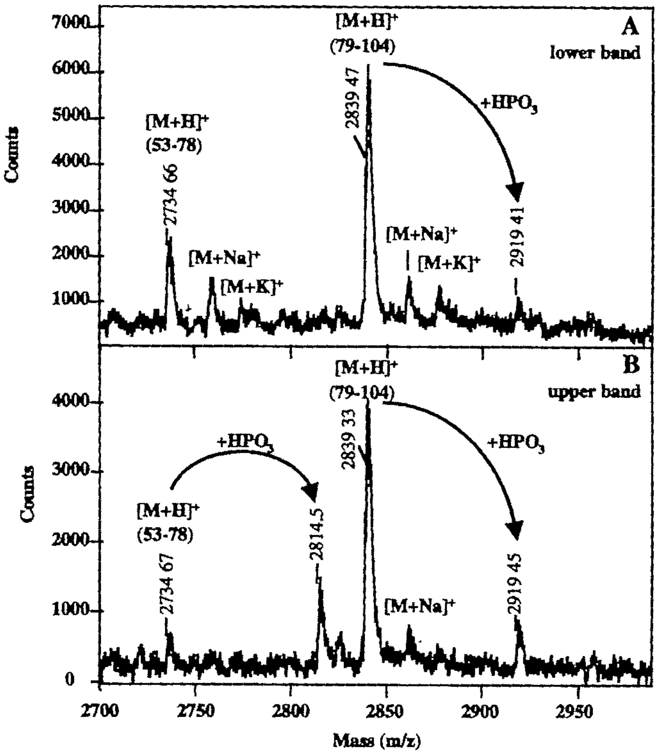

Figure 4 Differential peptide mass mapping of the TYMV 66K lower and upper band tryptic digests: identification of two phosphorylated peptides

Mass spectra obtained by MALDI–TOF MS in the mass range of 2700–3000 a m u of the tryptic peptides generated from the His-66K lower (**A**) and upper (**B**) band digestions The molecular ions were assigned to amino acid sequences of His-66K protein according to its sequence and the cleavage specificity of trypsin The amino acid sequences of the peptides corresponding to the molecular ions observed are indicated, as well as their corresponding sodium and potassium adducts ([M + Na]$^+$ and [M + K]$^+$) Amino acid residues were numbered according to the sequence of the native protein + HPO$_3$ indicates the addition of one phosphate group to each peptide (mass increment of 80 a m u)

the TYMV 66K protein, and suggests that some serine phosphorylation events may not affect the electrophoretic mobility of the protein.

Mapping of the phosphorylated region

To gain some insights into the identification of the phosphorylated sites, we searched for phosphorylated tryptic peptides using MALDI–TOF MS. Purified His-66K was subjected to SDS/PAGE, and after reverse staining, the two bands corresponding to the differently phosphorylated forms were excised from the gel and digested with trypsin. The generated peptides were submitted directly to peptide mass mapping using MALDI–TOF MS (results not shown). The molecular ions were assigned to amino acid sequences of the protein based on the His-66K sequence and cleavage specificity of trypsin. The identified peptides covered 70–80 % of the His-66K protein sequence.

Comparison of the mass spectra obtained for each band of the doublet revealed that two peptides clearly displayed a mass increment of 80 atomic mass units (a.m.u.) characteristic of the addition of a single phosphate group (Figure 4). The mass spectrum of the lower band tryptic digest (Figure 4A) revealed the presence of the non-phosphorylated forms of the peptides 53–78 and 79–104 (experimental [M + H]$^+$ values of 2734.66 and 2839.47 a.m u. respectively), and their corresponding sodium and potassium adducts. In addition, a minor peak with an increase in mass of 80 corresponding to the mono-phosphorylated form of the peptide 79–104 was also observed (experimental [M + H]$^+$ of 2919.41 a.m.u.). In the mass spectrum of the upper band digest (Figure 4B), this mono-phosphorylated form of the peptide 79–104 was still present, with a slightly increased intensity. Moreover, we also observed the mono-phosphorylated form of peptide 53–78 (experimental [M + H]$^+$ of 2814.5 a m.u.), which was more abundant than its non-phosphorylated form Both peptides are contiguous in the protein sequence and each encompass four putative phosphorylation sites: Thr-64, Ser-69, Thr-70 and Ser-71 for peptide 53–78 and Ser-80, Ser-90, Ser-102 and Thr-103 for peptide 79–104.

Evidence for ubiquitinylation of the TYMV 66K protein

Several of these putatively phosphorylated residues are contained within the longest sequence of contiguous PEST residues in the protein, which extends from amino acids 56 to 78 (see Discussion).

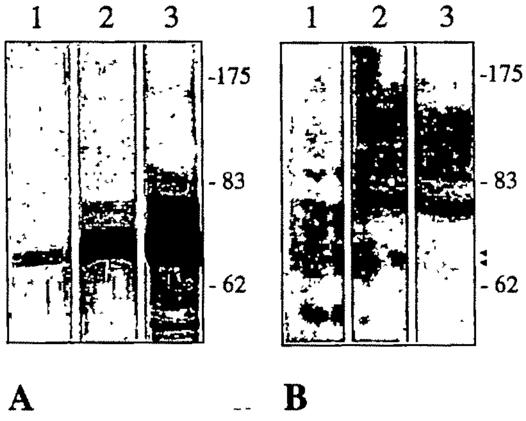

Figure 5 Evidence for the presence of TYMV ubiquitin–66K conjugates

(**A**) Increasing amounts of purified His-66K protein (30, 150 and 500 ng in lanes 1, 2 and 3 respectively) were analysed by SDS/PAGE (7% gel) and were revealed by Western blotting using the anti-66K antiserum (**B**) Total proteins from control baculovirus-infected cells (lane 1), Bac8AF-infected cells (lane 2) and purified His-66K (lane 3) were analysed by SDS/PAGE (7% gel) and were revealed by Western blotting using the monoclonal antibody FK2 directed against ubiquitin conjugates The position of the major His-66K doublet is indicated by arrowheads The positions of molecular-mass markers are indicated

PEST-rich sequences are potential degradation signals through the ubiquitin/proteasome degradation pathway, and it has been reported that phosphorylation of serine or threonine residues can activate latent PEST sequences. This prompted us to examine whether we could observe ubiquitinylated forms of the 66K protein.

On the conjugation of ubiquitin to a protein substrate, multiple bands are observed in SDS/PAGE, which consist of several molecules of ubiquitin linked to a single molecule of the protein When increasing amounts of His-66K protein were analysed by Western blotting using the anti-66K antiserum (Figure 5A), a set of larger products of discrete sizes was revealed, which appeared as a ladder of double bands. The size interval between each step of this ladder ($\approx$ 8 kDa) closely matches the molecular mass of ubiquitin, a result consistent with the formation of poly-ubiquitin conjugates

To ensure that these higher-molecular-mass species were actually covalent complexes between the TYMV 66K protein and ubiquitin, we carried out a Western-blot analysis using a monoclonal antibody (FK2) specific for ubiquitin conjugates [27]. When total proteins from control baculovirus-infected insect cells were analysed with this antibody (Figure 5B, lane 1), a number of proteins were revealed, reflecting the variety of proteins that are ubiquitinylated *in vivo*. However, when total proteins from 8AF-infected cells or purified His-66K protein were analysed similarly (Figure 5B, lanes 2 and 3), the same ladder of additional bands as observed in Figure 5(A) was specifically recognized by the FK2 monoclonal antibody. This recognition was specific because the excess amount of His-66K protein (indicated by arrowheads) gave only background signal. This demonstrates that the TYMV 66K protein is conjugated to ubiquitin in insect cells.

DISCUSSION

The high levels of expression that we obtained by using recombinant baculovirus–insect cell system accomplishes the first step in developing a system for the study *in vitro* of the TYMV RdRp. The observation that the purified protein appeared as a double band with both bands of equivalent intensity, combined with the extensive documentation relative to the ability of the baculovirus expression system to perform the appropriate post-translational modifications to recombinant proteins [32] prompted us to study the TYMV His-66K post-translational modifications. Additional experiments are in progress to characterize its biochemical properties further.

Our results demonstrate that the TYMV RdRp domain expressed in insect cells can be phosphorylated on both serine and threonine residues. This finding implies that phosphorylation may be involved in regulating the RNA polymerase activity of the TYMV 66K protein, as is the case with RNA polymerase II, whose processivity is regulated by such a post-translational modification of its C-terminal domain [33]. Interestingly, the RdRp domain of hepatitis C virus NS5B has also recently been shown to be phosphorylated [34], but its phospho amino acid residues have not yet been characterized. In addition to the RNA polymerase activity, the TYMV 66K protein is likely to participate in numerous other activities and to interact with other viral or cellular proteins in order to accomplish template specificity, chain initiation, regulation of plus- and minus-strand synthesis or membrane association of the replication complex Conceivably, any of these additional activities or interactions could be affected by modifications of amino acid residues in the RdRp.

In order to determine what role phosphorylation of the 66K protein may have in TYMV replication functions, we were interested in defining more precisely the phosphorylated peptides. MALDI–TOF MS allowed the identification of two contiguous mono-phosphorylated tryptic peptides (amino acids 53–78 and 79–104). Each of these two peptides contains four serine or threonine residues that may constitute possible phosphorylation sites. Analysis of kinase consensus recognition sites [35] revealed that Thr-70 and Ser-102 may constitute target sites for casein kinase II, whereas protein kinase C may use Ser-102 as a substrate More accurate characterization of phosphorylation sites requiring phosphopeptide purification and sequencing is the subject of further studies.

It should be noted that the MALDI MS analysis does not allow quantification of the amount of peptides present within the mixture, because the intensity of the signal is highly dependent on the nature of the polypeptide and can be significantly affected by a single amino acid change [36]. In particular, it has been reported that phosphopeptides often yield poor response in MALDI MS in positive-ion mode compared with non-phosphorylated peptides, most likely because of the negative charge of the phosphate group [37,38]. These differences in ion detection, which prevent possible quantification of the corresponding biomolecules, are further increased in complex peptide mixtures such as those obtained by tryptic digestion, due to either a ‘suppression effect’ or low ionization efficiency [37,39] As a consequence, we cannot exclude the existence of other minor phosphorylated peptides that would have been undetected in the MALDI–TOF mass spectra of either band of the doublet, which may also contribute to the anti-phosphoserine and anti-phosphothreonine antibodies’ reactivity.

Some regions of the RdRp domain are highly conserved among plus-strand RNA viruses [40], but the identified phosphorylated peptides are part of the N-terminal sequence, which is more divergent Amino acid sequence comparison among tymoviral RdRps (Figure 6A) revealed that none of the eight potential phosphorylated residues of TYMV 66K are present at conserved positions, with the exception of residue 80, which consists of either a serine or a threonine in all tymoviral sequences. Despite this lack of sequence conservation among tymoviral

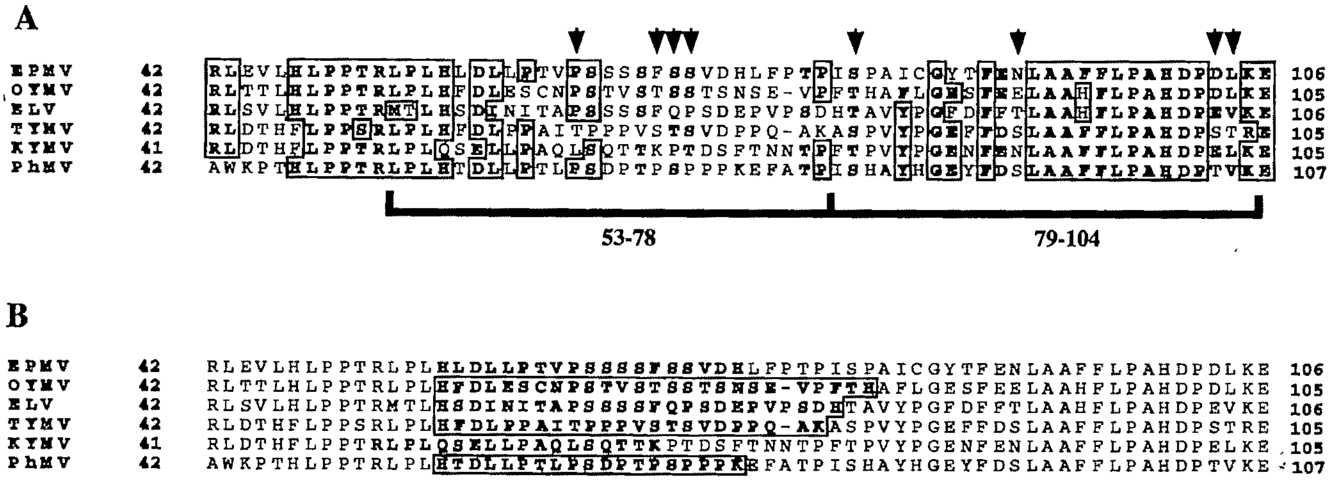
A
EPMV 42 RLEVLHLPPTRLPLHLDLLPTVPSSSSFSSVDHLFPTPISPAICGYTFENLAAFFLPAHDPDLKE 106
OYMV 42 RLTTLHLPPTRLPLHFDLESCNPSTVSTSSTSNSE-VPFTHAFLGHSFEELAAHFLPAHDPDLKE 105
ELV 42 RLSVLHLPPTRMTLHSDINITAPSSSSFQPSDEPVPSDHTAVYPGFDFFTLAAHFLPAHDPEVKE 106
TYMV 42 RLDTHFLPPSRLPLHFDLPPAITPPPVSTSVDPPQ-AKASPVYPGEFFDSLAAFFLPAHDPSTRE 105
KYMV 41 RLDTHFLPPTRLPLQSELLPAQLSQTTKPTDSFTNNTPFTPVYPGENFENLAAFFLPAHDPELKE 105
PhMV 42 AWKPTHLPPTRLPLHTDLLPTLPSDPTPSPPPKEFATPISHAYHGEYFDSLAAFFLPAHDPTVKE 107
53-78
79-104
B
EPMV 42 RLEVLHLPPTRLPLHLDLLPTVPSSSSFSSVDHLFPTPISPAICGYTFENLAAFFLPAHDPDLKE 106
OYMV 42 RLTTLHLPPTRLPLHFDLESCNPSTVSTSSTSNSE-VPFTHAFLGESFEELAAHFLPAHDPDLKE 105
ELV 42 RLSVLHLPPTRMTLHSDINITAPSSSSFQPSDEPVPSDHTAVYPGFDFFTLAAHFLPAHDPEVKE 106
TYMV 42 RLDTHFLPPSRLPLHFDLPPAITPPPVSTSVDPPQ-AKASPVYPGEFFDSLAAFFLPAHDPSTRE 105
KYMV 41 RLDTHFLPPTRLPLQSELLPAQLSQTTKPTDSFTNNTPFTPVYPGENFENLAAFFLPAHDPELKE 105
PhMV 42 AWKPTHLPPTRLPLHTDLLPTLPSDPTPSPPPKEFATPISHAYHGEYFDSLAAFFLPAHDPTVKE 107

Figure 6 Sequence alignment of tymovirus RdRps

(**A**) The N-terminal region of tymovirus RdRp was aligned using the CLUSTAL W computer program. Conserved amino acids are in bold type and highly conserved ones are boxed. The identified phosphorylated peptide sequences are underlined and the potential phosphorylation sites in TYMV 66K protein are indicated by arrows. (**B**) The PEST sequences identified using the PEST-FIND computer program are shown in bold type. Boxed residues indicate PEST regions displaying high PEST scores [+2.8 for TYMV, +6.7 for ononis yellow mosaic virus (OYMV), +10.3 for erysimum latent virus (ELV) and +14.1 for physalis mottle virus (PhMV)], whereas non-boxed residues indicate PEST regions displaying poor PEST scores [−10 for kennedya yellow mottle virus (KYMV) and −2 for eggplant mosaic virus (EPMV)]. Virus sequences (and accession numbers) used in the alignment were: TYMV (P10358), kennedya yellow mottle virus (P36304), eggplant mosaic virus (P20126), ononis yellow mosaic virus (P20127), erysimum latent virus (P35928) and physalis mottle virus (CAA76071). The numbering refers to amino acid positions in the RdRp protein.

RdRps, we observed that the amino acid composition within the region comprising amino acids 56–84 was rather similar, and displayed a particular enrichment for proline, serine, threonine and acidic residues. This finding led us to the hypothesis that this portion of the protein may consist of a so-called PEST region [41]. Using the PEST-FIND computer program, amino acids 56–78 within the TYMV 66K protein were indeed identified as being a putative PEST sequence (Figure 6B). Interestingly, PEST sequences were invariably identified in this particular region within the different tymoviral RdRp proteins (Figure 6B), although their PEST scores were highly variable (ranking from −10 for kennedya yellow mottle virus RdRp to +14 for physalis mottle virus RdRp).

PEST sequences were first identified as signals for protein instability [42] but it is likely that they function indirectly in degradation. Many PEST sequences are conditional signals, serving principally as sites for phosphorylation, which is necessary for further ubiquitinylation and degradation of some proteins [43–45]. Based on these observations, we propose that phosphate addition to particular Ser and Thr residues in the N-terminal region of TYMV 66K protein may serve for activating a latent PEST signal, thereby controlling the metabolic stability of the protein. In this respect, it should be noted that the TYMV 66K protein has been reported to be unstable when produced by translation *in vitro* in rabbit reticulocyte lysate, resulting in low and variable amounts of products [46]. A truncated protein of 32 kDa comprising the first 240 amino acids behaved similarly [46], whereas an internal deletion of amino acids 72–209 that covers part of the proposed PEST sequence was found to stabilize the protein product [7]. The corresponding protein domains encoded by other tymoviruses were also postulated to be rapidly degraded *in vitro* [47]. These observations support the implication of the PEST region in proteolytic targeting and instability of the tymovirus RdRps.

A considerable body of evidence supports the idea that PEST sequences target proteins for degradation by the ubiquitin/proteasome system. Ubiquitin is a 76-residue protein whose covalent conjugation to lysine residues of other protein substrates is a common means by which eukaryotic cells signal their subsequent degradation by the 26 S proteasome, a multiprotease complex (reviewed in [48]). Using monoclonal antibodies specific for ubiquitin conjugates, we were able to demonstrate that the TYMV 66K protein is conjugated to ubiquitin molecules when expressed in insect cells. These data provide a first step towards proving the involvement of the ubiquitin/proteasome system in TYMV 66K protein processing. Because the ubiquitin conjugates appeared as clearly resolved doublets, they provide evidence that the two forms of 66K can be ubiquitinylated, regardless of the difference in their phosphorylation status. Attempts to identify the ubiquitinylation site(s) by an MS approach have been unsuccessful so far, and therefore directed mutagenesis of lysine residues thought to be implicated in ubiquitin conjugation is the subject of further experiments.

Ubiquitinylation of recombinant proteins produced in the baculovirus–insect cell system has been described previously in a few cases [49,50]. The ubiquitin-dependent proteolysis pathway was reported to be functional in baculovirus-infected insect cells up to ≈ 24 h post-infection [50], the lack of ATP in the later stages of infection rendering it non-functional, which may explain our capability of observing stable ubiquitin–66K conjugates. Because some of the components of the ubiquitin/proteasome pathway have been characterized in plants (reviewed in [51]), it is tempting to speculate on the formation of poly-ubiquitin–66K conjugates in virus-infected plant cells, whose degradation may relate to the extremely low levels of 66K protein present during infection. Further studies are required to elucidate whether this is indeed the case.

Interestingly, the involvement of the ubiquitin proteolytic pathway has already been suggested regarding another member of the 'alpha-like' viral super-group: the Sindbis virus RdRp nsP4 protein [52]. It is produced by an endoproteolytic cleavage of the viral precursor polyprotein and, as with other alphavirus RdRps, it bears an N-terminal Tyr residue [53]. It has been reported that, both *in vitro* and *in vivo*, Sindbis nsP4 is degraded by the ubiquitin-dependent N-end rule pathway [54], a rule that relates the *in vivo* half-life of a protein to the identity of its N-terminal residue [55].

Indirect evidence therefore suggests that selective degradation of viral proteins by the ubiquitin-dependent proteolytic pathway may be a common feature of alpha-like viral RdRps Whether this reflects a strategy by which the virus regulates the intracellular levels of mature cleavage products or a host defence mechanism aimed at the elimination of viral proteins will be the subject of further studies.

We are grateful to M Cerutti, A -L Haenni and J. Rossier for their interest in the work and their kind hospitality during the course of these studies We thank K Séron and R. Haguenauer-Tsapis for the gift of antibodies, M Cerutti for providing the plasmid p10-119pst, G Beaud and J -M Galan for technical advice, R Haguenauer-Tsapis and J -M Galan for helpful discussions and L van Dinten for comments on the manuscript Specials thanks to J -P Le Caer for helpful discussions and expert assistance in MS. F.H. was the recipient of a fellowship from the Ministère de l'Education Nationale de la Recherche et de la Technologie (MENRT) and from the Association pour la Recherche sur le Cancer (ARC) The funding of ARC for MALDI–TOF MS equipment is gratefully acknowledged. This work was supported in part by grants from MENRT (Programme de Recherche Fondamentale en Microbiologie et Maladies Infectieuses et Parasitaires) and CNRS (Programme Jeunes Equipes) to I J

REFERENCES

1 Goldbach, R and Wellink, J (1988) Evolution of plus-strand RNA viruses Intervirology **29**, 260–267

2 Morch, M D, Boyer, J C and Haenni, A L (1988) Overlapping open reading frames revealed by complete nucleotide sequencing of turnip yellow mosaic virus genomic RNA Nucleic Acids Res. **16**, 6157–6173

3 Buck, K W (1996) Comparison of the replication of positive-stranded RNA viruses of plants and animals Adv Virus Res **47**, 159–251

4 Weiland, J. J and Dreher, T W (1989) Infectious TYMV RNA from cloned cDNA effects *in vitro* and *in vivo* of point substitutions in the initiation codons of two extensively overlapping ORFs Nucleic Acids Res **17**, 4675–4687

5 Morch, M D, Drugeon, G, Szafranski, P and Haenni, A L (1989) Proteolytic origin of the 150-kilodalton protein encoded by turnip yellow mosaic virus genomic RNA J Virol **63**, 5153–5158

6 Kadaré, G, Rozanov, M. and Haenni, A L (1995) Expression of the turnip yellow mosaic virus proteinase in *Escherichia coli* and determination of the cleavage site within the 206 kDa protein J Gen Virol **76**, 2853–2857

7 Bransom, K L, Wallace, S E and Dreher, T W (1996) Identification of the cleavage site recognized by the turnip yellow mosaic virus protease Virology **217**, 404–406

8 Garnier, M, Candresse, T and Bové, J M (1986) Immunocytochemical localization of TYMV-coded structural and nonstructural proteins by the Protein A-gold technique Virology **151**, 100–109

9 Weiland, J J and Dreher, T. W. (1993) Cis-preferential replication of the turnip yellow mosaic virus RNA genome Proc Natl Acad Sci U S A **90**, 6095–6099

10 Poch, O, Sauvaget, I, Delarue, M and Tordo, N (1989) Identification of four conserved motifs among the RNA-dependent polymerase encoding elements EMBO J **8**, 3867–3874

11 Joyce, C M and Steitz, T A. (1995) Polymerase structures and function variations on a theme? J Bacteriol **177**, 6321–6329

12 Mouchès, C, Bové, C. and Bové, J M (1974) Turnip yellow mosaic virus-RNA replicase partial purification of the enzyme from the solubilized enzyme-template complex Virology **58**, 409–423

13 Deiman, B A, Kortlever, R. M and Pleij, C. W. (1997) The role of the pseudoknot at the 3′ end of turnip yellow mosaic virus RNA in minus-strand synthesis by the viral RNA-dependent RNA polymerase J Virol **71**, 5990–5996

14 Gargouri-Bouzid, R, David, C and Haenni, A L (1991) The 3′ promoter region involved in RNA synthesis directed by the turnip yellow mosaic virus genome *in vitro* FEBS Lett **294**, 56–58

15 Singh, R N and Dreher, T W (1997) Turnip yellow mosaic virus RNA-dependent RNA polymerase initiation of minus strand synthesis *in vitro* Virology **233**, 430–439

16 Neufeld, K. L, Richards, O C and Ehrenfeld, E (1991) Expression and characterization of poliovirus proteins 3BVPg, 3Cpro, and 3Dpol in recombinant baculovirus-infected *Spodoptera frugiperda* cells Virus Res **19**, 173–188

17 Hong, Y and Hunt, A G (1996) RNA polymerase activity catalyzed by a potyvirus-encoded RNA-dependent RNA polymerase Virology **226**, 146–151

18 Behrens, S E, Tomei, L and De Francesco, R. (1996) Identification and properties of the RNA-dependent RNA polymerase of hepatitis C virus EMBO J **15**, 12–22

19 Neufeld, K L, Richards, O C and Ehrenfeld, E (1991) Purification, characterization, and comparison of poliovirus RNA polymerase from native and recombinant sources J Biol Chem **266**, 24212–24219

20 Ausubel, F M, Brent, R, Kingston, R E, Moore, D D, Seidman, J G, Smith, J A. and Struhl, K (1987) Current Protocols in Molecular Biology, Wiley, New York

21 Sambrook, J, Fritsch, E F and Maniatis, T (1989) Molecular Cloning a Laboratory Manual, Cold Spring Harbor Press, Cold Spring Harbor

22 Chaabihi, H, Ogliastro, M H, Martin, M, Giraud, C, Devauchelle, G and Cerutti, M (1993) Competition between baculovirus polyhedrin and p10 gene expression during infection of insect cells J Virol **67**, 2664–2671

23 Blanc, S, Schmidt, I, Kuhl, G, Esperandieu, P, Lebeurier, G, Hull, R, Cerutti, M and Louis, C (1993) Paracrystalline structure of cauliflower mosaic virus aphid transmission factor produced both in plants and in a heterologous system and relationship with a solubilized active form Virology **197**, 283–292

24 Laemmli, U K (1970) Cleavage of structural proteins during the assembly of the head of bacteriophage T4 Nature (London) **227**, 680–685

25 Castellanos-Serra, L., Proenza, W, Huerta, V, Moritz, R L and Simpson, R J (1999) Proteome analysis of polyacrylamide gel-separated proteins visualized by reversible negative staining using imidazole-zinc salts Electrophoresis **20**, 732–737

26 Deiman, B A, Seron, K, Jaspars, E M. and Pleij, C W (1997) Efficient transcription of the tRNA-like structure of turnip yellow mosaic virus by a template-dependent and specific viral RNA polymerase obtained by a new procedure J Virol Methods **64**, 181–195

27 Fujimuro, M, Sawada, H and Yokosawa, H (1994) Production and characterization of monoclonal antibodies specific to multi-ubiquitin chains of polyubiquitinated proteins FEBS Lett **349**, 173–180

28 Kamps, M P (1991) Determination of phosphoamino acid composition by acid hydrolysis of protein blotted to Immobilon Methods Enzymol **201**, 21–27

29 Duclos, B, Marcandier, S and Cozzone, A J (1991) Chemical properties and separation of phosphoamino acids by thin-layer chromatography and/or electrophoresis Methods Enzymol. **201**, 10–21

30 Wilm, M, Shevchenko, A, Houthaeve, T, Breit, S., Schweigerer, L, Fotsis, T and Mann, M (1996) Femtomole sequencing of proteins from polyacrylamide gels by nano-electrospray mass spectrometry Nature (London) **379**, 466–469

31 Sulkowski, E (1985) Purification of proteins by IMAC Trends Biotechnol **3**, 1–7

32 Fraser, M J (1989) Expression of eukaryotic genes in insect cultures In Vitro Cell Dev Biol **25**, 225–235

33 Payne, J M, Laybourn, P J and Dahmus, M E (1989) The transition of RNA polymerase II from initiation to elongation is associated with phosphorylation of the carboxyl-terminal domain of subunit IIa. J Biol. Chem. **264**, 19621–19629

34 Hwang, S B, Park, K J, Kim, Y S, Sung, Y C and Lai, M M (1997) Hepatitis C virus NS5B protein is a membrane-associated phosphoprotein with a predominantly perinuclear localization Virology **227**, 439–446

35 Bairoch, A, Bucher, P and Hofmann, K (1996) The PROSITE database, its status in 1995 Nucleic Acids Res **24**, 189–196

36 Redeker, V, Rossier, J and Frankfurter, A (1998) Posttranslational modifications of the C-terminus of alpha-tubulin in adult rat brain alpha 4 is glutamylated at two residues Biochemistry **37**, 14838–14844

37 Liao, P C, Leykam, J, Andrews, P C, Gage, D A and Allison, J (1994) An approach to locate phosphorylation sites in a phosphoprotein mass mapping by combining specific enzymatic degradation with matrix-assisted laser desorption/ionization mass spectrometry Anal Biochem **219**, 9–20

38 Asara, J M and Allison, J (1999) Enhanced detection of phosphopeptides in matrix-assisted laser desorption/ionization mass spectrometry using ammonium salts J Am Soc Mass Spectrom **10**, 35–44

39 Kratzer, R, Eckerskorn, C, Karas, M and Lottspeich, F (1998) Suppression effects in enzymatic peptide ladder sequencing using ultraviolet matrix assisted laser desorption/ionization mass spectrometry Electrophoresis **19**, 1910–1919

40 Koonin, E V (1991) The phylogeny of RNA-dependent RNA polymerases of positive-strand RNA viruses J Gen Virol **72**, 2197–2206

41 Rechsteiner, M. and Rogers, S W (1996) PEST sequences and regulation by proteolysis Trends Biochem Sci **21**, 267–271

42 Rogers, S, Wells, R and Rechsteiner, M (1986) Amino acid sequences common to rapidly degraded proteins the PEST hypothesis Science **234**, 364–368

43 Lin, R, Beauparlant, P, Makris, C, Meloche, S and Hiscott, J (1996) Phosphorylation of IkappaBalpha in the C-terminal PEST domain by casein kinase II affects intrinsic protein stability Mol Cell Biol **16**, 1401–1409

44 Lanker, S., Valdivieso, M H and Wittenberg, C (1996) Rapid degradation of the G1 cyclin Cln2 induced by CDK-dependent phosphorylation Science **271**, 1597–1601

45 Marchal, C, Haguenauer-Tsapis, R and Urban-Grimal, D (1998) A PEST-like sequence mediates phosphorylation and efficient ubiquitination of yeast uracil permease Mol Cell Biol **18**, 314–321

46 Bransom, K L, Weiland, J J. and Dreher, T W (1991) Proteolytic maturation of the 206-kDa nonstructural protein encoded by turnip yellow mosaic virus RNA Virology **184**, 351–358

47 Kadaré, G, Drugeon, G, Savithri, H S and Haenni, A L (1992) Comparison of the strategies of expression of five tymovirus RNAs by *in vitro* translation studies. J Gen Virol **73**, 493–498

48 Ciechanover, A (1998) The ubiquitin-proteasome pathway on protein death and cell life EMBO J **17**, 7151–7160

49 Cahoreau, C, Garnier, L, Djiane, J, Devauchelle, G and Cerutti, M (1994) Evidence for N-glycosylation and ubiquitination of the prolactin receptor expressed in a baculovirus-insect cell system. FEBS Lett. **350**, 230–234

50 Daniels, P R, Sanders, C M and Maitland, N J (1998) Characterization of the interactions of human papillomavirus type 16 E6 with p53 and E6-associated protein in insect and human cells J Gen Virol **79**, 489–499

51 Vierstra, R D (1996) Proteolysis in plants mechanisms and functions Plant Mol. Biol **32**, 275–302

52 Wellink, J and van Kammen, A (1988) Proteases involved in the processing of viral polyproteins Arch Virol **98**, 1–26

53 Strauss, J H and Strauss, E G (1994) The alphaviruses gene expression, replication, and evolution Microbiol. Rev **58**, 491–562

54 de Groot, R J, Rumenapf, T, Kuhn, R. J, Strauss, E G and Strauss, J H (1991) Sindbis virus RNA polymerase is degraded by the N-end rule pathway Proc Natl. Acad Sci. U S A **88**, 8967–8971

55 Varshavsky, A (1996) The N-end rule functions, mysteries, uses Proc Natl Acad Sci U S A **93**, 12142–12149

Received 6 January 2000/3 April 2000, accepted 3 May 2000

Interferons activate the p42/44 mitogen-activated protein kinase and JAK-STAT (Janus kinase-signal transducer and activator transcription factor) signalling pathways in hepatocytes: differential regulation by acute ethanol via a protein kinase C-dependent mechanism

Van-Anh T. NGUYEN, Jianping CHEN, Feng HONG, Edward J. N. ISHAC, and Bin GAO[1]
Department of Pharmacology and Toxicology, Medical College of Virginia, Virginia Commonwealth University, Richmond, VA 23298, U.S.A.

Interferons (IFNs) have been used in the treatment of viral hepatitis. However, their effectiveness is much reduced (< 10 %) in alcoholics. The mechanism underlying this resistance remains unknown. Here, we report that IFN-α/β and IFN-γ rapidly activate the JAK-STAT1 (Janus kinase-signal transducer and activator transcription factor 1) and p42/44 mitogen-activated protein kinase (p42/44 MAPK) in freshly isolated rat hepatocytes. Treatment of hepatocytes with 25–100 mM ethanol for 30 min inhibited IFN-β- or IFN-γ-induced STAT1 activation and tyrosine phosphorylation. The inhibitory effect of ethanol was not reversed by pretreatment with either sodium vanadate, a non-selective tyrosine phosphatase inhibitor, or with MG132, a specific proteasome inhibitor. This suggests that protein tyrosine phosphatases or the ubiquitin–proteasome pathway are not involved in the inhibitory action of ethanol. In contrast with the JAK-STAT signalling pathway, acute ethanol exposure significantly potentiated IFN-β or IFN-γ-induced activation of p42/44 MAPK, and caused marked activation of protein kinase C (PKC). Inhibition of PKC partially antagonized ethanol attenuation of IFN-induced STAT1 activation, suggesting that PKC may be involved. Taken together, these findings suggest that the ability of biologically relevant concentrations of ethanol (less than 100 mM) to markedly inhibit IFN-activated STAT1 is one of the cellular mechanisms responsible for the observed resistance of IFN therapy in alcoholics.

Key words: interleukin-6, proteasome, protein-tyrosine phosphatase, tyrosine phosphorylation, viral hepatitis.

INTRODUCTION

Type I (predominantly α/β) and type II (γ) interferons (IFNs) were first identified as inducible secretory proteins with antiviral and antitumor activities, and now have been used in the treatment of a wide variety of diseases [1], including various liver diseases [2–8]. For example, IFN-α/β and IFN-γ have been used in the treatment for viral hepatitis and liver fibrosis [2–8]. The primary form of treatment for viral hepatitis is interferon therapy alone or in combination with Ribavirin. Such therapy can reduce elevated serum alanine transferase levels, eliminate serum virus RNA and improve liver histology [2–8]. Unfortunately, however, less than 10 % of alcoholics are responsive to IFN therapy [9–12].

Type I (predominantly α/β) and type II (γ) IFNs signal through distinct but related pathways via binding to type I and type II receptors respectively. The binding of IFNs to their receptors activates the receptor-associated tyrosine kinases [JAK1 and TyK2 associate with the two chains of IFN-α/β receptor, JAK1 (Janus kinase 1) and JAK2 with the IFN-γ receptor chains]. This receptor–kinase complex interacts with, and activates, the SH2-containing cytoplasmic STATs (signal transducer and activator transcription factors) (IFN-α/β activates STAT1, STAT2 or STAT3, IFN-γ activates STAT1, STAT3 or STAT5, depending on cell type). Activated STAT proteins then form homo- or hetero-complexes that translocate to the nucleus to activate the transcription of many target genes (reviewed in [13–15]). In addition to the JAK-STAT signalling pathway, IFNs also activate p42/44 mitogen-activated protein kinase (p42/44 MAPK) [16–18] and insulin receptor substrate-1 (IRS1) [19,20]. The role of IFN-activated STAT1 in antiviral and antitumour activities is clearly demonstrated in STAT1 knockout mice [21,22]. In these mice, IFN signalling is defective and the innate response to viral or bacterial infection is absent. Furthermore, STAT1-deficient mice as well as IFN-γ-deficient mice have a higher incidence of tumours [21,22]. However, the roles of p42/44 MAPK and IRS1 in the function of IFNs are not clear.

Although IFNs have been widely used in the treatment of liver diseases, the IFN signalling pathway in the liver and the mechanisms for unresponsiveness to IFNs in alcoholics remain unknown. In the present study we demonstrate that IFNs activated both p42/44 MAPK and JAK-STAT signalling pathways in freshly isolated hepatocytes. These signalling pathways are differentially regulated by acute ethanol treatment. The ability of biologically relevant concentrations (less than 100 mM) of ethanol to inhibit IFN-activated STAT1 may, at least in part, account for the observed resistance of IFN therapy in alcoholic patients [9–12].

MATERIALS AND METHODS

Materials

STAT1, STAT3, and STAT5 antibodies were purchased from Upstate Biotechnology (Lake Placid, NY, U.S.A.). Anti-

---

Abbreviations used: JAK-STAT, Janus kinase-signal transducer and activator transcription factor, p42/44 MAPK, p42/44 mitogen-activated protein kinase, PKB/Akt, protein kinase B, IFN, interferon; IL-6, interleukin-6, IRS1, insulin receptor substrate-1, JNK, c-Jun N-terminal kinase, PKC, protein kinase C; DMSA, DNA gel-mobility-shift assay, SH, Src homology

[1] To whom correspondence should be addressed (e-mail bgao@hsc.vcu.edu)

phospho-STAT1 (Tyr^{701}), anti-phospho-p42/44 MAPK (Tyr^{204}), anti-[phospho-c-Jun N-terminal kinase (JNK)] (Thr^{183}/Tyr^{185}), anti-phospho-Akt (Ser^{473}) antibodies were obtained from Bio-lab (Beverly, MA, U.S.A.). The following reagents were purchased from Sigma Chemicals (St. Louis, MO, U.S.A.): ethanol, collagenase type IV, sodium vanadate, Nonidet P40. GF-109203X, and MG132 were obtained from Calbiochem (San Diego, CA, U S A.). IFN-α, IFN-β and IFN-γ were purchased from Bioscience International (Camarillo, CA, U.S.A.). Radiolabelled [γ-^{32}P]ATP was purchased from DuPont NEN (Boston, MA, U S A.).

Isolation of hepatocytes

Liver cells were isolated by a collagenase-perfusion protocol as described previously [23]. Isolated cells were washed twice and resuspended in Krebs–Henseleit solution (118 mM NaCl/4 7 mM KCl/1 2 mM $MgSO_4$/2.5 mM $CaCl_2$/1.2 mM KH_2PO_4/25 mM $NaHCO_3$/10 mM glucose) containing 1.5 % gelatin, and were further treated with drugs and/or ethanol and/or IFN.

DNA gel-mobility-shift assay (DMSA)

DMSA for STAT binding was described previously [24,25] The STAT binding site of oligo m67 (the high-affinity serum-inducible element m67) (5′-GTCGACATTTCCCGTAAATCGTCGA-3′) was used as a probe.

Western-blot analysis

Western-blot analysis was described previously [23] Hepatocytes were re-suspended in lysis buffer [30 mM Tris (pH 7.5)/150 mM NaCl/1 mM PMSF/1 mM Na_3VO_4/1 % Nonidet P40/10 % glycerol] and then centrifuged for 10 min at 4 °C. The protein concentration of the supernatant (protein fraction) was calculated using the Bio-Rad protein assay. An aliquot of 40 μg of protein was mixed with an equivalent volume of 2 × protein loading buffer, pH 7 4, containing β-mercaptoethanol and boiled for 5 min before loading on to an SDS/8 %-polyacrylamide gel. After electrophoresis, proteins were transferred on to nitrocellulose membranes and blotted against primary antibodies. Membranes were washed with TPBS (0.05 % Tween 20 in PBS, pH 7.4) and incubated with a 1:4000 dilution of horseradish peroxidase-conjugated secondary antibodies for 45 min. Protein bands were revealed by an enhanced-chemiluminescence (ECL$^{®}$) reaction (Amersham Pharmacia Biotech, Piscataway, NJ, U.S.A.).

P42/44 MAPK, JNK and protein kinase B (PKB/Akt) phosphorylation

P42/44 MAPK, JNK, and PKB/Akt phosphorylation were detected by Western-blot analysis using specific anti-phospho-p42/44 MAPK (Tyr^{204}), anti-phospho-JNK (Thr^{183}/Tyr^{185}), and anti-phospho-PKB/Akt (Ser^{473}) antibodies respectively.

Protein kinase C (PKC) assay

PKC activity was determined by measuring the transfer of ^{32}P from [γ-^{32}P]ATP to histone IIIs as described previously [26]. Briefly, the reaction was initiated by the addition of 50 μg of protein from the cytosol or membrane fraction to a reaction mixture (0.25 ml volume) containing 20 mM Tris/HCl, 0.75 mM $CaCl_2$, 20 mM magnesium acetate, 5 μg of leupeptin, 100 μg of histone IIIs, 100 μM (60 c.p.m./pmol) [γ-^{32}P]ATP at pH 7.5, in the absence or presence of 25 μg of phosphatidylserine (PKC cofactor) and 1 μg of diacylglycerol (PKC activator). Samples were incubated for 5 min at 31 °C and the reaction was terminated by the addition of 1 ml of 25 % (v/v) trichloroacetic acid. Tubes were centrifuged at 5000 *g* for 15 min and the pellet washed three times with 4 ml of cold trichloroacetic acid (10 %, v/v). Precipitates were solubilized with 0.5 ml of 2 M NaOH and transferred to vials for liquid-scintillation counting. PKC activity was calculated by subtracting the amount of ^{32}P incorporated in the absence of phospholipids (non-PKC) from the amount of ^{32}P incorporated in the presence of phospholipids, and this was expressed as pmol of ^{32}P incorporated into histone III/min per mg of protein at 31 °C. Enzyme activity was observed to be linear up to 15 min The cytosol and membrane fractions were prepared as described previously [26]. Briefly, hepatocytes were resuspended in 1 ml of homogenization buffer A (20 mM Tris/HCl/330 mM sucrose/2 mM EDTA/0.5 mM EGTA/2 mM PMSF, pH 7.5), homogenized with 30 strokes on ice and then centrifuged at 100000 *g* for 1 h The supernatant was used as the cytosol fraction. The remaining pellet was resuspended in 1 ml of buffer A containing 1 % Nonidet P40 and homogenized for ten strokes, incubated on ice for 30 min and then centrifuged at 100000 *g* for 15 min The supernatant was used as the membrane fraction.

RESULTS

IFN-α, IFN-β and IFN-γ activate the JAK-STAT1 signalling pathway in freshly isolated hepatocytes

As shown in Figure 1(A), exposure of freshly isolated hepatocytes to IFN-α, IFN-β, or IFN-γ for 20–50 min led to a significant increase in STAT binding to the specific m67 oligonucleotide probe (lanes 1–4, lanes 5–8 and lanes 9–12). To identify the STAT protein that was involved, a DNA gel supershift assay was performed (Figure 1B). As shown in Figure 1(B), STAT1 antibody, but not STAT3 or STAT5 antibody, was able to supershift the IFN-β-activated complex. Similar results were obtained with IFN-γ-activated complex (results not shown). These findings suggest that IFNs activate only STAT1, but not STAT3 or STAT5, in primary rat hepatocytes. Moreover, Western-blotting analysis in Figure 1(C) showed that IFN-β or IFN-γ activated STAT1, but not STAT3, tyrosine phosphorylation, while interleukin-6 (IL-6) induced both STAT1 and STAT3 tyrosine phosphorylation (lane 4). Furthermore, IFN-α, IFN-β and IFN-γ also activated STAT1 in human hepatocellular carcinoma HepG2 cells (results not shown). These findings indicate that IFN-α, IFN-β and IFN-γ activate the JAK-STAT1 signalling pathway in freshly isolated hepatocytes and HepG2 cells. Since IFN-α and IFN-β both act on the similar type I receptor [13–15], we only studied the effects of ethanol on one of the representative IFN-β signalling pathways described in the present paper.

Effects of IFN-α, IFN-β, and IFN-γ on p42/44 MAPK, PKB/Akt and p46/54 JNK in freshly isolated hepatocytes

As shown in Figure 2(A), treatment of freshly isolated hepatocytes with either IFN-α or IFN-β rapidly activated p42/44 MAPK, the peak effect occurring at 10 and 20 min respectively, and declined towards control levels after 60 min exposure. IFN-γ treatment also activated p42/44 MAPK in hepatocytes, with the peak activation at 5 min and declining towards control levels after 20 min treatment. Interestingly, upon IFN-γ incubation for 60 min, p42/44 MAPK phosphorylation increased again. Activation of p42/44 MAPK by IFN-α/β or IFN-γ was also observed in HepG2 cells (results not shown). Positive control

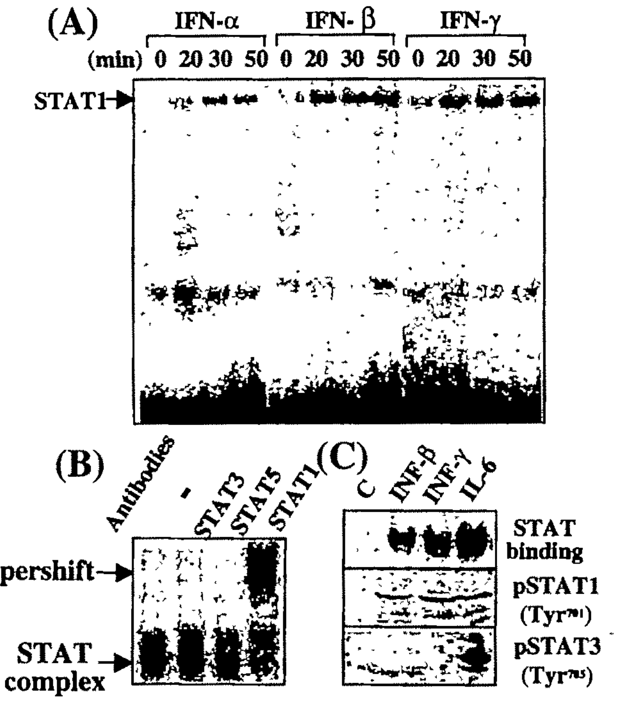

Figure 1 IFNs activate STAT1 in primary hepatocytes

(**A**) Freshly isolated hepatocytes were incubated with IFN-α (250 units/ml), IFN-β (250 units/ml) or IFN-γ (10 ng/ml) for various time periods as indicated. Whole-cell extracts were prepared and DMSA was performed using the m67 probe, as described in the Materials and methods section. (**B**) Hepatocytes were stimulated with IFN-β (250 units/ml) for 30 min. Whole-cell extracts were incubated with various STAT antibodies as indicated and subjected to a supershift assay. (**C**) Hepatocytes were stimulated with IFN-β ('INF-β') (250 units/ml), IFN-γ ('INF-γ') (10 ng/ml) or IL-6 (20 ng/ml) for 30 min. Whole-cell extracts were subjected to DMSA to examine STAT binding or Western-blotting analysis using anti-phosphotyrosine STAT1 (Tyr^{701}) or anti-phosphotyrosine STAT3 (Tyr^{705}). An autoradiogram representative of three independent experiments is shown in each panel.

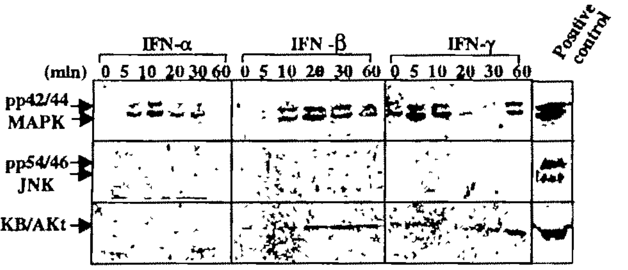

Figure 2 Effects of IFNs on p42/44 MAPK, PKB/Akt and JNK in primary hepatocytes

Freshly isolated hepatocytes were incubated with IFN-α (250 units/ml), IFN-β (250 units/ml) or IFN-γ (10 ng/ml) for various time periods as indicated. Whole-cell extracts were subjected to Western-blotting analysis using anti-phospho-p42/44 MAPK, anti-phospho-JNK or anti-phospho-PKB/Akt antibodies as indicated. Hepatocytes were stimulated with EGF (10 ng/ml), tumour necrosis factor-α (20 ng/ml) and phenylephrine (10^{-5} M) for 10 min as positive controls for p42/44 MAPK, JNK and PKB/Akt respectively. An autoradiogram representative of three independent experiments is shown in each panel.

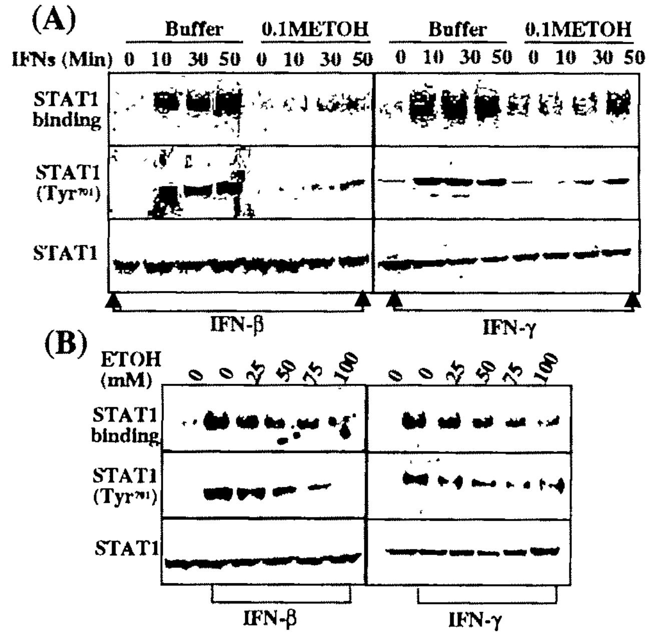

Figure 3 Acute ethanol inhibits IFN-induced STAT1 binding and tyrosine phosphorylation

(**A**) Freshly isolated rat hepatocytes were incubated with 100 mM ethanol or buffer for 30 min, then stimulated with IFN-β (250 units/ml) or IFN-γ (10 ng/ml) for various time periods as indicated. (**B**) Freshly isolated hepatocytes were incubated with various concentrations of ethanol for 30 min, followed by a 30 min stimulation with IFN-β (250 units/ml) or IFN-γ (10 ng/ml). In (**A**) and (**B**), after treatment, whole-cell extracts were prepared and subjected to DMSA to examine STAT binding or Western-blotting analysis using anti-phosphotyrosine STAT1 (Tyr^{701}) or anti-STAT1 antibodies. An autoradiogram representative of three independent experiments is shown in each panel.

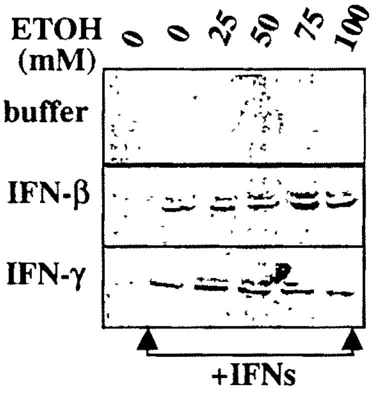

Figure 4 Acute ethanol potentiates IFN-activated p42/44 MAPK

Freshly isolated rat hepatocytes were pretreated with various concentrations of ethanol, followed by a 10 min stimulation with buffer, IFN-β (250 units/ml) or IFN-γ (10 ng/ml). Whole-cell extracts were then subjected to Western-blotting analysis using an anti-phospho-p42/44 MAPK antibody. The autoradiograms shown are representative of three independent experiments.

activation of p42/44 MAPK by epidermal growth factor (EGF) was 5-fold stronger than that observed with IFN.

Effects of IFNs on PKB/Akt and JNK were also examined. As shown in Figure 2, neither IFN-α, nor IFN-β and IFN-γ, activated p46/54 JNK, whereas positive control tumour necrosis factor-α significantly activated this kinase. IFN-β or IFN-γ, but not IFN-α, also slightly activated PKB/Akt in primary hepatocytes. Positive control phenylephrine markedly stimulated this kinase. Since IFNs did not significantly activate JNK and weakly activated PKB/Akt, effects of ethanol on these two kinases were not further studied here.

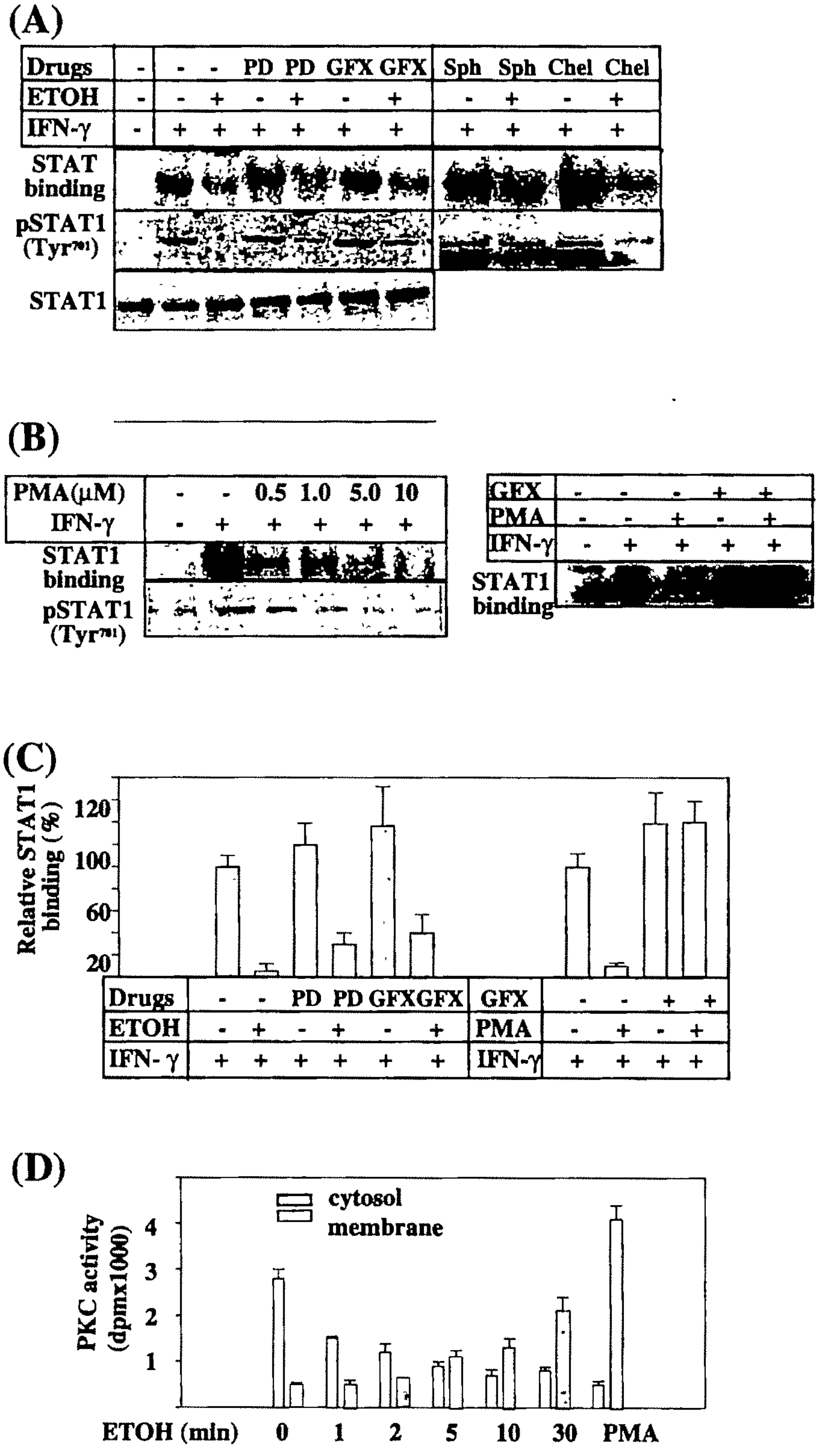

Figure 5 Evidence for the involvement of PKC in ethanol suppression of IFN-induced STAT1

(**A**) Freshly isolated rat hepatocytes were incubated with 50 μM PD98059 (PD), 2 μM GF109203X (GFX), 1 μM sphingosine (Sph) or 0.5 μM chelerythrine (Chel) for 30 min, then with 100 mM ethanol for 30 min, followed by a 30 min stimulation with IFN-γ (10 ng/ml) for 30 min. Cell extracts were then subjected to DMSA to detect STAT1 binding or Western-blot analysis using anti-phospho-STAT1 (Tyr^{701}) or anti-STAT1 antibodies. (**B**) In left panel, freshly isolated rat hepatocytes were incubated with PMA (0.5–10 μM) for 30 min, followed by a 30 min stimulation with IFN-γ (10 ng/ml). In the right panel, freshly isolated hepatocytes were incubated with 2 μM GF109203X for 30 min, then with 0.5 μM PMA for 30 min, followed by a 30-min stimulation with IFN-γ (10 ng/ml). Cell extracts in both left and right panels were subjected to DMSA to detect STAT1 binding. (**A**) and (**B**) are representative of three to seven independent experiments. (**C**). The autoradiograms were quantified by phosphorimaging from (**A**) and (**B**). Values shown are means ± S.E.M. for three to seven independent experiments, expressed as fold changes over control. (**D**) Freshly isolated hepatocytes were incubated with 100 mM ethanol for various time periods as indicated or with 1 μM PMA for 10 min. Cytosol and membrane protein fractions were prepared and subjected to the PKC assay described in the Materials and methods section.

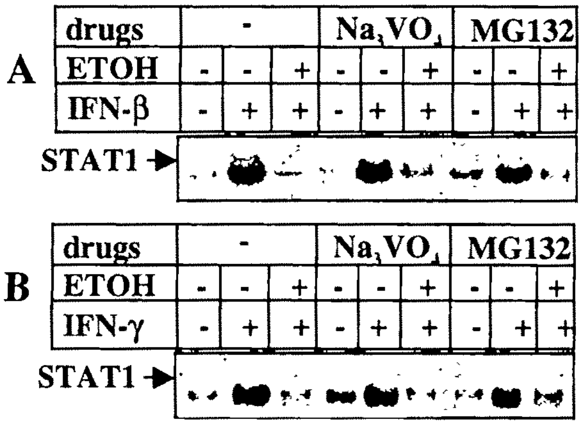

Figure 6 Tyrosine phosphatases and the ubiquitin–proteasome pathway are not involved in ethanol suppression of IFN-induced STAT1 activation

Freshly isolated rat hepatocytes were pretreated with buffer, sodium vanadate (0.2 mM) or proteasome inhibitor (50 μM MG132) for 30 min, followed by incubation with or without 100 mM ethanol for 30 min, and then stimulated with 250 units/ml IFN-β (A) or 10 ng/ml IFN-γ (B) for 30 min DMSA was performed using the m67 probe An autoradiogram representative of three independent experiments is shown in each panel

Acute ethanol inhibits IFN-β- or IFN-γ-induced STAT1 activation and tyrosine phosphorylation

To examine the effects of ethanol on IFN-induced STAT1 activation, freshly isolated hepatocytes were incubated with 100 mM ethanol for 30 min, followed by stimulation with IFNs for various time periods As shown in Figure 3(A), 100 mM ethanol almost completely abolished IFN-β- or IFN-γ-induced STAT1 binding to the m67 probe. Furthermore, IFN-β- or IFN-γ-induced STAT1 activation was inhibited by a 30 min pretreatment with ethanol in a concentration-dependent manner, with inhibition evident at 25 mM and complete inhibition at 100 mM ethanol (Figure 3B).

To examine whether rapid inhibition of IFN-β- or IFN-γ-induced STAT1 activation by ethanol was due to suppression of STAT1 tyrosine phosphorylation, Western-blot analysis was performed using an anti-phospho-STAT1 (Tyr^{701}) antibody. As shown in Figure 3(A), it was observed that either IFN-β or IFN-γ induced significant STAT1 tyrosine phosphorylation, and pretreatment of hepatocytes with 100 mM ethanol for 30 min abolished this activation. Ethanol inhibition of IFN-induced STAT1 tyrosine phosphorylation was also concentration-dependent, with inhibition evident at 25 mM (Figure 3B). Ethanol alone did not affect basal STAT1 tyrosine phosphorylation (results not shown). As illustrated in the bottom panels of Figures 3(A) and 3(B), the same ethanol treatment did not significantly affect the cellular level of the STAT1 protein expression. These findings suggest that acute exposure of hepatocytes to biologically relevant concentrations of ethanol markedly inhibits IFN-activated STAT1. The inhibitory effect of ethanol on IFN-activated STAT1 is not non-specific, since the same ethanol treatment potentiated IFN-activated p42/44 MAPK (see below).

Acute ethanol potentiates IFN-β- and IFN-γ-activated p42/44 MAPK

Effect of ethanol on p42/44 MAPK was examined. As shown in Figure 4(A), exposure of primary hepatocytes to various concentrations of ethanol for 30 min did not significantly affect the basal levels of p42/44 MAPK (top panel), but significantly potentiated IFN-β- and IFN-γ-activated p42/44 MAPK. Activation was most evident at 50–75 mM ethanol.

Activation of PKC is partially involved in ethanol inhibition of IFN-activated STAT1

Activation of PKC has been proposed to mediate several effects of ethanol, such as potentiation of p42/44 MAPK [27] or desensitization of receptor-mediated phospholipase C activation [28]. To test whether activation of PKC was involved in ethanol inhibition of IFN-activated STAT1, a highly specific PKC inhibitor, GF109203X, was used. As shown in Figure 5(A), blocking PKC activation with 2 μM GF109203X partially prevented ethanol inhibition of IFN-γ-induced STAT1. In this experiment, as well as seven replicate experiments with similar results, GF109203X partially (30 %) antagonized ethanol suppression of IFN-γ-activated STAT1 (Figure 5C). Other PKC inhibitors, such as sphingosine and chelerythrine, also partially antagonized ethanol suppression of IFN-γ-activated STAT1 (Figure 5A). Similar experiments with IFN-α/β and IL-6 were conducted and suggest that PKC is also partially involved in ethanol inhibition of IL-6-activated STAT3 and IFN-α/β-activated STAT1 (results not shown). Moreover, PD98059, a specific MEK1 inhibitor, also partially reversed ethanol inhibition of IFN-activated STAT1 (Figure 5A), suggesting that activation of p42/44 MAPK is partially involved.

To examine further the role of PKC in ethanol suppression of STAT activation, two experiments were carried out. First, we investigated whether the PKC activator PMA was able to inhibit STAT activation induced by either IFNs or IL-6. As shown in Figures 5(B) and 5(C), pretreatment of primary hepatoctyes with 0.5 to 10.0 μM PMA significantly inhibited IFN-γ-activated STAT1 binding and tyrosine phosphorylation. GF109203X, a highly selective PKC inhibitor, completely abolished PMA inhibition of STAT activation (Figures 5B and 5C). Similar experiments with IFN-α/β and IL-6 demonstrated that PMA attenuated IL-6-activated STAT3 and IFN-α/β-activated STAT1 (results not shown).

Secondly, we examined whether ethanol was able to induce PKC activation and membrane translocation. Freshly isolated hepatocytes were incubated with 100 mM ethanol for various time periods. Cytosol and membrane fractions of cell lysates were prepared and examined for PKC enzymic activity. Incubation of freshly isolated hepaotcytes with ethanol decreased PKC activity in the cytosol fraction and increased it in the membrane fraction (Figure 5D), suggesting that ethanol stimulates PKC translocation from cytosol to membrane after activation. Western-blotting analysis also showed that acute exposure of freshly isolated hepatocyte to ethanol slightly caused PKCα and PKCβ1 protein translocation from cytosol to membrane (results not shown), further supporting the notion that acute ethanol exposure slightly activates PKC.

Tyrosine phosphatases and the ubiquintin–proteasome pathway are not involved in ethanol suppression of IFN-induced STAT1 activation

The data from Figure 5 demonstrated that GF109203X completely antagonized PMA inhibition of STAT activation, but only partially (30 %) attenuated ethanol inhibition of STAT activation. This suggested that PKC could not fully explain the inhibitory action of ethanol. Thus the next obvious question was what other mechanisms are involved in ethanol suppression of STAT activation. Both tyrosine phosphatases and the ubiquitin–proteasome pathway have been implicated in inactivation of the JAK-STAT signalling pathway (reviewed in [29–31]); we wondered whether these pathways were involved in ethanol inhibition of IFN-activated STAT1. To test these possibilities, the non-selective tyrosine phosphatase inhibitor sodium orthovanadate and the specific proteasome inhibitor MG132 were used. As shown in Figures 6(A) and 6(B), neither sodium orthovanadate nor MG132 pretreatment antagonized ethanol suppression of IFN-β- or IFN-γ-activated STAT1, while the same treatment markedly reversed IL-1β suppression of IFN-α-activated STAT1 (X. Shen, Z. Tian, and B. Gao, unpublished work). This suggests that both tyrosine phosphatases and the proteasome-dependent pathway are not involved in ethanol suppression of IFN-induced STAT1 activation

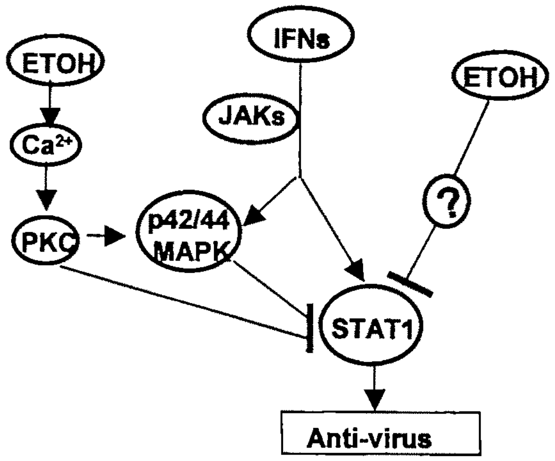

Figure 7 Model for ethanol suppression of IFN-induced STAT1 activation

IFN activates both p42/44 MAPK and STAT1 signalling pathways in primary hepatocytes, and activation of p42/44 MAPK negatively regulates STAT1 activation Acute exposure of hepatocytes to ethanol induces a rapid rise in cytosolic Ca^{2+} [28] and a consequent activation of PKC. Activated PKC can directly attenuate IFN-activated STAT1 or indirectly inhibit it by potentiation of IFN-activated p42/44 MAPK Other unknown mechanisms (?) may also be involved in ethanol suppression of IFN-activated STAT1 in freshly isolated hepatocytes

DISCUSSION

IFNs have been shown to activate various signalling pathways in many cell types [13–15], but their signalling pathways in primary hepatocytes have not been explored. Here we demonstrate that both IFN-α/β and IFN-γ are able to activate the JAK-STAT1, p42/44 MAPK, and PKB/Akt in rat primary hepatocytes. IFN-γ has been shown to activate specific STAT1, STAT3 and STAT5 in certain cell types. For example, IFN-γ activates only STAT1 in some cell types [32,33], both STAT1 and STAT3 in adipocytes [34], and only STAT5 in U937 cells [35]. Here we show that IFN-γ and IFN-β activate only STAT1 in rat primary hepatocytes (Figure 1). The inability of IFNs to activate STAT3 and STAT5 in hepatocytes could be due to difference in the receptor expression, binding affinities, the presence or absence of other signalling proteins, or STAT dimer composition.

It has been reported that IFNs are able to activate the p42/44 MAPK signalling pathway in certain cells, and here we demonstrate that both IFN-α/β and IFN-γ activate p42/44 MAPK, but not JNK, in primary hepatocytes (Figure 2) and in human hepatoma HepG2 cells (results not shown) Compared with EGF, IFNs are weak activators of p42/44 MAPK, as shown in Figure 2, where EGF activation of p42/44 MAPK was 5-fold stronger than IFN. The connection between the JAK-STAT1 and the p42/44 MAPK signalling pathways is not clear It has been shown that activation of p42/44 MAPK can specifically phosphorylate STAT3 on Ser^{727} in response to growth factor [36] and negatively regulate STAT3 activation [24,37] However, STAT1 appears to be a poor substrate for all MAPK superfamily members [36], and the kinase responsible for STAT1 Ser^{727} phosphorylation has not been identified. Here we demonstrated that blocking p42/44 MAPK activation by PD98059 slightly potentiated IFN-γ-induced STAT1 binding and STAT1 Tyr^{701} phosphorylation (Figure 5), suggesting that activation of p42/44 MAPK may antagonize IFN-γ-induced STAT1 activation. The role of p42/44 MAPK in the inactivation of STATs is not clear and requires further studies

An interesting finding in the present study is that, in freshly isolated rat hepatocytes, biologically relevant concentrations (less than 100 mM) of ethanol rapidly and dose-dependently inhibited IFN-β- or IFN-γ-induced activation of STAT1, but also potentiated IFN-β or IFN-γ-induced activation of p42/44 MAPK. Three lines of evidence suggest that activation of PKC is involved in this event. First, the specific PKC inhibitor GF109203X caused marked attenuation of ethanol suppression of IFN-induced STAT1 activation (Figures 5A and 5C). Secondly, activation of PKC by PMA blocked IFN-induced STAT1 activation (Figures 5B and 5C). Thirdly, acute ethanol treatment caused rapid and marked activation of PKC in primary hepatocytes (Figure 5D). Furthermore, Figures 5(A) and 5(C) showed that inhibition of p42/44 MAPK activation by PD 98059 only slightly potentiated IFN-activated STAT1 and partially antagonized ethanol inhibition of IFN-activated STAT1. This suggested that p42/44 MAPK may also be involved in the inhibitory effect of ethanol on STAT activation.

Interestingly, our (J. Chen and B. Gao) unpublished work demonstrated that biologically relevant concentrations of ethanol attenuated STAT activation in freshly isolated hepatocytes, but not in cultured hepatocytes or hepatocullular carcinoma HepG2 cells. Further experiments indicated that the lack of inhibitory effect of ethanol on cultured hepatocytes and HepG2 cells was not due to ethanol metabolism or proliferation status. These findings suggest that freshly isolated hepatocytes are more sensitive to ethanol inhibition of the JAK-STAT signalling pathway than cultured hepatocytes or HepG2 cells, which may be implicated in pathogenesis and progression of alcoholic liver diseases.

Inhibition of PKC by GF109203X completely abolished PMA attenuation of IFN-γ-activated STAT1 (Figures 5B and 5C), but only partially (about 30 %) blocked ethanol inhibition of IFN-activated STAT1 (Figures 5B and 5C) or IL-6-activated STAT3 (results not shown). These findings suggest that PKC is only partially involved in, and cannot fully account for, ethanol suppression of STAT activation. Several mechanisms responsible for inactivation of the JAK-STAT signalling pathway have been proposed (reviewed in [29–31]. For example, activated JAK-STAT can been attenuated by: (1) dephosphorylation by protein tyrosine phosphatases; (2) proteolytic degradation by the ubiquitin–proteasome pathway; (3) inhibitory molecules such as SOCS/JAB/SSI/CIS. In the present study the lack of effect of sodium vanadate and MG132 on the inhibitory action of ethanol on STAT1 activation suggests that protein tyrosine phosphatases and the ubiquitin–proteasome pathway are not involved The inhibitory molecules are also unlikely to be involved, because these proteins are newly synthesized after stimulation with IFN, whereas ethanol inhibitory action is rapid and does not require new protein synthesis (X. Shen, Z. Tian and B. Gao, unpublished work). Thus the molecular mechanisms responsible for ethanol inhibition of STAT activation are not fully understood and require further investigation.

Taken together, we have integrated each of our findings with a proposed model (summarized in Figure 7) that allows for cross-talk between ethanol, IFN-activated p42/44 MAPK and STAT1. In this model, acute exposure of hepatocytes to ethanol induces a rapid but transient activation of phosphoinositide-specific phospholipase C and a consequent rise in cytosolic Ca^{2+} and diacylglycerol [28], which can activate PKC. Activated PKC can directly attenuate IFN-activated STAT1 or indirectly inhibit it by potentiation of IFN-activated p42/44 MAPK. Ethanol may also inhibit IFN-activated STAT1 by some unknown mechanisms. We have previously shown that acute ethanol rapidly and significantly inhibited IL-6-activated STAT3 in freshly isolated hepatocytes [38], suggesting that ethanol may interfere with the phosphorylation of STAT protein in general and its molecular target may be conserved domains of STAT proteins, such as the Src homology 2 (SH2) domain. Indeed, it has been reported that several kinases containing SH2 domains can be affected by ethanol [39–42]. In view of the critical role of IFN-activated STAT1 as a protective agent in viral infection [21,22], ethanol suppression of IFN-activated STAT1 may, at least in part, account for the high incidence of viral hepatitis and unresponsiveness to IFN therapy in alcoholics.

We thank Dr Phillip Hylemon and Ms Patricia Bohdan for providing some of the freshly isolated hepatocytes This work was supported by National Institutes of Health Grants R03AA11823, R01AA12637 and R29CA72681 (to B G.).

REFERENCES

1 De Maeyer, E and De Maeyer-Guignard, J (1998) Interferons In Cytokine Handbook (Thomson, A, ed), pp. 491–516, Academic Press, San Diego

2 Davis, G L (1999) Combination therapy with interferon-α and ribavirin as retreatment of interferon relapse in chronic hepatitis C Semin Liver Dis 19, 49–55

3 Younossi, Z M. and Perrillo, R P (1999) The roles of amantadine, rimantadine, ursodeoxycholic acid, and NSAIDs, alone or in combination with α interferons, in the treatment of chronic hepatitis C Semin Liver Dis 19, 95–102

4 Gish, R G (1999) Standards of treatment in chronic hepatitis C Semin Liver Dis 19, 35–47

5 Lindsay, K L (1997) Therapy of hepatitis C overview Hepatology 26, 71S–77S

6 Keeffe, E B and Hollinger, F B. (1997) Therapy of hepatitis C. consensus interferon trials Consensus Interferon Study Group Hepatology 26, 101S–107S

7 Zein, N N (1998) Interferons in the management of viral hepatitis Cytokines Cell Mol Ther 4, 229–241

8 Christie, J M and Chapman, R W (1999) Combination therapy for chronic hepatitis C interferon and ribavirin Hosp Med 60, 357–361

9 Schiff, E R (1999) The alcoholic patient with hepatitis C virus infection Hepatology 26, 39S–42S

10 Ohnishi, K., Matsuo, S, Matsutani, K., Itahashi, M, Kakihara, K, Suzuki, K, Ito, S and Fujiwara, K (1996) Interferon therapy for chronic hepatitis C in habitual drinkers comparison with chronic hepatitis C in infrequent drinkers Am J Gastroenterol 91, 1374–1379

11 Okazaki, T, Yoshihara, H, Suzuki, K, Yamada, Y, Tsujimura, T, Kawano, K., Yamada, Y and Abe, H (1994) Efficacy of interferon therapy in patients with chronic hepatitis C Comparison between non-drinkers and drinkers Scand J Gastroenterol 29, 1039–1043

12 Mochida, S, Ohnishi, K, Matsuo, S., Kakihara, K and Fujiwara, K (1996) Effect of alcohol intake on the efficacy of interferon therapy in patients with chronic hepatitis C as evaluated by multivariate logistic regression analysis Alcohol Clin Exp Res 20, 371–377

13 Stark, G R, Kerr, I M, Williams, B R G, Silverman, R H and Schreiber, R D (1998) How cells respond to interferons. Annu Rev Biochem 67, 227–264

14 Platanias, L C and Fish, E N (1999) Signalling pathways activated by interferons Exp Hematol 27, 1583–1592

15 Haque, S J and Williams, B R (1998) Signal transduction in the interferon system Semin Oncol. 25, 14–22

16 Liu, M K, Brownsey, R W and Reiner, N E (1994) Gamma interferon induces rapid and coordinate activation of mitogen-activated protein kinase (extracellular signal-regulated kinase) and calcium-independent protein kinase C in human monocytes Infect Immun 62, 2722–2731

17 Stancato, L F, Yu, C R, Petricoin, E F and Larner, A C. (1998) Activation of Raf-1 by interferon gamma and oncostatin M requires expression of the Stat1 transcription factor J Biol Chem 273, 18701–18704

18 David, M, Petricoin, E, Benjamin, C, Pine, R, Weber, M J and Larner, A C (1995) Requirement for MAP kinase (ERK2) activity in interferon alpha- and interferon beta-stimulated gene expression through STAT proteins Science 269, 1721–1723

19 Uddin, S., Yenush, L, Sun, X J, Sweet, M E, White, M F and Platanias, L C (1995) Interferon-alpha engages the insulin receptor substrate-1 to associate with the phosphatidylinositol 3′-kinase J. Biol Chem 270, 15938–15941

20 Burfoot, M S, Rogers, N C, Watling, D, Smith, J M, Pons, S, Paonessaw, G, Pellegrini, S, White, M F and Kerr, I M. (1997) Janus kinase-dependent activation of insulin receptor substrate 1 in response to interleukin-4, oncostatin M, and the interferons J Biol Chem 272, 24183–24190

21 Durbin, J E, Hackenmiller, R, Simon, M C and Levy, D. E (1996) Targeted disruption of the mouse Stat1 gene results in compromised innate immunity to viral disease Cell 84, 443–450

22 Meraz, M, A., Whitem, J M, Sheehan, K C, Bach, E A, Rodig, S J, Dighe, A S, Kaplan, D H, Riley, J K, Greenlund, A C, Campbell, D et al (1996) Targeted disruption of the Stat1 gene in mice reveals unexpected physiologic specificity in the JAK-STAT signalling pathway Cell 84, 431–442

23 Gao, B, Jiang, L and Kunos, G (1996) Transcriptional regulation of alpha(1b)adrenergic receptors [alpha(1b)AR] by nuclear factor 1 (NF1) a decline in the concentration of NF1 correlates with the downregulation of alpha(1b)AR gene expression in regenerating liver Mol Cell Biol 16, 5997–6008

24 Nguyen, V T. and Gao, B (1999) Cross-talk between α_{1B}-adrenergic receptor (α_{1B}AR) and interleukin-6 (IL-6) signalling pathways Activation of α_{1B}AR inhibits IL-6-activated STAT3 in hepatic cells by a p42/44 mitogen-activated protein kinase-dependent mechanism J Biol Chem 274, 35492–35498

25 Chen, J P, Bao, H F, Sawyer, S, Kunos, G and Gao, B (1997) Effects of short and long term ethanol on the activation of signal transducer and activator transcription factor 3 in normal and regenerating liver Biochem Biophys Res. Commun 239, 666–669

26 Kraft, A S and Anderson, W B (1983) Characterization of cytosolic calcium-activated phospholipid-dependent protein kinase activity in embryonal carcinoma cells Effect of retinoic acid-induced differentiation of F9 cells to parietal endoderm J. Biol. Chem 258, 9178–9183

27 Roivainen, R, Hundle, B and Messing, O R (1995) Ethanol enhances growth factor activation of mitogen-activated protein kinases by a protein kinase C-dependent mechanism. Proc Natl Acad Sci U.S.A. 92, 1891–1895

28 Higashi, K and Hoek, J B (1991) Ethanol causes desensitization of receptor-mediated phospholipase C activation in isolated hepatocytes J Biol Chem. 266, 2178–2190

29 Starr, R and Hilton, D J (1999) Negative regulation of the JAK/STAT pathway Bioessays 47, 47–52

30 Yoshimura, A (1998) The CIS family negative regulators of JAK-STAT signalling Cytokine Growth Factor Rev 9, 197–204

31 Hilton, D J (1999) Negative regulators of cytokine signal transduction Cell Mol Life Sci. 55, 1568–1577

32 Schindler, C, Fu, X Y., Improta, T, Aebersold, R and Darnell, Jr, J E (1992) Proteins of transcription factor ISGF-3 one gene encodes the 91-and 84-kDa ISGF-3 proteins that are activated by interferon alpha Proc Natl Acad. Sci U S A 89, 7386–7389

33 Shuai, K, Schindler, C, Prezioso, V R and Darnell, Jr, J E (1992) A single phosphotyrosine residue of Stat91 required for gene activation by interferon-gamma Science 258, 1808–1812

34 Stephens, J M, Lumpkin, S. J and Fishman, J B (1998) Activation of signal transducers and activators of transcription 1 and 3 by leukemia inhibitory factor, oncostatin-M, and interferon-gamma in adipocytes J Biol Chem 273, 31408–31416

35 Meinke, A, Barahmand-pour, F, Wohrl, S, Stoiber, D and Decker, T (1996) Activation of different Stat5 isoforms contributes to cell-type-restricted signalling in response to interferons Mol Cell Biol 16, 6937–6944

36 Chung, J, Uchida, E, Grammer, T C and Blenis, J (1997) STAT3 serine phosphorylation by ERK-dependent and -independent pathways negatively modulates its tyrosine phosphorylation Mol Cell Biol 17, 6508–6516

37 Sengupta, T K, Talbot, E S, Scherle, P A and Ivashkiv, L B. (1998) Rapid inhibition of interleukin-6 signalling and Stat3 activation mediated by mitogen-activated protein kinases Proc Natl Acad Sci U S A. **95**, 11107–11112

38 Chen, J P, Kunos, G and Gao, B. (1999) Ethanol rapidly inhibits IL-6-activated STAT3 and C/EBP mRNA expression in freshly isolated rat hepatocytes FEBS Lett **457**, 162–168

39 Sasaki, Y and Wands, J R (1994) Ethanol impairs insulin receptor substrate-1 mediated signal transduction during rat liver regeneration Biochem. Biophys Res Commun **199**, 403–409

40 Xu, Y Y, Bhavani, K, Wands, J R and de la Monte, S. M (1995) Ethanol inhibits insulin receptor substrate-1 tyrosine phosphorylation and insulin-stimulated neuronal thread protein gene expression. Biochem J **310**, 125–132

41 Resnicoff, M., Rubini, M, Baserga, R and Rubin, R (1994) Ethanol inhibits insulin-like growth factor-1-mediated signalling and proliferation of C6 rat glioblastoma cells Lab Invest **71**, 657–662

42 Mohr, L, Tanaka, S. and Wands, J. R (1998) Ethanol inhibits hepatocyte proliferation in insulin receptor substrate 1 transgenic mice Gastroenterology **115**, 1558–1565

Received 10 January 2000/28 April 2000, accepted 10 May 2000

Biochem J (2000) 349, 435–441 (Printed in Great Britain)

Sp1-like activity mediates angiotensin-II-induced plasminogen-activator inhibitor type-1 (*PAI-1*) gene expression in mesangial cells

Masaru MOTOJIMA*[1], Takao Ando* and Toshimasa YOSHIOKA†

*Biomedical Research Laboratories, Kureha Chemical Industry Co, 3-26-2 Hyakunin-cho, Shinjuku-ku, Tokyo 169-8503, Japan, and †Department of Pharmacology, Tokyo Women's Medical University, School of Medicine, 8-1 Kawada-cho, Shinjuku-ku, Tokyo 162-8666, Japan

Angiotensin II (Ang II) up-regulates plasminogen-activator inhibitor type-1 (PAI-1) expression in mesangial cells to enhance extracellular matrix formation. The proximal promoter region (bp −87 to −45) of the human *PAI-1* gene contains several potent binding sites for transcription factors [two phorbol-ester-response-element (TRE)-like sequences; D-box (−82 to −76) and P-box (−61 to 54), and one Sp1 binding site-like sequence, Sp1-box 1 (−72 to −67)]. We studied this region to determine the transcription factor(s) that mediates Ang-II-induced transcriptional activation of the *PAI-1* gene. Various double-stranded decoy oligodeoxynucleotides (ODNs) corresponding to various sequences in the proximal promoter region were transfected to mesangial cells to examine the effects on Ang-II-induced PAI-1 mRNA expression. Transfection with the full-length decoy (bp −87 to −45, D-P-ODN) markedly attenuated Ang-II-induced PAI-1 mRNA expression by up to 70%. Transfection with D-ODN (−87 to −71) and P-ODN (−66 to −45), which correspond to each of the two TRE-like sequences, did not attenuate the expression. Gel-shift assays using nuclear extracts prepared from Ang-II-treated mesangial cells and D-P-ODN showed three specific complexes. The major complex was supershifted by anti-Sp1 antibody The methylation-interference experiment demonstrated that human recombinant Sp1 bound to the so-called GT box (TGGGTGGGGCT, −78 to −69), which contains the Sp1-box 1. The complex that migrated with anti-Sp1 antibody was enhanced in the cells treated with Ang II. Further, D-Sp1-ODN (−85 to −63) containing the GT box attenuated up-regulation of PAI-1 mRNA expression induced by Ang II to a level (68±9% inhibition) comparable to D-P-ODN, whereas ODN with four mutations in the GT box had no effect. Our findings suggest that binding of Sp1 or an Sp1-like transcription factor to the GT box in the PAI-1 promoter up-regulates *PAI-1* gene transcription in mesangial cells stimulated with Ang II. This transcription-factor binding site may be targeted to control Ang-II-dependent extracellular matrix formation by mesangial cells.

Key words: double-stranded decoy oligodeoxynucleotide, extracellular matrix, transcription, plasmin system.

INTRODUCTION

Mesangial expansion due to an accumulation of extracellular matrix is a hallmark of progressive glomerular diseases. Numerous studies indicate that angiotensin II (Ang II) mediates extracellular-matrix accumulation by a mechanism independent of its vasopressor effect [1]. Ang II stimulates production of extracellular-matrix proteins in glomerular mesangial cells, which are the major cells to produce mesangial extracellular matrix. Ang II has also been shown to reduce the degradation of matrix proteins by up-regulating plasminogen-activator inhibitors [2,3] Recent studies demonstrate that plasmin is a major regulator of mesangial cell matrix turnover [4]. Plasmin generation is regulated by a balance between plasminogen activator and plasminogen-activator inhibitors. Glomeruli isolated from animal models of proliferative glomerulonephritis showed an increase in plasminogen-activator inhibitor type-1 (PAI-1) deposition in the extracellular matrix, which suggests that PAI-1 is the one of key factors associated with mesangial matrix accumulation [5] The expression of the PAI-1 mRNA in mesangial cells has been shown to be up-regulated by Ang II, which activates the transcription of the *PAI-1* gene [6]. We have demonstrated previously that the protein kinase C (PKC)-dependent pathway is involved in the up-regulation of PAI-1 mRNA [7]. Further, PKC-activating phorbol ester markedly up-regulates PAI-1 mRNA expression in mesangial cells.

Phorbol esters have been reported to induce *PAI-1* gene transcription to up-regulate the mRNA level in many cells. Phorbol esters regulate the expression of many genes through the phorbol ester-response elements (TREs). The proximal promoter region of the human *PAI-1* gene close to the TATA box contains two TRE-like elements located at bp −82 to −76 (designated D-box) and −61 to −54 (P-box) upstream of the cap site [8]. The c-Jun homodimer (activator protein 1, AP-1) and c-Jun/c-Fos hetrodimer bind to the two TRE-like sequences to mediate phorbol ester response. There are two Sp1 binding site-like sequences at bp −72 to −67 (Sp1-box 1) and −45 to −40 (Sp1-box 2) in the proximal promoter region. Sp1 is a general transcription factor that binds to the so-called GC box and is expressed ubiquitously in many tissues [9]. The functional significance of these TRE-like and Sp1-box elements in Ang-II-induced PAI-1 mRNA up-regulation has not been identified. This study examined the molecular mechanisms by which Ang II induces up-regulation of *PAI-1* gene expression. For this purpose, a series of decoy oligodeoxynucleotides (ODNs) targeting the promoter region, TRE-like boxes and the Sp1 box of the human *PAI-1* gene was constructed and used to manipulate Ang-II-mediated transcriptional changes. Specific binding of the tran-

---

Abbreviations used Ang II, angiotensin II, PAI-1, plasminogen-activator inhibitor type 1, PKC, protein kinase C, TRE, phorbol ester-response element, ODN, oligodeoxynucleotide, DIG, digoxigenin, DTT, dithiothreitol, AP, activator protein, MAPK, mitogen-activated protein kinase

[1] To whom correspondence should be addressed (e-mail ct005@mb infoweb.ne jp).

scriptional factors to these ODNs was further evaluated by gel-shift and supershift assays.

EXPERIMENTAL

Mesangial cell culture

Rat mesangial cells were prepared as described previously [7]. Briefly, kidney cortices were isolated from 7-week-old male Sprague–Dawley rats. They were minced and passed through a series of sieves to isolate the glomeruli. Isolated glomeruli were treated with 1 mg/ml collagenase (Wako, Osaka, Japan) for 30 min, resuspended in RPMI 1640 medium containing 17% fetal bovine serum (Gibco-BRL, Grand Island, NY, U.S.A.), 0.1 units/ml insulin (Sigma, St. Louis, MO, U.S.A.) and antibiotics, and seeded in 100-mm plastic tissue-culture dishes. Outgrowing mesangial cells were maintained in the same medium, characterized by immunohistochemical staining of desmin, α-smooth-muscle actin and cytokeratin, and by low-density lipoprotein uptake. The cells were used in experiments between passages 4 and 7. The expression of Ang-II receptor was confirmed at each passage by a ^{125}I-Ang-II-binding assay.

For Ang-II stimulation, cells were rendered quiescent by culturing in serum-free medium for 24 h, and then stimulated with 100 nM Ang II (Sigma) for 3 or 6 h. In experiments using decoy ODNs, the cells were pretreated with ODN–lipofectin complex (molar ratio, 1:1, Gibco-BRL) at the indicated concentrations in a serum-free medium for 24 h as described elsewhere [10]. They were then stimulated with 100 nM Ang II for 6 h.

Northern blotting

An 877-bp fragment of rat PAI-1 cDNA and a 476-bp fragment of β-actin cDNA were labelled with digoxigenin (DIG) and used as probes for Northern blotting as described previously [7].

Total RNA was isolated using Isogen (Wako), 1 ml of which was added to mesangial cells cultured in a 60-mm dish. After cell lysis, the sample was collected in a tube, and total RNAs were extracted by chloroform and centrifuged. RNAs were precipitated with isopropanol, rinsed in 75% ethanol and resuspended in an appropriate amount of diethyl pyrocarbonate treated water.

Total RNA (10–20 μg) was fractionated by electrophoresis on a 1% agarose gel. The RNA was then transferred from the gel to a Hybond N$^+$ nylon membrane (Amersham, Little Chalfont, Bucks., U.K.) and immobilized by UV cross-linking. The membrane was prehybridized in a solution containing 4 × SSCP (where 1 × SSCP is 0.12 M NaCl/0.015 M sodium citrate/0.015 M Na_2HPO_4/0.005 M NaH_2PO_4), 1 × Denhardt's solution, 1% SDS, 50% formamide and 100 μg/ml salmon sperm DNA at 42 °C for 3 h. Hybridization was then performed in a solution containing 4 × SSCP, 1 × Denhardt's solution, 1% SDS, 5% dextran sulphate, 50% formamide, 100 μg/ml salmon sperm DNA and denatured DIG-labelled probe at 42 °C for 16 h. After hybridization, the membrane was washed twice with 1 × SSC (0.15 M NaCl/0.015 M sodium citrate) containing 0.1% SDS at room temperature for 15 min and then washed twice with 0.2 × SSC containing 0.1% SDS at 42 °C for 15 min. The hybridized probe was detected using a DIG-detection kit (Boehringer Mannheim, Mannheim, Germany) according to the manufacturer's instructions.

Preparation of nuclear extract

After stimulating rat mesangial cells with 100 nM Ang II for 3 h, the cells were trypsinized and washed with PBS. The cells were suspended in a buffer [10 mM Hepes (pH 7.6), 15 mM KCl, 2 mM $MgCl_2$, 0.1 mM EDTA, 1 mM dithiothreitol (DTT), 0.5 mM PMSF and 10 μg/ml leupeptin] and collected by brief centrifugation at 2000 *g*. The cells were lysed in the same buffer containing 0.2% Nonidet P40 and centrifuged again. The nuclei were isolated by suspending the pellet in a sucrose buffer [0.25 M sucrose, 10 mM Hepes (pH 7.6), 15 mM KCl, 2 mM $MgCl_2$, 0.1 mM EDTA, 1 mM DTT, 0.5 mM PMSF and 10 μg/ml leupeptin] and centrifuging at 2000 *g*. The nuclear protein was extracted by suspending the pellet in an extraction buffer [50 mM Hepes (pH 7.6), 400 mM KCl, 10% glycerol, 0.1 mM EDTA, 1 mM DTT, 0.5 mM PMSF and 10 μg/ml leupeptin] and incubating at 4 °C for 30 min. Insoluble materials were removed by centrifugation at 1000 *g* for 15 min.

Gel-shift assay

Gel-shift assay was performed using a DIG gel-shift kit (Boehringer Mannheim). Briefly, double-stranded ODN probes, as described in Figure 1, were 3′-end labelled with DIG using terminal transferase according to the manufacturer's instructions.

Proximal promoter region of human PAI-1 gene

–90 –80 –70 –60 –50 –40 –30
5′-TCCCAGAGCCAGTGAGTGGGTGGGGCTGGAACATGAGTTCATCTATTTCCTGCCCACATCTGGTATAAA-3′
D-box Sp1-box 1 P-box Sp1-box 2 TATA box

Oligodeoxynucleotides (ODNs)

D-P-ODN	**GCCAGTGAGTGGGTGGGGCTGGAACATGAGTTCATCTATTTC**
M D-P-ODN	**GCCAGTGAGTGGGTGGTTCTGGAACATGAGTTCATCTATTTC**
D-ODN	**GCCAGTGAGTGGGTGGT**
P-ODN	**GAACATGAGTTCATCTATTTC**
Sp1-ODN	**GGGTGGGGCTGGAACATG**
M Sp1-ODN	**GGGTGGTT CTGGAACATG**
D-Sp1-ODN	**CAGTGAGTGGGTGGGGCTGGAACA**
M D-Sp1-ODN	**CAGTGAGTGAATTCGGCTGGAACA**
Sp1 consensus	**AATCGAACTTCGGGGCGGGGCGAG**

Figure 1 Sequence of proximal promoter of the human *PAI-1* gene and ODNs used in the experiments

The proposed AP-1 and Sp1 binding sites are underlined according to the method of Knudsen et al. [8]. The sequences of ODNs used as decoys and for gel-shift assays are shown. Underlined bases indicate mutations created in the respective ODNs.

The labelled probes (20 fmol) were incubated with the nuclear protein preparation in a binding buffer [20 mM Hepes (pH 7.6) 30 mM KCl, 0.2 % (w/v) Tween 20, 1 mM EDTA, 1 mM DTT, 10 mM $(NH_4)_2SO_4$, 25 ng/μl poly d(I-C), 25 ng/μl poly d(A-T) and 50 ng/μl poly L-lysine] at room temperature for 30 min. For gel supershift assay, antisera to Sp1, Sp3, AP-1 or AP-2 (Santa Cruz Biotechnology, Santa Cruz, CA, U.S.A.) were added to the mixture and kept on ice for 1 h. After incubation, the protein–DNA complexes were separated by 5 % non-denaturing acrylamide gel electrophoresis. The protein–DNA complexes were transferred to a nylon membrane by electroblotting and were detected using the DIG-detection kit.

Methylation interference

A synthesized sense strand of D-P-ODN (the ODN spanning from D-box to P-box, see Figure 1) was 3′-end labelled with DIG by chemical modification (Japan Bioservice, Saitama, Japan) and then made double-stranded with an unlabelled antisense strand. The dimethyl sulphate reaction was started by adding 1 μl of dimethyl sulphate to a buffer containing 50 mM sodium acetate (pH 8.0), 1 mM EDTA and 33 pmol of the ODN, in a volume of 200 μl. After incubation at room temperature for 10 min, the reaction was stopped by adding 50 μl of the stop solution (1.5 M sodium acetate, pH 8.0, and 1 M β-mercaptoethanol). The ODN was precipitated with 750 μl of ethanol. The precipitate was resuspended in TE buffer (50 mM Tris/HCl, pH 8.0, and 1 mM EDTA) containing 100 mM NaCl. The ODN (200 fmol) was incubated with 1 fpu (footprint unit) of recombinant human Sp1 (Promaga, Madison, WI, U.S.A.) in the gel-shift binding buffer for 30 min. The Sp1–ODN complex was separated by electrophoresis on a 5 % non-denaturing acrylamide gel and transferred to DEAE paper by electroblotting. The DEAE paper was washed three times with TE buffer containing 50 mM NaCl. The labelled ODN was extracted with TE buffer containing 1 M NaCl and precipitated with ethanol. The precipitate was suspended in 1 M piperidine, incubated at 90 °C for 30 min and lyophilized. The digested ODN was electrophresed on a 12 % sequencing gel, transferred to a nylon membrane and detected using the DIG-detection kit.

Results are presented as means ± S.D. Student's *t* test was used for comparisons, with $P < 0.05$ considered statistically significant. Each experiment was performed at least in triplicate.

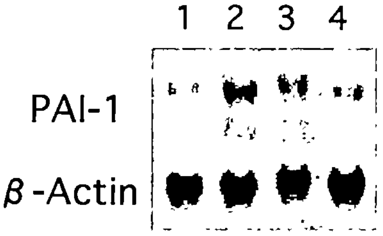

Figure 2 Effect of the decoy D-P-ODN on Ang-II-induced PAI-1 mRNA expression

Mesangial cells were transfected with D-P-ODN at different concentrations in a serum-free medium for 24 h, and then stimulated with 100 nM Ang II for 6 h The PAI-1 mRNA expression was analysed by Northern blotting using rat PAI-1 probe Lane 1, control, no treatment, lane 2, Ang II, lane 3, 1 μM D-P-ODN + Ang II, lane 4, 5 μM D-P-ODN + Ang II

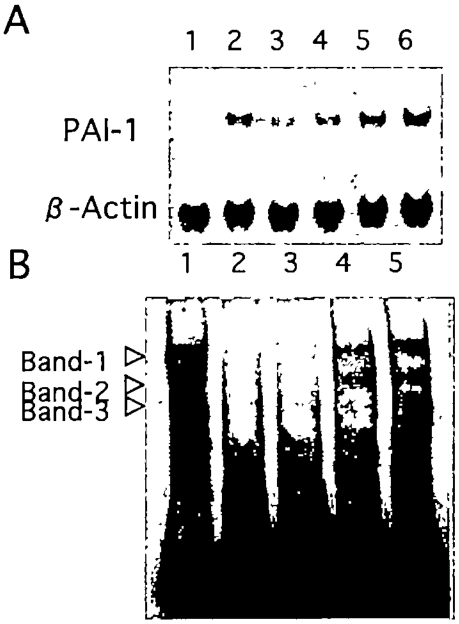

Figure 3 Effects of the decoy M D-P-ODN, D-ODN and P-ODN on Ang-II-induced PAI-1 mRNA expression

(**A**) Northern blotting. Mesangial cells were transfected with 5 μM D-P-ODN, M D-P-ODN, D-ODN or P-ODN in a serum-free medium for 24 h, and then stimulated with 100 nM Ang II for 6 h The PAI-1 mRNA expression was analysed by Northern blotting using rat PAI-1 probe Lane 1, control, no treatment, lane 2, Ang II, lane 3, D-P-ODN + Ang II; lane 4, M D-P-ODN + Ang II, lane 5, D-ODN + Ang II, lane 6, P-ODN + Ang II (**B**) Gel-shift assay 3′-End labelled D-P-ODN was incubated with nuclear extracts prepared from mesangial cells in the absence or presence of a 100-fold excess of unlabelled ODN The protein–DNA complexes were separated by 5% non-denaturing acrylamide gel electrophoresis Lane 1, control, no competitor, lane 2, 100-fold excess of unlabelled D-P-ODN, lane 3, 100-fold excess of unlabelled M D-P-ODN, lane 4, 100-fold excess of unlabelled D-ODN, lane 5, 100-fold excess of unlabelled P-ODN

RESULTS

PAI-1 gene promoter activity was studied by transfecting mesangial cells with double-stranded decoy ODNs to inhibit specific transcription factors. This experimental approach overcame the technical difficulties of transfecting mesangial cells with plasmid vectors to perform a functional reporter gene assay. Figure 1 shows the sequence of the human PAI-1 proximal promoter region [8] and the sequences of the decoy ODNs used in this study. The region between bp −79 and −44 in the human *PAI-1* gene is identical with the corresponding regions in the mouse and rat genes. The D-box and P-box are similar to the binding sites for AP-1 (TREs). The sequences with similarity to the general transcription factor Sp1 binding site are designated Sp1-box 1 and Sp1-box 2.

Initially, we assessed the effect of the decoy ODN spanning from D-box to P-box (D-P-ODN). D-P-ODN dose-dependently inhibited the Ang-II-induced PAI-1 mRNA up-regulation in rat mesangial cells (Figure 2). To examine which portion of D-P-ODN is responsible for the inhibition, ODNs corresponding to the D-box (D-ODN), the P-box (P-ODN) and D-P-ODN with mutations at the Sp1-box 1 (M D-P-ODN) were constructed (Figure 1). Cells transfected with the D-ODN and P-ODN showed no inhibition but rather enhanced signals of PAI-1 mRNA when treated with Ang II (Figure 3A). Transfection with M D-P-ODN inhibited the up-regulation induced by Ang II to a level comparable with that with the D-P-ODN. These data suggest that (i) both D- and P-boxes are necessary for inducing PAI-1 mRNA up-regulation by Ang II, or (ii) the mutation created in the Sp1-box 1 is not effective for inhibiting Sp1

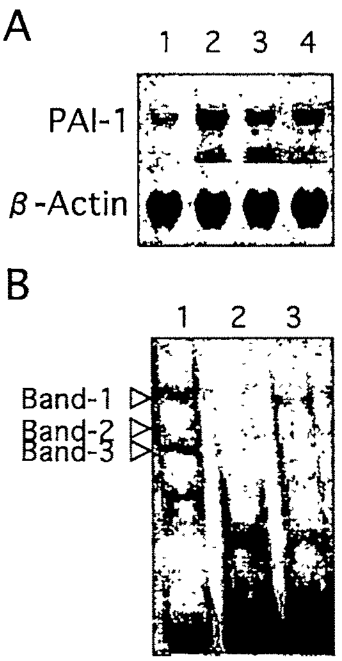

Figure 4 Effects of the decoy Sp1-ODN on Ang-II-induced PAI-1 mRNA expression

(**A**) Northern blotting Mesangial cells were transfected with 5 μM Sp1-ODN or M Sp1-ODN in a serum-free medium for 24 h, and then stimulated with 100 nM Ang II for 6 h The PAI-1 mRNA expression was analysed by Northern blotting using rat PAI-1 probe Lane 1, control, no treatment, lane 2, Ang II, lane 3, Sp1-ODN + Ang II, lane 4, M Sp1-ODN + Ang II (**B**) Gel-shift assay 3′-End labelled D-P-ODN was incubated with nuclear extract prepared from mesangial cells in the absence or presence of a 100-fold excess of unlabelled ODN The protein–DNA complexes were separated by 5% non-denaturing acrylamide gel electrophoresis Lane 1, control, no competitor, lane 2, 100-fold excess of unlabelled D-P-ODN, lane 3, 100-fold excess of unlabelled Sp1-ODN.

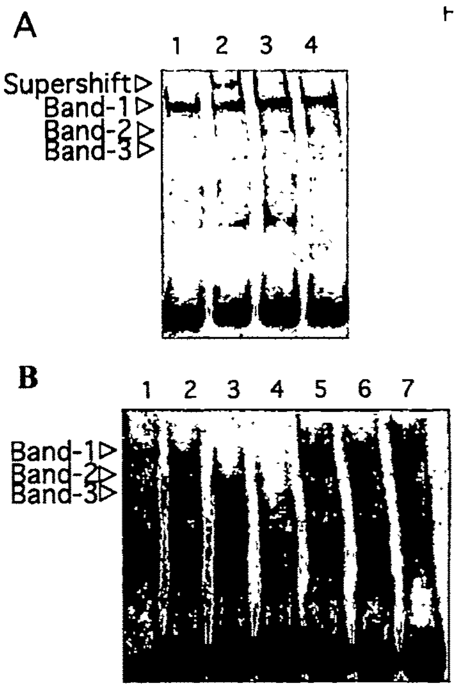

Figure 5 Molecular interaction of Sp1 or Sp1-like activity in mesangial cells with the D-P-ODN

(**A**) Gel supershift assay 3′-End labelled D-P-ODN was incubated with nuclear extracts prepared from mesangial cells Then, an antibody to Sp1, AP-1 or AP-2 was added to the reaction mixtures. The protein–DNA complexes were separated by 5% non-denaturing acrylamide gel electrophoresis Lane 1, control, no antibody; lane 2, anti-Sp1 antibody, lane 3, anti-AP-1 antibody, lane 4, anti-AP-2 antibody (**B**) Competition of gel shift by D-P-ODN or Sp1 consensus ODN 3′-End labelled D-P-ODN was incubated with nuclear extracts from mesangial cells in the presence of various concentrations of D-P-ODN or Sp1 consensus ODN The protein–DNA complexes were separated by 5% non-denaturing acrylamide gel electrophoresis Lane 1, control, no competitor, lane 2, 80 fmol of D-P-ODN (4-fold); lane 3, 400 fmol of D-P-ODN (20-fold), lane 4, 2000 fmol of D-P-ODN (100-fold), lane 5, 80 fmol of Sp1 consensus ODN (4-fold), lane 6, 400 fmol of Sp1 consensus ODN (20-fold), lane 7, 2000 fmol of Sp1 consensus ODN (100-fold)

binding. To address these questions, a gel-shift assay was performed using mesangial-cell nuclear extracts and the D-P-ODN. The gel-shift assay showed at least three specific bands, which were abolished by the addition of an excess of unlabelled D-P-ODN (designated bands 1–3 from the top, Figure 3B). Addition of the unlabelled M D-P-ODN to the reaction mixture abolished complex formation of all the three bands. However, addition of D-ODN or P-ODN exhibited only weak competition for these bands. These data indicate that M D-P-ODN has similar capability to D-P-ODN in competing for binding with transcription factors.

Since the decoy ODN with mutations in the Sp1-box 1 (M D-P-ODN) failed to inhibit transcription-factor binding, we synthesized another decoy, Sp1-ODN, to inhibit Sp1 transcriptional activity. Mesangial cells transfected with Sp1-ODN showed a weak attenuation of Ang-II-induced PAI-1 mRNA up-regulation (about 30% reduction, Figure 4A), whereas the mutated control M Sp1-ODN had little effect on the expression. The gel-shift assay showed that intensities of the three bands were decreased by the addition of excess Sp1-ODN, but it did not completely compete out these bands as D-P-ODN did (Figure 4B). Thus the affinity of Sp1-ODN for these factors was much lower than that of D-P-ODN. These data indicate that the weak affinity of Sp1-ODN for transcription factor resulted in weak inhibition of Ang-II-induced PAI-1 mRNA up-regulation.

To identify the transcription factors that bind to D-P-ODN we performed gel supershift assays with antibodies to AP-1, AP-2 and Sp1. The antibody to Sp1 supershifted band 1 (Figure 5A). The anti-AP-1 antibody also yielded a supershifted band, although we could not identify which of the three bands had been supershifted. The anti-AP-2 antibody did not cause supershifting. A competition assay using a putative Sp1 consensus sequence abolished binding of the three bands with an affinity comparable with the D-P-ODN (Figure 5B). These results indicate that Sp1 or an Sp1-like factor binds to a region of the *PAI-1* gene corresponding to the D-P-ODN.

To define the binding site of Sp1 in the *PAI-1* gene, we performed a methylation-interference experiment using DIG-labelled D-P-ODN and human recombinant Sp1. The methylated ODN interfered with Sp1 binding from bp −78 to −69 (Figure 6). Thus Sp1 binds to the ODN at the sequence TGGGTGGGGCT, which is the so-called GT-box sequence and contains Sp1-box 1 in the *PAI-1* gene. To verify the binding of Sp1 or Sp1-like activity to the GT box, D-Sp1-ODN, which contains the GT box, and a control, M D-Sp1-ODN, with four mutations in the GT box (TGGGTGGGGCT → TGAATTCGGCT, with the changes underlined), were synthesized. When D-Sp1-ODN was incubated with mesangial-cell nuclear extracts, three complexes were observed, as shown earlier with D-P-ODN, although the intensities of bands 2 and 3 were weak (Figure 7). These three bands were competed out when a 100-fold excess of D-Sp1-ODN

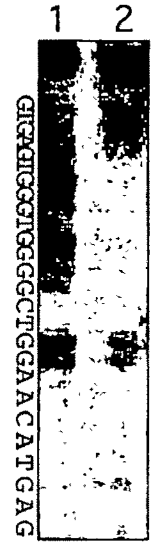

Figure 6 Methylation interference of recombinant human Sp1 binding

3′-End labelled D-P-ODN was methylated and incubated with recombinant human Sp1 The protein–DNA complexes were isolated and the DNA was digested by the Maxam–Gilbert reaction The DNA fragments were separated by electrophoresis on a 12% sequence gel Lane 1, control, no protein incubation, lane 2, incubated with recombinant human Sp1

was added to the reaction mixture; however, M D-Sp1-ODN had little effect on the three bands. The band-1 complex was supershifted with anti-Sp1 antibody. Thus the results indicate that the GT box in the PAI-1 promoter served as the binding site for Sp1 or an Sp1-like factor.

The nature of the band-1 complex in Ang-II-induced PAI-1 mRNA up-regulation was studied by a gel-shift assay. The intensity of the band-1 complex in nuclear extract from rat mesangial cells treated with Ang II for 3 h was compared with that from untreated control cells. The intensity of band-1 complex was substantially increased after 3 h of Ang II treatment (Figure 8). Densitometric analysis revealed a 2.36±0.05-fold increase in Sp1-like-factor binding by Ang II compared with non-treated control, whereas the intensities of bands 2 and 3 were comparable. The Ang-II-responsive component of band 1 was evaluated further. When an antibody to Sp3, which also belongs to the Sp1 family of transcription factors, was added to the system, it supershifted band 1. When both anti-Sp1 and anti-Sp3 antibodies were added to the system, the band-1 complex disappeared completely (Figure 9A). The results indicate that band 1 consists mainly of Sp1 and Sp3. Then the amount of Sp1 and Sp3 in the nuclear extracts from Ang-II-treated and non-treated cells was compared by adding each antibody to the system and the intensity of remaining band 1 was measured. When anti-Sp1 antibody was added to the system there was no significant difference in the intensities of remaining band 1 (Sp3 or Sp3-like)

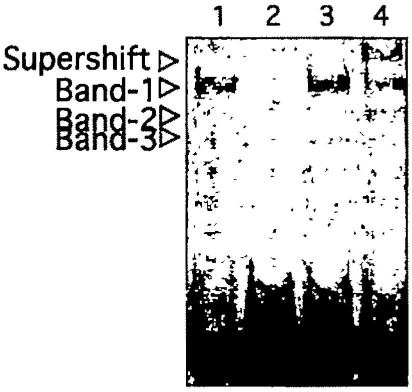

Figure 7 Molecular interaction of Sp1 or Sp1-like activity with the GT box

3′-End labelled D-Sp1-ODN was incubated with nuclear extracts from mesangial cells in the absence or presence of 100-fold excess of unlabelled ODN or anti-Sp1 antibody The protein–DNA complexes were separated by 5% non-denaturing acrylamide gel electrophoresis Lane 1, control, no competitor, lane 2, 100-fold excess of unlabelled D-Sp1-ODN, lane 3, 100-fold excess of unlabelled M D-Sp1-ODN; lane 4, gel supershift assay with anti-Sp1 antibody.

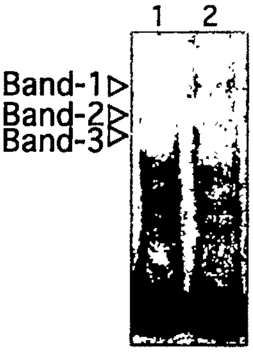

Figure 8 Activation of Sp1-like factor in Ang-II-treated mesangial cells

3′-End labelled D-Sp1-ODN was incubated with nuclear extracts of Ang-II-treated mesangial cells The protein–DNA complexes were separated by 5% non-denaturing acrylamide gel electrophoresis (Although not shown, Western-blot analysis of the nuclear extract from mesangial cells showed no apparent change in the Sp1 protein after the treatment with Ang II) Lane 1, control, untreated cells, lane 2, Ang-II-treated cells

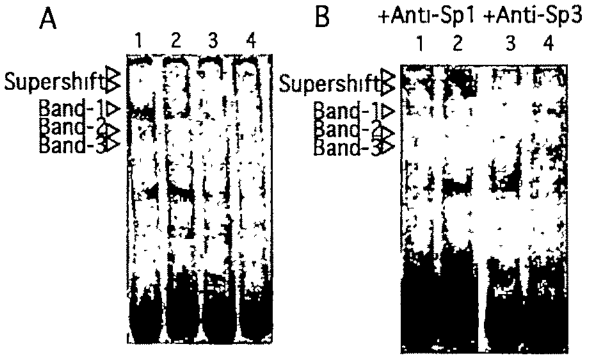

Figure 9 Binding of Sp1 and Sp3 in mesangial cells to the GT box

(A) Gel supershift assay 3′-End labelled D-Sp1-ODN was incubated with nuclear extracts prepared from mesangial cells Then, an antibody to Sp1 and/or Sp3 was added to the reaction mixtures The protein–DNA complexes were separated by 5% non-denaturing acrylamide gel electrophoresis Lane 1, control, no antibody, lane 2, anti-Sp1 antibody, lane 3, anti-Sp3 antibody, lane 4, anti-Sp1 and anti-Sp3 antibodies (B) Comparison of Sp1(-like activity) and Sp3(-like activity) in nuclear extracts from Ang-II-treated cells and non-treated cells 3′-End labelled D-Sp1-ODN was incubated with nuclear extracts from mesangial cells Then, an antibody to Sp1 or Sp3 was added to the reaction mixtures The protein–DNA complexes were separated by 5% non-denaturing acrylamide gel electrophoresis Lanes 1 and 2, supershifted with anti-Sp1 antibody, lanes 3 and 4, supershifted with anti-Sp3 antibody Lanes 1 and 3, control, non-treated cells, lanes 2 and 4, Ang-II-treated cells

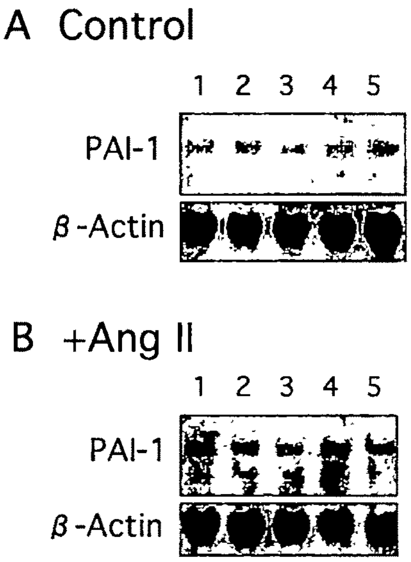

Figure 10 Effect of the decoy D-Sp1-ODN on Ang-II-induced PAI-1 mRNA expression

(**A**) Basal PAI-1 mRNA expression. (**B**) Ang-II-induced PAI-1 mRNA expression Mesangial cells were transfected with D-Sp1-ODN or M D-Sp1-ODN by incubation with indicated concentrations of the ODN in a serum-free medium for 24 h, and then stimulated with vehicle (Control, **A**) or 100 nM Ang II (**B**) for 6 h The PAI-1 mRNA expression was analysed by Northern blotting using rat PAI-1 probe Lanes 1, control, no ODN treatment, lanes 2, 1 μM D-Sp1-ODN, lanes 3, 5 μM D-Sp1-ODN, lanes 4, 1 μM M D-Sp1-ODN, lanes 5, 5 μM M D-Sp1-ODN

between the nuclear extract from Ang-II-treated and non-treated cells (Figure 9B, left-hand panel). In contrast, when anti-Sp3 antibody was added to the system, the intensity of remaining band 1 (Sp1 or Sp1-like) was enhanced in the nuclear extract from Ang-II-treated cells (Figure 9B, right-hand panel). There was a 2.99±0.38-fold increase in the density of the remaining band 1 in anti-Sp3-antibody-treated nuclear extract from Ang-II-treated cells compared with the non-treated control cells. Thus the element of band 1 that was enhanced by Ang II was supershifted by anti-Sp1 but not by anti-Sp3

The effect of transfection with D-Sp1-ODN in mesangial cells treated with Ang II was studied. D-Sp1-ODN inhibited the Ang-II-induced PAI-1 mRNA up-regulation in a dose-dependent manner, whereas the mutated control M D-Sp1-ODN had little effect on the induced expression (Figure 10). Densitometric analysis revealed a 68±9% ($n = 4$) reduction in Ang-II-induced PAI-1 mRNA expression in the cells transfected with 5 μM D-Sp1-ODN. Mesangial cells not treated with Ang II showed a 20±6% reduction in PAI-1 mRNA expression when transfected with 5 μM D-Sp1-ODN. M D-Sp1-ODN had little effect on both Ang-II-treated and non-treated cells Thus Sp1 or an Sp1-like factor that is supershifted with anti-Sp1 antibody is likely to be involved both in basal and Ang-II-induced PAI-1 mRNA expression.

DISCUSSION

Our previous study demonstrated that Ang II up-regulates PAI-1 mRNA through PKC activation in glomerular mesangial cells [7]. The present study examined the molecular mechanism of Ang-II-induced up-regulation of *PAI-1* gene expression. Up-regulation of the gene expression has been shown to be transcriptionally regulated by its proximal promoter region. The decoy ODN (D-P-ODN) of the promoter region, which contains two TRE-like sequences and one Sp1 binding site-like sequence, abolished the gene expression induced by Ang II.

The gel-shift assay, gel supershift assay and methylation-interference experiment in the present study suggest a unique protein–DNA interaction of *PAI-1* gene regulation in mesangial cells. These studies demonstrated that general transcription factors, Sp1 and Sp3, or factors that bind to the GT box and cross-react with anti-Sp1 and anti-Sp3 antibodies, bind to the proximal promoter region of the *PAI-1*-gene. In the gel-shift assay, anti-Sp1 and anti-Sp3 antibodies substantially supershifted the complex (band 1) of the D-P-ODN and the mesangial-cell nuclear extract The methylation-interference experiment revealed that the core sequence of the binding site for Sp1 is located in the so-called GT box, which contains the Sp1-box 1. Sp1 and Sp3 have been shown to regulate basal transcription of many genes [9] In the gel-shift assay, the intensity of the complex, which contains Sp1 or an Sp1-like factor, was significantly enhanced in nuclear extract from Ang-II-treated mesangial cells compared with untreated control cells. In contrast, the intensity of the Sp3 or Sp3-like factor was not significantly different between Ang-II-treated and non-treated cells The functional significance of the Sp1 and Sp3 binding to the GT box was examined by the use of decoys. The D-Sp1-ODN decoy, which masks the GT box, abolished the Ang-II-induced PAI-1 mRNA up-regulation, and a mutation in the D-Sp1-ODN resulted in a loss of the inhibitory effect of the D-Sp1-ODN. Transcription of the *PAI-1* gene is likely to be regulated by a balance between the activity of Sp1 and Sp3. Sp3 has been shown to repress transcriptional activity of Sp1 [9].

Several mechanisms for the activation of Sp1 or Sp1-like factor are postulated. Ang II has been reported to induce Sp1 protein in neonatal cardiac fibroblasts [11]. However, we did not observe induction of Sp1 protein by Ang II in rat mesangial cells (results not shown). Another mechanism of Sp1 activation is phosphorylation or dephosphorylation of the protein Sp1 has been reported to be activated by both phosphorylation and dephosphorylation [12–15]. Mitogen-activated protein kinase (MAPK) has been shown to activate Sp1 [16,17]. Ang II has been proposed to stimulate MAPK in a PKC-dependent manner [18,19]. Our previous data demonstrated up-regulation of *PAI-1* gene expression by Ang II through PKC and protein tyrosine kinases downstream of PKC [7]. Taken together, binding of Sp1 to the GT box may be increased by the PKC- and MAPK-dependent signalling pathway in response to Ang II.

It has been reported that the two TRE-like sequences in the proximal promoter region of the *PAI-1* gene mediate signals from the PKC activator, phorbol ester, in MCF-7 and HepG2 cells [8,20]. Thus, we initially anticipated that Ang-II-induced PAI-1 up-regulation was mediated by the two TRE-like sequences To our surprise, decoy ODNs encoding the two respective TRE-like sequences were not effective in blocking the induction. On the other hand, there was a weak but detectable supershift by anti-AP-1 antibody in the gel shift. Because of a weak affinity of the two TRE-like sequences for AP-1 compared with the TRE-consensus sequence [8], a larger amount of the decoy ODN may have been required to inhibit AP-1. In this regard, a decoy ODN containing an AP-1 consensus sequence showed a weak inhibitory effect (approx. 20%) on Ang-II-induced PAI-1 mRNA up-regulation (results not shown).

Nevertheless, the present study shows that Sp1, or an Sp1-like factor, is the effector of Ang-II-induced up-regulation of the *PAI-1* gene in mesangial cells. Since various decoy ODNs have been used successfully in experimental models of glomerular diseases [10,21], our approach to suppress extracellular matrix formation by mesangial cells may have clinical implication as a potential molecular pharmacological tool to control progressive renal diseases.

We thank Miss Erika Sugawara for her excellent technical assistance

REFERENCES

1 Matsusaka, T., Hymes, J and Ichikawa, I (1996) Angiotensin in progressive renal diseases theory and practice J Am Soc Nephrol. **7**, 2025–2043

2 Hamdan, A D, Quist, W C, Gugne, J. B. and Feener, E P (1996) Angiotensin-converting enzyme inhibition suppresses plasminogen activator-1 expression in the neointima of balloon-injured rat aorta Circulation **93**, 1073–1078

3 Oikawa, T, Freeman, M, Lo, W, Vaughan, D E and Fogo, A (1997) Modulation of plasminogen activator inhibitor-1 *in vivo* a new mechanism for the anti-fibrinotic effect of renin–angiotensin inhibition Kidney Int **51**, 164–172

4 Baricos, W H, Cortez, S L, El-Dahr, S S and Schnaper, H W (1995) ECM degradation by cultured human mesangial cells is mediated by a PA/plasmin/MMP-2 cascade Kidney Int **47**, 1039–1047

5 Tomooka, S, Border, W A, Marshall, B C and Noble, N A (1992) Glomerular matrix accumulation is linked to inhibition of the plasmin protease system Kidney Int **42**, 1462–1469

6 Kagami, S, Kuhara, T, Okada, K, Kuroda, Y, Border, W A and Noble, N A (1997) Dual effects of angiotensin II on the plasminogen/plasmin system in rat mesangial cells Kidney Int **51**, 664–671

7 Motojima, M, Kakuchi, J and Yoshioka, T. (1999) Association of TGF-β signaling in angiotensin II-induced PAI-1 mRNA upregulation in mesangial cells role of PKC Biochim Biophys Acta **1449**, 217–226

8 Knudsen, H, Olesen, T, Riccio, A and Ungaro, R. (1994) A common response element mediates differential effects of phorbol esters and forskolin on type-1 plasminogen activator inhibitor gene expression in human breast carcinoma cells. Eur J Biochem **220**, 63–74

9 Lania, L, Majello, B. and De Luca, P (1997) Transcriptional regulation by the Sp family proteins Int J Biochem Cell Biol. **29**, 1313–1323

10 Maeshima, Y., Kashihara, N, Yasuda, T, Sugiyama, H, Sekikawa, T, Okamoto, K, Kanao, K, Watanabe, Y, Kanwar, Y. S and Makino, H. (1998) Inhibition of mesangial cell proliferation by E2F decoy oligodeoxynucleotide *in vitro* and *in vivo* J Clin. Invest **101**, 2589–2597

11 Grohe, C, Kahlert, S, Lobbert, K, Neyses, L, van Eickels, M, Stimpel, M and Vetter, H (1998) Angiotensin converting enzyme inhibition modulates cardiac fibroblast growth. J. Hypertens **16**, 377–384

12 Black, A R, Jensen, D., Lin, S-Y and Azizkhan, J C (1999) Growth/cell cycle regulation of Sp1 phosphorylation. J Biol Chem **274**, 1207–1215

13 Armstrong, S. A., Barry, D A, Leggett, R W and Mueller, C R (1997) Casein kinase II-mediated phosphorylation of the C terminus of Sp1 decreases its DNA binding activity J Biol. Chem **272**, 13489–13495

14 Rohiff, C, Ahmad, S, Borellini, F, Lei, J and Glazer, R I (1997) Modulation of transcription factor Sp1 by cAMP-dependent protein kinase J Biol Chem **272**, 21137–21141

15 Daniel, S, Zhang, S, DePaoli-Roach, A A and Kim, K-H (1996) Dephosphorylation of Sp1 by protein phosphatase 1 is involved in the glucose-mediated activation of the acetyl-CoA carboxylase gene J Biol Chem **271**, 14692–14697

16 Merchant, J. L, Du, M and Todisco, A (1999) Sp1 phosphorylation by Erk 2 stimulates DNA binding Biochem Biophys Res. Commun **254**, 454–461

17 Milanini, J, Vinals, F, Pouyssegur, J and Pages, G (1998) p42/p44 MAP kinase module plays a key role in the transcriptional regulation of the vascular endothelial growth factor gene in fibroblasts J Biol Chem **273**, 18165–18172

18 Tian, Y, Smith, R D, Balla, T and Catt, K. J (1998) Angiotensin II activates mitogen-activated protein kinase via protein kinase C and Ras/Raf-1 kinase in bovine adrenal glomerulosa cells Endocrinology **139**, 1801–1809

19 Zou, Y, Komuro, I, Yamazaki, T, Aikawa, R., Kudoh, S, Shiojima, I, Hiroi, Y, Mizuno, T and Yazaki, Y (1996) Protein kinase C, but not tyrosine kinases or Ras, plays a critical role in angiotensin II-induced activation of Raf-1 kinase and extracellular signal-regulated protein kinases in cardiac myocytes J. Biol. Chem **271**, 33592–33597

20 Arts, J, Grimbergen, J, Bosma, P J, Rahmsdorf, H. J and Kooistra, T (1996) Role of c-Jun and proximal phorbol 12-myristate-13-acetate-(PMA)-responsive elements in the regulation of basal and PMA-stimulated plasminogen-activator inhibitor-1 gene expression in HepG2 Eur J Biochem **241**, 393–402

21 Morishita, R, Higaki, J, Tomita, N and Ogihara, T (1998) Application of transcription factor 'Decoy' strategy as a means of gene therapy and study of gene expression in cardiovascular disease Circ Res **82**, 1023–1028

Received 3 December 1999/5 April 2000, accepted 10 May 2000

Biochem J (2000) 349, 443–453 (Printed in Great Britain)

Tissue-specificity, functional characterization and subcellular localization of a rat ubiquitin-specific processing protease, UBP109, whose mRNA expression is developmentally regulated

Kyung Chan PARK*, Eun Jung CHOI*, Sang Won MIN*, Sung Soo CHUNG*, Hyun KIM†, Toshiaki SUZUKI‡, Keiji TANAKA‡, and Chin Ha CHUNG*[1]

*Division of Biological Sciences and Research Center for Cell Differentiation, College of Natural Sciences, Seoul National University, Seoul 151-742, Korea, †Department of Anatomy, Institute of Medical Genetics, College of Medicine, Korea University, Seoul 136-701, Korea, and ‡Tokyo Metropolitan Institute of Medical Science, CREST, Japan Science and Technology Corporation, Tokyo 113, Japan

A cDNA encoding an ubiquitin-specific processing protease, UBP109, in rat skeletal muscle was cloned and its product was characterized. Northern analysis revealed that UBP109 mRNA is highly expressed in testis and spleen, compared with other tissues. Furthermore, *in situ* hybridization showed that the level of UBP109 mRNA in liver, spinal cord and brain dramatically changed during embryonic development, indicating that the expression of UBP109 mRNA is developmentally regulated. UBP109 was expressed in *Escherichia coli* and purified to apparent homogeneity using a ^{125}I-labelled ubiquitin–peptide fusion as a substrate. The purified enzyme cleaved at the C-terminus of the ubiquitin moiety in natural and engineered fusions irrespective of their sizes. UBP109 also released free ubiquitin from poly-His-tagged penta-ubiquitin. Moreover, it released free ubiquitin from poly-ubiquitinated protein conjugates of rabbit reticulocytes. In addition, UBP109 localized to both the cytoplasm and the nucleus and, among three putative nuclear localization sequences, only the one located near the C-terminus is responsible for nuclear localization. These results suggest that UBP109 may play an important role in generation of free ubiquitin from its precursors and its recycling from poly-ubiquitinated protein conjugates, and hence in regulation of ubiquitin-mediated cellular processes, particularly related to embryonic development.

Key words: de-ubiquitinating enzyme, embryonic development, hUSP15, nuclear localization, UBP109.

INTRODUCTION

Covalent modification of proteins by the 76-residue ubiquitin (Ub) polypeptide is involved in many aspects of protein metabolism and cellular functions, including elimination of abnormal proteins, cell-cycle progression, signal transduction, transcription, and antigen presentation [1,2]. The known substrates of this ubiquitination pathway include protein kinase (Mos), cyclins, transcription factors (Matα2, GCN4, c-Jun, p53 and nuclear factor-κB), inhibitors of cyclin-dependent protein kinases (Sic1, Far1 and Rum1), and subunits of trimeric G-proteins [3,4]. Ubs are covalently ligated to proteins by the action of a multiple enzyme system consisting of E1 (Ub-activating), E2 (Ub-conjugating), and E3 (Ub-ligating) enzymes. Proteins ligated to multiple units of Ub are recognized by the 19 S regulatory complex of the 26 S proteasome. Proteins bound to the 19 S complex are then probably unfolded [5,6] and translocated into the central cavity of the 20 S proteasome, where they are degraded to small peptides in an ATP-dependent fashion [1–4,7].

Ubs are encoded by two distinct classes of genes, neither of which encodes a monomeric form of Ub [8,9]. One is a poly-Ub gene which encodes a linear polymer of Ubs that are linked through peptide bonds between the C-terminal Gly and N-terminal Met of contiguous Ub molecules. The other encodes a fusion protein in which a single Ub is linked to a ribosomal protein consisting of 52 or 76–80 amino acids [10]. Thus generation of free Ub from linear Ub polymers and Ub-fusion proteins and recycling of Ub from poly-ubiquitinated protein conjugates by de-ubiquitinating enzymes (DUBs) should be essential for the Ub-mediated cellular processes.

DUBs can be divided into two groups: Ub C-terminal hydrolases (UCHs) and Ub-specific processing proteases (UBPs) [11]. As far as the UCH family is concerned, a neuron-specific UCH in the marine snail *Aplysia* has been reported to be essential for long-term facilitation [12]. Recently, Leroy and co-workers have identified, in a German family with Parkinson's disease, a mutation in the UCH-L1 gene resulting in a change of Ile^{93} to Met, implicating the involvement of Ub pathway in Parkinson's disease [13]. Saigoh et al. [14] have found that, in the gracile-axonal-dystropy (*gad*) mouse showing ataxia, accumulation of amyloid β-protein and Ub-positive deposits occurs retrogradely along the sensory and motor nervous systems and that the *gad* mutation is caused by an in-frame deletion including exons 7 and 8 of UCH-L1. Johnston et al. [15] have determined the crystal structure of UCH-L3, which shows a central antiparallel β-sheet flanked on both sides by α-helices. This resembles the structure of the well-known papain-like cysteine proteases, with the greatest similarity to cathepsin B. As for the UBP family, many UBPs have been implicated in numerous cellular processes, such as eye development in the fly [16], transcriptional silencing [17], cytokine response [18], and growth regulation [18,19].

Abbreviations used Ub, ubiquitin; UCH, ubiquitin C-terminal hydrolase, YUH1, yeast ubiquitin hydrolase 1, gal, galactosidase, UBP, ubiquitin-specific processing protease, USP, ubiquitin-specific protease, Unp, ubiquitous nuclear protein, DUB, de-ubiquitinating enzyme, Ub-PESTc, ubiquitin-αNH-MHISPPEPESEEEEEHYC, CEP80, carboxyl extension protein 80, DHFR, dihydrofolate reductase, His-penta-Ub, poly-His-tagged penta-Ub, NLS, nuclear localization signal, Ni-NTA, Ni^{2+}-nitrilotriacetate, DTT, dithiothreitol, Rb, retinoblastoma protein

[1] To whom correspondence should be addressed (e-mail chchung@snu.ac kr)

In the mouse and human, cDNAs of ubiquitous nuclear protein (Unp) have been cloned. *unp* was originally identified during a survey of mouse genes near the Mpv20 retroviral insertion site. Analysis of the Unp cDNAs has revealed their sequence homology with the UBP family, and their products have been shown to be functional DUBs [20–22] In addition, the deduced amino acid sequences of the Unps contain putative nuclear localization signals (NLSs), based on their similarity to the NLS domain of the p53 protein [23], and the binding motifs for retinoblastoma protein (Rb) [24,25]. However, the subcellular localization of endogenous Unps has been controversial, since the mouse Unp has been reported to localize to the nucleus [26], while human Unp (Unph) has been shown to exist exclusively in the cytoplasm [27].

The mouse *unp* is related to the human oncogene *tre-2* [27]. Expression of *unp* from a highly active promoter results in tumorigenic transformation of NIH3T3 cells, and induces lung carcinomas when the cells are injected into athymic mice [26]. Unph mRNA levels are consistently elevated in small-cell tumours and adenocarcinomas of the lung, suggesting a possible causative role of Unps in the neoplastic process [21]. Two human Unp cDNAs, unpEL and unpES, have also been isolated from adult tissues [22] The UnpEL is longer at both N- and C-termini than Unph, and UnpES, which has an internal deletion, is shorter by 47 amino acids than UnpEL. This could be a tissue-specific isoform, presumably a product of alternative splicing The relative abundance of the Unp isoforms on Northern blots varies from tissue to tissue: in the brain, mRNA of UnpEL predominates, while in the testis, most of the Unp-specific signal came from mRNA of UnpES, and in the skeletal muscle, both are equally represented. Interestingly, the levels of UnpEL and UnpES are reduced in small-cell-lung-carcinoma cell lines, raising a possibility that Unps may be tumour suppressors. This contradictory observation for transforming potential and tumour-suppressing activity of Unps could be explained by an example of the tumour suppressor p53, which was originally identified as a proto-oncogene Recently, a human Ub-specific protease gene, *USP15*, has been identified [28]. The USP15 protein has the sequence most closely related to Unp, and its gene is localized to chromosome band 12q14, a different location from that of *unp* (3p21 3). It has been reported that breaks in a broad region of chromosome 12, 12q13-q15, occur in lipomas [29]. In addition, amplification of 12q14-15 and 12q14-21 sequences has been found in the neuroblastoma cell line NGP [30] and both mucinous ovarian neoplasmas and Brenner tumours respectively, which sometimes co-exist in the same patient [31].

In the present study, a UBP cDNA was isolated from rat skeletal-muscle cDNA library using an *Escherichia coli*-based *in vivo* screening method [32,33]. We expressed the enzyme in *E. coli*, purified it from the cells, and analysed its *in vitro* properties We also analysed the expression of its mRNA in rat embryos, various adult tissues and cancer cells by Northern blotting and/or *in situ* hybridization and determined its subcellular localization.

EXPERIMENTAL

Materials

The rat cDNAs in pBluescript II (pBS) were excised from the rat skeletal-muscle λ ZAPII cDNA library (Stratagene) by following the procedure recommended by the manufacturer. The cDNA plasmids were propagated in *E. coli* JM101 cells (*supE thi* Δ(*lac-proAB*)/*F′ tra*D36 *proA*$^+$ *proB*$^+$ *lacI*^{q} *lacZ*Δ*M*15) that had been transformed with pACUb-R-β-galactosidase (pACUb-R-β-gal) or pACUb-M-β-gal [34].

Ub-αNH-MHISPPEPESEEEEEHYC (Ub-PESTc), Ub-αNH-carboxyl extension protein of 80 amino acids (Ub-CEP80), and Ub-αNH-dihydrofolate reductase (Ub-DHFR) were purified as described previously [35]. A plasmid for poly-His-tagged penta-Ub (His-penta-Ub) was constructed as follows. The open reading frame of yeast UBI4 gene was amplified by PCR from the *Saccharomyces cerevisiae* genomic DNA, using specific primers with additional restriction-enzyme cleavage sites to facilitate insertion into pET-16b vector (Novagene). The His-penta-Ub protein was expressed in *E. coli* and then purified using a Ni^{2+}-nitrilotriacetate (Ni-NTA)–agarose affinity column by following the procedure recommended by the manufacturer The purified Ub-PESTc was radiolabelled with Na^{125}I using Iodo-Beads (Pierce) [36]. Ub was radiolabelled with Na^{125}I using chloramine-T. Ub-aldehyde was prepared by borohydride reduction of Ub in the presence of YUH1 as described in [37]. Reticulocytes were obtained by subcutaneous injections of phenylhydrazine into albino rabbits [38]. From the cells, fraction II, containing the Ub-conjugating system, was prepared as described in [39]. An anti-β-gal antiserum was obtained from Cappel (Durham, NC, U.S.A.).

Cloning of UBP109 cDNA

The *E. coli* JM101 cells carrying both the rat cDNA plasmids and pACUb-R-β-gal were plated on to agar plates containing 100 μg/ml ampicillin, 34 μg/ml chloramphenicol, and 40 μg/ml 5-bromo-4-chloroindol-3-yl β-D-galactoside ('X-Gal') They were then incubated at 37 °C for 14 h. Among 3×10^5 transformants, three appeared as white colonies, while the others were stained as blue. All the control cells (i.e. transformed with pBS vector only) developed a blue colour From the three white colonies, plasmids were isolated and again transformed into the *E. coli* JM101 expressing either Ub-R-β-gal or Ub-M-β-gal. Only one of the three colonies turned white when transformed with Ub-R-β-gal, but not with Ub-M-β-gal (i e. became blue), confirming that the white colony contains the plasmid carrying the rat cDNA specifying the UBP activity against the Ub-β-gal proteins. The plasmid was isolated, sequenced, and is referred to as pBS-Ubp109. The UBP109 cDNA was also cloned into pQE31 vector, and the resulting plasmid was referred to as pQE31-Ubp109.

In situ hybridization

In situ hybridization was performed essentially as described previously [40]. Radiolabelled riboprobes were synthesized by *in vitro* transcription using α-^{35}S-UTP. Frozen embryo and adult tissues were cut into 12 μm-thick slices and mounted on to gelatin-coated slides. The sections were fixed in 4% (w/v) paraformaldehyde, treated with 0.25% (w/v) acetic anhydride in 0.1 M triethanolamine, pH 8, containing 0.9% (w/v) NaCl to reduce non-specific hybridization due to electrostatic forces, dehydrated and defatted in ethanol and chloroform, and finally air-dried. The hybridization solution (2×10^7 c.p m./ml) was applied directly to each mounted section for 16 h at 52 °C. The sections were washed in 2 × SSC (1 × SSC is 0.15 M NaCl/0 015 M sodium citrate), treated with RNase A (20 μg/ml) for 30 min at 37 °C, and washed sequentially for 30 min in 1 × SSC and 0.5 × SSC at room temperature and 30 min in 0.1 × SSC at 60 °C After drying, the slides were exposed for 7 days to β-max Hyperfilm (Amersham–Pharmacia) for autoradiography.

Expression of UBP109 in *E. coli*

The XL-1/pQE31-Ubp109 cells were grown to mid-exponential phase in Luria broth at 37 °C Expression of UBP109 was then induced for 2 h by treating with 1 mM isopropyl thio-β-D-galactoside After the treatment, the cells were harvested and suspended in 50 mM phosphate buffer, pH 7.8, containing 0.3 M NaCl. The cell suspension was then disrupted in a French press at 96.6 MPa (14000 lb/in^2) and centrifuged at 100000 *g* for 2 h. The resulting supernatants are referred to as 'crude extracts'.

In vitro assays for UBP activity

The UBP activity was assayed by incubation of the reaction mixtures (0.1 ml) containing appropriate amounts of the enzyme fractions and 10 μg of ^{125}I-labelled Ub-PESTc [(1–2)×10^3 c.p.m./μg] in 100 mM Tris/HCl (pH 8)/1 mM EDTA/1 mM dithiothreitol (DTT)/5% (v/v) glycerol [35]. After incubation for appropriate periods at 37 °C, the reaction was terminated by adding 50 μl of 40% (w/v) trichloroacetic acid and 50 μl of 1.2% (w/v) BSA. The samples were centrifuged, and the resulting supernatants were counted for their radioactivity using a γ-radiation counter. The enzyme activity is expressed as a percentage of ^{125}I-labelled Ub-PESTc hydrolysed to acid-soluble products.

Preparation of poly-Ub–protein conjugates

To prepare poly-Ub-ϵNH–protein conjugates, 1 μg of the ^{125}I-labelled Ub [(1–2)×10^6 c.p.m.] was incubated with 720 μg of fraction II and an ATP-regenerating system [39]. The ATP-regenerating system consisted of 10 mM Tris/HCl (pH 7.8), 15 units/ml creatine phosphokinase, 6.5 mM phosphocreatine, 1.5 mM ATP, 1 mM DTT, 0.5 mM MgCl$_2$, and 1 mM KCl in a final volume of 0.3 ml. Incubations were performed for 2 h at 37 °C in the presence of 1 mM haemin to prevent proteolysis of the ubiquitinated protein conjugates by the 26 S proteasome. After incubation, the samples were heated for 10 min at 55 °C for inactivation of endogenous DUBs. The resulting samples were freed of excess ^{125}I-labelled Ub by treatment with 0.2 N NaOH and 100 mM DTT, followed by gel filtration on a Sephadex G-75 column equilibrated with 25 mM Tris/HCl buffer, pH 7.8, containing 1 mM DTT and 1 mM EDTA.

Separation of cytosolic and nuclear fractions

L6 myoblasts were suspended in the hypo-osmotic buffer consisting of 10 mM Hepes, pH 7.9, 0.1 mM EDTA, 0.1 mM EGTA, 1 mM DTT, 10 mM KCl, and 2 mM PMSF, and placed on ice for 15 min. The samples were homogenized twice in a Dounce homogenizer and centrifuged for 5 min at 500 *g* and then for 30 min at 15000 *g*. The resulting supernatants are referred to as the 'cytosolic fraction'. The pellets were resuspended in the same volume of the lysis buffer consisting of 20 mM Tris/HCl, pH 7.5, 150 mM NaCl, 2 mM EDTA, 1% Triton X-100 and 2 mM PMSF. The samples were then centrifuged for 30 min at 15000 *g*. The resulting supernatants are referred to as the 'nuclear fraction'.

Immunoblot analysis

To prepare polyclonal antiserum against UBP109, a multiple antigenic peptide, CSEMETDEPDDESSQDQE, derived from the internal sequence (625–641 residues) of the protein was synthesized (Nippon Roche Research Center, Kamacura City, Japan). This peptide, conjugated to keyhole-limpet haemocyanin, was subcutaneously injected into albino rabbits. From the antiserum, the anti-UBP109 IgGs were affinity-purified using the peptide linked to CNBr-activated Sepharose-4B (Sigma). For immunoblot analysis, SDS/PAGE was carried out using the cytosolic and nuclear fractions obtained from L6 myoblasts Proteins in the gels were transferred on to nitrocellulose membranes and incubated with the purified anti-UBP109 IgG [41]. The membranes were then incubated with the rabbit anti-IgG conjugated with horseradish peroxidase (HRP), and immunoreactive bands were detected using 4-chloro-1-naphthol or an enhanced chemiluminiscence (ECL®) kit (Amersham–Pharmacia)

Determination of subcellular localization of UBP109

In order to generate mutations in three putative NLSs of UBP109, mutagenesis was performed by PCR to replace ^{371}RKKP, ^{678}HKKR and ^{728}LKKR by RIDP, HEDP and IDER respectively, using oligonucleotide primers. The UBP109 cDNAs carrying each mutation were ligated into pcDNA3.1 and tagged with *myc* to their 5′-ends of the open reading frame. The resulting plasmids carrying the mutations in the first, second and third sites are referred to as pcDNAmyc109-1, -2 and -3 respectively, and the plasmid containing the wild-type UBP109 cDNA is referred to as pcDNAmyc109.

NIH3T3 cells and L6 myoblasts were cultured in Dulbecco's modified Eagle's medium supplemented with 100 units/ml of penicillin and 1 μg/ml of streptomycin. The culture medium also contained 10% (v/v) calf serum for NIH3T3 cells or 10% (v/v) fetal bovine serum for L6 myoblasts. Cells were then plated at 4×10^5 cells/ml density on gelatin-coated glass coverslips. After culturing for 24 h, the cells were transfected with the recombinant pcDNA3.1 plasmids using LipofectAMINE PLUS (Gibco BRL) by following the procedure recommended by the manufacturer. The transfected cells were cultured for 3 h, re-fed with the fresh culture medium supplemented with 10% serum, and further cultured for 24–48 h.

For cell staining, the cultured cells on coverslips were fixed for 10 min in 3.7% (w/v) paraformaldehyde buffered with PBS and permeabilized with PBS containing 0.5% (v/v) Triton X-100 for 5 min. The coverslips then were blocked with PBS containing 10% (v/v) goat serum and 0.1% (w/v) gelatin, and incubated for 1 h with anti-*myc* monoclonal antibody in PBS containing 1% BSA. They were washed three times with PBS containing 0.1% Triton X-100, incubated for 1 h with fluorescein-conjugated goat anti-mouse IgG, and washed three times with PBS containing 0.1% Triton X-100. Stained cells were mounted on slide glasses with Vectshield (Vector Laboratories, Burlingame, CA, U.S.A.) and observed with a laser scanning confocal microscope (Carl Zeiss LSM 510) [42]. Samples were excited by a 488 nm argon laser, and the images were filtered by a long-pass 505 nm filter.

RESULTS

Cloning of *ubp109*

Using an *E coli*-based *in vivo* screening methods, we isolated a cDNA expressing de-ubiquitinating activity from rat skeletal-muscle cDNA library. The open reading frame specifying the de-ubiquitinating activity was identified by subcloning and nucleotide sequencing of the cDNA and named *ubp109*, since it encodes a 109 kDa protein (GenBank accession number AF106657) This cDNA has a stop codon (TAG at −12) within the short 5′ untranslated region and Kozak consensus sequence (AAG-ATGG) [43]. The position of the start (ATG) codon of

```
                                                  GTCGCTGCCGCCTCCGCTACCGCTAGTGGAAGAAG   -1
ATGGCGGAAGGCGGAGCGGCGGACCTGGACACCCAGCGTTCTGACATCGCGACGCTGCTCAAAACCTCGCTCCGGAAAGGGGACACCTGG   90
 M  A  E  G  G  A  A  D  L  D  T  Q  R  S  D  I  A  T  L  L  K  T  S  L  R  K  G  D  T  W   30
TATCTAGTAGATAGTCGGTGGTTCAAACAGTGGAAAAAATATGTTGGCTTTGACAGTTGGGACAAATACCAGATGGGAGATCAAAATGTC  180
 Y  L  V  D  S  R  W  F  K  Q  W  K  K  Y  V  G  F  D  S  W  D  K  Y  Q  M  G  D  Q  N  V   60
TATCCTGGACCCATCGATAACTCTGGACTTCTCAAAGATGGCGATGCTCAGTCACTTAAGGAACACCTTATCGACGAGTTGGATTACATA  270
 Y  P  G  P  I  D  N  S  G  L  L  K  D  G  D  A  Q  S  L  K  E  H  L  I  D  E  L  D  Y  I   90
CTGTTGCCGACTGAGGGCTGGAATAAACTTGTCAGCTGGTACACACTGATGGAAGGCCAAGAGCCAATAGCAAGAAAGGTGGTAGAACAG  360
 L  L  P  T  E  G  W  N  K  L  V  S  W  Y  T  L  M  E  G  Q  E  P  I  A  R  K  V  V  E  Q  120
GGCATGTTTGTAAAGCACTGCAAAGTGGAAGTCTACCTCACAGAACTGAAGCTCTGCGAGAATGGGAACATGAACAATGTTGTAACTCGG  450
 G  M  F  V  K  H  C  K  V  E  V  Y  L  T  E  L  K  L  C  E  N  G  N  M  N  N  V  V  T  R  150
AGATTTAGCAAAGCTGACACAATAGACACAATTGAAAAGGAAATAAGAAAGATCTTCAATATTCCAGATGAAAAGGAGGCCAGACTGTGG  540
 R  F  S  K  A  D  T  I  D  T  I  E  K  E  I  R  K  I  F  N  I  P  D  E  K  E  A  R  L  W  180
AACAAGTATATGAGTAACACATTTGAGCCACTGAATAAGCCAGACAGCACCATCCAGGATGCCGGCCTATACCAAGGACAGGTGTTAGTG  630
 N  K  Y  M  S  N  T  F  E  P  L  N  K  P  D  S  T  I  Q  DA  G  L  Y  Q  G  Q  V  L  V  210
ATAGAACAAAAAAATGAAGACGGAACGTGGCCCAGGGGTCCCTCTGCTCCTAATGTGAAAAACTCCAATTATTGTCTCCCGTCATATACT  720
 I  E  Q  K  N  E  D  G  T  W  P  R  G  P  S  A  P  N  V  K  N  S  N  Y  C  L  P  S  Y  T  240
GCTTACAAGAACTATGATTATTCGGAACCTGGAAGAAACAATGAACAGCCAGGCCTGTGTGGCCTAAGTAACTTGGGAAACACATGTTTC  810
 A  Y  K  N  Y  D  Y  S  E  P  G  R  N  N  E  Q  P  G  L  C  G  L  S  N  L  G  N  T  C  F  270
ATGAACTCAGCCATTCAGTGTTTGAGCAACACACCTCCACTTACTGAATATTTCCTCAATGATAAGTACCAAGAAGAGCTGAATTTTGAC  900
 M  N  S  A  I  Q  C  L  S  N  T  P  P  L  T  E  Y  F  L  N  D  K  Y  Q  E  E  L  N  F  D  300
AATCCCTTAGGAATGAGAGGTGAAATAGCTAAATCATATGCTGAACTCATCAAGCAGATGTGGTCTGGAAAGTTTAGCTATGTCACTCCA  990
 N  P  L  G  M  R  G  E  I  A  K  S  Y  A  E  L  I  K  Q  M  W  S  G  K  F  S  Y  V  T  P  330
AGAGCATTTAAGACACAAGTAGGACGTTTTGCACCTCAGTTCTCTGGATATCAACAGCAAGACTGCCAAGAACTACTAGCTTTCCTATTA 1080
 R  A  F  K  T  Q  V  G  R  F  A  P  Q  F  S  G  Y  Q  Q  Q  D  C  Q  E  L  L  A  F  L  L  360
GATGGATTACATGAGGATTTGAATAGAATTAGGAAAAAACCATATATCCAGTTAAAAGATGCTGATGGAGGCCAGACAAGGTGGTTGCT 1170
 D  G  L  H  E  D  L  N  R  I |R  K  K  P| Y  I  Q  L  K  D  A  D  G  R  P  D  K  V  V  A  390
GAAGAAGCCTGGGAAAACCATTTAAAAAGAAATGATTCTATCATAGTAGATATATTTCATGGCCTTTTCAAGTCTACGTTAGTGTGTCCT 1260
 E  E  A  W  E  N  H  L  K  R  N  D  S  I  I  V  D  I  F  H  G  L  F  K  S  T  L  V  C  P  420
GAGTGTGCTAAGATCTCAGTGACCTTCGACCCTTTCTGTTACTTGACACTTCCATTGCCTATGAAAAAGGAACGTAGCTTAGAAGTTTAT 1350
 E  C  A  K  I  S  V  T  F  D  P  F  C  Y  L  T  L  P  L  P  M  K  K  E  R  S  L  E  V  Y  450
TTAGTTAGAATGGATCCACTTGCTAAACCTATGCAATACAAAGTCATTGTGCCCAAAATTGGAAATATACTAGACCTTTGTACAGCACTG 1440
 L  V  R  M  D  P  L  A  K  P  M  Q  Y  K  V  I  V  P  K  I  G  N  I  L  D  L  C  T  A  L  480
TCTGCTTTGTCGGGAGTACCTGCAGATAAGATGATAGTCACTGACATATATAATCATAGATTTCACAGGATATTTGCAATGGATGAGAAC 1530
 S  A  L  S  G  V  P  A  D  K  M  I  V  T  D  I  Y  N  H  R  F  H  R  I  F  A  M  D  E  N  510
CTGAGTAGTATTATGGAGCGGGATGATATTTATGTGTTTGAAATTAACATCAACAGGACAGAAGACACAGAACATGTGGTTATTCCTGTT 1620
 L  S  S  I  M  E  R  D  D  I  Y  V  F  E  I  N  I  N  R  T  E  D  T  E  H  V  V  I  P  V  540
TGCCTAAGAGAAAAGTTCAGACACTCAAGTTACACTCACCACACTGGCTCTTCACTGTTCGGCCAGCCTTTTCTTATGGCCGTGCCACGG 1710
 C  L  R  E  K  F  R  H  S  S  Y  T  H  H  T  G  S  S  L  F  G  Q  P  F  L  M  A  V  P  R  570
AACAATACTGAAGATAAACTCTACAATCTCCTGCTCTTGAGAATGTGCCGGTATGTCAAGATGTCTACTGAAACTGAGGAAACTGATGGA 1800
 N  N  T  E  D  K  L  Y  N  L  L  L  L  R  M  C  R  Y  V  K  M  S  T  E  T  E  E  T  D  G  600
CCCCTGCGTTGCTGTGAGGACCAGAATATTAATGGGAATGGTCCAAATGGCATACATGAAGAAGGCTCACCAAGTGAGATGGAGACAGAT 1890
 P  L  R  C  C  E  D  Q  N  I  N  G  N  G  P  N  G  I  H  E  E  G  S  P  S  E  M  E  T  D  630
GAACCAGATGATGAGTCCAGCCAGGATCAAGAGCTTCCCTCAGAAAATGAGAACAGTCAGTCTGAAGATTCAGTCGGAGGAGATAACGAT 1980
 E  P  D  D  E  S  S  Q  D  Q  E  L  P  S  E  N  E  N  S  Q  S  E  D  S  V  G  G  D  N  D  660
TCTGAAAATGGATTGTGTACTGAAGAAACATGCAAAGGTCGACTGACGGGACACAAAAAGCGATTGTTTACATTCCAGTTCAACAACTTA 2070
 S  E  N  G  L  C  T  E  E  T  C  K  G  R  L  T  G |H  K  K  R| L  F  T  F  Q  F  N  N  L  690
GGCAACACTGATATCAACTATATCAAAGACGACACCAGGCATATAAGATTTGATGATAGGCAGCTTCGGCTAGATGAAAGATCTTTTCTC 2160
 G  N  T  D  I  N  Y  I  K  D  D  T  R  H  I  R  F  D  D  R  Q  L  R  L  D  E  R  S  F  L  720
GCCTTGGACTGGGACCCTGACTTGAAGAAGAGATATTTTGATGAGAATGCTGCAGAGGATTTTGAAAAACATGAAAGCGTGGAATATAAA 2250
 A  L  D  W  D  P  D |L  K  K  R| Y  F  D  E  N  A  A  E  D  F  E  K  H  E  S  V  E  Y  K  750
CCTCCAAAAAGACCCTTTGTGAAGTTAAAAGACTGCATTGAACTTTTCACAACAAAAGAGAAGCTAGGTGCTGAAGACCCCTGGTATTGT 2340
 P  P  K  R  P  F  V  K  L  K  D  C  I  E  L  F  T  T  K  E  K  L  G  A  E  D  P  W  Y  C  780
CCAAATTGTAAAGAGCATCAGCAAGCCACCAAGAAATTAGATCTGTGGTCCCTGCCTCCCGTTCTTGTGGTGCATCTCAAGAGATTCTCC 2430
 P  N  C  K  E  H  Q  Q  A  T  K  K  L  D  L  W  S  L  P  P  V  L  V  V  H  L  K  R  F  S  810
TATAGTCGCTACATGAGAGACAAGCTAGATACATTAGTCGATTTTCCCATCAGTGACTTGGATATGTCGGAATTCCTAATTAACCCAAAT 2520
 Y  S  R  Y  M  R  D  K  L  D  T  L  V  D  F  P  I  S  D  L  D  M  S  E  F  L  I  N  P  N  840
GCAGGCCCTTGCCGCTATAATTTGATTGCTGTTTCCAATCACTATGGAGGGATGGGAGGAGGACATTATACTGCTTTTGCAAAGAACAAA 2610
 A  G  P  C  R  Y  N  L  I  A  V  S  N  H  Y  G  G  M  G  G  G  H  Y  T  A  F  A  K  N  K  870
GATGATGGAAAGTGGTACTATTTTGATGACAGTAGCGTCTCCAGTGCATCTGAAGACCAAATTGTGTCCAAAGCAGCATACGTGCTCTTC 2700
 D  D  G  K  W  Y  Y  F  D  D  S  S  V  S  S  A  S  E  D  Q  I  V  S  K  A  A  Y  V  L  F  900
TACCAGAGACAGGACACTTTCAGTGGAACTGGCTTCTTCCCTCTCGACCGAGAAACTAAAGGTGCTTCAGCTGCCACAGGTGTCCCCCTG 2790
 Y  Q  R  Q  D  T  F  S  G  T  G  F  F  P  L  D  R  E  T  K  G  A  S  A  A  T  G  V  P  L  930
GAAAGTGACGAAGACAGCAATGATAATGACAATGATCTAGAAAATGAAAACTGTATGCACACTAATTAATGAAAGTCCAAGAAGCCATAC 2880
 E  S  D  E  D  S  N  D  N  D  N  D  L  E  N  E  N  C  M  H  T  N  *                        952
GAGAGAGAGAGAAAGAGAGAGAGAGACTTTCCTGCCGGTGGTATCTGTGGAGACGGAGTTACCCACCGCATTAAACAGAGGTTTGAGAGG 2970
AGGCGTTTCAGATACCCGAATGTAAATCCTTTATCAGATTTTAAATTCTGCAGTACTTGCCGTGAAACACAATGAAAACTTTAACAGAAA 3060
TTGTTTTTTAAAACATTTACAGTTTTGTATTTACAAGCTAAATATATATATAGGAAATCACAAATAAATCCCTTTTAAGTTAAAAAAAAAAA 3150
AAAAAAAAAAAAAAAAAAAAAAAAAAAA                                                                3178
```

Figure 1 Nucleotide sequence of the UBP109 cDNA and deduced amino acid sequence of the UBP109 protein

The nucleotides are numbered on the right, beginning at A of the presumed start codon The amino acid residues are also numbered on the right The asterisk indicates the TAG stop codon The regions with the **bold** characters are the conserved Cys, Asp, and His domains, the boxed regions are the putative NLS motifs, and the underlined regions are the Rb-binding motifs

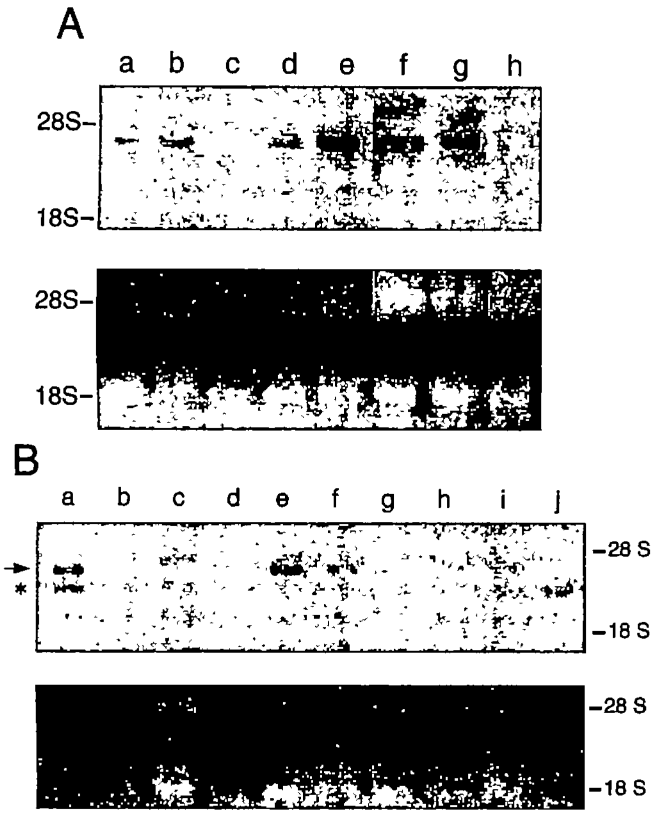

Figure 2 Expression of the UBP109 mRNA in various rat tissues and human carcinoma cells

(**A**) Northern-blot analysis for expression of UBP109 mRNA in various rat tissues Lane a, skeletal muscle, lane b, heart; lane c, brain, lane d, ovary, lane e, testis, lane f, kidney, lane g, spleen, lane h, liver (**B**) Northern-blot analysis for expression of UBP109 mRNA in various carcinomas Lane a, L6 (rat myoblast), lane b, HeLa, lane c, Jurkat; lane d, HepG2; lane e, U937 (human premyeloma), lane f, Hep3 (human squamous carcinoma), lane g, SH-SY5Y (neuroblastoma); lane h, H1299 (lung carcinoma), lane i, Saos-2 (human osteosarcoma), lane j, FLF (human primary fibroblast) The gels were also stained with ethidium bromide prior to autoradiography to reveal the ribosomal RNAs (lower panels)

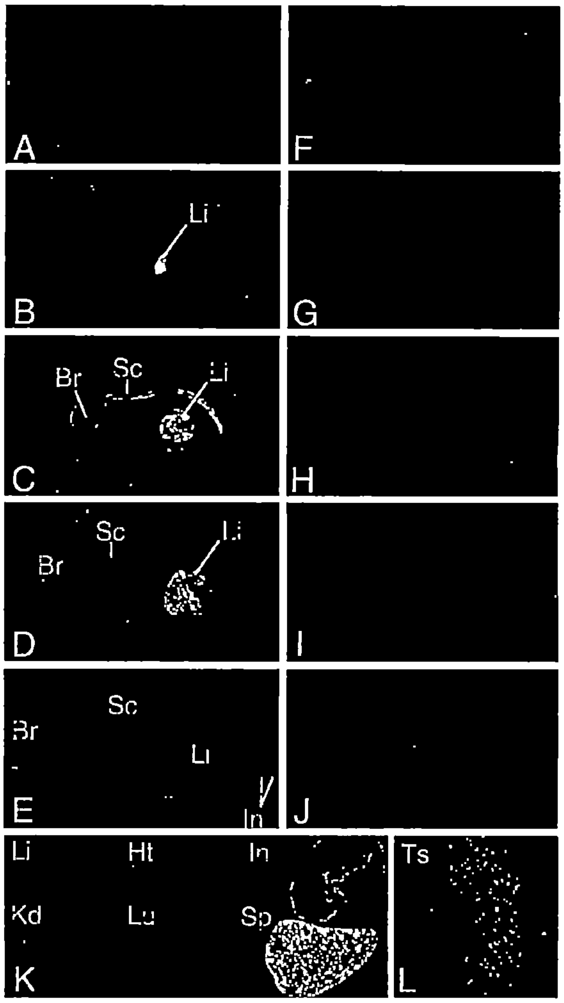

Figure 3 Localization of the UBP109 mRNA in rat embryos and rat adult tissues by *in situ* hybridization

Negative film image of *in situ* hybridization of a parasagittal section was developed for 12–20-day-old rat embryos (**A–J** respectively) with 2-day intervals and for rat adult tissues (**K** and **L**) An UBP109 antisense mRNA probe was used for (**A–E**), (**K**) and (**L**), and a sense probe was used for (**F**)–(**J**) Br, brain, Ht, heart, In, intestine, Kl, kidney, Li, liver, Lu, lung, Sc, spinal cord, Sp, spleen, Ts, testis.

ubp109 was inferred to yield the 2856 bp open reading frame, which encodes a protein consisting of 952 residues (109 255 Da) (Figure 1). From the deduced amino acid sequences, the pI was estimated to be 4.98.

Sequence alignment demonstrated that UBP109 had the Cys and His domains, which is typical for DUBs, and showed 98.2% amino acid sequence identity with USP15, which is a recently reported human UBP, and about 60% identity with Unps of human and mouse, which also are UBPs. Thus UBP109 is a rat homologue of human USP15. The deduced amino acid sequence contained three putative NLSs, based on their similarity to the NLS domain of p53 protein [23]. In addition, three motifs common to proteins that physically associate with Rb protein were also found (Figure 1).

Expression of UBP109 mRNA

To investigate the expression of UBP109 mRNA, Northern-blot analysis was performed using the ^{32}P-labelled 5′-region of Ubp109 (367 bp fragment) as a probe. A single transcript of about 3.7 kb was detected in various rat tissues. The size of the UBP109 cDNA, consisting of 2856 bp and poly(A) tail, corresponded well with the estimated size of the transcript (Figure 2A). Interestingly, expression of the UBP109 mRNA was the highest in testis and spleen, although it was also detected in the other tissues tested.

The UBP109 protein is the sequence most closely related to Unp, a candidate for tumour suppressor, sharing about 60% sequence identity. The gene for USP15, a human homologue of rat UBP109, is localized to chromosome band 12q14, a region where breakage or amplification in various carcinomas has been reported. In an attempt to determine the relationship of UBP109 with cancer, we examined the expression of UBP109 mRNA in various carcinoma cell lines (Figure 2B). The UBP109 mRNA was expressed to various extents among the samples, to high levels especially in lymphoma cells (U937), but there was little or no expression in cervical carcinoma (HeLa), hepatoma (HepG2) and neuroblastoma (SH-SY5Y) cells. Interestingly, an extra faint band was detected only in non-transformed cells, such as L6 myoblasts and FLF human primary fibroblast cells (indicated by an asterisk). However, it remains unknown whether the extra

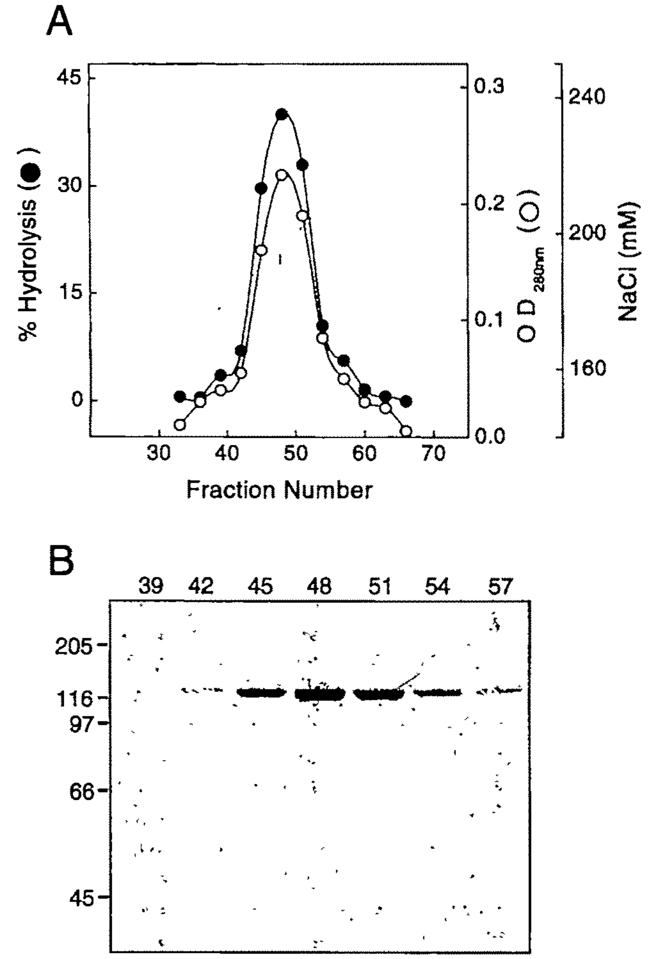

Figure 4 Purification of UBP109 from *E. coli*

(**A**) The UBP109 enzyme preparation obtained from the CM-Sepharose column was chromatographed on a Q-Sepharose column as described in the text. Fractions (1 ml each) were collected, and aliquots (5 μl) of them were assayed for their ability to hydrolyse 10 μg of ^{125}I-labelled Ub-PESTc (●). Incubations were performed for 1 h at 37 °C. Proteins were determined by their absorbance at 280 nm (○). The diagonal dotted line shows the linear gradient of NaCl. (**B**) Aliquots (50 μl each) of the peak fractions were subjected to SDS/PAGE on an 8% slab gel containing SDS and 2-mercaptoethanol, followed by staining with Coomassie Blue R-250.

Table 1 Summary of the purification of UBP109

A unit of the enzyme activity was defined as 1 μg of Ub-PESTc cleaved to acid-soluble products/h.

Step	Protein (mg)	Total activity (units)	Specific activity (units/mg)	Recovery (%)
Crude extract	1000	37024	37	100
NTA–agarose	15	12308	1026	33
DEAE-Sepharose	1.2	10837	9031	29
CM-Sepharose	0.5	6875	13750	18
Q-Sepharose	0.2	3080	15385	8.3

band represents an isoform of UBP109 or a differently spliced product.

Upon *in situ* hybridization we also localized the UBP109 transcript on the parasagittal whole-body sections of 12–20-day-old rat embryos (referred to as E12–E20), as well as on adult tissue sections (Figure 3). Expression of the UBP mRNA in the liver was dramatically increased during the E14–E16 stage (Figures 3B and 3C) and gradually reduced thereafter. In the spinal cord, the mRNA level reached a maximum at E16 (Figure 3C) and rapidly declined during the E18–E20 stage (Figures 3D and 3E). The signal in the brain was also detected from E16, but declined more slowly than that in the spinal cord at the later stage. On the other hand, the UBP109 mRNA began to appear in the intestine at E20 (Figure 3E). Little or no UBP109 mRNA was detected when the same experiments were performed using a sense probe (Figures 3F–3J). Interestingly, expression of the UBP109 mRNA was localized almost exclusively to the outer layer of the intestine in the adult tissue (Figure 3K) as well as in the embryo (Figure 3E). In accord with the Northern-blot data, both of the adult spleen and testis tissues strongly expressed the UBP109 transcript (Figures 3K and 3L). On the other hand, little or no signal was detected in the other adult tissues, unlike the results of Northern-blot analysis, which used concentrated RNA preparations. These results suggest that expression of the UBP109 mRNA is regulated during embryonic development and is tissue-specific in adults.

Purification of UBP109

To purify the UBP109 protein, crude extract (1 g) was prepared from 12 g of *E. coli* cells that had been transformed with pQE31-Ubp109. During purification, the enzyme activity was monitored by determining its ability to hydrolyse ^{125}I-labelled Ub-PESTc. The extracts were applied to an NTA–agarose column (1 cm × 5 cm) equilibrated with 50 mM phosphate (pH 7.8)/0.3 M NaCl. The column was washed with the phosphate buffer containing 35 mM imidazole, adjusted to pH 6.8. Proteins bound to the column were eluted with a linear gradient of 35–200 mM imidazole. Fractions with high activity were pooled and dialysed against buffer A (20 mM Tris/HCl/5 mM 2-mercaptoethanol/1 mM EDTA/10% glycerol, pH 7.8). The dialysed sample was applied to a DEAE-Sepharose column (1 cm × 5 cm) equilibrated with buffer A, and the column was washed with the same buffer. The bound proteins were eluted with a linear gradient of 0–300 mM NaCl. Fractions with high activity were pooled and dialysed against 20 mM phosphate buffer, pH 6.5, containing 5 mM 2-mercaptoethanol, 1 mM EDTA and 10% glycerol. The dialysed sample was applied to a CM-Sepharose column (1 cm × 5 cm) equilibrated with the phosphate buffer. After washing the column, proteins bound to the column were eluted with a linear gradient of 50–350 mM phosphate. Fractions with high activity were pooled and dialysed against buffer A. The dialysed sample was applied to a Q-Sepharose column (1 cm × 5 cm) equilibrated with buffer A, and the bound proteins were eluted with a linear gradient of 0–300 mM NaCl. Fractions under the symmetric peak of the Ub-PESTc-degrading activity (Figure 4A) were pooled, dialysed against buffer A, concentrated by ultrafiltration, and kept frozen at −70 °C until use. A summary of the purification protocol is shown in Table 1.

The size of the enzyme was estimated to be about 120 kDa upon chromatography on a Sephacryl S-300 column (1 cm × 30 cm) equilibrated with buffer A containing 0.1 M NaCl (results not shown). It also ran as a single protein of 118 kDa upon analysis by SDS/PAGE (Figure 4B). Since the enzyme was expressed as a poly-His-tagged fusion protein, it ran larger than 109 kDa under both non-denaturing and denaturing conditions. These results indicate that UBP109 consists of a single polypeptide.

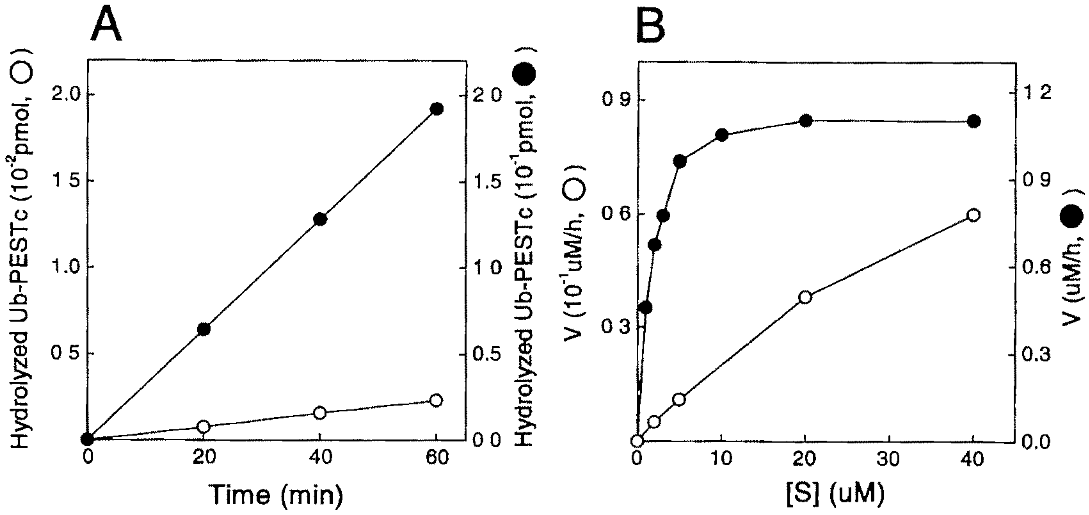

Figure 5 Hydrolysis of ^{125}I-labelled Ub-PESTc by the purified UBP109

(A) Reaction mixtures contained 10 ng of the purified UBP109 and 10 μg of ^{125}I-labelled Ub-PESTc [(0.5–1) × 10^3 c.p.m./μg)] in 100 mM Tris/HCl (pH 7.8)/1 mM EDTA/1 mM dithiothreitol/5% glycerol. The mixtures were incubated for various periods at 37 °C in the absence (○) or presence (●) of 10 μg of poly-L-Lys. (B) Assays were performed as described for (A), but in the presence of increasing concentrations of the substrate. Note that the scale on the *y*-axis in each panel is different.

Biochemical properties

To determine the time-dependent hydrolysis of ^{125}I-labelled Ub-PESTc by the purified UBP109, assays were performed by incubation of the enzyme at 37 °C for various periods. Poly-L-Lys has been shown to markedly stimulate the Ub-PESTc-hydrolysing activity of YUH1 as well as of most UCHs identified in chick skeletal muscle [35]. Therefore the enzyme assay was also performed in the presence of 10 μg of poly-L-Lys. As shown in Figure 5(A), the polycationic agent activated the enzyme activity nearly 100-fold. In addition, the rate of Ub-PESTc hydrolysis increased linearly with time at least for 1 h under the assay conditions. This extent of activation was much higher than that observed with any other DUBs, including YUH1 or chick UCH6 [35]. Using a double-reciprocal plot of the data, the K_m for Ub-PESTc was estimated to be 1.67 and 104 μM in the presence and absence of poly-L-Lys respectively (Figure 5B). On the other hand, little or no change was observed for the V_{max} value upon treatment with poly-L-Lys. These results indicate that the activation of the enzyme activity by poly-L-Lys is due to a marked increase in the affinity of the Ub-PESTc substrate to UBP109.

We also examined the effects of various protease inhibitors *N*-ethylmaleimide (1 mM), a thiol-group-blocking agent, almost completely blocked the activity of UBP109 against Ub-PESTc. Ub-aldehyde (1 μM), which is a specific inhibitor of DUBs, also strongly inhibited the enzyme activity. On the other hand, little or no effect was observed upon treatment with *o*-phenanthroline, a metal chelating agent, or PMSF, which is a serine-protease inhibitor (results not shown).

Hydrolysis of Ub precursors and poly-Ub–protein conjugates

In order to determine the substrate specificity of UBP109, the purified enzyme was incubated with various Ub-αNH-protein extensions, such as Ub-DHFR, Ub-CEP80 and His-penta-Ub. After incubation, the samples were subjected to SDS/PAGE using 4, 10, and 16% discontinuous slab gels as described previously [35], followed by staining with Coomassie Blue R-250. As a control, hydrolysis of Ub-PESTc was also determined under the same conditions. UBP109 was capable of generating free Ub from all of the substrates tested (Figure 6A). To determine whether UBP109 can release free Ub from Ub-M-β-gal under *in vitro* conditions, the purified enzyme was incubated with the extracts of *E. coli* MC1000 cells that had been transformed with pACUb-M-β-gal. The samples were then subjected to immunoblot analysis using an anti-β-gal antibody. Figure 6(B) shows that UBP109 can rapidly hydrolyse Ub-M-β-gal. These results indicate that the purified UBP109 is capable of cleaving the C-terminus of the Ub moiety in natural and engineered fusions irrespective of their sizes.

We then examined whether UBP109 could also release free Ub from poly-Ub-ϵNH-protein conjugates. The substrates were prepared using ^{125}I-labelled Ub and fraction II of rabbit reticulocytes and incubated with the purified UBP109 followed by SDS/PAGE. As shown in Figure 6(C), the amount of high-molecular-mass poly-Ub–protein conjugates was significantly decreased with a concomitant increase in the amount of Ub band upon incubation in the presence of the enzyme compared with that in its absence (Figure 6, lanes b and c respectively). On the other hand, treatment with *N*-ethylmaleimide (1 mM) or Ub-aldehyde (1 μM) almost completely prevented the generation of free Ub (Figure 6, lanes d and e respectively). These results indicate that UBP109 is capable of releasing free Ub from branched poly-Ub chains conjugated to proteins.

Subcellular localization of UBP109

UBP109 has three putative NLS motifs (see Figure 1). To determine the subcellular localization of UBP109, we first separated the lysates of cultured L6 myoblasts into cytosolic and nuclear fractions. The same aliquots of the fractions were then subjected to immunoblot analysis using the purified anti-UBP109 IgGs. As shown in Figure 7(A), the intensity of the UBP109 protein band in the cytosolic fraction was about the same as that in the nuclear fraction. Tubulin-β protein is shown as a cytosolic marker protein. These results strongly suggest that UBP109 localizes to both the cytoplasm and the nucleus.

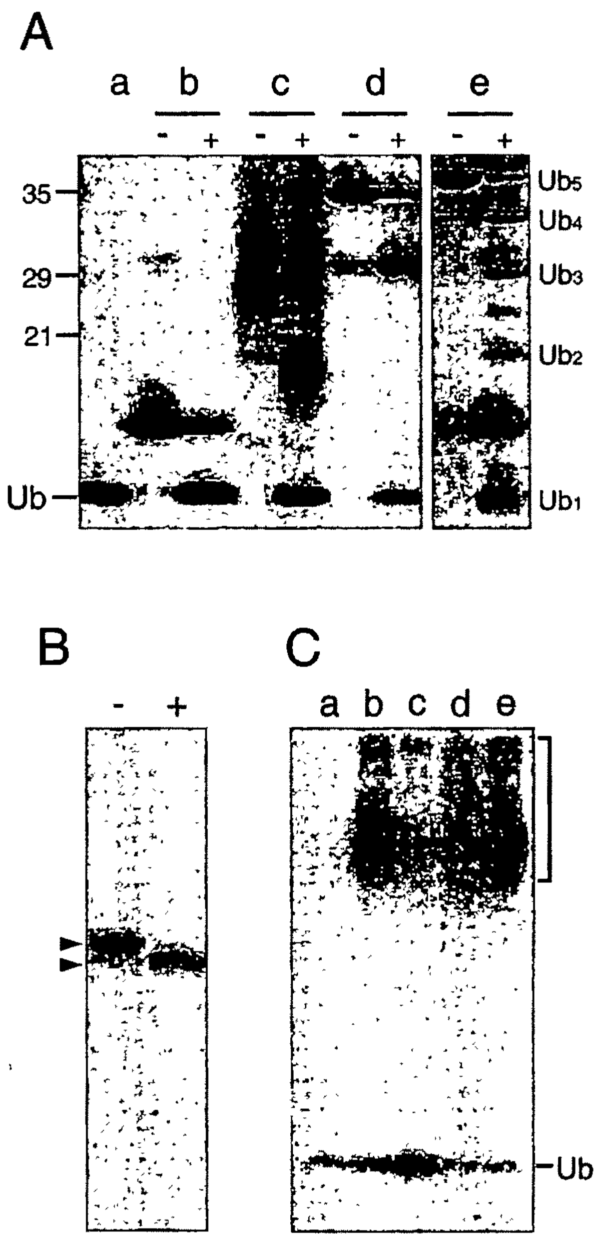

Figure 6 Hydrolysis of various Ub-αNH-protein extensions and the branched poly-Ub–protein conjugates by UBP109

(**A**) Aliquots (5 μg each) of the purified Ub-PESTc (lanes b), Ub-CEP80 (lanes c), Ub-DHFR (lanes d), and His-penta-Ub (lanes e) were incubated alone (— lanes) or with 0 2 μg of UBP109 (+ lanes) for 2 h at 37 °C As a control, Ub alone (lane a) was also incubated After incubation, the samples were subjected to SDS/PAGE on discontinuous gels Proteins in the gels were then revealed by staining with Coomassie Blue R-250. (**B**) The extracts (100 μg) obtained from *E coli* MC1000 cells expressing Ub-M-β-gal were incubated alone (— lane) or with 0 2 μg of UBP109 (+ lane) for 2 h at 37 °C After incubation, the samples were electrophoresed as in Figure 4, followed by immunoblot analysis using an anti-β-gal antibody. The arrowheads indicate Ub-β-gal (upper) and β-gal (lower) (**C**) Poly-Ub–protein conjugates were prepared by incubating ^{125}I-labelled Ub and reticulocyte lysate fraction II The ^{125}I-labelled-Ub–protein conjugates were then incubated alone (lane b) or with 0 2 μg of UBP109 in the absence (lane c) and presence of 1 mM *N*-ethylmaleimide (lane d) or 1 μM Ub-aldehyde (lane e) for 2 h at 37 °C After incubation, the samples were subjected to SDS/PAGE as in (**A**), followed by autoradiography Lane a indicates ^{125}I-labelled Ub incubated alone

In order to clarify further the localization of UBP109, NIH3T3 cells were transfected with pcDNAmyc109 expressing *myc*-tagged UBP109. The cells were then subjected to immunostaining with an anti-*myc* antibody, followed by confocal microscopy. Figure 7(B) shows that the cells are stained in the nucleus as well as in the cytoplasm, confirming that UBP109 is localized to both of the subcellular fractions. Similar data were obtained when the same experiment was performed using L6 myoblasts (results not shown). To find out which of the three putative NLS motifs is responsible for nuclear translocation of UBP109, we generated mutations in each of the motifs. The mutated cDNAs in pcDNA3.1 were transfected into NIH3T3 cells, followed by confocal microscopy. Transfection of pcDNAmyc109-1 and -2, in which ^{371}RKKP and ^{678}HKKR were replaced by RIDP and HEDP respectively, did not show any effect on the localization of UBP109 (Figures 7C and 7D respectively). Strikingly, the enzyme was exclusively localized to the cytoplasm of the cells transfected with pcDNAmyc109-3, in which ^{728}LKKR was substituted with IDER (Figure 7E). These results indicate that the third NLS motif (LKKR) is responsible for nuclear localization of UBP109.

DISCUSSION

In the present study we have cloned a cDNA that encodes the 109 kDa UBP protein, UBP109, from rat skeletal-muscle cDNA library. We have also purified the protein to apparent homogeneity upon expression in *E. coli* and demonstrated that the purified enzyme is capable of releasing free Ub, not only from linear Ub–protein conjugates, such as Ub-CEP80, Ub-DHFR, His-penta-Ub, and Ub-β-gal, but also from branched poly-Ub–protein conjugates. Thus it appears likely that UBP109 plays an important role in generation of free Ub molecules from its precursors and in recycling and/or 'trimming' of Ub from poly-Ub–protein conjugates. Of interest is the finding that poly-L-Lys dramatically stimulates the activity of UBP109 on Ub-PESTc. Its stimulatory effect appears to be due to an increase in the affinity of the substrate for the enzyme, perhaps through neutralizing the negative charge in the 'PEST' sequence of Ub-PESTc fusion. However, the mechanism for the activation of the UBP109 activity by poly-L-Lys remains unclear, because other polycationic agents, such as histone, spermine and putrescine, show little or no effect on the enzyme activity, similar to the chick UCH6 that is activated by poly-L-Lys but not the others [35].

Recently, Baker and co-workers [28] have cloned an UBP cDNA using KIAA0529 human cDNA and designated its product as USP15. They also showed that USP15 has about 60 % sequence identity with human and mouse Unps. Amino-acid-sequence analysis has revealed that the rat UBP109 shows as much as 98.2 % sequence identity with human USP15. Thus UBP109 is a homologue of human USP15, and these two enzymes are closely related to the human and mouse Unps but are not their homologues. Interestingly, all of these UBP enzymes contain three putative NLS motifs in addition to multiple Rb-binding sequences and the conserved Cys/His domains that are a characteristic of DUBs. Their short, putative NLS sequence is a typical XKKX, where X is any residue, as has been found in the RC3 and RC9 subunits of rat proteasome [44–46] and subunit YC7-α of yeast proteasome [47], and appears sufficient for their nuclear translocation [48]. The presence of this motif is consistent with our finding of UBP109 in the nuclear fractions of L6 myoblasts. However, contrary to the report that human Unp exclusively localizes to the cytosolic fraction of HeLa cells and that mouse Unp exists predominantly in the nucleus of NIH3T3 cells [22,26], UBP109 was found in both the nucleus and the cytoplasm of NIH3T3 cells, as well as of L6 myoblasts. Moreover, we found that, among the three putative NLSs only the one located nearest to the C-terminus was responsible for nuclear

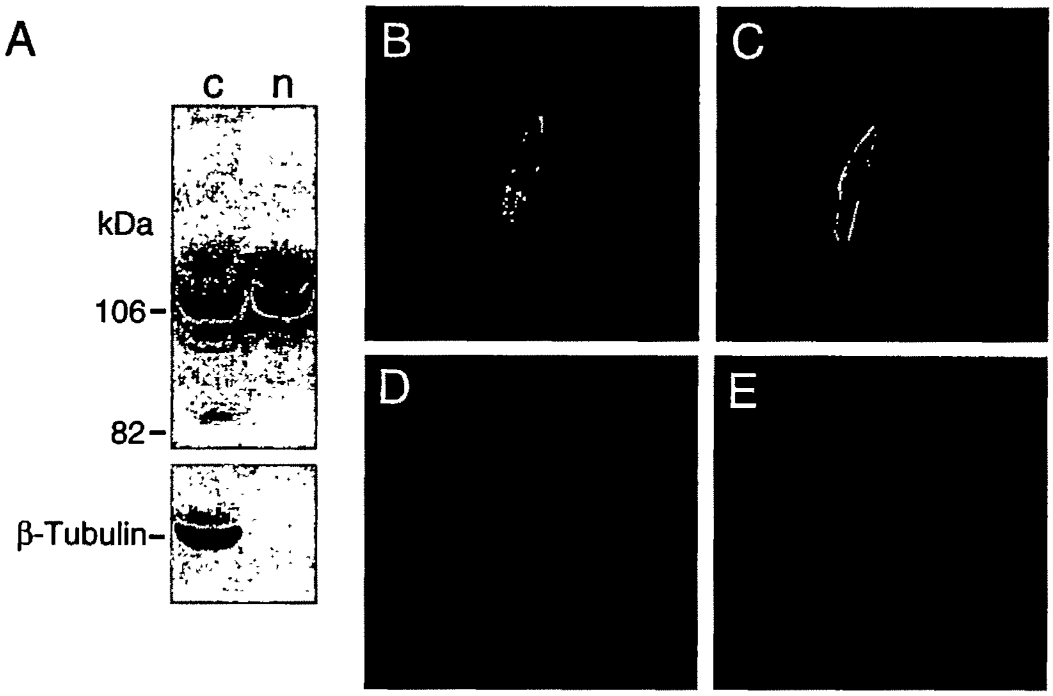

Figure 7 Subcellular localization of UBP109 in cells

L6 myoblasts cultured for 72 h (**A**) were harvested and fractionated into cytosolic and nuclear fractions as described in the Experimental section The same volume of each fraction was subjected to SDS/PAGE as in Figure 4, followed by immunoblot analysis using the purified anti-UBP109 IgGs Lane c and lane n indicate the cytosolic and nuclear fractions respectively β-Tubulin was also used as a cytosolic marker protein NIH3T3 cells were transfected with pcDNAmyc109 (**B**), pcDNAmyc109-1 (**C**), pcDNAmyc109-2 (**D**) or pcDNAmyc109-3 (**E**). After transfection, the cells were stained and observed under a confocal laser scanning microscope as described in the Experimental section

translocation of UBP109. Perhaps the different localization of the Unp and UBP109 family reflects the specific role of each enzyme in different tissues with different substrates.

Of particular interest is the finding that the expression of UBP109 transcript is developmentally regulated upon analysis by *in situ* hybridization. In the liver and the spinal cord, the UBP109 mRNA was strongly expressed during E12–E14 and disappeared at the later stage of embryonic development. In the brain, the signal began to appear at E16 and became more intense at the later stages. However, the UBP109 mRNA could be detected in none of the adult tissues. On the other hand, in the intestine, the UBP109 mRNA was detected from E20 and more intensely at adult stage. Thus it appears likely that the UBP109 enzyme plays an important role during embryonic development, although its specific function in each organ is unknown.

Moreover, the extremely high expression of UBP109 mRNA in specific adult organs such as the spleen and the testis implies specific functions of the enzyme in those tissues. As for the testis, UBP109 may be involved in cell proliferation or spermiogenesis. Recent evidence suggests that the Ub/proteasome system is involved in the loss of most of the cytoplasm occurring during spermiogenesis [49,50]. UBP109 may activate the proteasome-mediated degradation of the cytoplasmic proteins by generation of free Ub from its precursors and/or recycling or 'trimming' of Ub from poly-Ub–protein conjugates. The abundance of UBP109 mRNA in both the fetal liver and the adult spleen could also suggest its additional role in haematopoiesis. There have been several reports of DUBs involved in haematopoiesis, such as murine DUB-1, which shows significant similarity with Unps and is proposed to be a product of hematopoietic-specific immediate early gene induced by interleukin-3 and interleukin-5 [18,51]. In addition, the recently reported UBP43 [52], which is highly expressed in fetal liver, has also been suggested to play an important role in hematopoietic cell differentiation. UBP109 may also involve in hematopoiesis occurring initially in the fetal liver and then in adult spleen. Since during haematopoiesis a common stem cell becomes committed to differentiate along particular lineage by specific cytokines, and since specific cytokines induce specific genes, which include some UBP genes, it seems possible that different cytokines induce different UBPs with distinct substrate specificity and that the induced UBPs cleave different substrates involved in the formation of various types of the blood cells.

The gene for USP15, a human homologue of rat UBP109, has been shown to localize to chromosome band 12q14, a different location from that for human Unps (3p21.3). In many carcinomas, disturbance of chromosome 12 is frequently found. Breaks occur in a broad region of chromosome 12, 12q13-q15, in lipomas [29]. Amplification of 12q14-15 and 12q14-21 sequences has also been found in the neuroblastoma cell line NGP [30] and in both mucinous ovarian neoplasmas and Brenner tumours respectively, which sometimes co-exist in the same patient [31]. In addition, UBP109 was found to show approx. 60 % sequence identity with human Unph, which is proposed to be a proto-oncogene product related to tre-2, leading us to consider a possible involvement of UBP109 in tumorigenesis. Although we have no evidence connecting UBP109 to cancer, the expression of UBP109 mRNA was found to vary markedly among different carcinomas, compared with non-transformed cells, including human primary fibroblasts and rat L6 myoblasts. For example, the level of UBP109 mRNA is strongly expressed in human premyeloma (U937), whereas little or none is detected in cervical carcinoma (HeLa), hepatoma (HepG2) and lung carcinomas (H1299). In addition, it is noteworthy that a smaller transcript, which reacts with the UBP109 cDNA probe, is present in the non-transformed cells but not in any of the tumour cell lines tested (see Figure 2B). Thus it is tempting to speculate that UBP109 may be involved in the regulation of cell growth, although we do not have any evidence that there exists any aberration of the chromosome 12q14 region in the carcinoma cell samples we used.

The presence of Rb-binding motifs in UBP109 also suggests a possible role of the enzyme in cell-growth regulation. Recent evidence has shown that Rb is a target for ubiquitination [53]. UBPs containing Rb-binding motifs, including UBP109, may act as a proto-oncogene product through participation in the Rb degradation and in turn overcoming the inhibitory effect of Rb on the cell cycle. On the other hand, there is a report showing that the level of Unp in lung-carcinoma cell lines is rather decreased, compared with normal cells [22]. Moreover, Unp has been reported to interact with Rb in mouse cells as well as under *in vitro* conditions [28], suggesting a possibility that Unps are involved in stabilization of Rb rather than its degradation and hence in cell-growth regulation. Thus it is again tempting to speculate that UBP109 may also participate in regulation of cell growth through an Rb-mediated pathway, although the binding of UBP109 with Rb has not yet been corroborated.

We thank Mr Zee-Won Lee (Korea Basic Science Institute) for his help in confocal microscopy. We also thank Dr Martin Rechsteiner (Department of Biological Chemistry, University of Utah, Salt Lake City, UT, U.S.A.) for providing *E coli* strain AR13 carrying pNMHUB-PESTc, from which Ub-PESTc was purified, and Dr Rohan T Baker (Molecular and Biochemical Genetics Group, Australian National University, Canberra, ACT, Australia) for pACUb-R-β-gal and pACUb-M-β-gal E J C is the recipient of a BK fellowship This work was supported by grants from The Korea Science and Engineering Foundation through the Research Center for Cell Differentiation, the Korean Ministry of Education and CREST (Core Research for Evolutional Science and Technology), Japan Science and Technology Co-operation.

REFERENCES

1 Wilkinson, K D (1995) Roles of ubiquitinylation in proteolysis and cellular regulation Annu Rev Nutr. **15**, 161–189

2 Hershko, A and Ciechanover, A (1992) The ubiquitin system for protein degradation Annu Rev Biochem **61**, 761–807

3 Hochstrasser, M (1996) Ubiquitin-dependent protein degradation Annu Rev Genet **30**, 405–439

4 Finley, D and Chau, V (1991) Ubiquitination Annu Rev Cell Biol **7**, 25–69

5 Baumeister, W, Cejka, Z, Kania, M and Seemuller, E (1997) The proteasome a macromolecular assembly designed to confine proteolysis to a nanocompartment Biol Chem. **378**, 121–130

6 Braun, B C, Glickman, M, Kraft, R, Dahlmann, B, Kloetzel, P M, Finley, D and Schmidt, M. (1999) The base of the proteasome regulatory particle exhibits chaperone-like activity Nat Cell Biol **1**, 221–226

7 Coux, O, Tanaka, K and Goldberg, A L (1996) Structure and functions of the 20 S and 26 S proteasomes Annu Rev Biochem **65**, 801–847

8 Ozkaynak, E, Finley, D and Varshavsky, A (1984) The yeast ubiquitin gene head-to-tail repeats encoding a polyubiquitin precursor protein Nature (London) **312**, 663–666

9 Lund, P K, Moats-Staats, B M, Simmons, J G, Hoyt, E, D'Ercole, A J., Martin, F and van Wyk, J J (1985) Nucleotide sequence analysis of a cDNA encoding human ubiquitin reveals that ubiquitin is synthesized as a precursor J Biol Chem **260**, 7609–7613

10 Finley, D, Bartel, B and Varshavsky, A (1989) The tails of ubiquitin precursors are ribosomal proteins whose fusion to ubiquitin facilitates ribosome biogenesis Nature (London) **338**, 394–401

11 Wilkinson, K D (1997) Regulation of ubiquitin-dependent processes by deubiquitinating enzymes FASEB J. **11**, 1245–1256

12 Hedge, A N, Inokuchi, K, Pei, W, Casadio, A, Ghirardi, M, Chain, D G, Martin, K C, Kandel, E R and Schwartz, J H (1997) Ubiquitin C-terminal hydrolase is an immediate-early gene essential for long-term facilitation in *Aplysia* Cell **89**, 115–126

13 Leroy, E, Boyer, R, Auburger, G, Leube, B, Ulm, G, Mezey, E, Harta, G, Brownstein, M J, Jonnalagada, S, Chernova, T et al (1998) The ubiquitin pathway in Parkinson's disease Nature (London) **395**, 451–452

14 Saigoh, K, Wang, Y L, Suh, J G, Yamanishi, T, Sakai, Y, Kiyosawa, H, Harada, T, Ichihara, N, Wakana, S, Kikuchi, T and Wada, K (1999) Intragenic deletion in the gene encoding ubiquitin carboxy-terminal hydrolase in gad mice Nat Genet **23**, 47–51

15 Johnston, S C, Riddle, S M, Cohen, R E and Hill, C P (1999) Structural basis for the specificity of ubiquitin C-terminal hydrolases EMBO J **18**, 3877–3887

16 Huang, Y, Baker, R and Fischer-Vize, J A (1995) Control of cell fate by a deubiquitinating enzyme encoded by the fat facets gene Science **270**, 1828–1831

17 Moazed, D and Johnson, A D (1996) A deubiquitinating enzyme interacts with SIR4 and regulates silencing in *S cerevisiae* Cell **86**, 667–677

18 Zhu, Y, Carroll, M, Papa, F R, Hochstrasser, M and D'Andrea, A D (1996) DUB-1, a deubiquitinating enzyme with growth-suppressing activity Proc Natl Acad Sci U S A **93**, 3275–3279

19 Naviglio, S, Mattecucci, C, Matoskova, B, Nagase, T, Nomura, N, Di Fiore, P P and Draetta, G F (1998) UBPY a growth-regulated human ubiquitin isopeptidase EMBO J **17**, 3241–3250

20 Gupta, K, Copeland, N G, Gilbert D J, Jenkins, N A and Gray, D A (1993) *unp*, a mouse gene related to the *tre* oncogene Oncogene **8**, 2307–2310

21 Gray, D A, Inazawa, J, Gupta, K, Wong, A, Ueda, R and Takahashi, T (1995) Elevated expression of Unph, a proto-oncogene at 3p21 3, in human lung tumors Oncogene **10**, 2179–2183

22 Frederick, A, Rolfe, M and Chiu, M I (1998) The human UNP locus at 3p21 31 encodes two tissue-selective, cytoplasmic isoforms with deubiquitinating activity that have reduced expression in small cell lung carcinoma cell lines Oncogene **16**, 153–165

23 Shaulsky, G, Goldfinger, N, Ben-Ze'ev, A and Rotter, V (1990) Nuclear accumulation of p53 protein is mediated by several nuclear localization signals and plays a role in tumorigenesis Mol Cell Biol **10**, 6565–6577

24 Defeo-Jones, D, Huang, P S, Jones, R E, Haskell, K M, Vuocolo, G A, Hanobik, M G, Huber, H E and Oliff, A (1991) Cloning of cDNAs for cellular proteins that bind to the retinoblastoma gene product Nature (London) **352**, 251–254

25 Kaelin, W G, Krek, W, Sellers, W R, Decaprio, J A, Ajchenbaum, F, Fuchs, C S, Chittenden, T, Li, Y, Farnham, P J, Blanar, M A et al (1992) Expression cloning of a cDNA encoding a retinoblastoma-binding protein with E2F-like properties Cell **70**, 351–364

26 Gupta, K, Chevrette, M and Gray, D A (1994) The Unp proto-oncogene encodes a nuclear protein. Oncogene **9**, 1729–1731

27 Nakamura, T, Hillova, J, Mariage-Samson, R, Onno, M, Huebner, K, Cannizzaro, L A, Boghosian-Sell, L, Croce, C M and Hill, M (1992) A novel transcriptional unit of the *tre* oncogene widely expressed in human cancer cells Oncogene **7**, 733–741

28 Baker, R T, Wang, X, Woollatt, E, White, J A and Sutherland, G R (1999) Identification, functional characterization and chromosomal localization of USP15, a novel human ubiquitin-specific protease related to the UNP oncoprotein and a systematic nomenclature for human ubiquitin-specific proteases Genomics **59**, 264–274

29 Merscher, S, Marondel, I, Pedeutour, F, Gaudray, P, Kucherlapati, R and Turc-Carel, C (1997) Identification of new translocation breakpoints at 12q13 in lipomas Genomics **46**, 70–77

30 Van Roy, N, Forus, A, Myklebost, O, Cheng, N C, Versteeg, R and Speleman, F (1995) Identification of two distinct chromosome 12-derived amplification units in neuroblastoma cell line NGP Cancer Genet Cytogenet **82**, 151–154

31 Pejovic, T, Burki, N, Odunsi, K, Fiedler, P, Achong, N, Schwartz, P E and Ward, D C. (1999) Well-differentiated mucinous carcinoma of the ovary and a coexisting Brenner tumor both exhibit amplification of 12q14-21 by comparative genomic hybridization Gynecol Oncol **74**, 134–137

32 Baek, S H, Choi, K S, Yoo, Y J, Cho, C M, Baker, R T, Tanaka, K and Chung, C H (1997) Molecular cloning of a novel ubiquitin-specific protease, UBP41, with isopeptidase activity in chick skeletal muscle J Biol. Chem **272**, 25560–25565

33 Baek, S H, Park, K C, Lee, J I, Kim, K I, Yoo, Y J, Tanaka, K, Baker, R T and Chung, C H (1998) A novel family of ubiquitin-specific proteases in chick skeletal muscle with distinct N- and C-terminal extensions Biochem J **334**, 677–684

34 Tobias, J W and Varshavsky, A (1991) Cloning and functional analysis of the ubiquitin-specific protease gene UBP1 of *Saccharomyces cerevisiae* J Biol Chem **266**, 12021–12028

35 Woo, S K, Lee, J I, Park, I K, Yoo, Y J, Cho, C M, Kang, M-S, Ha, D B, Tanaka, K and Chung, C H (1995) Multiple ubiquitin C-terminal hydrolases from chick skeletal muscle J Biol Chem **270**, 18766–18773

36 Markwell, M A K (1982) A new solid-state reagent to iodinate proteins I Conditions for the efficient labeling of antiserum. Anal Biochem **125**, 427–432

37 Hershko, A and Rose, I A (1987) Ubiquitin-aldehyde. a general inhibitor of ubiquitin-recycling processes Proc Natl Acad Sci U S A **84**, 1829–1833

38 Etlinger, J D and Goldberg, A L (1977) A soluble ATP-dependent proteolytic system responsible for the degradation of abnormal proteins in reticulocytes Proc Natl Acad Sci U S A **74**, 54–58

39 Haas, A L and Rose, I A. (1981) Hemin inhibits ATP-dependent ubiquitin-dependent proteolysis role of hemin in regulating ubiquitin conjugate degradation Proc Natl Acad Sci U S A **78**, 6845–6848

40 Simmons, D M, Arriza, J L and Swanson, L W (1989) A complete protocol for in situ hybridization of messenger RNAs in brain and other tissues with radiolabeled single stranded RNA probes J Histotechnol **12**, 169–181

41 Blake, M S, Johnston, K H, Russell-Jones, G J and Gotschlich, E C (1984) A rapid, sensitive method for detection of alkaline phosphatase-conjugated anti-antibody on Western blots. Anal Biochem **136**, 175–179

42 Lee, Z W, Kweon, S M, Kim, B C, Leem, S H, Shin, I, Kim, J H and Ha, K S (1998) Phosphatidic acid-induced elevation of intracellular Ca^{2+} is mediated by RhoA and H_2O_2 in Rat-2 fibroblasts J Biol Chem **273**, 12710–12715

43 Kozak, M (1991) Structural features in eukaryotic mRNAs that modulate the initiation of translation. J Biol Chem **266**, 19867–19870

44 Tanaka, K, Fujiwara, T, Kumatori, A, Shin, S, Yoshimura, T, Ichihara, A, Tokunaga, F., Aruga, R, Iwanaga, S, Kakizuka, A and Nakanishi, S (1990) Molecular cloning of cDNA for proteasomes from rat liver primary structure of component C3 with a possible tyrosine phosphorylation site Biochemistry **29**, 3777–3785

45 Kumatori, A, Tanaka, K, Tamura, T, Fujiwara, T, Ichihara, A, Togunaga, F, Onikura, A and Iwanaga, S (1990) cDNA cloning and sequencing of component C9 of proteasomes from rat hepatoma cells FEBS Lett **264**, 279–282

46 Benedict, C. M and Clawson, G A (1996) Nuclear multicatalytic proteinase subunit RRC3 is important for growth regulation in hepatocytes Biochemistry **35**, 11612–11621

47 Fujiwara, T, Tanaka, K, Orino, E, Yoshimura, T., Kumatori, A, Tamura, T, Chung, C H, Nakai, T, Yamaguchi, K, Shin, S et al (1990) Proteasomes are essential for yeast proliferation cDNA cloning and gene disruption of two major subunits J Biol Chem **265**, 16604–16613

48 Roberts, B (1989) Nuclear location signal-mediated protein transport Biochim Biophys Acta **1008**, 263–280

49 Wing, S S, Bedard, N, Morales, C, Hingamp, P and Trasler, J (1996) A novel rat homolog of the *Saccharomyces cerevisiae* ubiquitin-conjugating enzymes UBC4 and UBC5 with distinct biochemical features is induced during spermatogenesis Mol Cell Biol **16**, 4064–4072

50 Rajapurohitam, V, Morales, C R, El-Alfy, M, Lefrancois, S, Bedard, N and Wing, S S (1999) Activation of a UBC4-dependent pathway of ubiquitin conjugation during postnatal development of the rat testis Dev Biol **212**, 217–228

51 Zhu, Y, Pless, M, Inhorn, R, Mathey-Prevot, B and D'Andrea, A D (1996) The murine DUB-1 gene is specifically induced by the betac subunit of interleukin-3 receptor. Mol Cell. Biol **16**, 4808–4817

52 Liu, L Q, Ilaria, Jr, R, Kingsley, P D, Iwama, A, van Etten, R A, Palis, J and Zhang, D E (1999) A novel ubiquitin-specific protease, UBP43, cloned from leukemia fusion protein AML1-ETO-expressing mice, functions in hematopoietic cell differentiation. Mol Cell Biol **19**, 3029–3038

53 Boyer, S. N, Wazer, D E and Band, V (1996) E7 protein of human papilloma virus-16 induces degradation of retinoblastoma protein through the ubiquitin-proteasome pathway Cancer Res **56**, 4620–4624

Received 28 March 2000, accepted 11 May 2000

Biochem. J (2000) 349, 455–461 (Printed in Great Britain)

Glutathione peroxidase-1 but not -4 is involved in the regulation of cellular 5-lipoxygenase activity in monocytic cells

Dietlind STRAIF*, Oliver WERZ*, Roland KELLNER†, Ute BAHR‡ and Dieter STEINHILBER*[1]

*Institute of Pharmaceutical Chemistry, University of Frankfurt, Marie-Curie-Str. 9, D-60439 Frankfurt, Germany, †Preclinical Research Department/GBT, Merck KGaA, D-64271 Darmstadt, Germany, and ‡Institute of Instrumental Analytical Chemistry, University of Frankfurt, Theodor-Stern Kai, 60590 Frankfurt, Germany

In contrast to neutrophils or B-lymphocytes, cells of the monocytic lineage like rat macrophages, human peripheral blood monocytes and Mono Mac 6 cells contain a strong inhibitor of 5-lipoxygenase (5-LO) activity, which scavenges hydroperoxides and inhibits 5-LO activity in broken-cell preparations in the absence of exogenously added thiols. Chromatographic purification of the inhibitor from the human monocytic cell line Mono Mac 6 and amino acid sequence analysis revealed that the inhibitory factor is glutathione peroxidase-1 (GPx-1). In contrast to the peroxidase activity of GPx-1, 5-LO inhibition by GPx-1 was supported by β-mercaptoethanol and there was no absolute requirement for millimolar concentrations of glutathione or dithiothreitol. These cofactor characteristics suggest that both activities address distinct catalytic properties of GPx-1. 5-LO inhibition by GPx-1 was not due to direct GPx–5-LO protein–protein interactions, since GPx-1 did not bind to immobilized 5-LO. Interestingly, 5-LO derived from granulocytes was significantly more resistant against GPx-1 inhibition than B-lymphocytic 5-LO, which correlates with the respective cellular 5-LO activities. In summary, the data suggest that, in addition to previously reported phospholipid hydroperoxide glutathione peroxidase (GPx-4), GPx-1 is an efficient inhibitor of 5-LO even at low thiol concentrations, and is involved in the regulation of cellular 5-LO activity in various cell types.

Key words: inflammation, leukotriene, B-lymphocyte, Mono Mac 6 cell.

INTRODUCTION

Leukotrienes are mediators of inflammatory responses that can be formed in a variety of cells of myeloid origin like granulocytes, monocytes/macrophages, mast cells and dendritic cells and in B-lymphocytic cells after stimulation. 5-Lipoxygenase (5-LO) catalyses the biosynthesis of leukotriene A_4 from arachidonic acid, which can be subsequently transformed into leukotriene B_4 or leukotriene C_4 by leukotriene A_4 hydrolase or leukotriene C_4 synthases, respectively [1,2]. In resting neutrophils, Mono Mac 6 cells and HL-60 cells, 5-LO is localized in the cytosol and it was shown for neutrophils that 5-LO translocates to the nuclear membrane after cell stimulation where it interacts with FLAP (5-LO-activating protein) [3–5]. The cellular capacity for leukotriene biosynthesis is upregulated during myeloid cell maturation. It has been shown that 5-LO mRNA and protein expression increases during differentiation *in vitro* of the human promyelocytic cell line HL-60 by DMSO or 1,25-dihydroxyvitamin D_3 (VD3) [5,6]. When expression of 5-LO protein and activity was studied in detail, it became evident that DMSO differentiation of HL-60 cells or differentiation of Mono Mac 6 cells with either transforming growth factor β1 (TGFβ) or VD3 induces expression of 5-LO protein but no or only low cellular 5-LO activity [7,8]. In HL-60 cells, addition of TGFβ is required for upregulation of cellular 5-LO activity during DMSO-induced differentiation [9]. Moreover, we could show that VD3 and TGFβ upregulate cellular leukotriene synthesis in DMSO-differentiated HL-60 cells by induction of a peroxidase-insensitive 5-LO catalytic activity [10]. B-lymphocytes and B-lymphocytic cell lines constitutively express 5-LO protein but there is no detectable enzyme activity after stimulation with ionophore and arachidonic acid. Recently, several groups including ours showed that the phospholipid hydroperoxide glutathione peroxidase (GPx-4) is responsible for the suppression of 5-LO activity in a variety of cell types like B-lymphocytes, A431 cells, RBL-2H3 cells and immature HL-60 cells [10–12]. In addition to their function in the regulation of cellular 5-LO activity, glutathione peroxidases (GPxs) also play an important role in the 5-LO inhibition by non-redox-type inhibitors. Recently, it was shown that the inhibitory potency of several non-redox-type 5-LO inhibitors strongly depends on GPxs and that increased peroxide levels lead to impaired efficacy of inhibitors like ZM 230487 or L-739,010 [13].

In contrast to neutrophils, cytosol from rat alveolar and peritoneal macrophages and from human peripheral blood monocytes contains a strong inhibitor of 5-LO activity [14,15]. Initial characterization of the inhibitor demonstrated that it is a protein that scavenges hydroperoxides. Accordingly, we observed a strong 5-LO inhibitory activity in the cytosol of Mono Mac 6 cells which inhibited 5-LO activity in broken-cell preparations in the absence of exogenously added thiols, as reported for various monocytic cell types [15]. Here, we show that the endogenous inhibitor is glutathione peroxidase-1 (GPx-1) and that this enzyme is a very effective suppressor of 5-LO activity in intact cells and in broken-cell preparations even at low concentrations of thiols.

Abbreviations used. 5-LO, 5-lipoxygenase, TGFβ, transforming growth factor β1, VD3, 1,25-dihydroxyvitamin D_3; DTT, dithiothreitol, GPx, glutathione peroxidase, GPx-1, glutathione peroxidase-1, GPx-4, phospholipid hydroperoxide glutathione peroxidase, FCS, fetal calf serum, MALDI-TOF, matrix-assisted laser-desorption ionization–time-of-flight, 5-HPETE, 5-hydroperoxyeicosatraenoic acid, TRAP-1, TGFβ-receptor-I-associated protein-1

[1] To whom correspondence should be addressed (e-mail steinhilber@em.uni-frankfurt.de)

MATERIALS AND METHODS

Materials

RPMI 1640 medium was from Gibco and fetal calf serum (FCS) was obtained from Boehringer Mannheim. Insulin was a gift from Aventis (Frankfurt, Germany). VD3 was kindly provided by Dr H. Wiesinger (Schering AG, Berlin, Germany). Human TGFβ was purified from outdated platelets according to [16]. HPLC solvents and β-mercaptoethanol were from Merck (Darmstadt, Germany). Dithiothreitol (DTT), bovine GPx-1 (G6137), human GPx-1 (G4013), glutathione reductase and selenium dioxide were purchased from Sigma (Deisenhofen, Germany). GSH and NADPH were obtained from Serva (Heidelberg, Germany). Polyclonal anti-human GPx-1/catalase antibody was purchased from Dunn Labortechnik (Asbach, Germany).

Cells

Mono Mac 6 cells were kindly provided by Dr H. W. L. Ziegler-Heitbrock (Institute for Immunology, University of Munich, Munich, Germany) and cultured in RPMI 1640 as described in [17]. Cultures were seeded at a density of 3×10^5 cells/ml. BL41-E95A cells were kindly provided by Dr Hans-Erik Claesson (Karolinska Institute, Stockholm, Sweden) and maintained in RPMI 1640 medium containing 10 % (v/v) heat-inactivated FCS, 100 μg/ml streptomycin and 100 units/ml penicillin. Cultures were seeded at a density of 2×10^5 cells/ml. All cell lines were maintained in a humidified atmosphere of air at 37 °C and 6 % CO_2. For serum-free culture of both cell lines, serum was replaced by 5 μg/ml human transferrin, 10 μg/ml bovine insulin [18] and 1 μg/ml catalase. Cells were cultured in serum-free medium for at least 2 passages before experiments were started (1 passage corresponds to 3 or 4 days). Granulocytes were isolated from human peripheral blood buffy-coat preparations derived from healthy donors at St. Markus Krankenhaus (Frankfurt, Germany) as described previously [19].

Determination of 5-LO activity

Homogenates and 100000-*g* supernatants were prepared and 5-LO activity was determined as described by Werz and Steinhilber [10]. 5-LO activity is expressed as ng of 5-LO metabolites/10^6 cells, which includes the all-*trans* isomers of leukotriene B_4, leukotriene B_4, and 5-hydroxy-6,8,11,14-eicosatetraenoic acid.

Determination of 5-LO inhibitory activity

As shown previously, 100000-*g* supernatants of Mono Mac 6 cells dose-dependently inhibit the 5-LO activity of BL41-E95A 100000-*g* supernatants in the presence of β-mercaptoethanol [20]. Thus inhibition of 5-LO activity of BL41-E95A 100000-*g* supernatants was used to monitor inhibitory fractions from Mono Mac 6 preparations. Aliquots of the fractions obtained during chromatographic purification of the inhibitor were added to 1 ml of BL41-E95A 100000-*g* supernatants (corresponding to 10^7 cells) and 5-LO activity was determined in the presence of 0.5 mM β-mercaptoethanol as described in [10].

Determination of GPx activity

Method A: GPx activity was measured by the indirect glutathione reductase-coupled method described by Wendel [21], and 1 unit of GPx activity was defined as the conversion of 0.5 μmol of NADPH to $NADP^+$ per min at 37 °C and 1 mM GSH. Cellular GPx activity is expressed as m-units/10^6 cells.

Method B: co-substrate specificity was determined by a slightly modified GPx assay described by Cha and Kim [22]. Reaction mixture (100 μl) containing 5 mM thiol and GPx (13 m-units) in PBS, pH 7.0, was incubated at 37 °C and the reaction was started by addition of 12.6 μl of cumene hydroperoxide (1.5 mM final concentration). After 1, 3, 5 and 7 min, 20 μl of the reaction mixture was added to 0.8 ml of a trichloroacetic acid solution (12.5 %, w/v) to stop the reaction. Subsequently, 0.2 ml of 10 mM $Fe(NH_4)_2(SO_4)_2$ and 0.1 ml of 2.5 M KSCN were added and the complex was developed for at least 3 min, giving a purple colour. Cumene hydroperoxide concentration was calculated after measuring the absorbance at 480 nm using a molar absorptivity of 8703. For each measurement, the non-enzymic reaction was assessed without GPx-1.

Purification of a cytosolic 5-LO inhibitor from Mono Mac 6 cells

Cells were cultured in FCS medium supplemented with Se^{4+} (5 ng/ml). After cell harvest, a 100000-*g* supernatant was prepared as described in [10] and applied directly to a Sephacryl S-200 column (1.6 cm × 62 cm) equilibrated with PBS/1 mM EDTA. The column was eluted at a flow rate of 0.5 ml/min and 3-ml fractions were collected and checked for inhibition of 5-LO activity of BL41-E95A supernatants. Inhibitory fractions were pooled and concentrated by ultrafiltration (YM 10 membrane, Amicon) to 2.5 ml. Then, the buffer of the concentrate was changed by gel-permeation chromatography on a prepacked Sephadex® G-25 column (PD-10 column, Pharmacia) which had been equilibrated with 0.005 M phosphate buffer (pH 8.0)/1 mM EDTA/2.5 mM β-mercaptoethanol (buffer DEAE-1). The resulting sample was further purified by anion-exchange chromatography using a Fractogel® EMD DEAE Tentakel column (Merck; bed volume, 5 ml) equilibrated with buffer DEAE-1. After the elution of unabsorbed material at 1.5 ml/min, the flow rate was increased to 2 ml/min and a linear gradient of 0–100 % 0.08 M phosphate buffer (pH 8.0)/1 mM EDTA/2.5 mM β-mercaptoethanol (over 13 min) was started. The UV absorbance was recorded at 280 nm. Fractions (2 ml) were collected and aliquots were tested for 5-LO inhibitory activity. Inhibitory fractions were combined and after addition of ammonium sulphate (1 M, final concentration) the solution was added to a RESOURCE® PHE column (6.4 mm × 30 mm, Pharmacia) equilibrated with 0.05 M phosphate buffer (pH 7.4)/1 mM EDTA/1 M $(NH_4)_2SO_4$/2.5 mM β-mercaptoethanol (buffer Phenyl-Superose-1). After elution of the column with 11.5 ml of Phenyl-Superose-1 buffer at a flow rate of 0.8 ml/min, a linear gradient (gradient volume 20 ml) from 1 M ammonium sulphate to pure buffer [buffer Phenyl-Superose-1 without $(NH_4)_2SO_4$] was used to elute the inhibitory enzyme at a flow rate of 1 ml/min. The elution of the inhibitory enzyme was complete after an additional 8 min of elution with pure phosphate buffer. Fractions (2 ml) were collected and elution of the 5-LO inhibitor was monitored by inhibition of 5-LO activity of BL41-E95A supernatants. The active fractions were pooled, supplemented with $(NH_4)_2SO_4$ (1.2 M final concentration) and applied directly on to a RESOURCE® ISO column (6.4 mm × 30 mm, Pharmacia) equilibrated with 0.05 M phosphate buffer (pH 7.0)/1 mM EDTA/2.5 mM β-mercaptoethanol containing 1.2 M $(NH_4)_2SO_4$ (buffer Isopropyl-Superose-1). Elution conditions, fraction collection and tests of 5-LO inhibition were the same as described for Phenyl-Superose chromatography. The inhibitory fractions were pooled and used for protein identification. All purification steps including centrifugation were performed at +4 °C. Prior to determination of 5-LO inhibitory activity, the buffer of each aliquot was changed to PBS/1 mM EDTA using Sephadex® G-25 columns (PD-10, Pharmacia) according to the manufacturer's instructions.

SDS/PAGE analysis

Protein purification was examined by reducing SDS/PAGE performed in 15 % slab gels (0.75 mm) according to [23]. Proteins were visualized by silver staining.

Protein analysis

For Western-blot analysis, SDS/PAGE was carried out as described above and blotting was done according to a previous protocol [24] using a Mini Trans-Blot® assembly (Bio-Rad). Amino acid sequencing was carried out after SDS/PAGE and in-gel trypsin digestion of the upper band of the 23-kDa doublet. Purification of the fragments and sequencing was performed as described in [25].

Matrix-assisted laser-desorption ionization–time-of-flight (MALDI-TOF) MS analysis was performed on a Voyager RPDE mass spectrometer (PerSeptive Biosystems, Framingham, MA, U.S.A.). The isolated and lyophilized protein was taken up in water, mixed with matrix solution (2,5-dihydroxybenzoic acid, 20 g/l), and spotted on to the probe slide. Following an air-dry step, spectra were obtained in the linear mode at an acceleration voltage of 25 kV. Carbonic anhydrase was used as external standard.

Partial purification of 5-LO

The 5-LO enzyme of BL41-E95A cells and granulocytes was partially purified by ATP-agarose affinity chromatography [26].

Data analysis

Statistical evaluation of the data was performed using Student's *t* test for unpaired observations. A *P* value of < 0.05 was considered significant.

RESULTS

Mono Mac 6 and BL41-E95A cells contain distinct selenium-dependent 5-LO inhibitors

Cellular 5-LO activity of BL41-E95A and Mono Mac 6 cells is strongly inhibited by selenium. Both cell lines show low cellular 5-LO activity after cultivation in FCS medium or in serum-free medium supplemented with 1 ng/ml Se^{4+} (13 nM) supplied as selenite (Figure 1). Transfer into serum-free medium for 2–3 passages lead to a strong increase in 5-LO activity of intact BL41-E95A and Mono Mac 6 cells. In BL41-E95A cells, 5-LO activity of the corresponding cell homogenates was hardly affected by the cellular selenium status.

However, in contrast to BL41-E95A cells, 5-LO activity in Mono Mac 6 cell homogenates strongly depended on the cell culture conditions. Cultivation of Mono Mac 6 cells in the presence of FCS or selenium strongly suppressed 5-LO activity in the cell homogenates whereas serum-free culture conditions resulted in high 5-LO activity.

Thus in contrast to GPx-4 that was previously identified as endogenous inhibitor in HL-60 cells and BL41-E95A cells [10], the selenium-dependent Mono Mac 6 inhibitor does not require addition of millimolar concentrations of thiols as co-substrate in order to inhibit 5-LO activity in cell homogenates or 100000-*g* supernatants (Figure 1) [10]. Determination of the apparent molecular size by gel-permeation chromatography revealed that the Mono Mac 6 inhibitor is larger than 66 kDa and has a much higher molecular mass than the 5-LO inhibitor (GPx-4) described previously in BL41-E95A cells (Figure 2). Thus it was of interest

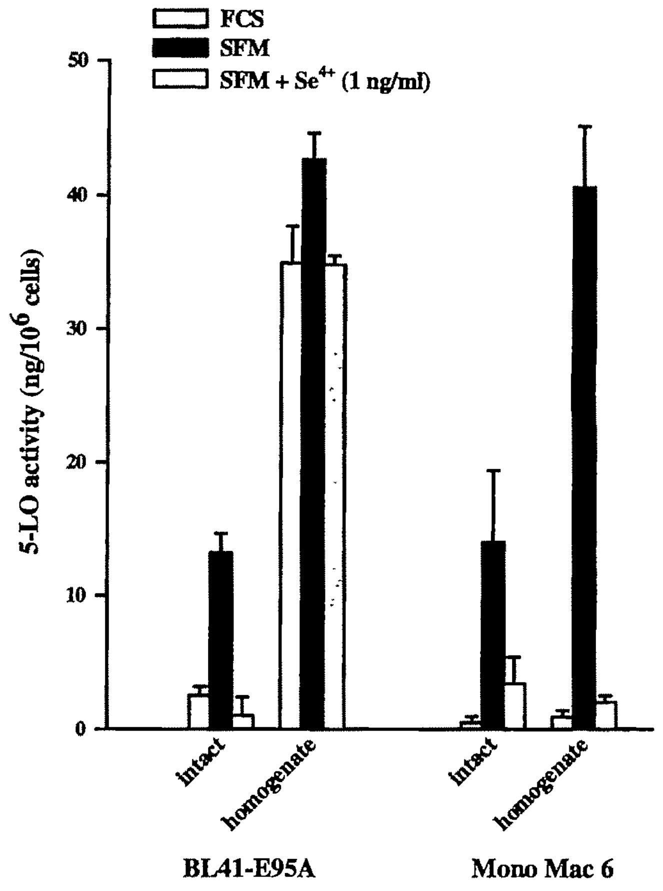

Figure 1 Selenium-dependent inhibition of 5-LO activity of intact cells and cell homogenates from BL41-E95A and Mono Mac 6 cells

Cells were cultured under the indicated culture conditions for 2 or 3 passages (SFM, serum-free medium) Mono Mac 6 were differentiated for 2 days with TGFβ (1 ng/ml) Then, 5-LO activity of intact cells and cell homogenates was determined in the absence of exogenously added thiols Results are expressed as means ± S E M of three independent experiments

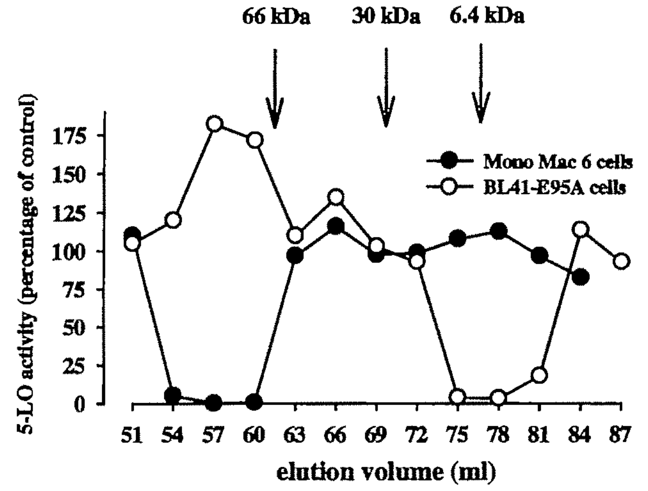

Figure 2 Gel-permeation chromatography of the endogenous 5-LO inhibitor from Mono Mac 6 and BL41-E95A cells

Each 100000-*g* supernatant was applied to a Sephacryl S-200 column, eluted as described in the Materials and methods section, and inhibition of 5-LO activity by the fractions was determined Data are representative of at least two independent experiments

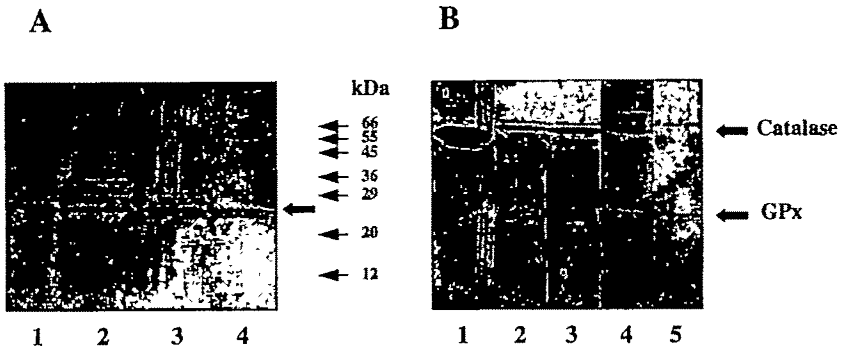

Figure 3 SDS/PAGE analysis (A) and Western-blot analysis (B) of the 5-LO inhibitor

Concentrated protein samples from different stages of purification were electrophoresed by reducing SDS/PAGE (15% gel) (**A**) Lane 1, sample from DEAE chromatography, lane 2, sample from Phenyl-Superose chromatography, lane 3, sample from Isopropyl-Superose chromatography; lane 4, bovine GPx (**B**) Lane 1, catalase; lanes 2 and 3, human GPx-1, lane 4, sample from DEAE chromatography, lane 5, sample from Isopropyl-Superose chromatography In (**A**) the position of human GPx-1 is indicated with a bold arrow

to identify the selenium-dependent inhibitor in Mono Mac 6 cells.

Purification of the 5-LO inhibitor and identification as GPx-1

Purification was performed as described in the Materials and methods section and the obtained fractions were tested for 5-LO inhibition and GPx activity. It became apparent that the 5-LO inhibitory activity co-eluted with the GPx activity during all chromatographic purification steps (results not shown).

Purification of the 5-LO inhibitor by chromatography on EMD DEAE, Phenyl-Superose and Isopropyl-Superose was monitored by SDS/PAGE analysis (Figure 3A, lanes 1–3). After the final Superose column-chromatography step only two protein bands were detectable following silver staining. One band was very faint, and the other, with a molecular mass of approx. 23 kDa, co-migrated in the gel with bovine GPx-1 (Figure 3A, lane 4).

Since experimental data indicated that the inhibitory enzyme might be a GPx distinct from GPx-4 but with a similar size to GPx-1, Western-blot analysis was performed using an antibody against human GPx-1/catalase (Figure 3B). The antibody recognized catalase (Figure 3B, lane 1), human GPx-1 reference (Figure 3B, lanes 2 and 3, two different concentrations) and the isolated protein band displaying the same mobility as GPx-1 (Figure 3B, lanes 4 and 5). These results strongly suggested that the enzyme responsible for 5-LO inhibition in Mono Mac 6 cells is GPx-1. It was interesting to note that the antibody recognized a double band when the human GPx-1 standard was analysed. The same double band was also detected in the SDS/PAGE analysis of the isolated enzyme in some of the enzyme preparations from Mono Mac 6 cells (results not shown). A possible explanation for the occurrence of a double band with identical immunological properties is that the second band represents a proteolytically processed form of GPx-1 as described previously [27]. The molecular masses of the double band of the isolated inhibitor were 22087 and 20290 Da, as determined by MALDI-TOF MS. Unfortunately, the precision of the MALDI MS analysis was limited since only rather broad signals could be obtained for these two peaks in the mass spectrum (results not shown). However, the data fit well with the calculated molecular mass of GPx-1 and a truncated form generated by proteolysis at a cleavage site between amino acids 15 and 16, giving molecular masses of 21768 and 20350 Da, respectively [28].

Table 1 Cellular GPx activities of Mono Mac 6, HL-60 and BL41-E95A cells

Cells were cultured under the indicated culture conditions for 2 passages Differentiation of Mono Mac 6 and HL-60 cells was induced by addition of TGFβ (1 ng/ml) and VD3 (50 nM) for 4 days GPx activity of the 100000-*g* supernatants was determined with the GPx assay (method A, see the Materials and methods section) and the results are expressed as m-units/10^6 cells (means ± S E M , $n = 3$)

	GPx activity (m-units/10^6 cells)		
	Mono Mac 6		
Cell-culture conditions	Undifferentiated	Differentiated	BL41-E95A
With serum	6 5±1 1	8.2±0 3	0 6±0 3
With serum + 1 ng/ml Se^{4+}	20 1±3 4	28 0±1 3	1 7±0 1
Serum-free medium	1 8±0 3	1 3±0 3	0 3±0 1

For final identification of the isolated enzyme, amino acid sequence analysis was performed. The protein was found to have a blocked N-terminus and was therefore submitted to in-gel trypsin digestion. Chromatographic separation of the fragments and sequencing of three peptides gave the sequences DYTQMNELQR, NEEILNSLKYVR and FLVGPDGVPLRR, corresponding to amino acids 53–62, 87–98 and 165–176 of GPx-1.

Mono Mac 6 cells have much higher GPx activities than BL41-E95A cells

Analysis of GPx-1 and GPx-4 mRNA expression by reverse transcriptase PCR showed that both genes are expressed in lymphocytes and in undifferentiated and differentiated myeloid cells [10]. To elucidate whether there are differences in cellular peroxidase activity between Mono Mac 6 and BL41-E95A cells and whether there are changes in cellular GPx activity related to Mono Mac 6 cell differentiation, GPx activity was determined in undifferentiated cells and in Mono Mac 6 cells differentiated in the presence of VD3 (50 nM) and TGFβ (1 ng/ml) for 4 days (Table 1). The data demonstrate that undifferentiated Mono Mac 6 cells show at least an 11-fold-higher GPx activity than BL41-E95A cells.

Addition of selenium (1 ng/ml) as selenite elevated GPx activity of all investigated cell lines about 3-fold, whereas serum-

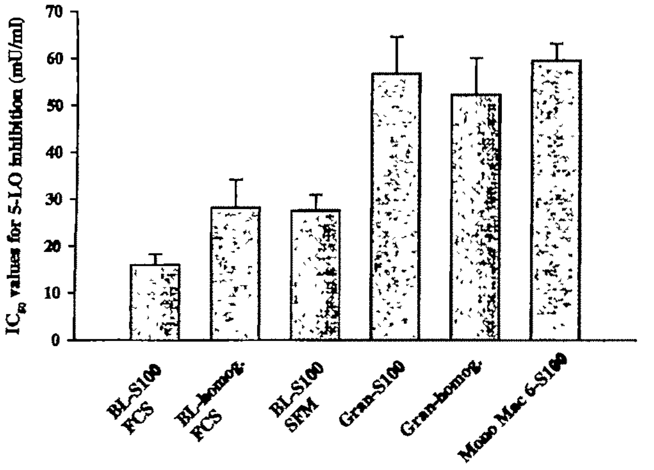

Figure 4 Inhibition of 5-LO activity of various cell types by undifferentiated Mono Mac 6 100000-*g* supernatants

IC_{50} values for inhibition of 5-LO activity were determined in the presence of 0.5 mM β-mercaptoethanol. Values given are means±S.E.M. for at least three independent experiments. S100, 100000-*g* supernatant, SFM, serum-free medium, Gran, granulocytes

Table 2 Effects of thiols on 5-LO inhibition by Mono Mac 6 100000-*g* supernatants and bovine GPx-1

IC_{50} values for 5-LO inhibition by Mono Mac 6 100000-*g* supernatants were determined in the presence of 0.5 mM of the indicated thiol, those of bovine GPx-1 were determined with 1 mM thiol. Endogenous low-molecular-mass thiols of the 100000-*g* supernatants were removed by gel filtration on a PD-10 column (Pharmacia). IC_{50} values for 5-LO inhibition are expressed as means obtained from at least two independent dose-response curves (±S.E.M.). n.d., not determined

	IC_{50} value (m-units/ml)	
Cofactor	GPx from Mono Mac 6 100000-*g* supernatants	Bovine GPx-1
GSH	11.5±0.5	10.7±2.7
DTT	20±10	14.2±3.6
β-Mercaptoethanol	35±5	51.8±12.1
Without thiol addition	215±15	84±2.5
Thiol removal	280±30	n.d.

free culture conditions led to very low cellular GPx activities. Differentiation of Mono Mac 6 cells did not result in significant changes in cellular GPx activity (Table 1).

Cell-dependent differences in stability of 5-LO catalytic activity against GPx-1

We have shown previously that upregulation of cellular 5-LO activity during differentiation of myeloid cells is due to a reduced sensitivity of the 5-LO catalytic activity against inhibition by peroxidases [10]. Therefore, it was of interest to compare the inhibitory effect of the Mono Mac 6 100000-*g* supernatant on 5-LO derived from BL41-E95A, granulocyte and differentiated Mono Mac 6 cells (Figure 4). Undifferentiated Mono Mac 6 cells used as the GPx source were grown in FCS medium containing 0.1 ng/ml Se^{4+} for 4 days. Granulocytes were isolated as described in the Materials and methods section, and BL41-E95A cells were cultured either for 4 days in FCS medium or for 2 passages in serum-free medium. Mono Mac 6 cells grown under serum-free conditions for 1 passage were differentiated by addition of VD3 (50 nM) and TGFβ (1 ng/ml) for 4 days [8]. IC_{50} values for 5-LO inhibition were determined from dose-response curves obtained by addition of increasing concentrations of GPx-1 derived from 100000-*g* supernatants of undifferentiated Mono Mac 6 cells to broken-cell preparations of BL41-E95A cells, TGFβ/VD3-differentiated Mono Mac 6 cells and granulocytes in the presence of 0.5 mM β-mercaptoethanol. As can be seen from Figure 4, higher GPx activities are required for inhibition of granulocyte or Mono Mac 6 5-LO than for B-lymphocytic 5-LO. Thus as shown previously for GPx-4, 5-LO derived from differentiated myeloid cell lines or granulocytes is significantly more resistant towards peroxidase inhibition than B-lymphocytic 5-LO (Figure 4).

Inhibition of 5-LO by GPx-1 is not due to direct protein–protein interactions

In order to investigate whether 5-LO inhibition by GPx-1 might be due to direct interactions between GPx-1 and 5-LO, 5-LO from BL41-E95A (grown in FCS medium) and granulocyte 100000-*g* supernatants was immobilized on ATP-agarose columns and the columns were washed in order to remove unbound materials. Then, GPx-1 from Mono Mac 6 100000-*g* supernatants (obtained from cells grown in FCS medium supplemented with 5 ng/ml Se^{4+}) was applied to each column. The resulting pass-through fraction was collected and three washing steps were performed as described for 5-LO isolation and collected. Then, 5-LO was eluted as described above (5-LO fraction). GPx activity was measured in the pass-through fraction, the three wash fractions and the 5-LO fraction. Interestingly, more than 98% of the GPx activity was recovered in the pass-through fraction and the first washing fraction but no GPx activity co-eluted with 5-LO from the ATP-agarose column. The data suggest that there is no direct binding of GPx-1 to 5-LO.

Thiol specificity of GPx-1

GPx-1 accepts GSH and to a lesser extent DTT as co-substrate, but not β-mercaptoethanol [29,30]. However, in our experiments, 5-LO inhibition by GPx-1 could also be observed in the presence of β-mercaptoethanol (e.g. Table 2). Interestingly, the presence of 2.5 mM β-mercaptoethanol was essential for the recovery of 5-LO inhibitory activity during DEAE, Phenyl- and Isopropyl-Superose column chromatography. No 5-LO inhibition could be detected after any of these purification steps if they were performed in the presence of 0.5 mM β-mercaptoethanol. Furthermore, 5-LO inhibition was more effective in the presence of elevated concentrations of β-mercaptoethanol [IC_{50} values for 5-LO inhibition were 16±2.3 and 8.5±1.9 m-units/ml in the presence of 0.5 and 2 mM β-mercaptoethanol, respectively (means±S.E.M.; $n = 3$)]. Similar results were obtained with bovine GPx [IC_{50} values were 27.7±1.8 and 17.7±4.4 m-units/ml, respectively, ($n = 3$)].

The effects of thiols (GSH, DTT and β-mercaptoethanol) on 5-LO inhibition by GPx are shown in Table 2. Inhibition of 5-LO activity was determined in 100000-*g* supernatants of BL41-E95A cells which were kept in serum-free medium for 2 passages in order to inhibit endogenous selenium-dependent peroxidases. 100000-*g* Supernatants of Mono Mac 6 cells that were cultured in FCS medium supplemented with 5 ng/ml Se^{4+} were used as a GPx source. IC_{50} values for 5-LO inhibition by Mono Mac 6-derived GPx-1 were determined in the presence or absence of 0.5 mM thiol and the IC_{50} values for bovine GPx were obtained in the presence of 1 mM thiol. As can be seen from Table 2, 5-

LO inhibition by the peroxidases was most effective in the presence of GSH and only 3-fold-higher GPx concentrations are required with β-mercaptoethanol. 5-LO inhibition still occurred in the absence of added thiols although 5–10-fold-higher GPx concentrations were required. Removal of endogenous GSH and other low-molecular-mass thiols by gel filtration on PD-10 columns (Pharmacia) equilibrated with PBS/1 mM EDTA (Table 2) slightly increased the IC_{50} values from 215 to 280 m-units/ml, indicating that even traces of thiol slightly enhance the inhibitory activity of GPx-1.

Next, the acceptance of thiols by GPx-1 for peroxidase activity was investigated. GPx-1 activity was determined with GPx assay method B in the presence of 5 mM GSH, DTT, β-mercaptoethanol or β-mercaptoethanol in combination of 10 μM GSH, respectively. GPx activity could only be detected in the presence of GSH (0.4 nmol of peroxide/min per m-unit) or DTT (0.1 nmol of peroxide/min per m-unit) but not with β-mercaptoethanol, even in the presence of low concentrations (10 μM) of GSH, thus confirming the data found in the literature [29,30]. Therefore, it can be concluded that β-mercaptoethanol does not serve as co-substrate for the peroxidase activity of GPx-1 but that it is able to support 5-LO inhibition by GPx-1.

DISCUSSION

In previous studies, GPx-4 was shown to be an efficient endogenous inhibitor of cellular 5-LO activity in a variety of cell types, like BL41-E95A cells, in the presence of thiols. In contrast to this, rat and human monocytic cells and the human monocytic cell line Mono Mac 6 contain a cytosolic, selenium-dependent 5-LO inhibitor that does not require the presence of millimolar concentrations of thiol for inhibition of 5-LO activity (Figure 1) [14,15]. Gel-filtration chromatography revealed that this inhibitor has a higher molecular mass than the previously characterized GPx-4-like inhibitor in BL41-E95A cells [10]. No 5-LO inhibition was detected in fractions corresponding to the molecular mass of GPx-4 (18 kDa). This demonstrated that this enzyme is not involved in regulation of 5-LO activity in Mono Mac 6 cells. Purification, Western-blot analysis and protein sequencing led to the identification of GPx-1 as endogenous 5-LO inhibitor in Mono Mac 6 cells. In accordance to this, it was found that Mono Mac 6 cells possess a cellular GPx-1 activity that is at least 10-fold higher than in BL41-E95A cells (Table 1), giving a reasonable explanation for the observed differences in the 5-LO inhibitory activity in the cytosols of these cell lines The 5-LO inhibitory potency in crude cell homogenates and in fractions obtained during purification correlated with the presence of GPx-1 and was practically identical to GPx-1 enzyme preparations, which were pure according to SDS/PAGE analysis (Table 2 and Figure 3A, lane 4), indicating that GPx-1 is the protein responsible for 5-LO inhibition

Interestingly, cellular GPx activity of Mono Mac 6 cells does not change during differentiation of the cells with TGFβ and VD3 (Table 1). This is in contrast to the changes in 5-LO activity observed after differentiation of Mono Mac 6 cells with TGFβ and VD3. As shown before, differentiation of Mono Mac 6 cells by TGFβ plus VD3 is required for upregulation of cellular 5-LO activity whereas differentiation of the cells with TGFβ alone leads to prominent expression of 5-LO protein but extremely low activity in intact cells and homogenates ([8] and Figure 1). One possible explanation, which is supported by recombination experiments with cytosols and 5-LO enzyme preparations from different sources [8,10] and by differences in peroxidase sensitivity of 5-LO enzymes derived from cells with high and low cellular 5-LO activity (Figure 4) is that VD3 and TGFβ induce a peroxidase-insensitive 5-LO catalytic activity. This could be due to post-translational modifications of the 5-LO protein or to interactions with other proteins induced or activated by TGFβ and VD3. Recently, TGFβ-receptor-I-associated protein-1 (TRAP-1) partial cDNA was identified in a yeast two-hybrid screening system and the expressed protein was shown to physically interact with 5-LO [31]. On the other hand, TRAP-1 specifically interacts only with the activated form of the type-I TGFβ receptor [32]. Therefore, a function of TRAP-1 could be the association of the 5-LO protein to the activated TGFβ receptor, thereby providing a link between TGFβ receptor activation and the observed effects of TGFβ and TGFβ/VD3 on cellular 5-LO activity and/or peroxidase sensitivity.

No physical interaction was observed between GPx-1 and 5-LO protein from granulocytes and BL41-E95A cells, which suggests that suppression of cellular 5-LO activity by peroxidases is rather due to their effects on cellular peroxide tone than to specific 5-LO/GPx interactions.

In contrast to GPx-4, GPx-1 inhibits 5-LO activity in the absence of millimolar concentrations of thiols (Figure 1). Moreover, β-mercaptoethanol, which does not significantly serve as co-substrate for the peroxidase reaction (see the Results section) supports 5-LO inhibition by GPx-1 (Table 2), indicating that GPx-1 does not require high turnover of peroxides for 5-LO inhibition. This could be due to the circumstance that 5-LO inhibition can be achieved by keeping the peroxide concentration in the assay mixture under a certain level, thus prolonging the lag phase and preventing the onset of the lipoxygenase reaction. Due to the low 5-hydroperoxyeicosatraenoic acid (5-HPETE) production during the lag phase, 5-LO inhibition by GPx rather requires rapid reaction rates than a high turnover of substrate, e.g. 5-HPETE. In its reduced selenol form, GPx-1 rapidly reduces peroxides to the respective alcohols, whereas the active-site selenol is oxidized to selenenic acid [33]. In subsequent steps, the active-site selenenic acid of GPx is reduced to its selenol form by oxidation of thiols, preferentially GSH. This mechanism was confirmed in a recent study where it was shown that selenols like selenocysteine efficiently reduce lipid hydroperoxides like 15-HPETE to alcohols [34]. Interestingly, the selenocysteine residue of GPx-1 is expressed at the surface, allowing easy access of substrates and thus high reaction rates with peroxides [33]. The lack of an absolute requirement for thiols for 5-LO inhibition and the loss of the 5-LO inhibitory activity of GPx-1 upon purification in thiol-free buffer can thus be explained by the assumption that the selenol form of GPx-1 is the species responsible for 5-LO inhibition and that the suppression of the onset of the 5-LO catalytic activity by GPx-1 rather requires rapid reduction of hydroperoxides than a high turnover of substrate.

In summary, we have shown that GPx-1 is an efficient, endogenous inhibitor of cellular 5-LO activity when it is expressed in sufficient quantities. This might be of relevance for the regulation of cellular 5-LO activity in various cell types and for the pharmacology of peroxidase-dependent non-redox inhibitors of 5-LO.

We thank Dr Olof Rådmark and Dr Michael Karas for helpful discussions and Dagmar Szellas for expert technical assistance This study was supported by grants from Deutsche Forschungsgemeinschaft (Ste 458/3-2 to D Steinhilber) and the Fonds der Chemischen Industrie

REFERENCES

1 Samuelsson, B, Dahlén, S-E, Lindgren, J-Å, Rouzer, C A and Serhan, C N (1987) Leukotrienes and lipoxins structures, biosynthesis, and biological effects Science **237**, 1171–1176

2 Ford-Hutchinson, A W, Gresser, M and Young, R N (1994) 5-Lipoxygenase Annu Rev Biochem **63**, 383–417

3 Kargman, S, Prasit, P and Evans, J F (1991) Translocation of HL-60 cell 5-lipoxygenase Inhibition of A23187 or N-formyl-methionyl-leucyl-phenylalanine-induced translocation by indole and quinoline leukotriene synthesis inhibitors J Biol Chem **266**, 23745–23752

4 Woods, J W, Evans, J F, Ethier, D, Scott, S, Vickers, P J, Hearn, L, Heibein, J A, Charleson, S and Singer, I I (1994) 5-Lipoxygenase and 5-lipoxygenase activating protein are localized in the nuclear envelope of activated human leukocytes J Exp Med **178**, 1935–1946

5 Reid, G K, Kargman, S., Vickers, P J, Mancini, J A, Léveillé, C, Ethier, D, Miller, D K, Gillard, J W., Dixon, R A F and Evans, J F (1990) Correlation between expression of 5-lipoxygenase-activating protein, 5-lipoxygenase, and cellular leukotriene synthesis J Biol Chem **265**, 19818–19823

6 Bennett, C F, Chiang, M-Y, Monia, B P and Crooke, S T (1993) Regulation of 5-lipoxygenase and 5-lipoxygenase-activating protein expression in HL-60 cells Biochem J **289**, 33–39

7 Steinhilber, D, Hoshiko, S, Grunewald, J, Rådmark, O and Samuelsson, B (1993) Serum factors regulate 5-lipoxygenase activity in maturating HL-60 cells Biochim Biophys Acta **1178**, 1–8

8 Brungs, M, Rådmark, O, Samuelsson, B and Steinhilber, D (1995) Sequential induction of 5-lipoxygenase gene expression and activity in Mono Mac 6 cells by transforming growth factor-beta and 1,25-dihydroxyvitamin D_3 Proc Natl Acad Sci USA **92**, 107–111

9 Steinhilber, D, Rådmark, O and Samuelsson, B (1993) Transforming growth factor beta upregulates 5-lipoxygenase activity during myeloid cell maturation Proc Natl Acad Sci. USA **90**, 5984–5988

10 Werz, O and Steinhilber, D (1996) Selenium-dependent peroxidases suppress 5-lipoxygenase activity in B-lymphocytes and immature myeloid cells – the presence of peroxidase-insensitive 5-lipoxygenase activity in differentiated myeloid cells Eur J Biochem. **242**, 90–97

11 Imai, H, Narashima, K, Arai, M, Sakamoto, H, Chiba, N and Nakagawa, Y (1998) Suppression of leukotriene formation in RBL-2H3 cells that overexpressed phospholipid hydroperoxide glutathione peroxidase J Biol Chem **273**, 1990–1997

12 Huang, H S, Chen, C J, Lu, H S and Chang, W C (1998) Identification of a lipoxygenase inhibitor in A431 cells as a phospholipid hydroperoxide glutathione peroxidase FEBS Lett **424**, 22–26

13 Werz, O, Szellas, D, Henseler, M and Steinhilber, D (1998) Nonredox 5-lipoxygenase Inhibitors require glutathione peroxidase for efficient inhibition of 5-lipoxygenase activity Mol Pharmacol **54**, 445–451

14 Coffey, M, Peters-Golden, M, Fantone, J C. and Sporn, P H S. (1992) Membrane association of active 5-lipoxygenase in resting cells – evidence for novel regulation of the enzyme in the rat alveolar macrophage J Biol Chem **267**, 570–576

15 Coffey, M J, Wilcoxen, S E, Sporn, P H and Peters-Golden, M (1998) Regulation of 5-lipoxygenase activity in mononuclear phagocytes characterization of an endogenous cytosolic inhibitor Prostagland Lipid Mediators **56**, 113–117

16 Werz, O, Brungs, M and Steinhilber, D (1996) Purification of transforming growth factor beta1 from human platelets Pharmazie **51**, 893–896

17 Ziegler-Heitbrock, H W L, Thiel, E, Futterer, A, Herzog, V, Wirtz, A and Riethmuller, G. (1988) Establishment of a human cell line (Mono Mac 6) with characteristics of mature monocytes. Int J Cancer **41**, 456–461

18 Breitman, T R, Collins, S. J and Keene, B. R (1980) Replacement of serum by insulin and transferrin supports growth and differentiation of the human promyelocytic cell line, HL-60 Exp Cell Res **126**, 494–498

19 Boyum, A (1968) Isolation of mononuclear cells and granulocytes from human blood Scand J Clin Lab Invest **97** (suppl 21), 77–89

20 Werz, O and Steinhilber, D (1998) Regulation of 5-lipoxygenase activity by selenium-dependent peroxidases Effects of transforming growth factor-beta and 1,25-dihydroxyvitamin D_3 in Recent Advances in Prostaglandin, Thromboxane and Leukotriene Research (Sinzinger, H, Vane, J R, Samuelsson, B, Paoletti, R, Ramwell, P W and Wong, P Y-K, eds), pp 383–386, Plenum Press, New York

21 Wendel, A (1981) Glutathione peroxidase Methods Enzymol **77**, 325–333

22 Cha, M K and Kim, I H (1996) Glutathione-linked thiol peroxidase activity of human serum albumin – a possible antioxidant role of serum albumin in blood plasma Biochem Biophys Res Commun **222**, 619–625

23 Laemmli, U K (1970) Cleavage of structural proteins during the assembly of the head of bacteriophage T Nature (London) **227**, 680–685

24 Towbin, H, Staehelin, T and Gordon, J (1979) Electrophoretic transfer of proteins from polyacrylamide gels to nitrocellulose sheets procedure and some applications Proc Natl Acad Sci USA **76**, 4350–4354

25 Kellner, R, Lottspeich, F and Meyer, H E (1998) Microcharacterization of proteins, Wiley-VCH, Weinheim

26 Zhang, Y Y, Lind, B, Rådmark, O and Samuelsson, B (1993) Iron content of human 5-lipoxygenase, effects of mutations regarding conserved histidine residues J Biol Chem **268**, 2535–2541

27 Gettins, P, Duwayne, D and Crews, B (1992) Selenium-dependent glutathione-peroxidases from ovine and bovine erythrocytes occur as longer chain forms than previously recognized Arch Biochem Biophys **294**, 511–518

28 Mullenbach, G T, Tabrizi, A, Irvine, B D, Bell, G I and Hallewell, R A (1987) Sequence of a cDNA coding for human glutathione peroxidase confirms TGA encodes active site selenocysteine Nucleic Acids Res **15**, 5484–5487

29 Flohé, L, Gunzel, W, Jung, G, Schaich, E and Schneider, F (1971) Glutathion-peroxidase, II Hoppe-Seyler's Z Physiol Chem. **352**, 159–169

30 Tappel, A L (1978) Glutathione peroxidase and hydroperoxides Methods Enzymol **52**, 506–513

31 Provost, P, Samuelsson, B and Rådmark, O (1999) Interaction of 5-lipoxygenase with cellular proteins Proc Natl Acad Sci USA **96**, 1881–1885

32 Charng, M-J, Zhang, D, Kinnunen, P and Schneider, M. D (1998) A novel protein distinguishes between quiescent and activated forms of the type I transforming growth factor receptor J Biol Chem **273**, 9365–9368

33 Epp, O, Ladenstein, R and Wendel, A (1983) The refined structure of the selenoenzyme glutathione peroxidase at 0 2 nm resolution Eur J Biochem **133**, 51–69

34 Bjornstedt, M, Hamberg, M, Kumar, S, Xue, J and Holmgren, A (1995) Human thioredoxin reductase directly reduces lipid hydroperoxides by NADPH and selenocystine strongly stimulates the reaction via catalytically generated selenols J Biol Chem **270**, 11761–11764

Received 6 October 1999/7 April 2000, accepted 28 April 2000

Esterification of free fatty acids in adipocytes: a comparison between octanoate and oleate

Wen GUO, Ji-Kyung CHOI, James L. KIRKLAND, Barbara E. CORKEY[1] and James A. HAMILTON

Obesity Research Unit, Department of Medicine and Biophysics, Boston Medical Center, Room 803, 650 Albany Street, Boston, MA 02118, U.S.A.

Medium-chain triacylglycerols (MCT) are present in milk, coconut oil and other foods, and are used therapeutically in special diets for certain disorders of lipid and glucose utilization. Recently, it has become apparent that MCT are not only oxidized in the liver, but are also present in lymph and fat tissue, particularly after chronic treatment. To evaluate the influence of MCT on metabolism in fat cells, we compared incorporation of octanoate and oleate into cellular triacylglycerols of 3T3-L1 adipocytes as well as their effects on preadipocyte differentiation. We found that less octanoate than oleate was stored and that more octanoate than oleate was oxidized. Octanoate was esterified to a greater extent at the *sn*-1,3 position of glyceryl carbons than at the *sn*-2 position, whereas the opposite was true for oleate. Glycerol release from fat cells pre-treated with octanoate was also greater than from cells pre-treated with oleate, presumably related to the preferential release of octanoate from the *sn*-1,3 position. Octanoate was not incorporated into lipids in undifferentiated cells and did not induce differentiation in these cells, whereas oleate was readily stored and actually induced differentiation. Incorporation of octanoate into lipids increased as cells differentiated, but reached a maximum of about 10% of the total stored fatty acids. If these effects *in vitro* also occur *in vivo*, substitution of octanoate for oleate or other long-chain fatty acids could have the beneficial effect of diminishing fat-cell number and lipid content.

Key words: differentiation, lipolysis, triacylglycerol storage.

INTRODUCTION

It has been demonstrated that medium-chain fatty acids (MCFA) are more efficiently oxidized than long-chain fatty acids (LCFA) at the whole-body level [1,2] and in isolated tissue or cells [3–7]. However, little is known about how MCFA are metabolized via pathways alternative to oxidation, and how this affects other metabolic events in cells.

On the other hand, medium-chain triacylglycerols (MCT) have been used as nutrients for patients with disorders of long-chain triacylglycerol (LCT) or glucose metabolism for decades. Several early studies demonstrated that MCT diets prevented weight gain in animals [8–10] without affecting plasma cholesterol or other physiological parameters [11,12]. Feeding MCT early in life influenced adipose-tissue development and resulted in fewer and smaller fat cells with less lipid [10]. Neurotoxicity [13] and ketosis [14] have only been reported after acute, high-dose MCT intravenous infusion in animals. Recent trials have demonstrated that the addition of MCT to human diets is of benefit for certain dyslipidaemic disorders including diabetes [15,16]. The rationale for these therapeutic benefits is not fully understood. The potential applications of MCT in the treatment of obesity have been reviewed in [17,18].

While it is generally accepted that MCFA are absorbed via the portal vein and are oxidized in the liver, a recent study shows that when fed enterally to rats, significant amounts of MCFA relative to LCFA appear in lymph [19]. Chylomicron triacylglycerols (TG) in human subjects consuming MCT diets also contained significant amounts of MCFA [20]. Infants fed MCT-enriched formulae accumulated substantial amounts of MCFA in their adipose tissues [21]. We also found that adipose tissues from young (2-week-old) rats contain levels of MCFA that are more than 2-fold higher than those in older ones (3-months old; W. Guo and B. E. Corkey, unpublished work). This is most probably due to storage of MCFA acquired from milk in the young rats and their loss after weaning. In pre-term infants, about 27% [22] to 50% [23] of the dietary MCT intake was oxidized. On the other hand, up to 82% and 90% of octanoate was recovered as CO_2 in fed and fasted rats after 6 h of intravenous infusion of octanoic acid [24]. These studies indicate that MCT may not be exclusively oxidized in the liver, especially after an extended feeding period. The impact of MCFA on metabolism in peripheral tissues may be more significant than previously appreciated.

To determine whether the ability of MCT diet to diminish fat stores could be reproduced *in vitro*, and to study the mechanism, we compared the incorporation of octanoate with that of oleate into lipids using differentiated 3T3-L1 cells as a fat-cell model. We also compared effects of octanoate with oleate on fat-cell differentiation in 3T3-L1 preadipocytes.

MATERIALS AND METHODS

Chemicals

1-^{13}C-Labelled free fatty acids (FFA) and deuterated solvent (chloroform) were purchased from Cambridge Isotope (Cambridge, MA, U.S.A.). Other organic solvents were of HPLC grade from Aldrich (Milwaukee, WI, U.S.A.). [1-^{13}C]Methyl palmitate was synthesized as described previously [25].

Cell-culture medium, fetal bovine serum, penicillin and streptomycin were purchased from Gibco (Grand Island, NY, U.S.A.). Methylisobutylxanthine, dexamethasone and insulin were purchased from Sigma (St. Louis, MO, U.S.A.).

Abbreviations used: TG, triacylglycerols; MCT, medium-chain triacylglycerols; LCT, long-chain triacylglycerols; MCFA, medium-chain fatty acids; LCFA, long-chain fatty acids; FFA, free fatty acids; G3PD, glycerol-3-phosphate dehydrogenase; DMEM, Dulbecco's modified Eagle's medium; MDI, methylisobutylxanthine/dexamethasone/insulin.

[1] To whom correspondence should be addressed (e-mail bcorkey@med-med1.bu.edu).

Cell culture

NIH-3T3-L1 cells were cultured in basal medium [Dulbecco's modified Eagle's medium (DMEM), fetal bovine serum (10%), penicillin (100 units/ml) and streptomycin (100 μg/ml)] until 2 days post-confluence. To induce differentiation, unless otherwise indicated, cells were exposed to basal medium supplemented with MDI [methylisobutylxanthine (120 μg/ml), dexamethasone (0.39 μg/ml) and insulin (10 μg/ml)]. Cells were washed 2 days later and then exposed to insulin (2.5 μg/ml)-supplemented basal medium. Medium was changed every 2 days. Lipid droplets were visible by phase-contrast microscopy 2 days after MDI treatment.

HepG2 cells were grown in DMEM with 10% fetal bovine serum containing the same concentrations of the above antibiotics and were used 2 days post-confluence.

Fatty acid induced differentiation

Cells were exposed to oleate or octanoate (1 mM in 0.2 mM BSA) and insulin (2.5 μg/ml) in basal medium 2 days after they had reached confluence. The 5:1 molar ratio of FFA/BSA promotes net transfer of FFA from BSA-binding sites to cells [26]. No MDI treatment was applied to these cultures.

Incubation with [1-^{13}C]FFA

A stock solution containing [1-^{13}C]octanoate or [1-^{13}C]oleate (1 mM in 0.2 mM BSA) was added to the cell culture during a regular medium change. At termination, cells were washed three times with an ice-cold solution (pH 7.4) containing sucrose (250 mM), Tris (10 mM) and 2-mercaptoethanol (1 mM), scraped into the above solution containing additional EDTA (0.2 mM) and homogenized. Aliquots of the homogenate were stored at −80 °C for DNA and TG analysis. Aliquots for glycerol-3-phosphate dehydrogenase (G3PD) analysis were centrifuged at 44000 *g* for 20 min and the supernatants were stored at −80 °C until analysis. The homogenates were then extracted for lipids for NMR studies as described previously [25,27].

Partitioning of [1-^{14}C]FFA between CO$_2$ production and TG incorporation

3T3-L1 cells were prepared in T25 culture flasks. After MDI treatment (4 days), cells were exposed to basal medium containing insulin (2.5 μg/ml) and 1 mM fatty acids (in 0.2 mM BSA) as described above but with a trace amount of [1-^{14}C]octanoate or [1-^{14}C]oleate (3 μCi). The incubation was terminated after 60 min. ^{14}CO$_2$ released from fatty acid oxidation was collected and quantified using a published protocol [4]. The cellular lipids were extracted and separated by TLC. The TG fraction was scraped off and dissolved in Ecosin-A solution for scintillation counting. The d.p.m. values of the reaction products (CO$_2$, TG) were converted into nmol by referring to the d.p.m. values of known concentrations of the starting materials ([1-^{14}C]octanoate and [1-^{14}C]oleate). Cellular DNA was measured in parallel cultures.

Measurement of basal lipolysis

After the MDI treatment (4 days), cells were incubated with [1-^{13}C]octanoate or [1-^{13}C]oleate for 16 h so that the intracellular TG pool was enriched with the corresponding isotope-labelled fatty acids. Control cultures were terminated at this time, and cells were homogenated for TG and DNA analysis. After aliquots were taken for these analyses, cellular lipids were extracted for NMR and GLC analysis. Parallel cultures were washed three times with PBS solution and incubated with serum-free DMEM containing 1% BSA, conditions that favour basal lipolysis. At the end of the incubation, media were aspirated and assayed for glycerol (Sigma procedure no. 337A [27]), and the cells were harvested for analysis as described above. The cell morphology examined before and after the incubation showed that more and/or larger lipid droplets appeared after 96 h of incubation. However, there was no microscopically detectable difference between the cells pre-treated with oleate or octanoate.

Quantification of ^{13}C label incorporation into cellular TG from the NMR peak intensity

The ^{13}C-NMR spectra were obtained at 125 MHz on a Bruker DMX-500 spectrometer with a 5-mm triple resonance probe (Bilerica, MA, U.S.A.). Other details have been described in our previous reports [25,27].

The absolute intensities of ^{13}C=O signals were measured by reference to an internal standard [25]. For cells incubated with [1-^{13}C]oleate, the ^{13}C=O signals from direct incorporation were very intense compared with those from unlabelled carbons (> 90-fold, Figure 1A). Therefore, the measured C=O peak intensity was taken to be equivalent to the [1-^{13}C]oleate in TG. For cells incubated with [1-^{13}C]octanoate, the signals from direct incorporation of [1-^{13}C]octanoate were less intense than the C=O signals from unlabelled TG (Figure 1B; signals from unlabelled saturated acyl chains overlapped those of esterified [1-^{13}C] octanoate, but were generally 30–40% of their unsaturated counterparts in control cultures). Therefore, the signal intensity from direct incorporation of [1-^{13}C]octanoate was obtained by subtracting the background signal from control. This may not be completely accurate when octanoate incorporation is very limited. Nevertheless, these partial errors do not affect the general conclusions from this study (see below).

Measurement of total cellular DNA, TG and G3PD activity

Duplicate aliquots of homogenate were taken for DNA assays [28] and TG measurement (Sigma procedure no. 337 [27]). G3PD was measured by following the disappearance of NADH during enzyme-catalysed dihydroxyacetone phosphate reduction under zero-order conditions [29].

Methylation of TG and GLC analysis of fatty acyl composition

The lipid components of cell extracts were separated by TLC (hexane/ethyl ether/acetic acid, 70:30:1). Methylation was performed by incubation in BF3-methanol solution (14%, v/v, BF3 in methanol) at 60 °C for 30 min. The fatty acid methyl ester was extracted into a hexane solution. The hexane solution was dried with anhydrous sodium sulphate. To avoid the evaporation of methyl octanoate, the hexane solution was used directly for GLC study without further condensation. GLC analysis was performed on a Shimuzu 14A gas chromatograph with a Supelco SP® -2380 capillary column with an initial oven temperature of 150 °C, final temperature of 240 °C, heating rate of 4 °C/min, injector temperature of 220 °C and detector temperature of 240 °C. Carrier gas (He) was at 50 kPa, make-up carrier gas (He) at 100 kPa, hydrogen gas at 55 kPa and compressed air at 50 kPa. The sample was injected in 1–1.5 μl with splitting rate of 1:25.

Statistical analysis

Except when indicated otherwise, experiments presented here were repeated 3–6 times. The results were analysed using Microcal Origin (Microcal Software, Northampton, MA, U.S.A.) and are presented as means ± S.E.M. Student's *t* test was performed for

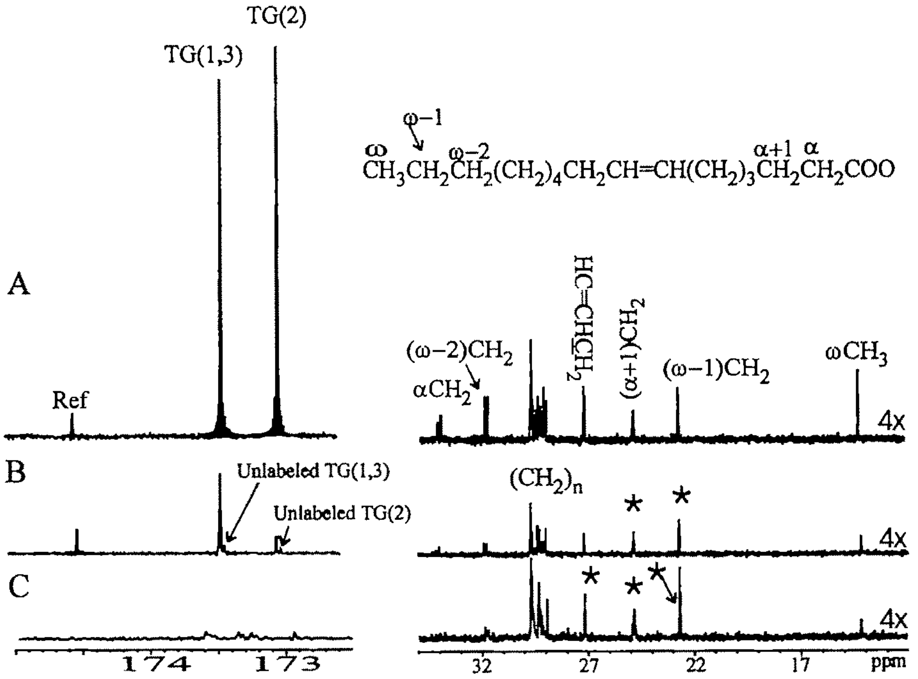

Figure 1 **^{13}C-NMR spectra of lipid extracts after cells were incubated with [1-^{13}C]fatty acids**

(**A**) Oleate and (**B**) octanoate in 3T3-L1 fat cells, and (**C**) octanoate in HepG2 cells. Above the spectra is shown a molecular formula of palmitoleate, a common end product of *de novo* synthesis of LCFA The spectrum was obtained with 2000 (**A**) and 4000 (**B** and **C**) scans

selected results, and the *P* values are presented in the corresponding Figures.

RESULTS

Partitioning of exogenous FFA between oxidation and storage

The partitioning of exogenous octanoate and oleate into the metabolic end products of CO_2 and TG is shown in Table 1. Incorporation of either octanoate- or oleate-derived ^{14}C isotopes into other lipid fractions (cholesterol, phospholipids and diglycerides) was much less extensive (results not shown). Our results show that under identical culture conditions, octanoate partitioned into CO_2 more extensively than TG, but the opposite was found for oleate. The total number of mol of exogenous fatty acids converted into TG plus CO_2 within 60 min was similar. Considering that each octanoyl chain only produces 8 CO_2 molecules (eight times values in Table 1) whereas oleate produces 18 CO_2 molecules (18 times value in Table 1), the actual the amount of CO_2 produced from octanoate was about 3-fold greater than that from exogenous oleate.

Table 1 **Exogenous octanoate and oleate incorporated into the metabolic end products in 3T3-L1 adipocytes detected as CO_2 and TG expressed as nmol of the corresponding fatty acids converted into each product (nmol/h per μg of DNA)**

Since part of the acetyl-CoA derived from octanoate may be re-utilized for *de novo* synthesis of LCFA and incorporated subsequently into TG (see below), the amount of isotope recovered in the TG fraction may be more than the actual amount of octanoyl chain esterified into TG However, since the amount partitioned into the *de novo* synthesis is less than 16% (as detected by ^{13}C-NMR, see below), the results shown here still reflect the amount of [1-^{14}C]octanoate esterified Furthermore, the inclusion of *de novo*-synthesized LCFA in TG only supports, rather than averts, the conclusion that octanoate was more oxidized than stored Means±S.E.M. are shown ($n = 3$)

Sample	TG	CO_2
Octanoate	0.9±0.1	8.4±1.2
Oleate	7.6±0.8	0.7±0.1

It is not possible to determine the endogenous fatty acid pool using this approach. This pool may also contribute to CO_2 production in cells exposed to octanoate and oleate. However, our results show that both octanoate and oleate are actively metabolized in 3T3-L1 adipocytes, and are in accord with previous observations that more octanoate is oxidized than stored in animal cells [1,3–6].

Direct incorporation of exogenous FFA into cellular lipids

The ^{13}C-NMR spectra of lipid extracts from 3T3-L1 adipocytes incubated with [1-^{13}C]octanoate or [1-^{13}C]oleate for 24 h are shown in Figures 1(A) and 1(B). For comparison, a spectrum of the lipid extract from HepG2 cells incubated with [1-^{13}C]octanoate for 24 h is shown in Figure 1(C). The carbonyl signals are shown in the left-hand panels and aliphatic carbon signals in the right-hand panels. Spectra obtained under other incubation conditions had similar general features with different peak intensities.

[1-^{13}C]Oleate and [1-^{13}C]octanoate were each found to be esterified to TG at the *sn*-1,3 as well as the *sn*-2 positions in fat cells (Figure 1), represented by the peaks arising from the corresponding carbonyl resonances, TG(1,3) and TG(2). Such

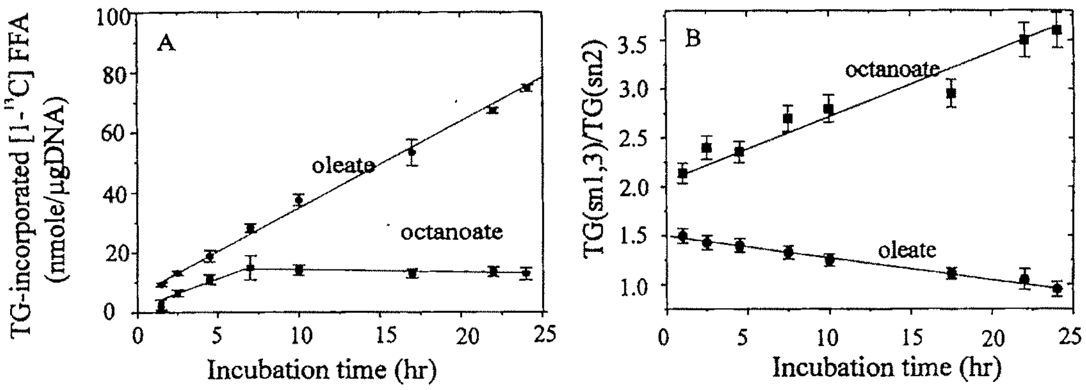

Figure 2 Time-dependent incorporation of fatty acids into cellular TG

(**A**) Incorporation of [1-^{13}C]oleate and [1-^{13}C]octanoate into cellular TG as a function of incubation time (**B**) The acyl chain-specific esterification of [1-^{13}C]oleate and [1-^{13}C]octanoate, as determined by the relative-peak-intensity ratio of the TG(1,3)/TG(2)

direct esterification of [1-^{13}C]octanoate was not detected in HepG2 cells (Figure 1C), whereas [1-^{13}C]oleate was directly esterified in HepG2 cells [30] to an extent similar to that in fat cells (results not shown). The amount of [1-^{13}C]oleate or [1-^{13}C]octanoate incorporated into phospholipids was insignificant, as evidenced by the lack of corresponding resonances [25].

Utilization of [1-^{13}C]FFA-derived [^{13}C]acetyl-CoA in *de novo* synthesis

In principle, the acetyl-CoA derived from the β-oxidation of [1-^{13}C]FFA can be used for *de novo* FFA synthesis. Any incorporation of [1-^{13}C]acetyl-CoA into the acyl methylene would be detected by NMR. In previous studies on fat cells treated with oleate or palmitate, partitioning of exogenous fatty acids into this pathway was not detected [25,27,31]. However, for cells incubated with octanoate, we found that the integrated intensities of some methylene peaks representing a single carbon ($\alpha+1$, $\omega-1$, etc.) were about 2-fold more intense than the ωCH_3 peak (Figures 1B and 1C), indicating selective labelling of the aliphatic region with ^{13}C isotope. Peaks for the αCH_2 and $(\alpha+1)CH_2$ generally were broader or split because of the magnetic shielding from *sn*-1,3 or *sn*-2 carbonyls. Therefore, the peak heights of these signals were lower than the signals arising from the other methylenes even though they may have had the same overall integral intensity.

We then separated the lipid mixtures (of 3T3-L1 or HepG2) by TLC, and examined the TG and phospholipid fractions by NMR. The spectra from the phospholipid fractions were very weak and did not reveal any ^{13}C signal enhancement. The spectra of the TG fractions were essentially the same as those before the separation, indicating that the signals detected in the spectra shown in Figure 1 were from the TG fractions. This also shows that part of the [1-^{13}C]acetyl-CoA derived from the β-oxidation of [1-^{13}C]octanoate was used for *de novo* fatty acid synthesis and then stored in cellular TG. Since the NMR signal intensity from each ^{13}C label is equivalent to that from ≈ 100 natural carbons, a 2–3-fold peak intensity corresponds to about 1–2% isotope enrichment. The observation that the $(\omega-1)CH_2$ peak is more intense than the ωCH_3 peak indicates that [1-^{13}C]acetyl-CoA can be used as the priming unit for the acyl chains. The peak intensity of ωCH_3 can be used as an intrinsic reference to detect the partitioning of ^{13}C-labelled substrates in the *de novo* synthesis pathway.

Octanoate was incorporated into TG less extensively than oleate

Within a 24-h period, the accumulation of oleate into TG increased with incubation time, whereas the accumulation of octanoate reached a plateau at ≈ 7 h (Figure 2A). In 24 h, about four times more total [1-^{13}C]oleate than [1-^{13}C]octanoate was incorporated into TG.

To determine if the low rate of incorporation of octanoate into TG was related to substrate availability, cells were incubated with various concentrations (1–5 mM) of [1-^{13}C]octanoate for 24 h. However, the incorporation of [1-^{13}C]octanoate into lipid did not vary significantly with respect to octanoate concentration, as determined by NMR (results not shown). Hence, substrate availability (within the range investigated) was not rate limiting for the esterification of octanoate, and it is likely that the process was saturated. In other experiments, we incubated cells with [1-^{13}C]octanoate for longer periods (up to 7 days), and did not find a substantial increase in the incorporation of [1-^{13}C]octanoate. Such saturation could be either due to limited incorporation or faster turnover of TG that contains octanoate.

Octanoate and oleate differ in the glyceryl position to which they are esterified

The extent of [1-^{13}C]fatty acid esterification at the *sn*-1,3 or *sn*-2 positions on glycerol can be determined by the peak intensity ratio of TG(1,3)/TG(2). A ratio of 2.0 corresponds to random access of exogenous fatty acids to the three glycerol carbons. For cells incubated with oleate, this ratio was lower than 2.0, and decreased with incubation time (Figure 2B), as found previously [27,31]. For cells incubated with octanoate, this ratio was higher than 2.0, and increased with incubation time (Figure 2B). Hence, these two types of fatty acids not only have different overall storage rates, but also have different esterification rates at the three acyl chain positions in TG. The observation that octanoate has a higher preference for *sn*-1,3 positions agrees with the acyl specificity in animal milk [32].

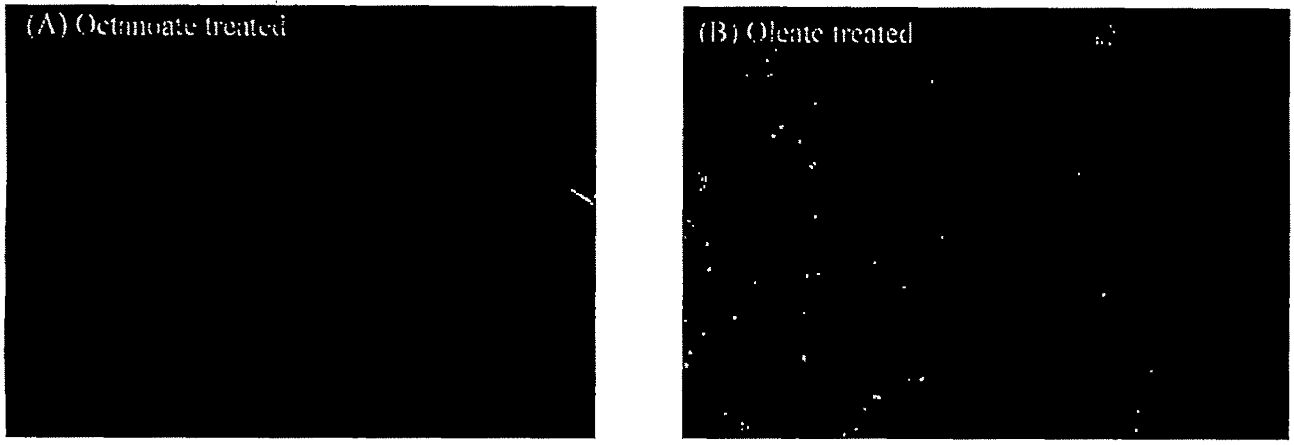

Figure 3 Micrographs (magnification ≈ 200) of 3T3-L1 cells after incubation for 9 days with basal medium containing insulin (2.5 μg/ml) in the presence of 1 mM octanoate (A) and oleate (B) in 0.2 mM BSA

These cells were not treated with methylisobutylxanthine or dexamethasone

Table 2 The cellular TG content and G3PD activity in 3T3-L1 cells with basal medium containing insulin (2.5 μg/ml) in the presence of octanoate and oleate (means ± S.E.M., $n = 3$)

Cells were not treated with methylisobutylxanthine or dexamethasone

	TG (μg/μg of DNA)		G3PD (nmol/min per μg of DNA)	
Sample	Day 6	Day 9	Day 6	Day 9
Control	0.3 ± 0.05	0.5 ± 0.03	0.12 ± 0.02	0.3 ± 0.02
Octanoate	0.1 ± 0.02	0.6 ± 0.04	0.09 ± 0.01	0.2 ± 0.01
Oleate	1.7 ± 0.2	5.1 ± 0.3	0.45 ± 0.02	1.7 ± 0.1

Octanoate and oleate differ in their effects in inducing fat-cell differentiation

When added to undifferentiated cells (not treated with MDI), lipid droplets began to appear in cells treated with oleate 3 days after the incubation. In octanoate-treated and control cells lipid droplets began to appear 6 days after incubation, but to a much lesser extent than in cells treated with oleate After 9 days of incubation, about 90 % of the cells contained lipid droplets The droplets in octanoate-treated cells (Figure 3A) were much smaller than those in oleate-treated cells (Figure 3B). After extended fatty acid incubation, there was about a 20 % cell loss in oleate-treated cultures, as shown by microscopic examination (Figure 3) and corroborated by DNA analysis. Such cell loss was less significant in octanoate-treated cells. Since the cells that lifted off were mostly differentiated fat cells (examined by microscopy), the cell loss was likely to be induced by the propensity of fat-laden cells to float rather than by fatty acid-related toxicity, although the rapid lipid accumulation in the presence of excess oleate may have accelerated this process. When cells were differentiated with MDI treatment and subsequently accumulated lipids mostly by *de novo* synthesis from glucose, cell loss was not significant up to 6 days after MDI treatment.

The total TG accumulated in oleate-treated cells was substantially greater than for cells treated with octanoate (Table 2). The TG thus accumulated contained mostly oleate (> 80 %) in oleate-treated cells, and mostly palmitate and palmitoleate in control or octanoate-treated cells (results not shown), indicating that the latter accumulate fat via a *de novo* pathway, as well documented in 3T3-L1 cells [33,34].

To confirm that the TG storage was a result of cell differentiation rather than non-specific accumulation of exogenous fatty acids [35], G3PD activity, a commonly recognized differentiation marker, was analysed in cells thus treated. The results showed a close correspondence between G3PD activity and total TG stored (Table 2). We concluded that incubation with oleate (in the presence of insulin) significantly promoted adipocyte differentiation in 3T3-L1 cells, resulting in higher storage of TG, whereas octanoate did not have such an influence.

Octanoate incorporation increased as differentiation progressed

Incorporation of [1-^{13}C]octanoate was nearly undetectable in undifferentiated cells. A gradual increase in direct esterification of [1-^{13}C]octanoate occurred as cells progressed to later stages of differentiation, using G3PD as a marker of differentiation (Figure 4). The incubation with octanoate in this experiment was performed from day 0 to day 6 after MDI treatment. Incorporation of octanoate at the *sn*-2 position reached a plateau early in differentiation whereas incorporation at the *sn*-1,3 position continued to increase, resulting in an increase in the TG(1,3)/TG(2) ratio (Figure 4, inset).

Glycerol release from cells pre-treated with oleate or octanoate

To compare the effects of oleate and octanoate on TG hydrolysis, cells pre-treated with the corresponding fatty acids were incubated with lipid-free DMEM (1 % BSA). The total DNA values per culture assayed at 0, 7, 48 and 96 h were essentially unchanged (139 ± 4 μg/culture), and there was no difference between cells treated with oleate or octanoate. Total cellular TG continued to increase, and slightly more than doubled in 96 h (Figure 5A) The slightly higher TG storage in oleate-treated cells was likely to be a result of more extensive storage of exogenous oleate than octanoate during the 16-h pre-treatment period. The steady rate at which stored TG increased thereafter indicates that *de novo* synthesis of LCFA was not affected differently by octanoate or oleate pre-treatment, and was not hampered by serum deprivation during the time course.

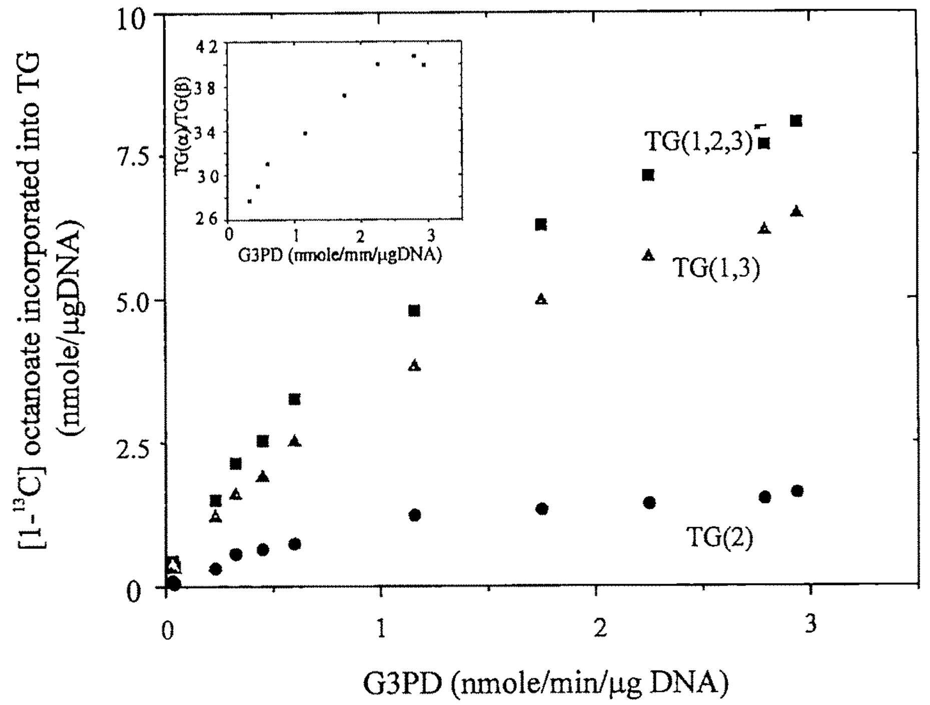

Figure 4 Quantitative incorporation of [1-^{13}C]octanoate into *sn*-1,3 [TG1,3)], *sn*-2 [(TG(2)] and total TG [TG(1,2,3)] as a function of cellular G3PD activity

Inset TG(1,3)/TG(2) ratio as a function of G3PD activity

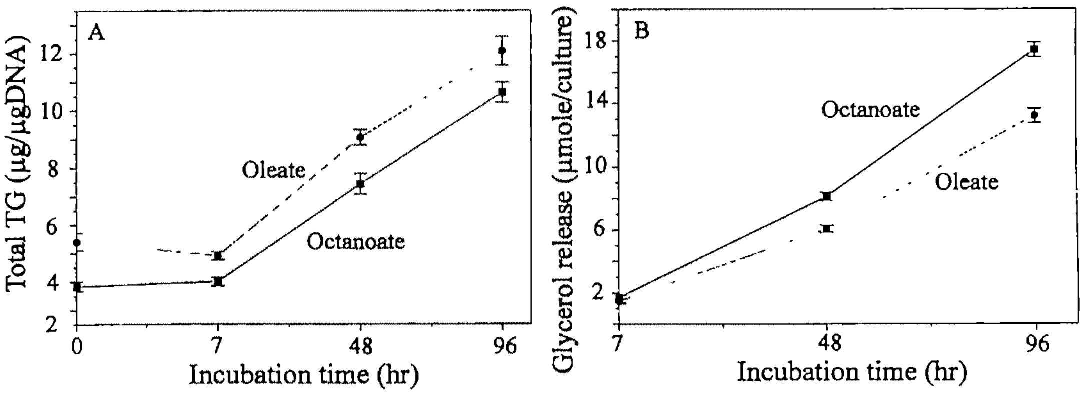

Figure 5 The total cellular TG before and after lipolysis (A) and the amount of glycerol released during the incubation (B)

Cells were pre-treated with oleate or octanoate as indicated The data points are connected by lines purely for visual examination of the results

Despite a slightly lower cellular TG content, cells treated with octanoate released more glycerol than cells treated with oleate after 48 and 96 h of incubation (Figure 5B). Glycerol release was linear with incubation time, and comparable with the reported values in basal lipolysis [33].

Octanoate turnover is faster than oleate during lipolysis

The turnover rate of [1-^{13}C]FFA incorporated in TG can also be measured by NMR. As shown in Figures 6(A) and 6(B), the total intensity of the [1-^{13}C]oleate signal was similar before and after the 96-h incubation with DMEM This indicates that most of the [1-^{13}C]oleate remained esterified to TG (including unhydrolysed and hydrolysed but re-esterified oleate), as reported previously [27]. Some of the [1-^{13}C]oleate released from the *sn*-1,3 positions may have been re-esterified at the *sn*-2 position, because the ratio of TG(1,3)/TG(2) decreased from about 1.2 (Figure 6A) to less than 1.0 (Figure 6B). Based on the integrated signal intensities, over 99 ± 3.3 % (±S.E.M.) of the [1-^{13}C]oleate remained in TG ($n = 3$).

On the other hand, incorporation of [1-^{13}C]octanoate was initially lower than oleate, but the absolute amount of incorporation was significant compared with the control (Figure 6C). After the 96-h incubation with DMEM, signals from [1-^{13}C]octanoyl chains were largely decreased at the *sn*-1,3 position, and completely depleted at the *sn*-2 position (Figure 6D). About

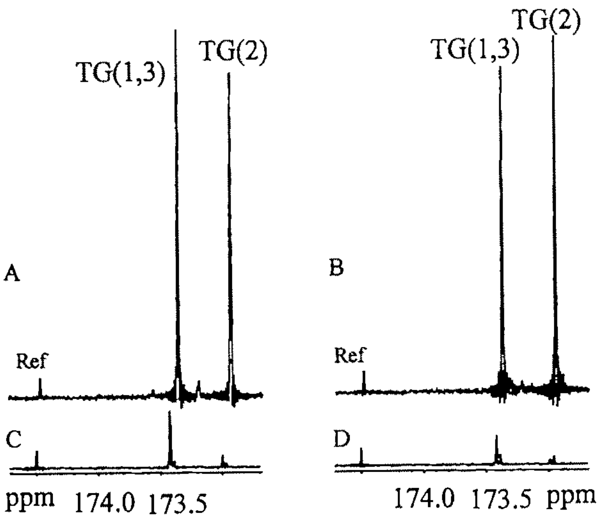

Figure 6 ^{13}C-NMR spectra (carbonyl region) of cellular lipids before (left) and after (right) 96 h of basal lipolysis of cells pre-treated with [1-^{13}C]oleate (A, B) and [1-^{13}C]octanoate (C, D)

The aliphatic regions (results not shown) of spectra (**C**) and (**D**) were both similar to that shown in Figure 1(B), implying no significant changes in the utilization of [1-^{13}C]octanoate for *de novo* synthesis of LCFA

Table 3 Fatty acid composition of cellular TG before and after 96 h of incubation with DMEM (1% BSA) in cells pre-treated with oleate and octanoate

Results are shown as percentages (means ± S.E.M., $n = 3$). The appearance of odd-number chain-length fatty acids is typical in 3T3-L1 fat cells as a result of *de novo* synthesis [50]. Other fatty acids, including $C_{18:2}$ and $C_{18:3}$, were also detected, but to a lower extent

	Oleate		Octanoate	
Acyl chains	Before	After	Before	After
8:0	0	0	10.33±0.3	0.99±0.05
14:0	2.84±0.09	3.28±0.02	3.74±0.04	3.88±0.21
14:1	4.75±0.08	5.48±0.03	5.56±0.29	5.78±0.11
15:0	1.02±0.04	1.36±0.02	1.43±0.14	1.63±0.17
15:1	0.81±0.01	1.24±0.09	1.4±0.14	1.41±0.09
16:0	20.01±0.36	23.65±0.03	24.62±0.35	24.45±0.03
16:1	27.34±0.29	38.65±0.2	38.61±0.2	47.64±0.34
17:0	0.82±0.03	0.75±0.03	0.9±0.03	0.85±0.096
17:1	3.31±0.26	3.98±0.07	3.89±0.1	4.73±0.12
18:0	0.38±0.04	0.41±0.02	0.49±0.02	0.51±0.16
18:1 n9	36.4±0.4	19.71±0.02	6.69±0.09	6.2±0.29
18:1 n11	1.35±0.07	1.51±0.12	2.34±0.05	1.95±0.13

21 ± 1.2 % (±S.E.M.) of the [1-^{13}C]octanoate remained esterified in TG ($n = 3$).

Table 3 shows the acyl chain composition in cellular TG fractions determined by GLC. For cells pre-treated with [1-^{13}C]oleate, the percentage of fatty acyl chains in cellular TG was in the order: oleate > palmitoleate > palmitate. The predominance of oleate corresponds to the rapid uptake and storage of exogenous [1-^{13}C]oleate. After the 96-h incubation with DMEM, this order changed to palmitoleate > palmitate > oleate. The proportion of oleate declined by ≈ 50 %. Since the amount of total TG was approximately doubled during this period of time, this result indicates that the absolute amount of oleate in TG did not change significantly. Instead, the reduction in the proportion of oleate was due to increases in palmitoleate and palmitate.

For cells pre-treated with [1-^{13}C]octanoate, the acyl chains of TG were predominantly palmitoleate and palmitate (Table 3). Octanoate incorporation amounted to 10 ± 0.9 % ($n = 3$) of total acyl composition. After the 96-h incubation with DMEM, the proportion of octanoate in total stored fatty acids was reduced to about 1 ± 0.1 % ($n = 3$). Considering that the total TG content doubled during this period (96 h), the absolute amount of octanoate that remained in TG was about 20 % of the original amount (10 %), a figure that agrees with the NMR results (Figures 6C and 6D).

To determine whether the released octanoate accumulated in the medium, the fatty acid composition of the incubation medium was analysed. The fatty acids detected were mainly palmitate and palmitoleate, with no detectable octanoate and only an insignificant amount of oleate. Together, these results suggested that when deprived of exogenous lipid supply, [1-^{13}C]oleate was largely conserved in the cellular TG [27], whereas [1-^{13}C]octanoate was largely dissipated, probably through oxidation.

DISCUSSION

Fatty acids of different chain lengths have different effects on cellular processes. Whereas the pathological roles of saturated compared with unsaturated LCFA are well established [36], the effects of MCFA have received far less attention. Goals of this study were to determine how much octanoate was stored, how it perturbed the molecular structure of TG, and how it affected cell differentiation. Our data document major differences between octanoate and oleate in their oxidation, esterification and release from TG and their influence on adipocyte differentiation.

It has been widely accepted that MCFA are mainly oxidized in cells through the carnitine-independent pathway whereas LCFA may be stored or oxidized depending on the economy of other fuels, as we have also found [37]. This argument has been used to explain the low storage rate of MCFA in fat cells [17]. However, there is evidence that MCFA can be esterified in TG in the liver [38] and fat cells [21,39], which we confirmed in this study.

First, we showed that octanoate was stored in differentiated fat cells but not in undifferentiated preadipocytes (Figure 4), although oleate can also be stored in undifferentiated fat-cell precursors [27]. Storage of octanoate increased as cells became more differentiated until a maximum level was reached. Whether the storage rate would continue to increase with further fat-cell enlargement (as found in obesity) remains to be determined. It is well known that MCFA have a low affinity for cytosolic acyl-CoA synthase [40], but can be readily activated within the mitochondrial matrix for oxidation. Both factors might lead to relatively low cytosolic substrate availability for esterification. However, these may not be the sole reasons for the low rate of MCFA storage, because increasing the substrate concentration of octanoate (up to 5-fold) and extending the incubation period did not increase the proportion of octanoate in stored fat. Another related factor may be the pool of carnitine, which is needed to transport octanoyl-CoA from the mitochondria to the cytosol, and the pool of CoA, which increases with differentiation (A. M. Richard and B. E. Corkey, unpublished work) and could lead to an increase of octanoyl-CoA concentration in the cytosol.

Secondly, we found that when stored, octanoate was mostly esterified at the *sn*-1,3 positions. Esterification of a medium chain to the *sn*-2 position may be thermodynamically unfavourable. Monoacylglycerol acyltransferase may have a higher affinity for LCFA than MCFA so that most of the acyl chains delivered to the *sn*-2 position are from LCFA, especially unsaturated LCFA

[41]. In addition, the incorporation of MCFA might be mostly accomplished via de-acylation/re-acylation of existing TG molecules, whereas incorporation of LCFA may also be accomplished via the synthesis of new TG molecules directly from free fatty acids and α-glycerolphosphate. This is particularly relevant since we found that MCFA are not esterified in cells that have not acquired a suitable amount of TG, whereas the storage of LCFA does not have such a pre-requisite. Since the turnover of *sn*-1,3 chains in TG is more active than *sn*-2 chains [31], it is not surprising that more MCFA are esterified at the *sn*-1,3 positions

Our observation that octanoate incorporation in fat cells becomes saturated and accounts for about 10 % of total fatty acids is consistent with previous studies *in vivo* [21]. When converted to a molar scale, this accounts for $\approx 20\,\%$ of the total acyl chains stored in fat cells, an amount that would be predicted to have substantial effects on cellular metabolism. In contrast to our observation that octanoate turnover was much faster than that of oleate (Figure 6), storage of MCFA in infant subcutaneous fat was rather stable and remained unchanged 1 week after switching to a MCT-free diet [21] This is probably because subcutaneous-fat turnover rate is intrinsically lower than that in visceral fat since it serves mainly as thermal insulation and mechanical cushioning [42]. Furthermore, visceral fat is affected more by dietary modulation than peripheral fat.

Thirdly, an interesting finding in our study was that fat cells pre-treated with octanoate have a significantly enhanced TG hydrolysis (Figure 5) To our knowledge, such a finding has not been reported before. It may be argued that less TG storage in cells pre-treated with octanoate results in smaller fat droplets and thus a larger surface area of lipids. However, the cells we used were well differentiated before they were treated with octanoate, and there were no microscopic differences in cell morphology or fat droplet size examined by phase contrast microscopy. The difference in total stored TG was rather small between cells pre-treated with octanoate or oleate, and could not account for the difference in glycerol release (Figure 5). Instead, our results suggested that incorporation of octanoate may facilitate TG hydrolysis. Since the hydrolysis product MCFA diffuses away from the site of reaction more rapidly than LCFA, the lipase efficiency is higher for MCT than LCT [43]. Furthermore, hydrolysis at the *sn*-1,3 position is the rate-limiting step in TG lipolysis [44]. Hence, our findings of the preferential incorporation of octanoate at the *sn*-1,3 position and the increased glycerol release in octanoate pre-treated fat cells fit together logically.

Finally, another important observation was that octanoate, in contrast to oleate, did not stimulate differentiation after an extended incubation period The eventual lipid accumulation was similar to that seen in control cells as a result of limited spontaneous differentiation in the presence of insulin and glucose [34]. In contrast, incubation with oleate rapidly induced differentiation with characteristic marked TG accumulation and increased G3PD activity. This is consistent with previous reports that LCFA induce the expression of genes involved in fatty acid metabolism [45–47]. This may explain the observation that weaning rats on MCT diets have lower fat-cell numbers as adults compared with their littermates on LCT diets [10]. Furthermore, long-chain CoA esters, but not short- or medium-chain CoA esters, are potent modulators of metabolic enzymes and signal transduction [48,49]. The fact that LCFA induces preadipocyte differentiation *in vitro* may also correlate with the observations that animals and humans on high-fat diets usually acquire more fat cells than controls [50–52]. Hence, replacement of part of the LCFA in conventional high-fat diets with MCFA at critical times in development may provide a means to control cell number and decrease lipid accretion.

This work was supported by grants AHA/GIA 13519967 to W G, AG/DK 13925 to J.L K, HL 26335 to J A H., and DK 46200 to W.G, J L.K, B E.C and J A.H.

REFERENCES

1 Metges, C C and Wolfram, G (1991) Medium- and long-chain triglycerides labeled with ^{13}C a comparison of oxidation after oral or parenteral administration in humans J Nutr. **121**, 31–36

2 Schwabe, A D., Bennett, L R and Bowman, L P. (1964) Octanoic acid absorption and oxidation in humans J Appl Physiol **19**, 335–337

3 Pegorier, J-P, Duee, P-H, Herbin, C, Laulan, P-Y, Blade, C, Peret, J and Girard, J. (1988) Fatty acid metabolism in hepatocytes isolated from rats adapted to high-fat diets containing long- or medium-chain triglycerides Biochem J. **249**, 801–806

4 Maragoudakis, M E, Kalinsky, H J and Lennane, J. (1975) Metabolism of octanoate and its effects on glucose and palmitate utilization by isolated fat cells Proc Soc Exp Biol Med **148**, 606–610

5 Crozier, G L (1988) Medium chain triglyceride feeding over the long term the metabolic fate of [^{14}C]octanoate and [^{14}C]oleate in isolated rat hepatocytes J Nutr **118**, 297–304

6 Christensen, E, Hagve, T A., Gronn, M and Christophersen, B O (1989) Beta-oxidation of medium chain (C8–C14) fatty acids studied in isolated liver cells Biochim Biophys Acta **1004**, 187–195

7 Binnert, C, Pachiaudi, C, Beylot, M, Hans, D., Vandermander, J, Chantre, P, Riou, J P and Laville, M. (1998) Influence of human obesity on the metabolic fate of dietary long- and medium-chain triacylglycerols Am J Clin Nutr **67**, 595–601

8 Kaunitz, H, Slanetz, C A., Johnson, R. E, Babayan, V K and Barsky, G (1958) Relation of saturated, medium- and long-chain triglycerides to growth, appetite, thirst and weight maintenance requirements. J Nutr **64**, 513–524

9 Geliebter, A, Torbay, N, Bracco, E F., Hashim, S A and Van Itallie, T B (1983) Overfeeding with medium-chain triglyceride diet results in diminished deposition of fat. Am J Clin. Nutr **37**, 1–4

10 Hashim, S A and Tantibhedyangkul, P (1987) Medium chain triglyceride in early life effects on growth of adipose tissue Lipids **22**, 429–434

11 Chanez, M, Bois-joyeuz, B, Arnaud, M. J and Peret, J (1991) Metabolic effects in rats of a diet with a moderate level of medium chain triglycerides J. Nutr **121**, 585–594

12 Wall, K M, Schade, D and Innis, S M (1994) Plasma and tissue lipids of piglets fed formula containing saturated fatty acids from medium-chain triglycerides with or without fish oil Am J Clin Nutr **59**, 1317–1324

13 Miles, J M, Cattalini, M, Sharbrough, F. W, Wold, L E, Wharen, R E, Gerich, J E and Haymond, M W (1991) Metabolic and neurologic effects of an intravenous medium-chain triglyceride emulsion J. Parenteral Enteral Nutr **15**, 37–41

14 Gordon, E E and Duger, J (1975) Experimental hyperosmolar diabetic syndrome Ketogenic response to medium-chain triglycerides Diabetes **24**, 301–306

15 Rouis, M, Dugi, K A, Previato, L., Patterson, A P, Brunzell, J D, Brewer, H B and Santamarina-Fojo, S (1997) Therapeutic response to medium chain triglycerides and w-3 fatty acids in a patient with the familial chylomicronemia syndrome Arterioscler Thromb Vasc Biol **17**, 1400–1406

16 Eckel, R, Hanson, A S, Chen, A Y, Berman, J N, Yost, T J and Brass, E P (1992) Dietary substitution of medium-chain triglycerides improves insulin-mediated glucose metabolism in NIDDM subjects Diabetes **41**, 641–647

17 Bach, A C, Ingenbleek, Y and Frey, A (1996) The usefulness of dietary medium-chain triglycerides in body weight control fact or fancy? J Lipid Res **37**, 708–726

18 Papamandjaris, A A, MacDougall, D E and Jones, P J (1998) Medium chain fatty acid metabolism and energy expenditure obesity treatment implications Life Sci **62**, 1203–1215

19 Sigalet, D and Martin, G (1999) Lymphatic absorption of glucose and fatty acids as determined by direct measurement. J Pediatr Surg **34**, 39–43

20 Swift, L L, Hill, J O, Peters, J C. and Greene, H L (1990) Medium-chain fatty acids evidence for incorporation into chylomicron triglycerides in humans Am J Clin. Nutr **52**, 834–836

21 Sarda, P, Lepage, G, Roy, C and Chessex, P (1987) Storage of medium chain triglycerides in adipose tissue of orally fed infants Am J Clin Nutr **45**, 399–406

22 Putet, G, Thelin, A and Arnaud, M J (1984) Oxidation metabolism of ^{13}C medium chain triglyceride (MCT) fed to preterm infants (PT) Pediatr Res **18**, 344 (abstract)

23 Carnielli, V P., Sulkers, E. J, Moretti, C, Wattimena, J L, van Goudoever, J. B, Degenhart, H J, Zacchello, F and Sauer, P J (1994) Conversion of octanoic acid into long-chain saturated fatty acids in premature infants fed a formula containing medium-chain triglycerides Metabolism **43**, 1287–1292

24 Lassow, W J and Chaikoff, I L (1955) Carbohydrate sparing of fatty acid oxidation Arch Biochem Biophys **57**, 23–28

25 Guo, W, Kirkland, J L, Corkey, B E and Hamilton, J. A (1998) A ^{13}C nuclear magnetic resonance study of free fatty acid incorporation in acylated lipids in differentiating preadipocytes. Lipids **33**, 449–454

26 Kamp, F and Hamilton, J A (1993) Movement of fatty acids, fatty acid analogues, and bile acids across phospholipid bilayers Biochemistry **32**, 11074–11086

27 Guo, W, Choi, J.-K, Kirkland, J L, Corkey, B E and Hamilton, J A (1999) Incorporation of [1-^{13}C]oleate into cellular triglycerides in differentiating 3T3L1 cells Lipids **34**, 825–831

28 Labarca, C. and Paigen, K (1980) A simple, rapid, and sensitive DNA assay procedure Anal Biochem **102**, 344–352

29 Kozakvak, L P. and Jensen, J. T (1974) Genetic and developmental control of multiple forms of glycerol-3-phosphate dehydrogenase J Biol Chem **249**, 7775–7781

30 Homan, R., Grossman, J E and Pownall, H J (1991) Differential effects of eicosapentaenoic acid and oleic acid on lipid synthesis and secretion by HepG2 cells J Lipid Res **32**, 231–241

31 Soma, M R, Mims, M P, Chan, M V, Rees, D and Morrisett, J D (1992) Triglyceride metabolism in 3T3–L1 cells An *in vivo* ^{13}C NMR study J Biol Chem **267**, 11168–11175

32 Lin, C. Y, Abraham, S and Smith, S (1976) Acyl specificity in triglyceride synthesis by lactating rat mammary gland J Lipid Res **7**, 647–656

33 Glenn, K C, Shieh, J. J and Laird, D M (1992) Characterization of 3T3–L1 storage lipid metabolism effects of somatotropin and insulin on specific pathways. Endocrinology **131**, 1115–1124

34 Green, H and Kehinde, O (1975) An established preadipose cell line and its differentiation in culture II Factors affecting the adipose conversion Cell **5**, 19–27

35 Shillabeer, G, Forden, J. M and Lau, D C (1989) Induction of preadipocyte differentiation by mature fat cells in the rat J Clin Invest **84**, 381–387

36 Jump, D B, Clarke, S D, Thelen, A, Liimatta, M, Ren, B and Badin, M V (1997) Dietary fat, genes, and human health Adv Exp Med Biol **422**, 167–176

37 Friedman, M. I and Tordoff, M G (1986) Fatty acid oxidation and glucose utilization interact to control food intake in rats. Am J Physiol **251**, R840–R845

38 Pahl-Wostl, C and Seelig, J (1987) Ketogenesis in the liver followed by ^{13}C NMR spectroscopy Infusion of [1-^{13}C]octanoate. Biol Chem **368**, 305–314

39 Knittle, J. L and Hirsch, J (1965) Effect of chain length on rates of uptake of free fatty acids during *in vitro* incubations of rat adipose tissue J. Lipid Res **6**, 565–571

Received 13 January 2000/22 March 2000, accepted 12 April 2000

40 Aas, M (1971) Organ and subcellular distribution of fatty acid activating enzymes in the rat. Biochim Biophys Acta **231**, 32–47

41 Brindley, D. N (1985) Metabolism of triacylglycerol, In Biochemistry of Lipids and Membranes (Vance, D E and Vance, J E, eds), pp. 213–241, Benjamin/Cumming Publishing Company, Reading, MA

42 Wertheimer, H E (1965) Adipose Tissue (Renold, A E and Cahill, Jr, G F, eds), pp 5–11, American Physiological Society, Washington DC

43 Deckelbaum, R J, Hamilton, J A, Moser, A, Bengtsson-Olivecrona, G, Butbul, E, Carpentier, Y, Gutman, A and Olivecrona, T (1990) Medium-chain versus long-chain triacylglycerol emulsion hydrolysis by lipoprotein lipase and hepatic lipase implications for the mechanisms of lipase action. Biochemistry **29**, 1136–1142

44 Belfrage, P, Fredrikson, G, Nilsson, N O and Strofors, P (1981) Regulation of adipose-tissue lipolysis by phosphorylation of hormone-sensitive lipase Int J Obes **5**, 635–641

45 Amri, E-Z, Ailhaud, G and Grimaldi, P-A (1994) Fatty acids as signal transducing molecules. involvement in the differentiation of preadipose to adipose cells J Lipid Res **35**, 930–937

46 Distel, R J., Robinson, G. S and Spiegelman, B. M (1992) Fatty acid regulation of gene expression transcriptional and post-transcriptional mechanisms J Biol. Chem **267**, 5937–5941

47 Schoonjans, K, Watanabe, M, Suzuki, H, Mahfoudi, A, Krey, G, Wahli, W, Grimaldi, P, Staels, B, Yamamoto, T and Auwerx, J (1995) Induction of the acyl-Coenzyme A synthetase gene by fibrates and fatty acids is mediated by a peroxisome proliferator response element in the C promotor J Biol Chem **270**, 19269–19276

48 Faergeman, N J and Knudsen, J. (1997) Role of long-chain fatty acyl-CoA esters in the regulation of metabolism and in cell signalling. Biochem J **323**, 1–12

49 Prentki, M and Corkey, B E (1996) Are the b-cell signaling molecules malonyl-CoA and cytosolic long-chain acyl-CoA implicated in multiple tissue defects of obesity and NIDDM? Diabetes **45**, 273–283

50 Faust, I. M, Johnson, P R, Stern, J S and Hirsch, J (1978) Diet-induced adipocyte number increase in adult rats a new model of obesity Am J Physiol **235**, E279–E286

51 Hirsch, J and Batchelor, B (1976) Adipose tissue cellularity and human obesity Clin Endocrinol Metab **5**, 299–311

52 Shillabeer, G. and Lau, D. C. W (1994) Regulation of new fat cell formation in rats the role of dietary fats J Lipid Res **35**, 592–600

Link peptide cartilage growth factor is degraded by membrane proteinases

Michael F. DEAN[1] and Paul SANSOM

Department of Veterinary Basic Sciences, The Royal Veterinary College, University of London, Royal College Street, London NW1 0TU, U.K.

The peptide DHLSDNYTLDHDRAIH (Link N), cleaved from the N-terminus of the link protein component of cartilage proteoglycan aggregates by the action of stromelysin, can act as a growth factor and stimulate synthesis of proteoglycans and collagen in articular cartilage [McKenna, Liu, Sansom and Dean (1998) Arthritis Rheum. **41**, 157–161]. The mechanism by which this biologically active peptide is degraded and inactivated was investigated using U937 monocytes as a model cell. Time-course experiments showed that two major proteases, an initial serine proteinase followed by a metalloproteinase, acted in sequence. Analysis of the resulting fragments showed that the serine endopeptidase cleavage was at the Leu^3–Ser^4 bond to produce the peptide SDNYTLDHDRAIH. The terminal serine could then be removed from the resulting peptide by an aminopeptidase. A second metallopeptidase liberated the peptides SDNYTL or DNYTL from DHDRAIH by cleavage at the Leu^9–Asp^{10} bond. The DNYTL peptide intermediate was degraded too rapidly to allow sequencing and sequential aminopeptidase cleavages removed further amino acids from the N-terminus of the remaining DHDRAIH peptide. The identical patterns of breakdown that occurred when either whole cells or purified plasma membranes were used indicated that proteolysis and inactivation of Link N was carried out entirely by membrane-associated enzymes.

Key words: cartilage, cell membranes, link peptide, proteinase.

INTRODUCTION

Normal articular cartilage is in a state of dynamic equilibrium, with turnover and repair regulated by the interaction of chondrocytes with a number of factors that may act during development, growth and maintenance. Among these are transforming growth factor β and insulin-like growth factor-1, which can up-regulate synthesis of aggrecan, collagen, link protein and hyaluronan [1–3]. Another growth factor, human osteogenic protein-1, can stimulate synthesis of proteoglycans and collagen type II in chondrocytes cultured in alginate beads [4]. In contrast, cytokines such as interleukin-1 and tumour necrosis factor α have opposite effects and can induce chondrocytes to down-regulate proteoglycan and type-II collagen synthesis [5,6] and increase synthesis of stromelysin and collagenase [7,8]. An imbalance in any of these control mechanisms can lead eventually to a loss of cartilage.

Synthesis and degradation of cartilage matrix may also be regulated by interaction of chondrocytes with matrix molecules themselves, or fragments derived from them by proteolysis. One of these is link protein, which comprises approx. 0.05 % of the wet weight of cartilage [9], is synthesized as a single gene product [10] and is glycosylated to generate two mature forms of 48 kDa and 44 kDa. Its primary role in articular cartilage is to stabilize the interaction of the proteoglycan aggrecan with hyaluronan [11]. As cartilage ages, a 41-kDa form of link protein resulting from cleavage of the His^{16}–Ile^{17} bond by the enzyme stromelysin accumulates [12,13]. We postulated that this cleaved N-terminal peptide, called the N-terminal link-protein peptide or Link N, may have an additional function as a cartilage growth factor [14]. Nanomolar concentrations of this peptide were shown subsequently to stimulate synthesis of proteoglycans and collagen in normal articular cartilage from a wide age range of subjects [15,16]. The newly synthesized proteoglycans had a normal composition and were therefore capable of being integrated into a viable cartilage matrix [17].

A number of other biologically active proteins involved in joint metabolism are synthesized as propeptides that require specific proteolysis to become active [18].These peptides have relatively short half-lives before they themselves are degraded and inactivated [19]. For example, substance P is found in increased levels in rheumatoid synovial fluid [20] and may contribute to early arthritis by activating inflammatory cells [21,22]. Its hydrolysis by the membrane proteinase CD10 produces a fragment (SP7-11) that can induce synthesis of collagenase by chondrocytes [23]. Another active peptide, neuropeptide Y, can increase the inflammatory response within joints [24] and may be degraded by cell-surface peptidases such as CD10 and CD26, which regulate its interconversion between receptor-selective forms and degraded inactive metabolites [25]. Many of these membrane peptidases are distributed widely [26], suggesting they have an important function in the regulation of peptide-mediated control of cell metabolism by either inactivating biologically active peptides or cleaving inactive peptides to form new active intermediates [27–30].

To determine whether link peptide is degraded by a similar mechanism, the sites of cleavage of link peptide were investigated using U937 monocytes because of the similarity of their proteinase profile to those of the main cell types found in synovial fluids during inflammatory episodes [31,32]. During these periods of inflammation degradation of Link N would be expected to be maximal. We now present data that show that link peptide itself is also rapidly degraded in a specific manner by plasma-membrane-associated peptidases. This may be the primary mechanism by which the effects of this peptide growth factor are controlled.

MATERIALS AND METHODS

Materials

Enzyme inhibitors were supplied by Sigma (Poole, Dorset, U.K.) and HPLC-grade solvents by Merck (Dagenham, Essex,

---

Abbreviations used: DFP, di-isopropylfluorophosphate; E64, *trans*-epoxysuccinyl-L-leucylamido-(4-guanido)butane; Link N, N-terminal link-protein peptide.

[1] To whom correspondence should be addressed (e-mail mdean@rvc.ac.uk).

U.K.). Tissue-culture medium, serum and Dulbecco's PBS were from Imperial Laboratories (Andover, Hants., U.K.). Protein assay reagents were obtained from Bio-Rad Laboratories (Hemel Hempstead, Herts., U.K.) and $Na^{125}I$ was from Amersham (Little Chalfont, Bucks., U.K.). All other reagents were from Sigma and were of analytical grade.

Synthetic peptides

The N-terminal peptide DHLSDNYTLDHDRAIH (Link N) was synthesized at the National Institute for Medical Research, Mill Hill, London, U.K., using stepwise solid-phase synthesis with Fmoc (fluoren-9-ylmethoxycarbonyl) chemistry on an Applied Biosystems 431a Automatic Peptide Synthesiser. Its homogeneity was determined by C_4 reversed-phase HPLC and fast-atom bombardment MS. It was purified on a Gilson HPLC fitted with a 250 mm × 4.6 mm Dynamax 300 Å C_{18} reversed-phase column (Rainin Instrument Co.) using a linear gradient of 0 1 % trifluoroacetic acid (solvent A) and acetonitrile/0.086 % trifluoroacetic acid (solvent B) at a flow rate of 1.0 ml/min. Unlabelled peptides were detected by peptide-bond absorption at 206 nm using a Gilson System Controller and the radioactivity of iodinated peptides measured with a Berthold LB-206 on-line monitor and flow cell. Column performance was monitored using standard samples of trypsinized horse cytochrome *c* eluted with a 5–45 % gradient of solvent B.

Radio-iodination of peptides

Iodo-beads were added to 500-μl aliquots of Link N dissolved at a concentration of 1 mg/ml in PBS. After 5 min, 500 μCi of $Na^{125}I$ was added, the mixture agitated for 30 min and the iodinated peptide solution removed and stored at 4 °C. Incorporation was routinely > 99.9 %, to produce a specific radioactivity of 1.0 mCi/mg of Link N. Working solutions of iodo-Link N were prepared by dilution of this stock peptide with RPMI 1640 culture medium or PBS.

Preparation of membranes

Samples of cells were washed with PBS and suspended at a concentration of 1×10^8 in 5 ml of buffer C (5 mM Tris/HCl, 1 mM sodium bicarbonate, 5 mM magnesium chloride, 1 mM calcium chloride, pH 7.4) for 20 min to allow swelling. After 20 min at a pressure of 65 psi ($\equiv$ 448.5 kPa) in a Nitrogen Bomb the cells were disrupted by cavitation and nuclei and cell debris removed by centrifugation at 1000 ***g***. The lysate was pelleted at 100000 ***g*** for 1 h (in a Beckman TL-100 ultracentrifuge), washed with 10 mM Tris/HCl, pH 7.4, and resuspended in 200 μl of 10 mM CHAPS/10 mM Tris/HCl, pH 7.4. Aliquots of this solution were used to measure the effects of whole-cell lysates on cleavage of Link N. Subcellular fractions were prepared on discontinuous sucrose gradients [33]. The lysate (A layer) was layered over a gradient of 2 ml of 20 % (w/v) sucrose (B layer), 42 % sucrose (C layer) and 70 % sucrose (D layer) in lysis buffer and centrifuged at 52000 ***g*** for 60 min. The microsomes (A/B interface), plasma membranes (B/C interface) and lysosomal fraction (C/D interface) were then diluted with buffer and pelleted at 100000 ***g*** for 60 min. The plasma-membrane fraction pellet was resuspended in 200 μl of Tris buffer, pH 7.4, and this stock was diluted when required for peptide-cleavage experiments to produce a membrane solution equivalent to 5×10^6 cells per 50 μl. The protein content of each fraction was determined with the Bio-Rad protein reagent using bovine serum globulin as a standard. This procedure successfully purified plasma membranes, resulting in a 5-fold enrichment of leucine aminopeptidase from 1.0 to 5.3 units/mg in a fraction that contained less than 10 % of the total protein. There was an accompanying 3-fold enrichment of β-D-glucuronidase from 1.0 to 2.7 units/mg in the lysosomal fraction.

Enzyme assays

To determine the leucine aminopeptidase activity of membranes, 50-μl aliquots were mixed with 150 μl of leucine *p*-nitroanilide (1 mg per ml in 10 mM Tris/HCl, pH 7.4) in a 96-well microtitre plate. Absorbance was read at 405 nm after 1 h at 37 °C and a unit of activity calculated as being equivalent to the increase in absorbance produced by 1 mg of membrane in 1 h. β-D-Glucuronidase activity was used as a marker of lysosomal membranes. For this, 10 μl of membrane were mixed with 2 ml of 1 mM 4-methylumbelliferyl β-D-glucuronide in 0.1 M sodium acetate, pH 4.5, at 37 °C for 30 min. The reaction was stopped with 3 ml of 0.4 M glycine buffer, pH 10.4, and the rate of release of methylumbelliferone measured on a Locarte fluorimeter. A unit of activity was equivalent to the change in fluorescence produced by 1 mg of membrane in 30 min.

Proteolysis of Link N by U937 monocytes

Human U937 monocytes were maintained as suspension cultures in RPMI 1640 medium containing 5 % heat-inactivated foetal bovine serum, 100 units/ml penicillin, 100 mg/ml streptomycin and 2 mM L-glutamine in a humidified atmosphere of 5 % CO_2 at 37 °C Cell viability routinely exceeded 95 % by Trypan-Blue exclusion. Aliquots of cells (50 μl, containing 10^6 cells in serum-free RPMI) were mixed with aliquots of iodinated Link N (0.1 μCi in 50 μl of RPMI) and incubated at 37 °C. For membrane experiments, aliquots of plasma membranes (50 μl, equivalent to 5×10^6 cells) were added to 50 μl of iodo-Link N and incubated at 37 °C. Proteolysis was terminated by the addition of 200 μl of 0.1 % trifluoroacetic acid followed by filtration of the samples (pore size 0.22 mm, Millipore) and proteolysis measured by HPLC. When proteinase inhibitors were used these were dissolved in ethanol or DMSO to produce 100-times-concentrated stock solutions. These were added to cell or membrane samples to give the required final concentrations 10 min before the addition of Link N. Control experiments used equivalent volumes of inhibitor solvents alone.

Sequence analysis of peptides

Degradation of Link N was measured by incubation of 100-μl samples of unlabelled peptide (1 mg/ml in PBS) at 37 °C with 10^7 U937 monocytes or with 50 μl of a 2 μg/ml solution of plasma membranes (equivalent to 2.5×10^7 cells). Incubation was terminated by adding 200 μl of 0.1 % trifluoroacetic acid and filtration through a 0.22-mm filter. The resulting peptides were separated by reversed-phase HPLC and analysed by solid-phase sequencing (Protein Sequencing Service at the National Institute for Medical Research). Some peptides were also analysed by fast-atom bombardment MS (Department of Chemistry, University of Manchester Institute of Science and Technology, Manchester, U.K.).

RESULTS

Proteolysis of Link N

Initial time-course experiments were carried out using U937 cells in RPMI medium, which contained components that interfered with the detection of peptides at both 206 nm and 280 nm. To

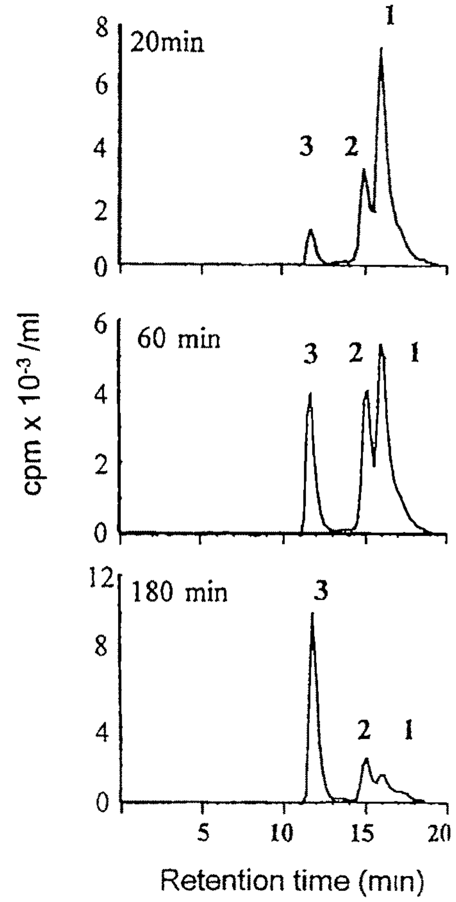

Figure 1 Processing of iodinated Link N by U937 cells

Iodinated Link N (0 2 μCi, equivalent to 200 ng of peptide) was incubated with 1 × 10^6 U937 cells in 100 μl of RPMI 1640 and aliquots taken for analysis by C_{18} reversed-phase HPLC Radiolabel was detected by on-line gamma counting and expressed as c p m /ml

Table 1 Effect of proteinase inhibitors on cleavage of iodinated Link N by U937 cells

U937 cells (1 × 10^6) were pre-incubated for 10 min with inhibitors prior to the addition of 0 2 μCi of iodinated Link N. Incubation was terminated after 60 min by addition of 0 2% trifluoroacetic acid, and aliquots analysed by C_{18} reversed-phase HPLC. Values are the percentage of total counts present in each peak Peak numbers are those indicated in Figure 1

Treatment	Peak 1 (% Total counts)	Peak 2 (% Total counts)	Peak 3 (% Total counts)
Control	45	27	28
0 2 mM PMSF	86	8	6
1 0 mM DFP	46	25	29
1 0 mM Phenanthroline	69	28	3
1 0 mM EDTA	45	35	20
1 0 mM E64	45	26	28
2 0 mM Iodoacetamide	78	18	4
2 0 mM Pepstatin A	45	27	28

avoid complications in interpretation of chromatographs due to these interfering components, an alternative method of peptide detection was used. It had been shown previously that ^{125}I could be incorporated into the Tyr^7 residue of Link N, and that this radiolabel could be used to measure cleavage [14]. Iodinated Link N peptides could be detected by gamma counting without interference from exogenous factors. Cleavage of this labelled peptide was rapid, resulting in conversion of Link N peptide (Figure 1, peak 1, retention time 16.0 min) into a single labelled product (Figure 1, peak 3, retention time 11.6 min) in less than 4 h under the conditions used (Figure 1). An additional peak with a retention time of 15.1 min accumulated and then disappeared, suggesting that there were two sequential cleavages; conversion of peak 1 into the intermediate 2, which was in turn converted into 3. Incubation of iodinated Link N in medium alone induced no breakdown of the peptide and medium that had been conditioned by prior incubation with monocytes also had no effect, indicating that the enzymes responsible for these cleavages were cell-associated and had not been secreted. Breakdown of

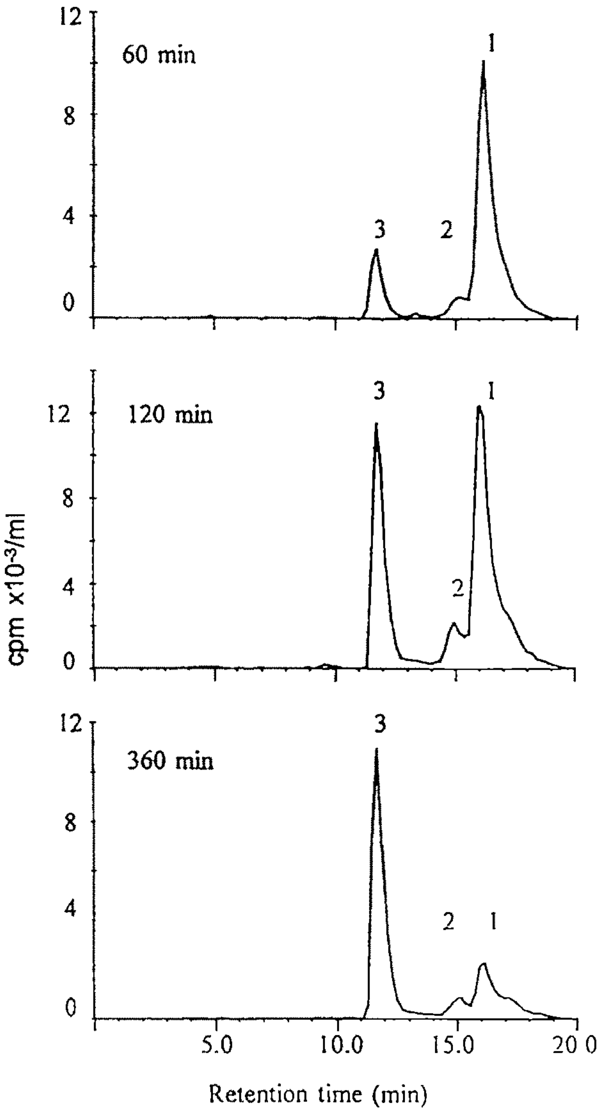

Figure 2 Processing of iodinated Link N by U937 plasma membranes

Iodinated Link N (0.2 μCi, equivalent to 200 ng of peptide) was incubated with a plasma-membrane fraction equivalent to 5 × 10^6 cells in a volume of 100 μl and aliquots taken for analysis by C_{18} reversed-phase HPLC Radiolabel was detected by on-line gamma counting and expressed as c p m /ml

Table 2 Effect of proteinase inhibitors on cleavage of iodinated Link N by U937 plasma membranes

U937 plasma membranes, equivalent to 5 × 10^6 cells, were pre-incubated for 10 min with inhibitors before the addition of 0.2 μCi of iodinated Link N. Incubation was terminated after 60 min by addition of 0.2% trifluoroacetic acid, and aliquots analysed by C_{18} reversed-phase HPLC. Values are the percentage of total counts present in each peak. Peak numbers relate to those indicated in Figure 2.

Treatment	Peak 1 (% Total counts)	Peak 2 (% Total counts)	Peak 3 (% Total counts)
Control	41	10	49
0.2 mM PMSF	80	5	15
1.0 mM DFP	42	9	49
1.0 mM Phenanthroline	83	16	1
1.0 mM EDTA	42	14	44
1.0 mM E64	41	10	49
2.0 mM Iodoacetamide	88	11	1
2.0 mM Pepstatin A	41	10	49

Link N was inhibited almost completely by the serine proteinase inhibitor PMSF, by the metalloproteinase inhibitor 1,10-phenanthroline and also by iodoacetamide (Table 1), although none of these prevented cleavage completely. In contrast, di-isopropyl-fluorophosphate (DFP), *trans*-epoxysuccinyl-L-leucylamido-(4-guanido)butane (E64) and pepstatin A had no effect. EDTA did not prevent breakdown of the starting peptide but did inhibit conversion of the intermediate peak 2 into peak 3, suggesting that different enzymes were responsible for each cleavage. The inhibitor solvents alone (DMSO or ethanol) did not inhibit proteolysis.

When whole-cell homogenates were tested on Link N before membrane fractionation, the peptide was degraded completely after 15 min of incubation. No clear sequence of cleavages could be deduced, unlike the distinct pattern of cleavages observed when whole cells were used. When purified plasma membranes in PBS were used in place of whole cells, however, an almost identical pattern of cleavage was seen. Link N (Figure 2, peak 1, retention time 16.0 min) was again converted into a single labelled final product (Figure 2, peak 3, retention time 11.7 min) in 6 h. An intermediate peak (Figure 2, peak 2, retention time 15.0 min) again accumulated but less rapidly, reaching a maximum of 15 % of the total label after 2 h of incubation, compared with a maximum of 40 % when the peptide was degraded by whole cells.

As with whole cells, breakdown of the peptide by membranes was inhibited by PMSF, 1,10-phenanthroline and iodoacetamide (Table 2). EDTA did not affect breakdown of the starting peptide but did inhibit further processing of the intermediate peak 2. Again, DFP, E64 and pepstatin A had no significant effect on either cleavage. These data showed that the pattern of proteolysis observed with intact cells was duplicated by plasma membranes and involved at least two sequentially acting enzymes. The relative activities of each of these had altered slightly during membrane preparation, giving rise to the small differences observed in the relative rates of cleavage. The specific inhibitors of membrane proteinases captopril and phosphoramidon (10 μM) had no measurable effect on cleavage of Link N but bestatin, an aminopeptidase inhibitor, reduced breakdown to less than 5 % of uninhibited controls.

Determination of cleavage sites

To produce sufficient quantities of peptides for direct amino acid analysis and mass analysis, microgram quantities of unlabelled Link N in PBS, which contained no interfering peptides, were used as a substrate to determine the sites of cleavage. Four major peaks were resolved when the peptide was degraded by intact cells (Figure 3). Peak c1, the parent peptide, was not sequenced. Peak c2 (retention time 14.0 min) and peak c3 (9.8 min) were both resolved as double peaks, which is often characteristic of a C-terminal histidine residue, which may be present as both D and L isomers that can be distinguished when peptides are detected by absorption at 206 nm. Peak c4 (6.8 min) was resolved as a single

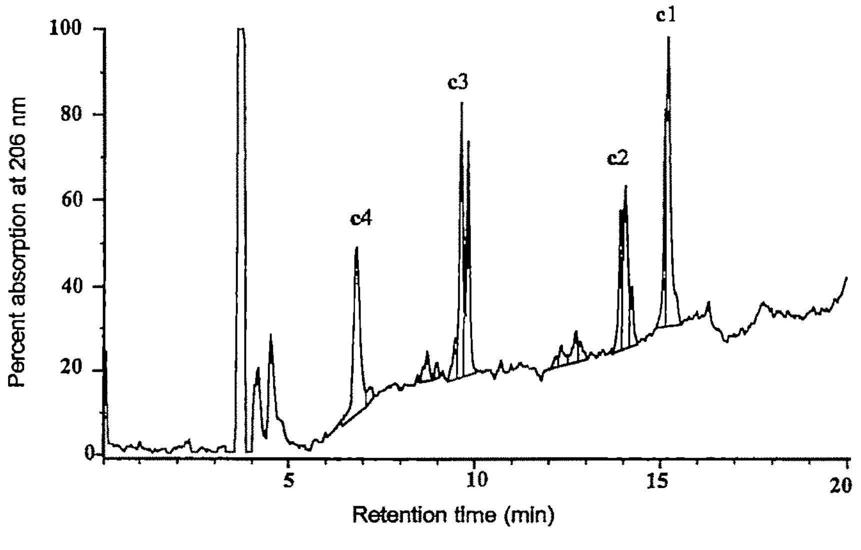

Figure 3 Cleavage of Link N by U937 cells

Link N (100 μg) was incubated for 4 h with 5 × 10^6 cells in 200 μl of PBS and the peptides separated for sequence analysis by C_{18} reversed-phase HPLC. Peptides were detected by absorbance of peptide bonds at 206 nm and expressed as a percentage of maximal absorption on an adjustable scale

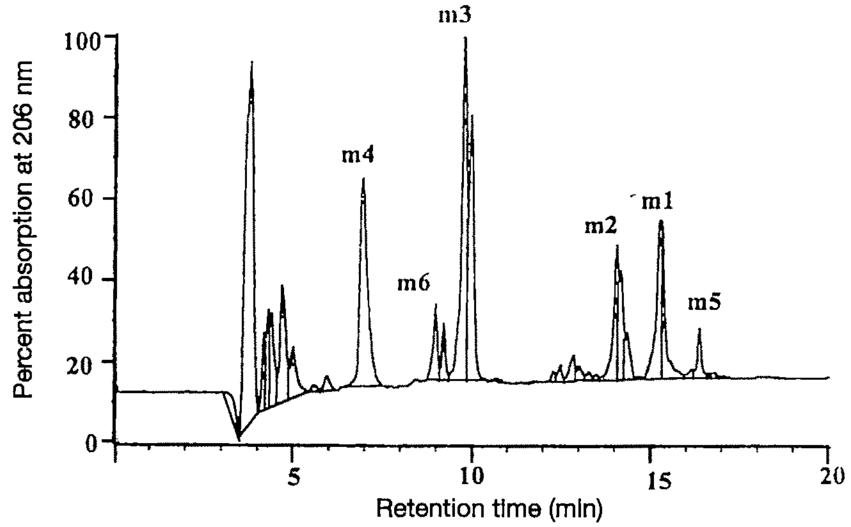

Figure 4 Cleavage of Link N by U937 plasma membranes

Link N (100 μg) was incubated for 24 h with plasma membranes equivalent to 1 × 10^7 cells in 200 μl of PBS and the peptides separated by C_{18} reversed-phase HPLC Peptides were detected by absorbance of peptide bonds at 206 nm and expressed as a percentage of maximal absorption on an adjustable scale

component and therefore did not contain sequences from the C-terminal end of the peptide. The supernatant solution from cells that had been incubated in PBS for 24 h contained no detectable peptides and there was no breakdown of Link N when it was incubated in PBS alone, showing that each of these components had been derived by cell-mediated proteolysis.

The similarity in retention times of peaks 2 and 3 (Figure 1) resulting from cleavage of either iodinated or unlabelled Link N suggested that they had identical sequences. Analysis of these products showed that peaks c2 and c3 were N-terminally truncated forms of Link N with sequences DNYTLDHDRAIH and DHDRAIH respectively. Although peak c3 did not contain any measurable tyrosine, its retention time corresponded to that of peak 3 derived from iodinated Link N, suggesting that it may have co-eluted with a minor tyrosine-containing peptide having an identical retention time. No clearly defined sequence could be assigned to peak c4 The identities of peaks c2 and c3 were confirmed by mass spectral analysis, which gave values of 1472 Da and 862 Da, respectively, identical to those predicted from their amino acid compositions.

Analysis of the peptides produced from Link N by isolated plasma membranes showed that the same three peaks (peaks **m2**, **m3** and **m4**, Figure 4), corresponding to peaks c2, c3 and c4 (Figure 3) were present. Peak **m2** (retention time 14.0 min) and peak **m3** (retention time 9.8 min) again had the double peak characteristic of a C-terminal histidine and corresponded to peaks 2 and 3 derived from iodinated Link N (Figure 2). Peak **m4** (retention time 6.8 min) was again present as a single peak and two further peptides, present in only trace amounts when whole cells were used, were resolved. Peptide **m5** had a retention time of 16.4 min, greater than that of the starting peptide and peak **m6** (retention time 9.0 min) had the double peak characteristic of a C-terminal histidine. These additional peaks may have been present in larger proportions than when whole cells were used because of the increased time of incubation used for membrane experiments.

Sequence analysis of the peptides produced by plasma membranes showed that there was a somewhat more complex mechanism of breakdown than had been observed with intact cells (Table 3). Peak **m2** was a mixture of three unresolved peptides with the same retention times but each with a different N-terminus. These consisted of the sequence DNYTLDHDRAIH together with two related peptides containing one more or one less amino acid. Peak **m3** was again identified as DHDRAIH and did not therefore contain tyrosine, although its retention time suggested that it may have corresponded to peak 3 derived from iodinated Link N. The new peak **m6** was a peptide from which two further N-terminal amino acids had been removed to produce the product DRAIH. Peak **m4** contained free tyrosine and leucine but peak **m5** could not be identified by direct sequence analysis.

Table 3 Sequences of Link N cleavage fragments produced by plasma membranes

The sequences of the cleavage fragments are those present in each of the components shown in Figure 4

Peak	Retention time (min)	Sequence
m2	14.0	SDNYTLDHDRAIH DNYTLDHDRAIH NYTLDHDRAIH
m3	9.8	DHDRAIH
m4	6.8	Y, L
m5	16.4	Not sequenced
m6	9.0	DRAIH

DISCUSSION

Earlier experiments have shown that the cartilage-derived growth factor Link N is rapidly degraded by a variety of different cell types, including chondrocytes and macrophages [14]. A similar method of inactivation has been described for a number of other small, biologically active peptides [26]. Proteinases not normally synthesized by chondrocytes have been identified in articular cartilage and are thought to originate from neutrophils, macro-

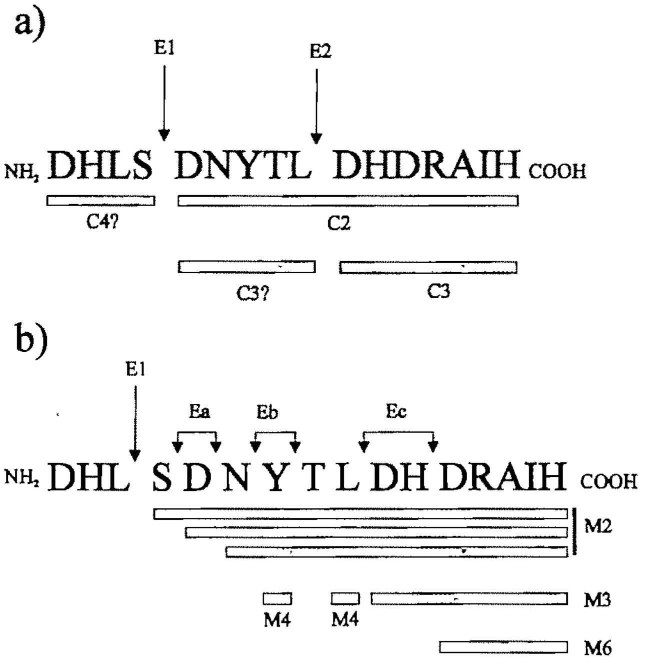
a)
E1
E2
NH₂ DHLS DNYTL DHDRAIH COOH
C4?
C2
C3?
C3
b)
E1
Ea
Eb
Ec
NH₂ DHL S D N Y T L DH DRAIH COOH
M2
M3
M4
M4
M6

Figure 5 Proposed scheme for cleavage of Link N

(**a**) The initial scheme proposed for cleavage of Link N by intact cells involved the first cleavage by a serine protease E1 at Ser^4–Asp^5 followed by a cleavage by the metalloprotease E2 at Leu^9–Asp^{10} **c**2 and **c**3 are peptides with known sequences, **c**3 and **c**4 are deduced assignments (**b**) The scheme proposed for cleavage of Link N by purified plasma membranes An obligatory initial cleavage by a serine protease E1 at Leu^3–Ser^4 is followed by sequential aminopeptidase cleavages Ea represents known sites of aminopeptidase cleavage and Eb sites of cleavage that must occur to liberate free tyrosine The endopeptidase represented by Ec corresponds to the EDTA-inhibitable enzyme E2 The peptides designated **m2**–**m6** correspond to peaks **m2**–**m6** depicted in Figure 4

phages, synoviocytes and lymphocytes [34]. One or more of these proteinases may be responsible for cleavage and inactivation of Link N. U937 monocytes were therefore chosen to investigate the mechanism and sites of cleavage because of the similarity of their proteinase profile to those of the main cell types found in synovial fluids during episodes of inflammation [31,32] when degradation of Link N would be expected to be maximal.

Time-course experiments using radio-iodinated Link N showed that at least two cell-associated proteinases were involved in its cleavage to produce a final labelled product Since PMSF abolished degradation of Link N almost completely, this first cleavage appeared to be essential before cleavage of the resulting intermediate radiolabelled peptide by the second, EDTA-sensitive, peptidase could take place. Phenanthroline inhibited both enzymes, suggesting that the enzyme responsible for the first cleavage may have been a metal-dependent serine protease. Although iodoacetamide also inhibited breakdown, the lack of action of E64, a specific thiol-protease inhibitor, indicated that this may have been a non-specific effect.

When unlabelled Link N was used as a substrate, several additional peptides that did not contain a labelled tyrosine were resolved. Sequencing of these suggested that the initial cleavage of the peptide at Ser^4–Asp^5 by an unknown serine proteinase E1 had released the peptide DHLS (corresponding to component **c**4) from Link N The subsequent cleavage of the remaining peptide DNYTLDHDRAIH at the Leu^9–Asp^{10} bond by the metalloproteinase E2, as depicted in Figure 5(a), released the remaining peptide DHDRAIH from DNYTL, which may have co-eluted with peak **c**3 but have been degraded too rapidly to be detected during sequencing. This would account for the presence of tyrosine in this fraction when iodinated peptide was used as a substrate.

The profile of Link N breakdown produced by U937 plasma membranes (Figure 4) was almost identical to but more complex than that seen with whole cells (Figure 3), indicating that the mechanism of degradation was essentially the same and involved membrane-associated proteinases. However, two additional minor peaks were detected that were present as trace amounts only when whole cells were used. Peak **m2** contained two additional peptides with either one more or one less amino acid in addition to the DNYTLDHDRAIH sequence. These data suggested that the initial serine proteinase E1 had removed a tripeptide DHL, not a tetrapeptide, and that the resulting sequence SDNYTLDHDRAIH had undergone further processing by the action of aminopeptidases. The sequence data for the breakdown of Link N by whole cells showed that trace quantities of serine were present as an alternative first residue to aspartate, indicating that when intact cells were used, cleavage of serine from the newly generated N-terminal of SDNYTLDHDRAIH was extremely rapid but was reduced when purified membranes were used. When the sequences of the peaks were determined, **m2** was shown to contain a Tyr^7 residue as expected and probably corresponded to the radiolabelled intermediate peak 2. However, **m3** was too truncated to contain tyrosine and it appeared that following cleavage of DHLS from Link N at Ser^4–Asp^5, the E2 cleavage liberated the peptide DNYTL from DNYTLDHDRAIH by cleavage at Leu^9–Asp^{10}. Although DNYTL was not detected by sequence analysis, it may have co-eluted with DHDRAIH, explaining the localization of the labelled peak **m3** derived from iodinated Link N to this region of the chromatograph. Peptide DNYTL was then degraded rapidly by the subsequent action of aminopeptidases and endopeptidases, as depicted in Figure 5(b). The initial cleavage by a serine-dependent protease was followed by a metallo-endopeptidase that cleaved the remaining peptide into two and sequential trimming by one or more aminopeptidases then released a series of sub-peptides.

The U937 cells used in these experiments express both elastase and cathepsin G, two proteinases that are important in the degradation of articular cartilage, either directly or through modulation of metalloproteinase activity [35–37]. Although these enzymes are normally lysosomal in origin, they have been purified from U937 plasma membranes [38] and either of these may have been responsible for this first cleavage. However, Link N was not cleaved by either a commercial preparation of human leucocyte elastase or by stromelysin itself (results not shown).

U937 plasma membranes also express a number of metallopeptidases. These include dipeptidyl peptidase IV (CD26), aminopeptidase N (CD 13), and angiotensin-converting enzyme [39,40]. A membrane-bound form of the metalloproteinase aggrecanase, which is inhibited by EDTA and the endopeptidase 24.11 (CD10) have also been described on chondrocytes [41,42]. Breakdown of Link N was not, however, inhibited by phosphoramidon, a specific inhibitor of endopeptidase 24.11, or by captopril, an inhibitor of angiotensin-converting enzyme. A membrane form of the thiol-dependent metalloendopeptidase thimet oligopeptidase has been described [43,44], athough it is not known whether this is expressed on U937 cells. This enzyme is able to cleave peptides ranging from 6 to 17 residues in length and like the Link N peptidases is inhibited by EDTA and phenanthroline but is unaffected by DFP or phosphoramidon [43]. Thimet oligopeptidase is known to inactivate a number of biologically active peptides including bradykinin, neurotensin, angiotensin, substance P and α endorphin and may therefore have been the enzyme responsible for one or more of the endopeptidase cleavages of Link N. Bestatin, a specific inhibitor of aminopeptidases, also inhibited cleavage of Link N, indicating that one or more of this group of enzymes may have been responsible for some of the additional N-terminal cleavages observed.

Membrane-peptidase-mediated inactivation of a large number of other biologically active peptides has been well documented [39,40]. Since data from previous experiments have shown that N- and C-terminally truncated link peptides with the sequences SDNYTLDHDR and DNYTLDHDR lost their ability to stimulate proteoglycan synthesis [15], it is probable that Link N was also inactivated by rapid specific cleavage mediated by membrane-associated proteinases.

We thank the Medical Research Council, Action Research and the Home of Rest for Horses for their financial support

REFERENCES

1 Hill, D J and Logan, A. (1992) Peptide growth factors and their interactions during chondrogenesis. Prog Growth Factor Res. **4**, 45–68

2 Malemud, C J (1993) The role of growth factors in cartilage metabolism Rheum Dis Clin. North Am **19**, 569–580

3 Trippel, S B (1995) Growth factor actions on articular cartilage J Rheumatol (**S43**) **22**, 129–132

4 Flechtenmacher, J, Huch, K, Thonar, E J-A, Mollenhauer, J. A, Davies, S R, Schmid, T., Puhl, W., Sampath, T K., Addelotte, M. B and Keuttner, K (1996) Recombinant human osteogenic protein 1 is a potent stimulator of the synthesis of cartilage proteoglycans and collagens by human articular cartilage Arthritis Rheum **39**, 1896–904

5 Arend, W P and Dayer, J-M (1995) Inhibition of the production and effects of interleukin-1 and tumour necrosis factor α in rheumatoid arthritis Arthritis Rheum **38**, 151–160

6 Goldring, M B, Birkhead, J, Sandell, L J, Kimura, T and Krane, S M (1988) Interleukin 1 supresses expression of cartilage specific types II and IX collagens and increases types I and III collagens in human chondrocytes J Clin. Invest **82**, 2026–2037

7 Hasty, K. A, Relfe, R A., Kang, A H. and Stuart, J M (1990) The role of stromelysin in the cartilage destruction that accompanies inflammatory arthritis Arthritis Rheum **33**, 388–397

8 Pelletier, J P, DiBattista, J A, Roughley, P, McCollum, R and Martel-Pelletier, J. (1993) Cytokines and inflammation in cartilage degradation Rheum Dis. Clin North Am. **19**, 545–568

9 Neame, P J and Barry, FP. (1993) The link proteins Experientia **49**, 393–402

10 Hering, T M and Sandell, L J (1990) Biosynthesis and processing of bovine cartilage link proteins. J Biol Chem **265**, 2375–2382

11 Hardingham, T E (1979) The role of link protein in the structure of cartilage proteoglycan aggregates. Biochem J **177**, 237–247

12 Mort, J S, Poole, A R and Roughley, P J (1983) Age-related changes in the structure of proteoglycan link proteins present in normal human articular cartilage Biochem J **214**, 269–272

13 Nguyen, Q, Liu, J., Roughley, P J. and Mort, J S. (1991) Link protein as a monitor *in situ* of endogenous proteolysis in adult human articular cartilage Biochem J **278**, 143–147

14 Martin, H and Dean, M F (1993) An N-terminal peptide from link protein is rapidly degraded by chondrocytes, monocytes and B cells Eur. J Biochem **212**, 87–94

15 McKenna, L A, Liu, H, Sansom, P. A and Dean, M F (1998) An N-terminal peptide from link protein stimulates proteoglycan biosynthesis in human articular cartilage *in vitro* Arthritis Rheum **41**, 157–161

16 Liu, H, McKenna, L A and Dean, M F (1999) An N-terminal link protein peptide stimulates biosynthesis of collagen by explants of human articular cartilage Trans 45th Orthop Res Soc (abstracts), p 17, Anaheim, U S A

17 Liu, H, McKenna, L A and Dean, M F (1999) The macromolecular characteristics of cartilage proteoglycans do not change when synthesis is upregulated by link protein peptide Biochim Biophys Acta **1428**, 191–200

18 Rangaraju, N S and Harris, R B (1991) Processing enzyme specificity is a consequence of pro-hormone precursor protein conformation Arch Biochem Biophys **290**, 418–426

19 Powell, M. F, Grey, H., Gaeta, F., Sette, A. and Colon, S. (1992) Peptide stability in drug development a comparison of peptide reactivity in different biological media J Pharmacol Sci **81**, 731–735

20 Matucci-Cerinic, M, Partsch, G, Marabini, S and Cagnoni, M (1991) High levels of substance P in rheumatoid arthritis synovial fluid and evidence that synoviocytes are not the major source of substance P Clin Exp Rheumatol **9**, 440–441

21 Lotz, M, Carson, D A. and Vaughn, J H (1987) Substance P activation of rheumatoid synoviocytes neutral pathway in pathogenesis of arthritis Science **235**, 893–895

22 Halliday, D. A, McNiel, J D and Scicchitano, R (1992) Failure of tachykinins including substance P and its fragments to influence proteoglycan and protein synthesis in bovine chondrocytes *in vitro* Biochim Biophys Acta **1137**, 29–33

23 Halliday, D A., McNeil, J D, Betts, W H and Scicchitano, R. (1993) The substance P fragment SP-(7–11) increases prostaglandin E2, intracellular Ca^{2+} and collagenase production in bovine articular chondrocytes Biochem J **292**, 57–62

24 Jorgensen, C and Sany, J (1994) Modulation of the immune response by the neuro-endocrine axis in rheumatoid arthritis. Clin Exp. Rheum **12**, 435–441

25 Medeiros, M S. and Turner, A J (1994) Post-secretory processing of regulatory peptides the pancreatic polypeptide family as a model example Biochimie **76**, 283–287

26 Turner, A. J and Barnes, K (1994) Neuropeptidases. candidate enzymes and techniques for study Biochem Soc. Trans **22**, 122–126

27 Matsas, R, Fulcher, I S, Kenny, A J. and Turner, A J (1983) Substance P and [Leu]enkephalin are hydrolysed by an enzyme in pig caudate synaptic membranes that is identical with the endopeptidase of kidney microvilli. Proc Natl Acad Sci U S A **80**, 3111–3115

28 Kenny, A J, O'Hare, M J. and Gusterson, B A (1989) Cell-surface peptidases as modulators of growth and differentiation Lancet **2**, 785

29 Naquet, P and Pierres, M (1991) Cell-surface enzymes and lymphocyte functions Curr Opin Immunol. **3**, 326–332

30 Rose, K., Savoy, L A, Muir, A V., Davies, J G., Offord, R E and Turcatti, G (1988) Insulin proteinase liberates from glucagon a fragment known to have enhanced activity against Ca^{2+}/Mg^{2+}-dependent ATPase. Biochem J **256**, 847–851

31 Moore, A R, Iwamura, H, Larbre, J P, Scott, D L and Willoughby, D A. (1993) Cartilage degradation by polymorphonuclear leucocytes: *in vitro* assessment of the pathogenic mechanisms Ann Rheum Dis. **52**, 27–31

32 Jensen, H S (1992) Elastolytic activity of human monocytes. rheumatological aspects Clin Exp Rheum **10**, 607–612

33 Chain, B M, Bou-Gharios, G and Olsen, I (1989) Endopeptidase activities associated with the plasma membrane compartment of an antigen-presenting B cell. Clin Exp. Immunol **75**, 87–92

34 Froelich, C. J., Zhang, X., Turbov, J, Hudig, D, Winkler, U. and Hanna, W L (1993) Human granzyme B degrades aggrecan proteoglycan in matrix synthesized by chondrocytes J Immunol. **151**, 7161–7171

35 Velvart, M. and Fehr, K (1987) Degradation *in vivo* of articular cartilage in rheumatoid arthritis and juvenile chronic arthritis by cathepsin G and elastase from polymorphonuclear leukocytes Rheumatol Int **7**, 195–202

36 Janusz, M J and Doherty, N S. (1991) Degradation of cartilage matrix proteoglycan by human neutrophils involves both elastase and cathepsin G J Immunol **146**, 3922–3928

37 McDonnell, J, Lobner, J M, Knight, W B, Lark, M W, Green, B, Poe, M and Moore, V L (1993) Comparison of the proteoglycanolytic activities of human leukocyte elastase and human cathepsin G *in vitro* and *in vivo* Connective Tiss Res. **30**, 1–9

38 Maison, C M., Villiers, C L and Colomb, M G. (1991) Proteolysis of C3 on U937 cell plasma membranes Purification of cathepsin G J Immunol. **147**, 921–926

39 Bauvois, B, Sanceau, J and Wietzerbin, J (1992) Human U937 cell surface peptidase activities. characterization and degradative effect on tumour necrosis factor-α Eur J Immunol **22**, 923–930

40 Laouar, A., Villiers, C, Sanceau, J, Maison, C, Colomb, M., Wietzerbin, J and Bauvois, B (1993) Inactivation of interleukin-6 *in vitro* by monoblastic U937 cell plasma membranes involves both protease and peptidyl-transferase activities. Eur J Biochem **215**, 825–831

41 Billington, C J, Clark, I M and Cawston, T E (1998) An aggrecan degrading activity associated with chondrocyte membranes Biochem J. **336**, 207–212

42 Kenny, A J, Bowes, M A, Gee, N. S and Matsas, R (1985) Endopeptidase-24 11 a cell surface enzyme for metabolising regulatory peptides. Biochem Soc Trans. **13**, 293–295

43 Dando, P M, Brown, M A and Barrett, A J (1993) Human thimet oligopeptidase. Biochem J **294**, 451–457

44 Barrett, A J and Brown, M A (1990) Chicken liver pz-peptidase, a thiol dependent metallo-endopeptidase Biochem J **271**, 701–706

Received 17 August 1999/16 March 2000, accepted 6 April 2000

Biochem J (2000) 349, 481–487 (Printed in Great Britain)

Evidence that 12-lipoxygenase product 12-hydroxyeicosatetraenoic acid activates p21-activated kinase

Yeshao WEN*, Jiali GU*, Ulla G. KNAUS†, Lisa THOMAS*, Noe GONZALES‡ and Jerry L. NADLER*[1]

*Division of Endocrinology and Metabolism, University of Virginia Health Sciences Center, MR4 Building Room 5150, Lane Road, Charlottesville, VA 22908, U.S.A., †Department of Immunology, The Scripps Research Institute, 10550 North Torrey Pines Road, La Jolla, CA 92037, U.S.A., and ‡Department of Diabetes, Endocrinology and Metabolism, City of Hope Medical Center, Gonda Building, 1500 East Duarte Road, Duarte, CA 91010, U.S.A.

The effect of 12-hydroxyeicosatetraenoic acid (12-HETE), an arachidonic acid metabolite of 12-lipoxygenase, to activate $p21^{Rac/Cdc42}$-activated kinase (PAK1) was studied in a Chinese hamster ovary fibroblast cell line overexpressing the rat vascular type-1a angiotensin II receptor (CHO-AT_{1a}). 12-HETE (0.1 μM) treatment induced a time-dependent activation of PAK1, with a peak effect at 10 min (335 ± 16 % of control; $n = 3$, $P < 0.001$). The stimulatory effect of 12-HETE on PAK1 activity was dose-dependent, with the maximal activation at 0.01 μM (350 ± 15 % of control; $n = 3$, $P < 0.001$). A PAK1 fragment encoding the Cdc42/Rac binding domain (amino acid residues 67–150 of hPAK1 termed PBD), was transfected into CHO-AT_{1a} cells. PBD transfection markedly reduced 12-HETE-induced PAK1 activation. Furthermore, transfection of dominant negative Cdc42 and Rac1 inhibited 12-HETE-induced PAK1, strongly suggesting that Cdc42 and Rac1 are the upstream activators of 12-HETE-induced PAK1 activation. Low concentrations (1.5 μM) of LY294002, a highly specific inhibitor of phosphoinositide 3-kinase (PI-3K), abolished 12-HETE-induced PAK1 activation, suggesting that PI-3K activation is upstream of 12-HETE-induced PAK1 activation. Transfection of dominant negative PAK1 blocked 12-HETE-induced PAK1, cJun N-terminal kinase (JNK1) and extracellular-signal-regulated kinase (ERK) activity, while transfection of constitutively active PAK1 stimulated PAK1, JNK1 and ERK activity, suggesting that PAK1 is an upstream activator of 12-HETE-induced JNK1 and ERK activation in these cells. We conclude that 12-HETE can activate Cdc42, Rac1 and PI-3K, which then participate as upstream signalling molecules for PAK1 and JNK1 activation.

Key words: Cdc42, phosphoinositide 3-kinase, Rac.

INTRODUCTION

p21-activated kinases (PAKs) are a novel group of 60–70 kDa serine/threonine kinases [1]. Several distinct members of the PAK family have been identified [2–5]. The C-terminal catalytic domain of PAKs is 60–70 % identical to *Saccharomyces cerevisiae* Ste20, an enzyme involved in linking pheromone-activated G protein-coupled receptors to a mitogen-activated protein (MAP) kinase cascade. The N-terminal segment of the PAK family of kinases contains a Cdc42/Rac interactive binding (CRIB) domain and several proline-rich sequences similar to canonical SH3 domain binding regions [6,7]. It has been demonstrated that glutathione S-transferase (GST) fusion proteins containing the SH3 domains of Nck and phospholipase Cγ can bind to PAK3 and PAK1 in an *in vitro* binding assay [6].

PAKs complex specifically with activated (GTP-bound) Cdc42 and Rac proteins, but not Rho proteins, leading to kinase autophosphorylation and activation, while GDP-bound forms of Rac and Cdc42 do not interact with the kinases [1]. The mechanism that underlies the stimulation of kinase activity by these GTP-binding proteins is not fully known. It is likely that the binding of the GTPase to an identified specific region, the CRIB domain, within the N-terminal half of the kinase releases a negative constraint [4]. New evidence shows that PAK proteins contain a basic region, consisting of three contiguous lysine residues (Lys^{66}-Lys^{67}-Lys^{68}) which lie outside of the previously identified CRIB and are required elements for Rac/PAK interaction [8]. It was also recently suggested that Rac functions downstream, instead of upstream, of phosphoinositide 3-kinase (PI-3K) in the insulin signalling cascade leading to activation of PAK65 [9].

Evidence has shown that Cdc42/Rac1 can activate the cJun N-terminal kinases (JNKs) and p38 MAP kinase in certain cell types upon co-transfection [10–13]. The potential candidates for coupling Cdc42/Rac1 to JNK are the PAK family, including PAK1, PAK2 and PAK3. PAK fragments that include the CRIB inhibit epidermal growth factor activation of JNK and interleukin-1 activation of p38. Moreover, constitutively active mutants of PAK1 or PAK3 activate JNK and p38 kinases upon co-transfection. However, the identity of the PAK substrate(s) that couple these kinases to stress-activated protein kinase/JNKs and p38 pathways and the mechanisms involved in this activation have not yet been elucidated [14].

The 12-lipoxygenase (12-LO) enzyme generates active lipids from arachidonic acid. The lipid products of 12-LO, including 12-hydroxyeicosatetraenoic acid (12-HETE), have been shown to lead to growth promoting or inflammatory changes in various types of cells. Our previous studies have demonstrated that 12-LO products can promote cell growth in Chinese hamster ovary fibroblasts stably overexpressing the angiotensin type Ia receptor (CHO-AT_{1a}) [15]. 12-HETE activates extracellular-signal-regulated kinase (ERK) [14] and JNK1 in CHO-AT_{1a} cells when added in the medium [16]. In the present study, we demonstrate for the first time that 12-LO products are able to activate PAK.

Abbreviations used: CHO-AT_{1a} cells, angiotensin II receptor-transfected Chinese hamster ovary cells; JNK, cJun N-terminal kinase; 12-HETE, 12-hydroxyeicosatetraenoic acid; LO, lipoxygenase; PAK, $p21^{Rac/Cdc42}$-activated kinase; PBD, $p21^{Rac/Cdc42}$ binding domain; CRIB, Rac/Cdc42 interactive binding domain; FBS, fetal bovine serum; DTT, dithiothreitol; MLK, mixed lineage kinase; PI-3K, phosphoinositide 3-kinase; ERK, extracellular-signal-regulated kinase; MKK, mitogen-activated protein kinase (MAPK) kinase; MEK, MAPK/ERK kinase.

[1] To whom correspondence should be addressed (e-mail jln2n@virginia.edu).

The data indicate that small-molecular-mass GTP-binding proteins are involved as upstream activators of PAK, and moreover, that PI-3K is involved in activating PAK in response to 12-HETE Finally, we demonstrate that PAK is an upstream activator of JNK and ERK in CHO-AT_{1a} cells.

MATERIALS AND METHODS

Reagents

Ham's F-12 medium and fetal bovine serum (FBS) were supplied by Irvine Scientific (Santa Ana, CA, U.S.A.). BSA (fatty acid free), leupeptin and aprotinin were from Sigma 12-HETE and LY294002 were from Biomol (Plymouth, Meeting, PA, U.S.A.). Wortmannin was from Alexis Corporation. Dr Michael Karin (UC San Diego, CA, U.S.A.) kindly provided the GST–cJun (amino acid residues 1–79) plasmid. JNK1 antibody was from Santa Cruz Biotechnology. [γ-^{32}P]ATP was from New England Nuclear Corp. (Bannockbure, IL, U.S.A.). PAK1 antibodies [2] and the following plasmids: pCVM6M–PBD (residues 67–150); wild-type PAK1; dominant negative PAK1, PAK1K299R, constitutively active PAK1, PAK1T423E; empty vector, pRK5; dominant negative Rac, pRK5–RacT17N; and dominant negative CDC42, pRK5–Cdc42T17N were used.

Cell culture and preparation of cell extracts

CHO-AT_{1a} cells were maintained in 100 mm dishes in Ham's F-12 media with 10% FBS, as described in [15–17] Cells were growth-arrested by incubation in depletion medium (Ham's F-12 medium containing 1 mg/ml BSA and 20 mM Hepes, pH 7.4, for 72 h prior to use. Cells were treated with 12-HETE in serum-free, BSA-containing medium. After washing twice with cold PBS, the cells were lysed by lysis buffer (50 mM Hepes, pH 7.5, 150 mM NaCl, 5 mM $MgCl_2$, 1 mM EGTA, 50 mM NaF, 10 mM sodium pyrophosphate, 1% Nonidet P40, 2.5% glycerol, and 1 mM sodium orthovanadate, containing the protease inhibitors PMSF, leupeptin and aprotinin) The lysate was centrifuged at 14000 × *g* at 4 °C for 10 min. Protein determination of lysate was done by the Bradford method.

Transient transfection in CHO-AT_{1a} cells

Plasmids used were endotoxin-free and prepared by EndoFree plasmid kit (Qiagen) using the standard protocol. The DNA-transfection method used was a cationic liposome-mediated transfection with DOSPER liposomal transfection reagent (Boehringer Mannheim) which followed the manufacturer's instructions. Briefly, the cells were plated the day before the transfection experiment at 3×10^6 cells per 100 mm dish. Next day, cells were washed with Opti-MEM® reduced-serum medium (Gibco BRL) and incubated in 5 ml of Ham's F-12 with 1% FBS. A 45 μg DOSPER/15 μg plasmid mixture was prepared and added to each dish After 5 h incubation the transfection medium was replaced and 8 ml of fresh depletion medium was added, containing 1% FBS, for overnight incubation. The cells were washed twice with depletion medium, incubated in the same medium for another 32 h, and harvested.

Immunoprecipitation and PAK1 activity assay

For immunoprecipitation, 300 μg of lysate protein was incubated with PAK1 antibody (1:20) [2] in the lysis buffer overnight at 4 °C, followed by incubation with 60 μl of a 50% slurry of Protein A beads for 60 min. After washing 3 times with lysis buffer and twice with kinase buffer, the kinase activity was measured in 60 μl of kinase buffer [50 mM Hepes, pH 7.4, 10 mM $MgCl_2$, 2 mM $MnCl_2$, and 0.2 mM dithiothreitol (DTT)] containing 2 μg of myelin basic protein and 20 μM ATP and 5 μCi of [γ-^{32}P]ATP. After incubation for 30 min at 30 °C, the reaction was stopped with 5 × Laemmli sample buffer and resolved on an SDS/12% polyacrylamide gel, followed by autoradiography.

Immunoprecipitation and Jun kinase assay

For immunoprecipitation, 50 μg of lysate protein in diluted WCE buffer (20 mM Hepes, pH 7.7, 75 mM NaCl, 2.5 mM $MgCl_2$, 0.1 mM EDTA, 0.05% Triton X-100, 0.5 mM DTT, 20 mM β-glycerophosphate, 0.1 mM sodium orthovanadate, 5 μg/ml leupeptin and aprotinin and 0.1 mM PMSF) was used, mixed with 10 μl of JNK-1 antibody, and the mixture was rotated at 4 °C overnight and added to 60 μl of Protein A–Sepharose. After 1 h incubation at 4 °C, the beads were washed 4 times with diluted WCE buffer, the pelleted beads were resuspended in 60 μl of kinase buffer, 20 mM Hepes at pH 7.6, 20 mM $MgCl_2$, 20 mM β-glycerophosphate, 20 mM *p*-nitrophenyl phosphate, 0.1 mM sodium orthovanadate and 2 mM DTT, containing 2 μg of GST–cJun (residues 1–79) and 20 μM ATP and 5 μCi of [γ-^{32}P]ATP. After 30 min at 30 °C, the reaction was stopped with 5 × Laemmli sample buffer and resolved on an SDS/12% polyacrylamide gel, followed by autoradiography. According to the manufacturer's data, the antibody JNK-1 is specific for the JNK-1 protein and does not react to any significant degree with JNK-2.

Immunoprecipitation and ERK assay

Immunoprecipitation and kinase assay were also used for ERK1 activity measurement. A 50 μg sample of lysate protein was added in 500 μl of ERK buffer [50 mM Hepes, pH 7.4, 1% Triton X-100, 80 mM β-glycerophosphate, 10 mM EGTA, 2 mM EDTA, 1 mM nitrophenyl phosphate, 10 mM NaF, 10 mM pyrophosphate, 1 mM sodium orthovanadate, 20 μg/ml of leupeptin and aprotinin, and 0.1 mM PMSF) and mixed with 10 μl of ERK1 antibody. The mixture was rotated at 4 °C overnight, then the solution was added to 60 μl of Protein A–Sepharose. After 1 h incubation at 4 °C, the beads were washed 4 times with diluted ERK buffer, the pelleted beads were resuspended in 60 μl of kinase buffer (20 mM Hepes at pH 7.4, 10 mM $MgCl_2$, 5 mM β-glycerophosphate, 20 mM *p*-nitrophenyl phosphate, 0.1 mM sodium orthovanadate, 2 mM DTT, 2 μg of myelin basic protein and 20 μM ATP and 5 μCi of [γ-^{32}P]ATP). After 30 min at 30 °C, the reaction was stopped with 5 × Laemmli sample buffer and resolved on an SDS/12% polyacrylamide gel, followed by autoradiography. The antibody against ERK1 was from Santa Cruz.

Detection of PAK1 and PAK2 in CHO-AT_{1a} cells by immunoblotting

A sample of protein (20–30 μg) from CHO-AT_{1a} cell lysate was resolved with SDS/7.5% PAGE, transferred on to nitrocellulose, and probed with antisera detecting both PAK1 and PAK2, as described in [2]

Data analysis

The results are expressed as means ± S.E.M. from combined experiments, as noted in each legend. ANOVA with Dunnett's, Tukey–Kramer's multiple comparisons tests, or Student's *t*-tests were used to analyse the data. Autoradiograms of the JNK activity studies were analysed with an automated computerized densitometer (SCISCAN 5000; USB, Cleveland, OH, U S.A.). Measurements were made in the linear range and the values expressed as arbitrary attenuance units or fold over control.

RESULTS

12-LO products activate PAK activity

The time frame for PAK1 activation induced by the 12-LO product, 12-HETE, was first assessed in CHO-AT$_{1a}$ cells serum depleted for 3 days. The data in Figure 1 show that 0.1 μM 12-HETE treatment elicited PAK1 activation as early as 5 min (140$\pm$11 % of control; $n = 3$) and the effect reached a peak at 10 min (335$\pm$16 % of control; $n = 4$, $P < 0.001$). PAK1 activation was sustained to 10 min (290$\pm$9 % of control; $n = 3$, $P < 0.001$) and decreased thereafter. However, 12-HETE still significantly activated PAK1 activity at 60 min (196$\pm$21 % of control, $n = 3$, $P < 0.01$).

The dose-dependent activation of PAK1 by 12-HETE was also studied. Concentrations of 12-HETE as low as 0.1 nM could activate PAK1 activity (183$\pm$20 % of control; $n = 3$, $P < 0.05$). The peak effect for activation was reached at 0.01 μM 12-HETE (350$\pm$15 % of control; $n = 3$, $P < 0.001$). These data indicate that 12-HETE can dose-dependently increase PAK1 activity in CHO-AT$_{1a}$ cells. To elucidate the particular PAK isoforms involved in 12-HETE activation, we first examined whether PAK1 or PAK2 is expressed in CHO-AT$_{1a}$ cells. Figure 2(a) represents a Western blot with an antibody which can detect both PAK1 and PAK2, showing bands at 67 and 62 kDa, indicating that the PAK1 and PAK2 isoforms are expressed in CHO-AT$_{1a}$ cells. A protein lysate from human neutrophils were taken as a control showing the same two bands. Figure 2(b) shows that 12-HETE activates predominantly PAK1. The antibody used was specific to PAK1 in the PAK1 activity assay, or specific to PAK2 in the PAK2 activity assay.

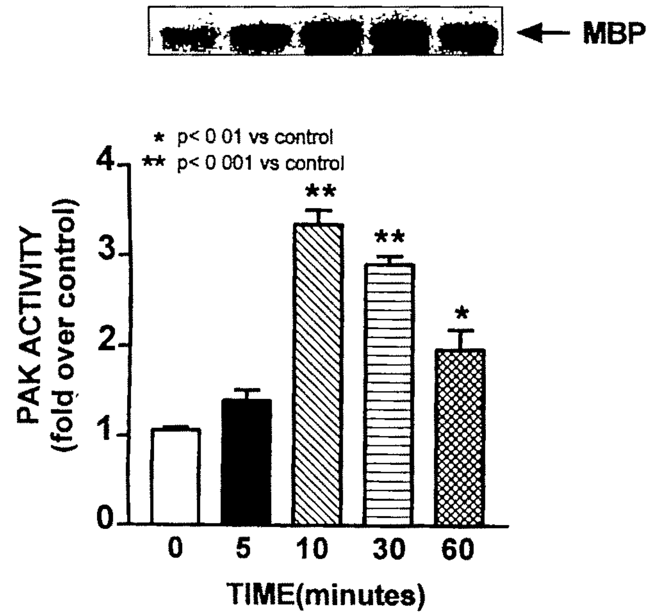

Figure 1 Time course of PAK1 activation by 12-HETE in CHO-AT$_{1a}$ cells

The cells were gently washed and placed in depletion medium for 72 h prior to use After incubation for 30 min, the cells were treated with 12-HETE (0.1 μM) or with ethanol The 12-HETE treatment was terminated by washing twice with PBS and adding 300 μl of lysis buffer as described in the Materials and methods section Top panel shows a representative autoradiogram of phosphorylated MBP bands from a gel PAK1 activity was measured with MBP as a substrate Bottom panel shows the densitometric quantification of PAK1 activity stimulated with 0.1 μM 12-HETE or ethanol in the control for the time indicated Each point is an average (means$\pm$S E M) from at least 3 separate experiments Results are expressed as stimulation over control.

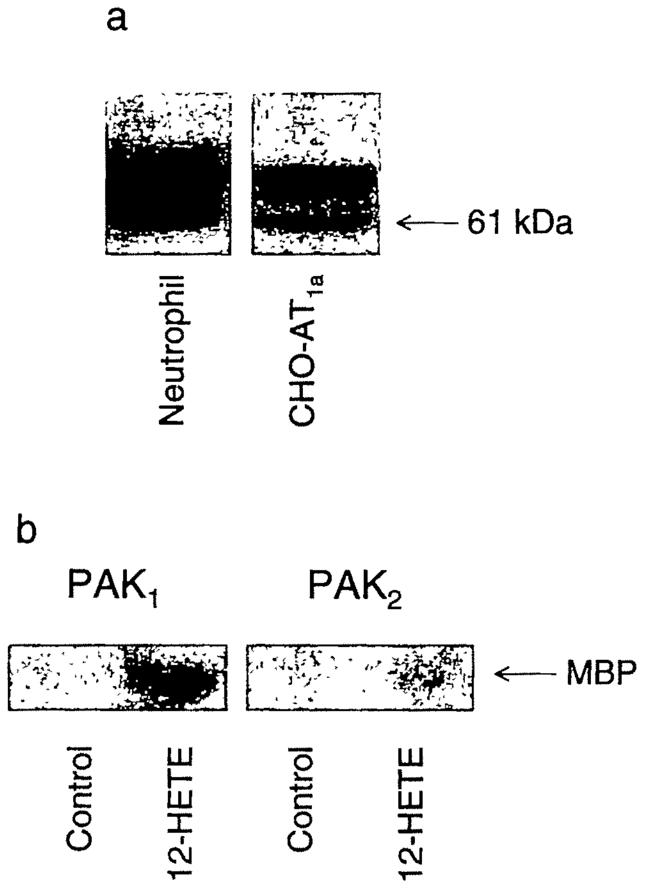

Figure 2 Western blot of PAK1 and PAK2 expression and 12-HETE activates PAK1 and PAK2 activity in CHO-AT1a cells

(a) Neutrophil cytosol protein (20 μg, left lane) or 30 μg of CHO-AT$_{1a}$ cell cytosol protein (right lane) was resolved by SDS/PAGE, transferred on to a nitrocellulose membrane, and probed with antisera recognizing PAK1 and PAK2 The upper band is located at 67 kDa, the lower band at 62 kDa (b) CHO-AT$_{1a}$ cells were treated with 0.1 μM 12-HETE or vehicle (ethanol) in the control for 10 min Detergent-containing lysates were immunoprecipitated with anti-PAK1 or anti-PAK2 antibodies Phosphorylation reactions were conducted with MBP as substrate The two left bands show the basal and 12-HETE-stimulated PAK1 activity, the right bands show the basal and 12-HETE-stimulated PAK2 activity Identical results were seen in 3 experiments

Small-molecular-weight GTP-binding proteins are the direct activators of PAK

To elucidate the mechanism of PAK1 activation by 12-HETE, a PBD plasmid encoding 84 amino acids (hPAK1, residues 67–150) which includes the CRIB domain was transfected into CHO-AT$_{1a}$ cells. Figure 3 illustrates that PBD transfection almost completely inhibited 12-HETE-induced PAK1 activation ($n = 4$, $P < 0.001$). PBD transfection itself had no effect on basal PAK1 activity. Cells were treated with the transfection reagents only in the non-PBD-transfected group (without empty vector) under the same conditions. Dominant negative Rac1 and Cdc42 GTPase mutants were used to confirm this result. Plasmids

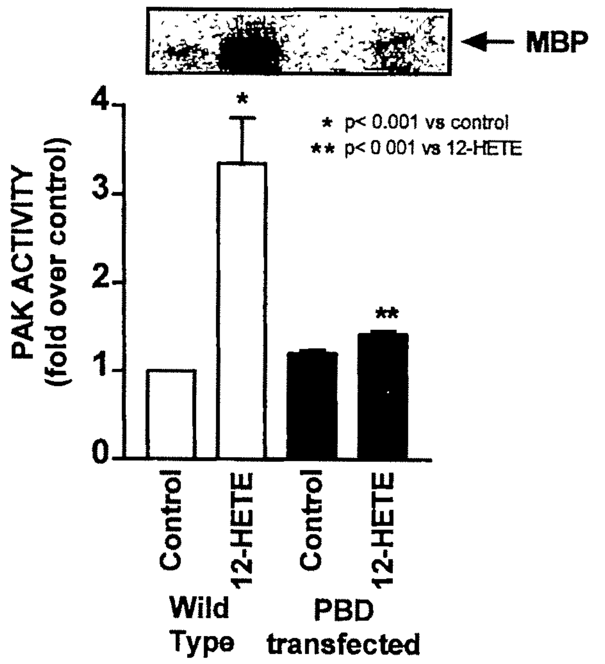

Figure 3 Inhibitory effect of transient transfection of PBD plasmid on 12-HETE-induced PAK1 activation

For the PBD-transfected group, CHO-AT$_{1a}$ cells were transiently transfected with 15 μg of PBD plasmid as described in the Materials and methods section For the non-PBD transfected group, CHO-AT$_{1a}$ cells were treated with the same transfection reagents as the PBD-transfected group Cells were then treated with 12-HETE or ethanol for 10 min The top panel illustrates a representative autoradiogram of phosphorylated MBP bands, the bottom panel illustrates the densitometric quantification Each point is an average (means ± S E M) of at least 3 separate experiments Results are expressed as stimulation over control The PAK1 activity was measured as described in the Materials and methods section

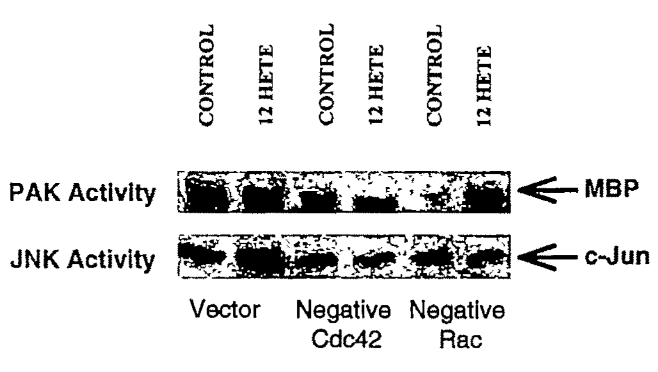

Figure 4 The effects of transfection of Rho GTPase mutants on PAK1 or JNK1 activity in CHO-AT$_{1a}$ cells

CHO-AT$_{1a}$ cells were transiently transfected with various dominant negative Rac1 and Cdc42 GTPases or empty vector as described in the Materials and methods section Cells then were treated with 12-HETE or ethanol (control) for 10 min Cell extracts were used for PAK1 and JNK1 activity measurement Similar results were obtained from two experiments

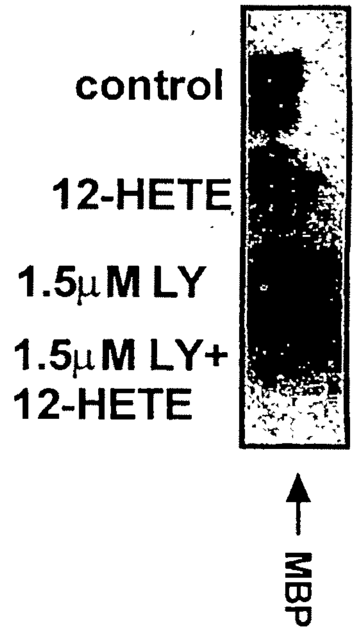

Figure 5 The PI-3-K inhibitor LY294002 inhibits 12-HETE-induced PAK1 activity

Cells were pretreated with different concentrations of LY294002 or DMSO in the control for 30 min, then treated with 12-HETE (0 1 μM) or ethanol in the control for 10 min. PAK1 activity was measured as described in the Materials and methods section The Figure shows a representative autoradiogram of phosphorylated MBP bands from 3 similar experiments

Rac1T17N, Cdc42T17N and empty vector pRK5 were transiently transfected into CHO-AT$_{1a}$ cells. The transfected cells of each construct were divided into two samples, treated with ethanol or with 12-HETE, then PAK1 and JNK1 activity of the lysates was measured as shown in Figure 4. The upper line of Figure 4 shows the effect of Rac and Cdc42 mutant transfection on 12-HETE-induced PAK1 activation. 12-HETE stimulated PAK1 activity in the cells expressing the empty vector compared with the PAK1 activity of cells treated with ethanol. The transfection of dominant negative Cdc42 (Cdc42T17N) completely attenuated 12-HETE-induced PAK1 activation. Interestingly, dominant negative Rac1 (Rac1T17N) significantly inhibited the basal PAK1 activity Although 12-HETE could still increase PAK1 activity, 12-HETE addition could not reverse PAK activity to the basal level seen in empty vector-transfected cells. These results clearly support the role of Cdc42 and Rac1 in 12-HETE-induced activation of PAK1. Dominant negative Cdc42 and Rac1 mutants were also used to further evaluate the role of GTPases in the response of JNK1 activation by PAK. Part of cell extract from the samples for measuring the effect of mutant transfection on PAK1 activity was used for measuring JNK1 activity. The results of these studies are seen on the bottom line of Figure 4. 12-HETE stimulated JNK1 activity in cells expressing empty vector. However, 12-HETE no longer activated JNK1 activity in cells expressing dominantly negative Cdc42 (Cdc42T17N) and negative Rac1 mutant (Rac1T17N), thus strongly suggesting that the 12-HETE activation pathway on JNK1 is mediated by Cdc42 and/or Rac1.

Evidence that PI-3K is an upstream activator of PAK

To evaluate whether PI-3K lies upstream of PAK1 in the 12-HETE-activated signalling pathway, the selective PI-3K inhibitor LY294002 was used. As shown in Figure 5, LY294002 at a concentration of 1.5 μM completely blocked 12-HETE-induced PAK activation. LY294002 had no detectable effect on basal PI-3K activity. Wortmannin, another inhibitor of PI-3K, at 100 nM also significantly reduced 12-HETE-induced PAK activation (results not shown).

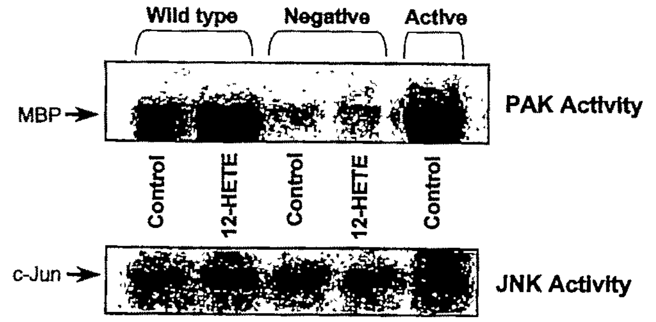

Figure 6 Effect of transient transfection of PAK1 mutants on 12-HETE-induced PAK1 and JNK1 activity

CHO-AT$_{1a}$ cells were transfected with wild-type PAK1, dominant negative PAK1 plasmid, or constitutively active PAK1 as described in the Materials and methods section. The transfected cells were treated with 12-HETE (0.1 μM) or ethanol (control) for 10 min. The same lysate was used for both PAK1 and JNK1 activity measurements. Shown are representative autoradiograms of phosphorylated MBP bands (top panel) and phosphorylated GST–cJun (residues 1–79) (bottom panel). Results are representative of 3 similar experiments.

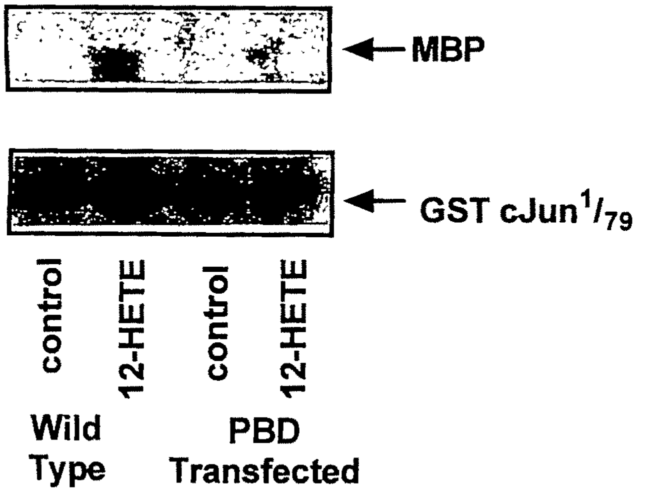

Figure 7 Effect of PAK1-PBD on 12-HETE-induced PAK1 and JNK1 activity

The transfection procedure was performed as described in the Materials and methods section. Cells were treated with 12-HETE (0.1 μM) or ethanol (control) for 10 min. The same lysate was used for both PAK and JNK activity measurements. Autoradiograms of phosphorylated MBP bands (top panel) and phosphorylated GST–cJun (residues 1–79) (bottom panel) are representative of results from 3 similar experiments.

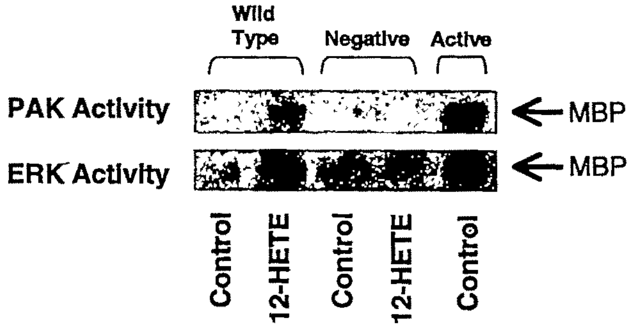

Figure 8 Effect of transient transfection of PAK1 mutants on 12-HETE-induced PAK1 and ERK1/2 activity

CHO-AT$_{1a}$ cells were transfected with wild-type PAK1, dominant negative PAK1 or constitutively active PAK1 respectively, as described in the Materials and methods section. The transfected cells were treated with 12-HETE (0.1 μM) or ethanol in the control for 10 min. The same lysate was used for both PAK1 and ERK1/2 activity measurements. The top panel shows PAK1 activity and the lower panel shows the ERK1/2 activity representative of results from 2 similar experiments. Both kinase assays used MBP as substrate.

PAK lies upstream of JNK in the 12-HETE-induced pathway

To further elucidate whether PAK1 is an upstream activator of JNK1 in the 12-HETE-induced pathway, PAK1 wild-type (PAK1wt), dominant negative PAK1 (PAK1K229R) [12] and constitutively active PAK1 (PAK1T423E) were transiently transfected into CHO-AT$_{1a}$ cells. After stimulation with 12-HETE or ethanol, the cells were lysed to measure PAK1 and JNK1 activity. As shown in top panel of Figure 6, 12-HETE treatment stimulated PAK1 activity in wild-type PAK1 transfected cells. In contrast, 12-HETE-induced PAK1 activity was clearly inhibited in dominant negative PAK1 transfected cells. PAK1 activity was increased in constitutively active PAK1 transfected cells in the absence of 12-HETE treatment. The same lysates from these transfection experiments were collected to analyse the effect of transfection of these PAK1 mutants on JNK1 activity. These results are shown in the lower panel of Figure 6. 12-HETE treatment stimulated JNK1 activity in wild-type PAK1 transfected cells compared with cells treated with vehicle alone. In addition, 12-HETE-induced JNK1 activity was inhibited in dominant negative PAK1 transfected cells. However, JNK1 activity was markedly increased in dominant active PAK1 transfected cells. Transient transfection of the PBD plasmid was also used to evaluate the role of GTPase and PAK kinase activity in JNK1 activation by 12-HETE. Figure 7 shows that PBD transfection almost completely blocked both 12-HETE-induced PAK1 activation and 12-HETE-induced JNK1 activation. The activities of both kinases could be stimulated by 12-HETE treatment in non-PBD-transfected CHO-AT$_{1a}$ cells, which were treated only with the transfection reagents, thus indicating that transfection agents alone were not responsible for the inhibition or the 12-HETE response.

PAK lies upstream of ERK activation in 12-HETE-induced pathway

To dissect the relationship between PAK1 and ERK1/2, transient transfection of the PAK1 mutants into CHO-AT$_{1a}$ cells was again utilized. The effect of PAK1 mutants on PAK1 activation is shown in the upper panel, and the effect on ERK1/2 activation is shown in lower panel, in Figure 8. The results clearly indicate that 12-HETE stimulates PAK1 and ERK1/2 activation in wild-type PAK1-transfected cells; however, the 12-HETE stimulation of ERK1/2 was partially blocked by dominant negative PAK1. Interestingly, constitutively active PAK itself could activate ERK1/2 activity, indicating that PAK1 can activate ERK1/2 in CHO-AT$_{1a}$ cells.

DISCUSSION

In this report we describe for the first time that an arachidonic acid metabolite of 12-LO, 12-S-HETE, can activate PAK1 activity in CHO fibroblasts. The 12-HETE-induced PAK1 stimulation was time-dependent, with activation seen as early as 5 min and a peak effect at 10 min. PAK1 activation was also sustained until 30 min and decreased thereafter. However, 12-HETE still significantly activated PAK1 activity at 60 min (Figure 1). The stimulatory effect of 12-HETE on PAK1 activity was also dose-dependent, with concentrations of 12-HETE as low as 0.1 nM exhibiting PAK1 activation. The maximal effect for activation was reached at 0.01 μM 12-HETE. Interestingly, the precursor of 12-HETE, arachidonic acid, does not stimulate PAK activity [18], indicating that 12-HETE stimulation of PAK1 activity is a specific response that is not due to non-specific hydrophobic- or detergent-like properties of this lipid. Current studies are underway to investigate whether 12-HETE acts by binding to a specific receptor.

It has been established that PAKs are regulated by three different mechanisms: (i) by the binding of GTP-bound Rac or Cdc42 to an N-terminal GTPase-binding domain, (ii) in the case of PAK2, by the caspase-mediated proteolytic removal of the regulatory N-terminus [19], and (iii) direct activation of PAK activity by three classes of lipids such as sphingolipid, phosphatidylinositol and phosphatidic acids [18]. Since 12-HETE is defined as a type of fatty acid with four double bonds, it was of interest to further define whether the 12-HETE action is mediated through small-molecular-weight GTP-binding proteins to PAK1 or by directly interacting with PAK1 similar to sphingosine or phosphatidic acid. The GTPase-binding domain was used to elucidate the role of Rac and Cdc42 in the process of PAK1 activation. PBD is a segment of 84 amino acid residues (hPAK1, residues 67–150) comprising the CRIB domain, which is a region of approx. 16 amino acid residues corresponding to amino acid residues 74–89 of rat $p65^{\mathrm{PAK}}\alpha$ [20]. When overexpressed in cells, PBD would compete for the binding site on GTP-bound active Cdc42/Rac1 with PAK1 molecules and thereby block PAK1 activation. The transfection of the PBD almost completely blocked the activation of PAK1 activity by 12-HETE (Figure 3). To further confirm this result, transfection of dominant negative Cdc42d and Rac1 GTPase mutants was performed and PAK1 activity measured The results in Figure 4 indicated that 12-HETE was able to activate PAK1 activity in cells expressing empty vectors. However, 12-HETE did not activate PAK1 activity in cells expressing negative Cdc42, suggesting that Cdc42 GTPases are the direct upstream activators for 12-HETE-induced PAK1 stimulation. Interestingly, negative Rac mutant significantly inhibited the basal PAK1 activity, while 12-HETE was able to increase PAK1 activity somewhat, but could not reverse it to the basal level in empty-vector-transfected cells. These results suggest that the regulation of PAK1 activation by Rac1 is somewhat different from that by Cdc42. New evidence from other laboratories suggests that Cdc42 and Rac have different mechanisms for activation of PAK. It appears that there are three domains on GTPases of the Rho family including Rac1. These three domains are the residues 26–45 [21], the insert region 124–135 [21], and an intact polybasic domain consisting of six contiguous basic amino acids (residues 183–188) at its C-terminus [8]. Cdc42 shares highly homology with Rac in the Ras-like effector region, residues 26–45 [21], while the insert region is not implicated in PAK activation [21]. New data show that mutation of six basic residues (183–188) to neutral amino acids in C-terminal polybasic domains of Rac 1 dramatically decreased the ability of Rac1 to bind PAK1, and almost completely abolished its ability to stimulate PAK1 activity [8]. This C-terminal polybasic domain is present in several members of the Ras superfamily of small GTP-binding proteins including Rac1 K-Ras4B, Rap1A and Rap1B [8]. These data clearly indicate that Cdc42 and Rac1 share a highly homologous N-terminal Ras-like effector region in regard to PAK activation. However, Rac1 possesses its own unique regions to bind and activate PAK1. Therefore this Rac unique region might account for the further inhibition of basal PAK activity by negative Rac1, while Cdc42 did not. To date, there have been no studies evaluating the possible stimulatory action of 12-HETE on Rac1. However, there is evidence showing that many biologically active lipids are regulators of the Rac–GDP-dissociation-inhibitor complex [22]. Additional studies will be needed to test this hypothesis.

To investigate the role of PI-3K in 12-HETE-introduced PAK1 activation, two distinct pharmacological inhibitors were used. Wortmannin decreased 12-HETE-induced PAK1 activation; but, since Wortmannin can also inhibit myosin light-chain kinase and other kinases, we also used LY294002, a more specific PI-3K inhibitor. At a concentration of 1.5 μM, LY294002 totally suppressed 12-HETE-induced PAK1 activation (Figure 5), clearly indicating that PI-3K is an upstream activator of PAK1. PI-3K products have been shown to play a role in the activation of Rac [23,24], indicating that PI-3K lies upstream of Rac1. However, there is also a report showing that PI-3K is the effector protein of Cdc42/Rac1 [25]. The present study did not evaluate whether PI-3K is upstream of Cdc42 or Rac1, or whether there are parallel, but separate, pathways linking the GTP-binding proteins and PI-3K to PAK1 activation. Further experiments will be needed to elucidate this mechanism.

To explore the role of PAK1 in 12-HETE-induced JNK1 activation in CHO-AT$_{1a}$ cells, dominant negative PAK1 was first used to interrupt the PAK1 activation pathway by 12-HETE. Transient transfection of dominant negative PAK1 blocked both 12-HETE-induced PAK1 and JNK1 activities. In contrast, PAK1 or JNK1 activity was markedly activated in cells overexpressing constitutively active PAK1 (Figure 6). Since we concluded that at least Cdc42 is a direct activator of PAK1, it is reasonable to suggest that JNK1 activity should be blocked if the pathway from Cdc42/Rac to PAK1 was inhibited using PBD. The results demonstrated that when PBD is expressed in the CHO-AT$_{1a}$ cells both 12-HETE induced PAK1 and JNK1 were blocked (Figure 7) The transfection of negative Cdc42 or Rac1 also blocked JNK1 activity (Figure 4). These results strongly suggest that PAK1 is an upstream activator of JNK1 in response to 12-HETE, and the activation pathway by 12-HETE should be 12-HETE → Cdc42 → PAK → JNK. The results also suggest the partial role of Rac in this response. The activation pathway Cdc42/Rac → PAK → JNK by other agonists has been demonstrated by others [26,27]. However, a new family of mixed lineage kinases (MLK) has been identified [28]. Notably, two members of this family, MLK2 and MLK3, possess an SH3 domain in their N-terminal region, and both have a functional CRIB domain which mediates GTP-dependent association with Rac1 and Cdc42 [29,30]. MLK3 has been demonstrated to activate mitogen-activated protein kinase (MAPK) kinase 4 (MKK4) and MKK7 *in vitro*, both are specific activators of JNK [30].

Our previous studies have shown that 12-HETE is a potent growth-promoting agent and stimulator of ERK1/2 activity in CHO-AT$_{1a}$ cells [15]. The link between cell growth and PAK activation has not been clarified. However, there are some clues supporting a role of PAK1 in cellular growth. New data demonstrates that PAK1 phosphorylates MAP/ERK kinase 1 (MEK1) on serine-298, a site important for binding of Raf-1 to MEK1 *in vivo* [30]. In the present study, we demonstrate that PAK1 is an upstream mediator in 12-HETE-induced ERK1/2 activation by transfection of PAK1 mutants. This conclusion is based on data showing that a negative PAK1 mutant suppresses 12-HETE-induced ERK1/2 activity, while constitutive active PAK1 mutant stimulates ERK1/2 activity without the presence of 12-HETE (Figure 8). These results suggest that PAK1 is an upstream activator of ERK1/2 in the 12-HETE-induced action pathway.

In summary, this study provides evidence for the first time that PAK1 is an upstream mediator in 12-HETE-induced JNK1 and

ERK1/2 activation. These results also provide evidence for the role of small GTP-binding proteins in PAK1 and JNK1 activation in a 12-HETE-induced signal transduction pathway. Therefore, 12-LO products should be considered as activators of the PAK pathway.

We thank Dr Gary M Bokoch for helpful discussions, Dr Eric Clauser for providing of CHO-AT$_{1a}$ cells, and Almira Fontanilla for secretarial assistance This work was supported by a Scientist Development Grant from the American Heart Association, Greater Los Angeles Affiliate (to Y W.), National Institutes of Health grant R01 DK-39721 and HL 55798 (to J L N and Y W.) and by R01 AI-35947 (to U G.K)

REFERENCES

1 Manser, E, Leung, T, Salihuddin, H, Zhao, Z-S and Lim, L (1994) Nature (London) **367**, 40–46
2 Knaus, U. G, Morris, S, Dong, H.-J, Chernoff, J and Bokoch, G. M (1995) Science **269**, 221–223
3 Manser, E, Chong, C., Zhao, Z-S., Leung, T., Michael, G, Hall, C and Lim, L (1995) J Biol Chem **270**, 25070–25078
4 Bagrodia, S, Taylor, S J., Creasy, C. L, Chernoff, J and Cerione, R. A (1995) J. Biol Chem. **270**, 22731–22737
5 Martin, G. A, Bollag, G, McCormick, F. and Abo, A (1995) EMBO J **14**, 1970–1978
6 Galisteo, M L, Chernoff, J, Su, Y-C, Skolnik, E Y and Schlessinger, J (1996) J Biol Chem **271**, 20997–21000
7 Bokoch, G. M, Wang, Y, Bohl, B P, Sells, M A., Quilliam, L A and Knaus, U G (1996) J Biol Chem **271**, 25746–25749
8 Knaus, U G., Wang, Y., Reilly, A M., Warnock, D and Jackson, J H. (1998) J Biol Chem **273**, 21512–21518
9 Tsakiridis, T, Taha, C, Grinstein, S and Klip, A (1996) J Biol Chem **271**, 19664–19667
10 Coso, O A., Chiariello, M, Yu, J-C., Teramoto, H., Crespo, P, Xu, N., Miki, T and Gutkind, J. S (1995) Cell **81**, 1137–1146
11 Minden, A, Lin, A, Claret, F-X., Abo, A and Karin, M. (1995) Cell **81**, 1147–1157
12 Zhang, S, Han, J, Sells, M A, Chernoff, J., Knaus, U. G, Ulevitch, R J and Bokoch, G M (1995) J. Biol. Chem **270**, 23934–23936
13 Bagrodia, S, Derijard, B, Davis, R J and Cerione, R A. (1995) J Biol Chem **270**, 27995–27998
14 Teramoto, H., Coso, O A., Miyata, H, Igishi, T, Miki, T. and Gutkind, T S. (1996) J Biol Chem **271**, 27225–27228
15 Wen, Y, Nadler, J L, Gonzales, N., Scott, S, Clauser, E and Natarajan, R (1996) Am J. Physiol **271**, C1212–C1220
16 Wen, Y, Scott, S, Liu, Y, Gonzales, N. and Nadler, J L (1997) Circ. Res **81**, 651–655
17 Teutsch, B, Bihoreau, C, Monnot, C, Bernstein, K. E, Murphy, J, Alexander, R W, Corvol, P and Clauser, E (1992) Biochem Biophys. Res. Commun **18**, 1381–1388
18 Bokoch, G. M, Reilly, A M, Daniels, R H, King, C C, Olivera, A, Spiegel, S and Knaus, U G (1998) J Biol. Chem. **273**, 8137–8144
19 Rudel, T and Bokoch, G M (1997) Science **276**, 1571–1574
20 Burbelo, P D., Drechsel, D. and Hall, A. (1995) J Biol Chem **270**, 29071–29074
21 Freeman, J L., Abo, A and Lambeth, J. D (1996) J. Biol Chem **271**, 19794–19801
22 Welch, H., Eguinoa, A, Stephens, L R and Hawkins, P T (1998) J. Biol. Chem. **273**, 11248–11256
23 Nimnual, A S, Yatsula, B A. and Bar-Sagi, D (1998) Science **279**, 560–563
24 Keely, P J, Westwick, J K, Whitehead, I P, Der, C J and Parise, L V (1997) Nature (London) **390**, 632–636
25 Coso, O A, Chiariello, M, Yu, J, Teramoto, H, Crespo, P, Xu, N, Miki, T and Gutkind, J S. (1995) Cell **81**, 1137–1146
26 Minden, A., Lin, A, Claret, F, Abo, A and Karin, M (1995) Cell **81**, 1147–1157
27 Merritt, S E., Mata, M, Nihalani, D, Zhu, C, Hu, X. and Holzman, L B (1999) J. Biol Chem **274**, 10195–10202
28 Nagata, K I., Puls, A, Futter, C., Schaefer, A. P, Nakata, T., Hirokawa, N. and Hall, A (1998) EMBO J **17**, 149–158
29 Teramoto, H, Coso, O. A, Miyata, H., Igishi, T, Miki, T and Gutkind, J S (1996) J Biol. Chem **271**, 277225–27228
30 Frost, J A, Steen, H., Shapiro, P, Lewis, T, Ahn, N, Shaw, P E and Cobb, M H. (1997) EMBO J **16**, 6426–6438

Received 3 March 2000, accepted 25 April 2000

Biochem J (2000) 349, 489–499 (Printed in Great Britain)

Activation of protein kinase C alters $p34^{cdc2}$ phosphorylation state and kinase activity in early sea urchin embryos by abolishing intracellular Ca^{2+} transients

Frank A. SUPRYNOWICZ*, Laurence GROIGNO†, Michael WHITAKER†, Frederick J. MILLER‡, Greenfield SLUDER‡, John STURROCK§ and Tim WHALLEY§[1]

*Laboratory of Cellular and Molecular Biophysics, National Institute of Child Health and Human Development, Bethesda, MD 20892, U S A, †Department of Physiological Sciences, University of Newcastle-upon-Tyne, Newcastle NE2 4HH, U K., ‡Worcester Foundation for Biomedical Research, Shrewsbury, MA 01545, U S A, and §Institute of Biological Sciences, University of Stirling, Stirling FK9 4LA, U.K

The $p34^{cdc2}$ protein kinase, a universal regulator of mitosis, is controlled positively and negatively by phosphorylation, and by association with B-type mitotic cyclins. In addition, activation and inactivation of $p34^{cdc2}$ are induced by Ca^{2+} and prevented by Ca^{2+} chelators in permeabilized cells and cell-free systems. This suggests that intracellular Ca^{2+} transients may play an important physiological role in the control of $p34^{cdc2}$ kinase activity. We have found that activators of protein kinase C can be used to block cell cycle-related alterations in intracellular Ca^{2+} concentration ($[Ca^{2+}]_i$) in early sea urchin embryos without altering the normal resting level of Ca^{2+}. We have used this finding to investigate whether $[Ca^{2+}]_i$ transients control $p34^{cdc2}$ kinase activity in living cells via a mechanism that involves cyclin B or the phosphorylation state of $p34^{cdc2}$. In the present study we show that the elimination of $[Ca^{2+}]_i$ transients during interphase blocks $p34^{cdc2}$ activation and entry into mitosis, while the elimination of mitotic $[Ca^{2+}]_i$ transients prevents $p34^{cdc2}$ inactivation and exit from mitosis. Moreover, we find that $[Ca^{2+}]_i$ transients are not required for the synthesis of cyclin B, its binding to $p34^{cdc2}$ or its destruction during anaphase. However, in the absence of interphase $[Ca^{2+}]_i$ transients $p34^{cdc2}$ does not undergo the tyrosine dephosphorylation that is required for activation, and in the absence of mitotic $[Ca^{2+}]_i$ transients $p34^{cdc2}$ does not undergo threonine dephosphorylation that is normally associated with inactivation. These results provide evidence that intracellular $[Ca^{2+}]_i$ transients trigger the dephosphorylation of $p34^{cdc2}$ at key regulatory sites, thereby controlling the timing of mitosis entry and exit.

Key words: cyclin B, embryonic cell cycle, Ins(1,4,5)P_3, mitosis, phorbol esters.

INTRODUCTION

In all eukaryotic cells that have been studied, protein phosphorylation serves as a key regulator of cell cycle events. Sequential phases of the cell cycle are induced by the sequential activation and inactivation of cyclin-dependent kinases, which in turn phosphorylate a wide range of cellular substrates [1]. Entry and exit from the M phase of the cell cycle are triggered universally by the activation and inactivation of $p34^{cdc2}$, a cyclin-dependent kinase that binds B-type mitotic cyclins. During interphase the association of $p34^{cdc2}$ with cyclin B causes $p34^{cdc2}$ to be phosphorylated at activating (Thr^{161}) and inhibitory (Thr^{14} and Tyr^{15}) sites, leading to the accumulation of inactive $p34^{cdc2}$–cyclin B complexes. Dephosphorylation of the inhibitory sites at the G2/M transition by the cdc25 phosphatase activates $p34^{cdc2}$, while the dephosphorylation of Thr^{161} and proteolytic destruction of cyclin B at the metaphase/anaphase transition inactivates $p34^{cdc2}$ [2].

The idea that Ca^{2+} is an important regulator of the M phase of the cell cycle is supported by studies showing that the intracellular Ca^{2+} concentration ($[Ca^{2+}]_i$) increases transiently at nuclear envelope breakdown (NEBD), anaphase onset and cytokinesis [3,4]. Further evidence that Ca^{2+} regulates cell division comes from studies in which Ca^{2+} chelators, or inhibitors of Ins(1,4,5)P_3-mediated Ca^{2+} mobilization, delay or prevent cell cycle progression [5–8]. The effects of the chelators are reversed by Ca^{2+} and, in some cases, cell cycle events are triggered prematurely by an experimentally induced $[Ca^{2+}]_i$ transient [9–12]. However, $[Ca^{2+}]_i$ transients are not observed in all cells under all conditions, suggesting that they may often be too localized to detect, or that they do not serve a regulatory function [11,13]

In oocytes arrested at meiotic metaphase, a key function of the fertilization $[Ca^{2+}]_i$ transient is to induce exit from meiosis by triggering cyclin B proteolysis and $p34^{cdc2}$ inactivation [14]. Ca^{2+} may control the activity of $p34^{cdc2}$ during mitotic cell cycles as well, based on our previous finding that the precocious elevation of $[Ca^{2+}]_i$ induces premature $p34^{cdc2}$ inactivation in permeabilized sea urchin embryos [15]. In addition, Ca^{2+} chelators block activation and inactivation of $p34^{cdc2}$ in interphase and mitotic extracts of *Xenopus* embryos [16]. However, because Ca^{2+}-induced $p34^{cdc2}$ inactivation is not correlated with cyclin B proteolysis in these studies [15,16], Ca^{2+} and $p34^{cdc2}$ may be linked by different mechanisms in mitosis and meiosis.

To determine the molecular basis for the regulation of $p34^{cdc2}$

Abbreviations used BAPTA, bis-(o-aminophenoxy)ethane-*N,N,N',N'*-tetra-acetic acid, $[Ca^{2+}]_i$, intracellular Ca^{2+} concentration, diC_8, 1,2-dioctanoyl-*sn*-glycerol, CFASW, calcium-free artificial sea water, DTT, dithiothreitol, NEBD, nuclear envelope breakdown, PKC, protein kinase C, PLC, phospholipase C, TCA, trichloroacetic acid

[1] To whom correspondence should be addressed (e-mail tdw1@stir ac uk)

activity by Ca^{2+} during mitotic cell cycles, we have experimentally inhibited cell cycle $[Ca^{2+}]_i$ transients in synchronous populations of early sea urchin embryos. Previously, it has been shown in a variety of cells that manipulations that activate protein kinase C (PKC) inhibit receptor-coupled mobilization of Ca^{2+} from intracellular stores [17–19]. We found that in early sea urchin embryos, activation of PKC eliminates cell cycle $[Ca^{2+}]_i$ transients without altering the normal resting level of $[Ca^{2+}]_i$. Using this approach, potential Ca^{2+} requirements for $p34^{cdc2}$ activation, inactivation, complex formation with cyclin B, and the phosphorylation state of important regulatory amino acids may be directly identified by biochemical analysis. In the present study our results provide evidence that $[Ca^{2+}]_i$ transients trigger the dephosphorylation of $p34^{cdc2}$ at key regulatory sites, thereby controlling $p34^{cdc2}$ activity and the timing of mitosis entry and exit.

MATERIALS AND METHODS

Reagents

PMA and 4αPMA were purchased from LC Laboratories (Woburn, MA, U.S.A). Stock solutions were prepared in DMSO at a concentration of 2 mM and were stored frozen under N_2 to inhibit oxidation. For experiments, aliquots were diluted to 20 μM with DMSO, so that 1 % (v/v) DMSO would be present to increase the solubility of the compounds in sea water at the final working concentration of 200 nM. 1,2-Dioctanoyl-*sn*-glycerol (diC_8), from Avanti Polar Lipids (Alabaster, AL, U.S.A.), dissolved in chloroform was dried under a stream of N_2 and dissolved in DMSO as a 100 × stock solution (5–10 mM) to be used the same day. Staurosporine and the Ca^{2+} ionophore A23187 (Calbiochem, La Jolla, CA, U.S.A.) were prepared as 100 × stock solutions in DMSO. Emetine (Sigma, St. Louis, MO, U.S.A.) was dissolved in sea water at a concentration of 10 mM. PKC(19–31) peptide (LC Laboratories) was dissolved in either intracellular buffer (see below) at a concentration of 1 mM, or in microinjection buffer (300 mM potassium gluconate, 300 mM glycine, 10 mM NaCl, 2 mM $MgSO_4$ and 2 mM EGTA, pH 7.2) at a concentration of 9 mM. Except for diC_8, the stock solutions were stored as aliquots at −70 °C. Protease inhibitors were obtained from Boehringer Mannheim (Lewes, East Sussex, U.K.). Antimycin, oligomycin, phosphocreatine and creatine phosphokinase were purchased from Sigma (Poole, Dorset, U.K.).

Embryo culture and micro-injection

Eggs were collected from the sea urchin *Lytechinus pictus* (Marinus, Long Beach, CA, U.S.A.) in artificial sea water (435 mM NaCl, 40 mM $MgCl_2$, 15 mM $MgSO_4$, 11 mM $CaCl_2$, 10 mM KCl and 5 mM Hepes/NaOH, pH 8.0) following intracoelomic injection of 0.5 M KCl. The eggs were harvested by centrifuging for 30 s at 250 *g* and were treated with sea water adjusted to pH 5.0 (with HCl) for 3 min to remove the jelly layer. These were then suspended to 1 % (v/v) in sea water and stirred continuously at 16 °C using a motorized paddle or shaking water bath. Fertilization was accomplished by introducing a few drops of sperm diluted with sea water. Batches of eggs exhibiting less than 95 % fertilization were discarded. For determinations of NEBD, embryos were fixed in ethanol/acetic acid (3 : 1, v/v) and were examined using differential interference contrast microscopy. A number of embryos (100) were evaluated per time point. Chromosomes were stained in fixed embryos using 70 % (v/v) acetic acid saturated with orcein (Sigma).

$[Ca^{2+}]_i$ was measured using a fluorescence ratio method [20] in embryos injected with fura 2 conjugated to 10 kDa dextran (Molecular Probes, Eugene, OR, U.S.A.), according to the method of Ciapa et al. [21]. The embryos were treated with PMA (or DMSO) 10 min after fertilization, while in suspension. After 20 min these were affixed to polylysine-coated cover slips for injection and measurements.

Injections of PKC(19–31) were performed as described by Sluder et al. [22]. Injection volumes were determined from the diameter of equivalent oil droplets used to cap the micropipettes Stock solution (9 mM) was introduced (4–12 pl), yielding an intracellular concentration of 50–150 μM for a hollow sphere equal to the embryo in diameter (110 μm).

Measurements of protein and DNA synthesis

To measure rates of protein synthesis, suspensions of eggs were pre-loaded with 15 μCi/ml $[^{35}S]$methionine (1200 Ci/mmol; Amersham, Arlington Heights, IL, U.S.A.) for 20 min. The eggs were then washed three times with sea water, suspended to 1 % (v/v) and fertilized. At intervals, samples were precipitated with 10 % (w/v) trichloroacetic acid (TCA; 60 min at 4 °C) and collected by centrifugation (5000 *g* for 2 min). Aliquots of the TCA-soluble supernatants were mixed with Aquasol (Packard Instruments, Meriden, CT, U.S.A.) for liquid-scintillation counting in order to determine the specific radioactivity of the intracellular methionine pool. TCA precipitates were washed three times with 10 % TCA containing 1 mg/ml methionine, solubilized in 1 M NaOH, and counted to determine ^{35}S incorporation. The incorporation is expressed as a percentage of the intracellular methionine pool. For determinations of cyclin B abundance, eggs were pre-loaded for 20 min with 25 μCi/ml $[^{35}S]$methionine and washed as above. Following fertilization, samples were analysed by SDS/PAGE and autoradiography [15].

To monitor DNA synthesis, 20 μCi/ml $[^{3}H]$thymidine (80 Ci/mmol; Amersham) was added to eggs 10 min before fertilization. At intervals after fertilization, samples were washed three times with sea water at 4 °C and precipitated with 10 % TCA containing 0.5 mg/ml thymidine. The precipitates were washed three times with 10 % TCA containing thymidine and were subsequently solubilized in 1 M NaOH. Aliquots of the TCA-soluble and TCA-insoluble fractions were analysed by liquid-scintillation counting to determine the percentage of incorporation, as above. The fraction of TCA-soluble radioactivity corresponding to $[^{3}H]$thymidine triphosphate is essentially constant at this stage of development.

Kinase assays

Embryos were washed and re-suspended to 1 % (v/v) in intracellular buffer [250 mM potassium gluconate, 250 mM *N*-methyl-D-glucamine, 50 mM Hepes/acetate (pH 7.2), 10 mM EGTA, 6.7 mM $MgCl_2$ and 1 mM dithiothreitol (DTT)] at 4 °C, and were lysed using three 10-s pulses of a Branson Sonifier fitted with a stepped micro-tip (Branson Ultrasonics, Danbury, CT, U.S.A.). $p34^{cdc2}$ kinase activity and protein concentrations were measured as described previously [15] except that 50 μM PKC(19–31) was included in the kinase assays.

Anti-phosphotyrosine immunoblots

Embryos were lysed in adsorption buffer (intracellular buffer without $MgCl_2$, supplemented with 5 mM EDTA, 1 mM Na_3VO_4, 1 μM microcystin-LR, 0.5 mM PMSF, 2 μg/ml leupeptin and 2 μg/ml pepstatin) using ultrasonic disruption. To enrich for $p34^{cdc2}$, volumes of lysate containing 1 mg of protein were adsorbed to 35 μl of $p13^{suc1}$–Sepharose beads for 60 min at 4 °C (5 mg of $p13^{suc1}$/ml of beads; Upstate Biotechnology, Lake Placid, NY, U.S.A.). After adsorption, the beads were washed three times with adsorption buffer and twice with buffer containing 50 mM Tris/HCl (pH 6.8), 50 mM NaCl, 2 mM EDTA, 1 mM DTT, 1 mM Na_3VO_4, 1 μM microcystin-LR, 0.5 mM PMSF, 2 μg/ml leupeptin and 2 μg/ml pepstatin. Bound proteins were eluted in 125 μl of SDS/PAGE sample buffer, resolved by SDS/PAGE, and transferred on to nitrocellulose membranes [15]. Transfers were blocked for 2 h at room temperature with TBS [10 mM Tris/HCl (pH 8.0)/150 mM NaCl] containing 5 % (w/v) BSA (Sigma; 'essentially fatty acid-free') and 1 % (w/v) ovalbumin, and were labelled overnight at 4 °C with an anti-phosphotyrosine monoclonal antibody diluted to 2 μg/ml in blocking solution (clone PY20; ICN, Costa Mesa, CA, U.S.A.). The transfers were subsequently labelled for 90 min at room temperature with affinity-purified rabbit anti-mouse IgG (Pierce, Rockford, IL, U.S.A.) at 1 μg/ml, followed by ^{125}I-labelled Protein A (Amersham) at 10 ng/ml, in blocking solution. After each labelling step, the transfers were washed four times with TBS (10 min per wash). Autoradiography was performed at −70 °C with an intensifying screen.

Measuring Ca^{2+} pumping and release in microsomes

Calcium homoeostasis in an endoplasmic reticulum preparation from sea urchin embryos was investigated essentially as described previously [23]. Microsomes were prepared from control or PMA-treated embryos 60 min after fertilization (200 nM 4αPMA or 200 nM PMA added 24 min after fertilization) PMA or 4αPMA was included at concentrations of 200 nM in all buffers used for microsome preparation and subsequent analysis. Embryos produced from the fertilization of 5 ml of eggs were collected by centrifugation and suspended in calcium-free artificial sea water (CFASW; 445 mM NaCl, 40 mM $MgCl_2$, 15 mM $MgSO_4$, 10 mM KCl, 1 mM EDTA, 2 mM EGTA and 10 mM Hepes/NaOH, pH 8.0). Eggs were washed twice with CFASW and then suspended 1:1 (v/v) in ice-cold isolation buffer (250 mM *N*-methyl glucamine, 250 mM potassium gluconate, 20 mM Hepes and 1 mM $MgCl_2$, adjusted to pH 7.2 with acetic acid). The embryos were homogenized with 10 strokes of a tight-fitting teflon pestle in a Potter homogenizer. The homogenate was centrifuged at 10000 *g* for 10 s and the pellet was discarded. The resulting microsome fractions were used immediately for analysis of calcium homoeostasis.

Embryo homogenate (1 ml) was added to 1 ml of fluorimeter buffer (a solution comprising isolation buffer supplemented with 1 mM NaN_3, 1 μg/ml oligomycin and antimycin, 0.1 mg/ml soybean trypsin inhibitor, 200 μg/ml leupeptin, 200 μg/ml aprotinin, 1 mM ATP, 10 mM phosphocreatine and 10 units/ml creatine phosphokinase). This mixture was incubated for 1 h at 16 °C. This was then added to 8 ml of fluorimeter buffer and the mixture was incubated at 16 °C for 4 h. Fluorimetry was performed using a Perkin Elmer Luminescence Spectrometer (LS50-B). A 3 ml aliquot of microsomes was added to a quartz cuvette and 1 μM fluo 3 (Molecular Probes) was added. The mixture was stirred at full speed using a stirring cuvette holder and the temperature was maintained at 16 °C. Fluorescence was measured using an excitation wavelength of 490 nm and an emission wavelength of 590 nm.

Phosphopeptide mapping and phospho amino acid analysis

Embryo suspensions were supplemented with 0.13 mCi/ml carrier-free $^{32}PO_4$ (Amersham), 20 min after fertilization. Samples were washed extensively, lysed in adsorption buffer and incubated with $p13^{suc1}$ beads as outlined above. Eluted proteins were resolved by SDS/PAGE, transferred on to Immobilon-P membranes (Millipore, Bedford, MA) in the presence of 20 % (v/v) methanol and 0.1 % SDS, and visualized by autoradiography. The band corresponding to $p34^{cdc2}$ was excised and digested with 2 × 4 μg of tosylphenylalanylchloromethane-trypsin (Pierce) according to the protocol of Luo et al. [24]. Peptide mapping was performed on ^{32}P-labelled tryptic digests as described by Boyle et al. [25]. Samples were applied to 100 μm thin-layer cellulose plates and were electrophoresed at pH 1.9 for 25 minutes at 1 kV. Separation in the second-dimension was by chromatography in phospho chromatography buffer. For phospho amino acid analysis, tryptic digests were hydrolysed in constant-boiling 6 M HCl for 6 h at 110 °C to enrich for phosphothreonine (see the Results section). Liberated phospho amino acids were separated by TLC [26] and quantified using a PhosphorImager (Molecular Dynamics, Sunnyvale, CA, U.S.A.). For each time point $p34^{cdc2}$-associated ^{32}P was normalized to account for the specific radioactivity of the intracellular TCA-soluble pool. The size of the intracellular ATP pool does not change during these experiments [27], and the turnover of the protein phosphate *in vivo* is rapid since the amount of ^{32}P incorporated into the TCA-insoluble fraction closely parallels the specific radioactivity of the intracellular ^{32}P pool (results not shown).

RESULTS

Activators of PKC block mitosis entry and exit

Embryos of the sea urchin *L. pictus* were treated at different stages of the cell cycle with 200 nM PMA, a potent activator of PKC [28]. As a control embryos were also treated with 200 nM 4αPMA, an isomer of PMA that does not activate PKC. When 4αPMA was applied during G1 phase (24 min after fertilization), embryos underwent multiple rounds of division (Figures 1A and 1E) with timing that was typical of untreated populations. In contrast, the application of PMA during G1 phase arrested the cell cycle at a stage preceding mitosis; NEBD (Figures 1B and 1F) and chromosome condensation (results not shown) were blocked for at least 2 h. The fact that DNA is replicated in the PMA-treated embryos (Figure 2B) indicates that the cell cycle is blocked in G2 phase.

When PMA was administered during prophase or pro-metaphase (72 min after fertilization), embryos entered mitosis but were unable to exit; nuclear envelope re-formation did not occur (Figures 1C and 1G), and chromosomes remained condensed (Figure 1H). The application of PMA during telophase (96 min after fertilization) did not interfere with the completion of mitosis, but arrested the cell cycle before the next mitosis (Figure 1D). Identical results were obtained with the PKC activator, diC_8, at concentrations of 50–100 μM (see below). The cell cycle arrest imposed by activators of PKC was not due to a general repression of cell metabolism, as neither protein nor DNA synthesis was inhibited (Figure 2). Thus activators of PKC block entry into or exit from mitosis, depending on the cell cycle stage at which they are applied.

Because PKC activation arrested the cell cycle, we determined the consequences of inhibiting PKC by injecting the selective peptide inhibitor PKC(19–31) [29] during interphase of the first cell cycle (25–50 min after fertilization). An intracellular concentration of 70–150 μM peptide was used, since $\geqslant$ 60 μM has been shown to block 98 % of the cytoplasmic alkalinization induced by PMA in unfertilized *L. pictus* eggs [30]. Embryos injected with PKC(19–31) divided at least three times, with the

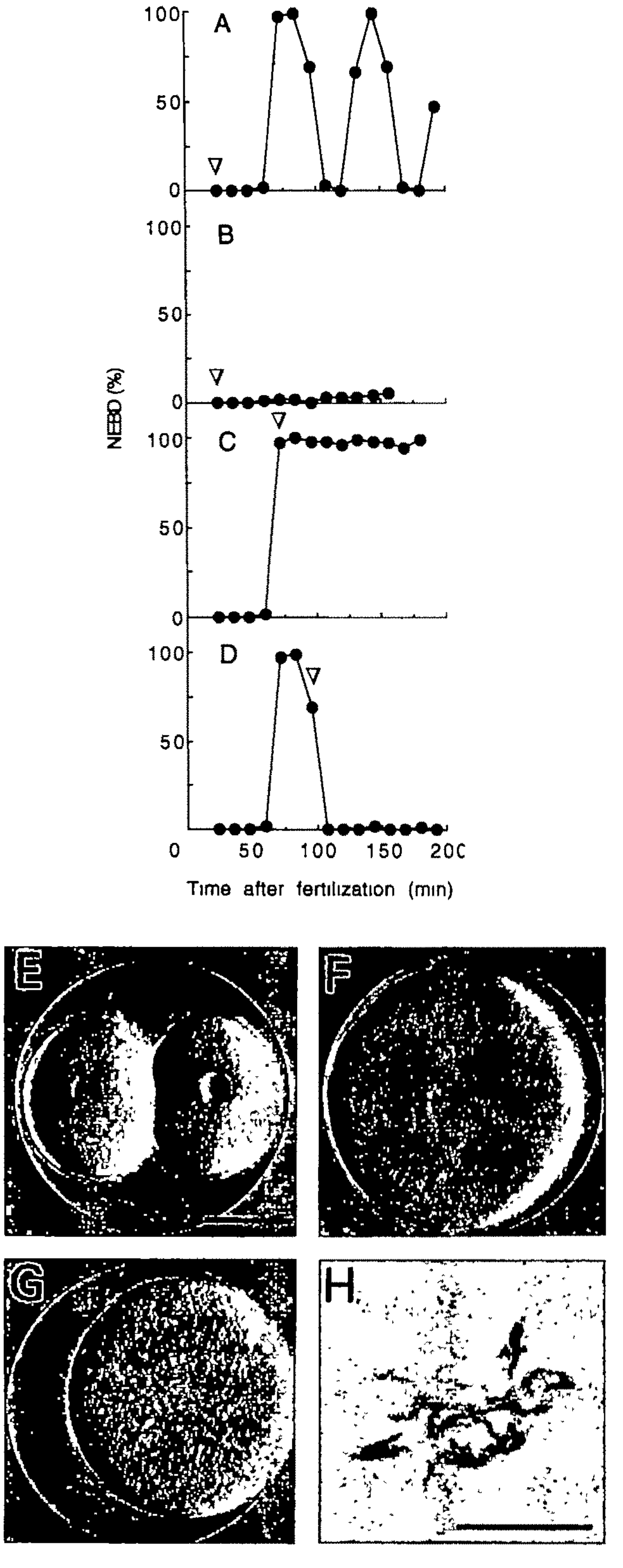

Figure 1 PMA blocks cell cycle progression in a stage-dependent manner

Embryos were treated with 200 nM 4αPMA (A) or 200 nM PMA (B–D) at the times indicated (arrows) At intervals, samples were fixed and examined microscopically to determine the kinetics of NEBD (E) Photomicrograph of (A) at 120 min (F) and (G) Embryos from (B) and (C) at 120 min (H) Embryo from (C) at 120 min stained to visualize chromatin Scale bars represent 50 μm in (E–G) and 10 μm in (H) Results typical of 5 experiments are shown

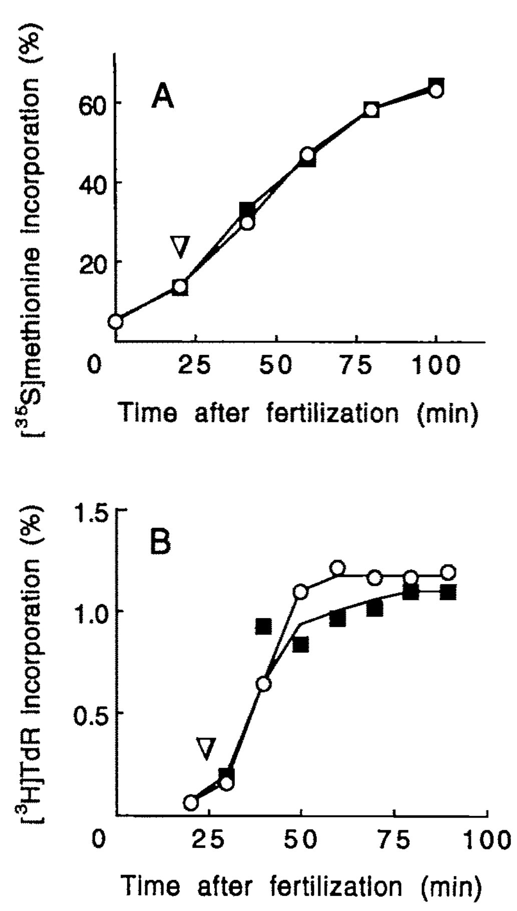

Figure 2 Effect of PMA on protein and DNA synthesis

PMA (■) or 4αPMA (○) (200 nM) was added to embryos during G1 phase (arrow) Protein synthesis (A) and DNA synthesis (B) were measured as described in the Materials and methods section Typical results are shown.

same timing as control embryos injected with buffer ($n = 12$). Therefore apart from its role in cytoplasmic alkalinization at fertilization [31,32], PKC is not essential for cell cycle progression in sea urchin embryos As diacylglycerol would be generated when Ins(1,4,5)P_3 is produced prior to each $[\mathrm{Ca}^{2+}]_i$ transient, one might also expect PKC to be activated at each $[\mathrm{Ca}^{2+}]_i$ transient. Our data suggest that this activation, if it takes place, is not essential for cell cycle progression. Perhaps PtdIns(4,5)P_2 hydrolysis is localized to regions of the cell where PKC is absent or, alternatively, it is possible that diacylglycerol is rapidly metabolized before PKC activation can take place.

PKC activation inhibits cell cycle $[\mathrm{Ca}^{2+}]_i$ transients

The fact that activators of PKC block the cell cycle in a manner similar to Ca^{2+} chelators [3], and the reported inhibition of receptor-coupled Ca^{2+} mobilization by PKC [17–19], suggested that PKC might inhibit cell cycle-related $[\mathrm{Ca}^{2+}]_i$ transients. To directly test this possibility, embryos were continuously treated with PMA (or with DMSO, as a control) beginning in G1 phase, and were injected with fura 2-dextran, so that $[\mathrm{Ca}^{2+}]_i$ could be measured in individual embryos using dual wavelength confocal microscopy. In the controls, $[\mathrm{Ca}^{2+}]_i$ fluctuated over the course of the cell cycle, exhibiting sustained increases (> 2 min) of 50–125 nM that were associated with NEBD, anaphase onset, and cytokinesis (Figure 3A), as reported previously [20,21]. PMA

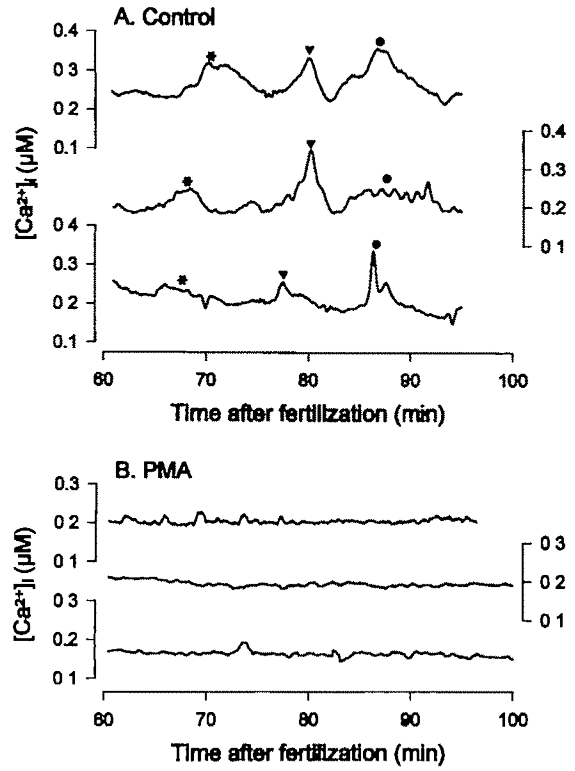

Figure 3 PMA eliminates cell cycle $[Ca^{2+}]_i$ transients

$[Ca^{2+}]_i$ was measured continuously in individual embryos that were treated with 1% DMSO (**A**) or 200 nM PMA (**B**) during G1 phase (10 min after fertilization) and subsequently injected with fura 20–dextran. Each recording in (**A**) is from an embryo of the same batch as the corresponding recording in (**B**). The results shown are representative of 9 trials in which the embryos remained viable throughout the course of the experiment. In four additional trials, the combination of PMA treatment and micro-injection resulted in distortion of the embryos, gross movements of the cytoplasm, and relocation of the nucleus to the cell periphery. Symbols indicate $[Ca^{2+}]_i$ transients associated with NEBD (∗) anaphase onset (▼) and cytokinesis (●).

treatment did not significantly alter the resting level of $[Ca^{2+}]_i$ in the embryos; however, it eliminated all sustained increases in $[Ca^{2+}]_i$ for at least 40 min (Figure 3B). In four out of four control experiments, an NEBD-associated calcium transient occurred 68.6±0.92 min after fertilization. Its peak height was 66±10 nM and its duration was 5.9±1.06 min. In seven experiments in which $[Ca^{2+}]_i$ was monitored from 30 to 90 min after fertilization, in embryos treated with PMA at 24 min, the largest and longest deviation in $[Ca^{2+}]_i$ from baseline was a 30 nM excursion of 1.1 min duration that occurred 40 min after fertilization. The mean of the excursions from baseline in PMA-treated embryos between 64.92 and 72.28 min after fertilization (two standard deviations either side of the mean time of occurrence of the NEBD transient in controls) was 22.5±4.66 nM. Analysis of the control and PMA-treatment NEBD $[Ca^{2+}]_i$ data using an unpaired t-test showed the differences to be significant at the $P \leqslant 0.001$ level. Thus it can be seen that activation of PKC leads to a suppression of cell cycle associated $[Ca^{2+}]_i$ transients. The absence of $[Ca^{2+}]_i$ transients might explain the arrest of the cell cycle in PMA-treated embryos.

We used an *in vitro* egg endoplasmic reticulum microsome preparation [23] to determine whether PMA treatment had any effect on either Ca^{2+}-pumping or Ins(1,4,5)P_3 sensitivity. Microsomes were prepared from control or PMA-treated embryos 60 min after fertilization (200 nM 4αPMA or 200 nM PMA added 24 min after fertilization) and both the Ca^{2+}-pumping rate and Ins(1,4,5)P_3 sensitivity were determined. As shown in Table 1 there was no difference in either parameter between the PMA-treated and control embryos.

Table 1 PKC activation does not affect Ca^{2+} pumping or sensitivity to InsP_3 in endoplasmic reticulum microsome homogenates

Embryos were treated with 4αPMA (control) or PMA 24 min after fertilization. Microsomes were prepared 36 min after these additions. $[Ca^{2+}]$ was monitored using fluo 3 fluorescence and when a steady baseline reading was achieved Ca^{2+} pumping rate and InsP_3 sensitivity were determined. Protein concentrations in control and PMA-treated microsomes were adjusted so that they were identical. The rate of Ca^{2+} pumping was determined by adding 10 nmol of Ca^{2+} and measuring the decrease in $[Ca^{2+}]$ over the following 10 min. InsP_3 sensitivity was determined by measuring the increase in $[Ca^{2+}]$ following the addition of 100 nM InsP_3. For both Ca^{2+} pumping and InsP_3 sensitivity determinations the data were obtained from duplicate experiments from three separate batches of embryos.

Condition	Rate of Ca^{2+} pumping by sea urchin embryo microsomes (nmol/min) means±S.E.M., $n = 6$	Extent of Ca^{2+} release in response to 100 nM InsP_3 (nmol), means±S.E.M., $n = 6$
Control	0.89±0.15	4.13±0.45
PMA-treated	0.92±0.13	3.99±0.34

PKC stimulation prevents $p34^{cdc2}$ activation and inactivation

Since entry and exit from mitosis are controlled by the $p34^{cdc2}$ protein kinase, we investigated whether the activation of PKC blocks cell cycle progression by interfering with the activation and inactivation of $p34^{cdc2}$. In this regard, it was important to establish that we could accurately measure the protein kinase activity of $p34^{cdc2}$ in embryos treated with activators of PKC, since PKC phosphorylates histone H1, the substrate used to assay $p34^{cdc2}$ activity. Therefore we determined the $[Ca^{2+}]$ dependence of sea urchin PKC in crude lysates using the selective peptide substrate, $[Ser^{25}]$PKC(19–31) [29]. We found that PKC activity was only 9.1±0.6% maximal (mean±S.D.) at 40 nM Ca^{2+}, the concentration present in $p34^{cdc2}$ kinase assays. This result is consistent with the previous identification of *L. pictus* PKC as a Ca^{2+}-requiring isoform based on biochemical properties [33] and sequence analysis [34]. As shown in Figure 4(A), the inclusion of 50 µM PKC(19–31) in $p34^{cdc2}$ kinase assays of PMA-treated embryos eliminated the low level of Ca^{2+}-independent PKC activity without inhibiting $p34^{cdc2}$.

When 4αPMA was applied to embryos during G1 phase, $p34^{cdc2}$ kinase activity underwent cyclical oscillations, increasing 8–10-fold prior to mitosis and then rapidly decreasing to the interphase level during mitosis (Figure 4B). In contrast, $p34^{cdc2}$ kinase activity increased only slightly over a period of 3 h when PMA was applied during G1 phase and entry into mitosis was blocked (Figure 4B). Thus the failure of these embryos to enter mitosis correlated with their inability to activate $p34^{cdc2}$.

When PKC was activated during prophase to block exit from mitosis, $p34^{cdc2}$ kinase activity remained at the elevated mitotic level for at least 2 h (Figure 4C). Thus the failure of these embryos to exit mitosis correlated with their inability to inactivate $p34^{cdc2}$. Elevated protein kinase activity was responsible for the

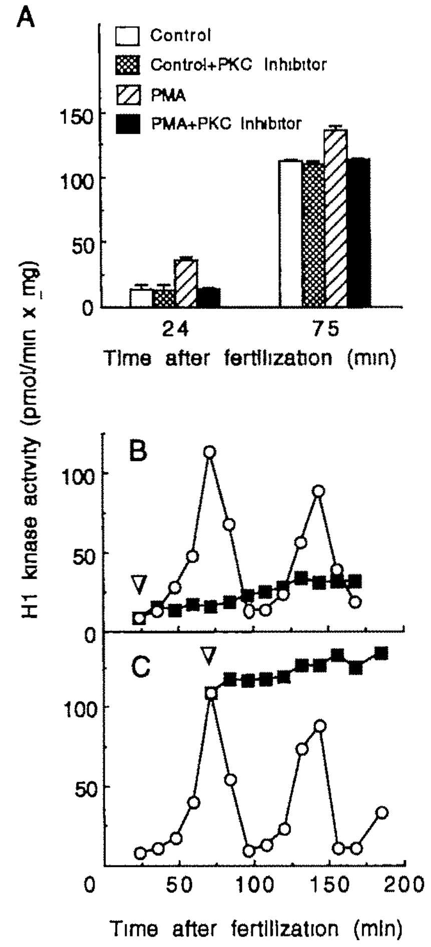

Figure 4 PMA blocks activation and inactivation of $p34^{cdc2}$

(**A**) Selectivity of the $p34^{cdc2}$ kinase assay Lysates were prepared from embryos treated with 200 nM PMA for 5 min, and from untreated embryos, during G1 phase (24 min after fertilization) and prophase (75 min after fertilization) In both cases, the phosphorylation of histone H1 was assayed in the presence and absence of 50 μM PKC(19–31) (**B**) PKC activation during G1 phase blocks $p34^{cdc2}$ activation $p34^{cdc2}$ kinase activity was measured in lysates prepared every 12 min from embryos which received additions of 200 nM PMA (■) or 4αPMA (○), 24 min after fertilization (arrow) Control (4αPMA-treated) embryos completed two cycles of NEBD and assembly, while those treated with PMA did not undergo NEBD (**C**) PKC activation during prophase blocks $p34^{cdc2}$ inactivation $p34^{cdc2}$ kinase activity was monitored in embryos which received additions of 200 nM PMA (■), or 4αPMA (○), 75 min after fertilization (arrow) Control embryos completed a second mitosis, whereas embryos treated with PMA did not exit from the first mitosis Typical results are shown

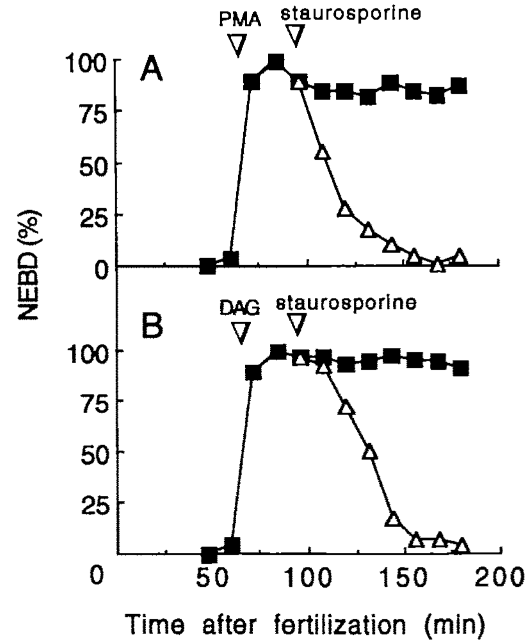

Figure 5 Reversibility of the mitotic arrest induced by activators of PKC

Embryos (■) were treated with 200 nM PMA (**A**) or 100 μM diC_8 (**B**) during prophase (first arrow). After 24 min (second arrow), 5 μM staurosporine was administered to half of each population (△) The percentage of embryos exhibiting NEBD was determined for all four populations Typical results are shown DAG, diC_8

block to mitosis exit, since it was reversed by staurosporine, an inhibitor of serine/threonine protein kinases. As shown in Figure 5 the addition of 5 μM staurosporine induced nuclear envelope re-formation in > 95 % of embryos arrested in mitosis as a result of PMA or diC_8 treatment.

Elevated $[Ca^{2+}]_i$ restores $p34^{cdc2}$ activation and inactivation in PMA-treated embryos

To establish that the effects of PMA on $p34^{cdc2}$ activation and inactivation were due to the absence of $[Ca^{2+}]_i$ transients, rather than to a direct effect of PKC (or PMA) on $p34^{cdc2}$, we used the Ca^{2+} ionophore A23187 to elevate $[Ca^{2+}]_i$ in PMA-treated embryos. As shown in Figures 6(A) and 6(B), the addition of Ca^{2+} ionophore to embryos blocked in interphase with low $p34^{cdc2}$ kinase activity led to an approximately 2-fold activation of $p34^{cdc2}$. When PMA was applied later in the cell cycle, to arrest embryos with elevated $p34^{cdc2}$ kinase activity, ionophore treatment triggered a 65 % decrease in activity (Figure 6C). Moreover, it is significant that the same ionophore treatment promoted activation of $p34^{cdc2}$ when activation was blocked by PMA, and induced inactivation of $p34^{cdc2}$ when inactivation was blocked by PMA. In both of these cases, while there was an alteration in the level of $p34^{cdc2}$ kinase activity upon addition of ionophore there was neither entry into nor exit from mitosis. This might be due to the fact that ionophore-induced $[Ca^{2+}]_i$ transients differ from normal cell cycle $[Ca^{2+}]_i$ transients, in terms of both magnitude and spatial localization. In an attempt to more faithfully replicate normal cell cycle $[Ca^{2+}]_i$ transients, Ins(1,4,5)P_3 (1 μM) was injected into embryos that had been arrested in interphase by the addition of PMA 24 min after fertilization. In 20 experiments, in 3 batches of embryos, microinjection of Ins(1,4,5)P_3 did not permit entry into mitosis as determined by scoring for NEBD (results not shown).

PKC activation uncouples $p34^{cdc2}$ activity and cyclin B abundance

Since the activation of $p34^{cdc2}$ requires its binding to cyclin B, while inactivation normally requires cyclin B proteolysis [35,36], we determined whether PKC activation had effects on the synthesis and destruction of cyclin B. Embryos were pulse-labelled with $[^{35}S]$methionine prior to fertilization and levels of cyclin B were monitored by SDS/PAGE and autoradiography. In control embryos, treated with 4αPMA during G1 phase, cyclin B migrated on SDS gels with an apparent molecular mass of 50 kDa, and was converted into a 53 kDa form during late G2 and early M phases (Figure 7A; control, 48–84 min) due to phosphorylation by $p34^{cdc2}$ [3,37]. During anaphase, cyclin B was completely destroyed (Figure 7A; control, 96–108 min), and

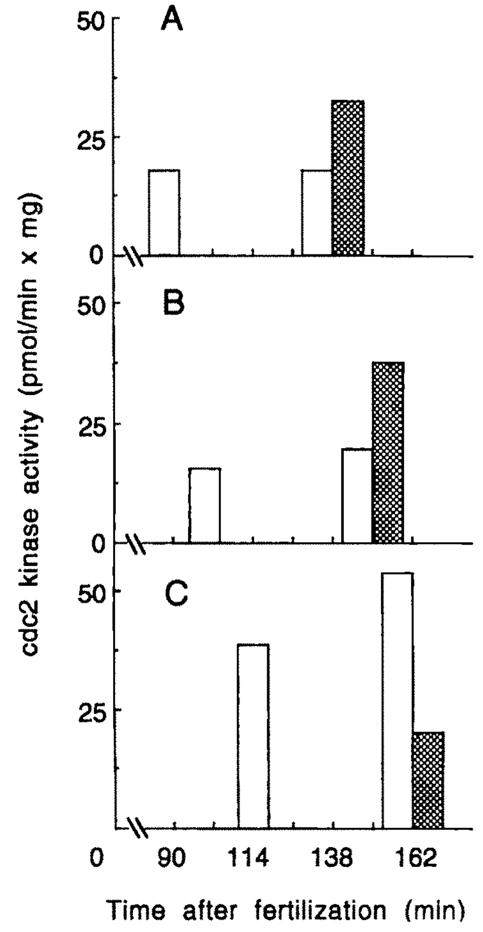

Figure 6 Ca^{2+} promotes p34^{cdc2} kinase activation and inactivation in PMA-blocked embryos

Batches of embryos were treated with 200 nM PMA at three successive stages of the cell cycle In each instance, p34^{cdc2} kinase activity was determined 12 min after the addition of PMA (first open bar) and 60 min after PMA (second open bar) Ca^{2+} ionophore, A23187 (5 μg/ml), was added to half of each batch 12 min after PMA addition, and p34^{cdc2} kinase activity was measured 48 min later (i e 60 min after PMA addition, solid bar) Times of PMA addition correspond to (**A**) anaphase and (**B**) telophase of the first mitosis, (**C**) interphase of the second cell cycle A typical result is shown

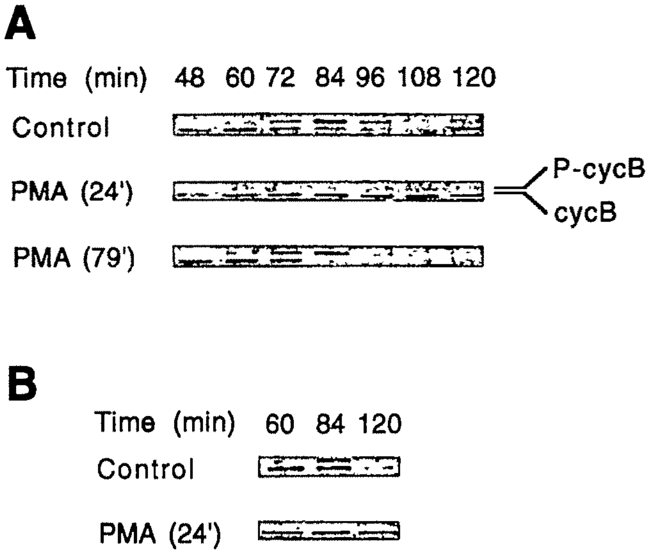

Figure 7 [Ca^{2+}]$_i$ transients are not required for the synthesis and destruction of cyclin B

(**A**) Levels of dephosphorylated and phosphorylated cyclin B (cycB and P-cycB) in control embryos treated with 200 nM 4αPMA during G1 phase (24 min after fertilization), and in embryos treated with 200 nM PMA during G1 phase or prophase (24 or 79 min after fertilization) The control embryos completed mitosis, while those treated with PMA at 24 min did not enter mitosis and those treated at 79 min did not exit mitosis (**B**) Levels of cyclin B bound to p34^{cdc2} were determined by adsorption to p13^{suc1}–Sepharose Typical results are shown

then began to re-accumulate in advance of the next mitosis (Figure 7A; control, 120 min). Cyclin B was synthesized at the same rate in embryos in which PKC was activated during G1 phase; however, it did not become phosphorylated (consistent with the block to p34^{cdc2} activation) and was not destroyed (Figure 7A; PMA added at 24 min). Furthermore, cyclin B co-adsorbed with p34^{cdc2} on to immobilized p13^{suc1} (Figure 7B), indicating that it was bound to p34^{cdc2} in the PMA-treated embryos. Therefore the activation of PKC during interphase inhibits the pathway controlling p34^{cdc2} activation at a step which follows formation of the p34^{cdc2}–cyclin B complex. Since we have shown that the application of Ca^{2+} ionophore activates p34^{cdc2} in embryos treated with PMA in interphase, the simplest interpretation of these data is that interphase [Ca^{2+}]$_i$ transients are required for activation of p34^{cdc2} following the formation of the p34^{cdc2}–cyclin B complex.

When PKC was activated during prophase in order to arrest the cell cycle in mitosis (with high p34^{cdc2} activity), cyclin B nevertheless was destroyed at the same time as in control embryos (Figure 7A; PMA added at 79 min). This result demonstrated that the destruction of cyclin B and inactivation of p34^{cdc2} could be temporally uncoupled in sea urchin embryos, such that p34^{cdc2} remained active in the absence of cyclin B. A similar result has been observed in frog oocytes treated with okadaic acid [36]. Since we have shown that artificially elevating [Ca^{2+}]$_i$ in embryos arrested in mitosis led to a decrease in p34^{cdc2} activity we conclude that Ca^{2+} is required to regulate the pathway controlling p34^{cdc2} inactivation at a step which is distinct from cyclin B proteolysis.

Ca^{2+} requirements for p34^{cdc2} dephosphorylation

The data presented so far suggest that PKC activation abolishes the cell cycle [Ca^{2+}]$_i$ transients that normally regulate p34^{cdc2} activation and inactivation. They also indicate that the cell cycle dynamics of cyclin B are not affected by the abolition of cell cycle [Ca^{2+}]$_i$ transients. A general paradigm for mitotic regulation is that the association of p34^{cdc2} with cyclin B during interphase promotes p34^{cdc2} phosphorylation at both inhibitory (Thr^{14} and Tyr^{15}) and activating (Thr^{161}) sites. Dephosphorylation of the inhibitory sites during G2 phase activates p34^{cdc2}, while dephosphorylation of the activating site during anaphase is essential for inactivation [36,38]. Since the cell cycle dynamics of cyclin B did not explain the Ca^{2+} requirement for p34^{cdc2} activation and inactivation in our study, we analysed how the elimination of [Ca^{2+}]$_i$ transients through PKC activation might influence the phosphorylation state of p34^{cdc2} at putative regulatory sites.

In early sea urchin embryos p34^{cdc2} undergoes cell cycle-dependent tyrosine phosphorylation, which is at least partially dependent on newly synthesized cyclin B [39]. As shown in

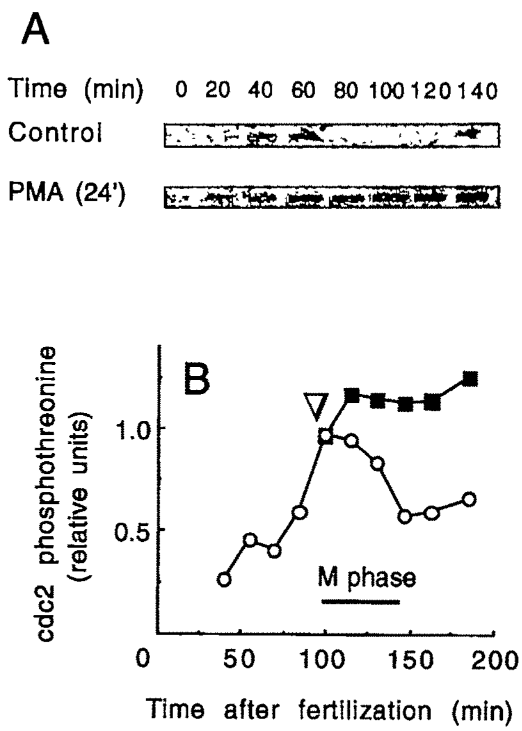

Figure 8 [Ca^{2+}]$_i$ transients are required for cell cycle-dependent p34^{cdc2} dephosphorylation

(A) Anti-phosphotyrosine Western-blot of p34^{cdc2} in embryos treated with 200 nM PMA or 200 nM 4αPMA during G1 phase (24 min after fertilization) The PMA-treated embryos did not undergo NEBD (B) Phosphothreonine content of p34^{cdc2} in embryos treated with 200 nM PMA and 100 μM emetine (■) during prophase (arrow), and in control embryos which were similarly treated with 4αPMA and emetine (○) The PMA-treated embryos did not exit from mitosis

Figure 8(A) (control), p34^{cdc2} exhibited a normal pattern of tyrosine phosphorylation and dephosphorylation over the course of the cell cycle in 4αPMA-treated control embryos. The phosphotyrosine content of p34^{cdc2} gradually increased after fertilization, and was maximal during interphase prior to p34^{cdc2} activation (0–60 min). Phosphotyrosine was absent during mitosis (80–100 min), but reappeared during the next interphase (120–140 min). In contrast, the level of p34^{cdc2} tyrosine phosphorylation continued to increase throughout the experiment when PMA was applied during G1 phase (Figure 8A; PMA). Therefore p34^{cdc2} did not undergo the tyrosine dephosphorylation necessary for activation in PMA-treated embryos that lacked interphase [Ca^{2+}]$_i$ transients.

To study whether or not Ca^{2+} was also involved in regulating p34^{cdc2} phosphorylation at an activating site, equivalent to Thr^{161}, two-dimensional phosphopeptide mapping and phospho amino acid analysis were performed on tryptic digests of p34^{cdc2} that were isolated from ^{32}P-labelled embryos. Interestingly, a Thr^{161}-containing phosphopeptide was not evident in two-dimensional maps; perhaps because Thr^{161} phosphorylation is difficult to detect by ^{32}P labelling *in vivo* [40], and because only 20 % of the p34^{cdc2}-associated ^{32}P was phosphothreonine (results not shown). Therefore we subjected ^{32}P-labelled sea urchin p34^{cdc2} to acid hydrolysis (6 M HCl at 110 °C) for 6 h, since the half-life of phosphothreonine under these conditions is > 25 h, while the half-lives of phosphoserine and phosphotyrosine are 8 h and 2 h respectively [41,42]. This procedure improved the yield of free phosphothreonine relative to phosphoserine and phosphotyrosine. Levels of ^{32}P-labelled phosphothreonine were measured using TLC As shown in Figure 8(B), the phosphothreonine content of p34^{cdc2} increased more than 2-fold prior to mitosis in control embryos, and decreased to a similar extent as the population returned to interphase. In contrast, phosphothreonine remained at the elevated mitotic level for at least 90 min when PMA was added during prophase to block p34^{cdc2} inactivation and exit from mitosis (Figure 8B). The addition of PMA did not induce extensive phosphorylation of p34^{cdc2} by PKC, since additional tryptic phosphopeptides were not present in two-dimensional maps of p34^{cdc2} isolated from PMA-treated embryos (results not shown). In addition, our results were not influenced by the re-phosphorylation of sites equivalent to Thr^{14} and Thr^{161} in preparation for the next mitosis. These events require cyclin B [36,38], and emetine was added to both the control and the PMA-treated embryos during prophase to block the *de novo* synthesis of cyclin B after it was destroyed. Therefore in PMA-treated embryos where PKC activation leads to an abolition of mitotic [Ca^{2+}]$_i$ transients, p34^{cdc2} does not undergo the threonine dephosphorylation that is normally associated with its inactivation following cyclin B degradation.

DISCUSSION

PKC activation causes cell cycle arrest in sea urchin early embryos

PKC has been implicated as a regulator of the cell cycle in many cell types. In oocytes, PKC activation has been shown to both inhibit [43–45] and stimulate [46,47] meiotic maturation. We examined the effects of activators of PKC on the early embryonic cell cycles of sea urchins. We found that treatment of sea urchin early embryos with activators of PKC (PMA or diC$_8$) resulted in cell cycle arrest that was dependent on the time of application of the inhibitor. The administration of PKC activators prior to the beginning of S phase blocked entry into mitosis, while administration during prophase blocked exit from mitosis. The concentration of PMA used in the present study (200 nM) is sufficient to activate PKC *in vivo*, since similar concentrations induce cytoplasmic alkalinization in unfertilized sea urchin eggs; a process that involves activation of a Na$^+$/H$^+$ antiporter by PKC [30–32]. To learn more about the inhibitory effects of PKC on the cell cycle we analysed the effects of PKC activation on [Ca^{2+}]$_i$, cyclin B levels, p34^{cdc2} kinase activity and its phosphorylation state.

PKC activation blocks cell cycle [Ca^{2+}]$_i$ transients

We have shown that the activation of PKC eliminates cell cycle [Ca^{2+}]$_i$ transients in populations of early sea urchin embryos without altering the normal resting level of [Ca^{2+}]$_i$. This method arrests the cell cycle in a manner similar to Ca^{2+} chelators injected into single cells [3,4] In our hands, PMA was more effective than the membrane-permeant Ca^{2+} chelator, bis-(*o*-aminophenoxy)ethane-*N*,*N*,*N*′,*N*′-tetra-acetic acid (BAPTA) tetrakis(acetoxymethyl ester), at blocking cell cycle progression in sea urchins. A number of our results show that it is unlikely that PMA arrests the cell cycle due to a non-specific toxic effect. First, the embryos arrest at different defined stages of the cell cycle depending on the time of PMA application. Second, the PMA isomer, 4αPMA, has no effect on cell cycle progression. Third, rates of protein and DNA synthesis are not altered by PMA treatment Fourth, PMA does not alter the resting level of [Ca^{2+}]$_i$.

How does the activation of PKC block cell cycle [Ca^{2+}]$_i$ transients? In early frog and sea urchin embryos, there is compelling evidence that these transients are generated by periodic increases in the intracellular concentration of Ins(1,4,5)P_3, which causes Ca^{2+} to be released from the endoplasmic reticulum [8,21]. In cultured cells, PKC activation blocks the production of Ins(1,4,5)P_3 by receptor-coupled PtdIns(4,5)P_2 hydrolysis in response to growth factors and other extracellular signals [17–19] This inhibition is due to PKC phosphorylating phospholipase C (PLC), the enzyme that catalyses PtdIns(4,5)P_2 hydrolysis, or to PKC phosphorylating the cell surface receptor. These phosphorylations prevent the subsequent activation of PLC by tyrosine phosphorylation [17,19] or G proteins [18]. It is intriguing in light of this finding that PMA-induced cell cycle arrest at G2/M in cultured mammalian cells involves PKC phosphorylation of the epidermal growth factor receptor [48]. We have shown that endoplasmic reticulum microsomes prepared from PMA-treated embryos sequester Ca^{2+} at the same rate as microsomes prepared from control embryos. Furthermore, endoplasmic reticulum microsomes prepared from PMA-treated embryos have the same sensitivity to Ins(1,4,5)P_3 as controls. These observations are consistent with the idea that PKC activation blocks [Ca^{2+}]$_i$ transients by reducing levels of Ins(1,4,5)P_3 during the cell cycle. In sea urchin embryos, the increases in Ins(1,4,5)P_3 during the cell cycle are probably due to the periodic activation of a PLCγ isoform [49] and this is clearly a potential target for phosphorylation by PMA-activated PKC.

[Ca^{2+}]$_i$ transients required for p34^{cdc2} activation and inactivation

We took advantage of the finding that PKC activation appeared to inhibit embryonic cell cycles by preventing normal [Ca^{2+}]$_i$ transients, to determine how [Ca^{2+}]$_i$ transients might affect levels of p34^{cdc2} kinase activity. In the first cell cycle of sea urchin embryos, [Ca^{2+}]$_i$ is transiently elevated at pro-nuclear migration (G1/S), NEBD, anaphase onset, and cleavage [3,8,20,21]. The capacity to eliminate these [Ca^{2+}]$_i$ transients using PMA has enabled us to directly show that Ca^{2+} is required *in vivo* for activation and inactivation of the key cell cycle regulatory protein, p34^{cdc2}. The effect of PMA on p34^{cdc2} activity is due to its effect on [Ca^{2+}]$_i$ transients, since both the activation and inactivation of p34^{cdc2} are partially restored in PMA-treated embryos when Ca^{2+} ionophore A23187 is used to elevate [Ca^{2+}]$_i$. Ca^{2+} may be required for the p34^{cdc2} activation pathway as early as the G1/S transition, since the administration of PKC activators at later stages of the cell cycle does not block mitosis entry. Therefore it is possible that one or both of the interphase [Ca^{2+}]$_i$ transients (G1/S and NEBD) participate in the activation of p34^{cdc2}.

Ca^{2+} is required for the inactivation of p34^{cdc2} at the metaphase/anaphase transition, since the administration of PKC activators during telophase does not block exit from mitosis This suggests that the metaphase/anaphase [Ca^{2+}]$_i$ transient participates in the p34^{cdc2} inactivation pathway. Although it is well established that elevated [Ca^{2+}]$_i$ triggers p34^{cdc2} inactivation in oocytes arrested at meiotic metaphase [14], there have been few reports of Ca^{2+} regulating p34^{cdc2} activity during mitosis. Activation and inactivation of p34^{cdc2} are inhibited by Ca^{2+} chelators in cell-free preparations of frog embryos [16], and elevated physiological levels of Ca^{2+} induce precocious inactivation of p34^{cdc2} in permeabilized sea urchin embryos [15]. The latter finding implies that the metaphase/anaphase [Ca^{2+}]$_i$ transient is not only required for p34^{cdc2} inactivation, but that it controls the timing of inactivation.

Although artificially elevating [Ca^{2+}]$_i$ by the application of ionophore led to a partial restoration of both activation and inactivation of p34^{cdc2}, this did not allow cell cycle progression to take place. Microinjection of Ins(1,4,5)P_3 into arrested embryos was similarly without effect. This might be because neither of these artificial methods of elevating [Ca^{2+}]$_i$ faithfully recreates the temporal and spatial aspects of cell cycle [Ca^{2+}]$_i$ transients that are required for entry into or exit from mitosis. Alternatively, it is possible that PKC activation might also inhibit cell cycle progression through alternative mechanisms in addition to its effect on cell cycle [Ca^{2+}]$_i$ transients. For example, it is possible that PKC activation might result in the abnormal sub-cellular distribution of key Ca^{2+}-binding proteins, such as calmodulin [50].

Mechanism of p34^{cdc2} activation by Ca^{2+}

In systems where it has been analysed, the activation of p34^{cdc2} involves several sequential events. In the first step, p34^{cdc2} binds to cyclin B and is phosphorylated at a site required for activity (Thr^{161}), and at sites that inhibit its activity (Thr^{14} and Tyr^{15}). In the second step, the cdc25 phosphatase activates p34^{cdc2} by dephosphorylating Tyr^{15} and Thr^{14} [2]. The amino acid sequence of sea urchin p34^{cdc2} has not been determined; however, it undergoes cycles of tyrosine phosphorylation during interphase and dephosphorylation at G2/M, consistent with the presence of an inhibitory site equivalent to Tyr^{15} ([39] and Figure 8A). We have shown in the present study that the elimination of interphase [Ca^{2+}]$_i$ transients does not inhibit cyclin B synthesis, formation of the cyclin B–p34^{cdc2} complex, or the phosphorylation of p34^{cdc2} on tyrosine. However, p34^{cdc2} is not activated and does not undergo the tyrosine dephosphorylation that normally accompanies activation. These results imply that elevated Ca^{2+} is required for the dephosphorylation of p34^{cdc2} at an inhibitory site equivalent to Tyr^{15} If so, the role of Ca^{2+} may be to increase cdc25 phosphatase activity, or to decrease the activity of Wee1, the protein kinase that phosphorylates p34^{cdc2} at Tyr^{15}. In HeLa cells, the human tyrosine phosphatase p54(cdc25-c) is phosphorylated at the G2/M phase transition through a Ca^{2+}/calmodulin-dependent pathway [51]. It is possible that in sea urchin embryos, cdc25 activity is affected by the [Ca^{2+}]$_i$ transient at the G2/M phase transition through a similar Ca^{2+}-dependent mechanism.

Mechanism of p34^{cdc2} inactivation by Ca^{2+}

The inactivation of p34^{cdc2} during M phase involves proteolytic destruction of its cyclin B subunit and dephosphorylation at Thr^{161} [36]. In frog oocytes arrested at meiotic metaphase, the fertilization [Ca^{2+}]$_i$ transient induces proteolysis of cyclin B and inactivation of p34^{cdc2} [14]. In permeabilized sea urchin embryos, elevated [Ca^{2+}]$_i$ induces p34^{cdc2} inactivation without cyclin B proteolysis, thereby demonstrating that these two processes can be uncoupled in a mitotic system, and that p34^{cdc2} inactivation, but not cyclin destruction, is controlled by Ca^{2+} [15]. This conclusion is supported by the work of Lindsay et al. [16], who found that the addition of Ca^{2+} to mitotic extracts prepared in the presence of the Ca^{2+} chelator, BAPTA, could induce rapid inactivation of p34^{cdc2} without cyclin B proteolysis. An important prediction of our hypothesis is that the elimination of mitotic [Ca^{2+}]$_i$ transients should block inactivation of p34^{cdc2} without blocking the destruction of cyclin B. In the present study, we show that this prediction is correct; the use of PMA to eliminate [Ca^{2+}]$_i$ transients during mitosis blocks p34^{cdc2} inactivation, but cyclin B is destroyed at the same time as in control embryos. This is further evidence that p34^{cdc2} inactivation and cyclin B pro-

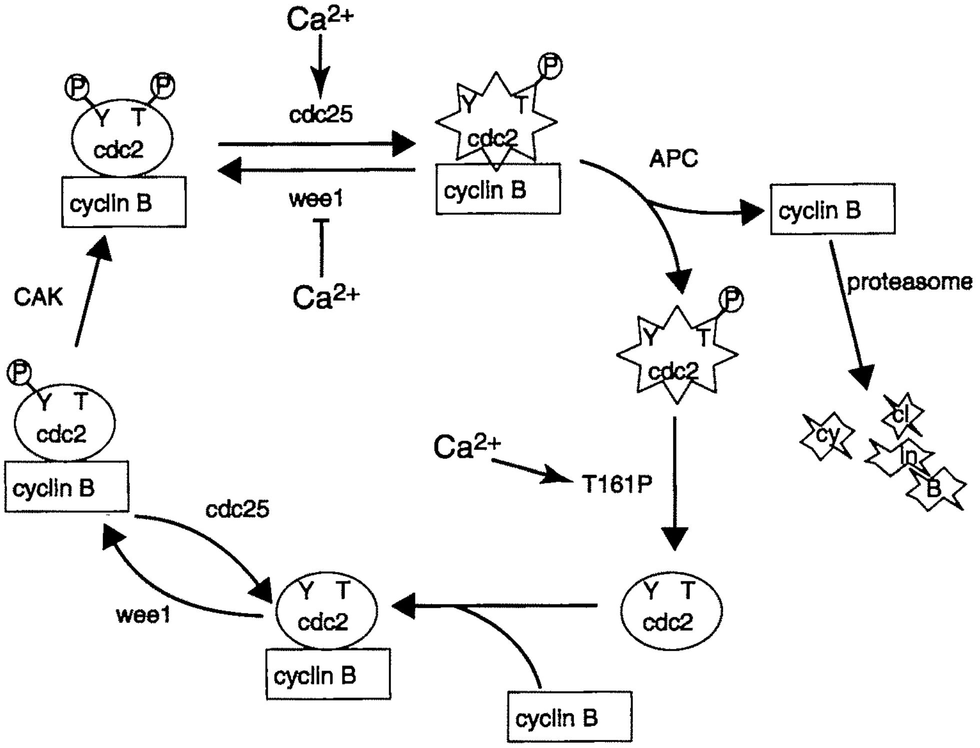

Figure 9 The effects of Ca^{2+} on p34^{cdc2} kinase activation and inactivation in embryonic cell cycles

The various p34^{cdc2}–cyclin B complexes formed during the early embryonic cell cycles are shown. Inactive p34^{cdc2} is shown as an oval and active p34^{cdc2} is shown as a star shape. In interphase, p34^{cdc2} and cyclin B associate and p34^{cdc2} is phosphorylated on Tyr^{15} (Y on the left side of cdc2) by Wee1 kinase. Thr^{161} (T on the right side of cdc2) is phosphorylated by cdc2-activating kinase (CAK). At the onset of mitosis, the conversion from inactive into active p34^{cdc2} kinase is accomplished through the dephosphorylation of Tyr^{15} by the tyrosine phosphatase cdc25. Activation of p34^{cdc2} kinase leads to the stimulation of the anaphase-promoting complex (APC) leading to cyclin destruction by proteasomes. As mitosis ends, p34^{cdc2} is rendered inactive by the activity of Thr^{161} phosphatase (T161P). The data presented in the present study suggest that Ca^{2+} is important in the activation of p34^{cdc2} kinase either through the activation of cdc25 or inactivation of Wee1. Ca^{2+} is also required for Thr^{161} phosphatase activation and thus p34^{cdc2} inactivation.

teolysis are distinct, separable processes during mitosis. In contrast, we show that in the absence of mitotic [Ca^{2+}]$_i$ transients, p34^{cdc2} does not undergo threonine dephosphorylation that is normally associated with its inactivation and exit from mitosis. Lorca et al. [36] previously reported that okadaic acid (an inhibitor of type 1 and type 2A serine/threonine protein phosphatases) blocked p34^{cdc2} inactivation, but not cyclin B proteolysis, in cell-free extracts of frog embryos. In their study, p34^{cdc2} remained active in the absence of cyclin B, because it did not undergo dephosphorylation at Thr^{161}. Our results provide evidence that the metaphase/anaphase [Ca^{2+}]$_i$ transient controls the timing of p34^{cdc2} inactivation in early sea urchin embryos by inducing the dephosphorylation of p34^{cdc2} at a site required for activity (the equivalent of Thr^{161}). A model of the possible interactions of Ca^{2+} with cell cycle control proteins in early embryonic cell cycles is shown in Figure 9.

If Ca^{2+} inactivates p34^{cdc2} via dephosphorylation, what is the role of cyclin B proteolysis? Since the phosphorylation of p34^{cdc2} at Thr^{161} requires p34^{cdc2} binding to cyclin B [36,38], and because the Thr^{161} kinase is constitutively active during early development [52], cyclin B proteolysis ensures that p34^{cdc2} remains inactive until the appropriate stage of the next cell cycle, when cyclin B has re-accumulated. This is especially important in view of the transient nature of the metaphase/anaphase increase in [Ca^{2+}]$_i$. A return of [Ca^{2+}]$_i$ to resting levels in the continued presence of cyclin B might be expected to re-activate p34^{cdc2} and thereby prevent the completion of mitosis, as occurs with non-degradable cyclin B mutants [35,53–55]. In permeabilized sea urchin embryos, elevated [Ca^{2+}]$_i$ inactivates p34^{cdc2} without cyclin B proteolysis; however, [Ca^{2+}]$_i$ is maintained at an elevated level throughout the course of these experiments by means of Ca^{2+}/EGTA buffers [15]. Although the phosphothreonine content of p34^{cdc2} was not determined in the present study, Ca^{2+} was found to induce dissociation of cyclin B–p34^{cdc2} complexes [15]. Since this complex is stabilized by the phosphorylation of p34^{cdc2} at Thr^{161} [56], its dissociation may well be a consequence of Ca^{2+}-induced Thr^{161} dephosphorylation. How Ca^{2+} plays a role in p34^{cdc2} activation at one stage of the cell cycle, and triggers inactivation at another stage, is an important question. The present study suggests that component(s) of the pathway that govern p34^{cdc2} dephosphorylation at Thr^{161} are not functional, or do not have access to p34^{cdc2}, during the NEBD [Ca^{2+}]$_i$ transient. In contrast, these component(s) are enabled, or are accessible to p34^{cdc2} at the time of the metaphase/anaphase [Ca^{2+}]$_i$ transient.

We thank Dr Joshua Zimmerberg for his support throughout the duration of this project. This work was supported in part by grants from the Royal Society and the University of Stirling Graduate's Association (to T. W.), and a programme grant from the Wellcome Trust (to M. W.)

REFERENCES

1 Norbury, C. and Nurse, P. (1992) Annu. Rev. Biochem. **61**, 441–470
2 Coleman, T. R. and Dunphy, W. G. (1994) Curr. Opin. Cell Biol. **6**, 877–882
3 Whitaker, M. and Patel, R. (1990) Development **108**, 525–542

4 Whitaker, M. (1995) Adv Second Messenger Phosphoprotein Res **30**, 299–310
5 Silver, R B. (1989) Dev Biol **131**, 11–26
6 Tombes, R M, Simerly, C, Bonsy, G G. and Schatten, G (1992) J. Cell Biol. **117**, 799–811
7 Miller, A L, Fluck, R A, McLaughlin, J. A and Jaffe, L F (1993) J Cell Sci **106**, 523–534
8 Groigno, L and Whitaker, M J. (1998) Cell **92**, 193–204
9 Steinhardt, R A and Alderton, J (1988) Nature (London) **332**, 364–366
10 Twigg, J, Patel, R and Whitaker, M (1988) Nature (London) **332**, 366–369
11 Kao, J P Y., Alderton, J M, Tsien, R Y. and Steinhardt, R A (1990) J. Cell Biol **111**, 183–196
12 Wilding, M, Wright, E M, Patel, R., Ellis-Davies, G and Whitaker, M (1996) J Cell Biol **135**, 191–199
13 Tombes, R M and Bonsy, G G (1989) J. Cell Biol **109**, 627–636
14 Lorca, T, Cruzalegui, F. H, Fesquet, D, Cavadore, J. C, Mery, J, Means, A and Doree, M (1993) Nature (London) **366**, 270–273
15 Suprynowicz, F. A, Prusmack, C and Whalley, T. (1994) Proc Natl. Acad Sci USA **91**, 6176–6180
16 Lindsay, H D, Whitaker, M J and Ford, C. C. (1995) J Cell Sci. **108**, 3557–3568
17 Decker, S J, Ellis, C, Pawson, T and Velu, T. (1990) J Biol Chem **265**, 7009–7015
18 Ryu, S. H, Kim, U. H, Wahl, M I, Brown, A B, Carpenter, G, Huang, K P and Rhee, S G (1990) J. Biol Chem **265**, 17941–17945
19 Park, D J, Min, H K and Rhee, S G (1992) J Biol Chem **267**, 1496–1501
20 Poenie, M, Alderton, J., Tsien, R Y and Steinhardt, R A (1985) Nature (London) **315**, 147–149
21 Clapa, B, Pesando, D, Wilding, M and Whitaker, M (1994) Nature (London) **368**, 875–878
22 Sluder, G, Miller, F. J. and Rieder, C L (1986) J Cell Biol **103**, 1873–1881
23 Galione, A, McDougall, A, Busa, W, Willmott, N, Gillot, I and Whitaker, M (1993) Science **261**, 348–352
24 Luo, K, Hurley, T. R and Sefton, B M (1991) Methods Enzymol **201**, 149–152
25 Boyle, W J, van der Geer, P and Hunter, T (1991) Methods Enzymol **201**, 110–149
26 Neufeld, E, Goren, H J and Boland, D (1989) Anal Biochem **177**, 138–143
27 Epel, D (1969) Exp Cell Res **58**, 312–319
28 Nishizuka, Y (1984) Nature (London) **308**, 693–698
29 House, C and Kemp, B E (1987) Science **238**, 1726–1728
30 Shen, S S and Buck, W. R (1990) Dev Biol **140**, 272–280
31 Swann, K. and Whitaker, M. (1985) Nature (London) **314**, 274–277
32 Lau, A F, Rayson, T C and Humphreys, T (1986) Exp Cell Res. **166**, 23–30
33 Shen, S S and Ricke, L A (1989) Comp Biochem Physiol, Part B· Biochem Mol Biol. **92**, 251–254
34 Rakow, T L and Shen, S S. (1994) Dev Growth Differ **36**, 489–497
35 Murray, A W, Solomon, M J and Kirschner, M W (1989) Nature (London) **339**, 280–286
36 Lorca, T, Labbe, J C, Devault, A, Fesquet, D., Capony, J P, Cavadore, J. C, Le Bouffant, F and Doree, M (1992) EMBO J **11**, 2381–2390
37 Meijer, L, Arion, D, Golsteyn, R, Pines, J, Brizuela, L, Hunt, T and Beach, D (1989) EMBO J **8**, 2275–2282
38 Solomon, M J., Lee, T. and Kirschner, M W. (1992) Mol Biol Cell **3**, 13–27
39 Edgecombe, M, Patel, R and Whitaker, M (1991) EMBO J **10**, 3769–3775
40 Krek, W and Nigg, E A (1992) New Biol **4**, 323–329
41 Bitte, L and Kabat, D. (1974) Methods Enzymol **30**, 563–590
42 Cooper, J A, Sefton, B. M and Hunter, T (1983) Methods Enzymol **99**, 387–402
43 Bornslaeger, E A., Poueymirou, W T, Mattei, P. and Schultz, R M (1986) Exp Cell Res **165**, 507–517
44 Lefevre, B, Pesty, A, Koziak, K and Testart, J (1992) J. Exp Zool. **264**, 206–213
45 Stith, B J, Goalstone, M L and Kirkwood, A J. (1992) Cell Signalling **4**, 393–403
46 Colonna, R, Tatone, C, Francione, A, Rosati, F, Callaini, G, Corda, D. and Di Francesco, L (1997) Mol Reprod Dev **48**, 292–299
47 Yoshimura, Y, Nakamura, Y, Ando, M, Jinno, M, Nanno, T, Oda, T, Koyama, N and Shiokawa, S (1992) Biol Reprod **47**, 118–125
48 Livneh, E, Dull, T J, Berent, E, Prywes, R, Ullrich, A and Schlesinger, J. (1988) Mol Cell Biol **8**, 2302–2308
49 Shearer, J, De Nadai, C., Emily-Fenouil, F, Gache, C, Whitaker, M and Ciapa, B (1999) Development **126**, 2273–2284
50 Torok, K, Wilding, M, Groigno, L, Patel, R and Whitaker, M J (1998) Curr. Biol **8**, 692–699
51 Patel, R., Holt, M, Philipova, R., Moss, S, Schulman, H., Hidaka, H. and Whitaker, M J (1999) J Biol Chem **274**, 7958–7968
52 Brown, A J, Jones, T and Shuttleworth, J (1994) Mol Biol Cell **5**, 921–932
53 Ghiara, J B, Richardson, H. E, Sugimoto, K, Henze, M, Lew, D J, Wittenberg, C and Reed, S I (1991) Cell **65**, 163–174
54 Luca, F C, Shibuya, E K., Dohrmann, C E and Ruderman, J V (1991) EMBO J **10**, 4311–4320
55 Gallant, P and Nigg, E A (1992) J Cell Biol **117**, 213–224
56 Ducommun, B, Brambilla, P., Felix, M A, Franza, Jr, B. R, Karsenti, E and Draetta, G (1991) EMBO J **10**, 3311–3319

Received 4 November 1999/30 March 2000, accepted 28 April 2000

Identification of active-site residues in *Bradyrhizobium japonicum* malonamidase E2

Hyun Min KOO, Sung-Ook CHOI, Hyun Mi KIM and Yu Sam KIM[1]
Department of Biochemistry, College of Science, Bioproducts Research Center, Yonsei University, Seoul 120-749, Korea

Malonamidase (MA) E2 was previously purified and characterized from *Bradyrhizobium japonicum* USDA 110. The gene encoding this enzyme has been cloned, sequenced and expressed in *Escherichia coli*. The recombinant MAE2 was purified to homogeneity from the transformed *E. coli*. The biochemical properties of the recombinant enzyme are essentially identical to those from wild-type *B. japonicum*. A database search showed that the MAE2 protein has a high sequence similarity with the common signature sequences of the amidase family. The only exception is that the aspartic residue in these signature sequences is replaced by a glutamine residue. In order to identify amino acid residues essential for enzyme activity, a series of site-directed mutagenesis studies and steady-state kinetic experiments were performed. Gln^{195}, Ser^{199}, Cys^{207} and Lys^{213} of the common signature sequences were selected for site-directed mutagenesis. Among the mutants, Q195D, Q195E and S199C showed less than 0.02 % of the k_{cat} value of the wild-type enzyme, and S199A, Q195L and Q195N exhibited no detectable catalytic activities. Mutants (K213L, K213R and K213H) obtained by replacement of the only conserved basic residue, Lys^{213}, in the signature sequences, also displayed significant reductions (approx. 380-fold) in k_{cat} value, whereas C207A kept full activity. These results suggest that MAE2 may catalyse hydrolysis of malonamate by a novel catalytic mechanism, in which Gln^{195}, Ser^{199} and Lys^{213} are involved.

Key words: glutamine, serine, lysine, site-directed mutagenesis, steady-state kinetics.

INTRODUCTION

Three malonamidases (MAs), MAE1a, MAE1b, and MAE2, have previously been purified and characterized from *Bradyrhizobium japonicum* [1]. These enzymes are known to catalyse all or some of the following reactions: malonyl transfer to hydroxylamine; hydroxylaminolysis of malonamate; and hydrolysis of malonamate. Among them, MAE2 is highly specific for hydroxylaminolysis and hydrolysis of malonamate. Its affinity for malonamate is 30- and 70-fold higher than that for MAE1a and MAE1b respectively [1]. These enzymes were first found in *B. japonicum* bacteroids and the plant cytosol of soybean nodules. It has been proposed that they may be involved in the transport of fixed nitrogen from bacteroids to the plant cell in symbiotic nitrogen metabolism [2].

Acylamide amidohydrolases (amidases; EC 3.5.1.4) catalyse hydrolysis of carboxylic acid amides to carboxylic acids and free ammonium. These enzymes are involved in nitrogen metabolism in cells and are widely distributed in living organisms: they have been found in both prokaryotic and eukaryotic cells. Among bacterial enzymes, amidases from *Brevibacterium* sp. R312 and *Pseudomonas aeruginosa* are well characterized. Based on the results of experiments performed with inhibitors, they have been classified as sulphydryl enzymes [3,4], which belong to an amidase signature family. This family has a highly conserved linear sequence rich in serine and glycine residues which spans nearly 50 amino acids in length (Figure 1) [5,6]. In addition to MAE2, more than 45 proteins containing the amidase signature sequence have been identified to date. They include many prokaryotic [6–12] and fungal enzymes [13–15], one avian enzyme [16], one mammalian enzyme [17] and three putative members from *Caenorhabditis elegans*. Recently, Kobayashi and his co-workers showed that the active-site residues of *Rhodococcus rhodochrous* J1 amidase were Asp^{191} and Ser^{195} rather than the generally accepted Cys^{203} residue [18]. The catalytic features of rat fatty acid amide hydrolase (FAAH), which is the only characterized mammalian member of the amidase family, were investigated through mutagenesis, affinity labelling and kinetic studies. Affinity labelling of FAAH with ethoxyoleoyl fluorophosphonate, a specific nucleophilic inhibitor, has demonstrated that the Ser^{241} residue is the enzyme's catalytic nucleophile [19]. In spite of significant progress in expanding our knowledge of amidases, little is known about their catalytic mechanism and/or tertiary structure.

In the present study we describe the molecular cloning of the *B japonicum MAE2* gene and the expression of the gene in *Escherichia coli*. Our results from mutagenesis and steady-state kinetic experiments clearly demonstrate that Gln^{195}, Ser^{199} and Lys^{213} are essential for MAE2 catalytic activity. Identification of the active-site residues demonstrates not only the specificity of the enzyme for malonamate, but also enhances our understanding of the enzyme's reaction mechanism.

EXPERIMENTAL

Strains and plasmids

B. japonicum USDA 110 was obtained from the Genetic Engineering Research Institute (Daeduck, Korea). *E. coli* XL-1 Blue MRA (P2) and MRA (Stratagene) were used to construct the genomic library of *B. japonicum*. For subcloning, *E. coli* XL-1 Blue MRF' (Stratagene) was used as a host strain. A pCR2.1

Abbreviations used: FAAH, fatty acid amide hydrolase, IPTG, isopropyl β-D-thiogalactoside, LB, Luria–Bertani, MA, malonamidase

[1] To whom correspondence should be addressed (e-mail yskim@bubble.yonsei.ac.kr)

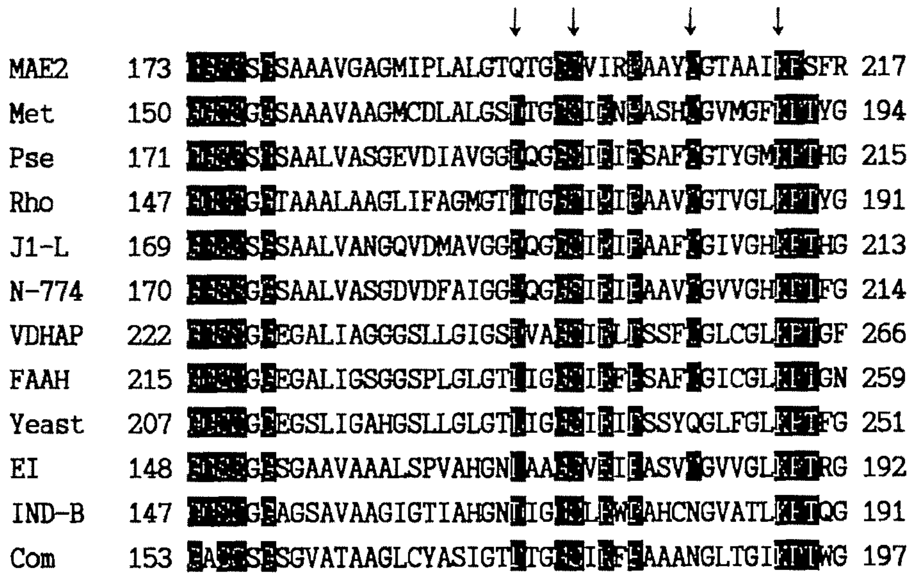

Figure 1 The amidase signature sequence region of all previously reported members of the amidase family

From top to bottom MAE2, malonamidase E2 from *B japonicum* USDA110 (GenBank AF012735), Met, amidase from *Methanobacterium thermoautotrophicum* [22], Pse, amidase from *Pseudomonas chlororaphis* [23], Rho, amidase from *Rhodococcus* sp [6], J1-L, amidase from *Rhodococcus rhodochrous* J1 [7], N-774, amidase from *Rhodococcus* sp. N-774 [8]; VDHAP, a vitamin D_3 hydroxylase-associated protein from cockerel [16], FAAH, oleamide hydrolase from rat [17], Yeast, putative amidase from *Saccharomyces cerevisiae* [24], EI (6-aminohexanoate-cyclic-dimer hydrolase), EI enzyme from *Flavobacterium* [9], IND-B, indoleacetamide hydrolase from *Bradyrhizobium japonicum* [26], Com, amidase from *Comamonas acidovorans* [27] Residues of the signature sequence region that are conserved among the amidase family members are shown on a black background and the relative amino acid position of the signature sequence in each amidase is given by the numbers preceding and following the sequence information Arrows indicate the amino acid residues that correspond to Gln^{195}, Ser^{199}, Cys^{207} and Lys^{213} of malonamidase E2 from *B japonicum* examined in this experiment

vector for cloning of PCR products was purchased from Invitrogen. The λ vector (λ DASH II/*Bam*HI vector kit) and the pBluescript KS II plasmid vector for subcloning of genes were purchased from Stratagene. The pUC18 plasmid for expression of genes was obtained from Pharmacia.

Enzymes and chemicals

Restriction enzymes and *Taq* DNA polymerase were purchased from Boehringer Mannheim. T4 DNA ligase and calf intestinal phosphatase were obtained from New England Biolabs (Beverly, MA, U.S.A.) Sequencing primers and the labelling system were purchased from Promega. ^{32}P-labelled nucleotides and nitrocellulose filters were from Amersham Pharmacia Biotech. The synthetic oligonucleotides were obtained from Bioneer Co., Chungbuk, Korea.

N-terminal amino acid sequence analysis of MAE2

MAE2 was purified by the method described previously [1]. One nmole of the protein was subjected to electrophoresis by SDS/PAGE (12 % polyacrylamide) and was then electroblotted on to a PVDF membrane according to the method of Matsudaira [20]. The N-terminal sequence of the protein was analysed by Edman degradation using a gas-phase protein microsequencer (PE Applied Biosystems; model 477A).

Purification and sequence determination of peptides generated by tryptic digestion of MAE2

The purified enzyme (300 μg) was denatured, reduced and digested with trypsin at 37 °C for 48 h. The resulting peptides were purified by HPLC on a Deltapak C_{18} reverse-phase column (3.9 mm × 200 mm) using a 0–80 % acetonitrile linear gradient. Three major peptide fragments were collected and subjected to automated sequence analysis on a Milligen 6600B Amino acid Sequencer from Applied Biosystems, Inc..

Preparation of total DNA from *B. japonicum*

Cells from a 200 ml culture, grown in yeast/mannitol at 30 °C, were harvested. Harvested cells were then suspended in 9 ml of Tris/EDTA buffer [10 mM Tris/HCl (pH 8.0)/1mM EDTA], and incubated with proteinase K (1 mg/ml) and 1 % (w/v) SDS overnight at 50 °C. The lysate was extracted twice with phenol/chloroform/isoamyl alcohol (25:24:1, by vol.) and twice with chloroform/isoamyl alcohol (24:1, v/v), and digested for 30 min at 37 °C with ribonuclease A (0.1 mg/ml). The ribonuclease-digested lysate was again extracted with phenol/chloroform/isoamyl alcohol (25:24:1, by vol.) and chloroform/isoamyl alcohol (24:1, v/v). The DNA was precipitated by the addition of 0 1 vol. of 3 M sodium acetate (pH 5.2) and 2 vol. of absolute ethanol. The precipitated DNA was spooled on to a glass rod, washed with 70 % ethanol, and resuspended in Tris/EDTA buffer (pH 8.0).

Preparation of the λ DNA library

The DNA isolated from *B. japonicum* was partially digested with *Sau*3AI and analysed on a 0.6 % agarose gel. Fractions containing fragments of 9–23 kb were pooled together, ligated to the λ DASHII/*Bam*HI vector that had been previously digested with *Bam*HI, and packaged using Gigapack III Gold packaging extract (Stratagene). The packaged λ phage were then used to infect *E. coli* XL-1 Blue MRA (P2).

Preparation of the probe

The N-terminal amino acid sequence of MAE2 is MISLADLQRRIETGELSPNAAI. A sense primer [5′-TGATCI(G/C)(G/C)(C/T)T(G/C)GC(G/C)GA(C/T)(C/T)T(G/A/T/C)CA-3′] of the N-terminal amino acid sequence (MISLADLQ) and an antisense primer [5′-GGT(G/C)GGCAT(A/G)TT(G/C)GC(G/A/T/C)GT(A/G)TC-3′] of an internal amino acid sequence (TDANMPT) were prepared to make a probe. By using the following PCR procedure and the degenerate primers, a PCR product was prepared. Reaction mixtures (100 μl) for PCR contained 100 ng of *B. japonicum* total DNA, 1.25 mM of each primer, 2.5 units of *Taq* DNA polymerase, 2 mM of each dNTP, and 1 μl of 10 × PCR buffer (Boehringer Mannheim). The PCR reaction was carried out in a Techne Progene programmable cycling heat block for 30 cycles of 50 s of denaturation at 95 °C, 30 s of annealing at 45 °C and 60 s of extension at 72 °C, followed by one cycle of 50 s of denaturation at 95 °C and 30 s of annealing at 45 °C, 7 min of extension at 72 °C. The 216-bp PCR product was purified from a 12% polyacrylamide gel, cloned into a pCR 2.1 vector (Invitrogen) according to the manufacturer's protocol and sequenced. The product was radiolabelled with [α-^{32}P]dCTP using a Prime-a Labeling system (Promega) and was subsequently used for screening the λ DNA library.

Cloning strategy and DNA sequence analysis

The λ library of *B. japonicum* total DNA was screened by plaque hybridization with the radiolabelled 216-bp PCR fragment as a probe. Positive plaques were isolated by successive plating, and a pure phage was purified using a plate lysate method A 2-kb *Bam*HI fragment inserted into the positive λ phage DNA was subcloned into pBluescript KS II (designated pBMAE2). Appropriate restriction fragments of the DNA were prepared for sequencing. These were sequenced using the ABI PRISM® Dye Terminator Cycle Sequencing Ready Reaction Kit (Perkin–Elmer) and the ABI 310 automated sequencer (Applied Biosystems Division of Perkin–Elmer).

Construction of expression plasmid with the *MAE2* gene

Since there were no suitable restriction sites upstream of the presumed ATG initiation codon, it was necessary to modify the sequence upstream of the ATG codon in order for expression to occur. Modification was achieved by using PCR with the recombinant plasmid (pBMAE2) as a template and the following two primers. Primer 1, GC**GGATCC**A*AGAAGG*GTATGAGCCatgatctcactcgccga, contained 4 segments: (1) a *Bam*HI recognition site (bold); (2) a ribosome-binding site (italicized); (3) a TGA stop codon (underlined); and (4) the *MAE2* structural gene that begins with the ATG start codon (lower-case letters). Primer 2, GC**GGATCC**gtgcgatgatcagtgc, contained 16 nucleotides of the gene complementary to nucleotides 1293–1308 (lower case letters) and a *Bam*HI recognition site (bold). The plasmid designated as pMAE2 was constructed by ligation of the PCR product with pUC18/*Bam*HI. This was then used to transform *E. coli* AD494 (DE3) (Novagen, Madison, WI, U.S.A.).

Construction of recombinant plasmid for the expression of MAE2 with a His-tag

Expression vector pRSET A (Invitrogen), which is designed to express proteins containing a His-tag at the N-terminal was used in order to facilitate the enzyme's recovery and subsequent purification. The *MAE2* gene was amplified with two oligonucleotides, 5′-GC**GGATCC**ATGATCTCACTCGCCGA-3′ and 5′-GC**GGATCC**GTGCGATGATCAGTGC-3′ (the *Bam*HI recognition site is shown in bold). For PCR amplification, 50 ng of pMAE2 was used as a template in a 50 μl reaction system containing 0.2 mM of each dNTP, 1.5 mM MgCl$_2$, 25 pmol of each primer, 1 × *Pfu* reaction buffer (Stratagene) and 2.5 units of *Pfu* DNA polymerase (Stratagene). The PCR reaction was carried out in a Techne Progene programmable cycling heat block for 25 cycles of 50 s of denaturation at 96 °C, 50 s of annealing at 52 °C and 3 min 30 s of extension at 72 °C, followed by one cycle of 50 s of denaturation at 96 °C, 50 s of annealing at 52 °C and 10 min of extension at 72 °C. The amplified product was digested with *Bam*HI and was subcloned into the *Bam*HI site of the expression vector pRSET A. The resulting plasmid was named pHMAE2.

Table 1 Oligonucleotides used for site-directed mutagenesis

Nucleotide sequences corresponding to the mutated amino acid residues are underlined

MAE2 gene allele	Mutagenic primer set
Q195D	CGAGCCGCCGGTATCGGTGCCCAGCGCCAGCGG GCGCTGGGCACCGATACCGGCGGCTCGGTGATC
Q195E	CGAGCCGCCGGTGAAGGTGCCCAGCGCCAGCGG GCGCTGGGCACCTTCACCGGCGGCTCGGTGATC
Q195L	CGAGCCGCCGGTCAGGGTGCCCAGCGCCAGCGG GCGCTGGGCACCCTGACCGGCGGCTCGGTGATC
Q195N	CGAGCCGCCGGTAATGGTGCCCAGCGCCAGCGG GCGCTGGGCACCATTACCGGCGGCTCGGTGATC
S199A	GGGCCGGATCACCGCGCCGCCGGTCTGGGTGCC CAGACCGGCGGCGCGGTGATCCGGCCCGCCGCC
S199C	GGGCCGGATCACTGCGCCGCCGGTCTGGGTGCC CAGACCGGCGGCGCAGTGATCCGGCCCGCCGCC
C207A	CCCGCCGCCTATCGCGGGACGGCCGCGATCAAG CGCGGCCGTCCCGCGATAGGCGGCGGGCCGGAT
K213L	GCGGAACGACGGCAGGATCGCGGCCGTCCCGCA ACGGCCGCGATCCTGCCGTCGTTCCGCATGCTG
K213H	GCGGAACGACGGATGGATCGCGGCCGTCCCGCA ACGGCCGCGATCCATCCGTCGTTCCGCATGCTG
K213R	GCGGAACGACGGCGCGATCGCGGCCGTCCCGCA ACGGCCGCGATCGCGCCGTCGTTCCGCATGCTG

Site-directed mutagenesis

Appropriate pairs of mutagenic primers (see Table 1) were synthesized and used to generate the mutated *MAE2* by PCR, according to the method of QuickChange site-directed mutagenesis from Stratagene. Here, the pHMAE2 was used as the template for *Pfu* DNA polymerase (Stratagene). Following PCR, the wild-type parental plasmid remaining in the PCR product was selectively digested by the *Dpn*I restriction enzyme (Boehringer Mannheim), and the resultant mixture was used to transform chemically competent *E. coli* XL-1 Blue MRF' (Stratagene). The desired mutants were sequenced to identify each mutation and confirm their fidelity.

Expression and purification of wild-type MAE2

MAE2 was expressed in *E. coli* AD494 (DE3) (Novagen) transformed with pMAE2. *E. coli* RNA polymerase recognized a Lac promoter on pUC18 that was used as a vector for subcloning. The transformed *E. coli* were cultured for 12 h in 3 ml of Luria–Bertani (LB) medium containing ampicillin (50 μg/ml), and then transferred into 200 ml of the same medium. The culture was incubated at 37 °C for 3 h and isopropyl 1-thio-β-D-galactoside (IPTG) (1 mM final conc.) was added, followed by incubating the culture at 37 °C for 16 h The cells were harvested and resuspended in 20 mM Tris/HCl (pH 7:4)/15 % (v/v) glycerol. The preparation of crude extract followed by Affi-Gel Blue column chromatography were performed by the method described previously [1]. The adsorbed proteins were sequentially eluted by the application of a 400-ml linear gradient of NaCl (0–2 M) in the same buffer and a 300-ml stepwise gradient of 2 M NaCl in 20 mM Tris/HCl (pH 7.4). Fractions were collected and assayed for MAE2 activity. Fractions containing the enzyme activity were pooled. $ZnSO_4$ was added to the enzyme solution to give a final concentration of 0.5 mM. This solution was subsequently applied to a Phenyl-Sepharose CL-4B column, equilibrated with 20 mM Tris/HCl (pH 7.4) containing 2 M NaCl and 2 mM $ZnSO_4$. After loading was completed, the unadsorbed materials were washed with 100 ml of the same Tris buffer containing 2 M NaCl and 2 mM EDTA. MAE2 was eluted by the application of a 300-ml linear descending gradient (2–0 M) of NaCl in 20 mM Tris/HCl (pH 7.4) containing 2 mM EDTA. Fractions containing the enzyme activity were pooled and dialysed twice against 2 litres of the same Tris buffer The dialysed solution was loaded on to Red-120 agarose, pre-equilibrated with the same buffer. As soon as the loading was completed, the adsorbed proteins were eluted by the application of a linear gradient of NaCl (0–2 M) in the same buffer. MAE2 was eluted at 1 7–1.9 M NaCl The MAE2 solution was dialysed against the same Tris buffer, stored at 4 °C, and used for all subsequent experiments.

Expression and purification of MAE2 and mutants with a His-tag

The expression and purification of MAE2 with a His-tag were accomplished according to the manufacturer's instructions (Novagen). *E coli* BL21 (DE3) pLysS (Novagen) transformed with pHMAE2 were cultured for 12 h in 3 ml of LB medium containing ampicillin (50 μg/ml), and were then transferred into 200 ml of the same medium. The culture was incubated at 37 °C for 2 h and IPTG (0.5 mM final conc.) was added. This was followed by incubating the culture at 25 °C for 20 h. The cells were harvested, resuspended in 8 ml of binding buffer [20 mM Tris/HCl (pH 7.9)/5 mM imidazole/500 mM NaCl] and sonicated. The cell lysates were put on to a His-Bind resin column. The protein bound to the matrix was eluted with elution buffer [20 mM Tris/HCl (pH 7.9)/400 mM imidazole/500 mM NaCl]. This protein was dialysed against 2 litres of 10 mM Tris/HCl (pH 8.0), stored at 4 °C, and used for all subsequent experiments. Each of the mutants was also expressed and purified under the same conditions.

CD spectroscopy

CD spectroscopy was used to compare the overall secondary structure of wild-type and selected mutant proteins. Measurements were recorded at room temperature from 190–250 nm under nitrogen using a JASCO J-720 spectropolarimeter with a 1 mm cell and 0 2 nm wavelength increments. Each spectrum was normalized for protein concentration and the observed ellipticity (θ) was background-corrected against the spectrum obtained for the dialysis buffer [10 mM Tris/HCl (pH 8.0)]

Enzyme assays and kinetic experiments

MAE2 activity was measured by the method described previously [1]. The method was based on hydroxylaminolysis of malonamate:

$$HOOCCH_2CONH_2 + NH_2OH \rightarrow HOOCCH_2CONHOH + NH_3$$

Reaction mixtures (500 μl) contain 100 mM Tris/HCl buffer (pH 8.0), 10 mM malonamate, neutralized 20 mM NH_2OH and enzyme After incubation for 30 min at 37 °C, the malonohydroxamate formed was determined by the same method described previously for malonyl-CoA synthetase [21] The K_m and k_{cat} values were measured as described above with various substrate concentrations (0.625–20 mM). The enzyme concentrations used in this experiment were 0.042 μM for the wild-type enzyme and 2.1 μM for each mutant. The rate of malonohydroxamate formation increased with increasing substrate concentration; demonstrating typical Michaelis–Menten saturation kinetic behaviour. The double-reciprocal plots were linear, and from these plots the kinetic parameters were determined. The error values reported reflect the standard deviation of at least three independent trials.

RESULTS

Cloning and nucleotide sequence of the *MAE2* gene from *B. japonicum* USDA 110

Degenerate oligonucleotides corresponding to the amino acid sequences of the N-terminal region of the protein and of internal peptides were synthesized and used to clone a 216-bp DNA fragment from *B. japonicum* total DNA. This partial clone was then used as a probe to screen a *B. japonicum* total DNA library for full-length clones. Clones containing the entire gene were isolated. The DNA prepared from these positive clones was subjected to restriction analysis and Southern-blot hybridization with the probe, which indicated the location of the *MAE2* gene. A 2-kb *Bam*HI DNA fragment that contained the entire gene was isolated and subcloned into pBluescript KS II, and the clone thus obtained was designated as pBMAE2. The nucleotide sequence of the *MAE2* gene was previously deposited at the GenBank database under the accession number AF012735. The *MAE2* gene encodes a polypeptide of 432 amino acids with a calculated molecular mass of 45635 Da. The N-terminal and three tryptic peptide sequences for MAE2 of *B. japonicum*, MISLADLQRRIETGELSPNAAI, DPTDTANMPT, WQPRHD, and AGASVQAIDL, match the nucleotide sequence in the MAE2 gene, thus confirming that the gene encodes MAE2.

A database search showed that the MAE2 protein sequence shares close homology to several amidase enzymes from organisms as diverse as *Methanobacterium thermoautotropicum* [22], *Pseudomonas chlororaphis* [23], *Rhodococcus* sp. [6,8], *R. rhodochrous* [7], *Saccharomyces cerevisiae* [24], *C. elegans* [25], *Flavobacterium* [9], *B. japonicum* [26], *Comamonas acidovorans* [27] and rat [17]. These amidases collectively make up an enzyme family whose members all share a common signature sequence (Figure 1).

Purification and characterization of MAE2 expressed in *E. coli*

When *E. coli* harbouring pMAE2 were cultured for 12 h at 37 °C in LB medium in the presence of 1 mM IPTG, the MAE2 activity in the supernatant of the sonicated cell-free extract of the transformant was 0 67 μmol/min per mg of protein, which was 3.4-fold higher than that in *B japonicum* USDA 110 (with malonamate as the substrate). The MAE2 was easily purified as described in the Experimental section. The enzyme from the Red-120 agarose gel was homogeneous on SDS/PAGE (results not shown) after approx. 386-fold purification with a recovery of approx 43 % (Table 2). The specific activity of the purified recombinant enzyme was 251 μmol/min per mg of protein, for malonamate, at pH 8.0 and 37 °C, corresponding well to the reported value of 269 μmol/min per mg of protein for the protein

Table 2 Purification of MAE2 from transformed *E. coli* harboring pMAE2

Starting material 8 g bacteria (wet mass). Enzyme activity was measured as described in the Experimental section.

Purification	Volume (ml)	Total protein (mg)	Total activity (μmol/min)	Specific activity (μmol/min per mg)	Recovery (%)	Fold
Crude extract	60	1432	954	0.67	100	1
Affi-Gel Blue	260	78	667	8.5	70	12.7
Phenyl-Sepharose	51	12.8	532	41.6	56	62
Red-120 agarose	53	1.58	410	259	43	386

purified from *B. japonicum*. The k_{cat} values of the recombinant enzyme were essentially identical to the parental enzyme from *B. japonicum* (2.2×10^3 s^{-1} and 2.1×10^3 s^{-1} respectively). The substrate specificity of the enzyme was examined by using other substrate analogues (malonate, succinate, acetate, succinnamate, malonamide and acetamide). However, these analogues could not be used as substrates, instead of malonamate, showing that the enzyme is highly specific for malonamate. These results indicate that the properties such as specific activity, molecular mass, substrate specificity and kinetic properties of the enzyme expressed in *E. coli* were more or less identical to those of the parental MAE2.

Identification of putative active-site residues

The amino acid sequence of MAE2 identified this enzyme as a member of the amidase family, as mentioned above. This enzyme family is defined by a highly conserved linear sequence which spans nearly 50 amino acids in length (Figure 1) [5,6]. MAE2 shows a sequence similarity with the common signature sequence except that, interestingly, a glutamine residue is located at the position corresponding to the conserved aspartic residue in the common signature sequences (Figure 1). So far, members of the amidase family have been generally classified as one of the sulphydryl enzymes [3,4]. Recently, two active-site amino acid residues, aspartic acid and serine, have been identified within these common signature sequences of the *R. rhodochrous* J1 amidase [18]. It was suggested that Asp^{191} of the *Rhodococcus* amidase may function as a general base drawing the proton from the Ser^{195} C^{γ} hydroxy group, allowing the serine to act as a nucleophile attacking the carbonyl group of the amide junction within the substrate. More recently, the corresponding serine (residue 199 in MAE2 numbering) in the FAAH sequence was identified as a catalytic nucleophile through mutagenesis and affinity labelling studies [19]. Considering the above results, the glutamine residue together with the serine residue was expected to be a candidate for the active-site amino acid residue of MAE2. We thus selected Gln^{195} and Ser^{199}, as well as Cys^{207}, for mutagenesis. To test the possibility that a highly conserved basic residue served as the catalytic base of MAE2, we also selected Lys^{213}, which is the only conserved basic residue in the signature sequence (Figure 1).

Kinetic properties of MAE2 mutants

In order to identify active-site residues essential for MAE2 function, wild-type MAE2 and its site-specific mutants were produced as His-tagged fusion proteins in *E. coli*. Ten different mutant enzymes (Q195D, Q195L, Q195N, Q195E, S199A, S199C, K213L, K213H, K213R and C207A), as well as wild-type MAE2, were prepared and their hydrolytic activities, with malonamate as substrate, were determined. The mutant enzymes were successfully produced in *E. coli* BL21 (DE3) pLysS and were purified under the same conditions as the wild-type MAE2. Their CD spectra in the far UV region were almost identical to that of the wild-type enzyme with a His-tag (Figure 2), indicating that no major changes occurred in the overall conformation of the mutant enzymes. Specific activities of S199A, Q195L and Q195N mutant enzymes were below the detection level ($\leqslant 0.01$ % of the original activity), even when large amounts of the enzymes were used in the reaction for 16 h. The specific activity of the wild-type enzyme with a His-tag was similar to that of the parental enzyme from *B. japonicum* (228 μmol/min per mg of protein and 269 μmol/min per mg of protein respectively). The k_{cat} values of the two enzymes were essentially identical (2.2×10^3 s^{-1} and 2.1×10^3 s^{-1} respectively), suggesting that the His-tag had no effect on the Michaelis–Menten parameters.

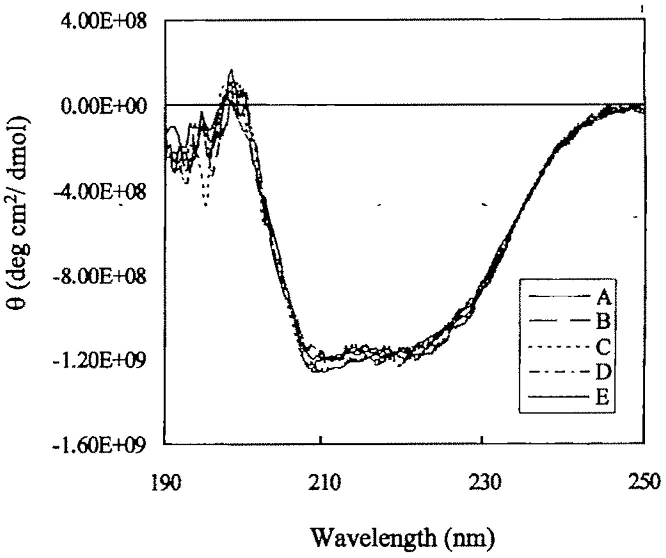

Figure 2 Circular dichroism spectra of purified wild-type and mutant MAE2 enzymes

The spectra were recorded in 10 mM Tris/HCl buffer, pH 8.0, in the far-UV region between 190 and 250 nm at 25 °C. Spectra of protein samples (approximately 0.3 mg/ml) were measured in a 300 μl quartz cell of 1 mm path length. The lines A–E represent wild-type, Q195E, S199A, K213H and C207A respectively. The CD spectra of the Q195D, Q195L, Q195N, S199C, K213L and K213R mutants were within error of the spectra shown but were omitted for clarity.

The steady-state kinetic analysis of the mutant enzymes showed that mutations of the three residues, Gln^{195}, Ser^{199} and Lys^{213}, resulted in MAE2 enzymes bearing significant catalytic defects (Table 3). The k_{cat} value for malonohydroxamate formation, which was 2200 s^{-1} in the wild-type, was decreased by approx. 7×10^3-fold in the Q195D and Q195E mutants, 1.2×10^4-fold in the S199C mutant and approx. 380-fold in the K213 mutants. The K_m of the Q195E mutant was 3-fold higher than that of the wild-type enzyme. The difference occurred due to the change of the ionization state caused by the substitution. Differences in the K_m values of other mutants were insignificant compared to that of the wild-type. This implied that the substitutions had no influence on substrate binding. The C207A mutant exhibited catalytic properties similar to those of wild-type MAE2 (Table 3). The results indicate that Ser^{199}, Lys^{213} and Gln^{195} are crucial to the catalytic activity of MAE2, whereas Cys^{207} is not. This is in agreement with the finding that the purified wild-type MAE2

Table 3 Kinetic properties of MAE2 mutants

Assay conditions were as described in the Experimental section Values represent means ± S D ($n \geqslant 3$)

Enzyme	K_m (mM)	k_{cat} (s^{-1})	k_{cat}/K_m ($M^{-1}\ s^{-1}$)
Wild-type	3.76 ± 0.4	2200 ± 160	585000
Q195E	12.1 ± 1.1	0.32 ± 0.04	26.4
Q195D	1.81 ± 0.2	0.30 ± 0.03	166
S199C	6.94 ± 0.7	0.18 ± 0.01	25.9
C207A	4.21 ± 0.1	2400 ± 270	570000
K213L	2.28 ± 0.2	5.8 ± 1.1	2540
K213H	2.03 ± 0.1	5.8 ± 0.9	2860
K213R	1.8 ± 0.4	5.7 ± 0.4	3170

shows a strong resistance to thiol reagents, such as *N*-ethylmaleimide and iodoacetamide (results not shown), and with the finding that Cys^{207} is not completely conserved in every member of the amidase family (Figure 1).

DISCUSSION

We have investigated the cloning and sequencing of the *MAE2* gene from *B. japonicum*, which allow the comparison of the amino acid sequence derived from its DNA with those of the amidase signature family reported so far. MAE2 shows sequence similarity with the common signature sequence of amidases. It is interesting to note that in MAE2 a glutamine residue occupies the position of the catalytic aspartic residue found in the common signature sequences (Figure 1). The present study also describes site-directed mutagenesis experiments on the MAE2 from *B. japonicum*.

MA was previously known to form a covalent intermediate during catalysis. The isolation of [^{14}C]malonyl-enzyme by gel-filtration and isotope-exchange experiments with [^{18}O]malonate indicated that the enzyme operates by an acyl-enzyme mechanism [1]. MAE2 is not inactivated by the serine-directed inhibitor, PMSF (results not shown). Although this result seems to be inconsistent with the crucial role of Ser^{199} as revealed by the site-directed mutagenesis experiments, such apparent inconsistency is known in several serine proteases. For example, leader peptidase, which removes signal peptides from exported proteins, is a serine protease, yet it is not sensitive to diisopropyl fluorophosphate ('DIFP') or PMSF [28]. It is also interesting to note that the S199C mutant showed some enzyme activity (approx. 0.025 % of the original activity), demonstrating indirectly the importance of Ser^{199} as a nucleophile. In support of this notion, the corresponding serine in rat FAAH was identified as the enzyme's catalytic nucleophile [19].

The amide bond ($CO-NH_2$) in the amide substrate is structurally not too far removed from a peptide bond (CO-NH-). Recently, Kobayashi and his co-workers proposed an evolutionary relationship between amide-bond cleaving enzymes (including amidases) and peptide-bond-cleaving enzymes (including aspartic proteinases) [18]. However, MAE2 deviates from the amidase signature sequence in that a conserved aspartic residue is replaced with a glutamine residue (residue 195 in MAE2 numbering). We should therefore consider the possibility that the catalytic mechanism of the enzyme might resemble that of serine proteases. The standard mechanism for proteases, especially serine proteases, which has evolved both by convergent and divergent evolution [29], involves a catalytic triad. The classical catalytic triad consists of a serine nucleophile, a histidine that acts as a general base to activate the hydroxy group of the serine, and an aspartate, which stabilizes the partial charge assumed by the histidine [30]. In the case of rat FAAH, the FAAH mutants H184Q, H358A and H449A, which involve the only three conserved histidine residues among rat, mouse and human FAAHs, retained almost full activity, suggesting that a histidine base does not participate in FAAH's catalytic mechanism [19]. As shown in Figure 1 there are no histidine or aspartic residues in the common signature sequence of MAE2, whereas there are both a highly conserved lysine residue and a serine residue. Moreover, we found that there are no conserved histidine or aspartic residues when the amino acid sequence of MAE2 is aligned with all previously reported members of the amidase family (results not shown). These results suggest that MAE2 does not contain a Ser-His-Asp catalytic triad commonly found in other serine hydrolytic enzymes. Among serine hydrolases, class A β-lactamases [31], the type I signal peptidases [32] and the Lex repressor [33] have been found to utilize a non-histidine base in catalysis. In these unusual cases, a lysine residue is thought to function as the general base to assist in nucleophilic attack by the serine hydroxy group. MAE2 has Lys^{213} that is highly conserved in the signature sequence of the amidase family. It is very interesting to note that when lysine is replaced by other amino acids in the three mutants we have examined, namely K213L, K213R and K213E, the mutants exhibit significant catalytic defects suggesting the importance of Lys^{213} in enzymic activity. Although the specific role of the lysine residue in MAE2 catalysis has not been established, it is most likely that Lys^{213} functions as a base in the activation of MAE2's serine nucleophile. Further characterization of MAE2's kinetic mechanism and high-resolution structural studies may elucidate the potential role of the lysine residue in MAE2's catalytic mechanism.

Mutation of Gln^{195} to glutamic acid, aspartic acid, leucine or asparagine in MAE2 revealed that it plays a significant role in catalysis. The reaction of amidases is thought to proceed via an acyl-enzyme intermediate like an oxyanion derivative of the peptide in serine protease catalysis [17,34]. We suggest that Gln^{195} may participate in the stabilization of the transition-state complex, by forming a hydrogen-bond to the oxyanion. A similar role for asparagine has been proposed in the catalytic mechanism of subtilisin from *Bacillus amyloliquefaciens* [34] and penicillin acylase from *E. coli* [35]. In the case of subtilisin, preventing formation of hydrogen-bonds in the oxyanion hole by mutating asparagine to alanine decreases its reaction rate by more than 1000-fold, which emphasizes the importance of this residue in hydrolysis.

In summary, we have sequenced, cloned and expressed the *B. japonicum* MAE2 in *E. coli*, and the Gln^{195}, Ser^{199} and Lys^{213} in the signature sequences were identified to be part of the active-site of the enzyme. This is the first report that an amidase having the common signature sequence catalyses hydrolysis of an amide by a novel catalytic mechanism in which serine, glutamine and lysine are involved. This finding will be instrumental for understanding the catalytic action of the amidase family.

We wish to thank Dr S W Kang (Laboratory of Cell Signaling, NHBLI/NIH, Bethesda, MA 20892, U S A) for providing the amino acid sequence We also thank Professor Heinz G Floss for critical review of the manuscript This work was supported by a grant from the Korea Science and Engineering Foundation (97-05-01-06-01-5)

REFERENCES

1 Kim, Y. S. and Kang, S. W (1994) Novel malonamidases in *Bradyrhizobium japonicum* Purification, characterization, and immunological comparison J Biol. Chem **269**, 8014–8021

2 Kim, Y. S and Chae, H Z (1990) A model of nitrogen flow by malonamate in *Rhizobium japonicum*-soybean symbiosis Biochem Biophys Res Commun **169**, 692–699

3 Thiery, A, Maestracci, M., Arnaud, A, Galzy, P. and Nicolas, M (1986) Purification and properties of an acylamide amidohydrolase (E C 3 5 1.4) with a wide activity spectrum from *Brevibacterium* sp R312 J. Basic Microbiol **26**, 299–311

4 Brammar, W. J and Clarke, P H (1964) Induction and repression of *Pseudomonas aeruginosa* amidase J Gen Microbiol **37**, 307–319

5 Chebrou, H, Bigey, F., Arnaud, A and Galzy, P (1996) Study of the amidase signature group Biochim Biophys. Acta **1298**, 285–293

6 Mayaux, J-F, Cerbelaud, E, Soubrier, F, Faucher, D and Petre, D (1990) Purification, cloning, and primary structure of an enantiomer-selective amidase from *Brevibacterium* sp strain R312 structural evidence for genetic coupling with nitrile hydratase J Bacteriol. **172**, 6764–6773

7 Kobayashi M, Komeda, H, Nagasawa, T, Nishiyama, M, Horinouchi, S, Beppu, T, Yamada, H and Shimizu, S (1993) Amidase coupled with low-molecular-mass nitrile hydratase from *Rhodococcus rhodochrous* J1. Sequencing and expression of the gene and purification and characterization of the gene product Eur J Biochem **217**, 327–336

8 Hashimoto, Y, Nishiyama, M, Ikehata, O, Horinouchi, S and Beppu, T (1991) Cloning and characterization of an amidase gene from *Rhodococcus* species N-774 and its expression in *Escherichia coli* Biochim Biophys Acta **1088**, 225–233

9 Tsuchiya, K, Fukuyama, S, Kanzaki, N, Kanagawa, K, Negoro, S and Okada, H (1989) High homology between 6-aminohexanoate-cyclic-dimer hydrolases of *Flavobacterium* and *Pseudomonas* strains J Bacteriol **171**, 3187–3191

10 Klee, H, Montoya, A., Horodyski, F, Lichtenstein, C, Garfinkel, D, Fuller, S, Flores, C, Peschon, J, Nester, E and Gordon, M (1984) Nucleotide sequence of the *tms* genes of the pTiA6NC octopine Ti plasmid: two gene products involved in plant tumorigenesis Proc Natl Acad Sci. U S A. **81**, 1728–1732

11 Curnow, A W, Hong, K-W, Yuan, R, Kim, S.-I, Martins, O., Winkler, W, Henkin, T M and Soll, D (1997) Glu-tRNAGln amidotransferase a novel heterotrimeric enzyme required for correct decoding of glutamine codons during translation Proc. Natl Acad Sci U S.A. **94**, 11819–11826

12 Boshoff, H I and Mizrahi, V (1998) Purification, gene cloning, targeted knockout, overexpression, and biochemical characterization of the major pyrazinamidase from *Mycobacterium smegmatis* J Bacteriol **180**, 5809–5814

13 Corrick, C M, Twomey, A P and Hynes, M J (1987) The nucleotide sequence of the *amdS* gene of *Aspergillus nidulans* and the molecular characterization of 5′ mutations. Gene **53**, 63–71

14 Gomi, K, Kitamoto, K and Kumagai, C (1991) Cloning and molecular characterization of the acetamidase-encoding gene (*amdS*) from *Aspergillus oryzae* Gene **108**, 91–98

15 Genbauffe, F S and Cooper, T G (1991) The urea amidolyase (DUR1, 2) gene of *Saccharomyces cerevisiae* DNA Sequence **2**, 19–32

16 Ettinger, R A and DeLuca, H F (1995) The vitamin D3 hydroxylase-associated protein is a propionamide-metabolizing amidase enzyme Arch. Biochem Biophys **316**, 14–19

17 Cravatt, B F, Giang, D K, Mayfield, S P, Boeger, D L, Lerner, R A and Gilula, N B (1996) Molecular characterization of an enzyme that degrades neuromodulatory fatty-acid amides Nature (London) **384**, 83–87

18 Kobayashi, M., Fujiwara, Y, Goda, M., Komeda, H and Shimizu, S (1997) Identification of active sites in amidase evolutionary relationship between amide bond- and peptide bond-cleaving enzymes Proc Natl Acad Sci U S A **94**, 11986–11991

19 Patricelli, M. P., Lovato, M A and Cravatt, B F (1999) Chemical and mutagenic investigations of fatty acid amide hydrolase evidence for a family of serine hydrolases with distinct catalytic properties Biochemistry **38**, 9804–9812

20 Matsudaira, P T (1989) A Practical Guide to Protein and Peptide Purification for Microsequencing, pp 53–59, Academic Press, Inc San Diego

21 Kim, Y S and Bang, S K (1988) Assays for malonyl-coenzyme A synthase Anal Biochem **170**, 45–49

22 Smith, D R, Doucette-Stamm, L A, Deloughery, C., Lee, H, Dubois, J, Aldredge, T, Bashirzadeh, R, Blakely, D, Cook, R, Gilbert, K. et al (1997) Complete genome sequence of *Methanobacterium thermoautotrophicum* δH functional analysis and comparative genomics J Bacteriol **179**, 7135–7155

23 Nishiyama, M, Horinouchi, S., Kobayashi M, Nagasawa, T., Yamada, H and Beppu, T (1991) Cloning and characterization of genes responsible for metabolism of nitrile compounds from *Pseudomonas chlororaphis* B23 J Bacteriol **173**, 2465–2472

24 Chang, T H. and Abelson, J (1990) Identification of a putative amidase gene in yeast *Saccharomyces cerevisiae* Nucleic Acids Res. **18**, 7180

25 Wilson, R., Ainscough, R, Anderson, K, Baynes, C., Berks, M, Bonfield, J, Burton, J, Connell, M, Copsey, T and Cooper, J (1994) 2 2 Mb of contiguous nucleotide sequence from chromosome III of *C. elegans* Nature (London) **368**, 32–38

26 Sekine, M, Watanabe, K and Syono, K (1989) Nucleotide sequence of a gene for indole-3-acetamide hydrolase from *Bradyrhizobium japonicum* Nucleic Acids Res **17**, 6400

27 Hayashi, T, Yamamoto, K, Matsuo, A., Otsubo, K., Muramatsu, S, Matsuda, A and Komatsu, K.-I. (1997) Characterization and cloning of an enantioselective amidase from *Comamonas acidovorans* KPO-2771–4 J Ferment Bioeng **83**, 139–145

28 Zwizinski, C, Date, T and Wickner, W (1981) Leader peptidase is found in both the inner and outer membranes of *Escherichia coli*. J. Biol. Chem **256**, 3593–3597

29 Paetzel, M. and Dalbey, R E (1997) Catalytic hydroxyl/amine dyads within serine proteases Trends Biochem Sci **22**, 28–31

30 Perona, J J and Craik, C S (1995) Structural basis of substrate specificity in the serine proteases. Protein Sci. **4**, 337–360

31 Strynadka, N C, Adachi, H, Jensen, S. E, Johns, K, Sielecki, A, Betzel, C, Sutoh, K and James, M N (1992) Molecular structure of the acyl-enzyme intermediate in beta-lactam hydrolysis at 1.7 Å resolution Nature (London) **359**, 700–705

32 Paetzel, M, Dalbey, R E and Strynadka, N C (1998) Crystal structure of a bacterial signal peptidase in complex with a beta-lactam inhibitor Nature (London) **396**, 186–190

33 Okada, H, Negoro, S., Kimura, H and Nakamura, S (1983) Evolutionary adaptation of plasmid-encoded enzymes for degrading nylon oligomers. Nature (London) **306**, 203–206

34 Carter, P and Wells, J (1988) Dissecting the catalytic triad of a serine protease Nature (London) **332**, 564–568

35 Duggleby, H J, Tolley, S P, Hill, C P, Dodson, E J, Dodson, G and Moody, P C (1995) Penicillin acylase has a single-amino-acid catalytic centre Nature (London) **373**, 264–268

Received 17 December 1999/20 March 2000, accepted 3 May 2000

Biochem J. (2000) 349, 509–518 (Printed in Great Britain)

NIMA-related kinase 2 (Nek2), a cell-cycle-regulated protein kinase localized to centrosomes, is complexed to protein phosphatase 1

Nicholas R. HELPS[1], Xinmei LUO[1], Hazel M. BARKER and Patricia T. W. COHEN[2]

Medical Research Council Protein Phosphorylation Unit, Department of Biochemistry, MSI/WTB Complex, University of Dundee, Dow Street, Dundee DD1 5EH, Scotland, U K

The cell cycle-regulated protein serine/threonine NIMA-related kinase 2 (Nek2), which shows a predominant localization at centrosomes, is identified as a protein which interacts with protein phosphatase 1 (PP1) using the yeast two-hybrid system. Complex formation between Nek2 and PP1 is supported by co-precipitation of the two proteins using transfected expression constructs of Nek2 and the endogenous Nek2/PP1 proteins. The sequence KVHF in the C-terminal region of Nek2, which conforms to the consensus PP1-binding motif, is shown to be essential for the interaction of Nek2 with PP1. Nek2 activity increases with autophosphorylation and addition of phosphatase inhibitors and decreases in the presence of PP1. PP1 is a substrate for Nek2 and phosphorylation of PP1γ_1 on two C-terminal sites reduces its phosphatase activity. The presence of a ternary complex containing centrosomal Nek2-associated protein (C-Nap1), Nek2 and PP1 has also been demonstrated, and C-Nap1 is shown to be a substrate for both Nek2 and PP1 *in vitro* and in cell extracts. The implications of kinase–phosphatase complex formation involving Nek2 and PP1 are discussed in terms of the coordination of centrosome separation with cell cycle progression.

Key words: centrosome, cell signalling, NIMA related kinase, protein serine/threonine phosphatase.

INTRODUCTION

Most cellular functions are regulated by reversible protein phosphorylation catalysed by protein kinases and protein phosphatases. Protein phosphatase 1 (PP1) is a major eukaryotic protein phosphatase that regulates a diverse range of cellular processes by dephosphorylation of serine and threonine residues [1,2]. The pleiotropic function of PP1 resides in the ability of the catalytic subunit of PP1 (PP1c) to associate with many different regulatory subunits *in vivo* that may target PP1c to specific subcellular locations, alter its substrate specificity and allow its activity to be modified by extracellular signals. Over 20 different regulatory or targeting subunits of PP1c have now been identified. For example, glycogen-binding subunits target PP1c to regulate the enzymes of glycogen metabolism, and myosin-targeting subunits enable PP1c to regulate myosin contractility [3,4] Several proteins that interact with PP1c permit this phosphatase to regulate specific nuclear processes. These include NIPP-1 (nuclear inhibitor of PP1) [5,6], p99/PNUTS (PP1 nuclear targeting subunit) [7,8] and the polypyrimidine tract-binding protein-associated splicing factor, PSF1 [9] (proteins that are likely to be involved in RNA processing and transport), and sds22 [supressor 2 of dis2 (PP1) mutant], a protein required for exit from mitosis [10]. Binding of PP1c to scaffold proteins may modulate ion channel activity [11] and other neuronal functions [12]. Complex formation of PP1c with other proteins, such as p53-binding protein 53BP2 [13], the ribosomal-binding protein RIPP1 [14], and a protein of herpes simplex virus 1 [15] that influences protein synthesis, may direct PP1c to specific substrates. PP1c also binds to a number of small inhibitor proteins, including inhibitor-1 and inhibitor-2, which inhibit PP1c activity at nanomolar concentrations [1,16].

Interaction of regulatory subunits with PP1c is usually mutually exclusive, an observation recently explained by the discovery that a short motif -(R/K)(V/I)XF- present in the majority (but not all) of these subunits is sufficient for binding to PP1c [4,17]. In the present study, we identify the protein serine/threonine NIMA-related 2 kinase (Nek2) as a protein that interacts with PP1c via the PP1c consensus-binding motif.

Nek2 is a mammalian kinase structurally related to the protein kinase NIMA of *Aspergillus nidulans* that is required for entry into mitosis [18–20] Temperature-sensitive mutations of NIMA reversibly arrest cells in late G2 [21], despite the presence of activated $p34^{cdc2}$ kinase activity, indicating that NIMA function plays an essential role downstream or parallel to $p34^{cdc2}$ for progression through mitosis [22]. Although phosphorylation of NIMA by $p34^{cdc2}$/cyclin B is not required for basal level NIMA kinase activity, it appears to be required for mitotic entry [23].

Evidence for a NIMA-like mitotic pathway in mammalian cells was suggested by the induction of G2 arrest in HeLa cells with dominant negative mutants of NIMA, although the arrest could be overcome by a constitutively active mutant of $p34^{cdc2}$ [24]. The most closely related mammalian kinase to NIMA is Nek2 (47% amino acid identity in the catalytic domain), and both kinases are expressed in a cell cycle-regulated manner [25]. However, expression of the Nek2 protein is low during M and G_1, but high during S and G_2 phases of the cell cycle, its serine/threonine kinase activity paralleling its abundance [26]. This suggests that Nek2 may function earlier in the cell cycle than NIMA (which accumulates in G_2), its expression is high during M phase, and it is degraded at the end of M phase. Nek2 shows an intense localization at centrosomes, the principal microtubule-organizing centre of mammalian cells [27]. Overexpression of Nek2 induces centrosome splitting, while more prolonged over-

---

Abbreviations used NIMA, never in mitosis in *Aspergillus nidulans*, Nek2, NIMA-related kinase 2, PP1, protein phosphatase 1, PP1c, protein phosphatase 1 catalytic subunit, C-Nap1, centrosomal Nek2-associated protein, GST, glutathione-S-transferase; MBP, maltose-binding protein, ATP[S], adenosine 5′-[γ-thio]triphosphate.

[1] These authors contributed equally to this work

[2] To whom correspondence should be addressed (e-mail p t.w.cohen@dundee ac uk)

expression of active or inactive Nek2 leads to dispersal of centrosomal material, suggesting that Nek2 is involved in centrosome separation at the G_2/M transition. A yeast two-hybrid screen with Nek2 as bait led to the isolation of centrosomal Nek2-associated protein (C-Nap1), a protein with extensive coiled-coil structure that was highly enriched in centrosome preparations. The C-terminal region of C-Nap1 was phosphorylated by Nek2 *in vitro*, as well as after coexpression of the two proteins *in vivo*. It was proposed that C-Nap1 could be a component connecting the proximal ends of the duplicated centrioles to each other that, upon phosphorylation by Nek2, would cause loss of centriole–centriole cohesion and permit centrosome splitting [28]. In the present article, we show that Nek2 and PP1 form a kinase–phosphatase complex that can influence the phosphorylation state of C-Nap1, and discuss the implications of the interactions for the regulation of centrosome separation and cell cycle progression

MATERIALS AND METHODS

General methods and the yeast two-hybrid analysis

Microbial strains and methods for the yeast two-hybrid screen are described in Helps et al. [13,29]. In order to isolate proteins capable of interacting with PP1, the yeast strain Y190 containing a pAS2-$PP1_{\gamma1}$ plasmid was transformed with DNA from a human peripheral B lymphocyte cDNA library in pACT. Ten colonies were obtained on selective media from which the pACT plasmids were recovered into *Escherichia coli* and their cDNA inserts sequenced

Oligonucleotides were synthesized by Miss Audrey Gough and Miss Kaera Maxwell (University of Dundee, Scotland, U.K.) on an Applied Biosystems model 394 DNA synthesizer DNA sequencing was performed using Taq dye terminator cycle sequencing on PE Biosystems automated DNA sequencers.

Construction of glutathione-S-transferase (GST) fusion vectors for the expression of Nek2 variants in mammalian cells

Reverse transcription was used to obtain the coding region of Nek2 5′ of PP1H5 (which encodes amino acid residues 227–445 of Nek2) using total RNA from a human breast adenocarcinoma cell line MCF7, mouse Moloney murine leukaemia virus reverse transcriptase (Promega) and oligo(dT) primers. The resulting cDNA served as template for a PCR using two specific primers, $Nek2_{1-21}$ (5′-GCGCGGATCCCATATGCCTTCCCGGGCTGAGGAC-3′) and $Nek2_{1105-1083}$ (5′-TCTCTTGCTTTGAGAGCTCGCTC-3′), containing the restriction sites *Bam*HI and *Sac*I respectively (underlined). The PCR product of 973 bp was digested with *Bam*HI and *Sac*I, purified using QIAquick Nucleotide Removal Kit (Qiagen) and inserted into pACT-PP1H5 cleaved with the same enzymes. The resulting construct, containing the full-length cDNA of Nek2 in a *Bam*HI–*Bgl*II fragment, was verified by DNA sequencing. For expression of Nek2 as a GST fusion protein in mammalian cells, the Nek2 cDNA was subcloned into the *Bam*HI site of the vector pEBG-2T [30] to produce the expression plasmid, pEBG-Nek2.

The construct pEBG–Nek2KD (kinase dead) was produced by mutating the codon for lysine-37 (AAA) in Nek2 to the codon for arginine (AGA). The mutation was performed by a two-step recombinant PCR method [31,32], using pEBG–Nek2 as template DNA with primer $Nek_{252-230}$ (5′-CAAGTTCTCTCCAAACTAATATC-3′) containing the desired mutation (underlined) and its reverse complement. The outside primers were $Nek2_{1-21}$ and $Nek2_{625-606}$ (5′-CTAGCTAGCCCAAAGTCTCC-3′), downstream of a *Hin*cII site. The PCR product was subcloned into pCR2.1-TOPO vector (Invitrogen, Leek, The Netherlands) and verified by DNA sequencing. A 0.4 kb *Bam*HI–*Hin*cII fragment containing the desired mutation was cleaved out and used to replace the corresponding fragment in pEBG–Nek2.

The construct pEBG–Nek2NB (non-binding) was produced by mutation of the codon for phenylalanine-386 (TTC) to alanine (GCC). The primer $Nek2_{747-766}$ (5′-TTGCTGTATGAGTTATGTGC-3′), which lies upstream of an *Eco*RI site, and primer $Nek2_{1337-1277}$ (5′-CTCAGAATTCTCACTCCTCATGATGTTCTCTTTACTTTCCCCACTGGCATGAACTTTCTTC-3′) containing an *Eco*RI site (double underlined) and the mutation (underlined), were employed using pEBG–Nek2 as a template in a PCR to obtain a fragment containing the desired mutation The 0 5 kb PCR fragment was digested with *Eco*RI and this fragment was substituted for the corresponding *Eco*RI fragment of Nek2 in pFASTBACHTb (Life Technologies), a vector that has no *Eco*RI sites. The *Bam*HI–*Kpn*I fragment of pEBG–Nek2 was replaced by the corresponding fragment from pFASTBACHTb–Nek2 to give pEBG–Nek2NB, the mutation being confirmed by DNA sequencing.

Expression of proteins in bacteria

C-Nap1 fused to maltose-binding protein (MBP)

DNA encoding the C-terminal amino acid residues 1851–2442 of C-Nap1 [28] was PCR-amplified from human testis Marathon-Ready cDNA according to the manufacturer's instructions (ClonTech, Palo Alto, CA,U.S.A.) using the oligonucleotide primers CCATATGACACTGAAGGAGCGTCATGG and TTCTAGATGAGAGGCAGTACATGTC, containing naturally occurring *Nde*I and *Xba*I sites (underlined) present within the cDNA. The PCR product was cloned into the pCR2.1 (TOPO) vector, its sequence was confirmed and the insert was subcloned into the MBP fusion vector, p-MAL-HA [pMAL-c2 (New England Biolabs) modified by Dr C. A. Armstrong to contain an HA tag and additional restriction enzyme sites including an *Nde*I site] using the *Nde*I site and a *Hin*dIII site (present in the pCR2.1 vector). The plasmid was transformed into *E. coli* BL21 (DE3) pLysS which were grown at 37 °C to D_{600} of 0.3, then expression was induced with 100 μM isopropyl β-D-thiogalactoside for 3 h at 37 °C. The cells were harvested by centrifugation, resuspended in ice-cold lysis buffer [50 mM Tris/HCl (pH 7.5), 0.1 mM EGTA, 0.1 % (v/v) 2-mercaptoethanol, 0.02 % (w/v) Brij 35, 5 % (v/v) glycerol, 1 mM EDTA, 200 mM NaCl], containing 0.1 mM PMSF and 1 mM benzamidine, and lysed by sonication. The lysate was centrifuged at 45000 *g* for 20 min and the supernatant was added to 1.5 ml of amylose resin (New England Biolabs) equilibrated in lysis buffer. After incubation with mixing at 4 °C for 1 h, the resin was washed three times with 20 ml of the same buffer, then placed in an Econpac (Bio-Rad) column. After further washing, the bound MBP–C-Nap1 protein was eluted from the column with buffer containing 10 mM maltose. The peak protein fractions were dialysed against 50 mM Tris/HCl (pH 7.5), 0.1 mM EGTA, 0.1 % (v/v) β-mercaptoethanol, 0.02 % (w/v) Brij 35, 5 % (v/v) glycerol and stored at −70 °C.

PP1H5 fused to GST and MBP

A *Bgl*II fragment encompassing the PP1H5 fragment of Nek2 was excised from the pACT plasmid and inserted into the *Bam*HI site of the expression plasmids pGEX-3X and pMAL-HA, which were expressed in *E. coli*. GST–PP1H5 was affinity purified on GSH–agarose [13] and MBP–PP1H5 was affinity-purified as described above for MBP–C-Nap1.

PP1 variants

Rabbit (identical sequence to human) PP1α and human PP1$_{\gamma1}$ [33] were expressed in *E. coli* and purified as described [34]. The PP1γ_1 cDNA in the pCW expression vector was mutated at histidine-125 to alanine by using the Quikchange mutagenesis system (Stratagene) and the complimentary oligonucleotides CAGAGGGAAC**GCT**GAATGTGCC and GGCACATTC**AGC**GTTCCCTCTG (mutated codons in **bold**). After verifying that the sequence was correct, the mutated PP1γ_1 protein was expressed and purified as described for PP1γ_1. The construction and expression of PP1$_{\gamma1}$ tagged with the epitope EFMPME(H)$_6$ is described in [13].

Production of antibodies

A 10 mg aliquot of GST–PP1H5 was cleaved with 0.1 mg of Factor Xa (New England Biolabs) in 50 mM Tris/HCl (pH 8.0)/ 100 mM NaCl/2 mM CaCl$_2$/1 mM dithiothreitol/0.5 mM EDTA/0.5 % Triton for 1 h at 23 °C. The pH was then adjusted to 7.5, the solution was made 2 mM in EGTA and the Factor Xa was removed by adsorption to *p*-aminobenzamidine–agarose beads. Free GST was removed from the PP1H5 by adsorption to GSH–agarose beads. The purified PP1H5 (C-terminal 219 amino acids of Nek2) was used to raise anti-Nek2 antibodies in sheep at the Scottish Antibody Production Unit (SAPU,. Carluke, Ayrshire, Scotland U.K.), which were affinity purified on a column matrix of MBP–PP1H5 covalently coupled to CNBr–Sepharose (Pharmacia). Affinity purified anti-Nek2 antibodies (1 mg) were coupled to Protein G–Sepharose (1 ml) using dimethylpimelimidate [35]. Anti-GST antibodies were obtained from Santa Cruz Biotechnology. Anti-PP1 antibodies were raised against the human PP1$_{\gamma1}$ in sheep by SAPU, affinity purified on a column matrix of PP1$_{\gamma1}$ coupled to CNBr–Sepharose and coupled to Protein G–Sepharose as described for Nek2 antibodies. Antibodies against the PP1$_{\gamma1}$ epitope tag EFMPME were coupled to Sepharose as described in [13]. Anti-C-Nap1 antibodies were raised in sheep by SAPU to the peptides CPHSHKTSPMEEQS, CQAPEATVLEAETRR and CLHPSPSTTQAASR, conjugated to keyhole limpet haemocyanin and affinity purified on peptide CH-Sepharose columns.

Transfection of 293 cells and preparation of cell extracts

Human embryonic kidney 293 cells were cultured in 10 cm-diameter dishes and transfected with pEBG constructs using a modified calcium phosphate method [36]. Cell lysates were prepared 48 h post-transfection after one medium change 24 h after transfection. Each dish of cells was lysed in 0.5 ml of ice-cold lysis buffer [50 mM Hepes (pH 7.5), 100 mM NaCl, 10 mM MgCl$_2$, 5 mM MnCl$_2$, 5 mM KCl, 5 mM EGTA, 2 mM EDTA, 0.1 % Nonidet P40] containing Complete Protease Inhibitor Cocktail (Boehringer Mannheim) and supplemented with 2 μM microcystin where stated. The lysate was centrifuged through a QIAshredder (Qiagen) for 10 min at 4 °C for homogenization. The cleared extract was snap-frozen in liquid nitrogen and stored at −80 °C.

Immunoprecipitation, glutathione- and amylose-affinity methods

Cell lysate containing 1 mg of protein in 0.5 ml of lysis buffer was used for each immunoprecipitation. The lysates were precleared at 4 °C for 1 h on a shaking platform with 10 μl of Protein G–Sepharose. The supernatants were incubated with 10 μl of Protein G–Sepharose coupled to 10 μg of anti-PP1 antibodies for 1 h at 4 °C. The immunoprecipitates were washed four times with lysis buffer and subjected to 10 % PAGE in SDS buffer. Glutathione-affinity and amylose-affinity sedimentations were performed in a similar manner from cell extracts and with purified proteins, except that anti-PP1–Sepharose was replaced by GSH–Sepharose (Pharmacia) and amylose resin respectively.

For immunoprecipitations using anti-Nek2 antibody, cell extracts at 1 mg/ml protein in lysis buffer were precleared for 30 min at 4 °C using pre-immune IgG covalently bound to Protein G–Sepharose, then transferred to anti-Nek2–Sepharose and incubated for 1 h at 4 °C. The immunoprecipitates were washed three times with lysis buffer and then used for SDS/PAGE or protein phosphatase assays.

In vitro kinase assays

Lysates from cells transfected with pEBG–Nek2 constructs were incubated at 4 °C for 1 h on a shaking platform with 10 μl of GSH–Sepharose. The beads were washed twice in lysis buffer containing 0.5 M NaCl, once with lysis buffer and once with kinase buffer [50 mM Tris/HCl (pH 7 5), 10 mM MgCl$_2$]. The standard Nek2 kinase assay (50 μl) contained washed GSH–Sepharose precipitate, 50 mM Tris/HCl (pH 7.5), 10 mM MgCl$_2$, 1 mM dithiothreitol, and 0.1 mM [γ-^{32}P]ATP (1000 c.p.m./ pmol). Myelin basic protein (Gibco Life Sciences, Paisley, Renfrewshire, Scotland, U.K.), dephosphorylated β-casein (Sigma), PP1 or C-Nap1 were included as exogenous substrates at 18 μM, 16 μM, 2.7 μM and 0.7 μM respectively. The assays were carried out for 15 min at 30 °C, with continuous agitation. Reactions were stopped by the addition of 10 μl of 6 × SDS/ PAGE loading buffer and heated at 95 °C for 5 min, following by separation of the reaction products by SDS/PAGE and detection by autoradiography. Alternatively, for reactions containing myelin basic protein, a 40 μl aliquot was removed, spotted onto a 2 × 2 cm square of phosphocellulose paper and immersed in 75 mM phosphoric acid. After washing four times in phosphoric acid and once in acetone, the papers were dried and the ^{32}P radioactivity determined by Cerenkov counting. One unit of kinase activity is that amount of enzyme that incorporates 1 nmol ATP into the substrate in 1 min.

Identification of Nek2 phosphorylation sites on PP1γ

GST–Nek2 protein was purified from 400 μg of protein from extracts of transfected 293 cells. A 1 μg portion of PP1γ(H125A) was then phosphorylated by this kinase preparation in 30 μl of reaction mixture containing 50 mM Tris/HCl (pH 7.5), 10 mM MgCl$_2$, 0.1 % (v/v) 2-mercaptoethanol and 100 μM [^{32}P]γATP for 1 h at 30 °C. The reaction products were separated by SDS/PAGE in 10 % gels and stained with Coomassie Brilliant Blue R250. The PP1γ band was excized from the gel, digested with trypsin and the peptides were separated by HPLC. ^{32}P-labelled peptides were analysed by Dr N. Morrice (University of Dundee, Scotland, U.K.) using matrix-assisted laser desorption ionization–time-of-flight MS on an Elite-STR mass spectrometer (PerSeptive Biosystems) in reflector mode with 4-hydroxy-α-cyanocinnamic acid (10 mg/ml in 50 % acetonitrile/0.1 % trifluoroacetic acid/49.9 % water) as the matrix. The sequences were confirmed by Edman degradation on an Applied Biosystems 476A sequencer. The sites of phosphorylation were determined by measuring the release of radioactivity following solid-phase Edman degradation of the peptides coupled to Sequelon-AA membrane (Milligen, Bedford, M.A. U.S.A.).

Protein phosphatase assays

^{32}P-labelled rabbit skeletal muscle glycogen phosphorylase was prepared using phosphorylase kinase to a stoichiometry of 1 mol phosphate/mol subunit by Dr H Y. L. Tung [37]. [^{32}P]-Labelled MBP–C-Nap1 was prepared as follows: GST–Nek2NB was purified from 1 mg of cell extract as described above and the washed GSH–Sepharose beads further washed once in reaction buffer [50 mM Tris/HCl (pH 7.5), 0.5 mM EGTA, 10% (v/v) glycerol, 0.5% (v/v) 2-mercaptoethanol]. The kinase (attached to the beads) was then used to label 1 mg of pure MBP–C-Nap1 in 1 ml of reaction buffer containing 10 mM $MgCl_2$, 100 μM [^{32}P]γATP, 150 mM NaCl and 20 μM microcystin YR. After incubation at 30 °C for 2 h, NaCl was added to 0.5 M and incubation continued for 10 min. The beads were then pelleted by centrifugation (6000 *g*, 1 min) and the supernatant loaded onto a 20 × 1 cm G50 superfine column equilibrated in reaction buffer. Fractions were collected and the peak of radiolabelled protein stored frozen at −20 °C. The specific activity of the [γ-^{32}P]ATP used for phosphorylations was 1000 c.p.m./pmol. Protein phosphatase assays were performed as described in [37,38] using phosphorylase (10 μM or 2.7 μM) or C-Nap-1 (2.7 μM). Immunoprecipitation phosphatase assays were performed in a similar manner, except that a shaking incubator was used. One unit of phosphatase activity was that amount of enzyme that catalysed the release of 1 μmol [^{32}P]phosphate/min from [^{32}P]-labelled substrate in the standard assay

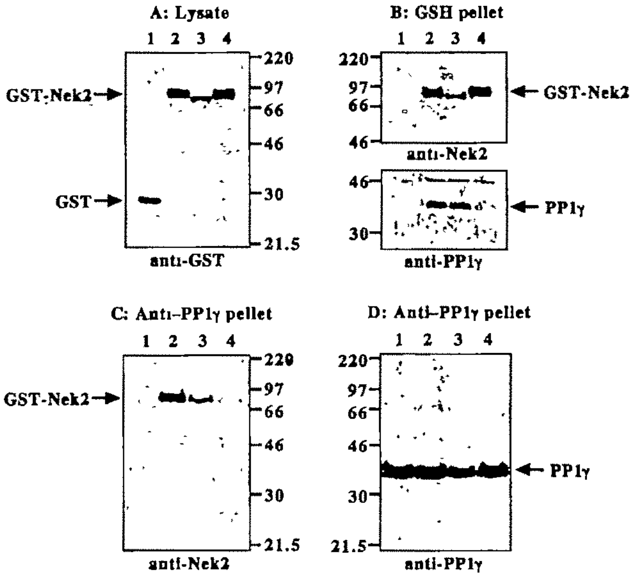

Figure 1 Co-sedimentation of GST-Nek2 with PP1

(**A**) Soluble protein (10 μg) from lysates of 293 cells overexpressing GST (lane 1), GST–Nek2 (lane 2), GST–Nek2KD (lane 3) and GST–Nek2NB (lane 4) was separated by SDS/PAGE, transferred onto a nitrocellulose membrane and then probed with anti-GST antibody. (**B–D**) Cell extracts as in (**A**), containing 1 mg of soluble protein, were precleared with 10 μl of Protein G–Sepharose and then incubated for 1 h at 4 °C with 10 μl of GSH–Sepharose (**B**) or 10 μl of anti-PP1 antibody linked to Protein G–Sepharose (**C**,**D**) The Sepharose beads were washed four times with lysis buffer and the bound proteins eluted with SDS/PAGE loading buffer and separated by SDS/PAGE (**B**) Immunoblotting was performed with anti-PP1 antibody (bottom pannel) and then, after stripping, the filter was reprobed with anti-Nek2 antibody (top panel) Immunoblotting was performed with anti-Nek2 antibody (**C**) and then, after stripping, with anti-PP1 antibody (**D**) The positions of the standard (Amersham Rainbow) marker proteins, myosin (220 kDa), glycogen phosphorylase (97 kDa), BSA (66 kDa), ovalbumin (46 kDa) and carbonic anhydrase (30 kDa) are indicated. Arrows mark the positions of the relevant proteins

RESULTS

Identification of Nek2 as a PP1-binding subunit

In order to identify proteins capable of interacting with PP1, a yeast two-hybrid screen was performed with PP1γ_1 as bait [29,39]. One of ten positive clones identified from a human B lymphocyte library contained a cDNA, termed PP1H5, that was found to encode the C-terminal region of the protein kinase Nek2 PP1H5 comprised 1294 bp, which encoded amino acids 227–445 and encompassed the entire 3′ untranslated region of Nek2. The sequence was identical with that reported previously [25]. The binding of the C-terminal region of Nek2 to PP1 was confirmed by co-immunoprecipitation of bacterially expressed GST–PP1H5 with bacterially expressed epitope-tagged PP1γ_1 (results not shown).

Full-length Nek2 (amino acids 1–445) was transiently expressed in 293 cells as a GST fusion protein (Figure 1A) The binding of Nek2 to PP1 was shown by sedimentation of GST–Nek2 followed by immunodetection of PP1 in the pellet (Figure 1B). Immunoprecipitation of PP1 followed by immunodetection of the GST–Nek2 fusion protein in the PP1 immunoprecipitates using anti-Nek2 antibody (Figure 1C) or anti-GST antibody (results not shown) confirmed the specificity of the Nek2–PP1 interaction. The band detected in lane 2 of Figure 1 (A, B and C) has an apparent molecular mass of 73 kDa, as expected for the fusion of Nek2 (47 kDa) and GST (26 kDa). This band cannot be seen in lane 1 of the same Figures, which contain the extract of cells transfected with pEBG-2T vector expressing only GST. The results indicate that the binding of GST–Nek2 to PP1 is caused by the interaction of Nek2 with PP1 and not by an interaction of GST with PP1.

The phenylalanine in the -(R/K)(V/I)XF- motif of Nek2 is essential for binding to PP1

The kinase domain of Nek2 encompasses the N-terminal 271 amino acids of Nek2, while the C-terminal region is non-catalytic. This region contains the sequence KVHF, at position 383–386, that conforms to the consensus sequence -(R/K)(V/I)XF- for binding of many regulatory subunits to PP1 [17]. We therefore sought to determine whether the sequence KVHF was responsible for the binding of Nek2 to PP1 by mutating phenylalanine-386 to alanine. Transient transfection of the construct pEBG–Nek2NB (non-binding), which encodes the mutation F386A, resulted in the expression of GST–Nek2NB as detected by immunoblotting (Figure 1A, lane 4). In contrast to the results with wild-type Nek2 (Figure 1C, lane 2), no binding of GST–Nek2NB to PP1 could be detected on immunoprecipitation of PP1 (Figure 1C, lane 4). Figure 1(D) shows that an equal amount of PP1 was precipitated from all lysates with anti-PP1 antibodies. No binding of GST–Nek2NB to PP1 was detected by pelleting GST–Nek2NB with glutathione beads followed by immunoblotting with PP1 antibodies (Figure 1B, lane 4). Although it is possible that the lack of co-sedimentation of GST–Nek2NB with PP1 could be caused by a conformational change in GST–Nek2NB, this is unlikely because the latter still retains its protein kinase activity (see Figure 3C and Figure 4). A catalytically inactive Nek2 mutant, termed GST–Nek2KD (kinase dead), in which lysine-37 had been changed to arginine, resulted in loss of Nek2 activity [26]. As expected, loss of kinase activity did not result in loss of PP1 binding (Figure 1B, lane 3 and Figure 1C, lane 3). The slightly lower levels of GST–Nek2KD compared with GST–Nek2 sedimented with PP1 are explained by the lower expression level of GST–Nek2KD compared with GST–Nek2 after transfection of the cells with equal amounts of each construct (Figure 1A). In

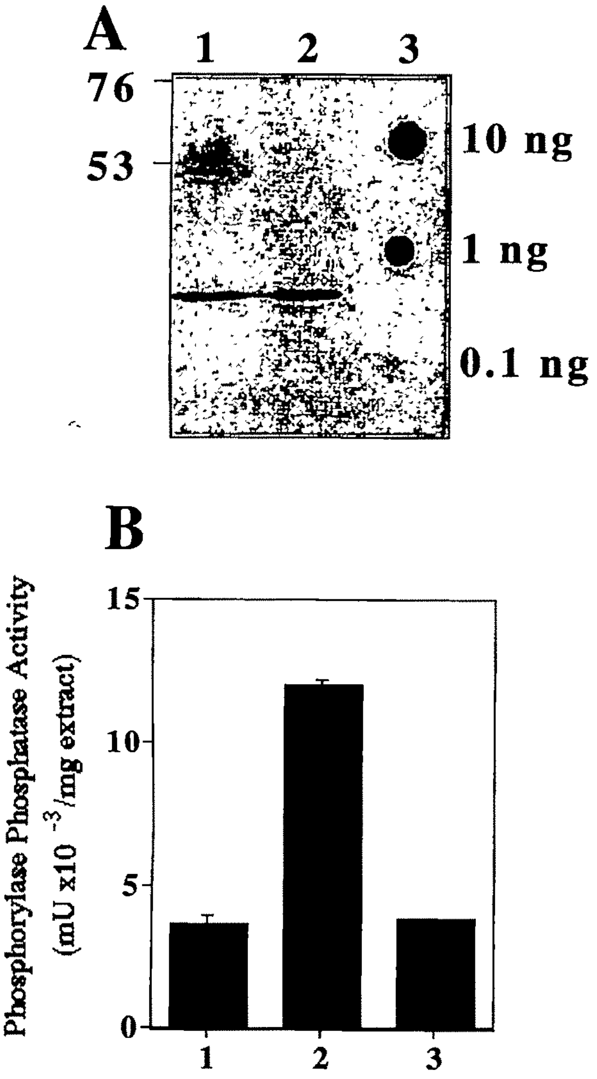

Figure 2 Identification of endogenous Nek2 and Nek2–PP1 complex

(**A**) Aliquots (200 μg) of protein from 293 cell extracts (non-transfected) were precleared with preimmune IgG beads, then incubated with either anti-Nek2 beads (lane 1) or pre-immune IgG beads (lane 2). The beads were washed with lysis buffer and the bound proteins separated by SDS/10% PAGE. After transfer to nitrocellulose, the Nek2 (47 kDa) was detected with biotinylated anti-Nek2 followed by avidin–horseradish peroxidase. Lane 3, Nek2 controls 10 ng, 1 ng and 0.1 ng of GST–Nek2. An unknown protein of lower molecular mass is detected in both lanes 1 and 2. (**B**) Phosphatase assays on Nek2-immunoprecipitates. A 100 μg aliquot of protein from 293 cell extracts (non-transfected) was precleared with preimmune IgG beads, then incubated with pre-immune IgG or anti-Nek2 beads. The beads were washed with lysis buffer, then the bound phosphatase activity assayed using [^{32}P]-labelled phosphorylase as substrate. 1, Pre-immune beads; 2, anti-Nek2 beads; 3, anti-Nek2 plus 100 nM inhibitor-2. The [^{32}P] released from the substrate was measured after extraction with molybdate [38] to ensure that the product of the reaction was P_i and not phosphopeptides released by proteinases present in the Nek2 immunoprecipitates.

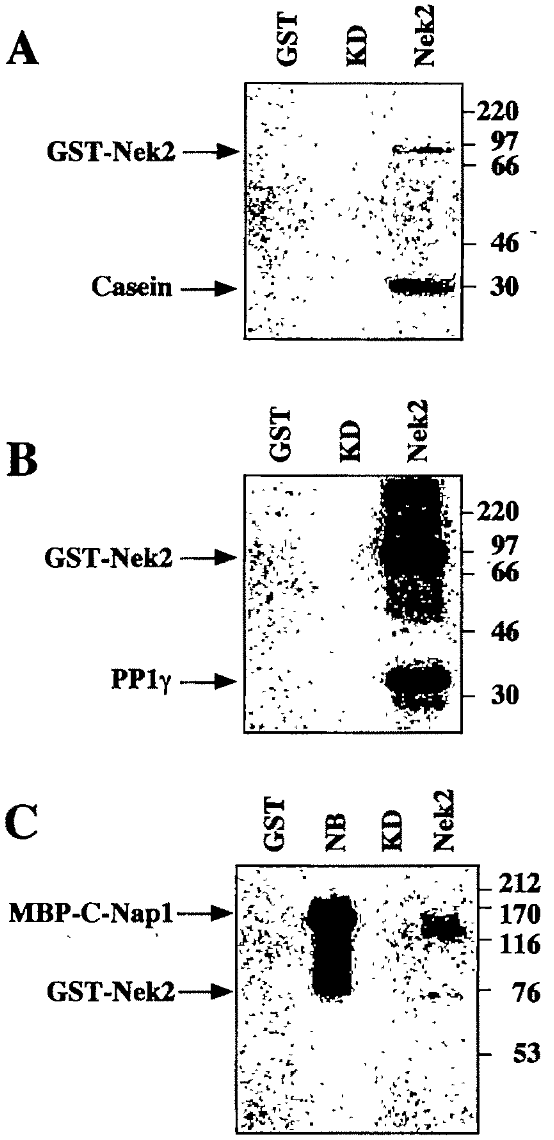

Figure 3 Protein kinase activities of GST fusion proteins towards casein (A), PP1 (B) and C-Nap1 (C)

Extracts containing 1 mg of soluble protein from 293 cells overexpressing GST, GST–Nek2KD (KD), GST–Nek2 (Nek2) and GST–Nek2NB (NB) were incubated with 10 μl of GSH–Sepharose at 4 °C for 1 h. After sedimentation and washing of the GSH–Sepharose pellets, the associated kinase activity was assayed in the presence of casein, PP1 or MBP–C-Nap1 as described in the Materials and methods section. The reactions were stopped by boiling in 10 μl of 6 × SDS/PAGE loading buffer. Proteins were separated on SDS/PAGE, the gels stained with Coomassie Blue, dried, and phosphorylated proteins detected by autoradiography. For (**A**) and (**B**), the positions of the standard marker proteins, indicated on the right, are as listed in Figure 1. For (**C**), the marker proteins are myosin (212 kDa), α-2-macroglobulin (170 kDa), β-galactosidase (116 kDa), transferrin (76 kDa) and glutamate dehydrogenase (53 kDa). Arrows mark the positions of the relevant proteins.

addition, phosphatase activity was consistently associated with GST–Nek2 and GST–Nek2KD bound to GSH–Sepharose, but not with GST–Nek2NB or GST (results not shown).

Interaction of the endogenous Nek2 and PP1 proteins

In order to investigate whether a complex is formed between endogenous Nek2 and PP1, we immunoprecipitated Nek2 from 293 cell extracts using anti-Nek2. Since the Nek2 protein and IgG heavy chain migrate similarly on SDS/PAGE, detection of the precipitated protein required use of biotinylated anti-Nek2 followed by avidin–horseradish peroxidase. Figure 2(A) shows that the Nek2 protein is bound specifically by the anti-Nek2 antibody (lane 1) and not pre-immune IgG (lane 2), but only approx. 1 ng of Nek2 protein was recovered from 200 μg of protein in 293 cell extracts. Lack of detection of Nek2 on immunoblots of whole cell lysates (results not shown) also suggested the level of Nek2 in the cell may be very low and would preclude detection of any associated PP1 by immunoblotting. We therefore assayed the Nek2 immunoprecipitates to detect the PP1 bound to Nek2. Figure 2(B) shows that significant phosphatase activity was present within the anti-Nek2 immunoprecipitate. This activity was blocked by inhibitor-2, a specific inhibitor of protein phosphatase 1 that does not inhibit other protein serine/threonine phosphatases, demonstrating that the activity was PP1.

GST–Nek2 undergoes autophosphorylation and can phosphorylate casein, PP1, myelin basic protein and C-Nap1

For all assays of Nek2 most of the bound PP1 was removed by washing the GSH–Sepharose pellets in buffer containing 0.5 M NaCl. GST–Nek2 was able to phosphorylate casein, PP1, C-Nap1 (Figure 3) and myelin basic protein (Figure 4A). As expected no activity could be detected in the precipitates from cells expressing GST–Nek2KD or GST. Figure 3(A) shows the autoradiograph of the components of a protein kinase assay separated on SDS/PAGE when casein was used as substrate. The upper band (73 kDa) is the expected size for GST–Nek2, and is phosphorylated. No band of the same size can be seen where GST–Nek2KD was assayed, indicating that the phosphorylation of GST–Nek2 resulted from autophosphorylation, rather than phosphorylation by traces of a contaminating kinase present in the assay. The position of the lower phosphorylated band corresponded to casein. Lack of casein kinase activity in GSH–Sepharose pellets from extracts expressing GST or GST–Nek2KD indicated that the phosphorylation of casein was also catalysed by Nek2 kinase, and that no other kinases capable of phosphorylating casein are present in the GST–Nek2KD pellet. Figure 3(B) shows that in the presence of the phosphatase inhibitor okadaic acid, PP1 could also be phosphorylated by GST–Nek2, but not by GST–Nek2KD. Again, the ^{32}P-labelled GST–Nek2 was consistently seen only in the GST–Nek2 and not in the GST–Nek2KD or GST assays. No phosphorylated bands (Nek2 or PP1) were seen in the absence of okadaic acid when PP1 was the substrate (results not shown).

Since C-Nap1 has been reported to be a protein that not only binds to Nek2 but also may be an *in vivo* substrate for this kinase [28], we examined the phosphorylation of a C-terminal fragment of C-Nap1 (amino acids 1851–2442) by the Nek2 proteins. Figure 3(C) shows that in the absence of PP1 inhibitors, C-Nap1 can be phosphorylated by GST–Nek2, but not by GST–Nek2KD. GST–Nek2NB had an enhanced activity towards C-Nap1 compared with that of GST–Nek2, presumably because dephosphorylation by Nek2-bound PP1 was eliminated.

GST–Nek2 and GST–Nek2NB, but not GST–Nek2KD, were also capable of phosphorylating myelin basic protein (Figure 4A). The activities of both GST–Nek2 and GST–Nek2NB were substantially increased when the protein serine/threonine phosphatase inhibitor, microcystin, was included in the cell lysis buffer. One interpretation of these results is that serine/threonine autophosphorylation of Nek2 leads to an increase in the protein kinase activity of Nek2. The fact that there was an approx. 3-fold increase in GST–Nek2 activity and a less than 2-fold increase in GST–Nek2NB activity in the presence of microcystin suggests that PP1 bound to GST–Nek2 is responsible, at least in part, for the dephosphorylation and partial inactivation of GST–Nek2. Figure 4(B) shows that GST–Nek2NB (lane 5) and a component of GST–Nek2 (lane 1) have a reduced electrophoretic mobility compared with GST–Nek2KD (lane 3), consistent with autophosphorylation of GST–Nek2 and GST–Nek2NB. In the presence of microcystin the mobility of GST–Nek2 (Figure 4, lane 2) and GST–Nek2NB (lane 6) is further decreased, consistent with additional phosphorylation underlying the increase in activity. Addition of excess PP1 to the lysates resulted in shifting the mobility of GST–Nek2 in lanes 1, 2, 5 and 6 (Figure 4) to that seen in lanes 3 and 4, consistent with the mobility shift being due to phosphorylation (results not shown).

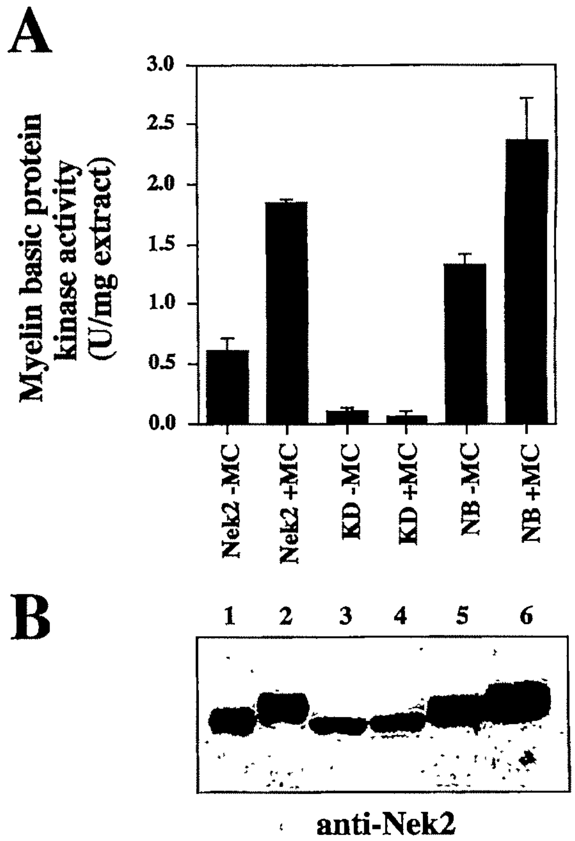

Figure 4 Protein kinase activities of GST–Nek2 fusion proteins using myelin basic protein as substrate

(**A**) Cell extracts containing 10 μg of soluble protein from 293 cells overexpressing GST–Nek2 (lanes 1 and 2), GST–Nek2KD (lanes 3 and 4) and GST–Nek2NB (lanes 5 and 6), prepared with lysis buffer without microcystin (MC) (lanes 1, 3 and 5) or containing microcystin (lanes 2, 4 and 6) were incubated with 10 μl of GSH–Sepharose for 1 h at 4 °C. After sedimentation and washing of the GSH–Sepharose pellets, the associated kinase activity was assayed by counting [γ-^{32}P]ATP incorporated into myelin basic protein. The data are presented as means ± S.E.M. for two separate experiments with each determination carried out in duplicate. (**B**) A 10 μg aliquot of the same cell extracts was separated on 7.5% PAGE and immunoblotting was performed with anti-Nek2 antibody.

Incubation of Nek2 with PP1 causes a reduction of Nek2 activity

In order to examine whether Nek2 activity could be altered by PP1, GST–Nek2 was incubated with or without bacterially expressed PP1 or with microcystin-inactivated PP1, prior to being subjected to protein kinase assays. Incubation of Nek2 with an equimolar amount of PP1 caused approx. 65 % inhibition of Nek2 activity in 2 min, but no further inhibition with longer incubation times (Figure 5). However, Nek2 inhibition could be further enhanced if the concentration of PP1 was increased (results not shown). Incubation of GST–Nek2 with microcystin-inactivated PP1 had no effect on Nek2 activity.

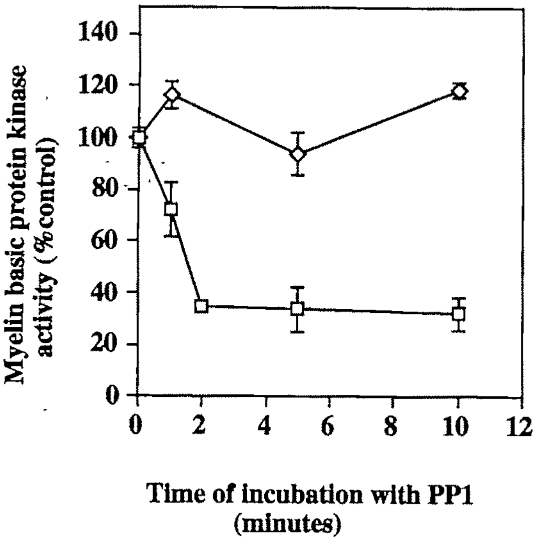

Figure 5 Effect of PP1 on the myelin basic protein kinase activity of Nek2

Assays were performed using GST–Nek2 eluted from GSH-Sepharose and myelin basic protein as substrate. Prior to the kinase assay, GST–Nek2 was incubated at 30 °C with active PP1 (□) or microcystin-inactivated PP1 (◇) for varying times. The incubation with active PP1 was then stopped by adding 5 μM microcystin. The ratio of Nek2/PP1 was equimolar as judged by Coomassie-stained PAGE. Kinase assays were carried out as described in the Materials and methods section. Microcystin-inactivated PP1 was prepared by incubation of PP1 with microcystin for 10 min at 30 °C. The complete inactivation was confirmed by protein phosphatase assay using [^{32}P]phosphorylase as substrate.

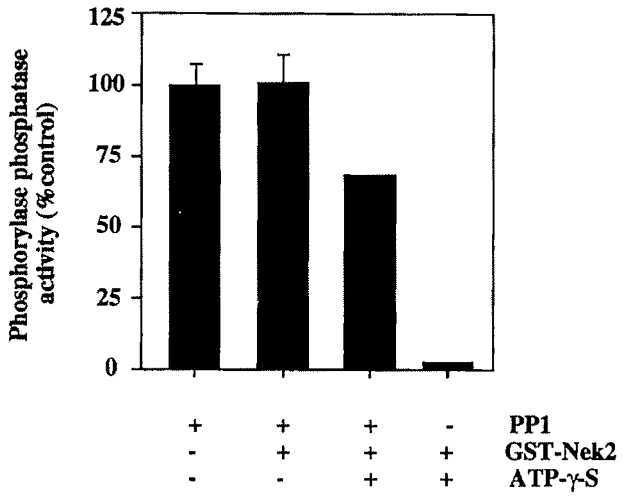

Figure 6 Effect of Nek2 on the phosphatase activity of PP1

GSH–Sepharose beads incubated with cell extracts (containing 2 μM microcystin) from control 293 cells or 293 cells overexpressing GST–Nek2 were washed twice with lysis buffer containing 0.5 M NaCl, once with lysis buffer and once in 50 mM Tris/HCl, pH 7.5. Phosphorylation reactions were carried out for 60 min at 30 °C in 40 μl containing 50 mM Tris/HCl (pH 7.5), 10 mM $MgCl_2$, 1 mM dithiothreitol, and 0.1 mM ATP[S], with PP1 being included at 3 μg/ml. Phosphatase assays were then performed immediately using 20 μl of [^{32}P]phosphorylase (final concentration 10 μM). Protein phosphatase activity was plotted as a percentage of the activity observed when GSH–Sepharose beads were incubated with the extract from control 293 cells, PP1 being included at 3 μg/ml. The data are presented as the means ± S.E.M. for two separate experiments with each determination carried out in duplicate.

Phosphorylation of PP1γ on two threonine residues by Nek2 reduces its phosphatase activity *in vitro*

Since PP1 could be phosphorylated by Nek2, we sought to investigate whether the enzymic activity of PP1 was changed upon phosphorylation. Addressing this problem is not straightforward. First, if PP1 and Nek2 were added together, Nek2 activity was reduced (Figure 5). Secondly, PP1 could autodephosphorylate itself after being phosphorylated by Nek2. In order to partially resolve these problems, the molar ratio of Nek2/PP1 was maintained at a high level ($> 3:1$) and the assay was performed with adenosine 5′-[γ-thio]triphosphate (ATP[S]) instead of ATP, since ATP[S] can be used as a substrate by kinases, but the thiophosphate is resistant to dephosphorylation by protein phosphatases. Under these experimental conditions, the enzymic activity of PP1 was found to be reduced by approx. 30% after incubation with Nek2 and Mg^{2+}-ATP[S], compared with controls in which either Nek2 or ATP[S] were excluded (Figure 6). Since this result could be achieved only with ATP[S], autodephosphorylation of PP1 must occur after it is phosphorylated by Nek2 using ATP.

Due to autodephosphorylation, active PP1 could not be used to determine phosphorylation sites. Also, PP1γ_1 inactivated by okadaic acid (Figure 3B) was not phosphorylated to a sufficient level to identify the phosphorylation sites. We therefore mutated the PP1γ_1 catalytic subunit at histidine-125. This residue acts as a general acid in the proposed catalytic mechanism of PP1 [40] and its mutation to alanine would be expected to dramatically reduce catalytic activity. Soluble PP1γ(H125A) protein was expressed, demonstrating that the mutation does not result in denaturation of the protein and, when assayed against ^{32}P-labelled phosphorylase in the standard phosphatase assay, showed essentially no activity (results not shown). Phosphorylation by Nek2 followed by matrix-assisted laser desorption ionization–time-of-flight MS and solid-phase sequencing revealed that this protein is phosphorylated on two C-terminal threonines. Threonine-307 and -318 appear to be equally well phosphorylated by Nek2 under the conditions used and a stoichiometry of approx. 2 moles phosphate/mol PP1γ was obtained. The consensus sequence for these two Nek2 phosphorylation sites is (R/K)XX(A/I)(phosphoT)(R/K) and supports previous studies using peptide substrates, which suggested that basic residues may contribute to substrate recognition by Nek2 [26]. Although PP1α and PP1β do not contain homologous serine/threonine residues to threonine-307, PP1α contains a serine residue and PP1β contains a threonine residue homologous to PP1γ threonine-318, with basic residues in the surrounding sequence. Nek2 was previously shown to phosphorylate serine residues in peptides and proteins [26]. We also found that MBP–C-Nap1 is an excellent substrate for Nek2. Approx. 13 moles of phosphate were incorporated/mol of C-Nap1 by Nek2 (results not shown).

Nek2, PP1α and C-Nap1 form a ternary complex *in vitro*

In order to ascertain whether Nek2, PP1α and C-Nap1 can form a ternary complex we performed amylose resin affinity binding experiments with GST–Nek2 variants, MBP–C-Nap1 and PP1α. Amylose resin has a high affinity for MBP, but no affinity for GST. Hence any complex containing GST–Nek2, MBP–C-Nap1 and PP1α must represent a ternary complex and not separate dimeric complexes. Figure 7 shows that all three proteins are present in the pellet when GST–Nek2 or GST–Nek2KD are used, confirming the presence of a ternary complex. However, the PP1α is not present when either GST–Nek2NB or GST are used. All three versions of the GST–Nek2 protein are recovered in the pellet, demonstrating that they can all bind to C-Nap1 and

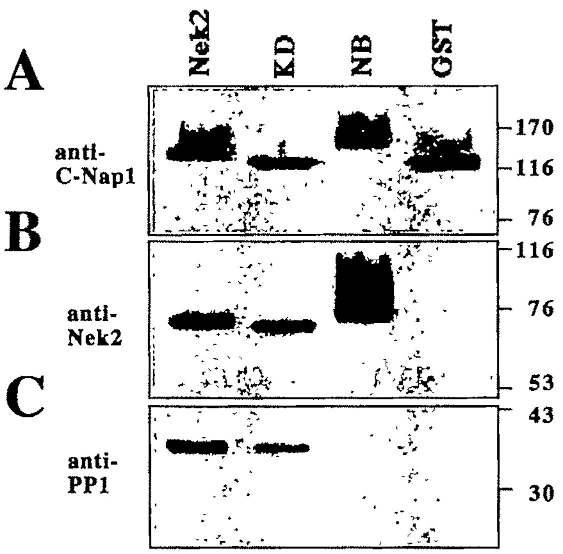

Figure 7 Co-sedimentation of Nek2, C-Nap1 and PP1.

293 cells were transfected with the Nek2 constructs indicated A 200 μg portion of protein from each cell extract was incubated with 2 μg of MBP–C-Nap1, 2 μg PP1α and amylose resin The beads were washed and bound proteins separated on either 7 5% acrylamide (for C-Nap1 and Nek2 blots) or 10% acrylamide (for PP1 blots) SDS/PAGE After transfer to nitrocellulose, the blots were incubated with the indicated antibodies and proteins visualized by ECL® (A) Anti-C-Nap1, (B) anti-Nek2, (C) anti-PP1γ In all panels lane 1, GST–Nek2, lane 2, GST–Nek2KD, lane 3, GST–Nek2NB, lane 4, GST only Size markers are in kDa

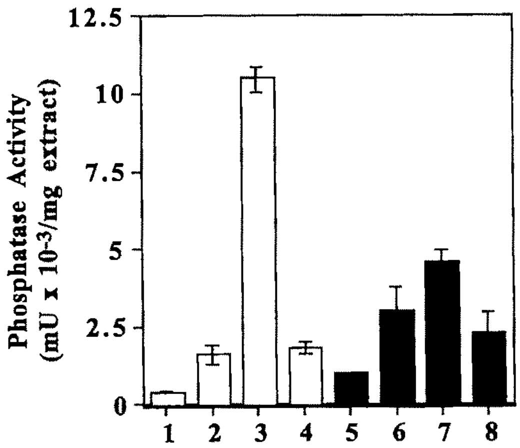

Figure 8 Characterization of Nek2–PP1 phosphatase activity

A 100 μg portion of 293 cell extract (non-transfected) was incubated with pre-immune IgG or anti-Nek2 beads. The beads were washed with lysis buffer, then the bound phosphatase activity measured 1 and 5, pre-immune beads, 2 and 6, anti-Nek2 beads, 3 and 7, anti-Nek2 beads plus 1 μM peptide 294 (GKRTNLRKTGSERIAMGMRVKFNPLALLLDSC), 4 and 8, anti-Nek2 beads plus 1 μM control peptide 575 (GKRTNLRKTGSERIAMGMRVKANPLALLLDSC) The PP1-binding motif is underlined Bars 1–4 were assayed using [^{32}P]phosphorylase as substrate (final concentration 2 7 μM) and bars 5–8 used phosphorylated MBP–C-Nap1 as substrate (final concentration 2 7 μM) Activity (after molybdate extraction) is stated as m-units $\times 10^{-3}$/mg of protein in the extract

that the PP1α is recovered in the pellet only because of its ability to bind to Nek2. The slightly lower level of GST–Nek2KD seen in the pellet fraction compared with the other tracks probably explains the slightly reduced amount of PP1α seen in this track. The mobilities of the GST–Nek2 variants are in accordance with those in Figure 4. Consistent with being a multiply phosphorylated substrate of Nek2 (see earlier), MBP–C-Nap1 shows a large decrease in mobility (approx. 20 kDa) in the presence of GST–Nek2NB compared with unphosphorylated C-Nap1 in the GST–Nek2KD and GST incubations.

Nek2-PP1 dephosphorylates C-Nap1

Immunoprecipitation of the endogenous Nek2–PP1 from 293 cell lysates using the anti-Nek2 antibody allowed us to test whether C-Nap1 phosphorylated by Nek2 could be dephosphorylated by the Nek2–PP1 complex, as suggested by the results in Figure 7(A). Assays using C-Nap1 as substrate and Nek2–PP1 immunoprecipitates as the source of phosphatase are compared with parallel assays with phosphorylase as substrate. Figure 8 shows that the Nek2–PP1 complex has an approx. 2-fold higher activity towards C-Nap1 than phosphorylase. The influence of Nek2 on the phosphatase activity was assessed by prior incubation of the PP1–Nek2 complex with peptide-294 (amino acids 773–810 of 53BP2), which has previously been shown to disrupt targetting subunit–PP1 complexes and, in many cases, to relieve inhibition of phosphorylase phosphatase activity caused by the targetting subunit [4] The activity towards phosphorylase was dramatically increased by prior incubation of PP1–Nek2 with peptide-294, while the control peptide-575, mutated in the PP1 binding site, had no effect. When C-Nap1 protein was used as substrate, addition of peptide-294 caused only a slight increase in phosphatase activity and the control peptide-575 again had no effect. These results indicate that binding of PP1 to Nek2 suppresses the phosphorylase phosphatase activity, resulting in a large increase in the C-Nap1/phosphorylase phosphatase activity ratio.

DISCUSSION

Although many proteins have been identified at centrosomes, the molecular mechanisms underlying the regulation of centrosome function are unclear. The processes by which centrosomes duplicate, nucleate microtubules and separate at mitosis to form the spindle poles all require elucidation. The protein serine/threonine kinase, Nek2, which exhibits predominant localization at centrosomes and causes splitting or dispersal of centrosomes when overexpressed [27], is shown here to form a complex with the protein serine/threonine phosphatase PP1. We demonstrate that the Nek2–PP1 complex occurs both *in vitro*, using bacterially expressed proteins, and in cell extracts through the motif KVHF at position 383–386 of Nek2, a sequence that conforms to the known PP1 consensus binding motif. Nek2 activity is not necessary for the formation of the Nek2–PP1 complex. We also demonstrate that at least two distinct isoforms of PP1 (PP1α and PP1γ_1) can interact with Nek2. Interestingly, PP1α has recently been reported to show a marked localization at centrosomes during mitosis [41]. These data point to a phosphorylation–dephosphorylation cycle catalysed by the Nek2–PP1 complex being important in centrosome function and most probably in centrosome separation. Other isoforms of mammalian NIMA-related kinases, namely Nek1 and Nek3, do not possess a consensus PP1-binding motif and there is no PP1-binding motif in *A. nidulans* NIMA that conforms to the mammalian or yeast consensus PP1-binding motifs [17].

Several kinase–phosphatase complexes have been postulated to mediate cellular signals, such as calmodulin kinase IV-PP2A [42] and extracellular-signal-regulated kinase 2/mitogen-activated protein kinase phosphatase 3 [43] Complex formation localizes both enzymes to a specific substrate and tight regulation of the kinase by the phosphatase and vice versa can explain how a kinase can be activated transiently in response to an extracellular signal. However, there is no evidence for an upstream kinase activating Nek2. Fry et al. [26] showed that the levels of Nek2 protein changed during the cell cycle, being high throughout S and G_2 phases and low during other phases of the cell cycle. We have demonstrated here that Nek2 is activated by autophosphorylation and that this activation can be at least partially reversed by PP1. The kinase activity of Nek2 may only become effective on exogenous substrates when its activity outstrips that of PP1, at which point it may also partially inhibit PP1 by phosphorylation. Once the activity of Nek2 falls below that required to inhibit PP1, the rise in PP1 activity would very rapidly dephosphorylate and switch off Nek2 activity. Such rapid molecular switching, proposed for kinase–phosphatase complexes involved in signalling, may be relevant here to rapidly and transiently switch on centrosome separation.

One possible mechanism by which the Nek2–PP1 complex could function is that Nek2 may phosphorylate a substrate protein and this is then followed by dephosphorylation of the substrate protein by PP1. Successive cycles of phosphorylation and dephosphorylation could result in centrosome separation in a process similar to muscle contraction. A more likely alternative is that phosphorylation of a substrate protein by Nek2 may allow centrosomes to move apart, and that PP1 may prevent the newly formed centrioles from separating until the G_2/M transition. A putative *in vivo* substrate is C-Nap1, previously shown to bind to Nek2 and to undergo phosphorylation *in vitro* [28]. Whereas Nek2 [27] and PP1α [41] localize to centrosomes in both interphase and mitosis, C-Nap1 was found to localize to centrosomes during interphase, but anti-C-Nap1 antibody interaction at centrosomes diminished at the onset of prophase and was lost during mitosis. C-Nap1, a protein with coiled coil structure, was therefore postulated to tether the proximal ends of centrioles together during interphase, and phosphorylation of C-Nap1 by Nek2 at G_2/M to cause depolymerization or degradation of C-Nap1 and thus centriole separation [28]. Our results support the idea that C-Nap1, Nek2 and PP1 could be involved in centrosome separation. We show that C-Nap1 is an *in vitro* substrate for both Nek2 and PP1 that is bound to Nek2. Additionally all three proteins can form a ternary complex *in vitro*. The very high level of phosphorylation on the C-terminal 592 amino acids of C-Nap1 could represent a method to facilitate centrosome separation through either a conformational change or a surface charge effect.

Assays comparing C-Nap1 and phosphorylase as substrates for the Nek2–PP1 complex showed that the phosphatase activity towards C-Nap1 was higher than towards phosphorylase. Addition of a peptide (294) that should disrupt the interaction of PP1 with Nek2, caused the phosphorylase phosphatase activity to increase approx. 7-fold, while there was only a marginal effect of the C-Nap1 phosphatase activity. These results indicate that PP1c has a much higher activity towards phosphorylase than C-Nap1. Binding of PP1c to Nek2 suppresses the phosphorylase phosphatase activity, while having little effect on the C-Nap1 phosphatase activity, an effect consistent with Nek2 being a regulatory subunit for PP1. Thus the interaction of PP1c with Nek2 increases PP1c specificity for C-Nap1 by enhancing the C-Nap1/phosphorylase phosphatase activity ratio. Combined with the highly specific location of Nek2 at the centrosome, this may minimize dephosphorylation of irrelevant substrates by the Nek2–PP1 complex.

Overexpression of active Nek2 in mammalian cells was shown to initially induce centrosome splitting, while more prolonged overexpression of active Nek2 led to dispersal of centrosomal material, as did overexpression of inactive Nek2 at all time points [27]. We found that overexpression of Nek2 mutated in the PP1-binding site (GST–Nek2NB) in a human fibroblast cell line (MCF7) also caused centrosome dispersal at even the earliest time points we could examine (results not shown). However, the kinase activity of Nek2NB is likely to be higher than that of Nek2 due to the absence of bound PP1, which would inhibit autophosphorylation. Consequently, overexpression of Nek2NB might be expected to cause more rapid centrosome dispersal than the overexpression of Nek2. In the light of our finding that Nek2 binds PP1, overexpression of Nek2KD might cause centrosomal dispersal because it brings to the centrosome active PP1 that, in excess, might interfere with many phosphorylation reactions.

Since centrosome separation must be coordinated with other cell cycle events it is likely that proteins regulating the Nek2–PP1 switch will be involved in initiating other aspects of cell division. Although, $p34^{cdc2}$ has been shown to phosphorylate further and activate *A. nidulans* NIMA subsequent to autophosphorylation [23], there is no evidence for $p34^{cdc2}$ activation of mammalian Nek2. However, it has been shown that both $p34^{cdc2}$-cyclinA and $p34^{cdc2}$-cyclinB are able to phosphorylate and inactivate PP1α on threonine-320 and the homologous threonine-311 in PP1γ_1 [44]. This site is distinct from the sites (threonine-307 and threonine-318) on PP1γ_1 that are phosphorylated by Nek2. Phosphorylation of PP1 by $p34^{cdc2}$ would enhance the ability of Nek2 to autophosphorylate and, consequently, to phosphorylate its target substrates such as C-Nap1. Furthermore, it has been shown that peak PP1 phosphorylation occurs at the G_2/M phase of the cell cycle [45]. This coincides with centrosome separation and a peak in Nek2 kinase activity [26]. A possible mechanism whereby the initiation of mitosis is coupled to centrosome separation at G_2-M is that $p34^{cdc2}$ phosphorylates and inactivates PP1, thereby allowing Nek2 kinase to phosphorylate the C-Nap1 protein thus causing centrosome separation. However, other kinases activated at G_2/M with similar substrate specificities, such as polo-like kinases [46], could have the same effect on PP1. We are currently attempting to test this hypothesis by studying the effect of phosphorylation by $p34^{cdc2}$-cyclinA and $p34^{cdc2}$-cyclinB and polo-like kinases on PP1 activity of the endogenous Nek2/PP1 complex.

While this paper was under review, Uto and Sagata [47] showed that *Xenopus* Nek2B, an alternatively spliced form of Nek2, is required for the assembly and/or maintenance of centrosomes in early *Xenopus* embryos in which centrosome cycles can occur autonomously. Interestingly, Nek2B does not contain the PP1-binding site that we identify here, an observation that may explain why Nek2B, in contrast with Nek2, does not cause centrosome splitting and functions at a time when the centrosome cycle is not coupled to nuclear events.

We are grateful to Nick Morrice for the analysis of the phosphorylation sites on PP1, Steve Elledge for the yeast two-hybrid system, and Agnieszka Kieloch for cell culture. The work was supported by the U.K. Medical Research Council. X.L. thanks the Training and Mobility in Research network (Contract ERBFMRXCT96-0041) for postdoctoral support.

REFERENCES

1 Cohen, P. (1989) The structure and regulation of protein phosphatases. Annu. Rev. Biochem. **58**, 453–508

2 Bollen, M. and Stalmans, W. (1992) The structure, role and regulation of type 1 protein phosphatases. Crit. Rev. Biochem. Mol. Biol. **27**, 227–281

3 Hubbard, M. J. and Cohen, P. (1993) On target with a new mechanism for the regulation of protein phosphorylation. Trends Biochem. Sci. **18**, 172–177

4 Johnson, D F, Moorhead, G, Caudwell, F B., Cohen, P, Chen, Y H, Chen, M X and Cohen, P T W. (1996) Identification of the protein phosphatase-1-binding domains on the glycogen and myofibrillar targetting subunits Eur J Biochem **239**, 317–325

5 Jagiello, I, Beullens, M., Vulsteke, V, Wera, S, Sohlberg, B, Stalmans, W, von Gerbain, A and Bollen, M (1997) Nipp-1, a nuclear inhibitory subunit of protein phosphatase-1 has RNA-binding properties J Biol Chem. **272**, 22067–22071

6 Trinkle-Mulcahy, L, Ajuh, P, Prescott, A, Claverie-Martin, F, Cohen, S, Lamond, A I and Cohen, P (1999) Nuclear organisation of NIPP1, a regulatory subunit of protein phosphatase 1 that assocorates with pre-mRNA splicing factors J Cell Sci **112**, 157–168

7 Kreivi, J-P, Trinkle-Mulcahy, L, Lyon, C E, Morrice, N. A, Cohen, P and Lamond, A I (1997) Purification and characterisation of p99, a nuclear modulator of protein phosphatase 1 activity. FEBS Lett **420**, 57–62

8 Allen, P B, Kwon, Y.-G, Nairn, A C and Greengard, P (1998) Isolation and characterization of PNUTS, a putative protein phosphatase 1 nuclear targeting subunit Proc Natl Acad Sci U S A **273**, 4089–4095

9 Hirano, K, Erdodi, F, Patton, J G and Hartshorne, D J (1996) Interaction of protein phosphatase type 1 with a splicing factor FEBS Lett **389**, 191–194

10 Stone, E M, Yamano, H., Kinoshita, N and Yanagida, M (1993) Mitotic regulation of protein phosphatases by the fission yeast sds22 protein Curr Biol **3**, 13–26

11 Westphal, R S, Tavalin, S J, Lin, J W, Alto, N M, Fraser, I. D C, Langeberg, L K, Sheng, M and Scott, J D (1999) Regulation of NMDA receptors by an associated phosphatase-kinase signaling complex Science **285**, 93–96

12 McAvoy, T, Allen, P B, Obaishi, H, Nakanishi, H, Takai, Y, Greengard, P, Nairn, A C and Hemmings, H C (1999) Regulation of neurabin I interaction with protein phosphatase 1 by phosphorylation Biochemistry **38**, 12943–12949

13 Helps, N R, Barker, H M, Elledge, S J and Cohen, P T W (1995) Protein phosphatase 1 interacts with p53BP2, a protein which binds to the tumour suppressor p53 FEBS Lett **377**, 295–300

14 Beullens, M, Stalmans, W and Bollen, M (1996) Characterisation of a ribosomal inhibitory polypeptide of protein phosphatase-1 from rat liver Eur J Biochem **239**, 183–189

15 He, B, Gross, M and Roizman, B (1997) The $\gamma_1$34.5 protein of herpes simplex virus 1 complexes to protein phosphatase 1α to dephosphorylate the a subunit of eukaryotic translation initiation factor 2 and preclude the shut of protein synthesis by double stranded RNA-activated protein kinase Proc Natl Acad Sci. U S A **94**, 843–848

16 Wera, S and Hemmings, B A (1995) Serine/threonine protein phosphatases Biochem J **311**, 17–29

17 Egloff, M-P., Johnson, F, Moorhead, G., Cohen, P T W, Cohen, P and Barford, D (1997) Structural basis for the recognition of regulatory subunits by the catalytic subunit of protein phosphatase 1 EMBO J **16**, 1876–1887

18 Fry, A M and Nigg, E A (1995) The NIMA kinase joins forces with Cdc2 Curr Biol **5**, 1122–1125

19 Lu, K P and Hunter, T (1995) The NIMA kinase a mitotic regulator in *Aspergillus nidulans* and vertebrate cells In Progress in Cell Cycle Research , vol. 1 (Meijer, L, Guidet, S and Tung, H Y L, eds), pp 187–205, Plenum Press, New York

20 Osmani, S A and Ye, X S (1996) Cell cycle regulation in *Aspergillus* by two protein kinases Biochem. J. **317**, 633–641

21 Oakley, B R. and Morris, N R (1983) A mutation in *Aspergillus nidulans* that blocks the transition from interphase to prophase J Cell Biol **96**, 1155–1158

22 Osmani, A H, McGuire, S L and Osmani, S A (1991) Parallel activation of the NIMA and p34cdc2 cell cycle-regulated protein kinases is required to initiate mitosis in *A nidulans* Cell **67**, 283–291

23 Ye, X S, Xu, G, Pu, R T, Fincher, R R, McGuire, S L, Osmani, A H and Osmani, S. A. (1995) The NIMA protein kinase is hyperphosphorylated and activated downstream of p34*cdc2*/cyclinB coordination of two mitosis promoting kinases EMBO J. **14**, 986–994

24 Lu, K P and Hunter, T (1995) Evidence for a NIMA-like mitotic pathway in vertebrate cells Cell **81**, 413–424

25 Schultz, S J, Fry, A M., Sutterlin, C, Ried, T and Nigg, E A (1994) Cell cycle-dependent expression of Nek2, a novel human protein kinase related to the NIMA mitotic regulator of *Aspergillus nidulans* Cell Growth Differ. **5**, 625–635

26 Fry, A M, Scultz, S J, Bartek, J and Nigg, E A (1995) Substrate specificity and cell cycle regulation of the Nek2 protein kinase, a potential human homologue of the mitotic regulator NIMA of *Aspergillus nidulans* J Biol Chem **270**, 12899–12905

27 Fry, A M, Meraldi, P. and Nigg, E A (1998) A centrosomal function for the human Nek2 protein kinase, a member of the NIMA family of cell cycle regulators EMBO J **17**, 470–481

28 Fry, A M, Mayor, T, Meraldi, P, Stierhof, Y-D, Tanaka, K and Nigg, E A (1998) C-Nap1, a novel centrosomal coiled-coil protein and candidate substrate of the cell cycle-regulated protein kinase Nek2 J Cell Biol **141**, 1563–1574

29 Helps, N R, Street, A J, Elledge, S J and Cohen, P T W (1994) Cloning of the complete coding region for human protein phosphatase inhibitor 2 using the two hybrid system and expression of inhibitor 2 in *E coli* FEBS Lett **340**, 93–98

30 Sanchez, I, Hughes, R. T, Mayer, B J, Yee, K, Woodgett, J R, Avruch, J, Kyriakis, J M and Zon, L I (1994) Role of SAPK/ERK kinase-1 in the stress-activated pathway regulating transcription factor c-Jun Nature (London) **372**, 794–798

31 Higuchi, R (1990) Recombinant PCR In PCR Protocols, a Guide to Methods and Applications (Innis, M A, Gelfand, D H, Sninsky, J J and White, T J, eds), pp 177–183, Academic Press, San Diego

32 MacKintosh, R W, Dalby, K N, Campbell, D G., Cohen, P T W, Cohen, P and MacKintosh, C (1995) The cyanobacterial toxin microcystin binds covalently to cysteine-273 on protein phosphatase 1 FEBS Lett **371**, 236–240

33 Barker, H M., Craig, S P, Spurr, N K and Cohen, P T W (1993) Sequence of human protein serine/threonine phosphatase 1 gamma and localization of the gene (PPP1CC) encoding it to chromosome bands 12q24 1-q24 2 Biochim Biophys Acta **1178**, 228–233

34 Alessi, D R, Street, A J, Cohen, P and Cohen, P T W (1993) Inhibitor-2 functions like a chaperone to fold three expressed isoforms of mammalian protein phosphatase-1 into a conformation with the specificity and regulatory properties of the native enzyme Eur J Biochem **213**, 1055–1066

35 Harlow, E and Lane, D (1988) Immunoaffinity purification In Antibodies: a Laboratory Manual, pp 511–552, Cold Spring Harbor Laboratory Press, Cold Spring Harbor, NY

36 Alessi, D R, Andjelkovic, M, Caudwell, B, Cron, P, Morrice, N., Cohen, P and Hemmings, B A (1996) Mechanism of activation of protein kinase B by insulin and IGF-1. EMBO J **15**, 6541–6551

37 Cohen, P, Alemany, S, Hemmings, B A, Resink, T J, Stralfors, P and Tung, H Y L (1988) Protein phosphatase-1 and protein phosphatase-2A from rabbit skeletal muscle. Methods Enzymol **159**, 390–408

38 MacKintosh, C (1993) Assay and purification of protein (serine/threonine) phosphatases In Protein Phosphorylation, a Practical Approach (Hardie, D G, ed), pp 197–230, IRL Press, Oxford

39 Durfee, T, Becherer, K, Chen, P-L, Yeh, S-H, Yang, Y, Kilburn, A E, Lee, W H and Elledge, S J (1993) The retinoblastoma protein associates with the protein phosphatase type 1 catalytic subunit Genes Dev. **7**, 555–569

40 Egloff, M-P, Cohen, P T W, Reinemer, P and Barford, D (1995) Crystal structure of the catalytic subunit of human protein phosphatase 1 and its complex with tungstate J Mol Biol **254**, 942–959

41 Andreassen, P R, Lacroix, F B, Villa-Moruzzi, E and Margolis, R L (1998) Differential subcellular localization of protein phosphatase-1 alpha, gamma1 and delta isoforms during both interphase and mitosis in mammalian cells J. Cell Biol **141**, 1207–1215

42 Westphal, R S, Anderson, K A, Means, A R and Wadzinski, B E (1998) A signaling complex of Ca^{2+}-calmodulin-dependent protein kinase IV and protein phosphatase 2A. Science **280**, 1258–1261

43 Camps, M, Nichols, A, Gillieron, C, Antonsson, B., Muda, M, Chabert, C, Boschert, U and Arkinstall, S. (1998) Catalytic activation of the phosphatase MKP-3 by ERK2 mitogen-activated protein kinase Science **280**, 1262–1265

44 Dohadwala, M, da Cruz e Silva, E F, Hall, F. L, Williams, R T, Carbonaro-Hall, D A, Nairn, A C, Greengard, P and Berndt, N (1994) Phosphorylation and inactivation of protein phosphatase 1 by cyclin-dependent kinases Proc Natl Acad Sci U S A **91**, 6408–6412

45 Kwon, Y-G, Lee, S Y, Choi, Y, Greengard, P and Nairn, A C (1997) Cell cycle-dependent phosphorylation of mammalian protein phosphatase 1 by cdc2 kinase Proc Natl Acad Sci U S A **94**, 2168–2173

46 Lane, H A and Nigg, E A (1997) Cell-cycle control POLO-like kinases join the outer circle Trends Cell Biol **7**, 63–68

47 Uto, K and Sagata, N (2000) Nek2B, a novel maternal form of Nek2 kinase, is essential for the assembly or maintenance of centrosomes in early *Xenopus* embryos EMBO J **19**, 1816–1826

Received 21 March 2000/26 April 2000, accepted 11 May 2000

Biochem J (2000) 349, 519–526 (Printed in Great Britain)

Kinetics and control of oxidative phosphorylation in rat liver mitochondria after chronic ethanol feeding

Ausra MARCINKEVICIUTE*†, Vida MILDAZIENE†‡, Sara CRUMM*, Oleg DEMIN*§, Jan B. HOEK* and Boris KHOLODENKO*[1]

*Department of Pathology, Anatomy and Cell Biology, Thomas Jefferson University, 1020 Locust St, Philadelphia, PA 19107, U.S.A., †Institute for Biomedical Research, Kaunas Medical University, Eiveniu 4, Kaunas LT-3007, Lithuania, ‡Vytautas Magnus University, Vileikos 8, Kaunas LT-3035, Lithuania, and § A. N. Belozersky Institute of Physico-Chemical Biology, Moscow State University, Vorobiovy Gory, Moscow 119899, Russia

---

Changes in the kinetics and regulation of oxidative phosphorylation were characterized in isolated rat liver mitochondria after 2 months of ethanol consumption. Mitochondrial energy metabolism was conceptually divided into three groups of reactions, either producing protonmotive force (Δp) (the respiratory subsystem) or consuming it (the phosphorylation subsystem and the proton leak). Manifestation of ethanol-induced mitochondrial malfunctioning of the respiratory subsystem was observed with various substrates; the respiration rate in State 3 was inhibited by 27±4% with succinate plus amytal, by 20±4% with glutamate plus malate, and by 17±2% with *N,N,N′,N′*-tetramethyl-*p*-phenylenediamine/ascorbate. The inhibition of the respiratory activity correlated with the lower activities of cytochrome *c* oxidase, the bc_1 complex, and the ATP synthase in mitochondria of ethanol-fed rats. The block of reactions consuming the Δp to produce ATP (the phosphorylating subsystem) was suppressed after 2 months of ethanol feeding, whereas the mitochondrial proton leak was not affected. The contributions of Δp supply (the respiratory subsystem) and Δp demand (the phosphorylation and the proton leak) to the control of the respiratory flux were quantified as the control coefficients of these subsystems. In State 3, the distribution of control exerted by different reaction blocks over respiratory flux was not significantly affected by ethanol diet, despite the marked changes in the kinetics of individual functional units of mitochondrial oxidative phosphorylation. This suggests the operation of compensatory mechanisms, when control redistributes among the different components within the same subsystem.

Key words: control coefficient, kinetic response, top-down control analysis.

INTRODUCTION

Chronic intake of large quantities of ethanol is associated with marked alterations in mitochondrial structure and function, both in humans and in experimental animals (reviewed in [1–4]). Abnormalities in mitochondrial morphology, e.g. deformed and enlarged mitochondria, often with paracrystalline inclusions, are evident in liver, muscle and other tissues. The most prominent site of ethanol-induced mitochondrial changes is the liver. Early studies [5,6] established that liver mitochondria isolated from rats fed an ethanol-containing diet for 3–5 weeks exhibited a decrease in NAD-linked respiration, both under conditions of active respiration (State 3, defined as the mitochondrial state in which ADP supply is saturating and excess substrate and P_i are available) and in uncoupled mitochondria. Subsequent studies (reviewed in [2]) demonstrated that these effects had their origin in a decrease in the activity of select components of the oxidative phosphorylation machinery, notably NADH dehydrogenase, cytochrome *b*, cytochrome oxidase and ATP synthase. Since all of these protein complexes contain one or more subunits encoded by mitochondrial DNA, a defect in mitochondrial protein synthesis may account, at least in part, for these altered activities, and there is evidence that the effects of chronic ethanol treatment may be due to dysfunctional mitochondrial ribosomes [7,8]. However, other mechanisms may contribute to the changes in electron transport and ATP synthase activity, e.g. the accumulation of dysfunctional proteins in the form of acetaldehyde adducts or through damage by free radical species, or changes in membrane structure associated with altered properties of mitochondrial cardiolipin [4]. By contrast, isolated mitochondria from heart, skeletal muscle and brain show less evidence of defects in these pathways [1,3,9,10]. The progression of ultrastructural changes in the heart is slower than in the liver, and the onset of biochemical alterations is much later.

Despite many studies indicating effects of chronic alcoholism on various mitochondrial enzyme activities, there is as yet neither a clear picture of the relative importance of such changes for overall mitochondrial respiration, nor a quantitative assessment of alterations in the kinetic responses and regulation. In the present paper, we investigate the effect of chronic ethanol treatment using an analysis known as 'top-down' metabolic control analysis (reviewed in [11,12]). In this context, the oxidative phosphorylation system is conceptually divided into three subsystems, either producing or consuming the protonmotive force (Δp). Δp is generated by the respiratory subsystem (*R*), which includes the substrate transport systems in the inner membrane, the tricarboxylic acid cycle enzymes and substrate dehydrogenases providing electrons to the respiratory chain, and the complexes of the electron transport chain. The remaining two blocks of reactions consume Δp: the phosphorylation subsystem (*P*) and the proton leak subsystem (*L*). The phosphorylation subsystem includes the phosphate transport systems, the ATP synthase, the adenine nucleotide translocator, and any reactions that may be present in the medium (or in the matrix) converting

---

Abbreviations used Δp, protonmotive force; TMPD, *N,N,N′,N′*-tetramethyl-*p*-phenylenediamine, TPP^+, tetraphenylphosphonium

[1] To whom correspondence should be addressed (e-mail Boris.Kholodenko@mail.tju.edu)

ATP into ADP. The proton leak unit represents uncoupled respiration (mainly the leak of protons across the mitochondrial membrane, but also any other non-phosphorylating ion fluxes that dissipate Δp)

The present paper analyses the dependencies of the fluxes through the respiratory subsystem (J_R), the phosphorylation subsystem (J_P) and the proton leak pathways (J_L) on Δp. Under conditions where changes in ΔpH can be negligible, the mitochondrial membrane potential ($\Delta\Psi$) may be considered instead of Δp. This simplification is valid as long as $\Delta\Psi$ is the major contributor to Δp, or there is a reasonably constant relationship between $\Delta\Psi$ and ΔpH [13]. In applying top-down analysis to mitochondria from the ethanol-fed and control rats, the present paper investigates how the functional units of the system are affected by chronic ethanol treatment.

In this work we quantified the changes in the kinetic responses of the functional units of the oxidative phosphorylation machinery (the respiratory subsystem, proton leak and phosphorylation subsystem) in rat liver mitochondria after 2 months of ethanol feeding, using different respiratory substrates: succinate, glutamate plus malate, and *N*,*N*,*N'*,*N'*-tetramethyl-*p*-phenylenediamine (TMPD) plus ascorbate. The oxidation of these substrates involves different mitochondrial enzymes, and the supply of reducing equivalents occurs at different levels of the electron transport chain. Using the plots of J_R, J_P and J_L versus $\Delta\Psi$, we determine the control exerted by the suppliers and consumers of the Δp over mitochondrial respiration in ethanol-fed and control rats. Our results demonstrate that in rat liver mitochondria, a 2-month treatment with ethanol diet suppresses both the respiratory and phosphorylation subsystems, but to a different degree depending on the substrate used; proton leak was not affected. Remarkably, despite the changes in the activity of respiratory complexes in the mitochondria from ethanol-fed and control animals, there were no significant changes in the control distribution.

We applied kinetic modelling in order to understand why the control distribution does not change, despite marked alterations in the kinetics of individual functional units of oxidative phosphorylation. Theoretical analysis demonstrated that simultaneous depression of the supply and demand blocks, as found in ethanol-affected mitochondria, can occur without a significant change in the control distribution. Moreover, the depression of the activity of the individual components within the same block can cause the control redistribution among these components, even though the net control exerted by the block does not change.

EXPERIMENTAL

We used male Sprague–Dawley rats (275–300 g) which were pair-fed according to the protocol of DeCarli and Lieber [14] for 5–7 weeks, with ethanol-fed animals receiving a diet containing 36% ethanol, and carbohydrate substituting for ethanol in the control diet. This dietary treatment results in a distinct pattern of changes in activity of respiratory chain components and ATP synthase, without causing overt liver disease [2].

Liver mitochondria were isolated in 5 mM Hepes (pH 7.4)-buffered sucrose (0.25 M), containing 3 mM EGTA and 0.2% BSA (HMS medium), using standard differential centrifugation procedures. The pellet of the first low-speed centrifugation step was resuspended in HMS medium and recentrifuged to recover mitochondria retained in the low-speed pellet. The final wash of the mitochondrial pellet was in EGTA-free HMS medium. The mitochondrial pellet was resuspended in the same medium, protein was adjusted to 50 mg/ml, and the preparation was stored on ice until use. Protein concentrations were determined by the biuret or Lowry methods. Previous studies have documented exhaustively that the mitochondrial content of the liver, and the relative purity of mitochondria, are comparable in ethanol-fed and control rats following 5–8 weeks of feeding acording to the Lieber–DeCarli protocol [15–18].

Mitochondria were incubated at 30 °C in a closed, stirred and thermostated 1.5 ml glass vessel, fitted with both a Clark oxygen electrode (Rank Brothers, Cambridge, U.K.) and a tetraphenylphosphonium (TPP^+)-selective electrode (A. Zimkus, Vilnius, Lithuania). The incubation medium contained Hepes (20 mM, pH 7.4), KCl (50 mM), sucrose (200 mM), KH_2PO_4 (3 mM), EGTA (0.1 mM), $MgCl_2$ (1 mM) and dithiothreitol (1 mM). TPP^+ (133–266 nM) was addded for membrane potential measurements Incubations were carried out under the following substrate conditions: 5 mM glutamate plus 5 mM malate, 5 mM succinate (plus 1 mM amytal, used for technical reasons in preference to rotenone, since we had difficulty washing out the relatively hydrophobic rotenone from the TPP^+-selective electrode, whereas the more polar amytal did not cause this problem.), or 10 mM ascorbate plus 350 μM TMPD. Mitochondrial protein was 0.5 mg/ml. The creatine kinase ADP-regenerating system (50 mM creatine, 1 mM ATP and 30 units/ml creatine kinase to obtain State 3 conditions) was used to clamp the ATP/ADP ratio and to maintain stationary respiration rates. The creatine kinase system does not itself control respiration [19], but enables the ATP/ADP ratio to be clamped at different respiratory states throughout the range from State 4 (the mitochondrial state in which oxidative phosphorylation is limited by lack of external ADP, but in the presence of ATP) to State 3. Control experiments demonstrated that the respiration rate was not limited by the amount of creatine kinase, therefore all control over respiration rate was exerted by mitochondrial enzymes. The rate of mitochondrial respiration corresponding to State 3 was registered after addition of 1 mM ATP to the incubation medium. The following inhibitor concentrations were used in titrations to establish the relationship of respiratory activities to membrane potential: 0.03–1 mM malonate, 1.3–10 nM rotenone, 5–75 μM KCN, and 15–150 nM carboxyatractyloside.

The membrane potential of mitochondria was calculated from the distribution of TPP^+ using a binding correction factor of 0.16. This correction was based on a series of experiments with isolated mitochondria in which the ratio of accumulation of Rb^+ and TPP^+ was compared over a range of membrane potentials, titrated by addition of KCl in the presence of valinomycin [20]. Control experiments established that the TPP^+-binding correction in liver mitochondria was not significantly affected by chronic ethanol consumption (results not shown).

Determination of mitochondrial volume and ΔpH

Mitochondrial volume was determined from the distribution of ^3H_2O and $[^{14}C]$sucrose, and ΔpH from the distribution of $[^3H]$acetate and $[^{14}C]$sucrose [20], under the same incubation conditions as mitochondrial respiration. The results show that in State 3 the matrix volume and ΔpH of isolated liver mitochondria oxidizing succinate/amytal were not significantly affected by 5–7 weeks of ethanol feeding. Matrix volume and ΔpH in the preparations from the ethanol-fed animals changed, compared with controls, from 0.89 ± 0.02 μl/mg to 0.84 ± 0.03 μl/mg, and from 31.3 ± 0.4 mV to 28.1 ± 1.8 mV respectively. Also, under the conditions used here (i.e. in the presence of excess P_i), ΔpH made only a modest contribution to the total Δp, and this contribution was not significantly affected by the inhibitor titrations (results not shown). Thus the conditions were appropriate for using membrane potential measurements as quantitative indicators of changes in Δp.

Measurements of ATPase, cytochrome oxidase and ubiquinol:cytochrome *c* (*bc*$_1$ complex) activities

ATPase and cytochrome oxidase activities were measured in fractured mitochondria from rat liver. Fractured mitochondria were made by rapidly freeze–thawing liver mitochondria (repeated three times). ATPase activity was measured at 30 °C by recording the pH changes in the incubation chamber during ATP hydrolysis reaction in the presence of 250 mM sucrose, 5 mM $MgCl_2$, 2.5 mM Tris (pH 8) and 1 mM ATP [21]. The buffering capacity of the reaction mixture was determined experimentally by adding a known amount of HCl (5 μl of 50 mM HCl $\equiv$ 250 nmol ions H^+) to the reaction mixture after each measurement, and recording the pH change induced by this addition. The ATPase activity was estimated from the initial rate of increase in H^+ concentration during ATP hydrolysis. Control experiments showed that H^+ formation was > 95 % inhibited by oligomycin (1.5 μg/ml).

Cytochrome oxidase activity was measured at 30 °C by monitoring the rate of oxygen consumtion by fractured mitochondria (0.4 mg protein/ml) in the presence of 0.35 mM TMPD, 10 mM ascorbate and 0.015 mM cytochrome *c*, under the same incubation conditions as for mitochondrial respiration.

Activity of the bc_1 complex was measured spectrophotometrically by following the kinetics of cytochrome c reduction. Measurements were carried out at 30 °C in the presence of KH_2PO_4 (35 mM pH 7.2), $MgCl_2$ (5mM), BSA (fatty acid-free, 2.5 mg/ml), KCN (0.2 mM), oxidized cytochrome *c* (20 μM), rotenone (4 μg/ml), fractured mitochondria (10 μg mitochondrial protein) and antimycine (0 or 10 μg/ml). Reactions were started by adding 20 μM decylubiquinol. Enzymic activity was measured at 550 nM for 2 min, with an absorption coefficient of 18.5 $mM^{-1} \cdot cm^{-1}$.

Statistical analysis

Data are expressed as means ± S.E M. of 3–7 experiments carried out on different mitochondrial preparations. Each point for every individual preparation is averaged from two or three repetitive runs.

RESULTS

Activities and kinetic responses of the components of oxidative phosphorylation in chronic alcoholism

We measured the activities of ubiquinol:cytochrome *c* reductase (bc_1 complex), cytochrome oxidase, and the hydrolytic activity of ATPase in submitochondrial particles, from the livers of control and ethanol-fed animals. The results presented in Table 1 demonstrate that 2 months of chronic alcohol treatment diminished the activities of the bc_1 complex, cytochrome oxidase and ATPase in rat liver mitochondria by 41 ± 5 %, 40 ± 6 % and 36 ± 4 % respectively (Table 1). These data are consistent with previous studies [5,10,22–26]. The alterations in the component activities bring about the differential responses of each block of reactions *R*, *L* and *P* to changes in $\Delta\Psi$ These responses were determined by a series of inhibitor titrations as follows: first, the dependence of the flux through the respiratory subsystem, J_R, on $\Delta\Psi$ was determined by titrating mitochondria in State 3 with an inhibitor of the phosphorylation subsystem (carboxyatractyloside or oligomycin). Inhibition of phosphorylation caused an increase in $\Delta\Psi$ (similar to that occuring during the State 3/State 4 transition), which was accompanied by a decreased rate of O_2 uptake. At steady state, J_R is equal to the sum of the rates of O_2 consumption needed to drive the phosphorylation subsystem (J_P) and the proton leak (J_L)· $J_R = J_P + J_L$. Secondly, the dependence of J_L on $\Delta\Psi$ was determined under conditions of complete inhibition of J_P by excess (1 μM) oligomycin, so that $J_R = J_L$ [27]. Mitochondria oxidizing succinate were titrated with malonate (an inhibitor of succinate dehydrogenase). Titrations with rotenone or KCN were used to inhibit oxidation of glutamate plus malate, and TMPD plus ascorbate respectively. Inhibition of the respiratory subsystem caused $\Delta\Psi$ to decrease, and J_L was detemined as the rate of O_2 consumption at different values of $\Delta\Psi$. Thirdly, a similar titration protocol with inhibitors of the respiratory subsystem (malonate and rotenone or KCN in the absence of oligomycin) was used to determine the dependence of J_P on $\Delta\Psi$. The phosphorylation flux at each $\Delta\Psi$ was calculated by substracting the proton leak J_L from J_R at corresponding $\Delta\Psi$ values ($J_P = J_R - J_L$).

Table 1 Activities of respiratory chain components and ATPase after chronic alcohol treatment

*Statistically significant effect of alcohol ($P < 0.05$)

Component	Control	Ethanol	Inhibition (%)
Cytochrome *c* oxidase (n-atoms O/min per mg)	504 ± 35	305 ± 38*	40 ± 6
ATPase (nmol H^+/min per mg)	64.4 ± 5.6	39.6 ± 1.9*	36 ± 4
bc_1 complex (μM cytochrome *c*/min)	2.16 ± 0.17	1.33 ± 0.20*	41 ± 5

Respiratory subsystem analysis

Generation of Δp with different substrates involves different mitochondrial enzymes and encompasses different segments of the electron transport chain, resulting in different numbers of protons pumped per pair of electrons. As a consequence, plots of J_R versus $\Delta\Psi$ vary with the oxidative substrate. Figure 1 shows the kinetic responses of the respiratory subsystems, J_R, in mitochondria from ethanol-fed and control rats oxidizing different substrates, which enter the respiratory chain at different levels.

The simplest substrate supply condition is when mitochondria oxidize TMPD plus ascorbate, where no substrate translocator system is involved and reducing equivalents enter the electron transport chain at the level of cytochrome *c*. At saturating TMPD/ascorbate concentrations, the flux through the respiratory subsystem is mainly (> 80 %) controlled by cytochrome *c* oxidase and no other respiratory complexes are involved. Figure 1(A) demonstrates an inhibition (15–19 %) of the respiratory subsystem over the entire membrane potential range in mitochondria from ethanol-fed animals compared with mitochondria from pair-fed control animals. This observation is in agreement with a decrease in cytochrome *c* oxidase activity following chronic ethanol consumption (Table 1) [2,6,7,24,26].

A somewhat different pattern was obtained with mitochondria respiring on succinate (Figure 1B). This substrate enters the mitochondrial matrix on the dicarboxylate translocator in exchange for malate. Reducing equivalents are derived from the substrate through succinate dehydrogenase, and enter the electron transport chain at the level of coenzyme Q. Excess amytal was added in these experiments in order to suppress the accumulation of oxaloacetate, a potent competitive inhibitor of succinate dehydrogenase. In State 3, mitochondria from ethanol-

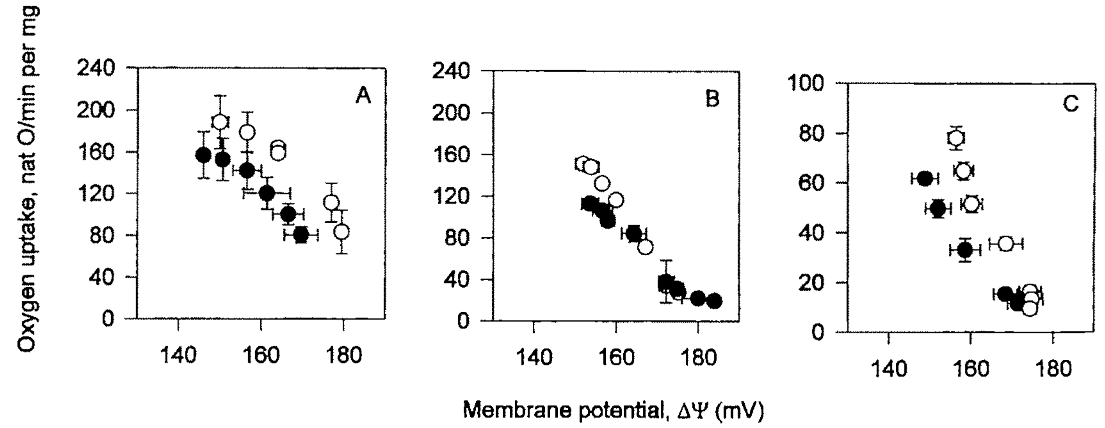

Figure 1 Kinetic response of the respiratory subsystem to changes in the membrane potential

Liver mitochondria oxidizing (A) TMPD (0.35 mM) plus ascorbate (10 mM), (B) succinate (10 mM) plus amytal (1 mM), (C) glutamate (5 mM) plus malate (5 mM). Control (○), ethanol-fed animals (●)

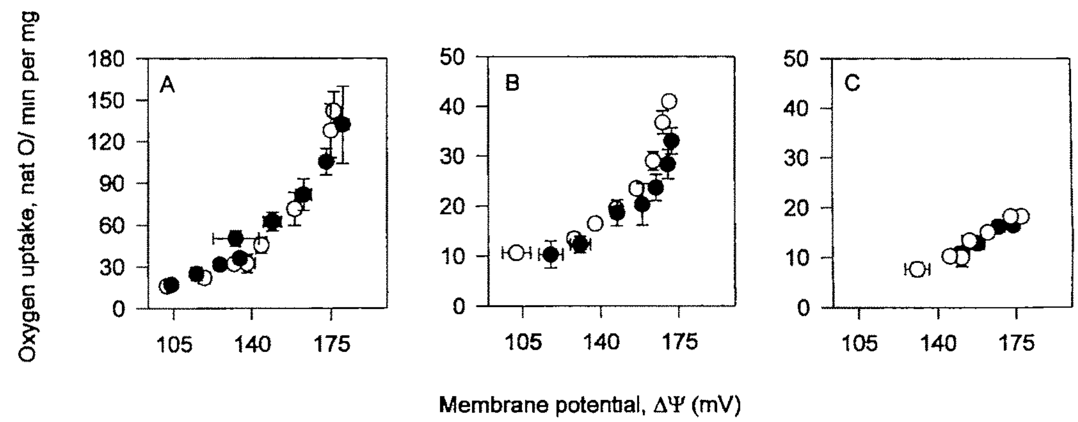

Figure 2 Dependence of the proton leak on the membrane potential

Liver mitochondria oxidizing (A) TMPD (0.35 mM) plus ascorbate (10 mM), (B) succinate (10 mM) plus amytal (1 mM), (C) glutamate (5 mM) plus malate (5 mM) Control (○), ethanol-fed animals (●)

fed rats exhibited lower succinate oxidation rates (by 26–33 %) than mitochondria from pair-fed control animals, in agreement with previous studies (data from 4 pairs receiving ethanol for 5–6 weeks). When succinate oxidation rates were decreased by titration with carboxyatractyloside, the difference between mitochondria from control and ethanol-fed rats in the activity of the respiratory subsystem declined as a function of the membrane potential under the conditions approaching State 4 (Figure 1B). These observations are in agreement with earlier findings that the flux of succinate oxidation is controlled primarily by components other than the electron transport chain under conditions of submaximal respiratory activity [19].

Glutamate plus malate oxidation follows more complex pathways, which supply reducing equivalents to the respiratory chain mostly in the form of NADH. When glutamate is oxidized in the presence of malate, glutamate traps oxaloacetate derived from malate to form aspartate and α-ketoglutarate. Aspartate is quantitatively exchanged for glutamate on the glutamate/aspartate translocator, whereas α-ketoglutarate can be either exchanged for extramitochondrial malate, or oxidized through α-ketoglutarate dehydrogenase. Hence the flux through malate dehydrogenase equals the sum of the fluxes through α-ketoglutarate dehydrogenase and the malate/α-ketoglutarate translocator. As shown in Figure 1(C), mitochondria from ethanol-fed animals oxidizing glutamate plus malate exhibited lower activities of the respiratory subsystem (by 11–35 %) than mitochondria from control animals over most of the range of ΔΨ, except under maximally inhibited conditions

Proton leak subsystem analysis

Figure 2 shows the kinetic response of the proton leak (J_L) to ΔΨ in mitochondria from ethanol-fed and control animals oxidizing different substrates. Mitochondria oxidizing TMPD plus ascorbate were titrated with KCN (Figure 2A), whereas malonate and rotenone were used to titrate succinate (Figure 2B) and glutamate plus malate (Figure 2C) oxidation respectively. Inhibition of the respiratory subsystem caused a decrease in ΔΨ. Proton leak is not directly affected by these inhibitors in the range of concentrations used [28].

Maximal rates of proton leak were obtained in State 4 where the membrane potential was maximal (no inhibitor added).

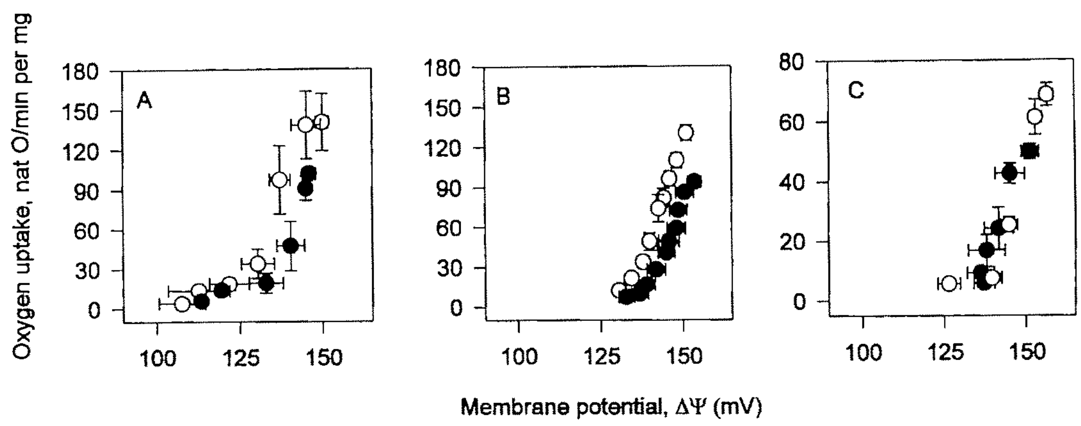

Figure 3 Kinetic response of the phosphorylation subsystem to changes in the membrane potential

Liver mitochondria oxidizing (**A**) TMPD (0.35 mM) plus ascorbate (10 mM), (**B**) succinate (10 mM) plus amytal (1 mM), (**C**) glutamate (5 mM) plus malate (5 mM) Control (○), ethanol-fed animals (●)

Titration with the inhibitor decreases respiratory rates and causes a decrease in ΔΨ. No significant differences were observed between mitochondria from ethanol-fed and control animals. Also, in State 4, the respiration rates were not significantly different between these preparations. Experiments in the presence of nigericin (1 μM), which equilibrates pH differences across the mitochondrial membrane in a K$^+$-containing medium, showed similar dependencies of J_L on the Δp, confirming that under our experimental conditions the effects of ΔpH can be neglected (results not shown). Also, addition of BSA (2 mg/ml) did not affect proton leak rates in these mitochondria, indicating that non-esterified fatty acids did not contribute to the proton leak in either preparation (results not shown). It should be noted that the mitochondrial isolation medium contained BSA in order to suppress possible differences between ethanol-fed and control animals due to endogenous fatty acids.

Phosphorylation subsystem analysis

Similar to the measurements of ΔΨ-dependence of the proton leak, inhibitors of the respiratory subsystem were used to determine the dependence of the phosphorylation flux on ΔΨ. In Figure 3, the flux through the phosphorylation subsystem was examined under State 3 conditions over a wide range of ΔΨ values. Results obtained with TMPD plus ascorbate (Figure 3A) and succinate (Figure 3B) as respiratory substrates were essentially similar, showing a significant inhibition of the phosphorylation subsystem in mitochondria from ethanol-fed animals over the entire range of ΔΨ values examined. In contrast, no inhibition was observed for mitochondria oxidizing glutamate plus malate at corresponding ΔΨ values (Figure 3C). The difference in sensitivity to chronic ethanol treatment is not unexpected and is related to different pathways of substrate oxidation. In mitochondria respiring on glutamate/malate, any substrate-linked phosphorylation associated with α-ketoglutarate oxidation contributes to overall ATP production. When this step is inhibited with arsenite, the ΔΨ dependence of phosphorylation resembles the findings with other substrates, showing the suppression of the ATP-producing subsystem after chronic ethanol treatment (results not shown). This suggests that substrate-linked phosphorylation can compensate to some extent for the defect in ATP synthase-mediated ATP production in ethanol-fed rats.

Table 2 Control coefficients of ΔΨ supply and ΔΨ demand processes over the respiration flux in State 3

	Control exerted by ΔΨ supply		Control exerted by ΔΨ demand	
Substrate	Control	Ethanol	Control	Ethanol
TMPD/ascorbate	0.68 ± 0.02	0.72 ± 0.09	0.32 ± 0.02	0.28 ± 0.09
Succinate/amytal	0.73 ± 0.08	0.67 ± 0.09	0.27 ± 0.08	0.33 ± 0.09
Glutamate/malate	0.48 ± 0.06	0.44 ± 0.03	0.52 ± 0.06	0.56 ± 0.03

Analysis of control parameters

We conceptually grouped the reactions of the phosphorylation subsystem and the proton leak into a single block of reactions consuming Δp. In this manner, the oxidative phosphorylation machinery is divided into two parts only: ΔΨ supply and ΔΨ demand processes. The control exerted by either of these two parts on mitochondrial respiration is quantified as the control coefficient of ΔΨ supply and ΔΨ demand processes, C_{supply} and C_{demand} respectively. The control coefficients are calculated from the elasticities, ϵ^{supply} and ϵ^{demand}, which are the normalized derivatives of the fluxes through the appropriate parts of the system with respect to ΔΨ [12]:

$$\epsilon^{supply} = \frac{\Delta\Psi}{J_R}\cdot\frac{\partial J_R}{\partial\Delta\Psi};\ \epsilon^{demand} = \frac{\Delta\Psi}{J_P+J_L}\cdot\frac{\partial(J_P+J_L)}{\partial\Delta\Psi}$$

These derivatives were determined from the kinetic dependencies shown in Figures 1–3 at ΔΨ values corresponding to State 3 respiration for each of the respiratory substrates examined. The control coefficients (C_{supply} and C_{demand}) of ΔΨ supply and ΔΨ demand processes were calculated as:

$$C_{supply} = \frac{\epsilon^{demand}}{\epsilon^{demand}-\epsilon^{supply}};\ C_{demand} = \frac{-\epsilon^{supply}}{\epsilon^{demand}-\epsilon^{supply}}$$

Table 2 demonstrates how control of State 3 respiration rate is distributed among the different subsystems generating and consuming Δp. In mitochondria from both control and ethanol-fed rats, the respiratory subsystem makes a predominant contribution to the flux control with TMPD/ascorbate (68 % and 72 % respectively) and with succinate/amytal (73 % and 67 % respectively), whereas it contributes only approx. 50 % when glutamate plus malate is used as substrate Remarkably, the State 3 control coefficients were not significantly different between preparations from control and ethanol-fed rats for any of these substrate conditions, despite the substantial inhibition of both the electron transport and the phosphorylation reactions, as reflected in the State 3 oxidation rates with all substrates. This finding suggests that the mitochondrial oxidative phosphorylation system may compensate for the inhibition of the electron transport components and the phosphorylation reactions to maintain a substrate-specific pattern of control distribution, despite the alterations in the enzymatic components that occurred after chronic ethanol consumption

DISCUSSION

The findings reported in this study illustrate how mitochondria adapt to simultaneous changes in multiple components of the energy conservation system following chronic ethanol consumption. Ethanol treatment causes tissue-specific changes in mitochondrial morphology and membrane physical properties, including effects on mitochondrial inner membrane phospholipids and alterations in the activity and kinetic properties of several mitochondrial enzymes (reviewed in [2,4]). Mitochondrially encoded subunits of electron-transport-chain complexes and ATP synthase are specifically affected, resulting in a decrease by 30–50 % in the activity of NADH dehydrogenase, cytochrome bc_1 complex, cytochrome oxidase and ATP synthase [1,6,24,26]. These changes in mitochondrial characteristics occur in liver over a period of 3–5 weeks of ethanol feeding by the Lieber–DeCarli protocol [14] and may be more extensive with other more invasive ethanol-feeding protocols. Despite detailed studies of the molecular basis of these changes in oxidative phosphorylation, the consequences for cellular energy metabolism have not been characterized. We employed top-down regulatory analysis to answer the question of how these changes in the activity of multiple inner-membrane components affect the overall pathway rates and the integrative control of the oxidative phosphorylation machinery in isolated mitochondria. Top-down control analysis not only characterizes changes in key bioenergetic parameters, but can also identify alterations in the regulatory characteristics of mitochondrial oxidative phosphorylation. Specifically, top-down analysis can distinguish how the kinetic consequences of the ethanol-induced changes in enzymic components are distributed between the mitochondrial respiratory subsystem, the proton leak, and the phosphorylation subsystem.

In agreement with previous studies that reported a decline in electron transport components [5,10,22–26], the rate of generation of Δp (the respiratory subsystem) with different substrates was inhibited after 2 months of ethanol consumption. With NAD^+-dependent substrates and TMPD/ascorbate a significant suppression of the respiratory subsystem was observed at all values of the mitochondrial membrane potential examined, with more pronounced inhibition in State 3 than State 4. Succinate oxidation was significantly suppressed in State 3 only, reflecting the predominant control of this pathway by succinate dehydrogenase, the activity of which is not affected by ethanol treatment [5]. Despite this decrease in the respiratory capacity, the response of the respiratory chain to changes in membrane potential (as reflected in the elasticity coefficient derived from the slope of the curves shown in Figures 1–3) was only modestly affected by ethanol treatment.

The Δp dependence of the proton leak rate did not differ in mitochondria from control and ethanol-fed rats for any of the substrate conditions studied. This finding suggests that the changes in phospholipids and membrane proteins that occur after 2 months of ethanol feeding did not affect the permeability of the mitochondrial membrane to protons. This conclusion conflicts with some earlier studies, but is in agreement with the data reported by Murphy and Tipton [29]. It is interesting to note that in other studies we found that longer term ethanol feeding (up to 18 months) may be associated with an enhanced proton leak rate, possibly due to the expression of uncoupling protein (results not shown).

Ethanol effects on the phosphorylation subsystem can be reliably determined using succinate or TMPD/ascorbate, since inhibitor titrations of succinate dehydrogenase or cytochrome oxidase do not affect the enzymes of the phosphorylation subsystem directly. The data obtained with mitochondria oxidizing either of these substrates demonstrated a suppression of the responses of the phosphorylation subsystem to $\Delta\Psi$ changes. We were unable to detect any significant inhibition of the phosphorylation subsystem in mitochondria oxidizing glutamate plus malate. However, the application of top-down analysis is more complicated for substrates such as glutamate plus malate, which involve the substrate-linked phosphorylation step of α-ketoglutarate dehydrogenase/succinate thiokinase, since an ATP-producing reaction appears both in the supply and demand blocks.

The distribution of control over the supply and demand processes is calculated from the elasticities of the phosphorylation and respiration subsystems. In State 3, mitochondria from ethanol-fed and pair-fed control rats did not show significant shifts in the distribution of control in favour of either the phosphorylation or respiration subsystem. (Table 2). The moderate changes that were observed, did not achieve statistical significance for any of the substrate conditions. This finding indicates that the control distribution in State 3 appeared relatively stable to substantial changes in the enzyme activities of both supply and demand blocks. Interestingly, this correlates with the findings of Brand and Kesseler [30], who showed that in potato tuber mitochondria, cadmium did not affect the control pattern at State 3 respiration, whereas it caused a progressive inhibition of the respiratory subsystem over the entire range of Δp between States 3 and 4.

How does the mitochondrial system at State 3 compensate for marked changes in activity of the enzyme systems of oxidative phosphorylation? Some insight can be obtained from a kinetic model of mitochondrial respiration published elsewhere [31,32]. This model implements all available kinetic knowledge concerning the individual enzymes and non-enzymic steps of the mitochondrial oxidative phosphorylation machinery. The estimated $\Delta\Psi$ dependency of the respiratory subsystem and the phosphorylation subsystem generated by this model accounts reasonably well for the experimentally observed traces shown in Figures 1–3 (see Figure 4, solid lines). Figure 4 illustrates a theoretical analysis of how the oxidative phosphorylation system would be affected by a decrease in the content of electron-transport-chain components and ATP synthase observed in the range of 36–41 % (Table 1) during oxidation of succinate/amytal (Figure 4, broken lines). It is evident that the response patterns obtained in the computational analysis qualitatively match the patterns obtained experimentally, both in 'normal' mitochondria and in the partly inhibited state. The kinetic model illustrates that the simultaneous depression of the supply and demand blocks found in ethanol-affected mitochondria did not change the mitochondrial membrane potential in State 3. Indeed, in

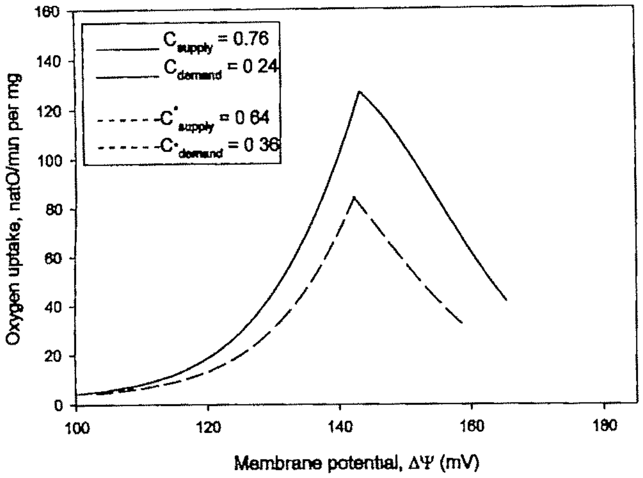

Figure 4 Simulated responses of the supply and demand blocks of oxidative phosphorylation to $\Delta\Psi$ changes in mitochondria with 'normal' and suppressed activities of electron transport chain and ATP synthase

Solid lines correspond to control mitochondria oxidizing succinate/amytal, and broken lines correspond to mitochondria with the ATP synthase activity inhibited by 36%, the bc_1 complex activity inhibited by 41% and the activity of cytochrome *c* oxidase inhibited by 40% The dotted extensions of the dashed lines illustrate how the response pattern would change if either ATP synthase or the electron transport chain activity were suppressed separately. The control coefficients of the supply block (the respiration subsystem) were 0 89 and 0 72 in control (C_{supply}) and inhibited (C^{*}_{supply}) mitochondria respectively The control coefficients of the demand block (which involves the proton leak and phosphorylation subsystem) are equal to one minus the control coefficients of the supply block

Figure 4 the points of intersections of the two solid lines (State 3 of normal mitochondria) and the two broken lines (State 3 of affected mitochondria) correspond to the same ΔΨ value of 141 mV. The dotted lines in Figure 4 illustrate the expected response patterns when only the ATP synthase or only the electron transport components are inhibited. The points of intersection of dotted and solid lines show that the State 3 membrane potential would change upwards if only the ATP synthase were inhibited by ethanol treatment, and downwards if only the respiratory chain were affected. As shown in Figure 4, the computed control coefficients appeared to be within the range of values observed experimentally, with a predominant fraction of the control being located in the respiratory subsystem. Inhibition of the activities of bc_1 complex, cytochrome oxidase and ATP synthase (Table 1) shifted the control away from the respiratory subsystem, towards the phosphorylation subsystem. However, the change in control distribution associated with the inhibited state was relatively modest, and would be difficult to identify experimentally.

How is it that the system requires so little compensation in control distribution for these marked changes in enzyme activity? We tried to answer this question using the model and calculating the control distribution, not only among the blocks of multiple reactions (as we did in our experiments), but also among the individual components within these blocks. In control mitochondria respiring on succinate/amytal at State 3, succinate dehydrogenase carries the major part (approx. 80%) of the control over respiration. The rest of the control is nearly equally distributed among the other components of the system: bc_1 complex, cytochrome oxidase, ATP synthase, adenine nucleotide translocator and proton leak. According to the data presented in Table 1, we calculated the control coefficients for each component in the system for mitochondria with suppressed cytochrome oxidase, bc_1 complex and ATP synthase activities. In this case, control shifted substantially from succinate dehydrogenase (now 30% of control) to bc_1 complex and cytochrome oxidase. However, the net control, exerted by the respiratory subsystem, remained almost the same, despite the substantial decrease in the activities of some of its components and the redistribution of the control within the subsystem. The conclusion from these theoretical observations is that, in chronic alcoholism, the suppressed capacities of some mitochondrial enzymes can cause a redistribution of the control among individual steps in the respiration pathway. However, ethanol-induced changes in control distriution are essentially undetectable in 'top-down' control analysis, where the number of reactions are conceptually grouped into complex blocks, and only the control distribution among these blocks is calculated. Thus compensation within each of the major blocks of oxidative phosophorylation can prevent the change in control distribution between these blocks.

Despite the lack of change in State 3 control distribution following chronic ethanol feeding, the compensations reflected in steady-state metabolite changes are likely to have important physiological ramifications, by making mitochondria much more susceptible to changes in energy demand. This may have significant implications for the performance of liver mitochondria from alcoholic animals under conditions of physiological stress, such as hypoxia or Ca^{2+} overload. This may account for an enhanced mitochondrial capacity to generate reactive oxygen intermediates, which is largely a reflection of steady-state levels of semiquinone [33]. Also, matrix ATP/ADP ratio may be more susceptible to stress. Interestingly, some reports have demonstrated that liver cells from ethanol-fed rats have a decreased capacity to maintain adequate ATP/ADP ratios under conditions of modest hypoxia, even though ATP levels can be maintained adequately under normal oxygen supply conditions [34]. Under these conditions it would be more difficult for mitochondria from ethanol-fed animals to maintain the necessary rates of ATP production in the liver. The impact of these defects may be further strengthened by the increased exposure to hypoxic conditions that occurs particularly in the pericentral zones in the liver *in vivo*, which may contribute to the liver damage associated with chronic ethanol consumption [35].

This work was supported by NIH grants AA11689, GM59570-01A1, AA01786, AA07215 and AA08714 O D thanks the Copernicus program for his support. We thank Professor J -P. Mazat (University Bordeaux II, France) for the bc_1 activity assay

REFERENCES

1 Cunningham, C C., Kouri, D. L , Beeker, K R and Spach, P I. (1989) Alcohol Clin Exp Res **13**, 58–65
2 Cunningham, C. C , Coleman, W B and Spach, P I (1990) Alcohol Alcohol. **25**, 127–136
3 Cunningham, C. C and Spach, P I. (1994) Alcohol Clin Exp Res **18**, 132–137
4 Hoek, J B (1994) Curr. Top. Bioenerg. **17**, 197–241
5 Bernstein, J D. and Penniall, R (1978) Biochem. Pharmacol. **27**, 2337–2342
6 Cederbaum, A I , Lieber, C. S and Rubin, E (1974) Arch Biochem. Biophys **165**, 560–569
7 Coleman, W B. and Cunningham, C C. (1991) Biochim Biophys Acta **1058**, 178–186
8 Cahill, A , Balo, D L , Ivester, P and Cunningham, C C (1996) Alcohol . Clin Exp Res. **20**, 1362–1367
9 Cardellach, F , Taraschi, T F , Ellingson, J S., Stubbs, C D , Rubin, E and Hoek, J B. (1991) Biochem J. **274**, 565–573
10 Thayer, W. S and Rottenberg, H (1992) Alcohol · Clin Exp Res **16**, 1–4
11 Quant, P. A (1993) Trends Biochem Sci **18**, 26–30
12 Brand, M D (1996) J. Theor. Biol. **182**, 351–360

13 Brown, G C, Hafner, R P and Brand, M. D (1990) Eur J Biochem **188**, 321–325
14 DeCarli, L M and Lieber, C S (1967) J Nutr **91**, 331–336
15 Thayer, W S and Rubin, E (1981) J Biol Chem. **256**, 6090–6097
16 Thayer, W S and Cummings, Jr, J J (1990) Biochim Biophys Acta **1016**, 333–338
17 Cederbaum, A I, Lieber, C. S, Toth, A, Beattie, D S and Rubin, E (1973) J Biol Chem **248**, 4977–4986
18 Bernstein, J. D. and Penniall, R (1978) Alcohol · Clin Exp Res. **2**, 301–310
19 Kholodenko, B., Zilinskiene, V, Borutaite, V, Ivanoviene, L, Toleikis, A and Praskevicius, A (1987) FEBS Lett **223**, 247–250
20 Brand, M D (1995) in Bioenergetics—A Practical Approach (Brown, G C. and Cooper, C E., eds), pp 39–62, Oxford University Press, Oxford, U K
21 Rottenberg, H, Robertson, D E and Rubin, E (1980) Lab. Invest **42**, 318–326
22 Schilling, R J and Reitz, R C (1980) Biochim Biophys. Acta **603**, 266–277
23 Thayer, W S (1987) Ann N Y Acad Sci **492**, 193–206
24 Thayer, W. S. and Rubin, E (1980) Adv Exp Med Biol **132**, 385–392
25 Thayer, W S, Ohnishi, T and Rubin, E (1980) Biochim Biophys Acta **591**, 22–36
26 Thayer, W S and Rubin, E (1979) J Biol Chem. **254**, 7717–7723
27 Brand, M D, Hafner, R P and Brown, G C (1988) Biochem J **255**, 535–539
28 Hafner, R P, Brown, G C and Brand, M D (1990) Eur J Biochem. **188**, 313–319
29 Murphy, M P and Tipton, K F (1992) Biochem Pharmacol **43**, 2663–2667
30 Brand, M. D and Kesseler, A (1995) Biochem Soc Trans **23**, 371–376
31 Kholodenko, B N and Ehrlich, L I (1985) Biophysics (Engl Transl) **30**, 911–919
32 Demin, O V, Kholodenko, B N and Skulachev, V P (1998) Mol Cell Biochem **184**, 21–33
33 Korshunov, S S, Skulachev, V P and Starkov, A A (1997) FEBS Lett **416**, 15–18
34 Spach, P I, Herbert, J S and Cunningham, C C (1991) Biochim Biophys Acta **1056**, 40–46
35 Arteel, G. E, Iimuro, Y, Yin, M, Raleigh, J A and Thurman, R G. (1997) Hepatology **25**, 920–926

Received 13 September 1999/7 April 2000, accepted 3 May 2000

Biochem. J. (2000) **349**, 527–537 (Printed in Great Britain)

Isolation and characterization of casein kinase I from *Dictyostelium discoideum*

Gema MORENO-BUENO, Carmela CALÉS, M. Margarita BEHRENS[1] and Margarita FERNÁNDEZ-RENART[2]
Instituto de Investigaciones Biomédicas 'Alberto Sols', UAM-CSIC, C/ Arturo Duperier 4, 28029 Madrid, Spain

---

In the present study, the molecular cloning and characterization of a 49-kDa form of casein kinase (CK)I from *Dictyostelium discoideum* is reported. The predicted amino acid sequence shares 70 % identity with the catalytic domain of the mammalian δ and ϵ isoforms, *Drosophila* CKIϵ and *Schizosaccharomyces pombe* Hhp1, and 63 % identity with Hrr25, a 57-kDa form of yeast CK involved in DNA repair. *D. discoideum* CKI (DdCKI) was expressed in vegetative asynchronous cells as well as in differentiated cells, as detected by Northern-blot analysis. The level of *DdCKI* expression did not change during the cell cycle. Antibodies raised against a truncated version of the protein recognized a 49-kDa protein from *D. discoideum* extracts. Protein expression paralleled the pattern found for the RNA. The expression of *DdCKI* in *Escherichia coli* resulted in an active enzyme that autophosphorylated and phosphorylated casein. Immunofluorescence assays showed that DdCKI was localized in the cytoplasm and nuclei of *Dictyostelium* cells. The lack of disruptants of the *CKI* gene suggests that this protein is essential for the vegetative growth of *D. discoideum*. Overexpression of *DdCKI* resulted in cells with increased resistance to hydroxyurea, suggesting a potential role for this kinase in DNA repair.

Key words: casein kinase, cDNA cloning, immunofluorescence, protein expression.

INTRODUCTION

Casein kinase (CK)I was among the first protein kinases to be described. It is an ubiquitous monomeric enzyme ranging in size from 25 to 55 kDa and is present in the plasma membrane, nuclei, cytoplasm and cytoskeleton of eukaryotic cells [1]. Once considered to represent a single entity, it is now known to comprise a family, which represents a distinct branch of the eukaryotic protein kinase. CKI homologues have been identified in organisms ranging from yeasts to humans [2]. All members of the CKI family contain a catalytic domain in the N-terminal portion of the protein. This domain structurally resembles that of other protein kinases. The main differences are observed in subdomain VIII, in which the common peptide triplet Ala-Pro-Glu is replaced by Ser-Ile/Val-Asn, and in subdomain XI, in which a normally invariant arginine residue is absent.

The substrate specificity is determined by acidic or phosphoryl groups located three to four residues upstream of the target residue. Some CKI isoforms can be classified as dual-specificity protein kinases, because they can phosphorylate tyrosine as well as serine or threonine residues [3,4]. Several CKI substrates have been identified, such as glycogen synthase, RNA polymerases I and II, p53, spectrin and NF-AT4, among others [2]. However, only in a few instances has phosphorylation by CKI been shown to correlate with changes in substrate function, such as in the case of the SV40 T antigen [5] or the NF-AT4 transcription factor [6].

CKI has been implicated in several aspects of cell regulation. In mammals it has been found associated with the adaptor protein Nck [7], and it can phosphorylate the 14-3-3 protein [8], suggesting a role in signal transduction. It has been shown recently, in *Xenopus* and *Caenorhabditis elegans*, that CKI is a component of the Wnt signaling pathway, which controls a variety of processes including cell growth and development [9]. A CKI gene (*Dbt*) has been cloned in *Drosophila* [10]. The DBT protein is essential for viability, and is involved in mantaining circadian rhythms. CKI homologues in budding and fission yeast may regulate aspects of cellular DNA metabolism and are involved in DNA repair [11,12]. *Saccharomyces cerevisiae* Hrr25 is involved in double-strand break repair, in sporulation and in the cell cycle, and it has also been shown recently to be involved in vesicle budding from the endoplasmic reticulum [13]. A pair of related CKI homologues, Hhp1 and Hhp2, play similar roles in DNA repair in *Schizosaccharomyces pombe*.

The *Sa. cerevisiae YCK1* and *YCK2* genes supply an activity essential for vegetative growth, and confer halotolerance when overexpressed [14], and *YCK2* also plays a role in cytokinesis [15]. Overexpression of *Cki2* in *Sch. pombe* leads to a severe growth defect and aberrant morphology [16]. Ultraviolet irradiation of early *Drosophila* embryos relocalizes CKI to the interphase nucleus, suggesting a possible requirement for this enzyme in mechanisms associated with DNA repair [17].

Dictyostelium discoideum is a simple eukaryote that shows, in the course of its life cycle, a period of cell differentiation and morphogenesis, which makes it an attractive system for addressing a wide variety of biological problems.

In this organism, development is triggered by the removal of the food source from vegetatively growing amoebae. Cells thereupon aggregate to form a multicellular mound, by means of chemotaxis to pulsatile cAMP signals acting through cell-surface

---

Abbreviations used: Bsr, blasticidin; CK, casein kinase; DdCKI, casein kinase I gene and gene products from *Dictyostelium discoideum*; IPTG, isopropyl-β-D-thiogalactoside; K38R, CKI mutation in which the lysine-38 residue is substituted with arginine.

[1] Present address: Department of Neurology and Center for the Study of the Nervous System Injury, Washington University School of Medicine, St. Louis, MO 63110, U.S.A.

[2] To whom correspondence should be addressed (e-mail mfernandez@mvax.fmed.uam.es).

The nucleotide sequence data reported will appear in DDBJ, EMBL and GenBank Nucleotide Sequence Databases under the accession number AF003547.

receptors [18]. cAMP is also involved in the expression of genes essential for aggregation, entry into the morphogenetic stage, pre-spore cell differentiation and culmination [19] Cellular differentiation ultimately gives rise to the spore and stalk cells of the fruiting body. All the internal cAMP responses are mediated by cAMP-dependent protein kinase [20].

In *D. discoideum*, the unique *CKII* gene has been shown to be essential for vegetative growth [21]. This CKII, unlike its higher eukaryotic counterparts, lacks the β subunit [21,22] Several CKI activities have been characterized on the basis of their biochemical and chromatographic properties [23]

In the present report we describe the isolation and characterization of a *CKI* gene from *D. discoideum* (*DdCKI*), the analysis of its expression in the life cycle of the organism, its intracellular localization and its genetic analysis.

MATERIALS AND METHODS

Growth and development of *D. discoideum*

AX-2 cells were cultured in exponentially modified HL-5 medium (peptone was substituted for tryptone) [24], and differentiated on nitrocellulose filters in Mes/PDF buffer (20 mM KCl, 1.2 mM MgSO$_4$, 7.5 mM Mes, pH 6.5).

For the developmental time-course assays, cells were plated on to sterile 4.5-cm diam. plates (0.5×10^8–1×10^8 cells/plate). At different time points, the cells were rapidly scraped from the plate and frozen in liquid N$_2$ until further use Synchronization experiments were performed as described previously [25].

Plating assay for sensitivity to DNA-damaging agents

For viability assays, 2×10^6 cells/ml were cultured for 20 h in modified HL-5 medium with 100 or 200 mM hydroxyurea (Sigma) or 100 μM cisplatin (*cis*-diamine-dichloroplatinum II) (Sigma). Control cells were kept for a similar time without the addition of drugs. In all treatments, a volume, equivalent to 350 cells of untreated control cells, was plated on to SM plates with a lawn of *Klebsiella aerogenes* to determine viability. The surviving colonies were monitored after three or four days. The percentage of viability was calculated as the number of colonies obtained following the various treatments compared with the number of control cells.

D. discoideum extracts and S-Sepharose chromatography

For Western-blot experiments, *Dictyostelium* cells were lysed by sonication (vegetative or early differentiated cells) or with glass beads (late differentiated cells) in a buffer containing 50 mM Tris/HCl (pH 7.5), 300 mM NaCl, 5 mM EDTA, 40 mM sodium pyrophosphate, 30 % (w/v) sucrose, 0.5 mg/ml leupeptin, 50 μg/ml aprotinin, 0.1 mM tosyl-lysylchloromethane (‘TLCK’) and 0.1 mM Na$_3$VO$_4$.

Cytosolic extracts, prepared in the same buffer without NaCl, were applied to an S-Sepharose (5 ml) column equilibrated in 50 mM Tris/HCl (pH 7.5), 2 mM EDTA, 5 mM 2-mercaptoethanol, 10 mM sodium pyrophosphate, 20 % (v/v) glycerol and 10 mM NaF After washing with 10 volumes of equilibration buffer, the bound proteins were eluted with a linear gradient of 0–1 M NaCl, and 10 μl aliquots from each fraction were assayed for casein kinase activity using casein as substrate. Nuclei were prepared as described previously [26].

Southern- and Northern-blot hybridization analysis

Southern- and Northern-blot hybridization were done using standard protocols [27]. Hybridization was performed at high stringency in buffer containing 50 % (v/v) formamide at 42 °C, or at 37 °C for low stringency conditions. DNA was obtained from vegetative cells as described in [28], and 1 μg was digested with various restriction enzymes, resolved on a 0.7 % (w/v) agarose gel and transferred to a nylon membrane for hybridization.

For Northern-blot analysis, total RNA from vegetative and differentiated cells was isolated by the method of Chomczynski et al. [29]. Poly(A)$^+$ mRNA was obtained as in [30] For reverse transcription-PCR, total RNA was prepared using Trizol (Gibco BRL), following the manufacturer's conditions.

Molecular cloning of *DdCKI*

PCR primers were designed using the yeast Yck2 sequence as a guide A forward primer (5′ CAACATATTCCGTACAGGGGA) and a reverse primer (5′ ATCGTCTCTTCTGGATTGTTC) were used to amplify a 99-bp fragment from yeast genomic DNA. This PCR product was sequenced and used as a probe to screen a *Dictyostelium* cDNA library from 4-h differentiated cells cloned in λgt11 (Clontech). Recombinant phages (160000) were screened, in duplicate, with the yeast probe labelled with random primers and [α-^{32}P]dATP (5000 Ci/mmol), Amersham). Hybridization was done under low stringency conditions, and positive clones were plaque purified. One of the positive clones (clone 1) was isolated and subcloned in pUC19. This clone contained a 1200-bp insert with a single open reading frame and a missing 5′ initiation codon. The 5′ initiation site was found by rescreening the cDNA library under stringent conditions using clone 1 cDNA as a probe (clone 2).

To obtain the complete gene (*pBS-CKI*), the *Eco*RI/*Pst*I fragment of clone 1 was replaced with the same fragment of clone 2 (the *Pst*I site in the clone 1 polylinker was previously eliminated by cutting, filling and ligation).

Recombinant DdCKI constructs

Three different constructs were obtained. First, in the pRSETc (Invitrogen) vector to express recombinant *CKI* in bacteria. For this construct, a *Pvu*II site was engineered to clone the complete CKI coding region in-frame with the His$_6$ tag present in the vector. Secondly, a fusion with the maltose binding protein, to obtain antibodies against CKI. This construct was made with an *Eco*RI/*Hin*dIII fragment of the *CKI* gene. Thirdly, a construct to express the *CKI* gene constitutively under the Act-15 *D. discoideum* promoter. We used the pDXA-HC vector [31] that gives protein tagged with the c-myc epitope in the C-terminus. The *CKI* gene was amplified with primers (sense, 5′ ACGTGGTACCGATTTAAGAATTGGTGG, and antisense, 5′ AACACAACAAGGCCACCAGCAAAGACTCGAGATCGG) in order to create *Kpn*I and *Xho*I sites repectively (underlined) to clone into the corresponding sites of the pDXA-HC vector. Finally, for gene replacement, the 1.4-kb blasticidin (Bsr)S cassette, obtained by digestion of pBsrS 2 [32] with *Sma*I and *Hin*dIII, was shunted and inserted into the *Nco*I site of the *CKI* gene. The 2.7 kb fragment of *DdCKI* harbouring the BsrS cassette was excised with *Eco*RI and used to transform *D. discoideum* cells.

D. discoideum transformation

Transformation was performed by electroporation, using 20–30 μg of the final constructs. Transformants were selected at 5 μg/ml G418 or 5 μg/ml BsrS, according to the construct used. Colonies became visible after about 15 days. The resistant clones were plated on to a lawn of *K. aerogenes* grown on SM nutrient agar plates. The plates were incubated at 23 °C, and individual colonies were removed, grown in a HL5 medium with 10 μg/ml G418 or 10 μg/ml BsrS and analysed.

Purification of His$_6$-tagged CKI

Wild-type *Dictyostelium* cells or cells expressing His$_6$–CK1 were cultured in modified HL5 medium and harvested at 4×10^6 cells/ml. After washing once with cold PBS, the cells were resuspended in lysis buffer A [20 mM Hepes (pH 7.5), 10 mM 2-glycerophosphate, 5 mM 2-mercaptoethanol, 1 mM Na_3VO_4, 20 mM imidazole, 0.1 % (v/v) Triton X-100] with 40 μg/ml aprotinin, 50 μg/ml leupeptin and 1 mM tosyl-lysylchloromethane. The cell extracts were centrifuged at 100000 *g* for 30 min at 4 °C. Equal amount of protein from the supernatants were loaded on to Ni^{2+}–agarose columns (2 ml) equilibrated with lysis buffer. After washing with 10 column volumes of the same buffer, the bound protein was eluted step-wise with 150 mM and 300 mM imidazole in the same buffer without Triton. The eluted fractions were used for Western-blotting and CK assays *in vitro*.

Purification of *CKI expressed* in bacteria

Escherichia coli strain BL21(DE3) was transformed with the pRSETc construct. A single colony was removed and grown at 30 °C to a D_{600} of 0.8. Isopropyl-β-D-thiogalactoside (IPTG) was added to 0.4 mM, and the cells were incubated for 1 h at 37 °C. The induced cells were harvested, washed and resuspended in 5 vol. of lysis buffer B [20 mM Tris/HCl (pH 7.9), 0.5 M NaCl, 10 % (v/v) glycerol, 5 mM imidazole) containing 1 mM PMSF and 25 μg/ml each of leupeptin, pepstatin and aprotinin. The cell suspension was sonicated and the resulting lysate was cleared by centrifugation at 15000 *g* for 20 min. The supernatant was loaded on to a 1 ml Ni^{2+}–agarose column pre-equilibrated in lysis buffer B containing 0.05 % (v/v) Nonidet P-40. The column was washed with 15 vol of the same buffer, and the proteins were eluted with sequential 5 ml volumes of lysis buffer B containing 0.02 % (v/v) Nonidet P-40 and 50, 100, 200 or 500 mM imidazole. The fractions collected were analysed for protein by Western-blotting and protein kinase activity.

Production of antibodies against CKI

E. coli strain TG1 was transformed with pMal-NCKI. Cells containing the pMal-NCK1 plasmid were grown at 37 °C to a D_{600} of 0.4–0.6. IPTG was added to 0.3 mM and the cells were incubated for 3 h. The induced cells were harvested, washed and resuspended in 5 vol of 10 mM Tris/HCl, pH 8, 200 mM NaCl, 1 mM EDTA, 1 mM dithiothreitol, with 10 mM NaF and 25 μg/ml each of leupeptin and aprotinin. The cell suspension was sonicated and the resulting lysate was cleared by centrifugation at 15000 *g* for 20 min. The recombinant protein was purified from the *E. coli* extracts by chromatography on an amylose column using standard protocols. To generate antibodies against DdCKI, rabbits were immunized with the purified maltose-binding-protein fusion protein, which had been excised and extracted from an SDS/polyacrylamide gel.

CK assays

Two different assays were used to measure CKI activity. In some assays p-81 paper was used to measure the ^{32}P-label incorporated into casein [23], and in others the radioactivity incorporated into casein was monitored by SDS/PAGE and autoradiography of the gels. The assay was performed in a final volume of 30 μl containing 50 mM Tris/HCl (pH 7.4), 10 mM $MgCl_2$, 0.2 mM Na_3VO_4, 2–20 μM [γ-^{32}P]ATP (800–1000 c.p.m./pmol), 10 mg/ml casein and 10–30 μg of the protein fraction to be assayed.

Immunofluorescence analysis

For staining intact cells, the following procedure was used. Cells (10^5) growing in modified HL-5 medium were spotted on to coverslips, which had been pre-treated with gelatin, and were centrifuged at 2000 *g* for 10 min in a Cyto-spin centrifuge. The harvested cells were washed once in PBS and fixed in 3.7 % (v/v) paraformaldehyde in PBS for 15 min, followed by incubation in 5 mM NH_4Cl in PBS for 5 min. After washing with PBS and permeabilization with 0.2 % (v/v) Triton for 8 min, the cells were washed once in PBS and blocked with 5 % (v/v) fetal-calf serum in PBS for 30 min The coverslips were then incubated with affinity-purified CKI antibody in PBS for 1 h at room temperature A pre-immune serum was used as a control. The coverslips were washed five times (10 min each) with PBS and then incubated for 1 h at room temperature with a fresh 1:200 dilution of Rhodamine-labelled goat anti-rabbit IgG (Dianova). Coverslips were washed as above and mounted in Mowiol. Some samples were stained with 0.1 μg/ml 4,6-diamidino-2-phenylindole ('DAPI') in PBS for 2–5 min.

Immunoblotting

Purified fusion proteins or 10–50 μg of protein from bacterial or *Dictyostelium* extracts were subjected to SDS/PAGE (10–12 % gels) and transferred to Immobilon filters (Millipore) in 12.5 mM Tris/HCl (pH 8.5), 86 mM glycine and 15 % methanol. Membranes were blocked in Tris-buffered saline containing 0.05 % (v/v) Tween-20 and 5 % (w/v) non-fat dried milk or, for the His$_6$tagged proteins, 3 % (w/v) BSA. Primary and secondary antibodies were diluted in the same buffer. Bound antibodies were detected by enhanced chemiluminescence according to the manufacturer's instructions (Amersham).

RESULTS

Characterization of a *D. discoideum* CK

The screening of a *D. discoideum* cDNA library with a 99-bp PCR product obtained from yeast yielded one positive clone. The cDNA insert of this clone (clone 1) was sequenced completely. Clone 1 represented a cDNA that encodes a sequence with high similarity to higher eukaryotes and yeast CKI, and did not contain the initiation site. The cDNA of clone 1 was used as probe to rescreen the cDNA library. Several additional clones were isolated, and three of them were analysed (clones 2, 3 and 4). The lengths of the clones were 1122, 1152 and 1140 nt respectively.

Clone 2 was truncated at the 3′ end and contained the initiation site, 84 nt of 5′-untranslated sequence and 1012 nt overlapping the sequence of clone 1. Clone 3 was also 3′ truncated and contained the initiation site, 26 nt of untranslated sequence and 1104 nt overlapping the sequence of clone 1 and clone 4 which was 5′ truncated. The complete coding sequence (pBS-CKI) was obtained as described in the Materials and methods section.

The putative ATG initiation codon lies within a translation initiation consensus sequence defined by Kozak [33], and it is immediately preceded by a stop codon in the same reading frame. Moreover, the predicted start site is consistent with that of other *CKI* isoforms. The stop codon present in the cDNA of clones 1 and 4 includes the first nucleotide of the *Eco*RI cloning

```
                10        20        30        40        50        60        70        80        90       100
                 |         |         |         |         |         |         |         |         |         |
DdCk1    M—DLRIGGKYRISRKIGGGSFGEIYLGTNISTNEEVAIKLEPAKAIHPQLLFESKLYKIFQGGIGIPAVKWFGFDGDYNIMVMDILGPSLEDIFNYCGR
hCKIε    .—E.V.N...LG...S....D...A..ASG.......CV.TK....HI...F..MM...V...SI..C.AE...V...E...........F.S.
hCKIδ    .—E.V.NR.LG...S....D....D.AAG.......CV.TK....HI...I..MM...V...TIR.C.AE...V...E...........F.S.
dDBT     .—E.V.N...LG...S....D....T.NPG.......CIRTK....HI...F..TM.......RII.C.SE...V...E...........F.S.
yHhp1    .AL.....N....G...S....D.....VVSG.......STRAK....EY.YRV.R.LS..V...FVR...VEC...A..............F.N.
yHhp2    .TV.IK.N....G...S....Q...L.TVNG.Q..V.....L..R.H...EY.FRV.N.LK.N....TIR...VTNS..A..............CY...
yHrr25   .—...V.R.F..G...S....D..H...LISG.......SIRSR....DY..RV.RYLS..V...FIR...REGE..A..I...........Y.H.

               110       120       130       140       150       160       170       180       190       200
                 |         |         |         |         |         |         |         |         |         |
DdCk1    KFSIKTVIMIGDQMLRRIEFIHSNNFIHRDIKPDNFLMGIGKRGHWNLIDFGIAKRYRDPKTHQHIPYR.HKNLTGTARYASINTHQGIEQSRRDDLES
hCKIε    .......L.A...IS...Y...K.....V.........L..K.NL.YI......K...AR.........N...........I...L............
hCKIδ    .......L.A...IS...Y...K.....V.........L..K.NL.YI......K...AR.........N...........I...L............
dDBT     R......L.A...IS..DY...RD...............L..K.NL.YI......KF..ARSIK......N...........I...L............
yHhp1    .......L.A..LIS.......KS.L..................NQ..I......KI..H...L......N...........I...L............
yHhp2    ..T....L.A..LIS...YV..KS.L............—-K.HSNV.TM......K...F...V....DN...........I...I............
yHrr25   R..F...I..AL..FC..QY..GRS..............V.R..ST.HV.....S.K...FN..R......N.S.........V...L............

               210       220       230       240       250       260       270       280       290
                 |         |         |         |         |         |         |         |         |
DdCk1    LGLVLMYFNRGSLPWQGLKAYTKRDRYEKICDKKAQTKIDTLCQGFPSEEATFINYTRFLKFEDKPDFLYLRKLLREMFVREGYRYDYMFDW
hCKIε    ..Y......L.........A...Q...R.SE..MS.P.EV..K.Y....S.Y...FC.S.R.D....YS...Q.F.NL.H.Q.FS...V...
hCKIδ    ..Y......L.........A...Q...R.SE..MS.P.EV..K.Y......Y...FC.S.R.D....YS...Q-F.NL.H.Q.FS...V...
dDBT     ..Y......L.A.......AN..Q...R.SE..LS.S.W...K......VNY...FC.QMH.DQR...YCH..K.F.NL.H.L.FT...V...
yHhp1    ..Y..V..CR.........T...KQ.....ME..IS.PTEV..R...Q..SIY......S.R.D....YA....K.F.DL.C.QS.EF......
yHhp2    ..Y..L..CR.......Q.D...EQ...QR.R.T.IG.PLEV..K.L.E..I.YMC....Q.S.TE..NYA....K.F.DLLI.K..Q...V...
yHrr25   ..Y..I..CK.........T...KQ...DR.ME..LNVSVE...S.L.L..QEYMA.CRN....DE...YLF.AR.FKDLSIKLE.HN.HL...
```

Figure 1 Alignment of *D. discoideum* CKI sequences

Comparison of the primary structure of the kinase domains of *D discoideum* (DdCk1), human (h) CKIε and CKIδ, yeast (y) kinases Hrr25, Hhp1 and Hhp2, and *Drosophila* CKIε (dDBT) Residues that are identical for all members of the CKI family are indicated with dots

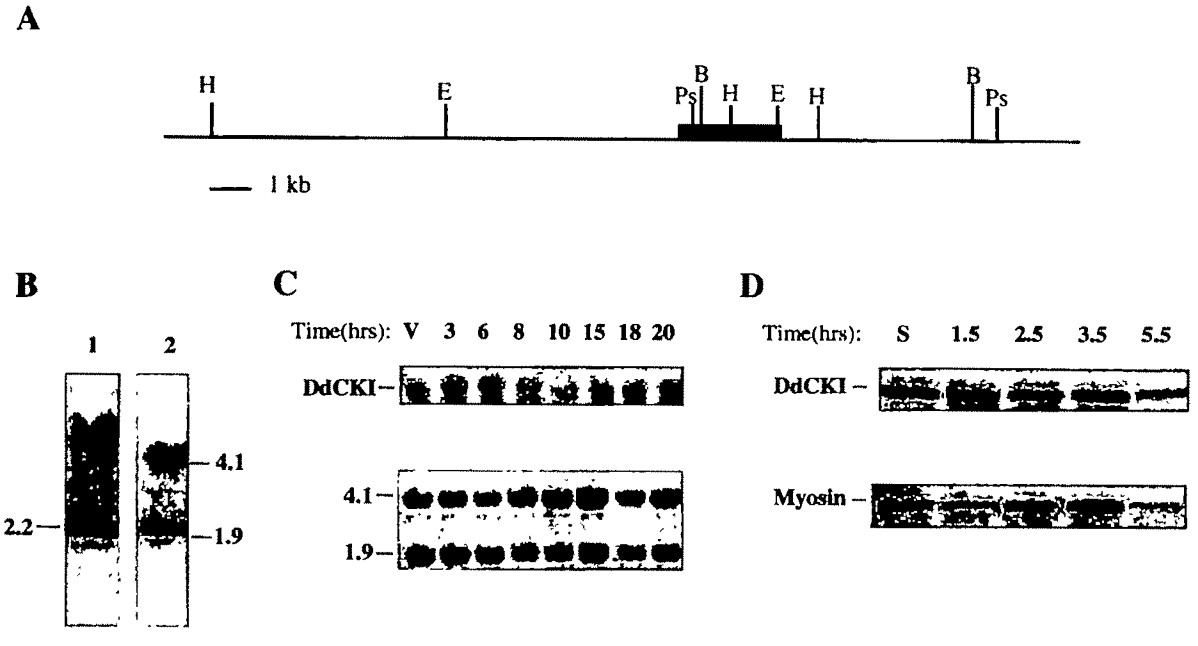

Figure 2 Southern- and Northern-blot analysis of DdCKI at different developmental stages

(**A**) Map of the *DdCKI* gene Genomic DNA was digested with *Eco*RI (E), *Hin*dIII (H), *Pst*I (Ps), and *Bgl*II (B) (**B**) Total RNA (30 μg, lane 1) or poly (A)$^+$ RNA (5 μg, lane 2) from 4 h-differentiated cells were resolved on an agarose/formaldehyde gel, transferred to a nylon membrane and probed with the insert of clone 1 labelled by random priming (**C**) Top panel total RNA (6 μg/lane) was prepared from samples taken at various times after cell starvation V, vegetative cells Bottom panel rRNA is shown as an indicator of gel loading (**D**) Top panel Poly(A)$^+$ RNA (5 μg/lane) was prepared from cells synchronized by the stationary phase release method Aliquots of cells were taken after resuspension in fresh medium for the indicated time periods S, stationary cells Bottom panel the same filter hybridized with a myosin probe as an indicator of gel loading

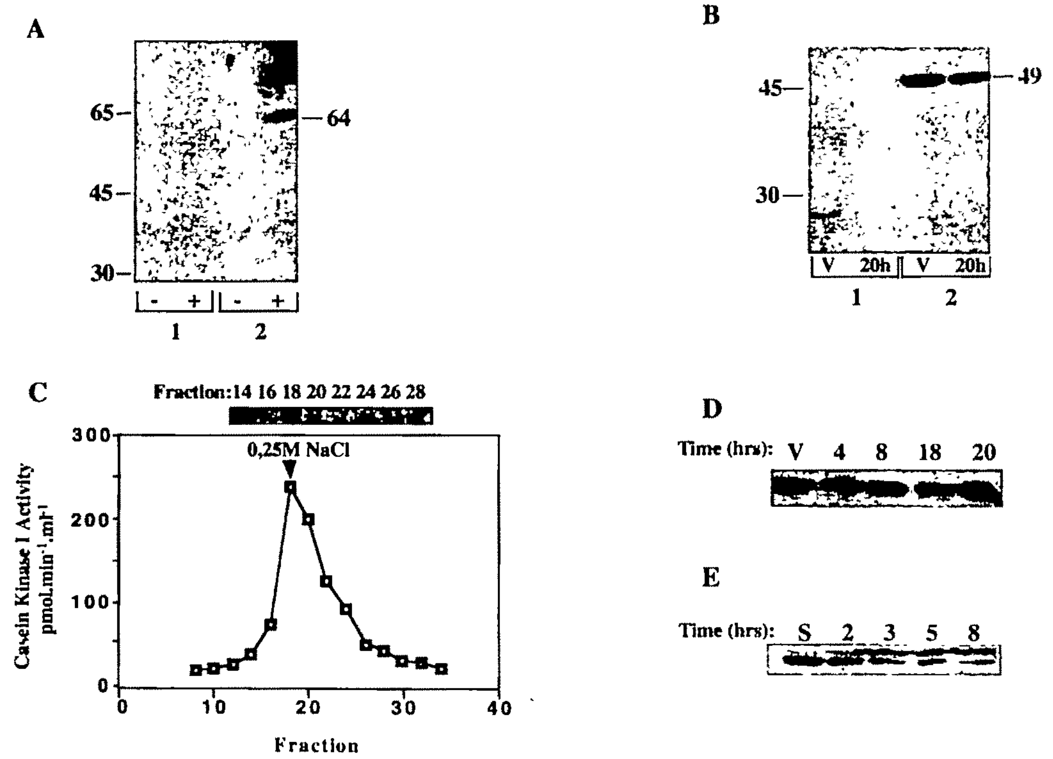

Figure 3 Immunoblot analysis of CKI

(**A**) pMal-CKI was grown in *E coli* strain TG1 and the cells were induced with IPTG (+) or left untreated (—) Cell extracts, purified by amylose chromatography, were resolved on SDS/PAGE (10% gel) and the proteins were transferred to Immobilon membranes and incubated with preimmune (1) or immune (2) serum produced against recombinant CKI Molecular mass markers (in kDa) are shown on the left, and the mass of the recombinant protein detected by the antibody is shown on the right (**B**) Soluble *Dictyostelium* extracts (5 μg), prepared as described in the Materials and methods section were resolved on SDS/PAGE (10% gel), and a Western blot analysis was performed as described for (**A**), 1, preimmune serum, 2, immune serum (**C**) CK activity assay in fractions eluted from S-Sepharose, performed as indicated in the Materials and methods section The upper part of the Figure shows a Western blot of the various fractions, using the DdCKI antibody (**D**) Soluble *Dictyostelium* extracts (10 μg) from cells differentiated for 4, 8, 18 or 20 h were used for Western-blot analysis as in (**A**) V, vegetative asynchronously growing cells (**E**) Soluble *Dictyostelium* extracts (10 μg) from synchronized vegetative cells were used for Western-blot analysis as described above S, stationary cells Time (hrs), time after resuspension in fresh axenic medium at which the samples were removed

site. Translation of the complete 1284 nt open reading frame predicts a 426-amino-acid polypeptide with a molecular mass of 48800. The predicted polypeptide has a calculated pI of 9.7.

The DdCKI contained the 12 conserved subdomains of protein kinases described by Hanks et al. [34] The N-terminal 300 amino acids of DdCKI show more than 50% identity with other CKI family members (Figure 1) The greatest similarity, when the catalytic domains are compared, has been found in *Drosophila* CKI ϵ (70%), human CKI ϵ and δ (71%) and yeast Hhp1 (65%).

The hydrophilic segment, located downstream of the catalytic domain, was difficult to align and corresponded to a poorly conserved region among the different family members. The DdCKI C-terminal region was extremely rich in glutamine, as is the case of yeast Yck1 and Yck2 and Hhp1 However, stretches of glutamine and asparagine are very frequent in *D. discoideum* proteins [35].

Analysis of the *DdCKI* gene

Southern-blot analysis, performed using the cDNA of clone 1 as probe under stringent conditions, gave single bands, suggesting that a single gene encodes *DdCKI* Only when the hybridization was performed at low stringency conditions were several bands observed, which may correspond to other related genes in *Dictyostelium* (results not shown). A physical map of the gene has been constructed using genomic DNA and a combination of restriction enzymes (Figure 2A). The enzymes selected did not excise or excised only once within the cDNA sequence As can be seen in Figure 2(B), the results obtained from the Southern-blot analysis indicate the presence of an *Eco*RI site at the end of the coding region.

Analysis of DdCKI mRNA expression

DdCKI expression was analysed with total or poly(A)$^+$ RNA from the different developmental stages of *D. discoideum*, using the cDNA of clone 1 as a probe. As shown in Figure 2(B), there was a major message at 2.2 kb. The expression level of the mRNA did not change during the developmental programme (Figure 2C).

To determine if the DdCKI mRNA levels were regulated in the different phases of the cell cycle, synchronized cells were used. As shown in Figure 2(D), there were no significant changes in DdCKI mRNA expression during the cell cycle.

Antibody to DdCKI recognizes a 49-kDa *D. discoideum* protein

In Western-blot assays the polyclonal antibody raised against the N-terminal fragment of DdCKI recognized the recombinant

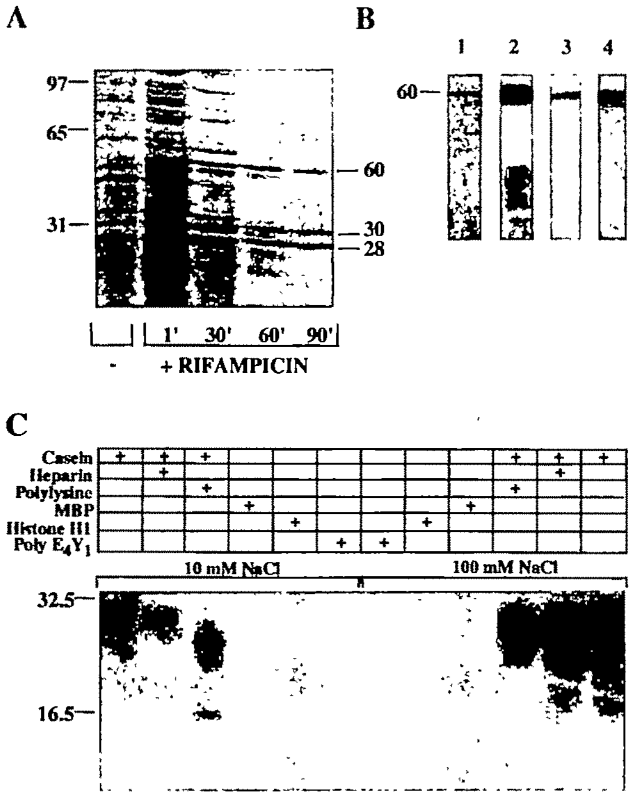

Figure 4 Expression and activity assay of DdCKI

(**A**) *E. coli* BL21(DE3) containing plasmid pLys was transformed with the expression vector pRSETc-CKI, as described in the Materials and methods section. After induction for 1 h with IPTG, cells were treated with 0.1 mg/ml rifampicin for the indicated time periods and labelled with 0.5 μCi of [^{35}S]methionine (Amersham) for 5 min. The cells were pelleted by centrifugation, lysed in sample buffer and analysed by SDS/PAGE and autoradiography. Molecular-mass markers (in kDa) are shown on the left, the molecular masses of the recombinant protein and of the major degradation products are shown on the right. (**B**) Recombinant DdCKI containing the His$_6$ tag was produced purified with Ni^{2+}–agarose chromatography, as described in the Materials and methods section, and prepared for SDS/PAGE and Western blotting. 1, Coomassie Blue staining of SDS/polyacrylamide gel, 2, immunoblot of sample 1 probed with anti-His$_6$-tag antibody, 3, immunoblot of sample 1 probed with anti-CKI antibody; 4, autoradiogram of sample 1 incubated in the presence of Mg^{2+} and [γ-^{32}P]ATP. (**C**) Phosphorylation of casein by DdCKI. Recombinant purified CKI was incubated with [γ-^{32}P]ATP with 5 μg of each putative protein substrate in kinase assay buffer. MBP, myelin basic protein. The phosphorylated proteins were resolved by SDS/PAGE (14% gel) and analysed by autoradiography.

protein induced and purified from bacteria as a maltose-binding-protein fusion (Figure 3A). This antibody also recognized a 49-kDa protein band in *Dictyostelium* extracts present in vegetative cells as well as in late differentiated cells (Figure 3B). Moreover, when *Dictyostelium* protein extracts were separated on S-Sepharose, the CK activity eluting at 0.25 M NaCl co-migrated with the 49-kDa band (Figure 3C).

Changes in protein levels during differentiation were not detected (Figure 3D). The protein level profile obtained for synchronized cells showed a slight decrease in the amount of protein after duplication of the cell numbers (Figure 3E).

Expression of *DdCKI* in *E. coli*

It appears that the CKI enzymes may interfere with bacterial cellular functions, as it was difficult to achieve high levels of *DdCKI* expression. Two different induction temperatures, 25 °C and 37 °C, were used and no differences in expression were found with either. Short inductions were performed, because the protein was proteolysed at longer induction times, giving rise to several defined proteolytic products (Figure 4A).

The high degree of similarity between *DdCKI* and other *CKI* isoforms strongly suggested that *DdCKI* encoded a CKI. To confirm this, a recombinant protein with a His$_6$ tag was obtained, as described in the Materials and methods section. After IPTG induction, affinity-purified extracts of cells carrying the DdCKI construct contained a 60-kDa protein that reacted with the His$_6$-tag antibody and with the anti-DdCKI antibody (Figure 4B).

When the purified recombinant DdCKI protein was incubated in the presence of [γ-^{32}P]ATP, the protein band identified by the CKI antibody appeared to be phosphorylated (Figure 4B). We then tested several CKI substrates (Figure 4C), and it was found that DdCKI phosphorylated casein but not myelin basic protein or histone, as was expected. Phosphorylation of the tyrosine-containing polymer poly-E$_4$Y$_1$ was not detected. The effect of heparin and polylysine, with casein as substrate, was tested in different experimental conditions. The effect of these two polycations varied depending on the NaCl concentration in the assay, when the NaCl concentration was high (0.1 M), heparin and polylysine behaved as slight activators, but when low (10 mM) NaCl concentrations were used, heparin inhibited CKI activity and polylysine modified the specificity of CKI for phosphorylation of different casein subunits.

Localization of DdCKI by immunofluorescence

Affinity-purified CKI antibodies were used to study the intracellular distribution of DdCKI in vegetative *D. discoideum* cells. The labelling specificity was confirmed in experiments where immunofluorescent staining was performed with a pre-immune serum. Cells treated with secondary antibodies alone showed no staining (results not shown). As shown in Figure 5 both cytoplasm and nucleus were stained by the antibodies, indicating that DdCKI is localized in both cellular compartments.

Genetic analysis of DdCKI function

The gene-expression data suggest that the CKI protein might be involved in different processes throughout the life cycle of *Dictyostelium*. We have attempted to determine the function of the gene in *Dictyostelium* by either disrupting or over-expressing the *CKI* gene.

To create a null strain for *CKI*, *Dictyostelium* cells were transfected with a gene replacement vector containing a BsrS cassette, as described in the Materials and methods section. Several attempts to obtain blasticidine-resistant clones with the *CKI* gene disrupted were unsuccessful.

In two independent experiments, seven blasticidine-resistant clones were obtained, and no homologous recombination was found when analysed by Southern blotting and PCR. Southern-blot analysis of one blasticidine-resistant clone (Figure 6A), showed that all the bands corresponding to the *CKI* wild-type gene were present (marked with crosses), indicating that the blasticidine-cassette containing construct had been inserted at different places of the genome. As can be seen in Figure 6(B), the clones obtained expressed the blasticidine-resistance gene, as well as the endogenous *CKI* gene.

A different strategy was adopted to study *CKI* gene function. The complete coding region of *CKI* downstream of the actin promoter was cloned, using the pDXA-HC vector. A similar construct was also used with the mutation Lys^{38} → Arg (K38R).

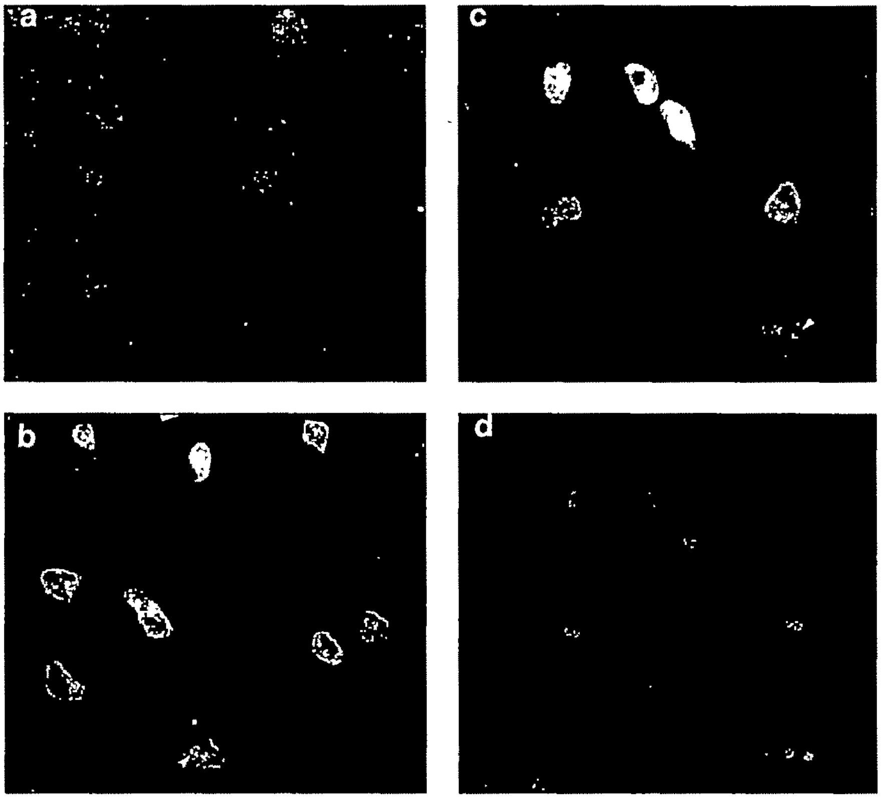

Figure 5 Immunolocalization of DdCKI in untransformed (AX-2) cells

Asynchronous cells were prepared as described in the Materials and methods section. (**a**) Cells stained with preimmune serum, (**b**) cells stained only with affinity-purified anti-CKI antibody; (**c**) cells stained with affinity-purified anti-CKI antibody; (**d**) the same field of cells as in (**c**) stained with 4,6-diamidino-2-phenylindole The arrowheads indicate the cells that show nuclear staining for CKI Magnification × 63

Lysine-38 is required for activity in other members of the CKI family, and has been shown to act as a dominant-negative form of the protein.

Cells resistant to G418 were selected, as described in the Materials and methods section. In order to check that the transfected constructs were expressed in the G418-resistant cells, total RNA was prepared and reverse transcription-PCR was performed. For the PCR, a sense oligonucleotide designed according to the CKI sequence, and an antisense oligonucleotide designed according to the vector sequence was used. Several clones expressed the construct containing the wild-type sequence, but none was obtained containing the K38R mutation after two independent transfection experiments (results not shown). The clones containing the wild-type cDNA of CKI were verified by Northern-blot analysis using cDNA of CKI as a probe (Figure 7A).

In order to analyse if a functional protein was being produced, cytoplasmic extracts were made from vegetative growing untransformed cells and cells containing clone 4 expressing the His_6-CKI–Myc tagged protein. Extracts containing an equal amount of protein were separated on Ni^{2+}–agarose, as described in the Materials and methods section. The presence of the recombinant protein was assayed using a human Myc antibody. As can be seen in Figure 7(B), a protein band of the expected mobility was clearly detected in the eluates from the CKI-expressing strain but not from the wild-type cells. The ability of the expressed protein to phosphorylate casein was assayed by incubating an aliquot of these fractions with casein and [γ-^{32}P]ATP; the products were separated by SDS/PAGE and detected by autoradigraphy (Figure 7B). The 150 mM imidazole fractions showed casein phosphorylating activity which was higher in eluates from the His_6-CKI-expressing cells than in the control. This result indicates that the CKI expressed in the transformed cells is a functional protein. Nuclei were prepared from untransformed cells and two different transformants and, as can be seen in Figure 7(C), the overexpressed protein was also found in the nuclear fraction of the cell.

When the phenotype of the cells overexpressing *DdCKI* was examined, no growth or developmental phenotype was observed, nor was any difference found in the migration of the slugs towards a luminous source.

The response to DNA-damaging agents, such as cisplatin and hydroxyurea, was also examined under conditions known to decrease the viability of *Dictyostelium* cells [36,37]. The transfected cells showed more resistance than untransfected control cells to treatment with hydroxyurea (Figure 7D); no difference was found after the cisplatin treatment.

DISCUSSION

Using a PCR strategy, we have cloned the first *DdCKI*. Several cDNA clones were isolated and analysed from a cDNA library. Sequence analysis of this cDNA indicated that it encodes a single reading frame comprising 426 amino acids. Two of the clones analysed have a stop codon in the *Eco*RI cloning site. We believe

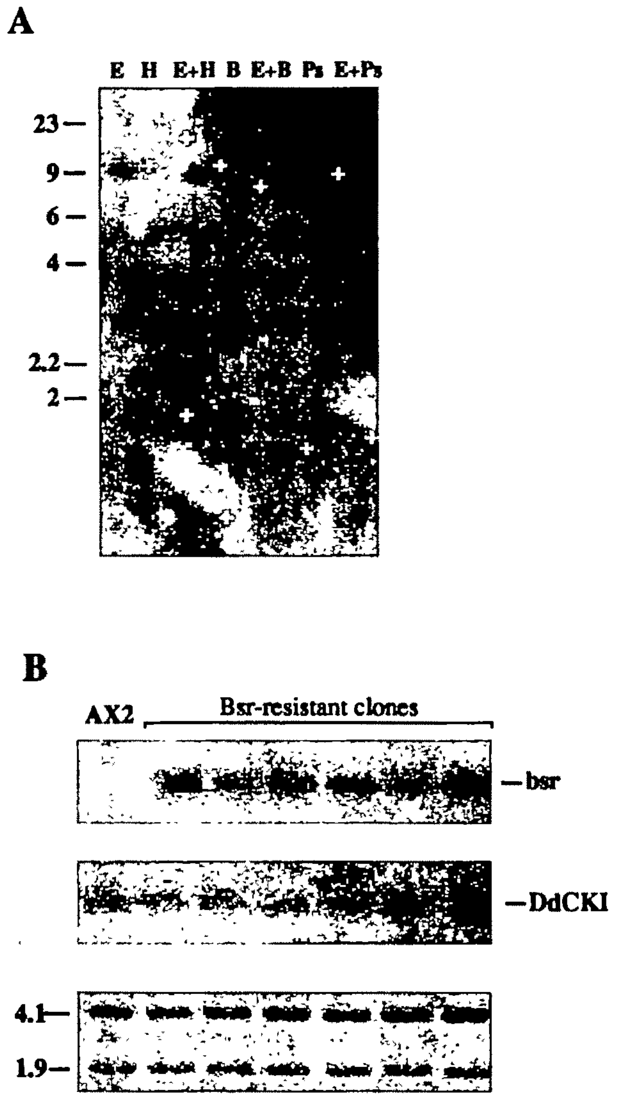

Figure 6 Southern- and Northern-blot analysis of blasticidine-resistant clones

(**A**) Genomic DNA from blasticidine-resistant clone 2 was cleaved with various restriction enzymes and probed with DdCKI cDNA. *Eco*RI (E), *Hin*dIII (H), *Eco*RI + *Hin*dIII (E + H), *Bgl*II (B), *Eco*RI + *Bgl*II (E + B), *Pst*I (Ps) and *Eco*RI + *Pst*I (E + Ps). Mass markers (in kb) are shown on the left. (**B**) Top panels: total RNA (6 μg/lane), prepared as indicated in the Materials and methods section from various Bsr-resistant clones or from untransformed cells (AX2), was resolved on an agarose/formaldehyde gel, transferred to a nylon membrane and probed with the cDNA of the BsrS cassette or the cDNA of DdCKI labelled by random priming. Bottom panels: rRNA is shown as an indicator of gel loading.

that this *Eco*RI site is a constituent of the gene for two reasons. First, Southern-blot analysis indicates that the *Eco*RI site located in the 3′-coding region is a true site and not a cloning artifact. Secondly, the size of the protein detected by the antibody matches the predicted molecular mass of the coded protein.

The cDNA described in the present work belongs to the CKI protein family. The members of this family share several well-conserved motifs, such as LLGPSLEDLF (residues 86–95), HIPXR (residues 166–170), EXSRRDD (residues 191–197) and LPWQGLKA (residues 213–220). Furthermore, this cDNA lacks the APE sequence in subdomain VIII, which is replaced by SLN (residues181–183). All these features are specific for CKI, and are probably important for protein–protein interactions.

On the basis of sequence identity, DdCKI is very close to the mammalian δ and ϵ isoforms and to the yeast Hhp1, Hhp2 and Hrr25, which are assumed to be located in the nucleus. This nuclear localization is postulated because of the sequence identity and because these isoforms contain a putative TKK/RQKY nuclear localization signal similar to the sequence thought to be involved in targeting other proteins, such as histone 2B, to the nucleus [38].

The C-terminal portion of DdCKI is rich in glutamine and proline residues. In *D. discoideum* a repetitive element, composed of the codon AAC, is found in developmentally regulated transcripts; these AAC sequences can be translated in all three reading frames in the proteins, giving rise to asparagine (ACC), threonine (ACA) or glutamine (CAA) [35]. Other proteins rich in glutamine and proline residues are a number of CKIs, such as Hrr25, Hhp1, Yck1 and Yck2, and transcription factors such as Sp1, PU1 or TAFII [39,40]. The function of these regions has been analysed in greater detail in transcription factors, where they have been shown to be involved in transcription trans-activation through interaction with regulatory proteins [39].

Our Southern-blot hybridization data suggest that CKI-related isoforms might be present in *Dictyostelium*. This is in agreement with our previous biochemical studies, based mainly on the chromatographic behaviour, which revealed the presence of several CKI isoforms in this organism [23].

CKI is expressed throughout the whole life cycle of *Dictyostelium*

The results of the Northern-blot analysis performed with RNA from differentiated cells show a major 2.2-kb transcript. Two species have been detected in the rabbit, one of 3.5 kb, which is detected in most tissues, and one of 1.9 kb with a high level of expression in testis and heart [41]. Several such messages are also found in human cells [42]. No changes were detected either throughout differentiation or during the cell cycle of *Dictyostelium*, suggesting that *CKI* may have a role in the development of the slime mould. In parallel with the expression of *DdCKI*, Western-blot analysis showed that the protein was present throughout the differentiation programme of *Dictyostelium*. The rat and rabbit *CKIδ*, which are the CKs most similar to *DdCKI*, have a widespread distribution and have been detected in all tissues examined [41].

Antibodies generated against the N-terminal region of DdCKI recognized a 49-kDa protein, which was close to the predicted molecular mass based on the cDNA. A protein with the same molecular mass was detected when *Dictyostelium* cell extracts were prepared in the presence of high leupeptin concentrations or when cells were directly resuspended in sample buffer for Western-blot analysis, which suggests that this 49-kDa protein was not a proteolytic product. A wide range of molecular masses, ranging from 30 to 60 kDa, has been described for CKI isoforms. High-molecular-mass forms have been isolated from nuclei. However, the protein mass is not indicative of localization within the cell, as the largest CKI isoforms, yeast Yck1 and Yck2 [14] and Cki1 and Cki2 [16], are cytoplasmic membrane-associated proteins, while the human 34-kDa CKIα has been found associated to kinetochore fibres in mitosis [43].

DdCKI expressed in bacteria has CK activity

DdCKI has been expressed in bacteria, and the recombinant protein was very sensitive to proteolysis. The purified recom-

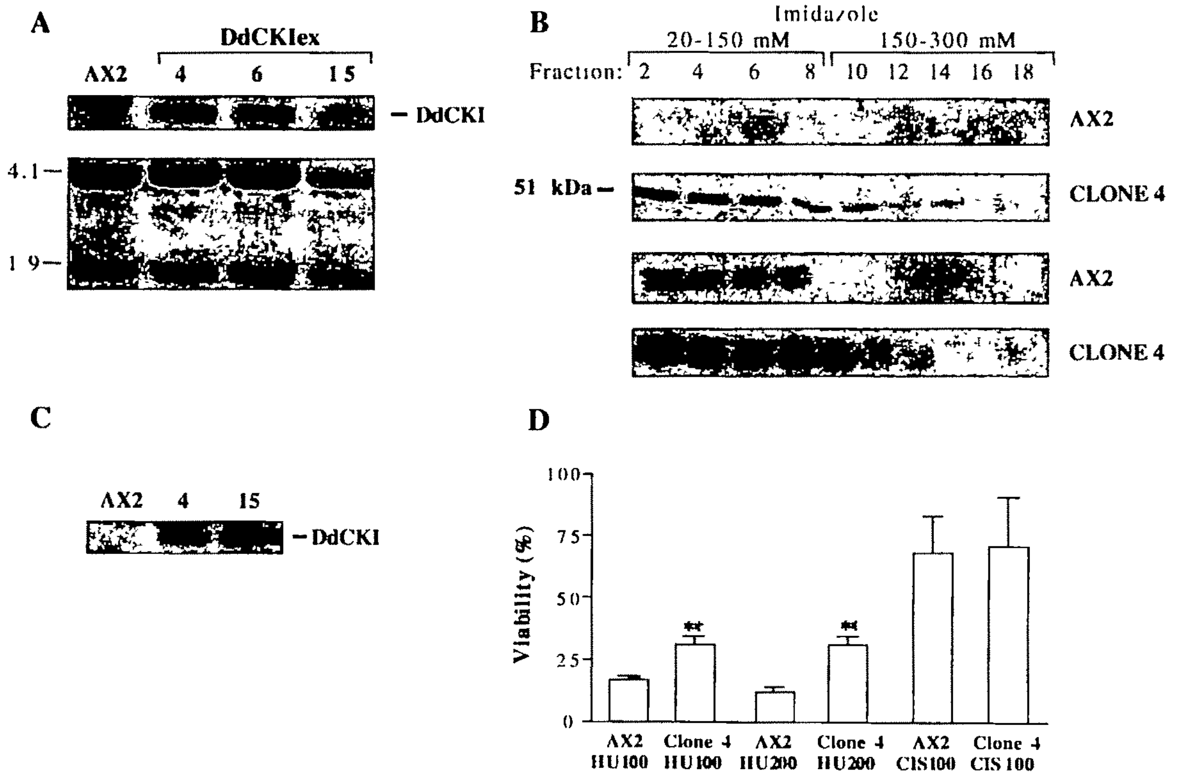

Figure 7 Expression of recombinant DdCKI in untransformed (AX2) cells

(**A**) Northern-blot analysis of RNAs (10 μg) isolated from untransformed vegetative cells (AX2) or from three geneticin-resistant clones. cDNA from DdCKI was used as a probe. (**B**) Wild-type strain (AX2) and one Act15-His$_6$ CKI–Myc overexpresser (clone 4) were harvested at 4×10^6 cells/ml and lysed by sonication. Soluble extracts containing equal amounts of protein were purified by Ni^{2+}–agarose as indicated in the Materials and methods section. Samples of the 150 mM or 300 mM fractions were used for immunoblotting or *in vitro* assay. Top panels: immunoblot probed with anti-Myc antibody. The mass of the recombinant protein detected by the antibody is shown on the left. Bottom panels: samples of the same fractions were used for *in vitro* phosphorylation of casein. (**C**) Nuclei from the wild-type strain (AX2) or from two clones (4 and 15) expressing ectopical *DdCKI* were prepared as indicated in the Materials and methods section. Nuclear extracts containing equal amounts of protein were used for Western blotting and probed with anti-Myc antibody. (**D**) Viability assay performed with 100 or 200 mM hydroxyurea (HU) or 100 μM cisplatin (CIS), as indicated in the Materials and methods section, using untransformed (AX2) or clone 4 cells. The data are the means (±S.E.M.) of triplicates for each treatment, determined by one-way analysis of variance ('ANOVA') and Tukey post-test. Control untreated cells = 100% viability. **, significantly different from AX2 cells, $P < 0.01$.

binant DdCKI autophosphorylated and phosphorylated casein, as expected, and did not phosphorylate basic proteins, such as myelin basic protein or histone H1. We have not detected phosphorylation of poly-E_4Y_1 under our assay conditions, in contrary to the recombinants Hhp1 and Hhp2 expressed in bacteria [3].

Studies on the effect of heparin on the activity of CKI from different sources have yielded inconsistent results. Inhibition was observed in some cases [44], whereas in others either no effect or activation was reported [45]. This also applies to the effect of polylysine on CKI activity; polylysine stimulates recombinant CKIα when assayed with D4 peptide, but no effect was detected when phosvitin was used as substrate [46].

When the effect of heparin on CKI activity was tested using casein as the substrate, we observed inhibition or activation depending on the salt concentration in the assay; a differential effect of polylysine at different salt concentrations was also observed. The experiments of Graves and Roach [47], using a truncated version of CKIδ, led them to postulate that the C-terminus of CKIδ was critical for the action of heparin, because the full-length enzyme was activated by heparin, whereas the mutant lacking the C-terminus was insensitive. Based on this observation, we suggest that the salt concentration probably affects the structure of the C-terminal portion of the enzyme, although a change in substrate structure cannot be ruled out.

Immunolocalization of DdCKI

During its vegetative phase, the cellular slime mould *D. discoideum* grows as unicellular, haploid eukaryotic amoebae. Our immunofluorescence experiments indicate that the endogenous CKI is distributed in the cytoplasm and the nuclei of the vegetative cells. The overexpressed *CKI* is also detected in both the cytoplasmic and nuclear fractions, suggesting that this CKI might be playing a nuclear role, as has been proposed for some CKIs of other organisms [10,17,48,49].

Genetic analysis of *DdCKI*

Our genetic analysis suggests that *DdCKI* may be an essential gene for growth. We were unable to disrupt the gene by homologous recombination, and also to express the *CKI* K38R mutant using the same vector that allowed the expression of the wild-type protein. This suggests that *CKI* K38R might indeed be acting as a dominant negative, and lends support to the proposition that *CKI* might be essential for *Dictyostelium*. *DdCKI* could be required to support the vegetative growth of the cells, in the same way that Hrr25 protein kinase is important for normal growth in yeast [11].

The observation that the cells from the overexpressing clone were more resistant to hydroxyurea treatment than the wild-type ones is consistent with a potential role of this protein in DNA repair mechanisms, as is the case in *Sch. pombe* [12] and *Sa. cerevisiae* [11].

One possible role for CKI would be in the Wnt signalling pathway, since CKIϵ (72% homology with DdCKI in the catalytic domain) has been shown recently to be a conserved component of this pathway [9], and is involved in a variety of processes, including cell growth and development. Glycogen synthase kinase 3, a component of this pathway in metazoa, also regulates cell fate during *Dictyostelium* development.

We are at present preparing constructs of dominant negative and constitutively active versions of *DdCKI* under the promoters specific for stalk and spore genes, with the aim of obtaining further information on the potential role of this kinase in cell differentiation.

We thank Dr Ana Camacho for help with the expression experiments, Dr Antonio Coloma for the cDNA library, Dr Jaime Renart for his continuous support, Dr Ricardo Escalante for a critical reading of the manuscript, and Carmen Domínguez for her technical assistance G M.-B. was the beneficiary of a fellowship from the Universidad Autónoma de Madrid This work has been supported by grants from the D G.C Y T

REFERENCES

1 Issinger, O. G (1993) Casein kinases pleiotropic mediators of cellular regulation Pharmacol Ther. **59**, 1–30

2 Gross, S D and Anderson, R A (1998) Casein kinase I spatial organization and positioning of a multifuntional protein kinase family Cell Signal **10**, 699–711

3 Hoekstra, M F, Dhillon, N, Carmel, G, DeMaggio, A J., Lindberg, R A, Hunter, T and Kuret, J (1994) Budding and fission yeast casein kinase I isoforms have dual-specificity protein kinase activity Mol Biol Cell **5**, 877–886

4 Pulgar, V, Tapia, C, Vignolo, P, Santos, J and Sunkel, C E (1996) The recombinant a isoform of protein kinase CK1 from *Xenopus laevis* can phosphorylate tyrosine in synthetic substrates Eur J Biochem **242**, 519–528

5 Cegielska, A and Virshup, D M (1993) Control of simian virus 40 DNA replication by the HeLa cell nuclear kinase casein kinase Mol Cell Biol **13**, 1202–1211

6 Zhu, J, Shibasaki, F, Price, R, Guillemot, J C, Yano, T, Dotsch, V, Wagner, G, Ferrera, P. and McKeon, F (1998) Intramolecular masking of nuclear import signal on NF-AT4 by casein kinase I and MEKK1 Cell **93**, 851–861

7 Lussier, G. and Larose, L (1997) A casein kinase I activity is constitutively associated with Nck J. Biol Chem **272**, 2688–2694

8 Dubois, T, Rommel, C, Howel, S, Steinhusson, U, Soneji, Y, Morrice, N, Moelling, K and Aitken, A (1997) 14-3-3 is phosphorylated by casein kinase I on residue 233 Phosphorylation at this site *in vivo* regulates Raf/14-3-3 interaction J Biol. Chem **272**, 28882–28888

9 Peters, J. M, Mckay, R M, Mackay, J P and Graff, J M (1999) Casein kinase I transduces Wnt signals Nature (London) **401**, 345–350

10 Kloss, B, Price, J L, Saez, L, Blau, J, Rothenfluh, A, Wesley, C S and Young, W (1998) The *Drosophila* clock gene double-time encodes a protein closely related to human casein kinase Iϵ Cell **94**, 97–107

11 Hoekstra, M F, Liskay, R M, Ou, A C, DeMagio, A J, Burbee, D G and Heffron, F (1991) HRR25, a putative protein kinase from budding yeast association with repair of damaged DNA Science **253**, 1031–1034

12 Dhillon, N and Hoekstra, M F (1994) Characterization of two protein kinases from *Schizosaccharomyces pombe* involved in the regulation of DNA repair EMBO J **13**, 2777–2788

13 Murakami, A, Kimura, K and Nakano, A (1999) The inactive form of a yeast casein kinase I suppresses the secretory defect of the sec12 mutant Implication of negative regulation by the Hrr25 kinase in the vesicle budding from the endoplasmic reticulum J Biol Chem **274**, 3804–3810

14 Robinson, L C, Menold, M M, Garret, S and Culbertson, M R (1993) Casein kinase I-like protein kinases encoded by Yck1 and Yck2 are required for yeast morphogenesis. Mol Cell Biol **13**, 2870–2881

15 Robinson, L C, Bradley, C, Bryan, J D, Jerome, A, Kweon, Y and Panek, H R (1999) The Yck2 yeast casein kinase 1 isoform shows cell cycle-specific localization to sites of polarized growth and is required for proper septin organization Mol Biol Cell **10**, 1077–1092

16 Wang, P. C, Vancura, A., Desai, A, Carmel, G and Kuret, J. (1994) Cytoplasmic forms of fission yeast casein kinase-1 associate primarily with the particulate fraction of the cell J Biol Chem **269**, 12014–12023

17 Santos, J A, Logarinho, E, Tapia, C, Allende, C C and Allende, J E (1996) The casein kinase 1α gene of *Drosophila melanogaster* is developmentally regulated and the kinase activity of the protein induced by DNA damage J Cell Sci **109**, 1847–1856

18 Firtel, R. A (1991) Signal transduction pathways controlling multicellular development in *Dictyostelium* Trends Genet **7**, 14875–14883

19 Williams, J G (1991) Regulation of cellular differentiation during *Dictyostelium* morphogenesis Curr Opin Genet. Dev **1**, 358–362

20 Wang, B and Kuspa, A (1997) *Dictyostelium* development in the absence of cAMP Science **277**, 251–254

21 Kikkawa, U, Mann, S K, Firtel, R A and Hunter, T (1992) Molecular clonning of casein kinase IIa subunit from *Dictyostelium discoideum* and its expression in the life cycle Mol Cell Biol **12**, 5711–5723

22 Ospina, B, Nuñez, A and Fernández-Renart, M (1992) Purification of a soluble casein kinase II from *Dictyostelium discoideum* lacking the β subunit regulation during proliferation and differentiation Mol Cell Biochem **118**, 49–60

23 Ospina, B and Fernández-Renart, M (1990) Characterization of three casein kinases type I from *Dictyostelium discoideum* Biochim Biophys Acta **1052**, 483–488

24 Watts, D J and Asworth, J M (1970) Growth of *Myxamoebae* of the cellular slime mould *Dictyostelium discoideum* in axenic culture Biochem J **119**, 171–174

25 Weijer, C J, Duschl, G and David, C D (1984) A revision of the *Dictyostelium discoideum* cell cycle J Cell Sci **70**, 111–131

26 Knetsch, M L, Epskamp, J P, Schenk, P W., Wang, Y, Segall, J E and Snaar-Jagalska, B E (1996) Dual role of cAMP and involment of both G-proteins and ras in regulation of ERK2 in *Dictyostelium discoideum* EMBO J **15**, 3361–3368

27 Sambrook, J D, Fritsch, E F and Maniatis, T (1989) Molecular Cloning A Laboratory Manual, 2nd edn, Cold Spring Harbor Laboratory, Cold Spring Harbor, NY

28 Nellen, W., Data, S, Reymond, C, Sivertsen, A, Mann, S, Crowley, T and Firtel, R A (1987) Molecular biology in *Dictyostelium* tools and applications Methods Cell Biol **28**, 67–100

29 Chomczynski, P and Sacchi, N (1987) Single-step method of RNA isolation by acid guanidium thiocyanate-phenol-chloroform extraction Anal Biochem **162**, 156–159

30 Vennstrom, B and Bishop, J M (1982) Isolation and characterization of chicken DNA homologous to the two putative oncogenes of avian erythroblastosis virus Cell **28**, 135–143

31 Manstein, D J, Schuster, H-P, Morandini, P and Hunt, D. M (1995) Cloning vectors for the production of proteins in *Dictyostelium discoideum* Gene **162**, 129–134

32 Adachi, H, Hasebe, T, Yoshinaga, K, Ohta, T and Sutoh, K (1994) Isolation of *Dictyostelium discoideum* cytokinesis mutants by restriction enzyme-mediated integration of the blasticidin S resistance marker Biochem. Biophys Res Commun **205**, 1808–1814

33 Kozak, M (1987) An analysis of 5′ non-coding sequences from 699 vertebrate messenger RNAs Nucleic Acids Res **15**, 8125–8130

34 Hanks, S K, Quinn, A M and Hunter, T (1988) The protein kinase family conserved features and deduced phylogeny of the catalityc domain Science **241**, 42–51

35 Shaw, D R, Ichter, H, Giorda, R, Ohmachi, T and Ennis, H L (1989) Nucleotide sequences of *Dictyostelium discoideum* developmentally regulated cDNAs rich in (AAC) imply proteins that contain clusters of asparagine, glutamine or threonine Mol Gen Genet **218**, 453–459

36 Yu, S-L, Lee, S-K, Alexander, H. and Alexander, S (1998) Rapid changes of nucleotide excision repair gene expression following UV-irradiation and cisplatin treatment of *Dictyostelium discoideum* Nucleic Acids Res **26**, 3397–3403

37 Freeland, T M, Guyer, R. B., Lind, A Z and Deering, R A (1996) Apurinic/apyrimidinic (AP) endonuclease from *Dictyostelium discoideum* cloning, nucleotide sequence and induction by sublethal levels of DNA damaging agents Nucleic Acids Res **24**, 1950–1953

38 Moreland, R B, Langevin, G L, Singer, R H, Garces, R L and Herford, L M (1987) Amino acid sequences that determine the nuclear localization of yeast histone 2B Mol Cell Biol **7**, 4048–4057

39 Fisher, R C, Olson, M C, Pongubala, J M R, Perkel, J M, Atchinson, M L, Scott, E W and Simon, M C (1998) Normal myeloid development requires both the glutamine-rich transactivation domain and the PEST region of transcription factor PU1 but not the potent acidic transactivation domain Mol Cell Biol **18**, 4347–4353

40 Saluja, D, Vassallo, M F and Tanese, N (1998) Distinct subdomains of human TAFII 130 are required for interactions with glutamine-rich transcriptional activators Mol Cell Biol **18**, 5734–5743

41 Graves, P R, Haas, D W, Hagedorn, C H, DePaoli-Roach, A and Roach, P J (1993) Molecular cloning, expression, and characterization of a 49-Kilodalton casein kinase I isoform from rat testis J Biol Chem **268**, 6394–9401

42 Rowles, J, Slaughter, C, Moomaw, C, Hsu, J and Cobb, M H (1991) Purification of casein kinase I and isolation of cDNAs encoding multiple casein kinase I-like enzymes Proc Natl Acad. Sci U S A **88**, 9548–9552

43 Brockman, J L, Gross, S D., Sussman, M. R. and Anderson, R. A (1992) Cell cycle-dependent localization of casein kinase I to mitotic spindles Proc Natl Acad Sci. U S.A **89**, 9454–9458

44 Singh, T J (1988) Polyamines stimulate the activity of glycogen kidney and different rat tissues Arch Biochem Biophys **267**, 167–175

45 Floyd, C C, Grant, P, Gallant, P E and Pant, H C (1991) Principal neurofilament-associated protein kinase in squid axoplasm is related to casein kinase I. J Biol. Chem. **266**, 4987–4994

46 Zhai, L., Graves, P. R., Longenecker, K. L, DePaoli-Roach, A A and Roach, P J (1992) Recombinant rabbit muscle casein kinase Iα is inhibited by heparin and activited by polylysine. Biochem. Biophys. Res Commun **189**, 944–949

47 Graves, P R and Roach, P J (1995) Role of COOH-terminal phosphorylation in the regulation of casein kinase 1δ J Biol Chem **270**, 21689–21694

48 Vancura, A, Sessler, A, Leichus, B and Kuret, J (1994) A prenylation motif is required for plasma membrane localization and biochemical function of casein kinase I in budding yeast J. Biol Chem. **269**, 19271–19278

49 Brockman, J. L and Anderson, R. A (1991) Casein kinase I is regulated by phosphatidylinositol 4,5 bisphosphate in native membranes J Biol Chem **266**, 2508–2512

Received 30 November 1999/16 March 2000, accepted 25 April 2000

Biochem. J. (2000) 349, 539–545 (Printed in Great Britain)

Hepatic intralobular mapping of fructose metabolism in the rat liver

Shamus P. BURNS*[1], Helena C. MURPHY*, Richard A. ILES*, Rosemary A. BAILEY† and Robert D. COHEN*

*Cell Regulation Unit, Department of Diabetes and Metabolic Medicine, 5th Floor Alexandra Wing, St Bartholomew's and The Royal London School of Medicine and Dentistry, Whitechapel Road, London E1 1BB, U.K., and †School of Mathematical Sciences, Queen Mary and Westfield College, London E1 4NS, U.K.

Detailed mapping of glucose and lactate metabolism along the radius of the hepatic lobule was performed *in situ* in rat livers perfused with 1.5 mM lactate before and during the addition of 5 mM fructose. The majority of fructose uptake occurred in the periportal region; 45% of fructose taken up in the periportal half of the lobular volume being converted into glucose. Periportal lactate uptake was markedly decreased by addition of fructose. Basal perivenous lactate output, which was derived from glucose synthesized periportally, was increased in the presence of fructose. During fructose infusion there was a small decrease in cell pH periportally, but acidification of up to 0.5 pH units perivenously. The evidence suggests that *in situ* the apparent direct conversion of fructose into lactate represents, to a substantial extent, the result of periportal conversion of fructose into glucose and the subsequent uptake and glycolysis to lactate in the perivenous zone of some of that glucose. ^{31}P NMR spectroscopy showed that the cellular concentration of phosphomonoesters changes very little periportally during fructose infusion, but there was an approximate twofold increase perivenously, presumably due to the accumulation of fructose 1-phosphate. It may be inferred that fructokinase activity is expressed throughout the hepatic lobule.

Key words: fructose 1-phosphate, hepatic glucose output, intracellular pH, lactate uptake.

INTRODUCTION

Addition of fructose to rat liver perfusions causes an immediate but temporary decrease in hepatic ATP and P$_i$, partly attributable to the accumulation of fructose 1-phosphate by the action of fructokinase (EC 2.7.1.4), degradation of adenine nucleotides to IMP and urate [1,2] and a simultaneous fall in hepatocyte intracellular pH (pH$_i$) [3]. Recovery of ATP is rapid but only partial, possibly because of irreversible degradation of adenine nucleotides. These phenomena have their counterparts in studies in man [4,5], and have had important implications for intravenous feeding regimes [2] and for the understanding of the metabolic disturbance in hereditary fructose intolerance [6]. The principal possible fates of fructose in the liver are conversion into glucose or glycogen, fructolysis to pyruvate and lactate, and oxidation. This description of overall events does not take into account intralobular metabolic heterogeneity, and the sites within the lobule of fructose uptake and conversion into glucose and lactate are unclear or controversial [7,8]. The overall fall in pH$_i$ measured by ^{31}P NMR spectroscopy appears to be less than when determined using intracellular microelectrodes [3,9].

We have described a method [10] for detailed mapping of metabolic events and metabolite concentrations along the radius of the hepatic lobule *in situ* in the isolated perfused rat liver. The technique does not depend on the preparation of isolated hepatocytes from different zones of the lobule, thus avoiding changes of metabolite content and loss of polarity and vascular relationships during isolation. A further advantage is the facility with which reaction sequences which commence periportally and are completed perivenously can be investigated. In the present study, we have adapted this method to map fructose metabolism along the lobular radius to determine whether heterogeneity of metabolism could resolve the controversies and anomalies referred to above.

MATERIALS AND METHODS

Animals

Male Wistar rats (320 g) fed on standard rat chow were used after a 48 h fast. Isolated liver perfusions were set up at 37 °C as previously described [11] using erythrocyte- and albumin-free perfusate consisting of Krebs bicarbonate buffer [12] gassed with 95% O$_2$/5% CO$_2$ to give pH 7.4. Sodium L(+)-lactate (1.5 mM) was included as exogenous substrate for the liver throughout the protocol. The flow rate was 10 ml/min per 100 g of rat.

Mapping of intralobular fructose metabolism

In the original method [10], sharply defined lobular destruction, in amounts which varied between individual livers, was produced by retrograde perfusion of digitonin, followed by resumption of antegrade perfusion. The functional and microscopic effects of digitonin have been previously summarized [10,13–15]. Briefly, a sharply demarcated zone of destruction of hepatocytes, sinusoidal and Kupffer cells, centred on the central venules, is produced. The radius of these zones is dependent on the duration of retrograde digitonin perfusion. There are no effects on zones more periportal to the demarcation, since digitonin is avidly bound on a first-pass basis to membrane cholesterol. The metabolic activity or overall metabolite concentration of the remaining unaffected part of the lobule, was expressed as a fraction of the pre-digitonin value and plotted against the mean fractional lobular volume remaining (FVR) unaffected by digitonin, determined as described in [10]. Curves were fitted to the data and transformed to give plots of point-by-point metabolic

---

Abbreviations used: pH$_i$, intracellular pH, FVR, fractional volume remaining, HGO, hepatic glucose output, PME, phosphomonoesters

[1] To whom correspondence should be addressed (e-mail S.P.Burns@mds.qmw.ac.uk)

activity or metabolite concentration along the radius of the lobule. In the present study, livers were subjected to retrograde digitonin destruction of varying degree. Baseline observations of glucose and other metabolite output or uptake, hepatocyte cell pH$_i$ and ATP in the unaffected part of the lobule were then made and plotted against FVR. Infusion of fructose was then commenced and the observations repeated. Thus the modification consisted of comparisons made during fructose versus baseline on previously digitonin-treated livers, rather than before and after digitonin. In addition, substrate and metabolite uptake and output were expressed in absolute terms, rather than as ratios between different phases of the protocol; this modification was necessary for interpretation of the data but produces some scatter, since variation between livers is not completely compensated for.

The point of establishment of perfusion was taken as zero time. The perfusion was non-recirculating throughout. After 5 min of antegrade perfusion, flow was stopped and digitonin (4 mg/ml in Tris buffer, pH 7.4) perfused in the retrograde direction at approx. 30 ml/min for times that varied in the different livers between 10 s and 2 min. Antegrade perfusion was then re-established and the preparation placed in the bore of the NMR spectrometer. Baseline samples of influent and effluent perfusate were obtained at 20 min, 25 min and 30 min for measurement of pH, $P\mathrm{CO}_2$, $P\mathrm{O}_2$, glucose, lactate and fructose; a baseline spectrum was collected for estimation of pH$_i$, intracellular P$_i$, ATP and phosphomonoesters (PMEs) over the period 29–33 min. D-Fructose was then infused to achieve a concentration in the portal influent of 5 mM over the period 33–45 min. Further spectra were collected over the period 33–45 min in 4 min blocks (i.e. three spectra), together with portal and hepatic venous samples at 38 min and 43 min. The liver was then fixed by perfusion of approx. 30 ml of 10 % formalin. Tissue blocks were removed for determination of FVR by semi-automated quantitative histomorphometry, as previously described [9].

^{31}P NMR studies

These were carried out in a Sisco 4.7T NMR spectrometer with a horizontal bore and a gradient insert of internal diameter 120 mm. A pulse repetition time of 0.33 s was used to saturate extracellular P$_i$ and thus eliminate P$_i$ signal from this source, as previously described [10]. Chemical shift of the P$_i$ resonance was referenced both to the α-ATP plus α-ADP peak, and then to an external standard of methylene diphosphonic acid placed under the liver, the chemical shift of which was used for subsequent calibration within each liver, before and during fructose infusion [10]. pH$_i$ was calculated by reference to a standard curve. NMR spectra were interpreted by Lorentzian-line-shape analysis, using the FITPLA program [16]. Three singlet peaks were fitted to the partially overlapping PME, phosphodiester and P$_i$ resonances in the baseline spectrum. The analysis was then repeated in the spectrum recorded during fructose infusion, assuming the parameters width at half-height and chemical shift were unchanged for the phosphodiester peak from the values obtained in the baseline spectrum. The methylene diphosphonate and β-ATP resonances were analysed in the same way, the width at half-height and chemical shift being fixed to the pre-fructose values obtained by FITPLA.

Analytical procedures

Samples were stored at −20 °C until analysis. Glucose [15] and lactate [11] were determined as previously described. Fructose was measured enzymically [17] using a modification of a kit supplied by Boehringer Mannheim. $P\mathrm{CO}_2$ and $P\mathrm{O}_2$ were determined immediately in an Instrumentation Laboratory 1304 blood gas analyser.

Calculations

The balance of glucose, lactate and fructose across the liver was calculated using the Fick principle. Curves were fitted to the data plots of glucose output versus FVR before and during fructose infusion, using the Levenburg–Marquandt algorithm [18]. It should be noted that each point on these data plots represents the change of function or metabolite concentration induced by fructose in the whole of the remaining liver unaffected by digitonin. The curves fitted to the data plots were then transformed using the procedure described previously (see Appendix 1 in [10]) to give point-by-point plots of glucose uptake or output before and during fructose infusion against location, defined either by fractional lobular volume or fractional radial distance from the lobular centre, assuming the lobules to be on average spherical. This procedure does not include a scaling factor, which is immaterial when point function is described in relative terms (as in our previous use of this technique [10,15,21]); however, in the present context, in which absolute values of function are needed, it requires modification. Appendix 1 in [10] describes the analysis in terms of a single lobule. Scaling to liver weight per 100 g rat weight (eqn. 2 of that Appendix) becomes:

$$y_x = -(1/4.2)(\mathrm{d}F/\mathrm{d}x)$$

where $\mathrm{d}F/\mathrm{d}x$ is the slope of the curve fitted to plots of function (F) in μmol/min per 100 g rat against FVR (denoted as x), and y_x the point function in units of activity (μmol/min per g) of tissue at a point where the fractional volume of the lobule periportal to it is x. The minus sign disappears when FVR is replaced by fractional volume from the centrilobular vein (Figure 1, top panel). We have assumed a liver weight in starved rats of 4.2 g per 100 g rat weight and liver specific gravity of unity. The above equation has been used to derive point function per g of liver tissue for glucose before and during fructose (Figure 1, bottom panel). As in our previous publications using this technique [10,15,19], the transformation has been confined to data limited by the highest (FVR = 0.2) and lowest (FVR = 0.93) degrees of digitonin destruction achieved. Above the former limit, extrapolation of the curve is uncertain; below the latter limit, the very small volumes of tissue involved, and uncertainties caused by the variable size of the central venule, inevitably decrease accuracy. Confidence limits for the transformed curves were derived as in [10]. The variance/covariance matrices for this purpose were calculated using Genstat® [20].

It should be emphasized that the fitted curves do not represent any preconceived model of metabolic events, but are merely vehicles for the transformation procedure. The transformation was not attempted for substrates or metabolites other than glucose, since the scatter in other variables precluded unambiguous curve fitting. As previously explained [10], it is in any case not possible to perform the transformation on the pH$_i$ data, notwithstanding this, it is possible to make some inferences about the distribution of pH$_i$ and changes in pH$_i$ from the data plots.

RESULTS AND DISCUSSION

Table 1 shows measurements in control livers (no digitonin) of the fractional change during fructose compared with baseline in P$_i$, PMEs, and estimates of ATP from the resonances of the β-phosphorus resonance. It may be seen that a reasonable steady

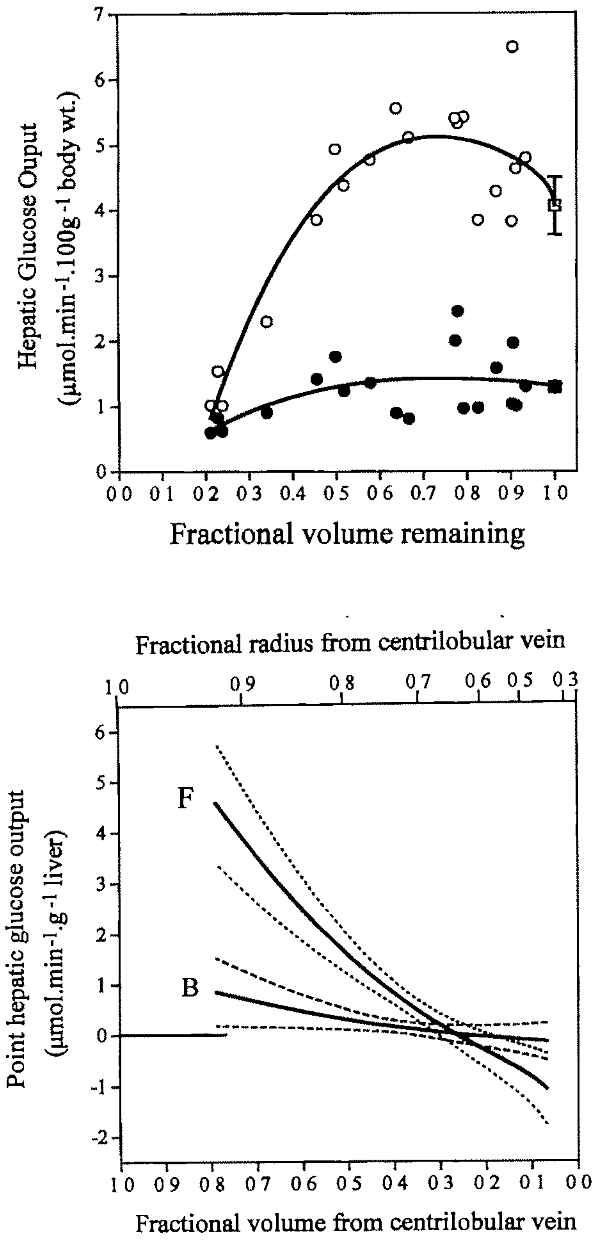

Figure 1 Zonal glucose handling by the perfused rat liver before and during fructose infusion

Top panel lactate (1 5 mM) was present throughout In this and subsequent Figures of this type, all data are from the same set of experiments and each pair of points at the same FVR represents data from a single liver, before and during fructose infusion Means ± S E M of data obtained in control studies in which digitonin was omitted are shown at FVR = 1 0 (□, ■, $n = 6$) The best fitting curves are before fructose (●)· $\mathrm{HGO} = 1\ 289 + 0\ 419(1-\mathrm{FVR})^{2/3} - 2\ 061(1-\mathrm{FVR})^{3}$ and during fructose (○) $\mathrm{HGO} = 4\ 054 + 2\ 465(1-\mathrm{FVR})^{0\ 5} - 11\ 03(1-\mathrm{FVR})^{3}$ All individual data points were used for curve fitting Bottom panel transformation of the curves (top panel) to show handling of glucose before (B, baseline) and during fructose (F) infusion by hepatocytes according to their position along the periportal-to-perivenous axis of the hepatic lobule The lower abscissa defines that position by indicating the fractional volume of the lobule more perivenous to it Thus a unit of lobular volume from the central venule of 0 2 indicates the position of a cell on a spherical shell which has 20% of the lobular volume more perivenous to it Because of spherical geometry, the radius of that shell is 58% of the radius of the whole lobule The upper abscissa is expressed in terms of radial position from the centre of the lobule Values above and below zero represent glucose output and uptake respectively The 95% confidence limits of the transformed curves are shown (calculated as described in Appendix 2 in [10]).

state was obtained in the last two 4 min periods of fructose infusion. There was an approximate twofold increase in PME, a 30% fall in β-ATP, and 25% fall in P_i during fructose.

Table 1 Fractional change in P_i, PME and ATP in isolated perfused liver, during 5 mM fructose infusion determined by ^{31}P NMR spectroscopy

Paired *t*-tests indicated that metabolite concentrations were significantly different ($P < 0\ 05$) to pre-fructose values except P_i at 10 min

	Fractional change in metabolite concentration during fructose infusion (means ± S E M., $n = 6$)		
Fructose infusion period (min)	P_i	PME	ATP
0	1	1	1
2	0 71 (0 08)	1.86 (0 29)	0.79 (0 04)
6	0 77 (0 10)	2.24 (0 42)	0 62 (0 10)
10	0 80 (0 14)	2 24 (0.35)	0 66 (0 09)

Figure 1 (top panel) plots hepatic glucose output (HGO) against the fractional volume of the hepatic lobule remaining unaffected after digitonin, before and during fructose infusion. In interpreting diagrams of this format, it should be borne in mind that the data at an FVR of, for example, 0 75 is generated by the whole of the lobular volume periportal to the limit of the digitonin destruction, which has involved the 25% of the lobular volume more perivenous to that limit. Curves have been fitted to the data as described in the Materials and methods section. Since hepatic glucose output before and during fructose is measured on the same livers, a paired *t*-test can be done without making assumptions about the fitted curves. This establishes that separate curves are needed ($P < 0.001$).

In whole perfused liver, mean glucose production during fructose is 3.1 times greater than baseline (i.e. data at FVR = 1.0). It may be seen that HGO is greater during fructose at FVR = 0.75 than at FVR = 1.0, indicating that some of the glucose (approx. 1 µmol/min per 100 g of rat) generated more periportally may be taken up by the more perivenous regions; therefore when those regions are destroyed, there is an increase in net glucose output [15]. In contrast, larger degrees of destruction (leaving smaller FVRs) produce a rapid decline of HGO, indicating that the glucose synthesized was derived from the more periportal 75% of the lobular volume.

To obtain a point-by-point map of glucose handling, the equations of best fit curves have been used to transform the data in Figure 1 (top panel) into a plot (Figure 1, bottom panel) of HGO in cells according to their location within the lobule, before and during fructose. Thus during fructose, point HGO in the extreme periportal region was approximately five times that before fructose. Point HGO declines in the periportal → perivenous direction until it reaches zero both before and during fructose, approx. 65% along the radius from the lobular centre; this means that the periportal 70% of lobular volume puts out glucose. Thereafter, at all points more perivenously, HGO is negative during fructose (i.e. glucose uptake is occurring), reflecting the negative gradient between FVRs of 0.75 and 1.0 of the curve fitted to the data during fructose in Figure 1 (top panel). The 95% confidence limits in Figure 1 (bottom panel) in the perivenous region encompass zero glucose flux before fructose.

We have previously shown that perivenous glucose uptake may occur with lactate as the sole substrate [15]. We have postulated that the relatively high concentration of perivenous glucokinase activity remaining in starved livers might be responsible for perivenous glucose uptake [15]. If glucokinase was responsible for this phenomenon then the high $S_{0\ 5}$, with respect

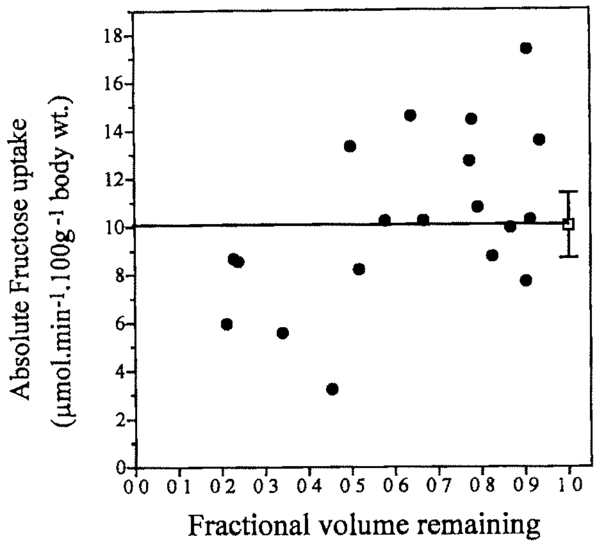

Figure 2 Fructose uptake plotted against FVR

Control studies with digitonin omitted (n = 6, means ± S E M) are shown at FVR = 1 0 (□) The horizontal line is drawn through the mean fructose uptake in control livers

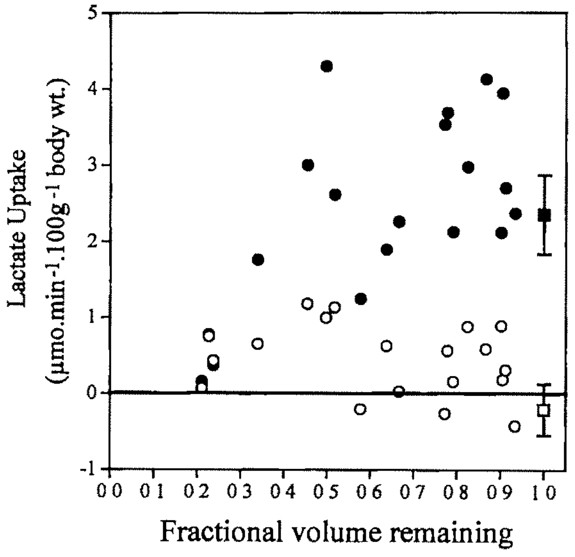

Figure 3 Hepatic lactate uptake before (●) and during (○) the infusion of fructose, plotted against the FVR after retrograde perfusion of digitonin

Control studies with digitonin omitted (n = 6, means ± S E M) are shown at FVR = 1.0 (□, ■) Symbols are as described Figure 1 The horizontal line is drawn through zero lactate balance

to glucose (approx. 8 mM), might be expected to result in increased perivenous glucose uptake during fructose, when the sinusoidal glucose concentration is highest. In this study, sinusoidal glucose concentration reaching the last 30 % of the lobular volume was approx. 0.2 mM before and 0.5 mM during fructose.

Data on fructose uptake using the same format (Figure 2) shows considerable scatter, but is most compatible with the major uptake of fructose being in the periportal half of the lobular volume, since there is no clear change in fructose uptake over a range of destructions over the FVR range of 0.5–1.0. By comparing the glucose and fructose data it may be calculated that the periportal region converts approx. 45 % of fructose taken up into glucose. The data below suggest that in the periportal region the fate of that fraction of fructose which is taken up, but not converted into glucose, is glycogen formation and/or oxidation, rather than conversion into lactate.

Figure 3 shows lactate uptake plotted against FVR, before and during fructose infusion. Before fructose, in the intact liver (FVR = 1.0) mean lactate uptake was 2.4 µmol/min per 100 g of rat; small destructions (FVR 0.7–1.0) increase net lactate uptake, so that at FVR = 0.75, the best estimate of lactate uptake is approx. 3.0 µmol/min per 100 g of rat. This suggests that perivenous cells located in the centrilobular 20 % of the lobule may produce lactate. Larger destructions (FVR range 0.2–0.8) produce a rapid decline in lactate uptake (Figure 3), consistent with the periportal site of lactate uptake and gluconeogenesis from lactate previously shown [10,15].

During fructose infusion in the continued presence of 1.5 mM lactate (Figure 3), mean lactate balance across the intact liver (FVR = 1) becomes slightly negative, indicating net lactate production in most cases (i.e. periportal lactate uptake is exceeded by perivenous lactate output). There is a clear separation of the data from that obtained before fructose in the FVR range 0.5–1.0, with lactate uptake much decreased in the FVR range 0.4–1.0 compared with that before fructose. A paired t-test establishes that lactate uptake during fructose is significantly different from that before fructose ($P < 0.001$). The positive slope in the FVR range 0.2–0.5 indicates that lactate uptake is still occurring, but since that slope is clearly less than in the same region before fructose, lactate uptake must be decreased by fructose. Linear-regression analysis of the data before and during fructose in the FVR range 0.8–1.0, indicates that a stronger trend toward a negative slope exists for the data during fructose (P = 0.07) than for the pre-fructose data (P = 0.23). This data suggests production of lactate by perivenous hepatocytes especially during fructose infusion, which is consistent with the net production of lactate during fructose infusion in the intact liver, despite continuing periportal lactate uptake.

Supporting this interpretation are the observations on hepatic cell pH$_i$. Figure 4 (top panel) shows pH$_i$ derived from the ^{31}P NMR P$_i$ peak before and during fructose. It may be seen that when FVR is low (i.e. a relatively thin periportal shell of viable cells remains), pH$_i$ is high (7.6–7 8). This is consistent with our previous observations [9], and we have attributed this phenomenon to the high rate of gluconeogenesis from lactate (a proton-consuming process [11,21]) in the periportal cells, with lactate as sole substrate. pH$_i$ in the perivenous region must be lower than the values in the region of high FVR in Figure 4 (top panel), because the latter values are contributed to by the high pH$_i$ of the periportal region. It may be noted that the points obtained before fructose lie above those during fructose infusion. Figure 4 (bottom panel) shows the change in recorded pH$_i$ (ΔpH$_i$) induced by fructose infusion. At high FVRs there is marked lowering of pH$_i$ during fructose, whereas at low FVR the change in pH$_i$ is small, resulting in a significant linear regression of ΔpH$_i$ versus FVR (P < 0 01). There must therefore be considerable perivenous acidification during fructose, accounting for the major part of the fall in pH$_i$ during fructose in the intact liver. The substantial fall in pH$_i$ perivenously during fructose strongly suggests fructolysis and/or glycolysis to lactate in this region, as inferred from the lactate data above. The lesser fall in pH$_i$ periportally may be due to the inhibition of gluconeogenesis from lactate observed during fructose infusion and its replacement by gluconeogenesis from fructose, a proton-neutral process.

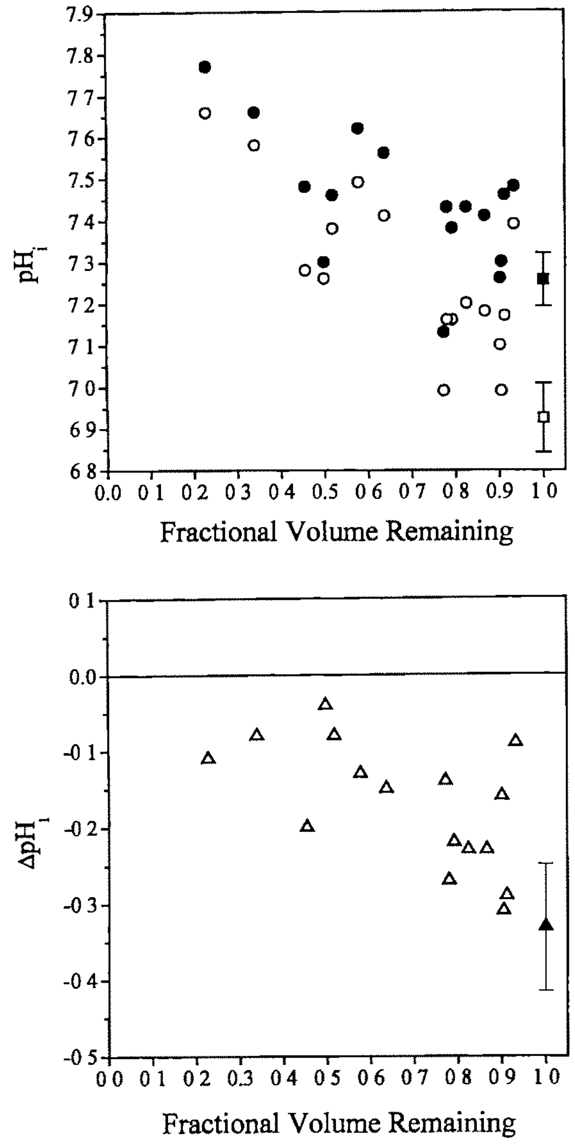

Figure 4 pHi in the perfused rat liver after retrograde digitonin destruction, before and after fructose infusion

Top panel: pH$_i$ in the remaining lobule after digitonin destruction before (●) and during (○) fructose infusion, plotted against FVR. Means±S.E.M. from control studies (digitonin omitted) before and during fructose are shown at FVR = 1.0 (□, ■). Bottom panel: change in pH$_i$ between the basal and fructose phases, calculated from the data in the top panel; control studies with digitonin omitted ($n = 6$, means±S.E.M.) are shown at FVR = 1.0 (▲).

The above data suggests that generation of lactate plus protons is taking place perivenously, in contrast to the situation periportally. We conclude that under the present conditions the more periportal zones convert almost half of the fructose taken up into glucose, with the fate of the remainder of the periportal fructose uptake being either glycogen synthesis or oxidation, but not lactate. The perivenous zones generate lactate plus protons from fructose and/or periportally synthesized glucose. Since, as indicated above, the perivenous uptake of fructose is likely to be small, it seems possible that most of the perivenous lactate output is derived from glucose originating periportally from fructose. Comparison of Figure 1 (top panel) and Figure 3 indicates that the perivenous uptake of glucose during fructose is more than sufficient to account for the lactate output in this region. Although fructose uptake is probably less perivenously than periportally, some at least must occur since fructose 1-phosphate accumulates predominantly in the perivenous zone (see below). Direct fructolysis within the same hepatocytes which originally take up fructose is also a potential source of perivenous lactate production. Though this doubtless occurs to some extent, its extent might be greatly overestimated by studies in mixed suspensions of isolated hepatocytes containing both periportal and perivenous cells, or in balance studies across whole liver perfusions, in which pathways commence periportally (e.g. fructose conversion into glucose) and continue perivenously (glucose conversion into lactate), might appear only as direct fructose conversion into lactate.

Figure 5 (top panel) shows the fractional change in PME during fructose infusion. It may be calculated from the data of Woods et al. [1] that approx. 85% of the increase in PME in whole perfused rat liver during fructose is attributable to the accumulation of fructose 1-phosphate, so the great majority of the PME increase shown in Figure 5 (top panel) is likely to arise from fructose 1-phosphate. When FVR is less than 0.5, there is very little change in PME, despite the major conversion of fructose into glucose in the periportal region. However, at FVR 0.5–1.0, and in controls (no digitonin), there are substantial increases in PME. Since fructose uptake may be less perivenously than periportally (Figure 2), these data suggest a relative impediment to the onward metabolism of fructose 1-phosphate in the perivenous region. Previous workers have identified smaller increments in PME and little change in pH$_i$ using ^{31}P NMR following fructose administration in rat models of hepatic centrilobular necrosis [22]. These observations are consistent with our findings that accumulation of PME and decreased pH$_i$ arise from glucose and fructose metabolism in the perivenous zone.

Figure 5 (bottom panel) shows the plot of fractional change in PME against the reciprocal of fractional change in ATP. The data shows considerable scatter but has a significant linear regression ($P < 0.01$), suggesting an inverse relationship of PME and ATP throughout the lobule. It therefore seems likely that the fall in ATP is caused by fructose 1-phosphate accumulation as previously suggested [1].

It can be concluded that fructokinase is expressed throughout the liver lobule, since periportal cells convert fructose into glucose and PME accumulates perivenously during fructose infusion. 'Fructolysis' is, however, limited perivenously, perhaps because of the intrinsically low expression of fructose 1-phosphate aldolase. Alternatively, the rate of provision of ATP for the fructokinase reaction may be limited perivenously by the low capacity of that zone for aerobic oxidation [19], leaving glycolysis as the main mechanism of ATP provision. Though perivenous falls in ATP during fructose might be expected to stimulate glycolysis by release of ATP inhibition of phosphofructokinase-1, that effect would be offset by the marked fall in pH$_i$ in this region (Figure 4) [23].

Fructose infusion at low portal concentrations (approx. 0.4 mM) has been shown to stimulate hepatic glycogen formation from glucose in dogs [24], possibly due to the accumulation of intracellular fructose 1-phosphate, which is known to release glucokinase from its regulatory protein at very low concentrations [25,26]. Fructose 1-phosphate may also contribute to glycogen accumulation by inhibition of glycogen phosphorylase [27]. Since in livers from 48-h starved rats glucokinase activity (and enzyme protein concentration [28]) are markedly concentrated in the most perivenous cells [15], where the accumulation of fructose 1-phosphate is greatest (Figure 5), glucokinase activation would occur primarily in those cells and present

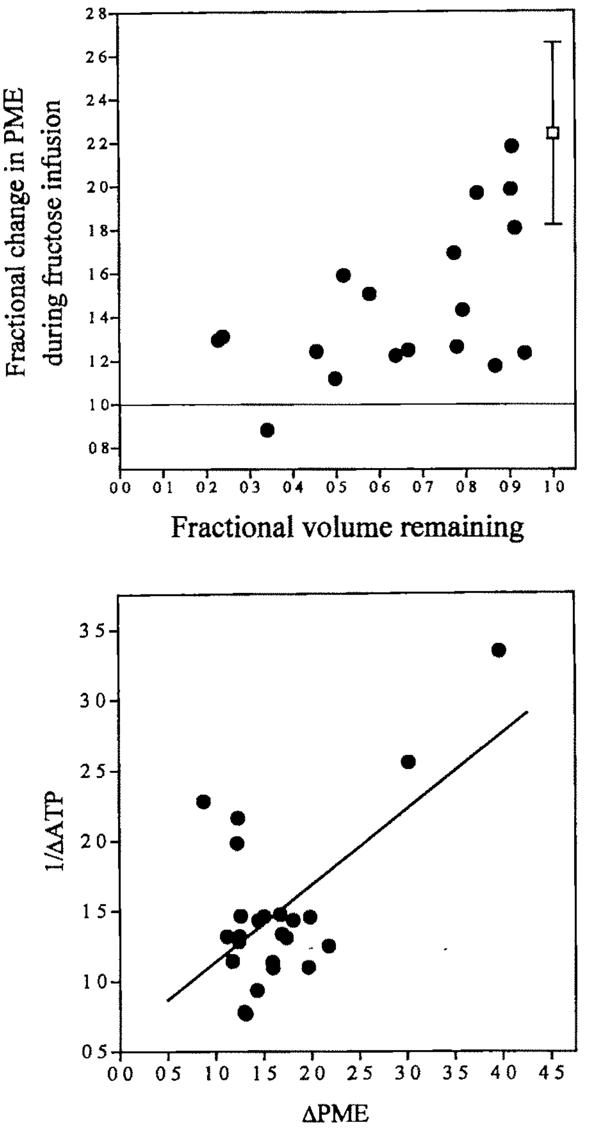

Figure 6 Fractional change in PME during fructose infusion, and the relationship to ΔATP

Top panel fractional change in PMEs (predominantly fructose 1-phosphate) concentration during fructose infusion (compared with pre-fructose), plotted against FVR Means ± S E.M of the fractional change seen in control studies (*n* = 6), i e with no digitonin destruction, is shown at FVR = 1 0 (□) Bottom panel 1/ΔATP plotted against ΔPME The regression line is 1/ΔATP = 0 60 + 0 54(ΔPME)

glucose 6-phosphate for glycolysis to lactate, as well as for glycogen synthesis.

Finally, the present study sheds some light on the relatively small changes in pH_i during fructose infusion, previously detected by ^{31}P NMR in whole liver [3]. The NMR-measured changes in the present study were rather greater than previously described; however, in whole livers, perivenous acidification would have been partially obscured by the lack of change in pH_i periportally. The larger falls in pH_i observed using pH-sensitive micro-electrodes [9] might be purely due to chance impalements of perivenous cells, in which marked falls in perivenous pH_i during fructose infusion are suggested by the present data, the apparent discrepancy being thus a manifestation of heterogeneity within the hepatic lobule.

This work was supported by a grant from the Wellcome Trust We are grateful to Dr P. Kinchesh, and the University of London Intercollegiate Research Service for access to NMR facilities, and to Professor D M Williams for the use of quantitative histomorphometry equipment and Professor C L Berry for histological facilities.

REFERENCES

1 Woods, H F, Eggleston, L V. and Krebs, H A (1970) The cause of hepatic accumulation of fructose 1-phosphate on fructose loading Biochem J **119**, 501–510

2 Woods, H. F and Alberti, K G G M (1972) Dangers of intravenous fructose Lancet **ii**, 1354–1357

3 Iles, R A., Griffiths, J R, Stevens, A N., Gadian, D G and Porteous, R (1980) Effects of fructose on the energy metabolism and acid–base status of the perfused starved-rat liver A ^{31}phosphorus nuclear magnetic resonance study. Biochem. J. **192**, 191–202

4 Sahebjami, H and Scalettar, R (1971) Effects of fructose infusion on lactate and uric acid metabolism Lancet **1**, 366–369

5 Oberhaensli, R D, Rajagopalan, B, Tylor, D J, Radda, G K, Collins, J E, Leonard, J. V, Schwarz, H and Herschkowitz, N. (1987) Study of hereditary fructose intolerance by use of ^{31}P magnetic resonance spectroscopy Lancet **i**, 931–934

6 Gitzelmann, R, Steinmann, B. and Van Den Berghe, G (1989) Disorders of fructose metabolism In The Metabolic Basis of Inherited Disease, vol 1 (Scriver, C R, Beaudet, A L, Sly, W S and Valle, D, eds), pp 407–425, McGraw-Hill, New York

7 Anundi, I, Kauffman, F C and Thurman, R C (1987) Gluconeogenesis from fructose predominates in periportal regions of the liver lobule J Biol Chem **262**, 9529–9534

8 Suzuki-Kemmelmeier, F, Ishii-Iwamoto, E L and Bracht, A (1992) The metabolism of fructose in the bivascularly perfused rat liver Biochim Biophys Acta **1116**, 275–282

9 Cohen, R D, Henderson, R. M, Iles, R A and Smith, J A (1982) Metabolic interrelationships of intracellular pH measured by double-barrelled micro-electrodes in perfused rat liver J. Physiol **330**, 69–80

10 Burns, S P, Cohen, R D, Iles, R A, Germain, J P, Going, T. C. H, Evans, S J W and Royston, P (1996) A method for determination *in situ* of variations within the hepatic lobule of hepatocyte function and metabolite concentrations Biochem J **319**, 377–383

11 Cohen, R D, Iles, R A, Barnett, D, Howell, M E O and Strunin, J The effect of changes in lactate uptake on the intracellular pH of the perfused rat liver. (1971) Clin. Sci **41**, 159–170

12 Krebs, H. A and Henseleit, K (1932) Untersuchungen uber die Harnstoffbildung im Tierkorper Hoppe-Seyler's Z Physiol Chem **210**, 33–36

13 Quistorff, B and Romert, P. (1989) High zone-selectivity of cell permeabilization following digitonin-pulse perfusion of rat liver A re-interpretation of the microcirculatory zones Histochemistry **92**, 487–498

14 Racine, L, Scoazec, J, Moreau, A, Bernuau, D. and Feldmann, G (1993) Effects of digitonin on the intracellular content of rat hepatocytes implications for its use in the study of intralobular heterogeneity J Histochem. Cytochem **7**, 991–1001

15 Burns, S P, Desai, M, Cohen, R D, Hales, C N, Iles, R A, Germain, J P, Going, T C H and Bailey, R A (1997) Gluconeogenesis, glucose handling, and structural changes in livers of the adult offspring of rats partially deprived of protein during pregnancy and lactation J Clin Invest **100**, 1768–1774

16 Ala-Korpela, M, Korhonen, A, Keisala, J, Horkko, S., Korpi, P, Ingman, L P, Jokisaari, J, Savolainen, M J and Kesaniemi, Y A (1994) ^{1}H NMR-based absolute quantitation of human lipoproteins and their lipid contents directly from plasma. J Lipid Res **35**, 2292–2304

17 Bergmeyer, H U and Bernt, E (1974) D-Fructose In Methods of Enzymatic Analysis (Bergmeyer, H. U ed), pp 1176–1179, Academic Press, New York

18 Press, W H, Flannery, B P, Teukolsky, S A, Vetterling, W T (1988) The Art of Scientific Computing: Numerical Recipes In C, Cambridge University Press, New York

19 Burns, S P, Cohen, R D., Iles, R A, Bailey, R A, Desai, M, Germain, J P and Going, T C H (1999) Zonation of gluconeogenesis, ketogenesis and intracellular pH in livers from normal and diabetic ketoacidotic rats. evidence for intralobular redistribution of metabolic events in ketoacidosis Biochem J **343**, 273–280

20 Payne, R W, Lane, P W, Digby, P G N, Harding, S A, Leech, P K, Morgan G W, Todd, A D, Thompson, R, Tunnicliffe Wilson, G, Welham, S J et al. (1993) Genstat 5 Release 3 Reference Manual, Clarendon Press, Oxford

21 Cohen, R. D. (1990) The metabolic background to acid–base homeostasis and some of its disorders In The Metabolic and Molecular Basis of Acquired Disease (Cohen, R D, Lewis, B., Alberti, K G M M and Denman, A M eds), pp 962–1001, Baillière Tindall, London

22 Bates, T E, Williams, S R, Busza, A L, Proctor, E and Gadian, D. G. (1988) A ^{31}P nuclear magnetic resonance study *in vivo* of metabolic abnormalities in rats with acute liver failure NMR Biomed **1**, 69–73

23 Ui, M (1966) A role of phosphofructokinase in pH-dependent regulation of glycolysis. Biochim Biophys. Acta **124**, 310–322
24 Shiota, M., Galassetti, P., Monohan, M, Neal, D. W and Cherrington, A. D (1998) Small amounts of fructose markedly augment net hepatic glucose uptake in the conscious dog Diabetes **47**, 867–873
25 Detheux, M., Vandercammen, A and Van Schaftingen, E (1991) Effectors of the regulatory protein acting on liver glucokinase: a kinetic investigation Eur J. Biochem **200**, 553–561
26 Agius, L and Peak, M. (1993) Intracellular binding of glucokinase in hepatocytes and translocation by glucose, fructose and insulin Biochem J. **296**, 785–796
27 Youn, J H, Youn, M S. and Bergman, R N (1986) Synergism of glucose and fructose in net glycogen synthesis in perfused rat livers J. Biol Chem **261**, 15960–15969
28 Toyoda, Y, Miwa, I, Kamiya, M, Ogiso, S, Nonogaki, N, Aoki, S and Okuda, J (1995) Tissue and subcellular distribution of glucokinase in rat liver and their changes during fasting–refeeding Histochem Cell Biol **103**, 31–38

Received 4 January 2000/11 April 2000, accepted 28 April 2000

Biochem. J (2000) 349, 547–557 (Printed in Great Britain)

Regulation of BAD by cAMP-dependent protein kinase is mediated via phosphorylation of a novel site, Ser^{155}

Jose M. LIZCANO[1], Nick MORRICE and Philip COHEN[2]

MRC Protein Phosphorylation Unit, Department of Biochemistry, MSI/WTB Complex, University of Dundee, Dow Street, Dundee DD1 5EH, Scotland, U.K.

The interaction of BAD (Bcl-2/Bcl-X$_L$-antagonist, causing cell death) with Bcl-2/Bcl-X$_L$ is thought to neutralize the anti-apoptotic effects of the latter proteins, and may represent one of the mechanisms by which BAD promotes apoptosis A variety of survival signals are reported to induce the phosphorylation of BAD at Ser^{112} or Ser^{136}, triggering its dissociation from Bcl-2/Bcl-X$_L$. Ser^{136} is thought to be phosphorylated by protein kinase B (PKB, also called Akt), which is activated when cells are exposed to agonists that stimulate phosphatidylinositol 3-kinase (PI3K). In contrast, Ser^{112} is reported to be phosphorylated by mitogen-activated protein (MAP) kinase-activated protein kinase-1 (MAPKAP-K1, also called RSK) and by cAMP-dependent protein kinase (PKA). Here we identify Ser^{155} as a third phosphorylation site on BAD. We find that Ser^{155} is phosphorylated preferentially by PKA *in vitro* and is the only residue in BAD that becomes phosphorylated when cells are exposed to cAMP-elevating agents. The phosphorylation of BAD at Ser^{155} prevents it from binding to Bcl-X$_L$ and promotes its interaction with 14-3-3 proteins. We also provide further evidence that MAPKAP-K1 mediates the phosphorylation of Ser^{112} in response to agonists that activate the classical MAP kinase pathway. However insulin-like growth factor 1, a potent activator of PI3K and PKB does not increase the phosphorylation of Ser^{136} in BAD-transfected HEK-293 cells, and nor is the basal level of Ser^{136} phosphorylation suppressed by inhibitors of PI3K.

Key words: apoptosis, Bcl-2, cAMP, MAP kinase, PKB

INTRODUCTION

Programmed cell death (apoptosis) is the process by which cells destroy themselves when they are damaged irrepairably by exposure to stressful stimuli or infectious agents, or when they no longer receive signals from specific survival factors [1]. The regulation of apoptosis is critical for many processes, including development, the defence against pathogens and the prevention of proliferation of transformed cells. Bcl-2 and related cytoplasmic proteins are key regulators of apoptosis [2], and there has been much interest focussed upon their regulation over the past few years. One member of this family is BAD (Bcl-2/Bcl-X$_L$-antagonist, causing cell death), a pro-apoptotic protein that binds to the anti-apoptotic proteins Bcl-2 and Bcl-X$_L$ [3]. This interaction is thought to neutralize the anti-apoptotic effects of Bcl-2/Bcl-X$_L$ and may represent one of the mechanisms by which BAD promotes apoptosis.

Zha et al. [4] were the first to report that treating lymphoid progenitor cells with interleukin-3 (IL-3) results in the phosphorylation of BAD. This causes BAD to interact with 14-3-3 proteins instead of Bcl-2 or Bcl-X$_L$, resulting in the liberation of these anti-apoptotic proteins, which can then interact with Bax to inhibit apoptosis.

Two sites on BAD, Ser^{112} and Ser^{136}, were reported to be phosphorylated *in vivo* [4]. Both sites lie in Arg-Xaa-Arg-Xaa-Xaa-Ser/Thr- sequences, which are preferred consensus sequences for several protein kinases, including protein kinase B (PKB) and mitogen-activated protein (MAP) kinase-activated protein kinase-1 (MAPKAP-K1, also called RSK) [5,6]. Subsequently, BAD was found to be phosphorylated at Ser^{136} by PKB (also called Akt) *in vitro* or when co-expressed with BAD in cells [7,8]. This protein kinase is reported to have strongly anti-apoptotic effects when constitutively active forms are over-expressed and to be activated *in vivo* when cells are stimulated with survival signals that activate phosphatidylinositol 3-kinase (PI3K), including IL-3 [9].

More recently, activation of the MAP kinase pathway was reported to induce the phosphorylation of BAD at Ser^{112}. Thus BAD phosphorylation induced by IL-3 or granolocyte–macrophage colony-stimulating factor (GMCSF) was partially suppressed by PD 98059 [10,11], an inhibitor of the activation of MAP kinase kinase-1 (MKK1) [12] Similarly, the phosphorylation of BAD at Ser^{112} induced by brain-derived neurotrophic factor (BDNF) in cerebellar granule neurons [13] or by PMA ('TPA') [14], epidermal growth factor (EGF) [15] or activated Ras or Raf [15] in transfected HEK-293 cells, was prevented by PD 98059. MAPKAP-K1, which is an immediate downstream target of the MAP kinases extracellular-signal-regulated kinases (ERKs) 1 and 2, was found to phosphorylate Ser^{112} in co-transfection experiments carried out in 293 cells [13–15]. These

---

Abbreviations used BAD, Bcl-2/Bcl-X$_L$-antagonist, causing cell death, BDNF, brain-derived neurotrophic factor, EGF, epidermal growth factor, ERK, extracellular-signal-regulated kinase, GMCSF, granulocyte–macrophage colony-stimulating factor, GST, glutathione S-transferase, IBMX, isobutylmethylxanthine, IGF1, insulin-like growth factor-1, IL, interleukin; MAP, mitogen-activated protein, MAPKAP-K1, MAP kinase-activated protein kinase-1, MKK1, MAP kinase kinase-1, MSK1, mitogen-and-stress-activated protein kinase-1, NEB, New England Biolabs, PDK1, 3-phosphoinositide-dependent protein kinase-1, PI3K, phosphatidylinositol 3-kinase; PKA, cAMP-dependent protein kinase, PKB, protein kinase B, PKC, protein kinase C, PKI, specific peptide inhibitor of PKA, PDGF, platelet-derived growth factor

[1] Present address Department de Bioquimica i Biologia Molecular, Facultat de Medicina, Universitat Autonoma de Barcelona, E-08193 Bellaterra, Barcelona, Spain

[2] To whom correspondence should be addressed (p cohen@dundee ac.uk).

observations suggest that MAPKAP-K1 is the protein kinase that mediates the phosphorylation of Ser^{112} *in vivo* by stimuli that activate the classical MAP kinase cascade.

cAMP-dependent protein kinase (PKA) was also reported to phosphorylate BAD at Ser^{112} and to be the major Ser^{112} kinase associated with a mitochondrial membrane fraction isolated from IL-3-stimulated cells. This appeared to be a particular form of PKA that was complexed to the PKA-anchoring protein ('AKAP') 84; this protein targets PKA to the mitochondrial outer membrane [16]. These observations contrasted with the suggestion that the IL-3-induced phosphorylation of Ser^{112} was mediated by MAPKAP-K1. Moreover forskolin, a cAMP-elevating agent, was reported to induce the phosphorylation of BAD at Ser^{112} in transfected 293 cells [14].

Here we report that the major site on BAD phosphorylated by PKA *in vitro* is not Ser^{112} or Ser^{136}, but Ser^{155}. Moreover, Ser^{155}, but not Ser^{112} or Ser^{136}, becomes phosphorylated when transfected 293 cells are stimulated by cAMP-elevating agents. The phosphorylation of Ser^{155} triggers the dissociation of BAD from Bcl-2 and Bcl-X$_L$ and promotes its interaction with 14-3-3 proteins.

MATERIALS AND METHODS

Materials

Tissue-culture reagents, EGF and insulin-like growth factor-1 (IGF1) were purchased from Gibco BRL (Paisley, Renfrewshire, Scotland, U.K.); complete protease cocktail and sequencing-grade trypsin were from Boehringer (Lewes, East Sussex, U.K.), H89, PD 98059, Ro 318220, rapamycin and Zwittergent 3-16 were from Calbiochem (Nottingham, U.K.), forskolin, isobutylmethylxanthine (IBMX), wortmannin and PMA were from Sigma (Poole, Dorset, U.K.), Protein G–Sepharose was from Pharmacia (Milton Keynes, U.K.), pEBG-BAD plasmid expressing glutathione S-transferase (GST)–BAD was from New England Biolabs (NEB) (Hitchin, Herts., U.K.) and [γ-^{32}P]ATP was from Amersham (Little Chalfont, Bucks., U.K.). An antibody that recognizes 14-3-3γ (SC-73) was obtained from Santa Cruz Biotechnology (Santa Cruz, CA, U.S.A.).

Buffer solutions

Buffer A comprised 50 mM Tris/HCl, pH 7.5, 1 mM EDTA, 1 mM EGTA, 1 % (w/v) Triton X-100, 1 mM sodium orthovanadate, 50 mM NaF, 5 mM sodium pyrophosphate, 0.27 M sucrose and 0.1 % β-mercaptoethanol. Cell-lysis buffer was Buffer A containing 2 μM microcystin-LR, 0.1 mM PMSF, 1 mM benzamidine. Buffer B comprised 50 mM Tris/HCl, pH 7.5, 1 mM EGTA, 0.1 % (v/v) β-mercaptoethanol and 0.05 % (w/v) Brij-35.

Expression of GST–BAD and His-Bcl-X$_L$ in *Escherichia coli*

A cDNA encoding full-length murine BAD was obtained by PCR from a mouse cDNA library and subcloned into a pGEX vector by Dr Antonio Casamayor in this Unit. The Ser^{112} → Ala/Ser^{136} → Ala double mutant was generated by using a PCR-based site-directed mutagenesis kit (Stratagene) and verified by DNA sequencing. The mutant constructs were transformed into BL21 DE3 (pLysS) *E. coli* and the GST fusion proteins purified on GSH–Sepharose. Each litre of bacterial culture yielded 1 mg of pure GST–BAD. A vector expressing the first 211 residues of Bcl-X$_L$ (lacking the C-terminal hydrophobic region) preceded by six histidine residues [17] was provided by Dr. Paul Clarke, Biomedical Research Centre, Ninewells Hospital, Dundee, Scotland, U.K. This was also expressed in *E. coli* and purified on Ni^{2+}-nitrilotriacetate–agarose. Each litre of bacterial culture yielded 4 mg of pure His-Bcl-X$_L$.

Isolation and assay of protein kinases

Protein kinases were provided by the members of this Unit indicated in parentheses: MAPKAP-K1b (RSK2) purified to near homogeneity from rabbit skeletal muscle [18] (Dr N. Morrice); the catalytic subunit of PKA purified to homogeneity from bovine cardiac muscle [19] (Dr C. Smythe); GST–mitogen-and-stress-activated protein kinase-1 (MSK1) activated by ERK2 [20] (Dr A. Paterson); His-tagged PKBα activated by 3-phosphoinositide-dependent protein kinase-1 (PDK1; Dr C. Armstrong). One unit of protein kinase activity was that amount which catalysed the phosphorylation of 1 nmol of phosphate in 1 min in the standard assay at 30 °C. MAPKAP-K1, MSK1 and PKB were assayed using the peptide Gly-Arg-Pro-Arg-Thr-Ser-Ser-Phe-Ala-Glu-Gly (Crosstide, 30 μM) and PKA using the peptide Leu-Arg-Arg-Ala-Ser-Leu-Gly (Kemptide, 30 μM)

Tryptic digestion of phosphorylated BAD

GST–BAD (2 μM) purified from bacterial extracts was phosphorylated by incubation for 90 min at 30 °C with GST–MSK1, MAPKAP-K1, PKA or PKB, each at 10 units/ml in Buffer B plus 10 mM $MgCl_2$ and 0.1 mM [γ-^{32}P]ATP (5000 c.p.m./pmol). After denaturation, electrophoresis on an SDS/10 % (w/v) polyacrylamide gel and Coomassie Blue staining, ^{32}P-labelled full-length GST–BAD was excised from the gel and digested for 18 h with 1 μg of trypsin at 30 °C in 0.3 ml of digestion buffer (0.05 % Zwittergent 3-16 in 50 mM ammonium bicarbonate). The digest was centrifuged for 10 min at 13000 *g*, extracted with a further 0.3 ml of digestion buffer and the supernatant, containing > 90 % of the ^{32}P radioactivity, chromatographed on a C$_{18}$ column as described in the Figure legends.

Production of antibodies that recognize BAD

Polyclonal antibodies that recognize specific phosphorylation sites in murine BAD were raised against the following peptides (one-letter code): RSRMSS*YPDRG (Ser^{112}), RGSRS*APPNL (Ser^{136}) and RELRRMS*DEFEGS (Ser^{155}), where S* denotes a phosphorylated serine residue. These peptides were coupled with keyhole-limpet haemocyanin, and each injected into a different sheep at the Scottish Antibody Production Unit (Carluke, Ayrshire, U.K.). A second injection was made 6 weeks later. After a further 2 weeks, serum was withdrawn and affinity-purified by sequential chromatographies on phosphopeptide–CH-Sepharose and dephosphopeptide–CH-Sepharose. A further antibody that recognizes phosphorylated and dephosphorylated BAD was raised against the synthetic peptide WDRNLGRGSAPSQ, which corresponds to residues 162–174 of BAD. The antibodies used in the present study may be obtained from UBI (Lake Placid, NY, U S.A.).

Cell culture

HEK-293 cells and monkey kidney COS1 cells were maintained in Dulbecco's modified Eagle's medium supplemented with 10 % (v/v) foetal-calf serum, at 37 °C, in an atmosphere of 5 % CO_2.

Transient transfections, stimulation and cell lysis

Dishes (10 cm diameter) of HEK-293 cells were transfected with 10 μg of the pEBG-BAD plasmid (NEB) using a modified

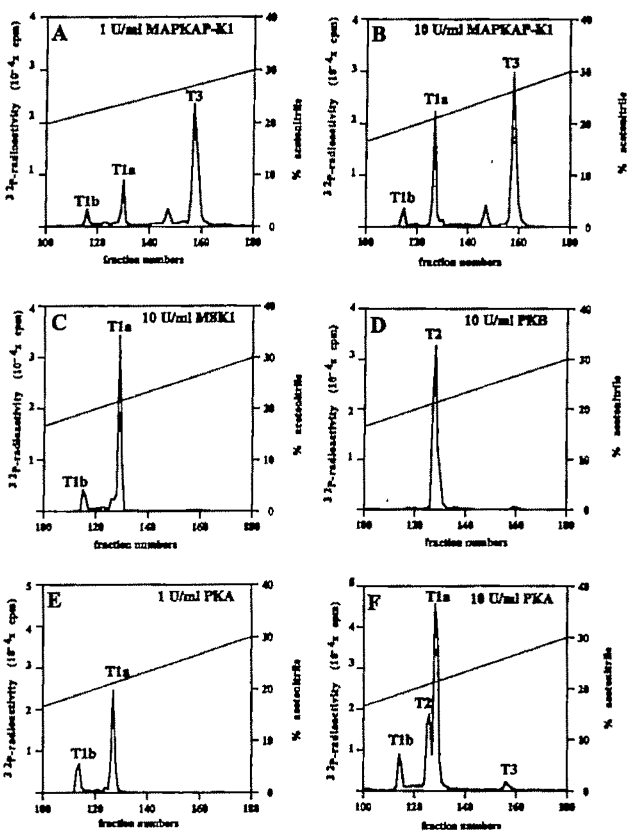

Figure 1 Separation of the tryptic phosphopeptides in BAD after phosphorylation *in vitro* by PKB, MSK1, MAPKAP-K1 and PKA

The ^{32}P-labelled peptides obtained by tryptic digestion of BAD phosphorylated by the protein kinases indicated (see the Materials and methods section) were chromatographed on a Vydac 218TP54 C_{18} column (Separations Group, Hesperia, CA, U.S.A.) equilibrated with 0.1% trifluoroacetic acid. The column was developed with a linear acetonitrile gradient in 0.1% trifluoroacetic acid (dotted lines). The flow rate was 0.8 ml/min, and fractions, 0.4 ml each, were collected. All 240 fractions were counted for ^{32}P radioactivity (continuous lines). Typically > 90% of the ^{32}P radioactivity applied to the column was recovered in the eluted fractions. The four major ^{32}P-labelled peptides eluted at fractions 116 (termed T1b), 128 (termed T2), 130 (termed T1a) and 158 (termed T3) are indicated. No ^{32}P radioactivity was detected in fractions 1–100 and 181–240 (results not shown). Similar results were obtained in three separate experiments for (**B**), (**C**) and (**F**) and two experiments for (**A**), (**D**) and (**E**)

calcium phosphate gel method [21]. After transfection (24 h), cells were serum-starved for 18 h, then stimulated for the times indicated with PMA, EGF, IGF1 or forskolin, with or without prior treatment for 1 h with PD 98059, U0126, Ro 318220, H89, wortmannin, LY 249002 or rapamycin, Each dish of cells was lysed in 1 ml of ice-cold lysis buffer, centrifuged at 4 °C for 10 min at 13000 g, and the supernatants frozen immediately in liquid nitrogen and stored at −80 °C until use. Protein concentrations were determined [22] using BSA as standard.

Immunoblotting of BAD

Extracts of cells overexpressing GST–BAD were fractionated by electrophoresis on SDS/10%-polyacrylamide gels and transferred to nitrocellulose membranes. Blots were blocked for 1 h at room temperature with 5% (w/v) non-fat dried milk in 20 mM Tris/HCl (pH 7.5)/150 mM NaCl/0.1% Tween 20, then incubated with primary antibody overnight at 4 °C, followed by incubation for 1 h with secondary antibody. Finally the blots were developed with enhanced chemiluminescence (ECL®) reagent (Amersham). All antibodies prepared in the present study were used at 0.1 μg/ml. Before use, all phosphospecific antibodies were preincubated with the dephosphorylated form of the relevant phosphopeptide immunogen (10–50 μg/ml). This was done to neutralize any antibodies present that might recognize the dephosphorylated form of BAD.

Bcl-X_L binding assay

GST–BAD (1 μg) was phosphorylated *in vitro* by incubation for 1 h at 30 °C with or without MSK1, MAPKAP-K1, PKA or PKB (each at 10 units/ml) in Buffer B containing 10 mM $MgCl_2$ and 0.1 mM [γ-^{32}P]ATP (500 c.p.m./pmol). The solutions (25 μl) were further incubated for 1 h at 4 °C with 5 μg His-Bcl-X_L in 50 μl of lysis buffer, and the BAD complexed to Bcl-X_L was captured on Ni^{2+}-nitrilotriacetate–agarose beads. After centrifugation for 5 min at 13000 g, the supernatants (S) were set aside and the pellets (P) washed five times with lysis buffer. The supernatants and final pellets were denatured in SDS, and the solubilized proteins electrophoresed on SDS/10%-polyacrylamide gels and transferred to nitrocellulose. The membranes were autoradiographed and further analysed by immunoblotting with the antibody that recognizes phosphorylated and dephosphorylated BAD equally well.

14-3-3 overlay

GST–BAD was phosphorylated for 1 h and 30 °C *in vitro* by incubation with 10 units/ml of GST–MSK1, MAPKAP-K1, PKA or PKB, in buffer B containing 10 mM $MgCl_2$ and 0.1 mM unlabelled ATP. Samples were denatured in SDS, electrophoresed on a SDS/10%-polyacrylamide gel and transferred to nitrocellulose. 14-3-3 overlay assay was performed using the mixed BMH1 and BMH2 isoforms of *Saccharomyces cerevisiae* 14-3-3 proteins each labelled with digoxygenin [23].

RESULTS

Phosphorylation of BAD *in vitro* by different protein kinases

MAPKAP-K1 is not the only protein kinase that is activated by the MAP kinase family members ERK1 and ERK2. In particular, MSK1 and the closely related MSK2 are also physiological substrates for ERK1/ERK2 [20] and are therefore candidates to mediate the phosphorylation of BAD at Ser^{112}. For this reason, we compared the phosphorylation of BAD by MAPKAP-K1 and MSK1 (Figure 1).

MAPKAP-K1 (1 unit/ml) or MSK1 (10 units/ml) both phosphorylated BAD to about 1 mol/mol of protein after 90 min. Digestion with trypsin, followed by chromatography on a C_{18} column revealed that MAPKAP-K1 had phosphorylated BAD at one major tryptic phosphopeptide termed T3 (Figure 1A), which was identified by MS (Table 1) and Edman sequencing (results not shown), as the peptide comprising residues 110–130 phosphorylated at Ser^{112}, as expected. In contrast, MSK1 phosphorylated a distinct tryptic peptide, T1a (Figure 1C), which was eluted at almost the same acetonitrile concentration as the single tryptic peptide phosphorylated by PKB (10 units/ml), termed phosphopeptide T2 (Figure 1D). Peptide T2 was identified by MS (Table 1) and Edman sequencing (results not shown) as the peptide comprising residues 134–146 of BAD, phosphorylated at Ser^{136} as expected. Surprisingly, however, peptide T1a was found not to be identical with peptide T2, but to comprise residues 153–163 of BAD (Table 1) phosphorylated at Ser^{155} (Figure 2A).

Table 1 Identification of tryptic phosphopeptides isolated from BAD phosphorylated with different protein kinases

The phosphopeptides from Figure 1 were analysed on a Perseptive Biosystems (Framingham, MA, U S A) Elite STR matrix-assisted laser-desorption-ionization–time-of-flight ('MALDI-TOF') mass spectrometer in the linear and reflector mode, using 10 mg/ml·α-cyanocinnamic acid as the matrix The asterisk (*) indicates a methionine sulphone derivative The sequences of peptides are T1a and T1b, RMSDEFEGSFK; T2, SRSAPPNLWAAQR, T3, HSSYPAGTEEDEGMEEELSPFR

			Mass	
Kinase	Phosphopeptide	Residues	Measured	Theoretical
MSK1	T1a	153–163	1428 49*	1428 59
	T1b	153–163	1428.56*	1428 59
PKB	T2	134–146	1533 58	1533.77
MAPKAP-K1	T1a	153–163	1428.52*	1428 59
	T1b	153–163	1428 56*	1428 59
	T3	110–131	2576 80	2577 00
PKA	T1a	153–163	1428 46*	1428.59
	T1b	153–163	1429.63*	1428 59
	T2	134–146	1535 12	1533 77
	T3	110–131	2576 34	2577 00

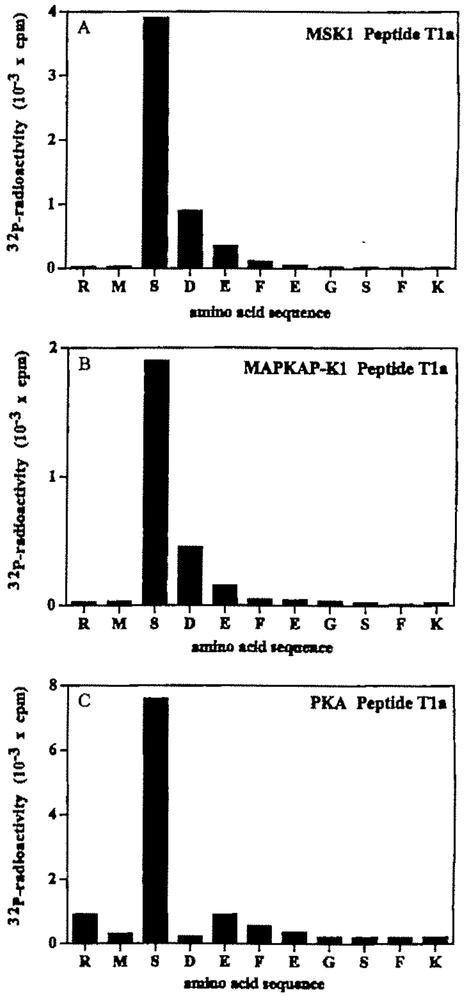

Figure 2 Identification of the phosphorylation sites in peptide T1a

Phosphopeptides T1a from Figures 1(B), 1(C) and 1(F) were sequenced by Edman degradation using an Applied Biosystems 492A protein sequencer ^{32}P radioactivity released after each cycle was measured in a separate experiment by solid-phase Edman degradation of the peptides coupled to a Sequelon-AA membrane (Milligen, Bedford, MA, U S A) as described previously [34]

Interestingly, the minor tryptic phosphopeptide phosphorylated by low concentrations of MAPKAP-K1 (1 unit/ml, Figure 1A) co-migrated with peptide T1a and also comprised residues 153–163 (Table 1) phosphorylated at Ser^{155} (results not shown). When the concentration of MAPKAP-K1 was increased to 10 units/ml, the phosphorylation of BAD approached 2 mol of phosphate/mol of protein, and peptide T1a was now phosphorylated at Ser^{155} to a much high stoichiometry (Figures 1B, 2B and Table 1). The molecular mass of the minor tryptic phosphopeptide T1b (Figures 1A, 1B and 1C) corresponded to that of T1a in which the methionine at residue 154 was partially oxidized to methionine sulphone (Table 1). Peptide T1a is likely to correspond to the unoxidized peptide, which becomes oxidized after its elution from the C_{18} column and before its analysis by MS.

The amino acid sequence surrounding Ser^{155} (Arg-Arg-Met-Ser) is the preferred consensus sequence for phosphorylation by PKA (reviewed in [24]), which prompted us to re-examine the phosphorylation of BAD by this protein kinase. At 1 unit/ml, PKA phosphorylated BAD at one major and one minor tryptic phosphopeptide, co-eluting with peptides T1a and T1b respectively (Figure 1E). MS (Table 1) and Edman sequencing (Figure 2C) confirmed that both peptides comprised residues 153–163 phosphorylated at Ser^{155}. At 1 unit/ml PKA there was no detectable phosphorylation of Ser^{112} or Ser^{136} after 90 min phosphorylation. However, only a low level of phosphorylation of peptide T2 (containing Ser^{136}) and trace phosphorylation of peptide T3 (containing Ser^{112}) was observed when the concentration of PKA was increased to 10 units/ml (Figure 1F). Further analysis of the traces of peptide T3 revealed that it was a mixture of two phosphopeptides, one phosphorylated at Ser^{111} and the other at Ser^{112} (results not shown). The results presented in Figures 1(E) and 1(F) were obtained using PKA purified from bovine heart in our Unit. However, identical results were obtained with PKA from porcine heart and bovine heart purchased from Sigma (results not shown), the source of the PKA used previously by others [16]. The phosphorylation of BAD by all preparations of PKA was prevented by inclusion of the specific peptide inhibitor of PKA (PKI) in the assays (results not shown).

Consistent with the results presented in Figures 1 and 2, the stoichiometry of phosphorylation of BAD by MSK1 (10 units/ml) was not decreased, and the phosphorylation of BAD by PKA (10 units/ml) only decreased from 2 mol/mol to 1 mol/mol when Ser^{112} and Ser^{136} were both mutated to Ala. In contrast, phosphorylation by PKB was abolished, as expected (results not shown).

Phosphorylation of BAD at Ser^{155} is stimulated by forskolin, but not by PMA, EGF or IGF1 in 293 cells

In order to study the site-specific phosphorylation of BAD in response to different agonists, we raised three different antibodies that recognize this protein only when it is phosphorylated at one of the three known sites. The specificity of these antibodies is

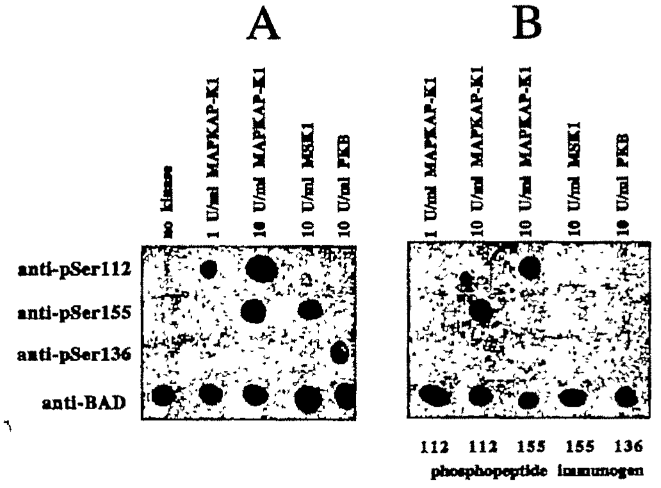

Figure 3 Generation of phosphospecific antibodies against BAD

(A) Bacterially expressed GST–BAD was incubated for 90 min with MgATP, and either 1 unit/ml MAPKAP-K1 or 10 units/ml MAPKAP-K1, or for 90 min with 10 units/ml MSK1 or 10 units/ml PKB, or left unphosphorylated. Aliquots containing 200 ng of BAD were then spotted to nitrocellulose membranes and immunoblotted with affinity-purified antibodies (0.1 μg/ml) raised against phosphopeptides corresponding to the sequences surrounding Ser^{112}, Ser^{136} and Ser^{155}, as well as a dephosphopeptide corresponding to residues 162–174 of BAD. Each piece of nitrocellulose paper was developed simultaneously for the same length of time using the same secondary antibody, and the times of exposure to the film were identical. The strength of the signals can therefore be compared directly. (B) The experiment was carried out exactly as in (A), except that the antibodies were preincubated before immunoblotting with 0.1 mg/ml of an indicated phosphopeptide immunogen used to raise a particular phosphospecific antibody.

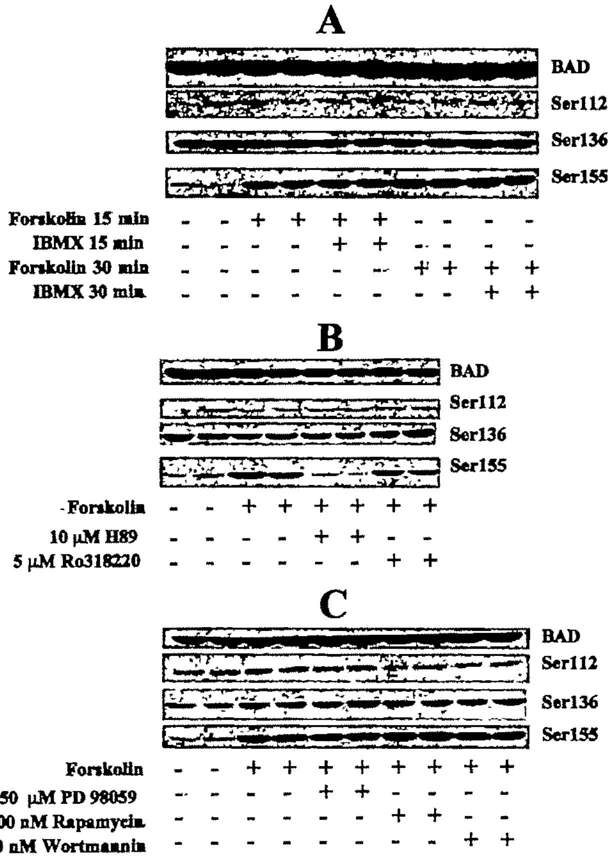
A
BAD
Ser112
Ser136
Ser155
Forskolin 15 min - - + + + + - - - -
IBMX 15 min - - - - + + - - - -
Forskolin 30 min - - - - - - + + + +
IBMX 30 min - - - - - - - - + +
B
BAD
Ser112
Ser136
Ser155
Forskolin - - + + + + + +
10 μM H89 - - - - + + - -
5 μM Ro318220 - - - - - - + +
C
BAD
Ser112
Ser136
Ser155
Forskolin - - + + + + + + + +
50 μM PD 98059 - - - - + + - - - -
100 nM Rapamycin - - - - - - + + - -
100 nM Wortmannin - - - - - - - - + +

Figure 4 Forskolin stimulates the phosphorylation of BAD at Ser^{155}, but not Ser^{112} or Ser^{136} in 293 cells

(A) 293 cells transfected with a plasmid encoding GST–BAD were stimulated for the times indicated with 20 μM forskolin alone or in combination with 10 μM IBMX. (B) Prior to stimulation with forskolin for 30 min, the cells were pretreated for 1 h with 10 μM H89 or 5 μM Ro 318220. (C) same as (B), except that the cells were pretreated with 50 μM PD 98059, 100 nM wortmannin or 100 nM rapamycin. Aliquots of cell lysate (25 μg of protein) were denatured in SDS, electrophoresed on SDS/10%-polyacrylamide gels and, after transfer to nitrocellulose, immunoblotted with the four antibodies used in Figure 3.

demonstrated in Figure 3. The antibody raised against a phosphopeptide corresponding to the sequence surrounding Ser^{112} recognized BAD only after phosphorylation by MAPKAP-K1, but not after phosphorylation at Ser^{136} by PKB or at Ser^{155} by MSK1 (Figure 3A). The recognition of Ser^{112} by this antibody was abolished when it was incubated with the phosphopeptide immunogen used to raise it, but not when it was incubated with the phosphopeptides used to raise the anti-Ser^{155} antibody (Figure 3B) or the anti-Ser^{136} antibody (results not shown). The specificities of the antibodies raised against phosphopeptides corresponding to the sequences surrounding Ser^{136} and Ser^{155} were established in analogous experiments (Figure 3). These antibodies were then used to examine the site-specific phosphorylation of GST–BAD in 293 cells. As indicated below, each antibody recognized a single 50 kDa protein in the transfected cells, corresponding to GST–BAD that was absent in control cells transfected with an empty vector (results not shown).

In unstimulated 293 cells transfected with GST–BAD, the level of phosphorylation of Ser^{155} was low, but increased strikingly in response to the adenylate cyclase activator forskolin and the cAMP phosphodiesterase inhibitor IBMX (Figure 4A), reaching a plateau at 5–15 min (results not shown). In contrast, forskolin (with or without IBMX) did not stimulate the phosphorylation of BAD at Ser^{112} or Ser^{136} up to 30 min using our phosphospecific antibodies (Figure 4).

Ro 318220 is a bisindoylmaleimide, originally developed as an inhibitor of protein kinase C (PKC), but which inhibits MAPKAP-K1 and MSK1 with similar potency to PKC *in vitro* [20,25]. In contrast, PKA and PKB are only inhibited by Ro 318220 at far higher concentrations [25]. Ro 318220 (5 μM) did not affect the forskolin/IBMX-induced phosphorylation of Ser^{155} (Figure 4B), a concentration that blocked PMA- or EGF-induced phosphorylation of Ser^{112} (see below). H89 is an isoquinoline derivative originally developed as an inhibitor of PKA, but which inhibits MSK1 with similar potency *in vitro* ([26]; S. Davies, H. Reddy and P. Cohen, unpublished work). This compound (at 10 μM) prevented the forskolin/IBMX-induced phosphorylation of Ser^{155} (Figure 4B), consistent with phosphorylation by PKA. The phosphorylation of BAD at Ser^{155} was not suppressed by PD 98059, wortmannin (an inhibitor of PI3K) or rapamycin [an inhibitor of the protein kinase 'mTOR' (mammalian target of rapamycin)] (Figure 4C).

Phosphorylation of BAD at Ser^{112} is stimulated by EGF and PMA

The classical MAP kinase cascade was maximally activated after 5 min (EGF) or 15 min (PMA), as judged by the activation of MAPKAP-K1 (Figures 5A and 5B). EGF and PMA both stimulated the phosphorylation of BAD at Ser^{112} at a rate consistent with the rate of activation of MAPKAP-K1 (Figures 5A and 5B). EGF and PMA did not stimulate the phosphorylation of BAD at Ser^{136} or Ser^{155} up to 30 min (Figure 5).

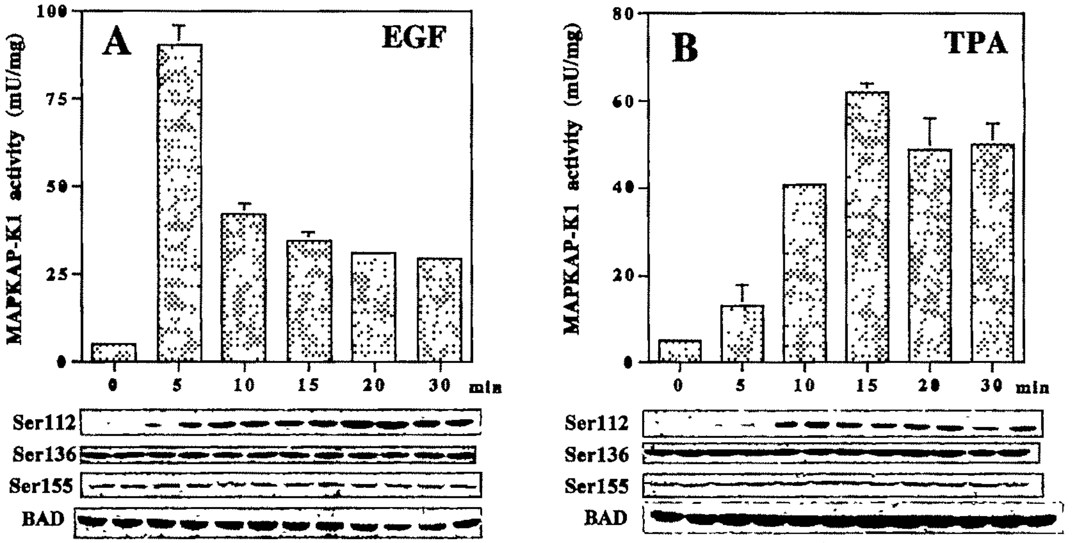

Figure 5 Phosphorylation of BAD at Ser^{112} by EGF and PMA correlates with the activation of MAPKAP-K1

293 cells transfected with a plasmid encoding GST–BAD were stimulated for the times indicated with 100 ng/ml EGF (A) or 400 ng/ml PMA ('TPA', (B). MAPKAP-K1 was immunoprecipitated from lysates [35] and assayed as described in the Materials and methods section The activities are presented as means ± S E M for three separate experiments Aliquots of the cell lysate (25 μg of protein) were then denatured in SDS, electrophoresed on SDS/10%-polyacrylamide gels and, after transfer to nitrocellulose, immunoblotted with the four antibodies used in Figure 3

The phosphorylation of Ser^{112} induced by EGF (Figure 6A) or PMA (Figure 6B) was prevented by PD 98059 or by U0126 (another specific inhibitor of the MAP kinase cascade [27]), but not by wortmannin or rapamycin. Ro 318220 completely prevented the PMA-stimulated phosphorylation of Ser^{112} at 1 μM (Figure 6B). EGF-stimulated Ser^{112} phosphorylation was unaffected at this concentration of Ro 318220, but strongly suppressed at 5 μM Ro 318220 (Figure 6A). H89 (10 μM) had no effect on the EGF-induced phosphorylation of Ser^{112} (results not shown), consistent with H89 being a much weaker inhibitor of MAPKAP-K1 than PKA or MSK1 ([26]; S. Davies, H. Reddy and P. Cohen, unpublished work).

Phosphorylation of BAD at Ser^{136} in transfected 293 cells is not affected by IGF1 or by inhibitors of PI3K

IGF1 induced a strong activation of PKB in 293 cells that was maximal after 5 min, sustained for at least 60 min and prevented by the PI3K inhibitor wortmannin [28] (Figure 7). IGF1 did not stimulate any increase in the phosphorylation of BAD at Ser^{112}, Ser^{136} or Ser^{155}, and nor was the basal level of phosphorylation of any of these sites in unstimulated cells affected by incubation for 1 h with 100 nM wortmannin (Figure 7) or overnight with 100 μM LY 294002 (results not shown), another inhibitor of PI3K.

Effect of site-specific phosphorylation on the interaction of BAD with Bcl-X$_L$ and 14-3-3 proteins

BAD was phosphorylated *in vitro* by incubation with Mg[γ-^{32}P]-ATP and concentrations of MAPKAP-K1, MSK1, PKA and PKB that produced near-stoichiometric phosphorylation of particular sites. A fivefold excess of His-tagged Bcl-X$_L$ was added and the proportion of BAD complexed to Bcl-X$_L$ was determined after pulling down the Bcl-X$_L$ on Ni^{2+}-nitrilotriacetate–agarose (Figure 8A). When BAD was not phosphorylated, it was entirely bound to Bcl-X$_L$ In contrast, no ^{32}P-labelled BAD was bound to Bcl-X$_L$ after phosphorylation by MAPKAP-K1, PKA or MSK1, as judged by immunoblotting or autoradiography. However, 50% of the ^{32}P-labelled BAD was still bound to Bcl-X$_L$ after phosphorylation to 1 mol/mol with PKB (Figure 8A).

In a separate experiment, BAD was phosphorylated as described above, but with unlabelled ATP. The BAD was electrophoresed on a polyacrylamide gel and, after transfer to nitrocellulose, the membranes were blotted with digoxygenin-labelled 14-3-3 proteins. An interaction with 14-3-3 proteins was detected after phosphorylation of BAD by MAPKAP-K1, MSK1, PKA or PKB. No 14-3-3 binding was detected before phosphorylation (Figure 8B). The interaction with 14-3-3 proteins was prevented by preincubating the 14-3-3 probe with a synthetic phosphopeptide corresponding to residues 149–161 of BAD phosphorylated at Ser^{155} (results not shown).

In order to examine whether agonist-stimulated phosphorylation of GST–BAD in 293 cells would induce its interaction with endogenous 14-3-3 proteins, we purified the GST–BAD from these cells and, after electrophoresis, tested for the presence of 14-3-3γ with a specific antibody. These experiments revealed a low level of 14-3-3γ associated with GST–BAD from control cells, which increased considerably when the cells were stimulated with EGF, PMA or forskolin (Figure 8C). The amount of 14-3-3γ was not, however, increased by stimulation with IGF1, consistent with the failure of this agonist to increase the phosphorylation of Ser^{136} or any other site (Figure 7).

Comparison of our Ser^{112}-phosphospecific antibody with that produced by NEB

Our finding that Ser^{155} is the only site that becomes phosphorylated in 293 cells exposed to cAMP-elevating agents (Figure 4) was in conflict with the results of other investigators who reported that forskolin induced the phosphorylation of Ser^{112} in 293 cells transfected with BAD [14]. Since the only obvious

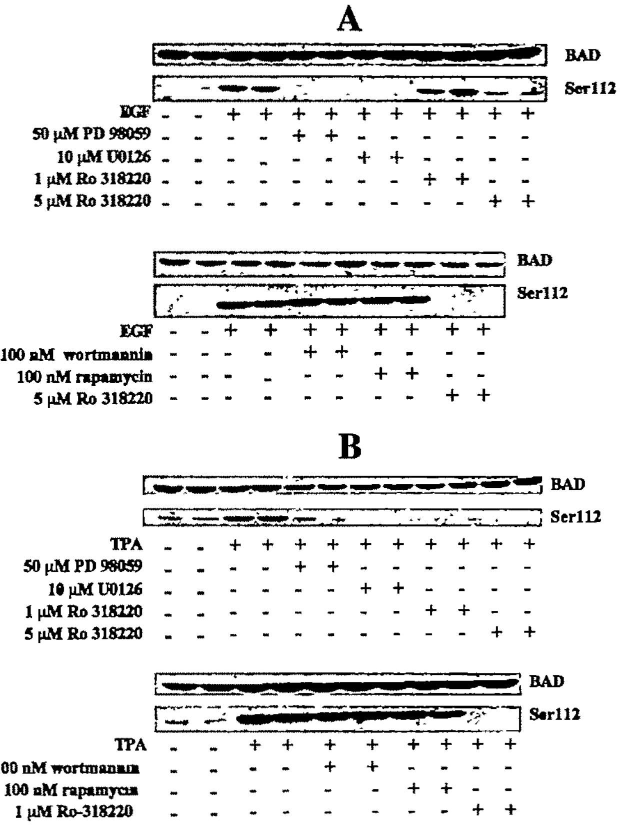

Figure 6 Effects of different protein kinase inhibitors on the EGF- and PMA-induced phosphorylation of BAD at Ser^{112} in 293 cells

293 cells transfected with a plasmid encoding GST–BAD were stimulated for 5 min with 100 ng/ml EGF (**A**) or for 15 min with 400 ng/ml PMA ('TPA', **B**) Prior stimulation with agonist, the cells were pretreated for 1 h with PD 98059, U0126, Ro 318220, wortmannin or rapamycin at the concentrations indicated Cell lysates (25 μg of protein) were denatured in SDS, electrophoresed on SDS/10%-polyacrylamide gels and, after transfer to nitrocellulose, immunoblotted with the antibody specific for BAD phosphorylated at Ser^{112} ('Ser112') The membranes were then stripped and re-probed with the antibody that recognizes phosphorylated and dephosphoryated BAD equally well ('BAD')

difference between these studies and our own was the source of the phosphospecific antibody, we compared the specificity of the anti-Ser^{112} antibody made by NEB with our own antibody. These studies revealed that the NEB antibody recognized BAD phosphorylated by PKB at Ser^{136} and BAD phosphorylated by MSK1 at Ser^{155}, albeit more weakly than BAD phosphorylated by MAPKAP-K1 at both Ser^{112} and Ser^{155} (Figure 9A). In contrast, our antibody only recognized Ser^{112} under the same conditions (Figure 3).

In order to see whether the lack of specificity of the NEB antibody was the cause of the discrepancy, we stimulated BAD-transfected 293 cells with forskolin or PMA, and then tested for BAD phosphorylation at Ser^{112}. As expected, our anti-Ser^{112} antibody recognized BAD only when the cells were stimulated with PMA and not when they were stimulated with forskolin. In contrast, the anti-Ser^{112} antibody from NEB recognized BAD after the cells were stimulated with PMA or forskolin (Figure 9B). The weaker effect of forskolin on 'Ser^{112} phosphorylation' is similar to that reported by Tan et al. [14] and is consistent with the weak recognition of the Ser^{155} site by the NEB 'anti-Ser^{112}' antibody.

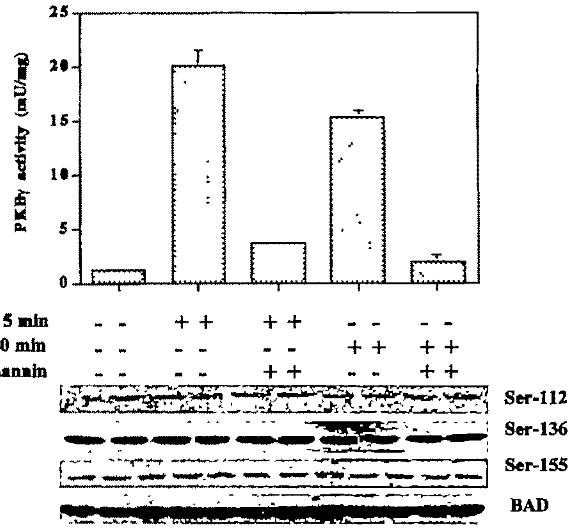

Figure 7 Phosphorylation of BAD at Ser^{136} does not correlate with PKB activation

293 cells transfected with a plasmid encoding GST–BAD were stimulated with 100 ng/ml IGF1 for 5 or 20 min Prior to stimulation with agonist, the cells were pretreated for 1 h with or without 100 nM wortmannin. PKBγ was immunoprecipitated from 50 μg of cell lysate [36] and assayed as described in the Materials and methods section The activities are presented as means ± S E M for three separate experiments Cell lysates (25 μg of protein) were denatured in SDS, electrophoresed on SDS/10%-polyacrylamide gels and, after transfer to nitrocellulose, immunoblotted with the four antibodies used in Figure 3

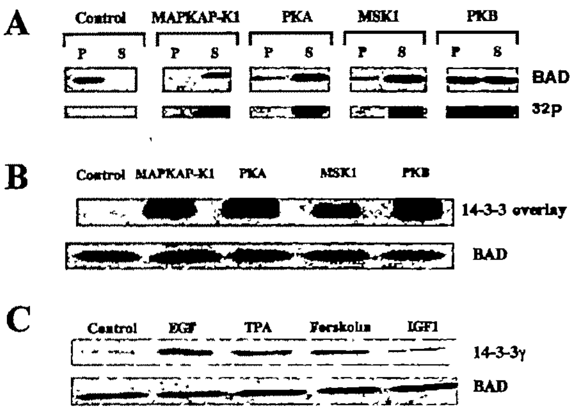

Figure 8 Effect of site-specific phosphorylation on the interaction of BAD with Bcl-X$_L$ and 14-3-3 proteins

(**A**) Interaction of BAD with Bcl-X$_L$ This was carried out as described in the Materials and methods section The membranes were autoradiographed (lower panels) and further analysed by immunoblotting with the antibody that recognizes phosphorylated and dephosphorylated BAD equally well (upper panels) (**B**) 14-3-3 overlay GST–BAD was phosphorylated and processed as in (**A**), but with unlabelled ATP. The 14-3-3 overlays (upper panel) were performed as described in the Materials and methods section using the BMH1 and BMH2 isoforms of *S cerevisiae* The membranes were then stripped and re-probed with the antibody that recognizes phosphorylated and dephosphoryated BAD equally well (lower panel) (**C**) Agonist-induced interaction of GST–BAD with endogenous 14-3-3γ 293 cells were transfected with GST–BAD, then stimulated with EGF (5 min), PMA ('TPA'; 15 min) or forskolin (30 min) or IGF1 (10 min) as in Figures 4, 5 and 7 After cell lysis, 20 μg of lysate was incubated for 1 h with 10 μl of packed GSH–agarose. After brief centrifugation, the supernatant was discarded and the beads washed four times with 1 ml of Buffer A containing 125 mM NaCl Finally, the pellet was denatured in SDS, the solubilized proteins electrophoresed, transferred to nitrocellulose and analysed by immunoblotting with an antibody that recognises 14-3-3γ (upper panel). The membrane was stripped and re-probed with the same anti-BAD antibody as in (**B**) (lower panel)

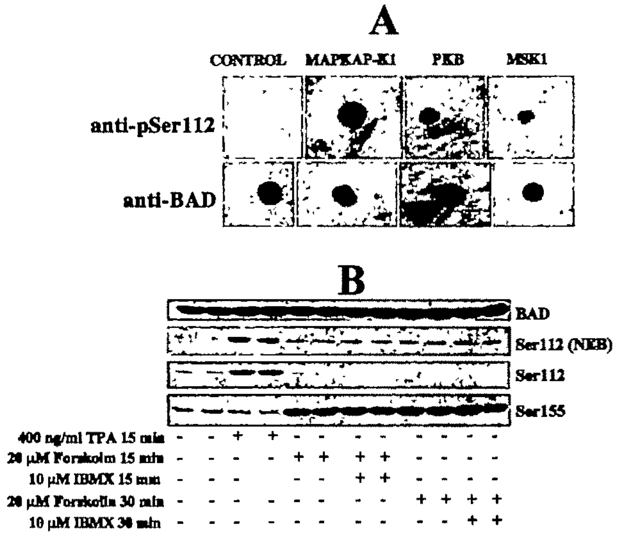
A
CONTROL
MAPKAP-K1
PKB
MSK1
anti-pSer112
anti-BAD
B
BAD
Ser112 (NEB)
Ser112
Ser155
400 ng/ml TPA 15 min - - + + - - - - - - - -
20 µM Forskolin 15 min - - - - + + + + - - - -
10 µM IBMX 15 min - - - - - + + - - - -
20 µM Forskolin 30 min - - - - - - - - + + + +
10 µM IBMX 30 min - - - - - - - - - - + +

Figure 9 Examination of the specificity of the anti-Ser^{112} antibody sold by NEB

(**A**) GST–BAD expressed in *E coli* was phosphorylated for 90 min with MAPKAP-K1, PKB or MSK1 (each at 10 units/ml) or left unphosphorylated ('CONTROL') Aliquots (200 ng) were spotted on to nitrocellulose membranes and immunoblotted with the anti-Ser^{112} antibody from NEB or our anti-BAD antibody that recognizes phosphorylated and dephosphorylated BAD equally well. Each piece of nitrocellulose paper was developed simultaneously for the same length of time using the same secondary antibody, and the times of exposure to the film were identical The strength of the signals can therefore be compared directly. (**B**) BAD-transfected 293 cells were stimulated with PMA ('TPA') or forskolin (alone or with IBMX) and, after cell lysis, the phosphorylation of Ser^{112} and Ser^{155} was examined by immunoblotting as in Figure 4, with the anti-Ser^{112} antibody from NEB and the anti-Ser^{112}, anti-Ser^{155} and anti-BAD antibodies made by our laboratory

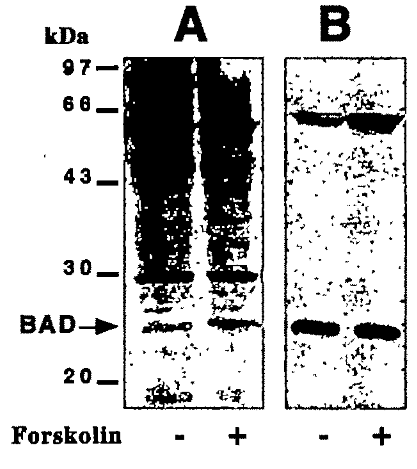

Figure 10 Forskolin induces phosphorylation of the endogenous BAD at Ser^{155} in COS1 cells

COS1 cells were stimulated for 30 min without or with 20 μM forskolin, then lysed and 200 μg of lysate protein was electrophoresed on a SDS/12.5%-polyacrylamide gel. After transfer to nitrocellulose, the membranes were blocked by incubation overnight with the blocking solution (see the Materials and methods section) (**A**) The membranes were immunoblotted for 24 h at 4 °C with the anti-Ser^{155} antibody (2 μg/ml) before detection with the ECL® system. The positions of BAD and the marker proteins glyocgen phosphorylase (97 kDa), serum albumin (66 kDa), ovalbumin (43 kDa), carbonic anhydrase (30 kDa) and soybean trypsin inhibitor (20 kDa) are indicated (**B**) same as (**A**), except that an anti-BAD monoclonal antibody B36420 (Transduction Laboratories), which detects phosphorylated and dephosphorylated BAD equally well, was used for immunoblotting.

Phosphorylation of endogenous BAD in COS1 cells

The analysis of the phosphorylation of BAD in 293 cells described so far was carried out using cells in which GST–BAD was overexpressed. It was therefore important to extend the work to examine whether the much lower levels of BAD present endogenously in mammalian cells were phosphorylated at Ser^{155} in response to cAMP elevation. After testing many cell lines we found that the level of BAD in COS1 cells was just sufficient to carry out this experiment. These studies showed that forskolin stimulates the phosphorylation of endogenous BAD at Ser^{155} (Figure 10A), confirming the results obtained in transfected 293 cells (Figure 4).

DISCUSSION

In the present paper we identify Ser^{155} as a novel phosphorylation site in BAD. This residue lies in an optimal consensus sequence for phosphorylation by PKA (Arg-Arg-Xaa-Ser) and is phosphorylated by this protein kinase at a far higher rate *in vitro* than any other site. Ser^{112} and Ser^{136} were only trace-phosphorylated, even after prolonged incubation with high concentrations of PKA (Figure 1F). Consistent with these findings, Ser^{155} was the only one of these three residues that became phosphorylated in transfected 293 cells (Figure 4) stimulated with the cAMP-elevating agents forskolin and IBMX. Moreover, the endogenous BAD in COS1 cells was phosphorylated at this site in response to the same agonists (Figure 10). Ser^{155} is also phosphorylated *in vitro* by MSK1 (Figure 1C) and, at a low rate, by MAPKAP-K1 (Figures 1A and 1B). However, neither of these protein kinases appear to be rate-limiting for the phosphorylation of Ser^{155} in 293 cells, because Ser^{155} phosphorylation was not induced by stimulation with agonists that activate the classical MAP kinase cascade (EGF, PMA) and hence activate MSK1 [20] and MAPKAP-K1 (Figure 5). Similarly, exposure to UV-C radiation or to the protein-synthesis inhibitor anisomycin, under conditions that strongly activate MSK1 in 293 cells via the SAPK2/p38 pathway [20], did not induce any phosphorylation of BAD at Ser^{155} (results not shown).

The specific phosphorylation of BAD at Ser^{155} by MSK1 *in vitro* (Figure 1C) triggered its dissociation from Bcl-X$_L$ even more effectively than the specific phosphorylation of BAD at Ser^{136} by PKB (Figure 8A) and induced a similar interaction with 14-3-3 proteins (Figure 8B). Moreover, the forskolin-induced phosphorylation of BAD at Ser^{155} promoted its interaction with the endogenous 14-3-3γ present in 293 cells (Figure 8C), in a similar manner to the PMA or EGF-induced phosphorylation of Ser^{112} (Figure 8C). Since forskolin stimulates the phosphorylation of Ser^{155}, but not Ser^{112} or Ser^{136} (Figure 4), this establishes that BAD can interact with 14-3-3 proteins when phosphorylated at Ser^{155}. However, unlike Ser^{112} and Ser^{136}, Ser^{155} does not lie in the sequence Arg-Xaa-Xaa-Ser(P)-Xaa-Pro, which is the canonical consensus for binding to 14-3-3 proteins. However, there are precedents for 14-3-3 proteins binding to phosphorylated sequences lacking proline at the +2 position. For example, the 14-3-3 binding sequence in protein tyrosine phosphatase H1, lies in the sequence **Arg**-Ser-**Leu**-**Ser(P)**-Val-**Glu** [29], which is similar to that surrounding Ser^{155} (**Arg**-Arg-**Met**-**Ser(P)**-Asp-**Glu**). The phosphopeptide comprising residues 149–161 prevented the interaction of Ser^{155}-phosphorylated BAD with 14-3-3 proteins (results not shown), demonstrating that this sequence does indeed bind to 14-3-3 proteins. In summary, our results show that the phosphorylation of BAD at Ser^{155} triggers the dissociation of BAD from Bcl-X$_L$ and its interaction with 14-3-3 proteins. This may contribute to the anti-apoptotic effects of cAMP-elevating

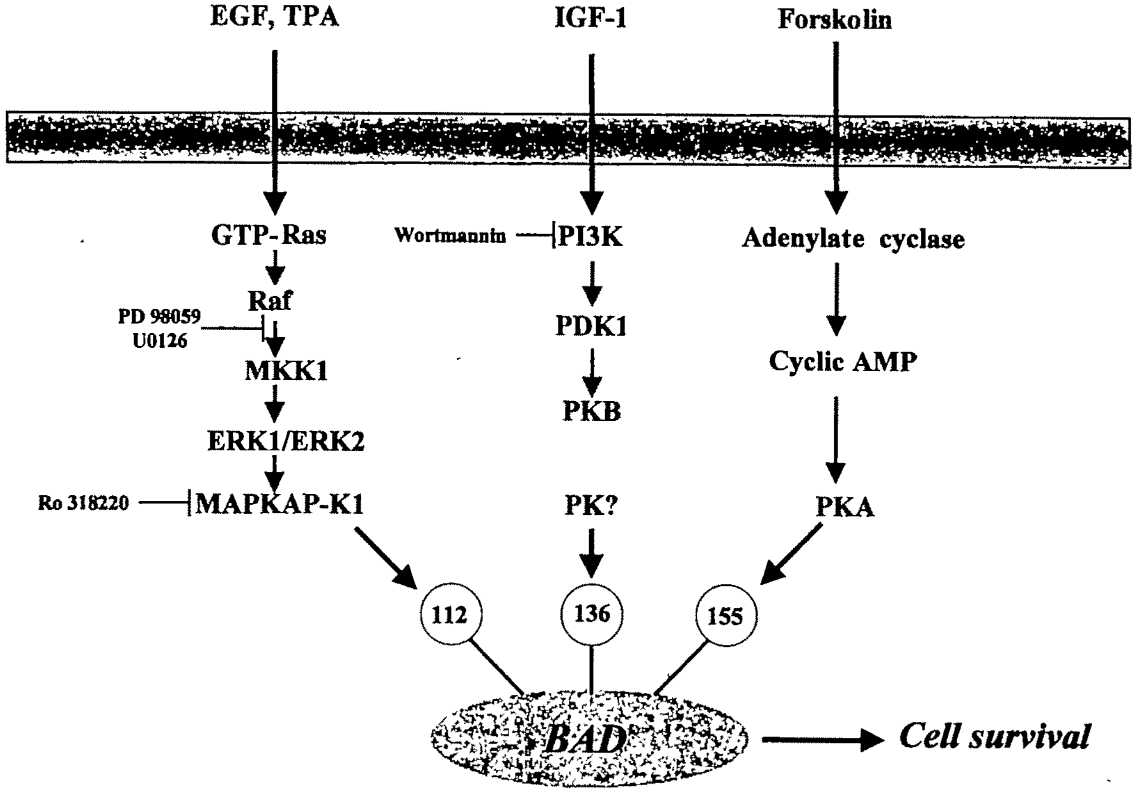

Scheme 1 BAD is phosphorylated at different sites in response to agonists that activate distinct signal-transduction pathways

The sites of action of the kinase inhibitors used in the present paper are indicated. PK? Indicates that phosphorylation of BAD at Ser^{136} in 293 cells is catalysed by a protein kinase that has not yet been identified. 'TPA' is PMA.

agents, which have been well documented in several systems, including cerebellar granule neurons [30], developing retina [31] and neutrophils [32].

Our results do not agree with those of Harada et al. [16], who reported that Ser^{112} was the major residue phosphorylated by the purified catalytic subunit of PKA, purchased from Sigma, and a form of PKA associated with a mitochondrial fraction isolated from IL-3-stimulated FL5.12 cells. However, in the studies by Harada et al., Ser^{112} was not identified directly, and phosphorylation was only inferred from the observation that phosphorylation was greatly reduced if Ser^{112} was mutated to Ala. The discrepancy between their results and ours is not explained by the source of the PKA, since we found that Ser^{155} was the major site phosphorylated with three different catalytic subunit preparations, including PKA from Sigma (see the Results section). These observations point to the importance of identifying phosphorylation sites directly by isolating and sequencing the relevant phosphopeptides, and highlight the potential dangers inherent in indirect methods that are based on decreased phosphorylation of mutant proteins.

Our results also disagree with those of Tan et al. [14], who reported that the phosphorylation of Ser^{112} in BAD-transfected 293 cells was stimulated by the cAMP-elevating agent forskolin. In the present study, no phosphorylation of Ser^{112} could be detected after stimulation by forskolin (Figure 4). This discrepancy appears to be explained by the anti-Ser^{112} antibody used by Tan et al. [14], which, in contrast with our antibody (Figure 3), recognized BAD phosphorylated at Ser^{136} and Ser^{155}, as well as BAD phosphorylated at Ser^{112} (Figure 9A). Thus, in their studies, the forskolin-induced phosphorylation of 'Ser112' was really measuring the phosphorylation of Ser^{155} (Figure 9B). Although phosphospecific antibodies can be extremely valuable, our findings illustrate the potential hazard of relying exclusively on such antibodies the specificity of which has not been established rigorously. It is also essential to establish that a phosphospecific antibody is neutralized by the phosphorylated peptide immunogen and not by the corresponding dephosphopeptide. This is not possible with phosphospecific antibodies marketed by NEB, since they do not sell the phosphopeptide antigen that they use to raise a particular antibody and will not even reveal its identity.

In the present study we showed that the phosphorylation of BAD at Ser^{112} was stimulated by exposure to agonists that activate the classical MAP kinase cascade (EGF, PMA; see Figure 5), and similar results were obtained by other investigators while our studies were in progress [14,15]. The agonist-induced phosphorylation of Ser^{112} was prevented by two structurally distinct inhibitors of the MAP kinase cascade, namely PD 98059 (Figure 6) [15] and U0126 (Figure 6). The failure of Tan et al. [14] to observe a strong inhibition of PMA-induced phosphorylation of Ser^{112}, may be explained by the lower concentration of PD 98059 used in their experiments. The difficulty of completely suppressing activation of the MAP kinase cascade by agonists that are particularly strong activators of this pathway has been discussed previously [12]. The phosphorylation of endogenous BAD at Ser^{112} via the classical MAP kinase cascade has also been demonstrated in IL-3-dependent MC9 cells [11] and BDNF-stimulated cerebellar granule neurons [13].

MAPKAP-K1 is the only identified protein kinase in the classical MAP kinase cascade that phosphorylates BAD at Ser^{112}

in vitro [13,14] (Figure 1) and in co-transfection experiments [13,14]. In the present study we also showed that the EGF-induced phosphorylation of Ser^{112} is strongly suppressed in 293 cells by 5 μM Ro 318220 (Figure 6A), a potent ATP-competitive inhibitor of MAPKAP-K1 [25], but not by H89 (10 μM), a weak inhibitor of this enzyme (results not shown). In contrast, forskolin-induced phosphorylation of Ser^{155} was suppressed by 10 μM H89, a strong ATP-competitive inhibitor of PKA, but not by 5 μM Ro 318220, a weak inhibitor of PKA (Figure 4B). These studies are consistent with Ser^{112} phosphorylation being catalysed by MAPKAP-K1. Ro 318220 at 1 μM did not inhibit the EGF-induced phosphoryation of Ser^{112}, but abolished PMA-induced Ser^{112} phosphorylation. This shows that Ro 318220 inhibits PKC *in vivo* at a lower concentration than that which inhibits MAPKAP-K1. This, in turn, implies that PKC activity is not rate-limiting for the EGF-induced activation of the MAP kinase cascade in 293 cells.

GST–BAD was phosphorylated at Ser^{136} in unstimulated 293 cells, and no agonist was found that could increase the basal phosphorylation of this site (Figures 4, 5 and 7). In particular IGF1, a potent activator of PI3K and PKB, had no effect on Ser^{136} phosphorylation (Figure 7) and did not increase the interaction of BAD with 14-3-3 proteins (Figure 8C) in 293 cells. Fang et al. [15] also failed to observe a significant effect of insulin or IGF1 on Ser^{136} phosphorylation in 293 cells transfected with BAD. These observations are consistent with those of Scheid and Duronio [10], who found that IL-4, a good activator of PKB, failed to induce the phosphorylation of the endogenous BAD in MC-9 cells. Indeed there are few studies where increased Ser^{136} phosphorylation of endogenous or transfected BAD has been demonstrated convincingly. A small increase in Ser^{136} phosphorylation of endogenous BAD was noted by Bai et al. [33] in IGF1-stimulated vascular smooth-muscle cells, while Datta et al. [7] observed that inhibitors of PI3K blocked the hyperphosphorylation of BAD induced by platelet-derived growth factor (PDGF) in balb/c 3T3 cells. However, the sites phosphorylated in response to PDGF were not identified in the latter study.

In summary, the basal level of phosphorylation of BAD at Ser^{136} is unaffected by prolonged treatment with inhibitors of PI3K in 293 cells, suggesting that an as-yet-unidentified protein kinase, distinct from PKB, mediates the constitutive phosphorylation of BAD at this site. MAPKAP-K1 mediates the phosphorylation of BAD at Ser^{112} induced by agonists that activate the classical MAP kinase cascade, while PKA mediates the phosphorylation of Ser^{155}, by agonists that elevate the intracellular concentration of cAMP (Scheme 1). Thus BAD represents a point of convergence of several different signal-transduction pathways that are activated by survival factors that inhibit apoptosis in mammalian cells.

Digoxygenin-labelled 14-3-3 proteins were a gift from Dr Mercedes Rublo and Dr Carol MacKintosh in this Unit, and bacteria expressing Bcl-X_L were generously provided by Dr Paul Clarke, Biomedical Research Centre, Ninewells Hospital Medical School, Dundee, Scotland, U K We thank Mrs Agnieszka Kieloch for cell culture and Dr Ana Cuenda for many valuable discussions The work was supported by the Medical Research Council, The Royal Society and the Louis Jeantet Foundation

REFERENCES

1 Kerr, J F, Wyllie, A. H and Currie, A R. (1972) Apoptosis a basic biological phenomenon with wide-ranging implications in tissue kinetics Br J Cancer **26**, 239–257
2 Adams, J. M. and Cory, S (1998) The Bcl-2 protein family arbiters of cell survival Science **281**, 1322–1326
3 Yang, E, Zha, J, Jockel, J., Boise, L H, Thompson, C. B and Korsemeyer, S J. (1995) Bad, a hetrodimeric partner for Bcl-X_L and Bcl-2 displaces Bax and promotes cell death Cell **80**, 285–291
4 Zha, J, Harada, H, Yang, E, Jockel, J and Korsemeyer, S J (1996) Serine phosphorylation of death agonist BAD in response to survival factor results in binding to 14-3-3 not Bcl-X_L Cell **87**, 619–628
5 Leighton, I A, Dalby, K N, Caudwell, F B, Cohen, P T W. and Cohen, P (1995) Comparison of the specificities of p70 S6 kinase and MAPKAP kinase-1 identifies a relatively specific substrate for p70 S6 kinase the N-terminal kinase domain of MAPKAP kinase-1 is essential for peptide phosphorylation FEBS Lett **375**, 289–293
6 Alessi, D R., Caudwell, F. B., Andjelkovic, M, Hemmings, B. A and Cohen, P (1996) Molecular basis for the substrate specificity of protein kinase B; comparison with MAPKAP kinase-1 and p70 S6 kinase FEBS Lett **399**, 333–338
7 Datta, S R, Dudek, H, Tao, X, Masters, S, Fu, H, Gotoh, Y and Greenberg, M A (1997) Akt phosphorylation of BAD couples survival signals to the cell-intrinsic death machinery Cell **91**, 231–241
8 del Peso, L, Gonzalez-Garcia, M, Page, C, Herrera, R. and Nunez, G. (1997) Interleukin-3-induced phosphorylation of BAD though the protein kinase Akt Nature (London) **278**, 687–689
9 Downward, J L (1998) Mechanisms and consequences of activation of protein kinase B/Akt Curr. Opin Cell Biol. **10**, 262–267
10 Scheid, M P and Duronio, V (1998) Dissociation of cytokine-induced phosphorylation of Bad and activation of PKB/akt involvement of MEK upstream of Bad phosphorylation. Proc Natl Acad Sci USA **95**, 7439–7444
11 Scheid, M. P, Schubert, K M and Duronio, V (1999) Regulation of Bad phosphorylation and association with Bcl-X_L by the MAPK/Erk kinase J Biol Chem **274**, 31108–31113
12 Alessi, D R., Cuenda, A, Cohen, P, Dudley, D T and Saltiel, A R (1995) PD98059 is a specific inhibitor of the activation of mitogen-activated protein kinase kinase *in vitro* and *in vivo* J. Biol Chem **270**, 27489–27494
13 Bonni, A, Brunet, A, West, A E, Datta, S R, Takasu, M A and Greenberg, M E (1999) Cell survival promoted by the Ras-MAPK signaling pathway by transcription-dependent and independent mechanisms Science **286**, 1358–1362
14 Tan, Y, Ruan, H., Demeter, M R and Comb, M J (1999) p90^{RSK} blocks Bad-mediated cell death via a protein kinase C-dependent pathway J Biol Chem. **274**, 34859–34867
15 Fang, X., Yu, S, Eder, A, Mao, M, Bast, R. C, Boyd, D and Mills, G B (1999) Regulation of BAD phosphorylation at Ser^{112} by the Ras-mitogen-activated protein kinase pathway Oncogene **18**, 6635–6640
16 Harada, H, Becknell, B, Wilm, M, Mann, M., Huang, I J, Taylor, S S, Scott, J D and Korsemeyer, S J (1999) Phosphorylation and inactivation of BAD by mitochondria-anchored protein kinase A Mol Cell **3**, 413–422
17 Cosulich, S C, Savory, P. J. and Clarke, P R (1999) Bcl-2 regulates amplification of caspase activation by cytochrome *c* Curr Biol **9**, 147–150
18 Sutherland, C, Campbell, D G and Cohen, P (1993) Identification of insulin-stimulated protein kinase-1 as the rabbit equivalent of rsk^{mo}-2 Eur J Biochem **212**, 581–588
19 Reimann, E M and Beham, R A (1983) Preparation of partially purified protein kinase inhibitor Methods Enzymol. **99**, 51–55
20 Deak, M, Clifton, A D, Lucocq, J M and Alessi, D. R. (1998) Mitogen- and stress-activated protein kinase-1 (MSK1) is directly activated by MAPK and SAPK2/p38, and may mediate activation of CREB EMBO J **17**, 4426–4441
21 Cuenda, A, Cohen, P, Buee-Scherrer, V and Goedert, M (1997) Activation of stress-activated protein kinase-3 (SAPK3) by cytokines and cellular stresses is mediated via SAPKK3(MKK6), comparison of the specificities of SAPK3 and SAPK2(RK/p38) EMBO J. **16**, 295–305
22 Bradford, M M (1976) A rapid and sensitive method for the quantitation of microgram quantities of protein utilizing the principle of protein–dye binding Anal Biochem **72**, 248–254
23 Moorhead, G, Douglas, P, Cotelle, V, Harthill, J, Morrice, N., Meek, S, Deiting, U, Stitt, M, Scarabel, M, Aitken, A and MacKintosh, C (1999) Phosphorylation-dependent interaction between enzymes of plant metabolism and 14-3-3 proteins Plant J **18**, 1–12
24 Cohen, P (1978) The role of cyclic AMP-dependent protein kinase in the regulation of glycogen metabolism in mammalian skeletal muscle Curr Top. Cell Regul **14**, 117–196
25 Alessi, D. R (1997) The protein kinase C inhibitors Ro 318220 and GF 109203X are equally potent inhibitors of MAPKAP kinase-1β (Rsk-2) and p70 S6 kinase. FEBS Lett **402**, 121–123
26 Thomson, S., Clayton, A L, Hazzalin, C A, Rose, S, Barratt, M J and Mahadevan, L C (1999) The nucleosomal response associated wih immediate early gene induction is mediated via alternative MAP kinase cascades: MSK1 as a potential histone H3/HMG-14 kinase EMBO J. **18**, 4779–4793
27 Favata, M F, Horiuchi, K Y, Manos, E J, Daulerio, A J, Stradley, D A, Feeser, W S, van Dyk, D E, Pitts, W. J, Earl, R A, Hobbs, F et al. (1998) Identification of a novel inhibitor of mitogen-activated protein kinase kinase J. Biol. Chem. **273**, 18623–18632

28 Alessi, D R., Andjelkovic, M, Caudwell, F B, Cron, P., Morrice, N, Cohen, P. and Hemmings, B A (1996) Mechanism of activation of protein kinase B by insulin and IGF1. EMBO J **15**, 6541–6551

29 Zhang, S-H, Kobayashi, R., Graves, P R, Piwnica-Worms, H and Tonks, N. K (1997) Serine phosphorylation-dependent association of the band 4.1-related protein tyrosine phosphatase PTPH1 with 14-3-3b protein. J. Biol Chem **272**, 27281–27287

30 Villalba, M, Bockaert, J. and Journot, L (1997) Concomitant induction of apoptosis and necrosis in cerebellar granule cells following serum and potassium withdrawal. NeuroReport **8**, 981–985

31 Varella, M. H., de Mello, F G and Linden, R (1999) Evidence for an anti-apoptotic role of dopamine in developing retinal tissue. J. Neurochem **73**, 485–492

32 Parvathenani, L K., Buescher, E S, Chacon-Cruz, E and Beebe, S. J. (1998) Type I cAMP-dependent protein kinase delays apoptosis in human neurophils at a site upstream of caspase 3 J. Biol. Chem **273**, 6736–6743

33 Bai, H-Z, Pollman, M J, Inishi, Y and Gibbons, G H (1999) Regulation of vascular smooth-muscle cell apoptosis; modulation of Bad by a phosphatidylinositol 3-kinase-dependent pathway. Circ. Res, **85**, 229–237

34 Stokoe, D, Campbell, D. G, Nakielny, S., Hidaka, H, Leevers, S. J., Marshall, C and Cohen, P (1992) MAPKAP kinase-2, a novel protein kinase activated by mitogen-activated protein kinase EMBO J **11**, 3985–3994

35 Dalby, K N, Morrice, N., Caudwell, F B, Avruch, J. and Cohen, P. (1998) Identification of regulatory phosphorylation sites in mitogen-activated protein kinase (MAPK)-activated protein kinase-1a/p90(rsk) that are inducible by MAPK J. Biol. Chem **273**, 1496–1505

36 Walker, K. S, Deak, M, Paterson, A., Hudson, K, Cohen, P. and Alessi, D R (1998) Activation of protein kinase B β and γ isoforms by insulin *in vivo* and by 3-phosphoinositide dependent protein kinase-1 *in vitro* comparison with protein kinase B α. Biochem J **331**, 299–308

Received 7 April 2000/26 April 2000; accepted 8 May 2000

The human breast carcinoma cell line HBL-100 acquires exogenous cholesterol from high-density lipoprotein via CLA-1 (CD-36 and LIMPII analogous 1)-mediated selective cholesteryl ester uptake

Pirkko J. PUSSINEN*[1], Barbara KARTEN*[2], Andrea WINTERSPERGER*, Helga REICHER*, Mark McLEAN†,
Ernst MALLE* and Wolfgang SATTLER*[3]

*Institute of Medical Biochemistry and Molecular Biology, University of Graz, Harrachgasse 21, 8010 Graz, Austria, and †Department of Obstetrics and Gynecology, University of South Florida, Tampa, FL 33606, U.S.A.

Aberrant cell proliferation is one of the hallmarks of carcinogenesis, and cholesterol is thought to play an important role during cell proliferation and cancer progression. In the present study we examined the pathways that could contribute to enhanced proliferation rates of HBL-100 cells in the presence of apolipoprotein E-depleted high-density lipoprotein subclass 3 (HDL_3). When HBL-100 cells were cultivated in the presence of HDL_3 (up to 200 μg/ml HDL_3 protein), the growth rates and cellular cholesterol content were directly related to the concentrations of HDL_3 in the culture medium. In principle, two pathways can contribute to cholesterol/cholesteryl ester (CE) uptake from HDL_3, (i) holoparticle- and (ii) scavenger-receptor BI (SR-BI)-mediated selective uptake of HDL_3-associated CEs. Northern- and Western-blot analyses revealed the expression of CLA-1 (CD-36 and LIMPII analogous 1), the human homologue of the rodent HDL receptor SR-BI. In line with CLA-1 expression, selective uptake of HDL_3-CEs exceeded HDL_3-holoparticle uptake between 12- and 58-fold. Competition experiments demonstrated that CLA-1 ligands (oxidized HDL, oxidized and acetylated low-density lipoprotein and phosphatidylserine) inhibited selective HDL_3-CE uptake. In line with the ligand-binding specificity of CLA-1, phosphatidylcholine did not compete for selective HDL_3-CE uptake. Selective uptake was regulated by the availability of exogenous cholesterol and PMA, but not by adrenocorticotropic hormone. HPLC analysis revealed that a substantial part of HDL_3-CE, which was taken up selectively, was subjected to intracellular hydrolysis. A potential candidate facilitating extralysosomal hydrolysis of HDL_3-CE is hormone-sensitive lipase, an enzyme which was identified in HBL-100 cells by Western blots. Our findings demonstrate that HBL-100 cells are able to acquire HDL-CEs via selective uptake. Subsequent partial hydrolysis by hormone-sensitive lipase could provide 'free' cholesterol that is available for the synthesis of cellular membranes during proliferation of cancer cells.

Key words: cancer cell, cell growth, human scavenger receptor class B type I.

INTRODUCTION

Numerous studies have implicated an important role for cholesterol during proliferation and progression of cancer. In principle, rapidly dividing cancer cells have two major possibilities to fulfil their need for cholesterol. The cellular requirements can be met by either *de novo* biosynthesis or uptake of exogenous lipoprotein-associated cholesterol and cholesteryl esters (CEs). In normal cells and tissues *de novo* cholesterol biosynthesis is under tight feedback regulation [1]. It has been suggested that this mechanism might be lost during neoplasia (reviewed in [2]), probably a reflection of the high cholesterol requirements of actively dividing tumour cells.

Whereas high levels of high-density lipoprotein (HDL) are clearly associated with a decreased risk for developing coronary artery disease (due to HDL-mediated removal of peripheral cholesterol), it has been suggested that high levels of HDL are associated with an increased risk of breast cancer development [3,4]. It has been reported that the proliferation rates of immortalized human breast cancer cells are increased by the presence of HDL in the culture medium, an effect that is more pronounced for oestrogen-receptor-positive cells as compared with oestrogen-receptor-negative cell lines [5].

Cellular uptake of exogenous cholesterol is facilitated by lipoprotein receptors, e.g. the 'classical' low-density-lipoprotein (LDL) receptor and a scavenger receptor of the B class (SR-BI), which was recently identified as an HDL receptor in rodents [6,7]. The major mechanisms by which HDL-associated CEs are transferred from the lipoprotein to the target cell are fundamentally different from the receptor-mediated endocytosis pathway (holoparticle uptake) used for the delivery of LDL cholesterol to the cell. The former mechanism, termed selective uptake of HDL-CE, involves HDL binding to a specific receptor, transfer of lipids (but not proteins) to the cell, and subsequent dissociation of CE-depleted HDL particles from the cell [6]. Once HDL-CEs are internalized via the selective-uptake pathway, they are rapidly hydrolysed in an extralysosomal compartment [8,9], probably by hormone-sensitive lipase (HSL [10]). The major expression sites of SR-BI are the liver and steroidogenic tissues, in which its expression is regulated by trophic hormones [11–13]. The tissue-specific expression of SR-BI reflects its involvement in the removal of excess cholesterol from peripheral tissue to the

---

Abbreviations used: ACTH, adrenocorticotropic hormone; CE, cholesteryl ester; CLA-1, CD-36 and LIMPII analogous 1, HDL, high-density lipoprotein; HDL_3, HDL subclass 3, HSL, hormone-sensitive lipase; LDL, low-density lipoprotein, SR-BI, scavenger receptor class BI; DMEM, Dulbecco's modified Eagle's medium, FCS, fetal calf serum; LPDS, lipoprotein-depleted serum; $[^3H]Ch_{16:0}$, $[^3H]$cholesteryl palmitate, SREBP, sterol-regulatory-element-binding protein.

[1] Present address: Institute for Dentistry, Mannerheimintie 172, 00300 Helsinki, Finland.

[2] Present address: MRC Group on the Molecular and Cell Biology of Lipids, University of Alberta, Edmonton, Canada.

[3] To whom correspondence should be addressed (e-mail Wolfgang.sattler@kfunigraz.ac.at)

liver (reverse cholesterol transport [14,15]) and as a receptor providing cholesterol in the form of CEs for hormone synthesis [16]. In more general terms, high SR-BI expression was found in a variety of cell models known to use large quantities of HDL-derived cholesterol [6,12,17]. Facilitation of bi-directional cholesterol flux is one of the unique features of SR-BI [18]. The human analogue of SR-BI, CLA-1 (CD36 and LIMPII analogous-1), has been identified as a member of the *CD36* gene family and is widely expressed [19]. Human CLA-1 and mouse SR-BI are highly similar (79 % amino acid sequence identity) [20] and share comparable biochemical functions and ligand-binding specificity [6,21,22].

To address more directly the role of exogenous HDL on proliferation rates of human breast carcinoma cells, we have investigated how HBL-100 cells acquire HDL-derived cholesterol. Our data indicate that CLA-1-mediated selective uptake of HDL-CEs and subsequent hydrolysis by HSL could provide a substantial contribution to the 'free' cholesterol pool in rapidly dividing HBL-100 breast carcinoma cells.

MATERIALS AND METHODS

Cell culture

During the present study HBL-100 human breast carcinoma cells were used and cultured as described in [23]. HBL-100 cells express the oestrogen and the LDL receptors [24]. Briefly, cells were grown in Dulbecco's modified Eagle's medium (DMEM) containing 10% (v/v) fetal calf serum (FCS) or lipoprotein-depleted serum (LPDS), 2 mM L-glutamine, 100 units/ml penicillin and 100 mg/ml streptomycin. Cells were cultured as monolayers in a humidified atmosphere of 95% air/5% CO_2 at 37 °C, and transferred or harvested at 70% confluency by addition of 0.25% trypsin, containing 1 mM EDTA, until the cells could be dislodged by tapping. Trypsin was inactivated by the addition of a 10-fold excess of fresh DMEM, and the trypsin/medium mixture was removed by low-speed centrifugation. Culture medium was changed routinely every 2 days.

Isolation of human plasma lipoproteins

Human HDL_3 (HDL subclass 3, $d = 1.125$–1.21 g/ml; containing apolipoprotein A-I as the major apolipoprotein) was prepared from fresh human plasma from normolipaemic donors by ultracentrifugation in a KBr gradient as described in [25]. After ultracentrifugation, the lipoproteins were dialysed against PBS (10 mM phosphate, pH 7.4, containing 150 mM NaCl) and stored at +4 °C under nitrogen. The protein content was determined according to Lowry et al. [26] using BSA as standard.

Labelling of lipoproteins

HDL_3 was iodinated with $Na^{125}I$ using *N*-bromosuccinimide as the oxidizing agent [27], resulting in specific radioactivities between 200 and 400 c.p.m./ng of protein. Labelling of the HDL_3-CE moiety was performed with [^{3}H]cholesteryl palmitate ([^{3}H]$Ch_{16\,0}$) essentially as described in [28]. Tracer (200 μCi in toluene) and 140 μg of phosphatidylcholine (in trichloromethane) were dried under N_2 in a round-bottomed flask (25 ml) and 1 ml of PBS (pH 7.4) was added to the flask (flushed with argon), which was kept rotating at 37 °C to resuspend the lipids. After 30 min the flask was sonicated for 10 min under argon in a bath-type sonicator and transferred to a Pyrex tube containing 960 μl of LPDS and 6 mg of HDL_3. The mixture was incubated at 37 °C (overnight, under N_2). Labelled HDL_3 was isolated by ultracentrifugation as described above and excess KBr was removed by size-exclusion chromatography on PD10 columns (Pharmacia, Vienna, Austria). Specific radioactivities of [^{3}H]$Ch_{16\,0}$-labelled HDL_3 were between 6 and 10 c.p.m./ng of protein.

Modification of lipoproteins

LDL and HDL_3 were oxidized in the presence of Cu^{2+} as described in [29]. Formation of conjugated dienes was assayed on-line by the increase in absorbance at 234 nm (within the first 3 h, $\Delta A_{234} \approx 0.8$–$0.9$). After 24 h, oxidation was stopped by the addition of EDTA (final concentration, 1 mg/ml). Acetylation of LDL was performed as described in [30]. Briefly, 1 ml of a solution containing 2.5 mg of LDL protein was added to 1 ml of a solution of saturated sodium acetate with continuous stirring on ice. Multiple 2-μl aliquots of acetic anhydride were added to the solution containing LDL in 2-μl aliquots within 1 h to give a mass 1.5 times higher than that of LDL. The solution was mixed for an additional 30 min, and dialysed against PBS.

Preparation of phosphatidylserine liposomes

Phosphatidylserine or phosphatidylcholine and cholesterol (all stock solutions 10 mg/ml chloroform) were mixed in a 1:1 molar ratio, the solvent was evaporated on a Rotavapor and the lipids were dried overnight. Tris/HCl (2 ml, 10 mM, pH 8.0, containing 0.1 M KCl and 1 mM EDTA) was added and kept rotating for 30 min at 37 °C. This mixture was sonicated for 5 min on ice, and dialysed against PBS. The phospholipid and cholesterol contents were analysed using commercially available enzymic test kits.

Determination of cholesterol in cellular lipid extracts

During all experiments the cells were counted in a haemocytometer in duplicate. After counting, the cellular lipids were extracted twice with 500 μl of hexane/2-propanol (3:2, v/v). After centrifugation at 14000 *g*, 500 μl of the organic phase was removed and hydrolysed in KOH [31]. The neutral lipids were extracted into hexane, dried and converted into the corresponding trimethylsilyl ether derivatives [80 μl of acetone/20 μl bis(trimethylsilyl)trifluoroacetamide containing 1% trimethylchlorosilane; 15 min at 50 °C]. Lipid extracts without prior hydrolysis were processed as described above to determine the intracellular unesterified cholesterol content The difference between the cholesterol contents of hydrolysed versus non-hydrolysed samples should reflect the contribution of selective CE uptake to the total cellular cholesterol content. The trimethylsilyl-ether derivatives were analysed by GC and quantified with 5α-cholestane as an internal standard [32].

Intracellular hydrolysis of HDL_3-CEs

After incubation of HBL-100 cells in the presence of [^{3}H]$Ch_{16\,0}$-labelled HDL_3 the cellular lipids were extracted as described above, dried under N_2 and resuspended in 150 μl of the mobile phase (hexane/ethanol/acetic acid, 98:1.995:0.005, by vol.). The cholesterol and CE contents in the samples were analysed on an EXSil100 silica column (5 μm of material, 200 mm × 4.6 mm; Activon, Sydney, Australia) at a flow rate of 1 ml/min on a Waters HPLC system (Waters, Vienna, Austria). Elution of [^{3}H]cholesterol and [^{3}H]$Ch_{16\,0}$ was monitored by radiometric detection (RadioMatic Flow One/Beta; Packard-Canberra, Vienna, Austria) at a liquid-scintillator flow rate of 2 ml/min.

Cell experiments

Prior to the uptake experiments the cells were preincubated (overnight) in DMEM containing LPDS (10%, v/v). Lipoprotein-uptake studies were performed in the presence of the

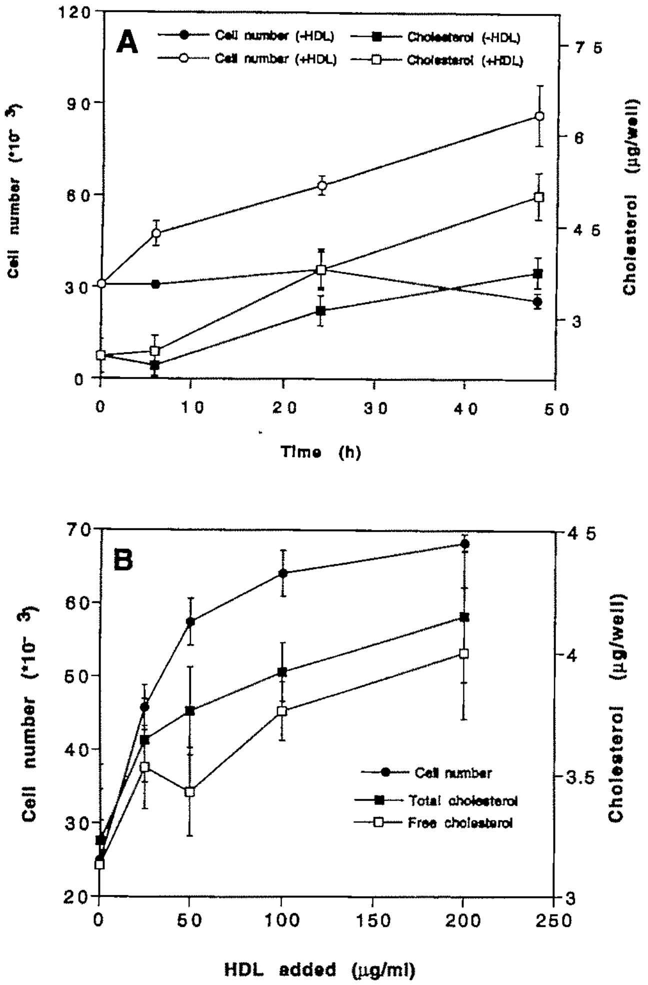

Figure 1 Effect of exogenous HDL$_3$ on HBL-100 growth rates and cellular cholesterol levels

(A) Cells (30000) were seeded in 6-well cluster trays and incubated in DMEM containing LPDS (10%, ■, ●) or in DMEM containing LPDS and 100 μg/ml HDL$_3$ (□, ○) At the indicated time points the cells were washed twice with PBS, trypsin-treated, and counted in a haemocytometer (○, ●) after 6, 24 and 48 h The cellular cholesterol content was analysed by GC prior to (□) and after (■) hydrolysis of the cellular lipids in ethanolic KOH, as described in the Materials and methods section Quantification was performed using 5α-cholestane as an internal standard (B) Cells (30000) were seeded in 6-well cluster trays and incubated in DMEM containing LPDS (10%) in the presence of the indicated concentrations of HDL$_3$ After 48 h, cell numbers (●) and the cellular cholesterol content (□, ■) were determined Data shown represent means ± S D for three independent experiments

indicated amounts of iodinated (^{125}I-HDL$_3$) or [^{3}H]Ch$_{18:0}$-labelled HDL$_3$ for the indicated times, the medium was aspirated and the cells were washed twice with Tris/HCl (50 mM/150 mM NaCl, pH 7.4/2 % BSA) and twice with the same buffer without BSA. Cells were then lysed in NaOH (0.3 M) and the radioactivity was counted. An aliquot of the hydrolysate was used to determine the cellular protein content [26]. In this study ^{125}I-HDL$_3$ uptake is termed holoparticle uptake, while [^{3}H]Ch$_{18:0}$-labelled HDL$_3$ uptake is referred to as apparent particle uptake (i.e. the amount of lipoprotein uptake that would account for [^{3}H]Ch$_{18:0}$ uptake is calculated from the specific radioactivity). This is necessary to be able to compare the two uptake pathways quantitatively. Selective uptake is calculated as the difference between apparent particle uptake and holoparticle uptake.

To determine intracellular hydrolysis rates of [^{3}H]Ch$_{18:0}$, the cellular lipids were extracted with hexane/2-propanol (2 × 1 ml), dried and analysed by HPLC with radiometric detection as described above. Competition experiments were performed in the presence of the indicated excess of the corresponding competitor. Binding constants were calculated by non-linear regression analysis using GraphPad.

Northern-blot analysis

RNA was isolated by the RNeasy Midi-kit (Qiagen, Vienna, Austria) from 2 × 10^6 HBL-100 cells. RNA (10 μg) was denatured at 65 °C for 5 min in sample loading buffer (20 mM Mops/ethidium bromide) and run through 1 % agarose/20 mM Mops/8 % formaldehyde gels (80 V) using 20 mM Mops as running buffer. The RNA was transferred to Hybond-N membrane (Amersham, Vienna, Austria) overnight in 10 × SSC (0.15 M NaCl/0.015 M sodium citrate), and fixed for 30 s under UV light. The membrane was probed with ^{32}P-labelled full-length rat SR-BI cDNA [33] overnight at +62 °C in 50 % formamide, 5 × SSPE (50 mM sodium phosphate, pH 7.4/750 mM NaCl/5 mM EDTA), 0.01 % BSA and 1 % SDS, and washed in 0.5 × SSC/0.1 % SDS at room temperature. The film was exposed for 5 days at −70 °C.

Western-blot analysis

Analysis of CLA-1 expression

HBL-100 cells were cultured in a T75 flask and incubated in DMEM containing FCS (10%, v/v) or LPDS (10%, v/v) overnight. The cells were washed twice with PBS (pH 7.4) containing 150 mM NaCl, 1 mM benzamidine, 20 μg/ml leupeptin and 20 μg/ml antipapain and scraped into 500 μl of the same buffer. Cells were sonicated on ice (10 s, 3 times) and centrifuged at 10000 g for 10 min The supernatant (100 μl) was mixed with 100 μl of sample buffer, heated to 98 °C (3 min) and 20 μl of the mixture was applied to a SDS/PAGE gel (8 %) and transferred electrophoretically on to nitrocellulose (150 mA, 4 °C, 90 min). Immunoreactive bands were detected with a polyclonal rabbit antiserum raised against a keyhole-limpet haemocyanin-coupled peptide corresponding to the cytoplasmic 15 C-terminal amino acids of SR-BI of the chinese hamster. Due to the sequence similarity in the C-terminal portion between SR-BI and CLA-1, the antibody also cross-reacts with CLA-1. Horseradish peroxidase-conjugated goat anti-rabbit IgG was used as a secondary antibody and visualization of immunoreactive bands was performed using the ECL® detection system (Amersham).

Analysis of HSL expression

HBL-100 cells of one T75 flask were washed twice with ice-cold PBS, scraped, centrifuged at 4000 g (10 min) and the pellets frozen at −70 °C. For electrophoresis the cells were resuspended in 200 μl of homogenizing buffer (20 mM Tris/HCl/0.25 M sucrose/1 mM dithiothreitol/1 mM EDTA/1 mM benzamidine/20 μg/ml leupeptin/20 μg/ml antipapain, pH 7.4). Cells were lysed by disruption with sonication (10 s, 3 times) and the homogenate was centrifuged for 10 min at 10000 g. For SDS/PAGE, 50 μl of SDS buffer and 12.5 μl of 10 % SDS were added to 50 μl of supernatant, boiled for 5 min, separated on a 7.5 % SDS gel and transferred on to nitrocellulose as described above. For immunoblotting polyclonal chicken anti-rat HSL (a kind gift of C. Holm, Department of Cell and Molecular Biology, Lund University, Lund, Sweden), rabbit anti-chicken IgG (Sigma) and alkaline phosphatase-conjugated affinity-purified goat anti-rabbit IgG (Sigma) were used. Homogenized mouse epididymal fat pads containing relatively high concentrations of HSL were used as a positive control.

RESULTS

Effects of exogenous HDL$_3$ on HBL-100 growth rates

The time- and concentration-dependent effect of exogenously added HDL on HBL-100 cell growth is shown in Figure 1. HBL-100 cells (30000 cells) were seeded in 6-well trays and incubated in DMEM (containing 10 % LPDS) in the absence or presence of human HDL$_3$ (100 μg/ml medium) for 6, 24 and 48 h. The addition of HDL$_3$ to the growth medium exhibited pronounced growth-stimulatory effects (an increase in cell numbers from 30000 to 85000 cells; Figure 1A). In contrast, cells cultured in LPDS-containing medium without HDL were in growth arrest. Also, the cellular cholesterol content was affected by the presence of HDL$_3$ in the culture medium. While the total cholesterol content of cells cultivated in the absence of HDL$_3$ increased from 2.3 to 3.8 μg of cholesterol/well (0 versus 48 h), the corresponding values for cells cultured in HDL$_3$-containing medium increased from 2.4 to 5.0 μg of cholesterol/well (Figure 1A). Proliferation rates of HBL-100 cells were dependent on the concentration of HDL$_3$ present in the culture medium (Figure 1B). Cell numbers increased with increasing HDL$_3$ content (from 30000 to 68000; 0–200 μg of HDL$_3$/ml). Also the cellular total cholesterol content increased from 3.2 to 4.2 μg of cholesterol/well in a manner dependent on the amount of exogenous HDL$_3$. When the cellular lipid extracts were analysed for the unesterified cholesterol content (i.e. without hydrolysis prior to derivatization and GC analysis) we have obtained consistently lower cholesterol concentrations (from 3.13 to 4.0 μg/well). These were, however, statistically not significantly different from values obtained from hydrolysed samples (Figure 1B, open versus filled squares). Whether this is a reflection of the relatively low capacity of the plasma-membrane bilayer for CE accommodation and rapid intracellular hydrolysis is presently not clear. However, from these experiments it is evident that the presence of HDL$_3$ in the culture medium affects both cell growth and the cholesterol content of HBL-100 cells.

Identification of CLA-1 and HSL by Northern- and Western-blot analyses

One mechanism that could contribute to HDL-mediated growth stimulation is the selective uptake of HDL-CE via CLA-1 and subsequent intracellular hydrolysis. This process would result in the generation of 'free' cholesterol in addition to the endogenously synthesized pool that could be utilized for the generation of new membrane surface area for rapidly dividing carcinoma cells.

In Northern blots the CLA-1 message was detected as a 2.8-kb species in both LPDS- and FCS-incubated cells with similar intensities (Figure 2A, lanes 1 and 2, respectively). In Western blots we could detect two bands in lysates of HBL-100 cells that were precultured in LPDS- (Figure 2B, lane 1) and FCS-containing medium (Figure 2B, lane 2). The apparent molecular masses of the immunoreactive bands were 82 and 78 kDa, respectively. The intensities of both bands were slightly higher (approx. 1.5-fold, as evaluated by densitometry) when cells were preincubated in LPDS in comparison with FCS. As a positive control for SR-BI expression we have used a rat liver homogenate (Figure 2B, lane 3).

One candidate that could facilitate intracellular hydrolysis of HDL-CEs which were taken up selectively is HSL. In line with intracellular CE hydrolysis within the 6-h time course (see below), we could detect a protein with an apparent molecular mass of 86 kDa using a polyclonal chicken anti-rat HSL as primary antibody (Figure 2C, lane 1). The apparent molecular mass of mouse fat HSL (Figure 2C, lane 2) was slightly lower (84 kDa), in line with data reported for HSL in different species [34].

Uptake mechanisms of HDL$_3$-CEs

In principle, cells can acquire HDL-associated lipids by either uptake of intact lipoprotein particles (holoparticle uptake) or a

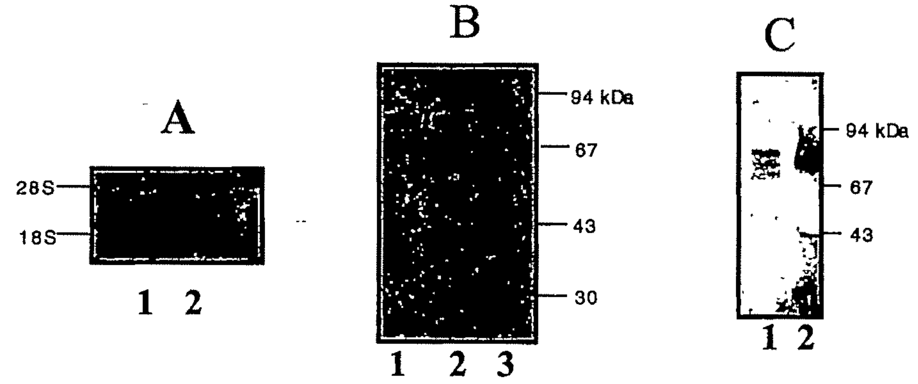

Figure 2 Northern- and Western-blot analyses of CLA-1 and HSL

(A) Northern-blot analysis of CLA-1 mRNA expression. RNA from HBL-100 cells cultured in DMEM containing LPDS (10%, lane 1) or FCS (10%; lane 2) was isolated, transferred to a Hybond membrane, and probed with a ^{32}P-labelled full-length rat SR-BI cDNA as described in the Materials and methods section. The migrations of 28 S and 18 S ribosomal RNAs are indicated. (B) Western-blot analysis of CLA-1 expression. HBL-100 proteins were separated on an SDS/PAGE gel (8%) under reducing conditions and transferred to nitrocellulose. CLA-1 was identified using a rabbit polyclonal antiserum (dilution, 1:1000) raised against a peptide corresponding to amino acids 496–508 of SR-BI. After addition of a peroxidase-conjugated goat anti-rabbit IgG (1:2000), immunoreactive bands were visualized with the ECL system. Prior to immunoblotting experiments, HBL-100 cells were cultured overnight in DMEM containing LPDS (10%, lane 1) or FCS (10%, lane 2). A rat liver homogenate was included as a positive SR-BI control (lane 3). Visualization was performed with the ECL method. (C) Western-blot analysis of HSL expression. HBL-100 cells were lysed as described in the Materials and methods section, separated on an SDS/PAGE gel (7.5%), and transferred to nitrocellulose. Western-blot analysis was performed with a polyclonal chicken anti-rat HSL primary antibody, followed by rabbit anti-chicken IgG and alkaline phosphatase-conjugated affinity-purified goat anti-rabbit IgG as secondary antibodies. Prior to Western blotting, HBL-100 cells were cultured overnight in DMEM containing FCS (lane 1). An infranatant of a homogenized mouse epididymal fat pad was used as positive HSL control (lane 2). For (B) and (C), the positions of the molecular-mass markers are indicated.

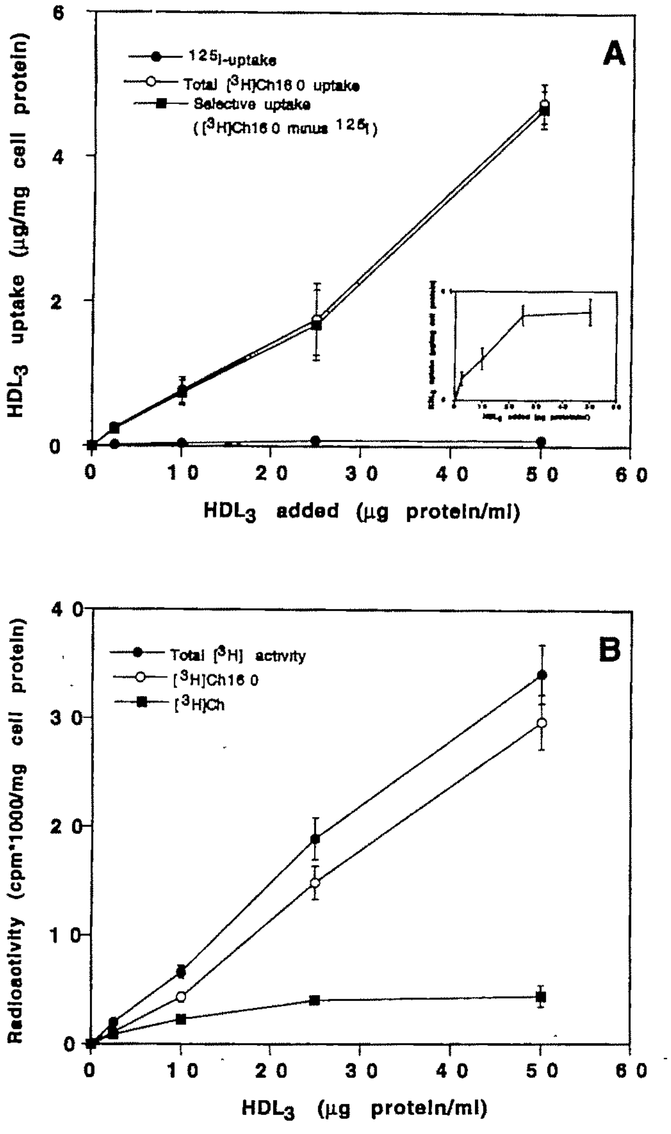

Figure 3 Uptake (A) and intracellular hydrolysis (B) of HDL$_3$-CE

(A) HBL-100 cells were seeded on 6-well plates and grown in DMEM/10% LPDS for 24 h before addition of HDL$_3$ The cells were then incubated for 6 h in the presence of increasing concentrations of ^{125}I-HDL$_3$ or [^{3}H]Ch$_{16\ 0}$-labelled HDL$_3$ in the absence or presence of a 10-fold excess of HDL$_3$ to differentiate between specific and non-specific uptake Holoparticle, apparent particle and selective uptake was calculated as described in the Materials and methods section After 6 h the medium was removed and the cells were washed, and analysed for radioactivity as described in the Materials and methods HDL$_3$ uptake was calculated from the specific radioactivities (c p m /ng of protein) of the lipoprotein preparations and the cell-associated radioactivity The inset shows uptake of ^{125}I-HDL$_3$ with the *y* axis drawn on a smaller scale (0–0 1 μg/mg of cell protein), and the *x* axis the same as the larger graph Results shown are specific uptake data and represent mean values ± S D from three independent experiments. (B) HBL-100 cells were grown on 6-well plates for 24 h in DMEM containing LPDS and increasing amounts of [^{3}H]Ch$_{16\ 0}$-labelled HDL$_3$ were added to the medium The cells were incubated for 6 h, washed, extracted and analysed for radioactive CE and cholesterol by HPLC with radiometric detection as described in the Materials and methods section Data shown represent means ± S D. for three independent experiments

combination of holoparticle-dependent and holoparticle-independent (selective) uptake. To compare the relative contribution of holoparticle and selective HDL-CE uptake with total CE uptake, HBL-100 cells were incubated in the presence of increasing concentrations of ^{125}I-HDL$_3$ and [^{3}H]Ch$_{16\ 0}$-labelled HDL$_3$. Results of these experiments are shown in Figure 3(A).

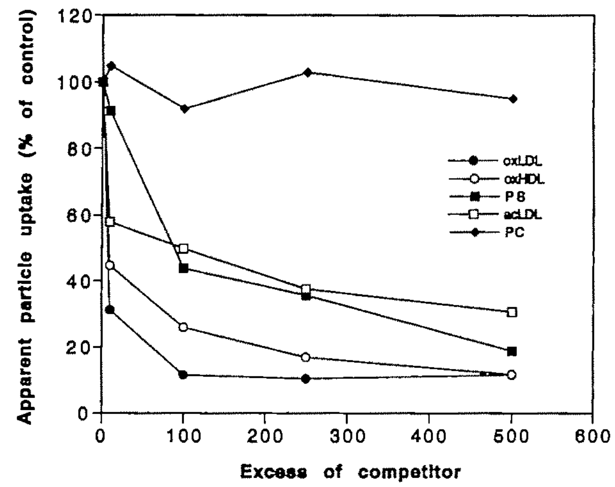

Figure 4 Competition of HDL$_3$ uptake by HBL-100 cells

HBL-100 cells were grown on 6-well plates for 24 h in DMEM containing LPDS before the competition experiments To each well, 10 μg of [^{3}H]Ch$_{16\ 0}$-labelled HDL$_3$ together with the indicated molar excess of competitors was added. The excess of phosphatidylserine (PS) and phosphatidylcholine (PC) liposomes was based on the phospholipid content of HDL$_3$. After a 6-h incubation the cells were washed, lysed and the radioactivity was measured on a β-counter Data shown represent means for three independent experiments (for more clarity error bars are not displayed, S D < 11%) oxHDL and oxLDL, oxidized HDL and LDL, acLDL, acetylated LDL

HDL$_3$ holoparticle uptake provided only a small contribution to total HDL$_3$-CE uptake (between 2 and 8 %), with a higher contribution at lower HDL$_3$ concentrations. Calculation of binding constants for ^{125}I-HDL$_3$ by non-linear regression analysis revealed a K_d of 28 μg of total HDL$_3$/ml (1.4×10^{-7} M) and a B_{max} of 220 ng of total HDL$_3$/mg of cell protein. The remaining HDL$_3$-CE uptake was attributable to selective uptake, exceeding HDL$_3$ holoparticle uptake by between 12- (2.5 μg/ml HDL$_3$) and 58-fold (50 μg/ml HDL$_3$). These findings underline the pronounced capacity of HBL-100 cells for selective HDL-CE uptake.

To investigate the intracellular fate of HDL$_3$-CEs taken up via the selective-uptake pathway, cells were incubated in the presence of [^{3}H]Ch$_{16\ 0}$-labelled HDL$_3$, and the cellular lipids were extracted and analysed by HPLC with radiometric detection as outlined in the Materials and methods section. As can be seen from Figure 3(B), HBL-100 cells acquired [^{3}H]Ch$_{16\ 0}$ in a dose-dependent manner in a near-linear process (1100–30000 c.p.m.). Part of the HDL$_3$-CE, which was taken up selectively, was subjected to intracellular hydrolysis, producing [^{3}H]cholesterol. Intracellular hydrolysis was dependent on the amount of HDL$_3$ present in the culture medium and decreased from 45 (2.5 μg) to 13 % (50 μg) of total cell-associated [^{3}H]Ch$_{16\ 0}$. Thus, selective uptake of HDL$_3$-CEs results in intracellular accumulation of unesterified cholesterol within the 6-h incubation period studied here.

Uptake specificity of HDL$_3$-CEs by HBL-100 cells

To verify further that CLA-1 is responsible for selective HDL-CE uptake by HBL-100 cells, we have performed a series of competition experiments with native and modified lipoproteins that are known substrates for CLA-1 (Figure 4). The most efficient competitors for HDL$_3$-CE uptake were oxidized LDL and HDL (> 50 % inhibition at a 10-fold excess of competitors), followed by acetylated LDL (50 % competition at a 100-fold excess). As anionic phospholipids like phosphatidylserine are also ligands for CLA-1, we have included phospholipids in these

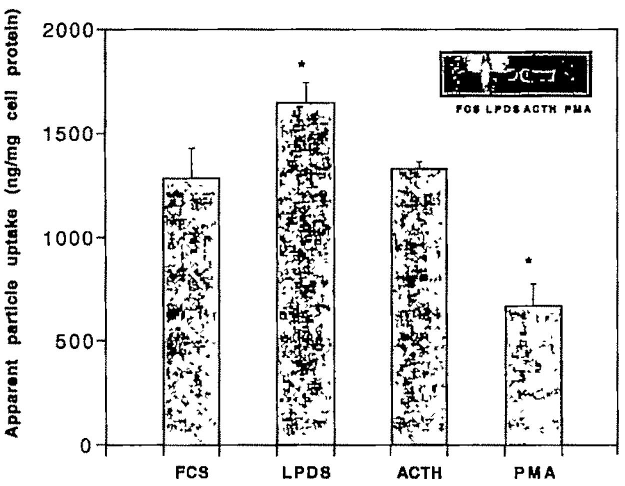

Figure 5 Regulation of HDL_3-CE uptake

HBL-100 cells were incubated overnight on 6-well plates in DMEM containing FCS (10%; v/v) or LPDS (10%; v/v) or DMEM/LPDS containing adrenocorticotropic hormone (ACTH, 1 μM) or PMA (100 nM) To each well, 20 μg of $[^3H]Ch_{16:0}$-labelled HDL_3 was added, the cells were incubated for 6 h, washed, lysed and counted in a β-counter Data shown represent means ± S D for three independent experiments. *$P < 0.001$, calculated by the Student's *t* test of independent samples, FCS versus LPDS, ACTH, PMA. The insert shows Western-blot analysis of CLA-1 protein expression after the corresponding treatments (with FCS, LPDS, ACTH and PMA)

competition studies. Phosphatidylserine competed for approx. 80% of selective HDL_3-CE uptake, whereas the addition of phosphatidylcholine did not impair selective HDL_3-CE uptake. This latter result is also indicative for CLA-1-mediated selective uptake of HDL_3-CE by HBL-100 cells.

It has been suggested that cellular levels of free cholesterol regulate SR-BI expression via a feedback loop [35]. To test whether HDL_3-CE uptake by HBL-100 cells is regulated by the cholesterol content of the medium, cells were preincubated in DMEM containing either FCS or LPDS (Figure 5). Incubation in LPDS-containing medium significantly up-regulated HDL_3-CE uptake (1280 versus 1650 ng/mg of cell protein; FCS versus LPDS conditions), findings in line with sterol-regulatory-element-binding protein (SREBP)-1a-regulated transcription of the *SR-BI* gene [36]. We have also investigated the effects of adrenocorticotropic hormone (ACTH) and PMA (Figure 5) on the efficacy of HDL_3-CE uptake by HBL-100 cells, since both agents are known to regulate SR-BI and CLA-1 expression [21,35]. While ACTH was without effect, PMA treatment of the cells significantly reduced the capacity for HDL_3-CE uptake (1330 and 668 ng/mg of cell protein; ACTH and PMA, respectively). The inset of Figure 5 shows Western-blot analysis of membrane-protein fractions obtained from the correspondingly treated cells. Densitometric evaluation of immunoreactive bands revealed that CLA-1 was up-regulated by LPDS and down-regulated by PMA (inset to Figure 5, lanes 2 and 4, respectively), reflecting the findings for HDL-CE uptake. In contrast, ACTH treatment up-regulated CLA-1 expression (Figure 5 inset, lane 3); however, this was not accompanied by increased uptake of HDL_3-CE.

DISCUSSION

In the present study we have investigated whether human HBL-100 cells acquire cholesterol from exogenous human HDL via the selective-uptake pathway. From our results it is conceivable that CLA-1-mediated selective uptake of HDL-CE and subsequent hydrolysis by HSL could contribute significantly to an accessible 'free' cholesterol pool. This pool might be used for the generation of new membrane surface area by rapidly dividing tumour cells or facilitate intracellular signalling pathways involved in the regulation of cell proliferation [37].

A number of studies have reported that cancer cells and solid tumours take up LDL more effectively than normal tissues (reviewed in [38]), which is probably a reflection of a higher cholesterol demand of dividing cells in contrast with differentiated cells. On the other hand, some tumours do not internalize great amounts of LDL. Thus it has been suggested that is important to show not only binding but also internalization of LDL [38]. While this is certainly true for LDL-based drug-targeting studies, the demonstration of internalization might be insufficient regarding cholesterol utilization by tumour cells. As a result of selective LDL-CE uptake (e.g. [39,40]), the utilization of LDL-derived cholesterol/CEs might be underestimated by the analysis of LDL holoparticle internalization.

It is interesting that HDL-derived cholesterol has received much less attention. This might be due to the fact that an HDL receptor was identified only recently [6]. In these studies, it was demonstrated that SR-BI mediates selective uptake of HDL-CE, is expressed in a tissue-specific manner and is under tight hormonal regulation [16]. The human homologue of SR-BI, CLA-1, shares ≈ 80% amino acid similarity with SR-BI, mediates comparable functions as does the rodent receptor [21,22], and is expressed predominantly in human tissues performing very active cholesterol turnover, i.e. the liver and steroidogenic tissues [22]. During the present study with HBL-100 cancer cells we have observed exceptionally high selective uptake of HDL-CEs. In our experiments selective HDL-CE uptake exceeded HDL holoparticle uptake by between 12- and 58-fold. In contrast with ^{125}I-HDL_3 holoparticle binding, selective HDL_3-CE uptake was not a saturable process, a phenomenon consistently observed during different studies (e.g. [6,41,42]). This might be a reflection of a continuous CE influx into the cells fuelled by dissociation of CE-depleted HDL particles from, and rebinding of HDL particles with 'normal' CE content to, CLA-1.

Northern- and Western-blot analyses have verified that HBL-100 cells express CLA-1, the human receptor facilitating selective HDL-CE uptake (see above). Although we could detect only a single 2.8-kb RNA species in Northern blots, Western-blotting experiments revealed other immunoreactive bands with molecular masses of 82 and 78 kDa. It is presently not clear whether or not this is a reflection of alternative mRNA splicing of a single precursor transcript, as reported for SR-BI/SR-BII biosynthesis [41,43]. The specificity of selective HDL-CE uptake by HBL-100 cells is similar to the ligand-binding specificity described for CLA-1 [21,22]. Selective uptake of HDL-CEs was up-regulated by depletion of intracellular cholesterol pools and down-regulated by PMA treatment, findings in line with SR-BI expression reported for hepatocytes [13,42] and CLA-1 expression by human monocytic THP-1 cells [21], respectively.

According to our findings, selective uptake of HDL-CEs via a CLA-1-mediated pathway could indicate the first step in providing cholesterol to HBL-100 cells, probably in a similar manner to that suggested for developing embryonic tissues [44]. However, it is clear that CEs must be hydrolysed by an intracellular esterase to be available for incorporation into newly formed membranes. CEs that have been taken up via the selective-uptake pathway are hydrolysed in an extralysosomal compartment, probably the cytosol [8,9]. One potential candidate that could facilitate CE hydrolysis after selective uptake is the neutral, multifunctional esterase HSL [45]. In addition to triacylglycerol lipase activity, HSL mediates neutral CE hydrolase activity [10,45]. Co-expression of high levels of SR-BI [6] and HSL [46] in steroidogenic tissues could reflect a functional relationship between these proteins in tissues with high cholesterol-turnover rates. The expression of HSL by HBL-100 cells could provide a plausible explanation for the relatively high intracellular hydrolysis rates of internalized CEs. Whether this is a reflection of a comparable inter-relationship between selective CE uptake via CLA-1 and subsequent hydrolysis by HSL in cancer cells remains to be established. It is important to note that a number of oestrogen-receptor-positive and oestrogen-receptor-negative human breast cancer cell lines express the peripheral-type benzodiazepine receptor (PBR) [37]. PBR facilitates transport of unesterified cholesterol into the nucleus, an observation associated with increased cellular proliferation rates of MDA-231 breast cancer cells [37]. As outlined in [37], it is not clear whether PBR-mediated cholesterol transport into the nucleus involves signalling via SREBPs.

An important question arising from our study is whether or not CLA-1 expression could be used for lipoprotein-mediated drug targeting in a similar manner as reported for the LDL receptor (reviewed in [38]). Lipoproteins and apolipoprotein-containing liposomes are applied as potential delivery systems for anti-tumour agents [47,48]. Lactosylated reconstituted HDL particles have been reported to be potential drug-carrier vehicles, which are subjected to hepatic uptake via the asialoglycoprotein receptor [48]. Incorporation of an elliptinium derivative into LDL improved the potency of this drug against B16 melanomas in mice [49]. As CLA-1 is a multi-ligand receptor, it could be useful to study HDL-mediated delivery of hydrophobic cytotoxic drugs which have a structural relationship to CEs.

There is general agreement that high HDL concentrations are associated with a decreased risk of the development of coronary artery disease [50], a process mediated in part by SR-BI [42,51–54]. However, the situation is less clear with regard to circulating HDL levels and the risk of developing breast cancer, a leading cause of death of women in Western societies. Some authors have reported an association between high HDL cholesterol and the incidence of breast cancer [3,4], a fact that is possibly related to oestrogen metabolism [55]. This could be a reflection of cholesterol supply via selective HDL-CE uptake (serving as precursors for hormone synthesis) or the result of other signalling pathways mediated by HDL [56,57].

Financial support was from the Austrian Research Foundation (P14109-GEN to W S. and P14186-MED to E M), the Austrian National Bank (project P8127 to W.S and P8132 to A W) and the Finnish Cultural Foundation (a personal grant to P J P)

REFERENCES

1 Goldstein, J. L and Brown, M S (1977) Low-density lipoprotein pathway and its relation to atherosclerosis Annu. Rev Biochem **46**, 897–930

2 Coleman, P. S , Chen, L C. and Sepp-Lorenzino, L (1997) in Cholesterol . its Function and Metabolism in Biology and Medicine (Bittman, R , ed), pp 363–435, Plenum Press, New York

3 Boyd, N. F and McGuire, V (1990) Evidence of association between plasma high-density lipoprotein cholesterol and risk factors for breast cancer J Natl Cancer Inst **21**, 460–468

4 Moorman, P G , Hulka, B S., Hiatt, R. A , Krieger, N , Newman, B , Vogelman, J H and Orentreich, N. (1998) Association between high-density lipoprotein cholesterol and breast cancer varies by menopausal status Cancer Epidemiol. Biomarkers Prev. **7**, 483–488

5 Rotheneder, M. and Kostner, G M (1989) Effects of low- and high-density lipoproteins in the proliferation of human breast cancer cells *in vitro* differences between hormone-dependent and independent cell lines Int. J Cancer **43**, 875–879

6 Acton, S , Rigotti, A , Landschulz, K T., Xu, S , Hobbs, H. H and Krieger, M (1996) Identification of a scavenger receptor SR-BI as a high density lipoprotein receptor Science **271**, 518–520

7 Acton, S L , Scherer, P E , Lodish, H F and Krieger, M (1994) Expression cloning of SR-BI, a CD36-related class B scavenger receptor J. Biol Chem **269**, 21003–21009

8 Sparrow, C P. and Pittman, R C. (1990) Cholesterol esters selectively taken up from high-density lipoproteins are hydrolyzed extralysosomally. Biochim Biophys Acta **1043**, 203–210

9 Sattler, W and Stocker, R (1993) Greater selective uptake by HepG2 cells of high-density lipoprotein cholesteryl ester hydroperoxides than that of unoxidized cholesteryl esters. Biochem J **294**, 771–778

10 Osuga, J , Ishibashi, S , Oka, T , Yagyu, H , Tozawa, R , Fujimoto, A , Shionoiri, F , Yahagi, N , Kraemer, F B , Tsutsumi, O and Yamada, N (2000) Targeted disruption of hormone-sensitive lipase results in a male sterility and adipocyte hypertrophy, but not in obesity Proc Natl Acad Sci U.S A **97**, 787–792

11 Azhar, S , Nomoto, A , Leers-Sucheta, S and Reaven, E (1998) Simultaneous induction of an HDL receptor protein (SR-BI) and the selective uptake of HDL-cholesteryl esters in a physiologically relevant steroidogenic cell model J Lipid Res **39**, 1616–1628

12 Rigotti, A , Edelman, E. R , Seifert, P , Iqbal, S N , DeMattos, R B , Temel, R E , Krieger, M. and Williams, D L (1996) Regulation by adrenocorticotropic hormone of the in vivo expression of scavenger receptor class B type I (SR-BI), a high density lipoprotein receptor, in steroidogenic cells of the murine adrenal gland J Biol Chem **271**, 33545–33549

13 Fluiter, K , van der Westerhuijzen, D. R and van Berkel, T J C. (1998) *In vivo* regulation of scavenger receptor BI and the selective uptake of high density lipoprotein cholesteryl esters in rat liver parenchymal cells and Kupffer cells J. Biol Chem **273**, 8434–8438

14 Fidge, N H (1999) High density lipoprotein receptors, binding proteins and ligands J Lipid Res **40**, 187–201

15 Rothblat, G H., de la LLera-Moya, M , Atger, V , Kellner-Weibel, G , Williams, D L and Phillips, M C. (1999) Cell cholesterol efflux integrations of old and new observations provides new insights J Lipid Res. **40**, 781–796

16 Rigotti, A , Trigatti, B , Babitt, J , Penman, M , Xu, S and Krieger, M (1997) Scavenger receptor BI–a cell surface receptor for high density lipoprotein. Curr Opin Lipidol. **8**, 181–188

17 Babitt, J , Trigatti, B., Rigotti, A , Smart, E J , Anderson, R G W., Xu, S and Krieger, M (1997) Murine SR-BI, a high density lipoprotein receptor that mediates selective lipid uptake, is N-glycosylated and fatty acid acylated and colocalizes with plasma membrane caveolae J Biol. Chem. **271**, 13242–13249

18 Williams, D L , Connelly, M A , Temel, R E , Swarnakar, S , Phillips, M C., de la Llera-Moya, M and Rothblat, G H (1999) Scavenger receptor BI and cholesterol trafficking Curr Opin Lipidol **10**, 329–399

19 Calvo, D , Dopazo, J and Vega, M. A (1995) The CD36, CLA-1 (CD36L1), and LIMPII (CD36L2) gene family· cellular distribution, chromosomal localization and genetic evolution Genomics **25**, 100–106

20 Calvo, D and Vega, M A (1993) Identification, primary structure, and distribution of CLA-1, a novel member of the CD36/LIMPII gene family. J. Biol Chem **268**, 18929–18935

21 Murao, K , Terpstra, V , Green, S R , Kondratenko, N , Steinberg, D and Quehenberger, O (1997) Characterization of CLA-1, a human homologue of rodent scavenger receptor BI, as a receptor for high density lipoprotein and apoptotic thymocytes J Biol. Chem **272**, 17551–17557

22 Calvo, D., Gomez-Coronado, D., Lasuncion, M A and Vega, M A (1997) CLA-1 is an 85-kD plasma membrane glycoprotein that acts as a receptor for both native (HDL, LDL and VLDL) and modified (OxLDL and AcLDL) lipoproteins Arterioscler Thromb Vasc Biol **17**, 2341–2349

23 Chajes, V., Sattler, W , Stranzl, A and Kostner, G M (1995) Influence of n — 3 fatty acids on the growth of human breast cancer cells *in vitro* relationship to peroxides and vitamin E Breast Cancer Res Treatment **34**, 199–212

24 Stranzl, A , Schmidt, H , Winkler, R and Kostner, G M (1997) Low-density lipoprotein receptor mRNA in human breast cancer cells: influence by PKC modulators Breast Cancer Res Treatment **42**, 195–205

25 Sattler, W., Mohr, D. and Stocker, R (1994) Rapid isolation of lipoproteins and assessment of their peroxidation by high-performance liquid chromatography postcolumn chemiluminescence Methods Enzymol **233**, 469–489

26 Lowry, O H., Rosebrough, N J , Farr, A L and Randall, R J (1951) Protein measurement with the Folin reagent. J Biol Chem **193**, 265–275

27 Sinn, H J., Schrenk, H H , Friedrich, E A , Via, D P and Dresel, H. A (1988) Radioiodination of proteins and lipoproteins using *N*-bromosuccinimide as oxidizing agent Anal. Biochem **170**, 186–192

28 Hough, J L and Zilversmit, D B (1984) Comparison of various methods for *in vitro* cholesteryl ester labeling of lipoproteins from hypercholesterolemic rabbits Biochim Biophys Acta **792**, 338–347

29 Karten, B, Boechzelt, H, Abuja, P M, Mittelbach, M and Sattler, W (1999) Macrophage-enhanced formation of cholesteryl ester-core aldehydes during oxidation of low density lipoprotein J Lipid Res **40**, 1240–1253

30 Basu, S K, Goldstein, J L, Anderson, G W and Brown, M S (1976) Degradation of cationized low density lipoprotein and regulation of cholesterol metabolism in homozygous familial hypercholesterolemia fibroblasts Proc Natl Acad Sci U S A **73**, 3178–3182

31 Sattler, W., Leis, H J, Kostner, G. M and Malle, E (1995) Quantification of 7-dehydrocholesterol in plasma and amniotic fluid by liquid chromatography/particle beam-mass spectrometry as a biochemical marker for the Smith-Lemli-Opitz syndrome Rapid Commun Mass Spectrom **9**, 1288–1292

32 Karten, B, Beisiegel, U., Gercken, G and Kontush, A (1997) Mechanisms of lipid peroxidation in human blood plasma a kinetic approach Chem Phys Lipids **88**, 83–96

33 McLean, M P and Sandhoff, T W (1998) Expression and hormonal regulation of the high-density lipoprotein (HDL) receptor scavenger receptor class B type I messenger ribonucleic acid in the rat ovary Endocrine **9**, 243–252

34 Holm, C, Belfrage, P and Fredrikson, G. (1989) Human adipose tissue hormone-sensitive lipase identification and comparison with other species Biochim Biophys. Acta **1006**, 193–197

35 Wang, N, Weng, W, Breslow, J L and Tall, A R. (1996) Scavenger receptor BI (SR-BI) is up-regulated in adrenal gland in apolipoprotein A-I knock-out mice as a response to depletion of cholesterol stores *In vivo* evidence that SR-BI is a functional high density lipoprotein receptor under feedback control J. Biol Chem. **271**, 21001–21004

36 Lopez, D and McLean, M. (1999) Sterol regulatory element-binding protein-1a binds to *cis* elements in the promoter of the rat high density lipoprotein receptor SR-BI gene Endocrinology **140**, 5669–5681

37 Hardwick, M., Fertikh, D, Culty, M., Li, H, Vidic, B and Papadopoulos, V (1999) Peripheral-type benzodiazepine receptor (PBR) in human breast cancer correlation of breast cancer cell aggressive phenotype with PBR expression, nuclear localization, and PBR-mediated cell proliferation and nuclear transport of cholesterol Cancer Res **59**, 831–842

38 Firestone, R A (1994) Low-density lipoproteins as a vehicle for targeting antitumor compounds to cells Bioconjugate Chem **5**, 105–113

39 Swarnakar, S., Reyland, M E, Deng, J, Azhar, S. and Williams, D L (1998) Selective uptake of low density lipoprotein-cholesteryl ester is enhanced by inducible apolipoprotein E expression in cultured mouse adrenocortical cells J Biol. Chem **273**, 12140–12147

40 Swarnakar, S, Temel, R E, Connelly, M A, Azhar, S. and Williams, D L (1999) Scavenger receptor class B, type I, mediates selective uptake of low density lipoprotein cholesteryl ester J Biol Chem. **274**, 29733–29739

41 Webb, N R., Connell, P M., Graf, G. A, Smart, E J, de Villiers, W S J., de Beer, F C and van der Westhuyzen, D. R (1998) SR-BII, an isoform of the scavenger receptor BI containing an alternate cytoplasmic tail, mediates lipid transfer between high density lipoproteins and cells. J Biol Chem **273**, 15241–15248

42 Fluiter, K, Sattler, W, De Beer, M. C, Connell, P. M, van der Westerhuyzen, D R and van Berkel, T J C (1999) Scavenger receptor BI mediates the selective uptake of oxidized cholesterol esters by rat liver J Biol Chem **274**, 8893–8899

43 Webb, N. R, de Villiers, W J S, Connell, P M, de Beer, F C and van der Westhuyzen, D R (1997) Alternative forms of the scavenger receptor BI (SR-BI) J Lipid Res **38**, 1490–1495

44 Hatzopoulos, A K, Rigotti, A, Rosenberg, R D and Krieger, M (1998) Temporal and spatial expression of the HDL receptor SR-BI during murine embryogenesis. J Lipid Res. **39**, 495–508

45 Osterlund, T, Danielsson, B, Degerman, E, Contreras, J. A, Edgren, G, Davis, R C, Schotz, M. C and Holm, C (1996) Domain-structure analysis of recombinant rat hormone-sensitive lipase Biochem. J **319**, 411–420

46 Holm, C, Belfrage, P and Fredrikson, G (1987) Immunological evidence for the presence of hormone-sensitive lipase in rat tissues other than adipose tissue. Biochem Biophys Res. Commun **148**, 99–105

47 Rensen, P C N, Schiffelers, R M, Versluis, A J, Bijsterbosch, M. K, van Kuijk-Meuwissen, M. E M J and van Berkel, T J C (1997) Human recombinant apolipoprotein E-enriched liposomes can mimic low-density lipoproteins as carriers for the site-specific delivery of antitumor agents Mol Pharmacol **52**, 445–455

48 Schouten, D, van der Kooij, M., Muller, J., Pieters, M N, Bijsterbosch, M K and van Berkel, T J C (1993) Development of lipoprotein-like lipid particles for drug targeting neo-high density lipoproteins Mol Pharmacol **44**, 486–492

49 Samadi-Baboli, M., Favre, G., Canal, P and Soula, G. (1993) Low density lipoprotein for cytotoxic drug targeting. improved activity of elliptinium derivative against B16 melanoma cells Br J Cancer **68**, 319–326

50 Stein, O. and Stein, Y (1999) Atheroprotective mechanisms of HDL Atherosclerosis **144**, 285–301

51 Varban, M L, Rinninger, F, Wang, N, Fairchild-Huntress, V, Dunmore, J H, Fang, Q., Gosselin, M L, Dixon, K L, Deeds, J D, Acton, S L et al (1998) Targeted mutation reveals a central role for SR-BI in hepatic selective uptake of high-density lipoprotein cholesterol Proc Natl Acad Sci U S A **95**, 4619–4624

52 Kozarsky, K F, Donahee, M H, Rigotti, A, Iqbal, S. N, Edelman, E R and Krieger, M. (1997) Overexpression of the HDL receptor SR-BI alters plasma HDL and bile cholesterol levels Nature (London) **387**, 414–417

53 Rigotti, A, Trigatti, B. L, Penman, M, Rayburn, H, Herz, J and Krieger, M (1997) A targeted mutation in the murine gene encoding the high density lipoprotein (HDL) receptor scavenger receptor class B type I reveals its key role in HDL metabolism Proc. Natl Acad. Sci U.S.A **94**, 12610–12615

54 Trigatti, A, Rayburn, H, Vinals, M, Braun, A, Miettinen, H, Penman, M., Hertz, M, Schrenzel, M, Amigo, L, Rigotti, A and Krieger, M (1999) Influence of the high density lipoprotein receptor SR-BI on reproductive and cardiovascular pathophysiology Proc Natl Acad Sci U S A **96**, 9322–9327

55 Ferraroni, M, Gerber, M, Decarli, A, Richardson, S., Marubini, E, Crastes de Paulet, P., Crastes de Paulet, A. and Pujol, H (1993) HDL-cholesterol and breast cancer a joint study in northern Italy and southern France Int J Epidemiol **22**, 772–780

56 Porn, I, Akerman, K. E O and Slotte, J P (1991) High-density lipoproteins induce a rapid and transient release of Ca^{2+} in cultured fibroblasts Biochem J **279**, 29–33

57 Walter, M, Reincke, H, Nofer, J R, Seedorf, U and Assmann, G (1995) HDL$_3$ stimulates multiple pathways in human skin fibroblasts Arterioscler. Thromb Vasc Biol. **15**, 1975–1986

Received 21 February 2000/13 April 2000, accepted 16 May 2000

Novel application of *S*-nitrosoglutathione–Sepharose to identify proteins that are potential targets for *S*-nitrosoglutathione-induced mixed-disulphide formation

Peter KLATT[1], Estela PINEDA MOLINA, Dolores PÉREZ-SALA and Santiago LAMAS

Department of Estructura y Función de Proteínas, Centro de Investigaciones Biológicas, Instituto Reina Sofía de Investigaciones Nefrológicas, Consejo Superior de Investigaciones Científicas, Velázquez 144, E-28006 Madrid, Spain

Site-specific S-glutathionylation is emerging as a novel mechanism by which *S*-nitrosoglutathione (GSNO) may modify functionally important protein thiols. Here, we show that GSNO–Sepharose mimicks site-specific S-glutathionylation of the transcription factors c-Jun and p50 by free GSNO *in vitro*. Both c-Jun and p50 were found to bind to immobilized GSNO through the formation of a mixed disulphide, involving a conserved cysteine residue located in the DNA-binding domains of these transcription factors. Furthermore, we show that c-Jun, p50, glycogen phosphorylase *b*, glyceraldehyde-3-phosphate dehydrogenase, creatine kinase, glutaredoxin and caspase-3 can be precipitated from a mixture of purified thiol-containing proteins by the formation of a mixed-disulphide bond with GSNO–Sepharose. With few exceptions, protein binding to this matrix correlated well with the susceptibility of the investigated proteins to undergo GSNO- but not diamide-induced mixed-disulphide formation *in vitro*. Finally, it is shown that covalent GSNO–Sepharose chromatography of HeLa cell nuclear extracts results in the enrichment of proteins which incorporate glutathione in response to GSNO treatment. As suggested by DNA-binding assays, this group of nuclear proteins include the transcription factors activator protein-1, nuclear factor-κB and cAMP-response-element-binding protein. In conclusion, we introduce GSNO–Sepharose as a probe for site-specific S-glutathionylation and as a novel and potentially useful tool to isolate and identify proteins which are candidate targets for GSNO-induced mixed-disulphide formation.

Key words: affinity chromatography, cysteine, glutathionylation, nitric oxide, nitrosothiol.

INTRODUCTION

The ubiquitous signalling molecule NO has been implicated in the regulation of key functions in the immune, cardiovascular, and nervous system [1]. The main source of NO in mammalian cells is the enzymic oxidation of L-arginine to L-citrulline and NO by NO synthases [2]. Alternatively, NO may be produced in ischaemic tissues by non-enzymic transformation of nitrite [3]. The reactivity and fate of NO in biological systems is governed by a complex, and as yet not completely elucidated, network of competing reactions with molecular oxygen, superoxide, transition metals and thiols [4–6]. These reactions yield a variety of NO-derived reactive nitrogen species (RNS) such as N_2O_3, peroxynitrite, nitrosyl–metal complexes and S-nitrosothiols. NO and other RNS react rapidly with GSH, the major intracellular low-molecular-mass antioxidant, to yield the S-nitrosothiol *S*-nitrosoglutathione (GSNO). GSNO has been identified in a variety of tissues and is considered to represent a functionally relevant signalling molecule which may act independently of homolytic cleavage to NO or be metabolized to other bioactive nitrogen oxides [6].

The best characterized effect of NO and other NO-derived signalling molecules is the activation of soluble guanylate cyclase by interaction with the haem group of the enzyme [7]. However, accumulating evidence suggests that the diverse biological effects of RNS [8] can be attributed, at least in part, to their potential to modify and regulate the activity of target proteins by tyrosine nitration, carbonyl formation at lysine and arginine residues, methionine oxidation [9], as well as through the oxidation and S-nitrosation of cysteine residues [10]. The modification of protein thiols by RNS has gained considerable attention because of its implication in the regulation of protein function in physiologically relevant signalling as well as in situations of nitrosative stress [11,12]. Depending on the microenvironment of the targeted protein thiol and the chemical reactivity of the NO-derived signalling molecule, protein cysteines may suffer S-nitrosation, or oxidation to sulphenic, sulphinic or sulphonic acid, as well as disulphide-bridge formation [10]. Interestingly, recent work linked the formation of GSNO to the regulation of proteins by mixed-disulphide formation. First suggestions that GSNO may act as an S-glutathionylating agent came from early work on the NO/GSH-dependent modification of yeast alcohol dehydrogenase [13]. A more recent study on the regulation of aldose reductase by GSNO shows that micromolar concentrations of the nitrosothiol inhibited the enzyme through site-specific mixed-disulphide formation at a conserved cysteine residue in the catalytic site [14]. A possible role of NO-induced protein thiolation in intact cells was highlighted by experiments demonstrating that endothelial cells respond to exogenous NO production with the transient thiolation of a number of, as yet unidentified, cellular proteins [15]. The concept of NO-dependent protein thiolation as a regulatory mechanism was further supported by very recent studies on the mechanisms of NO/GSH-dependent modification of H-ras and carbonic anhydrase [16], as

---

Abbreviations used: GSNO, *S*-nitrosoglutathione, AP-1, activator protein 1; NF-κB, nuclear factor κB, CREB, cAMP-response-element-binding protein; CP-1, CCAAT-binding protein 1, EMSA, electrophoretic mobility-shift assay, RNS, reactive nitrogen species, NP40, Nonidet P40, SOD, Cu,Zn superoxide dismutase; GAPDH, glyceraldehyde-3-phosphate dehydrogenase; GPDH, glycerol-3-phosphate dehydrogenase

[1] To whom correspondence should be addressed. Present address: Department of Immunology and Oncology, Centro Nacional de Biotecnología, Campus de Cantoblanco, E-28049 Madrid, Spain (e-mail pklatt@cnb.uam.es).

well as glyceraldehyde-3-phosphate dehydrogenase (GAPDH) [17], sarcoplasmic reticulum calcium-ATPase [18], and the cysteine proteases caspase-3 [19] and cathepsin K [20]. A recent report from our laboratory on the regulation of c-Jun DNA binding by NO extends these findings, suggesting a novel role for S-glutathionylation in the regulation of transcription [21]. This study provides evidence that NO inhibits the DNA-binding activity of the activator protein 1 (AP-1) subunit c-Jun *in vitro* in a reversible and redox-independent manner. The underlying mechanism was shown to involve the formation of a mixed disulphide at a conserved cysteine residue in the DNA-binding site of the transcription factor through a reaction which depends on the NO-mediated conversion of GSH into GSNO.

Although the molecular basis of GSNO-induced protein thiolation remains to be established, both previous data (reviewed in [22]) and molecular modelling of S-glutathionylated c-Jun [23] suggest that mixed-disulphide formation could be facilitated by specific interactions between the glutathionyl moiety and basic amino acid side chains which flank the targeted protein thiol. Given that not only c-Jun but a number of other transcription factors, such as members of the Fos, activating transcription factor/cAMP-response-element-binding protein (CREB) and Rel/nuclear factor κB (NF-κB) families, as well as various cytosolic proteins, including glycogen phosphorylase b, GAPDH and creatine kinase, contain potentially redox- and NO-sensitive cysteine residues surrounded by basic amino acids, it is attractive to speculate that GSNO-mediated S-glutathionylation may constitute a general mechanism by which the formation of NO and, consequently, GSNO may be transduced into a functional response at the transcriptional level. As yet, however, there are no methods available which allow a rapid and simple screening for proteins which are candidate targets for GSNO-induced S-glutathionylation. The aim of this study is to provide a novel methodological approach to address this issue. We show that GSNO covalently attached to Sepharose mimicks site-specific S-glutathionylation of the transcription factor c-Jun by free GSNO, and allows the isolation of transcription factors that are potentially modified by GSNO-mediated mixed-disulphide formation from HeLa cell nuclear extracts.

EXPERIMENTAL

Materials

Purified BSA, alcohol dehydrogenase (from baker's yeast), carbonic anhydrase (from bovine erythrocytes), creatine kinase (from rabbit muscle), GAPDH (from rabbit muscle), glycerol-3-phosphate dehydrogenase (GPDH, from rabbit muscle), Hb (from bovine erythrocytes), glycogen phosphorylase *b* (from rabbit muscle), and Cu,Zn superoxide dismutase (SOD, from bovine liver) were purchased from Sigma. S-nitrosated BSA was prepared by incubation of BSA in acidified nitrite, as described in [24]. The recombinant wild-type and mutant DNA-binding domains of human c-Jun (amino acid residues 233–327 of the translated sequence, GenBank accession number J04111) and truncated human p50 (amino acid residues 36–385, GenBank accession number M55643) were expressed in *Escherichia coli* as hexahistidine fusion proteins and purified as described in [25,26] (these constructs are referred to as c-Jun and p50 throughout the text). DNA-binding activities of the recombinant wild-type and mutant proteins were assessed by electrophoretic mobility-shift assay (EMSA). The protease inhibitor Pefabloc was obtained from Roche Molecular Biochemicals. Stock solutions of [^{3}H]GSH were prepared at a final concentration of 20 mM by the addition a freshly prepared solution of 22 mM unlabelled GSH (free acid, SigmaUltra) in water/[^{3}H]GSH [10:1, v/v (40–50 Ci/mmol, approx. 0.02 mM; DuPont New England Nuclear, Boston, MA, U.S.A.)], and stored in small aliquots at −80 °C. [^{3}H]GSNO (1 mM) was prepared by nitrosation of [^{3}H]GSH (1 mM) with sodium nitrite (1 mM) in 10 mM HCl. Unlabelled GSNO was purchased from Alexis Biochemicals. Cell culture products were from Gibco BRL, all other reagents from Sigma–Aldrich.

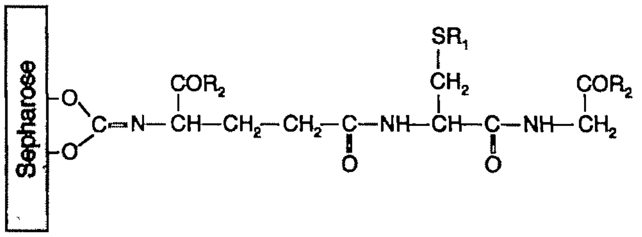

Scheme 1 Structure of GSH–Sepharose analogues used in this study

GSH–Sepharose (R_1 = H, R_2 = OH) was prepared by reduction of commercially available activated thiol–Sepharose 4B (R_1 = 2-thiopyridyl, R_2 = OH) GSNO Sepharose (R_1 = NO, R_2 = OH) was obtained by subsequent S-nitrosation of GSH–Sepharose with acidified nitrite At neutral pH, R_2 is deprotonised and adopts a negative charge The ethyl ester of GSNO–Sepharose (R_1 = NO, R_2 = OC$_2$H$_5$) was prepared by esterification of GSH–Sepharose in acidified ethanol prior to S-nitrosation Where indicated, GSNO–Sepharose was recovered from the GSNO–Sepharose ethyl ester by esterase treatment Details of the preparation procedures are provided in the Experimental section

Determinations of free thiol, S-nitrosothiol and protein concentrations

Free thiol and S-nitrosothiol concentrations were determined photometrically by previously described modifications of the Ellman and Saville assay [27] respectively. Protein concentrations were determined by the method of Bradford with BSA as standard protein [28].

Preparation of GSH–Sepharose analogues

GSH– and GSNO–Sepharose (Scheme 1) were prepared from 2,2′-dipyridyldisulphide-activated GSH–Sepharose ('activated thiol–Sepharose 4B', obtained from Amersham Pharmacia Biotech) according to a recently published method [29] with minor modifications. Briefly, activated thiol–Sepharose 4B was suspended in water, and the swollen gel was washed with 10 vol. of water prior to reduction of the activated thiol groups by incubation for 45 min at ambient temperature in 10 vol. of 0.3 M NaHCO$_3$ (pH 8.5) containing 1 mM EDTA and 5 % (v/v) 2-mercaptoethanol This procedure yielded reduced GSH–Sepharose, which was washed with 30 vol. of a 50 mM Tris/HCl buffer (pH 7.4) containing 250 mM NaCl and 1 mM EDTA.

To obtain GSNO–Sepharose, the GSH matrix was washed with 30 vol. of 10 mM HCl and resuspended in 2 vol. of 10 mM HCl prior to addition of 2 vol. of 10 mM NaNO$_2$ in water. The suspension was agitated thoroughly and incubated for approx. 15 min at ambient temperature. The obtained GSNO–Sepharose was washed with 30 vol. of a 50 mM Tris/HCl buffer (pH 7.4), containing 250 mM NaCl and 1 mM EDTA, and stored in this buffer at 4 °C under nitrogen in the dark. Under these conditions, GSNO–Sepharose was relatively stable, and the loss of S-nitrosothiol groups was less than 5 % and 15 % within 1 and 2 weeks respectively. As judged by the determination of HgCl$_2$-releasable NO (2.4 ± 0.3 µmol/ml of swollen gel, $n = 6$), the conversion of the GSH groups contained in GSH–Sepharose

(2.5 ± 0.5 μmol/ml of swollen gel, $n = 6$) to S-nitrosothiols was almost quantitative.

The ethyl ester of GSNO–Sepharose (Scheme 1) was prepared in analogy to a previously published procedure described for the preparation of GSH ethyl ester [30]. 2,2′-Dipyridyldisulphide-activated GSH–Sepharose (0.5 g) was suspended in 10 ml of anhydrous ethanol, containing 274 μl of concentrated H_2SO_4, and the incubation was suspended overnight under constant agitation at 30 °C. The Sepharose was rehydrated by subsequent washing steps with 10 vol. of 80, 60, 40, 20 and 0 % ethanol in water (v/v) prior to reduction and S-nitrosation as described above. Finally, the material obtained was washed with 30 vol. of a 50 mM Tris/HCl buffer (pH 7.4) containing 250 mM NaCl and 1 mM EDTA. The S-nitrosothiol content of this Sepharose preparation was determined as 2.1 ± 0.1 μmol/ml of swollen gel ($n = 4$). The content of GSH ethyl ester groups was 2.8 ± 1.1 μmol/ml of swollen gel ($n = 3$), as estimated from enzymic determination of ethanol [31], which was released from the matrix by treatment with porcine liver esterase (100 units/ml of swollen gel). Thus for unknown reasons, esterification was not quantitative, and reached only 56 % of the theoretical content of two ethyl groups per GSH molecule. For some control experiments, GSH–Sepharose was recovered from the GSNO ethyl ester–Sepharose by treatment with 100 units of esterase (purified from porcine liver, purchased from Sigma) per ml of swollen gel for 30 min at ambient temperature.

Precipitation of purified proteins by GSH–Sepharose analogues

To assay purified proteins for covalent binding to one of the GSH–Sepharose counterparts described above, the indicated proteins (10 μg, unless otherwise specified) were incubated at ambient temperature with the Sepharose (0.1 ml, unless otherwise specified) in a final volume of 0.5 ml of buffer A [50 mM Tris/HCl (pH 7.4) containing 250 mM NaCl, 1 mM EDTA and 0.01 % (v/v) Nonidet P40 (NP40)]. After 30 min, the Sepharose matrix was pelleted by short centrifugation (300 *g* for 1 min) and washed three times with 1 ml of buffer A. Bound protein was eluted in 0.4 ml of buffer A containing 1 % (v/v) 2-mercaptoethanol. Protein binding to the matrix was quantified by determining protein concentrations in the eluate. For some experiments, elution was performed with 0.1 ml of buffer A containing 1 % (v/v) 2-mercaptoethanol, and samples were analysed by SDS/PAGE on 13 % polyacrylamide gels. Gels were stained for protein with Coomassie Blue and dried.

Preparation of nuclear extracts from HeLa cells

HeLa cells were cultured in RPMI 1640 medium with L-Glutamine (Gibco BRL) containing 9 % (v/v) fetal bovine serum and antibiotics (90 units/ml penicillin and 90 μg/ml streptomycin). Exponentially growing (⩽ 75 % confluence) cells (12 culture dishes, 10 cm diameter) were washed with ice-cold PBS, scraped into PBS, pelleted by centrifugation, and resuspended in a final volume of 10 ml of a 10 mM Hepes buffer (pH 7.9) containing 10 mM NaCl, 1 mM EDTA, 1 % (v/v) glycerol, 0.1 % (v/v) 2-mercaptoethanol and 2 mM Pefabloc. Following incubation for 15 min on ice, NP40 was added at a final concentration of 0.6 %. Subsequently, the cell suspension was agitated vigorously for 10 s and centrifuged for 3 min at 20000 *g*. The pellet obtained was resuspended in a final volume of 1.5 ml of a 20 mM Hepes buffer (pH 7.9), containing 500 mM NaCl, 1 mM EDTA, 10 % (v/v) glycerol, 0.1 % (v/v) 2-mercaptoethanol and 2 mM Pefabloc, incubated on ice for 30 min, and agitated vigorously several times prior to centrifugation for 6 min at 20000 *g*. The obtained supernatant, which contained 1–2 mg/ml protein, was stored at −80 °C.

Isolation of nuclear proteins by covalent GSNO chromatography

Pooled nuclear extracts (10–15 mg of total protein) from exponentially growing HeLa cells were diluted 1 : 100 (v/v) in buffer A containing 1 mM of the protease inhibitor Pefabloc and 4–8 ml of thoroughly suspended GSNO–Sepharose. The suspension was incubated for 30 min at ambient temperature with occasional shaking prior to filtration over a fritted column (internal diameter of 1 cm). To the column flow-through containing unbound protein, 2-mercaptoethanol was added at a final concentration of 1 % (v/v), prior to concentration of the solution to a final volume of ⩽ 5 ml on Vivapore 20 concentrators (molecular mass cut-off 7500 Da; Vivascience, Binbrook, Lincoln, U.K.). Subsequently, the column was washed with 30 vol. of buffer A and eluted with three vol. of buffer A containing 1 % (v/v) 2-mercaptoethanol. The eluate was concentrated to ⩽ 1 ml on Vivapore 20 concentrators. The protein concentrates obtained were stored at −80 °C.

Detection of mixed-disulphide formation with [^{3}H]GSH

Mixed-disulphide formation between the indicated purified proteins and GSH was determined as dithiotreitol-labile, trichloracetic acid-precipitable incorporation of [^{3}H]-labelled GSH as described recently [23]. Briefly, the indicated proteins (2–10 μM) were incubated for 30 min at 37 °C in 0.1 ml of a 20 mM Tris/HCl buffer (pH 7.5), containing 50 mM NaCl, 5 mM $MgCl_2$, 1 mM EDTA, 5 % (v/v) glycerol, 0.01 % (v/v) NP40 and 3 mM [^{3}H]GSH ($6–9 \times 10^5$ c.p.m.) in the absence and presence of either 1 mM [^{3}H]GSNO or 10 mM diamide. Samples that were used to calculate blank values also contained 10 mM dithiotreitol.

To assay the protein fractions which had been obtained by GSNO–Sepharose chromatography of HeLa cell nuclear extracts, 2-mercaptoethanol contained in the protein preparations was replaced by GSH. For this purpose, the proteins were subjected to chromatography on Sephadex G-25 columns (NAP-10; Amersham Pharmacia Biotech) which had been equilibrated with buffer A containing 1 mM GSH. The protein-containing column fractions (0.6–0.8 ml) were pooled and concentrated to a final volume of approx. 0.3 ml on Vivapore 20 concentrators. Subsequently, the sample was assayed for mixed-disulphide formation, which was induced either by the addition of 1 mM [^{3}H]GSH (blank value), 1 mM [^{3}H]GSH and 10 mM diamide (diamide-induced S-glutathionylation), or 1 mM [^{3}H]GSNO (GSNO-induced S-glutathionylation), as described above. S-Glutathionylation reactions were stopped by the addition of 1 ml of 10 % (w/v) ice-cold trichloracetic acid. Samples were incubated on ice for 30 min prior to centrifugation at 4 °C for 10 min at 20000 *g*. The precipitated protein pellet was washed three times with 1 ml of 10 % (w/v) ice-cold trichloracetic acid prior to incubation with 0.1 ml of 1 N NaOH for 20 min at 70–80 °C. The NaOH-solubilized proteins were added to 14 ml of a standard liquid-scintillation cocktail (ReadySafe; Beckman Instruments, Madrid, Spain) to which 1 ml of 10 % (w/v) trichloroacetic acid was added, and assayed for incorporation of [^{3}H]GSH by liquid-scintillation counting.

Analysis of DNA-binding activity by EMSA

Protein fractions (0.5–2 μg of total protein), which had been obtained by chromatography on GSNO–Sepharose, were incubated in a 20 mM Tris/HCl buffer (pH 7.5) containing 50 mM NaCl, 5 mM $MgCl_2$, 1 mM EDTA, 5 % (v/v) glycerol, 0.01 %

(v/v) NP40, 0.2 mg/ml BSA and 0.1 mg/ml poly(dI-dC). One of the following ^{32}P-radiolabelled double-stranded oligonucleotides containing the DNA-binding sites for the transcription factors: AP-1 (5′-GGG CTT GAT GAG TCA GCC GGA GC-3′), NF-κB (5′-GGA GAG GGG ATT CCC TGC G-3′), CREB (5′-AGA GAT TGC CTG ACG TCA GAG AGC TAG-3′), CCAAT-binding protein 1 (CP-1; 5′-CCA CAA ACC AGC CAA TGA GTA ACT GCT GG-3′) or Sp1 (5′-ATT CGA TGC GGG CGG GGC GAG C-3′) were also added. Protein samples which were analysed for Sp1 DNA-binding activity were pre-incubated on ice for 30 min in the presence of 3 mM $ZnSO_4$ in order to restore zinc-dependent DNA binding of the transcription factor [32]. Where indicated, incubations additionally contained an approx. 50-fold excess of an unlabelled competitor oligonucleotide. Subsequent to incubation for 30 min on ice, samples were subjected to electrophoresis at 180 V on pre-electrophoresed 6 % non-denaturing polyacrylamide gels with 22 mM Tris/borate/0.5 mM EDTA as running buffer. Gels were dried and visualized by autoradiography.

Data representation

The number of protein cysteines, as well as the quantification of protein S-glutathionylation (mol GSH incorporated/mol protein) and molar protein concentrations given in the text, refer to the native quaternary structure of the respective protein, i.e. monomers (BSA, carbonic anhydrase, glutaredoxin and thioredoxin), homodimers (c-Jun, creatine kinase, GPDH, glycogen phosphorylase *b*, p50 and SOD), heterodimers (Hb), homotetramers (alcohol dehydrogenase and GAPDH) and heterotetramers (caspase-3). Unless otherwise indicated, data are given as means ± S.E.M., with the number of independent experiments (*n*) in parenthesis.

RESULTS

Binding of purified c-Jun DNA-binding domains to GSNO–Sepharose

Recently, we have shown that GSNO induces the formation of a mixed disulphide between the glutathionyl moiety of GSNO and a conserved cysteine residue in the DNA-binding domain of the transcription factor c-Jun [21]. In accordance with a molecular model of thiolated c-Jun [23], which suggested that specific GSNO–protein interactions facilitate mixed-disulphide formation, we speculated that GSNO–Sepharose might serve as a probe of protein thiols which are susceptible to GSNO-induced S-glutathionylation. To address this issue, we studied binding of recombinant c-Jun DNA-binding domains to the GSNO matrix. As shown in Figure 1(A), c-Jun bound to GSNO–Sepharose following saturation kinetics. Binding to 0.1 ml of GSNO–Sepharose, which contained 240 ± 30 nmol ($n = 6$) S-nitrosothiol groups (see also the Experimental section), was virtually quantitative (> 95 % of total protein) when the amounts of c-Jun were < 0.2 nmol, and approached saturation at > 1 nmol c-Jun. In the presence of saturating amounts of protein (2 nmol c-Jun), binding showed a linear dependency on the total amount of GSNO–Sepharose (Figure 1B). From the slope of this graph, the c-Jun-binding capacity of GSNO–Sepharose was calculated as 12 nmol c-Jun monomer/ml of swollen gel (i.e. per 2.4 μmol S-nitrosothiol groups). c-Jun binding to GSNO–Sepharose could not be reverted by high-salt (1 M NaCl) or detergent (5 % SDS), but was completely abolished by millimolar concentrations of thiol-reducing agents, such as 2-mercaptoethanol, GSH, and dithiotreitol (results not shown). These data suggest that c-Jun binds covalently to GSNO–Sepharose through mixed-disulphide bond formation with the thiol groups of the matrix.

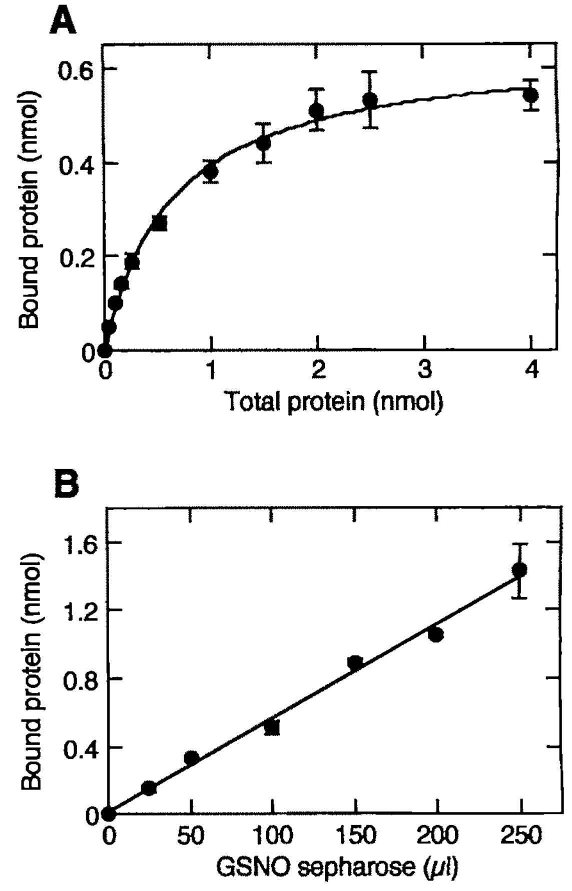

Figure 1 Binding of c-Jun to GSNO–Sepharose

Recombinant c-Jun DNA-binding domains were incubated in a final volume of 0.5 ml with GSNO–Sepharose and assayed for covalent binding to this matrix through mixed-disulphide formation as described in the Experimental section. The dependency of c-Jun binding on the total amount of c-Jun protein (**A**) was assayed with increasing amounts of c-Jun (0.05–4 nmol) and a fixed quantity (0.1 ml) of GSNO–Sepharose. To determine the dependency of c-Jun binding on the amount of GSNO–Sepharose (**B**), a fixed amount of c-Jun (2 nmol) was incubated with increasing amounts of GSNO–Sepharose (25–250 μl). Data are means ± S.E.M. of 4–12 different experiments.

GSNO–Sepharose precipitation of purified proteins susceptible to GSNO-induced S-glutathionylation

The above data, obtained with the cDNA-binding domain of c-Jun as model protein, encourage the view that mixed-disulphide formation between a given protein and GSNO–Sepharose might reflect its susceptibility to GSNO-induced S-glutathionylation. To address this issue, we compared structurally distinct proteins in terms of GSNO–Sepharose binding, as well as GSNO- and diamide-induced S-glutathionylation. In the first set of experiments, we chose p50, Hb and BSA because, similar to c-Jun, they contain critical cysteine residues which have been shown previously to be sensitive to GSNO or other NO donor compounds [24,33–35]. However, the question of whether GSNO may direct mixed-disulphide formation to these proteins has not been addressed so far. We compared GSNO–Sepharose binding

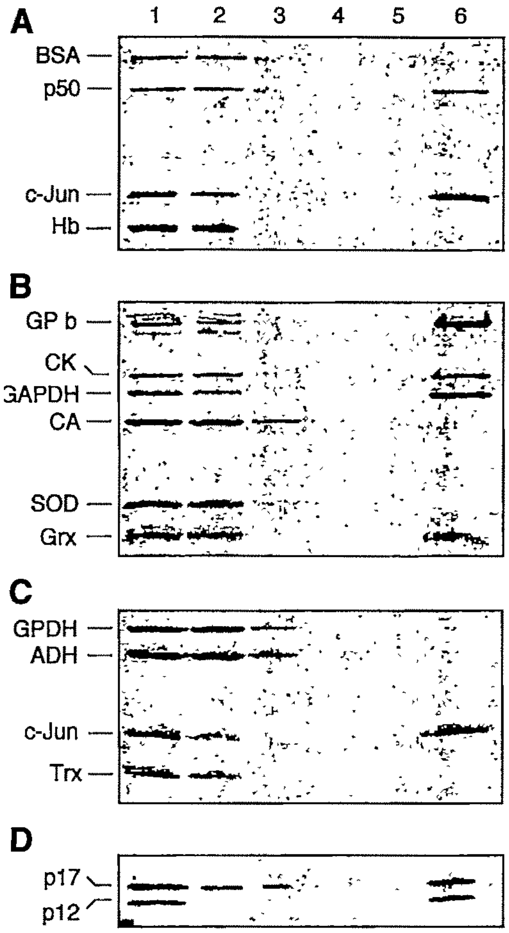

Figure 2 Binding of purified proteins to GSNO–Sepharose

A mixture of various purified proteins, i.e. BSA, p50, c-Jun and Hb (**A**), glycogen phosphorylase *b* (GP b), creatine kinase (CK), GAPDH, carbonic anhydrase (CA), SOD and glutaredoxin (Grx) (**B**), GPDH, alcohol dehydrogenase (ADH), c-Jun and thioredoxin (Trx) (**C**) and caspase-3 composed by the subunits p12 and p17 (**D**) was incubated in a final volume of 0.5 ml with 0.1 ml of GSNO–Sepharose for 30 min at ambient temperature, as described in the Experimental section. The amount of the individual proteins was 10 μg, with the exception of Hb and caspase-3, where the amount was 20 μg. Bound proteins were isolated by short centrifugation of the Sepharose matrix, which was washed three times with 0.5 ml of a 50 mM Tris/HCl buffer containing 250 mM NaCl, 1 mM EDTA and 0.01 % NP40 prior to elution with 0.1 ml of the washing buffer to which 1 % (v/v) 2-mercaptoethanol was added. Aliquots (25 μl) of the complete incubation mixture (lane 1), the supernatant containing unbound proteins (lane 2), the first (lane 3), second (lane 4) and third (lane 5) wash, as well as the Sepharose eluate (lane 6), were subjected to SDS/13 % PAGE, and gels were stained for protein with Coomassie Blue. The gels shown are representative of at least three similar experiments.

of p50, Hb and BSA with that of c-Jun (Figure 2A) by incubating a mixture of the purified proteins with the nitrosothiol matrix (lane 1). The supernatant (Figure 2, lane 2) was discarded, and non-specifically bound proteins were removed by excessive washing of the matrix (lanes 3–5) prior to reductive elution of covalently bound proteins (lane 6). The eluate contained c-Jun and p50, but only barely detectable amounts of Hb and BSA. GSNO–Sepharose binding of these proteins was further quantified in independent experiments by determining their amounts in the eluate with the Bradford assay (see the Experimental section). When 4 nmol of c-Jun and p50 were incubated with 0.1 ml of GSNO–Sepharose, the affinity matrix precipitated 0.54 ± 0.03 ($n = 3$) and 0.38 ± 0.04 ($n = 3$) nmol protein respectively, whereas binding of Hb and BSA was barely detectable [0.09 ± 0.01 ($n = 3$) and 0.07 ± 0.01 ($n = 3$) nmol protein respectively]. Qualitatively similar results were obtained under non-saturating conditions, i.e. when the amount of total protein was reduced to $\leqslant 0.1$ nmol (results not shown). These data correlated well with the GSNO-induced incorporation of [^{3}H]GSH into these proteins, which was considerably lower with Hb and BSA than with p50 and c-Jun (Table 1).

To exclude that lack of BSA and Hb binding to GSNO–Sepharose was due to the inaccessibility of the cysteine residues contained in these proteins to GSH, we used the non-selective thiol-oxidizing agent diamide to induce mixed-disulphide formation. As shown in Table 1, treatment of c-Jun with diamide in the presence of GSH resulted in the stoichiometric incorporation of one GSH molecule into each of the four c-Jun cysteines. In the p50 homodimer, four cysteine residues form intramolecular disulphide bridges, and two further cysteines do not appear to be solvent-accessible [36,37]. Accordingly, only 8 of the 14 cysteine residues were found to be available for mixed-disulphide formation. The Hb tetramer contains two cysteines, which have been shown to be susceptible to diamide-induced mixed-disulphide formation [38]. In fact, we found that both residues incorporated GSH upon diamide treatment. Previous studies on the reactivity of BSA thiols have shown that commercially available BSA contains only one single reactive cysteine residue [39]. In the present study, this is reflected by the diamide-induced GSH incorporation of approx. 1 mol GSH/mol BSA. Thus lack of GSNO–Sepharose binding of Hb and BSA is apparently not due to the lack of cysteine residues that can undergo S-glutathionylation, but rather reflects their low reactivity towards GSNO. Consistent with this hypothesis, activation of the GSH matrix by 2,2′-dipyridyldisulphide bound these four proteins with comparable efficacy (results not shown).

To further support the potential applicability of GSNO–Sepharose to the isolation of proteins that form mixed disulphides with GSNO, we analysed various purified cysteine-containing proteins for GSNO–Sepharose binding (Figure 2B–D) and compared the data obtained with results from [^{3}H]GSH-incorporation experiments (Table 1). To assay these proteins for the total amount of cysteine residues that are accessible to mixed-disulphide formation, [^{3}H]GSH incorporation was induced by diamide. Previous work indicates that glycogen phosphorylase *b* and creatine kinase [40], as well as carbonic anhydrase isoenzymes [41,42], GAPDH [43,44], SOD [45] and glutaredoxin [46], may be modified by redox- or free radical-induced mixed-disulphide formation. Furthermore, in the case of glycogen phosphorylase *b* and an isoform of carbonic anhydrase [16], as well as GAPDH [17], GSNO-induced S-glutathionylation has been reported. Figure 2(B) shows that glycogen phosphorylase *b*, creatine kinase, GAPDH and glutaredoxin bound to GSNO–Sepharose, whereas carbonic anhydrase and SOD apparently did not form mixed disulphides with the NO-activated thiol matrix. These findings fitted well with the differential susceptibility of these proteins to GSNO-induced S-glutathionylation (Table 1). Whereas GSNO-induced GSH incorporation into glycogen phosphorylase *b*, creatine kinase, GAPDH and glutaredoxin was comparable with that found for the GSNO–Sepharose binders c-Jun and p50 (0.9–2 mol GSH/mol protein), S-glutathionylation of carbonic anhydrase and SOD was similar to that found for BSA and Hb (0.1–0.2 mol GSH/mol protein), which, as shown above, could not be efficiently bound by the matrix.

In a previous study, it was speculated that alcohol dehydrogenase may be modified by GSNO-induced S-glutathionylation [13]. A further cysteine-rich enzyme that has been proposed to be regulated by GSH-dependent oxidation of critical cysteine

Table 1 Diamide- and GSNO-induced protein S-glutathionylation

The total number of protein cysteines was taken from the published amino acid sequences of the investigated wild-type proteins, and refers to their established quaternary structure as given in the Experimental section. Diamide- and GSNO-induced S-glutathionylation of the indicated purified proteins (2–10 μM) were determined in the presence of ^{3}H-labelled GSH (3 mM) and induced by 1 mM [^{3}H]GSNO or 10 mM diamide. Data are means ± S.E.M. for at least three independent experiments. n.d., not determined.

Protein	Number of cysteines	S-Glutathionylation induced by GSH/GSNO (mol/mol protein)	S-Glutathionylation induced by GSH/diamide (mol/mol protein)
c-Jun	4	1.96±0.14	3.83±0.06
Glycogen phosphorylase *b*	18	1.95±0.09	14.34±0.84
GAPDH	16	1.28±0.18	4.17±0.39
Caspase-3	14	1.22±0.12	n.d.
Creatine kinase	8	0.97±0.14	3.08±0.59
Glutaredoxin	4	0.88±0.02	1.02±0.02
p50	14	0.86±0.06	8.06±0.26
Alcohol dehydrogenase	32	0.43±0.01	16.94±0.59
GPDH	22	0.43±0.03	14.49±1.78
Hb	2	0.21±0.01	1.80±0.10
Thioredoxin	3	0.17±0.01	0.64±0.03
Carbonic anhydrase	1	0.11±0.05	0.43±0.03
SOD	6	0.16±0.01	0.34±0.01
BSA	35	0.07±0.01	0.84±0.01

Table 2 Site-specific binding of c-Jun and p50 to GSNO–Sepharose

Wild-type and mutant c-Jun and p50 DNA-binding domains (0.05–0.5 nmol), in which the cysteine located in the DNA-binding site (serine-269) and the adjacent leucine zipper (serine-320) of c-Jun or the cysteine in the DNA-binding site of p50 (serine-62) were substituted by serine, were precipitated by 0.15 ml of GSNO–Sepharose or 2,2′-dipyridyl disulphide-activated GSH–Sepharose, as described in the Experimental section. The amounts of mutant proteins bound to GSNO–Sepharose, which are expressed as a percentage of binding of the corresponding wild-type proteins, are means ± S.E.M. of at least three different experiments.

	Bound protein (% of wild-type)		
	c-Jun (serine-269)	c-Jun (serine-320)	p50 (serine-62)
GSNO–Sepharose	9±6	97±12	15±2
2,2′-Dipyridyl disulphide-activated GSH–Sepharose	84±4	90±5	87±3

residues is GPDH [47,48]. Baker's yeast alcohol dehydrogenase and rabbit muscle GPDH contain 32 and 22 cysteine residues, and incorporate 17 and 14 mole GSH/mol protein upon exposure to diamide respectively (Table 1). Nevertheless, these proteins did not bind to a significant extent to GSNO–Sepharose as compared with the GSNO–Sepharose binder c-Jun (Figure 2C). Both proteins, however, formed low, but significant, amounts (approx. 0.4 mol GSH per mol protein) of mixed disulphides when incubated with GSH/GSNO (Table 1). These data suggest that protein binding to GSNO–Sepharose is not only governed by the overall capacity of a protein to incorporate GSH upon GSNO treatment, but also by other, as yet unknown, factors. A further attempt to identify proteins which contain reactive and GSNO-accessible thiol groups was based on previous work on the thioredoxin system, suggesting that GSNO has free access to, and may react with, one of the active-site cysteines of thioredoxin [49]. As shown in Table 1, purified thioredoxin incorporated > 0.6 mol GSH/mol protein upon diamide treatment but < 0.2 mol GSH/mol protein in the presence of GSNO. In accordance with this relatively poor yield of GSNO-dependent GSH incorporation, we did not detect thioredoxin binding to GSNO–Sepharose (Figure 2C).

Very recent work suggests that the cysteine protease caspase-3 may be modified at various cysteine residues by NO-mediated S-glutathionylation [19]. In the present study, we found that GSNO oxidizes caspase-3 by S-glutathionylation of an overall amount of 1.2 cysteine residues/holoenzyme (Table 1). The susceptibility of the caspase to GSNO mixed-disulphide formation correlated with its capacity to covalently interact with immobilized GSNO (Figure 2D). Furthermore, in accordance with the reported localization of mixed disulphides on both caspase-3 subunits (p12 and p17) [19], we found that both p12 and p17 could be bound by GSNO–Sepharose.

Specificity of protein binding to GSNO–Sepharose

The above data indicate that GSNO-induced S-glutathionylation does not apparently affect each cysteine residue that is accessible to GSH, but may be specifically targeted to a subset of GSNO-sensitive thiols. The c-Jun DNA-binding domain contains two cysteine residues: cysteine-269, located in the basic domain of the protein which makes direct contact with its target DNA sequence; and cysteine-320, in the monomer–monomer interface [50]. However, only cysteine-269 forms a mixed disulphide upon GSNO treatment [21]. Here, we show that such site specificity of GSNO-induced S-glutathionylation is preserved when GSNO–Sepharose is used as the thiolating probe. As shown in Table 2, a cysteine-to-serine mutation at cysteine-269 almost completely abolished c-Jun binding to the immobilized nitrosothiol, whereas binding was virtually unaffected by a cysteine-to-serine mutation at cysteine-320, compared with the wild-type protein. The observed site-specificity was apparently not due to steric constraints which inhibit access of Sepharose-coupled GSNO to cysteine-320, since both the serine-320 and serine-269 mutants bound to 2,2′-dipyridyl disulphide activated GSH–Sepharose with comparable efficacy. These data correlated well with recently published results [21] showing that GSNO-induced S-glutathionylation was reduced to 16 ± 6 (5) % of the wild-type protein in the serine-269 mutant and virtually unaffected in the serine-320 mutant [107 ± 11 % ($n = 3$) of the wild-type protein].

Similarly, modification of a single cysteine residue (cysteine-62) has been shown to mediate inhibition of DNA binding of the NF-κB subunit p50 by diamide and NO [26,33]. In accordance with these studies, we found that GSNO inhibited DNA binding of purified p50 with a half-maximal effective concentration of approx. 0.1 mM, and that substitution of cysteine-62 by serine rendered p50 DNA binding insensitive to GSNO (results not shown). It is tempting to speculate, therefore, that cysteine-62 could be the target thiol for GSNO-induced thiolation. $[^3H]$GSH-incorporation experiments showed that GSNO-induced S-glutathionylation of p50 (Table 1) was markedly reduced in the serine-62 mutant [7 ± 4 % ($n = 4$) of the wild-type protein]. Site specificity of GSNO-mediated p50 mixed-disulphide formation was preserved in GSNO–Sepharose binding experiments. As shown in Table 2, point mutation of cysteine-62 to serine markedly reduced the capacity of p50 to bind to GSNO–Sepharose. Similar to c-Jun, site specificity of covalent binding to the thiol–Sepharose was almost completely lost when the GSH moiety of the matrix was activated with 2,2′-dipyridyl disulphide instead of NO (Table 2).

It was suggested that specific GSH–protein interactions may facilitate mixed-disulphide formation [22]. Molecular modelling of c-Jun encourages this view, proposing that electrostatic interactions between basic amino acids surrounding the targeted cysteine residue and negatively charged carboxylates of the GSH moiety may contribute to the susceptibility of protein thiols to S-glutathionylation [23]. To address the question of whether such ionic interactions may play a role in protein binding to GSNO–Sepharose, the negative charges of the matrix were neutralized by converting the carboxylates in the GSNO molecule into the neutral ethyl esters (Scheme 1). Glycogen phosphorylase *b*, creatine kinase, GAPDH and c-Jun were shown above to incorporate $\geqslant 1$ mol GSH/mol protein (Table 1) and to bind well to GSNO–Sepharose (Figure 2). However, as shown in Figure 3(A), binding to GSNO ethyl ester–sepharose was suppressed in the case of glycogen phosphorylase *b* and creatine kinase, and markedly impaired with GAPDH and c-Jun (see also Figure 2). To exclude that such loss of binding was caused by modifications of the matrix other than esterification during the preparation of this GSH Sepharose counterpart, GSNO ethyl ester–Sepharose was treated with esterase to remove the ester groups and, consequently, to recover the negatively charged carboxylate groups. This procedure, in fact, restored the capacity of the matrix to bind glycogen phosphorylase *b* and creatine kinase, and slightly increased c-Jun and GAPDH binding to the immobilized nitrosothiol (Figure 3B). These data indicate that ionic GSH–protein interactions may facilitate protein binding to GSNO–Sepharose. Saturation curves of c-Jun binding to GSNO ethyl ester–Sepharose before and after esterase treatment (results not shown) further corroborated this hypothesis. Maximal binding of c-Jun to these two Sepharose preparations was virtually identical [GSNO ethyl ester–Sepharose, 0.62 ± 0.03 ($n = 3$) nmol protein/0.1 ml of swollen gel; esterase-treated GSNO ethyl ester–Sepharose, 0.59 ± 0.05 ($n = 3$) nmol protein/0.1 ml of swollen gel], whereas the concentration of c-Jun required for half-maximal binding to 0.1 ml of Sepharose was approx. 4-fold higher with the ethyl ester [1.15 ± 0.16 ($n = 3$) nmol protein] as compared with the esterase-treated matrix (0.28 ± 0.07 ($n = 3$) nmol protein).

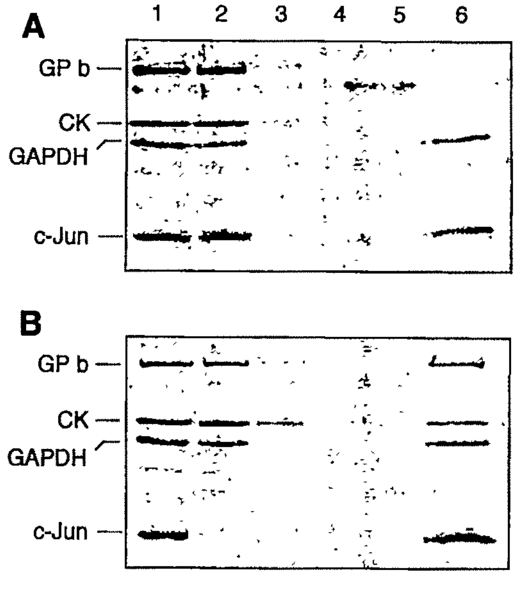

Figure 3 Binding of purified proteins to GSNO ethyl ester–Sepharose

A mixture of purified glycogen phosphorylase *b* (GP b), creatine kinase (CK), GAPDH and c-Jun (10 μg each) was incubated in a final volume of 0.5 ml with 0.1 ml of GSNO ethyl ester–Sepharose for 30 min at ambient temperature, as described in the Experimental section (**A**) The same experiment was repeated with GSNO ethyl ester–Sepharose which had been pretreated with esterase to convert the ethyl ester back into the free carboxylic acid (**B**) Bound proteins were isolated as described in the legend to Figure 2 Aliquots (25 μl) of the complete incubation mixture (lane 1), the supernatant containing unbound proteins (lane 2), the first (lane 3), second (lane 4) and third (lane 5) wash, as well as the Sepharose eluate (lane 6), were subjected to SDS/13% PAGE and gels were stained for protein with Coomassie Blue The gels shown are representative for three experiments

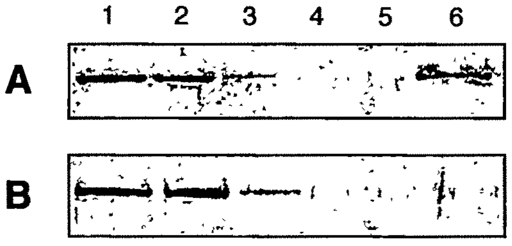

Figure 4 Binding of S-nitrosated BSA to GSH–Sepharose

S-Nitrosated BSA (10 μg) was incubated in a final volume of 0.5 ml with 0.1 ml of GSH–Sepharose for 30 min at ambient temperature, as described in the Experimental section (**A**) Incubations of unmodified BSA with GSNO–Sepharose (**B**) were performed under identical conditions Bound BSA was isolated as described in the legend to Figure 2 Aliquots (25 μl) of the complete incubation mixture (lane 1), the supernatant containing unbound BSA (lane 2), the first (lane 3), second (lane 4) and third (lane 5) wash, as well as BSA released from GSNO–Sepharose by elution under reducing conditions (lane 6), were subjected to SDS/13% PAGE, and gels were stained for protein with Coomassie Blue The gels shown are representative for three experiments

It is currently thought that GSNO-induced S-glutathionylation may involve either a direct nucleophilic attack of a protein thiol on GSNO or a two-step reaction in which the NO group is transferred to the protein thiol prior to reaction of the nitrosated protein with GSH [13,14,16,17,20,21]. Thus it could be argued that protein binding to GSNO–Sepharose depends on the activation of protein thiols via a *trans*-nitrosation reaction, rather

Table 3 Isolation of nuclear HeLa cell proteins that are susceptible to GSNO-induced S-glutathionylation

HeLa cell nuclear extracts were subjected to chromatography on GSNO–Sepharose, and the total extract, column flow-through and eluate were analysed for protein content and S-glutathionylation S-Glutathionylation was induced either by the addition of GSNO or diamide, as described in the Experimental section Data are means ± S.E.M of three different preparations

	Total extract	Flow-through	Eluate
Total protein (mg)	12 ± 3	11 ± 3	0.05 ± 0.01
GSNO-induced S-glutathionylation (nmol [^{3}H]GSH/mg of protein)	2 ± 2	3 ± 1	37 ± 14
Recovery of GSNO-reactive thiols (%)	100	138	8
Purification of GSNO-reactive thiols (-fold)	1	1	19
Diamide-induced S-glutathionylation (nmol [^{3}H]GSH/mg of protein)	53 ± 12	67 ± 19	122 ± 12
Recovery of diamide-reactive thiols (%)	100	116	1
Purification of diamide-reactive thiols (-fold)	1	1	2

than on specific GSNO–protein interactions that facilitate a direct reaction between the protein and GSNO. To address this issue, we attempted to study binding of S-nitrosated proteins to GSH–Sepharose. However, almost all of the proteins investigated in this study (listed in Table 1) did not stably incorporate significant amounts of NO (results not shown). One exception was BSA, which formed a relatively stable S-nitrosothiol. Similar to previous studies which reported the incorporation of approx. 0.8 mol NO/mol protein [24], we found that treatment of BSA with acidified nitrite yielded 0.55 ± 0.11 ($n = 6$) mol S-nitrosothiol groups/mol BSA. As shown in Figure 4(A), incubation of S-nitrosated BSA with GSH–Sepharose resulted in the formation of a mixed disulphide with the reduced thiol matrix Importantly, unmodified BSA does not bind to GSNO–Sepharose (Figure 4B, compare also with Figure 2A) indicating that GSNO–Sepharose rather selects for proteins which react directly with GSNO than for proteins that react with GSH through a GSNO-dependent *trans*-nitrosation reaction.

Isolation of nuclear transcription factors by GSNO–Sepharose chromatography

The above data encourage the view that GSNO–Sepharose might be useful for the isolation and identification of cellular proteins which are potential targets for GSNO-induced S-glutathionylation. When nuclear extracts from exponentially growing HeLa cells were subjected to GSNO–Sepharose chromatography, less than 0.5 % of the total amount of protein loaded on to the nitrosothiol–Sepharose bound to the matrix through mixed-disulphide formation (Table 3). As judged by Coomassie Blue-staining of SDS gels, the protein fraction isolated by this method displayed a substantially distinct protein pattern than the column flow-through (results not shown). Thus to investigate if chromatography on GSNO–Sepharose resulted in a significant enrichment of proteins susceptible to GSNO-induced thiolation, we performed [^{3}H]GSH-incorporation assays comparing unbound (GSNO–Sepharose flow-through) with bound (GSNO–Sepharose eluate) protein fractions. As shown in Table 3, the overall capacity of proteins to undergo GSNO-induced mixed-disulphide formation was 12-fold higher in the GSNO–Sepharose eluate than in the column flow-through. When glutathionylation was induced by diamide, the increase in total GSH incorporation into proteins of the eluate was less than twofold compared with proteins contained in the column flow-through. Thus despite the low yield of this method (8 % recovery of GSNO-sensitive protein thiols), these data suggest that GSNO–Sepharose chromatography may serve to enrich proteins that can be modified by GSNO-mediated incorporation of GSH

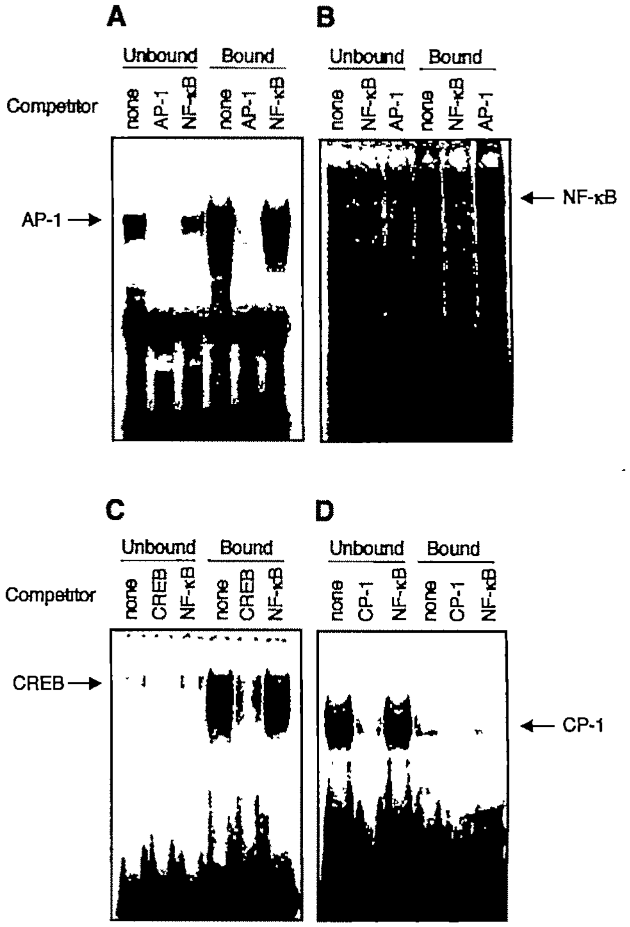

Figure 5 Isolation of AP-1, NF-κB, CREB and CP-1 DNA-binding activities from HeLa cells by GSNO–Sepharose chromatography

HeLa cell nuclear extracts were subjected to chromatography on GSNO–Sepharose The column flow-through (unbound) and eluate (bound) were analysed for AP-1 (**A**), NF-κB (**B**), CREB (**C**) and CP-1 (**D**) DNA-binding activities by EMSA, as described in the Experimental section Specificity of protein–DNA complex formation was confirmed by homologous and heterologous competition with a 50-fold excess of the indicated unlabelled oligonucleotides The gels shown are representative for four similar experiments

As yet, the only transcriptional activators known to be S-glutathionylated by GSNO *in vitro* are the AP-1 subunit c-Jun [21] and the NF-κB subunit p50 (the present study). Analysis of the GSNO–Sepharose column flow-through and eluate by EMSA revealed that both AP-1 (Figure 5A) as well as NF-κB (Figure 5B) DNA-binding activities bound almost quantitatively to the nitrosothiol matrix. Presence of c-Jun and p50 in the GSNO–Sepharose eluate was confirmed by Western blot (results not shown). We further analysed the column fractions obtained for DNA-binding activity of CREB, a transcription factor whose DNA-binding site is homologous to that of c-Jun. As shown in Figure 5(C), the column eluate was enriched in protein(s) which specifically bound to the consensus DNA sequence for CREB. In contrast, DNA-binding activity of the transcription factor CP-1, a cysteine-containing CCAAT-binding protein [51], was almost exclusively detected in the column flow-through (Figure 5D). Similarly, DNA-binding activity of Sp1, which binds to DNA through a Cys$_2$/His$_2$ zinc-finger motif [32], was not enriched in the GSNO–Sepharose eluate (results not shown).

DISCUSSION

The S-nitrosothiol GSNO has been implicated in the regulation of cellular functions through the modification of functionally critical cysteine residues in target proteins [10]. Recent data suggest that GSNO may play a role in the regulation of transcription by reversibly transferring its glutathione moiety to a cysteine residue in the DNA-binding site of the transcription factor c-Jun *in vitro* [21]. As yet, it remains unknown whether this modification is unique to c-Jun or if it is shared by other proteins. We addressed this issue using GSNO–Sepharose as a tool which should allow the isolation of proteins through site-specific GSNO–protein interactions, leading to the formation of a mixed disulphide with the immobilized nitrosothiol.

First, to investigate the potential usefulness of GSNO–Sepharose as a probe of GSNO-induced S-glutathionylation, we characterized the interaction between the matrix and the DNA-binding domain of c-Jun We provide experimental evidence that c-Jun binds to GSNO–Sepharose through the formation of a mixed-disulphide bond. Maximal protein binding to the matrix, however appears rather low comparing the maximal number of c-Jun molecules bound/ml of Sepharose (12 nmol) with the number of S-nitrosothiol groups contained in 1 ml of the matrix (2.4 μmol). This corresponds to a reaction of only 0.5 % of the total S-nitrosothiol groups with protein thiols under saturating concentrations. This low yield can be explained partly by the stringent assay conditions. We performed the binding assays in the presence of 0.25 M NaCl and 0.01 % NP40 to suppress the non-specific formation of mixed disulphides. When the assays were performed in the absence of NP40 and NaCl, binding of c-Jun was increased approx fivefold (results not shown). Furthermore, the low yield may be due to the low capacity of native proteins to bind to the Sepharose matrix because of steric constraints. In support of this, it was found that 1 ml of activated thiol–Sepharose, the starting material for the preparation of GSNO–Sepharose, bound a maximum of approx. 10–50 nmol of native proteins such as Hb, erythrocyte band III protein and collagen [52–54], whereas up to 200 nmol of denatured proteins and peptides could be retained by 1 ml of the same matrix [55] Of note is the fact that GSNO is coupled directly, i.e. without the introduction of spacer groups, to the Sepharose carrier through the terminal amino group of its γ-glutamate moiety (Scheme 1) It is conceivable, therefore, that the matrix might impair protein–GSH interactions and, therefore, will not work with proteins whose GSNO-sensitive cysteine residues are buried within the native-folded-protein structure. It remains to be investigated whether the introduction of flexible spacer groups could improve the efficacy of GSNO–Sepharose as a mixed-disulphide-forming matrix.

In accordance with previous data on c-Jun thiolation [21,23], we found that this protein bound to GSNO–Sepharose through the formation of a mixed disulphide with a single cysteine residue which was identified as cysteine-269 by site-directed mutagenesis. It is worth noting that site-specificity of c-Jun S-glutathionylation was not due to lack of accessibility or reactivity of the second pair of cysteine residues (cysteine-320) contained in the c-Jun homodimer. This conclusion is supported by the observation that cysteine-320 was quantitatively converted into a mixed disulphide when diamide was used to induce mixed-disulphide formation. Similarly, when the thiol group of glutathione–Sepharose was activated with 2,2′-dipyridyl disulphide instead of NO, both cysteine-269 and cysteine-320 bound equally to the thiol matrix, indicating that lack of c-Jun binding to GSNO–Sepharose through cysteine-320 was not due to steric constraints. Covalent protein binding to GSNO–Sepharose, therefore, apparently does not just simply detect the presence of reactive and freely accessible cysteine residues but rather reflects the particular reactivity of a protein thiol in terms of its susceptibility to undergo GSNO-induced S-glutathionylation. The basic environment of c-Jun cysteine-269 has been suggested to account for the particular reactivity and redox-sensitivity of this thiol [56]. Thus to investigate whether site-specific binding to GSNO–Sepharose is unique to c-Jun, or is shared by other DNA-binding proteins, we searched for another model transcription factor which contains functionally important cysteine residues but displays marked structural differences to c-Jun. Similar to c-Jun, the NO- and redox-sensitivity of the NF-κB subunit p50 maps to a single cysteine residue (cysteine-62) in its DNA-binding site [26,33]. Moreover, it has been speculated that redox-regulation of NF-κB DNA binding in intact cells could involve S-glutathionylation of cysteine-62 [57]. In the present study, we show that p50 can be precipitated by GSNO–Sepharose and that covalent binding to the immobilized nitrosothiol critically depends on one single cysteine residue. Site-directed mutagenesis revealed that cysteine-62 accounts for covalent binding of the NF-κB subunit to the matrix. [^{3}H]GSH-incorporation assays corroborate the suggestion that cysteine-62 of p50 may represent a novel target for GSNO-induced S-glutathionylation *in vitro*.

The observation that GSNO–Sepharose binds c-Jun and p50 through site-specific disulphide formation with a single thiol suggests that this matrix may permit the isolation of GSNO target proteins from a mixture of cysteine-containing proteins. As a first attempt to address this issue, we investigated the capacity of GSNO–Sepharose to precipitate c-Jun and p50 from a mixture of purified proteins which additionally contained BSA and Hb. It is noteworthy that both BSA and Hb contain reactive cysteine residues which are quantitatively thiolated by GSH/diamide and exhibit some reactivity in terms of mixed-disulphide formation with both solute and immobilized GSNO. When p50 and c-Jun were competing with BSA and Hb for covalent binding to GSNO–Sepharose, the NO-activated thiol matrix precipitated c-Jun and p50 with high specificity (Figure 2). Similarly, a number of other proteins have been shown in the present study to contain reactive cysteine residues that can be S-glutathionylated by GSNO *in vitro*. The data presented in Table 1 and Figure 2 suggest that, in general, GSNO–Sepharose binding reflects the susceptibility of a given protein to react with GSNO, and is not just simply the presence of cysteine residues that can be modified by diamide-induced S-glutathionylation. However, alcohol dehydrogenase and GPDH did not bind to the GSNO matrix despite their capacity to undergo some GSNO-induced S-glutathionylation in solution. As discussed above, this may be explained by steric constraints imposed by the structure of the proteins which does not allow access of the Sepharose to cysteine residues, that are not located on the protein surface. Moreover, in some cases, the interpretation of quantitative data as presented in Table 1 is compromised by the lack of information about the contribution of individual cysteine residues to the overall number of GSH molecules incorporated per protein. The targeted cysteine residues in c-Jun and p50 have been identified by site-directed mutagenesis, and it can be concluded that a single cysteine residue accounts for the major part of the observed S-glutathionylation in these proteins. In the case of alcohol dehydrogenase and GPDH, we found that 17 and 15 cysteine residues respectively can be modified by diamide-induced S-glutathionylation. However, only a total of 0.4 of these residues, which are available for mixed-disulphide formation, can be glutathionylated by GSNO. If GSNO-induced S-glutathionylation were not localized to one single protein thiol (i.e. 0.4 mol GSH/cysteine residue), but equally distributed over all of these residues (i.e. 0.03 mol GSH per cysteine residue), the degree of thiolation at the level of individual protein thiols would be even lower than that observed for BSA and Hb (0.07 and 0.21 mol GSH/mol protein respectively) and, therefore, might be too low to result in detectable GSNO–Sepharose binding. Definite conclusions, however, await further studies with the respective cysteine mutants.

So far, little is known about the molecular basis of GSNO-induced protein thiolation and about possible factors that confer site specificity to this modification. Initially, it was proposed that NO induces S-glutathionylation via a two-step mechanism which involves S-nitrosation of the target protein thiol and subsequent replacement of the NO group by the glutathionyl moiety [13]. Our data on the reaction of S-nitrosated BSA with GSH–Sepharose (Figure 4) confirm that this pathway may in fact lead to the formation of a mixed disulphide between a protein and immobilized glutathione. However, the observation that BSA neither incorporated GSNO in solution nor bound to GSNO–Sepharose render it unlikely that such a mechanism accounts for the apparent selectivity and specificity of GSNO-induced mixed-disulphide formation observed here. More recently, it has been suggested that GSNO-induced protein glutathionylation involves a nucleophilic attack of the protein thiol on the sulphur of GSNO [14,17,20,21]. Thus the site-specificity of GSNO-induced thiolation may be explained in part by the basic micro-environment of the target cysteine which lowers its pK_a value and thus increases the nucleophilicity and reactivity of the sulphur atom [58]. A comparison of the sequences and, where available, tertiary structures of the proteins that were found in the present study, both to incorporate GSH upon GSNO treatment and to bind to GSNO Sepharose, confirms that these proteins contain at least one cysteine residue that is surrounded by basic amino acids (results not shown). Finally, previous work on the molecular basis of protein S-glutathionylation suggests that the incorporation of GSH may be facilitated by protein–GSH interactions [22]. In support of this suggestion, kinetic data on the inhibition of aldose reductase by GSNO-mediated thiolation revealed that the reaction of the enzyme with GSNO is in fact preceded by tight-binding of the nitrosothiol to the active site of the enzyme [14]. Furthermore, molecular modelling of S-glutathionylated c-Jun would be compatible with stabilization of the mixed disulphide by electrostatic protein–GSH interactions, involving positively charged arginine and lysine residues in the protein and negatively charged carboxyl groups in the GSH moiety [23]. Similarly, a cluster of positively charged amino acids was proposed to facilitate S-glutathionylation of protein tyrosine phosphatase-1B [59]. We addressed this issue using GSNO ethyl ester–Sepharose as a probe for S-nitrosothiol-induced disulphide formation and show that loss of the positive charges at the carboxyl moieties of the GSH molecule reduces binding of some proteins to the matrix (Figure 4). Although it cannot be excluded that impaired binding of proteins to GSNO ethyl ester–Sepharose is caused by steric constraints imposed by the introduction of the ethyl ester groups, our results are compatible with the view that ionic interactions may contribute to GSNO-dependent S-glutathionylation.

One further step to establish immobilized GSNO as a tool to isolate and identify novel targets of GSNO-induced S-glutathionylation from more complex protein mixtures was to subject HeLa cell nuclear extracts to covalent GSNO–Sepharose chromatography [^{3}H]GSH-incorporation assays revealed that the proteins isolated by GSNO–Sepharose exhibit a > 10-fold higher capacity to undergo GSNO-induced mixed disulphide formation than the column flow-through (Table 3). Importantly, diamide-induced [^{3}H]GSH incorporation was of the same order of magnitude in both protein fractions, indicating that the observed differences, with regard to GSNO-induced thiolation, were not due to a difference in the number of reactive thiols in the compared protein fractions. In keeping with the idea that diamide-induced [^{3}H]GSH incorporation into a protein reflects the total number of cysteine residues that are accessible to mixed-disulphide formation, and assuming that the cysteine residues that undergo GSNO-induced [^{3}H]GSH incorporation are contained within this group of diamide-sensitive thiols (Table 1), the ratio of GSNO- versus diamide-induced [^{3}H]GSH incorporation should be a measure for the relative number of cysteine residues that can be modified by GSNO-induced S-glutathionylation. Thus from the data presented in Table 3, it can be estimated that in the GSNO–Sepharose flow-through one out of 22 diamide-sensitive cysteine residues (i.e. 3 versus 67 nmol [^{3}H]GSH/mg protein) is modified by GSNO-mediated glutathionylation, whereas in the bound protein fraction one out of three diamide-sensitive cysteine residues forms a mixed disulphide with GSH in response to GSNO treatment (i.e. 37 versus 122 nmol [^{3}H]GSH/mg protein). Thus the nitrosated matrix apparently selects for protein thiols susceptible to GSNO-induced mixed-disulphide formation (i.e. GSNO-induced thiolation) and not just simply for reactive thiol groups (i.e. diamide-induced thiolation). This is also reflected by the purification factors for proteins in the eluate that are susceptible to diamide and GSNO-inducible S-glutathionylation (2 versus 19 respectively). A potential limitation of this technique, however, is its poor yield. As evident from the data presented in Table 3, only 50 μg and 8 % of the total amount of HeLa cell protein thiols that are susceptible to GSNO-dependent S-glutathionylation can be precipitated by the matrix. Saturation of the matrix can be excluded as an explanation because, as estimated from Figure 1, the approx. 5 ml of Sepharose used in these purifications should bind about 1 mg of protein. One possible explication for this low yield may be residual 2-mercaptoethanol contained in the incubation. To inhibit oxidation of cysteine residues during the preparation of the cell extract, the isolation buffers contained 0.1 % 2-mercaptoethanol (see the Experimental section), which could both degrade the GSNO bond and reduce mixed disulphides. Although, the cell extract was diluted 100-fold in the final suspension with the GSNO–Sepharose, it should be taken into account that the final concentration of the thiol in the binding assay is approx. 100 μM. Although addition of 100 μM 2-mercaptoethanol to incubations of purified c-Jun and p50 with GSNO–Sepharose did not significantly lower the yield of bound proteins (results not shown), we cannot exclude the possibility that the same concentration of 2-mercaptoethanol interferes with binding of HeLa cell proteins. Nevertheless, our data indicate that nuclear proteins constitute a pool of, as yet, unidentified proteins which are susceptible to GSNO-induced thiolation We showed that purified c-Jun and p50, which are subunits of the AP-1 and NF-κB transcription factors respectively, bind to immobilized GSNO and can be S-glutathionylated by free GSNO *in vitro*. Consistent with these findings, analysis of the HeLa cell nuclear extracts by covalent GSNO–Sepharose chromatography and EMSA revealed that the DNA-binding activities of AP-1 and NF-κB can be precipitated by GSNO–Sepharose (Figure 5). The specificity of the nitrosothiol matrix was confirmed by the observation that the DNA-binding activity of CREB, which in terms of its DNA-binding site can be considered as a structural homologue of c-Jun, was retained by the matrix, whereas the transcription factors CP-1 and Sp1 did not bind. It is noteworthy that both CP-1 and Sp1 contain reactive cysteine residues in their DNA-binding domains.

In conclusion, these data support the potential applicability of covalent GSNO–Sepharose chromatography to the isolation of cysteine-containing cellular proteins, including nuclear transcription factors, that can be modified by GSNO-induced S-glutathionylation.

This work was supported by grants from the Comisión Interministenal de Ciencia y Tecnología (CICYT, SAF 97-0035), the Comunidad Autónoma de Madrid (CAM 08 4/0032/1998) and the European Community (BMH4-CT98-5052) We thank Dr Javier Rey (Centro de Investigaciones Biológicas, CSIC, Madrid, Spain) and Dr J. Alcamí (Instituto de Salud Carlos III, Madrid, Spain) for their donation of c-Jun and p50 cDNA respectively. Purified recombinant human glutaredoxin and thioredoxin were generously given by Dr José Antonio Bárcena (Universidad de Córdoba, Córdoba, Spain), and purified recombinant human caspase-3 was kindly provided by Dr Bernhard Brune (University of Erlangen-Nurnberg, Erlangen, Germany). We also thank Dr María del Pilar Ramos Alvarez (Universidad San Pablo CEU, Boadilla del Monte, Spain) for helpful suggestions and comments on the manuscript

REFERENCES

1 Mayer, B and Hemmens, B (1997) Biosynthesis and action of nitric oxide in mammalian cells Trends Biochem Sci **22**, 477–481

2 Marletta, M A (1994) Nitric oxide synthase aspects concerning structure and catalysis Cell **78**, 927–930

3 Zweier, J L, Samouilov, A and Kuppusamy, P (1999) Non-enzymatic nitric oxide synthesis in biological systems Biochim. Biophys Acta **1411**, 250–262

4 Koppenol, W H (1998) The basic chemistry of nitrogen monoxide and peroxynitrite Free Radical Biol Med **25**, 385–391

5 Wink, D A and Mitchell, J B (1998) Chemical biology of nitric oxide insights into regulatory, cytotoxic, and cytoprotective mechanisms of nitric oxide Free Radical Biol Med **25**, 434–456

6 Gaston, B. (1999) Nitric oxide and thiol groups Biochim Biophys Acta **1411**, 323–333

7 Denninger, J W and Marletta, M A. (1999) Guanylate cyclase and the NO/cGMP signaling pathway Biochim Biophys Acta **1411**, 334–350

8 Patel, R P, McAndrew, J, Sellak, H, White, C R, Jo, H J, Freeman, B. A and Darley-Usmar, V M (1999) Biological aspects of reactive nitrogen species Biochim. Biophys Acta **1411**, 385–400

9 Tien, M, Berlett, B S, Levine, R L, Chock, P B and Stadtman, E R (1999) Peroxynitrite-mediated modification of proteins at physiological carbon dioxide concentration pH dependence of carbonyl formation, tyrosine nitration, and methionine oxidation Proc. Natl Acad Sci. U.S A **96**, 7809–7814

10 Stamler, J S and Hausladen, A (1998) Oxidative modifications in nitrosative stress Nat Struct Biol **5**, 247–249

11 Stamler, J S (1994) Redox signaling nitrosylation and related target interactions of nitric oxide. Cell **78**, 931–936

12 Beckman, J S and Koppenol, W H (1996) Nitric oxide, superoxide, and peroxynitrite the good, the bad, and the ugly Am J Physiol **40**, C1424–C1437

13 Park, J W (1988) Reaction of S-nitrosoglutathione with sulfhydryl groups in proteins Biochem Biophys Res Commun **152**, 916–920

14 Chandra, A, Srivastava, S, Petrash, J M., Bhatnagar, A and Srivastava, S K (1997) Modification of aldose-reductase by S-nitrosoglutathione Biochemistry **36**, 15801–15809

15 Padgett, C M and Whorton, A R (1998) Cellular responses to nitric oxide role of protein S-thiolation/dethiolation Arch Biochem Biophys **358**, 232–242

16 Ji, Y B, Akerboom, T P M., Sies, H and Thomas, J A (1999) S-Nitrosylation and S-glutathiolation of protein sulfhydryls by S-nitroso glutathione Arch Biochem Biophys **362**, 67–78

17 Mohr, S, Hallak, H, de Boitte, A, Lapetina, E G and Brune, B (1999) Nitric oxide-induced S-glutathionylation and inactivation of glyceraldehyde-3-phosphate dehydrogenase J Biol. Chem **274**, 9427–9430

18 Viner, R I, Williams, T D and Schoneich, C (1999) Peroxynitrite modification of protein thiols: oxidation, nitrosylation, and S-glutathiolation of functionally important cysteine residue(s) in the sarcoplasmic reticulum Ca-ATPase Biochemistry **38**, 12408–12415

19 Zech, B, Wilm, M, van Eldik, R and Brune, B (1999) Mass spectrometric analysis of nitric oxide-modified caspase-3. J Biol Chem **274**, 20931–20936

20 Percival, M D, Ouellet, M, Campagnolo, C., Claveau, D and Li, C (1999) Inhibition of cathepsin K by nitric oxide donors: evidence for the formation of mixed disulfides and a sulfenic acid Biochemistry **38**, 13574–13583

21 Klatt, P, Molina, E P and Lamas, S (1999) Nitric oxide inhibits c-Jun DNA binding by specifically targeted S-glutathionylation J Biol Chem **274**, 15857–15864

22 Thomas, J A, Poland, B and Honzatko, R (1995) Protein sulfhydryls and their role in the antioxidant function of protein S-thiolation Arch Biochem Biophys **319**, 1–9

23 Klatt, P, Molina, E P, De Lacoba, M. G, Padilla, C A, Martinez Galisteo, E, Barcena, J A and Lamas, S. (1999) Redox regulation of c-Jun DNA binding by reversible S-glutathiolation. FASEB J **13**, 1481–1490

24 Stamler, J S, Simon, D I, Osborne, J A, Mullins, M E, Jaraki, O., Michel, T, Singel, D J and Loscalzo, J (1992) S-Nitrosylation of proteins with nitric oxide - synthesis and characterization of biologically active compounds Proc Natl Acad. Sci U S A **89**, 444–448

25 Xanthoudakis, S and Curran, T (1994) Analysis of c-Fos and c-Jun redox-dependent DNA binding activity Methods Enzymol **234**, 163–175

26 Matthews, J. R., Wakasugi, N, Virelizier, J L, Yodoi, J and Hay, R. T (1992) Thioredoxin regulates the DNA binding activity of NF-κB by reduction of a disulphide bond involving cysteine 62 Nucleic Acids Res **20**, 3821–3830

27 Gergel, D and Cederbaum, A I (1996) Inhibition of the catalytic activity of alcohol dehydrogenase by nitric oxide is associated with S-nitrosylation and the release of zinc Biochemistry **35**, 16186–16194

28 Bradford, M M (1976) A rapid and sensitive method for the quantitation of microgram quantities of protein utilizing the principle of protein-dye binding Anal Biochem **72**, 248–254

29 Liu, Z, Rudd, M A, Freedman, J. E. and Loscalzo, J (1998) S-transnitrosation reactions are involved in the metabolic fate and biological actions of nitric oxide. J Pharmacol Exp Ther **284**, 526–534

30 Anderson, M E and Meister, A (1989) Glutathione monoesters Anal. Biochem **183**, 16–20

31 Cornell, N W. and Veech, R L (1983) Enzymatic measurement of ethanol or NAD in acid extracts of biological samples. Anal Biochem **132**, 418–423

32 Kadonaga, J T, Carner, K R, Masiarz, F R and Tjian, R (1987) Isolation of cDNA encoding transcription factor Sp1 and functional analysis of the DNA binding domain. Cell **51**, 1079–1090

33 Matthews, J. R., Botting, C H, Panico, M, Morris, H R and Hay, R. T. (1996) Inhibition of NF-κB binding by nitric oxide Nucleic Acids Res **24**, 2236–2242

34 Stamler, J S, Jia, L, Eu, J. P, McMahon, T J, Demchenko, I T, Bonaventura, J, Gernert, K and Piantadosi, C A (1997) Blood flow regulation by S-nitrosohemoglobin in the physiological oxygen gradient Science **276**, 2034–2037

35 Nikitovic, D, Holmgren, A and Spyrou, G (1998) Inhibition of AP-1 DNA binding by nitric oxide involving conserved cysteine residues in Jun and Fos Biochem Biophys Res. Commun. **342**, 109–112

36 Ghosh, G, van Duyne, G, Ghosh, S. and Sigler, P B (1995) Structure of NF-κB p50 homodimer bound to a κB site Nature (London) **373**, 303–310

37 Muller, C. W., Rey, F A, Sodeoka, M, Verdine, G L and Harrison, S. C (1995) Structure of the NF-κB p50 homodimer bound to DNA. Nature (London) **373**, 311–317

38 Dafré, A L and Reischl, E (1998) Oxidative stress causes intracellular reversible S-thiolation of chicken hemoglobin under diamide and xanthine oxidase treatment. Arch Biochem. Biophys **358**, 291–296

39 DeMaster, E G., Quast, B J, Redfern, B and Nagasawa, H T (1995) Reaction of nitric oxide with the free sulfhydryl group of human serum albumin yields a sulfenic acid and nitrous oxide Biochemistry **34**, 11494–11499

40 Park, E. M. and Thomas, J A (1988) S-Thiolation of creatine kinase and glycogen phosphorylase *b* initiated by partially reduced oxygen species Biochim Biophys Acta **964**, 151–160

41 Kondo, T, Taniguchi, N, Hirano, T. and Kawakami, Y (1984) A novel low-activity form of carbonic anhydrase I in erythrocytes of patients with primary aldosteronism Evidence for the presence of a mixed disulfide with glutathione J Biol Chem **259**, 15517–15522

42 Chai, Y C., Jung, C H., Lii, C K, Ashraf, S S, Hendrich, S, Wolf, B, Sies, H and Thomas, J A (1991) Identification of an abundant S-thiolated rat liver protein as carbonic anhydrase III, characterization of S-thiolation and dethiolation reactions Arch Biochem Biophys **284**, 270–278

43 Ravichandran, V, Seres, T, Moriguchi, T., Thomas, J A. and Johnston, R B (1994) S-thiolation of glyceraldehyde-3-phosphate dehydrogenase induced by the phagocytosis associated respiratory burst in blood monocytes J Biol Chem **269**, 25010–25015

44 Schuppe-Koistinen, I, Moldéus, P., Bergman, T. and Cotgreave, I A (1994) S-Thiolation of human endothelial cell glyceraldehyde-3-phosphate dehydrogenase after hydrogen peroxide treatment Eur J Biochem **221**, 1033–1037

45 Schinina, M E, Carlini, P, Polticelli, F, Zappacosta, F, Bossa, F and Calabrese, L (1996) Amino acid sequence of chicken Cu, Zn-containing superoxide dismutase and identification of glutathionyl adducts at exposed cysteine residues Eur. J Biochem. **237**, 433–439

46 Yang, Y, Jao, S., Nanduri, S, Starke, D W, Mieyal, J J and Qin, J (1998) Reactivity of the human thioltransferase (glutaredoxin) C7S, C25S, C78S, C82S mutant and NMR solution structure of its glutathionyl mixed disulfide intermediate reflect catalytic specificity Biochemistry **37**, 17145–17156

47 Saéz, G T, Romero, F J and Viña, J. (1985) Effects of glutathione depletion on gluconeogenesis in isolated hepatocytes Arch Biochem Biophys **241**, 75–80

48 Smith, R. E and MacQuarrie, R. (1979) The role of cysteine residues in the catalytic activity of glycerol-3-phosphate dehydrogenase Biochim Biophys Acta **567**, 269–277

49 Nikitovic, D and Holmgren, A (1996) S-nitrosoglutathione is cleaved by the thioredoxin system with liberation of glutathione and redox regulating nitric oxide J Biol Chem. **271**, 19180–19185

50 Glover, J. N M and Harrison, S C (1995) Crystal structure of the heterodimeric bZIP transcription factor c-Fos-c-Jun bound to DNA Nature (London) **373**, 257–261

51 Morel, Y and Barouki, R (1998) Down-regulation of cytochrome P450 1A1 gene promoter by oxidative stress - critical contribution of nuclear factor 1. J. Biol Chem **273**, 26969–26976

52 Kahlenberg, A (1976) Preparative isolation of band 3, the predominant polypeptides of the human erythrocyte membrane Anal Biochem **74**, 337–342

53 De Bruin, S H, Joordens, J. J and Rollema, H S (1977) An isolation procedure for the native alpha chain of bovine hemoglobin. A study of the functional properties of this chain and its hybrid with the human beta chain Eur. J Biochem **75**, 211–215

54 Sykes, B. C (1976) The separation of two soft-tissue collagens by covalent chromatography FEBS Lett **61**, 180–185

55 Egorov, T A, Svenson, A, Ryden, L and Carlsson, J. (1975) A rapid and specific method for isolation of thiol-containing peptides from large proteins by thiol-disulfide exchange on a solid support Proc Natl Acad Sci. U S A **72**, 3029–3033

56 Abate, C, Patel, L, Rauscher, F J and Curran, T (1990) Redox regulation of Fos and Jun DNA-binding activity in vitro Science **249**, 1157–1161

57 Galter, D., Mihm, S and Droge, W (1994) Distinct effects of glutathione disulfide on the nuclear transcription factors κB and the activator protein-1 Eur J. Biochem **221**, 639–648

58 Snyder, G H, Cennerazzo, M J, Karalis, A J and Field, D (1981) Electrostatic influence of local cysteine environments on disulfide exchange kinetics Biochemistry **20**, 6509–6519

59 Barrett, W C., DeGnore, J P, Keng, Y F, Zhang, Z Y, Yim, M B. and Chock, P B (1999) Roles of superoxide radical anion in signal transduction mediated by reversible regulation of protein-tyrosine phosphatase 1B J Biol. Chem. **274**, 34543–34546

Received 4 January 2000/18 April 2000; accepted 11 May 2000

Biochem J (2000) 349, 579–586 (Printed in Great Britain)

Effect of inhibition of glutathione synthesis on insulin action: *in vivo* and *in vitro* studies using buthionine sulfoximine

Mogher KHAMAISI[1]*, Oren KAVEL[1]*, Moti ROSENSTOCK†, Michal PORAT*, Michal YULI‡, Nurit KAISER‡ and Assaf RUDICH[2]*†

*Department of Clinical Biochemistry, Faculty of Health Sciences, Ben-Gurion University of the Negev, Beer-Sheva, IL-84105 Israel,
†The S. Daniel Abraham Center for Health and Nutrition, Faculty of Health Sciences, Ben-Gurion University of the Negev, Beer-Sheva, IL-84105 Israel, and
‡Department of Endocrinology and Metabolism, P. O. Box 12000, Hebrew University, Hadassah Medical Center, Jerusalem, 91120 Israel

Decreased cellular GSH content is a common finding in experimental and human diabetes, in which increased oxidative stress appears to occur. Oxidative stress has been suggested to play a causative role in the development of impaired insulin action on adipose tissue and skeletal muscle. In this study we undertook to investigate the potential of GSH depletion to induce insulin resistance, by utilizing the GSH synthesis inhibitor, L-buthionine-[*S*,*R*]-sulfoximine (BSO). GSH depletion (20–80 % in various tissues), was achieved *in vivo* by treating rats for 20 days with BSO, and *in vitro* (80 %) by treating 3T3-L1 adipocytes with BSO for 18 h. No demonstrable change in the GSH/GSSG ratio was observed following BSO treatment. GSH depletion was progressively associated with abnormal glucose tolerance test, which could not be attributed to impaired insulin secretion. Skeletal muscle insulin responsiveness was unaffected by GSH depletion, based on normal glucose response to exogenous insulin, 2-deoxyglucose uptake measurements in isolated soleus muscle, and on normal skeletal muscle expression of GLUT4 protein. Adipocyte insulin responsiveness *in vitro* was assessed in 3T3-L1 adipocytes, which displayed decreased insulin-stimulated tyrosine phosphorylation of insulin-receptor-substrate proteins and of the insulin receptor, but exaggerated protein kinase B phosphorylation However, insulin-stimulated glucose uptake was unaffected by GSH depletion. In accordance, normal adipose tissue insulin sensitivity was observed in BSO-treated rats *in vivo*, as demonstrated by normal inhibition of circulating non-esterified fatty acid levels by endogenous insulin secretion. In conclusion, GSH depletion by BSO results in impaired glucose tolerance, but preserved adipocyte and skeletal muscle insulin responsiveness. This suggests that alternative oxidation-borne factors mediate the induction of peripheral insulin resistance by oxidative stress.

Key words. 3T3-L1 adipocytes, adipose tissue, insulin resistance, oxidative stress, skeletal muscle.

INTRODUCTION

Experimental and human diabetes is increasingly recognized as being associated with markers for increased oxidative stress. Despite methodological and conceptual difficulties in assessing increased oxidative stress *in vivo* [1], diabetic animals and humans display increased levels of oxidative products of lipids, DNA and protein [2–4]. Decreased antioxidant defence systems have been more difficult to demonstrate in diabetes. Assessment of the level of antioxidant vitamins and the activity of antioxidant enzymes have largely yielded conflicting results, attributable to cell type, patient selection and analytical methodology. Nevertheless, most available human studies have suggested decreased plasma vitamin C levels [5–7] and reduced activity of superoxide dismutase in leucocytes [8,9]. Moreover, a vast majority of the studies addressing the level of glutathione (either total or reduced form) demonstrate that glutathione levels in whole blood [10,11], platelets [12] and polymorphonuclear cells [13] are decreased in diabetic patients. In the streptozotocin-induced diabetic rat, GSH levels are also decreased in liver, kidney, heart and nerves [14–16]. As the major redox buffer of the cell, this decrease in the level of GSH may be viewed to reflect and/or contribute to the oxidative stress and redox imbalance which accompanies the diabetic milieu.

Defining whether increased oxidative stress plays a role in the pathophysiology of diabetes and its complications may be important both for understanding the disease processes, as well as for developing new therapeutic modalities. Various studies suggest that increased oxidative stress may play a role in the development of accelerated atherosclerosis in diabetes [17], in embryonal maldevelopment in diabetic pregnancies [18], and possibly in the pathophysiology of diabetic neuropathy, retinopathy and cataract formation [2,19]. The pancreatic beta-cell was also shown to be target for oxidative stress [20]. Expression of antioxidant enzymes is very low in pancreatic islets [21], making them rather sensitive to glycation-mediated reduction of insulin gene transcription and beta-cell apoptosis [20,22,23]. In addition, several lines of evidence suggest that increased oxidative stress may play a role in peripheral insulin resistance. These mainly include clinical studies, which correlated oxidative stress parameters with the metabolic control of patients [4,24,25]. Other studies reported beneficial metabolic effects of pharmacological doses of vitamin E [26], vitamin C [27], GSH [28] or lipoic acid [29], when administered to healthy volunteers or to diabetic subjects. A direct impairment in insulin responsiveness by reactive oxygen species has been demonstrated in cell culture systems [30–33]. In 3T3-L1 adipocytes, we have shown that micromolar H_2O_2 treatment impaired various metabolic effects of insulin, including the stimulation of glucose uptake activity. The cellular mechanism involved alterations in the expression and translocation capacity of the insulin-sensitive glucose transporter GLUT4 [34], and was associated with defective activation

---

Abbreviations used. BSO, L-buthionine-[*S*,*R*]-sulfoximine, NEFA, non-esterified fatty acid, GTT, glucose tolerance test, ITT, insulin tolerance test, PKB, protein kinase B, LMRT, low-molecular-mass reduced thiol

[1] These authors contributed equally to this work

[2] To whom correspondence should be addressed at the Department of Clinical Biochemistry (e-mail rudich@bgumail bgu ac il)

of protein kinase B (PKB) [32]. Since these studies demonstrate the potential causative relationship between oxidative stress and impaired insulin response, a crucial issue is to define which redox parameter acts as a biological mediator.

In the present study, we undertook to dissect out a potential role for decreased GSH levels in the development of impaired glucose homoeostasis and decreased response of insulin target tissues to its metabolic actions (insulin resistance). For this purpose, the γ-glutamylcysteine synthetase inhibitor L-buthionine-[S,R]-sulfoximine (BSO) was used to decrease tissue levels of GSH in normal rats, or to inhibit GSH synthesis in an insulin-responsive adipocyte cell line. Thereafter, glucose homoeostasis was assessed *in vivo*, and the cellular response to insulin was investigated either *ex vivo* or in the cultured cells. Our results suggest that the marked decrease in GSH levels was associated with impaired glucose tolerance, but with preserved insulin-responsiveness of skeletal muscle and adipocytes.

EXPERIMENTAL

Animal treatment

All protocols were approved in advance by the Ben-Gurion University Animal Studies Committee. Five-week-old male Sprague–Dawley rats were purchased from Harlan Laboratories (Jerusalem, Israel). They were kept on a 12-h light/dark cycle at 23 °C, housed four in a cage. Standard rat chow and tap water were provided *ad libitum* during the entire experiment. BSO (Sigma) was dissolved in saline and 2 mmol/kg body weight BSO or vehicle ($n = 8$ in each group) administered by a daily intraperitoneal injection between 9–11 a.m. for 20 days, following previously described protocols [35,36]. Glucose homoeostasis was evaluated during the treatment period by a glucose tolerance test (GTT) performed on days 8 and 16, following 18 h of fast (intraperitoneal injection of 2 g/kg glucose), and by an insulin tolerance test (ITT) performed on day 18 of the study after 4 h fast (intravenous administration of 0.5 unit/kg recombinant human insulin). Blood glucose levels during both the GTT and ITT were expressed for each rat as a percentage of its glucose level at $t = 0$, and plotted as a function of time. The area under the curve for each rat was calculated using the KaleidaGraph version 3.04 (Synergy Software, Reading, PA, U.S.A.), and the mean value ± S.E.M. calculated for each group

At 20 h after the final treatment (day 20), and following a 12-h fast, animals were weighed, anaesthetized with phenobarbital (80 mg/kg, intraperitoneal), and the soleus muscle dissected out for *ex vivo* 2-deoxyglucose uptake measurements. Blood was then drawn by cardiac puncture into EDTA-containing test tubes, and an aliquot was taken for determination of low-molecular-mass reduced thiols (LMRTs), as described below. The remaining blood was centrifuged at 4 °C, and the plasma stored frozen in aliquots at −70 °C. Gastrocnemius muscle and liver were rapidly dissected out and frozen immediately in liquid nitrogen for storage at −70 °C until used for further analyses. The pancreas was removed and cut into two parts, one was frozen at −70 °C for subsequent determination of immunoreactive insulin content, and the other fixed in 10 % phosphate-buffered formalin for immunohistochemical analysis.

LMRTs, GSH and GSSG determinations

Whole blood, liver and muscle LMRTs were measured spectrophotometrically according to Ellman's method [37], as previously described [38]. Liver GSH and GSSG were measured spectrophotometrically by the glutathione reductase recycling assay, following a method described by Anderson [39].

Pancreatic insulin content

Frozen pancreatic tissue was weighed and homogenized in 1 ml of ice-cold HCl/ethanol, as described in [40], followed by extraction for 24 h at 4 °C. The supernatant was removed following centrifugation and used for determination of insulin content after the appropriate dilution in RIA buffer (0.1 % BSA in PBS, pH 7.4).

Immunohistochemical studies

Pancreatic tissue was fixed in 10 % phosphate-buffered formalin and embedded in paraffin Multiple sequential sections (5 μm) were mounted on slides for immunohistochemical analysis. Deparaffinized sections were rinsed with PBS, and endogenous peroxidase blocked by exposure to 3 % H_2O_2 for 15 min at room temperature. For detection of islet hormones, sections were incubated with either guinea pig anti-insulin antibody at 1:100 (Sigma), or with rabbit anti-glucagon serum (Immustain®; DPC, Los Angeles, CA, U.S.A.), at 37 °C for 1 h followed by detection using a strepavidin–biotin peroxidase complex developed with aminoethylcarbazole substrate (Zymed Laboratories, San Francisco, CA, U.S.A.). Two sections per animal, containing 30–40 islets each, were evaluated by light microscopy at × 200 magnification.

2-Deoxyglucose uptake into isolated soleus muscle

Soleus muscles were dissected out immediately after the induction of anaesthesia, and incubated in the absence or presence of 2 m-units/ml human insulin, after which 2-deoxyglucose uptake was determined exactly as described in [41].

Cell culture and treatment

3T3-L1 pre-adipocytes (A.T.C C), were grown in six-well plates and differentiated to adipocytes, exactly as described in [30,34]. In all experiments, fully differentiated cells (10–12 days post-differentiation induction) were used. Cells were washed three times with PBS, and incubated for 18 h in serum-free medium, supplemented with BSA (0.5 % w/v, RIA grade), in the absence or presence of 0.5 mM BSO. Alternatively, cells were incubated after 16 h of serum deprivation for an additional 2 h with glucose oxidase (Sigma; 100 m-units/ml), which generated a constant medium H_2O_2 concentration of approx. 25 μM, as previously described [32]. Protein recovery and 3-(4,5-dimethylthiazol-2-yl)-2,5-diphenyl-2*H*-tetrazolium bromide (MTT) test confirmed cell viability At the end of the incubation period, cells were washed three times with PBS, and incubated with or without 100 nM human insulin for either 7 min (for cell lysate preparation) or 20 min for glucose transport activity. Hexose transport activity was evaluated by the uptake of 2-deoxy-[^{3}H]glucose (50 μM, 1 μCi/ml), during 10 min incubation of the cells, as previously described [30]. Non-specific uptake was determined with 50 μM cytochalasin B, which was added to the reaction mixture.

Membrane preparations, total cell lysates and Western-blot analysis

Gastrocnemius muscle total membranes were prepared as previously described [42]. Total membranes of 3T3-L1 adipocytes (a single well of a six-well plate per condition) were prepared exactly as we previously described [32]. SDS/PAGE (7.5 % or 10 %) and Western-blot analysis, for detecting total membrane GLUT4 content, were carried out using anti-GLUT4 antibody (Chemicon International, Temecula, CA, U.S.A.). PKB phosphorylation was detected in total cell lysates using serine-473

PKB antibodies (New England Biolabs), and tyrosine phosphorylation state using anti-phosphotyrosine (4G-10) antibodies (Upstate Biotechnology, Lake Placid, NY, U.S.A.). Blots were then incubated with horseradish peroxidase-conjugated anti-rabbit IgG (Amersham Life Sciences), after which luminescence was detected by enhanced chemiluminescence (Pierce, Rockford, IL, U.S.A.). Density values of the different bands were obtained after scanning the blots with video densitometry using the UVP-GDF 5000 system (UVP Inc , San Gabriel, CA, U.S.A.), followed by quantification using Image Quant version 3.3 (Molecular Dynamics, Palo Alto, CA, U.S.A.).

Other assays

Blood glucose was measured using a glucometer (Glucometer Elite; Bayer Diagnostic, Tarrytown, NY, U.S.A.). Insulin RIA was performed using anti-insulin coated tubes (ICN Pharmaceuticals, Costa Mesa, CA, U.S.A.), and ^{125}I-insulin from Linco Research, St Charles, MO, U.S.A.) Rat insulin was used as a standard. Protein was measured using the Bio-Rad protein assay [43]. Plasma non-esterified fatty acid (NEFA) concentration was determined using a commercial kit (Roche Molecular Biochemicals, Mannheim, Germany)

Statistical analysis

The non-parametric Mann–Whitney test was used to determine the U value for differences between the control (vehicle treated) and BSO-treated animals Student's t-test was used to determine significance of changes between treated and control cells. In both cases an α- or P-value of 0.05 was set as the threshold of statistical significance

RESULTS

Five-week-old rats were treated for 20 days with the γ-glutamylcysteine synthetase inhibitor BSO, by a daily intraperitoneal injection (2 mmol/kg per day), following a previously described protocol [36]. BSO treatment was not associated with mortality, diarrhea, or any noticeable adverse effects. Consistent with previous reports [36], weight gain during the 20 days of treatment was decreased by approx. 8 % in the BSO-treated animals (Table 1). As expected, BSO treatment resulted in decreased plasma and tissue levels of LMRTs, of which GSH is the major contributor. Whole blood and skeletal muscle LMRT levels were reduced to 63 ± 5 % and 14 ± 1 % respectively of the levels measured in the control group (Table 1). In liver, the effect of BSO treatment on LMRTs and on the GSH/GSSG ratio was evaluated. Only a mild 20 % decrease in LMRTs was observed in BSO-treated rats, whereas the GSH/GSSG ratio was not decreased, consistent with a previous report using the same BSO dose [36].

Table 1 Effect of 20 days BSO-treatment on weight gain, LMRT content and liver glutathione

Five-week-old rats were treated by a daily intraperitoneal injection of either vehicle or BSO for 20 consecutive days At the end of the experiment, rats were fasted for 12 h then weighed and anaesthetized, after which tissues and blood were collected, as described in the Experimental section Values are means ± S E M

	Control (vehicle, $n = 8$)	BSO ($n = 8$)
Weight gain (g)	128.3 ± 4 4	118 0 ± 2 5*
LMRTs		
Whole blood (μmol/g Hb)	12 20 ± 1 05	7 63 ± 0 57*
Gastrocnemius muscle (μmol/g)	0 74 ± 0 06	0 11 ± 0 01*
Liver (μmol/g)	5 40 ± 0 60	4 23 ± 0 60*
Liver glutathione (μmol/g)		
GSH	3.25 ± 0 44	1 9 ± 0.33*
GSSG	0 082 ± 0 001	0 040 ± 0 001*
GSH/GSSG	40 0 ± 5 2	50 0 ± 7 43

* $P < 0\ 05$ compared with control animals

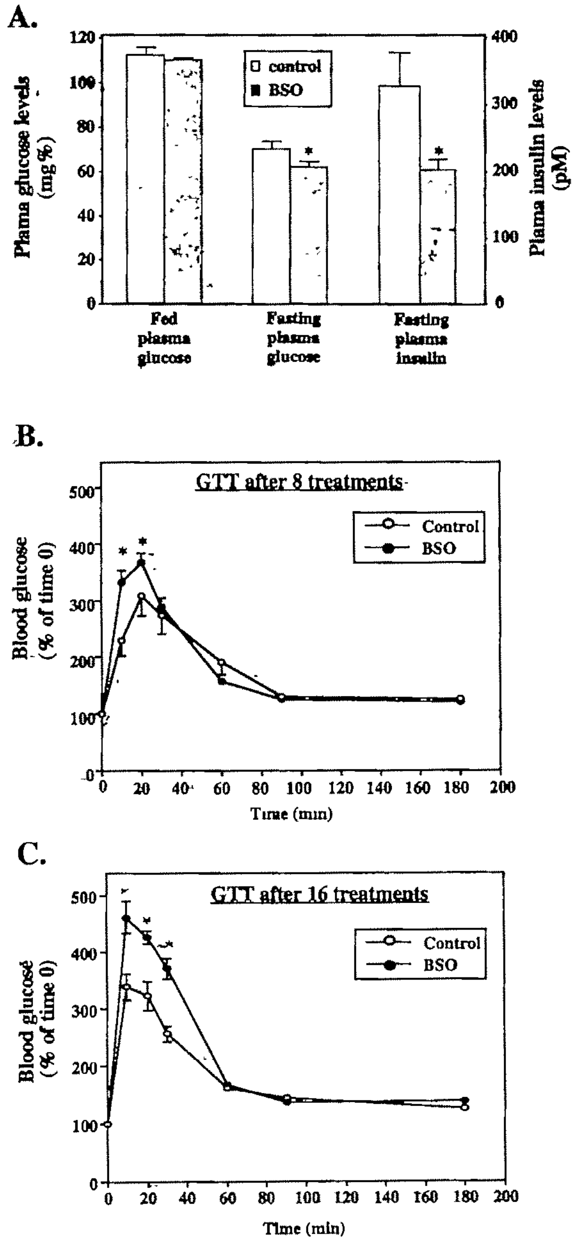

Figure 1 The effect of BSO treatment on steady-state glucose and insulin levels, and on the dynamic glucose levels during GTT

Five-week-old rats were treated with BSO or vehicle ($n = 8$ for each group) by a daily intraperitoneal injection (**A**) At the end of the experiment (day 20), fed-state glucose levels were measured in tail blood, and again following 12 h of fasting Fasting circulating insulin levels were also determined After the 8th or the 16th treatment (**B,C** respectively), animals were fasted overnight and 2 g/kg glucose administered as described in the Experimental section Glucose levels in tail blood was measured at the indicated times, and presented for each rat as % of the value at $t = 0$ (immediately before glucose administration) Each point is presented as means ± S E M *$P < 0.05$ compared with vehicle-treated animals at the same time point

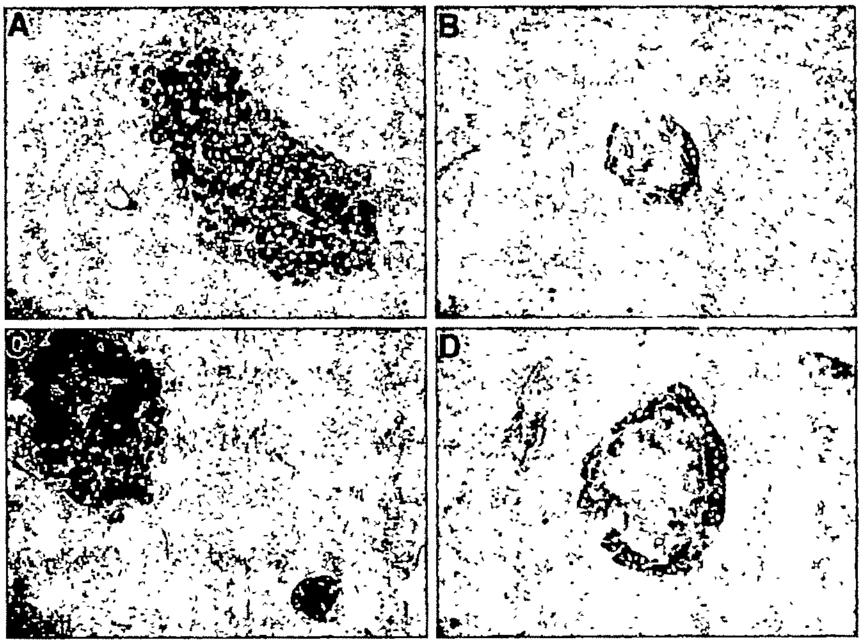

Figure 2 Photomicrographs of pancreatic sections from control and BSO-treated rats immunostained for insulin or glucagon

At the end of the experiment (see the Experimental section), control (**A**,**B**) and BSO-treated rats (**C**,**D**) were anaesthesized and the pancreas dissected out, followed by preparation of histological sections, and immunostaining with insulin (**A**,**C**) or glucagon (**B**,**D**) antibodies

In order to determine the potential causative role of GSH depletion on the induction of peripheral insulin resistance and impaired glucose homoeostasis, the following experiments were performed: (1) steady-state levels of blood glucose and plasma insulin were evaluated in the fed and fasting states, and the dynamic changes in blood glucose concentrations determined following administration of a glucose (GTT) or insulin load (ITT); (2) skeletal muscle responsiveness to insulin was studied by an *ex vivo* measurement of glucose uptake into soleus muscle in the absence or presence of insulin, and by measuring GLUT4 protein content in gastrocnemius muscle; and (3) adipose insulin sensitivity was evaluated *in vivo* by measuring the dynamic changes in circulating NEFAs during GTT, and *in vitro* by the use of the 3T3-L1 adipocytes cell line model.

The effect of 20 days of BSO treatment on the steady-state levels of glucose in the fed and fasting states are presented in Figure 1(A). As can be noted, GSH depletion was not associated with elevated blood glucose levels, and in fasting conditions was found to be lower than in control animals. Fasting plasma insulin concentrations were also significantly lower in the BSO-treated animals. Figures 1(B) and 1(C) demonstrate glucose levels following an intraperitoneal injection of 2 g/kg glucose (GTT) after 8 and 16 treatments respectively. As can be noted, following 8 days of treatment, the increase in glucose levels 10 min and 20 min after the glucose load was greater in the BSO group relative to control. Following 16 days of BSO treatment, this impairment in glucose tolerance became more pronounced, with glucose levels at the 30-min time point also significantly increased. At day 8, the calculated area under the curve was 12258±1560 and 13045±642 (arbitrary units) for the control and BSO-treated groups respectively. Following 16 treatments, the respective area under the curve values were 12198±1298 and 14990±718, a difference which reached statistical significance ($P = 0.001$). To exclude impaired insulin secretion as the cause for the abnormal GTT in BSO-treated rats, circulating insulin levels were measured during the GTT, and were found to be identical between the two groups at time points 5, 15 and 60 min (results not shown). Moreover, there was no change in pancreatic immunoreactive insulin content (18.5±4 4 and 19.8±4.5 nmol/g tissue in control and BSO-treated rats respectively), and islet architecture was found to be normal (Figure 2). Collectively, the data presented in Figures 1 and 2 demonstrate that GSH depletion was associated with impaired glucose tolerance, but not with impaired beta-cell function.

We further assessed whether the abnormal GTT resulted from skeletal muscle and/or adipose tissue (peripheral) insulin resistance. Insulin administration (0.5 unit/kg) resulted in a rapid decrease in blood glucose levels, that were restored to the basal levels after 60 min. BSO treatment was not associated with blunting of the glucose curve during ITT (Figure 3A). Skeletal muscle responsiveness to insulin was also assessed *ex vivo* by measuring 2-deoxyglucose uptake into isolated soleus muscle in the absence and presence of insulin. In control animals, exposure of soleus muscle to insulin augmented hexose uptake from 66±4 to 113±11 pmol/mg muscle per 20 min. Similarly, in BSO-treated rats 2-deoxyglucose uptake increased from 68±7 to 121±13 pmol/mg muscle per 20 min Both basal and insulin-stimulated glucose uptake values were not significantly different between the two groups. Accordingly, the protein content of the insulin-responsive glucose transporter GLUT4, previously shown to be reduced in gastrocnemius muscle membranes of diabetic rats [38,41], was not affected by BSO treatment (representative blot shown in Figure 3B).

The effect of GSH depletion by BSO on adipocyte insulin responsiveness was assessed both at the cellular level, by utilizing 3T3-L1 adipocytes, as well as *in vivo*. This cell line was selected since it is an acceptable model for adipose tissue, uniquely displaying both insulin signalling, as well as metabolic insulin

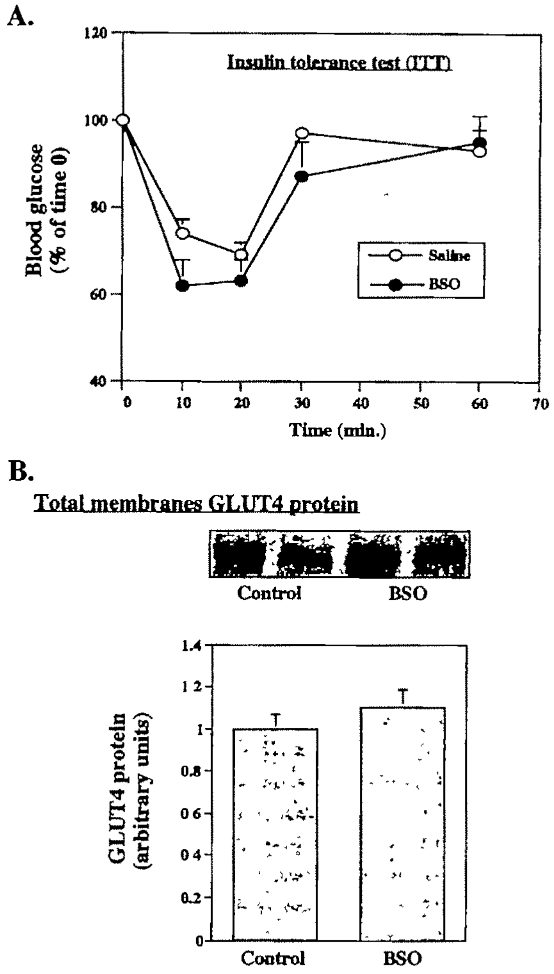

Figure 3 The effect of BSO treatment on dynamic glucose levels during ITT, and on gastrocnemius muscle total membrane GLUT4 protein content

(A) ITT was performed on BSO- or vehicle-treated animals ($n = 4$ in each group) after the 17th treatment, as described in the legend for Figure 1. At each time point, 250 μl of tail blood was collected, assayed for glucose and the data analysed (see the Experimental section). Results are means ± S.E.M. (B) Total membranes were prepared from gastrocnemius muscle, and GLUT4 protein content was assessed using Western-blot analysis. Shown is a representative blot, as well as densitometry analysis (means ± S.E.M., in arbitrary units) of GLUT4 content as measured in muscles of eight rats in each group.

Table 2 Cellular glutathione content in 3T3-L1 adipocytes treated with BSO or H_2O_2

Fully differentiated 3T3-L1 adipocytes were incubated for 18 h in serum-deprived medium with or without 0.5 mM BSO, or exposed for the last 2 h of incubation to approx. 25 μM H_2O_2 produced by adding glucose oxidase to the culture medium. Cells were then washed three times with PBS, and assessed for GSH and GSSG content, as described in the Experimental section. Results are means ± S.E.M. of three experiments, each performed in duplicates. UD, undetectable.

	Control	BSO (0.5 mM, 18 h)	H2O2 (25 μM, 2 h)
GSH (nmoles/mg of protein)	32.07 ± 2.28	5.40 ± 0.80†	18.65 ± 2.62*
GSSG (nmoles/mg of protein)	0.26 ± 0.06	UD	0.27 ± 0.04
GSH/GSSG	123.5 ± 18.5	–	69.3 ± 2.5*

* $P < 0.05$ compared with control cells
† $P < 0.001$ compared with control cells

responsiveness. In addition, we have previously shown in this cell line that oxidative stress, characterized by a significant decrease in cellular GSH, results in impaired insulin action [30,34]. As shown in Table 2, 18 h incubation with 0.5 mM BSO resulted in an 80% reduction in cellular GSH content, with GSSG levels below the detection limits of the glutathione reductase recycling assay. As expected, exposure of the cells for 2 h to approx. 25 μM H_2O_2 resulted in a significant decrease in GSH, but also in decreased GSH/GSSG ratio. The insulin-signalling cascade was analysed under these conditions. In control cells, insulin stimulated the tyrosine phosphorylation of the β-subunit of the insulin receptor (95 kDa band) and of insulin-receptor-substrate proteins (approx. 180 kDa). In BSO-treated cells, insulin-stimulated phosphorylation of these two major phosphotyrosine bands tended to decrease (Figure 4A). The effect of H_2O_2 treatment of the cells on insulin-stimulated tyrosine phosphorylation is shown as comparison. Incubation with H_2O_2 was associated with several phosphotyrosine bands, one of which is a high-molecular-mass (approx. 200 kDa) protein, as previously described [44]. Following insulin stimulation, an exaggerated, rather than decreased, tyrosine phosphorylation of insulin-receptor-substrate and the β-subunit of the insulin receptor could be observed. The effect of BSO on more distal events in the insulin-signalling cascade was addressed by measuring insulin-induced serine-473 phosphorylation of PKB, a key enzyme in the metabolic signalling pathway of insulin. As shown in Figure 4(B), BSO treatment resulted in a mild increase ($P > 0.05$) of insulin-induced phosphorylation, without affecting total PKB-α content (results not shown). In contrast, cells exposed to 25 μM H_2O_2 displayed increased basal PKB phosphorylation, as well as a significant reduction in the ability of insulin to stimulate PKB phosphorylation. Consistent with this observation were the findings on the effects of BSO and H_2O_2 on insulin-stimulated hexose transport activity. While GSH depletion by BSO did not significantly affect basal or insulin-stimulated 2-deoxyglucose uptake activity, H_2O_2 exposure significantly impaired the capacity of insulin to stimulate 2-deoxyglucose uptake (Figure 4C). Moreover, consistent with the data obtained in skeletal muscle, total membrane GLUT4 protein content in BSO-treated 3T3-L1 adipocytes was comparable with control cells (results not shown).

The *in vivo* relevance of these findings to adipose tissue insulin responsiveness was addressed by measuring plasma NEFA levels during GTT, since adipose tissue acutely responds to insulin by inhibition of lipolysis. As shown in Figure 4(D), fasting NEFA levels rapidly decreased following glucose administration and endogenous insulin secretion. In BSO-treated rats, this response was comparable with that observed in control rats, suggesting normal adipose tissue responsiveness *in vivo*. Collectively, these data indicate that skeletal muscle and adipocyte insulin-responsiveness remained intact, despite GSH synthesis inhibition and a significant depletion of tissue and cellular GSH.

DISCUSSION

This study addresses the hypothesis that decreased cellular or tissue levels of GSH could mediate the effects of oxidative stress on glucose homoeostasis and insulin responsiveness. Recent studies from several groups, including our own, have demonstrated that oxidative stress impairs the normal cellular response to insulin [30,31,33]. Decreased GSH levels were found in both 3T3-L1 adipocytes exposed to a H_2O_2-generating system [44], and also in blood and tissues of streptozotocin-induced diabetic rats [38], in which impaired peripheral insulin sensitivity was observed. These data established an association between decreased GSH content and impaired insulin response, raising the

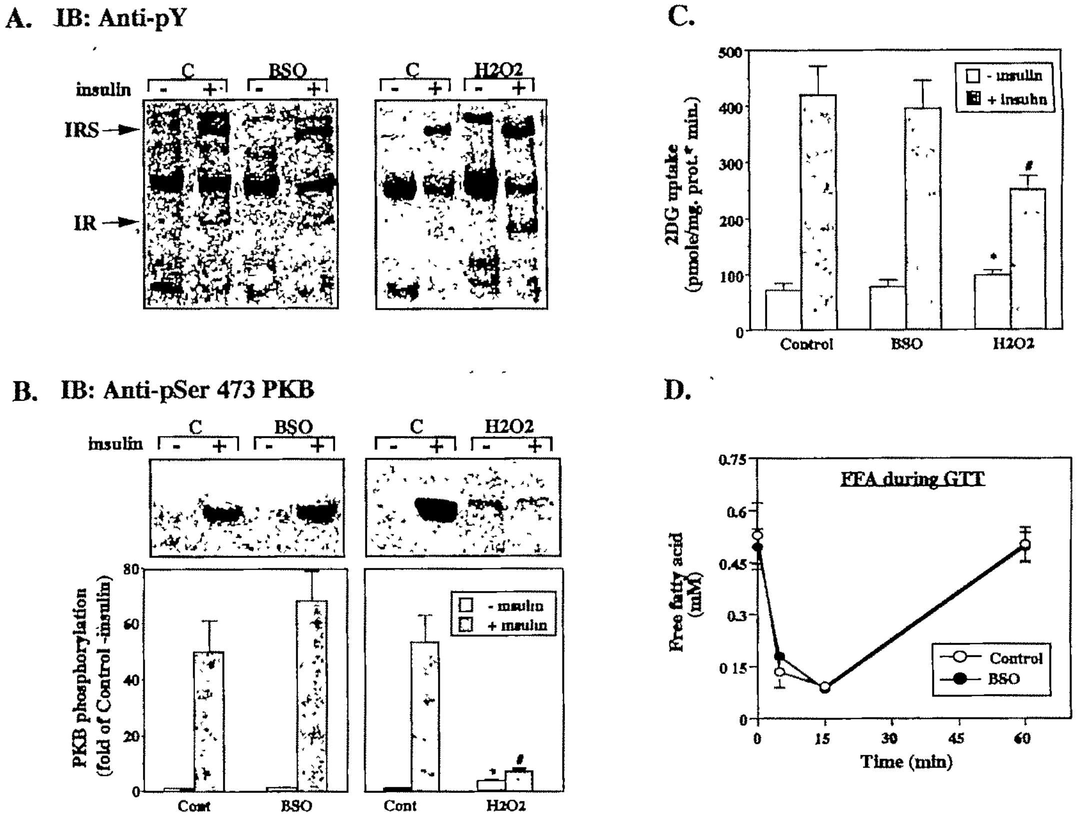

Figure 4 The effect of BSO treatment on adipocyte insulin sensitivity

(**A**,**B**) Differentiated 3T3-L1 adipocytes were either treated with 0.5 mM BSO in serum-free medium for 18 h or exposed for the last 2 h to glucose oxidase in the culture medium, generating H_2O_2 at a concentration of approx. 25 μM. Cells were then rinsed three times with PBS and incubated for an additional 7 min with or without 100 nM insulin, after which cell lysates and Western-blot analyses were performed as described in the Experimental section. Blots shown are representative of at least five different experiments yielding similar results. $^*P < 0.05$ compared with control cells (C) without insulin. $^\# P < 0.001$ compared with insulin-stimulated control cells. Abbreviations: Anti-pY, anti-phosphotyrosine, IR, insulin receptor, IRS, insulin-receptor substrate. (**C**) At the end of the BSO or H_2O_2 treatments, cells were rinsed and incubated for an additional 20 min with or without 100 nM insulin, after which 2-deoxyglucose uptake was assessed. Results are means ± S.E.M. of six independent experiments performed at least in duplicate. $^*P < 0.05$ compared with control cells without insulin. $^\# P < 0.001$ compared with insulin-stimulated control cells. (**D**) During a GTT performed after the 17th day of treatment, plasma NEFA (FFA) concentrations were measured at the indicated time points. Results are means ± S.E.M. of four animals in each group.

possibility that decreased GSH is causative in impairing insulin action.

Several potential cellular mechanisms, to explain how decreased GSH content would potentially affect peripheral insulin action, could be raised. Insulin stimulates glucose transport and metabolism in adipocytes and in skeletal muscle by inducing the translocation of glucose transporters (GLUT4) from internal membrane pools to the plasma membrane [45,46]. This complex process may potentially be affected by GSH depletion, modulating either the metabolic insulin signalling or GLUT4 protein expression.

3T3-L1 adipocytes exposed to oxidative stress characterized by decreased GSH and GSH/GSSG ratio ([44] and Table 2), demonstrated impaired insulin-stimulated glucose transport and GLUT4 translocation [34]. These could be attributed to impaired capacity of insulin to stimulate the phosphorylation and activity of PKB, a key enzyme in the metabolic signalling of insulin [32]. When cellular GSH content was increased by pretreating the cells with lipoic acid, these effects of oxidative stress were significantly prevented [44]. In addition, GLUT4 translocation has been demonstrated to depend on *N*-ethylmaleimide-sensitive proteins (reviewed in [45,46]), and SH reagents have been shown to affect the insulin signalling apparatus [47,48], providing additional potential targets for GSH depletion. In the present study, however, cellular depletion of GSH which was not associated with a decreased GSH/GSSG ratio (Tables 1 and 2), did not cause impaired capacity of insulin to trigger the serine phosphorylation of PKB (Figure 4B). Consistently, insulin-stimulated glucose transport activity, severely impaired by exposure to H_2O_2, was not significantly affected by BSO treatment (Figure 4C).

The importance of normal GLUT4 levels for maintaining glucose homoeostasis has been conclusively demonstrated using heterozygous GLUT4-knockout mice, which develop insulin resistance and a Type II diabetes-like syndrome [49]. 3T3-L1 adipocytes exposed for 18 h to micromolar H_2O_2 concentrations exhibit decreased GLUT4 protein and mRNA expression [30]. In skeletal muscle of streptozotocin-induced diabetic rats, GLUT4 protein levels were decreased, which was associated with decreased GSH content [38,41]. Moreover, multiple regression analysis demonstrated skeletal muscle GSH content as an independent predictor for GLUT4 protein levels [38]. Furthermore, when skeletal muscle GSH content was increased by treating diabetic rats with lipoic acid, GLUT4 protein content was increased [38,41]. Yet, in the present study, decreased GSH levels induced by inhibiting its synthesis by BSO (Table 1), were not associated with decreased GLUT4 protein content, neither in the cell line, nor in rat skeletal muscle (Figure 3B). This was despite the fact that the degree of GSH depletion achieved was at least comparable, if not greater than, GSH depletion observed following H_2O_2 treatment of the cells (Table 2), or in diabetes [38]. Thus the present study does not support the notion that GSH levels in themselves regulate GLUT4 protein levels.

Several interpretations of the data, demonstrating lack of effect of GSH depletion on peripheral insulin action, can be generated. Firstly, the degree or duration of GSH depletion achieved *in vivo* may not have been sufficient to produce an effect on insulin signalling However, GSH depletion in BSO-treated cells and animals was greater than that observed with H_2O_2-treated cells (Table 2) or in diabetic rats [38], both of which displayed impairment in insulin action Thus it is possible that other antioxidant defence mechanisms compensated for the decrease in GSH content under our experimental conditions At the cellular level, it could be speculated that GSH depletion by BSO did not occur at a cellular compartment critical for normal insulin responsiveness.

An alternative line of reasoning may be, that GSH depletion in itself is not the mediator of oxidative stress-induced insulin resistance, at least not as an independent factor. It is noteworthy, that BSO treatment at higher doses is associated with both vitamin E and vitamin C depletion and elevated lipid peroxidation products [50]. The dose used in the present study, however, allowed us to assess the isolated effect of GSH depletion without simultaneous generation of lipid peroxidation products [36]. Inhibiting GSH synthesis resulted in decreased GSH content, but also in decreased GSSG (Table 1), whereas oxidative stress is associated with increased formation of oxidized moieties, such as GSSG (manifested by a decreased GSH/GSSG ratio) and protein-SG. Oxidative- and lipid peroxidation-induced modification of proteins may alter their function, as well as their degradation through the proteasome protein-degradation system [51,52]. It is therefore suggested that isolated inhibition of GSH synthesis does not mimic the complex reactions associated with oxidative stress, in which oxidative modification of proteins and additional cell components occurs, each acting alone or in concert as the biologically significant mediator in the induction of insulin resistance.

Although GSH depletion did not cause measurable insulin resistance at the skeletal muscle and adipocyte level, progressive impairment of glucose tolerance did occur with BSO treatment (Figures 1B and 1C). Since no evidence for beta-cell dysfunction could be demonstrated, the reason for glucose intolerance induced by BSO treatment remains elusive. It could either reflect alterations in glucose utilization by tissues other than skeletal muscle and adipocytes addressed in this study (e.g. liver), or by tissues in which glucose utilization is not insulin dependent. In that sense, GSH depletion in itself may contribute to the overall impairment in glucose homoeostasis in diabetes.

In conclusion, this study demonstrates that decreasing cellular or tissue levels of GSH by inhibiting its synthesis, cannot reproduce the impaired insulin responsiveness of skeletal muscle and adipocytes that occurs in response to oxidative stress or to chronic hyperglycaemia. These data suggest that alternative or additional oxidation-borne factors function as biologically relevant mediators of oxidative stress-induced insulin resistance.

This study was supported by grants from the Israel Ministry of Sciences (to M K), the Israeli Academy of Sciences (to A R), and from The Juvenile Diabetes Foundation International (to N K)

REFERENCES

1 de Zwart, L L, Meerman, J H, Commandeur, J N and Vermeulen, N P. (1999) Biomarkers of free radical damage applications in experimental animals and in humans. Free Radical Biol Med **26**, 202–226

2 Baynes, J W and Thorpe, S. R (1999) Role of oxidative stress in diabetic complications a new perspective on an old paradigm Diabetes **48**, 1–9

3 Dandona, P, Thusu, K, Cook, S, Snyder, B, Makowski, J, Armstrong, D and Nicotera, T (1996) Oxidative damage to DNA in diabetes mellitus Lancet **347**, 444–445

4 Nourooz Zadeh, J, Rahimi, A., Tajaddini Sarmadi, J, Tritschler, H, Rosen, P, Halliwell, B and Betteridge, D J. (1997) Relationships between plasma measures of oxidative stress and metabolic control in NIDDM. Diabetologia **40**, 647–653

5 Sinclair, A J, Girling, A. J., Gray, L, Le Guen, C, Lunec, J and Barnett, A H (1991) Disturbed handling of ascorbic acid in diabetic patients with and without microangiopathy during high dose ascorbate supplementation Diabetologia **34**, 171–175

6 Will, J C, Ford, E S and Bowman, B A (1999) Serum vitamin C concentrations and diabetes findings from the Third National Health and Nutrition Examination Survey, 1988–1994 Am J Clin Nutr **70**, 49–52

7 Yue, D K, McLennan, S, McGill, M, Fisher, E, Heffernan, S, Capogreco, C and Turtle, J R (1990) Abnormalities of ascorbic acid metabolism and diabetic control differences between diabetic patients and diabetic rats Diabetes Res Clin Pract **9**, 239–244

8 Nath, N., Chari, S N and Rathi, A B (1984) Superoxide dismutase in diabetic polymorphonuclear leukocytes Diabetes **33**, 586–589

9 Muchova, J, Liptakova, A, Orszaghova, Z, Garaiova, I, Tison, P, Carsky, J. and Durackova, Z (1999) Antioxidant systems in polymorphonuclear leucocytes of Type 2 diabetes mellitus Diabetic Med. **16**, 74–78

10 Yoshida, K, Hirokawa, J, Tagami, S, Kawakami, Y., Urata, Y and Kondo, T. (1995) Weakened cellular scavenging activity against oxidative stress in diabetes mellitus regulation of glutathione synthesis and efflux Diabetologia **38**, 201–210

11 Samiec, P S, Drews Botsch, C, Flagg, E. W., Kurtz, J C, Sternberg, Jr, P., Reed, R. L and Jones, D. P. (1998) Glutathione in human plasma decline in association with aging, age-related macular degeneration, and diabetes Free Radical Biol Med **24**, 699–704

12 Thomas, G, Skrinska, V., Lucas, F V and Schumacher, O P (1985) Platelet glutathione and thromboxane synthesis in diabetes Diabetes **34**, 951–954

13 Chari, S. N, Nath, N. and Rathi, A B (1984) Glutathione and its redox system in diabetic polymorphonuclear leukocytes Am J Med Sci **287**, 14–15

14 Nagamatsu, M, Nickander, K K., Schmelzer, J. D, Raya, A, Wittrock, D. A., Tritschler, H and Low, P A (1995) Lipoic acid improves nerve blood flow, reduces oxidative stress, and improves distal nerve conduction in experimental diabetic neuropathy Diabetes Care **18**, 1160–1167

15 Loven, D, Schedl, H, Wilson, H, Daabees, T T, Stegink, L D, Diekus, M and Oberley, L (1986) Effect of insulin and oral glutathione on glutathione levels and superoxide dismutase activities in organs of rats with streptozocin-induced diabetes. Diabetes **35**, 503–507

16 Volkovova, K, Chorvathova, V., Jurcovicova, M, Koszeghyova, L and Bobek, P (1993) Antioxidative state of the myocardium and kidneys in acute diabetic rats Physiol Res **42**, 251–255

17 Giugliano, D, Ceriello, A. and Paolisso, G (1996) Oxidative stress and diabetic vascular complications. Diabetes Care **19**, 257–267

18 Eriksson, U J and Borg, L A H (1993) Diabetes and embryonic malformations Role of substrate-induced free-oxygen radical production for dysmorphogenesis in cultured rat embryos Diabetes **42**, 411–419

19 Wolff, S P (1993) Diabetes mellitus and free radicals Free radicals, transition metals and oxidative stress in the aetiology of diabetes mellitus and complications Br Med Bull **49**, 642–652

20 Kaneto, H, Fujii, J, Myint, T, Miyazawa, N, Islam, K N, Kawasaki, Y, Suzuki, K, Nakamura, M, Tatsumi, H., Yamasaki, Y and Taniguchi, N (1996) Reducing sugars trigger oxidative modification and apoptosis in pancreatic beta-cells by provoking oxidative stress through the glycation reaction Biochem J **320**, 855–863

21 Tiedge, M, Lortz, S, Drinkgern, J and Lenzen, S (1997) Relation between antioxidant enzyme gene expression and antioxidative defense status of insulin-producing cells Diabetes **46**, 1733–1742

22 Kaneto, H, Kajimoto, Y., I., M. J, Matsuoka, T, Fujitani, Y, Umayahara, Y, Hanafusa, T, Matsuzawa, Y., Yamasaki, Y and Hori, M (1999) Beneficial effects of antioxidants in diabetes. Possible protection of pancreatic cells against glucose toxicity Diabetes **48**, 2398–2406

23 Matsuoka, T, Kajimoto, Y, Watada, H, Kaneto, H, Kishimoto, M, Umayahara, Y, Fujitani, Y., Kamada, T, Kawamori, R and Yamasaki, Y (1997) Glycation-dependent, reactive oxygen species-mediated suppression of the insulin gene promoter activity in HIT cells J Clin. Invest. **99**, 144–150

24 Paolisso, G, D'Amore, A, Di Maro, G, Galzerano, D, Tesauro, P, Varricchio, M and

D'Onofrio, F (1993) Evidence for a relationship between free radicals and insulin action in the elderly Metabolism **42**, 659–663

25 Paolisso, G, D'Amore, A, Volpe, C, Balbi, V., Saccomanno, F., Galzerano, D., Giugliano, D, Varricchio, M. and D'Onofrio, F. (1994) Evidence for a relationship between oxidative stress and insulin action in non-insulin-dependent (type II) diabetic patients Metabolism **43**, 1426–1429

26 Caballero, B (1993) Vitamin E improves the action of insulin Nutr Rev. **51**, 339–340

27 Paolisso, G, D'Amore, A, Balbi, V, Volpe, C., Galzerano, D, Giugliano, D., Sgambato, S, Varricchio, M and D'Onofrio, F (1994) Plasma vitamin C affects glucose homeostasis in healthy subjects and in non-insulin-dependent diabetics Am J Physiol **266**, E261–E268

28 Paolisso, G, Di Maro, G, Pizza, G, D'Amore, A, Sgambato, S, Tesauro, P, Varricchio, M and D'Onofrio, F (1992) Plasma GSH/GSSG affects glucose homeostasis in healthy subjects and non-insulin-dependent diabetics Am. J. Physiol **263**, E435–E440

29 Jacob, S., Henriksen, E J, Schiemann, A L, Simon, I, Clancy, D. E, Tritschler, H J, Jung, W. I., Augustin, H J and Dietze, G J (1995) Enhancement of glucose disposal in patients with type 2 diabetes by alpha-lipoic acid Arzneim-Forschung **45**, 872–874

30 Rudich, A, Kozlovsky, N, Potashnik, R and Bashan, N (1997) Oxidant stress reduces insulin responsiveness in 3T3–L1 adipocytes Am J Physiol **272**, E935–E940

31 Hansen, L L, Ikeda, Y., Olsen, G S., Busch, A K. and Mosthaf, L (1999) Insulin signaling is inhibited by micromolar concentrations of H_2O_2 Evidence for a role of H_2O_2 in tumor necrosis factor-mediated insulin resistance. J Biol Chem **274**, 25078–25084

32 Tirosh, A, Potashnik, R., Bashan, N and Rudich, A (1999) Oxidative stress disrupts insulin-induced cellular redistribution of insulin receptor substrate-1 and phosphatidylinositol 3-kinase in 3T3–L1 adipocytes J Biol Chem. **274**, 10595–10602

33 Blair, A S, Hajduch, E, Litherland, G J and Hundal, H S (1999) Regulation of Glucose Transport and Glycogen Synthesis in L6 Muscle Cells during Oxidative Stress Evidence for cross-talk between the insulin and SAPK2/p38 mitogen-activated protein kinase signaling pathways J. Biol Chem **274**, 36293–36299

34 Rudich, A, Tirosh, A, Potashnik, R, Hemi, R, Kanety, H and Bashan, N (1998) Prolonged oxidative stress impairs insulin-induced GLUT4 translocation in 3T3–L1 adipocytes. Diabetes **47**, 1562–1569

35 Martensson, J, Jain, A., Stole, E, Frayer, W, Auld, P A and Meister, A. (1991) Inhibition of glutathione synthesis in the newborn rat a model for endogenously produced oxidative stress Proc Natl Acad Sci U.S A **88**, 9360–9364

36 Leeuwenburgh, C. and Ji, L L (1995) Glutathione depletion in rested and exercised mice biochemical consequence and adaptation Arch Biochem Biophys **316**, 941–949

Received 25 February 2000/7 April 2000, accepted 5 May 2000

37 Ellman, G L. (1959) Tissue sulphydryl groups. Arch Biochem Biophys **82**, 70–77

38 Khamaisi, M, Rudich, A., Beeri, I, Pessler, D, Friger, M., Gavrilov, V., Tritschler, H and Bashan, N (1999) Metabolic effects of gamma-linolenic acid–alpha-lipoic acid conjugate in streptozotocin diabetic rats Antiox Redox Signaling **1**, 523–535

39 Anderson, M E (1985) Determination of glutathione and glutathione disulfide in biological samples Methods Enzymol **113**, 548–555

40 Gadot, M, Leibowitz, G, Shafrir, E, Cerasi, E, Gross, D J and Kaiser, N (1994) Hyperproinsulinemia and insulin deficiency in the diabetic Psammomys obesus Endocrinology **135**, 610–616

41 Khamaisi, M, Potashnik, R., Tirosh, A, Demshchak, E, Rudich, A, Tritschler, H, Wessel, K and Bashan, N (1997) Lipoic acid reduces glycemia and increases muscle GLUT4 content in streptozotocin-diabetic rats Metabolism **46**, 763–768

42 Ramlal, T, Rastogi, S, Vranic, M and Klip, A (1989) Decrease in glucose transporter number in skeletal muscle of mildly diabetic (streptozotocin-treated) rats Endocrinology **125**, 890–897

43 Bradford, M. M (1976) A rapid and sensitive method for the quantitation of microgram quantities of protein utilizing the principle of protein-dye binding Anal Biochem **72**, 248–254

44 Rudich, A, Tirosh, A, Potashnik, R, Khamaisi, M and Bashan, N (1999) Lipoic acid protects against oxidative stress induced impairment in insulin stimulation of PKB and glucose transport in 3T3–L1 adipocytes Diabetologia **42**, 949–957

45 Holman, G D and Kasuga, M (1997) From receptor to transporter insulin signalling to glucose transport Diabetologia **40**, 991–1003

46 Rea, S and James, D. E (1997) Moving GLUT4 The biogenesis and trafficking of GLUT4 storage vesicles Diabetes **46**, 1667–1677

47 Frost, S C and Lane, M D (1985) Evidence for the involvement of vicinal sulfhydryl groups in insulin-activated hexose transport by 3T3–L1 adipocytes J Biol Chem **260**, 2646–2652

48 Begum, N. (1994) Phenylarsine oxide inhibits insulin-stimulated protein phosphatase 1 activity and GLUT4 translocation Am. J Physiol **267**, E14–E23

49 Stenbit, A E, Tsao, T S, Li, J, Burcelin, R, Geenen, D L, Factor, S M, Houseknecht, K, Katz, E B. and Charron, M J (1997) GLUT4 heterozygous knockout mice develop muscle insulin resistance and diabetes Nat Med **3**, 1096–1101

50 Sen, C K, Atalay, M and Hanninen, O (1994) Exercise-induced oxidative stress glutathione supplementation and deficiency J Appl Physiol **77**, 2177–2187

51 Okada, K, Wangpoengtrakul, C, Osawa, T, Toyokuni, S, Tanaka, K and Uchida, K (1999) 4-Hydroxy-2-nonenal-mediated impairment of intracellular proteolysis during oxidative stress Identification of proteasomes as target molecules J Biol Chem **274**, 23787–23793

52 Figueiredo Pereira, M. E, Yakushin, S and Cohen, G (1998) Disruption of the intracellular sulfhydryl homeostasis by cadmium-induced oxidative stress leads to protein thiolation and ubiquitination in neuronal cells J Biol. Chem **273**, 12703–12709

N-arginine dibasic convertase (nardilysin) isoforms are soluble dibasic-specific metalloendopeptidases that localize in the cytoplasm and at the cell surface

Véronique HOSPITAL*[1], Valérie CHESNEAU†, Agnès BALOGH*, Catherine JOULIE*, Nabil G. SEIDAH‡, Paul COHEN* and Annik PRAT*[1,2]

*Laboratoire de Biochimie des Signaux Régulateurs Cellulaires et Moléculaires, UMR 7631 CNRS, Université Pierre et Marie Curie, 96 Bd Raspail, 75006 Paris, France, †Ben May Institute for Cancer Research, University of Chicago, 5841 S Maryland, Chicago, IL 60637, U.S.A., and ‡Laboratory of Biochemical Neuroendocrinology, Clinical Research Institute of Montreal, 110 Pine Ave West, Montreal, Quebec, H2W 1R7 Canada

N-arginine (R) dibasic (NRD) convertase (nardilysin; EC 3.4.24.61), a metalloendopeptidase of the M16 family, specifically cleaves peptide substrates at the N-terminus of arginines in dibasic motifs *in vitro*. In rat testis, the enzyme localizes within the cytoplasm of spermatids and associates with microtubules of the manchette and axoneme. NRD1 and NRD2 convertases, two NRD convertase isoforms, differ by the absence (isoform 1) or presence (isoform 2) of a 68-amino acid insertion close to the active site. In this study, we overexpressed both isoforms, either by vaccinia virus infection of BSC40 cells or transfection of COS-7 cells. The partially purified enzymes exhibit very similar biochemical and enzymic properties. Microsequencing revealed that NRD convertase is N-terminally processed. Results of immunocytofluorescence, immunoelectron microscopy and subcellular fractionation studies argue in favour of a primary cytosolic localization of both peptidases. Although the putative signal peptide did not direct NRD convertase into microsomes in an *in vitro* translation assay, biotinylation experiments clearly showed the presence of both isoforms at the cell surface. In conclusion, although most known processing events at pairs of basic residues are achieved by proprotein convertases within the secretory pathway, NRD convertase may fulfil a similar function in the cytoplasm and/or at the cell surface

Key words: cell-surface biotinylation, extracellular endoprotease, M16 family, proprotein processing, testicular enzyme.

INTRODUCTION

Several members of the M16 family of metalloproteinases [1,2] have been implicated in the proteolytic processing of peptides or proteins. Examples include insulin-degrading enzyme (insulysin; EC 3.4.24.56 [3,4]), mitochondrial matrix-processing protease ([5], for a review see [6]) and chloroplast-processing endopeptidase [7,8], these two involved in the removal of the N-terminal transit peptide of nuclear-encoded proteins, yeast pro-a-factor-processing proteases, Axl1 and Ste23 [9,10], and N-arginine (R) dibasic convertase (NRD convertase, or nardilysin; EC 3.4.24.61).

First discovered in rat brain cortex [11,12], NRD convertase was purified from testis, where it is particularly abundant ([13], for reviews see [14,15]). *In vitro*, this metalloendopeptidase cleaves various peptides such as somatostatin-28 (S-28), dynorphin A and atrial natriuretic factor at the N-terminus of arginines within paired basic residues [13], canonical processing sites for secretory precursor proteins [16,17]. The analysis of the first NRD convertase cDNA obtained from rat testis [18] predicted an 1161-amino acid (aa)-long sequence containing a highly acidic stretch of 71 residues (79 % Glu and Asp) and an HXXEH motif found in the catalytic site of several metallopeptidases [19,20]. Recently, a second NRD convertase cDNA was identified in human and rat testis [21]. The deduced aa sequence, NRD2 convertase, differs from the originally characterized NRD1 convertase by a 68-aa insertion between the acidic stretch and the HXXEH motif. Using a specific probe for each NRD isoform, Northern-blot analyses demonstrated that the NRD2 convertase isoform represents 50 and 10 % of the total NRD convertase transcripts in human and rat testis, respectively [21]. However, since attempts to obtain rat NRD2 (rNRD2) convertase-specific antibodies remain unsuccessful, the ratio *in vivo* of the two protein isoforms in testis and other tissues could not be evaluated. In human, the gene encoding NRD convertase was localized to chromosome 1p32 [21].

Although NRD convertase expression was detected in most of the tissues analysed [13,21,22], testis remains its major expression site in the adult rat. In this tissue, NRD convertase synthesis is restricted to germ cells and is regulated during spermiogenesis [23] While detected at low levels in young spermatids, the protein accumulates in the cytoplasm of elongated spermatids with a noticeable concentration at the level of two microtubular structures, the manchette and the axoneme [23]. Its regulated expression during spermatogenesis and its concentration in the flagellum suggest a role in the differentiation of the male germ cell. Furthermore, murine NRD convertase transcripts were detected on embryonic day 10.5, almost exclusively within neural tissues, suggesting that the enzyme plays specific roles in neuronal development as well [22]. NRD convertase mRNAs were also detected in all cell lines analysed [21] Recently, this endopeptidase was rediscovered as a dynorphin-converting enzyme in

---

Abbreviations used: NRD convertase, N-arginine (R) dibasic convertase, rNRD convertase, rat NRD convertase, S-28, somatostatin-28, VV, vaccinia virus, IF, immunofluorescence, IEM, immunoelectron microscopy, ER, endoplasmic reticulum, aa, amino acid, NEP, neutral endopeptidase, D-PBS, Dulbecco's PBS, GFP, green fluorescent protein, β-Gal, β-galactosidase

[1] Present address Laboratory of Biochemical Neuroendocrinology, Clinical Research Institute of Montreal, 110 Pine Ave West, Montreal, Quebec, H2W 1R7 Canada.

[2] To whom correspondence should be addressed, at the Laboratory of Biochemical Neuroendocrinology (e-mail annik-prat@ircm.qc.ca)

the culture medium of the mouse thymus-derived cell line EL-4 [24]. Thus NRD convertase appears to be localized in the cytoplasm and/or to be secreted by some cell types, including the male germ cells [23]. Although the N-terminus of the protein shows some characteristics reminiscent of a signal peptide [25], its functionality remains to be established.

To study the potential differences existing between the two closely related NRD convertase isoforms, we overexpressed them by infecting BSC40 cells with recombinant vaccinia viruses (VVs). rNRD1 and rNRD2 convertases were then partially purified, and their biochemical and enzymic properties analysed. Their subcellular localization was investigated in transiently transfected COS-7 cells and/or infected BSC40 cells by immunofluorescence (IF), immunoelectron microscopy (IEM), subcellular fractionation and biotinylation of cell-surface proteins. The ability of the N-terminus of NRD convertase to function *in vitro* as a signal peptide was also assessed.

EXPERIMENTAL

Cell culture

BSC40 and COS-7 cells were respectively maintained in minimal essential medium (Gibco-BRL, Life Technologies, Paisley, Scotland) and Dulbecco's modified Eagle's medium containing 10% fetal bovine serum and 25 μg/ml gentamicin (all from Gibco-BRL) at 37 °C in 5% CO_2.

Plasmid constructions

The 3′-untranslated region of the rNRD1 convertase cDNA in pBluescript II SK$^+$ (pBlrNRD1 [18]) was shortened by replacing the *Nsi*I–*Hin*dIII digestion product with a PCR fragment that inserts a *Hin*dIII restriction site 26 bp downstream of the stop codon (pBlrNRD1exp3′). This modified cDNA was then subcloned as a *Sma*I–*Hin*dIII fragment into the *Eco*RV and *Hin*dIII sites of the mammalian expression vector pcDNA3 (Invitrogen, Leek, The Netherlands). The removal of the 5′-untranslated region was achieved in two steps. The 3592-bp *Sma*I–*Hin*dIII fragment was first digested with *Bst*UI to remove the whole 5′-untranslated region plus 16 bp of the open reading frame. This was then ligated with a 24-bp-long linker composed of two annealed oligonucleotides, 5′-TCGACAGAATGCTGAGGAGAGTCG-3′ and 5′-CGACTCTCCTCAGCATTCTG-3′, thereby introducing a *Sal*I site 4 bp upstream of the initiation codon and a nucleotide context respecting Kozak's rules [26] This ligation product was digested by *Sal*I and subcloned into the VV transfer plasmid pMJ601 [27] to generate pMJ601-rNRD1. The pMJ601-rNRD2 and pcDNA3-rNRD2 vectors were obtained by replacing the *Bgl*II fragment (nt 439–1290) with a *Bgl*II cassette containing the 204-bp insertion of rNRD2 convertase.

For *in vitro* translation experiments, the *Bam*HI fragment of pBlrNRD1, containing part of the polylinker and nt 1–1348 of rNRD1 convertase cDNA, was cloned into the *Bam*HI site of the mutagenesis vector tg131 (Sculptor, Amersham Pharmacia Biotech, Uppsala, Sweden). In order to introduce a *Hin*dIII site at position 45, the underlined nucleotides shown here were mutagenized by the use of the oligonucleotide 5′-CTAGAGCGGCCGCAAGCTTAGCGC-3′. The resulting *Hin*dIII–*Bam*HI fragment was subcloned in pBluescript II KS$^+$ to generate pBl5′rNRD1$\triangle$1-44. The vector containing the full-length cDNA of the rabbit neutral endopeptidase (NEP, or neprilysin; EC 3.4.24.11 [28]) under the control of the SP6 RNA polymerase promoter (pSP6NEP) was kindly provided by Dr G. Boileau (University of Montreal, Montreal, Quebec, Canada).

VV infections

The pMJ601 constructs were used to produce NRD convertase recombinant VV [27]. VV.mPC5* in which the active-site Ser^{354} of the proprotein convertase PC5 was mutated to Ala has been described previously [29]. VV:βGal expressed the *Escherichia coli* β-galactosidase (β-Gal). For enzyme preparation, subcellular fractionation and biotinylation, confluent BSC40 cells were infected at a multiplicity of infection of 5. Parallel plates were either not infected, or infected with the wild-type virus (VV:WT) or the recombinants VV.rNRD1, VV:rNRD2, VV:mPC5* or VV:βGal. Following 30-min infections at 20 °C in PBS containing 1 mM $MgCl_2$ and 0.01% BSA, the inoculum was replaced by minimal essential medium. Cells were incubated at 37 °C for either 16–18 h for enzyme preparation or 4–5 h for subcellular fractionation and biotinylation experiments. They were then scraped into a Dulbecco's PBS (D-PBS, Gibco-BRL) medium and collected by centrifugation (1000 *g* for 10 min) or treated with biotin.

Enzyme preparation

A single Wistar rat testis (Pelfreeze, Rogers, AR, U.S.A.) or pooled duplicate naïve or infected BSC40 cells (4×10^7 cells) were homogenized in 50 mM Tris/HCl, pH 7.5, containing 5 mM β-mercaptoethanol, and centrifuged at 14000 *g* for 15 min. The supernatant (homogenate) was applied to a DEAE-Trisacryl M ion-exchange column (10 ml bed volume; BioSepra, Villeneuve la Garenne, France) pre-equilibrated with 50 mM Tris/HCl, pH 7.5/150 mM KCl. After washing with 50 ml of the same buffer, the column was eluted with a 30-ml linear gradient from 150 to 400 mM KCl in 50 mM Tris/HCl, pH 7.5. Fractions (1 ml) were collected and assayed for enzyme activity. Pools of active fractions (post-DEAE pools) were concentrated and desalted on Ultrafree-30K (Millipore, Molsheim, France) and used in enzymic assays, analysis by SDS/PAGE (8% gel) and Western blotting or N-terminal sequencing. Purified NRD convertase was prepared from rat testis as described previously [13].

pH optima and inhibitor profiles

Routine enzyme assays were carried out by incubation of an aliquot of the enzyme preparation with either 5 μg of PRERKAGAKNY-NH_2 ([Ala^{17}, Tyr^{20}]S-28-(10-20)-NH_2, residues 10–20 from S-28, the 17th (Ala) and 20th (Tyr) residues being different from the wild-type sequence [11]) in 50 mM Tris/HCl, pH 8.9 (buffer A), or 3.5 μg of dynorphin A (Sigma, St. Louis, MO, U.S.A.) in 250 mM Tris/HCl, pH 7.5 (buffer B), in a 100-μl final volume. The reaction was stopped by adding 10 μl of concentrated acetic acid and analysed by reverse-phase HPLC on a μ-Bondapak C_{18} column, as described in [13]. For the inhibition study, enzymes were preincubated with the inhibitor for 15 min at 37 °C, prior to the addition of the substrate. A control incubation without inhibitor was defined as 100% endopeptidase activity. For pH-optima determinations, the substrate PRERKAGAKNY-NH_2 was digested in the following buffers 50 mM sodium phosphate, pH 5.8–7.6, 50 mM Tris/HCl, pH 7.5–8.9, and 50 mM glycine/NaOH, pH 8.7–10.5.

Transfections of COS-7 cells

The pcDNA3, pcDNA3-rNRD1, pcDNA3-rNRD2 and pIRES2-EGFP (Clontech, Palo Alto, CA, U.S.A.) vectors were transfected into COS-7 cells using Superfect (Qiagen, Hilden, Germany). Briefly, 24 h before transfection, cells were grown on 100-mm plates (10^6 cells), containing glass coverslips for IF experiments, or on 35-mm plates for ultrastructural studies (10^6 cells). The Superfect-DNA precipitate, prepared using either 10 or 2 μg of DNA and 60 or 20 μl of Superfect depending on plate size, was incubated with COS-7 cells for 2.5 h at 37 °C. The cells were washed successively with D-PBS and fresh Dulbecco's modified Eagle's medium containing 10 % fetal bovine serum and 25 μg/ml gentamicin was added. Later (24 h), cells were either harvested for Western-blot analysis or subcellular fractionation, fixed for immunocytochemistry or treated with biotin.

Subcellular fractionation of transfected COS-7 cells and infected BSC40 cells

Transfected or infected cells were scraped in D-PBS, gently pelleted at 500 *g*, put on ice and washed twice with PBS. They were then resuspended in a buffer (5 mM Tris/HCl, pH 7.5/250 mM sucrose/1 mM MgCl$_2$) containing various protease inhibitors (2.5 mM EDTA/2 mM β-mercaptoethanol/100 μg/ml PMSF/100 μM pepstatin/2 μg/ml leupeptin and aprotinin) and broken by repeated passages through a 25-gauge needle. Nuclei and cellular debris were removed by centrifugation at 2000 *g* for 10 min at 4 °C. The resulting supernatant (S1) was centrifugated at 100000 *g* for 30 min at 4 °C in a TLA 120-2 fixed-angle rotor (Beckman Instruments, Fullerton, CA, U.S.A.). The supernatant (S2), containing mainly cytoplasmic proteins, was collected. The pellet (P2), containing among others intact microsomes, was washed twice and resuspended in the above buffer after one freeze–thaw cycle. The proteins in the S2 and P2 fractions were analysed by Western blotting.

Antibodies

The calreticulin and PC5 polyclonal antisera used were directed against human recombinant calreticulin (both antigen and antibody were provided kindly by Dr L. Rokeach, University of Montreal) and the N-terminus of active mouse PC5 [30], respectively. For immunocytochemistry, the polyclonal NRD convertase antiserum [13] was purified as follows. Rat testis NRD convertase was electrophoresed on an 8 % SDS/polyacrylamide gel and transferred on to a nitrocellulose membrane After incubation with the anti-rNRD convertase immune serum, antibodies associated with the 140-kDa form were eluted from the membrane at 4 °C in 0.1 M glycine, pH 2.8, and neutralized with 2 M Tris/HCl, pH 8. Anti-green fluorescent protein (GFP) monoclonal antibodies and rabbit anti-*E. coli* β-Gal antibodies were purchased from Molecular Probes (Eugene, OR, U.S.A.) and Eppendorf-5Prime (Boulder, CO, U.S.A.) respectively.

IEM and IF

Transfected COS-7 were fixed in periodate/lysine/paraformaldehyde [31] for 2 h at room temperature, washed three times in PBS, preincubated for 30 min in 50 mM NH$_4$Cl, and permeabilized in PBS containing 0.2 % gelatin/0.005 % saponin for 1 h. After a 3-h incubation with purified anti-NRD convertase antibodies, cells were rinsed three times with PBS and incubated for 90 min with a goat Fab anti-rabbit IgG conjugated with peroxidase (Biosys, Compiègne, France) for IEM or with goat anti-rabbit IgG conjugated with FITC (Jackson Immuno-Research Laboratories, West Grove, PA, U.S.A.) for IF. For IEM, cells were postfixed in 1 % glutaraldehyde and the peroxidase activity was visualized using 3,3′-diaminobenzidine tetrahydrochloride. They were then fixed in 1 % osmium tetroxide, dehydrated and embedded *in situ* in epon [32]. Selected areas of immunoreactive cells were sectioned as described previously [33]. Ultrathin sections were examined at the electron microscope without further staining. For IF, cells were washed and examined with an epifluorescence microscope (Leica Microscopy, Heerbrugg, Switzerland).

Western-blot analyses

Whole-cell extracts were prepared as follows. Cell pellets were resuspended in 50 mM Tris/HCl, pH 7.4/150 mM NaCl/0 02 % sodium azide supplemented with the above cocktail of protease inhibitors. Crude extracts were then submitted to three cycles of freeze–thaw, homogenized through a 25-gauge needle, centrifuged at 12000 *g* for 30 min and the supernatants analysed Proteins from whole cell extracts, subcellular fractions or post-biotinylation immunoprecipitation were separated by 8 or 10 % SDS/PAGE (SE250 apparatus; Hoefer, San Francisco, CA, U.S.A.) and transferred on to nitrocellulose membranes (Optitran BA-S 85; Schleicher and Schuell, Dassel, Germany) using a semi-dry TE270 unit (Hoefer). Anti-NRD convertase, anti-calreticulin, anti-PC5 and anti-β-Gal polyclonal sera were used at final dilutions of 1/2000, 1/5000, 1/500 and 1/1000, respectively. The antigen–antibody complexes were revealed using a donkey anti-rabbit IgG horseradish peroxidase conjugate (ECLPlus Western blotting detection, Amersham Pharmacia Biotech). Monoclonal anti-GFP was used at a 1/400 final dilution and revealed using a sheep anti-mouse IgG horseradish peroxidase conjugate (Amersham Pharmacia Biotech). Prestained molecular-mass markers were purchased from New England Biolabs (Hitchin, Herts., U K) or from Amersham Pharmacia Biotech. Protein concentration was estimated as described previously [34]

Transcription-translation analyses *in vitro*

The plasmids pB15′rNRD1Δ1-44 and pSP6NEP were linearized with *Ssp*I and *Bst*XI, respectively, and transcribed *in vitro* using an RNA transcription-translation kit (Promega, Madison, WI, U.S.A.) RNAs (5 μg) were translated *in vitro* in the presence or absence of rough microsomes and [^{35}S]methionine. Where indicated, trypsin and Triton X-100 were added to 5 μg/ml and 1 % final concentrations respectively The translation products were analysed on SDS/PAGE (15 % gel) followed by fluorography (Amplify, Amersham Pharmacia Biotech).

Biotinylation of cell-surface proteins

Transfected COS-7 and infected BSC40 cells were washed three times with ice-cold PBS with 1 mM MgCl$_2$ and incubated for 1 h at 4 °C with 0.5 mg/ml sulpho-NHS-LC-LC-Biotin (Pierce, Rockford, IL, U.S.A.). Then, cells were washed three times with ice-cold PBS containing 1 mM MgCl$_2$, lysed in a buffer (20 mM Tris/HCl, pH 8.0/150 mM NaCl/1 % sodium deoxycholate/1 % Triton X-100) containing protease inhibitors (protease-inhibitor-cocktail tablets, Amersham Pharmacia Biotech) and centrifuged at 12000 *g* for 15 min at 4 °C. The supernatants were immunoprecipitated with antibodies directed against NRD convertase (1/250), β-Gal (1/200) or GFP (2 μg). Immunoprecipitated proteins corresponding to 2×10^6 transfected COS-7 or 10^6 infected BSC40 cells were resolved by SDS/PAGE (10 % gel) and transferred on to nitrocellulose membranes as described above. Biotinylated proteins were revealed with a streptavidin-horseradish peroxidase conjugate (Amersham Pharmacia Biotech).

RESULTS

Comparison of the biochemical properties of the two recombinant rNRD isoforms

Expression of enzymically active rNRD1 and rNRD2 convertases

To study the possible influence of the 68-aa insertion [21] on the catalytic properties of NRD2 convertase, we first expressed the two rat isoforms either by VV infection of BSC40 cells or by transient transfection of COS-7 cells. The expression of the recombinant proteins was monitored by Western-blot analyses of crude cell extracts (Figure 1). In both expression systems, the recombinant rNRD1 convertase migrated with an apparent molecular mass of 140 kDa, similar to that of rNRD convertase

Table 1 Inhibition profiles of rNRD convertase isoforms and rat testicular enzyme

Results are expressed as percentage inhibition, taking the control incubation as 0% inhibition. Quantities of enzyme introduced in the assay were adjusted for each enzyme preparation to obtain a 50% cleavage of the substrate in 15 min at 37 °C in the absence of inhibitor. Conditions were as follows. (**A**) 50 mM Tris/HCl, pH 8.9, and 5 μg of PRERKAGAKNY-NH_2, (**B**) 250 mM Tris/HCl, pH 7.5, and 3.5 μg of dynorphin A. The enzyme was preincubated with the inhibitor for 15 min at 37 °C and the reaction initiated by addition of the substrate. After 15 min of incubation, the reaction was stopped by addition of 10 μl of glacial acetic acid. The final volume of the assay was 100 μl.

(A)

	Inhibition (%)		
	Testicular rNRD	rNRD1	rNRD2
EDTA (100 μM)	32±5	56±2	46±4
1,10-Phenanthroline (500 μM)	59±4	100	100
N-Ethylmaleimide (1 mM)	18±4	11±4	0
Amastatin (200 μM)	25±3	86±1	100
Bestatin (500 μM)	0	0	0

(B)

	Inhibition (%)		
	Purified rNRD	rNRD1	rNRD2
EDTA (100 μM)	100	100	100
1,10-Phenanthroline (500 μM)	100	100	100
N-Ethylmaleimide (1 mM)	100	100	100
Amastatin (200 μM)	33±2	0	0
Bestatin (500 μM)	0	0	0

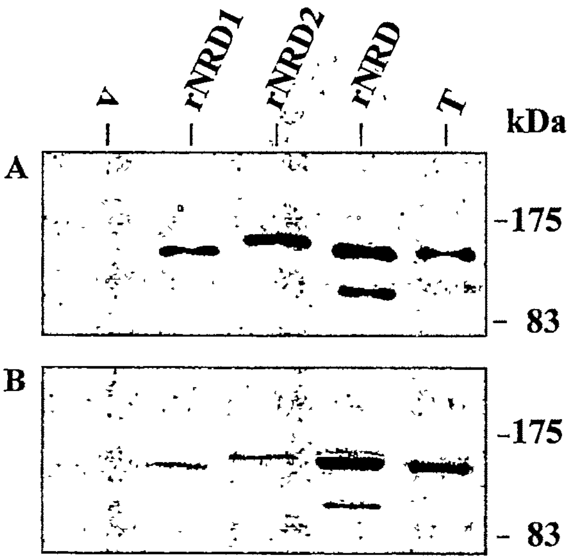

Figure 1 Overexpression of rNRD1 and rNRD2 convertases in infected BSC40 cells and transfected COS-7 cells

Western-blot analysis of crude protein extracts from (**A**) BSC40 cells infected with the wild-type VV (V, 9 μg), the recombinant VV rNRD1 (3 μg) and VV rNRD2 (9 μg), (**B**) and COS-7 cells transfected with pcDNA3 vector (V, 15 μg), pcDNA3-rNRD1 (5 μg) and pcDNA3-rNRD2 (15 μg) were separated by SDS/PAGE on an 8% polyacrylamide gel. Purified rat testis NRD convertase (rNRD, 0.67 μg) and crude testis extract (T, 10 μg) were also analysed.

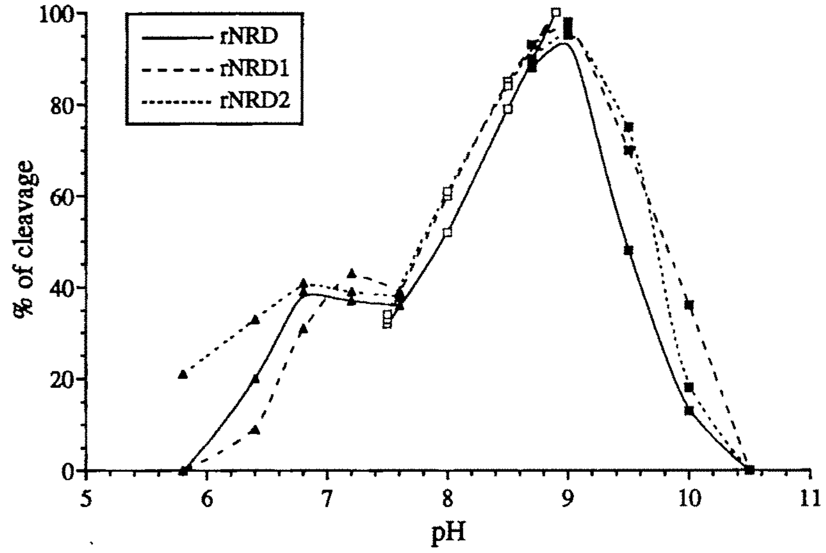

Figure 2 pH dependence of PRERKAGAKNY-NH_2 cleavage by recombinant rNRD convertase isoforms or the rat testis purified enzyme

The percentage of peptide cleavage was determined at various pH values (5.8–10.5) using the following buffers: 50 mM sodium phosphate (▲), 50 mM Tris/HCl (□) and 50 mM glycine/NaOH (■). The extent of cleavage at the pH optimum (8.9) was taken as 100%.

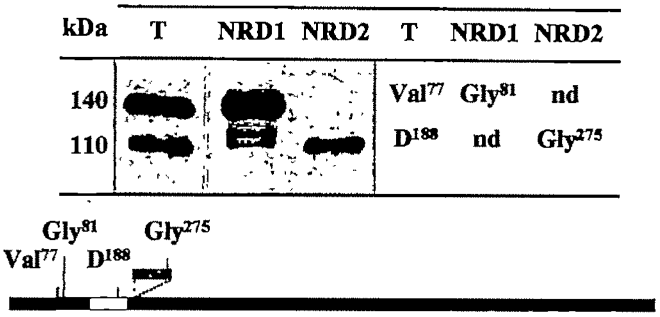

Figure 3 N-termini of rNRD convertase species

Western-blot analyses of post-DEAE concentrated pools from rat testis (T, 5 μg) and from BSC40 cells infected by VV rNRD1 (1 μg) or VV rNRD2 (2 μg) are shown. N-terminal sequencing of 140-kDa (rNRD and rNRD1) or 110-kDa (rNRD and rNRD2) species identified Val^{77} and Gly^{81}, and Asp^{188} and Gly^{275}, as N-termini, respectively. These are positioned on a schematic representation of the NRD convertase sequence below. The white box represents the 71-aa acidic stretch while the elevated hatched one represents the specific rNRD2 convertase 68-aa insertion.

purified from rat testis. rNRD2 convertase showed a slightly slower migration (≈ 145 kDa) in accordance with its additional 68 aa. Although rNRD2 convertase transcripts represent 10 % of the total NRD convertase mRNA in testis [21], we could not detect rNRD2 convertase in testicular extracts (Figure 1, rNRD and T). Since to date rNRD2 convertase-specific antibodies are not available, it is difficult to conclude whether this isoform is absent or scarcely present in this tissue. The 110-kDa immunoreactive protein detected in the rat testis crude extract and the purified enzyme preparation was identified as a degradation product of NRD convertase (see below). Also, neither rNRD1 nor rNRD2 convertases could be detected in culture media of either cell line (results not shown), suggesting that they are not secreted by these cells.

After partial purification on a DEAE-Trisacryl M ion-exchange column, both recombinant proteinases were shown to cleave the model peptide PRERKAGAKNY-NH$_2$. This synthetic peptide mimicking the dibasic processing site of pro-somatostatin had been previously used routinely to monitor the purification of NRD convertase [11,13]. As with the endoprotease isolated from rat testis, isoforms 1 and 2 produced the same proteolytic fragment (RKAGAKNY-NH$_2$). Finally, comparable percentages of cleavage were obtained when the same quantity of each enzyme was used (as estimated by silver staining of SDS/acrylamide gels). Control extracts from BSC40 cells not infected or infected by the wild-type VV, as well as those from COS-7 cells transfected with pcDNA3, were totally devoid of activity towards the model peptide. To further analyse the biochemical properties of each isoform, the VV overexpression system was chosen because of its higher expression rate.

pH optima and inhibition profiles

Using the same model substrate as above, an optimal pH of 8.9 was determined previously for the purified rat testis enzyme [13]. Since at this pH the optimal concentration in Tris was found to be 50 mM (results not shown), three 50 mM buffers covering a pH range from 5.8 to 10.5 were used. As seen in Figure 2, the same major optimal pH of 8.9 was obtained for the three enzyme preparations (done in triplicate). In addition, the three curves were superimposable. A similar shoulder was observed for each enzyme preparation around neutral pH. However, rNRD2

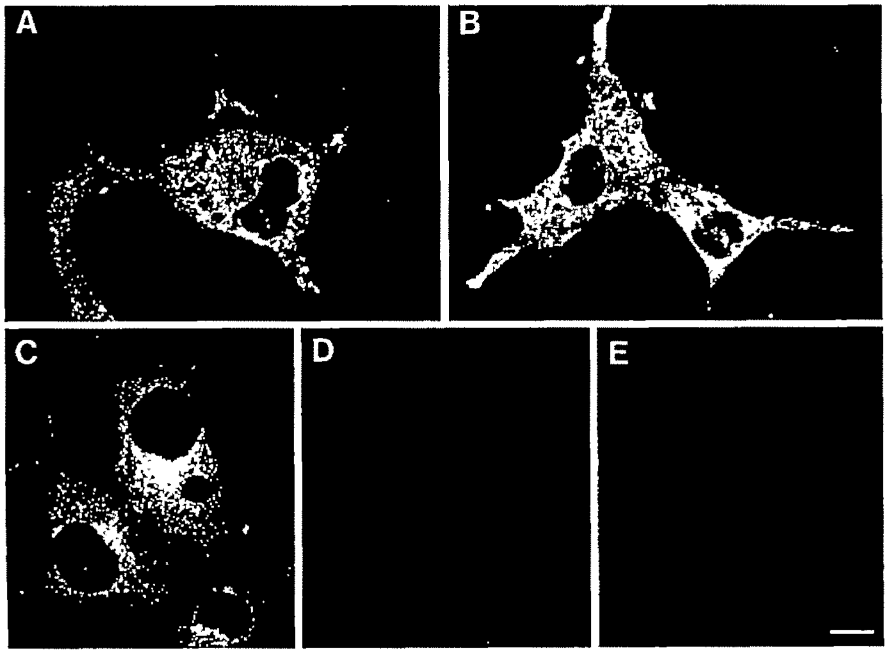

Figure 4 IF localization of rNRD convertase isoforms

Transfected COS-7 cells with either pcDNA3-rNRD1 (A) or pcDNA3-rNRD2 (B) or untransfected cells (C) were immunolabelled with rNRD convertase-purified antibodies (A, B) or anti-calreticulin (C). Negative controls consisted of either COS-7 cells transfected with pcDNA3 and revealed with anti-rNRD convertase (E) or COS-7 cells expressing rNRD1 convertase and labelled with rNRD convertase preimmune serum (D). Scale bar, 10 μm.

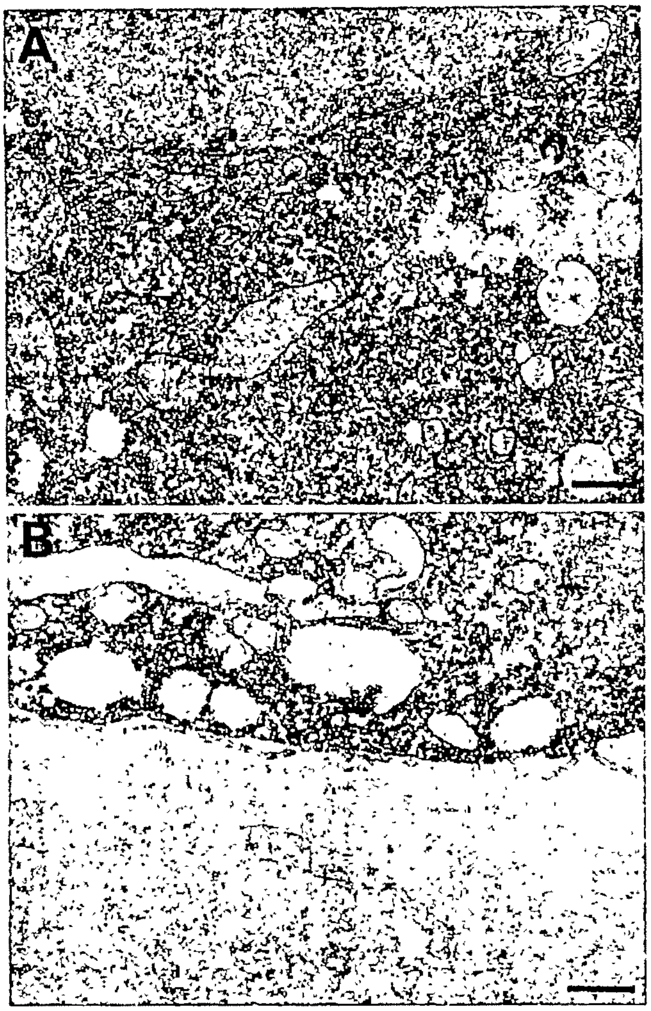

Figure 5 IEM

NRD convertase immunoreactivity in COS-7 cells transfected with pcDNA3-rNRD1 (**A**) or pcDNA3-rNRD2 (**B**) was visualized indirectly by peroxidase activity In (**B**), note the presence of transfected (upper) and untransfected (lower) cells present on the same section Scale bar, 1 μm

convertase seemed to conserve a higher activity at acidic pH.

To detect any differences between the enzymic properties of the two isoforms, various reagents reported to inhibit NRD convertase activity [13] were tested in two types of assay (Table 1A and 1B). The first one (Table 1A) was performed in 50 mM Tris/HCl, pH 8.9, with the model substrate PRERKAGAKNY-NH$_2$, whereas the second (Table 1B) was carried out in 250 mM Tris/HCl, pH 7.5, with dynorphin A as a substrate, as described previously [13] In both assays, the two isoforms showed very similar inhibitor sensitivities. However, except for 1,10-phenanthroline, the amounts of inhibitors needed to achieve 100% inhibition in assay B were 10 times higher than reported previously [13]. This discrepancy may be explained by the lower degree of purity of the enzyme preparation used here. The same explanation stands for the higher inhibitions observed for rNRD1 or rNRD2 convertases than for the rat testis enzyme (except in the case of *N*-ethylmaleimide). Indeed, the latter exhibits a lower specific activity. Curiously, whereas testis rNRD convertase showed comparable inhibitions by amastatin in both assays, the two isoforms were either not inhibited (assay B) or completely inhibited (assay A). Note that 500 μM bestatin, representing a 10-fold higher concentration than previously used, failed to inhibit any of the three enzymes.

N-terminal heterogeneity of the different NRD convertase immunoreactive species

Western-blot analysis of the partially purified enzyme preparations revealed a noticeable difference in the stability of the respective isoforms (Figure 3) While rNRD1 convertase remained relatively stable as a 140-kDa protein for several days at 4 °C, rNRD2 convertase was transformed rapidly into a 110-kDa protein. The disappearance of the 145-kDa rNRD2 form seemed to be concomitant with the loss of enzyme activity. Whereas the partially purified rNRD1 convertase samples showed comparable specific activities 2 or 10 days post-homogenization, rNRD2 convertase activity, which was easily measurable at day 2, could no longer be monitored at day 10. In addition to the major 140-kDa and minor 110-kDa forms, another minor 120-kDa immunoreactive protein is also observed in Figure 3 (lane NRD1) Only in BSC40 cell extracts did we observe similar levels of the 110- and 120-kDa forms. In testicular extracts, we rarely see the 120-kDa form. The nature of this intermediate is yet to be determined. The possible presence in the rNRD2 convertase preparation of a contaminant responsible for its degradation, and its absence in the rNRD1 convertase preparation, was ruled out by mixing the partially purified enzymes in various ratios. Indeed, the 140-kDa rNRD1 convertase remained stable in the presence of various quantities of rNRD2 convertase preparation. We thus hypothesize that rNRD2 convertase offers a specific fragile site. Concerning the rat testis enzyme, the formation of an inactive 110-kDa degradation product mainly occurred during the last hydroxyapatite purification process [13].

N-terminal sequencing of the 140-kDa species revealed that rat testis NRD convertase and recombinant rNRD1 convertase start at Val^{77} and Gly^{81}, respectively (Figure 3; sequence accession no. L27124) Due to the instability of the 145-kDa rNRD2 convertase, its N-terminus could not be elucidated. Sequence analysis of the 110-kDa forms of rNRD2 and testicular rNRD convertases showed that they start at Gly^{275} (i.e. within the 68-aa insertion; accession no. X93208) and at Asp^{188} (i.e within the last third of the acidic stretch), respectively (Figure 3). The identification of a rNRD2-specific residue (Gly^{275}) as the N-terminus of the 110-kDa rNRD2 species reinforces the above hypothesis of a fragile site specific to rNRD2 convertase Whether the corresponding cleavage, which occurs during the purification process, may have relevance *in vivo* or not remains to be determined.

Subcellular localization of recombinant rNRD1 and rNRD2 convertases

IF microscopy

To determine the intracellular localization of the rNRD convertase isoforms, an IF microscopy study was conducted in transiently transfected COS-7 cells. Similar staining patterns, consisting of a dense non-uniform perinuclear staining that extends up to the cell periphery, were observed in rNRD1 or rNRD2 convertase-expressing cells (Figures 4A and 4B). To check if this pattern indicates an endoplasmic reticulum (ER)-like localization, cells were also stained with an antiserum directed against calreticulin (Figure 4C), a soluble protein localized mainly

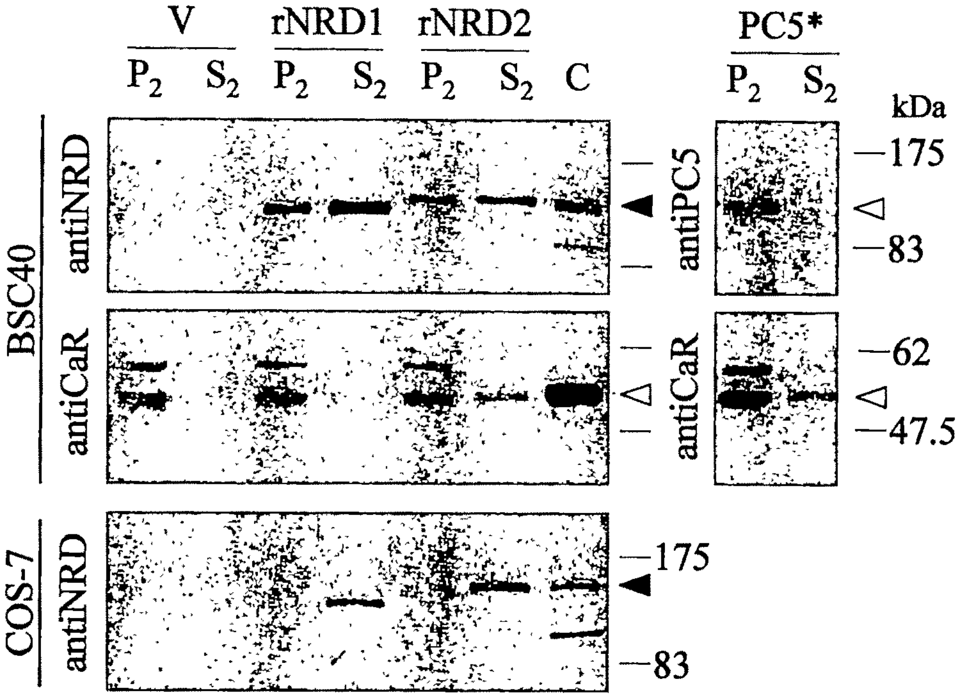

Figure 6 Distribution of overexpressed rNRD1 and rNRD2 convertases isoforms in subcellular fractions

Membrane (P2) and soluble (S2) fractions (15 μg) from BSC40 cells infected with the wild-type VV (V), VV rNRD1, VV rNRD2, VV PC5* (see text) or 20 μg of fractions P2 and S2 of transfected COS-7 cells with pcDNA vector (V), pcDNA3-rNRD1 and pcDNA3-rNRD2 were analysed by Western blotting using anti-rNRD convertase or anti-PC5 polyclonal sera BSC40 cell extracts were also probed with anti-calreticulin (antiCaR) antibodies. Lanes C consist of a mixture of 0 67 μg of purified testicular rNRD convertase and 0 1 μg of human recombinant calreticulin Black arrowheads show NRD convertase species in either BSC40 or COS-7 subcellular fractions (left-hand upper and lower panels), whereas white arrowheads indicate either to PC5-specific species (upper right panel) or calreticulin-specific species (middle left and lower right panels)

in ER [35]. Although rNRD convertase also presents a punctuate labelling, its staining is more diffused when compared with that of calreticulin. The two negative controls consisting of either rNRD1 convertase-transfected cells incubated with preimmune serum (Figure 4D) or COS-7 cells transfected with pcDNA3 (Figure 4E) did not show any labelling.

IEM

At the ultrastructural level (Figure 5), cells expressing either rNRD convertase isoform were characterized by the same dense labelling throughout the cytoplasm, whereas non-transfected cells were totally devoid of staining (Figure 5B). These data support the primary location of the enzyme as being within the cytoplasm.

Subcellular fractionation

Infected BSC40 cells and transfected COS-7 cells were homogenized in an isotonic buffer (0.25 M sucrose), and the resulting extract submitted to consecutive low- and high-speed centrifugations. Aliquots of the resulting high-speed pellets (P2) and supernatants (S2) were analysed by Western blotting (Figure 6). The fraction P2 was expected to contain primarily intact organelles and membrane-associated proteins. In both cell types, rNRD1 and rNRD2 convertases were found predominantly in the soluble S2 fractions. The ratio of either isoform in the soluble fraction to that in the membrane (S2/P2) was about 2 in BSC40 cells and 4 in COS-7 cells. As a control, the 54-kDa calreticulin was detected mainly in the P2 fractions of BSC40 cells. The calreticulin immunoreactive 58-kDa species, only observed in P2 fractions, were not identified. In order to eliminate the possibility that overexpression causes missorting of proteins, BSC40 cells were also infected by VV·mPC5*, encoding a catalytically inactive mutant of the proprotein convertase PC5 [29], which is retained as a zymogen in the lumen of the ER since it is unable to autocatalytically cleave its pro-segment (N. G. Seidah, unpublished work). As expected, mPC5* immunoreactivity was detected exclusively in the P2 fraction (Figure 6). Thus when compared with the absence of mPC5* or the limited amount of calreticulin in S2 fractions, the above data suggest that rNRD1 and rNRD2 convertases were present predominantly in soluble fractions, even though a significant portion was also present in membrane fractions.

Translation *in vitro* of rNRD1 convertase mRNA

The presence of NRD convertase prompted us to check the ability of its putative signal peptide to direct it to the ER lumen. Transcription *in vitro* of the 5′ region of rNRD1 (up to nt 1174 [18]) or NEP (up to nt 1004 [29]) cDNAs was performed and the resulting RNAs were used in an *in vitro* translation assay. In the absence of canine microsomes, the protein products showed apparent molecular masses of 42 and 36 kDa, respectively, in agreement with the sizes expected from each construct (Figure 7, lane 1). In the presence of canine microsomes, an increase in the size of the NEP product was observed (Figure 7, lane 4). This is in accordance with the presence of an N-terminal hydrophobic

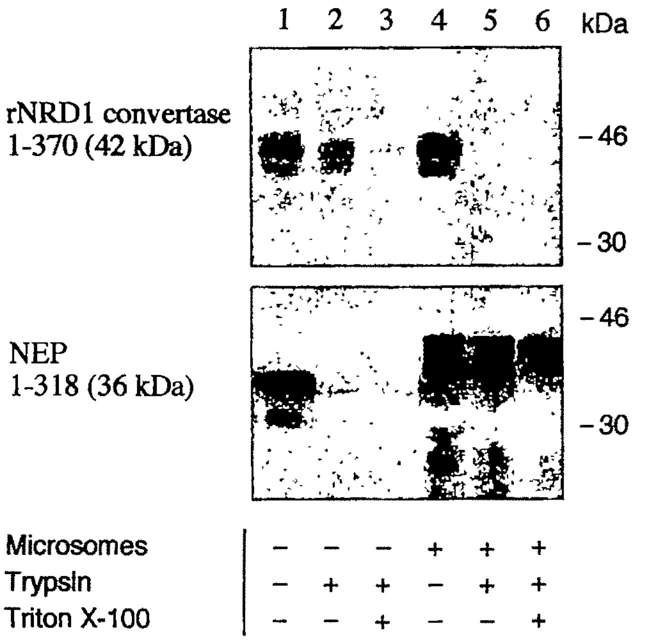

Figure 7 Translation and translocation assay *in vitro* of an N-terminal rNRD1 convertase polypeptide

In vitro-synthesized RNAs encoding N-terminal regions of rNRD1 convertase or NEP were translated *in vitro* using a rabbit reticulocyte lysate system in the absence (lanes 1–3) or presence (lanes 4–6) of dog pancreas microsomes. Aliquots of the translated products were assayed for sensitivity to trypsin digestion (lanes 2, 3, 5 and 6) in the absence (lanes 2 and 5) or presence (lanes 3 and 6) of Triton X-100.

signal peptide/membrane-anchor motif allowing an ER luminal location and N-glycosylation of NEP translation products. Under the same conditions, no apparent molecular-mass change was observed for the rNRD1 convertase products, in spite of the presence of two putative N-glycosylation sites (compare lanes 1 and 4 in Figure 7). In addition, whereas NEP translation products were sensitive to trypsin digestion only in the presence of Triton X-100, which lyses microsomes, rNRD1 convertase translation products were digested with trypsin even in the absence of Triton X-100 (Figure 7, lanes 2, 3, 5 and 6). With the caveat that this assay was conducted with a truncated form of rNRD1 convertase to facilitate the detection of potential changes in molecular mass, these results suggested that the N-terminus of NRD convertase did not function as a signal peptide and reinforce the proposal of a primary cytoplasmic location for the enzyme.

Biotinylation of the cell-surface proteins

The inability *in vitro* of NRD convertase to enter into microsomes was surprising, since it was reported to be secreted by spermatids [23] and EL-4 cells [24]. However, as mentioned above, it could not be detected in culture media of COS-7 or BSC40 cells, even when rNRD1 or rNRD2 convertases were overexpressed. Since the subcellular P2 fraction may also contain plasma membranes, the possible presence of the enzyme at the cell surface was assessed. Intact COS-7 or BSC40 cells overexpressing either rNRD1 or rNRD2 convertases, or control proteins, were biotinylated and then lysed. Immunoprecipitated proteins were analysed subsequently by Western blotting and revealed by either streptavidin (Figure 8, upper panel) or specific antibodies (Figure 8, lower panel). In either expression system, biotinylated rNRD1 and rNRD2 convertases were detected. On the other hand, the two control cytoplasmic proteins overexpressed by either infection of BSC40 cells (β-Gal, ≈ 110 kDa) or transfection of COS-7 cells (enhanced GFP, ≈ 28 kDa) did not show any streptavidin labelling, but were immunoprecipitated effectively (Figure 8, lower panel). Thus these results indicate clearly that both NRD convertase isoforms are present at the cell surface and that this localization cannot be attributed to their overexpression. No labelling of the cell surface in the immunohistochemical study (Figures 4 and 5) could be observed but this may be due to the fixation conditions and/or to a low cell-surface/cytoplasm ratio of the enzyme. However, it is worth noting that the pH

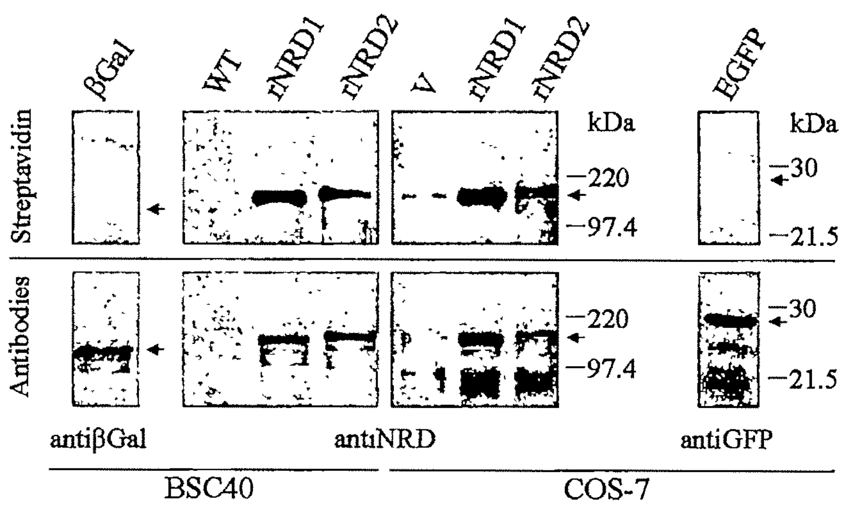

Figure 8 Biotinylation of cell-surface proteins

BSC40 and COS-7 cells overexpressing either rNRD1 or rNRD2 convertases, β-Gal or enhanced GFP (EGFP) were biotinylated. Immunoprecipitated proteins (see the Experimental section) were revealed by either streptavidin or specific antibodies. WT and V indicate that the cell extracts were obtained by wild-type VV infection or pcDNA3 transfection, respectively. Arrows indicate the expected positions of the different proteins analysed.

optimum of the enzyme is in favour of its activity being in the extracellular compartment.

DISCUSSION

Since the discovery of NRD convertase 10 years ago, its cellular localization has been unambiguously defined only in the testis, its major expression site, where it is associated with two microtubular structures of late spermatids [23]. Until now, the physiological function of NRD convertase has remained unresolved. In addition, it was recently shown that human and rat NRD convertases exist as two isoforms, NRD1 and NRD2 convertases [21]. They differ by the presence in NRD2 convertase of a 68-aa insertion close to the active site, which possibly confers a specific function to this isoform. In this report, we aimed at comparing the biochemical and enzymic properties as well as the subcellular distribution of overexpressed rNRD1 and rNRD2 convertases.

Purification of each recombinant enzyme following VV infections of BSC40 cells allowed the comparison of their properties *in vitro*. The data did not reveal any significant differences in their optimal pH towards a somatostatin-related undecapeptide substrate (Figure 2). Furthermore, their enzymic activities towards dynorphin A or the above peptide exhibited comparable sensitivities to inhibitors (Table 1). Parallel analyses showed that both recombinant enzymes behaved mostly like native NRD convertase purified from rat testis. Accordingly, this study did not allow us to establish significant variation between the enzymic properties of the two isoforms. The major difference observed resided in the instability of rNRD2 convertase, which was converted readily into a 110-kDa species (Figure 3). The corresponding cleavage occurs upstream of Gly^{275}, which lies within the 68-aa insertion. The physiological relevance *in vivo* of this observation is uncertain since the 110-kDa species could not be detected in fresh cellular extracts.

N-terminal sequencing of the purified testis enzyme and recombinant rNRD1 convertase revealed that the first ≈ 80 residues predicted from the cDNA sequence were missing. Indeed, the unique N-terminus identified for the testis NRD convertase suggested a cleavage at GlyArg$\downarrow$Val^{77}, whereas that of the recombinant rNRD1 convertase isolated from BSC40 cells revealed processing at ArgLeu$\downarrow$Gly^{81} (Figure 3). Alignment of the sequences surrounding these N-termini did not reveal any striking similarity and the candidate enzyme(s) involved remains to be identified. Such N-terminal variability may reflect a protease-sensitive region processed in a cell-specific manner *in vivo* or during the purification procedure. Future studies will address the question of the role of the N-terminal sequence and its effect on the activity of NRD convertase.

Whereas NRD convertase has been localized in the cytoplasm of spermatids [23], several elements prompted us to check for the possible localization of the enzyme, or one of its isoforms, in the secretory pathway: (i) detection of the enzyme in conditioned [23] or culture media [24]; and (ii) a cleavage selectivity reminiscent of that of the secretory proprotein convertases [36].

The present study shows that both NRD convertase isoforms localize primarily within the cytoplasm of BSC40 and COS-7 cells, although a significant fraction of these proteins is present at the cell surface. This was based on a compendium of results obtained by immunocytochemical analyses at both the light (Figure 4) and electron (Figure 5) microscopy levels, subcellular fractionations (Figure 6), translation *in vitro* (Figure 7) and biotinylation of cell-surface proteins (Figure 8). Altogether, these data are consistent with those obtained in the testis, which show that NRD convertase is present in the cytoplasm of spermatids and exported out of these cells [23].

It is thus revealing that an enzyme, which was isolated originally based on its ability to specifically cleave model peptides at the N-terminus of arginines in dibasic sequences [12,13], turns out to be primarily a cytosolic proteinase. Processed dibasic and monobasic sequences are normally found in secretory proteins including pro-hormones and proproteins [36,37]. A survey of the literature revealed that although several cytosolic proteinases have been studied extensively, such as those involved in the calcium-dependent (calpains) and ubiquitin/proteasome-dependent pathways [38,39] and the pro-apoptotic caspases [40], none of them presented a selectivity for pairs of basic residues Moreover, to our knowledge, no cytosolic precursors were reported to be processed specifically at dibasic sites, although, for most of them, the processing mechanism(s) as well as the precise cleavage sites remain to be elucidated. This is the case, for example, of the polyglutamine-containing proteins involved in neurodegenerative disorders such as huntingtin in Huntington's disease [41], and atrophin-1 in dentatorubropallidoluysian atrophy (DRPLA [42]). It remains to be seen if NRD convertase is involved in the metabolism of these and whether it may represent a new target for therapeutic intervention in some degenerative pathologies.

The presence of NRD convertase at the cell surface opens new perspectives concerning its biological function. NRD convertase's nearest neighbour, insulin-degrading enzyme, is the only M16 family member that has been reported to be possibly present at the cell surface, where it would degrade insulin [43]. Several members of other families of metallopeptidases have been involved in either post-secretory peptide inactivation, such as neprilysin [44] or meprin [45], or activation such as the more selective endothelin-converting enzyme [46] An example of a dibasic processing event occurring at the cell surface is the cleavage at Arg–Arg^{18} of glucagon-generating miniglucagon(19-29) [47]. However, if NRD convertase was implicated in such a cleavage, the presence of a surface aminopeptidase B-like activity [48] would be required to trim out the N-terminal arginine(s).

No transmembrane domain or canonical site for membrane anchorage was predicted from the primary structure, except the presence of an N-myristoylation site starting at Gly^{81} [49]. Since Gly^{81} constitutes the N-terminus of rNRD1 convertase overexpressed in BSC40 cells, this isoform, and possibly rNRD2 convertase, may thus be myristoylated in this cell type. It was reported recently that this type of acylation localized signalling-model proteins to specific intracellular membranes [50]. We may thus consider that, independently of its presence at the cell surface, NRD convertase may be myristoylated in the cytoplasm and then attached to intracellular membranes. This would be in agreement with the non-uniform perinuclear staining (Figure 4) and the rather high levels of NRD convertase (Figure 6) in BSC40 membrane fractions (about 30 %). Note, however, that the testis enzyme shows a different N-terminus (Val^{77}) incompatible with its myristoylation, suggesting that myristoylation of NRD convertase, if it occurs, may be cell-type dependent.

The export/secretion mechanism of NRD convertase is still obscure, and further studies are needed in order to elucidate this process. In that context, several proteins lacking conventional signal peptides and unambiguously localized outside the cell were described, without a clear-cut mechanistic explanation, e.g. interleukin-1α or β [51], basic fibroblast growth factor [52] or metalloendopeptidase EC 3.4.24.15 [53]

In conclusion, the present studies revealed for the first time that a dibasic-specific protease can be found both in the cytosol and at the cell surface. The identification of the cognate substrates of NRD convertase will surely open new avenues in our understanding of the limited proteolysis of precursors within these cellular compartments. In addition, it is also conceivable that NRD convertase may have another function, independent from its enzymic activity, as reported for the M16 family member Axl1 [9].

We thank Claude Tougard for her advice and microscope facilities We are very grateful to Marsha Rosner for her logistical support of V C., Guy Boileau for welcoming A P in his laboratory for the *in vitro* translation experiments and Luis Rokeach for the generous gifts of calreticulin and corresponding antibodies. This work was supported in part by CNRS and the University Pierre et Marie Curie (to UMR 7631) and by a Medical Research Council (Canada) program grant no PG-11474 V.H and V.C were recipients of the Association pour la Recherche sur le Cancer V H. was also supported by the Office Franco-Québécois pour la Jeunesse and A B was a CNRS post-doctoral fellow.

REFERENCES

1 Hooper, N M (1994) Families of zinc metalloproteases FEBS Lett **354**, 1–6

2 Barrett, A J., Rawlings, N D and Woessner, J. F (1998) Handbook of Protolytic Enzymes, Academic Press, London

3 Affholter, J A, Fried, V A and Roth, R A. (1988) Human insulin-degrading enzyme shares structural and functional homologies with *E coli* protease III. Science **242**, 1415–1418

4 Baumeister, H., Muller, D., Rehbein, M and Richter, D (1993) The rat insulin-degrading enzyme Molecular cloning and characterization of tissue-specific transcripts FEBS Lett. **317**, 250–254

5 Hawlitschek, G, Schneider, H, Schmidt, B, Tropschug, M., Hartl, F. U and Neupert, W (1988) Mitochondrial protein import. Identification of processing peptidase and of PEP, a processing enhancing protein Cell **53**, 795–806

6 Braun, H P and Schmitz, U K (1997) The mitochondrial processing peptidase Int J Biochem Cell Biol. **29**, 1043–1045

7 VanderVere, P. S, Bennett, T M, Oblong, J E and Lamppa, G K (1995) A chloroplast processing enzyme involved in precursor maturation shares a zinc-binding motif with a recently recognized family of metalloendopeptidase. Proc Natl Acad. Sci U S A **92**, 7177–7181

8 Richter, S and Lamppa, G K (1998) A chloroplast processing enzyme functions as a general stromal processing peptidase Proc Natl Acad Sci U.S A **95**, 7463–7468

9 Fujita, A, Oka, C, Arikawa, Y, Katagai, T, Tonouchi, A, Kuhara, S and Misumi, Y (1994) A yeast gene necessary for bud-site selection encodes a protein similar to insulin-degrading enzyme Nature (London) **372**, 567–570

10 Adames, N, Blundell, K, Ashby, M N. and Boone, C (1995) Role of yeast insulin-degrading enzyme homologs in propheromone processing and bud site selection Science **270**, 464–467

11 Gluschankof, P, Gomez, S, Morel, A and Cohen, P (1987) Enzymes that process somatostatin precursors A novel endoprotease that cleaves before the arginine-lysine doublet is involved in somatostatin-28 convertase activity of rat brain cortex J Biol Chem **262**, 9615–9620

12 Gomez, S, Gluschankof, P., Lepage, A and Cohen, P. (1988) Relationship between endo- and exopeptidases in a processing enzyme system activation of an endoprotease by the aminopeptidase B-like activity in somatostatin-28 convertase Proc Natl Acad Sci U S A **85**, 5468–5472

13 Chesneau, V, Pierotti, A R, Barré, N, Créminon, C, Tougard, C and Cohen, P (1994) Isolation and characterization of a dibasic selective metalloendopeptidase from rat testes that cleaves at the amino terminus of arginine residues J Biol Chem **269**, 2056–2061

14 Chesneau, V, Pierotti, A R., Prat, A, Gaudoux, F, Foulon, T and Cohen, P (1994) N-arginine dibasic convertase (NRD convertase): a newcomer to the family of processing endopeptidases An overview Biochimie **76**, 234–240

15 Cohen, P, Pierotti, A. R, Chesneau, V, Foulon, T. and Prat, A. (1995) N-arginine dibasic convertase Methods Enzymol **248**, 703–716

16 Tager, H S and Steiner, D F (1974) Peptide hormones Annu. Rev Biochem **43**, 509–538

17 Chrétien, M, Sikstrom, R, Lazure, C, Mbikay, M, Benjannet, S, Marcinkiewicz, M and Seidah, N G. (1989) Expression of the diversity of neural and hormonal peptides via the cleavage of precursor molecules, in Peptide Hormones as Prohormones (Martinez, J, ed), pp. 1–24, Ellis Horwood, Chichester

18 Pierotti, A R., Prat, A, Chesneau, V., Gaudoux, F., Leseney, A M, Foulon, T and Cohen, P (1994) N-arginine dibasic convertase, a metalloendopeptidase as a prototype of a class of processing enzymes Proc. Natl Acad Sci. U S A **91**, 6078–6082

19 Becker, A B. and Roth, R. A (1992) An unusual active site identified in a family of zinc metalloendopeptidases Proc. Natl Acad Sci. U S A. **89**, 3835–3839

20 Gehm, B D, Kuo, W L., Perlman, R K and Rosner, M. R (1993) Mutations in a zinc-binding domain of human insulin-degrading enzyme eliminate catalytic activity but not insulin binding J Biol Chem **268**, 7943–7948

21 Hospital, V, Prat, A, Joulie, C, Cherif, D, Day, R and Cohen, P (1997) Human and rat testis express two mRNA species encoding variants of NRD convertase, a metalloendopeptidase of the insulinase family. Biochem J **327**, 773–779

22 Fumagalli, P, Accarino, M, Egeo, A, Scartezzini, P, Rappazzo, G, Pizzuti, A, Avvantaggiato, V, Simeone, A., Arrigo, G, Zuffardi, O., Ottolenghi, S and Taramelli, R (1998) Human NRD convertase a highly conserved metalloendopeptidase expressed at specific sites during development and in adult tissues Genomics **47**, 238–245

23 Chesneau, V, Prat, A, Segretain, D, Hospital, V., Dupaix, A, Foulon, T, Jegou, B and Cohen, P. (1996) NRD convertase a putative processing endopeptidase associated with the axoneme and the manchette in late spermatids J Cell Sci. **109**, 2737–2745

24 Csuhai, E, Safavi, A and Hersh, L B (1995) Purification and characterization of a secreted arginine-specific dibasic cleaving enzyme from EL-4 cells. Biochemistry **34**, 12411–12419

25 Nielsen, H, Engelbrecht, J., Brunak, S and von Heijne, G (1997) Identification of prokaryotic and eukaryotic signal peptides and prediction of their cleavage sites Protein Eng **10**, 1–6

26 Kozak, M (1991) Structural features in eukaryotic mRNAs that modulate the initiation of translation J Biol Chem. **266**, 19867–19870

27 Davison, A J and Moss, B. (1990) New vaccinia virus recombination plasmids incorporating a synthetic late promotor for high level expression of foreign proteins Nucleic Acids Res **18**, 4285–4286

28 Devault, A, Lazure, C, Nault, C, Le Moual, H., Seidah, N G., Chretien, M., Kahn, P., Powell, J., Mallet, J, Beaumont, A et al (1987) Amino acid sequence of rabbit kidney neutral endopeptidase 24 11 (enkephalinase) deduced from a complementary DNA EMBO J **6**, 1317–1322

29 Campan, M, Yoshizumi, M., Seidah, N G, Lee, M E, Bianchi, C and Haber, E (1996) Increased proteolytic processing of protein tyrosin phophatase mu in confluent vascular endothelial cells: the role of PC5, a member of the subtilisin family. Biochemistry **35**, 3797–3802

30 De Bie, I, Marcinkiewicz, M., Malide, D., Lazure, C., Nakayama, K, Bendayan, M and Seidah, N G (1996) The isoforms of proprotein convertase PC5 are sorted to different subcellular compartments J Cell Biol **135**, 1261–1275

31 MacLean, I W and Nakane, P. K (1974) Periodate-lysine-paraformaldehyde fixation A new fixation for electron microscopy J Histochem Cytochem **22**, 1077–1083

32 Brinkley, B R, Murphy, P. and Richardson, L C (1967) Procedure for embedding *in situ* selected cells cultured *in vitro* J Cell Biol **35**, 279–283

33 Picart, R. and Tixier-Vidal, A (1974) Description d'une méthode permettant la sélection et l'étude ultrastructurale de plages cellulaires dans les monocouches hétérogènes cultivées en flacons de plastique J. Microsc. **20**, 80a

34 Schaffner, W and Weissmann, C (1973) A rapid, sensitive, and specific method for the determination of the protein in dilute solution Anal Biochem. **56**, 502–514

35 Fliegel, L, Burns, K., Opas, M and Michalak, M. (1989) The high-affinity calcium binding protein of sarcoplasmic reticulum Tissue distribution and homology with calregulin Biochim Biophys Acta **982**, 1–8

36 Seidah, N G and Chrétien, M (1999) Proprotein and prohormone convertases a family of subtilases generating diverse bioactive polypeptides Brain Res **848**, 45–62

37 Steiner, D F (1998) The proprotein convertases Curr Opin Chem Biol. **2**, 31–39

38 Johnson, G V and Guttmann, R P (1997) Calpains intact and active? Bioessays **19**, 1011–1018

39 Mykles, D L (1998) Intracellular proteinases of invertebrates calcium-dependent and proteasome/ubiquitin-dependent systems Int. Rev Cytol **184**, 157–289

40 Kidd, V. J (1998) Proteolytic activities that mediate apoptosis Annu Rev Physiol **60**, 533–573

41 Huntington's Disease Collaborative Research Group (1993) A novel gene containing a trinucleotide repeat that is unstable on Huntington's disease chromosomes Cell **72**, 971–983

42 Koide, R, Ikeuchi, T, Onodera, O, Tanaka, H, Igarashi, S, Endo, K, Takahashi, H, Kondo, R, Ishikawa, A, Hayashi, T et al (1994) Unstable expansion of CAG repeat in hereditary dentatorubral-pallidoluysian atrophy (DRPLA) Nat Genet **6**, 9–13

43 Seta, K A and Roth, R. A. (1997) Overexpression of insulin degrading enzyme cellular localization and effects on insulin signalling. Biochem Biophys. Res Commun **231**, 167–171

44 Erdos, E G and Skidgel, R A. (1989) Neutral endopeptidase 24 11 (enkephalinase) and related regulators of peptides hormones FASEB J **3**, 145–151

45 Bond, J S and Beynon, R J (1995) The astacin family of metalloendopeptidases Protein Sci **4**, 1247–1261

46 Barnes, K and Turner, A J (1997) The endothelin system and endothelin-converting

enzyme in the brain molecular and cellular studies Neurochem. Res **22**, 1033–1040

47 Mallat, A., Pavoine, C, Dufour, M., Lotersztajn, S, Bataille, D. and Pecker, F. (1987) A glucagon fragment is responsible for the inhibition of the liver Ca^{2+} pump by glucagon Nature (London) **325**, 620–622

48 Balogh, A, Cadel, S, Foulon, T, Picart, R, Der Garabedian, A, Rousselet, A, Tougard, C and Cohen, P (1998) Aminopeptidase B: a processing enzyme secreted and associated with the plasma membrane of rat pheochromocytoma (PC12) cells. J. Cell Sci **111**, 161–169

49 Towler, D. A, Gordon, J I, Adams, S P and Glaser, L (1988) The biology and enzymology of eukaryotic protein acylation Annu Rev Biochem **57**, 69–99

50 McCabe, J B. and Berthiaume, L G (1999) Functional roles for fatty acylated amino-terminal domains in subcellular localization -Mol. Biol. Cell **10**, 3771–3786

51 Rubartelli, A., Cozzolino, F., Talio, M. and Sitia, R. (1990) A novel secretory pathway for interleukin-1β, a protein lacking a signal sequence EMBO J **9**, 1503–1510

52 Kandel, J., Bossy-Wetzel, E., Radvanyi, F., Klagsbrun, M, Folkman, J. and Hanahan, D (1991) Neovascularization is associated with a switch to the export of bFGF in a multistep development of fibrosarcoma Cell **66**, 1095–1104

53 Crack, P. J, Wu, T J, Cummins, P M, Ferro, E S, Tullai, J W, Glucksman, M J. and Roberts, J L (1999) The association of metalloendopeptidase EC 3 4 24.15 at the extracellular surface of the AtT20 cell plasme membrane. Brain Res **835**, 113–124

Received 20 January 2000/24 March 2000; accepted 5 May 2000

Biochem. J. (2000) **349**, 599–604 (Printed in Great Britain)

Recovery of active medium-chain-length-poly-3-hydroxyalkanoate polymerase from inactive inclusion bodies using ion-exchange resin

Qun REN[1], Guy DE ROO, Birgit KESSLER and Bernard WITHOLT[2]
Institute of Biotechnology, ETH Hönggerberg, CH-8093 Zürich, Switzerland

A novel process for the purification of active medium-chain-length-polyhydroxyalkanoate (mcl-PHA) polymerase was developed. This process is based on solubilization and activation of inactive polymerase inclusion bodies by incubation with ion-exchange resin. The mcl-PHA polymerase 1 from *Pseudomonas oleovorans* was overproduced from the P*alk* promoter. Most of the polymerase produced was sequestered in the cytoplasm as an inactive form in insoluble aggregates. By incubating the protein aggregates with S-Sepharose ion-exchange resin in the presence of dithiothreitol and glycerol, the mcl-PHA polymerase could be extracted in an active and soluble form with a final yield of about 5.2 mg/g of cell dry weight. The solubilized polymerase was able to catalyse the *in vitro* synthesis of mcl-PHA without any additional cell components, suggesting its potential application for production of biopolymer. The procedure used here may be of general value in solubilizing and activating purified inactive labile enzymes.

Key words: *in vitro* synthesis of polymer, protein inclusion bodies, *Pseudomonas*, recovery of enzyme activity.

INTRODUCTION

Poly-3-hydroxyalkanoates (PHAs), which are produced as intracellular storage material by many bacterial species, have attracted considerable attention on account of their potential applications as biodegradable plastics and as sources of valuable chiral synthons (for reviews, see [1,2]). The best known variants, for which the genetics and enzymology have been studied in detail, and which have been produced industrially, are the homopolymer poly-3-hydroxybutyric acid (PHB) and the copolymer PHB/V, which contains 3-hydroxyvaleric acid in addition to 3-hydroxybutyric acid (see review [2]). Since both of these monomers are short-chain hydroxyalkanoic acids, PHB and PHB/V are referred to as short-chain-length (scl) PHAs (note that 'short chain length' is a characteristic of the monomer; the polymer may well be a very long molecule, as is generally the case for PHB). Most other PHAs are referred to as medium-chain-length (mcl) PHAs, because the monomers are generally consisting of six or more carbon atoms [3].

There are several enzymes involved in the synthesis of PHAs. Among these enzymes, the PHA polymerases (these are also called PHA synthases) are the key enzymes, which incorporate 3-hydroxyacyl moieties into nascent PHA chains, using CoA-activated precursors (see review [2]). Since the polymerase encoding gene was first identified in *Ralstonia eutropha* [4], many PHA polymerases or the corresponding genes have been studied thus far (see review [2]). There has been some work on the enzymology of PHA polymerases. However, to date, only PHB polymerase has been purified and studied *in vitro* in detail [5,6]. Several groups have attempted to isolate mcl-PHA polymerases, but so far no success has been reported. Although mcl-PHA polymerases have proved difficult to isolate, it would be useful to have such enzymes available, both to study structural and functional characteristics, and also to use polymerases in the synthesis of specific homo- and hetero-polymers *in vitro*. Thus there is a clear incentive to prepare active purified mcl-PHA polymerases.

Since very little PHA polymerase appears as free soluble protein in the wild-type *Pseudomonas* strains [7], we chose to overproduce this protein. In the present paper we describe the recovery of PHA polymerase activity from inclusion bodies which have been formed upon overexpression of the corresponding gene. The purified active polymerase allowed us to synthesize homopolymeric mcl-PHAs *in vitro*.

EXPERIMENTAL

Bacterial strains and plasmids

Pseudomonas putida GPp104 (PHA$^-$) [8] was used in the present study. pAlkVSVG1 [pGEM-5Zf(+), P*alk*, VSV G tag, Ap^r] [9] and pVLT35 (P*tac*/*lacI*^{q}, Mob$^+$, RSF1010 *ori*, Sm^r/Sp^r) [10] were used to construct pET701 and pET702. pAlkVSVG1 contains the P*alk* promoter, which originates from the *P. oleovorans* alkane-degradation system and is known to allow efficient gene expression in *Pseudomonas* strains [9], and a sequence coding for 12 C-terminal amino acids of the vesicular-stomatitis-virus glycoprotein (VSV G), to which monoclonal antibodies are available. Plasmid pGEc74 (pLAFR1, *alkST*, Tc^r) contains the regulatory gene for expression of the P*alk* promoter [11].

Recombinant DNA techniques

Isolation and analysis of plasmid DNA were carried out as described by Sambrook et al. [12]. Two oligonucleotide primers with the following sequences: AGCGTCGTACATGTCTAAC-

---

Abbreviations: DTT, dithiothreitol, DCPK, dicyclopropyl ketone, VSV G, vesicular-stomatitis-virus glycoprotein, PHB, poly-3-hydroxybutyric acid, PHB/V, co-polymer containing 3-hydroxyvaleric acid in addition to 3-hydroxybutyric acid, PHA, poly-3-hydroxyalkanoate, mcl- and scl-PHA, medium- and short-chain-length PHA, LB, Luria–Bertani; GC, gas chromatography, cdw, cell dry weight

[1] Present address: Institute of Microbiology, ETH Zentrum, CH-8092 Zurich, Switzerland

[2] To whom correspondence should be addressed (e-mail bw@biotech.biol.ethz.ch)

AAGAAC and ACGCTCGTGAACGTAGGTGCC were designed and synthesized (Microsynth G.m.b.H., Balgach, Switzerland) to perform site-directed mutagenesis (exchanged nucleotides are underlined) and to amplify the *phaC1*-containing fragment.

pET701 was constructed as follows. For integration of appropriate restriction sites, a site-directed mutagenesis was performed which resulted in a change of three base-pairs in *phaC1*, but the amino acid sequence of the PHA polymerase was not changed. Instead of introducing a *Nco*I site at the start codon of *phaC1*, an *Afl*III site (which produces cohesive ends compatible with the *Nco*I site) was generated because this led to fewer base-pair changes and because the *phaC1* gene does not contain an internal *Afl*III site, while it does contain several *Nco*I sites. The 1.7 kb PCR fragment was digested with *Afl*III, isolated and ligated into *Nco*I/*Eco*RV-digested pAlkVSVG1, resulting in the 5 kb plasmid pET701.

pAlkVSVG1 is derived from the ColE1-derived pGEM-5Zf(+) (Promega) and cannot replicate in *Pseudomonas*. pET702 was constructed from pVLT35, which contains a RSF1010 replicon and replicates both in *Escherichia coli* and in *Pseudomonas*. In order to remove the *tac* promoter, pVLT35 was digested with *Apa*I and *Pst*I, producing an 8.3 kb fragment. Since there are several *Pst*I sites inside *phaC1*, pET701 was digested with *Apa*I and *Nsi*I, generating cohesive ends compatible with *Pst*I. The 2-kb P*alk-phaC1-tag* containing fragment was then ligated to the *Apa*I/*Pst*I sites of pVLT35, resulting in the 10.3 kb plasmid pET702

Media, growth conditions and cell disruption

Luria–Bertani (LB) medium was used as rich medium [12]. For testing the expression system for PHA polymerase production, *Pseudomonas* recombinants were grown on E2 minimal medium [13]. As carbon source, 15 mM sodium octanoate was added. All recombinants were precultured in LB medium at 30 °C with appropriate antibiotics (tetracycline, 12.5 μg/ml; streptomycin, 100 μg/ml), then transferred into minimal medium in a 1:100 dilution.

To induce the P*alk* promoter, pGEc74 was always co-transformed with P*alk* expression plasmids, and dicyclopropyl ketone (DCPK) was added to 0.03 % (v/v) in the early exponential phase. Cell growth was monitored by measuring D_{450} [14].

Pseudomonas cells were harvested and washed once with Tris/HCl (50 mM, pH 8). The pellets were resuspended in the same buffer to a D_{450} of 40–50. Cells were disrupted by three passages through a French pressure cell at 75.8 MPa (11000 lbf/in^2) and 4 °C.

Protein analysis

Proteins were separated by gel electrophoresis as decribed by Laemmli [15]. The amount of PHA polymerase relative to total protein was determined by densitometric scanning (Molecular Dynamics). Total protein was assayed with a Lowry-based method (Bio-Rad detergent compatible assay) in the presence of SDS with BSA as the standard. Immunoblotting of polymerase was carried out as previously described [9].

N-terminal sequencing

Approx. 10 μg of protein was applied on a protein gel, followed by transfer on to a PVDF membrane (Immobilon-PSQ; Millipore Corp., Bedford, MA, U.S.A.) [12]. N-terminal sequencing of the appropriate band was carried out by the service laboratory in Molekularbiologie, ETH Hönggerberg, Switzerland.

Determination of PHA

To determine the polyester content and composition, samples were treated with chloroform and H_2SO_4/methanol (85:15, v/v) [16] and analyzed using a CP-Sil 5 CB column (Chrompack) on a gas chromatograph (Fisons) [16]. Gas-chromatography–MS (GC–MS) analyses were performed on a Fisons MD800 mass spectrometer, using electron impact at 70 eV [17].

Synthesis and purification of polymerase substrate 3-hydroxyoctanoyl-CoA

CoA was coupled to 3-hydroxyoctanoic acid (Sigma) by using acyl-CoA synthetase (Sigma) as described previously [18]. The product, 3-hydroxyoctanoyl-CoA, was purified over an ODS-2 reverse phase column by HPLC [18], dried using a SpeedVac apparatus, and then dissolved in 50 mM Tris/HCl, pH 8.

Isolation of PHA polymerase inclusion bodies

Inclusion bodies were isolated as described previously [19] with the following modifications: to separate PHA granules which contain active PHA polymerase from the polymerase inclusion bodies, the cell lysates were layered on to a 20 % (w/v) sucrose solution and ultracentrifuged at 110000 *g* for 2.5 h [20]. After this centrifugation, PHA granules remained on the top of the sucrose solution and the polymerase inclusion bodies were precipitated into the pellet fraction. The pellet fraction was then resuspended in washing buffer (0.5 % Triton X-100/1 mM EDTA) and centrifuged at 10000 *g* for 10 min to separate membrane proteins from inclusion bodies [19]. The pelleted inclusion bodies were washed at least three times with 50 mM Tris, pH 8.0, and finally resuspended in the same buffer to 1 mg/ml.

Solubilization of PHA polymerase

Solubilization or extraction of polymerase from the inclusion bodies was achieved by mixing 0.5 ml of buffer A [50 mM Tris/HCl (pH 7.5)/50 mM NaCl/1 mM EDTA/1 mM dithiothreitol (DTT)/1 mM PMSF/10 % (v/v) glycerol], containing about 20 μg of polymerase inclusion bodies, with an equal bed volume of Q- or S-Sepharose Fast Flow, equilibrated in buffer A, and shaking the suspensions gently at 4 °C for 2–3 h. As controls, either inclusion bodies, Q-Sepharose or S-Sepharose were/was omitted from the mixture. The suspensions were then centrifuged at 10000 *g* for 10 min to remove the resins. The pelleted resins were further resuspended in buffer A and 0.5 M NaCl, and were shaken at 4 °C for 2 h to elute adsorbed polymerase. The suspensions were centrifuged again at 10000 *g* for 10 min. The supernatants obtained after the two centrifugations were collected and used for polymerase studies.

In vitro polymerase activity assay

The polymerase activity was followed by monitoring the depletion of substrate 3-hydroxyoctanoyl-CoA by HPLC as described previously [20]. One unit is defined as 1 μmol of substrate depletion/min.

In vitro synthesis of polymeric mcl-PHA

The *in vitro* formation of mcl-PHA was followed by detecting the chloroform-extractable product. A typical reaction mixture contained the following components, in a final volume of 450 μl: 0.5 mM 3-hydroxyoctanoyl-CoA, 50 mM Tris, pH 8, and the soluble polymerase (0.5–1 μg). Assay mixtures were incubated at 30 °C, samples (60 μl) were taken at different time points, and the reactions were stopped by the addition of 140 μl of 1 % trichloroacetic acid. The solution was then extracted with 500 μl of chloroform, which contained 0.01 mg/ml methyl benzoate. A 400 μl sample of the chloroform phase was transferred to a Pyrex tube, mixed with 600 μl of chloroform (containing 0.01 mg/ml methyl benzoate) and 1 ml of H_2SO_4/methanol (85:15, v/v). The mixture was then analysed for the presence and composition of PHA as described previously [16].

RESULTS AND DISCUSSION

Overproduction of PHA polymerase

Previously we have found that, in the wild-type *P. oleovorans* or *P. putida* strains, PHA polymerase mainly appears as the PHA-granule-attached form [7,18] We have tried to isolate PHA polymerase from PHA granules with various extraction procedures. However, extraction of the PHA polymerase from PHA granules invariably resulted in activity loss of polymerase (G. de Roo and B. Witholt, unpublished work). We do not yet understand why PHA polymerase is inactivated by its removal from granules. It is possible that the polymerase is active only when bound to a hydrophobic surface, normally provided by the granule, perhaps there is a requirement for an initiator of polymerization, or perhaps the protein denatures on extraction from PHA granules. None of these explanations is particularly convincing, since PHB polymerase has been purified and is functional in aqueous buffers [5,21]. We therefore decided to overproduce the PHA polymerase and then recover the enzyme activity by refolding.

In our first attempts to reach high-level production of PHA polymerase, the corresponding encoding gene *phaC1* was cloned under the control of P*lac* and P*tac* promoters. Expression of these constructs, however, resulted in less than 0.1 % PHA polymerase of total cell protein in recombinant strains (results not shown). We therefore constructed the plasmid pET702 in which *phaC1* expression is under the control of the P*alk* promoter [9], and *phaC1* is tagged with a sequence coding for 12 C-terminal amino acids of VSV G [9], to which monoclonal antibodies are available. The construct was tested in the PHA polymerase-negative *P. putida* mutant GPp104. In the recombinant harbouring pET702 in combination with pGEc74 containing the *alkS* regulatory gene for P*alk* expression, induction led to the appearance of an extra band at about 62 kDa (Figure 1A, lane 3 versus lane 2). Western blotting using anti-(VSV G) antibodies showed that the PHA polymerase was absent in uninduced cells (lane 9) and clearly present in induced cells (lane 10), indicating that *phaC1* expression is tightly regulated by the P*alk* promoter. We typically obtained PHA polymerase levels of about 15–25 % of the total protein in *Pseudomonas*.

The VSV G-tagged polymerase was also tested for its ability to restore PHA accumulation in *P. putida* GPp104. Although the host is not capable of accumulating PHA [8], GPp104 carrying pET702 and pGEc74 produced about 30 % (w/w) PHA per cell dry weight (cdw). Without induction, only trace amounts of PHA (0.5 % PHA/cdw) were detected, demonstrating that the tagged PHA polymerase synthesized from pET702 is functional in *Pseudomonas*.

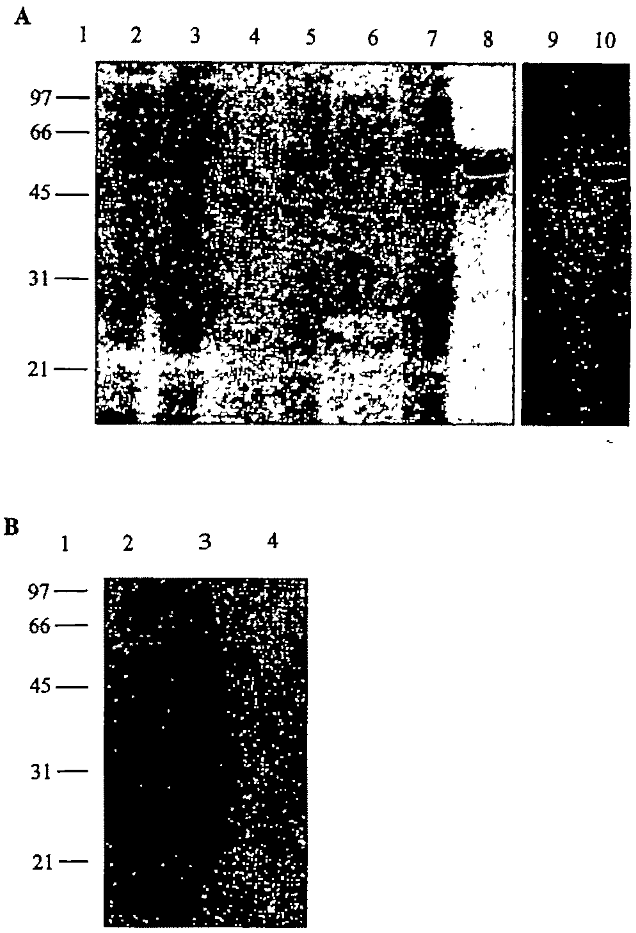

Figure 1 Expression, purification and solubilization of *phaC1*-VSV G

The *Pseudomonas* recombinant was grown in minimal medium E2 with octanoate as carbon sources at 30 °C DCPK (0.03%) was added in the early exponential phase, and incubation continued for 8 h Culture samples were analysed by SDS/12% -PAGE (**A**) Overproduction of PHA polymerase Lanes 1, protein size markers (kDa), 2, uninduced sample, 3, induced sample, 4 and 5, soluble and insoluble fractions after the cell lysate was centrifuged at 3000 ***g*** for 10 min, 6 and 7, soluble supernatant and insoluble pellet fractions of the whole cell lysate after centrifugation in 20% (w/v) sucrose at 110000 ***g*** for 2.5 h, 8, purified PHA polymerase inclusion bodies, 9 and 10, Western blotting of samples from lanes 2 and 3 respectively (**B**) Solubilization of polymerase from inclusion bodies Each sample corresponds to 4 μg of inclusion bodies Lanes. 1, protein size markers (kDa), 2, solubilized polymerase after inclusion bodies were incubated with S-Sepharose, 3, soluble fraction after S-Sepharose was incubated in buffer A, 4, solubilized polymerase after inclusion bodies were incubated in buffer without S-Sepharose

Purification of PHA polymerase inclusion bodies

When cells containing PHA polymerase were lysed, most of the polymerase precipitated into the pellet fraction after low-speed centrifugation (Figure 1A, lane 5 versus lane 4), suggesting that the enzyme might be present in inclusion bodies or insoluble aggregates. These inclusion bodies were separated from the PHA granule-attached polymerase and the majority of other proteins in the cell lysate by centrifugation through 20 % (w/v) sucrose at 110 000 ***g*** for 2.5 h. After this centrifugation, the polymerase accounted for more than 50 % of total pellet protein (Figure 1A, lane 7; Table 1). N-terminal sequencing confirmed the identity of the polymerase band. We further purified the pellet fraction by washing it with Triton X-100 to remove contaminating proteins. On the basis of SDS/PAGE, the final preparation contained more than 98 % pure polymerase (Figure 1A, lane 8; Table 1). The final yield of the purified PHA polymerase inclusion bodies was estimated to be 55.8 mg/g of cdw (Table 1). However, in these inclusion bodies no PHA polymerase activity was detected (Table 1).

Table 1 Purification of PHA polymerase from *P. putida* GPp104[pET702, pGEc74]*

Purification step	Total protein (mg)	PHA polymerase (% of total protein)‡	Polymerase activity (units)§	Specific activity (units/mg)§
Pellet fraction†	13.00	50	–	–
Inclusion bodies†	5.58	98	–	–
Solubilized polymerase†	0.52	100	2.29	4.40

* PHA polymerase was purified from 100 mg of cells (dry weight), the data presented in this Table are the averages from two independent experiments

† The pellet fraction was obtained by centrifugation of cell lysate in 20% (w/v) sucrose at 110000 *g* for 2.5 h; the inclusion bodies were obtained by washing the pellet fraction with Triton X-100 to remove contaminating proteins, soluble polymerase was obtained by incubating polymerase inclusion bodies with S-Sepharose as described in the Experimental section

‡ Polymerase levels were estimated by densitometric scanning of SDS/PAGE gels

§ The polymerase activity was determined with 3-hydroxyoctanoyl-CoA by substrate depletion as described previously [20]

Solubilization and activity recovery of PHA polymerase with ion exchange resin

To recover polymerase activity from the inclusion bodies, we first tried conventional methods in which inclusion bodies were dissolved in 8 M urea, followed by rapid dilution in several renaturation buffers [22]. However, no polymerase activity was obtained (results not shown). Previously it was reported that some protein inclusion bodies could be solubilized and activated by interacting with ion-exchange resins [23], and we therefore tested this approach with S- and Q-Sepharose Fast Flow. We were unsuccessful with Q-Sepharose, but we found that S-Sepharose partially solubilized the polymerase (Figure 1B, lane 2). About 10% polymerase was recovered from the inclusion bodies, leading to a final yield of the soluble enzyme of 5.2 mg/g cdw (Table 1). The solubilized polymerase exhibited a maximum specific activity of 4.40 units/mg with 3-hydroxyoctanoyl-CoA in the presence of 1 mg/ml BSA (Table 1). In all of our experiments, recovery of activity occurred only by exposure of polymerase inclusion bodies to S-Sepharose in buffer, but not by exposure to the buffer alone.

Factors affecting solubilization of polymerase and its activity

We have tested different conditions which might influence the recovery of polymerase from inclusion bodies. We noted that omission of DTT in buffer A led to essentially complete loss of the polymerase activity, omission of glycerol gave an approx. 6-fold reduced enzyme activity, omission of PMSF resulted in degradation of polymerase Furthermore it was found that the activity of polymerase solubilized from the inclusion bodies was time-dependent. Activity started to decrease after 3 h incubation in buffer A, and, after 8 h, no polymerase activity could be detected.

Different storage conditions were also investigated for retention of activity. We found that the soluble polymerase lost its activity completely by storage at −20 °C for 24 h in buffer A, even in the presence of DTT and glycerol, indicating that the soluble polymerase is rather unstable, as has also been found for solubilized PHB polymerase [5,21]. The reason for this is not clear at present. It is possible that there are component(s) which are necessary for stabilizing the polymerase and are abundant in the cells but are missing in purified soluble polymerase. Further optimization for recovery efficiency and improvement for polymerase stability by using different detergents are under investigation.

Various additives were tested on the basis of what we have recently reported for PHA-granule-attached polymerase [20] (Table 2) We found that the soluble polymerase was completely inactivated by the addition of 0.5% v/v) Triton X-100. A positive effect on polymerase activity was observed after the addition of BSA (1 mg/ml) or phospholipids (1 mg/ml), leading to about 1.5-fold higher activity compared with the control (Table 2). This is similar to what was reported for PHA-granule-attached polymerase [20]. Addition of NaCl (0.5 M) or EDTA (5 mM) did not lead to significant effects on polymerase activity.

In vitro synthesis of homopolymeric mcl-PHA by the soluble polymerase

3-Hydroxyoctanoyl-CoA was incubated with the solubilized polymerase for various time periods. The reactions were stopped by the addition of 1% trichloroacetic acid. The polymeric

Table 2 Effect of various additives on PHA polymerase activity*

Additive	Concentration	PHA polymerase activity (units/mg of polymerase)	Percentage of activity
None†	–	2.47	100
Triton X-100	0.5%, v/v	⩽ 0.01	0
BSA	1 mg/ml	4.40	180
phospholipids	1 mg/ml	3.71	150
NaCl	0.5 M	2.45	100
EDTA	5 mM	2.44	100

* The activity of soluble PHA polymerase in buffer A was taken as 100; the effect of additives on polymerase activity is shown relative to this activity

† A typical reaction mixture (100 μl) contained 0.4–0.6 mM 3-hydroxyoctanoyl-CoA, 50 mM Tris/HCl, pH 8, and 0.5–1 μg of soluble polymerase

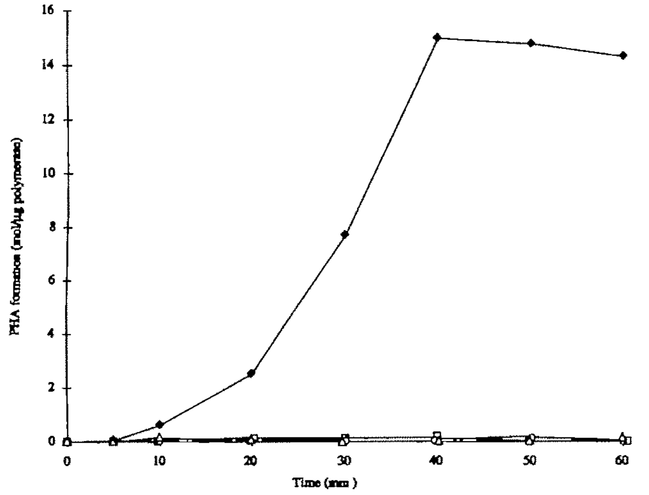

Figure 2 ***In vitro* formation of chloroform-extractable mcl-PHA by purified polymerase**

Purified soluble polymerase (1 µg) was exposed to substrate 3-hydroxyoctanoyl-CoA Samples were taken at different time points The formation of chloroform-extractable product was analysed by GC and GC–MS as described in the Experimental section ◆, soluble fraction recovered from inclusion bodies after incubation with S-Sepharose; △, □ and ○, Controls (□, control 1, no polymerase was added in the assay mixture, △, control 2, no substrate was added in the assay mixture, ○, control 3, soluble fraction recovered from inclusion bodies after incubation with buffer alone without S-Sepharose)

product was extracted into chloroform, and analysed by GC and GC–MS as described in the Experimental section. This procedure allowed us to detect only monomers derived from the chloroform-extractable PHA. It does not detect unchanged substrate (3-hydroxyoctanoyl-CoA) or 3-hydroxyoctanoic acid which might be formed in the assay mixture, since this substrate and the free acid remained in the water phase under our assay conditions. This was evidenced by using radioactively labelled monomers (results not shown).

No chloroform-extractable material was detected when substrate or polymerase was omitted from the reaction mixture (Figure 2). Chloroform-extractable material was also absent when inclusion bodies were used (Figure 2). PHA formation was only observed when substrate and the PHA polymerase solubilized from inclusion bodies were added to the assay mixture. From these data we can conclude that the formation of the chloroform-extractable material did not require other components except the polymerase and its substrate. The formation of PHA followed a sigmoidal curve, suggesting that there was an initial activation step before PHA synthesis could be observed. Ultimately, incubation of 1 µg of soluble polymerase led to the incorporation of 15 nmol of 3-hydroxyoctanoic acid into chloroform-extractable PHA (Figure 2). 3-Hydroxyoctanoate accounted for 99.9 % of this PHA and the PHA could therefore be regarded as a homopolymer. However, the exact physical state of the polymer produced (such as molecular mass, granule size, substrate specificity etc.) remains to be experimentally determined.

The finding that synthesis of polymer can occur in the presence of substrate and polymerase without any other additives is in accord with the previous findings of Gerngross and co-workers, who showed that PHB can be synthesized *in vitro* without additional factors except substrate and enzyme [6]. The kinetics of mcl-PHA production are also reminiscent of the kinetics seen with PHB polymerase, namely an initial low rate which accelerates as the synthesis proceeds. Further work has to be done to understand the nature of this activation during polymer synthesis. A likely possibility is that the nascent polymer chain improves the catalytic characteristics of the polymerase, perhaps by binding to the sites through which the enzyme binds to native PHA granules.

In the present study we have established an efficient process to obtain soluble, active mcl-PHA polymerase which had previously proved difficult to isolate in an active form. Ion-exchange resin was applied to recover the activity of inactive PHA polymerase produced as inclusion bodies. We anticipate that the procedure applied here may be of potential use in solubilizing and activating other inactive enzymes.

We thank Professor L Thony-Meyer for reading the manuscript before its submission, Dr M Nieboer for providing plasmid pAlkVSVG1, Professor H. Ploegh for providing monoclonal antibodies against the VSV G tag, and Dr G. Frank for doing the N-terminal sequencing.

REFERENCES

1 Hrabak, O. (1992) Industrial production of poly-β-hydroxybutyrate FEMS Microbiol Rev **103**, 251–256
2 Madison, L L and Huisman, G W (1999) Metabolic engineering of poly-(3-hydroxyalkanoates): from DNA to plastic. Microbiol Mol. Biol Rev **63**, 21–53
3 Steinbuchel, A and Valentin, H E (1995) Diversity of bacterial polyhydroxyalkanoic acids. FEMS Microbiol. Lett **128**, 219–228
4 Peoples, O P and Sinskey, A J (1989) Poly-β-hydroxybutyrate biosynthesis in *Alcaligenes eutrophus* H16: identification and characterization of the PHB polymerase gene (*phbC*). J. Biol Chem **264**, 15298–15303
5 Gerngross, T U, Snell, K D, Peoples, O. P., Sinskey, A. J., Csuhai, E, Masamune, S and Stubbe, J (1994) Overexpression and purification of the soluble polyhydroxyalkanoate synthase from *Alcaligenes eutrophus* evidence for a required posttranslational modification for catalytic activity. Biochemistry **33**, 9311–9320
6 Gerngross, T U. and Martin, D P. (1995) Enzyme-catalyzed synthesis of poly[(*R*)-(−)-3-hydroxybutyrate]· formation of macroscopic granules *in vitro* Proc Natl. Acad Sci. U.S.A **92**, 6279–6283
7 Kraak, M N, Smits, T H. M., Kessler, B and Witholt, B (1997) Polymerase C1 levels and poly-(*R*-3-hydroxyalkanoate) synthesis in wild-type and recombinant *Pseudomonas* strains J Bacteriol. **179**, 4985–4991
8 Huisman, G W, Wonink, E, Meima, R, Kazemier, B, Terpstra, P and Witholt, B (1991) Metabolism of poly-(3-hydroxyalkanoates) (PHAs) by *Pseudomonas oleovorans* J Biol. Chem. **266**, 2191–2198
9 Nieboer, M (1996) Overproduction of a foreign membrane monooxygenase in E. coli relation to membrane biogenesis. Ph D Thesis, University of Groningen
10 de Lorenzo, V., Eltis, L, Kessler, B and Timmis, K. N. (1993) Analysis of *Pseudomonas* gene products using *lacI*^{q}/P*trp-lac* plasmids and transposons that confer conditional phenotypes Gene **123**, 17–24
11 Eggink, G, Lageveen, R G, Altenburg, B and Witholt, B (1987) Controlled and functional expression of the *Pseudomonas oleovorans* alkane utilizing system in *Pseudomonas putida* and *Escherichia coli* J Biol Chem **262**, 17712–17718
12 Sambrook, J, Fritsch, E F and Maniatis, T (1989) Molecular Cloning· a Laboratory Manual, Cold Spring Harbor Laboratory Press, Cold Spring Harbor, NY
13 Huisman, G W, de Leeuw, O., Eggink, G and Witholt, B (1989) Synthesis of polyhydroxyalkanoates is a common feature of fluorescent pseudomonads. Appl Environ. Microbiol **55**, 1949–1954
14 Witholt, B (1972) Method for isolating mutants overproducing nicotinamide–adenine dinucleotide and its precursors J Bacteriol **109**, 350–364
15 Laemmli, U. K. (1970) Cleavage of structural proteins during the assembly of the head of bacteriophage T4. Nature (London) **227**, 680–685
16 Lageveen, R G, Huisman, G. W., Preusting, H, Ketelaar, P., Eggink, G and Witholt, B (1988) Formation of polyesters by *Pseudomonas oleovorans* effect of substrates on formation and composition of poly-(*R*)-3-hydroxyalkanoates and poly-(*R*)-3-hydroxyalkenoates. Appl Environ Microbiol. **54**, 2924–2932
17 Huijberts, G N M, de Rijk, T C, de Waard, P and Eggink, G (1995) ^{13}C nuclear magnetic resonance studies of *Pseudomonas putida* fatty acid metabolic routes involved in poly-(3-hydroxyalkanoate) synthesis J Bacteriol **176**, 1661–1666
18 Kraak, M N, Kessler, B and Witholt, B. (1997) *In vitro* activities of granule-bound poly[(*R*)-3-hydroxyalkanoate] polymerase C1 of *Pseudomonas oleovorans* development of an activity test for medium-chain-length-poly(3-hydroxyalkanoate) polymerases Eur. J Biochem **250**, 432–439
19 Nagai, K and Thogersen, H C (1990) Synthesis and sequence-specific proteolysis of hybrid proteins produced in *Escherichia coli* Methods Enzymol **153**, 461–481

20 de Roo, G., Ren, Q., Witholt, B. and Kessler, B (2000) Development of an improved *in vitro* activity assay for medium chain length PHA polymerase based on CoenzymeA release measurements J Microbiol Methods, in the press

21 Haywood, G. W., Anderson, A J and Dawes, E A (1989) The importance of PHB-synthase substrate specificity in polyhydroxyalkanoate synthesis by *Alcaligenes eutrophus* FEMS Microbiol Lett. **57**, 1–6

22 Harris, E L V and Angal, S. (1989) Protein Purification Methods a Practical Approach, Oxford University Press, Oxford

23 Hoess, A, Arthur, A K, Wanner, G. and Fanning, E. (1988) Recovery of soluble, biologically active recombinant proteins from total bacterial lysates using ion exchange resin Bio/Technology **6**, 1214–1217

Received 11 April 2000/22 May 2000, accepted 24 May 2000

Biochem J (2000) 349, 605–610 (Printed in Great Britain)

Phosphoinositide 3-kinase-dependent phosphorylation of the dual adaptor for phosphotyrosine and 3-phosphoinositides by the Src family of tyrosine kinase

Simon DOWLER*[1], Leire MONTALVO†, Doreen CANTRELL‡, Nick MORRICE* and Dario R. ALESSI*

*MRC Protein Phosphorylation Unit, Department of Biochemistry, MSI/WTB Complex, University of Dundee, Dow Street, Dundee DD1 5EH, Scotland, U.K., †Dpto Bioquímica y Biología Molecular, Facultad de Medicina, Campus Universitario, 28871 Alcalá de Henares, Madrid, Spain, and ‡Lymphocyte Activation Laboratory, Imperial Cancer Research Fund, Lincoln's Inn Fields, London WC2A 3PX, U.K.

We recently identified a novel adaptor protein, termed dual adaptor for phosphotyrosine and 3-phosphoinositides (DAPP1), that possesses a Src homology (SH2) domain and a pleckstrin homology (PH) domain. DAPP1 exhibits a high-affinity interaction with PtdIns(3,4,5)P_3 and PtdIns(3,4)P_2, which bind to the PH domain. In the present study we show that when DAPP1 is expressed in HEK-293 cells, the agonists insulin, insulin-like growth factor-1 and epidermal growth factor induce the phosphorylation of DAPP1 at Tyr^{139}. Treatment of cells with phosphoinositide 3-kinase (PI 3-kinase) inhibitors or expression of a dominant-negative PI 3-kinase prevent phosphorylation of DAPP1 at Tyr^{139}, and a PH-domain mutant of DAPP1, which does not interact with PtdIns(3,4,5)P_3 or PtdIns(3,4)P_2, is not phosphorylated at Tyr^{139} following agonist stimulation of cells. Overexpression of a constitutively active form of PI 3-kinase induced the phosphorylation of DAPP1 in unstimulated cells. We demonstrated that Tyr^{139} of DAPP1 is likely to be phosphorylated *in vivo* by a Src-family tyrosine kinase, since the specific Src-family inhibitor, PP2, but not an inactive variant of this drug, PP3, prevented the agonist-induced tyrosine phosphorylation of DAPP1. Src, Lyn and Lck tyrosine kinases phosphorylate DAPP1 at Tyr^{139} *in vitro* at similar rates in the presence or absence of PtdIns(3,4,5)P_3, and overexpression of these kinases in HEK-293 cells induces the phosphorylation of Tyr^{139}. These findings indicate that, following activation of PI 3-kinases, PtdIns(3,4,5)P_3 or PtdIns(3,4)P_2 bind to DAPP1, recruiting it to the plasma membrane where it becomes phosphorylated at Tyr^{139} by a Src-family tyrosine kinase.

Key words: PH domain, PP2 inhibitor, protein phosphorylation, SH2 domain, Src tyrosine kinases.

INTRODUCTION

Stimulation of cells with insulin and growth factors activates members of the phosphoinositide 3-kinase (PI 3-kinase) family, which phosphorylate PtdIns(4,5)P_2 at the D-3 position of the inositol ring to generate the lipid second messenger, PtdIns(3,4,5)P_3 [1] PtdIns(3,4,5)P_3 and its immediate breakdown product, PtdIns(3,4)P_2, also thought to be a second messenger, interact with proteins that possess a certain type of pleckstrin homology (PH) domain [2], leading to the recruitment of these molecules to the plasma membrane and the activation of signal transduction pathways that regulate cell growth, proliferation, survival, differentiation and cytoskeletal changes [3].

Proteins possessing PH domains that interact with PtdIns(3,4,5)P_3 include the serine/threonine protein kinases, protein kinase B (PKB) [4], 3-phosphoinositide-dependent protein kinase-1 (PDK1) [5], Bruton's tyrosine kinase (BTK) [6], the Rho/Rac GTP exchange factor Vav [7], the adaptor protein Gab1 [8] and the ADP-ribosylation factor GTP exchange factor GRP1 [9]. Interaction of PtdIns(3,4,5)P_3 with PKB, BTK, Gab1 and Vav induces their translocation to the cell membrane, which is necessary for their phosphorylation and activation by specific upstream protein-kinases. PKB is phosphorylated and activated by PDK1 [10], whereas BTK [6] and Vav [7] are phosphorylated and activated by members of the Src family of tyrosine kinases, and Gab1 is phosphorylated by receptor tyrosine kinases [8].

We [11] and subsequently others [12,13] have identified a widely expressed protein termed dual adaptor for phosphotyrosine and 3-phosphoinositides (DAPP1), which contains both a PH domain, that interacts specifically with PtdIns(3,4,5)P_3/PtdIns(3,4)P_2, as well as a phosphotyrosine-binding Src homology (SH2) domain. In the present paper, we demonstrate that the activation of PI 3-kinase in cells induces the phosphorylation of DAPP1 at Tyr^{139}, and provide evidence that a Src family of tyrosine kinase mediates the phosphorylation of DAPP1 at this site.

MATERIALS AND METHODS

Materials

Insulin was from Novo-Nordisk (Copenhagen, Denmark), insulin-like growth factor-1 (IGF1) and epidermal growth factor (EGF) were from Life Technologies, PP2 and PP3 were from Calbiochem, Protease inhibitor tablets were from Roche, and wortmannin, LY 294002 and anti-FLAG M2 antibody were from Sigma. Antibodies against phosphotyrosine (PY99), Lyn and Lck were from Santa Cruz; partially purified Src and Lyn and the anti-Src antibody were from Upstate Biotechnology, anti-CD2 antibody was from Plasminogen. Lck was expressed in Sf9 cells infected with baculovirus vectors by Dr Andrew

---

Abbreviations used: BTK, Bruton tyrosine kinase, DAPP1, dual adaptor for phosphotyrosine and 3-phosphoinositides, EGF, epidermal growth factor, GST, glutathione S-transferase, IGF1, insulin-like growth factor-1, PKB, protein kinase B, PDK1, 3-phosphoinositide-dependent protein kinase-1, PI 3-kinase, phosphoinositide 3-kinase, PH, pleckstrin homology; SH2, Src homology, Y139F, Tyr^{139} → Phe substitution

[1] To whom correspondence should be addressed (e-mail s.j.dowler@dundee.ac.uk)

Paterson (MRC Protein Phosphorylation Unit, University of Dundee, Dundee, Scotland, U.K).

General methods

Molecular-biology techniques were performed using standard protocols. Site-directed mutagenesis was carried out using the QuikChange kit (Stratagene), following instructions provided by the manufacturer. DNA constructs used for transfection were purified from *Escherichia coli* using the Qiagen plasmid Mega kit according to the manufacturer's protocol, and their sequences were verified using an automated DNA sequencer.

Plasmids

Constructs encoding wild-type and mutant DAPP1 with an N-terminal glutathione S-transferase (GST) tag followed by a FLAG epitope tag were subcloned into either pEBG2T, for expression in HEK-293 cells (as described previously [11]), or pGEX-4T-2, for expression in *E. coli*. The constructs expressing the wild-type and kinase-dead PI 3-kinase catalytic subunit fused to the transmembrane domain of rat CD2 (termed p110* and p110-KD), and the dominant-negative (Δp85α) PI 3-kinase, have been described previously [14]. Constructs expressing Lyn, Itk and Bmx (in the pSRα vector), JAK2 (in the pSVK3 vector), Btk (in the pRK5 vector) and FAK (in the pCMV5 vector) were gifts from Hiroyuki Mano (Jichi Medical School, Tochigi, Japan). The construct expressing Lck (in the pCDNA vector) was kindly provided by Dr Bart Sefton (The Salk Institute, La Jolla, CA, U.S.A.). The construct expressing c-Src (in the pUSEamp vector) was purchased from UBI.

Transfection, cell stimulation and immunoblotting

HEK-293 cells were cultured on 10-cm-diameter dishes in Dulbecco's modified Eagle's medium containing 10 % (v/v) fetal-bovine serum, and transfections were carried out using a modified calcium phosphate method [15]. In all experiments, 5 μg of DNA of the indicated construct was used per dish, except for experiments using the GST–DAPP1[W250L] mutant, in which 10 μg of DNA was used in order to obtain expression equal to that of the wild-type GST–DAPP1. At 24 h post-transfection the cells were serum-starved for 16 h and incubated in the presence or absence of inhibitors prior to stimulation, as described in the Figure legends. The cells were lysed in 1 ml of ice-cold lysis buffer [which consisted of 50 mM Tris/HCl (pH 7 5), 1 mM EGTA, 1 mM EDTA, 1 % (w/v) Triton X-100, 1 mM sodium orthovanadate, 50 mM sodium fluoride, 5 mM sodium pyrophosphate, 0.27 M sucrose, 1 μM microcystin-LR, 0.1 % (v/v) 2-mercaptoethanol and one tablet of protease inhibitor cocktail per 50 ml of buffer]. The lysates were cleared by centrifugation at 13000 *g* for 10 min at 2 °C, and aliquots of supernatant (50 μg of protein) were incubated for 1 h at 4 °C with 10 μl of GSH–Sepharose. The beads were washed twice in lysis buffer containing 0.5 M NaCl, followed by two further washes in Buffer B [50 mM Tris/HCl (pH 7.5)/ 0.1 mM EGTA/ 0.1 % (v/v) 2-mercaptoethanol]. The beads were resuspended in 1 vol. of sample buffer containing 100 mM Tris/HCl (pH 6.8), 4 % (w/v) SDS, 20 % (v/v) glycerol and 200 mM dithiothreitol, and the released proteins were subjected to SDS/PAGE. The gels were analysed by immunoblotting with the indicated antibodies. Briefly, membranes were blocked in 50 mM Tris/HCl (pH 7.5)/0.15 M NaCl/0.5 % (v/v) Tween 20 (TBST) containing either 3 mg/ml BSA (for anti-phosphotyrosine blots) or 10 % (w/v) skimmed milk (for all other blots). The nitrocellulose membranes were immunoblotted in the same buffer with anti-phosphotyrosine PY99 antibody (at a dilution of 1:2000), anti-FLAG monoclonal antibody (1:10000) and anti-Src, Lck, Lyn, CD2 antibody (1:1000). Detection was performed using horseradish-peroxidase-conjugated secondary antibodies and ECL* (Amersham).

Expression of GST–DAPP1 and GST–DAPP1[Y139F] (Tyr^{139} → Phe substitution) in *E. coli*

The pGEX-4T-2 constructs encoding wild-type DAPP1 and DAPP1[Y139F] were transformed into BL21 *E. coli* cells and a 0.5 l culture was grown at 37 °C in Luria broth containing 100 μg/ml ampicillin until the D_{600} was 0.6. Isopropyl-β-D-thiogalactoside (250 μM) was added and the cells were cultured for a further 16 h at 26 °C. The cells were lysed and the GST–DAPP1 fusion proteins purified by affinity chromatography on GSH–Sepharose beads, as described previously for ERK2 [16].

In vitro phosphorylation of DAPP1 by Src, Lyn and Lck

A solution (20 μl) containing bacterially expressed GST–DAPP1 or GST–DAPP1[Y139F] (1 μg), purified Src (1 unit), Lck (1 unit) and Lyn (1 unit), 5 mM manganese acetate, 5 mM magnesium acetate, 100 μM [γ-^{32}P]ATP, 50 mM Tris/HCl (pH 7.5) and 0.1 % (v/v) 2-mercaptoethanol was incubated for 30 min at 30 °C. The reactions were stopped by the addition of SDS and the samples were subjected to SDS/PAGE (7.5 % gel), and phosphorylation of DAPP1 was revealed by autoradiography. Src, Lyn and Lck were assayed using the peptide substrate KVEKIGEGTYGVVYK [17], and 1 unit of activity was determined as that which phosphorylates 1 nmol of peptide substrate in 1 min.

Mapping the residue phosphorylated in DAPP1 by Lck

A solution (50 μl) containing GST–DAPP1 (5 μg), 5 μg of Sf9 cell lysate expressing Lck (or Sf9 cell lysate not expressing Lck, as a control), 5 mM manganese acetate, 5 mM magnesium acetate, 100 μM [γ-^{32}P]ATP, 50 mM Tris/HCl (pH 7.7) and 0.1 % (v/v) 2-mercaptoethanol was incubated for 30 min at 30 °C. The reactions were stopped by the addition of SDS and 2-mercaptoethanol to final concentrations of 1 % (w/v) and 1 % (v/v) respectively, and heated for 5 min at 95 °C. After cooling to ambient temperature, 4-vinylpyridine was added to a concentration of 2.5 % (v/v), and the sample was kept on a shaking platform for 1 h at 30 °C to alkylate cysteine residues. The sample was then electrophoresed by SDS/PAGE (7.5 % gel), and the ^{32}P-labelled GST–DAPP1 was eluted from the gel and digested with trypsin and chromatographed on a reverse-phase C_{18} column as described previously for PKB [15]. DAPP1 was not significantly phosphorylated when incubated in the control Sf9 cell lysate not expressing Lck.

RESULTS

DAPP1 is phosphorylated at Tyr^{139} in HEK-293 cells

We sought to test whether DAPP1 was phosphorylated on tyrosine residues following stimulation of cells with extracellular agonists. Full-length human DAPP1 was expressed in human HEK-293 cells as a GST-fusion protein, the cells were serum-starved for 16 h, and then stimulated with either insulin, IGF1 or EGF. The cells were lysed, GST–DAPP1 was purified by affinity chromatography on GSH–Sepharose, and then GST–DAPP1

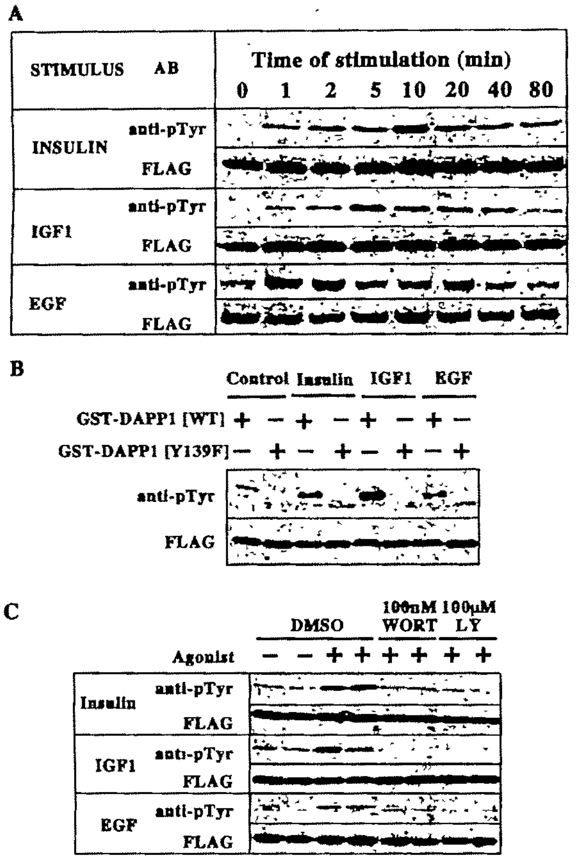

Figure 1 DAPP1 is phosphorylated at Tyr^{139} in stimulated cells

(**A**) HEK-293 cells were transiently transfected with DNA constructs expressing wild-type GST–DAPP1 At 24 h post-transfection the cells were serum-starved for 16 h and stimulated with insulin (100 nM), IGF1 (100 ng/ml) or EGF (100 ng/ml) for the indicated times The cells were lysed, and GST–DAPP1 was purified from aliquots of the supernatant by affinity chromatography on glutathione–Sepharose. The purified protein was separated by SDS/PAGE (7 5% gel) and immunoblotted using an anti-phosphotyrosine (anti-pTyr) or a FLAG antibody to detect GST–DAPP1 (GST–DAPP1 is also FLAG-epitope tagged [11]). (**B**) As in (**A**), except that the HEK-293 cells were transiently transfected with DNA constructs expressing wild-type (WT) GST–DAPP1 or the GST–DAPP1 [Y139F] mutant The cells were stimulated with insulin (10 min) and IGF1 (10 min) or EGF (5 min) (**C**) As in (**A**), except that the cells were incubated for 10 min prior to stimulation with 100 nM wortmannin (WORT) or 100 μM LY294002 (LY) or DMSO The cells were stimulated either for 10 min with insulin or IGF1 or for 5 min with EGF These results are representative of at least three independent experiments in (**A**) and (**C**) and two experiments in (**B**)

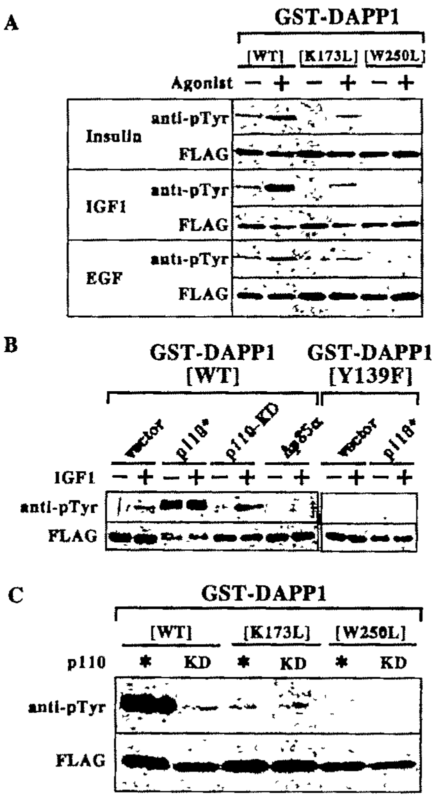

Figure 2 Phosphorylation of DAPP1 is dependent on the PH domain and requires PI 3-kinase

(**A**) HEK-293 cells were transiently transfected with DNA constructs expressing wild type (WT) GST–DAPP1 or mutants of GST–DAPP1 that do not interact with 3-phosphoinositides (GST–DAPP1[K173L] or GST–DAPP1[W250L]) At 24 h post-transfection the cells were serum-starved for 16 h prior to stimulation with 100 nM insulin (10 min), 100 ng/ml IGF1 (10 min) or 100 ng/ml EGF (5 min) The cells were lysed, and GST–DAPP1 was purified and immunoblotted using an anti-phosphotyrosine antibody (anti-pTyr) or a FLAG antibody to detect GST–DAPP1 (**B**) As in (**A**), except that HEK-293 cells were transiently co-transfected with DNA constructs expressing GST–DAPP1[WT] or GST–DAPP1[Y139F], together with constructs expressing membrane-targetted wild-type PI 3-kinase (p110*), membrane-targetted kinase dead PI 3-kinase (p110-KD), a dominant-negative PI 3-kinase (Δp85α) or empty pCMV5 vector (vector) At 24 h post-transfection the cells were serum-starved for 16 h and then left unstimulated (—) or stimulated with IGF1 for 10 min (+) The expression of PI 3-kinase constructs was verified by immunoblotting with anti-CD2 antibody p110* and p110-KD were expressed at similar levels, and Δp85α was expressed at a 5-fold higher level (results not shown) (**C**) As in (**A**), except that the cells were co-transfected with the indicated forms of PI 3-kinase The cells were lysed without stimulation. These results are representative of two separate experiments

was immunoblotted with an anti-phosphotyrosine antibody (Figure 1A). These agonists induced a rapid phosphorylation of DAPP1 within 1–2 min, which was sustained for 80 min after stimulation with insulin, but was more transient with IGF1 and EGF (Figure 1A).

Tyr^{139} of DAPP1 is located between the SH2 and PH domains of DAPP1 and is the only tyrosine residue in the DAPP1 protein not located in the SH2 or PH domains. To our knowledge no tyrosine residue in a SH2 or PH domain has previously been shown to be phosphorylated. We therefore speculated that Tyr^{139} was the site of phosphorylation on DAPP1. To investigate this we mutated Tyr^{139} → Phe (Y139F) and expressed this mutant in HEK-293 cells as a GST-fusion protein. Stimulation of cells with insulin, IGF1 or EGF failed to induce any detectable phosphorylation of the GST–DAPP1[Y139F] mutant (Figure 1B), indicating that Tyr^{139} was indeed the site of phosphorylation.

Phosphorylation of DAPP1 is downstream of PI 3-kinase

In order to establish whether the activation of PI 3-kinase was required for phosphorylation of DAPP1 at Tyr^{139}, we added the structurally unrelated PI 3-kinase inhibitors wortmannin (100 nM) or LY 294002 (100 μM) to the tissue-culture medium at concentrations that inhibit the insulin-induced activation of PKB in these cells [18] prior to stimulation of the cells. These inhibitors prevented tyrosine phosphorylation of DAPP1 induced by insulin, IGF1 or EGF (Figure 1C).

Two mutants of GST–DAPP1, which do not interact with 3-phosphoinositides {GST–DAPP1[K173L] (Lys^{173} → Leu) and GST–DAPP1[W250L] (Trp^{250} → Leu)} [11], were not significantly phosphorylated on tyrosine following stimulation of cells with insulin, IGF1 or EGF (Figure 2A). Overexpression of DAPP1

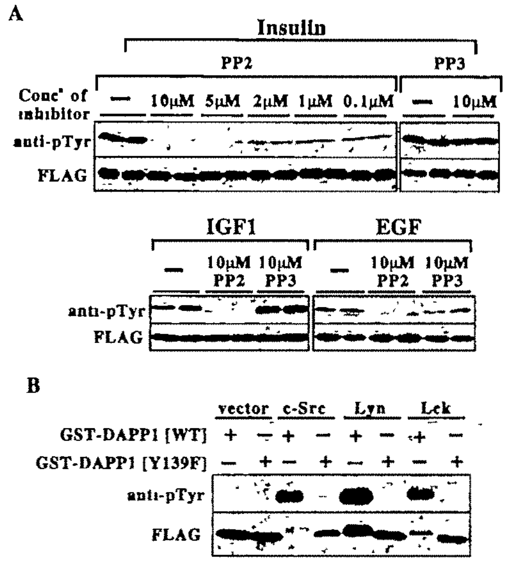

Figure 3 Phosphorylation of DAPP1 at Tyr^{139} by Src-family kinases *in vivo*

(**A**) HEK-293 cells were transiently transfected with DNA constructs expressing wild-type GST–DAPP1. At 24 h post-transfection, the cells were serum-starved for 16 h and incubated with DMSO (—) or the indicated concentrations of PP2 or PP3 for 20 min before stimulation with 100 nM insulin (10 min), 100 ng/ml IGF1 (10 min) or 100 ng/ml EGF (5 min). The cells were lysed and GST–DAPP1 was purified and immunoblotted using an anti-phosphotyrosine antibody (anti-pTyr) or a FLAG antibody to detect GST–DAPP1. (**B**) As in (**A**), except that HEK-293 cells were co-transfected with DNA constructs expressing wild-type (WT) GST–DAPP1 or GST–DAPP1[Y139F], together with constructs expressing Src, Lyn, Lck or empty pCMV5 vector (vector). At 24 h post-transfection, the cells were serum-starved for 16 h and lysed without stimulation. Expression of Src, Lyn and Lck was verified by immunoblotting of cell lysates with appropriate antibodies and these kinases were expressed at similar levels in cells expressing either GST–DAPP1 [WT] or GST–DAPP1 [Y139F] (results not shown). These results are representative of two separate experiments.

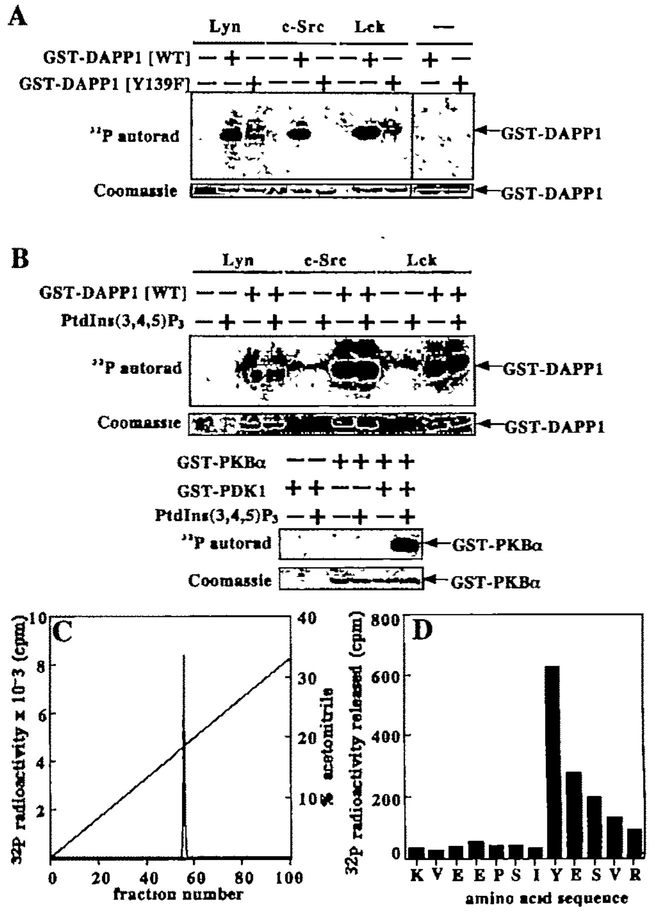

Figure 4 Phosphorylation of DAPP1 at Tyr^{139} by Src-family kinases *in vitro*

(**A**) The indicated Src-family tyrosine kinases were incubated with purified wild-type (WT) GST–DAPP1 or GST–DAPP1[Y139F] in the presence of [γ-^{32}P]ATP as described in the Materials and methods section. The proteins were separated by PAGE (7.5% gel), the gel was stained with Coomassie Blue and autoradiographed to detect phosphorylated DAPP1. (**B**) As in (**A**), except that the reactions were performed in the presence of lipid vesicles containing 100 μM phosphatidylcholine and 100 μM phosphatidylserine with (+) or without (—) 10 μM *sn*-1-stearoyl-2-arachidonoyl-D-PtdIns(3,4,5)P_3 (prepared as described in [28]). In a parallel reaction it was verified that GST–PDK1 only phosphorylated GST–PKBα in the presence of lipid vesicles containing PtdIns(3,4,5)P_3. (**C**) DAPP1, which had been phosphorylated with Lck using [γ-^{32}P]ATP to 0.8 mol of ^{32}P/mol of protein (see the Materials and methods section), was digested with trypsin and chromatographed on a Vydac 218TP54 C_{18} column (Separations Group, Hesperia, CA, U.S.A.), equilibrated with 0.1% (v/v) aqueous trifluoroacetic acid. The column was developed with a linear acetonitrile gradient (diagonal line) at a flow rate of 0.8 ml/min and fractions of 0.4 ml were collected. Of the radioactivity applied to the column 85% was recovered from the major ^{32}P-peptide eluting at 18.8% acetonitrile. (**D**) A portion of the major ^{32}P-peptide (5 pmol) was analysed on an Applied Biosystems 492A sequencer, and the phenylthiohydantoin amino acids identified after each cycle of Edman degradation are shown, using the single-letter code. A portion of this peptide (2000 c.p.m.) was also coupled covalently to a Sequelon arylamine membrane and analysed on an Applied Biosystems 470A sequencer, the ^{32}P radioactivity released was measured after each cycle of Edman degradation.

with a membrane-targetted, constitutively activated form of PI 3-kinase (termed p110* [14]) induced a high level of tyrosine phosphorylation of wild-type GST–DAPP1, but not of GST–DAPP1(Y139F), in unstimulated cells, which was not increased further by stimulation with IGF1 (Figure 2B). In contrast, a membrane-targetted, catalytically inactive mutant of PI 3-kinase (termed p110-KD) failed to induce tyrosine phosphorylation of DAPP1 and the overexpression of a dominant-negative mutant of PI 3-kinase (termed Δp85α) inhibited the IGF1-induced tyrosine phosphorylation of DAPP1 (Figure 2B). Moreover, overexpression of the constitutively activated form of PI 3-kinase did not induce tyrosine phosphorylation of the mutants of GST–DAPP1, which no longer interact with 3-phosphoinositides (GST–DAPP1[K173L] and GST–DAPP1[W250L]) (Figure 2C).

Phosphorylation of DAPP1 is prevented by inhibitors of the Src family of tyrosine kinases

Tyr^{139} of DAPP1 lies in a sequence motif Ile^{138}-Tyr-Glu^{140}, which is predicted to correspond to the optimal consensus motif for phosphorylation by Src-family tyrosine kinases [19]. We therefore tested the effect of PP2, a specific inhibitor for this class of tyrosine kinase, and PP3, a structurally related compound that does not inhibit Src-family tyrosine kinases [20,21]. PP2 inhibited the Src family kinase members tested with an IC_{50} of ≈ 5 nM *in vitro* and does not significantly inhibit any other class of tyrosine kinase tested [20,21] or 25 serine/threonine protein kinases tested (S. Davis, H. Reddy and P. Cohen, personal communication). PP2 potently inhibited the insulin-induced tyrosine phosphorylation of DAPP1 (Figure 3A), even at very low concentrations of this drug (0.1 μM). In contrast, PP3, even at a concentration of 10 μM, did not inhibit insulin-mediated tyrosine phosphorylation significantly (Figure 3A). PP2 also inhibited the tyrosine phosphorylation of DAPP1 induced by IGF1 and EGF (Figure 3A).

Expression of Src, Lck or Lyn in cells induces phosphorylation of DAPP1

HEK-293 cells were transfected with constructs expressing either the wild-type GST–DAPP1 or the GST–DAPP1[Y139F] mutant, together with constructs encoding the Src-family tyrosine kinases Src, Lyn or Lck. This resulted in the wild-type GST–DAPP1, but not the GST–DAPP1[Y139F] mutant, becoming tyrosine phosphorylated in unstimulated cells (Figure 3B). Phosphorylation was accompanied by a decrease in the electrophoretic mobility of DAPP1 and was not increased further by stimulating cells with insulin, IGF1 or EGF (results not shown). Expression of DAPP1 with other tyrosine kinases, including the focal adhesion kinase, Janus kinase-2 and the Tec tyrosine kinases (BTK, Itk and BMX), failed to induce phosphorylation of wild-type GST–DAPP1 (results not shown).

Src, Lyn and Lck phosphorylated wild-type GST–DAPP1 *in vitro*, but the GST–DAPP1[Y139F] mutant was either not phosphorylated or phosphorylated to a very low extent (Figure 4A). The phosphorylation of DAPP1 by Src, Lyn and Lck *in vitro* was not affected by the presence of lipid vesicles containing PtdIns(3,4,5)P_3. However, in parallel experiments, PDK1 only phosphorylated PKB in the presence of lipid vesicles containing PtdIns(3,4,5)P_3 (Figure 4B), as reported previously [22,23]. The site on DAPP1 phosphorylated by Lck was also mapped by phosphorylating DAPP1 with Lck to 0.8 mol of P_i/mol of protein, digesting the ^{32}P-labelled DAPP1 with trypsin and subjecting the resulting peptides to chromatography on a C_{18} column at pH 1.9. Only one major ^{32}P-labelled peptide, eluted at 18.8 % acetonitrile, was observed (Figure 4C). Its sequence commenced at residue 132 of DAPP1, and a single burst of radioactivity occurred after the eighth cycle of Edman degradation (Figure 4D). Its molecular mass (1515.66), determined by matrix-assisted laser-desorption ionization–time-of-flight ('MALDI-TOF') MS, was identical with that expected (1515.74) for the tryptic peptide comprising residues 132–143 and phosphorylated at a single position. These results demonstrate that DAPP1 is phosphorylated at Tyr^{139} *in vitro* by Lck.

DISCUSSION

In the present work we demonstrate that DAPP1 becomes phosphorylated at a single tyrosine residue (Tyr^{139}) following stimulation of HEK-293 cells with agonists such as insulin, IGF1 and EGF. The phosphorylation of DAPP1 on Tyr^{139} is likely to be downstream of PI 3-kinase as inhibitors of PI 3-kinase (Figure 1C) and expression of a dominant-negative PI 3-kinase mutant prevented agonist-induced DAPP1 tyrosine phosphorylation (Figure 2B). Furthermore, the expression of a constitutively active PI 3-kinase in cells induced phosphorylation of DAPP1 at Tyr^{139} in unstimulated cells (Figure 2B). DAPP1 mutants that are unable to interact with PtdIns(3,4,5)P_3/PtdIns(3,4)P_2 were not phosphorylated at Tyr^{139} in either stimulated cells (Figure 2A) or cells overexpressing active PI 3-kinase (Figure 2C), suggesting that DAPP1 needs to interact with PtdIns(3,4,5)P_3/PtdIns(3,4)P_2 in order for it to become phosphorylated at this site. Furthermore, the time course of DAPP1 phosphorylation (Figure 1A) closely parallelled the activation of PKB in these cells by insulin, IGF1 [18] and EGF (M. Shaw, personal communication). DAPP1 also possesses an SH2 domain at its N-terminus and, in order to investigate the role of this domain, we mutated a conserved Arg residue (Arg^{61} to a Glu) that, in principle, should prevent the SH2 domain of DAPP1 from binding to tyrosine-phosphorylated proteins. We observed that when the GST–DAPP1[R61E] mutant was expressed in unstimulated cells, it was phosphorylated on tyrosine at a low level. However insulin, IGF1, EGF or overexpression of constitutively active PI 3-kinase did not induce any further tyrosine phosphorylation of the GST–DAPP1[R61E] mutant (results not shown). This indicates that the SH2 domain of DAPP1 is likely to be playing a role in enabling DAPP1 to become phosphorylated at Tyr^{139} in response to agonists that induce PI 3-kinase activation Further work is required to identify the proteins with which the SH2 domain of DAPP1 interacts, and the role that they play in enabling DAPP1 to become phosphorylated at Tyr^{139}.

The Src family of protein kinases contain eight members, some which are broadly expressed (e g. Src) and others whose expression is restricted to certain tissues (such as Lck and Lyn, which are mainly expressed in haematopoietic cells) [24]. These kinases possess overlapping substrate specificities, are known to play key functions in regulating signal-transduction pathways and have also been shown to play a role in several human malignancies [25]. Src-family tyrosine kinases are activated by both receptor tyrosine kinases, as well as by receptors that are not protein kinases. Here we demonstrate that DAPP1 is likely to be a physiological substrate for the Src family of tyrosine kinase, as the Src-family inhibitor PP2 prevented agonist-induced tyrosine phosphorylation of DAPP1 in cells. HEK-293 cells express detectable levels of Src and Lyn (results not shown), which may be the kinases responsible for the phosphorylation of transfected GST–DAPP1 at Tyr^{139} observed in our experiments. Src, Lyn or Lck phosphorylated DAPP1 on Tyr^{139} *in vitro*.

Tyr^{139} is conserved in human, mouse and sea-squirt (*Halocynthia roretzi*) DAPP1 [National Center for Biotechnology Information (NCBI) accession number AV383515], which would be predicted if phosphorylation of this residue is of physiological importance. Furthermore, co-expression of DAPP1 with Src, Lyn or Lck induced a very high level of phosphorylation of DAPP1 at Tyr^{139}, even in unstimulated cells, which was not increased further by agonist stimulation of cells. As Src-family kinases activate the PI 3-kinase pathway in many cells [1], it is possible that the overexpression of Src, Lyn or Lck in HEK-293 cells induces the activation of PI 3-kinase, thereby promoting DAPP1 phosphorylation in unstimulated cells. As Src-family tyrosine kinases are located at the plasma membrane by virtue of myristoylation and palmitoylation of their N-termini [26], it is likely that the role of PtdIns(3,4,5)P_3 is to recruit DAPP1 to the cell membrane, where it can be phosphorylated with Src-family tyrosine kinases.

One of the general mechanisms by which PtdIns(3,4,5)P_3/PtdIns(3,4)P_2 functions in cells is to recruit PH-domain-containing proteins to the plasma membrane, enabling them to become phosphorylated and hence activated (see the Introduction). This also appears to be the case for DAPP1 which, like BTK, Vav and Gab1, becomes phosphorylated at tyrosine residues following its interaction with PtdIns(3,4,5)P_3/PtdIns(3,4)P_2 in cells. DAPP1, like BTK and Vav, is phosphorylated by Src-family kinases *in vitro* at a similar rate in the presence or absence of PtdIns(3,4,5)P_3 (Figure 4B), suggesting that the interaction of DAPP1 with 3-phosphoinositides does not induce a conformational change that converts it into a substrate for the Src family of tyrosine kinases. This is in contrast with PKB, which is converted into a substrate for PDK1 through its interaction with PtdIns(3,4,5)P_3 (Figure 4B) [27].

Consistent with the above model, Clark and colleagues [12] have recently demonstrated that transfected DAPP1 is recruited to the plasma membrane of cells through its PH domain following activation of PI 3-kinase. Those authors also showed that the endogenous DAPP1 in B cells is phosphorylated on a tyrosine residue(s) in response to activation of the B-cell receptor. They also present some evidence that DAPP1 may interact with phospholipase $C\gamma 2$ through its SH2 domain, and, when DAPP1 is overexpressed in cells, it negatively inhibits transcriptional responses, regulated by nuclear factor, of activated T cells [12]. It will be important to establish whether DAPP1 in B cells is also phosphorylated at Tyr^{139} by Src-family kinases following the activation of PI 3-kinase in response to activation of the B-cell receptor.

In summary, the results presented here indicate that DAPP1 is likely to be a direct cellular target for both PI 3-kinase and Src-family tyrosine kinases, and that the phosphorylation of DAPP1 at Tyr^{139} may play an important role in triggering signal-transduction pathways that lie downstream of both PI 3-kinase and the Src family of tyrosine kinases. Physiological processes regulated by phosphorylation of DAPP1 should therefore be inhibited by either PI 3-kinase or Src inhibitors.

We thank Andrew Paterson for the expression of Lck, and Hiroyuki Mano and Bart Sefton for providing plasmids expressing tyrosine kinases. S D is a recipient of a Medical Research Council (MRC) Studentship, and L M was supported by a travelling grant from the Spanish government This work was also supported by Diabetes UK (D R A.) and MRC (D R A)

REFERENCES

1 Vanhaesebroeck, B , Leevers, S J , Panayotou, G and Waterfield, M D. (1997) Phosphoinositide 3-kinases a conserved family of signal transducers. Trends Biochem Sci **22**, 267–272

2 Isakoff, S J , Cardozo, T , Andreev, J , Li, Z , Ferguson, K M , Abagyan, R , Lemmon, M A , Aronheim, A and Skolnik, E Y (1998) Identification and analysis of PH domain-containing targets of phosphatidylinositol 3-kinase using a novel *in vivo* assay in yeast. EMBO J **17**, 5374–5387

3 Rameh, L E and Cantley, L C (1999) The role of phosphoinositide 3-kinase lipid products in cell function J Biol Chem. **274**, 8347–8350

4 Coffer, P J , Jin, J and Woodgett, J. R. (1998) Protein kinase B (c-Akt) a multifunctional mediator of phosphatidylinositol 3-kinase activation Biochem J **335**, 1–13

5 Belham, C , Wu, S and Avruch, J (1999) Intracellular signalling PDK1a kinase at the hub of things Curr Biol **9**, R93–R96

6 Li, Z , Wahl, M I , Eguinoa, A , Stephens, L R , Hawkins, P T and Witte, O N (1997) Phosphatidylinositol 3-kinase-gamma activates Bruton's tyrosine kinase in concert with Src family kinases Proc. Natl Acad Sci U S A **94**, 13820–13825

7 Han, J , Luby-Phelps, K , Das, B , Shu, X , Xia, Y , Mosteller, R D , Krishna, U M , Falck, J. R., White, M A and Broek, D (1998) Role of substrates and products of PI 3-kinase in regulating activation of Rac-related guanosine triphosphatases by Vav Science **279**, 558–560

8 Rodrigues, G. A , Falasca, M , Zhang, Z , Ong, S H. and Schlessinger, J (2000) A novel positive feedback loop mediated by the docking protein Gab1 and phosphatidylinositol 3-kinase in epidermal growth factor receptor signaling. Mol Cell Biol. **20**, 1448–1459

9 Klarlund, J K , Rameh, L E , Cantley, L C , Buxton, J. M., Holik, J J , Sakelis, C , Patki, V , Corvera, S and Czech, M P (1998) Regulation of GRP1-catalyzed ADP ribosylation factor guanine nucleotide exchange by phosphatidylinositol 3,4,5-trisphosphate. J Biol. Chem **273**, 1859–1862

10 Vanhaesebroeck, B and Alessi, D R. (2000) The PI3K–PDK1 connection more than just a road to PKB Biochem J. **346**, 561–576

11 Dowler, S., Currie, R A , Downes, C P and Alessi, D R (1999) DAPP1 a dual adaptor for phosphotyrosine and 3-phosphoinositides Biochem J **342**, 7–12

12 Marshall, A. J , Niiro, H , Lerner, C G , Yun, T J , Thomas, S , Disteche, C M and Clark, E A (2000) A novel B lymphocyte-associated adaptor protein, Bam32, regulates antigen receptor signaling downstream of phosphatidylinositol 3-kinase J Exp Med. **191**, 1319–1332

13 Rao, V. R., Corradetti, M N., Chen, J , Peng, J , Yuan, J , Prestwich, G D and Brugge, J S (1999) Expression cloning of protein targets for 3-phosphorylated phosphoinositides J Biol Chem **274**, 37893–37900

14 Reif, K , Nobes, C D , Thomas, G , Hall, A and Cantrell, D A (1996) Phosphatidylinositol 3-kinase signals activate a selective subset of Rac/Rho-dependent effector pathways Curr Biol. **6**, 1445–1455

15 Alessi, D R , Andjelkovic, M , Caudwell, B , Cron, P , Morrice, N , Cohen, P and Hemmings, B A (1996) Mechanism of activation of protein kinase B by insulin and IGF-1 EMBO J **15**, 6541–6551

16 Alessi, D R , Cohen, P , Ashworth, A , Cowley, S , Leevers, S J and Marshall, C J (1995) Assay and expression of mitogen-activated protein kinase, MAP kinase kinase, and Raf Methods Enzymol **255**, 279–290

17 Cheng, H C , Nishio, H , Hatase, O , Ralph, S and Wang, J H (1992) A synthetic peptide derived from p34cdc2 is a specific and efficient substrate of src-family tyrosine kinases J Biol Chem **267**, 9248–9256

18 Shaw, M., Cohen, P and Alessi, D R (1998) The activation of protein kinase B by H_2O_2 or heat shock is mediated by phosphoinositide 3-kinase and not by mitogen-activated protein kinase-activated protein kinase-2 Biochem J **336**, 241–246

19 Songyang, Z and Cantley, L C (1995) Recognition and specificity in protein tyrosine kinase-mediated signalling. Trends Biochem Sci **20**, 470–475

20 Liu, Y , Bishop, A , Witucki, L., Kraybill, B , Shimizu, E , Tsien, J , Ubersax, J., Blethrow, J , Morgan, D O and Shokat, K M (1999) Structural basis for selective inhibition of Src family kinases by PP1 Chem Biol **6**, 671–678

21 Hanke, J. H., Gardner, J P , Dow, R L., Changelian, P S , Brissette, W H., Weringer, E J , Pollok, B A and Connelly, P A (1996) Discovery of a novel, potent, and Src family-selective tyrosine kinase inhibitor Study of Lck- and FynT-dependent T cell activation J Biol Chem. **271**, 695–701

22 Alessi, D. R , Deak, M , Casamayor, A , Caudwell, F. B., Morrice, N , Norman, D G , Gaffney, P , Reese, C B , MacDougall, C N , Harbison, D et al (1997) 3-Phosphoinositide-dependent protein kinase-1 (PDK1) structural and functional homology with the Drosophila DSTPK61 kinase Curr. Biol **7**, 776–789

23 Stephens, L , Anderson, K , Stokoe, D , Erdjument-Bromage, H , Painter, G F., Holmes, A B , Gaffney, P R , Reese, C B., McCormick, F , Tempst, P. et al (1998) Protein kinase B kinases that mediate phosphatidylinositol 3,4,5-trisphosphate-dependent activation of protein kinase B Science **279**, 710–714

24 Bolen, J. B., Rowley, R. B , Spana, C and Tsygankov, A. Y. (1992) The Src family of tyrosine protein kinases in hemopoietic signal transduction FASEB J **6**, 3403–3409

25 Ottenhoff-Kalff, A E , Rijksen, G , van Beurden, E A , Hennipman, A , Michels, A A and Staal, G E (1992) Characterization of protein tyrosine kinases from human breast cancer involvement of the c-src oncogene product Cancer Res **52**, 4773–4778

26 Resh, M D (1994) Myristylation and palmitylation of Src family members: the fats of the matter Cell **76**, 411–413

27 Alessi, D R and Downes, C. P (1998) The role of PI 3-kinase in insulin action Biochim. Biophys Acta **1436**, 151–164

28 Alessi, D. R , James, S R , Downes, C P., Holmes, A B., Gaffney, P R , Reese, C B and Cohen, P (1997) Characterization of a 3-phosphoinositide-dependent protein kinase which phosphorylates and activates protein kinase Balpha Curr Biol **7**, 261–269

Received 26 April 2000/19 May 2000; accepted 31 May 2000

Targeting and insertion of C-terminally anchored proteins to the mitochondrial outer membrane is specific and saturable but does not strictly require ATP or molecular chaperones

Ling LAN, Sandra ISENMANN and Binks W. WATTENBERG[1]

Division of Human Immunology, Hanson Centre for Cancer Research, Institute of Medical and Veterinary Sciences, Adelaide, South Australia 5000, Australia

A distinct class of proteins contain a C-terminal membrane anchor and a cytoplasmic functional domain. A subset of these proteins is targeted to the mitochondrial outer membrane. Here, to probe for the involvement of a saturable targeting mechanism for this class of proteins, and to elucidate the roles of chaperone proteins and ATP, we have utilized an *in vitro* targeting system consisting of *in vitro*-synthesized proteins and isolated mitochondria. To establish the specificity of targeting we have used a closely related protein pair. VAMP-1A and VAMP-1B are splice variants of the vesicle-associated membrane protein/synaptobrevin-1 (VAMP-1) gene. In intact cells VAMP-1B is targeted to mitochondria whereas VAMP-1A is targeted to membranes of the secretory pathway, yet these isoforms differ by only five amino acids at the extreme C-terminus. Here we demonstrate that, *in vitro*, VAMP-1B is imported into both intact mitochondria and mitochondrial outer-membrane vesicles with a 15-fold greater efficiency than VAMP-1A. We generated and purified bacterially expressed fusion proteins consisting of the C-terminal two-thirds of VAMP-1A or -1B proteins fused to glutathione S-transferase (GST). Using these fusion proteins we demonstrate that protein targeting and insertion is saturable and specific for the VAMP-1B membrane anchor. To elucidate the role of cytosolic chaperones on VAMP-1B targeting, we also used the purified, *Escherichia coli*-derived fusion proteins. ^{33}P-Labelled GST-VAMP-1B$_{61-116}$, but not GST-VAMP-1A$_{61-118}$, was efficiently targeted to mitochondria in a chaperone-free system. Thus the information required for targeting is contained within the targeted protein itself and not the chaperone or a chaperone–protein complex, although chaperones may be required to maintain a transport-competent conformation. Moreover, ATP was required for transport only in the presence of cytosolic chaperone proteins. Therefore the ATP requirement of transport appears to reflect the participation of chaperones and not any other ATP-dependent step. These data demonstrate that targeting of C-terminally anchored proteins to mitochondria is sequence specific and mediated by a saturable mechanism. Neither ATP nor chaperone proteins are strictly required for either specific targeting or membrane insertion.

Key words: import pathway, protein import, rat liver mitochondria, tail-anchored membrane protein, VAMP-1.

INTRODUCTION

C-terminally anchored proteins represent a unique subset of membrane proteins in the cell that play a number of critical roles [1]. Examples include the vesicle-associated membrane protein/synaptobrevin (VAMP) and syntaxin families of proteins, members of the soluble *N*-ethylmaleimide-sensitive-factor-attachment-protein receptor (SNARE) proteins, which are crucial elements of the vesicular trafficking system of the cell, and the Bcl-2 family of proteins, involved in apoptosis. These proteins share a domain structure consisting of an N-terminal cytosolic domain, the functional domain of the protein, and a stretch of hydrophobic residues at the extreme C-terminus of the protein that provides both the targeting signal and the membrane anchor. Because the membrane anchor is C-terminal the targeting of these proteins to their respective membranes must be post-translational rather than co-translational. The extent to which the targeting of these proteins is compartment-specific has been controversial. Early studies indicated that a prototypic member of this class of proteins, cytochrome b_5, could insert non-specifically into lipid membranes *in vitro* [2–4], suggesting that targeting would be relatively non-specific. More recently, however, it has been recognized that in some cases, but not all, localization is quite specific. For example, two closely related isoforms of the cytochrome b_5 gene have been found to have non-overlapping subcellular distributions. One isoform, rat outer mitochondrial membrane cytochrome b_5, is only present in mitochondria whereas the other, microsomal cytochrome b_5, is restricted to endoplasmic reticulum (ER) membranes [5]. Such restricted localization is not always observed for this class of proteins. Bcl-2 is found in the ER, the nuclear membrane and in mitochondria [6,7], bringing into question the specificity of the targeting apparatus. Yet even in the case of Bcl-2 the question remains whether the promiscuity of targeting is due to a lack of specificity in the targeting process, or the presence in one protein of multiple targeting signals. The bulk of evidence suggests that

---

Abbreviations used VAMP, vesicle-associated membrane protein/synaptobrevin, SNARE, soluble *N*-ethylmaleimide-sensitive-factor-attachment-protein receptor, pSU9$_{1-69}$-DHFR, fusion protein between matrix-targeting signal of F$_0$-ATPase subunit 9 and mouse dihydrofolate reductase; ER, endoplasmic reticulum, CCCP, carbonyl cyanide *m*-chlorophenylhydrazone, cpn$_{60}$, chaperonin heat-shock protein 60, Tom20, translocase of the outer membrane of mitochondria of 20 kDa; GST, glutathione S-transferase, SRP, signal-recognition particle, MSF, mitochondrial import stimulation factor, GRP$_{78}$, 78-kDa glucose-regulated protein

[1] To whom correspondence should be addressed (e-mail brian.wattenberg@imvs.sa.gov.au)

the only two membranes to which C-terminally anchored proteins can be targeted are the ER and the mitochondrial outer membrane [1,8,9]. Recently the identification of distinct targeting motifs of C-terminally anchored proteins for the ER [10] and mitochondria [11,12] has lent force to the notion that targeting is specific.

The targeting of mitochondrial matrix-targeted proteins has been well studied. Most of these proteins are nuclear-encoded, translated and transferred from the cytosol and imported into mitochondria by a post-translational mechanism [13] The targeting of these proteins to mitochondria involves both mitochondrial membrane components and cytosolic factors [14]. About nine components of the mitochondrial import machinery have been identified in the mitochondrial outer membrane [14]. Cytosolic chaperone proteins, including mitochondrial import stimulation factor (MSF) and Hsp70 can interact with, and stimulate the import of, proteins destined for mitochondrial matrix [15,16] It is unclear at present whether proteins targeted to the mitochondrial outer membrane by C-terminal signal/anchors utilize this same machinery, although there are some suggestions that at least some of the same components are employed [9]. The targeting signal for matrix-directed proteins is a cleavable N-terminal, amphipathic helix. This N-terminal targeting signal is not present in the C-terminally anchored proteins. Instead, the targeting signal is included in the membrane anchor itself. Mutagenesis studies suggest that this signal consists of a relatively short stretch of hydrophobic amino acids (less than 21), which is flanked at both ends by positively charged residues [11].

The mechanism of targeting C-terminally anchored protein to the outer membrane remains unclear. Based on several observations, a multi-step model for this mechanism has been proposed [9]. In this model the protein to be targeted associates with cytosolic chaperones during or shortly after translation. The chaperone-bound protein is then transferred to a hypothetical receptor protein on the mitochondrial surface. Finally, the receptor-bound protein is passed to an insertion complex that accomplishes integration of the protein into the bilayer. Here we focus on three major issues. First, we explore the specificity of targeting by testing for a saturable component of the targeting apparatus that is specific for the known targeting signal. The second issue is whether cytosolic chaperone proteins carry targeting information As noted above, chaperones have been implicated in the delivery of matrix-directed proteins by preserving a conformation in the targeted protein, but the chaperones themselves do not contain targeting information. For C-terminal signal/anchor proteins the situation is somewhat different, as the targeting signal is hydrophobic, and a chaperone may conceivably have signalling function. This would be in analogy to the signal-recognition particle (SRP), which recognizes a hydrophobic signal peptide in targeting to the ER In the case of SRP, which can loosely be considered a chaperone, the targeting receptor in the ER recognizes the SRP–signal-peptide complex, and therefore SRP is part of the recognition signal [17]. We wished to determine whether an SRP-like mechanism might be involved in targeting of C-terminally anchored proteins. A third issue is the requirement for ATP in protein import. Previous studies of C-terminal anchored protein targeting to mitochondria have demonstrated a requirement for ATP [9,18]. However, the import step that requires ATP has not been defined ATP may well be required for the transfer of targeted proteins from chaperones to the mitochondrial receptor(s). The requirement for ATP in this manner for matrix-directed proteins has previously been identified [19–21]. However, it has also been suggested that ATP has a post-receptor role, perhaps in the insertion step of transport [9]. A direct test of the role of ATP in the import process is therefore called for.

To answer these questions an *in vitro* approach is the most direct and compelling avenue. A methodological problem with this approach is the demonstration of specificity. Isolated mitochondria are incubated with *in vitro*-translated protein and the association of the translated protein with mitochondria is taken to represent targeting. It is especially important to distinguish specific from non-specific targeting in such a system because some C-terminally anchored proteins are known to spontaneously insert into membranes *in vitro* [4].

To address this issue we have utilized a novel pair of C-terminally anchored proteins, one of which is targeted to the ER/secretory pathway in cells, and the other of which is targeted to mitochondria. VAMP-1 was originally characterized as a SNARE protein involved in the regulated exocytosis of synaptic vesicles [22]. We recently identified a splice variant of VAMP-1, VAMP-1B, which differs by only five amino acids from the originally identified isoform, named VAMP-1A [11]. The sequence difference includes the truncation of the C-terminal hydrophobic anchor by four amino acids, and the addition of three charged amino acids at the extreme C-terminus. This small sequence change redirects VAMP-1B to the mitochondrial outer membrane rather than the ER. Here we use this pair to demonstrate that targeting of C-terminally anchored proteins to mitochondria *in vitro* is specific, involves a saturable process (presumably the targeting receptor), and that although chaperone proteins appear to assist transport and to confer ATP dependence to the process, the targeting apparatus recognizes the targeted protein directly rather than recognizing a chaperone–protein complex.

MATERIALS AND METHODS

General procedures

DNA manipulations were performed following standard protocols [23] and all plasmids were propagated in *Escherichia coli* strain DH5α except where indicated. SDS/PAGE was performed by standard procedures [24]. Western blots were performed using 1:10000 dilution of rabbit anti-cpn$_{60}$ (chaperonin heat-shock protein 60) antibody (a gift from Dr Nick Hoogenraad, La Trobe University, Melbourne, Australia) and 1:2000 dilution of horseradish peroxidase-conjugated secondary antibody (Amrad Biotech, Melbourne, Australia) An ER-specific protein maker, the 78-kDa glucose-regulated protein (GRP$_{78}$), was detected using 2 μg/ml goat anti-GRP$_{78}$ antibody and 1:2000 dilution of horseradish peroxidase-conjugated rabbit anti-goat antibody (Santa Cruz Biotechnology, Santa Cruz, CA, U.S.A.). Radioactivity analysis was performed using a PhosphorImager and ImageQuant software (Molecular Dynamics, Sunnyvale, CA, U.S.A.). The treatment of reactions with apyrase, hexokinase and trypsin (Sigma, St. Louis, MO, U.S.A.) was as described in the Figure legends

Plasmid constructions

The coding sequences for VAMP-1A and VAMP-1B were amplified separately by PCR from either rat brain or human HUVEC (human umbilical vein endothelial cell) cDNA libraries [11]. The PCR products were cut with *Eco*RI and ligated into the pGEM-4Z vector. The coding sequences for the C-termini of VAMP-1A (amino acids 61–118) and VAMP-1B (amino acids 61–116) were amplified by PCR using pGEM-4Z-VAMP-1A and pGEM-4Z-VAMP-1B as templates. The common upstream primer used for VAMP-1A and VAMP-1B was 5′-GATC-

GGATCCTTGCAGGCAGGAGCATCACA-3′, in which the restriction site for *Bam*HI is underlined. The downstream primers used for VAMP-1A and VAMP-1B were 5′-GACTGAATTC TTTCAAGTAAAAAAGTAGATTAC-3′ and 5′-GACTGAATTCAATCAGTCCCGCCTTACAAT-3′, respectively, in which the *Eco*RI sites are underlined For protein expression, the PCR fragments were digested with *Bam*HI and *Eco*RI and ligated into the *Bam*HI/*Eco*RI site of pGEX-2TK. DNA sequencing was performed to confirm that the VAMP-1A and VAMP-1B tails were fused to glutathione S-transferase (GST) in-frame.

Preparation of crude mitochondria, purified enriched mitochondria and mitochondrial outer-membrane vesicles

All of the following procedures were performed at 4 °C. Crude mitochondria were isolated from rat liver by the following method. Briefly, Dark-Agouti rat livers were cut up, homogenized in buffer A [20 mM Hepes, pH 7.5, 220 mM mannitol, 70 mM sucrose, 1 mM EDTA, 0.5 % BSA and 1 mM pefabloc (Boehringer Mannheim Biochemica, Mannheim, Germany)], and centrifuged in a Beckman JA-10 rotor at 3000 *g* to remove nuclear debris. The post-nuclear supernatant was centrifuged in a Beckman JA-10 rotor at 16000 *g* for 15 min, yielding a crude mitochondrial pellet and a post-mitochondrial supernatant The resulting crude mitochondrial pellet was resuspended with buffer B (buffer A minus 0.5 % BSA) and washed three times by centrifugation in a Beckman JA-10 rotor at 16000 *g* for 15 min. The resulting fraction is termed 'washed mitochondria'. For some experiments, these washed mitochondria were layered on a 30 % Percoll gradient in buffer B and centrifuged in a 55Ti rotor at 110000 *g* for 30 min. The resulting lower mitochondrial band (a light-brownish colour) was collected and precipitated by centrifugation in a JA-20 rotor at 9000 *g* for 10 min. Purified enriched mitochondria were obtained after washing the above pellet twice with buffer B to remove Percoll To isolate mitochondrial outer membrane vesicles, purified enriched mitochondria were swollen by stirring in 10 mM K_2HPO_4/KH_2PO_4 buffer, pH 7.4, for 30 min. The outer membrane was separated from mitoplasts by five strokes with a motor-driven Teflon/glass homogenizer A post-mitoplast supernatant was obtained by centrifugation of the homogenate in a JA-20 rotor at 17500 *g* for 10 min. Mitochondrial outer-membrane vesicles were precipitated by centrifugation of the post-mitoplast supernatant in a 55Ti rotor at 250000 *g* for 1 h, resuspended in buffer B, aliquoted and stored at −80 °C. The protein concentrations of the above organelles and membrane preparations were determined using the bicinchoninic acid reagent kit (Pierce, Rockford, IL, U.S.A.) using BSA as a standard

In vitro transcription, translation and mitochondrial import

VAMP-1A, VAMP-1B, Bcl-2 and pSU9$_{1-69}$-DHFR (the fusion protein between the matrix-targeting signal of F_0-ATPase subunit 9 and mouse dihydrofolate reductase) RNAs were synthesized by transcription *in vitro* (Promega, Madison, WI, U.S.A.) at 30 °C for 60 min Translation of VAMP-1A and VAMP-1B was performed in either a nuclease-treated rabbit reticulocyte lysate system or a cell-free wheatgerm system (Promega), using [^{35}S]-methionine (ICN Pharmaceuticals, Irvine, CA, U.S.A.) as a radioactive label following the manufacturer's instructions. Translation products were analysed by SDS/PAGE (15 % gel) and quantification of the dried gel was performed by direct radioactive analysis using a PhosphorImager. All mitochondrial targeting was performed using washed mitochondria except where indicated. Part (10–20 %) of the translation reaction containing ^{35}S-labelled protein was incubated with 100 μg of intact rat liver mitochondria at 30 °C with import buffer (20 mM Hepes, pH 7.5, 250 mM sucrose, 5 mM $MgCl_2$, 80 mM KCl, 10 mM sodium succinate and 1 mM dithiothreitol) for the times indicated in the Figure legends. The import reaction was layered on the top of a 220-μl 220 mM sucrose cushion in buffer B and mitochondria were recovered by centrifugation in a Biofuge 13 at 13000 *g* for 10 min at 4 °C. Alkaline extraction was performed by incubation of the mitochondrial pellet with freshly prepared 0.1 M Na_2CO_3, pH 11.5, on ice for 30 min with periodic vortexing. The membrane pellets were collected by centrifugation in an airfuge (Beckman Instruments, Carlsbad, CA, U.S.A.) at 30 psi (207 kPa) for 10 min. The radioactive proteins were analysed by SDS/PAGE and quantified using a PhosphorImager. The relative insertion is represented as the percentage input (the ratio of mitochondrially incorporated protein to input translation product).

GST-fusion-protein preparation

E. coli BL21/DE3 cells were transformed with pGEX-2TK encoding either GST or GST fused in-frame to amino acids 61–118 of VAMP-1A (GST-VAMP-1A$_{61-118}$) and 61–116 of VAMP-1B (GST-VAMP-1B$_{61-116}$). A 2 litre culture in superbroth (50 μg/ml ampicillin) was seeded with 100 ml of an overnight culture and grown for 2–3 h at 30 °C. The cells were induced with 1 mM isopropyl β-D-thiogalactoside once they reached an attenuance of 1.0 (at 600 nm). After 5 h, the cells were collected by centrifugation and resuspended in 10 ml of 50 mM Tris/100 mM NaCl/5 mM EDTA/10 μg/ml leupeptin/1 μM aprotinin/1 mM PMSF, pH 8.0. The cells were lysed by a probe sonicator (5 mm diameter) followed by the addition of Triton X-100 to 2 % and dithiothreitol to 5 mM. The supernatant was collected by centrifugation of the lysate at 12100 *g* for 10 min at 4 °C and then incubated with 2 ml of a 50 % slurry of glutathione-agarose beads (Pharmacia Biotech, Uppsala, Sweden) equilibrated with PBS buffer for 1.5 h at 4 °C with agitation. The beads were loaded into a 10-ml chromatography column (Bio-Rad, Hercules, CA, U.S.A.) and washed five times with 10 ml of ice-cold PBS/1 % Triton X-100, once with PBS/1 % Triton X-100/1 M NaCl, and once with PBS. The beads were resuspended with 1 ml of PBS/50 % glycerol, aliquoted and frozen in liquid nitrogen. The purity of the preparation and the yield of GST, GST-VAMP-1A$_{61-118}$ and GST-VAMP-1B$_{61-116}$ on the beads were assessed by SDS/PAGE and Coomassie Brilliant Blue staining. The full-length GST-fusion proteins presented as a major band in the gel were quantified by comparison with BSA. For competition experiments, GST-fusion proteins were eluted from the beads by incubation with the same volume of glutathione elution buffer (10 mM reduced glutathione in 50 mM Tris/HCl, pH 8.0, and 7 M urea) at room temperature (22–25 °C) for 10 min. The eluate was collected and pooled following three repeated elution and centrifugation steps, aliquoted and assessed by SDS/PAGE.

GST-fusion-protein radiolabelling

The glutathione-agarose beads bound with GST-fusion proteins were washed with 10 volumes of HMK buffer (20 mM Tris, pH 7.5/0.1 M NaCl/12 mM $MgCl_2$). The sedimented beads were incubated with 0.3 volumes of protein kinase reaction mixture {HMK buffer, 0.3 units of bovine heart kinase (Sigma) and 10 mCi/ml [γ-^{32}P]ATP} at 4 °C for 30 min. Following the addition of 10 volumes of stop solution (10 mM sodium phosphate, pH 8.0, 10 mM sodium pyrophosphate, 10 mM EDTA and

1 mg/ml BSA), the beads were sedimented by centrifugation and washed with 10 volumes of PBS buffer. Finally, the radiolabelled fusion proteins were eluted as described above and assessed by SDS/PAGE and PhosphorImager.

Radiolabelled GST-fusion-protein targeting

^{33}P-Labelled GST fusion proteins (final concentration 500 nM, quantified according to molecular mass) in elution buffer containing 7 M urea were incubated with 100 μg of rat liver mitochondria at 30 °C for 30 min. The final concentration of urea in the import reaction was 0.2 M. The recovery of the mitochondrial pellet, alkaline extraction and analysis and quantification of imported signal were performed as described above.

RESULTS

Differential targeting of VAMP-1 isoforms is reproduced *in vitro*

We wished to determine whether *in vitro* the mitochondrial outer-membrane-targeting system could distinguish between a C-terminally anchored protein that is targeted *in vivo* to mitochondria (VAMP-1B [11]) and a splice isoform that is not mitochondrially targeted (VAMP-1A). As shown in Figure 1(A), VAMP-1B is identical in sequence with VAMP-1A from residues 1 to 113. However, their sequences diverge at the C-terminus, the predicted transmembrane segment. VAMP-1B has a shorter transmembrane segment by four amino acids compared with VAMP-1A, and ends with three charged amino acids. After incubation of reticulocyte lysate containing radiolabelled VAMP-1A and VAMP-1B with washed rat liver mitochondria, only VAMP-1B efficiently binds to mitochondria membranes (Figure 1B, lanes 3 and 4). The majority of the mitochondrially associated VAMP-1B is resistant to alkali extraction (Figure 1B, lanes 5 and 6). Quantification, accomplished by comparison of the total amount of VAMP-1 protein added to the reaction (Input, lanes 1 and 2) with the amount of protein imported to the mitochondria, indicated that VAMP-1B was imported with 15-fold higher efficiency than VAMP-1A. The recovery of an alkali-resistant form of VAMP-1B in the pelletable fraction depends on the presence of mitochondria (Figure 1C, lanes 4 and 6), indicating that VAMP-1B is integrated into the mitochondrial membrane lipid bilayer, and is not simply aggregating. The amount of VAMP-1B insertion increases with an increase in mitochondria

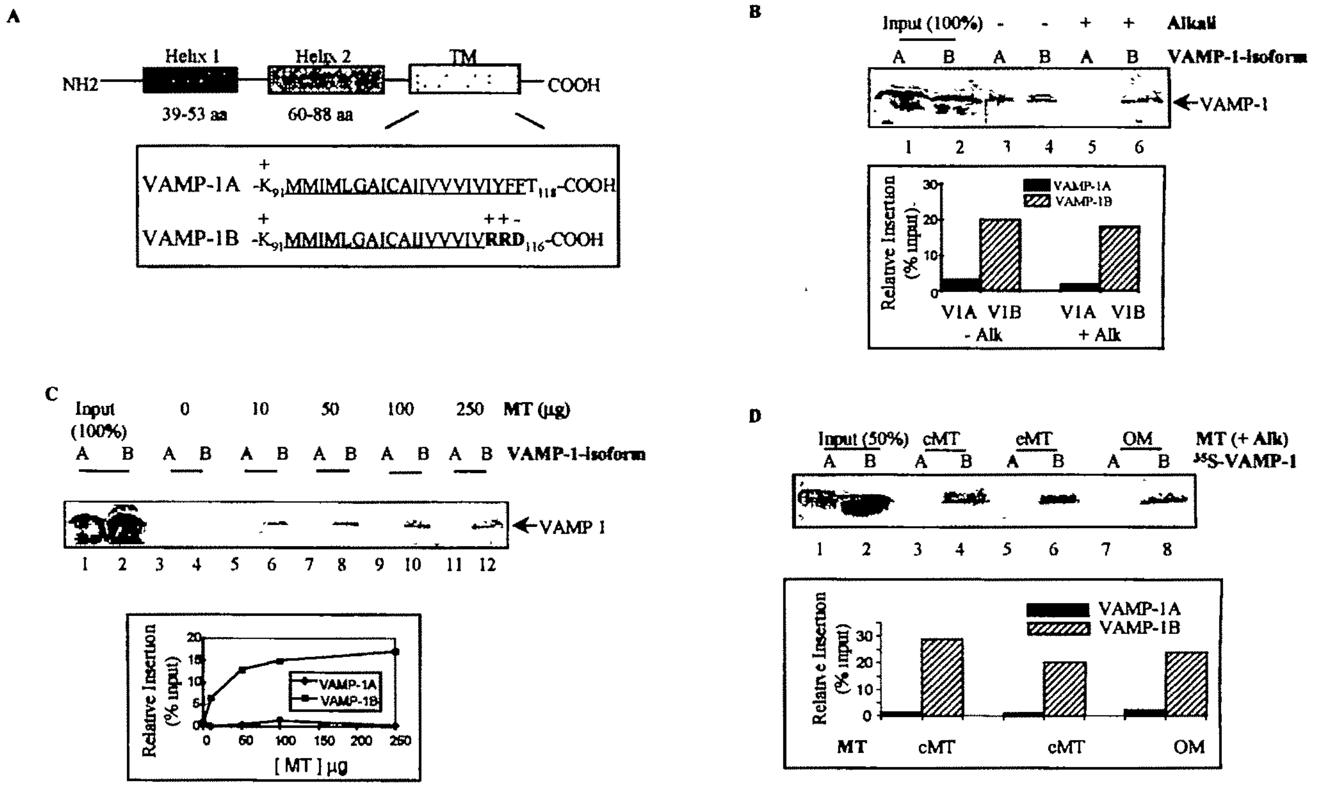

Figure 1 VAMP-1B is specifically targeted to mitochondria *in vitro*

(**A**) Scheme of VAMP-1 splice isoforms. VAMP-1 protein contains two putative helical domains and a transmembrane domain (TM). VAMP-1B is identical with VAMP-1A except for a slightly shorter hydrophobic domain and charged residues in its C-terminus. (**B**) *In vitro* import of VAMP-1 isoforms to mitochondria. ^{35}S-Labelled VAMP-1A and VAMP-1B were incubated with 100 μg of washed rat liver mitochondria at 30 °C for 30 min. Mitochondria were recovered and analysed by SDS/PAGE either directly or after extraction in 0.1 M Na_2CO_3, pH 11.5 (±alkali, Alk), as described in the Materials and methods section. The radioactivity of inserted VAMP-1 was quantified using a PhosphorImager. The relative Insertion was calculated as the percentage of total radioactive protein added to each assay (Input) recovered with the mitochondrial pellet. Input represents the amount of translation product in each import assay. (**C**) Mitochondria are not limiting for the specific targeting of VAMP-1B. [^{35}S]Labelled VAMP-1A and VAMP-1B were incubated with intact mitochondria (MT, 0–250 μg), at 30 °C for 30 min. Mitochondria were recovered and analysed after alkaline extraction. For (**B**) and (**C**), lanes 1 and 2 represent 100% of the [^{35}S]protein added to each assay. (**D**) Crude mitochondria (cMT, 100 μg), purified enriched mitochondria (eMT, 25 μg) and mitochondrial outer-membrane vesicles (OM, 5 μg) were incubated with [^{35}S]VAMP-1A and [^{35}S]VAMP-1B at 30 °C for 30 min. Mitochondria and outer-membrane vesicles were pelleted by spinning in an airfuge at 30 psi (207 kPa) for 10 min. After alkaline treatment mitochondria and outer membranes were recovered and analysed. Lanes 1 and 2 represent 50% of the [^{35}S]protein added to each assay.

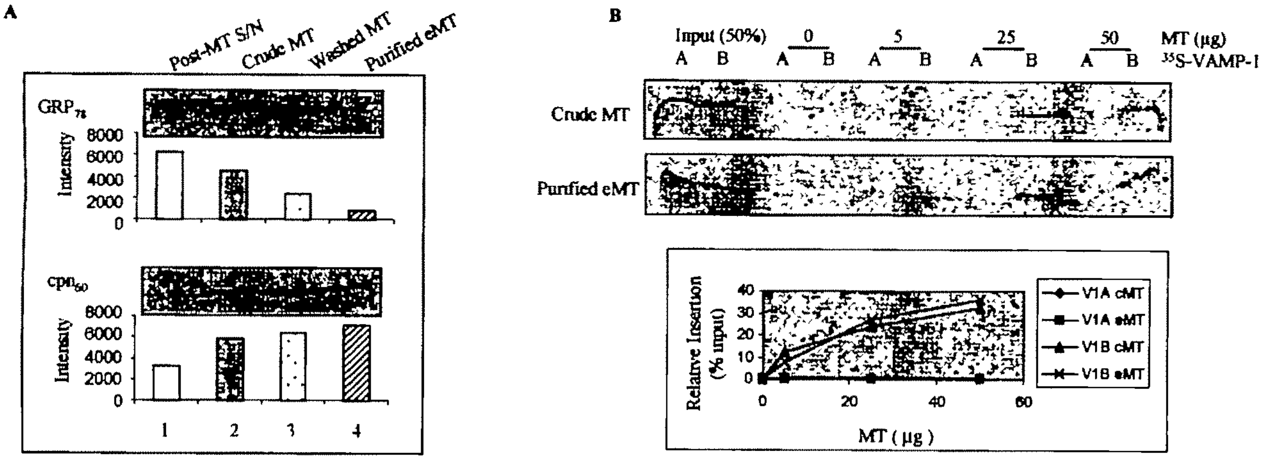

Figure 2 Insertion of VAMP-1B into mitochondria and highly purified mitochondria

(A) Comparison of the purity of mitochondrial preparations by Western blot (20 µg of protein/lane) using ER-specific marker (GRP$_{78}$) and mitochondrial matrix-protein marker (cpn$_{60}$). Microsome fractions isolated from rat liver post-mitochondrial supernatant (Post-MT S/N), crude mitochondria (MT), washed mitochondria and purified enriched mitochondria were normalized by protein concentration, analysed by SDS/PAGE and probed with anti-cpn$_{60}$ or anti-GRP$_{78}$ antibody. The intensity of the band detected by enhanced chemiluminescence was scanned and quantified by ImageQuant. (B) Comparison of relative insertion of VAMP-1B into crude mitochondria and purified mitochondria. [^{35}S]VAMP-1A and [^{35}S]VAMP-1B were incubated with 0, 5, 25 and 50 µg of crude mitochondria (cMT) or purified enriched mitochondria (eMT) at 30 °C for 30 min. The mitochondria were recovered and analysed after alkaline extraction as described in Figure 1. Lanes 1 and 2 represent 50% of the [^{35}S]protein added to each assay.

concentration and reaches a plateau (about 20% of input) with 100 µg of mitochondria per reaction (Figure 1C, lower panel). This level of efficiency of import is similar to that measured previously for C-terminally anchored proteins [18,25]. It is unclear why in this and other studies the efficiency of transport is not higher. However, this experiment demonstrates that levels of mitochondria are not limiting. VAMP-1A insertion was low at all levels of mitochondria added, illustrating that the differential targeting was preserved even with high concentrations of mitochondria. Differential targeting was observed with gradient-purified mitochondria and outer-membrane vesicles as well as with the mitochondria derived from differential centrifugation used routinely. As shown in Figure 1(D), 25 µg of gradient-purified enriched mitochondria (lanes 5 and 6) and 5 µg of an outer-membrane preparation (lanes 7 and 8), prepared by a standard technique, exhibited similar activity for VAMP-1B insertion as 100 µg of crude mitochondria (lanes 3 and 4). The differential targeting was reproduced in both purified enriched mitochondria and outer-membrane vesicles. Quantification showed that the relative insertion of VAMP-1B into both purified enriched mitochondria and mitochondrial outer-membrane vesicles was 20%, whereas that of VAMP-1A was only 1%.

To confirm that the targeting of VAMP-1B observed in the import assay was not due to non-mitochondrial membranes contaminating our mitochondrial preparations the purity of membrane and organelle fractions was monitored using the ER marker GRP$_{78}$ and the mitochondrial matrix protein cpn$_{60}$. Washing and gradient purification reduced the level of ER contamination to low levels (Figure 2A, upper panel) while, as expected, maintaining levels of the mitochondrial marker. Compared with cpn$_{60}$ protein (Figure 2A, lower panel), GRP$_{78}$ was reduced about 5-fold in purified enriched mitochondria (Figure 2A, compare lanes 4 in upper and lower panels). Whereas the ER contamination of the purified mitochondria was strongly reduced, the amount of VAMP-1B targeting was unaffected (Figure 2B). This indicates that membrane targeting detected here is indeed to mitochondrial membranes and not to contaminating ER membranes.

Characteristics of VAMP-1B targeting

The driving force for insertion of VAMP-1B into mitochondrial outer membrane remains unknown. To test the dependence of VAMP-1B targeting on inner-membrane potential, we used carbonyl cyanide *m*-chlorophenylhydrazone (CCCP), an uncoupler of inner-membrane electrochemical potential. ^{35}S-Labelled VAMP-1 and pSU9$_{1-69}$-DHFR [26] were incubated with intact washed mitochondria in either the absence or presence of 45 µM CCCP. Matrix targeting is marked by the proteolytic maturation of the protein by the matrix signal peptidase. While the import of the matrix-targeted protein pSU$_{1-69}$-DHFR was abolished by treatment with CCCP (Figure 3A, lanes 6 and 9), insertion of VAMP-1B into the mitochondrial outer membrane was unaffected by CCCP (Figure 3A, lanes 5 and 8). This demonstrates that, as has been shown previously for other outer-membrane-targeted proteins [18,25], the import of VAMP-1B (Figure 3A, lower panel) into mitochondria was independent of the mitochondrial electrochemical potential. To examine the topology of the inserted VAMP-1B, a proteolysis experiment was performed. Since the bulk of the protein is N-terminal to the membrane anchor, it is expected that if the protein is oriented with the N-terminus towards the cytosol the protein will be largely protease-sensitive when inserted into intact mitochondria, whereas if the N-terminus is oriented towards the inter-membrane space the protein will be protected from proteolysis by the mitochondrial outer membrane. After import, the bulk of the VAMP-1B protein was cleaved by exogenous trypsin (Figure 3B, lanes 4 and 6), indicating that VAMP-1B is anchored by the predicted transmembrane domain in the N_{cyto}–C_{in} orientation.

To characterize broadly the steps involved in transport, we wished to compare the targeting of VAMP-1B with that of another well-characterized C-terminally anchored mitochondrial

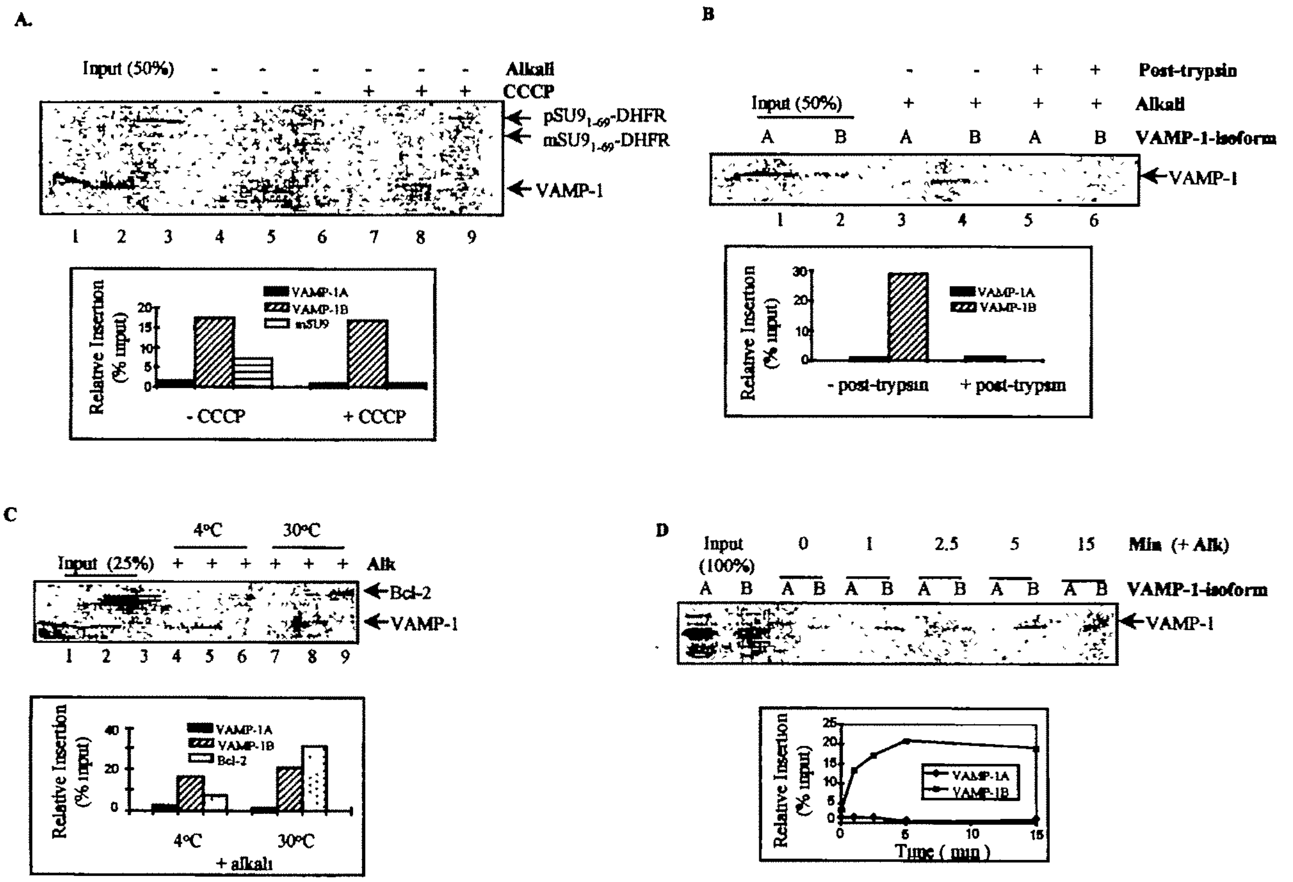

Figure 3 VAMP-1B insertion into mitochondria is independent of membrane potential, the protein is anchored in the outer membrane with its C-terminus and insertion is relatively temperature-insensitive and rapid

(A) CCCP inhibits pSU9$_{1-69}$-DHFR targeting but not VAMP-1B ^{35}S-Labelled VAMP-1A, VAMP-1B and pSU9$_{1-69}$-DHFR were incubated with intact washed mitochondria at 30 °C, in the absence (lanes 4–6) or presence (lanes 7–9) of 45 μM CCCP Mitochondria were recovered and analysed directly m, mature-size protein Lanes 1, 2 and 3 represent 50% of the [^{35}S]protein added to each assay (B) VAMP-1B is anchored in the outer membrane After import, mitochondria were treated with 30 μg/ml trypsin on ice for 30 min in the presence or absence of excess 100 μg/ml soya bean trypsin inhibitor (± post-trypsin) Mitochondria were recovered and analysed after alkaline extraction Lanes 1 and 2 represent 50% of the [^{35}S]protein added to each assay (C) Effect of temperature on VAMP-1 import ^{35}S-Labelled VAMP-1A, VAMP-1B and Bcl-2 were incubated with intact washed mitochondria at either 4 or 30 °C Mitochondria were recovered and analysed after alkaline extraction (Alk, lanes 4–9) Lanes 1, 2 and 3 represent 25% of the [^{35}S]protein added to each assay (D) Time course of mitochondrial targeting at 4 °C ^{35}S-Labelled VAMP-1A and VAMP-1B were incubated with intact washed mitochondria for 0, 1, 2 5, 5 and 15 min Mitochondria were recovered and analysed after alkaline extraction The relative insertion was plotted as a function of time Lanes 1 and 2 represent 100% of the [^{35}S]protein added to each assay

protein, Bcl-2, and to determine the temperature dependency of the transport reaction. The recovery of the membrane-inserted alkali-resistant form of Bcl-2 was greater at 30 °C than at 4 °C (Figure 3C, lanes 6 and 9) but the insertion of VAMP-1B was only slightly increased at 30 °C when compared with 4 °C (Figure 3C, lanes 5 and 8). About 20 % of the input VAMP-1B and 30 % of the input Bcl-2 were inserted into membrane at 30 °C (Figure 3C, lower panel). In three additional experiments the efficiency of insertion of VAMP-1B and Bcl-2 was found to be similar to one another (results not shown). These data illustrate that the import of VAMP-1B into mitochondria is similar in efficiency to Bcl-2 but is less sensitive to temperature This difference in temperature dependence could be at any one of several steps in transport (see Discussion).

The import of VAMP-1B at low temperature suggests that targeting is a high-affinity process To examine this more closely we measured the time course of targeting of VAMP-1B to mitochondria at 4 °C ^{35}S-Labelled VAMP-1A and VAMP-1B were incubated with intact washed mitochondria at 4 °C for 0, 1, 2.5, 5 and 15 min. Mitochondria were recovered and analysed after alkali treatment Unlike VAMP-1A, the insertion of VAMP-1B into mitochondria increases with time (Figure 3D). The amount of insertion reaches a plateau at 5 min (Figure 3D, lower panel), indicating that the uptake of VAMP-1B to mitochondria is rapid even at reduced temperature.

VAMP-1B targeting into mitochondria is saturable

One characteristic of a receptor-mediated process is saturability To test whether VAMP-1B targeting requires a mitochondrial receptor, we produced constructs for bacterial expression encoding the C-terminal half of VAMP-1A (residues 61–118) and VAMP-1B (residues 61–116) fused to the C-terminus of GST. The corresponding proteins were expressed in *E. coli*, and purified by affinity chromatography on glutathione-agarose. These purified, non-radioactive proteins were then added in mass amounts to transport assays to test for competition with the ^{35}S-labelled proteins produced by translation *in vitro* To prevent aggregation, the GST-fusion proteins were eluted in a buffer containing 7 M urea. When diluted into the assay mix the final urea concentration was 0.7 M. Control experiments indicated that this level of urea had no effect on targeting (results not shown), as had been shown

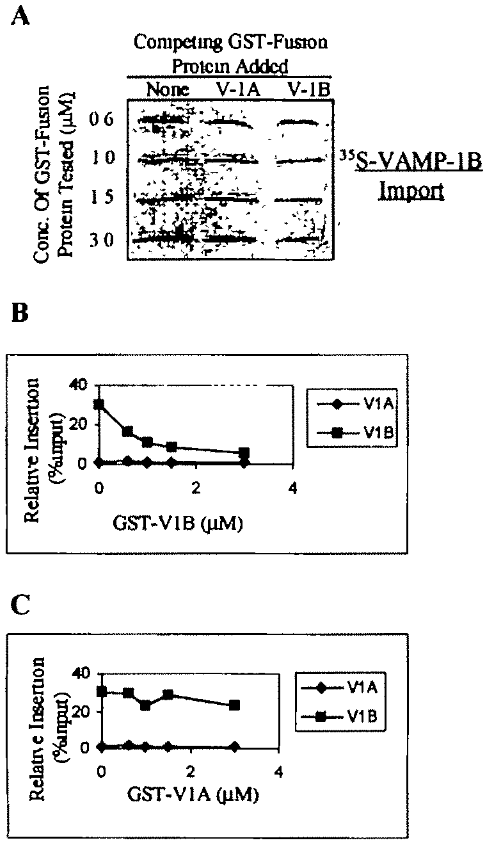

Figure 4 Inhibition of VAMP-1B insertion by purified GST-fused VAMP-1B

(**A**) In a series of import experiments purified GST-VAMP-1B$_{61-116}$ (V-1B) or GST-VAMP-1A$_{61-118}$ (V-1A, 0–3 μM) in 7 M urea were added to import mixtures containing 100 μg of intact washed mitochondria and ^{35}S-labelled VAMP-1B For each experiment a no-peptide control, with just urea added, was included The final concentration of urea in all reaction mixtures was 0 7 M After 30 min of incubation at 30 °C, mitochondria were recovered and alkaline extracted Recovered ^{35}S-labelled VAMP-1B and -1A (not shown in **A**) was analysed by SDS/PAGE and PhosphorImager analysis Imported VAMP-1 proteins were quantified and compared with the input to the import reaction (not shown in **A**) as described in the Materials and methods section (**B**) Quantification of inhibition of GST-VAMP-1B$_{61-116}$ (**C**) Quantification of inhibition of GST-VAMP-1A$_{61-118}$

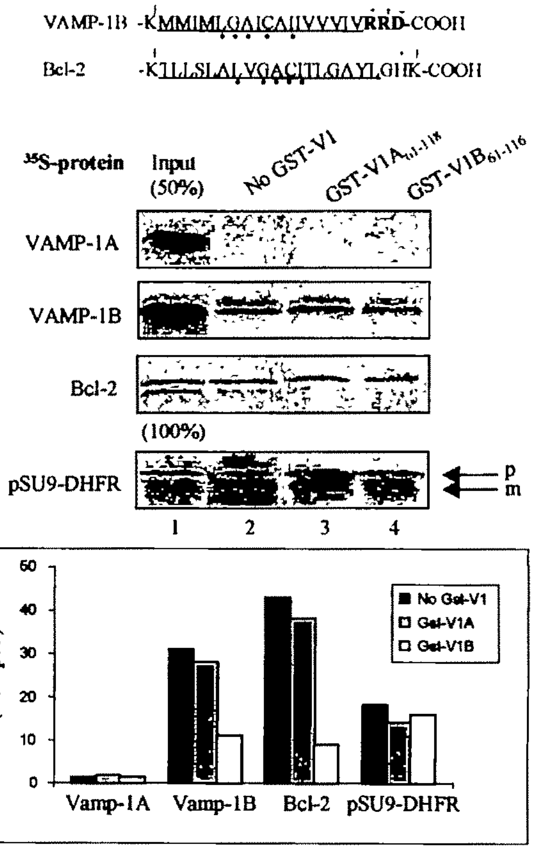

Figure 5 Competition of targeting of outer-membrane and matrix proteins to mitochondria by purified VAMP-1 protein chimaeras

VAMP-1B and Bcl-2 targeting into mitochondria is inhibited by GST-VAMP-1B$_{61-116}$ ^{35}S-Labelled VAMP-1A, VAMP-1B, Bcl-2 and pSU9$_{1-69}$-DHFR were incubated with 100 μg of washed mitochondria at 30 °C for 30 min in the absence of eluted GST-fusion protein (lanes 2), and in the presence of 3 μM GST-VAMP-1A$_{61-118}$ (lanes 3) or 3 μM GST-VAMP-1B$_{61-116}$, (lanes 4). The final concentration of urea in the import mixtures was 0 7 M Mitochondria were recovered after alkaline extraction and analysed as described in Figure 1 Lane 1 for panels VAMP-1A, VAMP-1B and Bcl-2 represents 50% of the [^{35}S]protein added to each assay and lane 1 for panel pSU9$_{1-69}$-DHFR represents 100% of the [^{35}S]protein added to each assay The dots below the VAMP-1B and Bcl-2 sequences indicate identical amino acids, p, precursor, m, mature.

previously for transport of proteins to the mitochondrial matrix [27]. The presence of GST-VAMP-1B$_{61-116}$ strongly inhibited the targeting and insertion of VAMP-1B into the mitochondrial outer membrane (Figure 4A). Inhibition was close to 80% at 3 μM GST-VAMP-1B$_{61-116}$, and was half-maximal at 1 μM. The corresponding protein derived from VAMP-1A had no significant effect on targeting and insertion at these levels (Figure 4B) These data demonstrate that VAMP-1B targeting to mitochondria is saturable and strongly implicate the involvement of a protein receptor in this process Consistent with this concept, we found that pre-treatment of mitochondria with trypsin to remove surface proteins significantly inhibited VAMP-1B targeting (results not shown). This protease-sensitivity result mirrors previous reports for Bcl-2 [28]. These results suggest that the mitochondrial targeting of VAMP-1B depends on a saturable surface receptor.

Structural similarities between the VAMP-1B signal/anchor sequence and that of other C-terminally anchored outer-membrane proteins, such as Bcl-2, suggest that they may share a common import pathway To test this directly the ability of GST-VAMP-1B to compete for the mitochondrial targeting of Bcl-2 was explored (Figure 5). In the presence of 3 μM GST-VAMP-1B$_{61-116}$, the insertion of both VAMP-1B and Bcl-2 were reduced by 65–75% (Figure 5, lanes 2–4). GST-VAMP-1A$_{61-118}$ had only a marginal effect. We have therefore established that VAMP-1B and Bcl-2 share a common uptake pathway that recognizes the structural similarities between the VAMP-1B and Bcl-2 targeting signals, but rejects the closely related VAMP-1A signal. The ability of GST-VAMP-1B to compete for targeting of a matrix-directed protein, pSU9$_{1-69}$-DHFR, was also tested Neither GST-VAMP-1A$_{61-118}$ nor GST-VAMP-1B$_{61-116}$ had a significant effect on the import of pSU9$_{1-69}$-DHFR, as judged by the proteolytic conversion of precursor pSU9$_{1-69}$-DHFR into the mature form in the mitochondrial matrix. These results indicate that whereas VAMP-1B may share the same receptor as Bcl-2, and presumably other C-terminally anchored proteins, matrix-targeted proteins use a different receptor system or, alternatively, that a different step in transport is rate-limiting.

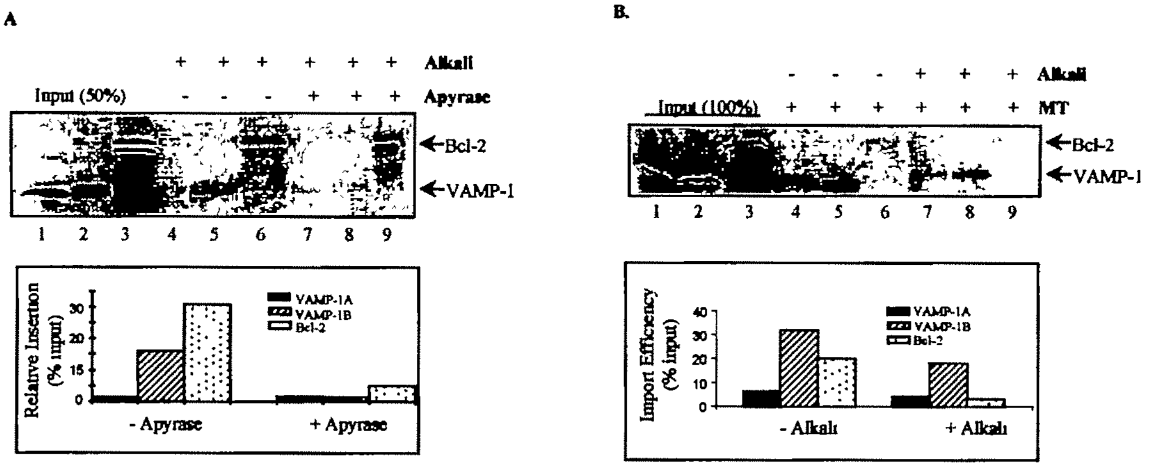

Figure 6 VAMP-1B targeting from reticulocyte lysates requires ATP

(**A**) Translation mixtures from reticulocyte lysate containing *in vitro*-translated VAMP-1A, VAMP-1B or Bcl-2, without (lanes 4–6) and with (lanes 7–9) 5 units of apyrase pretreatment at 24 °C for 20 min, were then incubated with 100 μg of washed mitochondria for 30 min at 30 °C Mitochondria were recovered following alkaline extraction Lanes 1 and 2 represent 50% of the [^{35}S]protein added to each assay (**B**) Import of C-terminally anchored proteins from wheatgerm extract translations to mitochondria ^{35}S-Labelled wheatgerm extract translated VAMP-1A, VAMP-1B and Bcl-2 were incubated with intact washed mitochondria (MT) at 30 °C for 30 min Mitochondria were recovered and analysed directly (lanes 4–6) or after alkaline extraction (lanes 7–9) The relative insertion was calculated as a proportion of input Lanes 1, 2 and 3 represent 100% of the [^{35}S]protein added to each assay

ATP-dependence of outer-mitochondrial membrane targeting

The involvement of ATP in VAMP-1B targeting was examined using apyrase to deplete ATP from the import reactions. When VAMP-1A, VAMP-1B and Bcl-2 were incubated with mitochondria, the targeting of VAMP-1B was completely abolished by ATP depletion (Figure 6A, lanes 5 and 8) and the targeting of Bcl-2 was significantly reduced (Figure 6A, lanes 6 and 9). Similar results were obtained when using hexokinase to deplete ATP (results not shown). These results are similar to those found previously for the ATP dependence of mitochondrial insertion of Bcl-2 [18].

Although the involvement of molecular chaperones in the import of C-terminally anchored proteins has not been demonstrated previously, molecular chaperones have been implicated in import of proteins to the mitochondrial matrix. Molecular chaperones require ATP for function, and the ATP dependence of import may therefore be due to the involvement of ATP-dependent chaperone proteins. An alternative role for ATP is in an ATP-dependent import or translocation event. These possibilities are explored below.

Import of VAMP-1B translated in a cell-free wheatgerm extract to mitochondria

Wheatgerm extract contains relatively few chaperones and does not contain the chaperone MSF that may have a specific interaction with proteins destined for import into mitochondria [15,29]. Therefore, to test the dependence of VAMP-1B targeting on MSF we measured the mitochondrial targeting of VAMP-1B translated in wheatgerm extract. VAMP-1B bound to mitochondria, as judged by the signal before alkaline extraction, and inserted into mitochondrial membrane with about 20% efficiency (Figure 6B, lane 5), as judged after alkaline treatment (Figure 6B, lane 8), similar to levels of insertion found when the protein was translated in reticulocyte lysate. No insertion of VAMP-1A was detected (Figure 6B, lanes 4 and 7). In contrast Bcl-2 was bound but not inserted into the membrane (Figure 6B, lanes 6 and 9). Adding reticulocyte lysate to the wheatgerm extract system did not increase import of VAMP-1B to mitochondria (results not shown). This indicates that wheatgerm extract contains sufficient levels of components required for VAMP-1B targeting and that MSF is not required for VAMP-1B targeting. Conversely, Bcl-2 insertion depends on a component of reticulocyte lysate not found in wheatgerm extract, possibly MSF. After depletion of ATP in the wheatgerm translation mixture with either apyrase or hexokinase, the import of VAMP-1B was reduced from 20% efficiency to 7%, but targeting was not completely abolished as it is in the reticulocyte lysate system (results not shown). This small, but significant, difference in the degree of ATP dependence between translation in wheatgerm and reticulocyte lysates suggests a relationship between the ATP dependence and cytosolic factors involved in the targeting process.

Cytosolic factor(s) are not required for selective VAMP-1B targeting

Are cytosolic chaperone proteins absolutely required for selective targeting of C-terminally anchored proteins? To test this we measured the import of VAMP-1A and VAMP-1B in the absence of any cytosolic proteins by utilizing the purified GST-fusion proteins GST-VAMP-1A$_{61-118}$ and GST-VAMP-1B$_{61-116}$. The fusion proteins were purified and maintained in 7 M urea to prevent aggregation. After purification, these proteins, which were engineered with an N-terminal protein kinase A phosphorylation site, were phosphorylated *in vitro* by incubation with protein kinase and [^{33}P]ATP. The ^{33}P-labelled proteins purified from *E. coli* extracts were diluted from the 7 M urea in which they were isolated and incubated in the absence or presence of intact mitochondria. [^{33}P]GST-VAMP-1B$_{61-116}$ efficiently targeted to and integrated into mitochondria whereas the corresponding VAMP-1A construct only slightly associated with mitochondria (Figure 7A, lanes 8 and 9). During GST-fusion-protein purification, both VAMP-1A and VAMP-1B were partially degraded (shown in Figure 7, lanes 2 and 3, lower bands). However, only the full-length VAMP-1B fusion protein was

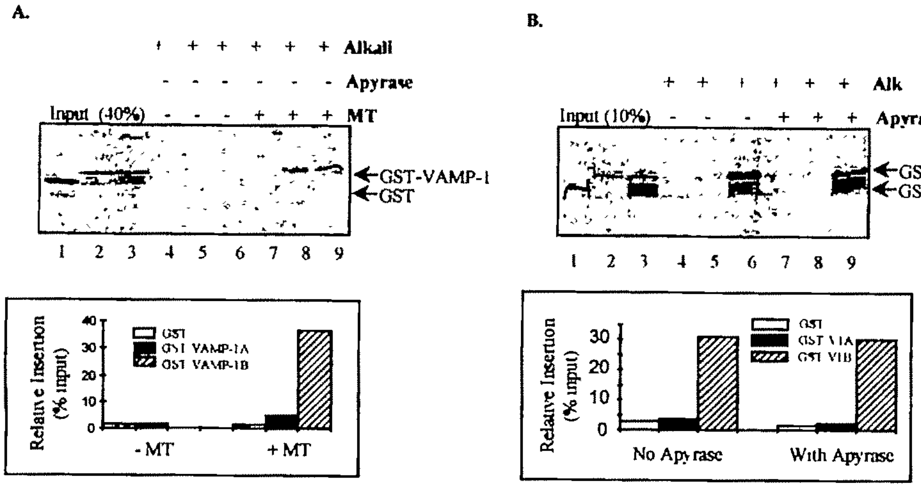

Figure 7 The VAMP-1B C-terminus mediates selective targeting to mitochondria in the absence of cytosolic proteins in an ATP-independent fashion

(**A**) Targeting of ^{33}P-labelled GST-fused VAMP-1 tails to mitochondria Bacterially expressed GST-fusion proteins were purified and radiolabelled with [^{33}P]ATP by phosphorylation on beads and eluted with 10 mM reduced glutathione elution buffer containing 7 M urea Radiolabelled GST (lanes 4 and 7), GST-VAMP-1A$_{61-118}$ (lanes 5 and 8) and GST-VAMP-1B$_{61-116}$ (lanes 6 and 9) in 7 M urea were incubated without (lanes 4–6) or with (lanes 7–9) washed mitochondria (MT) for 30 min at 30 °C. The final concentration of urea in the import mixture was 0 2 M Mitochondria were recovered after alkaline extraction, and import efficiency was calculated as a proportion of input Lanes 1, 2 and 3 represent 40% of the [^{35}S]protein added to each assay (**B**) Mitochondrial uptake of the GST-VAMP-1B$_{61-116}$ does not require ATP Radiolabelled GST (lanes 4 and 7), GST-VAMP-1A$_{61-118}$ (lanes 5 and 8) and GST-VAMP-1B$_{61-116}$ (lanes 6 and 9) were treated without (lanes 4–6) or with (lanes 7–9) 5 units of apyrase at 24 °C for 20 min before performing import Mitochondria were recovered after alkaline extraction and analysed as described above Lanes 1, 2 and 3 represent 10% of the [^{35}S]protein added to each assay

substantially inserted into the membrane. Not surprisingly, GST alone was not incorporated into the mitochondrial membrane. The selective targeting of chaperone-free VAMP-1B conclusively demonstrates that chaperones do not have a direct role in the targeting process. It does not rule out, however, that chaperones may assist the process *in vivo*, or *in vitro* in the absence of urea, by maintaining proteins in a transport-competent conformation. Because this system lacks any lysate-derived cytosolic proteins, it was possible to test whether the ATP dependence of import measured previously with *in vitro*-translated proteins was due to the involvement of cytosolic components. The treatment of eluted ^{33}P-labelled fusion proteins with apyrase and inclusion of apyrase in the import reaction did not diminish the import of [^{33}P]GST-VAMP-1B$_{61-116}$ to mitochondria (Figure 7B, lanes 6 and 9). Similar results were obtained with hexokinase treatment (results not shown). These experiments establish two important aspects of the targeting process. First, cytosolic proteins are not absolutely required, so all the information required for targeting must reside in the targeted protein itself interacting with the mitochondrial receptor. Secondly, the import process is fundamentally ATP-independent. However, when cytosolic proteins assist the process an ATP requirement is imposed on the system

DISCUSSION

The specificity of targeting of C-terminally anchored proteins to mitochondria

Current evidence indicates that the mitochondrial outer membrane and the ER are the only two sites in the cell competent for insertion of C-terminally anchored proteins. Here we have shown that whereas VAMP-1B is imported into the mitochondrial outer membrane efficiently, VAMP-1A is not. These experiments demonstrate that, *in vitro*, mitochondria could distinguish between two closely related proteins on the basis of the amino acid sequence in the C-terminal membrane anchor, mirroring results seen in intact cells [11]. The signal/anchor sequence of VAMP-1B closely matches in overall structure that of several other tail-anchored proteins of the mitochondrial outer membrane These proteins all contain hydrophobic membrane-anchoring segments of around 17 residues, flanked by positively charged amino acids. Furthermore, mutagenesis of this region of VAMP-1B has identified these sequence characteristics as being crucial for a functional targeting signal. VAMP-1A and -1B are therefore a useful pair of proteins to establish the specificity of targeting to the outer membrane. This specificity is difficult to reconcile with a spontaneous insertion mechanism, given the small difference in sequence between VAMP-1A and -1B To directly confirm that the targeting of C-terminally anchored proteins to mitochondria is specific, we demonstrate that the import pathway is saturable, but only by the VAMP-1B and not the VAMP-1A targeting sequence. As expected, the VAMP-1B targeting sequence also competes for uptake of Bcl-2, demonstrating that the mechanism being tested is general for C-terminally anchored proteins.

Like two other outer-membrane proteins, Bcl-2 [18] and the hybrid protein pOMD29-DHFR [30], VAMP-1B insertion is independent of membrane potential, indicating that the transport event is driven only by events in the outer membrane. The targeting of VAMP-1B is rapid and relatively temperature-insensitive. This is consistent with a transport mechanism that proceeds with high affinity and very high energy efficiency, much as has been observed for the targeting of the matrix proteins [26,31]. The difference in temperature dependence between VAMP-1B and Bcl-2 could conceivably be at the recognition step at the membrane surface or in a subsequent membrane-insertion step. We believe it is most likely that this difference reflects a distinction in how these proteins interact with cytosolic chaperones. As illustrated in Figure 6, VAMP-1B is transported efficiently when translated in wheatgerm lysates, whereas Bcl-2 is not. This is most probably because of a difference in chaperone interactions. Similarly the most temperature-sensitive step in transport could involve the ATP-dependent transfer of these proteins from chaperones to the mitochondrial receptor. The difference in temperature dependence may therefore reflect a difference in the strength of interaction of VAMP-1B and Bcl-2 with chaperones, or a difference in the spectrum of chaperones that are bound by these proteins in lysates.

Evidence for a specific targeting receptor for C-terminally anchored membrane proteins

The specificity and saturability of C-terminally anchored protein targeting is strongly suggestive of the involvement of a targeting receptor. Limited proteolytic digestion of the mitochondrial surface inhibits targeting of Bcl-2 to mitochondria [9,18], consistent with our evidence for a saturable, protein-mediated uptake mechanism. Is the receptor one of the receptor complexes identified previously for import of matrix-targeted proteins? Antibodies to one component, Tom20 (translocase of the outer membrane of mitochondria of 20 kDa), have been reported to reduce, but not eliminate, targeting of Bcl-2 to mitochondria [9]. However, it has not been shown conclusively that Tom20 is itself the relevant receptor, or whether other components, such as an insertion pore, are required for targeting and/or insertion. Resolution of this question will likely require a more definitive biochemical approach. The ability to achieve import in a fully reconstituted system [32] coupled with our greater understanding of the structure of the targeting sequence for both mitochondria and the ER holds great promise in this regard.

The role of chaperone proteins and ATP

It has been shown that cytosolic chaperones bind to matrix-destined preproteins post-translationally and prevent them from misfolding or aggregating, and preserve their import competence [14]. For matrix-directed proteins the chaperones are not thought to impart targeting information themselves. However this question has remained open for tail-anchored proteins. We therefore asked whether a cytosolic factor is required for selective delivery of VAMP-1B to mitochondria. Given the hydrophobic nature of the C-terminal anchor/signal sequence it is not surprising that chaperones might be involved in preventing aggregation. But do chaperones have a role in the selectivity of targeting? The classical route of protein import into the ER provides an interesting paradigm for hydrophobic targeting sequences In this system, soluble cytosolic SRP binds to a hydrophobic targeting signal peptide of the preprotein co-translationally, blocking translation, and transfers the translation apparatus to the ER by binding to the SRP receptor in the ER membrane [17]. In this case the targeting function is not provided directly by the signal peptide but indirectly by its interaction with SRP, which only targets to its receptor when bound to a signal peptide. To address the function of chaperones in specific mitochondrial targeting, it was essential to see whether mitochondrial import could be recreated in the absence of chaperones.

To accomplish this, transport of purified VAMP chimaeras, instead of VAMPs derived from *in vitro* translation, was tested. The chaperone-free VAMP-1B chimaera was indeed targeted efficiently to mitochondria. This demonstrates for the first time that targeting specificity does not reside in the interaction between the mitochondrial receptor and a chaperone, or chaperone–protein complex, but directly in an interaction with the targeted protein itself (Figure 7). It should be noted that these chimaeras were diluted from concentrated urea solutions to prevent aggregation of the hydrophobic membrane anchor It seems likely that in the cell chaperones would function to prevent this type of aggregation, but these studies demonstrate that they do not have a direct role in specific targeting. The observation that ATP is required in the presence, but not the absence of cytosolic factors is most readily explained by a requirement for ATP in chaperone action ATP is required for chaperones to release bound substrates and it is likely in this case that the release of the targeted protein from chaperones to the mitochondrial targeting receptor is the ATP-dependent step of transport. However, the participation of chaperones is only suggested indirectly by the present study. Which chaperones are involved and how they allow recognition of the targeting sequence by the mitochondrial receptor will require further investigation. The ATP-independent targeting of the chaperone-free VAMP-1B chimaera to mitochondria indicates that the interaction of the targeted protein with the mitochondrial outer membrane generates the driving force for translocation. The implication is that there is a gradient of affinity of the hydrophobic signal anchor sequence of tail-anchored proteins going from the targeting receptor to the insertion pore (if it is indeed involved) to the bilayer of the outer membrane. This gradient of affinity gives rise to an insertion mechanism that is independent of a chemical energy source.

Once the targeting receptor has been identified it will be of great interest to determine how the requirement to bind the signal/anchor sequence with adequate affinity to target the sequence from cytosol to mitochondria is balanced with the need to spontaneously release the same sequence to the insertion apparatus. The finding of mitochondrial targeting of [^{33}P]GST-VAMP-1B$_{61-116}$ also demonstrates that the VAMP-1B C-terminus (55 amino acids) contains sufficient information for selective targeting (including recognition by mitochondrial receptors and translocation into the membrane). Indeed we find that the sequence requirement for VAMP-1B-specific mitochondrial targeting resides solely in the transmembrane anchor sequence (L. Lan, S. Isenmann, O. Mckenzie and B. W. Wattenberg, unpublished work).

The data presented here demonstrate that mitochondrial surface proteins function as an apparatus for selective and direct interaction and translocation of tail-anchored proteins to mitochondria. Chaperones appear to assist but are not essential for selective targeting. Moreover, the insertion of C-terminally anchored proteins into the membrane does not require ATP. Further studies are ongoing to identify the components that recognize C-terminal mitochondrial targeting signals and insert them into the outer-mitochondrial membrane.

We thank Dr Nikolaus Pfanner for providing pSU9$_{1-69}$-DHFR cDNA and Dr Nick Hoogenraad for providing anti-cpn$_{60}$ antibody We appreciate the comments from Dr Trevor Lithgow and Dr Stuart Pitson This research was supported by a grant from the National Health and Medical Research Council (NHMRC)

REFERENCES

1 Kutay, U , Hartmann, E and Rapoport, T A (1993) A class of membrane proteins with a C-terminal anchor Trends Cell Biol **3**, 72–75

2 Enoch, H G , Fleming, P J and Strittmatter, P (1979) The binding of cytochrome b_5 to phospholipid vesicles and biological membranes Effect of orientation on intermembrane transfer and digestion by carboxypeptidase Y J Biol Chem **254**, 6483–6488

3 Anderson, D J , Mostov, K E and Blobel, G (1983) Mechanisms of integration of *de novo*-synthesized polypeptides into membranes signal-recognition particle is required for integration into microsomal membranes of calcium ATPase and of lens MP26 but not of cytochrome b_5 Proc Natl Acad Sci U S A **80**, 7249–7253

4 Kim, P K , Janiak-Spens, F., Trimble, W S , Leber, B and Andrews, D W (1997) Evidence for multiple mechanisms for membrane binding and integration via carboxyl-terminal insertion sequences Biochemistry **36**, 8873–8882

5 D'Arrigo, A , Manera, E , Longhi, R and Borgese, N (1993) The specific subcellular localization of two isoforms of cytochrome b_5 suggests novel targeting pathways J Biol Chem **268**, 2802–2808

6 Krajewski, S, Tanaka, S, Takayama, S., Schibler, M. J, Fenton, W and Reed, J C (1993) Investigation of the subcellular distribution of the bcl-2 oncoprotein residence in the nuclear envelope, endoplasmic reticulum, and outer mitochondrial membranes Cancer Res. **53**, 4701–4714

7 Lithgow, T., van Driel, R, Bertram, J F and Strasser, A (1994) The protein product of the oncogene bcl-2 is a component of the nuclear envelope, the endoplasmic reticulum, and the outer mitochondrial membrane Cell Growth Differ **5**, 411–417

8 Kutay, U, Ahnert-Hilger, G, Hartmann, E, Wiedenmann, B and Rapoport, T A (1995) Transport route for synaptobrevin via a novel pathway of insertion into the endoplasmic reticulum membrane EMBO J **14**, 217–223

9 Millar, D. G and Shore, G C (1996) Signal anchor sequence insertion into the outer mitochondrial membrane J Biol Chem **271**, 25823–25829

10 Kim, P K, Hollerbach, C, Trimble, W S, Leber, B and Andrews, D W (1999) Identification of the endoplasmic reticulum signal in vesicle associated membrane proteins J Biol Chem **274**, 36876–36882

11 Isenmann, S, Khew-Goodall, Y, Gamble, J, Vadas, M and Wattenberg, B W (1998) A splice-isoform of vesicle-associated membrane protein-1 (VAMP-1) contains a mitochondrial targeting signal Mol Biol Cell **9**, 1649–1660

12 Kuroda, R, Ikenoue, T, Honsho, M, Tsujimoto, S, Mitoma, J Y and Ito, A (1998) Charged amino acids at the carboxyl-terminal portions determine the intracellular locations of two isoforms of cytochrome b_5 J Biol Chem **273**, 31097–31102

13 Neupert, W, Hartl, F U, Craig, E A and Pfanner, N (1990) How do polypeptides cross the mitochondrial membranes? Cell **63**, 447–450

14 Pfanner, N, Craig, E A and Honlinger, A (1997) Mitochondrial preprotein translocase Annu Rev. Cell Dev Biol **13**, 25–51

15 Hachiya, N, Alam, R, Sakasegawa, Y., Sakaguchi, M., Mihara, K and Omura, T (1993) A mitochondrial import factor purified from rat liver cytosol is an ATP-dependent conformational modulator for precursor proteins EMBO J **12**, 1579–1586

16 Deshaies, R J, Koch B D, Werner-Washburne, M, Craig E A and Schekman, R (1988) A subfamily of stress proteins facilitates translocation of secretory and mitochondrial precursor polypeptides Nature (London) **332**, 800–805

17 Walter, P and Johnson, A E (1994) Signal sequence recognition and protein targeting to the endoplasmic reticulum membrane Annu Rev Cell Biol **10**, 87–119

18 Nguyen, M, Millar, D. G, Yong, V W., Korsmeyer, S J and Shore, G C (1993) Targeting of Bcl-2 to the mitochondrial outer membrane by a COOH-terminal signal anchor sequence. J Biol Chem **268**, 25265–25268

Received 14 January 2000/10 April 2000; accepted 3 May 2000

19 Hachiya, N, Mihara, K, Suda, K, Horst, M, Schatz, G and Lithgow, T (1995) Reconstitution of the initial steps of mitochondrial protein import Nature (London) **376**, 705–709

20 Komiya, T, Sakaguchi, M and Mihara, K (1996) Cytoplasmic chaperones determine the targeting pathway of precursor proteins to mitochondria EMBO J **15**, 399–407

21 Schatz, G (1996) The protein import system of mitochondria J Biol Chem **271**, 31763–31766

22 Trimble, W S, Cowan, D M and Scheller, R H (1988) VAMP-1 a synaptic vesicle-associated integral membrane protein. Proc Natl Acad Sci U.S.A **85**, 4538–4542

23 Sambrook, J, Fritsch, E F. and Maniatis, T (1989) Molecular Cloning a Laboratory Manual, 2nd edn, Cold Spring Harbor Press, Cold Spring Harbor

24 Laemmli, U K (1970) Cleavage of structural proteins during the assembly of the head of bacteriophage T4 Nature (London) **227**, 680–685

25 Zhuang, Z P, Marks, B and McCauley, R B (1992) The insertion of monoamine oxidase A into the outer membrane of rat liver mitochondria J Biol Chem **267**, 591–596

26 Pfanner, N, Muller, H K, Harmey, M A and Neupert, W (1987) Mitochondrial protein import involvement of the mature part of a cleavable precursor protein in the binding to receptor sites EMBO J **6**, 3449–3454

27 Eilers, M, Hwang, S and Schatz, G (1988) Unfolding and refolding of a purified precursor protein during import into isolated mitochondria EMBO J **7**, 1139–1145

28 Janiak, F, Leber, B and Andrews, D W (1994) Assembly of Bcl-2 into microsomal and outer mitochondrial membranes J Biol. Chem **269**, 9842–9849

29 Murakami, H, Pain, D and Blobel, G (1988) 70-kDa heat shock-related protein is one of at least two distinct cytosolic factors stimulating protein import into mitochondria J Cell Biol **107**, 2051–2057

30 McBride, H M, Millar, D. G, Li, J M and Shore, G C (1992) A signal-anchor sequence selective for the mitochondrial outer membrane J Cell Biol **119**, 1451–1457

31 Iwahashi, J, Takaichi, S, Mihara, K and Omura, T (1994) Reconstitution of import-competent outer membrane vesicles from mammalian mitochondria J Biochem **116**, 156–163

32 Schleiff, E, Silvius, J R and Shore, G C (1999) Direct membrane insertion of voltage-dependent anion-selective channel protein catalyzed by mitochondrial Tom20 J Cell Biol **145**, 973–978

pH-dependence of the fast step of maltose hydrolysis catalysed by glucoamylase G1 from *Aspergillus niger*

Ulla CHRISTENSEN[1]
Kemisk Laboratorium IV, Universitetsparken 5, DK-2100 Copenhagen, Denmark

The presteady-state kinetic parameters of the interaction of wild-type glucoamylase from *Aspergillus niger* (EC 3.2.1.3) with maltose were obtained and analysed in the pH range 3–7 with intervals of 0.25 pH units. In all cases the following three-step reaction scheme was found to apply.

$$E+S \overset{K_1}{\rightleftharpoons} ES_1 \underset{k_{-2}}{\overset{k_2}{\rightleftharpoons}} ES_2 \xrightarrow{k_{cat}} E+P$$

The general result of the analysis of the presteady-state kinetics is that glucoamylase G1 is affected by the protonation states of three groups, with pK_a values of 2.7, 4.5 and 5.7 in the free enzyme and of 2.7, 4.75 and 6.5 in the first enzyme–substrate complex. The protonation of the group in the enzyme–substrate complex with a pK_a 6.5 had no effect on k_2 (1640 s^{-1}) or k_{-2} (20 ± 4 s^{-1}), but resulted in a stronger enzyme–substrate interaction, due to a decrease of K_1 from 40 to 6.3 mM. In other words, when the substrate is bound, the pK_a of the acid group changes to increase the fraction of reactive enzyme. Since this pK_a parallels that of the Michaelis complex, known from the pH-dependence of k_{cat}, the group in question is most probably the catalytic acid Glu-179. Protonation of Glu-179 thus is of no importance in the second step, clearly indicating that this step represents a conformational change and not the actual hydrolysis step of the reaction. Protonation of the pK_a = 4.75 group leads to a small decrease in k_2 to 1090 s^{-1}, and also to minor changes in K_1. The group with pK_a = 2.7 leads to a major decrease of k_2, of which the limit may be zero, but shows no effect on K_1. Thus no difference is seen between the pK_a values of the free enzyme and of the first enzyme–substrate complex at low pH.

Key words: glucoamylase reaction mechanism, presteady-state kinetics.

INTRODUCTION

Glucoamylase (1,4-α-D-glucan glucohydrolase, EC 3.2.1.3) is an inverting exoglycosidase, producing β-D-glucose by hydrolysis of α-1,4-glucosidic bonds, and of α-1,6-bonds with much less efficiency, from the non-reducing end of starch and related oligo- and polysaccharides [1,2]. Glucoamylases from *Aspergilli* exist in two natural forms: G1 and G2. The G1 form from *Aspergillus niger* (Ala-1–Arg-616) consists of a catalytic and a starch-binding domain connected with a highly O-glycosylated linker region.

The three-dimensional structure of the catalytic domain and part of the linker region of glucoamylase from *A. awamori* var. X100 is known [3–8]. The sequences of the glucoamylases from *A. awamori* var. X100 and *A. niger* show 95% amino acid identity and the catalytic sites of the two glucoamylases show no differences [8a].

The proposed and generally accepted mechanism of hydrolysis involves proton transfer to the glycosidic oxygen of the scissile bond from a general acid catalyst, formation of an oxocarbonium ion-like transition state and a nucleophilic attack of water assisted by a general base catalyst [9–12]. Glu-179 and Glu-400 have been identified as, respectively, the general acid and the general base catalysts and the pH-dependencies of steady-state kinetic parameters are in accordance with a rate-determining hydrolysis involving these two catalytic residues [7,13–16].

We have undertaken presteady-state kinetic studies of the mechanism of the *A. niger* enzyme and mutants thereof [8a,17–19] and have found that analysis according to a three-step reaction mechanism (model 1, shown here) of substrate catalysis involving two intermediates showed excellent compatibility:

$$E+S \overset{K_1}{\rightleftharpoons} ES_1 \underset{k_{-2}}{\overset{k_2}{\rightleftharpoons}} ES_2 \xrightarrow{k_{cat}} E+P$$

It has been shown that the presteady-state kinetic results [19] are not in accordance with the classical model [2,21,22] of glucoamylase-catalysed reactions, which involves strong non-productive binding of substrates and intrinsic catalytic-constant values independent of the substrate length.

Figure 1 shows a stereoview of the active site of glucoamylase with bound D-*gluco*-dihydroacarbose. Mutations on the β-flank (as defined in Figure 1) primarily affect the second reaction step [8a]. We interpreted the step as a conformational change, where the substrate reaches the correct position for catalysis after the initial association, in which apparently the formation of hydrogen bonds to Arg-305 and to Glu-180 play important roles [8a]. This is also in accordance with a critical role of Glu-180 for the induction of a productive conformation of isomaltose [23].

We have seen further that mutations on the α-flank result primarily in almost total loss of catalytic turnover, $k_{cat} \rightarrow 0$, and have interpreted this as the lack of correct position of Glu-179 for catalysis in the second reaction step in these mutants. In contrast, it has been suggested that the fast second reaction step is the actual hydrolysis step and that the rate-determining step is a product-release step [24–26]. Clearly these conflicting conclusions need to be resolved. We have therefore studied the pH-dependencies of the presteady-state kinetic parameters in order to determine first of all whether or not the second reaction step shows a pH-dependence corresponding to that expected for a hydrolysis step.

EXPERIMENTAL

Enzymes and substrates

Glucoamylase G1 purified from the commercial preparation (AMG 200L) from Novo Nordisk A/S (Bagsvaerd, Denmark)

---

[1] E-mail u.christensen@pop.ki.ku.dk

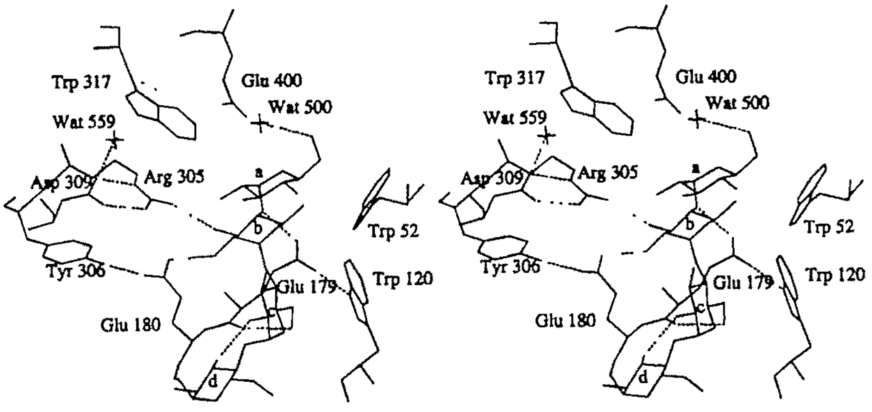

Figure 1 Stereoview of the active site of glucoamylase from *A. awamori* var X100 with bound D-*gluco*-dihydroacarbose [8]

The four rings of the substrate are marked a, b, c and d. Hydrogen-bond interactions less than 3.0 Å are represented by dashed lines, that of Trp-52–Glu-179 (3.04 Å [8]) therefore does not appear. We define the α-flank of the active site as that on the right side of the ligand and the β-flank as that on the left side in this representation. Wat, water

using affinity chromatography on acarbose–Sepharose, as described in [27], and separated from the G2 form by FPLC chromatography on High-Load Q-Sepharose, as described in [28], was a gift from Birte Svensson, Carlsberg Laboratory, Copenhagen, Denmark. Protein concentrations were determined by amino acid analysis [29]. Maltose was from Merck (Darmstadt, Germany). D-Glucose oxidase kits for glucose determination were obtained from Sigma (St. Louis, MO, U.S.A.).

Steady-state kinetics

Initial rates of hydrolysis of the maltose were determined at 8 °C in 0.05 M phosphate buffers, pH 6–7, using seven substrate concentrations in the range $0.125\times K_m$–$8\times K_m$. The final enzyme concentrations were 0.1–1 μM. Glucose released was determined by the glucose oxidase method using microtitre plates [16,30,31].

Stopped-flow fluorescence kinetics

Changes of intrinsic protein fluorescence as a result of ligand binding to glucoamylase in the presteady-state phase of the reactions were observed as described previously [8a,17–19]. Series of experiments were performed using 10 concentrations of maltose in an appropriate range dependent on the pH at 8 °C in 0.1 M sodium acetate buffers, pH 3–6.3 and 0.05 M phosphate buffers, pH 6–7, with 0.25-pH-unit intervals in a Hi-Tech Scientific PQ/SF-53 spectrofluorimeter equipped with a high-intensity xenon arc lamp. The excitation wavelength was 280 nm, the slit width 5 mm. The light emitted from the reaction mixture passed a cut-off emission filter (WG 320; 80 % transmittance at 320 nm). The final enzyme concentrations were in the range of 1.0–1.2 μM. After rapid mixing of enzyme and substrate (less than 1 ms), the time course of the intrinsic fluorescence intensity (arbitrary units, V) was recorded. In total, 400 pairs of data were taken and data from 2–4 experiments were averaged. The averaged stopped-flow data were fitted to several non-linear analytic equations using the Hi-Tech HS-1 Data Pro software. In all cases the single-exponential expression (eqn. 1) resulted in the best fit to the stopped-flow trace. The traces were similar to those obtained previously with the wild-type and mutants of *A. niger* glucoamylase [8a,17–19].

$$\Delta F([S],t) = \Delta F([S],\infty)[1-\exp(-k_{obs}\times t)] \qquad (1)$$

where k_{obs} is the observed first-order rate constant and $\Delta F([S],t)$ is the relative fluorescence change observed at the actual substrate concentration, [S], and time, *t*. $\Delta F([S],\infty)$ is the equilibrium change in fluorescence at a time, *t*, where no (or only negligible) hydrolysis has yet occurred. In no case have changes of the fluorescence corresponding to the pre-equilibrium of the first step in the reaction been observed. The usual control experiments, where the sum of the initial measured fluorescence of an enzyme–buffer mixture and a substrate–buffer mixture is compared with that obtained at zero time from the fit to eqn. (1) of the enzyme–substrate mixture in question, always showed identical values. According to model 1, when no initial change of fluorescence associated with ES_1 is observed, the fluorescence change is proportional to the concentration of ES_2 at any given time. Its final steady-state value at concentration [S] of the substrate, $\Delta F([S],\infty)$, is a hyperbolic function of [S] with the limit value $\Delta F_{max}([S],\infty)$, which is the maximal relative fluorescence change at saturation with the substrate, and with characteristic half-saturation substrate concentration, K_m [19]. The concentration-dependence of k_{obs} in all cases corresponded with the reaction scheme model 1 and provided values of K_1, k_2 and k_{-2} from eqn. (2):

$$k_{obs} = \{k_2/(1+K_1/[S])\}+k_{-2} \qquad (2)$$

The k_{-2} values obtained were almost constant, 20±4 s^{-1}.

Data analysis

The presteady-state and steady-state kinetic parameters were obtained from fits of the values of k_{obs}, $\Delta F([S],4)$ and initial rates as functions of the substrate concentration as described previously [8a]. The pH-dependencies of the parameter values obtained were similarly analysed using the non-linear least-squares fitting software GraFit from Erithacus Software or ENZFITTER from Elsevier BIOSOFT to fit the appropriate equations given below. Double-logarithmic plots were not used

RESULTS

Two carboxylic groups, those of Glu-179 and Glu-400, have been assigned as general acid and general base catalysts, respectively, in the assumed rate-determining hydrolytic reaction step of glucoamylase-catalysed reactions. These are results based on pH-dependencies of steady-state kinetic parameters with pK_a values of ≈ 6 for Glu-179 and ≈ 3 for Glu-400 [14–16], chemical-modification studies [13] and structural data [7]. Here the pH-dependencies of the presteady-state kinetic parameters of the reaction of glucoamylase G1 with maltose were determined.

Figure 2 illustrates the presteady-state results obtained at pH 7, with $k_{obs}-k_{-2}$ (eqn. 2) shown as a function of the maltose concentration. Similar saturation curves were obtained at all the pH values investigated. The resulting values of the parameters at pH 7 (0.1 μM [H^+]) obtained from the fit to eqn. (2) were: $K_1(H^+_{0\ 1\,\mu M})$ 33 mM and $k_2(H^+_{0\ 1\,\mu M})$ 1640 s^{-1}. The $K_1(H^+)$ value decreases in the pH range 7–4 and then becomes constant. At pH 4–3 $K_1(H^+_{0\ 1-1\,mM})$ was 3.8 mM, whereas the $k_2(H^+)$ value was constant in the range pH 7–6, $k_2(H^+_{0\ 1-1\,\mu M})$ = 1640 s^{-1}, and then decreased.

Scheme 1 illustrates the presteady-state reaction (the formation of ES_2 of model 1); just one protonation of the enzyme is taken into consideration. For Scheme 1 the experimentally obtained values of $k_2(H^+)$ and $K_1(H^+)$ are functions of the H^+ concentration, as described in eqns (3) and (4) [32]:

$$k_2(H^+) = k_{2,E} + (k_{2,EH} - k_{2,E})/(1 + K_{ESH}/H^+) \qquad (3)$$

which states that $k_2(H^+)$ changes from the $k_{2,E}$ level to the $k_{2,EH}$ level and follows a saturation curve as H^+ increases from $H^+ \ll K_{EHS}$ to $H^+ \gg K_{EHS}$. If $k_{2,E}$ is known, the difference $[k_2(H^+) - k_{2,E}]$ shows a simple saturation curve as a function of the H^+ concentration (eqn. 3) from which K_{EHS} may be determined. Similarly,

$$K_1(H^+) = K_{1,E} + (K_{1,EH} - K_{1,E})/(1 + K_{ESH}/H^+) \qquad (4)$$

Since, further, a relation exists between the K values (eqn. 5), all the parameters that describe the reaction of Scheme 2 may be obtained from an analysis using eqns (3–5).

$$K_{1,E} \cdot K_{ESH} = K_{1,EH} \cdot K_{EH} \qquad (5)$$

The $k_2(H^+)$ values obtained here decrease with increasing H^+ concentration, the $k_{2,E}$ value thus is larger than the $k_{2,EH}$ value, and the positive difference $[k_{2,E} - k_2(H^+)]$, the saturating value of which is the positive difference $(k_{2,E} - k_{2,EH})$, was analysed. Since $k_2(H^+)$ is constant in the range pH 7–6, the value of $k_{2,E}$ is known to be 1640 s^{-1}. The result of the fit is shown in Figure 3. The fitted curve yielded: $k_{2,EH}$ = 1090 s^{-1}, K_{ESH} = 18.8 μM and pK_a = 4.73 Values obtained at a pH lower than 4.25 did not fit this curve, indicating that a second protonation occurs at pH less than 4. Fitting of eqn. (3) using the value 1090 s^{-1} as $k_{2,E}$ of this second protonation resulted in a second K_{ESH}, of 2.2 mM, with pK_a = 2.7 and a final $k_{2,EH}$ value ≈ 0, as illustrated in Figure 4. These last values are rather poorly determined with standard errors ≈ 30 %, and would have been obtained with greater confidence had the enzyme been stable at a pH lower than 2.75, where it tended to aggregate after 10–15 min.

$K_1(H^+)$ immediately decreases with increasing [H^+] from pH 7, thus a $K_{1,E}$ value is not known, and the three parameters, $K_{1,E}$, $K_{1,EH}$ and K_{ESH}, were determined directly from fitting eqn. (4) to the data (Figure 5) in the pH range 7–5.5. The fitted curve yielded: $K_{1,E}$ = 40 mM, $K_{1,EH}$ = 6.3 mM and K_{ESH} = 0.3 μM, with pK_a = 6.5, and thus (eqn. 5) K_{EH} = 1.9 μM (pK_a = 5.7). Data in the pH range 2.75–5.25 did not fit this curve, indicating an influence of the group with pK_a 4.73 known from the analysis of the $k_2(H^+)$ results. Using the known final $K_{1,EH}$ value (3.8 mM) of this second protonation reaction the two parameters $K_{1,EH}$ and K_{ESH} were obtained from a fit of eqn. (4) to the $K_1(H^+)$ results obtained in the pH range 5–3 (Figure 6). This yielded $K_{1,EH}$ = 6.4 mM and K_{ESH} = 16.5 μM (pK_a = 4.78), each in good agreement with the result obtained from Figure 5 ($K_{1,EH}$ = 6.3 mM) and Figure 3 (K_{ESH} = 18.8 μM) respectively. Scheme 2 summarizes the results obtained. Three protonation reactions influence the presteady-state kinetics of glucoamylase-catalysed hydrolysis of maltose in the pH range 7–3. First protonization of an enzymic group with pK_a = 5.7 in the free enzyme and pK_a = 6.5 in the first enzyme–substrate complex makes the K_1 value decrease from 40 to 6.3 mM, but has no influence on k_2. The second reaction is equally fast, k_2 = 1640 s^{-1}, of the protonated ESH and the unprotonated ES. There next appears a pH effect, slightly decreasing both K_1 and k_2, with a pK_a value of 4.5 for the free enzyme and of 4.75 for the enzyme–substrate complex.

Finally, the k_2 value decreases and apparent H^+ saturation of this enzymic group with a pK_a of 2.7 leads to an apparent final value of k_2 = 0, whereas this process shows no influence on the K_1 value.

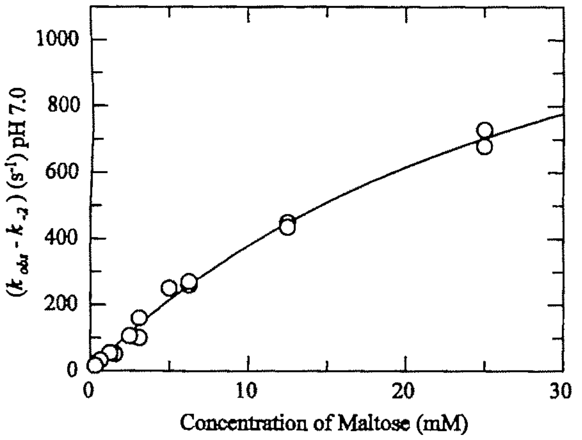

Figure 2 Presteady-state kinetic results of the reaction of glucoamylase G1 with maltose at pH 7

$k_{obs} - k_{-2}$ is shown as a function of maltose concentration The curve is that obtained from fitting eqn (2) to the data with the resulting values of the parameters K_1 = 33 mM and k_2 = 1640 s^{-1}

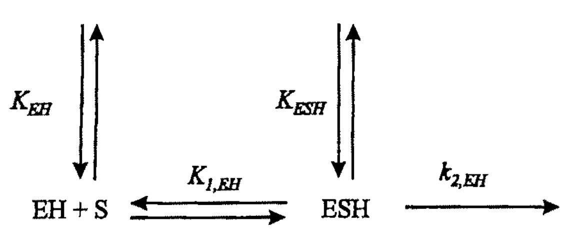

Scheme 1 Reaction scheme illustrating the presteady-state part of the glucoamylase mechanism taking into consideration one protonization of an enzymic group

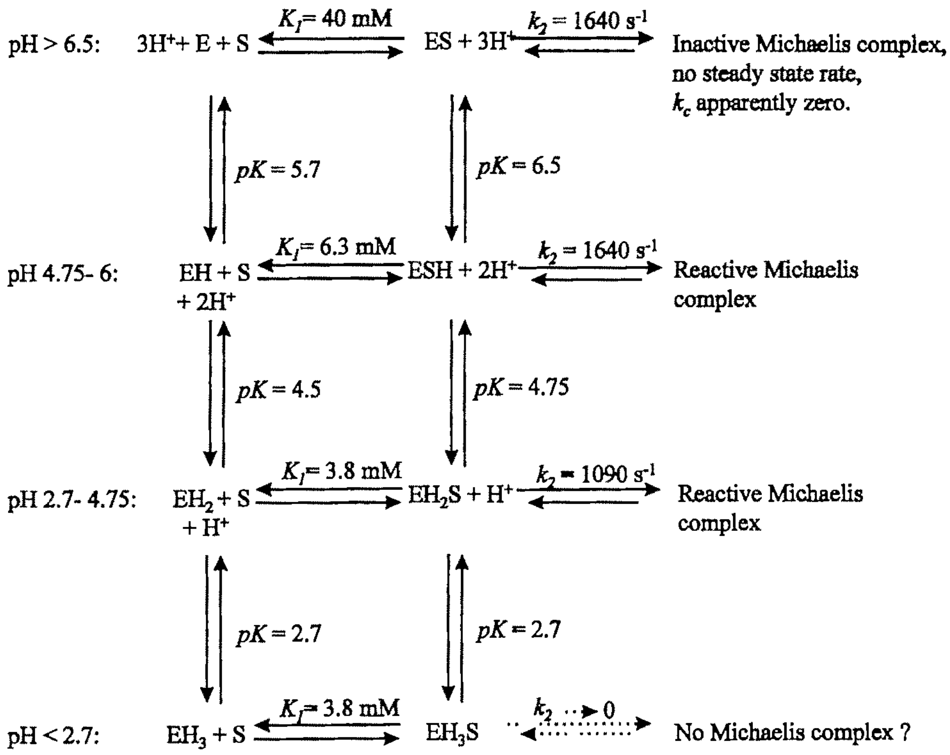

Scheme 2 Reaction scheme showing the pH-dependence of two of the three reaction steps of glucoamylase G1-catalysed hydrolysis of maltose

The dominating reaction(s) at a given pH is indicated. k_c, k_{cat}

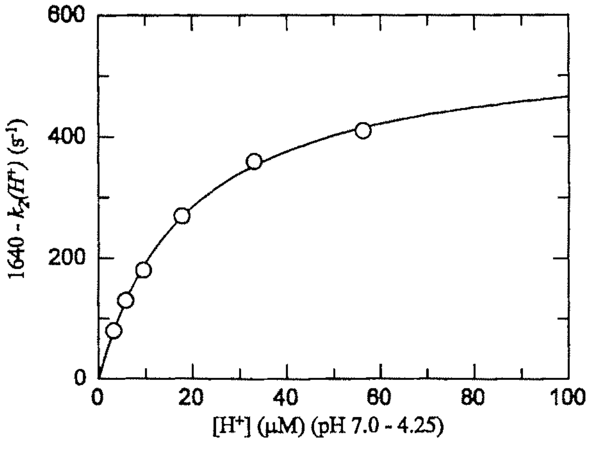

Figure 3 [H$^+$]-Dependence in the pH range 7–4.25 of the presteady-state kinetic parameter k_2(H$^+$) of glucoamylase G1-catalysed hydrolysis of maltose

As expected from eqn (3), the difference [1640 − k_2(H$^+$)] (in s^{-1}) follows a saturation curve when plotted against the concentration of [H$^+$]. The curve is that obtained from fitting eqn (3) to the data with the resulting values of the parameters $k_{2,EH} = 1090$ s^{-1} and $K_{ESH} = 18.8$ mM

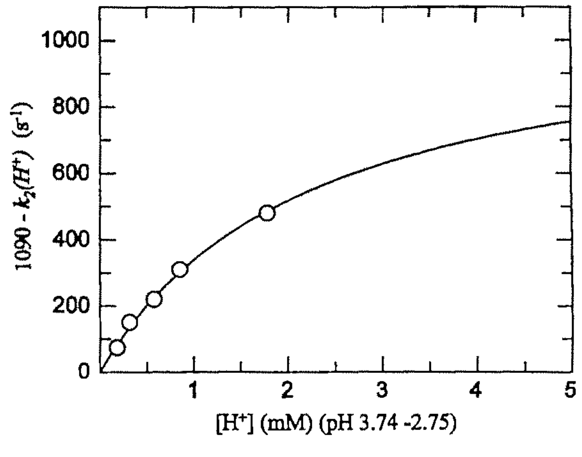

Figure 4 [H$^+$]-Dependence in the pH range 3.74–2.75 of the presteady-state kinetic parameter k_2(H$^+$)

In this range a second protonization is observed The curve shown results from fitting of eqn (3) using the final value of the first protonization 1090 s^{-1} as $k_{2,E}$

DISCUSSION

The generally accepted mechanism of hydrolysis catalysed by glucoamylases involves proton transfer to the glycosidic oxygen of the scissile bond from a general acid catalyst, formation of an oxocarbenium ion-like transition state and a nucleophilic attack of water assisted by a general base catalyst [9–12]. The catalysis occurs with inversion of the anomeric configuration in a single displacement mechanism and the distance between the catalytic acids is 9.2 Å, as is typical for inverting glycoside hydrolases [11,33]. Studies on mutant glucoamylases have shown further a number of other acid residues that affect the glucoamylase-catalysed reactions. Thus mutation of Asp-55 [34,35] and Glu-180 [19,23,36], respectively, show marked effects on the catalytic rate and on the substrate binding.

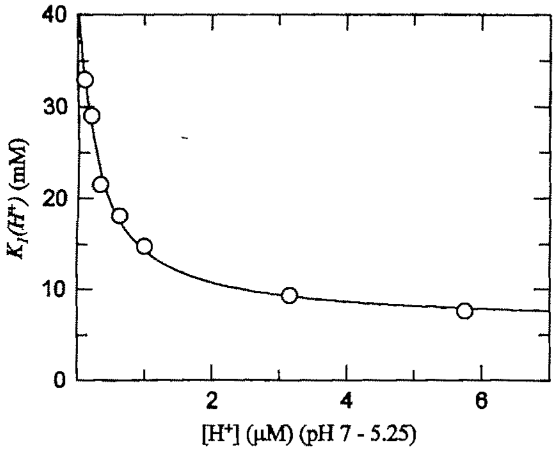

Figure 5 [H+]-Dependence in the pH range 7–5.25 of the presteady-state kinetic parameter $K_1(H^+)$ of glucoamylase G1-catalysed hydrolysis of maltose

The curve shown results from fitting of eqn (4) to the data

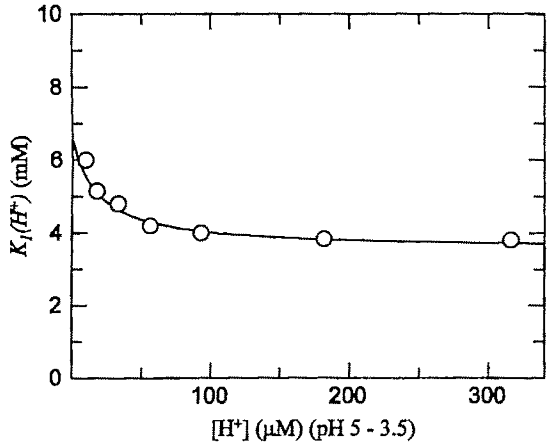

Figure 6 [H+]-Dependence in the pH range 5–3.5 of the presteady-state kinetic parameter $K_1(H^+)$ of glucoamylase G1-catalysed hydrolysis of maltose

The curve shown results from fitting of eqn (4) to the data

Here the pH-dependencies of the first and second steps of glucoamylase G1-catalysed hydrolysis of maltose have been investigated. The presteady-state kinetic parameters obtained show the participation of three groups ionizing in the pH range 7–2.5 (Scheme 2). The first one to be protonated when the H^+ concentration increases shows a pK_a of 5.7 for the free enzyme, E, and a pK_a of 6.5 for the enzyme–substrate complex, ES_1. Since it is found that k_2 is not influenced, and that k_{-2} is approximately the same, the pK_a value of this group is also ≈ 6.5 of the Michaelis complex, ES_2, and is thus the one that shows its effect on k_{cat}. This is in excellent agreement with the steady-state kinetic results, where a pK_a value of 6.4 was obtained from the dependence of k_{cat} on H^+ at 8 °C (results not shown) The group with $pK_a \approx 6.5$ is thus the one defined as the general acid catalyst of glucoamylase and identified as Glu-179. Protonation/deprotonation of this group has no effect on the rate of the second reaction step of model 1; k_2 does not change. We are therefore able to conclude that a conformational change and not hydrolysis of the substrate is occurring in the second reaction step. The rate-determining step of glucoamylase-catalysed reactions with the rate constant k_{cat}, which follows the second step and is dependent on a protonated form of Glu-179, must then be the hydrolysis step It is impossible that the hydrolysis step can be independent of the presence or absence of a protonated catalytic acid but totally govern the release of products, as has been claimed recently [24–26].

The other groups of $pK_a \approx 4.5$ and ≈ 2.75 found here to affect the presteady-state kinetics of glucoamylase are less easy to identify. Glu-400 immediately is a candidate at least for the group with $pK_a \approx 2.75$, whereas the observed effects are too small and relate to a weaker acid of the group of $pK_a \approx 4.5$. In our previous studies of the presteady-state kinetics of glucoamylase and mutants thereof [8a], the second step of the reaction, which, as can now be said with confidence, represents a conformational change resulting in the optimal enzyme–substrate configuration for hydrolysis, was shown to depend on side chains on the β-flank of the active site (Figure 1). Glu-180 plays an important role here, the pattern of hydrogen bonds between Arg-305, Asp-309, Tyr-306 and Glu-180 is disturbed when Glu-180 is mutated to Gln [8a] and protonation of Glu-180 most probably would result in the same effect with marked reduction of k_2. Asp-309 of course may be another candidate. Each of these may be the group with a pK_a of 2.75 (Scheme 2), which strongly affects the rate of the second reaction step, but not K_1. Protonation of this group actually seems to hinder the formation of the normal Michaelis complex to such an extent that this and not the protonation of the catalytic base would govern the decrease of the steady-state rates at very low pH, if the enzyme was stable here.

The presteady-state kinetic parameters are only slightly pertubated by the group of $pK_a \approx 4.5$, and this group does not affect the steady-state kinetics according to previous pH studies [1,13–16]. So this may be any acid group that is not of great importance, perhaps influencing the reaction slightly at a distance from the active site. Also, since the pK_a value in itself makes it possible that the effects stem from the buffer, an acetate ion or an acetic acid molecule may interact with the enzyme and lead to small kinetic effects.

A rate-determining hydrolysis step is supported in model 1:

$$E+S \overset{K_1}{\rightleftharpoons} ES_1 \underset{k_{-2}}{\overset{k_2}{\rightleftharpoons}} ES_2 \xrightarrow{k_{cat}} E+P$$

The claim that product dissociation and not hydrolysis should be the rate-determining step governed by k_{cat} [25,26], seems highly unlikely in the light of the known pH-dependency of k_{cat} [1,14–16], the weak binding of the product glucose [2] and results showing the slower, but nevertheless fast, second reaction steps of a number of mutants [8a,17–19]. The present study of the pH-dependence of the presteady-state kinetic parameters of the interaction of wild-type glucoamylase G1 and maltose has shown further that the k_2 value slightly increases in the range pH 5–7, and does not decrease with the pK_a of the catalytic acid, as would be the case if this step was the actual hydrolysis step.

I am grateful for support from the Danish Research Council's Committee on Biotechnology (grant no 9502014)

REFERENCES

1 Hiromi, K., Takahashi, K., Hamauzu, Z. and Ono, S. (1966) Kinetic studies on glucoamylase III The influence of pH on the rates of hydrolysis of maltose and panose glucosidic linkages J Biochem (Tokyo) 59, 469–475
2 Hiromi, K., Ohnishi, M and Tanaka, A (1983) Subsite structure and ligand binding mechanism of glucoamylase Mol Cell Biochem 51, 79–95

3 Aleshin, A E, Golubev, A., Firsov, L M and Honzatko, R B (1992) Crystal structure of glucoamylase from *Aspergillus awamori* var. X100 to 2 2-Å resolution J. Biol. Chem. **267**, 19291–19298

4 Aleshin, A E., Firsov, L M and Honzatko, R B (1994) Refined structure for the complex of acarbose with glucoamylase from *Aspergillus awamori* var X100 to 2 4-Å resolution J Biol Chem **269**, 15631–15639

5 Aleshin, A E, Hoffman, C, Firsov, L M and Honzatko, R B (1994) Refined crystal structures of glucoamylase from *Aspergillus awamori* var X100 J. Mol Biol **238**, 575–591

6 Aleshin, A E, Stoffer, B., Firsov, L M., Svensson, B and Honzatko, R B (1996) Crystallographic complexes of glucoamylase with maltooligosaccharide analogs relationship of stereochemical distortions at the nonreducing end to the catalytic mechanism Biochemistry **35**, 8319–8328

7 Harris, E M S., Aleshin, A E, Firsov, L M. and Honzatko, R B (1993) Refined structures for the complex of 1-deoxynojirimycin with glucoamylase from *Aspergillus awamori* var X100 to 2 4-Å resolution Biochemistry **32**, 1618–1626

8 Stoffer, B, Aleshin, A E, Firsov, L M, Svensson, B and Honzatko, R B (1995) Refined structure for the complex of D-gluco-dihydroacarbose with glucoamylase from *Aspergillus awamori* var X100 to 2 2-Å resolution. dual conformations for extended inhibitors bound to the active site of glucoamylase FEBS Lett **358**, 57–61

8a Christensen, T, Stoffer, B B, Svensson, B and Christensen, U (1997) Some details of the reaction mechanism of glucoamylase from *Aspergillus niger* Kinetic and structural studies on Trp52 → Phe and Trp317 → Phe mutants. Eur J Biochem **250**, 638–645

9 Sinnott, M L (1990) Catalytic mechanisms of enzymatic glycosyl transfer Chem Rev **90**, 1171–1202

10 Konstantinidis, A and Sinnott, M L (1991) The interaction of 1-fluoro-D-glucopyranosyl fluoride with glucosidases Biochem J **279**, 587–593

11 McCarter, J D and Withers, S G (1994) Mechanisms of enzymatic glycoside hydrolysis Curr Opin. Struct Biol **4**, 885–892

12 Tanaka, Y, Tao, W, Blanchard, J S and Hehre, E J (1994) Transition state structures for the hydrolysis of α-D-glucopyranosyl fluoride by retaining and inverting reactions of glycosylases J Biol Chem **269**, 32306–32312

13 Svensson, B, Clarke, A J, Svendsen, I and Møller, H (1990) Identification of carboxylic acid residues in glucoamylase that participate in catalysis and substrate binding Eur J Biochem **188**, 29–38

14 Sierks, M R, Ford, C, Reilly, P J and Svensson, B (1990) Catalytic mechanism of fungal glucoamylase as defined by mutagenisis of Asp176, Glu179 and Glu180 in the enzyme from *Aspergillus awamori* Protein Eng. **3**, 193–198

15 Bakir, U, Coutinho, P M, Sullivan, P A, Ford, C and Reilly, P. J (1993) Cassette mutagenesis of *Aspergillus awamori* glucoamylase near its general acid residue to probe its catalytic and pH properties Protein Eng. **6**, 939–946

16 Frandsen, T P, Dupont, C, Lehmbeck, J, Stoffer, B, Sierks, M R, Honzatko, R B and Svensson, B (1994) Site-directed mutagenesis of the catalytic base glutamic acid 400 in glucoamylase from *Aspergillus niger* and of tyrosine 48 and glutamine 401, both hydrogen-bonded to the gamma-carboxylate group of glutamic acid 400 Biochemistry **33**, 13808–13816

17 Olsen, K, Svensson, B and Christensen, U (1992) Stopped-flow fluorescence and steady-state kinetic studies of ligand-binding reactions of glucoamylase from *Aspergillus niger* Eur J Biochem **209**, 777–784

18 Olsen, K, Christensen, U., Sierks, M R and Svensson, B (1993) Reaction mechanisms of Trp120 → Phe and wild-type glucoamylases from *Aspergillus niger*. Interactions with maltooligodextrins and acarbose Biochemistry **32**, 9686–9693

Received 7 February 2000/3 April 2000, accepted 5 May 2000

19 Christensen, U, Olsen, K, Stoffer, B B and Svensson, B. (1996) Substrate binding mechanism of Glu180 → Gln, Asp176 → Asn, and wild-type glucoamylases from *Aspergillus niger*. Biochemistry **35**, 15009–15018

20 Reference deleted

21 Hiromi, K (1970) Interpretation of dependency of rate parameters on the degree of polymerization of substrate in enzyme-catalysed reactions Evaluation of subsite affinities of exo-enzyme Biochem Biophys Res Commun. **40**, 1–6

22 Hiromi, K (1995) Kinetic studies on the interaction of glucoamylase with substrates and analogues, In Enzyme Chemistry and Molcular Biology of Amylases and Related Enzymes (Yamamoto, T, ed.), pp. 112–136, CRC Press, Boca Raton

23 Frandsen, T P, Stoffer, B B, Palcic, M M, Hof, S and Svensson, B (1996) Structure and energetics of the glucoamylase-isomaltose transition-state complex probed by using modeling and deoxygenated substrates coupled with site-directed mutagenesis J Mol Biol **263**, 79–89

24 Sierks, M R and Svensson, B (1996) Catalytic mechanism of glucoamylase probed by mutagenesis in conjunction with hydrolysis of α-D-glucopyranosyl fluoride and maltooligosaccharides Biochemistry **35**, 1865–1871

25 Natarajan, S and Sierks, M R (1996) Identification of enzyme-substrate and enzyme-product complexes in the catalytic mechanism of glucoamylase from *Aspergillus awamori* Biochemistry **35**, 15269–15279

26 Sierks, M R, Sico, C and Zaw, M (1997) Solvent and viscosity effects on the rate-limiting product release step of glucoamylase during maltose hydrolysis Biotechnol Progr **13**, 601–608

27 Clarke, A J and Svensson, B (1984) Identification of an essential tryptophanyl residue in the primary structure of glucoamylase G2 from *Aspergillus niger* Carlsberg Res Commun. **49**, 559–566

28 Stoffer, B., Frandsen, T P, Busk, P K, Schneider, P, Svendsen, I and Svensson, B (1993) Production, purification and characterization of the catalytic domain of glucoamylase from *Aspergillus niger* Biochem J **292**, 197–202

29 Svensson, B, Larsen, K, Svendsen, I and Boel, E (1983) The complete amino acid sequence of the glycoprotein, glucoamylase G1 (EC 3 2 1 3), from *Aspergillus niger* Carlsberg Res Commun **48**, 529–543

30 Fox, J D. and Robyt, J F (1991) Miniaturization of three carbohydrate analyses using a microsample plate reader Anal Biochem **195**, 93–96

31 Palcic, M M, Skydstrup, T, Bock, K, Le, N. and Lemieux, R U (1993) Substrate recognition by amyloglucosidases evaluation of conformationally biased isomaltosides Carbohydr Res **250**, 87–92

32 Dissing, J, Rangaard, B and Christensen, U (1993) Activity modulation of the fast and slow isozymes of human cytosolic low-molecular-weight acid phosphatase (ACP1) by purines Biochim Biophys Acta **1162**, 275–282

33 Davies, G and Henrissat, B (1995) Structures and mechanisms of glycosyl hydrolases Structure **3**, 853–858

34 Sierks, M R and Svensson, B (1993) Functional roles of the invariant aspartic acid 55, tyrosine 306, and aspartic acid 309 in glucoamylase from *Aspergillus awamori* studied by mutagenesis Biochemistry **32**, 1113–1117

35 Frandsen, T P, Christensen, T, Stoffer, B., Lehmbeck, J, Dupont, C, Honzatko, R B and Svensson, B. (1995) Mutational analysis of the roles in catalysis and substrate recognition of arginines 54 and 305, aspartic acid 309, and tryptophan 317 located at subsites 1 and 2 in glucoamylase from *Aspergillus niger* Biochemistry **34**, 10162–10169

36 Sierks, M R and Svensson, B (1992) Kinetic identification of a hydrogen bonding pair in the glucoamylase-maltose transition state complex Protein Eng **5**, 185–188

Biochem J (2000) 349, 629–634 (Printed in Great Britain)

Identification of the differential distribution patterns of mRNAs and consensus binding sequences for mouse DAF-16 homologues

Tatsuo FURUYAMA*[1], Toru NAKAZAWA*, Itsuko NAKANO† and Nozomu MORI*†

*Laboratory of Genetics of Aging, Department of Molecular Genetic Research, National Institute for Longevity Sciences (NILS), 36-3 Gengo, Morioka, Oobu, Aichi 474-8522, Japan, and †CREST, Science and Technology Corporation of Japan (JST), 36-3 Gengo, Morioka, Oobu, Aichi 474-8522, Japan

daf-16 is a forkhead-type transcription factor, functioning downstream of insulin-like signals, and is known to be critical to the regulation of life span in *Caenorhabditis elegans*. Mammalian DAF-16 homologues include AFX, FKHR and FKHRL1, which contain a conserved forkhead domain and three putative phosphorylation sites for the Ser/Thr kinase Akt/protein kinase B (PKB), as well as for DAF-16. To assess the function of the homologues, we examined tissue distribution patterns of mRNAs for DAF-16 homologues in mice. In the embryos, expressions of AFX, FKHR and FKHRL1 mRNAs were complementary to each other and were highest in muscle, adipose tissue and embryonic liver. The characteristic expression pattern remained in the adult, except that signals of FKHRL1 became evident in more tissues, including the brain. In order to clarify whether each DAF-16 homologue had different target genes, we determined the consensus sequences for the binding of DAF-16 and the mouse homologues. The binding sequences for all four proteins shared a core sequence, TTGTTTAC, daf-16 family protein-binding element (DBE) binding protein. However, electrophoretic mobility shift assay showed that the binding affinity of DAF-16 homologues to the core sequence was stronger than that to the insulin-responsive element in the insulin-like growth factor binding protein-1 promoter region, which has been identified as a binding sequence for them. We identified one copy of the DBE upstream of the first exon of *sod-3* by searching the genomic database of *C. elegans*. Taken together, DAF-16 homologues can fundamentally regulate the common target genes in insulin-responsive tissues and the specificity to target genes of each protein is partially determined by the differences in their expression patterns.

Key words: forkhead-type transcription factors (AFX, FKHR, FKHRL1), gene regulation, longevity, *sod-3*.

INTRODUCTION

It has been reported that the life span is genetically controlled [1]. The mechanisms of genetic control of aging have been examined in several models, such as *Caenorhabditis elegans*. Friedman and Johnson [2] found a mutant, *age-1*, with a 60 % extension of life span in a screening programme for long-lived mutants. Kenyon et al. [3] exploited a temperature-sensitive dauer mutant, *daf-2*, which caused constitutive entry into diapause, even under conditions of plentiful food. They found that, by moving *daf-2* mutant organisms to a non-permissive temperature, they lived, as L4 larvae, for more than twice the normal life span. Moreover, *daf-2/age-1* double mutants lived no longer than *daf-2* mutants, suggesting that the two genes operate in the same signalling pathway. Life span extension resulting from either *age-1* or *daf-2* mutations is prevented by loss of functional mutations in the *daf-16* gene [3]. Therefore *daf-16* function is a prerequisite for life-span extension through the *daf-2* and *age-1* related signalling pathway. Recent molecular cloning analysis revealed that *daf-2*, *age-1* and *daf-16* encode the homologue of the insulin receptor, phosphatidylinositol 3-kinase and forkhead-transcription factor respectively [4–7]. These results suggest that an insulin-like signalling pathway controls life-span extension in *C. elegans*. More recently, Apfeld and Kenyon [8] revealed, by genetic mosaic analysis, that the daf-2 signalling pathway acts not as a cell-autonomous control system but as a systemic one. Thus, in mammals, DAF-16 homologues may control the transcription of certain intercellular signalling molecules, such as hormones, which are sent to systemic cells. The apparent similarity of the mammalian insulin-signalling pathway to that of the *C. elegans daf-2/age-1/daf-16* pathway raises the possibility that the systemic aging control mechanism may be conserved in evolution. If so, mammalian homologues of daf-16 may regulate an aging-related molecule.

In mammals, three members of the forkhead family of transcription factors, termed AFX, FKHR and FKHRL1, are most similar in amino-acid sequence to DAF-16 and represent the mammalian counterparts of daf-16. The human DAF-16 homologues were first identified at chromosomal breakpoints in human tumours [9–11]. They were reported recently to be phosphorylated by a Ser/Thr protein kinase, Akt/PKB, following insulin or insulin-like growth factor (IGF)-1 stimulation; and to bind the insulin-responsive sequence (IRS) in the insulin-like growth factor binding protein-1 (IGFBP1) promoter (BP-1) [12–18]. The IRS-related sequences also exist in the promoter region of other genes which are known to be down-regulated by insulin, such as phosphoenolpyruvate carboxykinase [19]. However, it is not clear which of the DAF-16 homologues more effectively binds to the IRS or IRS-related sequences. Moreover, if all homologues effectively bind to the sequences, it remains to be determined whether all homologues regulate the same genes *in vivo*.

To clarify these issues, we made two suppositions: (1) that temporally and spatially different expressions of DAF-16 homologues confer the differences in functions *in vivo*, and (2) that one of these homologues has higher affinities for some IRS or IRS-related sequences than the others. In the present study, to

---

Abbreviations used IRS, insulin responsive sequence, DBE, daf-16 family protein-binding element, IGF, insulin-like growth factor, IGFBP1, insulin-like growth factor binding protein-1, BP-1, insulin-responsive sequence in the IGFBP-1 promoter region; EMSA, electrophoretic mobility shift assay, Trx, thioredoxin; IRE, insulin-responsive element

[1] To whom correspondence should be addressed (e-mail tfuruyam@nils go.jp)

investigate the first possibility, we determined the tissue distribution of the mRNAs for these homologues in embryonic and adult tissues. We then identified the binding sequences of the mouse DAF-16 homologues to test the latter.

MATERIALS AND METHODS

cDNA cloning

cDNA clones for mouse DAF-16 homologues, AFX, FKHR and FKHRL1, were obtained by screening a mouse neonatal brain cDNA library (Stratagene) using a PCR fragment corresponding to the region between two amino acid sequences (QIYEWM and WT/STFRP), which is conserved among DAF-16 homologues, as a probe. Cloned cDNAs were edited, and a cDNA containing a full open reading frame for each homologue resulted. Nucleotide sequences were determined on an ABI Prism 377 sequencer using the Big dye sequence kit.

Northern-blot analysis

ICR mice were purchased from SLC (Hamamatsu, Japan). Total RNAs were purified from each tissue using Trizol reagent (Gibco BRL), and 20 μg of total RNA was electrophoresed and blotted on to Gene Screen Plus membranes (NEN). A 660–1604 bp fragment for AFX (database accession number AB032770), a 1107–2257 bp fragment for FKHR (database accession number AF114258) and a 811–2556 bp fragment for FKHRL1 (database accession number AF114259), which locate in the 3′ region to the forkhead domain and have few similarities in their DNA sequences, were labelled with [α-^{32}P]dCTP using a Megaprime labelling kit (Amersham) 18 S ribosomal RNA was used as an internal control. ExpressHyb solution (Clontech) was used under standard conditions of hybridization at 65 °C and the blot was washed at 65 °C in 0.1 × SSC (1 × SSC = 0.15 M NaCl, 0.015 M sodium citrate) containing 0.1 % (w/v) SDS. The blot was exposed to an X-OMAT autoradiography film (Kodak) for 3–7 days at −80 °C.

In *situ* hybridization

ICR mice were mated and the day when a vaginal plug was discovered was recorded as embryonic day zero. Embryonic day 15.5 tissues or tissues of adult mice were frozen using solid CO_2, stored at −80 °C, and 15 μm-thick cryostat sections were prepared just before the *in situ* hybridization procedure described previously [20]. The fragments used in the Northern-blot analysis were inserted into pBluescriptSK− and used as a template for RNA probes. Antisense or sense RNA probes were synthesized with [^{35}S]UTP by T3 or T7 RNA polymerases. Sections were dipped in emulsion NTB2 (Kodak) and exposed for 14–21 days. Sections were observed with OptiPhoto2 (Nikon). Sense probes showed no significant signals

Bacterial expression

The DNA fragment encoding the full sequence of the open reading frames of DAF-16, AFX, FKHR and FKHRL1 was amplified with specific primers with appropriate restriction enzyme sites. The PCR products were digested with *Eco*RI and *Xab*I for AFX, *Bam*H1 and *Xba*I for FKHR and *Bam*HI and *Xho*I for FKHRL1, and were cloned between the corresponding sites in pCDN3.1-myc-His-B (Invitrogen). The fragments excised from the expression vector with *Bam*HI and *Age*I were cloned between *Bam*HI and *Sma*I in the vector pET32a (Novagene), which is designed to produce thioredoxin (Trx)-fused proteins Cultures of *Escherichia coli* BL21 (DE3), harbouring the respective plasmids, were induced with 0.1 mM isopropyl β-D-thiogalactoside and cultured for a further 3–5 h at 37 °C. The bacteria were collected by centrifugation and resuspended in ice-cold buffer. The suspension was sonicated five times at 50 % power for 1 min each time. The lysed bacteria were cleared by centrifugation at 15000 *g* for 30 min at 4 °C. The plasmid proteins were purified using Talon beads (Clontech) using the manufacturer's protocol.

Electrophoretic mobility shift assay (EMSA)

DNA-binding reactions were performed in binding buffer [20 mM Hepes (pH 7.9), 50 mM KCl, 2 mM $MgCl_2$, 0 5 mM EDTA, 10 % (v/v) glycerol, 0.1 mg/ml BSA, 2 mM dithiothreitol] containing 50 ng/ml poly(dI·dC), a probe 5′-end labelled with [γ-^{32}P]ATP and approx. 50 ng of Trx-fusion proteins. After incubation for 15 min at 25 °C, the reaction products were separated by PAGE (4 % polyacrylamide gel) in 0.25 × TBE (22.5 mM Tris/borate, 0.5 mM EDTA) containing 5 % glycerol The gels were dried, exposed for 3–6 h to imaging plates and analysed on BAS2500 (Fuji Film).

Selection of binding sites

A 72-mer oligonucleotide in which the 32 central bases (N32) were completely degenerate, 5′-CGCTCGAGGGATCCGAATTC(N32)TCTAGAAAGCTTGTCGACGC-3′, was synthesized and purified with HPLC. A probe for use in the EMSA was generated using the 72-mer oligonucleotide as a template and primers 5′-GCGTCGACAAGCTTTCTAGA-3′ and 5′-GCGTCGACAAGCTTCTAGA-3′. Following binding to ~ 50 ng of each fusion protein, EMSA was performed and the location of the DNA–protein complexes within the gels was approximated, based on the mobility of complexes generated with the BP-1 probe. The sequence of the BP-1 probe used was 5′-GAGTGCTAGCAAGCAAAACAAACTTATTTTGAACACGGGGATCCAA-3′. Gel slices were homogenized and incubated in gel elution buffer (0.5 M ammonium acetate, 10 mM $MgCl_2$, 1 mM EDTA and 0.1 % SDS) at 37 °C for 3 h. Recovered oligonucleotides were extracted with phenol/chloroform, precipitated with ethanol, reamplified and subjected to the next round of binding. Following completion of the fourth selection–amplification cycles, PCR products were digested with *Eco*RI and *Xba*I and cloned between the corresponding sites in pBluescriptSK−. Between 21 and 25 inserts were sequenced for each DAF-16 homologue.

Transfections and reporter assays

The reporters described here were derived from the pGL3-basic firefly luciferase vector with a minimal TATA box (Promega). Reporters containing the DAF-16 family protein-binding element (DBE) or the BP1 sequences were generated by ligation of concatemerized oligonucleotides to *Bgl*II-digested pGL3 or *Bgl*II–*Nhe*I-digested pGL3 respectively. They were designated p2xDBE-luc (with two copies of the DBE), p4xDBE-luc (with four copies of DBE), p6xDBE-luc (with six copies of the DBE) and pBP1-luc (with one copy of the BP1). The complementary oligonucleotides used for pDBE-luc constructions were 5′-GATCAAGTAAACAACTATGTAAACAA-3′ and 5′-GATCTTGTTTACATAGTTGTTTACTT-3′, whereas those used for pBP-1-luc construction were 5′-GAGTGCTAGCAAGCAAAACAAACTTATTTTGAACACGGGGATCCAA-3′ and 5′-TTGGATCCCCGTGTTCAAAATAAGTTTGTTTTGCTTGCTAGCACTC-3′. NIH3T3 cells grown in 24-well dishes were transfected with 200 ng of each reporter vector, 20 ng of pRL-

TK *Renilla* luciferase vector, as an internal control, and FKHR or *LacZ* expression vectors using LipofectAMINE plus reagents (GIBCO-BRL). For dose–response analysis, 10, 50, 100, 150, 200 or 300 ng of FKHR expression vector were used. *LacZ* expression vector was included in samples to adjust the total expression vector transfected to 300 ng. FKHR (150 ng) or *LacZ* expression vectors were used for examining the effects of multiple copies of DBEs on transcriptional activity. At 24 h after transfection, 50 ng/ml IGF-1 (GIBCO-BRL) or 20 % (v/v) fetal-bovine serum (GIBCO-BRL) was added. Then, 24 h later the relative luciferase activity was determined (the firefly luciferase activity divided by the *Renilla* luciferase activity) using the Dual Luciferase Reporter Assay System (Promega). Statistical significances were calculated using the Student's *t* test.

RESULTS

We first examined the tissue distribution of mRNAs for DAF-16 homologues in the adult by Northern-blot analysis (Figure 1). A single band was detected at approx. 3.4 kb for AFX, approx 6.1 kb for FKHR and approx. 7.5 kb for FKHRL1. AFX mRNA was expressed at a higher level in the heart and skeletal muscle and at a moderate level in brown and white adipose tissues. FKHR mRNA was expressed at a higher level in brown adipose tissue, white adipose tissue and spleen, and a little was detected in liver and skeletal muscle. FKHRL1 mRNA was expressed at a higher level in heart, brain, spleen and kidney and at a moderate level in white adipose tissue and testis but, interestingly, little was detected in skeletal muscle and brown adipose tissue when compared with levels in heart and white adipose tissue. The expression of three genes were detected to a lesser extent in the liver.

The tissue distribution in the day 15.5 embryo was examined by *in situ* hybridization histochemistry (Figure 2). Interestingly, three members showed complementary distribution, and a high level of expression was detected in skeletal muscle for AFX (Figure 2A), in adipose tissue for FKHR (Figure 2B) and in the liver for FKHRL1 (Figure 2F)

We next examined the binding sequences of the three homologues. Each possesses a similar forkhead domain, although they

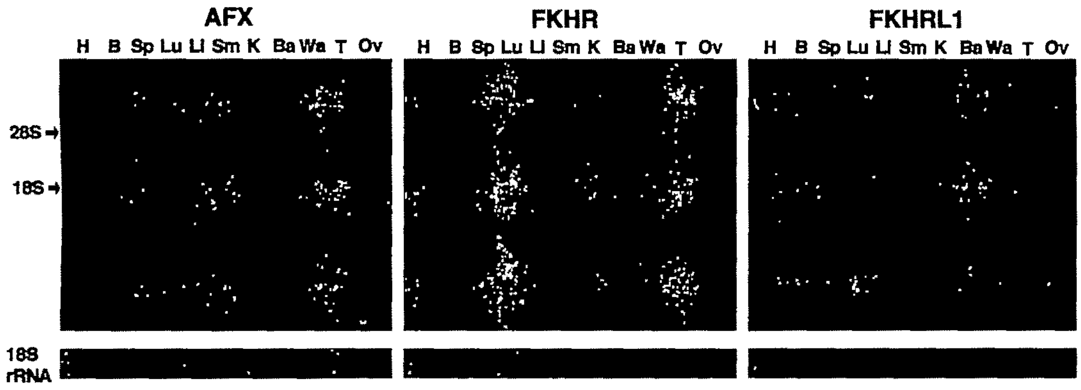
AFX
H B Sp Lu Li Sm K Ba Wa T Ov
FKHR
H B Sp Lu Li Sm K Ba Wa T Ov
FKHRL1
H B Sp Lu Li Sm K Ba Wa T Ov
28S
18S
18S rRNA

Figure 1 Northern-blot analysis of three DAF-16 homologues in adult mouse tissues

Top panel total RNA (20 μg), isolated from ICR mouse tissues, was subjected to electrophoresis and blotted on to a nylon membrane as described in the Materials and methods section The blots were hybridized with ^{32}P-labelled cDNA probes specific for mouse DAF-16 homologues AFX (left panel), FKHR (middle panel) and FKHRL1 (right panel) showed a 3 4-kb, 6 5-kb and 7 1-kb transcripts respectively H, heart, B, brain, Sp, spleen, Lu, lung, Li, liver, Sm, skeletal muscle; K, kidney, Wa, white adipose tissue, Ba, brown adipose tissue, T, testis, Ov, ovary Bottom panel 18 S ribosomal RNA served as an internal control

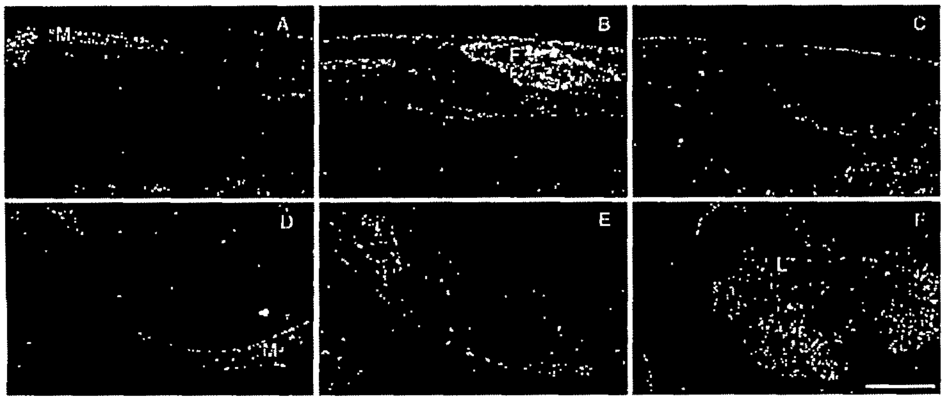

Figure 2 *In situ* hybridization histochemistry showing complementary tissue distribution among DAF-16 homologues in day 15.5 mouse embryos

(A,B) AFX, (C,D) FKHR, (E,F) FKHRL1 The highest expression levels of AFX, FKHR and FKHRL1 respectively were found in (A) skeletal muscles (M), (B) adipose tissue (F), and and (F) embryonic liver (L) Bar = 1 mm

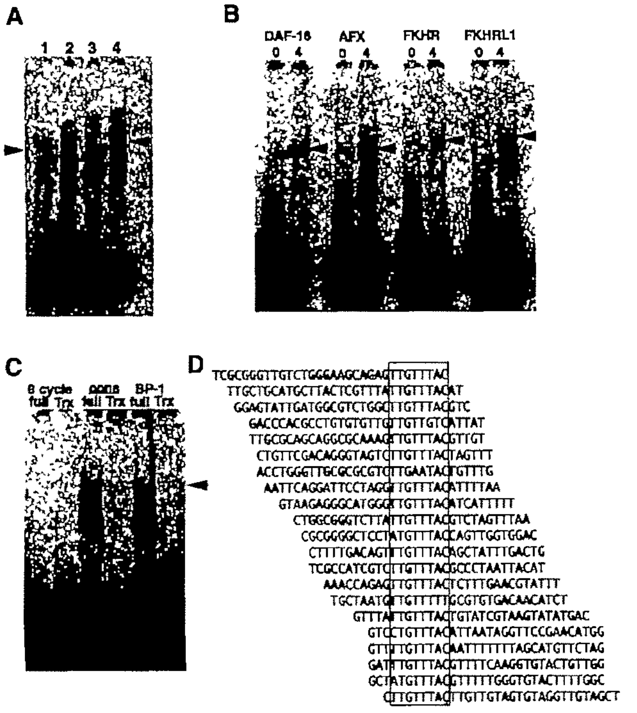

```
TCGCGGGTTGTCTGGGAAGCAGAGTTGTTTAC
   TTGCTGCATGCTTACTCGTTTATTGTTTACAT
    GGAGTATTGATGGCGTCTGGCTTGTTTACGTC
      GACCCACGCCTGTGTGTTGTTGTTGTCATTAT
      TTGCGCAGCAGGCGCAAAGTTGTTTACGTTGT
       CTGTTCGACAGGGTAGTCTTGTTTACTAGTTT
       ACCTGGGTTGCGCGCGTCTTGAATACTGTTTG
        AATTCAGGATTCCTAGGTTGTTTACATTTTAA
          GTAAGAGGGCATGGGTTGTTTACATCATTTTT
            CTGGCGGGTCTTATTGTTTACGTCTAGTTTAA
             CGCGGGGCTCCTATGTTTACCAGTTGGTGGAC
              CTTTTGACAGTTTGTTTACAGCTATTTGACTG
              TCGCCATCGTCTTGTTTACGCCCTAATTACAT
                AAACCAGAGTTGTTTACTCTTTGAACGTATTT
                 TGCTAATGTTGTTTTTGCGTGTGACAACATCT
                    GTTTATTGTTTACTGTATCGTAAGTATATGAC
                      GTCCTGTTTACATTAATAGGTTCCGAACATGG
                      GTTTTGTTTACAATTTTTTTAGCATGTTCTAG
                      GATTTGTTTACGTTTTCAAGGTGTACTGTTGG
                      GCTATGTTTACGTTTTTGGGTGTACTTTTGGC
                        CTTGTTTACTTGTTGTAGTGTAGGTTGTAGCT
```

Figure 3 Selection of binding sites for random-sequence oligonucleotides with Trx–DAF16, Trx–AFX, Trx–FKHR and Trx–FKHRL1 fusion proteins

(**A**) Binding of the BP-1 to DAF-16 and DAF-16 homologues: 1, Trx–DAF16, 2, Trx–AFX, 3, Trx–FKHR, 4, Trx–FKHRL1 (**B**) Enrichment of high-affinity binding sites following four cycles of sequential selection and amplification EMSA of the PCR products obtained after the fourth amplification (4) and the randomized oligonucleotides used as starting material for the selection (0). (**C**) Trx–FKHR fusion protein (cons) showed a shifted band as did the BP-1, but Trx alone did not bind to the consensus sequence. The arrowheads indicate the shifted bands which may be due to degraded products (**D**) Summary of sequences selected with Trx–FKHR The 32 nt, corresponding to the randomized segment of 21 selected PCR products, are shown The core sequence of the FKHR binding site is boxed

vary in their primary structure, suggesting that they may have different DNA binding specificities. First, we confirmed that DAF-16 and DAF-16 homologues could bind to the BP-1 (Figure 3A), as reported previously [12–18]. Binding was performed with a random pool of oligonucleotides, using a variety of PCR/selection strategies described previously [21]. After four rounds of selection and amplification, the enriched oligonucleotides were cloned and sequenced. For each DAF-16 homologue, 21–25 different sequences were compared and a consensus sequence was calculated. To rule out that the Trx moiety of the fusion proteins may have any affinity for the selected sequences, Trx protein alone and with the consensus sequence was also tested by EMSA, and no band shift was evident (Figure 3C). The sequencing results revealed that a related 8-bp sequence (5′-TTGTTTAC-3′) or its complement was present in each clone, for example sequences selected with FKHR (Figure 3D). DAF16, AFX and FKHRL1 also shared a consensus sequence identical to that obtained for FKHR (Figure 4). Moreover, DAF-16 and DAF-16 homologues exhibited different preferences in the 5′ flanking sequence of the consensus sequence, i e. GNA for FKHR and TNG for FKHRL1. In the 3′ flanking region of the consensus sequence they shared a similar sequence, NTTT. This consensus sequence was most similar to that of FREAC-3, another forkhead family member described previously [21].

DAF-16

				Core of binding site									
	-3	-2	-1	1	2	3	4	5	6	7	8	9	10	11
				T	T	G	T	T	T	A	C			
A	4	4	4	1	0	1	0	0	0	22	0	10	8	3
C	3	3	4	0	0	0	0	1	0	0	21	3	5	10
T	7	10	5	23	25	0	25	24	25	1	4	5	7	8
G	9	7	12	1	0	24	0	0	0	2	0	6	3	1

AFX

	-3	-2	-1	1	2	3	4	5	6	7	8	9	10	11
A	8	3	0	0	0	0	0	0	2	19	0	5	5	3
C	6	5	2	0	0	0	0	0	1	0	20	6	2	3
T	4	9	6	22	22	0	22	22	19	3	2	3	13	9
G	4	5	14	0	0	22	0	0	0	0	0	8	1	6

FKHR

	-3	-2	-1	1	2	3	4	5	6	7	8	9	10	11
A	4	4	3	2	0	0	1	1	0	19	0	7	3	0
C	1	2	6	1	0	0	0	0	0	0	20	1	3	5
T	4	10	5	18	21	0	20	20	20	2	1	5	11	10
G	11	4	7	0	0	21	0	0	1	0	0	7	3	2

FKHRL1

	-3	-2	-1	1	2	3	4	5	6	7	8	9	10	11
A	4	5	1	0	0	0	0	0	1	20	0	9	4	9
C	4	4	6	0	0	0	0	0	0	0	19	2	1	2
T	11	7	5	21	22	0	22	22	20	2	2	5	13	8
G	2	5	10	1	0	22	0	0	1	0	1	5	0	0

Figure 4 Summary of selected binding sequences for DAF16, AFX, FKHR and FKHRL1 proteins

The numbers represent the frequency of each nucleotide at each position The number of sequences on which this summary is based is 25 for DAF16, 22 for AFX, 21 for FKHR and 22 for FKHRL1. The core sequence, TTGTTTAC, was shared and the sequence is named as DBE

To test whether the 8-bp consensus sequence (DBE, for daf-16 family member binding element) was sufficient for binding to the DAF-16 homologues, complementary 20-bp oligonucleotide strands containing a single DBE and a single DBE with a single base-pair change of T or G to C (TCGTTTAC, TTCTTTAC, TTGCTTAC and TTGTCTAC) were synthesized and used in an EMSA. The DAF-16 homologues bound the probe containing native DBE, but the mutated probes bound to a much lesser extent or not at all (Figure 5A). The insulin-responsive element (IRE) in the BP-1 is 5′-TT(G/A)TTTTG-3′ and differs from the DBE in the last two bases. We examined for which of the two sequences DAF-16 homologues had a stronger affinity by EMSA with complementary oligonucleotides in which DBE was replaced by a single IRE. All the DAF-16 homologues bound more strongly to the DBE sequence than to the IRE, at least *in vitro* (Figure 5B).

To test whether the DBE recognized by DAF-16 homologues could function *in vivo*, we carried out a reporter assay with p2xDBE-luc, p4xDBE-luc, p6xDBE-luc and pBP1-luc using NIH3T3 cells and the FKHR expression vector. We first examined the dose response of the FKHR expression vector with p2xDBE-luc. The transcriptional activity of the FKHR expression vector increased in a dose-dependent manner and, with ⩾ 100 ng of FKHR expression vector, it was three-fold that with the LacZ vector (Figure 6A). The effects of numbers of copies of the DBE in the promoter region on the transcriptional activity was examined and FKHR showed approximately twice as much reporter activity as LacZ in p2xDBE-luc (Figure 6B). In addition, upon treatment of the cells with IGF-1 or serum, the activity decreased by half. The levels of reporter activity achieved with p4xDBE-luc and p6xDBE-luc were significantly increased to > 4- and 10-fold respectively when compared with that with the LacZ vector alone.

We searched for a candidate for target genes for DAF-16 using the BLASTN program in a genomic database of *C. elegans* (Sanger Center) and identified one copy of the DBE upstream of the first exon of *sod-3* (Figure 7).

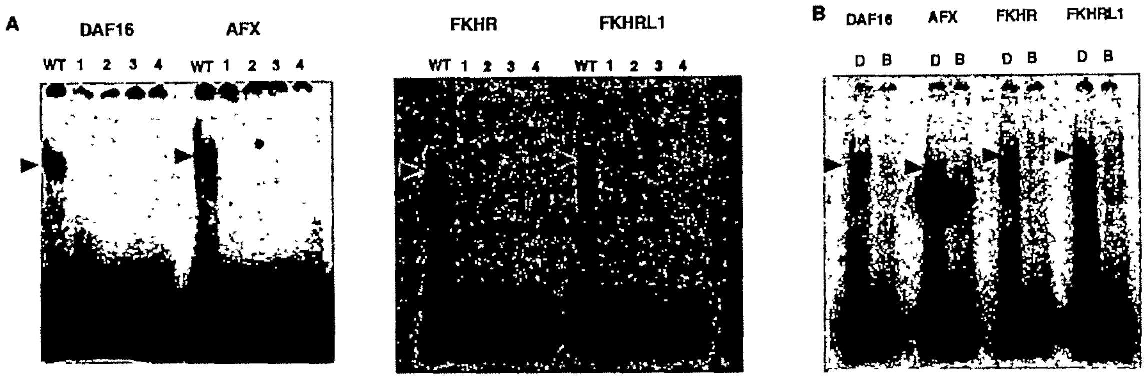

Figure 5 DBE oligonucleotides bind to DAF-16 homologues

(**A**) Examples of EMSA using the Trx-fused DAF-16 homologues and a ^{32}P-labelled DBE probe (WT) or similar probes in which each nucleotide, respectively, of TGTT in TTGTTTAC was changed to C (lanes 1, 2, 3 and 4 respectively) These mutations destroyed the complex of probes and DAF-16 homologues (**B**) EMSA using ^{32}P-labelled DBE (D) or ^{32}P-labelled BP-1 (B) as a probe for examining the affinity for each DAF-16 homologue DAF-16 homologues bound more strongly to the DBE than to the BP-1 Arrowheads indicate the shifted bands due to degraded products

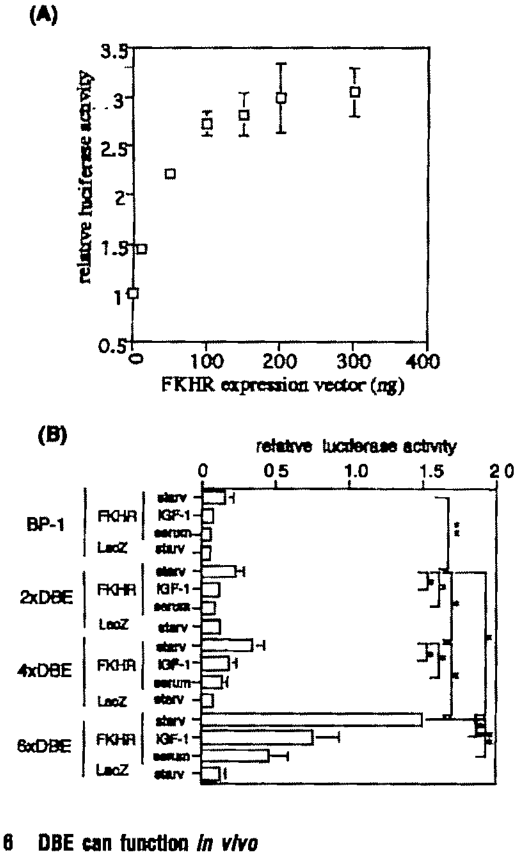

Figure 6 DBE can function *in vivo*

(**A**) The FKHR expression vector increased the relative luciferase activity of a p2xDBE-luc reporter gene in a dose-dependent manner The activity saturated at $\geqslant$ 100 ng of the FKHR expression vector. NIH3T3 cells were transfected with p2xDBE-luc, pRL-TK and various amounts of FKHR expression vector and 48 h after transfection the cells were harvested and assayed as described in the Materials and methods section The relative luciferase activity was determined as the firefly luciferase activity divided by the *Renilla* luciferase activity and the points shown represent the means ± S E M. of three experiments (**B**) NIH3T3 cells were transfected with the indicated plasmids (pBP-1-luc, p2xDBE-luc, p4xDBE-luc and p6xDBE-luc), pRL-TK and FKHR expression vector, and 24 h after the transfection were treated with or without 50 ng/ml IGF-1 or 20% bovine-fetal serum. The transcriptional activities were determined as described in (**A**) The values are the means ± S.E M. of three experiments. Asterisks show statistically significant differences calculated by Student's *t* test (**P* < 0 05 and ***P* < 0 01).

sod-3:

…

tctctttctctcaacaacaatgtgctggccttgcatgtttg
ccagtgcgggttgtttacgcgttttcaagatttttggtctc
ctatctaacgtcccgaaatgcatttttttcctttcatttggt
ttttttctgttcgagaaaagTGACCGTTTGTCAAATCTTCT
AATTTTCAGTGAATAAAATGCTGCAATCTACTGCTCGCACT
GCTTCAAAGCTTGTTCAACCGGTTGCGGGgtaagtcaaaat
gaaattttcgtttaaaaattggtttttttttggtattataga
taaaacttataccaaaacaaaacatatttagaaaaactttta
atagagaataattgtttaataattaatttttgcaagctcct
ttt…

Figure 7 *C. elegans sod-3* is a candidate target gene of DAF-16

One copy of DBE is located upstream of the first exon of *C elegans sod-3* The DBE is underlined and capital letters indicate the exon region

DISCUSSION

In ICR mice, the expression of DAF-16 homologues were detected at a high levels in the insulin/IGF-1 responsive tissues, such as muscle and adipose tissue in both adults and embryos. This was consistent with the regulation of the transcriptional activities of these proteins by insulin/IGF-1 ([12–18]; T. Furuyama, T. Nakazawa, I. Nakano and N. Mori, unpublished work). However, not all insulin responsive tissues expressed the DAF-16 homologues. The distribution pattern of the three DAF-16 homologues was similar in embryos, i.e. AFX, FKHR and FKHRL1 were expressed more strongly in muscle, adipose tissue and liver respectively. The characteristic distribution pattern remained in the adult and AFX mRNA was expressed at a higher level in muscle, and FKHR in brown and white adipose tissue. This suggested that each homologue plays an important role in the regulation of a target gene in a specific tissue. For example, FKHR may regulate a target gene in adipose tissues. However, the signal level of FKHRL1 was found to be higher in many adult tissues than that of embryonic tissues, so it may function in the mature tissues. Moreover, the distribution pattern in the embryos was also similar to that of Akt2 among Akt family members, suggesting that Akt2 is critical in phosphorylating DAF-16 homologues following insulin/IGF-1 stimulation [22]. It remains to be clarified whether Akt2 can phosphorylate DAF-16 homologues more efficiently than Akt1.

We next examined the possibility that each DAF-16 homologue recognized a specific sequence for DNA binding. The DBE selected by each DAF-16 homologue, using binding-site selection, was identical, and was 5′-TTGTTTAC-3′. This sequence includes the sequence conserved among forkhead family members, TRTTTAY. A change of any one base in TGTT to C caused the DAF-16 homologue to dissociate from the DBE. Similarly, the change of G or T to C in TRTTTAY was reported previously to prevent binding to the forkhead domain [21]. Taken together, this suggests that DAF-16 homologues also bind to DNA via a forkhead domain, and a variation from the typical forkhead domain, conserved among the family members, may determine the base pairs flanking TGTT in the DBE. Moreover, the binding-site selection revealed that each DAF-16 homologue exhibits different preferences in the 5′-flanking sequence of the DBE. This difference may determine which target genes each DAF-16 homologue regulates.

The BP-1 has been reported to be recognized by DAF-16 homologues [12–18]. The IREs are TT(G/A)TTTTC and are different from the DBE in the last two bases. EMSA revealed that DAF-16 homologues bound more strongly to the DBE than to the IRE in the BP-1. This finding is consistent with the fact that we detected the DBE sequence exclusively by its binding site. However, it is possible that the common regions flanking the IRE or the DBE in the oligonucleotide probes confer a more rigid affinity for the DBE. Indeed, the regions flanking TRTTTAY were reported to be critical for binding between DNA and the protein in another forkhead family member, FREAC-3 [21].

The reporter gene assays confirmed that the DBE could also function *in vivo*. Since the transcriptional activity was dose-dependent on the FKHR expression vector and copy-number dependent on the DBE, it suggests that DAF-16 homologues could also bind to the DBE *in vivo* and transactivate the reporter genes through the DBE. Moreover, the finding that the transcriptional activity with p2xDBE-luc was higher than that with pBP-1-luc suggests that the DAF-16 homologues bind more strongly to the DBE than the BP-1. In addition, the reporter-gene assay showed that the DBE alone is sufficient for repression by IGF-1 or serum. Indeed, FKHRL1 is phosphorylated by Akt/PKB following stimulation of insulin or serum and translocates to the cytoplasm from the nuclei, which results in a decrease in the amount of FKHRL1 proteins in the nuclei and repression of a target gene ([17]; T. Furuyama, T. Nakazawa, I. Nakano and N. Mori, unpublished work). The translocation in the cells is critical for the determination of transcriptional activities by DAF-16 homologues. However, the DBE is only 8-bp and is similar to a consensus sequence recognized by other forkhead members, and so the specificity may be low. Therefore it is likely that the specificity is increased by interaction with particular molecules and by the different tissue distribution patterns.

In the process of searching for a candidate for the target genes of daf-16 in the genomic database of *C. elegans*, we found one copy of DBE upstream of the first exon of *sod-3*. The product of *sod-3* is a Mn-containing superoxide dismutase and is localized in the mitochondria. It is reported that the expression level of *sod-3* is up-regulated in the dauer larva and the *daf-2* mutant and it disappears in the double mutant *daf-2*/*daf-16* [23]. Our study supports these findings and strongly suggests that DAF-16 directly regulates the expression level of *sod-3* through the DBE.

Recent studies have revealed that mammalian DAF-16 homologues play an important role downstream of the insulin/IGF-1 signalling pathway, as in *C. elegans* [12–18]. However, there is no evidence for a direct relationship between the DAF-16 homologues and the regulation of aging or life span in mammals. To explore the issue further, we need to identify the target genes for DAF-16 homologues and their functions. The DBE may be valuable as a marker in the search for the target genes.

In summary, DAF-16 homologues can fundamentally regulate the same target genes through the DBE, and the specificity of each homologue to the target genes is partially determined by the differences in their expression patterns.

We are grateful to Dr Y Naruse for technical advice regarding the binding-site selection and EMSA, and for useful discussions of our results, and to Dr H Yamashita for technical advice T N is a pre-doctoral fellow at Tohoku University School of Medicine, Japan. This work was supported, in part, by a grant for Longevity Sciences from the Ministry of Health and Welfare to N M

REFERENCES

1 Jazwinski, S M (1996) Science **273**, 54–59
2 Friedman, D. B and Johnson, T. E (1988) Genetics **118**, 75–86
3 Kenyon, C, Chang, J, Gensch, E, Rudner, A and Tabtiang, R (1993) Nature (London) **366**, 461–464
4 Morris, J Z, Tissenbaum, H A and Ruvkun, G (1996) Nature (London) **382**, 536–539
5 Kimura, K D, Tissenbaum, H A, Liu, Y and Ruvkun, G. (1997) Science **277**, 942–946
6 Ogg, S., Paradis, S., Gottlieb, S, Patterson, G I, Lee, L, Tissenbaum, H A and Ruvkun, G (1997) Nature (London) **389**, 994–999
7 Lin, K, Dorman, J B, Rodan, A and Kenyon, C. (1997) Science **278**, 1319–1322
8 Apfeld, J and Kenyon, C (1998) Cell **95**, 199–210
9 Galili, N, Davis, R J, Fredericks, W. J, Mukhopadhyay, S, Rauscher, F J. D, Emanuel, B. S, Rovera, G and Barr, F. G (1993) Nat Genet **5**, 230–235
10 Borkhardt, A., Repp, R, Haas, O A, Leis, T, Harbott, J., Kreuder, J, Hammermann, J, Henn, T. and Lampert, F (1997) Oncogene **14**, 195–202
11 Anderson, M J, Viars, C S, Czekay, S, Cavenee, W K and Arden, K C (1998) Genomics **47**, 187–199
12 Kops, G J., de Ruiter, N. D., De Vries-Smits, A M, Powell, D R, Bos, J L and Burgering, B. M. (1999) Nature (London) **398**, 630–634
13 Guo, S, Rena, G, Cichy, S, He, X, Cohen, P and Unterman, T. (1999) J Biol Chem. **274**, 17184–17192
14 Nakae, J, Park, B C and Accili, D (1999) J Biol. Chem. **274**, 15982–15985
15 Tang, E D, Nunez, G, Barr, F G and Guan, K L (1999) J Biol Chem **274**, 16741–16746
16 Biggs, 3rd, W H., Meisenhelder, J, Hunter, T, Cavenee, W K and Arden, K C (1999) Proc Natl Acad. Sci U.S A **96**, 7421–7426
17 Brunet, A, Bonni, A, Zigmond, M J, Lin, M Z, Juo, P., Hu, L S, Anderson, M J, Arden, K C., Blenis, J. and Greenberg, M E (1999) Cell **96**, 857–868
18 Rena, G, Guo, S, Cichy, S C, Unterman, T G and Cohen, P (1999) J Biol Chem **274**, 17179–17183
19 O'Brien, R M and Granner, D K (1996) Physiol Rev **76**, 1109–1161
20 Nishihara, E, Furuyama, T, Yamashita, S and Mori, N (1998) Neuroreport **9**, 3259–3263
21 Pierrou, S, Hellqvist, M, Samuelsson, L, Enerback, S and Carlsson, P (1994) EMBO J. **13**, 5002–5012
22 Altomare, D A, Lyons, G E, Mitsuuchi, Y, Cheng, J Q and Testa, J. R (1998) Oncogene **16**, 2407–2411
23 Honda, Y. and Honda, S. (1999) FASEB J **13**, 1385–1393

Received 25 October 1999/7 April 2000, accepted 9 May 2000

Biochem J. (2000) 349, 635–640 (Printed in Great Britain)

Substrate specificity of the expressed carotenoid 3,4-desaturase from *Rubrivivax gelatinosus* reveals the detailed reaction sequence to spheroidene and spirilloxanthin

Sabine STEIGER*, Chantal ASTIER† and Gerhard SANDMANN*[1]

*Biosynthesis Group, Botanical Institute, J W Goethe Universität, P.O Box 111930, D-60054 Frankfurt, Germany, and
†Centre de Génétique Moléculaire du CNRS (UPR 9061) associé à l'Université Pierre et Marie Curie, Bâtiment 24, Avenue de la Terrasse,
91198 Gif sur Yvette Cedex, France

Carotenoid biosynthesis in the photosynthetic bacterium *Rubrivivax gelatinosus* leads to the formation of hydroxyspheroidene and spirilloxanthin as the products of a branched pathway. In this study we investigated the role of the desaturase encoded by *crtD* which catalyses the introduction of C-3,4 double bonds into acyclic carotenoids. The desaturase was expressed in *Escherichia coli*, and the activity and the substrate specificity of the enzyme were evaluated *in vitro* by application of structurally different carotenoids. The results indicate that the enzyme is a 3,4-desaturase that converts 1-hydroxy carotenoids. The 3,4-desaturation reaction can only occur with mono-1-hydroxy carotenoids at a ψ-end group or with 1,1′-dihydroxy derivatives carrying a 3′,4′-double bond. In addition, 1-HO-ζ-carotene could also be converted by the desaturase. Enzyme kinetic studies showed a substrate preference of 1-HO-neurosporene over 1-HO-lycopene. Consequences from the biochemical data for the reaction sequence of hydroxyspheroidene and spirilloxanthin formation and the interconnection of both branches are discussed.

Key words: acyclic 1-hydroxy carotenoid 3,4-desaturase, *crtD* gene, enzyme kinetics, *in vitro* assay, spirilloxanthin biosynthesis.

INTRODUCTION

The purple photosynthetic bacteria belonging to the Rhodospirillaceae synthesize acyclic C_{40} carotenoids with C-3,4 conjugated double bonds, which are modified by hydroxy or methoxy groups at position C-1 and/or C-1′. The initial part of all the pathways includes the synthesis and desaturation of phytoene [1]. In *Rhodobacter capsulatus* a single enzyme mediates the desaturation to neurosporene [2], which is then converted by subsequent hydration, desaturation and methylation reactions into hydroxyspheroidene under anaerobic conditions or into the ketocarotenoid spheroidenone in the presence of oxygen [3,4].

In *Rubrivivax gelatinosus* a second branch leads to the biosynthesis of the maximally desaturated carotenoid spirilloxanthin, in addition to the spheroidene pathway [5]. It is not clear whether spirilloxanthin formation in *R gelatinosus* proceeds exclusively via lycopene and its 1- and 1′-hydroxy derivatives or also via spheroidene, which involves hydration of neurosporene. The route of spirilloxanthin biosynthesis has been established in different species of the Rhodospirillaceae, mainly in *Rhodospirillum rubrum* where spirilloxanthin is found as the major carotenoid, based on the identification of intermediates [3,6] and inhibitor studies [7,8] The creation of mutant strains by gene inactivation resulting in the accumulation of intermediates achieved further progress [9,10]. It is generally accepted that lycopene is an important precursor. It is converted into spirilloxanthin by a number of consecutive reactions that operate first at one end of the symmetrical lycopene molecule and then at the other [7]. Lycopene was detected in small amounts as a precursor in deletion mutants of *R. gelatinosus* [9] as well as in the light-harvesting complexes of this bacterium [11]. Nevertheless, an alternative spirilloxanthin pathway which by-passes the formation of 1-HO-lycopene and proceeds via the neurosporene route to spheroidene, as proposed by Eimhjellen and Liaaen-Jensen [6], may exist. In order to establish the precise reaction sequence leading to spirilloxanthin formation in *R. gelatinosus* enzymic studies are indispensable. Only the determination of the substrate specifities of the key enzymes involved in the *R. gelatinosus* spirilloxanthin branch using all putative intermediates will disclose the spirilloxanthin pathway. Several genes coding for the enzymes participating in the carotenoid biosynthesis pathways in the Rhodospirillaceae have been identified [9,12,13]. However, the characterization of the enzymes involved has only just started. Only two of the carotenogenic enzymes, a phytoene desaturase from *Rh. capsulatus* [14] and the 3,4-desaturase of *Rh. sphaeroides*, have been functionally characterized [15].

In this article we report the expression of the *R. gelatinosus crtD* gene in *Escherichia coli* to produce a functional enzyme. After production of putative substrate carotenoids by combination of different carotenogenic genes, detailed studies of the reactions involved in carotenoid biosynthesis were carried out. The definite reaction sequence of hydroxyspheroidene and spirilloxanthin formation in *R. gelatinosus* and the role of the 3,4-desaturase, CrtD, in this pathway could be established.

EXPERIMENTAL

Cultivation

Cells of wild-type *R. gelatinosus* and a mutant, SID2, lacking the *crtD* gene [9], were grown photoheterotrophically at 32 °C in a malate medium [16] for 4 days. *E. coli* JM101 cells containing plasmids with different combinations of carotenogenic genes were used for the production of marker carotenoids and various substrates for enzyme reactions. The plasmids are listed in Table 1, including the references where the constructions were described. Transformants were cultivated for 2 days at 28 °C in

---

[1] To whom correspondence should be addressed (e-mail sandmann@em uni-frankfurt de)

Table 1 Plasmid combinations in *E. coli* JM101 used for the production of substrate carotenoids

Abbreviations used. amp, ampicillin, chl, chloramphenicol, kan, kanamycin, tet, tetracycline Assignment of genes *crtE*, geranylgeranyl pyrophosphate synthase, *crtB*, phytoene synthase, *crtI*$_{Rc}$, phytoene desaturase from *Rhodobacter capsulatus*, *crtI*$_{Eu}$, phytoene desaturase from *Erwinia uredovora*, *crtC*$_{Rg}$, carotene hydratase from *R. gelatinosus*; *crtC*$_{Rc}$, carotene hydratase from *Rhodob capsulatus*; *crtD*$_{Rg}$, carotenoid 3,4-desaturase from *R. gelatinosus*, *al1*, phytoene desaturase from *Neurospora crassa*; *crtP*, phytoene desaturase, *crtY*, lycopene cyclase, *crtF*, 1-HO-carotenoid methylase

Plasmid	Resistance	Gene	Carotenoid formed
pACcrtEBI$_{Rc}$ [24] + pRKcrtC$_{Rc}$ [15]	chl, tet	*crtE*, *crtB*, *crtI*$_{Rc}$, *crtC*$_{Rg}$	1-HO-Neurosporene, 1,1′-(HO)$_2$-neurosporene
pACcrtEBI$_{Eu}$ [24] + pRKcrtC$_{Rc}$	chl, tet	*crtE*, *crtB*, *crtI*$_{Eu}$, *crtC*$_{Rc}$	1-HO-Lycopene, 1,1′-(HO)$_2$-lycopene
pACcrtEBI$_{Rc}$ + pRKcrtC$_{Rc}$ + pUCcrtF [15]	chl, tet, amp	*crtE*, *crtB*, *crtI*$_{Rc}$, *crtC*$_{Rc}$, *crtF*	1-(CH$_3$O)-Neurosporene
pACcrtEBI$_{Eu}$ + pSO50 [9]	chl, tet	*crtE*, *crtB*, *crtI*$_{Eu}$, *crtC*$_{Rg}$, *crtD*$_{Rg}$	1,1′-(HO)$_2$-3,4-Didehydrolycopene
pACcrtEBal1 [15] + pRKcrtC$_{Rc}$ + pSO53	chl, tet, kan	*crtE*, *crtB*, *al1*, *crtC*$_{Rc}$, *crtD*$_{Rg}$	1′-HO-3,4-Didehydrolycopene
pACcrtEBP [24] + pRKcrtC$_{Rc}$	chl, tet	*crtE*, *crtB*, *crtP*, *crtC*$_{Rc}$	1-HO-ζ-Carotene, 1,1′-(HO)$_2$-ζ-carotene
pACCAR16Δcrtx [25] + pRKcrtC$_{Rc}$	chl, tet	*crtE*, *crtB*, *crtI*$_{Eu}$, *crtY*, crtC$_{Rc}$	1-HO-γ-Carotene
PACcrtEBI$_{Rc}$ + pSO50 + pUCcrtF	chl, kan, amp	*crtE*, *crtB*, *crtI*$_{Rc}$, *crtC*$_{Rg}$, crtD$_{Rg}$, *crtF*	1′-HO-Spheroidene
PACcrtEBI$_{Rc}$ + pSO50	chl, kan	*crtE*, *crtB*, *crtI*$_{Rc}$, *crtC*$_{Rg}$, *crtD*$_{Rg}$	Demethylspheroidene, 1-HO-demethylspheroidene
PACcrtEBI$_{Rc}$ + pRKcrtC$_{Rc}$ + pSO53 + pUCcrtF	chl, tet, kan, amp	*crtE*, *crtB*, *crtI*$_{Rc}$, *crtC*$_{Rc}$, *crtD*$_{Rg}$, *crtF*	1-CH$_3$O-1′-HO-3,4-Didehydrolycopene
PaCcrtEBI$_{Eu}$ + pRKcrtC$_{Rc}$ + pSO50 + pUCcrtF	chl, tet, kan, amp	*crtE*, *crtB*, *crtI*$_{Eu}$, *crtC*$_{Rg}$, *crtD*$_{Rg}$, *crtF*	1-CH$_3$O-3,4-Didehydrolycopene

Luria–Bertani broth [17] in the presence of chloramphenicol (35 μg/ml), ampicillin (100 μg/ml), kanamycin (25 μg/ml) or tetracycline (25 μg/ml) according to the plasmids used.

Protein expression and *in vitro* enzyme reaction

E. coli strain JM101 was the host for the plasmid pSO53, which carries the desaturase gene *crtD* from *R. gelatinosus*. The pSO53 plasmid was constructed from the pSO50 plasmid. The pSO50 plasmid contained a 3-kb *SacI* fragment encoding *crtD–C* genes under the control of the *lac* promoter [18]. The downstream fragment from the *Bam*HI site to the end was deleted to keep only the *crtD* gene Cultures were grown in Luria–Bertani broth [17] containing kanamycin (25 μg/ml) at 37 °C until an attenuance (D_{600}) of 0.1 was reached. Protein expression was induced by addition of isopropyl β-D-galactoside to a final concentration of 0.4 mM and incubation at 28 °C overnight.

The cells were harvested by centrifugation at 6000 *g* for 15 min at 4 °C, resuspended 1:20 in 50 mM potassium phosphate buffer, pH 7.8, and broken by two passages through a French pressure cell at 95 MPa The homogenate was incubated with DNase (10 μg/ml) on ice for 10 min. After centrifugation at 40000 *g* for 20 min at 4 °C the supernatant (500 μl; approx. 6 μg of desaturase) was used for enzyme assays *in vitro* in a final volume of 1 ml. Purified carotenoids (3 μg) were added in lipid suspension (100 μg of soya-bean lipid/ml of buffer). To determine the K_m values carotenoid concentrations from 2 to 50 μM were used. Assays were incubated for 18 h under shaking at 28 °C in the dark.

The amount of the desaturase was estimated after SDS/PAGE on 15% gels [19] after staining the polypeptides with Coomassie Brilliant Blue Total protein was determined using the method of Bradford [20].

Carotenoid extraction and HPLC analysis

Carotenoids were extracted from freeze-dried *R. gelatinosus* cells and *E. coli* transformants by addition of methanol containing 6% KOH and heating for 20 min at 60 °C. Extracts were partitioned against 10% ether in petrol. The upper phase was collected and evaporated. Separation of the carotenoids was carried out by chromatography on aluminium oxide as described previously [15]. If necessary they were purified further by HPLC. The HPLC system used for purification and for separation of substrates from products after the enzymic reactions consisted of a Nucleosil C_{18} 3-μm column (Macherey-Nagel, Düren, Germany) with acetonitrile/methanol/2-propanol (75:17.5:7.5, by vol.) as eluent. Carotenoids were identified and quantified with authentic standards, by their retention times and their absorbance spectra, which were recorded from the elution peaks using a Kontron diode-array detector model 440 [15].

RESULTS

Comparison of the carotenoid content (Figure 1) of the *R. gelatinosus* wild-type cells and the mutant cells lacking *crtD* give a first indication of the role of the desaturase in the carotenoid

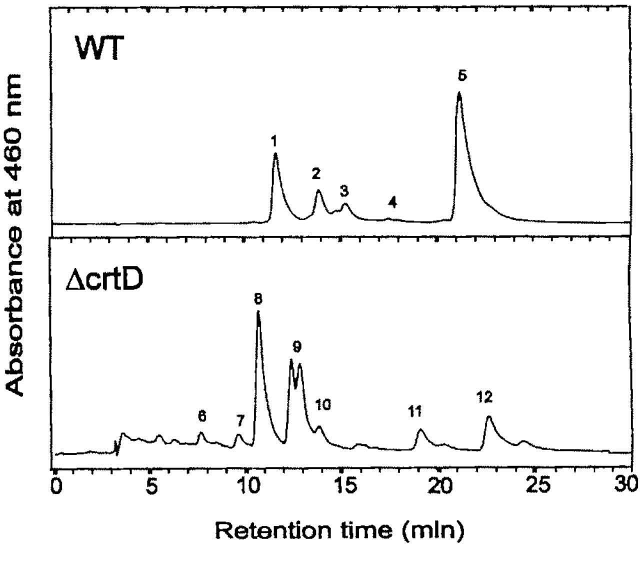

Figure 1 HPLC separation of the carotenoids of *Rubrivivax gelatinosus* wild-type (WT) and the mutant lacking a functional *crtD* gene

Peaks correspond to 1, 1′-HO-spheroidene, 2, spirilloxanthin, 3, 1-CH$_3$O-3,4-didehydrolycopene; 4, demethylspheroidene, 5, spheroidene, 6, 1,1′-(HO)$_2$-neurosporene, 7, 1-CH$_3$O-1′-HO-lycopene, 8, 1-CH$_3$O-1′-HO-neurosporene, 9, 1-HO-neurosporene, 10, 1-CH$_3$O-lycopene, 11, 1-CH$_3$O-neurosporene, 12, neurosporene

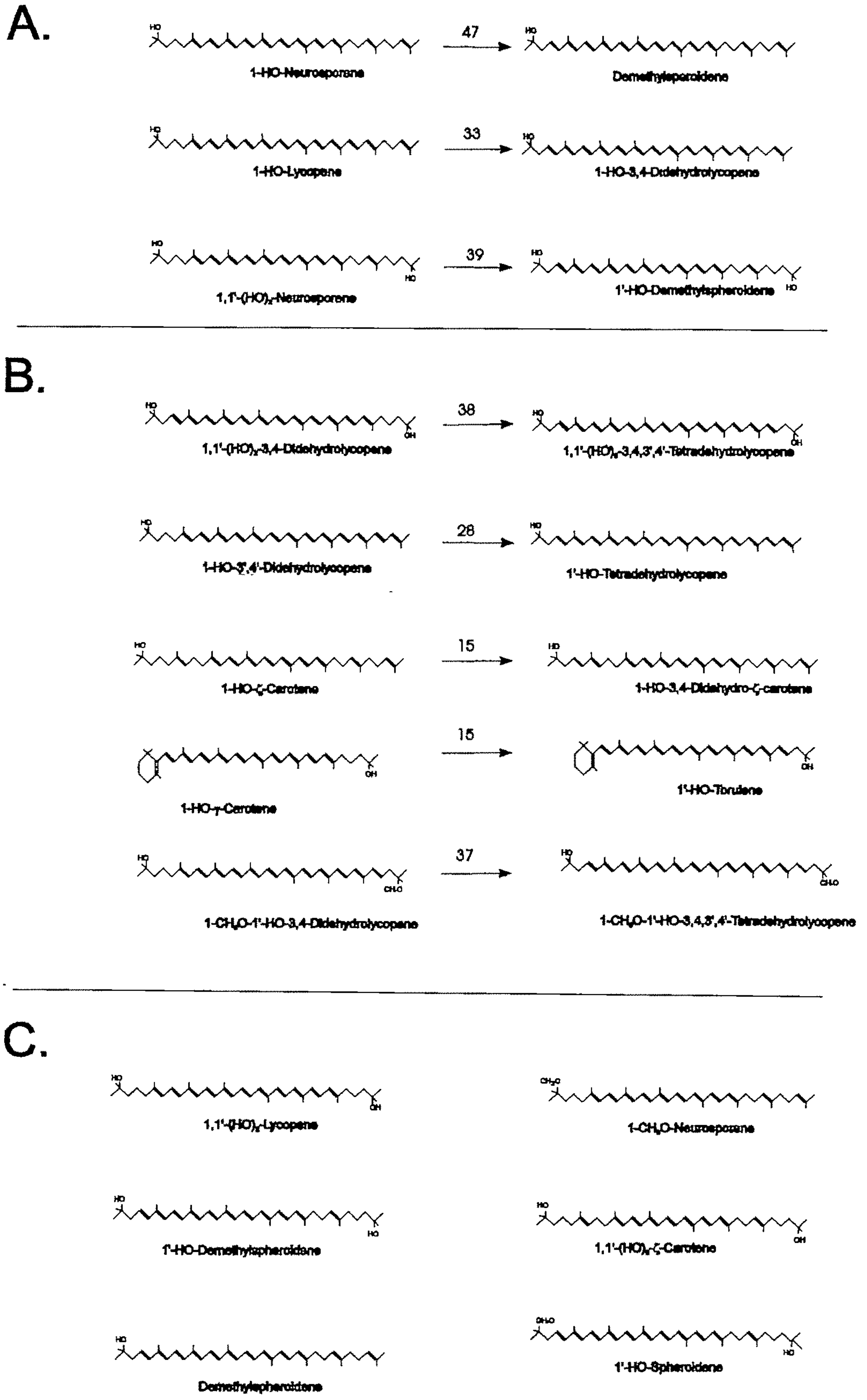
A.
HO
47
1-HO-Neurosporene
Demethylspheroidene
33
1-HO-Lycopene
1-HO-3,4-Didehydrolycopene
39
1,1'-(HO)$_2$-Neurosporene
1'-HO-Demethylspheroidene
B.
38
1,1'-(HO)$_2$-3,4-Didehydrolycopene
1,1'-(HO)$_2$-3,4,3',4'-Tetradehydrolycopene
OH
28
1-HO-3',4'-Didehydrolycopene
1'-HO-Tetradehydrolycopene
15
1-HO-ζ-Carotene
1-HO-3,4-Didehydro-ζ-carotene
15
1-HO-γ-Carotene
1'-HO-Torulene
37
1-CH$_3$O-1'-HO-3,4-Didehydrolycopene
1-CH$_3$O-1'-HO-3,4,3',4'-Tetradehydrolycopene
CH$_3$O
C.
1,1'-(HO)$_2$-Lycopene
1-CH$_3$O-Neurosporene
1'-HO-Demethylspheroidene
1,1'-(HO)$_2$-ζ-Carotene
Demethylspheroidene
1'-HO-Spheroidene

Figure 2 Substrate specificity and catalytic reactions of the carotenoid 3,4-desaturase, CrtD

Percentage conversions of 3 μg of the corresponding substrate with enzyme extracts containing 6 μg of desaturase for 18 h are shown above the arrows. (**A**) Substrates with the highest conversion of 40–50% under the reactions indicated in the Experimental section (**B**) Conversion of 20–40% (**C**) Carotenoids that where not converted by CrtD.

Table 2 Kinetic parameters for the most efficient substrates of CrtD from *R. gelatinosus*

K_m and V_{max} values are the means of at least three determinations obtained from double-reciprocal plots of the reaction rates versus the substrate concentrations with 5–8 data points and a correlation coefficient for linearity of > 0.98. The S.D. values for both parameters were in the range of 14–24% of the mean values.

Substrate	K_m (μM)	V_{max} (nmol·mg of protein^{-1}·h^{-1})	V_{max}/K_m ($\times 10^{-2}$)
1-HO-Neurosporene	25	1.35	5.4
1,1′-$(HO)_2$-Neurosporene	19	0.58	3.0
1-HO-Lycopene	40	0.69	1.7

pathway. The major carotenoids in the wild-type *R. gelatinosus* grown under anaerobic conditions were spheroidene (Figure 1, peak 5) and 1′-HO-spheroidene (peak 1), with absorption maxima at 430, 455 and 470 nm. Another product was spirilloxanthin (peak 2), a carotenoid with absorption maxima at 470, 495 and 515 nm. The intermediates were identified as 1-CH_3O-3,4-didehydrolycopene (peak 3) and demethylspheroidene (peak 4). The *R. gelatinosus* mutant showed a different carotenoid pattern. The neurosporene-related carotenoids 1-HO-neurosporene (peak 9), 1,1′-$(HO)_2$-neurosporene (peak 6), 1-CH_3O-1′-HO-neurosporene (peak 8) and 1-CH_3O-neurosporene (peak 11), with their typical absorption spectra of 410, 440 and 470 nm, were accumulated. In addition the lycopene derivatives 1-CH_3O-1′-HO-lycopene (peak 7) and 1-CH_3O-lycopene (peak 10), with typical absorption maxima of 440, 470 and 490 nm, were enriched.

Determination of the specificity of the carotenoid 3,4-desaturase CrtD for a range of substrates that may be alternatively involved as intermediates is the ultimate procedure for the study of the formation of spirilloxanthin in *R. gelatinosus*. For enzymic investigations, the functional expression of the 3,4-desaturase was optimized and monitored by SDS/PAGE. The yield of this protein was 3–5% of the total *E. coli* protein. After disruption of the *E. coli* cells under high pressure and centrifugation, the protein was enriched in the supernatant, and could be used without additional solubilization for enzymic characterization.

Structurally different carotenoids, which can all be considered putative substrates and which may play a possible role as intermediates in the carotenoid pathway of *R. gelatinosus*, were used for characterization of the enzyme *in vitro*. Figure 2 shows the carotenoid substrate specificity for 1-hydroxy derivatives and the catalytic reactions of the 3,4-desaturase. Among the carotenoids tested, 1-HO-neurosporene, 1-HO-lycopene and 1,1′-$(HO)_2$-neurosporene were the most efficient substrates for the 3,4-desaturase. Under our conditions, 47, 33 and 39%, respectively, of these substrate carotenoids were converted into demethylspheroidene, 1-HO-3,4-didehydrolycopene and 1′-HO-demethylspheroidene.

As 1-HO-neurosporene, 1-HO-lycopene and 1,1′-$(HO)_2$-neurosporene are putative branching products for the carotenoid pathway in *R. gelatinosus*, enzyme kinetic studies were performed using these substrates. K_m values were determined to be 25 μM for 1-HO-neurosporene, 40 μM for 1-HO-lycopene and 19 μM for 1,1′-$(HO)_2$-neurosporene. The corresponding V_{max} values were 1.35 nmol·h^{-1}·mg^{-1} for 1-HO-neurosporene, 0.69 nmol·h^{-1}·mg^{-1} for 1-HO-lycopene and 0.58 nmol·h^{-1}·mg^{-1} for 1,1′-$(HO)_2$-neurosporene, respectively (Table 2).

To determine the structural characteristics recognized by the desaturase, different carotenoids were used in the assay *in vitro*. Not only were the 3,4-didehydrolycopene derivatives 1,1′-$(HO)_2$-3,4-didehydrolycopene, 1-CH_3O-1′-HO-3,4-didehydrolycopene and 1′-HO-3,4-didehydrolycopene converted by 38, 37 and 28%, respectively, by the enzyme but also were 1-HO-ξ-carotene and 1-HO-γ-carotene, by 15% each. In contrast, the dihydroxy derivatives 1,1′-$(HO)_2$-lycopene and 1,1′-$(HO)_2$-ξ-carotene and the neurosporene derivatives 1-CH_3O-neurosporene, 1′-HO-demethylspheroidene and demethylspheroidene were not recognized as substrates by the 3,4-desaturase. For each enzyme preparation 1-HO-neurosporene was used as a positive control to ensure enzyme activity in the range of 42–48% conversion.

DISCUSSION

Substantial progress to elucidate the individual steps of carotenoid biosynthetic pathways can be made by the development of enzyme assays *in vitro* [21]. We followed this strategy for the carotenoid 3,4-desaturase CrtD from *R. gelatinosus*. Thus it was possible to express from the encoding gene a soluble form of this protein which due to its high activity was suitable for enzyme kinetic studies. The characterization of the enzymic properties of CrtD showed that this desaturase is able to convert structurally different substrates participating simultanously in the biosynthesis of hydroxyspheroidene as well as of spirilloxanthin. Furthermore, deletions of a single *crtD* gene in *R. gelatinosus* resulted in the accumulation of intermediates of both branches, all lacking the 3,4-double bond (Figure 1).

The results of Figure 2 indicate that generally a hydroxy group at position C-1 is required for the 3,4-desaturation reaction. But other structural features of the substrate molecule also determine acceptance by the enzyme. Substrate molecules derived from 1-HO-lycopene are converted, but only if no additional hydroxy group is located on the other end of the molecule in position C-1′. Thus, 1-HO-lycopene is converted into 1-HO-3,4-didehydrolycopene as well as 1-HO-γ-carotene, and 1′-HO-3,4-didehydrolycopene into 1′-HO-torulene and 1′-HO-tetradehydrolycopene, whereas 1,1′-$(HO)_2$-lycopene is not a substrate. However, conversion of dihydroxylycopene derivatives occurs only if one of the hydroxy or corresponding methoxy groups is accompanied by an additional double bond in position C-3,4, as in 1,1′-$(HO)_2$-3,4-didehydrolycopene or 1-CH_3O-1′-HO-3,4-didehydrolycopene. Unlike lycopene derivatives, 1-HO-neurosporenes are desaturated at position C-3,4 regardless of the presence or absence of a hydroxy group at the C-1′ end of the molecule. However, desaturation occurs only at the half of the molecule that resembles lycopene, as shown by the conversion of 1-HO-neurosporene into demethylspheroidene, and of 1,1′-$(HO)_2$-neurosporene into 1-HO-demethylspheroidene. When the 1-hydroxy group is replaced by a methoxy group, 3,4-desaturation is inhibited. Thus the C-3,4 desaturase from *R. gelatinosus* is functional as a 1-hydroxy carotenoid desaturase but not as a 1-methoxy carotenoid desaturase, as shown previously for the 1-HO-neurosporene desaturase from *Rh. sphaeroides* [15].

Taking the results presented in Figure 2 the individual steps of the reaction sequence to hydroxyspheroidene and also to spirilloxanthin in *R. gelatinosus* are outlined in Scheme 1. The general reaction sequence involving CrtD is hydration of the isopropylidene end group of lycopene or neurosporene, followed by a dehydrogenation to indroduce a C-3,4 double bond at the hydroxylated end and a final methylation of the hydroxy group. In case of hydroxyspheroidene synthesis the desaturation of hydroxyneurosporene leads to demethylspheroidene, followed by the methylation of the hydroxy group to spheroidene and addition of water to the double bond at C-1′,2′. The results

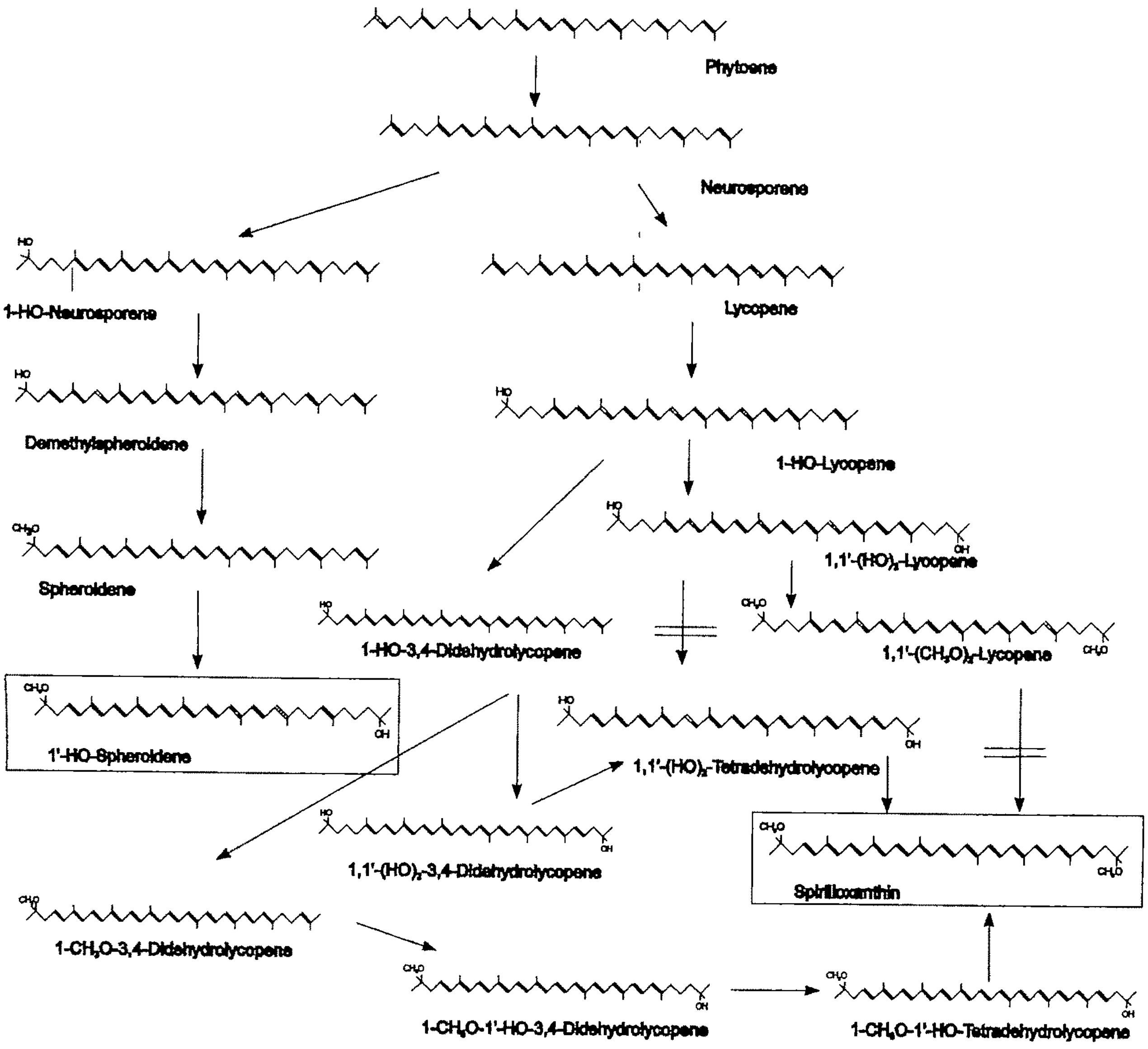
Phytoene
Neurosporene
1-HO-Neurosporene
Lycopene
Demethylspheroidene
1-HO-Lycopene
Spheroidene
1,1'-(HO)$_2$-Lycopene
1-HO-3,4-Didehydrolycopene
1,1'-(CH$_3$O)$_2$-Lycopene
1'-HO-Spheroidene
1,1'-(HO)$_2$-Tetradehydrolycopene
1,1'-(HO)$_2$-3,4-Didehydrolycopene
Spirilloxanthin
1-CH$_3$O-3,4-Didehydrolycopene
1-CH$_3$O-1'-HO-3,4-Didehydrolycopene
1-CH$_3$O-1'-HO-Tetradehydrolycopene
HO
OH
CH$_3$O

Scheme 1 Individual reactions involved in the biosynthesis of 1'-hydroxyspheroidene and spirilloxanthin in *R. gelatinosus*

exclude that the desaturation step occurs before the transfer of the methyl group. This finding is in contrast with the postulation by Davies [7] for *Rh. sphaeroides* that in spheroidene biosynthesis 3,4-dihydrospheroidene is an intermediate rather than demethylspheroidene, but confirms the pathway established by Liaaen-Jensen et al. [3].

The initial reaction for the biosynthesis of spirilloxanthin is the formation of 1-HO-lycopene. This direct route proceeds via 1-HO-didehydrolycopene in *R. gelatinosus* (Scheme 1). From 1-HO-didehydrolycopene onwards, the pathway branches by either formation of the 1'-hydroxy group or methylation of the 1-hydroxy group, yielding 1,1'-(HO)$_2$-didehydrolycopene or 1-CH$_3$O-3,4-didehydrolycopene, respectively. After establishment of the 1'-hydroxy group of the latter carotenoid, they are further desaturated by CrtD and metabolized to spirilloxanthin by methylation of the hydroxy group. Obviously, the generalization [7] that one side of the molecule should be processed completely before the other side is substituted is not absolutely strict for the spirilloxanthin pathway in *R. gelatinosus* and can be modified slightly in such a way that, after one 3,4-desaturation step, introduction of the second hydroxy group at C-1' may occur before the hydroxy group at C-1 is methylated. This reaction sequence can also be concluded for spirilloxanthin synthesis in *Rhodosp. rubrum* because 3,4,3',4'-tetrahydrospirilloxanthin was detected in a mutant with an inactivated *crtD* gene [10].

The formation of 1,1'-(HO)$_2$-lycopene, which is catalysed by the *crtC*-encoded hydratase from *R. gelatinosus* (S. Steiger and G. Sandmann, unpublished work), leads to a dead end of the spirilloxanthin biosynthetic branch. One of the expected hydroxy and methoxy products, 1-CH$_3$O-1'-HO-lycopene was found only in the mutant with the deleted *crtD* gene (Figure 1).

Our investigation gave no evidence for an additional reaction sequence to spirilloxanthin via the spheroidene branch. 1'-HO-Demethylspheroidene, demethylspheroidene and 1'-HO-spheroidene were not converted by CrtD. However, for a final conclusion that both branches operate independently, one has to wait for the availability of the *crtI* gene from *R. gelatinosus* and use it to evaluate whether the corresponding enzyme is able to desaturate the 7′,8′ position of 1′-HO-spheroidene.

When the neurosporene-derived spheroidene pathway of *R. gelatinosus* is compared with the lycopene-derived spirilloxanthin branch, it is obvious that the decisive difference is at the level of the phytoene desaturation. In addition to CrtI, the subsequent enzymes of the pathway have also adapted to simultanous spheroidene or spirilloxanthin synthesis. This is the case for CrtD from *R. gelatinosus* but enzyme kinetic studies revealed a higher affinity for 1-HO-neurosporene than for 1-HO-lycopene (Table 2). Furthermore, V_{max}/K_m ratios were determined for different substrates. These specificity constants indicate the substrate preference of an enzyme [22,23]. The $>$ 3-fold-higher value for 1-HO-neurosporene over 1-HO-lycopene demonstrates that this substrate is much better converted by CrtD.

The present investigation provided a better understanding of the existing and possible enzymic reactions involved in the hydroxyspheroidene and spirilloxanthin pathways of *R. gelatinosus* and of the separation of both metabolic branches. When other enzymes from this bacterium, especially its phytoene desaturase CrtI and hydratase CrtC, are available and accessible to enzymic studies, the detailed overall picture of hydroxyspheroidene and spirilloxanthin synthesis will be completed.

This work was supported by the Deutsche Forschungsgemeinschaft

REFERENCES

1 Goodwin, T W (1980) The Biochemistry of the Carotenoids, vol. 1, Chapman and Hall, London

2 Linden, H, Misawa, N, Chamovitz, D., Pecker, I, Hirschberg, J and Sandmann, G. (1991) Functional complementation in *Escherichia coli* of different phytoene desaturase genes and analysis of accumulated carotenes Z Naturforsch **46c**, 1045–1051

3 Liaaen-Jensen, S, Cohen-Bazire, G and Stanier, R Y (1961) Biosynthesis of carotenoids in purple bacteria a re-evaluation based on consideration of chemical struture Nature (London) **192**, 1168–1172

4 Scolnik, P, Walker, A. M A and Marrs, B. L (1980) Biosynthesis of carotenoid derivatives derived from neurosporene in *Rhodopseudomonas capsulata* J Biol Chem. **255**, 2427–2432

5 Schmidt, K (1978) Biosynthesis of carotenoids In The Photosynthetic Bacteria (Clayton, R K and Sistrom, W R, eds), pp. 729–750, Plenum Press, New York

6 Eimhjellen, K. E. and Liaaen-Jensen, S (1964) The biosynthesis of carotenoids in *Pseudomonas gelatinosa* Biochim Biophys Acta **82**, 21–40

7 Davies, B H (1970) Alternative pathways of spirilloxanthin biosynthesis in *Rhodospirillum rubrum* Biochem J **116**, 101–110

8 Singh, R. K, Ben-Aziz, A, Britton, G and Goodwin, T W (1973) Biosynthesis of spheroidene and hydroxyspheroidene in *Rhodopseudomonas* species experiments with nicotine as inhibitor. Biochem. J **132**, 649–652

9 Ouchane, S, Picaud, M, Vernotte, C, Reiss-Husson, F and Astier, C (1997) Pleiotropic effects of *puf* Interposon mutagenesis on carotenoid biosynthesis in *Rubrivivax gelatinosus* J Biol Chem **272**, 1670–1676

10 Komori, M., Ghosh, R, Takaichi, S, Hu, Y, Mizoguchi, T, Koyama, Y and Kuki, M (1998) A null lesion in the rhodopin 3,4-desaturase of *Rhodospirillum rubrum* unmarks a cryptic branch of the carotenoid biosynthetic pathway Biochemistry **37**, 8987–8994

11 Takaichi, S and Shimada, K (1999) Pigment composition of two pigment-protein complexes derived from anaerobically and semi-aerobically grown *Rubrivivax gelatinosus*, and identification of a new keto-carotenoid Plant Cell Physiol **40**, 613–617

12 Armstrong, G A (1994) Eubacteria show their true colors genetics of carotenoid pigment biosynthesis from microbes to plants J Bacteriol. **176**, 4795–4802

13 Gari, E, Toledo, J. C., Gibert, I. and Barbe, J (1996) Nucleotide sequence of the methoxyneurosporene dehydrogenase gene from *Rhodobacter spheroides* comparison with other bacterial carotenoid dehydrogenases FEMS Microbiol Lett **93**, 103–108

14 Raisig, A, Bartley, G P, Scolnik, P. and Sandmann, G (1996) Purification in an active state and properties of the 3-step phytoene desaturase from *Rhodobacter capsulatus* overexpressed in *Escherichia coli* J Biochem **119**, 559–564

15 Albrecht, M, Ruther, A and Sandmann, G (1997) Purification and biochemical characterization of a hydroxyneurosporene desaturase in the biosynthetic pathway of the carotenoid spheroidene in *Rhodobacter sphaeroides* J Bacteriol. **179**, 7462–7467

16 Agalidis, I, Rivas, E and Reiss-Husson, F (1990) Reaction center light harvesting B875 complexes from *Rhodocyclus gelatinosus*. characterization and identification of quinones Photosynth. Res. **23**, 249–255

17 Sambrook, J, Fritsch, E F. and Maniatis, T (1989) Molecular Cloning· a Laboratory Manual, 2nd edn, Cold Spring Harbor Press, Cold Spring Harbor

18 Ouchane, S., Picaud, M, Vernotte, C. and Astier, C (1997) Photooxidative stress stimulates illegitimate recombination and mutability in carotenoid-less mutants of *Rubrivivax gelatinosus*. EMBO J **16**, 4777–4787

19 Laemmli, U K (1970) Cleavage of structural proteins during the assembly of the head of bacteriophage T4. Nature (London) **227**, 680–685

20 Bradford, M. (1976) A rapid and sensitive method for the quantitation of microgram quantities of proteins utilizing the principle of protein-dye binding *Anal* Biochem **72**, 248–254

21 Sandmann, G (1997) High level expression of carotenogenic genes for enzyme purification and biochemical characterization Pure Appl Chem **69**, 2163–2168

22 Wu, W., Lui, Y, Riedel, B, Wissing, J, Fisch, A and Carman, G M (1996) Purification and characterization of diacylglycerol pyrophosphate phosphatase from *Saccharomyces cerevisiae* J Biol Chem **271**, 1869–1876

23 Ferri, S R. and Toguri, T (1997) Substrate specificity modification of the stromal glycerol-3-phosphate acyltransferase Arch. Biochem Biophys. **337**, 202–208

24 Linden, H, Misawa, N, Saito, T. and Sandmann, G. (1994) A novel carotenoid biosynthesis gene coding for ζ-carotene desaturase functional expression, sequence and phylogenetic origin Plant Mol Biol **24**, 369–379

25 Misawa, N, Satomi, Y, Kondo, K., Yokoyama, A, Kajiwara, S, Daito, T, Ohtani, T and Miki, W (1995) Structure and functional analysis of a marine bacterial carotenoid biosynthesis gene cluster and astaxanthin biosynthetic pathway proposed at the gene level J Bacteriol **177**, 6575–6584

Received 11 January 2000/12 April 2000, accepted 11 May 2000

Biochem J. (2000) 349, 641–649 (Printed in Great Britain)

Cloning and characterization of the 5′ flanking region of the sialomucin complex/rat *Muc4* gene: promoter activity in cultured cells

Shari A. PRICE-SCHIAVI[1], Aymee PEREZ[1], Roy BARCO and Kermit L. CARRAWAY[2]
Department of Cell Biology and Anatomy (R-124), University of Miami School of Medicine, PO Box 016960, Miami, FL 33101, U.S.A.

Sialomucin complex (SMC/Muc4) is a heterodimeric glycoprotein complex consisting of a mucin subunit ascites sialoglycoprotein-1 (ASGP-1) and a transmembrane subunit (ASGP-2), which is aberrantly expressed on the surfaces of a variety of tumour cells. SMC is transcribed from a single gene, translated into a large polypeptide precursor, and further processed to yield the mature ASGP-1/ASGP-2 complex. SMC has complex spatial and temporal expression patterns in the normal rat, suggesting that it has complex regulatory mechanisms. A crude exon/intron map of the 5′ regions of the SMC/*Muc4* gene generated from clones isolated from a normal rat liver genomic DNA library reveals that this gene has a small first exon comprising the 5′ untranslated region and signal peptide, followed by a large intron. The second exon appears to be large, comprising the 5′ unique region and a large part (probably all) of the tandem repeat domain. This structure is strikingly similar to that reported for the human *MUC4* gene. Using PCR-based DNA walking, 2.4 kb of the 5′-flanking region of the SMC/*Muc4* gene was cloned and characterized. Promoter-pattern searches yielded multiple motifs commonly found in tissue-specific promoters. Reporter constructs generated from this 2.4 kb fragment demonstrate promoter activity in primary rat mammary epithelial cells (MEC), the human colon tumour cell line HCT-116, and the human lung carcinoma cell line NCI-H292, but not in COS-7 cells, suggesting epithelial cell specificity. Deletion constructs of this sequence transfected into rat MEC or HCT-116 cells demonstrate greatly varying levels of activity, suggesting that there are positive and negative, as well as tissue-specific, regulatory elements in this sequence. Taken together, these data suggest that the rat SMC/Muc4 promoter has been identified, that it is tissue- (epithelial cell-) specific, and that there are both positive and negative, as well as tissue-specific, regulatory elements in the sequence.

Key words: glycoprotein, mucin, regulatory elements, transcriptional regulation.

INTRODUCTION

Mucins are large glycoconjugates with molecular masses ranging from 300 kDa to over 40000 kDa [1–3]. The most important characteristic of these molecules is that they contain serine- and threonine-rich domains, which can be extensively O-glycosylated [3–5]. Mucins are subdivided into three categories: secretory gel-forming mucins, like MUC2 and MUC5AC, form large oligomers through linkage of protein monomers via disulphide bonds in their N- and C-terminal domains; small, soluble mucins, like MUC7 [6], have smaller polypeptide backbones and do not form disulphide-crosslinked gels; and membrane-bound mucins, such as MUC1, have a hydrophobic membrane-spanning domain and also do not form disulphide-linked oligomers [1]. Because of its large extended structure and cell surface location, MUC1 has been assigned a number of possible functions. In normal and tumour tissue, MUC1 may create a barrier to cell–cell interactions, reduce adhesion of macromolecules to the cell surface, and provide resistance to natural killer and cytotoxic T-cell killing [7].

Sialomucin complex (SMC) is another well-characterized membrane mucin. It was originally discovered as the major cell surface glycoprotein complex of the highly malignant metastatic ascites 13762 rat mammary adenocarcinoma [8]. SMC consists of a peripheral, O-glycosylated glycoprotein [8,9], ascites sialoglycoprotein-1 (ASGP-1), which is tightly, but non-covalently bound to an N-glycosylated integral membrane glycoprotein, ASGP-2 [10]. The complex is encoded on a single gene, transcribed as a 9 kb transcript [11–13], and translated into a single large (approx. 300 kDa) polypeptide precursor that is proteolytically cleaved during its transit to the cell surface [11]. Both subunits of this complex have been cloned and sequenced. The ASGP-1 sequence predicts a protein of 2172 amino acids with a potential molecular mass of > 200000 [13]. It consists of three domains: an N-terminal unique sequence, a large repeat sequence rich in serine and threonine residues which can be O-glycosylated, and a C-terminal unique sequence [13]. ASGP-2 is a 120–140 kDa glycoprotein consisting of 744 amino acid residues [12]. Its deduced amino acid sequence encodes seven putative domains: two hydrophilic N-glycosylated domains, two epidermal growth factor (EGF)-like domains, a cysteine-rich domain, a transmembrane domain, and a small cytoplasmic domain [12].

Recent studies have shown that SMC is the rat homologue of human MUC4. Human MUC4 shows substantial similarities to rat SMC at both the N- and C-terminal portions of the molecules [14]. They differ in their repeat domains in that SMC does not have the 16 amino acid repeat cloned and sequenced in the original description of MUC4 [15]. Thus the similarity between the molecules was not observed previously. However, the 70% identity between the human MUC4 analogue of ASGP-2 and rat ASGP-2 provides strong evidence that they are homologous proteins.

Abbreviations used: SMC, sialomucin complex, ASGP, ascites sialoglycoprotein, EGF, epidermal growth factor; CAT, chloramphenicol acetyltransferase; MEC, mammary epithelial cells, HCT, human colon tumour.

[1] These authors contributed equally to this work

[2] To whom correspondence should be addressed (e-mail Kcarrawa@med.miami.edu).

Several functions have been proposed for SMC/MUC4. Through its highly O-glycosylated tandem repeat domain, ASGP-1 can act as a protective barrier to tumour cells and exposed epithelia. Indeed, SMC expression in transfected A375 tumour cells provides anti-recognition and anti-adhesive properties [8,16,17]. Furthermore, SMC expression in tumour cells reduces their killing by natural killer cells [18]. This anti-recognition property may be important to the high metastatic capacity of the 13762 ascites cells [16,18,19]. Further, the presence of SMC on exposed epithelia such as cornea, vagina and cervix suggests a protective role for SMC [20,21]. ASGP-2 has two EGF-like domains, which have all of the consensus residues present in active members of the EGF family [12]. Moreover, SMC has been shown to bind to, and modulate phosphorylation of, the receptor ErbB2 [22]. Thus the transmembrane subunit ASGP-2 is proposed to modulate signalling through the EGF family of receptors via its interaction with ErbB2 [22,23], the critical receptor for formation of active heterodimers of the class I receptor tyrosine kinases [24]. This interaction may play a role in the constitutive phosphorylation of ErbB2 in the 13762 ascites cells [25], and the rapid growth of these cells *in vivo*.

The expression patterns of both human MUC4 and rat SMC/Muc4 have been studied in detail. MUC4 is expressed in a broad range of secretory epithelial cells. By Northern blotting and/or *in situ* hybridization, human MUC4 mRNA has been detected in colon, stomach, cervix and lung [26,27], but not in normal pancreas, gall bladder and breast tissues. Western blot and immunohistochemistry reveal that rat SMC/Muc4 protein is expressed in a number of normal rat tissues including colon, small and large intestine, trachea, uterus, cornea and mammary gland [28]. SMC is overexpressed on the surface of the 13762 rat mammary adenocarcinoma ($> 10^6$ copies/cell) at a level approx. 100-fold higher than that in lactating mammary gland or approx. 10000-fold higher than that in normal virgin gland [8,16,29,30] Human MUC4 has also been shown to be aberrantly expressed in some tumours [31]. Thus SMC/Muc4 must be tightly regulated, since aberrant expression of this protein could have deleterious consequences.

In an effort to study regulation of SMC in normal cells and tumour cells, we have cloned and characterized the 5′ flanking region of the *SMC* gene. Although the new sequence apparently does not contain a TATA box, it does contain other motifs commonly found in tissue-specific promoters. The 5′ flanking sequence shows promoter activity in both rat mammary epithelial cells (MEC) and human lung and colon epithelial cell lines, but not in COS-7 cells, suggesting tissue specificity. Moreover, deletion mutants transfected into rat MEC and human colon tumour (HCT) cells display different patterns of activity, suggesting different regulatory mechanisms in different tissues. Taken together, these data suggest that the rat SMC/Muc4 promoter has been identified, it is tissue specific, and it has different regulatory mechanisms in different cell types

EXPERIMENTAL

Materials

COS-7, HCT-116 cells and NCI-H292 human lung carcinoma cells were obtained from A.T.C.C. Probe A2G2-#9, which comprises the 5′ 1.7 kb of SMC cDNA, has been described in [13] Anti-ASGP-2 mouse monoclonal antibody 4F12 has been described in [30]. Unless otherwise stated, all cell culture supplies were purchased from Gibco Life Technologies. The positive control vector for the p50 subunit of human DNA polymerase delta was generously given by Dr Marietta Lee.

Cell culture

Preparation and culture of normal rat MEC has been described previously in [29]. COS-7 cells were maintained in Dulbecco's modified Eagle's medium supplemented with 10% fetal bovine serum, 100 units/ml penicillin, and 100 μg/ml streptomycin. HCT-116 cells were maintained in McCoy's 5A medium supplemented with 10% fetal bovine serum, 1 mM L-glutamine, 100 units/ml penicillin, and 100 μg/ml streptomycin. Human lung carcinoma NCI-H292 cells were maintained in RPMI 1640 medium supplemented with 10% fetal bovine serum, 100 units/ml penicillin, and 100 μg/ml streptomycin.

Primer sequences

Oligonucleotide primers were synthesized from sequences in the 5′ unique region of SMC cDNA: L-19: 5′-AGTAGGGACAGGCTCACCTC-3′; A1-L: 5′-ACCTCTGTGCTGTGGAGATT-3′; R-85: 5′-CTCCCTCAGGAATCTCCACAGCACAGA-3′; A1-S: 5′-TTCTCTGGAGCCATGCGAGG-3′; R-173: 5′-GGCAAGAACACAGGCAGCTCAGACACA-3′; R-187: 5′-AGGTAGCAGGAGGAGGCAAG-3′; L-197. 5′ TCAACTACATCAGCCCCGAA-3′; R-339: 5′-GAAGTAACCATCGGTGATGC-3′.

Library screening

A normal rat liver EMBL3-SP-6/T7 library was obtained from ClonTech Laboratories (Palo Alto, CA, U.S.A.). Phage were plated on *Escherichia coli* K802 at a density of 50000 plaque forming units/150 mm plate, and incubated overnight at 37 °C. Phage were lifted on to positively charged nylon filters and denatured in 1.5 M NaCl, 0.5 M NaOH. Denatured DNA was crosslinked using a Stratalinker (Stratagene, La Jolla, CA, U.S.A.). The membranes were prehybridized for at least 2 h at 42 °C in prehybridization solution [50% formamide, 5 × SSC (where 1 × SSC is 0.15 M NaCl/0.015 M sodium citrate), 5 × Denhardt's reagent, 0.1% SDS, and 0.5 mg/ml salmon sperm DNA]. The probe A2G2-#9, a 1.7 kb probe which spans the 5′ unique region and four tandem repeats of SMC cDNA, was random primed labelled with $[^{32}P]$dCTP using a Random Primed Labeling kit (Boehringer Mannheim). The membranes were hybridized overnight at 42 °C in prehybridization solution containing 0.1 g/ml dextran sulphate and the labelled probe. Following hybridization, membranes were washed once at room temperature in 2 × SSC with 0.1% SDS for 15 min, twice at 50 °C in 2 × SSC with 0.1% SDS for 20 min each, and once at 50 °C in 0.1 × SSC with 0.1% SDS for 15 min. Signals were detected by exposure with Kodak XAR-5 X-ray film. Positive clones were confirmed on duplicate filters and purified to homogeneity through three more rounds of screening. Phage DNA was isolated using the manufacturer's protocol from the LambdaPhage DNA midiprep kit from Qiagen.

Southern blotting

PCR products or digested DNA samples were resolved on 1% agarose gels. Resolved DNAs were depurinated by soaking the gel in 0.25 M HCl for 15 min, then transferred to positively charged nylon membranes under denaturing conditions (0.4 M NaOH) overnight, and crosslinked using a Stratalinker. Hybridizations were carried out using the recommended protocols from the Boerhinger Mannheim Digoxigenin Labeling kit. Briefly, membranes were prehybridized in prehybridization buffer (5 × SSC, 1.0% blocking reagent, 0.1% *N*-lauroylsarcosine, 0.02% SDS) for 1 h at 63 °C, followed by hybridization for 4 h at 63 °C to oligonucleotides which were digoxigenin end-labelled The membranes were washed three times with 2 × SSC, 0.1 % SDS at 63 °C, and once with 0.5 × SSC, 0.1 % SDS at 63 °C. For development, the membranes were blocked for 30 min with blocking buffer [100 mM Tris/HCl (pH 7.5), 150 mM NaCl, 2 % blocking reagent], incubated with alkaline phosphatase-conjugated anti-digoxigenin antibody for 30 min in blocking buffer, and washed twice with wash buffer [100 mM Tris/HCl (pH 7.5), 150 mM NaCl]. Membranes were developed with Lumi-Phos 530 or disodium 3-(4-methoxyspiro-{1,2-dioxetane-3,2′-(5′-chloro)tricyclo[3.3.1.1.13,7]}decan-4-yl)phenyl phosphate (‘CSPD’, Boehringer Mannheim), and signals were detected by exposure to Kodak XLS film.

PCR-based DNA walking

A PromoterFinder PCR-based DNA walking kit was purchased from ClonTech Laboratories. High-molecular-mass genomic DNA was purified from 13762 MAT-C1 ascites cells or normal rat liver tissue, and its quality was determined by electrophoresis on a 0.5 % agarose gel. The isolated DNA was digested overnight with five different rare cutting blunt-end restriction enzymes: *Dra*I, *Eco*RV, *Pvu*II, *Sca*I and *Stu*I. After digestion, each sample of digested DNA was purified by phenol/chloroform extraction and ethanol precipitation. A portion of each purified DNA sample was ligated to an adapter provided in the PromoterFinder kit using the manufacturer’s recommended protocol. The resulting enzyme-digested, adapter-ligated genomic DNA pools were then ready to be used for PCR.

The first PCR reaction was performed using adapter primer-1, a primer from the ligated adapter region, and the gene-specific primer R-173. Cycling conditions were 94 °C for 30 s (1 cycle); 94 °C for 30 s, 59 °C for 30 s, 72 °C for 3 min (40 cycles); and 72 °C for 10 min (1 cycle). The second PCR reaction was performed on 1 μl of PCR product from the first round of PCR. The second set of primers, AP-2 (from the ligated adapter region) and R-85, were ‘nested’ completely within the region amplified by the first set of primers. Cycling conditions for the second round of PCR were 94 °C for 30 s (1 cycle); 94 °C for 30 s, 71 °C for 3 min (40 cycles); and 71 °C for 7 min (1 cycle). PCR products were resolved on 1 % agarose gels, and the resulting bands were confirmed by hybridization to digoxigenin-labelled oligonucleotide L-19

Constructs

Original constructs

The p10-Sal construct, which contains the entire phage insert from phage clone 10-2, was generated by excision of the entire SMC genomic insert with *Sal*I, which only cleaves in the phage multicloning region, not in the insert region. This insert was ligated into the *Sal*I-digested pSport vector (Gibco Life Technologies). The pCR2.1-EV plasmid was generated by cloning the major 600 bp PCR product produced in the *Eco*RV sample from PCR-based DNA walking into the T/A cloning vector pCR2.1 (Invitrogen, Carlsbad, CA, U.S.A.). The pCR2.1-NDI plasmid was generated by cloning the major 2400 bp PCR product from the *Dra*I sample from PCR-based DNA walking into the T/A cloning vector pCR2.1.

Reporter constructs

A *BamH*I–*Xba*I fragment from pCR2.1-EV was ligated to pCAT3Basic (Promega) digested with *Nhe*I–*Bgl*II to yield pFEcoRV. A *Kpn*I–*Xho*I fragment from pCR2.1-EV was ligated to pCAT3Basic (Promega) digested with *Kpn*I–*Xho*I to obtain pREcoRV. Similarly, *Kpn*I–*Xho*I and *Bam*HI–*Xba*I fragments from pCR2.1-NDI were ligated to pCAT3Basic digested with *Kpn*I–*Xho*I and *Nhe*I–*Bgl*II respectively, to create pF*Dra*I and pR*Dra*I. p*Sma*I was generated by inserting the *Sma*I–*Xho*I fragment from pCR2.1-NDI into pCAT3Basic, which was digested with *Sac*I, filled in with T4 DNA polymerase, and redigested with *Xho*I. pBamHI was obtained by digesting pCR2.1-NDI with *BamHI*, filling in the overhang with T4 DNA polymerase, and redigesting with *Xho*I. The resulting fragment was inserted into pCAT3Basic, which was digested with *Sac*I, filled in with T4 DNA polymerase, and redigested with *Xho*I. pEco47III was generated by inserting a *Eco*47III/*Xho*I fragment from pCR2.1-NDI into pCAT3Basic, prepared as described above. pNcoI was prepared by digesting pCR2.1-NDI with *Nco*I, filling in the overhang with T4 DNA polymerase, and redigesting with *Xho*I. The resulting fragment was ligated into pCAT3Basic prepared as described. pHindIII was constructed by digesting pCR2.1-NDI with *Hin*dIII, filling the overhang with T4 DNA polymerase and redigesting with *Xho*I. The resulting fragment was ligated into pCAT3Basic prepared as described. pEcoRI and pPstI were created by ligating *Eco*RI/T4 DNA polymerase and *Pst*I/T4 DNA polymerase fragments from pCR2.1-NDI to pCAT3Basic digested with *Sma*I and dephosphorylated with calf intestinal alkaline phosphatase.

The ligation mixtures were used to transform electro-competent INVα-F′ (Invitrogen) *E. coli*, and colonies were screened by filter hybridization to digoxigenin-labelled oligonucleotide L-19, or by restriction mapping from plasmid mini-preps. Plasmid preparations were performed for the appropriate clones with a Qiagen maxi-prep kit For reporter constructs XL-1 Blue *E. coli* (Stratagene) were chemically transformed and selected by convenient restriction digestion.

Transfections

HCT-116, NCI-H292 human lung carcinoma, or normal primary rat MEC were transfected with reporter vectors using the recommended protocol for LipofectAMINE (Gibco Life Technologies). Transfections were performed in triplicate. Cells and conditioned media were harvested 48 h after transfection. Briefly, cells were washed twice with Dulbecco’s PBS without calcium. To each well 300 μl of Reporter Lysis Buffer (Promega) was added. The cells were incubated in a shaker for 15 min at room temperature and scraped with a rubber policeman. The samples were centrifuged for 10 min at 4 °C and the resulting supernatants were utilized for subsequent chloramphenicol acetyltransferase (CAT) and β-galactosidase assays The β-galactosidase activity, used to monitor transfection efficiency per well, was performed as follows: 1 ml of 60 mM Na_2-PO_4, 40 mM NaH_2PO_4, 10 mM KCl, 1 mM $MgCl_2$, 50 mM β-mercaptoethanol, and 0.2 ml of *o*-nitrophenyl galactoside (2 mg/ml in 60 mM Na_2HPO_4, 40 mM NaH_2PO_4) were added to 15 μl (HCT 116), 100 μl (NCI H292), 50 μl (COS7) and 120 μl (MEC) of cell extract. The reaction was carried out at 37 °C, until a yellow shade was obvious, and stopped by adding 0.5 ml of 1 M Na_2CO_3, so that the absorbance at 420 nm ranged from 0.2 to 0.7. β-Galactosidase activity was expressed as $D_{420} \times 100$, and extrapolated to the reaction time in hours for the total of 300 μl of cell extract. Under these conditions the β-galactosidase activity obtained ranged from 200–600 units per well of HCT 116 cells, 200–450 units per well of COS-7 cells, 50–300 units per well of NCI H292 cells, and 30–250 units per well of MEC.

CAT assays were performed with the amounts of extracts corresponding to equal β-galactosidase activity, and then brought to 125 μl with lysis buffer (Promega); 5 μl of 25 mM acetyl-CoA and 0.5 μCi of ^{14}C-chloramphenicol (50 mCi/mmol, New England Nuclear) were added, and the reaction was performed at 37 °C. Considering that acetyl-CoA is rapidly degraded, it was added again in the reaction for MEC. The incubation time at 37 °C was usually 1 h but in the case of MEC the CAT reaction was left overnight. The reaction was stopped and the chloramphenicol was extracted with 1 ml of ethyl acetate. The solvent was dried, the pellet resuspended in 15 μl of ethyl acetate, and spotted on a silica gel thin-layer plate to separate the native chloramphenicol from its acetylated derivatives. Migration was in chloroform/methanol (19:1, v/v) for 1 h. After overnight autoradiography, the spots were cut out and counted to quantitate the amount of chloramphenicol converted into its acetylated forms.

Reporter construct results were calculated as the percent chloramphenicol converted from the normalized CAT assay. For transfection studies, results were calculated as the percent activity of the positive p50 control. For deletion mutant studies, results were calculated as the percent activity of the longest construct, pFDraI.

RESULTS

Characterization of SMC 5′ genomic clone

In an effort to isolate the promoter of the *SMC* gene, a rat liver genomic λ EMBL-3 SP-6/T-7 library was screened with ^{32}P-labelled A2G2-#9, which spans the 5′ 1.7 kb of the SMC cDNA and comprises the entire unique region and four repeats (Figure 1A). Two positive clones (10-2 and 7-1) were isolated and partially characterized. *Sal*I digestion of both clone 10-2 and clone 7-1 separated the entire insert fragment from the two phage arms of 21 kb and 9 kb. The insert sizes for clone 10-2 and clone 7-1 were approx. 18 kb and approx. 14 kb respectively, so the clones were different but overlapping. When clone 10-2 and clone 7-1 were probed with oligonucleotide R-339, which lies just 5′ of the repeat region, only clone 10-2 digests hybridized. This result suggests that the genomic insert of clone 7-1 stops within or at the 5′ end of the repeat region and that clone 10-2 contains more SMC/Muc4 5′ sequence.

For further characterization, the entire insert of clone 10-2 was subcloned into the pSport vector yielding p10-Sal. A partial restriction map of p10-Sal is shown in Figure 2. Long-range PCR between primer R-339 and T7 using p10-Sal as a template yielded a product of approx. 8.5 kb. Since primer R-339 is a right (3′-5′) primer, this result suggests that clone p10-Sal contains approx. 8.5 kb of SMC sequence upstream of this primer (Figure 2). The area of interest is the 5′-most region of the gene. Therefore to determine if clone p10-Sal contains any of the most 5′ coding region of the SMC/*Muc4* gene, *Sac*I digests of clone p10-Sal were subjected to Southern-blot analysis with several oligonucleotides from the 5′ region of the SMC cDNA: R-339, R-187, A1-S, A1-L, and L19 (see Figure 1B for positions of the oligonucleotide probes). Clone p10-Sal did not hybridize to any of the 5′ probes tested (results not shown), suggesting that this clone does not contain any of the 5′-most sequence of the *SMC* gene.

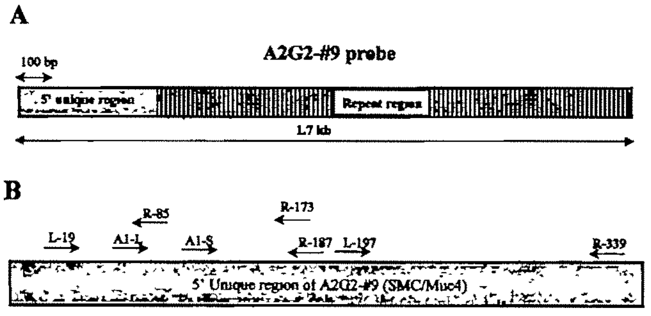

Figure 1 Probes and primers used in these studies

(A) Schematic representation of SMC/Muc4 probe A2G2-#9 (B) Relative positions of oligonucleotide primers used in these studies

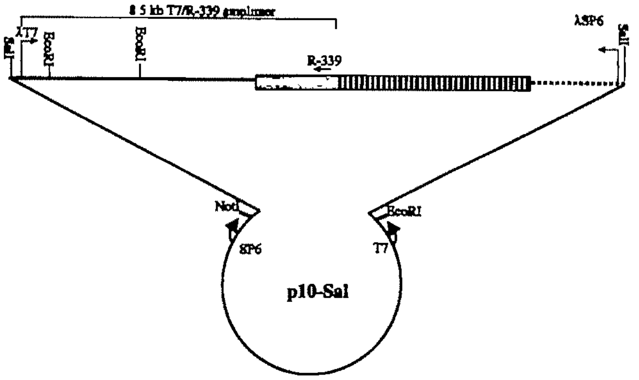

Figure 2 Characterization of phage clone 10-2

Restriction map and schematic representation of clone p10-Sal Box indicates coding sequence, striped region indicates repeat sequences

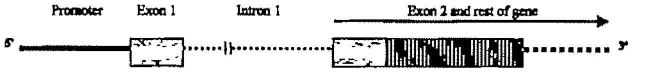

Figure 3 Preliminary genomic map of the 5′ regions of the rat SMC/*Muc4* gene

Striped region in exon 2 indicates repeat sequences

Clone p10-Sal was sequenced in the 5′ direction from the oligonucleotide primer R-339 to determine how much known coding sequence it contained. From R-339, the sequence was identical to 120 bases of the SMC/Muc4 cDNA sequence. After 120 bases, the sequences diverged, suggesting the presence of an intron. Only 196 bp of known sialomucin coding sequence lies upstream of the putative intron. In subsequent experiments, this 196 bp region is called exon 1. Sequence generated from the 5′ end of p10-Sal failed to align with the 5′-most 196 bp of the SMC/Muc4 coding region, again suggesting that this clone does not contain SMC/Muc4 exon 1 or any 5′ flanking sequence. Clone p10-Sal was also sequenced in the 3′ direction from primer L-197. For approx. 600 bp of sequence obtained, the genomic sequence was identical to the 5′ unique region and tandem repeat region originally described for the SMC cDNA, with no divergent sequence. This result suggests that exon 2 contains the bulk of the 5′ unique sequence, and at least part of the tandem repeat domain. The presence of divergent sequence and the lack of hybridization to any of the most 5′ oligonucleotide probes suggests that the phage clone p10 contains at least part of rat SMC/Muc4 exon 2 and at least part of a large intron but none of the 5′-most coding or flanking regions (Figure 3).

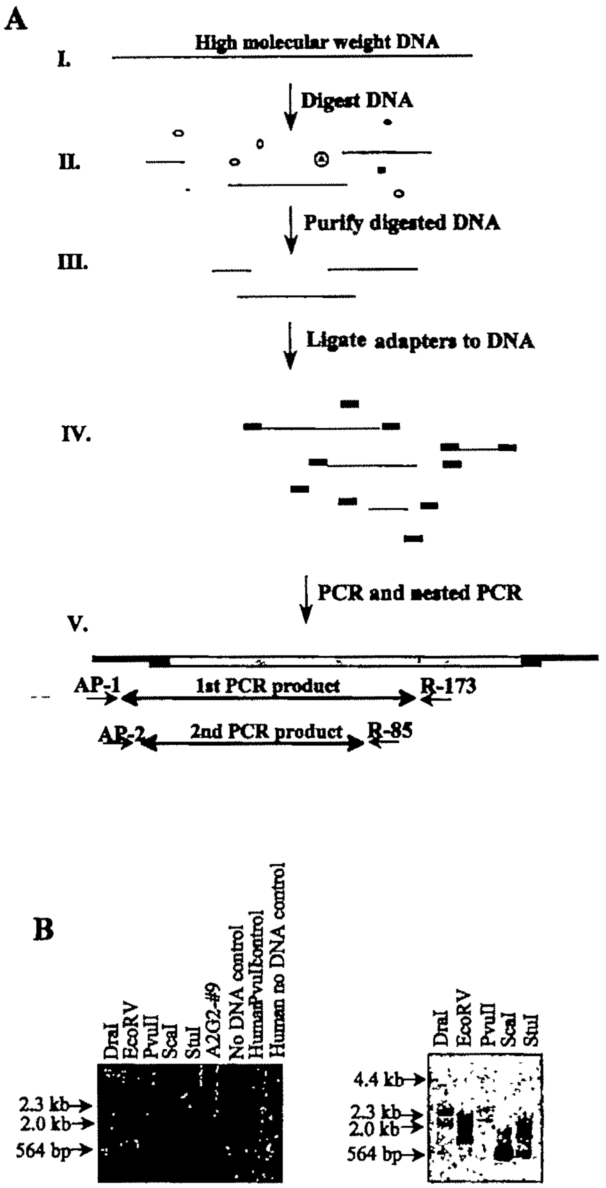

Figure 4 Cloning of SMC promoter

(A) Schematic representation of PromoterFinder PCR-based DNA walking (B) Oligonucleotide L-19 hybridization of DNA walking products derived from ascites tumour cells (left panel) and normal rat liver (right panel) DNA Samples are indicated at the top of the blots Molecular mass markers are indicated to the left of the blots

Cloning of the SMC promoter

After screening 3.5 x 10^6 phage with SMC/Muc4 5′ probes, no exon 1-containing phage clones were identified, suggesting that no exon 1-containing phage were present in the normal rat genomic library. Thus a new approach was used to identify the SMC promoter. Using PCR-based DNA walking with the ClonTech PromoterFinder Construction kit, 600 bp from ascites tumour DNA and 2.4 kb from normal rat liver DNA of new genomic sequence were isolated 5′ of the known SMC cDNA sequence. To accomplish this, five different genomic DNA preparations were used for PCR-based DNA walking by the scheme outlined in Figure 4(A). For each DNA preparation two rounds of PCR were performed. The first PCR reaction was performed using a primer from the ligated adapter region and a gene-specific primer. The second PCR reaction was performed using 'nested' primers for both the adapter and gene-specific regions. The gene-specific primers chosen for the two rounds of PCR for both the normal and tumour samples were 27-mers, R-173 and R-85, which are located in the putative first exon of the *SMC* gene (Figure 1B). The first round of PCR was carried out using a standard three-step protocol of 40 cycles, followed by a 7-min extension. On an ethidium bromide agarose gel, smears ranging from approx. 4 kb to 500 bp were visible for all the DNA preparations. For each DNA preparation, 1 μl of first-round PCR product was used as a template for the second-round 'nested' PCR. The second round of PCR was carried out using 40 cycles and a two-step protocol, where the annealing and extension steps were combined into one step. The T_m values of the gene-specific primers were high (72 °C), and the single step annealing and extension at 71 °C allowed for more specific product amplification.

On an ethidium bromide-stained agarose gel of the second-round PCR, discreet bands of approx. 600 bp in the *Eco*RV and 450 bp for *Sca*I samples were visible for the tumour DNA preparations. Several discreet bands, including 2.4 kb in *Dra*I, 600 bp in *Eco*RV, 2.0 kb in *Pvu*II, and 800 bp in *Stu*I samples, were visible for the normal DNA preparations. An A2G2-#9 positive control, prepared in a manner similar to that for the genomic samples, yielded a discreet product of approx. 3.0 kb for the first round of PCR, and a smear for the second round. A human positive control *Pvu*II library amplified with primers provided in the kit yielded the expected product of 1.5 kb, while all negative control samples showed no amplification. To confirm which bands were authentic, the products were probed with oligonucleotide L-19. All bands hybridized with this probe, suggesting that all the products contain 5′ SMC sequence (Figure 4B).

The 600 bp *Eco*RV band from the tumour DNA and 2.4 kb *Dra*I band from normal DNA were the largest products for each genomic DNA preparation tested. Therefore they were each cloned into the pCR2.1 vector using the Invitrogen TA cloning kit, yielding plasmid pCR2 1-EV for the tumour and plasmid pCR2 1-nDI for the normal. Plasmids pCR2 1-EV and pCR2.1-nDI were sequenced from the T7 promoter and a M13 reverse sequence contained in the vector. The insert sequences obtained for the tumour and normal samples aligned with the first 85 bases of the 5′ end of known SMC/Muc4 sequence, and contained approx. 500 bp or 2.4 kb of new sequence upstream respectively. The region between bases −700 and +1 has approx 50% GC content, while upstream the sequence gradually becomes more AT-rich. The new normal and tumour sequences are identical for the 600 bp they have in common. A pattern search yielded no TATA box close to the described transcription start site [13], but motifs were identified which are commonly found in promoters, such as a CAAT box, activator protein-1 and -2 sites, SP-1 transcription factor sites, GAS sequence, oestrogen response and glucocorticoid response half-sites (Figure 5).

Promoter activity of 600 bp and 2.4 kb clones

To determine if the 2.4 kb *Dra*I and 600 bp *Eco*RV fragments of new 5′ SMC sequence obtained from the normal rat have promoter activity, these sequences were subcloned into the reporter construct pCAT3-Basic in the forward and reverse directions to yield pFDraI and pRDraI for the 2 4 kb fragment and pFEcoRV and pREcoRV for the 600 bp fragment respectively. To test for promoter activity, these constructs along with pCAT3-Basic (with no insert as a negative control), p-βgal

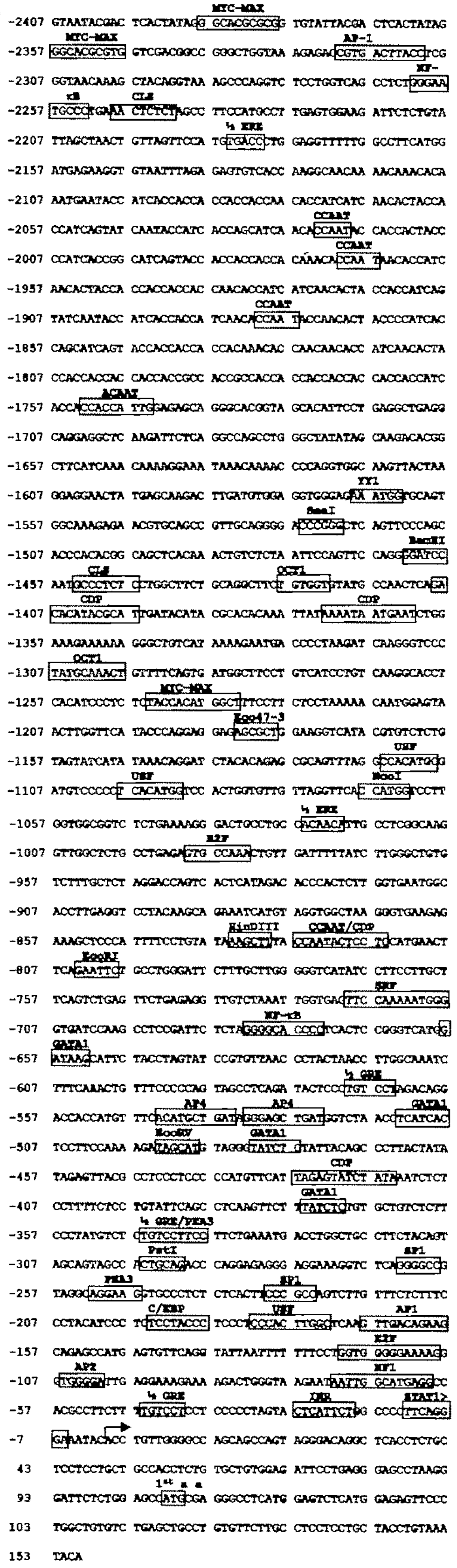

Figure 5 Sequence of 5′-flanking region of SMC/Muc4

Common promoter motifs and restriction sites are shown in **bold** above the corresponding sequence

```
                     10        20        30           40
                      *         *         *            *
Rat     AT---GTCTCT--GTCCTTCCTTCTGAAATGACCTGGCTGCC---TTCTA
         :   : : :   :::  ::: ::::      ::   :  :'   ::::
Human   GTACAGCCCCAAGGTCGCTCCCTCTG---GGCCCTTTCTTCCCCATTCTT
                50        60                    70
                 *         *                     *
Rat     C--AGTAGCAGTAGCCACTG------------CAGACCCAGGAGAGGGAG
        :  :: :::   :  : :::            :.: ::: :: ::.''::
Human   CCCAGCAGCCCAAAGCTCTGGTGGACAGGGGCAGCCCCTGGGGAGGGAG
        80        90       100        110       120
         *         *         *          *         *
Rat     GAAAGGTCTCAGGGGCCGTAGGC-AGGAAGGTGCCCTCTCTCACTTCCCG
           ::: : ::::  ::   ::: :::: :':  :. : : :: .::  :
Human   GAGAGGACCCAGGAACC--CGGCTAGGAGGGTGGCC-CACCCATTTCCAG
        130       140       150       160       170
          *         *         *         *         *
Rat     CCAGTCTTGTTTCTCTTTCCCTACATCCCTCTCCTACCCTCCCTCCCACT
           : : :::: :  :: ::: :  :: : :::: ' ::  ':  :''::
Human   TGTGACCTGTTCCCATTCCCCCATGTCTC-CTCCCATCCCTCCCGCCACT
        180       190        200       210       220
          *         *          *         *         *
Rat     TGGCTCAAGTTGAC-AGAAGCAGAGCCATGAGTGTTCAGGTATTAATTTT
          ::::: : :::  :::::::::.: : : ::::   ::: :   '':
Human   CAGCTCAGGCTGATGAGAAGCAGAGCAACGGGTGTATCGGTGT---TTTC
         230       240       250       260       270
           *         *         *         *         *
Rat     TTTCCTGGTGGGGAAAAGGGTGGGGATTGAGGAAAGAAAAGACTGGGTA
        ::::::.:::::' :    .::::::  :::::: ::::::    :::
Human   TTTCCTGGTGGGTAGTGGGTGGGG-CTGAGGAGAGAAAA----GGG--
         280       290       300       310       320
           *         *         *         *         *
Rat     AGAATAATTGGCATGAGGCCACGCCTTCTTTTGTCCTCCTCCCCCTAGTA
              ..: .: ': :::: ::': :::::::::::: ::::   ::
Human   ----TGATTAGCGTGGGGCCCCGCCCTCTTTTGTCCTCTTCCC---AG-G
         330       340       350        360       370
           *         *         *          *         *
Rat     CTCATTCTGGCCCCTTCAGGGAAATACACCTG-TTGGGGCCAGCAGCCAG
         :    ..:'::'' '. : ::::  ::: '. '  :::::::: ::: :
Human   TTC--CCTGGCCCCTTCGGAGAAACGCACTTGGTTCGGGCCAGCCGCCTG
          380       390       400       410       420
            *         *         *         *         *
Rat     TAGGGACAGGCTCACCTCTGCTCCTCCTGCTGCCACCTCTGTGCTGTGGA
          ::::: ::::::: ::::::::::   :::'  :  .:. :: :::::
Human   AGGGGACGGGCTCACGTCTGCTCCTCACACTGCAGCTGCTGGGCCGTGGA
          430       440       450         460
            *         *         *           *
Rat     GATTCCTGAGGGAGCCTAAGGGATTCT--CTGGAGCC
        : ::::  ::::'::.   :::: : :  : : :'::
Huamn   GCTTCCCCAGGGAGCCAGGGGGACTTTTGCCGCAGCC
```

Figure 6 Comparison of rat SMC/Muc4 and human MUC4 5′-flanking regions

Table 1 CAT conversion in promoter assays

Values given as %.

Cell line	pFDraI	pRDraI	pFEcoRV	pREcoRV	p50+	pCAT3-Basic
HCT-116	33	0.5	53	1	90	20
NCI-H292	6	0.5	9	0.5	12	1
COS-7	8	2	2	1	45	0.5

(as transfection efficiency control), and p50 (a housekeeping gene promoter as positive control) were transfected into HCT-116 and human lung carcinoma NCI-H292 epithelial cell lines. These cell lines were chosen for initial reporter construct analysis because they have been reported to express MUC4 [33,34]. The first approx. 450 bases of the new rat 5′ flanking region is approx. 70% homologous to that described for human MUC4 [35] (Figure 6), suggesting that the rat promoter may also have activity in MUC4-expressing human cell lines. The fibroblast cell line COS-7 was also used to test tissue specificity, as SMC/MUC4 has only been reported in epithelial cells rather than stromal (fibroblastoid) cells. Normalized CAT assays were performed (Table 1), and the results were plotted. The forward constructs of

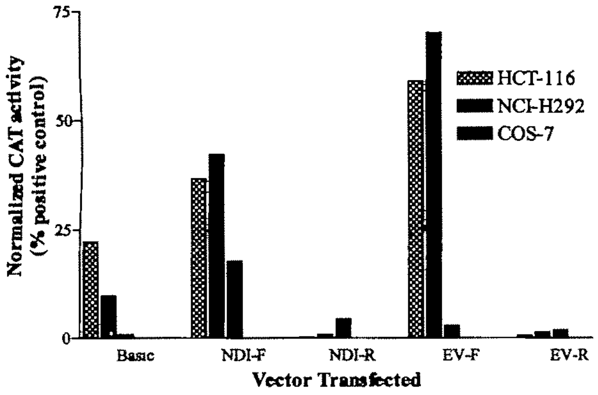

Figure 7 Promoter activity of rat SMC/Muc4 promoter sequence in transfected cell lines

Human lung carcinoma cell line NCI-H292, HCT-116 and COS-7 cells were transfected with empty vector (pCAT3Basic), positive control p50 subunit of DNA polymerase, or reporter constructs containing 2.4 kb (pFDraI and pRDraI) or 600 bp (pFEcoRV and pREcoRV) in forward and reverse orientations. Cells were co-transfected with β-galactosidase vectors to normalize for transfection efficiency. Normalized CAT assays were performed and CAT conversion for the p50 positive control was set at 100%. Results for reporter constructs were plotted as percent total activity of the positive p50 control

both the 2.4 kb and 600 bp fragments have much higher activity than the reverse constructs in both HCT-116 and NCI-H292 cell lines (Figure 7). Promoter activity from both constructs is substantially lower in COS-7 cells, suggesting that this promoter activity is tissue specific to epithelial cells, as expected. The level of CAT conversion in cells transfected with the pCAT3Basic vector is most likely due to an enhancer element present in this vector. However, the marked lack of CAT activity in cells transfected with the reverse promoter constructs indicates that the promoter activity detected with the forward promoter constructs is authentic. Moreover, the higher levels of promoter activity in cells transfected with pFEcoRV constructs suggests that elements which confer epithelial specificity are present in the proximal promoter. Taken together, these data indicate that at least part of the SMC promoter has been identified and that it is tissue specific.

The initial pattern search yielded several positive and negative regulatory elements in the SMC/MUC4 5′ flanking region (Figure 5). To further investigate promoter activity of the SMC/Muc4 5′ flanking sequence, deletion constructs initiating from bases −2407, −1523, −1462, −1180, −1067, −834, −802, −490 and −291 were produced in the pCAT3Basic vector (Figure 8). These constructs were transfected into rat primary MEC or HCT-116 cells and assayed for promoter activity. The activity of each deletion construct was plotted as a percent activity relative to that of the largest construct, pFDraI (Figure 8). Promoter activity was different in both cells types with the deletion constructs. MEC promoter activity was greatly enhanced in the longer (pSmaI, pBamHI, pEco47-3) and shorter (pEcoRV and pPstI) constructs. In HCT116 cells activity was enhanced in the pBamHI and the three shortest constructs. These data suggest that there are positive regulatory elements in both the proximal and distal SMC/Muc4 promoter and that there are negative regulatory elements in the intermediate and far distal regions of this promoter. Further, these data suggest that there are elements in the distal promoter region which confer cell specificity for MEC and colon.

DISCUSSION

The main goal of these studies was to isolate the SMC/Muc4 promoter to begin elucidating how this gene is transcriptionally regulated in normal tissues and how its misregulation may lead to aberrant expression in tumour cells. Genomic library screening did not produce the SMC/Muc4 promoter. However, it yielded a large clone containing the repeat domain, part of the 5′ unique sequence, and part of a large intron. Interestingly, the crude exon/intron map of SMC/Muc4 is strikingly similar to that described for human MUC4 [35]. The putative first exon of the rat *SMC* gene is approx. 190 bp, and encodes a 5′ untranslated region and 27 amino acids which comprise the putative signal peptide, followed closely by a large intron. The presence of both primers used for PCR-based DNA walking on the same small genomic DNA fragments, and the absence of any other sequence

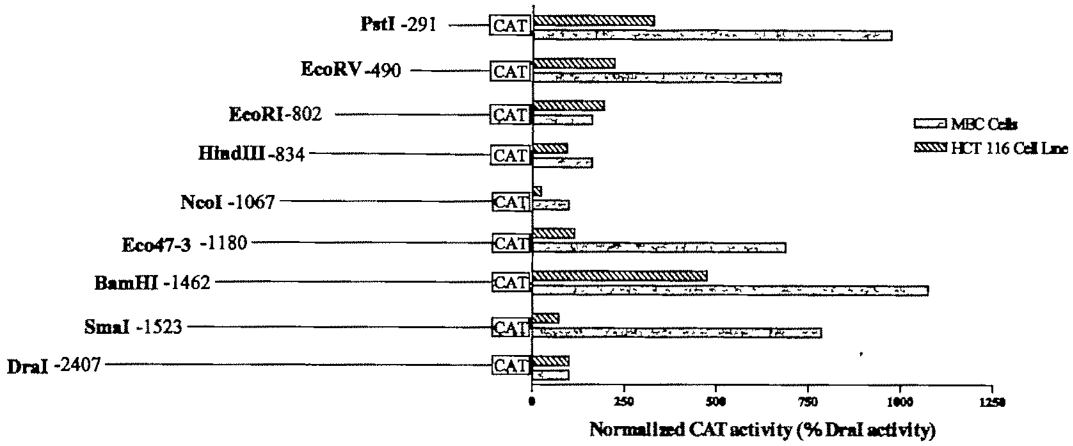

Figure 8 Activity of SMC/Muc4 promoter deletion mutants

Deletion mutants of the SMC/Muc4 promoter were generated by restriction digests of the new 5′ SMC flanking region as outlined in the Experimental section. Deletion mutants and β-galactosidase vectors (to normalize for transfection efficiency) were transfected into primary MEC or HCT-116 cells. Normalized CAT assays were performed, and CAT conversion for the largest construct pFDraI was set at 100%. Results for deletion constructs were plotted as percent total activity of the pFDraI reporter construct divergence within the first 85 bp of SMC cDNA and genomic DNA, suggests that this 190 bp is the first exon of the SMC/*Muc4* gene. Clone 10-2 contained ~ 8.5 kb of intron sequence and no exon 1 sequence, so the full size of rat SMC/Muc4 intron 1 is not known at this time. Like rat SMC/Muc4, the first exon of the human *MUC4* gene encodes the 5′ untranslated region and the first 27 N-terminal residues followed by a 15 kb intron [35]. The second exon of the human *MUC4* gene contains three large tandem repeats similar to those in rat SMC/Muc4, a 554 amino acid unique region, the large 16 amino acid tandem repeat domain, and another small unique sequence [35]. Sequencing in the 3′ direction from primer L-197 indicates that the second exon of the rat SMC/*Muc4* gene contains the bulk of the 5′ unique region and at least part of the tandem repeat region. Based on the striking similarity of the 5′ ends of the rat SMC/*Muc4* and human *MUC4* genes, we suggest that the second exon of the rat *SMC* gene contains the 5′ unique region, all of the tandem repeat domain, and at least part of the 3′ unique region of ASGP-1. It is interesting to note that the tandem repeat domains of several mucins are located on a single exon of their respective genes [36]. The exon/intron boundaries of the ASGP-2 subunit are as yet unknown. Thus a preliminary genomic map for rat SMC has been generated from these data, which shows strong similarity to that described for the human homologue of SMC, MUC4 [35].

Using an alternate PCR-based DNA walking protocol, PromoterFinder from ClonTech Laboratories, 600 bp and 2400 bp of new 5′ sequence were obtained from 13762 tumour cell and normal rat DNA respectively. Both of these fragments were sequenced, and for the 600 overlapping base pairs, the sequences were identical. A pattern search yielded no TATA box, but several important promoter motifs were identified. However, due to the small size of these sequences, their presence does not confirm that these DNA sequences contain the normal or tumour SMC/Muc4 promoter. Thus these sequences were cloned into the pCAT3Basic reporter vector in both forward and reverse orientations and transfected into HCT-116, NCI-H292, and COS-7 cells to test for promoter activity. The forward constructs had much higher activity than the controls and exhibited epithelial cell specificity, indicating that these fragments contain at least part of the epithelial-cell-specific SMC/Muc4 promoter. Moreover, transfection of deletion constructs into MEC and HCT-116 cells suggests complex regulation of this promoter, with positive regulatory elements in the proximal and distal promoter regions, and negative regulatory elements in the intermediate and far distal regions. This result is to be expected given the complex spatial and developmental expression patterns reported for the SMC/Muc4 protein [28]. Taken together, these data indicate that at least part of the SMC/Muc4 promoter has been identified and that it is tissue specific.

Not much is currently known about mucin gene promoters. The MUC1 promoter is the best studied of the mucin gene promoters. As in the SMC/Muc4 promoter, the MUC1 promoter contains two SP-1 sites. Mutation of these sites results in reduced transcription of reporter constructs in MUC1-expressing epithelial cell lines. However, mutation of the more proximal site increased transcription in non-epithelial cells lines, suggesting that this SP-1 site may be involved in tissue specificity [37]. The promoter of rat MUC2 also has an SP-1 site that has been proposed to be involved in tissue specificity of this gene [38]. SP-1 sites are found less frequently in tissue-specific promoters; however, other proteins, which are as yet unknown, can bind to the same core element (GGGCGG), suggesting that interactions of several factors may be involved in tissue-specific gene expression [37,39]. It remains to be seen if the SP-1 sites in the *SMC* gene promoter contribute to its tissue-specific regulation.

There are other regions of the *SMC* gene that will be of interest to study, such as the oestrogen response element and glucocorticoid response element half-sites. Ishikawa cells, a hormone-responsive human epithelial cell line, have been shown to express MUC4 (human SMC) [38]. Treatment of these cells with oestrogen or dexamethasone results in an increase in MUC4 RNA levels. Treatment with progesterone alone does not affect MUC4 RNA levels, but does inhibit MUC4 upregulation by oestrogen [38]. This is in agreement with SMC/Muc4 expression in rat uterus, which is strongly upregulated at the transcript level by oestrogen [40] However, upregulation of SMC/Muc4 by oestrogen appears to be an indirect effect mediated by uterine stromal cells (N. Idris and K. L. Carraway, unpublished work). In addition, we have shown that transforming growth factor-β downregulates SMC/Muc4 at the transcript level directly in uterine luminal epithelial cells. We have also recently demonstrated that in mammary epithlelial cells, SMC/Muc4 is partially regulated at the transcript level by an ERK-dependent pathway (X. Zhu, S. A. Price-Schiavi and K. L. Carraway, unpublished work) Thus it will be of interest to determine which areas of the SMC/Muc-4 promoter are involved in regulation of SMC in normal tissues and how it is misregulated in tumour cells.

This research was supported in part by Grant CA52498 from the National Institutes of Health and by the Sylvester Comprehensive Cancer Center of the University of Miami

REFERENCES

1 Corfield, A P, Carrington, S D, Hicks, S J, Berry, M. and Ellingham, R (1997) Ocular mucins purification, metabolism and functions Prog Retinal Eye Res **16**, 627–656

2 Hicks, S J., Carrington, S.D, Kaswan, R, Adam, S., Bara, J and Corfield, A (1997) Demonstration of discrete secreted and membrane-bound ocular mucins in the dog Exp Eye Res. **64**, 597–607

3 Strous, G J and Dekker, J (1992) Mucin-type glycoproteins Crit Rev Biochem Mol Biol. **27**, 57–92

4 Carlstedt, I, Sheehan, J K, Corfield, A P and Gallagher, J T (1985) Mucous glycoproteins a gel of a problem Essays Biochem **20**, 40–75

5 Forstner, J F and Forstner, G G (1994) Gastrointestinal mucus In Physiology of the Gastrointestinal Tract (Johnson, L K, ed), pp 1245–1283, Raven Press, New York

6 Bobek, L A, Tsai, H., Biesbrock, A R and Levine, M J (1993) Molecular cloning, sequence, and specificity of expression of the gene encoding the low molecular weight human salivary mucin (MUC7) J Biol Chem **268**, 20563–20569

7 Gendler, S J and Spicer, A P (1995) Epithelial mucin genes Annu Rev Physiol **57**, 607–634

8 Sherblom, A P and Carraway, K L (1980) A complex of two cell surface glycoproteins from ascites mammary adenocarcinoma cells J Biol Chem **255**, 12051–12059

9 Spielman, J., Rockley, N L and Carraway, K L (1987) Temporal aspects of O-glycosylation and cell surface expression of ascites sialoglycoprotein-1, the major cell surface sialomucin of 13762 mammary ascites tumor cells J Biol Chem **262**, 269–275

10 Hull, S R, Sheng, Z, Vanderpuye, O A, David, C and Carraway, K L (1990) Isolation and partial characterization of ascites sialoglycoprotein-2 of the cell surface sialomucin complex of 13762 rat mammary adenocarcinoma cells Biochem J **265**, 121–129

11 Sheng, Z, Hull, S R and Carraway, K L (1990) Biosynthesis of the cell surface sialomucin complex of ascites 13762 rat mammary adenocarcinoma cells from a high molecular weight precursor. J Biol Chem. **265**, 8505–8510

12 Sheng, Z, Wu, K, Carraway, K L and Fregien, N. (1992) Molecular cloning of the transmembrane component of the 13762 mammary adenocarcinoma sialomucin complex A new member of the epidermal growth factor superfamily J. Biol Chem. **267**, 16341–16346

13 Wu, K, Fregien, N. and Carraway, K L (1994) Molecular cloning and sequencing of the mucin subunit of a heterodimeric, bifunctional cell surface glycoprotein complex of ascites rat mammary adenocarcinoma cells. J. Biol Chem **269**, 11950–11955

14 Moniaux, N, Nollet, S, Porchet, N, Degand, P, Laine, A and Aubert, J-P (1999) Complete sequence of the human mucin MUC4 a putative cell membrane-associated mucin. Biochem. J **338**, 325–333

15 Porchet, N, Nguyen, V C, Dufosse, J., Audie, J P, Guyonnet Duperat, V, Gross, M. S, Denis, C, Degand, P, Bernheim, A and Aubert, J P (1991) Molecular cloning and chromosomal localization of a novel human tracheo-bronchial mucin cDNA containing tandemly repeated sequences of 48 base pairs Biochem Biophys Res Commun **175**, 414–422

16 Sherblom, A P, Buck, R L and Carraway, K L (1980) Purification of the major sialoglycoproteins of 13762 MAT-B1 and MAT-C1 rat ascites mammary adenocarcinoma cells by density gradient centrifugation in cesium chloride and guanidine hydrochloride J Biol Chem **255**, 783–790

17 Komatsu, M., Carraway, C A C, Fregien, N L and Carraway, K. L (1997) Reversible disruption of cell-matrix and cell-cell interactions by overexpression of sialomucin complex. J. Biol Chem **272**, 33245–33254

18 Howard, S C, Hull, S R, Huggins, J W, Carraway, C. A. C and Carraway, K L (1982) Relationship between xenotransplantability and cell surface properties of ascites sublines of a rat mammary adenocarcinoma J Nat Cancer Inst. **69**, 33–40

19 Carraway, K. L and Spielman, J (1986) Structural and functional aspects of tumor cell sialomucins Mol Cell Biochem **72**, 109–120

20 Price-Schiavi, S A, Meller, D, Jing, X, Merritt, J, Carvajal, M E, Tseng, S C G and Carraway, K L (1998) Sialomucin complex at the rat ocular surface a new model for ocular surface protection Biochem J **335**, 457–463

21 Idris, N. and Carraway, K L (1999) Sialomucin complex (Muc4) expression in the rat female reproductive tract Biol Reprod **61**, 1431–1438

22 Carraway, K L III, Rossi, E A, Komatsu, M, Price-Schiavi, S. A, Huang, D, Carvajal, M. E, Guy, P M, Fregien, N, Carraway, C. A. C and Carraway, K L (1999) An intramembrane modulator of the ErbB2 receptor tyrosine kinase that potentiates neuregulin signaling J Biol. Chem **274**, 5263–5266

23 Carraway, K L, Fregien, N, Carraway, C A C and Carraway, K. L. III (1992) Tumor sialomucin complexes as tumor antigens and modulators of cellular interactions and proliferation J Cell Sci. **103**, 299–307

24 Carraway, K. L. III and Cantley, L C (1994) A neu acquaintance for erbB3 and erbB4 a role for receptor heterodimerization in growth signalling Cell **78**, 5–8

25 Juang, S-H, Carvajal, M E, Whitney, M, Liu, Y and Carraway, C A C (1996) Tyrosine phosphorylation at the membrane-microfilament interface a p185neu-associated signal transduction particle containing Src, Abl and phosphorylated p58, a membrane- and microfilament-associated retroviral gag-like protein Oncogene **12**, 1033–1042

26 Audie, J P, Janin, A, Prochet, N, Copin, M C, Gosselin, B and Aubert, J P (1993) Expression of human mucin genes in respiratory, digestive, and reproductive tracts ascertained by in situ hybridization J Histochem. Cytochem **41**, 1479–1485

27 Audie, J. P., Tetaert, D., Pigny, P, Buisine, M P, Janin, A., Aubert, J P, Porchet, N and Boersma, A (1995) Mucin gene expression in the human endocervix Hum Reprod **10**, 98–102

Received 8 March 2000/18 April 2000, accepted 5 May 2000

28 Carraway, K L, Price-Schiavi, S A, Komatsu, M, Idris, N, Perez, A, Li, P, Jepson, S, Zhu, X, Carvajal, M E and Carraway, C A C (2000) Multiple facets of sialomucin complex/MUC4, a membrane mucin and Erbb2 ligand, in tumors and tissues (Y2K Update) Front Biosci **5**, 95–107

29 Price-Schiavi, S A., Carraway, C A C, Fregien, N and Carraway, K L. (1998) Post-transcriptional regulation of a milk membrane protein, the sialomucin complex (Ascites sialoglycoprotein (ASGP)-1/ASGP-2, rat muc4), by transforming growth factor beta J Biol Chem **273**, 35228–35237

30 Rossi, E A, McNeer, R, Price-Schiavi, S A, Komatsu, M, Van den Brande, J. M. H., Thompson, J F, Carraway, C A C, Fregien, N L and Carraway, K. L (1996) Sialomucin complex, a heterodimeric glycoprotein complex. Expression as a soluble, secretable form in lactating mammary gland and colon J Biol Chem **271**, 33476–33485

31 Walsh, M D, McGuckin, M. A, Devine, P L, Hohn, B G and Wright, R G (1993) Expression of MUC2 epithelial mucin in breast carcinoma J Clin Pathol. **46**, 922–925

32 Reference deleted

33 Berger, J. T, Voynow, J. A, Peters, K W and Rose, M C. (1999) Respiratory carcinoma cell lines MUC genes and glycoconjugates Am J Respir Cell Mol Biol **3**, 500–510

34 Ogata, S, Uehara, H, Chen, A and Itzkowitz, S H (1992) Mucin gene expression in colonic tissues and cell lines Cancer Res **52**, 5971–5978

35 Nollet, S, Moniaux, N, Maury, J, Petitprezk, D, Degand, P., Laine, A, Porchet, N and Aubert, J-P (1998) Human mucin gene MUC4 organization of its 5′-region and polymorphism of its central tandem repeat array Biochem J **332**, 739–748

36 Gum, J R, Ho, J. J.L, Pratt, W S, Hicks, J W, Hill, A. S., Vinall, L E, Roberton, A. M., Swallow, D M and Kim, Y S (1997) MUC3 human intestinal mucin Analysis of gene structure, the carboxyl terminus, and a novel upstream repetitive region J Biol Chem **272**, 26678–26686

37 Kovarik, A., Lu, P. J., Peat, N, Morris, J and Taylor-Papadimitriou, J (1996) Two GC boxes (Sp1 sites) are involved in regulation of the activity of the epithelium-specific MUC1 promoter J Biol Chem **271**, 18140–18147

38 Gollub, E G, Waksman, H., Goswami, S and Marom, Z (1995) Mucin genes are regulated by estrogen and dexamethasone Biochem Biophys. Res Commun **217**, 1006–1014

39 Nogami, H, Ohmori, H Li, J-D, Gallup, M Gum, J, Kim, Y and Basbaum, C (1997) Sp1 protein contributes to airway-specific rat MUC 2 mucin gene transcription. Gene **198**, 191–201

40 McNeer, R R, Carraway, C A C, Fregien, N. and Carraway, K L (1998) Characterization of the expression and steroid hormone control of sialomucin complex in the rat uterus: implications for uterine receptivity J. Cell. Physiol. **176**, 110–119

Biochem. J. (2000) **349**, 651–656 (Printed in Great Britain)

Enhancement of the thermostability and hydrolytic activity of xylanase by random gene shuffling

Hajime SHIBUYA*[1], Satoshi KANEKO† and Kiyoshi HAYASHI†

*Wood Chemistry Division, Forestry and Forest Products Research Institute, Kukizaki, Ibaraki, 305-8687, Japan, and †National Food Research Institute, Tsukuba, Ibaraki, 305-8642, Japan

The thermostability of *Streptomyces lividans* xylanase B (SlxB-cat) was significantly increased by the replacement of its *N*-terminal region with the corresponding region from *Thermomonospora fusca* xylanase A (TfxA-cat) without observing a decrease in enzyme activity. In spite of the significant similarity between the amino acid sequences of the two xylanases, their thermostabilities are quite different. To facilitate an understanding of the contribution of structure to the thermostability observed, chimaeric enzymes were constructed by random gene shuffling and the thermostable chimaeric enzymes were selected for further study. A comparative study of the chimaeric and parental enzymes indicated that the *N*-terminus of TfxA-cat contributed to the observed thermostability. However, too many substitutions decreased both the thermostability and the activity of the enzyme. The mutants with the most desirable characteristics, Stx15 and Stx18, exhibited significant thermostabilities at 70 °C with optimum temperatures which were 20 °C higher than that of SlxB-cat and equal to that of TfxA-cat. The ability of these two chimaeric enzymes to produce reducing sugar from xylan was enhanced in comparison with the parental enzymes. These results suggest that these chimaeric enzymes inherit both their thermostability from TfxA-cat and their increased reactivity from SlxB-cat. Our study also demonstrates that random shuffling between a mesophilic enzyme and its thermophilic counterpart represents a facile approach for the improvement of the thermostability of a mesophilic enzyme.

Key words: chimaera, biobleaching, *Streptomyces lividans*, *Thermomonospora fusca*, xylan.

INTRODUCTION

Xylan is the most abundant hemicellulose in the cell walls of terrestrial plants and is usually associated with the cellulosic and lignin components. Xylan consists of a backbone of β-(1,4)-D-xylopyranoside residues which are commonly substituted with acetyl, arabinose and 4-*O*-methyl-glucuronose residues. A wide variety of micro-organisms is known to produce xylan-degrading enzymes. The enzymic cleavage of β-1,4-xylosidic linkages is performed by xylanases (β-1,4-xylan xylanohydrolase, EC 3.2.1.8). On the basis of amino acid similarities, xylanases are classified into the glycosyl hydrolase families 10 and 11 [1]. Their biotechnological applications are of interest to the animal-feed, food-processing, and pulp-and-paper industries. In particular, xylanase has been found to be effective in reducing chlorine dosage requirements in the Kraft pulp-bleaching process [2]. The xylanases used in biobleaching applications are usually family-11 xylanases. This is because a low-molecular-mass enzyme is desirable for fibre penetration, and a lack of cellulase activity is required to maintain pulp yield and strength. In addition, it is desirable that xylanases used for biobleaching are stable and active under alkaline conditions at high temperatures. There has been a considerable amount of research devoted to identifying new xylanases and improving the properties of wild-types of xylanases to meet the requirements of the pulp-and-paper industry.

Thermomonospora fusca xylanase A is known as one of the most thermostable xylanases, retaining 96 % of its activity even after 18 h at 75 °C [3]. Xylanase A consists of a substrate-binding domain and a catalytic domain connected by a linker region. The amino acid sequence of the catalytic domain of the enzyme shows that it belongs to family 11 and it has 72 % identity with the catalytic domain of *Streptomyces lividans* xylanase B. However, the thermostabilities of the two xylanases are quite different – the stability of *S. lividans* xylanase B decreases gradually above 37 °C [4]. Thus *T. fusca* xylanase A is a thermostable homologue of *S. lividans* xylanase B and, as such, these two enzymes are suitable for studying the mechanistic aspects of thermostability.

DNA shuffling is a powerful approach for studying structure–function relationships. However, to our knowledge, no DNA shuffling work has previously been performed on xylanases. In the present study, we chose the random fragmentation and PCR reassembly method [5,6] and DNA coding from the catalytic domains of xylanase A from *T. fusca* (TfxA-cat) and xylanase B from *S. lividans* (SlxB-cat) to construct a pool of chimaeric xylanases. Resulting chimaeric enzymes displaying thermostability were selected, and the properties of these enzymes were compared with those of the parent enzymes.

MATERIALS AND METHODS

Preparation of TfxA-cat and SlxB-cat genes

The DNA encoding of the TfxA-cat was amplified from the plasmid pD731, which was kindly provided by Professor David B. Wilson (Section of Biochemistry, Molecular and Cell Biology, Cornell University, Ithaca, NY, U.S.A.). The PCR primers used were: TfA-N (5′-GTGGGATCCGCCGTGACCTCCAACGAGACCGGGTACC-3′) and TfA-CdB (5′-GTGCTGCAG*TTA*GCTGGTGCCCAACGTCACGTTCCAGGACCCGCTGCTCTG-3′). TfA-N includes the *Bam*HI recognition site (underlined), which occurs just before the first codon of the

---

Abbreviations used: TfxA-cat, catalytic domain of *Thermomonospora fusca* xylanase A; SlxB-cat, catalytic domain of *Streptomyces lividans* xylanase B; LB, Luria–Bertani; RBB-xylan, 4-*O*-methyl-D-glucurono-D-xylan–Remazol Brilliant Blue R.

[1] To whom correspondence should be addressed (e-mail bushi@ffpri.affrc.go.jp).

mature enzyme. TfA-CdB includes the *C*-terminal region of the catalytic domain; the termination codon is shown in *italics* and the *Pst*I recognition site is underlined. One base was intentionally changed and is shown in **bold** type. This base was changed to remove the *Bam*HI cleavage site which exists in the original gene.

The gene encoding the SlxB-cat was amplified from the genomic DNA of *S. lividans* 66 mycelium using the following PCR primers: SlB-N (5′-GTGGGATCCGACACGGTCGTCACGACCAACCAGGAGGGC-3′) and SlB-C(5′-GTGCTGCAG*TTA*CCCGCCGACGTTGATGCTGGAGCTGCC-3′). SlB-N includes the *Bam*HI restriction site (underlined), which is located just before the first codon of the mature enzyme. SlB-C includes the *C*-terminal region of the catalytic domain; the termination codon is in *italics* and the *Pst*I restriction site is underlined

Amplification of DNA was performed using a MiniCycler® (MJ Research, Watertown, MA, U.S.A.) employing the following temperature program: 5 min at 98 °C, 25 cycles of 1 min at 98 °C, 1 min at 65 °C, 1 min at 72 °C, followed by 10 min at 72 °C. After the first 5 min denaturation step the temperature program was paused, TaKaRa LA Taq® (1.25 units; Takara Shuzo, Shiga, Japan) was added to the reaction mixture (25 μl), and the temperature program was immediately continued. Using this method, GC-rich target genes were efficiently amplified. The PCR products were subcloned into pCR2.1 (Invitrogen) and the nucleotide sequences were confirmed. TfxA-cat and SlxB-cat genes were cleaved by *Bam*HI and *Pst*I and ligated with pQE30 (Qiagen) using the *Bam*HI and *Pst*I sites to obtain pTfxA-cat and pSlxB-cat respectively.

DNase I digestion and fragment reassembly

Approx. 6.0 μg of pTfxA-cat and pSlxB-cat were diluted to 90 μl with distilled water and 10 μl of 10 × DNase I buffer [0.5 M Tris/HCl (pH 7.4)/100 mM MgCl$_2$] was added. These plasmids were digested with DNase I (0.88 unit) at 25 °C for 15 min and the digests were electrophoresed on a 2%-(w/v)-agarose gel. DNA fragments (< 100 bp) were extracted from the gel and recovered in 50 μl of distilled water. The resultant DNase I digests were mixed (total 6.4 μl) and 1.0 μl of 10 × PCR buffer (Takara Shuzo), 1.0 μl of 25 mM MgCl$_2$ and 1.6 μl of dNTP mixture (2.5 mM each) were added The subsequent PCR program used was the same as described above, except that annealing was performed at 45 °C. A portion of this reaction mixture (8.0 μl) was added to 0.2 μl of 10 × PCR buffer, 0.2 μl of 25 mM MgCl$_2$ and 1.6 μl of dNTP mixture, and the PCR was repeated. This extra PCR step was necessary to complete the assembly of the DNA.

PCR amplification of the fragment reassembly products

PCR was carried out using 2.5 μl of the fragment reassembly products using the primers 30BU (5′-CTATGAGAGGATCGCATCACCATCACCATCACGGATCC-3′) and 30PL (5′-CAGGAGTCCAAGCTCAGCTAATTAAGCTTGGCTGCAG-3′), which correspond to the outer region of the *Bam*HI and *Pst*I sites of pQE30 respectively. The PCR products were digested with *Bam*HI and *Pst*I, purified by agarose-gel electrophoresis, then ligated into pQE30 between the *Bam*HI and *Pst*I sites. The recombinant plasmids were transformed into *Escherichia coli* M15[pREP4] (Qiagen) and plated on to Luria–Bertani (LB) agar containing 50 μg/ml ampicillin, 50 μg/ml kanamycin and 0.5% 4-*O*-methyl-D-glucurono-D-xylan–Remazol Brilliant Blue R (RBB-xylan; Sigma). The colonies which were capable of acting on RBB-xylan were picked for screening.

Screening for thermostable chimaeric enzymes

The colonies of recombinant *E. coli* were transferred on to an RBB-xylan plate [0.5% RBB-xylan and 1.5% agar in 0.4 × McIlvaine buffer (1 × McIlvaine buffer is 0.1 M citric acid/0.2 M Na$_2$HPO$_4$), pH 5.7] using toothpicks and the plate was incubated at 60 °C for 1 h The plate was then left overnight at room temperature. 'Successful' colonies were identified by their ability to form a distinct halo in the RBB-xylan-containing agar.

Enzyme production and purification

The recombinant *E. coli* was grown at 37 °C in 100 ml of LB medium containing ampicillin and kanamycin until an attenuance (D_{600}) of 0.7 was reached. A 100 μl portion of 1 M isopropyl 1-thio-β-D-galactoside was added and incubation was continued for a further 5 h. The cells were harvested by centrifugation at 10000 *g* for 15 min and resuspended in 50 mM phosphate buffer, pH 7.0 (5 ml). The cells were sonicated three times for 2 min each time in a Branson model 250D sonifier, and cell debris was removed by centrifugation. The supernatant was subjected to FPLC (Pharmacia Biotech FPLC system) using a column of HiTrap chelating resin charged with Ni^{2+} and equilibrated with 50 mM phosphate buffer, pH 7.0. After application of the enzyme, the column was washed with 50 mM phosphate buffer, pH 7.0, followed by the same phosphate buffer containing 100 mM imidazole. The enzyme was then eluted with 250 mM imidazole in the same phosphate buffer.

Assay of xylanase activity and protein determination

Soluble birchwood xylan (Fluka), prepared as described previously [7], was used in the determination of xylanase activity. Assays were performed in 0.4 × McIlvaine buffer, pH 5.7, containing 5 mg/ml soluble birchwood xylan and 0.1 mg/ml BSA. The pH value of the McIlvaine buffer was confirmed at room temperature After incubation at 50 °C for 30 min, the reducing power released was measured by the Somogyi–Nelson method [8], using D-xylose as the standard. Thermostability was tested by heating enzyme samples (10 ± 2 μg of protein/ml) containing 1.0 mg/ml BSA and 0.4 × McIlvaine buffer, pH 5.7, at 70 °C for various periods of time, then assaying the activity as described above. K_m and k_{cat} values were determined using substrate concentrations ranging from 0.4 to 10 mg/ml xylan. Assays were performed as described above, except that the reaction mixture was incubated for 5 min at 40 °C and the production of reducing sugar was measured by using *p*-hydroxybenzoic acid hydrazide [9] Protein concentration was measured using DC Protein Assay Reagents (Bio-Rad) with BSA as the standard

RESULTS

Construction and screening of chimaeric xylanases

The amino acid sequence similarities of TfxA-cat and SlxB-cat are shown in Figure 1. TfxA-cat and SlxB-cat consist of 189 and 191 amino acid residues respectively, with 148 residues being identical. The recombinant enzymes exhibit the same activity as the native enzymes when soluble xylan is used as the substrate. Both *T. fusca* xylanase A and *S. lividans* xylanase B are known to be composed of a catalytic domain, a binding domain and a linker region [3,10]. It has been reported previously that the removal of the substrate-binding domain from the native enzyme has no effect on the hydrolysis of soluble xylan [3,11]. Both TfxA-cat and SlxB-cat were functionally expressed in *E. coli* and showed similar properties to those reported for the native

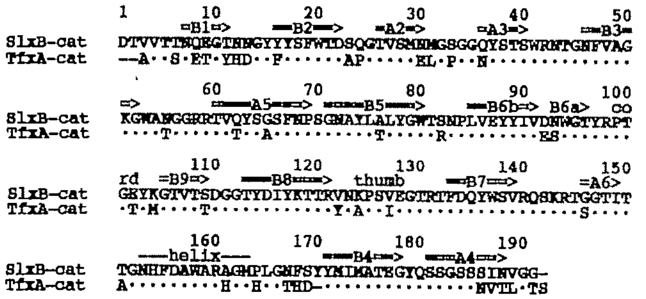
1
10
20
30
40
50
B1
B2
A2
A3
B3
SlxB-cat
TfxA-cat
--A··S·ET·YHD··F······AP·····EL·P··N···············
60
70
80
90
100
A5
B5
B6b
B6a
SlxB-cat
TfxA-cat
····T······T··A···········T·····R··········ES·······
110
120
130
140
150
rd
B9
B8
thumb
B7
A6
SlxB-cat
TfxA-cat
·T·M····T·············Y·A··I···················S····
160
170
180
190
helix
B4
A4
SlxB-cat
TfxA-cat
A··········H··H··THD-··················NVTL·TS

Figure 1 Amino acid sequence comparison of SlxB-cat and TfxA-cat

The SlxB-cat and TfxA-cat genes were amplified by PCR and the amino acid sequences shown were deduced from the nucleotide sequences. The amino acid numbering corresponds to SlxB-cat. The secondary-structure elements (arrows indicate β-strands and dotted lines indicate helices) refer to xylanase XYNII from *T. reesei* [19]. For TfxA-cat, only the amino acids which differ from SlxB-cat are shown.

enzymes [3,4]. Using the random-gene-shuffling technique, the DNA fragments encoding the catalytic domains TfxA-cat and SlxB-cat were used in the construction of a pool of chimaeric xylanase genes. Equimolar mixtures of DNase I digests of TfxA-cat and SlxB-cat genes were reassembled by PCR without primers. The resultant shuffled genes were digested with *Bam*HI and *Pst*I, and inserted into the expression vector pQE30, then transformed into *E. coli* by electroporation. For the selection of a chimaeric enzyme with higher thermostability than SlxB-cat, recombinant *E. coli* colonies produced by the random-gene-shuffling method were placed on to RBB-xylan plates and incubated at 60 °C for 1 h. Theoretically, colonies capable of acting on RBB-xylan after this treatment possessed either the TfxA-cat gene or were thermostable mutants, because these incubation conditions inactivated SlxB-cat. In cases where the recombinant enzyme is not stable at 60 °C, only a small halo, due to residual activity, is produced. A small halo may also indicate low specific activity, even if the enzyme is relatively thermostable at 60 °C. Using this screening method, 18 colonies were selected from a total of 48 colonies as thermostable mutants relative to SlxB-cat.

Sequence analyses of the chimaeric xylanases

The amino acid sequences of the chimaeric xylanases were determined and are shown in Figure 2(A), along with the halo sizes after 1 h incubation at 60 °C. The sequences indicate that DNA shuffling of the TfxA-cat and SlxB-cat genes was successful. From the 18 thermostable colonies, only 15 different chimaeric genes were obtained, since three colonies were found to share identical sequences and also another two colonies were found to

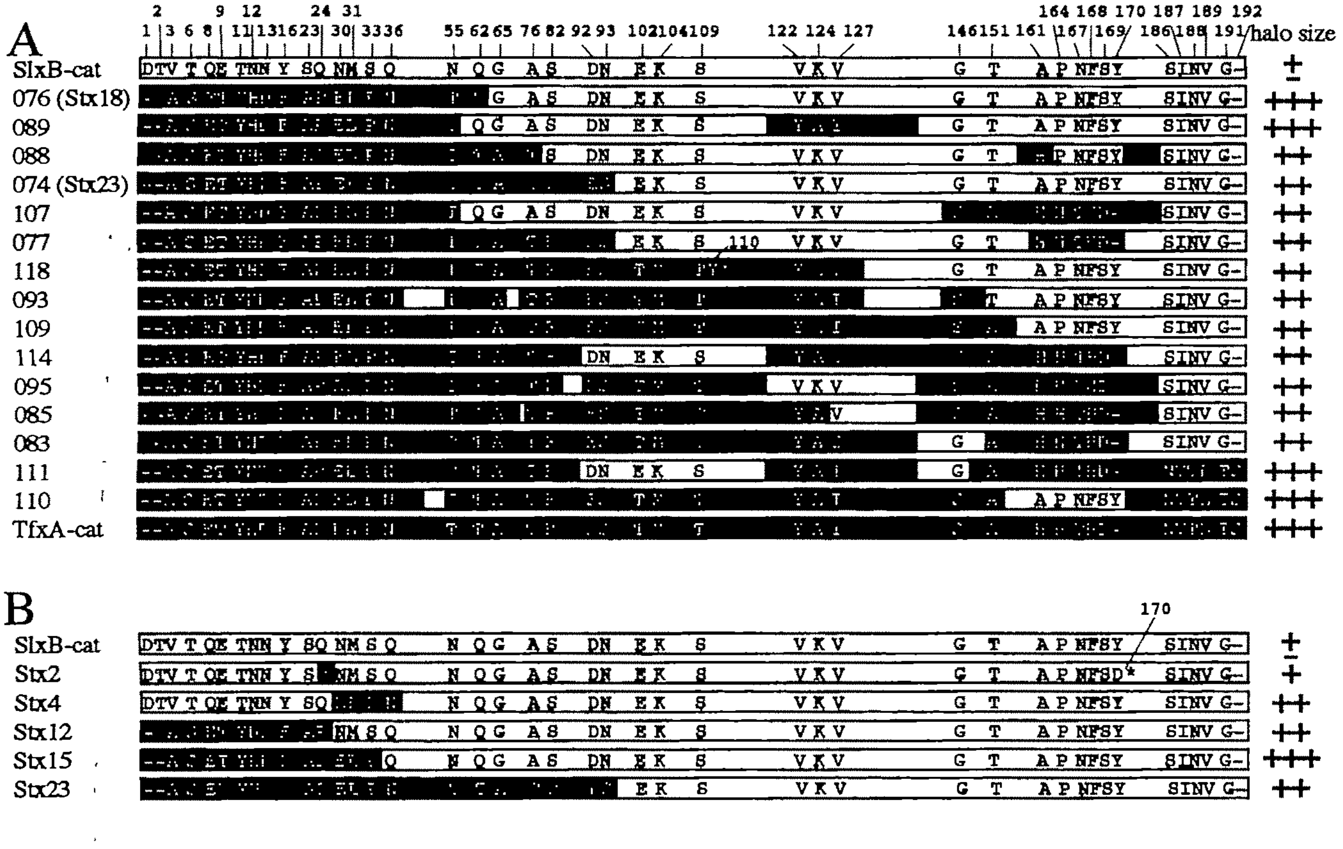

Figure 2 Schematic diagrams of parental and chimaeric enzymes and their residual activities on RBB-xylan plates

(A) DNA shuffling was carried out with an equimolar mixture of the DNase I digests of TfxA-cat and SlxB-cat genes. The colonies of recombinant *E. coli* were transferred on to an RBB-xylan plate. The plate was incubated at 60 °C for 1 h and then left overnight at room temperature. Colonies that were capable of acting on RBB-xylan after this treatment were selected. (B) DNA shuffling and the following screening methods were the same as described above except that SlxB-cat and Stx23 genes were used for the construction of a pool of chimaeric xylanase genes and were mixed in the ratio 3:1. The halo size is indicated as: ±, < 1 mm, +, 1–3 mm, ++, 3–5 mm, +++, > 5 mm. The 43 amino acids different between TfxA-cat and SlxB-cat are shown in the schematic diagrams. An asterisk (*) indicates a mutational change (D110Y and Y170D).

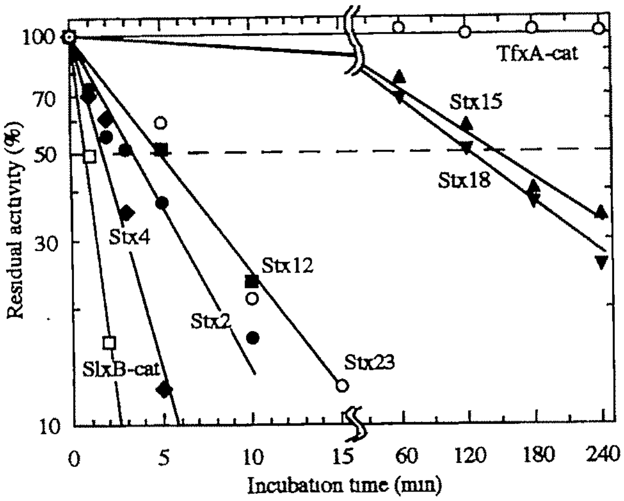

Figure 3 Heat-inactivation time courses of the parental and chimaeric enzymes

The parental and chimaeric enzymes were heated at 70 °C in 0.4 × McIlvaine buffer, pH 5 7, containing 1.0 mg/ml BSA. The residual activity was measured at 50 °C with 5 mg/ml soluble xylan in 0 4 × McIlvaine buffer, pH 5 7

Table 1 Kinetic constants for parental and chimaeric enzymes

Xylanase activities were determined at 40 °C using soluble xylan in 0 4 × McIlvaine buffer, pH 5.7 The concentration of soluble xylan employed ranged from 0 4 to 10 mg/ml

Enzyme	K_m (mg/ml)	k_{cat} (s^{-1})	k_{cat}/K_m
SlxB-cat	1 0	75	75
Stx2	1 9	67	35
Stx4	1 6	86	54
Stx12	1 4	88	63
Stx15	1 2	77	64
Stx18	1 1	77	70
Stx23	1 4	41	29
TfxA-cat	1 8	85	47

share the same sequence. In chimaera 118 a one-point mutation (D110Y) occurred, resulting in the amino acid change of Asp^{110} to Tyr.

All of the selected chimaeric enzymes possessed *N*-terminal regions derived from TfxA-cat, indicating that this segment of TfxA-cat was essential for demonstrating activity under the screening conditions. Although chimaera 076 produced the largest halo, it possessed the smallest number of amino acid substitutions relative to SlxB-cat. Amino acid substitutions in the region between the 50th and 100th amino acid residues appear to affect the size of the halo on the RBB-xylan plate For example, the difference between chimaeras 076 and 074 is due to five additional amino acid residue substitutions from TfxA-cat in chimaera 076, which are located in this region. The halo size produced by chimaera 074 was smaller than that of chimaera 076. By contrast, comparing the sequences of the chimaeric enzymes indicates that the various substitutions occurring between the 100th and the 170th amino acid residues had little effect on the halo size. These observations suggest that amino acid substitutions occurring in the *N*-terminal region are essential for activity at high temperature; however, substitutions in other regions have only minor or negative effects on the formation of haloes under the screening conditions employed.

To obtain additional chimaeric enzymes whose *N*-termini were partially replaced by the corresponding region of TfxA-cat, we constructed a pool of chimaeric genes between SlxB-cat and chimaera 074. DNase I digests of the SlxB-cat and chimaera 074 genes were mixed in a 3·1 ratio to decrease the chance of chimaera 074 reconstructing itself or producing mutants with only minor changes. Four colonies were selected from a total of 290 colonies using the same screening method described above, and the amino acid sequences of the four colonies were determined (Figure 2B). These chimaeric enzymes, namely Stx2, Stx4, Stx12 and Stx15, had one, four, 12 and 15 amino acid substitutions relative to SlxB-cat respectively. Stx2 also had another substitution, Y170D ($Tyr^{170} \rightarrow Asp$), resulting from a point mutation occurring in the PCR step. These four different enzymes were selected for further study, along with chimaeras 076 (Stx18) and 074 (Stx23).

Thermostability

TfxA-cat, SlxB-cat and the six chimaeric enzymes were purified to homogeneity by SDS/PAGE (results not shown) using a nickel-chelating FPLC column. The residual activities of these enzymes after heating at 70 °C are shown in Figure 3. TfxA-cat was stable at 70 °C, even after incubation for 240 min, in contrast with SlxB-cat, which lost 50 % of its activity after only 1 min. All of the six selected chimaeric enzymes were more stable than SlxB-cat. Stx2 exhibited 50 % of its initial activity after 3 min incubation at 70 °C, indicating that having only two amino acid substitutions relative to SlxB-cat increased the half-life of the enzyme three-fold. Stx4, having four amino acid substitutions relative to SlxB-cat, also displayed an increase in half-life under these conditions. Significant improvements in thermostability were achieved by Stx15 and Stx18, as they displayed half-lives of about 120 min. Stx12 and Stx23 also showed an improvement in thermostability, but the half-lives of these mutants were far less than those of Stx15 and Stx18.

Reducing-sugar productivity from soluble xylan

Kinetic constants for the parental and chimaeric enzymes are shown in Table 1. The k_{cat}/K_m values obtained for the Stx4, Stx12, Stx15 and Stx18 were intermediate between those of SlxB-cat and TfxA-cat, indicating that these mutants were as functional as the parent enzymes in performing the hydrolysis of xylan. In contrast, k_{cat}/K_m values for Stx2 and Stx23 were lower than the values for the parent enzymes. Both the K_m and k_{cat} values for Stx2 were inferior to the values obtained for the parent enzymes. The K_m value for Stx23 was not significantly different from that of the parent enzymes, but the k_{cat} value was about half that of the parent values.

The xylan-hydrolyzing activities of the chimaeric enzymes were determined at various temperatures and the results compared with those of the parent enzymes (Figure 4). Improvement in the thermostability of Stx4, Stx12, Stx15 and Stx18 was paralleled by an increase in the production of reducing sugar at elevated temperatures Stx4 and Stx12 were most active at 65 °C, 10 °C higher than the optimal temperature of SlxB-cat. It is noteworthy that Stx4 was significantly more active at 65 °C than SlxB-cat, and this difference is due to only four amino acid

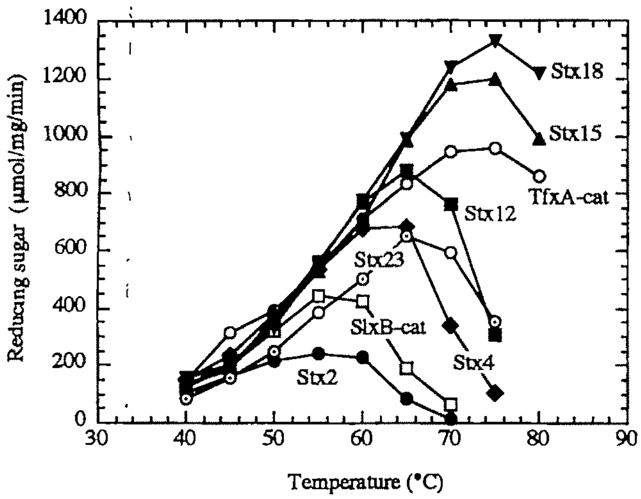

Figure 4 Reducing-sugar productivity of parental and chimaeric enzymes

Enzyme reactions were performed in 0.4 × McIlvaine buffer, pH 5.7, containing 0.1 mg/ml BSA. The data plotted are averages for three independent experiments.

substitutions. Stx15 and Stx18 exhibited maximal activity at 75 °C, which was 20 °C higher than displayed by SlxB-cat and was equal to that of TfxA-cat. Remarkably, Stx18 produced 1.4 times more reducing sugar than TfxA-cat at 75 °C, although SlxB-cat was inactivated at this temperature. For these four chimaeric enzymes (Stx4, Stx12, Stx15 and Stx18), the enhanced thermostability contributed to an increase in reducing-sugar production at elevated temperatures. Stx23 also exhibited a rise in the observed optimum temperature (65 °C); however, it was less active than the above four chimaeric enzymes when compared at 65 °C. Stx2, which was more stable than SlxB-cat at 70 °C, did not demonstrate an increase in the optimum temperature and showed poor reducing-sugar productivity compared with SlxB-cat. These results indicate that even if a mutant displays good residual activity after heating, it is not necessarily enzymically functional at that temperature.

DISCUSSION

Two thermostable family-11 xylanases were crystallized and structural contributions to their stabilities were predicted. The crystallographic structure of *Bacillus* D3 xylanase revealed that surface aromatic residues form hydrophobic clusters between molecules [12]. These intermolecular hydrophobic contacts induce aggregation at high protein concentrations and may contribute to the thermostability of the xylanase. The crystal structure of the thermostable xylanase from *Thermomyces lanuginosus*, a thermophilic fungus, has been also described [13]. Its thermostability was ascribed to an extra disulphide bridge and ion-pair interactions throughout the protein.

Attempts to improve the thermostability of family-11 xylanases have previously been reported [14,15], but have been only partly successful. These results showed that the increase in residual activity observed after heating does not always contribute to activity at high temperatures. Although the mutants were thermostable compared with the wild-type, they were less active at low temperatures. It is common for significant conformational changes to occur in enzymes during catalysis [16]. The conformational changes occurring in xylanase from *Trichoderma reesei* were studied on the basis of crystal structure [17,18]. Structural changes led to the opening and closing of the active site, and this probably plays a role in the function of the enzyme. Therefore amino acid substitution which enhances the thermostability of an enzyme may often change its molecular structure, causing a deterioration in the enzyme activity observed.

To facilitate an understanding of the contribution of structure to the thermostability, we constructed the chimaeric enzymes of TfxA-cat and SlxB-cat by random gene shuffling. Chimaeric and parental enzymes used in this study were purified to homogeneity on SDS/PAGE and the activity that is seen is directly comparable with that of the parental enzyme. As shown in Table 1, the k_{cat} values for the purified chimaeric enzymes were close to that of the parental enzymes, except for Stx23, indicating that these mutants were as functional as the parental enzymes.

In the present study we revealed that the *N*-terminus of TfxA-cat contributes to thermostability. Stx2, which has two amino acid substitutions, Q24P ($Gln^{24} \rightarrow Pro$) and Y170D, showed an enhancement in thermostability at 70 °C. Of the two amino acid substitutions, Q24P must be responsible for the enhancement of the thermostability, because it was found in all thermostable chimaeric enzymes in the present study, except for Stx4 (Figure 2). Pro^{24} is thought to be located between two β-strands, B2 and A2 [13,19], and seems likely to contribute to structural stability by reducing the entropy of the unfolded state [20]. Stx4, which consists of four amino acid substitutions relative to SlxB-cat, also displayed an enhancement in thermostability. Pro^{33}, which is located in the loop between β-strands A2 and A3 [13,19], is also thought to participate in the stabilization of the enzyme in a similar manner to Pro^{24}. Enhancement of the stabilities for Stx2 and Stx4 were, however, relatively small compared with the enhancements observed in chimaeras Stx15 and Stx18, indicating that proline substitution is only a minor factor in the stabilization of the enzyme.

Significant improvement in thermostability was achieved in Stx15 and Stx18. Stx15 has 13 amino acid substitutions and two eliminations, and can be regarded as a double mutant of chimaeras Stx12 and Stx4 (Figure 2). However, the half-life of Stx15 at 70 °C was much longer than those of Stx12 and Stx4 (Figure 3), indicating that there are other, additional, major stabilizing factors present between the substituted residues in Stx12 and Stx4. Of the 13 residues, 11, namely Ala^{3}, Ser^{6}, Glu^{8}, Thr^{9}, Tyr^{11}, His^{12}, Asp^{13}, Phe^{16}, Glu^{30}, Leu^{31} and Pro^{33}, are predicted to be closely located around the *N*-terminus. Therefore it is likely that these residues are involved in the structural stability of the *N*-terminal region, resulting in a significant increase in the half-life of enzymes containing these residues. The *N*-terminal sequence of *Cellulomonas fimi* xylanase D, another thermostable enzyme from xylanase family 11, is similar to that of TfxA-cat [21]. This also lends support to the importance of this region to thermostability. However, further analysis is required to determine the exact contributions of the *N*-terminal residues to the structural stabilization of xylanases.

For soluble xylan, the K_m value for SlxB-cat was 1.0 mg/ml, which is far less than that observed for TfxA-cat (1.8 mg/ml), although the k_{cat} values for SlxB-cat and TfxA-cat were similar (75 and 85 s^{-1}; Table 1). Stx15 and Stx18 displayed K_m values of 1.1 and 1.2 mg/ml respectively and k_{cat} values of 77 s^{-1} (Table 1). These results indicate that the catalytic capacities of Stx15 and Stx18 are similar to those observed for SlxB-cat. Therefore it can be said that Stx15 and Stx18 inherit their thermostability from TfxA-cat and their catalytic efficiency from SlxB-cat, resulting in an observed increase in reducing-sugar productivity at high temperatures.

Our results suggest that random shuffling between a mesophilic and a thermophilic enzyme is an effective approach for combining the activity and the stability from each of the parental enzymes. In general, the evolutionary-design approach produces an increase in the thermostability of a mesophilic enzyme far more readily than a rational approach [22]. In addition, the use of naturally occurring sequences increases the functional sequence diversity of the chimaeric library, allowing rapid searching of a large sequence space [23]. When a mesophilic and a thermophilic homologue are available as the starting genetic material, DNA shuffling of these enzymes is thought to be a facile approach for increasing the thermostability of the mesophilic enzyme without cost to its activity.

We are grateful for the presubmission editorial assistance of Dr Joanne B Hart in the preparation of this manuscript We also thank Ms Setsuko Koyana for her technical support throughout this work. This research was supported in part by a grant from the Program for Promotion of Basic Research Activities for Innovation Biosciences and Rice Genome Project PR-2208, Ministry of Agriculture, Forestry and Fisheries, Japan

REFERENCES

1 Henrissat, B (1991) Biochem J **280**, 309–316
2 Viikari, L, Kantelinen, A, Sundquist, J. and Linko, M (1994) FEMS Microbiol Rev **13**, 335–350
3 Irwin, D, Jung, E D and Wilson, D B (1994) Appl Environ Microbiol **60**, 763–770
4 Kluepfel, D., Vats-Mehta, S, Aumont, F., Shareck, F and Morosoli, R. (1990) Biochem. J. **267**, 45–50
5 Smith, G P (1994) Nature (London) **370**, 324–325
6 Stemmer, W. P C (1994) Nature (London) **370**, 389–390
7 Dupont, C, Roberge, M., Shareck, F., Morosoli, R and Kluepfel, D (1998) Biochem J **330**, 41–45
8 Somogyi, M (1952) J. Biol Chem **195**, 19–23
9 Lever, M. (1972) Anal Biochem **47**, 273–279
10 Shareck, F, Roy, C, Yaguchi, M, Morosoli, R and Kluepfel, D. (1991) Gene **107**, 75–82
11 Kaneko, S, Kuno, A, Muramatsu, M, Iwamatsu, S, Kusakabe, I and Hayashi, K (2000) Biosci. Biotechnol Biochem **64**, 447–451
12 Harris, G W, Pickersgill, R. W, Connerton, I, Debeire, P., Touzel, J P., Breton, C and Pérez, S (1997) Proteins **29**, 77–86
13 Gruber, K, Klintschar, G., Hayn, M, Schlacher, A, Steiner, W and Kratky, C (1998) Biochemistry **37**, 13475–13485
14 Arase, A, Yomo, T, Urabe, I, Hata, Y, Katsube, Y and Okada, H. (1993) FEBS Lett **316**, 123–127
15 Wakarchuk, W. W, Sung, W L, Campbell, R. L, Cunningham, A, Watson, D C and Yaguchi, M. (1994) Protein Eng **7**, 1379–1386
16 Gerstein, M, Lesk, A and Chothia, C (1994) Biochemistry **33**, 6739–6749
17 Havukainen, R, Torronen, A., Laitinen, T and Rouvinen, J (1996) Biochemistry **35**, 9617–9624
18 Muilu, J, Torronen, A, Perakyla, M and Rouvinen, J (1998) Proteins Struct Funct Genet **31**, 434–444
19 Torronen, A and Rouvinen, J. (1997) J Biotechnol **57**, 137–149
20 Schimmel, P R and Flory, P J (1968) J Mol Biol **34**, 105–120
21 Millward-Sadler, S J, Poole, D M, Henrissat, B, Hazlewood, G P, Clarke, J. H and Gilbert, H J. (1994) Mol Microbiol. **11**, 375–382
22 Arnold, F H (1998) Proc Natl Acad Sci U S A **95**, 2035–2036
23 Crameri, A, Raillard, S A, Bermudez, E. and Stemmer, W. P. C (1998) Nature (London) **391**, 288–291

Received 25 October 1999/4 April 2000, accepted 10 May 2000

Essential Reading
from Portland Press

Portland Press

The Biology of Nitric Oxide Part 7

Edited by S Moncada, Cruciform Project, London, UK, L Gustafsson, Karolinska Institute, Stockholm, Sweden, P Wiklund, Karolinska Hospital, Stockholm, Sweden and EA Higgs, Cruciform Project, London, UK

1 85578 142 5 Hardback March 2000 400 pages £110 00

The proceedings of the *Sixth International Meeting on the Biology of Nitric Oxide* held at Stockholm, Sweden on 5-8 September 1999.

This book provides an up-to-date overview of the current status of the field with contributions from over 400 specialists covering the following areas:

Molecular Biology, Biochemistry, Physiology, Pathophysiology, Inflammation, Tumours, Apoptosis, Novel Compounds and Clinical Aspects.

Nitric Oxide and the Peripheral Nervous System

Edited by N Toda, Shiga University of Medical Science, Ohtsu, Japan, S Moncada, Cruciform Project, London, UK, R Furchgott, State University of New York, USA and EA Higgs, Cruciform Project, London, UK

1 85578 139 5 Hardback June 2000 200 pages £85 00

This volume provides an overview of NO in the peripheral nervous system, covering aspects ranging from the molecular biology and distribution of neuronal nitric oxide synthase, through the physiological and pathophysiological roles of NO in various nitrergic systems (systems of nerves whose transmitter function depends on the release of NO).

Potential therapies that may arise from our increasing knowledge of this fascinating field of research are also reviewed.

Eicosanoids and Related Compounds in Plants and Animals

Edited by AF Rowley, University of Wales, Swansea, UK, H Kühn, Humboldt University of Berlin, Germany, and T Schewe, Free University of Berlin, Germany

1 85578 108 5 Hardback October 1998 240 pages £65 00

This book provides an up-to-date overview of the nature, modes of biosynthesis, and functions of eicosanoids and related compounds in plants and animals.

This volume draws together, for the first time, overviews describing the importance of eicosanoids in plants and animals. No other volume has attempted to consolidate such a diverse approach in a single volume. The uniformity of presentation is an unusual feature with the volume divided into two main sections: biochemical and functional sections. The first section deals with the diversity of eicosanoids generated and the nature of the enzymes and other factors associated with their biosynthesis. The second deals largely with the more functional aspects of eicosanoids. The volume should be of great interest to researchers in diverse fields including lipid biochemistry, molecular evolution, plant and animal physiology, and general biology.

Landmarks in Intracellular Signalling

Edited by RD Burgoyne and OH Petersen, University of Liverpool, UK

1 85578 101 8 Paperback 1997 278 pages £20 00

The idea behind Landmarks in Intracellular Signalling is to provide full reproductions of a set of key papers which have been chosen as landmark papers in the various aspects of intracelllular signalling. The selected papers have all resulted in significant advances in one or other aspect of intracellular signalling.

Readers of *Landmarks in Intracellular Signalling* will now have easy, ready available access to the original literature from one source. The papers are accompanied by commentaries that describe why the papers were significant, how the work came about and summarize the advances that have been made up to the present time as a consequence of the original paper.

Orders:
www.portlandpress.co.uk/books/orderinfo.htm

Portland Press, Commerce Way,
Colchester, CO2 8HP
t: 01206 796351
f: 01206 799331
e: sales@portlandpress.co.uk

Please add £2.50 per book
to a maximum of £7.50

In the USA and Canada
Princeton University Press
c/o California/Princeton Fulfillment
Services, Inc
1445 Lower Ferry Road,
Ewing, New Jersey 08618
t: 1-800-777-4726
f: 1-800-999-1958
e: orders@cpfs.pupress.princeton.edu

Postage: Please add $3.75 for first
book and US$1.00 for each
additional book

BAT/0500/F

The Bad Company

PHOSPHORYLATION
STATE-SPECIFIC ANTIBODIES

Determination of the phosphorylation state of individual signaling proteins is the next basic requirement for the study of cell signaling. Phospho peptide-directed antibodies report the phosphorylation state of serine, threonine or tyrosine in the context of a defined sequence of flanking amino acids. Positional specificity for defined phosphorylation motifs affords functional insights into signaling activities.

pAdducin
pAkt
pATF
pBad
pCaMK
pCREB
pEGF-R
perb B-2
pFAK
pFGF-R
pGluR
pGSK-3
pHistone
pHSP 27
pFKHRL1
pJAK-2
pJun
pKip
pLeptin-R
pMAPK
pMBP
pNR1
pPDGF-R
pPhospholamban
pPKC
pPP2A
pRaf1
pRsk 1
p(p70) S6 Kinase
pSKK
pSmad
pSrc

upstate
biotechnology
an Argonex Company

10 Old Barn Road • Lake Placid, NY 12946
800-233-3991 / www.upstatebiotech.com

[illegible]

Printed in Great Britain by the University Press, Cambridge